UNCLASSIFIED

AD NUMBER

AD006841

NEW LIMITATION CHANGE

TO

Approved for public release, distribution unlimited

FROM

Distribution authorized to U.S. Gov't. agencies and their contractors; Administrative/Operational Use; Sep 1950. Other requests shall be referred to the Office of Naval Research, 800 North Quincy Street, Arlington, VA 22217-5660.

AUTHORITY

ONR ltr, 4 Sep 2003

THIS PAGE IS UNCLASSIFIED

Reproduced by
Armed Se s Technical Information Agenc
IT SERVICE CENTER
BUILDING, DAYTON, 2, OHIO

AD-

6841

UNCLASSIFIED

Reproduced

FROM

LOW CONTRAST COPY.

ORIGINAL DOCUMENTS

MAY BE OBTAINED ON

LOAN

FROM

ARMED SERVICES TECHNICAL INFORMATION AGENCY
DOCUMENT SERVICE CENTER
U.B. BUILDING, DAYTON, 2, OHIO

PART OF THIS DOCUMENT NOT REPRODUCIBLE

UNDERWATER EXPLOSION RESEARCH

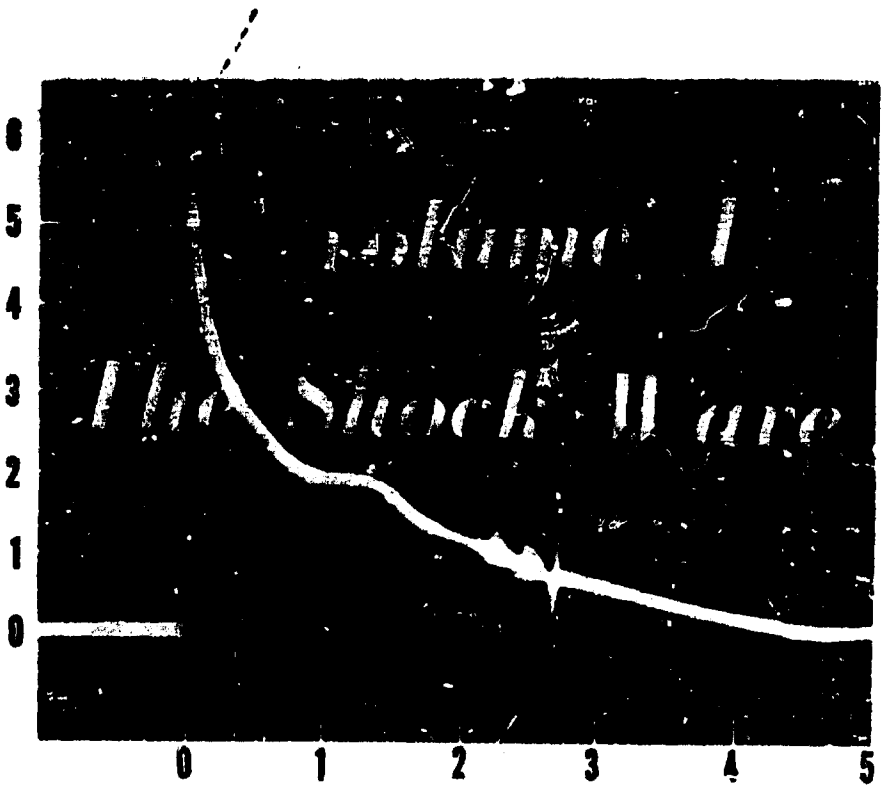
VOLUME I - THE SHOCK WAVE

OFFICE OF NAVAL RESEARCH - DEPARTMENT OF THE NAVY

NAVAL UNDERWATER EXPLOSION RESEARCH

A COMPENDIUM OF BRITISH AND AMERICAN REPORTS

1950



Best Available Copy

OFFICE OF NAVAL RESEARCH ★ DEPARTMENT OF THE NAVY

British Crown Copyright reserved. Reproduced with the permission of the Controller of His Britannic Majesty's Stationery Office.

Best Available Copy

Bibliography

Most of the papers in this volume contain references to further work, some of which may be included within this Compendium. Properly qualified persons may obtain additional references or material on application to the following establishments:

1. Secretary, Undex Sub-Panel
   Naval Construction Research Establishment
   Rosyth
   Fife
   Scotland

2. Chief of Naval Research
   c/o Navy Research Section
   Library of Congress
   Washington 25, D. C.

3. The Director
   David W. Taylor Model Basin
   Carderock, Maryland

4. The Commander
   U. S. Naval Ordnance Laboratory
   White Oak, Maryland

Best Available Copy

PREFACE

During the recent war there arose on both sides of the Atlantic among research workers in the field of underwater explosions the feeling that some of the problems posed by the conditions of undersea warfare had already presented themselves in the past and that various attempts had been made to solve them. Many of the records, however, had been lost or effectively hidden except for what had crept into open publications and consequently a whole new literature had to be developed at considerable cost in both time and money, encompassing both old and new problems. A corollary of this experience has been the firm conviction that this new literature should not suffer a similar fate. The idea of the joint publication of American and British research in the field of underwater explosions took form in the latter part of 1946 and the idea was further explored with the Bureau of Ordnance and the Bureau of Ships, United States Navy Department and with the British Admiralty. The Office of Naval Research, Navy Department, in its capacity of disseminator of scientific information undertook to sponsor the publication and has eventually seen the project through to its present form.

The Compendium has three major purposes: first, to give a greater availability to many papers which otherwise would exist in a very small number of copies, and to preserve and revive certain rare items, the scarcity of which was due to wartime shortages rather than to any deficiencies in the papers themselves; second, to present a representative summary of original source material and to display the scope of this material in a manner which might make it of more universal interest to schools and colleges as a branch of applied science; and third, to stimulate interest in this field for the general benefit of the sciences of Naval Architecture and Naval Ordnance and to provide those working in these fields with ready reference material on many of the important problems which they must face in their work.

The scheme of the Compendium is as follows: All of the papers selected, which represent between 10 and 20 percent of the total quantity of material known to exist, have been divided into three volumes. The first volume is devoted to the primary underwater shock wave, the second to the hydrodynamical effects falling under incompressible theory including the oscillations and behaviour of the gas globe formed by the explosion products, and the third to the effects of all of these phenomena on structures and to the measurement and calculation of the resulting damage. Three papers have been selected with the object of summarizing the knowledge over the field within the scope of the Compendium; these papers, which are placed in the first volume, serve to introduce the subject both in general terms, and also with some mathematical detail.

The allocation of the original papers to the different volumes has, in a few cases, not been obvious and the editors must assume full responsibility for any arbitrary assignments. A far greater responsibility of the editors has lain in the selection of the papers and in this, various considerations have had a voice.

Many of the older papers have been included for their historical interest. Some papers have been used to provide suitable introductory or background material. Most of the other papers have been included intact and represent the opinions of the authors at the time of writing. A few of the papers have been reworked and consist of new material incorporated into the older original papers, or consist of a summary of several progress reports which were too repetitive for economical inclusion without condensation. Papers which have been rewritten are so marked with the new date affixed. In general, selections have been made in an effort to give the best review of the entire subject in order to convey the most, and the best information within the space limitations imposed by the exigencies of publication, and within the scope permitted by considerations of security. Both these features prevent this compilation from being exhaustive, and the latter feature prevents many successful workers in this field from receiving recognition here.

The editors believe that this Compendium is a new venture in international co-operation and hope that this effort may prove useful in pointing the way for other similar joint enterprises which may be considered desirable.

Best Available Copy

It is our desire to acknowledge the continued interest of Dr. A. T. Waterman, Deputy Chief, Office of Naval Research, Navy Department, without whose help these volumes could not have been produced, to thank Mr. Martin Jansson of the Technical Information Division, Office of Naval Research, and his capable staff for their painstaking and careful work in preparing the material for reproduction. We also acknowledge the guidance afforded by the British Undex Panel, particularly Dr. A. R. Bryant and Dr. E. N. Fox (a former member), the assistance of Mr. T. Aves of the Department of Research Programmes & Planning and Miss E. Lord of the Department of Physical Research in the preparation of the British contribution, and to thank Dr. T. L. Brownyard of the Bureau of Ordnance Navy Department for his help in some of the correspondence and in some of the problems of security clearance.

G. K. Hartmann
Chief, Explosives Research Department
U. S. Naval Ordnance Laboratory.

E. G. Hill
Department of Physical Research
Admiralty

TABLE OF CONTENTS

VOLUME I

THE SHOCK WAVE

Page

Preface v

SUMMARY PAPERS

A REVIEW OF UNDERWATER EXPLOSION PHENOMENA (B)*
E. N. Fox, Cambridge University 1

EXPERIMENTS ON THE PRESSURE WAVE THROWN OUT BY SUBMARINE EXPLOSIONS (B)
H. W. Hilliar, Admiralty Experimental Station 85

REPORT ON UNDERWATER EXPLOSIONS (A)*
E. H. Kennard, David W. Taylor Model Basin 159

DETONATION THEORY

THE HYDRODYNAMIC THEORY OF DETONATION AND SHOCK WAVES (A)
G. B. Kistiakowsky, E. Bright Wilson, Jr., Harvard University; R. S. Halford, Columbia University 209

NOTE ON THE LATERAL EXPANSION BEHIND A DETONATION WAVE (B)
G. I. Taylor and M. Jones, Cambridge University 263

PROPAGATION THEORY

THE PRESSURE-TIME CURVE FOR UNDERWATER EXPLOSIONS (B)
W. G. Penney, Imperial College, London 273

PRESSURE-TIME CURVES FOR SUB-MARINE EXPLOSIONS (SECOND PAPER) (B)
W. G. Penney and H. K. Dasgupta, Imperial College, London 289

AN APPROXIMATE CALCULATION OF THE PRESSURES PRODUCED BY DETONATING LINE CHARGES UNDERWATER (B)
G. Charlesworth and A. R. Bryant, Road Research Laboratory, London 301

PROPOSAL AND ANALYSIS OF A NEW NUMERICAL METHOD FOR THE TREATMENT OF HYDRODYNAMICAL SHOCK PROBLEMS (A)
John Von Neumann, Institute of Advanced Study, Princeton, N. J. 311

CALCULATION FROM THERMODYNAMICAL AND HYDRODYNAMICAL CONSIDERATIONS OF UNDERWATER SHOCK-WAVES FOR SPHERICAL CHARGES (B)
H. N. V. Temperley and J. Craig, Admiralty Undex Works, Rosyth, Scotland 347

HYDRODYNAMIC PROPERTIES OF SEA WATER AT THE FRONT OF A SHOCK WAVE (A)
J. M. Richardson, Cornell University, N. Y.; A. B. Arons, and R. R. Halverson, Underwater Explosives Research Laboratory, Woods Hole Oceanographic Institution . 373

* (A) American Contribution
(B) British Contribution

Page

THEORY OF THE SHOCK WAVE PRODUCED BY AN UNDERWATER EXPLOSION (A)
Stuart R. Brinkley, Jr., Bureau of Mines, Department of the Interior; John G. Kirkwood, California Institute of Technology 383

EXPERIMENTAL TECHNIQUES - ELECTRICAL

NATURE OF THE PRESSURE IMPULSE PRODUCED BY THE DETONATION OF EXPLOSIVES UNDER WATER. AN INVESTIGATION BY THE PIEZO-ELECTRIC CATHODE-RAY OSCILLOGRAPH METHOD (B)
A. B. Wood, Admiralty Research Laboratory 497

A MEASUREMENT OF THE PRESSURE CLOSE TO AN EXPLOSIVE UNDER WATER (B)
G. I. Taylor and R. M. Davies, Cambridge University 549

INSTRUMENTATION FOR THE MEASUREMENT OF UNDERWATER EXPLOSION PRESSURES (A)
M. A. Greenfield and M. M. Shapiro, David W. Taylor Model Basin 563

THE ELECTRIC POTENTIALS PRODUCED IN THE CONDUCTORS OF A SUBMERGED CABLE BY UNDERWATER EXPLOSIONS (B)
A. H. Bebb and R. V. Bundy, Naval Construction Research Establishment, Rosyth, Scotland 623

ELECTRICAL INSTRUMENTS FOR STUDY OF UNDERWATER EXPLOSIONS AND OTHER TRANSIENT PHENOMENA (A)
R. H. Cole, David Stacey, and R. M. Brown, Underwater Explosives Research Laboratory, Woods Hole Oceanographic Institution 635

THE MEASUREMENT OF UNDERWATER EXPLOSIONS FROM SERVICE WEAPONS AT THE UNDERWATER EXPLOSIVES RESEARCH LABORATORY (A)
J. S. Coles, Underwater Explosives Research Laboratory, Woods Hole Oceanographic Institution 703

PIEZO-ELECTRIC GAUGES - DEVELOPMENT OF THE MINIATURE TYPE (B)
A. H. Bebb, D. R. J. Wallace, and D. W. Taylor, Naval Construction Research Establishment, Rosyth, Scotland 799

DESIGN AND USE OF PIEZOELECTRIC GAUGES FOR MEASUREMENT OF LARGE TRANSIENT PRESSURES (A)
A. B. Arons and R. H. Cole, Underwater Explosives Research Laboratory, Woods Hole Oceanographic Institution 831

A STUDY OF PIEZOELECTRIC GAUGE CABLE TERMINATION (A)
Otto Meier, Jr., Naval Ordnance Laboratory 839

EXPERIMENTAL TECHNIQUES - MECHANICAL

THE THEORY OF PISTON GAUGES (A)
K. Finkelstein, Bureau of Ordnance, Navy Department 859

RESPONSE OF THE BALL CRUSHER GAUGE TO VARIOUS DRIVING FUNCTIONS (A)
A. B. Arons, Underwater Explosives Research Laboratory, Woods Hole Oceanographic Institution 907

Page

EXPERIMENTAL TECHNIQUES - OPTICAL

NOTE ON THE WATER FORMATION PRODUCED BY AN UNDERWATER EXPLOSION ON THE MODEL SCALE (B)
A. J. Harris, Road Research Laboratory, London 935

TRANSMISSION OF A SHOCKWAVE FROM WATER TO AIR AT NORMAL INCIDENCE (B)
A. J. Harris, Road Research Laboratory, London 943

THEORY OF PEAK PRESSURE AND TIME CONSTANT DETERMINATION FOR SHOCK WAVES BY THE METHOD OF OPTICAL DISTORTION (A)
R. R. Halverson, Underwater Explosives Research Laboratory, Woods Hole Oceanographic Institution 947

PHOTOGRAPHY OF UNDERWATER EXPLOSIONS, I (A)
J. E. Eldridge, P. M. Fye, and R. W. Spitzer, Underwater Explosives Research Laboratory, Woods Hole Oceanographic Institution 969

EXPERIMENTAL MEASUREMENTS

THE DECAY OF PLANE, CYLINDRICAL AND SPHERICAL SHOCK WAVES (B)
A. J. Harris, Road Research Laboratory, London 1053

PRESSURES PRODUCED BY THE UNDERWATER EXPLOSION OF LINE CHARGES (B)
G. Charlesworth, Road Research Laboratory, London 1057

DECAY OF SHOCK WAVES IN WATER (B)
A. J. Harris, Road Research Laboratory, London 1065

MEASUREMENT OF THE SHOCK-WAVE VELOCITY IN AIR ABOVE A WATER SURFACE, DUE TO THE DETONATION OF A SUBMERGED CHARGE (B)
D. Croney and R. D. Davies, Road Research Laboratory, London 1069

MEASUREMENT OF THE SHOCK-WAVE VELOCITY IN AIR ABOVE A WATER SURFACE DUE TO THE DETONATION OF 16-LB. SPHERICAL CHARGES OF T.N.T. (B)
D. Croney, Road Research Laboratory, Lonoon 1073

SHOCK-WAVE PARAMETERS FROM SPHERICAL TNT CHARGES DETONATED UNDER WATER (A)
J. S. Coles, E. A. Christian, J. P. Slifko, C. R. Niffenegger, and M. A. Rogers, Underwater Explosives Research Laboratory, Woods Hole Oceanographic Institution . 1095

SHOCK-WAVE PARAMETERS MEASURED OFF THE ENDS AND PERPENDICULAR BISECTOR OF LINE CHARGES 25 FT. LONG CONTAINING 50 LB. OF FLEXE. TNT (A)
J. S. Coles, R. H. Cole, P. C. Cross, J. P. Slifko, C. R. Niffenegger, A. E. Christian, and M. A. Rogers, Underwater Explosives Research Laboratory, Woods Hole Oceanographic Institution 1107

ENERGY PARTITION IN UNDERWATER EXPLOSION PHENOMENA (A)
A. B. Arons and D. R. Yennie, Underwater Explosives Research Laboratory Woods Hole Oceanographic Institution 1137

Page

SHOCK INTERACTIONS

THE PRESSURE AND IMPULSE OF SUBMARINE EXPLOSION WAVES ON PLATES (B)
G. I. Taylor, Cambridge University 1155

THE REFLECTION OF A SPHERICAL WAVE FROM AN INFINITE PLATE (B)
E. N. Fox, Admiralty Undex Works, Rosyth, Scotland 1175

THE EFFECT OF STRATIFICATION OF SEA-WATER ON THE PROPAGATION OF AN EXPLOSION PULSE (B)
H. N. V. Temperley, Admiralty Undex Works, Rosyth, Scotland 1189

MEASUREMENTS ON PRESSURE WAVES IN REGION OF TWO OBLIQUELY INTERSECTING UNDERWATER SHOCK WAVES (A)
A. M. Shanes, Underwater Explosives Research Laboratory, Woods Hole Oceanographic Institution 1197

THE MULTIPLE CHARGE EFFECT (B)
A. G. Booker and C. Harrington, Mine Design Department, Admiralty 1211

THE MULTIPLE CHARGE EFFECT, PART III (B)
A. G. Booker and C. Harrington, Mine Design Department, Admiralty 1221

THE NORMAL REFLECTION OF A SHOCK WAVE (A)
R. Finkelstein, Bureau of Ordnance, Navy Department 1247

INTERACTION OF SHOCK-WAVES IN WATER-LIKE SUBSTANCES (A)
H. Polachek and R. J. Seeger, Bureau of Ordnance, Navy Department 1269

THE REFLECTION OF SMALL-CHARGE SHOCK WAVES FROM A FREE SURFACE (A)
G. M. Sokol, Underwater Explosives Research Laboratory, Woods Hole Oceanographic Institution 1389

BOUNDARY OF DISTURBANCE FOR NON-LINEAR REFLECTION OF UNDERWATER SHOCK WAVES AT A FREE SURFACE (A)
Alfred H. Keil, Underwater Explosions Research Unit, Norfolk Naval Shipyard 1423

LONG RANGE SHOCK PROPAGATION IN UNDERWATER EXPLOSION PHENOMENA II (A)
A. B. Arons, D. R. Yennie, and T. P. Cotter, Jr., Underwater Explosives Research Laboratory, Woods Hole Oceanographic Institution, ... 1473

INDEX OF AUTHORS
. 1585

A REVIEW OF UNDERWATER EXPLOSION PHENOMENA

E. N. Fox
Cambridge University

British Contribution

1947

This review was originally prepared in the light of knowledge on the subject at the end of World War II. During the course of publication certain sections (distinguished by an asterisk to the paragraph number) have been amended or inserted, at the suggestion of W. G. Penney, to take account of some of the more recent advances in knowledge.

LIST OF CONTENTS

INTRODUCTION

	Para.
Resolution of the damage problem	1

PHENOMENA IN OPEN WATER

The general sequence of events	5
The pressure pulse	12
Variation of pressure with time and distance	12
Variation of pressure with time (distance constant)	13
Variation of pressure with distance (time constant)	15
Particle velocity	18
Impulse per unit area	19
Energy associated with the pressure pulse	20
Empirical data for the pressure pulse	22
Effects of finite amplitude of the pulse	35
Reflection of pulse at the sea surface	39
Reflection of pulse at the sea-bed	48
Charge well away from sea-bed	50
Charge on sea-bed	56
The gas bubble	62
Oscillation and rise of bubble in mid-water	62
Behaviour of bubble near free and rigid surfaces	69
Motion of bubble near sea surface	71
Motion of bubble near sea-bed	72
Visible surface phenomena	74
Spray dome	75
The plume	81

INTERACTION BETWEEN TARGET AND WATER PHENOMENA DUE TO NON-CONTACT EXPLOSIONS

Pressure pulse incident on infinite plane air-backed plate	85
Water sticks to plate and does not cavitate	88
Water exerts no tension on plate and does not cavitate	89
Water exerts no tension on plate and cavitates after plate leaves water	91
Pressure pulse incident on a yielding diaphragm in an infinite unyielding baffle	103
Bodily motion of targets due to pressure pulse	114
Behaviour of gas bubble in presence of target	121

THE NATURE OF DEFORMATION OF THE TARGET

Yielding of steel targets	127
Fundamental assumptions of plastic yielding of steel	131
Plastic bending of a beam	137
Dishing of a thin panel of plating	139
Plastic deformation under dynamic loads	145
Rupture of steel	161
Notch brittleness	163
Shape and size of steel specimen or target	164
Speed of loading	167

Best Available Copy

APPENDIX A

Theory of small-amplitude sound pulses

APPENDIX B

Theory of gas bubble motion

APPENDIX C

Effects of pressure pulse normally incident on an infinite plane plate

APPENDIX D

Deformation of a rectangular plastic panel by suddenly applied pressure

APPENDIX E

Deflection of a uniform elastic beam on spring supports

APPENDIX F

Air blast from underwater explosions

APPENDIX G

Gravity waves in the sea caused by explosions

LIST OF ILLUSTRATIONS

	Fig.
Surface showing variation of pressure with time and distance ...	1
Curves showing variation of pressure with time at two fixed points	2
Curves showing variation of pressure with distance at two fixed times	3
Empirical curve showing pressure/time variation	4
The reflection of the pressure pulse at an air/water surface ...	5
Pressure/time variations for a point below the sea surface ...	6
Pressure/time variations at large angles of incidence with a free surface	6a
Reflection of pulse at sea-bed	7
Pressure/time variation at a point near the sea-bed	8
Glancing incidence reflection of pulse at sea-bed	9
Curves showing calculated bubble motion	10
Calculated pressure/time variation of first bubble pulse ...	11
Curves showing the distribution of pressure with depth immediately above the explosion	12
Resultant velocity of projected water	13
Variation in thickness of the initial layer of spray dome ...	14
Surface effects of shallow explosions	14a
Pressure pulse incident on unit area of infinite plate	15
Pressure on plate when there is no cavitation at plate or in water	16
Diagrammatic representation of successive stages when plate leaves water and subsequently cavitates	17
Energy transferred to target from pressure pulse	18
Essential features of box and drum models	19
Pressure pulse incident on yielding piston in infinite unyielding wall	20
Central plastic deflections of box model target plate	21
Static stress - strain curve for mild steel	22
Simplified stress - strain curve	23
Symmetrical section of beam	24
Plastic bending of simply-supported beam by concentrated central load	25

Best Available Copy

UNDERWATER EXPLOSIONS

INTRODUCTION

Resolution of the damage problem

1. The effect of an underwater explosion against a vessel will depend on both the proximity of the explosion to the vessel and the way in which the vessel is constructed. These effects may be sub-divided into:-

(1) the effect of contact explosions against single-hulled vessels,
(2) the effect of non-contact explosions against vessels with some form of multi-bulkhead protection,
(3) the effect of contact explosions against multi-bulkhead protected vessels,
(4) the effect of non-contact explosions against single-hulled vessels.

For case 1, a very small underwater charge is sufficient to hole a single-hulled vessel when in contact or near-contact and little theory is necessary. For case 2, however, non-contact explosions from normal types and sizes of charges will do little damage to a multiple protective system except when the outer skin is air-backed; this may be considered in the same way as the shell of a single-hulled vessel. Little theoretical treatment has yet been found possible for contact explosions in case 3. Therefore, the main theory to be discussed will be concerned with the problem of a single thickness of air-backed plating subjected to non-contact explosions sufficiently distant for the damage to be appreciable, but not catastrophic.

2. For such non-contact explosions the phenomena can be conveniently considered under the following main headings:-

(1) The phenomena in the water which are proper to the explosion itself,
(2) the interaction of these water phenomena with the target, this interaction depending on both target and explosion properties,
(3) the nature of the deformation of the target insofar as it depends on the properties of the target.

3. The treatment of the material in the main text is such that a knowledge of mathematics beyond interpretation of simple formulae is not required. Where it has been thought necessary, mathematical relationships have been illustrated graphically. Results quoted in the main text without proof are deduced in Appendices and are referred to by the appropriate equation number. An equation prefixed by a letter is derived in the Appendix of that letter.

4. The terms "open water" and "mid-water" will be used frequently. Open water is understood to mean the conditions which usually exist on the high seas where the only factors (external to the charge) which influence the explosion are the surrounding water and the presence of the sea surface and sea bottom. Mid-water is understood to involve the further restriction that the point of explosion is sufficiently far from both sea surface and sea bottom for neither of these to exert a direct influence on the explosion. The most convenient explosive for underwater experimental work is T.N.T. and, therefore, the term 'charge' implies a charge of T.N.T. However, results observed for T.N.T. charges can be applied to charges of other explosives by means of a conversion factor. In particular, from the standpoint of underwater explosive effects, a 100 lb. charge of torpex is equivalent to 145 lb. charge of T.N.T. and the weight conversion factor of 1.45 is reasonably constant for torpex charges of any size.

PHENOMENA IN OPEN WATER

The general sequence of events

5. Consider for simplicity an unconfined spherical charge initiated from the centre. On initiation, a detonation wave will travel out radially from the centre with a velocity characteristic of the explosive. Within the region traversed by this wave, the explosive is converted into incandescent gas at a very high pressure. In front of the detonation wave the explosive remains uncharged, being "unaware" of the initiation. In T.N.T. for example, the detonation wave travels at approximately 23,000 ft. per sec. so that a charge of 400 lb. T.N.T. occupying a sphere of about one foot radius would be all converted into incandescent gas at a pressure of the order of several hundred tons per sq.in. in the very short time of about 40 microseconds.

6. The high pressure gas bubble then tries to expand and the first result is a compression of the spherical layer of water immediately surrounding the charge. This layer in turn compresses a further layer and so on. In this way, a wave of compression is propagated through the water radially outwards from the explosion. This wave is usually termed the pressure pulse.

7. The velocity of propagation of the pressure pulse at first decreases as the pulse travels outwards until, at a comparatively short distance from the explosion, it becomes approximately constant at the normal velocity of sound about 5,000 ft. per sec. in sea water. Except for a small inner region surrounding the charge, the pressure pulse obeys the usual acoustic laws, the intensity decreasing steadily with increasing distance until, at very large distances, the pulse becomes simply a noise. The persistence of the pulse is demonstrated by the fact that the detonation of a charge of only 9 oz. guncotton can be detected at a distance of 40 miles. The characteristics of the pressure pulse will be considered in detail later, but one feature is that the pressure in the pulse can be treated as essentially positive, any subsequent suction in the pulse being unimportant. This is in marked contrast to blast in air where a phase of positive pressure is followed by an appreciable suction phase.

8. While the pressure pulse is travelling outwards to large distances, the original gas bubble expands. The pressure in the gas bubble, therefore, decreases and becomes ultimately of the same order as the hydrostatic pressure in the water. Except in the initial stages, this expansion takes place relatively slowly and the motion of the surrounding water is in the nature of a general bodily flow, as opposed to the compression of successive layers associated with the pressure pulse. This outward flow involves a considerable mass of water with large kinetic energy and, as a result, the flow overshoots the equilibrium position in which the pressure in the gas bubble is equal to the hydrostatic pressure in the surrounding water. When the outward expansion ceases, therefore, the pressure in the bubble is less than the hydrostatic pressure for equilibrium and the bubble commences to contract with resulting inward flow of water. This return flow also over-shoots the equilibrium position and the bubble contracts to a small volume at a pressure which is fairly high, although not nearly as high as the original pressure at detonation. This small bubble then behaves effectively as a second explosion and the whole process is repeated, a second compression wave being sent out as the bubble commences to expand again.

9. Simple theory predicts that the oscillation of the bubble would continue indefinitely in an unlimited mass of water, the original explosion producing in effect a series of successive explosions. In practice, however, energy is dissipated to the surrounding water and the pressure in succeeding pulses decays so that each explosion becomes intrinsically weaker than its predecessor. Moreover, at a later stage, the bubble tends to break up into smaller bubbles with further dissipation of energy and the process terminates after a few oscillations.

10. As a further effect, the gas bubble rises and in practice the gases will eventually break surface. Depending on the size of charge and its depth below the surface, this venting may occur either before or after the original bubble has disintegrated into smaller bubbles with a resulting variation in the surface effects.

11. The primary phenomena associated with an underwater explosion after detonation can, therefore, be summarised thus. First, the propagation of a pressure pulse to a great distance. Secondly, oscillations of the gas bubble with the associated production of additional pulses each intrinsically feebler than the preceding one. Thirdly, the rise of the bubble under the indirect influence of gravity. These phenomena will now be considered in detail together with the modifications and additional phenomena introduced by the presence of the sea surface and the sea-bed.

The pressure pulse

Variation of pressure with time and distance

12. For most purposes, the pressure pulse behaves simply as an intense sound pulse beyond a relatively small distance from the explosion. Therefore, the standard theory for the propagation of sound waves will be applicable to a study of the behaviour of the pressure pulse. Those points which are specially relevant to an understanding of the pressure pulse are treated in detail at Appendix A where it is shown that at a point distant r from the charge centre:-

$$p = \frac{\rho}{r} f(t - \frac{r}{c}) \quad \ldots \quad \ldots \quad \ldots \quad \ldots \quad \ldots \quad \ldots \quad \ldots \quad \ldots \qquad (1)$$

where

- t = time interval after the initiation of the explosive charge
- ρ = mass density of water
- c = velocity of sound in water
- p = pressure in pulse (additional to the hydrostatic pressure existing prior to the pulse)

Equation 1 gives the pressure p as a function of the two variables, r and t. Such a relationship can be represented graphically by a surface in a three co-ordinate system. The dependence of p upon r and t is illustrated by the surface of arbitary shape shown in fig. 1.

However, it is instructive to study the variation of p with change in only one of the two variables, the other remaining constant. Thus the plane curve ABC gives the variation of pressure with time at a constant distance r_1 from the explosion. Similarly, the variation of pressure with distance at a constant time t_1 after the explosion can be studied from the plane curve, PED.

Variation of pressure with time (distance constant)

13. To understand the physical significance of equation 1, let p_1 denote the pressure at time t_1 and distance r_1 and let p_2 denote the pressure at time t_2 and greater distance r_2. Then from equation 1

$$p_1 = \rho/r_1 \, f(t_1 - \frac{r_1}{c}) \quad \ldots \quad \ldots \quad \ldots \quad \ldots \quad \ldots \quad \ldots \quad \ldots \qquad (2)$$

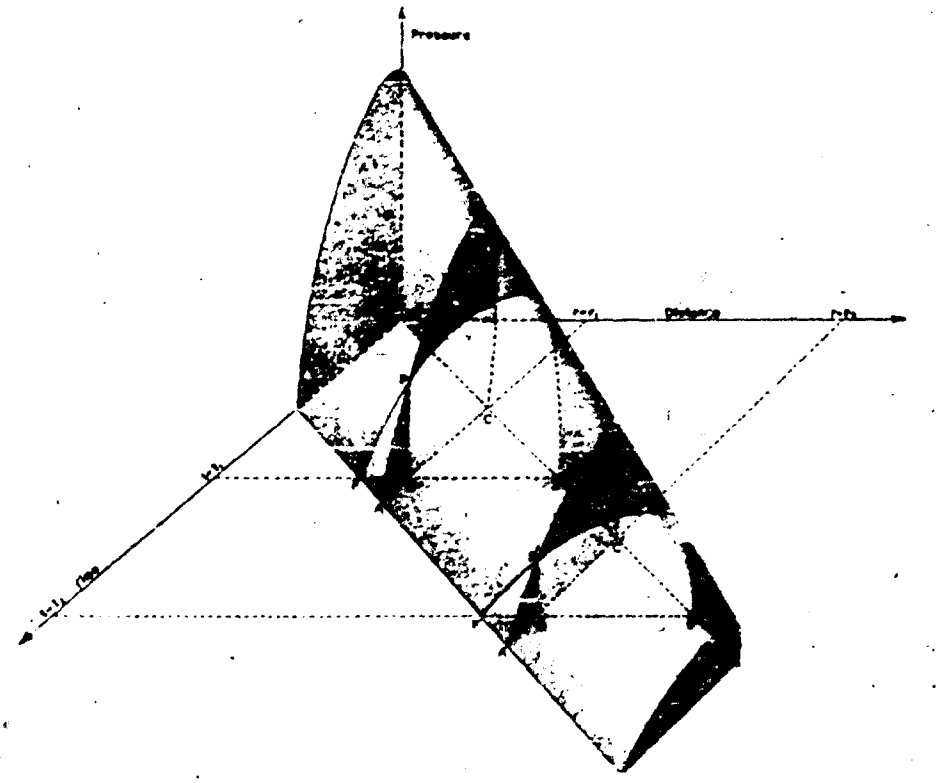


Fig. 1 - Surface showing variation of pressure with time and distance

$$p_2 = \rho/r_2 f(t_2 - \frac{r_2}{c}) \quad \ldots \quad \ldots \quad \ldots \quad \ldots \quad \ldots \quad \ldots \quad \ldots \quad (3)$$

If times and distances are now related by

$$t_2 - t_1 = \frac{(r_2 - r_1)}{c} \quad \ldots \quad \ldots \quad \ldots \quad \ldots \quad \ldots \quad \ldots \quad \ldots \quad (4)$$

Then from equations 2, 3, and 4

$$p_1 r_1 = p_2 r_2 \quad \ldots \quad \ldots \quad \ldots \quad \ldots \quad \ldots \quad \ldots \quad (5)$$

If two points of given r_1 and r_2 are considered, then for varying t_1 and t_2, equations 2 and 3 give the two pressure/time curves at these points. For any spherical sound pulse let these pressure/time curves be represented by ABC and A'B'C' in fig. 2. These curves are drawn of arbitrary shape.

Best Available Copy

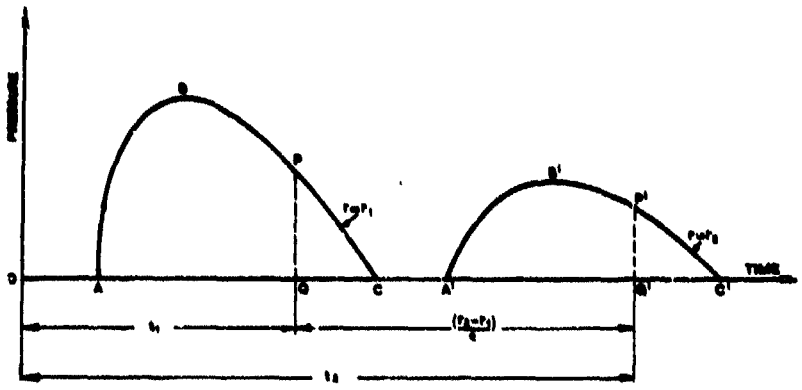


Fig. 2 - Curves showing variation of pressure with time at two fixed points

For times satisfying equation 4 the respective ordinates are a constant time apart and, therefore

$$P'Q' = r_1/r_2 PQ \quad \ldots \quad \ldots \quad \ldots \quad \ldots \quad \ldots \quad \ldots \quad \ldots \quad (6)$$

It follows that the curve A'B'C' can be obtained from the curve ABC by displacing curve ABC a distance $(r_1 - r_2)/c$ to the right and reducing all the pressure ordinates in the same ratio r_1/r_2. The two curves can, therefore, be made of the same shape by changing only the pressure scale.

14. Expressed physically, the pressure/time variation at any distance r_1 is repeated on a reduced pressure scale r_1/r_2 at greater distance r_2 at a time $(r_2 - r_1)/c$ later. Subject to the reduction in magnitude, the pressure in the pulse thus travels a distance $(r_2 - r_1)$ in time $(r_2 - r_1)/c$ which corresponds to a constant velocity of propagation, c independent of r_1 or r_2. Equation 1 thus represents a wave travelling outwards with constant velocity c and giving pressure/time variations at different points similar to those illustrated in fig. 2.

Variation of pressure with distance (time constant)

15. Now consider the variation of the pressure in the pulse with distance. This variation is illustrated in fig. 3 for two given times t_1 and t_2 by the curves DEF and D'E'F' respectively.

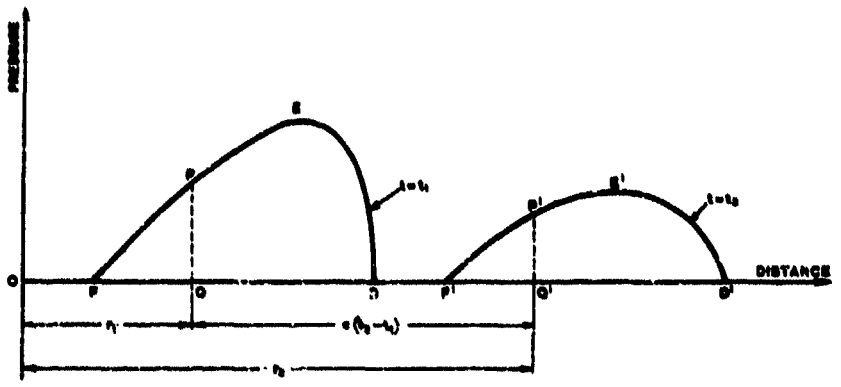


Fig.3 - Curves showing the variation of pressure with distance at two fixed times

Pairs of ordinates such as PQ and P'Q' in fig. 3 which satisfy equation 6 will then be a constant distance $c(t_2 - t_1)$ apart corresponding to a constant velocity of propagation c. The reduction ratio r_1/r_2, however, is not a constant for the two curves but will vary for each pair of ordinates. Unlike the pressure/time variation, the curves for pressure distribution with distance cannot be made strictly of the same shape by changing the pressure scale. However, if the effective length DF (= D'F') is small compared with r_1, the ratio r_1/r_2 will be approximately constant for the two curves DEF and D'E'F' which can then be made approximately the same shape as the curves in fig. 2 for pressure/time variation by a suitable choice of scales. Thus, choosing the origin of time so that the pressure pulse starts from its centre at time t = O, the point A in fig. 2 corresponds to time r_1/c and the shape of the curve ABC is given by

$$PQ = \frac{\rho}{r_1} f\left(t - \frac{r_1}{c}\right) = \frac{\rho}{r_1} f(AQ) \quad \ldots \quad \ldots \quad \ldots \quad \ldots \quad \ldots \quad \ldots \quad (7)$$

Similarly, the point D in fig. 3 corresponds to the extreme distance ct reached by the pulse in time t and the shape DEF is given by

$$PQ = \frac{\rho}{r} f\left(t_1 - \frac{r}{c}\right) = \frac{\rho}{r} f\left(\frac{OD}{c}\right) \quad \ldots \quad \ldots \quad \ldots \quad \ldots \quad \ldots \quad \ldots \quad (8)$$

If DF is now small compared with OD the factor ρ/r in equation 8 is sensibly constant over the curve DEF and equations 7 and 8 indicate that by a suitable choice of scales, the curves ABC and DEF would be approximately the same, although reversed with respect to the origins of time and distance.

16. This similarity of the pressure/time and pressure/distance curves becomes increasingly more accurate as the pulse travels outwards to great distances. The essential assumption is that the factor $1/r$ in equation 1 may be treated as constant when phenomena over distances small compared with r are concerned. This assumption corresponds to neglecting curvature of the spherical wave front and treating the pulse as a plane wave. This approximation will be frequently used in the succeeding analysis for the effects due to the pressure pulse.

17. In addition to the pressure, other quantities of interest in the study of underwater explosions are the particle velocity, the impulse per unit area and the energy associated with the pressure pulse. Formulae for these quantities are derived in Appendix A. The relative significance of these quantities will depend on the mechanism of damage.

Particle velocity

18. The particle velocity is the outwards radial velocity u communicated to the water by the pulse. It is essential to distinguish clearly between the wave-velocity c and the particle velocity u. As a very crude analogy, the pressure pulse from an explosion can be regarded as "news" of the explosion transmitted through the water; the wave velocity c is then simply the speed of transmission of this news whereas the particle velocity u and pressure p represent contents of the news. It is shown in Appendix A that the pressure p is related to the particle velocity u by the approximate equation

$$p = \rho c u \quad \ldots \quad \ldots \quad \ldots \quad \ldots \quad \ldots \quad \ldots \quad \ldots \quad \ldots \quad (9)$$

Equation 9, which is exact for a plane wave, becomes increasingly accurate for a spherical pulse as it travels outwards and is one of the basic relations which will be assumed in much of the succeeding analysis for the effects of the pressure pulse from an underwater explosion.

Impulse per unit area

19. The impulse per unit area I transmitted by the pulse across the spherical surface at radius r is equal to the area of the pressure/time curve and varies simply as the inverse of the distance.

Energy associated with the pressure pulse

20. The energy associated with the pulse is defined as the energy per unit area $\mathcal{E}$ transmitted by the pulse across the spherical surface at radius r. This energy varies inversely as the square of the distance if the relation in equation 9 is assumed to be accurate. Theoretically, the total energy E transmitted across the spherical surface is constant and is independent of distance. In practice, however, some of the energy is left behind as kinetic energy of the water after the pulse has passed. Nevertheless, at distances for which the pressure pulse from an underwater explosion can be considered as a sound pulse, these afterflow effects are small and will be neglected in the succeeding analysis.

21. All the preceding theory of sound pulses depends essentially on the assumption that the amplitude of the waves is small. The necessary criterion for the validity of this assumption is that the ratio u/c should be small. From equation 9 this indicates that the pressure p must be small compared with ρc^2 which is about 150 tons per sq. in. for water. Hence, the pressure pulse can involve pressures of the order of several tons per sq. in. and still be regarded as of small amplitude for theoretical analysis. In contrast, it is interesting to note that for air ρc^2 is only of order 20 lb. per sq. in. Thus, pressures which can be regarded as of small amplitude for blast in water are about 10,000 times greater than pressures of waves which may be considered to be of small amplitude for blast in air. This factor is largely responsible for the present emphasis on small amplitude waves for the pressure pulse in water as opposed to the emphasis on waves of finite amplitude for blast in air (Part 1, Chapter 4 of this Textbook).

Empirical data for the pressure pulse[3]

22. The theory of small-amplitude sound pulses is sufficient to describe the propagation of the pressure pulse except in the immediate neighbourhood of the charge. For a T.N.T. charge, the maximum pressure in the pulse becomes of order 2 tons per sq. in. or less at distances beyond about 12 charge diameters from the explosion. However, this simple theory gives no indication of the shape of the pulse, that is the form of the function f in equation 1, since this shape depends on the course of events in the inner region round the charge. Nevertheless, for distances at which the pressure pulse behaves to a reasonable approximation as a sound pulse of small amplitude, the simple theory can be used in conjunction with experimental evidence to deduce the shape of the pulse.

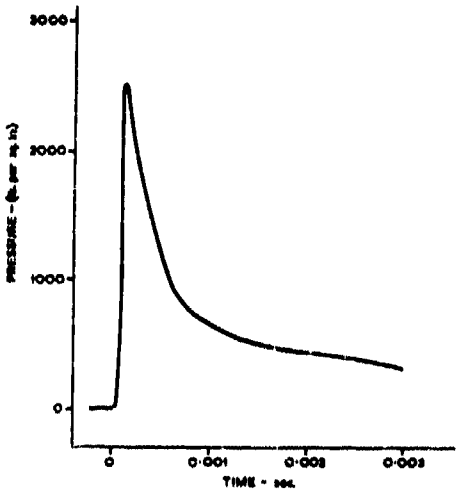


Fig.4 - Empirical curve showing the pressure/time variation

23. Fig.4 is a typical experimental record, obtained by a tourmaline gauge and shows the variation of pressure with time in the pulse. The curve indicates an initial vertical front, corresponding to a sharp instantaneous rise of pressure to a maximum value, followed by decreasing pressure. Unlike blast in air, the pressure remains positive throughout with no evidence of any subsequent appreciable suction phase. Empirical analysis of experimental results indicates that the initial decreasing portion following the front is exponential in shape, but that in the final "tail" the pressure decays more slowly than predicted by the exponential curve which fits the initial portion of the empirical curve. However, it seems fairly certain that the final tail is relatively unimportant so far as the damaging power of the pulse is concerned. Therefore, it is usual for theoretical analysis of damage to assume the pressure/time curve to be of the exponential form

$$p = p_m e^{-nt'} \quad \ldots \quad \ldots \quad \ldots \quad \ldots \quad \ldots \quad \ldots \quad \ldots \quad \ldots \quad (10)$$

where p_m is the maximum pressure in the pulse, n determines the rate of decay of pressure, and t' is time measured from the arrival of the pulse at any point under consideration.

24. It is found that for distances beyond which p_m is of the order of 2 tons per sq.in. or less, measurements are in reasonable agreement with the preceding acoustic theory which predicts that p_m should vary inversely as the distance and that n should be independent of distance. Empirical formulae for p_m, n and related quantities have been proposed[4] from data derived from underwater experiments with the large type tourmaline strip gauge. With such a recording technique, measurements were necessarily confined to distances greater than 100 times the charge radius. However, in recent years, an experimental technique[5,6] which depends on amplification of signals from very much smaller and simpler tourmaline gauges has been developed and it is now possible to investigate underwater effects at exceedingly small ranges. Using this technique, data for pressure, momentum and energy have been obtained for the whole range of distances including

measurements when the gauge was in contact with the charge. The results of these experiments indicate that at close ranges (between 85 and 13 times the charge radius), the original empirical formulae are not strictly true and, therefore, revised formulae have been proposed.[M] In addition to fitting results obtained at close ranges, these revised formulae also give a better fit for early results. At even closer ranges, further work indicates that these revised formulae have to be further modified. Nevertheless, in order to indicate the general nature of the formulae, it is instructive to quote the original empirical results for T.N.T. These results will be reasonably accurate for distances greater than about 100 times the charge radius. Let

W = weight of T.N.T. charge in lb.

D = distance from charge in feet

then the following empirical formulae were proposed from the early experimental data

$$p_m = 7 \frac{W^{\frac{1}{3}}}{D} \text{ tons per sq. in.} \quad \ldots \quad (11)$$

$$I = 1.9 \frac{W^{\frac{1}{3}}}{D} \text{ lb. sec. per sq. in.} \quad \ldots \quad (12)$$

$$\Omega = 2.8 \times 10^4 \frac{W}{D^2} \text{ ft. lb. per sq. ft.} \quad \ldots \quad (13)$$

$$E = 4\pi D^2 \Omega = 3.5 \times 10^5 \times W \text{ ft. lb.} \quad \ldots \quad (14)$$

It should be emphasised that these formulae were derived from data obtained at distances for which p_m is of order of 2 tons per sq. in. or less and are not accurate[M] for distances closer to the charge. The outer region in which these formulae are applicable is the region in which the pulse should behave sensibly as a small amplitude wave. These empirical formulae confirm that the form of variation of the respective quantities p_m, I and Ω with distance and the constancy of E for the pulse from a given charge agrees with that predicted by the theoretical equations in the outer region.

25. Since the shape of the pressure/time curve is not exactly exponential, it is necessary to decide which features of the actual pulse are to be most accurately simulated when using equation 10 to represent the pulse for damage purposes. For this purpose, the quantities p_m, I and Ω can be used but, in general, only two of the three equations 11, 12 and 13 can be accurately satisfied by a curve of the form given by equation 10 which involves only two parameters.

26. If the maximum pressure be chosen as a first criterion, then equation 11 is used to give p_m in equation 10. Therefore, either equation 12 or 13 can be used to determine an appropriate value of n for T.N.T. charges.

27. If impulse is the second criterion to be adopted for fitting the experimental results by using equation 10; then from equations A15 and 10

$$I = \frac{p_m}{n} \quad \ldots \quad (15)$$

Hence, substituting for p_m and I from equations 11 and 12 in equation 15

$$\frac{1}{n} = \frac{W^{\frac{1}{3}}}{8250} \text{ sec.} \quad \ldots \quad (16)$$

[M]

$p_m = 17{,}570 \left\{\frac{W^{\frac{1}{3}}}{D}\right\}^{1.13}$ lb. per sq. in.

$I = 2.279 \frac{W^{\frac{2}{3}}}{D}$ lb. sec. per sq. in.

$\Omega = 30{,}660 \frac{W}{D^2}$ ft. lb. per sq. ft.

$E = 385{,}200\ W$ ft. lb.

28. Alternatively, if energy is adopted as the criterion, then for an exponential shape of pulse, equations A17 and 10 give

$$\Omega = \frac{p_m^2}{2\rho c n} \quad \ldots \quad \ldots \quad \ldots \quad \ldots \quad \ldots \quad \ldots \quad \ldots \quad \ldots \quad (17)$$

Taking c = 5,000 ft. per sec. for sea water of density 64 lb. per cu. ft. and substituting for p_m and Ω in equation 17 by use of equations 11 and 12 then,

$$\frac{1}{n} = \frac{W^{\frac{1}{3}}}{9150} \text{ sec.} \quad \ldots \quad \ldots \quad \ldots \quad \ldots \quad \ldots \quad \ldots \quad \ldots \quad (18)$$

29. Yet another alternative is to make the exponential form give impulse and energy corresponding to equations 12 and 13 whilst disregarding equation 11. Then, by substituting from equations 12 and 13 in equations 15 and 17 respectively, and solving for p_m and n, the values to be used in equation 10 for T.N.T. charges would be

$$p_m = 6.3 \frac{W^{\frac{1}{3}}}{D} \text{ tons per sq. in.} \quad \ldots \quad \ldots \quad \ldots \quad \ldots \quad \ldots \quad (19)$$

$$\frac{1}{n} = \frac{W^{\frac{1}{3}}}{7400} \text{ sec.} \quad \ldots \quad \ldots \quad \ldots \quad \ldots \quad \ldots \quad \ldots \quad \ldots \quad (20)$$

30. Thus, using variously the empirical formulae 11, 12 and 13, three alternative pairs of formulae can be obtained for use with equation 10, namely, either (a) equations 11 and 16, (b) equations 11 and 18, or (c) equations 19 and 20. The three sets of formulae agree for a charge weight of about 130 lbs., and generally for medium weight charges of this order of size, the choice of formulae for p_m, I and n will not be of vital importance. Damage produced by a pressure pulse can depend primarily on any one of the three quantities p_m, I and Ω. The choice of formulae for p_m, I and n will, therefore, depend on the mechanism of damage. Where the damage is not specially dependent on any one of p_m, I and Ω equation 16 has the merit of giving values of n intermediate to those given by equation 18 and 20. In general, the simplicity of the exponential form of equation 10 for theoretical analysis more than offsets the attendant uncertainty as to the best values to be used for p_m and n.

31. Experimental measurements have, in general, been confined to measuring the pressure/time variation in the pulse at given points. However, the corresponding distribution of pressure in space at a given time can be deduced by using the preceding relationship between the pressure/time and pressure/distance curves for distances at which the pulse is of small amplitude. Thus in fig. 4, corresponding pressure/space distribution at the time when the front of the pulse reaches the distance r = 40 ft. will be given approximately by the pressure/time curve. The time scale would then be replaced by a distance scale with time 0 becoming r = 40 ft., time 0.001 becoming r = 35 ft., time 0.002 becoming r = 30 ft. and so on, the charge centre lying off the figure to the right.

32. Since the pulse has an indefinite tail there is strictly neither a definite duration of pulse at a given point nor a definite length of the pulse in space at a given time. However, for theoretical analysis using the exponential representation of equation 10, the parameter n determines the rapidity with which the pressure in the pulse drops to unimportant magnitudes. The reciprocal 1/n, which has the dimensions of time, gives a measure of the order of time for which the pressure is important and is the time constant for the pressure pulse.

33. In theoretical analysis, this time θ_n tends to play much the same role for an exponential pulse as does the duration for a pulse of finite duration. Similarly, a corresponding measure of the characteristic length of the pulse in space is provided by the quantity c/n which has the dimensions of a length. A measure of the characteristic duration of the pulse from T.N.T. charges can thus be obtained by using one of the alternative formulae 16, 18, and 20. The same formulae can be used to provide a measure of the characteristic length of the pulse by calculating c/n. For example, using equation 16 and taking $c = 5{,}000$ ft. per sec. then

$$\frac{c}{n} = 0.60\, W^{\frac{1}{3}} \text{ ft.} \quad \ldots \quad \ldots \quad \ldots \quad \ldots \quad \ldots \quad \ldots \quad \ldots \quad (21)$$

An estimate of the maximum particle velocity u occurring at the pulse front is given by using equation 11 and the approximate equation 9. For T.N.T. charges,

$$u = 230 \left(\frac{W}{D}\right)^{\frac{1}{3}} \text{ ft. per sec.} \quad \ldots \quad \ldots \quad \ldots \quad \ldots \quad \ldots \quad \ldots \quad (22)$$

34. The use of the principle* of dynamical similarity has not, in general, been employed in the empirical analysis of underwater explosion data to the same extent as for the problem of blast in air. Although the particular formulae 11 to 14 satisfy this principle, it should be noted that the experimental data from which they were derived can be rather better represented by formulae not satisfying dynamical similarity. It is not yet certain whether this departure from similarity is a true effect due to the fact that different size charges are never perfect scaled replicas, or whether it is mainly a spurious result arising from defects in the methods of measurement.

Effects of finite amplitude of the pulse

35. The simple theory of small-amplitude pulses is sufficient to account for the propagation of the pressure pulse at distances where the maximum pressure is of order 2 tons per sq. in. or less. At much smaller distances from the charge the simple theory becomes completely inadequate and a more elaborate theory is necessary.

36. Reasonably successful attempts have been made to calculate what happens in the neighbourhood of the charge. In particular, the theory predicts a form and order of magnitude of the pressure pulse in good agreement with experimental results and the theory serves to indicate the magnitude of the pressures near the explosion where it is difficult to take measurements. Such more complete theory for underwater explosions is essentially similar to that for blast in air and it will suffice here only to emphasise some effects connected in particular with the sharp-fronted nature of the pulse.

37. The passage of a finite amplitude pulse involves, in general, an irreversible heating of the water and a consequent dissipation of energy by conduction of heat through the water and by internal friction or viscosity. Both these effects are most pronounced in the steep front of the pulse where the most rapid changes occur and both tend to decrease the pressure in this front. On the other hand, the fact that larger pressures travel faster than smaller pressures (as in air) implies a building up of the pressure at the front. These conflicting effects tend to strike a balance and theory indicates that the thickness of the shock front, that is, the distance in which the pressure in the water rises from its undisturbed value in the front of the pulse to its maximum value in the pulse, is of the order of a few millionths of a centimetre; this corresponds to a time

* Recent work has, however, shown that for shock waves, the principle of dynamic similarity does hold.

of rise for the pressure at any point of the order of 10^{-11} sec. The time of rise has yet to be accurately measured but recent work indicates that it is at least as small as 10^{-8} sec. Such a time of rise can be regarded as instantaneous so far as the ultimate problem of damage to ships is concerned.

38. It may be finally noted that the energy dissipated as heat in the water during the early propagation of the pressure pulse can account for about 2% of the total energy of the explosion. The corresponding energy E, given in equation 14 which remains in the pressure pulse at large distances is also about 2% of the total energy liberated by the explosion. The pressure pulse thus only accounts for about 50% of the total energy and the remaining 50% is left behind as energy in the gas bubble and kinetic energy of motion in the water in the immediate neighbourhood of the explosion. This motion will be considered later (para. 62).

Reflection of pulse at sea surface

39. The inevitable presence of the sea surface can lead to important modifications of the pressure due to an underwater explosion. In considering the modification due to reflection of the pressure pulse, it is assumed that the explosion is sufficiently deep (about 12 charge diameters or more for conventional explosives) for the pressure pulse to behave simply as an intense sound pulse on arrival at the sea surface.

40. When a sound pulse arrives at a boundary between two different media it will produce in general a transmitted pulse and a reflected pulse. For an underwater pressure pulse arriving at the sea surface there will thus be a transmitted pulse or blast in the air and a reflected pulse in the water, this latter being additional to the original pulse. However, owing to the large difference between both the density and the compressibility of air and water, the pressure of the transmitted blast in the air is very small compared with the pressure in the underwater pulse and it is a very good approximation to neglect this transmitted pulse. The sea surface can thus be taken as a surface where the pressure effectively remains undisturbed and for this to be true the pressure in the reflected pulse at the surface must be equal but of opposite sign to the pressure at the surface due to the original pulse.

41. The pressure at any point below the surface due to the combined original and reflected pulses can be conveniently calculated by using the concept of images. In fig.5, E represents the explosion centre at a depth d below the sea surface A B and E' the image of E in the Plane A B. The pressure pulse sent out from E can then be taken as given by equation 1 where the distance r is measured from E. The reflected pulse can similarly be considered to originate simultaneously from E' and to contribute a pressure, p' where p' is given by

$$p' = -\rho/r' f(t - \frac{r'}{c}) \quad \ldots \quad \ldots \quad \ldots \quad \ldots \quad \ldots \quad (23)$$

where r' denotes the distance from E'. The reflection of the pressure pulse at the sea surface as a tensile pulse corresponds in effect to an equal but "negative" explosion at E'. The pressure at P due to both the incident and reflected pulses will then be given by

$$p = \frac{\rho}{r} f(t - \frac{r}{c}) - \frac{\rho}{r'} f(t - \frac{r'}{c}) \quad \ldots \quad \ldots \quad \ldots \quad \ldots \quad (24)$$

For any point on the sea surface, r = r' and equation 24 gives zero pressure corresponding to the condition that the pressure at this surface remains unchanged by the pressure pulse.

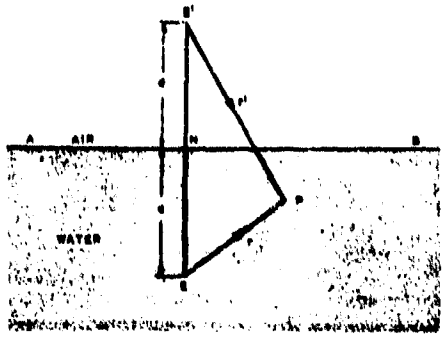


Fig. 5 - The reflection of the pressure pulse at an air/water surface

42. For a point P below the sea surface, r'>r, and the pressure given by equation 24 will be the difference between the two curves O C D and O'C D' in figure 6a. These curves are essentially of the same shape but differ in magnitude by the ratio r/r'. The time difference OO' = (r' - r)/c corresponds to the longer time taken for the reflected pulse to travel effectively from E', as compared with the time taken by the original pulse to travel from E. The resultant pressure at P given by equation 24 is then of the form O C O' C' F in fig. 6b.

43. Such use of equation 24 leads to negative pressures in the water which could be of much the same order as the maximum pressure in the original pulse. Some qualification is obviously necessary to allow for the fact that water cannot, in general, withstand large tensions. Experimental evidence on the tensile strength of water is somewhat contradictory. Under laboratory conditions, with all air bubbles removed as far as possible, ordinary water can apparently withstand static tensions of the order of 500 lb. per sq. in, whilst water nearly saturated with air can withstand static tensions to about 80 lb. per sq. in. Under dynamic conditions, the strength is probably less and drops to an almost negligible value if the flow becomes turbulent.

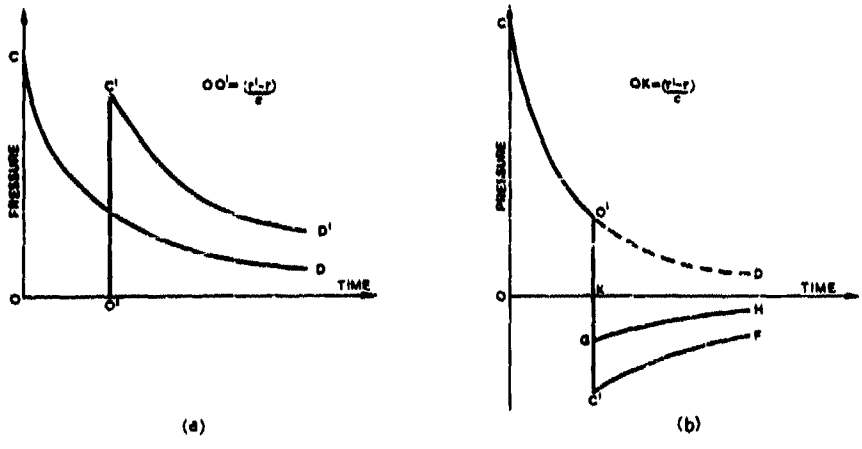


Fig. 6 - Pressure/time variations for a point below the sea surface

44. For the present problem, if the maximum pressure in the pulse is much greater than a few hundred lb. per sq.in. it seems fairly certain that the reflected pulse will cause some cavitation or breaking of the water. This cavitation will be most pronounced for points near N in fig.5 where it leads to the formation of the spray dome. For the present, attention will be confined to points such as P in fig.5 at some horizontal distance from E N; at such points the main effect of cavitation will be to replace the portion K C' P of the pressure/time curve in fig.6b by a portion K G H. The resultant curve O C O' K G H corresponds to the type of record observed experimentally for the pressure pulse as modified by the proximity of the sea surface. Since, in general, the tensile phase K G H is relatively small compared with the pressure phase O C O' K, it is reasonable and customary approximation to neglect the tensile phase and regard the pressure/time curve to be given by O C O' K.

45. The reflection of the pressure pulse at the sea surface with subsequent cavitation of the water can be taken into account theoretically by a simple "surface cut-off" effect. It is only necessary to evaluate r and r', the respective distances of any point P in fig.5 from the explosion E and its image E'. The pressure pulse from E is then considered to cease abruptly at time OO' = (r - r')/c after its commencement. This replaces any use of equation 24 which is invalidated by cavitation.

46. The surface cut-off does not affect the maximum pressure in the pulse but it can modify appreciably the transmitted impulse and energy. Assuming the exponential form given by equation 10 for the original pulse O C D to be correct, the surface cut-off decreases the transmitted impulse by the fractional amount

$$\frac{KO'}{OC} = e^{-\frac{\theta}{a}(r'-r)} \quad \ldots \quad \ldots \quad \ldots \quad \ldots \quad \ldots \quad \ldots \quad \ldots \quad (25)$$

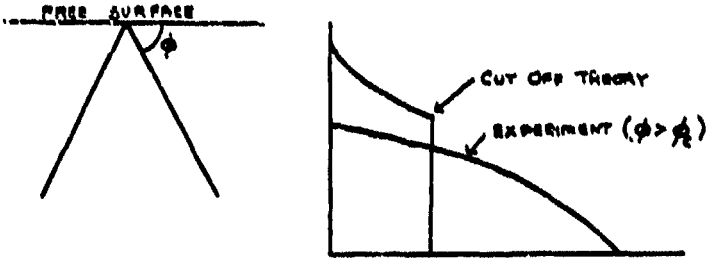
The transmitted energy is decreased by the fractional amount

$$\frac{KO'}{OC}^2 = e^{-2\frac{\theta}{a}(r'-r)} \quad \ldots \quad \ldots \quad \ldots \quad \ldots \quad \ldots \quad \ldots \quad \ldots \quad (26)$$

The length a/n depends on the size of the charge. For example, equation 21 gives a/n for a T.N.T. charge. The distance (r' - r) depends on the position of any target-point P in fig.5 relative to the explosion and the sea surface.

* The effect of reflection of the pressure pulse at a free surface has so far been treated by the methods of the theory of sound. The second order terms in the hydrodynamical equation, which are neglected in the theory of sound, are nevertheless of decisive importance when the incident pulse reaches the surface at nearly glancing angles.

A mathematical discussion 12a has shown that if the peak pressure in the shock wave, in pounds per sq.in., reaches the free surface at an angle of incidence less than a critical angle = (90 - 0.21)°, then the cut-off theory is approximately accurate. Should the angle of incidence be greater than the critical angle, then the cut-off theory is not correct in that it predicts too high a value of the peak pressure near the surface, and too short a duration. The failure of the simple cut-off theory becomes of practical importance when consideration is given to large explosions in relatively shallow water.



47. For a given charge at a given depth, the fractional decreases in impulse and energy will become greater as (r' - r) decreases; this will occur as the depth of P from E N increases. The resulting influence of surface cut off on the variation of damage with distance and orientation of explosion relative to the target is discussed later. Therefore it follows that damage to a surface vessel by the pressure pulse should tend to be less near the water line than near the bottom of the vessel, subject of course to the effect of any marked difference in strength of the ship's structure at different levels.

Reflection of the pulse at the sea-bed.

48. Pressure-time records of underwater explosions often show a pressure pulse, following, and partly superimposed on, the main pulse. The obvious interpretation of the second pulse is that it represents the reflection of the main pulse on the bottom. The time delay between the direct pulse and the reflected pulse agrees with expectations, but the magnitude of the reflected pulse is extremely variable, although it correlates in a general way with the hardness of the bottom. Thus the peak pressure in the reflected wave from a rock bottom might be as large as 30-50% of the direct pulse, while for a muddy bottom, the reflected pulse might be altogether absent. Should the bottom consist of a layer of mud or sand over rock, the reflection appears to occur on the rock surface.

49. The sea bed is so variable that it is difficult to make quantitative predictions of the reflected pulse. Indeed, no satisfactory theory has so far been developed except in two elementary limiting cases. The first limiting case is that where the sea bed is so very soft that it behaves exactly the same as water itself, and therefore gives no reflection. The second limiting case is that where the sea bed is completely rigid, and the reflected wave is therefore (in the theory of sound approximation at any rate) identical with the incident pulse. No actual sea bed is rigid, but a rock bottom might behave as an almost perfect reflection for very weak pulses (i.e. of order a few hundred p.s.i. peak pressure).

Charge well away from sea-bed

50. First, the explosion will be assumed sufficiently far from the sea-bed for the initial events in the inner region round the charge to be unaffected by the sea-bed. The pressure pulse sent out by the explosion will then be the same as for a charge in mid-water independent of the sea-bed and on reaching the sea-bed the pressure in the pulse will be assumed small enough for the simple linear theory of sound pulses to apply.

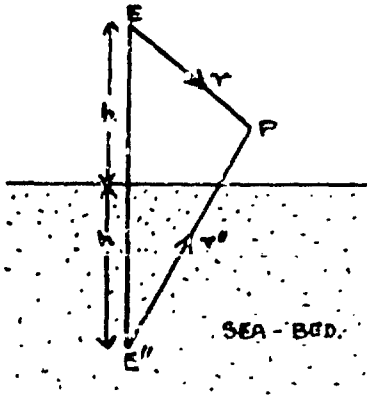


Fig.7 - Reflection of pulse at sea-bed

51. For a plane rigid sea-bed the necessary boundary condition is that there is no particle velocity of the water perpendicular to the sea-bed. This condition is satisfied if the effect of the sea-bed is considered equivalent to an image explosion at E'', equal in every respect to the actual explosion at E in fig. 7.

52. The pressure/time curve at any point P due to the original pulse and the reflected pulse would then be of the form O C C' C F, in fig.8, corresponding simply to the addition of pressure/time curves of the form O C D and O' C' D' in fig. 6a, from a single explosion at distances E P and E'' P respectively.

53. In practice, no sea-bed is completely rigid and the reflected pulse is smaller in magnitude than that indicated by the preceding assumption of complete reflection. Moreover, the sea-bed may distort the shape of the reflected pulse. In fig. 8 the portion O' C F would then be replaced by the smaller and more rounded bump O' G H.

Best Available Copy

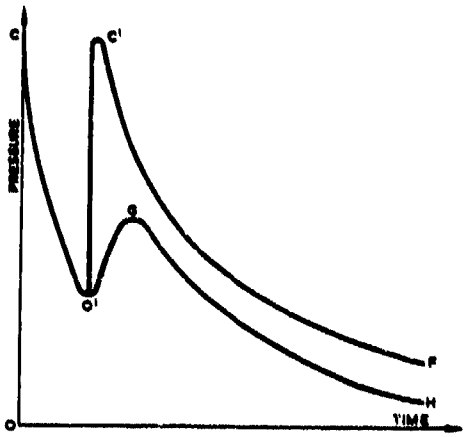


Fig.8 - Pressure/time variation at a point near the sea-bed

54. For a point Q on the sea-bed in fig.7, the theory of complete reflection gives a reflected pulse from E'' exactly equal and synchronous with the incident pulse from E and the resultant pressure/time curve is simply the original pulse doubled in pressure. In practice, such doubling is not attained but the maximum pressure, for example, at a point on a chalk sea-bed, may be 50% more than for a point in mid-water at the same distance from a similar charge.

55. Summing up, for a charge at some distance from the sea-bed, the effect of the sea-bed is positive in character leading to additional pressure which is largest in general at points on the sea-bed. An upper limit to such a sea-bed effect can be obtained by assuming complete reflection to occur, the pressure in the reflected pulse then corresponding to that from a charge in open water at the image E'' in fig. 7. As a final point, there is some limited experimental evidence that the reflection becomes more complete at more distant points to the side corresponding to near glancing incidence.

Charge on sea-bed

56. When the charge is on or near the sea-bed the events in the inner region, where the pulse is "born", are themselves affected by the presence of the sea-bed and the direct pulse sent out from the charge is no longer the same as for a similar charge well away from the sea-bed.

57. For the theoretical case of an infinitely rigid sea-bed it would still seem permissible, however, to assume that the presence of the sea-bed is equivalent to an equal charge at the image point, the new effect being that the charge and image charge interfere with one another. For the limiting case of a hemispherical charge of weight W on the sea-bed, theory would predict the same effects as a spherical charge of weight 2 W in mid-water. Equations 11 and 16 would then indicate a resultant pulse from the charge on the sea-bed having both pressure and time scale increased by a factor $\sqrt{2} = 1.26$ as compared with the same charge in open water. The corresponding energy per unit area of pulse front would, by virtue of equation 13, be simply doubled. This does not, of course, mean any change of <u>total</u> energy in the pulse since this is propagated out through a hemisphere when the charge is on the sea-bed and not through a sphere round the charge as in open water far from the sea-bed. These theoretical results for an infinitely hard sea-bed are subject to modification for actual sea-beds.

58. In practice, soft mud sea-beds behave effectively as further water, that is, the pulse is unaffected by the presence of the sea-bed and is the same as for a charge at the same distance in mid-water.

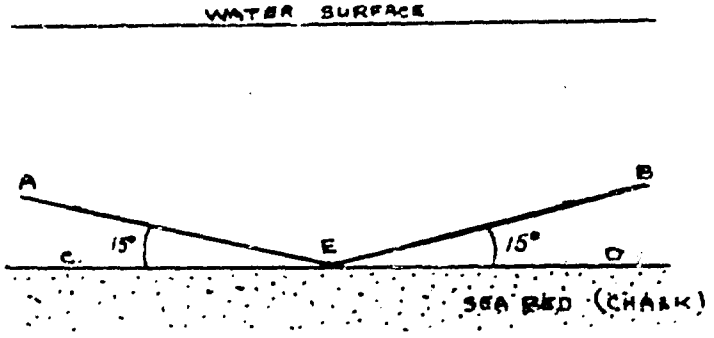


FIG. 8.

59.* A mathematical explanation of the "blind band" has not so far been given, no doubt because of the complexity of the problem. However, fast cine photographs of the motion caused by an electric spark (to simulate an explosion) made at the interface of two liquids, the lower one having a slightly greater density than the upper, show a bubble of very peculiar form. The collapsing stages are indeed remarkable, but what is more important for the present considerations is that the bubble in the upper liquid even in the very early stages is slightly elliptical, with the vertical radius greater than the horizontal. The lower liquid throws a degenerate type of circular curtain up into the upper bubble and the inner regions of the interface move upwards. Now these peculiar bubble shapes must imply that the associated pressure pulses in the two liquids also are not hemi-spherically symmetrical. One would anticipate that the pressure pulse near the interface would be anomalous, as indeed is observed. The blind band and the cavity, or crater, in the lower medium are in fact correlated manifestations of the same mechanical phenomena, and both are generated in the very early stages of the expansion of the explosive gases. Accepting this view, one would not expect artificial obstructions on the sea bed to produce "screening", i.e. a blind band. This is found to be the case. Furthermore, one would not expect to be able to detect a "blind band" in the air blast from an explosion on the ground, except very close-in, because the non-linear terms in the hydrodynamics of air blast are so very much more important than they are for water blast, and the departure from "geometrical optics" is correspondingly far greater.

60.* Two mathematical investigations, one supported by cognate experimental evidence relating to the reflection of pressure pulses at an interface, may be briefly mentioned here. The first is limited to weak pulses, so that the theory of sound is applicable, and is due largely to Arons and co-workers at Woods Hole. The second is purely mathematical(2) and relates to a finite step pulse in one medium meeting a second medium at a plane interface.

According to the usual theory of wave motion, when an infinite train of plane harmonic waves moving through a "lighter" medium in which the wave velocity is c meets the plane interface with a "denser" medium in which the wave velocity is C, reflection and refraction occur, and the refractive index is

$$\mu = C/c$$

Angles of incidence greater than or equal to the "critical angle" $\theta = \operatorname{cosec}^{-1}$, induce total reflection. Notice that depends only on the ratio of the two wave velocities and not on the frequency.

Best Available Co

By means of a Fourier transform, a pulse of any form may be expressed as a synthesis of various harmonic waves. The pulse shape of interest for underwater explosions has a sharp front and decays exponentially, and a manageable Fourier integral can be found for this case. Since the critical angle of reflection is independent of requency, such a pulse should be reflected completely for angles greater than the critical angle.

The interesting point arises, however, that each component in the incident pulse experiences a change of phase, the value of which is independent of the frequency. If all the components of a Fourier transform suffer the same change of phase, the resultant shape of pulse is changed, especially in the region of a steep front.

This simple but important conclusion agrees with experiment but recent work at Woods Hole has shown that the reflected wave can only be reproduced by the mathematical analysis if an appreciable absorption of energy is assumed in the reflecting medium. Particularly interesting is the work, both theoretical and experimental, on the multiple wave system in shallow water (12b).

The considerable algebraic and computational difficulties of the problem of the reflection and refraction of finite pressure pulses meeting an interface are demonstrated in an article by Taub (12c). A step pulse, lead by a shock wave, incident obliquely at an interface with a "denser" medium, always gives a shock in the denser medium, and a reflected Mach or a regularly reflected wave, depending on the angle of incidence and the mechanical parameters, in the lighter medium. A general solution has not been obtained.

61. To sum up, for soft sea-beds the presence of the sea-bed may in general be neglected and the explosion assumed to take place in an infinite depth of water so far as the pressure pulse is concerned. For hard sea-beds the effects differ appreciably according as the charge is well away from the sea-bed or not. If the charge is not near the sea-bed the latter acts as a partially reflecting surface and the maximum effect of the sea-bed occurs for points on the sea-bed. On the other hand, a charge of weight W on a hard sea-bed can be equivalent to a charge of weight 2 W in mid-water so far as the pulse arriving at points well away from the sea-bed is concerned At the same time, it can behave as of weight less than W for the pulse at points on the sea-bed. This phenomenon has yet to be satisfactorily explained.

<u>The gas bubble</u>

Oscillation and rise of bubble in mid-water

62. After the pressure pulse has been propagated well away from the explosion the motion of the gas bubble and the surrounding water take place relatively slowly in comparison with the initial events producing the pulse. Hence, whilst the compressibility of the water is an all important factor for the pressure pulse, it is quite a good approximation to neglect this compressibility during most of the bubble motion. The mathematical treatment is, therefore, based primarily on the ordinary laws for incompressible flow as given in standard text books of hydrodynamics.

63. Although the oscillation of the bubble had been predicted,[13] little significance was attached to bubble motion until World War II when interest was revived by the appearance of two important papers, one British,[5] the other American;[6] these two papers have formed the basis for most of the subsequent theory of bubble motion. An outline of the basic theory in the British form is given in Appendix B. Equations B8, B9 and B10 enable the bubble motion to be computed. Fig.10 shows graphically the results calculated for a small charge of 4.65 lb. of T.N.T. exploded at a depth of 20 ft. below the sea surface.

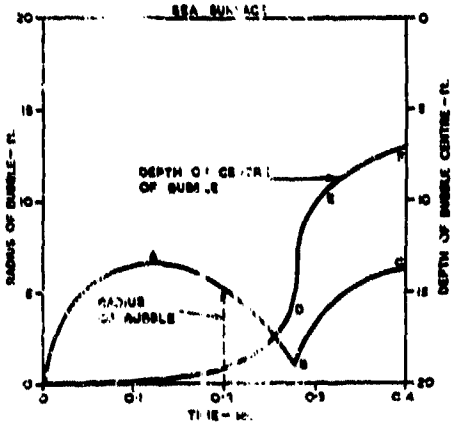


Fig.10 - Curves showing calculated bubble motion

64. The curve O A B C in fig.10 shows that the bubble first expands to a maximum radius of 5 - 6 ft. and then contracts to a radius rather less than 2 feet before commencing to expand again. At the same time, the bubble tends to rise, at first very slowly while the bubble is expanding, and then very quickly when the bubble becomes of small radius again. This rise is represented by the curve O D E F.

65. Using Bernoulli's equation, the pressure in the water associated with the bubble motion is found to be completely negligible except when the bubble is near its minimum radius. The pressure then rises sharply to give the effect of a second explosion emanating from the position of the bubble at this time. The resulting pulse will be termed the "first bubble pulse". If the pressure at a fixed distance from the bubble be considered, the first bubble pulse is relatively feeble compared with the original pressure pulse. On the other hand, since the bubble is moving upwards, a target point above the original explosion may be relatively close to the bubble at its first minimum and the resulting bubble pulse may have a damaging effect comparable with that of the original pressure pulse emanating from the more distant centre of the original explosion. For a fixed point 6 ft. below the sea surface and 14 ft. directly above a charge of 4.65 lb. T.N.T. exploded at a depth of 20 ft. the calculated pressure in the first bubble pulse is shown in fig. 11.

For comparison it may be noted that the original pressure pulse would have a maximum pressure of about 2,000 lb. per sq. in. and a time constant, 1/n of about 0.0002 sec. The bubble pulse is thus of much lower pressure but has a longer effective duration than the original pulse.

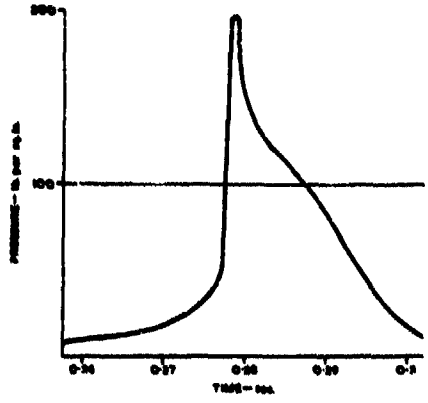


Fig.11 - Calculated pressure/time variation of first bubble pulse

66. Underwater photography and piezo-electric gauges have been used to obtain considerable empirical data on bubble motion resulting from small explosions in experimental tanks. Qualitatively, experiment confirms the theoretical predictions that the bubble will oscillate while rising and that it will send out a pulse at each minimum, the pressures in each pulse being small compared with those in the original pressure pulse but of longer effective duration. Quantitatively, the theory has given good predictions of observed period of first oscillation and the rise during this period. The theory cannot, however, predict with much accuracy the form and magnitude of the first bubble pulse and the curve shown in fig.11 should not be regarded as an accurate quantitative prediction. This defect of the theory was expected since the collapsing bubble tends to become unstable and depart from spherical shape and may even split into separate smaller bubbles which coalesce into a single bubble again on re-expansion. Further, near the minimum radius where changes are rapid it is no longer a good approximation to neglect the effects of compressibility. In general, therefore, the theory cannot be expected to predict with accuracy any quantity depending primarily on events when the bubble is near its minimum radius. It may be noted that although in fig.10 the most pronounced rise occurs near the minimum radius, this rise depends mainly on upward momentum acquired when the bubble is large. (The force producing the momentum is the buoyancy of the bubble which increases with the size of the bubble). The breakdown of the theory when the bubble is small does not, therefore, invalidate its use for estimating the rise of the bubble in the first oscillation.

67. With suitable sizes of charge and depths of explosion, several oscillations of the bubble may take place before it breaks surface or degenerates into smaller bubbles. The period of the second and later oscillations and the associated rise owing to the net hydrostatic force cannot, in general, be predicted with the same accuracy as the initial oscillation and rise. This further defect of the theory is undoubtedly associated with loss of energy during oscillation due to such causes as turbulence which are not allowed for in the theory. Due to this loss of energy, the later oscillations tend to become more rapid. For example, in an experiment with 1 oz. charge of Polar Ammon Gelignite exploded at a depth of 7 ft. in 15 ft. of water the periods of the first, second and third oscillations were found to be 0.072, 0.049 and 0.035 sec. respectively. The associated energies of the bubble motion would then be about 9000, 3000 and 1000 calories for the successive oscillations indicating that for this case about two-thirds of the energy was dissipated in each oscillation.

68. The main qualitative features of the bubble motion in mid water as predicted by theory and observed experimentally, can be summarised as follows:-

(1) an oscillation of the gas bubble,

(2) the rise of the bubble due to the net hydrostatic force, and

(3) the production of bubble pulses subsequent to the original pressure pulse.

The initial explosion is followed, in effect by subsidiary feebler explosions. If the explosion takes place well to the side of the target these "explosions" are relatively unimportant. If a charge is exploded vertically below a target, however, the rise of the bubble under gravity may cause one of the later explosions to occur very close to the target and contribute appreciable damage. This phenomenon of enhanced damage when an explosion takes place beneath a target instead of to the side, has been observed experimentally and is possibly the most important practical consequence of the bubble motion.

Behaviour of bubble near free and rigid surfaces

69. Possibly the most remarkable features of bubble behaviour are those associated with the presence of nearby surfaces. One extreme aspect is the behaviour of the bubble at the free surface of the sea where there is virtually no resistance to flow and where the pressure remains constant. The second extreme feature is the behaviour of the bubble at a completely rigid surface preventing any flow perpendicular to it. The effects of such surfaces have been both predicted mathematically and observed experimentally on the smallscale.* Briefly they are as follows:-

(1) A free surface exerts, in effect, a weak attraction for the bubble while it is expanding followed by a strong repulsion when the bubble is small and contracting. The net effect is that the bubble tends to move away from a free surface during a complete oscillation.

(2) A rigid surface exerts a weak repulsion for the bubble while it is expanding followed by a strong attraction when the bubble is small and contracting. The net effect is that the bubble tends to move towards a rigid surface and stick to it when in contact.

In both cases the attractions and repulsions increase with decreasing distance from the surface, subject in case 1 to the bubble not breaking surface on its expansion.

70. The repulsion from a free surface and the attraction to a rigid surface are in the nature of what is known mathematically as a second-order effect. It is not possible, therefore, to give any short account of the underlying theory[7] and attention will be concentrated on the qualitative results in connection with the effects of the sea surface and the sea-bed on the motion of the bubble.

---

* The reader is strongly recommended to see ciné-films of bubble motion.

Motion of bubble near sea surface

71. The sea surface behaves as a free surface and repels the bubble downwards. For an explosion near the sea surface there are, therefore, two opposing effects; the repulsion of the bubble by the sea surface, and the tendency for the bubble to rise under the net hydrostatic force. Consider similar charges exploded at different depths, excluding extremely shallow depths for which the bubble vents on its first expansion. As the charge depth decreases the repulsion of the free surface increases; the gravity rise will also increase, but more slowly because the operative "depth" affecting this rise is measured from a point 33 ft. above sea level (since the atmospheric pressure is equivalent to a head of 33 ft. of sea water.) For a shallow charge the repulsion can be the stronger effect and the bubble will sink, whilst for a deep charge the surface effect will be small and the bubble will rise. At some intermediate depth the two effects can exactly cancel and the bubble neither rises nor falls. Therefore, the major effect of the proximity of the sea surface on the motion of the bubble is a downwards repulsion tending to lessen and even reverse the upwards motion due to gravity.

Motion of bubble near sea-bed[16].

72. Experiments suggest that sea-beds in fact behave <u>qualitatively</u> like a rigid surface in the sense that they tend to attract the bubble. With very soft sea-beds and/or charges some distance from the sea-bed, this downwards attraction is weak and manifests itself only as a small decrease in the rise due to the net hydrostatic force. With charges close to, or in contact, with hard sea-beds, the attraction is strong and the bubble tends to stay on or near the sea-bed until it breaks up into small bubbles.

73. An important additional effect observed experimentally is that the proximity of the sea-bed tends to suppress the oscillations and the bubble pulses. Thus with 1 oz. charges and a gravel sea-bed three bubble pulses were detected for an explosion at 8 ft. from the sea-bed whereas explosions at 1 ft. 6 in. or less from the sea-bed gave only a single bubble pulse. Experiments with 1 oz. charges and an artificial (steel plate) rigid sea-bed showed a similar qualitative effect but the second pulse was evident at a charge distance of 1 ft. though not at a charge distance of 6 in. Charges of 1 lb. to 5 lb. exploded on or near a mud sea-bed also indicated this suppression as the position of the charge approached the sea-bed, and with the charge actually on the sea-bed there was rarely more than one bubble pulse which was of a broken nature. Therefore, the major effects of the proximity of the sea-bed on the bubble motion are first, a downwards attraction tending to lessen or even reverse the upwards motion due to net hydrostatic force, and secondly, a suppression of the later oscillations and bubble pulses.

<u>Visible surface phenomena</u>

74. The visible surface effects, often very spectacular, consist essentially of a spray dome produced by the pressure pulse and a subsequent plume produced by venting of the gas bubble. The dome and plume are not of direct significance in connection with damage. However, a knowledge of surface phenomena may enable the expert to estimate the size and depth of an explosion if photographs of the dome and plume are available. This can be of operational value.

Spray dome

75. The spray dome depends on the pressure pulse being reflected as a tensile pulse at the surface with subsequent cavitation of the water. To understand the mechanism of the formation of the dome it is first assumed that the pulse can be treated as a small-amplitude plane wave.

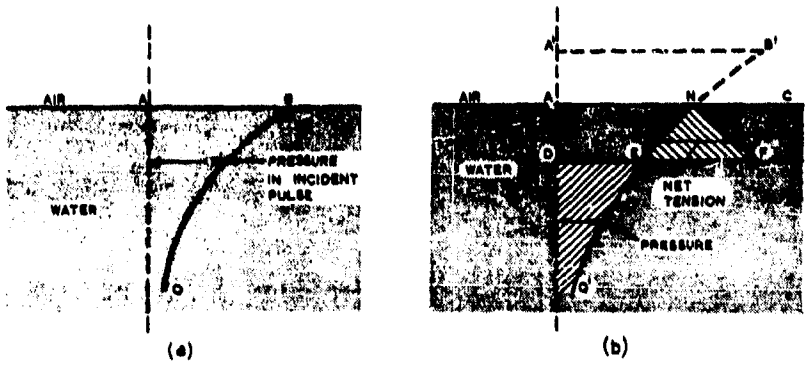


Fig.12 - Curves showing the distribution of pressure with depth immediately above the explosion

In fig.12a, the curve A B Q represents the distribution of pressure with depth immediately above the explosion at the instant when the front of the pulse reaches the surface. At a later time the pulse, which would have reached the position A' B' Q', in fig.12b if there were no surface, is instead reflected as a tensile pulse. The tensions in this wave are given by the curve A N F D which is the image in A C of the portion A' B' N A of the original pulse which has ceased to exist. The pressure in the water (apart from the hydrostatic pressure which is negligible in comparison with pulse pressures) is then given by the difference between the curve A N Q' representing the remaining original pulse and the curve A N F D representing the reflected pulse. Over the depth A D the net result is a tension in the water increasing from zero at the surface to a magnitude E F' at the depth D. Let the instant depicted in fig. 12b be so chosen that E F is equal to the greatest tension that the water can withstand. At this instant, therefore, the water will cavitate at the depth D and the layer of thickness A D will be projected upwards. The top D F of the water below will then behave as a new free surface from which the remaining pulse D E Q' is reflected as a tensile wave and the whole process can be repeated. If E F, representing the tensile strength of the water, is small compared with D F, representing the maximum pressure in the original pulse, a succession of thin layers is projected upwards each of which will break into drops.

76. The reflected pulse is produced in effect by a "negative" charge above the water tending to suck the water towards it. The particle velocity in the water due to the reflected pulse is thus upwards, that is, in the same direction as that due to the original pulse. If the cavitation tension E F is very small, the tension in the reflected pulse will be approximately uniform throughout the thin layer A D and equal to the pressure, similarly uniform, due to the original pulse. Each pulse will then contribute approximately equal particle velocities and the total particle velocity will be approximately twice that due to the original pulse. Considering the first very thin layer and using equation 17 the velocity of upwards projection of this first layer will be

$$v_o = \frac{2p_m}{\rho c} \quad \ldots \quad \ldots \quad \ldots \quad \ldots \quad \ldots \quad \ldots \quad \ldots \quad \ldots \quad (27)$$

where p_m is the pressure at the pulse front. For the next layer the same type of formula would hold but P_m, represented by D F in fig. 12b, is replaced by the slightly smaller pressure represented by D E. Since the pressure in the original pulse decreases steadily each successive layer will be projected with slightly smaller velocity than the preceding layer. In particular, therefore, the top of the dome is formed by drops from the first initial layer and attention will be concentrated on this layer.

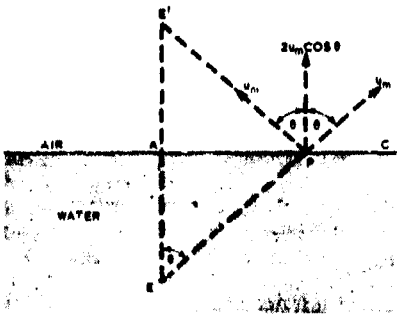


Fig.13 - Resultant velocity of projected water

77. So far, only a point immediately above the explosion has been discussed. In fig.13, E represents the charge and E' its image in the sea surface A C. Consider a point P in the direction E P making angle θ with the vertical. Due to the original pulse, the initial particle velocity at P is u_m in the direction E P, whilst due to the reflected pulse it is u_m directed along P E'. The resultant velocity v of the water projected initially at P is thus

$$v = 2u_m\cos\theta = \frac{2p_m}{\rho c}\cos\theta \quad \ldots \quad \ldots \quad (28)$$

where p_m refers to the maximum pressure at P. Since p_m and u_m vary inversely as the distance E P, the variation of v along the surface for a given weight and position of charge is of the form

$$v \propto \cos^2\theta \quad \ldots \quad \ldots \quad \ldots \quad (29)$$

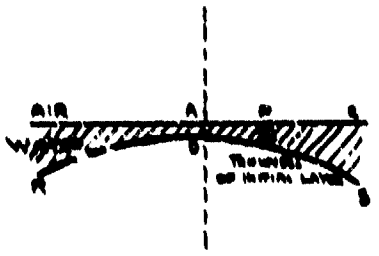


Fig.14 - Variation in thickness of the initial layer of spray dome

The initial upwards velocity of the drops thus decreases steadily as the horizontal distance from A increases and leads to a dome-shaped contour. With the assumption made, the dome would extend to infinity but the introduction of a finite value for the tension at which water cavitates would restrict the dome to a finite area of surface as observed in practice. Further, for a finite cavitation tension, the thickness of the initial layer projected at P in fig.14 will be greater than at A, the variation of thickness with distance A P being qualitatively of the shape R D S. As the layer increases in thickness a stage will be reached where it no longer breaks up to be projected as spray and an edge will be formed to the visible dome.

78. Beyond the dome there is thus a region in which rupture occurs below the surface to form a relatively thick top layer in a state of tension. It is observed in practice that the spray dome is surrounded by a "black ring", the outer radius of which is fully double that of the dome. If a given size of charge is exploded below a certain depth there is no spray dome, the maximum pressure being insufficient to cause cavitation in thin layers. Empirically, this depth for T.N.T. charges occurs when the maximum pressure p_m in the pulse on arrival at the surface is less than about 1/3 ton per sq. in. Thus, for example, there is no spray dome if a 300 lb. charge is exploded deeper than about 140 ft.

The precise mechanism of the surface phenomena has not been finally elucidated. Spark photographs of small sub-surface explosions, show that the free surface, as it is thrown upwards, breaks into a very large number of "needles or spikes". The tops of the needles peel off as drops. The implication of this result is that an instability of the interface has appeared at some early stage in the upward motion. This agrees with some mathematical and experimental investigations of G.I. Taylor and D.L. Lewis. They have proved that if a system composed of two media, with a common interface containing small irregularities (i.e. ripples), is accelerated in the direction from the denser medium to the lighter medium, the irregularities grow exponentially with time. The shock wave striking the free surface is a limiting case of this phenomenon, in that it causes a finite change in velocity instantaneously. The effect is to cause the crests of any small irregularities to shoot ahead of the main bulk of the water.

The initial velocity of the "profile" of these water drops is greater than the velocity v, considered in equation (29). Were this not so, measurements of the initial velocity distribution of the dome would permit one to calculate the exact depth of the explosion, and the peak pressure-distance relationship. Such calculations have in fact been made with reasonable success; and one must therefore conclude that the instability in the very early part of the motion of the dome is soon absorbed in the bulk motion, which thereafter proceeds as if the instability had never existed.

The magnification of surface ripples by the underwater shock decreases rapidly with horizontal distance away from the point on the surface above the explosion. Cine photographs of the surface show a darkening effect before anything else can be seen (18a). The exact size of this "black ring" depends on many factors, especially the lighting conditions, but there can be no doubt that the fundamental explanation is to be found in Taylor's ideas on the instability of an accelerated interface, in contrast with other explanations which relate the darkening to cavitation below the surface.

79. The spray dome is not of direct interest in connection with damage since it represent energy wasted from the attacker's point of view. However, the theory of its formation, using equations 27 and 28 or more complicated analogous formulae allowing for a finite tensile strength of water, can be of some use for subsidiary purposes in conjunction with experimental measurements from cine films of spray velocity, size and shape of the dome. In particular, the depth of explosion of charges dropped from aircraft can be estimated whilst on the more fundamental side such measurements can be used to obtain empirical data for the maximum pressure p_m in the pulse.

80. Occasionally, it is possible to distinguish a later secondary spray dome due to the first bubble pulse. The effect is generally indistinct because for deeper charges the bubble pulse and the resulting secondary dome are small, whilst for shallower charges this dome tends to be obscured by the plumes breaking through very soon afterwards. For charges near enough to the surface for the bubble to break surface on its first expansion, for example, 20 ft. or less for an amatol depth charge, there is of course no bubble pulse and no secondary dome.

The plume

81. The second phase of the visible surface effects is the eruption, through the dome of the water displaced bodily by the bubble motion. The resulting plume is somewhat variable in character and time of appearance but it has been possible in some instances to relate, at least approximately, the plume phenomena with the bubble motion. For a 500 lb. T.N.T. charge exploded at a depth of 50 feet, the first sign of plume appears 1½ sec. after the first appearance of the spray dome. For shallower depths of explosion the interval becomes shorter until finally the plume and dome become indistinguishable. On the other hand, as the charge depth increases, the interval becomes longer and the effects decrease. At a depth for which the spray dome no longer occurs, all that appears of the plume is a churning of the surface some seconds after the explosion as the residual gases stream up, the gas bubble having degenerated into small bubbles with little internal pressure.

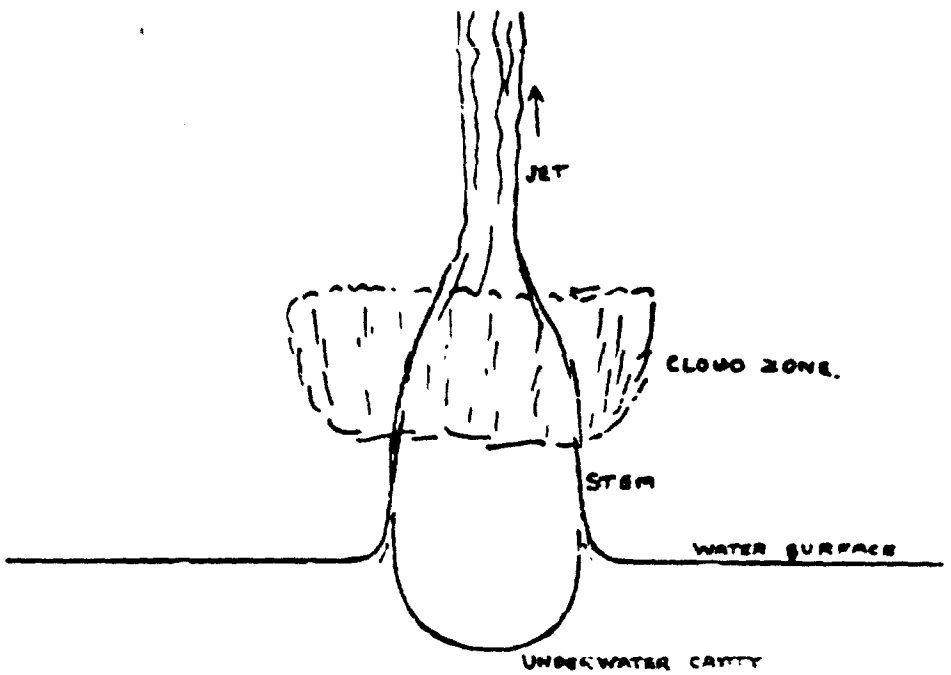
82. A remarkable plume results from the detonation of a charge close to the surface when the gas bubble vents through the surface with a high efflux velocity. The plume structure from a normal type of explosive of weight W lbs. detonated at a depth D feet, where $W^{\frac{1}{3}}/D$ is about 4 lbs.$^{\frac{1}{3}}$ feet^{-1}, i.e. a charge with its centre at about one charge diameter below the surface, is shown in the diagram. This illustrates the typical behaviour of such shallow underwater explosions.

When the gas bubble vents, the gas rapidly overexpands, entraining water from the region of venting into the brush-like cloud some which consists of finely divided water and gas, and so tends to disperse rapidly. Meanwhile the detonation impulse imparted below the surface generates an expanding cavity which is almost hemispherical. The water close to the free surface is, however, unconstrained and peels upwards to form the stem of the plume, the base of the stem keeping in step with the expanding cavity. The hollow nature of the stem sheath has been confirmed by pulse X-ray photographs. The gas pressure within the stem rapidly falls to a sub-atmospheric value as the stem expands and the excess pressure of the outside atmosphere makes the fluid in the stem reconverge into a jet which moves upwards with a high velocity. A tall slender column ensues which reaches a relatively great height and is characteristic of such shallow explosions.

If the depth of detonation D is increased slightly the initial appearance of the plume is slightly changed because the gas pressure on venting is reduced. The dimensions of the cloud zone diminish with the respect to the diameter of the stem until for a depth of detonation D where $W^{\frac{1}{3}}/D$ is about 1.5 $lb.^{\frac{1}{3}}$ $feet^{-1}$ the cloud zone width equals that the stem at maximum growth, i.e. about 20 charge diameters. The mechanism of stem and jet formation is, however, fundamentally unaltered. For geometrically similar shallow underwater explosions of different scales, the dimensions of the various plume features scale roughly as the linear dimensions of the experiment or as the cube root of the charge weight.

Some idea of the heights attained by the jets from such shallow underwater explosions is afforded by the following figures. A 10 lbs. charge of P.E. No. 2 at a depth of 1.6 feet, i.e. where $W^{\frac{1}{3}}/D = 1.3$ forms a jet which reaches a height of over 200 feet. A 300 lbs. depth charge fired at 5 ft. below the surface, i.e. $W^{\frac{1}{3}}/D = 1.4$ forms a jet which reaches over 600 feet and is only about 30 to 40 feet in diameter.

Fig. 14a



Best Available Copy

INTERACTION BETWEEN TARGET AND WATER PHENOMENA DUE TO NON-CONTACT EXPLOSIONS

83. So far in this chapter, the explosion has been assumed to take place in open water with no target present and attention has been concentrated on the resulting pressure in the water. However, the presence and behaviour of the target modifies this pressure so that it is not possible to make the simple assumption that the target is subjected to the pressure which would occur in the absence of the target. The important and rather difficult problem of the interaction between target and explosion effects must, therefore, be considered.

84. First, the effects associated with the pressure pulse will be studied. Existing theories for the interaction between the pressure pulse and a target have followed two basic lines depending on two different simple types of target:-

(1) the target is assumed to be plane and of infinite extent but capable of yielding.

(2) the target is considered to be plane but only a finite area is assumed to yield, the remainder of the target being fixed and rigid.

In general, the first type of theory is more relevant to actual ship targets whilst the second type of theory is especially relevant to special types of single-plate targets used in small-scale research.

Pressure pulse incident on infinite plane air-backed plate

85. The dimensions of actual ship targets are usually large compared with the effective length of the pulse and the curvature of the ship's plating is small. Therefore, it is not unreasonable to regard the hull plating to be an infinite plane plate. As a further simplication, the resistance to deformation of the hull is represented by a resistance distributed uniformly over the plane area, the movement of any element of area being opposed by a force proportional to displacement* of the element.

---

*Such a resistance is usually associated with an elastic spring but, as explained later, this linear relation holds also for plastic stretching of a plate; it is the latter rather than the former which is being simulated, since elastic deformation itself involves no permanent damage.

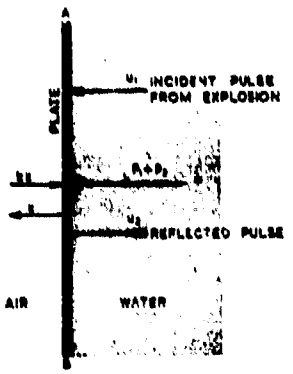


Fig. 15 - Pressure pulse incident on unit area of infinite plate

86. For the simplest case, the pressure pulse arrives at normal incidence and the explosion is sufficiently far away for the pulse to be treated as a plane wave. Every element in the plane plate then behaves in the same way and attention can be fixed on unit area. The incident pressure pulse from the explosion will then give rise to a reflected pulse, the form and magnitude of which will depend on the motion of the plate. Fig. 15 shows the pressure pulse incident on unit area of infinite plate. Expressions for the displacement of the plate and the pressure on it are derived at Appendix C where it is shown that if

t = time measured from the first arrival of the pulse at the plate
x = displacement of plate
k = resistance to motion for unit area per unit displacement of the plate
p_1 = pressure in incident pulse
p_2 = pressure in reflected pulse
p = pressure on plate
p_o = maximum pressure in incident pulse (at time $t = 0$)
u_1 = particle velocity due to the incident pulse in water touching plate
u_2 = particle velocity due to the reflected pulse in water touching plate
ρ = mass density of water
c = velocity of sound in water
m = mass of plate per unit area of surface
n = exponential parameter determining rate of decay of pressure

Then
$$x = \frac{2p_o}{mn^2(\varepsilon-1)\varepsilon}\left\{\varepsilon-1+e^{-n\varepsilon t}-\varepsilon e^{-nt}\right\} \quad \ldots \quad \ldots \quad \ldots \quad (30)$$

$$p = p_1+p_2 = \frac{2p_o}{\varepsilon-1}\left\{\varepsilon e^{-n\varepsilon t}-e^{-nt}\right\} \quad \ldots \quad \ldots \quad \ldots \quad (31)$$

where
$$\varepsilon = \frac{\rho c}{mn} \quad \ldots \quad \ldots \quad \ldots \quad \ldots \quad \ldots \quad \ldots \quad (32)$$

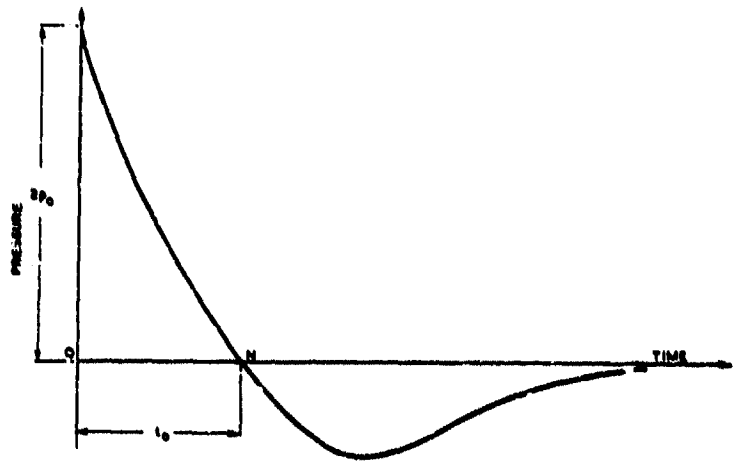


Fig. 16 - Pressure on plate when there is no cavitation at plate or in water

Fig. 16 illustrates the pressure/time variation of equation 31 diagrammatically and shows that the pressure acting on the plate will be initially $2p_o$ which corresponds to instantaneous complete reflection. The pressure then decreases to zero, followed by negative values which will ultimately tend to zero asymptotically.

87. This occurrence of tensions between the water and the plate raises immediately the question as to whether any appreciable tension can in fact be sustained between water and paint or steel. Further, if the preceding theory were correct, after tension develops between the plate and the water, there will also be tension in the water for some distance away from the plate. Can water withstand these tensions? Moreover, even if the water does not break, can it exert an appreciable tension on the plate? The answers to these questions, affect vitally the whole problem of damage to air-backed plates by the pressure pulse. Three cases will be considered:-

(1) The water sticks to the plate and does not cavitate.

(2) The water cannot exert any tension on the plate, but does not itself cavitate.

(3) The water cannot exert any tension on the plate and itself cavitates after the plate leaves the water.

Water sticks to plate and does not cavitate

88. Equation 30 holds for any value of time and the maximum value of the displacement, which occurs when t becomes infinitely large, is given by

$$x_{max} = \frac{2p_o}{mn^2\epsilon} = \frac{2p_o}{\rho cn} \quad \ldots \quad \ldots \quad \ldots \quad \ldots \quad \ldots \quad \ldots \quad (33)$$

This maximum displacement is independent of the target properties, being in fact simply twice the displacement associated with the pulse in mid-water with no target present. It indicates, for example, that at 50 ft. from a charge of 300 lb. T.N.T. the maximum deflection of the plating would only be about 0.4 in. This is certainly too small in comparison with observed damage to single-hulled surface vessels having plating about 1/4 in. thick. In general, therefore, the assumptions of this case seem unlikely to be relevant in the practical problem of damage.

Water exerts no tension on plate but does not cavitate

89. The solution given by equation 30 is now valid only for the initial period t_o in fig. 16 during which the pressure on the plate is positive. At $t = t_o$ the plate will leave the water and will subsequently be brought to rest by the resistance kx. Putting $p = 0$ in equation 31, the time t_o is given by

$$nt_o = \frac{1}{\xi - 1} \log \xi \quad \ldots \quad \ldots \quad \ldots \quad \ldots \quad \ldots \quad (34)$$

and thence by use* of equation 30 the velocity v_o of the plate at this time is

$$v_o = \frac{2p_o}{\rho c} \xi^{\frac{1}{1-\xi}} \quad \ldots \quad \ldots \quad \ldots \quad \ldots \quad \ldots \quad (35)$$

this is the velocity with which the plate leaves the water. Whilst it may be permissible under most relevant practical conditions to neglect the stiffness term kx during the time t_o in order to derive equation 35, it is essential to introduce this resistance during the subsequent motion since it is then the only mechanism which brings the plating to rest. The subsequent maximum displacement x_{max} is easily obtained from the energy equation

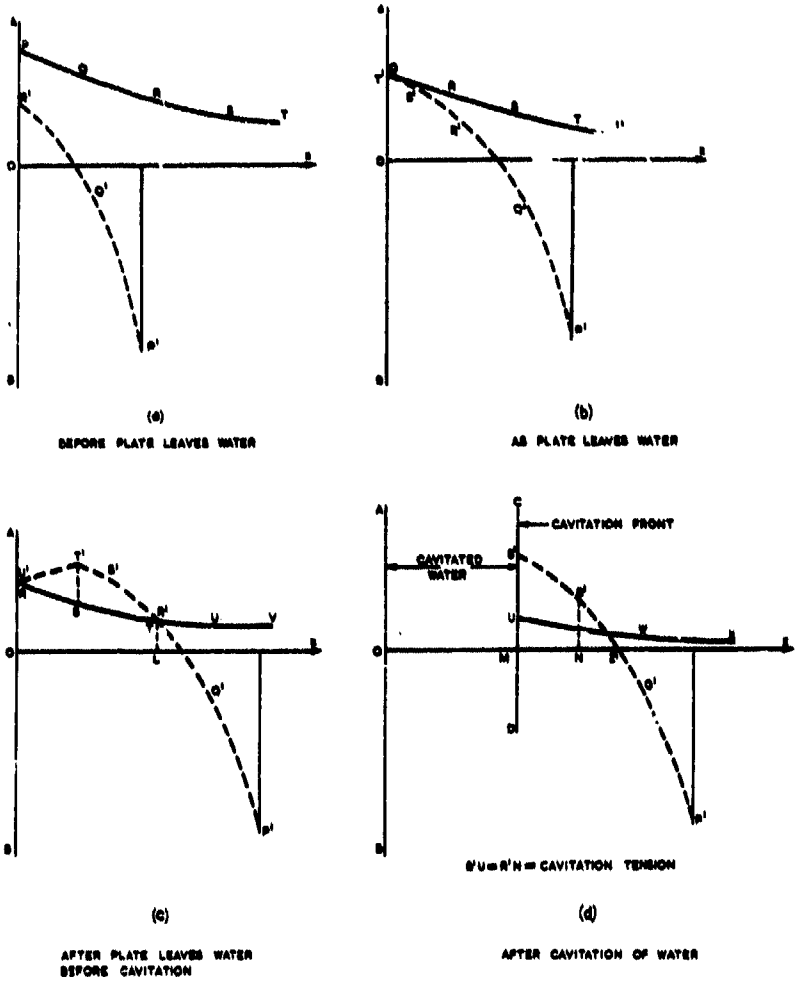
$$\frac{1}{2} k x_{max}^2 = \frac{1}{2} m v_o^2 \quad \ldots \quad \ldots \quad \ldots \quad \ldots \quad \ldots \quad (36)$$

The maximum displacement given by equations 35 and 36 will be greater than that given by equation 33 for case 1, the stiffness k being restricted to values small enough for it to be neglected, as assumed in deriving both equations 33 and 35. For example, with 1/4 in. plate and typical stiffness, the explosion of 300 lb. T.N.T. at a distance of 50 ft. would produce a deflection of about 1.2 in. on the assumptions of case 2 as compared with the estimate of 0.4 in. for case 1. The damage (as indicated by maximum displacement) estimated on the assumptions of case 2 is still, however, on the small side in comparison with observed damage in many cases. It is desirable, therefore, to see whether the remaining case 3 will lead to greater estimates of damage.

---

* Equation 35 is obtained by differentiating equation 30 with respect to time that is,

$$v_o = \left(\frac{dx}{dt}\right)_{t=t_o}$$



P'U' = R'N = CAVITATION TENSION

Notes

Full curves lettered P-X show incident wave travelling to left, pressure positive above Ox
Broken curves lettered P'U' show refected wave (plotted negatively) travelling to right, pressure positive below Ox

AB indicates original plate position

Fig. 17 - Successive stages when plate leaves water which subsequently cavitates

90. For comparison with case 3 it is convenient to express the results for the present case 2 in terms of the fraction of the energy of the incident pulse which is communicated to the plate. Writing,

$$\Omega' = \tfrac{1}{2}mv_o^2 \quad = \text{energy communicated to unit area of plate} \quad \ldots \quad (37)$$

$$\Omega_i = \frac{p_o^2}{2\rho a n} \quad = \text{energy in the pressure pulse, incident on unit area of the plate} \quad \ldots \quad (38)$$

then from equations 35 and 32 it follows that

$$\frac{\Omega'}{\Omega_i} = 4\epsilon^{\frac{1+\epsilon}{1-\epsilon}} \quad \ldots \quad \ldots \quad \ldots \quad \ldots \quad \ldots \quad \ldots \quad \ldots \quad \ldots \quad (39)$$

Water exerts no tension on plate and cavitates after plate leaves water

91. Consider the general case where the water cavitates at some finite tension. The conditions in the water at various stages of the motion are then illustrated diagrammatically in fig. 17 which shows in each stage the incident pulse, lettered P to X, moving to the left and the reflected pulse, lettered P' to U', moving to the right; the latter is plotted negatively since it is easier to see at a glance the resultant pressure or tension as the difference rather than as the sum of the ordinates of two curves. Fig. 17a illustrates the conditions prior to the plate leaving the water, the net pressure, given by the difference between the curves PQRST and P'Q'R', being positive everywhere. (Fig. 17a applies also for the previous cases 1 and 2).

92. Fig. 17b illustrates conditions at the instant the plate breaks away from the water, the net pressure being zero at the plate and positive elsewhere. Fig. 17c illustrates the conditions after this instant but prior to any cavitation in the water. The water is subjected to a net tension over the range OL and to a net pressure for greater distances from the original plate position. The plate is now ahead of the water, that is to the left of AB, with a gap between. The abrupt change of slope at T' in fig. 17c corresponds to the change-over as the plate leaves the water, from reflection of the incident pulse at the accelerating plate to reflection at the subsequent free water surface AB. (The conditions shown in fig. 17c represent also the water conditions in case 2).

93. Fig. 17c will continue to represent the events in the water until the greatest net tension T'S exceeds the tensile strength of the water. The resultant particle velocity in the water is represented (to arbitrary scale) by the sum of the full and broken curves in fig. 17. In particular, therefore, the water to the left of T'S in fig. 17c is moving to the left and if T'S becomes just greater than the tensile strength of water, the layer to the left will break away and follow up the plate.

94. For a finite tensile strength of water, this first layer will be of finite thickness, but due to the shape of the curves for the incident and reflected pulses, subsequent layers of infinitesimal thickness will be projected after the plate and in effect a "cavitation front" is propagated back through the water away from the original plate position. The subsequent conditions following such cavitation in the water are illustrated in fig. 17d where the cavitation front at position CD separates the water on the left, which has cavitated and is following up the plate, from the water on the right which has not yet cavitated.

95. The cavitation front travels back through the water with a velocity greater than the velocity of the individual pulses, and finally the only part of the reflected pulse which "escapes" from the neighbourhood of the plate is the part P'Q'R' in fig. 17d in which the pressure is either positive or, if negative, of magnitude less than the tension R'N to cause cavitation.

96. Summing up, the essential features of the motion according to these assumptions are first the plate is projected away from the water, secondly, the water cavitates and follows up the plate and thirdly, only the initial portion P'Q'R' of the reflected pulse escapes to large distances from the plate.

97. The velocity v_0 with which the plate leaves the water is greater than the velocity of the water which follows up, but as the plate is slowed down by the resistance kx of the supporting structure, the first layer of water will catch up the plate. As the succeeding layers of water also catch up, the plate will have an increasing thickness of water moving with it as it is slowed down by the resistance of the supporting structure. Some of the kinetic energy of the water which follows up will be lost on impact as each layer catches up the plate and water ahead, but the rest of this kinetic energy must ultimately be absorbed by the resistance of the supporting structure. The final maximum displacement of the plate, representing "damage", will thus be greater in case 3 when the water follows up than in the previous case 2 where there was no such phenomenon. To illustrate the potential magnitude of such increase in damage, the simplest case where the water cavitates at zero tension is considered, the energy lost on impact as the successive layers catch up the plate and water ahead being neglected.

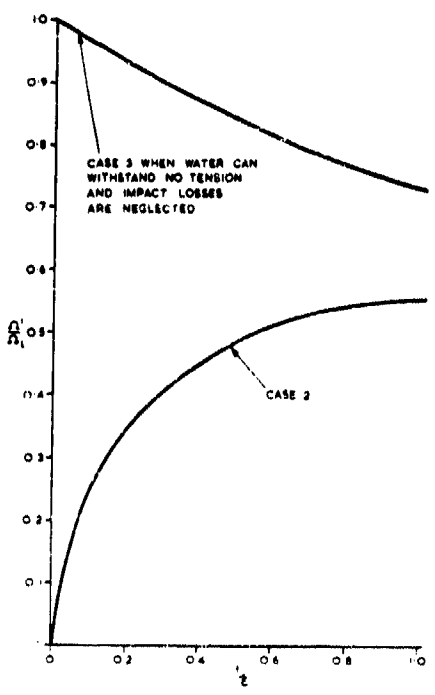


Fig. 18 - Energy transferred to target from pressure pulse

98. With the above simplifying assumptions, the total energy to be absorbed by the resistance kx is the total energy Ω_1 of the original incident pulse less the energy Ω_+ of the positive portion P'Q'Z' in fig. 17d of the reflected pulse which travels away to large distances from the plate. With the assumed neglect of kx in the initial stages of the motion when the positive portion of the reflected pulse is produced, the energy Ω_+ in this positive portion depends only on ξ and the remaining fraction of the incident energy which is to be absorbed by the resistance kx is shown plotted as the upper curve in fig. 18 against an abscissa $1/\xi \leq 1$. For most practical conditions of non-contact explosions against single-hulled vessels the value of ξ is relatively large corresponding to small values of the abscissa, less than 0.2 in fig. 18. The upper curve indicates that for such cases, over 90% of the incident energy has to be absorbed by the resistance of the plate to displacement. For comparison, the lower curve in fig. 18 shows the fraction of the incident energy given to the plate, according to equation 38, for case 2 where there is no follow-up effect. For practical cases corresponding

to small abscissae in fig. 18 it is seen that in case 3 the energy communicated to the plate is about three times or more than the corresponding communicated energy in case 2. More damage is thus to be expected in case 3 than in case 2.

99. The upper curve of fig. 18 is based on the neglect of the energy lost by impact as the cavitated water catches up the plate. A more rigorous analysis, allowing for such impact losses, suggests that for practical cases of large ξ, the energy finally transferred to the target is about two-thirds of the incident energy. This communicated energy is still, however, considerably greater than that given by the lower curve (case 2) in fig. 18 for small abscissae corresponding to large ξ.

100. The actual mechanism of cavitation as indicated by underwater photographs of air-backed plates subjected to small-scale explosions is the formation of bubbles in the water which at first grow in size and later collapse as the water piles up on the decelerating plate. Whilst the preceding simpler picture of the bombardment of the plate by successive layers is thus not strictly correct, the main conclusions already given are not invalidated. The essential feature from the damage aspect is that cavitation enables the water to follow-up the plate and transfer appreciable extra energy from the water to the target. It appears to be relatively unimportant whether such follow-up takes place by the water splitting into layers which bombard the plate or whether it occurs by the water "stretching" due to the formation of bubbles which subsequently collapse as the water piles up on the plate and moves forward with it.

101. The effect of a plane pulse arriving at an oblique angle instead of at normal incidence can be taken into account quite simply. If χ be the angle between the pulse front and the plate ($\chi = 0$ for normal incidence), then first, equations 30 to 35 can be simply generalised by writing $p_o \cos\chi$ for p_o and $u \cos\chi$ for u. In particular, equation 32 becomes

$$\xi = \frac{\rho_o}{m_n \cos\chi} \quad \ldots \quad \ldots \quad \ldots \quad \ldots \quad \ldots \quad \ldots \quad \ldots \quad (40)$$

Secondly, the energy incident on unit area of the plate is no longer the same as the energy per unit area of the pulse front, the two unit areas making angle χ with one another. It is the former energy which is relevant and equation 38 is replaced by

$$\Omega_i = \frac{p_o^2 \cos\chi}{2\rho_o m_n} \quad \ldots \quad \ldots \quad \ldots \quad \ldots \quad \ldots \quad \ldots \quad (41)$$

Thus, if ξ and Ω_i are defined by equations 40 and 41, the curves of fig. 18 hold, in general, for oblique incidence as well as normal incidence. Taking into account impact losses, the general result that about two-thirds of the incident energy is transferred to the target still holds for oblique incidence, the only effect of incidence being the decrease of Ω_i, the energy incident per unit area of plate, with increasing obliquity*.

---

* For glancing incidence, it is possible that anomalous results occur but such cases are usually unimportant since Ω_i is then so small.

Best Available Copy

102. The fact that the pulse front is spherical and not plane has also been investigated[11] and it was concluded that up to the time at which the plate leaves the water the assumption of a plane wave is a reasonable approximation. Beyond this time, that is when cavitation sets in, the analysis for the spherical pulse is also invalid. However, it seems likely that in practical cases the curvature of the pulse front will still have little effect. In general, it seems probable that the mechanism of transfer of energy from water to target envisaged in case 3, involving cavitation and follow-up of the water is the most common process for single-hulled ships subjected to the pressure pulse from non-contact explosions, especially when the conditions are such that appreciable deformation or even rupture of the hull occurs.

Pressure pulse incident on a yielding diaphragm in an infinite unyielding baffle

103. A considerable amount of experimental work, both empirical and fundamental, has been carried out by using targets consisting of a single circular or rectangular air-backed plate to represent a panel of ships' plating. In a ship, any one panel of plating dishing under the action of the pressure pulse, is restrained from pulling in round its edges by the surrounding panels of plating.

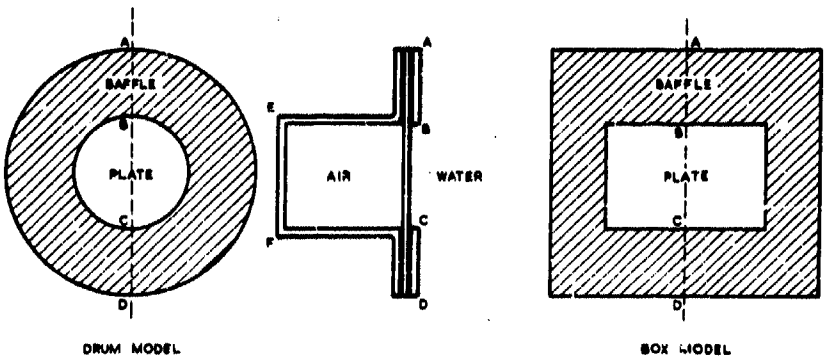


Fig. 19 - Essential features of box and drum models

Fig. 19 shows a typical single plate target, the air-backed plate BC forming one face of a strong box BEFC. To simulate the resistance of the surrounding panels and to prevent damage to the box (which can then be used for many experiments) the plate is much larger than the face of the box and is fastened by bolts or by welding to a thick rigid baffle indicated in section by AB and CD For the present discussion, the essential feature of this type of target is that the large surrounding baffle is relatively unyielding, being not only very stiff itself but also water-backed. The presence of the baffle can modify appreciably the transfer of energy from the water to the effective target plate BC. Much theoretical analysis has been carried out for such targets but it will suffice here to give only the analysis[12] for the simplest assumptions since this serves to bring out the essential differences between this type of theory and the infinite plate theory already discussed.

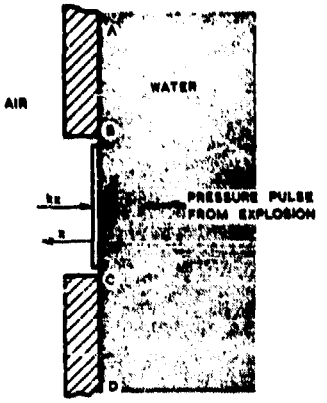


Fig. 20 - Pressure pulse incident on yielding piston in infinite unyielding wall

104. The yielding plate BC of fig. 19 is represented in fig. 20 by a rigid piston BC whose motion is resisted by a force proportional to displacement. The baffle is considered to be effectively infinite in extent and completely fixed and rigid. The pressure pulse is taken to be a plane pulse of small amplitude arriving at normal incidence to reach the target at time t = 0, the pressure in the pulse varying with time according to the exponential form of equation 10. The problem can be considered in two stages:-

(1) if the piston BC be held fixed then the whole plane ABCD in fig. 20 is fixed and rigid and the pressure pulse undergoes complete reflection. In particular, the pressure on BC will then be twice that in the incidence pulse, namely:-

$$\text{pressure with BC fixed} = 2p_o e^{-\eta t} \quad \ldots \quad \ldots \quad (42)$$

(2) the effect of the motion of the piston must now be added and as an approximation the compressibility of the water can be neglected so far as this motion is concerned. The second stage of the problem is thus to consider the incompressible flow associated with the motion of a rigid piston in an aperture of a rigid wall. So far as the piston motion is concerned, this flow results in an increase of the effective mass of the piston by the addition of a virtual mass M', the magnitude of which depends on the size and shape of the aperture.

105. For a circular piston of radius a in an aperture of a rigid wall in water of mass density , the virtual mass M' is given by[*]:-

$$M' = \frac{8}{3}\rho a^3 \quad \ldots \quad \ldots \quad \ldots \quad \ldots \quad \ldots \quad \ldots \quad \ldots \quad (43)$$

This mass of water M' effectively moves with the piston of mass M and exerts a drag on the piston which decelerates it. In addition, the resistance kx on the back of the piston also resists the movement of the piston caused by the incident pulse. The equation of motion[*] for the piston can, therefore, be formed from these three forces. The resistance kx is small in the initial stages, that is, when the force due to the incident pulse is not small. If the resistance kx is neglected, an approximate relation for the velocity v communicated by the pulse to the piston is given by

$$v = \frac{2\pi a^2 p_o}{(M+M')\eta} \quad \ldots \quad \ldots \quad \ldots \quad \ldots \quad \ldots \quad \ldots \quad (44)$$

---

[*] The equation of motion is:- $(M+M')\frac{d^2x}{dt^2} + kx = 2\pi a^2 p_o e^{-\eta t}$

If the term kx is neglected the solution for the velocity v is:-

$$v = \frac{dx}{dt} = \frac{2\pi a^2 p_o}{(M+M')} \int e^{-\eta t}\, dt = \frac{2\pi a^2 p_o}{(M+M')\eta}$$

The corresponding energy given to the piston and the entrained water of mass M' is then

$$\tfrac{1}{2}(M+M')v^2 = \frac{2\pi a^4 p_0^2}{(M+M')n^2} \quad \ldots \quad \ldots \quad \ldots \quad \ldots \quad \ldots \quad \ldots \quad (45)$$

This energy has ultimately to be absorbed by the spring resistance and is the energy communicated from the water to the target.

106. For comparison with the previous infinite plate theory it is convenient to express the results in terms of unit area of the piston. If

$$m = \frac{M}{\pi a^2} = \text{mass per unit area of piston} \quad \ldots \quad \ldots \quad (46)$$

$$\Omega' = \frac{(M+M')v^2}{2\pi a^2} = \text{energy transferred per unit area of piston} \quad (47)$$

$$\Omega_i = \frac{p_0^2}{2\rho c n} = \text{energy } \underline{\text{directly}} \text{ incident on unit area of piston} \quad \ldots \quad \ldots \quad \ldots \quad \ldots \quad \ldots \quad (48)$$

then using equation 43 for M' it then follows from equations 45 to 48 that

$$\frac{\Omega'}{\Omega_i} = \frac{3\pi}{2}\left(\frac{c}{na}\right)\left\{\frac{1}{1+\frac{3\pi m}{8\rho a}}\right\} \quad \ldots \quad \ldots \quad \ldots \quad \ldots \quad \ldots \quad (49)$$

In equation 49, the fraction $3\pi m/8\rho a$ is always small for practical ratios of plate thickness to plate diameter. The main factor determining the magnitude of Ω'/Ω_i is thus the ratio of c/n, the characteristic length of the pulse as given for example by equation 21, to the plate radius a. For a given target, that is given a, the ratio Ω'/Ω_i will increase steadily as c/n increases, that is as the size of the charge increases and there will be a particular size of charge for which $\Omega' = \Omega_i$. For larger charges giving longer pulses, the communicated energy Ω' will become greater than the energy Ω_i in that portion of the pulse which is directly incident on the target. What happens physically is that the pulse striking the baffle round the piston or plate is reflected without any absorption of energy and the pressure in front of the baffle is higher than in front of the yielding piston. Equalisation of pressure then tends to set in by the formation of a diffraction wave starting out from the periphery of the piston. This wave contributes an increase of pressure on the piston and a decrease of pressure on the baffle. In this way, some of the energy of the pulse incident on the baffle is diffracted on to the piston. The diffraction of sound pulses of small amplitude in water is similar to diffraction in air discussed in Part 1 Chapter 4 of this Textbook where it is pointed out that long pulses are subject to greater diffraction than short pulses. This same effect is evident in the present problem and is responsible for the steady increases of Ω' with increasing length of pulse.

107. The preceding simple theory has been extended by a number of refinements of which the most important is the consideration of the effect of the compressibility of the water. The assumption of incompressible flow implies that the water everywhere in contact with the piston knows immediately of the reflection of the pulse at the surrounding baffle and

modifies its motion accordingly. In fact, the news of such reflection travels through the water with the velocity c of sound and takes time a/c to reach the centre of the piston by way of the water. Moreover, the assumption of a rigid piston implies that the effect of any increase of pressure near the edge of the piston is shared out instantaneously over the whole piston; in fact, appreciable effects travel relatively slowly from the edge to the centre of a thin plate - more slowly than the velocity c of effects in the water. The net result is that in an actual drum target the element of the plate at its centre is unaware of the existence of the baffle until time a/c and up to this time it will behave as part of an infinite plate and the theory of para. 89-102 is relevant.

108. From equations 34 and 32 it can be shown that t_c increases as n decreases, that is as the length of the pulse c/n increases; this time t_c corresponds to the first occurrence of tensions with possible cavitation in the water. Hence, in the present problem, with a sufficiently long pulse the diffraction wave from the edge will reach the centre of the plate (in the time a/c) before the occurrence of any tension. The increase of pressure due to this diffraction wave may prevent any tensions developing. For a sufficiently long pulse, therefore, cavitation will not occur and the ultimate motion of the piston will be the same as that indicated by the assumption of incompressible flow. The effect of compressibility is then merely to produce a decaying oscillation superimposed on the motion for incompressible flow.[14]

109. For the other extreme of a very short pulse, the position is quite different. In this case, the process of case 3 involving cavitation will be virtually complete at the centre of the plate before the diffraction wave arrives from the edge and since the diffracted pressure is feeble for a short pulse it can have little effect on the amount of energy communicated to the target.

110. For intermediate lengths of pulse, there may be both appreciable cavitation and appreciable diffraction.[15] Physically, in such cases cavitation will tend to commence at the centre of the plate and spread back through the water as a beard of bubbly water, the bubbles being subsequently closed up both by the diffracted pressure from the baffle and by the water piling up on the decelerated plate. Quantitatively, this process is difficult to analyse,[16] but qualitatively it seems fairly certain that the effect of the diffraction from the baffle must be to communicate more energy to the target than that deduced for the preceding case 3 on infinite plate theory. The previous estimate for case 3 that about two-thirds of the directly-incident energy is transferred to the target should thus form a lower limit for single-plate targets of box or drum type subjected to explosives causing appreciable damage. On the other hand for the longer pulses where equation 49 indicates an energy transfer in excess of the lower limit, the use of this equation should provide an upper limit since it neglects any impact losses associated with the closing up of the cavitated water.

111. The assumption that the baffle is infinite in extent will be a reasonable approximation for a baffle of finite size only if the baffle width is large compared with the length of the pulse. For actual drum targets the outer diameter of the baffle is usually about twice the diameter of the air-backed plate and the assumption of an infinite baffle will not be justified for pulses of length comparable with, or greater than, the plate radius. Most experiments with drum targets have, however, been carried out with small charges for which the length of the pressure pulse is only about one-fifth of the plate radius so that the assumption of an infinite baffle is a fair approximation. As an exception, gauges[17] composed essentially of a stout cylindrical body closed at each end by a copper diaphragm with a small baffle, have been used for many years in trials with full-scale charges, the volume of dishing of the diaphragms being taken as an empirical measure of the potential damaging power of the

explosion. In such trials with large charges, for example, 300 lb. T.N.T., the pulse length is long compared with the size of the gauge and the preceding theory for an infinite baffle is not applicable. A very similar approximate theory can, however, be used. Thus if the pulse is very long compared with the gauge dimensions it can be argued that if the diaphragms be held fixed, diffraction round the sphere will rapidly equalise the pressure all over the gauge and this pressure will be approximately the same as that in the incident pulse. This corresponds simply to dropping the factor 2 in equation 42 and the remaining argument can then proceed as for the infinite baffle. In particular, equation 49 will then be modified by the insertion of a factor 0.25 on the right-hand side, that is the transferred energy Ω is only 25% of the similar energy for the case of an infinite baffle. Even so, with a sufficiently long pulse giving a large value of c/na it is still possible for the transferred energy Ω to be many times the directly incident energy, although reflection from a baffle plays no part in the theory. In this case, the yielding of the diaphragm reduces the pressure in its neighbourhood below the incident pressure, and energy is diffracted on to the diaphragm from the surrounding water which is effectively much more unyielding than the diaphragm. It must therefore be realised that whilst the presence of a baffle can increase considerably the energy transferred to a plate, it is by no means essential to have a baffle in order that the transferred energy can be greater than the directly incident energy.

112. Summing up, the main importance of the present theory involving diffraction effects is that it indicates a mechanism by which the energy transferred from the pressure pulse to a target can be greater than that estimated on the previous infinite plate theory. The present theory is most relevant to special types of single plate target used in small-scale experiments because for structural reasons they usually involve a baffle. For actual ships, it would appear that, whilst the infinite plate theory is in general more relevant, some increase of damage due to diffraction effects is possible. For example, the hull plating may be stiffened locally by seatings for machinery and some of the energy incident on these stiffer areas will tend to be diffracted on to unstiffened panels in the vicinity. A similar effect can take place in the vicinity of panels forming one wall of a water or fuel oil storage compartment. In general, such effects are unlikely to be large and if some allowance is to be made for them, the simplest correction is to replace the previous estimate (case 3, para. 99) that about two-thirds of the directly-incident energy is transferred, by the criterion that all this energy is transferred, that is $\Omega = \Omega_i$. Insofar as any simple criterion can be used for the complex problem of damage by underwater explosions, this hypothesis $\Omega = \Omega_i$ is most in accord with experimental results.

113. Finally, for both the infinite plate and the finite plate theories, it may be noted that by expressing results in terms of the energy transferred to the target, the stiffness constant k only enters insofar as it has been assumed effectively small. Generally, provided the resisting force remains small in comparison with inertia forces whilst most of this energy is transferred, the exact nature of this resistance, for example, whether it is constant or varies linearly with displacement, is not important. To this extent, the mechanism by which the damaging effect of the explosion is transferred from the water to the target is independent of the precise nature of the deformation of the target. This greatly simplifies the general problem and enables the transfer process to be discussed broadly without the added complication of a simultaneous consideration of the nature of the deformation of the target.

Bodily motion of targets due to pressure pulse

114. Besides damage to the hull, a ship or target will tend to move as a whole under the action of the pressure pulse from an underwater explosion. Such bodily motion would be expected to decrease, if anything, the damage

Best Available Copy

to the hull. For ships, this effect is probably small, but for small-scale targets, which usually only simulate a typical part of the ship's structure, the bodily motion will be proportionately larger and it is of some importance to estimate whether it is likely to affect the damage.

115. The one theoretical problem for which the bodily motion due to a small-amplitude pulse has been completely solved is that of a rigid sphere and then only on the assumption (usually justified) that the motion is small compared with the radius of the sphere. The analysis cannot easily be condensed and attention will therefore be concentrated on the general conclusions. The bodily motion of the sphere depends on the twin processes of reflection and diffraction, the former tending to increase the motion whilst diffraction of the pulse round to the back of the sphere tends to decrease the bodily motion. If a is the radius of the sphere, x is the distance of the explosion from the centre of the sphere and c/n is the characteristic length of the pulse (assumed exponential), the qualitative results depend on the ratios of these three lengths. The terms long pulse and short pulse will be used to denote the two extreme cases where c/n is large or small, respectively, compared with the radius a of the sphere. For long pulses the analysis and conclusions are restricted to the case where x/a is also large since otherwise the assumption that the pulse is of small amplitude will be violated. Since long pulses correspond to large explosions for most practical targets, this condition that x/a is large will usually be satisfied if catastrophic damage is to be avoided. For short pulses, the theory is not restricted to large values of x/a and in practical cases if the damage is not to be negligible the relevant values of x will usually be of order 2a.

116. The main conclusion from the analysis for a rigid sphere is that the bodily motion of a target is unlikely to affect the damage appreciably in the cases of either:-

(1) a long pulse from a distant large explosion or

(2) a short pulse from a small explosion fairly near the target, for example, $x = 1.25\ a$.

117. For a long plane pulse from a distant large explosion diffraction round the sphere (target) will tend to equalise the pressure on the front and back and this equalisation will be hastened by the actual bodily motion as the sphere moves away from the explosion. Measuring time from the instant at which a plane pulse first strikes the nearest point of the sphere, the diffracted pressure will reach the furthest point on the back of the sphere in time $t = (1+\sqrt{2})a/c = 2.57a/c$ and the analysis in fact indicates that equalisation is virtually complete by this time. Subsequent to this time the residual resultant force on the sphere as a whole is small and negligible. For long pulses, this time of about $2.5\ a/c$ is small compared with the characteristic time $1/n$ of the pulse and in effect only a small initial portion of the pulse produces any appreciable bodily motion. In contrast, the effect of the equalisation of pressure is that all elements of the surface are subjected to a pressure approximating to that in the incident pulse and it is on this relatively long duration pressure that the damage to the target will depend. In general, therefore, the bodily motion has little effect on the damage due to a long pulse from a large distant explosion.

118. For a short pulse from a relatively near small explosion the same conclusion is reached on somewhat different grounds. Here the most relevant fact is that the mass of the target is large in relation to the size of charge and only a small velocity of the target can be produced. In contrast, most of the effect of the pressure pulse will be concentrated on a small portion of the target nearest the explosion and quite large local velocities can be produced. For example, it was estimated that for

a sphere simulating some half-scale targets, the maximum bodily velocity would be only about 12 ft. per sec. whereas the corresponding velocity of the plating nearest the explosion, as deduced from equation 35, was about 380 ft. per sec. The bodily motion may thus be expected to be unimportant for such a case. It will be noticed, that whereas the sphere was assumed rigid in the analysis for estimating bodily motion, the results were used to derive conclusions concerning damage, which automatically implies some yielding of the surface. However, it seems reasonable to expect that the bodily motion of a yielding target will be less than of a rigid target and since the theoretical conclusions refer to cases where the bodily motion is expected to be unimportant, the use of an over-estimation for the bodily motion is justified. However, for cases where the theory of the rigid sphere indicates appreciable bodily motion it would be necessary, for practical application, to revise the theory to include some allowance for yielding. This problem is extremely difficult but some progress for specific targets can be made by approximate methods.[19]

119. The problem of bodily motion and the previous problem of copper diaphragm gauges represent cases where the effect of diffraction round an obstacle can be of importance. This effect is also of some importance for piezo-electric gauges used to measure the pressure/time variation in the pressure pulse. For this purpose it is desirable that the presence of the gauge, which is necessarily of finite size, should not modify appreciably the pressure in the water. The effects of diffraction round the gauge and bodily motion assist in this purpose by tending to equalise the pressure round the gauge.

120. For actual ship targets, questions of diffraction do not arise to a great extent in underwater explosion theory, especially in comparison with the similar effects in air. Thus the typical naval target is usually relatively isolated and questions of screening of one target by another rarely arise. Similarly, the diffraction of air blast into a building via broken windows has no real parallel for the underwater target.

Behaviour of gas bubble in presence of a target

121. The attraction of the gas bubble to a rigid surface and its repulsion by a free surface have already been described. A target which suffers damage by an underwater explosion represents an intermediate case of a yielding surface. The analysis of the behaviour of the bubble near a yielding surface is very difficult, especially as some allowance must be made for the prior effect of the pressure pulse on the target. Since bubble motion is relatively much more important on the small-scale, theoretical and experimental attention has been mainly concentrated on the behaviour of the bubble for small explosions against box and drum model targets.[21] An early theoretical analysis[22] for this problem suggested that the model might behave qualitatively as a free surface at one stage of the plate deflection and as a rigid surface at another stage with appreciable motion both away and towards the target. A later revised theory, however, suggested that repulsions effects were negligible and that the target behaved essentially as a rigid surface with a resultant attraction of the bubble towards the target. In the meantime, this latter conclusion had been deduced from experimental observations[23] of the bubble motion near a small box model which showed clearly the attraction of the bubble to the target. The magnitude of these displacements were in reasonable agreement with theoretical values calculated on the assumption that the flat target plate and surrounding baffle could be treated as a rigid disc of equal area. In general, therefore, it appears that small-scale box and drum model targets behave effectively as rigid surfaces and attract the gas bubble.

122. The bubble pulses are intrinsically much feebler than the initial pressure pulse but due to the attraction of the bubble to the target, the bubble pulses emanate from a source nearer to the target and can thus contribute appreciably to the damage.

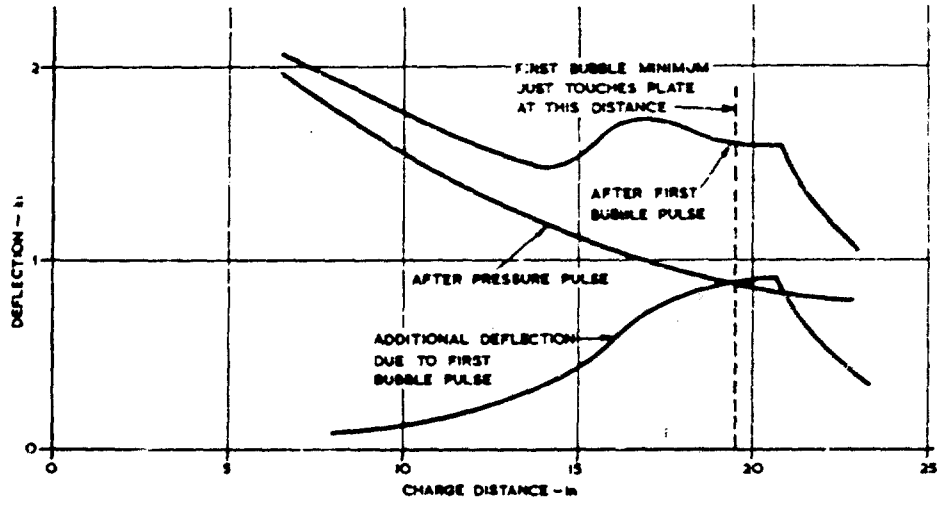


Fig. 21 - Central plastic deflections of box model target plate

Fig. 21 shows the results[35] deduced from the displacement/time records of the central deflection for a small-scale box model involving rectangular air-backed target plate 1 ft. 6 in. by 1 ft. subjected to the explosion of 1 oz. P.A.G. charges. The curves shown refer to permanent deformation excluding transient plastic contributions to the deflection. It is seen from fig. 21 that as the charge distance decreases below 2½ in. the additional deflection due to the first bubble pulse at first increases faster than the deflection due to the initial pressure pulse and the two contributions become approximately equal for a charge distance of about 19 in.. This distance corresponds to the critical case in which the attraction of the target is such that the bubble arrives at the plate when it is of minimum size and the pressures are highest. For closer charge distances the bubble contribution to central deflection in fact decreases and tends to become small compared with that due to the pressure pulse. This decrease of the additional deflection produced by the bubble is probably due to two main causes:-

(1) as the original deflection due to the pressure pulse increases, the pressure necessary to stretch the plate still further will also increase.

(2) at the closer distances the bubble arrives at the target plate while it is still fairly large and the presence of the plate tends to prevent the bubble from contracting to the same extent as it would in the absence of the target; this larger minimum volume implies lower bubble pressures[a] In support of this explanation, it should be noted that for the critical charge distance, the damage due to the bubble pulse is concentrated near the centre of the plate. The final overall damage to the target as measured by the mean deflection of the plate over its area does not show any pronounced bump at the critical distance corresponding to the bump in the upper curve of fig. 21. The bubble pulses subsequent to the first bubble pulse contributed little to the final damage.

---

[a] This is similar to the result that the sea-bed tends to suppress the bubble pulses.

Best Available Copy

123. At distances greater than the critical distance, the first bubble pulse originates from a source away from the target and its interaction with the target can be treated along the lines indicated for the pressure pulse in para. 102-113. The main point to be noted is that the bubble pulse is fairly long compared with both the target plate and baffle dimensions. The discussion concerning long pulses is thus especially relevant to the bubble pulse in these box model experiments and diffraction effects lead to a transferred energy some two to four times the energy in the part of the bubble pulse directly incident on the target plate.

124. Summing up, in small-scale experiments with box or drum models both the attraction of the bubble to the target and diffraction effects enhance the importance of the bubble which can produce damage comparable with that due to the initial pressure pulse. The relative importance of the bubble is greatest when the charge is a certain critical distance from the target corresponding to the bubble arriving at the target when it is of minimum radius and the resulting bubble damage tends to be concentrated locally on the target plate.

125. For actual ship targets the importance of the bubble in causing damage is much more problematical. For small charges fairly close to a target vessel it seems likely that the bubble can contribute appreciably to damage; this is relevant to the attack of submarines by a large number of small charges (one of which may explode close to the target) rather than one large charge. On the other hand, for large charges the movement of the bubble towards the target will in general be small, this movement increasing much slower than the scale of the explosion, and it is doubtful whether bubble damage is of importance for such full-scale non-contact charges against single-hulled vessels. A possible exception is the enhanced effect already mentioned for charges directly beneath the ship's bottom, this effect depending primarily on the rise of the bubble due to gravity though it may be assisted by the target attraction as the bubble approaches the ship's bottom.

NATURE OF DEFORMATION OF THE TARGET

126. For theoretical consideration, it is convenient to consider separately the behaviour of the target prior to rupture and the conditions governing rupture. Existing theory relates primarily to the yielding of targets, whilst the rupture of targets has been mainly investigated experimentally. The major part of the present section will, therefore, be concerned with yielding without rupture. Since nearly all naval targets have steel hulls, attention will be concentrated on targets constructed of steel.

Yielding of steel targets

127. It is first necessary to recognise an essential difference between the usual problem of designing structures under static loads and the problem of designing to resist impulsive loading produced by an underwater explosion. The full curve of fig. 22 illustrates diagrammatically the typical shape of the static stress-strain curve for a mild steel specimen tested in simple tension. The main features are the initial elastic portion AB, the upper and lower yield points C', C, the relatively flat portion CD, the strain hardening portion DEF and the final failure after the ultimate load has been reached at F.

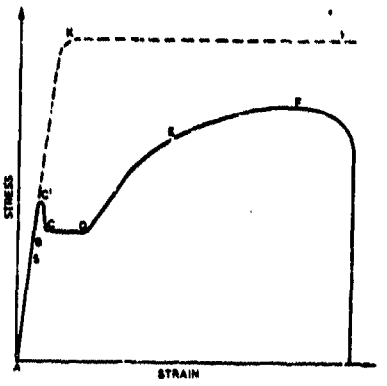


Fig. 22 - Static stress-strain curve for mild steel

128. In the normal problem of design under static loads the maximum loads to which the structure is to be subjected are given and the traditional method is to design so that for example, the maximum tensile stress corresponds to a point S in the elastic range. This design criterion means that it is reasonably certain that inaccuracies in the method of design will not result in the actual stress exceeding the yield point. It is important to note that, since load is the given criterion, the elastic range covers more than half the total range of load up to failure. Accordingly, in traditional design[17] the extra saving of steel by designing to a stress beyond the yield has not in general, been considered sufficient to warrant the extra risk of rupture and the potential inconvenience of permanent distortion. Problems of static loading have thus been primarily a design question of elastic deformations.

129. On the other hand, for the problem of impulsive loading due to an underwater explosion, the cumulative evidence already discussed suggests that the basic criterion is one of energy rather than load, that is, the structure has to absorb a given amount of energy rather than to withstand a given maximum load. Now in the static tension test the energy absorbed is proportional to the area under the full curve of fig. 22; the energy

---

[17] For certain types of structure the actual static load at collapse may be many times the load at which the elastic limit is first exceeded locally in the structure. It seems probable that plasticity will become increasingly important in static design problems in the future.

absorption in the elastic range being small compared with the energy absorbed plastically. The full curve relates to a normal static tension test at a low rate of strain. For higher rates of strain due to impulsive loading both yield stress and ultimate stress tend to increase, the former to the greater relative extent, and under high rates of strain the limited available evidence suggests that the curve tends to be of the form AKF'. The elastic absorption of energy is still small compared with the plastic absorption.[x] Since it is not practicable to construct vessels with hulls which can absorb sufficient energy elastically to withstand any likely scale of attack, the much greater energy absorption in plastic yielding is of paramount importance.

130. Summing up, therefore, whereas the traditional design of engineering structures under static loads is based essentially on the theory of elasticity, the present problem of structures submitted to underwater explosions is primarily a question of the theory of plasticity. The basic laws and simplifying assumptions involved in the theory of the plastic yielding of steel will, therefore, now be discussed.

Fundamental assumptions for plastic yielding of steel

131. As a first simplification, yielding in a simple tension test will be assumed to take place at a constant stress. For static loads this involves neglecting the difference between the upper and lower yield points and limiting consideration to strains up to the point D in fig. 22. For high rates of strain where the true curve becomes more of the shape AKF', the assumption of a flat topped stress-strain curve tends to be relatively accurate for strains right up to failure. The second simplification is to neglect the initial elastic portion so that finally the assumed curve is that shown in fig. 23. This refers to the condition of simple tension and it is now necessary to consider the general case of any system of stresses.

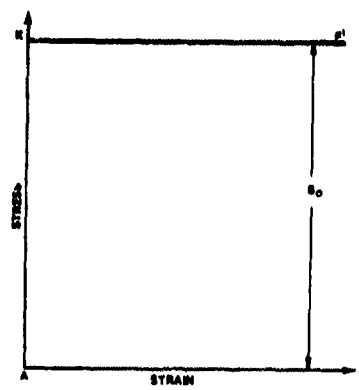


Fig. 23 - Simplified stress-strain curve

132. Let σ_1, σ_2, σ_3, denote the three principal stresses and e_1, e_2, e_3 the corresponding principal strains. Tensile stresses will be taken as positive and σ_1 will refer to the greatest algebraic stress and σ_3 to the least algebraic stress, that is, $\sigma_1 \geqslant \sigma_2 \geqslant \sigma_3$. For the simple tension test the assumed relation of fig. 23 then corresponds to

$$\left.\begin{aligned} \sigma_1 &= \text{constant} = \sigma_0 \\ \sigma_2 &= 0 \\ \sigma_3 &= 0 \end{aligned}\right\} \quad \ldots \quad \ldots \quad \ldots \quad (50)$$

For more general conditions of stress, several different theories have been advanced for the condition of plastic yielding, but only two of these simple theories have survived the test of time and experiment.

---

x Provided brittle fracture does not take place.

One hypothesis due to Mohr states that plastic yielding commences when the maximum shear stress reaches a definite value which is independent of the nature of the stress system. Since the maximum shear stress is half the greatest principal stress difference, this hypothesis may be written as

$$\sigma_1 - \sigma_3 = \text{constant} = s_0 \quad \cdots \quad \cdots \quad \cdots \quad (51)$$

in which the constant is chosen to agree with the notation of equation 50 for the special case of simple tension. This hypothesis is often referred to as the maximum stress-difference or maximum shear stress hypothesis.

133. An alternative hypothesis is that yielding commences when

$$(\sigma_1 - \sigma_2)^2 + (\sigma_2 - \sigma_3)^2 + (\sigma_3 - \sigma_1)^2 = \text{constant} = 2s_0^2 \quad \cdots \quad (52)$$

in which the constant is again conveniently expressed in terms of the yield stress s_0 for simple tension by substituting from equation 50 in equation 51. This hypothesis can be given a physical significance by considering the elastic deformation prior to yielding. The energy U stored per unit volume due to a purely elastic deformation obeying Hooke's law can be written if E is Young's Modulus and μ is Poisson's ratio in the form

$$U = \frac{(1-2\mu)}{6E}\left\{\sigma_1+\sigma_2+\sigma_3\right\}^2 + \frac{(1+\mu)}{6E}\left\{(\sigma_1-\sigma_2)^2 + (\sigma_2-\sigma_3)^2 + (\sigma_3-\sigma_1)^2\right\} \quad (53)$$

in which the first term represents the work done in increasing or decreasing volume whilst the second term is the remaining energy stored in change of shape. Hence, equation 52 states that yielding will commence when the energy involved in change of shape, that is distortion, reaches a certain definite magnitude independent of the stress system. This hypothesis is attributed variously to von Mises, Hencky, and Huber and is usually known as the maximum energy of distortion hypothesis or the maximum shear strain energy theory.

134. Both equations 51 and 52 refer only to the condition for the commencement of yielding and the constant s_0 refers to varying stress systems rather than to varying strain after yielding. For use in the present problem the constant in either case will be taken as holding throughout yielding and since elastic strain is to be neglected, equation 51 or equation 52 will then be assumed to hold from zero strain up to failure. Experimental evidence indicates that the assumption of equation 52 is more accurate than that of equation 51. However, equation 52 is a non-linear relation which frequently leads to intractable mathematics and it is necessary to use equation 51 or even more drastic approximations. So far as energy absorption is concerned, equations 51 and 52 differ quantitatively at the most by about 15% whilst for qualitative deductions the two hypotheses are unlikely to lead to any essential differences. It may be noted that both depend essentially on yielding due to shear stresses since when $\sigma_1 = \sigma_2 = \sigma_3$ and there are no shear stresses, neither hypothesis can be satisfied; that is, both indicate no plastic yielding under hydrostatic tension or compression. In general, neither equation 51 nor equation 52 is sufficient to determine what happens after yielding and two further basic assumptions are necessary.

135. The second basic assumption, known as the "Law of Yielding", relates the principal stress-differences and principal strain-differences by a proportionality rule, namely

$$\frac{\sigma_1 - \sigma_2}{e_1 - e_2} = \frac{\sigma_2 - \sigma_3}{e_2 - e_3} = \frac{\sigma_3 - \sigma_1}{e_3 - e_1} \geqslant 0 \quad \cdots \quad \cdots \quad (54)$$

There is little evidence to substantiate the validity of this law of yielding but experiments[39] have shown that, while not exact, it is at least a fair overall approximation in the range of stresses covered by these experiments.

136. A third basic assumption is that under plastic yielding the steel is incompressible, that is, there is no change in volume of the steel so that to the first order in strains

$$e_1 + e_2 + e_3 = 0 \quad \ldots \quad \ldots \quad \ldots \quad \ldots \quad (55)$$

This assumption is reasonably accurate. Equations 54, 55 and either equations 51 or 52 give three basic equations for the simple theory of plastic yielding in steel. Together with the three equations of equilibrium in a static problem or the three equations of motion in a dynamic problem a total of six equations is thus obtained to determine the six unknowns σ_1, σ_2, σ_3, e_1, e_2, e_3. In addition, there are the usual relations depending only on geometry which connect the strains e_1, e_2, e_3, with displacements. These latter can be introduced as convenient in any specific problem if the equations are thereby simplified. The hull structure of a ship may be considered broadly as composed of two simple units, namely, a beam and a panel of plating. To illustrate the implications of the preceding theory of plastic yielding, two relatively simple static problems will first be considered.

Plastic bending of a beam

137. Fig. 24 represents a beam of symmetrical section bent in a plane of symmetry. Assume, as in the simple theory of elastic bending, that plane sections remain plane and that the beam may be considered as composed of fibres each of which is stressed either in simple tension or simple compression. In this case, either equation 51 or equation 52 gives the result that the fibre stress is s_o for a fibre in tension or $-s_o$ for a fibre in compression. Hence, neglecting any elastic region, the stress is s_o everywhere above the neutral axis and $-s_o$ below this axis. For pure bending with no resultant axial force the area above the neutral axis must be equal to the area of the cross-section below this axis; this determines the position of the neutral axis for any given shape of cross section bent plastically. Having fixed this axis, the resultant moment G due to the fibre stresses can be shown to depend only on s_o and the shape of the cross-section; G will be independent of the amount of bending. Thus, on this simple theory which neglects elastic effects, the plastic resisting moment for any given beam is a constant G_o.

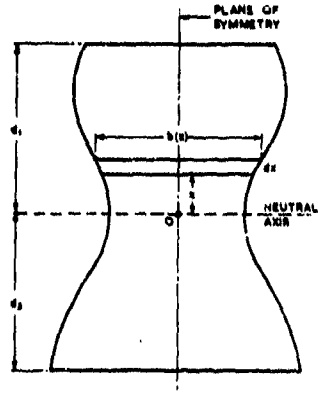


Fig. 24 - Symmetrical section of beam

138. Consider in particular that the beam is simply supported on a span of length l and subjected to a central concentrated load W. The bending moment in the beam is then $Wl/4$ at the centre decreasing linearly to zero at each end. Hence, if W is increased steadily from zero, then while $W < 4G_o/l$ the bending moment is everywhere less than the value G_o necessary

---

m The resultant bending moment G is given by:-

$$G = \int_0^{d_1} s_o b(x)\, x\, dx - \int_{-d_2}^{0} s_o b(x)\, x\, dx$$

where the symbols have the meaning indicated in fig. 24

to cause plastic yielding and, since elastic defects are being neglected, the beam remains undeflected. When $W = 4G_0/l$ however, the moment is G_0 at the centre and plastic yielding commences at the centre. Away from the centre the moment is still less than G_0 so that the beam remains unbent and tends, therefore, to deflect in the shape shown in fig. 25a, consisting of two

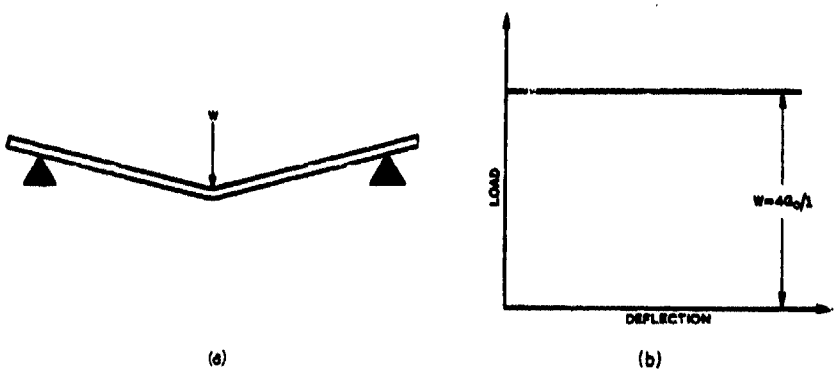


Fig. 25 - Plastic bending of simply supported beam by concentrated central load

straight line portions with a concentrated bend at the centre. Since the resisting moment G_0 is independent of the amount of bending it follows that the deflection will take place under the constant load $W = 4G_0/l$. The load deflection curve is thus of the flat-topped shape shown in fig. 25b, being similar to that assumed initially for the stress-strain relation in simple tension (or compression) illustrated in fig. 23. Experiments on the plastic bending of beams of various sections have shown that this simple theory is substantially correct.

Dishing of a thin panel of plating

139. Consider a thin circular plate, initially flat, rigidly fixed round its circumference and subjected to uniform lateral pressure. For appreciable plastic dishing, the bending resistance can be neglected in comparison with the resistance to stretching since the latter involves far more energy absorption for a thin plate. Secondly, the lateral pressure will in general be small compared with the yield stresses in the plane of the plate so that the problem becomes approximately one of two-dimensional stress with one principal stress, normal to the plane of the plate, equal to zero. By virtue of symmetry the principal stresses will then be

$\sigma_z = 0$, normal to plate

σ_r , radial in plane of plate

σ_t , circumferential in plane of plate.

On these assumptions, with use of the previous plasticity equations and neglecting elasticity the problem has been solved. The most important result which follows whether equation 51 or equation 52 is taken as the condition of plastic yielding, is that

$$\sigma_r = \sigma_t = s_0 \quad \ldots \quad \ldots \quad \ldots \quad \ldots \quad \ldots \quad (56)$$

This result implies that the stress in the plane of the plate is an equal tension in all directions, that is, it behaves like a soap bubble.

140. The solution[40] has also been given for an elliptically shaped panel of plating. In this case, if the major and minor axes of the ellipse are taken as co-ordinate axes Ox, Oy, it is found that the principal stresses in the plane of the plate at any point are σ_x and σ_y parallel to the axes. Both σ_x and σ_y are separately constant over the panel, but are not in general equal to one another, their ratio depending on the ratio of the minor and major axes of the ellipse. However, although strictly $\sigma_x \neq \sigma_y$, if it be assumed as an approximation that the elliptical panel behaves as a soap bubble with $\sigma_x = \sigma_y = s_0$, it can be shown that the energy absorbed by the plate according to this approximation differs by only a small fraction from the energy calculated by the more exact solution. Using equation 51 this error varies from 0 to 8% as the ellipse varies between the extreme cases of a circle and an infinitely long panel, whilst if equation 52 is used, the corresponding error varies from 0 to 12%.

141. This result for the elliptical panel illustrates a result which can be shown to be generally independent of the shape of the panel. Thus, for any element of plating subjected to a two-dimensional principal stress system σ_1 and σ_2 producing principal strains e_1, e_2 in the plane of the plate, the energy U absorbed per unit volume by plastic stretching can be evaluated by using either equation 51 or equation 52 together with equations 54 and 55 and these values of U can be compared with the soap bubble approximation $\sigma_1 = \sigma_2 = s_0$ which gives

$$U = s_0(e_1 + e_2) \quad \ldots \quad \ldots \quad \ldots \quad \ldots \quad \ldots \quad (57)$$

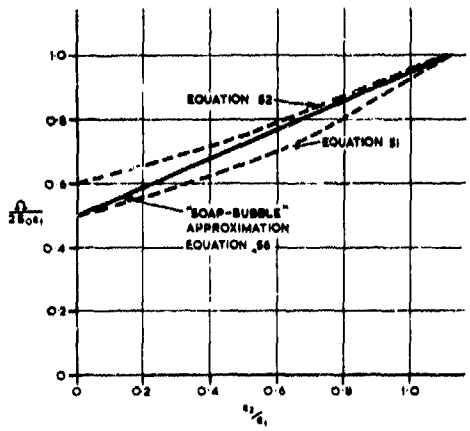


Fig. 26 - Energy absorbed in plastic stretching of thin plate

Fig. 26 shows the resulting comparison for different ratios e_2/e_1 of the two tensile strains in the plane of the plate (The remaining principal strain $e_3 = -e_1 - e_2$ corresponds to thinning of the plate). For a given state of strain, not only does the soap bubble approximation give an energy absorption differing by relatively small amounts from that deduced from equations 51 or 52 but it also gives an intermediate estimate.

142. The assumption that the plate behaves as a soap bubble exerting uniform tension s_0 in all directions thus appears to be a reasonable average approximation to equations 51 and 52. In particular, the practically important case of a rectangular panel, which has yet to be solved by using equation 51 or equation 52 can be easily solved by using the soap bubble approximation. Provided the central deflection is not excessive, that is less than one sixth of

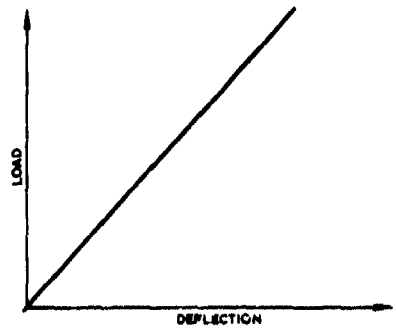


Fig. 27 - Plastic stretching of panel by lateral load

the smaller span, the load-deflection curve for the plate under any given distribution of static pressure will then be of the straight line form indicated in fig.27. The linear load-deflection relation more usually associated with elastic problems[x], thus holds for dishing of a panel of plating which is stretching plastically. It is this result which is the essential justification for the linear resistance assumed in the theories discussed earlier.

143. In this discussion of plastic yielding many approximations have been introduced and it might fairly be asked - may not the cumulative error be so large as to make the final results valueless? The answer to this question lies in experiment. Using a large box model with an unsupported plate area 6 ft. x 4 ft., a steel plate $\frac{1}{8}$ in. thick was tested under uniform static pressure applied hydraulically from the inside of the box.[41] The results were in good agreement with the soap bubble approximation, the shape of the dished plate being similar to that expected of a soap bubble and, apart from a small stiffening effect (attributed to some strain hardening), the pressure/deflection curve was sensibly linear. Further confirmation of the theory was obtained by a static test on a $\frac{1}{4}$ scale replica of the large box model.[42]

144. It is important to notice that the soap bubble approximation is only valid in problems such as that of the clamped panel of flat plating in which the plate is stretching in both directions. For a curved panel of plating such as a submarine pressure hull, in which the plate may be compressing in one direction and stretching in the other direction due to lateral pressure, then either equation 51 or 52 leads to an energy absorption approximately equal to S_0 times the numerically greater strain. This approximation has been suggested as of possible application to the problem of the submarine pressure hull but no serious attempt to do this has yet been made.

Plastic deformation under dynamic loads

145. The only problems of plastic yielding under dynamic loads which are at all amenable to exact theoretical treatment are simple cases in which the motion is effectively one-dimensional. The one case which has been treated fairly exhaustively is that of a long wire fixed at one end and subjected to a suddenly applied load at the other end. The basic analysis for this case was given independently in this country[43] and in America.[44,45] This case is not of direct application to the present problem of beams and plates but two general qualitative results are of some interest. First, if the stress-strain relation under dynamic loading is concave to the strain axis, for example AKF' in fig.22, the higher the stress the more slowly is it propagated along the wire. Fig.28 illustrates a plastic wave travelling along the wire tending to become less steep as it progresses. The stress distribution curve ABC becomes the curve A'B'C' as the wave travels to the right. This is the opposite effect to that holding for the shock wave in water where the wave tends to become more steep as

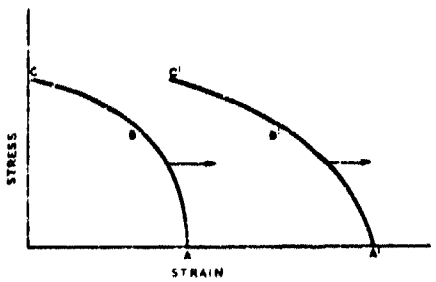


Fig.23 - Plastic wave in wire

---

x A linear resistance is not always obtained in elastic problems. In particular for the present case of a panel dished by lateral pressure, elastic stretching of the plate introduces a non-linear term in the resistance.

it progresses. A second result for the plastic wave in a wire is that no plastic wave can transmit a particle velocity greater than a certain critical value; thus if a long wire is hung from a fixed point and a weight is dropped on to a yoke at the lower end of the wire it is found that if the weight is dropped from above a certain height there is little or no plastic strain in the wire except very close to the yoke where it would break. This result is more especially relevant to the question of rupture discussed later.

146. For lateral loads on beams, one case which has been solved, including strain hardening effects, is that of an infinitely long beam subjected to a concentrated dynamic load at one section.[16] The more practical case of a beam of finite length presents greater difficulties. However, using the preceding simplified theory that the beam yields under a constant bending moment, it is possible to solve some simple special cases. Consider, for example, a simply supported beam given an initial triangular impulsive distribution of velocity which is zero at each end and rises linearly to a maximum at the centre. In this case the deflection at any time is also of triangular shape, that is, of the shape given in fig.25, and all the initial kinetic energy is ultimately absorbed by plastic bending at the centre. For a given amount of energy communicated as initial velocity in this particular way, the maximum central deflection of the beam can easily be calculated by equating this given energy to the energy absorbed in central bending, which is simply G_0 times the angle of bend at the centre; this angle is thus determined and hence the central deflection can be calculated.

147. For a panel of plating dished plastically by lateral loads, it has been seen that the assumption of a uniform tension in all directions in the plane of the plate is a reasonable approximation for static loads. This approximation can also be applied to solve certain special cases of dynamic loading. In particular, if a circular panel of plating fixed round its circumference is given an initial distribution of uniform velocity corresponding to a very large uniform pressure acting for a negligibly short time, then the cross section of the deformed panel at any time t is shown in fig.29. Here the outer annulus AB, A'B' (in section) has been deformed into the cone frustrum AC, A'C', (in section) which is at rest whilst the central portion BB' has moved to CC' and is still undeformed and moving with its initial velocity v. At a later time the deformed shape is similarly ADD'A' where DD' is undeformed and moving with velocity v whilst AD, A'D' is stretched and at rest.



Fig.29 - Section through deformed circular panel

148. Effectively, a plastic wave travels inwards from the fixed edge leaving behind it a stretched portion at rest whilst the central portion ahead of it is undeformed. This plastic wave travels in fact with a constant velocity $c_1 = \sqrt{S_0/\rho}$ where S_0 is a yield stress as defined previously and ρ is mass density. For steel, c_1 is about 570 ft. per sec. and is therefore not only small compared with the velocity of elastic waves in steel (about 17000 ft. per sec.) but also in comparison with the velocity of the pressure pulse in water (about 5000 ft. per sec.).*

* This result is relevant to the question of whether cavitation in the water occurs with a finite panel of plating.

When this plastic wave reaches the centre of the panel, the whole plate has become stretched into the form of a cone, ARA' in section, which is at rest and no further deformation or motion will occur, the whole of the original kinetic energy having been converted into permanent plastic stretching of the plate. For a rectangular panel of plating given an initial uniform velocity, the corresponding final deformation would be of the roof-top shape shown in fig.30, with the sloping sides equally inclined to the base; the same shape with the top cut off gives the intermediate shape whilst deforming, a central flat portion being undeformed and moving with its original velocity whilst the outer stretched portion would be at rest.



Fig.30 - Shape of deformed rectangular panel

149. Other special cases which can be solved are analogous to problems of an elastic membrane subjected to dynamic loading. Such membranes have certain definite shapes (theoretically infinite in number) in each of which they can vibrate with a certain definite frequency. Such a vibration is known as a normal mode.[47] For the analogous plastic panel, solutions can be obtained if the applied impulsive pressure is distributed over the panel in the shape corresponding to any one definite normal mode, provided also that variation of the overall magnitude of the pressure with time is such that the plate continues at all points until the final deformed shape is obtained by the plate coming to rest at all points simultaneously. In fig.31, for example, a rectangular panel of plating of sides 2a and 2b with axes Ox, Oy parallel to the sides and with origin at O is subjected to a suddenly applied pressure distribution of $p_o \cos \pi x/2a \cos \pi y/2b$. It is shown at Appendix D that if such a plate is fixed around the periphery and the deflections are relatively small compared with the smaller span (one sixth or less) then

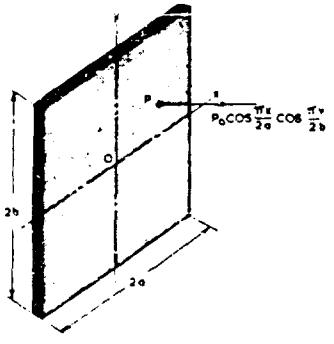


Fig.31 - Rectangular plate subjected to impulsive pressure distribution

$$w(t) = w_o(t) \cos \frac{\pi x}{2a} \cos \frac{\pi y}{2b} \quad \ldots \quad \ldots \quad \ldots \quad (58)$$

$$w_o(t) = K/2 \, (1 - \operatorname{cosec} t) \quad \ldots \quad \ldots \quad \ldots \quad (59)$$

where
- $w(t)$ = deflection of point (x,y) in the plate at time t
- $w_o(t)$ = central deflection of plate at time t
- h = plate thickness
- s, = uniform membrane stress
- t = time

Best Available Copy

$$K = \frac{\beta}{\pi^4 \sigma_0 h} \left\{ \frac{a^2 b^2}{(a^2 + b^2)} \right\} \quad \ldots \quad \ldots \quad \ldots \quad \ldots \quad (60)$$

$$\alpha^4 = \frac{\pi^2 \sigma_0}{4\rho} \left\{ \frac{1}{a^2} + \frac{1}{b^2} \right\} \quad \ldots \quad \ldots \quad \ldots \quad \ldots \quad (61)$$

The final solution given by equations 58, 59, 60, and 61 will be valid so long as the plate is stretching, which is true up to $t = \pi/\alpha$. At this instant $w_0(t) = w_0 = K$ and the plate is at rest everywhere with no velocity and a deflected shape w at any point (x,y) is given by

$$w = K \cos \frac{\pi x}{2a} \cos \frac{\pi y}{2b} \quad \ldots \quad \ldots \quad \ldots \quad \ldots \quad (62)$$

This represents permanent deformation and the plate will in fact remain in equilibrium thereafter since the applied pressure $p_0 \cos \pi x/2a \cos \pi y/2b$ is insufficient to cause further stretching. Equation 62 with K defined by equation 60 is therefore the final plastic dishing produced by the suddenly applied pressure $p_0 \cos \pi x/2a \cos \pi y/2b$.

150. The relative simplicity of the preceding example lies in the fact that the plate deflects in a constant shape throughout the motion. Similar results can be obtained for a pressure distribution of the more general normal mode type, namely, a pressure distribution of the type $p_0 \cos m\pi x/2a \cos n\pi y/2b$ where m and n are any odd integers. The resulting deflection is then of similar shape. Up to the time of maximum deformation these solutions for a plastic plate are separately identical with those for an elastic membrane. For the elastic membrane, the solution for any distribution of suddenly applied pressure can be simply obtained by superposition of the previous solutions for the separate normal modes. However, for plastic deformation the principle of superposition cannot, in general, be used. Thus, if more than one mode is involved in the elastic case the membrane will in general stop stretching and start contracting at one point in the membrane whilst it is still stretching at another point. This introduces no difficulties if the strain is elastic since the same equations hold both for an increase and a decrease in stretching. For the plastic plate this is not true, the soap bubble approximation being only valid when the plate is stretching in both directions; if the plate ceases to stretch it may remain inextensible or tend to compress in one or more directions and the fundamental assumptions and equations must be changed. For any general type of impulsive loading on a plastic plate, it would thus be necessary, when seeking an exact solution with any given plasticity assumptions, to watch, in effect, every point in a plate and change the basic equations locally whenever the plate stopped stretching. Such an allowance for the difference between loading and unloading is complicated enough in the simpler case of a plastic wire subjected to dynamic loads; for the plate problem it has yet to be carried out successfully.

151. The difficulty introduced by the irreversibility of the plastic deformation can be avoided by further approximation. For the previous special cases of loading by pressure distributions of the normal mode type $p_0 \cos m\pi x/2a \cos n\pi y/2b$ the simplicity of the analysis depends essentially on the fact that the plate deflects in a constant shape throughout the deformation so that all points of the plate cease to stretch and become at rest simultaneously. The irreversibility of the plastic deformation simply implies that the plate remains in this deformed state without further motion. This suggests as an approximation for the case of loading by an underwater explosion that the plate be assumed to deflect in some constant shape. This assumption has been termed proportional motion since the deflections of any two points remain in constant ratio throughout the motion. Thus for a rectangular panel of plating of sides 2a, 2b, and thickness h,

fixed round the periphery, the deflection w(t) at time t would be assumed to be of the form

$$w(t) = w_0(t)\, f(x,y) \quad \ldots \quad \ldots \quad \ldots \quad \ldots \quad (63)$$

where f(x,y) is any suitable shape which vanishes round the edge of the plate and is unity at the centre so that $w_0(t)$ is the central deflection at time t. For practical purposes, the final permanent deflection representing damage is of particular importance and it is natural to choose f(x,y) to correspond approximately to final observed dishes in box model experiments. These are in general more pointed that the relatively flat soap bubble shape obtained in static tests under uniform pressure and a reasonable approximation to the observed dishes is

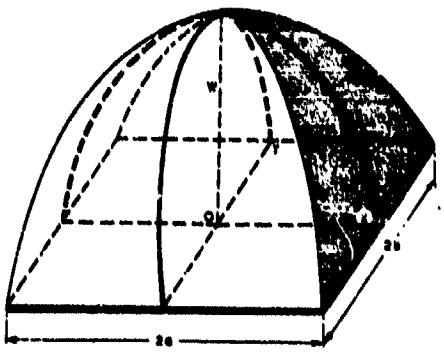


Fig.32 - Empirical shape of a deformed rectangular plate

$$f(x,y) = \left\{1 - \frac{x^2}{a^2}\right\}\left\{1 - \frac{y^2}{b^2}\right\} \quad \ldots \quad \ldots \quad \ldots \quad (64)$$

corresponding to parabolic sections parallel to the sides as shown in fig.32.

152. Using the membrane approximation of a uniform tension s_0, and assuming that the deflections are reasonably small compared with the smaller span, expressions for the energy Ω_p absorbed in plastic deformation by stretching from the flat plate to the dished shape, the total energy $\mathcal{T}$ of the deforming plate and the work W done by the pressure in deforming the plate are derived at Appendix D. In particular, it is shown that for the parabolic shape of equation 64

$$\Omega_p = \frac{64}{45}\left\{\frac{a}{b} + \frac{b}{a}\right\} s_0 h w_0^2 \quad \ldots \quad \ldots \quad (65)$$

153. The assumptions of proportional motion and a uniform membrane stress in the plate lead to a motion[x] analogous to that of a mass M on a spring of stiffness k subjected to a dynamic load F(t). There is of course the important proviso that the plastic deformation is irreversible; subject to certain restrictions on the variation of F(t) with time, this can simply be taken into account by assuming the motion to cease when $w_0(t)$ reaches its maximum value w_0 corresponding to zero velocity of the plate.

---

x This is valid in particular, if the pressure distribution remains constant after application or if the pressure is transient and ceases while the plate is still deflecting.

154. The preceding discussion indicates an approximate method of treating the plastic dishing of a plate under a given dynamic pressure. For the dishing of plates by underwater explosions the pressure on the plate is not known, ab initio, since as previously discussed it depends on the motion of the plate and, in particular, on whether cavitation occurs in the water. The problem is then more complicated, but the assumptions of proportional motion and uniform membrane stress have, in general, been the main simplifying assumptions (so far as the plate is concerned) in the more complicated analyses[49] allowing for the interaction of target and water phenomena. These analyses lead to the conclusion that in many cases, the pressure pulses from explosions tend to communicate a certain definite quantity of energy which is approximately equal to the energy directly incident on a deforming target plate. If this is so, the final dishing of the plate can be estimated without intermediate calculation of the actual motion. Thus using an assumed deflected shape of the type of equation 64 the total energy absorbed in plastic deformation is given by equation 65 and hence, by equating energy absorbed to energy communicated,

$$\Omega_i = \frac{64}{45}\left(\frac{a}{b} + \frac{b}{a}\right) s_0 h w_0^2 \quad \ldots \quad \ldots \quad \ldots \quad (66)$$

where w_0 is the final central deflection. The directly incident energy depends on the charge weight and the geometry of the target and the relative position of the charge; if bubble damage is appreciable the contributions to Ω_i from the subsequent bubble pulses must be added to that from the pressure pulse.[7]

155. Equations of the type 66 have been the most common simple basis of comparison of theory and experiment for box model and drum model tests. One minor point which may be noted is that for different assumed shapes $f(x,y)$ of proportional motion, the energy absorbed varies less for a given mean deflection than for a given central deflection. Thus if $\bar{w}$ is the mean deflection, the energy absorbed can be expressed in the form

$$\Omega_p = \tfrac{1}{2} k' \bar{w}^2 \quad \ldots \quad \ldots \quad \ldots \quad \ldots \quad (67)$$

and if this is equated to the incident energy Ω_i an estimate of $\bar{w}$ instead of w_0 is obtained. Such estimates of $\bar{w}$ vary less for different assumed shapes than do corresponding estimates of w_0. For this reason, results of box or drum model tests are often expressed in terms of the mean deflection rather than the maximum deflection.

156. The use of an assumed shape for calculating the final absorbed energy Ω_p in the preceding manner does not, of course, depend on the assumption of proportional motion, but only on the more general assumption that the plate stretches throughout its deformation so that the uniform membrane stress may be assumed as a reasonable approximation. The assumption of proportional motion is, however, of importance since it is involved in analyses forming the theoretical basis for the conclusion that approximately all the incident energy Ω_i is communicated to the target.

157. The preceding type of analysis is especially relevant to experimental investigations using box or drum models embodying a single plate fixed in a relatively rigid frame. For an actual ship the supporting framework of the panels cannot necessarily be assumed rigid and the basic system is rather a panel of plating supported by yielding beams. This more difficult problem is likely to defy exact analysis for a long time but using an approximate method[50] the deflection of any section of the beam and the deflections of the ends of the beams can be estimated. This method is of general application to problems of dynamic loading of structures but is especially relevant to the present type of problem since it enables the difficulties introduced by the irreversibility of plastic deformation to be overcome.

158. Essentially, the method is based on Hamilton's principle, which may be regarded as the fundamental basis of classical dynamics, and on an assumption of proportional motion for each separate unit of a system. Thus for a plate supported on yielding beams, the shape of the deflecting beams would be assumed and also the shape of the plate deflection relative to the beams, but the overall magnitudes of beam deflection and plate deflection would not be restricted and would not necessarily be in a constant ratio to one another. If Hamilton's principle is applied to the motion when so restricted, the problem is analogous to one of particle dynamics and the approximate solution is given by Lagrange's equations. A detailed description of this method and its application is too lengthy for discussion but the main steps when the method is applied to a simple elastic problem are outlined at Appendix E.

159. For problems of plastic deformation the application of the method is necessarily complicated by consideration of the irreversibility of the deformation, but, in general, this is not too difficult, involving mainly a consideration of the motion in several distinct stages.[71] The potential accuracy of the approximate method has been assessed by applying it to elastic problems and comparing the resulting solutions with nominally exact solutions.[72] Reasonable agreement was obtained. Further, in one plastic problem to which the method has been applied the approximate solution was in reasonable agreement with experimental results.[73]

160. Summing up, existing theory of the plastic deformation of targets by underwater explosions depends to a large extent on approximate plasticity assumptions and approximate methods of analysis. In spite of this, a certain measure of agreement between theory and experiment has been obtained and, pending more accurate theory, approximate methods may reasonably be expected to throw light in particular on the qualitative behaviour of a ship's hull structure subjected to underwater explosions. For example, the important question of the optimum distribution of weight of steel between plating and supporting framework for maximum resistance to impulsive loading is essentially a qualitative question in the sense that the answer can reasonably be expected not to depend greatly on the precise magnitude of the loading.

Rupture of steel

161. The onset of rupture in steel undoubtedly depends on many factors such as chemical composition, microstructure, the presence of flaws, size and geometrical shape of specimen, rate of loading, and temperature. Much research is at present being carried out to investigate the relative importance of these factors but at present there is no well-established quantitative theory which can be used to predict rupture. Attention will therefore be concentrated on the qualitative points which seem of most importance in connection with the problem of underwater explosion damage.

162. Broadly speaking, two main types of fracture may occur in steel, first, ductile fracture in which considerable deformation precedes rupture and secondly, brittle fracture in which little deformation occurs. In the former type, the energy absorbed in the steel prior to fracture is much greater than in the brittle type of fracture. Since, as previously discussed, damage by underwater explosions depends to a large extent on the ability of a structure to absorb energy it is obviously desirable from the ship designer's viewpoint that brittle fracture should be avoided. The ductile fracture is usually associated with a sliding process in the steel due to shear whereas the brittle fracture is considered to be a tearing apart of the metal due to tension. The type of fracture will thus depend not only on the relative inherent strengths of the steel to sliding and tearing but also on the type of stress system to which the steel is subjected; for example with uniform tension in all directions there would be no shear in a uniform material and failure would take place by tearing and be of the brittle type.

54

Notch brittleness

163. Minute imperfections or cracks in the steel can give rise to high local stresses and, in particular, there is reason to believe that triaxial tensions may be developed locally at the end of a sharp crack with a consequent tendency to brittle fracture. This has been investigated extensively by testing specimens with notches cut in them and it is found that brittle fractures can then occur when similar unnotched specimens exhibit a ductile fracture. In view of this, the term notch brittleness has become a general term to describe brittle fracture where it is suspected to be due to stress concentrations arising from cracks or local inhomogeneity of the material. There seems little doubt that such notch brittleness is one of the most important factors which influence rupture. In particular, it seems clearly established that notch brittleness increases with decreasing temperature, so that for example a notch specimen may fail with a relatively ductile fracture at a room temperature of 60°F whereas a similar specimen tested in an ice-bath may exhibit a brittle fracture. With regard to chemical composition there is some evidence that manganese is beneficial in tending to inhibit brittle fracture and that a minimum manganese content of 0.50% is desirable, especially for ships' plates over $\frac{1}{2}$ inch thick.

Shape and size of steel specimen or target

164. When a normal tensile specimen is tested and exhibits a ductile fracture it is well known that up to a certain load, the specimen tends to stretch uniformly but then develops a concentrated local neck where rupture finally occurs. The energy absorbed in the specimen can be considered broadly as composed of two parts,

(1) the energy used in uniform extension of the specimen

(2) energy absorbed in local necking.

For specimens of given diameter but varying length made from the same steel, the former energy will tend to increase in proportion to the length whereas the local necking energy absorption will remain relatively constant provided all specimens are reasonably long compared with diameter. The shape of the specimen as defined by the length/diameter ratio thus influences the average amount of energy absorbed per unit volume of the steel even though the applied load is nominally uniform throughout the specimen.

165. A second effect is the size effect which occurs for specimens of geometrically similar shape differing only in overall dimensions, each specimen being a smaller or larger scale replica of the other specimens. Thus, if similar notched specimens are submitted to similar static bending conditions up to fracture it is found that the larger the specimen the smaller is the relative deformation at fracture as measured, for example, by the ratio of central deflection to span if the specimens are supported at each end and subjected to a central load. Correspondingly, the energy absorbed per unit volume up to fracture decreases as the size of specimen increases. The precise mechanism for this size effect has yet to be established but it is undoubtedly related to the fact that although the specimens are true scale replicas on a macroscopic scale their microscopic structure has not similarly been scaled.

166. This size effect has also been observed in underwater explosion effects using different sizes of drum model targets constructed as scaled replicas and subjected to scaled charge conditions. Here it was found, that whereas deformations prior to rupture scaled reasonably well, large targets ruptured when dished (relatively) to a less extent than small targets at rupture. It has in fact long been known from empirical observation that damage by underwater explosions to full-scale targets tended to be greater than in corresponding small-scale trials. This size effect on rupture is thus especially relevant to quantitative interpretations of model tests.

Speed of loading

167. Fundamentally, speed of loading may be conveniently considered to have two effects. First, there is a possible effect of the microscopic behaviour of the steel, the resistance to sliding tending to increase with increasing rate of strain. As a result high rates of strain are conducive to the brittle type of failure with small energy absorption. Where the fracture does remain ductile, experiments with short specimens have shown that very high rates of strain can lead to a large increase in the yield point of mild steel and the energy absorbed up to fracture can also be larger than in a static test. Secondly, there is a possible macroscopic effect depending on the dynamics of the method by which impact stresses are applied. Thus experiments have been carried out on long wires with a tup at the lower end subjected to the impact of a weight at different velocities. Above a certain critical velocity (about 100 ft. per sec. in these experiments) it was found that the energy absorption to fracture suddenly decreased. This phenomenon depends on the propagation of plastic waves up the wire.

168. For a normal ductile material with a given stress/strain curve concave to the strain axis it is possible to analyse the simple one-dimensional propagation of plastic strain up the wire and it is in fact found that there is a limit to the particle velocity which can be transmitted. In the experiments under consideration, at the lower speeds the effect of the velocity given to the end of the wire could be propagated up the wire whereas above the critical speed the velocity of the tup was greater than the maximum particle velocity that could be propagated. It was in fact found that, whereas below the critical speed fracture could occur anywhere in the specimen, above the critical speed, fracture was always at the impact end with the rest of the wire relatively unstrained. Thus a low energy absorption may be associated with high speeds of loading even though the fracture itself is essentially ductile.

169. This type of localised fracture with low total energy absorption may be of some importance in connection with the behaviour of ship's plating when subjected to underwater explosions. Thus a panel of plating will in general be given a higher velocity normal to itself than the framework to which it is attached and round the edges the resultant lateral velocity of stretching may be greater than can be propagated through the plate. The panel can thus fail round the edges with relatively little energy absorption in the main body of the plate. This effect of edge restraint is relatively unexplored but is probably of considerable importance in actual ship targets.

APPENDIX A

Theory of small-amplitude sound pulses

A1. Pressure in pulse

Let t = time interval after the initiation of the explosive charge
ρ = mass density of water
c = velocity of sound in water
p = pressure in pulse (additional to the hydrostatic pressure existing prior to the arrival of the pulse)
V = velocity potential
r = distance of point from the centre of the charge

Assuming the pulse is of small amplitude and retaining only the first order term, the pressure is related to the velocity potential V by the equation

$$p = -\rho \frac{\partial V}{\partial t} \quad \ldots \quad (A1)$$

The partial differential is used since p and V will vary in general, both with time and with space co-ordinates defining the position of any point in the water. The velocity potential V can be shown to satisfy the wave equation

$$\nabla^2 V = \frac{1}{c^2} \cdot \frac{\partial^2 V}{\partial t^2} \quad \ldots \quad (A2)$$

where in rectangular co-ordinates

$$\nabla^2 V \equiv \frac{\partial^2 V}{\partial x^2} + \frac{\partial^2 V}{\partial y^2} + \frac{\partial^2 V}{\partial z^2} \quad \ldots \quad (A3)$$

Transforming equation A2 to spherical polar co-ordinates (r, θ, ϕ)

$$\frac{1}{c^2}\frac{\partial^2 V}{\partial t^2} = \frac{1}{r^2}\frac{\partial}{\partial r}\left(r^2\frac{\partial V}{\partial r}\right) + \frac{1}{r^2 \sin\theta}\frac{\partial}{\partial \theta}\left(\sin\theta \frac{\partial V}{\partial \theta}\right) + \frac{1}{r^2 \sin^2\theta}\frac{\partial^2 V}{\partial \phi^2} \quad \ldots \quad (A4)$$

But for any point distant r from this centre, both p and V will be functions of t and r only and equation A4 can be written

$$\frac{1}{c^2}\frac{\partial^2 V}{\partial t^2} = \frac{\partial^2 V}{\partial r^2} + \frac{2}{r}\frac{\partial V}{\partial r} \quad \ldots \quad (A5)$$

Equation A5 can be written in the form

$$\frac{\partial^2 (rV)}{\partial r^2} = \frac{1}{c^2}\frac{\partial^2 (rV)}{\partial t^2} \quad \ldots \quad (A6)$$

One solution of equation A6 is

$$V = \frac{F\left(t - \frac{r}{c}\right)}{r} \quad \ldots \quad (A7)$$

where F can, in general, be any function.

From equations A1 and A7 the pressure is given by

$$p = \frac{\rho}{r} f\left(t - \frac{r}{c}\right) \quad \ldots \quad \ldots \quad \ldots \quad \ldots \quad \ldots \quad \ldots \quad \ldots \quad \text{(A8)}$$

where - f denotes the derivative of F with respect to t as defined by

$$f(t) = -\frac{d}{dt}\left\{F(t)\right\} \quad \ldots \quad \ldots \quad \ldots \quad \ldots \quad \ldots \quad \ldots \quad \text{(A9)}$$

A2. Particle velocity. The particle velocity u can be derived from the velocity potential V by the relation

$$u = \frac{\partial V}{\partial r} \quad \ldots \quad \ldots \quad \ldots \quad \ldots \quad \ldots \quad \ldots \quad \ldots \quad \ldots \quad \text{(A10)}$$

From equations A7 and A10

$$u = \frac{1}{cr} f\left(t - \frac{r}{c}\right) - \frac{1}{r^2} F\left(t - \frac{r}{c}\right) \quad \ldots \quad \ldots \quad \ldots \quad \ldots \quad \text{(A11)}$$

where f is defined as before by equation A9.

The first term in equation A11 is similar to the expression for the pressure in equation A8 and decreases inversely as the distance, whereas the second term decreases more rapidly as the inverse square of the distance. At large distances this second term, sometimes called the afterflow, becomes negligible compared with the first term and to a first approximation

$$u = \frac{1}{cr} f\left(t - \frac{r}{c}\right) \quad \ldots \quad \ldots \quad \ldots \quad \ldots \quad \ldots \quad \ldots \quad \ldots \quad \text{(A12)}$$

Using the approximate relation of equation A12 and equation A8 the pressure and particle velocity are related by

$$p = \rho c u \quad \ldots \quad \ldots \quad \ldots \quad \ldots \quad \ldots \quad \ldots \quad \ldots \quad \ldots \quad \text{(A13)}$$

A3. Impulse per unit area. The impulse per unit area I transmitted by the pulse across the spherical surface at radius r is given by the area of the pressure/time curve at any distance. If the origin of time be taken from the instant at which the sound pulse starts from the centre, so that it arrives at radius r at time r/c then from equation A1

$$I = \int_{\frac{r}{c}}^{\infty} p \, dt = \frac{\rho}{r} \int_{\frac{r}{c}}^{\infty} f\left(t - \frac{r}{c}\right) dt \quad \ldots \quad \ldots \quad \ldots \quad \ldots \quad \text{(A14)}$$

Therefore

$$I = \frac{\rho}{r} \int_{0}^{\infty} f(t') \, dt', \text{ where } t' = \left(t - \frac{r}{c}\right) \quad \ldots \quad \ldots \quad \ldots \quad \text{(A15)}$$

Since the shape of f(t') is independent of distance, the impulse per unit area varies as the inverse of the distance.

A4. Energy associated with pulse. The energy per unit area Ω transmitted by the pulse across the spherical surface at radius r is given by

$$\Omega = \int_{\frac{r}{c}}^{\infty} p\, u\, dt \quad \ldots \quad \ldots \quad \ldots \quad \ldots \quad \ldots \quad \ldots \quad \ldots \quad (A16)$$

The integrand in equation A16 is the rate at which work is done per unit area by the water within the sphere of radius r on the water outside this sphere.

From the approximate relation of equation A13 and equation A8

$$\Omega = \rho c \int_{\frac{r}{c}}^{\infty} p^2\, dt = \frac{\rho}{cr^2} \int_0^{\infty} \left\{ f(t') \right\}^2 dt' \quad \ldots \quad \ldots \quad \ldots \quad (A17)$$

The total energy E transmitted across the spherical surface of radius r is given by

$$E = 4\pi r^2 \Omega = \frac{4\pi\rho}{c} \int_0^{\infty} \left\{ f(t') \right\}^2 dt' \quad \ldots \quad \ldots \quad \ldots \quad \ldots \quad (A18)$$

The use of equation A13 in deriving equations A17 and A18 corresponds to neglecting the second term in equation A11. If this latter term is taken into account, the energy E is no longer independent of distance, and even when the pulse is strictly finite in duration, some energy is left behind as kinetic energy of the water after the pulse has passed.

APPENDIX B

Theory of gas bubble motion

B1. The gas bubble is assumed to remain spherical throughout the motion but oscillates in size and rises under the influence of gravity. The motion is considered to take place in an unlimited mass of water. The free surface is taken to be sufficiently far away as to have no direct effect on the motion. (The surface will, however, enter indirectly, in so far as its position determines the hydrostatic pressure in the neighbourhood of the bubble).

B2. The motion of the gas bubble involves two well-known types of incompressible flow. The first type is the bodily motion of a sphere through water in a fixed direction, namely upwards for the gas bubble in the present problem. The second type of incompressible flow is the pure radial motion of the gas bubble corresponding to an expanding or contracting spherical cavity.

B3. The following notation will be used for the analysis of the motion.

t	=	time interval after the initiation of the explosive charge
ρ	=	mass density of water
a	=	radius of bubble
g	=	acceleration due to gravity
z	=	depth of bubble centre below a point 33 ft. above the water surface
p	=	pressure inside the bubble
v	=	volume of bubble
$G(a)$	=	potential energy of gas in bubble. This is equal to the work which would be done by the gas on the walls of the bubble if expanded adiabatically from radius a to infinite radius
Q_b	=	total energy associated with the bubble motion

B4. It is a standard result that a sphere moving linearly in water can be regarded as having, in addition to its own mass, a virtual mass equal to half the mass of the displaced water. Therefore, neglecting the weight of gas in the bubble the total effective mass of the bubble is the virtual mass, $2/3\pi\rho a^3$. The upwards velocity of the gas bubble is $-dz/dt$ so that the upward momentum is $-2/3\pi\rho a^3 dz/dt$. This upward momentum is produced by the net hydrostatic force on the bubble. Neglecting the weight of the gas in the bubble, this force is simply the weight of the displaced water, $4/3\pi a^3\rho g$. Therefore, by Newton's second law of motion

$$\tfrac{4}{3}\pi\rho a^3 g = \frac{d}{dt}\left\{ -\tfrac{2}{3}\pi\rho a^3 \frac{dz}{dt} \right\} \quad \ldots \quad \ldots \quad \ldots \quad \ldots \quad \ldots \qquad (B1)$$

Integrating equation B1 gives

$$-\frac{dz}{dt} = \frac{2g}{a^3}\int a^3\, dt \qquad \ldots \quad \ldots \quad \ldots \quad \ldots \quad \ldots \quad \ldots \qquad (B2)$$

B5. Another relation between a and z can be derived by forming the energy equation of the motion. First, the kinetic energy in the water round the bubble due to the combined radial and linear motion is given by

$$2\pi\rho a^3\left(\frac{da}{dt}\right)^2 + \tfrac{1}{3}\pi\rho a^3\left(\frac{dz}{dt}\right)^2$$

Secondly, changes in gravitational potential energy of the water can be simply allowed for by taking the bubble as having a negative weight equal to the weight of the displaced water. The potential energy due to gravity can thus be written as $4/3\pi a^3 \rho z$. Finally, the potential energy of compression in the gas has been defined as $G(a)$ whilst the total energy of the motion is Q_b. Hence the energy equation can be written

$$Q_b = 2\pi\rho a^3\left(\frac{da}{dt}\right)^2 + \frac{1}{3}\pi\rho a^3\left(\frac{dz}{dt}\right)^2 + \frac{4}{3}\pi a^3\rho g z + G(a) \quad \ldots \quad \ldots \quad (B3)$$

B6. The values of $G(a)$ and Q_b will depend on the nature of the explosive. For T.N.T. it was deduced from early measurements[x] of the period of oscillation of the gas bubble that $Q_b = 0.5Q$ where Q is the total chemical energy liberated by the explosive which can be taken as about 880 calories per gram for T.N.T. In C.G.S. units the energy Q_b of bubble motion for a T.N.T. charge of mass M grams is given by

$$Q_b = 1.85 \times 10^{10} \text{ M ergs} \quad \ldots \quad \ldots \quad \ldots \quad \ldots \quad \ldots \quad \ldots \quad (B4)$$

B7. An expression for $G(a)$ can be obtained by using the relevant adiabatic relationship between pressure and volume for gaseous products of the explosion. Using the relationship calculated by Jones and Miller for T.N.T. it is found that

$$G(a) = 2.189 \times 10^{10} \times \frac{M^{\frac{4}{3}}}{a^4} \quad \ldots \quad \ldots \quad \ldots \quad \ldots \quad \ldots \quad \ldots \quad (B5)$$

where a is measured in cm. and M in grams.

B8. Equations B2, B3, B4, and B5 can be used to determine a and z, for a T.N.T. charge of given size. However, for calculation purposes it is convenient to put these equations in non-dimensional form. This can be done by introducing a length L defined by

$$L = \left(\frac{Q_b}{g\rho}\right)^{\frac{1}{3}} \quad \ldots \quad \ldots \quad \ldots \quad \ldots \quad \ldots \quad \ldots \quad \ldots \quad \ldots \quad (B6)$$

Hence writing

$$\left.\begin{aligned} a &= a'L \\ z &= z'L \\ t &= t'\sqrt{\frac{L}{g}} \end{aligned}\right\} \quad \ldots \quad \ldots \quad \ldots \quad \ldots \quad \ldots \quad \ldots \quad \ldots \quad \ldots \quad (B7)$$

the equations for a' and z' are

$$\left(\frac{da'}{dt'}\right)^2 = \frac{1}{2\pi a'^3}\left\{1 - \frac{G(a)}{Q_b}\right\} - \frac{1}{6}\left(\frac{dz'}{dt'}\right)^2 - \frac{2}{3}z' \quad \ldots \quad \ldots \quad (B8)$$

$$-\frac{dz'}{dt'} = \frac{2}{a'^3}\int a'^3 dt' \quad \ldots \quad \ldots \quad \ldots \quad \ldots \quad \ldots \quad \ldots \quad (B9)$$

---

[x] Later results suggest that a better estimate is: $Q_b = 0.4\ Q$

For T.N.T. the ratio $\frac{G(a)}{Q_b}$ can be expressed as

$$\frac{G(a)}{Q_b} = 0.0177\, L^{\frac{1}{4}}\left(\frac{1}{a'}\right)^{\frac{3}{4}} \quad \ldots \quad \ldots \quad \ldots \quad \ldots \quad \ldots \quad \ldots \quad \text{(B10)}$$

where L is in centimetres.

B9. Equations B8, B9, and B10 are sufficient to determine a' and s' as functions of time subject to given initial values. For most purposes it is sufficient to take a' = 0 when t = 0 and if the charge is exploded at a depth s_0 below the level 33 ft. above the sea surface, the initial conditions can be written

$$\left.\begin{aligned} a' &= 0 \\ s' &= \frac{s}{L} = s'_0 \end{aligned}\right\} \text{ when } t = 0 \quad \ldots \quad \ldots \quad \ldots \quad \ldots \quad \ldots \quad \text{(B11)}$$

Since equations B8 and B9 are non-linear, they can in general only be solved by a numerical step-by-step process. Moreover, equation B10 involves L explicitly and since L varies with the size of charge, each calculation must be carried out separately for a particular size of charge and a given depth.

Secondly, changes in gravitational potential energy of the water can be simply allowed for by taking the bubble as having a negative weight equal to the weight of the displaced water. The potential energy due to gravity can thus be written as $4/3\pi a^3 \rho z$. Finally, the potential energy of compression in the gas has been defined as $G(a)$ whilst the total energy of the motion is Q_b. Hence the energy equation can be written

$$Q_b = 2\pi\rho a^3\left(\frac{da}{dt}\right)^2 + \frac{1}{3}\pi\rho a^3\left(\frac{dz}{dt}\right)^2 + \frac{4}{3}\pi a^3\rho g z + G(a) \quad \ldots \quad \ldots \qquad (B3)$$

B6. The values of $G(a)$ and Q_b will depend on the nature of the explosive. For T.N.T. it was deduced from early measurements[x] of the period of oscillation of the gas bubble that $Q_b = 0.5Q$ where Q is the total chemical energy liberated by the explosive which can be taken as about 880 calories per gram for T.N.T. In C.G.S. units the energy Q_b of bubble motion for a T.N.T. charge of mass M grams is given by

$$Q_b = 1.85 \times 10^{10} \text{ M ergs} \quad \ldots \quad \ldots \quad \ldots \quad \ldots \quad \ldots \quad \ldots \qquad (B4)$$

B7. An expression for $G(a)$ can be obtained by using the relevant adiabatic relationship between pressure and volume for gaseous products of the explosion. Using the relationship calculated by Jones and Miller for T.N.T. it is found that

$$G(a) = 2.189 \times 10^{10} \times \frac{M^{\frac{5}{4}}}{a^{\frac{1}{4}}} \quad \ldots \quad \ldots \quad \ldots \quad \ldots \quad \ldots \quad \ldots \qquad (B5)$$

where a is measured in cm. and M in grams.

B8. Equations B2, B3, B4, and B5 can be used to determine a and z, for a T.N.T. charge of given size. However, for calculation purposes it is convenient to put these equations in non-dimensional form. This can be done by introducing a length L defined by

$$L = \left(\frac{Q_b}{g\rho}\right)^{\frac{1}{4}} \quad \ldots \quad \ldots \quad \ldots \quad \ldots \quad \ldots \quad \ldots \quad \ldots \quad \ldots \qquad (B6)$$

Hence writing

$$\left.\begin{aligned} a &= a'L \\ z &= z'L \\ t &= t'\sqrt{\frac{L}{g}} \end{aligned}\right\} \quad \ldots \quad \ldots \quad \ldots \quad \ldots \quad \ldots \quad \ldots \quad \ldots \quad \ldots \qquad (B7)$$

the equations for a' and z' are

$$\left(\frac{da'}{dt'}\right)^2 = \frac{1}{2\pi a'^3}\left\{1 - \frac{G(a)}{Q_b}\right\} - \frac{1}{6}\left(\frac{dz'}{dt'}\right)^2 - \frac{2}{3}z' \quad \ldots \quad \ldots \qquad (B8)$$

$$-\frac{dz'}{dt'} = \frac{2}{a'^3}\int a'^3 dt' \quad \ldots \quad \ldots \quad \ldots \quad \ldots \quad \ldots \quad \ldots \qquad (B9)$$

---

[x] Later results suggest that a better estimate is: $Q_b = 0.4\,Q$

For T.N.T. the ratio $\frac{Q(a)}{Q_1}$ can be expressed as

$$\frac{Q(a)}{Q_1} = 0.0177\, L^{\frac{1}{3}}\left(\frac{1}{a}\right)^{\frac{2}{3}} \quad \ldots \quad \ldots \quad \ldots \quad \ldots \quad \ldots \quad \ldots \quad (B10)$$

where L is in centimetres.

B9. Equations B8, B9, and B10 are sufficient to determine a' and s' as functions of time subject to given initial values. For most purposes it is sufficient to take a' = 0 when t = 0 and if the charge is exploded at a depth s_0 below the level 33 ft. above the sea surface, the initial conditions can be written

$$\left.\begin{aligned} a' &= 0 \\ s' &= \frac{1}{L} = s'_0 \end{aligned}\right\} \text{ when } t = 0 \quad \ldots \quad \ldots \quad \ldots \quad \ldots \quad \ldots \quad (B11)$$

Since equations B8 and B9 are non-linear, they can in general only be solved by a numerical step-by-step process. Moreover, equation B10 involves L explicitly and since L varies with the size of charge, each calculation must be carried out separately for a particular size of charge and a given depth.

APPENDIX C

Effects of pressure pulse normally incident on a plane plate

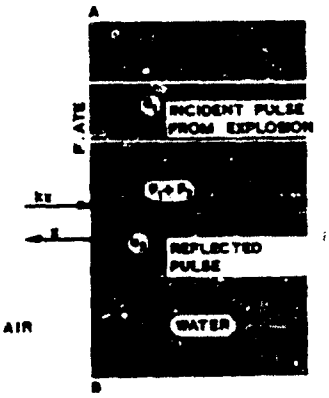


Fig.C1 - Pressure pulse incident on unit area of infinite plate

C1. Fig.C1 shows the pressure pulse normally incident on unit area of an infinite plate. Let

- t = time measured from the first arrival of the pulse at the plate
- x = displacement of the plate
- k = resistance to motion for unit area per unit displacement
- p_1 = pressure in incident pulse
- p_2 = pressure in reflected pulse
- p = pressure on plate
- p_0 = maximum pressure in pulse
- u_1 = particle velocity due to the incident pulse in water touching the plate
- u_2 = particle velocity due to the reflected pulse in water touching the plate
- ρ = mass density of water
- c = velocity of sound in water
- m = mass of plate per unit area of surface

The plate can reasonably be assumed thin enough to neglect elastic waves within it and can be treated as moving bodily with velocity dx/dt. The particle velocities are taken in the direction of travel of the respective waves. The total particle velocity of the water in the x direction is therefore $u_1 - u_2$. Assuming in the first instance that the plate and water move together, the continuity of velocity implies:-

$$\frac{dx}{dt} = u_1 - u_2 \qquad \ldots \quad (C1)$$

Now equation A13 holds generally for a plane wave or pulse travelling in any direction, the particle velocity being taken as measured in the direction of travel of the wave. Hence

$$p_1 = \rho c u_1, \qquad p_2 = \rho c u_2, \qquad \ldots \quad (C2)$$

Substituting in equation C1

$$\rho c \frac{dx}{dt} = p_1 - p_2 \qquad \ldots \quad (C3)$$

The equation of motion for unit area of plate is:-

$$m\frac{d^2x}{dt^2} = p_1 + p_2 - kx \qquad \ldots \quad (C4)$$

Substituting for p_2 from equation C3

$$m\frac{d^2x}{dt^2} + \rho c\frac{dx}{dt} + kx = 2p_1 \qquad \ldots \quad (C5)$$

Best Available Copy

Equation 05 relates the displacement of the plate to the pressure p_i in the incident pulse, that is the pressure in open water in the absence of the target. It is convenient to use the exponential form[2] for this pressure

$$p_i = p_0 e^{-\alpha t} \quad \ldots \quad \ldots \quad \ldots \quad \ldots \quad \ldots \quad \ldots \quad (06)$$

Substituting in equation 05

$$m\frac{d^2x}{dt^2} + \rho c\frac{dx}{dt} + kx = 2p_0 e^{-\alpha t} \quad \ldots \quad \ldots \quad \ldots \quad \ldots \quad (07)$$

Equation 07 can be solved for the initial conditions which correspond to the plate being at rest before the explosion, that is

$$\left.\begin{aligned} x &= 0 \\ \frac{dx}{dt} &= 0 \end{aligned}\right\} \text{ when } t = 0 \quad \ldots \quad \ldots \quad \ldots \quad \ldots \quad (08)$$

For most practical cases to which the theory is all applicable, it is sufficiently accurate, in the first instance, to neglect the term kx in equation 07. The solution for the displacement at any time is then

$$x = \frac{2p_0}{m\alpha^2(\xi-1)\xi}\left\{\xi - 1 + e^{-\alpha\xi t} - \xi e^{-\alpha t}\right\} \quad \ldots \quad \ldots \quad (09)$$

where ξ is a non-dimensional quantity defined by

$$\xi = \frac{\rho c}{m\alpha} \quad \ldots \quad \ldots \quad \ldots \quad \ldots \quad (010)$$

Corresponding to the solution 09 for the displacement, the pressure on the plate can be obtained from equations 03, 06 and 09 in the form

$$p = p_i + p_1 = \frac{2p_0}{\xi-1}\left\{\xi e^{-\alpha\xi t} - e^{-\alpha t}\right\} \quad \ldots \quad \ldots \quad (011)$$

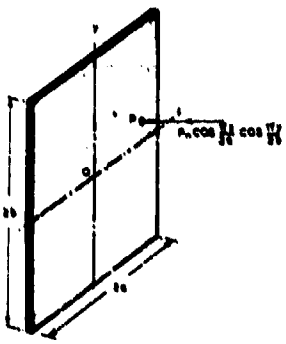
Now, whatever positive value be assigned to ξ, solution 011 indicates that the pressure acting on the plate will be initially $2p_0$, corresponding to instantaneous complete reflection and will then decrease to zero, followed by negative values which will ultimately tend to zero asymtotically.

---

[2] The symbol p_0 is used rather than p_m of equation 10 to avoid confusion with the latter suffix and the symbol m for the mass per unit area of plating.

APPENDIX D

Deformation of rectangular plastic panel by suddenly applied pressure



In fig. D1 a rectangular panel of plating of sides 2a, 2b with axis Ox, Oy parallel to the sides and having origin at O, the plate centre, is subjected to a suddenly applied pressure distribution $p_0 \cos \frac{\pi x}{2a} \cos \frac{\pi y}{2b}$.

If now

- h = plate thickness
- σ_0 = uniform membrane stress
- ρ = mass density of plate
- t = time
- $w(t)$ = deflection of point (x,y) in plate at time t
- $w_0(t)$ = central deflection at time t

Fig. D1 - Rectangular plate subjected to impulsive pressure distribution

then for deflections which are relatively small compared with the small span (one sixth or less), the equation of motion of the plate is

$$\rho h \frac{\partial^2 w(t)}{\partial t^2} = p_0 \cos \frac{\pi x}{2a} \cos \frac{\pi y}{2b} + \sigma_0 h \left\{ \frac{\partial^2 w(t)}{\partial x^2} + \frac{\partial^2 w(t)}{\partial y^2} \right\} \quad \ldots \quad \ldots \quad \ldots \quad (D1)$$

If the plate is fixed around the periphery the solution of equation D1 is

$$w(t) = w_0(t) \cos \frac{\pi x}{2a} \cos \frac{\pi y}{2b} \quad \ldots \quad \ldots \quad \ldots \quad \ldots \quad \ldots \quad \ldots \quad \ldots \quad (D2)$$

where $$\rho h \frac{d^2 w_0(t)}{dt^2} = p_0 - \frac{\sigma_0 h \pi^2}{4} \left\{ \frac{1}{a^2} + \frac{1}{b^2} \right\} w_0(t) \quad \ldots \quad \ldots \quad \ldots \quad (D3)$$

Subject to the initial conditions that the plate is flat and at rest, the solution of equation D3 is

$$w_0(t) = K/2 \, (1 - \cos \alpha t) \quad \ldots \quad \ldots \quad \ldots \quad \ldots \quad \ldots \quad \ldots \quad \ldots \quad (D4)$$

where $$K = \frac{\delta}{\pi^2 \sigma_0 h} \left\{ \frac{a^2 b^2}{a^2 + b^2} \right\} \quad \ldots \quad \ldots \quad \ldots \quad \ldots \quad \ldots \quad \ldots \quad \ldots \quad (D5)$$

$$\alpha^2 = \frac{\pi^2 \sigma_0}{\rho} \left\{ \frac{1}{a^2} + \frac{1}{b^2} \right\} \quad \ldots \quad \ldots \quad \ldots \quad \ldots \quad \ldots \quad \ldots \quad \ldots \quad (D6)$$

The final solution given by equations D2, D4, D5 and D6 will be valid so long as the plate is stretching, which is true up to $t = \pi/\alpha$. At this instant, $w_0(t) = w_0 = K$ and the plate is at rest everywhere with no velocity and has a deflected shape given by

$$w = K \cos \frac{\pi x}{2a} \cos \frac{\pi y}{2b} \quad \ldots \quad \ldots \quad \ldots \quad \ldots \quad \ldots \quad \ldots \quad \ldots \quad (D7)$$

where $w_o = K$ is the permanent central deflection (that is of O) and w is the permanent deflection of any point (x, y). Equation D7, therefore, represents permanent deformation and the plate will remain in equilibrium thereafter since the applied pressure $p_o \cos\frac{\pi x}{2a} \cos\frac{\pi y}{2b}$ is insufficient to cause further stretching. Thus, equation D7 with K defined by equation D5 is the final plastic dishing produced by the suddenly applied pressure $p_o \cos\frac{\pi x}{2a} \cos\frac{\pi y}{2b}$.

Energy absorbed in plastic deformation

D2. The energy Ω_p absorbed in plastic deformation by stretching from the flat plate to the dished shape is $\sigma_o h$ times the increase in area of the plate. If proportional motion of the deforming plate be assumed, that is the plate deforms in a constant shape throughout the motion, then the deflection w(t) for any point (x, y) in the plate at time t would be of the form

$$w(t) = w_o(t)\, f(x, y) \quad \ldots \quad \ldots \quad \ldots \quad \ldots \quad \ldots \quad \ldots \quad \ldots \quad (D8)$$

where $w_o(t)$ is the central deflection at time t

$$\text{therefore} \qquad \Omega_p = \tfrac{1}{2}\sigma_o h\, w_o^2(t) \int_{-a}^{a}\int_{-b}^{b}\left[\left(\frac{\partial f}{\partial x}\right)^2 + \left(\frac{\partial f}{\partial y}\right)^2\right] dy\,dx \qquad \ldots \quad (D9)$$

In particular, if the plate is assumed to deform in the empirical parabolic shape given by

$$f(x, y) = \left\{1 - \frac{x^2}{a^2}\right\}\left\{1 - \frac{y^2}{b^2}\right\} \quad \ldots \quad \ldots \quad \ldots \quad \ldots \quad \ldots \quad (D10)$$

$$\text{then} \qquad \Omega_p = \frac{64}{45}\left\{\frac{a}{b} + \frac{b}{a}\right\} \sigma_o h\, w_o^2(t) \quad \ldots \quad \ldots \quad \ldots \quad \ldots \quad \ldots \quad (D11)$$

Kinetic energy of deforming plate

D3. The total kinetic energy $\mathcal{T}$ of the deforming plate at time t is

$$\mathcal{T} = \tfrac{1}{2} h\rho \iint\left[f^2(x,y)\right]^2 dy\,dx \left(\frac{dw_o(t)}{dt}\right)^2 \quad \ldots \quad \ldots \quad \ldots \quad (D12)$$

For the shape given by equation D10 this gives

$$\mathcal{T} = \frac{128}{225}\rho h\, a\, b \left(\frac{dw_o(t)}{dt}\right)^2 \quad \ldots \quad \ldots \quad \ldots \quad \ldots \quad \ldots \quad (D13)$$

Work done by pressure

D4. If the motion is produced by some given pressure distribution $p(t, x, y)$ which varies in a known manner with t, x, y, the work W done by this pressure is

$$W = \int_0^t \int_{-a}^{a} \int_{-b}^{b} p(t, x, y) f(x,y) \frac{dw_o(t)}{dt} \, dydxdt \quad \ldots \quad \ldots \quad \ldots \quad (D14)$$

which may be written

$$W = \int_0^t P(t) \frac{dw_o(t)}{dt} \, . \, dt \quad \ldots \quad \ldots \quad \ldots \quad \ldots \quad \ldots \quad \ldots \quad (D15)$$

where $$P(t) = \int_{-a}^{a} \int_{-b}^{b} p(t,x,y) f(x,y) \, dydx \quad \ldots \quad \ldots \quad \ldots \quad \ldots \quad (D16)$$

D5. For a given pressure p and any assumed form for the deforming plate such as equation D10, the function $P(t)$ is known. Hence, equating the combined plastic and kinetic energy to the work done, that is

$$W = \Omega_p + \mathcal{T}$$

gives from equations D11, D13 and D15 an equation of the form

$$\tfrac{1}{2} M \left\{ \frac{dw_o(t)}{dt} \right\}^2 + \tfrac{1}{2} k w_o^2(t) = \int_0^t P(t) \frac{dw_o(t)}{dt} \, dt \quad \ldots \quad \ldots \quad (D17)$$

$$\left.\begin{aligned} \text{where} \quad M &= \tfrac{256}{225} \rho hab \\ k &= \tfrac{128}{45} \left(\frac{a}{b} + \frac{b}{a} \right) \sigma_o h \end{aligned}\right\} \quad \ldots \quad \ldots \quad \ldots \quad \ldots \quad \ldots \quad \ldots \quad (D18)$$

The energy equation D17 can be differentiated with respect to time to give

$$M \frac{d^2 w_o(t)}{dt^2} + k w_o(t) = P(t) \quad \ldots \quad \ldots \quad \ldots \quad \ldots \quad \ldots \quad (D19)$$

Thus the assumptions of proportional motion and a uniform membrane stress in the plate lead to a motion analogous to that of mass M on a spring of stiffness k subject to a dynamic load $P(t)$.

D6. For different assumed shapes $f(x,y)$ of proportional motion, the energy absorbed by the plate as given by equation D9 varies less for a given mean deflection than for a given central deflection. Thus if $\bar{w}(t)$ is the mean deflection

$$\bar{w}(t) = \frac{w_o(t)}{4ab} \int_{-a}^{a} \int_{-b}^{b} f(x,y)\,dy\,dx \quad \ldots \quad \ldots \quad \ldots \quad \ldots \quad \ldots \quad (D20)$$

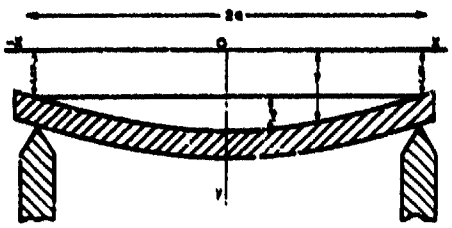
The energy absorbed by the plate can be expressed in the form

$$\Omega_p = \tfrac{1}{2} k' \bar{w}^2(t)$$

If Ω_p is equated to the incident energy Ω_i, an estimate of $\bar{w}(t)$ instead of $w_o(t)$ is obtained. Such estimates of $\bar{w}(t)$ vary less for different assumed shapes than do corresponding estimates of $w_o(t)$. For this reason, results of box or drum model tests are often expressed in terms of the mean deflection rather than the maximum deflection.

APPENDIX E

Deflection of a uniform elastic beam on spring supports



E1. Fig.E1 represents a uniform elastic beam of length 2a supported on spring supports and subjected to a uniformly distributed load w suddenly applied per unit length of the beam. Under these conditions, the deflection of any section of the beam distant x from the centre at time t is taken as y, and the deflection of the ends of the beam at this time is denoted by ξ. The deflection of the centre of the beam relative to the ends of the beam is represented by η while the mass per unit length of the beam is denoted by m.

Fig.E1. Deflection of uniform elastic beam on spring supports

First, the beam is assumed to deflect in the constant shape

$$y = \xi + \eta \cos\frac{\pi x}{2a} \quad \ldots \quad \ldots \quad \ldots \quad \ldots \quad \ldots \quad \ldots \quad \ldots \quad \ldots \quad (E1)$$

Equation E1 satisfies the necessary conditions that

$$\left.\begin{aligned} y &= \xi \\ \text{Bending moment } EI\frac{\partial^2 y}{\partial x^2} &= 0 \end{aligned}\right\} \text{ at ends when } x = \pm a \quad \ldots \quad \ldots \quad \ldots \quad (E2)$$

The problem is now reduced to finding ξ and η as functions of time. The kinetic energy of the beam $\mathfrak{T}$ is

$$\mathfrak{T} = \tfrac{1}{2}\int_{-a}^{a} m\left(\frac{\partial y}{\partial t}\right)^2 dx \quad \ldots \quad \ldots \quad \ldots \quad \ldots \quad \ldots \quad \ldots \quad \ldots \quad \ldots \quad (E3)$$

Whilst the total potential energy H of the system is

$$H = \tfrac{1}{2}k_1\xi^2 + \tfrac{1}{2}\int_{-a}^{a} EI\left(\frac{\partial^2 y}{\partial x^2}\right)^2 dx \quad \ldots \quad \ldots \quad \ldots \quad \ldots \quad \ldots \quad \ldots \quad (E4)$$

where the first term represents the contribution of the two end springs and the second term is the elastic energy of bending of the beam. Thirdly, the virtual work of the applied load w due to any small variation δy in the deflection is

$$\delta W = \int_{-a}^{a} w\,\delta y\, dx \quad \ldots \quad \ldots \quad \ldots \quad \ldots \quad \ldots \quad \ldots \quad \ldots \quad \ldots \quad (E5)$$

Using the assumed deflected shape of equation E1, equations E3, E4 and E5 become of the form

$$\left.\begin{aligned} \mathcal{T} &= \tfrac{1}{2} A \dot{\xi}^2 + B \dot{\xi} \dot{\eta} + \tfrac{1}{2} C \dot{\eta}^2 \\ \Pi &= \tfrac{1}{2} k_1 \xi^2 + \tfrac{1}{2} k \eta^2 \\ \delta W &= P \delta \xi + Q \delta \eta \end{aligned}\right\} \quad \ldots \quad \ldots \quad \ldots \quad \ldots \quad (E6)$$

where A, B, C, P, Q and k are constants depending on the beam and spring properties and the applied load w. For the two unknowns ξ and η, Lagrange's equations are

$$\frac{d}{dt}\left(\frac{\partial \mathcal{T}}{\partial \dot{\xi}}\right) + \frac{\partial \Pi}{\partial \xi} = P \quad \ldots \quad \ldots \quad \ldots \quad \ldots \quad \ldots \quad (E7)$$

$$\frac{d}{dt}\left(\frac{\partial \mathcal{T}}{\partial \dot{\eta}}\right) + \frac{\partial \Pi}{\partial \eta} = Q \quad \ldots \quad \ldots \quad \ldots \quad \ldots \quad \ldots \quad (E8)$$

which, when applied to equation E6 gives

$$A \ddot{\xi} + B \ddot{\eta} + k_1 \xi = P \quad \ldots \quad \ldots \quad \ldots \quad \ldots \quad \ldots \quad (E9)$$

$$B \ddot{\xi} + C \ddot{\eta} + k \eta = Q \quad \ldots \quad \ldots \quad \ldots \quad \ldots \quad \ldots \quad (E10)$$

Initially, the system is at rest so that

$$\left.\begin{aligned} \xi &= \dot{\xi} = 0 \\ \eta &= \dot{\eta} = 0 \end{aligned}\right\} \text{ when } t = 0 \quad \ldots \quad \ldots \quad \ldots \quad \ldots \quad (E11)$$

The ordinary simultaneous differential equations E9 and E10 can be solved subject to conditions of equation E11 and hence the method determines ξ and η

APPENDIX F. *

Airblast from underwater explosions

Not a great deal is known about the airblast caused by charges exploding below the surface in water. The few measurements which have been made have shown that if the charge is just above the surface of the water, the blast wave is the same as that from a similar charge resting on the ground. If the centre of the charge is a depth D expressed in units of the "charge radius", the blast wave in the air is believed to be approximately hemi-spherical in shape and intensity, centred at a point in the water surface above the charge, and to be roughly the same as that caused by a charge of weight SW exploded on the ground, where the reduction factor S is shown in the following graph as a function of D.

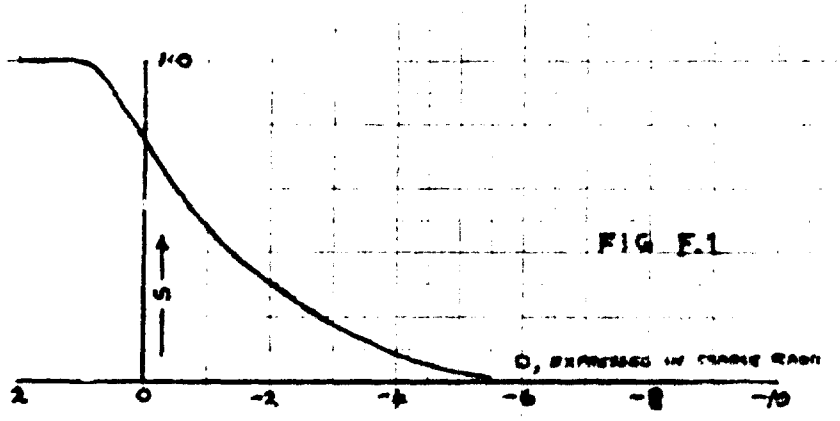


FIG F.1

If part of the charge is above the water surface, and part below, then it seems necessary to integrate over the charge, allowing for the depth of each element, in order to find the equivalent charge. For example, in the case where a cylindrical charge, long compared with its diameter, is detonated with the length vertical, part under water and part above, the part below water is very appreciably muffled, as is clear from an inspection of the curve S above.

An explosion which causes a strong airblast wave over the surface of water throws up spray. A layer of water is stripped off the surface and breaks up into droplets which move in the turbulent boundary layer. It can be shown that the height to which the spray reaches is approximately I/30 ft., where I is the positive impulse in the blast wave, measured in pounds weight milliseconds/in^2. This formula will begin to fail for small charges (1 lb. or less), but should be roughly valid for larger charges. The failure is due to the finite time taken for instabilities to develop in the water surface (of the order 1 millisecond), a time which is independent of the scale of the explosion.

Best Available Copy

APPENDIX G.*

Gravity waves in the sea caused by explosions

If a small charge, say a few ounces, is exploded just above or below a water surface, an impressive wave system is generated. The scaling laws from small to large charges, however, are such that large charges generate disappointingly small wave systems, particularly if the charge is exploded above the water surface.

The waves caused by an explosion below the surface is supposed to result mainly from the creation of a cavity which breaks near its maximum. The largest cavity is caused when the depth of the charge is about 70-80% of the maximum bubble radius, a result which allows the optimum depth to be calculated. The wave height at distances proportional to the linear dimensions of the bubble (or cavity) are directly proportional to the linear dimensions of the cavity. Since the bubble is created against a pressure which is the sum of atmospheric pressure and a head of water equal to the depth, the size of the cavity increases less rapidly with charge weight than does the linear dimensions of the charge.

When the charge is exploded a few charge radii above the water surface, the wave system is generated by the impulse given to the water surface. In this case, the scaling law is that the wave height at distances proportional to the linear dimensions of the charge is proportional only to the sixth root of the charge weight. Comparatively enormous charges (e.g. the atomic bomb) cause waves only a few inches high at a distance of 1,000 yards.

If the depth of water is only of the order of a few charge radii, the waves near the centre are comparable in height with the depth of water, and therefore probably break. The theory of small wave heights is no longer applicable, and the waves must be considered more analogous to a tidal bore.

Broadly speaking, gravity waves caused by explosions are of little operational interest, but there are two possible exceptions (a) where the charge is enormous (several thousands of tons, in relatively shallow water), (b) where multiple charge arrays, giving a "beam", are employed.

LIST OF REFERENCES

Ref.No.	Para.No.	Title	Reference
1	12	Theory of Sound Vol.II, Chapter XI Rayleigh.	Macmillan & Co. London.
2	12	Underwater Explosions R.H. Cole.	Princeton University Press (U.S.A)
3	22	Experiments on pressure wave thrown up by submarine explosions H.W. Hillyer.	D.S.R. Report R.E. 142/1919
4	24	Report on nature of the pressure impulse produced by the detonation of explosives underwater. A.B. Wood.	A.R.L. Report S1?
5	25	Report of the development of a standardised tourmaline pressure gauge	AUW/TRI.37/RP42
6	25	Report on use of amplifiers with piezo-electric gauges	N.C.R.E.R/10
7	25	Piezo-electric gauges - development of miniature type	N.C.R.E.R/28
8	26	Continuation of measurements of pressure momentum and energy close to exploding charges	N.C.R.E.R/42
9	36	Pressure/time curves for submarine explosions W.G. Penney.	Ministry of Home Security Report R.C.14
9	36	Pressure/time curves for submarine explosions W.G. Penney and H.K. Dasgupta.	Ministry of Home Security Report R.C. 333
10	36	Theory of propagation of shock waves from explosive sources in air and water. Kirkwood and Brinkley.	O.S.R.P.4814 and 5649 U.S.A.
11	36	Calculation from thermodynamical and hydrodynamical considerations of underwater shockwaves for spherical charges. H.N.V. Temperley and J. Craig.	Admiralty Report Under 136
12	37	The thickness of a shock front in a gas. George Cowan and D.F. Hornig.	Office of Naval Research (U.S.A) N.R-061-041
12a	46	Penney and Pile	Report on Progress in Physics, 1949.
12b	60	Arons and Collaborators	J.Accoust.Soc.Amer.
12c	60	Taub	Phys.Rev.72, p.51; 74, p.328.
13	63	Underwater explosions. Report on theoretical shape of the pressure/time curve and the growth of the gas bubble. S. Butterworth.	A.R.L. Report S5 1924

Ref.No.	Para.No.	Title	Reference
14	43	The behaviour of water under hydrostatic tension I. H.N.V. Temperley and Ll. G. Chambers.	Proc. Phys. Soc. LVIII p240 1946
15	63 182	"Vertical motion of spherical bubble and the pressure pulse surrounding it". G.I. Taylor.	Ministry of Home Security Report S.W.19
16	63	"The behaviour of an underwater explosion bubble". Conyers Herring.	N.D.R.C. Report C4-Sr20-010 (U.S.A) (U.S.A).
17	70	A simplified theory of the effect of surfaces on the motion of an explosion bubble A.R. Bryant.	Admiralty Report Undex 115
18	72	The effect of the bottom on underwater explosion phenomena	Admiralty Report Undex 158
18a	78	Splashes from underwater explosions Kolsky, Lewis, Sampson, Shearman and Snow.	P.R.S. Vol.196A 1949
19	87	"The pressure and impulse of submarine explosive waves on plates" G.I. Taylor	Ministry of Home Security Report R.C.235
20	99	"Theoretical investigation of cavitation phenomena occurring when an underwater pressure pulse is incident on a yielding surface. Part 1". H.N.V. Temperley	Admiralty Report Undex 99
21	102	"The reflection of a spherical wave from an infinite plate" E.N. Fox	Ministry of Home Security Report S.W.18
22	103	"Damage to ships plates by underwater explosions" S. Butterworth	Admiralty Report ARL/S10 and Undex 17
23	105	Theory of Sound, Vol.II, para.302 Rayleigh.	Macmillan & Co. London

Ref.No.	Para.No.	Title	Reference
24	108	Note on a motion of finite plate due to an underwater explosion S. Butterworth.	Admiralty Report AM/N1/24 and Under 17
25	110	"Interim report on measurement of motion of structures under impulsive loading" Part II, IV and V J.H. Linford.	Admiralty Reports Under 181, 182 and 210
26	110	"Theoretical investigation of cavitation phenomena when an underwater explosive is incident on a yielding surface" Parts II and III H.N.V. Temperley and L.L.G. Chambers.	Admiralty Reports Under 126 and 150
27	111	"Theoretical analysis of the dishing of six inch diameter copper diaphragm gauges by underwater explosions" E.N. Fox and W.T. Rollo.	Admiralty Report Under 217
28	115	"The bodily motion of a sphere subjected to the pressure pulse from an underwater explosion" E.N. Fox.	Admiralty Report Under 12
29	118	"The effect of its bodily motion on the dishing of a 'paddle-wheel' target" L.L.G. Chambers.	Admiralty Report Under 218
30	119	"Effect of reflection, diffraction and bodily motion on the recording of a pressure pulse by a peizo-electric gauge of finite size" E.N. Fox.	Admiralty Report Under 211
31	121	"The behaviour of the gas bubble formed by an underwater explosion in the presence of a deformable target" H.N.V. Temperley.	Admiralty Report Under 92
32	121	"The effect of an adjacent deforming target upon the bubble due to a submarine explosion" L.L.G. Chambers.	Admiralty Report Under 207
33	121	"Photographic measurements of the attraction of an underwater explosion bubble to the Road Research Laboratory Box Model target" A.R. Bryant.	Admiralty Report Under 185
34	121	"The attraction of an underwater explosion bubble to a rigid disc" A.R. Bryant.	Admiralty Report Under 135
35	122	"The effect of varying the charge distance in Box Model tests using 1/10" thick target plates" G. Charlesworth and J.E. Eaton.	Admiralty Report Under 177
36	123	"Diffraction effects in bubble damage to Box Model plates. Energy considerations" G. Charlesworth.	Admiralty Report Under 179

Ref.No.	Para.No.	Title	Reference
37	128	"The analysis of Engineering Structures" Chapter 24 Pippard and Baker.	Edward Arnold & Co., London 2nd. Edition 1943
38	129	"Stress-strain relationships in impact" G.I. Taylor.	Ministry of Home Security Report R.C.36
39	135	"The plastic distortion of metals" Taylor and Quinney.	Phil. Trans. Roy. Soc. A. 230
40	140 142	"The distortion under pressure of a diaphragm which is clamped along its edge and stressed beyond the elastic limit" G.I. Taylor.	Ministry of Home Security Report S.W.24
41	143	"Preliminary static test of a box model target plate" E.N. Fox.	Admiralty Report Undex 34
42	143	"The deflection of a box model plate under static loads" G. Charlesworth.	Admiralty Report Undex 24
43	145	"The plastic wave in a wire extended by an impact load" G.I. Taylor.	Ministry of Home Security Report R.C. 329
44	145	"On the propagation of plastic deformation in solids"	N.D.R.C. Report No. A29, 1942
45	145	"The propagation of plastic deformation in solids" T. von Karman and Pol. Duwez.	U.S.A. Sixth International Conference of Applied Mechanics Paris 1946
46	146	"The behaviour of long beams under impact loading" Duwez, Clark, Wood and Bohnenblust.	O.S.R.D. Report 1828 Sept. 1943 U.S.A.
47	149	"Theory of Sound" Vol.I, Chapter X Rayleigh.	Macmillan & Co. London
48	154	"Theoretical investigation of cavitation phenomena when an underwater explosive is incident on a yielding surface Parts II and III H.N.V. Temperley and L.L.G. Chambers.	Admiralty Report Undex 150
49	154	"Box Model tests with 1/10" and 1/16" target plates. Energy relationships" G. Charlesworth.	Admiralty Report Undex 178
50	157	"Note on an approximate method for the solution of dynamical problems" E.N. Fox.	Admiralty Report Undex 48

Ref.No.	Para.No.	Title	Reference
51	159	"The optimum distribution of weight between plating and stiffeners for maximum resistance to impulse loading: First theoretical analysis" E.N. Fox and J. Craig.	Admiralty Report Undex 104
52	159	"Some extensions of the Ritz method for the solutions of variational problems in mathematical physics" E.N. Fox	Admiralty Report Undex 212
53	159	"Analysis of pull-in at edge fixings in Box Model Plates" E.N. Fox.	Admiralty Report Undex 180
54	163	"Brittle fracture in mild steel plates" Various Authors.	Report of Conference of Brit. Iron & Steel Res. Assn. Cambridge Oct. 1945

EXPERIMENTS ON THE PRESSURE WAVE THROWN OUT BY SUBMARINE EXPLOSIONS

H. W. Hilliar
Admiralty Experimental Station

British Contribution

1919

EXPERIMENTS ON THE PRESSURE WAVE THROWN OUT BY SUBMARINE EXPLOSIONS.

CONTENTS.

PART I.—RESULTS.

Section.		Page.
1.	Origin and purpose of the experiments	3
2.	Scope of the results	4
3.	Nature and genesis of the pressure wave	4
4.	Effect of a 300-lb. charge of 40/60 Amatol at a distance of 50 feet	6
5.	Regularity and symmetry of the pressure wave	7
6.	Velocity of the pressure wave	8
7.	Variation of pressure with distance	9
8.	Surface effects	9
9.	Comparison of large and small charges	11
10.	Bottom effects	13
11.	Effect of surrounding the charge with an air chamber	14
12.	Comparisons of different explosives	14
13.	Gunpowder charges	14
14.	Composite charges	15
15.	Influence of the shape of the charge	15
16.	Damaging power of different pressure waves	16

PART II.—METHODS.

17.	Gauges for measuring the time-integral of the pressure	20
18.	Gauges for determining the complete time-pressure curve	21
19.	Gauges for measuring the maximum pressure	26
20.	Gauges for empirical comparisons of pressure (piasticine gauges)	30
21.	Methods of laying out the charge and gauges in the water	31
22.	Alternative methods for determining the time-pressure curve: Hopkinson's pressure-bar method: Sir J. J. Thomson's piezo-electric method	33
23.	Measurements of the velocity of the pressure wave	35
24.	Measurements of the echo reflected from the bottom	36

APPENDIX I.—SCHEDULE OF CHARGES AND SHOTS.

25.	List of charges	38
26.	List of shots	39

APPENDIX II.—CALIBRATION EXPERIMENTS.

27.	Apparatus	40
28.	Results	41

APPENDIX III.—MISCELLANEOUS.

29.	Some general points in the theory and use of pressure gauges	43

PART I.

RESULTS.

(1) Origin and Purpose of the Experiments.

The development of depth charges and non-contact mines as a means of destroying submarines has made it necessary to investigate as fully as possible the effects of different charges under water, at different distances, and under different conditions of depth, &c. The damage inflicted by a non-contact charge is due to a pressure wave transmitted through the water, and it is the law of action of this pressure wave that requires investigation.

The most fundamental way of attacking the problem is to make an exact physical study of the pressure wave springing from different charges, and then, as a second step, to determine the relation between the physical constants of the pressure wave and its damaging power.

This has been a recognised aim of investigation since observation mines were introduced in the American Civil War, and in fact the most extensive experiments on the subject, up to the present, were those made between 40 and 50 years ago by Lieut.-Col. H. L. Abbot, U.S. Engineers ("Experiments to develop a system of submarine mines, &c."—No. 23 of the professional papers of the Corps of Engineers of U.S. Army). Abbot's work, however, suffered from the limitation that the only quantity which he attempted to measure was the intensity of the pressure at different points in the water; there were no means for determining the duration of the pressure or the character of its rise and fall, though these are factors which may be of equal importance as regards the effect on a ship. The same remark applies to the continuation of Abbot's work in recent years by Lieut. Schuyler, U.S.N. Moreover, present knowledge shows that, even as regards maximum pressure, the gauges used by Abbot and Schuyler were too sluggish to give correct results (Section 19).

The necessity for fuller investigation, taking account of time as well as pressure, was urged on the Board of Invention and Research in 1917 by Sir R. Threlfall, and at his instance an attempt was made by the writer to develop gauges that would give more complete information. In the first half of 1918 a successful system of gauges

PRECEDING PAGE BLANK

was evolved depending on the use of soft copper plugs to register the momentum acquired by steel pistons exposed at their outer ends to the pressure in the water and free to move inwards towards an anvil. The construction, theory, and use of the gauges are described in Part II. of this report, Part I. dealing only with the results obtained, and it is sufficient to say here that the measurements from a set of gauges enable a stepped diagram to be drawn, representing the average pressure during different periods at a given place in the water, as illustrated for example in Fig. 1. A curve drawn through the steps in such a way as to take in as much as it leaves out is assumed to represent the time-history of the pressure. The maximum pressure was determined separately by a somewhat different type of gauge.

Some preliminary experiments were made at Portsmouth, but as soon as the gauges had passed out of the experimental stage approval was obtained for carrying out a systematic programme of investigation in deeper water. The locality selected was Troon, on the Firth of Clyde, and H.M. Drifter "Malapert" was allocated for the purpose. The experiments at Troon commenced in August 1918 and were concluded in the following April. A list of the charges fired is given in Appendix I., they were mostly of regular Service types and ranged from 40 lbs. of explosive to 1,900 lbs. One hundred and seven shots were fired altogether, amounting to about 21 tons of explosive.

The executive arrangements and the working party and ship were under the direction of Lieut.-Commander D. Errington, R.N.

(2) Scope of the Results.

Broadly summarised, the experiments have shown that the pressure wave from a submerged charge of high explosive is a very regular and symmetrical phenomenon. In the region investigated, that is to say, at distances between 25 and 100 feet from a 300-lb. charge and corresponding distances from other charges, the pressure wave follows very approximately the simple laws of sound, the velocity of the wave being the same as that of sound and the pressure falling nearly in simple proportion to the distance. All the principal features can be explained from the standpoint of acoustic theory. For example, the influence which the surface of the water exercises on the pressure at any given point can be completely accounted for by assuming that the pressure wave is reflected from the surface as a wave of tension.

The pressure wave from a big charge is more intense and more sustained than that from a small charge, the two pressure waves being connected by a definite relationship deduced from the principle of dynamic similarity.

Other questions examined include a comparison of various high explosives (T.N.T., 40/60 amatol, 80/20 amatol, guncotton and ammonium perchlorate) and also of some powder charges; the effect of surrounding a charge with a large air space, as in a buoyant mine; the effect of exploding a charge on the sea-bottom instead of in mid-water; the influence of the shape of the charge as affecting the symmetry of the pressure wave; and the effect of composite charges, made by lashing together several charges, of which only one is primed and fired.

By observing the deformation of standard mine cases suspended at known distances from various charges a beginning has been made in the investigation of the relative damaging power of different pressure waves, and it has been proved that the extent to which a structure is damaged is not entirely determined by the maximum intensity of the pressure, but also by the period for which the pressure is sustained.

(3) Nature and Genesis of the Pressure Wave.

Before describing the results in detail it is useful to picture what probably happens at the moment when a submarine charge is fired. Assume that the charge is a sphere of T.N.T., weighing 300 lbs. and therefore 22 inches in diameter, and that detonation is initiated at the centre. The velocity of detonation in T.N.T. is 23,000 feet a second, so that in about four hundred thousandths of a second the whole of the explosive is transformed into incandescent gas under enormous pressure. The globe of gas expands rapidly (but much less rapidly than it would in air, because it has the additional inertia of the surrounding water to overcome) and in a thousandth of a second the volume of gas has probably expanded 5 or 10 times and the pressure fallen to 2 or 3 per cent. of its first intensity. As the pressure falls the gases expand more slowly. In the first few hundredths of a second levitation has no time to lift them

appreciably; afterwards they begin to rise and to lose their sperical form. What happens to them eventually depends on the depth at which the charge was fired. If it was fired at a moderate depth, say 30 or 50 feet, the gases rise and vent themselves at the surface before their pressure is completely spent, throwing up tall plumes of smoke and spray. But at a greater depth, say 200 feet, the pressure of the gases is entirely spent before they can reach the surface; probably after several seconds the pressure falls to less than the normal hydrostatic pressure, owing to condensation of steam and other causes; after this the gases are churned up with the surrounding water into an emulsion, which, being of lower specific gravity than sea-water, pours up slowly to the surface.

The supposed history of the explosion products has been traced to a conclusion because it is of interest to account for the effects observed at the surface, but it is only during the first thousandth of a second or so that the effective part of the pressure wave is generated. At the moment when the wave of detonation reaches the surface of the exploding sphere the charge may be supposed still to occupy exactly its original volume (Section 9), and the water in contact with it, which until that moment was under normal pressure, is instantaneously subjected to a pressure probably exceeding 200 tons per square inch. The first layer of water is compressed and thrown outwards, compressing the next layer, and so on, and in this way there is generated the front of a pressure wave, which springs away with a velocity that at first exceeds and then rapidly approximates to that of sound in water. The globe of gas, expanding much less rapidly than the pressure wave, feeds the rear of the wave with a continually falling pressure. At any instant the pressure in the water at different points along a radius increases continuously from the boundary of the gases to the front of the wave, where the pressure is a maximum.

The pressure wave is, of course, nothing but a very strong sound wave; the mechanism of its propagation is essentially the same as that of sound, the difference is only in the intensity of the pressure transmitted. According to elementary acoustic theory the pressure in a spherically diverging sound wave falls off in simple proportion to the distance from the source, the time-pressure curve at distance D_1 being a copy of the curve at distance D_2 with the pressure altered in the ratio $\frac{D_2}{D_1}$. The velocity of propagation is independent of the distance. This theory, however, is only exact in the case of infinitely weak waves, since it rests on the assumption that the compression of the medium is indefinitely small. At a very great distance from a submarine explosion this condition will be approximately fulfilled, and the experiments made by Mr. Boulding in connexion with submarine sound ranging have proved that at distances of several miles the velocity of the pressure wave is the same as that of sound in sea-water.

On the other hand the simple laws of sound cannot be expected to apply in the region near the charge, where the very intense pressure produces considerable compression of the water. In this region the velocity of propagation of the pressure wave must be greater than that of sound (Section 23). Moreover, the front of the pressure wave, where the pressure is greatest, must travel faster than the subsequent parts of the wave, where the pressure is less, and this involves a tendency for the crest of the wave to become flattened, the maximum pressure falling more than in simple proportion to the distance. At the same time, if the energy of the wave is conserved, the time integral of the pressure must fall less than in proportion to the distance.

The present investigation was confined almost entirely to distances at which the pressure did not exceed about 2 tons per square inch (25 feet and upwards from a 300-lb. charge and corresponding distances from other charges). Under this pressure 100 volumes of sea-water are reduced to 98·7 volumes, that is to say, the "condensation" is only ·013. which is a small quantity though not of an infinitesimal order. It was therefore expected that the pressure wave would behave not very differently from an ordinary sound wave, both as regards velocity and in other respects, and the experimental results proved this view to be correct.

There must be a great difference in this respect between, the propagation of explosion pressure waves in water and in air, for the pressures necessary to produce the same small condensation in these two fluids are in the ratio 23,000 : 1. An explosion pressure wave in air must certainly deviate widely from the simple acoustic laws for a great distance from the charge.

(4) Effect of a 300-lb. Charge of 40/60 Amatol at a distance of 50 feet.

Towards the end of 1917 Mining School carried out a series of experiments in which H.M. Submarine D. 1 was attacked at different distances with depth charges containing 300 lbs. of 40/60 amatol. Roughly speaking, the result of these experiments was to show that at distances above 50 feet the damage was not very heavy, while at smaller distances the damage was vital. The gauges for the present experiments were accordingly designed to be suitable for the region between 25 and 100 feet from a charge of this type, and the pressure at a distance of 50 feet was made the first object of investigation.

The result is shown in Fig. 1, which represents the average of five shots. The pressure rises to its maximum intensity (·80 ton per square inch) almost instantaneously, at most in a few hundred-thousandths of a second; it falls in a thousandth of a second to a quarter of its maximum intensity, and afterwards continues to fall more and more slowly; after five thousandths of a second there still remains a very small pressure.

The time integral of the pressure

$$(= \int p dt = \text{the area of the time-pressure curve})$$

up to five thousandths of a second is $I\ (t = 5 \times 10^{-3}) = \cdot 68$, a pressure of one ton per square inch for a thousandth of a second being taken as the unit. The whole-time integral of pressure, up to the moment when the pressure ceases or becomes negative, can only be very slightly greater than this. More than half the time integral of pressure occurs in the first thousandth of a second, and more than four fifths in three thousandths of a second, $I\ (t = 10^{-3}) = \cdot 40$, $I\ (t = 3 \times 10^{-3}) = \cdot 60$.

A time-pressure curve such as that shown in Fig. 1 gives complete information as to what happens in the water when the pressure wave passes. For example, the velocity of a particle of the water at any moment is

$$\frac{p}{a\rho},$$

a being the velocity of the pressure wave (Section 6) and ρ the density of sea-water, or 33 p, if the velocity is expressed in feet per second and p in tons per square inch. The particle-velocity is greatest in the front of the wave, where the pressure is greatest, and there amounts, in the present case, to 26·4 feet per second. Again, the displacement of a particle from its original position is

$$\frac{1}{a\rho} \int p dt, \text{ or } 0 \cdot 40 . I,$$

if the displacement is expressed in inches and the time integral of pressure I in the dimensions defined above; thus in the present case the total displacement of a particle by the pressure wave is ·27 inch.

The flux of energy, that is to say, the energy which crosses each unit surface of a sphere with the charge at its centre, is

$$F = \frac{1}{a\rho} \int p^2 dt, \text{ or } F = 7 \cdot 4 \times 10^6 \int p^2 dt$$

if F is expressed in foot-pounds per square inch and p in tons per square inch. In the present case $F\ (t = 10^{-3}) = 14 \cdot 0$, $F\ (t = 3 \times 10^{-3}) = 15 \cdot 7$, $F\ (t = 5 \times 10^{-3}) = 16 \cdot 0$. Since nearly nine-tenths of the energy passes in the first thousandth of a second, which corresponds to a radial distance of about 5 feet, it is clear that nearly all the energy of the pressure wave is concentrated in the front of the wave in a layer only a few feet thick. The whole energy of the pressure wave, assuming that it springs from the charge with equal strength in all directions, is $4 \pi D^2 F = 72 \times 10^6$ foot-pounds, or $\cdot 24 \times 10^6$ foot-pounds per pound of explosive. Since the total energy liberated by the

Best Available Copy

explosion of 1 lb. of 40/60 amatol is roughly 10^8 foot-pounds, it appears that about a quarter of the whole energy of the explosion gets away in the pressure wave.

(5) Regularity and Symmetry of the Pressure Wave.

A mass of evidence was collected showing that the pressure wave from a high-explosive charge under water is very regular and symmetrical; the pressure wave springs away from the charge with practically the same strength in all directions, and when similar charges are fired under similar conditions the results are nearly identical.

The time-pressure curves illustrating this report represent in most cases the average of several shots. In only one instance (referred to in Section 10) did the results of any individual shot differ by more than about 5 per cent. from the group average. Three typical groups are shown in the following table, and some other figures are given at the end of Section 18.

TABLE I.

D = distance in feet from centre of charge to gauges.

P = maximum pressure, in tons per square inch.

I ($t = 3$) = time integral of pressure for the first three thousandths of a second, in units of 1 ton per square inch for one thousandth of a second.

Charge.	Shot.	D.	P.	I ($t = 3$).
1,600 lbs. 80/20 amatol - - -	85	63½	1·18	1·25
	86		1·13	1·15
	87		1·15	1·22
	Average.		1·15	1·21
272 lbs. R.D. No. 30 mixture - -	69	50	·68	·62
	71		·65	·61
	94		·68	·65
	Average.		·67	·63
312 lbs. guncotton - - - - -	60	50	·62	·53
	63		·63	·54
	67		·59	·52
	Average.		·61	·53

The symmetry of the pressure wave was tested, in a very large number of shots, by comparing the indications of two groups of gauges at equal distances from the charge in opposite directions, one group on the side away from the "Malapert," the other on the near side, and in some cases a third group of gauges was hung at an equal distance vertically underneath the charge. The ratios of the results in these three directions are shown in Table II. When copper gauges were not available for this purpose, use was made of the plasticine gauges described in Section 20. The distance of the gauges from the charge was in nearly all cases 50 feet from a 300-lb. charge and corresponding distances (Section 9) from other charges. It will be seen that there was only one instance of pronounced dissymmetry (Shot 27); in all other cases the differences are slight, averaging only about 5 per cent. Considering that the differences recorded in the table must be partly due to errors of the gauges and inexactness of the measured distances it is clear that the strength of the pressure wave is generally very nearly the same in all directions.

The special case of a charge of very elongated shape is dealt with in Section 15.

TABLE II.

P = maximum pressure.

$I(c)$, $I(p)$ = time integral of pressure measured by copper gauges and plasticine gauges respectively.

The arrows represent three directions from the charge, → being the direction from the charge towards the "Malapert."

Shot.	P.			I (c).		I (p).		
	←	→	↓	←	→	←	→	↓
17	—	—	—	—	—	100	100	—
20	—	—	—	—	—	100	103	—
22	—	—	—	—	—	100	91	—
23	—	—	—	—	—	100	97	—
25	—	—	—	—	—	100	95	—
27	—	—	—	—	—	100	92	133
29	—	—	—	—	—	100	—	100
30	—	—	—	—	—	100	90	98
32	—	—	—	—	—	100	108	
33	—	—	—	—	—	100	104	—
34	—	—	—	—	—	100	97	97
35	—	—	—	—	—	100	98	103
36	—	—	—	—	—	100	96	—
37	—	—	—	—	—	100	105	—
38	—	—	—	—	—	100	88	94
44	—	—	—	—	—	100	96	106
45	—	—	—	—	—	100	88	94
46	100	106	—	100	103	100	101	—
47	—	—	—	—	—	100	102	—
49	100	100	—	100	96	—	—	—
50	100	95	—	100	98	—	—	—
51	—	—	—	—	—	100	111	—
52	—	—	—	—	—	100	88	—
53	100	94	—	100	95	—	—	—
55	—	—	—	—	—	100	98	—
56	—	—	—	—	—	100	108	—
57	100	95	—	100	94	—	—	—
58	100	96	—	100	100	—	—	—
59	—	—	—	—	—	100	103	—
60	100	100	—	100	104	—	—	—
61	100	106	—	100	102	—	—	—
62	100	105	—	—	—	100	104	—
63	100	101	—	100	95	—	—	—
65	100	103	—	—	—	—	—	—
66	100	96	—	100	100	—	—	—
67	100	98	—	100	98	—	—	—
68	100	104	—	—	—	100	108	114
69	100	104	—	100	108	—	—	—
71	100	100	—	100	105	—	—	—
72	100	—	104	—	—	—	—	—
74	100	—	104	—	—	—	—	—
81	100	—	106	—	—	—	—	—
84	100	95	—	100	94	—	—	—
85	100	107	—	—	—	—	—	—
86	100	102	—	—	—	—	—	—
87	100	103	—	—	—	—	—	—
88	100	100	—	—	—	—	—	—
90	100	108	—	—	—	—	—	—
94	—	—	—	100	97	—	—	—
95	100	97	—	100	95	—	—	—
98	100	101	—	—	—	—	—	—
100	100	106	—	—	—	—	—	—
103	100	102	—	—	—	—	—	—
104	100	105	—	—	—	—	—	—

(6) Velocity of the Pressure Wave.

The experiments described in Section 23 proved that the velocity of the pressure wave is, within a few per cent., the same as that of sound in sea-water, or about 4,900 feet per second.

(7) Variation of Pressure with Distance.

This was investigated by hanging gauges at different distances D in the same radial direction from the charge. The results, which are recorded in Table III., were calculated in the form—

$$\frac{\text{Pressure (or time integral of pressure) at distance } D_1}{\text{Pressure (or time integral of pressure) at distance } D_2} = \left(\frac{D_2}{D_1}\right)^x$$

It will be seen that the maximum pressure appears to fall off slighty more than in proportion to the distance ($x > 1$), but roughly speaking the time-pressure curve at distance D_2 is a copy of the curve at distance D_1 with all the ordinates altered in the proportion $\frac{D_1}{D_2}$. Examples are shown in Figs. 14 to 18, 20 and 23.

The results indicate that the wave spreads with very little dissipation of its energy.

TABLE III.

D = distance in feet from centre of charge to gauges.
P = maximum pressure in tons per square inch.
$I(t = 1)$, $I(t = 3)$ = time integral of pressure for the first thousandth of a second and for the first three thousandths of a second, in units of one ton per square inch for one thousandth of a second.

Charge.	Shot.	D.	P.	x	I(t = 1)	x	I(t = 3)	x
1,900 lbs. 50/50 Amatol	Average of 88, 90	46	1·77	1·08	—		1·96	1·03
		92½	·85		—		·96	
		185	—		—		·47	1·03
1,600 lbs. 80/20 Amatol	Average of 85, 86, 87	63½	1·15	1·04	—		1·21	·99
		127	·56				·61	
1,000 lbs. T.N.T.	55	75	—		·53	1·03	·86	1·09
		250	—		·145		·23	
1,000 lbs. T.N.T.	Average of 32, 33	75	—		·34	1·01	·86	·95
		120	—		·335		·55	
820 lbs. 40/60 Amatol	Average of 36, 37	69	—		·48	1·02	·74	·91
		111	—		·295		·48	
820 lbs. 10/60 Amatol	52	69	—		·455	·95	·74	1·05
		169	—		·195		·29	
300 lbs. T.N.T.	Average of 17, 25	30	—		·64	1·07	·97	·94
		50	—		·37		·60	
300 lbs. 40/60 Amatol	29	50	—		—		·60	1·00
		120	—		—		·25	
300 lbs. 40/60 Amatol	Average of 105, 106, 107..	12	4·00	1·16				
		28	1·50	1·08	—		—	
		40	1·02	1·01				
		70	·58					

(8) Surface Effects.

When a charge is fired at moderate depth the effect observed at the surface is always twofold. Take, for example, the case of a 300-lb. amatol charge at a depth of 31½ feet. At the instant of firing (actually a few thousandths of a second after detonation) the surface above the charge begins to rise into a white dome of broken water, which reaches a height of about 35 feet on a diameter of 140 feet. About a second later the top of the dome is broken through by a rush of gas, which carries up plumes of spray to a height of 100 to 200 feet. The first effect signalises the arrival of the pressure wave at the surface; it has nothing to do with the products of the explosion, in fact there is "solid" water between the exploded charge and the surface at the moment when the dome begins to form. The second effect represents the venting of the explosion gases.

A large number of measurements of the dome and plumes are recorded in Section 26. The plumes are very variable, as might be expected; they generally appear as a broad bush-like eruption, but sometimes take the form of a single thin spout, rising to a much greater height (*e.g.*, Shots 51 and 65). The dome measurements are more regular, and might have been even more so if it had been possible

Best Available Copy

to take cinematograph records; the actual measurements are from photographs, and cannot be regarded as very accurate, since it is difficult to expose the camera at exactly the right moment. The significance of the dome measurements is discussed in Section 22. Some photographs of typical domes and plumes are reproduced at the end of this report.

When a charge is fired at a great depth the dome and plume effects appear in an entirely different form. For example, when a 300-lb. Amatol charge is fired at a depth of 200 feet the surface above the charge, over an area about 200 feet in diameter, is observed to quiver, and a slight flicker of spray is thrown up, but the surface as a whole does not rise at all and there is no sign of the whiteness caused by disintegrated water—on the contrary, if the sea is perfectly smooth the surface appears darkened, as still water is darkened by a catspaw of wind. Nothing further is seen until about 25 seconds later, when a large volume of creamy green fluid begins to pour up at the surface, consisting of an emulsion of bubbles and water, the residue of the explosion products.

The fact that the surface in this case is not broken at the moment of explosion is a proof that the energy of the pressure wave is completely reflected (except a minute fraction which passes into the air) and since it is a case of reflection in a dense medium at the surface of a light medium the pressure wave must be reflected as a wave of tension. The pressure in the wave front when it reaches the surface is 0·2 ton per square inch, and the reflected wave starts downward with a tension expressed by the same figure; it is clear therefore that the water is able to support a momentary tension of this amount without breaking. To discover how much tension sea water is capable of supporting, a series of 40-lb. and 300-lb. amatol charges were fired at different depths. The point dividing complete reflection on the one hand and complete disintegration of the surface on the other is not very distinct, and depends moreover on the state of the sea, the surface breaking more readily when there is any lop, but approximately the minimum depth for complete reflection at a flat calm surface was found to be 60 to 80 feet for a 40-lb. charge and 125 to 150 feet for a 300-lb. charge, corresponding in both cases to a pressure of about 0·3 ton per square inch, and it may be concluded that this is about the greatest tension that sea-water is capable of supporting, even momentarily.

The idea of the reflected tension wave leads to a simple theory of the effect which the surface exercises on the pressure at any given point in the water. Assume, to begin with, that the pressure wave is completely reflected, without breaking the surface. The effect at a point B, Fig. 2, is found by superimposing the effects of the pressure wave X direct from the charge A and the reflected tension wave Y, arriving by the path A C B. The tension wave is weaker than the pressure wave in the ratio

$$\frac{AB}{A'B}$$

and arrives later by an interval

$$\frac{A'B - AB}{a},$$

a being the velocity of sound in sea-water. The result is (as shown at Z) that the first part of the pressure wave arrives at B entirely unaffected by the proximity of the surface, but after a certain interval the remaining pressure is obliterated by the arrival of the tension wave.

If the pressure is strong enough to break the surface the matter is not so simple, but there is reason for believing that the same rule holds, at all events very nearly. To take an imaginary case, suppose that a plane wave of the form shown in Fig. 1 travels vertically to the surface, and that it disintegrates the water to a depth of 2 feet. This means that the first 4 feet of the pressure wave (from $t = 0$ to $t = \cdot 8 \times 10^{-3}$, Fig. 1) fails to get reflected, its energy being spent in giving an upward momentum to the disintegrated water. The remainder of the pressure wave, from $t = \cdot 8 \times 10^{-3}$, is reflected from the new surface, 2 feet below the original surface, as a wave of tension. The point to observe in the present connexion is, that while the tension wave has been shorn of its first 4 feet it has also 4 feet less distance to travel, and the moment of arrival of the front of the reflected wave at any given point in the water is therefore the same as it would have been if complete reflection had occurred at the original surface. It may be concluded therefore that the rule stated in the preceding paragraph still gives the correct moment for the obliteration of the pressure at any given

point in the water, and closer consideration shows that the rule is applicable in the region of disintegration itself, as well as below.

To test this theory, four 207-lb. charges of 80/20 amatol were fired at a depth of 34½ feet, and pressure measurements were made at depths of 1½ feet, 2½ feet, 5½ feet, 10 feet, and 34½ feet below the surface, the direct distance from the centre of charge to the gauges being 50 feet in every case. The time-pressure curve at a depth of 34½ feet is shown in Fig. 7, which represents the average of the four shots. The results at other depths are shown in Figs. 8 to 11; in these figures the rectangular steps represent the experimental results, but the curves are simply copies of the curve in Fig. 7, with the pressure cut off at times corresponding to the theory; for example, with the gauges at a depth of 10 feet the difference between the direct and reflected paths AB and ACB, Fig. 2, is 12·2 feet, corresponding to $2·5 \times 10^{-3}$ second, and the pressure is represented as ceasing at this moment. The good agreement between the curves drawn in this way and the rectangular steps derived from the experimental results is evidence of the correctness of the theory.

Further confirmation was obtained by firing a 1,000 lb. T.N.T. charge at a depth of 51½ feet and measuring the pressure at a point 40 feet below the surface and 250 feet distant from the charge. The experimental results are shown by the rectangular steps in Fig. 23, while the curve in the same figure is derived from the curve shown in Fig. 20, which represents the pressure from the same charge at a distance of 75 feet, by reducing the ordinates in the ratio $\frac{75}{250}$. The difference between the direct and reflected paths is 16 feet, and the pressure is therefore represented as ceasing at the moment $t = 3·25 \times 10^{-3}$. It will be seen that in this case also there is good agreement between the experimental rectangles and the theoretical curve.

The effect of varying the depth of the charge is covered by the same principle. At whatever depth a charge is fired, within practical limits, the pressure wave springing from it must have exactly the same character, for even at a depth of 1,000 feet the hydrostatic pressure is less than 2 ton per square inch, and the density and elasticity of the water are practically the same as at the surface. The only effect of firing the charge deep is to remove it far from the reflecting action of the surface.

A comparison of Figs. 1, 3, 4 and 5, all of which refer to 300 lb. charges of 40/60 Amatol, shows that the pressure wave is the same whether the depth of the charge is 34½ feet or 20 feet; with the charge at a depth of 10 feet the first part of the pressure wave is the same, but after $2·3 \times 10^{-3}$ seconds the reflected tension wave arrives at the gauges and obliterates the remaining pressure; with the charge at a depth of 5 feet the pressure is all over in about 1½ thousandths of a second.

To complete this series of experiments a charge of the same sort was fired on the surface, slung between two barrels so as to be about three-quarters submerged. The result is shown in Fig. 6. The maximum pressure reaches nearly its full value, but the pressure disappears very quickly, being practically all gone in half a thousandth of a second.

In many instances the gauges gave direct evidence that the pressure in the water is followed by a state of tension or cavitation—*see*, for example, Figs. 4 to 6 and 8 to 11. Attention may also be drawn to the figures for Shot 55 in Table VI. (Section 18), from which it will be seen that the pistons in the last gauge of the series were practically brought to rest before reaching the end of their travel, owing to the state of tension following the pressure wave. The tensions recorded were never very high however, the most that was observed being ·044 ton per square inch, or 6·7 atmospheres (Fig. 11). It is probable that cavitation occurs more readily at the surface of the gauges than in the water itself, so that the gauges record less than the full tension. The zero pressure line in the diagrams represents the normal hydrostatic pressure at the depth at which the gauges are hung; in Fig. 11 for example, the gauges being at a depth of 10 feet the normal pressure is 1·3 atmosphere or ·008 ton per square inch, and a pressure indicated as ·044 ton per square inch below normal represents only ·036 ton per square inch actual tension, or 5·4 atmospheres negative.

(9) Comparison of Large and Small Charges.

The experiments on this point were based on the following theory. Suppose that detonation is started simultaneously at corresponding points in two charges which are exactly similar except that the linear dimensions of one are R times as great as the

other; there are very strong reasons for expecting that the dynamical conditions in and around the small charge after a time t will be geometrically and dynamically similar to those in and around the big charge after a time Rt; that is to say, any two correspondingly situated particles at distances D and RD from the points at which detonation was started will have equal velocities and will be subject to equal pressures at moments t and Rt.

It can be demonstrated that if this rule is true for any one pair of moments subsequent to complete detonation it must remain true thereafter. For if the rule holds good at moments t and Rt every particle in the big system has the same velocity as the corresponding particle in the small system; the displacement of any particle in the big system is R times that of the corresponding particle in the small system; on the other hand the pressure gradient operating on a particle of the small system, and therefore the acceleration of the particle, is R times as great as for the corresponding particle in the big system; consequently, after infinitesimal increments of time dt and Rdt corresponding particles in the two systems will have acquired equal increments of velocity, but the increment of displacement of the particle in the big system will be R times as great as in the small system; the rule therefore will still hold good at moments $t + dt$ and $Rt + Rdt$, and by an extension of the same reasoning it will hold good at all subsequent times T and RT. To complete the proof of the rule it is necessary to show that it also holds good during detonation, when forces are being liberated by chemical change. The difficulty here is that the nature and laws of detonation are not yet fully understood, and any picture of the process must be to some extent hypothetical. Detonation, then, may be roughly conceived as a wave of chemical transformation which progresses from point to point with constant velocity, completing itself at each point practically instantaneously; each layer of explosive is detonated by the temperature and pressure of the next layer within and generates a temperature and pressure of its own, which on the one hand maintains the temperature and pressure of the next inner layer and on the other hand produces detonation in the next outer layer; the front of the detonation wave divides a region of unchanged explosive, which no pressure has yet reached, from a region of transformed explosive under uniform intense pressure. On this provisional view, the similarity rule obviously holds good during detonation and would consequently be valid at all stages. It will be seen therefore that it is possible to go a long way towards a complete proof of the rule, though not quite all the way. It may also be pointed out that very natural conclusions result from accepting the rule, such as, that the energy radiated from a charge is proportional to the weight of the charge, that the rate of decay of the pressure is inversely proportional to the linear dimensions of the charge, &c.

In dealing with charges of different sizes it is convenient to speak of distances in the ratio R as "corresponding distances." For example, 50 feet from a 300-lb. charge and 25½ feet from a 40-lb charge are corresponding distances, since—

$$\frac{50}{25{\cdot}5} = \frac{\sqrt[3]{300}}{40}.$$

According to the above theory, when the pressure waves from a big and a small charge are compared at corresponding distances the maximum pressure should be the same in both cases, but the pressure from the big charge should be R times as sustained, that is to say, it takes R times as long in falling to any given fraction of its maximum intensity. The whole time-integral of pressure should be R times as great for the big charge as for the small one, and the time-integral of pressure of the big charge for any period Rt should be R times the time-integral of pressure of the small charge for the corresponding period t. In short, the time-pressure curve of the big charge should be a copy of that of the small charge with all the abscissæ increased in the ratio R.

To put the theory to a satisfactory test it is necessary to make comparisons with charges differing very widely in magnitude. Experiments were therefore made with charges weighing 10 lbs. and 1 900 lbs., giving a scale ratio R = 3·62. The small charges were of 40/60 amatol and the large ones of 50/50 amatol, but these two mixtures may be regarded as giving identical effects (*see* Section 12). With gauges at distances of 25½ feet and 92½ feet, which correspond to 50 feet from a 300-lb. charge, results were obtained which are shown in Figs. 13 and 15. It will be seen that the maximum pressure from the small charge (·78 ton per square inch) is about 8 per cent. lower than that from the big charge (·85 ton per square inch), but the

greater part of this discrepancy is probably due to the gauges, which tend to underestimate the maximum pressure from a small charge, as explained in Section 19. The time taken for the pressure to fall to ·2 ton per square inch is $\cdot 60 \times 10^{-3}$ second in one case and $1 \cdot 80 \times 10^{-3}$ in the other, giving a ratio 3·0, which is fairly near the scale ratio R = 3·62. The time-integral of pressure of the small charge for a period $t = 10^{-3}$ second is 0·30, while that of the big charge for a period $Rt = 3 \cdot 62 \times 10^{-3}$ is 1·02, giving a ratio 3·4, which is very close to the scale ratio. The results with 300-lb. charges at 50 feet (Fig. 1) are in equally good agreement with the theory, and so are the comparisons between other large and small charges shown in Figs. 12 and 20, 7 and 17, 1 and 29. The small discrepancies between theory and results may be imputed to experimental errors and to differences in the make-up of the charges.

Putting together the results described in the last three sections, it will be seen that when once the time-pressure curve has been determined for a given charge at a given distance it is possible to construct the time-pressure curve for a similar charge of any size under any conditions of distance and depth. For example, suppose it is required to know what effect will be produced at a point 10 feet below the surface by the explosion of a 5-ton charge of 50/50 amatol 100 feet below the surface and 200 feet away horizontally. The curve for a 1,900-lb. charge at a distance of $92\frac{1}{2}$ feet is shown in Fig. 15; the corresponding distance for a 5-ton charge is

$$92\tfrac{1}{2} \times \sqrt[3]{\frac{11200}{1900}} = 167 \text{ feet},$$

and the time-pressure curve for a 5-ton charge at this distance is obtained from Fig. 15 by increasing all the abscissæ in the ratio

$$\sqrt[3]{\frac{11200}{1900}} = 1 \cdot 81;$$

the ordinates of this curve are then diminished in the ratio $\frac{167}{219}$, giving the time-pressure curve of a 5-ton charge at a distance of 219 feet, which is the direct distance from the centre of the charge to the point of reference; finally, since the difference between the direct and reflected paths from the charge to the point of reference, by the construction shown in Fig. 2, is 9 feet, the pressure is cut off after $1 \cdot 8 \times 10^{-3}$ second. The result is shown in Fig. 19. Other examples of predicted pressure curves are shown (in broken lines) in Figs. 17, 22, 24, and 20.

If the effect of the surface is left out of account, the maximum pressure P, the time-integral of pressure I, and the energy flux F from a charge of weight W at distance D can be expressed in the form—

$$P = K_1 \frac{W^{\frac{1}{3}}}{D}$$

$$I = K_2 \frac{W^{\frac{1}{3}}}{D}$$

$$F = K_3 \frac{W}{D^2}$$

K_1, K_2, and K_3 being constants depending on the nature of the explosive and its container. Neither these formulæ nor the above method of predicting the time-pressure curve can properly be applied in the region near the charge, where the pressure exceeds 2 tons per square inch, this region being outside the scope of the present investigation.

(10) Bottom Effects.

The experiments described in Section 24 show that the pressure wave is reflected from a mud bottom with much diminished intensity; the time-integral of the reflected pressure is less than half what it would be if complete reflection occurred.

Another point that was investigated was the effect of firing a charge on the bottom, instead of in mid-water. It is natural to expect that a stronger pressure wave would be generated, the difference should be more marked the greater the elastic resistance and density of the bottom, both these factors making it relatively unyielding to a sudden pressure, with the result that the radiated energy is concentrated in the water. In the limit, when the bottom is perfectly unyielding, the radiation of energy would be entirely confined to the water, and the pressure wave

from a hemispherical charge resting on the bottom would obviously be the same as that from a spherical charge of the same diameter in mid-water, that is to say, the charge on the bottom would give the same effect as a charge twice as heavy with water all round it. A hard rock bottom should approximate to this extreme, while sand or mud should give a similar but smaller effect.

Experiments were made by firing three 1,000-lb. T.N.T. charges on a sand bottom in 10 fathoms, about 1½ miles off Irvine; the pressure wave was measured at a distance of 75 feet from the centre of the charge, in a direction making an angle of about 60° with the vertical. In the case of shot 78 (Fig. 22) the result approximates to the calculated effect of a 2,000-lb. T.N.T. charge in mid-water; in shot 75 (Fig. 21) the pressure was considerably less, but still greatly in excess of the effect of the same charge in mid-water (Fig. 20); the third shot gave results intermediate between the other two.

The differences between the results of these three shots fired on the bottom were much greater than was ever observed in the case of shots fired in mid-water; this is not altogether surprising, seeing that the local configuration of the bottom and the depth of sand covering the underlying rock were quite likely different in all three cases.

(11) Effect of surrounding the charge with an Air Chamber.

Fig. 28 shows the time-pressure curve at a distance of 50 feet from the centre of an H 2 mine (a spherical mild steel shell 38 inches in diameter and ¼ inch thick, with a charge of 320 lbs. of 40/60 amatol in a central container, as shown in Fig. 46). Comparing Fig. 28 with Fig. 1 it will be seen that both the maximum pressure and the time-integral of pressure of the air-surrounded charge are slightly less than for the naked charge, but the difference in both respects is not much more than 5 per cent. This is rather surprising, seeing that the volume of air is nearly four times the volume of explosive.

Some H 2 mines filled with an additional 500 lbs. of 40/60 amatol (as at X 7, Fig. 46) gave the result shown in Fig. 29, which is very nearly the same as the calculated effect of the same charge in naked form.

(12) Comparison of different Explosives.

Figs. 12, 1, and 7 give a comparison between T.N.T. (tri-nitro toluene), 40/60 amatol (ammonium nitrate 40, T.N.T. 60) and 80/20 amatol (ammonium nitrate 80, T.N.T. 20). It will be seen that T.N.T. gives practically the same effect as 40/60 amatol, except that the maximum pressure is about 5 per cent. lower. Allowing for the slight difference in the weight of explosive, 80/20 amatol and T.N.T. give practically identical results. A comparison between 300-lb. charges of 40/60 amatol and 50/50 amatol showed no difference.

Figs. 30 and 31 show results obtained with guncotton and ammonium perchlorate charges. These results are not directly comparable with Figs. 1, 7 and 12, as the charges were made up in very thick walled mines (spherical mild steel shells, 38 inches in diameter and $\frac{3}{16}$ to ¼ inch thick). The maximum pressure in both cases, but especially for the guncotton charge, is a good deal lower than for amatol; this may be partly due to the thickness of the mine shell. On the other hand it is noticeable that the pressure of the ammonium perchlorate charge is very well sustained; the whole time-integral of pressure is decidedly higher than for amatol; with charges of equal weight and similar make-up the difference would be even more marked.

(13) Gunpowder Charges.

Fig. 32 shows the results obtained with some 500-lbs. charges of E.X.E. powder. This is a very slow-burning powder, density 1·8, pressed into hexagonal prisms 1¼ inches across the flats and with a central hole about ·4 inch in diameter. The charge was built up of these prisms in layers, and was fired by a central igniter,

consisting of a tin containing fine grain powder with a fulminate of mercury detonator. The time-pressure curve of this charge is an interesting contrast to that of a high explosive such as amatol. The pressure builds up slowly to a maximum which is not much more than $\frac{1}{5}$th of the maximum pressure given by an equal weight of amatol at the same distance; on the other hand the pressure lasts much longer; it does not reach its maximum until a time when the pressure from the amatol charge would practically have disappeared.

The surface above the charge showed no sign of breaking at the moment of explosion; the usual white dome was entirely absent; the tension in fact was too weak to break the water and the pressure wave was completely reflected. It was possible therefore to observe the first stages of the arrival of the burnt gases at the surface, which is masked, in the case of high explosives, by the dome of broken water thrown up by the pressure wave. The first effect, which appeared at a distinct interval after the moment of explosion, was the heaping up of a small mound of green water (Fig. 56); this was probably a sort of water-piston pushed up ahead of the ascending gas bubble; a moment later the gases burst through, forming plumes not unlike those given by a high-explosive charge (Fig. 57).

(14) Composite Charges.

Some composite charges were made by lashing together three 300-lb. charges of 40/60 amatol. Each 300-lb. charge was a cylinder 28 inches long and 18 inches in diameter; the three charges were lashed with their axes horizontal and parallel, so as to give a figure of three touching circles in cross-section; only the top charge was primed, the two others being fired by the explosion of the first. The result, shown in Fig. 24, approximates very closely to the calculated effect of a single 900-lb. charge.

(15) Influence of the Shape of the Charge.

Experiments on this point were made by lashing together three 300-lb charges of 40/60 amatol end-to-end. Each charge was a cylinder 28 inches long and 18 inches diameter, so that the composite charge had a length of nearly five diameters. Owing to the dished shape of the ends of the charges there was an average distance of about 3 inches between the amatol in one charge and the amatol in the next. One of the end charges was primed, the other two being fired by the explosion of the first. The composite charge was hung horizontally, and pressure measurements were taken in three directions, (1) in line with the axis of the charge from the primed end towards the unprimed end, (2) in line with the axis of the charge from the unprimed end towards the primed end, (3) at right angles to the axis of the charge. All three sets of gauges were at the same distance from the centre of the charge. The results are shown in Figs. 25, 26, and 27. It will be seen that the pressure is strongest but least sustained in the broadside direction, and weakest but most sustained in the direction opposite to that in which detonation proceeds.

These results admit of a simple explanation; in the broadside direction the effects of the three charges arrive simultaneously, or nearly so, while in the endwise directions they arrive more or less in turn; but there is a difference between the two endwise directions, because in the direction in which detonation proceeds the effects of the three charges arrive more nearly simultaneously than in the opposite direction, the time taken by detonation in travelling from one end of the charge to the other being in the first case subtracted from and in the second case added to the time taken by the pressure wave in travelling the same distance in water.

Comparing Figs. 25, 26, 27 with Fig. 24, it appears that the three charges lashed end-to-end give on the whole a less powerful effect than when bunched together. It is probable that, for general purposes, the best disposition of a given weight of explosive is in spherical form, which most nearly enables the effects of all its parts to arrive at any given point simultaneously. On the other hand, if a maximum effect is desired in a single direction the best shape would probably be a flat disc, the effect of which should be greatest in the direction of its axis.

(16) Damaging Power of different Pressure Waves.

For the practical application of the results described in the foregoing sections it is necessary to know what it is that determines damage, whether it is simply the maximum intensity of the pressure, or the whole time-integral of pressure, or some intermediate function such as the energy flux. The best way to investigate this question is to determine the relative distances at which big and little charges inflict the same damage on a given structure. It has been shown in Section 9 that the maximum pressure from a charge is proportional to

$$\frac{W^{\frac{1}{3}}}{D},$$

W being the weight of explosive and D the distance from the centre of the charge: consequently if damage is determined simply by the maximum pressure the damaging range of a charge will be proportional to $W^{\frac{1}{3}}$; the energy flux is proportional to $\frac{W}{D^3}$, so that if damage is determined by energy flux the damaging range will be proportional to $W^{\frac{1}{3}}$; the time-integral of pressure is proportional to

$$\frac{W^{\frac{1}{3}}}{D},$$

so that if damage is determined by time-integral of pressure the damaging range will be proportional to $W^{\frac{1}{3}}$.

During the first half of the experiments a great many observations were made by Mr. Robert Royds (on behalf of the Mining School) on the damage sustained by H 4 mine cases at different distances from various charges; afterwards these observations were extended by the writer to a greater range of charges, and a bottom line was used, as described in Section 21, to ensure accuracy of distance. An H 4 mine case is a sphere of mild steel $\frac{1}{4}$th inch thick and 31 inches in diameter; it is made in two halves, joined by an equatorial weld, and the lower half is fitted with a heavy plate carrying the mechanism of the mine. These mine cases, used as damage gauges, gave more constant results than had been anticipated; the central weld was the most variable part of the structure, and no great weight was attached to its behaviour. The damage varies very rapidly with the distance from the charge; there is a critical distance at which moderate damage is inflicted (damage 2 on the scale given below) and this distance can be estimated with a fair degree of accuracy, because a small change one way or the other gives either heavy damage or no damage at all; if 100 represents the distance at which the mine case is just not damaged at all, it is only necessary to bring it in to distance 75 or 70 to inflict fairly heavy damage (3 or 4 on the scale below). The damage begins with the formation of shallow dents, or places where the surface is pushed in and its curvature reversed; at closer range these dents become larger and deeper; finally they overlap each other and produce a general crumpling and folding of the mine case, and at this stage the metal is often more or less extensively torn; it should be noted, however, that (apart from the weld) the damage never shows any sign of beginning with a crack—when the metal is torn it is always as a result of excessive folding. The different degrees of damage were measured by the following scale:—

0. No damage (Fig. 63).
1. Shallow dents, not more than $1\frac{1}{2}$ inches below the original surface.
2. Large deep dents, say 3 or 4 inches below the original surface.
3. Very large overlapping dents, producing crumpling and folding of the metal.
4. Mine case very severely crushed and the metal torn (Fig. 64).

Experiments were made with these mine cases at different distances from 40-lb. charges of 40/60 amatol, 300-lb. charges of 40/60 amatol, 1,600-lb. charges of 80/20 amatol, and 1,900-lb. charges of 50/50 amatol. The differences in the composition of the amatol can be left out of account, for the corresponding differences

of pressure are too small to affect the conclusions. The results are recorded in the following table :—.

TABLE IV.

Charge.	Shot.	Depth of Charge. (Feet.)	Depth of Mine Case. (Feet.)	Centre of Charge to Nearest Point of Mine Case. (Feet.)	Damage.
40 lbs.	47	18	18	29	0 to
				29	0 to
	51	18	18	29	1½ (*see* note below)
				29	0
	56	18	18	29	1½ (*see* note below)
				29	0
	62	18	28	26	1
				26	1½
	63	18	28	26	1
				26	½
300 lbs.	8	34½	34½	70	1
	44	20	20	70	1
				70	1
	45	20	20	70	1
				70	1
1,600 lbs.	85	60	60	126	4 (*see* Fig. 64)
				189	0
	86	60	60	126	3
				189	0
	87	60	60	126	2½
				189	0
1,900 lbs.	88	64	64	157	2
				184	½
	89	64	64	157	3
				184	0
	90	64	64	157	2
				184	½

Note.—In shot 51 the damage to the first mine case was almost entirely along the equatorial weld; in shot 56 the whole damage to the first mine case was along the same weld, which had opened round half the circumference of the mine; in both cases, apart from the weld, the damage would have been very slight.

It will be seen that the distance at which a 40-lb. charge just ceases to inflict any damage on the mine case is about 30 feet. Taking distances in the ratio of the cube root of the weight of explosive, a distance of 126 feet from a 1,600-lb. charge corresponds to 37 feet from a 40-lb. charge, so that if the damaging range of a charge is proportional to $W^{\frac{1}{3}}$ the damage should be the same in these two cases; actually, the mine case is heavily damaged at 126 feet from a 1,600 lb. charge, while it would certainly be quite untouched at 37 feet from a 40-lb. charge. Again, if the damaging range is proportional to $W^{\frac{1}{3}}$, a 1,600-lb. charge at 189 feet should have the same effect as a 40-lb. charge at 16 feet; actually, the big charge at 189 feet causes no damage at all, while the damage from a 40-lb. charge at 16 feet would certainly be very heavy. It is clear, therefore, that the damaging range is proportional to something between $W^{\frac{1}{3}}$ and $W^{\frac{1}{2}}$, and the experiments with 1,900-lb charges show that it is very approximately proportional to $W^{\frac{1}{2}}$; for it may be inferred from the results in the table that a 1,900-lb. charge at 170 or 175 feet would produce the same damage as a 40-lb. charge at 26 feet, and on the assumption that the damaging range is proportional to $W^{\frac{1}{2}}$, a distance of 179 feet from the big charge corresponds to 26 feet from the small charge. On the same assumption the same damage should result from a 300-lb. charge at 71 feet, which is in good accordance with the observations.

These results bring out clearly that it is neither maximum pressure nor time-integral of pressure that determines this kind of damage, but something intermediate; a high maximum pressure is no use if it is not sufficiently sustained to deform the structure beyond its power of elastic recovery, and a high time-integral of pressure is no use if the pressure is less that the structure is able to resist. The

results are consistent with the supposition that the damaging power of a pressure wave is determined by its energy flux; on this view an H 4 mine case begins to be damaged when the energy flux exceeds about 5 foot-pounds per square inch; but, at best, this can only be true approximately and within limits, for it is possible to conceive of a very prolonged pressure wave with an energy flux exceeding 5 foot-pounds per square inch but with a maximum pressure much lower than the mine could withstand under statical conditions, and such a pressure wave would obviously have no effect. It is much more probable that damage is a function of the time-integral of the excess of pressure over a fixed value,

$$\int (p-k)\,dt,$$

k depending on the strength of the structure; for example, if k is taken as 0·1 ton per square inch,

$$\int (p-k)\,dt$$

has nearly the same value (about 0·2) for a 40-lb. charge at 26 feet, for a 300-lb. charge at 68 feet, and for a 1,900-lb. charge at 175 feet, which is in good agreement with the results in Table IV.; on this view an H. 4 mine case begins to be damaged when

$$\int (p-0{\cdot}1)\,dt$$

exceeds about 0·16, p being expressed in tons per square inch and t in thousandths of a second.

On general considerations, and quite apart from the above results, it is very difficult to suppose that the kind of damage at present in question can be determined simply by the maximum intensity of the pressure. A crack, such as is produced by a guncotton slab detonated in contact with a steel plate, may take only a few millionths of a second to form, but the damage actually inflicted is not of this kind; it is in the nature of deformation, and must take a relatively considerable time to become at all serious; the pressure on the mine case is only of the order of 1 ton per square inch, and the formation of even a shallow dent 1 inch deep must take at least several ten-thousandths of a second, in which time the pressure has fallen very much below its maximum intensity; it is clear, therefore, that the extent of the damage will depend very much on the rate at which the pressure falls. It is an instructive fact that an H 4 mine case is generally not damaged at all by a 40-lb. amatol charge at a distance of 29 feet, though the pressure at this distance (apart from any increase by reflection) is 0·7 ton per square inch, which is many times as great as the mine case could stand under statical conditions; the only possible explanation is that the pressure does not last long enough to deform the structure beyond its power of elastic recovery.

Damage to a hull by a distant charge will probably be governed by much the same considerations as damage to a mine case; deformation will be the primary effect, and where the metal is torn or rivets sheared, this will be a secondary effect arising out of the other; the rate of decay of pressure will have just the same importance in determining the extent of the damage.

It is very desirable that any experiments that may be made against hulls should include (1) a determination of the time-history of the movement of the hull itself at the point nearest to the charge, (2) a measurement by gauges of the time-pressure curve in the water just outside the hull at the same point.

Experimental results on the damage sustained by a given structure can be applied to similar structures of different dimensions by means of a rule first stated by Hopkinson. This rule is as follows:—the damage inflicted on a given structure by a given charge at a given distance will be reproduced to scale if the linear dimensions of the charge and structure and the distance between them are all increased or diminished in the same ratio. For example, it is known that a 300-lb. charge of amatol at a distance of 70 feet produces dents about 2 inches deep in a spherical mild steel shell 31 inches in diameter and $\frac{1}{8}$ inch thick; consequently it may be predicted that a 2,400-lb. charge at a distance of 140 feet will produce dents about 4 inches deep in a shell 62 inches in diameter and $\frac{1}{4}$ inch thick. This rule provides a link between the effects of a small charge on a small structure and of a big charge on a big

structure, but it gives no information as to the relative effects of big and small charges on the same structure. If a second rule can be established covering this side of the problem, the two together will obviously cover a very wide ground.

Hopkinson's rule can be deduced theoretically as an extension of the principle described in Section 9. Its validity has been proved experimentally for charges differing very widely in magnitude. The rule is obviously of great value in enabling full-scale inferences to be drawn from model experiments.

PART II.

METHODS.

(17) Gauges for measuring the Time-integral of the Pressure.

When the development of new gauges was undertaken, it was recognised that the ideal to be aimed at was an apparatus that would give the complete time-history of the pressure at a given point in the water, but it was difficult to see any way of arriving at this result. Hopkinson's pressure-bar method (Section 22) did not seem suitable, especially under sea conditions, for measuring pressures which it was estimated would endure for several thousandths of a second, while on the other hand this period was too short to give much hope of success with any form of mechanical chronograph. First attempts were therefore limited to the more moderate aim of producing gauges that would measure (1) the maximum intensity of the pressure, and (2) the time-integral of the pressure, or in other words the duration of the pressure multiplied by its average intensity.

After several failures, which need not be described, a successful time-integral gauge was produced in the form shown in Fig. 34 (Type G). This gauge was designed with a view to the greatest possible mechanical simplicity and absence of friction. It is based on the principle that the momentum acquired by a body is equal to the time-integral of the force that has acted on it. The working part is an easy-fitting steel piston, which rests on the rim of a small washer, with its bottom end exposed to the water. The top end of the piston carries a small copper cylinder, sprung into a thin corrugated metal jacket which keeps it centred. The central hole in which the piston works communicates with four others which act as an air reservoir. The air chamber is necessary both to prevent the piston from being forced up by hydrostatic pressure and to reduce the cushioning effect when the piston is driven in (Section 29).

The pressure set up by an explosion acts on the bottom end of the piston and shoots it inwards, and after travelling a distance of 2 inches the piston hammers the copper against the eyebolt of the gauge, which acts as an anvil. The energy of the piston is absorbed by the copper, which is shortened to an extent determined by micrometer measurements. By aid of calibration experiments the momentum of the

piston at the moment of impact can be deduced from the shortening of the copper, and this gives a measure, in definite units, of the time-integral of the pressure in the water.

Groups of these gauges gave exceedingly uniform results, but the question remained whether these results represented the whole time-integral of the pressure, because any pressure persisting after the moment of impact would fail to contribute to the momentum of the pistons and would be left out of account. It is obvious that no general answer is possible on this point, because the gauges might be able to catch the whole of the pressure from a given charge at a given distance but not from another charge or from the same charge at another distance. The question was investigated, for the case of a 300-lb. Amatol charge at a distance of 50 feet, by putting down a series of gauges with pistons having different amounts of free travel, and it was proved that in this particular case nearly the whole of the pressure was taken into account by a 3-inch piston with a 2-inch travel, as in Fig. 34.

These experiments suggested a method by which similar gauges might be made to yield the complete time-history of the pressure.

(18) Gauges for determining the complete Time-pressure Curve.

Suppose it were possible to measure the velocity of the piston of the gauge shown in Fig. 34 at different distances from its starting point; it would clearly be a simple matter to reconstruct the history of the pressure from these measurements. Take any two successive measurements, velocity v_1 at distance s_1, and velocity v_2 at distance s_2; the average velocity during the intervening period may be taken as $\frac{1}{2}(v_1 + v_2)$—this is not absolutely exact unless $v_2 - v_1$ is infinitesimal, but in practice the error is altogether negligible; the time of travel from s_1 to s_2 = distance divided by velocity

$$= \frac{2(s_2 - s_1)}{v_1 + v_2};$$

the average acceleration during the same period = change of velocity divided by time

$$= \frac{(v_2 - v_1)(v_1 + v_2)}{2(s_2 - s_1)};$$

and the pressure in the water = the acceleration of the piston multiplied by its mass and divided by its cross-sectional area

$$= \frac{M(v_2 - v_1)(v_1 + v_2)}{2A(s_2 - s_1)}.$$

Calculating all the measurements in this way, the result can be drawn diagrammatically as a series of rectangular steps, each representing a certain average pressure lasting a certain time, and a smooth curve drawn through all the steps in such a way as to leave out as much space as it takes in represents the reconstructed time-history of the pressure.

In practice it is hardly possible to measure the velocity of a single piston at different stages of its travel, but a practical alternative which gives exactly the same information is to use a series of gauges with similar pistons having different amounts of free travel, the velocity of each piston at the end of its travel being measured by the effect of its impact on a copper, as in Fig. 34. When it came to designing a series of gauges for this purpose it was found convenient to use comparatively long pistons in the gauges with the largest amount of free travel and short pistons in the gauges with least free travel. The difference in the mass of the pistons causes no difficulty; if a piston of mass M has a velocity V after travelling a distance S, a piston of unit mass acted on by the same pressure would have a velocity MV after travelling a distance MS; the results obtained with a series of pistons of unequal mass can therefore be translated to the basis of a series of pistons all of unit mass.

The gauges (types GX, GY, GZ, GA, and GB) which were designed for trying this method are illustrated in Figs. 35 and 36. They differ from the G gauge principally in being in nested form, the GX, GY, and GZ gauges taking six pistons each and the GA and GB gauges three. The only other difference worth noting is the annular form of the air chamber. Each of the five types of gauge takes two sizes of

piston, making a total of ten steps in the time scale; one extreme is a piston ¾ inch long with a free travel of $\frac{1}{10}$ inch, the other extreme is a 6½-inch piston with a 4-inch travel. Each gauge is filled with pistons of one size only, so that ten gauges must be put down to get a complete time-pressure curve. The six or three coppers in each gauge are merely to check one another, the average shortening of the coppers in each gauge being taken as the basis of calculation.

While these gauges were being made, the coppers were carefully calibrated by attacking them with pistons of known mass and velocity, both these factors being varied over a wide range. These experiments, which are described in Appendix II., proved that the shortening of the copper is entirely a function of energy; two pistons with the same kinetic energy produce exactly the same shortening, though one may be many times heavier than the other. The relation between shortening and energy, shown in a table in Appendix II., is the basis on which all the gauge results were calculated. The coppers in these calibration experiments behaved with great uniformity, an observation that was borne out by the whole of the subsequent sea trials, in which many thousands of them were expended.

When the gauges were tried they at once gave successful results, which can best be illustrated by quoting the complete figures of an actual experiment. This will also serve to explain the way in which the calculations are made, including various corrections which it has been convenient to leave out of sight in describing the simple theory of the method. The charge consisted of 300 lbs. of 40/60 amatol (Shot 4) at a depth of 34½-feet below the surface, and the gauges were hung in a vertical line, 1 foot apart, at a horizontal distance of 50 feet, the middle gauges being at the same depth as the charge. Referring to Table V., L represents the length, S the nominal free travel, and M the mass of the ten sizes of piston. The mass M includes not only the steel piston but also the copper, and the water which follows the piston into its bore up to the moment of impact, since these contribute their share to the inertia and energy of the moving system. Another point which has to be taken into account is the downward impulse which the pressure communicates to the whole gauge. It is clear that the body of the gauge is acted on by a force equal and opposite to that which propels the group of pistons, and that at each moment it has an acceleration, velocity, and displacement $\frac{1}{x}$ times that of the pistons, x being the ratio of the mass of the body of the gauge to that of the group of pistons. The momentum of the gauge is equal to that of the pistons, but its kinetic energy is less in the ratio $\frac{1}{x}$. At the moment of impact the momentum on both sides is cancelled, and the energy on both sides is absorbed by the coppers. The energy contributed by the pistons is therefore less than the total kinetic energy in the ratio $\frac{x}{x+1}$. The real travel S′ of the pistons up to the moment of impact is less than the nominal travel S in the same ratio. The equivalent travel of a 1-oz. piston, that is to say, the distance a 1-oz. piston would be moved if acted on by the same pressure up to the same moment, is $s = MS'$.

Thus far the figures in the table are merely characteristic of the gauges, and would be the same for any experiment; the figures which follow are special to this particular shot.

Δ represents the shortening of the coppers and E the corresponding energy, ascertained from the calibration table. The energy which a copper registers is principally kinetic, but not entirely, because the pressure existing in the water at the moment of impact does a certain amount of work on the copper while the latter is being shortened. The work done in this way is equal to the pressure multiplied by the cross-sectional area of the piston multiplied by the shortening of the copper, $= \cdot 036\, p\, \Delta$ foot-pounds, if p is expressed in tons per square inch. To apply this correction it is necessary to guess the pressure p; if the event shows that the guess was a bad one it may be necessary to repeat the calculation to a second approximation, but it is generally possible to make a good enough guess by comparing the figures for Δ with cases previously worked out. The remaining energy, $E' = E - \cdot 036\, p\, \Delta$, is from kinetic sources, and the part derived from the piston is $E'' = \frac{xE'}{x+1}$. Knowing the mass M and the kinetic energy E″ of the piston it is a simple matter to calculate its velocity V at the moment of impact, and the equivalent velocity of

a 1-oz. piston, that is to say, the velocity it would have if acted on by the same pressure up to the same moment, is $v - MV$. The results are now in the form postulated in the first paragraph of this section, expressing the velocities v that a 1-oz. piston would have acquired at distances s from its starting point, and the rest of the calculation is quite straightforward.

The result is shown graphically in Fig. 33 as a series of rectangular steps through which a curve has been drawn in such a way as to leave out as much as it takes in. It will be seen that the steps form a very regular series (as they do also in the numerous diagrams illustrating Part I. of this report), and that they provide a thoroughly definite basis for the greater part of the curve representing the decay of pressure. On the other hand, it is clear that the steps in Fig. 33 do not give any positive indication of the form of the pressure curve during the first two ten-thousandths of a second, when the pressure is a maximum. This part of the curve might have been drawn, without inconsistency, in quite a different way from that shown; for example it might have been drawn as indicated by the dotted lines. The determination of this part of the curve was effected by gauges of a rather different type, which are dealt with in the next section.

It may be pointed out that it is not always necessary or desirable to make use of all the 10 sizes of piston shown at the top of Table V. The GB gauges, with the $8\frac{3}{4}$-inch and $6\frac{1}{4}$-inch pistons, were generally omitted, being unnecessary except in the case of very big charges, and experience also showed that nothing was lost in most cases by omitting the $\frac{3}{4}\frac{3}{2}$-inch piston.

For comparison with Table V., the results of a number of other shots, all giving time-pressure curves of quite different character, are shown in a condensed form in Table VI.

Table V.

Gauge.	G X 1.	G X 2.	G Y 1.	G Y 2.	G Z 1.	G Z 2.	G A 1.	G A 2.	G B 1.	G B 2.	—
L	$\frac{3}{4}$	$\frac{11}{16}$	$1\frac{1}{16}$	$1\frac{5}{32}$	$2\frac{1}{8}$	$1\frac{5}{8}$	$4\frac{1}{2}$	3	$8\frac{3}{4}$	$6\frac{1}{8}$	Inches.
S	$\frac{1}{32}$	$\frac{11}{160}$	$\frac{5}{32}$	$\frac{11}{32}$	$\frac{3}{8}$	$\frac{7}{8}$	$\frac{3}{4}$	2	$1\frac{1}{2}$	4	„
M	·886	·815	1·421	1·278	2·134	1·752	4·05	3·09	8·10	6·18	Ounces.
$\frac{x}{x+1}$	·955	·96	·94	·945	·925	·94	·94	·955	·925	·94	——
$S' = S\frac{x}{x+1}$	·0478	·1380	·1469	·3219	·3468	·8224	·7050	1·910	1·387	3·760	Inches.
$s = M S'$	·0423	·1125	·2086	·4152	·7401	1·441	2·856	5·911	11·24	23·27	„
Δ	18·4	30·6	28·6	39·4	35·5	48·8	35·9	50·7	—	—	Thousandths of an inch.
E	1·49	3·32	3·06	5·26	4·42	7·54	4·50	8·02	—	—	Foot-pounds.
p	·55	·42	·33	·24	·18	·11	·07	·04	—	—	Tons per square inch.
$·036\, p\, \Delta$	·37	·45	·34	·34	·22	·19	·09	·07	—	—	Foot-pounds.
$E' = E - ·036\, p\, \Delta$	1·12	2·87	2·72	4·92	4·20	7·35	4·41	7·95	—	—	„
$E'' = E'\frac{x}{x+1}$	1·06	2·75	2·56	4·65	3·88	6·91	4·15	7·60	—	—	„
v	31·1	48·0	61·2	78·3	92·4	111·7	131·7	155·7	—	—	Feet per second.

$v_1 + v_2$	31·1	79	109	139	171	204	243	287	Feet per second.
$v_2 - v_1$	31·1	16·9	13·2	17·1	14·1	19·3	20·0	24·0	„ „
$s_2 - s_1$	·0423	·0702	·0961	·2066	·3249	·7009	1·415	3·055	Inches.
$t_2 - t_1 = ·67\frac{s_2 - s_1}{v_1 + v_2}$	·225	·15	·145	·245	·315	·57	1·04	1·80	Thousandths of a second.
t	·225	·375	·52	·765	1·08	1·65	2·69	4·49	„ „
$p = \frac{26·6 \times 10^{-4}}{\frac{(v_2 - v_1)(v_1 + v_2)}{s_2 - s_1}}$	·61	·51	·40	·31	·20	·15	·085	·06	Tons per square inch.

TABLE VI.

300-lb. Charge of 40/60 Amatol on Surface; Gauges 50 feet away. (*See* Fig. 6.)

Shot.	Gauge.	G X 1.	G X 2.	G Y 1.	G Y 2.	G Z 1.	G Z 2.
—	L	¾	1¼	1¼	1¾	2½	1⅝
64	Δ	16·9	23·4	19·5	19·2	12·3	9·4
—	*v*	30·0	40·2	46·8	44·8	40·3	30·4
—	*t*	·235	·40	·585	·96	1·60	3·25
—	*p*	·57	·27	·16	—·024	—·031	—·027

267-lb. Charge of 80/20 Amatol; Gauges 50 feet away and near the Surface. (*See* Fig. 9.)

Shot.	Gauge.	G X 1.	G Y 1.	G Y 2.	G Z 1.	G Z 2.	G A 1.
—	L	¾	1¼	1¾	2½	1⅝	4¼
28	Δ	17·7	26·5	32·9	23·9	26·5	14·5
—	*v*	30·8	57·7	69·5	68·0	67·6	63·6
—	*t*	·23	·545	·815	1·21	2·07	3·87
—	*p*	·60	·38	·195	—·017	—·002	—·010

1,000-*lb. Charge of T.N.T.; Gauges 250 feet away.* (*See* Fig. 23.)

Shot.	Gauge.	G X 1.	G Y 1.	G Y 2.	G Z 1.	G Z 2.	G A 1.	G A 2.
—	L	¾	1¼	1¾	2½	1⅝	4¼	3
55	Δ	7·6	12·0	16·6	15·5	20·0	10·2	0·7
—	*v*	17·6	32·0	39·3	47·4	53·7	48·8	—
—	*t*	·40	·96	1·44	2·07	3·23	5·54	—
—	*p*	·195	·115	·067	·058	·024	—·010	

300-lb. Charge of T.N.T.; Gauges 50 feet away. (*See* Fig. 12.)

Shot.	Gauge.	G X 1.	G Y 1.	G Y 2.	G Z 1.	G A 1.	G A 2.
—	L	¾	1¼	1¾	2½	4¼	3
11	Δ	17·7	26·2	35·3	33·9	33·1	47·2
17	Δ	17·3	27·4	36·3	34·3	34·8	47·5
25	Δ	18·3	27·8	36·0	34·1	35·3	49·0
Average	Δ	17·8	27·1	35·9	34·1	34·4	47·9
—	*v*	30·5	58·4	74·1	88·0	121·8	141·2
—	*t*	·23	·54	·80	1·14	2·86	4·79
—	*p*	·59	·40		·185	·08[illegible]	·045

1,900-lb. Charge of 50/50 Amatol; Gauges 46½ feet away. (See Fig. 14.)

Shot.	Gauge.	G X 2.	G Y 2.	G Z 2.	G A 2.	G B 1.
—	L	¾	1 7/16	1⅝	3	8½
88	Δ	68·8	99·5	128·6	147·4	106·6
90	Δ	69·7	100·1	133·7	150·2	107·3
Average	Δ	69·2	99·8	131·1	148·8	106·9
—	v	88·3	138·3	244·6	375·2	450·8
—	t	·32	·425	·96	2·05	3·18
—	p	1·76	1·55	·91	·49	·31

1,900-lb. Charge of 50/50 Amatol; Gauges 92½ feet away. (See Fig. 15.)

Shot.	Gauge.	G X 4.	G Y 3.	G Z 3.	G A 3.	G A 4.	G B 2.
—	L	⅜	1 1/16	2⅛	4½	8	8½
88	Δ	23·4	37·5	51·4	55·5	60·0	51·7
90	Δ	23·0	38·7	52·6	54·5	77·7	51·7
Average	Δ	23·2	38·1	52·0	55·0	78·8	51·7
—	v	36·1	78·3	124·4	185·8	222·0	251·9
—	t	·195	·448	·89	2·03	3·28	5·15
—	p	·82	·70	·495	·24	·13	·07

1,900-lb. Charge of 50/50 Amatol; Gauges 185 feet away. (See Fig. 16.)

Shot.	Gauge.	G X 6.	G Y 6.	G Z 6.	G A 5.	G A 6.
—	L	¾	1 7/16	1⅝	4½	3
88	Δ	20·8	29·5	38·5	29·8	37·4
90	Δ	20·9	28·1	36·6	27·4	36·9
Average	Δ	20·8	28·8	37·5	28·6	37·1
—	v	36·2	60·5	89·6	108·8	120·1
—	t	·52	1·04	2·18	3·37	5·59
—	p	·31	·21	·113	·072	·023

(19) Gauges for measuring the Maximum Pressure.

It is necessary to supplement the gauges described in the last section by others capable of measuring the maximum intensity of the pressure. What is wanted for this purpose is a gauge that will operate in the smallest possible time. If the gauge is to be of the same general type as those already described, that is to say, with a steel piston acting on a copper crusher, the obvious line of development is to reduce as much as

possible the weight of the piston and the extent of its movement. In the limit the piston becomes a flat plate held close up against the copper, so that the only movement is that which takes place during the actual crushing of the copper. The theory of this type of gauge requires separate consideration.

Let A be the area of the plate exposed to the pressure in the water, r the resistance of the copper when the plate has been moved inwards a distance s, Δ the amount by which the copper is finally shortened, E the corresponding quantity of energy, as shown in the calibration table, and R the resistance of the copper when $s = \Delta$. The energy registered by the copper is equal to the work done by the pressure in moving the plate—

$$E = \int r ds = A \int p \, ds.$$

There are two cases to consider (compare Sarrau and Vieille, Comptes Rendus, 1882); suppose in the first place that the pressure rises so gradually to its maximum intensity P that the gauge is able to keep step with it, the resistance of the copper at each instant being equal to the pressure on the plate; in this case obviously—

$$P = \frac{R}{A}.$$

The other extreme case is when the pressure rises instantaneously to its maximum intensity P and remains constant until the gauge has come to rest; in this case—

$$\int p \, ds = P\Delta,$$

so that—

$$P = \frac{E}{A\Delta};$$

if P is expressed in tons per square inch, E in foot-pounds, A in square inches, and Δ in thousandths of an inch—

$$P = 5{\cdot}36 \frac{E}{A\Delta} \quad . \quad . \quad . \quad . \quad . \quad . \quad . \quad . \quad . \quad . \quad . \quad (1)$$

In the pressure wave from a submerged high-explosive charge the conditions approximate much more closely to the second of these two cases than to the first; the pressure rises to its maximum intensity almost instantaneously, certainly in a time smaller than the time-constant of any gauge that it has been possible to construct; it does not however remain constant but rapidly commences to fall. In this case—

$$\int p \, ds$$

is approximately equal to $P'\Delta$, P' being the average pressure during the time of operation of the gauge; consequently equation (1) can be used, substituting P' for P.

The remaining part of the problem is to determine the time-constant T of the gauge, that is to say, the time during which the plate is in motion when subjected to a steady pressure. This depends on the inertia of the system, which is seated not only in the plate but also to some extent in the copper; it is easily shown that the mass of the plate must be added to one-third of the mass of the copper to get the total effective mass M. The equation of movement is—

$$M \frac{d^2s}{dt^2} + r = pA.$$

It is shown in Section 28 that for moderate crushings r = (approximately) $r_0 + ks$, where r_0 = 400 lbs. and k = 62 lbs per 10^{-3} inch. Consequently—

$$M \frac{d^2s}{dt^2} + r_0 + ks = pA.$$

Assuming that the pressure is constant the solution is—

$$s = \tfrac{1}{2}\Delta \left(1 - \cos \sqrt{\frac{k}{M}} \cdot t\right)$$

The movement therefore ceases when—

$$t = \pi \sqrt{\frac{M}{k}},$$

which represents the time-constant T of the gauge. Expressing T in thousandths of a second and M in ounces—

$$T = \cdot 16\sqrt{M} \quad . \quad . \quad . \quad . \quad . \quad . \quad . \quad . \quad . \quad . \quad (2)$$

The gauge therefore has a time-constant which depends on the inertia of the moving parts, but is independent of the extent to which the copper is crushed.

It is desirable to examine to what extent the time-constant is affected by the fact that the pressure in the water falls off instead of remaining constant, as assumed above. Suppose that the pressure decays linearly from its initial intensity, falling to P $(1 - j)$ during the nominal period T of the gauge. Then—

$$M\frac{d^2s}{dt^2} + r_o + ks = PA\left(1 - \frac{jt}{T}\right).$$

The solution is—

$$s = a + b \sin ct - a \cos ct - bct$$

where—

$$a = \frac{PA - r_o}{k}, \; b = \frac{jPA}{\pi k}, \; c = \sqrt{\frac{k}{M}}.$$

The movement ceases when—

$$\cos ct + \frac{a}{b} \sin ct = 1.$$

This moment is always earlier than the nominal period—

$$T = \frac{\pi}{c},$$

the difference being determined by the factor—

$$\frac{a}{b} = \frac{\pi}{j} \cdot \frac{PA - r_o}{PA}.$$

The ratio of the actual period T′ to the nominal period T for different values of this factor is as follows—

$\frac{\pi}{j} \cdot \frac{PA - r_o}{PA} =$	∞	10	5.
$\frac{T'}{T} =$	1	·935	·875.

For example, if the pressure falls 21 per cent. in the nominal period of the gauge, so that—

$$\frac{\pi}{j} = 15,$$

and if the initial pressure is PA = 1,200 lbs. = 3 r_o (which implies that Δ = about 20×10^{-8} inch) the actual period of the gauge is 6½ per cent. less than the nominal period. To take a second case, if the pressure falls 31½ per cent. in time T, so that—

$$\frac{\pi}{j} = 10,$$

and if PA = 800 lbs. = 2 r_o (which implies that Δ = about 10×10^{-8} inch) the difference between the nominal and actual periods is 12½ per cent. Roughly speaking, therefore, it may be said that a gauge of this type will have an actual period falling short of its nominal period by not more than about 10 per cent., provided the period is such that the pressure does not fall more than about 30 per cent. during the operation of the gauge, and provided the copper is crushed not less than 10×10^{-8} inch.

The form in which this type of gauge was finally embodied is shown in Fig. 37 (type GF). There are two plates in each gauge, and each plate is clamped by a central screw against a tripod of coppers. The mass of each plate is ·96 ounce and of each copper ·20 ounce, so that the total effective mass associated with each copper is M = ·39 ounce. The time-constant of the gauge is therefore, by formula (2), $T = 10^{-4}$ second. The pressure registered by each tripod of coppers is found by means of formula (1), E being the sum of the energies recorded by the three coppers, Δ the average shortening of the three coppers, and A the area of the plate not covered by the screw-head. At the same time a parallel form of gauge (type GH) was used,

which differed from type GF only in having plates $\frac{3}{8}$ inch thick instead of $\frac{1}{4}$ inch, and with a time-constant therefore twice as great, $T = 2 \times 10^{-4}$.

These gauges gave remarkably consistent results; the difference between the pressures recorded by the two tripods in each gauge averaged only 2 per cent., and in only one or two cases exceeded 5 per cent.

The GF and GH gauges are suitable for pressures from ·6 ton per square inch ($\Delta = 10 \times 10^{-3}$ inch) to 1·8 ton per square inch ($\Delta = 61 \times 10^{-3}$ inch). In the few instances in which higher pressures were measured a modified form of gauge (type GJ) was used, with a plate $\frac{3}{8}$ inch thick operating on a ring of 9 coppers. This gauge, which has a time-constant $T = 10^{-4}$ second, is suitable for pressures from 1·8 ton per square inch ($\Delta = 10 \times 10^{-3}$ inch) to 5·4 ton per square inch ($\Delta = 61 \times 10^{-3}$ inch).

The results from the GF and GH gauges proved that a time-constant of 10^{-4} second is small enough to give the true maximum pressure, provided the charge is not too small. (This was very fortunate, as it would have been impossible to design a gauge of the same type, that is to say, using the same coppers, with a time-constant substantially smaller). The proof rests on a comparison of the results obtained with very big charges. Taking the average of 3 shots of 1,600 lbs. 80/20 amatol the ratio of the pressures recorded by the GF and GH gauges was 100 : 99·1, and taking the average of 3 shots of 1,900 lbs. 50/50 amatol the ratio was 100 : 100·1, that is to say, the pressure recorded by a gauge with a time-constant of 10^{-4} second was the same, within the limits of error of the gauge, as the pressure recorded by a gauge with a time-constant of 2×10^{-4} second. The pressure therefore cannot have fallen more than a very small fraction during the first two ten-thousandths of a second. Taking the average of 11 shots of 300 lbs. 40/60 amatol the ratio of the pressures recorded by the GF and GH gauges was 100 : 94·6; and taking the average of 8 shots of 40 lbs. 40/60 amatol the ratio was 100 : 91·1. These figures illustrate the more rapid decline of the pressure from a small charge. Since the pressure from a 1,600-lb. charge does not fall appreciably in 2×10^{-4} second it may be concluded, from the considerations set out in Section 9, that the pressure from a 200-lb. charge falls equally little in half the time, i.e., in 10^{-4} second; consequently a gauge with a time-constant of 10^{-4} second may be assumed to be rapid enough for the correct determination of the maximum pressure from a charge of 200 lbs. or over. On the other hand, since a gauge with a time-constant of 2×10^{-4} second underestimates the maximum pressure from a 300-lb. charge by 5 or 6 per cent., it may be concluded that a gauge with a time-constant of 10^{-4} second will underestimate the pressure from a 40-lb. charge by about the same amount.

The gauges with free pistons described in the previous section differ from those dealt with in the present section in having no definite time-constant; the time from the first onset of pressure to the striking of the copper depends on the intensity of the pressure. It is possible, however, in certain cases to compare the results given by the two types of gauge, and it is always found that the pressure registered by the free-piston gauge is from 10 to 15 per cent. lower than the pressure registered by the other type of gauge. For example, at a distance of 92½ feet from a 1,900-lb. charge of 50/50 amatol a GX gauge with a ¾-inch piston registers a pressure of ·82 ton per square inch, the time of operation of the gauge being $1·95 \times 10^{-4}$ second (Table VI.). Under the same conditions a GH gauge, with a time-constant of 2×10^{-4} second, registers ·95 ton per square inch. Similarly, at 50 feet from a 300-lb. charge of 40/60 amatol a GX gauge with a ¾-inch piston registers ·75 ton per square inch, the time of operation being $2·2 \times 10^{-4}$ second, while a GH gauge registers ·84 ton per square inch. It is hardly surprising that there should be a small systematic difference between the results of the two kinds of gauge, but the discrepancy gives rise to a difficulty in drawing the time-pressure curve. If this curve is started from a maximum pressure corresponding to the indications of the GF gauge it is impossible to make the curve fall evenly through the rectangular steps calculated from the GX, GY, &c., gauges except by representing the initial decline of the pressure to be much more rapid than can be reconciled with the results described in the preceding paragraph. Some sort of accommodation had to be made, and it was decided to reduce the indications of the GF gauges in every case by 10 per cent. It should be understood therefore that wherever the "maximum pressure" is quoted in Part I. of this report, or in the diagrams illustrating it, the expression denotes the pressure recorded by a GF (or GJ) gauge *minus* 10 per cent.

The methods that have been described are not capable of determining the form of the rising part of the pressure curve; it can only be inferred that the pressure

takes no more than a few hundred-thousandths of a second to reach its maximum. In the time-pressure diagrams the pressure has been represented as rising to its maximum instantaneously; in the absence of fuller knowledge this seems a reasonable supposition, for the pressure in the exploded charge is no doubt greater immediately after detonation than at any subsequent moment, and the part of the wave in which the pressure is greatest may be expected to travel fastest (Section 23) and to remain in front. It should be pointed out, however, that the mathematical theory of an intense pressure wave with a vertical front has not proved soluble up to the present. (Rayleigh, "Theory of Sound," § 251.)

It will be recognised that the crusher gauge commonly used for measuring the pressure developed in ordnance by the propellant belongs to the type discussed in this section. A similar gauge with lead cylinders (Eley's lead crushers) in place of coppers is employed for measuring the lower pressures developed in shot-guns, and was used by Abbot and Schuyler for their investigations on explosion pressures in water. It is impossible, however, with lead crushers to get nearly so small a time-constant as with coppers. As shown in Section 28, the value of k for Eley's lead crushers is about 5·6 lbs. per 10^{-3} inch, compared with $k = 62$ for the coppers used in the present experiments, so that the time-constant of a gauge using these leads is—

$$T = \cdot 53\sqrt{M} \text{ (in thousandths of a second),}$$

that is to say, with pistons of equal mass the time-constant for leads is more than three times that for coppers. The pistons used by Abbot appear also to have been much more massive than was necessary, and although Abbot's description of his gauges is very incomplete it may be gathered that they had time-constants ranging from 4×10^{-4} to 8×10^{-4}; they were therefore far too sluggish to give anything like correct indications of the maximum pressure; the more transient pressures from small charges would be relatively under-estimated compared with the more sustained pressures from big charges. Moreover, the gauges for measuring low pressures had larger pistons and a higher time-constant than those for measuring high pressures, with the result that low pressures were relatively underestimated. These considerations are probably sufficient to account for the fact that Abbot found the pressure to vary, roughly speaking, as $\frac{W^{0\cdot7}}{D^{1\cdot4}}$, while the present investigation shows that the maximum pressure varies as $\frac{W^{\frac{1}{3}}}{D}$ (Section 9).

(20) Gauges for Empirical Comparisons of Pressure (Plasticine Gauges).

The simple gauge shown in Fig. 38 was designed for certain auxiliary purposes which required only an empirical measurement of the pressure, especially for investigating the symmetry of the pressure wave in different directions round the charge. The working element is a cup of plasticine, exposed at one face to the pressure in the water, which squeezes part of the plasticine through a narrow neck into an air-chamber forming the body of the gauge. The extruded plasticine is cut off and weighed.

Very consistent results are obtained from groups of these gauges if they are carefully prepared, the variability being only about 2 per cent. The batch of plasticine is thoroughly mixed by repeated rolling and folding. In filling the cups special care is taken to avoid including any air. Each cup, with the plasticine heaped up a little, is clamped in a vice, the plasticine is hammered until a length of one or two inches has been extruded through the neck, and the superfluous plasticine at top and bottom of the cup is shaved away flush. After an experiment the exposed face of the plasticine is scraped clean and heaped up with some more plasticine from the same batch, which is hammered through as before, and the gauge is ready for use again.

A comparison of the results given by these gauges under widely varying conditions leads to the conclusion that the weight of extruded plasticine is proportional to the time-integral of the pressure as long as the pressure exceeds about ·30 ton per square inch, but that when the pressure falls below this value it is unable to overcome the static resistance of the plasticine. Figures supporting this conclusion are shown in the following table. The time-integral of pressure $I(p > \cdot 30)$ is calculated in each case from the time-pressure curve indicated in the next column, or from a curve derived from this curve by diminishing all the ordinates in pro-

portion to the distance D. The table is divided into two groups of shots fired in October and January respectively. The ratio shown in the last column is fairly constant in each group, considering the wide range which the results cover, but is higher for the October shots than for those fired in the winter month. The results of shot 66 are of special interest, and strongly support the suggested theory of the action of the gauges.

TABLE VII.

d_1 = depth of charge (feet).
d_2 = depth of gauges (feet).
D = distance from charge to gauges (feet).
y = weight of extruded plasticine (grams).

Charge.	Shot.	d_1.	d_2.	D.	$1(\rho>0{\cdot}3)$.	Fig.	y.	$\frac{y}{1(\rho>0{\cdot}3)}$
October.								
267 lbs. 80/20 Amatol	27	34½	30	50	·265	7	·88	3·32
" " "	27	34½	5½	50	·265	10	·86	3·24
" " "	28	34½	30	50	·265	7	·85	3·21
1,000 lbs. T.N.T.	32	51½	40	120	·235	20	·73	3·11
" "	33	51½	40	120	·235	20	·72	3·06
" "	33	51½	40	75	·53	20	1·54	2·92
40 lbs. 40/60 Amatol	34	18	12	26½	·160	13	·52	3·25
" " "	33	18	12	26½	·160	13	·50	3·12
January.								
1,000 lbs. T.N.T.	55	51½	40	75	·53	20	1·19	2·25
" "	59	51½	40	75	·53	20	1·10	2·08
40 lbs. 40/60 Amatol	56	18	10	31	·115	13	·27	2·35
" " "	62	18	21	25	·170	13	·34	2·00
300 lbs. 40/60 Amatol	66	34½	74½	40	·442	1	·98	2·22
" " "	66	34½	94½	60	·225	1	·53	2·35
" " "	66	34½	114½	80	·120	1	·263	2·19
" " "	66	34½	134½	100	·060	1	·115	1·92
" " "	66	34½	154½	120	·032	1	·072	2·25

For the purpose of the symmetry test for which these gauges were principally designed it is not very important to know what they actually measure, but it is necessary to take account of the fact that the results do not vary in simple inverse proportion to the distance from the charge, as they would (approximately) with a gauge which measured either the maximum pressure or the whole time-integral of the pressure. The symmetry tests (Section 5) were carried out in nearly all cases with the plasticine gauges at a distance of 50 feet from a 300-lb. charge and at corresponding distances from charges of different size, and under these conditions a difference of 10 per cent. in the plasticine measurements represents a difference of only 7 per cent. in the whole time-integral of pressure. The results recorded in Table II. were therefore corrected in this ratio. For example, in the case of Shot 37 the two groups of plasticine gauges at opposite sides of the charge gave results in the ratio 100 : 107 ; this was corrected to 100 : 105, which represents the ratio of the distances at which the two groups of gauges would have given equal results.

It is of interest to note that plasticine gauges hung a few feet below the surface of the water give evidence of the abrupt cessation of the pressure due to the reflected tension wave (Figs. 8, 9, and 10), the extruded plasticine being torn by its own momentum right out of the neck of the gauge, like a plant pulled up by the root. When the gauges are at a somewhat greater depth the stalk of plasticine is generally broken off a little outside of the neck, and at still greater depths the stalk remains entire.

(21) Methods of laying out the Charge and Gauges in the Water.

The method adopted in all but a few cases was to hang the charge and gauges from floats lashed to a grass hawser at measured intervals. The "Malapert" being laid with the wind on her starboard quarter the gear was paid out on that side and dropped astern with the drift of the vessel. When the inboard end of the grass was

made fast the drift was sufficient to keep everything taut and in line, except on flat calm days, when a touch of the screw was needed. After the first few shots it was found that in even moderate breezes the drift was sufficient to draw the gauge lines somewhat out of the vertical, with the result that the distances from charge to gauges became inaccurate; this was remedied by introducing a light hemp bottom-line at a level just above the charge. The general arrangement will be seen from the example shown in Fig 40. A diagram of this sort was made out for each shot, for record and for the guidance of the working party. It is obviously not to scale, but all distances are shown by figures; for example, the first gauge line is 91½ feet beyond the charge, and carries two gauges GF3, G111 at depths of 53 feet and 54 feet. Beyond the four gauge lines are two H IV. mine cases, serving as damage gauges; these also are correctly distanced by the bottom-line.

The floats are not shown in the diagram. Fishermen's buffs proved to be the most convenient floats for supporting the gauge lines, but the charge was generally hung from a cask; heavy charges were hung from an empty Mark III. mine case, or, when necessary, from a pair of these cases. The gauges were shackled by their eyebolts to grommets in the gauge lines (Fig. 65), which were 1½-inch steel wires. The gauges were usually hung one foot apart and as nearly as possible at the same level as the charge. The bottom-line also was shackled to a grommet on each gauge line, but its attachment to the charge line was by means of a shackle embracing the charge line in such a way that the charge could spin without twisting up the bottom-line. The charge was generally hung by a 1½-inch steel wire but was lowered by a separate hemp line; after the charge was lowered the hemp line was left hanging slack, with its end bent on to the grass about 20 feet from the charge line, to provide for the recovery of the charge in case of misfire; a similar line was attached to the sinker of each of the H IV. mines; these ropes, as well as the firing-circuit, are omitted from the diagram for the sake of clearness. The "Malapert" was generally 300 feet from the charge, but this distance was increased for charges of more than 300 lbs.

The arrangement illustrated in Fig. 40 is typical of the great majority of the shots fired, though many of them were much simpler; frequently there were only two gauge lines at equal distances on opposite sides of the charge. On some occasions gauges were hung directly beneath the charge, as in Fig. 43. The experiments with long charges, described in Section 15, required special provision for keeping the axis of the charge parallel to the grass hawser; this was effected by a bifilar suspension, as shown in Fig 41, the suspension wires being bent on to the ends of a 12-foot plank, lashed to the grass, with a barrel at each end. Gauge lines were hung from the grass on both sides of the charge, with bottom-lines secured to the ends of the charge, and a third gauge line was hung from a transverse surface line, consisting of a light hemp rope with small floats, which was kept at right angles to the grass by the ship's dinghy, the bottom-line from this gauge line being secured to the middle of the charge.

The experiments in which charges were fired on the bottom (Section 10) required an entirely different scheme. The arrangement is shown in Fig. 42 The gauges were threaded by their eyebolts on a copper tube and lashed in position about one foot apart A steel wire was rove through the tube and bent on to the ends of a plank, the length of wire being such as to support the tube at a distance of 50 feet from the plank. The middle of the plank was lashed to the grass hawser, with bridles to its ends to keep it square. The charge consisting of 1,000 lbs. T.N.T., was lowered to the bottom in 10 fathoms by a hemp line, with marks at 75 feet and 105 feet from the centre of the charge. As soon as the charge reached bottom the hemp was made fast, so as to anchor the ship, while the two marks were lashed to the middle of the gauge tube and plank respectively. The gear was then let go and the "Malapert" allowed to drift until 450 feet of grass had been veered, when the hawser was made fast. The firing of the charge was delayed until two fishermen's buffs on the ends of the plank were observed to show signs of submerging, owing to the strain put on the grass hawser by the vessel's drift; by this means it was ensured that the system was thoroughly taut and the distance of the gauges correct at the moment of firing.

The plank and cross-bar device described in the previous paragraph was also used in some of the experiments described in Section 8, when a line of gauges had to be supported at a depth of only a few feet below the surface.

The foregoing brief description gives no account of the difficulty of handling so much gear with the restricted facilities of a small drifter. Plenty of opportunities for fouling and confusion presented themselves when the lines were being streamed, and it was due to the skill and experience of the working party that everything went without a hitch in all except two or three shots.

In any future trials it is recommended that the drifting method of suspension should be adopted, with a bottom-line as described in the first part of this section. The system is convenient to lay out and gives accurate distance, and it renders the experiments independent of tide. Suppose that a new explosive is to be tested against a standard, such as T.N.T., the following conditions would be suitable:—weight of charge, of each kind, 300 lbs.; number of charges, of each kind, 3; the charges should be in depth-charge form, not surrounded by an air chamber; depth of charge, not less than 30 feet; two gauge lines, one each side of charge, at a horizontal distance of 50 feet from centre of charge; gauges on each line as follows—GF, GX ($\frac{3}{4}$-inch piston), GY ($1\frac{1}{16}$-inch piston), GY ($1\frac{3}{16}$-inch piston), GZ ($2\frac{1}{2}$-inch piston), GZ ($1\frac{5}{8}$-inch piston), GA ($4\frac{1}{2}$-inch piston), GA (3-inch piston); gauges 1 foot apart, middle gauge at same depth as charge; the depth of water should not be less than 20 fathoms.

(22) Alternative Methods for determining the Time-pressure Curve; Hopkinson's Pressure-bar Method; Sir J. J. Thomson's Piezo-electric Method.

The results obtained with the gauges described in Sections 18 and 19 are so consistent and lead to such coherent conclusions that there is no doubt in the writer's mind of their substantial correctness; at the same time it is very desirable to check them if possible by some entirely different method. Two other methods are known for determining the time-pressure curve of an explosion. The first of these is Hopkinson's pressure-bar method, described in the Philosophical Transactions of the Royal Society, 1913. In this method the pressure to be investigated is allowed to act on one end of a steel bar, in which it generates a corresponding pressure wave, which travels with the velocity of sound in steel, about 17,000 feet per second. At a given moment the space-distribution of pressure along the bar is a copy of the time-distribution of the pressure which has acted on the end of the bar. The steel bar is divided toward its further end, the opposed faces of the cut being carefully surfaced and held in firm contact. The compression wave passes this joint unaltered, and reaching the end of the bar beyond the joint is reflected as a wave of tension. At a given moment the pressure at any section of the bar is the algebraic sum of the effects of the forward-travelling compression wave and the returning tension wave. As long as the amplitude of the compression wave at the joint exceeds that of the tension wave the part of the bar beyond the joint, known as the time-piece, is held in contact, but as soon as the amplitude of the tension wave at the joint equals that of the compression wave the time-piece is free to separate, and flies forward with a definite momentum. This momentum, which is determined by a ballistic pendulum, is a measure of the time-integral of the force (pressure multiplied by area) that has acted across the joint up to the moment of separation. By a series of experiments with time-pieces of different lengths it is possible to determine the whole time-integral of the pressure, the maximum intensity of the pressure, and the time during which the pressure exceeds any given value. The results do not give the exact form of the time-pressure curve; they give no information for example as to the relative rapidity of the rise and fall of the pressure; if, however, the pressure is assumed to reach its maximum intensity instantaneously, as is probably very nearly the case, this limitation disappears and the time-pressure curve is definitely determined.

Hopkinson's method has been extensively used for investigating the pressure in the immediate neighbourhood of small charges, say, a few ounces or a few pounds of guncotton; it is in fact the only accurate method available for the purpose. In these cases, however, the pressure is of the order of 100 tons per square inch and is all over in a ten-thousandth of a second or less, while the present problem is to measure pressures of the order of one ton per square inch lasting several thousandths of a second. The difference in both respects is against the method. With a pressure so low as 1 ton per square inch the velocity of the time-piece would be very small,

only about 30 inches per second, and its measurement would be a matter of very great difficulty under sea conditions. On the other hand, to explore the pressure for several thousandths of a second would require pressure-bars of enormous length; even for one-thousandth of a second the time-piece alone would have to be 8½ feet long. It is feared that the utility of Hopkinson's method will be confined to tank experiments with very small charges. Work on these lines is in hand at the Research Department, Woolwich.

The dome of broken water which is thrown up at the surface when a submerged charge is fired (Section 8) is a phenomenon closely parallel with Hopkinson's experiment. The pressure wave of the explosion is reflected from the surface as a tension wave, and the excess of tension over pressure causes separation of the upper layers of water, which rise with a certain amount of trapped momentum. If it could be assumed that the water separates at the least excess of tension, the velocity U with which the uppermost layer begins to rise above the surface would afford a measure of the maximum intensity P of the pressure (that is to say the maximum pressure that would exist at a point in the surface directly above the charge if the wave went on instead of undergoing reflection). It is easily shown that

$$U = \frac{2P}{a\rho},$$

a being the velocity of the pressure wave and ρ the density of sea-water; or U = 66P, if U is expressed in feet per second and P in tons per square inch. With a 300-lb. charge of 40/60 amatol at a depth of 34½ feet the gauge measurements show that P = about 1·2, so that the uppermost layer of water should begin to rise with a velocity of 79 feet per second, and under the action of gravity alone the dome should reach a height of nearly 100 feet. Actually the observations recorded in Section 26 show that it rises only to about 35 feet. A 40-lb. charge at a depth of 18 feet and a 1,900-lb. charge at a depth of 64 feet should also give an initial velocity of 79 feet per second, but in these two cases the actual height of the dome is about 25 feet and 55 feet. The observed height is always much less than the calculated height, and the difference is greater for small than for big charges. The most probable explanation is the resistance of the air; this would make all the results low, but would have less effect in the case of big charges because they throw up a greater volume of water. By means of cinematograph records it may be possible to make direct determinations of the initial velocity U, and it will be interesting to see whether results obtained in that way agree better with the gauge results. In any case, however, the assumption on which the calculation is based is not entirely correct, since it has been shown in Section 8 that sea-water is able to bear considerable momentary tensions without breaking.

Another method for determining the time-pressure curve, due to Sir J. J. Thomson, depends on the property possessed by quartz, tourmaline, and some other crystals, of liberating an electric charge under the action of pressure. The charge liberated at any instant is proportional to the pressure at that instant. A pair of electrodes on the crystal are connected to plates in a cathode-ray tube, producing an electrostatic field which deflects the cathode ray to an extent proportional to the pressure on the crystal. The movement of the ray is recorded on a photographic plate. An alternating magnetic field, of about a hundred cycles per second, produces a second movement of the ray, at right angles to that imparted by the piezo-electric action of the crystal, so as to draw out the deflection of the ray into the form of a loop, from the shape of which the whole time-history of the pressure can be deduced. This method has been developed at Shandon by Mr. David Keys, and successful experiments have already been made with miniature charges. No great difficulty is anticipated in applying the method under conditions parallel to those of the present experiments, and the results should be a valuable check on the gauge measurements. It may be hoped that this method will enable the time-pressure curve to be studied more closely and in detail than is possible by any other means at present known. For example, it is probable that the time-pressure curve of a charge surrounded by a big air-chamber is less simple than that of a naked charge; it very likely has secondary peaks or irregularities, and the same may be true of charges fired on the bottom. The present gauges are not well adapted to show these features, and if they exist it is probable that they can only be brought to light by methods giving a continuous trace of the pressure.

(23) Measurements of the Velocity of the Pressure Wave.

The velocity of the pressure wave was measured by means of the spark chronograph described in Section 27. As the pressure wave passed two contacts at measured distances from the charge it closed each in turn and operated the chronograph. The lay-out of one of these experiments is shown in Fig. 43, and the circuits in Fig. 44. Each contact consisted of a pair of brass springs built up with rubber strips into a watertight unit (Fig. 45). The time for the contact to close under a pressure of 1 ton per square inch was estimated to be about 3×10^{-6} second. The two contacts were lashed to a hemp line at distances of 50 feet and 60 feet from the charge. It will be seen from the lay-out diagram that as the "Malapert" drifted the resistance of the charge kept the hemp line taut. Above and between the contacts was a floating box containing the chronograph and its associated sparking-circuits. This box was connected to the "Malapert" by a 4-wire cable, so that the charging of the spark condensers and the speed of the chronograph could be controlled from the ship. The firing of the shot was delayed until the condensers had been charged and the chronograph brought to correct speed. Each condenser charging circuit included a high resistance, which gave it a charging period of several seconds, so that the chronograph would be unaffected by the rapid reclosing of a contact, such as might be occasioned by the reflected wave from the bottom. For the sake of simplicity only two contacts have been shown in Fig. 44, but actually these contacts and their associated circuits were in duplicate, so that as the pressure wave passed each contact position it operated two contacts and made a double record on the chronograph. The results of four shots, in all of which the contacts were at 50 feet and 60 feet from a 300-lb. amatol charge, were as follows. The mean result is probably within 5 per cent. of the truth.

Shot.	Velocity (feet per second).
72	5,180
74	4,820
105	4,830
106	4,730
Mean	4,890

The velocity of sound in water was determined by Colladon and Sturm in the Lake of Geneva in 1826 as 4,709 feet per second. The modulus of compressional elasticity—

$$\frac{\rho dp}{d\rho}$$

of sea-water is 8¼ per cent. higher than that of fresh water (Tait, Challenger Reports, 1888) and its density (ρ) is 3 per cent. higher, so that the velocity of sound—

$$\sqrt{\frac{dp}{d\rho}}$$

should be 2¾ per cent. higher, or 4,830 feet per second. The experiments of Mr. Boulding, off Culver, Isle of Wight, in 1917 gave the velocity as 4,940 feet per second (B.I.R. 34853/17). The water in the Clyde estuary between Arran and the mainland has nearly the full salinity of the open sea (three samples collected on different days gave 3·18, 3·16, and 3·20 grams NaCl per 100 c.c.), so that the velocity there may be taken as about 4,900 feet per second. This is practically identical with the figure found for the velocity of the pressure wave.

The velocity of sound in a medium is the velocity of an infinitely weak pressure wave. The theory of the velocity of a strong pressure wave has been considered by Rayleigh (Theory of Sound, § 251), whose observations may be paraphrased as follows:—Consider a small portion of the medium occupied by the pressure wave at a given moment, and imagine an infinitely weak secondary wave to be superposed; the secondary wave will travel, relatively to the medium, with the velocity a' of sound—not the velocity of sound in the undisturbed medium but the velocity of sound in the medium as modified by the pressure of the main wave; but the medium itself is in motion with a velocity u, depending on the pressure of the main wave, so that the whole velocity of the secondary wave is $a' + u$; what has been said of the secondary wave applies also to the parts of the main wave, so that the velocity of the main wave at the point considered may be taken as $a' + u$. We have to apply

Best Available Copy

this theory to the pressure wave from a 300-lb. amatol charge at a distance of 55 feet from the charge, where the maximum pressure is about 0·7 ton per square inch. Under this pressure the density (ρ) of the sea-water is 0·5 per cent. higher than normal, and the modulus of compressional elasticity—

$$\frac{\rho dp}{d\rho}$$

is about 4·5 per cent. higher (Tait, Challenger Report), so that the velocity a' of sound in the compressed medium is 2 per cent. higher than in the undisturbed water. The velocity of the medium itself is—

$$u = \frac{p}{a\rho} = 23 \text{ feet per second,}$$

or 0·5 per cent. of the velocity of sound. Consequently the velocity of the pressure wave, $a' + u$, should be 2·5 per cent. higher than the velocity of sound. Theoretical considerations therefore confirm the experimental results in indicating that the velocity of the pressure wave does not exceed that of sound by more than a few per cent. In the region near the charge the difference is no doubt greater.

Thirty years ago Threlfall and Adair made a series of experiments on the velocity of the pressure wave generated by small charges in sea-water (Proceedings of the Royal Society, 1889). Sensitive contact makers were mounted on piles at approximately 30 and 200 yards respectively from the charge, and the closure of the contacts was recorded on a pendulum chronograph. With a 9-oz. charge of guncotton they found a velocity of 5,700 feet per second, and with a 4-lb. charge of guncotton the velocity was 6,600 feet per second. It is difficult to reconcile these results, which among themselves were very consistent, with those obtained in the present experiments. Sir R. Threlfall has informed the writer that the possibility of a disturbance having been propagated through the sea-bottom and the supporting piles was carefully weighed and rejected at the time of the experiments.

The determination of the velocity of the pressure wave is of more than theoretical interest; it is a factor which has to be known in estimating the effect of the surface on the pressure at a point in the water (Section 8); moreover, the demonstration that the velocity is practically the same as that of sound strengthens the argument that the pressure wave in all respects approximately obeys the simple acoustic laws.

(24) Measurements of the Echo reflected from the Bottom.

All that was attempted in this direction was a measurement of the whole time-integral of the pressure in the reflected wave. For the purpose of this measurement it was necessary to modify one of the gauges described in Section 18 in such a way that the main pressure wave would have no effect except to set the gauge in readiness to be operated by the reflected wave. The bottom of a GZ gauge (Fig. 35) was fitted with a shutter A, Fig. 39, held by a powerful spring B against a detent C in one of the piston holes; the pressure of the main pressure wave forces in the detent C against a spring and also holds the shutter against the bottom of the gauge; when the pressure of the main wave ceases the shutter is pulled round by the spring against a stop D, in the next piston hole to the detent C, and exposes two piston holes E containing working pistons, which are afterwards operated by the reflected wave. The two remaining piston holes were blocked. The time-constant of the shutter was measured by the spark chronograph described in Section 27, and was found to be about 7×10^{-3} second. The working pistons were $\frac{3}{4}$ inch long, with $1\frac{3}{4}$ inch free travel. Lead crushers were used in place of coppers.

In one typical experiment with this gauge, the charge (300 lbs. 40/60 amatol) was $34\frac{1}{2}$ feet deep; the gauge was 40 feet deep and 50 feet away from the charge; the bottom, which was mud, was at 21 fathoms. The time-integral of pressure at a distance of 50 feet from this charge is I = ·68 (Section 4); the distance travelled by the reflected wave, from charge to bottom and from bottom to gauge, was 184 feet, so that if complete reflection occurred the time-integral of pressure of the reflected wave would be ·185; actually the gauge gave it as only ·068, corresponding to a coefficient of reflection of 0·37. In three similar experiments the values found for this coefficient were 0·29, 0·47, 0·47. It may be concluded therefore that reflection of a pressure wave from a mud bottom reduces the time-integral of pressure to less than half its incident value.

Reckoning time in thousandths of a second from the moment of detonation, the order of events in the above experiment is as follows:—The main wave reaches the gauge at $t = 10$ and forces in the detent, at the same time holding the shutter from movement; the tension wave from the surface arrives at the gauge at $t = 18$, and takes the pressure off the shutter; the shutter then begins to turn and completes its movement at $t = 25$; the reflected wave from the bottom arrives at the gauge at $t = 37$, and drives in the two pistons; the crushing of the leads indicates that the velocity of the pistons at the moment of impact is about 15 feet per second, so that impact must occur after $t = 47$, but probably not later than $t = 50$; the period of ten thousandths of a second during which the piston is in movement should be ample to cover the duration of the wave; finally, the wave reflected from the bottom reaches the surface and is reflected as a wave of tension, which arrives at the gauge at $t = 52$, just after the pistons have hammered the leads.

APPENDIX I.

SCHEDULE OF CHARGES AND SHOTS.

(25) List of Charges.

TABLE VIII.

Type of Charge.	Weight and Nature of Explosive.	Displacement (cubic feet)	Number fired.	Description.
G.	40 lbs. 40/60 Amatol.	0·7	23	Small depth charge: cylindrical mild steel casing with dished ends, 1 foot 9 inches long, 9 inches diameter, $\frac{1}{16}$ inch thick; explosive arranged as at G, Fig. 46.
D.	300 lbs. 40/60 or 50/50 Amatol.	3½	31	Depth charge; cylindrical mild steel casing with dished ends, 2 feet 3¾ inches long, 1 foot 5½ inches diameter, $\frac{1}{8}$ inch thick, completely filled with explosive except central primer tube.
D*	120 lbs. 40/60 Amatol.	3½	1	Depth charge; casing same as D but only partly filled with explosive.
DX	267 lbs. 80/20 Amatol.	3½	5	Depth charge; similar to D.
AD	300 lbs. T.N.T.	3½	6	American depth charge; similar to D.
X1	600 lbs. 40/60 or 50/50 Amatol.	7	1	Two D charges lashed side by side.
X2	900 lbs. 40/60 or 50/50 Amatol.	10½	3	Three D charges lashed together so as to give three touching circles in section.
X3	900 lbs. 40/60 or 50/50 Amatol.	10½	2	Three D charges lashed end-to-end.
M	1,000 lbs. T.N.T.	16	8	Ground mine; concrete casing, about 2 inches thick, as at M, Fig. 46.
X4	1,900 lbs. 50/50 Amatol.	21	3	Special charge; cylindrical mild steel casing with convex ends, 4 feet long, 2 feet 8 inches diameter, $\frac{5}{16}$ inch to $\frac{1}{4}$ inch thick; completely filled with explosive except central primer tube.
X5	1,600 lbs. 80/20 Amatol.	21	3	Similar to X4.
X6	500 lbs. Gunpowder (E.X.E. prism powder).	8	3	Special charge; cylindrical mild steel casing with convex ends, 3 feet 3 inches long, 1 foot 9½ inches diameter, $\frac{1}{8}$ inch to $\frac{5}{16}$ inch thick; completely filled with explosive except central primer tube.
H2	320 lbs. 40/60 Amatol.	16½	6	Buoyant mine; spherical mild steel casing, 3 feet 2 inches diameter, $\frac{1}{8}$ inch thick, explosive in central container as at H2, Fig. 46.
X7	820 lbs. 40/60 Amatol.	16½	4	H2 mine with 500 lbs. additional explosive filled in as at X7, Fig. 46.
X8	272 lbs. R.D. No. 30 mixture (ammonium perchlorate, 78; aluminium powder, 6; paraffin wax, 16).	16½	4	Special mine; spherical mild steel casing, 3 feet 2 inches diameter, $\frac{5}{16}$ inch to $\frac{1}{4}$ inch thick; explosive central, as in H2.
X9	312 lbs. wet guncotton	16½	3	Special mine; similar to X8.
P	2½ lbs. dry guncotton	0·04	1	Guncotton primer.

The primer employed for the majority of the charges contained 2½ lbs. of guncotton; the primer for the H2 mine had ¾ lb. C.E. and 2½ lbs T.N.T.; that for the M, X4, and X5 charges had 4 lbs. of tetryl.

(26) List of Shots.

TABLE IX.

Shot Number.	Type of Charge.	Date.	Depth of Centre of Charge. (Feet.)	Depth of Water. (Fathoms.)	Wind.	Sea (Trough to Crest in Feet).	Height of "Plumes." (Feet.)	Diameter of "Dome." (Feet.")	Height of "Dome." (Feet.)
1	D	27.8.18	34½	32	S.W. 3	3	—	—	—
2	G	29.8.18	34½	29	N.W. 3	2	60	120	11
3	D	29.8.18	34½	25	W.N.W. 2	2	160	—	—
4	D	30.8.18	34½	25	N.W. 5	4	120	140	—
5	D*	31.8.18	34½	25	N.W. 4	2	90	140	23
6	AD	3.9.18	34½	39	N.W. 2	2	140	140	30
7	D	4.9.18	34½	30	E. 3	½	70	160	30
8	D	5.9.18	34½	27	S.E. 1	0	80	150	30
9	D	6.9.18	31½	23	0	0	90	—	—
10	DX	7.9.18	34½	24	S.W. 1	1	90	—	—
11	AD	9.9.18	34½	30	S.W. 2	1	85	120	34
12	G	11.9.18	31½	30	W.N.W. 1	1	70	—	10
13	G	12.9.18	14½	26	N.W. 4	3	90	—	—
14	D	13.9.18	10	27	N.W. by N. 3	2	300	—	—
15	D	14.9.18	5	25	E. 3	1	400	—	—
16	P	18.9.18	4	2	—	0	—	—	—
17	AD	20.9.18	34½	30	S.W. 2	3	190	145	30
18	G	23.9.18	34½	22	N.W. 4	3	45	—	—
19	G	24.9.18	34½	25	S.W. 6	7	—	—	—
20	H2	26.9.18	34½	26	W.S.W. 2	1	150	120	25
21	G	30.9.18	34½	25	N.N.W. 3	1½	40	80	10
22	G	1.10.18	34½	26	N.W. by N. 2	½	60	80	11
23	G	4.10.18	34½	29	W.N.W. 3	2	45	90	10
24	H2	11.10.18	• 200	45	W.S.W. 1	½	—	—	0
25	AD	11.10.18	34½	30	N.W. by N. 2	½	130	—	—
26	H2	12.10.18	200	45	N.N.W. 2	½	—	—	0
27	DX	12.10.18	34½	25	N.N.W. 2	½	170	—	35
28	DX	13.10.18	34½	30	S.S.W. 3	2	170	140	35
29	D	14.10.18	34½	27	S.W. 3	2	260	—	—
30	DX	15.10.18	31½	29	0	½	160	—	—
31	D	16.10.18	5	26	N.W. by W. 3	2	450	—	—
32	M	23.10.18	51½	30	N.N.W. 1	½	220	220	48
33	M	25.10.18	51½	26	N.N.W. 3	2	190	205	60
34	G	27.10.18	18	27	0	0	85	60	24
35	G	27.10.18	18	27	S.W. 1	0	90	65	26
36	X7	29.10.18	47½	25	0	0	125	150	40
37	X7	1.11.18	47½	30	E. 2	1	190	230	46
38	DX	12.11.18	34½	27	0	0	130	125	28
39	G	12.11.18	150	45	0	0	—	—	0
40	G	12.11.18	100	45	0	0	—	—	0
41	G	14.11.18	80	22	S.S.E. 2	½	—	—	? 0
42	G	14.11.18	60	22	S.S.E. 2	½	—	—	?
43	G	14.11.18	50	22	S.S.E. 2	½	—	—	6
44	D	20.11.18	20	25	S. 3	2	230	—	—
45	D	23.11.18	20	25	S. 3	2½	190	—	—
46	X1	29.11.18	34½	25	N.W. 3	1	250	170	70
47	G	3.12.18	18	22	S.W. 1	0	85	—	—
48	X7	10.12.18	47½	28	N.N.W. 3	1½	—	—	—
49	H2	11.12.18	34½	27	N.E. by E. 2	½	170	120	35
50	X2	17.12.18	49½	28	S.W. 3	1½	200	170	43
51	G	31.12.18	18	22	N.E. 2	½	160	—	—
52	X7	3.1.19	47½	26	0	0	175	170	39
53	H2	4.1.19	34½	27	N.E. 2	½	100	115	29
54	X2	6.1.19	49½	31	S.W. 2	½	160	195	55
55	M	7.1.19	51½	32	E. by N. 3	1½	260	—	—
56	G	8.1.19	18	22	S.S.E. 3	1½	70	—	—
57	H2	14.1.19	34½	26	S.W. 1	½	150	105	34
58	X2	18.1.19	49½	28	N.N.W. 1	0	160	180	55
59	M	20.1.19	51½	30	S.S.E. 3	1½	280	200	52
60	X9	21.1.19	34½	26	S.S.E. 1	½	180	105	39
61	D	22.1.19	10	26	S.S.E. 2	1½	250	—	—
62	G	23.1.19	18	21	S. by E. 2	1	65	—	—
63	X9	28.1.19	34½	24	E. 1	½	170	115	37
64	D	29.1.19	½	26	N.E. 3	1	300	—	—
65	G	30.1.19	18	17	E. 2	1	200	—	—
66	D	31.1.19	34½	13	N.E. 2	1	250	150	38

Shot Number	Type of Charge	Date	Depth of Centre of Charge (Feet)	Depth of Water (Fathoms)	Wind.	Sea (Trough to Crest in Feet).	Height of "Plume." (Feet.)	Diameter of "Dome." (Feet.)	Height of "Dome." (Feet.)
67	X3	3.2.19	34½	28	E. 1	0	130	110	30
68	D	5.2.19	18	13	E. 4	1	180	95	28
69	X3	10.2.19	34½	25	E.N.E. 2	½	300	115	42
70	D	12.2.19	10	20	E.N.E. 1	½	—	—	—
71	X3	13.2.19	34½	26	0	0	170	—	—
72	D	14.2.19	10	25	0	0	400	—	—
73	M	17.2.19	60	10	E. 4	1	250	400	40
74	D	19.2.19	10	21	E. by S. 1	1	400	—	—
75	M	20.2.19	60	10	E. 2	½	180	240	38
76	M	21.2.19	60	10	E. by S. 2	1	195	290	55
77	D	21.2.19	125	25	E. by S. 2	1	—	—	? 0
78	M	22.2.19	60	10	E.N.E. 1	½	140	—	—
79	D	24.2.19	125	27	0	0	—	—	? 0
80	D	24.2.19	150	30	0	0	—	—	0
81	X3	25.2.19	49½	29	E.S.E. 3	1½	—	—	—
82	D	26.2.19	10	23	E.N.E. 4	1½	400	—	—
83	X3	28.2.19	49½	30	W. by S. 3	1½	—	—	—
84	AD	1.3.19	34½	27	S.S.E. 3	2	180	—	—
85	X3	4.3.19	60	39	N.W. 1	0	210	—	—
86	X3	5.3.19	60	40	W.N.W. 1	0	180	190	52
87	X3	12.3.19	60	40	N.E. by E. 3	2	210	—	—
88	X4	13.3.19	64	45	E. by S. 2	1	220	—	—
89	X4	14.3.19	64	51	0	0	200	300	53
90	X4	15.3.19	64	55	E. by N. 1	½	240	—	58
91	X6	17.3.19	34½	23	N.W. by N. 4	2	80	—	0
92	X6	18.3.19	40	27	S.E. by S. 3	½	90	—	0
93	X6	19.3.19	40	27	S.E. 5	3½	110	—	0
94	X8	20.3.19	34½	21	E.S.E. 3	2	175	—	—
95	AD	21.3.19	31½	21	E. 3	1½	195	—	—
96	D	22.3.19	200	48	E.N.E. 2	½	—	—	0
97	D	24.3.19	5	22	E. 1	½	—	—	—
98	D	25.3.19	34½	21	0	0	160	—	—
99	D	25.3.19	5	21	0	0	650	—	—
100	D	31.3.19	34½	22	N.N.W. 4	1½	—	130	40
101	D	31.3.19	34½	23	N.N.W. 4	1½	—	—	—
102	X8	31.3.19	34½	22	N.N.W. 4	1½	150	—	—
103	G	1.4.19	18	13	E.S.E. 2	½	—	—	—
104	G	1.4.19	18	14	E.N.E. 2	½	—	—	—
105	D	2.4.19	34½	33	W. by S. 2	½	—	—	—
106	D	3.4.19	34½	40	W. by S. 1	0	—	—	—
107	D	4.4.19	34½	42	S.W. by W. 2	1	—	120	40

Shots 73, 75, 76, and 78 were fired on a sand bottom about 1½ miles off Irvine; all other shots were fired approximately in a line between Troon and Holy Island, over a mud bottom.

APPENDIX II.

CALIBRATION EXPERIMENTS.

(27) Apparatus.

The copper cylinders which formed the measuring-element of the principal gauges were calibrated by firing steel pistons at them from a pneumatic gun, the velocity of the pistons being measured by an electric chronograph, which was developed for the purpose. The gun, shown in Fig. 47, consisted of a shot-gun barrel mounted vertically over a massive anvil. The piston was hung by a loop of fine wire from a cross-pin, resting in two notches in the upper end of the barrel, so that when compressed air was admitted above it it was blown off its support and projected on to a copper on the anvil. The top of the barrel was closed

by a screw cap, connected by a rubber tube to a reservoir of compressed air. The rubber tube was normally blocked by a metal blade acting as a pinch-valve, but this could be tripped at any moment so as to admit the compressed air to the gun barrel. By charging the reservoir to different pressures a wide range of velocities could be obtained. Four sizes of pistons were used, weighing 22½, 4½, 3, and 1½ ounces. The lightest of these pistons was hollow, as shown in the figure. With the reservoir charged at 75 lbs. per square inch above atmospheric pressure the lightest piston could be given a velocity of 150 feet per second, corresponding to 33 foot-pounds of energy, and the heaviest piston could be given a velocity of 50 feet per second, corresponding to 35 foot-pounds. For velocities from 11 to 16 feet per second compressed air was not used, the piston being dropped from different heights inside the barrel. For velocities lower than 11 feet per second the piston was dropped from the end of the barrel, which was brought down to a suitable height above the anvil.

When the piston was dropped from the end of the barrel its energy at the moment of impact was calculated from its weight and the height of its fall, but in all other cases the velocity was measured by a pair of electric contacts connected with a chronograph. Each contact consisted of a very light aluminium lever just projecting into the line of flight, with a copper brush about $\frac{1}{100}$-inch below it, so that contact was closed by the passage of the piston. The two contacts were exactly 1 foot apart, the upper one being about 1 foot below the end of the gun barrel and the lower one ½ inch above the point of impact. If T is the time recorded by the chronograph, x the distance between the contacts, y the distance from the lower contact to the point of impact, and g the acceleration due to gravity, the velocity of the piston at the moment of impact is—

$$\sqrt{\left(\frac{x}{T} + \frac{1}{2}gT\right)^2 + 2gy}.$$

The chronograph was a high-tension spark apparatus. The closure of each contact completed the circuit of a charged condenser (4 microfarads, 200 volts) through the primary of a transformer (a small induction coil) causing a spark in the secondary circuit between a fixed discharge point and a drum rotating at a known speed. A paper strip on the drum was perforated by the sparks, and the distance between the perforations, measured lengthwise on the paper strip, indicated the time-interval between the closure of the two contacts. The construction of the chronograph is shown in Fig. 48 and the circuits in Fig. 49. The method adopted for running the chronograph at correct speed was as follows: A soft iron cog-wheel, with 10 teeth, was fixed on the chronograph shaft so that the teeth rotated past a permanent magnet wound with a coil connected to a telephone; this arrangement produced an audible note corresponding to the speed of the drum; in a branch of the same circuit were a battery, a "button" microphone, and another wound magnet, the microphone and magnet being combined with a tuning-fork in the well-known way to constitute a retro-active system, producing a sustained pure tone; the speed of the chronograph motor was adjusted by a rheostat until slow steady beats were heard in the telephone, not more than one every second; the frequency of the tuning-fork (by comparison with a fork determined at the National Physical Laboratory) was 511, so that when the above adjustment had been made it was known that the drum was running at 51·1 ± 0·1 revolutions per second. The circumference of the drum, over the paper strip, was 12·60 inches, so that 1 inch corresponded to $\frac{1}{51}$ second.

The primaries of the transformers had an inductance of about 3 milli-henries; the calculated time for the condenser discharge current to reach its maximum was therefore $\frac{1}{3000}$ second, but the time necessary to establish a sparking potential was no doubt determined almost entirely by the time constant of the secondary circuit, and must have been far less than this; experiment in fact showed that the moment of sparking was the same, within 10^{-5} second, whether the capacity in the primary circuit was 2 microfarads or 8 microfarads. Whatever may have been the actual lag of the chronograph action it was only the variability that mattered. A large number of experiments were made on this point, four condensers being discharged simultaneously through separate transformers by closing a single contact, and it was found that the average difference between the four individual chronograph perforations and the mean of the four was only about 10^{-5} second, or less than $\frac{1}{500}$ inch. The variations were due to wandering of the sparks more than to real differences in the time of discharge.

(28) Results.

The copper cylinders were cut from rods of pure electrolytic copper, cold-drawn to diameter ·320 inch, the length of each piece being from ·499 inch to ·501 inch. As all measurements were made to the nearest ten-thousandths of an inch it was necessary for the ends to be cut perfectly square. The cut pieces were annealed in an electric muffle furnace at 600° C., the furnace being packed with sand to avoid oxidation. The coppers were allowed to cool slowly in the furnace, but quenching them in water seems a better plan; quenched coppers are cleaner and more convenient to measure and their resistance is almost exactly the same.

The uniformity of these coppers was tested by subjecting 116 of them (cut from 29 different rods) to a standard blow of 2·96 foot-pounds; the average shortening was $27·4 \times 10^{-3}$ inch, the extreme variation being $26·6 \times 10^{-3}$ to $27·9 \times 10^{-3}$; the average difference between the mean and individual results was $0·2 \times 10^{-3}$, or less than 1 per cent., a very remarkable degree of consistency.

The calibration experiments proved that the shortening of a copper measures the energy of the blow; a light and a heavy piston endowed with equal amounts of energy produce the same shortening. This is illustrated in Fig. 50, which shows two sections of the calibration curve with the actual results given by pistons of different weights. It was observed that there was generally no appreciable rebound of the piston, from which it may be concluded that the whole of its energy was absorbed by the copper; the exception was in the case of the lightest piston at very high velocities, when there was a very perceptible rebound, but even in this case the energy of rebound was only about 1 per cent. of the incident energy. The relation between the shortening Δ and the impressed energy E is shown in the following table.

TABLE X.

Δ = shortening of the copper, in thousandths of an inch.
E = energy in foot-pounds.

Δ	E	Δ	E	Δ	E	Δ	E
6	0·22	22	1·98	39	5·17	80	16·78
6	0·29	23	2·13	40	5·40	85	18·69
7	0·36	24	2·29	41	5·68	90	20·48
8	0·43	25	2·45	42	5·86	95	22·47
9	0·51	26	2·62	43	6·10	100	24·50
10	0·59	27	2·79	44	6·34	105	26·48
11	0·68	28	2·96	45	6·58	110	28·53
12	0·77	29	3·14	46	6·83	115	30·75
13	0·87	30	3·32	47	7·08	120	33·02
14	0·97	31	3·51	48	7·33	125	35·40
15	1·08	32	3·70	49	7·58	130	37·88
16	1·19	33	3·90	50	7·84	135	40·48
17	1·31	34	4·10	55	9·15	140	43·20
18	1·44	35	4·31	60	10·50	145	46·06
19	1·57	36	4·52	65	11·93	150	49·04
20	1·70	37	4·73	70	13·46	155	52·08
21	1·84	38	4·95	75	15·08	160	55·20

The fact that the shortening of a copper is entirely determined by the energy of the attacking piston can only be explained by supposing that the resistance of the copper at any moment is independent of the rate at which it is being shortened, and depends only on the extent to which it has been shortened. On this view the resistance of the copper for a given shortening Δ is

$$\frac{dE}{d\Delta}$$

and can be determined from the calibration results. If these results are analysed it will be found that for small values of Δ the resistance is approximately $r = r_0 + k\Delta$, where $r_0 = 400$ lbs. and $k = 62$ lbs. per 10^{-3} inch. For higher crushings, above $\Delta = 50 \times 10^{-3}$, the resistance is less than this formula indicates. The increase of resistance which accompanies shortening of the copper is due almost entirely to hardening of the metal, and in only a very small degree to enlargement of girth; for example, a copper crushed 40×10^{-3} inch has a resistance twice as great as a copper crushed 17×10^{-3} inch, though its cross-sectional area is only 5 per cent. greater.

For measuring very light impacts, less than 0·5 foot-pound, coppers are too hard and lead cylinders must be used. Eley's lead crushers were calibrated for this purpose, and the results are shown in Table XI. These leads are ·500 inch long and ·325 inch diameter. The relation between E and Δ is independent of the weight of the piston, so that it must be concluded, as in the case of coppers, that the resistance of a lead is independent of the rate at which it is being shortened. As in the case of coppers, the increase of resistance which accompanies shortening of the lead is due mainly to hardening of the metal, but there is this difference, that whereas the copper keeps its acquired hardness the lead swiftly reverts to its original softness (H. W. R. Mason, Arms and Explosives, Jan. 1, 1918). The self-annealing process occupies a matter of seconds or minutes, and it certainly has no time to take effect in the very brief duration of the impact of a piston, which is of the order of 10^{-3} second, but the phenomenon is worth noting since it invalidates any statical method for determining the resistance of the lead, and explains the "creeping" or gradual yielding of the lead which has been observed whenever it has been attempted to apply such methods. Calculated from the energy data the resistance of the lead is

$$r = \frac{dE}{d\Delta} = \text{(for small crushings) approximately } r_0 + k\Delta,$$

where $r_0 = 130$ lbs. and $k = 5{\cdot}6$ lbs. per 10^{-3} inch.

TABLE XI.

Δ = shortening of the lead, in thousandths of an inch.
E = energy in foot-pounds.

Δ	E	Δ	E	Δ	E	Δ	E
5	0·052	30	0·535	55	1·22	80	2·10
10	0·127	35	0·655	60	1·38	85	2·30
15	0·212	40	0·785	65	1·55	90	2·51
20	0·310	45	0·922	70	1·72	95	2·72
25	0·420	50	1·07	75	1·91	100	2·94

APPENDIX III.

MISCELLANEOUS.

(29) Some general Points in the Theory and Use of Pressure Gauges.

There is a general question which arises in connexion with any form of gauge for measuring the pressure in a pressure wave. The measurement required is the pressure that would exist in the water if the gauges were absent; to what extent are the gauge results vitiated by the modification of pressure due to the presence of the gauge? The presence of the gauge modifies the pressure in two ways. In the first place the gauge as a whole, regarded as an approximately rigid heavy body, increases the pressure on its front face (the side towards the oncoming wave) by reflection, and diminishes the pressure on its back face by shadowing. The seriousness of this effect depends on the relation between the size of the gauge and the thickness of that part of the pressure wave which it is supposed to measure. As regards the present gauges the effect will be most serious in the case of Type GF (Fig. 37); the linear dimensions of this gauge average about 3 inches and it has a time-constant of 10^{-4} second, corresponding to a 6-inch thickness of the wave in the water. The question was examined experimentally for this type of gauge by putting down 3 gauges near one another at equal distances from the charge, the working face of the first gauge being directed towards the charge, of the second at right angles, and of the third away from the charge; in three experiments of this kind, with gauges 40 feet away from 300-lb. charges of amatol or T.N.T., the pressures recorded were in the ratio:—

	105 : 100 : 96
	105 : 100 : 97
	108 : 100 : 96
Average - - -	106 : 100 : 96

These results show that so far as the present gauges are concerned the effects of reflection and shadowing are not large even in the most unfavourable case; it must also be remembered that throughout the investigation, with a few exceptions, the gauges were hung in the second of the above three positions, with the axis of the gauge at right angles to the direction of the charge, so that neither reflection nor shadowing would come into play to any appreciable extent.

In the second place every gauge has a part which yields to the pressure; how far is the pressure in the water reduced by the relief thus afforded to it? In dealing with this question it is convenient to have in mind an actual example; take the case of a G gauge (Fig. 34) at a distance of 50 feet from a 300-lb. amatol charge; this gauge has a piston 3 inches long and $\frac{1}{4}$ inch in diameter, with a free travel of 2 inches before it hammers the copper; from the moment when the pressure wave reaches it the piston moves with a continually increasing velocity until, after about five-thousandths of a second, it reaches the end of its travel with a velocity of about 50 feet per second. The movement of the piston propagates a secondary tension wave which spreads in all directions with the velocity of sound in water, and at any moment the pressure at a given point in the water is the algebraic sum of the pressure that would exist if the gauge were absent and the tension due to the movement of the piston. What we have to find is the extent to which the pressure is relieved at the mouth of the piston hole; this can be approximately estimated as follows: under a steady pressure p, water is forced through an unobstructed aperture with a velocity—

$$V = \sqrt{\frac{2p}{\rho}}, \text{ or } V = 570\sqrt{p},$$

if V is expressed in feet per second and p in tons per square inch; conversely, if a piston is withdrawn into a gauge with velocity V the pressure at the mouth of the piston hole will be relieved by an amount $p = 31 \times 10^{-7} V^2$. In the example stated above V is only 50 feet per second, so that the relief of pressure is less than ·01 ton per square inch, which is too small to be of any consequence. Taking the whole range of the experiments the velocity of the pistons was generally of the order of 50 feet per second or less; in a few instances it was of the order of 100 feet per second, or even a little higher, but this was only when the driving pressure was very great, so that the relief of pressure was still proportionately small. It may be concluded therefore that the movement of the piston does not reduce the driving pressure in any serious degree. The above way of looking at the matter is only justified when the diameter of the piston is small compared with the thickness of wave measured by the gauge, as it always is in the present gauges; if the diameter of the piston were large compared with the thickness of wave measured by the gauge entirely different considerations would apply, and the effect of the velocity of the piston in reducing the pressure would be far greater.

In calculating the results given by the gauges the pistons are assumed to be rigid. This assumption is roughly justified by the fact that the time required for a pressure wave to travel from one end of the piston to the other is always very small compared with the time during which the piston is receiving momentum from the external pressure. The most unfavourable case is the GX gauge (Fig. 35) with $\frac{1}{4}$-inch pistons; in this case the time required for a pressure wave to travel from one end of the piston to the other is about four millionths of a second, while the time during which the piston is receiving momentum from the external pressure is of the order of 2×10^{-4} second, or 50 times as long. It is perhaps desirable to go into this matter a little more fully. The movement of the piston at any moment can be resolved into (1) a uniform movement of translation, with a momentum equal to the time-integral of the force that has acted on the end of the piston, and (2) a state of distributed momentum, of which

the algebraic sum for the whole piston is zero, corresponding to an oscillation which travels up and down in the piston. If pressure has been applied to the end of the piston long enough for a wave to travel up and down the piston a number of times, the second movement will be very small compared with the first. The energy of movement (2) is gradually dissipated, a small fraction being communicated at each oscillation to the water in contact with the exposed face of the piston, in which it produces alternate condensations and rarefactions, but this dissipation of energy does not involve any loss in the algebraic total momentum of the piston, which is entirely comprised in movement (1), and it is only this momentum that the gauge is required to measure.

When the pistons of a gauge are driven in, the air in the gauge is compressed and offers a certain resistance to the movement. It is necessary to show that this effect is negligible. As a typical example one may take the case of a GZ gauge with 1½-inch pistons; the volume of air in this gauge is 8 cubic inches; if the gauge is hung at a depth of 33 feet in the water the volume of air is reduced to 4 cubic inches; when the six pistons are driven in, the volume of air is further reduced to 3 cubic inches; if this second compression is assumed to take place adiabatically it absorbs 3·05 foot-pounds of energy; the greater part of this work, 2·45 foot-pounds, is supplied by the normal external hydrostatic pressure, and it is only the difference, 0·6 foot-pounds, that is taken from the kinetic energy of the pistons, amounting to a loss of 0·1 foot-pound by each piston; this is a very small fraction of the energy of the piston, which in practice was generally from 5 to 10 foot-pounds. In most cases the error due to the cushioning effect of the air was less than in the above example; it was generally smaller than 1 per cent.

When a gauge of the kind described in Section 18 is put more than 50 or 60 feet deep, the water inside the gauge rises above the tops of the pistons. The gauges can, however, be used at greater depths if a few pellets of lead-sodium alloy (6 parts of lead to 1 of sodium by weight) are dropped into the air-chamber. This alloy reacts with water to generate hydrogen, and so keeps the air-chamber full of gas. The same device was used with the gauges described in Section 19, when these were at a depth of more than 40 feet.

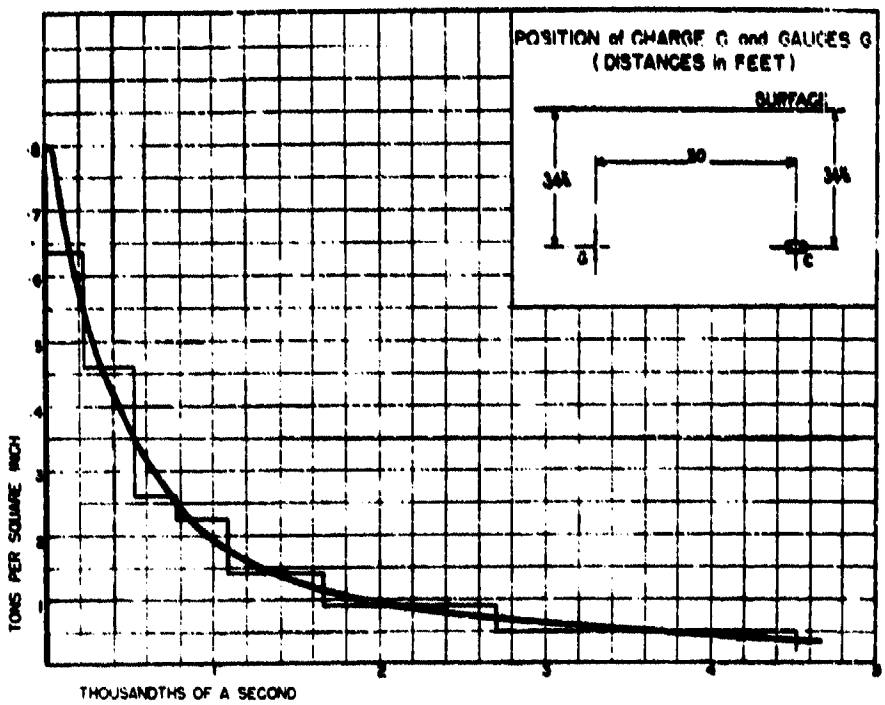


Fig. 1. 300 lbs. of 40/60 Amatol (D, Table VIII.); average of Shots 4, 8, 9, 29, 66; gauges 50 feet from centre of charge; maximum pressure = .80.

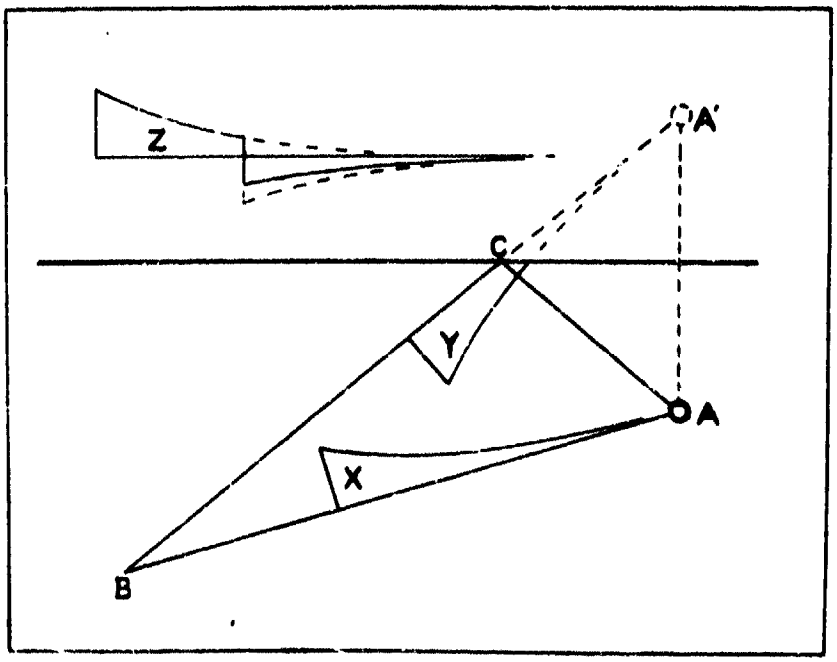


Fig. 2. Diagram illustrating the effect of the tension wave reflected from the surface.

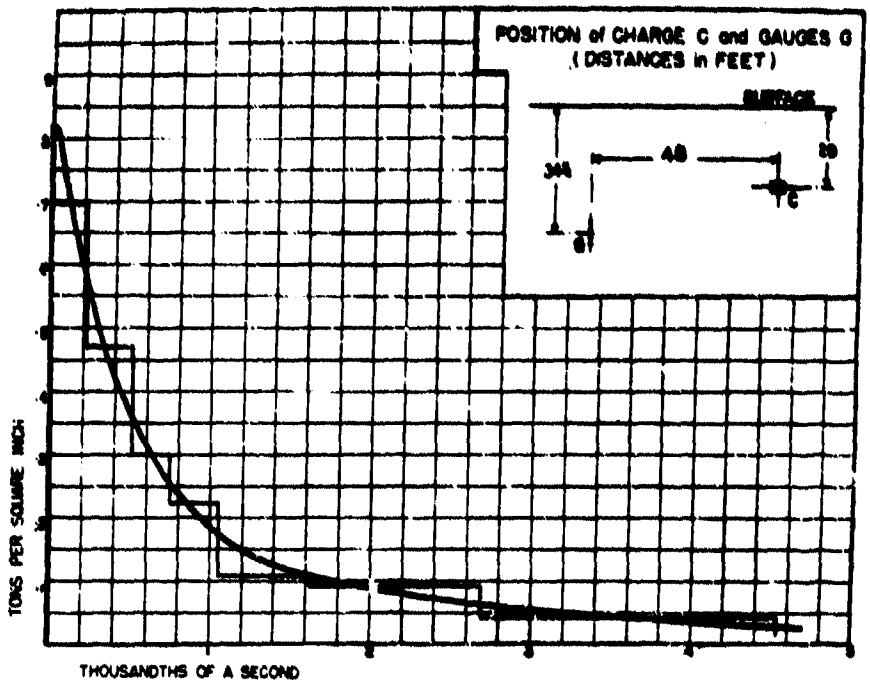


Fig. 3. 300 lbs. of 40/60 Amatol (D, Table VIII.); average of Shots 44, 45; charge not so deep as in Fig. 1; gauges 50 feet from centre of charge; maximum pressure = .82.

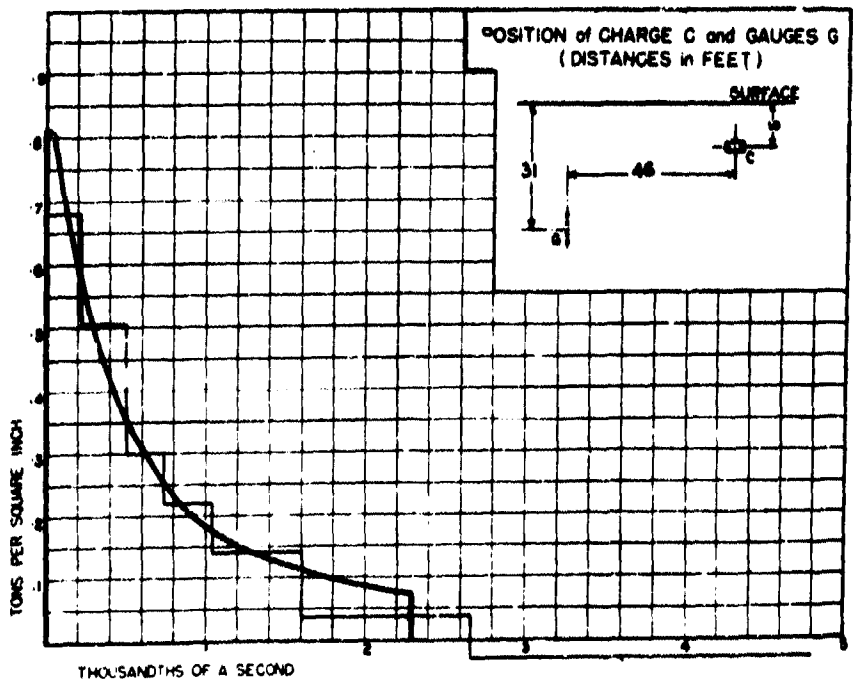


Fig. 4. 300 lbs. of 40/60 Amatol (D, Table VIII.), average of Shots 14, 61, 72, 74, 82; charge not so deep as in Fig. 3; gauges 50 feet from centre of charge; maximum pressure = .82.

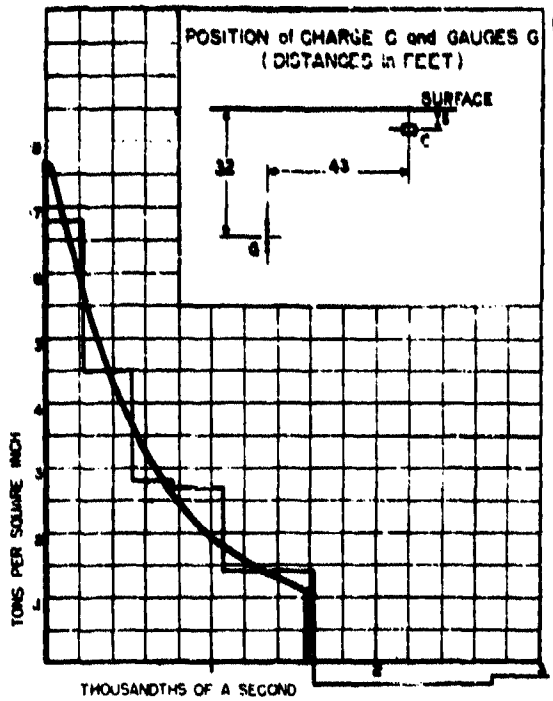


Fig. 5. 300 lbs. of 40/60 Amatol (D, Table VIII.); average of Shots 15, 97, 99; charge still shallower than in Fig. 4; gauges 50 feet from centre of charge; maximum pressure = .77.

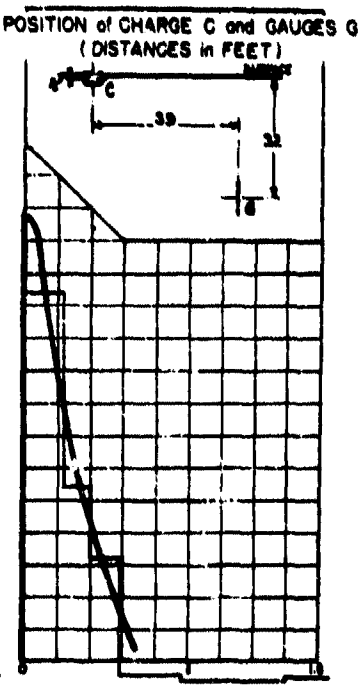


Fig. 6. 300 lbs. of 40/60 Amatol (D, Table VIII.); from Shot 64; charge on surface; gauges 50 feet from centre of charge; maximum pressure = .68.

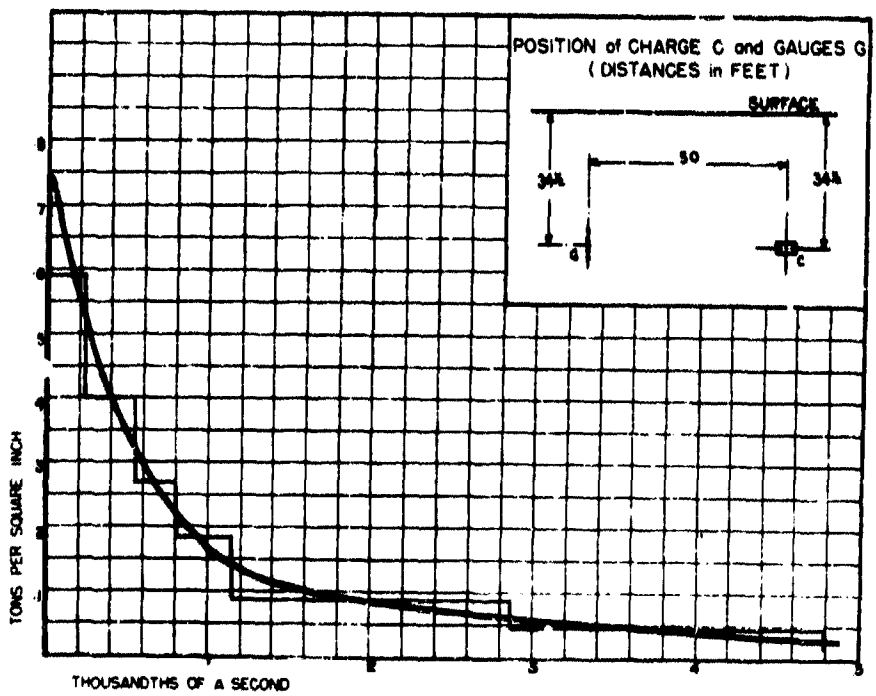


Fig. 7. 401 lbs. of 80/20 Amatol (IX, Table VIII.); average of Shots 27, 28, 30, 38; gauges 50 feet from centre of charge; maximum pressure = .74.

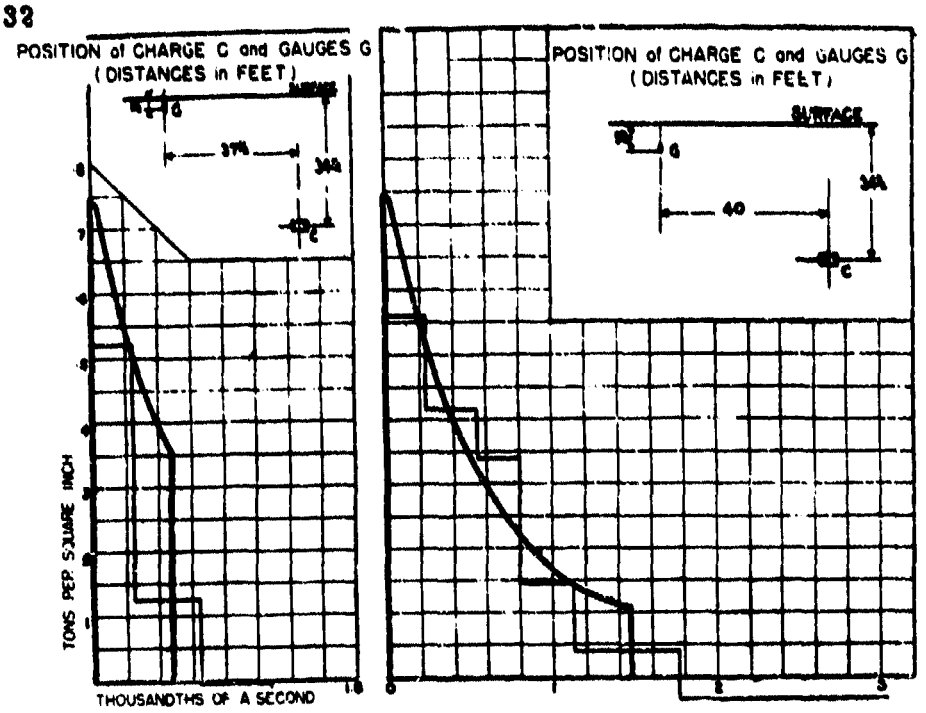


Fig. 8. 267 lbs. of 80/20 Amatol (DX, Table VIII.); Shot 38; gauges 50 feet from centre of charge and just below surface; the rectangular steps show the experimental results, the curve represents the effect predicted by theory.

Fig. 10. 267 lbs. of 80/20 Amatol (DX, Table VIII.); Shot 27; gauges 50 feet from centre of charge and deeper than in Fig. 9; the rectangular steps show the experimental results, the curve represents the effect predicted by theory.

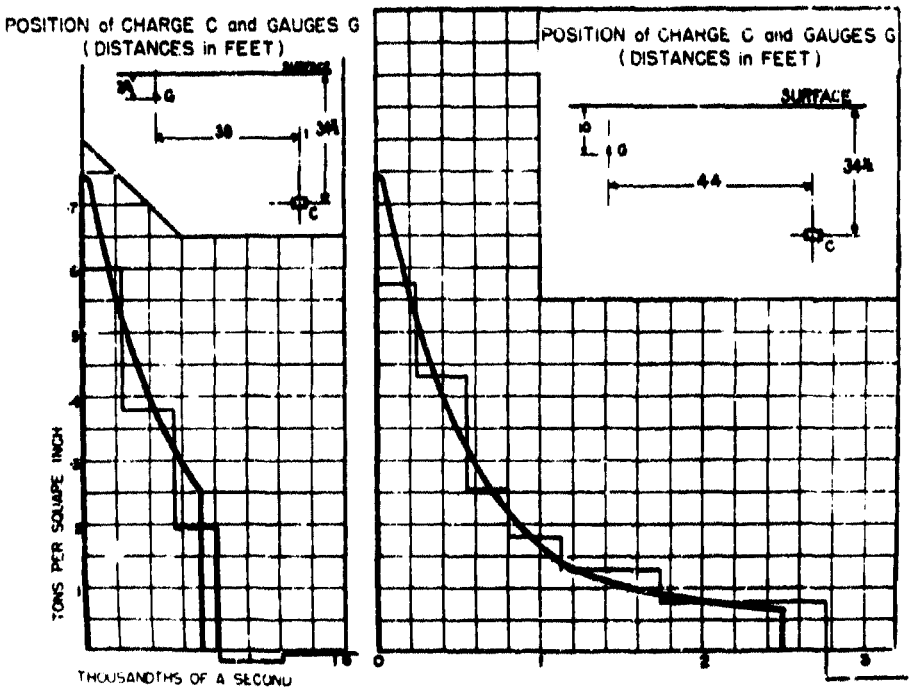


Fig. 9. 267 lbs. of 80/20 Amatol (DX, Table VIII.); Shot 28; gauges 50 feet from centre of charge and a little deeper than in Fig. 8; the rectangular steps show the experimental results, the curve represents the effect predicted by theory

Fig. 11. 267 lbs. of 80/20 Amatol (DX, Table VIII.); Shot 30; gauges 50 feet from centre of charge and deeper than in Fig. 10 but not so deep as in Fig. 7; the rectangular steps show the experimental results, the curve represents the effect predicted by theory.

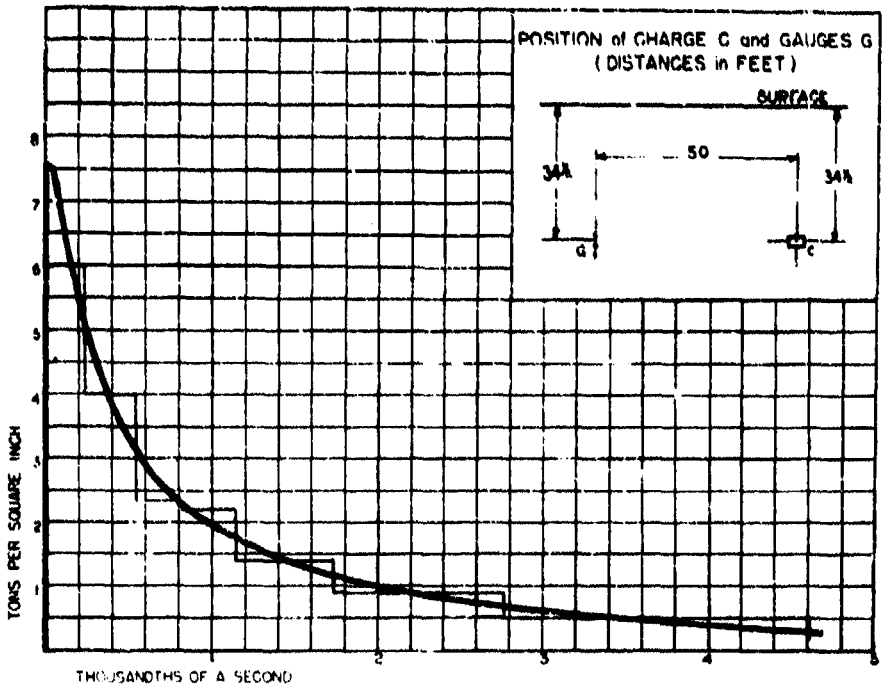


Fig. 12. 300 lbs. of T.N.T. (AD, Table VIII.); average of Shots 11, 17, 25; gauges 50 feet from centre of charge; maximum pressure = .76.

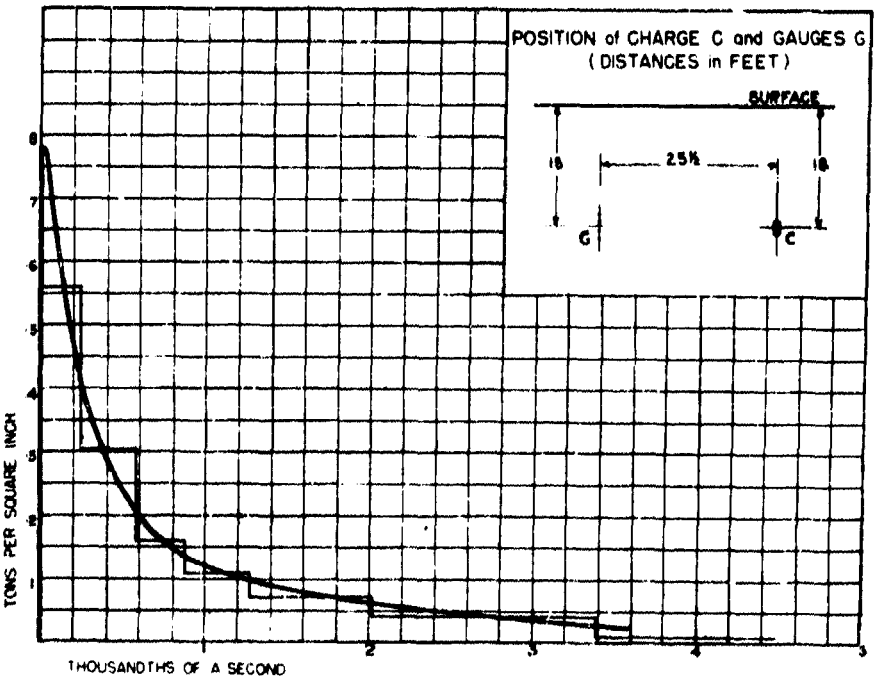


Fig. 13. 40 lbs. of 40/60 Amatol (G, Table VIII.); average of Shots 34, 35, 62, 65, 68; gauges 25 1/2 feet from centre of charge; maximum pressure = .78.

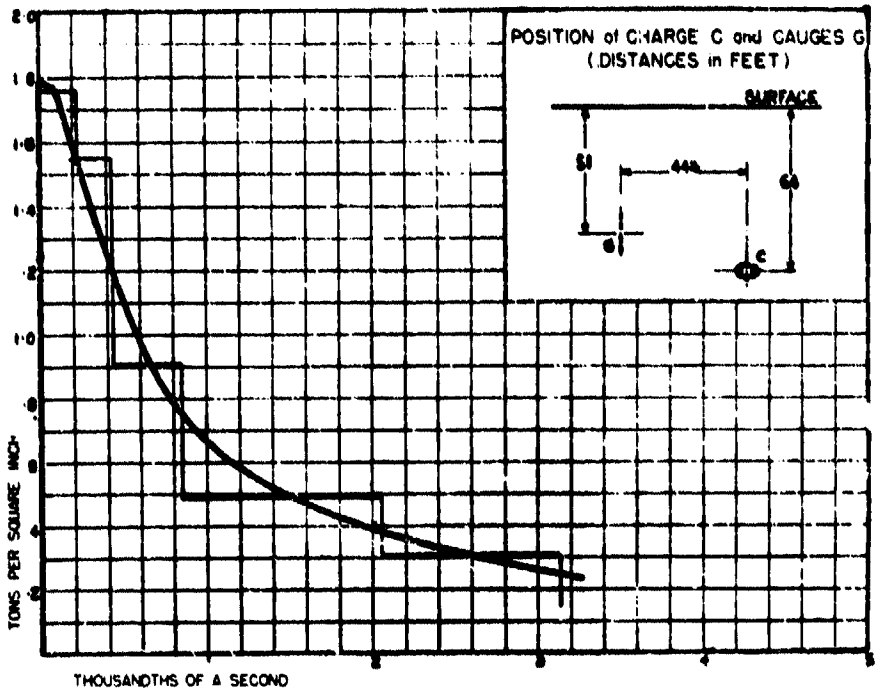


Fig. 14. 1900 lbs. of 50/50 Amatol (X4, Table VIII.); average of Shots 88, 90; gauges .6 1/4 feet from centre of charge; maximum pressure = 1.77.

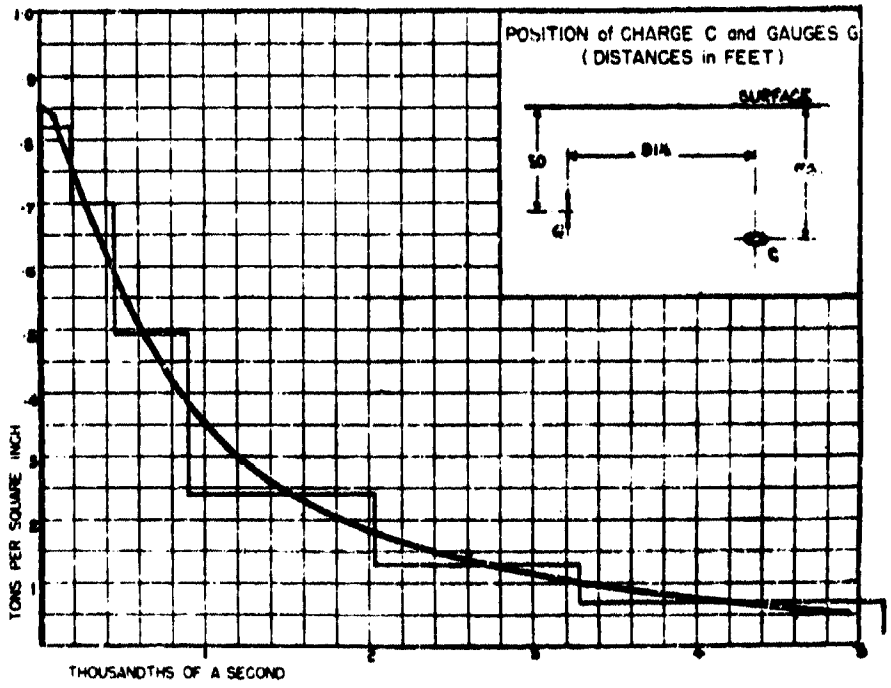


Fig. 15. 1900 lbs. of 50/50 Amatol (X4, Table VIII.); average of Shots 88, 90; gauges 92 1/2 feet from centre of charge; maximum pressure = .85.

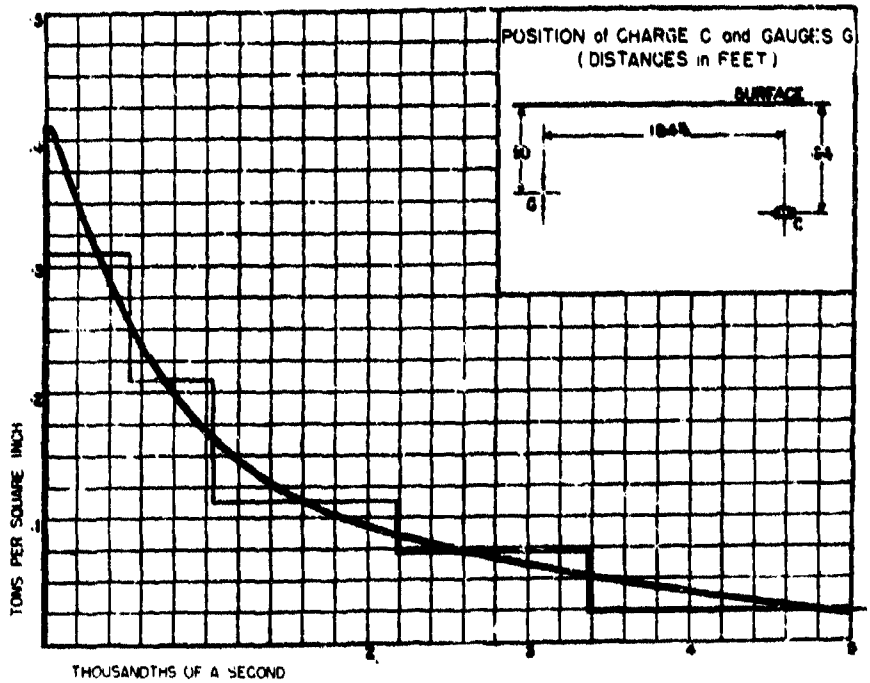


Fig. 16. 1,950 lbs. of 50/50 Amatol (X4, Table VIII.); average of Shots 88, 90; gauges 185 feet from centre of charge.

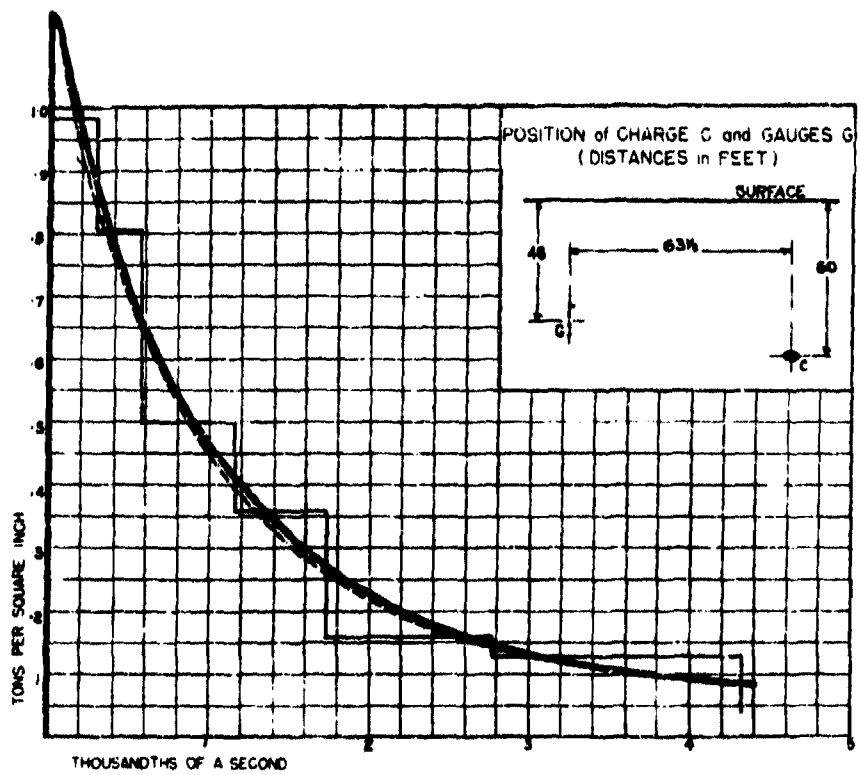


Fig. 17. 1,600 lbs. of 80/20 Amatol (X5, Table VIII.), average of Shots 85, 86, 87; gauges 63 1/2 feet from centre of charge; maximum pressure = 1.15; the broken line shows the curve for this size of charge at this distance predicted from the curve in Fig. 7.

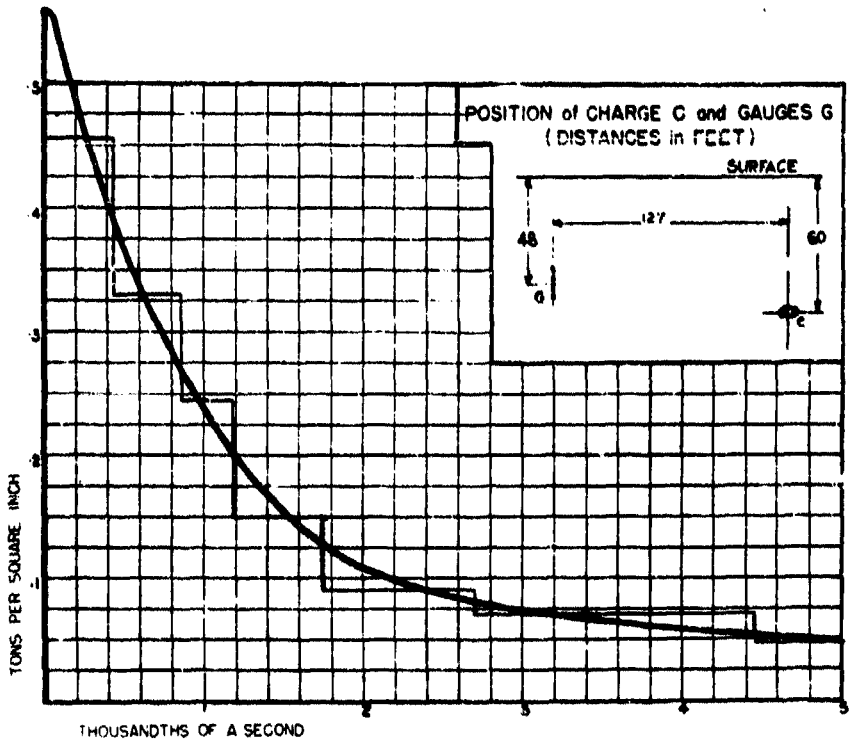


Fig. 18. 1600 lbs. of 80/20 Amatol (X5, Table VIII.); average of Shots 85, 86, 87; gauges 127 feet from centre of charge; maximum pressure = .56.

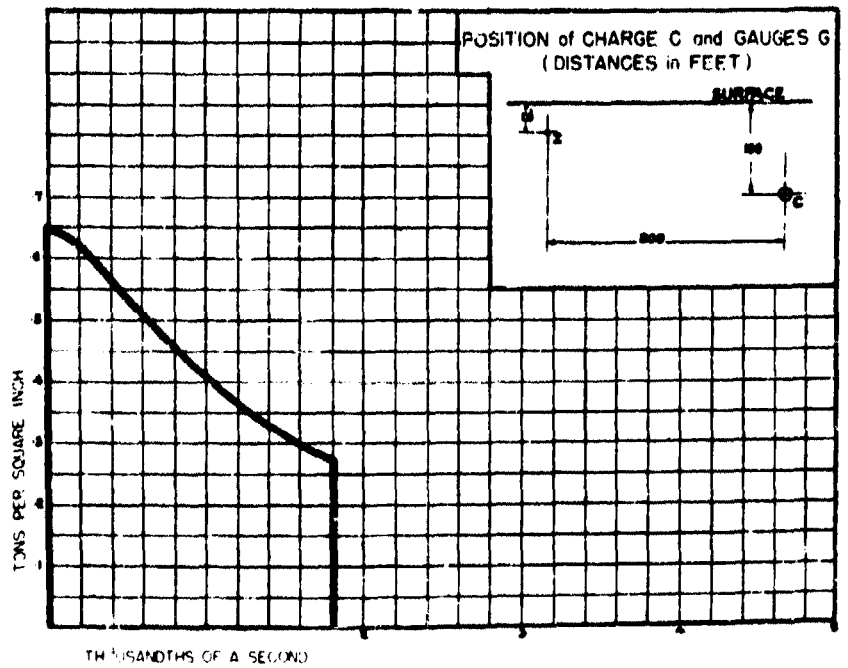


Fig. 19. Calculated effect of a 5 ton charge of 50/50 Amatol under the conditions shown in the inset diagram, the pressure being taken at the point G.

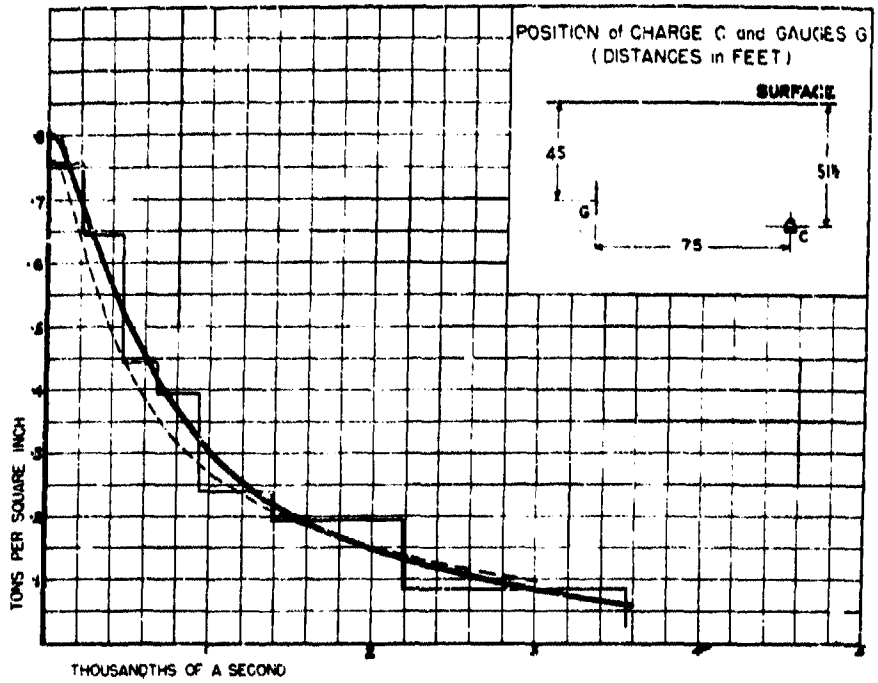


Fig. 20. 1,000 lbs. of T.N.T. (M, Table VIII.); average of Shots 32, 33, 55, 59; gauges 75 feet from centre of charge; maximum pressure = .80; the broken line shows the curve for this size of charge at this distance predicted from the curve in Fig. 12.

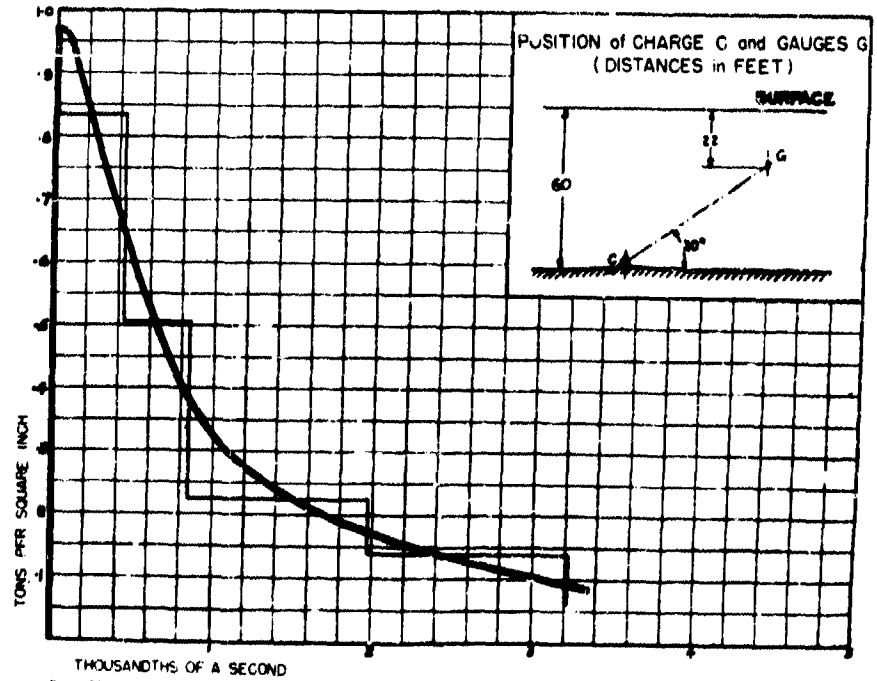


Fig. 21. 1,000 lbs. of T.N.T. (M, Teble VIII.) on the bottom; Shot 75; gauges 75 feet from centre of charge: maximum pressure = .97.

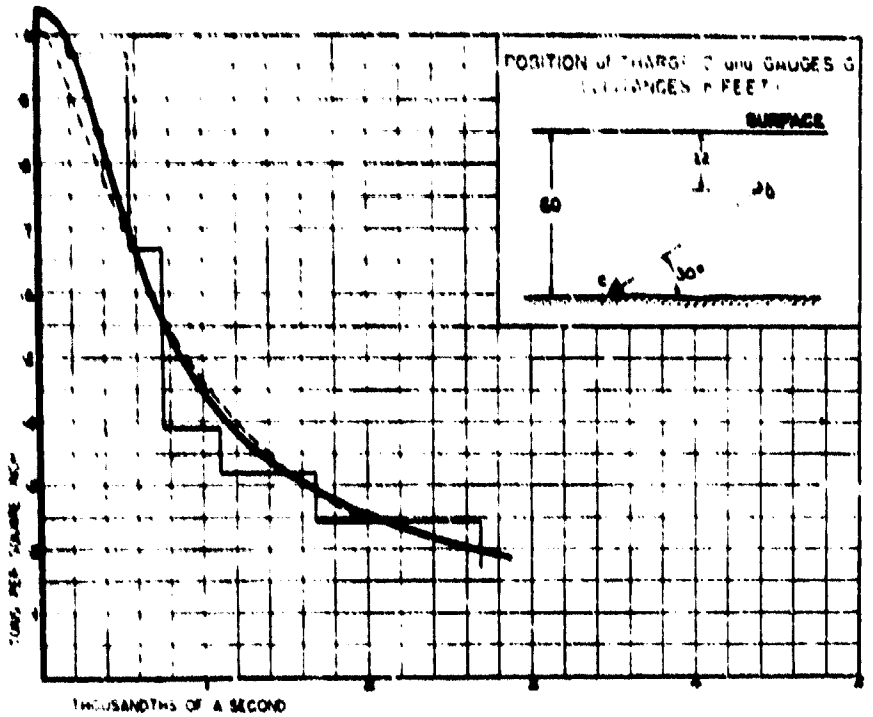


Fig. 22. 1,000 lbs. of T.N.T. (M, Table VIII.) on the bottom: Shot 78; gauges 75 feet from centre of charge. Maximum pressure = 1.33; the broken line shows the effect of a 2,000 lb. charge of T.N.T., in mid-water, at the same distance, calculated from the curve in Fig. 23.

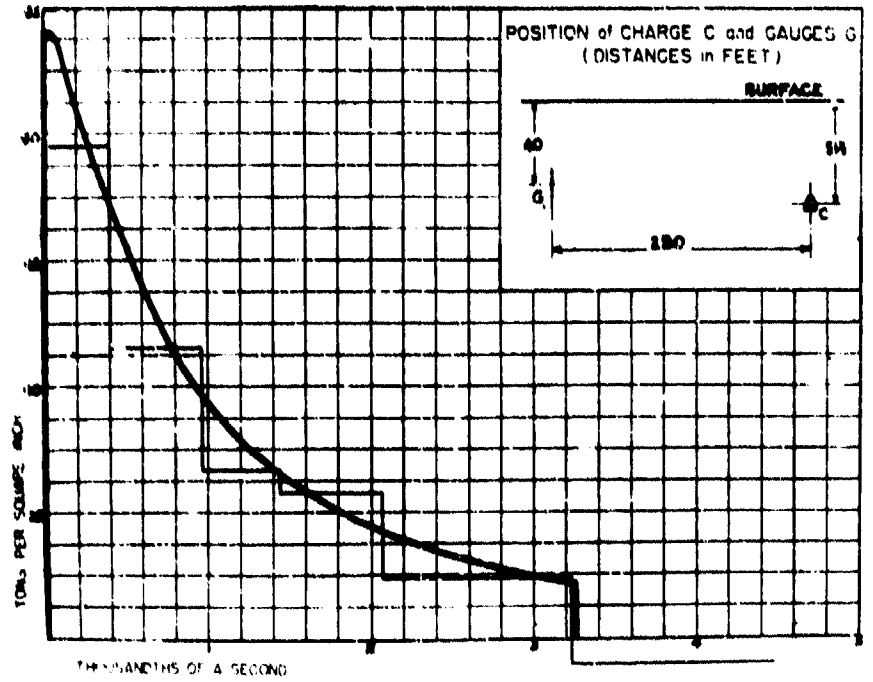


Fig. 23. 1,000 lbs. of T.N.T. (M, Table VIII.); Shot 95; gauges 250 feet from centre of charge; the rectangular steps show the experimental results, the curve represents the effect predicted by theory.

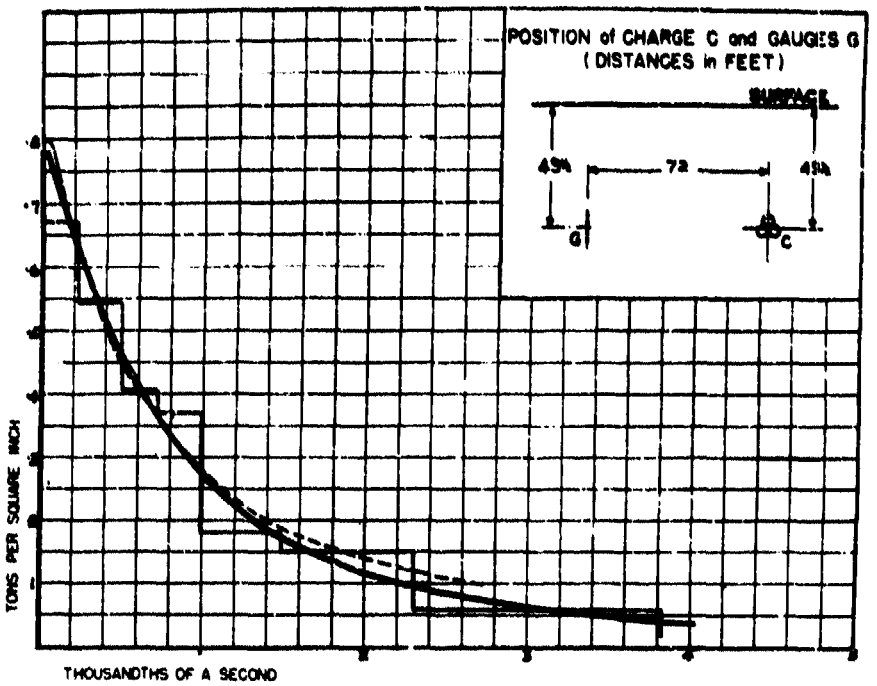


Fig. 24. Three 300 lb. charges of 40/60 Amatol lashed together in a bunch (X2, Table VIII.); average of Shots 50, 58; gauges 72 feet from centre of charge; maximum pressure = .78; the broken line shows the effect of a single 900 lb. charge, at the same distance, calculated from the curve in Fig. 1.

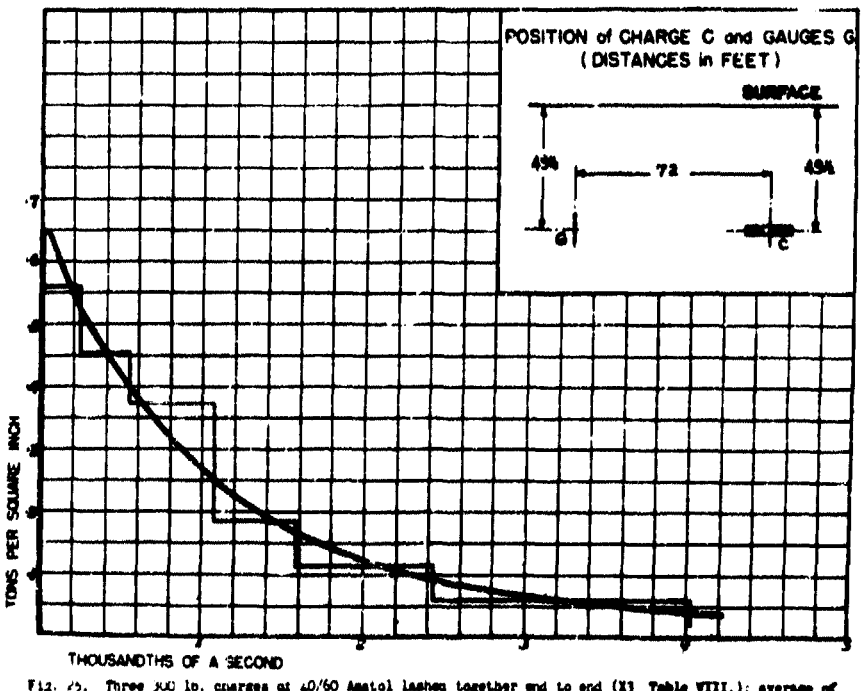


Fig. 25. Three 300 lb. charges at 40/60 Amatol lashed together end to end (X3 Table VIII.); average of Shots 61, 63; gauges 72 feet from centre of charge and in the direction of the length of the charge from the primed end towards the unprimed end; maximum pressure = .65.

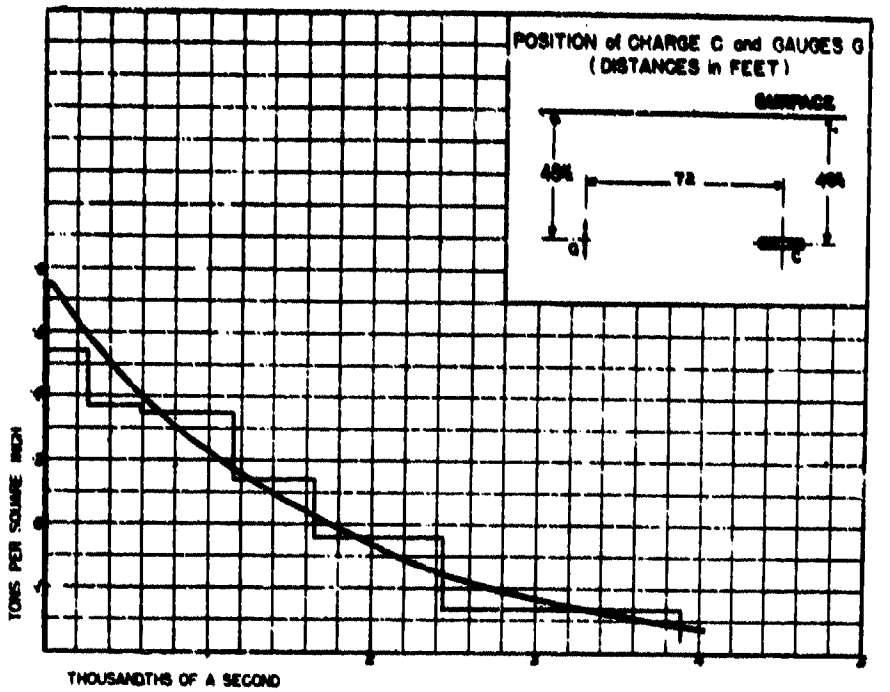


Fig. 26. Three 300 lb. charges of 40/60 Amtol lashed together end to end (X), Table VIII.); average of Shots 81, 83; gauges 72 feet from centre of charge and in the direction of the length of the charge from the unprimed end towards the primed end; maximum pressure = .58.

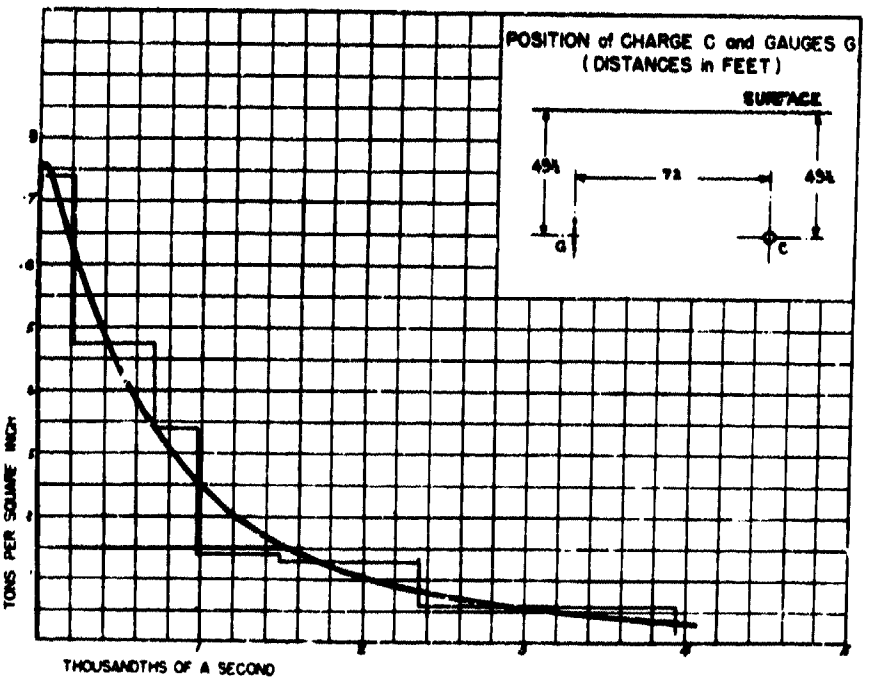


Fig. 27. Three 300 lb. charges of 40/60 Amtol lashed together end to end (X), Table VIII.); average of Shots 81, 83; gauges 72 feet from centre of charge and in a direction at right angles to the length of the charge; maximum pressure = .75.

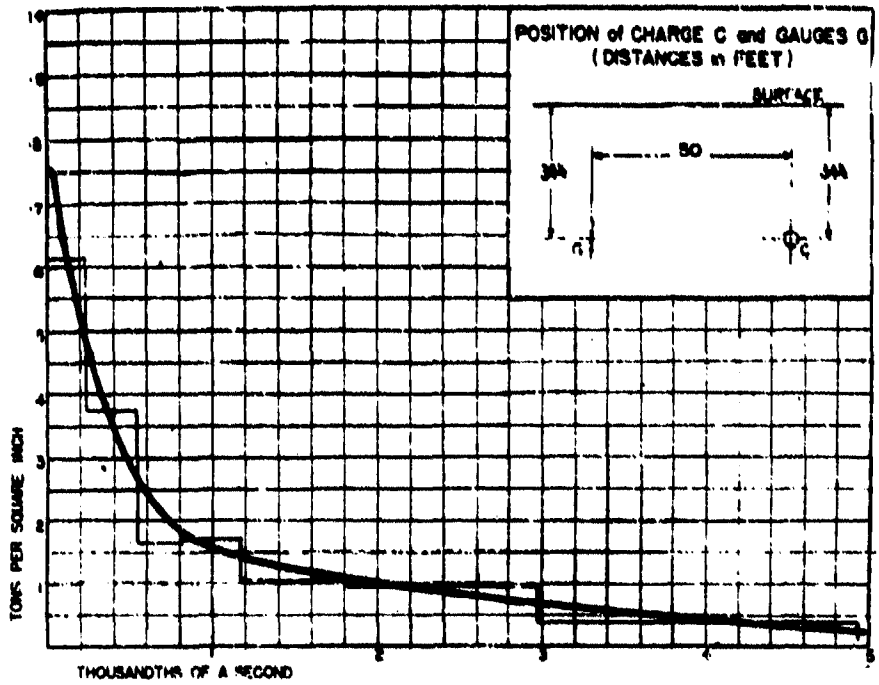


Fig. 28. 320 lbs. of 40/60 Amatol surrounded by an air chamber (M2, Table VIII.); average of Shots 20, 49, 53, 57; gauges 50 feet from centre of charge; maximum pressure = .76.

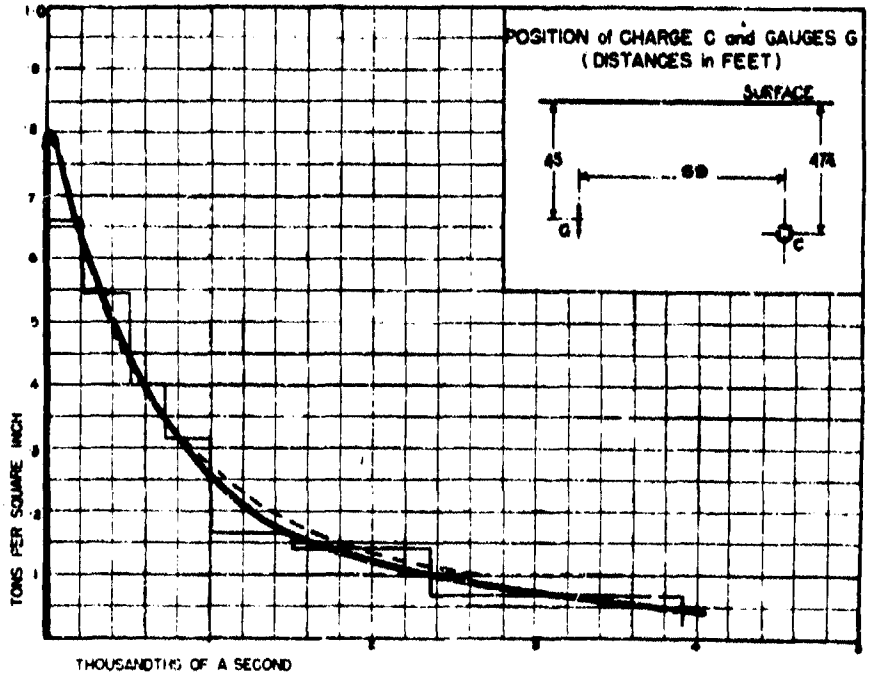


Fig. 29. 820 lbs. of 40/60 Amatol (X7, Table VIII); average of Shots 35, 37, 48, 52; gauges 59 feet from centre of charge; maximum pressure = .79; the broken line shows the effect of an 820 lb. charge at this distance calculated from the curve in Fig. 1.

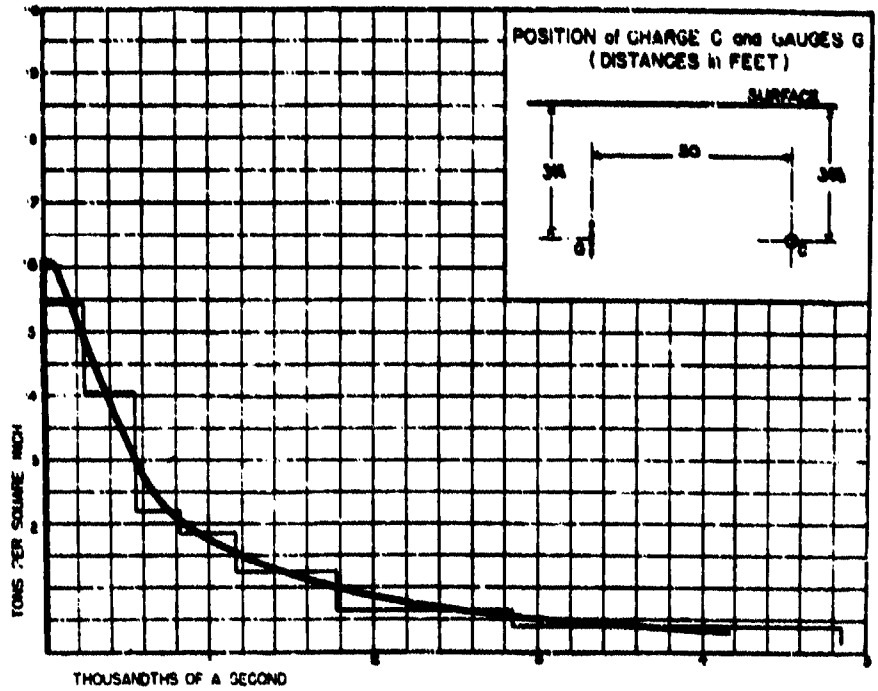


Fig. 30. 312 lbs. of wet guncotton surrounded by an air chamber (X9, Table VIII.); average of Shots 60, 63, 67; gauges 50 feet from centre of charge; maximum pressure = .61.

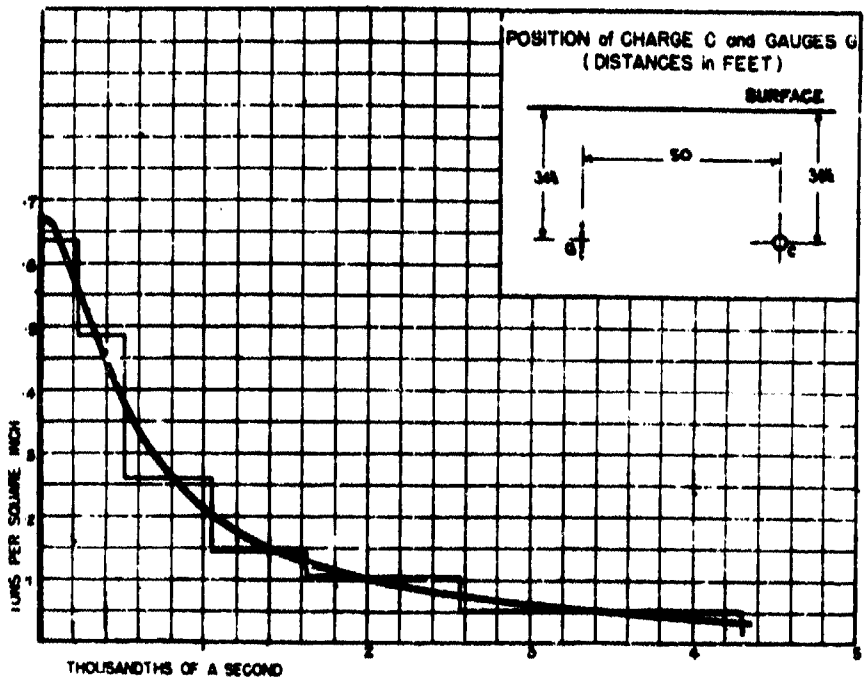


Fig. 31. 272 lbs. of R.D. No. 30 Mixture (Ammonium perchlorate 78, aluminium powder 6, paraffin wax 16) surrounded by an air chamber (X8, Table VIII.); average of Shots 69, 71, 94; gauges 50 feet from centre of charge; maximum pressure = .57.

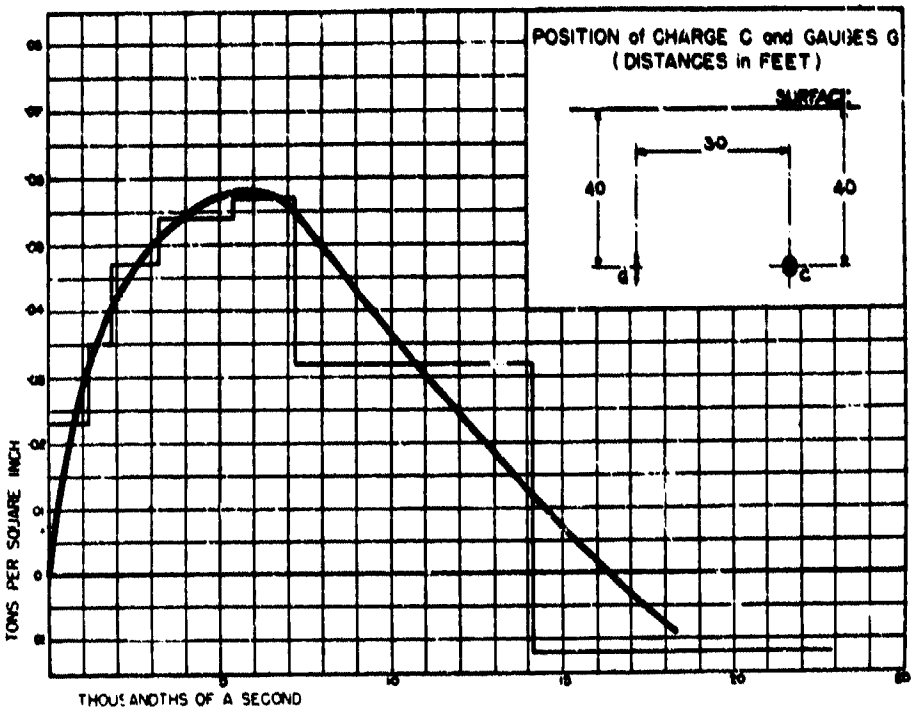


Fig. 32. 500 lbs. of gunpowder (X6, Table VIII.); average of Shots 92, 93; gauges 30 feet from centre of charge.

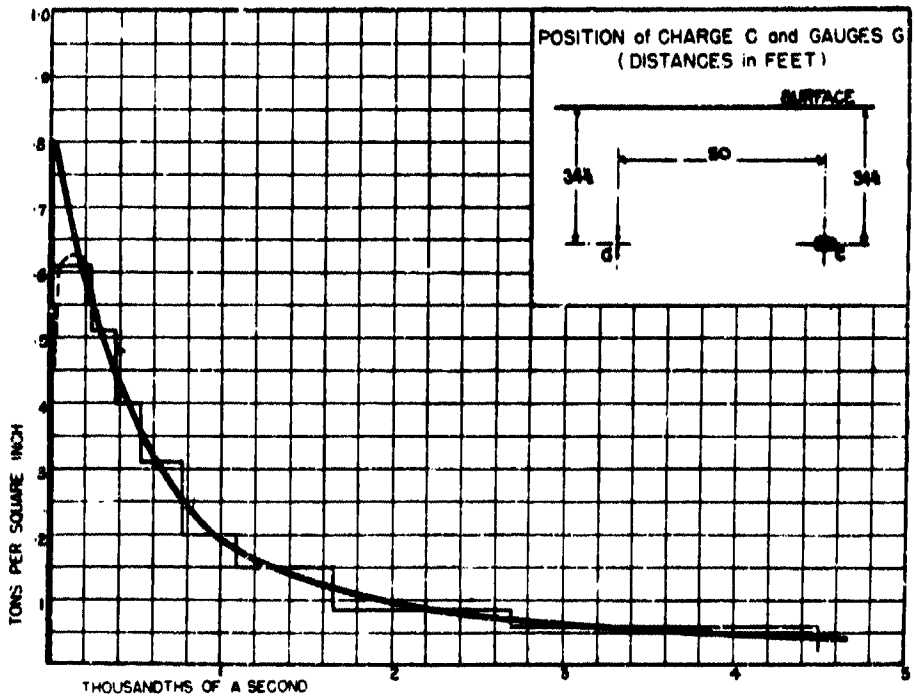


Fig. 33. 300 lbs. of 40/60 Amatol (D, Table VIII.); Shot 4; gauges 50 feet from centre of charge.

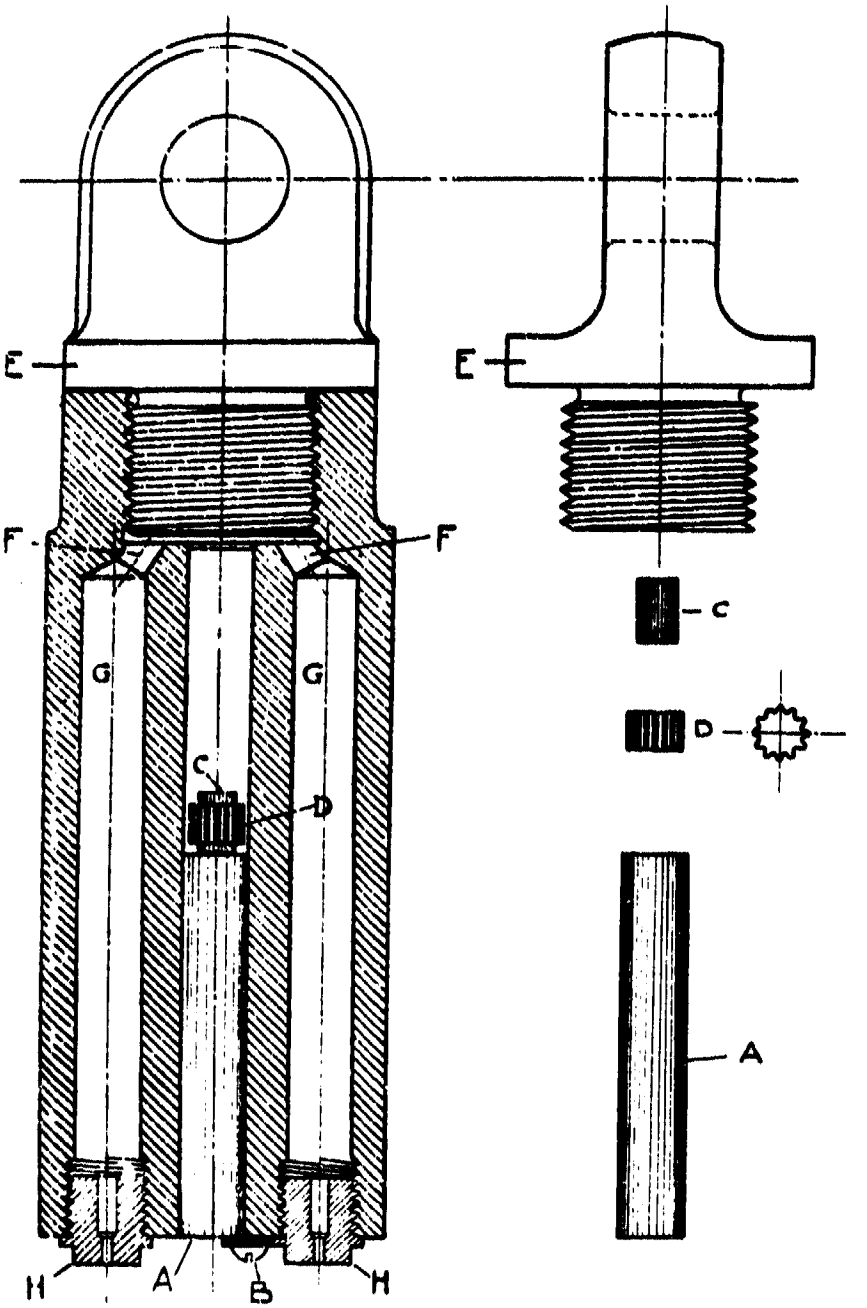


Fig. 34

G gauge; A, piston of tool steel, hardened and tempered blue and ground to size, with sharp edges removed, length 3 inches, diameter .498 inch; this piston works in a central 1/2-inch hole must both be cleaned quite free from oil before use: B, screw and two steel washers (No. 7 BA) projecting 1/32 inch over piston hole to support piston; C, annealed copper cylinder, .5 inch long, .32 inch diameter; D, corrugated jacket made from sheet brass .004 inch thick, length 5/16 inch, internal diameter 5/16 inch, external diameter 7/16 inch; in addition to centering the coppers, these jackets serve to attach paper slips printed with identification numbers; when expanded by use these jackets are restored to size by passing through a cone; E, eyebolt, which acts as an anvil; when this is screwed home its face is 5 1/2 inches from the bottom of the gauge; F, air-tunnels 1/4-inch diameter, communicating with G, four holes, 5 inches long, 1/2 inch diameter, closed at the bottom by H, screw stoppers, each pierced by an aperture, 1/16 inch diameter, through which water enters until the internal and external pressures are equal. The body of the gauge is of mild steel, the eyebolt of tool steel.

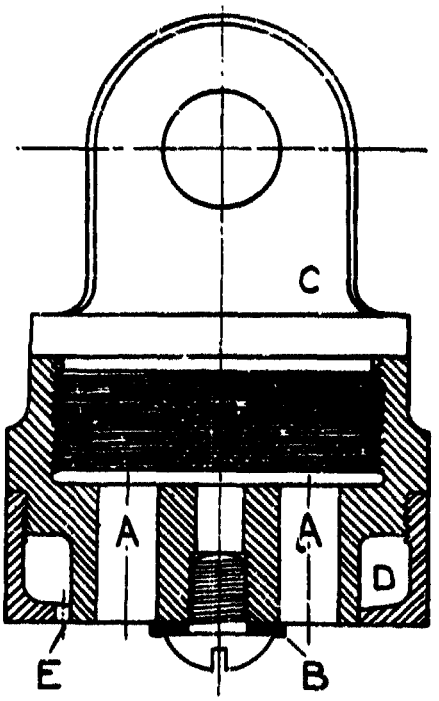
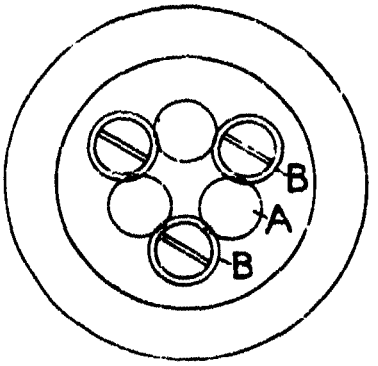


Fig. 35

GX, CY and GZ gauges; A, six piston holes, 1/2 inch diameter; B, self-centreing steel washer, overlapping all the piston holes 1/32 inch; C, eyebolt; the anvil face is 1.3 inches from the bottom of the gauge; D, annular air-chamber, 5/8 inch from top to bottom, 13/32 inch from inner to outer radius; this chamber communicates with the space below the anvil by six tunnels, 1/4 inch diameter, which are staggered between the piston holes; E, aperture, 1/8 inch diameter, for admitting water to the air-chamber. The foregoing dimensions refer to the GX gauge, which is shown in the figure; the GY and GZ gauges are similar but longer, differing only in the following dimensions--in the GY gauge the air chamber is 7/8 inch from top to bottom and the anvil face is 2 inches from the bottom of the gauge; in the GZ gauge these two dimensions are 1 5/8 inch and 3 inches respectively. The pistons used in the GA gauge are 3/4 inch or 21/32 inch long; in the GY gauge 1 11/32 inch or 1 5/32 inch; in the GZ gauge 2 1/8 inch or 1 5/8 inch. Except as regards length, the pistons are similar to those used in the G gauge, Fig. 34.



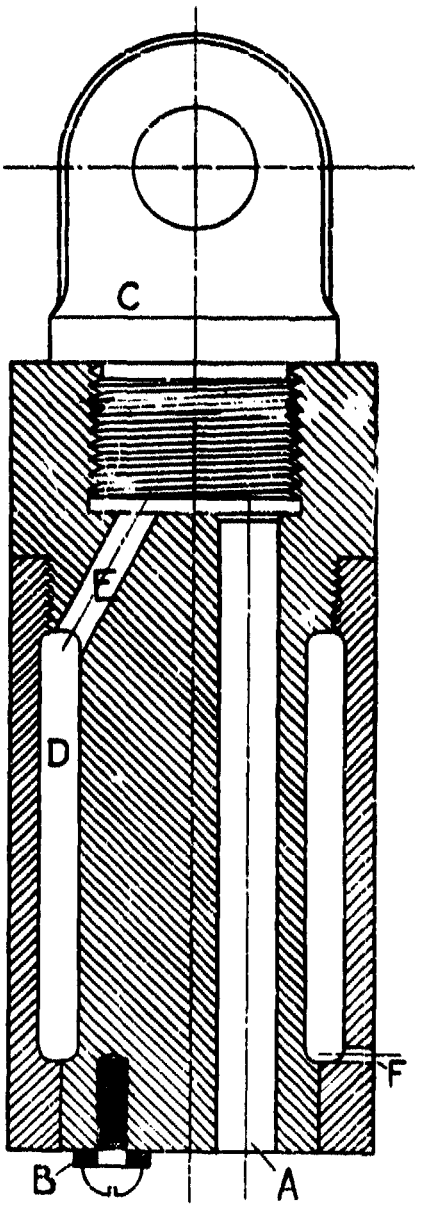
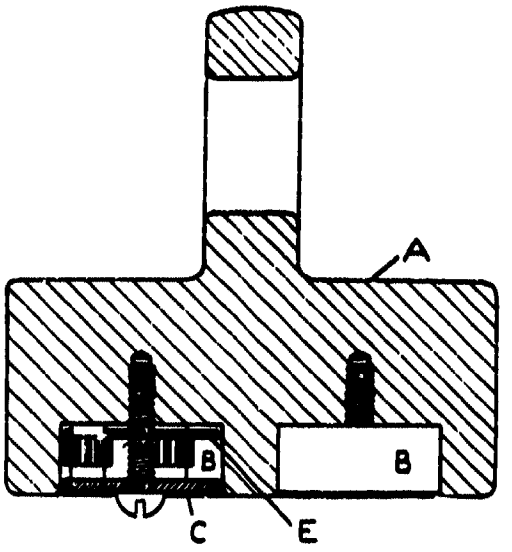
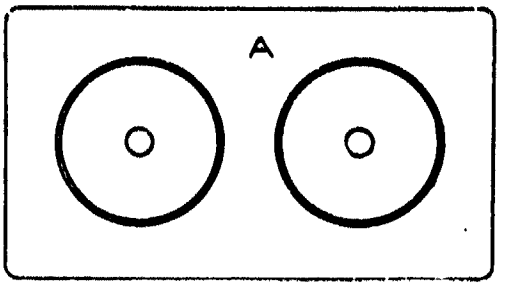


Fig. 36

GA and GB gauges; A, three piston holes, 1/2 inch diameter; B, three pairs of steel washers (No. 0 BA), each pair positioned to overlap two adjacent piston holes 1/50 inch; C, eyebolt; the anvil face is 5 1/2 inches from the bottom of the gauge; D, annular air-chamber, 3 5/8 inches from top to bottom, 5/16 inch from inner to outer radius; E, three air tunnels, 5/16 inch diameter, staggered between the piston holes, connecting the air chamber with the space below the anvil; F, aperture, 1/8 inch diameter, for admitting water to the air chamber. The foregoing dimensions refer to the GA gauge, which is shown in the figure; the GB gauge is similar but longer, the air chamber being 9 inches from top to bottom, and the anvil face 10 3/4 inches from the bottom of the gauge; also, in the GB gauge, the air chamber has a central flange to guard against collapse of the outer wall under strong external pressure; this flange is mutilated to give ample air connexion between the upper and lower halves of the chamber; the pistons used in the GA gauge are 4 1/4 inches or 3 inches long, in the GB gauge 8 3/4 inches or 6 1/4 inches.





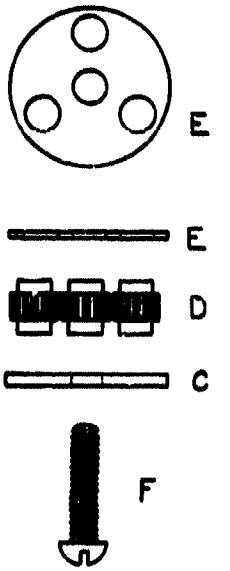


Fig. 37.
GF, GZ and GJ gauges; A, rectangular steel bed; B, two recesses, 1 1/2 inch diameter, .05 inch deep; C, steel steel plate, 1.498 inch diameter, 1/8 inch thick, with central 1/8 inch hole; D, three jacketed coppers (as in Fig. 34) in each recess; E, brass spacing plate, with three 23/64 inch holes on a 1 inch pitch circle for positioning the coppers; F, 1/4 inch steel screw, diameter of head 15/32 inch, for clamping the steel plate against the three coppers. The foregoing dimensions refer to the GF gauge, which is shown in the figure; the GZ gauge is similar but has plates 5/8 inch thick and recesses 1.15 inch deep; the GJ gauge has plates 1/8 inch thick, and a ring of 9 coppers in each of the two recesses, which are .9 inch deep.

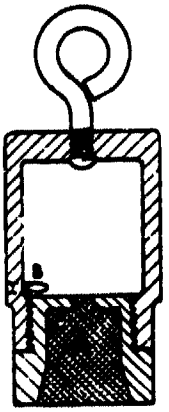


Fig. 38
Q, gauge; A, plasticine; B, oblique aperture, 1/16 inch diameter, for equalising internal and external pressure.

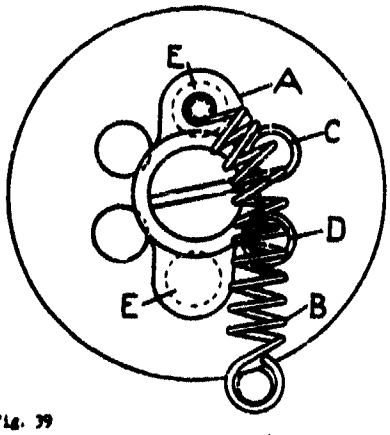


Fig. 39
GZ gauge modified for measuring the pressure wave reflected from the sea-bottom; the figure is a view of the bottom of the modified gauge.

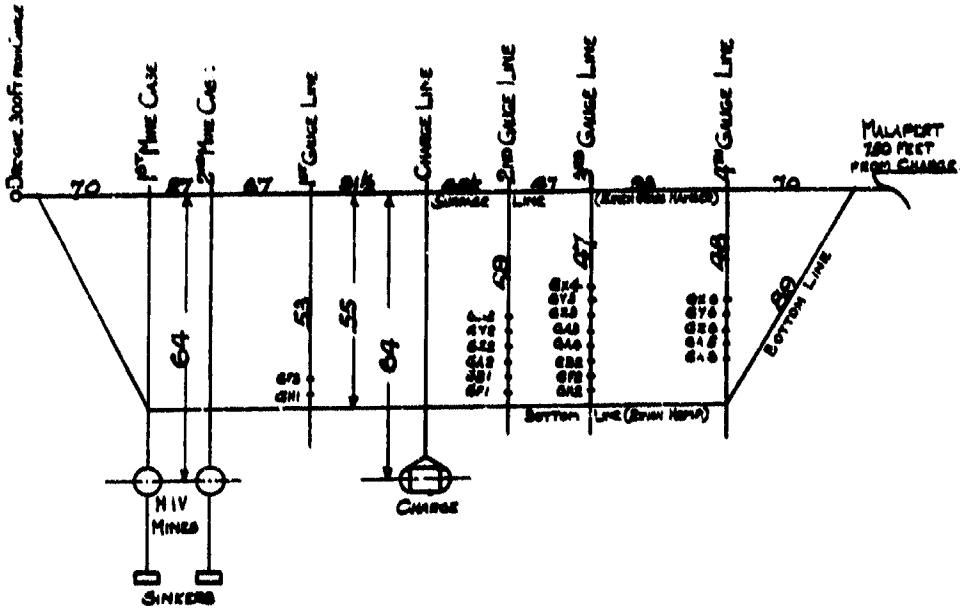


Fig. 40. Diagram showing the layout of Shots 88, 90 (1900 lbs. of 50/50 Amatol); all distances are marked in feet.

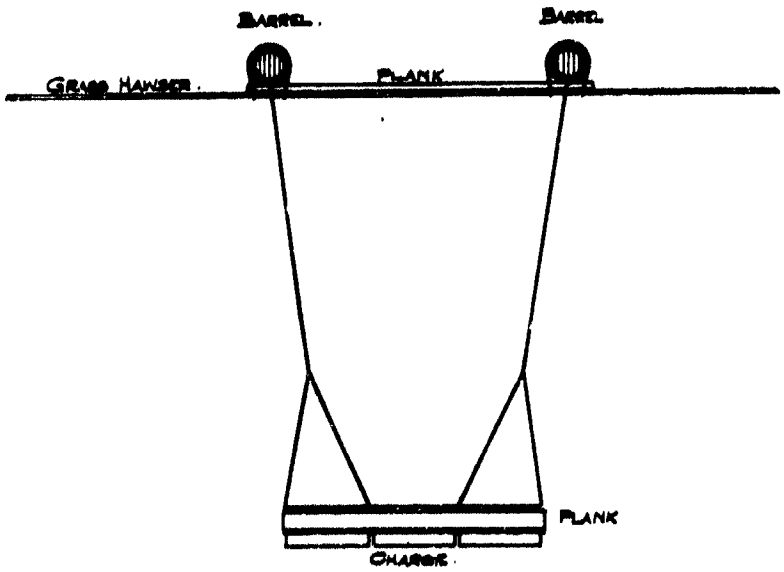


Fig. 41. Method of suspending a long charge (Shots 81, 83).

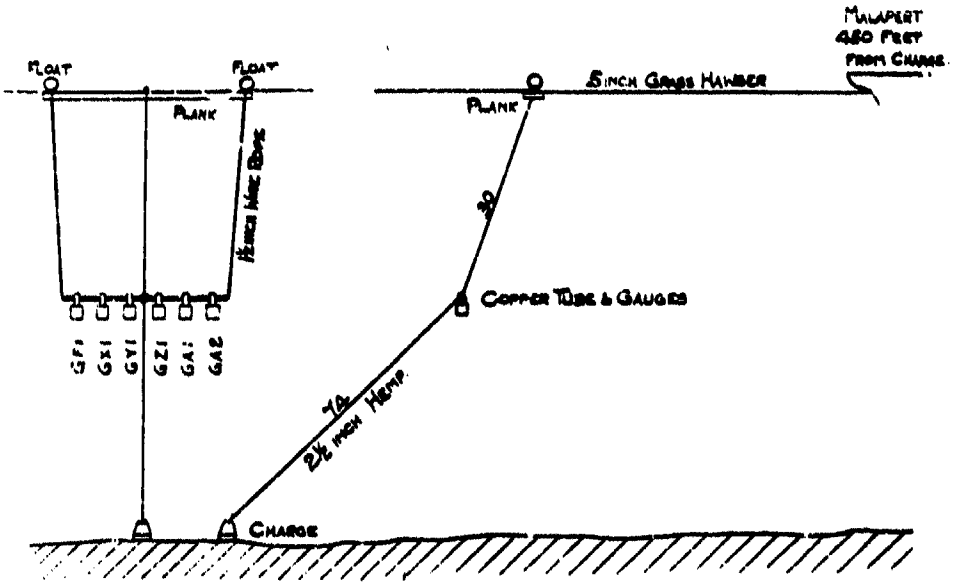


Fig 42. Diagram showing the layout of a bottom shot (Shots 75, 76, 78); all distances are marked in feet.

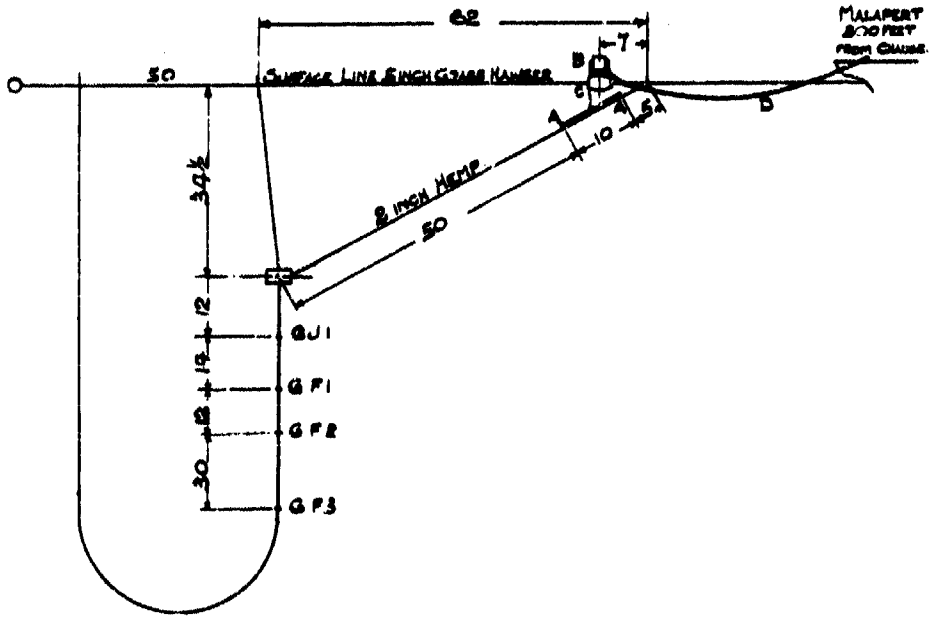


Fig. 43. Diagram showing the layout of Shot 105, for measuring the velocity of the pressure wave; A, A, contacts; B, water-tight box containing chronograph, etc.; C, raft consisting of a plank lashed across a pair of barrels; D, 4-wire cable from box to ship; all distances are marked in feet.

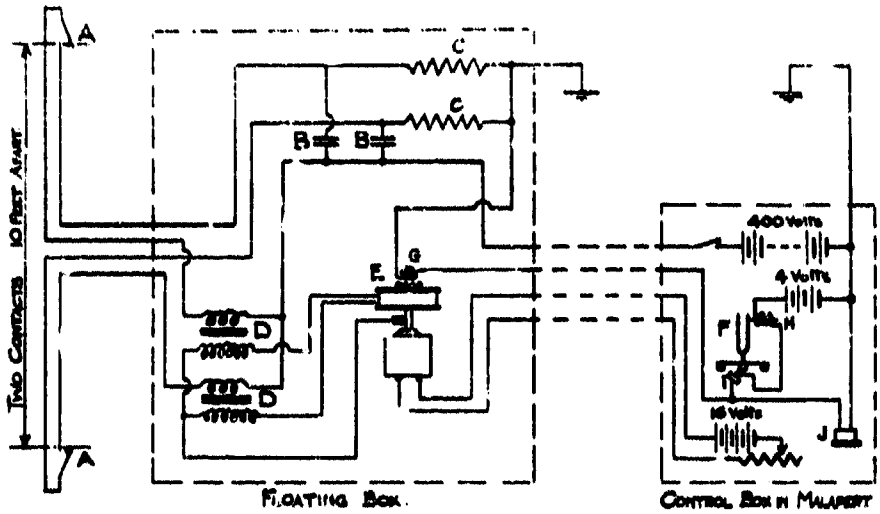


Fig. 44. Circuit arrangements of Shot 105 ; they are generally similar to those shown in Fig. 49.

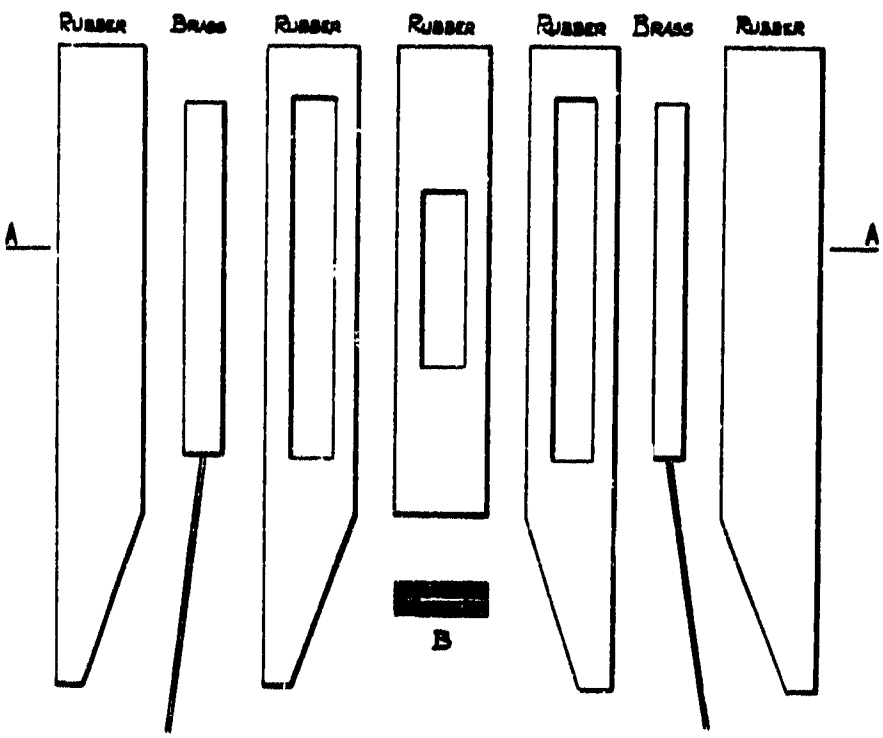


Fig. 48. Contact used in velocity measurements ; strips of brass and rubber were assembled in the order shown, the rubber strips being cemented together by painting them with naphtha ; B, is a section of the assembled contact on the line A, A, the thickness being much exaggerated ; actually the contact was about ¾ inch wide and 5/32 inch thick.

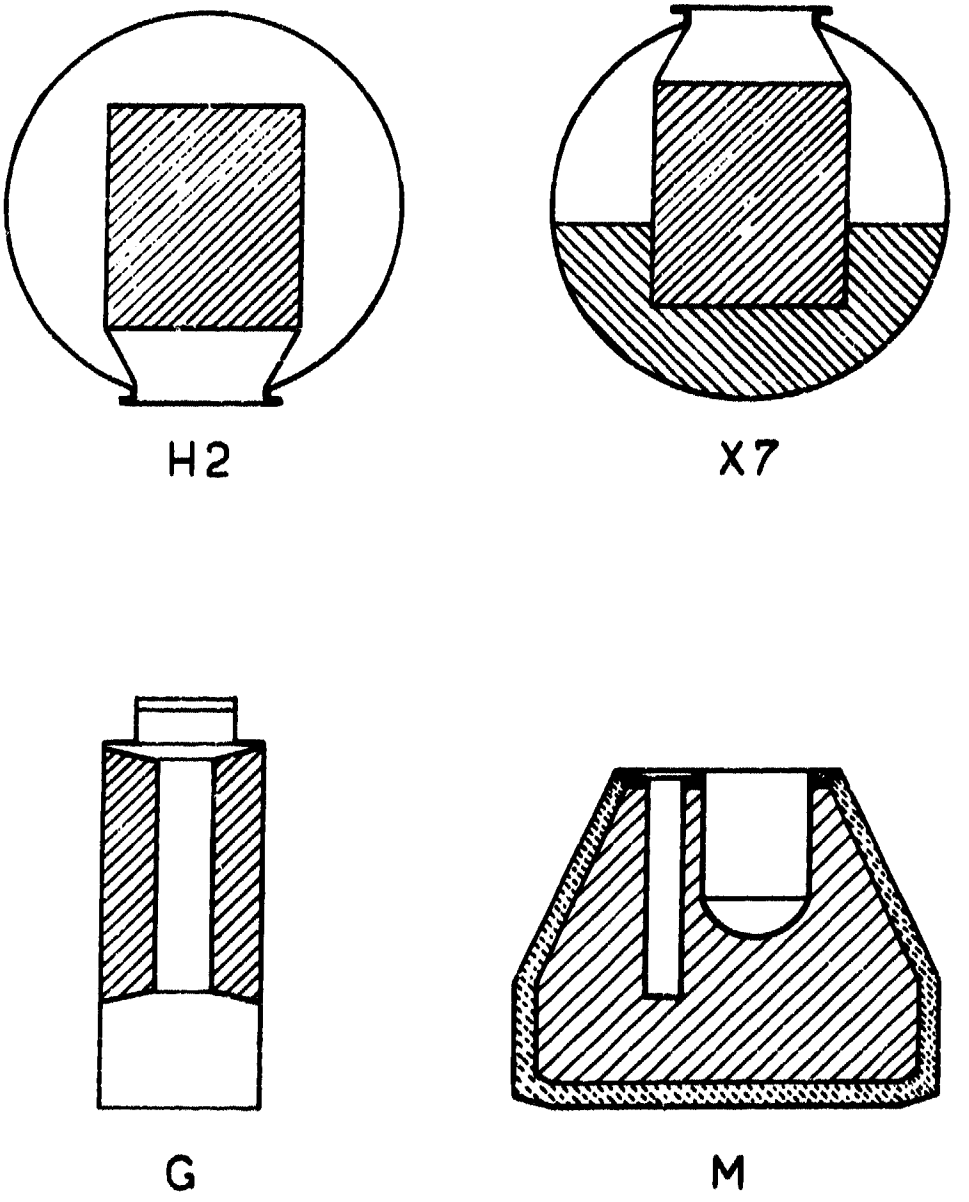


Fig. 46. Diagram showing the disposition of the explosive in some of the charges listed in Table VIII.

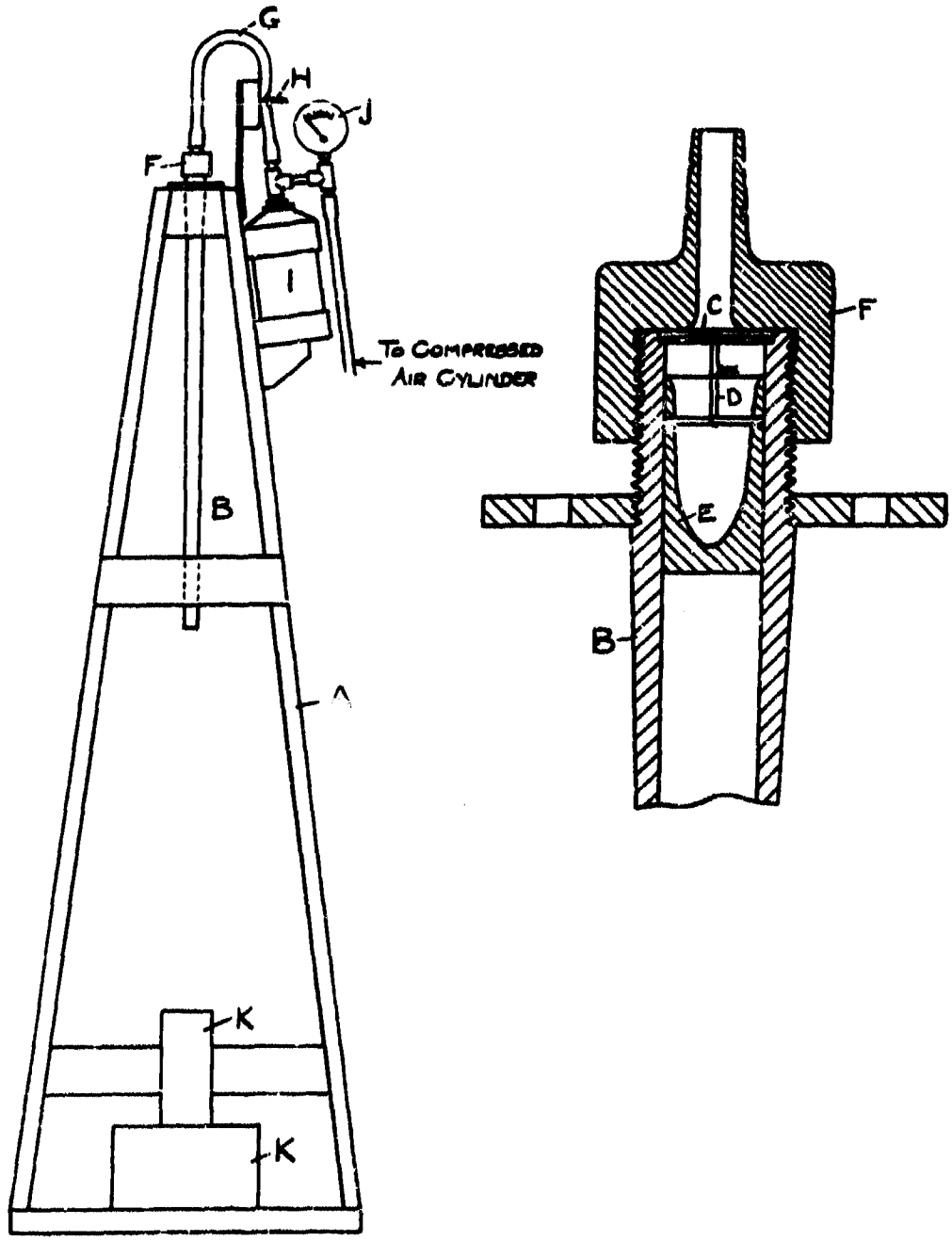
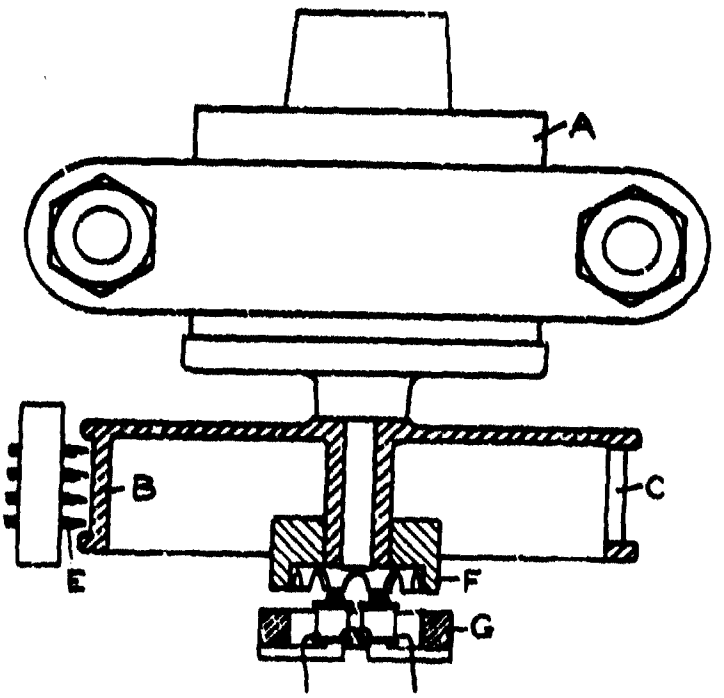


Fig. 47. Pneumatic gun; A, wooden frame; B, shot-gun barrel, 30 inches long, ·726 inch internal diameter; C, cross-pin; D, loop of fine wire; E, piston; F, screw-cap; G, rubber tube; H, pinch-valve; I, air reservoir, about 50 cubic inches; J, pressure gauge; K, anvil weighing 140 lbs.



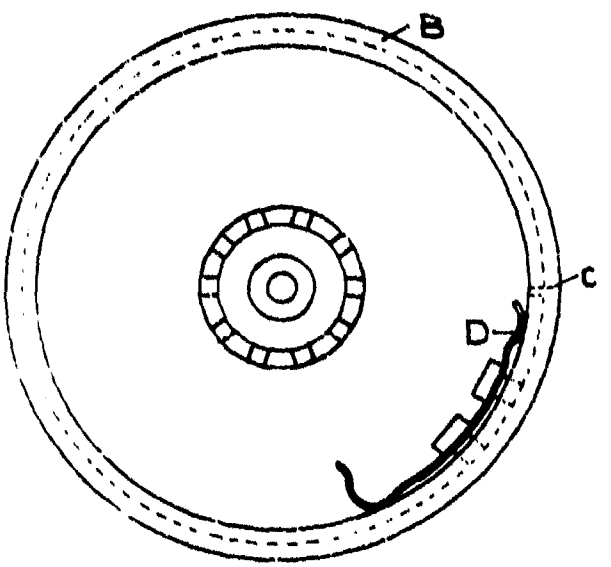


Fig. 48. Spark chronograph: A, electric motor. B, flanged chronograph drum; a strip of paper is fitted round the drum and the ends are passed through a slot C and clamped by a sliding spring clip D; the most suitable paper is the black surfaced kind used for lining books. E, four spark-points, 1/32 inch clear of drum. F, iron crown wheel with 10 teeth. G, magnet and coil.

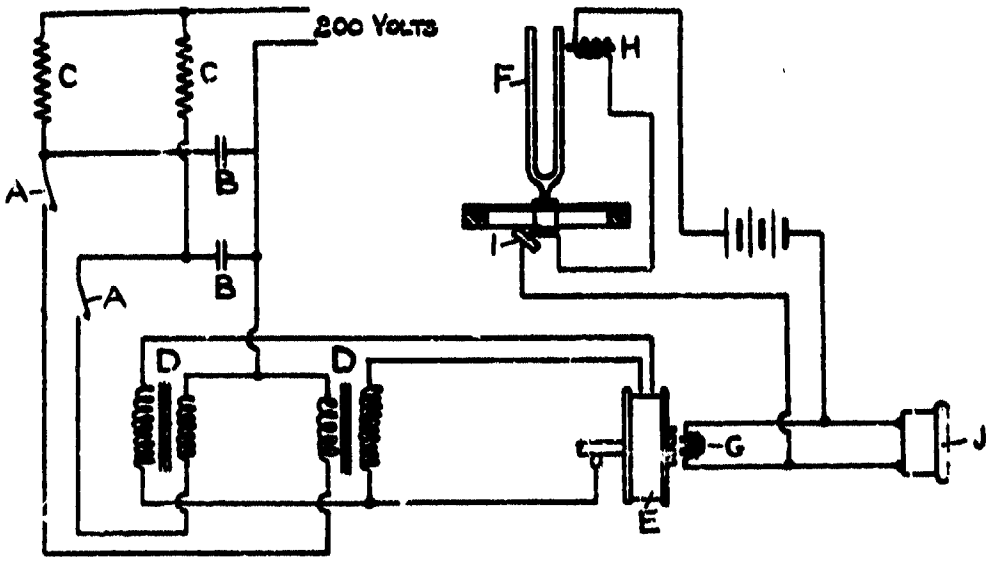


Fig. 49. Chronograph circuits; A, contacts; B, condensers (4 microfarads each); C, resistances (10^6 ohms each); D, transformers; E, spark chronograph; F, tuning-fork; G, H, wound magnets; I, microphone; J, telephone.

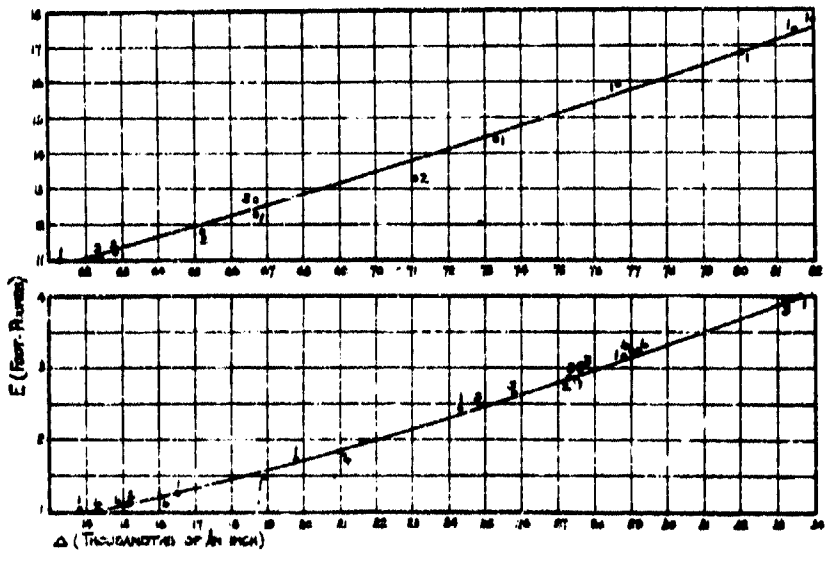


Fig. 50. Two sections of the copper calibration curve, showing the actual calibration results with pistons of different weights, (1) 22½ ounces (2) 4½ ounces, (3) 3 ounces, (4) 1½ ounces.



FIG. 51.—Shot 102: photograph of the "plumes" (150 feet high) thrown up by a 272-lb. charge of Ammonium perchlorate 31½ feet below the surface.



FIG. 52.—Shot 98: photograph of the "plumes" (160 feet high) thrown up by a 300-lb. charge of 40/60 Amatol 31½ feet below the surface.

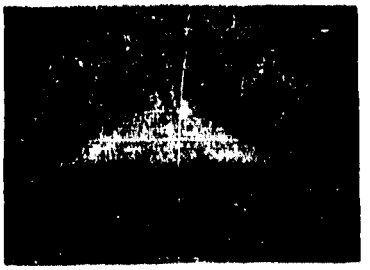


FIG. 53.—Shot 69: photograph of the "dome" (29 feet high) thrown up by a 272-lb. charge of Ammonium perchlorate 31½ feet below the surface.



FIG. 54.—Shot 14: 200-lb. charge of 40/60 Amatol 10 feet deep: the photograph shows the "plumes" beginning to break through the "dome" before the latter has reached its full height: at the moment shown the upheaval is 75 feet high, it eventually rose to 300 feet.



FIG. 55.—Shot 34: photograph of the "plumes" (85 feet high) thrown up by a 40-lb. charge of 40/60 Amatol 18 feet below the surface.

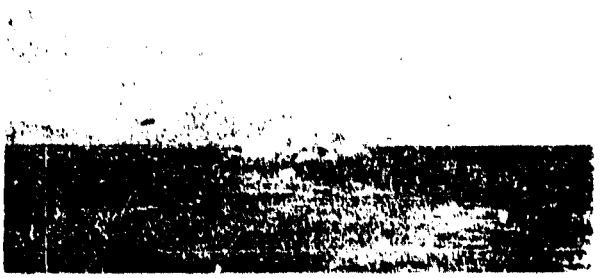


FIG. 56.—Shot 91; 500-lbs. of gunpowder 34½ feet below the surface, showing the first effect of the arrival of the burnt gases at the surface; the mound of water is 18 feet high.



FIG. 57.—Shot 92; showing the "plumes" (90 feet high) thrown up by a 500-lb. charge of gunpowder 10 feet below the surface.



FIG. 58.—Shot 64; 500-lb. charge of 40/60 Amatol 6red on the surface; the cloud, which is 100 feet high in the photograph, eventually rose to 300 feet.

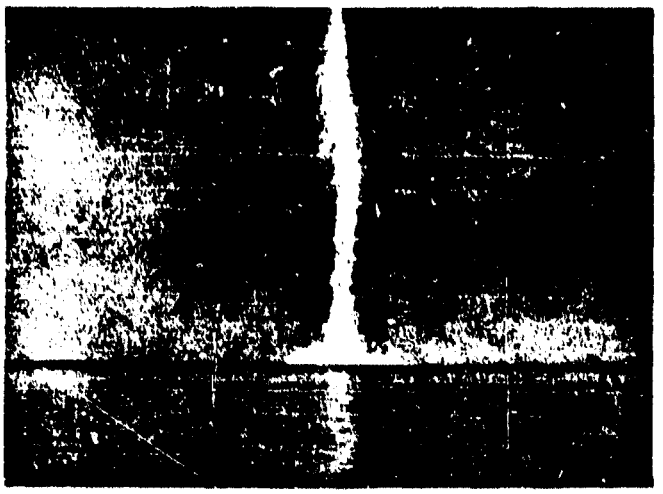


FIG. 59.—Shot 99; 300-lb. charge of 40/60 Amatol 5 feet below the surface; the "Malapert" (on left) is at the same distance as the spray-fountain, which is 650 feet high.

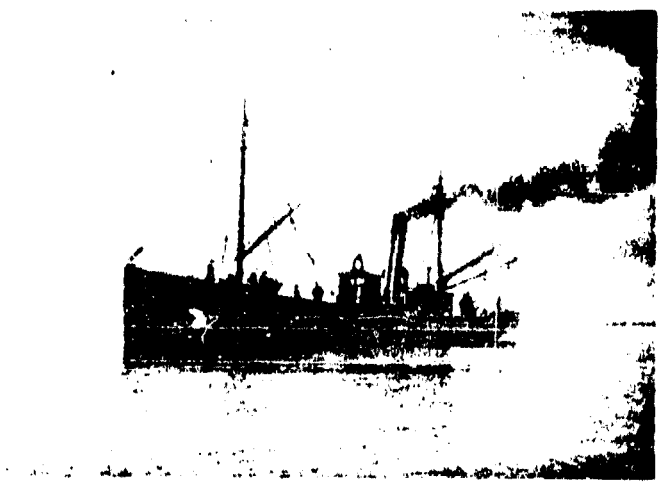


FIG. 60.—H.M. Drifter "Malapert."

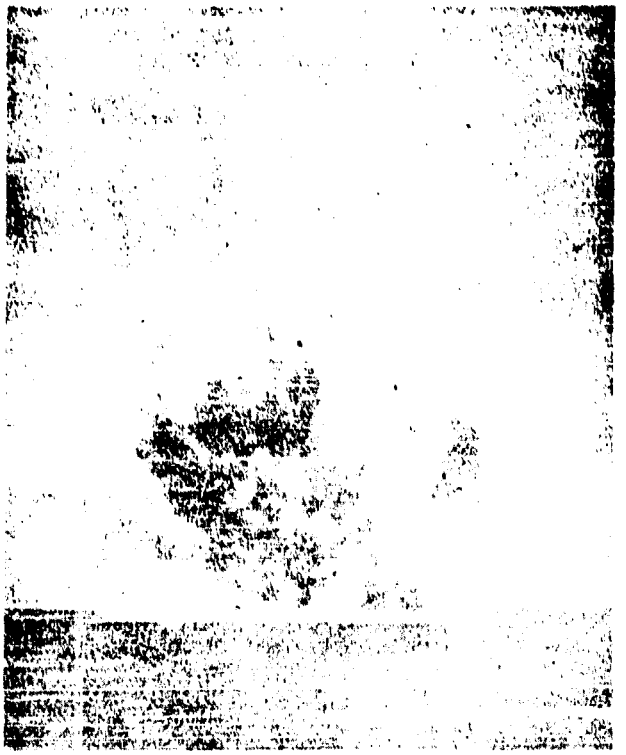


FIG. 61.—Shot 88; 1,900-lb. charge of 50/50 Amatol 64 feet below the surface; the "plumes" are 220 feet high.



FIG. 62.—Shot 89; 1,900-lb. charge of 50/50 Amatol 64 feet below the surface; the "dome" is 53 feet high.



FIG. 63.— Photograph of an H 4 mine case.

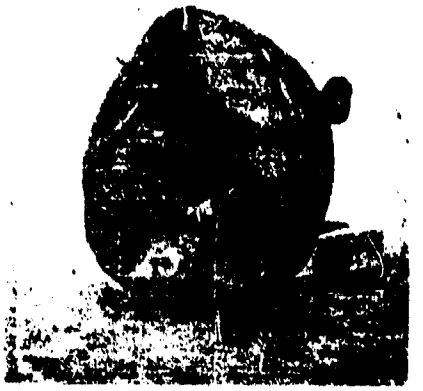


FIG. 64.—Photograph of an H 4 mine case which had been put down at a distance of 126 feet from a 1,600-lb. charge of 80/20 Amatol. (Shot 86.)



FIG. 65.—Photograph showing the method of hanging the gauges on a wire rope.

REPORT ON UNDERWATER EXPLOSIONS

E. H. Kennard
David W. Taylor Model Basin

American Contribution

October 1941

TABLE OF CONTENTS

	page
INTRODUCTION	1
UNITS	1
I. GENERAL SURVEY	1
1. COMPRESSIVE AND NON-COMPRESSIVE MOTION OF WATER	1
2. SEQUENCE OF EVENTS DUE TO AN UNDERWATER EXPLOSION	2
3. THE AFTERFLOW	3
II. THE EXPLOSION	4
III. THE PRESSURE WAVE AND AFTERFLOW IN THE WATER	5
1. OBSERVATIONS ON THE PRESSURE WAVE	6
2. MULTIPLE PRESSURE WAVES	9
3. QUALITATIVE THEORY OF THE PRESSURE WAVE	9
4. THE LAW OF SIMILARITY	12
5. A CALCULATION OF THE FIRST IMPULSE	12
6. THEORY OF THE SECONDARY IMPULSES	13
7. TURBULENCE	16
IV. EFFECTS OF THE PRESSURE WAVE ON AN OBSTACLE	17
1. MODE OF ESTIMATING EFFECTS	17
2. TARGET SMALL RELATIVE TO THE SCALE OF THE WAVE	18
3. TARGET LARGE RELATIVE TO THE SCALE OF THE WAVE	21
4. REFLECTION AT AN IMMOVABLE INTERFACE	21
5. STEEP-FRONTED WAVES	23
6. TARGET WITH INTERNAL INTERFACES	23
7. IMPACT OF A PLANE PRESSURE WAVE ON A FREE THIN UNIFORM PLATE	24
8. TARGET, A THIN UNIFORM PLATE WITH ELASTIC SUPPORT	26
9. EFFECTS ON A SHIP	29
10. ENERGY-MOMENTUM CONSIDERATIONS	30
11. OBSERVATIONS OF DAMAGING RANGE	31
V. SURFACE PHENOMENA OVER AN EXPLOSION	32

APPENDIX I

SMALL AMPLITUDES

I. WAVES OF SMALL AMPLITUDE - THE LINEAR THEORY	37
1. UNIFORM VELOCITY	37
2. UNIFORM FORM	37
3. SUPERPOSABILITY	37
4. PRESSURE AND PARTICLE VELOCITY	38

page

5. ENERGY AND MOMENTUM 39

II. REFLECTION OF SMALL-AMPLITUDE WAVES 39

1. OBLIQUE INCIDENCE 40

III. WAVES OF FINITE AMPLITUDE 41

IV. SHOCK FRONTS 42

APPENDIX II

RADIAL NON-COMPRESSIVE FLOW ABOUT A CENTRAL CAVITY

I. FUNDAMENTAL EQUATIONS 45

II. OSCILLATIONS OF A BUBBLE IN INCOMPRESSIBLE LIQUID 46

1. SMALL OSCILLATIONS 47

2. LARGE OSCILLATIONS 47

III. PRESSURE AND IMPULSE IN THE LIQUID 48

REMARKS ON THE THEORY OF SECONDARY IMPULSES
by Conyers Herring, Ph.D. 51

REPORT ON UNDERWATER EXPLOSIONS

INTRODUCTION

The purpose of this report is to collect in compact form what is known concerning certain practically important aspects of underwater explosions and their effects. After a few remarks concerning the role played by density changes in the motion of water, the typical sequence of events in an underwater explosion will be sketched. Then the principal parts of the sequence will be discussed in detail. For convenience of reference, the relevant parts of the theory of elastic waves in fluids are summarized in Appendix I. A bibliography of the most important publications on underwater explosive phenomena is given at the end of the report.

UNITS

Except where otherwise specified, all equations and mathematical expressions will be written in terms of absolute units, which may be thought of either as cgs units or as English gravitational, i.e., foot-slug-second units. When the English gravitational units are used, all pressures must be converted into pounds per square foot, and masses in pounds must be divided by $g = 32.2$. Numerical results will be cited always in English units. The density of water of specific gravity 1 is

1.940 slugs per cubic foot

For convenience a few equivalents are given here

1 kilogram per square centimeter = 14.22 pounds per square inch
10^6 dynes per square centimeter = 14.50 pounds per square inch
1 meter = 3.281 feet
1 pound = 453.6 grams
1 English ton = 2240 pounds

I. GENERAL SURVEY

1. COMPRESSIVE AND NON-COMPRESSIVE MOTION OF WATER

The motion of water usually involves changes in its density. These changes may or may not have to be taken into consideration in discussing the motion.

For the sake of convenience, the term *compressive motion* will be applied to motion in which the changes of density play a prominent role. The typical example of such motion is sound waves, which consist of alternate compressions and rarefactions propagated through the water at high speed.* The particle velocity, or velocity

* About 4930 feet per second in sea water at 15 degrees centigrade or 59 degrees fahrenheit.

of the water itself, is usually much less than the speed of propagation of the waves. In a train of waves traveling in one direction, the water in a region of compression is moving momentarily in the direction of propagation of the waves; in a rarefaction, the particle velocity is backward (opposite to the direction of propagation). The variations of pressure involved in ordinary sound waves are very small.

It is always possible to regard changes in the pressure of water as propagated through the water by a succession of small impulses moving with the speed of sound. In many types of motion, however, the time required for the propagation of such an impulse is so short as to be negligible, and the changes of density themselves may also be unimportant.

The term *non-compressive* may be applied to motion of such character that it is sufficiently accurate, first, to treat the medium as incompressible, and second, to assume that pressure applied to the boundary of the medium is propagated instantaneously to all points of the interior. Examples are the motion of water around a ship, or the flow of water in pipes that are not too long.

As a convenient criterion it may be said that the motion of water will be essentially non-compressive whenever the motion changes little during the time required for a sound wave to traverse the scene of action. At the opposite extreme, whenever a mass of water changes its motion considerably during the time required for a sound wave to traverse the mass, changes in density must usually be allowed for and the laws of compressive motion must be applied.

2. SEQUENCE OF EVENTS DUE TO AN UNDERWATER EXPLOSION

We are far from possessing complete experimental or theoretical knowledge of what occurs in an underwater explosion. The general sequence of events appears to be as follows.

When a mass of explosive material detonates, it almost instantly becomes gas under a very high pressure (1 or 2 million pounds per square inch), without appreciable increase in volume. The exploded gas then begins to expand and compresses the layer of water next to it; at the same time this layer of water is given a high velocity outward, perhaps 3000 feet per second. The layer of water, moving outward, then compresses the next layer and also accelerates it outward, and so on. In this way a state of high pressure and large particle velocity is propagated outward as the front of an impulsive wave.

The gas globe, pressing continually on the water, can be imagined to send out a succession of impulses of this sort, all of these impulses blending into a continuous wave. The pressure of the gas falls as the gas expands, however. Hence the maximum pressure and maximum particle velocity occur at or near the front of the wave,

as indicated roughly in Figure 1. The impulsive wave or *pressure wave*, as it is commonly called, travels eventually at the speed of sound, and may then be regarded as an intense sound wave; but at first its velocity should be much greater than the ordinary speed of sound. As the wave moves outward, both the pressure and the particle velocity in it decrease; when the distance r from the center exceeds about 10 times the radius of the mass of explosive material, the decrease is nearly in proportion to $1/r$, as in ordinary sound waves, but at first the rate of decrease should be much greater. The length of the pressure wave in the water, according to Hilliar's measurements, (1),* is of the order of 10 times the radius of the original mass of explosive; hence at a given point the duration of the pressure is one to several milliseconds.

The form of the pressure wave as indicated by Hilliar's measurements is shown in Figures 1 and 2. Figure 1 refers to a brisant explosive such as TNT. Figure 2 shows the wave from black powder, in which the rise of pressure is more gradual.

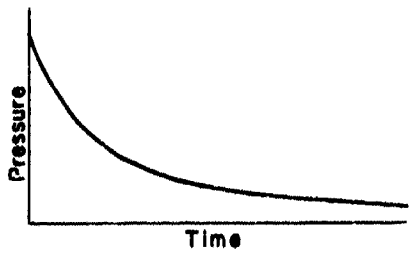


Figure 1 - From a Brisant Explosive

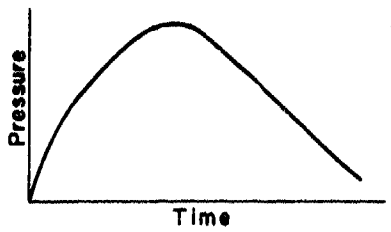


Figure 2 - From Black Powder

The ordinate shows the pressure in the impulsive wave as observed at a given point in the water, as a function of the time t.

The same figures also serve to represent the distribution of pressure in the water at a given instant, in a wave being propagated toward the left.

The true curves, however, are doubtless more or less wavy or even oscillatory. Furthermore, several lines of evidence point toward the occurrence of repeated impulses, following each other at intervals much longer than the time occupied by one impulse. These impulses are believed to be due to oscillations of the globe of exploded gas.

3. THE AFTERFLOW

It is well known that in a spherical wave the particle velocity consists of two components (Appendix I, Section 1; topic: Spherical Waves). One component

* Numbers in parentheses indicate references at the end of this report.

is exactly proportional to the excess pressure, as in plane waves. The second component represents an additional motion that is left in the water by the wave as it travels outward. This component, possibly representing the "surge" of some writers but called here the afterflow, tends to be inversely proportional to the square of the distance from the point of origin of the waves. The afterflow is important, therefore, only close to the source.

II. THE EXPLOSION

It will be assumed that the explosion process is of the type called *detonation*. In such a process a *detonation wave*, initiated at one point, sweeps through the explosive material. The front of the detonation wave is extremely steep. Each particle of the material, as the front passes over it, undergoes a sudden and fairly complete chemical change, its temperature and pressure rising to very high values; at the same time the intense pressure gradient in the detonation front imparts to the material a high forward particle velocity. Behind the detonation front, the pressure, temperature and particle velocity tend to fall off gradually to lower values, which are determined in part by conditions elsewhere in the exploded material.

The velocity of propagation of the detonation wave, or *detonation velocity*, D, is a constant for a given kind and density of material, provided the dimensions of the mass are not too small. Observed values of D for several substances, and a few estimates (not very reliable) of the maximum pressure p_m and centigrade temperature t_m in the detonation front, are as follows (1), (2) and (13) [cf. also (20)]:

	Guncotton	Picric Acid (1.63 g/cm³)	TNT (1.59 g/cm³)	Mercury Fulminate
D, feet per second	20,700	23,700	22,700	14,800
p_m, pounds per square inch		1.61×10^6	1.42×10^6	
t_m, degrees centigrade		3[illegible]	3360	

When the detonation wave reaches the surface of separation between the explosive and the water, it is partly continued as a wave of high pressure in the water, partly reflected as a wave of expansion traveling back through the exploded gas. The initial pressure in the water wave, however, should be considerably less than the pressure in the detonation wave itself.

The waves set up in the gas globe may strike the surface of separation between gas and water repeatedly, and in this way oscillations may be produced in the pressure wave that is sent out through the water. Furthermore, in actual cases, the detonation wave may reach different parts of the surface of the explosive at different times, depending upon the shape of the mass of explosive and the location of the

point of firing. The order of magnitude of the period of oscillations due to such causes may be estimated very roughly by dividing twice the diameter L (in feet) of the mass of explosive by an estimated average velocity of 10,000 feet per second, giving a period of $2L/10^4$ seconds, or about 10^{-4} seconds for ordinary heavy charges.

The statements made in this section concerning the explosion process represent, for the most part, theoretical conclusions. Little is known experimentally beyond the values of the detonation velocity D, nor have many theoretical calculations been made. Plausible equations, differential and algebraic, can be set up, but their solution requires numerical integration.

The calculation of G. I. Taylor deserves mention (3). He considers the case of a sphere of TNT in which the detonation is initiated at the center. The resulting distribution of pressure p and of outward particle velocity u are shown in Figure 3. The abscissa represents $z = r/R$, or the ratio of the distance r from the center of the sphere to the distance R of the detonation front from the center. Material for which $r > R$ is not yet detonated. The same plot holds good at all times, until the detonation front reaches the surface of the sphere of explosive. As time goes on, the point $r = R$ moves outward at the detonation velocity D. At any instant the exploded material is at rest within a sphere whose radius is 2/5 that of the detonation front. No experimental evidence exists to check these results.

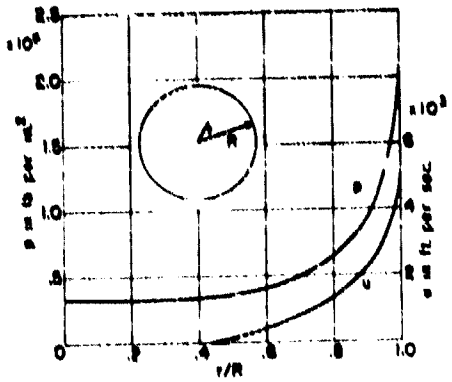


Figure 3 - Detonation of TNT Sphere

III. THE PRESSURE WAVE AND AFTERFLOW IN THE WATER

Only a few observations and calculations have been made of the wave produced in water by an explosion. Experimental observations are made difficult by the fact that the density of the material composing the instrument is necessarily comparable with the density of the medium in which the wave exists, in contrast with the case of blast waves in air. Theoretical calculations are hampered both by lack of knowledge of the properties of matter under very high pressure and by mathematical difficulties.

Properly to understand the phenomena requires familiarity with certain physical ideas and theoretical results concerning compressive waves. For convenience of reference, these ideas and results are collected together in Appendix I, and familiarity with the material in that section will be assumed.

1. OBSERVATIONS ON THE PRESSURE WAVE

ABBOT'S OBSERVATIONS (1869-1881), (4), the first extensive investigation, are chiefly of historical interest, because the interpretation of his data is open to question. The following conclusions from his work may be cited.

(a) Gunpowder gave erratic results, but the results produced by dynamite or guncotton were very consistent.

(b) The "mean" pressure in the water was found by Abbot to vary in proportion to the linear dimensions of the charge, and as $1/r^{1.4}$ where r is the distance of the point of observation from the center of the explosion (more recent work indicates a variation as $1/r$).

The following remark may also be quoted from his report as constituting early evidence pointing toward a multiplicity of some sort in the pressure wave: "It is a general characteristic of small and deeply submerged charges of the explosive compounds, and of some quick-acting explosive mixtures as well, that at the instant of detonation, before any disturbance of the water at the surface is visible, three sharp sounds are heard . . . . of nearly equal intensity," the interval of time between the last two being shorter than that between the first two. He states also that successive impulses are felt by a person standing in a boat.

HILLIAR'S OBSERVATIONS, (1), published by the English Department of Scientific Research and Experiment in 1919, are the best so far available. The report includes observations of the pressure wave, of the surface effects, and of relative damage to targets.

The pressure wave was studied chiefly by means of what might be called "impulse crusher gauges." The working part was a steel piston several inches long and half an inch in diameter, set in motion by the water pressing on the outer end. After traveling a known distance, the piston struck a short cylinder of copper. From the shortening produced in the copper the final velocity and momentum of the piston were calculated. The momentum was taken as a measure of the impulse $\int p dt$ in the wave from the start up to the instant at which the piston struck the copper. The coppers were calibrated by striking them with pistons moving at measured velocities. The shortening was found to be proportional to the energy of the blow, regardless of the weight of the piston. By using several gauges with pistons having various distances of free travel, all mounted at the same distance from the explosion, various portions of the total impulse could be measured; and from the calculated values of the final velocities of the pistons and their distances of travel, the times could be calculated.

Maximum pressures were also measured with a crusher gauge in which a plate, actuated by the water, crushed a copper with which it was initially in contact.

There is a possible source of error in the use of such gauges which is not discussed by Hilliar. Since the pistons moved parallel to the wave front (vertically), they would be caused to press against the wall of the hole owing to acceleration of

the gauge by the pressure gradient in the water, and so would be retarded by friction; furthemore, elastic oscillations in the gauge may be set up, with the same result. The indications of the gauge would thus be made too small. As a matter of fact, a systematic discrepancy of 10 to 15 per cent was noted between the indications of the impulse and the maximum-pressure gauges. This was overcome by arbitrarily reducing the indications of the maximum-pressure gauges by 10 per cent. Perhaps the correction should have been reversed.

For comparative observations, use was also made of simpler gauges in which a mass of plasticine was extruded through a hole by the pressure of the water, this mass being subsequently weighed.

A typical curve thus obtained, representing the average from 3 shots, is shown in Figure 4. The curve is drawn by estimation through the rectangles, which correspond to successive portions of $\int p dt$. The gauges were 50 feet from the charge.

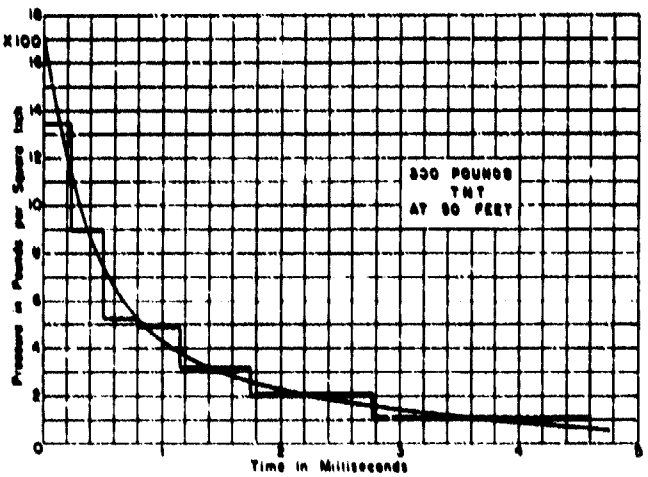


Figure 4

The following features of the behavior of the pressure wave were inferred from the observations:

(a) Law of Similarity. Charges of various sizes produce equal pressures at distances and at times which are in proportion to the linear dimensions of the charges.

(b) Variation with Distance. The magnitude of the pressure wave decreases in the inverse ratio of the distance r from the charge, at least if r lies between 30 and 120 times the radius of the charge.

Because of these simple features, it can be deduced from the observations that the maximum pressure due to W pounds of amatol or TNT at a distance of r feet is about

$$p_m = 13{,}000 \frac{W^{\frac{1}{3}}}{r} \text{ pounds per square inch}$$

(c) Velocity. The velocity of the wave is nearly that of sound, within the range specified.

(d) Regularity and Symmetry. The pressure wave does not vary much from one charge to another of the same kind and size, and it is spherically symmetrical, provided the charge is approximately symmetrical. When the charge is decidedly elongated or flattened, the pressure wave is not quite the same in different directions from the charge. The observed differences due to this cause, or to initiation of the detonation on one side, can be explained qualitatively by imagining the pressure wave to be made up of component waves emitted by the various parts of the charge, and then allowing for the differences in the time of travel of the component waves. Thus the wave from a long rod detonated at one end would be strongest but of shortest duration at points lying on the prolongation of the axis and in the direction of travel of the detonation wave, and weakest but of greatest duration in the opposite direction. If a maximum effect were desired in a particular direction, the best shape would probably be a curved disk, concave toward the side of the given direction, detonated at the center.

Surrounding a 320-pound charge of amatol with four times its own volume of air at atmospheric pressure produced little effect on the pressure wave.

(e) Reflections. When the charges were fired rather close to the surface of the water, the pressure wave was observed to be cut off at a time corresponding to the arrival of the wave reflected from the surface of the water. According to acoustic theory, the reflected wave should consist of a rarefaction which is the mirror image in the pressure axis of the incident pressure wave, atmospheric pressure being taken as zero.

Actually, although the positive pressure instantly disappeared at the calculated moment of arrival of the reflected wave, the maximum negative pressure observed did not exceed 90 pounds per square inch below the hydrostatic pressure at the level of the gauge. There is known to be a rather low limit to the negative pressure that water can stand, without the occurrence of cavitation, when it is in contact with solid objects. Very likely cavitation occurred around the gauges used in these observations and the true negative pressure occurring in the water was not indicated.

Reflection from the bottom was also observed. The pressure reflected from a mud bottom was only 0.4 times that in the incident wave. On the other hand, when a charge of 1000 pounds of TNT was laid directly on a sand bottom at 10 fathoms, the pressure wave was not much less than that to be expected from a 2000-pound charge surrounded by water. This is understandable, for the situation in question could be imitated roughly by passing a rigid diaphragm through the center of a 2000-pound

charge and the surrounding water and then removing the charge and water on one side of the diaphragm.

(f) Various Explosives. Amatol and TNT were found to emit very similar pressure waves. Guncotton and ammonium perchlorate gave considerably lower pressures, but the pressure from ammonium perchlorate was observed to fall off with time much less rapidly than that from TNT.

Gunpowder gave a pressure curve of rounded form, without a steep front, as in Figure 2. The pressures were also much less.

Hilliar's report has been summarized rather extensively here because no other comparable series of observations has been reported, and there is no evidence as yet of large errors in any of his conclusions.

III. PRESSURE WAVE
2. MULTIPLE WAVES

2. MULTIPLE PRESSURE WAVES

Considerable evidence has accumulated showing that an underwater explosion produces not one but several pressure waves of comparable magnitude. Besides the common observation that several sounds are heard, repeated impulses have been seen on oscillograph records. It was observed that the periods between successive impulses grew shorter; also that the period diminished with increasing depth of the point of explosion below the surface of the water. Moving pictures of a model boat, below which a charge was detonated, showed the boat to be kicked upward several times, at intervals of about 1/20 second.

The multiple impulses are probably due to oscillations of the gas globe. Such oscillations have been observed to occur, but the observations of Ramsauer (5) and of Ottenheimer (6) will not be discussed here because their interpretation is not wholly clear and the problem is under investigation at the present time.

Observations of the pressure wave need to be extended to cover these secondary parts of the pressure wave. It is important to find out whether the second impulse is larger than the first, and whether there is a difference in wave form.

III. PRESSURE WAVE
3. QUALITATIVE THEORY

3. QUALITATIVE THEORY OF THE PRESSURE WAVE

An exact theory of the motion of the water produced by an explosion can be constructed only by laborious methods of numerical integration. The main features to be expected in the phenomenon can be predicted, however, by means of reasoning based on the elementary principles of compressive waves and of hydrodynamics. The qualitative theory thus obtained will first be described, for purposes of orientation. Then the important phases of the process will be discussed in more exact terms.

When the detonation wave in the explosive reaches the surface of separation between explosive and water, it compresses the adjacent layer of water almost instantaneously and at the same time gives to it a high velocity outward. The outward rush of this layer then compresses the next layer, and at the same time the high pressure in the first layer gives a high velocity to the next layer. Continuation of this process results in the propagation of a state of high pressure and large particle velocity outward as the front of a diverging spherical pressure wave in the water. As the wave moves outward and becomes spread out over progressively larger areas, its intensity decreases, ultimately in inverse ratio to the distance from the center. Meanwhile, the gas maintains the water next to it at a high pressure, and the state of pressure and of motion in this water is continually propagated outward to form subsequent portions of the pressure wave.

As the gas expands, however, its pressure falls; the expansion should be nearly adiabatic, because of the rapidity of the expansion. The laws of ideal gases will not apply at first, however, because the density is then almost equal to that of the solid explosive. In the pressure wave, therefore, the pressure and the particle velocity should decrease behind the front. Thus a short time after the explosion occurs the distribution of pressure p and of outward particle velocity u in the water should be somewhat as shown in Figure 5, provided elastic oscillations within the gas globe itself are ignored; the abscissa r represents distance outward from the center of the original explosive mass, which is assumed spherical. The distance marked "gas" is the radius of the globe of gas at the instant in question; pressure and particle velocity within the gas are not shown. The distance marked "original solid" is the radius of the original sphere of explosive material.

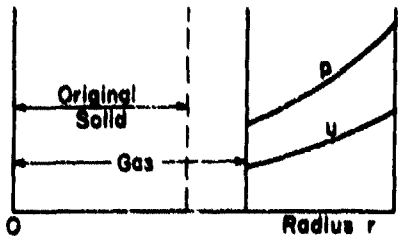


Figure 5

As the gas continues to expand, its pressure will eventually sink to the hydrostatic pressure p_0 proper to the depth at which the explosion occurs. If we were dealing with a one-dimensional case and hence with plane waves, the particle velocity u would now be zero and the expansion of the gas globe would cease.

In the case of diverging waves, however, we have to reckon with the "afterflow," described in Appendix I, Section 1, topic: Spherical Waves. The passage of a spherical pressure wave through the water leaves the water flowing outward, with a velocity roughly proportional to the inverse square of the distance from the center. Perhaps the pressure wave itself is to be identified with the Phase A of some writers, and the afterflow with Phase B or the "surge." The term *afterflow* is preferred here because, after all, even in the pressure wave there occurs a powerful, albeit short-lived, forward "surge" of the water. The distribution of pressure p and of resultant particle velocity u, including the velocity of afterflow, at the instant when p

has sunk to p_0 at the gas globe, should be, therefore, somewhat as shown in Figure 6, in which the scale of abscissas is reduced relative to that of Figure 5.

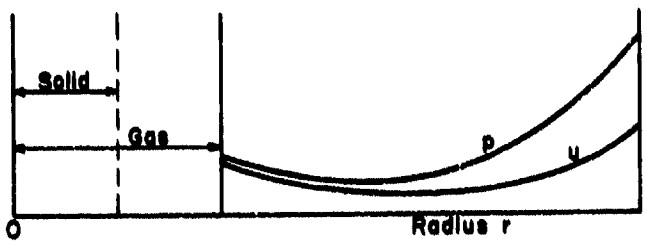


Figure 6

The afterflow has two effects:

The motion of the water due to the afterflow tends to modify the distribution of pressure roughly as if by adding to it a component proportional to $-\frac{1}{2}\rho u^2$ (ρ = density, u = particle velocity), as in the Bernoulli equation of ordinary hydrodynamics. Since u decreases in an outward direction, this effect tends to increase the pressure in the water as compared to that of the gas and so to prolong the pressure impulse. It can be said that an excessive amount of momentum is taken up at first by the water near the gas and is then paid out as this water moves outward and slows down.

The second effect of the afterflow will be that a large part of the energy originally in the exploded material is not carried off by the pressure wave but remains behind in the water in the form of kinetic energy. Hence the water will continue to flow outward after the gas pressure has sunk below the hydrostatic pressure; it will flow outward until, after the lapse of a comparatively long time, it is brought to rest by the action of the hydrostatic pressure.

The gas pressure having now become very small, the hydrostatic pressure will start the water moving inward, and the gas globe will thus be compressed again. During this second stage of compression, a second intense pressure wave will be emitted. The gas globe may oscillate in this fashion a number of times. The situation may be compared to a mass, representing the inertia of the water, mounted on two opposing springs, a powerful one, the gas, that ceases to act beyond a short distance, and a very weak one, the hydrostatic pressure. The weak spring will undergo large displacements, but, given time, it will get the mass moving inward again and so will eventually restore the initial state of high compression of the strong spring.

During each of the expansion phases, negative pressures (relative to the hydrostatic pressure as zero) will be transmitted to a distance. Thus we are led to expect that observation at a distance will reveal a succession of strong pressure impulses, separated by relatively long periods, during which both positive and negative pressures of moderate amplitude occur. The first impulse should have a steep front, whereas the subsequent ones should have rounded tops and should be progressively weaker.

The theoretical picture of the pressure as a function of the time thus obtained is sketched in Figure 7. It appears to agree at least roughly with the facts.



Figure 7

4. THE LAW OF SIMILARITY

The exact equations for the motion of non-viscous fluids lead to the same law of similarity that was established experimentally by Hilliar (Section 1, preceding). If the linear dimensions of the exploding charge are changed in the ratio s, without other change, the pressure curve previously obtained at a distance r from the center of the charge should now be obtained at a distance sr, except that all times will likewise be changed in the ratio s. The energy and the impulse, $\int p dt$, carried by the wave will, therefore, also be s times as great. Since the wave covers a spherical surface s^2 times as great, the total amount of energy is thus proportional to s^3 or to the weight of the charge.

5. A CALCULATION OF THE FIRST IMPULSE

The only available quantitative calculation of the first pressure wave seems to be that made in England by Penney (7). He starts with a spherical mass of TNT having a radius of 1 foot and hence a weight of 390 pounds (specific gravity = 1.565). Instead of solving the detonation problem, however, Penney substitutes an idealized initial condition; he assumes that at a certain instant the TNT is all exploded within its original volume, the exploded gas being at rest but under a pressure of 1,300,000 pounds per square inch. The genesis and propagation of the pressure wave in the water, and the motion of the globe of exploded gas are then worked out by numerical methods, for times up to 0.7 millisecond from the start.

In the beginning, the pressure at the interface between the exploded gas and the water is found to drop instantaneously to about 500,000 pounds per square inch, the water and gas at the interface acquiring simultaneously an outward velocity of about 3000 feet per second. A shock wave then proceeds outward into the water while an expansion wave travels back into the gas. After the lapse of 0.7 millisecond, the distribution of pressure p and of particle velocity u (taken positive

when directed outward), as a function of the distance r from the center of the gas globe, are found to be as shown in Figure 8. The long dotted line shows the instantaneous position of the interface between gas and water. The distance marked "initial solid" represents the radius of the original sphere of solid TNT.

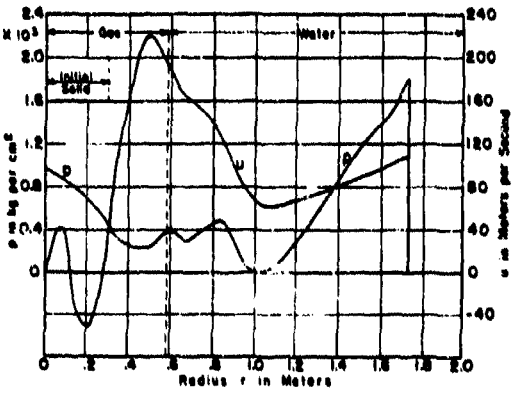


Figure 8

For times exceeding 0.7 millisecond, Penney uses a rough method of calculation, primarily for the purpose of discovering how the pressure may be expected to change with distance. He concludes that no marked change should occur in the shape of the pressure wave as it proceeds outward, but its intensity should decrease. Beyond a distance of 50 feet from the charge, the pressure in the wave should fall off like that of ordinary sound waves, nearly in inverse ratio to the distance, but at first the rate of decrease should be more rapid. At a distance r feet from the center (i.e., r times the radius of the original sphere of explosive) the pressure is x times as great as it would be if it varied as $1/r$, where x has, for example, these values:

r = 3	5	13	50
x = 2.5	2	1.3	1

In conclusion Penney shows a comparison of his curve for the pressure at 50 feet from 300 pounds of TNT with an experimental curve, which is almost the same as that published by Hilliar. The two curves agree in showing an initial pressure of 1800 pounds per square inch, but Penney's curve drops off more rapidly. The oscillatory feature in Penney's curve may be due to the peculiar initial condition from which he starts his calculation, or it may be that such features are missed in current methods of observation.

6. THEORY OF THE SECONDARY IMPULSES

In the absence of an exact theory of the oscillations of the gas globe and of the pressure impulses produced by them in the water, some light may be thrown upon the phenomena by developing a theory in which compression of the water is ignored. As a matter of fact, the actual motion must approximate closely to the non-compressive type except during the phase of intense compression of the gas.

Let us start with a sphere of compressed gas of negligible density surrounded by incompressible water at rest, and neglect gravity. During the motion, the pressure p and particle velocity u of the water at a distance r from the center will be given by Equations [8] and [2] of Appendix II.

$$p = \frac{r_g}{r}\left(p_g + \frac{1}{2}\rho u_g^2 - p_0\right) - \frac{1}{2}\rho u^2 + p_0,$$

$$u = \left(\frac{r_g}{r}\right)^2 u_g,$$

in which r_g is the radius of the sphere of gas, $u_g = dr_g/dt$, p_g is the pressure of the gas, p_0 is the hydrostatic pressure, ρ is the density of water. At a great distance the Bernouilli term, $\frac{1}{2}\rho u^2$, is negligible. Near the center, however, this term is not negligible; it causes the pressure transmitted to a distance to be determined, not by the pressure p_g of the gas alone, but by the quantity $p_g + \frac{1}{2}\rho u_g^2$. As the gas expands, p_g decreases but u_g^2 increases. The pressure impulses are thus made broader than would be expected from the variation with time of the gas pressure alone.

It is evident that oscillations will now occur in the general manner described in Section 3 preceding. Since no energy is lost here, however, the gas must return at each collapse to its initial pressure; hence all secondary pressure waves will be alike, and each one will be symmetrical about its center. The first pressure wave will be only a half-wave, arising from a single outstroke, whereas each subsequent wave is due to instroke plus outstroke. The impulse at distant points due to each secondary wave will thus be twice that due to the primary wave.

For the period of the oscillations an expression is readily obtained in the form of an integral (see Appendix II, Equations [17], [19], [22]). In two extreme cases the value of the integral is easily found.

The period T_0 of small radial oscillation of a gas bubble about its equilibrium size, with its pressure oscillating slightly above and slightly below hydrostatic pressure, is given by Minnaert's formula (8):

$$T_0 = 2\pi r_0 \sqrt{\frac{\rho}{3\gamma p_0}}$$

in which r_0 is the equilibrium radius of the bubble, ρ the density of the surrounding liquid, p_0 the hydrostatic pressure, and γ the ratio of the specific heats of the gas at constant pressure and at constant volume, respectively. For air in sea water, at a depth h, roughly

$$T_0 \approx \frac{1}{10}\, r_0 \sqrt{\frac{34}{34 + h}} \text{ seconds},$$

where r_0 and h are expressed in feet. That the oscillations can occur so rapidly becomes plausible when one recalls that the velocity of efflux of water under a pressure of only one atmosphere is 47 feet per second.

As the amplitude of oscillation increases, the period increases. When the maximum radius becomes 6 times the minimum, if $\gamma = 1.4$, a numerical integration

indicates that $T = \frac{4}{3} T_0$, approximately. Finally at very large amplitudes the period is given approximately by Willis' formula:

$$T = 1.83\, r_m \sqrt{\frac{\rho}{p_0}} = 1.14\, \rho^{\frac{1}{2}} p_0^{-\frac{5}{6}} W_1^{\frac{1}{3}}$$

where r_m is the maximum radius of the bubble or W_1 is the maximum energy of the gas, moving adiabatically, during an oscillation. The gas need not be assumed to behave as an ideal gas. In all cases the theory indicates a decrease in the period with increasing hydrostatic pressure, as is actually observed for the intervals between the secondary impulses. For a gas expanding adiabatically from a given state, r_0 is proportional to $p_0^{-1/3\gamma}$ where γ is the ratio of the specific heats of the gas. Hence, according to the small-amplitude formula, T_0 is proportional to $p_0^{-[\frac{1}{2}+\frac{1}{3\gamma}]}$, whereas according to the large-amplitude formula T is proportional to $p_0^{-\frac{5}{6}}$.

The total impulse, $\int p\,dt$, is very simply related to the particle velocity in non-compressive radial motion (e.g., in Equation [3] of Appendix I, Section 1, let the velocity of sound c become infinite). When the amplitude of oscillation is large, the total positive impulse at a distance r from the center, i.e., $\int p\,dt$ taken over the part of the cycle during which the pressure p exceeds the hydrostatic pressure p_0, is given by the formula (Appendix II, Equation [25]):

$$\int (p - p_0)\, dt = \frac{0.43}{r}\, \rho^{\frac{1}{2}}\, p_0^{-\frac{1}{6}}\, W_1^{\frac{2}{3}}$$

When compressibility of the water is taken into account, all of these results require modification and, unfortunately, the theory can be worked out only by methods of numerical integration.

Whereas the motion of an incompressible liquid is all afterflow, in a compressible liquid the particle velocity contains an additional component that is proportional to the pressure and hence in phase with it (the term $p/\rho c$ in Equation [3] in Appendix I, Section 1). The effect is both to modify the motion of the gas and to cause a radiation of energy. Such effects should become appreciable in water at pressures exceeding 1000 pounds per square inch.

Because of the loss of energy, the gas will collapse less completely in each successive oscillation, and the maximum pressure and the total impulse will decrease from one secondary wave to the next. It may even happen that the first secondary impulse is smaller than the primary impulse. Furthermore, the interval between oscillations will decrease slowly, as is actually observed for the intervals between secondary impulses. Exact calculations for the secondary waves are needed.

There is ample reason to believe that the loss of energy will be relatively large. It can be shown that a pressure curve such as that obtained when the water is treated as incompressible would involve, in actual water, a loss of energy in each oscillation comparable in magnitude with the energy of the gas. From his observations, Hilliar (1) concluded that the part of the primary pressure wave which was

covered by his measurements carried off about 1/4 of the energy available in exploded TNT.

The total impulse at distant points must in any case be measured by the velocity of the afterflow, as stated in the foregoing; for at a distance the compression of the water is always negligible. This fact furnishes an easy method of connecting the impulse with the energy of the afterflow, as was pointed out by W. C. Herring (9). Estimates thus made in actual cases come out surprisingly large. Thus, in the case of 300 pounds of TNT exploded 34.5 feet under the surface, if we insert in the formula given in the foregoing for $\int(p-p_0)dt$, W_1 = 300 x 1,200,000/2 foot-pounds, representing half of the initial energy that is available by expanding the exploded TNT to zero density, also ρ = 1.99 slugs per cubic foot and p_0 = 2 x 14.7 x 144 pounds per square foot, and then divide by 2 in order to have the impulse due to an outstroke alone, we find for the impulse in the primary wave, at a distance of 50 feet from the charge, 3.3 pound-seconds of impulse per square inch.

For comparison, the part of the pressure wave, 4 milliseconds in extent, that was measured by Hilliar represents an impulse of only 1.45 pound-seconds per square inch. The reason for this discrepancy is not clear. The observed pressure wave accounts for only a quarter of the energy in the TNT, so that the calculated value of 3.3 should be an underestimate. Perhaps an appreciable impulse may result from small pressures acting over relatively long times during a later phase than that covered by the measurements.

It may be remarked that spherical symmetry has been assumed in the foregoing discussion. If the motion is asymmetrical, the collapse may occur in such fashion as to break up the gas globe. Evidence of such occurrences in the case of small explosions has been secured by cinematic photography.

7. TURBULENCE

The question may arise whether the motion of the water produced by an explosion is turbulent or not. Turbulence can be produced only through the action of friction; and it seems that friction should have time to produce appreciable turbulence only near solid objects, such as fragments of a burst case. There exists no mechanism by which turbulence so produced can be propagated outwards with the pressure wave.

IV. EFFECTS OF THE PRESSURE WAVE ON AN OBSTACLE

1. MODE OF ESTIMATING EFFECTS

In the pressure wave there are four physical magnitudes of interest:

(a) pressure

(b) forward particle velocity

(c) momentum, of total magnitude $\int \rho u dx$ (ρ = density, u = particle velocity, x = coordinate in the direction of propagation)

(d) energy.

The effect of the wave upon an obstacle, which we shall hereafter call the "target" can always be calculated in terms of the pressure exerted upon it by the water. To do this, however, we must know the extent to which the presence of the obstacle in turn modifies the pressure in the water. Because of this complication, it may be more convenient to consider the process in terms of one or more of the foregoing magnitudes other than the pressure. The most advantageous choice of a mode of approach will depend largely upon the relation between the dimensions of the obstacle and the effective length of the pressure wave.

Misconceptions may easily arise from carrying over into the dynamic field modes of thought that are appropriate to the static field only. The following general principles may be noted:

A. *Strength of materials* may be of little importance in determining the effects of explosions. For example, it is unimportant that a pressure of 10,000 pounds per square inch is required to rupture a metal structure if 50,000 pounds per square inch is available in the pressure wave.

The action of explosives upon objects near at hand will depend more upon their relative inertia than upon their cohesive strength. At greater distances, on the other hand, cohesive strength may be the chief determining factor.

B. The *path of least resistance* will not be favored by explosive forces to the same degree as by forces of smaller magnitude but longer duration.

For example, a charge detonated in contact with a metal plate may punch a hole through the plate, although the path of least resistance would lie through the air. The air is accelerated outward with extreme rapidity by the high pressure, but the adjacent part of the plate is likewise given a considerable acceleration, sufficient to cause rupture. A dense object placed over the explosive, such as water or earth, increases the effect on the plate because of its inertia, the time of action of the explosive being thereby lengthened. Water on the opposite side of the plate, on the other hand, diminishes the effect somewhat.

C. *Large-scale effects* tend to be very much less severe than the local effects close to the charge. This is a consequence of the short time of action of the forces.

Violent effects may be produced on a small quantity of target material near the charge, but after the momentum given to this material has been distributed over a much larger mass, the velocities generated may be moderate.

These principles are well illustrated in the familiar example of a small charge detonated under a few feet of water in a tank. The explosion ruptures the tank, for which a static pressure of 4000 pounds per square inch would be required; yet the water is projected no higher than it would be if issuing from a water main at a pressure of 50 pounds per square inch. The pressure that acts on the tank may be close to 50,000 pounds per square inch, lasting a ten-thousandth of a second. Against such a pressure, a tensile strength of 4000 pounds is hardly distinguishable from no strength at all. On the water, however, the same general effect can be produced by the weak pressure in the main because the time of action is much longer, of the order of 0.1 second.

Viewed from another angle, the water illustrates the contrast between large-scale and local effects. The layer of water next to the charge experiences a momentary force of nearly a million pounds per square inch and is given a velocity of something like 10,000 feet per second. After 0.01 second, however, the pressure wave will have completed several trips back and forth through the entire mass of water, being reflected repeatedly at its boundaries, and as a consequence the momentum will have become distributed over the whole mass, with a very great reduction in the velocity of the water.

The problem of determining precisely the effects of a pressure wave upon a target is comparatively simple only in cases of extreme simplicity. Several such cases will be discussed in detail in order to throw light upon the general problem.

2. TARGET SMALL RELATIVE TO THE SCALE OF THE WAVE

Suppose, first, that over any distance equal to the largest linear dimension of the target, conditions in the pressure wave are nearly uniform. Then, to a first approximation, the flow of the water near the target can be treated as non-compressive, and the pressure can be treated as if it were static.

This is easily understood on the principle, applicable to all cases, that the flow of the water is accommodated to the presence of an obstacle by means of impulses propagated through it with the speed of sound. These impulses serve to modify in the proper manner the distribution of pressure and of particle velocity. If conditions in the wave undergo little variation over a distance equal to the greatest diameter of the target, the impulses have ample time to keep the flow around the target adjusted from moment to moment to the slowly varying conditions imposed by the oncoming wave.

The pressure upon a small target can conveniently be resolved into two parts:

(a) the pressure p that would exist at the same point if the target were replaced by water, and

(b) an additional "dynamic" pressure, positive or negative, caused by motion of the water relative to the target.

The magnitude of this additional pressure can scarcely exceed ρu^2, where ρ is the density and u is the particle velocity in the wave.

Thus, a pitot tube, small as compared with the thickness of the pressure wave and turned toward the side from which the wave approaches, would read the value of

$$p + \tfrac{1}{2}\rho u^2$$

Again, if the target has an axis of symmetry in the direction of propagation of the wave (this axis constituting, therefore, a streamline), the pressure at the point on the front face where the axis cuts the surface of the target will be $p + \rho u^2$.

In pressure waves in water, however, ρu^2 is much smaller than p. If, as is usually the case, the linear or small-amplitude theory can be used for the wave, and if for the moment we neglect the afterflow, we have $p = \rho c u$ (c is the speed of sound), hence

$$\frac{\rho u^2}{p} = \frac{u}{c}$$

In practical cases u is much smaller than c. For example, at 25 feet from 300 pounds of TNT, $u < 50$ feet per second, hence $u/c < 50/4930 = 1/100$. In blast waves in air, on the other hand, ρu^2 tends to equal p.

The afterflow velocity at the point just mentioned can be estimated from the third term in Equation [3] in Appendix I. The value of $\int p'dt'$ at that point is about 2 x 1.45 x 144 pound-seconds per square foot, $r = 25$ feet, and $\rho = 1.94$ slugs per cubic foot, hence the term in question gives an afterflow velocity of only 8 feet per second. Thus even at 25 feet from 300 pounds of TNT, which is well within its damaging range, dynamic effects of the afterflow or "surge" will usually be small.

One effect of the wave is a tendency to set the target in motion in the direction of propagation of the wave. The acceleration results from the combined action of the pressure gradient in the wave and, if there is relative motion between target and water, of the dynamic pressure ρu^2 and of viscosity. Minute suspended objects will tend to undergo the same displacement as does the water itself. Larger objects, if free to move, will be displaced less.

If the target can be crushed, its deformation will be determined almost wholly by the major component of the pressure on the target, which is the pressure in

the incident wave itself, and this pressure can be treated as static. Paradoxical as it may seem, parts of a small target may undergo displacements many times larger than the displacements of the water particles in the undisturbed wave. A particle of water is accelerated, first, forward as the pressure rises to its maximum, then backward as the pressure sinks, the pressure gradient being now reversed, and in the end the water is left at rest except for motion due to the afterflow. If part of the target is movable, however, it experiences a positive impulse of magnitude $\int p dt$ and so may be left in rapid motion by the passage of the wave. The water will follow this local motion of the target approximately according to the laws of non-compressive flow, provided the velocities involved do not become excessive.

In this way, for example, displacements of the piston of Hilliar 3 gauges could occur amounting to several inches, without causing much distortion of the pressure in the water, although the displacement produced by the wave in unobstructed water should have been only a fraction of an inch.

To take another example, suppose a wave like that at 50 feet from 300 pounds of TNT passes over a light, hollow metal sphere of 6 inches diameter; the maximum pressure of 1700 pounds per square inch is far more than enough to crush the sphere. The resistance of the metal will, therefore, play only a minor role in determining the initial phase of the motion. If we neglect this resistance altogether, it is easily calculated from Equation [6] in Appendix II that the water will start rushing toward the center of the sphere with a velocity of over 300 feet per second. The local motion involved is on a small scale as compared with the 5-foot effective length of the wave. The inward motion will continue until the kinetic energy of the water has been spent in deforming the sphere.

We may consider also the 31-inch mine case shown in Figure 64 of Hilliar's report (1). At a distance of 126 feet, a 1600-pound charge of amatol would produce a maximum pressure of about

$$13000 \ \frac{(1600)^{\frac{1}{3}}}{126} = 1180 \text{ pounds per square inch}$$

and hence a maximum water velocity of

$$\frac{1180}{\rho c} = \frac{1180}{68} = 17 \text{ feet per second}$$

From Hilliar's Figure 1 it can be calculated that the total (observed) impulse from 300 pounds at 50 feet is equivalent to the maximum pressure acting for 0.85 millisecond. The time for the larger charge would be $0.85 \times (1600/300)^{\frac{1}{3}} = 1.48$ millisecond; and 0.00148×17 foot per second $\times 12 = 0.3$ inch for the displacement of the unobstructed water. Yet the mine case is indented at least 15 inches. Even an object 31 inches in diameter should be small enough relative to a wave 5 to 10 feet long for the small-target theory to be partially applicable.

It may be of interest to consider the afterflow, also. An upper limit can be set to the displacement produced by it in unobstructed water in the following way.

From Equation [21b] in Appendix II we find that a gas globe from 1600 pounds of amatol under 60 feet of water might perhaps expand to a maximum radius of 30 feet. Then we have $4\pi \times 30^3/3$ cubic feet of water displaced outward over a sphere of radius 126 feet, requiring a linear displacement of the water of magnitude

$$\frac{4\pi \cdot \frac{30^3}{3}}{4\pi \cdot 126^2} = 0.57 \, foot = 7 \, inches$$

This displacement is of the same order of magnitude as the indentation in the mine case. Nevertheless, the afterflow cannot have had anything to do with the crushing action, for it occurs in too leisurely fashion, requiring over a quarter of a second. The pressures due to the afterflow must have been quite negligible.

3. TARGET LARGE RELATIVE TO THE SCALE OF THE WAVE

At the opposite extreme, when the target is large as compared to the thickness of the wave, the water has no time to escape sideways, and adjustment to the presence of the target must be made on the spot. Relatively large modifications of the water pressure may then occur. The appropriate ideas to use in considering the impact of the wave upon a large target are those associated with the reflection of waves.

In order to throw some light upon the complicated phenomena to be expected, a number of simplified cases will be discussed which are amenable to analytical treatment.

4. REFLECTION AT AN IMMOVABLE INTERFACE

Consider a plane wave in water falling at an angle of incidence θ upon the plane face of a target consisting of homogeneous material of a different sort, gaseous, liquid, or solid. Let the wave be of sufficiently low intensity so that acoustic theory can be used.

Then at the interface between water and target the incident wave will divide into two, a transmitted wave which continues into the target at an angle of refraction θ', and a reflected wave which returns into the water. Let the pressure and particle velocity in the incident wave be p, u, in the transmitted wave p', u', in the reflected wave p'', u''. Let the density and the speed of sound in water be ρ_1 and c_1, respectively, and in the material of the target, ρ_2 and c_2 (Figure 9).

Then according to the usual laws for the reflection of sound waves (Appendix I, Section 2, Equations [9a], [9b] and [10]),

$$c_2 \sin\theta = c_1 \sin\theta' \qquad [1]$$

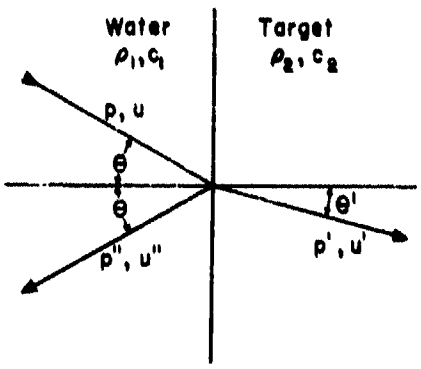


Figure 9

$$\frac{p'}{p} = \frac{2\rho_2 c_2 \cos\theta}{\rho_2 c_2 \cos\theta + \rho_1 c_1 \cos\theta'}, \qquad [2]$$

$$\frac{p''}{p} = \frac{\rho_2 c_2 \cos\theta - \rho_1 c_1 \cos\theta'}{\rho_2 c_2 \cos\theta + \rho_1 c_1 \cos\theta'}, \qquad [3]$$

The reflection coefficient is thus

$$R = \left(\frac{p''}{p}\right)^2 = \left(\frac{\rho_2 c_2 \cos\theta - \rho_1 c_1 \cos\theta'}{\rho_2 c_2 \cos\theta + \rho_1 c_1 \cos\theta'}\right)^2 \qquad [4]$$

The ratio of the total pressure on the interface to the incident pressure is

$$N = \frac{p + p''}{p} = \frac{p'}{p} = \frac{2\rho_2 c_2 \cos\theta}{\rho_2 c_2 \cos\theta + \rho_1 c_1 \cos\theta'}, \qquad [5]$$

The pressure measures the rate of transmission of momentum across a surface (so long as the amplitude of the waves is small); hence the value of N is also the ratio of the momentum absorbed by the target to the momentum brought up by the incident wave.

These equations hold so long as Equation [1] can be solved for θ'. If, however $c_2 \sin\theta > c_1$, total reflection occurs, with $p'' = p$ and $R = 1$, $N = 2$.

We note that if $c_1 = c_2$, $\rho_1 = \rho_2$, then $R = 0$ and $N = 1$, that is, the wave merely continues into the target without reflection. If $\rho_2 c_2 = 0$ (e.g. for vacuum), $R = 1$ and $N = 0$; also $p'' = -p$. In this case the incident wave is completely reflected with change of phase, compressions becoming rarefactions and vice versa; the particle velocity has the same direction in the reflected wave as in the incident wave, so that the reflected wave carries all of the incident momentum back into the water. If $\rho_2 c_2 \to \infty$, on the other hand, as for an extremely dense or rigid material, $N = 2$. Although the reflection of energy is again total ($R = 1$), the motion of the water is reversed by the reflection and the momentum given to the target is double that brought up by the incident wave. In this latter case the pressure in the water at the face of the target is likewise doubled.

At normal incidence the equations become

$$\frac{p'}{p} = \frac{2\rho_2 c_2}{\rho_2 c_2 + \rho_1 c_1}, \quad \frac{p''}{p} = \frac{\rho_2 c_2 - \rho_1 c_1}{\rho_2 c_2 + \rho_1 c_1} \qquad [6a, b]$$

$$R = \left(\frac{\rho_2 c_2 - \rho_1 c_1}{\rho_2 c_2 + \rho_1 c_1}\right)^2 \qquad [7]$$

$$N = \frac{2\rho_2 c_2}{\rho_1 c_1 + \rho_2 c_2} = 1 + \frac{\rho_2 c_2 - \rho_1 c_1}{\rho_2 c_2 + \rho_1 c_1} \qquad [8]$$

The effects of reflection at normal incidence depend only upon the ratio of the acoustic impedances, $\rho_1 c_1$ and $\rho_2 c_2$, in the two mediums. The pressure on the target is greater or less than that in the incident wave according as $\rho_2 c_2 > \rho_1 c_1$ or $\rho_2 c_2 < \rho_1 c_1$. In Figure 10, R and N are plotted as functions of the ratio $\rho_2 c_2 / \rho_1 c_1$,

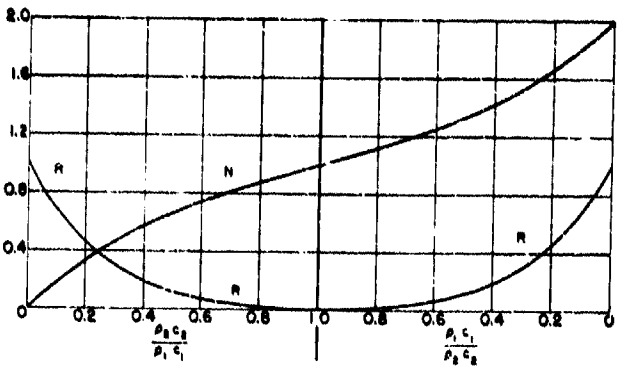


Figure 10

for $\theta = 0$, in a double plot whose mode of construction is sufficiently obvious. Values for three target materials in contact with sea water, for $\theta = 0$, are as follows:

	Steel	Copper	Air
p''/p	0.92	0.91	-0.99946
$N = (p+p'')/p$	1.92	1.91	0.00054
$R = p''^2/p^2$	0.85	0.82	1 - 0.00109

5. STEEP-FRONTED WAVES

If the incident wave has an extremely steep front, as has the pressure wave in water resulting from a detonating explosive, the wave transmitted into the target will also have a steep front. Waves of this character are easily produced in solid material by impact, and there is no evidence that they possess any special tendency to rupture or distort the material. It may be concluded that the precise shape of the steep front of the pressure wave is probably of no practical interest. Nor should the effects of the secondary impulses be altered much by the mere fact that they probably have no steep fronts at all.

The general form of the pressure wave may, however, be of importance, in some cases because of resonance effects.

6. TARGET WITH INTERNAL INTERFACES

The simplest type of a non-homogeneous target is one in which internal interfaces occur, as at the inner surface of a ship's plating. Additional reflections

will then occur at these interfaces. The reflected waves thus produced, returning to the outer surface, will be partly transmitted there and partly re-reflected back into the target; in part they will again be reflected at the internal interfaces; and so on. If the various interfaces are close together, however, as in a ship's skin, the interplay by repeated reflection goes on so rapidly that the various waves quickly blend together. Then other methods of analysis become sufficiently accurate and are more convenient.

Even if the target contains laterally dispersed structures, such as braces, the analysis in terms of waves is still applicable, but it becomes much more complicated.

7. IMPACT OF A PLANE PRESSURE WAVE ON A FREE THIN UNIFORM PLATE

By a thin plate is meant one so thin that the time required for an elastic wave to traverse the thickness of the plate is much less than the time required for the pressure in the incident wave to change appreciably. This condition may not be satisfied at the very front of the wave, but the small error so caused will be ignored. Under these circumstances it is sufficiently accurate to treat the plate as a rigid body.

As before, let p, u denote excess pressure (above hydrostatic) and particle velocity of the water in the incident wave, and p'', u'' the same quantities in the reflected wave. Let m denote mass per unit area of the plate, and x its position measured from any convenient origin in the direction of propagation of the wave, which we suppose to be perpendicular to the face of the plate (Figure 11). Then the equation of motion of the plate under the influence of the water pressure is

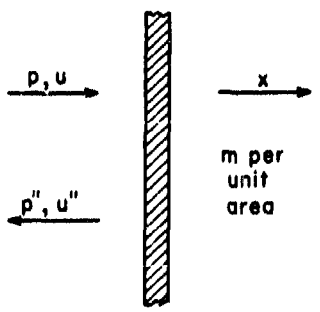


Figure 11

$$m \frac{d^2x}{dt^2} = p + p'' \qquad [9]$$

Air pressure on the opposite side of the plate is supposed to balance the hydrostatic pressure. Since the plate and water remain in contact, we have also

$$\frac{dx}{dt} = u + u'' = \left(\frac{p - p''}{\rho c}\right)$$

where ρ and c denote density and velocity of sound in the water; for $p = \rho c u$, $p'' = -\rho c u''$ (Appendix I, Section 1, Equation [2]). Eliminating p'':

$$m \frac{d^2x}{dt^2} + \rho c \frac{dx}{dt} = 2p \qquad [10]$$

Here p is a function of the time which may be denoted by $p(t)$. The equation can be solved for x when $p(t)$ is known. We shall consider in detail only a simple type of

wave bearing a rough resemblance to observed pressure waves (Figure 12).

Exponential Wave

Suppose that

$p(t) = 0$ for $t < 0$

$p(t) = p_0 e^{-\alpha t}$ for $t > 0$

Then it is easy to verify by substitution that a solution of [10] is, for $t > 0$,

$$\frac{dx}{dt} = \frac{2p_0}{\rho c - \alpha m} \left(e^{-\alpha t} - e^{-\beta t}\right), \quad \beta = \frac{\rho c}{m}$$

This solution also satisfies the necessary boundary condition that $(dx/dt) = 0$ at $t = 0$, the plate being at rest before the wave strikes it. (If $\rho c = \alpha m$, the solution is

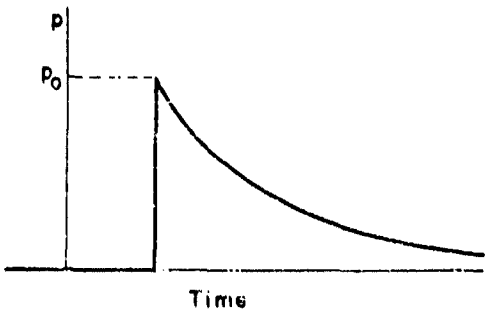


Figure 12

$$\frac{dx}{dt} = \frac{2p_0}{m} te^{-\alpha t}.)$$

Since the plate obviously comes to rest eventually, it follows from the conservation of energy that the wave must be totally reflected from it. The total displacement of the plate is finite and equal to

$$\Delta x = \int_0^\infty \frac{dx}{dt}\, dt = \frac{2p_0}{\alpha \rho c}$$

This may be compared with the net displacement undergone by an unobstructed water particle as the incident wave passes over it, which is

$$\int u\, dt = \int \frac{p}{\rho c}\, dt = \int_0^\infty \frac{p_0}{\rho c}\, e^{-\alpha t}\, dt = \frac{p_0}{\alpha \rho c}$$

Thus we have the following important conclusions:

1. The plate completely reflects the wave;

2. The total displacement of the plate is finite and is just twice the displacement produced in unobstructed water by the incident wave.

These conclusions are independent of the mass of the plate. A heavy plate acquires a smaller velocity but retains it longer. It can be shown that the same conclusions hold for a wave of any form. Furthermore, it can be shown that the same conclusions should hold generally for any target provided that

1. its characteristics vary only in one dimension, in the direction of incidence of the wave;

2. there is a light medium, like air, beyond the target;

3. the target is elastically connected throughout and does not break loose from the water.

The point of the last proviso lies in the fact that, since the target must be negatively accelerated during the later stages, negative pressures may occur in the water and cavitation may result.

It appears to follow from this analysis that if the skin of a ship were plane and held in place only by air pressure, the explosion of 300 pounds of TNT 20 feet from the ship would merely shift its skin inward an inch or so and leave it at rest. That damage actually results from such an explosion must be due either to the presence of stiff bracing or, perhaps, to cavitation in the water, so that the negative pressure during later stages fails to arrest the rapid inward motion of the skin.

The case of oblique incidence of the waves is much more complicated than that of normal incidence and will not be considered here. It involves questions as to bending of the plate.

The next case studied will be designed to throw light on the effect to be expected from bracing.

8. TARGET, A THIN UNIFORM PLATE WITH ELASTIC SUPPORT

Let the thin plate just described be held in position by springs or an equivalent support, with water on one side and vacuum or air on the other. The strength of the springs can most conveniently be specified by assigning the value of the frequency ν_0, with which the plate would vibrate, moving one-dimensionally in a direction perpendicular to its faces, if the water were absent. As before, we assume a plane pressure wave to fall at normal incidence upon the plate. Then, as the equation of motion of the plate, we may write in place of [9] or [10],

$$m\frac{d^2x}{dt^2} + 4\pi^2\nu_0^2\, mx = p + p''$$

$$m\frac{d^2x}{dt^2} + \rho c\,\frac{dx}{dt} + 4\pi^2\,\nu_0^2\, mx = 2p \qquad [11]$$

Thus, if $\rho c = 0$ and $p = 0$, the solution is $A\sin(2\pi\nu_0 t + a)$, representing an oscillation at frequency ν_0.

The left-hand member of Equation [11] is of the type encountered in dealing with linearly damped harmonic oscillations. The equation may be rewritten in a convenient generalized form thus:

$$\frac{d^2x}{dt^2} + 2\gamma\,\frac{dx}{dt} + \mu_0^2\, x = \frac{2p}{m} \qquad [12]$$

where in the present instance

$$\gamma = \frac{\rho c}{2m}, \quad \mu_0 = 2\pi\nu_0 \qquad [13a, b]$$

Damped Free Oscillations

If $p = 0$, the plate can execute oscillations damped because of radiation of its energy into the water, the energy being carried away by compressive waves. The solution of [12] when $p = 0$ is, according to circumstances:

if $\gamma > \mu_0$ (overdamped): $x = A_1 e^{-\gamma_1 t} + A_2 e^{-\gamma_2 t}$, $\gamma_1 = \gamma + \sqrt{\gamma^2 - \mu_0^2}$; $\gamma_2 = \gamma - \sqrt{\gamma^2 - \mu_0^2}$

if $\gamma < \mu_0$ (underdamped): $x = Ae^{-\gamma t}\sin(2\pi\nu t + a)$, $\nu = \nu_0\sqrt{1 - \left(\frac{\gamma^2}{\mu_0^2}\right)}$

Here A_1, A_2, A, a denote arbitrary constants.

Effect of a Pressure Wave

If a pressure wave strikes such a plate, it is evident from conservation of energy that the final result must be complete reflection of the incident energy. The point of practical interest is the maximum displacement of the plate, to which corresponds the maximum strain in the springs or other elastic support. The maximum displacement can be determined by solving Equation [12] if the pressure p in the incident wave is known as a function of the time.

Consider, for example, the exponential type of wave already employed:

$$p = 0 \text{ for } t < 0, \quad p = p_0 e^{-\alpha t} \text{ for } t > 0$$

Suppose that the plate is initially at rest and in equilibrium, with $x = 0$. The appropriate solution of [12] is most conveniently written in terms of the two auxiliary constants

$$x_s = \frac{p_0}{m\mu_0^2}, \quad \beta = \frac{\gamma}{\mu_0}, \quad n = \frac{\alpha}{\mu_0}$$

The constant x_s represents the static displacement of the plate under the maximum pressure p_0 (as may be seen by putting in Equation [12] $2p = p_0$, $d^2x/dt^2 = 0$, $dx/dt = 0$). The value of β determines the character of the free oscillations; and n can be regarded as the ratio of the natural time scale of the plate to the time scale of the exponential wave.

$\beta > 1$ (overdamped)

$1 - 2n\beta + n^2 \neq 0$:

$$x = \frac{2x_s}{1 - 2n\beta + n^2}\left[e^{-n\mu_0 t} - \frac{1}{2}\left(1 + \frac{n-\beta}{\sqrt{\beta^2 - 1}}\right)e^{-(\beta + \sqrt{\beta^2 - 1})\mu_0 t} - \frac{1}{2}\left(1 - \frac{n-\beta}{\sqrt{\beta^2 - 1}}\right)e^{-(\beta - \sqrt{\beta^2 - 1})\mu_0 t}\right]$$

$1 - 2n\beta + n^2 = 0$:

$$x = \frac{x_s}{\beta - n}\left[\mu_0 t\, e^{-n\mu_0 t} - \frac{1}{2(n-\beta)}\, e^{-\beta\mu_0 t}\left[e^{(n-\beta)\mu_0 t} - e^{-(n-\beta)\mu_0 t}\right]\right]$$

$\beta = 1$ (critically damped)

$$n \neq 1: \quad x = \frac{2x_s}{(n-1)^2}\left[e^{-n\mu_0 t} - e^{-\mu_0 t} + (n-1)\mu_0 t\, e^{-\mu_0 t}\right]$$

$$n = 1: \quad x = x_s(\mu_0 t)^2 e^{-\mu_0 t}$$

$\beta < 1$ (underdamped)

$$x = \frac{2x_s}{1-2n\beta+n^2}\left[e^{-n\mu_0 t} - \sqrt{\frac{1-2n\beta+n^2}{1-\beta^2}}\, e^{-\beta\mu_0 t}\sin\left(\sqrt{1-\beta^2}\,\mu_0 t + \tan^{-1}\frac{\sqrt{1-\beta^2}}{\beta-n}\right)\right]$$

Here $\tan^{-1}\sqrt{1-\beta^2}/(\beta-n)$ is to be taken in the first or second quadrant.

The equations for x as written still contain the constant μ_0, but this constant serves only to specify a time scale for the whole process. Otherwise all features are determined by the values of β and n. All of the equations represent the plate as returning ultimately to its position of equilibrium, as would be expected.

A plot showing certain values of x_m/x_s, the ratio of the maximum displacement x_m of the plate to its static displacement x_s under the initial pressure p_0, is shown in Figure 13. Only a few points were calculated, because of the laboriousness of the work; these points are indicated by crosses on the plot. Based on these points, roughly correct contours were drawn by estimation corresponding to various values of x_m/x_s, as indicated near the contours. The abscissa of each point on the plot represents a value of πn or $\frac{\alpha}{2\nu_0}$; for values above 1, however, distances along the axis are laid off in proportion to the reciprocal of πn, starting from 0 at the right-hand end of the plot. Similarly, the ordinate represents values of β up to 1, then of $1/\beta$ from 1 to 0, i.e., of β from 1 to ∞. Values of x_m/x_s for points between the contours can be estimated by interpolation.

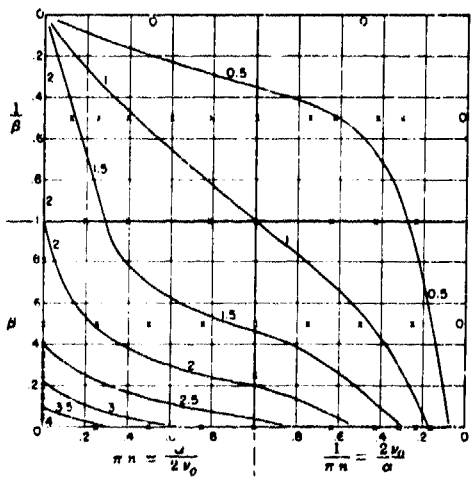


Figure 13

The largest value, $x_m/x_s = 4$, occurs when $n = \beta = 0$, i.e., for no damping and for a steady pressure beginning suddenly at a given moment. The value of x_m/x_s decreases with decrease in the natural frequency of the plate (decrease in μ_0), or with decrease in the length of the wave (increase in α); either of these changes makes the effective time of action of the wave less adequate for the production of a maximum effect. In an actual case the plate would probably be heavily overdamped by the radiation of waves into the water. Thus for a steel plate 1 inch thick in contact with sea water, $\gamma = 3900$ (i.e., 68.2 x 144 x 12/2 x 7.8 x 1.94), so that for $\nu_0 < 600$ cycles per second $\beta = \gamma/\mu_0 = \gamma/2\pi\nu_0 > 1$ and overdamping exists. The plate is not loaded by the water, however; its frequency of oscillation ν is modified by contact with the water only because of the damping action.

For the conclusions of this section to be valid, the lateral dimensions of the plate must be large as compared with the wave length of the compressive waves emitted into the water.

9. EFFECTS ON A SHIP

Oscillations of the type just described might correspond roughly to oscillations of a ship in which one of its sides moves in and out as a whole, against the elasticity of the bulkheads. The natural frequency for such oscillations should be of the order of 100, corresponding to $\mu_0 = 600$; but, with a weight of 50 pounds per square foot in the skin, $\gamma = 3200$ (i.e., 68.2 x 144 x 32.2/2 x 50), so that $\beta = \gamma/\mu_0 = 5$. Thus the oscillations should be heavily overdamped. For a pressure wave with $\alpha = 1200$, as in practical cases, $n = \alpha/\mu_0 = 2$. A glance at Figure 13 shows that x_m/x_s is small, the maximum displacement being much less than the static displacement due to the maximum pressure in the wave.

The same mathematical theory should be applicable to all modes of oscillation of a ship's side. It is only necessary to substitute in the formulas suitable values of the damping constant γ and of the undamped frequency ν_0. In all other cases than that of the infinite plane plate, however, ν_0 is altered as if the vibrating body were loaded to a certain extent by the water. As a rough rule, it may be said that damping by emission of compressive waves will be large or small according as the lateral dimensions of the vibrating segment of the ship are large or small as compared with the wave length in the water. Thus, the commonly studied oscillations of a single panel, at a frequency of perhaps 10, corresponding to a wave length of 500 feet, should be only slightly damped, as observed.

It should be remarked, however, that the time required for the propagation of elastic impulses along the bulkheads should also be taken into consideration.

10. ENERGY-MOMENTUM CONSIDERATIONS

In designing a structure to resist damage by an explosion wave, it may be more helpful to view the effect on the structure in terms of energy and momentum rather than in terms of pressure. The energy and the momentum brought up by the wave must be either reflected back into the water or absorbed by the structure.

If the structure is rigid, the energy is completely reflected. Since, however, compressions are reflected as compressions, the particle motion in the reflected wave has the opposite direction to that in the incident wave; hence the momentum taken up by the structure is twice that brought up by the incident wave. Furthermore, the process of reflection occurs in this case simultaneously with that of incidence. Hence the doubled absorption of momentum requires doubled stresses and strains in the structure (in addition to a possible further increase due to resonance effects).

To decrease the absorption of momentum, the structure must yield to the wave. If it yields, however, a fresh complication arises; for then it will take on part or all of the incident energy. Two alternatives are then open.

The energy may be converted into heat by means of friction and permanently retained in this form in the structure. If this is done, perhaps by the use of non-elastic materials, the impact of the explosion wave is handled somewhat as is the recoil of a gun, whose energy of backward motion is absorbed in dashpots.

If, on the other hand, the structure is made resilient, the energy will be returned into the water in a reflected wave, accompanied by the usual amount of momentum. As in the case of rigidity, therefore, the total amount of momentum absorbed by the structure will be twice that brought up by the incident wave. With the resilient structure, however, the process of reflection occurs partly or wholly after the incidence of the wave. Hence the doubling of the maximum stress is avoided. The general concussion of the vessel may be about the same in either case; but with the resilient structure the probability of rupture or deformation should be less. This conclusion appears to be illustrated by the case of an ice breaker sheathed with 4 feet of wood, against which a mine was exploded. The general damage throughout the ship was appreciable, but the local damage to the sheathing and to the steel hull was negligible.

As to the desirable amount of yielding, the theoretical answer is, *the more yielding the better*. The results deduced from calculation in the foregoing simple cases indicate that as the yielding increases to large values the absorption of energy decreases again; the absorption both of energy and of momentum tend ultimately toward zero (see Figure 10). The ideal procedure would be, therefore, to make the skin of a ship easily movable in directions perpendicular to its surface and to support it only by means of very flexible springs or by air pressure. Then, as the calculation for a thin plate shows, the pressure wave would be completely reflected, its only effect on the ship's skin being to displace it inward an inch or so. No damage would result, and the concussion would be negligible.

Aside from the practical difficulty of adopting such a mode of construction, the following consideration raises doubts as to its complete efficacy. From a highly yielding structure, a compression wave is reflected as a wave of almost equal rarefaction. There is a limit, however, to the tension which water will stand, especially when in contact with solid objects. During the later phases of the motion, therefore, the water may pull loose from the yielding structure, with the result that the structure will not be brought entirely to rest during the rarefaction phase but will be left with a high inward velocity. Or, cavitation may occur in the water, with the result that a layer of water next to the structure will also be left moving inward. The supports may or may not be adequate to check this motion without damage. Little is known concerning the magnitude of the tension that natural sea-water can stand momentarily without breaking.

Direct experiments on the effect of pressure waves upon highly yielding structures should be illuminating.

11. OBSERVATIONS OF DAMAGING RANGE

In Hilliar's report (1) extensive observations are recorded of the damage inflicted upon empty H4 mine cases, made of mild steel 1/8 inch thick and 31 inches in diameter. The degree of damage was found to vary rapidly with distance from the exploding charge, being heavy at a distance equal to three-quarters of the minimum distance D at which no damage at all is produced. Thus it becomes of special importance to determine the critical range D as a function of the weight W of the charge.

A partial answer is furnished by Hopkinson's rule of similarity: "The damage inflicted on a given structure by a given charge at a given distance will be reproduced to scale if the linear dimensions of the charge and structure and the distance between them are all increased or diminished in the same ratio." This rule can be deduced theoretically, and "its validity has been proved experimentally for charges differing very widely in magnitude."

As the result of extensive observations, Hilliar concludes that, for a given structure, the damage range D is approximately proportional to the square root of the weight of the charge.

By combining this result with Hopkinson's rule, a general formula can be deduced. Letting L stand for a convenient linear dimension of the structure, we have from Hilliar's result that

$$D = W^{\frac{1}{2}} f(L)$$

where f is a function not yet known. Changing all linear dimensions in the ratio r, we must have then

$$rD = (r^3 W)^{\frac{1}{2}} f(rL)$$

Hence

$$f(rL) = \frac{f(L)}{r^{\frac{1}{2}}}, \quad f(L) = D_0 L^{-\frac{1}{2}}$$

in which D_0 is a constant. Thus on similar structures

$$D = D_0 \left(\frac{W}{L}\right)^{\frac{1}{2}}$$

For a structure like an H4 mine case, of diameter L feet, and a charge of W pounds of TNT or amatol,

$$D = 7.6\, W^{\frac{1}{2}} L^{-\frac{1}{2}} \ feet$$

Or, we can say that the damage on any structure distant R from the charge is

$$F\left(\frac{W}{R^2 L}\right)$$

where F is a function depending on the type of structure.

Seeking a physical basis for Hilliar's result, we note that neither the pressure nor the impulse varies as $W^{\frac{1}{2}}$. It could be stated, however, that an H4 mine case "begins to be damaged when the energy flux exceeds about 5 foot-pounds per square inch." Hilliar is of the opinion, nevertheless, that this relation with the energy is fortuitous and that the significant quantity is more likely to be the time integral of the excess of pressure over a fixed value, $\int (p - k)\, dt$, where k depends upon the structure. On this view, an H4 mine case begins to be damaged when $\int (p - 200)\, dt$ exceeds about 360, p being in pounds per square inch and t in milliseconds.

V. SURFACE PHENOMENA OVER AN EXPLOSION

The surface of the water over an explosion behaves in a manner that is full of interest and often spectacular. These phenomena are of comparatively little practical importance, however, and will only be summarized here very briefly.

Three distinct effects are noted:

(a) At the instant of the explosion, the surface of the water seems to be agitated, and a light spray may be thrown up. This effect is not noticeable if the explosion is very deep.

(b) During the next second or two after the explosion, the water rises into a flattish "dome" which is often whitish in color and may attain a height of 50 feet or more. As the depth of the explosion is increased, the maximum height of the dome diminishes, and finally no dome is formed (e.g., there is none from 40 pounds of TNT or amatol 60 feet deep or 300 pounds 150 feet deep).

(c) Plumes of spray may be thrown up. If the charge is only a few feet below the surface, the plumes break through the dome while the latter is still rising, and

may attain a maximum height of as much as 500 feet. As the depth of the explosion is increased, the plumes become less marked and also appear later; they may break through the dome at the instant when the latter has attained its greatest height, or when it is sinking again, or the plumes may not appear until after the dome has disappeared. Finally, at great depths, no plumes are formed, but a minute or so after the explosion a mass of creamy water pours up to the surface.

All writers agree that the initial agitation of the surface is produced directly by the pressure wave, and that the plumes are thrown up by the exploded gases as they escape through the surface. Various theories have been offered, however, as to the cause of the dome.

Hilliar views the dome as an indirect effect of the pressure wave, arising from the fact that water can stand only a limited amount of tension. In the process of reflection from the surface, the pressure wave first gives to the water a high upward velocity, then endeavors to jerk it to rest again as tension develops below the surface. Bits of the surface may thus be jerked off, forming the initial spray that is sometimes observed. The water may also become broken to a depth of several feet, and in this case it will retain part of its upward velocity and will rise until checked by the action of gravity; a temporary dome of water, filled with bubbles or vacuous crevices, will thus be formed.

The explanation of the dome just described sounds plausible. Upon reflection at a free surface, the particle velocity of the water should be doubled. Hilliar's report lists 43 domes due to charges fired a long way above the bottom of the water. In all cases, calculation shows that the velocity required to project an object against gravity to the maximum height of the dome is less by at least 20 per cent than twice the calculated maximum velocity due to the reflected pressure wave at the surface of the water.

A final remark may be added concerning the explanation of the great height to which the plumes sometimes rise. Hilliar records a height of 140 feet due to 300 pounds of TNT fired at a depth of 34.5 feet. As the gas approaches the surface, it will occupy a volume which, if spherical, might have a diameter of 20 feet. Even if this were flattened down to 10 feet, we should have the pressure due to a water head of 10 feet transmitted upward through the gas against the last layer of water, a foot or so thick, so that this water would experience a momentary acceleration of the order of 10g and would be thrown violently upward. It is plausible that actions of this kind would be capable of projecting water to the heights observed.

REFERENCES

(1) "Experiments on the Pressure Wave thrown out by Submarine Explosions," by H. W. Hilliar, Research Experiment 142/19, 1919.

(2) "Ueber die Energie und Arbeitsfähigkeit von Explosivstoffen bei der Detonation," (On the Energy and Power of Explosives on Detonation), by A. Schmidt, Zeitschrift für das gesamte Schiess- und Sprengstoffwesen, vol. 30, p. 33, 1935, and "Ueber die Detonation von Sprengstoffen und die Beziehung zwischen Dichte und Detonationsgeschwindigkeit," (On the Detonation of Explosives and the Relation between Density and Speed of Detonation), by A. Schmidt, Zeitschrift für das gesamte Schiess- und Sprengstoffwesen, vol. 31, p. 364, 1936.

(3) "Detonation Theory and a Calculation for a TNT Sphere," by G. I. Taylor, Research Committee 178, 1941.

(4) "Report on a System of Submarine Mines," by Lt. Col. H. L. Abbot, USA, Professional Papers of the Corps of Engineers, U.S. Army, No. 23, Government Printing Office, Washington, 1881.

(5) "Massenbewegung des Wassers," (Mass Movement of Water), by Carl Ramsauer, Annalen der Physik, vol. 72, p. 265, 1923.

(6) "Etude theoretique des gerbes produites par les explosions sous-marines," (Theoretical Study of Jets produced by Underwater Explosions), by M. J. Ottenheimer, Memorial de l'artillerie francaise, vol. VIII, p. 325, 1929, "Sur le deplacement du front de gaz dans l'eau au cours d'une explosion sous-marine," (On the Displacement of the Interface during an Underwater Explosion), by M. J. Ottenheimer, ibid., vol. XII, pp. 75 and 980; "Sur la mechanique du choc sur l'eau," (On the Mechanics of Shock in Water), by M. J. Ottenheimer, ibid. vol. XII, p. 419.

(7) "The Pressure-Time Curve for Underwater Explosions," by W. G. Penney, (Research Committee 142), Civil Defense Research Committee, Home Ministry of Security, 1940, CONFIDENTIAL.

(8) "On Musical Air Bubbles and the Sounds of Running Water," by M. Minnaert, Philosophical Magazine 16, p. 235, 1933.

(9) Dr. W. Conyers Herring, oral communication, 1 August 1941.

(10) "Fortpflanzung ebener Luftwellen von endlicher Schwingungsweite," (Propagation of Plane Atmospheric Waves of Finite Amplitude), by Bernhard Riemann, Königliche Gesellschaft der Wissenschaften zu Göttingen, Gesammelte Werke VIII, 1860.

(11) "Aerial Waves of Finite Amplitude," by Lord Rayleigh, Royal Society Proceedings, vol. 84, p. 247, 1910.

(12) "Impact Waves and Detonation." Parts I and II. By R. Becker, Zeitschrift für Physik, vol. 8, p. 321, 1922. Translated in N.A.C.A. Techical Memorandums 505, 506.

(13) "Explosion und Explosionswellen," (Explosions and Explosion Waves), by Erwin Bollé, Handbuch der physikalischen und technischen Mechanik, VI, 1927.

(14) "On the Air Resistance of Projectiles," by Paul S. Epstein, National Academy of Sciences, Proceedings, 17, p. 532, 1931.

(15) "Propagation du mouvement dans les corps," (Propagation of Movement in Solids), by H. Hugoniot, Journal de l'ecole polytechnique, vol. 57, p. 3, 1887, and vol. 58, p. 1, 1889.

(16) "Fortpflanzungsgeschwindigkeit und Impulsstärke von Verdichtungsstössen," (Speed of Propagation and Strength of Impulse of Shock Waves), by Reinhold Rüdenberg, Artilleristische Monatshefte, 237, 285, 1916.

(17) "Explosions sous l'eau," (Underwater Explosions) by Divis and Röthing, Memorial de l'artillerie francaise, vol. XI, p. 515, 1932.

(18) "Resistance of Structures to Explosive Load," account of the Conference of 19 September 1940 issued by the David Taylor Model Basin, November 1940.

(19) "Final Report on the Hydrodynamical Theory of Detonation and Shock Waves," by G. B. Kistiakowsky and E. Bright Wilson, Jr., National Defense Research Council, Division B, Serial Number 52, 1941.

(20) National Defense Research Council Conference Report C4-Series 20-010 by Dr. W. Conyers Herring.

APPENDIX I
SMALL AMPLITUDES

For convenience of reference a summary will be given here of certain parts of the theory of compressive waves. For references see especially, besides books on sound, Lamb's Hydrodynamics and references to Riemann (10), Rayleigh (11), Becker (12), Bollé (13), and Epstein (14) at the end of the report.

It is convenient to divide compressive waves arbitrarily into three types, which will be discussed in turn. It will be assumed, except where stated, that effects due to heat conduction, viscosity, and thermal hysteresis are negligible.

I. WAVES OF SMALL AMPLITUDE - THE LINEAR THEORY

As the amplitude of compressive waves is made progressively smaller, the waves come to possess more perfectly certain simple properties; in the differential equations describing them, certain terms become negligible and the equations are then of the type called linear. The stock example is ordinary sound waves. The properties in question, predicted by theory and confirmed by experiment, are:

1. UNIFORM VELOCITY

The velocity c at which the waves travel through the medium is given by the formula

$$c = \sqrt{\frac{dp}{d\rho}} \qquad [1]$$

where p is the pressure in the medium and ρ is its density. The value of c is independent of wave length, and the relation between p and ρ follows the adiabatic law.

In water, c increases slightly with rise of temperature or with increase of pressure. Some values of c at 15 degrees centigrade (59 degrees fahrenheit) and 1 atmosphere, expressed in feet per second, are:

	Pure Water	Average Sea Water	Steel	Copper	Air
c =	4810	4930	16,400	11,670	1120 ft/sec

2. UNIFORM FORM

The Form of a plane wave does not change as the wave progresses.

3. SUPERPOSABILITY

Small waves can be superposed on each other, as occurs when two trains of waves meet. The resultant pressure is the sum of the component pressures, the resultant particle velocity is the vector sum of the particle velocities. The energy, however, exhibits the familiar phenomenon of interference, in exact analogy with light waves.

4. PRESSURE AND PARTICLE VELOCITY

Pressure and particle velocity are definitely related to each other in progressive waves.* The form of this relationship is somewhat different, however, in plane and in spherical waves.

In *plane* waves the "pressure" p (i.e., the excess of pressure above normal) and the particle velocity u are related by the equation

$$p = \rho c u \qquad [2]$$

where ρ is the density of the undisturbed fluid.

The coefficient ρc may be called the acoustic or radiative impedance of the fluid (also called "acoustic resistivity," although no dissipation of mechanical energy is involved). Some values of ρc are as follows, expressed for convenience in units suggested by the relation, $\rho c = p/u$, the pressure p being expressed in pounds per square inch and the velocity c in feet per second:

	Pure Water	Average Sea Water	Steel	Copper	Air (15 degrees Centigrade, 76 cm)
$\rho c \left(\frac{\text{lb}}{\text{in}^2}/\frac{\text{ft}}{\text{sec}}\right)$	64.8	68.17	1720	1400	0.0185

In English gravitational units, the values of ρc are equal to those given here multiplied by 144. The value of ρc is more than 3000 times as great in water as it is in air, because both the density and the elasticity are much greater. In a sound wave, where the pressure is 1 pound per square inch above normal, the particle velocity is less than 1/5 inch per second in water but 54 feet per second in air.

As a *spherical* wave moves outward from a center, the magnitude of the excess pressure, positive or negative, decreases in inverse ratio to the distance r from the center. The particle velocity, however, does not possess a unique relationship to the pressure at the same point, as it does in plane waves. The reason is that the decrease in magnitude of the pressure as r increases gives rise to an additional component in the pressure gradient, over and above that component which is involved in the propagation of the wave; and because of this additional pressure gradient, a compression accelerates the water outward while passing through it, whereas a rarefaction accelerates it inward. The additional acceleration thus produced by spherical waves is proportional to p/r.

The particle velocity u in a train of spherical waves spreading out from a center, at a point where the excess pressure is p, is given by the formula

$$u = \frac{p}{\rho c} + \frac{1}{\rho r}\int_{t_0}^{t} p'dt' + u_0 \qquad [3]$$

Here u is called positive when its direction is outward. The symbol u_0 stands for the particle velocity at the point in question at a time t_0 at which $p = 0$; and $\int_{t_0}^{t} p'dt'$

* The term "progressive" is meant to imply a disturbance traveling in a definite direction, as opposed to "standing" waves or any other admixture of progressive wave trains.

is the integral of the excess pressure with respect to the time, or the impulse, at the point in question from time t_0 up to the time t to which u and p refer. Since p itself falls off as $1/r$ as the wave moves outward, the additional velocity represented by the second term on the right in [3] varies from point to point as $1/r^2$. This term is thus of importance only near the source of the waves.

The name afterflow will be given to the part of the velocity represented by the second term on the right in Equation [3]. Each part of the pressure wave, as it passes outward from the center, makes a contribution to the afterflow whose magnitude is proportional to $1/r^2$.

5. ENERGY AND MOMENTUM

In plane progressive waves of small amplitude the energy at any point is half kinetic and half potential. If E is the energy density or energy per unit volume, and M is the momentum per unit volume,

$$E = \rho u^2 = \frac{p^2}{\rho c^2}, \qquad M = \rho u = \frac{p}{c} \qquad [4a,b]$$

If I is the intensity of the wave, or the energy transferred across unit area per second as the wave advances,

$$I = cE = \rho c u^2 = \frac{p^2}{\rho c} \qquad [5]$$

In sea water, if I_{in} denotes I expressed in foot-pounds per square inch per second, and if p_{in} denotes p expressed in pounds per square inch,

$$I_{in} = \frac{1}{68.2}\, p_{in}^2 \qquad [6]$$

In small waves the energy transferred equals the work done by the pressure p on the water moving with speed $u = p/\rho c$.

II. REFLECTION OF SMALL-AMPLITUDE WAVES

When a plane wave encounters a plane surface at which the nature of the medium changes abruptly, the wave divides into two waves, one of which travels into the second medium as a transmitted wave, while the other returns into the first medium as a reflected wave. The conditions to be satisfied at the interface are that the net pressure and particle velocity must be the same on both sides of the interface.

Let the incidence be normal, and let p, p', p'' denote the excess pressure (above normal) in the incident, transmitted, and reflected waves, respectively (Figure 14). Let the particle velocity be measured positively in the direction of propagation of the incident wave. Then, if u, u', u'' denote the corresponding particle velocities, and if ρ_1, c_1 and ρ_2, c_2 denote density and speed of sound in the first and second mediums, respectively, we have $p = \rho_1 c_1 u$, $p' = \rho_2 c_2 u'$, $p'' = -\rho_1 c_1 u''$ (the negative sign because of the reversed direction of propagation). At the interface

$$p + p'' = p', \quad u + u'' = u'$$

or

$$\frac{p}{\rho_1 c_1} - \frac{p''}{\rho_1 c_1} = \frac{p'}{\rho_2 c_2}$$

Solving,

$$p' = \frac{2\rho_2 c_2}{\rho_1 c_1 + \rho_2 c_2}\, p, \quad p'' = \frac{\rho_2 c_2 - \rho_1 c_1}{\rho_1 c_1 + \rho_2 c_2}\, p \qquad [7a,b]$$

The *reflection coefficient*, or fraction of the incident energy that is reflected, is

$$R = \left(\frac{p''}{p}\right)^2 = \left(\frac{\rho_2 c_2 - \rho_1 c_1}{\rho_1 c_1 + \rho_2 c_2}\right)^2 \qquad [8]$$

We note that everything depends upon the acoustic impedances of the medium. If these are equal ($\rho_1 c_1 = \rho_2 c_2$), no reflection occurs. If $\rho_1 c_1 < \rho_2 c_2$, p'' and p have the same sign, that is, compressions are reflected as compressions and rarefactions as rarefactions; if $\rho_1 c_1 > \rho_2 c_2$, p'' and p have opposite signs, so that compressions are reflected as rarefactions, and vice versa. If $c_2 = 0$, or if $\rho_2 = 0$ as for vacuum, $R = 1$, reflection being total.

Some numerical values for waves in sea water reflected from various mediums are:

	Steel	Copper	Air
R	0.85	0.82	1 - 0.0011
p'/p	0.92	0.91	- 0.99946

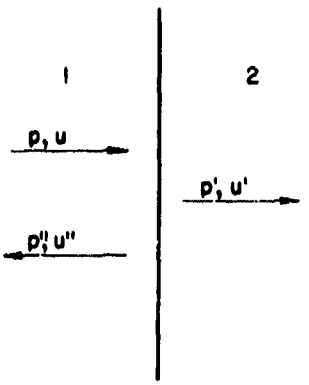


Figure 14

1. OBLIQUE INCIDENCE

If a plane sound wave falls upon a plane interface at an angle of incidence θ (Figure 15), the problem of reflection is easily treated provided one medium can be assumed to slide without friction over the other. Then, equating components of the particle velocity perpendicular to the interface in the two mediums, we obtain

$$\frac{p'}{p} = \frac{2\rho_2 c_2 \cos\theta}{\rho_2 c_2 \cos\theta + \rho_1 c_1 \cos\theta'},$$

$$\frac{p''}{p} = \frac{\rho_2 c_2 \cos\theta - \rho_1 c_1 \cos\theta'}{\rho_2 c_2 \cos\theta + \rho_1 c_1 \cos\theta'} \qquad [9a,b]$$

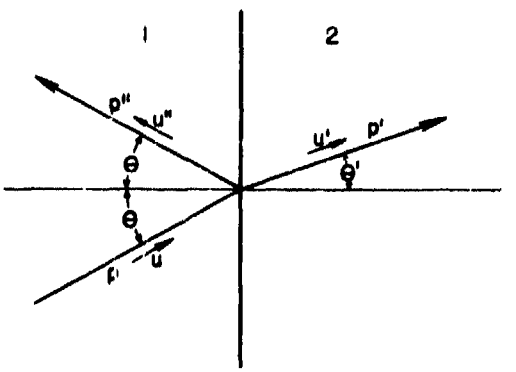


Figure 15

θ' being the angle of refraction so that

$$c_2 \sin\theta = c_1 \sin\theta' \qquad (10)$$

As before, the coefficient of reflection is $R = (p''/p)^2$.

If, however, as in all actual cases, sliding between the mediums does not occur, the boundary conditions cannot be satisfied merely by superposing upon the incident wave a reflected and a refracted one. A local disturbance must then occur near the interface, which involves shearing motion in both mediums. There should, however, be no appreciable effect upon the waves, so long as the amplitude remains small. If the waves are not spherical, or if $c_2 \sin\theta > c_1$, so that total reflection occurs, the phenomena at the interface are more complicated. Special effects due to this cause are utilized in geophysical sound-ranging.

III. WAVES OF FINITE AMPLITUDE

Waves of appreciable amplitude should possess none of the properties listed for waves of indefinitely small amplitude, except in approximate degree as the amplitude becomes rather small. In water, effects of finite amplitude should be appreciable at wave pressures exceeding 2000 pounds per square inch.

The various parts of a wave of finite amplitude travel at different speeds for two reasons. In the first place, the wave is carried along by the medium in its motion; and in the second place, the wave velocity itself usually increases with increasing density of the medium. Hence regions of higher pressure are propagated through space faster than regions of lower pressure. Consequently, a compression, as it advances should become progressively steeper at the rear, as suggested in Figure 16. There is some experimental evidence in support of this conclusion from theory, at least in the case of sound waves in air.

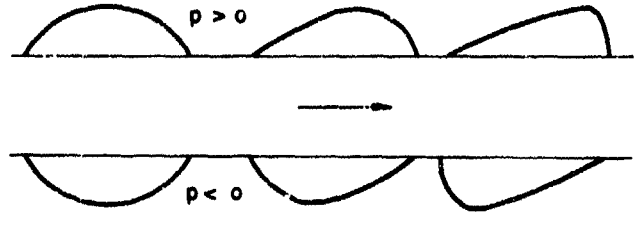


Figure 16

The final result of such a process would obviously be the production of infinite gradients, i.e., discontinuities of pressure and of particle velocity. When a discontinuity comes into existence, however, the ordinary laws of hydrodynamics fail. A special theory for the further propagation of such discontinuities has been given by Riemann (10) and Hugoniot (15). This theory will next be described.

IV. SHOCK FRONTS

Let P be a plane dividing the medium into two parts, and let the total pressure in the medium be p_1 on one side of this plane, and p_2 on the other side. Let the corresponding densities of the medium be ρ_1 and ρ_2. Let the medium on the first side be moving with velocity u_1, and that on the second side with velocity u_2, the motion being perpendicular to the plane and the positive direction for u being taken from medium 2 toward medium 1 (Figure 17). Thus at P a discontinuity may exist not only in the pressure and the density, but also in the particle velocity. It was shown by Riemann that the laws of the conservation of matter and of momentum could be satisfied by assuming that the discontinuity at P propagates itself from medium 2 into medium 1 at at a velocity U given by Equation [11], provided u_1 and u_2 have values such that Equation [12] is satisfied. Such a self-propagating discontinuity is called a *shock front*.

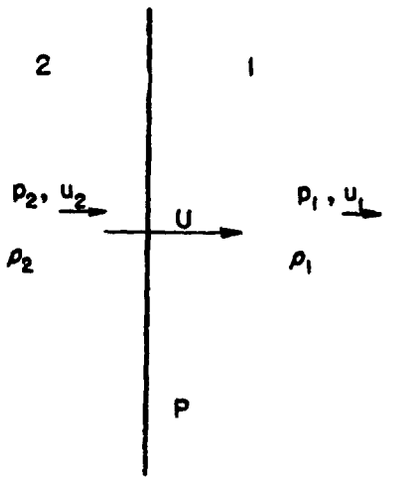


Figure 17

As the shock front advances, successive portions of the medium undergo a discontinuous change from density ρ_1 and pressure p_1 to ρ_2 and p_2, at the same time being accelerated from velocity u_1 to u_2. It was pointed out by Hugoniot that a certain change in the energy of the medium would also be required by the law of the conservation of energy. He showed that if E_1, E_2 denote the internal energy per unit mass of the medium in the two regions, then the difference, $E_2 - E_1$, must have the value given by Equation [13]. In ordinary sound waves E varies with ρ according to the law that holds for adiabatic changes of density, the change of E representing the work done by the pressure in compressing or rarefying the medium. To satisfy Equation [13], E must vary with ρ more rapidly than according to the adiabatic law.

Now in the phenomena of viscosity and of the conduction of heat we are familiar with irreversible processes by which the internal energy of a medium can be increased, with an accompanying increase in its entropy. No process can be imagined by which the energy might be decreased; probably such a process would violate the second law of thermodynamics. Hence it is assumed that a continuous irreversible conversion of mechanical energy into heat occurs in the shock front, of sufficient magnitude to make Equation [13] hold. The energy thus converted is brought up to the shock front as it progresses by the ordinary processes of mechanical transmission of energy through the medium.

It can be shown that positive amounts of energy will be delivered to the shock front only if $\rho_2 > \rho_1$, and hence $p_2 > p_1$. Thus only shock fronts of compression can occur.

In such a shock front the medium undergoes a sudden compression, and its temperature rises by an amount greater than the rise of temperature due to an adiabatic compression of the same magnitude.

A further condition for the existence of a shock front may be derived from Equation [12], in which the positive square root is meant and hence it is necessary that $u_2 > u_1$.

Thus we have for the velocity U with which the shock front travels in the direction toward medium 1, the change in internal energy of the medium produced by its passage, and the necessary conditions for its existence:

$$U = u_1 + \sqrt{\frac{p_2}{\rho_1}\,\frac{p_2 - p_1}{\rho_2 - \rho_1}} = u_2 + \sqrt{\frac{\rho_1}{\rho_2}\,\frac{p_2 - p_1}{\rho_2 - \rho_1}} \qquad [11]$$

$$u_2 - u_1 = \sqrt{\frac{1}{\rho_1 \rho_2}\,(p_2 - p_1)(\rho_2 - \rho_1)} \qquad [12]$$

$$E_2 - E_1 = \frac{1}{2}\,(p_1 + p_2)\left(\frac{1}{\rho_1} - \frac{1}{\rho_2}\right) \qquad [13]$$

$$u_2 > u_1,\ \rho_2 > \rho_1,\ p_2 > p_1 \qquad [14]$$

Equation [13] is known as the *Hugoniot relation*.

From Equation [11] it can be shown that the shock front advances through medium 1 faster than does an ordinary sound wave in that medium, whereas its speed relative to medium 2 is less than the speed of sound in that medium, i.e., if c_1, c_2 are the respective speeds of waves of small amplitude in the two mediums,

$$\sqrt{\frac{\rho_2}{\rho_1}\,\frac{p_2 - p_1}{\rho_2 - \rho_1}} > c_1, \quad \sqrt{\frac{\rho_1}{\rho_2}\,\frac{p_2 - p_1}{\rho_2 - \rho_1}} < c_2$$

It follows that no effects from the shock front can be propagated into medium 1, and the values of ρ_1, p_1, u_1, will therefore be determined by conditions elsewhere in that medium. Effects of conditions elsewhere in medium 2, on the other hand, propagated with the speed of sound, can overtake the shock front. We can regard these effects as furnishing one condition for fixing the values of ρ_2 and u_2 just behind the front. Equations [12] and [13] furnish two other conditions for the determination of the four quantities ρ_2, u_2, p_2 and E_2; and a fourth relation is furnished by the functional relation between E, p and ρ that is characteristic of the medium.

Since the existence of a shock front involves a continual dissipation of energy, it may be expected that shock fronts will usually weaken as they advance and ultimately disappear. As the ratio p_2/p_1 or ρ_2/ρ_1 approaches unity, a shock front approximates to an ordinary sound wave, and its velocity of propagation U reduces to the speed of sound.

In a *physical medium*, actual discontinuities are doubtless impossible. If the theory is amplified so as to allow for the influence of viscosity and of heat conduction, which are ignored in the ordinary theory of compressive waves, it is found

that there is a limit to the steepness of the pressure gradient that can be propagated through a medium (11), (12). Waves of intense steepness can occur, however, in which conditions on the two sides of the steep gradient are related by the shock-front Equations, [11] to [14]. Such waves might be called *physical shock fronts*, in contrast to the mathematical shock fronts just discussed. The thickness of a physical shock front should be of microscopic magnitude (for the method of estimating, see Reference (12)).

The theoretical determination of the distribution of pressure within an intense physical shock front presents a difficult problem because the ordinary theory of viscosity and of the conduction of heat may be expected to fail when the thickness of the front ceases to be large as compared with the distances between molecules. Furthermore, various forms of thermal hysteresis are likely to occur.

A certain amount of experimental evidence exists in support of the theory of shock fronts, especially as to the occurrence of speeds of propagation much exceeding that of ordinary sound waves.

Detonation waves in explosives are believed to be shock waves in which a chemical transformation occurs almost instantaneously as the wave passes. Because of the chemical change, an enormous rise of temperature occurs, and the pressure increases, as the wave passes, much more than it would owing to the increase in density alone.

APPENDIX II
RADIAL NON-COMPRESSIVE FLOW ABOUT A CENTRAL CAVITY

I. FUNDAMENTAL EQUATIONS

When incompressible homogeneous liquid flows with radial symmetry about a point O, its velocity u outward from O can be written

$$u = \frac{u_n}{r^2} \qquad [1]$$

where r denotes radial distance from O, and u_n the velocity at $r = 1$, which may be a function of the time. Suppose the space within a sphere of radius r_g about O is free from liquid; it may be empty or it may contain gas. Let u_g denote the value of u at $r = r_g$. Then $u_g = u_n / r_g^2$ and we can also write

$$u = u_g \left(\frac{r_g}{r}\right)^2 \qquad [2]$$

Because of this simple distribution of the velocity, it is possible to integrate the equation of motion of the liquid,

$$\frac{\partial u}{\partial t} + u \frac{\partial u}{\partial r} = -\frac{1}{\rho} \frac{\partial p}{\partial r} \qquad [3]$$

where p is pressure, t is time, ρ is density. From [1]

$$\frac{\partial u}{\partial t} = \frac{1}{r^2} \frac{d}{dt} u_n \qquad [4]$$

Hence we can write [3] in the form

$$\frac{1}{r^2} \frac{d}{dt} u_n + \frac{1}{2} \frac{\partial}{\partial r} u^2 + \frac{1}{\rho} \frac{\partial p}{\partial r} = 0$$

Taking $\int_r^\infty dr$ of each term in this equation and noting that

$$\int_r^\infty \frac{dr}{r^2} = \frac{1}{r}, \quad \int_r^\infty \frac{\partial p}{\partial r} dr = p_0 - p$$

where p_0 is the pressure at infinity and p that at distance r, we obtain

$$\frac{1}{r} \frac{d}{dt} u_n - \frac{1}{2} u^2 + \frac{1}{\rho} (p_0 - p) = 0$$

$$p = \rho \left(\frac{1}{r} \frac{d}{dt} u_n - \frac{1}{2} u^2\right) + p_0 \qquad [5]$$

This equation can be written in two other useful forms by using [4] or by writing, from [1], $u_n = r_g^2 u_g$:

$$p = \rho \left(r \frac{\partial u}{\partial t} - \frac{1}{2} u^2\right) + p_0 \qquad [6]$$

$$p = \rho \left[\frac{1}{r} \frac{d}{dt} (r_g^2 u_g) - \frac{1}{2} u^2\right] + p_0 \qquad [7]$$

Equation [6] expresses the pressure p at any point in terms of the velocity near that point. Equation [7] connects p with conditions at the cavity. Another expression for p, containing the pressure p_g at the cavity, is obtained if we write down [5] for $r = r_g$, namely,

$$p_g = \rho \left(\frac{1}{r_g} \frac{d}{dt} u_n - \frac{1}{2} u_g^2\right) + p_0$$

and eliminate u_s between this equation and [5]

$$p = \frac{r_s}{r}\left(p_s + \tfrac{1}{2}\rho u_s^2 - p_0\right) - \tfrac{1}{2}\rho u^2 + p_0 \qquad [8]$$

The impulse at any point distant r from the center can be found from [6] or [7]

$$\int (p - p_0)\,dt = \rho r \Delta u - \frac{1}{2}\rho \int u^2 dt = \frac{\rho}{r}\Delta(r_s^2 u_s) - \frac{1}{2}\rho \int u^2 dt \qquad [9]$$

where Δ denotes the change of a quantity during the time of integration. If r is large, $\int u^2 dt$ can be neglected.

II. OSCILLATIONS OF A BUBBLE IN INCOMPRESSIBLE LIQUID

Suppose now that the cavity contains gas of negligible mass; let the gas behave adiabatically, losing or gaining energy only by doing work upon the liquid. An equation of motion for the bubble of gas can be obtained by putting in [7] $p = p_s$, $r = r_s$ and $u = u_s$, carrying out the differentiation, and noting that $u_s = dr_s/dt$:

$$p_s = \rho\left[\frac{3}{2}\left(\frac{dr_s}{dt}\right)^2 + r_s\frac{d^2 r_s}{dt^2}\right] + p_0 \qquad [10]$$

Multiplying this equation through by $r_s^2\,dr_s/dt$ and then integrating with respect to the time, we obtain successively

$$p_s r_s^2 \frac{dr_s}{dt} = \rho\left[\frac{3}{2}\,r_s^2\left(\frac{dr_s}{dt}\right)^3 + r_s^3\,\frac{dr_s}{dt}\,\frac{d^2 r_s}{dt^2}\right] + p_0 r_s^2\,\frac{dr_s}{dt}$$

$$\int p_s r_s^2\,dr_s = \frac{1}{2}\rho r_s^3\left(\frac{dr_s}{dt}\right)^2 + \frac{1}{3}p_0 r_s^3 + const. \qquad [11]$$

Now the volume of the gas is

$$v_s = \frac{4\pi r_s^3}{3} \qquad [12]$$

hence

$$p_s r_s^2\,dr_s = \frac{1}{4\pi}\,p_s\,dv_s = -\frac{dW}{4\pi} \qquad [13]$$

where W is the energy of the gas. Thus we can write

$$\int p_s r_s^2\,dr_s = -\frac{W}{4\pi} + const.$$

Then Equation [11] can be written

$$\left(\frac{dr_s}{dt}\right)^2 = \frac{C}{r_s^3} - \frac{W}{2\pi\rho r_s^3} - \frac{2}{3}\,\frac{p_0}{\rho} \qquad [14]$$

where C is an arbitrary constant dependent on the initial conditions. If the gas is ideal, and if the ratio γ of its specific heats is also constant,

$$W = \frac{p_s v_s}{\gamma - 1}\,,\quad p_s v_s^\gamma = A = const.$$

and, using [12] we find

$$-\frac{W}{2\pi\rho r_s^3} = -\left(\frac{3}{4\pi}\right)^{\gamma-1}\frac{A}{2\pi\rho(\gamma-1)}\,\frac{1}{r_s^{3\gamma}} \qquad [15]$$

In any case, let the constant of integration in W be so chosen that $W>0$.

Since $W \to \infty$ as $r_g \to 0$, the right-hand member of [14] is negative at $r_g = 0$ and at $r_g = \infty$. If C is large enough, however, it will be positive between two values $r_g = r_1$ and $r_g = r_2$ which are the roots of

$$\frac{C}{r_g^3} - \frac{W}{2\pi\rho r_g^3} - \frac{2}{3}\frac{p_0}{\rho} = 0 \qquad [16]$$

Then the bubble will oscillate between the radii r_1 and r_2 with a period T given by

$$T = 2\int_{r_1}^{r_2} \left(\frac{dr_g}{dt}\right)^{-1} dr_g \qquad [17]$$

the integrand being given in terms of r_g by [14]. Even if the gas is ideal, the integration involves, in general, unfamiliar functions.

1. SMALL OSCILLATIONS

Let r_0 be the value of r_g at which the bubble is in equilibrium, with its pressure $p_g = p_0$. If it is slightly disturbed from this position, it will execute simple harmonic oscillations about $r_g = r_0$. For such motions, we can neglect $(dr_g/dt)^2$ in Equation [10] and also put $r_g = r_0$ obtaining

$$\frac{d^2 r_g}{dt^2} = \frac{1}{\rho r_0}(p_g - p_0)$$

Since $p_g - p_0$ is small, we can write

$$p_g - p_0 = (r_g - r_0)\frac{dp_g}{dr_g}$$

The period of the oscillation is, therefore, from the usual formula for harmonic oscillations,

$$T_0 = 2\pi(\rho r_0)^{\frac{1}{2}}\left(-\frac{dp_g}{dr_g}\right)^{-\frac{1}{2}} \qquad [18]$$

the derivative being evaluated at $r_g = r_0$.

If the gas is ideal, so that $p_g v_g^\gamma = p_g\,(4\pi r_g^3/3)^\gamma = \text{const.}$,

$$p_g = p_0\left(\frac{r_0}{r_g}\right)^{3\gamma}, \quad \frac{dp_g}{dr_g} = -\frac{3\gamma p_0}{r_g}\left(\frac{r_0}{r_g}\right)^{3\gamma-1}$$

Hence

$$T_0 = 2\pi r_0\sqrt{\frac{\rho}{3\gamma p_0}} \qquad [19]$$

2. LARGE OSCILLATIONS

As the amplitude of the oscillation increases, the period, given by [17], increases slowly. For $r_2/r_1 = 5.9$, numerical integration gives $T = 1.30\ T_0$ (20). When the ratio r_2/r_1 becomes large, a good approximation can be obtained as follows:

At $r = r_1$ the term containing W in [16] or on the right in [14] cannot exceed the term containing C, else the whole would be negative. As r increases from r_1, the W term decreases faster than the C term. Hence, if r_2/r_1 is large, the W term is

negligible over most of the range from r_1 to r_2 and especially near $r_0 = r_2$. Let us, therefore, drop this term altogether. Then [16] gives

$$C = \frac{2}{3}\frac{p_0}{\rho} r_2^3 \qquad [20]$$

Furthermore, since the range of integration greatly exceeds r_1, little error will result if we also extend the range back to $r_0 = 0$. Then [17], [14] and [20] give

$$T = 2\left(\frac{3\rho}{2p_0}\right)^{\frac{1}{2}} \int_0^{r_2} \frac{dr_0}{\left[\left(\frac{r_2}{r_0}\right)^3 - 1\right]^{\frac{1}{2}}}$$

Write

$$r_0 = r_2 \sin^{\frac{2}{3}}\theta, \quad dr_0 = \left(\frac{2}{3}\right) r_2 \sin^{-\frac{1}{3}}\theta \cos\theta\, d\theta$$

Then

$$T = \frac{4}{3}\left(\frac{3\rho}{2p_0}\right)^{\frac{1}{2}} r_2 \int_0^{\frac{\pi}{2}} \sin^{\frac{2}{3}}\theta\, d\theta$$

The integral can be expressed in terms of gamma functions or evaluated numerically; its value is 1.124.

In the applications, however, it is more convenient to express T in terms of the maximum energy W_1 of the gas, which is its energy at minimum size, when $r_0 = r_1$. Since r_2/r_1 is assumed large, it is evident from [20] that, when $r_0 = r_1$, the first term in [16] is much larger than the third and must, therefore, be nearly equal to the second. Hence, with the help of [20],

$$\frac{W_1}{2\pi\rho} = C = \frac{2}{3}\frac{p_0}{\rho} r_2^3, \quad r_2 = \left(\frac{3}{4\pi}\frac{W_1}{p_0}\right)^{\frac{1}{3}} \qquad [21a,b]$$

approximately. Thus, evaluating the constants,

$$T = 1.83\, r_2 \sqrt{\frac{\rho}{p_0}} = 1.14\, \rho^{\frac{1}{2}} p_0^{-\frac{5}{6}} W_1^{\frac{1}{3}} \qquad [22]$$

valid for large r_2/r_1 (perhaps $r_2/r_1 > 10$).

APPENDIX II
3. PRESSURE AND IMPULSE

III. PRESSURE AND IMPULSE IN THE LIQUID

The pressure p at any point in the liquid, as the bubble oscillates, is given by [8] in terms of the pressure p_0 of the gas and the velocity u_0 or dr_0/dt of the interface, which is given in turn by [14]. Or, in Equation [7] the pressure is given in terms of r_0 and u_0. To find p as a function of the time, Equation [14] must be integrated.

Expressions for the impulse in the liquid are easily obtained from [6] and

[7]. At large r, the Bernouilli term $(1/2)\rho u^2$ can be neglected. Hence, integrating, we obtain

$$\int (p - p_0)\,dt = \rho r \Delta u = \frac{\rho}{r}\,\Delta(r_g^2 u_g) \qquad [23]$$

where u denotes the velocity of the liquid at the point in question, and Δ the total change during the time covered by the integration. The value of r is held constant here whereas r_g varies with the time.

The total positive impulse during an oscillation can then be found, provided we know the maximum value of $r_g^2 u_g$. From [14]

$$r_g^2 u_g = \left(C r_g - \frac{W}{2\pi\rho}\, r_g - \frac{2}{3}\,\frac{p_0}{\rho}\, r_g^4\right)^{\frac{1}{2}} \qquad [24]$$

This is a maximum for such a value of r_g that

$$C - \frac{W}{2\pi\rho} - \frac{8}{3}\,\frac{p_0}{\rho}\, r_g^3 = 0$$

In the case of large oscillations, i.e., large r_2/r_1, this last equation can be solved approximately. For then we can write it, using [20],

$$\frac{2}{3}\,\frac{p_0}{\rho}\, r_2^3 - \frac{8}{3}\,\frac{p_0}{\rho}\, r_g^3 = \frac{W}{2\pi\rho}$$

The value, $r_g = 4^{-\frac{1}{3}} r_2$, is too large, for it makes the left side of this equation zero; but for such values of r_g, as we have seen, $W/2\pi\rho$ is small as compared with C or $(2p_0/3\rho)\, r^3$. Hence a small decrease in r_g will satisfy the equation. Neglecting this decrease, we have, therefore, approximately,

$$r_g = \frac{r_2}{4^{\frac{1}{3}}}$$

Inserting this value of r_g in [24], dropping the term in W, and using [21a,b], we find

$$(r_g^2 u_g)_{max} = \left(\frac{2}{\rho}\right)^{\frac{1}{2}} p_0^{-\frac{1}{6}} \left(\frac{3 W_1}{16\pi}\right)^{\frac{2}{3}}$$

Inserting twice this value for $\Delta(r_g^2 u_g)$ in [23], we obtain finally for the total positive impulse, during the part of the oscillation in which $p > p_0$, at a large distance r from the center,

$$\int_+ (p - p_0)\,dt = \frac{0.432}{r}\, \rho^{\frac{1}{2}}\, p_0^{-\frac{1}{6}}\, W_1^{\frac{2}{3}} \qquad [25]$$

THE HYDRODYNAMIC THEORY OF DETONATION AND SHOCK WAVES

G. B. Kistiakowsky, E. Bright Wilson, Jr.
Harvard University

and

R. S. Halford
Columbia University

American Contribution

1941

THE HYDRODYNAMIC THEORY OF DETONATION AND SHOCK WAVES

by

G. B. Kistiakowsky, E. Bright Wilson, Jr.
Harvard University

and

R. S. Halford, Columbia University

1941

Abstract

The fundamental equations of the hydrodynamic theory of one-dimensional shock waves, i.e. the equations of conservation of mass, momentum and energy, are developed. These are used to calculate the properties (velocity, mass-velocity, temperature and pressure rise) in shock waves in air and water. With one additional equation, they suffice to permit a calculation of detonation velocities in gaseous and solid explosives. Predictions of detonation velocities as a function of loading density are thereby achieved, accurate to a few percent. Pressures, temperatures and mass-velocities inside the explosive are also computed. The question of the rarefaction wave following the detonation front in the explosive is investigated. The initial velocity, pressure etc. of the shock wave produced at the end of a stick of explosive are calculated successfully. The dying away of shock waves, problems of reflection etc. are also discussed briefly.

TABLE OF CONTENTS

Part I. Basic Principles

Sec.		Page
1.	Introduction	1
2.	Basic Differential Equations	3
3.	Conditions at a Discontinuity	4
4.	Simple Shock Waves in an Ideal Gas	5

Part II. Calculation of Detonation Velocities

5.	Chapman-Jouget Condition for Detonation Velocity	8
6.	Gaseous Explosions	12
7.	Solid Explosives	15
8.	The Equation of State	17
9.	Practical Calculation of the Ideal Detonation Velocity	18
10.	Calculation of D/D_1	21
11.	Determination of Covolumes and Comparison with Experiment	24

Part III. Properties of Shock and Rarefaction Waves

12.	Integration of the Energy Equation	27
13.	Riemann's Form of the Fundamental Equations	28
14.	Solution for Progressive Waves	30
15.	Simple Rarefaction Waves	31
16.	Simple Shock Waves in Air and in Water	32
17.	Rarefaction Wave Following Shock Wave	34
18.	Rarefaction Wave Following a Detonation Wave	36
19.	Phenomena at Boundaries: Reflection	38
20.	Calculation of the Velocity of the Shock Wave from an Explosion	40
21.	Some Remarks about Work in Progress	46

Tables

Properties of Shock Waves in Air (constant γ)	7
Comparison of calc. and obs. Detonation Velocities in H_2, O_2 mixtures	14
Effect of Equilibria on Ideal Detonation Rates	17
Covolume Constant vs. Density of Loading for PETN	25
Covolume Constants for Various Explosives	25
Properties of Shock Waves in Air (Variable γ)	33
Properties of Shock Waves in Water	33
Calc. and obs. Initial Shock Wave Velocities in Air	45
Mean Heat Capacities of Product Gases	47
Covolume Constants for Product Gases	47
Auxiliary Table for Calculation of Detonation Velocities	48
Auxiliary Table for Calculation of Shock Wave Velocities from Explosion	49
Table of Pressures, etc. in Some Common Explosives	49

References

50

Symbols

* On an equation no., means for ideal gases only.
1,2 as subscripts, refer to initial and final state.
a velocity of sound in ideal gas at P_1, V_1.
b Cv/nR (Sec. 20).
c velocity of sound.
c_v, c_p specific heats at constant V and P.
d differential symbol.
e base of exponentials.
f arbitrary function, Eq. (103).
G $1-\alpha z/b$ (Sec.20).
h arbitrary function of T (Sec. 20).
i subscript, meaning ideal state.
k constant in Eq. (89), also subscript for kth product.
n_1, n_2 no. of moles of gaseous products from M grams of explosive
q no. of carbon atoms
r no. of hydrogen atoms
s no. of oxygen atoms
t no. of nitrogen atoms, also time
v volume occupied by M grams
w piston velocity
x cartesian coordinate, also abbreviation for Kh/v.
y abbreviation, Eq. (35).
z abbreviation, Eq. (73).
A coef. in heat capacity Eq. (54).
B " " " " " "
C heat capacity at constant volume (M grams), $\bar{C}$ mean heat capacity.
D detonation or shock wave velocity.
E internal energy per unit mass.
F function of x, usually $1 + xe^{\beta x}$.
H subscript meaning differentiation along Hugoniot curve.
Hf heat of formation
K covolume constant, Eq. (51).
M molecular weight.
P pressure (usually c.g.s. units).
Q heat absorbed at constant volume per M grams.
R gas constant per mole.
S entropy per gram.
T absolute temperature.
T' constant of integration (Sec. 20).
U mass velocity.
V specific volume.
X coordinate of piston
α constant in Eq. of state.
β " " " " "
γ c_p/c_v
η abbreviation Eq. (15).
μ " Eq. (14).
δ thickness of slice.
ρ density.
τ time for piston
ϕ angle in Eq. (21).
ω abbreviation, Eq. (90).

PART I. BASIC PRINCIPLES

1. Introduction

a. The detonation velocity. When a stick of explosive is detonated from one end, the chemical reaction which occurs takes a very short, but nevertheless finite, time to travel to the other end. This velocity of propagation of the chemical reaction is called the detonation velocity (D) and is a constant for a given material and density, provided that some conditions are satisfied, e.g.: the stick is not too narrow, the particle size not too large, initiation was strong enough, etc.. The progress of the explosion down the stick is accompanied by an immediate and very large increase in pressure and temperature. In fact the pressure in the burnt gases immediately behind the detonation front may be as great as one hundred thousand atmospheres and the temperature may run from 3,000 to 5,000 degrees Centigrade. In addition, the burnt gases acquire a very high forward velocity. Whereas the detonation velocity, which is the velocity of progress of a condition and not of any matter, may run from 3,000 to 8,000 meters per second (ca. 7,000 to 18,000 mph!), the actual material velocity falls in the range 1,000 to 2,000 meters per second.

b. The reaction zone. The time required for the explosive to react essentially completely to the burnt gases is, under favorable conditions, so short that the zone in which reaction is taking place at any instant is apparently very narrow. Consequently a mathematical plane dividing the untouched explosive from the burning material travels along the stick with velocity D, followed very closely by the plane which divides the burning material from the essentially completely reacted gases. The rise in pressure, temperature and material velocity takes place in this narrow reaction zone. Little quantitative information is available about the thickness of this zone except that it must be quite narrow. It may well be that this thickness, which measures the steepness of the rise in pressure, is an important measure of the ability of the explosion to cause destruction. However, for the purpose of calculating the velocity of detonation its exact value is not important and for mathematical simplicity, the zone is assumed to be infinitely narrow.

c. Rarefaction behind the detonation. Even when the explosive is strongly confined in a pipe with the end containing the initiator closed, the region of high pressure, temperature and material velocity must be followed by a region in which the pressure and temperature are falling to somewhat lower values while the material velocity falls to zero. Such a travelling region of falling pressure is called a rarefaction wave. Its front moves with approximately the velocity D but its back surface moves somewhat more slowly, actually with the velocity of sound in the burnt gases in the condition in which they are left after the passage of the rarefaction wave. It will be shown that the detonation velocity D is equal to the velocity of sound in the heated, compressed gases in front of the rarefaction wave plus the material velocity of these gases. The rarefaction wave thus continually spreads out.

The rarefaction wave may affect the observed detonation velocity if the rarefaction wave follows so closely on the detonation front that the region of reaction is overlapped by the rarefaction. This phenomenon has been little studied but may account for the lower velocity observed in narrow tubes, in which the radial expansion also produces a rarefaction wave.

d. Theory of finite waves. Many of the above statements can be verified by direct experiment, while others are consequences of the hydrodynamic theory of detonation and shock waves, the subject of this report. This theory has been developed over the past century by many investigators and is now quite universally accepted as a valid treatment of the general features of the problem. The theory originally arose from a consideration of sound waves of finite amplitude so that it is worth while discussing these here.

The ordinary theory of sound is applicable only to waves of infinitesimal amplitude. Investigation shows that that part of a compressional pulse which is of greater amplitude travels faster than the parts of lower amplitude. Therefore the shape of the pulse changes as it moves along, the top tending to catch up with the front. The pulse thus becomes steeper and steeper. If viscosity and thermal conduction (and the finite time required to establish equilibrium) are neglected, the pulse will ultimately acquire an infinitely steep front; i.e. a discontinuity in pressure and temperature will be formed. This is called a shock wave. The material behind the shock wave also acquires a forward material velocity.

The formation of a discontinuous shock wave may be made to seem reasonable by the following qualitative argument. Let a piston in a long tube be given a sudden small velocity. A sound pulse will be formed which advances ahead of the moving piston with the velocity of sound in the medium. The gas in front of the piston and behind the sound pulse will be moving with the velocity of the piston. Now increase the velocity of the piston by another sudden small increment. A second pulse will start travelling with the velocity of sound relative to the moving gas and therefore actually travelling with the velocity of sound plus the previous velocity of the piston. This pulse will thus catch up to the first one. Carry this procedure further and it is clear that a piling up of pulses will occur which will produce a discontinuity.

e. Rarefaction waves contrasted with shock waves. Reversing the above arguments, we see that rarefaction waves of finite amplitude will tend to spread out instead of piling up. In the absence of viscosity etc., rarefaction waves are thermodynamically reversible phenomena, i.e., no change of entropy is involved and the ordinary laws of adiabatic expansion can be applied. Shock waves on the other hand are irreversible; there is a continual dissipation of energy into heat. This may seem strange when viscosity, etc., are neglected but if the shock front is infinitely steep, dissipation can be caused by infinitely small values of the viscosity and heat conduction.

f. Basic principles of hydrodynamic theory. It is assumed that everywhere in the material there is conservation of mass and energy and that all motions are governed by Newton's laws. Furthermore, for simplicity it is usually but not necessarily assumed that the viscosity, thermal conduction

and wall conduction are negligible. In any numerical calculation it is also necessary to have equation of state and specific heat data for the materials involved. Upon these simple and unquestionably valid foundations it is possible to build a theory which is capable of predicting a considerable fraction of the observed facts and in addition providing information not yet capable of direct observation.

2. Basic Differential Equations

In regions of space and time in which no discontinuities occur, the basic equations of conservation of mass, momentum and energy can be expressed as differential equations.

a. Conservation of mass. Consider a very thin slice of the material in the tube. Let the thickness of the slice be ξ, its pressure P, its density ρ and the absolute velocity U at any instant. The position of the slice along the length of the tube is given by the coordinate x. If the matter in the back face of the slice moves forward with the velocity U while that in the front face has the velocity $U + \frac{\partial U}{\partial x}\xi$, then the thickness of the slice will change with time as follows:

$$\frac{d\xi}{dt} = \xi \frac{\partial U}{\partial x} \tag{1}$$

The slice is a definite portion of matter so that its mass must remain constant. Therefore:

$$\frac{d}{dt}(\xi\rho) = 0, \tag{2}$$

or, combining equations (1) and (2),

$$\frac{d\rho}{dt} = -\rho \frac{\partial U}{\partial x}, \tag{3}$$

an equation which is an expression of the law of conservation of matter.

b. Conservation of momentum. Newton's law of motion can be expressed as follows. The force on the back face of the slice is P (for unit cross-section) while the force on the front face is $-P-\frac{\partial P}{\partial x}\xi$. Consequently the law of motion becomes

$$\rho \frac{dU}{dt} = -\frac{\partial P}{\partial x}, \tag{4}$$

where ξ has been cancelled from both sides.

c. Conservation of energy. The law of conservation of energy can be stated in the form: the increase in the internal energy and kinetic energy of the slice in unit time equals the net work done on the slice by the forces on its faces in that time. The work done on the back face is the force times

the distance it moves in one second, or PU. Consequently the energy equation is

$$\rho \frac{d}{dt} (E + 1/2\, U^2) = - \frac{\partial (PU)}{\partial x}, \tag{5}$$

where ρ has again been omitted from both sides. E is the internal energy (chemical and thermal) per unit mass. This equation may be expanded and then simplified by combining it with Eq. (3) and (4). The result is

$$\frac{dE}{dt} = (P/\rho^2) \frac{d\rho}{dt} . \tag{6}$$

Eq. (3), (4) and (6) are the fundamental equations which must be satisfied by ρ, P, E and U.

3. Conditions at a Discontinuity

The differential equations of Sec. 2 govern the situation wherever no discontinuities occur, but if there is a discontinuity in ρ, P or U the conditions of conservation limit the values of the density etc. across the discontinuity.

a. Basic equations. In a time dt an amount of mass $\rho_1(D - U_1)\, dt$ is brought up to a moving discontinuity (velocity D) from the right, if the subscript 1 denotes the properties immediately to the right of the discontinuity. The cross-sectional area is unity. The mass $\rho_2(D - U_2)\, dt$ is taken away on the left in the same time. When dt is made very small so that the layers on either side are infinitesimal, the matter brought up on the right must equal that removed on the left so that

$$\rho_1(D - U_1) = \rho_2(D - U_2), \tag{7}$$

even if D is not a constant.

Similarly, the change in momentum of a very thin slice of matter of mass $\rho_1(D - U_1)$ upon the passage of the discontinuity can be equated to the force acting; i.e.

$$\rho_1(D - U_1)(U_2 - U_1) = P_2 - P_1 . \tag{8}$$

Finally the work done on the slice by the forces acting must equal the increase in energy so

$$P_2U_2 - P_1U_1 = \rho_1(D - U_1)(E_2 - E_1 + \tfrac{1}{2} U_2^2 - \tfrac{1}{2} U_1^2), \tag{9}$$

where E is the internal energy per unit mass.

b. Another form for basic equations. From the above equations by straight algebra one obtains (if $V = 1/\rho$)

$$D = U_1 + V_1\sqrt{(P_2 - P_1)/(V_1 - V_2)}, \tag{10}$$

$$U_2 = U_1 + \sqrt{(P_2 - P_1)(V_1 - V_2)}, \tag{11}$$

$$E_2 - E_1 = \tfrac{1}{2}(P_1 + P_2)(V_1 - V_2). \tag{12}$$

Knowledge of the equation of state and heat capacity enables one to calculate $E_2 - E_1$ as a function of P_2 and V_2 so that Eq. (12) becomes a relation between P_2 and V_2 (for given P_1, V_1). This is called the Rankine[13] Hugoniot[7] relation. A typical curve of this kind is shown in Fig. 3-1. It should be noted that this curve

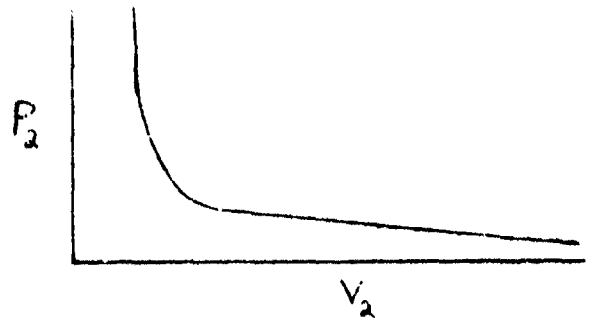


Fig. 3-1

is not the same as either the adiabatic or isothermal P-V curves.

Since there are three equations involving the quantities, P_1, V_1, U_1, D, P_2, V_2, U_2, a knowledge of P_1, V_1, U_1 and one of the others enables all to be computed.

A special type of discontinuity satisfying the above equations is worth noting. It is one in which $D=U_1=U_2$, $P_2=P_1$, but $V_1\neq V_2$ and $T_2\neq T_1$. Such a discontinuity (which may be a boundary between different kinds of gases, for example) would not be stable for long if heat conduction and diffusion were considered, but is of practical importance in the short time intervals of interest here.

The solution of a given problem is therefore determined if values of P, V and U can be found which satisfy the differential equations (3,4,6) wherever the properties are continuous, fit the relations (10-12) at all discontinuities, and are such that U equals U of the pistons, if any, closing the ends of the tube.

4. Simple Shock Waves in an Ideal Gas

a. General considerations. A simple and yet important application of the basic equations is to the problem of a shock wave produced in a perfect gas in a tube by a piston suddenly accelerated to a constant velocity w. Th

situation is shown in Fig. 4-1 in which the ordinate represents distance along the tube and the abscissa represents the time. The full line gives the position of the piston as a function of the time, while the dashed line shows the progress of the shock wave initiated by the sudden acceleration of the piston.

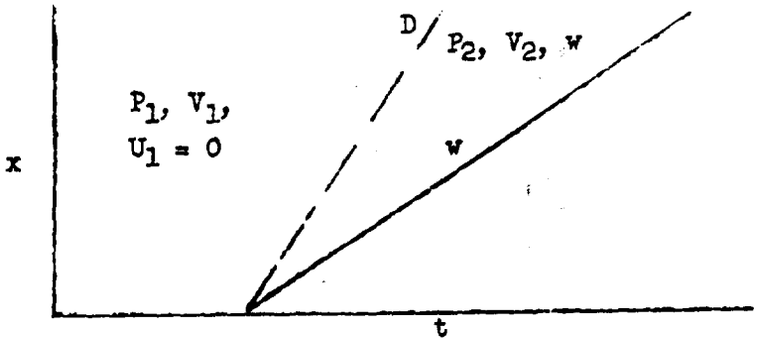


Fig. 4-1

The region in front of the gas is at rest with pressure P_1 and specific volume V_1. The gas behind the shock wave is at the higher pressure P_2, lower specific volume V_2 (higher density), and is moving with the uniform velocity w, that of the piston. The values of P_2, V_2, w, P_1 and V_1 are connected by the three basic equations of Sec. 3. The motion of the gas on other side of the shock wave must satisfy the differential equations of Sec. 2. Obviously, a mass of gas of uniform density and pressure moving at a uniform velocity does satisfy these equations. The three equations at the discontinuous shock front are just sufficient to specify the unknowns D, P_2 and V_2 in terms of the piston velocity w.

b. Application to an ideal gas.* If the heat capacity is assumed to be constant, the energy of a perfect gas is

$$E_2 - E_1 = c_v (T_2 - T_1), \qquad (13)^*$$

where c_v is the specific heat at constant volume and T the absolute temperature. Insertion of this and the equation of state

$$PV = RT/M$$

(R is gas constant per mole and M the molecular weight) into the basic equations of Sec. 3 leads to the following results.

$$D = a\left\{\mu + \sqrt{1 + \mu^2}\right\} \qquad (14)^*$$

$$= \eta + \sqrt{\eta^2 + \gamma P_1 V_1}\,, \qquad (15)^*$$

where $\mu = (1 + \gamma)w/4a$, $\eta = 1/4\ (1 + \gamma)w$,

and $a = \sqrt{\gamma RT_1/M} = \sqrt{\gamma P_1 V_1}$.

* Equations valid for ideal gases only will be marked with the symbol *.

Here $\underline{a}$ is the velocity of ordinary sound in the original medium, and $\gamma = c_p/c_v$, the ratio of the specific heats at constant pressure and volume. This expression reduces to D=a for w=0, as it should, and to

$$D \longrightarrow \tfrac{1}{2}(1+\gamma)\, w \qquad (16)^*$$

for w large. Furthermore, accurately,

$$P_2 - P_1 = Dw/V_1 \ , \qquad (17)$$

$$(V_2/V_1) = 1 - (w/D) \quad \underline{w \to \infty} \quad (\gamma-1)/(\gamma+1), \qquad (18)^*$$

and

$$T_2 - T_1 = \tfrac{1}{2}\left[(P_2 + P_1)/(P_2 - P_1)\right] w^2/c_v \ . \qquad (19)^*$$

The table shows the results of some calculations for shock waves in air, based on these equations. Here $a = 3.4\ 10^4$ cm./sec., $\gamma = 1.4$, $V_1 = 880$ cc. per gram, $c_v = 0.9 \times 10^7$ ergs/g./deg., $R/M = 2.87 \times 10^6$ ergs/deg./gram, $P_1 = 1$ atm.

w/a	=	0.5	1	5	10	20	
D/a	=	1.34	1.77	6.16	12.1	24	
P_2	=	1.87	3.3	41	158	625	atm.
V_2/V_1	=	0.63	0.44	0.19	0.17	.167	
$T_2 - T_1$	=	33°	120°	1720°	6500°	25500°	C.

These results are obviously only illustrative, since the variation of specific heat with temperature should be taken into account. They do, however, show that very high temperatures and velocities are accompanied by relatively low pressures, which is in agreement with the fact that shock waves in air are not particularly destructive compared with similar waves in water.

More accurate results for air are given in Sec. 16a where the variation of specific heat is taken into account.

PART II. CALCULATION OF DETONATION VELOCITIES

5. Chapman[4]-Jouget[9] Condition for Detonation Velocity

A detonation wave differs from a shock wave in that it is self-sustaining. The energy equation must include the chemical energy released by the explosive on decomposition. Furthermore, the velocity of the detonation, D, is not controlled by the velocity of the piston, nor indeed is a piston necessary. There are therefore four unknown quantities, D, P_2, V_2 and U_2 and only three conditions (mass, momentum and energy). A fourth condition is therefore necessary. No entirely satisfactory proof of this fourth condition has been given, but it is generally accepted that it is

$$D = U_2 + c_2 , \tag{20}$$

where c_2 is the velocity of sound in the gas behind the detonation wave and U_2 is the mass-velocity of this gas. This is equivalent to taking D as the minimum velocity compatible with the other conditions, as will be shown.

Chapman merely postulated Eq. (20), but it can be partially supported by the following arguments: The detonation velocity D, being given by (Eq. (10))

$$D = V_1 \sqrt{(P_2 - P_1) / (V_1 - V_2)} ,$$

is therefore also equal to

$$D = V_1 \sqrt{\tan \varphi} , \tag{21}$$

where φ is the angle between the line A Z and the negative V axis in Fig. 5-1. Z is the final point P_2, V_2 and A is the initial point P_1, V_1, which does not lie on the Hugoniot curve in the detonation case. The point J is the

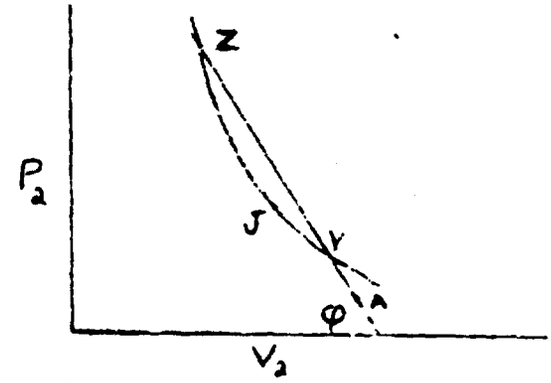


Fig. 5-1

point of tangency of lines from A and is therefore the final state P_2, V_2 which gives the minimum value of D.

If the final P and V correspond to a point on the Hugoniot curve higher than the point J, it will be shown that the velocity of sound in the burnt

gases is greater than the velocity of the detonation wave relative to the burnt gases. Consequently, if a rarefaction wave, due to any of a number of causes, starts behind the detonation wave, it will catch up with the detonation front. The rarefaction will then reduce the pressure, causing the final P and V to move down the curve toward the point J of Fig. 5-1. This explains why points above J on the curve are not stable. The rarefaction wave might be started by a deceleration of the piston, by turbulence back of the detonation front, or by loss of heat in the burnt gases through conduction, etc. At the point J, the velocity of the detonation wave is equal to the velocity of sound in the burnt gases plus the mass velocity of those gases, so that rarefaction waves will not then catch up with the detonation.

The argument which is used to exclude points on the Hugoniot curve below J is based on the entropy of the products. Consider the two points Y and Z on the same straight line from A (Fig. 5-1). Both Y and Z correspond to the same detonation velocity D by Eq. (21). It will be shown that the products of combustion have a greater entropy at Z than at Y. Consequently Z is a more probable state than Y. This is true for all pairs Y and Z on a line from A until Y and Z coincide at J. Therefore points above J are more probable than points below J but points above J slide down to J because of the effect of the rarefaction wave, so that J represents the stable and point. The condition of tangency therefore provides the additional condition required to specify the detonation velocity D uniquely.

The statements made above remain to be proved mathematically and this will now be done. First consider the velocity of rarefaction waves. The velocity of sound in a medium is given by

$$c_2 = V_2 \sqrt{-(dP_2/dV_2)_S}, \tag{22}$$

the subscript S denoting that the entropy is held constant. It is therefore important to investigate $(dP_2/dV_2)_S$ for various points on the Hugoniot curve. In general

$$T_2 dS_2 = dE_2 + P_2 dV_2 \tag{23}$$

and by differentiation of the Hugoniot expression, Eq. (12),

$$E_2 - E_1 = \tfrac{1}{2}(P_1 + P_2)(V_1 - V_2), \tag{24}$$

holding P_1, V_1 constant, one gets

$$dE_2 = -\tfrac{1}{2}(P_1 + P_2)dV_2 + \tfrac{1}{2}(V_1 - V_2)dP_2, \tag{25}$$

so that

$$T_2\left(\frac{dS_2}{dV_2}\right)_H = \tfrac{1}{2}(V_1 - V_2)\left\{\left(\frac{dP_2}{dV_2}\right)_H - \left[(P_1 - P_2)/(V_1 - V_2)\right]\right\}, \tag{26}$$

the subscript H denoting the derivative along the H curve. Now suppose that at some point along the H curve the adiabatic expansion curve (P-V curve

with S constant) passing through the point has the same slope as the H curve. Then $dS_2 = 0$ there and, from Eq. (26)

$$\left(\frac{dP_2}{dV_2}\right)_H = \left(\frac{dP_2}{dV_2}\right)_S = \frac{P_1 - P_2}{V_1 - V_2} = -\tan \varphi . \tag{27}$$

φ is the angle made by the line AZ and the negative V axis. Therefore, at this point, (J of Fig. 5-1), AZ is tangent to the H curve and the velocity of detonation is given by

$$D = V_1 \sqrt{(P_1 - P_2)/(V_2 - V_1)} = V_1 \sqrt{(dP_2/dV_2)_S} \tag{28}$$

$$= (V_1/V_2)c_2 .$$

From Eq. (7), $\rho_2/\rho_1 = V_1/V_2 = D/(D-U_2)$

whence

$$D = U_2 + c_2$$

as stated above. Furthermore, the entropy S_2 is an extremal (since $dS_2 = 0$). Actually S_2 is a minimum at this point, since by solving Eq. (26) for dS_2/dV_2 and differentiating with respect to V_2 at the point J one gets

$$\left(\frac{d^2S}{dV_2^2}\right)_H = \frac{V_1 - V_2}{2T_2}\left(\frac{d^2P}{dV_2^2}\right)_H \tag{29}$$

But $$dS = \left(\frac{dS}{dV}\right)_P dV + \left(\frac{dS}{dP}\right)_V dP \tag{30}$$

so that $$0 = \left(\frac{dS}{dV}\right)_P + \left(\frac{dS}{dP}\right)_V \left(\frac{dP}{dV}\right)_S , \tag{31}$$

and $$\left(\frac{dS}{dV}\right)_H = \left(\frac{dS}{dV}\right)_P + \left(\frac{dS}{dP}\right)_V \left(\frac{dP}{dV}\right)_H \tag{32}$$

Therefore,

$$\left(\frac{dP}{dV}\right)_H - \left(\frac{dP}{dV}\right)_S = \left(\frac{dS}{dV}\right)_H \Big/ \left(\frac{dS}{dP}\right)_V = -\left(\frac{dS}{dV}\right)_H \left(\frac{dT}{dV}\right)_P , \tag{33}$$

from which one finds that

$$\left(\frac{d^2P}{dV^2}\right)_H - \left[\frac{d}{dV}\left(\frac{dP}{dV}\right)_S\right]_H = \left(\frac{d^2P}{dV^2}\right)_H - \left(\frac{d^2P}{dV^2}\right)_S = -\left(\frac{d^2S}{dV^2}\right)_H \left(\frac{dT}{dV}\right)_P \qquad (34)$$

at the point J, since there the subscripts S and H are interchangeable for the outer differentiation. Combination of this result with Eq. (29) shows that

$$\left(\frac{d^2S}{dV_2^2}\right)_H = \frac{V_1 - V_2}{2T_2}\left(\frac{d^2P}{dV_2^2}\right)_S \Bigg/ \left[1 + \frac{V_1 - V_2}{2T_2}\left(\frac{dT}{dV}\right)_P\right]. \qquad (35)$$

In general $(d^2P/dV_2^2)_S > 0$ (i.e., adiabatic expansion curves have positive curvature) and for compression waves $V_1 > V_2$, so that $(d^2S/dV_2^2)_H > 0$, showing that S_2 is a minimum at J.

Eq. (26) shows that

$$\left(\frac{dP_2}{dV_2}\right)_H - \frac{P_1 - P_2}{V_1 - V_2} = \frac{2T_2}{V_1 - V_2}\left(\frac{dS_2}{dV_2}\right)_H \qquad (36)$$

Combination of this with Eq. (33) shows that

$$-\left(\frac{dP}{dV}\right)_S - \frac{P_2 - P_1}{V_1 - V_2} = -\left(\frac{dS}{dV}\right)_H \left\{\left(\frac{dT}{dV}\right)_P + \frac{2T_2}{V_1 - V_2}\right\}. \qquad (37)$$

For points above J (e.g. Z) $(dS/dV)_H$ is negative from Eq. (29) so that for those points

$$V_2\sqrt{-\left(\frac{dP}{dV}\right)_S} > V_2\sqrt{\frac{P_2 - P_1}{V_1 - V_2}} \qquad (38)$$

or $c > D - U_2$, where U_2 is the mass velocity of the burnt gas.

Now consider the entropy at points Z and Y of Fig. 5-1. Becker[1] points out that an ordinary shock wave with initial P and T those at Y and final P and T those at Z would have the same velocity as the detonation wave with P_2 and V_2 at either Z or Y. In the shock wave the entropy is higher behind the wave than in front of it so that S is higher at Z than at Y, as previously asserted.

There have been other arguments advanced for the particular choice of detonation velocity on the H curve, for example those of Scorah.[17] However, the whole question of the theoretical justification of Chapman's condition does not seem to be in a very satisfactory state, although there appears to be little doubt of its correctness.

6. Gaseous Explosions

Explosions of gaseous mixtures such as hydrogen and oxygen provide the best experimental test of the validity of the theory. This is true because the pressures attained in these explosions are sufficiently moderate so that we can use the perfect gas law and the available knowledge of gaseous equilibria. Furthermore, results with these mixtures throw considerable light on the question of whether equilibrium is really established in the detonation process.

a. Equations. Since the equations used for ideal gases will later prove useful as a first step in the treatment of solid explosives, they will be fully developed here. Consider first the Chapman-Jouget condition (see Eq. (28)).

$$D = V_1 \sqrt{-\left(\frac{dP_2}{dV_2}\right)_S} \tag{39}$$

For ideal gases, the adiabatic expansion law (S constant) is

$$P_2 V_{2i}^{\gamma_{2i}} = \text{const.}, \tag{40}*$$

(the subscript i will denote the ideal gas state). Therefore,

$$D_i = (V_1/V_{2i}) \sqrt{\gamma_{2i} P_2 V_{2i}} = (V_1/V_{2i}) \sqrt{n_2 \gamma_{2i} R T_{2i}/M}, \tag{41}*$$

in which n_2 is the number of moles of gas per M grams of burnt gases. Furthermore, U_2 can be eliminated from the equations for mass and momentum (Eq. (7) and (8)), giving the general result (if $U_1 = 0$):

$$P_2 - P_1 = D^2 (V_1 - V_2) / V_1^2 \ . \tag{42}$$

In the cases of interest P_1 can be neglected[+] compared with P_2. Then substitution of Eq. (41) for D yields

$$\frac{V_{2i}}{V_1 - V_{2i}} = \gamma_{2i} \tag{43}*$$

This expression may be used to reduce the Hugoniot equation (Eq. (12)) to a useful form, by elimination of $V_1 - V_2$. The result is

$$E_2 - E_1 = \tfrac{1}{2} P_2 V_{2i} / \gamma_{2i} = \tfrac{1}{2} n_2 R T_{2i} / \gamma_{2i} M \tag{44}*$$

For a perfect gas,

$$M(E_2 - E_1) = Q + C_i (T_{2i} - T_1), \tag{45}*$$

*Equations valid for ideal gases only will be marked with the symbol *.
[+]This is only a fair approximation for ordinary gas explosions but is very good for solids.

where Q is the heat of reaction at constant volume (heat absorbed) per M grams at the initial temperature T_1, while $\bar{C}_i$ is the mean heat capacity at constant volume of M grams of the burnt gases from T_1 to T_2. It should be noted that Q and $\bar{C}_i$ are to be computed on the basis of the final composition at T_{2i}, not the composition at T_1.

Eq. (44) and (45) can be combined into an equation for determining T_{2i}:

$$\tfrac{1}{2} n_2 RT_{2i}/\gamma_{2i} = Q + \bar{C}_i (T_{2i} - T_i). \qquad (46)^*$$

If the reaction went quantitatively so that shifts of the equilibrium with temperature and pressure did not enter, this equation could be solved for T_{2i}, given the dependence of $\bar{C}_i$ and γ on T_{2i}. However, in practice n_2 and Q depend indirectly on T_{2i} because the equilibrium composition of the products depends on T_{2i}. This complicates the calculations considerably but does not alter the principles involved. Having found T_{2i}, one can compute D_i from the following combination of Eq. (41) and (43):

$$D_i = (\gamma_{2i} + 1)\sqrt{n_2 RT_{2i}/\gamma_{2i}M} \qquad (47)^*$$

b. Comparison with experiment. These methods have been applied to mixtures of hydrogen and oxygen by Lewis and Friauf [12]. These authors chose for their calculations the best values available at that time for the heat capacities of the several substances involved. They are mostly four-constant empirical equations which could be somewhat improved with the modern data available. The resultant numerical changes in the results would be very slight however. The data on the equilibria $2H_2 + O_2 = 2\ H_2O$ and $H_2 = 2H$ seem also to be reliable, but the equilibrium $H_2O + \tfrac{1}{2} O_2 = 2OH$, which becomes important in mixtures rich in oxygen, cannot be calculated even at present with high precision because of the uncertainty in the heat of this reaction. The equilibrium $O_2 = 2O$ was not allowed for by the authors and they did not take into account the excess heat capacity of oxygen molecules due to electronic excitation. Both these omissions are not important. All in all it appears that similar calculations undertaken today with the aid of the most modern thermal data available would give results differing from those of Lewis and Friauf only insignificantly.

The following Table 6-1. gives a comparison of the theory with the observations of Dixon and others on gases at atmospheric pressure and room temperature, confined in tubes of more than 20 mm. diameter.

Table 6-1.

Calculated Detonation Velocity

Composition of the mixture	Quantitative reaction	Equilibria allowed for	Measured	Deviation %
$(2H_2 + 1\ O_2)$	3278 meters/sec.	2806	2819	-0.4
$+ 1\ N_2$	2712	2378	2407	-1.2
$+ 3\ N_2$	2194	2033	2055	-1.1
$+ 5\ N_2$	1927	1850	1822	+1.1
$+ 1\ O_2$	2630	2302	2319	-0.7
$+ 3\ O_2$	2092	1925	1922	+0.2
$+ 5\ O_2$	1825	1735	1700	+2.0
$+ 2\ H_2$	3650	3354	3273	+2.5
$+ 4\ H_2$	3769	3627	3527	+2.8
$+ 6\ H_2$	3802	3749	3532	+6.1

The following Table 6-2. shows a comparison of the theory with experiments of Lewis and Friauf on stoichiometric mixtures of hydrogen and oxygen with additions of helium and argon. As the authors state, their measurements were not very accurate and in the case of the stoichiometric mixture they obtained a detonation velocity lower than that found by Dixon. This may be due to a rather narrow tube (19 mm.) used in their experiments.

Table 6-2.

Calculated Detonation Velocity

Composition of the mixture	Quantitative reaction	Equilibria allowed for	Measured	Deviation %
$(2H_2 + O_2)$				
+ 1.5 He	3772	3200	3010	+6.2
+ 3 He	3990	3432	3130	+9.6
+ 5 He	4083	3613	3160	+14.5
+ 1.5 A	2500	2117	1950	+8.4
+ 3 A	2212	1907	1800	+6.1
+ 5 A	1992	1762	1700	+3.9

The results of these calculations must be considered as an unqualified success for the theory. With one exception the differences between calculated and observed values in the first table are all within the experimental errors of velocity measurements. This is very impressive when it is considered that the results of calculation could have been easily of an entirely wrong order of magnitude. The second table is less satisfactory but it may partially be explained by a systematic constant error of velocity determinations. Another explanation of the discrepancies, advanced by the authors, is that in detonation waves traveling at particularly high speed and in which the temperature is relatively low because of additions of foreign gases, the explosive reaction is too slow and the equilibrium is not fully established. However this may be, the results prove rather conclusively that one should calculate detonation velocities under the assumption that the various equilibria involved in the reaction mixture had time to be established. Such calculations should give the upper limit for the velocity of detonation, which agrees closely with experiments unless the conditions of detonation are exceptionally unfavorable.

It has been shown that when heat conductance and viscosity of gases are included in the calculation, the length of the shock wave front is calculated to be less than 10^{-5} cm. The detonation passes this layer in less than 10^{-10} seconds and it is of course entirely impossible that the complex reactions occurring in a hydrogen oxygen mixture can reach equilibrium within such a short time. The calculations of Lewis and Friauf show therefore that the hydrodynamic detonation theory correctly describes the observations even though detonation is not a near discontinuity in the medium but rather is a gradual wave of many times the length calculated from heat conductance and viscosity data. For the propagation of the wave not the shape of its front but the state of the medium at the crest--ahead of the rarefaction wave--must be of decisive importance.

7. Solid Explosives

If P_1 is ignored with respect to P_2, the only properties of the unburnt material entering the basic equations are the energy and density. The hydrodynamic theory has therefore been applied to solid as well as to gaseous explosives. There is, however, a serious difficulty. The greater density leads to much higher pressures in the solid case and our knowledge of the equation of state and equilibrium constants of substances under these conditions of temperature and pressure is rather scanty. Nevertheless, it is possible to obtain very useful results. The first step is to discuss the question of the composition of the burnt gases.

a. Free atoms. Dissociation into atoms and free radicals is fortunately not of importance because of the high pressures in detonation waves of solid explosives at ordinary densities of loading. Consider for example the dissociation $H_2 = 2\,H$. At 5000°K (rather high for most explosives) the dissociation constant has been calculated statistically to be 44.7 Atm. The concentration of free hydrogen does not exceed 10% by volume with most explosives and if the total pressure is 10^5 Atm. it is readily found that 2% of hydrogen is dissociated into atoms. This means an absorption of heat roughly equal to 3 Kcal per Kg of explosive, whose total heat of explosion

is normally of the order of 1000 Kcal/Kg. Thus T_2 is lowered by the inclusion of this dissociation to the extent of 0.3% but at the same time the mole number is increased and hence the pressure is greater. This effect is of the order of 0.10% and hence the total effect on the detonation rate is (because of the square root relation) $(\frac{1}{2})(0.3-0.10)\% = 0.10\%$. Similar calculations show that the water dissociations: $2H_2O = H_2 + 2OH$ and $2H_2O = O_2 + 2H_2$ are of small importance. Dissociations of oxygen and nitrogen are still more insignificant.

b. Polyatomic molecules. Various polyatomic molecules have been reported in the gas samples withdrawn from bombs after detonation. Thus Schmidt reports CH_4, C_2H_2, HCN, C_2N_2, NH_3 in variable but small amounts from almost all explosives. To allow for equilibrium formation of all these molecules seems mathematically an almost impossible task, particularly when it is considered that the thermodynamic functions of most of these molecules are not too accurately known at the high temperatures in question. Approximate calculations using ideal gas laws made on some of those which are found in greatest amounts indicate that the observed concentrations are in excess of equilibrium existing under the conditions of the detonation wave. In all probability these molecules are formed during the cooling process after detonation. But even when it is supposed that the analytical data represent the true conditions in the detonation wave, the formation of all these complex molecules does not alter greatly the results of calculation.

Taking as an example the particularly unfavorable case of TNT for which the oxygen deficiency is large and the complex products particularly abundant according to Schmidt,[16] one finds that in the formation of all complex products reported by Schmidt a total of 8.7 Kcal of heat is absorbed per Kg. of TNT, while the total heat evolution is 875 Kcal. At the same time the mole number of gaseous products is reduced from 32.6 to 30.7 and therefore the total effect on the detonation rate is approximately represented by the factor: $[(30.7/32.6)(875/866.3)]^{(1/2)} = 0.965$. The neglect of the complex products thus overestimates the rate by 3.5%, but it is believed that in general the corresponding error is smaller.

c. Free hydrogen and carbon. The formation of free hydrogen in the detonation wave in the absence of solid carbon can be neglected because the equilibrium constant of the reaction $H_2O + CO = CO_2 + H_2$ ranges from 0.2 at 3000° to 0.07 at 5000°K. Thus the greater part of the hydrogen is present as water and the formation of a few moles of free hydrogen per Kg of explosive is of little effect on the detonation rate. This follows because there is no mole number change in the reaction and the heat evolution is only 4.5 Kcal. per mole at 3000° and is less at 5000°. The neglect of hydrogen in the absence of solid carbon causes therefore an underestimation of the rate by a few percent at most.

In the presence of free carbon, on the other hand, the formation of free hydrogen will proceed almost quantitatively. The equilibrium constant of the reaction $C + H_2O = CO + H_2$ is about 10^5 Atm. at 3000°K and may be estimated as 5×10^6 Atm. at 5000°. Since the pressure (or fugacity, to be more correct) of carbon monoxide in the detonation wave seldom rises

to 10^5 Atm., the ratio P_{H_2}/P_{H_2O} is greater than unity so long as carbon is present. The assumption that the reaction goes completely to the right means an overestimation of the detonation rate because the heat absorption is overcompensated by an increased mole number of gaseous products. The following examples in Table 7-1 demonstrate the magnitude of the effect on D of the extreme assumptions concerning this equilibrium. It is seen that ideal rates calculated with no carbon and those calculated with no hydrogen differ only by 3% or less. In actuality the first case is approached closely almost always and hence the error resulting from the extreme assumption must be small.

Table 7-1. Effect of equilibria on ideal detonation rates.*

Compound	Decomposition equation	T_1°K	D_1 m/sec.
Picric Acid	$6\ CO + H_2O + \frac{1}{2}\ H_2 + 1\frac{1}{2}\ N_2$	3440	2140
	$5\frac{1}{2}\ CO + 1\frac{1}{2}\ H_2O + \frac{1}{2}C + 1\frac{1}{2}\ N_2$	3615	2120
TNT	$6\ CO + 2\frac{1}{2}\ H_2 + C + 1\frac{1}{2}\ N_2$	2830	2070
	$3\frac{1}{2}\ CO + 2\frac{1}{2}\ H_2O + 3\frac{1}{2}\ C + 1\frac{1}{2}\ N_2$	3650	2005
Tetryl	$7\ CO + H_2O + 1\frac{1}{2}\ H_2 + 2\frac{1}{2}\ N_2$	3950	2360
	$5\frac{1}{2}\ CO + 2\frac{1}{2}\ H_2O + 1\frac{1}{2}\ C + 2\frac{1}{2}\ N_2$	4245	2290

d. Summary. Summing up the results of this discussion it is found that the effects of chemical equilibria in the detonation wave are divers and altogether may effect a decrease of the rate with increasing pressure (or density of loading) amounting to perhaps 10 or at the very most 15%. This conclusion is interesting from the theoretical point of view since it indicates that the study of detonation rates for solids does not provide crucial evidence as to whether chemical equilibria are established in the wave or not. For the detonation to comply with the present theory it is only necessary to postulate that the reaction is "complete" in the sense that the oxygen combines with all the carbon to form CO, the excess oxygen combines with hydrogen to form water and if any is still left over, it combines with CO to form CO_2.

8. The Equation of State

If the ideal gas law is used, the calculated detonation velocity does not depend on the density of loading, as is seen from Eq. (47). This is found

* Calculated using ideal gas law.

to be true experimentally for gaseous explosions but it is not true for solids. Instead D increases sharply with increasing loading density, sometimes up to four times the ideal value. This rise is to be explained by deviations of the extremely dense burnt gases from the ideal state.

In Part II of our preliminary report[10] we described the very successful calculations of D for solid explosives, made by Dr. R. S. Halford in cooperation with us. There the equation of state

$$PVM = n_2 RT (1 + xe^x), \tag{48}$$

$$x = K/T^{1/3}VM \tag{49}$$

was used. M is the molecular weight of the original explosive, and K a constant characteristic of the composition of the burnt gases. More recently these calculations have been improved by Dr. D. P. MacDougall and Dr. L. Epstein of the High Explosives Research Laboratory of the Bureau of Mines, so that the results of Part II, though satisfactory, should now be considered obsolete. In the new calculations fewer approximations have been employed and a more general equation of state tried, namely:

$$PVM = n_2 RT (1 + xe^{\beta x}) \tag{50}$$

with

$$x = K/T^{\alpha} VM \quad . \tag{51}$$

Various values of α and β have been tried but very satisfactory results have been obtained with

$$\beta = 0.3, \ \alpha = 0.25.$$

The results with other values of α and β and the comparison of this equation of state with Bridgman's experimental measurements on the volumes of gases at high pressures will not be discussed here as they will be fully treated in Dr. MacDougall's report. Instead, the above equation will be assumed and applied to the calculation of detonation velocities.

9. Practical Calculation of the Ideal Detonation Velocity

a. Definition of ideal state. As a practical matter it is convenient to carry out the calculation of the detonation velocity of a solid explosive in two steps. The first is the calculation of a purely hypothetical D_1, for which the following properties are chosen:

(1) All product gases are ideal and the volume occupied by solid or liquid products may be neglected.
(2) All dissociations into free radicals and atoms are non-existant.
(3) Only solid carbon, CO, CO_2, H_2O, H_2, O_2, N_2 (and HCl, Cl_2, gaseous sulfur, SO_2, metals or metallic oxides, insofar as the corresponding

elements are present in the explosive) are formed.

(4) Oxygen reacts quantitatively with carbon to form CO, the excess forms quantitatively H_2O and what is left over reacts to form CO_2.

The question of whether a real pressure and temperature range exists in which all these assumptions hold is entirely immaterial for the following, because D_i and other "ideal" quantities resulting from these calculations are merely convenient steps to reach the real detonation velocity D.

The second step is the calculation of D/D_i. In this step any inadequacy of the conditions defining the ideal state must be corrected. The discussion in Sec. 7 shows that the ideal state should agree quite well with the real condition of the burnt gases except for the use of ideal gas behavior.

b. Decomposition equations. The detailed procedure for the numerical calculation of D_i will now be given. This is particularly simple for a special class of compounds with general formula

$$C_qH_rO_sN_t \text{ such that } q \leqslant s \leqslant 2q + r/2.$$

This class includes most of the common organic explosives, except TNT and nitroglycerin. Then the application of the general rules shows that such compounds will decompose according to one of the following equations.

Case A. $q + r/2 \geqslant s.$ $\quad n_2 = \frac{1}{2}(2q + r + t).$

$$C_qH_rO_sN_t = qCO + (q-s+r/2)H_2 + (s-q)H_2O + t/2\ N_2. \tag{52}$$

Case B. $q + r/2 \leqslant s.$ $\quad n_2 = \frac{1}{2}(2q+r+t).$

$$C_qH_rO_sH_t = (s-q-r/2)CO_2 + (2q-s+r/2)\ CO + (r/2)H_2O + t/2\ N_2. \tag{53}$$

For explosives not of this type the general rules above must be applied in each case in order to determine the composition of the products.

c. Heat capacity equations. In order to calculate the ideal temperature T_{2i} it is necessary to know the mean heat capacity of the products as a function of temperature. Fortunately the heat capacities of simple molecules can be calculated theoretically with considerable accuracy. The available information has been incorporated in empirical formulas of the type.

$$\bar{C}_i = \frac{1}{T_2-300}\int_{300}^{T_2} C_v dT = A+BT_2, \tag{54}*$$

in which A and B are numerical constants given in Table I of the Appendix. These equations are correct to about 1% for the temperature range 2000 to 5000°. From these tabulated constants for the individual gases, constants A and B for the mixture can be obtained as explained in Table I.

d. Calculation of the ideal temperature. If the empirical formula given above is substituted for $\bar{C}_i$ in Eq. (46) and this equation is solved for T_{2i}, the result is

$$T_{2i} = \frac{-Q + AT_1}{-(n_2R/2\gamma_{2i}) + A + B(T_{2i}-T_1)} \qquad (55)^*$$

Here the subscript i denotes the ideal state. In the above equation T_{2i} occurs on the right so that the equation is properly a quadratic equation but it is easier to solve it by successive approximations. A trial value of T_{2i} (say 4000°) is inserted in the denominator and the right hand side evaluated. The value of T_{2i} thus obtained is substituted in the denominator in place of the original trial value and a new value of T_{2i} obtained. Usually two trials are sufficient.

Strictly speaking, γ_{2i} will vary with T_2 and also with the composition. In practice, however, γ_{2i} has a range of only 10% for the substances considered in this report. Furthermore the term $n_2R/2\gamma_{2i}$ has a value only about 10% of the total denominator. Therefore, less than 0.5% error in T_{2i} will be introduced if the constant mean value of 0.80 is used for $R/2\gamma_{2i}$ in Eq. (55).

The heat of reaction Q can be obtained from the heat of formation Hf_o of the explosive, since

$$-Q = Hf_o - \sum_k n_k \, Hf_k \quad , \qquad (56)$$

where Hf_k denotes the heat of formation of the k^{th} product species (per mole) and n_k the number of moles of that species. The heats of combustion of most explosives are known so that the heats of formation are available.

e. Calculation of D_i. Eq. (47) can now be used to calculate the ideal detonation velocity D_i. The heat capacity ratio γ_{2i} could be determined directly from the known heat capacities of the products and the temperature, but this is rather tedious so an approximation has been adopted which yields values of D_i about 2% low. This error is largely removed by the method in which D/D_i is determined. The approximation consists in calculating γ using the mean value $\bar{C}$ instead of the heat capacity at T_{2i}. A very convenient equation is

$$\gamma_{2i} \cong 1 + \frac{n_2R}{A + BT_{2i}} \quad , \qquad (57)$$

A and B having been obtained already for use in Eq. (55).

With the values of T_{2i} from Eq. (55) and γ_{2i} as given above, D_i is easily computed from Eq. (47), repeated below:

$$D_1 = (\gamma_{2i} + 1) \sqrt{n_2 R T_{2i} / \gamma_{2i} M} \quad .$$

f. Formulation for cases A and B. For the special classes of compounds (A and B) mentioned in Sec. 9b, the heat capacity coefficients and the heats of formation of the products can be introduced numerically into the above equations, yielding the following formulas.

$q + r/2 \geq s$

$$T_{2i} = \frac{Hf_o - 30,500q+917r+59,055s+957t}{(1.86q+2.06r+2.95s+2.37t) + (-0.04q+0.15r+0.25s+0.11t).10^{-3}T_{2i}} \quad . \tag{58}$$

$q + r/2 \leq s$

$$T_{2i} = \frac{Hf_o - 40,724q-4,218r+69,249s+957t}{(0.26q+1.26r+4.55s+2.37t) + (-0.04q+0.15r+0.25s+0.11t).10^{-3}T_{2i}} \quad . \tag{59}$$

For both cases the equivalent of Eq. (47) becomes:

$$D_1 = \frac{\gamma_{2i} + 1}{\gamma_{2i}} \left(\frac{t/2 + r/2 + q}{12q+r+16s+14t} \cdot 8.31 \ \gamma_{2i} T_{2i}.10^{-3} \right)^{\frac{1}{2}} 10^3 \text{ m/sec.} \tag{60}$$

10. Calculation of D/D_1

a. General Equations. In order to calculate D when the burnt gases are imperfect, the analysis of Sec. 6 must be repeated in some general form. From pure thermodynamics we obtain the relation

$$\left(\frac{dP}{dV}\right)_S = - \left(\frac{dP}{dT}\right)_V \left(\frac{dT}{dS}\right)_V \left(\frac{dS}{dT}\right)_P \left(\frac{dT}{dV}\right)_P = \gamma \left(\frac{dP}{dV}\right)_T \quad . \tag{61}$$

From the equation of state

$$PV = nRT \ (1 + xe^{\beta x}) \ / \ M \tag{62}$$

with $x = K/MVT^{\alpha}$,

one obtains the result

$$\left(\frac{dP}{dV}\right)_T = - \frac{Py}{VF} \tag{63}$$

where $F = 1+xe^{\beta x}$, (64)

and $y = 1+2xe^{\beta x} + \beta x^2 e^{\beta x} = F+x(dF/dx)$. (65)

Substitution of these into the basic equation for D, Eq. (39), yields the expression

$$D=V_1\sqrt{P_2\ \gamma_2 y_2/V_2F_2} = (V_1/V_2)\sqrt{\gamma_2 n_2 R T_2 y_2/M}. \tag{66}$$

This equation can be substituted into Eq. (42) for P_2 to obtain

$$P_2 = P_2\ \gamma_2 y_2(V_1-V_2)\ /\ V_2F_2$$

or

$$(V_1/V_2) = (x_2/x_1) = 1 + (F_2/y_2\ \gamma_2), \tag{67}$$

where the subscripts 1 and 2 indicate the initial and final states, respectively. This equation is very useful in connecting x_2 and x_1.

b. Ratio D/D_1. Division of Eq. (66) for D by Eq. (47) for D_1 gives

$$D/D_1 = \frac{(\gamma_{21}+1)\ V_1}{V_2}\sqrt{\frac{\gamma_2}{\gamma_{21}}\ \frac{T_2}{T_{21}}\ y_2}\ . \tag{68}$$

It should be noted that V_2, T_2 and γ_2 differ in the ideal and real final states. It is found that tables of D/D_1 can be constructed so that it is not necessary to carry out a detailed calculation for each explosive and density.

c. Calculation of γ_2/γ_{21}. From thermodynamics one obtains the following equation for the actual heat capacity in terms of the ideal heat capacity C_{v1} (per M grams).

$$C_v = C_{v1} + MT\ \int_{\infty}^{V}(d^2P/dT^2)_V dV. \tag{69}$$

Also

$$\gamma = 1 - \frac{TM}{C_v}\left(\frac{dP}{dT}\right)_V^2 \Big/ \left(\frac{dP}{dV}\right)_T\ . \tag{70}$$

When the equation of state (62) is inserted in these expressions, the result is

$$C_v = C_{v1} + n\alpha(z-1)R, \tag{71}$$

and

$$\gamma = 1 + nR(z^2/C_v y)\ , \tag{72}$$

in which

$$z = F - \alpha x\ (dF/dx) = 1+(1-\alpha)xe^{\beta x} - \alpha\beta x^2 e^{\beta x}\ . \tag{73}$$

From these equations, γ_2/γ_{21} can be computed as a function of x_2, and therefore as a function of x_1 (essentially the density of loading) through Eq. (57), provided that C_{v1} is given. Fortunately the final ratio D/D_1 is not very sensitive to C_{v1}/n so that tables for three different values of C_{v1}/n are adequate for all the explosives considered.

d. Calculation of T_2/T_{21}. For imperfect gases the analogue of Eq. (42) is

$$M(E_2-E_1) = Q + \bar{C}_1 (T_2-T_1) + M \int_{\infty}^{V_2} (dE/dV)_{T_2} dV, \tag{74}$$

which expresses the application of the first law of thermodynamics. The reaction is first carried out to the final temperature at a large volume, such that the product gases are ideal, and these gases are then compressed to their final volume with a resultant energy term because of the gas imperfection.

Using the equation of state (52) and standard thermodynamics, one obtains

$$\left(\frac{dE}{dV}\right)_T = T\left(\frac{dP}{dT}\right)_V - P = -\frac{nRT\alpha x}{MV}\frac{dF}{dx} \tag{75}$$

so that

$$M\int_{\infty}^{V_2} (dE/dT)_{T_2}\, dV = +\, n_2RT_2\alpha\int_0^{x_2}(dF/dx)dx$$

$$= n_2RT_2\,\alpha\, x_{2\beta}^{\beta x_2} = n_2RT_2\,\alpha\,(F_2-1). \tag{76}$$

Eq. (57) can be rearranged to read

$$(V_1-V_2) = F_2V_2/y_2\,\gamma_2, \tag{77}$$

with which the Hugoniot equation (12) becomes

$$E_2-E_1=\tfrac{1}{2}P_2F_2V_2/y_2\,\gamma_2 = \tfrac{1}{2}n_2RT_2F_2^2/y_2\,\gamma_2M \tag{78}$$

Therefore, from Eq. (74), (75) and (78)

$$Q+\bar{C}_1(T_2-T_1)+n_2RT_2\,\alpha\,(F_2-1) = \tfrac{1}{2}n_2RT_2F_2^2/y_2\,\gamma_2. \tag{79}$$

Rearrangement of this yields

$$T_2\left[\bar{C}_1+n_2R\,\alpha\,(F_2-1) - \tfrac{1}{2}(n_2RF_2^2/y_2\,\gamma_2)\right] = -Q+\bar{C}_1T_1, \tag{80}$$

compared with

$$T_{21}\left[\bar{C}_1-\tfrac{1}{2}(n_2R/\gamma_{21})\right] = -Q+\bar{C}_1T_1 \tag{81}$$

for the ideal case (see Eq. (46)). Equating these expressions, one obtains

$$\frac{T_2}{T_{21}} = \frac{\bar{C}_1 - (n_2 R/2\ \gamma_{21})}{\bar{C}_1 + n_2 R\ \alpha (F_2 - 1) - (n_2 R F_2^{\,2}/2 y_2\ \gamma_2)} \qquad (82)$$

Strictly speaking the value of $\bar{C}_1$ in the denominator should be evaluated at T_{21} and that in the numerator at T_2, but these values differ so little that the value at T_{21} can be used for both.

e. Tables of D/D_1. The above results have been incorporated in Eq. (68) for D/D_1 and tables computed of D/D_1 vs x_1, (x_1 is proportional to the density of loading) for three values of $\bar{C}_1/n_2$. The results are sufficiently insensitive to $\bar{C}_1/n_2$ so that these three tables are sufficient. These tables also give T_2/T_{21}. They are included in the appendix, as calculated by Dr. D. P. MacDougall and Dr. L. Epstein. In order to compute D for a given explosive, the procedure is therefore to calculate D_1 first, then to get D/D_1 for the given density of loading from the appropriate table. In order to do this, however, it is necessary to know the value of K, the "covolume constant", which enters the equation of state. The evaluation of K will be discussed in the next section.

11. Determination of Covolumes and Comparison with Experiment.

a. Method of evaluating K. It is difficult to obtain sufficiently accurate values of the "covolume constant" K from direct experiments on gases because the equation of state used does not apply very well at easily attainable temperatures, where attractive forces play an important part. From a practical viewpoint, it is better to use the available data on experimental detonation velocities and work backwards to obtain a rule for evaluating the constant K. This rule can then be used to compute K and then D for a new substance.

b. Effect of density of loading. As a first test of the theory, the values of K which bring the calculated and observed values of D into agreement, were computed for a large number of different densities of loading of PETN by Dr. MacDougall and Dr. L. Epstein of the Bureau of Mines. The experimental measurements of three observers were included. If the basic theory, the form of the equation of state, the various approximations made, and the experimental measurements were all satisfactory, the K's so obtained should be the same. Table 11-1 shows how nearly this ideal result is achieved.* The worst deviation of any value of K from the average is 7% and the great majority of the deviations are less than 3%. The experimental error is at least that great, as judged by the disagreements between the different investigators. Similar constancy of K is found in other cases also. This gives us considerable confidence in the method.

c. Different explosives. Next K was calculated for a number of different explosives. Its value should depend on the composition of the burnt

* Actually $K/T_2^{1/4}$ is plotted but $T_2^{1/4}$ varies only slightly over the range of densities used.

Table 11-1. Covolume Constant vs. Density of Loading for PETN.

ρ_i	D/D_i	$K\rho_i/MT_2^{1/4}$	$K/T_2^{1/4}$	Dev.%	Observer
.50	1.355	.74	460	+2.0	Friedrich
.65	1.340	.95	462	+ .7	"
.80	2.050	1.17	462	+ .7	"
1.00	2.300	1.425	450	-2.0	"
1.20	2.554	1.77	466	+1.5	"
1.40	2.97	2.09	472	+2.8	"
1.60	3.305	2.385	471	+2.6	"
.75	2.015	1.13	476	+3.7	Roth
.91	2.210	1.345	467	+1.7	"
1.04	2.397	1.53	465	+1.3	"
1.45	3.085	2.19	477	+3.9	"
1.72	3.369	2.44	448	-2.4	"
.50	1.664	.75	474	+3.3	Cairns
.51	1.622	.705	457	-4.8	"
.53	1.664	.75	447	-2.6	"
.70	1.835	.945	427	-7.0	"
.80	1.995	1.11	439	-4.4	"
.81	2.020	1.135	443	-3.5	"
.91	2.220	1.35	469	+2.2	"
.92	2.230	1.365	469	+2.2	"
1.00	2.31	1.44	455	- .9	"
1.18	2.535	1.675	449	-2.2	"

Table 11-2. Covolume Constants for Various Explosives.

Substance	T_i	$K/T_2^{1/4}$	Kobs	Kcalc.	% dev.
PETN	4930	459	3046	3879	+0.9
Cyclonite	4350	319	2635	2622	- .5
Tetryl	3950	418	3313	3330	+ .5
Picric Acid	3440	346	2663	2643	- .6
DiPETN	4650	675	5569	5860	+5.2
Nitroglycerin	3230	344	2930	2805	-4.3
Nitropentanone	3350	597	4941	4953	+ .3
Nitropentanol	3970	627	4978	5115	+2.8
Nitrohexanone	2880	671(648)	4915(4749)	4736	- .2(-3.6)
Nitrohexanol	3515	739	5694	5290	-6.9
TNB	3350	294	2272	2451	+7.9
Nitroglycol	5300	233	1989	1896	-4.6
51%PETN etc.	4050	7517	12107	12523	+3.4

gases. The assumption was then tried that K is an additive function of K's characteristic of the different product molecules. The principal product species are N_2, CO, O_2, CO_2, H_2O, H_2 and solid carbon. It was found that values of K_k could be assigned to these substances so that very satisfactory agreement is obtained between the values of K obtained from the measured velocities and those computed from the additive rule:

$$K = \sum_k n_k K_k \,. \tag{33}$$

Table 11-2 shows the nature of this agreement, while Table II of the Appendix gives the values of K_k used. This success is quite pleasing since it gives us confidence that this method can be used to predict detonation velocities for other substances made of similar components.

d. Calculation of pressure, etc. Furthermore, this success gives us faith in the calculations of pressure, temperature, density and mass velocity in the explosion which can be made using the theory. The necessary auxiliary quantities K, x_2, D etc., can be calculated theoretically from a knowledge of the composition as shown above, or if D has been measured for the given density, the following scheme may be used. First calculate D_1 (see Sec. (9)). Then from D/D_1 work backwards in Table III (Appendix) to x_2, T_2/T_{21} and x_1. Then, from the definition of x ,

$$(KT^{-\alpha}) = Mx / \rho \,. \tag{34}$$

The pressure can be obtained from either the equation of state

$$P_2 = n_2 R T_2 x (1+x\varepsilon^{\beta x})/(KT^{-\alpha}), \tag{35}$$

or from Eq. (42)

$$P_2 = D^2 \rho_1 (1-x_1/x_2), \tag{35a}$$

which should give the same value (units are dynes/sq.cm if c.g.s. units are used for D, ρ_1).

The mass-velocity of the burnt gases is given by

$$U_2 = D(1-x_1/x_2) \tag{36}$$

which comes from the law of conservation of mass, Eq. (7), with $U_1=0$. Values of P_2, U_2, and T_2 for some important explosives are given in Table V of the Appendix.

e. Limitations. It should be stated here that this method does not work too well when solids or liquids are present in the hot decomposition products. This means that the results are somewhat in error for TNT and TNB, for example. This defect can doubtless be eliminated and efforts are being made to do so.

f. Acknowledgement. We should like to repeat at this point that the method described above is based on that given in Part II of our preliminary report, which was developed to a considerable extent by Dr. R. S. Halford. The numerical results, tables, etc., are, however, taken from a report by Dr. Duncan MacDougall and Dr. L. Epstein of the U. S. Bureau of Mines, which uses the modified equation of state. This report, (which will be available through the N.D.R.C.) should be consulted for further details.

PART III. PROPERTIES OF SHOCK AND RAREFACTION WAVES

We now return to motions which involve no release of chemical energy. These motions can be divided into two categories; shock waves and rarefaction waves. It is particularly important to be able to compute the properties of the shock wave initiated in the surrounding medium by an explosion, since this shock wave is one of the factors causing damage. It is necessary, however, to understand rarefaction waves before the other problem can be treated. In what follows only the one-dimensional case will be considered, but it is hoped to report on the three-dimensional case later.

12. Integration of the Energy Equation

So long as no discontinuities occur, it will be shown that the pressure of a given material point is a definite function of the density alone. This function may, however, be different for different material points but should not change with time (if one follows the material point in its motion) unless a discontinuity occurs. In general the function will change from one definite form to another on the passage of a discontinuity. If a given material point has a given $P(\rho)$ at time t_1 and another material point has the same $P(\rho)$ at any time t_2 then evidently the two will always have the same $P(\rho)$, barring discontinuities.

The proof involves the combination of the equation of state with the energy equation (6). From the equation of state and the heat capacity, etc., one can obtain $E = E(P, \rho)$. Then

$$\frac{dE}{dt} = \frac{\partial E}{\partial P}\frac{dP}{dt} + \frac{\partial E}{\partial \rho}\frac{d\rho}{dt} = \frac{P}{\rho^2}\frac{d\rho}{dt} \quad , \tag{87}$$

an equation connecting dP/dt with $d\rho/dt$ and known functions of P and ρ.

$$\therefore \frac{\partial E}{\partial P}\frac{dP}{dt} = \left(\frac{P}{\rho^2} - \frac{\partial E}{\partial \rho}\right)\frac{d\rho}{dt}$$

or
$$\frac{dP}{d\rho} = \left(\frac{P}{\rho^2} - \frac{\partial E}{\partial \rho}\right) \Big/ \frac{\partial E}{\partial P} \tag{88}$$

If the initial values of P and ρ are given, the solution of this equation satisfying these initial conditions is the desired function $P - P(\rho)$.

For an ideal gas this procedure gives the adiabatic law

$$P \rho^{-\gamma} = k, \text{ a constant,} \tag{89}$$

where $\gamma = C_p/C_v$. It should be noted that for a given material point, i.e. for a given point moving with the gas, k will remain a constant only while no discontinuity occurs. It will change on the passage of a shock wave. Furthermore, in the general case k may be different for different material points.

13. Riemann's Form of the Fundamental Equations

Whenever there is a portion of the x-t plane in which no discontinuities occur and in which all the material is on the same adiabatic, it is possible to transform the fundamental differential equations of Sec. 2 to another form of considerable value which is due to Riemann.[15] Under the restrictions given, the argument of the last section shows that P is a definite function of ρ alone. Then also c, the velocity of sound, is a function of ρ alone. Introduce a mathematical quantity

$$\omega = \int_{\rho_0}^{\rho} c \, d\rho / \rho, \tag{90}$$

where $c = (dP/d\rho)^{\frac{1}{2}}$ is the velocity of small amplitude sound waves under the given conditions. ρ_0 is the initial density. Then

$$c \frac{\partial \omega}{\partial x} = \frac{c^2}{\rho} \frac{\partial \rho}{\partial x} = \frac{1}{\rho} \frac{dP}{d\rho} \frac{\partial \rho}{\partial x} = \frac{1}{\rho} \frac{\partial P}{\partial x}, \tag{91}$$

$$\frac{\rho}{c} \frac{\partial \omega}{\partial t} = \frac{\partial \rho}{\partial t} . \tag{92}$$

Since $\frac{d}{dt} = \frac{\partial}{\partial t} + U \frac{\partial}{\partial x}$, the equations of conservation of mass and momentum, Eq. (3) and (4), can be expressed as

$$\frac{\partial \omega}{\partial t} + U \frac{\partial \omega}{\partial x} = - c \frac{\partial U}{\partial x}, \tag{93}$$

$$\frac{\partial U}{\partial t} + U \frac{\partial U}{\partial x} = - c \frac{\partial \omega}{\partial x} . \tag{94}$$

Addition and subtraction of these equations yields the new pair:

$$\left\{ \frac{\partial}{\partial t} + (U + c) \frac{\partial}{\partial x} \right\} (\omega + U) = 0 , \tag{95}$$

$$\left\{ \frac{\partial}{\partial t} + (U - c) \frac{\partial}{\partial x} \right\} (\omega - U) = 0 \tag{96}$$

These signify that the quantity $\omega + U$ appears to be constant to an observer moving along the tube with a velocity $U + c$ while the quantity $\omega - U$ appears constant to an observer moving with the velocity $U - c$. (These velocities are not necessarily constant.)

When applicable these equations enable one to see the nature of the solution. Two kinds of lines can be drawn in the x-t plane: "r lines", $dx/dt = U + c$, along which

$$r = \tfrac{1}{2}(\omega + U) \text{ is constant,}$$

and "s lines", $dx/dt = U - c$, along which

$$s = \tfrac{1}{2}(\omega - U) \text{ is constant.}$$

These lines have certain useful properties:

1. There is a line of each type through each point of the x, t plane.

2. If the values of $\underline{s}$ and $\underline{r}$ on the lines passing through a given point are known, then U and ω are known there. From these ρ and P can be found from Eq. (90).

3. If lines of a given kind having different values of $\underline{r}$ (or $\underline{s}$) come together at a point, there will be a discontinuity in U, ρ at that point.

4. If in a given region $\underline{s}$ has the same value along adjacent $\underline{s}$ lines, the $\underline{r}$ lines are straight in that region. For $\underline{r}$ is constant along an $\underline{r}$ line (which will cross the $\underline{s}$ lines) and if $\underline{s}$ is also constant along the $\underline{r}$ lines, both U and ω, therefore U and c, therefore the slope of the $\underline{r}$ lines must be constant.

5. Likewise if $\underline{r}$ has the same value along adjacent $\underline{r}$ lines in a given region, the $\underline{s}$ lines will be straight in this region.

6. For a perfect gas, at least, the curvature of an $\underline{r}$ or an $\underline{s}$ line is positive if U increases along the line.

Proof: (r case) curvature is determined by

$$d(U + c) = dU + (dc/d\omega)\, d\omega . \tag{97}$$

But $$\frac{dc}{d\omega} = \frac{dc}{d\rho}\,\frac{d\rho}{d\omega} = \frac{\rho}{c}\,\frac{dc}{d\rho}$$

and $$c^2 = dP/d\rho \quad \text{so } 2c(dc/d\rho) = d^2P/d\rho^2 ,$$

so $dc/d\omega = \rho\,(d^2P/d\rho^2)/2c^2$, a positive quantity. But along an $\underline{r}$ line $\omega + U$ is constant so $d\omega = -dU$. Therefore

$$d(U + c) = \left[1 - \rho\,(d^2P/d\rho^2)/2c^2\right] dU . \tag{98}$$

For a perfect gas $P = k\rho^{\gamma}$, $d^2P/d\rho^2 = k\gamma(\gamma - 1)\rho^{\gamma-2}$,

$$c^2 = k\gamma\rho^{\gamma-1},$$

$$\therefore \quad \left[1 - \rho(d^2P/d\rho^2)/2c^2\right] = 1 - \tfrac{1}{2}(\gamma - 1) > 0. \tag{99}$$

Presumably this result will still be true for imperfect gases. We do not know what the result will be for water. A similar result is obtained for $\underline{s}$ lines.

7. Only in exceptional circumstances ($U \pm c$ = velocity of piston) can $\underline{s}$ or $\underline{r}$ lines run parallel to the piston curves (in x, t plane). Ordinarily these lines will end on the piston curves. At these ends, U = U of piston. Therefore if $\underline{s}$ (or $\underline{r}$) is known for a line, U, ω, ρ, c and P are determined by U of the piston at the point where the line ends or begins at a piston.

14. Solution for Progressive Waves.

In certain cases $\underline{s} = \frac{1}{2}(\omega - U)$ is constant over a region. The $\underline{r}$ lines are then straight as already mentioned. Furthermore the solutions of Riemann's equations are readily obtained for such a region. For if

$$s = \tfrac{1}{2}(\omega - U) = \text{const.}, \tag{100}$$

then $$\omega = 2s + U = U + \text{const.}, \tag{101}$$

so that Eq. (95) becomes

$$\frac{\partial U}{\partial t} + (U + c)\frac{\partial U}{\partial x} = 0 \quad . \tag{102}$$

The solution of this equation (Rayleigh)[14] is

$$U = f[x - (U + c)t] \quad , \tag{103}$$

where f is an arbitrary function. The proof of this is

$$\frac{\partial U}{\partial x} = \left[1 - t\left(1 + \frac{dc}{dU}\right)\frac{\partial U}{\partial x}\right] f' \quad ,$$

$$\frac{\partial U}{\partial x} = f'/\left[1 + tf'\left(1 + \frac{dc}{dU}\right)\right] \quad , \tag{104}$$

where f' is the derivative of f. Also

$$\frac{\partial U}{\partial t} = -\left[(U + c) + t\left(1 + \frac{dc}{dU}\right)\frac{\partial U}{\partial t}\right] f' \quad ,$$

$$\therefore \quad \frac{\partial U}{\partial t} = -(U + c)f'/\left[1 + tf'\left(1 + \frac{dc}{dU}\right)\right] \quad , \tag{105}$$

from which Eq. (102) follows.

This solution implies that c is a function of U alone. That this is correct follows from the fact that P and therefore c is a function of ρ only and that ρ is a function of U through Eq. (90) and (101). However, c will be a different function of U for different (constant) values of s.

15. Simple Rarefaction Waves.

a. Graphical method. One of the simplest applications is to the case of an infinite tube, closed at one end by a movable piston. Everything is initially at rest and at time $t = t_1$ the piston begins to move backwards, thus initiating a rarefaction wave which travels down the tube to the right, away from the piston. Fig. 15-1 shows the path of the piston and the s and r lines.

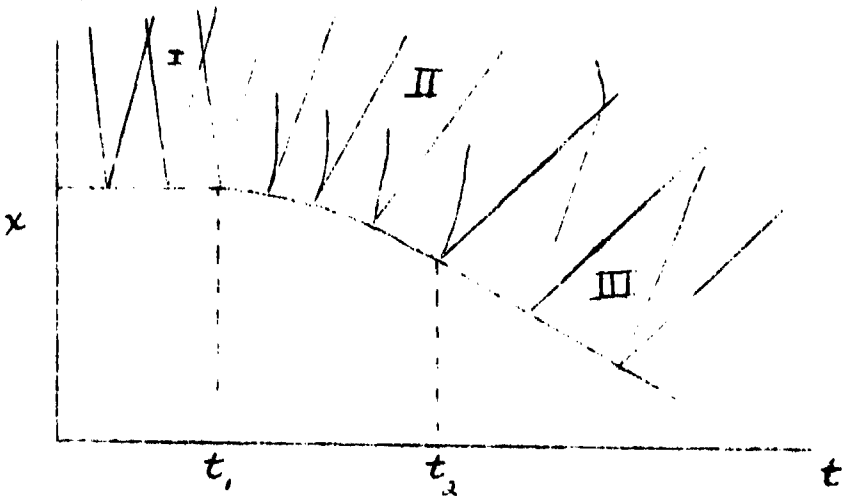


Fig. 15-1

Since at $t = 0$ the fluid is assumed to be uniform and at rest, U and $\omega = 0$ at $t = 0$(ρ_0 is taken as initial density). Therefore s and r = 0 in the region I so that both sets of lines are straight. The s lines from region I cover the whole x - t plane, since the tube is infinitely long. Therefore s = 0 everywhere and the r lines are straight everywhere and are really contour lines for U. The value of U for any r line equals the value of U of the piston at the starting point of the line. The lines starting before $t = t_1$ thus have U = 0. Between t_1 and t_2 the piston has a negative acceleration so the r lines slope less and less steeply and correspond to values of U decreasing from U = 0 to U = - w (-w is final velocity of piston, attained at $t = t_2$). Since r is changing from line to line in region II, the s lines are curved as shown ($dU < 0$). In region III, U is again constant (=-w) so that both sets of lines are straight in this region.

b. Analytical method. The analytic solution is obtained as follows. Let X and τ represent x and t for the piston. Then the coordinates x, t of an r line of value U starting from the piston point X, τ are related by the

equation

$$x = X + (t - \tau)(U + c) . \qquad (106)$$

Let $X = X(\tau)$, then $U = dX/d\tau = X'(\tau)$ at time τ. Also c is a known function of U, therefore of τ. Consequently, Eq. (106) can be converted into an equation involving only x, τ and t, or by solving $U = dX/d\tau = X'(\tau)$ for τ in terms of U, an equation involving only x, t and U can be obtained. Solution of this for U gives U as a function of x and t, and therefore also ρ, P and c as a function of x and t, the complete solution of the problem. Rayleigh gives some explicit results when the acceleration of the piston is constant from t_1 to t_2.

It will be noted that the front of the rarefaction wave propagates with the velocity of sound in the original medium, while the back propagates with the velocity of sound in the final rarefied medium plus the (negative) mass velocity of the final medium. The rarefaction wave therefore broadens out as it passes down the tube, and no discontinuities are produced.

16. Simple Shock Waves in Air and in Water.

If the piston is instantaneously accelerated to its final velocity w, the problem is readily soluble, as was shown in Sec. 4a, where the fluid was assumed to be a perfect gas with constant heat capacity.

a. Air, variable heat capacity. The heat capacity of air actually varies with temperature. [illegible] and Teller[2] have carefully investigated shock waves in air, taking this into account. Their results are given below in Table 16-1.

These investigators also studied very carefully the effect of the finite time required for translation, rotation, vibration and dissociation to come to equilibrium. These lags, especially that of dissociation, alter the shape of the pressure and temperature rise. In Table 16-1, there are two sets of entries. The first is calculated on the assumption that all degrees of freedom, including dissociation into free atoms, are in equilibrium. The second set is calculated on the assumption that there is no time for dissociation or vibration to change. Comparing the two cases, one sees that if equilibrium is established, the shock velocity D is less; the density higher, the temperature lower, and the pressure less than in the case when equilibrium is not completely established. Presumably the equilibrium values are the proper ones to use unless there is a rarefaction wave or some other phenomenon immediately behind the shock front.

At the present time Table 16-1 is being extended to higher velocities.

b. Shock waves in water. Shock waves in water differ greatly from those in air. If the pressure difference is the same, the shock velocity and the mass velocity are considerably less, and the temperature rise is enormously less. If the piston velocity (equals mass velocity) is the same

Table 16-1. Properties of Shock Waves in Air.

(adapted from Bethe and Teller)
$a = 344$ m./s. is velocity of sound at 1 atm., 300° K.

Equilibrium Case				Both	No Dissociation or Vibration			
U_2/a	ρ_2/ρ_1	P_2/P_1	T_2	D/a	T_2	P_2/P_1	ρ_2/ρ_1	U_2/a
0.725	1.907	2.543	400	1.523	400	2.530	1.904	.723
1.238	2.659	4.432	500	1.984	501	4.425	2.347	1.234
1.640	3.225	6.450	600	2.377	604	6.42	3.109	1.630
1.981	3.663	8.547	700	2.725	709	8.49	3.591	1.966
2.283	4.015	10.707	800	3.041	813	10.62	3.904	2.262
2.558	4.314	12.94	900	3.331	925	12.77	4.146	2.527
2.815	4.540	15.23	1000	3.611	1038	15.01	4.346	2.780
3.399	5.069	21.12	1250	4.235	1320	20.72	4.706	3.335
3.917	5.454	27.27	1500	4.797	1616	26.66	4.945	3.807
4.383	5.746	33.52	1750	5.307	1925	32.7	5.090	4.266
4.811	5.970	39.85	2000	5.770	2222	38.8	5.236	4.674
5.598	6.359	53.01	2500	6.645	2848	51.4	5.409	5.414
6.338	6.655	67.05	3000	7.433	3510	64.6	5.521	6.103
7.147	7.122	84.09	3500	8.315	4300	80.5	5.615	6.834
8.039	7.697	106.02	4000	9.297	5300	100.6	5.691	7.663
9.168	8.385	134.40	4500	10.410	6570	126.2	5.754	8.601
10.326	9.156	168.38	5000	11.595	8030	155.6	5.804	9.598

Table 16-2. Properties of Plane Shock Waves in Water.

(P_1 = 1 Kg./cm.^{2} , T = 293° K.)

U_2 material velocity behind wave front (meters/sec.)
D shock wave velocity "
P_2 pressure behind wave front (kg./cm^2)
ΔT temperature increment through wave front.

U_2	P_2	ΔT	D
61	1000	2°	1607
115	2000	5	1710
163	3000	8	1804
206	4000	12	1901
247	5000	16	1989
284	6000	20	2070
320	7000	24	2144
354	8000	28	2216
413	10000	36	2345
477	12000	45	2490

in air and in water, then the shock velocity is considerably higher, the pressure difference very much higher and the temperature rise lower in the water case.

In order to get these results quantitatively, we first put the Rankine-Hugoniot equation (Eq. (12)) in a rather general form. From purely thermodynamical considerations, one obtains the result that

$$E_2 - E_1 = \int_{T_1}^{T_2} \left(\frac{dE}{dT}\right)_{P_1} dT + \int_{P_1}^{P_2} \left(\frac{dE}{dP}\right)_{T_2} dP$$

$$= \int_{T_1}^{T_2} C_{p_1} \, dT - P_1 \int_{T_1}^{T_2} \left(\frac{dV}{dT}\right)_{P_1} dT - T_2 \int_{P_1}^{P_2} \left(\frac{dV}{dT}\right)_{T_2} dP$$

$$- \int_{P_1}^{P_2} P\left(\frac{dV}{dP}\right)_{T_2} dP \quad , \tag{107}$$

The second integral can be evaluated and the last one can be integrated by parts. If this is done and the result inserted in the Rankine-Hugoniot equation $E_2 - E_1 = \frac{1}{2}(P_1 + P_2)(V_1 - V_2)$, the result is

$$-\tfrac{1}{2}(P_2 - P_1)(V_1 + V_2) + \int_{T_1}^{T_2} C_{p_1} dT - T_2 \int_{P_1}^{P_2} \left(\frac{dV}{dT}\right)_{T_2} dP$$

$$+ \int_{P_1}^{P_2} V(T_2) \, dP = 0. \tag{108}$$

This equation should be quite general for any fluid to which the fundamental equations are applicable. In applying it to water, empirical data for V as a function of P and T can be used. This data has been obtained by Bridgeman.

Professor J. G. Kirkwood[9] has devised a very effective method of solving this equation numerically for water using successive approximations. He inserts the value of $P_2 - P_1$ and an assumed value of T_2 into a modified form of the equation and obtains a better value of T_2. From P_2 and T_2, V_2 comes from Bridgeman's results. Table 16-2 shows the values of P_2, V_2, T_2 and D computed by Kirkwood.

17. Rarefaction Wave Following Shock Wave.

Suppose that the piston is accelerated instantaneously to a constant velocity w, so that no difficulties arise over the initiation process, but that later the piston is gradually brought to rest, as shown in Fig. 17-1.

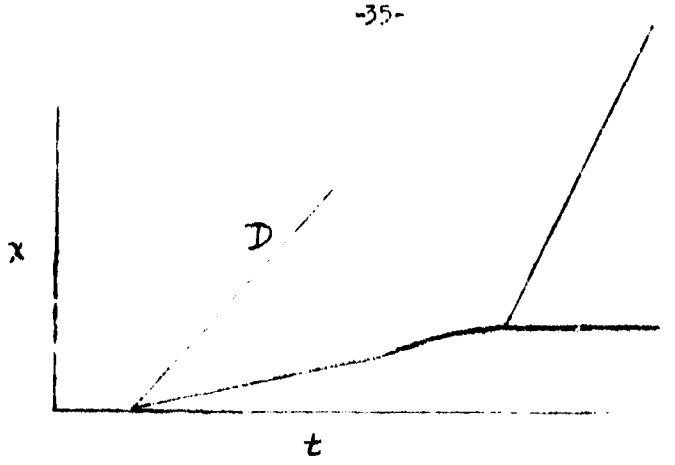


Fig. 17-1

Then it will be shown that the rarefaction wave which is started by the deceleration of the piston will overtake the shock wave and weaken it. The shock wave will therefore travel with constant velocity until overtaken by the front of the rarefaction wave, whereupon its velocity and intensity will be continuously reduced, presumably until an ordinary sound wave results. Therefore, even a plane shock wave in a medium with no viscosity or thermal conduction will die out unless it is continuously supported by a moving piston. This result may not be new, but we have not noticed it so far in the literature. The spherical case has not been treated but presumably would show a falling off greater than the inverse square.

Two arguments support this conclusion for plane shock waves. The first is a thermodynamic one. The compression of the medium which occurs when the shock front passes a given material point is an irreversible process---the material is shifted from one adiabatic to another in the process. Consequently energy is continually being degraded. But if the piston is ultimately brought to rest, only a finite amount of work is done by the piston on the column of material so that this work must ultimately be degraded to heat by the irreversible process. The shock wave cannot therefore continue indefinitely unaltered.

The second argument is more detailed. The rarefaction wave should behave exactly as the simple rarefaction discussed in Sec. 15 except that the velocity w is superimposed. Its front should thus propagate with a velocity w + c, where c is the velocity of sound in the compressed, heated gas back of the shock front. The shock wave itself travels with a slower speed than this. This is shown for the perfect gas case by inspection of Table 4-1, in which $(D/a) - (w/a) < 1$ or $D - w < a$. But $c > a$ because of the higher temperature. For a more general proof reference may be made to Sec. 5. There it was shown that if the final state of the medium is above the point of tangency J on the Hugoniot curve, the velocity of detonation is less than w + c. But in the shock wave case the initial point A (Fig. 5-1) lies on the Hugoniot curve, rather than below it as in the detonation problem. Consequently the only point of tangency is A itself so that the final state for any shock wave must be above the point of tangency and therefore the velocity is less than w + c and consequently less than that of the rarefaction wave. Duhem has also discussed this.

When the rarefaction catches up, reflection will presumably ensue. At this point the simple Riemann theory will no longer apply because when the shock wave amplitude is reduced the medium back of the reduced shock wave is not on the same adiabatic as the medium through which the undiminished shock wave passed.

Although it may be quite difficult to calculate the exact law of decay, it is clear that the shock wave must decay and that the way in which it will decay will depend on the time during which the piston is moving and the way in which the piston is decelerated. This problem is under consideration.

Incidentally, it is at least conceivable that more effect could be produced at a long distance by a gradual acceleration of the piston than by a sudden acceleration. During the initiation period the processes occurring are reversible until a discontinuity is produced. By a slow acceleration the distance in front of the piston at which discontinuity occurs is increased and therefore the degradation of energy is postponed.

There have been many criticisms of the Hugoniot treatment (Lamb,[11] Rayleigh),[14] the difficulty being connected with the idea that the passage of the shock front is an irreversible process although there is no viscosity or thermal conduction. As Rayleigh points out, perhaps one should consider the Hugoniot equations as limiting equations for very small viscosity, etc. Then the existence of a very steep shock front could result in a finite dissipation of energy even though the effect of viscosity, etc., could be neglected elsewhere.

18. Rarefaction Wave Following a Detonation Wave.

In this section detonation waves initiated by a single impulse from a piston will be discussed. At the discontinuous detonation frontthe Hugoniot conditions must again be satisfied, with the modification that the change in chemical energy due to the reaction must appear in ΔE. In the shock wave the velocity (U_2) of the gas back of the wave was that of the piston and all the energy came from the piston. Now, however, the detonation itself supplies energy and there is no reason why U_2 should equal w. There is another condition which must be satisfied at the detonation front, a condition which was discussed in Sec. 5. Upon the introduction of this condition, P_2, V_2, and U_2 become fixed without reference to the piston speed, so that in order to keep the product gases at a constant velocity, the piston velocity w must be specified, instead of being one of the independent variables as in the shock wave case.

Therefore if it is assumed that the detonation reaction starts instantly, the situation is quite simple when the piston is instantly accelerated to the proper final velocity w. Fig. 18-1 shows this case.

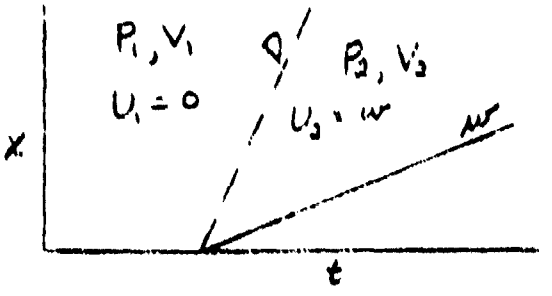


Fig. 18-1

In this case, if the piston is later brought to rest, a rarefaction wave is started which should behave the same way as the rarefaction wave in the corresponding shock wave case, i.e. according to Fig. 18-2, except that it does not catch up with the detonation wave since here D = c + w.

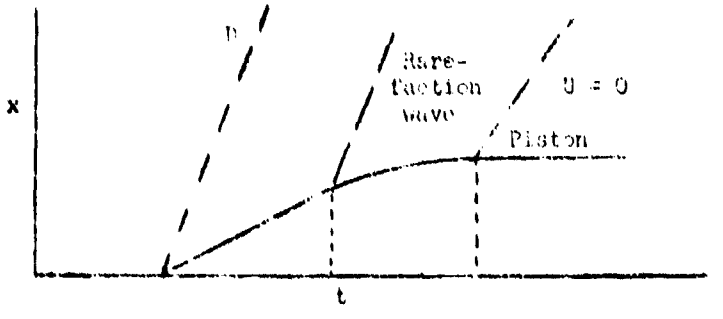


Fig. 18-2

If the time during which the piston is being slowed down is decreased, in the limit a situation such as shown in Fig. 18-3 should prevail.

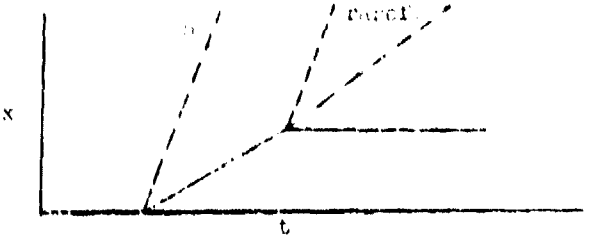


Fig. 18-3

Now suppose the length of time the piston travels to be reduced to a minimum. In the limit, the situation would look like Fig. 18-4.

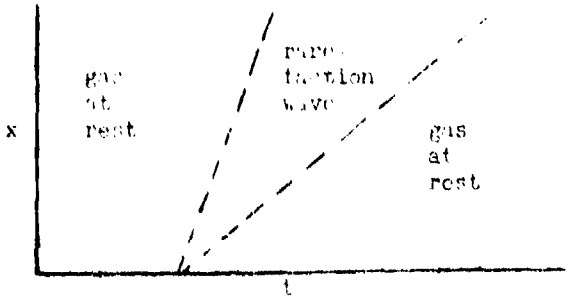


Fig. 18-4

Here the sharp detonation front is immediately followed by the rarefaction wave. The gas in front of the detonation front is at rest, immediately behind it has the velocity w, and this velocity falls off until the end of the rarefaction wave is reached, after which the gas is at rest.

It should be pointed out that this limiting case provides no mechanism for starting the detonation. It does illustrate, however, a situation close to that of an explosive detonated by a short sharp blow on an end otherwise blocked off by an immovable partition.

Another difference from the usual shock wave case is the fact that the products of an explosion are ordinarily mixtures in which various chemical equilibria can occur. As the gas cools off on decompression, these equilibria will shift, at least until the temperature falls so low that the equilibria become "frozen". These shifts cause changes in C_v, the heat capacity.

If the detonation front is not infinitely steep, and it of course can not be in reality, there is the possibility that the rarefaction wave may so cool the gases that the reaction is stopped before complete detonation has taken place, thus weakening the explosion. This may be the reason why the mode of detonation is important. Poor detonation may cause the rarefaction wave to follow too closely behind the detonation front. If the rarefaction does cut off the end of the detonation, it should reduce the detonation velocity, because it prevents complete chemical reaction.

As the detonation proceeds down a stick of explosive, the detonation front should be unchanged but the width of the rarefaction wave increases. This may account for observed differences in effect for different lengths, since the region of high pressure and velocity will increase in length as the detonation proceeds.

Quantitatively, the rarefaction wave back of the detonation wave can be treated by a procedure exactly similar to the simple rarefaction wave discussed in Sec. 15. Provided the equation of state of the product gases is known a complete solution can be obtained for any given deceleration of the piston. Practically, though, the qualitative results already outlined contain most of the useful information, inasmuch as the "deceleration of the piston" in the actual case is unknown and is determined by the mode of initiation of the detonation.

19. Phenomena at Boundaries: Reflection

Reflection plays a very important role in the initiation of shock waves by an accelerating piston, in the dying out of a shock wave due to its overrunning by a rarefaction wave, in the effect of shock waves on an obstacle, and on the initiation of a shock wave by an explosion. In this section will be given the beginnings of the treatment of reflections.

The simplest case is that of a compressional shock wave reflected from a rigid wall. The solution which satisfies all the requirements is shown in

Fig. 19-1. The reflected wave is also a compressional shock wave but it moves against the mass motion of the fluid and leaves the fluid behind it at rest. Its velocity is given by the expressions

$$D_{ref.} = -\left[-w + V_2\sqrt{(P_3 - P_2)/(V_2 - V_3)}\right],$$

$$0 = -w + \sqrt{(P_3 - P_2)(V_2 - V_3)}\ , \quad E_3 - E_2 = (1/2)(P_2 + P_3)(V_2 - V_3), \tag{109}$$

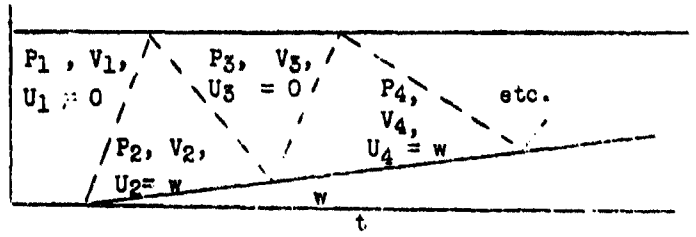


Fig. 19-1

Further reflections will take place from the piston, if it is rigid, as shown. The waves going in the negative direction will have lower speed (relative to fixed axes) than the forward waves, because they go in the direction opposite to the piston motion. As the fluid becomes more and more compressed (note that it does so in discontinuous steps in this case), the velocity of the waves increases.

If the rigid wall is replaced by a second medium of infinite extent, a shock wave will be transmitted into this second medium and either a shock or a rarefaction wave will be reflected. Across the boundary there must be equality of pressures and of mass velocities.

Let w be the mass velocity and P_2 the pressure in the first medium before reflection and let P_3 be the pressure which would be produced in medium II by a piston with velocity w. Then:

If $P_3^{II} > P_2$, shock wave reflected

If $P_3^{II} < P_2$ rarefaction wave reflected.

This result has been proven rigorously for ideal gases by von Newmann[18] but seems reasonable for any media.

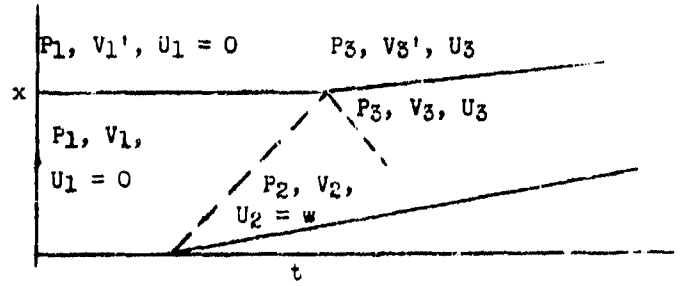


Fig. 19-2

The Hugoniot conditions must be satisfied at the dotted lines and equality of pressure and velocity maintained at the interface. The fluid in contact with the piston must have the velocity w of the piston. These conditions are just sufficient in number to specify all the free variables.

20. Calculation of the Velocity of the Shock Wave Produced by an Explosion

a. Basic principles. When the detonation wave travelling down a stick of explosive reaches the end, reflection occurs and two new waves are produced. One is the shock wave in the air at the end of the stick; the other is a rarefaction wave moving backward through the burnt gases. The boundary between the burnt gases and the outer air will also move forward, though not as fast as the shock wave in air.

The problem is treated most simply if the forward-moving rarefaction wave which inevitably follows the detonation wave (see Sec. 18) is ignored; i.e. the case of a semi-infinite stick is treated. The effect of this rarefaction may be added later.

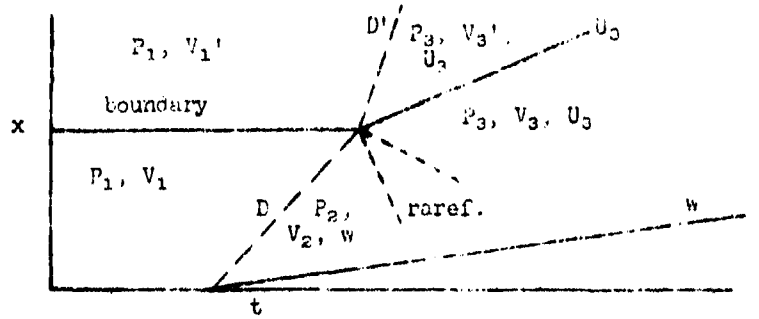


Fig. 20-1

The situation is then as shown in Fig. 20-1. It is assumed that across the boundary between the explosive and the air the pressures must remain equal and also the mass velocities. If the properties of the explosive are known, P_2, V_2, w and D can be calculated as shown in Part II. The values of P_3, V_3 and U_3 across the reflected rarefaction wave are calculated as seen below if one of them is known. That is, P_3, say, is a known function of P_2, V_2, w and U_3. Likewise from the theory of shock waves already given, P_3, V_3' and U_3 back of the shock wave are connected so that P_3 is a known function of U_3, P_1, and V_1. It is then merely necessary to combine these two equations connecting P_3 with U_3 to solve for both P_3 and U_3, and therefore D', etc.

Using the method of Sec. 13, we see that (since the stick is infinitely long) the whole region in the burnt gases is covered by r type lines originating in the region of uniform pressure and velocity (P_2,w) back of the detonation front. These lines run parallel to the detonation front in this region and curve upward on passing through the rarefaction wave. Consequently, since $r = \frac{1}{2}(w + U)$ is everywhere the same (in the burnt gases),

$$U_3 = -(\omega) + \text{const.} \tag{110}$$

$$\text{where } \omega = \int_{\rho_0}^{\rho} (c/\rho)\, d\rho . \tag{111}$$

On choosing $\rho_0 = \rho_2$, the const. becomes w, the mass-velocity back of the detonation front.

To summarize: the burnt gas expands reversibly, at the same time increasing its forward velocity and reducing its pressure and temperature. The air is compressed and acquires a forward velocity. The solution is assumed to be the situation reached when the pressures and velocities are equal across the boundary.

b. Use of a general equation of state. The equation of state will be written in the general form

$$Pv = nRTF(x) , \tag{112}$$

$$\text{where } x = (K/v)\, h(T) , \tag{113}$$

in which P is the pressure (c.g.s.), v the volume occupied by the gases resulting from the explosion of M grams of explosive, v=VM, n is the number of moles of products (all products are assumed to be gases), R is the gas constant per mole (c.g.s.), F(x) is some function of x, K is a constant for a given composition of the gases and for the given quantity M, and h(T) is a function of the temperature T. It will be assumed that the composition (therefore n and K) is independent of T and P.

The velocity U_3 of the burnt gases is connected with the density through the equation

$$U_3 = w - \int_{\rho_2}^{\rho} \sqrt{(dP/d\rho)_S}\; d\rho/\rho \tag{114}$$

as shown above. It is convenient to write the integral in the form

$$\int_{x_2}^{x} \left(\frac{dP}{d\rho}\right)_S^{\frac{1}{2}} \left(\frac{d\rho}{dx}\right)_S \frac{dx}{\rho} , \tag{115}$$

in which the integrand is expressed as a function of x. We therefore need $(dP/d\rho)_S$ and $(d\rho/dx)_S$. In addition we shall want P as a function

of x, and T as a function of x, the latter as an auxiliary quantity because T will appear in the integrand above. P will be obtained by integrating $(dP/dx)_S$ and T by integrating $(dT/dx)_S$.

From pure thermodynamics we obtain the following relations:

$$\left(\frac{dT}{dv}\right)_S = -\frac{T}{C_v}\left(\frac{dP}{dT}\right)_v \tag{116}$$

$$\left(\frac{dP}{dv}\right)_S = \gamma\left(\frac{dP}{dv}\right)_T \quad , \tag{117}$$

$$\gamma = 1 - \frac{T}{C_v}\left(\frac{dP}{dT}\right)_v^2 \Big/ \left(\frac{dP}{dv}\right)_T \quad , \tag{118}$$

$$C_v = C_{v_i} + T\int_{\infty}^{v}\left(\frac{d^2P}{dT^2}\right)_v dv \quad , \tag{119}$$

in which C_{v_i} is the heat capacity of the M grams of burnt gases at the temperature T treated as ideal gases, C_v the same quantity for the real gases at T and v. γ is C_p/C_v for the real gas.

The density ρ equals M/v so

$$\frac{d\rho}{dv} = -M/v^2 \ . \tag{120}$$

Also, from the definition of x,

$$dx = -(x/v)\,dv + (xh'/h)dT \quad , \tag{121}$$

$$\left(\frac{dx}{dv}\right)_S = \frac{-x}{v} + \frac{xh'}{h}\left(\frac{dT}{dv}\right)_S = -\frac{x}{v} - \frac{xh'T}{hC_v}\left(\frac{dP}{dT}\right)_v$$

$$= -x\,\frac{hC_v + vh'T\,(dP/dT)_v}{h\,v\,C_v} \tag{122}$$

These equations may now be combined to give the results desired, i.e.

$$\left(\frac{dT}{dx}\right)_S = \left(\frac{dT}{dv}\right)_S\left(\frac{dv}{dx}\right)_S = \frac{h\,v\,T}{x[hC_v\,(dT/dP)_v + vh'T]} \quad , \tag{123}$$

an expression which can be integrated to give T as a function of x, for given T_2 , x_2.

Also $\left(\frac{dP}{dx}\right)_S = \left(\frac{dP}{dv}\right)_S\left(\frac{dv}{dx}\right)_S = -\frac{\gamma\,h\,v\,C_v\,(dP/dv)_T}{x\,[h\,C_v + vh'T\,(dP/dT)_v]}$ (124)

which can be integrated to give P as a function of x if P_2 and x_2 are known.

Finally,

$$\frac{1}{\rho}\left(\frac{dP}{d\rho}\right)_S^{\frac{1}{2}}\left(\frac{d\rho}{dx}\right)_S = \frac{v}{M}\left(\frac{dP}{dv}\right)_S^{\frac{1}{2}}\left(\frac{d\rho}{dv}\right)^{\frac{1}{2}}\left(\frac{dv}{dx}\right)_S$$

$$= \sqrt{-\frac{\gamma}{M}\left(\frac{dP}{dv}\right)_T}\ \frac{hvC_v}{x\,[hC_v + vh'T\,(dP/dT)_v]} \qquad (125)$$

so that

$$U_3 = w - \int_{x_2}^{x} \sqrt{-\frac{\gamma}{M}\left(\frac{dP}{dv}\right)_T}\ \frac{hvC_v}{x[hC_v + vh'T\,(dP/dT)_v]}\,dx. \qquad (126)$$

In all these expressions C_v and γ should be considered as functions of x with S constant. The quantities $(dP/dv)_T$ and $(dP/dT)_v$ are given by the expressions

$$\left(\frac{dP}{dv}\right)_T = \frac{nRT}{v^2}\,(F + F'x) = -\frac{P}{vF}\,(F + F'x) \qquad (127)$$

$$\left(\frac{dP}{dT}\right)_v = \frac{nR}{v}\,(F + x'T'h'/h) \quad , \qquad (128)$$

in which $h' = dh/dT$, $F' = dF/dx$.

The above equations give U_3 and P_3 as functions of x, so that P_3 can be plotted against U_3. The intersection of this curve with the corresponding one for the shock wave gives the value of U_3 (and P_3) expected.

c. Use of a special equation of state. The equation of state used in Sec. 8 is a special case of the above general form. It is

$$Pv = nRT\,(1 + xe^{\beta x}) \qquad (129)$$

where $x = K/vT^{\alpha}$, $\alpha = 0.25$, $\beta = 0.3$, (130)

i.e. $F = 1 + xe^{\beta x}$, $h = T^{-\alpha}$, so

$$F' = e^{\beta x}(1 + \beta x),\quad h' = -\alpha h/T$$

and $$\left(\frac{dP}{dv}\right)_T = -\frac{P}{vF}\,(1 + 2xe^{\beta x} + \beta x^2 e^{\beta x}) = \frac{-Pv}{vF} \qquad (131)$$

where $y = F + F' = 1 + 2x + \beta x + \beta x^2 e^{\beta x}$.

Also $$\left(\frac{dP}{dT}\right)_V = \frac{nR}{v}(F - \alpha x F') = \frac{nRz}{v} , \quad (132)$$

where $$z = F - \alpha x F' = 1 + x e^{\beta x} - \alpha x e^{\beta x} - \alpha \beta x^2 e^{\beta x} . \quad (132)$$

Then $$\left(\frac{dT}{dx}\right)_S = \frac{Tz}{x(b - \alpha z)} \qquad \text{with } b = C_v/nR.$$

$$\therefore \quad \ln\frac{T}{T'} = \int \frac{z}{b\ g\ x}\, dx , \quad (133)$$

in which T' is a constant of integration and $g = 1 - (\alpha z/b)$.

From the general equation for C_v, we get in this case

$$b = b_1 + \alpha(z - 1) , \quad (134)$$

where $b_1 = C_{v1}/nR$; i.e. the ideal value of b. Also

$$\gamma = 1 + (z^2/by). \quad (135)$$

The pressure is obtained from the integral

$$\ln\frac{P}{P'} = \int \frac{\gamma y}{F\ g\ x}\, dx , \quad (136)$$

while $$U_3 = w - \sqrt{\frac{nRT'}{M}} \int_{x_2}^{x} \frac{\sqrt{\gamma y\, T/T'}}{g\ x}\, dx , \quad (137)$$

in which T/T' is taken from the previous calculation.

A rather exact treatment could be carried out using these equations, which enable the velocity U_3 and the pressure P_3 of the expanded burnt gases to be tabulated as a function of x. From this U_3 vs. P_3 is plotted and compared with U_3 vs P_3 for the shock wave in air, taken from Table 16-1. The intersection of the curves gives the solution for P_3 and U_3, so that the shock velocity D' can be read from Table 16-1. At the present time, however, the above equations have not yet been applied rigorously.

d. <u>An approximate procedure.</u> In the calculations so far carried out certain simplifications have been used. First T_2, P_2, w and x_2 were calculated for the burnt gases directly back of the detonation front by the methods of Part II. Then the variation of heat capacity with temperature was ignored in applying Eq. (134) and (133). It was thus possible to

tabulate T/T' as a function of x for a fixed value of b_1 (Cv_1/nR). From this and a knowledge of T_2 and x_2, T' can be read. This table is found in the appendix (Table A-IV). Likewise, the variation of b_1 with temperature was ignored in computing $\log P/P'$ as a function of x from Eq. (136). This is also tabulated in the appendix (Table A-IV). From it and a knowledge of P_2 and x_2, $\log P'$ is read off. Eq. (137) can next be employed to obtain U_3 as a function of x. The integral in Eq. (137) can be tabulated (Table IV), so that little labor is involved in carrying out these computations. When U_3 and P_3 have been computed for several values of x, P_3 can be plotted against U_3, and this curve compared with the corresponding curve for shock waves.

The approximation of ignoring the variation of heat capacity is probably not too serious. At the high temperatures involved the variation is not great; furthermore its effect partly cancels out.

e. A sample calculation. As an example consider tetryl at a density of 1.2 g./cc. Here M = 287, h = 11.5, T_1 = 3950 and $D_1 = 2.35\ 10^5$ cm./sec., according to the methods of Part II. We could also compute the other required properties theoretically but to avoid compounding errors, it is better to make use of the measured detonation velocity, $D = 5.9 \times 10^5$, at $\rho_1 = 1.2$. Then $D/D_1 = 2.50$. Examination of the heat capacity of the products shows that Table A-III with $Cv_1 = 7$ is the right one to use, whence we get $x_1 = 1.67$, $x_2 = 2.246$, $T_2 = 3520$. From Eq. (85b), $P_2 = 10.7 \times 10^{10}$ dynes/sq. cm. (over 10^5 atm.!). Then using Table A-IV we get $\log P' = 8.38427$ and $T' = 1180$. Also $w = 1.51 \times 10^5$ cm./sec. from Eq. (86).

These numbers may now be inserted in Eq. (137), making use of Table A-IV to obtain the values of the integral. The result is a Table of values of U_3 against the final x. From Table A-IV also one can obtain $\log P_3$ vs x knowing $\log P'$. Therefore $\log P_3$ can be plotted against U_3, as shown in Fig. 20-1. On the same plot is shown $\log P_3$ vs U_3 for the shock wave in air, these points being from Table 16-1.* The intersection of the shock wave curve with that for the burnt gases gives the predicted mass-velocity U_3, which enables D' to be found, again from Table 16-1. The result in this case is $D' = 7\,30$ meters/sec. for air. The experimental value is 7900 m./sec. It should be emphasized that these are only the initial shock wave velocities; they will decrease as the shock wave proceeds.

f. Other results. Little experimental data exists with which to compare calculations of initial shock wave velocities. Some of the available data is summarized in Table 20-1 below, together with the velocities computed as above. The agreement is all that could be expected.

Table 20-1. Calculated and observed Initial Shock Wave Velocities in Air. (Experimental results from Cairns)[3]

Explosive	Density	D'calc.	D'obs.	%
PETN	0.5	6120	6500	5.8
"	1.2	7880	8100	2.7
Tetryl	1.0	7500	7700	2.6
"	1.2	7750	7900	2.2

* For values beyond the limits of Table 16-1, the table in Sec. 4b was provisionally used.

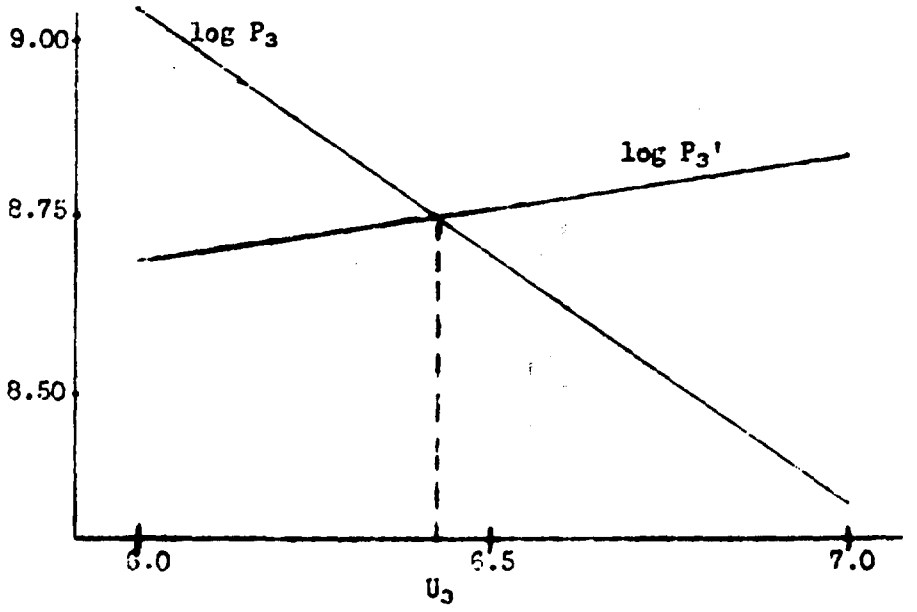


Fig. 20-1

21. Some Remarks about Work in Progress

At present the work described in this report is being carried further and it is hoped to be able to extend it to three dimensions. The question of the dying away of shock waves is being studied now and it is hoped ultimately to be able to calculate to a practical degree of accuracy all the phenomena associated with an explosion.

APPENDIX

Table A-I

Mean Heat Capacities

$$\bar{C} = [1/(T_2-300)] \int_{300}^{T_2} C_v dT = A + BT_2$$

Substance	A	B	Coef. Case A	Coef. Case B
C (solid)	3.94	0.27×10^{-3}		
CO	5.61	0.21×10^{-3}	q	2q-s+r/2
CO_2	10.16	0.46×10^{-3}		s-q-r/2
H_2	4.91	0.30×10^{-3}	q-s+r/2	
H_2O	7.86	0.55×10^{-3}	s-q	r/2
N_2	5.54	0.21×10^{-3}	t/2	t/2

The mean heat capacity of a mixture is also given by the equation

$$\bar{C} = A + BT_2, \text{ (calories per gram-mole)}$$

in which A and B are obtained from the individual values given above by multiplying each by the number of moles of that constituent and adding. The number of moles for the simple cases A and B of Sec. 9b are given in the fourth and fifth columns. The results above are accurate to 1% over the range 2000 to 5000° for T_2.

Table A-II

Covolume Constants for Individual Product Gases.

Gas	K_k (c.c.)	Gas	K_k (c.c.)
N_2, CO	316	H_2	54
CO_2	549	H_2O	241

For a mixture $K = \sum n_k K_k$

For cases A and B, the coefficients n_k are given in the previous table.

Table A-III. D/D_1, T/T_2 etc. vs. x_1.

(1) C_{v1} = 7 cals./deg.

x_1	x_2		γ/γ_1	T_2/T_{21}	D/D_1		x_1	x_2		γ/γ_1	T_2/T_{21}	D/D_1	
.20	0.324	290	.976	.982	1.178	172	1.80	2.398	238	.965	.886	2.627	210
.40	0.614	273	.968	.968	1.350	172	2.00	2.636	237	.964	.879	2.837	223
.60	0.887	265	.964	.955	1.522	172	2.20	2.875	240	.963	.875	3.060	238
.80	1.152	253	.963	.942	1.694	176	2.40	3.113	238	.962	.875	3.298	260
1.00	1.408	250	.963	.930	1.870	180	2 60	3.351	233	.960	.881	3.558	290
1.20	1.658	252	.964	.917	2.050	186	2.80	3.584	232	.958	.894	3.848	328
1.40	1.910	247	.964	.906	2.236	192	3.00	3.816	242	.955	.910	4.176	392
1.60	2.157	241	.965	.895	2.423	199	3.20	4.058		.952	.958	4.568	

(2) C_{v1} = 8.5 cals./deg.

x_1	x_2		γ/γ_1	T_2/T_{21}	D/D_1		x_1	x_2		γ/γ_1	T_2/T_{21}	D/D_1	
.20	0.328	292	.980	.985	1.131	174	1.80	2.414	242	.975	.899	2.648	210
.40	0.620	277	.978	.978	1.355	174	2.00	2.656	239	.975	.891	2.858	219
.60	0.897	266	.971	.965	1.529	175	2.20	2.895	235	975	.884	3.077	232
.80	1.163	258	.971	.952	1.704	179	2.40	3.130	240	.974	.880	3.309	247
1.00	1.421	254	.971	.941	1.883	183	2.60	3.370	236	.973	.878	3.556	266
1.20	1.675	251	.972	.930	2.066	188	2.80	3.606	234	.971	.881	3.822	294
1.40	1.926	245	.973	.920	2.254	194	3.00	3.840	230	.969	.890	4.116	326
1.60	2.171	245	.974	.909	2.448	200	3.20	4.070		.967	.907	4.442	

(3) C_{v1} = 10 cals./deg.

x_1	x_2		γ/γ_1	T_2/T_{21}	D/D		x_1	x_2		γ/γ_1	T_2/T_{21}	D/D_1	
.20	0.331	295	.983	.988	1.182	176	1.80	2.426	242	.981	.911	2.665	210
.40	0.626	277	.977	.977	1.358	175	2.00	2.668	240	.982	.902	2.875	219
.60	0.903	267	.975	.968	1.533	177	2.20	2.908	236	.982	.894	3.094	229
.80	1.170	261	.976	.959	1.710	181	2.40	3.144	239	.982	.887	3.323	242
1.00	1.431	254	.976	.950	1.891	186	2.60	3.383	237	.981	.882	3.565	257
1.20	1.685	251	.978	.940	2.077	190	2.80	3.620	235	.980	.880	3.822	276
1.40	1.936	246	.979	.930	2.267	196	3.00	3.855	231	.978	.882	4.098	302
1.60	2.182	244	.980	.920	2.463	202	3.20	4.086		.976	.888	4.400	

Table A-IV. Properties of Burnt Gases from Explosion.

(Int. = $\sqrt{R\gamma}\int_{x_2}^{x}\sqrt{yT/T^1}\,dx/gx$ with $\gamma = 1.23$)

x	T/T^1	log. P/P^1	Int.	x	T/T^1	log. P/P^1	Int.
0.1	1.000	0	0	1.5	2.303	2.1628	56725
0.2	1.181	0.4449	9030	1.6	2.389	2.2456	59834
0.3	1.306	0.7169	15040	1.7	2.470	2.3180	62860
0.4	1.414	0.9303	20000	1.8	2.560	2.3962	66024
0.5	1.505	1.0992	24170	1.9	2.646	2.4646	69126
0.6	1.594	1.2526	28080	2.0	2.742	2.5392	72377
0.7	1.674	1.3815	31590	2.1	2.833	2.6044	75584
0.8	1.757	1.5063	35040	2.2	2.936	2.6763	78952
0.9	1.832	1.6137	38250	2.3	3.033	2.7390	82294
1.0	1.913	1.7216	41480	2.4	3.144	2.8087	85809
1.1	1.987	1.8154	44530	2.5	3.249	2.8694	89315
1.2	2.068	1.9121	47650				
1.3	2.143	1.9965	50650				
1.4	2.225	2.0852	53650				

Table A-V. D, P_2, T_2, ρ_2 and U_2 for Some Common Explosives

Explosive	ρ_1	ρ_2	D(obs.)	P_2(atm.)	T_2(°K)	U_2(m/s)
PETN	.5	.73	4000	15,000	4740	1274
	1.2	1.63	6100	115,000	4520	1602
Cyclonite	1.2	1.62	6310	122,000	4220	1633
	1.56	2.04	7890	226,000	4100	1876
Tetryl	1.0	1.36	5500	78,000	3560	1444
	1.2	1.57	5900	106,000	3520	1513
Picric Acid	1.03	1.39	5150	70,000	3080	1332
	1.63	2.11	7210	189,000	3020	1632
Nitroglycerin	1.6	2.15	7400	222,000	4660	1899

NOTE ON THE LATERAL EXPANSION BEHIND A DETONATION WAVE

G. I. Taylor and M. Jones
Cambridge University

British Contribution

May 1942

NOTE ON THE LATERAL EXPANSION BEHIND A DETONATION WAVE

G. I. Taylor and M. Jones

May 1942

* * * * * * *

When a detonation wave travels along the length of a cylindrical explosive charge, the front seems to be a surface which is nearly perpendicular to its direction of motion, i.e. to the surface of the charge. Immediately behind the detonation front the products of combustion can expand laterally. If the explosive is contained in a tube the inertia of this tube is in most cases sufficient to ensure that the pressure across any section of the expanding tube is nearly uniform. When the wall of the tube is very light or when the charge is uncased the conditions are more complicated and the lateral as well as the longitudinal component of velocity in the expanding gas must be considered. Though the motion of the expanding gases from a cylindrical explosive cannot be described completely without great complexity of analysis, the motion in the region close to the point where the detonation wave meets the surface of the cylinder can be analysed.

The problem is simplified in the following way. We consider a semi-infinite block of explosive bounded by, and lying below, the xy-plane. Co-ordinates are taken moving with the uniform detonation velocity U_0 in the positive x direction. The lower half of the yz-plane then represents the detonation wave front and the motion of the expanding gases is steady relative to these moving axes. On account of the Chapman condition, we know that, referred to this system, the products of the detonation wave front are moving in the direction of the negative x - axis with the local velocity of sound C. The flow of the hot gases and the position of the shock wave which is produced in the surrounding medium can readily be calculated by the methods described by Taylor and Maccoll (Aerodynamic Theory, W.F. Durand Vol.III). To obtain numerical results the law for the adiabatic expansion of the explosion products must be known, and this has been given by Jones and Miller, and Jones for T.N.T. at densities 1.5 gm/cm^3 and 1.0 gm/cm^3 respectively.

Referring to Figure (1), OA denotes the detonation wave front, which is at rest in the co-ordinates considered, with gas passing through from right to left with velocity c where

$$c^2 = \left(\frac{dp}{d\rho}\right)_o \qquad (1)$$

p is the pressure and ρ the density, and the suffix o denotes values taken over the plane OA.

The equations of motion for two dimensions are

$$u\frac{\partial u}{\partial r} + \frac{v}{r}\frac{\partial u}{\partial \theta} - \frac{v^2}{r} = \frac{1}{\rho}\frac{\partial p}{\partial r}, \qquad (2)$$

$$u\frac{\partial v}{\partial r} + \frac{v}{r}\frac{\partial v}{\partial \theta} + \frac{uv}{r} = -\frac{1}{\rho}\frac{\partial p}{r\partial \theta} \qquad (3)$$

where r and θ are polar co-ordinates with respect to O and the reference line OA, and u and v are the components of the velocity parallel and perpendicular to r respectively.

We assume the existence of a solution (verifiable a posteriori) in which p, u and v are functions of θ only. Equation (2) then becomes

$$v = \left(\frac{du}{d\theta}\right) \qquad (4)$$

and (3), together with the equation of continuity,

$$u\rho + \frac{d}{d\theta}(v\rho) = 0,$$

gives .....

Best Available Copy

gives

$$v^2 = \frac{dp}{d\rho} \tag{5}$$

Also (3) and (4) with the condition that when $p = p_0$, $u = u$ and $v = c$ give

$$u^2 = c^2 - v^2 - 2\int_{p_0}^{p} \frac{1}{\rho}\, dp \tag{6}$$

From tabulated adiabatic p, v relations, the values of $\frac{dp}{d\rho}$ and $\int_{p_0}^{p} \frac{1}{\rho}\, dp$ have been calculated for various pressures. Thus the values of u and v for a given pressure are obtained from equations (5) and (6). The angle specifying the radius vector along which these values of u, v and p occur is given by equation (4) which may be rewritten

$$\theta = \int_0^u \frac{1}{v}\, du \tag{7}$$

This integral has to be evaluated numerically.

The direction of the stream lines is denoted by the angle ϕ relative to OA as reference line, which is given therefore by

$$\phi = \theta + \tan^{-1}\frac{v}{u} \tag{8}$$

Tables (1) and (2) give the angles θ and ϕ and also u and v for various pressures below the initial value p_0, for the loading densities 1.5 and 1.0 respectively. Curves in Figures (2) and (3) show the angles θ and ϕ plotted against $\log_{10} p$.

The Shock Wave in the Surrounding Medium.

When the expansion takes place into a medium such as air or water the solution can be obtained as follows. The solution already given holds over the region AOB. Along OB, the pressure is constant and the stream lines are all parallel to OD, i.e. the angle AOD is the value of ϕ corresponding to the value of θ AOB. In the region BOD the pressure is constant and the stream lines are straight and parallel to OD. OE represents the shock wave front in air; the angle EOA we denote by ψ. It is known from the theory of oblique shock waves (cf Taylor and Maccoll loc. cit.) that behind OE the stream lines are straight and the pressure is constant. The solution is determined therefore by the following two conditions. First, the constant pressure in the region EOD must be equal to that in BOD, and secondly, the direction of the stream lines behind OE must be given by ϕ, i.e. they must be parallel to OD. There is a tangential discontinuity in the velocity along OD.

Let U(p) be the velocity with which a shock wave is propagated into the outside medium in the direction of the normal to its plane when the pressure behind the shock wave front is p and the medium in front of the shock wave is at rest. Let u(p) be the corresponding particle velocity behind the shock wave front. The first condition may then be expressed by the equation

$$\sin\left(\psi - \frac{\pi}{2}\right) = \frac{U(p)}{U_D} \tag{9}$$

Since the velocity of the medium relative to the shock wave is $U(p) - u(p)$ the second condition is expressed by $U(p) - u(p) = U_D \cos\left(\frac{\pi}{2} - \psi\right) \tan(\psi - \phi)$ or $\sin\left(\psi - \frac{\pi}{2}\right) - \cos\left(\psi - \frac{\pi}{2}\right) \tan(\psi - \phi) = \frac{u(p)}{U_D}$ or it may be written in the form

$$\tan(\psi - \phi) = \frac{U(p) - u(p)}{(U_D^2 - u^2(p))^{\frac{1}{2}}}. \tag{10}$$

The functions U(p) and u(p) depend upon the medium into which the expansion takes place. For a perfect gas at pressure p_a in which the velocity of sound is c_o we have

U(p) .....

Best Available Copy

$$U(p) = c_0 \left\{ \frac{\gamma+1}{2\gamma} \left(\frac{p}{p_a} \right) + \frac{\gamma-1}{2\gamma} \right\}^{\frac{1}{2}} \qquad (11)$$

$$u(p) = \frac{c_0 \left(\frac{p}{p_a} - 1 \right)}{\gamma} \left\{ \frac{\gamma+1}{2\gamma} \left(\frac{p}{p_a} \right) + \frac{\gamma-1}{2\gamma} \right\}^{-\frac{1}{2}} \qquad (12)$$

where γ is the ratio of the specific heats.

For water, tables of the functions U(p) and u(p) have been kindly supplied to us by Dr. Penney. These functions are shown in Figure (4) in which U(p) and u(p) are plotted against $\log_{10} p$ where p is expressed in atmospheres.

To determine the shock wave we take a given value for p and from the known value of U(p) we find ψ from equation (9) and also ϕ from equation (10). The points ϕ, log p so determined are plotted in Figures (2) and (3). Curves (a) and (b) relate to air and water respectively. The intersections of the ϕ, log p curves obtained in this way with those obtained from the values of tables (1) and (2) determine the angle and the pressure of the shock wave maintained in the given medium by the adiabatic expansion of the explosion products.

A solution of this type in which the shock wave passes through the point O, Figure 1, is no always possible. In a gas, for high values of the pressure such as we consider here, $(1 - u(p)\, U(p))$ tends to a constant value $(\gamma - 1)/(\gamma + 1)$. Thus, if we denote for brevity $\tan(\phi - \frac{\pi}{2})$ by η and $\tan(\psi - \frac{\pi}{2})$ by ξ, equations (9) and (10) give

$$\xi - \eta = \left(\frac{\gamma-1}{\gamma+1} \right) \xi \ (1 + \xi\eta) \qquad (13)$$

The greatest value of η for which this equation has a real root in ξ is given by

$$\eta_{max} = \tan\left(\phi_{max} - \frac{\pi}{2}\right) = 1/\sqrt{(\gamma+1)(\gamma-1)}\ , \qquad (14)$$

and the co responding value of ψ is given by

$$\tan\left(\psi_{max} - \frac{\pi}{2}\right) = \sqrt{\frac{\gamma+1}{\gamma-1}} \qquad (15)$$

For air, assuming $\gamma = 1.4$ we find $\phi_{max} = 135$ degrees 35 minutes. Thus if the curve (a) Figures (2) and (3) has not cut the ϕ, log p curve when ϕ has reached this limiting value no solution of the type sought is possible. The effect is similar to that of the formation of a shock wave by a moving wedge. When the angle of the wedge exceeds a certain critical value, the shock wave no longer passes through the vertex of the wedge but moves ahead. Figures (2) and (3) show that for T.N.T. in air the angles ϕ are less than the critical values so that solutions of the form shown in Figure (1) are possible.

If the surrounding medium were helium gas $(\gamma = 1.67)$ the limiting value of ϕ would be 126.9 degrees so that in this case the shock wave would be ahead of the detonation wave for both densities.

It is interesting to find the angle X at which the particles of the surrounding medium are thrown forward in the shock wave, i.e. with respect to the explosive at rest. X is the angle between the direction of motion of the particles and the direction of the detonation wave normal. The horizontal and vertical components of the particle velocity in the shock wave (i.e. perpendicular and parallel to OA Figure (1)) are respectively

$$\frac{U_D \sin(\psi - \frac{\pi}{2}) \sin(\phi - \frac{\pi}{2})}{\cos(\psi - \phi)} \qquad (16)$$

and

$$\frac{U_D \cos(\psi - \frac{\pi}{2}) \sin(\phi - \frac{\pi}{2})}{\cos(\psi - \phi)} \qquad (17)$$

Thus $\tan X = \cot(\psi - \frac{\pi}{2})$ or $X = \pi - \psi$

The .....

Best Available Copy

The numerical results are summarised below:

T.N.T. density 1.5 gm/cm^3 u_0 = 6790 milliseconds.

In Air

θ = 124 degrees 24 minutes ϕ = 129 degrees 30 minutes ψ = 141 degrees 24 minutes χ = 38 degrees 36 minutes. Pressure in the shock wave = 300 atms.

In water

θ = 63 degrees ϕ = 100 degrees 36 minutes ψ = 127 degrees . minutes χ = 82 degrees 54 minutes. Pressure in the shock wave = 30,249 atms.

T.N.T. density 1.0 gm/cm^3 u_0 = 5266 milliseconds.

In Air

θ = 125 degrees 6 minutes ϕ = 131 degrees 42 minutes ψ = 145 degrees 21 minutes χ = 34 degrees 48 minutes. Pressure in the shock wave = 200 atms.

In water

θ = 57 degrees ϕ = 99 degrees 6 minutes ψ = 124 degrees 6 minutes χ = 50 degrees 54 minutes. Pressure in the shock wave = 31,620 atms.

The stream lines of the flow relative to the detonation wave are shown in Figure (1) for air and in Figure (5) for water. The line OO separating the explosion products from the surrounding air or water is shown clearly in both figures. As might be expected the expansion is much more rapid in air than in water. The degree of confinement obtained by surrounding the explosive with air and water respectively may be judged by comparing the pressure at the surface of separation between the products of combustion and the surrounding medium. In air this is only 300 atmospheres while in water it is 36,000.

This pressure may be compared with the initial pressure at the interface between water and a spherical explosive, calculated by Penney as 36,000 atmospheres. In Penney's case, the explosion products were assumed at rest before being suddenly released. A higher figure would have been obtained if the motion of the gas in the detonation wave had been taken into account.

The angles of the interface shown in Figures (1) and (5) are those which would actually be seen in an instantaneous photograph if the detonation process did in fact take place in a thin layer.

Among other things which might be the subject of experimental test is the prediction that the shock wave from a bare charge of T.N.T. would travel ahead of the detonation wave if exploded in helium but not in air.

TABLE 1.

T.N.T. density 1.5

p dynes/cm^2	θ degrees	ϕ degrees	u cm/sec.	v cm/sec.
15.84 x 10^{10}	0	90°	0	4.57 x 10^5
7.809 "	53° 42'	9° 24'	3.973 x 10^5	3.80 "
4.371 "	68° 48'	102° 54'	4.917 "	3.33 "
2.299 "	81° 30'	107° 42'	5.599 "	2.76 "
8.479 x 10^9	96° 48'	113° 6'	6.234 "	1.82 "
4.314 "	106°	117° 12'	6.476 "	1.28 "
1.947 "	113° 12'	121° 18'	6.611 "	0.937 "
7.98 x 10^8	119° 6'	125° 24'	6.696 "	0.736 "
2.800 "	124° 24'	129° 30'	6.758 "	0.608 "
8.707 x 10^7	129° 30'	133° 54'	6.808 "	0.521 "
1.994 "	134° 48'	138° 30'	6.852 "	0.463 "
2.816 x 10^6	140° 48'	143° 48'	6.894 "	0.360 "
0			6.979 "	0

Table II .....

TABLE II.

T.N.T. density 1.0

p dynes/cm^2	θ degrees	ϕ degrees	u cm/sec.	v cm/sec.
8.241×10^{10}	0	90°	0	3.703×10^5
4.606 "	45° 30'	95° 6'	2.851×10^5	3.346 "
2.748 "	62° 30'	100° 18'	3.789 "	2.937 "
1.734 "	74° 3 0'	104° 18'	4.362 "	2.503 "
1.213 "	82° 24'	107° 1P'	4.684 "	2.173 "
6.607×10^9	93° 36'	111° 54'	5.057 "	1.675 "
9.333×10^8	114° 54'	123° 42'	5.528 "	.854 "
4.867 "	120° 3 6'	127° 54'	5.605 "	.721 "
5.689×10^6	144° 1 8'	148° 48'	5.638 "	.461 "
0			6.028 "	0

Figure (1) Diagram showing the stream lines for T.N.T. density 1.5 gm/cm^3 detonating in air. Line OD separates the products of the explosive and the air of the explosive and the air of the shock wave with wave front OE.

Figure (2) T.N.T. density 1.5 gm/cm^3. Explanation in text.

Figure (3) T.N.T. density 1.0 gm/cm^3. Explanation in text.

Figure (4) Shock waves in water. Data supplied by Penney.

Figure (5) Stream lines for T.N.T. density 1.5 gm/cm^3 detonating in water. Region EOD is the water shock wave. DOA is region containing the products of the exploding T.N.T.

Best Available Copy

Fig 1

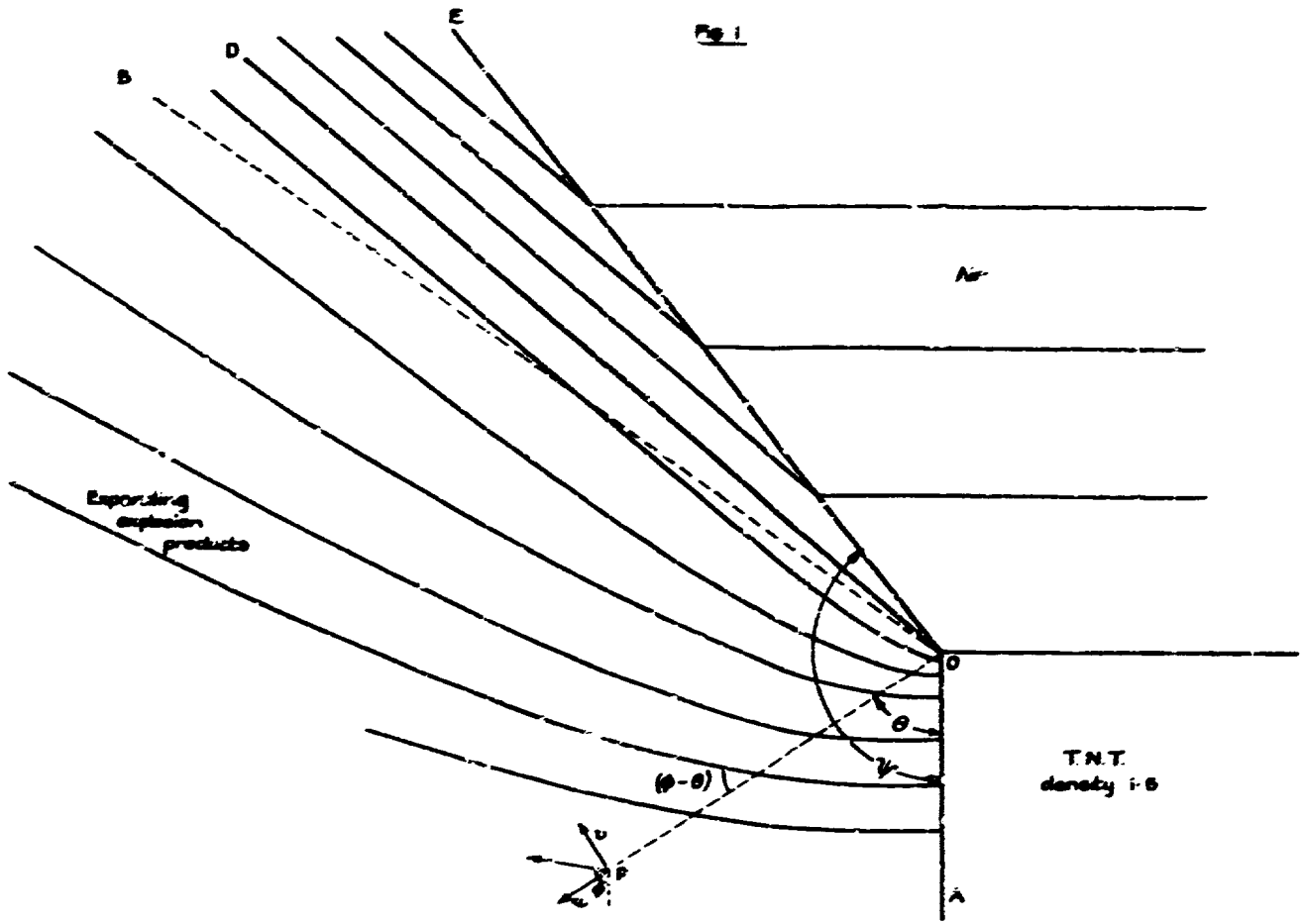
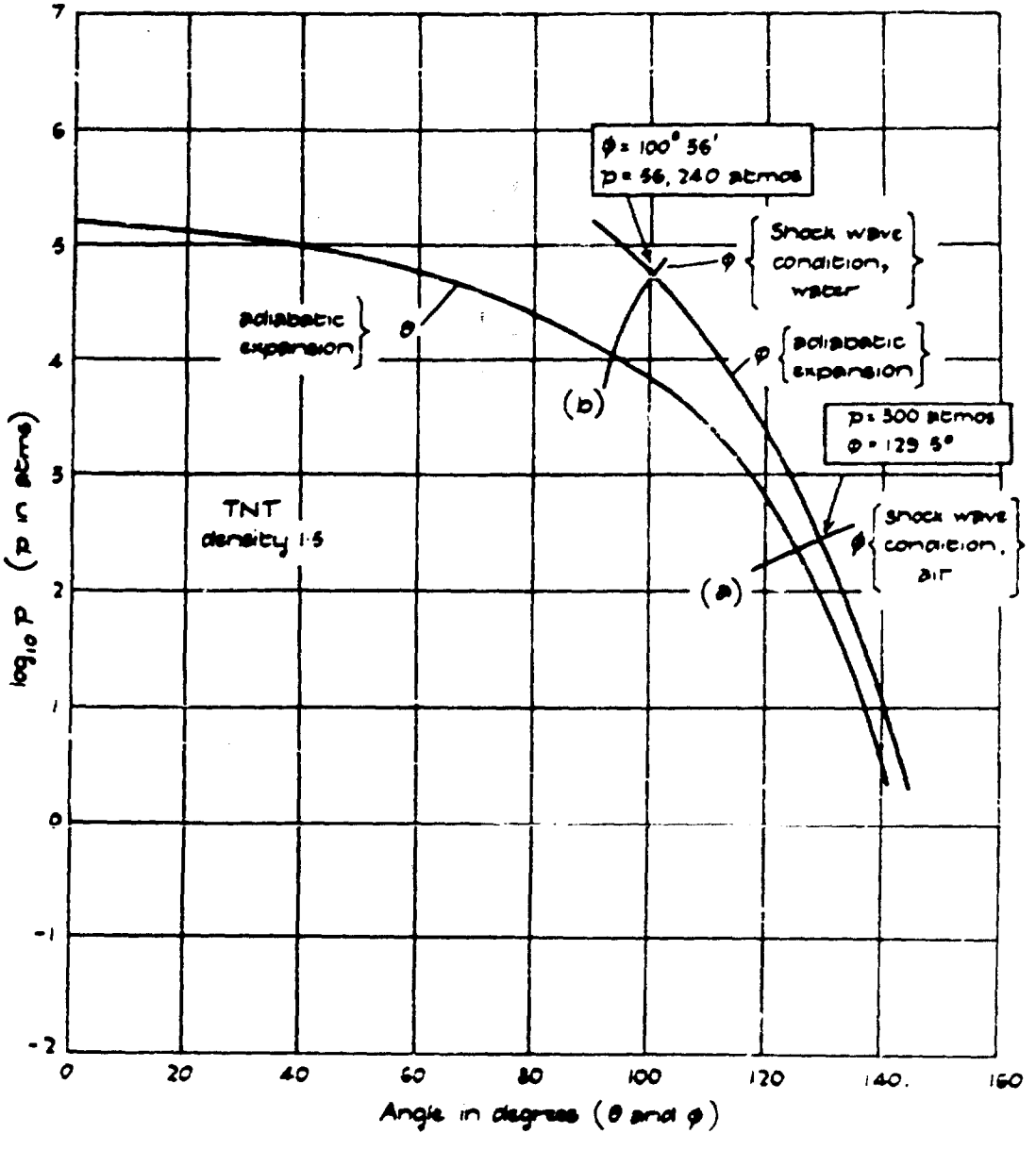

E
D
B
Air
Expanding
explosion
products
O
θ
ψ
(φ-θ)
T.N.T.
density 1·6
A

Fig. 2



Best Available Copy

No 3

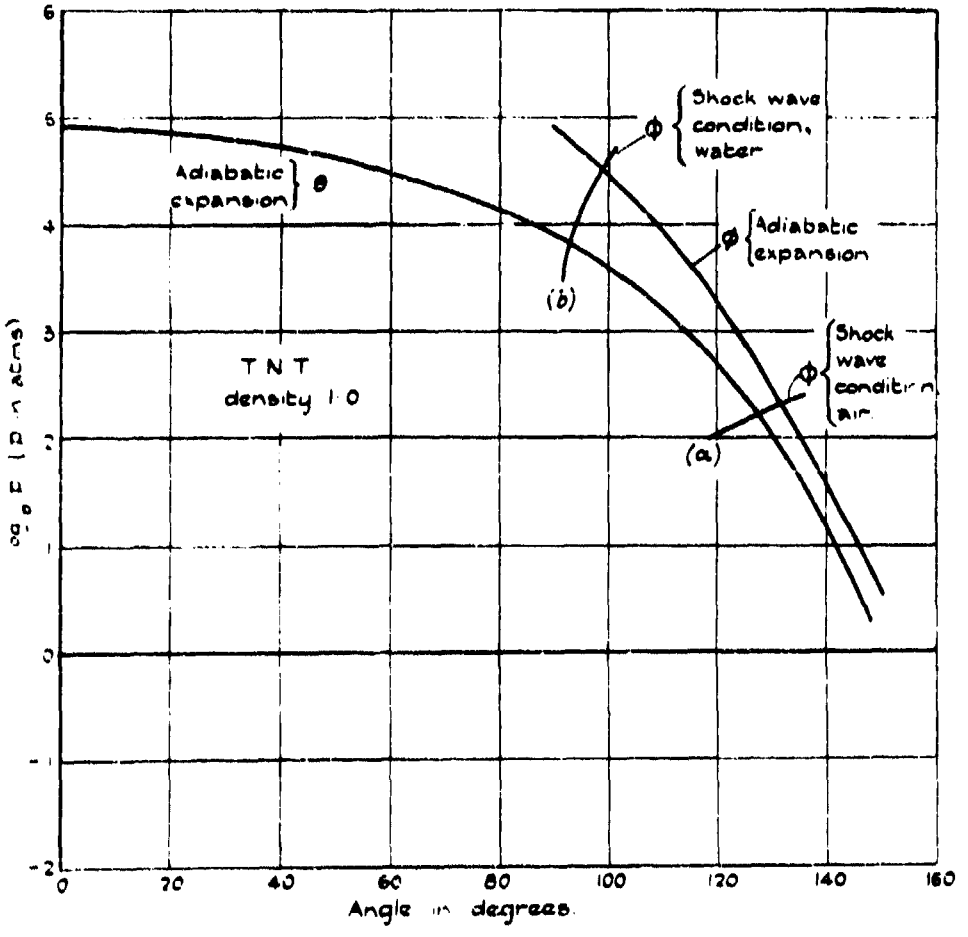

Shock wave condition, water
Adiabatic expansion
Adiabatic expansion
Shock wave condition, air
Adiabatic expansion
θ
Φ
φ
Φ
(b)
(a)
T N T
density 1·0
log10 P (P in atms)
Angle in degrees
6
5
4
3
2
1
0
-1
-2
0
20
40
60
80
100
120
140
160

Fig. 4

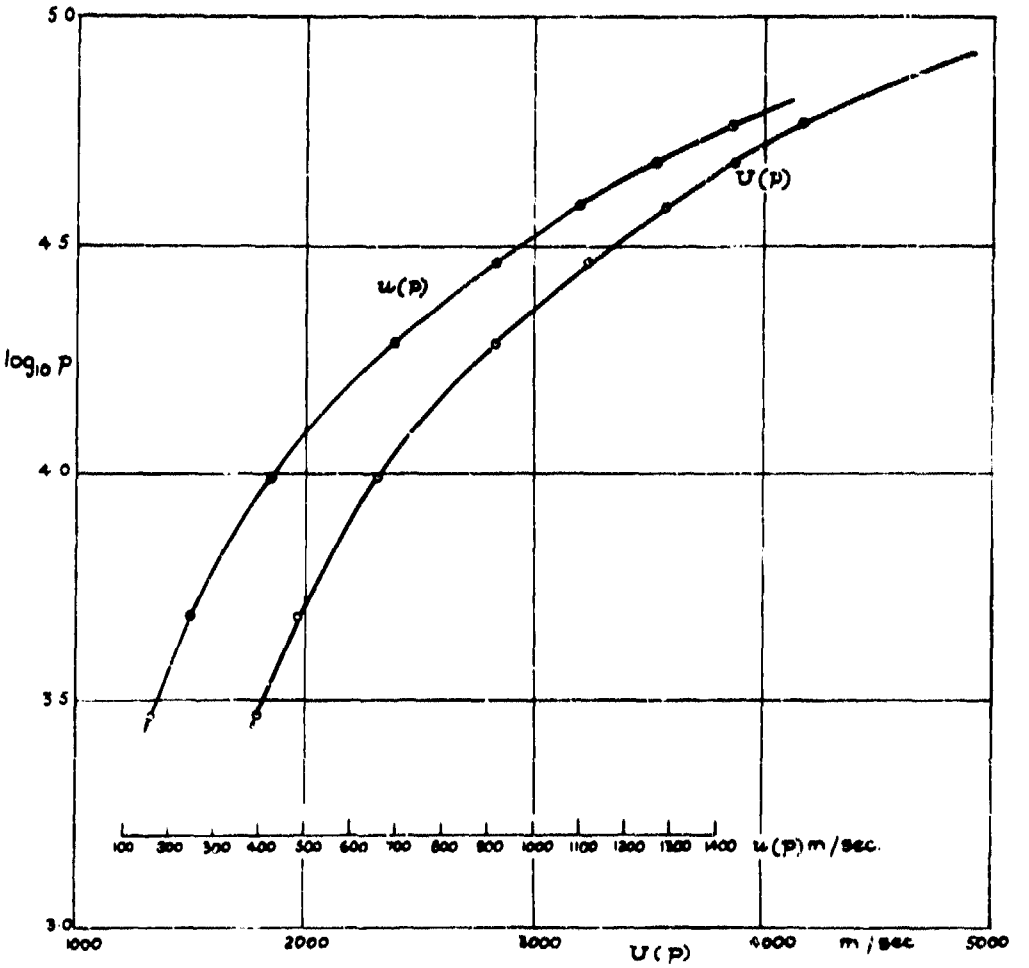
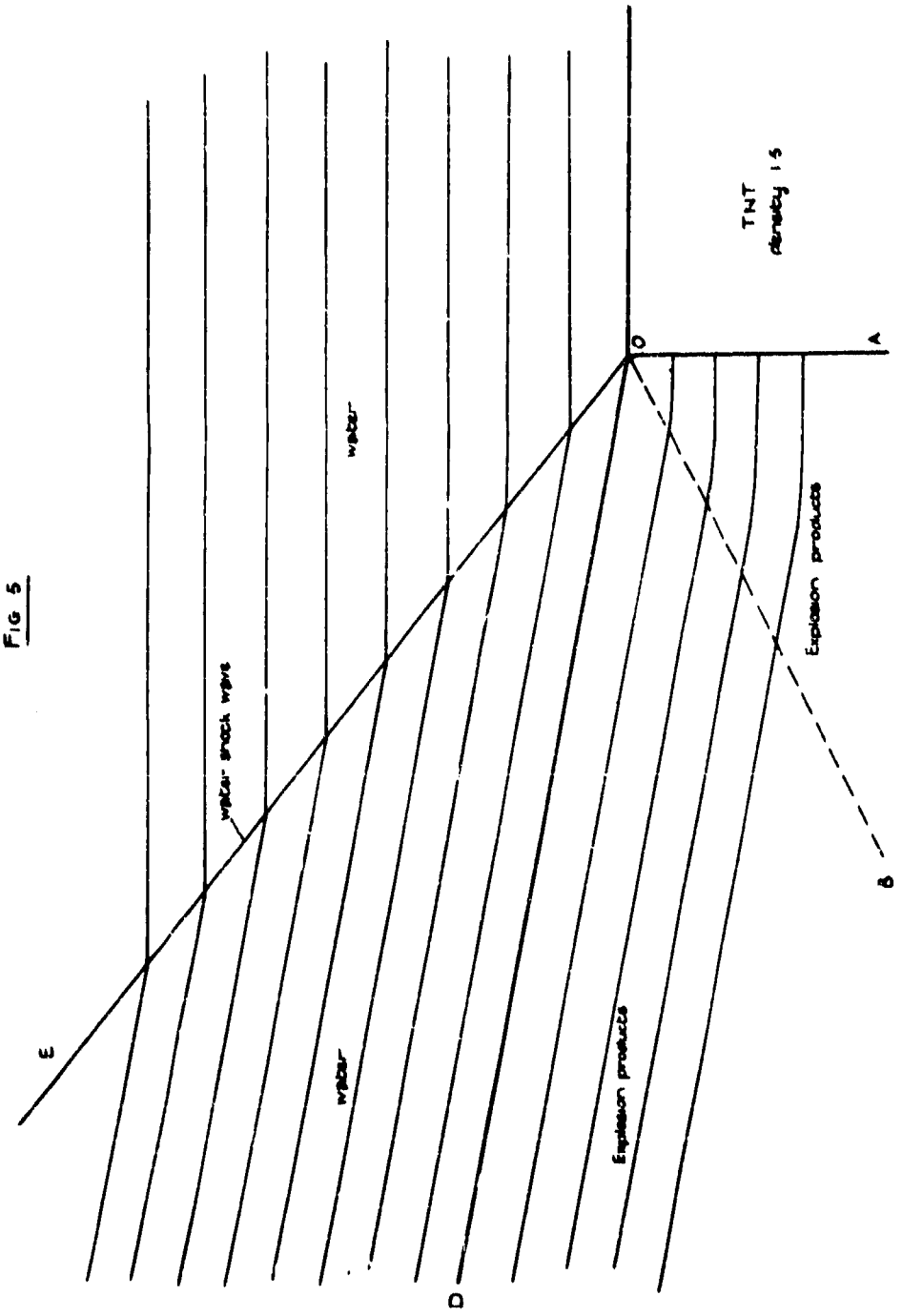

5.0
4.5
4.0
3.5
3.0
log10 P
u(p)
U(p)
100 200 300 400 500 600 700 800 900 1000 1100 1200 1300 1400 u(p) m/sec.
1000
2000
3000
4000
5000
U(p) m/sec

FIG 5


TNT
density 1·5
O
A
B
D
E
water
water
water-shock wave
Explosion products
Explosion products

THE PRESSURE-TIME CURVE FOR UNDERWATER EXPLOSIONS

W. G. Penney
Imperial College, London

British Contribution

November 1940

THE PRESSURE-TIME CURVE FOR UNDERWATER EXPLOSIONS

W. G. Penney

November 1940

* * * * * * * * *

The purpose of this mathematical investigation is to estimate the time variation of the pressure at various distances from the centre of an explosion of a spherical charge of T.N.T. surrounded by water. The results of some measurements are available for comparison, and the agreement is satisfactory. Confidence may therefore be placed in the values given by the theory for the pressures at positions so close to the charge that the force of the explosion prevents measurements from being made.

A rough description of the various events that occur is as follows. The explosive is supposed to be detonated, and for want of more detailed and accurate information we assume that the resulting hot gases are instantaneously at rest, and that the temperature, pressure and chemical composition are uniform. Thus, at the initial instant of time, we have a sphere of hot gas at a very high pressure, surrounded by water at atmospheric pressure. A shock wave of great intensity sets off into the water, and a rarefaction wave starts off into the gas. At the same time, the water and the gas in the immediate neighbourhood of the gas-water interface acquires a high velocity (of the order 1000 m./sec.). By the time the rarefaction wave has reached the centre of the gas, all parts of the gas are moving outwards, but the speeds in different spherical shells are different. Similarly, in the water, various shells up to the shock wave front are moving at different speeds, and there is a considerable variation of pressure throughout the system. As the gas expands, it does work, and the temperature, and hence the chemical composition, change. The pressure everywhere drops, but nowhere so quickly as at the centre of the gas, the origin, immediately the rarefaction wave reaches there. The next stage, therefore, is one where the pressure at the origin is very low and rising more or less uniformly to a maximum at the shock wave front. The pressure gradient near the origin soon stops the gas in this region from further expansion, and in fact soon causes gas to rush back again to the origin, restoring the pressure as it does so. The pressure gradient at the origin then becomes reversed, and gas rushes out again. The order of magnitude of the speeds at which the gas near the origin rushes in and out is 200 or 300 m./sec. The effect of the pulsation of the gas in the central region passes out into the rest of the gas and thence into the water as rarefaction and compression waves. Another set of waves is continually being generated at the gas-water interface, and the net result of all these waves, going in and out, is to average out most of them. Nevertheless, the pressure-time curve due to the explosion, even at considerable distances from the bomb, should show fluctuations. Because of the involved nature of the motion of the gas near the origin, it is not possible without very lengthy investigation to proceed to times much in excess of 0.6×10^{-3} seconds after the initial instant. Fortunately, most of the events which interest us have occurred by then, and are being propagated outwards.

One interesting fact brought out by the calculations is the rapid decrease of the shock wave intensity with distance. If the theory of sound were a valid approximation, the pressure drop at the shock wave front would vary like $1/r$, where r is the distance from the origin, and of course this will hold for very large values of r. Figure 4 shows how the pressure drop at the shock wave depends on r, for values of r up to about 25 charge diameters.

Our calculations may conveniently be separated into different sections. Section I describes a step-by-step method for dealing with a disturbance of spherical symmetry in a fluid. Section II deals with the numerical construction of certain auxiliary functions formally introduced in the previous section. Section III considers shock waves in water. Section IV gives the results of the calculations. Section V considers the extrapolation of the results to the position at which measurements were made, and compares the results with those observed.

Best Available Copy

Section I.....

SECTION 1. THE HYDRODYNAMICAL EQUATIONS.

Consider an invicid fluid in which pressure changes are occurring so fast that thermal conductivity may be neglected, and such that every element of the fluid conforms to the same adiabatic equation. Thus, we are assuming that the fluid could be reduced by suitable local adiabatic pressure changes in different regions into a condition in which the pressure, density and temperature are all uniform. When this is so, the pressure may be taken to depend on density only.

For a state of spherical symmetry, the equation of continuity and the equation of motion are

$$\frac{\partial \rho}{\partial t} + u\frac{\partial \rho}{\partial r} = -\rho\left[\frac{\partial u}{\partial r} + \frac{2u}{r}\right] \qquad (1)$$

$$\frac{\partial u}{\partial t} + u\frac{\partial u}{\partial r} = -\frac{1}{\rho}\frac{dp}{d\rho}\frac{\partial \rho}{\partial r} \qquad (2)$$

Following the well-known solution of Riemann for the corresponding one-dimensional case, we introduce two new functions P and Q, both of which involve an arbitrary function $f(\rho)$, whose precise definition we choose later, to suit our convenience.

$$P = f(\rho) + u, \quad Q = f(\rho) - u$$

Multiply (1) by $f'(\rho)$, and add to (2).

$$\frac{\partial P}{\partial t} + u\frac{\partial P}{\partial r} = -\frac{1}{\rho}\frac{dp}{dr}\frac{\partial \rho}{\partial r} - \rho f'(\rho)\frac{\partial u}{\partial r} - \rho f'(\rho)\frac{2u}{r} \qquad (3)$$

Write

$$[\, f'(\rho)\,]^2 = \frac{1}{\rho^2}\frac{dp}{d\rho}$$

thereby determining $f(\rho)$, apart from an arbitrary constant. This constant may be conveniently chosen by making the value of $f(\rho)$ zero for some standard state, denoted by suffix zero,

$$f(\rho) = \int_{\rho_0}^{\rho} \frac{1}{\rho}\sqrt{\frac{dp}{d\rho}}\, d\rho = \int_{v_0}^{v} \sqrt{-\frac{dp}{dv}}\, dv \qquad (4)$$

Using the definition of $f'(\rho)$ in (3), we obtain

$$\frac{\partial P}{\partial t} + u\frac{\partial P}{\partial r} = -\rho f'(\rho)\frac{\partial P}{\partial r} - \frac{2u\rho}{r} f'(\rho) \qquad (5)$$

Now P is a function of two independent variables only, r and t. Hence

$$dP = \frac{\partial P}{\partial r}\, dr + \frac{\partial P}{\partial t}\, dt$$

Making use of (5), this becomes

$$dP = \frac{\partial P}{\partial r}\, dr - dt\left[u\frac{\partial P}{\partial r} + \rho f'(\rho)\frac{\partial P}{\partial r} + \frac{2u\rho}{r} f'(\rho)\right]$$

$$= \frac{\partial P}{\partial r}\left[\, dr - \{\, \rho f'(\rho) + u \,\}\, dt \,\right] - \frac{2u\rho}{r} f'(\rho)\, dt$$

Now .....

See Lamb's Hydrodynamics.

$\rho f'(\rho)$ is the local velocity of sound V. Hence for a point moving with the velocity

$$\frac{dr}{dt} = \rho f'(\rho) + u = V + u,$$

$$dP = -\frac{2uV}{r} f'(\rho)\, dt = -\frac{2u}{r} V dt \qquad (6)$$

Thus, if the values of ρ and u are known everywhere at time t, thus determining the values of P and Q everywhere at this time, the value of P everywhere at time $t + \tau$ may be found from (6). All that we have to do is move the value of P at point r to point $r + (V + u)\tau$, and decrease the value by $2uV\tau/r$. A similar procedure gives the new function Q, as the following analysis shows.

Multiply (1) by $f'(\rho)$ and subtract (2). Then

$$\frac{\partial \rho}{\partial t} + u\frac{\partial \rho}{\partial r} = -\rho f'(\rho)\frac{\partial u}{\partial r} + \frac{1}{\rho}\frac{dp}{d\rho}\frac{\partial \rho}{\partial r} - \frac{2uV}{r} f'(\rho)$$

$$= \rho f'(\rho)\frac{\partial \rho}{\partial r} - \frac{2uV}{r} f'(\rho)$$

$$dQ = \frac{\partial Q}{\partial r} dr + \frac{\partial Q}{\partial t} dt$$

$$= \frac{\partial Q}{\partial \rho}\left[dr + \{ \rho f'(\rho) - u \}\, dt \right] - \frac{2u}{r} f'(\rho)\, dt$$

Hence for a point moving with velocity

$$\frac{dr}{dt} = \rho f'(\rho) - u = -V + u, \quad dQ = -\frac{2uV}{r} f'(\rho)\, dt = -\frac{2u}{r} V dt \qquad (7)$$

To find the new function Q, therefore, at time $t + \tau$, we move the value of Q at point r to point $r - (V-u)\tau$, and decrease Q by $2uV\tau/r$.

From the new values of P and Q, the values of ρ and u are everywhere determined. Thus at any point

$$u = \tfrac{1}{2}(P - Q), \quad f(\rho) = \tfrac{1}{2}(P + Q),$$

and from the curve giving $f(\rho)$ as a function of ρ, the value of ρ may be read off.

In the problem which we are considering there are two fluids involved. The analysis given above applies in both fluids, with the appropriate functions P, Q, V, etc. The boundary conditions at the interface are that the pressure and velocity should be continuous. The boundary condition at the origin is that the velocity is zero, and the boundary condition at the outer limit of the disturbance in the water may be expressed as a relation between ρ and u. This last condition we shall discuss later, when we consider the details of the step-by-step calculation.

SECTION II. NUMERICAL VALUES OF AUXILIARY FUNCTIONS.

We now consider how to estimate the values of the functions $f(\rho)$ and V in terms of the pressure as independent variable, both for water and the exploded gases. Clearly what is required is the relation for v, the specific volume (i.e. $1/\rho$), in terms of p in both cases.

The Exploded Gas.

First let us obtain $f(\rho)$ for the exploded gases. We make use of some results obtained by Dr. H. Jones for the adiabatic of the gases, the initial T.N.T. having a density 1.565 gm./cc. Jones gives numerical values of the pressure in terms of the volume, the initial volume being 145 cc.

A few .....

A few specimen figures from Jones' results are given in the following table.

TABLE 1.

v	145	150	160	200	280	400	900	3069
p	92	83	67	35	9.6	3.6	0.81	0.141

The volumes v are in cc., and the pressures p are in units 10^3 kgm/cm^2.

For values of v between 145 and 280, the above values are fitted fairly well by the equation

$$(p + 15.65)(v - 112.3) = 4390 \qquad (8)$$

and between the limits just quoted the equation is useful for theoretical work.

Before we go any further we must decide on a value for the initial radius of the charge. For convenience we take this to be 30 cm., so that the weight is 176 kgm, or 390 lb. By suitable scale changes, described when we come to consider the experimental results, our results may be easily modified to apply to any initial radius.

The appropriate modification of the above relation between p and v, valid for $92 \geqslant p \geqslant 9.6$ is

$$(p + 16.65)(v - 0.495) = 19.3 \qquad (9)$$

where v is the specific volume, i.e. the volume per gm. or $1/\rho$, where ρ is the density.

From this equation it is easy to find the velocity of sound V,

$$V = \sqrt{30/\rho} = (1950 + 35.2p) \text{ metres per second,}$$

valid for $p \geqslant 10$.

For lower values of p, the simplest way to get V is probably by numerical differentiation. We find values shown in Table 2.

The function $f(\rho)$ may also be obtained in the higher pressure regions immediately from the use of (9), and we find

$$f(\rho) = 1380 \log_e [\, 1 + p/16.65 \,] \text{ m./sec.}$$

For the lower pressure regions direct numerical differentiation and then integration must be made. The values we find are shown in Table 2.

As we have already mentioned, absolute values of $f(\rho)$ are of no consequence; all that matters is differences. The zero which we choose for $f(\rho)$ corresponds with $p = 0$ in (9), and therefore has no physical significance, but is nevertheless convenient.

TABLE 2. ($p \geqslant 10$)

p	10	20	30	40	50	60	70	80	90
V	2302	2604	3006	3358	3710	4062	4414	4766	5118
$f(\rho)$	649	1079	1424	1690	1921	2110	2280	2430	2562

Table 2 .....

TABLE 2. (p ≤ 10)

p	0.0674	0.137	0.24	0.43	0.79	1.40	2.00	4.0	6.0	8.0
V	490	540	570	630	705	790	900	1240	1540	1860
$f(\rho)$	-1740	-1470	-1190	-930	-670	-440	-240	60	350	610

The units for V and $f(\rho)$ are metres per second in every case.

Water.

Bridgeman has made accurate measurements of v for various values of p and T for water, but the maximum value of p which he was able to reach was p = 12. Now the most important region for our calculations is undoubtedly covered by his measurements, but nevertheless we do require to know the relation between p and v along an adiabatic for pressures as high as 40,000 kgm/cm^2. The best that we can do is to fit the adiabatic obtained from Bridgeman's figures up to p = 12 with a suitable equation, and then apply this equation up to p = 40.

From his measurements, Bridgeman was able to construct curves showing the adiabatic rise in temperature caused by a sudden small increase in pressure in water at various temperatures and pressures. These curves enable one to construct curves for water at various initial temperatures showing the rise in temperature as the pressure is increased adiabatically. Such curves are for the most part smooth, but do exhibit peculiar bumps, associated with the anomalous maximum density of water at atmospheric pressure at 4°C. We have made no effort to take such fine details into consideration; by assuming that the water was initially at 20°C, however, an adiabatic curve singularly free from bumps is obtained. From Bridgeman's results we find that for the adiabatic for water which is at 20°C for pressure one atmosphere, the following equation between p and v holds within about 1% over the pressure range $1 \leq p \leq 12{,}000$ atmospheres.

$$(p + 7.82)(v - 0.6807) = 2.493 \qquad (10)$$

the error being worst at the low pressure end.

This is the relation which we use over the entire pressure range with which we have to deal.

For initial temperatures greater than 20°C, we find the following adiabatic relation holds quite well

$$(p + 7.82)\left[v - 0.6807 - 0.00035\,(T_0 - 20) \right] = 2.493 + 0.0016\,(T_0 - 20),$$

where T_0 is the temperature at atmospheric pressure.

Direct calculation shows that the velocity of sound is given by

$$V = 1550 + 111\,p \quad \text{metres per second.}$$

The function $f(\rho)$ works out at

$$f(\rho) = 496 \log_e \left[1 + p/7.82 \right] \text{ m./sec.}$$

For small values of p we may expand

$$f(\rho) = 63.5p + \ldots$$

Table 3 shows values of V and $f(\rho)$, for comparison with those of Table 2. It will be seen that if our calculations are valid at the very high pressures, the velocity of sound is appreciably greater in water than in the exploded gas.

TABLE 3 .....

TABLE 3.

p	0.001	1	2	6	10	20	30	40
V	1550	1660	1770	2220	2660	3770	4980	5990
f(p)	0	60	113	283	410	630	780	890

Once again the units for V and f(p) are metres per second.

SECTION III. SHOCK WAVES IN WATER.

The theory of Hugoniot and others on shock waves in air may be modified to apply to water. There is no need to consider anything but plane waves because the shock wave is of negligible thickness, and the shock wave equations only express conservation theorems for various properties from the fluid on one side to the other.

Let the shock wave velocity be U, the mass velocity, pressure, temperature and specific volume on the high pressure side be u, p, T and v respectively, and the corresponding variables on the low pressure side by 0, p_0, T_0 and v_0 respectively.

The conservation of mass gives

$$(U - u)\, v_0 = Uv, \tag{11}$$

and the conservation of momentum

$$Uu = (p - p_0)\, v_0, \tag{12}$$

where the units of velocity are cm/sec. and of pressure are dynes/cm^2.

Write U = xu, and take the unit of velocity as metres/sec., and of pressure as 10^3 kgm/cm^2. Then the equivalent forms of (11) and (12) are

$$U = xu = 315\sqrt{(xp)}$$

$$x = v_0/(v_0 - v)$$

Clearly, we need one further equation to determine x before it is possible to find all variables in terms of p.

The usual argument of the piston in the cylinder shows that the increase in internal energy per unit mass of fluid in passing from the low pressure side to the high pressure side is $p(v_0 - v) - \frac{1}{2}u^2$. Using (11) and (12) we obtain the usual Hugoniot equation

$$\Delta E = \tfrac{1}{2}(p + p_0)(v_0 - v) \tag{13}$$

In order to put this equation in a form from which v may be found, we proceed as follows. Evaluate the work done in an adiabatic expansion from the initial state p,v to the state p_0,v_1, where v_1 is the volume corresponding to the pressure p_0 on the adiabatic containing p,v. Supply heat at constant pressure until the volume has increased to v. Then by the first law of thermodynamics

$$\Delta E = \int_{T_1}^{T} C_p\, dT - \int_{v}^{v_1} p\, dv - p_0\,(v - v_1)$$

$$= \tfrac{1}{2}(p + p_0)(v_0 - v)$$

Substituting .....

Best Available Copy

Substituting the known equation for the adiabatic, and putting in a numerical coefficient to express C_c in mechanical work units, we obtain

$$0.767 \int_{T_1}^{T} C_p dt = \tfrac{1}{2}p(v_0 + v - 2v_1) - 45 \log_e (v_0 - .0807)/(v_1 - .0807) + 7.62(v_0 - v_1) \qquad (14)$$

where T_1 is the temperature at state p_0, v_1.

This equation might be solved by trial and error. Thus a value might be assumed for v; the equation of state then fixes T, and direct substitution, assuming C_p known as a function of temperature, would show how closely the equation was satisfied. Subsequent attempts could be made nearer and nearer to the true solution. Fortunately, we do not need such great accuracy, and for our purpose it is sufficient to take C_p as unity. Bridgeman's results show that this is a good approximation.

Then

$$\int_{T_1}^{T} C_p dT = (T - T_1)$$

This simplification helps considerably in solving (14) by successive approximation. The first approximation is to put $v = v_1$ in the right hand side. Equate this value to $0.767\ (T - T_1)$ to find a value for T. From Bridgeman's results read off a corresponding value for v. Using this value of v, substitute in the right hand side of (14); equate to $0.767\ (T - T_1)$, and so on. The process converges rapidly. Of course, in the higher pressure regions, Bridgeman has no data, and the best that one can do is to study the trend of his results and make an inspired guess. As we have already stated, the pressure in our problem starts very high, but drops rapidly into the region covered by Bridgeman, and errors due to faulty approximations in the initial stages cannot seriously affect the later course of the motion.

For pressures up to about 2×10^3 kgm/cm., or roughly 13 tons/inch the shock wave velocity and the mass velocity increase linearly with p.

We find

$$U = 1550 + 99\rho + \ldots \qquad u = 63.5\rho\ (1 - \rho/15.6) + \ldots,$$

where the units of velocity are metres per second, and the units of ρ are 10^3 kgm/cm. Thus for small p, u and $f(\rho)$ are the same to first order.

The following table gives the shock wave velocity, the mass velocity behind the shock wave, ΔT, the rise in temperature from the initial state to the state behind the shock wave, and δT, the rise in temperature due to an adiabatic compression from the initial state to the pressure behind the shock wave.

TABLE 4.

p	0.001	4	8	12	20	30	40
U	1550	1920	2210	2490	3000	3560	4210
u	0	205	354	474	655	830	930
ΔT	0	30	45	61	94	152	212
δT	0	29	42	55	80	112	144

We have now enough information to describe how the actual calculations are made.

Section IV .....

SECTION IV. THE CALCULATIONS.

Section I has described a step-by-step method by which the propagation of the disturbance may be followed, provided that all parts of the fluid belong to the one adiabatic. This is not the case in the problem we wish to consider, because the shock wave raises the temperature more than does adiabatic compression to the same pressure. Thus, if the pressure difference on the two sides of the shock wave were 30,000 kgm/cm^2, the excess rise of temperature over that of the adiabatic compression, from Table 4, is 46°. The shock wave, as it passes outwards, expands and rapidly becomes less intense; as a result, the excess rise in temperature becomes rapidly less. For example, when the difference in pressure has dropped to 20,000 kgm/cm^2, the excess rise in temperature is only 14°.

We estimate that the shock wave has moved only about 12 cm. (and is therefore at radius 42 cm.) before the pressure difference on the two sides has dropped to 20,000 kgm/cm^2.

The physical properties of water at very high pressures in so far as they affect the transmission of pressure waves cannot vary very much in a few degrees. We therefore neglect the heating caused by the shock wave in excess of the adiabatic heating, and this approximation enables us to make use of the simple mathematical process described in Section I.

At time t = 0 seconds, therefore, we have a sphere of exploded gas at rest, of radius 30 cm., at uniform pressure, temperature and density, and surrounded by water at 20°C and atmospheric pressure. A rarefaction wave sets off into the gas and a shock wave sets off into the water. We wish to find the pressure at the interface. Clearly, it is somewhere between 92, the initial pressure in the gas, and 0.001, the initial pressure in the water. Since the initial densities are about the same (1.565 and 1.0), we anticipate something about the average, say p = 45. The proper value may be found as follows.

Let us for the moment consider only the one-dimensional Riemann problem and therefore ignore the changes in the functions P and Q caused by the "spherical" term $2\rho u/r$ in the equation of continuity. Then in the narrow strip of gas in the neighbourhood of the interface there will be very rapid changes of pressure and velocity, but the pressure and velocity are connected by the relation

$$P_2 = u + f_g(p) = f_g(90), \qquad (15)$$

where the suffix g stands for gas, since the value of P in this region is that which was originally in the undisturbed part of the gas.

Now the pressure and velocity are continuous across the interface, and from our work on shock waves in water (Section III) we know the values of u corresponding with values of p. We therefore try various values of p and get the corresponding value of u. By trying these values in (15) we soon get the proper solution. The solution is

$$p = 37.4, \qquad u = 960.$$

The corresponding shock wave velocity is

$$U = 4040.$$

After time τ seconds, where τ is a very short interval (we took 10^{-5} seconds) the shock wave has moved to $30 + U\tau$, and the interface has moved to $30 + u\tau$, and the pressure and mass velocity between these two radii are constant, and are given by (16).

The pressure and velocity distribution in that part of the gas which has been affected during the time τ may be obtained by the following arguments. From (15), at any point in the gas where the pressure at a particular instant is p, the mass velocity u is $f_g(92) - f_g(p)$. Now the injoing Q wave at this point has velocity V − u, where V is the velocity of sound at this pressure. Hence the value of Q corresponding with a particular p is propagated inwards with a velocity depending only on p, namely $V - f_g(92) + f_g(p)$ or $1950 + 35.2p + f_g(p) - f_g(92)$, making use of the expression for V obtained in Section II. The form of the function Q after time τ may therefore be found. The value of P everywhere in the gas is $f_g(92)$. Hence p and u may everywhere be determined.

As a .....

As a particular example, let us take $\rho = 60$. Then, using the results described in Section II we find $u = 480$, $Q = 1630$. After time 10^{-5} seconds, the Q value 1630 has moved to $r = 26.42$. Hence at time 10^{-5} seconds, the value of ρ at $r = 26.42$ is 60, and the value of u is 480, the units of Q and u being metres/second, and of ρ, 10^3 kgm/cm^2.

Figure 1 shows the distribution of pressure and velocity obtained by the above approximations, after time 10^{-5} seconds. The step-by-step process may now be applied to obtain the distribution at later times. There are three points that need further explanation. They are the fitting of the boundary conditions at the interface, the shock wave and the origin. Let us take the conditions at the interface first.

Suppose that the interface is at radius r at time t, and that the pressure and velocity there at this time are ρ and u respectively. After a small further time τ, the interface, to first order of small quantities, has moved to $r + u\tau$. The step-by-step method, using the functions P and Q, enables us to get the pressure and velocity throughout the main bulk of both fluids, but not in the narrow strip on either side of the interface, bounded by radius $r + u\tau - V_g\tau$ on the inside and radius $r + u\tau + V_w\tau$ on the outside, where V_g and V_w are the local velocities of sound in gas and water respectively. The velocity and pressure distribution curves, however, may be extended backwards into the strip from both sides in such a way that they join up smoothly.

Let us now take the conditions at the shock wave. If the shock wave radius at time t is R, and the velocity is U, then after a small further time τ, the shock wave has moved to $R + U\tau$. There is no difficulty about constructing the P curve at the new time, because the P curve moves outwards, and the rate of movement of any P value, according to the ideas of Section I, is $V + u$, where V is the local velocity of sound and is greater than U. The Q curve in the neighbourhood of the shock wave is not immediately obtainable, because the Q wave is moving inwards, and the value of Q is not conserved in passing through the shock wave. However, in compensation for the lack of knowledge about Q, we have the dynamical equations of the shock wave which give us a relation between ρ and u. Thus, at the new radius of the shock wave $R + U\tau$ we have the value of P, i.e. one relation between ρ and u, while another relation is provided by the shock wave equations. The two equations for ρ and u may be solved, and therefore the new value of Q at the shock wave found. By joining up this new Q point to the neighbouring Q curve obtained by the usual method, the complete Q curve is found. For low values of ρ, it will be seen that the Taylor's expansion for u and $f_w(\rho)$ begin with the same term in ρ. Hence Q at the shock wave begins with a term in ρ^2. Even for $\rho = 4$, Q at the shock wave is less than 1 m./second.

The condition at the origin is that $u = 0$, and therefore that $P = Q$. There is no especial difficulty about getting Q at the origin, but in some of the steps the arithmetic was lengthy, because of the term $2uVT/r$ in dQ. This term, of course, is always finite, but u changes very rapidly as the rarefaction reaches the centre, and several interpolated steps were made in the region of the origin, to improve the accuracy of the values obtained for Q and P in this region. Even so, we do not claim much in the way of accuracy, particularly as time proceeds, in this region. The steps should be taken very much smaller than we have taken. Nevertheless, an error in this region will not affect the pressure-time curves at distance 50 feet from the charge until about 0.6×10^{-3} seconds after the shock wave has passed.

In all we carried through 27 complete steps, and many intermediate steps over a small region of r when this seemed necessary. As a result we obtained the pressure as a function of radius at time 0.70×10^{-3} seconds. At this time, the shock wave radius is 174 cm., and the interface radius 58 cm. The pressure difference at the two sides of the shock wave is 1.92 in our units, or 12.6 tons per square inch.

Figure 2 gives graphically the results at the end of the 27th step ($t = 0.7 \times 10^{-3}$ second) Notice the changes in the sign of the velocity u, and the fluctuations in the pressure curve. The pronounced minimum in the pressure curve near $r = 100$ cm. has arisen from the great release in pressure in the water near the interface accompanying the expansion of the interface in the earlier stages of the motion. (In the earlier stages near the interface the pressure is such that water is appreciably less compressible than the exploded gas).

Section V.....

Best Available Co

SECTION V. EXTRAPOLATION OF THE STEP-BY-STEP RESULTS AND COMPARISON WITH EXPERIMENT.

The next problem is to take the pressure and velocity distribution curves at the end of the 27th step, and extrapolate to very much greater radii, and later times. This can be done fairly accurately without much trouble, because the ordinary theory of sound is now not a bad approximation. Some modification at the shock wave front is however necessary.

Let P_0 be the pressure difference at the shock wave front when the radius is R_0, as obtained by the last step in the step-by-step calculations. Then, if the theory of sound applied exactly to the pressure discontinuity at the shock wave, the pressure difference P at the shock wave when the radius was R, $R > R_0$, would be

$$P = P_0 R_0 / R \qquad (16)$$

The value of P given by this formula may be taken as a first approximation to the true value. Better approximations may be obtained by the following arguments.

The speed at which a particular value of the pressure at a point just behind the shock wave is passing up into the shock wave, thereby determining the pressure there, by the results of Section III, is V + u - U, or 74P metres per second. Hence by the time the shock wave has reached radius R, the pressure at the shock wave has come from a point which was distance d behind the shock wave when the latter was at R_0.

$$d = \int_{R_0}^{R} (V + u - U)\, dt,$$

the limits of t being those corresponding with the passage of the shock wave from R_0 to R. Now, with good approximation, we may replace dt by dR/U, and take only the leading term of U, namely 1.55×10^5. Similarly V + u - U may be replaced by 7400P. Moreover, P is given approximately by (16). Thus

$$d' = \rho_0 R_0 (7400/1.55 \times 10^5) \int_{R_0}^{R} dR/R = 0.048\, P_0 R_0 \log_e R/R_0 \qquad (17)$$

d', R_0 and R are in cm., and ρ_0 is in 10^3 kgm/cm. We have used the symbol d' instead of d to remind us of the approximate nature of the calculation by which it was obtained. Clearly d' is an upper limit to d because the value of P given by (16) is too large, and this error swamps all the other errors.

From the pressure-radius curve obtained in the last step of the step-by-step calculations, the pressure at distance d' behind the shock wave may be read off. Let this be p(d'). Then a second approximation for the pressure at the shock wave front when the wave has reached r is

$$P' = (R_0 - d')\, p\,(d')/r \qquad (18)$$

To get another approximation, we use this expression instead of (16) and repeat the calculations to get another approximation d" to d. Clearly

$$d'' = 0.048\, (R_0 - d)\, p\,(d')\, \log R/R_0$$

The value d" is probably as much below d as d' is above. Thus the average of d" and d' should be a very good approximation to d. We take

$$d = (d'' + d')/2.$$

Using this expression for d, we use an equation similar to (18) for the shock wave pressure at radius R, namely

$$P = (R_0 - d)\, p\,(d)/R \qquad (19)$$

This equation, together with the results of the last step in the step-by-step calculations, enables us to calculate the pressure of the shock wave at any later time.

In order .....

In order not to put too great a strain on the accuracy of (19), we first take a comparatively small value of R, namely R = 274, i.e. 100 cm. greater than that of the last step in the step-by-step calculations. The rest of the pressure-radius curve, for want of something better, we get from applying the ordinary theory of sound to the pressure-radius curve of the 27th step. Actually the error caused by this approximation appears to be insignificant

Having obtained the pressure-radius curve when the shock wave is at R = 274, we may now repeat the argument and get the curve at a later stage and so on. By proceeding in three or four steps we finally reach a stage where the shock wave is at R = 1665 cm. Table 5 gives our results for the difference in pressure on the two sides of the shock wave as a function of the radius of the wave. The units are 10^3 kgm/cm^2 for pressure and cm. for radius. For purposes of changing the units, 1 kgm/cm^2 = 0.97 atmos. = 6.4 tons/in^2.

TABLE 5.

R	90	86	100	174	274	574	1665
P	37.4	12.5	4.88	1.92	1.01	.412	.122
u	960	500	240	109	60	24	7.8

We have also included u, the mass velocity at the shock wave front, the units being metres per second.

Figure 4 shows a plot of PR against R. If the theory of sound were a valid approximation at all values of R, then PR would be constant.

Comparison with Experiment.

The results of some measurements on the pressure due to the explosion of 300 lb. of T.N.T. surrounded by water are given in the "Compilation of data resulting from trials to determine the explosive effects of aircraft bombs" (Research Department, Woolwich). The measurements were made at a distance of 50 feet. Our figures refer to a spherical charge of mass 390 lb. To convert our results into a form in which they may be directly compared with the experimental values we must divide our time scale by $\sqrt[3]{(390/300)} = 1.091$, and divide our radius scale by this same factor. Now 50' = 1540 cm.; hence, to get the pressure and velocity at this distance from a 300 lb. charge, all that we need is to get the pressure and velocity in our case at R = 1665 cm. From Table 5 we see that the initial pressure, attained on the arrival of the shock wave, is 0.122, or 0.8 tons/inch^2. This agrees perfectly with the experimental results.

Figure 5 shows the time variation of the pressure at 50' from the 300 lb. charge. The experimental curve is also shown. The agreement here is not good, but there is a rough similarity between the two curves. The difference may in part be due to the experimental charge not being quite spherical; this would cause fluctuations in the pressure-time curve to be smeared out. In any case, the theoretical curve does seem definitely to drop more rapidly than the experimental. As we have already explained, it is very difficult to get the pressure at times later than about 0.7×10^{-3} seconds after the arrival of the shock wave, because the pressure then corresponds with the very complicated sequence of events that occur near the centre of the charge after the main rarefaction wave has passed and the pressure is oscillating rapidly.

The very good agreement between the initial pressures gives one confidence that the variation of the shock wave pressure with radius is roughly right.

Acknowledgement.

The problem whose approximate solution is described in this paper was suggested to the writer by G.I. Taylor.

Best Available Copy

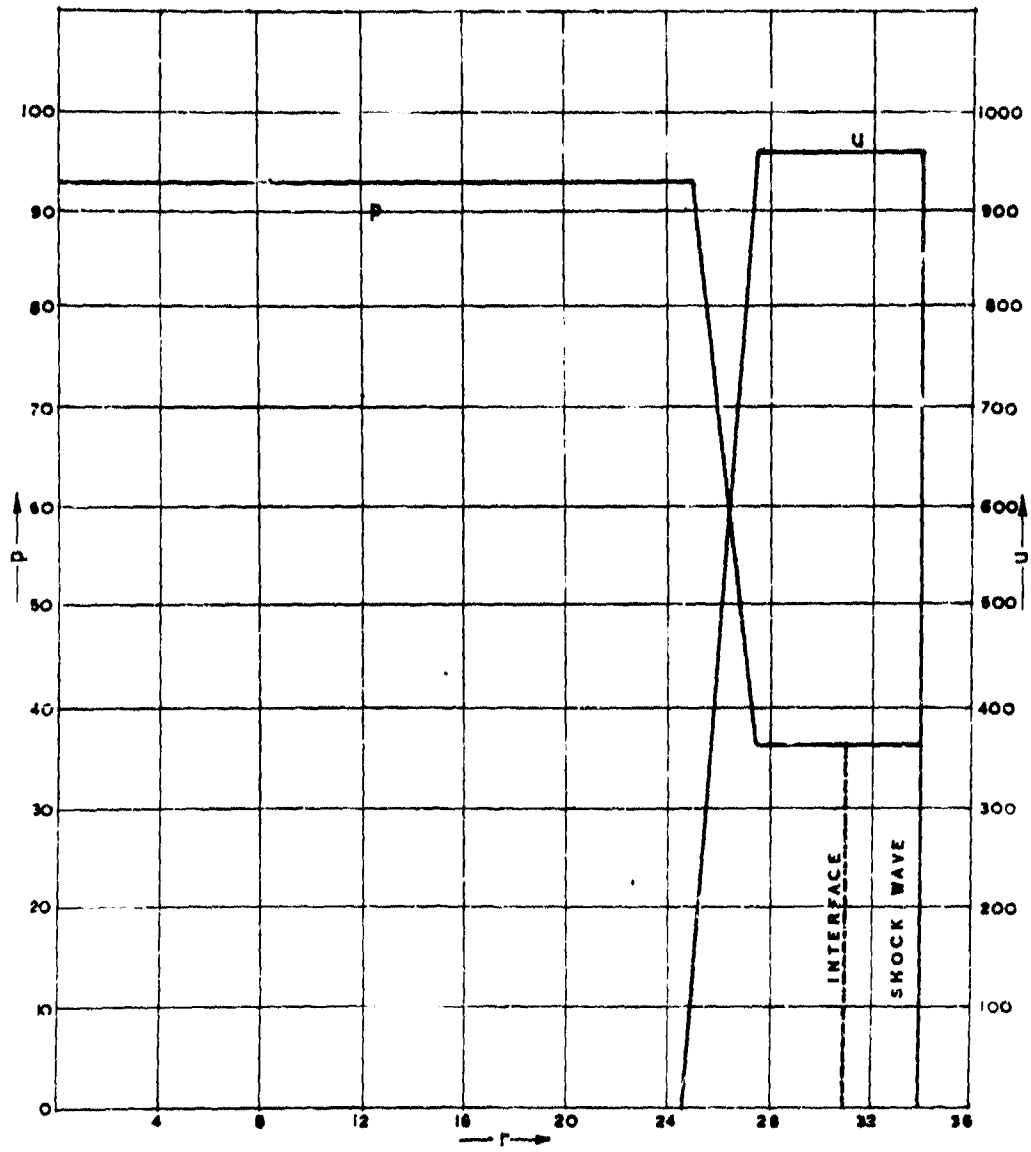


FIG · 1 · PRESSURE AND VELOCITY DISTRIBUTIONS AFTER 10^{-5} SECS ·
(UNITS : 10^{3} kgm/cm^{2} for p, cms. for r, and metres/sec for u)

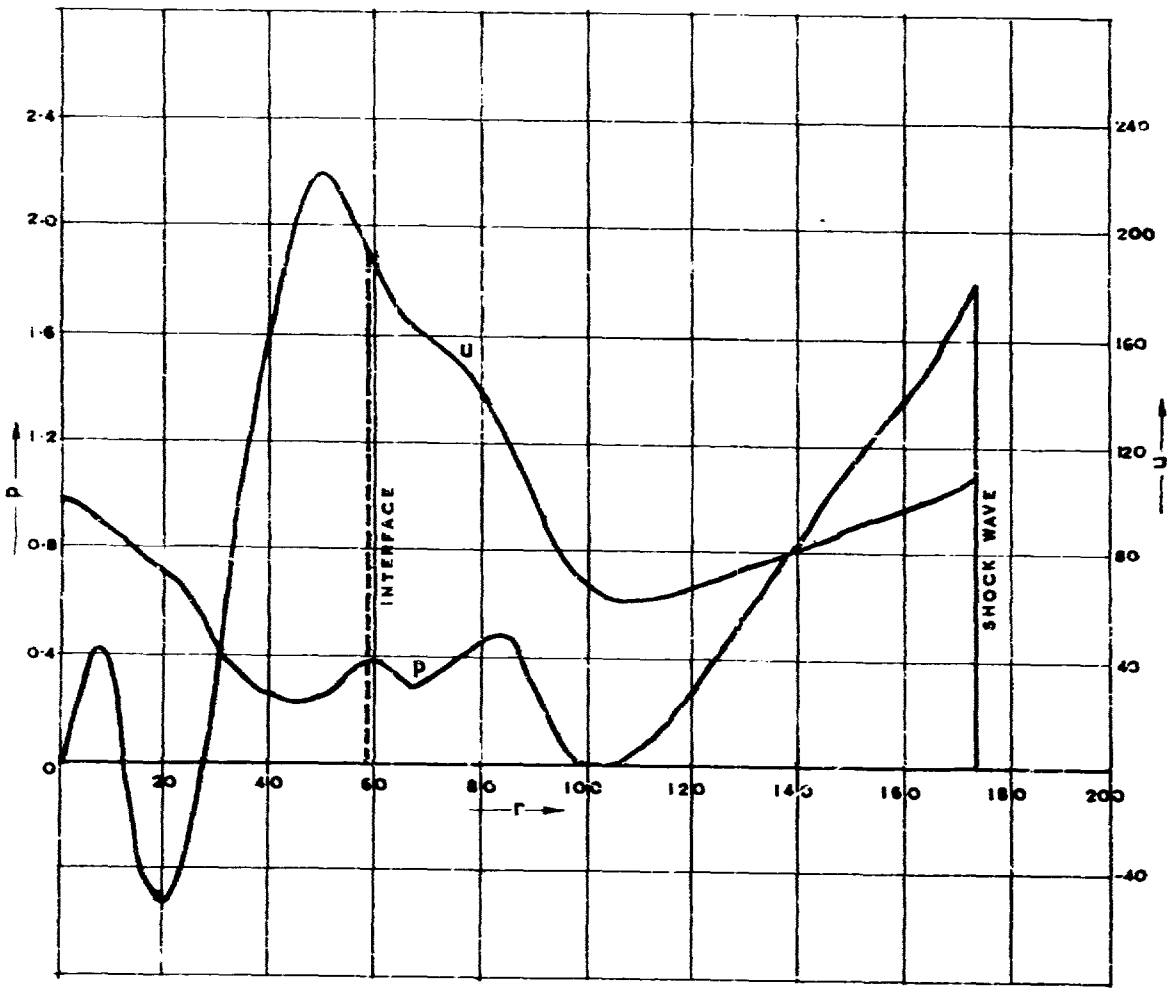


FIG ·2· PRESSURE AND VELOCITY DISTRIBUTIONS AT THE END OF 27th STEP ($t = 0.7 \times 10^{-3}$ secs). UNITS AS IN FIG ·1·

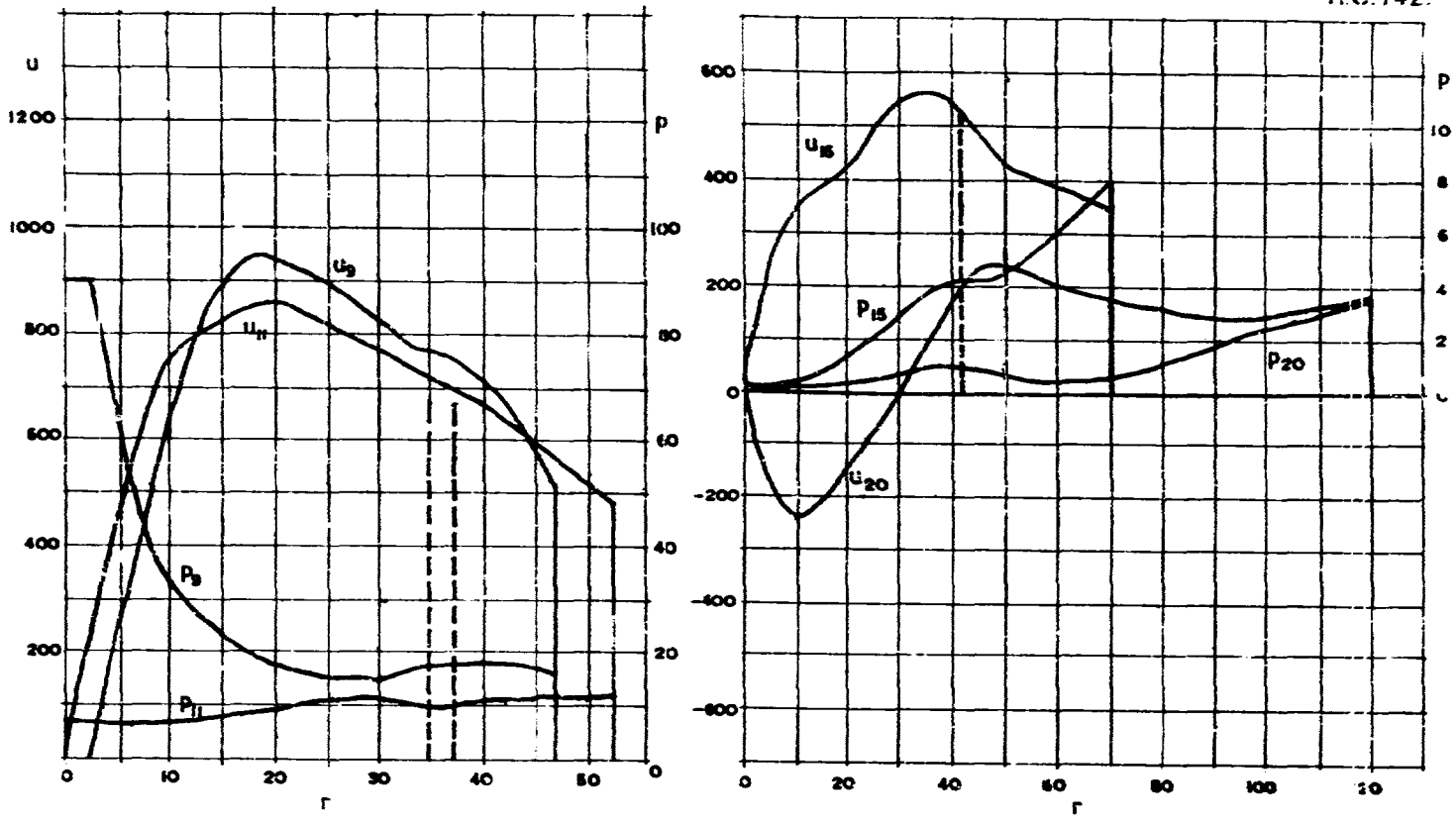
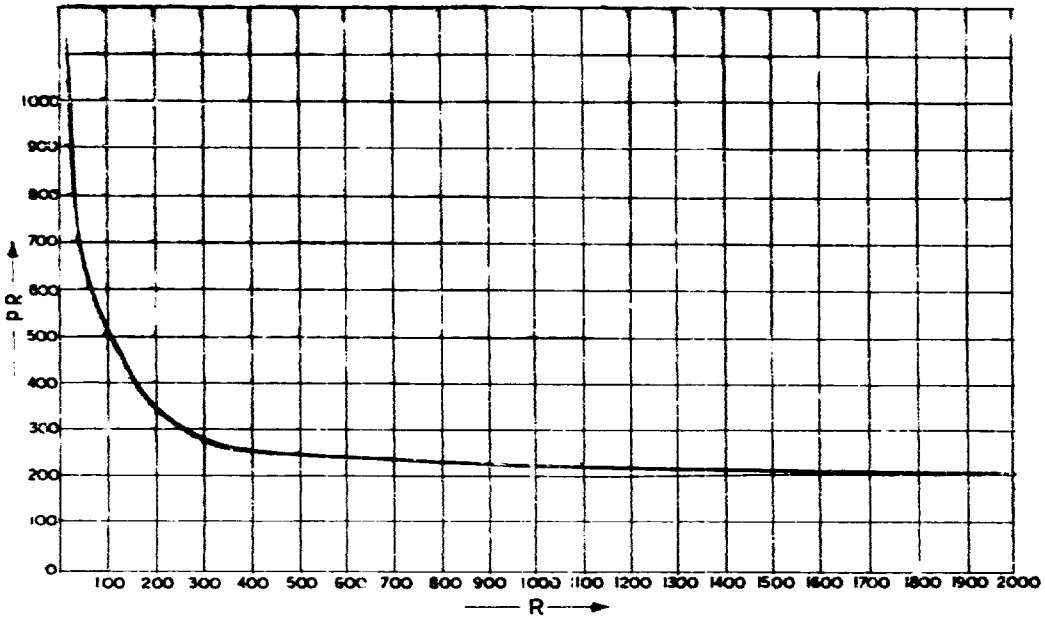
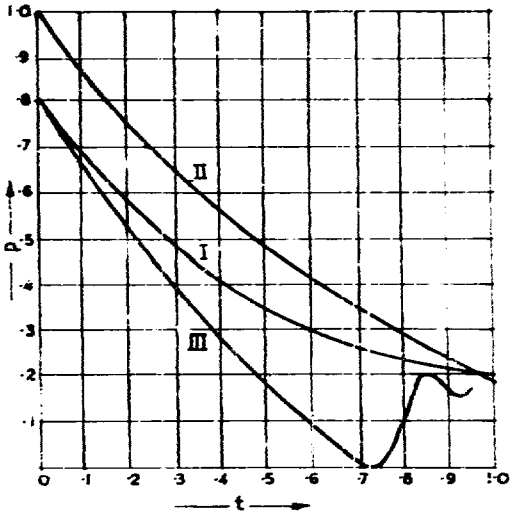


FIG. 3. PRESSURE AND VELOCITY CURVES AT THE END OF THE 9th. STEP ($t = 5{\cdot}4 \times 10^{-5}$ secs.) THE 11th. STEP ($t = 7{\cdot}4 \times 10^{-5}$ secs.) THE 15th. STEP ($t = 15 \times 10^{-5}$ secs.) AND THE 20th STEP ($t = 40 \times 10^{-5}$ secs.) IN THE 15th. AND 20th. STEPS THE PRESSURE DROP IN THE WATER JUST OUTSIDE THE EXPLODED GAS IS PLAINLY VISIBLE. UNITS AS IN FIGS. 1. AND 2.



FIG·4· PLOT OF PR AGAINST R FOR A 390 SPHERICAL CHARGE OF TNT
(P is shock wave pressure, R is radius. Units as before.)



FIG·5· PRESSURE AT 50·0' FROM 300lb. CHARGE.

I EXPERIMENTAL TNT·
II EXPERIMENTAL 40/60 AMATOL·
III THEORY TNT·
Units Tons/in^2 for p. Secs x 10^{-3} for t

PRESSURE-TIME CURVES FOR SUB-MARINE EXPLOSIONS (SECOND PAPER)

W. G. Penney and H. K. Dasgupta
Imperial College, London

British Contribution

July 1942

PRESSURE-TIME CURVES FOR SUB-MARINE EXPLOSIONS (SECOND PAPER)

W. G. Penney and N. K. Dasgupta

London, July 1942.

* * * * * * * *

Summary.

Numerical step-by-step calculations have been made on the development of an underwater disturbance caused by the spherical detonation of a T.N.T. charge of density 1.5. The theoretical pressure-time curves at a distance agree satisfactorily with those observed. If P tons/square inch is the peak pressure at D feet from a charge W lb., the theoretical values of P fit the formula

$$P = \frac{6.3\, W^{1/3}}{D} \exp\left(-0.274\, W^{1/3}/D\right)$$

The experimental values at a distance for charges of density 1.57 are about 10% higher. The discrepancy may be due to many causes, the two main ones being (1) the initial densities were not quite the same, (2) the assumed pressure and velocity curves in the spherical detonation wave were not quite correct, and correspond with a chemical energy release of 800 calories per gramme (a better value would be 1000).

The most interesting result of the calculation is the energy distribution throughout the system. In the early stages, the water surrounding the charge picks up energy very rapidly; the outward velocity is about 1400 metres/second. Roughly 30% of the energy of the charge has been given irreversibly to the water as heat by the time that the peak pressure is 1 ton/square inch.

This paper describes an attempt to improve on the calculations of the underwater pressure-time curves described in the report "The Pressure-time Curve for Underwater Explosions" (hereafter called Report "A"). The results, however, are very much the same as before. Agreement with experiment is very good, having regard to the extreme difficulty of maintaining accuracy through a long series of step-by-step calculations.

The method used is a modification of that used before, and for brevity we shall therefore write this paper on the understanding that it is to be read in conjunction with Report "A". Certain improvements in the values of the velocity of sound and the shock wave variables in water as functions of the pressure have been made. The initial conditions in the gas bubble have now been taken to be those behind the spherical detonation wave in T.N.T., derived by Taylor in R.C.178. Considerable difficulty was experienced in getting a start on the step-by-step calculations, because the pressure and velocity gradients at the detonation wave front are infinite. After some cogitation we decided that the regime shown in Figure 2 must be roughly right. The guiding principle which we used in averaging out the infinite gradients of the detonation wave front was to keep the energy balanced. Strictly speaking our initial conditions should be considered to be those of Figure 2 rather than those given by Taylor.

Adiabatics and shock waves in water.

Expressing pressures p in units 1000 kgm./sq.cm., and volumes v of 1 gm. of water in c.c., it was suggested in Report "A" that the adiabatics of water passing through the state T = 20°C at atmospheric pressure are given by the equation

$$(p + 7.32)(v - 0.6807) = 2.403 \qquad (1)$$

A reconsideration of the data of Bridgeman (Proc.Amer.Acad.Sci., Wash.66, 185, 1931) up to p = 12, and some further new data up to p = 50 which he has kindly supplied have led us to adopt a different equation. We now use

$$v(p + 3.000)^{0.139} = 1.166 \qquad (2)$$

The .....

The maximum error in v apparently occurs in the range $3.5 \leq p \leq 5$ and is less than 2 parts in 1000. For pressures in the ranges $.001 \leq p \leq 3.5$ and $5 \leq p \leq 12$ the error is smaller by a factor 3. At very high pressures, say $p = 50$ or more, the error may be several per cent but the experimental data are not at present sufficiently complete to state what the values of v are, within a few per cent.

Shock waves in water.

Consider a plane shock wave in water. Suppose that the pressure on the low pressure side is atmospheric, p_1, that the volume per gramme is v_1 and the temperature is 20°C. Let p_2 be the pressure and v_2 the volume on the high pressure side.

The shock wave equations are

$$U = v_1 \sqrt{(p_2 - p_1)/(v_1 - v_2)}, \tag{3}$$

$$u = \sqrt{(p_2 - p_1)(v_1 - v_2)}, \tag{4}$$

where v_2 is to be found for any specified p_2 from the Hugoniot equation

$$E_2 - E_1 = \tfrac{1}{2}(p_1 + p_2)(v_1 - v_2) \tag{5}$$

No simple exact expression is available for E_2, although the data of Bridgeman are complete enough to enable values of $E_2 - E_1$ to be constructed numerically for shock wave pressures up to 12. We shall require the solution of shock wave equations up to much higher pressures, and extrapolation of his results is necessary.

Figure 1 shows diagrammatically four points A, B, C, D on a $p - v$ diagram; A represents the initial state of the water before it enters the shock wave, and C is the state after it has passed through. There are two convenient reversible paths by which the water may be taken from A to C. The first is ABC; this corresponds to raising the pressure adiabatically to p_2 and then supplying heat along BC at constant pressure p_2. The second is ADC; this corresponds to supplying heat at atmospheric pressure until the water reaches C, and then raising the pressure adiabatically till C is reached.

The coefficient of thermal expansion at high pressures is appreciably smaller than it is at atmospheric pressure, and $v_2 - v'_2$, even at $p_2 = 50$, is not more than two parts in a thousand. Consequently, the path BC is unimportant compared with AB, and AB is known from (1). In contrast, the route ADC involves a different adiabatic for every value of p_2. Thus route ABC is much more convenient for our calculations than ADC.

From the first and second laws of thermodynamics, it follows that

$$E_2 - E_1 = \int_B^A p\,dv + \int_B^C C_p dT - p(v_2 - v'_2), \tag{6}$$

where C_p is the specific heat at constant pressure p_2.

The leading term on R.H.S. of (6) can be evaluated accurately with the aid of (1). Performing the integration, and putting $p_1 = 0$, it is found that (5) and (6) lead to

$$\tfrac{1}{2} p_1(v'_2 - v_2) + \int_B^C C_p dT = (v_1 - v'_2)(\tfrac{1}{2} p_2 + 3.4803) - 0.1600 v\, p_2 v'_2 \tag{7}$$

where v_1 corresponds with $p_1 = 0$.

The solution of (5) for v_2 given p_2 is most easily found by iteration. The process cannot be carried far because C_p and the coefficient of expansion at high pressures are not known accurately.

The .....

The first approximation is to assume the shock wave reversible, so that in Figure 1, B and C are supposed to coincide. Then $v_2 = v'_2$ and v'_2 follows immediately from (1).

Now we obtain a first approximation to $T_2 - T'_2$ from (7) by neglecting $v'_2 - v_2$ on L.H.S. For simplicity, assume that $C_p = 1$ cal./gm. Then

$$0.0426\,\theta = (v_1 - v'_2)(\tfrac{1}{2} p_2 + 3.4803) - 0.18009\, p_2\, v'_2 \qquad (8)$$

where θ is $T_2 - T'_2$ and the factor 0.0426 has arisen from expressing cal./gm. in mechanical units pv, p being 10^3 kgm./sq.cm. and v in c.c.

Using the experimental value of the coefficient of expansion at pressure p_2 over the range $T_2 - \theta$ to T_2, we then get a second approximation to v_2. Second approximations to U and u follow immediately. The iteration process converges so rapidly that further approximations are not warranted by the accuracy of the experimental data.

If $p < 1$, the heating θ in °C, above the adiabatic heating, is given by the formula

$$\theta = 0.0342p^3 - 0.0122p^4 + 0.0038p^5 - 0.0011p^6 + \ldots, \qquad (9)$$

The velocity of sound in any thermodynamic state of water lying on the adiabatic through A is obtained by differentiation of (1). Expressing c in metres per second

$$c_A = 1461\,(1 + p/3)^{0.431} \qquad (10)$$

Thus, the velocity of sound in water at 20°C and atmospheric pressure is estimated at 1461 m./second. This agrees exactly with the experimental value, within the limits of experimental error.

The following table gives a selection of values of U, u, $v_1 - v_2$, T'_2, T_2 and c_A for various p_2.

TABLE 1.

p_2	1	4	6	10	15	20	30	50
$v_1 - v_2$	.0389	.1101	.1403	.1822	.2151	.240	.277	.317
T'_2	21.81	30.18	36.46	46.67	65	85	155	325
T_2	21.84	31.10	38.20	54.45	77	104	192	400
U	1591	1891	2052	2324	2621	2850	3266	3493
u	61.7	208	288	423	563	688	893	1229
c_A	1655	2106	2347	2760	3164	3517	4109	5080

Units: p in kgm./sq.cm. = 6.35 tons/square inch, $v_1 - v_2$ in c.c., T'_2, T_2 in °C, U and u in m./second.

The values given in Table 1 agree well with those given in Report "A", except that the θ values have been improved, and with those quoted by Kistiakowsky and Wilson (Final Report on the hydrodynamics of shock waves, N.D.R.C.) The temperatures given in this last report, where they differ from those above, are probably more accurate than those quoted here, because they allowed for the variation of C_p with temperature. The difference never exceeds 1°C. The values of θ were not calculated by Kistiakowsky and Wilson, and their values extend only up to p = 12.

In the step-by-step calculations described in following paragraphs, the entropy gradient terms in the hydrodynamic equations were omitted. Thus, the calculations were made on the assumption that the temperature difference θ was insignificant as far as the propagation of pressure waves is concerned. To be consistent throughout, we have therefore calculated U, u, v, c behind the shock wave on the assumption that B and C in Figure 1 are consistent. Table 2 gives the numerical values.

TABLE 2 .....

TABLE 2.

p	.001	1	2	3	4	5	6	7	8	9	10
c	1462	1655	1822	1971	2106	2231	2347	2456	2559	2657	2750
u	0	61.9	118.7	168.1	208.3	249.5	288.2	328.6	369.9	398.8	424.1
U	0	1589	1700	1798	1887	1970	2046	2120	2191	2258	2316

p	12.5	15	20	25	30	35	40	45	50	55	60	65
c	2967	3164	3517	3828	4109	4366	4603	4829	5040	5239	5429	5611
u	499.2	568.5	694.1	807.7	911.8	1009	1100	1186	1268	1347	1421	1489
U	2460	2595	2832	3041	3235	3410	3573	3728	3878	4013	4170	4278

The Riemann function f is a numerical multiple of c.

$$f = \int^{p} \sqrt{-dp/dv}\,.\,dv = 0.3202\,c.$$

This relation is extraordinarily convenient in the numerical work because it means that c can be found by merely multiplying (P + Q) at any point by 0.1601.

Energy wastage in shock waves.

Shock waves, of course, are irreversible, and it is impossible without employing perfect heat engines to regain in mechanical form all of the energy being used in maintaining a shock wave of pressure p_2. The water on the high pressure side has kinetic energy, already in mechanical form, and in virtue of its pressure, may be made to do mechanical work by adiabatic expansion to atmospheric pressure against a full resistance. The water will then be hotter than it was originally (20°C) and the heat excess may be termed the "wastage". The wastage per gramme of water will be almost exactly θ calories. A very small correction should be applied, because the temperature difference between O and A in Figure 1, the true wastage, is not quite the same as the difference between C and B, called θ above. However, θ has not been calculated accurately enough to justify making a correction of this type.

Reflexion and stagnation pressures.

According to the theory of sound, an infinitesimal plane pressure pulse $p_0 + p_1$, incident normally on a plane rigid wall, is reflected, and the pressure on the wall is $p_0 + 2p_1$. This effect is usually known as "doubling by reflexion". If the plane wall is of finite area, the pressure instantaneously is doubled, but soon falls to $p_0 + p_1$ because of diffraction. When the incident pulse is of finite intensity, variations are possible. First, the instantaneous pressure excess over p_0 is not doubled, but is increased by a factor greater than 2 according to the medium and the precise value of p_1. Second, the mass velocity of the fluid u associated with the original pressure pulse may be less than, equal to, or greater than the velocity of sound c in the fluid carrying the pulse. If $u < c$, the situation is described as sonic; if $u > c$ the situation is described as supersonic. Details will be found in Rayleigh, Scientific Papers V, p.608; a helpful summary, together with numerical examples for air ($\gamma = 1.4$), will be found in R.C.118 (Taylor).

Consider now a plane shock wave in water about to impinge normally on a finite plane rigid wall. The first point to notice is that conditions near the wall are sonic up to pressures well beyond 50 (say 300 tons square inch). This may be seen from Tables 1 or 2, where c is always much greater than u. The pressure at the stagnation point, i.e. the point at which the stream has zero velocity, may be calculated from the pressure and velocity in the main stream by the use of Bernoulli's theorem. The instantaneous pressure on the wall may be found by introducing a reflected shock wave of sufficient intensity to reduce the mass velocity to zero. The following values have been computed to illustrate how the ordinary laws of sound reflexion apply reasonably well in water even at enormous pressures.

TABLE 3 .....

TABLE 3.

p_2	0.5	1	2	5	10	20	30	50
$\frac{p_r}{p_2}$	2.0870	2.1570	2.2993	2.5925	2.9112	3.389	3.688	3.915
$\frac{p_s}{p_2}$	1.0112	1.0205	1.0386	1.080	1.1262	1.1868	1.2278	1.2847

p_2 is the pressure (10^3 kgm./sq.cm. = 6.38 tons/square inch) behind the incident shock wave; p_r is the instantaneous reflected pressure, and p_s is the stagnation pressure.

The thickness of the shock waves in water.

The Admiralty records of the pressure pulses of underwater explosions (e.g. Wood, "Nature of the pressure impulse produced by the detonation of explosives under water. An investigation by the piezo electric cathode-ray oscillograph method", hereafter called "Report "B") all show a finite time of rise τ of the pressure to its peak value; the observed values of τ range from 50 to 100 microseconds. Even when correction is made for the finite dimensions of the gauges, it still appears that τ measures a real effect, whose exact nature is uncertain.

If the time of rise is 50 microseconds, the peak pressure lags by about 7 cm. behind the leading edge. We have estimated the thickness of shock waves in water of intensity less than 1000 atmospheres, to see if τ may be partly attributed to the thickness of the shock waves.

The calculations are only rough, and follow those of Taylor and MacColl for shock waves in air. (Durand - Aerodynamic Theory, Vol. 3, p.218).

The equation of energy is

$$\frac{d}{dx}\left[-pu + \frac{4}{3}\mu u \frac{du}{dx}\right] + J\,\frac{d^2\theta}{dx^2} = n\frac{dE}{dx} + \frac{m}{2}\frac{du^2}{dx^2}$$

The equation of continuity is

$$\rho u = m$$

The equation of state may be taken as

$$v = v_0 (1 + \alpha\theta - \beta p)$$

The adiabatic may be taken as

$$(p + p_0)^\gamma = C_0 \rho$$

where p_0 and C_0 are functions of θ, and γ is constant.

Solving the equations in a similar way to that devised by Taylor and MacColl, it is found that 80% of the change of velocity on the two sides of the shock wave occurs within the thickness T

$$T = x/(u_1 - u_2)$$

$$D = \left\{\frac{8}{3}\,\frac{2-\gamma}{1-\gamma}\,\frac{\mu}{\rho_1} - \frac{kJ}{\alpha}\left[\frac{\rho_0}{\rho_1^2 u_1^2} - \beta\right]\right\}\Big/\frac{3-3\gamma}{2(1-\gamma)}$$

The numerical values of the parameters are

$\alpha = .00084$, $\beta = .0256 \times 10^{-9}$, $\mu = .01004$, $k = .00138$, $\gamma = .138$, so that

$$T = x/(u_1 - u_2)$$

where $x = .001$ if $p = 1000$ kgm./sq.cm. and $x = .0105$ if $p = 4000$ kgm./sq.cm.

Thus .....

Best Available Co

Thus the thickness works out at about 10^{-6} cm. The calculation is practically meaningless, except in so far as it shows that the pulse thickness is less than the smallest thickness for which the calculation would be a reasonable representation of the facts.

The step-by-step calculations.

A modification of the method described in Report "A" was used.

The first eight steps were performed in exactly the same way as described in Report "A". The course of the disturbance was followed by means of local distortions and displacements of an outward moving curve P and an inward moving curve Q. In a small interval τ

$$dP = dQ = -2uc\tau/r.$$

Unfortunately, the values of τ needed to follow the disturbance to 6 charge radii in about 30 steps require values of τ rather too large for the second order corrections to P and Q to be inappreciable. We therefore modified the procedure after 8 very small steps to

$$dP = -2\,(uc\tau/r)_P$$

$$dQ = -2\,(uc\tau/r)_Q$$

where the average values were found by a two forward one backward scheme.

Suppose that the steps up to $(n-1)$ are complete, and have been accepted as correct. The nth and the $(n+1)$th steps are then made by the Report "A" procedure. From the $(n+1)$ values, the dP values in the nth step are corrected, by taking the average of $2uc\tau/r$ in the nth step and $2uc\tau/r$ in the $(n+1)$th step, the values in the latter case being found at the points to which the P curve had moved. Similarly, the dQ values are corrected. From the adjusted nth step, adjustments were then made in the $(n+1)$ step, and the $(n+2)$ step done by Report "A". A step backwards from $(n+2)$ to $(n+1)$ then gave the corrected $(n+1)$th step. Then $(n+2)$ was corrected, and $(n+3)$ begun. Thus every step was in fact performed three times, being averaged from information provided from steps on either side. It is much quicker to make the corrections than it would be to take τ one third as small, and perform three steps, because many of the columns do not change, and only one sheet of graph paper is needed for the three phases of one step.

Results.

The results of the calculations are shown in Figures 3, 4, 5, 6 and 7. Figures 3, 4 and 5 have been given in a form that applies to a 1800 lb. charge; simple scale changes by the cube root law would give the corresponding curves for any other weight of charge. The pressure and velocity distributions in the inner regions of the bubble are not shown because the calculated values are not reliable. All that can be said is that in the later stages of the calculations, the pressure in the bubble was rapidly tending towards uniformity, and that the gas radial velocity did not anywhere exceed about 200–300 m./second.

The calculated shock wave pressure in tons/square inch at x charge radii over the range $1 \leq x \leq 6$ fits closely to the law

$$p = \frac{46}{x}\, e^{2/x}$$

Thus P at D feet from a charge W lb. should be

$$P = \frac{9.2\, W^{1/3}}{D} \exp\left\{ 0.274\, W^{1/3}/D \right\}$$

The pressure at 80 feet from a 300 lb. charge is calculated to be 1940 lb./square inch, compared with the experimental value 2100 lb./square inch. (Report "B").

The asymptotic formula for P as $D \to \infty$ is

$$P = 18000\, W^{1/3}/D \quad \text{lb./square inch.}$$

compared with the experimental formula (Wood)

$$P = 12000\, W^{0.38}/D \quad \text{lb./square inch}$$

Correcting .....

Correcting this last formula to make P depend on $W^{4/3}$, the best interpretation of the experimental results is obtained with the formula

$$P = 16000\ W^{-4/3}/D \quad \text{lb./square inch.}$$

Since the theory cannot be relied on to within 10 or 20%, the agreement with experiment is quite satisfactory.

An approximate calculation of the pressure-time curve for a 300 lb. charge at 80 feet, based on Figure 8, gives results agreeing very closely with the experimental data, as shown in Figure 6. Figure 7 shows some of the pressure and velocity distribution curves at various steps.

Energy distribution throughout the system.

Although the close agreement between the theoretical and experimental pressure-time curves is extremely satisfactory, the accuracy of the experimental curves was more in question.

The theory, however, does provide valuable new information about the energy distribution throughout the system. All that is known experimentally is that roughly one-quarter of the chemical energy of the charge resides in the pressure pulse at the stage where the peak pressure is down to 1 ton/square inch. (See, for example, Wood, Report "B").

At any stage in the motion, the energy may be sub-divided as follows:-

(1) Kinetic energy of water (T_1)
(2) Potential energy of water (V_1)
(3) Irreversible heating of water, or wastage (w)
(4) Kinetic energy of gas (T_2)
(5) Potential energy of gas (V_2)

Of these, (1) and (4) call for no comments; (2) merely represents the energy stored as compression in the water; (4) also may be regarded as energy stored by compression, but the ultimate seat of energy here includes chemical as well as pressure energy because the chemical composition of the gas varies along the adiabatic; (3) is the ordinary wastage associated with shock waves (an account of the wastage associated with shock waves in water is given earlier in this paper).

The following table has been constructed to show the energies of the five categories when the shock wave front is at x-charge radii (initial density of charge 1.6), the units being calories per grams of T.N.T.

TABLE 4.

x	T_1	V_1	w	T_2	V_2
1.00	0	0	0	46	754
1.088	48	22	10	49	472
1.319	72	43	44	-	-
2.94	151	72	148	-	-
4.37	190	101	177	-	-
6.08	232	96	192	~ 8	~ 176

The sum of the energies along any row should, of course, equal the total energy of the explosive (here taken to be 800 cal./gm.), but because of the difficulty of maintaining accuracy in the inner regions of the bubble, the values of T_2 and V_2 in the latter stages are only rough. The first three columns, however, are reasonably accurate.

Figure 8 shows how the water acquires useful energy (i.e. $T_1 + V_1$) as a function of x. The remarkable feature of the curve is the extremely rapid rise near the beginning (x = 1). One

might .....

might regard the thin layer of compressed water as a casing; certainly its velocity and energy is comparable with that of a steel case surrounding a similar charge. At x = 4.088 charge radii, the water is compressed from its original thickness .088 to .056 and its average velocity is about 1450 m./second.

The additional wastage between x = 6.08 and x = 88 is only 66 cal./gm. Thus we have that the energy wastage at the limit of damaging range is 30% of the chemical energy, and is therefore roughly equal to that of the energy of the pulse at the same range.

It will be noticed that the total energy of the T.N.T. is taken as 800 cal./gm. This is perhaps on the low side. Jones, in R.C.212, estimates the chemical energy released per gm. of T.N.T. at loading density 1.5 gm./c.c. to be 1090 cal./gm. However, the adiabatic used by Taylor, R.C.178, was only approximate, and the total energy per gram., assuming Taylor's pressure and mass velocity curves together with Jones' adiabatics, R.C.212, works out at 800 cal./gm. A recalculation of the spherical detonation waves in T.N.T. for loading densities 1.5 and 1.0 is in progress, and a report on the results will be made shortly.

The energy of the disturbance at the end of the step-by-step calculations is 700 cal./gm. Most of the errors certainly occur in the inner regions.

Radius of bubble and velocity of interface.

Table 5 gives the radius of the bubble in cm. at times t microseconds, for a charge initially 50 cm. radius. The radial velocity in metres per second is also given.

TABLE 5.

t	0	5	10	20	30	40	50	70	90	110	130
r	51.6	56.9	60.8	67.3	73	78.2	82.9	91.2	98	103.9	109.4
u	1430	820	675	560	510	475	440	368	310	275	248

The overtaking effect and time of rise.

As mentioned earlier, the records of underwater explosions appear to show a finite time of rise τ to the peak pressure. If this effect is real (apparently there is still some doubt about it), the origin of τ might be sought in any of the followings-

(1) the effect of the case,
(2) detonation not spherical, so that the gauge records a series of elementary pulses building up to a maximum,
(3) change of phase of water.

The following table indicates that (1) and (2) taken separately are unlikely to provide the full explanation of τ. We have calculated a distance D in terms of the shock wave radius R cm. for a charge of initial radius 50 cm. At the instant that the spherical detonation wave reaches the surface of the charge an expanding sound pulse in the water has its leading edge at 50 + D; D is then chosen so that the shock wave overtakes the sound pulse at radius R.

TABLE 6.

R	56.58	65.93	91.8	147.0	200.5	271	304
D	5.56	10.09	22.8	41.5	54.1	65.8	70

Thus, if the sound wave had a start of 500 microseconds over the shock wave, the sound pulse would just be masked by the shock wave at distance 304 cm. Adjusting the scale to a 300 lb. charge gives the start as 270 microseconds. To give an observed τ of, say, 86 microseconds requires that the sound wave must be given a start 320 microseconds. This seems too large to be attributed to the effect of the case or non-spherical detonation.

Discussion ....

Discussion.

The calculations described above agree better with the observations than did those described in Report "A". The pressure-time curve falls away much more slowly with time, and it seems likely that the theoretical curve is monotonic. Probably the most interesting feature of the present calculations is the energy distribution of the disturbance in the early stages. About 61% of the energy is carried by the water by the time that the shock wave front has reached 6 charge radii; 41% is useful work and 2% is unavailable.

Similar calculations could be made on other, more powerful explosives, but in the meantime it seems clear that the useful work given to the water will increase with the chemical energy of the explosive, but less rapidly than linearly because the wastage goes up faster. It seems most unlikely that an explosive with great energy release will cause energy to be dissipated in the first few charge radii so rapidly that its "damaging effect" (or more precisely, the useful work left in the water) will be less at greater distances than that given by a less powerful explosive.

Measurements of the pressure-time curves at a distance cannot be used to determine the very early stages of an explosion, because of the overtaking effect, described earlier. It seems safe to say that whatever occurs within 100 microseconds of the detonation wave in a 300 lb. charge reaching the surface of the charge is completely undetectable by measurements at 80 feet. The question arises whether the best results at 80 feet might be obtained by preparing the explosive in such a way that the pressure does not build up to its maximum until 100-200 microseconds after the detonation wave has reached the surface. In other words, if aluminium is present in an explosive mixture for use at a distance under water, there may well be an upper and a lower limit to the size of aluminium particles required.

Description of diagrams.

Figure 1. Two reversible paths ABC, ADC by which water may be taken from the initial state to the final state of the shock wave transition.

Figure 2. The pressure and velocity distributions 10 microseconds after complete detonation of a 50 cm. sphere of T.N.T., density 1.6, surrounded by water. Shock wave at 54.4 cm.; interface at 51.6 cm.

Figure 3. The final version of the 17 step. The two forward, one backward procedure gives a tripling of each P and Q curve, but the scale of the diagram is not sufficient to show all the curves. The Q_w curve is practically the same in all cases; the P_w curves vary by about 10 m./second.

Figure 4. Velocity distribution curve after 24 complete steps ($t = 1.28 \times 10^{-3}$ seconds).

Figure 5. Pressure distribution curve after 24 complete steps.

Figure 6. The pressure-time curves for a 300 lb. charge at 50 feet. E experimental; T theoretical. The accuracy of the theoretical curve is not high since it is obtained by an extrapolation of uncertain validity.

Figure 7. Pressure and velocity distributions at various times t in 10^{-6} seconds for a charge of initial radius 50 cm.

Figure 8. The useful work and the wastage given to the water in cal./gm. of T.N.T., as a function of the radius of the shock wave x, expressed in charge radii. (A 300 lb. charge, density 1.6, has a radius approximately 11 inches).

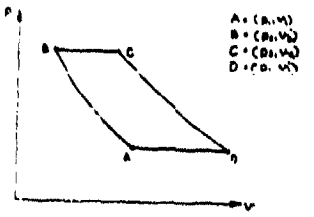


FIG. 1.

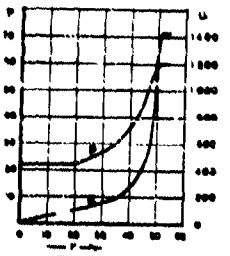


FIG. 2.

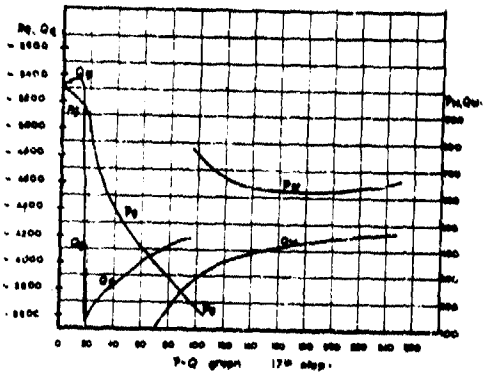


FIG. 3.

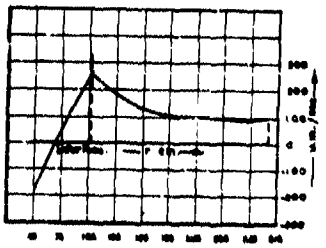


FIG. 4.

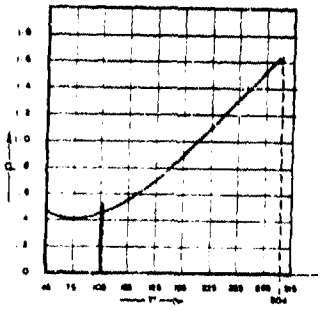


FIG. 5.

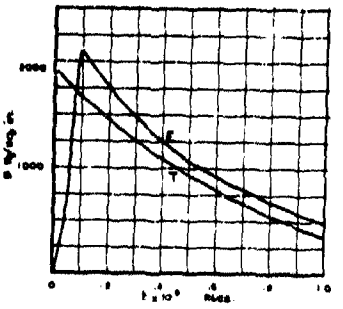


FIG. 6.

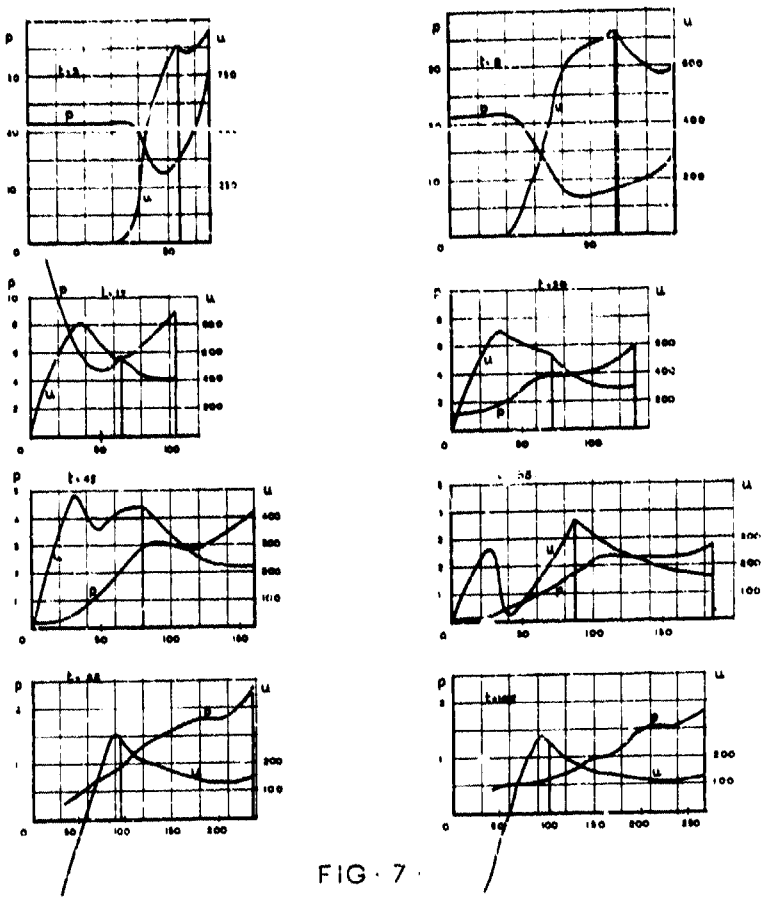


FIG · 7 ·

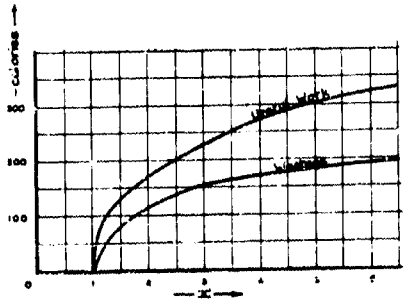


FIG · 8 ·

AN APPROXIMATE CALCULATION OF THE PRESSURES PRODUCED BY DETONATING LINE CHARGES UNDERWATER

G. Charlesworth and A. R. Bryant
Road Research Laboratory, London

British Contribution

December 1943

AN APPROXIMATE CALCULATION OF THE PRESSURES PRODUCED BY DETONATING LINE CHARGES UNDERWATER

G. Charlesworth and A. R. Bryant

December 1943

* * * * * *

Summary

Calculations have been made of the forms of the pressure-time curves produced by the detonation underwater of line charges, on the assumption that the line charge is equivalent to a number of elemental sources of pressure such that the pressure due to unit element at a point distant r from it is of the form $\frac{p_o e^{-kt}}{r}$.

The pressures produced by straight line charges at points on the perpendicular bisector and also on the axis of the charge in the direction of and in the opposite direction to that of detonation have been evaluated. The pressures produced by a circular arc and by an arc of an equiangular spiral of charge at the centres of the circle and spiral respectively, have also been calculated. Numerical examples have been considered for an arbitrary value of $k = 60{,}000$ sec.$^{-1}$ and the results have been compared with experimental values obtained using Cordtex charges.

It is concluded that the theory predicts to a first approximation the form and relative magnitudes of the pressure-time curves produced by line charges. It has been noted that the theory is limited by the uncertainty in the values to be assigned to p_o and k in any particular case and by the breakdown of the simple acoustic approximation at points near the charge.

Introduction

The purpose of this note is to attempt to calculate by approximate methods the distribution of the pressure effects produced by the explosion underwater of line charges.

General

The analysis used may best be illustrated by considering the special case shown in Figure 1, where the line OL represents the charge and O is the point of initiation. It is assumed that each element of the charge length δx produces at a point P distance r from it a pressure

$$\frac{p(t)\,\delta x}{r}$$

where p(t) is a function of time measured from the instant at which the element was detonated. It is also assumed that the pressures are simply additive.

Let c_1 be the detonation velocity of the charge

c_2 be the velocity of sound in water

where $c_1 > c_2$

Let $t = 0$ at the instant of detonation at O

Consider the effect at time t at a point P due to an element δx distant x from the end of the charge at which detonation commences. The element δx produces no effect at P until a time

$$\frac{x}{c_1} + \frac{r}{c_2}$$

The .....

Best Available Copy

The pressure at P due to this element is thus

$$p = 0 \qquad t < \frac{x}{c_1} + \frac{r}{c_2}$$

$$p = \frac{1}{r} \rho_0^2 \left(t - \frac{r}{c_1} - \frac{r}{c_2}\right) \delta x \qquad \left(t > \frac{x}{c_1} + \frac{r}{c_2}\right)$$

The total pressure at P will be the integrated effect of all the elemental sources. Until some time t_0 there will be no effect at P. At any instant after this time all the elements do not necessarily contribute to the pressure at P. Let the effective elements lie between l_1 and l_2, where l_1 and l_2 are the roots of

$$\frac{x}{c_1} + \frac{r}{c_2} = t$$

Then for this condition the pressure at P is

$$p = \int_{l_1}^{l_2} \frac{1}{r} \rho^2 \left(t - \frac{x}{c_1} - \frac{r}{c_2}\right) dx$$

After some later time t_1, the whole line will be contributory at P and the limits of integration will be 2L and 0 respectively where 2L is the total length of charge.

Special Cases.

Some particular cases of line charges will now be considered. In all these cases the function for pressure has been assumed as

$$p(t) = p_0 e^{-kt}$$

and the total length of line is 2L.

A *Rectilinear Charges*

Case 1 P on the perpendicular bisector of OL. (Figure 1b).

The first effect at P is produced by the element at X where XP is normal to the wave front at P and

$$\sin\theta = \frac{c_2}{c_1}$$

For this case $t_0 = \frac{L - d\tan\theta}{c_1} + \frac{d\sec\theta}{c_2}$ where d is the distance of P from the nearest point of the charge

$$t = \frac{2L}{c_1} + \frac{(L^2 + d^2)^{\frac{1}{2}}}{c_2}$$

The values of l_1 and l_2 are given respectively

$$l = \frac{c_1}{c_1^2 - c_2^2}\left[Lc_1 - tc_2^2 \mp c_2^2 (L - c_1 t)^2 - d^2 (c_1^2 - c_2^2)^{\frac{1}{2}}\right] \quad \text{for } t_0 < t < t_1$$

with the conditions that $l_1 \neq 0$

$l_2 \neq 2L$

when .....

when $t = t_o \quad l_1 = l_2$

r is given by

$$r = \left[(L - x)^2 + d^2 \right]^{\frac{1}{2}}$$

The pressure at P is thus

$$p = 0; \qquad \text{for } 0 < t < t_o$$

$$p = p_o \int_{l_1}^{l_2} \frac{e^{-k(t - \frac{x}{c_1} - \frac{r}{c_2})}}{r} dx \qquad \text{for } t_o \leq t \leq t_1 \text{ where } l_1 \leq 0, \; l_2 \geq 2L$$

$$p = p_o \int_{l_1}^{2L} \frac{e^{-k(t - \frac{x}{c_1} - \frac{r}{c_2})}}{r} dx \qquad \text{for } t_1 \leq t$$

Case 2 P on the axis of the charge in the direction of detonation (Figure 1c)

$$t_o = \frac{2L}{c_1} + \frac{d}{c_2}$$

$$t_1 = \frac{2L + d}{c_2}$$

$$l_2 = 2L \qquad \text{for } t_o \leq t$$

$$l_1 \left(\frac{1}{c_2} - \frac{1}{c_1} \right) = t_1 - t \qquad \text{for } t_o \leq t \leq t_1$$

$$r = 2L - x + d$$

The pressure at P is

$$p = 0, \qquad \text{for } 0 < t < t_o$$

$$p = p_o \int_{l_1}^{2L} \frac{e^{-k(t - \frac{x}{c_1} - \frac{r}{c_2})}}{r} dx \quad \text{for } t_o < t < t_1$$

$$p = p_o \int_{o}^{2L} \frac{e^{-k(t - \frac{x}{c_1} - \frac{r}{c_2})}}{r} dx \quad \text{for } t_1 \leq t$$

Case 3 P on the axis of the charge in the opposite direction to detonation (Figure 1d)

$$t_o = \frac{d}{c_2}$$

$$t_1 = \frac{2L}{c_1} + \frac{2L + d}{c_2}$$

$$l_1 = 0, \qquad \text{for } t_o < t$$

$$l_2 \left(\frac{1}{c_2} + \frac{1}{c_1} \right) = t - t_o \quad \text{for } t_o < t < t_1$$

$$r = d + x$$

The .....

Best Available Copy

The pressure at P is

$$p = 0, \qquad \text{for } 0 < t < t_0$$

$$p = p_0 \int_0^{l_2} \frac{e^{-k(t - \frac{x}{c_1} - \frac{r}{c_2})}}{r}\, dx \qquad \text{for } t_0 \leq t \leq t_1$$

$$p = p_0 \int_0^{2L} \frac{e^{-k(t - \frac{x}{c_1} - \frac{r}{c_2})}}{r}\, dx \qquad \text{for } t_1 \leq t$$

2. *Curvilinear Charges*

Case 1 Circular arc of charge, P at the centre of the circle.

This case is shown in Figure 2(a). Using the same notation as before, it is seen that

$$t_0 = \frac{r}{c_2}$$

$$t_1 = \frac{2L}{c_1} + \frac{r}{c_2}$$

$$l_1 = 0$$

$$l_2 = c_1 (t - t_0) \qquad \text{for } t_0 \leq t \leq t_1$$

In this case the equation for the pressure at P may be integrated directly to give

$$p = 0 \qquad t < t_0$$

$$p = \frac{p_0 c_1}{\pi r} \left(1 - e^{-k(t - t_0)}\right) \qquad t_0 \leq t \leq t_1$$

$$p = \frac{p_0 c_1}{\pi r} \left(e^{\frac{2kL}{c_1}} - 1\right) e^{-k(t - t_0)} \qquad t_1 < t$$

Case 2 Charge forming part of an equiangular spiral, P at the centre of the spiral.

This example, given in Figure 2(b) is that for which all the elements start to be effective at P at the same instant. If S be the length along the charge from the point of detonation O to some point Q and PQ = r

$$\frac{s}{c_1} + \frac{r}{c_2} = t_0$$

and the charge is thus part of an equiangular spiral.

Putting r_0 equal to the distance from P to the point of detonation,

$$t_0 = \frac{r_0}{c_2}$$

The pressure at P, after integration has been performed is

$$p = 0, \qquad t < t_0$$

$$p = \ldots\ldots$$

Best Available Copy

$$p = p_0 \frac{c_1}{c_2} e^{-k(t - t_0)} \log \left(\frac{c_1 t_0}{c_1 t_0 - 2L} \right) \qquad t_0 < t$$

Numerical Values

The forms of the pressure-time curves for these cases have been evaluated for particular values of the various parameters. For all cases

c_1 = 20,000 ft./sec.

c_2 = 5,000 ft./sec.

$2L$ = 6 ft.

k = 60,000 sec.$^{-1}$, p_0 = 5,000 lb./sq.in.

For cases A1, A2 and A3

d = 5 ft.

For cases B1 and B2

r = 5 ft.

r_0 = 5 ft.

respectively.

The forms of the various pressure-time curves are shown in Figure 3(a), (b), (c) and Figure 4(a) and (b) together with curves observed using piezo electric gauges and Cordtex charges of the same lengths and in the same positions as those in the calculations. The integrals for cases A1, 2 and 3 were computed numerically. In Figure 3 and 4 the time after detonation to the arrival of the wave is assumed to be the same for the observed curves as for the calculated curves, since these times were not observed experimentally. For underwater explosions of Cordtex, the values of c_1 and c_2 correspond approximately with those used in the calculations.

It is not known what values should be taken for the pressure p_0, at 1 foot from the explosion and for k which determines the rate of decay of the shock wave pressure, in order that they may correspond with the Cordtex. It is seen, however, that for values for p_0 of 5,000 lb./sq.in. and for k of 60,000 sec.$^{-1}$, the relative shapes and magnitudes of the calculated curves are not very dis-similar from those observed. The agreement is even better than is apparent in Figure 3 and 4. Thus the sharp cut-off of pressure in Figure 3(b) and 3(c) which occurred about 0.6 milliseconds after the start of the waves was due to the reflected tension wave from the free surface. The high peak pressure in Figure 3(c) was probably due to the added effect of the detonator. The gradual rise of the pressure shown in the record in Figure 4(b) was almost certainly due to the effect of the finite size of the gauge. If it is assumed that the actual wave reaching the gauge was shock-fronted and approximate calculation estimates the true peak to be about 4,500 lb./sq.in. instead of just over 2,000 lb./sq.in. which is more in accord with theoretical predictions.

From Figure 3(a), 4(a) and 4(b) it is seen that relatively small alterations in the shape of the charge produced considerable changes in the forms of the pressure-time curves. For these cases, however, the impulses were not very different and it is therefore possible that the damage produced by these charges would not be very dependent on the shape of the charge.

The report therefore indicates the extent to which the forms of the waves produced by line charges can be predicted to a first approximation, by the simple theory given in this note. It is to be noted, however, that the use of the theory is limited by uncertainty in the choice of values for p_0 and k. Further, the effects near to the charge will not be represented by the simple state of affairs assumed in the theory since the finite amplitude of the waves will result in their interaction in a more complicated manner than for waves of acoustic intensity. Thus, although the acoustic approximation may be valid at points more remote from the charge, the form of the waves reaching such points will have been determined to a certain extent by the condition obtaining near the charge.

Best Available Copy

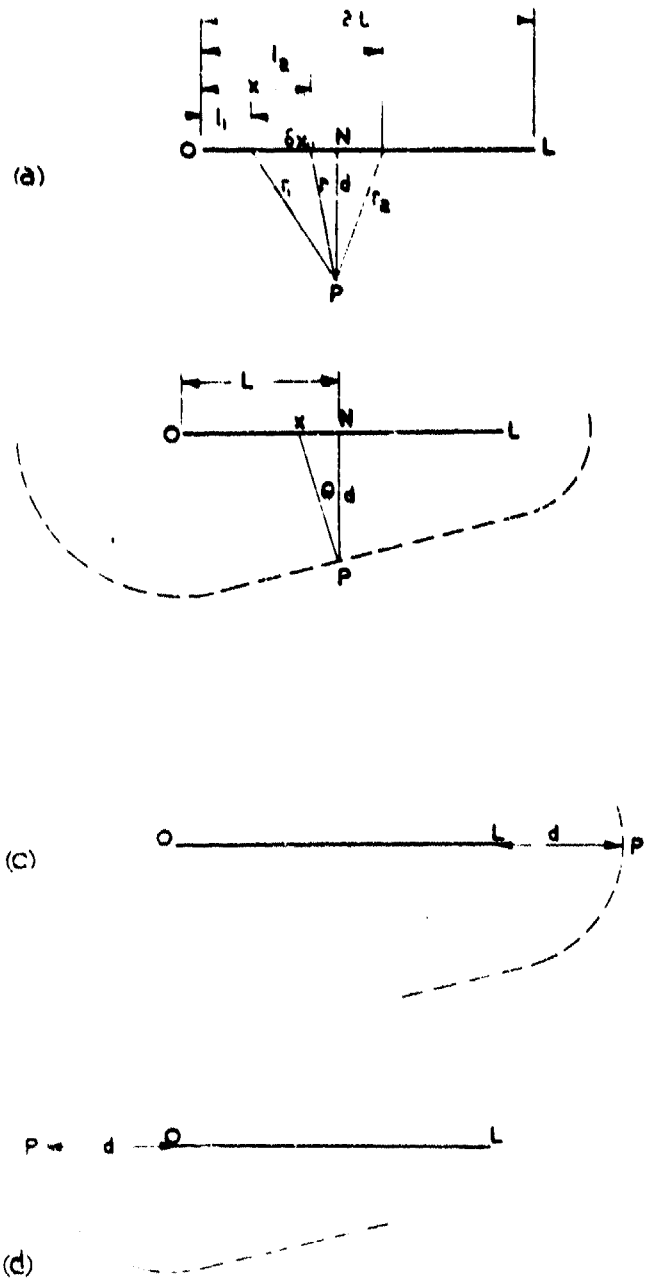
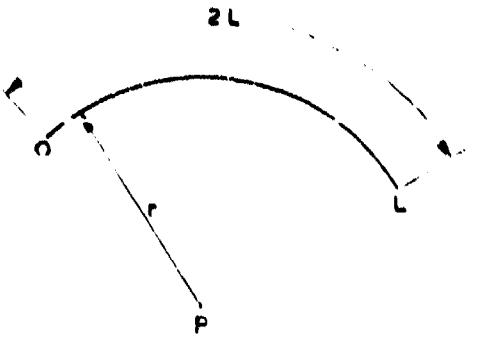
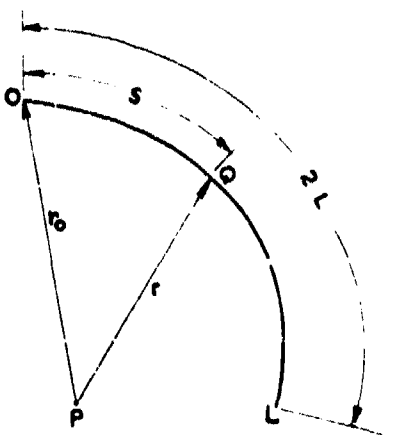


FIG. 1. RECTILINEAR CHARGES. O IS THE POINT OF DETONATION, OL THE CHARGE AND P THE POINT OF MEASUREMENT

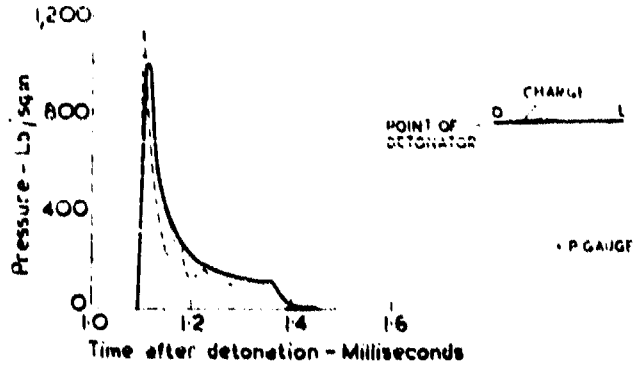


(a) CIRCULAR ARC.

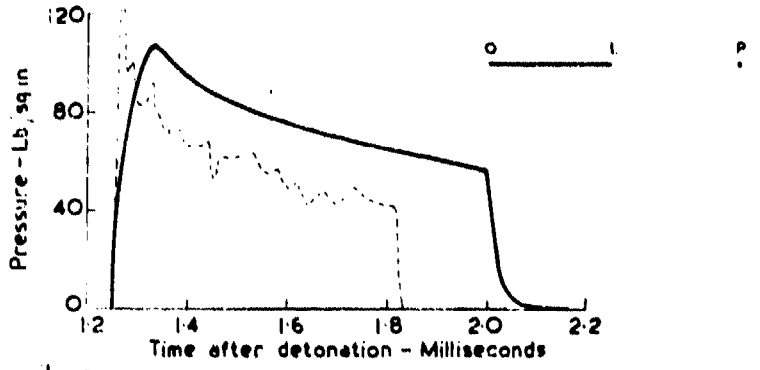


(b) ARC OF EQUIANGULAR SPIRAL.

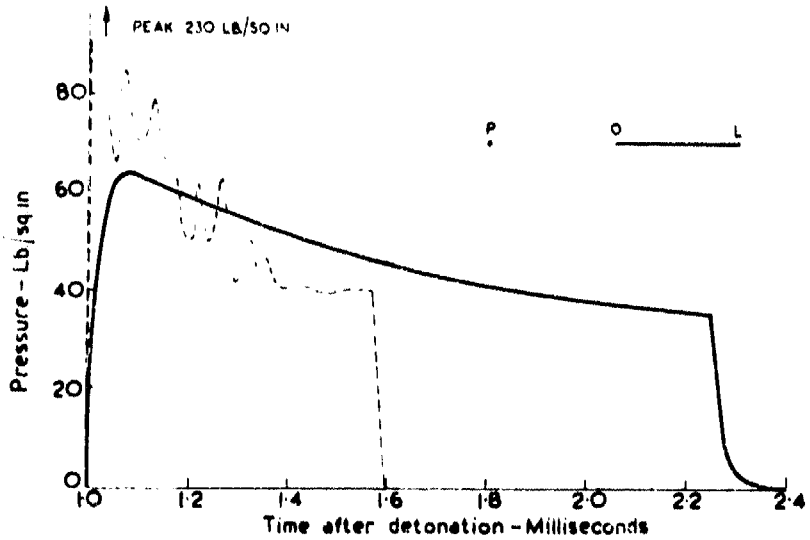
FIG.2. CURVILINEAR CHARGES. O IS THE POINT OF DETONATOR, OL THE CHARGE AND P THE POINT OF MEASUREMENT.



a P 5ft from charge on perpendicular bisector

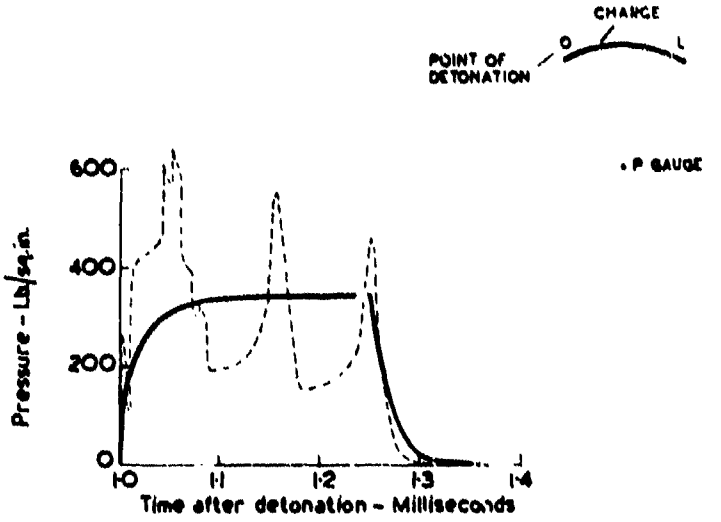


b P on the axis of the charge, 5ft. from the charge in the direction of detonation

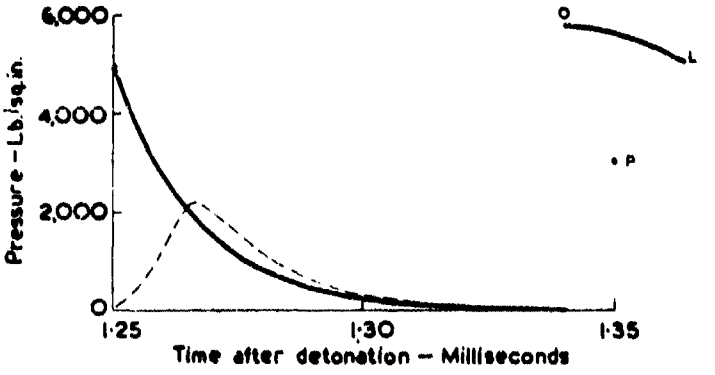


C P on the axis of the charge, 5ft. from the charge in the opposite direction to that of detonation

Fig.3. PRESSURE-TIME CURVES FOR STRAIGHT LINE CHARGES 5ft. LONG. FULL CURVE CALCULATED FOR P_0 = 5,000 LB./SQ.IN, K = 60,000 SEC, DASHED CURVE OBSERVED FOR CORDTEX. TIME AFTER DETONATION OF THE DASHED CURVE ASSUMED THE SAME AS FOR THE FULL CURVE



(a) Circular arc of charge, radius 5ft. P at the centre of the circle



(b) Charge forming arc of an equiangular spiral. P at the centre of the spiral 5ft. from the nearest point of the arc

Fig.4. PRESSURE-TIME CURVES FOR CURVILINEAR CHARGES 5ft. LONG FULL CURVE CALCULATED FOR P_o=5,000 LB./SQ.IN., K=60,000 SEC.$^{-1}$ DASHED CURVE OBSERVED FOR CORDTEX. TIME AFTER DETONATION OF THE DASHED CURVE ASSUMED THE SAME AS FOR THE FULL CURVE

PROPOSAL AND ANALYSIS OF A NEW NUMERICAL METHOD FOR THE TREATMENT OF HYDRODYNAMICAL SHOCK PROBLEMS

John Von Neumann
Institute of Advanced Study, Princeton, N. J.

American Contribution

March 1944

Analytical Table of Contents

	Page
Summary	1
§1. The equations of hydrodynamics, allowing for compressibility, but neglecting viscosity and heat conduction. The Lagrangeian form. One-dimensional case	4
§2. The conservation of energy and the principle of isentropy	5
§3. The formation of shocks	5
§4. The shock equations of Rankine and Hugoniot. Shocks and entropy	6
§5. Mathematical complications caused by the presence of shocks	7
§6. The idea of a simplified numerical approximative procedure. Discussion of a special case. The degradation of energy	9
§7. Expressions for the degradation of energy	11
§8. Physical interpretation of the proposed numerical approximative procedure	12
§9. Continuation	12
§10. The behavior of energy	14
§11. Discussion of an example	15
§12. The oscillations caused by shocks	16
§13. Mathematical interpretation. Weak convergence	18
§14. Statement of the program. Choice of Δq and Δt	18
§15. Procedure. Criteria by which the computations can be controlled. The importance of "experimental" problems	20
§16. The three problems which were solved at the Ballistic Research Laboratory at Aberdeen, Maryland. Description	22
§17. Continuation	25
§18. Continuation	25
§19. Analysis and interpretation of the results	27
§20. Conclusions. Proposed extensions of the program	28
§21. The spherically symmetric case	29
§22. Two- and three-dimensional problems	30
Figures 1 and 2	

PROPOSAL AND ANALYSIS OF A NEW NUMERICAL METHOD FOR THE TREATMENT OF HYDRODYNAMICAL SHOCK PROBLEMS

Summary

A. The differential equations of (compressible, non-viscous, non-conductive) hydrodynamics are of a not too complicated type as long as the motion is continuous and isentropic. It is known, however, that almost all hydrodynamical setups cause a development of discontinuities, so-called shocks, sooner or later. These shocks almost never remain "straight", and as soon as they are "curved" or intersect each other, isentropy ceases. The mathematical problem then becomes one of a most unusual and altogether intractable type: A differential equation in a domain with an unknown, "free", boundary along which "supernumerary" boundary conditions hold, and in many cases the coefficients of the differential equation will themselves depend on the (unknown) boundary.

A rigorous treatment of such a problem is only possible in a few exceptional cases. The direct computational procedures for its treatment are very complicated and lengthy.

B This report suggests a computational treatment which corresponds to the original differential equations, completely ignoring the possibility of shocks. Arguments are brought forth to support the view that this computational treatment will always produce (arbitrarily) good approximations of the rigorous theory which allows for shocks. That is, even when shocks are formed, and the motion ceases to be isentropic.

It is shown that the suggested treatment corresponds to a return from the continuum (hydrodynamical) theory to a kinetic (molecular) theory, using, however, a very simplified quasi-molecular model. The essential sim-

Best Available Co

plifications are these:

a) The number of molecules N ("Loschmidt's number" for a mol of substance) is "scaled down" from its actual value $\sim 10^{19}$ to sizes of 10 to 100.

b) The intramolecular forces are correspondingly "scaled up" so as to approximate the correct hydrodynamical situation.

c) The intramolecular forces are essentially simplified in various other respects.

C. The envisaged computations appear to be well suited to be efficiently carried out on punch-card equipment. The use of such equipment was made available for the exploration of certain problems of this type by the Ballistic Research Laboratory of the Ordnance Research Center, Aberdeen, Maryland. A number of these problems have already been solved, under the direction of Mr. L. E. Cunningham of that laboratory. Among these three "experimental" problems are discussed in this report. They lead to very encouraging results.

Specifically: In one-dimensional shock problems values of $N \sim 14$ or 29 (that is, 14 to 29 "molecules") and a Δt about one-half of its maximum allowable value (for details cf. section 18) produced results of highly satisfactory precision. The duration of the computations, including their setting up, was very reasonable.

D. The report contains an analysis of these computations, and of the main viewpoints in connection with further computations of this type. Physical aspects of the problems, like the hydrodynamical theory of the propagation of disturbances (sound) and the conservation of the total energy as well as its partial "degradation" by shocks, play an important role in discovering errors and keeping the equipment under control.

The possibilities of extending this method to spherically symmetric problems, and to "truly" many-dimensional problems, are discussed.

It is proposed to treat in the future various problems concerning the development, interaction, reflection, refraction and decay of shocks, by this method and its extensions.

Best Available Copy

§1. The considerations which follow apply to any gas or liquid in which compressibility is taken into account, but viscosity and heat conduction are neglected. From the point of view of gas dynamics such a substance is conveniently characterized by its caloric equation of state, which specifies the internal energy U as a function of two characteristic parameters, preferably of the specific volume v and the specific entropy S :

(1) $$U = U(v, S)$$

Then the density ρ is

(2) $$\rho = \frac{1}{v} ,$$

and the pressure p and temperature T are given by the equations

(3) $$p = -\frac{\partial U}{\partial v} , \qquad T = \frac{\partial U}{\partial S} .$$

The equations of motion will be stated in the Lagrange-ian form, for the main part of this discussion one-dimensionally. Then each elementary volume of the substance is characterized by a label a, its position being x at the time t. The purpose of the equations of motion is to determine x as a function of a, t.

(4) $$x = x(a, t)$$

It is convenient to choose the label a in such a manner that the substance contained in the interval $a, a + da$ has the mass da . I.e. that the "density in the label space" is identically 1. This being understood, it is immaterial whether the label a is also the position x at some "initial instant" t_0 (which is frequently the case) or not.

With the above convention concerning the label, the specific volume v is simply given by

(5) $$v = \frac{\partial x}{\partial a}$$

The conservation of momentum states that

(6) $$\frac{\partial^2 x}{\partial t^2} = -v \left(\frac{\partial p}{\partial x}\right)_{t = \text{const.}}$$

i.e. by (3) and (5)

(7) $$\frac{\partial^2 x}{\partial t^2} = -\frac{\partial}{\partial a} p\left(\frac{\partial x}{\partial a}, S\right) .$$

The conservation of energy, on the other nand, gives a relation which is easily transformed with the help of (3) and (7) into

(8) $$\frac{\partial S}{\partial t} = 0 .$$

In all these equations a, t are the independent variables.

§2. Equation (8) implies that if S is constant at some initial instant $t = t_0$, then it stays constant at all times, and so (8) can be replaced by

(9) $$S = S_0 = \text{Constant.}$$

This principle of isentropy then makes (7) the sole equation governing the motions, and renders the problem amenable to analytical or numerical treatment.

It is essential to realize that the decisive equation (8) expresses the conservation of energy, and nothing else. Thus, although it involves the specific entropy alone, it expresses nevertheless the first, and not the second law of thermodynamics. Furthermore, since (8) secures the constancy of specific entropy along the world line of each elementary volume, the second law, which requires that specific entropy should never decrease along that line, does not now impose any additional restriction.

§3. It is well known that a motion satisfying (7), (8), develops sooner or later a discontinuity of the first derivatives $\frac{\partial x}{\partial a}$, $\frac{\partial x}{\partial t}$. More precisely: apart from exceptional and degenerate cases, no solution can be

continued beyond some finite $t = t_s$, and the singularity at this t_s sets in by $\frac{\partial^2 x}{\partial a^2}$, $\frac{\partial^2 x}{\partial a \partial t}$ becoming infinite. At the next instant x can only be kept one-valued by permitting first-order discontinuities in $\frac{\partial x}{\partial a}$, $\frac{\partial x}{\partial t}$.

It has been established experimentally that this strange behavior of the solutions corresponds to a certain extent to the facts: In typical situations like those referred to above, real substances do indeed develop "discontinuities",- i.e. rapid changes of the specific volume $v = \frac{\partial x}{\partial a}$ and of the velocity $V = \frac{\partial x}{\partial t}$, which are discontinuities in the same approximation in which viscosity and heat conduction can be neglected, and are called <u>shocks</u>. These shocks appear even if the state of the substance at the initial instant $t = t_0$ was perfectly continuous, they develop as far as can be observed at the times $t = t_s$ at which the solution of (7), (8) becomes discontinuous, and as far as the motion stays continuous (7), (8) seem to be satisfied.

§4. After shocks have formed, the motion is still governed by the same conservation principles (of momentum and energy) on which (7), (8) are based. Hence (7), (8) still hold in the regions of space which contain no shocks, but beyond this it is necessary to apply those same conservation principles to the shocks themselves.

Let a shock at $a = \bar{a}(t)$ be formed by the states $\frac{\partial x}{\partial a} = v = v_1$, $\frac{\partial x}{\partial t} = V = V_1$, p_1, S_1, U_1 at $a = \bar{a} - 0$ and $\frac{\partial x}{\partial a} = v = v_2$, $\frac{\partial x}{\partial t} = V = V_2$, p_2, S_2, U_2 at $a = \bar{a} + 0$. The position of the shock is $\bar{x} = x(\bar{a}(t), t)$, its velocity $D = \frac{d\bar{x}}{dt}$; $\frac{d\bar{a}}{dt} = M$ is the <u>flow of mass across the shock</u>. Then the conservation theorems of mass

(which is an identity in the Lagrange-ian form, and was therefore not referred to explicitly in §1, but which is better made use of now), momentum and energy give successively

$$\frac{D - V_1}{v_1} = \frac{D - V_2}{v_2} = M = \pm \sqrt{\frac{p_2 - p_1}{v_1 - v_2}} , \tag{10}$$

$$\frac{p_1 + p_2}{2} = \frac{U_2 - U_1}{v_1 - v_2} . \tag{11}$$

Equations (10) are based on the conservation of mass and of momentum alone, (11) expresses (with the help of (10)) the conservation of energy. These are the familiar equations of Rankine and Hugoniot.

It is well known that (11) (together with (1), (3) for p_1, v_1, S_1, U_1 and p_2, v_2, S_2, U_2) necessitates in general that $S_1 \neq S_2$. As was shown by C. Duhem, H. Bethe, and H. Weyl, for the most important equations of state (1),

$$\operatorname{sign} (S_2 - S_1) = \operatorname{sign} (p_2 - p_1) \cdot \operatorname{sign} (\pm \text{in (10)}) . \tag{12}$$

Now the second law of thermodynamics forbids a decrease of the specific entropy S along the world line of each elementary volume; i.e. it requires

$$\operatorname{sign} (S_2 - S_1) = \operatorname{sign} M \quad (\text{for } S_1 \neq S_2, \ M \neq 0) \tag{13}$$

hence by (13)

$$\operatorname{sign} (\pm \text{in (10)}) = \operatorname{sign} (p_2 - p_1) \tag{14}$$

Summing up: When a world line crosses a shock, the specific entropy S changes, and the second law imposes the additional restriction (14).

§5. The general motion is thus described by (7), (8) in the regions where the derivatives are continuous, and by (10), (11) with (14) on the discontinuity surfaces. Accordingly the specific entropy S is con-

stant along each world line while it moves in the regions of continuity, but it undergoes a discontinuous increase each time a surface of discontinuity is crossed. The second law of thermodynamics is automatically fulfilled in the former regions, but it excludes 50 per cent of the solutions at the latter surfaces.

This is a most remarkable, and at first sight rather paradoxical violation of Hankel's principle of the "conservation of formal laws", but the investigations of W. Rayleigh, G. I. Taylor, and R. Becker on one hand, and extensive experimental material on the other, make it impossible to question these conclusions.

From a mathematical point of view the emergency of shocks, and the addition of (10), (11), (14) to (7), (8) represent an extreme complication. Without shocks there is usually isentropy, i.e. (8) implies (9), and (7) can be written as

$$\frac{\partial^2 x}{\partial t^2} = -\frac{\partial}{\partial a} p_0 \left(\frac{\partial x}{\partial a} \right) \tag{15}$$

where

$$p_0(v) \equiv p(v, S_0) \tag{16}$$

may be considered a known function. Then (15) is a hyperbolic differential equation of a familiar type, and can be treated adequately by Riemann's classical method of integration. If shocks are present, however, the situation changes radically. They act as unknown boundaries for the regions in which (7), (8) hold, and along these boundaries (10), (11), (14) must be fulfilled. The latter are easily seen to contain twice as many equations as a natural boundary condition (on a known boundary) for such a differential equation should, and this superdetermination along the unknown boundary should lead to its determination. Such problems with a "free boundary" are difficult at best, but in the present case an additional difficulty inter-

venes. The change of specific entropy S at the shock $a = \bar{a}(t)$ depends by (11) on the trajectory of the shock, i.e. on the unknown boundary $a = \bar{a}(t)$.

Now S enters explicitly into the differential equation (7). Hence we are dealing here with a "free boundary" problem where the coefficients of the differential equation themselves depend explicitly on the unknown, "free", boundary.

Problems of this type have never been treated in any generality, and appropriate analytical methods to deal with them are entirely unknown. Rigorous solutions have only been determined in very special cases, where the trajectories of the shocks could be guessed by other means, up to a few numerical parameters. Analytical approximative methods (e.g. expansions) or numerical ones are also very difficult and restricted to very few special cases. Furthermore the approximative numerical procedures do not seem to lend themselves for problems of this type to efficient mechanization.

§6. The idea which will be discussed here is to treat the continuous case (7), (8) with an approximative, numerical method, and to ignore the possibility of shocks, (10), (11), (14).

In order to diagnose the character and the implications of this idea, let us consider a special case of the equations of state (1), (3), which is itself of not inconsiderable practical importance.

Assume that there exists an absolute relation of the form

(17) $$p = p_0(v) \quad ,$$

where $p_0(v)$ is a known, fixed function. That is that the source of (17) is not (16) and (9) — that the differential equation (7) assumes the form (15) without (9), i.e. without isentropy. Owing to (3), (17) can hold only if the caloric equation of state has the form

(18) $$U = U(v, S) \equiv U_*(v) + U_{**}(S)$$

in which case (3) gives

$$(19)\qquad \begin{cases} p = -\dfrac{\partial U}{\partial v} = -\dfrac{d\,U_*(v)}{dv} \equiv p_0(v), \\ T = \dfrac{\partial U}{\partial S} \equiv \dfrac{d\,U_{**}(S)}{dS} \equiv T_0(S). \end{cases}$$

I.e.: In order that the pressure p be determined by the specific volume v alone, the same need not be true for the internal energy U, but U must be the sum of two terms U_*, U_{**}, of which U_* depends on the specific volume v alone and U_{**} on the specific entropy S alone -- and there can be no "interaction energy" involving v, S together.

In many compression and shock problems involving solids and liquids those can be treated as such "interactionless" substances.

In this case the specific entropy S disappears from the differential equation of the continuous case, which assumes the form (15), and also from the shock conditions (10), (14). These equations are sufficient to determine the variation of x, v, p, V, i.e. the visible motion of matter and the mechanical forces acting upon it. They depend only on the U_* term of the inner energy U (cf. (18)). U_{**} and S, T come in only in (11), which becomes

$$(20)\qquad \begin{cases} U_{**2} - U_{**1} = \dfrac{(p_1+p_2)(v_1-v_2)}{2} - (U_{*2} - U_{*1}) \\ \qquad\qquad = \dfrac{(p_1+p_2)(v_1-v_2)}{2} - \displaystyle\int_{v_2}^{v_1} p\,dv \end{cases}$$

Thus (3) is not needed in the case of continuous motion, and (11) is not needed in the case of shocks. However (8) and (11) express the conservation of energy, so we see: For an "interactionless" inner energy (18) the visible motion and the mechanical forces can be determined by themselves, without using the conservation of energy.

The latter then determines S, T by (8) and by (11), i.e. (20), respectively.

§7. $U_{**} = U_{**}(v)$ is the potential energy, $U_{***} = U_{***}(S)$ is the thermic energy. The total energy is made up of the kinetic, the potential, and the thermic energies. Since the total energy of the entire substance is conserved, and since in the case of continuous motion the thermic energy is conserved in each element by (8), so in this case the kinetic plus potential energy of the entire substance is conserved too. In the case of shocks proceed like this: Let the shock be oriented in the direction of the flow of substance, i.e. $M > 0$. Then $S_1 < S_2$ by (13); hence $U_{***1} < U_{***2}$. All sides of (20) are hence positive, and so the last expression in (20) necessitates $v_1 > v_2$ ($p = p_0(v)$ is usually convex from below as a function of v). (10) now necessitates $p_1 < p_2$. Since the thermic energy increases in each element by the above, the kinetic plus potential energy for the entire substance decreases.

So we see: If the thermic energy is left out of account, then the conservation of energy is still valid for the continuous motion, but it is replaced by a loss of energy for shocks.

This explains the apparent conflict between the mechanical conservation of energy and the principles of thermodynamics in the earlier forms of the theory of shocks.

According to the above, this loss of energy is better described as a degradation of energy. The specific degradation of energy (i.e. per unit mass) is

(21) $$\Delta_s = U_{***2} - U_{***1},$$

the rate of degradation of energy (i.e. per unit time) is

(22) $$\Delta_r = M \Delta_s$$

(21), (22) must be evaluated with the help of (10), (20).

§8. In carrying out numerical approximations of the hyperbolic differential equation (15), the continuous independent variables a, t must be replaced by discrete ones. For various reasons it is advantageous to carry this out in two successive steps, and to begin by making a alone discrete. One of these reasons is that a is really a discrete quantity, which was made artificially continuous by the classical transition from the kinetic theory to the continuous, hydrodynamical one: the elementary volumes of the substance, for which a is a label, should be naturally discrete entities. Thus the label a is "naturally" discrete, while the coordinates x, t are "naturally" continuous. (Note that in this setup the Lagrange-ian form is preferable to the Euler-ian, since the latter deals with x, t only, without a.) Making a discrete, and leaving x, t continuous, has therefore a certain physical meaning, and this will turn out to be very helpful presently.

Accordingly, let a run over a sequence of equidistant values, which may as well be normalized so as to be the integers:

$$a = \ldots -2, -1, 0, 1, 2, \ldots \tag{23}$$

It is also advantageous to write for x

$$x = x(a, t) \equiv x_a(t) . \tag{24}$$

The hyperbolic (partial) differential equation (15) can now be replaced by the approximative system of (total) differential equations

$$\frac{d^2 x_a}{dt^2} = p_a (x_a - x_{a-1}) - p_{a+1} (x_{a+1} - x_a) . \tag{25}$$

§9. It is an essential circumstance concerning the equations (25) that they are not only mathematical approximations of the rigorous equation (15), but also the rigorous equations of another physical system,

which is a physical approximation of that one underlying (15). Indeed, the system (25) is that one of the equations of motion of an ordinary (point) mechanical system with the coordinates $\dots, x_{-2}, x_{-1}, x_0, x_1, x_2, \dots$ and with the total energy

$$(26) \qquad \frac{1}{2} \sum_a \left(\frac{dx_a}{dt} \right)^2 + \sum_a U_a (x_a - x_{a-1}) .$$

This is a system of mass points Nos. $\dots, -2, -1, 0, 1, 2, \dots$ the point No. a having the coordinate x_a, the mass 1, and any two neighbors x_{a-1} and x_a being connected by a "spring" which has the potential energy $U_a = U_a(v)$ when its length is $v = v_a = x_a - x_{a-1}$.

Now this system of "beads on a line, connected by springs" is clearly a reasonable physical approximation of the substance which the hydrodynamical equation (15) describes. It corresponds to a quasi-molecular description of this substance, where the mass ascribed to one "bead" (i.e. the one elementary volume) is the mass of a "molecule". We chose to treat this as the unit mass, but it may nevertheless correspond to any desired real mass. Clearly this is not the "true" molecular description of the substance: For any workable computing scheme the number of these "molecules", i.e. of elementary volumes, will be much smaller than the actual number of molecules. Thus if a gram-mol of a real substance is considered, the true number of molecules in it is Loschmidt's number $N \sim 6 \cdot 10^{23}$, while for a practical computing scheme some number of "molecules" N between 10 and 10^6 will be appropriate. However, the actual value of Loschmidt's number N never figures in hydrodynamics; all that is required for the validity of (15) is that N should be a great number. The actual $N \sim 6 \cdot 10^{23}$ is certainly great, but much smaller numbers N may already be sufficiently great. Thus there is a chance that $N \sim 10^2$ will suffice.

So the replacement of (15) by (25) amounts to the introduction of a quasi-molecular description with a Loschmidt number N chosen for computing purposes, and therefore much too low. Reality is not (15) either; it is molecular with the correct $N \sim 6 \cdot 10^{23}$. Hence (25) is an aeceptable approximation if this "scaling down" of N from $6 \cdot 10^{23}$ to the value used, say 10^{4}, is acceptable. At this point two more remarks are in order:

First: This "scaling down" of N requires a corresponding "scaling up" of the "intramolecular forces", to produce the correct hydrodynamical forces. This has indeed been done: The potentials in (26), i.e. the forces in (25), were chosen so as to approximate just the correct forces in (15).

Second: The actual intramolecular forces are of course much more complicated than those of the simple "beads and springs" model used in (25), (26). However, the classical derivations of hydrodynamics from molecular-kinetic models have established that these more subtle details of the intramolecular forces are immaterial for this part of hydrodynamics: It can be derived from the "beads and springs" model just as well as from one where those details are taken into consideration.

§10. The above considerations make it plausible that the system (25) is a good approximation of the hydrodynamical equation (15), even for moderate values of the number of elementary volumes N. The minimum size of N which will give acceptable approximations must, of course, be determined by effective computation, and it may vary from problem to problem. We expressed above the surmise that values between 10 and 100 will usually suffice.

All these considerations are, however, only plausible as long as (15) describes reality without any further complications, i.e. in a continu-

ous motion. When shocks appear, the situation seems considerably less favorable. These two remarks suggest themselves immediately:

First: In the presence of shocks the real motion is not described by (15) alone, but by (15) together with (10), (14). Now while (25) is clearly an approximation of (15), it is not at all clear whether it is also one of (10), (14).

Second: Actually there are reasons to expect that something must go wrong with this latter approximation. Indeed, we saw in §7 that the total kinetic plus potential energy is not conserved in hydrodynamics when shocks are present, but that it is continuously degraded (i.e. decreasing) according to (22). On the other hand the expression (26) represents precisely the total kinetic plus potential energy -- no thermic energy makes its appearance in this expression, and there is indeed no room for a separate thermic energy in such a quasi-molecular model. And since (25) is the system of the ordinary (point) mechanical equations of motion belonging to the total energy (26), therefore (25) must conserve this energy.

Thus (25) must conserve (26), while (15) with (10), (14) does not conserve the analogue of (26). How then can (25) be an approximation of (15) with (10), (14)?

§11. Nevertheless it is hard to see how (25) can fail to describe the equivalents of shocks in certain situations. E.g. let the "beads and springs" model of §9 collide with a rigid wall; in this situation the wall would send a shock into a compressible substance (in hydrodynamical theory), and something similar must happen to the "beads and springs" model. The boundary conditions which describe this are easy to specify: For $t = 0$ the substance is in its normal state (i.e. each $v_\alpha = x_\alpha - x_{\alpha-1} = 1$, hence $x_\alpha = \alpha + \text{const.}$, e.g. $x_\alpha = \alpha$) and is moving uniformly

to the left:

$$(27)\qquad \begin{cases} \text{For } t = 0 \quad \text{all } x_\alpha = \alpha, \quad \dfrac{dx_\alpha}{dt} = -\alpha, \\ \text{with a given} \quad \alpha > 0. \end{cases}$$

For $t > 0$ the wall stops the molecule $\alpha = 0$ at $x = 0$:

$$(28)\qquad \text{For all } t \geq 0 \qquad x_0 = 0.$$

Clearly (27) should only apply to the right half, i.e. to $\alpha = 1, 2, \ldots$

Now (25) conserves the energy (26), i.e. the total kinetic plus potential energy, while (11) i.e. (20), excludes such a conservation. And the laws of Rankine and Hugoniot, on which (11) is based, are merely applications of the basic conservation principles, which hold for (25) too. How then can (25) still conserve the energy (26)?

The plausible answer is that (25) will produce something like a shock under the conditions specified, but that the motion of the x_α beyond the shock will not be the smooth hydrodynamical one, but rather one with a superposed oscillation. This oscillation should contain, as a kinetic energy, that degraded energy which can only be accounted for in the hydrodynamical case ((15) with (10), (14)) by introducing a separate thermic energy U_{**}. Indeed, (25) describes a quasi-molecular model, and in such a model the thermic energy appears necessarily as a part of the kinetic energy.

§12. These considerations suggest the surmise that (25) is always a valid approximation of the hydrodynamical motion, i.e. of (15) with (10), (14), but with this qualification: It is not the $x_\alpha = x_\alpha(t)$ of (25) which approximates the $x = x(a, t)$ of (15), but the average of the x_α over an interval (of sufficient length) of contiguous α's. The x_α themselves perform oscillations around these averages, and these oscillations do not tend to zero, but they make finite contributions to the total energy (26).

Indeed, these contributions are continuously increasing when shocks are present, and they account for the degradation of energy according to (21), (22).

The velocities produced by these oscillations are easy to estimate. Denoting such a velocity by V_{osc} amplitudes (maxima) by $^{a.m.}$ and averages by $\bar{\ }$, clearly

$$\overline{\tfrac{1}{2}(V_{osc})^2} = \Delta_S = \frac{(p_1+p_2)(v_1-v_2)}{2} - \int_{v_2}^{v_1} p\,dv$$

(use (21), (20)), and assuming that the oscillations are essentially harmonic,

$$\overline{(V_{osc})^2} = \frac{1}{2}\left(V_{osc}^{a.m.}\right)^2$$

From these

$$(29)\qquad \left(V_{osc}^{a.m.}\right)^2 = 4\left(\frac{(p_1+p_2)(v_1-v_2)}{2} - \int_{v_2}^{v_1} p\,dv\right)$$

Actually (29) should be corrected inasmuch as Δ_S may not be entirely kinetic energy: If the oscillations are of finite size, the non-linearity of the potential energy $U_a = U_*(v)$ will cause $\overline{U_*(x_a - x_{a-1})}$ to be different from $U_*(\overline{x_a - x_{a-1}})$, and while the hydrodynamical energy contains the first expression, (26) contains the second one. Thus $\overline{U_*(x_a - x_{a-1})} - U_*(\overline{x_a - x_{a-1}})$ too contributes to the specific dissipation Δ_S. If the oscillation of $v_a = x_a - x_a$ is v_{osc}, then this term is approximately

$$\frac{1}{2}\frac{d^2U_*}{dv^2}(v_{osc})^2 = -\frac{1}{2}\frac{dp}{dv}(v_{osc})^2 = \frac{1}{2}\frac{c^2(v_{osc})^2}{v^2}$$

where

$$(30)\qquad c = \sqrt{\frac{dp}{d\frac{1}{v}}} = v\sqrt{-\frac{dp}{dv}}$$

is the <u>local sound velocity</u>. The average is

$$\frac{1}{2}\,\frac{c^2\,\overline{(V_{osc})^2}}{v^2}$$

Assuming harmonicity

$$\overline{(V_{osc})^2} = \frac{1}{2}\left(V_{osc}^{am}\right)^2.$$

So the left-hand side (29) should be replaced by

(31) $$\left(V_{osc}^{am}\right)^2 + \frac{c^2\left(V_{osc}^{am}\right)^2}{v^2}$$

§13. In the mathematical terminology the surmise of §12 means that the quasi-molecular kinetic solution ((25)) converges to the hydrodynamical one ((15) with (10), (14)), but in the weak sense. I.e. that only the averages converge numerically. (Even this requires a slight qualification due to what was observed above concerning the U_* -averages, but there is no need to consider such details already here.)

A mathematical proof of this surmise would be most important, but it seems to be very difficult, even in the simplest special cases. The procedure to be followed here will therefore be a different one: We shall test the surmise experimentally by carrying out the necessary computations for certain moderate values of N (cf. §§9, 10), on problems where the rigorous hydrodynamical solution ((15) with (10), (14)) is known, and produces shocks. The comparison of the computed, approximate motion with the rigorous, hydrodynamical one will then be the test.

§14. It is worth while to state once more what we propose to do: The system (25) is a computational approximation of (15). (15) describes continuous hydrodynamical motions, but not shocks. It is nevertheless expected that the approximation (25) will prove itself better than its original

(15), and give adequate approximate descriptions of shocks.

In order to evaluate the system (25) by effective computation it is now necessary to carry out the second step mentioned at the beginning of §8, i.e. to make the remaining independent variable t discrete too. Choosing for t a sequence of equidistant values

(32) $t = s \cdot \tau, \qquad \tau$ fixed and $> 0, \qquad s = \cdots, -2, -1, 0, 1, 2, \cdots,$

a certain care in choosing τ is necessary.

First, we amplify (24) by writing

(33) $$x = x(a,t) \equiv x_a(t) \equiv x_a^s .$$

Second, the system of total differential equations (25) must now be replaced by the system of difference equations

(34) $$\frac{x_a^{s+1} - 2x_a^s + x_a^{s-1}}{\tau^2} = p_0\left(x_a^s - x_{a-1}^s\right) - p_0\left(x_{a+1}^s - x_a^s\right) .$$

Third, it is clear that in the recursion of (34) x_a^{s+1} is determined by x_{a-1}^s, x_a^s, x_{a+1}^s, x_a^{s-1} i.e. x_a^s by x_{a-1}^{s-1}, x_a^{s-1}, x_{a+1}^{s-1}, x_a^{s-2}. So x_a^s is determined by a family of $x_{a'}^{s'}$'s with

$$|a' - a| \leqq |s' - s| .$$

I.e. $x(a,t)$ is determined by a family of $x(a',t')$'s with

(35) $$|a' - a| \leqq \frac{1}{\tau} |t' - t| .$$

On the other hand the underlying hyperbolic partial differential equation (15) has a definite way to propagate influences: along the characteristic lines. The equation of those lines is

$$(da)^2 = -\left(\frac{dp}{dv}\right) \cdot (dt)^2$$

i.e. the area in which a change made at a, t makes itself felt is given by

$$|da| \leqq \sqrt{-\frac{dp}{dv}} \; |dt|$$

or, using (30), by

(36) $$|d'a| \leq \frac{c}{v}\,|da|\,.$$

Note that c was the velocity of sound in the physical space x, t, while $\frac{c}{v}$ is the velocity of sound in the label space a, t. Equivalently, $\frac{c}{v}$ is the flow of mass across the sound wave.

Now as R. Courant pointed out first for a more general class of problems, the computation cannot give significant results unless the dependences (35) which it permits contain the dependences (36) which the underlying problem demands. Consequently it is necessary that

$$\frac{1}{\tau} \geq \frac{c}{v}$$

i.e. that

(37) $$\tau \leq \frac{v}{c}\,.$$

Practically even a certain "factor of safety" in (37) will be advisable.

§15. The system of difference equations (34) is well suited to mechanization. Specifically, it can be solved with punch-card equipment, with s being the number of each one of the successive stacks of cards produced, and a the current number of each card within its stack. However, the following points must be emphasized:

First: We expect that after crossing the equivalent of a shock, a "molecule" a will develop an oscillation of x_a^s, which represents thermic agitation. The period of this oscillation will be of the order 1 in a, i.e. of the "grain size" introduced by the numerical approximation, by the operation of making the continuous a discrete.

Now by the usual standards of numerical computing, the appearance of such oscillations (of a period which is imposed by the "grain size" of the approximation, and not by some quantity derived from the underlying differen-

Best Available Copy

tial equation (15)) is a symptom of some inadequacy of the computing setup. It is therefore important to visualize that in the proposed setup this criterion must be abandoned: As soon as a shock has been crossed such oscillations must develop, and they have a perfectly good physical significance. They represent the thermic agitation caused by the degradation of energy through the shock.

Second: Since this important criterion for spotting errors or inadequacy of the computing setup is lost, we must see what other criteria remain. For errors there is always effective numerical checking, but it is practically difficult to get along without additional criteria of a more intrinsic significance, and they are also necessary in order to judge the adequacy of the entire setup.

The following criteria suggest themselves:

(A) Any conspicuous feature which appears in the initial conditions or anywhere later in the solution, will be propagated by the computation according to (35), while hydrodynamics cause propagation according to (36). The signal of (35) is the numerical or false signal, while the signal of (36) is the hydrodynamical or true signal. According to (37) the false signal must always be ahead of the true signal. Hence an actual computation can only be significant if the false signal is very weak (it should become weaker than any specified amount for a sufficiently small "grain size"), and if the essential changes arrive with the true signal.

(B) Since (25) conserves the total energy (26), therefore (34) should approximately conserve the equivalent of (26), i.e.

$$(38) \qquad \frac{1}{2\tau^2} \sum_a \left(x_a^{s+1} - x_a^{s-1} \right)^2 + \sum_a U_* \left(x_a^s - x_{a-1}^s \right).$$

Of course (38) will oscillate, since this conservation is only an approximate one. But after the average statistical behavior has been determined, any excessive deviation is an indication of some error of computation. Any clear trend of (38) with ζ is an indication of an inadequacy of the computing setup, particularly if it is in the direction (decrease) and of the order of magnitude of the shock degradation of energy according to (21), (22). Here the numerical rate of degradation is the significant quantity, i.e. the degradation of energy while ζ increases by 1, i.e. during τ units of time. By (21), (22) this is

$$\Delta_{n\tau} = \tau \Delta_\tau = \tau M \Delta_\zeta . \tag{39}$$

Hence oscillations and trends of (38) must be judged by comparing them in size with this $\Delta_{n\tau}$.

(C) It is advisable to acquire some general routine regarding the adequacy of computing setups, by dealing first with some selected experimental problems, i.e. simple problems in which the hydrodynamical solution is known. The comparison of the approximate, numerical solution with the (known) rigorous, hydrodynamical one will clearly be of considerable orienting value. The problems should be chosen in such a manner as to make it sure that shocks will develop, and preferably also other characteristic features of continuum hydrodynamics, such as Riemann rarefaction waves, wave reflections and intersections, etc.

§16. The Ballistic Research Laboratory of the Ordnance Research Center, Aberdeen, Maryland, is carrying out explorations of the suitability of its punch-card equipment for certain computations of the type described. This work began in early March 1944 and is continuing at the present time, under the direction and following the setups of Mr. L. E. Cunningham of the laboratory. The author wishes to take this opportunity to express his

thanks to the laboratory and to Mr. Cunningham, whose active interest made the decisive tests possible.

Three experimental tests of the kind described above, which were made at Aberdeen, will be discussed in §§16-20 which follow.

The precise formulation of these problems is this:

The equations of state which correspond to (19) are assumed to be as simple as possible without impairing the significance of the results, in order to facilitate the computations. Specifically

(40) $$p = p_0(v)$$

is assumed to be a polynomial. It is well known from hydrodynamics that in order to be realistic, the curve (40) must be convex from below. Accordingly

(41) $$p = p_0(v) \equiv 1 - v + \tfrac{1}{4} v^2$$

was chosen. This "substance" "collapses" (i.e. $v = 0$) for $p = 1$, and it "cavitates" (i.e. $p = 0$) for $v = 2$; however it behaves reasonably in the intervals

(42) $$0 < v < 2, \qquad 1 > p > 0,$$

and

(43) $$v = v_1 = 1; \qquad p = p_1 = 0.25$$

was used as the "normal", initial state of the substance. By (30) the sound velocity is

(44) $$c = v\sqrt{1 - \tfrac{1}{2} v},$$

hence the "normal", initial value is

(45) $$c_1 = \sqrt{\tfrac{1}{2}} = 0.707$$

The boundary conditions correspond to the collision of this substance with a wall, as described at the beginning of §11. It is preferable, however, to have a definite finite number of particles, i.e. of values of a,

(46) $a = 0, 1, 2, \cdots, a_0 - 2, a_0 - 1, a_0,$

and to place rigid walls at the two ends:

(47) For all $t \geq 0$ $\quad x_0 = 0, \quad x_{a_0} = a_0.$

This corresponds to (28). The initial state of the substance is as in (27), i.e. "normal" specific volume $v = 1$ and uniform motion to the left:

(48) For $t = 0$ $\quad x_a = a, \quad \frac{dx_a}{dt} = -\alpha$

for all $a = 1, 2, \cdots, a_0 - 2, a_0 - 1$

with a given $\alpha > 0$.

As the system of total differential equations (25) is replaced by the system of difference equations (34), the boundary conditions (47), (48) are to be replaced by

(49) For all $s = 0, 1, 2, \ldots$ $\quad x_0^s = 0, \quad x_{a_0}^s = a_0.$

(50) For all $a = 1, 2, \ldots, a_0 - 2, a_0 - 1$ $\quad x_a^0 = a$

$x_a' = a - \alpha\tau.$

The following remarks are now in order:

First: Of the $a_0 + 1$ "molecules" $a = 0, 1, 2, \ldots a_0 - 2, a_0 - 1, a_0$ the first and the last, $a = 0, a_0$, represent the two walls. Hence the substance proper consists of the $a_0 - 1$ molecules $a = 1, 2, \ldots, a_0 - 2, a_0 - 1$.

Second: The initial velocity $-\alpha$ points to the left (towards $a = 0$, away from $a = a_0$), hence there will be a compression wave originating at the wall $a = 0$, and an expansion wave at the wall $a = a_0$. I.e. the former will be a shock, and the latter a Riemann rarefaction wave.

Third: In order to have a way to estimate the significance of a given initial velocity α on an absolute scale, it is best to compare it with the "normal" sound velocity c_1 of (45). This gives as a measure

(51) $$\mu = \frac{\alpha}{c_1} = \sqrt{2}\,\alpha = 1.414\,\alpha,$$

the Mach number of the initial motion.

§17. The problems considered correspond to the choices

(52) $\alpha = 0.2, \quad 0.4, \qquad$ i.e. $\mu = 0.283, \quad 0.566.$

With these initial conditions (and the equation of state (41)) simple hydrodynamical considerations allow determination of the rigorous, hydrodynamical solutions. The results are these:

(A) At the wall $a = 0$ a shock originates. The velocity of this shock is $D = 0.555, \quad 0.400$; the state behind it is given by $v = 0.735, \quad 0.500$ and $p = 0.400, \quad 0.625$ and mass velocity 0.

(B) At the wall $a = a_0$ a Riemann rarefaction wave originates. The velocity of the front of this wave is $D' = 0.907, \quad 1.107$; the velocity of its back is $D'' = 0.770, \quad 0.646$; the state behind it is given by $v = 1.310, \; 1.718$ and $p = 0.119, \quad 0.020$ and mass velocity 0.

(C) The waves of (A) and (B) meet at the time $t = \frac{a_0}{D' + D''}$. At this instant the rarefaction wave begins to undergo a refraction on the shock, and its front continues behind the shock with the velocity $D^* = 0.584, \quad 0.433.$

(D) The shock of (A) has the specific dissipation of energy $\Delta_s = 0.00077, \quad 0.00521$, and the rate of dissipation of energy $\Delta_v = 0.00058, \quad 0.00417.$

§18. The choice of τ in each problem is governed by (37). The upper limit of (37) is the smallest $\frac{v}{c}$ which occurs in the problem, i.e. by (44) the smallest $\frac{1}{\sqrt{1 - \frac{1}{2}v}}$ I.e. the $\frac{1}{\sqrt{1 - \frac{1}{2}v}}$ belonging to the

smallest v. This is clearly the v behind the shock, hence by (A) above $v = 0.125, \quad 0.500$, and so $\frac{1}{\sqrt{1+v}} = 1.26, \quad 1.15$. Thus the requirement of (37) is $\tau \leq 1.26, \quad 1.15$, and therefore $\tau = 0.5$ would seem to be a safe value.

We can now state the three problems for which the solutions were computed:

Problem 1: $\alpha = 0.2$, i.e. the first choice of §17. $a_0 = 15$, i.e. $N = a_0 - 1 = 14$ "molecules". $\tau = 0.5$. Calculation carried until $s = 31$, i.e. $t = 15.5$.

Problem 2: Same as Problem 1, but $\tau = 0.25$ (as a check), calculation carried until $s = 51$, i.e. $t = 12.75$.

Problem 3: $\alpha = 0.4$, i.e. the second choice of §17. $a_0 = 30$, i.e. $N = a_0 - 1 = 29$ "molecules". $\tau = 0.5$, calculation carried until $s = 61$, i.e. $t = 30.5$.

As pointed out at the beginnings of §§15 and 16, the computations were carried out on the punch-card equipment of the Ballistic Research Laboratory at Aberdeen, Maryland. They produced very encouraging results. Such difficulties as presented themselves were all overcome by the very complete and efficient punch-card equipment of the Ballistic Research Laboratory under the direction of Mr. Cunningham. The actual computations on each problem required 6-12 working hours net, and the entire program (setting up, etc.), insofar as these three problems were concerned, took less than ten days.

A detailed analysis of the numerical material obtained was undertaken, and it gave very valuable pointers for the further development of this method. It will not be attempted to give here a detailed account of this analysis. We shall, however, point out some of the main features, and attach some graphical representations.

§19. First: The results obtained in Problems 1 and 3 are represented by Figures 1 and 2 respectively. The results in Problem 2 agree so well with those in Problem 1 that a graphical representation of the former would not have been distinguishable from one of the latter, i.e. from Figure 1 (except for the halving of τ, i.e. the doubling of ς).

In each figure the abscissae are the a, and the ordinates are the ς. The full lines, originating at $\varsigma = 0$ and $a = 1, 2, \cdots, a_0 - 1, a_0$, are the world lines of the corresponding "molecules". The dash-dash lines represent the main hydrodynamical features, that is, the loci where the rigorous, hydrodynamical solution places them according to (A)-(C) in §17: the line originating at the lower left corner is the shock, the two lines originating at the lower right corner are the front and the back of the Riemann rarefaction wave, and the refracted front of the rarefaction wave on the shock is also indicated.

Second: Both figures show that the initial motion, which is a family of parallel straight lines in the a, ς-plane, is significantly modified only when the shock or the front of the rarefaction are reached. These are the true signals in the sense of (A) in §15; the false signals are at the lines $\varsigma = a$ or $\varsigma = a_0 - a$, i.e. well ahead of the true ones, and at the false signals nothing visible happens. (The numerical material shows this in more precise quantitative detail.) Also, the change of direction at the shock is rather sudden, while that at the rarefaction is gradual and continuous. Summing up, the criterion of (A) in §15 is satisfied, and even the details of the compression and the expansion caused by the two walls are those which the rigorous, hydrodynamical solution leads one to expect.

Third: The numerical material shows that in all three problems the shocks are followed by oscillations of a more lasting nature than those which

Best Available Cop

accompany the rarefaction. In Problems 1, 2 these are too small to show on Figure 1, but in Problem 3 they are considerably greater and Figure 2 shows them accordingly. That figure makes it quite clear that the shock, but not the rarefaction, is followed by strong "thermic agitation" due to the degradation of energy which is caused by the shock alone.

Fourth: The values of v obtained in (A), (B) in §17 for the regions behind the shock and the rarefaction can be compared with the compression and the expansion shown on Figures 1, 2. The quantitative agreement is excellent. The world lines of individual "molecules" are also in good agreement with those obtained from the rigorous, hydrodynamical solution, if allowance is made for the post-shock oscillations.

Fifth: The numerical rate of degradation of energy is, by (39) in (B) in §15 together with (D) in §17 and the τ-values of §18, found to be

$$(53) \qquad \Delta_{\lambda\tau} = \tau\,\Delta_{\tau} = 0.00029,\quad 0.00015,\quad 0.00208,$$

for Problems 1, 2, 3, respectively.

As discussed in (B) in §15, this is the quantity which provides the significant standard of size for the oscillations and trends of the approximate energy (38).

Computations of (38) show that its total oscillations never exceed the quadruple of (53) in either problem, and that the overall trend of (38) is less per unit of ξ than one-twentieth of (53). This makes the significance of our computing procedure very plausible, and permits an easy spotting of computing errors with the help of the oscillations of the approximate energy (38).

§20. A more detailed inspection of the numerical results in Problem 3 allows also locating the course of the shock across the rarefaction. This is shown by the dash-dot line on Figure 2. It should be noted that

this represents already a result which cannot be obtained by classical methods in the rigorous, hydrodynamical theory: the "collision" of a shock and a rarefaction.

It is proposed to extend this method to more problems of this latter type, involving more complicated one-dimensional interactions of shocks and rarefactions. The experience with Problems 1, 2, 3 shows that a "substance" with 14 or 29 "molecules" is fully adequate to describe the finer nuances of hydrodynamic motion. We believe therefore that the possibilities which are opened up by this method are considerable.

The equation of state (41)

$$p = 1 - v + \tfrac{1}{4} v^2$$

must of course be replaced by more realistic ones. Actually non-polynomial equations, e.g. the "adiabatic"

(54) $$p = v^{-\gamma}$$

can be handled by the punch-card equipment through appropriate arrangements quite simply and efficiently.

All these problems, as well as the extension from the special equation of state (18), (19) to the general one (1), (3), will be dealt with in subsequent reports.

§21. Among more-than-one-dimensional problems, those of spherical symmetry suggest themselves first. Here x and a may be viewed as the distances from the center of symmetry of the physical space or the label space. This replaces the hydrodynamical partial differential equation (15) by

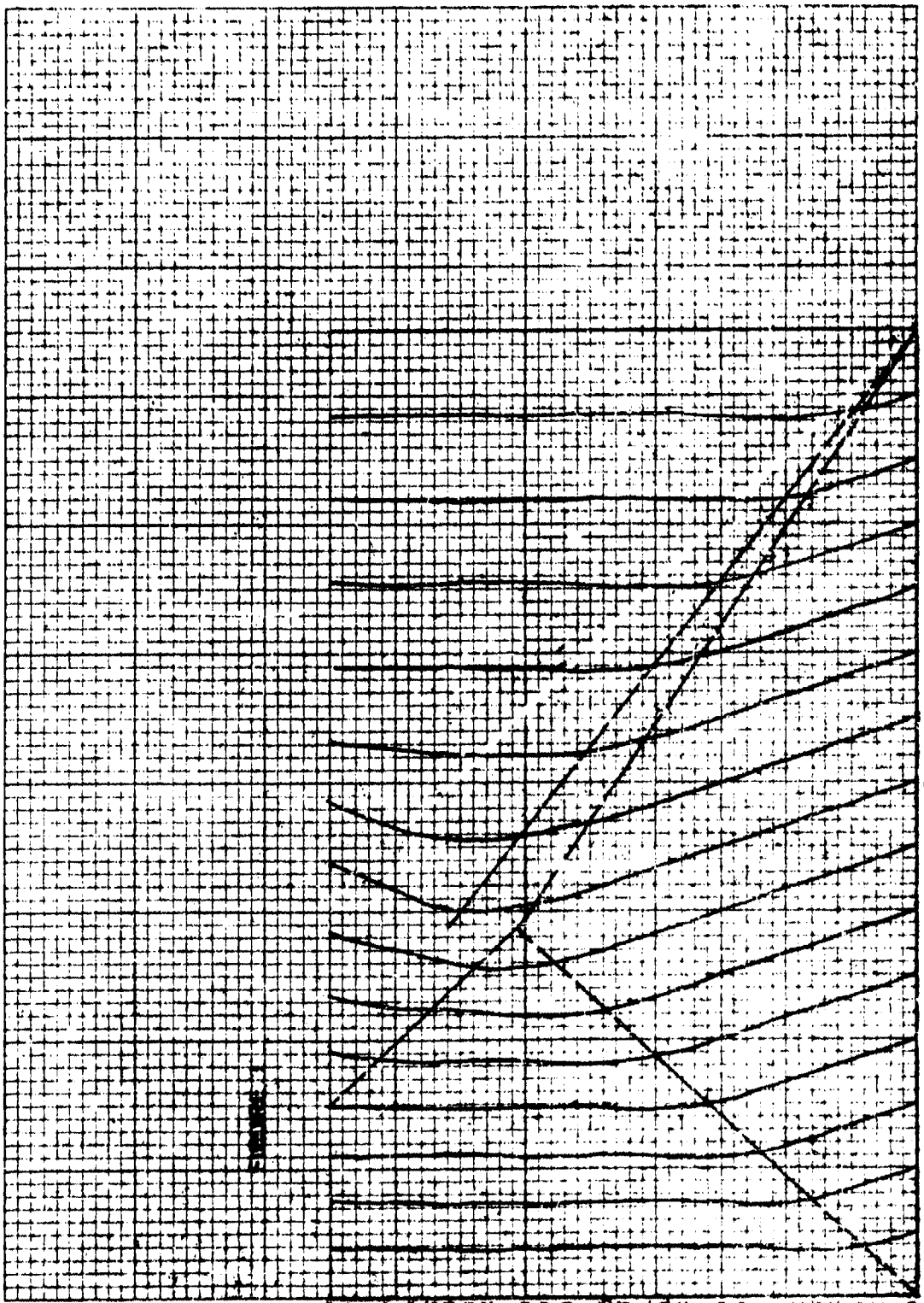
(55) $$\frac{\partial^2 x}{\partial t^2} = - \frac{x^2}{a^2} \frac{\partial}{\partial a} p_3 \left(\frac{x^2}{a^3} \frac{\partial x}{\partial a} \right),$$

which is of a very similar nature. Our approximative, numerical procedure applies to (55) in essentially the same way as to (15) in the one-dimensional case.

Numerical investigations of (55) are very desirable, since such problems as the decay of a spherical shock belong in this class. This subject will also be considered in subsequent reports.

§22. Truly two- or three-dimensional problems without the symmetries used in §21 are more difficult to handle. Our general approximative procedure still applies, but there seem to be reasons to fear that here the necessary number of "molecules" becomes inconveniently large. As pointed out in §20, 14 or slightly more "molecules" may suffice in one dimension, but this suggests that $14^2 \sim 200$ and $14^3 \sim 3\,000$ may be needed in truly two- or three-dimensional problems. These numbers seem too high for the existing machines, although 200 "molecules" are perhaps not altogether beyond capacity. The subject will be investigated further, particularly in view of the great importance of the hydrodynamical problems which a success in this direction would make accessible.

In the truly many-dimensional cases the possibility of using other types of machines will also have to be investigated. In this respect the relay-selector type machines seem very promising among the "digital" ones. The exploration of the "non-digital", "physical analogy" type machines is also being undertaken; some of these seem to be quite promising, although of lower precision than the "digital" machines.



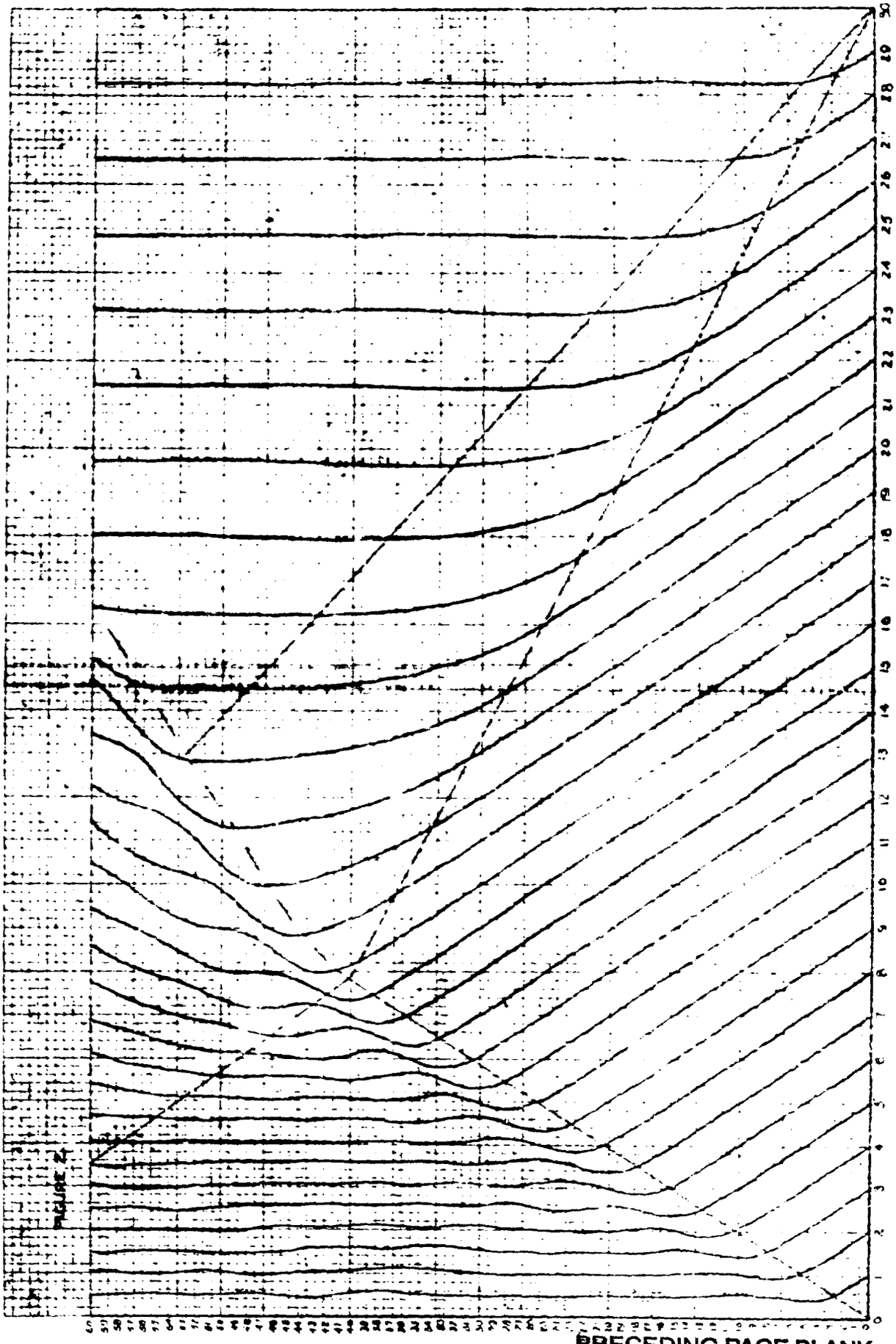


FIGURE 21

PRECEDING PAGE BLANK

CALCULATION FROM THERMODYNAMICAL AND HYDRODYNAMICAL CONSIDERATIONS OF UNDER-WATER SHOCK-WAVES FOR SPHERICAL CHARGES

H. N. V. Temperley and J. Craig
Admiralty Undex Works, Rosyth, Scotland

British Contribution

April 1945

CALCULATION FROM THERMODYNAMICAL AND HYDRODYNAMICAL CONSIDERATIONS OF UNDERWATER SHOCK-WAVES FOR SPHERICAL CHARGES

H. N. V. Temperley and J. Craig

April 1945

* * * * * * * * * *

Summary.

The results of calculations of the pressure pulses produced in water by spherical charges of T.N.T. and T.N.T./Aluminium 85/15 are presented. The equations of state for the explosion products were those calculated by Booth, while the equation of state for water was that used by Penney and Dasgupta which is practically identical with that used by Kirkwood and others(3). The gases are initially assumed to be at rest and at uniform pressure, as is done by Kirkwood and others(3) and in Penney's original calculations.

The results of the various theories are compared with experiment and the calculations now available enable the causes of some of the discrepancies between the various theories to be traced. With one or two exceptions, the experiments seem in good agreement with theory. The most serious discrepancy between theory and experiment seems to be in the single result obtained from the pressure-bar(1), which suggests a time constant much larger than the theory indicates. The most serious discrepancy between the theories seems to be the differing effects of the addition of aluminium to T.N.T. according to Kirkwood's theory and according to the present calculations. We have confirmed Kirkwood's assumption that the main portion of the pressure pulse is exponential, but it seems probable that Kirkwood's method of obtaining the constants in the exponential expression is too crude.

Introduction

It is desirable in explosion research to have some idea of the form of an underwater explosion pulse very close to the charge, say up to distances of 10 charge radii for a spherical charge. With the possible exception of Taylor and Davies' pressure bar(1), (which so far has only been used for one shot) no instrument has been devised which will stand up to the very high pressures in this region, although there are indirect methods of inferring the peak pressure which we shall discuss later on. It is therefore necessary to resort to theory in order to gain some idea of the pressures to be expected from contact or near-contact explosions, to assist both in the design of instruments for measuring these large pressures and in the design of structures to resist such explosions.

Methods available.

Two methods suggest themselves. One might start with experimental results at great distances from the charge and attempt to extrapolate inwards or one might start from the equations of state of the explosion products and of the water and, assuming reasonable initial conditions, follow hydrodynamically the variations with time of the pressure in the water and in the gas sphere. In this report we shall not use the first method, which has recently been used by Kirkwood and others(2) but we shall concentrate on the second. The success of this method naturally depends on the accuracy of our data. The equation of state of water over the pressure range required may now be regarded as fairly well known, covered as it is by recent experiments of Bridgman and others. The equation of state, of the explosion products cannot be observed directly, but must be calculated thermodynamically. This has been done by various workers. Even if one takes proper account of chemical equilibrium during the early stages of the expansion of the explosion products, it soon appears that the temperature falls rapidly during the expansion, and at some stage the explosion products will no longer be in equilibrium. Thus, at least one arbitrary assumption is involved in this calculation. A second difficulty is that explosives such as T.N.T. form solid carbon, and it is difficult to decide whether or not it should be considered to be in thermal equilibrium with the gases. A similar question arises with the aluminium oxide that is formed when aluminised explosives are detonated. Penney has also suggested that the aluminium might actually burn in the water near the charge. Fortunately, however, it

appears .....

Best Available (..

appears from the calculations of Kirkwood(3) and others, to be discussed later, that small changes in the chemistry of the decomposition make surprisingly little difference to the final results. In this report we shall use the adiabatics for T.N.T. and (T.N.T./Aluminium 85/15) obtained by Booth.

We may therefore take it that the two equations of state are known with sufficient accuracy for practical purposes. A more difficult question is to decide the initial conditions from which to start our hydrodynamical calculations. It is known from Taylor's theoretical work that a spherical detonation wave is a theoretical possibility, but there is no definite evidence that it really exists. We have therefore two possible choices. We might take the gas to be initially at rest at a high, but uniform, pressure, or we might take initial conditions based on the assumption of a spherical detonation wave. It is desirable to obtain data using both assumptions.

Calculations already carried out.

The first attempt was made at this problem by Penney. He obtained results which give the correct value for the peak pressure at great distances, but the wrong form for the pressure-time curve, the pressure very quickly dropping to zero, then rising again, an effect which is not observed experimentally. In a second attempt Penney and Dasgupta attacked the problem again, obtaining a curve very like those observed experimentally. It is difficult to compare these two reports directly, because, although in both substantially the same method of following the changes in pressure is used (a step-by-step method based on the Riemann hydrodynamical equations) two of the assumptions are changed. In the first paper the initial conditions are those of a gas at rest at uniform pressure, in the second those proper to the region just behind a detonation wave. In addition, different equations of state for water are used in the two papers. It was partly in order to sort out the effects of these two changes that the present calculations were undertaken.

Independently, Kirkwood and others(3) have attempted to obtain a theory of the propagation of the pressure pulse which shall enable results to be obtained in analytic form for different explosives, without having to report the laborious step-by-step process for each one. In all cases the initial conditions assumed are the same as those of Penney's original paper (gases initially at rest), but the equation of state for water is practically identical with that used by Penney and Dasgupta, so that here again no direct comparison is possible. Kirkwood(3) and his collaborators have carried out the work for a large range of explosives, and have also examined the effect of small variations in the equation of state of the gaseous products, and of temperature and salinity variations in the water. It appears that the effect of all these can be neglected for practical purposes.

The calculations actually carried out, the results of which are presented in this report, used the step-by-step method described by Penney. To try to maintain accuracy the steps were kept quite small, so that in 30 - 40 steps the shock front at the head of the pressure pulse had attained a radius of about six times the original radius of the charge (taken for convenience as 50 cm.). These results were extrapolated to greater distances by a method suggested by Dasgupta, to be described later. The equation of state for water was that used by Penney and Dasgupta and was practically identical with that used by Kirkwood and others(3). The equation of state for the gas was that calculated by Booth, while the initial conditions were that the gas was at rest at uniform pressure. In addition to T.N.T., the calculations were carried out for a T.N.T./Aluminium 85/15 mixture, to obtain a direct assessment of the effect of adding aluminium to a high explosive, and for comparison with Kirkwood's(3) work.

With these calculations available, we are in a position to make the following comparisons:-

(a) To ascertain the reason for the discrepancy between Penney's earlier results and Penney and Dasgupta's later results.

(b) To make a direct comparison between the step-by-step and Kirkwood methods.

(c) To obtain an assessment of the effect of adding aluminium to a high explosive.

Criticism of the methods.

The methods have both been fully described elsewhere, so that it is sufficient to say here that the step-by-step method is based on the equations:-

$\frac{\partial p}{\partial t}$ .....

Best Available

Best Available Copy

$$\frac{\partial P}{\partial t} + (c + u)\frac{\partial P}{\partial r} = -\frac{2uc}{r} \qquad (1)$$

$$\frac{\partial Q}{\partial t} - (c - u)\frac{\partial Q}{\partial r} = -\frac{2uc}{r} \qquad (2)$$

where u is the particle velocity, t the time co-ordinate and r the distance co-ordinate, and $P = f + u$, $Q = f - u$ and f is the Riemann function $f = \int_{\rho_0}^{\rho} \frac{c}{\rho} d\rho$. c is the velocity of sound, ρ the density and ρ_0 the density at atmospherical pressure. Kirkwood's(3) method is based essentially on two assumptions:-

(a) That the function $G = r\left[\int_{\rho_0}^{\rho} \frac{p}{\rho} + \frac{1}{2} f^2\right]$ is propagated outwards unchanged with a velocity $c + f$. (In the earlier reports f was replaced by u in these expressions). A similar function is propagated inwards into the gas.

(b) That the important part of the pressure pulse can be regarded as exponential.

In both methods due account has to be taken of the fact that at the shock front energy is being dissipated because the shock-front travels slightly slower than and thus "eats" up the remainder of the pulse, the relation between shock front pressure and velocity being determined by the Rankine-Hugoniot equations. The dissipation of energy due to this "overtaking effect" represents the effects of viscosity and thermal conductivity, which cannot be neglected at the steeply-sloped shock-front, even if they can be neglected in the remainder of the pulse.

The objection to the step-by-step method is that if the steps are made too small errors accumulate, while if they are taken too large the second-order terms are not negligible. Penney and Dasgupta attempted to allow for these second order terms by their "backwards and forwards" process. This process was not used in the present calculations, because it was considered that the additional labour and possibility of error entailed by working over three very similar sets of figures was likely to counterbalance any gain in accuracy. It was preferred to keep the steps small at stages where special difficulties occurred (at the beginning, at the instant when the rarefaction wave in the gas first reaches the origin and at the instant when a discontinuity in the Q function is about to set in, as described later), and to obtain a rough check on the over-all accuracy by computing the kinetic and potential energies of gas and water at a number of instants, adding to them the energy dissipated at the shock-front and seeing how nearly the total remained constant. The results suggest that the accuracy remains fairly good, at least in the early stages of the work, and are given in Tables I and II.

TABLE I.

Energy balance for T.N.T., expressed in calories per gram of explosive.

Position of Shock-Front. (Charge Radii).	1.00	1.03	1.12	1.84	2.16	2.92	3.68
P.E. of Gas	1028	1007	752	537	471	336	204
K.E. of Gas	0	8	112	158	102	25	8
P.E. of Water	0	5	45	80	97	110	113
K.E. of Water	0	9	94	176	201	265	269
Wastage	0	3	32	76	101	144	171
Total	1028	1032	1035	1027	972	880	765

Table II .....

Best Available Co

TABLE II.

Energy balance for T.N.T./Aluminum expressed in calories per gram of explosive.

Position of Shock-Front. (Charge Radii).	1.00	1.04	1.21	1.58	1.93	2.38	3.40
P.E. of Gas	1377	1350	1200	909	745	641	377
K.E. of Gas	0	10	72	187	194	103	1[illegible]
P.E. of Water	0	6	29	69	96	120	136
K.E. of Water	0	10	57	152	226	290	337
Wastage	0	2	27	78	118	160	222
Total	1377	1378	1385	1395	1379	1314	1087

The discrepancies in the energy in the latter stages of the work are due to a systematic cause explained in Section 6. It must not be assumed that the work has suddenly become less accurate.

The method of calculating these energies is fairly obvious. The potential energies of gas and water were computed as functions of pressure from the equation of state (by means of the familiar integral $\rho \int_{\rho_c}^{\rho} \frac{p d\rho}{\rho^2}$ which gives the potential energy per unit volume). The kinetic energy per unit volume is given simply by $\frac{1}{2} \rho u^2$, and u being known at every point, so that one can obtain the total kinetic energies by integrating this over the whole volume of the gas and the disturbed volume of the water, the weighting factor being $4\pi r^2 dr$. Similar integrations give the two potential energies. The total wastage was calculated from the figures given in Penney and Dasgupta's paper Table I, relating θ, the rate of wastage, to shock-wave pressure. The relations between time and position of shock-wave and value of shock-wave pressure being known, the wastage while the shock-wave moves from R_0 to R_1 is given by $4\pi \int_{h_0}^{h} r^2 \theta \rho dr$.

Kirkwood(3), by a process that is not explicitly stated, concluded that his results were not likely to be in error by more than 20%, and that they would be too high. This conclusion seems to be borne out by the comparison between theory and experiment, as will be seen later. Penney has questioned the validity of some of Kirkwood's assumptions and Kirkwood has replied answering some of the points raised. The only serious difficulty still outstanding is to decide to what extent one can replace, as Kirkwood does, the state of affairs represented by equations (1) and (2) by his rather simpler scheme of things, in which the outgoing wave in the gas and the ingoing wave in the water are both neglected. Calculations in fact show that the ingoing wave in the water is very far from negligible. It occurs for two reasons. First, because of the term $-\frac{2uc}{r}$ in equation (2), which causes the Q function to build up negatively as the wave travels inwards. Secondly, because the shock-front acts in some ways as a reflector owing to the overtaking effect, so that Q is not precisely zero even just behind the shock-front. In Kirkwood's first paper (O.S.R.D.588) it was erroneously stated that the theory implies neglect of the Q function. This is not so, because Kirkwood's function $\frac{c}{f}$ is not precisely the same as the Riemann function P, and Kirkwood has pointed out that his results in fact imply values of Q of the same order of magnitude as those given by the step-by-step calculations. However, the procedure of replacing two waves proceeding in opposite directions by a single wave cannot be carried out even in the simple case of a stretched string, so it is hard to see how it can be valid here. The comparative success of Kirkwood's theory is probably due to two main causes:-

(a) It is definitely a better approximation than "acoustic" theory.

(b) Substitution in the hydrodynamic equations shows that the first-order correction terms vanish, at all events for water.

Best Available C

A .....

A check on Kirkwood's theory of the propagation of the pressure pulse in water has been made by Road Research Laboratory by comparing the time and space derivatives of the pressure just behind the shock-front, as it can be shown that these are connected by a unique relation. It reveals discrepancies of up to 30% in the values obtained from Kirkwood's assumptions in the very high pressure region occurring initially near the charge. This check is a sensitive one, and does not imply that values of peak pressure, etc., show errors of this order.

The extrapolation process.

As stated, the step-by-step process was used until the shock-front had reached a point about 5 – 6 charge radii from the centre, and the pressure had dropped from its original high value of the order of 40 kilobars to about 2 kilobars. Some specimen values of P and Q and the pressure are given in Table III.

TABLE III.

Values after the final step.

	T.N.T.				T.N.T./Aluminium				
	r cms.	p kilobars	P metres/sec.	Q metres/sec.	r cms.	p kilobars	P metres/sec.	Q metres/sec.	
Shock front	268	2.25	260	0	313	2.25	255	0	Shock front
	248	2.05	255	– 10	280	1.65	215	– 15	
	216	1.55	220	– 30	248	1.20	195	– 35	
	184	1.00	195	– 65	216	.70	160	– 60	
	152	.65	200	– 115	184	.40	145	– 85	
Inter-face	107	.30	315	– 265	152	.25	175	– 135	
					121.3	.30	265	– 215	Inter-face

Original radius of charge was 50 cms. in both cases.

It will be seen that, even at these comparatively low pressures, the function Q is still not negligible except in the region just behind the shock-front. An attempt to carry the step-by-step process further (we need values at least 10 charge radii to get a satisfactory comparison with experiment) might lead to an unacceptable piling up of errors, while any extrapolation process involves the neglect of the ingoing wave. It was considered, however, that the application of such a process would give a better answer than either further application of the step-by-step method or Kirkwood's method, which amounts virtually to an application of extrapolation starting from an instant just after the pressure-pulse has begun to form. In particular, it should give a sufficiently good answer for the variation of peak pressure at various positions of the shock-front, and for the portion of the pressure-time curve immediately behind the shock-front. On the assumption that Q is zero, we have:-

$$u = f \qquad (3)$$

Also $P = f + u \left(\frac{dr}{dt}\right)_\rho = c + u$ from equation (1).

Therefore .....

Best Available Cor

Therefore $dt = -\frac{2}{p}\frac{dp}{dt}\,dt = -\frac{2}{c(c+u)}\,dr$ (for corresponding points in the pulse at different times). (4)

where $p = f + g = 2f = 2u$ which on substitution in equation (4) gives:-

$$\frac{df}{f} + \frac{dc}{c} = -\frac{dr}{r} \tag{5}$$

The adiabatic relation between pressure p and density ρ for water is given by:-

$$\frac{(p + p_0)^{\frac{1}{n}}}{\rho} = \text{constant}$$

whence $f = \int_{\rho_0}^{\rho} \frac{c}{\rho}\,d\rho = \frac{2}{n-1}(c - c_0)$ (6)

where $\frac{2}{n-1} = .3202$; c_0 = velocity of sound in water at atmospheric pressure.

Substitution of equation (6) in equation (5) gives

$$\frac{dc}{c - c_0} + \frac{2}{n-1}\frac{dc}{c} = -\frac{dr}{r}$$

or after integration

$$rc^{\frac{2}{n-1}}(c - c_0) = M \tag{7}$$

where M is constant for corresponding points on the pulse at different times.

Further, since

$$\frac{dr}{dt} = (u + c) = (f + c) = \frac{2}{n-1}(c - c_0) + c = \frac{n+1}{n-1}c - \frac{2}{n-1}$$

therefore from equation (7)

$$dt = -M\frac{dc}{c^{\frac{n+1}{n-1}}(c - c_0)^2}$$

which, after integration, gives

$$t_2 - t_1 = -M\int_{c_1}^{c_2} \frac{dc}{c^{\frac{n+1}{n-1}}(c - c_0)^2}$$

Substitute $\frac{c - c_0}{c_0} = x$.

Thus $t_2 - t_1 = -\frac{M}{c_0^{\frac{2n}{n-1}}}\int_{x_1}^{x_2} \frac{dx}{(1+x)^{\frac{n+1}{n-1}}x^2}$

whence by writing $\int_{x_2}^{2} \frac{dx}{(1+x)^{\frac{n+1}{n-1}}x^2} = I(x_2)$

$$t_2 - t_1 = -\frac{M}{c_0^{\frac{2n}{n-1}}}\left\{ I(x_2) - I(x_1) \right\} \tag{8}$$

In .....

In addition to the formulae already derived, it is neceessry, as will be explained later, to have an expression for the distance $r_2 - r_1$ moved by the shock front in the interval $t_2 - t_1$.

For this purpose, U, the shock wave velocity, has to be introduced in the expression $\int_{t_1}^{t_2} U\,dt$. The decrease of U with time is not known, but it is related to the pressure by the following relation, which is satisfactory for small pressures:-

$$U = c_0 (1 + \alpha x) \text{ where } \alpha = \tfrac{1}{3}.$$

As given above:-

$$dt = -\frac{A\,dc}{c^{\frac{n+1}{n-1}}(c - c_0)^2} = -\frac{M\,dx}{c_0^{\frac{2n}{n-1}}(1+x)^{\frac{n+1}{n-1}}x^2}$$

$$\int_{t_1}^{t_2} U\,dt = r_2 - r_1 = -\int_{x_1}^{x_2} c_0(1+\alpha x)\frac{M\,dx}{c_0^{\frac{2n}{n-1}}(1+x)^{\frac{n+1}{n-1}}x^2}$$

$$= -\frac{M}{c_0^{\frac{n+1}{n-1}}}\left[\int_{x_1}^{x_2}\frac{dx}{(1+x)^{\frac{n+1}{n-1}}x^2} + \alpha\int_{x_1}^{x_2}\frac{dx}{(1+x)^{\frac{n+1}{n-1}}x}\right]$$

$$r_2 - r_1 = \frac{M}{c_0^{\frac{n+1}{n-1}}}\left[J(x_2) - J(x_1)\right] \qquad (9)$$

where $J(x_2) = \int_{x_2}^{2}\frac{dx}{(1+x)^{\frac{n+1}{n-1}}x^2} + \alpha\int_{x_2}^{2}\frac{dx}{(1+x)^{\frac{n+1}{n-1}}x}$

The upper limit of 2 in the integrals has no special significance, but is introduced in order to simplify tabulation.

Method of Calculation.

Knowing the pressure (p_1) distribution in water when the shock-front has moved out to a distance R_1 in time t_1, we then assume the shock-front to have moved to a further distance R_2 and use equations (5), (6) and (7) to find the pressure distribution in the new position at time t_2.

The various steps of the calculations are as follows:-

(a) The integrals I(x) and J(x) are tabulated for a series of values of $x < 2$.

(b) Knowing p_1 hence c_1 at R_1 for the shock-wave, we can find M by using equation (7) with $r = R_1$ $c = c_1$.

(c) At this stage it cannot be assumed that the leading point of the shock-front at time t_1 will always remain the leading point (the pressure thus decreasing according to equation (5)) and on this assumption use R_2 and the value of M found by (b) to find the value of c_2 in equation (7). In actual fact the velocity U of the shock-wave is rather less than that of the leading point, so that the method just described would eventually give p_2 at a point beyond the actual position of the shock-wave. Instead, we must make use of equation (7) which was evolved from an expression for U. Thus, knowing $R_2 - R_1$, M and x_1, we find $J(x_2)$, hence x_2 c_2 and p_2 at R_2.

(d) The next step is to find $t_2 - t_1$ by equation (8) using the values of M, x_1, x_2 now known. The time $t_2 - t_1$ is a fixed time basis for all further calculations.

So .....

Best Available Copy

So far we have found the pressure at the new position of the shock-front. We now have to find the pressure distribution in the region behind the shock-front. For this purpose, we select a range of values of c_1 at distances r_1 when the shock-front is at R_1. Each pair of values (r_1, c_1) is then extended to the new values (r_2, c_2) by the following methods:-

(e) As before, knowing r_1 c_1 hence x_1, we find the corresponding M from equation (7).

(f) Using the fixed time basis $t_2 - t_1$ already found, equation (6) gives $f(x_2)$ hence x_2, c_2, p_2.

(g) Returning to equation (7) in the form $r_2 c_2^{.3202} (c_2 - c_o) = M$, we can therefore find r_2.

Thus, the conditions at r_1 have been translated into the corresponding conditions at r_2.

This method is repeated for each chosen r_1 until the pressure-distance relationship for the shock-wave in its new position R_2 has been completed.

As before, most of the complications are due to the fact that we still have to take due account of the overtaking effect even at comparatively low pressures. The extrapolation process is based on the constancy of the quantity $rc^{\frac{2}{n-1}} (c - c_o)$ for corresponding points on the pressure curve at different times. It is interesting to compare this with Kirkwood's method. The function that Kirkwood assumes to be constant is given by:-

$$G = r \left[\int_{\rho_o}^{\rho} \frac{dp}{\rho} + \frac{1}{2} f^2 \right]$$ where f is the Riemann function, defined as before.

Again using the equation of state for water, we find that this function is given by:-

$$G = r \left[\frac{c^2 - c_o^2}{n - 1} + \frac{2}{(n-1)^2} (c - c_o)^2 \right] \qquad (10)$$

For low pressures, c is nearly equal to c_o, and the main variation of the quantities G and M will be due to the variation of $c - c_o$, which occurs to the first power in both quantities, the second term in equation (10) being negligible compared with the first. It thus follows that in this limiting case the extrapolation process we have used is equivalent to Kirkwood's. For pressures of the order of 2 kilobars $c - c_o$ is about 30% of c_o, so that the peak pressures would have to be greater than this for the two methods to give significantly different results. Simple acoustic theory would give nearly as good an approximation.

It was found that the pressures dropped to low values at points more than a few charge radii behind the shock-front, so that c became nearly equal to c_o and the extrapolation process became inaccurate. Thus, apart altogether from the fact that Q was not negligible, it was not possible to apply the extrapolation process to points in the region of the water near the gas bubble. On the other hand, the overtaking effect continually destroyed the front of the pressure pulse. It was, therefore, not practicable to carry the extrapolation process beyond 30 charge radii, which, however, is enough to give us a satisfactory comparison with experiment and with the results of other workers.

Difficulties encountered in the calculations.

We have already mentioned the difficulties connected with the extrapolation. In the calculations proper, some further difficulties were encountered.

(a) Once the rarefaction wave passing into the gas had reached the origin, it became difficult to maintain accuracy on account of the term $-\frac{2uc}{r}$ which remains finite at the origin but cannot be determined graphically with any accuracy. For points near the origin $\frac{u}{r}$ was replaced by $\frac{du}{dr}$, but this quantity was also difficult to evaluate on account of the fact that the curve of u against r ends at the origin and ordinary

Best Available C

methods .....

methods of numerical differentiation are not applicable. An attempt to maintain the accuracy, by keeping the first few steps after the arrival of the rarefaction wave at the origin small, was made but it is difficult to assess the error due to this cause. However, events at the origin are unlikely to affect the main portion of the pressure pulse for a reason that we shall discuss immediately.

(b) The step-by-step method broke down in the gas shortly after the reflection of the rarefaction wave at the origin, a discontinuity in the Q function appearing about half-way between the origin and the interface. A similar effect seems to have occurred with Penney and Dasgupta calculations, but it is understood that it did occur in Penney's original calculations. The effect might be interpreted as the incipient formation of a shock-wave travelling inwards, but it is difficult to see why a rarefaction wave should suddenly reverse its direction of propagation and thus become a shock-wave. Such effects are usually associated with a boundary reflection, but no boundary is anywhere near. In another report we have described the phenomenon in detail, and have suggested that it may be an instance of an apparent "negative shock-front", such as has been observed by Libessart though the persistence of such a phenomenon for any finite time also leads to serious difficulties.

For the purpose of these calculations, it is important not so much to elucidate the exact nature of the effect but to decide what effect it is likely to have on conditions in the water. For this purpose the calculations were continued in the following way (after we had first satisfied ourselves, by repeating part of the calculations with a reduced size of step, that the appearance of the discontinuity was a real phenomenon). A continuation of the calculation, accepting the Riemann theory literally, would have given us a Q curve with two branches overlapping one another and connected by an S-shaped portion, so that, for certain values of r there would have been three possible values of Q. The lower part of the curve, starting from the origin, was retained up to the point at which the S-shaped portion began to bend backwards, and all of the upper branch of the curve overlapping this portion was erased. It is clear that this procedure will lead to the total energy being under-estimated if the real phenomenon is (say) an ingoing shock-wave, and we find indeed from Tables I and II that there is a marked decrease in the total energy in the latter steps, the decrease in fact practically coinciding with the appearance of the discontinuity in Q.

Our reason for adopting this method of calculation was to try to find out whether the rarefaction wave could reach the interface, and thus affect conditions in the water, possibly producing a pronounced minimum in the pressure-time curve of the kind found by Penney. We obtained the reassuring result that, even with our extreme assumption, the discontinuity in Q was only propagated with a speed comparable with the advance of the gas-water interface, so that it would be a long time before it could affect conditions in the water. In fact, the discontinuity in Q was still far behind the interface when the main portion of the pressure pulse had formed and the step-by-step calculations were broken off. Thus it would appear that conditions at the origin are not likely to have any important effect on the pulse in the water.

Summary of results.

In Tables IV and V the relation between pressure and time, which is what would be measured by a gauge at a fixed position in space, is given for distances of approximately 2, 3, 4 and 5 charge radii for both explosives. In Figures 1 and 2 the same data are plotted logarithmically, and it will be see that, with the exception of the case $\frac{R}{a} = 3.08$ for T.N.T., the pressure-time curve is a reasonable exponential even quite close to the charge, thus proving some justification for Kirkwood's second assumption. The time-constants of the exponentials given by the slopes of these curves are also given in the Tables. Owing to the "eating-up" of the pressure pulse by the shock-front, it is not possible to obtain satisfactory figures for the time constants beyond 5 charge radii. A rough comparison with Kirkwood's figures is made in Table VI.

In Figure 3 peak pressure multiplied by number of charge radii is plotted against distance for T.N.T. and T.N.T./Aluminium according to the present calculations, and according to Kirkwood's(2) latest figures (O.S.R.D.2022). Also included for comparison is Penney's earlier work on T.N.T. All these curves are based on the assumption that the gas is at rest initially. Penney and Dasgupta's calculations include the effect of a detonation wave, and cannot therefore be compared directly with the others. The following differences between the various calculations must also be noted:-

(a) .....

Best Available Copy

(a) In Penney's curve the equation of state for water differs from that used in the other work.

(b) The density of T.N.T. was 1.59 gms./cc. in Kirkwood's(2) work, 1.565 in Penney's work and 1.50 in the present calculations. The differences so introduced are not present calculations. The differences so introduced are not likely to be serious. They can be estimated by comparison of Kirkwood's results for T.N.T. of densities 1.59 and 1.40.

In Figure 4 a comparison is made of the present calculations with those of Penney and Dasgupta to see the effect of introducing a detonation wave. The equation of state for water is identical in the two cases, the equation of state for the gas not significantly different, but it should be noted that the initial conditions assumed by Penney and Dasgupta are such that the gas initially has a total energy of 800 calories per gram of explosive, as against 1028 calories per gram for the present calculations. This difference is partially counterbalanced by the fact that Penney and Dasgupta use a T.N.T. of higher density (1.565 instead of 1.50), but this still leaves a discrepancy of 19% in the energy for a charge of the same volume. No attempt has been made to introduce any correction for this in Figure 4.

Figure 5 includes all the theoretical curves of peak pressure against distance for T.N.T. Figures 6, 7 and 8 show the distribution of pressure and particle velocity as functions of distance for a T.N.T. charge at 3 different instants, while Figures 9, 10 and 11 give similar data for a T.N.T./Aluminium charge. The data for the conditions in the gas are only given between the interface and the first discontinuity in Q, for which region it will be unaffected by the behaviour of the discontinuity.

TABLE IV.

P - t Relationships for T.N.T.

$\frac{R}{a_0}$ = 2.06		$\frac{R}{a_0}$ = 3.08		$\frac{R}{a_0}$ = 3.91		$\frac{R}{a_0}$ = 5.04	
P	t	P	t	P	t	P	t
11.75	0	5.95	0	3.90	0	2.55	0
10.65	20	4.85	50	3.10	70	2.05	90
10.00	40	4.00	100	2.55	150	1.65	180
8.90	60	3.60	150	2.00	230		
7.60	90	2.90	210	1.55	310		
6.50	120	2.20	280	1.10	400	θ = 410 μ s	
5.55	150	1.55	360	.80	490		
4.90	190	1.10	440				
4.05	230	.90	520				
3.40	280	.65	610	θ = 325 μ s			
2.60	330	.40	700				
1.85	380						
1.60	440						
1.25	510	θ = 260 μ s					
.85	590						
.70	670						
θ = 220 μ s							

Table V. .....

Best Available Cop

TABLE V.

P – t Relationships for T.N.T./Aluminium

$\frac{R}{a_o}$ = 1.98		$\frac{R}{a_o}$ = 3.0		$\frac{R}{a_o}$ = 4.07		$\frac{R}{a_o}$ = 5.01	
P	t	P	t	P	t	P	t
14.85	0	7.60	0	4.5	0	3.2	0
14.00	15	6.40	45	3.6	70	2.1	150
12.90	35	5.40	95	2.85	150	1.20	350
12.00	55	4.40	145	2.20	250	.55	550
10.35	80	3.60	200	1.35	400		
9.10	110	2.85	260	.55	600	θ = 360 μ s	
7.85	140	2.25	330	.15	800		
6.70	175	1.65	410				
5.40	215	1.15	510	θ = 330 μ s			
4.35	260	.60	660				
3.40	310	.25	860				
2.75	360						
1.90	415	θ = 265 μ s					
θ = 220 μ s							

TABLE VI.

Comparison of Time-Constants with Kirkwood's Values.

	Density	$\frac{R}{a_o}$	1.00	2.06	3.08	3.91	5.04	7.51	10.0
T.N.T.	1.50	θ (present calculations)	–	220	260	325	410	–	–
	1.59	θ (Kirkwood)	172	(260)	(330)	(400)	(460)	560	695
	Density	$\frac{R}{a_o}$	1.00	1.98	4.00	4.07	5.01	7.71	10.0
T.N.T/Al.	1.765	θ (present calculations)	–	220	265	330	360	–	–
	1.694	θ (Kirkwood)	203	(280)	(360)	(450)	(520)	612	725

All values refer to a charge of 50 cm. radius, and are given in microseconds.

NOTE: The figures in brackets are taken as accurately as possible off Kirkwood's curves. Unbracketed figures are obtained from values quoted numerically.

Comparison .....

Best Available Copy

Comparison with experiment.

Figure 5 includes all the theoretical curves for T.N.T., although it is emphasised again that they do not originate in precisely the same assumptions. In addition, experimental information on pressures very near the charge is included, taken from various published reports. It is believed that this covers practically all results that have been reported, at all events within 15 – 20 charge radii. The following is a list of instruments and methods used.

(a) Piezo-electric gauge (Wood's Hole)(2) U.S. Report U.E. 24.

(b) Pressure-bar (Taylor and Davies)(1)

(c) Spray-velocity and air-shock wave (Road Research Laboratory)

(d) Spray-velocity (Wood's Hole) U.S. Report U.E. 27.

(e) Optical method (effect on refractive index of water) (Wood's Hole) U.S. Report U.E. 23.

In addition, two empirical lines have been included, one according to the law recently suggested in the U.S.A. (nomogram issued by Princeton University Station and stated to be based on data supplied by U.E.R.L.), and the other according to Wood's formula(4). This latter formula is based on measurements at comparatively large distances. As it does not scale up exactly with radius of charge, it has been drawn in for a 300 lb. charge.

The following comments are made on the various experimental points:-

(a) The line drawn through the points obtained with the piezo-electric gauge was obtained by Kirkwood's extrapolation method(2), of which a preliminary account is given in U.S. Report U.E. 24.

(b) Although the one point obtained from the pressure-bar gives reasonable agreement with the theoretical curves, the experiment indicated a time-constant much greater than 100 microseconds, whereas theory indicates a time-constant of the order of 50 microseconds.

(c) The pressure was inferred by two distinct methods, by the velocity of surface spray and by the velocity of the shock-front rising into the air from the water surface. These two methods agree well except at the 2 charge radii position, where the shock-front is probably obscured by the spray. The lower point is obtained on the assumption that the shock-front velocity in air is the same as the spray velocity. These experiments were with C.E. and 5% has been arbitrarily deducted from the readings to give a comparison with T.N.T.

(d) The spray velocity method is applied in this case to T.N.T.

(e) In the optical method the shock-wave was used as a lens. The explosive was Tetryl, which according to Kirkwood's(3) figures has a theoretical peak pressure distance curve almost identical with T.N.T. of density 1.59. According to experimental work quoted by Kirkwood (in O.S.R.D. 2022), Tetryl has a peak pressure distinctly above the theoretical, at all events for points near the charge (see Figure 1 of that Report). This is in sharp contrast with T.N.T., for which the peak pressures are below Kirkwood's curve as is clear from Figure 5 of this report. (One would expect Kirkwood's theory to over-estimate the pressure somewhat). It is therefore not clear by what factor the Tetryl results should be corrected in order to give a comparison with T.N.T.

Discussion.

With the exception of the strange result on the time-constant revealed by the pressure-bar, it may be stated that the disagreements between theory and experiment are no greater than the discrepancies between the various theories, also that the various methods of measurement agree well among themselves. We are, however, now in a position to trace at any rate some of the causes of these discrepancies, and to infer the approximate effect that they have. We may list them for convenience under a number of headings.

(a) .....

Best Available Co

(a) Variations of loading densities and energy release.

By interpolating between Kirkwood's curves(3) for T.N.T. density 1.59 and T.N.T. density 1.40, we conclude that an overall reduction of the order of 10% should be made in the peak pressures for a density of 1.59 to compare them with a density of 1.50. This would give much better agreement with the step-by-step results, but we ought logically to apply a similar correction process to the T.N.T./Aluminium results, and this would worsen the agreement because Kirkwood's density is less. It is difficult to know how to correct Penney and Dasgupta's curve to allow for the fact that they assumed too small an energy content. The discrepancy in energy was 19%, so the discrepancy in peak pressure is unlikely to be more than 10%, and will probably be less, owing to the fact that the wastage of energy in the shock-wave increases faster with peak pressure than does the energy given to the water.

(b) Variations of the equation of state of the gas.

We may deduce from Kirkwood's(2) work that variations in the composition, equilibrium, etc., of the exploded products makes relatively little difference to the pressure in the water. The step-by-step calculations give no evidence on this point.

(c) Variations of the equation of state of the water.

It will be seen from Figures 3 and 5, comparing Penney's original work with the present calculations, that the peak pressure distance curve is only affected by the change in the equation of state in the region very near the charge. However, the pronounced minimum in the pressure-time curve, which was such a disquieting feature of Penney's original results, has disappeared. It was suggested by one of us that this minimum had appeared due to Penney's original equation of state giving too small a compressibility of water at high pressures, which surmise seems to be confirmed.

Kirkwood's(3) work indicates that minor changes in the constants of the equation of state, due to temperature and salinity changes, are of practically no importance.

(d) Variations of the assumed initial conditions.

Figure 4 gives a straight comparison of our calculations with those of Penney and Dasgupta. Apart from the fact that the equation of state for the gas is slightly different, the only change that has been made is that we have replaced the "detonation wave" conditions by the assumption that the gas is initially at rest. It will be noted that Penney and Dasgupta's curve crosses ours twice, and this would remain true even if one made a correction of the order of 5 or 10% to allow for the energy difference already referred to. On account of the fact that higher peak pressure in the water involves a more than proportional rate of wastage of energy at the shock-front, it is clear that this phenomenon of crossing over is to be expected. In another report it has been suggested by one of us that an affect of this kind (different detonation velocities and pressures) may account for the anomalous results observed with Torpex and Minol II, Torpex being apparently better at great distances, while Minol II gives bigger deflections on the box model (small distances). An attempt is made to correlate this with the detonation properties, Torpex being a sensitive explosive, whereas Minol II is difficult to detonate.

(e) The effect of adding Aluminium.

Neither our calculations nor Kirkwood's(2) throw any light on the question of whether or not the effect of aluminium is due to "after-burning", i.e., to the time of reaction of the Aluminium with the other explosion products being comparable with the time of expansion of the gas bubble. In the calculations of the adiabatics it is assumed that the reaction of the Aluminium is virtually completed before the expansion begins. Leaving aside this point, it is clear from Figure 3 and Table VI that Kirkwood finds that the addition of Aluminium has hardly any effect on the peak pressure but lengthens the time-constant, while we find an appreciable increase in the peak pressure but practically no effect on the time-constant. Indeed, at 5 charge radii the time-constant for the aluminised explosive drops below that for T.N.T., this presumably being associated with the fact that the ratio of peak pressure is increasing in this region. At 30 charge radii our curves for peak pressure are approaching one another rapidly, and we should expect this decrease in the peak pressure ratio to be associated with an increase in the ratio of time constants, although we have no definite figures to bear this out. If so, it means that the step-by-step and Kirkwood methods give similar predictions at large distances, in agreement with the experiments, which indicate practically no effect of the Aluminium on the peak pressure, but an increase in the time constant.

At .....

Best Available Copy

At small distances, however, the two theories are in fundamental disagreement as to what exactly the effect of adding Aluminium is. This disagreement is particularly serious because, in each pair of results, nothing has been changed except the adiabatic of the explosion products so that it is clear that either one or the other theory cannot be relied on near the charge, even for comparison purposes.

(f) The effect of neglecting the ingoing wave in the water.

Comparison of the two sets of curves indicates at once that Kirkwood's(3) theory tends to give too high values for both peak pressure and time constant, but that the correction involved may well differ considerably for different explosives.

(g) The effect of Kirkwood's exponential assumption.

Kirkwood's theory apparently involves a straight assumption that the pressure-time curve is exponential. The constants are determined by the initial conditions of continuity of pressure and velocity at the gas-water interface, and once this has been done the subsequent behaviour of the pressure pulse is determined entirely by the properties of water, the properties of the gas having no further chance of influencing the answer. We think that our results, showing as they do that the predicted form of the pulse is exponential, represent a distinct improvement, and also that there may be some way of determining the time constant which shall take account, by some averaging process, of part of the early history of the gas bubble, as distinct from the conditions at the initial instant only. At later instants, the Q function in the water will have to be considered explicitly. This point will be investigated further.

Conclusions.

Apart from the exceptions noted above, it will be seen that the various theories are in reasonable agreement with one another and with experiment, and that the causes of many of the apparent discrepancies can be traced. The step-by-step calculations justify Kirkwood's(3) assumption of an exponential pressure pulse, but indicate that the determination of the constants of the exponential curve needs some method more elaborate than that used by Kirkwood(3), even if only comparisons of different explosives are wanted. It is probable that this method will need to take explicit account of conditions at the surface of the gas bubble at instants other than the initial one. The Q function in the water is then not negligible near the gas bubble, and will probably have to be allowed for also.

References.

(1) Taylor and Davies. "A Measurement of the Pressure close to an Explosive Underwater"

(2) Kirkwood and Others. U.S. Report U.E. 24

(3) Bethe, Kirkwood et al. "The Pressure-wave produced by an Underwater Explosion". A series of reports beginning with O.S.R.D. 588. Most of the information is summarised in O.S.R.D. 2022 which supersedes some of the earlier reports.

(4) Wood. "Nature of the Pressure Impulse produced by the detonation of explosives under water. An investigation by the Piezo-electric cathode-ray oscillograph method".

Best Available Copy

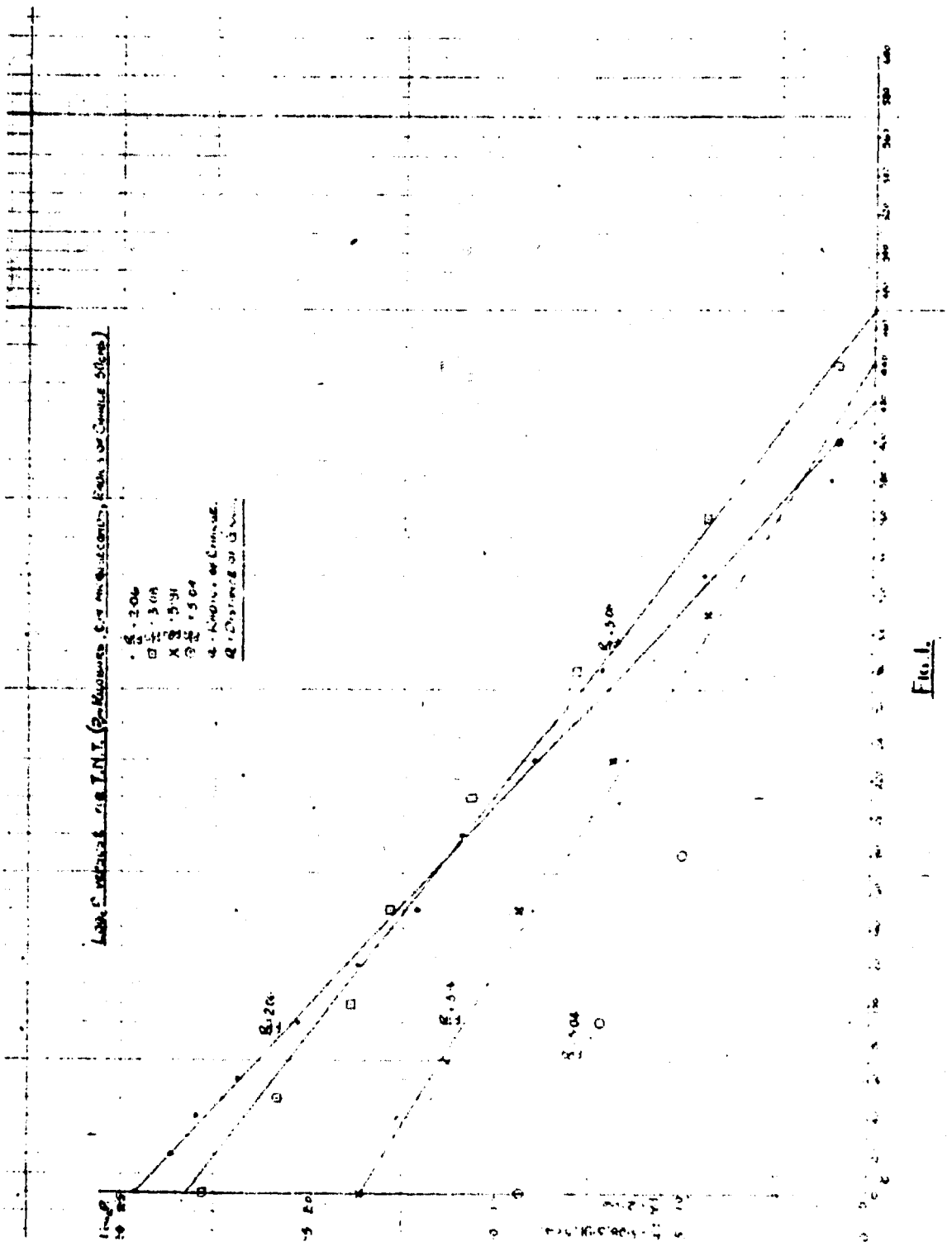


Fig. 1.

Best Available Copy

Fig. 2

Best Available Copy

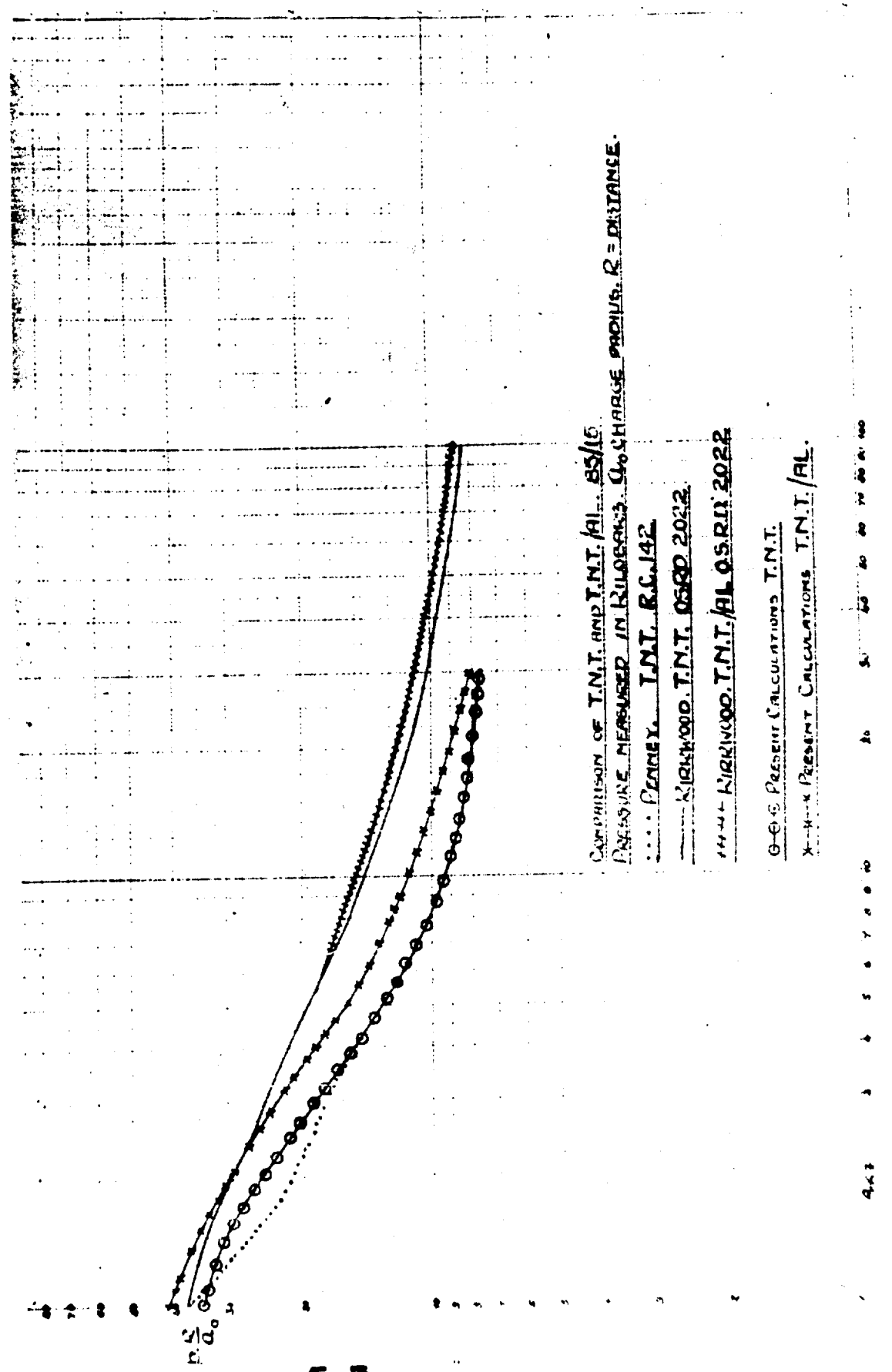


FIG. 3.

Best Available Copy

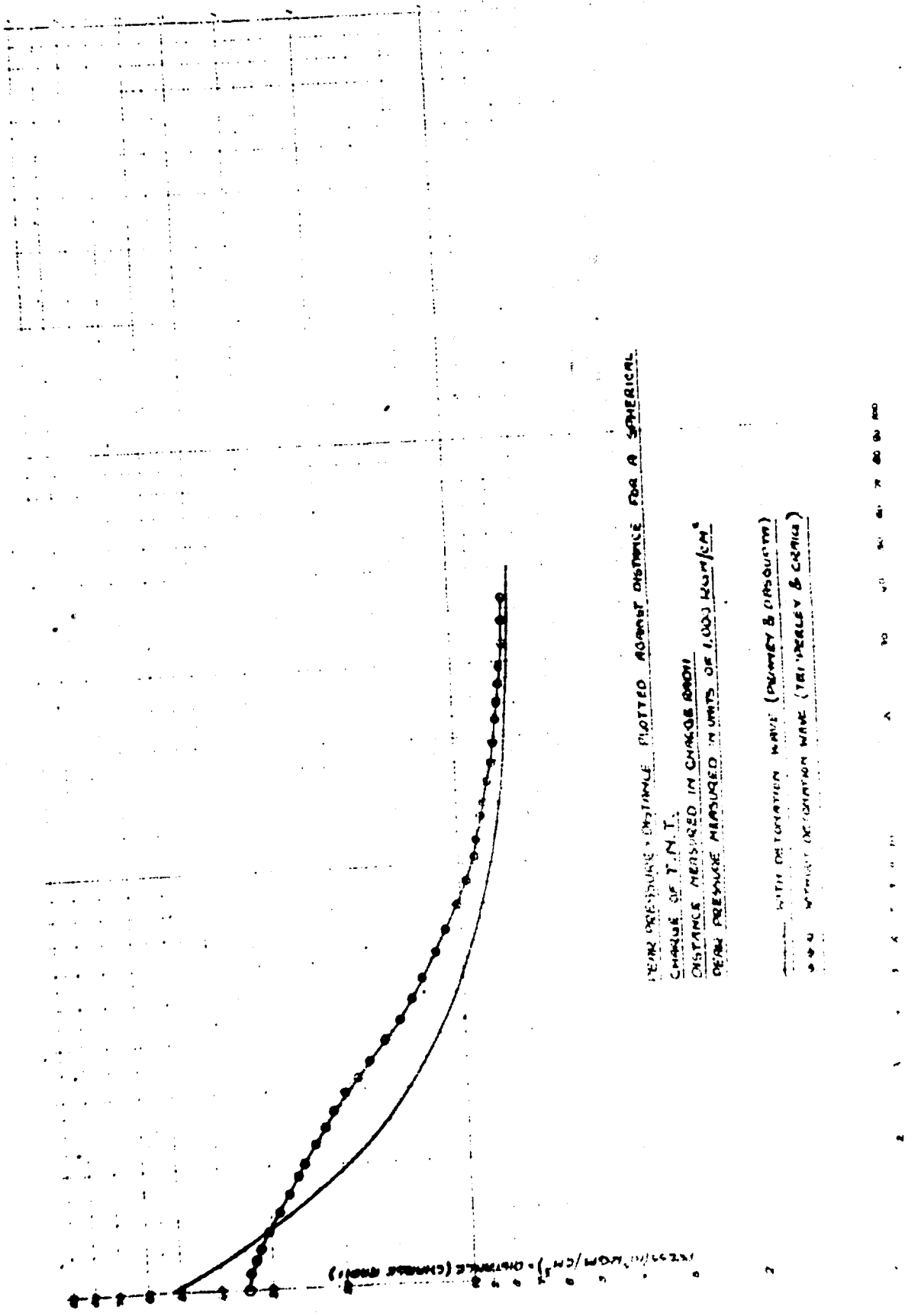


Fig. 4.

Best Available Co

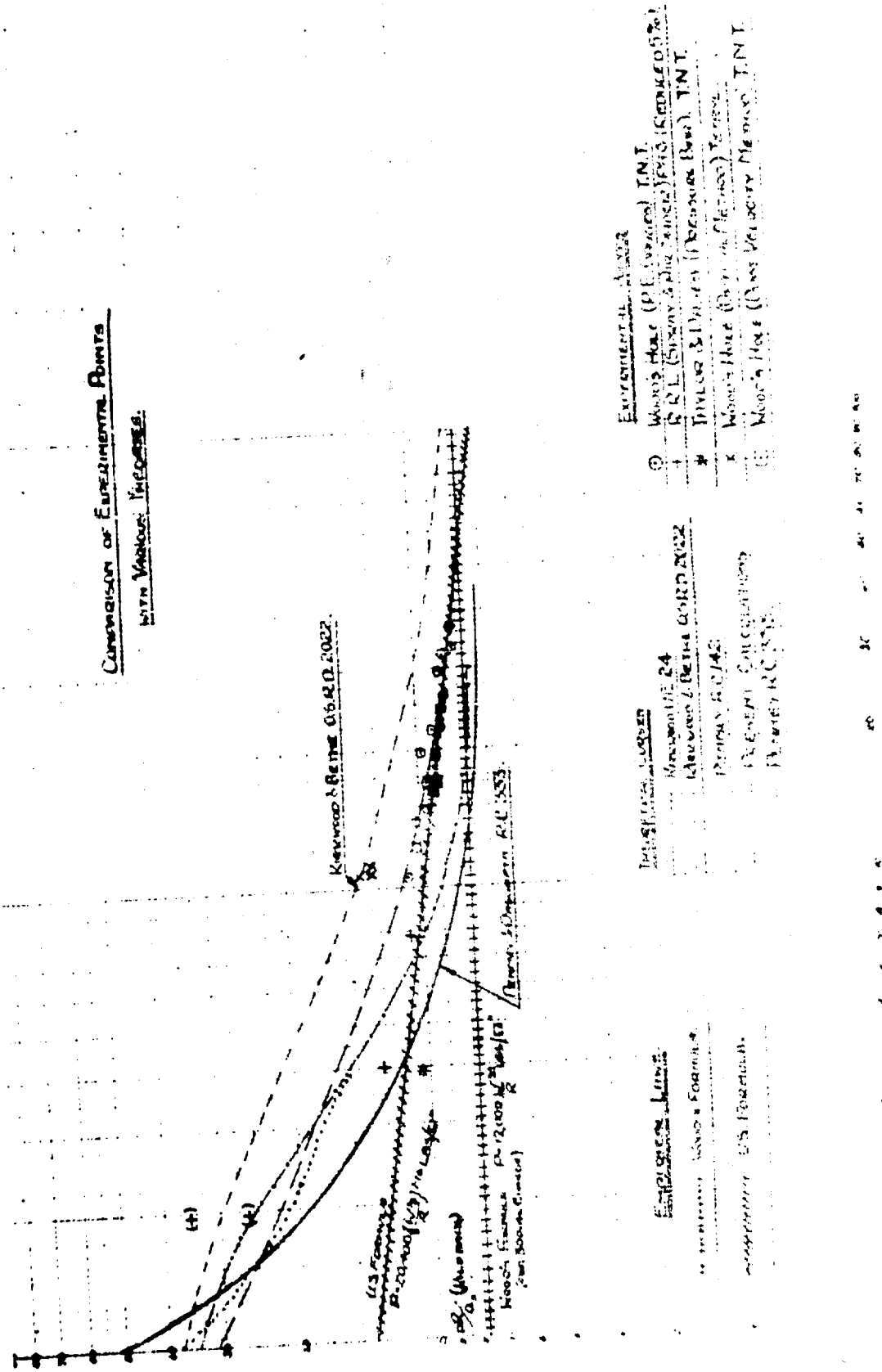

Comparison of Experimental Points
with Various Theories
Kenwood Report 05.12.2022
Experimental Data
Best Available Co

Fig. 5

Best Available Copy

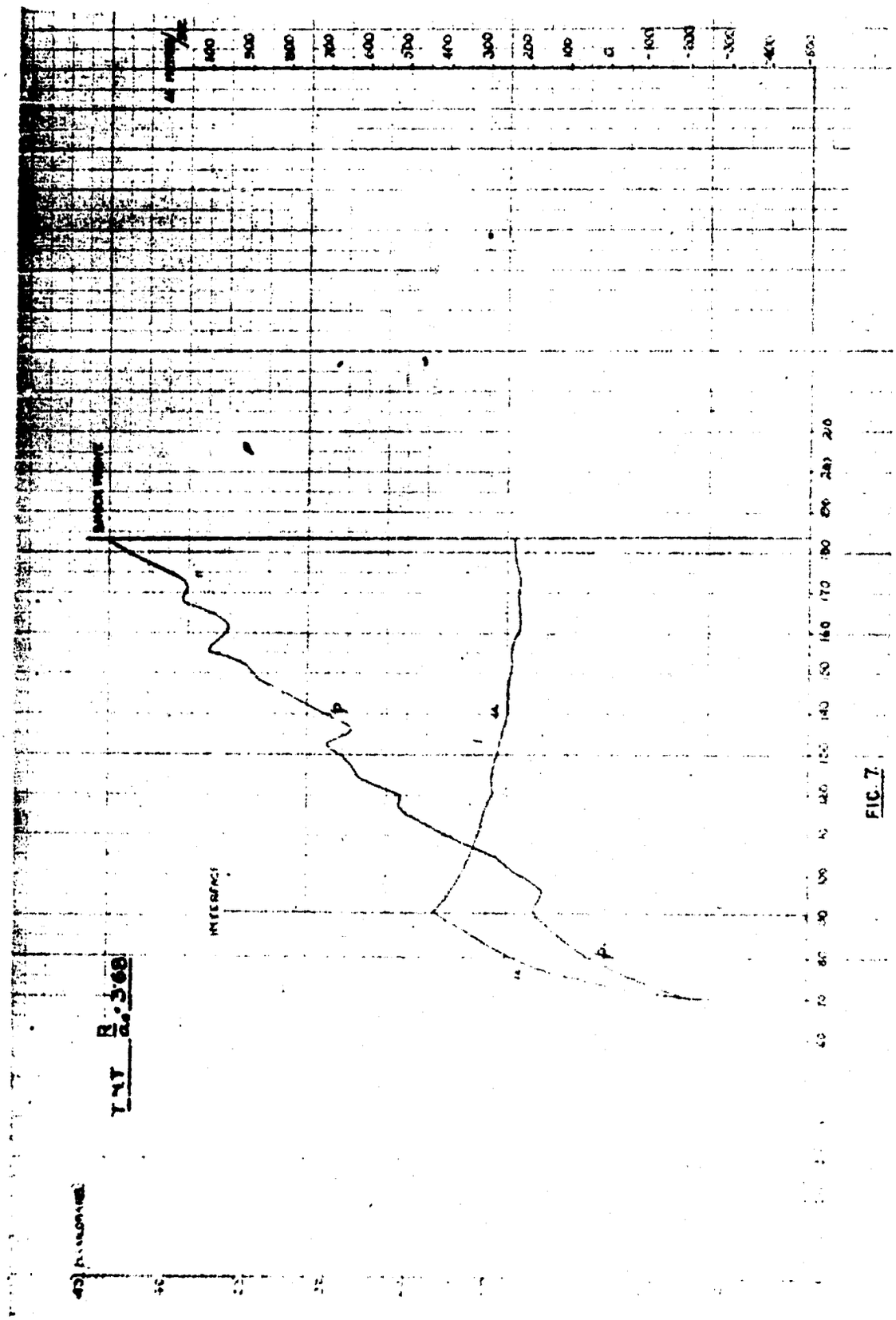
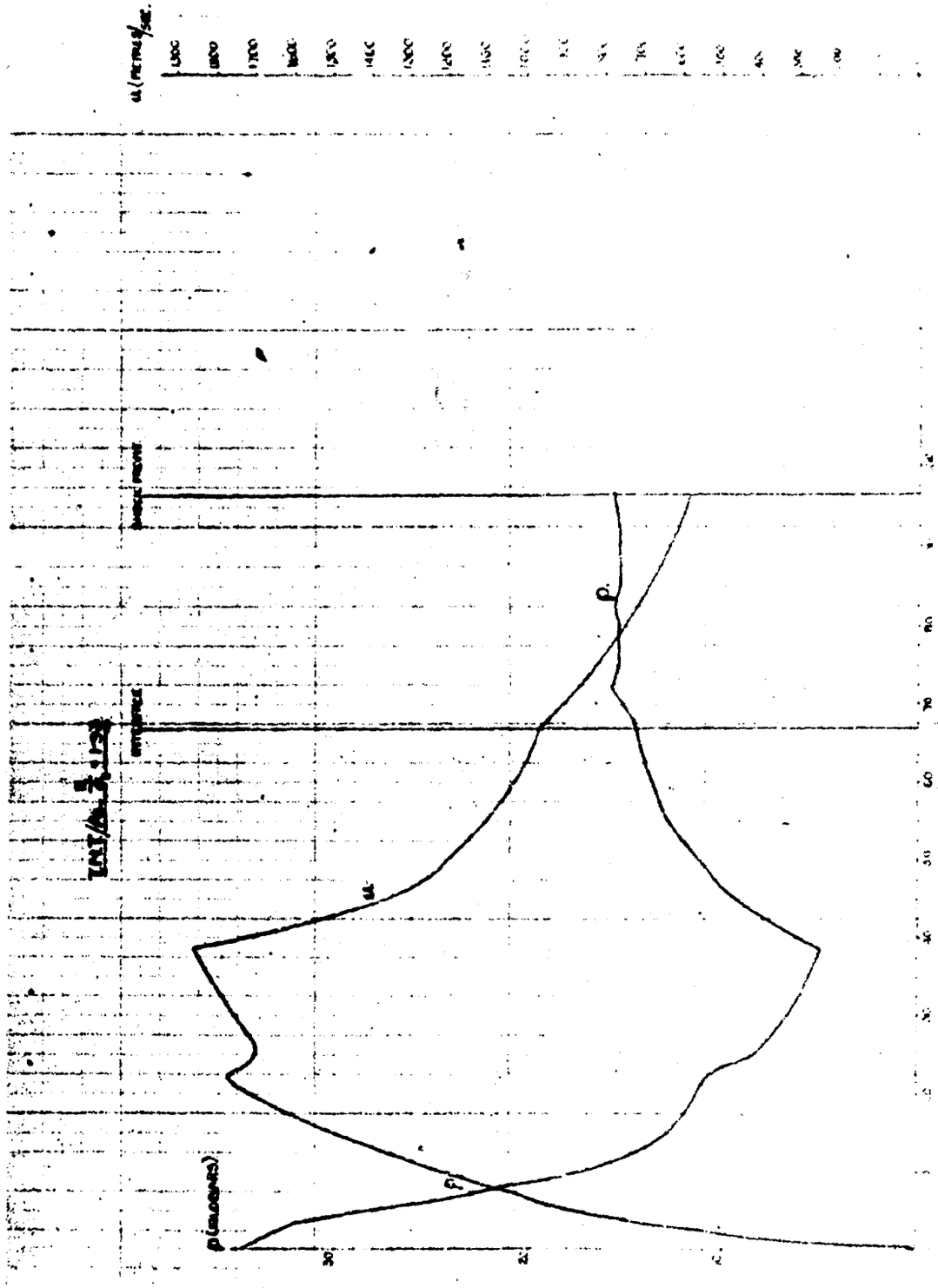


FIG. 7

Best Available Copy

Best Available Copy



Best Available Copy

FIG 10

Best Available Copy

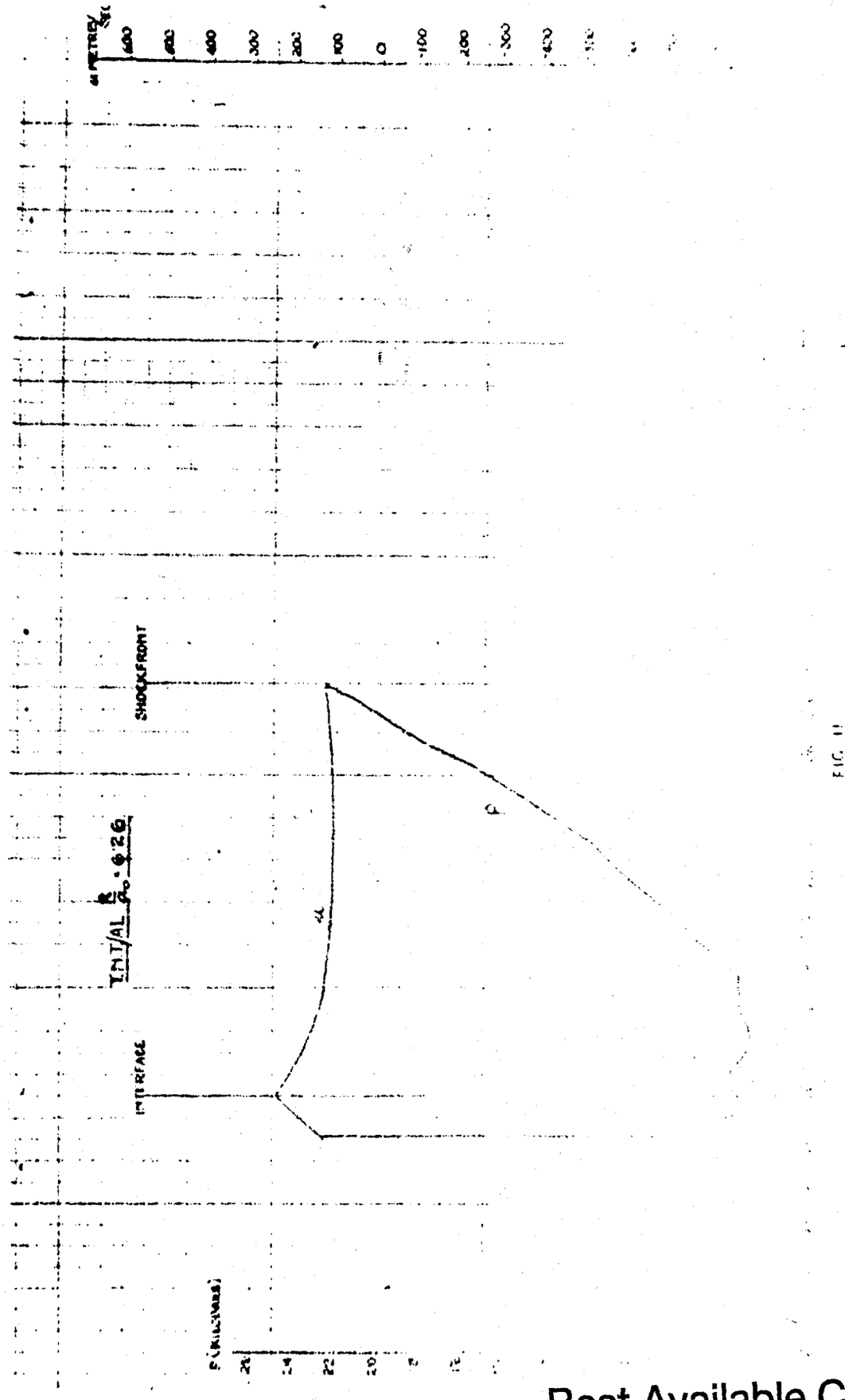


FIG. 11

Best Available Copy

HYDRODYNAMIC PROPERTIES OF SEA WATER AT THE FRONT OF A SHOCK WAVE

J. M. Richardson
Cornell University, N. Y.

and

A. B. Arons and R. R. Halverson
Underwater Explosives Research Laboratory
Woods Hole Oceanographic Institution

American Contribution

2 June 1947

Reprinted from THE JOURNAL OF CHEMICAL PHYSICS,
Vol. 15, No. 11, pp. 785-794, November 1947

Reprinted from THE JOURNAL OF CHEMICAL PHYSICS, Vol. 15, No. 11, 785–794, November, 1947
Printed in U. S. A.

Hydrodynamic Properties of Sea Water at the Front of a Shock Wave*

J. M. RICHARDSON**
Baker Laboratory, Cornell University, Ithaca, N. Y.

AND

A. B. ARONS*** AND R. R. HALVERSON****
Underwater Explosives Research Laboratory, Woods Hole Oceanographic Institution, Woods Hole, Massachusetts

(Received June 2, 1947)

The Rankine-Hugoniot relations have been applied to appropriate equation-of-state data in order to calculate the propagation velocity, particle velocity, enthalpy increment, Riemann function, etc. at shock fronts of various amplitudes in sea water. One set of tables provides values over a wide pressure range (up to about 80 kilobars) and is principally intended for use in conjunction with theories of propagation of shock waves originated by underwater explosions. A second set of tables contains values which are closely spaced up to pressures of 14 kilobars. These are calculated with somewhat greater precision and are intended for use in connection with experimental measurements of particle and propagation velocities, etc.

I. INTRODUCTION

IT has long been recognized that the velocity of propagation of sound waves of finite amplitude in a fluid medium is a function of the pressure in the wave. Lamb[1] ascribes the early development of the theory to independent investigations of Earnshaw and Riemann. Qualitatively this work indicated that, since the higher pressure portions of a wave travel with greater velocity, an arbitrarily-shaped pressure pulse of finite amplitude must, during propagation, alter its shape in such a manner as to build up into a shock front. By applying the laws of conservation of mass, energy, and momentum to the transfer of matter across the shock front, Rankine and Hugoniot obtained a set of three relations among the five variables: pressure, density, particle velocity (u), shock front

* The work described in this report was performed under National Defense Research Committee Contracts OEMsr-121 with Cornell University and OEMsr-569 with the Woods Hole Oceanographic Institution.
** Present address: Bell Telephone Laboratories, Inc., Murray Hill, N. J.
*** Present address: Department of Physics, Stevens Institute of Technology, Hoboken, N. J.
**** Deceased.
[1] H. Lamb, *Hydrodynamics* (Cambridge University Press, London, 1932) 6th Ed., p. 481.

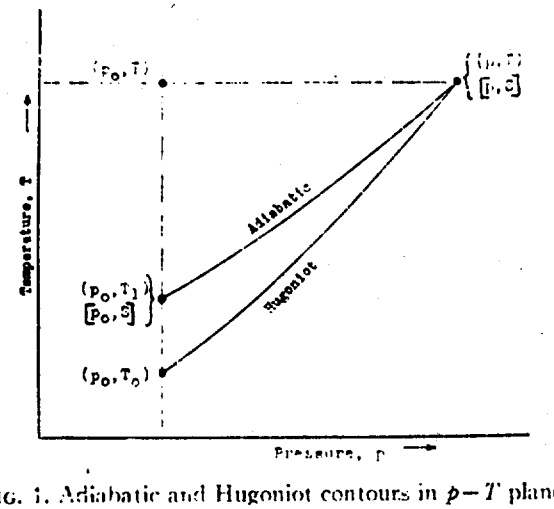


FIG. 1. Adiabatic and Hugoniot contours in $p-T$ plane.

velocity (U), and enthalpy increment (ΔH). These relations, when applied to data on the equation-of-state and specific heat, make it possible to calculate u, U, and ΔH and to evaluate certain other functions applicable to the theory of the formation and propagation of shock waves originated by explosions.[2]

Precise knowledge of u and U also makes it possible to calculate shock wave pressures in cases where the particle velocity or propagation velocity can be measured. The purpose of the calculations described below was to apply the Hugoniot relations to appropriate equation-of-state data for sea water in order to provide (a) tables of the desired functions up to very high pressures (*ca.* 80 kilobars) for use in the theory of propagation of underwater explosion waves,[2] and (b) tables of particle and propagation velocity at fairly close pressure intervals in a lower pressure region (up to *ca.* 14 kilobars).

II. OUTLINE OF THE THEORY AND COMPUTATIONAL PROCEDURES

In this section we give an account of the hydrodynamical and thermodynamical relations, and the computational procedures leading to the numerical results tabulated in Sections III and IV. For the convenience of the reader a glossary of symbols is presented in Appendix III.

When a shock wave advances with velocity U into a stationary fluid of unperturbed pressure p_0 and specific volume v_0, the pressure p, specific volume v, and particle velocity u of the fluid behind the shock front are determined by the Rankine[3]-Hugoniot[4] conditions, which express the conservation of mass, momentum, and energy of an element of fluid passing through the front. For the purposes of this paper, these conditions may conveniently be written

$$u=[(p-p_0)(v_0-v)]^{\frac{1}{2}}, \tag{2.1}$$

$$U=v_0[(p-p_0)/(v_0-v)]^{\frac{1}{2}} \tag{2.2}$$

$$\Delta H=(1/2)(p-p_0)(v+v_0). \tag{2.3}$$

In the last equation, ΔH is the specific enthalpy increment of an element of fluid when it passes through the front. The specific enthalpy is defined as the sum of the internal energy per gram and the pressure-volume product, pv.

Given equation of state and specific heat data for the fluid, any three of the variables p, v, U and u may be determined as functions of the fourth. Here we shall regard p as the independent variable. For certain hydrodynamic applications we must have, in addition to v, U, and u as functions of p, the sound velocity

$$c=(\partial p/\partial \rho)^{\frac{1}{2}}{}_S; \quad \rho=1/v, \tag{2.4}$$

the Riemann σ-function†

$$\sigma=\int_{p_0}^{p}[v[p', S]/c[p', S]]dp', \tag{2.5}$$

and the undissipated enthalpy

$$\omega=\int_{p_0}^{p}v[p', S]dp', \tag{2.6}$$

where S is the entropy.

In practice, one must resort to successive approximations to effect a reduction of the Hugoniot conditions, combined with equation-of-state and specific heat data, to a set of relations expressing u, U, and v as functions of p. To this

[2] J. G. Kirkwood and H. Bethe, *The Pressure Wave Produced by an Underwater Explosion* (Dept. of Commerce Bibliography No. PB 32182, OSRD Report No. 588, Part I.

[3] W. J. M. Rankine, Trans. Roy. Soc. London, **A160**, 277 (1870).

[4] H. Hugoniot, J. de l'ecole polyt. **51**, 3 (1887); **58**, 1 (1888).

† The Riemann σ-function occurs in Riemann's form of the hydrodynamical equations, which, for the case of spherical symmetry, may be written (see reference 1):

$$[(\partial/\partial t)+(c+u)(\partial/\partial r)](\sigma+u)=-2cu/r,$$
$$[(\partial/\partial t)-(c-u)(\partial/\partial r)](\sigma-u)=0,$$

where t is the time and r is the radial coordinate. The other quantities have already been defined.

Best Available Co

end, it is expedient first to consider certain quantities as functions of pressure and temperature, p and T, or pressure and entropy, p and S. Before proceeding to a more detailed discussion of the calculations it may perhaps help to orient the reader if we consider, qualitatively, contours of some pertinent quantities in the p–T plane. In Fig. 1, the possible states of a given fluid just behind the shock front lie along a single curve, which we have labeled "Hugoniot." An element of fluid initially in the state (p_0, T_0) which has attained a state (p, T) just behind the shock front finally returns to a state (p_0, T_1) along the adiabatic, so labeled in the figure. Also included are the designations of a few points on a p–S basis using square brackets according to the convention introduced in Part b of this section. In general, T_1 is larger than T_0 because of the dissipation occuring at the front. The central part of our problem is the determination of the Hugoniot curve.

We shall consider in Part a the calculations due to Arons and Halverson[5] which are intended to be accurate in the range of relatively low pressure (*ca.* 0 to 20 kilobars). These results as stated in the introduction are intended for the determination of the peak pressure of a shock wave from measured values of the shock front velocity U or particle velocity u. In Part b, we shall consider the calculations of Kirkwood and Richardson,[6] the results of which were originally intended for the applications of the shock wave propagation theory of Kirkwood and Bethe[2] which required data over a higher range of pressures (*ca.* 20 to 50 kilobars).

a. Calculations of Arons and Halverson

Here we outline the calculations[7] suitable for the relatively low pressure range (*ca.* 0 to 20 kilobars) based upon the equation-of-state and specific heat data discussed in detail in Appendix I. For the range 0 to 1.5 kilobars, the Ekman equation-of-state was used; in the range 0 to 25 kilobars, the Tait equation-of-state,

$$v(0, T)-v(p, T)/v(0, T) = (1/n)\log[1+p/B(t)], \quad t=(T-273.16)^\circ\text{C}. \tag{2.7}$$

In the first case, the initial temperature was $t_0=15^\circ$C; in the second, $t_0=25^\circ$C. In both cases, the initial pressure $p_0=0$. Neither of the two equations-of-state are complete in the sense that $v_0=v(0, T)$ must be determined by auxiliary thermal expansion data (also discussed in Appendix I).

We express the enthalpy and volume increments

$$\begin{aligned}\Delta H &= H(p, T)-H(0, T_0),\\ \Delta v &= v(p, T)-v(0, T_0),\end{aligned} \tag{2.8}$$

in terms of line integrals, first along an isobar from $(0, T_0)$ to $(0, T)$ and, secondly, along an isotherm from $(0, T)$ to (p, T) (see Fig. 1). For the enthalpy increment we obtain

$$\begin{aligned}&\Delta H=\Delta_p H+\Delta_T H,\\ &\Delta_p H=\int_{T_0}^{T} C_p(0, T')dT'=\bar{c}_p\Delta T,\\ &\Delta_T H=\int_0^p\left[v(p', T)-T\frac{\partial v(p', T)}{\partial T}\right]dp',\\ &\Delta T=T-T_0,\end{aligned} \tag{2.9}$$

where $c_p(0, T)$ is the specific heat extrapolated to zero pressure and $\bar{c}_p$ is the mean of c_p over the temperature range ΔT.

For the volume increment we obtain

$$\begin{aligned}&\Delta v=\Delta_p v+\Delta_T v,\\ &\Delta_p v=v(0, T)-v(0, T_0)=\bar{\beta}_0\Delta T,\\ &\Delta_T v=v(p, T)-v(0, T),\end{aligned} \tag{2.10}$$

where $\bar{\beta}_0$ is the mean thermal expansion at zero pressure over the temperature range ΔT.

From the last Hugoniot condition, Eq. (2.3), and Eq. (2.9) we obtain

$$\Delta T=\frac{[v(0, T_0)+(1/2)(\Delta_T v)]p-\Delta_T H}{\bar{c}_p-(1/2)(\bar{\beta}_0 p)}, \tag{2.11}$$

where $\Delta_T H$ is to be calculated by means of the third of Eq. (2.9) and the appropriate equation-of-state, and where $\Delta_T v$ is to be obtained from compressibility data. The right-hand side of Eq. (2.11) depends, of course, on the temperature T. The determination of ΔT is accomplished by the method of successive approximations. A trial

[5] A. B. Arons and R. R. Halverson, *Hugoniot Calculations for Sea Water at the Shock Front*, OSRD Report No. 6377, NDRC No. A-469.

[6] J. G. Kirkwood and J. M. Richardson, *The Pressure Wave Produced by an Underwater Explosion, Part III*, OSRD Report No. 813 (Dept. of Commerce Bibliography No. PB 32184).

[7] J. G. Kirkwood and E. Montroll, *Pressure Wave Produced by an Underwater Explosion, II*, OSRD Report No. 676 (Dept. of Commerce Bibliography PB-32183).

TABLE I. $U-c_0/c_0$, u, and ΔH in low pressure region (based on Ekman equation-of-state). Sea water: Initial temperature 15°C; salinity 32 parts per thousand (3.79 wt. percent NaCl); $c_0 = 4922.8$ ft/sec = 1500.5 m/sec.

A				B			
$p-p_0$ (kbar)	$\frac{U-c_0}{c_0}$ (%)	u (m/sec)	ΔH (cal/gm)	$p-p_0$ (lb/in²)	$\frac{U-c_0}{c_0}$ (%)	u (ft/sec)	ΔH (cal/gm)
0.00	0.00	0.0	0.0	0	0.00	0.0	0.0
.25	2.07	15.1	5.8	2,000	1.14	29.1	3.2
.50	4.03	31.2	11.5	4,000	2.27	57.6	6.4
.75	5.93	46.2	17.2	6,000	3.35	85.5	9.6
1.00	7.81	60.5	23.0	8,000	4.43	112.9	12.7
1.25	9.65	74.4	28.5	10,000	5.48	139.7	15.9
1.50	11.44	87.7	34.1	12,000	6.53	166.0	19.0
				14,000	7.56	191.8	22.1
				16,000	8.58	217.1	25.2
				18,000	9.59	242.0	28.3
				20,000	10.57	266.5	31.3
				22,000	11.55	290.6	34.5

TABLE II. $U-c_0/c_0$, u, and ΔH in intermediate pressure region (1.5 to 25 kilobars) (based on Tait equation-of-state; $n = 7.800$, $B = 3.012$). Sea water: Initial temperature 25°C; salinity 32 parts per thousand (3.79 wt. percent NaCl): $c_0 = 5014.7$ ft/sec = 1528.5 m/sec.

A				B			
$p-p_0$ (kbar)	$\frac{U-c_0}{c_0}$ (%)	u (m/sec)	ΔH (cal/gm)	$p-p_0$ (lb/in²)	$\frac{U-c_0}{c_0}$ (%)	u (ft/sec)	ΔH (cal/gm)
0.0	0.00	0.0	0.0	0	0.0	0	0.0
1.0	8.18	59.2	23.0	20,000	11.0	258	31.3
1.5	11.88	85.5	31.2	30,000	15.8	375	46.6
2.0	15.39	110.1	45.3	40,000	20.5	483	62.0
2.5	18.71	135.0	56.3	50,000	24.7	584	77.0
3.0	21.86	157.8	67.2	60,000	28.7	676	92.0
4.0	27.84	200.5	88.8	70,000	32.5	767	107.0
5.0	33.39	240.2	110.1	80,000	36.0	853	121.0
6.0	38.59	277.5	131.2	90,000	39.1	937	135.0
8.0	48.13	346.1	172.9	100,000	42.8	1014	150.0
10.0	56.73	408.9	214.0	120,000	49.2	1168	178.0
12.0	64.70	466.9	254.8	140,000	55.2	1312	207.0
14.0	72.25	510.9	295.2	160,000	60.8	1445	235.0
25.0	108.40	769.1	514.4	180,000	66.3	1564	263.0
				200,000	71.5	1662	291.0

value of ΔT is used in evaluating the right-hand side giving a more accurate value of ΔT on the left-hand side, and the process is repeated until the results of two successive steps differ by a sufficiently small amount. One or two steps generally suffice.

We have thus obtained T as a function of p along the Hugoniot curve (see Fig. 1). It is now possible to calculate immediately the particle velocity u, the propagation velocity U, and the specific volume v as functions of p behind the shock front. The results using the Ekman equation-of-state and the Tait equation-of-state are tabulated in Tables I and II, respectively, of Section III.

b. The Calculations of Richardson and Kirkwood

Here we outline the calculations[4] intended for the applications of the shock wave propagation theory of Kirkwood and Bethe.[3] These are based upon the equation-of-state and specific heat data discussed in detail in Appendix II. We use a modified Tait equation-of-state connecting $v(p, T)$ and $v(0, T)$ to be discussed below. In most respects, the data is made to fit the properties of an aqueous 0.7 molal NaCl solution assumed to be roughly equivalent to sea water of salinity $s = 32$ parts per thousand (see Section 1 of Appendix I).

In these calculations the initial pressure p_0 is taken to be zero, and several different initial temperatures T_0 are used: 0°C, 20°C, and 40°C.

Before indicating the precise nature of the modification of the Tait equation, it is desirable to mention that in this part two different pairs of independent variables will be used: pressure and temperature (p, T), and pressure and entropy $[p, S]$. Consequently, in order to indicate which pair are used in a function, we will use parenthesis to indicate the first pair and square brackets to indicate the second, i.e. $v(p, T)$ and $v[p, S]$.

The modified form of Tait equation introduced by Kirkwood[2,6] is

$$\log(v_1/v) = (1/n)\log(1+p/A[S]), \quad (2.12)$$

where

$$v = v[p, S] = v(p, T[p, S]), \quad v_1 = v[0, S],$$

(see Fig. 1) n is an empirical constant, and the function $A[S]$ is related to the function $B(t)$ in the original isothermal form of the Tait equation, Eq. (2.7), as follows,

$$A[S] = B(t[0, S]), \quad t = (T-273.16)°\text{C}. \quad (2.13)$$

The reasons for introducing this modification of the Tait equation are at least twofold: (1) the anomaly of a vanishing specific volume $v(p, T)$ at a finite pressure along a given adiabatic (which does not differ markedly from the Hugoniot curve in the case of water) is removed to a higher pressure by replacing $[v(0, T)-v(p, T)]/[v(0, T)]$

TABLE III. Values of $U-c_0/c_0$ for different temperatures and salinities at a shock wave peak pressure of 1.00 kilobar.

Salinity (parts per thou)	Temperature (°C)	$\frac{U-c_0}{c_0}$ (%)
32	15	7.81
32	25	7.81
35	15	7.76

by $\log(v[0, S]/v[p, S])$, and (2) the calculation of quantities defined by line integrals along adiabatics is greatly simplified by taking S instead of T as one of the independent variables.

The function $A[S]$ is related simply to c_1, the sound velocity at zero pressure and entropy S according to Eq. (2.4) as follows

$$A[S]=c_1^2/nv_1; \quad c_1=c[0, S]. \tag{2.14}$$

On the basis of Bridgman's p–v–T data for pure water, an average value of n equal to 7.15 has been selected for the present calculations. In Section 2 of Appendix II, it is shown that n deviates from this value by less than 4 percent in a large pressure-temperature field bounded by adiabatics starting at zero pressure and temperatures of 20°C and 60°C, respectively, and extending to pressures of 25,000 kg/cm². We assume that n has the same value for an aqueous 0.7 molal NaCl solution as for pure water, and we obtain by interpolation the required values of $B(t)$ from R. E. Gibson's values of $B(t)$ for dilute aqueous NaCl solutions (see Appendix II, Section 1). The appropriate heat capacity and thermal expansion data are discussed in Section 1 of Appendix II.

We now proceed to the calculation of the quantities u, U, c, σ, and ω. We first express these quantities with use of Eq. (2.12) in terms of p,

$$v=v(p, T)=v[p, S], \quad v_0=v(0, T_0),$$

$v_1=v(0, T_1)=v[0, S]$, and $c_1=c(0, T_1)=c[0, S]$ (see Eqs. (2.1)–(2.6), also Fig. 1) as follows:

$$u=[p(v_0-v)]^{\frac{1}{2}}, \tag{2.15}$$

$$U=pv_0/u, \tag{2.16}$$

$$c=c_1(v_1/v)^{(n-1)/2}, \tag{2.17}$$

$$\sigma=\frac{2c_1}{n-1}[(v_1/v)^{(n-1)/2}-1], \tag{2.18}$$

$$\omega=\frac{c_1^2}{n-1}[(v_1/v)^{n-1}-1], \tag{2.19}$$

Once the temperature T_1, to which an element of fluid returns along the adiabatic intersecting the Hugoniot curve at (p, T), is determined, all of the above quantities may be determined as functions of p. To accomplish this, the enthalpy increment, ΔH, occurring in the third Hugoniot condition, Eq. (2.3), is written as the sum of two line integrals, the first along an isobar from $(0, T_0)=[0, S_0]$ to $(0, T_1)=[0, S]$ and the second along an adiabatic from $(0, T_1)=[0, S]$ to $(p, T)=[p, S]$ (see Fig. 1), giving:

$$\Delta H=\omega+h,$$

$$\omega=\int_0^{p} v[p', S]dp', \tag{2.20}$$

$$h=\int_{S_0}^{S} T[0, S']dS'=\int_{T_0}^{T_1} c_p(0, T')dT',$$

where ω is the undissipated enthalpy already defined by Eq. (2.6) with $p_0=0$ and given explicitly in terms of c_1, v_1, and v in Eq. (2.19). The dissipated enthalpy h can be determined as an explicit function of T_0 and T_1 from specific heat data (Appendix II, Section 1). Combining the third Hugoniot condition, Eq. (2.3), with Eqs. (2.19) and (2.20) we obtain the relation

$$\frac{h}{c_1^2}=\frac{1}{2n}\left[y-\frac{n+1}{n-1}(y^{(1-1/n)}-1)-y^{-1/n}\right]-\frac{v_1-v_0}{2nv_1}(y-1), \tag{2.21}$$

TABLE IV. Properties of sea water at a shock front. (Initial temperature 0°C; salinity 0.7 m NaCl; $C_0=1443$ m/sec.)

p (kilobar)	u (m/sec)	U (m/sec)	c (m/sec)	σ (m/sec)	$\omega\times10^{-6}$ (m/sec)²	h (Joule/gm)	v (cm³/gm)
0	0	—	—	0	0	0	0.9915
5	257.0	1930	2190	253.5	0.4565	6.740	.8593
10	433.0	2290	2720	420.5	0.8720	25.80	.8040
15	575.0	2585	3145	552.0	1.270	54.40	.7710
20	697.5	2845	3510	664.0	1.655	86.55	.7483
25	805.5	3075	3835	763.5	2.030	122.5	.7319
30	905.0	3285	4125	855.5	2.405	160.5	.7186
35	997.0	3480	4395	940.5	2.770	201.5	.7075
40	1080	3665	4640	1020	3.140	244.0	.6989
50	1240	4000	5095	1175	3.860	331.0	.6842
60	1385	4300	5495	1315	4.575	419.0	.6728
70	1515	4585	5870	1455	5.285	509.0	.6641
80	1635	4855	6225	1585	6.000	595.5	.6579
90	1740	5120	6570	1705	6.730	676.0	.6542

TABLE V. Properties of sea water at a shock front. (Initial temperature 20°C; salinity 0.7 m NaCl; $C_0=1517$ m/sec.)

p (kilobar)	u (m/sec)	U (m/sec)	c (m/sec)	σ (m/sec)	$\omega\times10^{-6}$ (m/sec)²	h (Joule/gm)	v (cm³/gm)
0	0	—	—	0	0	0	0.9929
5	251.0	1975	2230	248.5	0.4395	5.570	.8668
10	425.5	2335	2785	415.5	0.8790	23.45	.8120
15	567.0	2630	3175	549.0	1.280	49.35	.7787
20	689.0	2880	3515	663.0	1.670	80.05	.7555
25	798.0	3110	3853	765.0	2.050	115.0	.7381
30	897.5	3320	4140	859.0	2.425	152.5	.7251
35	990.0	3510	4405	946.5	2.795	192.0	.7150
40	1075	3697	4650	1030	3.160	233.0	.7064
50	1235	4020	5100	1185	3.885	317.5	.6930
60	1380	4325	5505	1330	4.605	404.5	.6765
70	1510	4610	5880	1465	5.320	489.5	.6659
80	1625	4885	6240	1600	6.030	573.5	.6626

TABLE VI. Properties of sea water at a shock front. (Initial temperature 40°C; salinity 0.7 m NaCl.)

p (kilobars)	u (m/sec)	U (m/sec)	c (m/sec)	σ (m/sec)	$\omega \times 10^{-6}$ (m/sec)^2	h (joule/gm)	v (cm^3/gm)
0	0	—	—	0	0	0	0.9991
5	249.5	2005	2255	247.0	0.1630	5.59	.8749
10	423.5	2360	2775	415.0	0.4870	22.75	.8198
15	566.5	2645	3195	550.0	1.290	48.30	.7859
20	699.0	2900	3550	666.5	1.685	79.70	.7621
25	798.5	3130	3865	770.5	2.065	113.5	.7451
30	899.0	3335	4150	866.0	2.445	151.0	.7298
35	992.0	3525	4415	955.5	2.815	189.5	.7179
40	1080	3705	4660	1040	3.185	230.5	.7080
50	1240	4035	5110	1200	3.915	315.0	.6926
60	1380	4340	5515	1345	4.640	400.5	.6813
70	1510	4635	5900	1485	5.370	483.0	.6737

where $y=(v_1/v)^n$. With the aid of tables of n/c_1^2 and v_1 as functions of T_1 and T_0, Eq. (2.21) may be solved by successive approximations giving T_1 as a function of the parameter y. Since the equation of state, Eq. (2.12), may be expressed simply as $p=B(T_1-273.16)[y-1]$, the temperature T_1 may be determined as a function of the pressure p by a tabular elimination of y. By graphical interpolation, T_1 is finally determined for the desired integral values of p (in kilobars), and the functions u, U, c, σ, and ω are then computed as functions of p by means of Eqs. (2.15)–(2.19).

III. NUMERICAL RESULTS OF ARONS AND HALVERSON

In fundamental shock wave studies, it is frequently necessary to know values of $U-c_0/c_0$ and u at given pressure levels to the highest possible degree of accuracy. With this object in view, the calculation methods described in Section 2A were applied to the best available equation-to-state data. The numerical results are given in Tables I and II. A critical discussion of the equation-of-state data will be found in Appendix I together with references to the sources from which they were obtained.

Table I gives results for the "low pressure" region, covering shock wave peak pressures of from 0 to 1.50 kilobars (*ca.* 22,000 p.s.i.). The calculations in this table were based upon the Ekman equation-of-state for sea water (see Appendix I) which is used in the calculation of sound velocity for echo-ranging tables.

Since the Ekman equation deviates appreciably from experimental compressibility data at pressures exceeding 2 kilobars, this equation was abandoned in the "intermediate pressure" region. The results in Table II are applicable principally to the region between 1.5 and 14 kilobars (*ca.* 200,000 p.s.i.) and are based on a careful fit of the Tait equation to Adams's experimental compressibility data (see Appendix I).

Tables I and II were computed for certain specific values of temperature and sea water salinity (equivalent to 0.675 molal NaCl), and it is shown in Table III that the value of $U-c_0/c_0$ is not very sensitive to changes in these variables.

IV. NUMERICAL RESULTS OF KIRKWOOD AND RICHARDSON

In Tables IV to VI, the particle velocity u, the shock front velocity U, the sound velocity c, the Riemann σ-function, the undissipated enthalpy ω, the dissipated enthalpy h, and the specific volume v of sea water (0.7 molal NaCl solution) are presented as functions of pressure p along three Hugoniot curves, starting at zero pressure and the temperatures 0°C, 20°C and 40°C, respectively. These results have been calculated by the procedures of Part b of Section 2 and the data of Appendix II. The results above 30 kilobars represent extrapolations beyond the range of experimental data: consequently the validity of the results above, say, 50 kilobars, is questionable.

In closing this discussion of the calculations, the authors wish to acknowledge their gratitude and appreciation to Professor J. G. Kirkwood of Cornell University for his contributions in initiating the work and in supplying valuable guidance and advice.

APPENDIX I††

1. Salinity and Temperature Conditions

All calculations were made for sea water having a salinity of 32 parts per thousand (the average salinity of sea water at Woods Hole, Massachusetts). Salinity is defined in terms of directly measured chlorinity as:

$$s=0.030+1.8050\ \mathrm{Cl}$$

where s and Cl are expressed in parts per thousand.

It was calculated from the average composition

†† Equation-of-state data used in computation of Tables I and II.

Best Available Co

of sea water that (on the basis of *ionic strength*) a salinity of 32 parts per thousand is equivalent to an NaCl solution having a molality of 0.675 or a weight percentage of 3.79 percent NaCl.

Table I was computed for an initial temperature of 15°C because this temperature is a rough average of conditions normally encountered in experimental work. Table II was computed for an initial temperature of 25°C because this was the temperature quoted for the available compressibility data.[8] Table III shows that the results are not sensitive to small variations in temperature and salinity.

2. Specific Volume and Coefficient and Thermal Expansion

The best sources of data seem to be the oceanographical tables of Knudsen.[9] Second power equations in t(°C) were fitted to the data tabulated for $s=32$:

For Table I:

$$v(t)=0.97709+2.05\times10^{-4}(t-15)+4\times10^{-6}(t-15)^2.$$

For Table II:

$$v(t)=0.97956+2.85\times10^{-4}(t-25)+4\times10^{-6}(t-25)^2.$$

3. Heat Capacity

The heat capacity data used in computing Tables I and II are those quoted by S. Kuwahara:[10]

$$C_p=C_{p'}-0.0004226t+0.000006321t^2 \text{ cal./gm°C},$$

TABLE VII. Comparison of experimentally measured sound velocity with calculations based on the Ekman Compressibility Equation. (Salinity = 31.7 parts per thousand.)

Temperature (°C)	Velocity of sound (ft/sec) Measured	Calculated	Deviation (%)
10.9	4887.7	4875.6	0.26
11.6	4885.8	4883.8	0.04
11.6	4 93.1	4883.8	0.19
11.5	4902.4	4882.5	0.41
11.1	4888.3	4878.5	0.20

[8] Adams, J. Am. Chem. Soc. **53**, 3769 (1931).
[9] *Oceanographical Tables*, Comissariat of Agriculture, USSR, Moscow, 1931. (A general compilation of oceanographic data by N. N. Zubov.)
[10] S. Kuwahara, *Velocity of Sound in Sea Water and Calculation of the Velocity for Use in Sonic Sounding* (Hydrographic Dept. I.J.N. Tokyo, 1938).

TABLE VIII. Comparison of Adams's experimental compressibilities and the empirical fit given by the Ekman and Tait equations

	$(v_0-v)/v_0$				
	Adams (experimental)		Ekman equation	Tait* equation	
P (kbar)	Pure H_2O	3.79% NaCl	$S=32$ (Table I)	$n=7.800$ $B=3.012$ (Table II)	$n=7.445$ $B=3.156$
0.0	0.0000	0.0000	0.0000	0.0000	0.0000
0.5	.0212	.0196	.0198	.0197	.0198
1.0	.0393	.0368	.0370	.0368	.0370
1.5	.0555	.0522	.0522	.0518	.0522
2.0	.0699	.0658	.0655	.0653	.0659
3.0	.0945	.0894	.0871	.0887	.0897
4.0	.1152	.1091	—	.1083	.1095
5.0	.1330	.1265	—	.1254	.1275
6.0	.1485	.1417	—	.1405	.1431
7.0	.1622	.1552	—	.1540	.1569
8.0	.1746	.1670	—	.1662	.1695
9.0	.1858	.1781	—	.1775	.1812
10.0	.1964	.1886	—	.1876	.1917
11.0	.2059	.1980	—	.1972	.2017

* $(v_0-v)/v_0=(1/n)\log(1+p/B)$.

where

$$C_{p'}=1.005-0.004136s+0.0001098s^2-0.000001324s^3.$$

In the above equations, t is temperature in °C and s is salinity in parts per 1000. These data are in good agreement with those used by Kirkwood and Richardson, quote in Appendix II.

4. Compressibility Data for Low Pressure Region (Table I)

The following equation was used in computing Table I:

$$10^5\mu=\frac{4886}{1+0.183p}-[227+28.33t-0.551t^2+0.004t^3]+p[105.5+9.50t-0.158t^2]-1.5p^2t-\left(\frac{\gamma-28}{10}\right)[147.3-2.72t+0.04t^2-p(32.4-0.87t+0.02t^2)]+\left(\frac{\gamma-28}{10}\right)^2[4.5-0.1t-p(1.8-0.06t)],$$

where p is pressure in kilobars, t is temperature in degrees centigrade, and μ is defined by:

$$v=v_0(1-\mu p),$$

γ is defined by:

$$\gamma=-0.069+1.4708\,\text{Cl}-0.001570\,\text{Cl}^2+0.0000398\,\text{Cl}^3.$$

The above empirical equation for sea water compressibility is due to Ekman[11] and has been widely used for computation of sound velocity in sea water.[10,12] The validity of the Ekman equation for sound velocity calculations was verified experimentally as indicated in Table VII.

Experimental sound velocity measurements were made by recording with a rotating drum camera the signals applied to a cathode ray oscilloscope by two very small piezoelectric gauges placed a known distance apart. The sound source was a No. 8 detonator cap placed far enough away from the gauges so that the effect of finite pressure amplitude was less than 0.03 percent. An error of about 0.2 percent was inherent in the experimental work owing to slight errors in the alignment of the two recording gauges with the sound source. This accounts for the magnitude and systematic nature of the discrepancy apparent in Table VII.

Further verification of the applicability of Ekman's equation in the region up to 1.50 kilobars is given in Table VIII where values obtained from the equation are compared with the experimental values of Adams for NaCl solutions.

5. Compressibility Data for Intermediate Pressure Region (Table II)

As indicated in Part 1 of this appendix, a sea water salinity of 32 parts per thousand corresponds to a 3.79 weight percent solution of NaCl. The compressibility of NaCl solution of this concentration was obtained by graphical interpolation of Adams's data.[8]

The Tait equation in the form:

$$v(0, T) - v(p, T)/v(0, T) = (1/n)\log[1 + p/B(t)], \qquad t = (T - 273.16)°\text{C}$$

was then fitted to Adams's data. In an effort to

TABLE IX. Values of n computed from p–v–t data using $n = 7.15$ in computation of ΔT.

t_0* (°C)	p (kg/cm²) 5000	15,000	25,000
20	7.211	7.183	7.130
40	7.360	7.126	6.969
60	7.411	7.054	6.868

* t_0 = centigrade temperature through which the adiabatic for S passes at zero pressure.

[11] V. W. Ekman, *Publications de Circonstance No. 43 Conseil Permanent International Pour L'Exploration de la Mer*, November 1908).

[12] Matthews, *Tables of the Velocity of Sound in Pure Water and Sea Water for Use in Echo Sounding and Sound Ranging* (Hydrographic Dept., Admiralty, H.D. No. 282).

check the Tait equation against the Ekman equation used for computation of Table I, a fit was first made to the lower pressure region. Values of n and $B(25°\text{C})$ were so selected that the equation not only fitted the data of Adams with adequate precision but also yielded the correct velocity of sound in the limit of zero pressure. This additional restriction (that the equation give $c_0 = 1528$ m/sec. at 25°C and $s = 32$) required that $nB(25°\text{C}) = 23.497$, the latter relation being obtained from the thermodynamic equations:

$$\left(\frac{\partial v}{\partial p}\right)_T = -\frac{v_0^2}{c_0^2} - \frac{T}{c_p}\left(\frac{\partial v}{\partial T}\right)_p^2,$$

$$\left(\frac{\partial v}{\partial p}\right)_T = -\frac{v_0}{nB(t)} \text{ at } p = 0.$$

In this case n was taken as 7.445 and $B(25°\text{C})$ as 3.156 kilobars, and the resulting equation fits the data of Adams quite closely up to pressures of about 4 kilobars as shown in Table VIII. For purposes of further calculation, the temperature *variation* of B was assumed to be the same as that used by Kirkwood and Richardson on the basis of a private communication from Gibson (see Appendix II). Calculation of $U - c_0/c_0$ at 1.00 kilobar yielded a value of 7.85 percent, in good agreement with the value of 7.81 percent obtained from the Ekman equation.

Having verified the accuracy of results obtained from the Tait equation when fitted as described above, the same technique was used to fit the equation to the intermediate pressure range (up to values for 11 kilobars quoted by Adams; it was assumed safe to extrapolate the resulting equation to pressures of 14 or 15 kilobars). It was found that the best fit of the data as well as a correct value for the velocity of sound were obtained by taking $n = 7.800$ and $B(25°\text{C}) = 3.012$, the temperature variation of B again being assumed to be that mentioned above. The Tait equation containing these parameters was then used for the computation of Table II. The fit of the equation to Adams's data is shown in Table VIII.

APPENDIX II

1. Data Employed in the Computations of Part B of Section II

In the modified Tait equation, Eq. (2.12), the function $A[S] = B(t)$, where $t = T[0, S] - 273.16$,

is determined from the empirical values of $B(t)$, fitting the original isothermal Tait equation, Eq. (2.7), to experimental data. R. E. Gibson[13] gives third-degree t-expansions of $B(t)$ for various molalities of NaCl. By interpolating the coefficients (the constant term numerically and the other graphically) for a molality of 0.7, one obtains $B(t) = 3.134 - 1.65\times10^{-3}(t-55) - 1.181\times10^{-4}(t-55)^2 + 5.32\times10^{-7}(t-55)^3$ kilobars.

The specific heat $c_p(0, T)$ for a 0.7 molal NaCl solution was obtained by interpolation from the values quoted in the *International Critical Tables* and *Physikalischchemische Tabellen*. The resulting set of values is fitted adequately by the expression

$$c_p(0, t+273.16) = 3.9644 + 6.24\times10^{-4}t \text{ joule/gm. deg.}$$

From Gibson and Loeffler[14] a set of values of $v(0, T)$ covering the range from 25°C to 95°C inclusive was obtained for a 0.7 molal NaCl solution by means of empirical equations giving $v(0, T)$ as a function of concentration for each temperature. In extrapolating to higher temperatures, the relation,

$$v(0, t+273.16) = 0.994150 + 2.929\times10^{-4}(t-25) + 3.241\times10^{-6}(t-25)^2 \text{ cm}^3/\text{gm.}$$

was used; for lower temperatures ($t<10$°C),

$$v(0, t+273.16) = 0.991442 + 6.025\times10^{-6}(t-3.8)^2 \text{ cm}^3/\text{gm.}$$

2. Test of the Modified Tait Equation with Bridgman's Data for Pure Water. Determination of the Characteristic Constant n.

The modified Tait equation-of-state, Eq. (2.12), may for our present purposes be written in the form

$$\log(v[0, S]/v[p, S]) = (1/n)\log(1+p/A[S]) \quad (11\text{-}1)$$

where $A[S]$ is related to the $B(t)$ in the original isothermal equation of state as follows,

$$A[S] = B(t_0), \quad t_0 = T_0 - 273.16, \quad T_0 = T[0, S]. \quad (11\text{-}2)$$

According to the convention introduced in Part B of Section II, parentheses ( ) after a function denotes that the independent variables are p and T, whereas square brackets [ ] denote that they are p and S.

Now we wish to test Eq. (11-1) with Bridgman's[15] p-v-T data for pure water with the ultimate object of finding the best value for n. We assume implicitly that n does not vary rapidly with NaCl concentration. To make the comparison, we first must know the values of the temperature T corresponding to the various points $[p, S]$, the calculation of which we consider below.

Letting $T(0, S] = T_0$, $T[p, S] = T$, and $T - T_0 = \Delta T$, we have

$$\Delta T = \int_0^p \frac{\partial T[p, S]}{\partial p}dp = \int_0^p \frac{\partial v[p, S]}{\partial S}dp. \quad (11\text{-}3)$$

Using Eq. (11-1), a simple calculation yields

$$\Delta T = \frac{G}{(1+p/A)^{1/n}}[(1+D)(1+p/A) - (n+D)(1+p/A)^{1/n} + n - 1], \quad (11\text{-}4)$$

where

$$A = A[S] = B(t_0),$$

$$G = \frac{A'[S]v[0, S]}{n-1} = \frac{T_0B'(t_0)\cdot v(0, T_0)}{(n-1)\cdot c_p(0, T_0)},$$

$$D = \frac{nA[S]\dfrac{\partial v[0, S]}{\partial S}}{A'[S]v[0, S]} = \frac{nB(t_0)\beta_0}{B'(t_0)v(0, T_0)},$$

$$\beta_0 = \left(\frac{\partial v(0, T)}{\partial T}\right)_{T=T_0}.$$

To calculate T, given a specified p and $T_0 = T[0, S]$, a tentative value of $n = 7.15$ was chosen for use in Eq. (11-4). The corresponding value of $v[p, S] = v(p, T)$ was obtained by interpolation from Bridgman's[15] p-v-T data. Inserting these values of $v[p, S]$ in Eq. (11-1), and knowing the values of $v[0, S] = v(0, T_0)$ and $B(t_0)$ for pure water, a set of values of n was calculated for $p = 5{,}000$, $15{,}000$, $25{,}000$ kg/cm²

[13] Private communication.
[14] Gibson and Loeffler, J. Am. Chem. Soc. **53**, 443 (1941).
[15] Bridgman, J. Chem. Phys. **3**, 597 (1935) and private communication.

and $t_c = T_0 - 273.16 = 20°, 40°, 60°C$, the results summarized in Table IX.

Additional data (for pure water) used in Eqs. (II-1) and (II-4) were

$$B(t) = 2.996 + 7.285 \times 10^{-3}(t-25) - 1.790 \times 10^{-4}(t-25)^2 + 6.13 \times 10^{-7}(t-25)^3 \text{ kilobars},^{13}$$

and

$$\frac{1}{2.303}\frac{\partial \log v(0, 273.16+t)}{\partial t} = \frac{2(t-3.98)}{244{,}860+15{,}040(t-3.98)^{0.62}} - \frac{(0.62)(15{,}040)(t-3.98)^{1.62}}{[244{,}860+15{,}040(t-3.98)^{0.62}]^2}$$

obtained from Ipatov's[16] empirical equation for v by differentiation.

The average value of n is 7.146. In the present calculations this value has been rounded off to 7.15.

The entries in Tables IV, V, and VI therefore contain more significant figures than the test justifies. On the basis of the test, the errors associated with the use of the modified Tait equation are of the order of several percent. In particular, the results obtained for low pressures will disagree with known data by several percent.

[16] I. V. Ipatov, J. Phys. Chem. (U.S.S.R.) **5**, 1230 (1934).

APPENDIX III

Symbols

$A[S]$ = parameter in modified ("adiabatic") Tait equation-of-state.
$B(t)$ = parameter in isothermal Tait equation-of-state.
c = local velocity of sound.
c_0 = velocity of sound at zero pressure.
c_p = specific heat at constant pressure.
h = dissipated enthalpy increment: $\int_{T_0}^{T} c_p(0, T')dT'$.
ΔH = enthalpy increment: $\Delta H = \omega + h$.
n = characteristic constant in Tait equation-of-state.
p_0 = initial pressure ahead of shock front, $p_0 = 0$, in these calculations.
p = pressure behind shock front
S = entropy.
s = sea water salinity.
t = temperature in °C.
T = absolute temperature.
u = particle velocity behind shock front.
U = shock front propagation velocity.
v_0 = specific volume of medium ahead of shock front.
v = specific volume of medium behind shock front.
$\bar{\beta}_0$ = mean compressibility at zero pressure over temperature range ΔT.
ρ = density.
σ = Riemann function: $\int_{p_0}^{p} \frac{v[p', S]}{c[p', S]}dp'$.
ω = undissipated enthalpy increment: $\int_{p_0}^{p} v[p', S]dp'$.

THEORY OF THE SHOCK WAVE PRODUCED BY AN UNDERWATER EXPLOSION

Stuart R. Brinkley, Jr.
Bureau of Mines, Department of the Interior
and
John G. Kirkwood
California Institute of Technology

American Contribution

1950

Editors Note:

This paper summarizes and condenses a large amount of theoretical work carried on during the war and referred to in the text. The paper was written in order to combine and unify the presentation of this theoretical work for this Compendium.

CONTENTS

Abstract

1. INTRODUCTION 1

2. SPECIFICATION OF INITIAL CONDITIONS 7

3. PROPAGATION OF THE KINETICS ENTHALPY BY AN UNDERWATER SHOCK WAVE 15

4. MOTION OF SURFACE OF GAS SPHERE 29

5. DISSIPATION AND SPREAD PARAMETERS 38

6. ASYMPTOTIC BEHAVIOR OF PRESSURE WAVE 49

7. CALCULATION OF PRESSURE-TIME CURVE 59

8. SIMILARITY RESTRAINT PROPAGATION THEORY 62

9. THE SHOCK WAVE FOR CYLINDRICAL SYMMETRY 85

10. COMPARISON WITH THE EXPERIMENT 97

THEORY OF THE SHOCK WAVE PRODUCED BY AN UNDERWATER EXPLOSION

By Stuart R. Brinkley, Jr. and John G. Kirkwood

ABSTRACT

The effect of an underwater shock wave from an explosive source upon a target structure is determined by the amplitude and duration of the shock wave. The theoretical description of an underwater shock wave is thus of importance in the determination of the effectiveness of different explosives for use in underwater ordnance.

The kinetic enthalpy propagation theory of Kirkwood and Bethe is developed from the assumption that level values of a function $G = r\,(w + u^2/2)$ are propagated outward from the generating charge with a velocity $\tilde{c} = c + u$, where r is the distance from the charge, w the enthalpy increment of the water for pressure p, u the particle velocity, and c the sound velocity at pressure p. Kirkwood and Bethe have estimated an upper bound of the error resulting from their basic assumption and have developed the relations necessary for the calculation of underwater shock-wave parameters as functions of distance from the charge.

In the similarity restraint propagation theory of Kirkwood and Brinkley, the explicit integration of the equations of hydrodynamics is avoided by the assumption of an exponential Lagrange energy-time curve and the utilization of the second law of thermodynamics to determine at an arbitrary distance from the charge the partition of the initial shock-wave energy between dissipated energy residual in the fluid already traversed by

the shock wave and energy available for further propagation. There result a pair of ordinary differential equations for peak pressure and shock-wave energy as functions of distance from the charge that are easily integrated with simple numerical procedures.

In the present report, these two theories are developed in detail for the shock wave of spherical symmetry. The shock wave of cylindrical symmetry from an infinite cylinder of explosive is treated by the methods of Kirkwood and Brinkley. Calculations of the shock-wave parameters for several explosives by the two theories are compared with each other and with the results of experiment.

THEORY OF THE SHOCK WAVE PRODUCED BY AN UNDERWATER EXPLOSION

1. Introduction

When a spherical charge of explosive submerged in a large body of water is detonated at its center, the following sequence of events occurs. A detonation wave travels from the center toward the surface of the charge, converting the explosive into certain decomposition products. At the instant of arrival of the front of the detonation wave at the boundary of the charge, a shock wave advances into the water, the boundary of radius a(t) moves forward, and a reflected wave recedes into the gas sphere, composed of the products of the explosion. The reflected wave, according to the circumstances, may initially be a shock wave, but it must rapidly become a wave of rarefaction in the region behind the advancing boundary a(t)

1/ Physical Chemist, Explosives Branch, Bureau of Mines, U. S. Department of the Interior.
2/ Professor of Chemistry, California Institute of Technology, Pasadena, California.

between the two mediums. The shock wave with a profile consisting of practically infinite steepness and a tail of diminishing intensity is propagated into the water and produces the initial pressure pulse in the environment of the explosive. After a relatively long period following emission of the shock wave, a series of secondary pressure pulses of considerable breadth and low intensity is emitted. The secondary pulses arise from oscillations of the gas sphere, which withdraw energy for their production from the slowly diminishing tail of the shock wave. Although the secondary pulses may play a certain role, the damage to marine structures produced by an underwater explosion must be principally attributed to the initial pressure pulse. Because of its probable role in producing damage to structures, the theoretical and experimental investigation of the intensity and duration of the initial pressure pulse is of considerable importance.

The hydrodynamical analysis of the initial pressure pulse emitted by the expanding gas sphere presents certain rather formidable difficulties. Although the wave approaches acoustical behavior at large distances from the charge, neither the acoustical approximation nor the incompressible approximation is adequate to describe the motion of the water in the neighborhood of the gas sphere in the initial stages, owing to the high pressures and large particle velocities involved. For example, in the case of TNT, the initial pressure in the shock front is of the order of 30,000 atmospheres and the initial particle velocity of the order of 1000 meters/second. Furthermore, an analysis of the initial stages of the motion is necessary to predict the amplitude and duration of the shock wave, even in its later acoustical phase at large distances from the charge.

Lamb[3] has presented a solution of the problem in the incompressible approximation, remarking that a more elaborate analysis appears hopeless. The moderately good agreement of Lamb's theory with available experimental data for TNT is completely removed when an appropriate equation of state such as that of Wilson and Kistiakowsky[4] is employed for the gas sphere instead of the ideal gas equation of state. Lamb's theory has been improved somewhat by Butterworth,[5] who attempts to fit an acoustical solution of the hydrodynamical equations for large distances to the incompressible solution for small distances at a distance equal to several times the radius of the gas sphere. A thorough analysis of the problem has been given by Penney.[6] Penney's calculations are based upon the numerical integration of the Riemann equations, valid if dissipation terms in the equation of motion of the fluid can be neglected. This direct method suffers from the disadvantage that a laborious process of numerical integration must be repeated for each explosive.

Kirkwood and Bethe[7] have developed an explicit theory of the shock wave produced by an underwater explosion. The theory can be employed to calculate the pressure-time curve of the shock wave at any distance from a spherical charge of explosive, given the thermodynamic properties of the

---

3/ H. Lamb, Phil. Mag., 45, 259 (1923).
4/ G. B. Kistiakowsky and E. B. Wilson, Jr., OSRD Report No. 114 (1941).
5/ S. Butterworth, British Report, S.R.E., Summary No. M.S. 594/36 (1936).
6/ W. G. Penney, Btitish Report RC 142 (1941). W. G. Penney and H. K. Dasgupta, British Report RC 333 (1942).
7/ J. G. Kirkwood and H. A. Bethe, OSRD Report No. 588 (1942).

explosive and those of water. A description of the theory divides itself naturally into three parts: The specification of the initial conditions at the boundary between the water and the gaseous products of the explosion; the formulation of a new and adequate theory of propagation of the spherical shock wave in water; the investigation of the motion of the surface of the gas sphere composed of the explosion products. Our discussion follows closely the exposition of the original paper.[2]

In the section 2, initial conditions are formulated and a method is outlined for calculating p_1 and u_1, the initial pressure and initial particle velocity at the surface of the gas sphere. In section 3, the theory of propagation of the spherical shock wave in water is developed. It is found that to an adequate approximation a quantity $r\Omega$ is propagated outward from the surface of the gas sphere with a velocity c+u, where r is the distance from the center of the charge, c the local velocity of sound, and u the particle velocity of the water. The function Ω, called the kinetic enthalpy, is equal to $\omega + u^2/2$, where ω is the enthalpy increment ΔH relative to the undisturbed water ahead of the shock front. Owing to the fact that c+u exceeds the velocity of the shock front, the crest of the pressure wave is progressively destroyed as the disturbance travels outward. Also, owing to the fact that c+u depends upon the local intensity of the wave, the wave profile is progressively broadened as it travels outward.

In the section 4, the motion of the gas sphere surface is investigated, and the quantity $G_a(t)$, equal to $a(t)\Omega_a(t)$, is determined as a function of time t, a(t) being the radius of the gas sphere at the time

t and $\Omega_a(t)$ the kinetic enthalpy of the water at this surface. Due to the rapid decrease of $G_a(t)$, it can be adequately represented by the peak formula,

$$G_a(t) = G_1 e^{-t/\theta_1},$$
$$\theta_1 = a_0 / c_0, \qquad (1.1)$$
$$c_0 = \frac{\omega_1}{w_1} \frac{\rho_1^* c_1^* (J_1^* c_1^* + J_1 c_1)}{\rho_1 c_1 + \rho_1^* c_1^*},$$

where the subscript 1 denotes initial values of the several quantities on the gas sphere surface of initial radius a_0; w_1, ρ_1, c_1 are the enthalpy, density, and sound velocity in the water, ρ_1^*, and c_1^* the density and sound velocity in the gas, and J_1 and J_1^* are factors of magnitude unity for which explicit formulas are given in the text. All quantities are functions of the initial pressure p_1. After long times the peak formula ceases to be valid, and $G_a(t)$ varies as $(1 + t/\theta_2)^{-4/5}$, but this behavior affects only the tail of the shock wave.

In the section 5, the development of the kinetic enthalpy propagation theory is completed by the evaluation of the spread parameter and the dissipation parameter. The significance of these quantities is described in the text. In section 6, the asymptotic behavior of the pressure wave is discussed. At distances exceeding about 25 charge radii from the center of the charge, the pressure p is given by the asymptotic formula

$$p = \chi \frac{a_0}{R} p_0 e^{-t'/\theta},$$
$$p_0 = \rho_0 \Omega_1, \quad \chi = \chi(R/a_0), \qquad (1.2)$$
$$\theta = \theta_1 \gamma(R/a_0),$$

where t' is the time measured from the instant of arrival of the wave at R. The dissipation parameter $\chi(R)$ and the spread parameter $\gamma(R)$ are slowly varying functions of R, for which simple algebraic formulas are given, and

ρ_0 is the density of water at zero pressure. In the discussion of the asymptotic behavior of the wave at large distances, the relation between the destruction of the wave crest and the dissipation of energy at the wave front is clarified. In the section 7, the method of calculating the pressure-time curve of the shock wave is outlined, the necessary formulas are assembled, and typical results of the application of the theory to service explosives are exhibited.

In the development of the kinetic enthalpy propagation theory all elements of the fluid are assumed to be on the same adiabatic. This is not strictly true, since the entropy increment of an element of fluid at a shock front of changing intensity depends upon the time at which it passes through the front. Kirkwood and Brinkley[8] have developed a propagation theory which takes proper account of the finite entropy increment in the fluid resulting from the passage of the shock wave. The partial differential equations of hydrodynamics and the Hugoniot relation between pressure and particle velocity are used to provide three relations between the four partial derivatives of pressure and particle velocity, with respect to time and distance from the source, at the shock front. An approximate fourth relation is set up by imposing a similarity restraint on the shape of the energy-time curve of the shock wave and by utilizing the second law of thermodynamics to determine, at an arbitrary distance, the distribution of the initial energy input between dissipated energy residual in the fluid already traversed by the shock wave and energy available for further propagations. The four relations are used to formulate a pair of ordinary differential equations for peak pressure and shock-wave energy as functions of distance from the source and in addition

8/ J. G. Kirkwood and S. R. Brinkley, Jr., OSRD Report No. 4814 (1945). S. R. Brinkley, Jr. and J. G. Kirkwood, Phys. Rev., 71, 606 (1947).

to determine the initial slope of the pressure-time curve of the shock wave. This theory permits using the exact Hugoniot equations of the fluid in the numerical integration of the propagation equations. While less flexible than the propagation theory of Kirkwood and Bethe, the approximations employed are less drastic than those of the latter authors. In section eight, this alternative propagation theory is described in detail for the case of underwater shock waves of spherical symmetry.

In section 9, we discuss briefly the results obtained by Rice and Ginell[9] in their application of the methods of Kirkwood and Bethe to the shock wave of cylindrical symmetry generated by an infinite cylinder of explosive detonated simultaneously at all points of its axis. These results are less satisfactory than for the case of spherical symmetry because the propagation velocity of the kinetic enthalpy is not well approximated by $c+u$. The shock wave of cylindrical symmetry can be satisfactorily described by the methods of Kirkwood and Brinkley,[10] and we describe their application to the shock wave generated by an infinite cylinder of explosive in which the detonation wave travels in the axial direction.

2. Specification of Initial Conditions

In this section, we wish to examine the initial conditions at the boundary between explosive and water leading to the emission of the shock wave. When the detonation front arrives at the surface of the sphere of radius a, forming the boundary between the initially intact explosive and the water, a shock wave travels into the water and the following boundary conditions are established.

$$p^*(a,t) = p(a,t), \quad u^*(a,t) = u(a,t), \tag{2.1}$$

9/ O. K. Rice and R. Ginell, OSRD Report No. 2023 (1943), OSRD Report No. 3950 (1944).

10/ S. R. Brinkley, Jr., and J. G. Kirkwood, OSRD Report No. 5659 (1945), Phys. Rev., 72, 1109 (1947), Proc. Symposia App. Math., 1, 48 (1949).

where p^* and u^* are the pressure and particle velocity of the gas interior to the spherical boundary a; p and u the pressure and particle velocity of the water exterior to the surface a.

At the shock front in the water, the Rankine-Hugoniot[11] conditions are always satisfied,

$$\begin{aligned} \rho(U-u) &= \rho_0 U , \\ p - p_0 &= \rho_0 u U , \\ \Delta E &= \tfrac{1}{2}(p+p_0)\left(\tfrac{1}{\rho_0} - \tfrac{1}{\rho}\right) , \end{aligned} \tag{2.2}$$

where p and ρ are the pressure and density of the water behind the shock front, p_0 and ρ_0 the pressure and density ahead of it, and U the velocity of propagation of the front. The internal energy increment at the shock front, ΔE, is a function of p, ρ, p_0, and ρ_0, which may be explicitly calculated from the equation of state of the fluid. Eqs. 2.2 thus provide three relations between the four variables p, ρ, u and U, from which any three of them may be determined as functions of the remaining variable. An alternative form of Eqs. 2.2 which frequently proves useful is the following,

$$\begin{aligned} u &= \sqrt{(p-p_0)\left(\tfrac{1}{\rho_0} - \tfrac{1}{\rho}\right)} , \\ uU &= \Delta H + u^2/2 , \\ \Delta H &= \tfrac{1}{2}(p-p_0)\left(\tfrac{1}{\rho_0} + \tfrac{1}{\rho}\right) , \end{aligned} \tag{2.3}$$

where ΔH is the enthalpy increment at the shock front, $\Delta E + p/\rho - p_0/\rho_0$. At the instant $t = 0$, when the shock front is coincident with the boundary

---

[11] W. J. M. Rankine, Phil. Trans. 160, 277 (1870).
H. Hugoniot, J. de l'École Polyt., 57, 3 (1887); 58, 1 (1888).

of the gas sphere, the Hugoniot conditions Eqs. 2.2 or 2.3 provide one relationship,

$$u_1 = F(p_1),$$
$$u_1 = u(a_0, 0),\ p_1 = p(a_0, 0), \tag{2.4}$$

between the initial pressure p_1 and initial velocity u_1 at the surface of the gas sphere.

To obtain a second relation between p_1 and u_1 to be used in conjunction with Eq. 2.4, we must consider what is happening in the interior of the gas sphere. At precisely the initial instant of time the situation is rather complicated. The front of the advancing detonation wave is coincident with the spherical surface a_0, and its tail extends back into the gas in the interior. Near the detonation front both pressure and particle velocity are high, although the pressure does not greatly exceed the equilibrium pressure p_e corresponding to adiabatic conversion at constant volume of the solid explosive into its decomposition products. According to G. I. Taylor,[12] the detonation wave is of appreciable intensity only in an outer spherical shell bounded by radii $3a_0/5$ and a_0, the gas in the interior being at rest. The velocity of the detonation wave is in general of the order of 5000 meters/sec. Thus the time width of the head of the wave is quite small, of the order of $10^{-4}\, a_0$, if a_0 is expressed in meters. We shall find that θ_0, equal to a_0/c_0 where c_0 is the velocity of sound in water at zero pressure, is a convenient unit of time to employ in discussing underwater explosions. The breadth of the head of the detonation

12/ G. I. Taylor, British Report RC 178 (1941).

wave is about $\theta_0/6$ in the typical case. We may reasonably expect that after an interval of time of this magnitude, the head of the detonation wave will have disappeared in the gas sphere by transmission of a shock wave to the water and by the smoothing effect of receding rarefaction waves.

In the theory of propagation of the shock wave in water, we shall find that the crest of the shock wave is progressively destroyed as it advances outward and that the wave emitted from the gas sphere before a certain time $\tau_0(R)$ is dissipated before the shock front arrives at a distance R from the center of the charge. In the typical case of TNT, τ_0 is about $\theta_0/2$ at a distance of $25a_0$. Thus, except in the immediate neighborhood of the charge, we may assume that the initial details of profile impressed upon the shock wave by transmission of the head of the detonation wave into the water are not extremely important. We therefore specify initial conditions in the gas sphere which are closely approximated after the very short initial period of time $\theta_0/6$. These are the same conditions as those employed by Penney. At time $t = 0$, the gas sphere is assumed to be at a uniform pressure p_e^*, the equilibrium pressure corresponding to adiabatic conversion at constant density of the solid explosive into its decomposition products. The pressure p_e^* may be calculated from the heat of the explosion reaction and the heat capacity and equation of state of the products.

The pressure discontinuity $p_e^*-p_0$ at the boundary a_0 is at once propagated into the water, the boundary conditions 2.1 are established, and Eq. 2.4 is satisfied. At the same time a rarefaction wave starts into the gas. By the Riemann theory, the value of a certain function Ψ is initially

zero for such a receding rarefaction wave

$$\begin{aligned} F_1 &= \sigma_1^* + u_1 = 0 , \\ \sigma^*(p) &= \int_{\rho_e^*}^{\rho^*} (c^*/\rho)\, d\rho , \\ \rho^* &= \rho^*(p, S_e^*) , \end{aligned} \tag{2.5}$$

where c^* is the velocity of sound in the gas. The integral defining the function σ_1^* is to be taken along the initial adiabatic of the gas from its initial density ρ_e^* to a density ρ_1^* determined as a function of p_1 along the adiabatic of entropy S_e^* by the equation of state of the gas. Eqs. 2.5 therefore provide a second relation between p_1 and u_1,

$$\sigma^*(p_1) + u_1 = 0 . \tag{2.6}$$

Simultaneous solution of Eqs. 2.4 and 2.6 determines the initial values of p_1 and u_1 on the gas sphere. This solution is most conveniently carried out by graphical determination of the intersection point of the curves $F(p)$ and $-\sigma^*(p)$. The pressure p_1 is generally much less than p_e^*.

The calculation of the pressure p_e for adiabatic constant volume conversion of the explosive to its products is a straightforward problem in thermodynamics. For this process,

$$\sum n_i E_i - E_o = \bar{C}_v (T_e - T_o) + \int_{\infty}^{1/\rho_e^*} \left(\frac{\partial E}{\partial v}\right)_{T_e} dv , \tag{2.7}$$

where E_i is the molar heat of formation at constant volume and temperature T_o of the i-th product constituent, E_o is the specific heat of formation at constant volume and temperature T_o of the intact explosive, n_i is the number of moles of the i-th product constituent per gram of explosive, and $\bar{C}_v$ is the zero-pressure specific mean heat capacity over the temperature range of

the explosion products. We may employ the Kistiakowsky-Wilson[4] equation of state,

$$p^*/\rho^* = nRT(1 + \chi e^{\beta\chi}),$$
$$\chi = \Sigma n_i k_i \rho^*/T^\alpha, \tag{2.8}$$

where n is the total number of moles of products per gram of explosive, k_i is an empirical parameter characteristic of the i-th constituent with dimensions of volume which can be called a covolume, and α and β are empirical constants. Then

$$\int_\infty^{V/p} \left(\frac{\partial E}{\partial V}\right)_T dv = nRT\alpha\chi e^{\beta\chi}. \tag{2.9}$$

We may represent with adequate accuracy the mean heat capacity as a linear function of T in the form

$$\bar{C}_v = \Sigma n_i A_i + T\Sigma n_i B_i, \tag{2.10}$$

where A_i and B_i are constants characteristic of the i-th constituent. With Eqs. 2.9 and 2.10, Eq. (2.7) can be written in the form

$$\Sigma n_i E_i - E_0 = (\Sigma n_i A_i + T_e \Sigma n_i B_i)(T_e - T_0) + nRT_e\alpha\chi_e e^{\beta\chi_e}, \tag{2.11}$$

which can be solved numerically for the temperature T_e of the adiabatic constant volume explosion state if the composition of the products is known. The pressure p_e^* corresponding to temperature T_e and density ρ_e^* can then be determined at once from the equation of state. The specific entropy $S^*(\rho^*, T)$ is given by

$$S^*(\rho^*, T) = \Sigma n_i S_i(T) - R\Sigma n_i \log n_i \rho^* RT + \int_\infty^{1/\rho^*} \left[\left(\frac{\partial p}{\partial T}\right)_\rho - nR\rho\right] dv, \tag{2.12}$$

where S_i^c is the molar entropy at unit pressure of the i-th constituent. With the equation of state 2.8, we obtain,

$$S^*(\rho^*, T) = \Sigma n_i S_i^c(T) - nR\left[\log \rho^* + \tfrac{1}{3}(e^{3\varkappa} - 1) - \alpha\varkappa e^{\beta\varkappa}\right], \quad (2.13)$$

which can be employed for the determination of the entropy of the adiabatic constant volume explosion state and which then suffices for the construction of the adiabatic $p^* = p^*(\rho_e^*, S_e^*)$ if the composition of the explosion products is known along the adiabatic expansion curve. In the construction of this curve, it is convenient to employ the temperature as the independent variable and to determine,

$$\begin{aligned} p^* &= p^*(T, S_e^*) \quad , \\ \rho^* &= \rho^*(T, S_e^*) \quad . \end{aligned} \quad (2.14)$$

The function $\sigma^*(p)$ can be calculated by numerical methods from a tabular presentation of relations 2.14.

In the calculation of $p_e^* = p^*(\rho_e^*, S_e^*)$ and the construction of the curve $p^* = p^*(\rho^*, S_e^*)$ it is necessary at each stage of the computations to know the composition of the fluid composed of the explosion products. The calculations are carried out iteratively. The state (T, ρ^*) is determined by the appropriate relation for an approximate composition. The composition (n_i) is then calculated for this state by standard thermodynamic methods. This composition is then employed in the determination of a second approximation of the state, and the process is continued to convergence.

The composition is determined by solving the requisite number of equations expressing the conservation of each kind of element

simultaneously with mass action expressions of the form

$$K = \prod n_i^{\nu_i} \tag{2.15}$$

for equilibrium of the chemical reaction

$$\sum \nu_i Y^{(i)} = 0 \quad , \tag{2.16}$$

where $Y^{(i)}$ denotes the formula of the i-th product constituent and K is the value of the mass action constant. We discuss here the evaluation of K for the pressures characteristic of the explosion process. A discussion of techniques for the calculation of the equilibrium composition of systems of many constituents has been published elsewhere.[13]

The specific work content $A(\rho^*,T)$ is given by standard thermodynamics as

$$A(\rho^*,T) = \sum n_i \mu_i^0 + RT\left[n \log \frac{V^*}{n} + \sum n_i \log n_i - n\right] + \int_0^{\rho^*} \frac{p}{\rho^2}\, d\rho \quad . \tag{2.17}$$

The chemical potential μ_i is defined as

$$\mu_i = \left(\frac{\partial A}{\partial n_i}\right)_{T,\rho,n_j \neq n_i} \quad . \tag{2.18}$$

Employing the equation of state 2.8, we obtain

$$\mu_i = \mu_i^0 + RT\left[\log n_i + \log \frac{R^*}{n} + \frac{1}{\beta}(e^{\beta x} - 1) + (nk_i / \Sigma n_i k_i) x e^{\beta x} - \log (1 + x e^{\beta x})\right], \tag{2.19}$$

13/ S. R. Brinkley, Jr., J. Chem. Phys., 15, 107 (1947).

For equilibrium of reaction 2.16,

$$\Sigma \nu_i \mu_i = 0 \quad , \tag{2.20}$$

and

$$K = K_p \Gamma \quad , \tag{2.21}$$

where

$$-RT \log K_p = \Sigma \nu_i \mu_i^{\circ} \quad , \tag{2.22}$$

is the thermodynamic equilibrium constant for reaction 2.16, and

$$\log \Gamma = \left[\log \frac{b^*}{n} + \frac{1}{\beta}(e^{\beta x}-1) - \log(1+x e^{\beta x})\right] \Sigma \nu_i + \left(\Sigma \nu_i k_i / \Sigma x_i k_i\right) n x e^{\beta x} . \tag{2.23}$$

3. Propagation of the Kinetic Enthalpy by an Underwater Shock Wave[14/]

In this section it is our purpose to investigate the form of the pressure wave in water emitted by the expanding gas sphere. This wave is contained in the region between the gas sphere of radius a(t) and the shock front of radius R(t). Under the initial conditions prescribed in the foregoing section, a and R are coincident with a_o, the radius of the intact charge of explosive, at the instant t = 0, and a(t) advances with the velocity $u_a(t)$, R(t) with the velocity U(t). Our first task is to relate the motion of the shock front and the form of the wave behind it to the motion of the gas sphere surface a(t).

14/ See Reference 7, Section 2.

In describing the motion of the water in the spherical shell between a(t) and R(t), it is convenient to use the Eulerian form of the hydrodynamical equations of continuity and motion. With the neglect of stresses arising from viscosity, these equations are:

$$\frac{1}{\rho}\frac{D\rho}{Dt} = -\nabla\cdot\underline{u}\ ,$$

$$\frac{D\underline{u}}{Dt} = -\frac{1}{\rho}\nabla p\ , \qquad (3.1)$$

$$\frac{D}{Dt} = \frac{\partial}{\partial t} + \underline{u}\cdot\nabla\ ,$$

where ρ is the density, p the pressure, and u the particle velocity. Eqs. 3.1 must be supplemented by the equation of state of the fluid, which provides a relation between pressure, density, and entropy, and the equation of entropy transport

$$\frac{DS}{Dt} = 0\ , \qquad (3.2)$$

where S is the specific entropy of the fluid (entropy per gram). The entropy transport equation is based upon the assumption that the fluid experiences only reversible adiabatic changes of state behind the shock front, which is true if the influence of heat conduction and diffusion can be neglected in the time interval during which an element of fluid is traversed by the wave. At this point it is not assumed that all elements of fluid are on the same adiabatic; and, indeed this is not strictly true, since at a shock front of changing intensity, the entropy increment of an element of fluid at the shock front depends upon the time at which it passes through the front.

It is convenient to eliminate p and ρ from equations 3.1 and 3.2 with the introduction of the enthalpy or heat content H, defined as

$$H = E + p/\rho , \tag{3.3}$$

where E is the internal energy per gram of fluid. We shall denote by ω the enthalpy increment

$$\omega = H - H_0 , \tag{3.4}$$

where H_0 is the enthalpy of the undisturbed fluid in front of the shock wave. The fundamental thermodynamic equation for H yields

$$d\omega = T\,dS + dp/\rho . \tag{3.5}$$

where T is the absolute temperature. The enthalpy increment ω may be written in the form,

$$\omega = \int_{p_0}^{p} \frac{dp'}{\rho(S, p')} + \int_{S_0}^{S} T(p_0, S')\,dS' , \tag{3.6}$$

where p_0 and S_0 are the pressure and entropy of the undisturbed fluid, and the line integrals are on paths of constant entropy, S, and pressure, p_0, respectively. Introduction of Eq. 3.5 into Eq. 3.1 with the use of Eq. 3.2 yields

$$\begin{aligned} &\nabla \cdot \underset{\sim}{u} = -\frac{1}{c^2}\frac{D\omega}{Dt} \quad , \quad \frac{DS}{Dt} = 0 , \\ &\frac{\partial \underset{\sim}{u}}{\partial t} - \underset{\sim}{u} \times (\nabla \times \underset{\sim}{u}) = -\nabla\Omega + T\nabla S , \\ &\Omega = \omega + u^2/2 \quad , \quad c^2 = \left(\frac{\partial p}{\partial \rho}\right)_S \quad . \end{aligned} \tag{3.7}$$

where Ω may be called the kinetic enthalpy and c is the velocity of sound in the fluid in state (p,S). Numerical calculations based upon the equation

of state of water and the entropy increments at the shock front demanded by the Hugoniot conditions show that up to pressures of 50,000 atmospheres the dissipated enthalpy $\int_{S_0}^{S} T(p_0,S')\,dS'$ amounts to only a few percent of the total enthalpy ω. We are therefore justified in approximating ω by

$$\omega = \int_{p_0}^{p} \frac{dp'}{\rho(S_0,p')} \quad , \tag{3.8}$$

and in neglecting the dissipative term in Eqs. 3.7. With this simplification Eqs. 3.7 become

$$\begin{aligned} \nabla \cdot \underset{\sim}{u} &= -\frac{1}{c^2}\frac{D\omega}{Dt} \quad , \\ \frac{\partial \underset{\sim}{u}}{\partial t} - \underset{\sim}{u} \times (\nabla \times \underset{\sim}{u}) &= -\nabla \Omega \quad . \end{aligned} \tag{3.9}$$

In this approximation the entropy transport equation becomes irrelevant. The initial conditions correspond to irrotational flow, and Eqs. 3.9 then demand that $\nabla \times \underset{\sim}{u}$ remain zero for all times. Moreover, for purely radial flow which we shall have to consider, $\nabla \times \underset{\sim}{u}$ is zero under any conditions. We may therefore introduce a velocity potential ψ,

$$\underset{\sim}{u} = -\nabla \psi \quad . \tag{3.10}$$

Introduction of 3.10 into Eq. 3.9 yields

$$\begin{aligned} \nabla^2 \psi &= \frac{1}{c^2}\frac{D\omega}{Dt} \quad , \\ \Omega &= \frac{\partial \psi}{\partial t} \quad . \end{aligned} \tag{3.11}$$

Elimination of ω between Eqs. 3.11 gives the wave equation

$$\nabla^2\psi - \frac{1}{c^2}\frac{\partial^2\psi}{\partial t^2} = \frac{1}{c^2}\left[\frac{1}{2}\underline{u}\cdot\nabla u^2 - \frac{Du^2}{Dt}\right], \qquad (3.12)$$

$$\underline{u} = -\nabla\psi, \quad \Omega = \partial\psi/\partial t.$$

For the case of spherical symmetry, which we shall consider, Eqs. 3.12 take the form

$$\psi = \varphi/r, \quad \Omega = G/r,$$

$$u = \frac{\varphi}{r^2} - \frac{1}{r}\frac{\partial\varphi}{\partial r}, \quad G = \frac{\partial\varphi}{\partial t}, \qquad (3.13)$$

$$\frac{\partial^2\varphi}{\partial r^2} - \frac{1}{c^2}\frac{\partial^2\varphi}{\partial t^2} = \frac{r}{c^2}\left[\frac{u}{2}\frac{\partial u^2}{\partial r} - \frac{Du^2}{Dt}\right].$$

Ω and u are related in the following manner,

$$u = \frac{\varphi}{r^2} + \frac{\Omega}{c_\varphi}, \qquad (3.14)$$

$$c_\varphi = (\partial r/\partial t)_\varphi,$$

where c_φ is the velocity of propagation of the function $\varphi(r,t)$.

An alternative formulation of the hydrodynamical equations 3.1 is the well-known Riemann formulation.[15] Since we shall use the Riemann equations in an auxiliary capacity in investigating the solutions of Eq. 3.13, we present them here. If a function σ is defined as

$$\sigma = \int_{\rho_0}^{\rho} \frac{c}{\rho}\, d\rho \qquad (3.15)$$

taken along the initial adiabatic S_0, and dissipative terms can be neglected, Eqs. 3.1 take the form for the case of spherical symmetry,

$$\frac{\partial\sigma}{\partial t} + u\frac{\partial\sigma}{\partial r} + c\frac{\partial u}{\partial r} + \frac{2uc}{r} = 0, \quad \frac{\partial u}{\partial t} + c\frac{\partial\sigma}{\partial r} + u\frac{\partial u}{\partial r} = 0. \qquad (3.16)$$

15/ B. Riemann, Nachr. Ges. Wiss. Göttingen, 8, 43 (1860

Introduction of the new variables,

$$\bar{r} = (\sigma + u)/2 \quad ,$$
$$\bar{s} = (\sigma - u)/2 \quad , \tag{3.17}$$

yields the Riemann equations

$$\frac{\partial \bar{r}}{\partial t} + (c + u)\frac{\partial \bar{r}}{\partial r} = -\frac{uc}{r} \quad ,$$
$$\frac{\partial \bar{s}}{\partial t} - (c - u)\frac{\partial \bar{s}}{\partial r} = -\frac{uc}{r} \quad . \tag{3.18}$$

The kinetic enthalpy Ω is related to the Riemann functions $\bar{r}$ and $\bar{s}$ in the following manner

$$d\Omega = (c + u)\,d\bar{r} + (c - u)\,d\bar{s} \quad , \tag{3.19}$$

a relation we shall presently use.

It is instructive to review the integration of Eqs. 3.13 in two limiting cases, the incompressible approximation and the acoustical approximation. The incompressible approximation is obtained in the limit $c' \to \infty$, and Eq. 3.13 becomes

$$\frac{\partial^2 \varphi}{\partial r^2} = 0 \quad , \tag{3.20}$$

which with the boundary condition $\Omega \to 0$ as $r \to \infty$, leads to the result $\varphi = \varphi(t)$, and

$$\Omega = G(t)/r \quad , \quad G(t) = \varphi'(t),$$
$$u = \varphi(t)/r^2 \quad . \tag{3.21}$$

In this case we note that $r\Omega$ is propagated outward with infinite velocity.

The acoustical approximation is obtained by suppressing nonlinear terms in Eq. 3.13;

$$\frac{\partial^2 \varphi}{\partial r^2} - \frac{1}{c_0^2}\frac{\partial^2 \varphi}{\partial t^2} = 0 \quad , \tag{3.22}$$

with the solution,

$$\varphi = \varphi(t - r/c_0),$$

where c_0 is the asymptotic sound velocity for waves of vanishing amplitude in the undisturbed fluid, the solution $\varphi(t - r/c_0)$ being appropriate for an outgoing progressive wave. For Ω and u, we obtain

$$\Omega = G(t - r/c_0)/r \quad , \quad G(t) = \varphi'(t),$$
$$u = \varphi(t - r/c_0)/r^2 + \Omega/c_0 . \tag{3.23}$$

In this case, we note that $r\Omega$ is propagated outward with the finite and constant velocity c_0. The acoustical approximations to the Riemann functions $\bar{r}$ and $\bar{s}$ are of interest. For an outgoing spherical wave, they are

$$\bar{r} = \frac{\varphi'(t - r/c_0)}{c_0 r} + \frac{\varphi(t - r/c_0)}{2r^2},$$
$$\bar{s} = -\frac{\varphi(t - r/c_0)}{2r^2} . \tag{3.24}$$

We note also that in the incompressible approximation, Lim $(c \to \infty)$ $\sigma = 0$, we have

$$\bar{s} = -\frac{\varphi(t)}{2r^2} . \tag{3.25}$$

Thus the function, h, defined as

$$h = \bar{s} + \varphi/2r^2 , \tag{3.26}$$

vanishes both in the acoustical and in the incompressible domains of flow. It is also vanishingly small in the region behind the shock front in the initial stage of its formation, since $\bar{s}$ is always small just behind the shock front and φ is equal to $r\int_0^t \Omega(r,t')\,dt'$.

Since in the incompressible and acoustical limits $r\Omega$ or G is propagated outward in the one case with infinite velocity and in the

other case with constant velocity C_0, we are led to ask whether the spherical shock-wave problem possesses solutions corresponding to an outgoing progressive wave in which r, τ or G is propagated behind the shock front with a variable velocity $\bar{c}$ depending upon the intensity of the wave. To investigate this possibility, we consider the characteristics of G with the differential equations,

$$(\partial r/\partial t)_a = \bar{c}, \tag{3.27}$$

shown schematically in Figure 3.1.

It is assumed that the characteristics $r(t,G)$ are monotonic curves with finite positive slope $\bar{c}$, which do not intersect at any point behind the shock front. We then define a function $\tau(r,t)$ by the relation,

$$G_a(\tau) = G(r,t), \tag{3.28}$$

where for the present G_a is an arbitrary function except for the requirement that τ be a single-valued function of G. Eq. 3.27 may therefore be written as

$$\bar{c} = \left(\frac{\partial r}{\partial t}\right)_\tau . \tag{3.29}$$

We now integrate Eq. 3.29 along a path of constant τ in the form

$$\tau = t - \int_{a(\tau)}^{r} \frac{dr'}{\bar{c}(r',\tau)} , \tag{3.30}$$

where $a(t)$ is the radius of the expanding gas sphere at time t. We remark that τ has been assigned the dimensions of a time and that the integration constant in Eq. 3.30 has been so chosen that

$$\tau[a(t),t] = t . \tag{3.31}$$

Eqs. 3.29 and 3.31 then determine the arbitrary function $G_a(t)$ as

$$G_a(t) = G[a(t),t] . \tag{3.32}$$

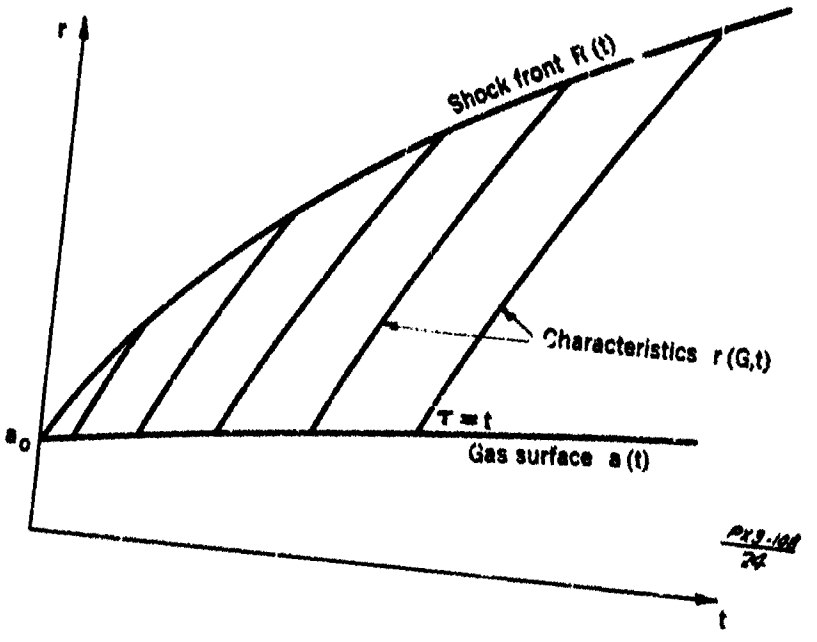


FIGURE 3.1 - Characteristics of Eq. 3.27. The characteristics r(G,t) are contours of constant G and of constant τ.

Thus $G_a(t)$ is the value of the function G on the surface of the gas sphere at time t. We are now provided with the following relation between the kinetic enthalpy Ω at any point (r, t) and the value of G on the surface of the gas sphere, $G_a(\tau)$ at a retarded time τ determined by Eq. 3.30,

$$\Omega(r, t) = G_a(\tau)/r = a(\tau)\Omega_a(\tau)/r , \qquad (3.33)$$

where $\Omega_a(t)$ is the value of Ω on the surface of the gas sphere at time t.

At first glance it might seem that the solution 3.33 would differ from the incompressible solution, Eq. 3.21, only in the detail that the wave requires a finite interval of time to reach a given point r. However, if $\bar{c}$ diminishes with diminishing Ω and if the value of $\bar{c}$ at the shock front exceeds the wave-front velocity, U, then there are other important differences. There will occur a progressive destruction of the crest of the wave at the shock front and, when $G_a(t)$ is a monotone decreasing function of t, a progressive broadening of the profile of the wave as it advances outward.

To illustrate these points, we consider the value of $\tau^*(R)$ at the shock front, given by Eq. 3.30,

$$\tau^* = \int_{a_0}^{R} \frac{dr'}{U[r', \tau_0(r')]} - \int_{a(\tau_0)}^{R} \frac{dr'}{\bar{c}(r', \tau_0)} , \qquad (3.34)$$

where the integral $\int_{a_0}^{R} dr'/U$ is the time t_0 required for the shock front to travel to the point R. We remark that if $\bar{c} > U$, τ_0, initially zero, is an increasing function of R. Thus at a specified point

R, only that part of the wave emitted by the gas sphere after the time $\tau_0(R)$ is realized, the crest of wave emitted in the interval $0 \leq t \leq \tau_0$ being destroyed at the shock front as the wave progresses outward.

For small intervals of time t' after the wave front has passed a point R, we may expand τ in a Taylor series,

$$\begin{aligned} \tau &= \tau_0 + t'/\gamma , \\ t' &= t - t_0 , \\ \frac{1}{\gamma} &= \left(\frac{\partial \tau}{\partial t}\right)_R , \end{aligned} \tag{3.35}$$

where t_0 is the time at which the front reaches the point R, and $1/\gamma$ is the partial time derivative of τ at time t_0. An expansion of this type could be made not only at the shock front R but also at an arbitrary point r behind the front, if desired. From Eq. 3.30, we obtain for γ,

$$\gamma = 1 - \frac{u_a(\tau)}{\bar{c}_a(\tau)} - \int_{a(\tau)}^{R} \frac{1}{\bar{c}^2}\left(\frac{\partial \bar{c}}{\partial \tau}\right)_{r'} dr' . \tag{3.36}$$

It is to be expected that $\bar{c}$ is a decreasing function of τ at constant r since it is a decreasing function of Ω and $G_a(t)$ is in our applications a decreasing function of time. Thus γ will be greater than unity for sufficiently large r. This means that the t' scale is broadened relative to the $\tau - \tau_0$ scale, and the wave profile at R is broadened relative to the time profile of the wave during emission from the gas sphere surface.

At sufficiently large distances R from the center of the charge, $\Omega(R,t)$, though not of course $\Omega_a(\tau)$, can be approximated in acoustical form by p/ρ_0, where ρ_0 is the density of water at zero pressure. With this approximation and the approximation, Eq. 3.35, Eq. 3.33 becomes

$$\begin{aligned} p &= (a_0/R)\, P(\tau_0 + t'/\gamma) , \\ P(t) &= \rho_0 \frac{a(t)}{a_0} \Omega_0(t) . \end{aligned} \tag{3.37}$$

These relations, together with Eqs. 3.34 and 3.36, provide an an asymptotic relation for the pressure as a function of time t' at a fixed point R in terms of the radius of the gas sphere $a(t)$ and the enthalpy of the water at this surface at time $\tau_0 + t'/\gamma$.

The foregoing analysis reduces the problem of propagation of the shock wave from the gas-sphere surface $a(t)$ to an investigation of the slopes $\bar{c}$ of the characteristics of G. An exact determination of $\bar{c}$ or even a rigorous proof that $\bar{c}$ has the properties hypothetically ascribed to it appears to be prohibitively difficult. However, it is possible to get information about the asymptotic behavior of $\bar{c}$, to assign a reasonable approximation to $\bar{c}$, and to estimate the error entailed in this approximation. From the acoustical approximation, Eq. 3.23, we remark that $\bar{c}$ approaches c_0, the sound velocity at zero pressure, as r increases. The asymptotic value c_0 is not adequate for our purposes. As a possible approximation to $\bar{c}$, the local sound velocity $c + u$ in the moving medium suggests itself as reasonable. In order to investigate this approximation, we write,

$$\bar{c} = (\partial G/\partial t)/(\partial G/\partial r),$$

$$g = \frac{\partial G}{\partial r} + \frac{1}{c+u}\frac{\partial G}{\partial t}, \tag{3.38}$$

where g is the variation of G along the contours of slope $c + u$. Expressing $\partial G/\partial r$ in terms of $\partial G/\partial t$ and g, writing $\partial G/\partial t$ as $G_a'(\tau)(\partial\tau/\partial t)$, and using Eqs. 3.13 and 3.19 for the calculation of g, we finally obtain

$$\bar{c} = (c+u)\left[1 - \frac{(c+u)\,q}{G_a'(\tau)\,\tau_t'}\right]^{-1},$$

$$g = \Omega - uc + r(c-u)\left[\frac{\partial \bar{s}}{\partial r} + \frac{1}{c+u}\frac{\partial \bar{s}}{\partial t}\right], \tag{3.39}$$

$$G_a'(\tau) = \frac{DG_a}{D\tau}, \quad \tau_t' = \left(\frac{\partial \tau}{\partial t}\right)_r.$$

A further reduction of g with the aid of Eqs. 3.13, 3.16, 3.17, and 3.24 yields,

$$g = \frac{c+3u}{2(c+u)}\left(\omega + \frac{3\sigma^2}{2} - c\sigma\right) - \frac{2u(\sigma^2 - \bar{s}^2)}{c+u} - g\bar{s}^2$$
$$+ (c-u)\left[\frac{\partial(rh)}{\partial r} + \frac{1}{c+u}\frac{\partial(rh)}{\partial t}\right], \tag{3.40}$$

$$h = \bar{s} + \varphi/2r^2.$$

We have already remarked (Eqs. 3.24 and 3.36) that h vanishes in regions in which the flow is either incompressible or accustical, a circumstance which makes the form, Eq. 3.40, especially convenient as an expression for g.

From Eqs. 3.23 and 3.26, we remark that σ and u behave asymptotically as $1/r$ and $\bar{s}$ as $1/r^2$. If c is a continuous function of density, we may assume it to be an analytic function of σ of the form $c_0 + c_1\sigma + \cdots$. Since ω is equal to $\int_0^\sigma c\,d\sigma$, it has the power series $c_0\sigma + c_1\sigma^2/2 + \cdots$. Thus the sum of the first three terms of the expression for g, Eq. 3.40, is at most of order σ^2 and thus of order $1/r^2$ in its asymptotic behavior. In

regard to the last term of Eq. 3.40, we remark that an alternative expression for h is

$$h = \frac{1}{2}\left(\sigma - \Omega/c_\varphi\right), \qquad c_\varphi = \left(\partial r/\partial t\right)_\varphi , \tag{3.41}$$

where c_φ is the propagation velocity of $\varphi(r,t)$. From Eq. 3.22 we see that $c_\varphi \to c_0$ in the acoustical approximation and thus, since $\Omega \to c_0\sigma$, h will consist of terms of the order of σ^2 and u^2 and higher. Since $\bar{s}$ or $(\sigma - u)/2$ is of order $1/r^2$, we may consider the dominant term in h to be of the order $\bar{r}^2/c_0$. Using the Riemann equations 3.18 to compute the derivatives of $r\bar{r}^2/c_0$, we get

$$(c-u)\left[\frac{\partial(rh)}{\partial r} + \frac{1}{c+u}\frac{\partial(rh)}{\partial t}\right] = O(\bar{r}^2) = O(1/r^2). \tag{3.42}$$

Thus the remainder term g is of order $1/r^2$. In the pure acoustical approximation, we note that $\tau \to t - r/c_0$ and τ'_t tends to unity. Therefore

$$(c+u)\,g/G'_a(\tau)\,\tau'_t = O(1/r^2). \tag{3.43}$$

A more refined analysis than the pure acoustical theory, based upon the expression,

$$\left(\frac{\partial\tau}{\partial t}\right) = 1 - \frac{u_a(r)}{\bar{c}_a(\tau)} - \int_{a(\tau)}^{r} \frac{1}{\bar{c}^2}\left(\frac{\partial\bar{c}}{\partial\tau}\right)_{r'} dr', \tag{3.44}$$

shows that if $\bar{c}$ contains terms of order $1/r$ then

$$\frac{\partial\tau}{\partial t} \longrightarrow -\log r \quad \text{as} \quad r \longrightarrow \infty . \tag{3.45}$$

The asymptotic behavior described by Eq. 3.45 arises from the fact that there is some spreading of the wave profile even in the acoustical limit.

Therefore, we have been able to show that with increasing r,

$$(c+u)\, g / G_a'(\tau)\, \tau_t' = O(\log r / r^2), \tag{3.46}$$

where $O(\log r/r^2)$ denotes terms diminishing as $(\log r)/r$ or more rapidly. Thus, we have the asymptotic result,

$$\bar{c} = c + u + O(\log r / r^2). \tag{3.47}$$

We shall find it sufficient to adopt $c+u$ as an approximation to $\bar{c}$.

The corresponding approximation to the retarded time τ of Eq. 3.28 then becomes

$$\tau = t - \int_{a(\tau)}^{r} \frac{dr'}{c+u}, \tag{3.48}$$

where the integral is again taken along a path at constant τ. The error in $G(r,t)$ arising from the use of the approximate τ of Eq. 3.48 can be expressed in the following manner. With this definition of τ, $(\partial G/\partial r)_\tau$ is no longer zero but has the value

$$\left(\frac{\partial G}{\partial r}\right)_\tau = \frac{\partial G}{\partial r} + \frac{1}{c+u}\frac{\partial G}{\partial t} = g(r,\tau), \tag{3.49}$$

where $g(r,\tau)$ is given by Eq. 3.46. Since the approximate τ becomes equal to t when r is equal to $a(t)$, we obtain by integrating 3.49 along a path at constant

$$G(r,t) = (1+\epsilon)\, G_a(\tau),$$
$$\epsilon = \frac{1}{G_a(\tau)} \int_{a(\tau)}^{r} g(r',\tau)\, dr'. \tag{3.50}$$

We shall find that water is a particularly favorable case for the application of the approximate theory. Numerical estimates of an upper bound

to the error ϵ in examples to which the theory is to be applied indicate that it does not exceed 20% in the most unfavorable cases and probably is much less than this. Since ϵ is algebraically negative, the approximate theory in which it is neglected yields an upper bound to G.

4. Motion of Surface of Gas Sphere[16]

According to the initial conditions described in Section 2, we have at the instant $t = 0$ a gas sphere of radius a_0 at a uniform pressure p_e, the equilibrium pressure of the product gases arising from adiabatic conversion of the solid explosive at constant volume. The water surrounding the gas sphere is at a uniform pressure p_0 (1 atm. or for practical purposes zero). The discontinuity in pressure $p_e - p_0$ at the boundary between water and gas is removed instantaneously with the establishment of a pressure p_1 and velocity u_1 on the sphere $r = a_0$. At the same time, an advancing shock wave starts in the water and a receding rarefaction wave starts in the gas sphere. The motion of the surface $a(t)$ is controlled by these two waves. The propagation theory that we have developed for the wave in water can be applied with slight modification to the wave in the gas sphere, since in a rarefaction wave the requirement of no dissipation is satisfied exactly. However, in setting up the equations of motion of the gas-sphere surface, we shall restrict our considerations to an initial period of time during which the wave just interior to the surface $a(t)$ is a simple recessive rarefaction wave.

After a period certainly greater than $2a_0/c_1^*$ where c_1^* is the initial velocity of sound in the gas, a reflected wave will arrive at the sphere surface, after which the rarefaction wave becomes compound. A

16/ See Reference 7, Section 3.

solution of the compound rarefaction wave involves the spherical analog of the Lagrange ballistic problem and is very complicated. We believe that the complication introduced by successive reflections of the rarefaction wave between the center and surface of the gas sphere is not of great practical importance for two reasons. First, the major part of the water shock wave is emitted in an interval of the order of $2\,a_0/c_0^*$, so that the first reflected wave would at most disturb its tail at all distances of practical interest. Second, due to the attenuating effect of the factor $1/r$ in a spherical wave and the fact that the gas sphere will have expanded to several times its initial radius before the first reflected wave arrives at the surface, the pressure will already be so low when it arrives that it will have little accelerating effect on the surface. Nevertheless, it is possible that the successive reflected waves in the gas sphere will produce small pulsations in the tail of the shock wave, which we shall ignore in the present theory.

At the surface $a(t)$, we have continuity of pressure and material velocity and therefore of the total time derivatives of these quantities. Making use of the continuity condition, we may write the equations of continuity exterior and interior to $a(t)$ in the form,

$$\begin{aligned} \frac{1}{c^2\rho}\frac{Dp}{Dt} &= -\frac{\partial u}{\partial r} - \frac{2u}{a}, \\ \frac{1}{c^{*2}\rho^*}\frac{Dp}{Dt} &= -\left(\frac{\partial u}{\partial r}\right)^* - \frac{2u}{a}, \end{aligned} \tag{4.1}$$

where c and ρ refer to the water just exterior to the surface; c^* and ρ^* to the gas just interior to the surface. The partial derivatives $(\partial u/\partial r)$ and $(\partial u/\partial r)^*$ are in general different. To eliminate them from Eqs.

4.1, we must make use of the theory of propagation of the shock and rarefaction waves emitted by the moving sphere surface. The advancing shock wave in water, we treat according to Section 3 as a wave in which $r\Omega$ or G is propagated outward with a velocity $\bar{c}$. The receding rarefaction wave before the arrival of reflections from the center of the sphere, we treat as a recessive wave in which $r\Omega$ or G is propagated from $a(t)$ with velocity $-\bar{c}^*$.

To illustrate the procedure, we outline the elimination of $\partial u/\partial r$ from the first of Eq. 4.1. From the theory of propagation, the equation of motion, and the definition of G, we have

$$\begin{aligned} &\frac{\partial G}{\partial t} + \bar{c}\,\frac{\partial G}{\partial r} = 0 \ , \\ &\rho \frac{Du}{Dt} + \frac{\partial p}{\partial r} = 0 \ , \\ &dG = \Omega\, dr + r\, dp/\rho + r u\, du. \end{aligned} \tag{4.2}$$

Eqs. 4.2 lead to the following relation,

$$u(\bar{c}-u)\frac{\partial u}{\partial r} + \frac{1}{\rho}\frac{Dp}{Dt} - (\bar{c}-2u)\frac{Du}{Dt} = -\frac{\Omega \bar{c}}{r} \ . \tag{4.3}$$

Elimination of $\partial u/\partial r$ between Eq. 4.3 and the first of Eqs. 4.1 yields at the surface $r = a$,

$$\frac{1}{\rho c}\frac{Dp}{Dt} = \frac{c(\bar{c}-2u)}{c^2 - u\bar{c} + u^2}\frac{Du}{Dt} - \frac{c}{a}\,\frac{\bar{c}(\omega - 3u^2/2) + 2u^3}{c^2 - u\bar{c} + u^2} \ . \tag{4.4}$$

In an exactly similar manner, we obtain from the propagation equation for the gas on the interior of the sphere

$$\begin{aligned} &\frac{1}{\rho^* c^*}\frac{Dp}{Dt} = -\frac{c^*(\bar{c}^* - 2u)}{c^{*2} - u\bar{c}^* + u^2}\frac{Du}{Dt} + \frac{c^*}{a}\,\frac{\bar{c}^*(\omega^* - 3u^2/2) + 2u^3}{c^{*2} - u\bar{c}^* + u^2} \ , \\ &\omega^* = \int_{\rho_e^*}^{\rho^*} c^2\, d\rho/\rho \ , \end{aligned} \tag{4.5}$$

where ω^* is to be computed along the initial adiabatic of the gas. Eqs. 4.4 and 4.5 constitute a system of differential equations for p and u, the solution of which together with the initial values of these functions determines p and u on the gas sphere as functions of time, the velocities c, $\bar{c}$, c^*, and $\bar{c}^*$ being determined as functions of p and of u along the initial adiabatics of the two fluids by their respective equations of state. In the present discussion, we shall suppress the subscript a used to denote values of functions on the surface $a(t)$ in Section 3, since all equations of this section refer to this surface alone.

We now introduce the approximations $c+u$ and c^*-u for $\bar{c}$ and $\bar{c}^*$ into Eqs. 4.4 and 4.5. The error introduced in the rarefaction wave in the gas by approximating $\bar{c}^*$ with c^*-u is of the same relative magnitude as the corresponding approximation in water, although perhaps numerically a little larger due to the fortunate cancelation of certain terms in the remainder for water. With these approximations, Eqs. 4.4 and 4.5 reduce to

$$\begin{aligned}
\frac{1}{\rho c}\frac{Dp}{Dt} &= \frac{Du}{Dt} - J\frac{uc}{a}, \\
\frac{1}{\rho^* c^*}\frac{Dp}{Dt} &= -\frac{Du}{Dt} - J^*\frac{uc^*}{a}, \\
J &= \frac{1}{uc}\left[\frac{c+u}{c-u}\omega - \frac{3u^2}{2} - \frac{u^3}{c-u}\right], \\
J^* &= \frac{1}{uc^*}\left[-\frac{c^*-u}{c^*+u}\omega^* + \frac{3u^2}{2} - \frac{u^3}{c^*+u}\right].
\end{aligned} \tag{4.6}$$

From Eqs. 3.5, we obtain by rearrangement,

$$\begin{aligned}
\frac{Dp}{Dt} &= -\rho\rho^* c c^* \frac{Jc + J^* c^*}{\rho c + \rho^* c^*}\frac{u}{a}, \\
\frac{Du}{Dt} &= \frac{J\rho c^2 - J^*\rho^* c^{*2}}{\rho c + \rho^* c^*}.
\end{aligned} \tag{4.7}$$

Since ω is positive and ω^* is negative, J and J^* are initially positive quantities of order of magnitude unity. If oscillations of the gas sphere, which occur only after a long period of time are ignored, J^* remains positive, but J may become negative, though never sufficiently so to make Dp/Dt positive.

From Eqs. 4.7, we infer that Dp/Dt is initially large in absolute magnitude and negative in sign. Although decreasing somewhat in magnitude, it remains negative during the initial phase of the motion. The peak approximation is therefore appropriate for p as well as for the functions ω and σ.[17] The derivative Du/Dt may initially have either sign, depending upon the equations of state of the two mediums. For a boundary between water and typical gas mixtures resulting from explosion products, Du/Dt is initially large and positive, but diminishes rapidly to zero and becomes negative. As a more detailed investigation will show, u depends

---

17/ A function F(t), described by the peak approximation, is supposed to have an exponential decay of the form,

$$F(t) = F_1 e^{-t/\theta_F}$$

where $F_1 = F(0)$, and $-1/\theta_F$ is the initial value of the logarithmic derivative of F with respect to t.

$$-1/\theta_F = [d \log F(t)/dt]_{t=0}$$

θ_F may be called the time constant. The function $F(t)$ is thus represented by a two parameter curve, an approximation that is appropriate when $F(t)$ is initially a rapidly decreasing function of t.

asymptotically on time as $(1 + t/\theta_2)^{-2/\lambda}$, where θ_2 is a characteristic time. The initial peak approximation to the term $a u^2/2$ in $G_a(t)$ is therefore poor, but due to the rapid change in sign of Du/Dt, $a(t)$ may be treated as a slowly varying function of time.

The peak approximation to the enthalpy ω is to be obtained as follows,

$$\omega_a(t) = \omega_1 e^{-t/\theta_1} ,$$
$$1/\theta_1 = -\left[D \log \omega / Dt\right]_{t=0} , \qquad (4.8)$$
$$= -(1/\rho_1 \omega_1)\left[Dp/Dt\right]_{t=0} ,$$

where ω_1 is the initial value of $\omega_a(t)$ on the gas sphere. Using the first of Eqs. 4.7 to get the limit on the right-hand side of Eq. 4.8, we obtain

$$\theta_1 = a_0/c_{\theta_1} ,$$
$$c_{\theta_1} = \frac{\rho_1'' c_1^* u_1}{\omega_1} \frac{J_1 c_1 + J_1^* c_1^*}{\rho_1 c_1 + \rho_1^* c_1^*} c_1 , \qquad (4.9)$$

where the subscript 1 denotes as usual initial values of the quantities on the gas sphere surface. Since $a(t)$ is a slowly varying function of time, the appropriate peak approximation to $a(t)\,\omega_a(t)$ is

$$a(t)\,\omega_a(t) = a_0 \omega_1 e^{-t/\theta_1} . \qquad (4.10)$$

Eq. 4.10 therefore determines the first term in $G_a(t)$, equal to $a(t)\left[\omega_a(t) + u_a^2/2\right]$, as a function of time and of parameters depending upon the initial conditions at the gas sphere surface.

In order to investigate the manner in which $u(t)$, the velocity of the gas sphere surface depends upon time, we return to Eqs. 4.6, the first of which may be written in the alternative form

$$a\frac{Du}{Dt} + \frac{3}{2}u^2 - B(t) = 0 ,$$

$$B(t) = \frac{c+u}{c-u}\omega + \frac{a}{\rho c}\frac{Dp}{Dt} - \frac{u^2}{c+u} . \qquad (4.11)$$

The incompressible approximation to $B(t)$ is the following,

$$\lim\ (c \to \infty)\ B(t) = \omega = (p - p_0)/\rho_0 .$$

In this approximation, Eq. 4.11 becomes

$$a\frac{Du}{Dt} + \frac{3u^2}{2} - \frac{p - p_0}{\rho_0} = 0 . \qquad (4.12)$$

Eq. 4.12 was employed by Lamb[3] in his theory of underwater explosions to describe the motion of the gas sphere. To integrate Eq. 4.12, he neglected p_0 and assumed p to be the equilibrium pressure of the uniformly expanding gas sphere of volume $4\pi a^3/3$. If the term p_0 is retained in the last term of Eq. 4.12, one finds that instead of a monotonic increase in $a(t)$, oscillations of the gas sphere occur a long time after the emission of the shock wave. Butterworth[5] and Herring[18] have given a satisfactory treatment of these oscillations and the secondary pressure pulses arising from them. Since they have no appreciable influence on the shock wave, we shall approximate the asymptotic value of $B(t)$ at long times by zero instead of p_0/ρ_0.

In order to integrate Eq. 4.11 for the initial stages of the motion of the gas sphere, we recall that the peak approximation is suitable for p and ω as long as their magnitude is of any significance for our purposes. Applying the peak approximation to the factors ω and Dp/Dt in the first two terms of $B(t)$ and neglecting the relatively small term $u^2/(c-u)$, we obtain

18/ C. Hering, NDRC Division 6 Report C4-sr 20 (1941).

$$a\frac{Du}{Dt} + \frac{3u^2}{2} = \left(\frac{a_0}{a}\right)^{1/2} B_1 e^{-t/\theta_1} ,$$

$$\theta_1 = \frac{a_0}{c_1}\frac{\omega_1}{u_1\rho_1^* c_1^*}\frac{A a_1 + \rho_1^* c_1^*}{J_1 c_1 + J_1^* c_1^*} , \qquad (4.13)$$

$$B_1 = \omega_1\left(\frac{c_1 + u_1}{c_1 - u_1} - \frac{a_0}{c_1\theta_1}\right) ,$$

where the slowly varying factor $(a_0/a)^{1/2}$ is retained in $B(t)$ for convenience in integration. Writing Da/Dt for u and integrating once, we obtain

$$a^{3/2}u = a_0^{3/2}u_1\left[1 + \mu_0\mu_1(1 - e^{-t/\theta_1})\right] ,$$

$$\mu_0 = B_1/u_1^2 , \quad \mu_1 = u_1\theta_1/a_0 . \qquad (4.14)$$

Again writing Da/Dt for u and integrating Eq. 4.14, we get

$$\left(\frac{a}{a_0}\right)^{5/2} = \left(1 - \frac{5}{2}\mu_0\mu_1^2\right)\left[1 + \frac{t}{\theta_2} + \frac{5\mu_0\mu_1^2}{2 - 5\mu_0\mu_1^2}e^{-t/\theta_1}\right] ,$$

$$\theta_2 = \frac{2}{5}\frac{a_0}{u_1}\frac{1 - 5\mu_0\mu_1^2/2}{1 + \mu_0\mu_1} . \qquad (4.15)$$

The asymptotic forms of Eqs. 4.14 and 4.15 at large times are

$$a^{3/2}u = a_0^{3/2}u_1(1 + \mu_0\mu_1) ,$$

$$(a/a_0)^{5/2} = (1 - 5\mu_0\mu_1^2/2)(1 + t/\theta_2) . \qquad (4.16)$$

The asymptotic constancy of $a^{3/2}u$ and variations of a/a_0 as $t^{2/5}$ hold rigorously when p_0 is zero and p tends to zero more rapidly than $1/t^2$. The constancy of $a^{3/2}u$ implies conservation of the kinetic energy integral of the fluid. At all times of significance to us p_0 may be treated as zero, since we are not concerned with the secondary pulses which have already been adequately treated by others.

The second term $a(t)u(t)^2/2$ in $G_a(t)$ becomes, with the use of Eqs. 4.14 and 4.15,

$$\frac{a u^2}{2} = \lambda \frac{a_0 u_1^2}{2} \frac{\left[1 - e^{-t/\theta_1}/(1+\mu_0\mu_1)\right]^2}{\left[1 + t/\theta_2 + 5^{-}\mu_0\mu_1^2 e^{-t/\theta_1}/(2 - 5^{-}\mu_0\mu_1^2)\right]^{4/5^{-}}}$$

$$\lambda = \frac{(1+\mu_0\mu_1)^2}{(1 - 5^{-}\mu_0\mu_1^2/2)^{4/5^{-}}} \qquad (4.17)$$

where properly terms of the order e^{-2t/θ_1} and $t\,e^{-t/\theta_1}$ should be dropped to be consistent with the peak approximation to $B(t)$. If we add Eq. 4.17 to the peak formula for $a\omega$ of Eq. 4.10 and suppress such terms, the resulting expression for $G_a(t)$ is slightly in error for $t = 0$. Since, however, $u^2/2$ is small relative to ω in the initial stages of the motion, a suitable interpolation formula for $G_a(t)$, accurate for $t = 0$ and for long times, and consistent with the peak approximations of Eq. 4.10 and 4.17 is the following,

$$G_a(t) = a_0 \Omega_{10} e^{-t/\theta_1} + a_0 \Omega_{11} (1 + t/\theta_2)^{-4/5^{-}},$$

$$\Omega_{10} = \omega_1 + (1-\lambda) u_1^2/2 \,, \quad \Omega_{11} = \lambda u_1^2/2 \,. \qquad (4.18)$$

Since Ω_{11} is in general small relative to Ω_{10}, the complete peak approximation,

$$G_a(t) = G_1 e^{-t/\theta_1},$$

$$G_1 = a_0(\omega_1 + u_1^2/2) = a_0 \Omega_1 \,, \qquad (4.19)$$

may be used for small values of t when $5\theta_2/4$ does not differ greatly from θ_1. If Eq. 4.19 is employed to represent $G_a(t)$, the tail of the shock wave will of course be distorted since the exponential differs widely

from $t^{-4/5}$ for long times. A suitable compromise between Eqs. 4.18 and 4.19 appears to consist in using Eq. 4.19 for calculating τ_e and γ, the retarded time and time spread, and then using Eq. 4.18 for the explicit calculation of the pressure behind the front for $\tau > \tau_e$. However, the complete theory based upon Eq. 4.19 yields surprisingly satisfactory results and is probably adequate for most engineering calculations requiring an estimate of the intensity and duration of the initial pressure pulse produced by an underwater explosion.

Equations 4.18 and 4.19 together with the propagation theory of Section 2, provide a complete description of the shock wave emitted by a spherical charge of explosive in terms of the initial conditions on the boundary between the gaseous products of the explosive and the water.

5. Dissipation and Spread Parameters[19]

In this section, we wish to complete the evaluation of the retarded time τ_e of the shock front and of the time-spread parameter γ for use in the propagation theory, Eq. 3.33, and in the asymptotic theory of Eq. 3.37. The latter theory is appropriate for the calculation of the pressure-time curve of the shock wave at distances from the charge exceeding about 25 charge radii, and it forms a basis for the discussion of the limiting properties of the shock wave at great distances from the charge. In this section, we shall explicitly employ several properties of water that are derivable from the equation of state, and it is necessary at this point to introduce a particular equation of state.

The Tait[20] equation may be written in the form

19/ See Reference 7, Section 2.

20/ P. G. Tait, "Report on Some of the Physical Properties of Fresh Water and Sea Water." The Physics and Chemistry of the Voyage of H.M.S. Challenger., vol. II, Part IV, S. P. LXI (1888).
See also R. E. Gibson, J. Am. Chem. Soc., 56, 4 (1934); 57, 284 (1935).

$$\frac{1}{\rho^2}\left(\frac{\partial \rho}{\partial p}\right)_T = \frac{1}{n[p + B(T)]} , \qquad (5.1)$$

where n is a constant and B a function of T only. This equation has been shown by Gibson and Bridgman to represent compressibility data for water at pressures up to 350,000 lb/in.^{2}. For our purposes, we employ a modified form of the Tait equation along an adiabatic in the form,

$$\frac{1}{\rho}\left(\frac{\partial \rho}{\partial p}\right)_S = \frac{1}{n[p + B(S)]} . \qquad (5.2)$$

Eq. 5.2 is of a more reasonable form than the isothermal Tait equation for use at very high pressures, since the latter permits a state of zero volume for finite pressure and in consequence must overestimate the sound velocity at high pressures. The adiabatic of sea water (taken to be 0.7 molal HCl solution) passing through 1 atmosphere and 20° C. is adequately represented by Eq. 5.2 with $n = 7.15$, $B = 3.047$ kilobars.[21] Eq. 5.2 permits the calculation by straightforward methods of the shock-front conditions (Eq. 2.2) and of the enthalpy ω, acoustic velocity c, and Riemann function σ as functions of the shock-front pressure. The results for sea water initially at 20° C. are listed in Table 5.1 for shock-front pressures up to 80 kilobars.[22]

In the further discussion of the propagation theory, it is necessary to employ various explicit relations for the various variables behind the

---

21/ The quantities n and B were supplied by R. E. Gibson.

22/ J. G. Kirkwood and J. M. Richardson, OSRD Report No. 813 (1942). See also J. M. Richardson, A. B. Arons, H. H. Halverson, J. Chem. Phys., 15, 785 (1947).

TABLE 5.1 - Properties of strong shock fronts in salt water initially at 20° C.

P (kilobars)	u_p (m./sec.)	σ (m./sec.)	U (m./sec.)	c (m./sec.)
0	0	0	(1465)	(1465)
5	251	249	1975	2230
10	426	416	2335	2755
15	567	549	2630	3175
20	689	663	2880	3535
25	796	765	3110	3655
30	898	859	3320	4140
35	990	947	3510	4405
40	1075	1030	3690	4650
50	1235	1185	4020	5100
60	1380	1330	4325	5505
70	1510	1465	4610	5880
80	1625	1600	4885	6240

shock front. Eq. 5.2 provides a relation that is convenient for this purpose. Although the shock-front conditions should properly be calculated from the Rankine-Hugoniot relations, Eq. 2.2, the small value of the entropy change at the shock front makes it possible to assume an adiabatic change. Since the pressure p_0 of the undisturbed fluid can be neglected compared to the parameter B, we note that

$$B = \rho_0 c_0^2 / n, \tag{5.3}$$

where ρ_0 is the density and c_0 the velocity of sound in the undisturbed fluid. Using Eq. 5.2, we find the following important relations,

$$\begin{aligned} p &= \frac{\rho_0 c_0^2}{n}\left[\left(\frac{\rho}{\rho_0}\right)^n - 1\right], \\ c &= c_0\left(\frac{\rho}{\rho_0}\right)^{(n-1)/2} = c_0\left(1 + \frac{np}{\rho_0 c_0^2}\right)^{(n-1)/2n}, \\ \sigma &= \frac{2c_0}{n-1}\left[\left(\frac{\rho}{\rho_0}\right)^{(n-1)/2} - 1\right] = \frac{2c_0}{n-1}\left[\left(1 + \frac{np}{\rho_0 c_0^2}\right)^{(n-1)/2n} - 1\right], \\ c &= c_0 + \frac{n-1}{2}\sigma, \end{aligned} \tag{5.4}$$

where p is the pressure, c sound velocity, and c_0 sound velocity at zero pressure. The enthalpy ω, equal to $\int_0^\sigma c\, d\sigma$, with neglect of dissipation is

$$\omega = c_0\sigma + \frac{n-1}{4}\sigma^2. \tag{5.5}$$

Moreover, if the Riemann function $\bar{s}$ is small at the shock front, the wave front velocity U is related to σ in the following manner,

$$U = c_0 + \frac{n+1}{4}\sigma . \qquad (5.6)$$

Detailed numerical calculations, based upon the isothermal Tait equation and the Hugoniot conditions, have been carried out for the properties of water at the shock front up to a pressure of 50 kilobars (1 kilobar = 986.9 atmospheres). They show that $\tilde{s}$ is very small in comparison with u and that the change in adiabatic along the Hugoniot curve is slight. Except for the sound velocity c at the higher pressures, the approximate formulas 5.4, 5.5, and 5.6, based upon the modified Tait equation 5.2 integrated along the initial adiabatic, yield results which are not significantly different from the numerical calculations based on Eq. 5.1. Since the Hugoniot curve for water crosses the liquid-ice VII phase boundary at about 25,000 atm., extrapolation into a metastable liquid region inaccessible to measurement is necessary. The occurrence of the transition during the short time of passage of a shock wave seems entirely excluded on the basis of Bridgmen's experiments.

We return now to the asymptotic theory of the pressure-time curve. The retarded time $\tau_0(R)$ at the shock front is given by

$$\tau_0(R) = \int_{a_0}^{R} \frac{dr'}{U(r', \tau_0')} - \int_{a(\tau_0)}^{R} \frac{dr'}{c+u} , \qquad (5.7)$$

obtained from Eq. 3.34 with the substitution $\bar{c} = c+u$. The time-spread parameter γ, a measure of the broadening of the $t - t_0$ scale relative to the $\tau - \tau_0$ scale, was defined by

$$\gamma = \left(\frac{\partial t}{\partial r}\right)_R . \tag{3.35}$$

The asymptotic propagation equation, valid when $\Omega(R,t)$ can be approximated in acoustical form by p/ρ, has been shown to be

$$p = (a_0/R)\, P(\tau_0 + t'/\gamma), \quad t' = t - t_0(R),$$
$$P(t) = p_0 \frac{a(t)}{a_0}\, \Omega_a(t). \tag{3.37}$$

We remark again that at the shock-front numerical calculation shows $\bar{s}$ never to exceed a few percent of u. Therefore at the shock front or in a region immediately behind it, we can safely approximate $\bar{s}$ by zero and u by σ. We shall employ this approximation in calculating τ_0 and γ. Although the second integral of Eq. 5.7 defining τ_0, is taken along a path extending behind the shock front, it is easy to see that no point of this path lies very far behind the front. This is because the shock front $R(t')$ moves only slightly more slowly than the wave of constant τ_0, that is, the point $r'(t', \tau_0)$. The time elapsing between the passage of the shock front and of the wave of constant τ_0 at any given point r' is of the order of τ_0 or smaller, and for our theory only small values of τ_0 are important. Therefore the Riemann $\bar{s}$ has no time to build up to appreciable values. With the neglect of $\bar{s}$, we may write, using Eqs. 5.4, 5.5, and 5.6,

$$\begin{aligned} c + u &= c_0(1 + 2\beta\sigma), \\ U &= c_0(1 + \beta\sigma), \\ \Omega &= c_0\sigma(1 + \beta\sigma), \\ \beta &= (n+1)/4c_0 . \end{aligned} \tag{5.8}$$

From the equation of propagation, 3.32, σ' and τ satisfy the relation,

$$G_a(\tau) = c_0 \tau' \sigma (1+\beta\sigma). \tag{5.9}$$

Change of variable from τ' to σ in the integral of Eq. 3.48 and use of Eq. 5.9 gives

$$\begin{aligned} \tau &= t - \chi(\tau,\sigma), \\ \chi(\tau,\sigma) &= \frac{G_a(\tau)}{c_0^2} \int_0^{\sigma_a} \frac{d\sigma'}{\sigma'^2(1+\beta\sigma')^2}, \\ &= \frac{\beta G_a(\tau)}{c_0^2}\left[z - z_a - \left(\frac{1}{z} - \frac{1}{z_a}\right) - 2\log\frac{z}{z_a}\right], \\ z &= 1 + 1/\beta\sigma, \quad \sigma_a = \sigma_a(\tau), \end{aligned} \tag{5.10}$$

where the subscript a denotes the value of a function on the surface of the gas sphere at time τ. By differentiation of Eq. 5.10, we at once obtain the time-spread parameter γ of Eq. 3.35

$$\gamma = 1 - \frac{1}{\beta c_0}\frac{1}{z_a+1} - \frac{2\beta}{c_0^2} G_a'(\tau_0)\left[\log\frac{z}{z_a} - \frac{4(z-z_a)}{(z+1)(z_a+1)}\right], \tag{5.11}$$

$$G_a'(\tau_0) = dG_a/d\tau_0,$$

where z and z_a are defined in Eq. 5.11 as $1+1/\beta\sigma$ and $1+1/\beta\sigma_a$, respectively.

To determine the retarded time τ_0 at the wave front, we consider the time t_0 required for the wave front to reach the point R.

$$t_0 = \int_{a_0}^{R} \frac{dr}{U[r, \tau_0(r)]}, \tag{5.12}$$

where $\tau_0(r)$ corresponds to a position of the front at point r. Change

of variable from r to σ and τ_0 in the integral of Eq. 5.12, use of Eq. 5.9, and substitution in Eq. 5.10 yields, after an integration by parts,[22]

$$\tau_0 = \frac{\beta}{c_0^2}\left[\int_\sigma^{\sigma_1} \frac{2G_a(\tau_0) - G_a(\tau_0')}{\sigma'(1+\beta\sigma')^3}\,d\sigma' + \frac{G_a(\tau_0) - G_1}{\sigma_1(1+\beta\sigma_1)^2} + J_0(\tau_0)G_a(\tau_0)\right],$$

$$J_0 = \frac{1}{\beta}\int_{\sigma_a}^{\sigma_1} \frac{d\sigma'}{\sigma'^2(1+\beta\sigma')^2} = Z_a - Z_1 - \left(\frac{1}{z_a} - \frac{1}{z_1}\right) - 2\log\frac{z_a}{z_1}, \quad (5.13)$$

$$\tau_0' = \tau_0(\sigma'),$$

---

[23] To obtain Eq. 5.13 we proceed as follows. From Eq. 5.9 we get by differentiation

$$dr = -\frac{G_a}{c_0}\frac{1+2\beta\sigma}{\sigma^2(1+\beta\sigma)^2}\,d\sigma + \frac{1}{c_0}\frac{dG_a}{\sigma(1+\beta\sigma)}.$$

Employing this result together with Eq. 5.8 for U in Eq. 5.12, we obtain

$$\tau_0 = \frac{1}{c_0^2}\left[\int_\sigma^{\sigma_1} \frac{G_a(\tau_0')(1+2\beta\sigma')\,d\tau'}{\sigma'^2(1+\beta\sigma')^2} - G_a(\tau_0)\int_\sigma^{\sigma_a} \frac{d\sigma'}{\sigma'^2(1+\beta\sigma')^2} + \int_{G_1}^{G_a} \frac{dG_a}{\sigma'(1+\beta\sigma')^2}\right].$$

Integration of the last term by parts, division of the interval of integration in the second term

$$\int_\sigma^{\sigma_a} = \int_\sigma^{\sigma_1} - \int_{\sigma_a}^{\sigma_1}$$

and partial integration of the term

$$\int_\sigma^{\sigma_1}$$

yields Eq. 5.13.

where c_1, σ_1, and Z_1 refer to the initial values of these variables on the gas sphere at time $t = 0$. Introduction of a new variable y, defined as

$$y = \int_{\sigma}^{\sigma_1} \frac{d\sigma'}{\sigma'(1+\beta\sigma')^2}, \qquad (5.14)$$
$$= \log \frac{Z}{Z_1} + 2\left(\frac{1}{Z} - \frac{1}{Z_1}\right) - \frac{1}{2}\left(\frac{1}{Z^2} - \frac{1}{Z_1^2}\right),$$

into Eq. 5.13 and differentiation with respect to τ_0 gives the following linear differential equation,

$$\frac{dy}{d\tau_0} + \frac{2G_a'(\tau_0)}{G_a(\tau_0)} y = \frac{c_0^2}{\beta} \frac{1+N'(\tau_0)}{G_a(\tau_0)}, \qquad (5.15)$$
$$N(\tau_0) = \frac{1}{c_0^2}\left[\frac{G_1 - G_a}{\sigma_1(1+\beta\sigma_1)^2} - G_a J_0\right].$$

Solution of Eq. 5.15 yields the result[24],

$$y = \frac{c_0^2}{\beta G_a^2}\int_0^{\tau_0} G_a(t)\,dt + \frac{1}{2\beta}\frac{G_1^2 - G_a^2}{G_a^2}\frac{1}{\sigma_1(1+\beta\sigma_1)^2} - \frac{J_0}{2}$$
$$- \frac{a_0 c_0 G_1}{\beta G_a^2}\frac{J_1}{2}, \quad J_1 = \frac{c_0}{\Omega_1}\int_{\sigma_a}^{\sigma_1} (c/a_0)^2\,d\sigma_a. \qquad (5.16)$$

---

[24] To obtain Eq. 5.16 we first integrate the linear equation 5.15 in standard form, using the condition $y = 0$ for $\tau_0 = 0$. Then

$$y = \frac{c_0^2}{\beta G_a^2}\int_0^{\tau_0} G_a(t)\left[1 + N'(t)\right]dt,$$
$$N'(t) = -\frac{1}{c_0^2}\left[\frac{G_a'(t)}{\sigma_1(1+\beta\sigma_1)^2} + \frac{d}{dt}G_a(t)J_0(t)\right].$$

Integrating the first term of $G_a(t)N'(t)$ directly and the second term by parts, we obtain Eq. 5.16.

When $G_a(t)$ is known as a function of time, Eq. 5.16 determines τ_0 as a function of σ' at the shock front, since y is a function of σ alone by Eq. 5.14. By Eq. 5.9, σ' may in turn be expressed as a function of R and τ_0 and thus Eq. 5.16 determines τ_0 as a function of R. In order to put this relationship into a more explicit form, we introduce the following definitions,

$$\theta_a(\tau_0) = \frac{1}{G_1 - G_a(\tau_0)} \int_0^{\tau_0} G_a(t)\, dt ,$$

$$\chi(\tau_0) = G_a(\tau_0)/G_1 , \qquad (5.17)$$

$$x_q = R/a_0 .$$

From Eq. 5.9 and the definition of Z as $1 + 1/\beta\sigma$, we find that Z is a function of q alone,

$$Z = 1 + \frac{q}{2\Gamma_1} + \left[\frac{q}{\Gamma_1} + \left(\frac{q}{2\Gamma_1}\right)^2\right]^{1/2} , \qquad (5.18)$$

$$\Gamma_1 = \beta \Omega_1 / c_0 ,$$

where Ω_1 is the initial value $\Omega_a(0)$ of the kinetic enthalpy of the water at the gas sphere surface. Since y is a function of Z alone, it is by Eq. 5.18 a function of q alone. In fact, for large q we get the asymptotic relation,

$$y = \log q - \Gamma_0 ,$$

$$\Gamma_0 = 2 \log \frac{Z_1}{Z_1 - 1} + \frac{2}{Z_1} - \frac{1}{2}\frac{1}{Z_1^2} . \qquad (5.19)$$

The definition of the characteristic time $\theta_a(\tau_0)$ is particularly useful when we employ a peak approximation to $G_a(t)$.

With the definitions of Eq. 5.17, Eq. 5.16 may be written in the form

$$K_1/\chi^2 - 1/\chi - \alpha K_0(q) = 0 \quad ,$$

$$K_1 = 1 + \alpha(Z_1 - 1)/2 Z_1 - \alpha J_1^-/2 \quad ,$$

$$K_0(q) = (Z_1 - 1)/2 Z_1 + I_1^-[y(q) + J_0/2] \quad , \qquad (5.20)$$

$$\alpha = \theta_0/\theta_a \quad , \quad \theta_0 = a_0/c_0 .$$

We may call $\chi(\tau_0)$ the dissipation factor, since it specifies the ratio of the peak value $G_a(\tau_0)$ at the point R to the initial value $G_a(0)$ of $G_a(t)$ on the gas-sphere surface. The part of the wave emitted from the gas-sphere surface in the time interval τ_0 is destroyed before the wave reaches the point R. Solution of Eq. 5.20 yields

$$\chi(\tau_0) = \frac{2K_1}{1 + [1 + 4\alpha K_1 K_0(q)]^{1/2}} \quad . \qquad (5.21)$$

Eq. 5.21 is strictly a transcendental equation for τ_0, since α depends upon τ_0 through θ_a, and K_1 and K_0 depend upon τ_0 through the integrals J_1 and J_0^-. Given $G_a(t)$, one may solve it exactly by graphical methods or by successive approximation. However, in most cases of interest to us, J_0 and J_1 can be neglected in comparison with the other terms in K_0 and K_1 without significant error. Moreover when the peak formula,

$$G_a(t) = G_1 e^{-t/\theta_1} \quad , \qquad (4.21)$$

discussed in Section 4, is employed for $G_a(t)$, we have

$$\theta_a = \theta_1 \quad , \quad \alpha = \theta_0/\theta_1 \quad , \qquad (5.22)$$

and α is a constant. Under these circumstances, Eq. 5.21 is particularly convenient, since it at once determines the dissipation factor χ as a function of q, and therefore of χq or R/a_0.

When the peak approximation, Eq. 4.21 can be employed for the time spread parameter γ of Eq. 5.11 assumes the simple form,

$$\gamma = 1 - \frac{1}{\beta c_0}\frac{1}{Z_a+1} + 2\alpha\chi\Gamma_1\left[\log\frac{Z}{Z_a} - \frac{4(Z-Z_a)}{(Z+1)(Z_a+1)}\right],$$

$$Z_a = 1 + q_a/2\Gamma_1 + \left[q_a/\Gamma_1 + (q_a/2\Gamma_1)^2\right]^{1/2}, \qquad (5.23)$$

$$q_a = a(\tau)/a_0\chi,$$

where it is usually adequate to approximate q_a by χ.

We now employ the definitions of Eqs. 3.35, 4.19, and 5.17 to express the equation of propagation, Eq. 3.33 in its final form,

$$\Omega(R,t) = \chi\frac{a_0}{R}\Omega_1 e^{-t'/\theta},$$

$$\theta = \gamma\theta_1, \qquad (5.24)$$

where t' is the time measured from the instant t_0 at which the wave front arrives at point R. The dissipation parameter χ is to be calculated by means of Eq. 5.21 and the spread parameter γ is to be calculated by means of Eqs. 5.23.

6. Asymptotic Behavior of Pressure Wave[25]

We have pointed out that the kinetic enthalpy propagation theory is considerably simplified at large distances from the charge. At distances great enough so that the kinetic enthalpy can be represented by its acoustical approximation, the theory reduces to a description of the propagation of the pressure, thus facilitating calculation of the pressure-time

25/ See Reference 7, Section 5.

curve of the shock wave. The intensity and shape of the wave are determined by the dissipation parameter χ and the spread parameter γ. These quantities take on particularly simple forms at large distances from the charges, $R/a_0 \gg 1$. An examination of their asymptotic forms permits a clearer grasp of the physical characteristics of the pressure wave than is to be obtained from the more exact but more complicated formulae of the preceding discussion.

The propagation equation has been written in the form

$$\Omega(R,t) = \chi(a_0/R)\,\Omega_1 e^{-t'/\theta},$$
$$\theta = \theta_1 \gamma, \quad t' = t - t_0, \tag{5.24}$$

where t_0 is the time at which the wave front arrives at point R, and where the dissipation parameter χ and spread parameter γ are given by Eqs 5.21 and 5.23. At distances at which $\Omega(R,t)$ can be represented by its acoustical approximation p/ρ_0, Eq. 5.24 yields for the pressure,

$$p = \chi(a_0/R)\, P_0\, e^{-t'/\theta},$$
$$P_0 = \rho_0 \Omega_1, \quad \theta = \theta_1 \gamma(R/a_0), \tag{6.1}$$
$$\chi = \chi(R/a_0),$$

where ρ_0 is the density of water at zero pressure. For most explosives, p/ρ_0 is an entirely adequate approximation to Ω at distances exceeding twenty-five charge radii.

At large distances from the charges, $R/a_0 \gg 1$, the wave propagates with nearly acoustic velocity c_0, and a sufficient approximation for the particle velocity u (cf. Eq. 3.23) is

$$u = \frac{G_2(\tau)}{c_0 R} + \frac{\varphi}{R^2}.$$

The afterflow term φ/R^2 is negligible relative to the first term at large distances for a long period of time after passage of the wave front. In fact, we may define the initial pulse as the region behind the wave front in which φ/R^2 is negligible. It becomes the dominant term in the afterflow region which does not concern us here.

The asymptotic expressions for the dissipation and spreading parameters, χ and γ, at large distances are the following,

$$\chi = (\rho_0 c_0/\beta)^{1/2} (\alpha P_0 \log R/a_0)^{-1/2},$$
$$P_0 = \rho_0 \Omega_1, \quad \alpha = \theta_0/\theta_a, \tag{6.2}$$
$$\gamma = -2\beta \frac{G_a'(\tau)}{c_0^2} \log R/a_0,$$

if we approximate K_1 by unity, from which it differs only slightly. The peak pressure at the shock front p_m is given by the asymptotic formula

$$p_m = \frac{a_0}{R} \left(\frac{\rho_0 c_0}{\beta}\right)^{1/2} \left(\frac{P_0}{\alpha \log R/a_0}\right)^{1/2}. \tag{6.3}$$

Eqs. 6.2 and 6.3 have several interesting features. The peak pressure does not decrease exactly as $1/R$ as required by the elementary acoustical approximation, but slightly more rapidly because of the logarithmic factor, $(\log R/a_0)^{-1/2}$ in x. This factor varies, of course, very slowly in comparison with $1/R$. Its presence is due to the progressive destruction of the head of the wave at the shock front (increase of τ_0) which persists even at large distances. The difference between local sound velocity and wave-front velocity, which gives rise to destruction of the wave front, is connected in an interesting way with the energy dissipation at the shock front, as we shall presently see.

The peak pressure at large distances is not proportional to the initial pressure at the gas sphere surface, roughly P_0 or $\rho_0 \Omega_1$, but varies only as the square root of this quantity $P_0^{1/2}$. Since the peak pressure contains the factor θ_a, which measures the time of decay on the surface, it will be larger the more sustained the pressure is at the surface of the gas sphere. In the asymptotic peak-pressure formula, the explosive is completely characterized by the ratio P_0/α or $\theta_a P_0/\theta_0$. Recalling the definition of θ_a, Eq. 5.17, we find

$$\frac{P_0}{\alpha} = \frac{\rho_0 c_0}{a_0} \int_0^{\tau_0} G_a(\tau)\, d\tau \tag{6.4}$$

for times τ_0 sufficiently large to permit the neglect of $G_a(\tau_0)$ in comparison with G_1 in the expression for θ_a. With the use of Eq. 6.4, the peak-pressure Eq. 6.3 may be written in the form

$$\begin{aligned} p_m &= \frac{a_0}{R} \rho_0 c_0^2 \left(\frac{\pi}{\log R/a_0} \right)^{1/2}, \\ \pi &= \frac{1}{\beta a_0^2 c_0^2} \int_0^{\tau_0} G_a(\tau)\, d\tau \,. \end{aligned} \tag{6.5}$$

The peak pressure is thus determined by π, the time integral of $G_a(\tau)$ over the interval τ_0, and not by the initial value G_a on the gas sphere. The result is independent of the form of $G_a(\tau)$.

After a time τ_0 long in comparison with the time of decay of the pressure at the gas sphere surface, we might expect π to approach a constant value π_m. This is not quite correct since the afterflow term $a u^2/2$ in

$G_a(\tau)$ prevents the integral κ from converging as $\tau_0 \to \infty$. However, the afterflow term contributes only a slowly varying term of the order of $\tau_0^{1/5}$ to κ. If τ_m is a time long in comparison with the time of decay of the pressure on the surface of the gas sphere but short relative to the time of decay of the afterflow term $a u^2/2$, κ will approach the value κ_m

$$\kappa_m = \frac{1}{\beta a_0^2 c_0^2} \int_0^{\tau_m} G_a(\tau)\, d\tau \simeq \frac{P_0 \theta_1}{\beta a_0 \rho_0 c_0^2} \tag{6.6}$$

and remain nearly constant for all distances at which the peak pressure in the initial pulse has practical interest. In the peak approximation, Eq. 4.21 κ is of course independent of ε_0 and has the value $P_0\theta_1/\beta a_0 \rho_0 c_0^2$ at all times.

We turn now to the time scale of the pressure wave at the point R. The parameter γ, Eqs. 5.23 and 6.2, measures the spread of the time scale. Waves generated at the gas sphere in the short interval τ are spread out over the much longer interval $\gamma\tau$ when they arrive at a distant point R. We first consider the asymptotic form for γ appropriate to the peak approximation, Eq. 4.21. In this approximation, the second of Eqs. 6.2 becomes

$$\gamma = 2/\kappa . \tag{6.7}$$

In other words, γ is proportional to the reciprocal of the dissipation parameter κ. As a consequence of Eq. 6.7, we find that the asymptotic duration Θ of the pulse, equal to $2\theta_1/\kappa$, does not depend directly on the time θ_1 of emission of the wave from the bubble surface. Instead θ depends only on the properties of water and the peak pressure p_m at the point R.

From Eqs. 6.2 and 6.7, we easily obtain the interesting but of course rough estimate of θ ,

$$\theta = 0.125\ R\, p_m \log R/a_0 , \qquad (6.8)$$

if θ is expressed in milliseconds, R in meters, and p_m in kilobars. The factor 0.125 is to be replaced by 0.017 if R is expressed in feet, p_m in tons/in.^{2} and common logarithms are used.

Thus far we have considered the parameter γ as constant throughout the pulse. This is not strictly true, and in fact the approximation formulas of Section 7 are somewhat inaccurate as a result. At small values of $G_a'(\tau)$, γ approaches unity and the distortion of the time scale is removed. Thus, while the crest of the initial pulse will be considereably spread out in time, its tail will arrive with practically the same time scale as that with which it originated on the gas-sphere surface.

A rough approximation to the time scale without use of the peak approximation may be obtained in another way. Remembering that γ is $(\partial t/\partial \tau)_R$ and integrating the second of Eqs. 6.2, we get

$$\begin{aligned} p(R,t) &= p_m (1 - t'/\theta) , \\ \theta &= \frac{2\beta R p_m}{\rho_0 c_0^2} \log R/a_0 , \\ t' &= t - t_0 , \end{aligned} \qquad (6.9)$$

where θ is identical with the time of decay of Eq. 6.8. Although the linear decay of pressure as a function of time, embodied in Eq. 6.9, is too crude an approximation for practical purposes, it is of some interest in showing that there is no reason to believe that a very

sharp pressure peak exists immediately at the shock front. If such a peak existed at the gas sphere surface during the generation of the wave, it would be wiped out by subsequent development of the wave, accompanied by destruction of the wave crest and spreading of the time scale.

An important quantity characterizing the wave is the time integral I of the pressure, which we may call the impulse. The values of I and p_m are useful in characterizing the duration and intensity of the initial pulse. We define I as follows,

$$I = \int_{t_0}^{t_m} p(R,t')dt' , \tag{6.10}$$

where t_0 is the time of arrival of the wave front at R and $t_m - t_0$ is a finite time long relative to the duration of the initial pulse. Due to the afterflow, I fails to converge for $t_m \to \infty$ unless the oscillations of the gas sphere are taken into account. From the equation of propagation, we get

$$I = (a_0/R)\, I_0 ,$$

$$I_0 = \frac{\rho_0}{a_0}\int_{t_0}^{t_m} G_a(t)\,dt = \frac{\rho_0}{a_0}\int_{\tau_0}^{\tau_m} \gamma G_a(\tau)\,d\tau , \tag{6.11}$$

With the use of the asymptotic relations, Eqs. 6.2, we obtain,

$$I_0 = P_0 \theta_a = a_0 \beta \rho_0 c_0^k \kappa . \tag{6.12}$$

We remark that the momentum integral I_0 is asymptotically determined

by the same parameter π as is the peak pressure p_m. In the peak approximation I_0 is equal to $P_0\theta_1$. It is interesting to notice that I_0 is conserved, that is, it is unaffected by dissipation at the front. The latter statement holds not asymptotically, but can be proved to be true at any distance R from the charge.

Another important quantity characterizing the initial pulse is the total energy flux E_f at a distance R from the charge. Quite generally, the energy current density at a point in the water is $\rho u \Omega$. The total energy flux through the sphere R is therefore given by

$$E_f = 4\pi R^2 \int_{t_0}^{\infty} \rho u \Omega \, dt . \qquad (6.13)$$

At large distances, $u \approx \Omega / c_0$, and the theory of propagation gives

$$E_f = \frac{4\pi\rho_0}{c_0} \int_{\tau_0}^{\infty} \tau G^2(\tau) \, d\tau . \qquad (6.14)$$

With the use of the asymptotic relations, Eq. 6.2, we obtain

$$E_f = \frac{4\pi a_0^2}{3\beta_0 c_0} \chi \theta_a P_0^2$$

$$= \frac{4\pi \beta \rho_0 c_0^3 a_0^3}{3} \pi^{3/2} (\log R/a_0)^{-1/2} . \qquad (6.15)$$

The asymptotic energy flux again depends upon the properties of the explosive only through the single parameter π, which also determines the peak pressure and momentum of the wave. We remark that the energy E_f is not conserved, since it contains the factor x which decreases monotonically with increasing distance from the charge.

The decrease of the energy flux with increasing distance from the charge allows us to give a physical interpretation to the quantity x, which justifies its designation as the dissipation parameter. We shall in fact show that, although we have neglected dissipation terms in the equation of motion behind the shock front, our theory implicitly takes into account energy dissipation at the shock front and does so in the correct way. Differentiation of Eq. 6.15 and use of Eq. 6.2 yields

$$\frac{dE_f}{dR} = -\frac{4\pi R^2}{3}\frac{\beta p_m^3}{\rho_0^2 c_0^3} \qquad (6.16)$$

$$p_m = (\varkappa a_0/R)P_0$$

The rate of dissipation of E_f at the shock front is therefore proportional to β, the coefficient of σ^2 in the shock-front velocity, $U = c_0(1+\beta\sigma)$. It can also be shown that for shock waves of low intensity, the parameter β determines the entropy increment ΔS experienced by unit mass of water in passing through a shock front of peak pressure p_m.

$$\Delta S = \frac{p_m^3}{12 T_0}\left(\frac{\partial^2 v}{\partial p^2}\right)_S ,$$

$$U = c_0\left[1 + \frac{\rho_0^3 c_0^3}{4}\left(\frac{\partial^2 v}{\partial p^2}\right)_S \sigma\right], \qquad (6.17)$$

where v is the specific volume of water. Thus we may write,

$$T_0\Delta S = \frac{\beta}{3\rho_0^3 c_0^3} p_m^3 \qquad (6.18)$$

As the shock front advances a distance dR, the water in a volume

$4\pi R^2 dR$ experiences an entropy increment per unit mass given by Eq. 6.18. As a result an amount of energy $-dE_f$ equal to $4\pi R^2 \rho_0 T_0 \Delta S\, dR$ is dissipated and remains bound in the water after the passage of the shock wave and return of the pressure to the value zero. The rate of dissipation is therefore given by

$$-\frac{dE_f}{dR} = \frac{4\pi R^2}{3}\frac{\beta p_m^3}{\rho_0^2 c_0^3}, \tag{6.19}$$

which agrees exactly with Eq. 6.16 obtained from our theory of propagation.

Since all the quantities p_m, θ, I_0, and E_f depend upon the explosive producing the wave only through the parameter κ, it is desirable to summarize the formulas relating them to this parameter, cf. Eqs. 6.3, 6.9, 6.12, and 6.15.

$$\begin{aligned} p_m &= \frac{a_0}{R}\rho_0 c_0^2 (\log R/a_0)^{-1/2}\, \kappa^{1/2}, \\ \theta &= 2\beta a_0 (\log R/a_0)^{1/2}\, \kappa^{1/2}, \\ I_0 &= \beta a_0 \rho_0 c_0^2 \kappa, \\ E_f &= \frac{8\pi\beta\rho_0 c_0^3 a_0^3}{3}(\log R/a_0)^{-1/2}\, \kappa^{3/2}. \end{aligned} \tag{6.20}$$

The peak pressure and time of duration of the pulse are thus propor-

tional to $\chi^{1/2}$, the momentum to χ, and the energy flux to $\chi^{3/2}$. In order to estimate χ, it is, of course, necessary to use the details of the theory of the preceding discussion since χ is not specified in any way by the asymptotic theory.

7. Calculation of Pressure-Time Curve.

We now proceed to outline on the basis of the theory of the propagation of the kinetic enthalpy a scheme for calculating the pressure-time curve of the shock wave produced at a distance R from an explosive and to list typical results of such calculations. The formulas necessary for this calculation can be assembled at once from the foregoing sections of this report. We shall restrict ourselves to the peak approximation to $G_a(t)$, since, although it distorts the tail of the shock wave somewhat, it leads to a particularly simple set of formulas which are probably adequate for engineering calculations requiring estimates of the intensity and duration of the initial pressure pulse. More elaborate formulas based upon the more refined expression for $G_a(t)$ of Eq. 4.18 may be readily set up when desired.

The peak formula for $G_a(t)$ is obtained in complete form from Eqs. 4.9 and 4.19,

$$
\begin{aligned}
&G_a(t) = G_1 e^{-t/\theta_1}, \\
&G_1 = a_0 \Omega_1, \quad \theta_1 = a_0/c_{\theta_1}, \\
&c_{\theta_1} = \frac{u_1 c_1}{\omega_1} \frac{(\rho_1^* c_1^*)(J_1 c_1 + J_1^* c_1^*)}{\rho_1 c_1 + \rho_1^* c_1^*}, \\
&J_1 = \frac{1}{u_1 c_1}\left[\frac{c_1+u_1}{c_1-u_1}\omega_1 - \frac{3u_1^2}{2} - \frac{u_1^3}{c_1-u_1}\right], \\
&J_1^* = \frac{1}{u_1 c_1^*}\left[-\frac{c_1^*-u_1}{c_1^*+u_1}\omega_1^* + \frac{3u_1^2}{2} + \frac{u_1^3}{c_1^*+u_1}\right],
\end{aligned}
\tag{7.1}
$$

where u_1 and Ω_1 are the initial values of material velocity and kinetic enthalpy of the water at the gas-sphere surface a_o; ρ_1, c_1, ω_1, the initial density, sound velocity, and enthalpy of the water at a_o; ρ_1^*, c_1^*, ω_1^* the initial values of the same quantities in the gas just interior to the sphere surface a_o.

The equation of propagation, Eq. 5.24, has been written in the form,

$$\Omega(R,t) = \chi\left(\frac{a_o}{R}\right)\Omega_1 e^{-t'/\theta}, \tag{7.2}$$

where t' is the time measured from the instant t_o at which the wave front arrives at point R. At distances at which $\Omega(R,t)$ can be represented by its acoustical approximation, we have obtained (Eq. 6.1)

$$p = \chi\left(\frac{a_o}{R}\right)P_o e^{-t/\theta},$$
$$P_o = \rho_o \Omega_1, \quad \theta = \theta_1 \gamma, \tag{7.3}$$

where ρ_o is the density of water at zero pressure. For most explosives, the acoustical approximation to Ω is entirely adequate at values of $R/a_o \geq 25$. For smaller values of R/a_o, it is preferable to use Eq. 7.2 rather than Eq. 7.3.

In order to calculate the dissipation parameter x and the time-spread parameter, γ, we again introduce the variable q

$$R/a_o = \chi q. \tag{7.4}$$

Neglecting the relatively small terms in J_o and J_1, Eqs. 5.20 yield

$$x = \frac{2K_1}{1+[1+4\alpha K_1 K_0(q)]^{1/2}},$$

$$K_1 = 1+\alpha(Z_1-1)/2Z_1,$$

$$K_0(q) = (Z_1-1)/2Z_1 + \Gamma_1' y(q), \qquad (7.5)$$

$$y(q) = \log Z/Z_1 - 2(1/Z_1 - 1/Z) + (1/Z_1^2 - 1/Z^2)/2,$$

$$Z = 1 + q/2\Gamma_1' + [q/\Gamma_1' + (q/2\Gamma_1')^2]^{1/2},$$

$$Z_1 = 1 + 1/\beta\sigma_1, \quad \Gamma_1' = \beta\Omega_1/c_0, \quad \alpha = a_0/c_0\theta_1.$$

Eqs. 7.5 suffice to determine x as a function of q for given initial values of Ω_1, σ_1, and θ_1. After Ω_1, σ_1, and θ_1 have been determined for a given explosive, x is conveniently determined as a function of R/a_0 by first calculating it as a function of q by Eq. 7.5 for several appropriate values of q, plotting or tabulating these values of x against xq (equal to R/a_0 by Eq. 7.4) and interpolating from the graph or table to obtain x for a desired value of R/a_0.

To calculate the time-spread parameter γ, we employ Eq. 5.23 and approximate qa by x.

$$\gamma = 1 - \frac{1}{\beta c_0}\frac{1}{1+Z_a} + 2\alpha x\Gamma_1'\left[\log\frac{Z}{Z_a} - \frac{4(Z-Z_a)}{(Z+1)(Z_a+1)}\right], \qquad (7.6)$$

$$Z_a = 1 + \frac{1}{2\Gamma_1' x} + \left[1/\Gamma_1' x + (1/2\Gamma_1' x)^2\right]^{1/2}.$$

Eq. 7.6 determines the parameter γ as a function of q and x(q). It is convenient to calculate γ for those values of q employed in the calculation of x(q), and to plot or tabulate the resulting values of γ against xq. From such a graph or table one may at once interpolate γ for a desired value of R/a_0. We remark that at large values of R/a_0, the last term of Eq. 7.6 is the dominant one in γ. It contains as a factor α or θ_0/θ_1, where θ_0 is a_0/c_0. Thus at large distances the time of decay, $\gamma\theta_1$, is controlled by θ_0, a time characteristic of water rather than of the explosive, although of course the second factor in this term

in γ depends on the characteristics of the explosive.

The results of the calculation by the methods of this section of the shock-wave parameters for the underwater explosion of spherical charges of TNT and Pentolite are listed in Tables 7.1 and 7.2. Figure 7.1 shows the variation with distance from the charge of the peak pressure p_m and the time constant θ for TNT. Figure 7.2 shows the variation with distance for the same substance of the dissipation parameter χ and the spread parameter γ. Theoretical predictions have been made for 48 different explosive combinations comprising 13 different explosives. Reference should be made to the original reports for the complete tabluations of the results of the theory.[26]

8. Similarity Restraint Propagation Theory[27]

In this section, we describe an alternative theory of the propagation of shock waves from the underwater explosion of spherical charges of explosive. The theory to be described results in the formulation of a pair of ordinary differential equations for peak pressure and shock-wave energy as functions of distance from the source. These equations can be integrated numerically for specified initial conditions, and they provide a particularly simple method for the extrapolation to points close to the charge of experimental peak pressure-distance curves, measured at large distances from the charge. Although less convenient than the analytical theory that has been described in the previous sections and less instructive

---

26/ J. G. Kirkwood, S. R. Brinkley, Jr., and J. M. Richardson, OSRD Report No. 2022 (1943); OSRD Report No. 3949 (1944). Calculations in earlier reports by Kirkwood et al. are superseded by these reports.

27/ See Reference 8.

TABLE 7.1 - Calculated shock-wave parameters for TNT, density 1.59

R/a_o	X	γ	θ/a_o (10^{-5} sec./cm.)	P_m (kilobars)
1	1.00	1.00	0.344	37.1
10	.399	4.04	1.39	1.39
25	.300	6.43	2.21	.421
50	.258	8.11	2.79	.181
100	.231	9.55	3.29	.0807

TABLE 7.2 - Calculated shock-wave parameters for Pentolite (PETN/TNT 50/50), density 1.60

R/a_o	X	γ	θ/a_o (10^{-5} sec./cm.)	P_m (kilobars)
1	1.00	1.00	0.310	41.8
10	.372	4.37	1.37	1.46
25	.277	7.09	2.22	.435
50	.237	8.96	2.81	.187
100	.211	10.6	3.33	.831

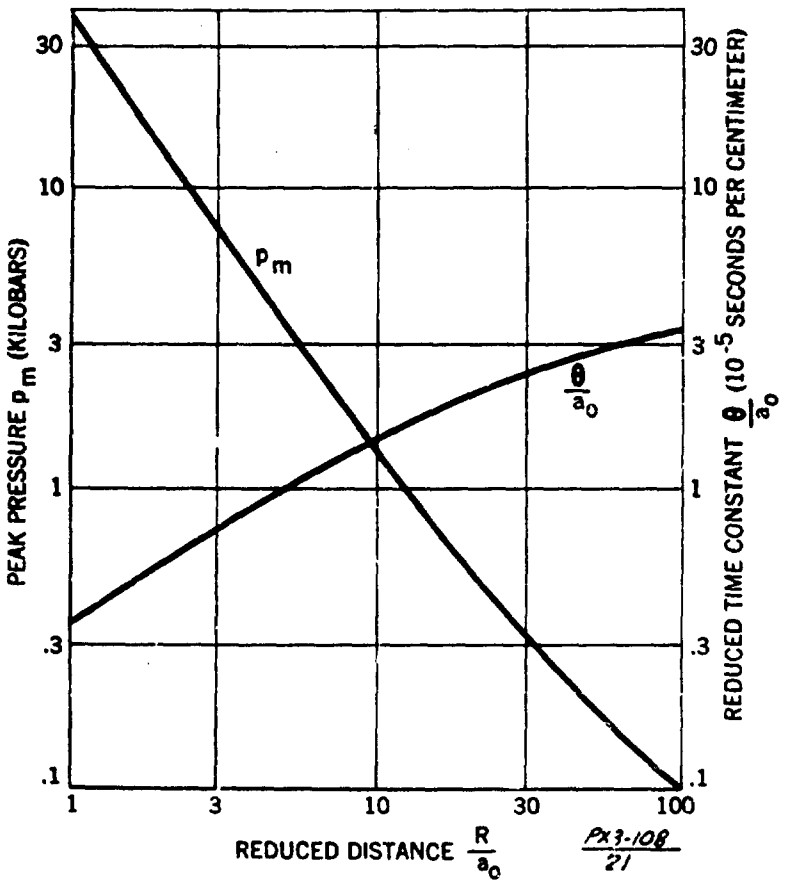


FIGURE 7.1 - Calculated peak pressures and time constants for TNT, density 1.59.

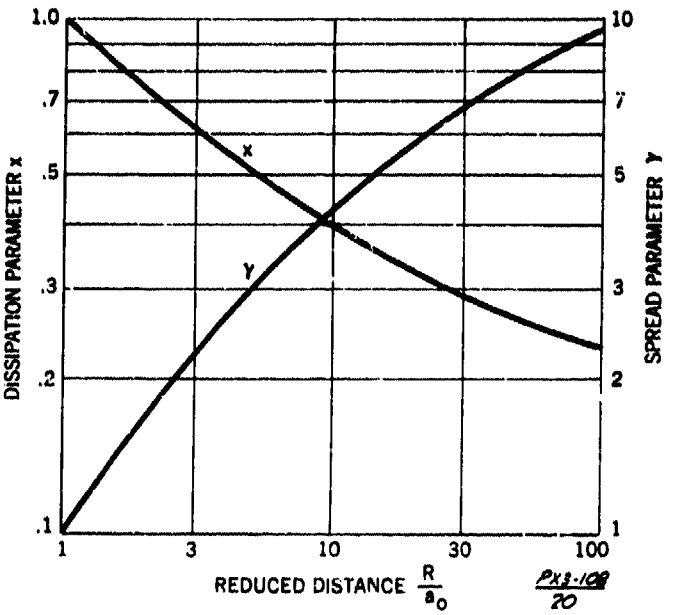


FIGURE 7.2 - Calculated dissipation and spread parameters for TNT, density 1.59.

as to the physical features accompanying the decay of the shock wave, the theory of this section requires fewer assumptions than does the former theory. Since these assumptions are quite different in nature from those of the former theory, the comparison of the two theories is of considerable interest.

The partial differential equations of hydrodynamics and the Hugoniot relation between pressure and particle velocity may be used to provide three relations between the four partial derivatives of pressure and particle velocity, evaluated at the shock front, with respect to time and distance from the source. If a fourth such relation could be formulated, it would then be possible to formulate an ordinary differential equation for the peak pressure as a function of the distance from the source.

$$\frac{dp}{dR} = F(p,R), \tag{8.1}$$

On mathematical grounds, it is, of course, futile to seek a fourth relation between the partial derivatives which does not involve an integral of the fundamental equations of hydrodynamics. However, we shall show that an approximate relation of the desired form can be formulated by imposing a similarity restraint on the shape of the energy-time curve of the shock wave and by utilizing the second law of thermodynamics to determine at an arbitrary distance the distribution of the initial energy input between dissipated energy residual in the fluid already traversed by the shock wave and energy available for further propagation.

The Eulerian equations of hydrodynamics, Eqs. 3.1, for spherical symmetry are

$$\rho\frac{Du}{Dt} = -\frac{\partial p}{\partial r}, \quad \frac{1}{\rho c^2}\frac{Dp}{Dt} + \frac{\partial u}{\partial r} = -\frac{2u}{r}. \tag{8.2}$$

The development of the theory is most easily carried out in terms of the label (Lagrange) coordinate r_0, the position in the undisturbed fluid of density ρ_0 of a volume element which at time t has the position r. The transformation from the Eulerian coordinate r to the Lagrangian coordinate r_0 is effected by means of the definition,

$$\left(\frac{\partial r}{\partial t}\right)_{r_0} = u , \tag{8.3}$$

and the Lagrangian equation of continuity, which is

$$\left(\frac{\partial r}{\partial r_0}\right)_t = \frac{\rho_0 r_0^2}{\rho r^2} \tag{8.4}$$

for spherical symmetry. Eqs. 8.2 are thus transformed to

$$\begin{aligned} &\frac{\rho r^2}{\rho_0 r_0^2}\frac{\partial u}{\partial r_0} + \frac{1}{\rho c^2}\frac{\partial p}{\partial t} = -\frac{2u}{r} , \\ &\rho_0 \frac{\partial u}{\partial t} + \frac{r^2}{r_0^2}\frac{\partial p}{\partial r_0} = 0 , \\ &\frac{\partial}{\partial t} = \left(\frac{\partial}{\partial t}\right)_{r_0} , \end{aligned} \tag{8.5}$$

where u is the particle velocity, p the pressure in excess of the pressure p_0 of the undisturbed fluid, ρ the density, ρ_0 the density of the undisturbed fluid, t the time, and r the Euler coordinate at time t of an element of fluid with Lagrange coordinate r_0. Eqs. 8.5 are supplemented by the equation of state of the fluid and the entropy transport equation $\partial S/\partial t = 0$, the latter of which we shall not explicitly use. Eqs. 8.5 are of a hybrid form in that we use the Lagrange coordinates r_0 and t as independent

variables but retain the Euler equation of continuity. Eqs. 8.5 are to be solved, subject to initial conditions specified on a curve in the (r_0, t)-plane, and to the Rankine-Hugoniot conditions (Eqs. 2.2) at the shock front,

$$\begin{aligned} p &= \rho_0 u U, \\ u &= U\left(1 - \frac{\rho_0}{\rho}\right), \\ \Delta H &= \frac{p}{2}\left(\frac{1}{\rho_0} + \frac{1}{\rho}\right), \end{aligned} \tag{8.6}$$

where ΔH is the specific enthalpy increment experienced by the fluid in traversing the shock front, and U is the velocity of the shock front. The Hugoniot conditions constitute supernumerary boundary conditions, compatible with the differential equations and specified initial conditions, only if the shock front follows an implicitly prescribed curve $R(t)$ in the (r_0, t)-plane. Having thus stated the mathematical problem, we shall describe an approximate method of avoiding the explicit integration of the partial differential equations.

We shall denote a derivative in which the shock front is stationary by

$$\begin{aligned} \frac{d}{dR} &= \left(\frac{\partial}{\partial r_0}\right)_{R(t)} = \left[\frac{\partial}{\partial r_0} + \frac{dt}{dR}\frac{\partial}{\partial t}\right]_{r_0 = R}, \\ &= \left[\frac{\partial}{\partial r_0} + \frac{1}{U}\frac{\partial}{\partial t}\right]_{r_0 = R}. \end{aligned} \tag{8.7}$$

If the operator d/dR is applied to the first of the Hugoniot relations (Eqs. 8.6), and if Eqs. 8.5 are specialized for the shock front, $r_0 = R$, we obtain the following three relations for the four partial derivatives $\partial p/\partial t$,

$\partial u/\partial t$, $\partial p/\partial r_0$, and $\partial u/\partial r_0$ at the shock front, where $r(t,R) = R$,

$$\frac{\rho_m}{\rho_0}\left(\frac{\partial u}{\partial r_0}\right)' + \frac{1}{\rho_m c_m^2}\left(\frac{\partial p}{\partial t}\right)' = -\frac{2u_m}{R},$$

$$\left(\frac{\partial u}{\partial t}\right)' + \frac{1}{\rho_0}\left(\frac{\partial p}{\partial r_0}\right)' = 0,$$

$$\left(\frac{\partial u}{\partial t}\right)' + U\left(\frac{\partial u}{\partial r_0}\right)' - \frac{g}{\rho_0 U}\left(\frac{\partial p}{\partial t}\right)' - \frac{g}{\rho_0}\left(\frac{\partial p}{\partial r_0}\right)' = 0, \qquad (8.8)$$

$$\rho_m = \rho(p_m),\ u_m = u(p_m),\ c_m = c(p_m),$$

where $g = \rho_0 U\, du_m'/dp_m = 1 - d\log U/d\log p_m$ and where the prime indicates that the partial derivatives are to be evaluated at the shock front. The derivative g is to be calculated from the first of the Hugoniot relations, Eqs. 8.6. All coefficients in Eqs. 8.8 can be expressed as functions of pressure alone by means of the Hugoniot conditions and the equations of state of the fluid.

We now desire to establish a supplementary relation to permit the formulation of an ordinary differential equation for the peak pressure as a function of distance from the charge without explicit integration of the fundamental equations of hydrodynamics. The physical basis for the supplementary relation to be established lies in the fact that the nonacoustical decay of waves of finite amplitude is closely associated with the entropy increment experienced by the fluid in passing through the shock front and the accompanying dissipation of energy. As a shock wave passes through a fluid, it leaves in its path a residual internal energy increment in each element of fluid determined by the entropy increment produced in it by the passage of the shock front. As a consequence, the energy propagated ahead by the shock wave decreases with the distance it has traveled from the source.

The work $W(R)$ done by a spherical shock wave on the fluid exterior to a sphere of radius R is

$$W(R) = 4\pi \int_{t(R)}^{\infty} [r(R,t)]^2 u (p + p_0)\, dt, \qquad (8.9)$$

where p and u denote excess pressure and particle velocity behind the shock front, $t(R)$ the time of arrival of the shock front at point R, and $r(R,t)$ the Euler coordinate of a particle of initial Lagrange coordinate R. The integral is along a path of constant Lagrange coordinate R. By the second law of thermodynamics, we assume that after the shock wave has traveled to infinity, the work $W(R)$, delivered to the fluid beyond R, is dissipated to internal energy of the fluid, each particle of fluid returning adiabatically to a state of thermodynamic equilibrium of pressure p_0 and an entropy exceeding its initial entropy by the increment corresponding to the peak pressure at which the shock front crossed it.

The adiabatic work W_0 (equal to the energy of explosion) done by a spherical charge of explosive of initial radius a_0 on the exterior fluid is

$$\frac{W_0}{4\pi} = \int_{a_0}^{R} \rho_0 r_0^2 E[p_m(r_0)]\, dr_0 + \int_{t(R)}^{\infty} r^2 u (p + p_0)\, dt, \qquad (8.10)$$

where E is the specific energy increment of the fluid at pressure p_0 and for an entropy increment corresponding to shock-front pressure p_m. Now,

$$p_0 \int_{t(R)}^{\infty} u r^2 dt = p_0 \int_{a_0}^{R} \left(\frac{\rho_0}{\rho} - 1\right) r_0^2\, dr_0 + \frac{p_0 \Delta V}{4\pi}, \qquad (8.11)$$

where ρ is the final density of the fluid, and ΔV is the volume increment of the gas sphere composed of the explosion products. Using Eq. 8.11, we combine the last term of the time integral with the first integral to obtain

$$\frac{W_0}{4\pi} = \int_{a_0}^{R} r_0^2 \rho_0 h[p_m(r_0)]\, dr_0 + \frac{p_0 \Delta V}{4\pi} + \int_{t(R)}^{\infty} r^2 u p\, dt, \qquad (8.12)$$

where the dissipated enthalpy $h = E + p_0 \Delta(1/\rho)$ is the specific enthalpy increment of an element of fluid, traversed by a shock wave of peak pressure p_m, after return to pressure p_0 on its new adiabatic. Assuming the time integral to vanish at $R = \infty$, we have

$$\frac{W_0}{4\pi} = \int_{a_0}^{\infty} r_0^2 \rho_0 h[p_m(r_0)]\, dr_0 + \frac{p_0 \Delta V}{4\pi} . \qquad (8.13)$$

Subtracting Eq. 8.13 from Eq. 8.12 and transposing, we obtain

$$D(R) = \int_{t(R)}^{\infty} r^2 u p\, dt ,$$
$$D(R) = \int_{R}^{\infty} r_0^2 \rho_0 h[p_m(r_0)]\, dr_0 . \qquad (8.14)$$

To exclude contributions of second shocks arising from possible oscillations of the gas sphere, we may within the limits of approximation of incompressive hydrodynamic theory apply Eqs. 8.13 and 8.14 up to the time the gas sphere reaches maximum radius instead of to infinity. ΔV then represents the volume increment of the gas sphere to maximum radius, and $p_0 \Delta V$ the part of the energy of explosion available for secondary pulses, which may eventually develop into shocks.

The integral of the energy-time curve, $D(R)$, is thus expressible, through Eq. 8.14, in terms of the peak pressure-distance curve of the shock wave at distances beyond R. It is to be remarked that Eq. 8.14 and the dissipation assumption do not violate conservation of momentum, since, through spreading of the wave, it is possible for the total momentum to remain finite while the particle velocity everywhere and the total kinetic energy tend to zero. Our dissipation assumption breaks down if the first shock wave can be overtaken by second shocks built up in its rear. This will not be the case if the pressure-time curve is initially monotone, decreasing with asymptotic value p_0. If the excess pressure p has a negative phase, a second shock will develop in the negative part of the pressure-time curve but cannot overtake the initial positive shock. In this case our theory will apply to the positive phase if the time integrals of Eqs. 8.9 to 8.14 are extended not to infinity but to the time t, at which the excess pressure in the positive phase vanishes. The general theory of shock waves is not sufficiently developed to permit one to say that there is proof for the foregoing statements, or even that a spherical shock is stable, but the statements can nevertheless be accepted with some assurance as plausible.

We now shall express the energy-time integral in reduced form,

$$
\begin{aligned}
&D(R) = R^2 p_m u(p_m) \mu \nu, \\
&-\frac{1}{\mu} = \frac{1}{p_m}\left(\frac{\partial p}{\partial t}\right)' + \frac{1}{u(p_m)}\left(\frac{\partial u}{\partial t}\right)' + \frac{2u(p_m)}{R}, \\
&\nu = \int_0^\infty f(R, \vartheta)\, d\vartheta, \quad \vartheta = \frac{t - t(R)}{\mu}, \\
&f(R, \vartheta) = r^2 p u / R^2 p_m u(p_m).
\end{aligned}
\tag{8.15}
$$

The function $f(R, \vartheta)$ is the energy-time integrand, normalized by its peak value $R^2 \rho_m u(\mu)$ at the shock front, expressed as a function of R and a reduced time ϑ which normalizes its initial slope to -1 if μ does not vanish. Thus $f(R, \vartheta)$ is a function having the properties,

$$f(R, 0) = 1,$$
$$[\partial f / \partial \vartheta]_{\vartheta = 0} = -1. \tag{8.16}$$

We also assume f to be a monotone decreasing function of ϑ. Elimination of μ between the first two of Eqs. 8.15 yields the desired fourth relation between the partial derivatives at the shock front supplementing Eqs. 8.8. It, of course, involves integrals of Eqs. 8.5 for the knowledge of the reduced energy-time function $f(R, \vartheta)$. However, if $f(a_0, \vartheta)$ is initially a monotone decreasing function of ϑ, $f(R, \vartheta)$ will remain so, and in fact will at large R become asymptotically a quadratic function of ϑ corresponding to the linear form of the pressure-time curve shown in section 6 to be asymptotically stable. This means that ν is a very slowly varying function of R, for which sufficiently accurate estimates for many purposes can be made without explicit integration of the hydrodynamic equations, Eqs. 8.5.

The assignment of a constant value, independent of R, to ν is equivalent to imposing a similarity restraint on the energy-time curve of the shock wave. This type of approximation is equivalent in principle to that underlying the Rayleigh-Ritz method for solving vibration problems, although we have not, of course, developed a variational procedure designed to carry the result to any desired degree of approximation.

The initial pressure-time, and also energy-time curve, of an explosion wave is rapidly decreasing. An expansion of the logarithm of the

function in a Taylor series in the time, the well-known peak approximation, is appropriate for an initial estimate of ν. This corresponds to an exponential $f(\vartheta)$,

$$f = e^{-\vartheta}, \qquad \nu = 1 . \tag{8.17}$$

For the asymptotic quadratic energy-time curve, corresponding to the linear pressure-time curve of the positive phase of a shock wave,

$$f = (1 - \vartheta/2)^2, \quad \vartheta \leq 2, \qquad f = 0, \quad \vartheta \geq 2, \qquad \nu = 2/3. \tag{8.18}$$

As a convenient empirical interpolation formula between the two extreme values of ν, we have found the following expression to be satisfactory.

$$\nu = 1 - \frac{2}{3} e^{-p_m/p_0} . \tag{8.19}$$

For explosion waves in water, the value $\nu = 1$ is suitable for all but very great distances from the charge, $R \gg$ 100 charge radii.

Elimination of μ between the first two of Eqs. 8.15 and combination with Eqs. 8.8 yield a set of four equations for the four partial derivatives $(\partial p/\partial t)'$, $(\partial u/\partial t)'$, $(\partial p/\partial r_0)'$, and $(\partial u/\partial r_0)'$ at the shock front,

$$\frac{1}{p_m}\left(\frac{\partial p}{\partial t}\right)' + \frac{1}{u_m}\left(\frac{\partial u}{\partial t}\right)' + \frac{2u_m}{R} = -\nu \frac{R^2 p_m u_m}{D(R)} ,$$

$$\frac{\rho_m}{\rho_0}\left(\frac{\partial u}{\partial r_0}\right)' + \frac{1}{\rho_m c_m^2}\left(\frac{\partial p}{\partial t}\right)' = -\frac{2u_m}{R}, \quad \left(\frac{\partial u}{\partial t}\right)' = -\frac{1}{\rho_0}\left(\frac{\partial p}{\partial r_0}\right)', \tag{8.20}$$

$$\left(\frac{\partial u}{\partial t}\right)' + U\left(\frac{\partial u}{\partial r_0}\right)' = \frac{1}{\rho_0 U}\left(\frac{\partial p}{\partial t}\right)' + \frac{1}{\rho_0}\left(\frac{\partial p}{\partial r_0}\right),$$

where the coefficients are determined as functions of p_m by the Hugoniot relations, Eqs. 8.6. By differentiation of the second of Eqs. 8.19 we obtain a total differential equation relating D to p_m and R,

$$\frac{dD}{dR} = -R^{\nu} \rho_0 h(p_m) . \tag{8.21}$$

Equations 8.20 and 8.21 are exact, although in using them we shall employ the similarity restraint in estimating the slowly varying function ν. We remark that Eqs. 8.20 are valid for plane and cylindrical shock waves when the terms $2u_m/R$ are replaced by zero and u_m/R, respectively.

Solution of the equations 8.20 for $(\partial p/\partial t)'$ and $(\partial p/\partial r_0)'$ and the application of Eq. 8.7 yields the desired total differential equation for dp_m/dR along the shock front. This equation is to be solved simultaneously with Eq. 8.21. The final differential equations can be written in the form,[28]

28/ We remark that if these methods are applied to the one-dimensional cases of the plane shock wave and the cylindrical shock wave resulting from adiabatic constant volume conversion of an infinite cylinder of explosive to its products, the resulting propagation equations can be written in the form,

$$\frac{dp_m}{dR} + \frac{\alpha p_m}{2R} N(p_m) = -\nu \frac{R^{\alpha} p_m^3}{D(R)} \left[\frac{1}{\rho_0 U^2} \frac{\sigma}{2(1+\sigma) - \sigma} \right],$$

$$\frac{dU}{dR} = -\rho_0 R^{\alpha} h(p_m),$$

where $\alpha = 0$ for the plane wave and $\alpha = 1$ for the cylindrical wave, and where

$$D(R) = \int_R^{\infty} \rho_0 r_0^{\alpha} h[p_m(r_0)] dr_0 .$$

The shock-wave energy per unit area of initial generating surface is equal to $a_0^{-\alpha} D(R)$. Eqs. 8.22 for the spherical wave are obtained with $\alpha = 2$. It may also be noted that the theory has not required the approximation of adiabatic flow employed in the kinetic enthalpy propagation theory. The exact Hugoniot curves of the fluid may be employed in the numerical integration of the propagation equations. As a result, the present theory is applicable to blast waves in air as well as to explosion waves in water.

$$\frac{dp_m}{dR} + \frac{p_m}{R} N(p_m) = -\frac{\gamma R^2 p_m^3}{D(R)} \left[\frac{1}{\rho_0 U^2} \frac{G}{2(1+g)-G}\right],$$

$$\frac{dD}{dR} = -\rho_0 R^2 h(p_m), \tag{8.22}$$

where $$N(p_m) = \frac{4\rho_0/\rho_m + 2(1-\rho_0/\rho_m)G}{2(1+g)-G},$$

$$G(p_m) = 1-(\rho_0 U/\rho_m c_m)^2,$$

$$g(p_m) = 1 - d\log U/d\log p_m .$$

By means of the Hugoniot relations, Eqs. 8.6, and the equation of state, the coefficients of Eqs. 8.22 can be determined as functions of peak pressure only.

For the solution of the propagation equations by numerical integration with specified initial conditions, it is convenient to transform Eqs. 8.22 to the dimensionless variables,

$$P = p_m R/B a_0 ,$$

$$Q = \left(\frac{12 n^2}{n+1}\right) \frac{D}{a_0^2 \rho R} , \tag{8.23}$$

where n and B are the parameters of the Tait equation of state,

$$p = B\left[\left(\frac{\rho}{\rho_0}\right)^n - 1\right] , \quad B = \rho_0 c_0^2/n . \tag{5.4}$$

The resulting propagation equations may be written in the form,

$$-\frac{dP}{d(R/a_0)} = \frac{a_0 P}{R}\left[N(p_m) - 1 + \frac{P^2}{Q} M(p_m)\right]$$

$$\frac{dQ}{d(R/a_0)} = \frac{a_0 Q}{R}\left[N(p_m) - 1 + \frac{P^2}{Q} L(p_m)\right] \tag{8.24}$$

where

$$L(p_m) = \left(\frac{12n^2}{n+1}\right)\left[\frac{B^2}{p_m}\frac{\nu}{\rho_0 U^2}\frac{G}{2(1+g)-G} - \frac{\rho_0 B^2 h(p_m)}{p_m^2}\right],$$

$$M(p_m) = \left(\frac{12n^2}{n+1}\right)\left[\frac{B^2}{p_m}\frac{\nu}{\rho_0 U^2}\frac{G}{2(1+g)-G}\right].$$

The quantities $L(p_m)$, $M(p_m)$, and $N(p_m)$ are listed in Table 8.1 as functions of p_m/B, and the auxiliary quantities $G(p_m)$, $g(p_m)$, ρ_m/ρ_0, and U/c_0 are listed in Table 8.2 as functions of the same argument.[29] The integration of Eqs. 8.24 by numerical methods is easily carried out by standard procedures.[30]

It is of interest to examine at once the asymptotic form of the solutions of Eqs. 8.22 or 8.24 for small excess pressure p_m. The normalisation of the coefficients of Eqs. 8.24 has been so arranged that

$$\text{Lim}\,(p_m \to 0)\; L(p_m) = 0,$$
$$\text{Lim}\,(p_m \to 0)\; M(p_m) = 1,$$
$$\text{Lim}\,(p_m \to 0)\; N(p_m) = 1.$$

The asymptotic equations are

$$-R\frac{dP}{dR} = \frac{P^2}{Q}, \qquad \frac{dQ}{dR} = 0, \tag{8.25}$$

with the integrals,

$$Rp_m = P_1[\log R/R_1]^{-1/2}, \qquad Q = 2P_1^2, \tag{8.26}$$

29/ S. R. Brinkley, Jr., and J. G. Kirkwood, OSRD Report 5649 (1949). Tabulated values of the impulse (infra) listed in this report contain a systematic numerical error. The shock-wave impulse should be separately calculated by Eq. 8.34.

30/ For example, see J. B. Scarborough, Numerical Mathematical Analysis; Johns Hopkins Press, Baltimore, Md. (1930), pp. 218 ff.

TABLE 8.1. - Functions for the integration of the propagation equations in sea water

$L(p_m)$	$M(p_m)$	$N(p_m)$	p_m/B
0.5000	1.5000	0	0
.4950	1.4843	0.001495	0.01
.4882	1.4670	.002924	.02
.4839	1.4524	.004355	.03
.4778	1.4363	.005725	.04
.4721	1.4207	.007075	.05
.4665	1.4054	.008424	.06
.4600	1.3871	.009774	.07
.4560	1.3759	.01112	.08
.4510	1.3617	.01247	.09
.4462	1.3479	.01380	.1
.3984	1.2175	.02622	.2
.3576	1.1058	.03745	.3
.3215	1.0095	.04763	.4
.2939	.9305	.05676	.5
.2673	.8555	.06581	.6
.2450	.7923	.07388	.7
.2268	.7378	.08156	.8
.2102	.6886	.08867	.9
.1945	.6439	.09517	1.0
.1404	.4793	.1235	1.5
.1133	.3844	.1416	2.0
.0889	.3123	.1563	2.5
.0690	.2524	.1696	3.0
.0536	.2048	.1815	3.5
.0428	.1695	.1919	4.0
.0366	.1465	.2009	4.5
.0345	.1348	.2085	5.0
.01276	.05140	.2506	10
.00694	.02770	.2678	15
.00452	.01731	.2848	20
.00359	.01242	.3143	25

TABLE 8.2 - Auxiliary functions for shock waves in sea water

P_m/B	U/c_o	$\varepsilon(p_m)$	$G(p_m)$	ρ/ρ_o
0.01	1.003	0.9971	0.005654	1.001393
.02	1.006	.9944	.01121	1.002774
.03	1.008	.9917	.01669	1.004142
.04	1.011	.9890	.02211	1.005502
.05	1.014	.9863	.02737	1.006846
.06	1.017	.9838	.03258	1.008180
.07	1.020	.9812	.03773	1.009499
.08	1.023	.9787	.04278	1.01082
.09	1.025	.9762	.04777	1.01213
.1	1.027	.9737	.05266	1.01342
.2	1.054	.9512	.09779	1.02584
.3	1.072	.9316	.1371	1.03738
.4	1.103	.9147	.1706	1.04818
.5	1.126	.8995	.2011	1.05835
.6	1.148	.8859	.2283	1.06797
.7	1.170	.8738	.2525	1.07705
.8	1.191	.8627	.2748	1.08568
.9	1.211	.8526	.2949	1.09392
1.0	1.231	.8435	.3130	1.1018
1.5	1.321	.8069	.3862	1.1368
2.0	1.407	.7654	.4500	1.1673
2.5	1.486	.7408	.4975	1.1935
3.0	1.555	.7298	.5192	1.2136
3.5	1.619	.7241	.5296	1.2302
4.0	1.682	.7110	.5515	1.2478
4.5	1.742	.6998	.5682	1.2630
5	1.797	.6906	.5799	1.2762
10	2.272	.6381	.6593	1.3720
15	2.462	.6149	.6944	1.4294
20	2.961	.5943	.7142	1.4687
25	3.252	.5638	.7255	1.4945

where P_1 and R_1 are constants. Eqs. 8.26 are in agreement with the asymptotic result of the kinetic enthalpy propagation theory Eq. 6.3.

The most important parameters of the pressure-time curve in the analysis of damage to structures by explosion waves are the peak pressure, energy, and impulse of the wave. Since the energy is most simply related to our propagation theory, we shall discuss it first. The energy of the shock wave when it arrives at a point R is by definition the work done on the fluid exterior to the sphere R. Thus, the shock-wave energy per unit area of the initial sphere of explosive is $D(R)/a_c^2$. If we denote by $\epsilon(R)$ the shock-wave energy per gram of the initial explosive charge, we find

$$\epsilon(R) = \left(\frac{n+1}{4n^2}\right) \frac{a_0}{R} \frac{Q p_m}{\rho_e}, \tag{8.27}$$

where ρ_e is the density of loading of the explosive. For the shock-wave energy delivered to unit area, $\epsilon(R)$ is to be divided by $4\pi R^2 w$, where w, the weight of explosive, is to be expressed in grams/ and R in centimeters.

The impulse I of the shock wave has been defined by Eq. 6.10. We may approximate the Euler pressure-time curve of the shock wave by the peak approximation,

$$p = p_m e^{-t/\Theta}, \tag{8.28}$$

where the Euler time constant Θ of the wave is defined as

$$-\frac{1}{\Theta} = \frac{1}{p_m}\left[\left(\frac{\partial p}{\partial t}\right)_r\right]_R \tag{8.29}$$

In terms of Lagrangian partial derivatives, the time constant is given by

$$\frac{1}{\Theta} = \frac{u_m}{p_m}\frac{\rho_m}{\rho_0}\left(\frac{\partial p}{\partial r_0}\right)' - \frac{1}{p_m}\left(\frac{\partial p}{\partial t}\right)' , \tag{8.30}$$

or

$$\frac{1}{\Theta} = \frac{1}{p_m}\frac{\rho_m}{\rho_0}\left[u_m \frac{dp_m}{dR} - \left(\frac{\partial p}{\partial t}\right)'\right] . \tag{8.31}$$

Employing Eqs. 8.20, we obtain

$$-\frac{1}{\Theta} = \frac{U}{R}\left\{\frac{2}{G} + \left[\left(\frac{1+g}{G}\right)\frac{\rho_m}{\rho_0} + 1 - \frac{\rho_m}{\rho_0}\right]\frac{R}{p_m}\frac{dp_m}{dR}\right\} . \tag{8.32}$$

All quantities in the expression for Θ may be expressed in terms of the integrals of the equations for the shock wave, Eqs. 8.22 or 8.24, with the aid of the Hugoniot relations.

For an exponential pressure-time curve consistent with the peak approximation and exponential energy-time curve, the impulse is given by

$$I = p_m \Theta , \tag{8.33}$$

and therefore

$$\frac{I}{B a_0} = \frac{P}{U}\left\{\frac{G}{\left[(1+g)(\rho_m/\rho_0) - G(1-\rho_m/\rho)\right]\left(-\frac{R}{p_m}\frac{dp_m}{dR}\right) - 2}\right\} . \tag{8.34}$$

Eqs. 8.24 require the specification of two constants of integration for their explicit integration, which is to be carried out by numerical procedures. The constants of integration may be determined either by the theoretical calculation of the initial peak pressure and energy of the generating pulse from thermodynamic information concerning the explosion products or from experimental measurements of the shock-wave parameters. The former method makes possible an a priori determination of the peak

pressure-distance curve of a given explosive. The latter method is useful in providing an extrapolation of an experimental peak pressure-distance curve, measured over a limited range of distances, to smaller or larger distances from the charges.

The constants of integration may be taken to be P_1 and Q_1, the initial values of the reduced pressure and energy variables. The initial pressure p_1 for the instantaneous detonation state corresponding to adiabatic isometric conversion of the explosive charge to its products is determined by Eqs. 2.4 and 2.6. The initial value of the reduced energy variable is then determined by Eq. 8.23.

$$P_1 = p_1 / B.$$

In order to determine Q_1, given by

$$-\frac{1}{Q_1} = \left(\frac{n+1}{12n^2}\right)\frac{a_0}{u_1}\left[\frac{1}{p_1}\left(\frac{\partial p}{\partial t}\right)_1 + \frac{1}{u_1}\left(\frac{\partial u}{\partial t}\right)_1 + \frac{2u_1}{a_0}\right], \qquad (8.35)$$

it is necessary to determine the partial derivatives $(\partial u/\partial t)_1$ and $(\partial p/\partial t)_1$. The equations of hydrodynamics in the gas sphere and in the exterior medium yield four relations,

$$\frac{\rho_1}{\rho_0}\left(\frac{\partial u}{\partial r_0}\right)_1 + \frac{1}{\rho_1 c_1^2}\left(\frac{\partial p}{\partial t}\right)_1 = -\frac{2u_1}{a_0}, \quad \frac{1}{\rho_0}\left(\frac{\partial p}{\partial r_0}\right)_1 = -\left(\frac{\partial u}{\partial t}\right)_1,$$

$$\frac{\rho_1^*}{\rho_0^*}\left(\frac{\partial u}{\partial r_0}\right)_1^* + \frac{1}{\rho_1^* c_1^{*2}}\left(\frac{\partial p}{\partial t}\right)_1 = -\frac{2u_1}{a_0}, \quad \frac{1}{\rho_0^*}\left(\frac{\partial p}{\partial r_0}\right)_1^* = -\left(\frac{\partial u}{\partial t}\right)_1, \qquad (8.36)$$

between the six partial derivatives $(\partial u/\partial r_0)_1$, $(\partial u/\partial r_0)_1^*$, $(\partial p/\partial r_0)_1$, $(\partial p/\partial r_0)_1^*$, $(\partial u/\partial t)$, and $(\partial p/\partial t)$, where the asterisked quantities refer to the gas and the unasterisked to the exterior medium and the subscript denotes the initial value of the quantity. The two Lagrange time derivatives are identical in gas and exterior medium because of continuity of pressure and particle velocity. Two further relations are provided by the shock-front stationary time derivative of the Hugoniot relation between p_m and u in the exterior medium and by the initial condition, $\partial \bar{r}^*/\partial r_0$, on the gas sphere,

$$\left(\frac{\partial u}{\partial t}\right)_1 + U_1\left(\frac{\partial u}{\partial r_0}\right)_1 = \frac{g_1}{\rho_0 U_1}\left(\frac{\partial p}{\partial t}\right)_1 + \frac{g_1}{\rho_0}\left(\frac{\partial p}{\partial r_0}\right)_1 ,$$
$$\frac{1}{\rho_1^* c_1^*}\left(\frac{\partial p}{\partial r_0}\right)_1^* + \left(\frac{\partial u}{\partial r_0}\right)_1^* = 0 . \qquad (8.37)$$

Solution of Eqs. 8.36 and 8.37 for $(\partial u/\partial t)_1$ and $(\partial p/\partial t)_1$ and substitution in Eq. 8.35 yields the desired expression for q_1 as a function of p_1,

$$q_1 = \left(\frac{6n^2}{n+1}\right)\left(1-\frac{\rho_0}{\rho_1}\right)\left\{\frac{(2-\eta_1)(1+g_1) - G_1}{[2(1+g_1)-G_1](1-\rho_0/\rho_1)(c_1^*/u_1 - 1) + \eta_1[1+g_1(1-\rho_0/\rho_1)]}\right\}, \qquad (8.38)$$

where

$$\eta_1 = 1 - \frac{\rho_0 U_1}{\rho_1^* c_1^*} ,$$

and where the necessary thermodynamic properties of the explosion products are calculated as functions of p_1 by methods outlined in section 2.

When the bubble of explosion products has expanded to maximum radius, it has a potential energy equal to $p_0 \Delta V$, where ΔV is the difference in volume between the bubble at maximum radius and the intact charge of explosive of radius a_e . The energy associated with the explosion products after emission of the shock wave can thus be estimated from experimental measurements of the maximum bubble radius. For TNT, it is known that the energy associated with the gas bubble at its first maximum is approximately 480 cal./gm., a figure which is 45 percent of the estimated energy of explosion of 1060 cal./gm. The bubble energy at the first maximum is quite generally about one half the energy of explosion.[31] The assumption that $\epsilon_1 = \epsilon_e / 2$, where ϵ_1 is the initial shock-wave energy and ϵ_e the energy of explosion, makes possible the formulation of an alternative method of determination of Q_1 , the initial value of the reduced energy variable. Making use of Eq. 8.27, we obtain

$$Q_1 = \left(\frac{2n^2}{n+1} \right) \frac{\rho_e \epsilon_e}{p_1} . \qquad (8.39)$$

The disadvantages of the approximate nature of Eq. 8.39 are to some extent minimized by the circumstance that except in the immediate vicinity of the charge the shock-wave parameters are not very sensitive to the initial energy of the wave.

Calculated values of the shock-wave parameters for the underwater explosion of TNT at a density of 1.59 gm./cm.^{3} are listed in Table 8.3. The initial pressure, p_1 = 37 kilebars, was calculated by Eqs. 2.4 and 2.6 and

---

31/ A. B. Arons and D. R. Yennie, Phys. Rev., 20, 519 (1948).

TABLE 8.3 - Peak pressures and shock-wave energies for the underwater explosion of TNT, density 1.59

R/a_0	P_m (kilobars)	ϵ (joules/gm.)
1	37.0	2390
5	3.07	1590
10	1.14	1320
25	.347	1110
50	.152	1020
100	.0680	955

is identical with that employed for the calculation by the theory of Kirkwood and Bethe. The initial value of the reduced energy variable, $Q_1 = 25.0$, was calculated by means of Eq. 6.78.[32] This value corresponds to the value $\mathcal{E}_1 = 572$ cal./gm. or, with an explosion energy of 1060 cal./gm., to an energy of the gas bubble at its first maximum of 478 cal./gm. The remarkably good agreement of the latter figure with experiment is probably fortuitous.

The calculated peak pressure-distance curve is compared with the predictions of the kinetic enthalpy propagation theory of Kirkwood and Bethe in Figure 8.1. At large distances, the results obtained by the similarity restraint theory are about 18 percent lower than those obtained by the kinetic enthalpy propagation theory. In view of the very different nature of the two theories, it may be concluded that the two theories are in satisfactory agreement.

The application of the similarity restraint theory to the calculation of the shock-wave parameters for particular explosives has been facilitated by the preparation of tables of the integrals of Eqs. 8.24 for a number of initial values of the peak pressure and reduced energy variable.[29] These tables permit the immediate evaluation of the shock-wave parameters for particular explosives after the initial conditions have been computed, and they may be employed with curve-fitting techniques for the extrapolation of experimental results, measured over a limited range of distance, to larger or smaller distances from the charge.

32/ The thermodynamic properties of the explosion products of TNT were taken from a tabulation by J. G. Kirkwood, S. R. Brinkley, Jr., and J. M. Richardson, OSRD Report 2022 (1943).

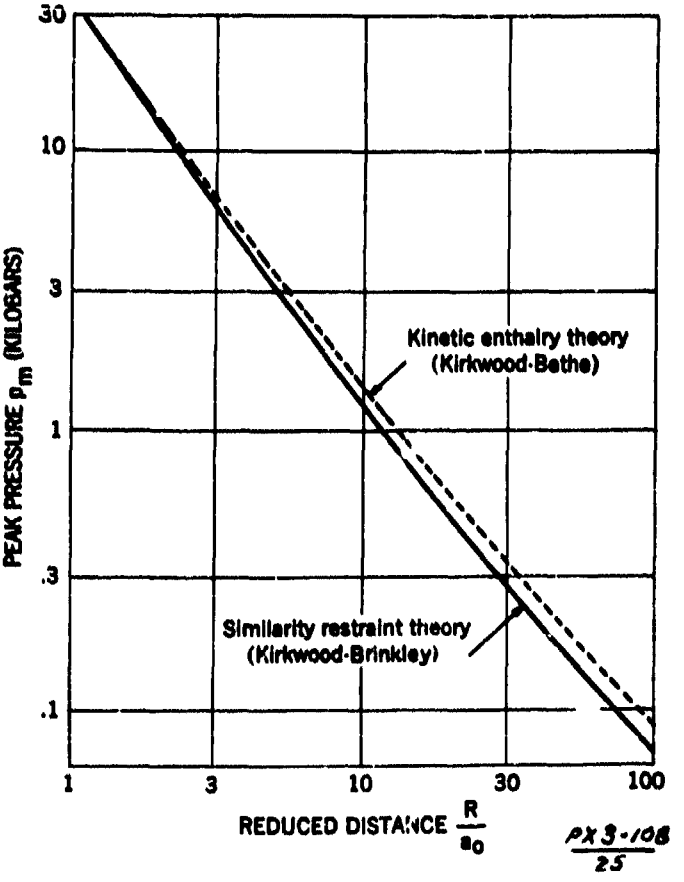


FIGURE 8.1 - Calculated peak pressures for TNT, density 1.59.

9. The Shock Wave for Cylindrical Symmetry

The theoretical description of underwater shock waves has so far been limited to the case of spherical symmetry. This case is the simplest one that corresponds to a situation that can be realized experimentally, and it is a good approximation, particularly at large distances, to the shock wave produced by charge shapes commonly employed. However, the theoretical investigation of shock waves of different symmetry is of interest for the information that it can give on the effect of symmetry upon the wave.

The methods of the kinetic enthalpy propagation theory of Kirkwood and Bethe have been employed by Rice and Ginell[9] for a theoretical treatment of the one-dimensional case of an infinite cylinder of explosive undergoing instantaneous adiabatic isometric conversion to its products. The shock-front conditions of Rankine and Hugoniot and the equation of state are the same as for the spherical case, the differences between spherical and cylindrical symmetry appearing in the fundamental equations of hydrodynamics. The initial conditions resulting from adiabatic constant volume explosion are also unaffected by the symmetry.

In the acoustic approximation, cylindrical waves undergo a change of type as they are propagated, and the variation of some property of the fluid, such as pressure, as $r^{-1/2}F(t - r/c_0)$, where F, is an arbitrary function, is valid only asymptotically. The corresponding variation as $r^{-1}F(t - r/c_0)$ for an acoustic spherical wave is valid at any distance. A finite amplitude theory, in which the approximations are suggested by the acoustic case, will therefore be less simply related to the wave. In the

theory of Rice and Ginell, it is assumed that level values of a function $G = r^{1/2}\Omega$ are propagated outward with a velocity $c + u$. Asymptotically, this assumption is equivalent to the basic assumption underlying the treatment of the spherical wave. However, detailed calculations showed the assumption to be increasingly in error at decreasing distances from the charge, and somewhat more satisfactory results were obtained by taking $G = r^{\alpha}\Omega$ with α equal to 4/10 instead of 1/2.

In view of the fact that the shock wave from an infinite cylinder of explosive is satisfactorily treated in a direct manner by the methods of the similarity restraint theory, an extended discussion of the theory of Rice and Ginell will not be given here, reference being made to their reports for the details of their treatment.

We consider two cases in the application of the similarity restraint propagation theory to the shock wave from infinitely long cylinders of explosives.[33] The assumption of adiabatic isometric conversion of the explosive charge to its decomposition products results in a one-dimensional theory in which the shock-wave parameters are functions of time and radial coordinate. The consideration of the shock wave produced by a stationary detonation wave traveling in the axial direction of the cylinder with a finite velocity leads to a two-dimensional theory in which the shock-wave properties are functions of time and radial coordinate only, since the axial and radial coordinates are connected by a relation $Z = Z(R)$. The basic assumptions of the theory as applied to the cylindrical wave are identical with those of the previous section, the treatment differing in detail due to the change in symmetry.

33/ See Reference 10.

The shock wave generated by a stationary detonation wave traveling in the axial direction of an infinite cylinder of an explosive is stationary in a coordinate system with origin in the detonation wave. Therefore, the Eulerian form of the equations of motion, Eqs. 3.1, is the preferred formulation for the development of the theory. They may be written in the form

$$\frac{1}{\rho c^2}\frac{Dp}{Dt} = -\nabla\cdot\underset{\sim}{u}\ , \quad \frac{D\underset{\sim}{u}}{Dt} = -\frac{1}{\rho}\nabla p\ , \tag{9.1}$$

where $\underset{\sim}{u}$ is the vector particle velocity, p the pressure in excess of the pressure p_0 of the undisturbed fluid, ρ the density, and c the Euler sound velocity. They are to be solved subject to initial conditions specified on a curve in the $(\underset{\sim}{r},t)$-space ($\underset{\sim}{r}$ is the Euler position vector), and to the Rankine-Hugoniot conditions, Eqs. 2.2, which constitute supernumerary boundary conditions at the shock front that are compatible with the equations of hydrodynamics and the prescribed initial conditions only if the shock front is an implicitly prescribed curve $\underset{\sim}{R}(t)$ in the $(\underset{\sim}{r},t)$-space. These relations are supplemented by the entropy transport equation, which we shall not use explicitly, and by an equation of state of the fluid that permits, in combination with the Hugoniot relations, evaluation of all of the properties of the shock front as functions of the peak pressure p_m. The particle velocity u of the Hugoniot relations, Eqs. 2.2, is here taken to be the component of particle velocity normal to the shock front, and the shock velocity U is the velocity of the shock front in the direction of its normal.

For the system with axial symmetry, we denote an operator which follows the shock front by

$$\frac{d}{dR} = \left[\underset{\sim}{1}_r\cdot\left(\nabla_0\underset{\sim}{r}\cdot\nabla + \frac{n}{U}\frac{D}{Dt}\right)\right]_{r=R}\ , \tag{9.2}$$

where R is the radial coordinate of the shock front, $\underset{\sim}{1}_R$ and $\underset{\sim}{n}$ are unit vectors in the radial direction and in the direction of the normal to the shock front, respectively, and $\nabla_0 \underset{\sim}{r}$ is the deformation-rotation dyadic. The components of $\nabla_0 \underset{\sim}{r}$ are easily found at the shock front from the fact that the medium experiences a pure strain of magnitude $\rho_0/\rho - 1$ in a direction normal to the shock front as the result of the passage of the wave. If the operator d/dR is applied to the Hugoniot relation between the pressure and particle velocity normal to the shock front and to the relation describing continuity of the tangential component of particle velocity at the shock front, there result

$$g \frac{d p_m}{dR} = \rho_0 U \left(\underset{\sim}{u}_m \cdot \frac{d \underset{\sim}{n}}{dR} + \frac{d \underset{\sim}{u}}{dR} \cdot \underset{\sim}{n} \right),$$

$$\frac{d \underset{\sim}{u}}{dR} \cdot (\underset{\sim}{1}_\varphi \times \underset{\sim}{n}) = \underset{\sim}{u}_m \cdot \left(\frac{d \underset{\sim}{n}}{dR} \times \underset{\sim}{1}_\varphi \right), \qquad (9.3)$$

$$g = g(p_m) = 1 - d \log U / d \log p_m .$$

The derivation of the approximate energy relation which avoids the explicit integration of the equations of hydrodynamics is analogous to that of section 8. The adiabatic work w_0 per unit area of initial generating surface done on the fluid exterior to a generating cylinder is given by

$$2\pi a_0 \, dz_0 \, w_0 = \int_{a_0}^{R} \rho_0 E\left[p_m(r_0)\right] 2\pi r_0 \, dz_0 \, dr_0 + (R, Z) \int_{t(R)}^{\infty} (p + p_0) \, \underset{\sim}{u} \cdot d\underset{\sim}{A} \, dt , \qquad (9.4)$$

where $\underset{\sim}{u}$ and p denote particle velocity and excess pressure behind the shock front, $t(R)$ is the time of arrival of the shock front at the point with Lagrange cylindrical coordinates $r_0 = R$, $z_0 = Z(R)$, $E(p_m)$ is the specific energy increment of the fluid at pressure p_0 for the entropy incre-

ment corresponding to peak pressure p_m, a_0 is the radial Lagrange coordinate of the generating surface, and $d\underline{A}$ is the Euler area element into which the Lagrange area element $2\pi r_0 dz_0 \frac{1}{\rho_0}$ is transformed by the passage of the shock wave. Now

$$(R,Z)\int_{t(R)}^{\infty} \underline{u}\cdot d\underline{A}\,dt = (R,Z)\int_{R}^{r(R,Z,\infty)} d\underline{r}\cdot d\underline{H} \quad , \tag{9.5}$$

where $\underline{r}$ is the Euler position vector of the area element, $r(r_0, z_0, t)$ is the Euler radial coordinate at time t, and where the variable of integration is restricted by the path and the definition of $d\underline{A}$ to the radial coordinate. The integrand of equation 9.5 can be shown to be an exact differential of r_0 and t along any path of constant z_0. Accordingly, the path of integration can be changed to

$$[t(R),Z]\int_{R}^{a_0} + (a_0,Z)\int_{a_0}^{r(a_0,Z,\infty)} + (t,Z)\int_{r(a_0,Z,\infty)}^{r(R,Z,\infty)} .$$

Now,

$$[t(R),Z]\int_{R}^{a_0} d\underline{r}\cdot d\underline{A} = -\int_{a_0}^{R} 2\pi r_0\, dz_0\, dr_0 \quad ,$$

since Euler and Lagrange coordinates are identical at or ahead of the shock front, and

$$(t,Z)\int_{r(a_0,Z,\infty)}^{r(R,Z,\infty)} d\underline{r}\cdot d\underline{A} = \int_{a_0}^{R} |\nabla_0 \underline{r}|\, 2\pi r_0\, dz_0\, dr_0 \quad .$$

With the equation of continuity, $\rho_0 = |\nabla_0 \underline{r}|\rho$ Eq. 9.5 becomes

$$(R,Z)\int_{t(R)}^{\infty} \underline{u}\cdot d\underline{A}\,dt = (a_0,Z)\int_{t(a_0)}^{\infty} \underline{u}\cdot d\underline{A}\,dt + \int_{a_0}^{R}\left(\frac{\rho_0}{\rho}-1\right)2\pi r_0\, dz_0\, dr_0 \quad . \tag{9.6}$$

Combining Eq. 9.6 with Eq. 9.4 and introducing the dissipated enthalpy $h(p_m) = E(p_m) + p_0 \Delta(1/\rho)$, one obtains

$$2\pi r_0 dz_0 w_\infty - \int_{t(r_0)}^{\infty} p_0 \, d\underset{\sim}{A} \cdot \underset{\sim}{u} \, dt = \int_{w_0}^{R} \rho_0 h[p_m(r_0)] 2\pi r_0 dz_0 dr_0 + \int_{t(R)}^{\infty} p \, \underset{\sim}{u} \cdot d\underset{\sim}{A} \, dt . \tag{9.7}$$

The time integral of the right member may be assumed to vanish for $R = \infty$. If one subtracts from Eq. 9.7 the expression obtained from that equation for $R = \infty$, there results the relation

$$2\pi dz_0 D(R) = \int_{t(R)}^{\infty} p \, \underset{\sim}{u} \cdot d\underset{\sim}{A} \, dt , \tag{9.8}$$

where

$$D(R) = \int_{R}^{\infty} \rho_0 h[p_m(r_0)] r_0 dr_0 . \tag{9.9}$$

Now, $d\underset{\sim}{A} = 2\pi r \, ds \, \underset{\sim}{n}$, where $\underset{\sim}{n}$ is the unit normal to $d\underset{\sim}{s}$ into which $dz_0 \underset{\sim}{1}_z$ is transformed by the passage of the wave, and therefore,

$$d\underset{\sim}{A} = 2\pi r \, dz_0 \, \underset{\sim}{1}_\varphi \times (\underset{\sim}{1}_z \cdot \nabla_0 \underset{\sim}{r}) .$$

Eq. 9.8 becomes

$$D(R) = \int_{t(R)}^{\infty} r p \, \underset{\sim}{u} \cdot [\underset{\sim}{1}_\varphi \times (\underset{\sim}{1}_z \cdot \nabla_0 \underset{\sim}{r})] \, dt . \tag{9.10}$$

The energy-time integral can be expressed in reduced form,

$$D(R) = F_m \mu \nu , \quad 1/\mu = -[(D/Dt) \log F]_{t(R)} ,$$

$$F = \underset{\sim}{u} \cdot [\underset{\sim}{1}_\varphi \times (\underset{\sim}{1}_z \cdot \nabla_0 \underset{\sim}{r})] r p , \quad \vartheta = [t - t(R)]/\mu , \tag{9.11}$$

$$f(R, \vartheta) = F/F_m , \quad \nu = \int_0^\infty f(R, \vartheta) \, d\vartheta .$$

The function $f(R,\vartheta)$ is the energy-time integrand, normalized by its peak value at the shock front, expressed as a function of R and a reduced time ϑ which normalizes its initial slope to -1 if μ does not vanish.

At the shock front, $\underset{\sim}{1}_\varphi \times \underset{\sim}{1}_z \cdot \nabla_0 \underset{\sim}{r} = \underset{\sim}{n} \sin\theta$, where θ is the angle between the tangent to the wavefront and the r-axis. The desired energy-equation is obtained by eliminating μ between the first two of Eqs. 9.11 and making use of the Hugoniot relations. As the result, one obtains

$$\left(\frac{D\underline{p}}{Dt}\right)_{r=R} + \rho_0 U \underset{\sim}{n} \cdot \left\{\frac{D\underline{u}}{Dt} + \underset{\sim}{1}_\varphi \times \left[\left(\underset{\sim}{1}_z \cdot \nabla_0 \underset{\sim}{r}\right) \cdot \nabla_0 \underline{u}\right]\right\}_{r=R} = -u \sin\theta \left[\frac{\mathcal{D} R p_{in}^2}{D(R)} + \frac{p_{rr}}{R}\right], \tag{9.12}$$

where $\nabla_0 \underline{u}$ is the Euler rate of strain dyadic, and where each term is evaluated at the shock front. The shock-wave energy at R per unit area of initial generating surface is $D(R)/a_0$, where a_0 is the Lagrange radial coordinate of the generating surface and $\mathcal{D}(R)$ is given by

$$\frac{dD}{dR} = -\rho_0 R h(p_{in}), \tag{9.13}$$

obtained by differentiation of the definition of the energy variable $D(R)$, Eq. 9.9.

As in the case of the spherical wave, $\nu = 1$ for the peak approximation to the Lagrange energy-time curve, and the assignment of this value, independent of the coordinates, is equivalent to imposing a similarity restraint on the energy-time curve.

In order to obtain the propagation equations for the one-dimensional wave, the origin of the radial coordinate r is taken to be

the axis of the generating cylinder. Eqs. 9.1, specialised to the shock front $r = R$, together with Eqs. 9.3 and 9.12, provide four nonhomogeneous, linear relations between the four nonvanishing time and distance derivatives of pressure and particle velocity, evaluated at the shock front, with coefficients that can be expressed as functions of distance and peak pressure through Eqs. 2.2 and the equation of state. The equations can be solved for the derivatives and an ordinary differential equation, $dp_m/dR = F(p_m, R)$, formulated with the aid of Eq. 9.12. An additional ordinary differential equation for the shock-wave energy is provided by Eq. 9.13. The results are

$$\frac{dp_m}{dR} = -\left\{\frac{p_m}{2R} N(p_m) + \frac{\rho R p_m^3}{D(R)} m(p_m)\right\}, \qquad (9.14)$$

where

$$N(p_m) = \frac{4\rho_0/\rho_m + 2(1-\rho_0/\rho_m)G}{2(1+q) - G},$$

$$m(p_m) = \frac{1}{\rho_0 U^2} \frac{G}{2(1+q) - G},$$

$$G(p_m) = 1 - (\rho_0 U/\rho_m c_m)^2.$$

Eqs. 9.13 and 9.14 may be integrated numerically, employing tables of the functions $h(p_m)$, $m(p_m)$, $N(p_m)$, which can be constructed by numerical methods from the exact Hugoniot curves for the fluid. Eqs. 9.13 and 9.14 are identical with the relations obtained with the simpler considerations of the last section.[23]

The asymptotic forms of Eqs. 9.13 and 9.14 are

$$\frac{dD}{dR} = \left(\frac{n+1}{12n^2}\right)\frac{R\,p^2}{B^2}\,,$$
$$\frac{dp_m}{dR} + \frac{p_m}{2R} = -\left(\frac{n+1}{12n^2}\right)\frac{R\,p^4}{DB^2}\,, \tag{9.15}$$

with the integrals

$$\sqrt{R}\,p_m = P_1\left[\sqrt{R} - \sqrt{R_1}\right]^{-1/2}\,,$$
$$D = \left[(n+1)/6n^2B^2\right]P_1^2\sqrt{R}\,p_m\,, \tag{9.16}$$

where P_1 and R_1 are constants.

To obtain the propagation equations for the two-dimensional wave, we let r and z be the cylindrical coordinates relative to an origin in the detonation front with the Z-axis coincident with the axis of the cylinder. The velocity of the detonation wave relative to a stationary origin in the negative Z-direction is U_D. The profile of the shock wave is a surface of revolution $Z = Z(R)$ with the differential equation

$$\frac{dZ}{dR} = \tan\theta\,. \tag{9.17}$$

Since the distance traveled by the shock front in time dt in the direction of its normal is $U\,dt$ and in the same time, the origin of the coordinate system travels a distance $U_D\,dt$ in the negative Z-direction,

$$\cos\theta = U/U_D\,. \tag{9.18}$$

Taylor[34] has shown that the Chapman-Jouguet[35] conditions can be satisfied at the front of a stationary detonation wave by solutions of the equations of hydrodynamics which depend only on $\underset{\sim}{r}/t$. For solutions of the Taylor type,

$$D/Dt = (\underset{\sim}{u} - \underset{\sim}{r}/t)\cdot\nabla \quad . \tag{9.19}$$

The solutions of Eqs. 9.1 and 9.19 for the exterior medium are compatible with the conditions on the boundary between explosion products and the exterior medium if solutions of the Taylor type are valid in the explosion products behind the detonation wave.

At any finite distance from an infinite cylinder of explosive, $\underset{\sim}{r}/t = 0$, and

$$D/Dt = \underset{\sim}{u}\cdot\nabla \quad . \tag{9.20}$$

Eq. 9.20 can be employed to provide three relations between the derivatives with respect to time and the distance coordinates of the pressure and the components of the particle velocity. These relations and Eqs. 9.1, specialized to the shock front, together with Eqs. 9.3 and 9.12, provide nine nonhomogeneous linear equations between nine partial derivatives with coefficients that are functions of R, U_D, and ρ_m. The equations can be solved for the derivatives and an ordinary differential equation, $d\rho_m/dR = F(\rho_m, U_D, R)$ formulated with the aid of Eq. 9.2. The result is

$$-\frac{d\rho_m}{dR} = \Phi(\rho_m, U_D)\left\{\frac{\rho_m}{2R}N(\rho_m) + \frac{2R\rho_m^3}{D(R)}M(\rho_m)\right\}, \tag{9.21}$$

34/ G. I. Taylor, British Report RC-178 (1941).

35/ H. L. Chapman, Phil. Mag. (5) 47, 90 (1889).
E. Jouguet, Comptes rendus, 132, 573 (1901).
See also S. R. Brinkley, Jr., and J. G. Kirkwood, Proc. Third Symposium on Combustion, Flame, and Explosion Phenomena, Williams and Wilkins Co. Baltimore (1949), p. 586.

where

$$\Phi(p_m, U_D) = \left[1 - \frac{\rho_e}{\rho_m} \frac{2(1+g) + G}{2(1-g) - G} \frac{U^2}{U_D^2 - U^2} \right]^{-1}, \tag{9.22}$$

and where $D(R)$ is given by Eq. 9.13 and $m(p_m)$, $N(p_m)$ have been given for the one-dimensional case. When $p_m(R)$ is known, the profile $Z(R)$ of the shock front can be obtained by an auxiliary integration

$$Z(R) = \int_{R_0}^{R} \left\{ \frac{U[p_m(r_0)]^2}{U_D^2} - 1 \right\}^{1/2} dr_0 . \tag{9.23}$$

We note that $\lim (U_D \to \infty)\ \Phi = 1$, and Eq. 9.21 is identical with Eq. 9.14 in this limit. Also, $\lim (p_m \to 0)\ \Phi = 1$, and the asymptotic solutions of Eqs. 9.14 and 9.21 have the same form.

The two constants of integration can be determined from the thermodynamic properties of the explosive and those of its products in the Chapman-Jouguet detonation state or in the instantaneous detonation state. The constants of integration may be conveniently selected as p_1 and ϵ_1, the initial values of the peak pressure and the total shock-wave energy delivered by the explosion products from unit mass of explosive.

The initial excess pressure p_1 and particle velocity u_1, continuous at the boundary, are determined by the relations,

$$\sigma^*(p_1) = \frac{U_D}{c_0} \left[U_D - \frac{p_1}{\rho_0} \frac{1}{U_D} \right] - \frac{U_D}{c_0} p_1 \left[\frac{1}{U_1^2} - \frac{1}{U_D^2} \right]^{1/2},$$

$$u_1 = p_1 / \rho_0 U_1 , \quad U_1 = U(p_1) , \tag{9.24}$$

where σ^* is the Riemann function in the gas sphere and $U(p_1)$ is the shock velocity in the exterior medium, determined as a function of pressure by the Hugoniot conditions. The asterisked quantities refer to the explosion products and the unasterisked to the exterior medium. The subscript D refers to the Chapman-Jouguet detonation state. The first of Eqs. 9.24 expresses the fact that the Riemann-$\bar{r}^*$, computed normal to the generating surface, initially vanishes in the receding rarefaction wave.

In the limit of infinite detonation velocity, the first of Eqs. 9.24 reduces to

$$\sigma^*(p_1) + u_1 = 0 , \tag{9.25}$$

which is in agreement with the expression of section 2 for the determination of the initial pressure from the instantaneous constant volume explosion state.

In the development of the propagation equations, the rate of energy delivery has been approximated by an exponential function of time. As in section 8, we may assume that the integral of this exponential function is equal to about one-half the total energy of explosion. The disadvantages of this procedure are minimized by the circumstance that except in the immediate vicinity of the charge, the shock-wave parameters are not very sensitive to the initial energy. Accordingly, the initial value of the energy variable D is taken to be

$$D_1 = \frac{a_0^2}{\gamma} \beta \rho_0 \zeta_1 , \tag{9.26}$$

where β, the fraction of the total explosion energy delivered to the first shock, can be estimated from measurements of the maximum bubble radius from spherical charges, or in the absence of such information, roughly approximated by the value 1/2. A more refined analysis for the determination of the initial shock-wave energy, similar to that for the spherical shock wave, has not been carried out for the cylindrical case.

10. Comparison with the Experiment

We conclude the discussion of the theory of the propagation of underwater shock waves by comparing with experimental values the results of the calculation of shock-wave parameters by the two theoretical procedures which have been outlined for two typical explosives. The kinetic enthalpy propagation theory and the similarity restraint propagation theory are based on entirely different theoretical assumptions, and it is therefore of interest to compare the predictions of the two theories and also to compare the theoretical predictions with experiment. A discussion of the techniques for the experimental determination of shock-wave parameters will be found elsewhere in this work.[16]

The use of the peak approximation to the kinetic enthalpy on the gas surface in the kinetic enthalpy propagation theory and the assumption of an exponential Lagrange energy-time curve in the similarity restraint propagation theory results for each theory in the prediction of an exponential form of the Euler pressure-time curve. The exponential pressure-time

16/ See also R. H. Cole, Underwater Explosions, Princeton University Press, Princeton, New Jersey (1948).

curve is a good approximation to the initial portions of the experimentally obtained pressure-time curves of underwater shock waves from explosive sources. It is not, however, a good representation of the latter portions of the experimental curve. In the later portions of the curve, the decay is much slower than that predicted for an exponential wave, the tail of the wave being the result of essentially incompressive motion exterior to the gas surface. The excess pressure associated with this motion becomes zero only at that time at which the gas pressure becomes equal to the hydrostatic pressure. This time is of the order of one-tenth of the period of pulsation of the gas bubble and is many times the time constant of the initial high-pressure portion of the wave. However, the peak approximation to the pressure-time curve provides a good representation of that portion of the wave for which the pressure is appreciable. In Figure 10.1, the experimental pressure-time curve obtained at 20 feet from a 300-lb. charge of TNT[37] is compared with the exponential pressure-time curves predicted by theory. It is evident that the exponential approximation is a good representation of the initial part of the curve.

Although the comparison of theoretical and experimental values of shock-wave peak pressure is unambiguous, a difficulty arises in the comparison of parameters which result from the integration of the pressure-time curve. The experimental form of the shock wave is such that the impulse, I, the integral under the pressure-time curve, does not converge rapidly to a limiting value with increasing values of the time. It is not therefore practical to define an upper limit of the time for which the impulse is

37/ R. H. Cole, loc. cit., p. 231.

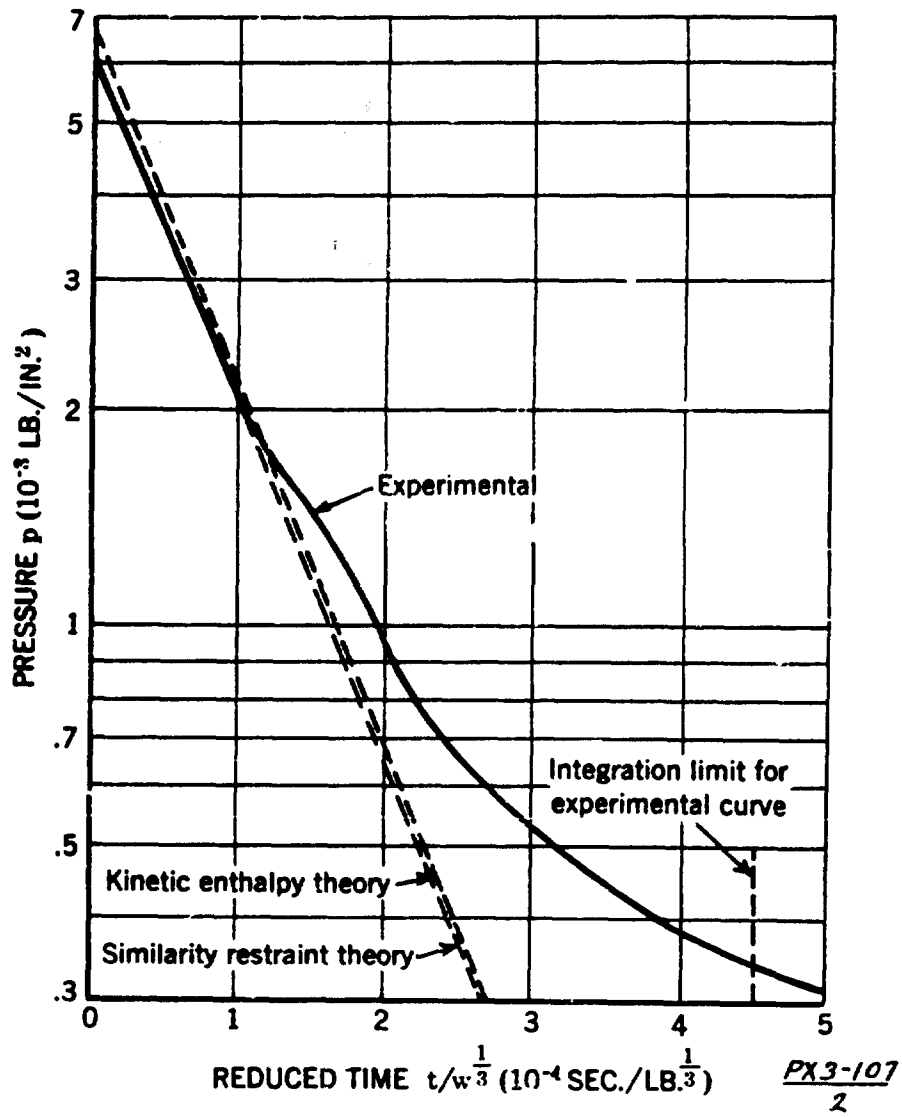


FIGURE 10.1 - Pressure-time curves for TNT (density 1.52) at $R/W^{1/3}$ = 3 ft./lb.$^{1/3}$.

obtained. For this reason the experimental impulse of a shock wave is customarily obtained by an integration over only the initial high-pressure region of the pressure-time curve to an arbitrarily assigned upper limit of time. It has been found that the figures obtained in this way for the impulse are entirely satisfactory for the comparison of the effectiveness of different explosives if the integration is carried to a time equal to five times the initial time constant of the wave. Although the experimental determination of the energy density is less ambiguous, a similar situation, described in detail by Cole, exists in this case also. Since the theoretical values of the impulse and energy density are obtained by integrating to infinite time an exponential pressure-time curve, the comparison of theoretically predicted values of the impulse and energy with the experimental values is somewhat arbitrary, and agreement as to absolute magnitude is to a certain extent fortuitous.

In Table 10.1, we list the result of the calculation of the peak pressure, impulse, and energy by the kinetic enthalpy propagation theory and by the similarity restraint propagation theory for underwater shock waves generated by spherical charges of TNT of density 1.52 gm./cm.^{3} and Tetryl of density 0.92 gm./cm.^{3}. The theoretical predictions of the kinetic enthalpy propagation theory have been obtained by interpolation of the values listed in a report by Kirkwood, Brinkley, and Richardson.[26] The initial conditions for the calculation of the shock-wave parameters by the similarity restraint propagation theory were obtained from Eqs. 2.4, 2.6, and 8.38, employing the tables of the thermodynamic properties of the explosion products given by Kirkwood, Brinkley, and Richardson.[26] The

TABLE 10.1 - Calculated and observed underwater shock-wave parameters for spherical TNT and Tetryl charges

$R/W^{1/3}$ (ft./lb.$^{1/3}$)	TNT (Density 1.52) (1)	(2)	(3)	Tetryl (Density 0.92) (1)	(2)	(3)
	Peak Pressure p_m (10^4 lb./in.^{2})					
1	2.99	2.62		2.55	2.56	
2	1.16	1.04	0.987	1.06	1.11	0.964
3	.691	.629	.624	.644	.679	.605
5	.367	.334	.351	.348	.372	.336
10	.162	.148	.160	.156	.169	.152
13	.120	.109	.119	.115	.126	.112
	Reduced Impulse $I/W^{1/3}$ (lb. sec./in.^{2}/lb.$^{1/3}$)					
1	1.41	1.35		1.47	2.00	
2	.840	.786	0.788	0.843	1.19	0.902
3	.606	.556	.549	.603	.862	.607
5	.385	.360	.349	.376	.554	.368
10	.204	.192	.188	.193	.299	.186
13	.161	.151	.149	.171	.232	.144
	Reduced Energy $E/W^{1/3}$ (10^3 in. lb./in.^{2}/lb.$^{1/3}$)					
1	3.75	3.93		3.33	6.36	
2	.865	.856	0.582	.795	1.46	0.700
3	.372	.357	.254	.345	.624	.299
5	.126	.120	.0889	.116	.211	.102
10	.0294	.0277	.0215	.0268	.0499	.0238
13	.0172	.0160	.0126	.0174	.0286	.0137

(1) Calculated with the kinetic enthalpy propagation theory.

(2) Calculated with the similarity restraint propagation theory.

(3) Experimental, calculated by equations 10.1.

calculations by the two different theories are thus based upon the same determination of the thermodynamic properties of the explosion products. The theoretical predictions by the similarity restraint propagation theory were obtained by the use of the tabulated integrals of the propagation equation, Eq. 8.24.[29] The theoretical results have been expressed in the English system of units that is commonly employed to record experimental results. The shock-wave energy E is the energy flux at distance R through unit area. In accordance with principles of similitude, the distance R, impulse I, and energy E, are reduced by the cube root of the charge weight. The experimental results for spherical TNT charges and cylindrical loose Tetryl charges were obtained at the Underwater Explosives Research Laboratory, Woods Hole, Mass., and are cited by Cole.[38] The experimental results were fitted to empirical expressions of the form

$$\begin{aligned} P_m &= k\,(W^{1/3}/R)^{\alpha}, \\ I/W^{1/3} &= l\,(W^{1/3}/R)^{\beta}, \\ E/W^{1/3} &= m\,(W^{1/3}/R)^{\gamma}, \end{aligned} \qquad (10.1)$$

where k, l, m, α, β, and γ, are empirical constants and where the distance and time scales have been reduced, in accordance with principles of similitude, by the cube root of the charge weight, W. These relations have been used for the calculation of the experimental values given in Table 10.1.

The data of Table 10.1 are also shown in Figures 10.2 to 10.4. In each of the figures, the function plotted as the ordinate has been

---

38/ R. B. Cole, loc. cit., p. 241.

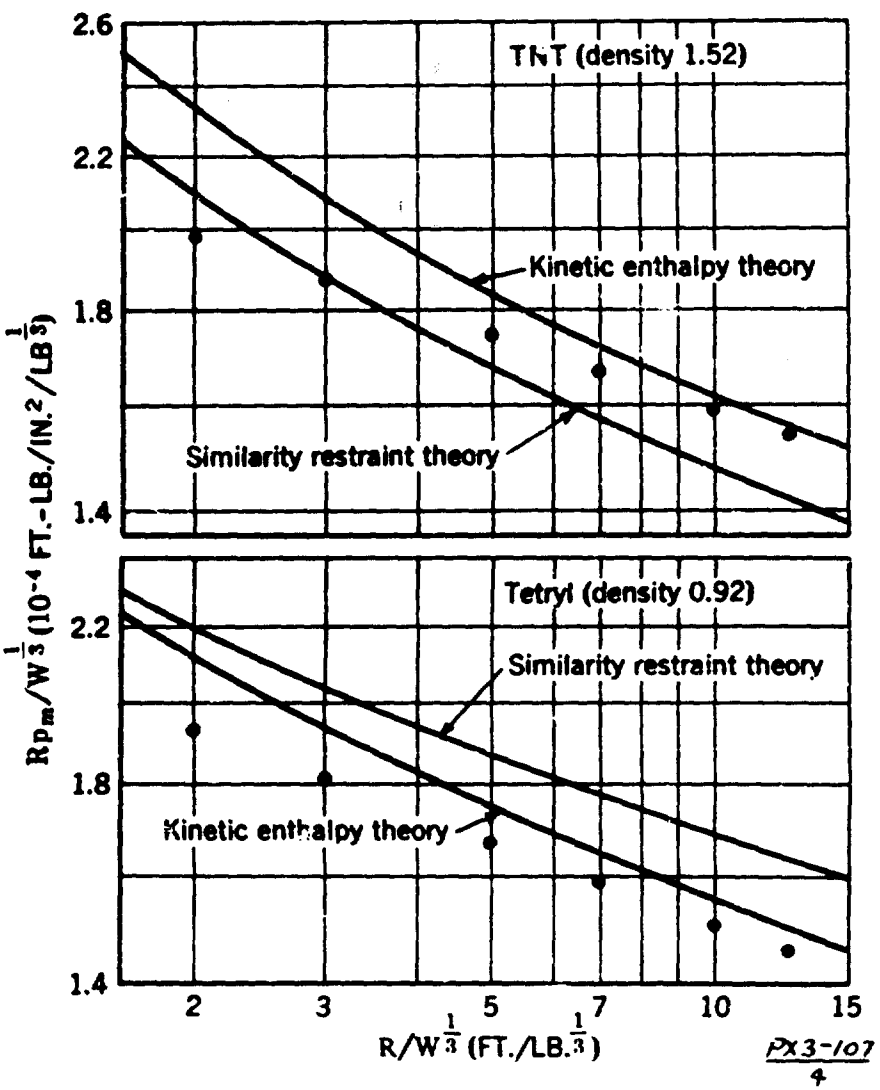


FIGURE 10.2 - Theoretical and experimental peak pressure-distance curves.

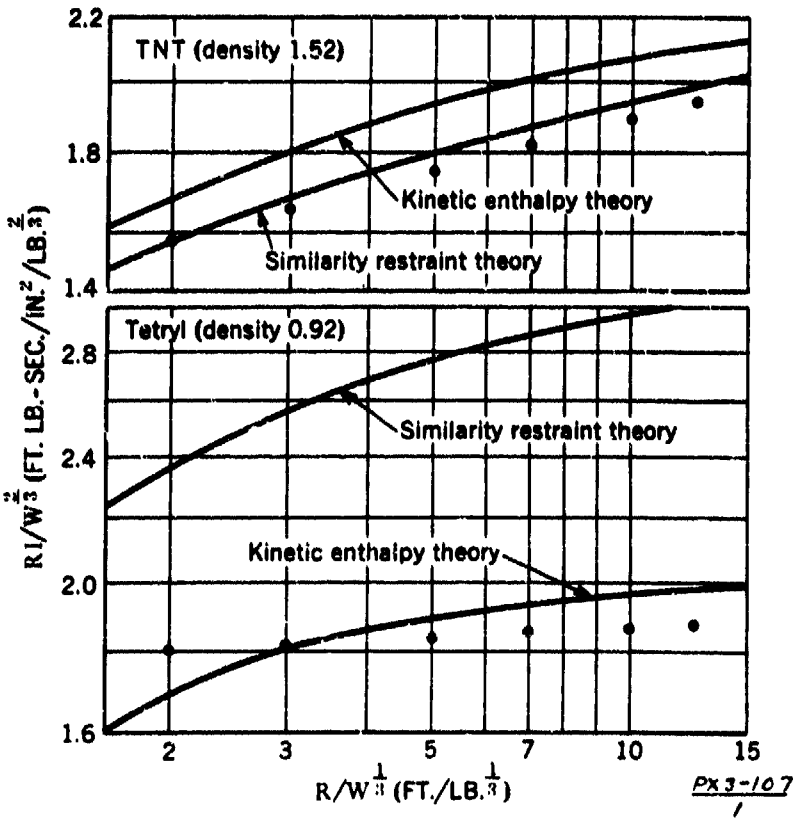


FIGURE 10.3 - Theoretical and experimental impulse-distance curves.

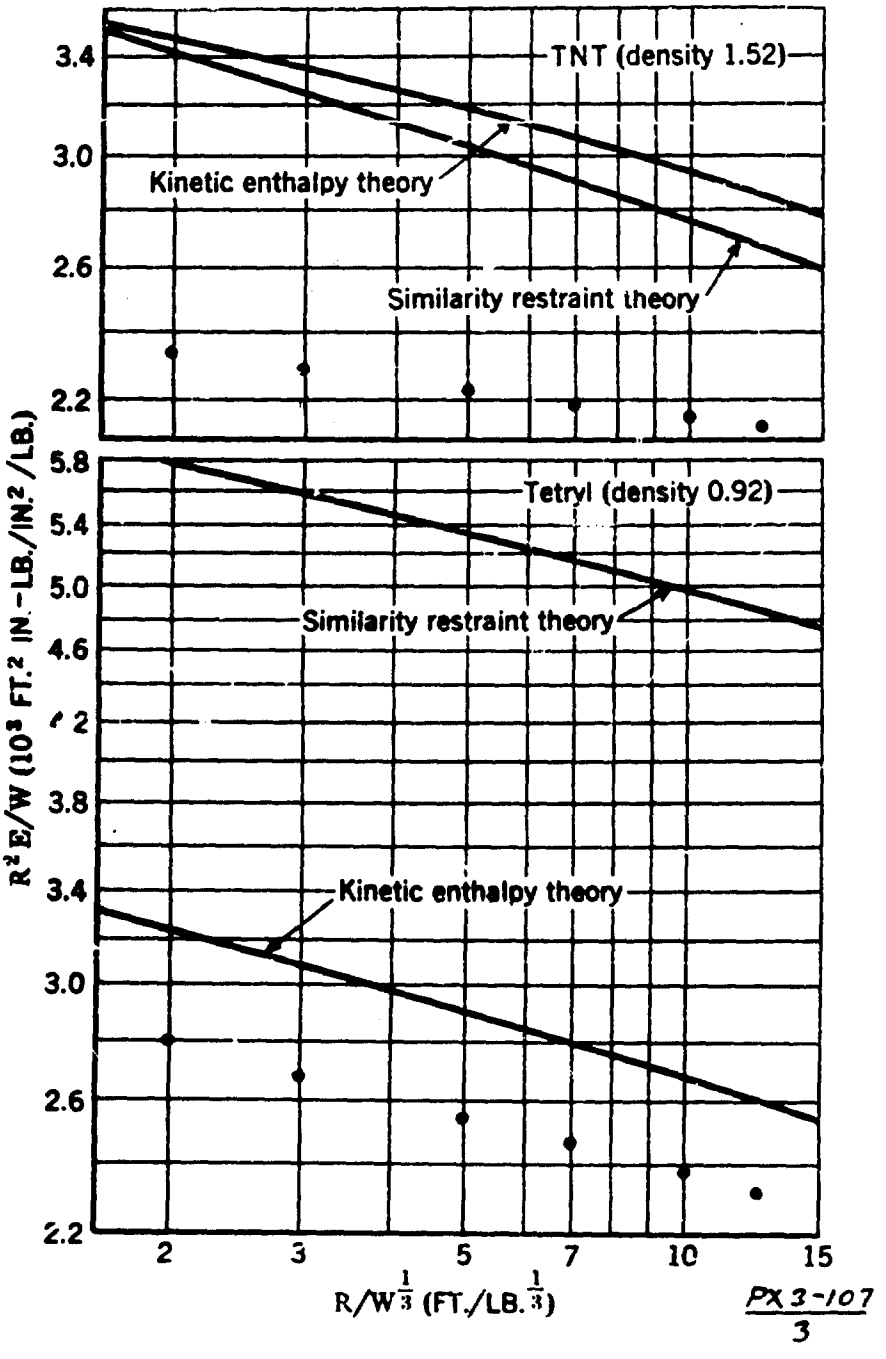


FIGURE 10.4 - Theoretical and experimental energy density-distance curves.

selected to display the nonacoustical nature of the decay of the function with distance. The predictions of the similarity restraint theory for the case of Tetryl reflect the fact that the calculated initial value of the shock-wave energy is somewhat in excess of the most probable value, determined from the maximum bubble radius.

It may be concluded that the two different theories are in satisfactory agreement and that they give, on the whole, a good account of the experimental observations. The theoretical curves are very sensitive to the initial conditions, determined by the thermodynamic properties of the products of explosion. Although the calculation of the initial conditions is straightforward, it requires a knowledge of an applicable equation of state for the explosion products. These products exist at a high temperature and very high pressure, a state that is inaccessible to direct experimental study, and the equation of state is subject to considerable uncertainty. The calculations given in this section have been based upon thermodynamic properties of explosion products determined with the aid of an equation of state of a form proposed by Kistiakowsky and Wilson.[4] The parameters of this equation were determined from observed velocities of detonation for a series of explosives by methods which have been described elsewhere.[39] Unfortunately, more recent experiment has resulted in a revision of the experimental detonation velocities which were employed for the evaluation of the equation of state parameters, and the equation of state is presently in need of revision. It appears probable that consistently satisfactory theoretical prediction of underwater shock-wave parameters could be achieved if an accurate equation of state for the explosion products were known.

39/ S. R. Brinkley, Jr., and E. B. Wilson, Jr. OSRD Report No. 905 (1942).

NATURE OF THE PRESSURE IMPULSE PRODUCED BY THE DETONATION OF EXPLOSIVES UNDER WATER. AN INVESTIGATION BY THE PIEZO-ELECTRIC CATHODE-RAY OSCILLOGRAPH METHOD

A. B. Wood
Admiralty Research Laboratory

British Contribution

November 1924

NATURE OF THE PRESSURE IMPULSE PRODUCED BY THE DETONATION OF EXPLOSIVES UNDER WATER. AN INVESTIGATION BY THE PIEZO-ELECTRIC CATHODE-RAY OSCILLOGRAPH METHOD

A. B. Wood

November 1924

* * * * * * * * * * *

Introduction

Part A. Methods and Apparatus.

Part B. Experimental Results.

Summary.

OBJECTS OF THE EXPERIMENTS

The experiments described in the report which follows are part of a series of practical and theoretical investigations. When complete these investigations will give data for determining the damage which will be done to a ship's structure by an underwater explosion without the necessity of carrying out large scale trials.

A first step in determining the deformation which a structure will undergo, when subjected to to the effects of an explosion, is to ascertain the magnitude of the forces due to the explosion, and in what manner these forces vary in the short interval of time during which they act.

It is apparent, after slight consideration, that there are numerous factors which may affect the pressures generated at a point in the water, and their manner of variation, and which will therefore have to be taken into account in any attempt to predict the effects of an explosion under water.

The chief factors are:-

(a) The weight and nature of the charge.

(b) The distance of the charge from the gauge (or point at which the measurements are made).

(c) The distances of the charge and the gauge from the surface and bottom of the sea, and from bodies or surfaces which might modify the effect of the explosion.

(d) The nature of the charge container (mine-case, torpedo warhead, etc.), the shape of the charge and the position of the point or points of initiation.

A sequence of different water-pressures due to an underwater explosion is completely described if we are able to state how long the abnormal pressures have endured and what was the excess of pressure over the normal at each instant during the time of operation of the effects of the explosion. It is therefore the object of this report to exhibit some of the relations between the shape of the curve showing water-pressures plotted against time, and the factors (a), (b), (c) and (d) above.

There is one further point which should be mentioned. Ultimately it is the effects of large explosions about which we desire information. The greater number of the experiments described in this report were made with small charges in the hope of discovering laws by which the effects of large explosions could be calculated. Larger charges were fired to check the laws derived from an examination of the results of experiments with small charges. The case of contact charges is outside the scope of this report.

Results .....

RESULTS OF THE EXPERIMENTS.

The object of the experiments, it has been stated above, was to express, if possible, the under-water pressure-time curve to an explosion in terms of certain distances, weights, etc., which could easily be measured or assumed. Many pressure-time curves have now been completely determined by the methods described in the report, but, from the point of view of expressing the damaging capacity of an explosion, it has been found easier to speak of the numerical values of the maximum pressure, momentum and energy of the pressure-train, and of the times taken for the pressure to rise to its maximum and to die away, rather than of the somewhat cumbersome mathematical formulae which can be used to express the shape of the pressure-time curve. The five quantities, maximum pressure, momentum, energy and times of rise and fall of pressure, have some clear relations with damaging power, while the equation of the pressure-time curve has no obvious interpretation in terms of damage, nor has it yet been found possible to refer any given amount of damage definitely to the numerical factors which determine mathematically the shape of the pressure time curve.

Shape of the Pressure Time Curve.

In general, the pressure-time curves due to under-water explosions show a rapid rise of pressure to a maximum value, followed by a fall lasting about twenty times as long. These times are clearly related to the rate of growth and collapse of the bubble of hot gases produced in the water by the explosion, and the results of experiments are in good agreement with a theoretical investigation which has been made into the movements of the surface of the bubble. The time taken for the pressure to rise to its maximum, and the maximum pressure reached, may be modified by the presence of air in the case containing the charge, the mechanical properties of the case, and the method of initiating the explosion. The average time of rise of pressure for all charges of the high explosives tested of weights between 2½ and 1000 lbs. is about five hundred-thousandths of a second, and the average time of fall is about one thousandth of a second.

Measurements of the time taken for the pressure to fall to a definite fraction of its maximum value indicate that this time is approximately proportional to the linear dimensions of the charge, i.e. to $\omega^{\frac{1}{3}}$. The shape of the curve is often seriously irregular and the departures from smoothness have been traced to irregularities in the charge and its case, and to bodies in the neighbourhood which may reflect or absorb the pressures in the water.

The relations between maximum pressure, momentum and energy, and weight of explosive and distance

The mean of a large series of observations made with charges whose weights varied between 2½ lbs. and 2000 lbs. may be expressed as follows -

(1) Maximum Pressure $= 12000 \left(\frac{W}{D}\right)^{1.38}$ lbs. per sq. in.

(2) Momentum $= 1.90 \left(\frac{W}{D}\right)^{1.65}$ lbs. secs. per sq. in.

(3) Total Energy of the spherical wave due to an explosion under water $= 3.5 \times 10^5 \, W$ ft. lbs.

or Energy per sq. ft. of wave front at a distance D from origin $= 2.79 \times 10^4 \left(\frac{W}{D^2}\right)$ ft. lbs.

where W = weight of charge in lbs.

D = distance, in feet between the centre of charge and the point at which the pressures are measured.

These .....

These formulae apply to T.N.T. Amatol, or Guncotton in the region where the maximum pressure does not exceed two tons per square inch, provided the charge and gauge are both more than 10 feet from the surface or bottom of the water and are sufficiently removed from other bodies or air spaces. Relation (3) above shows that about one quarter of the chemical energy of a charge of these explosives is converted into mechanical energy in the form of a pressure pulse in water. The values of (1), (2) and (3) above are little affected by the methods of filling the charge or, except in extreme cases, by the method of initiation or, except as stated above, by the depth of the charge.

Reflexion of the pressure train by the surface and bottom of the sea or by the hull of a ship

Records have been obtained or reflected pressure-trains in water. Observations of surface reflexions indicate that sea water can probably support a momentary tension not greater than 200 lbs. per square inch. Tensions of 100 lbs. per square inch and 170 lbs. per square inch have been observed for water in bulk and at a water-steel surface respectively. Records of bottom reflexions show that the ratio of the maximum pressures of the reflected and primary pressure waves is about 1:2 for a bottom composed of mud and sand. As a result of this phenomenon, the maximum pressure developed near a mine laid on the bottom of the sea will be greater than that developed by a similar mine moored in mid-water by about 50%. A record was obtained during the "Gorgon" trials which showed a sudden drop in the pressure at the gauge, due to the arrival of the reflected pressure-train from the hull.

Additional observations.

The experimental methods used in obtaining the above data were used to determine the velocity with which the disturbance due to an explosion is propagated in sea water. No certain difference between the velocity of these high pressure waves and that of ordinary sound waves was detected. Preliminary experiments were also made with a method for determining experimentally the rate of growth of the bubble of hot gases produced by an underwater explosion

BEARING OF THIS WORK ON FUTURE EXPERIMENTS.

The experimental methods elaborated for the work described in this report will be used, with others, in the series of model experiments which is to be carried out on the damaging capacity of pressure-waves due to explosions. The work which has been done has given us reasonably reliable means of predicting the form of the pressure-time curve under different conditions, and of calculating its more important characteristics. The next step is to link this information with "damage done" to different types of structure. One difficulty in working out estimates of damage is to arrive at a satisfactory numerical assessment of damage done, but already the theoretical investigation of this question has given encouraging results, and the model experiments, with possibly one or more large trials, should give information which, when taken into conjunction with our knowledge of the characteristics of pressure-time curves, will be of great value in determining what explosions can safely be withstood by the hull of a vessel.

Introduction and object of investigation.

For a considerable number of years efforts have been made by numerous physicists and engineers to obtain information, on the form, magnitude and destructive effect of the pressure wave produced by an underwater explosion but the results achieved are often very conflicting and throw little or no light on the problem. On the other hand certain experiments, notably by H. W. Hilliar, and Dr. G. W. Walker have cleared up many obscure points and have placed the whole problem on a more scientific basis. Hilliar's work, using the 'copper crusher-gauge' method, has yielded data not only regarding the maximum pressure developed in the explosive wave but also as to the form of the pressure-time relation. Walker's 'spray method' has given a means of determining maximum pressure, but throws no light on the question of the variation of pressure within the pulse. The 'copper diaphragm method', originally proposed by Walker is a promising form of 'damage indicator', but the interpretation of results is difficult at this stage. None of the above methods, however, gives a direct indication or record of the pressure-time relation in the explosive pulse. Hilliar's method gives indirectly an indication of the rate of fall of pressure

from .....

Best Available Co

from its maximum value but it supplies no information regarding the rise of pressure or regarding small fluctuations of pressure in the 'fall' curve. Again, all the above methods are based on certain assumptions relative to inertia in the mechanical system which indicates the pressure. Thus in Hilliar's method, assumptions are made regarding the inertia lags in the steel pistons (with added water) and in the coppers. In Walker's 'spray method', assumptions are made relative to the size of the spray 'droplets' and to the forces retarding their motion through the air. In the 'copper diaphragm' method also, theory is faced with difficulties mainly concerned with the motion of a metal plate strained beyond its elastic limit. It is not proposed at this stage, however, to discuss these methods beyond the point of showing how necessary it is to utilize a more perfect means of indicating the form and magnitude of the explosion pulse. Such a method must be free from all mechanical time-lags and must give a 'true' record of the actual time-pressure variation within the explosive pulse. The nearest approach to such an ideal method is that originally proposed by Sir J. J. Thomson* which utilizes the piezo-electric properties of certain crystalline substances, e.g. tourmaline, with a cathode ray oscillograph to record the variations of electric charge developed on the tourmaline when subjected to the pressure pulse produced by the explosion of a charge. The feasibility of the method was first demonstrated by D. A. Keys ø at Admiralty Experimental Station, Shandon. Since that time, the method and apparatus employed have been considerably improved and during the past two years a large mass of data has been obtained with the improved apparatus and technique. It is the object of this report to describe the method and apparatus employed during the past two years for obtaining automatic photographic records of the pressure-time curve of explosion impulses, and to consider the more important results obtained. It is also a matter of interest, and considerable practical value, to compare these results with those deduced by the Hilliar 'crusher gauge' method, and to provide a standard of comparison for any other methods (such as the 'copper diaphragm' method) which might prove of practical value in the service as 'damage' indicators.

The records obtained not only indicate the pressure-time sequence of the pulse, with the derived momentum-time and energy-time sequences, but also supply information relating to the reflection of the wave from the surface and bottom of the sea and also from the hull of a ship. Relations are obtained between the pressure, momentum and energy of the wave, and the size and distance of the charge from the piezo-electric gauge. Determinations have also been made of the velocity of the explosion wave in the neighbourhood of the charge, and a method has been developed for recording at high speed the initial stages of the explosion wave in order to obtain accurate data relating to the time of rise of pressure and the fine structure of the pressure pulse.

Part A. Method and Apparatus.

In this section it is proposed to deal with the more important details of technique and apparatus employed in obtaining photographic records of the explosion p/t curve, and to the methods of calibrating the piezo-electric gauge and the cathode-ray oscillograph. Consideration will also be given to certain precautions which must be observed in order to obtain 'true' records.

1. *General Outline of Method.*

Certain crystals e.g. tourmaline, quartz, rochelle salt etc. possess the property of exhibiting electrical charges on their faces when mechanical pressure is applied in certain directions ∠. The quantity of electricity liberated is found to be exactly proportional to the total pressure applied *. Hence a crystal of tourmaline may serve as a pressure gauge when used in conjunction with a suitable indicator of the electrostatic charge on its faces. If the pressure is of an impulsive character, as in the case of that developed by an under-water explosion, then it is essential that the indicator or recorder must be quick-acting and dead-beat. The cathode-ray oscillograph fulfils the required conditions, for the moving element

(the .....

* Sir J. J. Thomson Engineering Vol. 107, 1919, pp. 543-544.

ø D. A. Keys, Phil. Mag. 42, pp. 473-488, October (1921)

∠ This phenomenon was termed 'piezo-electricity' by Curie who discovered the effect in 1880.

* This is true up to the point of fracture of the crystal.

Best Available Co

(the cathode-ray stream) possesses negligible inertia, and is capable of responding instantaneously to electrostatic changes. The oscillograph is quite free from resonance, being equally sensitive at all frequencies, and will therefore indicate faithfully the fluctuations of electric charge produced by an impulsive pressure on the faces of the piezo-electric crystals. The cathode-ray oscillograph consists essentially of an evacuated tube in which a beam of cathode rays (high speed negatively charged electrons), is generated by means of a hot filament and suitable accelerating potential. A fine pencil of these rays passes between a pair of electrostatic deflecting plates and the poles of an electro-magnet, and ultimately falls on a phosphorescent observing screen or a photographic plate. The electrostatic deflecting plates are connected to the faces of the piezo-electric crystal and consequently the cathode stream is deflected in proportion to the magnitude of the charge on the crystal faces i.e. to the pressure applied. The electro-magnet is employed to deflect the rays at a known rate and in a direction at right angles to the electrostatic deflection, i.e. to generate a 'time-axis' for the pressure-time* record. The linear deflection of the cathode-rays is obtained by making use of the rise of current in the magnet circuit containing suitable inductance, resistance and voltage. In the early stages the rise of current is practically linear and the corresponding deflection of the cathode-rays is, to the required degree of accuracy, also a linear function of time. The timing arrangements, to bring the pressure-time (p/t) record to the middle of the plate, are rendered automatic by means of a pressure-switch in the sea situated between the charge and the p.e. gauges and connected in series with the above magnet circuit.

The distances of the switch from the gauge and the speed of traverse of the spot are adjusted according to the circumstances of the record to be obtained. When the charge is fired the pressure wave first closes the pressure switch, thereby starting the cathode-rays on their traverse across the plate, and then reaches the p.e. gauge which develops an electric charge and consequently deflects the cathode-rays in a direction at right angles to the time axis.

In this manner, knowing the pressure-sensitiveness of the p.e. gauge and the rate of traverse of the time axis, we obtain a p/t record on the photographic plate. It is of course necessary to calibrate the crystal vessel at known pressures and to determine the sensitivity and speed of the 'spot' of the cathode-ray oscillograph under different conditions.

With this information the explosion records obtained by the method just outlined give at once the pressure-time curve for the explosion pulse.

2. *Apparatus.*

The cathode ray oscillograph used throughout the investigation is of a particularly robust type suitable for use on board a rolling ship with engines throbbing - it has now been in continuous use in a ship for 2 years, and on several occasions under very severe weather conditions, without breakdown. The piezo-electric gauge and the pressure switch have also been specially designed to withstand the forces near underwater explosions of large charges.

(a) The Cathode Ray Oscillograph.

The cathode ray oscillograph used in these experiments is illustrated in the Figure. The cathode consists of a spiral of tungsten or lime-coated platinum wire, which is heated by means of an insulated battery. The hot spiral is supported inside a cylindrical sheath which exerts a focussing action on the cathode rays as they travel towards the anode. The rays are accelerated by means of an applied voltage of 3000, the positive end being connected to the anode and earthed. After passing through the pinhole tube in the anode the cathode rays travel through parallel electrostatic and magnetic fields and ultimately fall on the phosphorescent screen. Removal of this screen exposes a photographic plate to the action of the rays.

The .....

* We shall use p/t as an abbreviation for 'pressure-time' and p.e. for 'piezo-electric'.

Best Available Copy

The oscillograph is described in Proc. Phys. Soc. Vol. 35. February 15, 1923. It will be seen from the illustrations that the instrument is of very robust construction, consisting mainly of strong metal parts and a minimum amount of glass. The oscillograph is evacuated to a pressure less than 0.001 mm of mercury by means of a Gaede mercury pump with suitable backing pump (a Fleuss hand pump or a rotary oil 'box' pump). Under normal conditions the desired vacuum can be obtained after about 10 to 20 minutes continuous pumping, commencing at atmospheric pressure. The high tension D.C. supply is obtained from a 5000 volt generator. An automatic cut-out is provided which prevents the space current in the tube from rising above 20 milliamps, and incidentally protects the operator. The vacuum conditions in the apparatus are examined qualitatively by means of an auxiliary test bulb and spark coil.

A question of considerable importance in using the oscillograph for photographic purposes is that of the most suitable photographic plate. Since cathode rays of velocity corresponding to 3000 volts can only penetrate extremely thin films of matter, e.g. 10^{-4} mm. of gelatine, it is important that the energy of the ray should be expended in the most efficient manner. Consequently a special type of photographic plate, known as the Schumann plate*, has been employed in preference to the ordinary gelatine-coated plate. Analysis of the film to determine the ratio of Ag Br to gelatine in an ordinary plate and a Schumann plate has shown that the Schumann plate has about 100 times the proportion of Ag Br to gelatine that is found in the ordinary plate. On these grounds it would be anticipated that the cathode rays would produce much greater photographic effect in a Schumann plate than in the ordinary gelatine-coated plate, and this is strikingly borne out in practice. The Schumann plate gives excellent photographic results even when the cathode rays are deflected at the highest speeds. For comparatively slow records, however, Paget Half Tone plates have been found to give fairly satisfactory results.

The electro-magnet shown in the Figure is used to deflect the rays at a known rate across the plate i.e. to generate the time axis of the p/t record. For certain reasons it is not convenient, and in some cases it is impossible, to generate a time axis by mechanical movement (translation or rotation) of the photographic plate in a direction at right angles to the pressure axis of the record. The same result is obtained much more simply by passing a current which varies in a known manner through the electro-magnet. Thus if A.C. is applied to the magnet winding the cathode ray spot oscillates sinusoidally on the plate. It is, however, preferable that the time scale should be linear, since the photographic record is then the true p/t record and no further analysis is necessary. To generate a linear time axis the magnet is wound with an auxiliary coil which carries a steady current sufficient to deflect the spot from a position in the middle of the plate to a point just off the left-hand edge. If now a more powerful current is switched on the primary winding, and in opposition to that in the auxiliary winding, the spot will be swept across the plate from left to right. The speed of traverse depends of course on the magnitudes of inductance, resistance and voltage in the circuit of the primary winding. By reducing inductance and increasing voltage the speed can be increased as desired. In the early stages the growth of current is very nearly linear, and the deflection of the cathode rays will thus be a linear function of time.

On certain occasions two cathode ray oscillographs were employed simultaneously.

(b) The Piezo-Electric Gauge.

In selecting a suitable piezo-electric crystal for use in measuring explosion pressures it is necessary to bear in mind the experimental conditions. Tourmaline, quartz and rochelle salt all give strong piezo-electric effects but on general grounds tourmaline was considered to be the most suitable crystal to use for the investigation of explosion pressures. Its piezo electric sensitivity is greater for hydrostatic pressures than for lateral pressures ♯, it is strong mechanically and is not attacked by sea water. For use in explosion gauges the crystals are cut into slabs, usually 1 cm. thick ⁎. The piezo-electric gauge, as used in the explosion research, consists essentially of a mosaic of such slabs of tourmaline

(varying .....

* Originally invented by Schumann for photography of the ultra-violet spectrum.

♯ The crystalline structure of tourmaline differs from that of quartz.

⁎ The charge produced by a given pressure is independent of the thickness of the crystal slice - the choice of thickness therefore is decided by other conditions to be fulfilled in the design e.g. the greater the thickness the smaller the capacity etc.

Best Available Copy

(varying in shape and size) suitably mounted - care being taken to observe that all the pieces have their polarity in the same direction. The design of the gauge itself is a matter of considerable importance, as we shall see later, both the material and the dimensions of the mounting having an important bearing on the results obtained. Experiments have been made with a number of different types of gauge, but in all cases the following important considerations have been kept in mind in the design:-

(Note:- In the original paper follows a detailed discussion of the following points:-

(i) Insulation

(ii) Absence of air cavities

(iii) Material of the mounting

(iv) Dimensions of gauge)

(c) The Pressure Switch.

As we have already stated in the general outline of the p.e. method, the function of the pressure switch is to close the magnet deflecting circuit in the oscillograph, thereby starting the cathode rays in their traverse across the plate. It is essential that the switch should close quickly (in a time of the order of 10^{-4} second) should not re-open, and should be sufficiently robust to withstand the blow of the explosion wave at a short distance from the charge. The type of pressure-switch finally adopted is shown in figure 6a. It consists essentially of a pair of stainless steel coned points, electrically connected by means of a twin-core cable to the ship, mounted in a massive brass cylinder as shown. A lead disc $\frac{1}{32}$ inches thick is clamped by a screwed cap in the end of the cylinder and just clear of the tips of the stainless steel points. The body of the gauge behind the points is filled with ebonite and insulating compound, the whole being water-tight and free from air cavities. The lead disc is sufficiently stiff to prevent making contact across the points by average hydrostatic pressure (say up to 40 feet depth of water), but is easily forced into contact by the explosion pressure which often reaches 2000 lbs/sq. inch or more. These large pressures shear the lead disc at the clamping edge and impale it on the steel points, thus closing the magnet deflecting circuit of the oscillograph. The pressure-switch can be used again for the next explosion, after cleaning and fitting with a new lead disc. In the majority of cases the pressure-switch was arranged at a distance of 8 to 10 feet from the gauge on the side nearer the charge. Taking the velocity of the explosion wave as 5000 feet per second this gives a time interval between 1 and 2 thousands of a second before the pressure pulse reaches the p.e. gauge. Combined with a knowledge of the rate of traverse of the spot across the plate this provides the necessary information to localise the p/t record in a suitable position on the photographic plate. In special cases, of course, it was often necessary to vary the distance of the pressure switch from the gauge, time intervals being reckoned as before, i.e. 5 feet per .001 second (allowing 2 or 3 x 10^{-4} second for the lag in closing the pressure switch). On account of an element of uncertainty in the electrical resistance of the pressure switch, which would throw doubt on the actual rate of traverse of the spot across the plate it was considered advisable to insert a quick-acting relay* in the circuit, the 'local' contacts of the relay to act in parallel with the pressure switch. The operation of the pressure switch in this case not only starts the cathode ray moving across the plate but also actuates the relay, the local of which closes (and remains closed) at least .001 second before the pressure wave reaches the p.e. gauge. In this manner the time constant of the deflecting circuit during the p/t record is rendered perfectly definite and any complications due to a possible re-opening of the pressure-switch are obviated.

(Note:- In the original paper follows

(d) Description of the electrical circuits and auxiliary apparatus, including

(1) .....

* A converted Brown reed telephone with a lag, under the conditions of working, of not more than .0005 second.

Best Available Copy

(1) Cathode ray circuit

(2) Pressure switch circuit

(3) Piezo-electric gauge and testing circuits

(4) Calibration circuits:-

(i) Pressure calibration circuits - A.C., Rotating potentiometer, and inductive time base methods.

(ii) Time calibration circuits.

(e) An estimation is made of the mechanical and electrical lags in the piezo-electric gauge and its associated circuits.

(f) Explosive Charges.

Much of the preliminary work of the investigation (testing gauges, pressure switches, electrical circuits etc. etc.) was carried out by means of small gun cotton charges either 2½ lb. primer tins of Dry G.C. or 16½ lb. tins of wet G.C. primed with 2½ lb. tins of dry G.C. When larger charges were required for test purposes 300 lb. Amatol depth charges were used. In the main part of the investigation a special series of T.N.T. charges was employed, those charges being filled, to Vernon 'M' instructions, at Woolwich. These special T.N.T. charges were 'poured' fillings from the same 'melting' of T.N.T. to ensure uniformity of composition and density. The charges were made up in 'similar' cylindrical cases (length - diameter) to the following approximate weights:- 20, 60, 100, 150, 250, 500, 750, 1000 and 2000 lbs. A certain number of block-filled 100 lb. T.N.T. charges were fired also for comparison with the 100 lb. poured-filled charges. The T.N.T. charges were primed with C.E. pellets and a standard detonator was used.

In order to compare different method of priming and detonating some of the 100 lb. T.N.T. charges were detonated near one end of the cylinder whilst in the other the detonation was initiated centrally.

The small gun cotton charges were found extremely useful also in examining certain theories of explosion pressure and the behaviour of the p.e. gauge under different conditions. Measurements of the time of rise of pressure, velocity of pressure wave, surface and bottom reflections were made with these gun cotton charges.

The 2½ lb. Dry Gun Cotton Charge - consists of 4 cylindrical slabs of dry gun cotton, each 9 ozs. packed in cylindrical watertight containers 10⅛ inches long, 3½ inches diameter and .62 inches thick in the wall. Two No. 9 service detonators are fitted in parallel at one end and a watertight gland serves to seal the tin and bring out the firing leads. See Figure 8. Charge No. (12).

The 18½ lb. G.C. charge - consists of 16½ lbs. of wet gun cotton (with 20% added water) packed in a cylindrical container (nett weight 13 lbs.) 10¼ inches diameter x 10¼ inches long, having two cylindrical holes into one of which (the axial hole) is fitted a 2½ lb. dry G.C. primer, the other hole being left open to the sea. The primer is fired as before with 2 No. 9 service detonators in parallel. The thickness of the outer wall of the charge is $\frac{1}{16}$ inches. Reference to the diagram No. (13) in Figure 8 shows that the charge case is only partly filled with wet gun cotton the spaces between the cylincrical slabs being filled with air.

Depth Charges. These are of the standard service pattern shown in Figure 8 No. (11) containing 300 lbs. of 40/60 Amatol. For the purposes of the present experiments they were prepared for electrical firing being fitted with C.E. primers and standard detonators. These charges are practically free from air cavities.

M.II .....

Best Available Co

M.II Mines. These are of the standard service pattern shown in Figure 8 No. (12), fitted with an inner case containing 320 lbs. of 40/60 Amatol. This inner case is surrounded by an air space of considerable volume and a further iron container of spherical form having a diameter of 38 inches. The thickness of the wall of the inner charge is $\frac{1}{8}$ inch and of the outer spherical shell $\frac{1}{8}$ inch. The influence of the large air space is referred to in Section IV of the report. In this case also the mine was fitted with a C.E. primer and standard electrically-fired detonator.

Special T.N.T. Charges. A number of specially designed T.N.T. poured filled charges were prepared by Woolwich for the main purpose of explosion research - using all forms of gauge under widely conditions. Reference has already been made to the principal features of these charges which are shown diagrammatically to scale in Figure 8. It will be observed that the charge cases are completely filled with T.N.T. the linear dimensions of the inside of the case being approximately proportional to the cube root of the weight of the charge. The density of the T.N.T. filling is 1.47 app. Three sizes of primer, of the same type and fitted with the same standard detonator, are shown in Figures 8, No. 8, 9 and 10 and also fitted to the T.N.T. charges Nos. (1) to (7).

3. *Capacity and Insulation of the Piezo Electric Circuit.*

The voltage V developed in the circuit when a pressure p lbs/sq. in. is applied to a total area A sq. ins. of tourmaline crystals is

$$V = 8.65 \times 10^{-8} \frac{p.A}{C}$$

where C is the capacity of the circuit measured in farads. Since the deflection δ of the cathode rays is directly proportional to V it will be seen that this relation has an important bearing on the interpretation of the oscillograph record. Not only is it necessary that the value of C should be known accurately, but it is also important that it should be kept as small as possible so that the oscillograph deflections $\delta \propto V$ should provide an accurate measure of the pressure. Since C is determined mainly by the length of cable between the gauge and the ship carrying the oscillograph, this latter condition implies that the cable should be as short as possible. Against this, however, is the fact that the charge must be placed at a distance from the ship not less than the 'minimum safe distance' (determined by experience). The 'safety' limit, fixes the minimum length, and consequently capacity, of cable * to be used. This being known, sensitivity must be increased by increasing the area of tourmaline crystals or the sensitivity of the oscillograph. For certain reasons, the latter method was not practicable, consequently the diameter of the gauge generally employed was fixed at 7 inches, the effective area of crystals in this case giving sufficient sensitivity whilst meeting the conditions relating to the safety of the ship.

The type* and length of cable having been decided upon it is necessary to know accurately the value of the capacity of the circuit at the time of firing the charge. This quantity is measured immediately before and after firing on every occasion - the A.C. bridge shown in Figure 7a being employed for the purpose. Capacity measurements are considered accurate within 1%.

Now the total electrical charge generated on the tourmaline crystals is a very small quantity although the explosion pressure is high. Thus the explosion of 100 lb. T.N.T. at a distance of 40 feet from a 7 inches p.c. gauge develops a charge of the order of 10^{-6} coulombs, a very small electrical quantity. This charge only exists for a period less than 0.001 second during which it must be conveyed, without loss, to the oscillograph on the ship. It is evident, therefore, that the insulation of the circuit must be good in order that as little as possible of this charge shall leak away. From the point of view of leakage it is indeed fortunate that the electrical charge only exists for a very short period and that the capacity of the circuit is considerable. Thus if V_c is the voltage ($\propto Q \propto \rho$) in the circuit at any instant and V_t is its value at a time 't' after.

$$V_t =$$

* Aerials were avoided wherever possible on account of the difficulties involved in fitting at sea.

* The cable used with the p.c. gauges is pattern No. 1389A. M.T. cable, having a capacity to earth of .0042 mfd. per 100 feet, the insulation resistance being very high.

Best Available C

$V_t = V_0 e^{-\frac{1}{C R} t}$ (not considering the fluctuations of V due to pressure changes in the interval) where C is the capacity, R insulation resistance, and e the base of Naperian logarithms. It will be seen from this relation that the larger the values of C and R, the more nearly will $V_t/V_0 = 1$, i.e. the less charge will leak away. The following table gives an idea of the quantities involved:-

$C = 10^{-8}$ farad $t = .0001$ second

	R	$\frac{1}{C R}$	V_t/V_0	Loss due to leakage
(1)	100 megohms	1	1	—
(2)	10 "	10	1	—
(3)	1 "	100	0.99	1%
(4)	0.1 "	1000	0.90	10%

$C = 10^{-9}$ farad $t = .0001$ second

(1)	100 megohms	10	1	—
(2)	10 "	100	0.99	1%
(3)	1 "	1000	0.90	10%
(4)	0.1 "	10000	0.37	73%

These values show that even in a time as short as 10^{-4} second there may be appreciable leakage if the capacity is small (e.g. 10^{-9} farad) and the insulation poor. The effect of such leakage on an actual p/t curve (taken from Mr. Hilliar's report) is illustrated in Figure 9. It will readily be seen from inspection of the deduced 'leaky circuit' curves that it is of great importance to secure good insulation. Otherwise the following errors may be introduced:-

(i) The pressure-time curve recorded is not the true curve for the explosion.
(ii) The maximum pressure recorded is less than the actual maximum.
and (iii) When negative charges* are recorded, they do not necessarily indicate negative pressures.

In all cases, therefore, where the record is considered reliable, it has been carefully observed that the insulation resistance is sufficiently high (when considered in relation to capacity). In general the capacities employed were of the order of 10^{-8} farad and the insulation resistance not less than 40 megohms. In 10^{-4} second the leakage is in such a case considerably under 0.1%. Certain records have been obtained, however, under conditions where charges were fired when the insulation resistance was known to be low (.5 megohm). In these cases the record shows false 'negative' pressures - compare Figure 9 curves C and D, with records c, d and e, Sheet II. In every explosion experiment therefore careful measurements of capacity and insulation were made immediately before and after firing the charge. Records f and g on Sheet II are reproduced to compare with records c, d, e, as showing the effects of good and bad insulation respectively.

4. *Calibration of Apparatus.*

Before the pressure-time curve recorded by the oscillograph can be interpreted it is necessary to know the sensitivity of the various parts of the apparatus and the speed at which the rays have traversed the plate.

The voltage sensitivity of the oscillograph and the pressure sensitivity of the p.e. gauge are, under the experimental conditions, interlinked but it is a matter of some importance to know the oscillograph sensitivity independently, so that corrections may be applied under circumstances slightly different from the standard conditions.

(a) .....

* The negative charge referred to in (iii) begins to appear when the positive charge, due to the increasing pressure of the explosion pulse, has leaked off, further diminution of pressure (in the falling pressure region of the pulse) resulting in a negative charge being produced.

(a) Electro-Static Sensitivity of the Oscillograph.

It can easily be shown on theoretical grounds that the deflection δ of a stream of cathode rays of velocity v, charge e and mass m,* after passing between a pair of electrostatic deflecting plates of length λ and distance apart d, is given by the expression

$$\delta = \frac{a}{m} \frac{E}{v^2} \frac{\lambda}{d} \left(l + \frac{\lambda}{2}\right) \qquad (1)$$

where E is the p.d. applied across the deflecting plates and l is the subsequent length of path of the rays from the end of the deflecting plates to the photographic film. The velocity v can be expressed in terms of voltage V generating the rays,

$$v = 5.95 \sqrt{V} \times 10^7 \text{ cms/sec.} \quad V \text{ measured in volts.}$$

whence we find

$$\delta = \frac{E}{2V} \cdot K \left\{\frac{\lambda}{d}\left(l + \frac{\lambda}{2}\right)\right\} \qquad (2)$$

where K is the oscillograph constant and E and V are expressed in volts.

It will be seen from (2) that the deflection δ is directly proportional to the voltage applied to the deflecting plates and inversely proportional to the voltage generating the rays. These theoretical results have been verified experimentally. It is important to note, however, that the vacuum conditions in the oscillograph must be good for equation (2) to be strictly correct. If gas is present, the cathode rays are reduced in velocity by collision and consequently the sensitivity is increased, δ being larger than the value determined by (2)**. If therefore, the vacuum tube is soft when a record is made (this condition of course being avoided in general) it is necessary to make an independent voltage calibration of the oscillograph. Generally speaking, however, when the vacuum is good, relation (2) is strictly applicable and there is no need to make this special voltage calibration. Under these conditions a standard value of V is taken in practice, viz. 3000 volts, and all observations of deflections δ are reduced to this standard, δ being taken as inversely proportional to V.

The time axis of the oscillograph record is calibrated according to the method outlined in section II iv.b above. The circuit of the deflecting magnet is in this case identical with that used in making the explosion record. In certain cases the time calibration was recorded on the same plate as the actual explosion record but any slight advantage of this method over that in which a second plate is used, is lost in the increased risk of fogging and possibility of spoiling the explosion record itself. Consequently the general practice has been to expose a separate plate after the explosion has been recorded. Attempts were made to 'dot' the p/t record at regular time intervals but the results obtained were not very satisfactory. A relay system was devised also whereby a voltage calibration of the oscillograph was recorded at the end of the p/t record - see Record h Sheet II but this was only employed in a few cases. Various experimental devices of this nature were designed and tested but on the whole it was found more satisfactory to make calibrations on separate plates, rather than run the risk of spoiling a valuable explosion record by additional complications. Typical time scales are shown on Sheet I Records a, b, c and d.

(b) Pressure Calibration of Piezo-Electric Gauges

The calibration of the gauge is a matter of fundamental importance to the method and involves certain difficulties of a theoretical nature which must first be dealt with. When used to indicate explosion pressures, the gauge is subjected to a rapidly varying pressure and the conditions are essentially adiabatic in character. A static calibration of the gauge, under isothermal conditions, is therefore at least open to question. Keys ♯ has dealt with this point thermodynamically and has arrived at the conclusion that

the .....

$\frac{e}{m} = 5.316 \times 10^{17}$ E.S. Units for cathode rays.

** Variations due to this cause have occasionally been noticed when the tube is very 'soft' - changes of sensitivity of a few per cent being observed. Under these conditions, however, the indications of softness of the tube are obvious.

♯ Keys - Phil. Mag. Vol. xiii, p.473 (1921) (adiabatic and Isothermal Piezo Electric Constants of Tourmaline).

Best Available C

the error introduced in using a tourmaline gauge adiabatically (as in an explosion) and calibrating the gauge isothermally does not exceed 0.3% - negligible quantity. No experimental verification is given. In spite of this reassuring theoretical deduction, however, it is desirable that the experimental calibration method should, as far as possible, approach the ideal adiabatic condition. Towards this end, the pressure apparatus shown in Figure 10(a) and (b) has been designed. The pressure vessel consists of a heavy wrought iron cylinder capable of withstanding a steady hydrostatic pressure of the order of ½ ton per square inch. This cylinder is fitted with a watertight gland, for the cable of the p.e. gauge, and a special device for suddenly releasing the pressure on the gauge. This release consists essentially of an annealed copper disc (1⅛ inches diameter effective, and .007 inches thick) closing a hole on the lid of the pressure vessel. The copper disc, whilst making a good pressure joint is held between the jaws of a circular cutting punch - a slight rotation (30°) of a hand screw causing this punch to shear the copper disc completely around its circumference. Pressure is applied to the p.e. gauge in the pressure vessel, by means of a hydrostatic piston pump (with non-return valve) hand operated, the pressure being indicated on a Bourdon pressure gauge* 0 - 1200 lbs./sq.in. When all joints are tight the pressure vessel holds a steady pressure of 1000 lbs./sq.in. without leakage. If now the copper diaphragm is sheared by rotation of the cutting arm the pressure in the water filling the vessel is suddenly released through an aperature 1½ inches diameter. This sudden release develops a charge on the p.e. gauge proportional to the change of pressure. The records indicate that the time involved in the fall of pressure is a little under 0,01 second. Although this time may be considered large compared with the time of rise of pressure, viz., .0001 second, in an explosion impulse, it must still be regarded as of short duration when we are considering adiabatic and isothermal effects. It seems reasonable to suppose therefore that this method of calibration is essentially adiabatic, and the piezo-electric sensitivity of the gauge thus obtained is applicable without correction, to the case of the explosion record.

In making a calibration record it is important of course to measure the capacity and insulation of the p.e. circuit and to observe the voltage generating the cathode rays. The time axis of the record is made by one of the methods described in Section II iv. a. The rotating potentiometer method and the slow traverse method have both proved satisfactory and much superior to the older A.C. method. Records illustrating the three methods are shown on Sheet I. Records e, f, g and h. From such records as these the sensitivity of the gauge is determined. The pressure sensitivity of a gauge is usually expressed in terms of the pressure required to produce 1 cm. deflection of the cathode rays when the generating voltage V is 3000 volts and the capacity of the circuit is 0.01 μ farad**. All observations are therefore reduced to these standard conditions, making use of the information that $\delta \propto \frac{P}{C V}$* where P is the pressure in lbs./sq.in., C capacity in microfarads and V the generating voltage of the cathode rays.

The graphs shown in Figure 11 were experimentally determined in this manner and indicate:-

The deflection of the cathode rays is

(I) Directly proportional to the pressure applied and
(II) Inversely proportional to the capacity of the circuit.

In both cases the generating voltage V is kept constant, in (I) the capacity C is kept constant whilst P is varied and in (II) P is kept constant whilst C is varied.

In Section II (b) (iv) above it was pointed out that the voltage E developed in the p.e. gauge circuit is proportional to the area A of tourmaline crystals ($E = \frac{k \rho A}{C}$). Gauges of different sizes have been constructed and this point also has been verified experimentally - a 7 inches diameter gauge having approximately double the sensitivity of one 5 inches diameter. Slight differences between gauges of the same size have of course been observed as the crystals mounted in the gauges are irregular and do not completely cover the surface of the supporting metal plate. To summarise, - the theoretical relation $\delta \propto \frac{P A}{C V}$ has been experimentally verified.

The .....

* This gauge is calibrated at intervals and has been found to remain correct.

** These values of voltage and capacity were chosen as standard since they represent average values over the whole working period.

* $Q \propto P \quad E \propto \frac{P}{C} \quad \delta \propto \frac{E}{V} \quad \delta \propto \frac{P}{C V}$

The values of δ in the p/t record of an explosion, after reduction to standard circuit conditions (C = .01 mfd. V = 3000 volts), can at once be plotted in terms of pressure when the constant of the gauge is known.

5. *Lay-out of Charge and Gauges in the Sea.*

When firing large charges of the nature with which we are concerned in this report, the place chosen for the experiment must be at a considerable distance from the shore and in reasonably deep water. A point of vital importance is the distance of the gauges from the charge, whilst a secondary, though not unimportant, point relates to the depth of the charge and the gauges below the surface and their distance from the sea-bed. The majority of the charges fired in this investigation were situated at a point in the 'prohibited area' off Ryde, Isle of Wight - the depth of water being approximately 17 fathoms. For the purpose of the large-scale experiments two vessels are required, on one of which ('Carstairs' and later 'M.22') is installed the oscillograph recording apparatus and accessories. The second vessel ('Skylark' or 'Redwing') lays the 'trot', i.e. the system of buoys, wire, gauges and charge, as it gradually drifts away from the first vessel (at anchor), a steel hauser and a grass line connecting the two vessels. It should be mentioned at this point that in the large-scale trials the p.e. gauge was only one of a large number of other gauges (these being essentially mechanical in character) laid at the same time. A series of buoys attached at definite points of the steel cable connecting the two ships support the weight of the charge and a number of steel girder-section frames which carry the gauges. Supporting wires, which suspend these frames from the main steel trot-wire, are cut to definite lengths thereby locating the frames (and consequently the gauges which they carry. With respect to the charge. At the moment of firing the charge the second vessel starts her engines and pulls on the trot-wire. In this manner the trot is straightened out and the frames hang at their scheduled distances from the charge. With this arrangement of heavy frames and measured lengths of wire it is not possible that errors of distance due to tidal action on the frames can be of serious importance. The distances are considered accurate within ± 1 foot.

Large scale experiments were only carried out when the sea was moderately calm.

In addition to the above mentioned large scale trials, however, a considerable number of small charges (2½ lbs. and 18½ lbs. G.C.) were fired for other purposes. With these smaller shots the second vessel was unnecessary, all gauges etc. being laid from the first ship (e.g. M.22) at anchor, the tension on the trot-wire being maintained by a small boat or by a large buoy. It should be observed that in these cases the heavy iron girder frames were not used and the gear on the trot was comperatively light. Extra precautions (additional wires, etc.) were taken to ensure that the charge-gauge distancee were correct. Particular attention was also paid to the method of slinging the p.e. gauges to ensure that they were oriented in a definite direction with respect to the line of the charge, and that they were situated at an appreciable distance from resonant metal bodies (other gauges or frames) and from air cavities (e.g. diaphragm gauges).

In certain cases, e.g. where it was desired to record surface or bottom reflections of the explosion pulse, the gauge and charge were necessarily suspended on long wires. In such circumstances the spread of the 'V' to the two supporting buoys was very small. In these cases the charge was fired at slack water to ensure the gauge and charge hanging vertically and at the correct depths and distances apart. Reference will be made later to certain observations of the velocity of the explosion wave. In these experiments the two p.e. gauges used were bolted at a definite distance apart (known to .05 inches) on a 6 feet iron girder, the charge and pressure switch being arranged about 10 feet away on an extension of the line of the girder.

Occasional large charges (300 lb. M.II mines or depth charges) were fired in connection with other work of Vernon M, and in some of these cases it was possible also to obtain p.e. records. In these circumstances it was not always convenient to employ the usual trot arrangement to ensure accuracy of distance, and less accurate methods were adopted.

In general, however, the distances in the experiments were known, as stated above within ± 1 foot.

6.....

Best Available Co

6. *Method of Experiment.*

Whilst the trot is being laid the oscillograph is evacuated and adjusted until a suitable recording 'spot' is obtained. A general preliminary test of the various circuits-deflecting magnet, relay, E.S. plates etc. is then made. When the trot is laid and the p.e. cable and pressure switch cable joined to their respective circuits, after leaving a sufficient length in the sea to ensure the ship being at a safe distance from the charge, a careful measurement is made of the insulation and capacity of the complete p.e. circuit.

The insulation must be good (say > 50 megohms) and the capacity must be adjusted, by adding standard capacity, until it is estimated from the experimental conditions that the deflection of the cathode rays will be satisfactory. A final test of insulation and capacity is made just before firing the charge, after all cables have been made fast and the capacity is steady. The deflecting magnet circuit is adjusted to the required speed of traverse of the spot and a signal given 10 seconds before firing. At this signal the second vessel keeps the trot wire at a steady tension, a kinema* is started, and an operator stands by the firing key which is in the oscillograph room. At another signal the door of the oscillograph camera is opened and immediately afterwards the charge is fired. The insulation and capacity of the p.e. circuit are now checked - if possible, for very frequently the cables break and an 'earth' appears - before the trot is weighed. A record is also made of the time scale (at known frequency) the conditions of the deflecting circuits remaining exactly as in the explosion experiment. The operation of opening camera door, firing and reclosing the door should not take more than a fraction of a second. The longer the door is open, the greater is the danger of fogging the plate from diffuse cathode radiation.

In some cases where a very slow traverse of the spot (e.g. .01 to .1 second) is to be made, as in a bottom echo record, it is necessary to employ an auxiliary switch, closing with the firing switch, to cause the spot to jump on the left-hand edge of the plate at, or before, the instant of firing. This switch introduces a resistance shunting the auxiliary deflecting magnet, thus reducing the initial deflection of the spot to the left. In this manner, the spot is on the plate for a short interval just before the pressure switch is closed. Otherwise, it would not, in many cases be possible for the pressure switch to bring the spot on the plate before the arrival of the pressure wave at the gauge. This device has proved very serviceable in many cases where the pressure switch alone would have been of little use.

On certain occasions simultaneous records have been made with two cathode ray oscillographs.

Section B. Experimental Results.

After a preliminary series of experiments with small charges during which the technique of the method was greatly improved, it was possible to count on obtaining a satisfactory record of almost every shot and to examine the effect of the size and orientation of the gauge on the recorded pressure-time curve, and of the proximity of air cavities or resonant structures near the gauge.

1. *Variation of Maximum Pressure, Momentum and Energy in the Pressure Pulse with Weight and Distance of Charge.*

Data obtained from a large number of small charges were examined to eliminate accidental irregularities in the charges and were used as a check on the results obtained from a number of large charges. The latter series of large charges consisted of specially designed T.N.T. charges of weights varying from 20 to 2000 lbs. and a few 300 lb. amatol depth charges and H.2 mines. The special charges were all prepared from the same melt of T.N.T. of density 1.67 and every effort was made to render them similar.

The experimental results given in what follows refer only to the region where the maximum pressure developed in less than 2 tons per square inch.

(a) .....

* In some cases a kinema is used to photograph the spray and 'plume' phenomena accompany the explosion. Otherwise the 10 second signal is not required except as a general warning signal.

(a) Variation of P. max with Distance.

Two distinct methods of determining the variation of maximum pressure with distance from the charge have been employed. In the first method a number of charges are fired and records made with a piezo-electric gauge at different distances from the charge. From measurements of the maximum deflections of the individual records it is possible therefore to plot a curve connecting P max and distance. As we have already pointed out, however, the maximum pressure varies considerably from charge to charge (apparently similar) and it is necessary to make a number of records at each distance in order to obtain a reliable average.

Observations with a large number of 2½ lb. and 18½ lb. gun-cotton charges and a number of larger T.N.T. charges, indicate that the pressure falls off inversely as (distance)$^{1.0}$ within the limits of experimental error.

In view of the fact that charges are so variable and that slight errors in calibration of gauges and the oscillograph might affect the deductions, it seemed very desirable to devise a method which is quite independent of the differences between one charge and another and eliminates any assumption with regard to the gauge sensitivity or the oscillograph circuit. The method involves only a knowledge of the distances of the gauge from the charge and the deflections on the oscillograph record.

The principle of the second method is as follows:-

Two gauges A and B, connected to one oscillograph, are laid at distances D_1 and D_2 respectively from a charge, and a 'slow-traverse' record is taken when the charge is fired. Each gauge will record its pressure peak on the plate in the oscillograph. Suppose δ_1 and δ_2 are the measured amplitudes of these peaks. Then, assuming the pressure to vary as D^x we have

$$\delta_1 = aK_1 D_1^x \quad , \quad \delta_2 = aK_2 D_2^x$$

where a involves all the parameters external to the gauges (charge, oscillograph sensitivity, capacity of circuit) and K_1, K_2 depend only on the gauges, dividing δ_1 by δ_2 we eliminate a and obtain

$$\frac{\delta_1}{\delta_2} = \frac{K_1}{K_2}\left(\frac{D_1}{D_2}\right)^x \qquad (1)$$

Similarly, if a second shot be recorded with the gauges A B at distance D_3 D_4 giving peak amplitudes δ_3 and δ_4 respectively

$$\frac{\delta_3}{\delta_4} = \frac{K_1}{K_2}\left(\frac{D_3}{D_4}\right)^x \qquad (2)$$

Dividing (1) by (2) we have

$$\frac{\delta_1}{\delta_2}\,\frac{\delta_4}{\delta_3} = \left(\frac{D_1}{D_2}\,\frac{D_4}{D_3}\right)^x \qquad \text{thereby eliminating } K_1 K_2$$

whence

$$x = \log\left(\frac{\delta_1}{\delta_2}\,\frac{\delta_4}{\delta_3}\right) \Big/ \log\left(\frac{D_1}{D_2}\,\frac{D_4}{D_3}\right) \qquad (3)$$

In the practical application of this method three similar gauges A B C were employed simultaneously, and three 18½ lb. G.C. Charges $\alpha\beta\gamma$ were fired, the gauges being interchanged (ABC, CAB, BCA) in the respective shots. This was done to obtain as much data as possible with the fewest shots. The results are given in the following table:-

Shots .....

Best Available Copy

Shots	Gauges	D_1	D_2	D_3	D_4	1	2	3	4	
	B.C.	30	45	45	20	1.40	1.83	1.10	2.10	0.965
"	A.B.	20	30	30	45	1.10	1.40	0.85	1.10	"
"	A.C.	20	45	30	20	1.10	0.83	0.85	2.10	1.00
	A.C.	20	30	30	45	2.10	0.85	1.05	0.38	"
"	A.B.	30	45	45	20	0.95	1.10	0.38	1.70	1.02
"	B.C.	20	45	30	20	2.10	1.10	1.05	1.70	0.93
	A.B.	20	30	45	20	1.10	1.40	0.38	1.70	1.035
"	B.C.	30	45	20	30	1.40	0.83	1.70	1.05	"
	A.C.	20	45	45	30	1.10	0.83	0.38	1.05	1.06
	" indeterminate since $D_1 D_4 = D_2 D_3$					mean x = 1.00				

These results indicate quite definitely that the law of variation of P max with distance is given by $P_{max} \propto \frac{1}{D}$ for an 18½ lb. charge over a range from 20 to 45 feet. It should be noted, in applying the above method, that the accuracy diminishes as $\left(\frac{D_1}{D_2} \frac{D_4}{D_3}\right)$ approaches unity, and its logarithm zero, when the value of x (in formula 3, page 15) becomes indeterminate. In order to obtain an accurate result, the value of $D_1 \times D_4$ should be great compared with $D_2 \times D_3$ consistent with the condition that the values of $\delta_1 \delta_2 \delta_3 \delta_4$ should all be sufficiently great to be capable of accurate measurement.

It is considered that the relation between $P_{max} \propto D$ obtained in this manner is considerably more reliable than that obtained by the statistical average method referred to above. It is regretted, however, that no opportunity occurred during the investigation, of repeating the triple-gauge experiment with larger charges – only isolated observations having been made in such cases. The experiment appears to be well worth doing, however, to establish if the inverse distance law, which holds so exactly for 18½ lb. charges, is equally accurate for larger charges. Except in the region very close to the charge, perhaps, there appears to be no physical reason why this should not be so. Typical records are shown on Sheet 11 Records a and b. Record 'a' was obtained from an 18½ lb. G.C. charge, whilst in 'b' a 100 lb. T.N.T. charge was used.

(b) Variation of P_{max} with weight of Charge.

This relation is one which is considerably more difficult to determine for now we can rely only on the average of a number of shots. Individual variations of maximum pressure for charges of the same weight and composition and packed in similar containers are considerable. Thus for the specially prepared T.N.T. shots variations in P_{max} from the mean value for a particular weight of charge were, in extreme cases, as high as 20%; the mean variations of course were considerably less. Then again, with small gun cotton charges the extreme variation of P_{max} was approximately 30%, the mean variation being about 5 or 10%. The necessity for firing a large number of charges to obtain a reliable average value of P_{max} is apparent.

In order to reduce all charges and records to the same basis of comparison the inverse distance law has been assumed. As we have seen in (a) above this is probably true for all sizes of charge at the distances with which we are mainly concerned (viz. 10 to 60 feet from the charge). In Figure 16a are plotted the values of log P_{max} (at unit distance, 1 foot from charge) as a function of log W, obtained from the analysis of 148 p.c. records. The number of individual observations, of which each point on the curve is an average is indicated. Considerable weight must be attached to the points corresponding to 2½ lbs., 19½ lbs. and 100 lbs. charges, for these represent mean values of 38, 70 and 24 observations respectively. It will be observed that all the points lie on or close to, a straight line represented by the relation

$$\log P_{max} = 0.38 \log W + 4.08$$

or $$P_{max} = 12{,}000\ W^{.38}$$ lbs/sq.in. at 1 foot distance from a charge of weight W lbs. of T.N.T. gun cotton or amatol

or .....

Best Available Copy

or combining this with the inverse distance law, we have

$$P_{max} = \frac{12,000}{D} w^{.38} \text{ lbs/sq.in.}$$

(at distance D feet)

The relation obtained by plotting Hilliar maximum pressure gauge (G.F) observations* is identical with this - see Figure 16b. Now the simple theory of explosion pressures, as outlined by Hilliar (p.12 R.E.182/19) indicates that P_{max} should be proportional to $w^{.33}$ - see dotted line in Figure 16b. The difference between the two curves shown is quite outside the limits of experimental error. It has not been possible, however, to obtain a definite physical explanation of this difference between experimental results and simple theory, but it must be realised in the first place that the simple theory given by Hilliar does not include all the facts. The resistance offered by the charge case, for example, is ignored - it is probable that the elastic constants and dimensions of the charge case exert a definite influence on the maximum pressure imparted to the water. The question has been examined by Mr. Butterworth† who gives a rough theoretical estimate that on this account the recorded pressure will be about 6% lower than without the above - the correction being practically the same for all sizes of charge since the thickness of the metal cases employed increases in proportion to the linear dimensions of the charge (see Figure 11). It would appear therefore that under these circumstances the difference between the experimental result $P_{max} \propto w^{.38}$ and the theoretical deduction $P_{max} \propto w^{.33}$ remains unexplained.

Again it is probable that air cavities in, or near, the charge affect P_{max} - but such an effect would probably be of an irregular nature and would affect all charges, large and small, by about the same extent. It is realised, of course, that the method of recording P_{max} is open to criticism, for the p.e. gauges used have a finite size and measure only <u>average</u> pressure around the point of maximum compression in the pulse. On this account a positive correction, increasing as the size of the charge (and consequently the thickness of pulse) diminishes, must be applied to the recorded pressures. This would tend towards the cube root law but would require positive corrections to the observed values of 32% for 2½ lbs. 17½% for 18½ lbs. and 11% for 100 lbs. charges, assuming no appreciable correction is necessary in the record of a 1000 lb. charge.

This question of correction to the recorded values of P_{max} will be dealt with more fully in a later section where the form of the p/t curve is discussed. (See Section 4).

A point of some interest and importance in connection with the experimental results shown graphically in Figures 16a and b, is the fact that observations of P_{max} with gun cotton and amatol charges lie on the same straight line as the observations with T.N.T. charges. The results indicate therefore that there is no appreciable difference in maximum pressure developed by equal weights of these three explosives.

(c) <u>Momentum ($\int pdt$) and weight of charge</u>.

As in the case of maximum pressure, it has been found that the value of momentum, as measured by the area of the p/t curve, for a given size of charge is a very variable quantity. It is only by taking the average of a large number of observations therefore that reliable data can be obtained. With this end in view a careful analysis has been made of 116 records the area of the p/t curve being in each case measured by means of an Amsler integrator. It was necessary for this purpose first of all to analyse the original records and plot on an enlarged scale the graph of the pressure-time curve.

These graphs were then used in the planimeter measurements of area. Since it is impossible to extend the measurement to infinity along the time axis it was decided to measure areas up to a definite time 't' which is taken as proportion to $\sqrt[3]{w}$ ‡ a value of $t = 2.00 \times 10^{-3}$ second being adopted as a

standard .....

* The Hilliar gauge results used in this curve were obtained simultaneously for the same shots and are directly comparable with the p.e. records. The difference between 'G.F.' (3 copper) and 'G.J.' (9 copper) gauges has been dealt with in a report by Mr. Butterworth. See appendix.

† See appendix 8.

‡ Any small error involved in this assumption, only affects the result in the second order of small quantities.

Best Available Copy

standard in the case when W = 100 lbs. Under these conditions a correction of 4% may be required to all measured areas to give the true area up to infinity; i.e. $\int_0^\infty p\,dt = 1.04 \int p\,dt$ approximately. Thus for a 2½ lbs. charge the area of the p/t curve was measured up to a time 0.565×10^{-3} second, whereas in the case of a charge weighing 1000 lbs. the measurement of area extended to $t = 4.30 \times 10^{-3}$ second. In plotting results it is necessary first of all to bring all the observations to a standard distance of 1 foot and for this purpose the inverse distance law has been assumed. All the experimental evidence available supports the view that this law applies to momentum M as well as to P_{max}. In Figure 17 are plotted the values of $M \left(= D \int_0^t p\,dt \right)$ as a function of W the weight of charge – the logarithms of those quantities being used as a convenient means of determining x (in $M \propto W^x$) the slope of the line in the graph. It will be seen that the experimental points (each the mean of all reliable observations) lie well on the straight line given by

$$\log M = 0.65 \log W + 0.26$$

$$M = \frac{1.82}{D} W^{.65}$$

M – momentum in lbs/sec. per sq. in.
W – weight of charge in lbs.
D – distance in feet.

This has still to be corrected to bring the area observations to infinite time, i.e.

$$M = \frac{1.90}{D} W^{.65} \quad \text{lbs/sq in. secs.}$$

It will be seen that in this case the experimental result is in good agreement with theory, that momentum is proportional to the 2/3 power of weight of charge. The experimental result now obtained is regarded as very reliable, for in this case there is no doubtful gauge correction to apply, the area of the recorded p/t curve being exactly equal to that of the actual curve, since $\int p\,dt$ is independent of the gauge dimensions.

(d) Energy and weight of charge.

The p.e. records and graphs referred to in (c) above were also used in the measurement of energy which is proportional to $\int p^2\,dt$. All observations were reduced to the standard distance of 1 foot taking $E = D^2 \int p^2\,dt$ the law of inverse square of distance being assumed since the experimental data supports this law. In Figure 18 the results of all reliable observations are plotted in terms of log $E = \log D^2 \int p^2\,dt$ and log W – the number of individual observations at each point being indicated. It will at once be seen that the points lie well on a straight line, which can be expressed by the relation $\log E = 1.00 \log W + 4.12$ or $E = 13200\ W$

$$\text{i.e.} \quad E = \frac{13200\ W}{D^2}$$

W – lbs. weight of charge
p – lbs/sq.in.
D – feet
t – secs.

i.e. the energy in the pressure pulse is directly proportional to the weight of the charge. It will be observed also that in all cases, P_{max} M or E, the experimental observations for gun cotton and amatol lie well on the same straight line as those for T.N.T. (see Figures 16, 17 and 18) – an important point in dealing with the practical application of these results.

A matter of some importance arising from the above experimental relation connecting energy and weight of charge, is the calculation of the proportion of the available chemical energy of the charge which ultimately appears in the pressure pulse. If p is the pressure at a point at a distance D from the charge, v the particle velocity and ρ the density of the water, and C the velocity of elastic waves in the water, then the energy per unit area in the wave is $\int_0^\infty p\,v\,dt$. Since $p = \rho C v$ approximately this is equal to $\frac{1}{\rho C} \int_0^\infty p^2\,dt$. That is, the total energy passing across the surface of a sphere of radius D is $\frac{4\pi D^2}{\rho C} \int_0^\infty p^2\,dt$. Now our experiments indicate that $D^2 \int_0^\infty p^2\,dt = 13200$ per lb. weight of explosive,

the .....

Best Available Copy

the distance D and pressure p being measured in feet and lbs/sq.in. respectively.

Converting to C.G.S. units $D^2 \int_0^\infty p^2\,dt = 5.85 \times 10^{16}$ per lb. wt. of explosive. Whence we see that the total energy in the pressure wave is $\frac{4\pi}{\rho c} \times 5.85 \times 10^{16} = \underline{4.72 \times 10^{12}}$ ergs. per lb. weight of charge.

Comparing this with Sir R. Robertson's statement (Journal Chemical Society Vol. 119 Part I 1921) that the chemical energy per gram of T.N.T. is 924 calories, corresponding to 17.5×10^{12} ergs. per lb., we at once obtain the interesting result that 27% of the chemical energy of the T.N.T. appears in the pressure wave.

It is also interesting to observe that the relative chemical energies per gram of T.N.T. amatol (40/60) and gun cotton, are given as 924, 920 and 892 respectively. These values only differ by about 3%. It will be seen from the graph in Figure 18 that the energies in the pressure waves from T.N.T. Amatol and gun cotton are almost the same - a result in good agreement with the chemical data.

Summarising the principal experimental results to which reference has been made in this section, we find that the piezo electric-records indicate

(1) $P_{max} = 12.000\ W^{.38}/D^{1.00}$

(2) $\int_0^\infty p\,dt = 1.90\ W^{.68}/D$

(3) $\int_0^\infty p^2\,dt = 13200\ W^{1.00}/D^2$

where W is weight of charge in lbs., distances D are measured in feet and pressures in lbs/sq.in.

(Note - Momentum $= \int_0^\infty p\,dt$ Energy $= \frac{4\pi D^2}{\rho c} \int_0^\infty p^2\,dt$)

(4) About one quarter of the chemical energy of the explosive appears in the pressure wave.

(5) Relations (1) (2) (3) and (4) are equally applicable for T.N.T. Amatol (40/60), or gun cotton.

2. *Effect of Depth of Charge and Gauge.*

In the foregoing experiments on the variation of P_{max} M and E with weight of charge W, particular care was taken to ensure that the charges and gauges were suspended at a known depth below the surface. For the purpose of comparison of charges of different weights it was considered desirable, on general grounds, that the depth of submergence of the charge and gauges should be approximately proportional to the cube root of the weight of the charge taking 23 feet for 100 lb. charge as standard. Previous to this, however, it had been ascertained that, except at very small depths, the influence of depth on the pressure was almost if not entirely negligible. It will be seen in what follows that this was confirmed by subsequent experiments. It is to be expected, of course, that as the depth of the charge or the gauge becomes small in comparison with their distance apart, the 'negative' wave reflected from the surface will interfere with the direct positive wave received by the gauge. As the depth diminishes this effect will become more and more serious but it will only be at very shallow depth that the pressure maximum will be affected, as we shall see. The experimental observations may be divided into two sections.

(i) In which the depth of the charge is kept constant whilst the depth of gauge is varied.

and (ii) In which the depth of gauge is kept constant and the depth of charge is varied.

In .....

In the first series (i) 104 lbs. G.C. charges were used. Here it was found that P_{max} is only very slightly affected by depth; when the gauge is one foot from the surface the value of P_{max} is only 10% lower* than at 15 feet depth. The effect on momentum and energy is, however, more serious at such shallow depths, for the reflected pulse arrives near the point of maximum pressure and a considerable area of the pulse is therefore cancelled. At depths greater than 5 feet, however, the values of $P_{max} \int p\,dt$ and $\int p^2\,dt$ are practically independent of depth of the gauge.

In the second series (ii) 100 lbs. T.N.T. charges poured filled, were used, the depth of the gauge in all cases being greater than 10 feet. It was found as in the previous case, that the values of P_{max} M and E are practically constant so long as the depth of the charge exceeds about 5 feet. The effect of surface reflection is most marked in relation to momentum, since after a certain interval, depending on the difference between the direct and reflected paths of the wave, has elapsed the pressure is suddenly cut off by the surface-reflected wave. Unless the depth and difference of path are small, however, (less than 5 or 10 feet) this effect becomes negligible.

As a result of these experiments therefore, we may conclude that the depths of the charge and the gauge are practically immaterial provided they exceed a minimum of value of about 10 feet †. In this statement it is of course implied that bottom reflections are negligible, the bottom also being at a minimum distance of 10 feet from either gauge or charge.

The discussion of surface and bottom reflections is reserved for a later section (see Section 5).

3. *Comparison of Explosives, Poured and Block Filling, 'End' and 'Central' initiation.*

T.N.T., Amatol 40/60 and gun cotton charges of the same weight give equal values of P_{max}, momentum and energy.

A comparison of 'poured' and 'block' fillings, and of 'end' and 'central' initiation revealed no certain difference in these quantities.

4. *The Form of the Pressure Pulse.*

Before going on to discuss the experimental evidence relating to the form and magnitude of the pressure-time sequence in the explosion wave emanating from different sizes of charge under varying conditions, it may be of some assistance to consider the probable course of events when a charge is detonated under water. We shall assume in the first place that the charge is a sphere of radius 'r' centrally detonated and enclosed in a metal case of known elasticity, density and thickness. If the rate of detonation is taken as 7000 metres/second M the time taken for the whole of the charge to detonate will be $r/7000$ seconds for a 100 lbs. T.N.T. charge of radius approximately 0.2 metres this time is 2.9×10^{-5} second. It might reasonably be assumed that the velocity of detonation if not greater than, is at any rate equal to the velocity of propagation of an elastic pressure pulse through the charge. Consequently it would seem probable that the pressure on the inside of the charge case will rise instantaneously to its maximum value at the instant when all the charge is detonated and is converted into incandescent gas. The charge case and surrounding water now begin to move radially, starting from zero velocity and rapidly rising to a maximum. That is, the pressure pulse transmitted into the water will have a finite time of rise to its maximum value, this time of rise probably depending on a number of factors viz: (1) the maximum pressure instantaneously applied to the inner wall of the charge case, (2) the strength (elastic constants) of the material of the charge case, (3) the inertia of the charge case and surrounding water which is set in motion; it is probable also that the viscous resistance of the water plays an important part in the 'degradation' of the pressure pulse near the charge where the displacement amplitude is large. G. W. Walker formulated a theory of rise of pressure. His estimate of the time of rise of pressure in an M.2 mine cases is surprisingly near the

observed .....

* This is based on a single observation. It should be noted that under similar conditions individual variations up to 30% have been observed.

† This statement strictly speaking applies only to such distances apart of charge and gauge as are met with in the present investigation.

M

T.N.T.	6950	metres per sec.
Dry G.C.	7998	" " "
Wet "	5820	" " "

Best Available Copy

observed value in the present investigation viz. 0.6 x 10^{-4} second.

S. Butterworth* has more recently examined this question theoretically by a different process and also finds that the time of rise of pressure as affected by the presence of charge case and surrounding water is of the order 0.5 x 10^{-4} second.

After the charge-case has burst, the bubble of high pressure gas will rapidly expand with consequent fall of pressure. In the present investigation we are not concerned with the expansion of the bubble after a time of the order of .001 second, when it rises to the surface and expends its remaining pressure in throwing masses of water into the air in the form of a spray and plumes.

From such general considerations it is to be anticipated that the pressure pulse passing through the water at a point some distance from the charge will have a short, but finite, time of rise to a maximum value followed by a more gradual fall of pressure to zero again at a rate determined by the expansion of the gas bubble. A glance at typical explosion records at once reveals these characteristics, the time of rise being usually of the order of 10^{-3} second whilst the time of fall, of the order of 10^{-2} second, depends on the size of the charge. In what follows we shall deal in more detail with the principal characteristics of the records. It is our purpose also to determine as far as possible how nearly the recorded p/t curve represents the actual pressure-time variations taking place at that point in the water in which the p.e. gauge is situated.

(1) Time of Rise and Maximum Pressure.

In the original paper follows a detailed discussion of (a) the effect of the charge case, and (b) the effect of the finite size of the piezo electric gauge and the weight of the charge.

(2) Rate of Fall of pressure. Variation with Weight of Charge.

The question of expansion, with consequent fall of pressure of the gas bubble has been dealt with mathematically ∮ by Professor H. Lamb the deductions being in general agreement with the experimental results now obtained. Considerations of the rate of growth of the gas bubble indicate that the rate of fall of pressure is inversely proportional to the radius of the charge, i.e., to the cube root of the weight of the charge.

$$\frac{\delta P}{\delta t} \propto \frac{1}{\sqrt[3]{W}}$$

Measurements of the time 't' in which P_{max} falls to 0.25 of its initial value (taken from records of charges varying in weight from 2½ to 1000 lbs.) indicate that this deduction is experimentally verified. The results of observations are plotted in Figure 23 where it is seen that

$$\log \; = \; 0.32 \; W \text{ or } t \propto W^{.32}$$

$$\text{i.e. } \frac{\delta P}{\delta t} \propto W^{.32} \quad *$$

which relation within experimental limits, indicates that the rate of fall of pressure varies inversely as the linear dimensions of the charge. Taking m_1 as the rate of rise of pressure and m_2 as the rate of fall, the following are approximate mean experimental values of the ratio m_1/m_2 for 2½, 18½, 100 and 1000 lbs. charges, viz. 2, 4, 7 and 16 respectively. These values were employed to calcuate the correction to the Hilliar maximum pressure gauge G.F. It will be seen that the ratios vary approximately as the cube root of the weight of the charge.

(3) .....

* S. Butterworth. See Appendix B.

∮ Phil. Mag. January 1923. H. Lamb.

* Note - This result is obtained by assuming an exponential fall of pressure. The form of the pressure is more accurately expressed by the difference between two exponential functions but the slight change in $\delta P/\delta t$ involved from P = 1 to P = 25 between the above expression and the more accurate one is negligible.

Best Available C

(3) Irregularities in P/T Records.

In addition to the regular rise and fall of pressure which alone has been considered up to this point, the majority of p/t records exhibit irregularities of a more or less serious character. These irregularities have in some cases been found to originate in the charge itself, it others in the p.e. gauge, whilst in others they have been traced to the influence of bodies external to both the charge and the gauge. The irregularities are classified as periodic and non-periodic.

(i) The periodic fluctuations of pressure in the records have been traced to the following causes.

(α) Resonant vibrations in the gauge mounting. When the tourmaline crystals are mounted inside a cast brass ring (as in Figure 4a) it was found in every instance that the p/t record showed a superposed damped oscillation of frequency about 4000/second. The initial amplitude of this oscillation was a considerable proportion (10% or so) of the total pressure amplitude applied directly to the tourmaline. With a gauge mounting of ebonite or Xylonite these oscillations, if present at all, are negligible. Record g Sheet 3 shows the result obtained with an 'ebonite' and a 'brass' gauge exposed to the same shot (18½ lbs. G.C.). The oscillations due to the brass gauge are very pronounced.

(β) Resonant oscillation of the tourmaline slabs. A certain number of records, but not all, show indications of high frequency small amplitude oscillations which may possibly be ascribed to longitudinal oscillations of the tourmaline slabs in the direction of the electric axis. These oscillations are shown in Record a b c e f h j and k on Sheet 3. In a b c e and f the gauge used was 7 inches circular broadside-on; in 'h' the gauge was a 'strip' 15 inches long used end-on; in j 'strip' and 7 inches circular both broadside on; and in 'k' 7 inches circular edge-on and 7 inches circular broadside-on.

It will be seen therefore that the high frequency oscillations indicated by 'dots' on the record, occur whatever the orientation of the gauge with respect to the charge. In some cases, but not in all, it is possible to reconcile the frequency of these oscillations with the simple theory of resonant oscillations in the tourmaline slabs. Thus in record 'j' the period of the dots in the first peak is 0.31×10^{-6} second. Taking 6000 metres/second as the velocity of elastic waves in tourmaline and the thickness involved 2.2 cms. the calculated period should be 0.37×10^{-6} second in fair agreement with the record. Such agreement, however, is not always obtained and we must look for other causes also. It is interesting to note, in passing, that the dots in records a b c Sheet 3 appear in pairs.

It is difficult to explain why these oscillations should appear in some records but not in others - it is possible that some slight initial variation in the form of the incident p/t pulse may produce resonance in the tourmaline on one occasion but not in another. An examination of this point and a test of gauges having tourmaline slabs of different thicknesses would be interesting.

(γ) Electrical Resonance in p.e. Circuit. A possible cause of high frequency oscillation on the p/t record is the existence of inductance and capacity in the electrical circuit of the p.e. gauge and oscillograph. The inductance (calculated) of the single core cable with earth return as used in the present experiments is approximately 0.5×10^{-3} henry per 100 feet. With a 300 feet length of cable, of total capacity of 10^{-8} farad, the frequency of the superposed oscillations will be 10^5 ~/second approximately, which is of the same order of frequency as the oscillations due to resonance in the tourmaline slabs (see (β) above). The cause of the high frequency oscillations recorded may, therefore, be due either to (β) or (γ) or both, and can only be distinguished with certainty by varying L and C or by varying the thickness of the tourmaline. A simple test would be to use two gauges, having tourmaline of different thickness, in the same circuit for a record of the same shot.

In any case the amplitude of these oscillations is too small to have any practical significance, as the records show.

(ii) .....

Best Available Copy

(ii) Non-periodic irregularities. Effect of Air Cavities and Charge Case.

Even in the case where the mounting of the gauge is non-resonant many of the p/t records still exhibit irregularities which must be ascribed to other causes. A large number of records have been obtained in which two different p.e. gauges have been used - the oscillograph record consisting of two peaks corresponding to the passage of the pressure pulse over the two gauges. A comparison of such pairs of records reveals many interesting features some of which we have mentioned already (e.g. variation of τ and P_{max} with size of gauge). Apart from the influence of the gauge itself it is at once evident that many of the peculiarities occurring in one record of a pair appear also in the other. A large amount of evidence of this nature makes it clear that the charge itself is responsible for a large proportion of these irregularities. For example, it has been found that the p/t records of 18½ lb. charges are very variable, some records being comparatively smooth whilst others show very serious irregularities. Such irregularities and differences between individual charges receive an explanation when it is remembered that the 18½ lb. G.C. charge contains air cavities of considerable volume and somewhat irregular distribution, 2½ lb. charges are also somewhat variable but not quite as bad as the 18½ lbs. - they also contain some air but only a small volume. In order to eliminate entirely the possibility that such irregularities were due to a particular gauge or oscillograph a number of records were made using two independent oscillographs and three p.e. gauges (strip and two circular (one Broadside, 7 inches one edge 1 inch)). In all cases the three p/t peaks recorded were practically identical (making allowance for any differences arising from the difference in the sizes of the gauges used). Many of the irregularities occurring in the records of T.N.T. poured filled charges are probably due also to the presence of air cavities in the explosive - about 30 or 40% of the records are, however, practically "smooth" Records a and b Sheet 5 are a typical example of a smooth record reproduced on 3 different gauges and with two different oscillographs. In this case the charge was 100 lbs. block-filled T.N.T.

As was anticipated, the general effect of increasing size of p.e. gauge (from 1 inch (7 inches broadside) to 7 inches edge on) was to smooth the recorded p/t curve. This effect was strongly marked in the comparison of gauge records, the broadside-on gauge sometimes revealing very sharp pressure peaks which were smoothed out almost entirely by the edge-on gauge.

In certain of the earlier T.N.T. shots it was observed that the fall of pressure was irregular, but showed the same general features in all the records. It was then noticed that in these cases certain large diaphragm gauges containing air (cylinders 6 inches to 12 inches diameter) were laid at a certain distance (about 1½ feet further from the charge) from the p.e. gauge. These large air cavities constitute a 'sink' of energy for the pressure pulse and the reflected tension wave neutralises a portion of the primary pressure passing over the p.e. gauge. Repeating the experiment, after removing the diaphragm gauges, records comparatively free from irregularity were obtained. It appeared from such results as these that air cavities have a very powerful influence on the distribution of pressure at appreciable distances away. In order to test the point directly a 3-gauge 2-oscillograph comparison was made with an 18½ lbs. G.C. charge placing an empty primer tin about 2 feet above the charge. The same irregularities appeared in the second oscillograph record. A similar experiment (with a 2 gallon petrol tin near the charge) using two gauges recording on one oscillograph gave the result shown in Sheet 5 record 'g'. In both cases it will be seen that the air cavity introduces very definite irregularities into the form of the pressure pulse. The effect of the two gallon petrol tin is very pronounced and occurs at an instant coinciding with the difference of path traversed by the primary wave to the gauge and the wave which is reflected from the empty tin. The earlier irregularities on the p/t curve of the circular gauge which do not appear on the 'strip' record are probably due to the fact that the second record commences before the first is finished - this statement applies to many of the records where pairs of gauges were used a few feet apart.

In .....

In further illustration of the effect of air cavities it may be of interest to compare the record of an ordinary 300 lb. Amatol depth charge (Figure 8 (11)) with that of a typical H.11 mine 320 lbs. Amatol (Figure 8 (12)). The H.11 mine in every case exhibits a second subsidiary peak of pressure which does not occur in the depth-charge record. The secondary peak has on the average a P_{max} about 12% of that of the primary peak and occurs about 1.1 thousandths of a second afterwards. The momentum in the secondary is about 10% of that in the primary pulse. It seems probable therefore that about 90% of the momentum is communicated directly to the water through the ends of the charge case whilst the remaining 10% follows subsequently through the spherical mine shell via the air-space. The time of passage of secondary wave through the air space (about 1 foot) would probably be of the order of a thousandth of a second as the records indicate).

The record shown on Sheet 5 'h' is interesting. In this case the charge (100 lbs. G.C.) was lashed to the end of a spar of soft wood (about 3 inches diameter). It is observed that the maximum pressure recorded is abnormally low, the customary peak of the curve having been cut off. It is difficult to reconcile this result, however, with the fact that the maximum pressure developed by a 320 lb. H.11 mine or an 100 lb. G.C. charge is practically normal in spite of the presence of a large surrounding volume of air. In these cases it should be observed that the irregularities produced by the air cavities frequently occur subsequently to the maximum pressure being reached.

5. *Reflection of Pressure Pulse from Surface and Bottom of the Sea. Reflection from the Hull of "Gorgon".*

It is a matter of importance in considering the effect of the explosion of a charge under the water to determine not only the magnitude and form of the direct impulse but also the impulses reflected from the surface and bottom of the sea. In the case of surface reflection we are dealing with the transmission of a pressure pulse from a denser to a lighter medium in which case the reflected wave is similar to the primary wave but reversed in phase - i.e. the reflected pulse appears as a wave of tension. The actual process of reflection of a pressure pulse of large amplitude is complicated by the facts that water is incapable of transmitting a large tension and that the surface breaks up into spray at the onset of the primary pressure wave. Reflection from the bottom is comparatively simple but presents certain difficulties with which we shall deal later. In this case the pulse is travelling from a lighter to a denser medium so that the reflected wave has the same phase as the incident wave, i.e. the bottom reflection is a wave of positive pressure similar to that of the primary pulse.

(a) Bottom Reflection

When the cathode stream is traversed sufficiently slowly across the plate it is possible to record not only the primary pressure pulse which reaches the p.e. gauge directly but also the reflected pulses from the surface and the bottom of the sea. From geometrical considerations it is a simple matter to determine the most suitable rate of traverse to record these reflected pulses. Typical records showing bottom reflections are reproduced on Sheet 8 a to d.

The following table includes the results of measurements of records of this character. In the table h_1 and h_2 are the distances of the charge and p.e. gauge respectively from the bottom, the charge being 15 feet from the gauge in each case.

Table .....

No.	Weight of charge lbs.	h_1 Feet	h_2 Feet	Length of path		Maximum Pressure amplitude (cms. on record)		Ratio of amplitudes of reflected and incident pressure waves
				Direct Feet	Reflected Feet	Direct	Reflected	
1	18½	6	5	15	19.2	2.5	none recorded	-
2	2½	11	11	15	26.6	1.76	0.53	51%
3	2½	42	42	15	43	1.90	0.15	45%
4	2½	66	66	15	133	1.85	0.11	50%
5	2½	66	66	15	133	1.40	0.08	50%
6	2½	80	80	15	165	2.30	0.15	70%
7	2½	80	80	15	165	1.5	0.10	70%
(8)	2½	80	80	15	165	2.4	0.11	45%
9	100	80	80	15	165	2.7	0.14	57%

The values of efficiency of reflection given in the last column of the above table were obtained by referring the reflected pressure to the same distance, 15 feet, as the primary pulse assuming the inverse distance law of pressure variation. Thus in shot No. 2 the observed reflected pressure amplitude is 0.53 cms. the reflected path being 26.6 feet. Referring this value to a distance of 15 feet we obtain 0.90% cms. which is 51% of that produced by the direct pressure pulse at this distance. Shots (2) and (3) in the above were fired over a soft mud bottom in Portsmouth Harbour whilst the others, except No. 1, were fired in Spithead at a point where the bottom is hard mud and sand. The mean of all observations indicates an efficiency of reflection of 55% approximately from a bottom of mud and sand. This result has an important bearing on the use of bottom mines of the 'M' type. the maximum pressure, and presumably the momentum, developed by such mines being consequently 50% greater than the corresponding values for ordinary mines moored in midwater. Similarly the result is of importance in relation to echo methods of depth sounding where a small amplitude pressure pulse is reflected from the sea-bed.

(b) Surface Reflection. Reflection from the hull of H.M.S. "Gorgon".

The question of the reflection of a large-amplitude pressure wave from a water-air surface is much more difficult than might at first be supposed from a consideration of the work of earlier investigators, in particular of Hilliar and Walker. Thus both assume that the pressure pulse is completely reflected at the surface, but reversed in phase, the effects at any point in the water being simply determined by a superposition of the positive direct and negative reflected waves, making due allowance for the time difference in arrival at the point in question. It will be shown that such is not the case. In order to determine the critical depth at which the surface was only just broken (or just not broken, as we chose) into spray, charges were fired by these observers at different depths. On the basis of such experiments it was found that the maximum pressure applied to the water surface was about 0.3 ton/sq.in. at the critical stage when spray is just beginning to form. Consequently it was stated that the wave of this pressure amplitude is perfectly reflected, but it was erroneously concluded from this observation that water is capable of withstanding a tension of this amount. It will be shown in what follows that such is not the case. It has been rightly supposed, however, that the surface is capable of reflecting large pressure amplitude (of the order of 0.3 ton per sq. inch) but it must be remembered that at the instant of reflection the water below the surface is still under compression from the 'tail' of the advancing pressure pulse. The effect of the reflected pulse therefore is merely to neutralise this positive pressure (either totally or in part) but not necessarily to produce a large tension in the water.

Typical records showing surface reflections are reproduced in Sheet 7, whilst the experimental results for a number of 2½, 18½ and 100 lb. charges are included in the following table.

Table .....

Best Available Copy

TABLE

SURFACE REFLECTION

Charge 1.	Depth Feet: Charge 2.	Depth Feet: Gauge 3.	Length of path feet: Direct 'd' 4.	Length of path feet: Reflected 'r' 5.	Time difference of second calc. 6.	Maximum Pressure recorded: Direct lbs./sq.in. 7.	Maximum Pressure recorded: Reflected lbs./sq.in. 8.	Negative Pressure lbs./sq.in. 9.
(1) 18½ lbs. G.C.	15	15	20	36	.0032	1765	75	53
(2) (a "	15	15	30	442	.0024	1165	93	50
(b "	15	15	45	54	.0018	800	60	50
(3) (a "	15	15	30	42	.0024	1460	100	68
(b "	15	15	45	54	.0018	980	83	60
(4) (a "	15	15	30	42	.0024	1170	93	80
(b "	15	15	45	54	.0018	750	60	60
(5) (a "	15	15	20	36	.0032	2000	92	64
(b "	15	15	40	50	.002	107.	58	30
(c "	15	15	61	68	.0034	642	40	20
(6) "	15	1'°	24.5	25.7	.0003	1200	600 lbs. indef-inite	60
(7) "	15	2'°	23.8	26.2	.0005	1315	500 lbs. indef-inite	53
(8) 2½ lbs.	30	30	15	52	.008	1190	20	20
(9) "	30	30	15	52	.008	955	15	15
(10) "	60	60	15	120	.020	910	15	15
(11) "	15	15	15	33.6	.0038	1390	60	42
(12) "	14	14	15	33	.0038	1150	30	30
(13) "	14	14	15	33	.0038	1020	30	30
(14) "	14	14	15	33	.0038	1580	40	40
(15) "	11	11	15	26.6	.0023	1300	55	None
(16) 100 lbs. (S.16) T.N.T.	10	13	40	46	.0012	1779	320	None
(17) 100 lbs. (S.22) T.N.T.	23	23	60	74	.0028	895	150	100
(18) G.M 250 lbs. ó T.N.T.	15' from surface	15" from surface	47	50	.0006	(2600)	570	170

In all cases (1) to (17) the actual values of tension must be regarded as approximate only. The value in (18) is fairly accurate.

The conditions of reflection in these cases when the gauge is practically in the surface - are rendered uncertain by surface irregularities and the presence of the air floats near the gauge. The records indicate, however, a considerable drop in maximum pressure and momentum.

ó The reflection in this case took place from the steel hull of H.M. Ship "Gorgon".

A glance .....

Best Available Copy

A glance at the above table reveals a number of outstanding points. In the first place the maximum tension recorded under any circumstances is 170 lbs. per square inch; in the majority of cases the tension is of the order of 50 lbs./square inch. It seems improbable that the actual tension attained at any point in the water ever exceeds 200 lbs./square inch. On the other hand, the maximum pressure amplitude of the reflected pulse may reach 600 lbs. per square inch - see Column 8 of above table, in which case only a small fraction (sometimes zero) appears as tension. When the total reflected pressure amplitude is small the proportion of tension is usually great.

The results included in the table cannot possibly be explained on any theory of simple reflection from the surface, for the reflected pressure amplitudes recorded are, as a rule, only a few per cent (4 or 5 usually) of the expected values if perfect reflection is assumed. In certain cases, however, e.g. shots (6) (7) (16) and (18) in table, the reflected pressure is much greater than usual and in one of these cases (16) there is no tension recorded. In order to explain these apparently widely varying results the following qualitative theory (deleted) is suggested. It is assumed that perfect reflection takes place at the water-air surface and that the tension at any point in the water cannot exceed 'p' lbs./square inch without rupture and the consequent formation of a new water-air (or vacuum) surface.

The experimental results are in general conformity with the above theory of critical layers and multiple reflecting surfaces.

It seems not improbable also that this theory will explain certain large discrepancies still outstanding between the 'spray method' of measuring explosion pressure (see G.W. Walker's reports) and other methods such as Hilliar and the p.e. method now described. The question of the spray phenomena on these grounds requires further consideration.

To summarise the results of this section it appears that,

(1) The value of the maximum tension which sea-water can support momentarily is probably less than 200 lbs./square inch. Values of 100 lbs./square inch in 'water-in bulk' and of 170 lbs./square inch between water and steel are the highest tensions recorded.

(2) The maximum recorded pressure reflected from the sea surface is about 600 lbs./square inch but there is no reason to suppose that this is the maximum possible.

(3) A qualitative theory is proposed to explain these results. On this theory it appears that when the depths of charge and gauge are greater than certain critical values (depending on the size of charge and distance from gauge) the reflected pressure amplitude cannot exceed a certain small value of the order of 200 lbs./square inch.

(4) In the circumstances stated in (3) the practical effect of the 'negative-momentum' reflected from the surface of the sea is negligible.

6. *Velocity of the Pressure Wave.*

Experiments carried out at St. Margarets Bay S/R Station* in 1920 and 1921 gave an accurate value of the velocity of small amplitude explosion waves over a base line of the order of 10 miles. The velocity at different temperatures was expressed by the formula

$$V_t = 4756 + 13.8\,t - 0.12\,t^2 \text{ feet/second}$$ at a salinity of 35‰

Hilliar in 1919 measured the velocity of large-amplitude pressure waves (close to large charges) by means of two contacts at a known small distances apart and a chronograph running at a known speed. His experiments yielded the result that, within a few per cent, the velocity of the explosion wave (of pressure amplitude 0.7 ton/sq.in.) is the same as that of sound waves in water, or about 4900 feet/second. The temperature of the sea at the time of the measurements is not specified.

In the .....

* Proc. Roy. Soc. A, 103, p.284, 1923.

Best Available Copy

In the present investigation an attempt was made to determine the velocity of the pressure wave near the charge as accurately as possible in order to obtain the variation of velocity with pressure-amplitude. The method finally adopted employed two exactly similar circular p.e. gauges placed broadside-on to the charge and fixed on a rigid iron bar (of girder section) at a distance apart usually 5 feet (approx.) which could be accurately measured. The pair of gauges were suspended at a known distance from the charge on a continuation of the line of the bar passing through the charge. The depth of the charge, 18# G.C. and the gauges was kept constant at 15 feet the distances of the two gauges being 15 and 20 feet respectively from the charge. The gauges were connected in parallel to the oscillograph recording plates, the usual circuits containing the pressure switch being employed to traverse the spot across the plate. In order to obtain an accurate measure of the time-interval between the two pressure peaks (due to the two gauges) to be recorded, the potential variations in a valve circuit oscillating at a frequency of 2000 ~ (or in some cases 1000 ~/second) were applied to one of the deflecting plates of the oscillograph whilst the record was being made. In this manner the record consists of an oscillation of 2000 ~/second on which the two pressure peaks are superposed. Since the rise of pressure is very sudden, the instant of arrival of the explosion wave at each gauge can be read off the record very accurately. The frequency of oscillation was standardised at the time of firing the charge by comparison with a tuning fork* of frequency 1000 ~/second. A steel tape graduated in feet (tenths and hundredths) was employed to measure the distance apart of the gauges. It is considered that the distance apart of the gauges is probably correct to 1 part in 1000. The probable error in measurement of the velocity due to errors measurements of length of base is not greater than ± 0.1%, i.e. to ± 5 feet in a velocity of the order of 5000 feet/second. It must be pointed out at this stage, however, that the probable error of the final result is considerably greater than this due to errors introduced in the actual measurement of the records. Further reference to this will be made later. Temperature observations, using a reversing thermometer were made on each occasion of firing a charge. The preliminary observations by the method indicated above gave a value which agreed closely with the ordinary velocity of small amplitude waves, i.e. in accordance with the St. Margarets Bay results. This unexpected result led us to suspect a possible error due to the movement of the iron girder-bar which carried the gauges, in the direction of the pressure wave, such movement being transmitted (at a velocity higher than that in the water) through the bar itself to the second gauge. Such a movement would have two effects, (1) to increase the effective length of the base line between the gauges and, (2) to develop a small pressure on the second gauge before the arrival of the pressure pulse through the water. The entire absence of (2) made it seem improbable that (1) was of a serious nature. In order to leave no room for doubt, however, the experiment was repeated with the two gauges suspended freely (though at a definite distance apart) by means of spunyarn from short cross bars fixed on the girder bar. The values of the velocity were, however, unaffected by the change in the method of mounting the gauges, thereby eliminating the possibility of the error mentioned above. Further measurements were therefore made with the gauges rigidly clamped to the iron girder-bar.

The velocity observations may conveniently be divided into two series viz. (1) those made March – May 1923 when the sea temperature was about 10°C and, (2) those made in December 1923 the temperature then being 7°C approx. In the first series of observations the time scale was generated by an oscillation of 2000 ~/second with high harmonics (see Sheet 8 Records a to d), it was thought possible in this manner to obtain 't' the time interval between the gauges more accurately on account of the increased probability of obtaining sharply defined turning points on the time scale occurring at or near the instants of commencement of the pressure rise at the two gauges. In this case it was arranged that the 'pressure deflection' on the record should be large compared with the A.C. oscillations. The frequency of oscillation was adjusted to 2000 ~/second by tuning aurally to a 1000 ~/second fork. It is estimated that the error introduced in this manner does not exceed 1 in 250 in frequency, i.e. ± 20 feet in velocity. In the second series of experiments a large amplitude sine wave of 1000 ~/second was used as the time scale, the pressure deflection being kept relatively small (see Sheet 8 Records e, f and g). The frequency in this case was adjusted to that of the fork by beats and is considered accurate to 1 in 1000, equivalent to ± 5 feet in velocity. The results of all observations are included in the following table, where a comparison is made with the values of velocity for small-amplitude waves at the same temperatures. The distances of the two gauges from the 18# lbs. charges were in all cases 15 feet and 20 feet respectively, corresponding to a value of P_{max} at the mid point of the base-line of 2000 lbs /sq.in.

Table .....

*This fork had previously been standardised by direct comparison with a similar fork having an N.P.L. certificate its frequency being 1000.35 at 16°C.

TABLE

Record No.	Temperature °C	Length of base feet	Velocity V feet per second	Corresponding 'v' for small amplitude waves ft./sec.	Difference (V-v) ft./sec.
V.2	9.5	4.996	4862		
4	9.5	4.990	4875		
6	9.5	4.989	4880		
7	10.8	4.977	4880		
8	12.0	5.010	4877		
Mean	10.3°C		Mean 4875 ft./sec.	4886 ft./sec.	-10
V.16	6.8	4.997	4886		
17	7.0	4.997	4910		
18	7.0	4.833	4940		
19	7.2	4.825	4925		
20	6.7	4.825	4875		
22	6.7	4.828	4898		
Mean	6.9°C		Mean 4906 ft./sec.	4846 ft./sec.	+60
Mean of all records	8.5°C		4890 ft./sec.	4865 ft./sec.	+25

The chief source of error in the velocities given in the above table is that involved in the actual measurement of the records. In the first series V2 to Vg, for example, the probable error due to this cause in individual measurements is ± 30 ft./sec. by taking a series of independent measurements of each record, however, the error may be reduced. Taking into consideration all the above mentioned sources of error it seems probable that the velocity 4875 ft./sec. at 10.3°C is correct within limits of ± 40 ft./sec. Similarly it was considered that the value 4906 ft./sec. at 6.9°C obtained in the second series is also correct within the limits ± 30 ft./sec. It will be observed, however, that whilst the average of the first series gives a value of velocity of 10 ft./sec. lower than the known value for small amplitude waves, the average of the second series is 60 ft./sec. higher. It is difficult to account for this difference. Taking the mean of all observations the velocity of the large-amplitude pressure pulse is 4890 ft./sec. at 8.5°C as compared with 4865 ft./sec. for waves of very small amplitude. The difference between these values is small and uncertain.

Growth of Gas Bubble.

Reference has already been made above to the experimental observation that the rate of fall of pressure is proportional to the radius of the charge. This of course implies that the gas bubble formed at the instant of complete detonation expands approximately in accordance with ordinary gas laws. It is a matter of some theoretical and probably practical importance to measure the rate of expansion of the bubble, and consequently the rate of displacement of the water surrounding it, by more direct methods.

This question has already been examined by Ramsauer* by the following method. A number of steel points at known distances from the charge are connected through insulated leads to corresponding electromagnets which are arranged to control markers on a chronographic drum. Normally, direct current passes through the points and returns through a large earth plate. When the charge is exploded, however, and the expanding gas bubble touches one of the points the current is cut off and the corresponding electro-magnet records the instant on the chronograph. Similarly for the other points. In this way the chronograph record indicates the arrival of the bubble at the successive points, where it is possible to deduce the velocity and acceleration of the boundary of the gas bubble. Using charges of dry gun cotton of 1 to 5 lbs. weight, it was found that the maximum displacement of the boundary was

given ....

C. Ramsauer (Ann. der Physik 4 vol. 72 Heft 4. p.p. 265-284 August 1923) and Admiralty Technical Records Ac. 117.

given by $\gamma_{max} = 189.3 \sqrt[3]{\frac{W}{P}}$ cms.

where W is weight in grams and P is the total external pressure (atmospheric + head of water). In the case of a particular charge of 16.10 grams of dry G.C. fired at a depth of 500 cms. it was found that the radius of the bubble passed through the values 50, 100, 200, 300 and 400 cms. at times corresponding to 44, 60, 106 and 125 x 10^{-4} second respectively from the instant of detonation. From observations of this nature the speed of water displacement at varying distances and depths was determined.

Using piezo electric records of the p/t sequence of explosions, Butterworth has dealt with the question of expansion of the gas bubble theoretically. Ramsauer's experimental results are in good agreement with the theoretical deductions.

Experiments were commenced during the present investigation to test a modification of Ramsauer's method but no opportunity offered for completing the work. It may be of interest, however, to outline the method for future use with large charges - Ramsauer has only applied his method to charges up to about 6 lbs. weight. In the proposed modification a number of points in the sea are supplied with A.C. of known frequency. The potential drop across the points and earth return is indicated on the cathode ray oscillograph. As the bubble passes each point in succession the voltage changes corresponding are indicated by a change of amplitude of the A.C. wave on the oscillograph. Traversing the spot in the usual manner therefore should give an A.C. record showing a 'stepped' appearance, each 'step' indicating the arrival of the bubble at one of the points. The instant of firing the charge is indicated by the spot commencing to move when the pressure switch is closed. The time-intervals between the steps are known from the knowledge of the A.C. frequency. The preliminary tests of the method indicated, however, that the phenomena are not so simple as was at first supposed. Thus it was found that the bubble on arriving at the first 'point' instead of increasing the effective resistance of the point actually reduced it to a very small value, thereby masking the effect of the progress of the bubble over the succeeding points. There can be no doubt that the interior of the bubble in these early stages of expansion is a good electrical conductor, this being due, no doubt, to the intense ionisation due to the high temperature of the newly formed gas°. With a little modification, however, to meet such practical difficulties, there appears to be no serious reason why the method should not be developed so as to be of service in measuring the rate of growth of bubble for large charges.

APPENDIX A.

1. *Piezo Electric Constants and Other Properties of Tourmaline*

(a) Chemical Composition.

17 Al_2O_3, 9 Fe O, $2NO_2$, 24 SiO_2, $6B_2O_3$, $7H_2O$.

(b) Specific Inductive Capacity = 6.75 (A.R.L. measurement) of 'Black' Tourmaline.

(c) Piezo Electric Constants.

(1) Pressure applied along the electric axis $K_1 = -5.72 \times 10^{-8}$ E.S.U.

(2) Pressure applied along the optic axis. $K_2 = 0$.

(3) Pressure applied in the 3rd Direction. $K_3 = -0.88 \times 10^{-8}$ E.S.U.

(4) Hydrostatic Pressure. $K = K_1 K_2 K_3 = -6.6 \times 10^{-8}$ E.S.U.

and $Q = K p A$ where Q is the charge developed in E.S.U. 'p' is pressure in dynes per sq.in. and A is the area of crystal free at right angles to electric axis.

(d) Velocity of Sound in Tourmaline slab. } 6000 metres/second (Provisional only)

(e) Density of Black Tourmaline } 3.0 to 3.2

2. *Piezo Electric Constants of Quartz and Rochelle Salt.*

	Quartz
K_1	6.45×10^{-8}
K_2	0
K_3	-6.45×10^{-8}
$K = K_1 + K_2 + K_3$	0

Rochelle salt responds only to shearing forces and consequently gives no effect on application of hydrostatic pressure.

3. *Data Relating to Cathode Ray Oscillograph.*

(a) Velocity of Cathode Rays.

$$v = 5.95 \sqrt{V}.10^7 \text{ cms/sec.}$$

where V is the p.d. (in volts) accelerating the cathode rays.

(b) Voltage Sensitivity of Cathode Ray Oscillograph.

Deflection $\delta = \frac{1}{2V} \frac{\lambda}{d} \left(l + \frac{\lambda}{2} \right)$ cms. per volt.

where l = distance from mid-point of deflecting plates to screen.
λ = length of deflecting plates.
d = distance apart of deflecting plates.

(c) .....

According to "Tables of Physical Constants" published by French Physical Society, the composition is very variable.

(c) Magnetic Sensitivity of Cathode Ray Oscillograph.

Deflection $\delta = 0.5 \frac{H}{\theta} \lambda \left(l + \frac{\lambda}{2} \right)$ cms.

where H = strength of magnetic field.
λ = length of magnetic field traversed by the cathode rays.
and l = distance from mid-point of magnet to screen.

4. *Capacities of Cable, p.e. Gauges etc.*

(a) Single Core cable in sea (Pattern 1389A as used with p.e. gauges)

$$C = \frac{k}{4.60 \log \frac{R_2}{R_1}} \text{ cms.}$$



k = 2.5 for rubber

capacity = 0.0042 μfd. per 100 feet

(b) p.e. gauge (7 inches diameter) capacity 0.00035 μfd. (approx.)

(c) Oscillograph Deflecting Plates capacity a few cms. only.

(d) Aerial Wire

$$C = \frac{l}{2 \log_e \frac{4h}{d}} \text{ cms.}$$

d = diameter of wire
h = height above earth
l = length cms.

5. *Velocity of Explosion Waves** (Small Amplitude)

$$V_t = 4756 + 13.8t - 0.12t^2 \text{ feet/second.}$$

where t is the temperature of the sea in degrees Centigrade and the salinity of the sea is 35‰.

6. *Some Properties of Explosives* †

(a) Rates of Detonation.

Explosive	Density of Loading	Velocity metres/sec.
T.N.T.	1.57	6950
Gun cotton (dry)	1.2	7300
Amatol 40/60	1.55	6470
Mercury Fulminate	loose	3000

(b) Heat and Gases on Detonation.

Explosive	Calories per gram water gaseous	Total gases c.c. per gram.
T.N.T. (Δ = 1.5)	924	728
Gun cotton	982	875
Amatol 40/60 (Δ = 1.3)	885	886

Proc. Roy Soc. A.

† See Journal Chem. Soc. Vol. 119 p.1. Sir R. Robertson. Part 1921

Best Available Copy

APPENDIX B.

NOTE ON THE EFFECT OF A THIN STEEL PLATE IN THE PATH OF AN UNDERWATER EXPLOSION WAVE

S. Butterworth

If a small amplitude wave of any type passes normally through the surface of separation of two media having densities ρ_1 ρ_2 and characteristic velocities of propagation C_1, C_2 then at the surface of separation there will be produced a reflected and transmitted wave whose pressure amplitudes are obtained from that of the incident wave by multiplying by co-efficients r, s such that

$$r = \frac{\rho_2 C_2 - \rho_1 C_1}{\rho_2 C_2 + \rho_1 C_1} \qquad \text{and } s = 1 + r$$

In these formulae the incident wave is suppose to be travelling in the medium of density ρ_1. If the direction of travel be reversed the reflection and transmission co-efficients are r_1, s_1 where $1 = -r$, $s_1 = 1 + r_1$. In the case where the media are water and steel we find $r = 0.932$.

If this result be applied to the case of a thin steel plate placed normally in the path of an explosion wave we find that the emerging wave is built up of a succession of waves each of the same form as the incident wave but delayed in time by internal to and fro motion between the surfaces of the plate. Thus the first wave emerging is of amplitude ss_1 (the incident wave being assumed unity) and is followed by similar waves of amplitudes $ss_1 r_1^2$, $ss_1 r_1^4$, $ss_1 r_1^6$ ... at intervals 2τ, 4τ, 6τ where τ is the time taken to pass across the plate with the velocity appropriate to steel.

If, as is approximately the case for an explosion wave, we assume the incident wave to be represented by ϵ^{-t} (when the time t') and zero when t negative the emerging wave is given by

$$ss_1 \epsilon^{-t} \left\{ 1 + r_1^2 \epsilon^{-2\tau} + r_1^4 \epsilon^{-4\tau} + \cdots\cdots + (r_1^2 \epsilon^{2\tau})^{n-1} \right\} = ss_1 \epsilon^{-t} \frac{1 - (r_1^2 \epsilon^{2\tau})^n}{1 - r_1^2 \epsilon^{2\tau}}$$

when t lies between $2(n-1)\tau$ and $2n\tau$. Thus the merging wave varies by jerks at intervals 2τ. If these intervals are short as is the case with thin plates we can obtain the general course of the wave with time by putting

$$2n\tau = t, \quad r_1^{\frac{1}{\tau}} = \epsilon^{-\beta}$$

and the emerging wave is then $\rho (\epsilon^{-t} - \epsilon^{-\beta t})$

where $\rho = \frac{ss_1}{1 - r_1^2 \epsilon^{2\tau}}$ $\qquad \beta = \frac{1}{\tau} \log_\epsilon \frac{1}{r_1}$

The maximum pressure in the emergent wave occurs when $t = \frac{1}{\beta - 1} \log_\epsilon \beta$ and has the value $p_{max} = \rho (\beta - 1)/\beta \beta/\beta - 1$. In illustration suppose the incident wave to fall to 1/e in 10^{-3} second (as is approximately the case for a wave developed by a 500 lb. charge of T.N.T.) and let the steel plate considered be 1 cm. in thickness. Then since the unit of time is 10^{-3} second and the velocity of propagation in steel is 5×10^5 cm. per second, $\tau = 0.002$ and with $r_1 = 0.932$, $\beta = 36$, $\rho = 1$ giving $p_{max} = 0.877$ and $t = 0.102 \times 10^{-3}$ second.

The theory given above is of course only accurately applicable to waves of small amplitude. It has, however, been used in the text to estimate the effect of the mine-case in altering the form of the pressure wave. Since in these applications the alteration is small for a small amplitude wave, it may be fairly safely concluded that the effects for large amplitudes waves will also be small.

For simplicity the unit of time is chosen to be the time taken for the wave to fall to 1/e.

APPENDIX C.

CORRECTION ON PIEZO-ELECTRIC RECORDS DUE TO FINITE SIZE OF GAUGE

S. Butterworth

It is assumed that the pressure recorded at any instant is the mean pressure over the surface of the gauge.

The gauge is Edge On to the wave and the law for Pressure-Space is taken to be

$$\rho = Pe^{-\mu x}$$

$$= P\,(1 - \mu x + \tfrac{1}{2}\mu^2 x^2 - \tfrac{1}{6}\mu^3 x^3 + \ldots\ldots) \qquad (1)$$

Let the radius of the gauge be a and consider the moment when the wave front has reached the position A B in Figure 1 (Appendix C). Let A B subtend an angle 2ϕ at the centre of the gauge and let a narrow strip C D of width δx parallel to A B subtend an angle 2θ. Then the contribution of C D to the total pressure is

$$\rho.CD.\,\delta x = -2a^2 p \sin^2\theta\,\delta\theta \qquad (2)$$

since $CD = 2a\sin\theta$, $x = a(\cos\theta - \cos\phi)$, $\delta x = -a\sin\theta\,\delta\theta$

Integrating from $x = 0$ to $x = c$ [$= a(1 - \cos\phi)$] that is from $\theta = \phi$ to $\theta = 0$, we have for the integral pressure $2a^2\int_0^{\phi} \rho \sin^2\theta\, d\theta$ where ρ is expressed in terms of θ by replacing

x by $a(\cos\theta - \cos\phi)$ in (1)

Making this substitution in the series in (1), integrating term by term and dividing by πa^2 we find for the mean pressure

$$Pm = P(A + \mu a B + \mu^2 a^2 C + \ldots\ldots) \qquad (3)$$

where A, B, C are functions of ϕ viz:-

$$A = \frac{1}{\pi}(\phi - \tfrac{1}{2}\sin 2\phi)$$

$$B = \frac{1}{\pi}\left\{(\cos\phi - \tfrac{1}{2}\sin 2\phi) - \tfrac{2}{3}\sin^3\phi\right\} \qquad (4)$$

$$C = \frac{1}{\pi}\left\{\tfrac{1}{2}\cos^2\phi\,(\phi - \tfrac{1}{2}\sin 2\phi) - \tfrac{2}{3}\cos\phi\sin^2\phi + \tfrac{1}{8}(\phi - \tfrac{1}{4}\sin 4\phi)\right\}$$

The formulae give the following values for A, B, C.

ϕ.	A	B	C	$\frac{c}{a} = (1 - \cos\phi)$
0°	0	0	0	0
30°	0.029	0.001	0.00	0 .134
60°	0.196	0.040	0.01	0.500
90°	0.500	0.212	0.06	1.000
120°	0.805	0.540	0.24	1.500
150°	0.971	0.866	0.50	1.866
180°	1.000	1.000	0.62	2.000

By means of this table and equation (3), the course of the pressure-time curve recorded by the gauge up to the moment the wave fromt has traversed the gauge diameter may be obtained for any given values of μ and a, for if τ_0 is the time to traverse the gauge diameter and t the time to traverse the distance $t/\tau_0 = c/2a$.

Thus .....

Thus, when $\mu a = 0.2$ we obtain the following results

$\mu a = 0.2$

$t/\tau_0 = c/2a =$	0.067	0.250	0.500	0.750	0.933	1.000
$P_m/P =$	0.029	0.188	0.460	0.707	0.818	0.828

During this interval the recorded pressure is rising practically the whole time. When t exceeds τ_0 the recorded pressure must necessarily fall and will follow the law

$$P_m = P m_0 e^{-m(t-\tau_0)} \qquad (5)$$

where P_{m_0} is the value of Pm when $t = \tau_0$ and m gives the rate of decay of the true pressure with time. As a first approximation we may take the maximum pressure as occurring at $t = \tau_0$ and as given by the formula

$$P_{max} = P(1 - \mu a + 0.62 \mu^2 a^2) \qquad (6)$$

We will now obtain a more accurate expression for P_{max} since the time to reach the maximum is slightly less than τ_0. Assuming the maximum to occur when ϕ differs from π by a small angle ψ put $\phi = \pi - \psi$ in equations (4) and expand in ascending powers of ψ then

$$A = 1 - \frac{2}{3\pi}\psi^3 + \ldots\ldots \text{ to order } \psi^3$$

$$B = -1 + \tfrac{1}{2}\psi^2 + \ldots\ldots \text{ to order } \psi^2 \qquad (7)$$

$$C = -\frac{5}{8} + \ldots\ldots \text{ to order } \psi$$

D (co-efficient of $\mu^3 a^3$) $= \frac{7}{24}$ to order unity.

Substituting in (3)

$$P_m = P\left\{1 - \frac{2}{3\pi}\psi^3 - (1 - \tfrac{1}{2}\psi^2)\mu a + \tfrac{5}{8}\mu^2 a^2 - \tfrac{7}{24}\mu^3 a^3 + \ldots\ldots\right\} \qquad (8)$$

in the neighbourhood of $\phi = \pi$

To find the maximum, differentiate with respect to ψ and equate to zero. The maximum occurs when $\psi = \frac{\pi}{2}\mu a$ and has the value

$$P_{max} = P\left\{1 - \mu a + \tfrac{5}{8}\mu^2 a^2 + \frac{\pi^2 - 7}{24}\mu^3 a^3 \ldots\ldots\right\} \qquad (9)$$

and occurs at a time τ such that

$$\frac{\tau}{\tau_0} = 1 - \frac{\pi^2}{16}\mu^2 a^2 \qquad (10)$$

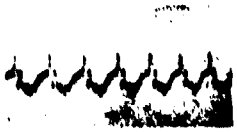
Equation (9) gives the following values for P_{max} and τ

μa	0	0.05	0.10	0.15	0.20	0.25	0.30	0.35	0.40
P_{max}/P	1	0.951	0.906	0.864	0.826	0.791	0.759	0.731	0.708
τ/τ_0	1	0.998	0.994	0.986	0.976	0.962	0.946	0.926	0.904

Sheet I



(a) Time Scale
~ 1000 per/sec.



(b) Time Scale
~ 2000 per/sec.



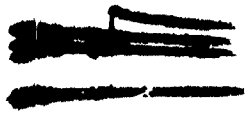
(c) Time Scale
~ 10,000 per/sec.



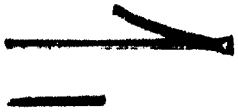
(d) Time Scale
~ 10,000 per/sec.



(e) Pressure Calibration
A.C. Method.

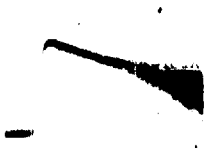


(f) Pressure Calibration
Rotating Potentiometer
method.



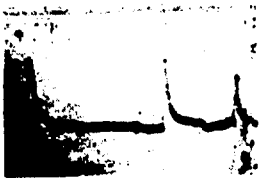
(g) Pressure Calibration
Inductive Method.

(Note also voltage
calibration)



(h) Pressure Calibration
Inductive Method.

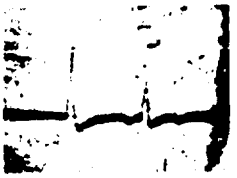
Sheet II



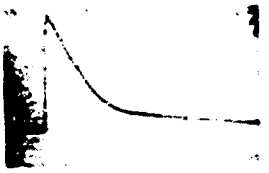
(a) Variation of P with distance $18\frac{1}{2}$ lbs. G.C. Gauges A.D. & C. at 20, 40 and 60 feet. (Note surface reflections.)



(b) Variation of P with D 100 lbs. T.N.T. charge Gauges at 15, 40 and 60 feet X_2, E_1 and X_1 (Note surface and bottom reflections).



(e) Record showing electrical leakage. $18\frac{1}{2}$ lbs. G.C. charge. (Note surface reflections).



(g) Good insulation $18\frac{1}{2}$ lbs. G.C. charge at 20 feet. 3.0 cms. = .001 sec.



(a) 18½ lb. G.C. charge at 13 ft. 8 cms. = .001 sec. (Note pairs of dots on rising pressure line).



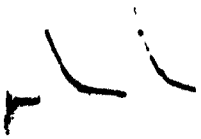
(b) 18½ lbs. G.C. at 13 feet. 8 cms. = .001 second. (Note dots on rising press).



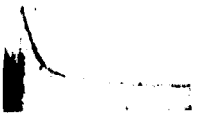
(j) 18½ lbs. G.C. Strip and Circular (7") gauges Broadside-on at 15' and 20 feet. Empty primer tin 2 feet above charge. (Note (i) dotted rise of pressure (ii) irregularities due to empty primer tin).



(k) 18½ lbs. G.C. Two circular 7" gauges Edge-on at 15' and Broadside on at 20 feet respectively. (Note H.F. Dots on rising pressure).



(a) 100 lbs. T.N.T. (Block Filled). Strip Broadside 36 ft. Car Broadside 42 ft. 1.35 cms. = .001 sec. Record on Oscillograph A.



(b) 100 lbs. T.N.T. (Block Filled). Car Edge-on 36 ft. 1.3 cms. = .001 sec. Record on Oscillograph B.

((a) and (b) are records of same shot).

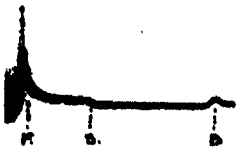


(g) Effect of Air Cavity near charge. 18½ lbs G.C. Strip Broadside 15 ft. Car Broadside 20 ft. (Note effect of empty 2 gall. petrol tin at 2 ft. above charge).

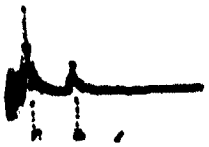


(h) 18½ lbs. G.C. Car Broadside 15 ft. Strip Broadside 20 ft. (The charge in this case was lashed to a spar of soft wood).

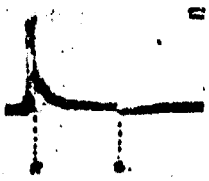
SURFACE AND BOTTOM REFLECTIONS



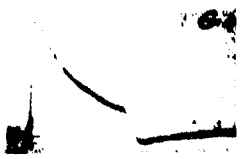
(c) 2½ lbs. G.C. at 15 ft.
Charge and gauge to surface = 11 ft.
Charge and gauge to bottom = 21 ft.
Both surface and bottom reflections shown clearly.



(d) 2½ lbs. G.C. at 15 ft.
Charge and gauge to surface = 21 ft.
Charge and gauge to bottom = 11 ft.
Note large amplitude bottom reflection.



(g) 18½ lbs. G.C. at 20 ft.
Depth of charge and gauge 15 ft.
0.5 cm. = .001 sec.
Note surface reflection.



(h) 250 lbs. T.N.T. at 47 ft. from p.e. gauge. The latter hung 1½ ft. from hull of ship ("GORGON").
Note marked hull reflection and slight tension developed.
(Upper part of main peak accidentally cut off in original record).

P. . Primary Pressure.
S. . Surface Reflection.
B. . Bottom Reflection.

VELOCITY RECORDS

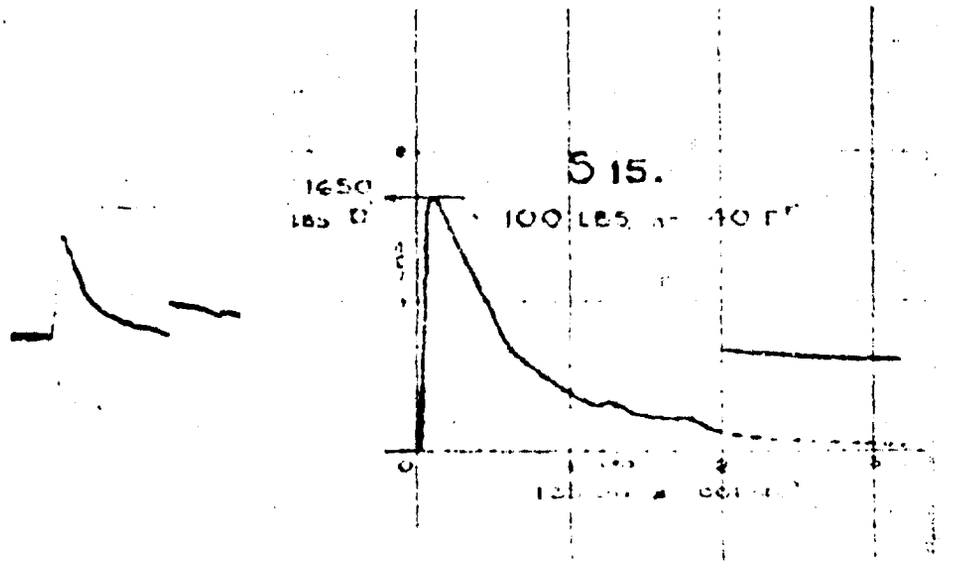


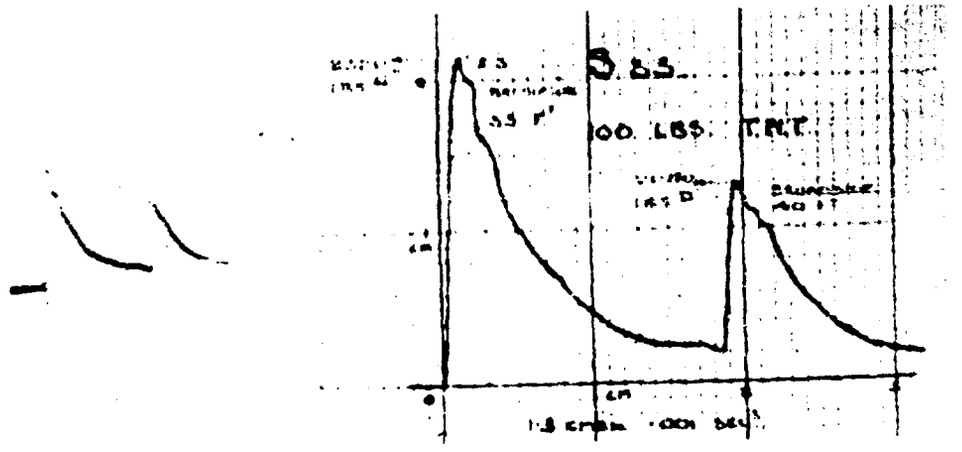
(a) Time Scale 2,000 per sec. with large number of harmonics.



(d) Repeat of (a).

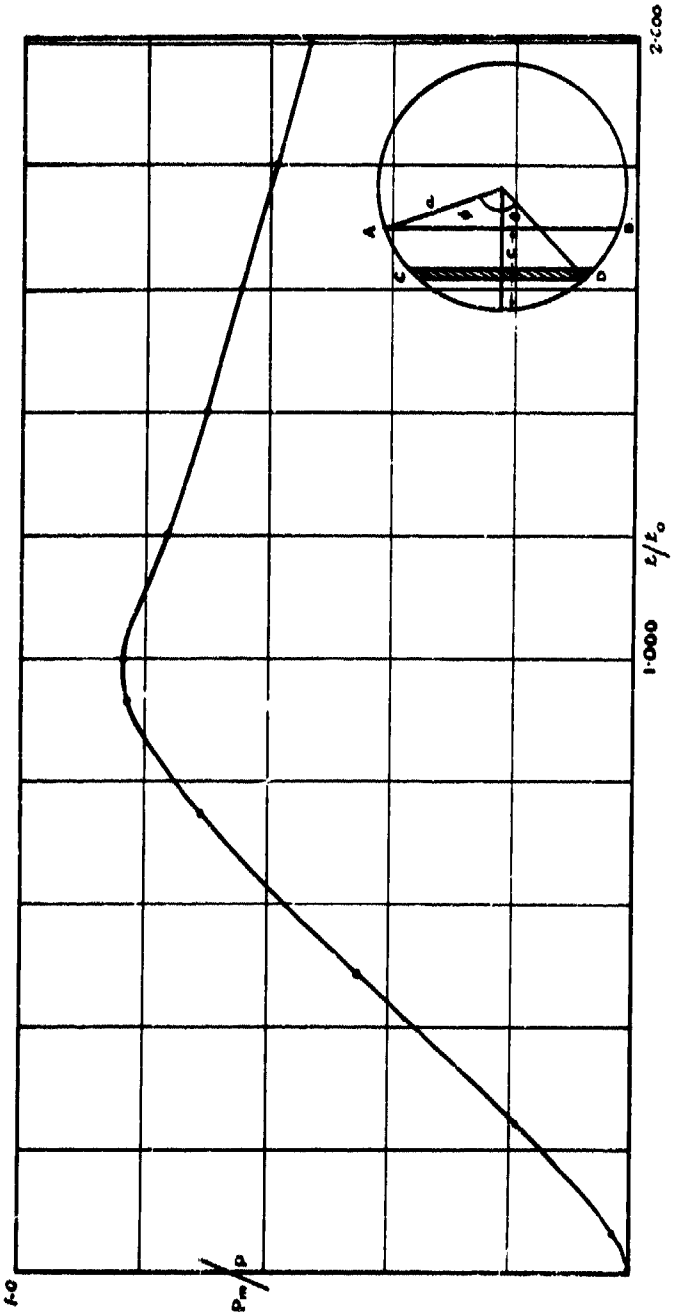
RECORDS OF SPECIAL T.N.T. CHARGES





Best Available Copy

Fig. 1.
Appendix. C.



P.E. Gauges. Curve for Correction of

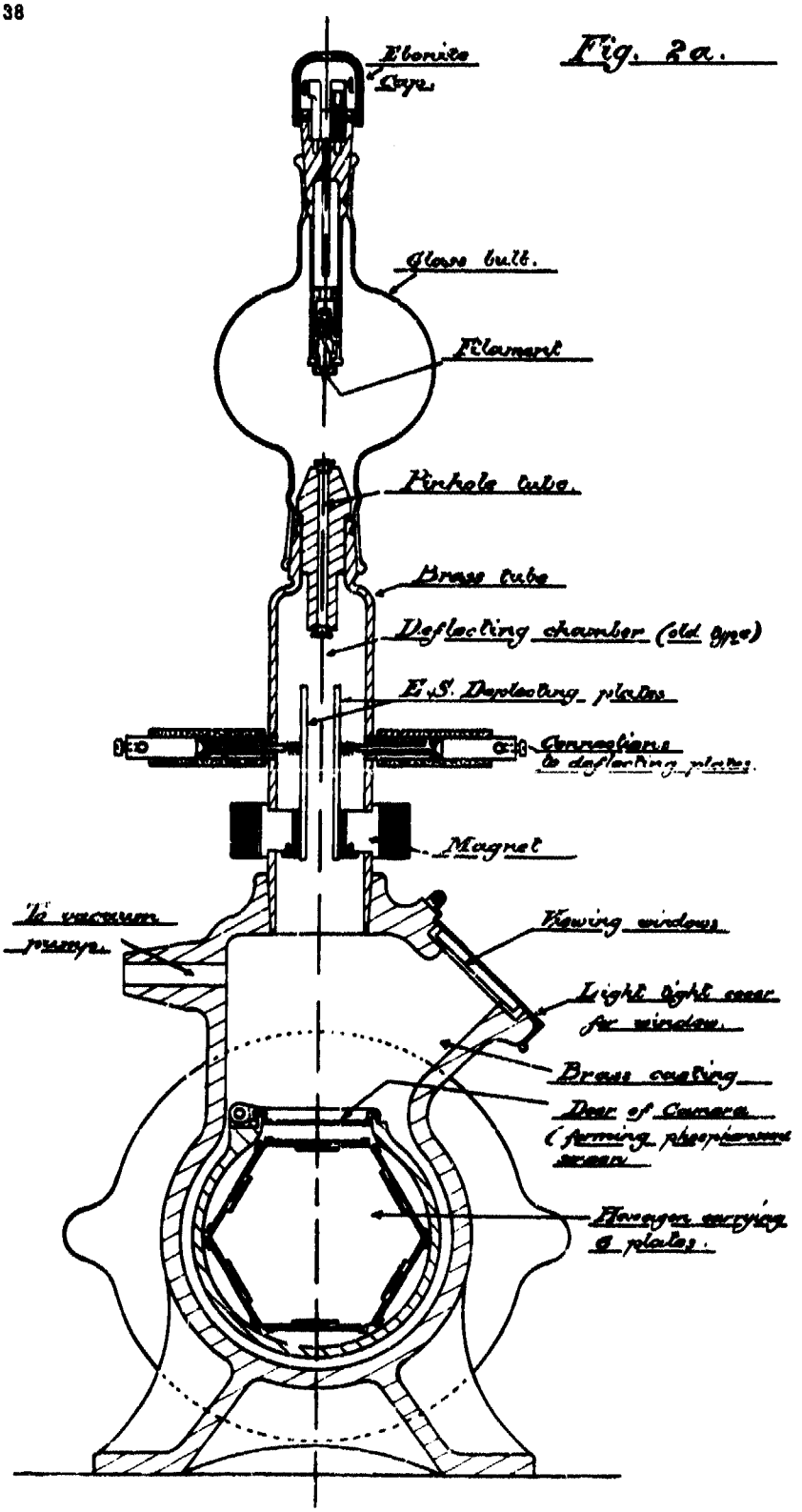

Ebonite Caps.
Glass bulb.
Filament
Pinhole tube.
Brass tube
Deflecting chamber (old type)
E.S. Deflecting plates
Connections to deflecting plates.
Magnet
To vacuum pumps.
Viewing windows
Light tight cover for window.
Brass coating
Door of Camera (forming photographic screen)
Tungsten carrying a plates.

Fig. 2a.

Fig. 2 b.

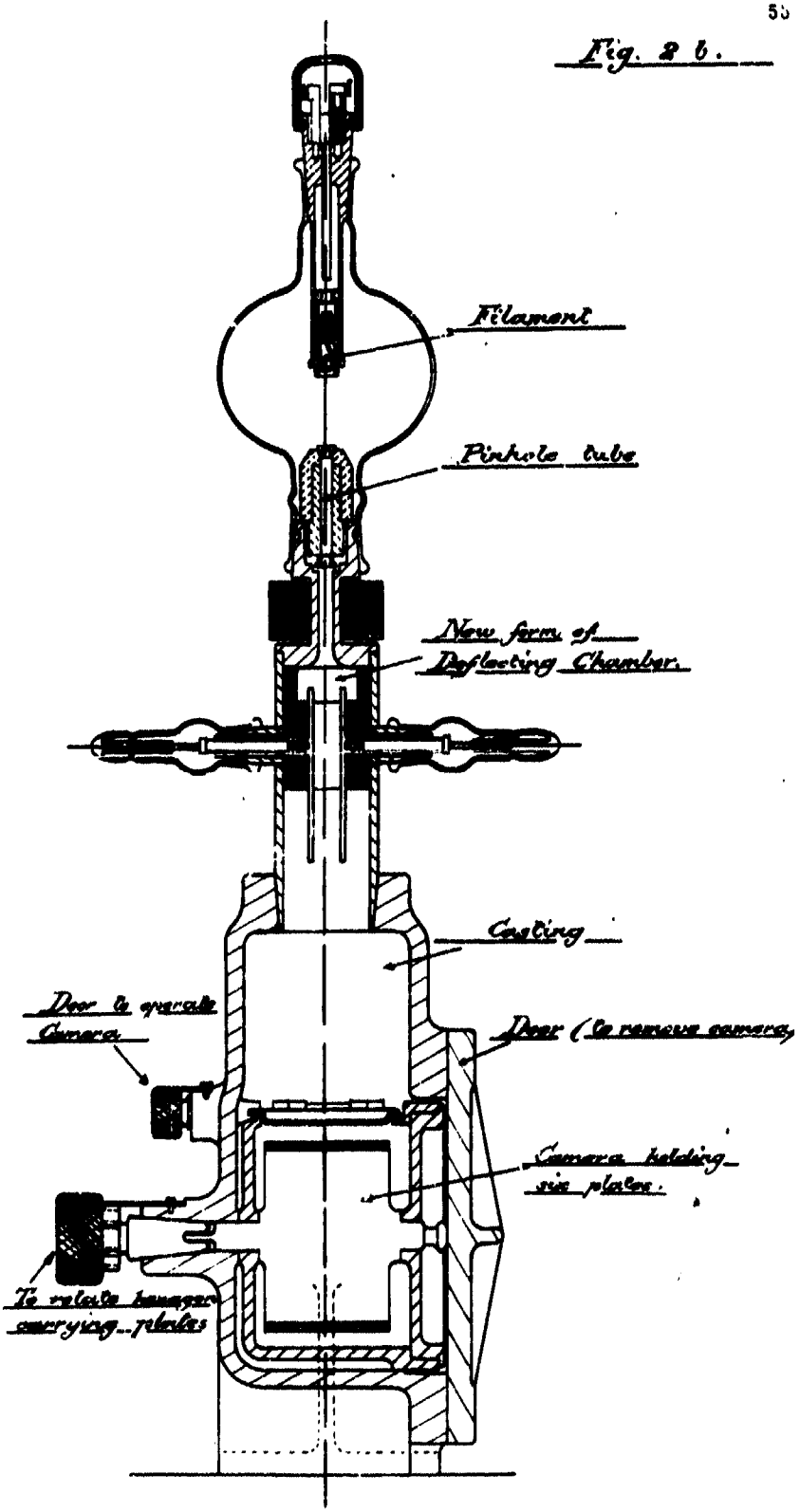
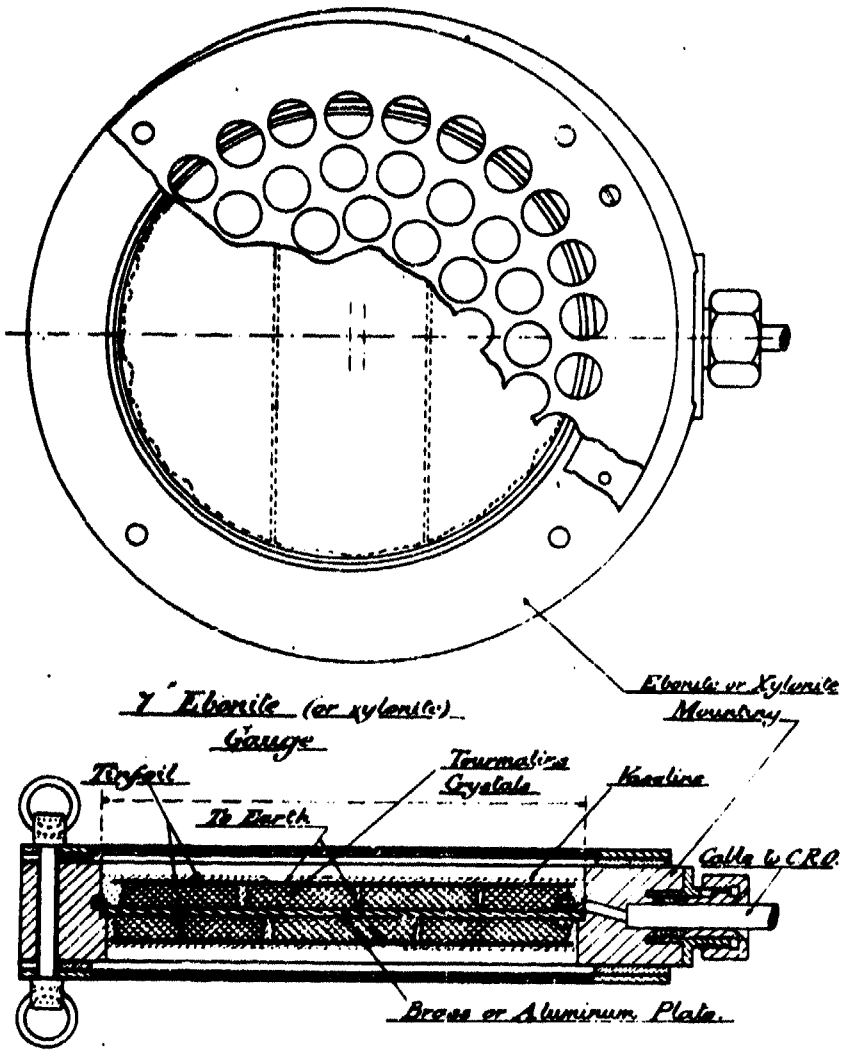

Filament
Pinhole tube
New form of
Deflecting Chamber.
Casting
Door to gravity
Camera.
Door (to remove camera)
Camera holding
six plates.
To rotate hanger
carrying plates

Fig. 9a.


Ebonite or Xylonite Mounting
7" Ebonite (or xylonite) Gauge
Tinfoil
Tourmaline Crystals
Kaolins
To Earth
Cable to C.R.O.
Brass or Aluminium Plate.

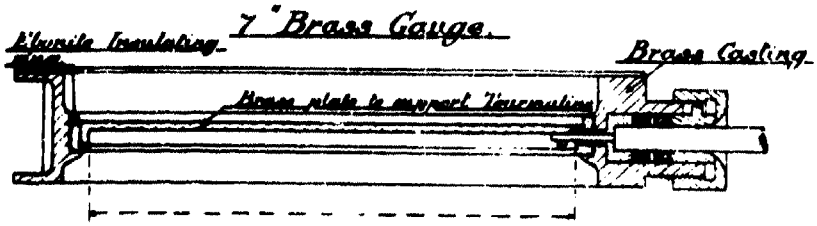

7" Brass Gauge.
Ebonite Insulating
Brass Casting
Brass plate to support Tourmalines

Fig. 4 b.

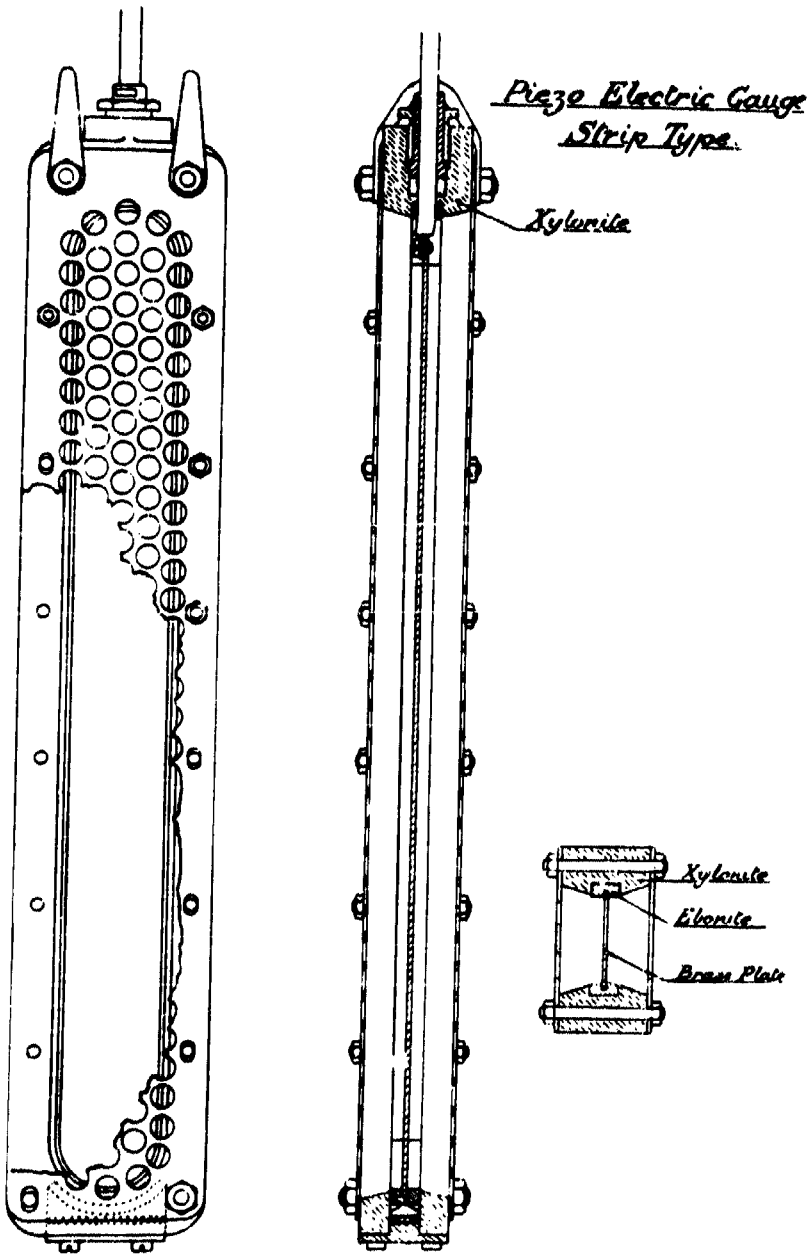
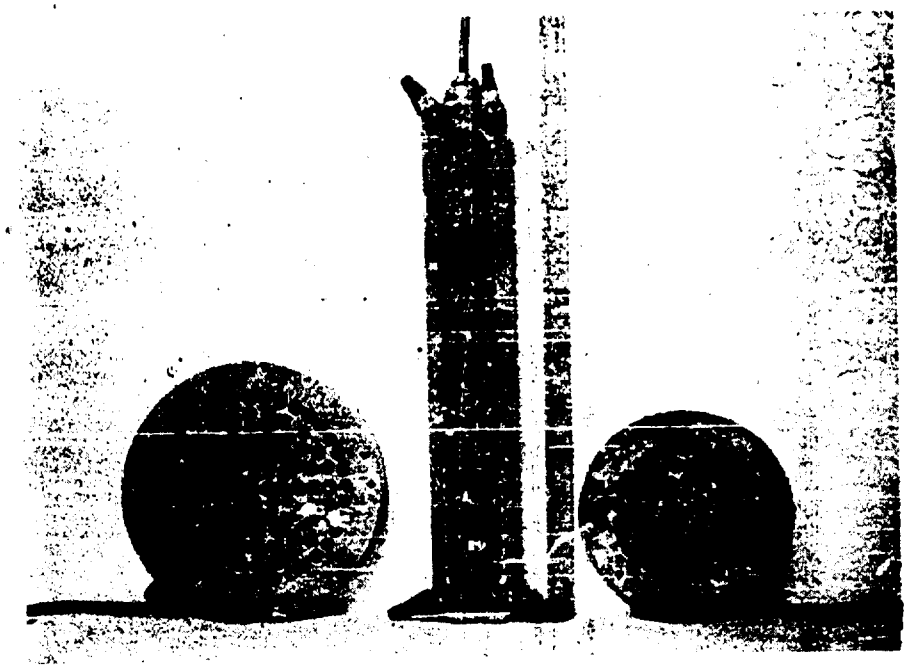

Piezo Electric Gauge
Strip Type.
Xylonite
Xylonite
Ebonite
Brass Plate

Fig.4.c



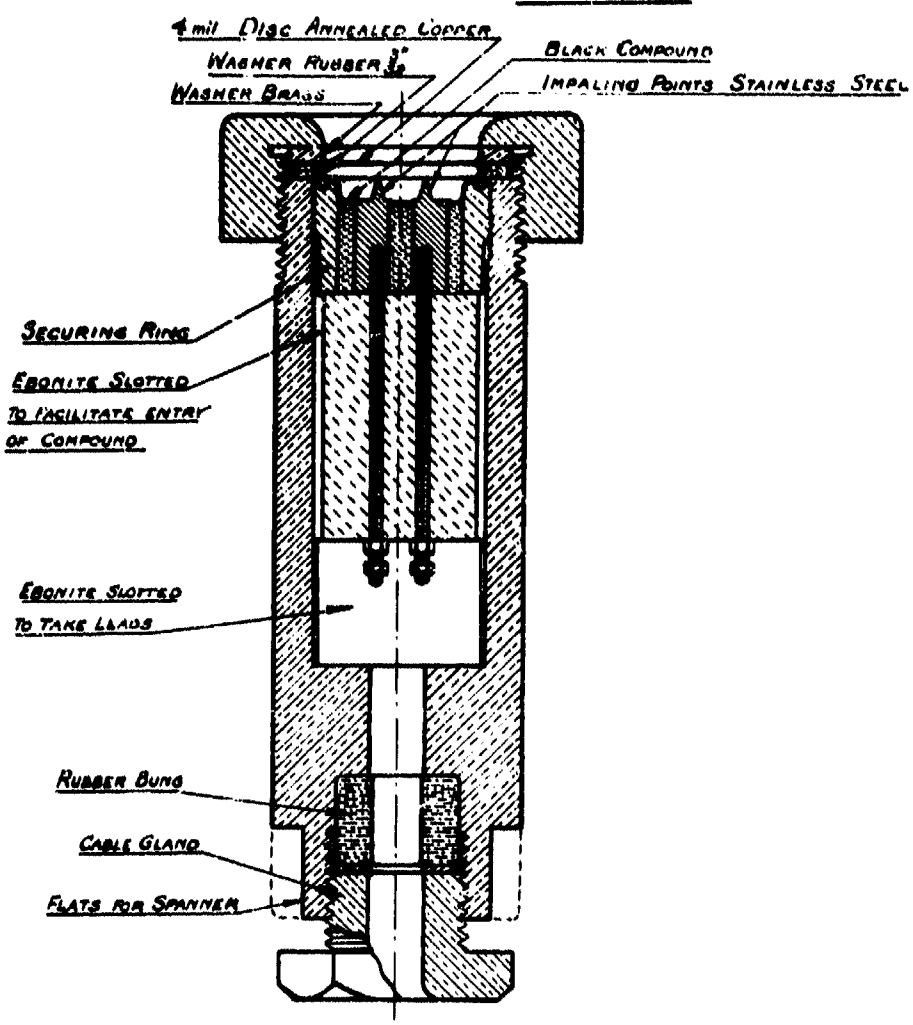
7" Circular 15" Strip 5" Circular

TYPES OF PIEZO ELECTRIC GAUGE

PRESSURE SWITCH

Fig. 6a.

Scale ~ Full Size.



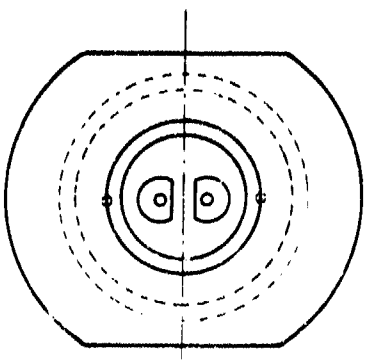


Fig. 8

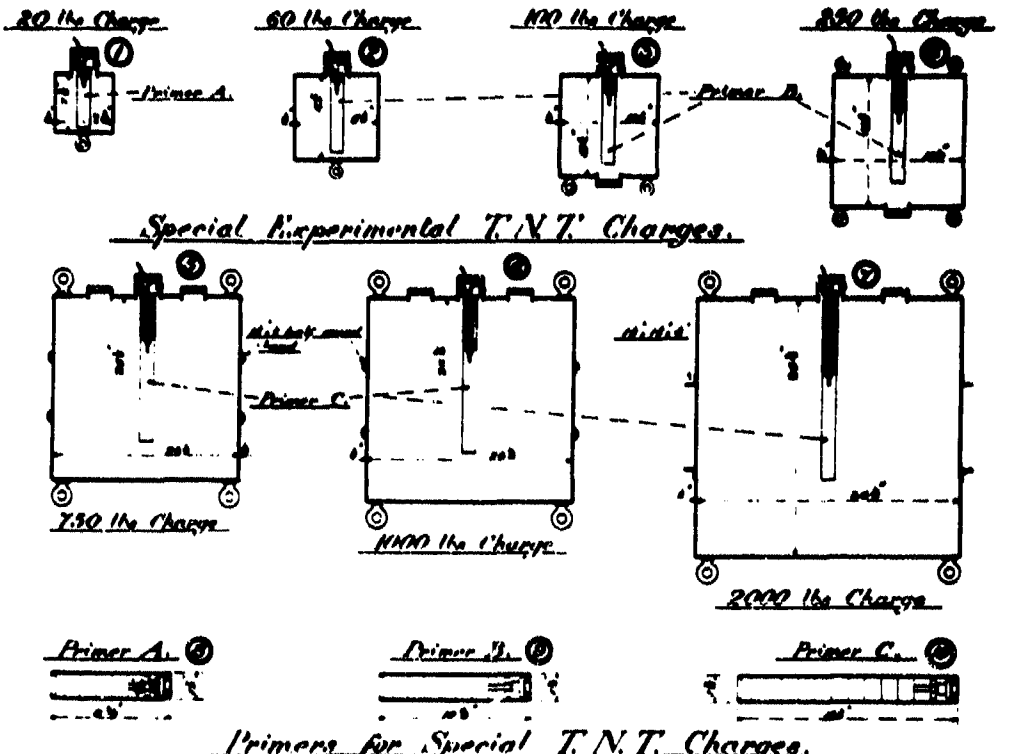
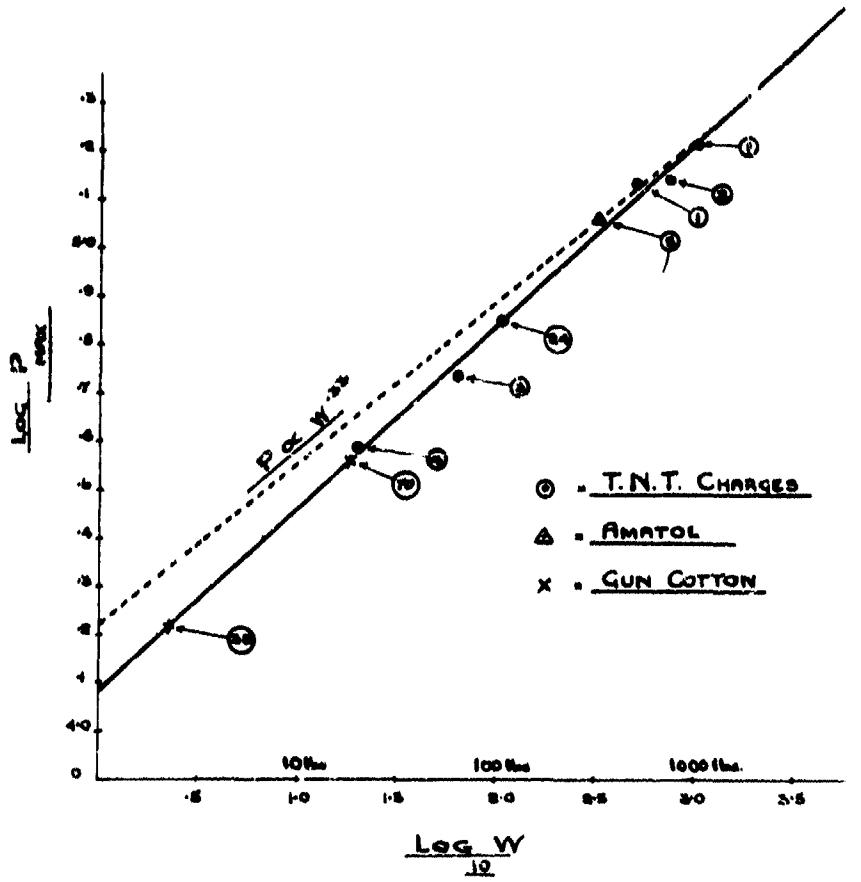

20 lbs Charge
60 lbs Charge
100 lbs Charge
250 lbs Charge
Primer A.
Primer B.
Special Experimental T.N.T. Charges.
Primer C.
750 lbs Charge
1000 lbs Charge
2000 lbs Charge
Primer A.
Primer B.
Primer C.
Primers for Special T.N.T. Charges.
Filled with Standard C.E. Pellets
168 lbs Charge Chee
Depth Charge
H.M.S. Mine
Amatol 320 lbs.
24" Diameter
24 lbs Primer Tin
Section of above.

Fig. 16 a.

Maximum pressure & weight of charge

(Piezo Electric Gauge)

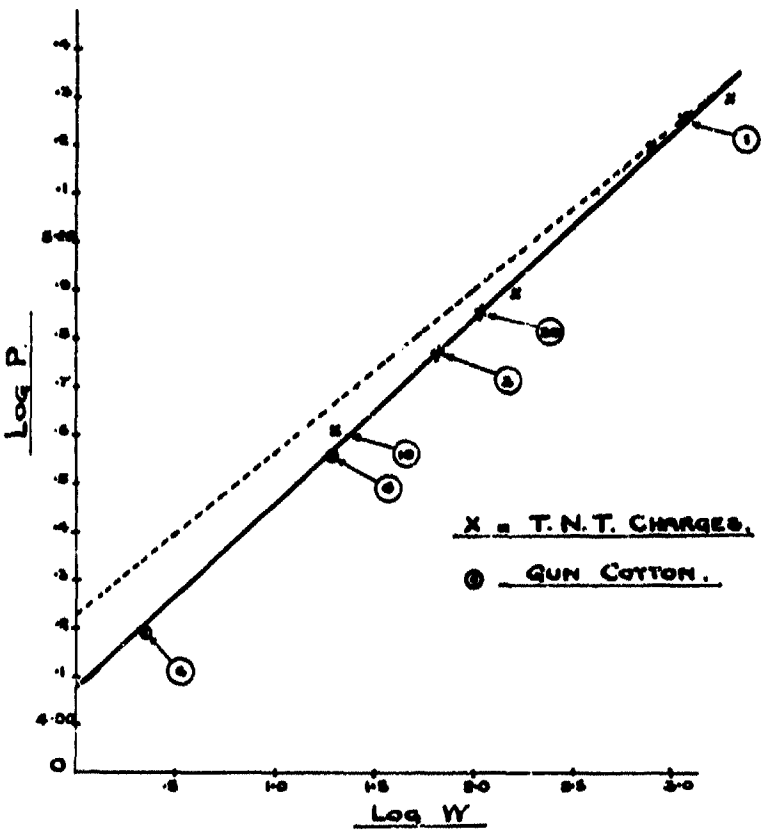


$$\frac{\text{Log } P}{\text{MAX}} = \cdot 38 \text{ Log } W + 4\cdot08 .$$

Fig. 16 b.

Maximum pressure & weight of charge

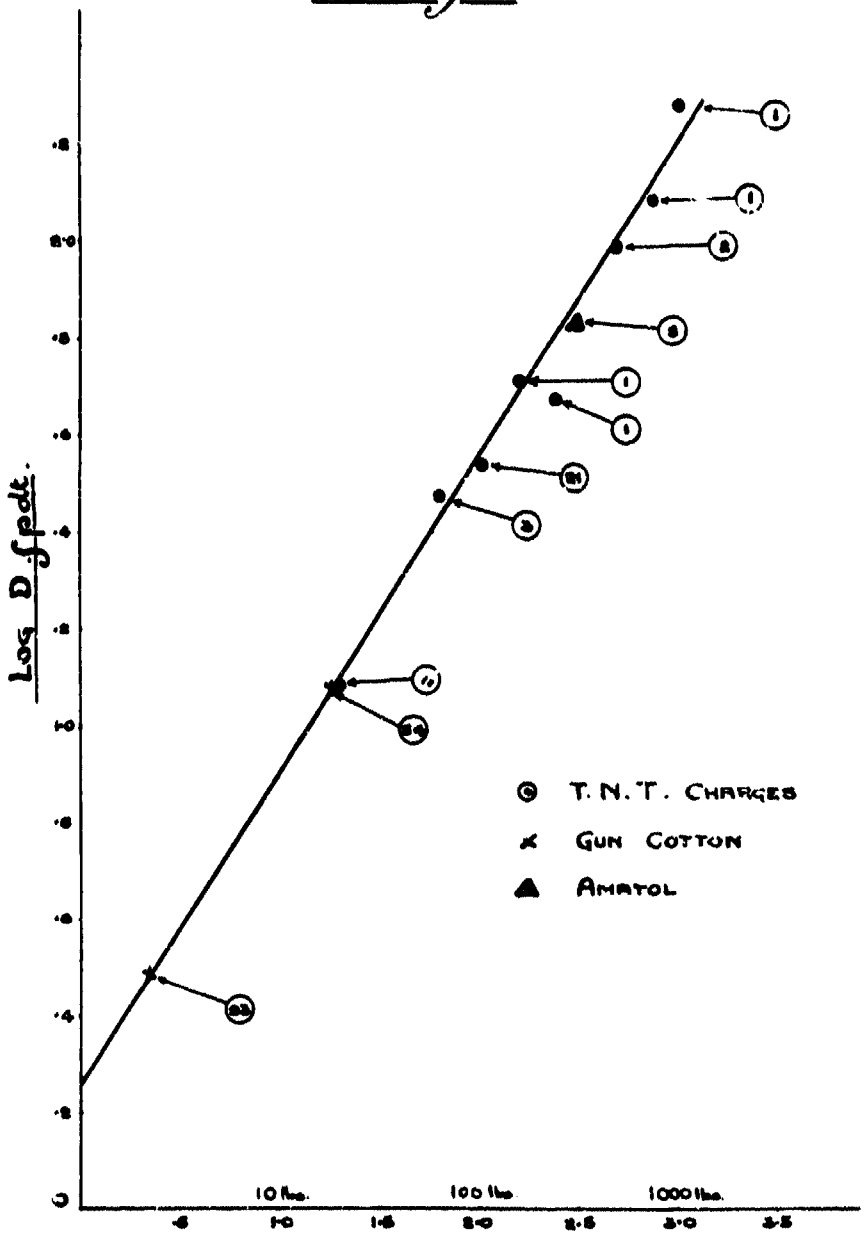
(Hilliar C.F. Gauge.)



$$\text{Log}_{10} P = .38 \text{ Log } W + 4.08.$$

Fig. 17.

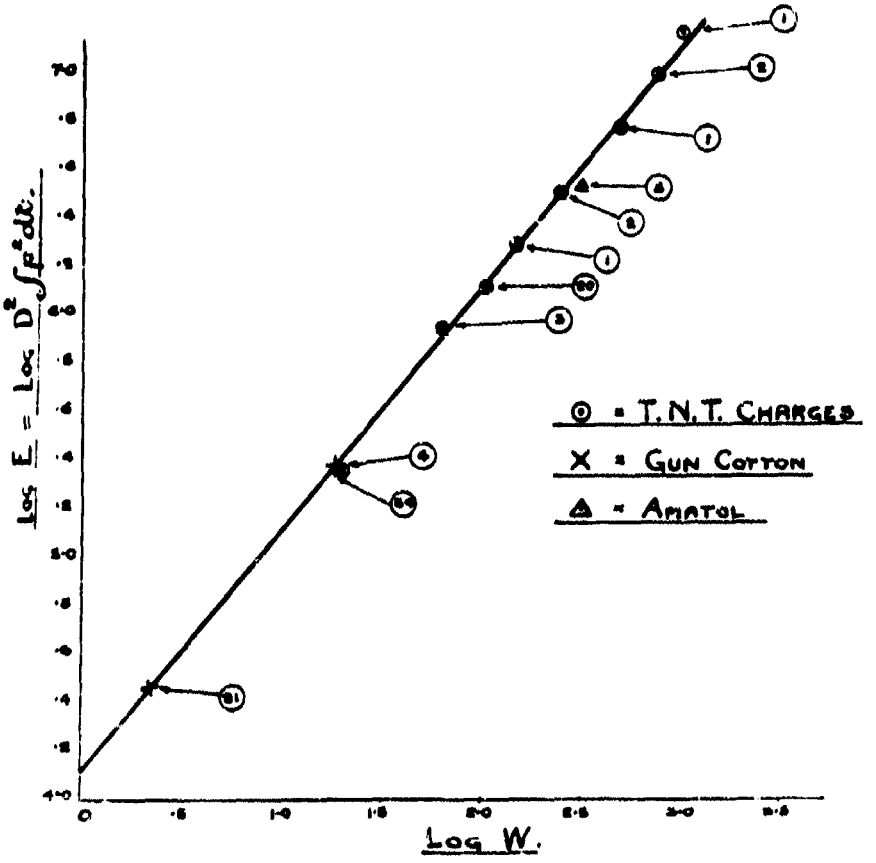
Momentum & Weight of Charge



Log M = ·65 Log W + ·86

Fig. 18.

Energy & Weight of Charges.



A MEASUREMENT OF THE PRESSURE CLOSE TO AN EXPLOSIVE UNDER WATER

G. I. Taylor and R. M. Davies
Cambridge University

British Contribution

June 1944

A MEASUREMENT OF THE PRESSURE CLOSE TO AN EXPLOSIVE UNDER WATER

G. I. Taylor and R. M. Davies
The Engineering Laboratory, Cambridge.

June 1944

* * * * * * *

Summary

This Report describes an experiment in which an electrical modification of the Hopkinson pressure bar was used to measure the pressure developed by a charge of 1.765 lb. T.N.T., primed with 0.05 lb. C.E., and exploded under water with the pressure end of the bar at a distance of 7.79 inches from the centre of the charge.

The record obtained in the experiment can be interpreted as giving an intial pressure of about 17 tons/sq. in. which remains constant for about 0.08 to 0.10 milliseconds; for the conditions of the experiment, the calculations of Penney and Dasgupta give an initial pressure of about 20 tons/sq. in., dropping to half-value in about 0.07 milliseconds. The agreement between the theory and our experiment is not good. It must, however, be remembered that the theoretical result is for a spherical detonation wave, whereas the experiment was carried out with a cylindrical charge; at the same time, difficulties arise in calculating the pressure from the oscillogram on account of the disturbing effects of dispersion in the pressure bar and of the normal pressure acting on its cylindrical surface when the shock wave is propagated outwards.

1. *Introduction.*

In two recent official reports we have described an electrical modification of the Hopkinson pressure bar which can be used to measure high transient pressures; the apparatus has been adapted to measure the pressure near a charge exploded under water and the present report gives the results of an experiment carried out with this apparatus in Portsmouth dockyard in February, 1942. The oscillogram which was obtained in the course of the experiment showed a number of unexpected features, some of which might have been caused by the dispersion of the elastic waves in the pressure bar; the publication of the results of the experiment was therefore postponed until the theoretical study of the propagation of elastic waves in bars had been completed.

2. *Description of the Apparatus.*

The general arrangement of the pressure bar, etc., is shown schematically in Figure 1. The pressure bar was made from a bar of tool steel, 1½ inches diameter and 22 feet long; the duration of the longest pulse which can be recorded by a bar of this length without overlapping due to reflected pulses is about 2½ milliseconds.

The bar was supported vertically in a girder frame attached to a crane, so that in the experiment, the bar was immersed to a depth of about 15 feet; the total depth of water was about 30 feet.

It is important to support the bar with rubber or some similar material, so as to insulate the bar as far as elastic waves are concerned. For this purpose, two horizontal steel shelves, about 3 feet apart in a vertical direction, were provided in the girder frame; a hole 1⅛ inches diameter was drilled in the lower shelf and a hole 2½ inches diameter in the upper shelf. A short length of rubber hose-pipe of suitable diameter was clamped to the bar by a "Jubilee" worm-drive hose

clip .....

clip and the bar was inserted in the frame so that the lower surface of the hose-pipe rested on the lower shelf when the arrangement was vertical. The bar was adjusted centrally relative to the hole in the lower plate, so as to give an all-round clearance of $\frac{1}{8}$ inch, and with the bar in this position, the gap between the bar and the hole in the upper shelf was packed with strips of sheet rubber so as to prevent lateral motion of the bar.

The ring switch, used to trigger the sweep of the oscillograph spots, was of the type previously described; it was situated a few inches above the lower shelf in the girder frame. The sweep circuit was adjusted so that the displacement of the measuring end of the bar was recorded on the return trace.

The bar condenser unit was a cylindrical unit measuring the longitudinal displacement of the end of the bar. The locating tube of the unit was an easy sliding fit on the pressure bar, and the unit was suspended from the girder frame by three adjustable weak springs as shown in Figure 1; these arrangements, together with the rubber cylinders supporting the insulated cylinder of the unit, ensured that the latter remained at rest during the upward motion of the measuring end of the pressure bar due to the explosion. The girder frame was covered with a wooden box (not shown in Figure 1) which protected the apparatus from damage by water.

The charge consisted of 1.765 lb. of T.N.T., together with 0.79 oz. C.E. primer, contained in a cylindrical charge case of mild steel plate, $\frac{1}{16}$ inch thick. The charge case was suspended from lugs attached to the lower end of the girder frame by spun yarn slings, approximately $\frac{5}{16}$ inch diameter, the distance between the lower end of the bar and the upper surface of the charge case being $6\frac{5}{8}$ inches in air. When the bar was lowered into the water, the spun yarn contracted and a separate experiment showed that the contraction under the conditions of this experiment was 1 mm. per foot length of spun yarn; the contraction in a length of 15 foot was thus 1.5 cm. = 0.59 inches, so that the true distance between the pressure end of the bar and the upper surface of the charge case was 6.04 inches.

3. *Experimental Results.*

The oscillogram of the p.d. developed across the input terminals of the amplifier in the experiment is shown in the lower trace in Figure 2; the upper trace in this figure was produced by a timing wave of period 0.0525 milliseconds. The analysis of the oscillogram of Figure 2 is given in curve (A) of Figure 3, where the displacement ξ of the measuring end of the bar is plotted as ordinate, and time t, reckoned from the arrival of the stress pulse at this end, is taken as abscissa; the values of ξ and t calculated from the readings of the measuring microscope are indicated by dots in Figure 3.

Assuming that dispersion effects in the bar are negligible and that a uniform pressure P is applied over the lower plane surface of the bar, the cylindrical surface being free from stress, the value of P corresponding to the point (t, ξ) in Figure 3 is given by equation

$$P = \tfrac{1}{2} \rho c \dot{\xi} = 2.05 \times 10^6 \dot{\xi} \quad \ldots \quad \ldots \quad \ldots \quad \ldots \quad \ldots \quad \ldots \qquad (3.4)$$

where ρ is the density of the material of the pressure bar, c is the velocity of extensional waves of infinite wavelength in the bar and $\dot{\xi}$ is the slope of the (ξ, t) curve at the point considered. Since the values of ρ and c were not determined for the particular bar used in this experiment, the value of ρc (4.10×10^6 gm./sq.cm.sec.), found in earlier experiments for the same type of steel, has been adopted for calculating P from the (ξ, t) curve.

Figure 3 curve (A), shows that, after an initial curved portion, the (ξ, t) curve is sensibly linear over the region t = 0.035 milliseconds to t = 0.183 milliseconds. If this linear portion is produced backwards to cut the t - axis, the length of the intercept on this axis corresponds to about 0.024 milliseconds. It can be shown that when the length of this intercept is not zero, the finite length can be due to three causes:- (1) the finite time taken by the applied pressure to rise from zero to a finite value, (2) the distortion of the pressure pulse due to dispersion in the bar, (3) the distortion of the p.d. developed across the bar condenser unit, due to imperfections in the

amplifier .....

Best Available Co

amplifier. Since the length of the intercept caused by imperfections in the amplifier used in these experiments is of the order of 0.4 microseconds, i.e. 0.0004 milliseconds, it is clearly legitimate to neglect the effect of distortion in the amplifier. The length of the intercept caused by distortion in the bar can be estimated and calculations show that the approximately linear portion of the $(k'\xi/e_g, t)$ curve for bar B, if produced backwards, will cut the t - axis at t = +3 microseconds approximately. Since the ordinate of this curve begins to differ from zero at about t = - 20 microseconds, the length of the intercept is about 23 microseconds = 0.023 milliseconds, which is of the same order as that actually found here in Figure 3. It should be remembered that the errors in the theory on which the calculations are based are likely to be greatest in the neighbourhood of t = o; it is nevertheless clear that the initial curvature of the curve of Figure 3 may be caused by dispersion in the pressure bar and that it is difficult to decide from experiments with a bar of this length and diameter, whether the applied pressure does or does not rise instantaneously from zero to a finite value.

Considering next the portion of the (ξ, t) curve of Figure 3 lying between t = 0.035 milliseconds and t = 0.143 milliseconds, the equation to the straight line of closest fit drawn through the experimental points is found, by Awbery's method*, to be

$$\xi = 1.3856t - 0.0328 \quad \ldots \quad \ldots \quad \ldots \quad \ldots \quad (3.5) \quad (\xi \text{ in cm., } t \text{ in milliseconds}).$$

The curve shown in Figure 3 has been drawn using this equation between the limits of t for which it applies and, on the scale of this figure, it is worth noticing that, apart from the point at t = 0.111 milliseconds, the scatter of the experimental points around the straight line is small.

From equation (3.5), it follows that, over the linear portion of Figure 3, $\dot{\xi} = 1.356 \times 10^3$ cm./sec., and hence, from equation (3.4),

$$P = 2.05 \times 10^6 \times 1.356 \times 10^3 = 2\,780 \times 10^9 \text{ dynes/sq.cm.}$$

$$P = 2.780 \times 10^9 \text{ dynes/sq.cm.} = 18.01 \text{ tons/sq.in.}$$

When t exceeds 0.143 milliseconds, the (ξ, t) curve shows a maximum when t = 0.164 milliseconds, followed by a minimum when t = 0.225 milliseconds, and a gradual, irregular rise which extends as far as t = 0.46 milliseconds; finally, this rise is followed by a series of irregular peaks.

The maximum and the minimum in the region extending from t = 0.164 to t = 0.225 milliseconds, are probably due to dispersion effects in the bar, associated with a decrease in the applied pressure. Whilst it is true that the effect only becomes prominent with a parallel plate condenser unit if the applied pressure undergoes very sudden variation, it must be remembered that the (response frequency) curves for a cylindrical condenser unit show that this type of unit magnifies and reverses the signs of the high frequency components in a pulse, relative to the low frequency components. It follows that dispersion effects will show up more prominently in a record taken with a cylindrical condenser unit than in one taken with a parallel plate unit. For these reasons, it is difficult to make any quantitative deductions from the (ξ, t) curve when t exceeds 0.14 milliseconds.

The periods of the small oscillations superposed on the record when t exceeds 0.225 milliseconds are of the order which one would expect from considerations of the propagation of a pulse consisting of extensional waves, on group velocity theory. This is shown by the agreement between these periods and the periods of the dominant groups which have been calculated, and which are represented to scale in Figure 3 by the lengths of the small sine-curves, C, placed at intervals of 0.05 milliseconds. As to the series of irregular peaks which occur when t exceeds 0.46 milliseconds, it was once thought that they might be due to flexural or transverse vibrations of the pressure bar, caused for example by an asymmetry of the charge relative to the pressure end of the bar; the investigation of the propagation of a pulse of flexural vibrations in a cylindrical bar, given in the appendix, shows however, that the fastest possible group of this type will not reach the measuring end of the bar within the time covered by the record of Figure 3. It may be that the peaks in question are caused

by .....

* J. H. Awbery, Proc. Phys. Soc., Vol. 41, p.384, (1929).

by the impact of fragments of the charge case against the pressure end of the bar.

4. *Discussion of the results and comparison with theory.*

The results of the experiment within the limits t = 0.035 and t = 0.143 milliseconds can be compared with previous calculations of Penney and of Penney and Dasgupta. The calculations given relate to a spherical charge of T.N.T. of radius 50 cm. packed to a density of 1.5 gm./c.c.; with this value for the density of T.N.T., the volume of our charge is 548.8 c.c , whilst the internal volume of the charge case used in this experiment is about 550 c.c. These two values of the volume of the charge are in good agreement and the radius of a sphere of volume 548.8 c.c. is 5.08 cm. = 2 inches; this sphere is shown in section in Figure 1 by the circle drawn in dotted lines with its centre at the centre of the charge case. The ratio of the radii of the charge used in the experiment and in Penney's calculation is 10.16; when comparing the results of the experiment with the calculation, it will be sufficiently accurate to take this ratio to be 10.00, since the errors in the experiment and in the calculation both exceed 1.6%.

Let P_1 and v be the values of a pressure and a velocity at time t' (say) reckoned from the beginning of an explosion and at a distance r (say) from the centre of the charge when the radius r_o (say) of the charge is 50 cm.; it follows from the similarity relationship that if r_o = 5 cm., the pressure and the velocity will have the values P_1 and v when the time is t'/10 and the distance is r/10.

Using this relationship, the curves shown in Figure 4, relating to r_o = 5 cm , have been calculated from the data given elsewhere. In this diagram, time t', reckoned from the instant of detonation is plotted as abscissa, and distance r from the centre of the charge as ordinate. The horizontal straight lines of ordinates 5.08 cm. and 19.79 cm. represent respectively the surface of the charge, assumed spherical, and the pressure end of the bar. The curve labelled "shock wave" gives the relationship between time t' and the distance r of the shock wave surface from the centre of the charge. This curve has been calculated from the values of the shock wave velocity u given by Penney and Dasgupta, the value of the shock wave pressure P_1 (say) corresponding to a given value of r being calculated from the equation

$$P_1 = \frac{46 r_o}{r} \frac{e^{2r_o}}{r^2} \quad (P_1 \text{ in tons/in.}^2) \quad \ldots \quad \ldots \quad \ldots \quad \ldots \qquad (4.1)$$

The curve labelled "interface" in Figure 4 shows the relationship between time t' and the distance, from the origin, of the interface separating the gas bubble and the water; the data for this curve is taken from Penney's calculations.

Figure 4 shows that the shock wave arrives at the pressure end of the bar when t' is approximately 0.065 milliseconds; the corresponding value of P_1 calculated from equation (4.1) is 19.7 tons/sq.in. The time of arrival of the bubble at the pressure end of the bar cannot be calculated with any degree of accuracy since the data available does not extend beyond t' = 0.130 millisecond, and as t' increases the radial velocity of the interface decreases. If, however, we assume that the radial velocity of the interface remains unchanged at the value (245 m./sec.) corresponding to t' = 0.130 milliseconds, then the bubble would reach the pressure end of the bar at time t' = 0.49 milliseconds.

The subsidiary curves (1) ... (4) of Figure 4 show the distribution of pressure over the lower portion of the bar when the shock wave has travelled different distances from the pressure end; curve (1), for example, relates to time t' = 0.085 milliseconds, and the pressures (in tons/sq.in.) at the different points on the bar at this instant are represented by the horizontal distances between the curve and the vertical line through O_1. Curves (1), (2) and (3) have been derived from the last two curves in Figure 7. Curve (4) has been extrapolated from curve (3), assuming that the shock wave pressure is given by equation (4.1) and that the pressure behind the shock wave falls off according to the ordinary theory of sound. The curves (1) ... (4) show that as t' increases from t' = 0.065 millisecond, the pressure distribution along the bar undergoes considerable variations. When t' = 0.065 millisecond, the cylindrical surface of the bar is free from stress whilst the plane end-surface facing the charge is subjected to a normal pressure of

19.7 tons/sq.in. On the other hand, when t' = 0.186 millisecond, the cylindrical surface of the bar is subjected to a normal pressure, which varies from 7.4 tons/sq.in. at the shock wave front to about 2.1 tons/sq.in. at a distance of 3.2 cm. from the pressure end of the bar; the plane end surface of the bar is subjected to a normal pressure of about 1.6 tons/sq.in.

Thus, after the arrival of the shock wave at the measuring end of the bar, a portion of the cylindrical surface of the bar is stressed normally, the length of the stressed portion increases non-linearly with time, and the value of the pressure at any point in this part of the bar decreases as time increases; in addition, the plane end surface of the bar is subjected to a normal pressure which is less than the shock-wave pressure and which decreases as time increases. In these circumstances, equation (3.4) giving the applied pressure in terms of the velocity of the measuring end of the bar, ceases to be true, and it is difficult to derive the relationship which will hold between the two quantities under the actual conditions of the experiment. It is, however, possible to investigate the simple case of a cylindrical pressure bar, subjected to a constant, uniform hydrostatic pressure along a portion of its length, assuming that the length of the stressed portion increases uniformly with time.

In Figure 5 let Ox represent the axis of a cylindrical pressure bar, the origin O being taken at the pressure end of the bar. We shall assume that the bar is sufficiently long to avoid overlapping of direct and reflected pulses, and that the radius of the bar is sufficiently small to enable dispersion effects to be neglected. Suppose that the pressure on the bar is initially zero and that a region of uniform hydrostatic pressure P_1 moves with a uniform velocity U in the positive direction of the x - axis; let the boundary between this region and the region where the pressure is zero, i.e. the shock wave front in the experiment, arrive at O at time t' = 0. Exaggerating the changes in the radius of the bar, the state of affairs at time t' may be represented diagramatically by Figure 5, where the shock wave front has reached the point A ($OA = Ut'$), whilst the front of the stress pulse in the bar, which starts from O at time t' = 0, has reached the point D ($OD = c_o t'$). The bar thus consists of three regions, - the region of uniform hydrostatic pressure, P_1 - region (1), say - the region of the stress pulse, in which the bar is strained in the direction Ox, the cylindrical surface being free from stress - region (2), say - and finally, the undisturbed region - region (3), say.

Let u_1, u = the particle velocities in regions (1) and (2)

P = the pressure (in the direction Ox) in region (2),

A_1, A, A_o = the area of cross-section of the bar in regions (1), (2), (3) respectively,

ρ_1, ρ, ρ_o = the density of the material of the bar in regions (1), (2), (3) respectively,

it follows that:

$$P = \rho c_o u \quad \ldots \quad \ldots \quad \ldots \quad \ldots \quad \ldots \quad \ldots \quad (4.2)$$

If we superpose a velocity U in the negative direction of Ox on the bar, the boundary BC is brought to rest and the particle velocities in regions (1) and (2) become $(U - u_1)$ and $(U - u)$ respectively.

Under these conditions, conservation of mass at the boundary BC gives

$$\rho_1 A_1 (U - u_1) = \rho A (U - u) \quad \ldots \quad \ldots \quad \ldots \quad \ldots \quad (4.3);$$

conservation of momentum at this boundary gives

$$P_1 A_1 - PA = \rho A (U - u)(u_1 - u) = \rho_1 A_1 (U - u_1)(u_1 - u) \ldots \quad \ldots \quad (4.4).$$

In order to find the relationship between P, P_1, U and c_o, it is necessary to eliminate u_1, ρ, ρ_1 and A_1 from equations (4.3) and (4.4). For this purpose, consider a portion of the bar in the unstrained state (region (3) of Figure 5) of length l_o, radius r_o and cross-sectional

area .....

area A_0. Let l be the length of this portion, r the radius and A the cross-sectional area when it is subjected to a longitudinal compressive stress P, the cylindrical surface being free from stress.

If σ be Poisson's ratio for the material of the bar, then

$$\frac{l}{l_0} = 1 - \frac{P}{E}; \qquad \frac{r}{r_0} = 1 + \sigma\frac{P}{E}.$$

The quantities P/E, $\sigma P/E$ and similar quantities are strains which we assume to be sufficiently small to allow squares and higher powers to be neglected. It follows that

$$\frac{A}{A_0} = \frac{r^2}{r_0^2} = 1 + \frac{2\sigma P}{E} \quad \ldots \quad \ldots \quad \ldots \quad \ldots \quad \ldots \quad \ldots \qquad (4.5a)$$

and, from the conservation of mass,

$$\frac{\rho A}{\rho_0 A_0} = \frac{l_0}{l} = 1 + \frac{P}{E} \quad \ldots \quad \ldots \quad \ldots \quad \ldots \quad \ldots \qquad (4.5)$$

Next suppose that the compressive stress P is removed and that a uniform hydrostatic pressure, P_1, is applied to the portion of the bar, and that its length, radius and cross-sectional area become l_1, r_1 and A_1 respectively. We now have

$$\frac{l_1}{l_0} = \frac{r_1}{r_0} = 1 - \frac{P_1}{E}(1 - 2\sigma)$$

so that

$$\frac{A_1}{A_0} = \frac{r_1^2}{r_0^2} = 1 - \frac{2P_1}{E}(1 - 2\sigma) \quad \ldots \quad \ldots \quad \ldots \quad \ldots \qquad (4.6a)$$

and

$$\frac{\rho_1 A_1}{\rho_0 A_0} = \frac{l_0}{l_1} = 1 + \frac{P_1}{E}(1 - 2\sigma) \quad \ldots \quad \ldots \quad \ldots \quad \ldots \qquad (4.6)$$

From equation (4.3)

$$\frac{U - u_1}{U - u} = \frac{\rho A}{\rho_1 A_1} = \frac{1 + P/E}{1 + \frac{P_1}{E}(1 - 2\sigma)} \quad \ldots \quad \ldots \qquad (4.7)$$

from equations (4.5) and (4.6).

Neglecting squares and higher orders of the small quantities P/E ... u_1/U, u/U, equation (4.7) becomes

$$u_1 - u = -\frac{U}{E}\left[P - P_1(1 - 2\sigma)\right] \quad \ldots \quad \ldots \quad \ldots \quad \ldots \qquad (4.8)$$

From equation (4.4)

$$u_1 - u = \frac{P_1 A_1 - PA}{\rho A(U - u)} = \frac{P_1\left[1 - \frac{2P_1}{E}(1 - 2\sigma)\right] - P\left[1 + \frac{2\sigma P}{E}\right]}{\rho_0\left(1 + \frac{P}{E}\right)\left(1 - \frac{u}{U}\right)} \quad \ldots \quad \ldots \qquad (4.9)$$

from .....

clip and the bar was inserted in the frame so that the lower surface of the hose-pipe rested on the lower shelf when the arrangement was vertical. The bar was adjusted centrally relative to the hole in the lower plate, so as to give an all-round clearance of $\frac{1}{8}$ inch, and with the bar in this position, the gap between the bar and the hole in the upper shelf was packed with strips of sheet rubber so as to prevent lateral motion of the bar.

The ring switch, used to trigger the sweep of the oscillograph spots, was of the type previously described; it was situated a few inches above the lower shelf in the girder frame. The sweep circuit was adjusted so that the displacement of the measuring end of the bar was recorded on the return trace.

The bar condenser unit was a cylindrical unit measuring the longitudinal displacement of the end of the bar. The locating tube of the unit was an easy sliding fit on the pressure bar, and the unit was suspended from the girder frame by three adjustable weak springs as shown in Figure 1; these arrangements, together with the rubber cylinders supporting the insulated cylinder of the unit, ensured that the latter remained at rest during the upward motion of the measuring end of the pressure bar due to the explosion. The girder frame was covered with a wooden box (not shown in Figure 1) which protected the apparatus from damage by water.

The charge consisted of 1.765 lb. of T.N.T., together with 0.79 oz. C.E. primer, contained in a cylindrical charge case of mild steel plate, $\frac{1}{16}$ inch thick. The charge case was suspended from lugs attached to the lower end of the girder frame by spun yarn slings, approximately $\frac{5}{16}$ inch diameter, the distance between the lower end of the bar and the upper surface of the charge case being $6\frac{5}{8}$ inches in air. When the bar was lowered into the water, the spun yarn contracted and a separate experiment showed that the contraction under the conditions of this experiment was 1 mm. per foot length of spun yarn; the contraction in a length of 15 foot was thus 1.5 cm. = 0.59 inches. so that the true distance between the pressure end of the bar and the upper surface of the charge case was 6.04 inches.

3. *Experimental Results.*

The oscillogram of the p.d. developed across the input terminals of the amplifier in the experiment is shown in the lower trace in Figure 2; the upper trace in this figure was produced by a timing wave of period 0.0525 milliseconds. The analysis of the oscillogram of Figure 2 is given in curve (A) of Figure 3, where the displacement ξ of the measuring end of the bar is plotted as ordinate, and time t, reckoned from the arrival of the stress pulse at this end, is taken as abscissa; the values of ξ and t calculated from the readings of the measuring microscope are indicated by dots in Figure 3.

Assuming that dispersion effects in the bar are negligible and that a uniform pressure P is applied over the lower plane surface of the bar, the cylindrical surface being free from stress, the value of P corresponding to the point (t, ξ) in Figure 3 is given by equation

$$P = \tfrac{1}{2}\rho c \dot{\xi} = 2.05 \times 10^6 \dot{\xi} \quad \ldots \quad \ldots \quad \ldots \quad \ldots \quad \ldots \quad \ldots \qquad (3.4)$$

where ρ is the density of the material of the pressure bar, c is the velocity of extensional waves of infinite wavelength in the bar and $\dot{\xi}$ is the slope of the (ξ, t) curve at the point considered. Since the values of ρ and c were not determined for the particular bar used in this experiment, the value of ρc (4.10×10^6 gm./sq.cm.sec.), found in earlier experiments for the same type of steel, has been adopted for calculating P from the (ξ, t) curve.

Figure 3 curve (A), shows that, after an initial curved portion, the (ξ, t) curve is sensibly linear over the region t = 0.035 milliseconds to t = 0.143 milliseconds. If this linear portion is produced backwards to cut the t - axis, the length of the intercept on this axis corresponds to about 0.024 milliseconds. It can be shown that when the length of this intercept is not zero, the finite length can be due to three causes:- (1) the finite time taken by the applied pressure to rise from zero to a finite value, (2) the distortion of the pressure pulse due to dispersion in the bar, (3) the distortion of the p.d. developed across the bar condenser unit, due to imperfections in the

amplifier .....

Best Available Copy

Appendix. The propagation of a pulse of flexural waves in a cylindrical bar.

If the forces applied to the pressure end of a bar are unsymmetrical with respect to the axis of the bar, the forces are equivalent to a longitudinal force along the axis, together with a couple; the longitudinal force gives rise to a stress pulse composed of longitudinal or extensional waves and the couple to a pulse consisting of flexural or transverse waves. Since a cylindrical condenser unit can respond to flexural waves, it is important to find whether an oscillogram, such as that shown in Figure 2, is affected by this type of wave, and this appendix deals with the propagation of a flexural wave pulse from the standpoint of the method of stationary phase, following the lines of the discussion for extensional wave pulses.

The differential equations, which have been used for describing flexural vibrations in a bar, fall into two classes, - the exact equations, due to Pochhammer and to Chree, derived from the general equations of the theory of elasticity, and the simpler less exact equations, derived in a more elementary manner from a consideration of the stresses in the bar. The former have been summarised by Love*, and calculations, based on these equations giving the phase velocity of flexural waves for different wavelengths, have been published recently by Hudson §.

The simpler equations, and the assumptions on which they are based have been summarised by Timoshenko #; more recently, a very thorough discussion of the problem has been given by Prescott ##.

Considering a cylindrical bar of radius a, let the axis of the bar (assumed straight when in equilibrium) be taken as the axis of x, and let the direction of the displacement of the bar in flexural or transverse vibration be taken as the axis of y. It will be assumed that the bar is uniform and that the displacements are small.

Let u_y = flexural displacement at time t at a cross-section of abscissa, x.

ρ = density of the material of the bar.

E = Young's modulus of the material of the bar.

μ = modulus of rigidity of the material of the bar.

σ = Poisson's ratio of the material of the bar.

$c_0 = \sqrt{\frac{E}{\rho}}$ = velocity of extensional waves of infinite wavelength in the bar.

c, c_g = phase and group velocities respectively of waves of wavelength λ in the bar.

$\kappa = \frac{\lambda}{2}$ = radius of gyration of the cross-section of the bar about an axis through the centre of gravity, perpendicular to the xy plane.

R = a non-dimensional constant, depending on the shape of the cross-section of the bar. (For a circular cross-section, R = 10/9).

$\epsilon = RE/\mu = 2R\ (1 + \sigma)$

λ, T = wavelength and period of a flexural wave.

Y = ...

* A.E.H. Love "Mathematical Theory of Elasticity", Art. 201 (4th Ed.) Cambridge (1934).

§ G.E. Hudson, Phys. Rev., Vol. 63, p.46, (1943).

S. Timoshenko, "Vibration Problems in Engineering", Arts. 40-43 New York, (1928).

J. Prescott, Phil. Mag., Vol. 33, p.703, (1942).

$$\gamma = \frac{2\pi}{\lambda} \quad : \quad \omega = \frac{2\pi}{T} = \gamma c = \frac{2\pi c}{\lambda}$$

The simplest theory of the flexural vibrations of a bar assumes that the displacement of an element of the bar consists solely of translation parallel to Oy; the differential equation may be written in the form

$$c_0^2 \, K^2 \, \frac{\partial^4 u_y}{\partial x^4} + \frac{\partial^2 u_y}{\partial t^2} = 0 \quad \ldots \quad \ldots \quad \ldots \quad \ldots \quad \ldots \qquad (A.1)$$

For sinusoidal waves of unit amplitude, u_y will be of the form

$$u_y = e^{i(\gamma x + \omega t)} \quad \ldots \quad \ldots \quad \ldots \quad \ldots \quad \ldots \quad \ldots \qquad (A.2)$$

and, substituting in equation (A.1), it is easy to show that the phase velocity c of sinusoidal flexural waves of wave-length λ is given by the equation

$$c = \gamma c_0 K = \pi c_0 \frac{a}{\lambda} \quad \ldots \quad \ldots \quad \ldots \quad \ldots \quad \ldots \quad \ldots \qquad (A.3)$$

The corresponding value of the group velocity, c_g, given by the equation

$$\frac{c_g}{c_0} = \frac{c}{c_0} + \frac{a}{\lambda} \, \frac{d\,(c/c_0)}{d\,(a/\lambda)} \quad \ldots \quad \ldots \quad \ldots \quad \ldots \qquad (A.4),$$

is here

$$c_g = 2c = 2\pi \, c_0 a/\lambda \quad \ldots \quad \ldots \quad \ldots \quad \ldots \quad \ldots \qquad (A.5)$$

This theory leads to a result which is physically absurd, namely that a wave-packet consisting of waves of infinitely short wave-lengths will be propagated with an infinite velocity; it also follows that a wave-packet consisting of waves of infinitely long wave-lengths will be propagated with an infinitesimally small velocity.

When the elements of the bar are considered to undergo rotation (without distortion) in addition to lateral displacement, the differential equation (A.1) is modified to the form (due apparently to Rayleigh) *

$$c_0^2 \, K^2 \, \frac{\partial^4 u_y}{\partial x^4} - K^2 \, \frac{\partial^4 u_y}{\partial x^2 \partial t^2} + \frac{\partial^2 u_y}{\partial t^2} = 0 \quad \ldots \quad \ldots \quad \ldots \qquad (A.6)$$

The effect of the rotation of the elements of the bar is represented by the term

$$- K^2 \, \frac{\partial^4 u_y}{\partial x^2 \partial t^2}$$

Proceeding as before, it may be shown that the phase and group velocities, derived from this equation, are given by

$$c = \frac{c_0}{\sqrt{1 + \frac{\lambda^2}{\pi^2 a^2}}} \; ; \quad c_g = \frac{c_0}{\sqrt{1 + \frac{\lambda^2}{\pi^2 a^2}}} \left\{ 1 + \frac{1}{1 + \frac{\pi^2 a^2}{\lambda^2}} \right\} \quad \ldots \qquad (A.7)$$

When $\frac{a}{\lambda}$ is small, the values of c and c_g given by this equation become equal to those given in equation (A.6); where $\frac{a}{\lambda}$ is large, both c and c_g approach the value c_0 asymptotically, so that

a wave- .....

* Lord Rayleigh, ("Theory of Sound" Vol. 1, p. 294, London (1894).

a wave-packet consisting of waves of infinitely short wavelengths will be propagated not with infinite velocity but with a velocity equal to the velocity of extensional waves of infinite wavelength.

When the shearing, the rotation and the lateral displacements of the elements of the bar are taken into account, the differential equation takes the form given by Timoshenko # and by Prescott (loc. cit.)

$$c_0^2 \kappa^2 \frac{\partial^4 u_y}{\partial x^4} + \frac{\partial^2 u_y}{\partial t^2} - \kappa^2 (1 + \epsilon) \frac{\partial^4 u_y}{\partial x^2 \partial t^2} + \frac{\epsilon \kappa^2}{c_0^2} \frac{\partial^4 u_y}{\partial t^4} = 0 \quad \ldots \quad (A.8)$$

This equation differs from equation (A.7) by the terms involving the non-dimensional parameter ϵ as a factor.

It can be shown that the phase and group velocities derived from equation (A.8) are given by the relationships

$$\left.\begin{aligned} \frac{c_0^2}{c^2} + \epsilon \frac{c^2}{c_0^2} &= 1 + \frac{\lambda^2}{\pi^2 a^2} + \epsilon \\ \frac{c_g}{c_0} &= \frac{c}{c_0}\left[1 - \frac{1}{1 + \frac{\pi^2 a^2}{\lambda^2}\left(1 + \epsilon - 2\epsilon \frac{c^2}{c_0^2}\right)}\right] \end{aligned}\right\} \quad \ldots \quad \ldots \quad (A.9)$$

For a given value of a/λ the first of these equations becomes a quadratic in c^2/c_0^2; the two roots are real, the larger giving a value of c which exceeds c_0 except in the limiting case where $a/\lambda = \infty$, whilst the smaller gives a value of c which is always less than c_0. The larger root does not appear to have any physical significance under ordinary conditions of experiment (c.f. Prescott, loc. cit.), and moreover the exact theory shows that c/c_0 is a single-valued function of a/λ; we shall therefore ignore this root, and, with this restriction, it follows that the values of c/c_0 and c_g/c_0 given by equation (A.9) reduce to those given by equations (A.3) and (A.5) when a/λ is small. When a/λ is large, c/c_0 and c_g/c_0 approach the value $1/\sqrt{\epsilon}$ asymptotically.

Assuming that $\sigma = 0.29$, the variation of c/c_0 and c_g/c_0 with a/λ given by equations (A.3), (A.5), (A.7) and (A.9) is shown graphically in Figures A.1. and A.2.; the values given by equations (A.3) and (A.5) are shown in the broken-line curve labelled "Flexural waves - Elementary Theory", those given by equation (A.7) in the chain-dotted curve labelled "Flexural waves - Rayleigh Theory", and those derived from equation (A.9) by the points marked by crosses. These diagrams also show the values of c/c_0 and c_g/c_0 deduced from the data given by Hudson; these values are given by the curve labelled "Flexural waves (exact theory)" and, for purposes of comparison, the values of c/c_0 and c_g/c_0, for extensional waves (1st mode, exact theory) have been included in the curves marked "Extensional waves". The curves given in these diagrams show a number of points of interest. When a/λ is small, the elementary theory gives the correct result. As a/λ increases from zero, the values of c/c_0 and c_g/c_0 given by the elementary theory and by the Rayleigh theory are greater than those given by the exact theory. When a/λ becomes large, the phase and group velocities become infinite on the elementary theory and equal to c_0 on the Rayleigh theory, whereas on the exact theory, they become equal to c_R, the velocity of the Rayleigh surface waves. One interesting feature of the curves is the degree of agreement between the values of c/c_0 and c_g/c_0 given by the exact theory and by the Timoshenko theory, and even when the error is a maximum, i.e., when a/λ is very large, the error of the Timoshenko theory is not excessive, since the limiting values of c/c_0 and c_g/c_0 (when $\sigma = 0.29$) are 0.8763 on the exact theory and 0.8906 on the Timoshenko theory. This feature of the Timoshenko theory justifies its use in dealing with problems, such as the determination of the frequency of lateral vibrations of bars, where the exact theory cannot be employed because of its complexity.

For .....

S. Timoshenko, Phil. Mag., Vol. 41, p.744, (1921)

For the purpose of discussing the propagation of a pulse of flexural vibrations, consider a bar which is stressed initially so that the flexural displacement is zero everywhere except at a certain cross-section where it is infinite; this cross-section will be taken as the origin of x. If the stress is released at time $t' = 0$, the period T_p of the dominant group in the disturbance at a cross-section of abscissa x at time t' can be deduced by group-velocity methods. It is convenient to take the non-dimensional ratio $t'/\frac{1}{2}T_0$ as the independent variable and the non-dimensional ratio T_p/T_a as the dependent variable, t_a and $\frac{1}{2}T_0$ being equal to the times taken by an extensional wave of infinite wave-length to traverse the distances a and x respectively. Since

$$\frac{T_p}{T_a} = \frac{\Delta}{a}\frac{c_0}{c} \quad \text{and} \quad \frac{t'}{\frac{1}{2}T_0} = \frac{c_0}{c_g} \qquad \ldots\ \ldots\ \ldots\ \ldots\ \ldots \qquad (A.10)$$

the values of these non-dimensional variables can be derived from the curves of Figures A.1. and A.2.

The $(T_p/T_a,\ t'/\frac{1}{2}T_0)$ curves deduced in this way are shown in Figure A.3. According to the elementary theory, $T_p/T_a = \lambda^2/\pi a^2$, $t'/\frac{1}{2}T_0 = \frac{\Delta}{\pi a}$; the $(T_p/T_a,\ t'/\frac{1}{2}T_0)$ curve is thus a parabola passing through the point $t'/\frac{1}{2}T_0 = 0$ and symmetrical about the axis of T_p/T_a passing through this point. This implies, as has already been pointed out, that wave-packets consisting of infinitely short waves arrive at the cross-section of abscissa x at the instant at which the disturbance departs from the origin. As a/λ decreases, the values of T_p/T_a and $t'/\frac{1}{2}T_0$ both increase, and for large values of a/λ (outside the range of Figure A.3) the curve given by the elementary theory coincides with the curves given by the more exact theories.

According to the curve given by the Rayleigh theory wave-packets consisting of infinitely short flexural waves take the same time to travel through a given distance as wave-packets composed of infinitely long extensional waves. As T_p/T_a increases (or a/λ decreases) $t'/\frac{1}{2}T_0$ decreases until it reaches a minimum value at $t'/\frac{1}{2}T_0 = 0.92$, when T_p/T_a is about 3 and a/λ is about 0.8; beyond this point $t'/\frac{1}{2}T_0$ decreases as T_p/T_a increases. Thus, according to this theory, when an infinitely intense flexural disturbance initially concentrated at the origin is released, the first components to arrive at a given point do so at time $t' = 0.92\ t_0/2$; their period is about $3T_a$ and their wavelength is about $1.25a$. In the interval between the arrival of these components and time $t' = T_0/2$, two groups of different wavelengths and period arrive simultaneously at each instant; finally when t' exceeds $T_0/2$, only one group arrives at a given instant, the period and the wavelength of the group increasing as t' increases.

Considering the results of the exact theory, it is clear that the faster components, originating in an infinitely intense disturbance at the origin, arrive at the cross-section of abscissa x at time $t' = 1.568\ T_0/2$; the period of these components is $5.29\ T_a$ and their wavelength is equal to $2.7a$. Between this value of t' and $t' = 1.735\ T_0/2$, two groups of different wavelengths and periods arrive simultaneously at each value of t'; at $t' = 1.735\ T_0/2$, the Rayleigh surface waves and waves of period $17.3\ T_a$ arrive simultaneously. When t' exceeds $1.735\ T_0/2$, only one group will arrive at each instant.

It is clear that the elementary theory and the Rayleigh theory give results which are very wide of the truth, and any solutions based on these theories of problems of the action of transient flexural stresses on bars are unlikely to be accurate unless it happens that the disturbances are such that waves of short wavelength are unimportant. Again, it is interesting to notice that the results derived from the Timoshenko theory are in excellent agreement with those deduced from the exact theory.

As far as the present experiment is concerned, the main interest of the curves of Figure A.3. is that they show that, on the exact theory, no flexural displacements will occur at the cross-section of abscissa x until $t' \geqslant 1.568\ T_0/2$, i.e. $t' \geqslant 1.568\ x/c_0$; remembering that the record in a given experiment begins when extensional displacements of infinite wavelengths arrive at the cross-section, i.e. when $t' = T_0/2 = x/c_0$, it follows that displacements due to flexural waves will not appear on the record until a time $0.568\ x/c_0$ after the beginning of the record. For the bar used in this experiment, $x = 670.5$ cm., $c_0 = 5.26 \times 10^5$ cm./sec., so that $0.568\ x/c_0 = 0.725$ millisecond, which is outside the range of time covered by the record.

Best Available Copy

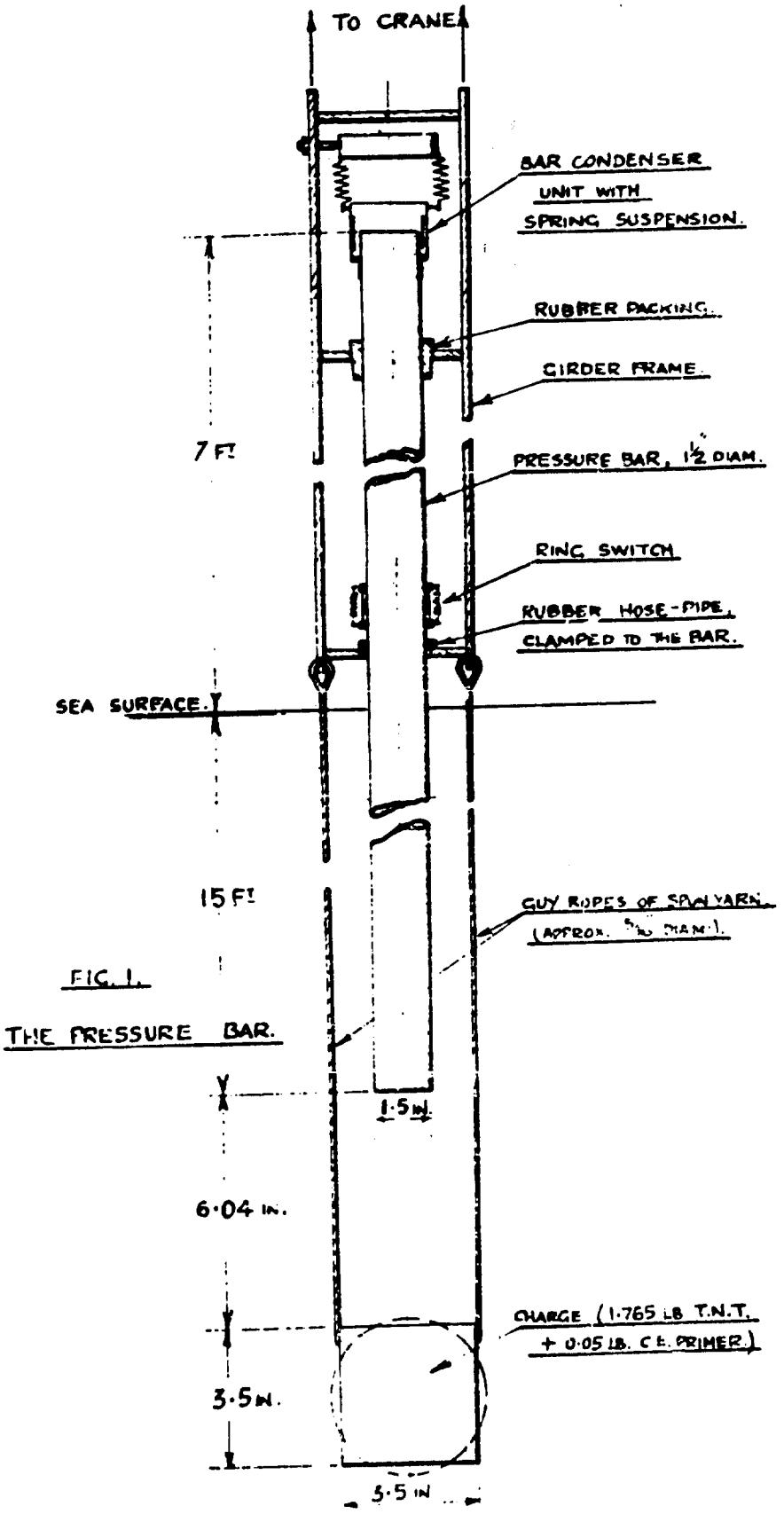


FIG. 1.

THE PRESSURE BAR.

FIG. A.1.

PHASE VELOCITY, c, OF EXTENSIONAL AND FLEXURAL WAVES OF WAVE-LENGTH Λ IN CYLINDRICAL BARS OF RADIUS a.

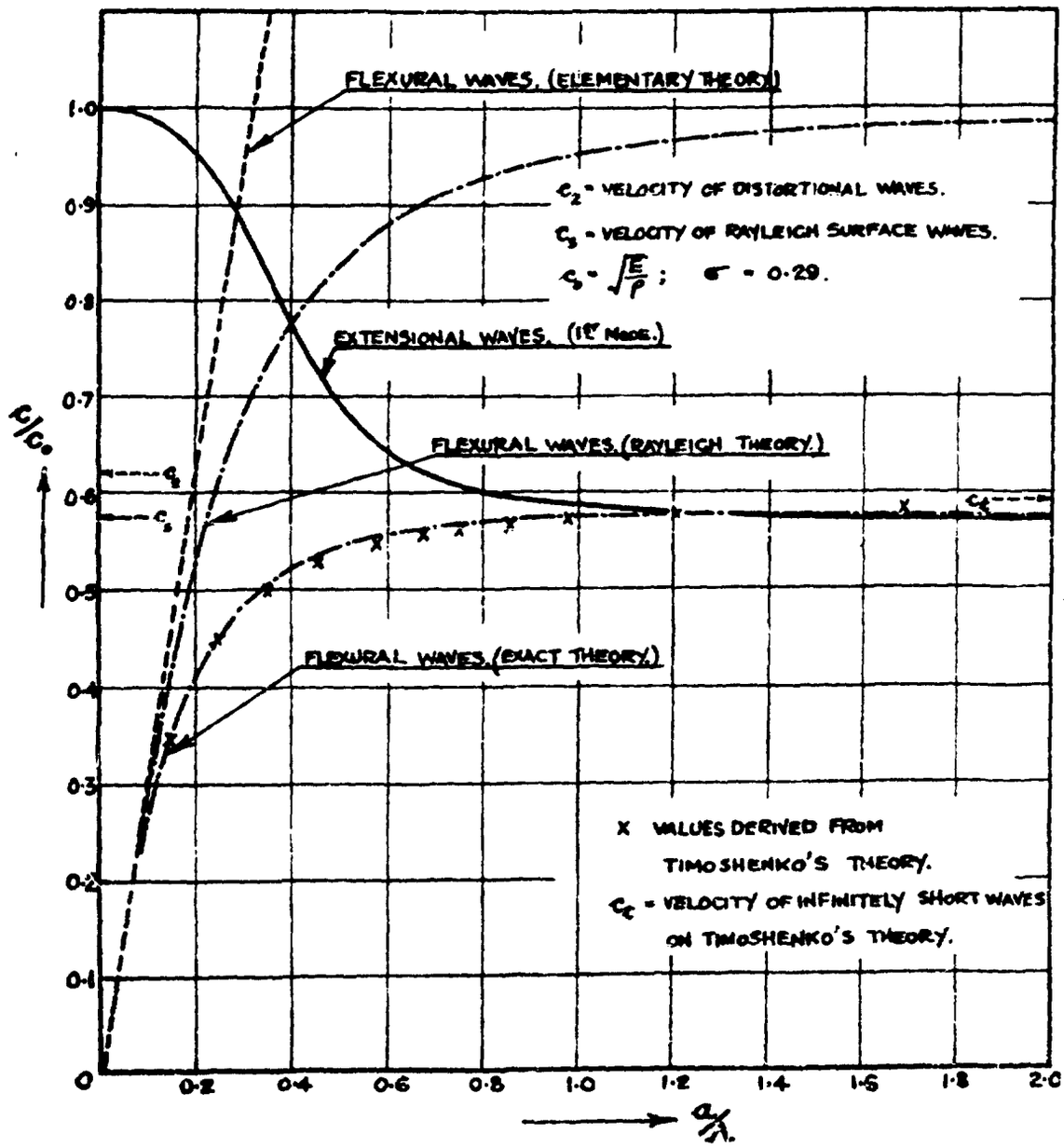


FIG. A.2.

GROUP VELOCITY, c_g, OF EXTENSIONAL AND FLEXURAL WAVES OF WAVELENGTH λ IN CYLINDRICAL BARS OF RADIUS a.

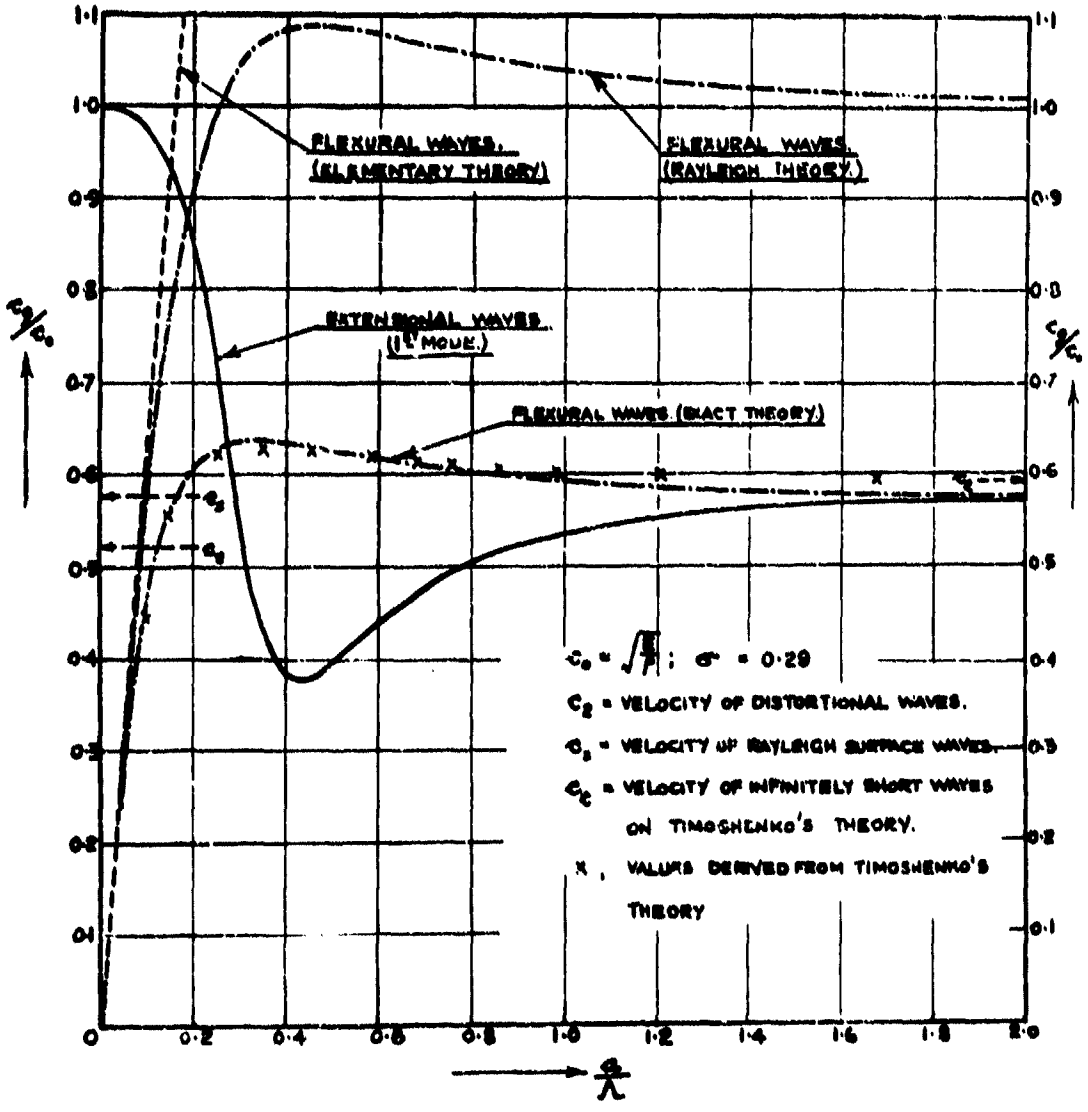
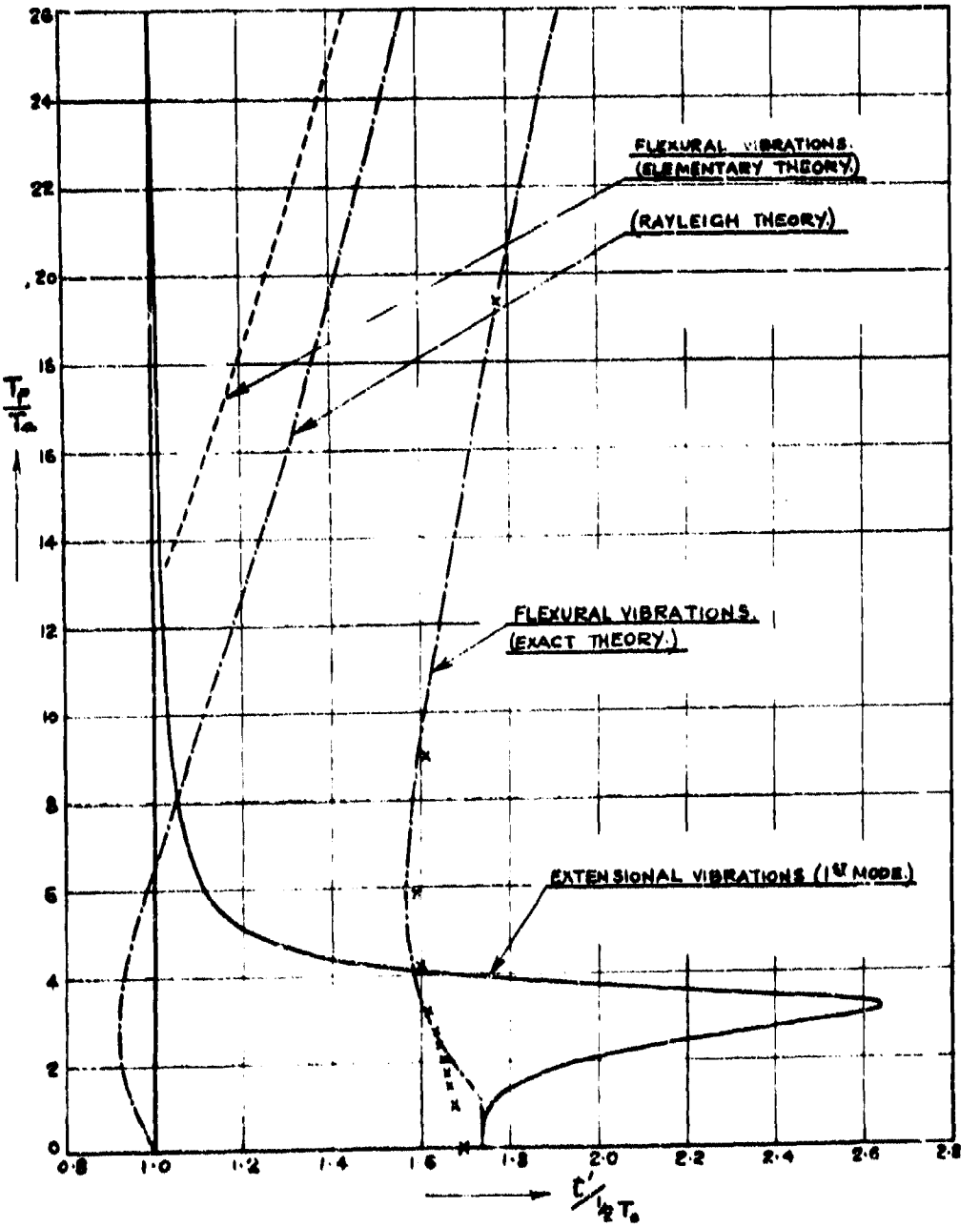


FIG. A.3.

THE PERIODS, T_p, OF THE DOMINANT GROUPS IN A BAR OF LENGTH l, RADIUS a, AT A POINT ABSCISSA x, AT THE TIME t' AFTER THE DEPARTURE OF AN INFINITELY THIN PULSE FROM THE ORIGIN.

$T_a = \frac{2a}{c_0}$; $\frac{1}{2}T_0 = \frac{l}{c_0}$.

X VALUES DERIVED FROM TIMOSHENKO'S THEORY.



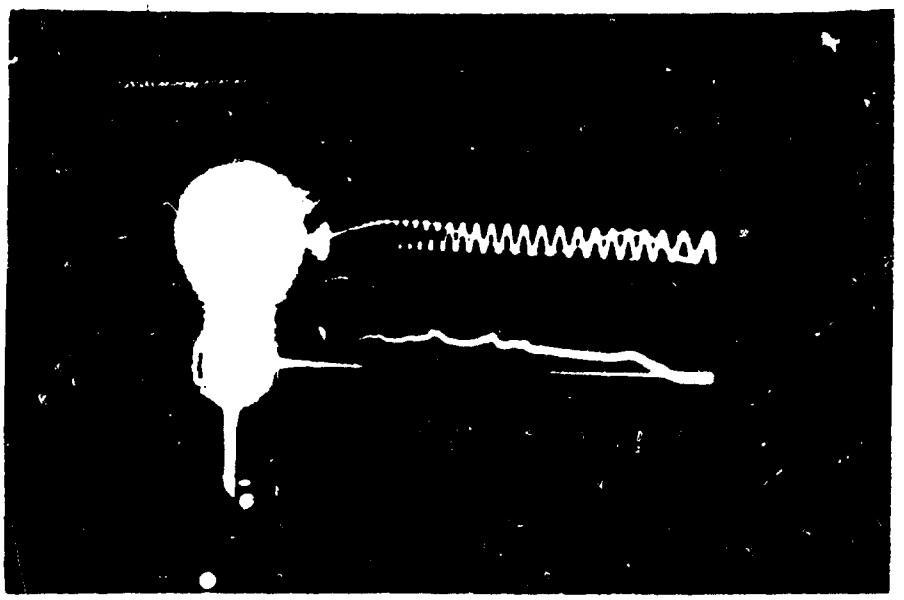


Fig. 2.

Oscillogram of the pulse due to a submarine explosion.

Pressure bar :- length = 22 ft.; diameter = 1½ inch.

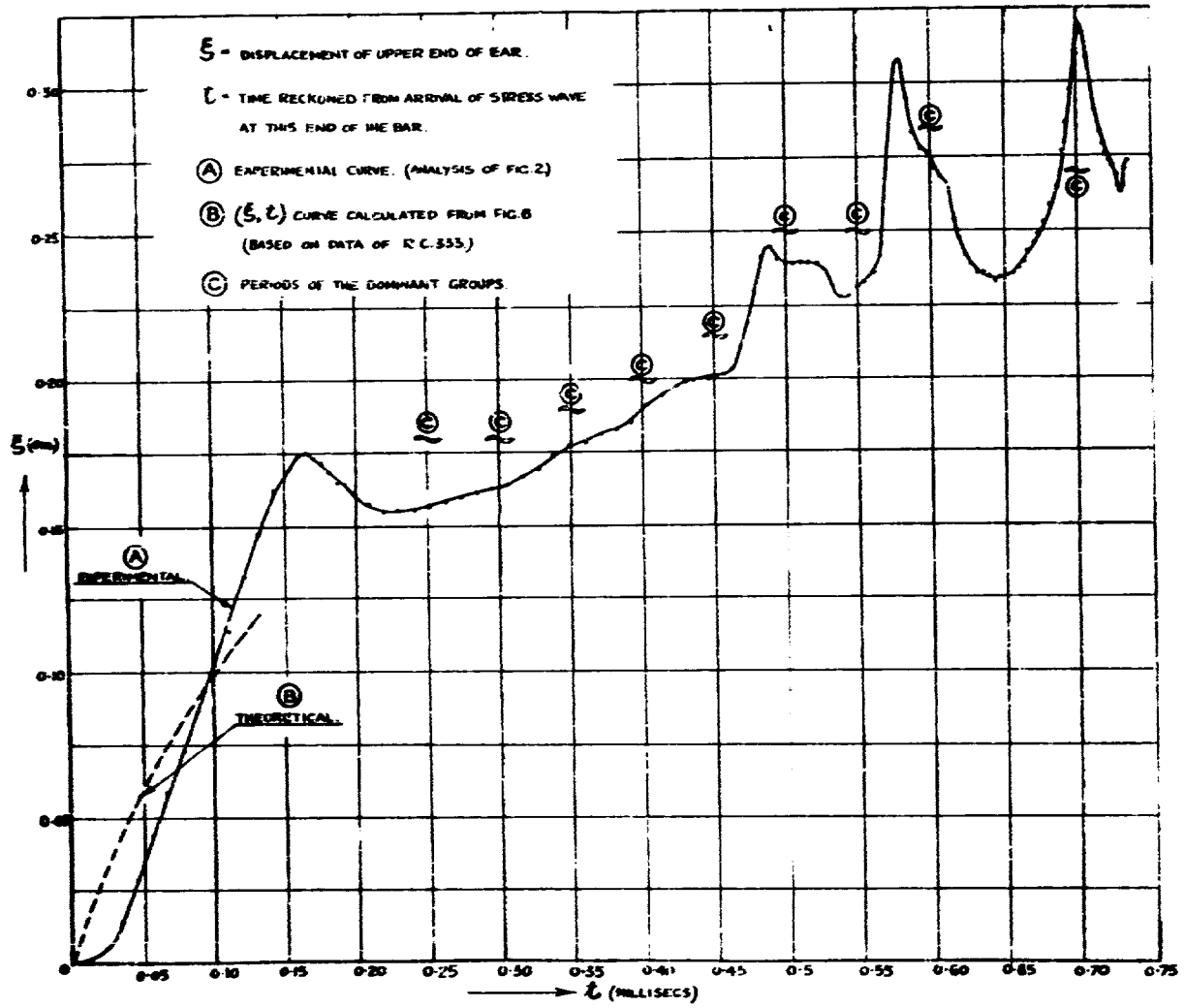
Condenser unit :- cylindrical type, measuring the longitudinal displacement of the end of the bar.

Upper trace :- timing wave of period 0.0525 millisecs.

Lower trace :- amplified p.d. from condenser unit.

FIG. 3.

ANALYSIS OF FIG. 2.



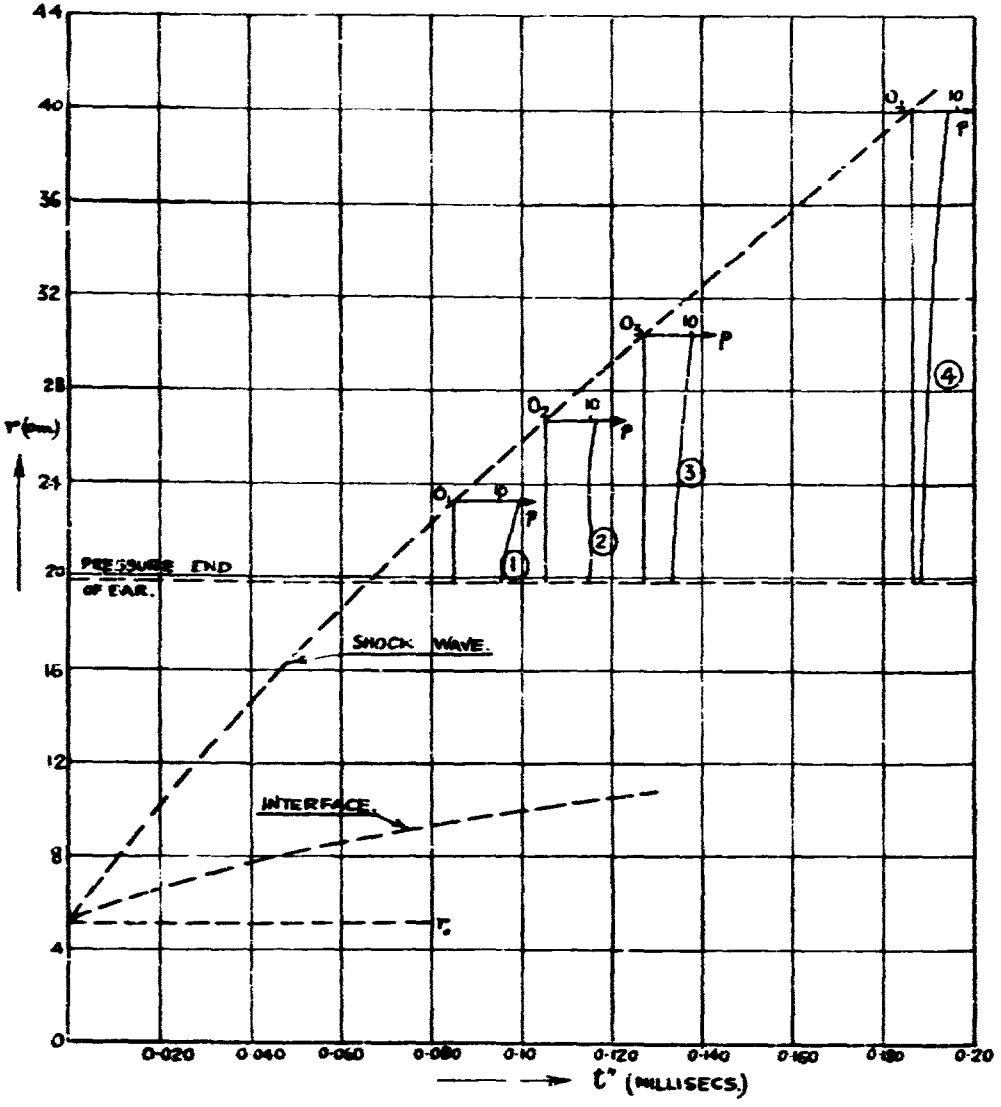


FIG. 4.

THE RELATION BETWEEN THE DISTANCE r" OF THE SHOCK WAVE AND THE GAS-WATER INTERFACE FROM THE CENTRE OF THE CHARGE, AND TIME t" RECKONED FROM THE INSTANT OF DETONATION. (BASED ON R.C 333.)

r_0 = RADIUS OF CHARGE, ASSUMED SPHERICAL.

WEIGHT OF CHARGE, (T.N.T.) = 1·815 LB.

CURVES ① - ④ :- {PRESSURE, DISTANCE}
CURVES FOR t" = 0·085, 0·105, 0·127, AND 0·186 MILLISECS.
PRESSURE, p, IN TONS/SQ. INCH.

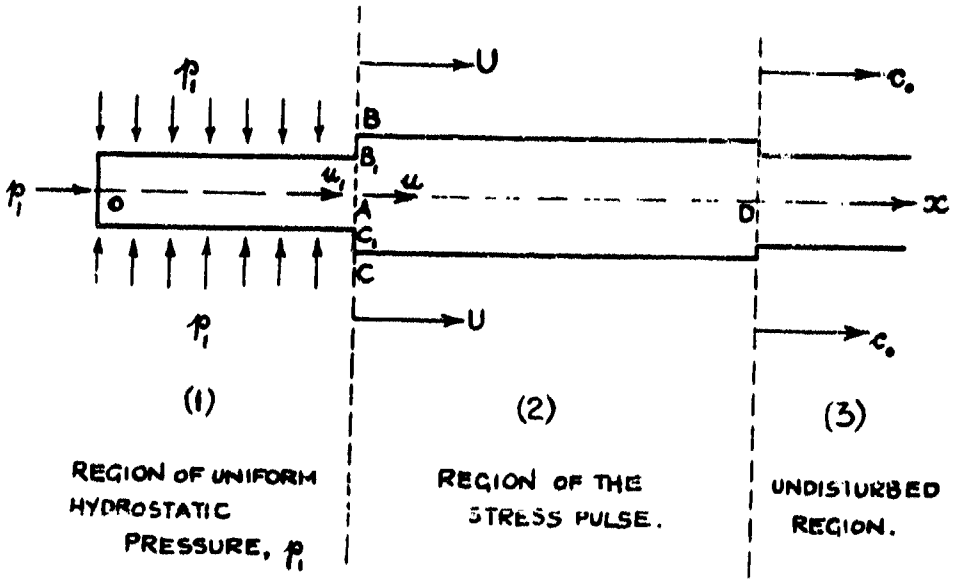


FIG. 5.

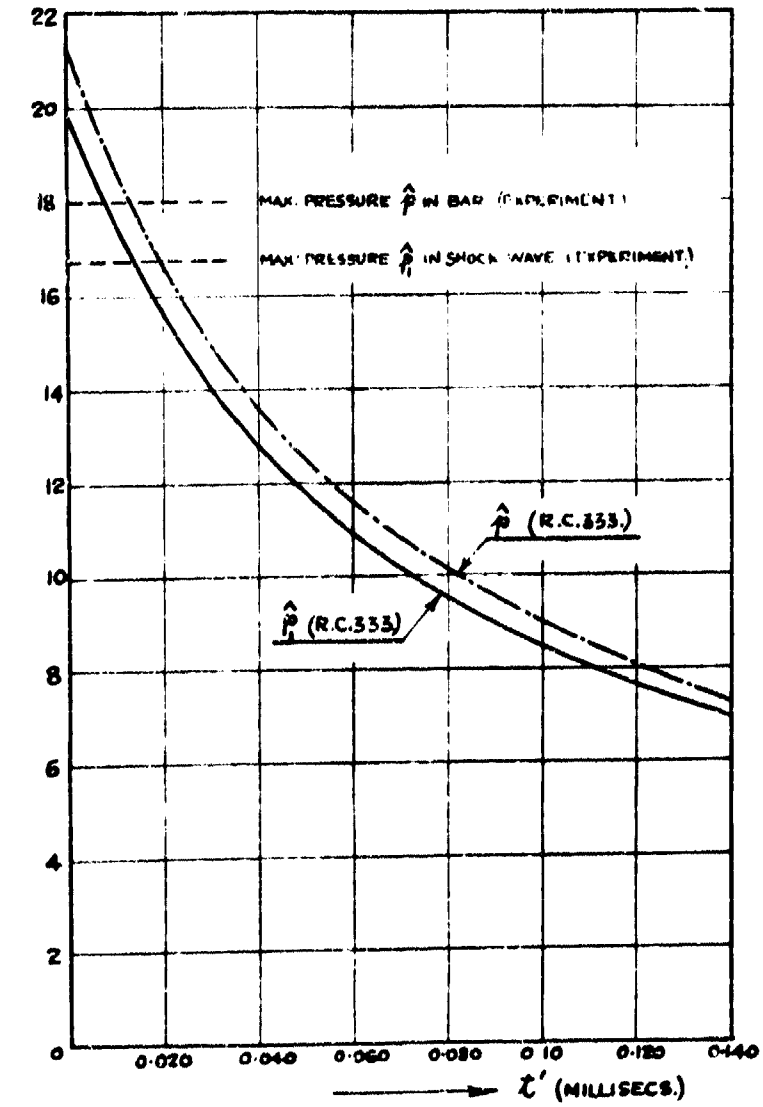
PRESSURE BAR SUBJECTED TO A HYDROSTATIC PRESSURE WHICH TRAVELS ALONG THE BAR WITH UNIFORM VELOCITY U.

FIG. 6.

THE RELATION BETWEEN PRESSURE $\hat{p}$, $\hat{p}_1$ (CALCULATED FROM R.C.333) AND TIME t', RECKONED FROM THE INSTANT OF THE ARRIVAL OF THE SHOCK WAVE AT THE PRESSURE END OF THE BAR.

$\hat{p}_1$ = SHOCK WAVE PRESSURE.

$\hat{p}$ = PRESSURE IN THE STRESS WAVE IN THE PRESSURE BAR. (MAX: VALUES)



INSTRUMENTATION FOR THE MEASUREMENT OF UNDERWATER EXPLOSION PRESSURES

M. A. Greenfield and M. M. Shapiro
David W. Taylor Model Basin

American Contribution

September 1944

TABLE OF CONTENTS

	page
ABSTRACT	1
INTRODUCTION	1
PART 1. GENERAL SPECIFICATIONS	2
EARLIER PIEZOELECTRIC GAGES	3
PART 2. TMB PICKUP ELEMENTS	4
THE TMB QUARTZ GAGE	4
THE TMB TOURMALINE GAGE	7
PRECAUTIONS IN THE USE OF PIEZOELECTRIC GAGES	9
THE TMB RESISTANCE GAGE	10
PART 3. CABLES AND RECORDING CHANNELS	12
TYPES OF DISTORTION OF A GAGE SIGNAL	12
DISTORTIONS DUE TO THE TRANSMISSION LINE	12
DISTORTIONS DUE TO MECHANICAL DISTURBANCE OF THE CABLE	18
DISTORTION DUE TO INSUFFICIENT TIME CONSTANT	24
DISTORTIONS DUE TO FREQUENCY RESPONSE OF AMPLIFIERS	27
THE TMB RECORDING CHANNEL	32
PART 4. CALIBRATION OF THE PRESSURE GAGES	33
PRESSURE APPARATUS	34
CIRCUITS FOR MEASURING THE OUTPUT OF THE GAGES	34
CALIBRATION OF THE PIEZOELECTRIC GAGES	34
Oscillographic Recording	36
Quadrant Electrometer	38
Microcoulometer	39
Program for Further Piezoelectric Calibration Studies	40
CALIBRATION OF THE GLASS RESISTANCE GAGE	41
PART 5. GAGE PERFORMANCE IN TESTS	41
UNDERWATER EXPLOSION TESTING	41
PRESSURES IN OPEN WATER	42
PRESSURES AT A SURFACE OF AN UNDERWATER STRUCTURE	44
USE OF THE TOURMALINE GAGE IN STUDYING A SLOWER PRESSURE CHANGE	45
REFERENCES	47
APPENDIX - CONSTRUCTION OF THE QUARTZ PIEZOELECTRIC GAGE	49
DESCRIPTION OF THE PRINCIPAL PARTS	49
ASSEMBLY OF THE GAGE	50
STATIC TESTING OF THE GAGE	51
SURFACE-PRESSURE MODIFICATION OF THE QUARTZ GAGE	51

INSTRUMENTATION FOR THE MEASUREMENT OF UNDERWATER EXPLOSION PRESSURES

ABSTRACT

The David Taylor Model Basin, in its efforts to provide instruments for the measurement of underwater explosion pressures, has developed three pressure gages, two of the piezoelectric and one of the resistance type. The construction and operation of the gages are described in detail.

The most important causes of distortion of a gage signal are analyzed, and the measures taken to overcome them are described. In particular the mechanical disturbance of a gage cable by an underwater explosion gives rise to a spurious signal which is large when ordinary coaxial cables are used. An investigation of this effect has resulted in the development of a coaxial cable which has many advantages over any other type that was investigated, and which permits accurate measurements of momentum.

Several techniques for calibrating the various gages are discussed. The best of these methods gives results which agree closely with those obtained by workers in other laboratories.

The gages were subjected to explosion tests with charges of about one ounce of tetryl, in which pressure-time records were obtained. Only the tourmaline gage has been tested with larger charges, of 100 grams or more. These tests yield records which exhibit a high degree of reproducibility.

INTRODUCTION

When intensive research into the fundamentals of underwater explosion phenomena was started in the United States less than four years ago, one of the first problems encountered was to find a satisfactory gage for measuring the high-intensity short-duration pressures in the water.

A number of gages had been developed by previous experimenters in this field, some of them mechanical and some electrical, but none of them were satisfactory for the new work being undertaken. Mechanical gages such as the Hilliar gage (1) (2)* were not fast enough to indicate the rate of rise and the peak pressures accurately, and the piezoelectric tourmaline crystal gage suggested by Sir J.J. Thomson (3) and used by Keys (4) was, like the Hilliar gage, so large that it was suitable only for work with large or service charges.

The rapid progress which had been made in the development of electronic instruments in the decade preceding 1940 suggested the use of some

---

* Numbers in parentheses indicate references on page 47 of this report.

PRECEDING PAGE BLANK

sort of electrical gage with oscillographic recording. Studies made with various types of electrical gages demonstrated that, at least for the small charges being used in the new series of experiments, the gage had likewise to be small in physical dimensions.

In view of the importance of the project and the necessity for devising an accurate and satisfactory gage before much real progress could be made on the research program, a number of different agencies began work on gages and carried it along simultaneously until all were satisfied that the desired result had been achieved. This is a case where duplication of effort, if it may be called by that name, was not only justifiable but necessary.

The David Taylor Model Basin was one of the agencies which engaged in this program of development. This report has been prepared to give an outline of the history of the project and a rather complete description of the results as they stand to the time of writing. All of the work in question has been done with electrical gages; two of the final designs are of the piezoelectric type and one is of the electrical resistance type.

For the convenience of the reader, the report is divided into five parts, giving first the general specifications for the gages, then in turn describing the pickup or sensitive elements and the cables and recording channels. The manner of calibrating the gages is described, and the report concludes with a description of the performance of the various designs during laboratory and field tests.

PART 1. GENERAL SPECIFICATIONS

The pressure of a shock wave resulting from the underwater detonation of a small charge of high explosive reaches its peak value in less than a microsecond (1×10^{-6} second); this peak value may be several thousand pounds per square inch. For explosive charges less than 1 pound, the duration* of the pressure wave is less than 70 microseconds. The characteristics of a typical wave are shown in Figure 1.

The pickup has to follow the pressure variations occurring in this time interval, and the period of its lowest mode of vibration must be small compared to the duration. For example, if this period is required to be less than 1/10 the duration, then the fundamental frequency of the pickup must exceed 1.5×10^5 cycles per second. This in turn means that none of the physical dimensions of the pickup may exceed about 1/2 inch.** The frequency

---

* The duration is defined as the time required for the pressure to drop to $1/e$, or 36.8 per cent of its peak amplitude.

** For example, at the lowest mode a freely suspended steel disk 0.25 inch thick and 0.8 inch in diameter vibrates at a frequency of approximately 1.5×10^5 cycles per second.

should in fact be even higher than 1.5×10^5 cycles per second to prevent the pickup from overshooting the peak pressure.

The pickup must be free of hysteresis and have good mechanical properties. It must not be brittle or have a low tensile strength or be soluble in fresh or sea water. It must operate without permanent deformations and it must respond linearly to the pressure.

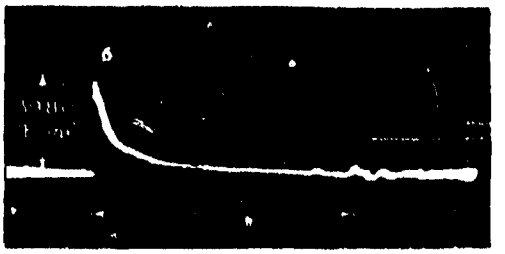


Figure 1 - Typical Pressure Record from an Underwater Explosion

This record was obtained by a tourmaline gage supplied by the Underwater Explosives Research Laboratory at Woods Hole; the charge was 150 grams of tetryl at 3 feet from the gage.

Finally, some way must be provided for transforming the mechanical variations of the pickup dimensions into electrical variations of voltage so that a record can be obtained with a cathode-ray oscillograph.

Both high- and low-impedance pickups were developed, to provide a check on the validity of the pressure measurements. The two types supplement each other, as will be discussed later in greater detail.

EARLIER PIEZOELECTRIC GAGES

Before the TMB gages and the manner in which they fulfill these requirements are described, the background of development should be filled in somewhat more completely than was done in the Introduction. As mentioned there, Sir J.J. Thomson was probably the first to suggest the use of piezoelectricity for the measurement of explosion pressures. An early form of piezoelectric manometer was devised by Keys, who used a dozen tourmaline crystals mounted in mosaic fashion inside a brass pressure vessel 6 inches in diameter. So large a voltage was developed by these crystals that the output could be impressed directly on the deflection plates of a cathode-ray oscillograph; no prior amplification was necessary.

A more recent and much smaller tourmaline crystal pressure gage was devised by Professor E.B. Wilson, Jr., and developed in collaboration with Dr. R.H. Cole of the Underwater Explosives Research Laboratory at the Woods Hole Oceanographic Institution, Woods Hole, Massachusetts (5). It consists of a single tourmaline crystal in the form of a thin plate, with two copper-plated faces or electrodes to which the cable leads are soldered. The pickup is insulated from the water by a thin protective coating, usually of Bostik cement. Typical overall dimensions of the crystal are about 0.6 inch by 0.3 inch by 0.08 inch. A shielded, rubber-insulated Belden cable connects the pickup to the amplifier.

Because the crystal is small, the output must be amplified before it is fed into a cathode-ray tube. However, this gage has the advantage that it can be used to study explosions of charges smaller than those required with the Keys type of gage.

PART 2. TMB PICKUP ELEMENTS

Two materials which satisfy all of the specified requirements for a high-impedance pickup are quartz and tourmaline crystals. Their piezoelectric properties are described in detail in References (6) to (14).

Quartz crystals have been used in the measurement of rapidly changing pressures in internal combustion engines (15). More recently the Naval Ordnance Laboratory has been developing a quartz indicator for the measurement of underwater explosion pressures (16). The two types of Taylor Model Basin piezoelectric gages use quartz and tourmaline, respectively.

THE TMB QUARTZ GAGE

When an "X-cut" plate of quartz* is subjected to a compressional force normal to its parallel faces, equal and opposite charges proportional to the force appear at these faces. Quartz is not sensitive to isotropic pressure and a quartz crystal forming the sensitive element of a pressure gage must be housed in a case so that the pressure will act only on the faces perpendicular to the electric axis. Quartz plates have been subjected to pressures up to 50,000 pounds per square inch in a testing machine, and the relationship between charge and pressure has been found to be linear over this full range (17).

The present TMB quartz gage has passed through several stages in its evolution. The earliest form had a large crystal and a plastic housing; a subsequent model used a double crystal and a brass housing; the gage described in this report is considerably smaller than the previous models and is of the single-crystal type. The techniques applied in the construction and assembly of a quartz gage at the Taylor Model Basin are described in the Appendix.

An idea of the progressive reduction in size, to obtain a high natural frequency of vibration for the quartz-mount system, is presented in Figure 2. In its present form the pickup element consists of a cylindrical quartz crystal 1/16 inch thick and 1/4 inch in diameter, housed in a brass cylindrical mount 7/32 inch high and 1/2 inch in diameter; see Figure 3. A brass tube, integral with this cylinder, contains the wire conductor attached

* A plate of quartz is said to be "X-cut" if its plane is perpendicular to an electric axis of the crystal.

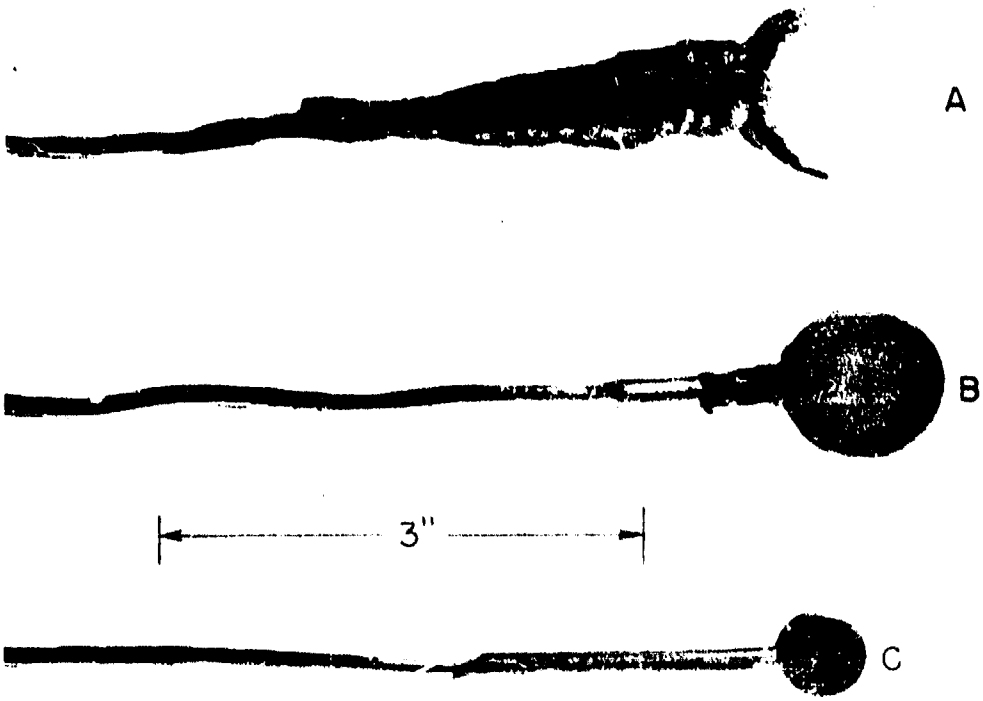


Figure 2 - Three Stages in the Evolution of the TMB Quartz Pressure Gage

A is an early model with plastic mount;
B is a double-crystal model with brass mount; and
C is a single-crystal model, shown in greater detail in Figure 3.
All three of the gages are reproduced here in approximately their natural size.

to one electrode on the quartz; the other side of the crystal is grounded to the mount. The brass tube is soldered to a long copper tube which serves as a cable.

The sensitivity of the pickup is determined by the area of the crystal and its total capacitance, the distributed cable capacitance, and any lumped capacitance that may be added. The output of the quartz crystal used is approximately

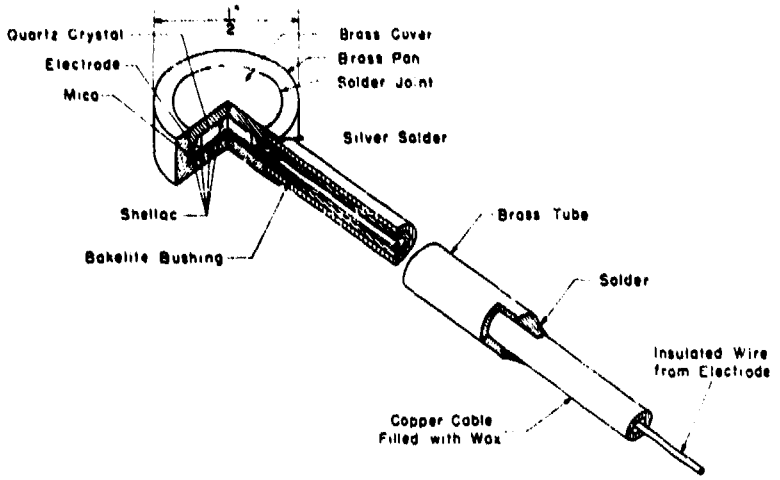


Figure 3 - Components of the TMB Quartz Piezoelectric Gage

The brass housing consists of three parts: a "pan" which contains the crystal; a cover; and a brass tube which is silver-soldered to the pan. A cylindrical, X-cut quartz crystal is cemented on one side to an electrode consisting of a thin copper disk, and on the other to the cover of the brass housing, through which it is grounded. The use of a copper disk for the electrode obviates the trouble of electroplating. Laterally the crystal is surrounded by an air gap which is required because quartz is insensitive to isotropic pressure. It is the need for this air gap which makes a housing necessary.

$$\frac{\Delta Q}{\Delta P} = KA = 5 \times 10^{-13} \ \frac{\text{coulombs}}{\text{pounds per square inch}}$$

where ΔQ is the charge produced, in coulombs,

ΔP is the pressure applied, in pounds per square inch,

K is the piezoelectric constant for quartz, about 1.03×10^{-11} coulombs per pound, and

A is the area of one side of the crystal, in square inches.

If a capacitance of 5000 micromicrofarads is used with a crystal 0.05 square inch in area, the voltage sensitivity is

$$\frac{KA}{C} = \frac{\Delta V}{\Delta P} = \frac{5 \times 10^{-13}}{5 \times 10^{-9}} \ \frac{\text{volt}}{\text{pounds per square inch}} = 10^{-4} \ \frac{\text{volt}}{\text{pounds per square inch}}$$

For a pressure of 4000 pounds per square inch the signal ΔV is 0.4 volt. The voltage variation across the capacitance is led through an amplifier into the input of a cathode-ray oscillograph. Then the record produced on the fluorescent screen can be photographed.

In any quartz gage intended for work under water, it is essential to have a watertight mount which will provide an air gap surrounding the lateral surface of the crystal. Rapid leakage of charge between the two electrodes must also be prevented. The leakage resistance of the TMB piezoelectric quartz gages is usually several thousand megohms.

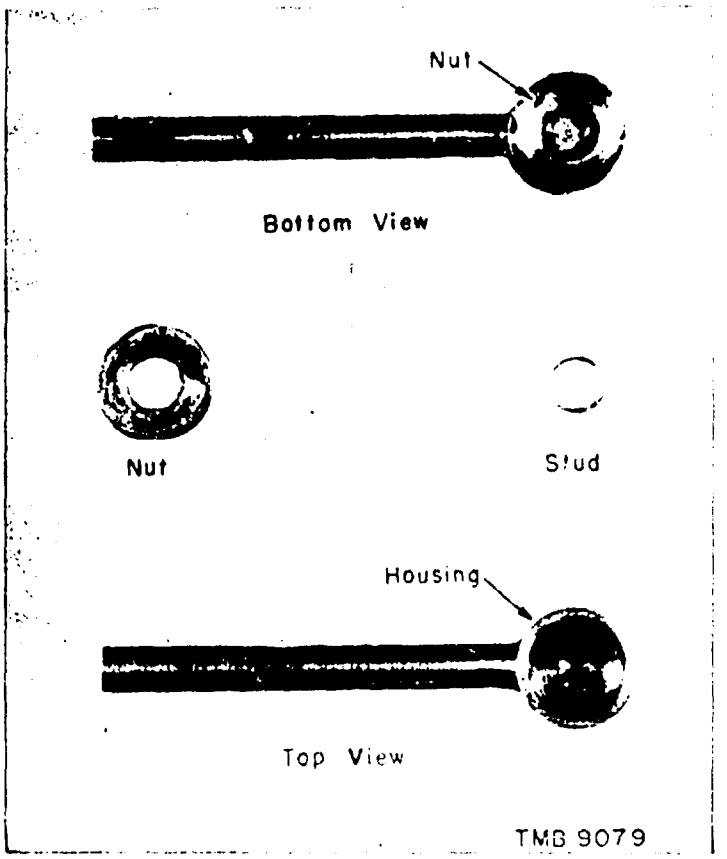


Figure 4 - Modification of Quartz Gage for Attachment to a Surface

A nut is soldered to the bottom of the housing, and a threaded stud is soldered to the surface at which the pressure is to be measured.

The brass housing of the quartz gage lends it great durability, and thus the gage will last for a very large number of explosions. This advantage is offset by the vibrations set up in the quartz mount when the gage is subjected to explosions. The observed frequency of the mount is of the order of 7×10^4 cycles per second, not high enough to prevent the introduction of an error in the determination of the peak pressure. A quartz gage of modified design which should possess a considerably higher natural frequency is under construction at the Taylor Model Basin.

The quartz mount can be readily adapted to the measurement of explosion pressures at the surface of an underwater structure. This is accomplished by silver-soldering a nut to the bottom of the mount, and attaching a threaded stud to the surface in question; see Figure 4.

THE TMB TOURMALINE GAGE

The TMB form of tourmaline pressure gage differs from the one developed by the Underwater Explosives Research Laboratory at Woods Hole chiefly

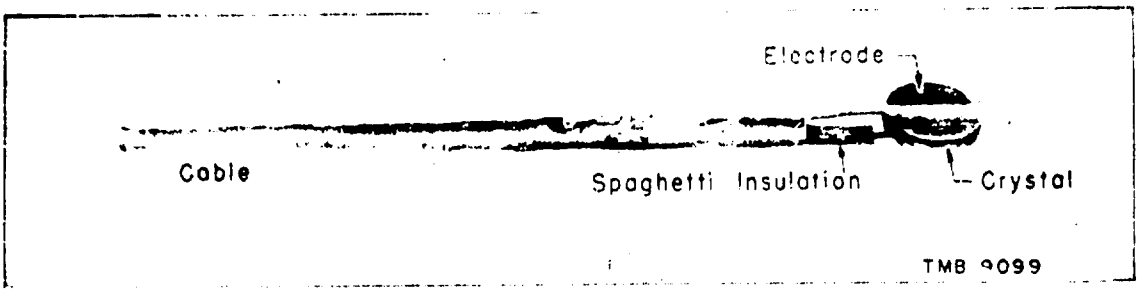


Figure 5a

This is a view of the gage element before the rubber coating is molded around the crystal.

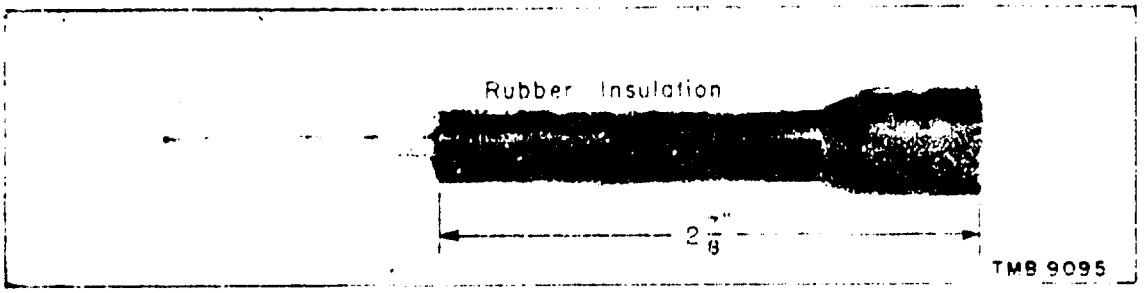


Figure 5b

This is a view of the completed gage.

Figure 5 - TMB Tourmaline Gage for Determining Underwater Explosion Pressures

in the type of insulation and cable employed. The construction of this gage and of a TMB copper cable have been described in detail elsewhere (18); they are shown here in the photographs, Figures 5a and 5b. Tourmaline is sensitive to isotropic pressure and therefore requires no mount. Thus the frequency of the lowest mode of vibration of the tourmaline gage is much greater than that of the quartz gage. The crystals employed have approximately the same area and sensitivity as the quartz crystals. The tourmaline crystals are insulated by molding a sheath of rubber with a low sulphur content about the crystal and that part of the cable to which it is attached.

A modified form of this gage has been used to obtain load-time records at a surface of an underwater structure exposed to explosive loading. The rubber insulation is not only molded about the crystal and the copper cable but also to a brass plate; see Figure 6. This plate is then bolted to the structure. The structure must be heavy enough to be unaffected in its deformation or its motion by the screws or by the weight of the brass plate. Pressure records obtained in this manner are compared with "open-water" records later in this report.

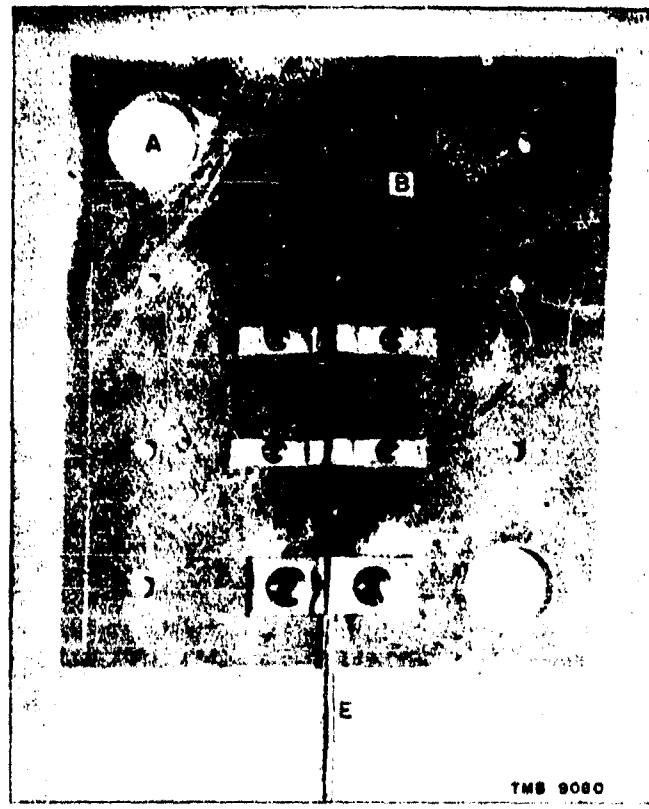


Figure 6 - Adaptation of Tourmaline Gage to Surface Pressure Measurements

A. Hole for alignment of brass plate with mold
B. Rubber insulation surrounding tourmaline crystal
C. Drilled hole to admit bolt for attaching brass plate to structure
D. Clamp to secure gage in cavity of brass plate
E. Wax-filled cable of copper tubing

In use, the entire assembly is bolted to the facing plate of the structure being tested.

PRECAUTIONS IN THE USE OF PIEZOELECTRIC GAGES

Inasmuch as piezoelectric gages are high-impedance sources, certain precautions must be taken in their use. If the cable leading from the pickup to the amplifier input is too long, then it acts as a transmission line with attendant frequency distortion of the signal. This is due to the fact that the high impedance of the gage does not match the low surge impedance of the cable; the latter is generally less than 100 ohms. This will be discussed in greater detail in the section headed "Cables and Recording Channels," pages 12 to 18.

The time constant of the gage is defined as the product of the total capacitance in parallel with the gage and the input resistance of the amplifier into which the gage output is sent. It is necessary that piezoelectric gages have a large time constant compared to the duration of the pressure under study. If the time constant is not sufficiently large, the signal will leak through the input resistance of the amplifier and will acquire a corresponding distortion; see pages 24 to 27, inclusive, for detailed calculations which provide practical criteria for the magnitude of the time constant needed.

Care must be exercised in the selection of a cable for piezoelectric pickup elements. It was found in the Taylor Model Basin tests that most cables, when subjected to an explosion, generate a signal of their own which has a low amplitude and long duration compared to the true signal. If the cable signal is not removed, measurements of momentum in the pressure field are particularly unreliable. A comparison of the signals produced by various cables is given in the section beginning on page 12. The cable finally selected (18) consists of an annealed copper tube with an outside diameter of 1/8 inch and a wall thickness of 1/32 inch. The central conductor is a Number 20 or Number 24 copper wire insulated with enamel and a double layer of glass fiber.* The space between the central conductor and the wall of the copper tube is filled with ceresin or paraffin. The wax prevents vibration of the central conductor inside the copper tube when the pressure pulse from an explosion strikes the cable.

THE TMB RESISTANCE GAGE

It was felt desirable to supplement the piezoelectric gages with a gage of the low-impedance type of approximately 100 ohms. Such a gage is particularly convenient if a very long line is required between the pickup element and the amplifier, or if a signal of long duration is to be studied. Since the impedance of the gage matches the surge impedance of the cable, there is no frequency distortion of the signal by the cable no matter how great its length.

The principle upon which the resistance gage operates is that its ohmic resistance changes when the pickup element is subjected to pressure. This change in resistance affects the current in a ballast circuit. The corresponding variation in voltage across part of the ballast resistance is recorded by the cathode-ray oscillograph. It is evident that insofar as the pickup element is concerned, there is no limitation on the maximum duration

* This wire is manufactured by the Anaconda Wire and Cable Company under the trade name of DVE wire. "DVE" wire signifies double vitrotex enameled.

of signal that may be studied. The low impedance of the pickup also serves to eliminate cable signal.

An early form of a resistance gage, constructed at the Massachusetts Institute of Technology, consisted of a 250- or 500-ohm resistor* imbedded in a rubber sheath. The pressure changed the average distance between the carbon particles on the glass tube in the resistor, thus producing a change in resistance. This gage was found to be fairly sensitive when connected to a 1500-ohm ballast resistance in series with a 45-volt battery; the voltage sensitivity was then about $5 \times 10^{-6} \frac{\text{volts}}{\text{pounds per square inch}}$, of the same order of magnitude as the sensitivity of a piezoelectric pickup.

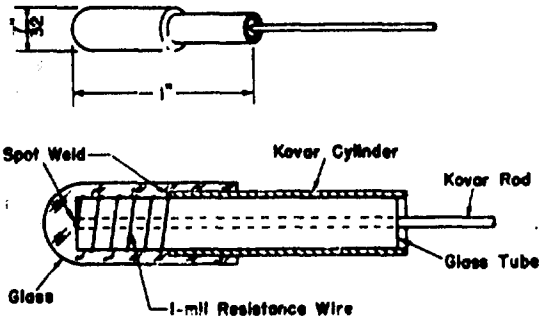


Figure 7 - Glass Resistance-Type Pickup

In the upper diagram the gage is shown in its natural size. The element is made of 705 glass as manufactured by the Corning Glass Company. Kovar is used for the metal parts because it has the same coefficient of expansion as glass over a large range of temperatures. The Kovar rod is slipped into a glass tube, and the tube is put into a Kovar cylinder. 1-mil Advance wire is then wrapped about the glass tube and the two ends of the wire are spot-welded to the Kovar wire and cylinder, respectively. A small glass tube is then slipped over the end of the assembly at which the Advance wire is spot-welded to the rod. The entire unit is heated with an oxygen-hydrogen torch until the glass parts and the Kovar are fused into an integral unit. After the element is annealed it is ready to be assembled on a cable.

However, these resistor gages showed high hysteresis. The calibrations of some of them varied by as much as 20 to 50 per cent after the element had been exposed to a number of explosions.

A gage was then developed at the Taylor Model Basin, which is elastic and which shows little hysteresis in the range of pressures encountered in underwater explosions. This gage consists of a glass element in which approximately 100 ohms of 1-mil Advance wire is imbedded; see Figure 7. The ends of this fine wire are spot-welded to a cylinder and a rod of an alloy which has equal thermal expansion with the glass, known by the trade name of Kovar. The overall dimensions of the glass element are about 1 inch by 7/32 inch. The Kovar cylinder and rod are set coaxially to prevent electrical leakage between them through the water. These elements can be calibrated in a static pressure chamber by measuring their resistance change with a Wheatstone bridge for a given applied pressure. They possess linear calibrations and show little hysteresis.

This resistance gage has the disadvantage of very low sensitivity compared to the piezoelectric gages. When a 100-ohm resistance element in

* As manufactured by the International Resistance Company.

series with a 100-ohm ballast resistor and four 6-volt storage batteries is subjected to a pressure of 3000 pounds per square inch, the voltage across the element changes by 5 millivolts. Furthermore, the gages are fragile compared to the piezoelectric elements and they seldom withstand more than half a dozen explosions.

When long lines and signals of long duration are encountered, it is desirable to use the resistance element as a check on the piezoelectric gages. The resistance gage may also be useful in determining whether or not cable signal has been eliminated from a piezoelectric gage; this is particularly important in the case of explosions of large charges. Long lines are then used so that the operating personnel and the amplifiers will be at a safe distance. Thus successive parts of the cable are subjected to the pressure wave over a relatively long period of time; i.e., the time required for sound in water to traverse the cable length. If any signal resulted from this pressure on the cable, the tail of the true pressure curve would be obscured. The resistance element should show no cable signal under these circumstances. This is important particularly if the momentum as well as the peak pressure in the pressure pulse is being investigated.

At the time of writing, the resistance element is not sufficiently rugged to be used as a field gage.

The sensitivity of the glass elements to pressure changes varies from 1.4 to 1.8×10^{-7} $\frac{1}{\text{pounds per square inch}}$. It is interesting to note that the compressibilities of various types of glass range from about 1 to 2×10^{-7} $\frac{1}{\text{pounds per square inch}}$.

PART 3. CABLES AND RECORDING CHANNELS

TYPES OF DISTORTION OF A GAGE SIGNAL

It has been mentioned in Part 2 that a long cable will act as a transmission line. Thus a signal propagated by such a cable will at a given instant possess different phases at different points along the line. This may give rise to distortion of the gage signal. Moreover, there are other causes of signal distortion, such as mechanical disturbance of the cable, insufficiently large time constant of the circuit, and inadequate frequency response of the amplifiers. These will be discussed in turn.

DISTORTIONS DUE TO THE TRANSMISSION LINE

The usual equations (19) describing a transmission line are included here for the reader's convenience.

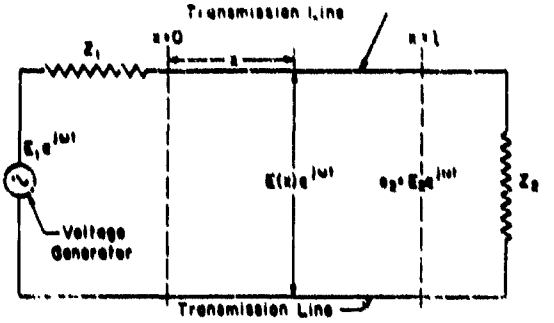


Figure 8 - Schematic Diagram of a Transmission Line Circuit

In Figure 8 $E_1 e^{j\omega t}$ is the voltage produced by a generator,

Z_1 is the impedance of the generator,

x is a distance along the transmission line, varying from 0 to l,

$E(x)e^{j\omega t}$ is the voltage at x between the pair of conductors which constitute the transmission line,

Z is the combined impedance of the resistances, inductances, and capacitances as used in particular cases,

$e_2 = E_2 e^{j\omega t}$ is $E(l)e^{j\omega t}$, the output voltage,

Z_2 is the terminating impedance, and

ω is the frequency of the impressed voltage, in radians per second.

These quantities are related by the equation

$$E(x) = \frac{Z_0 E_1 \left[\epsilon^{\alpha(l-x)} + r_2 \epsilon^{-\alpha(l-x)}\right]}{\left[Z_1 + Z_0\right]\left[\epsilon^{\alpha l} - r_1 r_2 \epsilon^{-\alpha l}\right]} \qquad [1]$$

where $Z_0 = \sqrt{\frac{R + jL\omega}{G + jC\omega}}$ is the surge impedance of the cable, defined as that impedance which must terminate both ends of a dissipationless line to make it a distortionless line,

R is the resistance per unit length of the line, with both conductors in series,

G is the leakage conductance from one conductor to the other, per unit length,

L is the distributed inductance per unit length,

C is the distributed capacitance per unit length,

$\alpha = \sqrt{(R + jL\omega)(G + jC\omega)}$ is the propagation function of the line,

$$r_1 = \frac{Z_1 - Z_0}{Z_1 + Z_0} \quad \text{and}$$

$$r_2 = \frac{Z_2 - Z_0}{Z_2 + Z_0}$$

It is the quantity $E(l)$ which is equal to E_2 that is important. This represents the output voltage of the cable and therefore the input voltage for the amplifiers.

$$E_2 = \frac{E_1 Z_0 (1 + r_2)}{(Z_1 + Z_0)(\epsilon^{\alpha l} - r_1 r_2 \epsilon^{-\alpha l})} \qquad [2]$$

The assumption will now be made that the line has no dissipation; i.e., $R = G = 0$.* Since C is approximately 40×10^{-12} farad per foot, G is unimportant above 20 or 30 cycles per second. The approximation is not as good for R since this quantity is approximately 0.01 ohm per foot for Number 20 copper wire, while L is approximately 1.2×10^{-7} henry per foot. However, good agreement with experiment is obtained even when R is neglected. This approximation simplifies the equation considerably.

$$\alpha = j\omega\sqrt{LC}; \quad Z_0 = \sqrt{\frac{L}{C}} \qquad [3]$$

Z_0 is now a pure resistance.

$$E_2 = \frac{E_1 Z_0 (1 + r_2)}{\left(Z_1 + Z_0\right)\left(\epsilon^{j\omega l\sqrt{LC}} - r_1 r_2 \epsilon^{-j\omega l\sqrt{LC}}\right)} \qquad [4]$$

It is to be noted that even for a dissipationless line there will be frequency distortion; i.e., E_2 is still a function of the frequency $\omega/2\pi$. However, if the line were terminated at both ends by impedances equal to the surge impedance, i.e., if $Z_1 = Z_2 = Z_0$, then $r_1 = r_2 = 0$.

$$E_2 = \frac{E_1}{2} \epsilon^{-j\omega l\sqrt{LC}} \qquad [5]$$

and

$$e_1 = E_2 \epsilon^{j\omega t} = \frac{E_1}{2} \epsilon^{j\omega(t - l\sqrt{LC})} \qquad [6]$$

The amplitude is now independent of the frequency, while the phase is altered only by having a constant subtracted from the time. Thus if the dissipationless line is terminated by its surge impedance, it becomes a

* $G \leqq 10^{-11}$ mho per foot for the cables used.

distortionless transmission system. It may be noted that the phase of the original signal has been altered by subtracting a constant time, $l\sqrt{LC}$. Since $\sqrt{LC} = 1/v$, where v is the phase velocity, $l\sqrt{LC}$ represents a time lag which is independent of the frequency. It is the time required for a sinusoidal component of the signal, as in a Fourier analysis, to traverse the length of the cable. If a nonsinusoidal voltage is impressed on the line, all the harmonic components will be subjected to the same amplitude and phase changes during the transmission. Thus a replica of the impressed voltage will arrive at the receiving end. This addition of the harmonic components is possible since all the differential equations are linear.

The important question that remains is the following. What magnitude of error is introduced by having the terminations Z_1 and Z_2 not equal to Z? The following analysis will give criteria for the length of line and the size of terminating impedance that will keep the distortion below a specified amount.

Substituting the values of r_1, r_2, and $l\sqrt{LC} = lC\sqrt{L/C} = lCZ_0 = C_cZ_0$ into Equation [4], we obtain

$$E_2 = \frac{E_1 Z_0 Z_2}{Z_0(Z_1 + Z_2)\cos\omega Z_0 C_c + (Z_0^2 + Z_1 Z_2)\, j \sin\omega Z_0 C_c} \qquad [7]$$

$C_c = lC$ is the distributed capacitance of the whole cable.

In this problem the pressure pulse gives rise to the generator voltage $E_1 e^{j\omega t}$ of the piezoelectric gage. The generator has an internal impedance

$$Z_1 = \frac{1}{j\omega C_g}$$

where C_g is the capacitance of the piezoelectric pickup element. If q is the charge generated by the gage then

$$q = E_1 C_g$$

and therefore

$$E_2 = \frac{q Z_0 Z_2}{Z_0\left(C_g Z_2 + \frac{1}{j\omega}\right)\cos\omega Z_0 C_c + \left(Z_0^2 C_g + \frac{Z_2}{j\omega}\right) j \sin\omega Z_0 C_c} \qquad [8]$$

It is customary to terminate the cable with a capacitance to control the output voltage. Therefore let

$$Z_2 = \frac{1}{j\omega C_2}$$

where C_2 is the terminating capacitance. Then Equation [8] becomes

$$E_2 = \frac{q}{(C_g + C_2)\cos\omega Z_0 C_c + \left(1 - \omega^2 C_2 C_g Z_0^2\right)\left(\frac{\sin\omega Z_0 C_c}{\omega Z_0 C_c}\right)C_c} \qquad [9]$$

This result has been obtained by Lampson (20).

The order of magnitude of the various parameters may be compared. C_g is very small, probably less than 40×10^{-12} farad. C_2 usually varies from 10^{-9} farad to 10^{-7} farad. $C_c = lC$ where C is approximately 40×10^{-12} farad per foot and l ranges from 20 feet to 1000 feet. Z_0 is the surge impedance and ranges from 50 to 70 ohms for ordinary microphone cables. The range of frequencies $\omega/2\pi$ of interest in underwater explosion work extends up to several hundred kilocycles, say 3×10^5 cycles per second.

If the length of the cable l is small, then $\sin\omega Z_0 C_c/\omega Z_0 C_c$ and $\cos\omega Z_0 C_c$ may be replaced by unity. In that event

$$E_2 = \frac{q}{C_g + C_2 + C_c(1 - \omega^2 C_g Z_0^2 C_2)} \qquad [10]$$

If the terminating capacitance C_2 is not large, then

$$E_2 = \frac{q}{C_g + C_2 + C_c} \qquad [11]$$

This value for the output voltage of the line is valid for short lines and for terminating capacitances C_2 that are not too large.

A comparison of Equations [11] and [9] shows that the effect of a large value for C_2 or for l is to increase the value of E_2 over that which would be obtained from Equation [11].

The effect of finite lengths of line can be easily estimated. Suppose it is desired that the value of E_2 should vary by no more than 4 per cent for a range of frequencies up to 3×10^5 cycles per second; assume that C_c and C_2 are approximately equal and that C_g is negligible. Then Equation [9] can be rewritten

$$E_2 = \frac{q}{C_2\left(\cos\omega Z_0 C_c + \frac{\sin\omega Z_0 C_c}{\omega Z_0 C_c}\right)} \qquad [9a]$$

For small values of the argument $\omega Z_0 C_c$ we can write

$$\cos\omega Z_0 C_c = 1 - \frac{(\omega Z_0 C_c)^2}{2}$$

$$\frac{\sin\omega Z_0 C_c}{\omega Z_0 C_c} = 1 - \frac{(\omega Z_0 C_c)^2}{6}$$

Thus the prescribed maximum variation of 4 per cent in E_2 will occur if $\cos \omega Z_0 C_c$ is allowed to deviate from unity by 0.03, and $\sin \omega Z_0 C_c / \omega Z_0 C_c$ by 0.01. Then

$$1 - \frac{(\omega Z_0 C_c)^2}{6} = 0.99$$

and therefore

$$\omega Z_0 C_c = 0.245$$

Let $Z_0 = 55$ ohms and $C = 40 \times 10^{-12}$ farad per foot. Then

$$l = \frac{C_c}{C} = \frac{\omega Z_0 C_c}{\omega Z_0 C} = 59 \text{ feet}$$

This is the maximum length of line that may be used under the stated conditions.

Similarly the effect of C_2 in causing distortion may be estimated. Let the deviation of $1 - \omega^2 C_c Z_0^2 C_2$ from unity be 3 per cent for the range of frequencies up to 3×10^5 cycles per second. Let $C_c = 30 \times 10^{-12}$ farad, and $Z_0 = 55$ ohms. Then

$$\omega^2 C_c Z_0^2 C_2 < 0.08$$

Therefore

$$C_2 < 0.11 \times 10^{-6} \text{ farad}$$

A 0.1-microfarad terminating capacitor is thus the largest that could be employed under the given conditions.

This is not a serious limitation on the attenuation of signal voltage. Capacitors larger than 0.1 microfarad may be employed to obtain greater attenuation by using two capacitors in series on the end of the line. If one capacitor is kept below the limit of 0.1 microfarad, the other capacitor may be as large as needed to secure the desired attenuation. The signal would then be taken from the larger capacitor. The combination would be an equivalent capacitor whose capacitance is less then the smaller of the pair and hence less than 0.1 microfarad.

It is more difficult to compensate for the use of a very long line to avoid distortion of the signal. There are two methods of dealing with this problem. One method is to use a preamplifier on the end of a line; for example, in the case just discussed the line was less than 59 feet long. The preamplifier is so designed that its output impedance is low enough to match the surge impedance of the cable. A line of any length can then be used from the output of the preamplifier to the input of the next amplifier. Such a preamplifier has been designed and tested in conjunction with 500 feet of

single conductor cable with a surge impedance of 72 ohms. The frequency-response curve of this preamplifier and 500 feet of cable is essentially flat between 100 cycles per second and one megacycle per second.

Another method consists in terminating the cable, at least approximately, in its surge impedance. This method has been described by Lampson (21). Other work has been done at the Taylor Model Basin on this problem (22).

DISTORTIONS DUE TO MECHANICAL DISTURBANCE OF THE CABLE

In Part 2 it was pointed out that the type of cable used with a gage is one of the factors which determine the degree of distortion of the signal obtained. In testing a piezoelectric gage at the Taylor Model Basin it was observed that mechanical disturbance of the cable modified the voltage signal perceptibly. It was evident that in using the gage to study the pressure-time variation near an underwater explosion, a spurious signal produced in the cable could introduce an appreciable error. Preliminary tests confirmed this conjecture. A series of tests was undertaken to compare the voltage signals from various types of shielded, single-conductor cables exposed without other pickup to an underwater explosion. An attempt was then made to improve one of the best of these, a coaxial copper-tube cable, so as to reduce its distortion of a gage signal. Finally, certain relevant properties of the modified cable were studied: The reproducibility of its voltage signal, and the effects of change in its orientation and configuration.

Each cable under investigation was prepared for immersion by insulating the wire at one end, both from the concentric shield and from the water, by rubber tape coated with Bostik cement. The other end was connected to the input of an amplifier. The cable was then taped to a plank and lowered diagonally into the water to a depth of 3 feet, as shown in Figure 9. Both cable and charge were mounted on suitable frames by means of which their depth and relative position could be accurately adjusted.

A Number 8 detonator was exploded, and the voltage output of the cable as a function of time was recorded with a Du Mont Type 208 cathode-ray oscillograph and an auxiliary camera. The time axis on the cathode-ray screen was swept out by a TMB sweep generator, and synchronized with the explosion by a trigger circuit. Voltage and time scales were calibrated with a General Radio Microvolter and an oscillator by impressing a sine wave of known amplitude and frequency on the screen of the cathode-ray tube. The photographic records were enlarged, and peak voltages were read off.

A detailed description of the cables, including the capacitance of each, and a tabulation of the results will be found in Tables 1 and 2, respectively. The peak voltages generated by the different cables range from

TABLE 1

Description of Cables Subjected to Underwater Explosions, and Peak Voltages Produced by These Cables

Serial Letter	Manufacturer's Designation	Central Wire B&S Gage	Insulation	Shield	Sheathing	Nominal Outside Diameter inches	Capacitance per foot μμf	Wall Thickness of Copper Tubes inches	Peak Voltage* millivolts
A	Belden 8421	20	Rubber	Copper Stranding	Rubber	0.260	44		136 ± 12
B	Belden 8401	26	Rubber	Copper - Phosphor-Bronze Stranding	Rubber	0.245	25		108 ± 10
C	Belden 8216	14	Rubber	Copper Stranding	Rubber	0.435	25.5		80 ± 9
D	Precision	20	Fiber-glass	Copper Tube	None	0.100	108	0.007	10 ± 2
E	Cable E	20	Fiber-glass	Copper Tube	None	0.125	57	0.034	13 ± 2
F	Precision	20	Fiber-glass and Celluloid	Copper Tube	None	0.218	107	0.013	40 ± 5
G	Belden 1637	20	Rubber	Copper Tube	None	0.256	161	0.012	21 ± 3
H	Belden 8863	20	Rubber, Cotton	Copper Stranding	None	0.225	33		26 ± 3

* The peak voltage was determined from at least four trials with each cable.

10 to 136 millivolts. Greater signals were produced by the rubber-sheathed cables than by the unsheathed ones, the former ranging from 80 to 136 millivolts, the latter from 10 to 40 millivolts. Typical durations of the signals were 2 or 3 milliseconds.

These large cable signals may give rise to important errors when used in conjunction with a crystal pickup in measurements on the initial part of the pressure pulse in an underwater explosion. Even larger relative errors will result, however, in pressure determinations during the ensuing period of several milliseconds characterized by distinctly lower pressures. The character of the tail of the curve corresponding to this later period may be completely masked by cable distortion. When measuring impulse or momentum the area under the pressure-time curve must be determined, and since the duration of the cable pulse is long compared to that of the true pressure pulse, a tail area of considerable size would make a large spurious contribution, say as large as 20 per cent, to the measured impulse.

The lowest signals, 10 and 13 millivolts, were produced by the cables designated as D and E respectively, see Table 1. The shielding in both consists of copper tubing rather than stranding; they have fiber-glass insulation, their outside diameter is small, 0.100 inch and 0.125 inch respectively, as compared to those of the other copper-tube cables tested, and

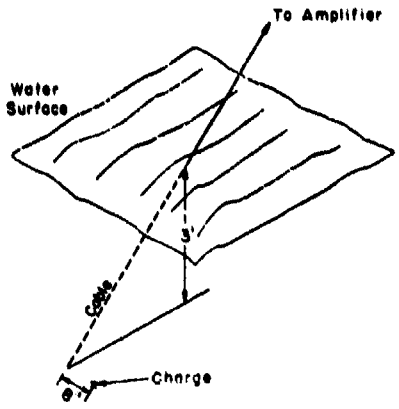


Figure 9a - Sidewise Orientation

The charge is offset from the cable, to produce lateral movement of the latter.

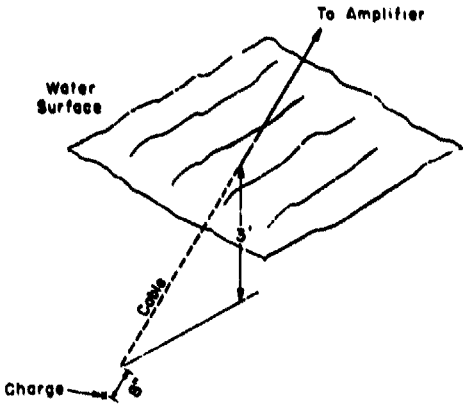


Figure 9b - Endwise Orientation

The charge is in line with the end of the cable.

Figure 9 - Orientations of Cable Relative to Charge in the Early Cable Tests

they are unsheathed. In Cable D, prepared by the Precision Tube Company, the copper tubing is placed over the insulation by a drawing operation. The resulting hardness of the tubing cannot be removed by annealing because this would damage the insulation. In Cable E, prepared at the Taylor Model Basin, Number 24 wire covered with fiber-glass insulation is inserted into tubing with a wall thickness of 0.034 inch. Because the tubing in the latter cable can be annealed *before* the wire is inserted, it has the advantage of flexibility. However, since the central wire is rather loose (this cable was made up without wax) it is capable of motion relative to the concentric tube. Hence the cable signal shows high-frequency oscillations due to the vibration of the wire; see Figure 10b.

To determine how much reduction in the peak voltage of Cable E could be effected by reducing the relative motion of the central wire, a test was made with a charge placed on an extension of the axis of the cable; see Figure 9b. The distance between the immersed end of the cable and the charge was kept fixed. The resulting peak voltage was 2 millivolts, compared to 13 millivolts when the charge was in the position shown in Figure 9a.

It appeared that of all the cables tested Cable E would be the most satisfactory for use in explosion gages, provided that it could be made insensitive to orientation. To accomplish this, it was decided to fill the space between the tube and the wire with wax (18). The modified cable, hereafter called the "TMB Cable," gave satisfactory results, as shown in Table 2,

Figure 10b

Figure 10c

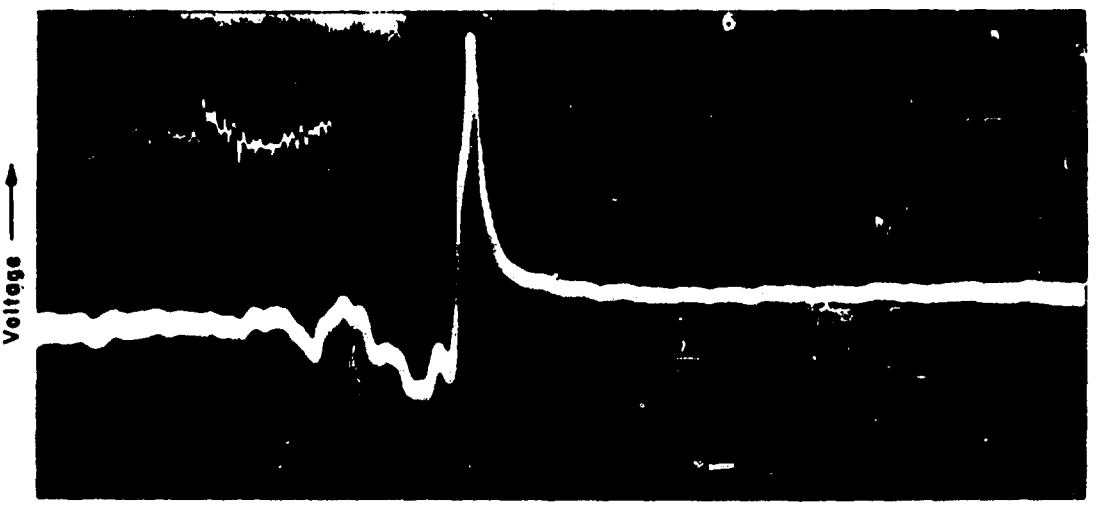


Figure 10a

Figure 10 - Voltage Signals Produced by Three Cables Subjected to the Underwater Explosion of a Detonator

Figure 10a shows a signal from a rubber-sheathed cable; Figure 10b, a signal from a coaxial copper-tube cable; and Figure 10c, a signal from a wax-filled TMB cable.

Figures 10b and 10c were originally taken at larger amplifications than those exhibited here, to permit accurate measurement. They have been reduced to show the three cable signals approximately to the same voltage scale. The apparently sharper focus in Figures 10b and 10c is due to this reduction. The time scales are different. The total time on each oscillogram is the same, 12 milliseconds.

TABLE 2

Comparison of Peak Voltages of TMB Wax-Filled Cable and Unmodified Cable

Cable	Peak Voltage, millivolts	
	Sidewise Orientation Figure 9a	Endwise Orientation Figure 9b
E	12.9	2.0
TMB	3.4	2.6

which gives the peak voltages obtained with the original and the modified cables for the positions shown in Figure 9. The capacitance of the TMB cable was 50 micromicrofarads per foot.

Figure 10 is a comparison of voltage-signal records from a rubber cable, from the unmodified copper-tube cable, and from the TMB cable. It

should be noted that although the time scales are different in the three records, the voltage scales are the same.

The TMB cable possesses the following advantages:

a. Compared to the unmodified Cable E, it is relatively insensitive to orientation.

b. For sidewise orientation, Figure 9a, it gives a peak signal less than 1/3 as large as does the unmodified copper cable, and about 1/30 of that produced by commercial rubber-sheathed cables.

c. High-frequency voltage oscillations due to vibration of the wire in the unwaxed copper-tube cable are eliminated; compare Figures 10b and 10c.

d. It is very flexible, since the copper tubing remains in the annealed condition after the central wire is inserted.

e. The use of copper tubing as a shield makes it easy to lead the gage cable into a pressure chamber for calibration. With rubber cable it is difficult to seal the gage inside the pressure chamber so that it will hold high pressure without damaging the rubber insulation.

f. It has a relatively low dielectric absorption. Consequently, its capacitance shows a negligible change with frequency, as compared with variations as high as 15 per cent observed for rubber-sheathed cables between 150 cycles per second and 30,000 cycles per second.

Because of these characteristics the TMB cable appears to be better suited for use with underwater explosion-pressure gages than any of the others tested. It has been adopted for all such gages recently constructed at the Taylor Model Basin.

In addition, two other features of the cable were investigated; the reproducibility of the voltage signal and the effect of changing the configuration of the cable in the pressure field. In a series of five detonations under nominally identical conditions, the peak voltage signal from the cable alone was found to be reproducible to within a probable deviation of 4 per cent. To test the effect of departure from a linear configuration, the cable was bent into a circle with the charge at its center. There was little change in the resulting cable signal.

Further tests of the relative merits of the TMB cable and a rubber-sheathed cable were subsequently made at the Underwater Explosives Research

Laboratory at Woods Hole, in connection with the use of larger charges. These experiments differed from the earlier ones mainly in two respects: charges of 250 grams of tetryl were exploded instead of detonators, and each of the cables tested was part of a complete piezoelectric gage assembly. The crystal signal was delayed so as to separate it from the initial part of the cable signal. This was done by bending the cable into the shape of an isosceles triangle with the crystal at its vertex 30 inches from the base; see Figure 11. The charge was placed at the same distance on the other side of the base. Hence the pressure pulse struck the cable about half a millisecond before reaching the crystal.

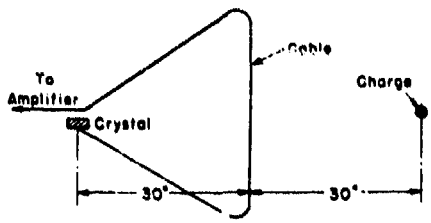


Figure 11 - Positions of Cable and Crystal Relative to Charge in the Cable

Cable signals obtained simultaneously from a Belden Series 8400 rubber-sheathed cable and from a TMB cable are shown in Figures 12 and 13. In these pictures the time sweep proceeds from left to right; thus the first disturbance at the left is that due to the cable. The steep signal which follows is produced by the crystal,* and the peculiar appearance of the subsequent portion of the curve was probably caused by the output of the crystal overloading the amplifier. Pairs of such records from ten explosions were obtained. These show a steady change in the condition of the rubber cable as

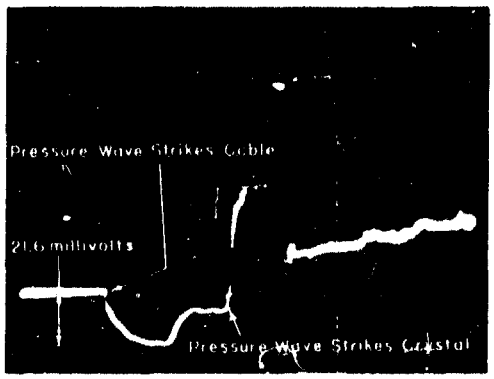


Figure 12 - Voltage Signal Produced by a Rubber Cable Subjected to an Underwater Explosion of 250 Grams of Tetryl

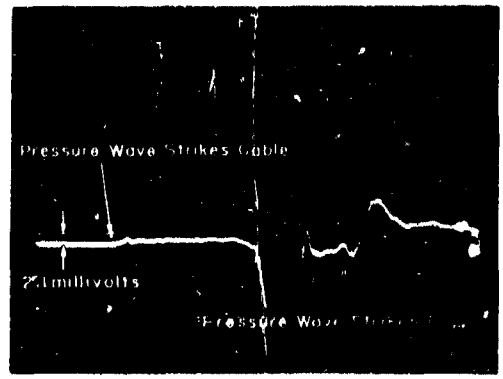


Figure 13 - Voltage Signal Produced by a TMB Cable Subjected to an Underwater Explosion of 250 Grams of Tetryl

* The amplifier was overloaded [illegible] signal was much too high for the crystal signal.

it is subjected to additional explosions. The peak voltage in the cable signal decreased from 22 millivolts in the first explosion to 6 millivolts in the tenth, while that in the TMB cable fluctuated between 1 and 2 millivolts. This effect of "aging" on the rubber cable, due to repeated explosions, had been observed previously at the Underwater Explosives Research Laboratory. The investigators at that laboratory report that the change is reversible; if an "aged" cable is put aside for a week or two it reverts to its former state and again gives rise to large signals. Other rubber-sheathed cables showed the same features in even greater degree.

When large numbers of gages with copper cables were used simultaneously on a ship, the noise level became objectionably high, probably as a result of eddy currents through the copper tube which serves as a return lead. One way to overcome this difficulty may be to replace the present combination of single conductor and grounded copper tube with a double conductor enclosed in a copper tube, the latter acting only as a shield.

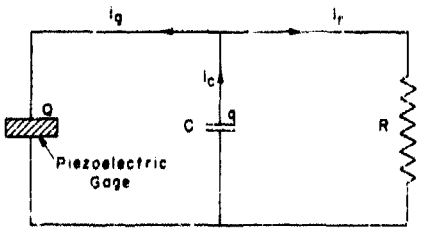
DISTORTION DUE TO INSUFFICIENT TIME CONSTANT

Another type of distortion of the gage signal occurs when the time constant of the circuit is too small compared to the duration of the signal. The following analysis provides practical criteria for the magnitude of the time constants needed to reduce this kind of distortion to a given percentage.

A piezoelectric gage circuit may be represented as in Figure 14.

To minimize distortion caused by leakage of the signal charge through the input resistance of the amplifier, the time constant of the circuit expressed by the product RC must be large compared to the duration of the signal.

The piezoelectric gage generates a charge which is proportional to the applied force. Since the peak pressure due to an underwater explosion occurs almost instantaneously, the peak charge is generated at the very start. As the pressure decreases, the crystal reabsorbs as much charge as it previously generated; this reverses the original current.



$Q(t)$ is the charge produced by the crystal; i.e., the true gage response which it is desired to measure,

$q(t)$ is the observed charge on the capacitor,

C is the combined distributed capacitance of the cable plus the terminating lumped capacitance,

R is the input resistance of the amplifier,

RC is the time constant of the circuit, and

i_g, i_r, and i_c are the instantaneous currents in the indicated branches of the circuit.

Figure 14 - Simplified Equivalent Circuit of a Piezoelectric Gage

Thus at first the charge is produced and thrown on the capacitor plates. Then as the pressure diminishes the capacitor discharges into the crystal and through the resistance R. It is apparent that if the resistance were infinite the voltage on the capacitor would follow the original pressure faithfully. However, the presence of a finite resistance causes a leakage through that as well as back into the crystal. Thus the voltage across the capacitor is always less than it would otherwise be. In fact, even if the original pressure were always positive, it would be possible, because of the leakage through R, for the capacitor to reverse its charge and indicate an apparent negative force. The distortion of the signal from a piezoelectric gage due to leakage is shown in Figure 15, in which V_0 is the observed voltage and V_t is the voltage to be expected for zero leakage.

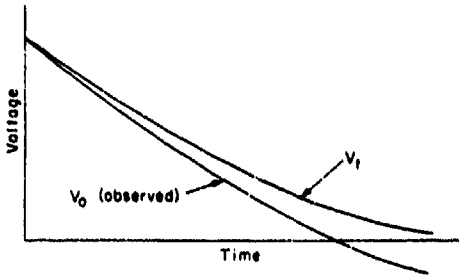


Figure 15 - Distortion of a Piezoelectric Gage Signal Due to RC Leakage

V_t is the value which would be obtained if the leakage were zero.

It is apparent that the relative error $(V_t - V_0)/V_t$ increases as time progresses. Thus if it is desired to study the late phases of the record, it is necessary to make the product RC quite large. This requirement is more severe than if the peak value alone were being investigated. An analysis of the distortion is given below.

Let $i_c = -dq/dt$ be the total current flowing out of the capacitor, $i_g = -dQ/dt$ be the current flowing into the crystal, and $i_r = q/RC$ be the current flowing through the resistance R. Then

$$i_c = i_g + i_r \qquad [12]$$

or

$$-\frac{dq}{dt} = \frac{q}{RC} - \frac{dQ}{dt}$$

and

$$\frac{dq}{dt} + \frac{q}{RC} = \frac{dQ}{dt}$$

$$q(t) = e^{-\int d\tau/RC}\left[\int \frac{dQ}{d\tau}\, e^{\int d\tau/RC}\, d\tau + c\right]$$

$$= e^{-t/RC}\left[Q(t)\, e^{t/RC} - \frac{1}{RC}\int_0^t Q(\tau)\, e^{\tau/RC}\, d\tau + C\right]$$

The initial conditions are that $q(0) = Q(0) = Q_i$, the initial charge produced. Therefore

$$q(t) = Q(t) - \frac{1}{RC} e^{-t/RC} \int_0^t Q(\tau)\, e^{\tau/RC}\, d\tau$$

where τ is the variable of integration. The relative error is

$$\frac{Q(t) - q(t)}{Q(t)} = \frac{\Delta Q}{Q} = \frac{1}{RC} \frac{\int_0^t Q(\tau)\, e^{\tau/RC}\, d\tau}{Q(t)\, e^{t/RC}} \qquad [13]$$

Thus far the expression for the charge produced by the crystal has been an arbitrary function. Now two special forms for $Q(t)$ will be considered.

$$\text{Case 1} \quad Q(t) = Q_0 e^{-t/t_0} \qquad [14]$$

$$\text{Case 2} \quad Q(t) = Q_0\left(1 - \frac{t}{t_0}\right) \qquad [15]$$

where $t_0 = RC$ is the time constant of the discharge.

For what time ought the relative error to be calculated? It is seen that the error increases with time. As a practical choice the comparison may be made for the time at which

$$\frac{t}{t_0} = 1 \text{ in Case 1}$$

and

$$\frac{t}{t_0} = \frac{2}{3} \text{ in Case 2}$$

In both cases $Q(t)$ is reduced to approximately 1/3 of its original value.

Table 3 is based on Equation [13]. It gives the relative error $\Delta Q/Q$ as a function of RC/t_0.

The conclusion to be drawn in each of the two cases is substantially the same. If the error is not to exceed 10 per cent, the time constant should be 10 to 15 times as

TABLE 3

Relative Error $\frac{\Delta Q}{Q}$ as a Function of $\frac{RC}{t_0}$ for Case 1 and Case 2

Case 1		Case 2	
$\frac{RC}{t_0}$	$\frac{\Delta Q}{Q}$	$\frac{RC}{t_0}$	$\frac{\Delta Q}{Q}$
1	1.00	1	0.92
2	0.65	2	0.55
3	0.47	3	0.39
4	0.37	4	0.31
5	0.31	5	0.25
6	0.26	8	0.13
7	0.23	10	0.11
10	0.16	16	0.07
15	0.11	.	.
20	0.08	.	.
.	.	.	.
.	.	.	.
.	.	.	.
∞	0	∞	0

large as the period of time which is of interest. Thus if the time of interest is 20 milliseconds, the time constant must exceed 250 milliseconds.

DISTORTIONS DUE TO FREQUENCY RESPONSE OF AMPLIFIERS

Thus far distortions associated with the cable and those due to inadequate time constant have been discussed. Another kind of signal distortion arises from inadequate frequency response of the amplifiers. There are several ways of describing this frequency response. The following are three methods in common use.

Let $E_1 \sin\omega t$ represent a standard sinusoidal signal going to the input of the amplifier. Then the output will have the form

$$E \sin(\omega t - \theta)$$

E is the amplitude of the output. If it is a function of the frequency ω, i.e., $E = E(\omega)$, then the amplifier has amplitude distortion. θ is the change in phase introduced by the amplifier. If θ is either a constant or a linear function of the frequency, i.e., $\theta = \theta(\omega) = \alpha\omega + \beta$, where α and β are constant, then there is no phase distortion. If θ is a nonlinear function of ω, then the amplifier has introduced phase distortion. In the case of the properly terminated cable treated in an earlier section, see Equation (5),

$E(\omega) = \frac{E_1}{2}$, which is independent of signal frequency ω;

$\theta(\omega) = j l\sqrt{LC}\,\omega$, which is a linear function of ω.

Thus the properly terminated cable is an example of a distortionless system. When $E(\omega)$ and $\theta(\omega)$ are determined experimentally, the frequency response is completely known.

A second method involves obtaining the response of the amplifier to a periodic square wave.

A third method is to obtain the response of the amplifier to a unit pulse; see Figure 16.

These modes of description are essentially equivalent, and any one may be derived from any other (23). Each may be useful for some specific purpose. Thus, for example, if it is desired to learn the effect of some parameter, such as the value of a resistance

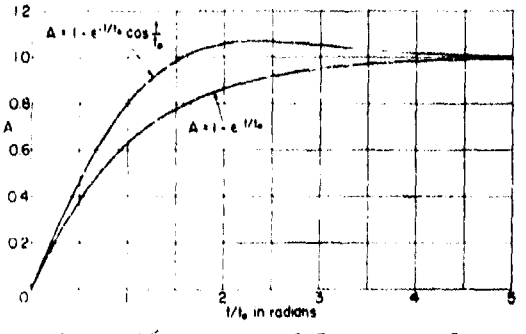


Figure 16 - Types of Response of Amplifiers to a Unit Pulse

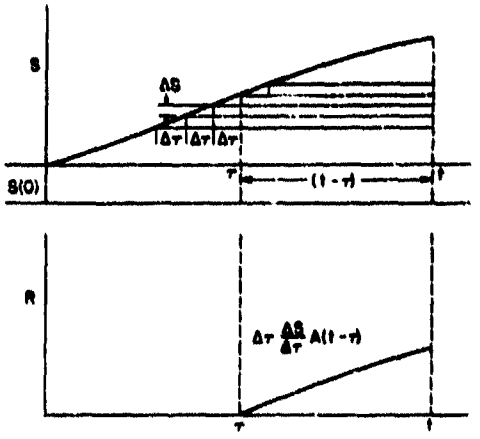


Figure 17 - Illustration of the Duhamel Integral

or capacitance, on the frequency response, then the response to a square wave may be "stopped" on the screen of a cathode ray oscillograph, and the change in the response can be observed visually and continuously as the resistance, or capacitance, is altered. Thus the square-wave method is valuable to anyone building an amplifier. Once the amplifier is built it may be necessary to determine the response to a given input transient signal. It is difficult to derive mathematically the response to a transient signal in terms of a known response to a square wave (23). This question may, however, be answered very conveniently if the response to a unit pulse is known, and for studying distortion, the square wave of adequate duration is sufficiently equivalent to it. The following analysis (24) shows how the response of any amplifier to a given signal may be calculated provided the response to a unit pulse is known. Let

$E(t)$ be 1 for $t \geq 0$; be 0 for $t < 0$ } the unit pulse,

$A(t)$ be the response to the unit pulse, usually called the indicial admittance,

$S(t)$ be the input or excitation signal, and

$R(t)$ be the response of the amplifier to $S(t)$.

It will be assumed that the amplifier is a linear system, i.e., it is describable by linear differential equations. In that case the principle of superposition may be used. It is also necessary to assume that the coefficients of the differential equations of the system (amplifier) are constants. This means that the response is only a function of $(t - \tau)$ where τ is the time at which the unit pulse is applied, and t is the time at which the response is desired.

Consider the input signal S as represented in Figure 17. The signal is to be considered as the sum of many rectangular pulses. Each pulse starts at a time $\Delta\tau$ after the previous one. The height of the pulse is given by

$$\Delta S = \frac{\Delta S}{\Delta \tau}\,\Delta \tau$$

Thus a pulse of height ΔS is applied at the time τ, while at a time $\Delta\tau$ later another pulse is applied, and so on. It is desired to find the effect of all these pulses at the definite time t. The response of any one of them is pictured in the lower half of Figure 17, and is given by

$$\frac{\Delta S}{\Delta \tau}\,\Delta \tau \cdot A(t-\tau)$$

There is also the contribution of the pulse whose height is $S(0)$. The corresponding response is given by the product

$$S(0) \cdot A(t)$$

The total response is obtained by adding all the steps. This yields

$$R(t) = S(0)\,A(t) + \sum \frac{\Delta S}{\Delta \tau}\,A(t-\tau)\,\Delta\tau$$

In the limit as $\Delta\tau \to 0$, the summation is replaced by the following expression, known as the Duhamel integral

$$R(t) = S(0)\,A(t) + \int_0^t \frac{dS(\tau)}{d\tau}\,A(t-\tau)\,d\tau$$

This formula gives the response for a given input signal $S(t)$ provided the response to a unit pulse. i.e., $A(t)$, is known; see Figure 16 and the upper half of Figure 17.

A specific case will be worked out in detail to illustrate the method.

Assume for instance that the response to a unit pulse has been obtained experimentally and is representable by the empirical equation

$$A(t) = 1 - \epsilon^{-t/t_0}$$

t_0 is a measure of "the time of rise" of the amplifier.* Let the input signal be that due to an underwater explosion. This may be represented fairly well by the form**

$$S(t) = \epsilon^{-t/T}$$

where T is the duration of the signal. Thus

---

* The response of actual amplifiers frequently approximates this form.

** For simplicity, $S(0)$ is chosen as unity, and $S(t)$ and $R(t)$ are dimensionless.

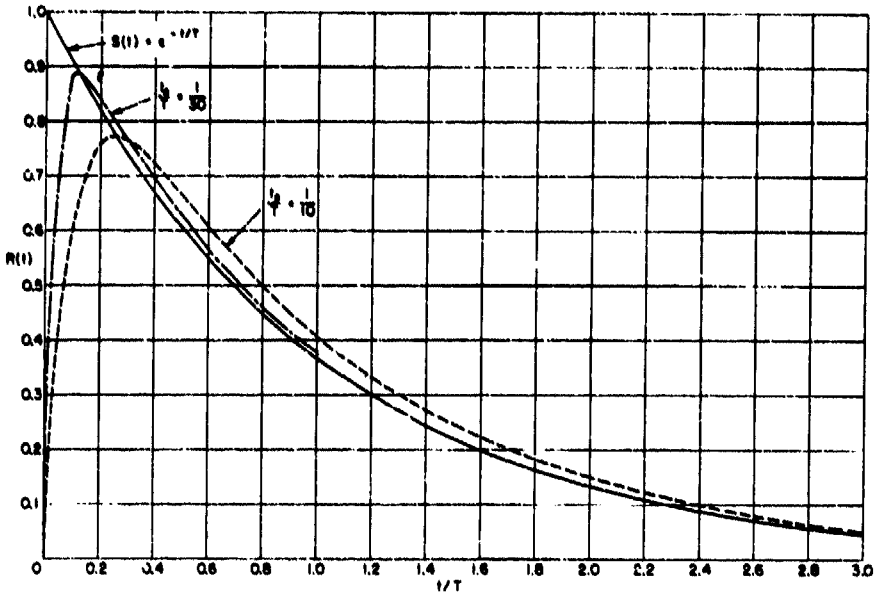


Figure 18 - Response of an Amplifier to an Input Signal of the Form $\epsilon^{-t/T}$

The amplifier in question is one which shows the response to a unit pulse depicted by the lower curve in Figure 16. The response is expressed by Equation [17] and is plotted for two values of t_0/T.

$$R(t) = 1 - \epsilon^{-t/t_0} - \int_0^t \frac{1}{T}\, \epsilon^{-\tau/T}\left(1 - \epsilon^{-(t-\tau)/t_0}\right) d\tau \qquad [16]$$

$$R(t) = \frac{T}{T - t_0}\left(\epsilon^{-t/T} - \epsilon^{-t/t_0}\right) \qquad [17]$$

See Reference (5).

The original signal $S(t)$ and response $R(t)$ are plotted for the indicated values of t_0/T in Figure 18. It is apparent that the response approaches the input signal more closely as t_0/T approaches zero. There is a considerable loss of peak signal even for small values of t_0/T; for example, a loss of 7.5 per cent for $t_0/T = 1/50$.

It is useful to obtain the peak response as a function of t_0/T. The t_0/T necessary for a given allowable loss of peak response for the assumed type of signal can then be specified. Differentiating Equation [17] yields

$$R'(t) = \frac{T}{T - t_0}\left[-\frac{1}{T}\,\epsilon^{-t/T} + \frac{1}{t_0}\,\epsilon^{-t/t_0}\right]$$

Setting this expression equal to zero, we obtain

$$\frac{1}{T}\,e^{-t_m/T} = \frac{1}{t_0}\,e^{-t_m/t_0}$$

where t_m is the time at which the maximum response occurs. The maximum response R_m at this time is given by

$$R_m = \frac{T}{T - t_0}\left(e^{-t_m/T} - e^{-t_m/t_0}\right) \qquad [18]$$

Let $X = t_0/T$. Then

$$R_m = \frac{1}{1 - X}\left(e^{-t_m/T} - e^{-t_m/t_0}\right)$$

but, from the preceding

$$e^{-t_m} = X^{t_0/(1-X)}$$

Eliminating t_m, we obtain

$$R_m = \frac{1}{1 - X}\left(X^{X/(1-X)} - X^{1/(1-X)}\right)$$

and

$$R_m = X^{X/(1-X)} \qquad [19]$$

This is the desired function giving the peak response to be expected from a given value of $X = t_0/T$. For values of X less than 1/20 we may use

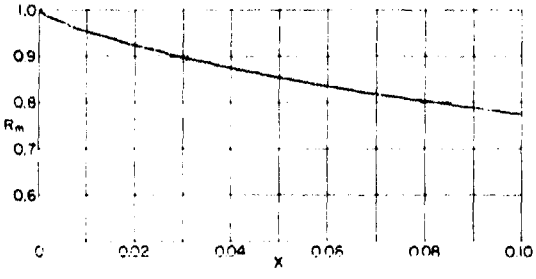


Figure 19 - Peak Response as a Function of $X = t_0/T$

The maxima of the family of curves in Figure 18 are plotted against the parameter t_0/T. This graph is a plot of Equation [19].

$R_m = X^X$ with an error which is less than 1 per cent. A plot of Equation [19] is given in Figure 19.

As a numerical example of the use of this result, suppose the amplifier is required to record 97 per cent of the peak pressure due to the underwater explosion of an ounce of tetryl. What time of rise should the

amplifier have? The duration of the pressure from an ounce of tetryl is approximately 35 microseconds. Thus

$$T = 35$$

$$R_m = 0.97 = X^X$$

Then

$$X = \frac{1}{170} = \frac{t_0}{T}$$

Therefore

$$t_0 = \frac{35}{170} = 0.2 \text{ microsecond}$$

This imposes a severe requirement upon the amplifier, as can be seen from the following example. Suppose that the frequency response of an available amplifier falls off by 8 per cent at 300 kilocycles. It then has a time of rise equal to 3/4 microsecond, a time too large to give the desired accuracy for an explosion of an ounce of tetryl.

It may be asked, what is the smallest charge for which the cited amplifier will record 97 per cent of the peak pressure? The duration of the pressure varies as the cube root of the mass of the charge. Therefore, the desired value of weight W of the charge may be obtained if the required duration is known. In this case

$$R_m = 0.97$$

$$t_0 = 0.75$$

$$X = \frac{1}{170} = \frac{t_0}{T}$$

Therefore

$$T = 0.75 \times 170 = 127 \text{ microseconds}$$

Comparing this time with the duration of an explosion of one ounce of tetryl, we have

$$\frac{W}{1} = \left(\frac{127}{35}\right)^3 = 47.8 \text{ ounces of tetryl}$$

Therefore the required charge is 3 pounds or more of tetryl.

If valid measurements are to be made it is necessary to take such precautions as working with relatively large charges or using very high fidelity amplifiers and cables which are not too long.

THE TMB RECORDING CHANNEL

The Taylor Model Basin recording channel consists of a series of units as indicated by the block diagram in Figure 20. The amplifier was designed by members of the staff and responds to frequencies up to 300

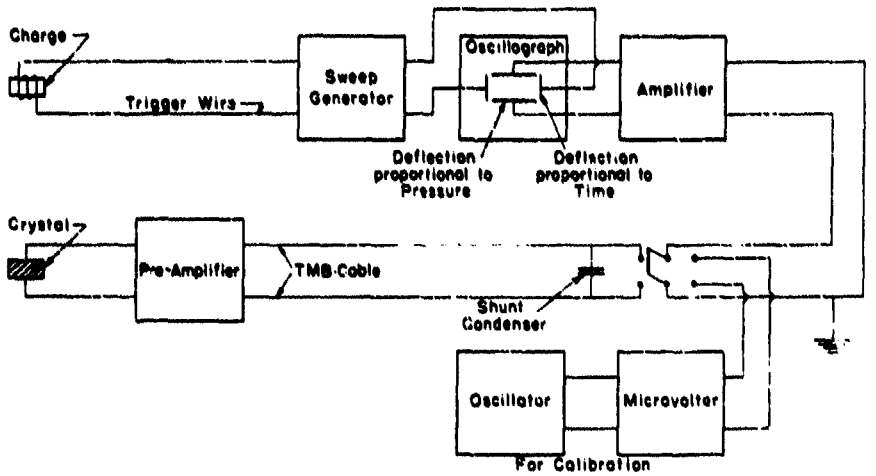


Figure 20 - Schematic Diagram of Channel used in Underwater Explosion Tests at the Taylor Model Basin

kilocycles. Its output goes directly to the vertical deflecting plates of a Du Mont Type 208 cathode-ray oscillograph. A high-vacuum type of sweep generator is used, which produces either single or continuous sweeps. A Hewlett-Packard oscillator and General Radio Microvolter are employed for time and voltage calibrations. A 35-mm Eastman Ektra camera using an f 1.9 lens records calibrations and explosion pressures. The sweep is initiated when a fine wire wrapped around the charge is broken by the explosion.

PART 4. CALIBRATION OF THE PRESSURE GAGES

The usefulness of a pressure gage for underwater explosions is manifestly limited by the accuracy and reliability of its calibration. This involves a precise determination of the electrical output of the gage when it is subjected to a known change in pressure. In this section the apparatus employed in applying a pressure change to the gage will be described first, then the circuit used in measuring its output by each of several different methods. Finally, the results obtained from the various calibrations will be compared with one another, with values of piezoelectric constants found in the literature, and with values obtained for the same crystals by two other laboratories.*

---

* The Underwater Explosives Research Laboratory at the Oceanographic Institution, Woods Hole, Massachusetts, and the Exploration Laboratory of the Stanolind Oil and Gas Company, Tulsa, Oklahoma.

PRESSURE APPARATUS

Calibration pressures are developed inside a cylindrical steel pressure chamber* filled with a rust-inhibiting solution of potassium dichromate and sodium carbonate. Oil is not used, since upon repeated immersion in oil at high pressures the rubber insulation on the tourmaline gages would be damaged. The crystal end of the gage is sealed into the pressure vessel by neoprene washers sandwiched between split brass washers. The latter fit snugly around the copper-tube cable, and the neoprene washers are compressed by a retaining screw through which the cable emerges from the chamber. The pressure is raised to some predetermined value which is read on a Bourdon-tube gage. Three such gages with ranges up to 2000, 5000, and 10,000 pounds per square inch have been used. These have been calibrated twice at the National Bureau of Standards. They can be read to within 1/4 to 1/2 of one per cent at the usual test pressures.

In the calibration of the piezoelectric gages, a rapid change in pressure is required. Therefore, once the desired pressure has been attained, it is released by one of the following two methods. A release valve is suddenly opened, permitting a return to atmospheric pressure in approximately 0.05 second; or a thin brass diaphragm, sealed into the chamber on the opposite side from the gage, is punctured, releasing the pressure in 0.2 to 0.3 millisecond. The diaphragm must be thick enough to withstand a given pressure, but thin enough to be readily punctured with, say, a thrust of a screwdriver. In practice, the diaphragms are made of brass, 1.12 inch in diameter and 0.003 inch to 0.008 inch thick, depending upon the pressure to which they are to be subjected. It requires but a few minutes to remove a punctured diaphragm and replace it with a new one.

Unlike the transient character of a piezoelectric gage calibration, that of a glass resistance gage is static; i.e., the pressure remains at a predetermined value while the change in the gage resistance is measured.

CIRCUITS FOR MEASURING THE OUTPUT OF THE GAGES

For a piezoelectric gage the output to be measured is a quantity of charge, whereas for a resistance-type gage the output is a change in resistance. Accordingly, different circuits must be used in calibrating the two types.

CALIBRATION OF THE PIEZOELECTRIC GAGES

The charge ΔQ developed by a piezoelectric crystal under load is proportional to the change ΔF in the total force acting on the electrode

* This apparatus was designed by Lt. Denrison Bancroft, USNR, of the David Taylor Model Basin staff.

surfaces, i.e., $\Delta Q = K\Delta F$, where K is the piezoelectric constant of the crystalline material along the electric axis. When a piezoelectric gage is subjected to hydrostatic pressure, it is convenient to write $\Delta Q = KA\,\Delta P$. The change in pressure ΔP acting over area A determines the total force transmitted to the electrode surface. From the constant KA of a particular gage, the change in pressure responsible for a given output of charge is inferred.

Since values of K are given in the literature, it may be inquired why calibration is necessary; why not simply multiply K by A? There are several reasons. The piezo constant is not the same for various specimens of tourmaline. It is difficult to know which of the values found in the literature is a correct value for the sample used in the gage.

In the case of the quartz gage there are two sources of possible error in computing KA rather than in determining it experimentally. In the first place, few quartz crystals are altogether free from "twinning" of right-handed and left-handed quartz. Twinning reduces the effective K of the crystal, since the two types of quartz show opposite polarities. Secondly, A is not known precisely. As pointed out in the Appendix, it is necessary that an air gap surround the quartz crystal laterally. The brass cover which transmits the external pressure to the crystal is supported partly by the crystal and partly by the cylindrical wall of the housing; see Figure 3 on page 6. Moreover, a portion of the brass cover lies over the air gap. Thus the effective area A subjected to pressure differs from the electrode surface of the crystal alone. Though it is possible to estimate approximately how much of the area over the air gap is supported by the crystal, it is not easy to compute this exactly. However, if the gage is calibrated, it is not necessary to know A, since the product KA is obtained directly.

For these reasons it is desirable to determine experimentally the constant KA of each gage. Now for any particular method of calibration, results of high internal consistency are not incompatible with the occurrence of a systematic error. To ensure reliable KA values, therefore, it is important to compare the results obtained by a given method of calibration with those obtained by another method, and, if possible, by an independent observer. At the Taylor Model Basin, in addition to the alternative methods of applying a pressure change which have already been described, experiments have been made with several different circuits for measuring the charge. One of these has proved especially successful, yielding results which not only show internal consistency but which agree closely with those obtained for the same crystals in other laboratories. Experiments have also been performed by two other methods of calibration. One of these used a Compton quadrant electrometer; the other utilized a "microcoulometer" or high-impedance current

amplifier and a moving-coil galvanometer. These latter two methods have the disadvantage of requiring exceedingly high gage impedance, at least 30,000 megohms, for successful operation. The oscillographic method, on the other hand, requires an impedance of only about 10 megohms. The various calibration techniques will now be described.

Oscillographic Recording

In this method of calibration the pressure is released by a bursting diaphragm, and the output is recorded on the screen of a cathode-ray tube. The gage is shunted by a mica capacitor and connected into the amplifier of a Du Mont Type 208 cathode-ray oscillograph. A horizontal time sweep is provided by a TMB sweep generator and synchronized with the pressure release by a simple trigger circuit. The output of the crystal as it is subjected to a pressure change appears as a voltage-time curve on the screen of the cathode-ray tube; see Figure 21. It is photographed with an Ektra camera, and the film records are measured with a micrometer microscope. The time required to release the pressure by puncturing a diaphragm, about 0.2 to 0.3 millisecond, makes the process especially amenable to oscillographic recording. The event is fast enough so that the required *RC* is not inconveniently large; on the other hand, it is slow enough so that the demands of flat frequency response on the amplifier and adequate beam intensity on the cathode-ray tube are not excessive. The slow descent of the portion of the curve to the right of the peak gives an indication of the large *RC*, 40 milliseconds, which was used. This time constant is so large compared to the time required for the release of the pressure that the leakage error in the measurement of peak pressure, as in Figure 15 on page 25, is less than 1 per cent. For time calibration a sine wave of known frequency is fed into the amplifier from a Hewlett-Packard oscillator. The amplitude is calibrated by putting a step voltage from a potentiometer into the amplifier of the Du Mont oscillograph.



Figure 21 - Calibration Record Obtained with the Direct Oscillographic Method

The pressure inside a calibration chamber is released by puncturing a thin brass diaphragm. The time scale runs from left to right.

Table 4 gives the results of a typical set of calibrations on five tourmaline crystals. Each *KA* value cited in Column 3 is the result of the number of determinations or "trials" indicated in Column 2. Thus the *KA* value

TABLE 4

Piezoelectric Calibration Constants of Typical Tourmaline Gages

1	2	3	4	5	6	7	8
Gage	Number of Trials	$KA \times 10^{13}$ coulombs per pounds per square inch		Per Cent Difference in KA	Area square inches	$K \times 10^{11}$ coulombs per pound	
		TMB	Stanolind			TMB	Stanolind
275	36	9.16 ± 0.08	9.21	0.5	0.0865	1.058	1.064
282	30	9.02 ± 0.06	8.87	1.7	0.084	1.074	1.058
284	17	9.10 ± 0.11	9.02	0.9	0.085	1.070	1.061
285	28	7.85 ± 0.18	7.89	0.5	0.074	1.061	1.066
XT-503	41	11.82 ± 0.11	12.06	2.0	0.112	1.053	1.074

for Gage 275 is based on the measurement of 36 oscillograms like the one in Figure 21. The deviation given in Column 3 is in every instance the standard deviation. It will be seen that the KA determinations for a given gage are internally consistent to within one or two per cent.

It is interesting to compare these KA values with those obtained for these same crystals by the Exploration Laboratory of the Stanolind Company,* from whom the plated crystals are procured. Their figures are listed in Column 4, and the percentage differences between these values and those obtained at the Taylor Model Basin are given in Column 5. The TMB calibrations differ from those of Stanolind by 2 per cent or less. It should be emphasized that the two sets of calibrations were performed by independent observers using different techniques. One of these gages, XT-503, was previously calibrated by the Underwater Explosives Research Laboratory at Woods Hole; the value obtained there is in agreement with Stanolind's within 1 per cent.

From the value of KA and the measured area of A of the crystals listed in Column 6, the piezoelectric constant K of the tourmaline used in these gages is computed. The values of K deduced from the Taylor Model Basin determinations and from those of the Stanolind Laboratory are listed in Columns 7 and 8 respectively. These figures may be compared with those computed from piezoelectric moduli given in the International Critical Tables (19). Using the moduli of Riecke and Voigt found in these tables, the piezoelectric constant of tourmaline along its electrical axis when the crystal is subjected

---

* Dr. Daniel Silverman of the Stanolind Company carried out these calibrations with a microcoulometer.

to hydrostatic pressure is computed to be 1.078×10^{-11} coulombs per pound. If the moduli determined by Röntgen are used, a value 1.087×10^{-11} coulombs per pound is obtained. The agreement with either of these values is thus quite satisfactory.

Quadrant Electrometer

An alternative method of calibrating the piezoelectric gage utilizes the Compton quadrant electrometer.* This instrument possesses much higher sensitivity than that required to measure the typical output of a TMB piezoelectric gage. By shunting the gage with a total capacitance of about 0.01 microfarad, as illustrated in Figure 22, a potential difference of about 0.1 volt was impressed on the quadrants. Although the instrument is capable of many refined sensitivity adjustments, it was found possible to get the desired range of sensitivities merely by varying the needle potential between 45 and 65 volts. Because of the high capacitance in parallel with the gage, the instrument was usually stable and free from excessive drift. However, for satisfactory operation the impedance of the electrometer system had to be kept high, of the order of 50,000 megohms. Gages of lower impedance could not be calibrated with the electrometer. To prevent moisture from collecting on the insulation, a small quantity of calcium chloride was kept inside the casing of the electrometer as well as inside the box which shielded the switches and capacitors.

Gages were calibrated in the following manner: After the needle potential was adjusted for the desired sensitivity, the "floating" quadrants were grounded by momentarily closing switch K_1; see Figure 22. Then, with K_2

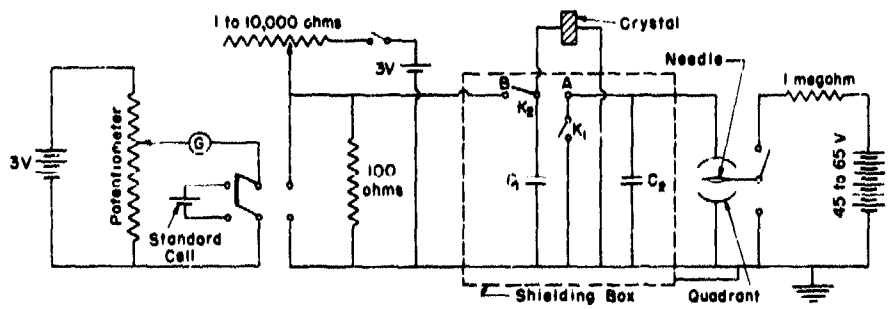


Figure 22 - Electrometer Calibration Circuit with Potentiometer

The deflections of a Compton quadrant electrometer are calibrated by putting a known voltage on the needle with a Leeds and Northrup Type K potentiometer.

* The electrometer was obtained on loan through the courtesy of Dr. L.E. Curtis of the Radioactivity Section, National Bureau of Standards.

in position A, the pressure on the crystal was released. The corresponding ballistic deflection was read on a scale about 1 meter from the electrometer. This was repeated for various pressures.

Voltage calibration of the scale was carried out as follows: First K_1 was momentarily closed. Then K_2 was thrown to position B, charging up a mica capacitor C_1 to a potential difference which was precisely determined with a Leeds and Northrup Type K potentiometer. By reversing K_2 the known voltage was impressed upon C_2 and the quadrants. Deflections of the needle were observed for a suitable range of voltages.

Voltages ΔV were plotted against corresponding pressure changes ΔP and a "best line" was drawn. Usually the experimental points were so nearly collinear that the slope $\Delta V/\Delta P$ could be determined without recourse to the method of least squares. The piezoelectric constant KA of the gage is given by $C(\Delta V/\Delta P)$, where C is the total capacitance in parallel with the gage. C was measured with a Schering capacitance-bridge circuit manufactured by the General Radio Company.

The results obtained with this method of calibration are described at the end of the next section.

Microcoulometer

A third calibration technique makes use of an impedance coupler, Figure 23, with a large time constant, together with a voltmeter consisting of a moving-coil galvanometer* in series with a suitable resistance. This circuit has been called a microcoulometer. It has an input impedance of 30,000 megohms and an input capacitance of 10^{-8} farad. Hence its time constant, about 200 seconds, is long in comparison with the time of deflection of the galvanometer coil, which is about 2 seconds. By the switch K_1, Figure 24, either the piezoelectric crystal or a potentiometer may be

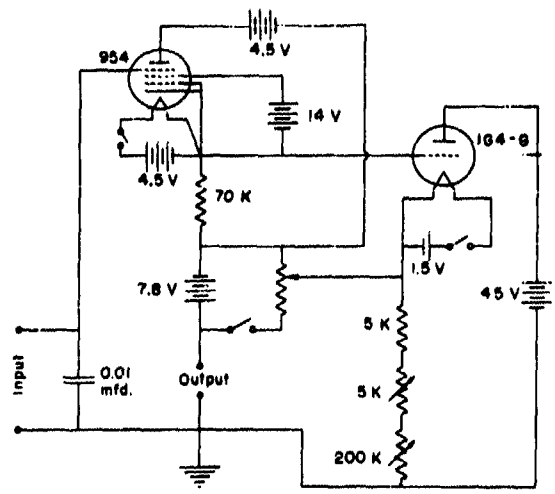


Figure 23 - Piezoelectric Gage Impedance Coupler with Large Time Constant, Termed a Microcoulometer

* The galvanometer employed is manufactured by the General Electric Company under Serial Number 320.

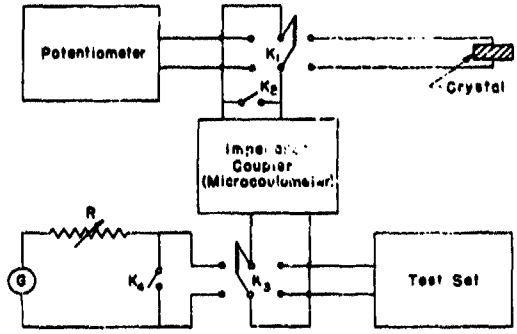


Figure 24 - Calibration Circuit Employing the Microcoulometer

The circuit in Figure 23 is represented by the box labeled "Impedance Coupler." The "input" and "output" of Figure 23 correspond to connections K_1 and K_3, respectively. The galvanometer G together with the series resistance R constitute the voltmeter.

connected to the input of the impedance coupler. With K_3 the output can be fed either into the galvanometer or into a Simpson test set.

The following calibration procedure is used: First the gage is momentarily shorted by the switch K_2. Then the variable resistor in the impedance coupler is adjusted until the output potential is zero. For preliminary adjustment of the output, the test set is a convenient indicator. In the interest of uniformly high accuracy, it is desirable to get nearly full-scale deflections of the galvanometer for each release of pressure. This is achieved by varying the series resistance R, which controls the galvanometer's voltage sensitivity.

To translate galvanometer deflections into volts, the potentiometer is employed in much the same manner as that described for the electrometer. Several voltages are applied to the microcoulometer for each value of R previously used, and the corresponding galvanometer deflections are noted. With these data it is possible to plot voltage against pressure change and as before, KA is determined from C and the slope $\Delta V/\Delta P$ of the curve.

The values of the calibration constant KA obtained with the electrometer and the microcoulometer are between 7 and 13 per cent lower than those determined with the oscillographic recording technique. The oscillographic values are judged to be correct within the experimental error, inasmuch as they have been independently substantiated by workers in two other laboratories. Moreover, they lead to a value of K which agree closely with that found by both Voigt and Röntgen. Both the electrometer and microcoulometer methods offer considerable difficulty because of the high input impedance which must be maintained for successful operation; the former is especially troublesome as it requires an impedance of 50,000 megohms. The discrepancy of 7 to 13 per cent has recently been accounted for (25).

Program for Further Piezoelectric Calibration Studies

Several important questions concerning piezoelectric calibrations remain to be answered. Some observers have found an indication of a difference between the KA value determined with a "bare" crystal, i.e., before the

insulation is coated on, and the value obtained after the gage has been coated with rubber. This question is being investigated.*

It is also planned to study the effect, if any, on KA when the gage is subjected to a series of explosions. In this connection it should be observed that the oscillographic calibration technique has a great advantage over the other methods, in that it can be applied to a gage after repeated explosions. It is found, for example, that the impedance of a gage after several explosions usually drops well below the 30,000 megohms required for calibration with the microcoulometer. Hence recalibration by this method is impossible. On the other hand, the oscillographic method does not demand an impedance of more than about 10 megohms, and the gage resistance seldom drops below several hundred megohms. When it does, the gage becomes useless in any event, for the RC of the gage circuit is then too small.

CALIBRATION OF THE GLASS RESISTANCE GAGE

The glass resistance gage is calibrated with a Wheatstone bridge. The gage is sealed into the pressure chamber in the same way as are the piezoelectric gages, except that a brass washer soldered to the cable above the glass element facilitates the closure.

A series of pressure increments ΔP up to 6000 pounds per square inch are then applied to the gage, and the change ΔR_g in its resistance is measured. Displacements on the galvanometer scale, which are proportional to the resistance changes ΔR_g, are plotted against ΔP. From the slope of the resulting line the calibration constant of the gage $1/R_g\ (\Delta R_g/\Delta P)$ is obtained. Values of this constant are of the order of 1.5×10^{-7} $\frac{1}{\text{pounds per square inch}}$. Since R_g is about 100 ohms, ΔR_g is of the order of 0.015 ohm for a change in pressure of 1000 pounds per square inch.

PART 5. GAGE PERFORMANCE IN TESTS

UNDERWATER EXPLOSION TESTING

It was thought desirable to test the piezoelectric gages under a variety of circumstances, using larger charges than could be fired at the Taylor Model Basin at the time this work was done. Tests were therefore conducted by Taylor Model Basin personnel at the Underwater Explosives Research Laboratory, Woods Hole. Considerable work on explosion pressures had been done by investigators at that laboratory with tourmaline gages manufactured by the Stanolind Company, and some of these gages were available for direct comparison with TMB tourmaline gages. Therefore it was decided to concentrate

* Dr. A. Borden reports that preliminary experiments indicate a difference of less than 1 per cent between the bare and the coated crystals.

initially on testing the performance of the tourmaline gage rather than that of the other gages. The recording facilities at Woods Hole were generously made available. The overall frequency response of the cable and amplifier was good to 300 kilocycles per second.

PRESSURES IN OPEN WATER

A welded ring 9 feet in diameter of 1 1/2-inch steel pipe was used for the mounting of charges and gages; see Figure 25. The charges, which ranged from 50 to 250 grams of loose tetryl, were placed in the center of the steel ring. The gages were mounted in the plane of the ring 36 inches from the charge. The charge and the gages were secured by vertical and horizontal wires. The wires in turn were attached to vertical steel rods passed through drilled holes in the 9-foot ring.

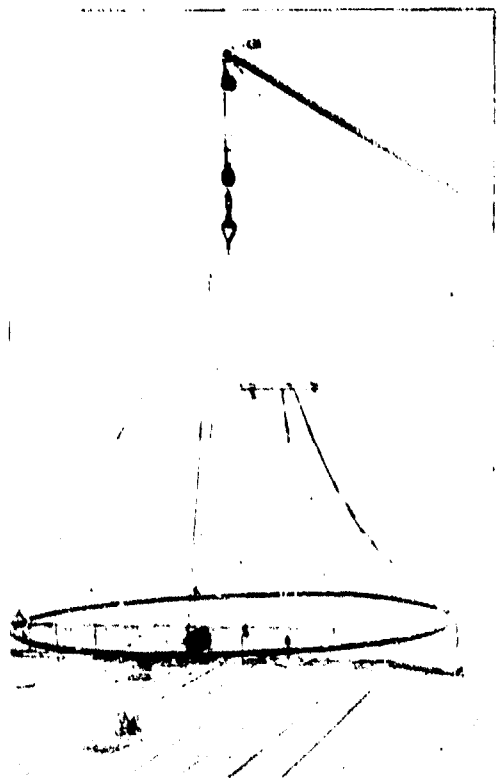


Figure 25 - Welded Steel Ring Used for Mounting Charges and Pressure Gages

This ring was used by TMB personnel in tests at the Underwater Explosives Research Laboratory at Woods Hole.

Three gages and recording channels were ordinarily employed; these gave at least two good records for each explosion. Two of the gages were usually the TMB copper-cable tourmaline type, whereas the third was a similar tourmaline gage mounted on a Belden 8400 rubber-sheathed cable; the latter gage was supplied by the Underwater Explosives Research Laboratory. The tetryl was detonated by firing a Number 8 detonator cap placed in the center of the charge.

Figure 26 shows photographic reproductions of some typical records. Table 5 summarizes some of the results obtained. Peak pressures recorded by the two types of gages generally agreed within 3 per cent. The average deviation of the pressures recorded by a single gage was also about 3 per cent.

After the consistent operation of the tourmaline gages when used with charges of this size had been established, it was decided to test their

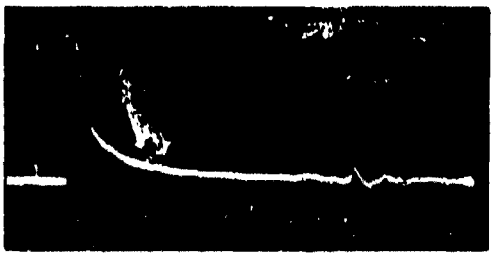


Figure 26a - Record Obtained with a TMB Tourmaline Pressure Gage

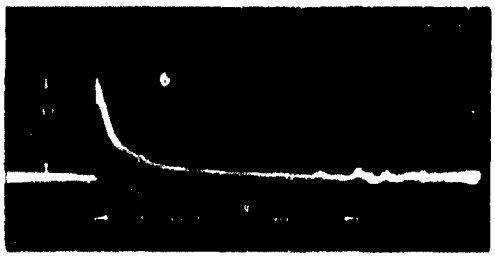


Figure 26b - Record Obtained with a Gage Supplied by the Underwater Explosives Research Laboratory

Figure 26 - Pressure-Time Oscillograms Obtained with Two Tourmaline Gages in Open Water

150 grams of tetryl 3 feet from the gage was used in each of the two explosions.

TABLE 5

Peak Pressure and Duration of Explosions as Registered by Tourmaline Piezoelectric Gages

The distance from the gages to the charge was 36 inches, plus or minus 1 inch.

Tetryl grams	Gage		Number of Records	Peak Pressure pounds per square inch	Duration microseconds
100	XT-C2	TMB*	9	3140 ± 110	55.4 ± 6.2
100	S-300	UERL**	8	3010 ± 120	52.3 ± 4.8
150	XT-C2	TMB	7	3840 ± 140	63.3 ± 2.2
150	XT-C4	TMB	11	3840 ± 50	58.9 ± 2.0
150	XT-B13	TMB	6	3740 ± 125	52.2 ± 1.7
150	S-300	UERL	14	3880 ± 65	54.5 ± 2.3

* "TMB" refers to a Taylor Model Basin gage.

** "UERL" refers to a gage belonging to the Underwater Explosives Research Laboratory.

performance when used with explosions of 1 ounce or less of tetryl.* In addition a comparison of the records obtained with tourmaline gages with those of the quartz and glass gages has been undertaken. These investigations are still in progress, and the results will be given in a subsequent report. Experience in these tests has shown clearly that the task of obtaining valid pressure-time records of explosions is greatly complicated when small charges are employed. For reasons set forth elsewhere in this report, the shorter

* The upper limit of 1 ounce was imposed by the fact that these tests were to be performed at the Taylor Model Basin, where facilities for larger explosions were then not available.

duration of such explosions imposes requirements upon the pickup, amplifier, sweep generator, and cathode-ray tube which are much more stringent than for explosions of larger charges.

PRESSURES AT A SURFACE OF AN UNDERWATER STRUCTURE

A modified form of the tourmaline gage has been used to obtain pressure-time records at a surface. The rubber insulation is molded about the crystal and also in a cavity sunk in a brass plate. The latter is bolted to the surface of an underwater structure; see Figure 6 on page 9. Thus far only preliminary comparisons have been made between this surface type of gage and the usual open-water type.

The brass plate was bolted to the center of a piece of plywood 2 feet square by 1.5 inch thick. The plywood was supported only by a rope so that it was free to move in the water. A 22-gram charge of tetryl was placed 20 inches from the surface gage so that the line joining the gage and the charge was perpendicular to the plane of the plywood. An open-water type of tourmaline gage, also placed 20 inches from the charge, served as a comparison pickup.

Figures 27a and 27b show a typical pair of comparison records. Two interesting differences always appear in these comparisons. The surface gage shows a higher peak pressure than is observed in open water; the ratio of these peak pressures is somewhat less than 2. The time histories of the two records are strikingly different. In Figure 27b the pressure indicated by the surface gage has dropped to zero in a time interval during which the pressure indicated by the open-water gage has decayed only to approximately 1/3 of its peak value.



Figure 27a - Explosion Pressures in Open Water

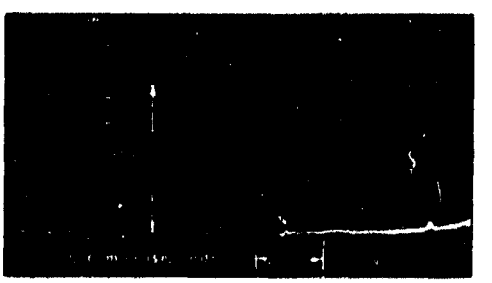


Figure 27b - Explosion Pressures on a Surface of an Underwater Structure

Figure 27 - Comparison of Explosion Pressures on a Surface of an Underwater Structure and in Open Water

The record in Figure 27a was obtained with the usual type of open-water gage; that in Figure 27b with a surface-type of tourmaline gage sunk into a brass plate. The return to zero pressure is much more rapid on the surface than in open water.

The approximate doubling of the peak pressure is to be expected because of the reflection of the pressure wave that takes place at the surface of the brass plate. Professor Kennard of the Taylor Model Basin staff has offered the following explanation for the rapid fall of the pressure to zero which is indicated by the surface gage. The pressure wave impinges upon the brass plate and causes it to move initially as if it were backed by air, because of the small acoustic impedance of the plywood. The brass plate undergoes very large accelerations and after a certain time t_1 cavitation occurs in the water. If we assume that cavitation sets in at zero pressure, and that the form of the shock wave is given by $e^{-\alpha t}$, then the time t_1 at which the record should indicate zero pressure is (26)*

$$t_1 = \frac{1}{\alpha} \frac{1}{x - 1} \ln x$$

where

$$x = \frac{\rho c}{\alpha m}$$

ρc is the specific acoustic impedance of the water; m is the mass per unit area of the brass plate.

α was determined from the open-water record given by Gage 280 in Figure 27a. It is approximately 28,300 seconds^{-1} if t is in seconds; m is 0.075 pound per square inch. This gives

$$t_1 = 35.3 \text{ microseconds}$$

Direct measurement on the curve in Figure 27b gives 35 microseconds for the time required to reach zero pressure.

USE OF THE TOURMALINE GAGE IN STUDYING A SLOWER PRESSURE CHANGE

The duration of an explosion of 100 grams of tetryl is about 50 microseconds. Recently the TMB tourmaline gage has been used to study pressure changes which are a thousand times as slow as this, i.e., about 50 to 100 milliseconds in duration.

The phenomenon under investigation was the load on an experimental 6-inch, 47-caliber, high-angle turret due to the recoil of the guns when they were fired. The shock of recoil is absorbed by a hydraulic brake or buffer. A 1/3-scale model of the turret at the Philadelphia Navy Yard was used for this test. The load due to recoil was simulated by the impact of a 2000-pound car rolling down an inclined track, and striking the piston of the buffer (28) (29).

* See also Reference (27), which deals with the explosive load on underwater structures as modified by bulk cavitation

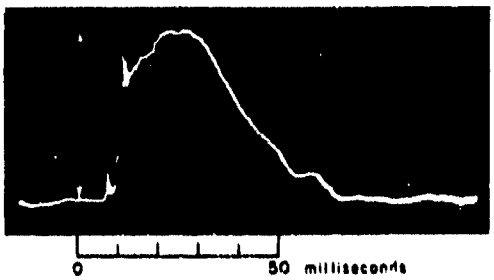


Figure 28 - Oscillogram Showing Pressure as a Function of Time Inside a Hydraulic Brake or Buffer

This record was obtained with a TMB tourmaline gage. The duration of this phenomenon is about 1000 times that of typical explosions described in this report.

From a measurement of the peak pressure inside the buffer the peak load can be deduced. This measurement has usually been made with a Crosby high-pressure engine indicator. It was desired to calibrate this instrument against a tourmaline gage.

The gage was sealed into the buffer by a special adapter. An RC constant of 1 second was provided by shunting the gage with a 0.01-microfarad capacitor and using a cathode follower with an input impedance of 100 megohms. A trigger circuit was designed in which a capacitor discharge, actuated by mechanical contact of two wires, set off the sweep. Contact was made at a predetermined time before impact when a bolt projecting from the moving car pushed one wire against the other. To record the pressure-time curve, a Du Mont Type 208 cathode-ray oscillograph was used together with the auxiliary equipment usually employed in recording transient pressures at the Taylor Model Basin.

The car was released from various heights up to 20 feet, and a pressure-time curve was obtained for each impact. Figure 28 shows a typical record for a 15-foot drop. The initial, sharp pulse is due to a shock-pressure wave transmitted through the buffer. This is followed by the main-peak portion of the curve which shows the variation of pressure inside the cylinder as the piston moves through it.

In an effort to check the validity of the pressure-time curve, the change in momentum mv of the car due to impact was compared with the total impulse $\int F dt$ deduced from the area under the pressure-time curve.* m is the mass of the car; v its velocity at the initial moment of impact; $F = Pa$, where P is the pressure recorded by the gage at time t, and a is the area of the piston. The integration, performed with a planimeter, is extended over a time from the initial moment of impact until the pressure returns to zero. The impulse measured in this way agreed with the calculated change in momentum to within 5 per cent.

Thus, besides its usefulness in explosion research, the TMB tourmaline gage appears to be equally suitable for the measurement of much slower pressure changes.

* The recoil velocity of the car is negligible.

REFERENCES

(1) "Experiments on the Pressure Wave Thrown Out by Submarine Explosions," by H.W. Hilliar, Department of Scientific Research and Experiment, R.E. 142/19, 1919.

(2) "The Hilliar Gage," by G.K. Hartmann, Ph.D., TMB CONFIDENTIAL Report 531, in preparation.

(3) "Piezoelectricity and Its Applications," by Sir J.J. Thomson, Engineering, Vol. 107, Number 2782, April 1919, pp. 543-544.

(4) "LVI. A Piezoelectric Method of Measuring Explosion Pressures," by David A. Keys, Philosophical Magazine, Vol. 42, Number 250, October 1921, p. 473.

(5) "Progress Report on Measurement of Underwater Explosion Pressures to April 1, 1942," by E.B. Wilson, Jr., and R.H. Cole, OSRD Report 523, Serial 226, April 1942.

(6) "Lehrbuch der Kristallphysik" (Textbook of Crystal Physics), by W. Voigt, Teubner, Leipzig, 1928.

(7) "Piezoelektrizität des Quarzes" (Piezoelectricity of Quartz), by A. Scheibe, Theodore Steinkopf, Dresden, 1938.

(8) "Quartz Oscillators and Their Applications," by P. Vigoureux, His Majesty's Stationery Office, London, 1939.

(9) "Le quartz piézoelectrique, et ses applications à la T.S.F." (Piezoelectric Quartz and Its Application to Wireless Communication), by F. Bedau, Hermann and Company, Paris, 1931.

(10) International Critical Tables, McGraw-Hill Book Company, New York, N.Y., Vol. 6, 1929, pp. 208-212.

(11) "Bibliography on Piezoelectricity," by W.G. Cady, Proceedings of the Institute of Radio Engineers, Vol. 16, 1928, p. 521.

(12) "A Survey of Piezoelectricity," by W.G. Cady, The American Physics Teacher, Vol. 6, 1938, p. 227.

(13) "Quartz and Tourmaline," by Peter Modrak, The Wireless Engineer, Vol. 14, Number 162, March 1937, p. 127.

(14) "Quartz and Tourmaline," by Peter Modrak, The Wireless Engineer, Vol. 14, Number 163, April 1937, p. 175.

(15) "Weiterentwicklung des piezoelektrischen Messverfahrens" (Progress in Methods of Piezoelectric Measurement), by S. Meurer, Forschung auf dem Gebiete des Ingenieurewesens, Vol. 11, 1940, p. 237.

(16) "Progress Report on Electrical Pressure Indicator," Naval Ordnance Laboratory Memorandum 2355, September 1942.

(17) "A Piezoelectric Method for the Instantaneous Measurement of High Pressures," by J.C. Karcher, Scientific Papers of the Bureau of Standards, Vol. 18, Number 445, 1922, p. 257.

(18) "A Tourmaline Crystal Gage for Underwater Explosion Pressure," by A.R. Cohen and B. Stiller, TMB Report R-157, December 1943.

(19) "Communication Networks," by E.A. Guillemin, Wiley and Sons, Vol. II, 1935, p. 42.

(20) "The Measurement of Transient Stress Displacement and Pressure," by C.W. Lampson, NDRC CONFIDENTIAL Report A-73, OSRD Number 756, July 1942.

(21) "Cable Compensation for Piezoelectric Gages," by C.W. Lampson, NDRC Armor and Ordnance CONFIDENTIAL Memorandum A-63M, January 1943.

(22) "Progress Report on Underwater Explosion Research, Bureau of Ships Symbol E139 - Part 9 - The Termination of Transmission Lines Used with Piezoelectric Gages," by J.J. Donoghue and R.B. Baxter, TMB CONFIDENTIAL Report R-244, April 1944.

(23) "Analysis of Systems with Known Transmission-Frequency Characteristics by Fourier Integrals," by W.L. Sullivan, Electrical Engineering, Vol. 61, 1942, p. 248.

(24) "Mathematical Methods in Engineering," by Th. von Karman and M.A. Biot, McGraw-Hill Book Company, New York, N.Y., 1940, p. 403.

(25) "Progress Report on Underwater Explosion Research, Bureau of Ships Symbol E139 - Part 11 - Errors Encountered in Calibrating Piezoelectric Gages with Slow-Recording Instruments," by A. Borden, TMB CONFIDENTIAL Report R-248, May 1944.

(26) "Effects of Underwater Explosions, General Considerations," by Professor E.H. Kennard, TMB CONFIDENTIAL Report 489, September 1942.

(27) "Explosive Load on Underwater Structures as Modified by Bulk Cavitation," by Professor E.H. Kennard, TMB CONFIDENTIAL Report 511, May 1943.

(28) "Tests of Turret Models under Dynamic Loading - Progress Report," by R.T. McGoldrick, TMB CONFIDENTIAL Report R-40, August 1941.

(29) "Theory of the Hydraulic Brake or Buffer," by B.L. Miller, Ph.D., TMB Report 482, January 1942.

APPENDIX

CONSTRUCTION OF THE QUARTZ PIEZOELECTRIC GAGE

Figure 3 is a view of the quartz gage with a section cut away to show the various components. The principal parts of the gage will first be described, then the details of its construction.

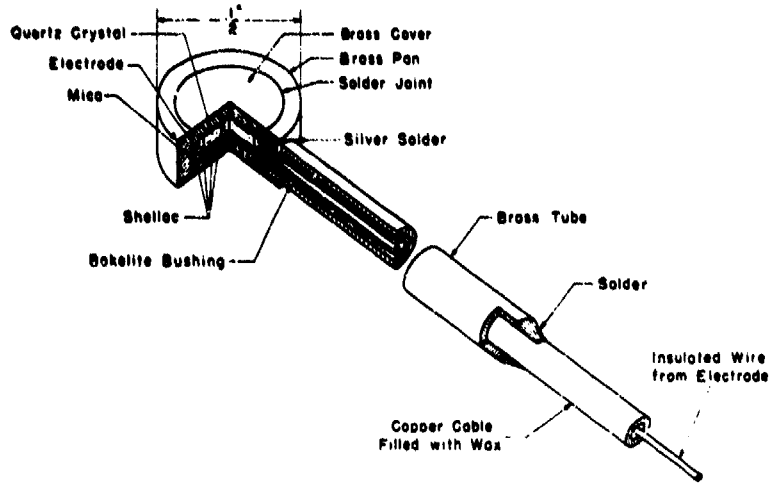


Figure 3 - Components of the TMB Quartz Piezoelectric Gage

The brass housing consists of three parts: a "pan" which contains the crystal; a cover; and a brass tube which is silver-soldered to the pan. A cylindrical, X-cut quartz crystal is cemented on one side to an electrode consisting of a thin copper disk, and on the other to the cover of the brass housing, through which it is grounded. The use of a copper disk for the electrode obviates the trouble of electroplating. Laterally the crystal is surrounded by an air gap which is required because quartz is insensitive to isotropic pressure. It is the need for this air gap which makes a housing necessary.

DESCRIPTION OF THE PRINCIPAL PARTS

The copper electrode is insulated from the brass pan by a thin sheet of mica. It is connected to the central lead wire, which is covered with enamel and a double layer of glass fiber. The space between this insulated wire and the concentric copper tube is filled with ceresin wax. Near its entrance into the pan the wire is insulated from the brass tube by a bakelite bushing. The crystal is so oriented that a compressional force produces a negative charge on the surface next to the copper electrode. When the gage is in use, the electrode is connected to the grid of an amplifier tube; thus the grid is charged negatively during compression. The brass housing is sealed watertight by soft-soldering the cover to the pan.

ASSEMBLY OF THE GAGE

Before assembly the various components of the gage are prepared as follows: an annealed copper-tube single-conductor cable is filled with wax, using a technique developed at the Taylor Model Basin (18). The outer surface at one end of this cable, as well as the inner surface of the brass tube to which it will be soldered, are tinned. The lateral surface of the cover is also tinned to prepare it for soldering to the pan. Pure orange shellac crystals are heated until they just melt; then thin coats of shellac are applied to the inside surfaces of the cover and pan, as well as to both surfaces

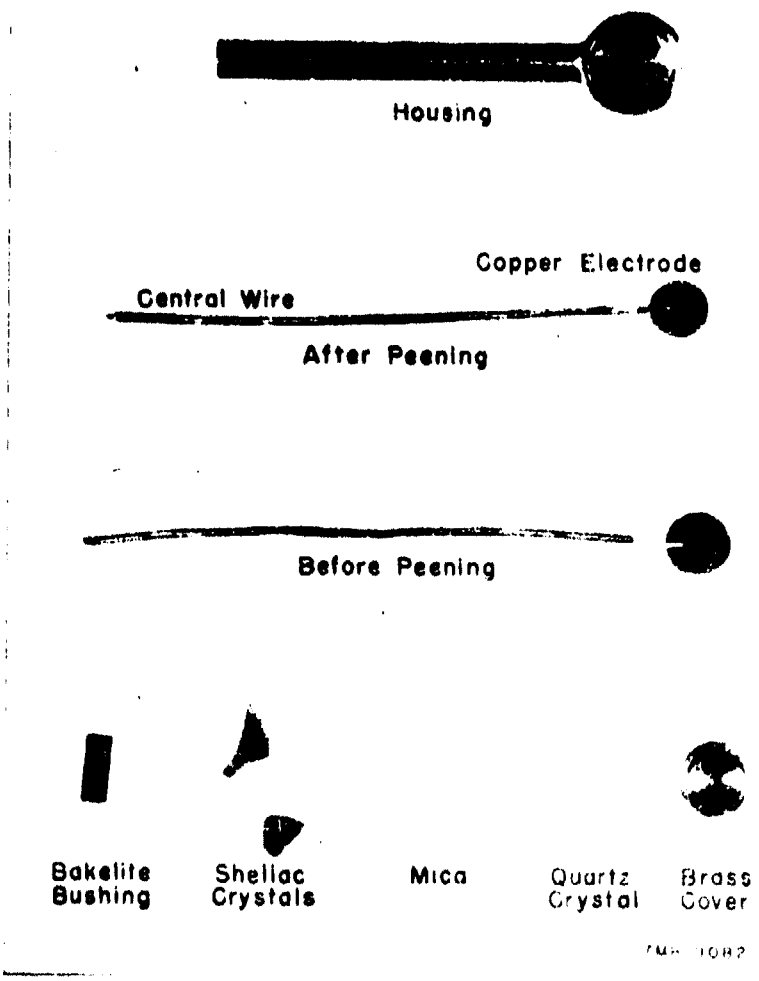


Figure 29 - Details of Assembly of the Quartz Gage

of the quartz crystal and mica.* Before the shellac has dried, the mica is cemented to the pan; similarly, the crystal is attached centrally to the cover. The slight depression in the cover serves a dual purpose: It helps in aligning the crystal, and later when the gage is finally assembled, the wall of the depression prevents the crystal from slipping sidewise off the electrode; this ensures that the full area of the crystal is utilized.

Before the wire is connected to the electrode, the copper cable is pushed into the brass tube farther than it will be in the completed gage, so that the wire emerging from it protrudes beyond the pan. A bakelite bushing is then slipped over this wire. The end of the wire is bared and attached to the electrode at the slit with a peening hammer, see Figure 29. A tight friction joint results; the short length of wire in the slit becomes virtually a part of the electrode. Then, while the bakelite bushing is inserted into the brass tube, the cable is pulled back until the copper electrode lies concentrically over the mica. The cover with the attached crystal is forced into the pan with a small C-clamp, and presure is maintained by this clamp while the cover is soft-soldered to the pan. During the soldering the shellac films remelt; thus, upon cooling, the various components are bound firmly together. Finally, the copper cable is soldered to the brass tube. The C-clamp is removed only after the metal has cooled. In both soldering operations great care is taken to keep the surfaces clean, so that the joints will be impervious to water under explosion pressures. If all the work has been done properly, the gage is now complete and ready for testing.

STATIC TESTING OF THE GAGE

At this stage the impedance of the gage is measured. For calibration with the microcoulometer described elsewhere in this report, the impedance should be at least 30,000 megohms. Next, to make sure that the gage is watertight, it is sealed in a pressure chamber and subjected to hydrostatic pressures up to 3000 pounds per square inch. Once more the impedance is measured. If the latter has dropped below its pre-immersion value, then the soldered joints may be leaky. If, on the other hand, the impedance is still high, the gage is ready for calibration.

SURFACE-PRESSURE MODIFICATION OF THE QUARTZ GAGE

The housing of the quartz gage has been successfully adapted to the measurement of explosion pressures on the surface of an underwater structure.

---

* When the crystal is subjected to a change in pressure the opposite charges developed on its two faces are transmitted by induction to the central electrode and the grounded cover, respectively, through the layers of shellac.

Best Available Copy

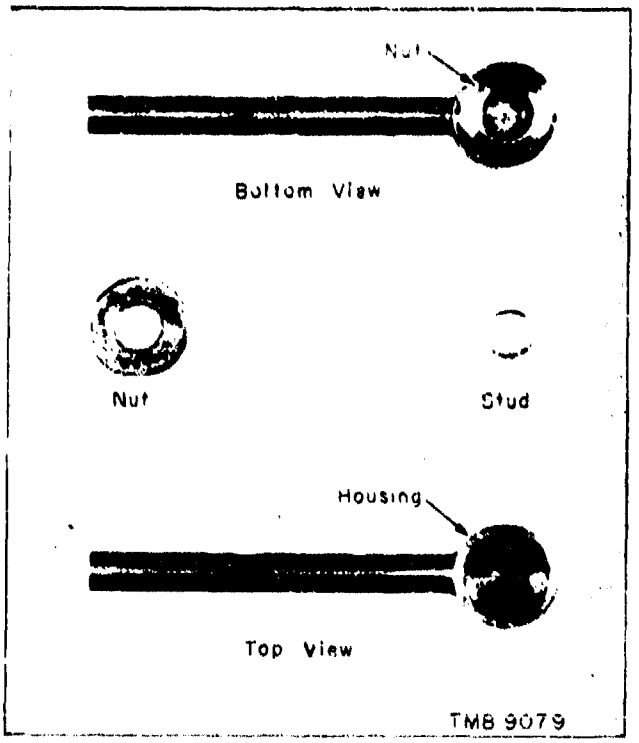


Figure 4 - Modification of Quartz Gage for Attachment to a Surface

A nut is soldered to the bottom of the housing, and a threaded stud is soldered to the surface at which the pressure is to be measured.

A brass nut whose outside diameter is the same as that of the pan, 1/2 inch, and whose inside diameter is 1/4 inch, is silver-soldered to the bottom of the housing. Since this nut is only 0.08 inch thick, it does not add excessively to the size or mass of the gage. A brass stud 1/4 inch in diameter and 0.075 inch thick is threaded to fit the nut. This stud is soldered to the surface under investigation, and the gage is then screwed down securely over the stud. Figure 4 shows the brass mount before and after adaptation to the surface type of gage, together with the nut and stud used in the conversion.

This type of "surface gage" has been designed so that it can be firmly attached not only to a rigid surface, but also to the surface of a diaphragm subjected to explosive loading. In the latter case the brass-plate type of tourmaline gage illustrated in Figure 6, on page 9, is inapplicable, as it is much too massive.

THE ELECTRIC POTENTIALS PRODUCED IN THE CONDUCTORS OF A SUBMERGED CABLE BY UNDERWATER EXPLOSIONS

A. H. Bebb and R. V. Bundy
Naval Construction Research Establishment
Rosyth, Scotland

British Contribution

October 1945

THE ELECTRIC POTENTIALS PRODUCED IN THE CONDUCTORS OF A SUBMERGED CABLE BY UNDERWATER EXPLOSIONS

A. H. Bebb and R. V. Bundy

October 1945

* * * * * * * * *

SUMMARY.

An account is given of a method of measuring the spurious signals contributed by the length of cable to the piezo-electric record of an underwater explosion.

The origin of "cable signals" has been qualitatively analysed and methods of treating the cable are discussed with the object of reducing these signals. One specified treatment has been shown to effect a reduction of 500 times.

INTRODUCTION.

Reference has previously been made to the effect of spurious cable signals upon the reliability of the use of miniature piezo-electric gauges to record pressure-time signatures in underwater explosions and an account of the cable developed for use with large piezo-electric gauges was given. This cable has now been further modified, the central or inner conductor consisting of seven copper strands 0.012" each in diameter and surrounded by telcothene or polythene to a diameter of 0.29". The outer conductor consists of a tinned copper wire braid and is surrounded by a second layer of polythene, the outside diameter of which is 0.43". This is further covered with a tough rubber sheath, and the overall diameter of the cable is nominally 0.56".

The constants of this cable are as follows:-

(a) Inductance: 0.43 μ H per metre;
(b) Capacity: 59 $\mu\mu$ F per metre;
(c) Surge impedance: 85 ohms;
(d) The variation of capacity with frequency up to 1 megacycle/second is negligible.

It is found that the cable described above gives a very consistent cable signal which, unlike that due to most cables, does not vary with time or with repeated subjection to explosion pressures. The cable signal in itself is not negligible and is in fact greater than that obtained with most cables; effective means of reducing it have, however, been developed, and this report is concerned with a description of its measurement and of the method applied in reducing its value, so as to be able to use the cable, in particular, with miniature gauges.

A reduction of some 500 times has been achieved by coating the inner telcothene core of the above cable with graphite or aqua-dag: this, of course, is the surface which is in intimate contact with the outer conductor of tinned copper braid.

Work on this subject was started in this Establishment early in 1944, and was continued throughout the year. In January 1945 it was learnt that similar investigations had been started independently in January 1944 by

Road .....

Road Research Laboratory working on the theory that cable signal arises from frictional charges in the cable dielectric.

The cable based on this research, was produced by Messrs. Callender and was tried here, but, although apparently entirely suitable for blast and small scale underwater work, it provided unsuitable for the conditions of trial required in this Establishment.

The present report therefore deals with the continuation of the research, applying the general principle to the particular cable defined above.

The principle used in measuring cable signal is as follows; the cable is sealed at one end and a length of several feet is subjected to hydrostatic pressure. The pressure is suddenly released by bursting a copper diaphragm and the signal received, amplified by means of a two-valve amplifier, and then recorded on a cathode ray oscillograph. The amplifier had a reasonably flat response between 100 c/s and 50 kc/s.

The use of long cables, properly terminated, together with the design of an amplifier for use with both large and small gauges, is being proceeded with; but in this connection it need only be stressed that for the tests described in this report the length of cable was kept approximately constant and as short as possible, and that the same amplifier and recording equipment was used throughout these tests.

It will be shown that the minimum size of gauge that can be used for pressure-time measurements of an underwater explosion is entirely dependent upon the cable signal reduction that can be achieved. To use small gauges without reducing cable signal to the order of 1% of the peak pressure expected from the explosion wave can cause incorrect interpretation of the records, particularly in impulse and energy determination because of the long duration of the cable signal. The cable signal value for any cable used with piezo-electric gauges must therefore be known. If it is not small, a correction for it may cause considerable ambiguity in determining the three main properties from an explosion wave record.

EXPERIMENTAL PROCEDURE AND RESULTS.

The work that has been carried out on cable signal has been intermittent. For example, the cable developed for use with piezo-electric gauges has been brought to this final design for reasons explained in the report already referred to in the introduction; other cables of a standard type have been tested also for cable signals, in order to aim at an understanding of the causes of cable signal. Reference to those will not be made except where evidence helps to explain this phenomenon.

(a) Test with "standard" cable; tough rubber sheath outer covering (T.R.S)

Omitting the graphite layer, Plate 1 illustrates the cable used in the test. One end was completely sealed. The central conductors were sealed inside the inner telcothene core, and the braid inside the outer telcothene core. The outer tough rubber sheath was then rubber taped to prevent water from seeping through to the surface of the outer telcothene layer. The insulation resistance of the cable under test (capacity 0.001μF) was infinite, both between the central conductor and the braid, and between the braid and the outside pressure calibration pot or laboratory earth as measured by a 2500 volt megger. Eighteen feet of the cable was placed inside the pressure pot and then subjected to a pressure of 1000 lbs./in.^{2}. The cable had to be shunted with a capacity of 0.075 μF so that the deflection on the cathode-ray tube, expressed in volts, did not exceed the linear output voltage of the 2 valve amplifier (amplification 625). Later as the cable was withdrawn from the pressure pot, the shunting capacity was reduced to 0.020 μF. The cable signal records obtained by a sudden release of pressure, i.e. by bursting the copper diaphragms, are shown in

Plate 2 .....

Plate 2; the spare spot on each oscillogram representing a sine wave oscillation of period 0.001 sec. The deflections have been measured and Table 1 gives the results obtained. Graph 1 shows how the cathode ray deflection varies with the length of cable subjected to pressure for the two values of circuit capacity.

From either of these two curves, the cable signal per foot of cable can be determined. Both curves give practically the same value, and this can be expressed by stating that if the cable capacity were 2500 $\mu\mu$F, and no amplifier were used, the voltage produced across the cathode ray plates would be 0.172 volts if 1 foot of cable were subjected to a pressure of 1000 lbs./in.^{2}.

(b) Test with standard cable; a P.V.C. outer covering

A cable similar to the "standard" type but having a plyvinyl chloride covering instead of rubber was used to examine the variation of signal with pressure. Graph 2 gives the results obtained. For a cable capacity circuit of 2500$\mu\mu$F the voltage produced across the cathode ray plates would thus be 0.121 volts if 1 foot of cable were subjected to a pressure of 1000 lbs./in.^{2}. It is interesting to note here that the commencement of cable signal measurements, about 30 feet of this cable (i.e. with the P.V.C. covering) was subjected to a release pressure of 1000 lbs./in.^{2} when the cable was connected direct to the cathode ray plates in a circuit of approximately 2500 $\mu\mu$F capacity, a deflection of about $\frac{1}{4}$ mm. was obtained. This figure is now confirmed of course by the more elaborate results obtained later and given above. (C.R.O. film sensitivity = 15.85 volts/mm).

(c) Test with Admiralty Pattern rubber covered cable.

Primarily with the object of obtaining evidence as to the cause of cable signal, and also with a view to determining the signal given by such rubber covered cable as were used by former workers with large piezo-electric gauges, Admiralty Pattern 1888 cable was next examined. This consists of 19 strands of tinned copper wire, each strand being 0.018" in diameter, bound with a tough rubber sheath to an overall diameter of approximately 0.35"; a photograph of this cable appears on Plate 1.

The results obtained showed that under the same conditions of subjecting 1 foot of cable to a pressure of 1000 lbs./in.^{2} in a circuit of capacity 2500 $\mu\mu$F. the voltage developed across the plates of the cathode ray tube would be 0.040 volts, but the direction of the cable signal was opposite to that obtained for the two telcothene cables.

The conclusions to be drawn from these tests and the curves illustrated in Graphs 1 and 2 are that the cable signal voltage is (1) directly proportional to the pressure to which the cable is subjected, and (2) directly proportional to the length of cable subjected to pressure. In the case of the cable developed for use with piezo-electric gauges at Admiralty Undex Works, the cable signal is quite large, in the opposite direction to and about 4 times greater than that of one of the standard Admiralty Cables, Admiralty Pattern 1888. Moreover the cable signal for the "standard cable" is in the same direction and nearly 1½ times that of an identical cable where the tough rubber sheath has been replaced by a polyvinyl chloride covering.

THE MAGNITUDE OF CABLE SIGNAL.

At this stage it is necessary to compare the effect of the "standard" cable signal with that of the gauge signal. The piezo-electric gauges being developed at Admiralty Undex Works are of three types, (i) the large two-ply type of dimensions 40 cms. x 4 cms. x 1 cm.; (ii) the medium two-ply type 1" in diameter, $\frac{1}{2}$" thick; and (iii) the small two-ply type $\frac{1}{2}$" in diameter, $\frac{1}{4}$" thick. Eight gauges of type (i) have been completed, each fitted with 250 yards of "standard" cable, but modified to reduce cable

signal .....

signal in the manner described later. Type (ii) is being proceeded with together with the development of amplifier, and the solution of the cable termination problem is being pursued. Type (iii) is being considered but at the moment is in abeyance, pending the practicability of reducing cable signal even if its physical interpretation cannot be explained completely.

In the case of the type (i) gauge, its capacity is about 200 $\mu\mu$ F; and if the gauge is connected by 250 yards of "standard" cable directly to the cathode ray oscilloscope, the total capacity of the circuit will be about 14000 $\mu\mu$ F. The piezo-electric constant of the tourmaline used was about 2.2×10^{-17} coulombs/dyne. Knowing this value, and assuming that the gauge is required to record a pressure of 1000 lbs./in.^{2} from an explosion pulse, it can be calculated that the voltage developed across the cathode ray plates will be 33.3 volts. For the same length of cable, and assuming 30 feet of it to be subjected to the same pressure all in phase, the cable signal will be $\frac{2500}{14000} \times 30 \times 0.172$ volts = 0.92 volts. Hence the cable signal is approximately 3% of the gauge signal, the direction being opposite to that of the pressure pulse. Since the duration of cable signal is long, its effect on impulse and energy is very large with this cable.

To consider the type (ii) gauge, its capacity is only about 20 $\mu\mu$ F, and under similar conditions to those already described, the voltage developed across the cathode ray plates will be only 1.11 volts. It is now seen that the cable signal may be of the same order as the crystal signal.

It need only be pointed out that the voltage developed across the type (iii) gauge can be calculated to be approximately 0.20 volts under similar conditions. The cable signal voltage will therefore be over 3 times as large as that developed by the crystal.

It should be noted that the untreated "standard" cable referred to in this report exhibits a rather large cable signal but the order of magnitude of the effect is the same over the range of untreated cables so far examined. The form of signal obtained with the "standard" cable whether the outer covering be T.R.S. or P.V.C. is almost identical to the signal obtained in calibrating large piezo-electric gauges in the pressure pot, except for direction or polarity.

FURTHER TESTS WITH CABLE (b).

In order to try and elucidate the properties of cable signal, it was next decided to try to protect the cable in the pressure pot. Two and a half feet of the cable with the outer P.V.C. covering was sealed inside a strong canvassed rubber tubing $\frac{3}{4}$" internal diameter and $1\frac{1}{2}$" external diameter with a seal at either end to prevent any trace of water seeping through. A column of air would therefore surround the portion of cable under test. The reduction in cable signal was only 20% and therefore insignificant. (It is remarked that probable a metal tube as outer cover to protect the cable might have given a better result, since it could withstand the subjected pressure without deformation).

The reinforced canvassed tube was next removed, as well as $2\frac{1}{2}$ ft. of P.V.C. thus exposing the outer layer of telecothene to the water. The cable signal was sensibly of the same order of magnitude although a 20% increase was observed, in two tests.

A length of cable✓ was then obtained from the manufacturer, closely resembling cable (b) except that (i) the P.V.C. outer covering was removed, (ii) the thickness of the outer telecothene layer was increased to make the overall diameter approximately the same as cable (b), and (iii) a lapping of copper foil 0.0015" thick was taped over the outer surface of the inner telcothene core, i.e. underneath the braid. The cable signal was still not significantly reduced, the value obtained being about $\frac{1}{3}$ of that obtaining for cable (b).

At .....

✓ The explanation for this test is given later.

At this stage it was thought that balanced-line cables might be selected to give a cable signal of the order of some 10% of the maximum cable signal of a single-conductor cable. But from considerations of the magnitude of cable signal as compared to the gauge signal, already calculated and described above, it was realised that the order of reduction which might be achieved by the use of balanced-line cables was not sufficiently significant, in particular, due to the difficulty in obtaining electrical balance.

TESTS ON OTHER CABLES.

In order to gather evidence about the origin of cable signal, tests were carried out on other cables. Details are not given but the following general conclusions were drawn from the tests.

(1) In the case of telcothene cables, unless the braid was also covered with telcothene, the cable signal appeared to be inconsistent in value for identical repeat shots even though the insulation resistance between the braid and earth was kept high by choice of a water-proof P.V.C. covering.

(2) When the braid was exposed to the water, the polarity of cable signal was reversed: this was also accompanied by some reduction in the value of cable signal.

(3) On one particular occasion, the cable signal reversed in polarity and increased considerably in magnitude, without any trace of water being able to penetrate to the braid through the P.V.C. covering; the only change made was in washing the pot and refilling with new water.

(4) A similar cable to (3) but with a considerably less overall diameter showed a reduction of 2 : 1 in cable signal voltage between observations over two successive days.

(5) One non-telcothene cable in particular was tested - a cable being used extensively, it is believed, by experimenters working with miniature gauges. It consisted of several central conductors enclosed in a soft synthetic thermo-plastic or rubber-like composition, the outside of which is bound with cloth; a tinned copper braid surrounded this and a cotton tape was wound over it, and then apparently a soft P.V.C. compound served as an outer covering.

With successive subjecting to hydrostatic pressure the cable signal exhibited a form of hysteresis effect, becoming gradually worse. When water penetrated to the braid, the cable signal reversal and decrease was again observed. The cable signal varied in value between 1/30th and 1/10th of that obtained for the "standard" cable.

DISCUSSION OF RESULTS.

It was realised that the problem of cable signal was a most difficult one, and might mean a long-term research programme with special facilities for its elucidation. But by the following reasoning, an attack was made which enabled a practical solution to be achieved and a reduction of cable signal by a factor of some 500.

The pressure applied to the "standard" telcothene cable apparently caused an electrostatic charge to be induced, and thus a potential difference to be developed between the central conductor and the braid. This electrostatic charge was shown from the experiments already described to be directly proportional both to the length of cable subjected to the pressure, and to the pressure itself. Also it was found that the

Best Available Copy

potential .....

potential difference developed, as registered by the cathode ray, depended upon the charge induced and on the total circuit capacity.

With high leakage resistance, the charge remained for a long time as indicated in the records. This long period may affect measurements of impulse and energy in the pressure pulse to a large and unknown degree.

In the case of the cable under heading (5) in "Tests on other Cables", it was concluded that the frictional charging effects in the rubber composition dielectric were reduced by the cloth and tape fillings either side of the braid. Water penetrating to the braid produced a reversal of the signal.

It was concluded also from the telephone cable results that the cable signal in the main was produced between the inner core dielectric and the braid. Consequently, it was presumed that if the braid made a more intimate contact with the dielectric, a marked reduction might be obtained. Hence, although it was not considered altogether sound to have a cable constructed similar to the "standard" cable but without an outer covering altogether, since an outside rubber covering had worsened cable signal as compared to a polyvinyl chloride covering, yet on the other hand, tests had revealed that the cable signal was about the same with or without a P.V.C. covering: consequently to save time such a sample length was manufactured with a copper foil lapped underneath the braid. The result was disappointing although a three-fold reduction in cable signal was definite.

This naturally led to the further consideration that if the inner dielectric core of the cable was covered with say aqua-dag or graphite, success might very well result.

FINAL TESTS ON "STANDARD TREATED" CABLE.

The inner telcothene core of the "standard" cable with its outer rubber covering was now subjected to an aqua-dag or graphite treatment; that is, the outer surface of the inner core in intimate contact with the braid was covered with this conducting layer uniformly sprayed over it.

Tests carried out with sample lengths of cable gave very satisfactory cable signal reduction. These tests are still not quite completed but it is anticipated that they will prove to be completely satisfactory, when the cable is produced on a large scale. Results at present have proved that hand-made sample lengths have given a greater reduction (of the order of 3 times) than cable produced in long lengths of 250 yards for example. This discrepancy is being pursued and has been taken up with the manufacturer. But it can be stated that at the present stage of production, the reduction is such that when 1 ft. of cable is subjected to a pressure of 1000 lbs./in.^{2} and the circuit capacity is maintained at 2500 $\mu\mu$F, the voltage developed is 1 millivolt compared to 0.172 volts for the same cable untreated. Hand-made samples, where by inspection, the aqua-dag has been thicker and more uniformly sprayed has given a reduction to $\frac{1}{4}$ millivolt under the same conditions, so that the reduction has been of the order of 500 and 170 times respectively for the hand-made and the bulk method of manufacturing the "standard" treated cable.

RE-CONSIDERATION OF THE MAGNITUDE OF CABLE SIGNAL.

Taking the lower cable signal reduction factor of 170, for the three types of gauges already described, the following results are obtained:-

Cable signal = 0.92 volts (under conditions already specified, namely 30 ft. of cable subjected to 1000 lbs./in.^{2} in a trial where 250 yards of standard cable of total capacity 14000 $\mu\mu$F is used).

Hence cable signal now = $\frac{0.92}{170}$ = 0.0054 volts.

Best Available Copy

(1) .....

(1) For the large two-ply gauge of dimensions 40 cms. x 4 cms. x 1 cm.,
Gauge signal = 33.3 volts.

$$\text{Ratio } \frac{\text{Cable signal}}{\text{Gauge signal}} = \frac{.0054}{33.3} \doteq 0.02\%$$

(2) For the medium two-ply gauge of dimensions 1" diameter and $\frac{1}{8}$" in thickness,
Gauge signal = 1.11 volts.

$$\text{Ratio } \frac{\text{Cable signal}}{\text{Gauge signal}} = \frac{.0054}{1.11} \doteq 0.5\%$$

(3) For the miniature two-ply gauge of dimensions $\frac{1}{8}$" in diameter and $\frac{1}{4}$" in thickness,
Gauge signal = 0.28 volts.

$$\text{Ratio } \frac{\text{Cable signal}}{\text{Gauge signal}} = \frac{.0054}{0.28} \doteq 2\%$$

If, as expected, the cable manufacturer can produce in bulk, "standard treated" cable, similar to the samples, the percentages given above will be reduced three-fold.

CONCLUSIONS.

The "standard treated" cable developed and referred to in this account appears to be highly satisfactory for use with both large and miniature gauges. These gauges are being produced at this Establishment together with piezo-electric recording equipment.

The variation of capacity with frequency is negligible up to 1 megacycle for this particular cable. Cable signal has been reduced to a reasonably small portion of the gauge signal.

TABLE 1 /

SIGNALS RECORDED FOR VARIOUS LENGTHS OF "STANDARD" CABLE WHEN SUBJECTED TO RELEASE PRESSURES OF 1000 lbs./in^2.

RECORD NO.	*LENGTH OF CABLE IN PRESSURE POT (ft)	TOTAL CIRCUIT CAPACITY AT AMPLIFIER INPUT (μ F)	CATHODE RAY DEFLECTION IN MILLIMETERS
1	18	0.076	4.15
2	18	0.076	4.0
3	13½	0.076	3.0
4	9	0.076	2.1
5	4½	0.076	1.05
6	4½	0.021	3.45
7	3	0.021	2.45
8	1½	0.021	1.05

TABLE 2 X

SIGNALS RECORDED FOR A CONSTANT LENGTH (24 ft.) OF CABLE WHEN SUBJECTED TO VARYING PRESSURES.

RECORD NO.	RELEASE PRESSURES (lbs./in^2)	TOTAL CIRCUIT CAP. AT AMPLIFIER INPUT (μ F)	CATHODE RAY DEFLECTION IN MILLIMETERS
9	987½	0.060	4.7
10	497½	0.060	2.3
11	270	0.060	1.2
12	245	0.060	1.1
13	500	0.060	2.3
14	975	0.060	4.7

/ Cable with outer covering of rubber

X Cable with outer covering of P.V.C.

ADDENDUM

THE ELECTRIC POTENTIALS PRODUCED IN THE CONDUCTORS OF A SUBMERGED CABLE BY UNDERWATER EXPLOSIONS.

SUMMARY.

Further work on the lines of this report has resulted in the practical elimination of unwanted signals induced directly by underwater explosions in cables used for piezo-electric measurements.

DISCUSSION OF RESULTS.

(1) Further development has proceeded with a view to reducing "cable signal" in the case of the cable shown in Plate 1 of the above report. Two changes have been made, namely, (a) graphiting the outer surface of the inner core of the cable underneath the braid with a much thicker coating than hitherto, and (b) graphiting the inner surface of the inner core which is in contact with the central conductors.

(2) The manufacturers producing specimens of this cable for experimental research at this Establishment have now been able to manufacture on production scale an equally satisfactory cable as a hand-made specimen.

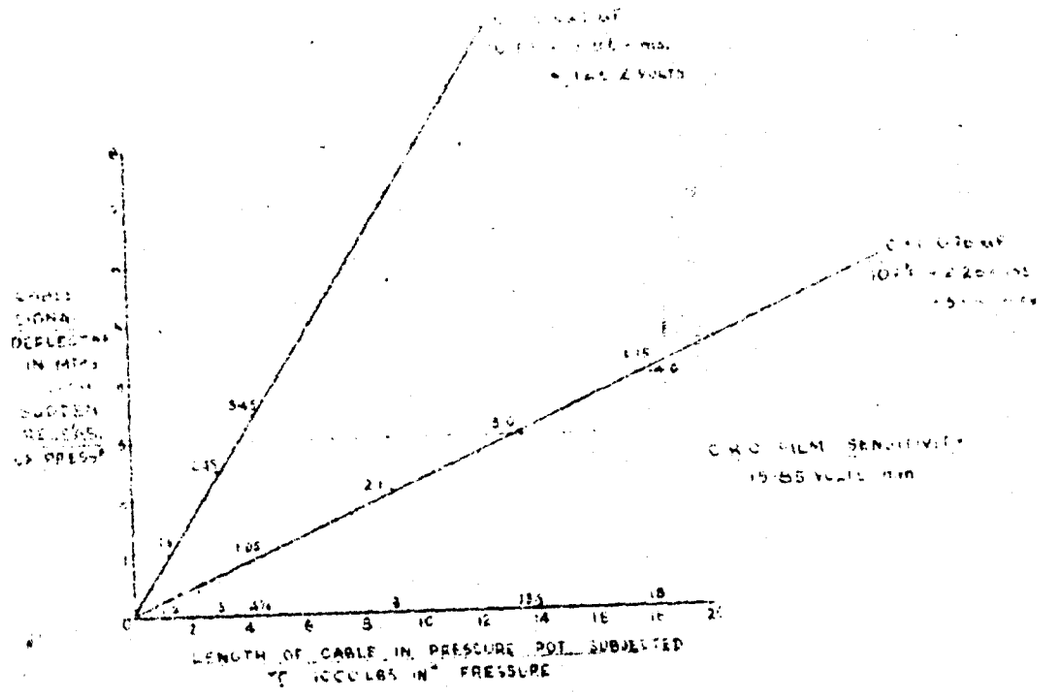
(3) The magnitude of the cable signal for 1 ft. of this cable when subjected to 1000 lbs./in.^{2} pressure in a circuit of capacity 2500 $\mu\mu$F was found to be 0.172 volt. In the previous report it was observed that this value had been reduced to 1 millivolt for a production length whereas a hand-made length gave a value of about $\frac{1}{4}$ millivolt. The new figure achieved is of the order of 40 microvolts under the same pressure and circuit conditions when both effects (a) and (b) above have been introduced, showing a reduction in "cable signal" of some 4000 times compared with untreated cable. The method of carrying out the tests is the standardised one described in the above report.

(4) The implications of this improvement may be illustrated by the following calculations. Assuming a total length of cable 250 yards (capacity 14000 micro-micro farads) of which 30 ft. is immersed and subjected to a pressure of 1000 lbs. per square inch is used with a two ply gauge $\frac{1}{2}$" in diameter and $\frac{1}{4}$" thickness then the ratio of cable signal to gauge signal will not exceed 0.1%. If the crystal dimensions are reduced to 3/16" diameter and 3/32" thickness the ratio will be about 0.5%.

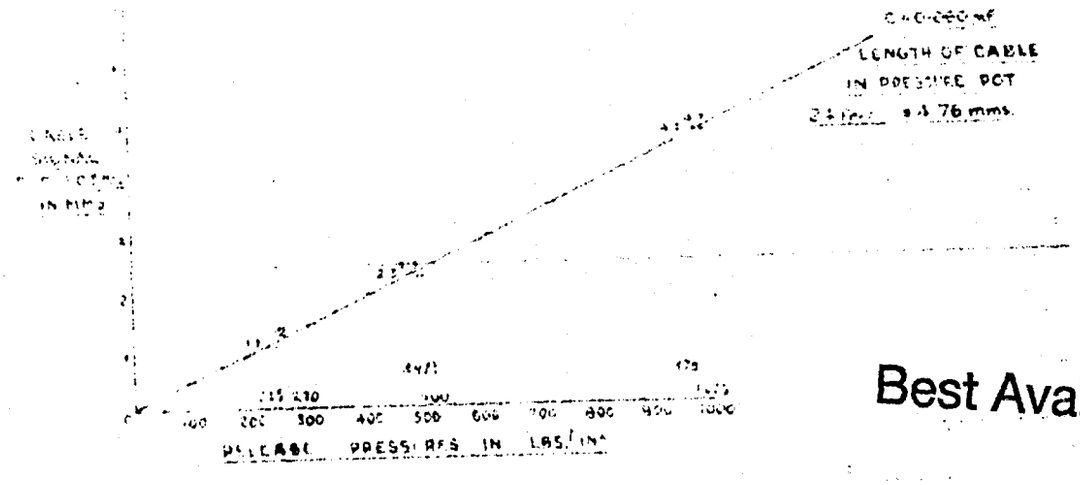
CONCLUSIONS.

The investigations reported in the report and this addendum have resulted in the production of a cable in which the unwanted parasitic signals due to the impact of the explosive pressure on the cable have been reduced to negligible dimensions.

2. This work may be regarded as a necessary and successful preliminary to the development of piezo-electric gauges of dimensions small enough to be regarded as suitable for recording the pressure history at a point.



GRAPH 1

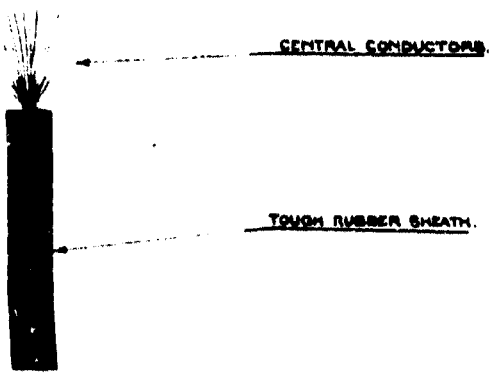


GRAPH 2

Best Available Copy

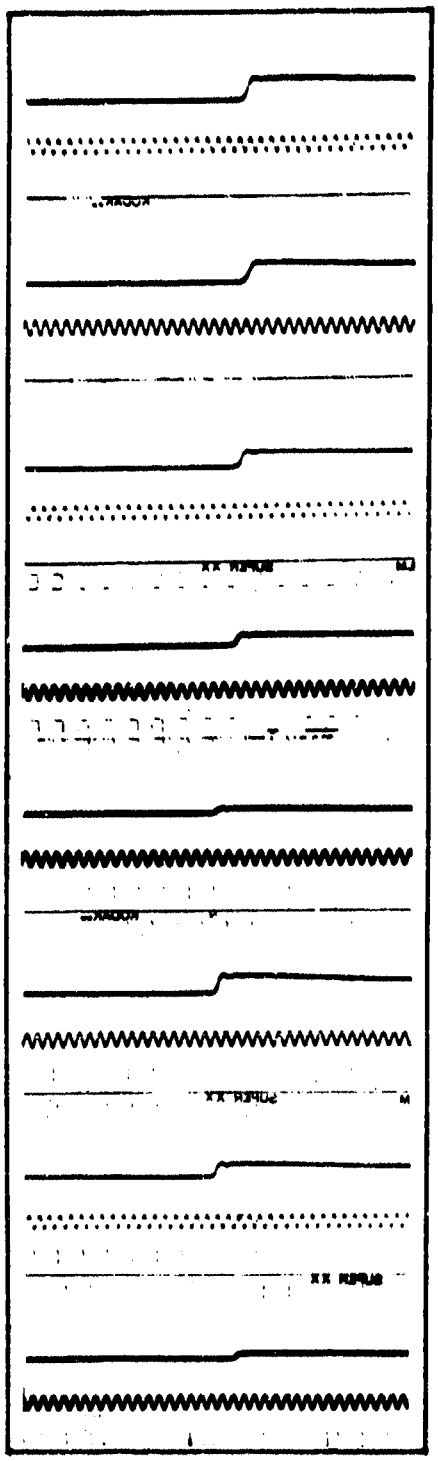


STANDARD TREATED CABLE.



CABLE ADMIRALTY PATTERN 1888.

PLATE. I.



VARIOUS LENGTHS OF "STANDARD" CABLE SUBJECTED TO 1000 LBS/IN^2 PRESSURE.
CIRCUIT CAPACITY REDUCED (SEE TABLE 1) FOR LAST THREE RECORDS.

ELECTRICAL INSTRUMENTS FOR STUDY OF UNDERWATER EXPLOSIONS AND OTHER TRANSIENT PHENOMENA

R. H. Cole, David Stacey, and R. M. Brown
Underwater Explosives Research Laboratory
Woods Hole Oceanographic Institution

American Contribution

30 November 1945

Personnel

The work described in this report has been carried out by a number of people working both individually and as groups during the past three years. As a result, it would be a difficult and complicated task to assign due credit to all persons involved in any specific development, and no attempt at such specific acknowledgement is made here.

The work has been done under the general supervision of R. H. Cole; David Stacey has been in charge of most of the electronics development and maintenance; the personnel involved has included R. M. Brown, C. P. Slichter, and R. L. Kaye. Others who have assisted for varying lengths of time are P. F. Smith, W. A. Adcock, A. F. Redfield, and B. Coggins.

This report was written by R. H. Cole, David Stacey, and R. M. Brown.

Paul C. Cross
Underwater Explosives Research Laboratory
Woods Hole Oceanographic Institution
Woods Hole, Massachusetts
October 31, 1945

CONTENTS

	Page
Abstract	1
Part	
I. INTRODUCTION	1
II. BASIC ELECTRONIC EQUIPMENT	5
1. Amplifiers	5
(a) Frequency-response characteristics	5
(b) Input impedance	15
(c) Linearity and stability	15
(d) Amplifier circuits; diagrams and descriptions	15
2. Cathode-ray tubes and supplies	26
(a) Cathode-ray tubes	27
(b) Power supplies	27
(c) Intensity-modulation coupling circuits	29
3. Time bases and synchronization circuits	31
(a) Linear time base	32
(b) Time delay and beam brightener	35
(c) Trigger-circuit beam brightener	36
(d) Synchronization circuits	36
III. PHOTOGRAPHIC RECORDING	41
IV. CALIBRATION EQUIPMENT	45
4. Transient voltage standards	46
(a) Standard voltage sources	46
(b) Step-function generators	47
5. Time standards	51
(a) Multivibrators	52
(b) Tuning forks	54
(c) Stabilized oscillator	54
(d) Miscellaneous circuits	54
6. Impedance standards	54
(a) Capacitance bridge	56
(b) Q-step calibration	58

PRECEDING PAGE BLANK

Part		Page
V.	MISCELLANEOUS	61
	7. Alternating-current power	61
	8. Master control panels	61
	9. General considerations in instrumentation	62

List of Figures

Figure		Page
1.	Block diagram of equipment for transient recording	2
2.	Transient response to an exponential pulse; high-frequency attenuation	9
3.	Peak response and time of response to exponential pulse	10
4.	Transient response to an exponential pulse; low-frequency attenuation	14
5.	Diagram of modified DuMont type 208 oscillograph amplifier	17
6.	Frequency-response curve: modified DuMont type 208 cathode-ray oscillograph	18
7.	Exponential transient-response curve	18
8.	View of four-channel oscillograph amplifier unit	21
9.	Diagram of four-channel oscillograph amplifier unit	22
10.	View of four-channel oscillograph amplifier and cathode-ray tube panels	23
11.	Diagram of four-channel oscillograph cathode-ray tube circuits	24
12.	Diagram of four-channel oscillograph amplifier supply	25
13.	Diagram of regulated 1300-volt supply	28
14.	Diagram of voltage-level shifter	30
15.	Diagram of linear time base, trip, and sweep circuits	33
16.	Diagram of linear time base, power supply, and beam brightener	34
17.	Diagram of time-delay beam brightener	37
18.	Diagram of trigger-circuit beam brightener	38
19.	View of camera hood and camera backs	43
20.	View of camera hood and rotating-drum camera back in place on oscillograph	44
21.	Diagram of high-current standard-voltage source	47
22.	Diagram of relay step-function generator	49

Figure		Page
23.	Diagram of electronic step-function generator	50
24.	Diagram of crystal-controlled multivibrator	53
25.	Diagram of stabilised L-C oscillator	55
26.	Diagram of capacity bridge	57
27.	Connections for Q-step calibration	59
28.	Diagram of master control panel	63

Abbreviations

In the circuit diagrams the following abbreviations are employed:

(a) μsec = microseconds. msec = milliseconds.
kc = kilocycles/second.

(b) Resistance values are in ohms unless followed by suffixes K or M to indicate thousands or millions of ohms. For example 3K = 3000 ohms. Resistances are ½ watt unless otherwise indicated. WW means wirewound.

(c) Capacity values are in microfarads (μf) unless otherwise indicated.

(d) Inductance values are in henries (h) or millihenries (mh).

ELECTRICAL INSTRUMENTS FOR STUDY OF UNDERWATER EXPLOSIONS AND OTHER TRANSIENT PHENOMENA

Abstract

This report contains diagrams and brief descriptions of electronic circuits used at the Underwater Explosives Research Laboratory for recording transients: amplifiers for cathode-ray tubes, time bases, time delays, and calibration equipment. Most of these circuits are intended primarily for use with piezoelectric pressure gauges but are readily adaptable to other types of gauge or pickup. Related pieces of apparatus, such as master control units, cameras, and special firing circuits, are also described. The requirements to be met by equipment used in recording transients are discussed at some length.

I. INTRODUCTION

In order to examine the properties of underwater explosions and their effects it is very desirable to be able to obtain a continuous record in time of such quantities as pressure, acceleration, and deformation. The most powerful class of tool for doing this is an appropriate electrical "transducer" for developing electrical signals proportional to the mechanical quantity. This is followed by a recording cathode-ray oscillograph together with appropriate auxiliary equipment for its operation. The purpose of this report is to make available details of circuits which have been successfully used at the Underwater Explosives Research Laboratory (UERL), together with some discussion of the requirements for such circuits and their operation. Very little of the equipment described is wholly original -- some of it having been adapted from commercially available instruments — and much of it has room for improvement. It has, however, been developed sufficiently to obtain useful results in field work with reasonable precision. This report is written in the hope that information about such equipment will be of use to others.

The block diagram (Fig. 1) represents the various elements involved in recording transients by a cathode-ray tube. The signal from the gauge or pickup is ordinarily too small to be applied directly to the cathode-ray tube without an intermediate amplifier, and a voltage calibration of the amplifier and tube is necessary. For a permanent record of deflection

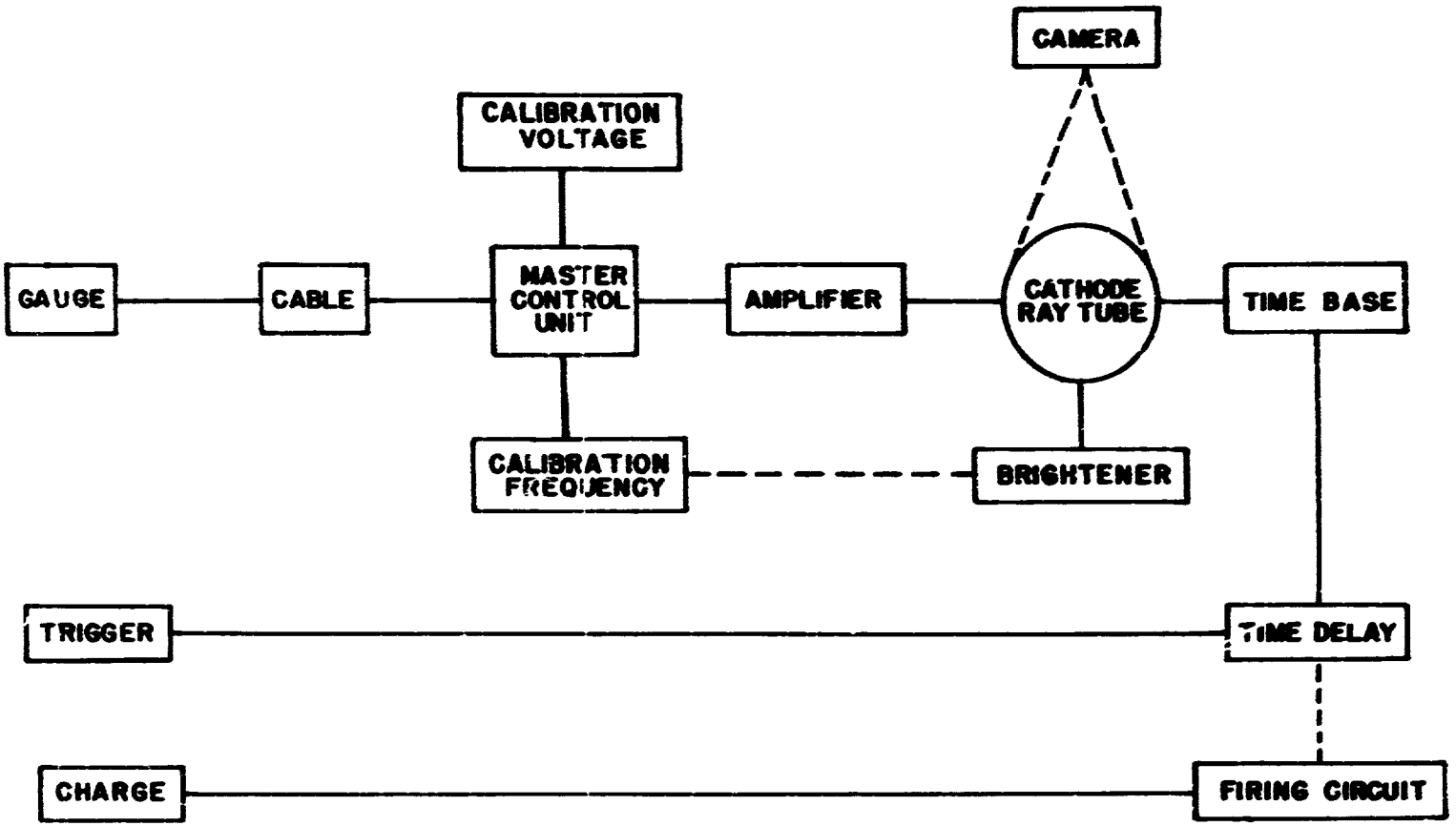


FIG. 1.
BLOCK DIAGRAM OF EQUIPMENT
FOR TRANSIENT RECORDING.

against time, photographic recording of the spot is made. The spot may be moved across the screen at a uniform rate and a still picture taken, or the film may be moved past the image of the spot at constant speed. If a linear sweep (time base) is used to move the spot, the starting of this tracer must be synchronized properly with the event to be recorded by some trigger signal; it is convenient in some cases to add a controlled interval between the two by a time-delay circuit. Further, it is nearly always necessary to increase the cathode-ray spot intensity for a suitable time interval and again turn it off, because mechanical camera shutters are usually too slow and inaccurate. Some sort of calibration of the speed of the spot or film is also necessary and can be supplied to the tube from a reference oscillator either as a deflection signal or as a modulation (dotting) of the spot intensity.

Auxiliary equipment is also necessary to provide suitable power for operation and, if much routine recording is to be done, master control (switching) circuits for the various operations are a great time saver.

It should be noted that the equipment described in this report was developed for use in the underwater explosion research at this laboratory. The instrumentation for air-blast work is to be described separately in NDRC Report A-373 (OSRD-6251).

II. BASIC ELECTRONIC EQUIPMENT

1. Amplifiers

The requirements of an amplifier for recording transient signals depend, of course, on the nature of the transient: its magnitude, the impedance of the gauge or pickup circuit, the maximum rate of change, and the duration of the signal. For example, shock pressures or accelerations rise very rapidly to a large peak value and fall to a very small value in a few milliseconds, whereas displacements or bubble-pulse pressures may have only a gradual smooth rise over a comparatively long time interval. In the first case, severe demands are imposed on the high-frequency response; in the second, the response must be good at long times after application of a signal if distortion is not to result. An amplifier to be used with a piezoelectric gauge or other high-impedance device must have a high input impedance in order not to distort the signal, and under some conditions it is essential that it not be microphonic as a result of shock. No matter what its use, the amplifier should have sufficient undistorted output to provide an adequate range of deflection voltage for the cathode-ray tube plates, and its gain should remain constant over a period of time sufficient for recording and calibration.

(a) Frequency-response characteristics. -- The frequency-response requirements for recording transients can best be appreciated by considering specific cases. An analysis which has proved useful in work at UERL is that of the effect of simplified response functions, which approximate the characteristics of resistance-coupled amplifiers, on a transient pulse having the form of a discontinuous rise followed by an exponential decay. The results[1] are sufficiently simple to bring out clearly the design problems and properties of circuit transient response and to give an approximate idea of the errors to be expected in practical cases.

---

[1] These results have been reported elsewhere in less detail; see Measurement of underwater explosion pressures, by E. B. Wilson and R. H. Cole, OSRD-523.

(i) High-frequency response. In an ordinary resistance-coupled amplifier stage, the high-frequency response falls to zero with increasing frequency because of the shunting capacity of circuit elements (tubes, resistors, wiring) in parallel with the load resistor across which the response signal is developed.

The relative response of this circuit to a signal of frequency f is given by

$$F(\omega) = [1 + (\omega\tau)^2]^{-\frac{1}{2}}, \tag{1}$$

where $\omega = 2\pi f$ and the "time constant" $\tau = RC$ — where R is the load resistance and C is the total circuit capacitance in parallel with it. The quantity τ can be evaluated from the response curve, as it is equal to $1/2\pi f_c$, where f_c is the frequency at which the response has fallen to 70 percent of its value at lower frequencies. The admittance function, of which the response $F(\omega)$ is the modulus, is

$$F(p) = \frac{1}{1 + p\tau}, \tag{2}$$

where $p = i\omega$ and $i = \sqrt{-1}$. The transient response resulting from the action of this or any other admittance function on a transient pulse F(t) is most easily obtained by the use of Fourier transforms, or pairs, if these can be found for the functions involved. An extensive table of these pairs compiled by Campbell and Foster,[2/] hereafter referred to as C-F, simplifies this procedure.

An applied transient S(t) in the form of a negative exponential

$$S(t) = Ae^{-t/\theta} \tag{3}$$

has the transform

$$M[S(t)] = A/(p + 1/\theta). \quad [C\text{-}F, \text{ Pair } 438]$$

[2/] G. A. Campbell and R. A. Foster, Fourier integrals for practical applications, Bell Telephone System Monograph B-584.

The response R(t) resulting from the admittance function [Eq. (2)] is then the transform

$$R(t) = M\left[F(p)\, M\,[S(t)]\right]$$

$$= M\left[\frac{1}{1 + p\tau} \cdot \frac{A}{p + 1/\theta}\right].$$

Therefore

$$R(t) = \frac{A}{1 - \frac{\tau}{\theta}}\left[e^{-t/\theta} - e^{-t/\tau}\right]. \qquad \text{[C-F, Pair 11d]} \tag{4}$$

The result [Eq. (4)] is plotted in Fig. 2 as a function of the reduced time t/θ for various values of the ratio θ/τ. If $\theta \longrightarrow \infty$, corresponding to an input pulse in the form of a stepwise charge of infinite duration, the response is $R(t) = A\left[1 - e^{-t/\tau}\right]$, and it is evident that τ is the time constant of the rise to the limiting value A. Unless this time constant τ is much smaller than the time constant θ of the applied pulse ($\theta/\tau \gg 1$) it is evident from Fig. 2 that considerable distortion of the initial part of the curve and loss of peak height result. From the plot it can be seen that the maximum of the response curve lies on the true response curve (the curve marked $\theta/\tau = \infty$ in Fig. 2). This is readily shown by the usual means from Eq. (4): setting the derivative of Eq. (4) equal to zero gives for time t_M of the maximum

$$t_M = -\frac{\tau}{1 - \frac{\tau}{\theta}} \log_e\left(\frac{\tau}{\theta}\right), \tag{5}$$

and substitution of this value in Eq. (4) gives for the maximum response

$$R(t_M) = A\left(\frac{\tau}{\theta}\right)^{-\frac{\tau/\theta}{1 - \tau/\theta}}. \tag{6}$$

It is easily seen from Eq. (6) that $R(t_M) = Ae^{-t_M/\theta} = S(t_M)$.

Plots of $R(t_M)/A$ and t_M/θ as functions of the time-constant ratio θ/τ are shown in Fig. 3. It can be seen that the maximum response $R(t_M)/A$ approaches unity asymptotically as θ/τ approaches infinity, and that this

ratio must be very large if appreciable reduction in peak height is to be avoided. For example, a loss of only 2 percent of the peak requires that $\theta/\tau = 300$. If a pulse of time constant $\theta = 50\ \mu$sec is to be recorded with this accuracy, $\tau = 0.17\ \mu$sec, and the amplifier stage should have 70 percent of its midband response at a frequency $f_c = 1/2\pi\tau = 950$ kc.

Another property of the response characteristic is that the area under the response curve for any value of θ/τ is equal to that under the applied transient if the integration is extended to infinite time. This appears reasonable from Fig. 2 and is easily proved by direct integration of Eqs. (3) and (4):

$$\int_0^\infty R(t)\,dt = \frac{A}{1 - \frac{\tau}{\theta}} \left[\theta\left(1 - e^{-t/\theta}\right) - \tau\left(1 - e^{-t/\tau}\right)\right]_0^\infty = A\theta,$$

$$\int_0^\infty S(t)\,dt = A\left[\theta\left(1 - e^{-t/\theta}\right)\right]_0^\infty = A\theta.$$

It is interesting to consider the area under the response curve for more general conditions. Let the response curve of the applied signal $F(t)$ be $R(t)$, and the response to an applied step signal be $S(t)$. If the system is linear, the response $R(t)$ may be expressed as a function of $F(t)$ and $S(t)$ by the superposition theorem.[3/]

The relation may be written

$$R(t) = S(0)\ F(t) + \int_0^t F(x)S'(t - x)\,dx, \tag{7}$$

where the prime superscript indicates differentiation with respect to the argument of the function. In the present case $S(0)$, the response at zero time to a step voltage, can be taken as zero. If we integrate from $t = 0$ to $t = t'$, the area $A(t')$ under the response curve is

---

3/ For a discussion of the superposition theorem, see Gardner and Barnes, Transients in linear systems (1942).

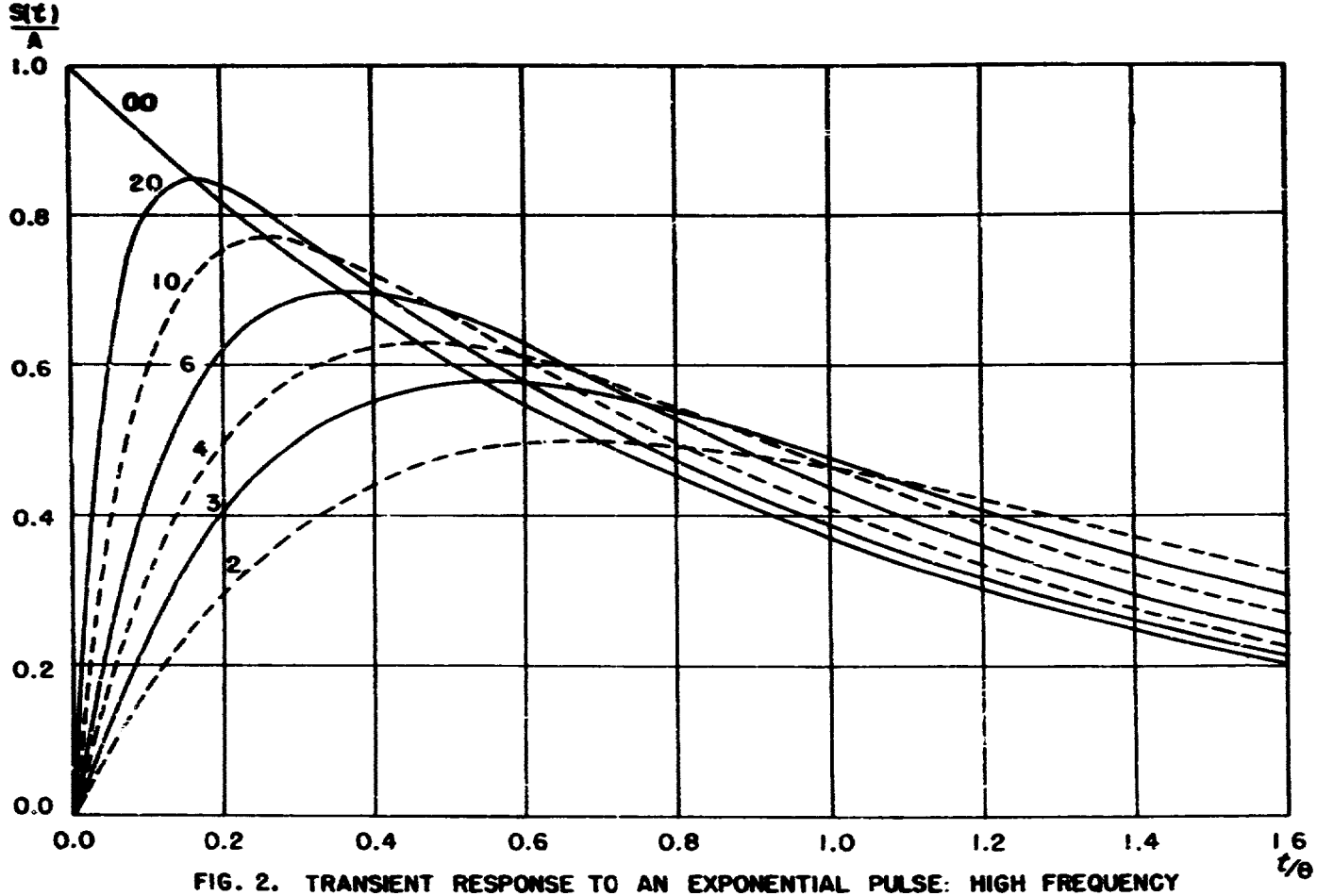


FIG. 2. TRANSIENT RESPONSE TO AN EXPONENTIAL PULSE: HIGH FREQUENCY ATTENUATION. EACH CURVE IS IDENTIFIED BY ITS VALUE OF θ/τ.

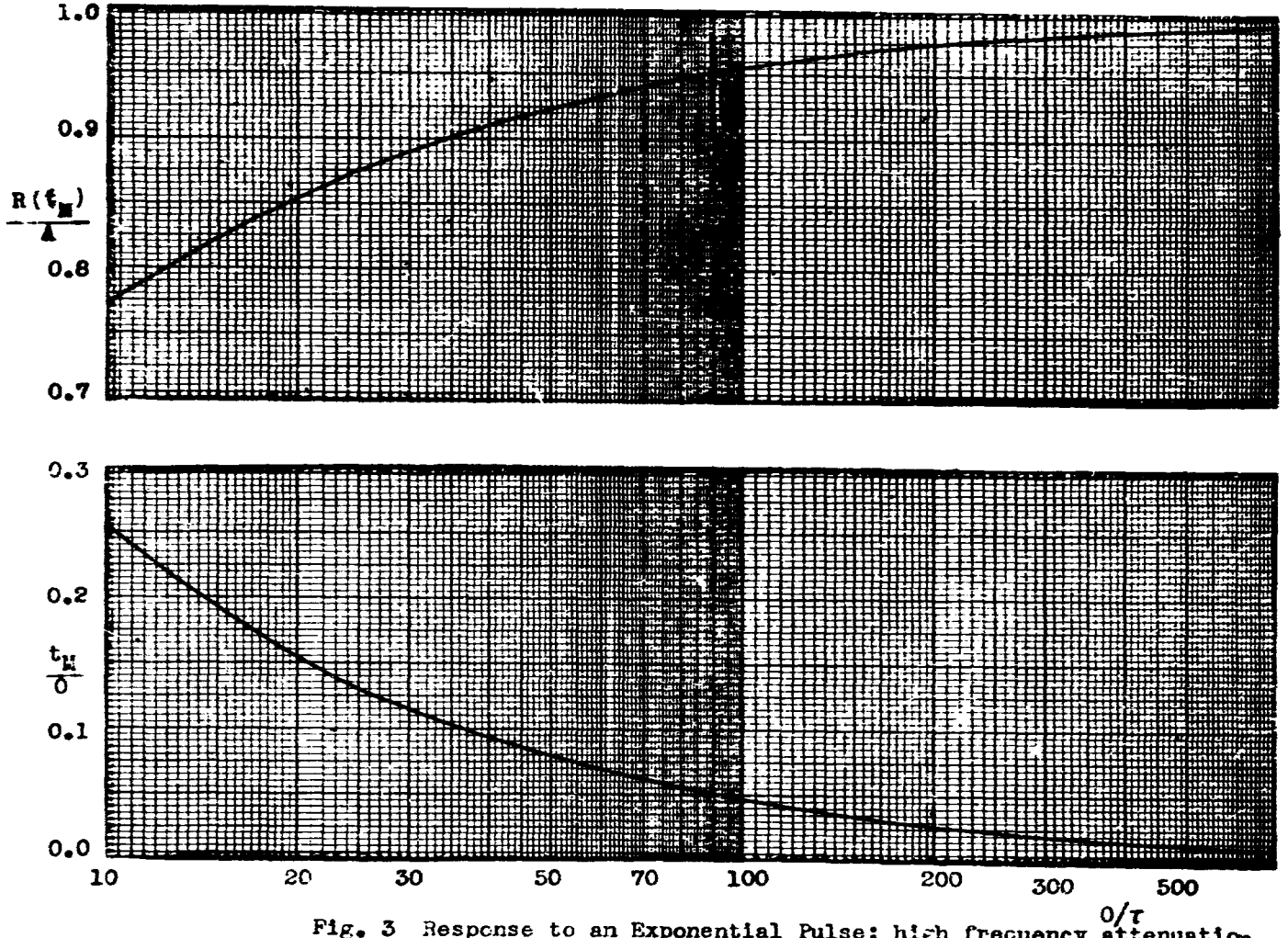


Fig. 3 Response to an Exponential Pulse; high frequency attenuation. Upper curve: peak response. Lower curve: time of response.

649

$$A(t') = \int_0^{t'} R(t)\,dt = \int_0^{t'} \int_0^{t} F(x)\, S'(t-x)\,dx\,dt.$$

Interchanging the order of integration and integrating over t, we obtain

$$(8) \qquad \begin{cases} A(t') = \displaystyle\int_0^{t'} F(x) \int_0^{t'} S'(t-x)\,dt\,dx \\ \qquad\quad = \displaystyle\int_0^{t'} S(t'-x)\, F(x)\,dx\,, \quad \text{if } S(0) = 0. \end{cases}$$

If the applied function F(x) becomes negligible in a time somewhat less than t' and the step response is essentially flat over the remaining interval, the area A(t') is determined essentially by the limiting value of the step response at long time. For example, if the step response S(t) has a limiting, or shoulder, value $S(\infty)$ as $t \to \infty$, and the applied function is significant over a limited time range, the appropriate response value for use in area calculations is $S(\infty)$. The limiting response area under the response curve as t' approaches infinity is

$$(9) \qquad A(\infty) = \lim_{t' \to \infty} \int_0^{t'} S(t'-x)\, F(x)\,dx.$$

If interchanging the integration and limiting processes is legitimate,

$$(10) \qquad A(\infty) = \int_0^{\infty} \lim_{t' \to \infty} S(t'-x)\, F(x)\,dx.$$

For functions S(X) and F(X), which converge sufficiently rapidly to limiting values $S(\infty)$ and zero, respectively, as X approaches infinity, this becomes

$$A(\infty) = S(\infty) \int_0^{\infty} F(x)\,dx.$$

Under such conditions, the area under the response curve is independent of the high-frequency response characteristics and is, except for the instrument factor $S(\omega)$, equal to the area under the applied signal. It is difficult to state any very general condition on the functions S(X) and F(X) sufficient to insure this result, but its legitimacy can be readily determined for any fairly definite set of conditions.

(ii) Low-frequency response. The failure of electrical circuits to have a finite response as the frequency approaches zero is usually due to the presence of capacitance in the circuit as a series element.[4] In the case of conventional voltage amplifiers, successive stages are coupled by condensers in order not to cascade operating potentials of the tubes. If the plate of one stage is coupled to the next grid by a capacitor C in series with the grid resistor R, the signal applied to the grid has the magnitude

$$F(\omega) = \frac{\omega}{\left[1 + (\omega\lambda)^2\right]^{\frac{1}{2}}}$$

relative to the signal across the network, where $\lambda = RC$. The admittance function is then

$$F(p) = \frac{p\lambda}{1 + p\lambda}.$$

The response R(t) to an applied exponential transient $S(t) = S(0)e^{-t/\theta}$ is given by the Fourier transform

$$R(t) = M\left[F(p)\ M\left[S(t)\right]\right] = S(0)\ M\left[\frac{p\lambda}{1 + p\lambda} \cdot \frac{1}{p + 1/\theta}\right].$$

The solution of this equation is

$$R(t) = S(0)\ \frac{e^{-t/\theta}}{1 - \frac{\theta}{\lambda}}\left[1 - \frac{\theta}{\lambda}\, e^{-\left(\frac{1}{\lambda} - \frac{1}{\theta}\right)t}\right]. \tag{11}$$

---

[4] Gauges which have an internal impedance equivalent to a capacitance will also have zero response at zero frequency if shunted by any resistance element. These conditions occur, for example, with a piezoelectric gauge shunted by the input resistance of an amplifier circuit. The analysis of the case is similar to that for the amplifier-coupling circuit.

This expression is plotted in Fig. 4 as a function of t/λ for a ratio $\theta/\lambda = 1/10$ (that is, amplifier time constant ten times that of the pulse). It is seen that, while the response curve has the same general form as the applied signal, it falls increasingly below the true curve as the time increases.[2/]

If one integrates Eq. (11) to infinite time, one finds that the total area under the response curve is zero. Hence the curve must go negative and remain so for a considerable interval, this interval increasing as the time constant λ increases. The result of zero total area is to be expected quite generally on the basis of the superposition theorem derivation carried out above. It was shown that the response area is determined primarily by the limiting value of the step-response characteristic at infinite time, which is zero for conventional amplifiers and circuits involving capacitative couplings (as already noted, piezoelectric or simple capacitance-type gauges have equivalent circuits of this form).

The error in area measurements for an exponential pulse can be calculated from the integral of Eq. (11). If the time t' to which the integration is carried is not greater than one-tenth the time constant λ of the circuit, the fractional error $\Delta A/A$ in the area $A(t')$ is approximately given by

$$\frac{\Delta A}{A} \approx \frac{t' - \theta}{\lambda}, \qquad \text{if } t' < 10\lambda. \tag{12}$$

If this error is to be less than 5 percent, the amplifier time constant must be at least twenty times that of the pulse. Equation (12), although approximate, is very useful as a guide in circuit design.

It must be remembered that the analysis leading to Eq. (12) is based on the assumption that the low-frequency response is that of a single R-C circuit. If low-frequency compensation is provided in the amplifier, the response can be improved over a limited range of frequencies in the cutoff region. This can be expressed in terms of an equivalent time constant, based

---

[2/] If the time constant λ of the circuit is much longer than the time constant θ of the signal, the correction term can be approximated by a series expansion. The first-order correction, neglecting the square and higher powers of (t/λ), is then

$$R(t) \approx S(0)e^{-t/\theta}\left[1 - \left(1 - \frac{\theta}{\lambda}\right)\left(\frac{t}{\lambda}\right)\right]$$

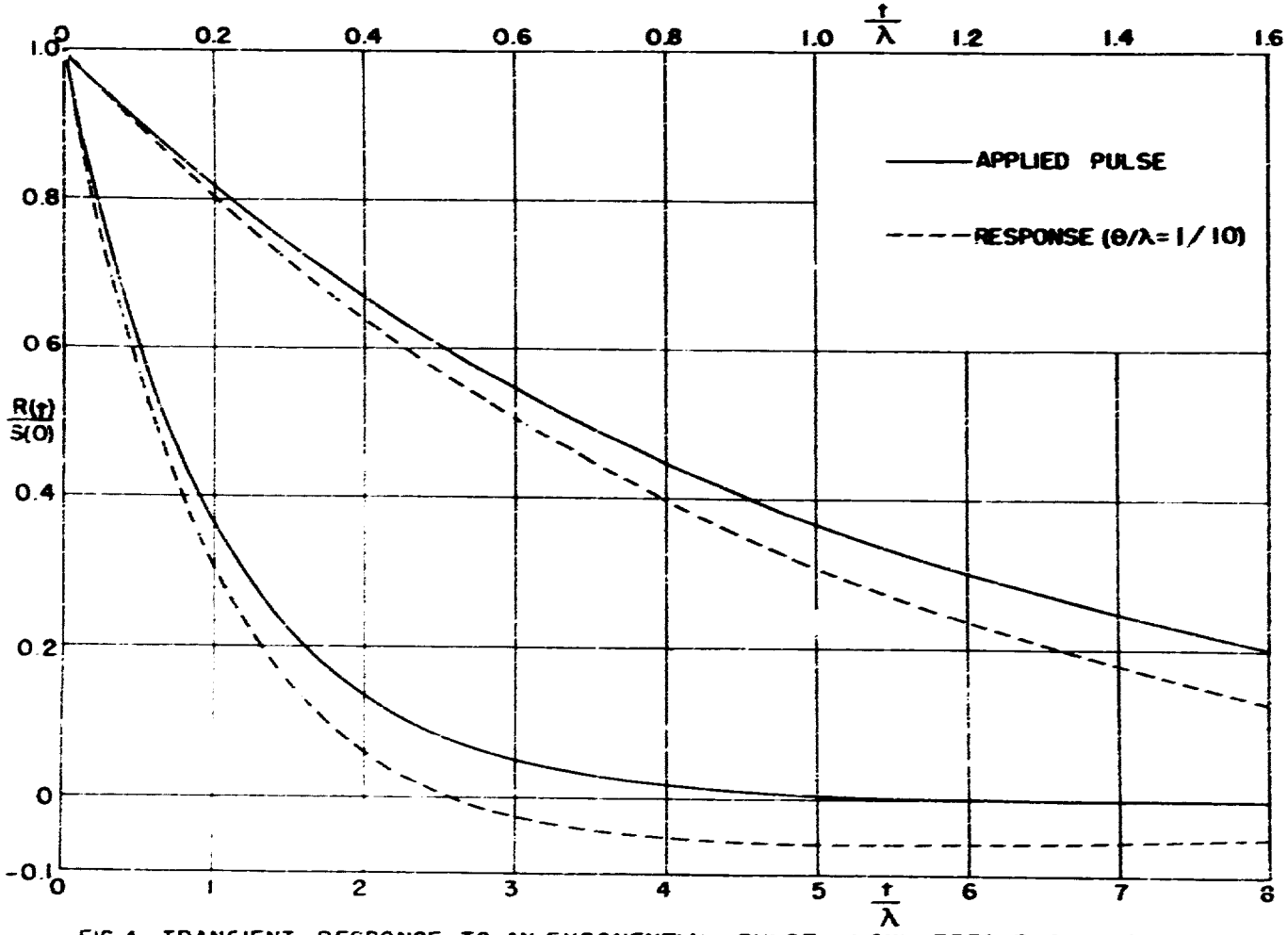


FIG 4 TRANSIENT RESPONSE TO AN EXPONENTIAL PULSE: LOW FREQUENCY ATTENUATION
THE TIME SCALE OF THE LOWER CURVES IS ENLARGED FIVE TIMES FOR THE UPPER CURVES

653

on the initial rate of decay in response to a step voltage. This can be made much greater than the value for an uncompensated amplifier, but is applicable only if the time of measurement t' does not exceed the time for which the compensation is effective.

Although the analyses of response characteristics carried out here have been rather simplified and specialized, it is believed that the requirements for other types of applied signal and response are best considered along similar lines, to which the present discussion may act as a guide.

(b) Input impedance. -- For certain applications, particularly use with piezoelectric gauges, an important factor in determining the low-frequency response characteristics is the input impedance. The low-frequency time constant of a piezoelectric-gauge circuit of capacitance C together with an input impedance R is given by the product RC, which must be of the order 50 to 100 times the interval over which a faithful record of the transient gauge signal is required.

The necessary input impedance so determined is usually several megohms for necessary or desirable values of the gauge-circuit capacitance C. Grid-circuit impedances of this magnitude frequently require special designs of the input stage. Usually these designs involve selected tube types and operating conditions in cathode-follower circuits, examples of which will be found in circuits described in the following.

(c) Linearity and stability. -- If accurate measurements are to be taken from records of transient output signals from an amplifier and indicating circuit, it is necessary that the sensitivity of the combination remain constant over at least short intervals, and that the output signal be a linear function of the applied voltage. It is usually desirable to use regulated supply voltages, particularly in the low-level stages, together with considerable degeneration of the well-known types. Linearity and stability are both improved with use of push-pull or balanced amplifier stages, which are virtually essential in high-level stages. In the interests of linearity these stages should also be considerably overdesigned as compared to commercial practice.

(d) Amplifier circuits; diagrams and descriptions. -- (i) Modified DuMont type 208 oscillograph. In much of the work which has been done at this laboratory, it has been found possible to adapt the DuMont type 208 oscillograph and make it a usable instrument for recording transients. The

necessary modifications include changes in the vertical or signal amplifier, increase in accelerating voltages, and modification of the deflecting-plate connections. The modifications of the amplifier circuit are:

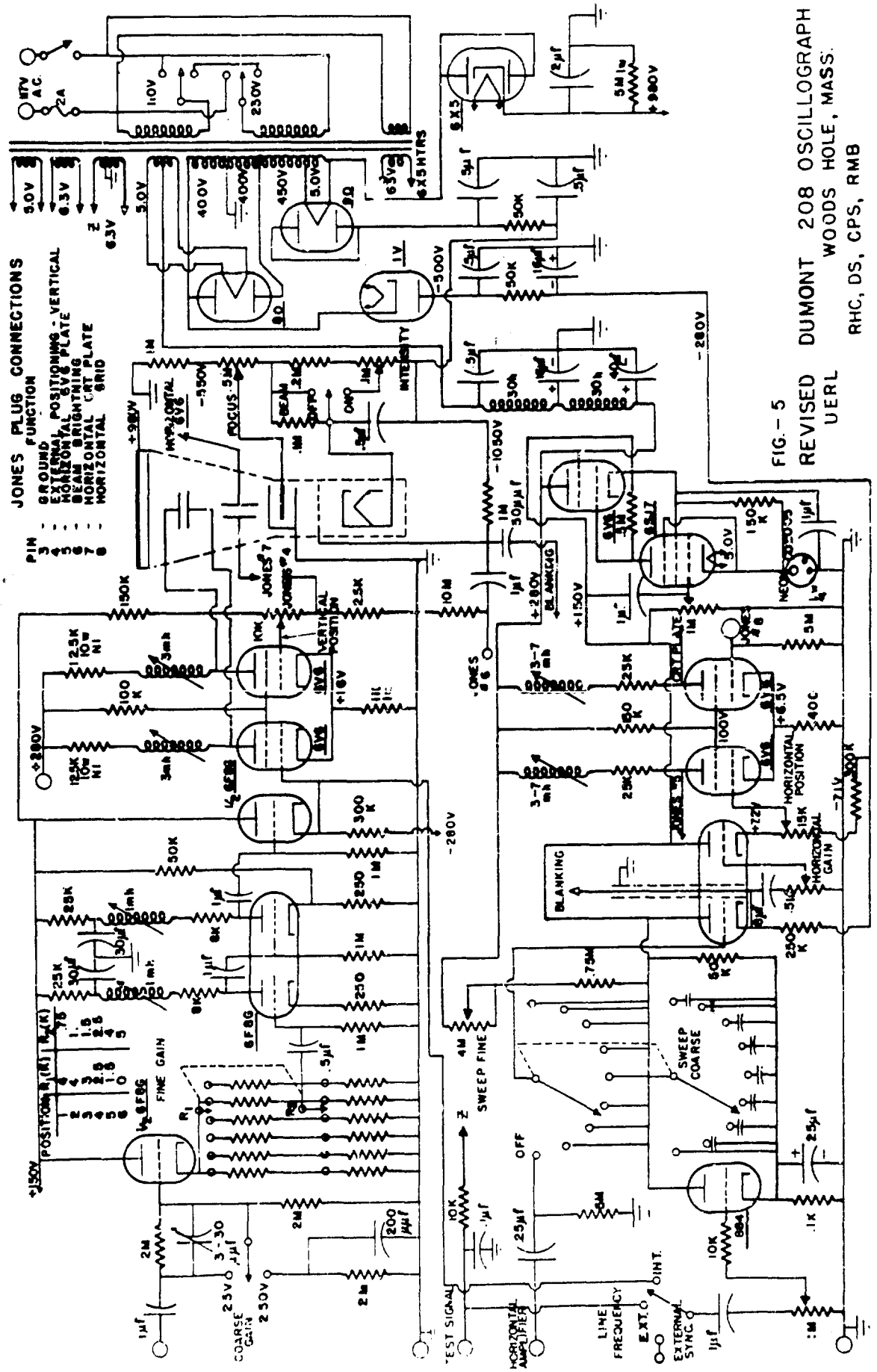
(1) the use of a low-impedance compensated step attenuator;
(2) minor changes in frequency-compensation circuits;
(3) redesigned position-control circuit;
(4) decreased load resistance and direct plate to cathode-ray tube connections in the output stage.

These changes were made to improve the frequency-response range under all conditions of gain and spot position, and to provide known gain settings which can be reproduced. The schematic circuit diagram is shown in Fig. 5.

Fine control of attenuation, without change in frequency response, is obtained by the use of a low-impedance voltage divider and a step switch which has very low stray capacitance. The amplifier response is further improved by the omission of a 0.005-μf condenser in the cathode of the first amplifier stage, the alteration of the vertical positioning circuit which reduces output impedance, and the redesign of the output stage to reduce load resistance and stray capacitance. Adjustment of the four compensating inductances requires care and understanding of the principles involved. Often turns must be taken from the output-stage inductances to reduce their value.

For use in recording transients, an eight-pin Jones plug permits patch-cord connection of the oscillograph to other control units. Single-sweep and beam-brightening voltages and control of cathode-ray spot position may thus be provided by external units.

In the routine testing of this instrument, a check sheet is used and a test film is made to determine the performance of the oscillograph. The high-frequency response is first measured visually with a sine-wave input at the following frequencies: 10, 30, 100, 150, 200, 300, and 400 kc/sec. To be acceptable, the oscillograph must be flat within plus or minus 2 percent up to 300 kc/sec and show no rise at 400 kc/sec. The frequency-response curve of a typical instrument is shown in Fig. 6. A photograph is then made to determine how well the oscilloscope will reproduce signals with an infinitely sharp rise and exponential decay. Four signals are used with time constants corresponding to 50 μsec, 150 μsec, 500 μsec, and infinite time



Best Available Copy

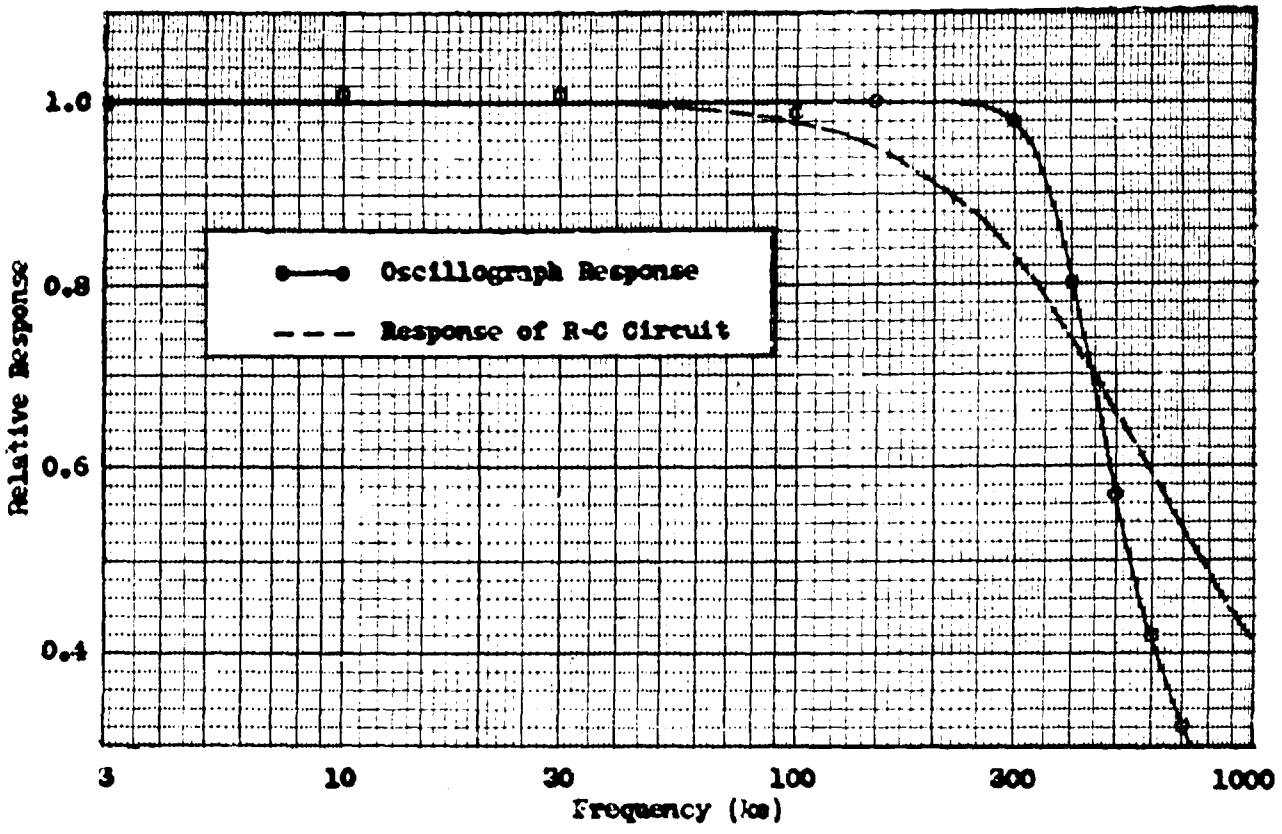


Fig. 6. Frequency Response: modified DuMont 208 oscillograph.

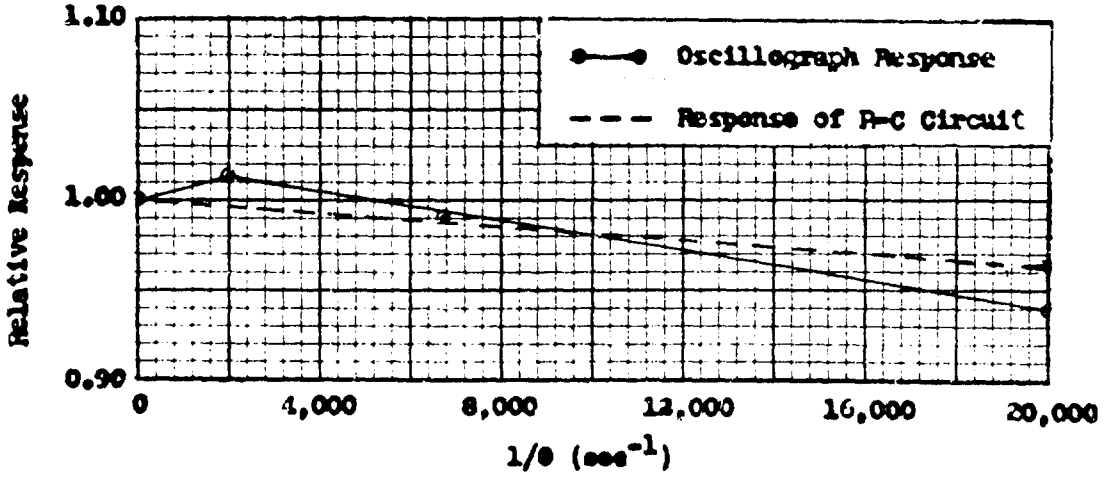


Fig. 7. Exponential Transient Response Curve.

Best Available Copy

constant. The ratio of the response for time constant θ to the response for infinite time constant is plotted against the reciprocal of the time constant θ, as shown in Fig. 7. Over the range of interest, the curve is approximately a straight line. This curve can be compared with a specified standard of performance, and also provides a convenient means of determining the error in recording a negative exponential of stated duration. The dashed curve is calculated from Eq. (6), assuming an equivalent amplifier time constant τ of 0.36 μsec. This value is obtained from the frequency-response curve for the same instrument, which shows a 30-percent drop in response at a frequency of 440 kc/sec [see Fig. (6)]. The agreement between the two curves is fairly good, in view of the simplified analysis leading to Eq. (6).

The compensated low-frequency response is checked by a voltage step on the test film, which has rarely shown any variation greater than 1 percent over the 25-msec interval used. On a typical unit, the time to fall 30 percent is 160 msec, corresponding to a frequency of 0.99 cycle/sec.

The sensitivity is 50 mv d.c. per inch at maximum gain and may be decreased in steps of approximately 35 percent to a minimum of 5 volts per inch deflection on the tube screen. The linearity is measured from the test film which has steps of $\frac{1}{2}$-in., 1-in., $1\frac{1}{2}$-in., and 2-in. deflection on the screen. To pass the test, scopes must have the ratio of deflection to voltage agree to 1 percent up to $1\frac{1}{2}$-in. deflection. The gain stability is tested during use and is usually better than 1 percent provided the a-c line is stable.

The troubles encountered with the type 208 oscillograph are usually due to tube or mechanical failures. The most common are: noisy input 6F8 tube, bad focus of the cathode-ray tube due to age, a broken wire in the output-stage inductances, loose cathode-ray tube socket, and occasionally a very high-frequency oscillation in the regulated 150-volt supply. This last trouble may be cured by installing a 0.01-μf condenser from the plate of the input 6F8 to ground.

Up to this time, 18 oscillographs have been modified as outlined in the foregoing, and have been in use for periods up to three years.

(ii) Four-channel oscillograph. This unit was designed to fill the need for a compact multichannel oscillograph recording on moving film. It has a flat frequency response from direct current to 100 kc/sec; a maximum

sensitivity of 50 mv d.c. per inch deflection on the cathode-ray tube screen, and negligible drift during a day's operation.

(1) Description of operation. There are five units in the oscillograph -- a camera assembly, an amplifier chassis, a cathode-ray tube chassis, and two power supplies. These can be installed in any standard relay rack of sufficient height, and then interconnected by patch cords.

Each amplifier (see Fig. 8) is built on a small chassis which is then plugged into a shock-mounted relay rack unit which holds all four amplifiers. This quick-change unit has many advantages, including mass production and easy replacement of a faulty unit. The electronic part of the system can be understood by referring to Fig. 9. The input is a cathode follower operating with reduced plate current and plate voltage. For direct-coupled operation, 20 megohms is a reasonable input impedance. If a coupling condenser is used, 1000 megohms may be used in the grid return if care is taken to eliminate leakage currents. The amplifier stage employs a conventional delta-type attenuator in the cathode circuit. The problem of zero signal drift was found to be reduced by the use of 6SH7 tubes rather than 6AC7 tubes, which were originally tried. Initial differences in tubes are compensated for by the use of a 50-ohm variable resistor (fine gain balance). The next stage is used to shift the d-c level of the signal from +72 volts to -62 volts and at the same time to provide positioning control of the cathode-ray spot. The output amplifier is conventional, but the use of a cathode-follower output is necessary when the amplifiers are at a distance from the cathode-ray tubes. This has the further advantage of lessening the capacitative load on the output amplifier. An unexpected phenomenon was observed in the initial design when the high-frequency response fell off at large deflections. This was because the cathode follower was originally working too close to cutoff on the extreme of the signal swing.

The cathode-ray tube chassis (see Figs. 10 and 11) is extremely compact and has nothing unusual in it except for a level shifter which allows a beam-brightening signal at ground potential to be applied direct-coupled to the grids of the cathode-ray tubes at a level of -1000 volts as described in Sec. 2(g). On the front panel there are individual intensity and focus controls, individual beam on-off switches, and a master intensity control. A Sylvania R1130 crater tube is included to give a time scale on the record.

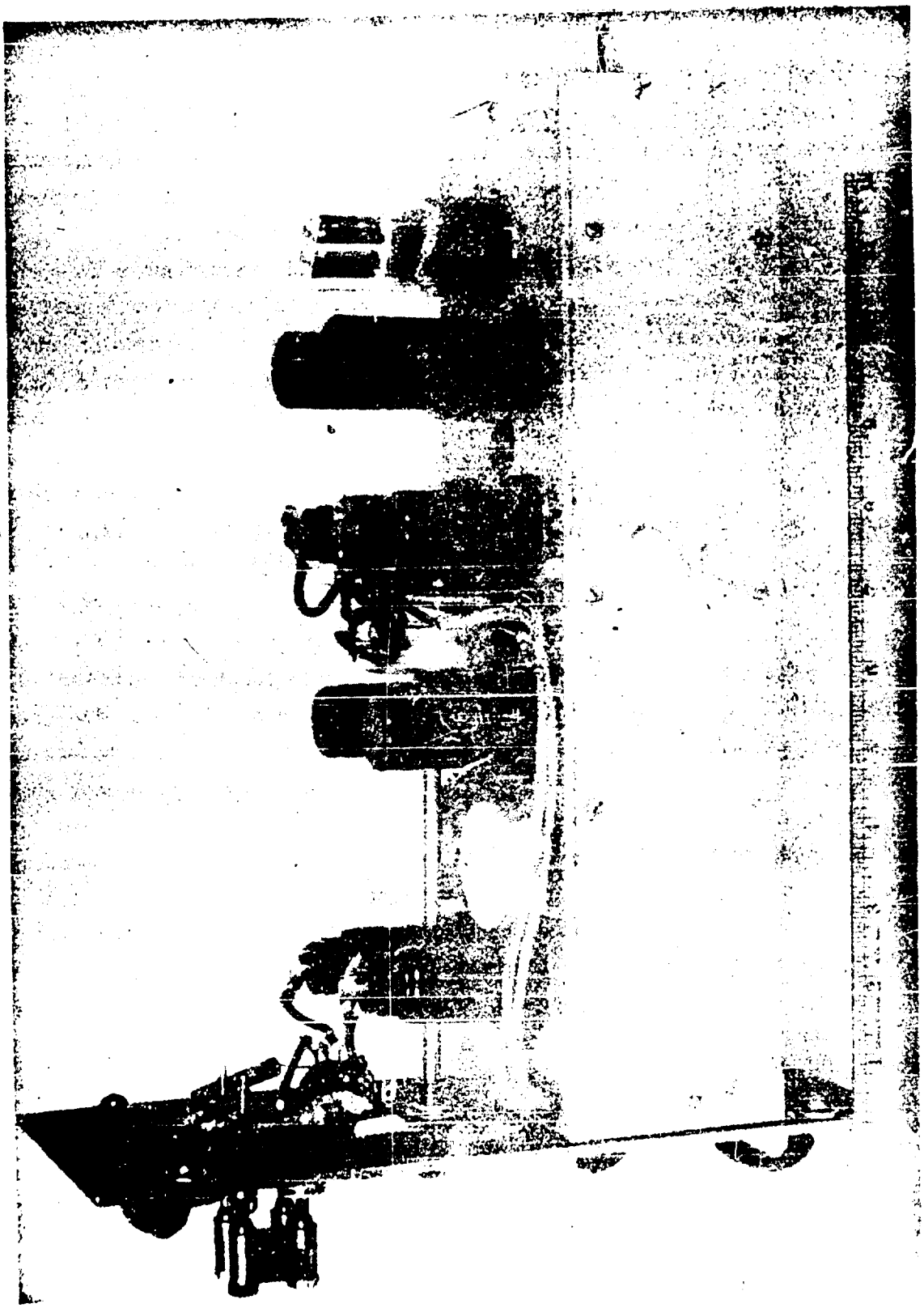


Fig. 8. View of four-channel oscillograph amplifier unit.

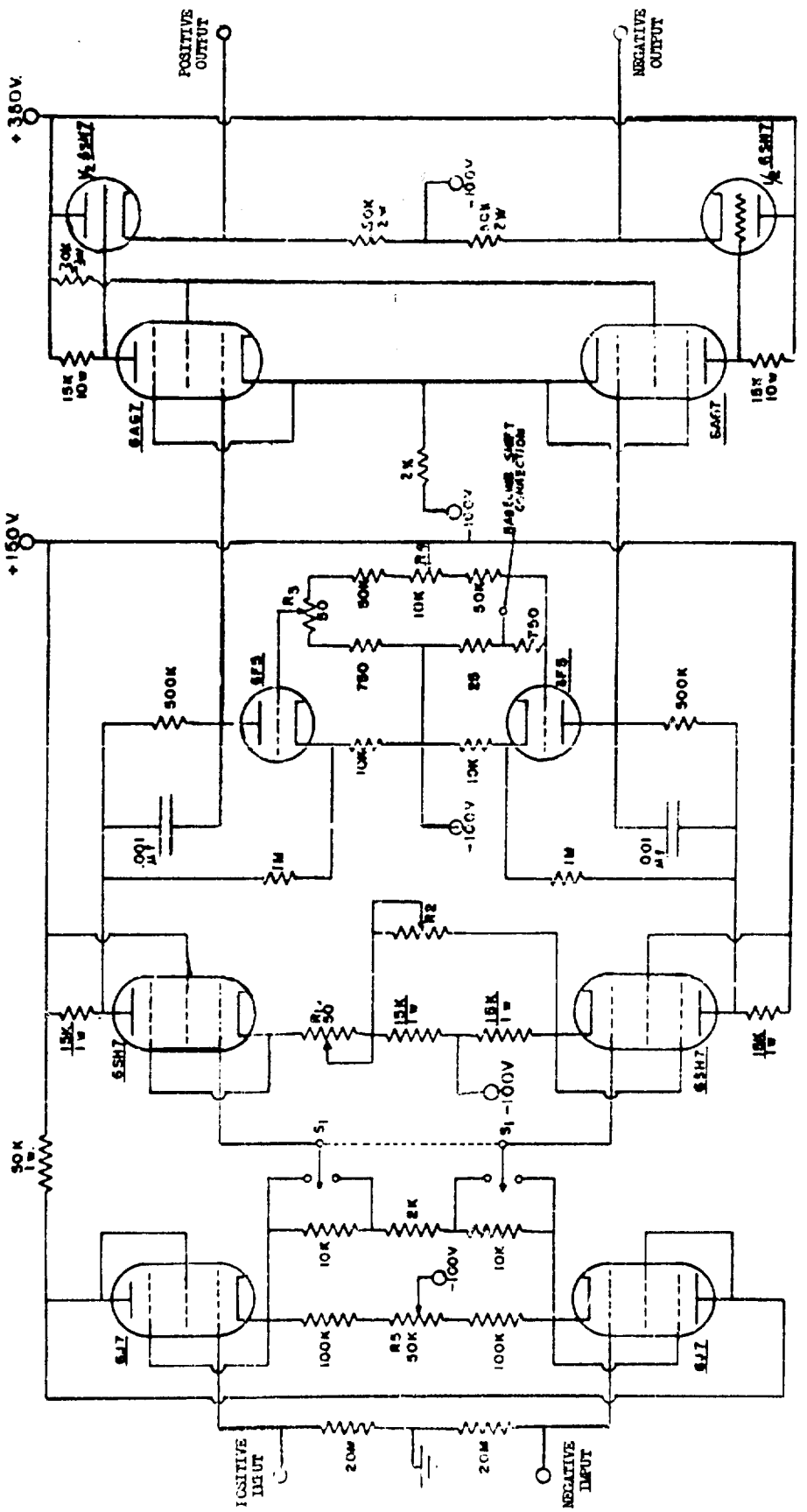


FIG. 9
BALANCED D.C. AMPLIFIER UNIT
FOR
FOUR CHANNEL OSCILLOGRAPH, MODEL III
C.E.C. DWG. NO. 7-51-48
USRL WOODS HOLE, MASS.

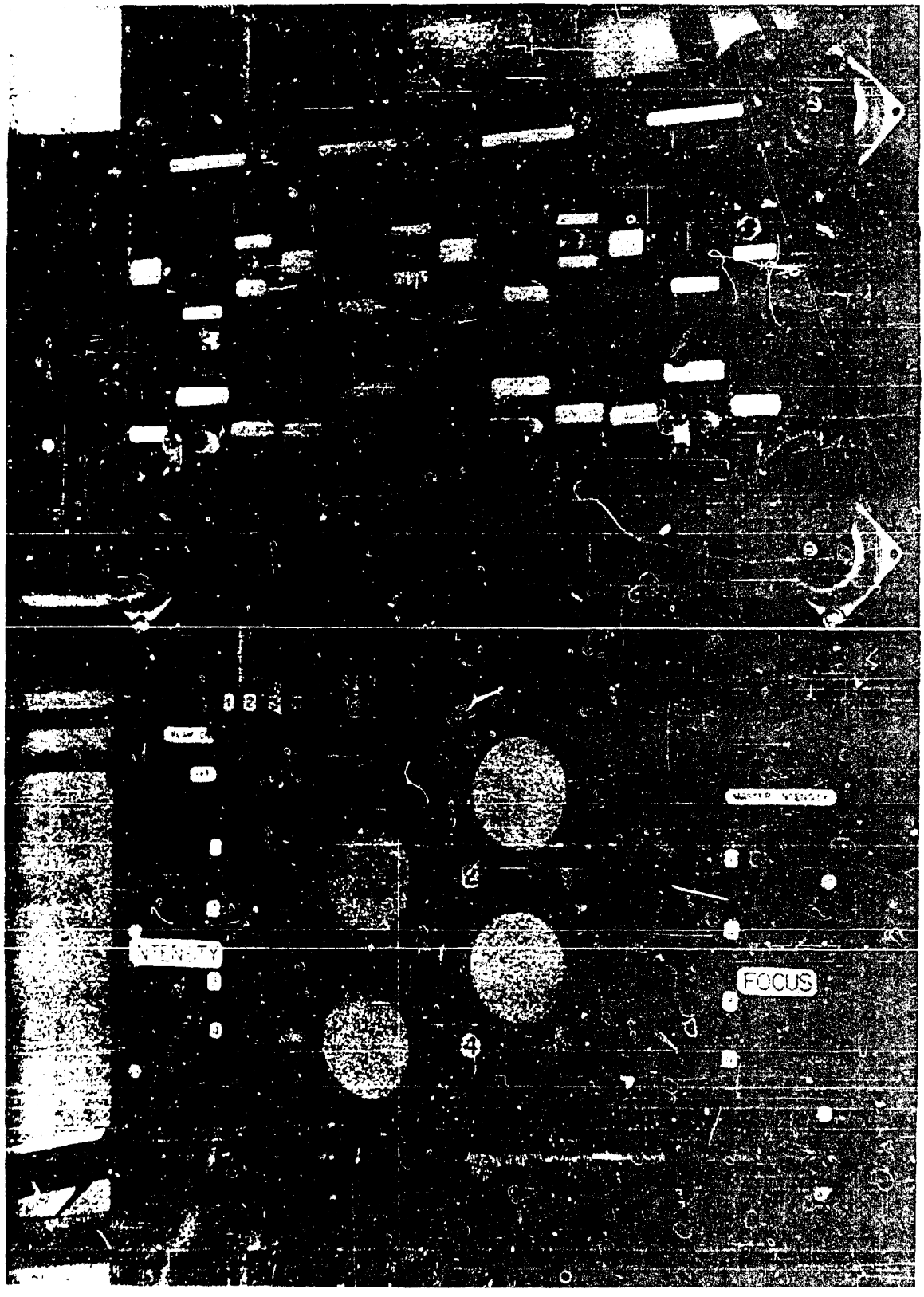


Fig. 10. View of four-channel oscillograph amplifier and cathode-ray tube panels.

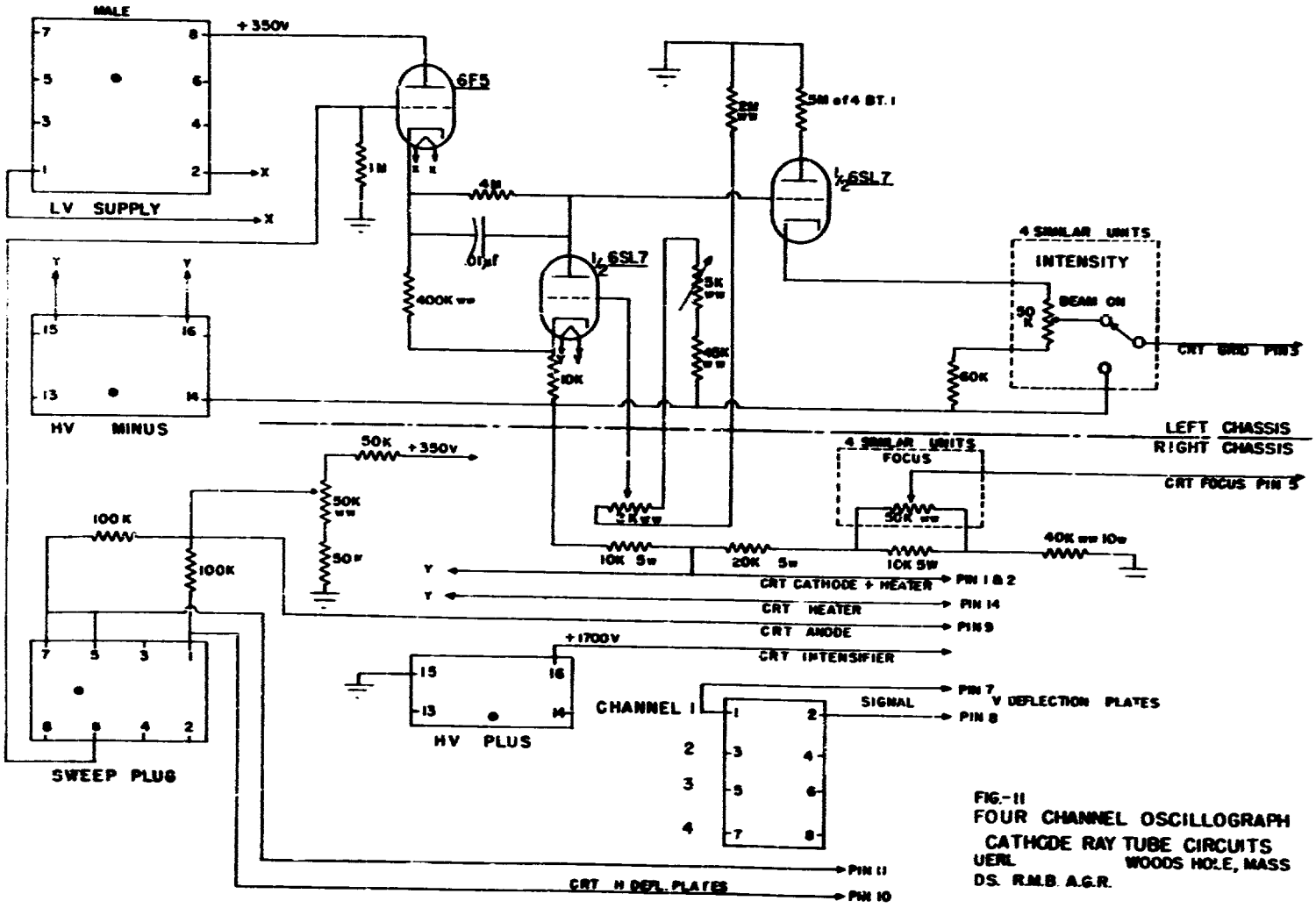


FIG.-11
FOUR CHANNEL OSCILLOGRAPH
CATHODE RAY TUBE CIRCUITS
UERL WOODS HOLE, MASS
DS. R.M.B. A.G.R.

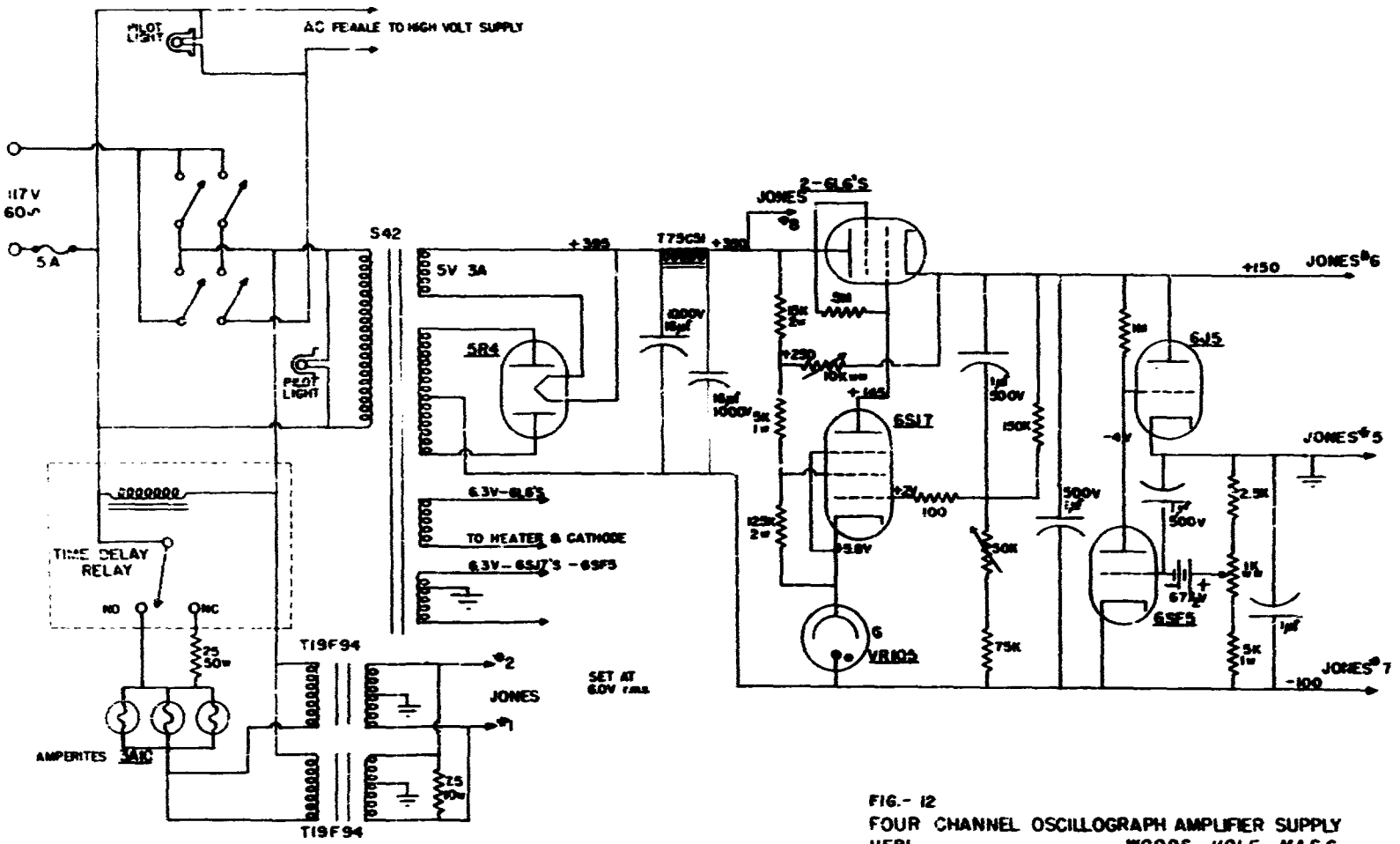


FIG.- 12
FOUR CHANNEL OSCILLOGRAPH AMPLIFIER SUPPLY
UERL WOODS HOLE, MASS.
RMB – DS.

The low-voltage supply (see Fig. 12) is a conventional regulated power supply of the cathode-follower type. Of interest, however, is the divider network supplying the screen of the 6SJ7 amplifier tube. This allows the screen to work at a respectable voltage and still supply perfect compensation for input voltage fluctuations. The use of Amperite ballast tubes to regulate the heaters of the amplifier tubes is a great improvement. Even more improvement can be obtained by increasing the working voltage drop across the Amperites by the use of a transformer rated for higher output voltage. A regulated negative supply delivers 1000-volt accelerating potential to the cathode-ray tube circuits. The circuit is similar to that described in Sec. 2(b) and shown in Fig. 13, except that a half-wave rectifier without doubling is used. The other half wave from the supply transformer is used as power source of a 1700-volt positive supply for the cathode-ray tube intensifier electrodes. This is a conventional half-wave supply with type 2X2 rectifier and condenser input filter.

The camera unit consists of a hood which is bolted to the front of the relay rack. This hood has fittings so that either a General Radio oscillograph camera or a rotating-drum camera (see Part III) may be used.

(2) Testing of oscillograph. The unit is tested in essentially the manner described in Sec. 1(d). However, much more care is necessary in the checking for base-line drift. This is usually caused by a difference in the characteristics of the first amplifier tubes (6SH7).

One unit has been in use for six months and has given very satisfactory service.

2. Cathode-ray tubes and supplies

The requirements imposed on cathode-ray tubes used for recording transients are more stringent than when the tubes are used for observation of stationary patterns, particularly when high writing speeds are needed. In the first place, higher accelerating voltages are required to give a sharper, more intense spot. Second, a means must usually be provided for modulating the spot intensity. The intensity-control grid is usually operated at a high negative potential, which makes necessary a coupling device from the brightener circuit [see Sec. 2(c)], and in addition, it is important to avoid undesired modulation of the intensity by 60-cycle or other pickup. A third consideration is the fact that the deflection factor of the tube (voltage

required to produce a given deflection) is directly proportional to the applied accelerating voltage. As a result, supply-voltage variations may produce serious changes in sensitivity of the recording system.

(a) Cathode-ray tubes. -- Most of the oscillographs developed at this laboratory have used one of three DuMont cathode-ray tube types: 5LP5, 5CP5, or 3FP5. All of these tubes have blue screens and the DuMont intensifier electrode for additional acceleration of the beam after deflection. The short-persistence blue screen is virtually essential for moving-film recording at speeds greater than about 100 in./sec, and the intensifier circuit permits greater spot intensity for a given deflection sensitivity. The first two types are 5-in. tubes, while the 3FP5, with 3-in. screen diameter, permits a more compact unit and has been found very satisfactory. The negative second-anode voltages used range from 1100 to 2200 volts, and positive intensifier voltages from 1100 to 3000 volts are used.

(b) Power supplies. -- (i) Modified type 208. The stock DuMont type 208 oscillograph does not provide adequate writing speed for most recording of transients. It can, however, be used at sweep speeds up to about 2 in./msec by increasing the intensifier voltage. This is done by addition of a half-wave rectifier tube and heater transformer, the high voltage being supplied from the original power transformer.[6]

It should be noted that the accelerating voltages of the type 208 oscillograph are very susceptible to line-voltage variations, since a condenser input filter without a filter choke is used. This type of filter responds very rapidly to increases in rectified input voltage and has a rather short time constant for decreases in input voltage. As a result, these oscillographs must be used on a well-regulated power line if the sensitivity is to be kept constant. With a good power source the over-all sensitivity of the oscillograph is reproducible to less than 1 percent over a period of an hour or more.

(ii) Regulated high-voltage supply. A 1300-volt regulated power-supply circuit which has been used for multichannel oscillographs and other high-voltage requirements is shown in Fig. 13. It is capable of delivering upwards of 15 ma at 1300 volts with good load and input-voltage regulation and negligible ripple.

---

[6] This circuit was originally developed at the David Taylor Model Basin.

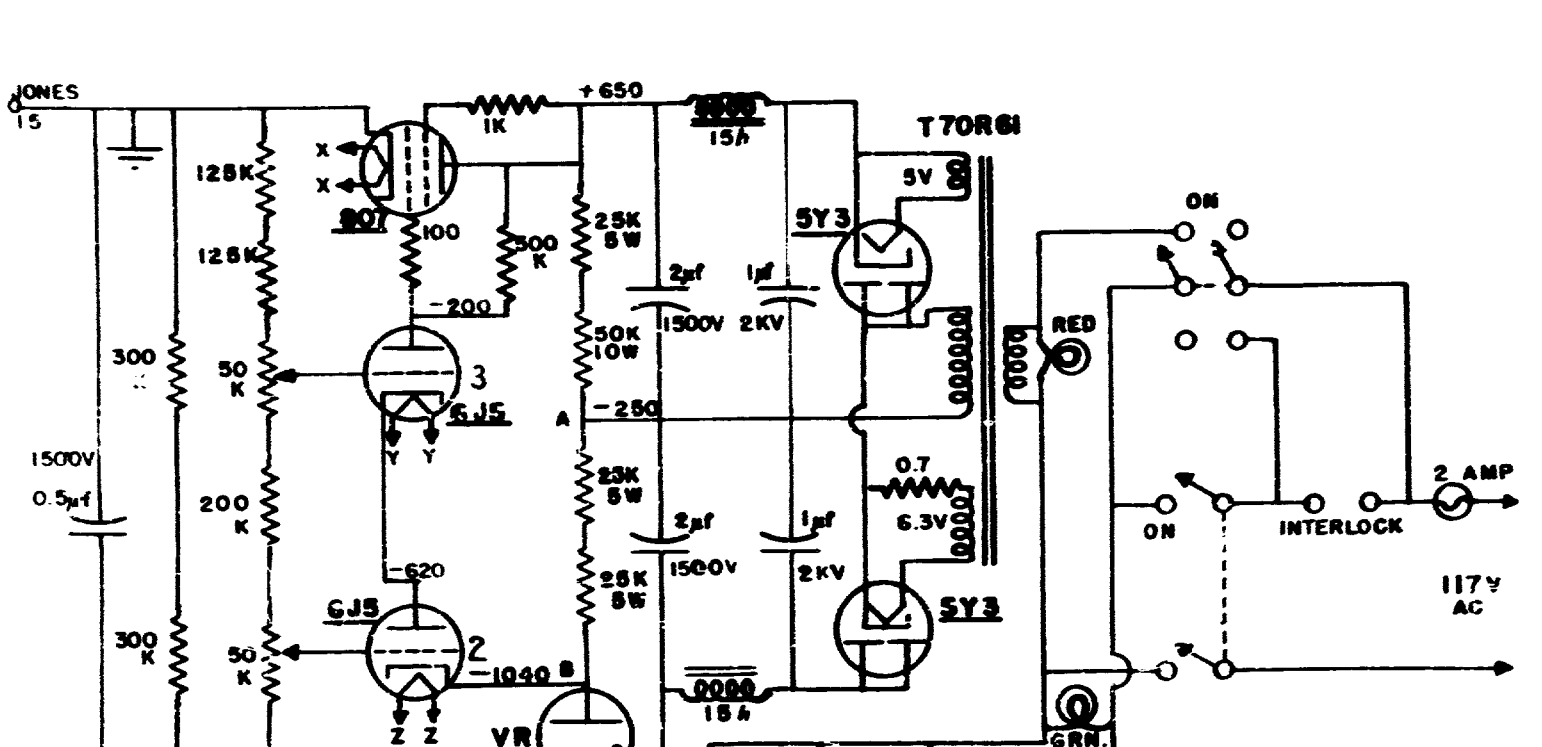


FIG.-13
REGULATED 1300 VOLT SUPPLY
UERL WOODS HOLE, MASS.
R.H.C.

The circuit employed is basically a degenerative stabiliser with amplified control voltage applied to the type 807 series tube. The amplifier is a so-called "cascode" circuit,[7] consisting of tubes 6J5, Nos. 2 and 3, controlled by output-circuit variations coupled to their grids by the dividers in the plate circuit of the constant-current tube 6J5 No. 1 (see Sec. 3). Reference voltages for this tube and the cascode are supplied by the gas regulator tubes VR105 and VR150. The interlock connection in the power circuit is intended for connection with other equipment to prevent premature application of voltage. The lining up and operation of the circuit are straightforward and require no comment.

The output voltage changes less than 2 volts when the a-c line is varied from 90 to 125 volts and the peak-to-peak ripple in the output is less than 0.5 volts. The internal impedance of the supply is less than 500 ohms.

(c) Intensity-modulation coupling circuits. -- The requirements for cathode-ray tube beam modulation are: (i), a means of applying a positive voltage of 20 to 100 volts to the grid of the tube for intervals of from a few milliseconds to seconds, the d-c level of the grid being 1000 volts or more below ground potential; (ii), freedom from 60-cycle or other pickup.

Two simple coupling methods can be employed successfully -- condenser coupling to the grid, or applying a much larger brightener voltage to the top of a potentiometer circuit on which the grid is tapped. The first is the most easily constructed circuit of all, but suffers from two disadvantages. First, the time constant of the grid circuit must be much greater than the time the beam is to remain on if the intensity is to remain essentially constant. If this duration is longer than, say, 100 msec a condenser of high capacity and voltage rating is required and some time must be allowed between brightening cycles to permit the circuit to recover.

A second drawback to use of condenser coupling is that the condenser effectively connects the cathode-ray tube grid to the brightener as far as fluctuations or ripple is concerned, while the cathode follows accelerating voltage-supply variations. The result is that any ripple in this supply appears as an undesired intensity modulation. Though the effect is not always serious and a good high-voltage supply will eliminate it, it is a basic difficulty.

---

[7] Hunt and Hickman, Rev. Sci. Inst. 10, 6 (1939).

669

The divider, or potentiometer, method suffers from the disadvantage of being wasteful in that only a small fraction of the large positive voltage which must be applied at the top of the divider is used. This places special requirements on the driving circuit. Also, some of the accelerating voltage must be wasted to provide bias for the tube.

More satisfactory coupling circuits for brightening can be provided at the expense of added tubes and components. One fairly simple method is to use a constant-current tube, as shown in Fig. 14. The plate current of tube T_2 can be made independent of its plate voltage by giving resistor R_1 the value μR_2, where μ is the amplification factor.[8] A signal applied at the grid of tube T_1 will therefore appear unchanged except for d-c level at the plate of T_2 or any intermediate point on the plate load resistor R_3. The by-pass condenser C is included to insure rapid response.

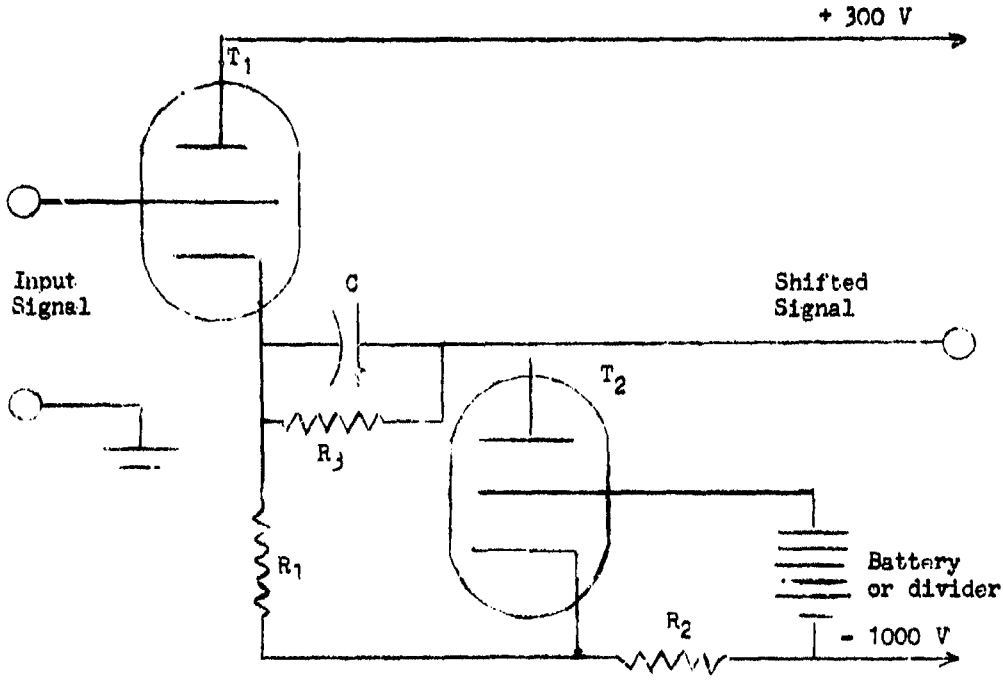


Fig. 14. Voltage-level shifter.

[8] This circuit is not original, but the proper person to credit is not known. The same circuit is used in the regulated high-voltage supply already described [see Sec. 2(b)].

The "level-shifter" circuit just described has the disadvantage of drawing current from the high-voltage supply. Its operation is also critical to the grid potential of tube T_2. Small variations due to resistor changes may thus cause drift in intensity over a period of time. A coupling method which is preferable for high accelerating voltages consists in putting the whole brightener circuit and its power supply at the potential level of the cathode-ray tube grid. With such a circuit the only coupling to circuits at ground potential required is for synchronizing pulses, which can be applied by a low-capacity condenser, and the power required is obtained from a source independent of the accelerating voltage supply. A circuit of this kind is described subsequently [Sec. 3(c)].

3. Time bases and synchronization circuits

In any recording of transients it is necessary to switch on the cathode-ray tube spot for a controlled interval after application of a signal which is properly synchronized with the event to be recorded. If time resolution is obtained by moving the cathode-ray tube spot across the screen, it is necessary also to provide a properly synchronized linear single-sweep circuit. In many cases it is desirable to provide a controlled time delay between the synchronizing pulse and the operation of these circuits. The time-delay circuit should provide accurately known intervals, the brightening circuit should provide uniform intensity of the electron beam, the sweep circuit should displace the trace at a constant rate across the screen, and all units should trigger reliably on readily obtainable pulses. The circuits which have been developed to meet these needs are described in the following.

An important practical consideration in underwater-explosion recording is the means of obtaining a synchronization pulse. The simplest solution is, of course, to eliminate the need of accurate synchronization by use of a continuous-film movie camera, which is started manually just before the time of interest. This method has also the advantage of being able to give a virtually unlimited time duration, but if any very great time resolution is required, large quantities of film are required, with increased expense and problems in film processing as a result. In some cases, however, use of such a camera may be the best solution.

Several means of synchronizing linear-sweep and rotating-drum recording of underwater explosions have been used at this laboratory, involving either the firing circuit or the pressure wave from the explosion. The details of these methods are described at the end of this section.

(a) Linear time base. -- The main function of a linear time base is to move the spot of a cathode-ray tube across the screen at a constant and predetermined rate. This forms the time axis for the recorded transient. Other functions include the initiation of the sweep by a trip pulse, turning on the spot or beam at the same time, and turning off the beam at the end of the time. For convenience, a continuous sweep is available, as well as a self-tripping single sweep.

The operation of the sweep may be understood by reference to Figs. 15 and 16. A positive pulse (2 volts or greater) applied at the trip input terminals is amplified and operates a trigger circuit of the "flip-flop" type.[9] This cuts off a switch tube, which allows the timing condenser to charge through a highly degenerated triode. With the aid of feedback from the succeeding cathode follower through a 200,000-ohm resistor,[10] the output is a voltage whose decay is highly linear with respect to time.

A cathode-follower output circuit is used to reduce the possibility of modulation by outside sources. For continuous sweep a portion of the sweep signal is fed back to make a self-oscillatory circuit. Self tripping at 2-sec intervals is obtained from the pulses of a neon-tube oscillator.

Turning the cathode-ray tube beam on and off is accomplished by means of two signals fed into a mixer stage. The first pulse turns the beam on when the sweep starts, and the second turns the beam off when the sweep has reached its end. The regulation of the voltage supplies is rather critical, and vacuum-tube regulators are used for both positive and negative supplies.

The troubles that have been encountered in the course of a year's use are as follows. If the tripping pulse is followed by a large negative signal (about 10 volts at full gain) the sweep can be stopped in midrange. This

---

[9] This and other principles are described in an excellent book by O. S. Puckle, Time bases (New York, 1943).

[10] This circuit is essentially an integrator, and the feedback method applied to it is the analogue of a differentiator circuit described by Schmitt and Tolles, Rev. Sci. Inst. 13, 115 (1942).

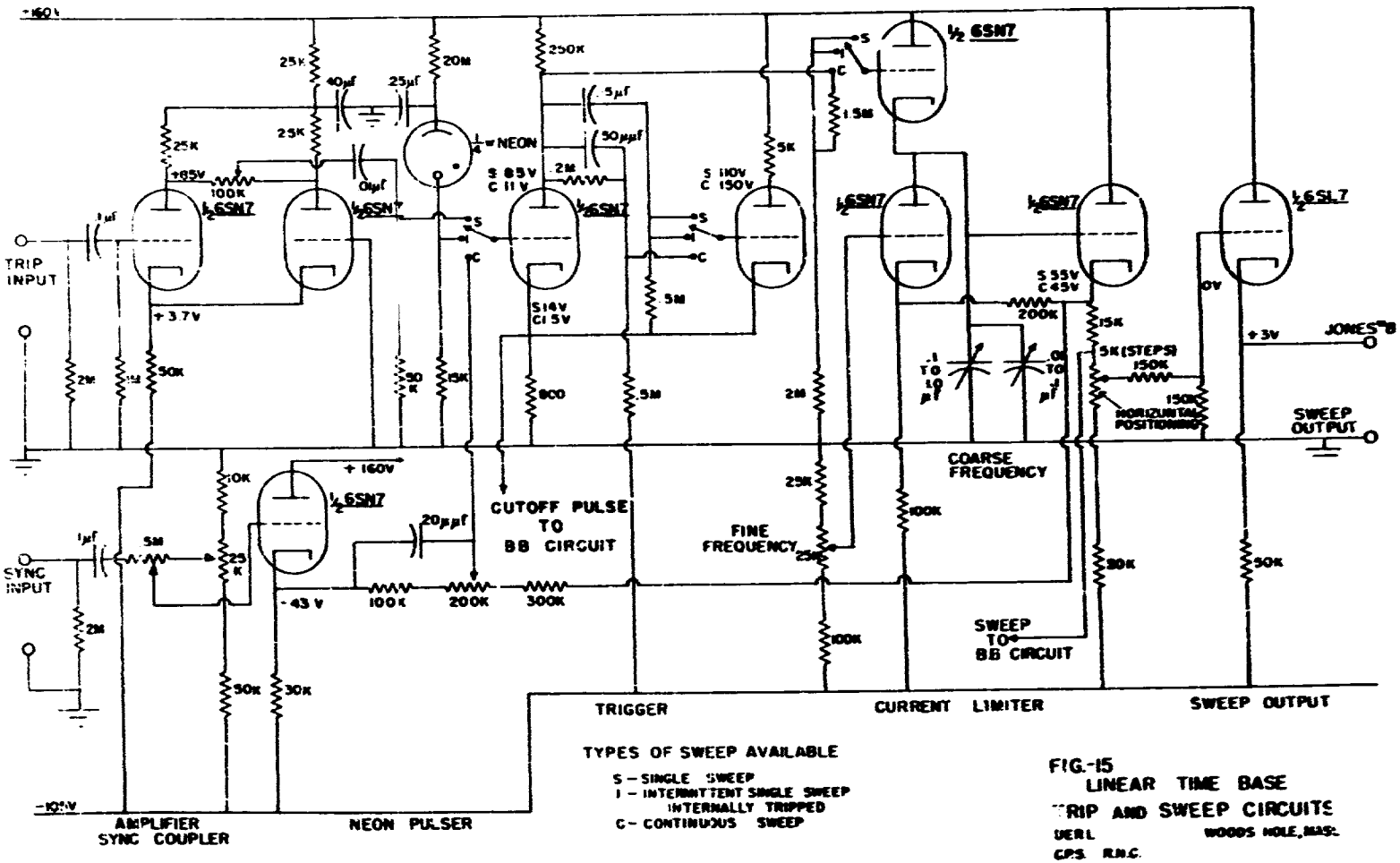
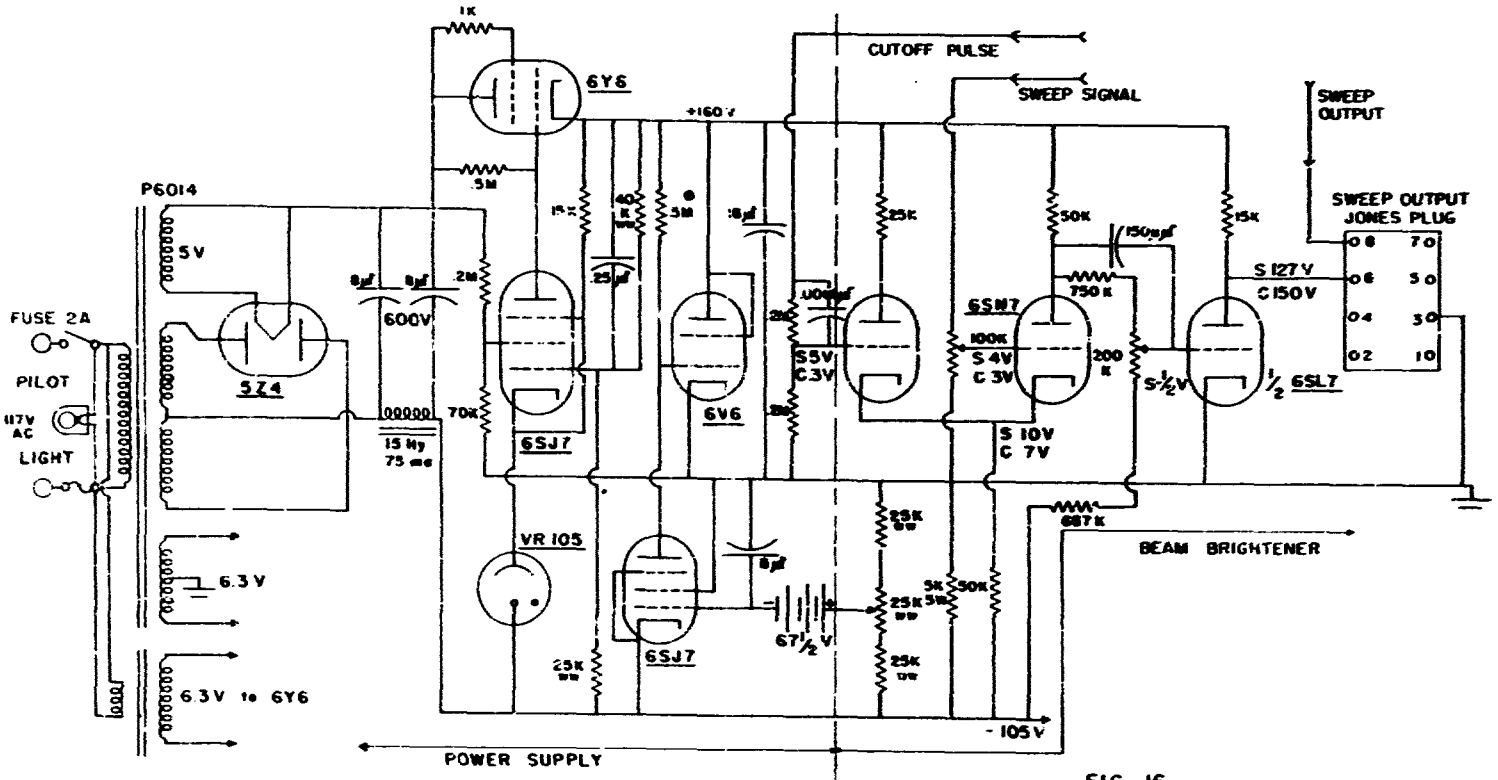


FIG.-15
LINEAR TIME BASE
TRIP AND SWEEP CIRCUITS
UERL WOODS HOLE, MASS.
CPS R.N.C.



BEAM BRIGHTENER ADJUSTMENT

IF DURATION IS TOO LONG - MOVE 100 K POTENTIOMETER UP AND SET 6SJ7 BIAS AT -½ V

SHORT- DOWN

FIG. 16

LINEAR TIME BASE

POWER SUPPLY AND BEAM BRIGHTENER

UERL WOODS HOLE, MASS.

CPS RHC

could be eliminated by the use of a thyratron in the input. When the timing condensers or wiring thereto show appreciable leakage, the linearity is affected. The beam-brightening circuit is direct-coupled and is likely to drift under extreme conditions of heat, humidity, or tube and resistor drift. Finally, the regulated supplies require wire-wound resistors in the amplifier-tube grid circuits to assure voltage stability.

In operation this design has given very good service. The linearity, in terms of time-displacement ratio, is better than 1 percent and is constant over a period of time which is long compared to the time required for a single measurement. The range in speeds is from 0.5 msec to 50 msec for a 4-in. trace on a DuMont type 208 oscillograph.

(b) Time delay and beam brightener. — This unit fills a double function. Upon the reception of a tripping signal, it produces one pulse at a variable time later, and then a second pulse at a variable time after the first pulse. The other function of the unit is to provide a variable time delay after the tripping signal and then produce a beam-brightening signal of variable duration.

The description of the operation may be followed by reference to Fig. 17. The tripping signal is fed into the first thyratron through a cathode follower to remove the effect of thyratron-grid current upon the tripping circuit. The required tripping signal may be varied from +0.3 to +7 volts by adjusting the thyratron-grid bias. The heart of the time-delay system is the next circuit. When the first thyratron fires, it changes the next tube from full conduction to full cutoff. The timing condenser C proceeds to charge toward the potential of the positive supply, and when it reaches -3 volts the second thyratron fires. The starting voltage for this charging process is substantially independent of tube constants because of the large plate resistor (5 megohms), and the charging action takes place with the tube cut off. With regulated supply voltages, the time to fire the second thyratron is determined only by the resistance and capacitance. When this action is over, the same process is repeated in the second delay circuit. A neon glow lamp indicates when this process has taken place. A manual reset button prepares the circuit for the next operation by cutting off the thyratron supply voltage.

The delay pulses may be taken from terminals on the front panel of the unit. The same pulses are fed into a mixer which gives a square beam-brightening pulse whose delay is controlled by the first timing circuit and whose duration is controlled by the second timing unit. Except for leakage in the timing condensers, this circuit has caused no trouble over an operating period of a year. The accuracy of timing, when checked, has been better than 1 percent.

(c) Trigger-circuit beam brightener. -- The purpose of this unit is to turn on the beam of a cathode-ray tube upon the reception of a positive pulse (any duration) and turn it off when a negative pulse is received. Operation from 1-msec duration to infinite duration is possible. The unit (see Fig. 18) is part of a complete oscillograph, but the description is included here as an example of a useful method. In practice it is activated by the time delay and beam brightener described in the previous section.

The operation is based on a flip-flop type of circuit with two stable conditions. A positive pulse of short (or long) duration makes the first tube conducting and the second tube nonconducting. The positive swing of the second plate is applied to a level shifter and thence to a cathode follower for the output controls. A positive pulse returns the circuit to its original condition. As the whole unit is operated at the level of the cathode-ray tube cathodes, this makes a convenient way to control the electron-beam intensity.

This unit has been in use for approximately six months and has required readjustment only when the 6SN7 tube was changed.

(d) Synchronization circuits. -- (i) Use of firing line. It is evident that the voltage required to fire an electric detonator cap provides a signal related to the time of explosion. In order to make use of this signal several difficulties must be kept in mind. First, a delay of several milliseconds occurs between application of the firing voltage and detonation of the cap. This interval may or may not be reproducible, depending on the particular cap used and the current in the circuit. If this variable delay is unimportant, a simple switch arrangement can be used to provide the desired pulse. One precaution must often be observed, namely, that the firing line be left ungrounded in order to prevent ground loops with the signal cables. These, if present, may induce considerable signal because of fluctuations in the firing-line current. Because of this, it is usually necessary or desirable that the

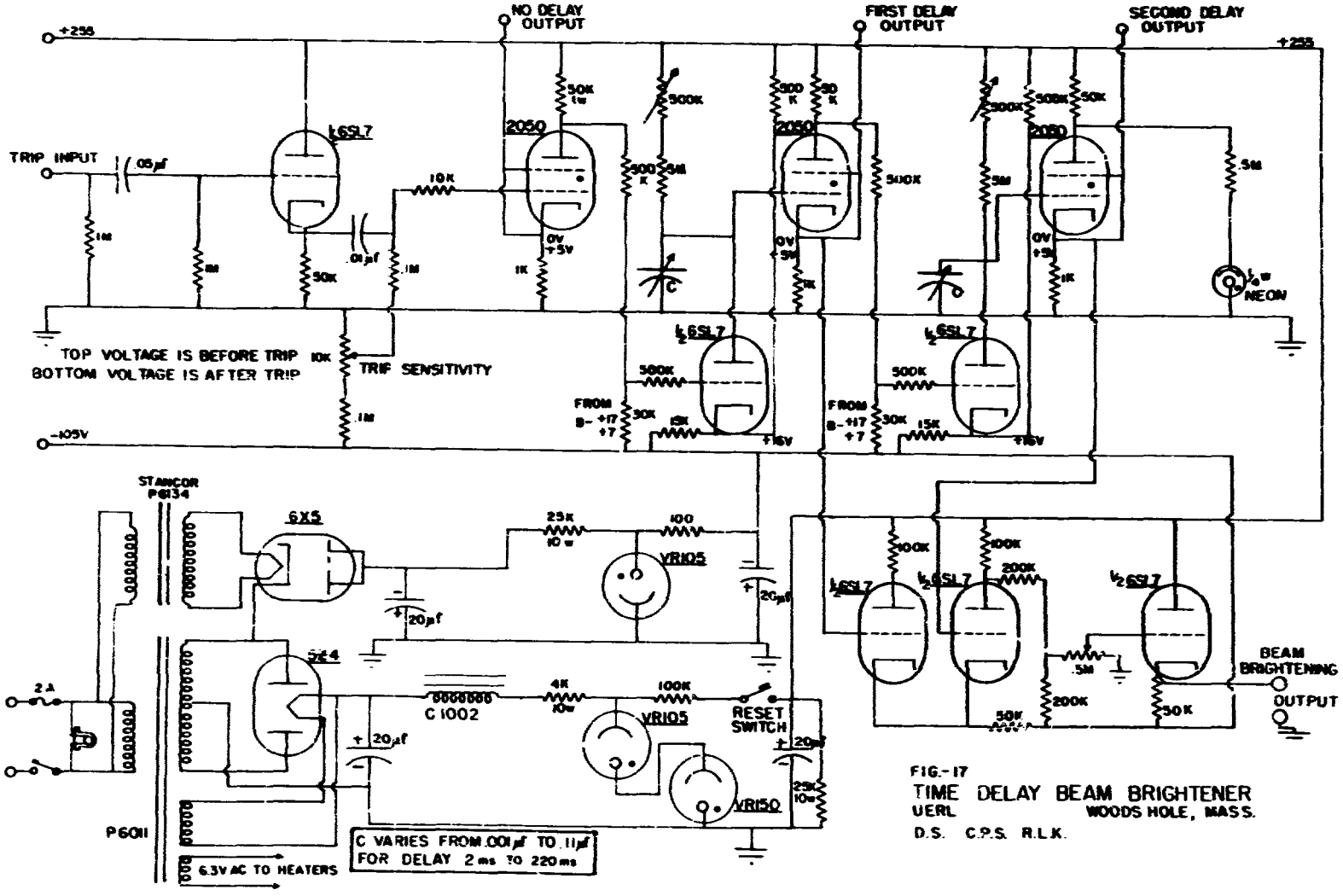
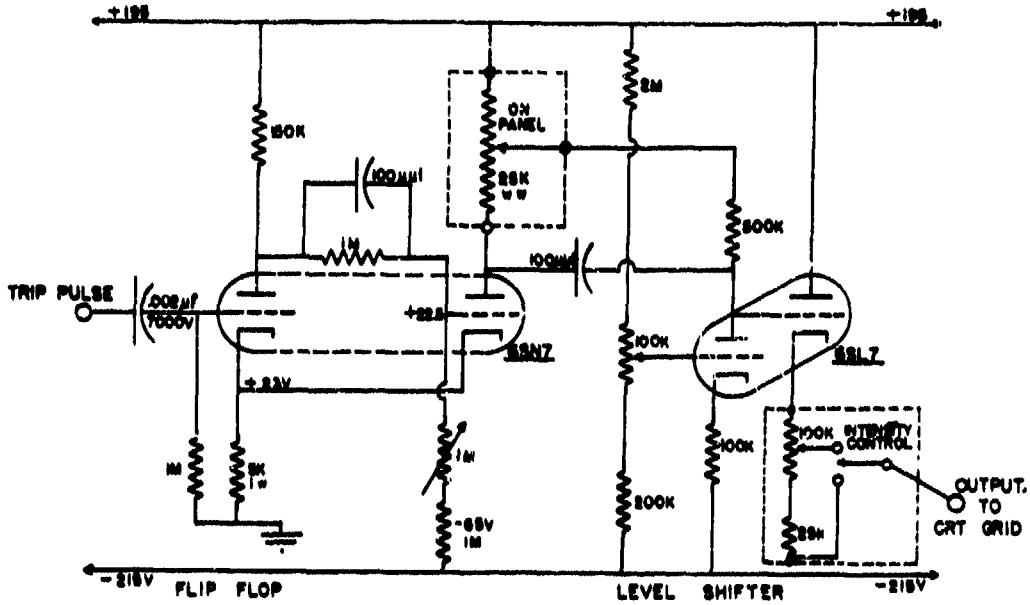


FIG.-17
TIME DELAY BEAM BRIGHTENER
UERL WOODS HOLE, MASS.
D.S. C.P.S. R.L.K.



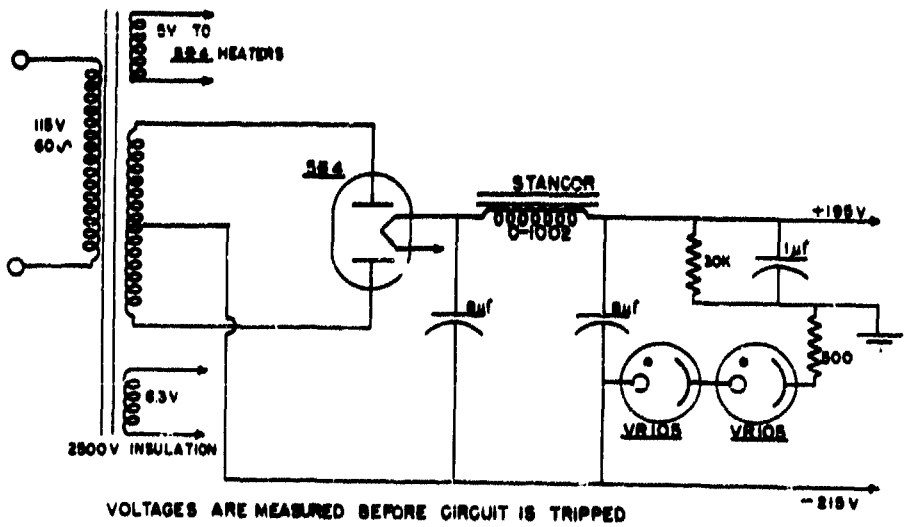


FIG. 18
TRIGGER CIRCUIT BEAM BRIGHTENER
UERL WOODS HOLE, MASS.
D. S. RL.K.

firing line be isolated from the other circuit grounds. A firing pulse can, in this case, be obtained from the firing circuit by inserting an isolation transformer in series with one side of the firing line, the trigger pulse being taken from the transformer secondary, one side of which may then be grounded.

Another method is to use a switch mechanically coupled to the firing switch but electrically independent of it. Any switch will have a time difference between closing of the two circuits, and in many switches this interval is of the order of milliseconds and not very reproducible. It has been found that some ordinary a-c tumbler switches as used in house wiring give a time difference between the two circuits of less than 100 μsec, which has been found reproducible to less than 10 μsec.

Another means of synchronization utilizes the change in firing-line current when the circuit is broken by detonation of the blasting cap. Several practical problems arise in application of this method. First, the circuit must be arranged to prevent the possibility of extraneous voltages triggering the circuits prematurely. Such signals may be developed by chatter in closing of the firing switch or change in firing-circuit resistance due to heating of the blasting-cap fuze wire before it burns out. Second, the breaking of the blasting-cap circuit is not necessarily coincident with the instant that detonation begins. Seismographic caps are especially designed to insure this coincidence and can be used successfully in small-charge work. A great deal of difficulty was experienced with early attempts to use the break of the cap circuit in detonating service weapons. These difficulties were never completely explained, but it is suspected that ionization of the gas sphere after detonation of the charge gave rise to conduction in the circuit which prevented satisfactory operation.

(ii) Pressure switches. In general, attempts to use the break of the firing circuit have given unsatisfactory results. Methods that work properly for a while break down when one begins to have confidence in them. As a result, this type of synchronization has been abandoned in favor of more dependable methods. The first of these used at this laboratory was a simple switch, consisting merely of a lead disk -- supported at its edge -- which was driven against a steel pin by force of the shock wave. This switch functioned reliably but had the disadvantage of requiring reassembly for each

shot and of being damaged to some extent (loosened threads, packing washers). A less troublesome system is simply to use a piezoelectric gauge of sufficiently rugged and waterproof construction. Such a gauge develops a reproducible signal, is easily tested, and unless damaged requires no maintenance. It can be placed at almost any desired position in relation to the charge and other equipment, thus providing considerable freedom in timing without need of auxiliary delay circuits.

For some experiments, it is desirable to fire one or more detonator caps with a minimum time delay. A condenser discharge circuit can be used to fire two or more caps in series with short delay and a difference in firing times of 5 to 10 μsec.

III. PHOTOGRAPHIC RECORDING

The camera has the function of recording permanently the movement of the spot on the cathode-ray tube. In some cases the spot movement contains the time base as well as the desired signal. For this type of record a camera with cut film or 35-mm film may be used in the conventional manner. In other types of recording, the time base is supplied by the movement of the film, and a rotating-drum or streak-film camera is used.

The operation of all cameras involves the following components: a hood to keep out stray light, a lens and shutter combination, a film back, film, and lastly a means of viewing the object photographed. The units used on a DuMont type 208 oscillograph are shown in Figs. 19 and 20.

For recording several channels on a single film special camera hoods are constructed to take the standard camera backs and film holders.

The standard hood is hinged at both front and rear for inspection of the cathode-ray tube screen. Inside the hood is a manually operated shutter and on top is a viewing hole with prism. The section that swings open holds a lens (1/2.0, focal length 50 mm), a Wollensak shutter, and clamps to hold any of the three standard film backs. The cut-film back takes a standard 6½ × 9 cm film holder, and gives four exposures as the back is removed and rotated. The roll-film back contains a rebuilt Argus camera which gives exposures on 35-mm film. The rotating-drum back carries approximately 10 in. of 35-mm film and may be driven from a constant-speed motor, either by a flexible-shaft drive or by a pully drive.

The film used is not extremely critical, but the best records have been obtained with Eastman Fluorographic film. A typical development uses D-19 for 6 min at 18°C. It has been found that an increase in time or temperature will raise the background fog more than would normally be expected. Other fast films and contrasty developers have been used with almost equivalent results.

Using this equipment, it has been routine to photograph with good readability a single trace in the form of an exponential pulse with a time constant of 50 μsec, which crosses a 5-in. cathode-ray tube screen,[11] in 1 msec.

---

[11] Accelerating potential and intensifier electrode potentials each 1100 volts.

The only trouble encountered has been with cable releases of diaphragm shutters; hence the manual shutter is used for important shots.



Fig. 19. View of camera hood and camera beside.

Best Available Co

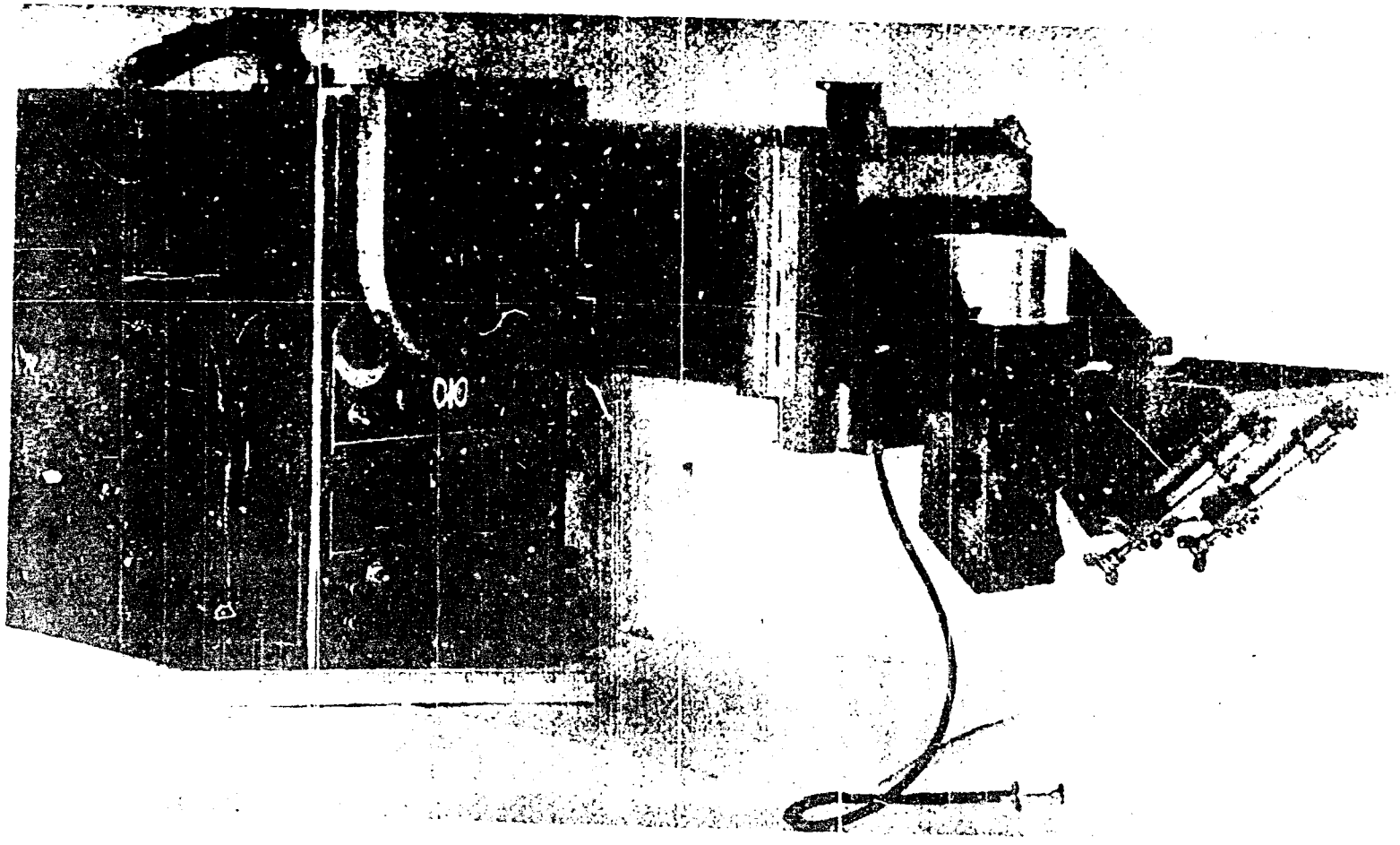


Fig. 20. View of camera hood and rotating-drum camera back in place on oscillograph.

683

IV. CALIBRATION EQUIPMENT

In the use of any system for recording transients, it is necessary to have an accurate calibration of its sensitivity and time resolution. It is also highly desirable to have a means of determining its transient response to an input signal of known form. In recording piezoelectric-gauge signals with long coupling cables, it is also necessary to determine the characteristics of these cables.

It is common practice in much oscillograph recording to calibrate both voltage and time scales by means of a sine wave of known frequency and amplitude determined by an a-c voltmeter of some sort. While this combination of functions is economical of time, it has the disadvantage that neither calibration is made in a fundamentally satisfactory manner for precision measurement. A sine wave is not ideally suited for interval measurements, as it is a smooth curve without discontinuities or other convenient reference points, and it is difficult to maintain accurate voltage calibrations of a-c meters.

It has been standard procedure at this laboratory to attack the calibration problem in a different way. The timing signal is shaped to have a sharply peaked wave form easily and accurately measured. No attempt is made to use this signal for voltage calibration, but rather a step voltage of known amplitude is applied separately. This step voltage is not only easily measured if the recording system has a good response, but also serves as a calibration of the transient response characteristics of the system. This additional information could be obtained from steady-state signals only at the expense of using a wide range of test frequencies, a procedure not practical in field work.

The concept of a routine calibration and transient-response test can be extended to include the impedance characteristics of any coupling network between the gauge and amplifiers. This is done, for example, in the "Q-step" calibration principle,[12] in which, in effect, a known quantity of charge,

---

[12] The Q-step principle, and its application to cable response testing, is described in NDRC Report A-306 (OSRD-4561). A brief description of the method is included for convenience in Sec. 6(b).

corresponding to charge developed by a piezoelectric gauge, is impressed on the coupling circuit and amplifier. In this use, the Q-step eliminates the need for an impedance bridge in determining cable response characteristics, as well as providing the necessary information in a more useful form.

4. Transient voltage standards

The requirements of a voltage standard are that it develop accurately known, dependable range of voltage values. It is very desirable also to have an internal means of checking these voltages at least approximately. If the same circuit is to be used as a generator of transients, it is necessary that the transient be of known and reproducible form adapted to calculation of response errors. The best single function for such a purpose is a voltage step, or Heaviside Unit Function, which jumps from one voltage level to another in a time ideally zero, practically small compared with any intervals involved in the measurement. Although a square wave is an approximation to such a step function much used in commercial practice, it has not been employed for testing of transient response at this laboratory because it gives no information at frequencies below the repetition rate, and because no good way of insuring the accuracy of its amplitude was seen. Instead, attention has been concentrated on development of step-function generators that would provide step functions of known displacement either by manual control or automatic triggering at regular intervals, and would provide a synchronizing pulse preceding the step by an adjustable time interval. These generators may be resolved into two parts: a standard voltage source, and a switching method for producing the step function.

(a) Standard voltage sources. -- The requirements placed on a calibration voltage standard are that it remain reasonably constant over time intervals between checking and that it be capable of supplying adequate power to the external circuit without disturbing the calibration -- in other words, that it permit low-impedance output from the source. It is usually difficult to satisfy both requirements simultaneously; most sources compromise between stability and power capability.

(1) Dry cells. The simplest standard voltage source is a dry cell operating under constant but low current drain. A circuit employing a Burgess type 4FA 1½-volt cell, operating with a drain of 1 ma requires recalibration once every two weeks. This is quite satisfactory if the moderately high output impedance can be tolerated.

(ii) Gaseous voltage-regulator tubes. If a gaseous voltage-regulator tube is operated under constant current, its terminal voltage will remain quite constant. The amount of stability is a function of the type and the individual tube. It has been found possible to select type VR105 tubes with a stability better than 0.1 percent. The noise level is less than 1 mv.

For selection the tubes are warmed up for one half hour, under their normal operating conditions, before being tested. Instability exhibits itself in rapid fluctuations during continual operation or in voltage jumps after the current is interrupted momentarily. Usually any voltage change is accompanied by a shift in the glow discharge over the cathode.

The circuit employed in this laboratory is shown in Fig. 21. It operates from an ordinarily filtered power supply. One voltage-regulator tube, type VR150, is employed to filter out any supply variations, thus maintaining constant current through the VR105. This circuit will provide adequate power for most calibrations as well as maintain accurate voltage.

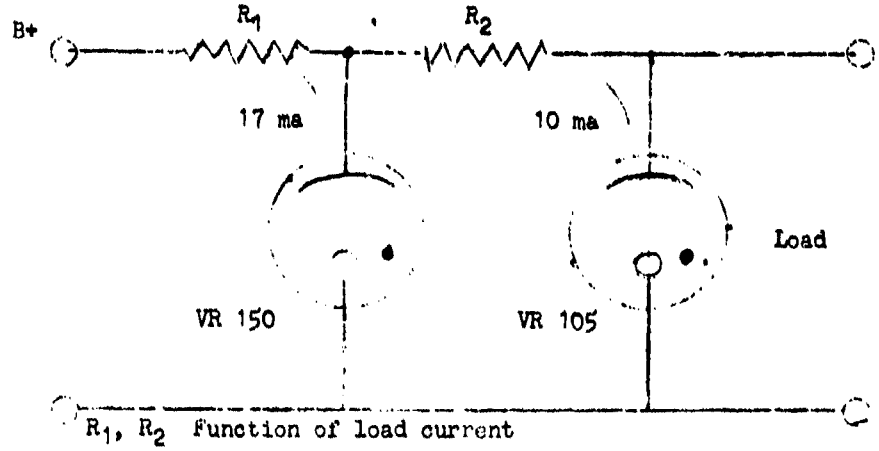


Fig. 21. High-current standard-voltage source.

(b) Step-function generators. -- (i) Relay step-function generator. Although it is possible to obtain clean voltage changes by mechanical switching, the mechanical devices tried here have always suffered to some extent from

one or more of the following difficulties:

(1) lack of reproducibility, time of closing variable, voltage not always clean;
(2) failure to remain in adjustment, necessitating cleaning of the contacts and "tinkering";
(3) tedious to use, requiring manual resetting.

The most satisfactory semi-mechanical device of this kind used here employs the opening of a relay contact, the relay being energized by a vacuum-tube circuit which also provides the synchronizing pulse for triggering the time-base or brightening circuits, and a regulated voltage source.

A simple circuit found adequate at this laboratory is shown in Fig. 22. The relay placed in the cathode of a flip-flop is normally energized. The trip pulse, after passing through a variable time-delay circuit, trips the flip-flop, de-energizing the relay. A Sigma type 4AH, 500-ohm plug-in relay was used here.

Because of its simplicity, very little trouble has arisen with this type of generator. It was found necessary, however, to keep the voltage difference between the relay coil windings and the relay frame as low as possible to eliminate electrolysis through the insulation. Furthermore, at recording speeds faster than 1 msec/in., even faster releasing relays exhibit some chatter and rounding of the step base. This makes difficult accurate measurement of the step height from photographic records in oscilloscope calibration. However, at slower recording speeds, units of this type have performed quite satisfactorily.

(ii) Electronic step-function generator. When the speed of recording is so fast that the chatter in a mechanical step-function generator cannot be tolerated, it is necessary to employ electronic means to generate the step function. The method developed here involves a rapid cutoff of the current to a voltage-regulator tube network such as described above, resulting in a drop in the output voltage which can appear as a positive or negative step function, depending on the method of connection to the recording circuit. The step function generated in this manner is quite clean.

The circuit developed at this laboratory is shown in Fig. 23. A type 6AG7 tube supplies the power to the VR network, operating in push-pull with another 6AG7 to maintain a constant drain on the power supply. For step-function generation the 6AG7 supplying the VR network is abruptly cut off,

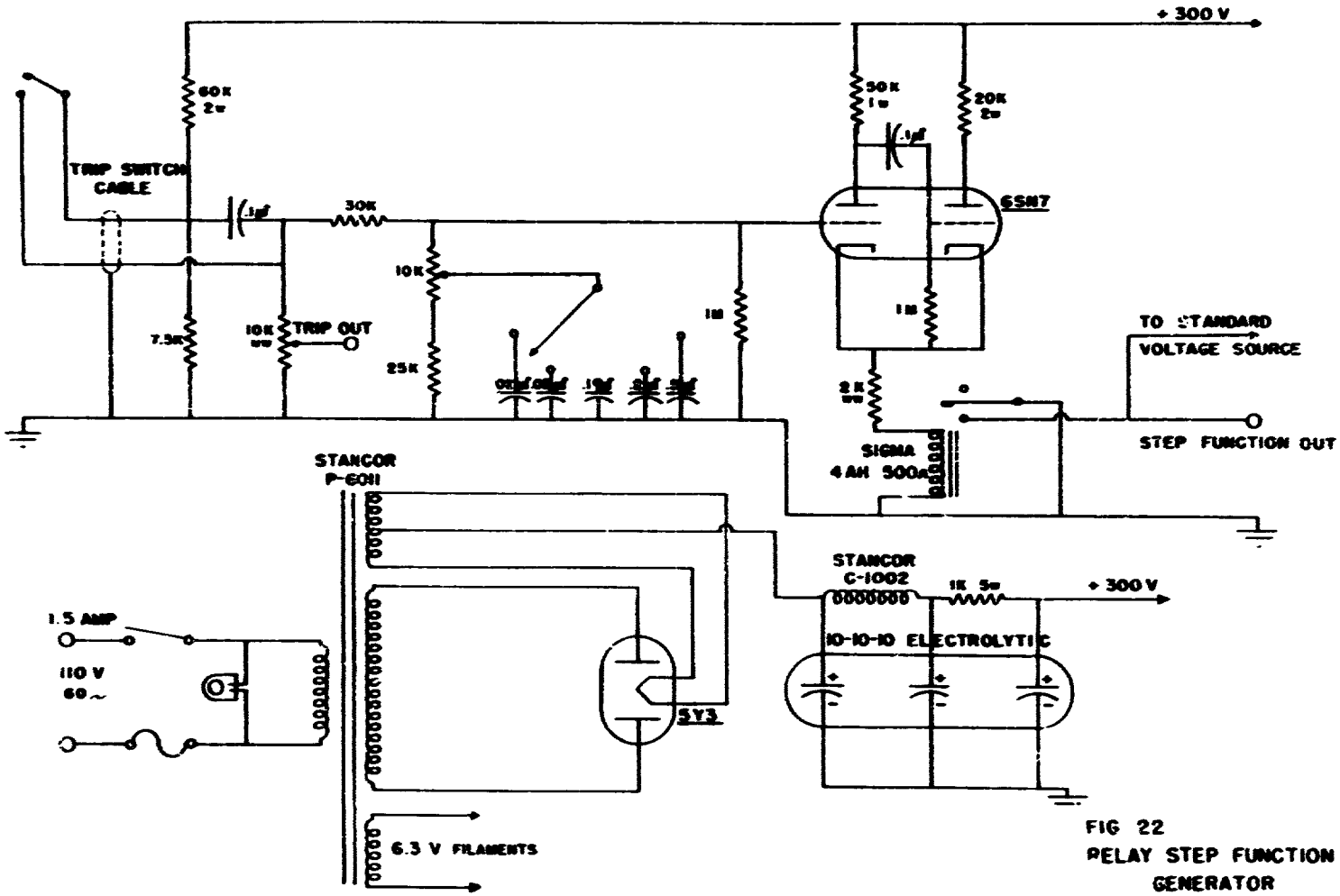


FIG 22
RELAY STEP FUNCTION GENERATOR

UERL WOODS HOLE, MASS.
RMB RLK

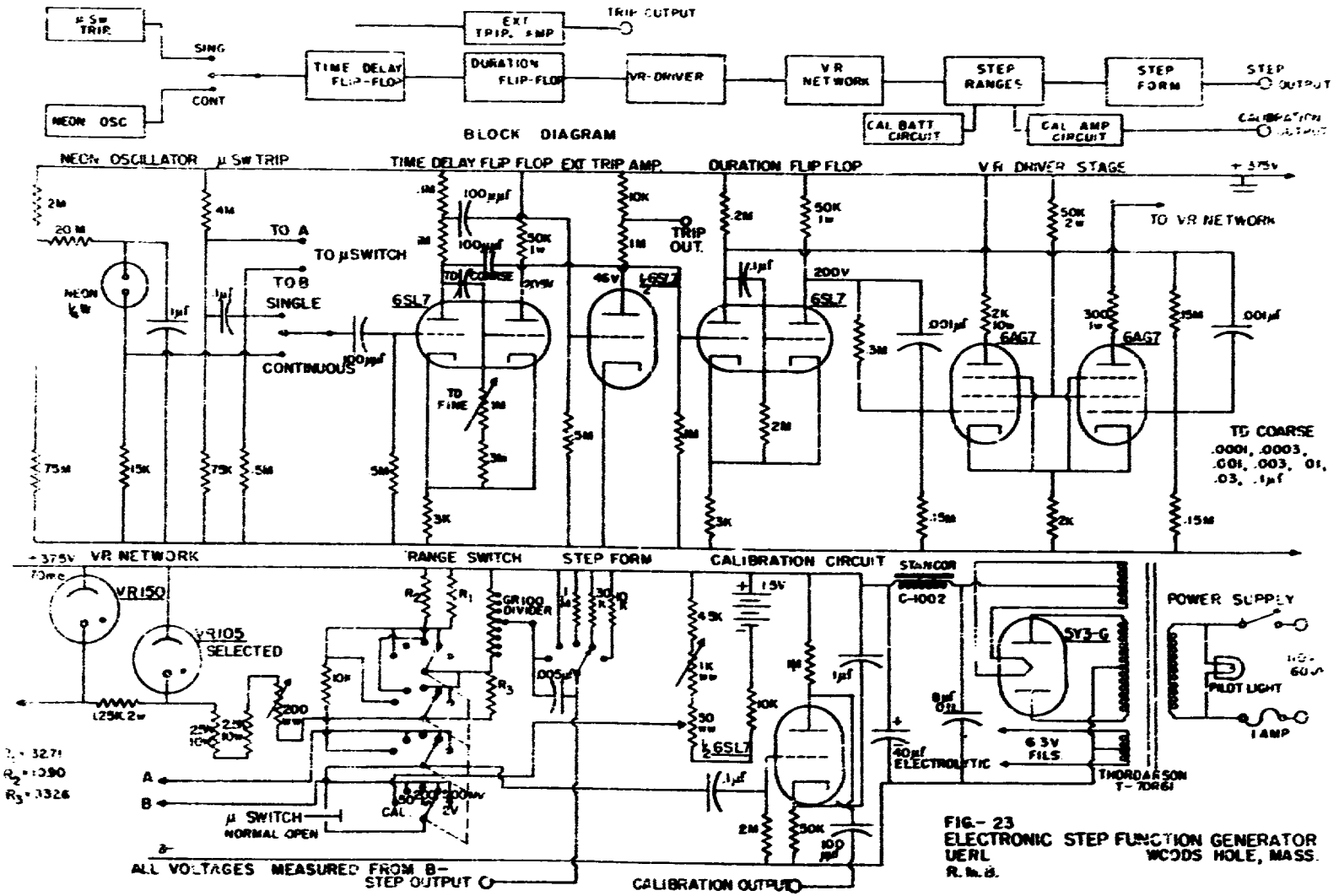


FIG.- 23
ELECTRONIC STEP FUNCTION GENERATOR
UERL WOODS HOLE, MASS.
R. In. 6.

6R9

while the other 6AG7 is driven to full current. Use of the Step Duration Flip-flop [see Sec. 3(a)] to drive the 6AG7 stage insures a sharp voltage change and provides a means for controlling the duration of the step function.

The operation is initiated by the closing of an external switch or by an internal oscillator. The pulse, so derived, trips the Time-delay Flip-flop which, on the initial flip, produces a pulse for actuation of the external recording mechanism, and on the return flop provides the pulse for tripping the Step Duration Flip-flop. The time delay between pulses may be adjusted over the range 100 μsec to 2 sec.

The output covers a range from 5 mv to 2 volts in four decades. Besides the step function, provision is also made for the generation of exponentially decaying functions of 50-, 150-, and 500-μsec time constant, through use of an R-C circuit.

For field calibrations a circuit is provided to check the standard voltage output at one point against a 1½-volt dry cell. The battery network is preadjusted to give a convenient fixed voltage; this is connected through a series resistance and switch to a point of presumably equal voltage on the standard voltage range. On closing the switch, any difference in the two voltages appears across the series resistance in a step form. Amplified in a condenser-coupled amplifier and viewed on an external oscilloscope, the voltage difference appears as an exponentially decaying function. A small adjustment of the battery voltage is provided for estimation of small differences in voltage.

The main difficulties encountered with this circuit have been in selecting the VR tubes and in combating leakage problems. Since the B+ is grounded to obtain positive direction of the step, considerable care must be taken to prevent leakage to the high-impedance grid circuits from affecting the operation, particularly that of the flip-flops. Care in wiring will eliminate most of this, however.

Four units of this type have been in calibration use for over six months, and aside from the difficulties mentioned, have given excellent service.

5. Time standards

For calibration of the time scales, an accurate, reliable, and easily calibrated time standard is required; an output wave form easily measurable

Best Available Cop

from photographic records is also desirable for some uses. To cover the range of time scales employed at this laboratory, several types of time standards have been used.

(a) Multivibrators. -- For time scales requiring time standards of frequency greater than 100 cycle/sec, the multivibrator is the most reliable and convenient. In this circuit, a frequency standard, usually a crystal oscillator, generates an accurate time signal, whose frequency is divided down to the values desired for calibration.

The circuit, shown in Fig. 24, is a multivibrator designed at this laboratory to generate output frequencies of 1, 5, 10, and 25 kc/sec, obtained from two multivibrator stages synchronized with a 100-kc/sec crystal-controlled oscillator. The output signal consists of very sharply spiked pulses.

The fundamental oscillator is a modified Colpitts circuit, electron-coupled and controlled by a Bliley 300-100 crystal. Small variable ceramic condensers afford small adjustments of the oscillator frequency over a range of approximately 100 cycle/sec.

The multivibrators are the conventional type employing 6SN7 tubes; the first multivibrator stage, operating at 25 and 10 kc/sec, is synchronized with the 100-kc/sec oscillator; the second, operating at 5 and 1 kc/sec, with the 10-kc/sec output of the first. The synchronization pulses are sharply peaked and applied across a resistor common to both multivibrator grids, in order to assure equal synchronization of both sides. The frequency-range switching is accomplished by changing the grid circuit elements, while the fine adjustments of each range utilize variable resistors in the grids.

The output signal of each multivibrator is peaked by a grid-leak biased amplifier. Variable negatively and positively spiked output voltages are available with a maximum output impedance of 500 ohms at the ends of the range.

The oscillator is adjusted by beating its signal on an ordinary receiver with the 5-kc/sec carrier of Station WWV of the National Bureau of Standards. The variable trimmer condensers should be adjusted together, to keep the two capacitances equal.

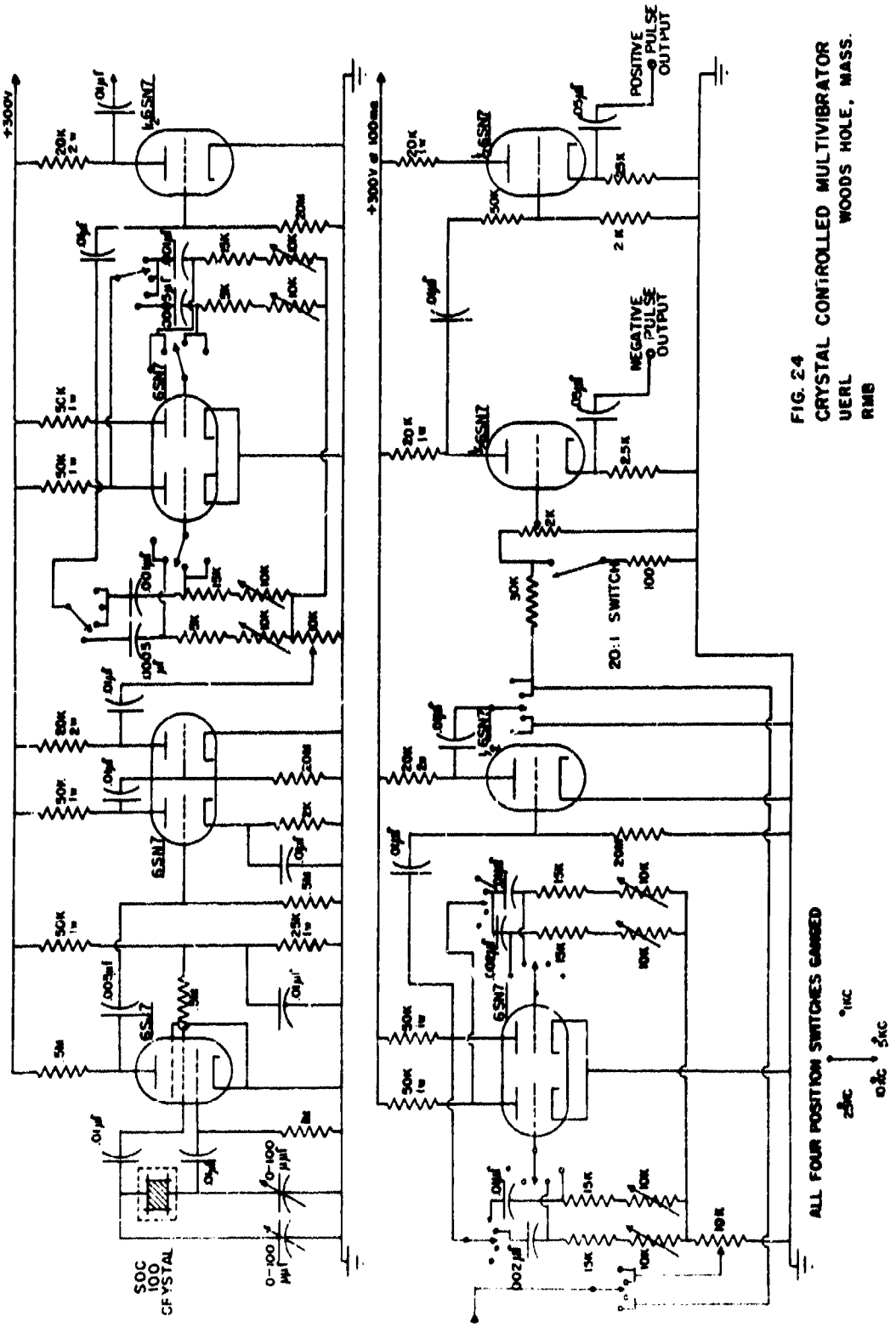


FIG. 24
CRYSTAL CONTROLLED MULTIVIBRATOR
UERL WOODS HOLE, MASS.
RMB

Adjustment of the multivibrators is best accomplished by adjusting their unsynchronized frequency to roughly 0.95 of the desired value, by means of the variable resistances in the grids; the synchronization voltage is then adjusted to give the correct frequency. Proper adjustment can most easily be observed by placing an oscilloscope across the common grid resistance; the input impedance of the oscilloscope has no effect on the operation because of the low impedance of this resistance. The voltage across this resistance shows the grid swings of both sides with the synchronization pulses superimposed on them.

The high-frequency components in the multivibrator and output signals necessitate careful planning of lead and tube locations to avoid cross pickup. Other than this, these instruments have caused little trouble in field use. They are particularly stable to line-voltage fluctuations, some maintaining their accuracy at input line voltages as low as 70 volts rms. Multivibrators of this type have been in service for almost a year and have proved quite reliable.

(b) Tuning forks. -- For time standards below 1 kc/sec, tuning forks are the most convenient. Most forks must be carefully shock mounted and oriented horizontally in order not to disturb their calibration. The General Radio type 813A and 815C forks have performed quite satisfactorily here when operated correctly. It should be noted that the larger forks, especially, are vulnerable to shock and should be used with caution in the region of an explosion.

(c) Stabilized oscillator. -- For field checks on the frequency standards, a number of battery-operated, resistance-stabilized L-C oscillators were constructed. These were stable to 0.1 percent and could have been used as standards if more accurate standards were not available. The circuit for these is shown in Fig. 25.

(d) Miscellaneous circuits. -- The Eccles-Jordan type counter circuits have been used to divide down the frequency from some other standard, such as a tuning fork or multivibrator, when the standard frequency was inconvenient. The time units so produced are usually not simple numbers, a fact which is inconvenient in measuring timing records.

6. Impedance standards

It is virtually essential that any laboratory which attempts to make quantitative electrical measurements have reference standards of impedance

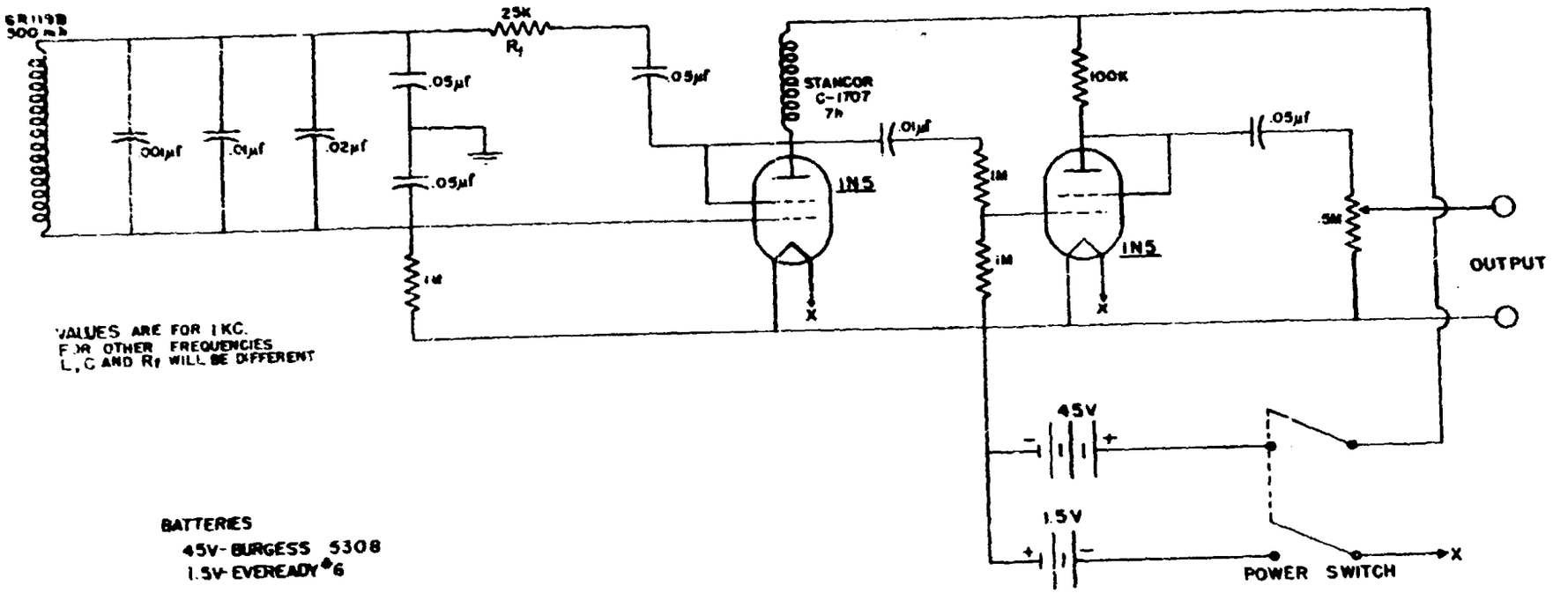


FIG.–25
STABILIZED L–C OSCILLATOR
UERL WOODS HOLE, MASS.
D.S.

and precise methods of impedance measurement.. The work of this laboratory has involved extensive development and use of piezoelectric pressure gauges, in which the charge developed on the crystal is proportional to the pressure. As ordinarily used, these gauges are shunted by large capacitances,[13] which must therefore be known if the charge resulting from pressure changes is to be determined from measured terminal voltages.

This laboratory has been fortunate enough to have the use of a wide-range resistance-capacitance bridge of considerable accuracy, which has been described elsewhere in detail.[14]

The bridge arms and other impedances are checked periodically against General Radio type precision fixed condensers. In order to standardize levels of measurements, interlaboratory checks of reference capacitors have occasionally been made.

For capacitance measurements in the field, a bridged-T capacitance comparison circuit has been developed. The development of the "Q-step" calibration method described in Sec. 6(b) has provided a better means of calibrating piezoelectric gauge circuits in terms of a fixed condenser.

(a) Capacitance bridge. — This bridge is used primarily to measure capacitances of electrical cables for fault location and to check condensers used in the "Q"-calibration procedure [see Sec. 6(b)].

The operation of the bridge is based on a substitution method in a bridged-T network (see Fig. 26). This network has zero transmission at a frequency determined by the two balance conditions:[15]

---

[13] Calibration and use of piezoelectric gauges for transient pressure measurements are discussed in forthcoming OSRD Reports.

[14] K. S. Cole and H. J. Curtis, Rev. Sci. Inst. 8, 333 (1937). The bridge and associated equipment were made available for this work through Konneth S. Cole and The College of Physicians and Surgeons, Columbia University, to whom this laboratory is greatly indebted.

[15] The balance conditions are readily determined from the fact that for zero transmission, the sum of the short-circuit transfer impedances of the two parallel paths from oscillator to detector must be zero. For a discussion of bridged and parallel T-networks, see W. N. Tuttle, Proc. I.R.E. 28, 23 (1940).

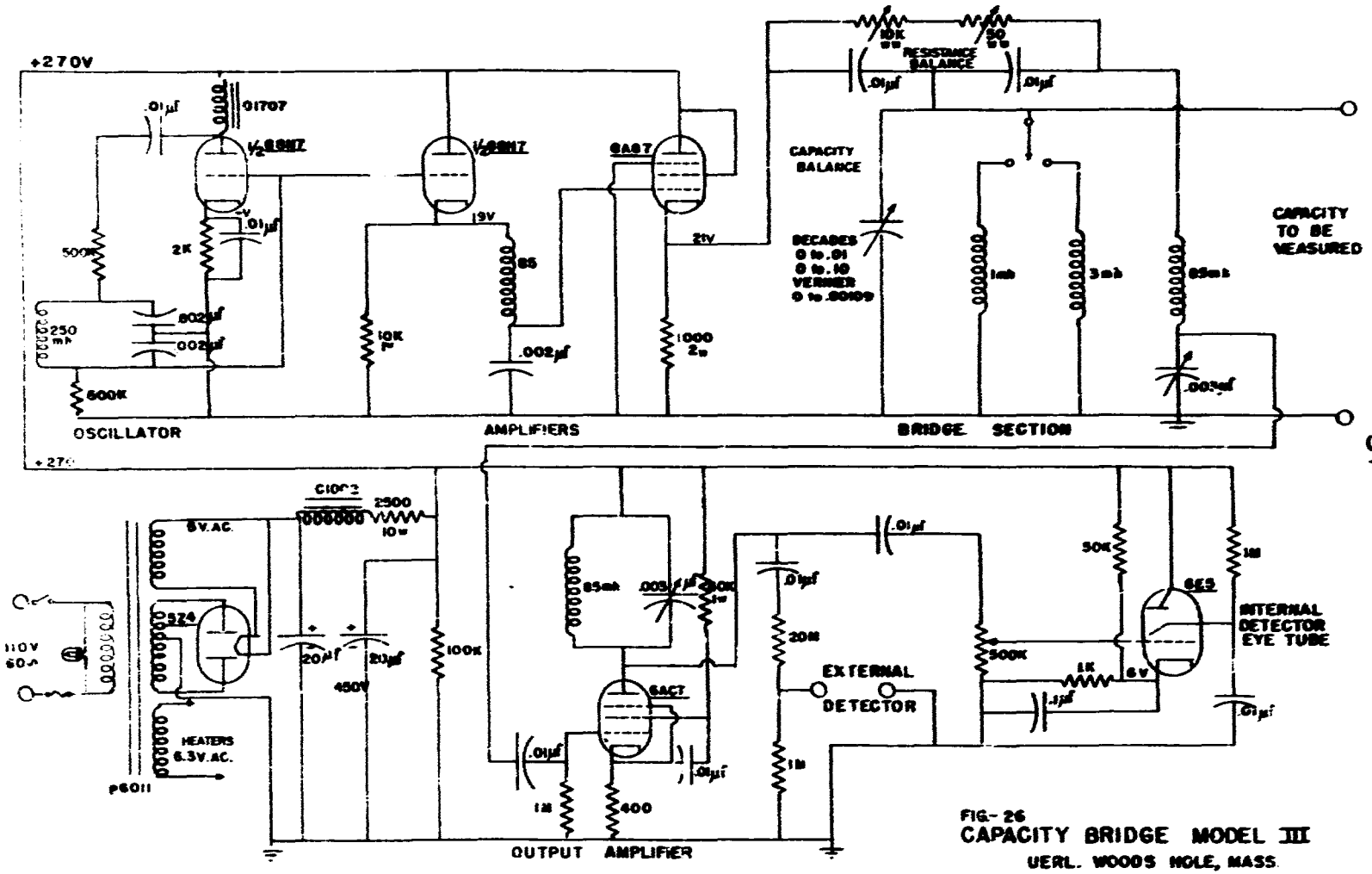


FIG- 26
CAPACITY BRIDGE MODEL III
UERL. WOODS HOLE, MASS.
D.S. R.L.K.

$$R_x = R_s/(R_s C\omega)^2,$$

$$C_x = 1/\omega^2 L - C_s - 2C.$$

If an unknown impedance is connected in parallel with C_s, its capacitance C_x is equal to the amount by which the condenser C_s must be decreased to rebalance the network, and its resistance R_x is determined by the change in R_s necessary for rebalance. These two balances are independent. In the design used, a nominal driving frequency of 10 kc/sec is employed, and capacitance ranges of 0 to 100,000 $\mu\mu$f, 0 to 10,000 $\mu\mu$f are obtained by suitable values of inductance L.

The driving frequency is provided by a resistance-stabilized oscillator, the output of which is amplified in a tuned L-C circuit driven by a cathode follower, and coupled to the T-network by a second cathode follower. At balance, no signal appears at the output of the network, and this balance condition is determined by an electron-ray (magic-eye) tube. This tube is operated with its triode amplifier section biased to cutoff; an a-c signal applied on the grid produces a d-c voltage on the ray-control electrode which changes the shaded area on the fluorescent target. For greater sensitivity a cathode-ray oscillograph or other indicating instrument may be connected to the terminals provided.

The T-network used has the advantage, as compared to a bridge circuit, that both input and output voltages and the unknown impedance have one side grounded. The balance is, however, frequency dependent; hence a stable oscillator frequency with pure wave form must be provided to prevent drift and balance errors from harmonic frequencies passed by the network. Good quality air and mica condensers should be used in the network.

The balance drifts while the oscillator is warming up and is affected by large line-voltage variations, but these errors are usually not serious. Except for condenser drift or failure, the accuracy of capacitance balance is 0.1 percent of full scale. Units of this and earlier types have been in service for two and one-half years with satisfactory results.

(b) Q-step calibration. -- The Q-step calibration procedure is, in effect, a means by which a known quantity of charge can be applied to a

capacitative circuit, the charge being determined in terms of a voltage and fixed capacitance. If a step voltage is applied, the method also determines the transient response of the system.

Consider the network of Fig. 27(a). If the admittance of the gauge and coupling impedance in parallel is $Y(i\omega)$, the voltage developed at the recorder is given by $V_p = Q_p/[C_s + Y(i\omega)/i\omega]$, where Q_p is the charge developed by the piezoelectric gauge. If, to calibrate the system, a known

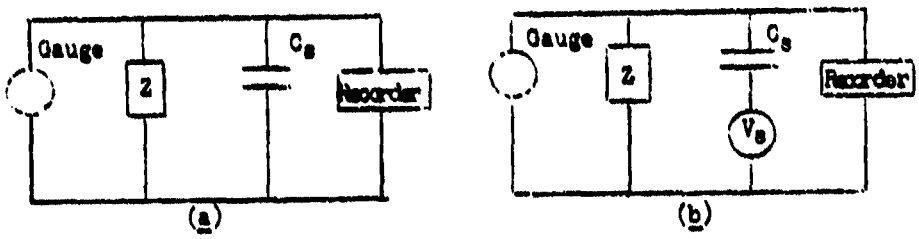


Fig. 27. Connections for Q-step calibration.

voltage V_s is applied as shown in Fig. 27(b), the resultant voltage V_o at the recorder is given by

$$V_o = C_s V_s/[C_s + Y(i\omega)/i\omega].$$

Eliminating the admittance $Y(i\omega)$, we have for the charge Q:

$$Q = C_s V_s(V_p/V_o).$$

Hence the gauge output Q is determined in the terms of the fixed capacitance C_s, the voltage V_s, and a ratio of voltages (or deflections) indicated by the recording system. Both the gauge circuit and recording system are calibrated in the one operation and the procedure is valid for any frequency or time characteristic of the applied voltage as long as the gauge circuit can be regarded as a two-terminal network.[16] In work at this laboratory, the voltage V_s is ordinarily applied by a step-function generator [see Sec. 4(b)], and the transient response of the cable and recording system is thereby determined.

---

[16] If the gauge circuit includes a coupling cable, this restriction will not be satisfied for transients occurring in intervals of the order of the transit time for the length of cable.

V. MISCELLANEOUS

7. Alternating-current power

The electronic equipment of this laboratory is designed to run on 117 volts rms at 60 cycle/sec. The equipment designed here will work over a plus or minus variation of 10 volts from this rated value and show no variation in performance. However, the DuMont type 208 oscillographs show a linear variation in sensitivity with respect to line voltage. This is due to the use of unregulated supplies for the cathode-ray tube, and it has been found impractical to install regulation. Therefore for a reproducibility of 1 percent, when the DuMont type 208's are used, the power-line voltage may not drift more than 1 volt during the period required for calibration and shooting. With oscillographs such as the four-channel oscillograph, the line drift may be 10 volts. All the instruments are comparatively insensitive with respect to frequency.

There are three sources of a-c power commonly used. The power supplied by the local power and light company has wide variations in voltage owing to changing load. This is eliminated when necessary by the use of a Sola constant-voltage transformer. There is, however, a frequency variation of 0.1 cycle/sec average to 0.2 cycle/sec maximum, which produces a voltage variation from the regulator of 0.3 to 0.6 percent.

Gasoline-engine generators, such as the Delco or Onan 5-kw, four-cylinder units, are capable of giving very good regulation under constant load. For example, one generator has a drift of approximately 1 volt during a day's work, with random variations of less than $\frac{1}{4}$ volt. If an engine is in poor condition, variations of 10 volts are not uncommon.

Battery-driven converters in the range of 500 to 1500 watts are capable of very good regulation. A typical marine installation has 20 storage batteries of 100-amp-hr capacity. These are recharged by rectifiers using generator or commercial a-c power. When batteries are in poor condition they may cause trouble.

Power distribution is controlled by a panel which has two channels. Voltage step-up or step-down is controlled by Variac transformers, and voltage, current, and frequency are shown by meters.

8. Master control panels

In the recording of a shot, switching problems are facilitated and human error made less likely by the use of a "Master Control Panel." By

use of a single knob, all electric switching is accomplished for the three photographs required for one shot, namely time-scale calibration, Q-step calibration, and the actual transient. Also included in the panel is a meter which measures the gauge cable resistances, a space for the "plug-in" cable compensation networks, and an interlocking firing-switch system which prevents the operator from firing the charge when the master switch is in the wrong position.

The circuit for the master control is given in Fig. 28. The design is a matter of switching and layout to give a maximum utility and freedom from error.

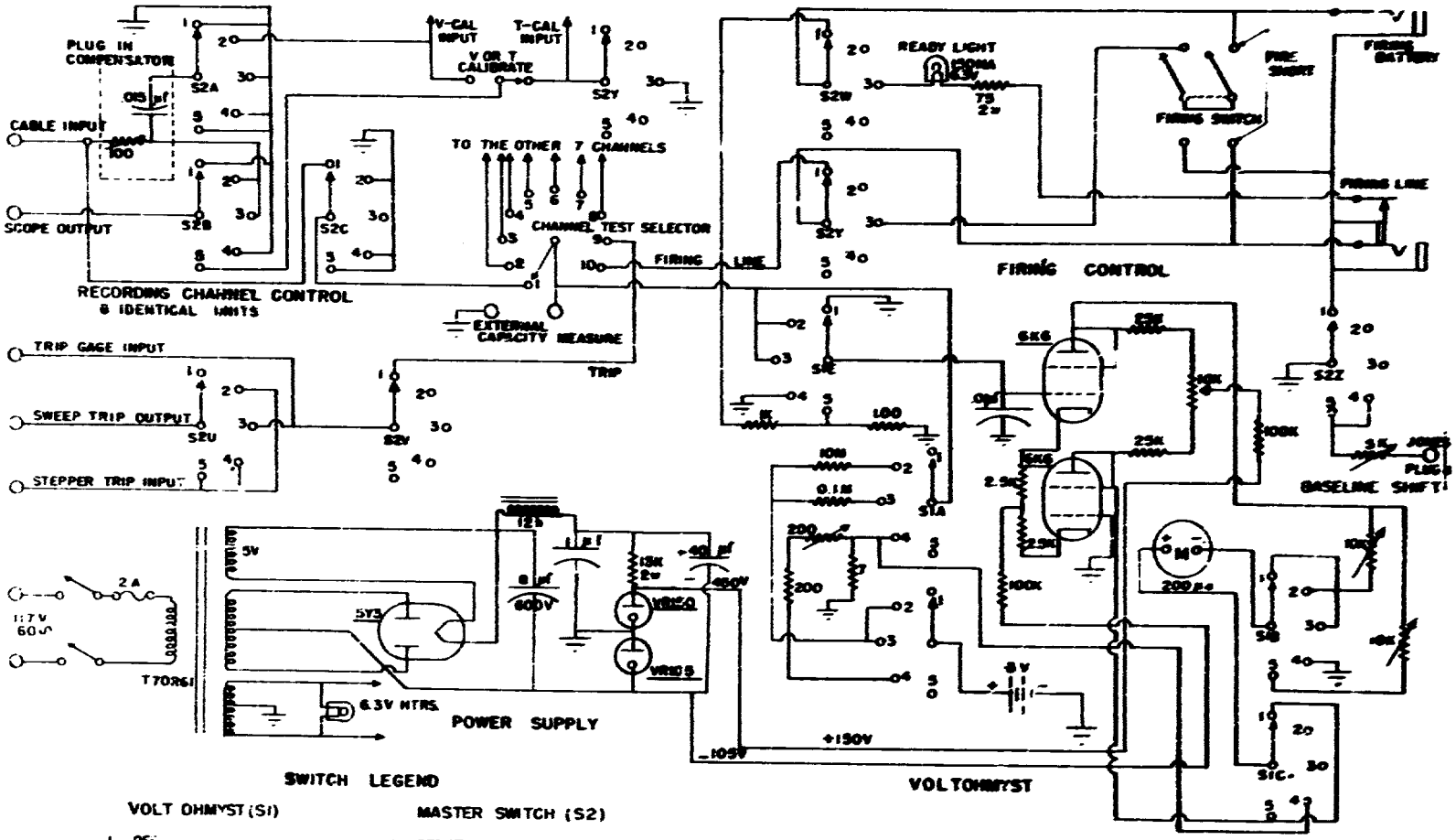
A master control unit of this type is useful primarily for work in which a considerable number of similar operations are to be conducted. In these circumstances, the time saving and increase in efficiency due to simplicity of operation and freedom from human error are very great, and can perhaps be properly appreciated only by those who have to operate a complicated array of equipment and by those who have to analyze the records.

9. General considerations in instrumentation

A background of four years' experience in design and construction of instruments for recording transients in the field has shown the importance of factors which are of less concern in laboratory work. These considerations are doubtless familiar enough to all who have made such measurements, but the following discussion is included as a possible help to those who may be called upon to plan equipment for field tests.

Field measurements of underwater explosions must frequently be made under adverse conditions, both for the operator and for the equipment. It is therefore important that the equipment function properly under unfavorable combinations of temperature, humidity, and primary power-supply variations. For the sake of the operator, it is also important that the necessary controls be simple and straightforward, and that proper functioning of the equipment be easily determinable. The possible need for repair in the field with limited facilities should also be taken into account.

A particularly important consideration is the fact that explosions occur once and may involve considerable amounts of time, effort, and money. In these circumstances, equipment which works 95 percent of the time may be worse than useless.



SWITCH LEGEND

VOLT OHMYST (S1)

1 OFF
2 RESISTANCE X 1 meg
3 X 10,000
4 X 1
5 FIRING BATTERY VOLTS

MASTER SWITCH (S2)

1 RESISTANCE OR CAPACITY TEST
2 Q-STEP CALIBRATION
3 READY TO FIRE
4 BASELINE
5 VOLTAGE OR TIME CALIBRATION

FIG-28
MASTER CONTROL PANEL - MODEL III

UERL WOODS HOLE, MASS
BS CPS AGR

These difficulties of field work underline the importance of mutual understanding on the part of the man who develops the equipment and the man who uses it. The former should know what will be required of the equipment, and should have field experience; the operator should have some knowledge of the basic principles of the equipment in order to use it intelligently. When a new type of measurement is to be undertaken, the design of needed electronic equipment must be based on knowledge of field requirements and what is reasonably possible.

The actual design should then be developed to meet the requirements with a minimum of adjustments and a maximum of reliability. Large safety factors should be allowed, to take account of such things as tube variations, tolerances of component parts, leakage currents. Good mechanical layout and construction and clean wiring may mean the difference between servicing in the field and stopping work until laboratory repairs can be made. It is also worth while to use standard and readily available components as far as possible.

The completed instrument should be tested under actual or simulated conditions and these results kept recorded as a part of the service record, on the instrument. Routine tests and inspections of all equipment are valuable in maintaining it at peak performance and avoiding breakdown.

THE MEASUREMENT OF UNDERWATER EXPLOSIONS FROM SERVICE WEAPONS AT THE UNDERWATER EXPLOSIVES RESEARCH LABORATORY

J. S. Coles
Underwater Explosives Research Laboratory
Woods Hole Oceanographic Institution

American Contribution

March 1946

Personnel

For a research program of the magnitude of that undertaken in measuring underwater explosions of full-scale weapons, many people contributed ideas and work. Listed below are a few out of the many who were directly responsible for much of the work: W. Adcock, R. M. Brown, J. D. W. Churchill, B. Coggins, R. H. Cole, J. S. Coles, G. Duys, A. Ferris, F. M. Fye, R. L. Kaye, J. Y. Kennedy, D. E. Kirkpatrick, J. Lacey, P. Newmark, C. R. Niffenegger, E. L. Patterson, Capt. S. E. Poole, W. S. Shultz, J. P. Slifko, D. S. Stacey, D. T. Tassinari, and A. H. Vine.

TABLE OF CONTENTS

		Page
Abstract		1
Part		
I.	INTRODUCTION	1
II.	GENERAL DESCRIPTION OF GEAR USED	3
	1. Vessel and equipment	3
	2. The "one-dimensional" fore and aft rig	3
	3. The "two-dimensional" paravane rig	3
	4. Instrumentation	4
	(a) Piezoelectric-gauge instrumentation	4
	(b) Mechanical-gauge instrumentation	5
III.	TYPE OF RESULTS OBTAINED	7
	5. Comparison of weapons with different explosive fillings	7
	(a) Procedure followed in analysis of data	7
	(b) Conversion from one type of explosive ratio to another	8
	6. Other types of data obtained	10
	(a) Effect of charge orientation	10
	(b) Booster effects	10
	(c) Shape effects	11
	(d) Similitude laws	11
	(e) Multiple charges	11
	(f) Surface effects	11
IV.	DETAILS OF INSTRUMENTATION	12
	7. Piezoelectric gauges and associated equipment	12
	(a) Gauges	12
	(b) Electrical cables	13
	(c) Recording equipment	14
	(d) Analysis of records	19
	(e) General comments concerning piezoelectric instrumentation	23
	8. The UERL diaphragm gauge	23
	(a) Description	23
	(b) Measurement of explosive effectiveness	23
	(c) Theory	24
	(d) Weight and distance exponents	25
	9. The Naval Ordnance Laboratory ball-crusher gauge	25
	(a) Description	26
	(b) Measurement of sphere deformation	26
	(c) Theory	27
	(d) Weight and distance exponents	28

PRECEDING PAGE BLANK

Part		Page
	10. The Bureau of Ships Modugno gauge	28
	(a) Description	28
	(b) Measurement of deformation	29
	(c) Weight and distance exponents	29
	11. Hilliar-type gauges	29
	(a) General theory	29
	(b) Single piston gauges	30
	(c) Multiple-piston gauges	30
	12. Summary of RELIANCE instrumentation	31
V.	DETAILS OF GEAR	32
	13. Gauge mounts	32
	(a) Large composite gauge blocks	32
	(b) Light diaphragm-gauge blocks	33
	(c) Small crusher-gauge mounts	33
	(d) Momentum- and Hilliar-gauge mounts	34
	(e) Piezoelectric-gauge mounts	34
	14. Gauge and charge spacing	35
	(a) Vertical components	35
	(b) Horizontal components	36
	15. Electrical cables and their suspension	37
VI.	SETTING AND RETRIEVING GEAR	38
	16. "One-dimensional" fore and aft rig	38
	(a) Setting the gear	38
	(b) Retrieving the gear	39
	17. "Two-dimensional" (paravane) rig	41
	(a) Setting the gear	41
	(b) Retrieving the gear	42

Appendix

I.	Use of the UERL Diaphragm Gauge	43
II.	Use of the NOL Crusher Gauge	45
III.	Use of the Hartmann Momentum Gauge	47
IV.	Use of the Improved Hilliar Gauge	49
V.	Electric Power for Schooner RELIANCE	52
VI.	Data for Lot V Steel Plates	53
VII.	Dynamic Calibration of Copper Crusher Spheres and Cylinders with Freely Falling Weights	54
VIII.	Static Calibration Curve Modugno-Gauge Disks	112
IX.	Beam Brightening and Firing Synchronizer	56

THE MEASUREMENT OF UNDERWATER EXPLOSIONS FROM SERVICE WEAPONS AT THE UNDERWATER EXPLOSIVES RESEARCH LABORATORY (UERL)

by

J. S. Coles, March 1946

Abstract

The instruments and methods used for measuring the effectiveness of and obtaining other data pertinent to underwater explosions of full-scale service weapons is described in detail. The theory and use of mechanical gauges, including the UERL-diaphragm, NOL ball-crusher, BuShips Modugno, and momentum gauges, are discussed; the practical application of piezoelectric gauges to full-scale measurements is illustrated. The highly specialized techniques involved in handling such a combination of heavy with friable equipment at sea is described.

I. INTRODUCTION

The comparison of various explosives in full-scale service weapons was begun by the Underwater Explosives Research Laboratory (UERL) in December 1942 at the request of the Bureau of Ordnance of the United States Navy. The very early work was done under great pressure and made use of the existing facilities at the UERL, which required the rather cumbersome coordination of several vessels. This work has been described previously [1]* When it became apparent after the first series of tests that there would be a large amount of such full-scale testing to be done, a special vessel was purchased for this purpose and converted into a floating laboratory. This vessel, Schooner RELIANCE, has been in continuous use since that time and is fully equipped for the recording of the signals from eight piezoelectric gauges, as well as servicing the mechanical-type gauges in use at UERL.

The measurement of the underwater effectiveness of an explosive ultimately involves the determination of damage to an actual target. In practice, this is best accomplished by measuring certain parameters of the shock wave resulting from an underwater explosion, and by measuring the actual damage to small targets such as small steel diaphragms.

The variation of pressure with respect to time (Fig. 1) may be measured at a given point in the water by means of a piezoelectric gauge; from this pressure-time curve, the peak pressure P_m, momentum or impulse I, and the energy E of the shock wave may be obtained. For most cases, the pressure-time curve may be represented by

$$P = P_m e^{-t/\theta}$$

*The list of references has been deleted.

Best Available Copy

over the regions from $t = 0$ to $t = \theta$, where t is the time measured from the peak and θ is the time constant of the shock wave. The response of mechanical gauges to the shock wave is some function of the initial portion of the pressure-time curve out to a time t corresponding to the completion of action of the particular gauge. Thus mechanical gauges with a response time that is short relative to the duration of the shock wave measure quantities associated closely with the peak pressure, while gauges with long response time measure quantities related more to the impulse of the shock wave. These measurements are with respect only to the primary shock wave, and are not affected by secondary pulses resulting from oscillations of the "bubble" in the water, although the piezoelectric gauges may be used for this purpose when so desired.

Due to the urgency of the work at the time it was undertaken it was impossible to complete the instrumentation before the actual comparison of explosives was begun. Thus during the early experiments only 2 piezoelectric gauges and a few diaphragm, ball-crusher and Modugno gauges were used on each shot, while in later experiments as many as 8 piezoelectric gauges, 25 ball-crusher, 8 diaphragm, 8 Modugno, and 8 Killiar-type momentum gauges were used. While the early work may have suffered somewhat because of the small amount of instrumentation, it was nevertheless possible to produce useful results that could not otherwise have been obtained.

The greater part of the work of the RELIANCE has been in the comparison of various explosives in standard service weapons, such as depth bombs, depth charges, and aircraft-dropped mines. Other types of more fundamental research have been done whenever possible, including the determination of similitude curves from spherical charges, the study of the pressure field about line charges and multiple charges.

II. GENERAL DESCRIPTION OF GEAR USED[1]

1. Vessel and equipment

The RELIANCE was a 76-ft Gloucester-type fishing schooner converted into a research vessel, equipped with an electronics cabin and a mechanical-gauge cabin, as well as the necessary sources of power for the work to be done. A two-way radio telephone and a recording fathometer were a part of the standard equipment. In addition to these scientific accomodations there were a galley, quarters for the crew, and a general workshop (Figs. 2 and 5).

Deck space was available for the necessary gear and other equipment, including a large power-driven reel for the piezoelectric-gauge cables.

2. The "one-dimensional" fore and aft rig

Practically all of the work in comparing explosives was done by locating the various gauges used on a straight line fore and aft through the charge and parallel to the surface of the water (Fig. 3). At the after end of this line was the sea anchor used for maintaining tension. In the middle was located the charge, while the forward end of this line was attached to a tow line leading up to the vessel RELIANCE. The gauges and charge were usually 40 ft below the surface and were suspended from surface floats. These components were attached to one another by means of the steel spacer cable which was kept stretched out by the strain of the sea anchor as the gear was towed through the water. Electrical cables for firing and for transmission of piezoelectric-gauge signals back to the electronics cabin were led to the surface and then to the RELIANCE by means of a surface line supported by special floats.

3. The "two-dimensional" paravane rig

A great disadvantage of the "one-dimensional" rig was that it allowed measurements to be made for a single charge in only two directions that were opposed by 180°. To obtain a measure of the explosion field in four directions from a charge, the two-dimensional or paravane rig was developed (Fig. 4). As with the one-dimensional rig the gauges and charge were suspended at the same fixed depth below the surface, with a line running from a sea anchor at the aft end of the gear through the charge to the tow line leading to the RELIANCE. In addition to this part of the gear, which is the same as for the one-dimensional rig cited above, there were also gauges mounted on two lines that were attached to the charge at an angle of 90° to the fore and aft line. These side lines were held out by means of two paravanes[2] attached to the gauge blocks at the ends.

There are many difficulties inherent with this paravane gear. It must be set in perfect balance, otherwise the paravanes do not behave properly

---

[1] Details will be found in Parts IV, V.

[2] A paravane here refers to a flat surface so suspended that it pulls out and down as it is towed through the water. Opposing these two forces is the force from the opposite paravane and the force upward due to a surface buoy.

and may foul the rig and even bring the vessel into serious trouble. There is always some bow in the side spacer cables due to the drag of the water, which causes an uncertainty with respect to the angle between the gauges and the charge and the gauge-to-charge distances. However, this uncertainty in gauge-to-charge distance may be overcome by comparing the results for an asymmetrical charge to results for a symmetrical charge fired under identical conditions. For the piezoelectric gauges used off the sides of the charge there must be a separate return line along the surface to carry the gauge cables.

The difficulties encountered with the paravane rig probably outweigh the advantage in obtaining values regarding the pressure field in two dimensions. The same results could be obtained more rapidly and with less trouble by using the one-dimensional rig and firing twice as many charges.

4. Instrumentation

The instrumentation may be generally divided into two types — piezoelectric and mechanical. The piezoelectric instrumentation gives rather complete fundamental information about the explosive shock wave in the water but is difficult to maintain and operate. On the other hand the mechanical-gauge instrumentation is easy to maintain and operate and is very reliable, but the results are much harder to interpret in terms of the shock-wave parameters.

(a) Piezoelectric-gauge instrumentation. — The instrumentation with piezoelectric gauges consisted of the following groups: gauges, transmission lines with their compensating networks, amplifying and recording equipment, time- and voltage-calibrating equipment.

(i) Gauges. The piezoelectric gauges used in this work were composed of 1, 2, or 4 tourmaline elements [2,3]. The ones usually employed were of the doublet type with a gauge constant of roughly 4 $\mu\mu$coulomb/(lb/in^2).

(ii) Transmission of gauge signals. The transmission system for bringing gauge signals to the RELIANCE consisted of the following elements: a copper tube with central conductor attached to the gauge and running directly back in the opposite direction from the charge for a distance of 20 ft where it was spliced to a Miller plug. From the other side of the Miller plug Army-Navy Type RG-41/U concentric cable ran up to a surface buoy. The length of this section of the cable varied from 40 to 80 ft depending upon the particular location of the gauge. This cable terminated in a second Miller connector at the surface buoy, where there was inserted a compensating patch cord containing a resistance-capacitance network which was a part of the double-ended cable compensation used with the RELIANCE-type gear. (Such compensation is necessary to correct for frequency response and dielectric absorption on long cables [4].) This patch cord was connected in turn to a 600-ft length of RG-41/U cable which ran back along the surface to the recording vessel, terminating at the large cable-reel on the deck. A 20-ft section of the same cable carried the signal from the reel down to the input of the compensating network in the master control panel.

(iii) Recording of gauge signals. The signal from the master control panel was fed directly into the vertical amplifiers of the cathode-ray oscilloscope. The trace of this signal on the Y-axis of the cathode-ray tube was recorded either by a rotating-drum camera or a still-film camera. In the former case no signal was used on the X-axis, while in the latter case a linear sweep was introduced in the X-axis. For each record a time calibration must calibrate the drum or sweep speed, and a voltage (V-step) or charge (Q-step) calibration must be put on the film to calibrate the electrical and photographic amplification of the trace. If a voltage step is used for this, the capacitance of the cable and gauge system must be measured separately on a capacitance bridge, while if a charge calibration is used independent determinations of the capacitance and voltage are unnecessary.

(iv) Interpretation of records. The photographic records so obtained were analysed by transforming them into absolute units of pressure and time from comparison with the V- or Q-step and the time calibration. This was formerly done by measuring the records on a movable-stage micrometer microscope, but more recently the pressure-time curves have been projected on photographic paper simultaneously with a two-dimensional grid which has been adjusted for the X-axis to read in absolute time units and for the Y-axis to read absolute pressure units, according to the time and voltage calibrations (see Fig. 1). After the pressure-time curves have been transformed into their absolute units, the peak pressure may be read off directly and the impulse and energy factor may be integrated graphically. The energy factor obtained by this simple graphical integration does not include the after-flow energy, which is important for spherical shock waves. Other pertinent data which are apparent on the pressure-time curves may also be noted at this time.

(b) Mechanical-gauge instrumentation. — (i) The UERL diaphragm gauge. The gauge that has proved itself to be the most reproducible for all routine measurements of explosive effectiveness has been the UERL diaphragm gauge [5]. This gauge consists essentially of a steel pot 3-1/2 in. in diameter on the face of which is mounted a thin diaphragm. The diaphragm materials and thicknesses vary, but for large-scale measurements 14-gauge (B and S) steel was generally used. Explosives were compared by taking ratios of the maximum deflections of the diaphragms after being subjected to the explosive shock wave. For large charges these diaphragm gauges read a quantity that corresponds to peak pressure, although the finite time of gauge action is longer than for the ball-crusher or Hodgnc gauges. The gauges were mounted in pairs, sometimes in a heavy gauge block and other times in a very light gauge block.

(ii) The Naval Ordnance Laboratory ball-crusher gauge. The Naval Ordnance Laboratory ball-crusher gauge [6] was used in very large numbers because of its operational simplicity and small size. A 1/2-in. diameter piston rests directly on a copper sphere which is supported by an anvil. When the piston is struck by the explosive shock, the copper sphere is deformed, the amount of deformation being a measure of the explosive effectiveness. The spheres used for most work were 3/8 in. in diameter, although the gauge was so designed that 5/32-in. diameter spheres could also be used.

A rather detailed theory has been presented for the action of this gauge [7,9] and its reproducibility has been summarized [8]. However, while it is possible to calculate the response of the gauge from a known pressure-time curve, it is not possible to determine the form of a pressure-time curve from the gauge response. Deformations of the copper spheres can be transformed to values for peak pressure provided the form of the pressure-time curve is previously known [10].

(iii) The Modugno gauge. The Bureau of Ships has developed a diaphragm type of gauge known as the Modugno gauge [11]. The effective diaphragm diameter is 1 in., and the diaphragm may be of various materials and thicknesses. Those used at UERL were either of approximately 0.065-in. copper or 0.050-in. thick cold-rolled steel. Comparison of the maximum deflection of these plates after being subjected to an explosive shock wave gave the relative effectiveness of the explosives. For large charges these gauges measured approximately peak pressure, having a somewhat shorter action time than the UERL diaphragm gauge but longer than the NOL ball-crusher gauge. The theory for these gauges has not been worked out to allow a computation of peak pressure from the gauge deflection, even when the form of the pressure-time curve is known, nor a calculation of the maximum deflection from a known pressure-time curve.

(iv) Hilliar-type gauges. Mechanical gauges that integrate the pressure-time curve to give the impulse in the shock wave have been designed following the principles laid down by Hilliar [12]. In this type of gauge the water transfers its impulse to a freely moving piston which at the end of its travel strikes a copper cylinder or copper sphere, and from the deformation of the cylinder or sphere the energy of the moving piston at the time of impact can be calculated. From this energy and the dimensions of the gauge the total impulse imparted to the piston by the shock wave may be determined, as well as the travel time of the piston before striking the copper cylinder or sphere (equivalent to the time of integration over the pressure-time curve).

(1) The improved Hilliar gauge. A modification by Hartmann of the original Hilliar gauge incorporated seven pistons of different sizes and travel times into the same gauge body [13]. One of the pistons has zero travel distance since it is in contact with a copper sphere (essentially the same as a ball-crusher gauge). From the gauge dimensions and cylinder deformations the average pressure of the water shock wave during different time intervals may be calculated, and by plotting these average pressures against time a pressure-time curve may be drawn. While this gauge is somewhat difficult to assemble and operate, and the calculations necessary to obtain a pressure-time curve are rather lengthy, it is possible to obtain a qualitative idea of such a curve without the use of electronic equipment.

(2) The Hartmann momentum gauge. A Hilliar type of gauge using a single piston of large mass with only a small area exposed to the shock wave, will measure the impulse over the major portion of the pressure-time curve. This gauge is much simpler to assemble and operate than the improved Hilliar gauge mentioned above, and the calculations of the "total momentum" may be made by reference to a graph of impulse versus deformation. However, it does not give any information regarding the form of the pressure-time curve.

III. TYPE OF RESULTS OBTAINED

5. Comparison of weapons with different explosive fillings

Concurrent with the continued development of better instruments for measuring the effects of explosions, the major portion of the work of the RELIANCE was in comparing different explosive fillings in various weapons. Because of unknown variables and variables not subject to control it was necessary to make all comparisons against a standard fired under identical conditions. Thus any uncertainty of the explosive effectiveness due to change in the absolute level as measured by the RELIANCE instruments was eliminated. Such changes in absolute level were inevitable with the continual evolution of the instrumentation. Since charges were usually at least in duplicate, a given series was usually divided into two or more strings with one charge of each type being fired in each string for the purpose of comparing the primary variable. If there were secondary or tertiary variables, such as orientation effects or booster effects, these could be compared from one string to another [14].

(a) Procedure followed in analysis of data. — The principal results obtained in comparing explosive fillings and other effects were ratios of gauge readings for a particular explosive to those for standard explosive, usually TNT. However since the effort necessary to obtain the data was so great, a rather elaborate statistical analysis was carried out which eliminated many gross errors and at the same time ensured that all good data were usable.

After the experimental data had been entered in tabular form, according to the distance from the charge and the type of measurement (that is, ball-crusher, Modugno and UERL-diaphragm deformation, piezoelectric peak pressure, momentum and energy, and Hilliar or Hartmann momentum), the percentage difference between the reading of two gauges forming a pair of a given type at a given distance was calculated. The standard deviation between two gauges was determined from the percentage differences for all pairs of a given type of gauge. When the percentage difference between two gauges forming a particular pair exceeded three times the standard deviation between two gauges of that type for that whole string, one of these two gauges was considered to be suspect. Examination of the gauge itself or comparison of its results with the results of other gauges would usually determine which gauge of the suspect pair was giving anomalous results, so that that particular gauge value could be eliminated from consideration.

For each string the ratio of the reading of a single individual gauge on a given explosive to the reading obtained by the same gauge for the standard explosive was calculated. These ratios were then averaged for all gauges of a given type and the standard deviation of the individual ratios from the mean was obtained. The ratios for each gauge type from the various strings were compared to one another for reproducibility between the strings and then were averaged over all strings and the standard deviation of the ratios from the mean and the standard deviation of the mean calculated. (At any point in the analysis where an individual gauge ratio deviated from the mean

of all gauge ratios by an amount greater than three times the standard deviation from the mean, that ratio was considered suspect and gauge readings for the two shots were examined individually for possible errors. Usually suspect values found in this manner were also suspect on the basis of the analysis of percentage difference between the two gauges of a given pair.) The mean of the ratios so obtained gave the average difference between the two explosives for an equal volume of charge measured at equal distances from the charge. This particular type of comparison may or may not have been the one desired for a particular application but other types of ratios could be calculated as discussed below provided the weight and distance exponents and the densities of the various explosives were known.

When secondary variables were being studied it was necessary to go through similar analysis comparing the results from the same explosive between the different strings. When it was not desired to study the effect of secondary variables it was the practice to change the charge-to-gauge distances between strings so as to give a good logarithmic distribution of the values of $W^{1/3}/R$, where W is the charge weight and R is the charge-to-gauge distance. This allowed a well-distributed series of points when the results were plotted on log-log paper.

The standard deviations calculated in the above analyses gave an estimate of the significance of the results obtained. The 5-percent significance level was usually employed at UERL (a significant difference between two values must exceed twice the standard deviation of the difference between these values). This level of significance was obtained by using from 40 to 50 mechanical gauges and 8 piezoelectric gauges on two or three strings, and it was usually possible to distinguish between two explosives which differed by as little as 2 percent. By increasing the number of gauges on each shot, or by increasing the number of strings it would be possible to obtain a higher level of significance or make closer distinctions. However the large increase in the number of gauges or number of shots necessary to appreciably raise the significance level was not deemed warranted for this work.

(b) Conversion from one type of explosive ratio to another. -- The directly determined experimental ratios from the RELIANCE work were usually the ratios of the gauge readings for equal volumes of explosives at equal charge-to-gauge distances (D_{Vd}). (For convenience, ratios are designated in the form $_{D}V_{d}$, where the letter on the line indicates the ratio and the subscripts indicate the quantities which remain constant. In particular, D_{Vd} means the ratio of the gauge readings D for equal volumes of explosives V at equal charge-to-gauge distances d.) For certain purposes it was desirable to compare explosives on a different basis. For example, in aircraft where the pay load is the limiting factor it would be desirable to compare the explosive powers from equal weights of explosives at equal distances (D_{Wd}). Also it is often desired to determine the weight of a particular standard explosive that is necessary to do the same damage at the same distance from the charge as a unit weight of some new explosive. The ratio of the weights (W_{Dd}) is referred to as "equivalent weight."

The various ratios are defined as follows:

Symbol	Equivalent	Definitions
D_{Vd}	$(D_2/D_1)_{V,d}$	The ratio of the gauge readings for equal volumes at equal distances.
D_{Wd}	$(D_2/D_1)_{W,d}$	The ratio of the gauge readings for equal weights at equal distances.
W_{Dd}	$(W_1/W_2)_{D,d}$	The weight ratio for equal gauge readings at equal distances. ("equivalent weight").
V_{Dd}	$(V_1/V_2)_{D,d}$	The volume ratio for equal gauge readins at equal distances.
d_{DV}	$(d_2/d_1)_{D,V}$	The distance ratio for equal gauge readings from equal volumes.
d_{DW}	$(d_2/d_1)_{D,W}$	The distance ratio for equal gauge readins from equal weights.
W_V	$(W_1/W_2)_V$	The weight ratio of charges of equal volume (density ratio).

where

D = gauge reading
W = charge weight
d = charge-to-gauge distance
V = charge volume

If it is assumed that the gauge readings follow the law

$$D = k \frac{W^m}{d^n}$$

where m and n are constants determined by the properties of the diaphragm, conversions from one type of ratio to another are fairly simple. The equations for conversion are as follows:

$$D_{Wd} = W_V^m D_{Vd} \qquad V_{Dd} = D_{Vd}^{1/m}$$

$$W_{Dd} = D_{Wd}^{1/m} \qquad d_{DV} = D_{Vd}^{1/n}$$

$$d_{DW} = D_{Wd}^{1/n}$$

Table I will be found convenient for making conversions from one ratio to another.

Table I. Conversion from one type of ratio to another.

Ratio: Known / Wanted	D_{Vd}	n_{Wd}	W_{Dd}	V_{Dd}	d_{DV}	d_{DW}
D_{Vd}		$W_V^{-m} D_{Wd}$	$W_V^{-m} W_{Dd}^{m}$	V_{Dd}^{n}	d_{DV}^{n}	$W_V^{-m} d_{DW}^{n}$
D_{Wd}	$W_V^{m} D_{Vd}$		W_{Dd}^{m}	$W_V^{m} V_{Dd}^{m}$	$W_V^{m} d_{DV}^{n}$	d_{DW}^{n}
W_{Dd}	$W_V D_{Vd}^{1/m}$	$D_{Wd}^{1/m}$		$W_V V_{Dd}$	$W_V d_{DV}^{n/m}$	$d_{DW}^{n/m}$
V_{Dd}	$D_{Vd}^{1/m}$	$W_V^{-1} D_{Wd}^{1/m}$	$W_V^{-1} W_{Dd}$		$d_{DV}^{n/m}$	$W_V^{-1} d_{DW}^{n/m}$
d_{DV}	$D_{Vd}^{1/n}$	$W_V^{-m/n} D_{Wd}^{1/n}$	$W_V^{-m/n} W_{Dd}^{m/n}$	$V_{Dd}^{m/n}$		$W_V^{-m/n} d_{DW}$
d_{DW}	$W_V^{m/n} D_{Vd}^{1/n}$	$D_{Wd}^{1/n}$	$W_{Dd}^{m/n}$	$W_V^{m/n} V_{Dd}^{m/n}$	$W_V^{m/n} d_{DV}$	

Extreme caution must be exercised in converting from one type of ratio to another, due to the high sensitivity of the conversions to weight and distance exponents. The weight and distance exponents for the mechanical gauges are not constant for different charge weights and different charge-to-gauge distances, since the gauge reading is dependent on the decay constant of the shock wave. Any determination of gauge exponents suffers from very low precision,[3] originating in uncontrolled variables (such as loading variations) over the large number of shots necessary, and, to a certain extent, in the inherent difficulties discussed above.

6. Other types of data obtained

Data were obtained in the course of these studies in addition to the comparison of the effectiveness of various explosives. Among these were:

(a) Effect of charge orientation. — The asymmetry of the shock wave resulting from the explosion of an asymmetrical charge was determined, usually as a secondary variable in an explosives comparison series. This information was useful in ascertaining whether or not a major portion of the explosive energy was being released in a direction which was not likely to include a target.

(b) Booster effects. — The size, composition and location of boosters were also studied, both as primary variables in series especially designed to study booster effects, and as secondary variables in explosives comparison series.

---

[3] See Sec. 8(d).

(e) Shape effects. — Charges of various shapes were fired and the shock wave studied in various orientations from these charges. These different shapes were confined to spheres, and to cylinders with different ratios of length to diameter.

(d) Similitude laws. — The relationships between the reading of a given gauge and the charge weight and charge-to-gauge distance were determined. This work was much more difficult due to the fact that it involved the absolute level of the various quantities. It was not until the instrumentation was fairly well stabilized that it was desirable to publish such results, and even then it has been necessary to revise the absolute levels reported on occasion.

(e) Multiple charges. — A study of the effects of subdividing a charge into smaller units of the same total weight as a given single charge, and the comparison of the results so obtained, was carried out in preliminary experiments. In this work it was extremely important to consider the various measured parameters in different directions from the charge.

(f) Surface effects. — The effect of the air-water interface and the bottom in producing reflected rarefaction and pressure waves has been studied under various experimental conditions.

In Part III the type of work which was done on the RELIANCE has been summarized. The details of the results are being reported elsewhere [15].

IV. DETAILS OF INSTRUMENTATION

7. Piezoelectric gauges and associated equipment

Eight separate channels were used to transmit, amplify, and record the signals from eight tourmaline gauges. The eight cables for the gauge signals, [illegible] for the pilot gauge signal (when still-film cameras were used) and the firing-line cable, were all made up into a unit for convenience in paying out. The pilot gauge cable was interchangeable with those of the recording gauges, and under certain conditions could serve as a spare. Writing speeds for the oscillographs from over 300 μsec/in. with the electronic sweep and still-film cameras down to less than 100 msec/in. with the rotating-drum cameras were available. Block diagrams showing the connections of the various components for both types of recording are given in Figs. 6 and 7. The individual components were so designed that one type of recording may be substituted for the other in less than 30 minutes by changing patch-cord connections and camera backs.

(a) Gauges. — (i) Crystal elements. The piezoelectric gauges used for RULLANDER [illegible] were constructed from tourmaline wafers of approximately 1/8-in. thickness and 1/2-in. diameter (Fig. 8). Electrodes were attached to the faces of these elements by various means, the more successful of which have been the Brashear silver-electrolytic copper and the baked silver spray process [2,3].

(ii) Assembly of crystal elements. The crystal elements with electrodes attached were assembled into doublet gauges (Type A) or quadruplet gauges (Type B) [2]. In the Type A assembly the positive faces of the two crystals were sweated together and attached to the central conductor which was led off through a copper tube, while extensions of the copper tube were fastened to the two outside negative faces of the two crystals. In the Type B assembly (Fig. 8) two doublet elements similar to Type A were fastened on either side of a central steel tab. The two outside faces and the two central faces of the crystals were negative and were connected electrically to this tab which was then fastened rigidly to the copper tube. The two positive electrodes were connected to the central conductor which was led through the copper tube. Due to the use of much thinner crystal elements in Type B it was possible to employ quadruplet gauges with an over-all thickness no greater than 1/8 in.

(iii) Waterproofing the completed gauge. Various methods of waterproofing these gauges have been found to be satisfactory. Among the materials used were moulded rubber, rubber tape and Bostik cement, Tygon and Zophar wax G276. The last material mentioned was found to be the most satisfactory in warm weather, but rubber tape and Tygon were better in cold weather. Good coatings on guages must be mechanically strong, have satisfactory dielectric properties, be free of bubbles, be adhesive, be free of electrical signal, be thin and easy to apply.

Best Available Copy

(iv) Calibration. The amount of charge developed by a given gauge per unit change in applied pressure was determined by means of a "static" microcoulometer technique [2]. The assembled but unmounted gauge element was subjected to 3000 lb/in^2 pressure which could be suddenly released, and the charge developed by the gauge read on a microcoulometer. Calibration of unmounted elements by this technique was reproducible to better than 2 percent but owing to the following factors the absolute value of the gauge constant in actual use was not necessarily represented by this precision: (1) the static calibration did not subject the gauge to a progressive shock wave simulating that which the gauge is used to measure; (2) the gauge constant may have been modified during mounting and coating; (3) cable signal[4] may have caused a variable apparent gauge constant different from the actual gauge constant; (4) gauges may have been unknowingly damaged during use thus altering their constants.

(b) Electrical cables. — The transmission of the gauge signal from the gauge to the recording vessel was a major problem in studying large explosive charges. The electrical signal produced by the gauge was small, and the long cables necessary caused attenuation of this signal and did not have a linear frequency response. In addition to this it was found that concentric cables themselves gave off a signal when subjected to mechanical stress. These problems have been dealt with in detail by R. H. Cole elsewhere [4] but are presented below particularly with view to the RELIANCE work.

(i) Cable signal. When a coaxial cable is struck by a shock wave an electrostatic charge is developed between the shield and central conductor. In a high impedance system such as encountered in using piezoelectric gauges the magnitude of the charge so developed may be large relative to the charge developed by the gauge itself. If the cable is leading directly away from the gauge, this signal does not affect the peak pressure value obtained, since the shock wave will not have struck the cable before the peak has been recorded. However, if it is desired to obtain the complete pressure-time curve this signal may introduce serious distortion, either positive or negative. As it was not practicable to construct gauges with a higher voltage output, it was necessary to overcome this problem by the use of cables with very small cable signal.

The cable used at UERL for this purpose was the type developed by the Taylor Model Basin [16]. This consisted of a copper tube of 1/8-in. outer diameter and 1/16-in. inner diameter through which was led a fiber-glass insulated enameled wire which served as the central conductor. Hot ceresin wax was drawn into the space between the central conductor and the tube. The cable signal developed by this tube was small compared with the gauge signal. The piezoelectric gauges were attached to 20 ft of the tube for most work which, since it lead directly away from the gauge in the direction of the propagation of the shock wave, gave a 4-msec interval during which the cable signal was as low as possible. When pressure-time curves over

---

[4] See Sec. 7(bi).

longer time intervals were required, longer lengths of copper tubes were used. These copper tubes stood up well with the normal handling on the RELIANCE but they did "wear out" with time (that is after they had been in use for considerable periods of time they gave larger spurious signals when struck by a shock wave). Between the end of the copper tubes and the recording equipment it was satisfactory to employ commercial shielded cable, such as microphone cable or Army-Navy type RG-41/U, since the shock wave did not strike this cable until after the desired signal had been recorded.

(ii) Frequency response of cables. In addition to the distortion of the signal due to the finite size of the gauge and to cable signal, further distortion may be caused by lack of linear frequency response. This may be due either to impedance mismatch between the cable and gauge or cable and oscilloscope, or to the dielectric absorption of the cable. Both of these difficulties can be overcome by the use of the proper terminating networks at the end of the cable [4].

For the early work done on the RELIANCE (previous to shot RE-125) the cables were compensated by a resistance-capacitance-inductance network at the input to the amplifiers of the cathode-ray oscilloscope (Fig. 9).

This compensation circuit is familiarly referred to as "single-ended" compensation. After shot RE-136, "double-ended" compensation was used. For this a resistance-capacitance network is placed at the input of the cathode-ray oscilloscope and also at the far end of the cable as shown in Fig. 10. With the double-ended system of compensation the steady-state response of the cable is flat within ± 3 percent up to 100 kc/sec and the rise time for a step-impulse input is 2 μ sec and the overshoot not more than 3 or 4 percent compared to the step height at 1 msec.

The compensating network at the far end of the cables is inserted in the form of a small patch cord between the cables leading up to the surface and the 600-ft surface cables leading back to the RELIANCE. These units were suject to frequent failure from mechanical stress until the type of construction shown in Fig. 11 was adopted. These patch cords for the different cables were all interchangeable, so that in case of failure they could be quickly replaced with a spare patch cord. The compensating network at the oscilloscope end of the cable was located at the input to the master control panel. These networks were also identical and were of the plug-in type, so that one network could be quickly removed and another one plugged in. The condenser in the latter network also served as the standard condenser for the Q-calibrations.5/

(c) Recording equipment. — After the signal had been brought to the recording vessel, it was necessary to make a permanent record of the transient voltage produced by the shock wave crossing the gauge. Cathode-ray oscilloscopes were used with photographic recording for this purpose. Associate equipment involved voltage-step sources for calibrating amplifier

---

5/ See Sec. 7(cv).

sensitivity and camera magnification, a capacitance bridge for measuring cable capacitance when the Q-step was not used, standard frequency sources for the time calibration of the sweep or film speed depending on whether still-film or rotating-drum cameras were used, electronic sweeps for still-film cameras, and the necessary cameras.

All of this equipment was efficiently housed in the electronics cabin built into the hold of the RELIANCE, the plan for which is shown in Fig. 2. The arrangement of the various electronic components is shown in Figs. 12, 13, and 14. The panels forming the cabin bulkhead behind this equipment were removable to allow minor servicing and the changing of patch-cord connections (Fig. 15).

(i) Master control. For routine shooting, where many channels are used, the length of time and large chance for error involved in connecting and disconnecting gauge lines, steppers, frequency sources, sweeps and tripping devices into the oscilloscopes make it imperative that some form of master control panel be used [17]. With this master control panel all switching operations were made by turning a single knob. Positions were available for voltage step, Q-step, time calibration, and firing, as well as for resistance and capacitance tests of cables. The circuits were interlocked so that it was not possible to fire the charge unless the master control panel was in the firing position. A meter was available on the master control panel by which the various cable resistances could be measured by turning a selector switch. There was also space in the back of the panel to provide for the plug-in cable compensation network.

(ii) Oscilloscope and amplifiers. The Dumont 208 oscilloscopes were used as the recording equipment with certain modifications. A low-impedance, compensated, step attenuator was inserted to give reproducible amplification settings. The frequency-compensation circuits were modified so that the oscilloscope had a frequency response flat to within ± 2 percent from about 5 cycle/sec up to 300 kc/sec, with no rise at 400 kc/sec. The accelerating voltage of the cathode-ray tube was increased enough to allow writing speeds up to 3 in./msec. Beam brightening and positioning could be controlled externally, and a single, repeating single, or continuous sweep was provided externally. The sensitivity range was from 5 v/in. deflection minimum up to 50 mv/in. deflection. The deflection-voltage ratio agreed to within 1 percent up to 1-1/2 in. deflection. Type 5LP5 tubes were used originally and later 5CP5 tubes were used. These tubes had short enough persistance so that they could be used successfully with rotating-drum cameras.

(iii) Voltage stepper. To calibrate the amplifier sensitivity and the magnification factor of the camera, it was necessary to place a known voltage on the plates of the oscilloscope and measure the resultant deflection recorded by the camera. This was done by changing the voltage level on the vertical plates when the trace was part way across the tube (in the case of the still-film camera) which resulted in a step. The use of Q-step network[6] allowed an estimate of both the high- and low-frequency response of

---

[6] See Sec. 7(cv).

Best Available Copy

the system by noting the rise of the step and its decay. Voltage steppers which have been employed at this laboratory have used as standard voltage sources both battery and regulated electronic power supplies [17]. Steppers using a battery as a source of standard potential have the inherent difficulty of being high-impedance devices. The electronic stepper which depends upon voltage regulator tubes as the source of standard potential has a low impedance output which is essential for use with the Q-step. The voltage stepper involved a time delay and a switching circuit. The time delay was so adjusted that the potential was switched from one level to another after the spot had progressed a certain distance across the screen. Any one of several standard voltages was selected so that the step height corresponded roughly to the expected peak height of the pressure-time curve. The steppers were also provided with an exponentially decaying step which approximates the form of the shock wave. This proved to be very useful for determining the frequency response of the oscilloscope as well as checking focus and intensity settings. On the later model electronic steppers a voltage-standardization check was provided by checking the potential source from the VR tubes against the potential of a dry cell. Periodic checks of both the electronic and battery sections were necessary with a standard cell and potentiometers. A triggering pulse, emitted with the initiation of the time delay for the stepper, was used to start the single sweep for the still-film cameras, or to brighten the beam on rotating-drum cameras.

(iv) Capacitance bridge. When the voltage calibration was used it was also necessary to determine the capacity of the gauge and cable system in order to calculate the gauge output. A capacitance bridge, included with the RELIANCE equipment for this purpose, was based on a substitution method in a bridged-T network [17]. The nominal driving frequency for the bridge was 10 kc/sec. This bridge was also used to aid in locating faults in cables as well as for measuring the standard condensers used in the Q-step.

(v) Q-step calibration network. By applying a known voltage in series with a known capacitance across the cable used, it was possible to eliminate the necessity of independent voltage and capacitance determinations [4,17]. The principle of this is illustrated in Fig. 16. For recording signals the connection is as shown in Fig. 16(a) and the output voltage V_t is

$$V_t = \frac{C_o V_o}{C^* + C_t}$$

where $C_o V_o$ is the charge developed by the gauge and C_o is much smaller than C^*, the cable capacity. For calibrating the cable and indicating instruments, the connection shown in Fig. 16(b) is used and a step voltage V_s is applied. The output voltage under these conditions is

$$V_c = \frac{C_t V_s}{C^* + C_t} .$$

Solving these two equations for C_oV_o we have

$$C_oV_o = C_t V_s \frac{V_t}{V_c} .$$

The unknown charge C_oV_o may therefore be determined from a known quantity of charge C_tV_s and the ratio of the voltage outputs. This voltage ratio is the ratio of the displacements on the cathode-ray oscillograph screen as recorded by the camera. In actual practice the standard condenser C_t was a part of the cable terminating circuit (corresponding to C_2 in Fig. 10). In addition to the greater ease in calibrating, the Q-step allows an estimate of the cable response characteristics. For example, if the cable had low impedance due to dielectric or salt-water leakage, the Q-step fell off exponentially. The conditions under which the records were actually made were thus known, and pressure-time curves could be corrected when necessary from the Q-step record by the superposition theorems.

(vi) Time standard. The standard frequency source commonly used on the RELIANCE for calibrating the time base was a multivibrator which was driven by a 100 kc/sec crystal-controlled oscillator [17]. Frequencies of 25, 10, 5 and 1 kc/sec were available. Some of the earlier circuits for this multivibrator would allow it to lock in on some sub-multiple of the oscillator frequency other than the one desired but later designs overcame this difficulty. The multivibrators were checked in the field by a battery-operated, resistance-stabilized L-C oscillator which was stable to 0.1 percent, thus allowing any major discrepancy in frequency (due to the wrong interlocking) to be detected. These frequency standards were checked against the standard frequency of radio station WWV.

(vii) Still-film cameras. The still-film cameras employed were mounted in a specially built camera hood fitted on the Dumont 208 oscillograph [17]. An f/2.0, 50-mm focal length lens was used with a manual flap swinging in front of the lens as a shutter. Diaphragm-type shutters were not found satisfactory because of trouble with the cable releases. The flap type shutter was very satisfactory since it was positive in action and shutters on several cameras could be very easily ganged to operate as one unit. Cut film 2-1/4 × 3-1/4 in. was used in a Recomar holder fitting into a camera back which could be rotated to give four different exposures on a single film.

(viii) Sweep. When a still-film camera was used the cathode-ray spot had to move across the screen at a uniform speed. This was done by means of a linear time base which swept across the screen once after being triggered, at the same time brightening the beam so that it recorded on the photographic film. Sweep speeds were available from 125 μsec/in. to 12.5 msec/in. For purposes of adjustment, both automatic intermittent single sweeps and continuous sweeps, in addition to triggered single sweeps, could be obtained from this linear time base [17].

The sweep speed was calibrated by placing the output of the time standard described in paragraph (vi) on the vertical plate of the cathode-ray tube; this calibration was done immediately before the shot was recorded in order to minimize any possible drift in sweep speeds.

The most reliable method for tripping the sweep was by the use of a pilot gauge at some point between the recording gauge and the charge. The signal resulting as the shock wave struck the pilot gauge actuated both the sweep and beam brightener. The distance between the pilot gauge and recording gauge determined the time interval between the beginning of the trace and the peak of the pressure-time curve.

(ix) Time delay. For recording several phenomena which occur within a few milliseconds of each other, only one sweep circuit need be used, the X-axis positioning control being adequate to cause the record of the desired phenomena to occur at the proper position on the cathode-ray tube screen. However, if these phenomena occur at times differing by more than a few milliseconds, more than one sweep must be used. Such a situation exists when gauges are used for recording the shock wave at several distances from an explosion. As additional pilot gauges for tripping the additional sweeps would require additional cables for transmitting the tripping pulse back to the vessel, it is more convenient to use a circuit capable of producing pulses for tripping the later sweeps at fixed time intervals after receiving the pulse from the trip gauge. A time delay circuit which would give one pulse with zero time delay, and two other independent pulses at any desired time from 0 to 100 msec after the trip pulse input was used routinely with still-film cameras on the RELIANCE. The two gauge pairs at the two closest gauge positions all operated on a sweep tripped at zero delay, the third gauge pair on a second sweep tripped by the first time delay, and the fourth gauge pair on a third sweep tripped by the second time delay.

(x) Rotating-drum cameras. Camera backs fitted with rotating drums of 10.0-in. circumference were also used on the regular camera tubes mounted on the oscillographs (Fig. 17). For the eight channels on the RELIANCE these cameras were driven by means of flexible shafts from a common drive shaft. Also driven from this common drive shaft were the synchronizing control cams and tachometer in the sequence beam brightener panel. These synchronizing cams fired the charge at a time so that the record would not come on the break in the film, brightened the cathode-ray beams at the beginning of the revolution and shut them off at the end, and also caused the crater tubes to flash for one revolution. These crater tubes are driven by the multivibrator described above.

Among the advantages of the rotating-drum camera for this work are the following: (1) the time calibration can be recorded simultaneously with the pressure-time curve; (2) there is no difficulty in reading the records due to nonlinearity of sweep speeds; (3) it is not necessary to use a trip gauge or other device near the charge to brighten the beam for recording, since this is done by control cams; (4) non-orthogonality of the cathode-ray tube plates need not be considered; (5) a large range of recording speeds is easily obtained and by means of the tachometer the approximate

recording speed being used is known in advance; (6) by means of the sequence beam brightener, the several different channels may be made to record at several widely different times; (7) the length of a single trace can be as much as 10 in., which is 10 times greater than the usable trace obtained with a still-film camera.

The sequence beam brightener, in conjunction with the control cams, brightens the beam for various intervals as indicated in Table II.

Table II. Duration of beam brightening for various sequence beam brightener settings.

Master Control →	Firing	Q-Step	V-Step
Beam-Brightener Setting	Interval of Beam Brightening* (degrees)		
1	0 - 360	0 - 180	180 - 360
2	180 - 540	180 - 360	360 - 540
3	360 - 720	360 - 540	540 - 720

*Angle of rotation from zero positions of the control cams.

The displacement of the base lines for these calibration steps from the base line of the pressure-time curve is interlocked with the switching in the master control panel.

(xi) Crater tubes. For placing the timing frequency from the multivibrator on the film, 8 Sylvania type R-1130B tubes ("crater" tubes) were used. Each one was mounted inside the individual camera tubes and the image of the spot placed in the plane of focus of the camera by means of a prism (Fig. 17). A power unit driven by the multivibrator was necessary to operate the crater tubes. It was found that the crater tubes would not start properly in total darkness, so a 1/4-watt neon bulb was placed adjacent to each one to photosensitize it.

(xii) Record identification. A minor but very essential part of making a record is in its identification. This should be done while the film is in the camera, at the time the record is made. A device found well-suited for this purpose was designed by J. P. Slifko, and consisted of a small portable projector with adjustable numbers, which, when placed over the viewing eye piece on the camera tube, would throw the image of the desired numbers on the screen of the cathode-ray tube. This image was then photographed on the film in the camera. When used with rotating-drum cameras, the drums must be stopped before this can be done.

(d) Analysis of records. — The cathode-ray oscilloscope trace of the pressure-time curve recorded on the film must be transposed into absolute units of pressure and time by comparing it with the Q-step and time calibrations. The pressure is given by

$$P = \frac{C_t V_s}{KA} \frac{h_b}{h_c}$$

where KA [μcoulomb/(lb/in^2)] is the constant for the gauge used, h_b and h_c the pressure height and step height, respectively, and the other quantities are as defined previously. When the voltage step is used in place of the Q-step calibration, C_t becomes C, the total capacity in the gauge circuit. The determination of the impulse and energy factor involves the evaluation of $\int P\,dt$ and $\int P^2\,dt$, usually by means of the trapezoidal rule. This requires recording the values of the pressure at a large number of times from the pressure-time curve. The following methods have been found most satisfactory for this work on a routine basis.

(i) Micrometer microscope. A micrometer microscope with a calibrated stage for moving the film at right angles to the micrometer in the eyepiece was formerly used for analysis of all records. The film was aligned on the stage so that the pressure axis was measured by the micrometer eyepiece and the time axis was measured by the scale on the stage. The ocular units of the eyepiece were transposed to pressure units by comparison with the height of the step, while the time units of the stage scale were transposed into time units by comparison with the standard timing wave on each film.

These records were usually integrated graphically in terms of the ocular and stage units and transformed into absolute units after integration. When desired the set of points was plotted on graph paper in terms of absolute units.

(ii) "Harp". A device was developed for obtaining a photographic projection of the pressure-time curve superimposed on a two-dimensional grid adjusted to read absolute pressure and time units. This device, which is known as the "Harp" (Fig. 18), consists of a photographic enlarger with one fixed and one adjustable grid at right angles, immediately over an easel holding a sheet of photographic enlarging paper. The film is placed in the enlarger with the pressure axis parallel to the fixed grid lines, and the enlargement factor is adjusted until the fixed grid reads convenient units of the time scale. This involves comparison with the time base which was placed on the record at the time the shot was made.

After the time scale is adjusted, the image of the Q-step is thrown on the paper and the adjustable grid is moved so that it will read in convenient pressure units. This is done by calculating the pressure that corresponds to the step height, using the formula:

$$P = \frac{C_t V_s}{KA} .$$

In cases where the voltage step is used, C_t becomes the capacitance C of the gauge-circuit cable. The adjustment of the horizontal grid is made so that the step reads that particular pressure in absolute units on the grid.

As this adjustable type of grid has proved to be extremely useful and has not been reported elsewhere by Division 2, it will be described in greater detail. It was first developed at the Woods Hole Oceanographic Institution by Ewing and Vine for use in the analysis of bathythermograph records. On two opposite sides of a parallelogram are placed strips with holes equally spaced. Thread or wire is strung through these holes to form the grid. The most satisfactory material found for use with this particular instrument has been black nylon filament. As the parallelogram is closed or opened, the spacing between the grid strings becomes smaller or greater.

This was adapted to the Harp by adding a fixed grid mounted immediately below the strings of the adjustable grid. Small angular adjustments are allowed for slight deviations from 90°, correcting for any non-orthogonality of the cathode-ray tube plates. The whole assembly may be rotated, or moved in a vertical or horizontal direction to allow the base line and origin of the pressure and time axes to be set to correspond with that on the image of the pressure-time curve. These adjustments are all made by means of screws whose controls are conveniently located for the operator. After adjusting the Harp so that the pressure and time grids read in absolute units, and the origin and base lines are properly aligned, the front of the assembly is raised to allow the photographic paper to be placed below the grid. The back of the assembly is rigidly hinged so that it cannot get out of adjustment during this process. The assembly is returned to its rest position, a mask is placed around the edges of the paper to identify the axes and place a form in the upper right hand corner of the projection for recording pertinent data. The timing calibration shows directly on this projection, allowing a check of the units of the time axis at any later time. A projection of the calibration step is also made which allows the units of the pressure axis to be checked later if necessary.

The Harp reproduces photographically an exact graph of the original trace of the pressure-time curve. This obviously has many advantages: (1) the tedious readings on the micrometer microscope have been eliminated; (2) time and pressure calibrations may be checked directly on the prints; (3) the process is photographic which means that the original piezoelectric record may be inspected in detail in its enlarged form, and fine structure which may be present may be immediately detected. This is not the case with micrometer microscope readings since the fine structure is often too detailed to record point for point. A very important advantage of Harp projection is that the projected records themselves indicate the uncertainties in values due to poor traces, width of trace, and so forth. This was not possible when the records were read on the micrometer microscope by technicians.

Peak pressures may be read directly from the records and the impulse and energy integrals may be calculated by the trapezoidal rule as they were from the micrometer microscope readings. With regard to the Q-step there is a small overshoot at the beginning which amounts to from 1 to 3 percent (compared to the step height at 1 msec) due to the frequency response of the system. Since the major portion of the pressure-time curve is used for measuring impulse and energy, the Harp is set on the Q-step 1 msec after the

step. This gives a good average setting. However, for measuring peak pressure a downward correction corresponding to the difference between the setting of the step and the value for the step at t = 0 must be made. The peak pressure read directly from the Harp projection is always high due to this factor. This illustrates another value of using the Q-step calibration since the cable response, being the same for the pressure record as it is for the step record, is taken into account in reading the pressure, impulse, and energy.

(iii) The mechanical evaluation of the impulse and energy integrals. Even with Harp records the integration of the pressure-time curve for impulse and energy by the trapezoidal approximation was still a time-consuming process. Linear planimeters were available for evaluating the impulse, but quadrate planimeters for the energy integral were not available. For this reason a mechanical integrator which would simultaneously evaluate both the impulse and energy functions under the pressure-time curve was designed and constructed [18]. By the use of this integrator the impulse and energy intervals may be rapidly evaluated using either the Harp projection, or the original film in conjunction with an internally contained projector.

(iv) General considerations of the integration of pressure-time curves. The question as to how far out on the time axis the integration should be carried is one which can be answered only by compromise. Since most of the RELIANCE work was done for the purpose of comparing explosive effectiveness, it has been felt that the amount of energy or impulse delivered in a time comparable with the time of damage of the target is the important factor. For this reason the pressure-time curves were integrated to some constant time value which was the same for all of the particular charges being compared in a given series. The value used was usually from 4 to 8 times the time constant of the shock wave. Integration to these times included almost all of the energy in the shock wave but did not include nearly so large a proportion of the impulse. This integration to a constant time could not be used where it was desired to obtain similitude curves for the different explosives. For this purpose it was necessary to obtain the time constant for the particular value of $W^{1/3}/R$ involved and to integrate to some exact multiple of this value. The time constant must be taken from the curve of $\theta/W^{1/3}$ versus $W^{1/3}/R$, which is the best line drawn through values from all charges and gauges of a given series. Otherwise errors due to the low precision in measuring the time constant will exaggerate the errors in impulse and energy being integrated.

The integral $\int P^2\,dt$ is transformed into the energy of the shock wave by means of the factor $A/\rho_o c_o$. The quantity A is

$$A = 1 - 1.67 \times 10^{-6}\, P_m - 4.9 \times 10^{-12}\, P_m^2 ,$$

while $\rho_o c_o = 5.58 \times 0.0065T$, where T (°C) is the temperature of the sea water, valid for T = 0 to 20°C [19].

For spherical shock waves the energy factor calculated from $\int P^2\,dt$ does not include the entire shock wave energy. A better approximation to this is given by the $\int P\{\int P\,dt\}\,dt$. This takes into account the after-flow correction due to the spherical form of the wave, which may amount to as much as 25 percent of the value of the energy factor at distances of less than 20 charge radii.[7] Hence the energy calculated from $\int P^2\,dt$ which is reported for RELIANCE results is referred to as the "energy factor."

(c) General comments concerning piezoelectric instrumentation. The rather comprehensive information concerning the pressure-time relationships resulting from an underwater explosion which can be obtained by the use of piezoelectric gauges is invaluable but at the same time requires much work and infinite patience when compared to the ease with which results may be obtained from mechanical gauges. To maintain 8 channels in operating condition the following personnel requirements must be met: maintenance and repair of gauges and cables, 3 semi-skilled persons; checking and operating equipment on board vessel, 1 technician (college training or equivalent) with help from cable men; development, construction, repair, maintenance, and laboratory checking of electronics equipment, 1 to 3 college-trained electronicians; analysis of piezoelectric records and working up results, 1 college girl with major in mathematics or physics and 2 assistants with college training; supervision of all work, correlating field work, laboratory work, and record reading, trouble shooting, planning and execution of experiments, 1 college trained man experienced in electronics, physics, and underwater explosion phenomena. The above is the staff required for average loads, and does not include seamen to set the charge and gear. Under peak loads additional help is necessary.

6. The UERL diaphragm gauge

The first gauge to be successfully used at this laboratory for comparing explosives was the UERL diaphragm gauge [1,5,20] (Fig. 19).

(a) Description. -- This gauge is constructed by welding a 3-in. length of 4-in. double extra strong steel pipe (finished to an inner diameter of 3.270 in.) to a square base of 1/2-in. plate. A top plate in which there is a hole of the same diameter as the inner diameter of the pipe is welded on. A copper or steel diaphragm is then placed over this top plate, a cover plate slipped over the diaphragm, held in place by 8 cap screws. Diaphragms which have been used have been of No. 14 B and S gauge electrolytic copper, No. 20 and No. 14 U.S. standard gauge hot-rolled steel. The 14-gauge steel diaphragms were the ones commonly used, the tensile strength being about 60,000 lb/in^2. Small variations in the thickness of the steel made it necessary to correct all deformations to a standard thickness of 0.085 in. Thickness corrections were made according to Kirkwood theory, and later according to empirical results obtained during shooting with small charges.

(b) Measurement of explosive effectiveness. -- The relative effectiveness of various explosives is measured with the diaphragm gauge in terms of the maximum depression of the steel diaphragm caused by the shock wave. The

[7] A. B. Arons, private communication.

Best Available Co

effectiveness may also be measured in terms of volume of the depression, but this measurement does not lend itself to as great precision and is also more difficult to perform. Dial-type depth gauges with a 6-in. base are used to measure this maximum depression to the nearc t 0.001 in. During shooting the gauges are mounted roughly face-on toward the charge, and it has been found that the maximum depression is not too dependent upon the angle of incidence of the shock wave. The tilt of the gauge away from the charge must be great enough so that the diaphragm is deformed unsymmetrically before the depression is affected.

(i) Precision of results for large charges. The UERL diaphragm gauge has been the most precise gauge used by this laboratory, the standard deviation per gauge being roughly 1.5 to 2 percent (calculated from differences between the two members of a pair of gauges).

(c) Theory. — The theory of the UERL diaphragm gauge has been worked out in detail by Kirkwood [5,21], who has also summarized the work done on the problem of the plastic deformation of circular diaphragms by G. I. Taylor, Kirkwood, Goranson, and Rennard. For steel diaphragms the equations given in this section which Kirkwood obtained from his parabolic treatment have proved to predict the maximum depression to within 5 percent of the value obtained experimentally. The symbols used in the equations are as follows:

Symbol	Unit	Definition
R_o	in.	Radius of circular diaphragm
a_o	in.	Thickness of diaphragm
ρ	gm/cm^3	Density of diaphragm
σ_o	lb/in^2	Yield stress of diaphragm
ρ_o	gm/cm^3	Density of liquid medium
R_1	in.	Radius of baffle of diaphragm
C_o	ft/sec	Velocity of sound in the liquid medium
ω		Plastic frequency of the diaphragm
θ	msec	Decay constant assuming the shock wave to decay exponentially ($P = P_m e^{-t/\theta}$, where P is the pressure at any time t after the peak pressure of the shock wave P_m)
I	lb-sec/in^2	Impulse of the shock wave; for exponentially decaying shock waves $I = P_m\theta$
Z_m	in.	Maximum central deflection
t_m	sec	Time of deflection

Maximum deflection Z_m is given by

$$Z_m = \frac{103.4}{(\rho\sigma_o)^{\frac{1}{2}}} \frac{R_o}{a_o} \frac{Ig(\beta)}{\left(1 + \frac{2}{3}\frac{\rho_o R_o}{\rho a_o}\right)^{\frac{1}{2}}} .$$

Time of deflection t_m is

$$t_m = \frac{\beta}{\omega} .$$

where

$$g(\beta) = \sin\beta - \frac{1}{2}\sin\left(\beta - R_1\frac{\omega}{C_o}\right)$$

$$\beta = \tan^{-1}\alpha + \cos^{-1}\gamma$$

$$\alpha = -\omega\theta - \frac{(1+\omega^2\theta^2)\sin(\omega R_1/C_o)}{2 - \cos(\omega R_1/C_o) + \omega\theta\sin(\omega R_1/C_o)}$$

$$\gamma = \frac{\left(2 - e^{R_1/C_o\omega}\right) e^{-\beta/\omega\theta}}{\left\{(1+\omega^2\theta^2)\left[1 + 8\sin^2\left(\frac{\omega R_1}{2C_o}\right)\right]\right\}^{\frac{1}{2}}}$$

$$\omega = \frac{0.2068}{R_o}\left(\frac{\sigma_o}{\rho}\right)^{\frac{1}{2}}\left(1 + \frac{2\rho_o R_o}{3\rho a_o}\right)^{-\frac{1}{2}}$$

It will be noted that in order to calculate the damage it is necessary to know that the pressure-time curve falls off exponentially at least as far out as the time of action of the gauge, and to have the maximum pressure and the time constant, which are usually obtained from piezoelectric data.

(d) Weight and distance exponents. — For 0.085-in. steel diaphragms, the distance exponent is 1.2, and the weight exponent 0.5.[8]

9. The Naval Ordnance Laboratory ball-crusher gauge

The NOL ball-crusher gauge [6] has been used on all RELIANCE shots. Various sizes of copper spheres were employed in the gauge and the gauge was mounted in various types of blocks and orientations.[2]

---

[8] See Sec. 5(b).

[2] See Sec. 13(c).

(a) Description. — (i) For 5/32-in. spheres. The gauge (Fig. 20) consits of a base of 1.5-in. diameter which includes the anvil against which the copper sphere is pressed, a stud by which the gauge is screwed into the mounting block, and a steel or brass body in which these two pieces are mounted. In some versions of the gauge these pieces of the base are made as one unit. The upper part of the base is threaded to accept the brass head (cap and piston guide in Fig. 20) of the gauge (also 1.5-in. diameter). The center hole of the brass head accepts the piston of the gauge, which is 0.5 in. in diameter and 0.5 in. long. The base of the piston, which rests against the copper sphere, has a 0.625-in. diameter ridge to allow a bearing surface for the small spring that holds the piston in contact with the copper sphere at all times. The copper sphere is placed in a rubber centering washer and inserted between the piston and anvil before the head is screwed on to the base of the gauge. When completely assembled the gauge is 1-3/4 in. in over-all length.

(ii) For 3/8-in. spheres. This same gauge may be used with 3/8-in. spheres by inserting an adaptor ring of 0.218-in. thickness between the head and the base before assembling. This allows the larger sphere to be inserted, and at the same time keeps the piston flush with the outer face of the gauge.

(b) Measurement of sphere deformation. — The deformation of the copper spheres may be obtained from micrometer measurements of the diameter before deformation and the distance between the two flat faces after deformation. Since the orientation of the copper sphere within the gauge can not be controlled, these spheres must have an out-of-roundness which is less than the desired precision of the measured deformations. Another factor affecting the reproducibility of the results is the hardness of the spheres; all spheres must be annealed dead soft. The hardness was checked for all spheres used at UERL with a drop test machine.[10]

Because of the large number of 3/8-in. spheres used on each shot, it was found convenient to set up a standard measuring procedure for them. The spheres were first subjected to one hundred percent inspection with go-no go gauge to keep any variations in out-of-roundness and diameter to within 0.0003 in. of the average diameter for the particular lot of spheres being used. This inspection made it unnecessary to measure and record the diameter of each individual sphere and identify each sphere with a particular gauge. After the spheres were deformed they were placed in envelopes marked to identify them with the gauge and its position during the shot. The deformation was measured by means of a bench-type dial gauge set to read zero deformation for a sphere of average diameter for the particular lot. The deformations of the damaged spheres were read directly from the dial. The uncertainty in this measurement was the tolerance allowed in the average diameter and resulted in somewhat lower precision in the results. However, the efficiency gained in servicing the gauges by this procedure made it possible to greatly increase the number of gauges that could be used on each shot.

---

[10] See Appendix VII.

(i) Precision. The standard deviation of a single ball-crusher gauge on a single shot was from 2 to 3 percent, calculated from the difference of readings of the two gauges in the same pair for a number of shots. A detailed analysis of many ball-crusher results from different sources by Brown [8] is in agreement with this estimate.

(c) Theory. — The ball-crusher gauge was designed and constructed by the Naval Ordnance Laboratories and used by them to evaluate underwater explosion effectiveness empirically in terms of the deformation of the copper sphere. Static calibrations of deformation in terms of applied pressure on the gauge were also available. Later, Hartmann developed the theory for the ball-crusher gauge to enable the calculation of the absolute value for the peak pressure. This involved the solution of the differential equation,

$$M\ddot{x} + kx = A\,P_m e^{-\mu t}$$

for the gauge. Here M is the mass of the moving parts (piston, water behind it, and a portion of the copper), x the piston displacement, $\ddot{x}$ the piston acceleration, k the force constant of the copper sphere, A the piston area, P_m the peak pressure and $\mu\,(= 1/\theta)$ the decay constant of the shock wave, and t the time measured from the incidence of the shock wave on the gauge. The solution is:

$$\frac{x}{P_m} = \frac{A}{M\omega^2 + k}\left(\frac{\mu}{\omega}\sin\omega t - \cos\omega t + e^{-\mu t}\right)$$

where

$$\omega = \sqrt{\frac{k}{M}}.$$

A partially analytical treatment of this equation has been carried through by E. B. Wilson, Jr. [22], who found that the equation

$$\frac{P_m}{P_a} = 0.500 + 0.806\left(\frac{M}{k}\right)^{1/2}\mu$$

expresses the relation with sufficient accuracy over the range $(M/k)^{1/2}\mu$ from 0 to 1.0. P_a is the apparent peak pressure calculated from the force constant of the sphere and its deformation according to $P_a = kx/A$. Substitution yields

$$\frac{P_m}{x} = \left[0.500 + 0.806\left(\frac{M}{k}\right)^{1/2}\mu\right]\frac{k}{A}.$$

For 3/8-in. diameter copper spheres with a force constant of 3.49×10^5, the equation becomes $P_m/x = 74.5 + 6.72\mu$ where x is in 10^{-3} in. and P is lb/in^2 [23].

Peak pressures calculated from ball-crusher deformations, according to the above theory, assuming an exponentially decaying shock wave and using the decay constant obtained from piezoelectric-gauge results, give fairly good agreement with the piezoelectric peak pressures. In one series of tests where the gauges were mounted face-on to the charge, ball-crusher peak pressures averaged 3 percent higher than piezoelectric peak pressures. In another series of tests where the ball-crusher gauges were mounted side-on to the charge, ball-crusher peak pressures averaged 8 percent lower than piezoelectric peak pressures. The latter case covered a wide range of distances and the rate of decay with distance of ball-crusher peak pressures was equal to that of piezoelectric peak pressures within the limits of error of observation [24,25].

Calculation of sphere deformation from the pressure-time curve has also been made by an iterative method [9], and Halverson and Slichter [10] by means of the superposition theorem have calculated the gauge response for shock waves which were not exponential. General considerations of the gauge have been given by Finkelstein [7], who found that the infinite baffle thickness for steel is from 3 to 4 m.

(d) Weight and distance exponents. — For 3/8-in. copper spheres, the distance exponent for gauges in the composite blocks (baffled) is 1.2, and for those in other mounts (unbaffled) is 1.0. Independent of the method of mounting the weight exponent is 0.4.[11]

10. The Bureau of Ships Modugno gauge

A diaphragm type of gauge developed by the Bureau of Ships from the gauge described by Dr. Francesco Modugno of the Royal Italian Navy has been used routinely for most of the RELIANCE measurements. This gauge offers no particular advantages over the ball-crusher or UERL-diaphragm gauge and is somewhat more difficult to use than the crusher gauge. No adequate theory has yet been developed for the Modugno gauge.

(a) Description. — The guage (Fig. 21) consists of a steel cylinder 1-9/16 in. in diameter, in the end of which there is a hemispherical cavity of 1-in. radius. a circular diaphragm is placed over the end of the cylinder, and a cap with a circular opening 1-in. in diameter is screwed over the diaphragm and the end of the cylinder. The flat surfaces of the cap and cylinder outside the hemispherical cavity have lands and grooves which aid in holding the diaphragm securely. The opposite end of the cylinder (below the spherical cavity) is machined down to a 1-in. threaded stud 2-9/16 in. long.

(i) Diaphragms used. Diaphragm thickness varied from 0.024 to 0.067 in. depending upon the pressure region in which the gauge was used and upon the material from which the diaphragm was made. Materials used were both soft copper and stainless steel. Each lot of disks used has been calibrated statically to allow corrections to be made for variations in hardness or tensile strength from lot to lot (Appendix VIII).

---

[11] See Sec. 5(b).

(b) Measurement of deformation. — The Bureau of Ships recommends [11] that the diaphragm deformation be measured in the gauge by taking the difference between the position of the center of the diaphragm before and after the shot. While this was done for all RELIANCE shots, "out-of-gauge" readings of deformation were also made by placing a depth gauge across the edges of the deformed plate and measuring the maximum depression. Out-of-gauge readings were consistently lower than in-gauge readings, but the precision of the reading was not markedly different. For the comparison of explosives the out-of-gauge readings were equivalent to in-gauge readings, and are much more convenient since it was not necessary they be made in the field nor need the gauges be carried back and forth to the laboratory.

(i) Precision. The Modugno gauge is about as precise as the ball-crusher gauge; that is, the standard deviation per gauge per shot is 2 to 3 percent, calculated from differences between the two members of a pair of gauges. However, because of the greater difficulty in handling Modugno gauges over ball-crusher gauges, they cannot be used in as great numbers and therefore the same degree of precision is not so easily attainable as with crusher gauges.

(c) Weight and distance exponents. — For 0.065-in. copper disks, the distance exponent is 1.0, and the weight exponent 0.3.[12]

11. Hilliar-type gauges

(a) General theory. — During World War I, Hilliar developed in England a mechanical gauge which would integrate the pressure-time curve over a range of times [12]. In this gauge a free piston was accelerated by the force due to the pressure of the water shock wave. After travelling a given distance this piston struck a copper cylinder. The kinetic energy of the piston at the moment of impact could then be calculated from the deformation of the copper cylinder. The impulse of the water shock wave transferred to the piston up until the time of impact was then determined from the relationship,

$$I = \frac{1}{A} \sqrt{2 \frac{M}{g}} \sqrt{E}$$

where I = the momentum of the water shock wave
M = the mass of the piston
g = the acceleration due to gravity
A = the area of the face of the piston
E = the energy corresponding to the deformation of the copper cylinder.

The time t over which the gauge integrated is equal to the time of travel of the piston. This may be represented by $t = L M/g I A$, where L is the length of travel.

---

[12] See Sec. 5(b).

12. Summary of RELIANCE instrumentation

The instruments which give the greatest and most comprehensive information for measuring explosions from large charges are the piezoelectric gauges and associated equipment, from which complete records of pressure and time may be obtained. However, this type of instrumentation is very difficult to maintain and operate as outlined in Sec. 7(a).

In contrast with the piezoelectric gauges, as regards difficulty of operation, are the mechanical gauges, particularly the ball-crusher gauge. One man can handle as many as 24 ball-crusher gauges on the vessel, and the measurement of the deformation of the copper balls can be done in the laboratory by other technicians. The Modugno and UERL-diaphragm gauges are somewhat more difficult to handle, especially the latter. However, the UERL-diaphragm gauge has greater precision than the Modugno or ball-crusher gauge, so that not as many of them are required on each shot. These three mechanical gauges give very little information about the form of the shock wave. Only the ball-crusher gauge is capable of having its reading transformed easily into peak pressure, and even this requires information regarding the form and decay constant of the shock wave.

The Hartmann momentum gauge, which integrates the pressure-time curve, is more difficult to handle than the above mechanical gauges, and the composite Hilliar gauge, which gives a rough form of the pressure-time curve, is the most difficult of the mechanical gauges to operate. The amount of information obtained by the use of each gauge is apparently in proportion to the difficulty of its operation.

V. DETAILS OF GEAR

13. Gauge mounts

The manner in which the mechanical gauges and the piezoelectric gauges were mounted was found to have an important bearing upon the results, both with respect to the absolute level and the reproducibility. The very early work was done with the gauges hanging on free suspension from various cables. This manner of mounting was abandoned soon, however, because of the large scatter in results from shots fired under identical conditions. From then on the work was done with the gauges rigidly mounted in blocks.

(a) Large composite gauge blocks. — The first gauge block successfully used and the one used most generally was the large composite gauge block holding two UERL-diaphragm gauges, two NOL crusher gauges and two Modugno gauges (Fig. 3B,24). It will be noted that the ball-crusher gauges were mounted with their faces flush with the face of the block. The Modugno gauges were screwed into the block so that the face of the gauge plate was roughly 1 in. in front of the face of the block. The diaphragm gauges were mounted in the lower half of the block so that their face plates were flush with the block. The overall dimensions of the block were 14 × 14 × 4 in., and fastened to the bottom of the block was a piece of 4-in. channel iron 4 ft long which attached to the spacer cable in such manner that the face of the gauge block was always perpendicular to the line of propagation of the shock wave. The block was suspended by a chain bridle from the back plate of the block so that it was fairly well balanced when hanging freely. The first blocks made weighed over 250 lb with all the gauges in place. Later on these were lightened so that they weighed from 195 to 200 lb with all gauges in place. No difference could be found in either absolute level or reproducibility of results as a result of this lightening of the blocks. Since the effective diameter of a baffle is the distance from the center of a gauge to the nearest edge, the UERL-diaphragm gauges were not baffled any more in these blocks than they were when suspended individually. However, the centers of the Modugno gauges were 3-1/2 in. from the edge of the block which gave them a greater baffle than they would ordinarily have had. The exact effect of this baffle on the Modugno gauges was complicated by the fact that the gauge plates were 1 in. in front of the face of the block proper, so that the baffling was not effective until 30 to 35 μ sec after the shock wave had struck the Modugno gauge plate. The distance from the center of the ball-crusher gauges to the nearest edge of the block was 2 in. so that the effective baffle of these gauges had a 2-in. radius.

(i) Effect of baffling on ball-crusher gauges in the composite blocks. To study the effect of the baffling of the ball-crusher gauges in these composite blocks, a pair of ball-crusher gauges were mounted on 1-in. brass rods in the Modugno-gauge hole in the block. The faces of the crusher gauges were 8-1/4 in. in front of the face of the block itself. This prevented the wave reflected from the face of the block from striking the gauges until about 270 μ sec after the shock wave had struck the gauges. As the ball-crusher gauge action for large charges is completed in from 150 to 200 μ sec, these gauges were effectively unbaffled. After correcting for the difference

and charge-to-gauge distances between the unbaffled and baffled ball-crusher gauges in these gauge blocks, it was found that the ratio of the deformation of the spheres in the unbaffled gauges to the deformation in the baffled gauges was 0.835. No significant difference in the scatter between the two members of the pair of baffled or unbaffled gauges was observed.

(b) Light diaphragm-gauge blocks. — A gauge block was designed to hold two diaphragm gauges, keeping the size and mass of the entire assembly as small as possible. These gauges were mounted by their back plates and a piece of steel pipe about 4 ft long was used to keep them oriented toward the charge. Effectively there were two diaphragm gauges side by side, facing the charge. The weight of the entire mount including the gauges was 70 lb compared with 200 lb for the composite gauge block. No difference in absolute deformation or in reproducibility of deformation was observed between the two types of blocks.

(c) Small crusher-gauge mounts. — Due to the simplicity of operation of the ball-crusher gauges and the known theory of their operation, it was desirable to use as many of this type of gauge on each shot as possible. To this end, a number of different types of small ball-crusher gauge mounts were designed and tested. Effects of the different types of mounting upon absolute level and reproducibility were noted.

(i) Vertical drop-line mounts. Two vertical gauges were mounted (distance between centers 1-7/8 in.) pointing downward on one of the 3-1/4 in. × 1-in. faces of a piece of steel 13-1/2 × 3-1/4 × 1 in. (weight 14 lb) which was fastened to the drop line supporting one of the composite gauge blocks. The gauges were 4 ft above the level of the spacer line. A similar mount was constructed with gauges mounted in the same position except that the length of the block was such that the total weight was 1/2 lb. No significant differences were found in absolute level or reproducibility of ball-crusher gauge reading due to the different weight of mounting. Comparison of the side-on orientation of unbaffled gauges in these vertical mounts with the face-on baffled gauges mounted in the composite gauge blocks (after correcting for differences in gauge-to-charge distances) gave a ratio of from 0.80 to 0.82 for the unbaffled deformation to the baffled deformation. No correction was made for the difference in gauge orientation. This result was consistent with that reported for baffling in Sec. 13(ai).

(ii) Crusher-gauge mount on the momentum-gauge frame. A pair of ball-crusher gauges was mounted face-on toward the charge and a second pair mounted side-on toward the charge (face downward) in the momentum gauge frame. These gauges were all effectively unbaffled but there was the possibility of reflection from the momentum gauges on the frame to the ball-crusher gauges. For one series of tests the ratio of the side-on gauge deformation to the face-on gauge deformation was 1.05, while for another series of tests this ratio was 1.07.

(iii) Small block face-on versus side-on mounts. Further tests of side-on versus face-on gauge orientations and of the weight of backing of ball-crusher gauges were made by constructing small blocks which clamped

directly to the spacer cable. Two gauges were mounted face-on parallel with the spacer cable with the center of each gauge 1-1/8 in. from the cable. The side-on gauges were mounted near the end of this block so that their axes were perpendicular to the spacer cable. The weight of the small block and the gauges was 5 lb (Fig. 26). A block with the gauges mounted in identical positions but of greater length was also constructed so that the total weight was 22 lb (Fig. 25). The ratio of the damage as measured by the side-on gauges to that measured by the face-on gauges was 0.95. The difference in the mass of the backing had no effect on absolute damage or scatter. Since in previous tests on the momentum-gauge mount, the side-on gauges had shown greater deformation than the face-on gauges, it was thought that there might be an effect due to the close proximity of the spacer cable to the face-on gauges.

Another type of mount was built with the centers of the face-on gauges 9 in. from the spacer cable and those of the side-on gauges about 12 in. from the cable. These mounts were built in models of two different weights; one weighed 5-3/4 lb (including gauges) and the second 23 lb. Using these mounts the ratio of the side-on gauge readings to the face-on gauge readings was about 1.04. No difference in absolute magnitude or scatter resulted from the difference between the masses of the two gauge mounts.

(iv) Quadrilateral ball-crusher side-on mount. As a result of the above tests, an extremely compact mount, holding four gauges side-on toward the charge (perpendicular to the spacer line) and easily moved from one position to another along the spacer line, was constructed. This mount (Fig. 34) consisted of a square of 1-1/2 in. steel plate 2-1/2 × 2-1/2 in., with the four ball-crusher gauges screwed into the four rectangular sides of this plate. The steel plate was divided diagonally to allow it to slip over the spacer cable, and this diagonal cut was notched to receive the cable. By loosening the screws holding the two halves of the plate together this mount could be slid along the cable to any desired position. The faces of the ball-crusher gauges in this mount were 3 in. from the spacer cable. This type of block was used for mounting crusher gauges after shot RE-155 and proved very satisfactory.

(d) Momentum- and Hilliar-gauge mounts. — The first Hilliar-gauge mounts were made by placing a cross bar at right angles to the spacer line and fastening the gauges at the end of this cross bar. This would not withstand the explosion and had to be repaired or renewed after each shot. Consequently a triangular suspension frame was constructed, which mounted five Hilliar or momentum gauges and four ball-crusher gauges. Later on this frame was replaced by the cross trussed rectangular frame as shown in Fig. 30. This frame would mount four momentum or Hilliar gauges at the four corners plus one at the intersection of the cross truss, and proved to be exceptionally sturdy in use. Bridles were used to keep all of these frames horizontal so that the gauges were always face downwards.

(e) Piezoelectric-gauge mounts. — (i) H-frames. Piezoelectric gauges were normally mounted on an H-frame, the cross bar of which was attached at mid-point to the spacer cable. Two piezoelectric gauges were

attached to the two sides of the H. (Fig. 3E). The distance between the two gauges was originally 24 in. then later 18, and finally 12 in. The 12-in. spacing was found to be satisfactory, easier to use, and more resistant to damage.

(ii) Other methods of mounting. Piezoelectric gauges were sometimes attached directly to the spacer cable. This was usually not satisfactory because of reflections or signals picked up from this cable. However, for certain types of measurement it was necessary to know the exact location of the gauges with the respect to the cable and to each other, and under these circumstances the H-frames could not be used since they were free to rotate about the cable as it twisted and untwisted with the strain of the gear.

In connection with mounting piezoelectric gauges there are certain points which should be made. It was noted that when gauges were placed at four different locations with all piezoelectric gauge cables leading directly back along the spacer cable, the large mass of these cables caused spurious signals to be produced in the gauges at the greatest distance from the charge. These spurious signals were eliminated when the four cables from the first two gauge positions were led up to the surface before reaching the third and fourth gauge positions. It was also found necessary to metallically ground by means of a long wire the copper tubes of the gauges at the four different gauge positions when the distances between positions were large. Before this metallic grounding was used, various disturbances were noted on the records of the far gauges at the time the shock wave struck the near gauges.

14. Gauge and charge spacing

One of the most important details of any explosive measurement is to set up and maintain the desired orientation between the charge and the various measuring instruments. For RELIANCE work this has been done entirely with flexible cables.

(a) Vertical components. — Various instruments and other gear were maintained vertically by means of drop lines and masses sufficient to hold them reasonably straight. The drop lines (usually 5/16-in. wire rope) were suspended from surface floats. The size of the surface floats depended upon the weight which had to be supported (Fig. 27). These surface floats were kept as small as possible consistent with the required buoyancy, so that the minimum drag on the floats was produced as the gear was towed through the water. Surface floats have consisted of 30- and 50-gal oil drums, of empty Mark 4 or Mark 6 mine cases, or of mooring buoys of various sizes. The mooring buoy most commonly used was the 21-in. spherical buoy. Spherical floats of 14-gauge steel (manufactured by the Chicago Float Works) have also proved extremely durable. However, the largest size in which these could be obtained had a 14-in. diameter and was not sufficient for supporting heavy gear. For supporting the charge, oak barrels were ordinarily used. These were less expensive than steel drums and their breakage did not matter since in this position directly over the charge even steel drums could usually be used but once. The Mark 4 or Mark 6 spherical mine cases were very resistant to shock wave damage, but it was extremely difficult to attach

the drop line securely since the fastenings on these mine cases failed easily. These cases were modified so that the strain from the drop line was assumed by the top of the mine case rather than by a weld at the bottom (Fig. 28A). Another advantage of this modification was that it allowed the insertion of a shock absorber to take up the shock occurring when the shock wave struck the mine case. In attaching the drop lines to the steel oil drums it was found best to make two bands of iron which completely circled the drum at two points, running a bridle between these two bands and attaching the line to this bridle. Much difficulty was experienced with having the drop line snap under the impact of the shock wave. Steel cable 5/16 in. in diameter has a breaking strength of roughly 6,000 lb and the heaviest weight put upon these cables was not more than 200 lb. However, the upward component on the float due to the pressure and the shock wave gave sufficient acceleration to break these cables. This was overcome by the use of some sort of shock absorber which would take up this instantaneous acceleration. Two modifications which have been used successfully are shown in Fig. 28.

In addition to the steel drop lines, manila safety lines were employed so that in case a drop line parted the gear was not lost. The manila lines were also used for lowering gear (snubbing around a cleat on the deck) and for retrieving gear since they could be brought in over a winch head. It was customary to attach these to independent fastenings both on the float and on the gear which was being suspended so that in case of failure of either fastening the gear was not lost.

The backward drag of the surface float caused variations in the depth of the gauges from the actual measured length of the various drop lines. This was not serious for the type of measurement being made on the RELIANCE since an arbitrary limit of variations in depth up to 3 ft was allowed. However, if depth must be maintained exactly, modifications to the type of rig here described must be made.

(b) Horizontal components. — Horizontal distances were maintained by keeping the horizontal spacer cable under strain at all times. This strain was the result of the 18-in. sea anchor at the stern end of the gauge spacer cable reacting against the 1 to 1.5-knot velocity of the gear as it was towed through the water. Near the sea anchor was a weight suspended from a surface float at the depth which it was desired to maintain. From this weight a manila line ran to the sternmost gauge block and 5/16-in. steel cable was used for spacer lines from this block forward to other blocks. From the foremost gauge block the steel spacer cable ran forward to a 200-lb lead weight suspended at the proper depth and from here the tow line ran back to the RELIANCE at the surface. The mass of the lead weight was sufficient to overcome the upward component of the tow line. The drag on the tow line at the vessel was estimated to be 400 to 500 lb. The general layout of the gear for a fore and aft shot was modified from time to time, and the four main modifications are shown in Fig. 29 and 3.

No lowering of gauge deformations due to the "shadow" of one composite gauge block on a second further from the charge was found at the time Modification C was adopted. However, to minimize the possibility of any such shadowing, the rear block was hung on the opposite side of the spacer cable from the front block with a distance of at least 10 ft between the two.

For the two-dimensional paravane rig, the vertical suspension was as described for the one-dimensional rig. The horizontal spacer lines were also the same, with the exception that to maintain the distance at right angles to the direction of the spacer line, paravanes were used at the extreme ends. These produced an outward drag which pulled the gauge blocks away from the charge. Distances determined in this direction were not certain because of the bow introduced into the cables by their resistance to the water as they moved through it.

15. Electrical cables and their suspension

The electrical cables were led back from the pilot gauge and from the two piezoelectric gauges nearest to the charge by attaching them to the spacer line at intervals with friction tape. At a point 20 ft forward (toward the RELIANCE) from the second piezoelectric gauge (Fig. 3) the cables were led to the surface along a drop line from a surface buoy, and then back to the connection barrel supporting the lead weight. Electrical cables from the two piezoelectric gauges farthest from the charge were led forward (away from the charge) to a point 30 ft from the farthest gauge and then were led to the surface along the drop line supporting the lead weight. At the surface float (connection barrel) the cables were connected to patch cords and were lead back to the vessel along the surface attached to a manila line which took the strain of the gear. Fourteen-in. spherical steel floats at intervals of about 60 ft buoyed the rope line and the electrical cables. At the RELIANCE the electrical cables were attached to a large reel (Fig. 30) where connecting patch cords leading to the electronics cabin were plugged in.

VI. SETTING AND RETRIEVING GEAR

16. "One-dimensional" fore and aft rig

As has been mentioned previously most of the work was done with a one dimensional fore and aft rig, which allowed gauges to be placed on two sides of the charge on two straight lines 180° apart. This rig was very simple to set and recover even in the event of a misfire.

(a) Setting the gear. — For setting the gear all the various components were laid out from stern to bow on the port side of the RELIANCE in the order in which they would go overboard (Fig. 31). The heavier components such as the composite gauge blocks were lifted over the side and snubbed just above the water line by means of the manila recovery line. The charge was armed and prepared for launching. Then it was lifted by the hoisting boom by means of a pendant led through the supporting ring for the charge with the two ends of the charge hooked on to the hoisting boom tackle. When these preparations were complete, the large float nearest the sea anchor was thrown over-board and allowed to drift back away from the vessel. During the entire operation of setting the gear the vessel was kept underway and also steered slightly to port to keep the gear away from the propeller. After the sea anchor ball had been payed out the sea anchor itself was put over-board and opened. The small weight near the sea anchor was then put over, and that part of the gear was payed out by the line which lead up to the sternmost gauge block. When small ball-crusher gauge blocks were located at great distances from the charge, the line was made of .5715-in. wire rope. However, when such gauge blocks were not used, the line was usually of manila. When the line became taut on the sternmost gauge block, the block was slowly lowered by means of the manila safety line snubbed around a cleat on the deck of the RELIANCE. Due to the proximity of this gauge block to the next composite gauge block forward, the spacer cable between the two soon became taut and the lowering of the second composite gauge block was begun, snubbing with the rope recovering line over a cleat as in the first case. As these two gauge blocks were being lowered the strain came on the sternmost of the momentum gauge rigs. These momentum-gauge rigs were then lifted over the sides and lowered, snubbed again by means of the manila recovery line.

Before the strain reached it the charge was lifted by means of the hoisting boom tackle and swung over the side. The weight of the charge was then taken up by a manila snubber line, and the pendant by which the charge had been lifted was removed. Another rope snubber line, one end of which was made fast to the vessel, was passed through an iron ring just forward of the forward momentum-gauge rig, and was used to take the strain of the after part of the gear until the charge was fairly well down in the water.

As the gauge blocks and charges neared their final depth, their supporting floats were thrown overboard, and the snubber lines quickly thrown off the cleats. While the charge was being lowered the other components were lowered simultaneously, keeping all lines tight. The spacer line forward of the charge (carrying the piezoelectric gauges, and for the early

shots two composite gauge blocks) was carefully lowered and then snubbed by the safety line from one of the composite gauge blocks or the recovery line running to the connection buoy. Lowering was continued and the various components cast off as they reached their final depth. The connection buoy (which also supported the lead weight) was then made ready to go overboard, and the lead weight lowered by means of the main towing cable which ran from the drum on the winch. As this gear dropped astern of the boat the piezoelectric gauge lines which ran along the surface were payed out. Since the large reel holding these lines was on the starboard side of the boat amidships, these cables previously had been led around the stern of the boat and up the port side outside of all rigging to the bow (Fig. 5 and 31). They were then payed out until there was no slack to the drum; the cables were reeled off the drum as the gear dropped astern. A manila line to take the strain from the electrical cables was made fast to the connection barrels and was payed out with the electrical cables. At intervals of approximately 60 ft a spherical surface buoy was attached connecting the electrical cables and the rope line together by means of a snap hook passing through grommets on these two lines. This gear was payed out as quickly as possible, synchronizing the rate for the electrical cables with the rate for the towing cable from the main drum (Fig. 32). When the charge was about 600 ft from the vessel it was in position for firing. With smaller size charges (less than 50 lb) it was not necessary to pay out the entire amount of cable before firing the charge.

After securing the main towing cable and the rope line taking the strain from the electrical cables, the patch cords were plugged in to the Miller connectors on the large reel. All patch cords were color coded for plugging into the big reel to minimize the possibility of error in connecting the proper gauge to the proper oscillograph recording channel. After the calibration of the electrical and recording equipment was made the charge was fired from the electronics cabin. Coordination was necessary at all times between the electronics cabin and the master of the vessel to be sure that the water was of sufficient depth, and also that no traffic was near the point at which the charge was being fired. An intercommunication system was used for this purpose.

(b) Retrieving the gear. -- (1) After firing the charge. When the charge was fired the gear was cut into two halves, split at the position formerly occupied by the charge. The stern part of the gear drifted off with the tide, while the forward part of the gear was still attached by means of the tow line and the electrical surface line to the vessel. The main towing cable was reeled in on the winch drum in coordination with the electrical cables being brought in by pulling the manila strain line on a gypsy head. As the electrical cables were separated from the manila strain line they were reeled onto the large reel, where the patch cords had been previously disconnected. This large reel was driven by an electric motor and a Graham adjustable speed transmission. (Power drive for this reel was necessary because of the great weight of the cables. Before power drive was installed it required two men to turn this reel by hand and one man to lead the cables onto the reel. After power drive was installed one man could control the reel and lead the cables onto it without additional help.)

When the gear was recovered to the lead weight and the connecting barrel supporting it, these were brought aboard and the connecting barrel was led forward to its usual position on the deck of the vessel. The electrical cables were fastened around the stern of the vessel and up the port side high up in the rigging to keep them out of the way of further operations. The rope recovery line strung from the connection barrel to the point 20 ft forward from the second piezoelectric-gauge pair was then brought in by means of the gypsy head. Simultaneously the steel spacer cable (to which the two piezoelectric-gauge pairs farthest from the charge were attached) was pulled in by hand and placed in its proper position on the deck. In turn the second connection barrel was brought aboard and placed in its position on the deck, and then the remainder of the spacer cable with the two piezoelectric-gauge pairs nearest to the charge was brought aboard. Except for any damage caused by the explosion, the gear was in a position ready to go overboard for the succeeding shot.

With the forward half of the gear retrieved the vessel picked up the after half of the gear. During weather of good visibility the after half was easily found, particularly since the ocean currents were well known by the master of the vessel. If the visibility was bad, or if it was after dark, special precautions had to be taken. In some cases a man put overboard in a dory immediately after the firing of the charge attached the dory to one of the surface floats of the stern half of the gear. When the vessel was ready to pick up the stern half of the gear, he signalled his position by means of a fog horn, or a light if visibility permitted. Another scheme was to attach a small flag (or light, if after dark) to a mast on the sea anchor ball before it was put overboard. This usually permitted easy location if visibility was good.

In retrieving the stern part of the gear the sea anchor ball was first picked up and the anchor spilled by a special line. The sea anchor was brought aboard and then the line running forward from the sea anchor weight to the sternmost gauge block was pulled in. The sternmost gauge block was lifted aboard and then the second gauge block and momentum gauges with their respective surface buoys. All of this gear was placed in its proper position on the deck ready for the next shot.

The ball-crusher, Modugno, and momentum or Hilliar gauges were removed from the rig and taken to the mechanical gauge cabin for servicing in preparation for the succeeding shot. The diaphragm gauges were serviced in the composite blocks on the deck. Any repairs to this part of the gear or replacements of surface floats damaged during the explosion were made at this time.

(ii) <u>After a misfire</u>. When the charge had not fired successfully the recovery of the gear was much more difficult. In these cases, a period of about one hour was allowed to elapse before recovery was attempted, to be sure that the misfire was not a hangfire which could have exploded after some time had elapsed. The gear was then brought aboard in roughly the reverse order in which it went out. Since the distances between gauge blocks and between gauge blocks and the charge were less than the depth at which

the gear was set, it was necessary to pick up the various components almost simultaneously in order to keep strain off the charge, and also to keep the total weight on any one line small enough to be handled. This was analagous to the procedure in setting out the gear and was one of the main difficulties of this operation. When the various gauges and other components had been lifted sufficiently for the charge to be placed on deck, the charge was disarmed and an investigation was made as to the cause of the misfire.

17. "Two-dimensional" (paravane) rig

(a) Setting the gear. — The two-dimensional paravane rig was used in order to obtain more information about the distribution of the shock wave around a charge without the necessity of firing additional charges. The various parts of this paravane rig are shown in Fig. 4. These were arranged on the stern of the RELIANCE, roughly in the order in which they were to go out. The charge was hung directly over the stern and the sternmost gauge block was hung on the starboard quarter of the vessel. Just forward of this was the starboard gauge block while the port gauge block was hung on the port quarter, and just forward of this was the forward gauge block. The two paravanes were kept on the starboard and port sides, respectively, just aft of the main rigging. As the gear was set, the sea anchor, its weight, and supporting ball were payed out until the strain came on the sternmost gauge block. This was then lowered, together with the momentum-gauge rig, until the strain came on the charge, when its lowering also was begun. The stern gauge block and its buoy were cast off as soon as the block reached the desired depth. As the strain from the two side spacer cables came on the starboard and port gauge blocks, these were lowered simultaneously with the charge until the cables running to the paravane became tight. At this point the two paravanes were payed out very slowly and in good balance. It was important to bear in mind that the greatest strain on the paravanes had to come from their towing lines. If the strain came from the line running to the gauge block, the paravane would shoot in toward the center of the rig, rather than pulling out from the charge. When the paravanes were properly set and pulling, the various components were lowered further, including the forward gauge block which by this time had begun to take part of the strain of the charge. As soon as possible the charge was cast off, and the two side gauge blocks were later cast off simultaneously. The forward gauge block was payed out and cast off. The paravanes were allowed to drop back as the main towing cable was payed out (Fig. 33), at such a rate that the two side gauge blocks were always somewhat forward of a line through the charge. This condition was maintained until the charge was at the proper distance from the boat for firing, and then the two side gauge blocks were allowed to drop back until they were exactly opposite the charge. It was extremely important for all these manouvers to be carefully coordinated during the setting of this gear. Due to the short distances between the various components compared with the depth at which the gear was set, they all had to be lowered almost simultaneously and exact horizontal symmetry had to be maintained. One paravane pulling harder than the other would cause the gear to become askew. If either paravane tended to shoot in, the gear became hopelessly tangled around the charge, and when working with non-standard booster systems or loadings, there would be danger of accidental detonation.

(b) Retrieving of gear. — (i) After firing the charge. After the charge had been fired the paravane rig was separated into four sections at the point formerly occupied by the charge. The stern section drifted off with the tide, the starboard and port sections swung far out due to the action of the paravanes, while the forward quarter remained directly astern of the vessel. The starboard paravane and gauge block were first taken aboard since two piezoelectric gauges were attached. The port paravane and gauge block were taken aboard, and then the main towline, the forward gauge block, and associated piezoelectric gauges. The same principles held during this procedure as were described in Sec. 16(bi). The stern portion of the gear was then retrieved as previously described.

(ii) After a misfire. Due to the complexity of the rig, retrieving a charge after a misfire was very difficult. However, this was usually accomplished by allowing the starboard paravane and gauge block to drop back beside the stern part of the gear and by pulling the port paravane and gauge block ahead beside the forward part of the gear. This brought all components into one line and they were then brought aboard in a fashion similar to that described for the one dimensional rig. At times when the gear became badly tangled, due to mishandling of the paravanes, it was necessary to retrieve without attempting to fire. Under these circumstances it was not always possible to retrieve this gear in an orderly fashion, and it was brought up in the safest manner feasible.

APPENDIX I

Use of the UERL Diaphragm Gauge

by C. R. Niffenegger

The UERL diaphragm consists of:

A. The main body of the gauge: The face of the body is a ground surface which has 8 tapped (1/2 in., N.C. 13-thread) holes equally spaced around it. Through the back plate of the gauge are four tapped holes which are used to hold the gauge to its support. The number of the gauge is stamped on one edge of the face.

B. The face plate: In the center of the face plate is a circular hole (3.432 in. in diameter) with a beveled edge. One side of the face plate is a ground surface with 8 holes drilled through to correspond with the tapped holes through the front face of the body. The face plate, also, is numbered on one edge.

C. The diaphragm: There are two thicknesses of diaphragm in use: 14 gauge (about 0.085 in. thickness) and 20 gauge (about 0.038 in. thickness). Eight holes are drilled through the plates to correspond with the holes in the face plate and the face of the main body of the gauge. The diaphragms are numbered according to lot number, sheet number, and individual plate number within the sheet.

D. Twelve bolts (1/2 in. N.C. 13-thread: 1 in. long). Assembling the gauge: First of all the inside of the main body, the ground surfaces, and the diaphragm must be thoroughly cleaned. The ground surfaces and diaphragm should then be checked for burrs. If any are found, be sure to remove them as they will allow leakage of water into the gauge.

A thin layer of Kasson water-proof grease is spread completely over both sides of the diaphragm. This waterproofs the gauge and, also, prevents rusting of the exposed part of the diaphragm. The diaphragm is then placed between the front face of the body and the ground surface of the face plate, so the numbers stamped on all three are on the same side of the gauge and so the numbered side of the diaphragm is towards to face plate. The bolts are then placed in position and all 8 bolts screwed in evenly until the diaphragm and face plates are just held in place. (If any of the bolts cannot be screwed in with the fingers, the hole should be tapped out or the bolt replaced.) They are then tightened with a torque wrench to 35 lb in. The gauge is then securely fastened to the support and is ready for use.

Measuring the diaphragms: Before the gauge is assembled, the thickness of each plate must be measured with a micrometer at the three unnumbered sides to get the average thickness. These thicknesses are recorded.

After the shot a dial depth gauge is used to measure the depressions in the diaphragms. Because the edges of the thin diaphragms assume a twist after deformation, a means must be used to hold these edges flat.

Since the plates are not of uniform thickness, a correction factor is applied to the depressions. Diaphragms of 14-gauge thickness are corrected to 0.085-in. thickness and 20-gauge diaphragms to 0.038-in. thickness.

APPENDIX II

Use of the NOL Crusher Gauge

[Adapted from Navy Department,
BuOrd (Re2c) Technical Note No. 15.]

Arrangement of the gauge: The gauge when ready for operation, consists of the following pieces:

1. The base, consisting of (a) the anvil against which the copper ball is pressed, (b) a stud by means of which the gauge is screwed into the mounting block, and (c) a steel or brass body in which these two pieces are mounted. In some versions of the gauge these pieces are combined into one unit.

2. The copper ball, which should measure 0.375 in. in diameter.

3. A rubber centering washer for the copper ball.

4. The piston, a mushroom shaped piece of steel, which is used to deform the copper ball.

5. A small spring, somewhat like a section of a corkscrew, which is designed to fit around the smaller portion of the piston and, by pressing against the piece described next (6), to hold the piston lightly against the copper ball.

6. A brass head for the gauge, into which the piston, spring, ball, and washer may be inserted as described below, which is screwed into the base, completing the assembly of the gauge.

7. A spacing ring, for use with gauges in which a 0.375-in. copper ball is used.

Preparing gauges for use:

1. Copper spheres of 3/8-in. or 5/32-in. diameter should be obtained from a lot which has been sampled and tested for uniformity of hardness. Spheres should be within $\pm$0.0003 in. of the mean diameter of the spheres in the particular lot, and their out-of-roundness should not exceed $\pm$0.0003 in.

2. Determine the number of gauges to be used in the test. Procure that number of each of the (7) pieces described above. Be sure that all parts of the same gauge bear the same serial number.

Check the gauge with a sphere in place to be sure the piston (and spacer ring, if 3/8-in. balls are used) is of the proper dimension so that the face of the piston is flush with the face of the gauge.

The piston must be free moving, without side play, in the body of the gauge.

The rubber washers should fit snugly into the cavity provided for them. After a washer has been used for some time it tends to swell. This leads to improper functioning of the gauge and is not desirable. Only washers in good condition should be used.

The small springs tend to lose their elasticity after a time and become ineffective. It is important that resilient springs be used.

3. Arrange the items in rows as follows:

Farthest from the gauge operator, line up the bases. The studs should stick up in the air. Slip the spacer rings over the base; friction will hold them in place. In the next row, place the heads. The internal portions of the heads should be exposed. Make sure that the numbers on the various pieces correspond.

The third row should consist of the pistons. These may best be arranged with the larger surfaces down. Again make sure that the piston numbers correspond to the other pieces.

The fourth row should consist of the springs.

The fifth row should consist of the rubber washers. This row is nearest the gauge operator.

Finally, in each washer place one of the measured copper balls, making sure that the washer fits around a diametric plane.

Now, place the springs from the fourth row on the pistons in the third row. Invert these two pieces as a unit, and insert them in the head pieces in the second row.

At this stage, one has left only three rows of materials.

Next, insert the rubber washer and the copper ball as a unit into the head piece. Make sure that the washer fits snugly into the cavity, and that the piston slides freely in the head.

The last step consists of screwing this complete head assembly onto the base assembly; that is, combining the elements in the farthest two rows.

When the final assembly of the head has been made, and it is being screwed onto the base, the ball and washer unit should not be permitted to become loose.

4. The completely assembled gauge should be checked by pressing on the piston. If the spring and washer are in proper condition, no play should be observed. If any play is observed the gauge as assembled is unsatisfactory and may give a deformation that corresponds to a higher pressure than actually existed in the shock wave. It should be reassembled using a spring or washer in good condition.

Cleaning the gauge: All parts of the gauge should be carefully cleaned after each use. The parts made of steel should be immersed in oil to prevent corrosion. Remove all oil before assembling the gauge for re-use.

APPENDIX III

Use of the Hartmann Momentum Gauge

[Adapted from Navy Department,
BuOrd (RE2c) Technical Note No. 15.]

Arrangement of the gauge: The gauge, when ready for operation, consists of the following pieces:

1. The body of the gauge, into which all the other pieces fit.

2. The cap of the gauge, which screws into the body of the gauge, and also into the mounting cap.

3. The piston, into which all the remaining pieces are placed.

4. The copper pellet, which should be 0.500 in. long.

5. The rubber washer, which centers the pellet in the cavity provided for it on the piston.

6. Two small cylindrical stop pins, and a spring, which fit into a cylindrical hole extending horizontally through the piston.

In additon to the item present in the gauge, certain additional devices are required to assist in the assembly of the gauge. These are mentioned below.

Preparing the gauge for use:

1. Copper pellets should be selected from lots of uniform hardness and diameter, and the length of each individual pellet should be recorded to 0.0001 in.

2. Determine the number of gauges to be used in the test. Procure that number of each of the six pieces or sets of pieces described above. Be sure all parts of the same gauge bear the same serial number.

Check to be sure the piston travels freely in the gauge.

Be sure spring catches do not stick in the body of the gauge.

3. Arrange the items in rows as follows:

In the row farthest from the operator place the bodies of the gauges with the small opening upward. The purpose of arranging the bodies upside down is to provide a stand for the pistons. Place the appropriate piston in the corresponding hole, so that the large part of the piston rests on the bottom of the gauge body.

In the next row, immediately in front of the row of bodies and pistons, place the corresponding top caps of the gauges.

Now distribute one copper pellet, one rubber centering washer, two pins and a spring to each gauge, making three rows of materials.

Each pellet should have inscribed upon it the number of the gauge in which the pellet is to be put. Slip the rubber centering washer over the pellet and insert both in the cavity so that the pellet is correctly positioned.

Next, insert the pins into the piston, and slip the retaining cylinder over the piston. Remove the piston from the body of the gauge, invert the gauge body, and slide the piston into the gauge body. Do not drop the piston. Make sure that the piston is properly seated, and the pellet is in place.

Screw on the cap, and the gauge is assembled. (A thin layer of grease may be applied to the surfaces which rub, if desired.)

4. It is necessary to waterproof the gauges when they have been assembled. To accomplish this the following procedure should be carried out.

(a) Sealing the top part of the gauge. Clean off any grease that may be present on the outside of the gauge. Wrap one layer of scotch tape around the gauge so the join between the body and the cap is covered. Paint over with waterproofing (Tygon primer and 2 coats of Tygon black).

(b) Sealing the bottom part of the gauge. Place one strip of scotch tape over the opening at the bottom. Paint with waterproofing.

(c) After the gauge is waterproofed every precaution should be taken to avoid puncture of the watertight seal. When it is necessary to unscrew the gauge from its mounting before it is used (which is the case when difficulty is encountered in screwing the gauge into the mounting and the gauge must be removed to permit cleaning, lubricating, and/or chasing of the threads) the body may rotate with respect to the cap and thus destroy the seal. Gauges must not be set on their faces; since this may puncture the waterproofing over the piston.

Cleaning the gauge: All parts of the gauge should be carefully cleaned after each use. A slight coat of oil should be used to prevent corosion of the steel parts. Keep oil off the rubber washer. Remove all oil before assembling the gauge for re-use.

Precautions: When the momentum gauge fails to function, it is nearly always due to water leaking into the gauge. If leaks occur, any information obtained is unreliable. The instruction found herein is designed not only to assist in the proper assembling of the gauge, but also to assure that the gauge after assembly will be and remain watertight until subjected to a shock wave.

APPENDIX IV

Use of the Improved Hilliar Gauge

[Adapted from Navy Department, Buord (Re2c) Technical Note No. 15.]

Arrangement of the gauge: The gauge, when ready for operation, consists of the following pieces:

1. The body of the gauge, which is used as a housing for most of the other pieces.

2. A cap for the gauge.

3. Six anvils, numbered 1 through 6.

4. Seven pistons, numbered 0 through 6, and corresponding springs.

5. One small retaining plate with three holes.

6. One sheet of cellophane.

7. One rubber gasket.

8. One ridge ring, with slots to fit pins on the body of the gauge.

9. One threaded clamp ring designed to hold the ridge ring.

10. Six copper cylinders, 0.500 in. long, and one copper ball 0.375 in. in diameter.

11. One rubber centering washer for copper ball.

Preparing the gauge for use:

1. Copper pellets and spheres should be selected from lots of uniform hardness and diameter. The length of each individual pellet should be recorded to 0.0001 in. The diameter of each sphere should be recorded to 0.0001 in., and the out-of-roundness should not exceed ± 0.0003 in.

2. Determine the number of gauges to be used in the test. Secure sufficient parts, as described above, to constitute that number of gauges. Be sure all parts of the same gauge bear the same serial number.

Check that all pistons travel freely in the gauge.

Since the cellophane disk serves as the waterproof seal for the bottom of the gauge its preparation is important. This disk should be cut with the cutter (biscuit type) designed especially for this purpose. Scissors should never be used to trim cellophane to size as this is likely to produce

out-of-roundness sufficient to cause leaks. Before any cellophane disk is used on a gauge all ravelings and any grit on the surface should be removed. If any creases or pin holes are present the cellophane should be discarded.

Line up the seven pistons in numerical order and cement on the appropriate pellets, each of which must be inscribed with the number of the piston to which it is to be cemented. This step is done first in order to give the cement time to harden before using the gauge.

NOTE: EXTREME CARE MUST BE TAKEN TO INSURE THAT THE PELLETS ARE CENTERED ON THE PISTONS. IF THEY ARE EVEN SLIGHTLY OFF CENTER, THE RESULTS OF THE TEST ARE RENDERED DOUBTFUL, SINCE THE PELLETS ARE THEN SQUEEZED BY THE SPRINGS.

Place the corresponding anvils and springs beside the pistons.

The next step consists of waterproofing the face, or exposed end, of the gauge. This is accomplished in the following manner.

Place one circle of cellophane over the face of the gauge, centering it properly. Lay the rubber gasket and the steel ridge ring around the edges, screw on the clamp ring hand tight, and then tighten it slightly (1/8 of a turn) with a wrench. The cellophane should be unwrinkled. Make 3 holes in the cellophane over the screw holes for the central plate, and place one drop of waterproofing on each. Put the retaining plate on, place another drop on each small hole in the plate and secure the plate with the screws provided. The face of the gauge should now be watertight.

The subsequent stage consists of the insertion of the pistons. Slip the small spring over the zero piston and insert it the entire distance, using a small wooden dowel, 1/4 in. in diameter and about 10 in. long. Lay the gauge on its side and slide the remaining six pistons into their proper holes. Use the wooden dowel, not a sharp metal instrument which may mar the pellets.

When all the pistons are installed, insert the springs. Make sure that no spring touches a pellet. Also insert one copper ball and its centering washer in the zero channel. Slide — do not drop — it in.

Now place the six anvils in their corresponding holes, and screw on the cap. It will be necessary to hold down anvils 4, 5 and 6 with a plate, such as the blade of a putty knife.

The final stage consists of waterproofing the top, following the same procedure as that outlined for the momentum gauge.

When the retainer plate, the pistons, and sometimes the gauge body develop sharp edges which bear against the cellophane disk, puncture of the cellophane is likely to occur. On new gauge parts sharp edges are prevalent. To prevent leaks from any such punctures these parts should be polished smooth with crocus cloth. The same precautions for maintaining watertightness which apply to the momentum gauge also apply to the Hilliar gauge.

Cleaning the gauge: All parts of the gauge should be carefully cleaned after each use. The metal parts should be oiled to prevent corrosion. Before reuse, the gauge should again be cleaned to remove all the oil.

Precautions: When the Hillior gauge fails to function, it is nearly always due to water leaking into the gauge. If leaks occur any information obtained is unreliable. The instruction found herein is designed not only to assist in the proper assembling of the gauge but also to assure that the gauge after assembly will be and remain watertight until subjected to a shock wave.

Thin layers of cement often cling to the bottom of the pellets. This layer and other dirt should be removed before the disks are measured.

APPENDIX V

Electric Power for Schooner RELIANCE

by J. P. Slifko

Both a-c and d-c sources of power in 115 v and 120 v respectively were used aboard the schooner RELIANCE. The d-c source consisted of 20 6-v automobile storage batteries of about 120 amp hr rating. This source was used on a 0.75 KVA inverter which supplied quite steady a-c current at 115 v for DuMont oscilloscopes. The d-c source was also used on the ship's lights when an a-c source was not available.

The model 50 AA1 Delco generator aboard the schooner supplied 5 KVA at 115 v, single phase, 60 c/sec. When the RELIANCE was tied at the dock, either 60 c/sec, 115-v, single-phase power from the Cape and Vineyard Electric Company, or the above mentioned Delco power, was used as an a-c source.

Since the voltage regulation for the Delco plant was poor, no loads were switched during calibration and shooting. Furthermore, gasoline for the Delco-plant engine was filtered twice to insure a steady flow of gasoline free from impurities and water into the carburetor.

To further insure steady a-c voltage for the RELIANCE electronic gear, a Sorenson model 1750 automatic voltage regulator was used. The manufacturer claimed a 0.2 percent automatic voltage regulation for a pre-set voltage independent of variations in input voltage, power factor, load or frequency, providing input voltage is between 95 and 130 v at 50 to 60 c/sec and load was between 800 and 2000 v amp. They also claimed stability and a complete recovery of voltage within from 1 to 6 cycles depending upon the magnitude of the voltage change.

APPENDIX VI

Data for Lot V Steel Plates

	Lot V Thick	Lot V Medium	Lot V-A Thin	Lot V-B Thin
Nominal Thickness (B and S)	9 gauge	14 gauge	20 gauge	20 gauge
Date Received at UERL	Oct. 1943	Oct. 1943	Oct. 1943	Dec. 1943
Values Supplied by Manufacturer (Armco)				
Longitudinal				
Yield point (lb/in^2)	48,000	41,200	35,100	39,500
Tensile strength (lb/in^2)	63,200	67,000	59,700	60,900
Elongation (percent)				35
Transverse				
Yield point (lb/in^2)	46,350	41,600	35,800	38,850
Tensile strength (lb/in^2)	69,200	68,000	59,400	66,800
Elongation (percent)				32
Values Supplied by Taylor Model Basin				
Yield point (lb/in^2)	40,310 ± 1,014	50,149 ± 629	42,608 ± 2,336	
Tensile strength (lb/in^2)	69,324 ± 704	72,803 ± 462	59,355 ± 2,467	
Values Supplied By MIT (Mehringer)				
Yield strength (lb/in^2)		46,590	36,800	
Ultimate strength (lb/in^2)		69,880	59,630	
Elongation (percent)		32.3	35.2	
Young's modulus ($10^6 \times lb/in^2$)		28.5	25.5	

APPENDIX VII

Dynamic Calibration of Copper Crusher Spheres and Cylinders with Freely Falling Weights

by P. Newmark and C. R. Niff negger

Several sizes of steel weights were released by an electromagnet from various heights and allowed to fall freely on copper spheres or cylinders which in turn rested on a hardened steel anvil. Plots of the energies required to produce given deformations against the deformations are shown in Figs. VII-2, VII-3, VII-4. The curves fit quite closely the following empirical equations in terms of E = energy (ft-lb) and D = deformation (10^{-3} in.).

For 3/8-in. spheres,

$$E = (330D + 0.27D^2)^2 \times 10^{-8}$$

for values of $D = 40 \times 10^{-3}$ in. through 150×10^{-3} in.

For 5/32-in. spheres,

$$E = (190D + 0.87D^2)^2 \times 10^{-8}$$

for values of $D = 30 \times 10^{-3}$ in. through 110×10^{-3} in. For copper cylinders (0.33-in. diameter, 1/2 in. long),

$$E = (700D + 0.46D^2)^{1.6} \times 10^{-6.4}$$

for values of $D = 40 \times 10^{-3}$ in. through 110×10^{-3} in.

The calibrations were made on the machine shown in Fig. VII-1, or on one similar to it. No significant differences could be noticed between the calibrations from different machines, provided the concrete base is sufficiently large.

Weights varying from 1/4 lb to 10 lb, dropped from heights up to 4 ft, were used in the present calibrations. Strain rates varied from 48.1 sec^{-1} to 195.0 sec^{-1} for the cylinders and from 62.3 sec^{-1} to 257.5 sec^{-1} for the spheres.

In almost all cases the two faces of the deformed specimens were not parallel, the extent to which the faces were not parallel varied. Micrometer measurements of deformations were taken across the centers of the two faces, and were reproducible to a high degree.

Rebounds of the weights were studied by motion pictures at a speed of 64 frames/sec and were found to be significant. As the energy availabe from the dropping weight just before impact (input energy) was increased,

there was a decrease in the percentage of that energy manifested in the rebound. About 3-1/2 percent of the input energy was manifested as rebound energy at the 1 ft-lb level, whereas at 34 ft-lb the rebound energy was but 1 percent. Cylinders gave about 10 percent greater rebound energy than spheres. Nevertheless, a correction for rebound was omitted from the energy versus deformation curves because the calibrating machine operates in a manner comparable to the gauges in which the copper crushers are used (momentum, Hilliar and ball-crusher gauges) and comparable rebounds probably occur in the gauges.

As in the earlier calibration studies, no definite speed effect was noted over the range of strain rates used.

The barreling effect (barreled rather than cylindrical shape of deformed cylinders which rough surfaces of anvil and piston will produce by constraining the motion of the cylinder faces) noted by Winslow and Bossey (High-Speed Compression Testing of Copper Crusher Cylinders and Spheres, II, Final Report, NDRC Report A-324 (OSRD-5039), p. 18) was noted in the present tests. It was most pronounced with large deformations of 0.1 in. or more. An examination of cylinders deformed by momentum and Hilliar gauges showed the same phenomenon. This indicates the need for maintaining smoothly finished surfaces on the anvils and pistons of all crusher-type gauges.

APPENDIX IX

Beam Brightening and Firing Synchronizer

This unit synchronizes the firing of the charge with the beam brightening for three separate groups of Dumont Oscilloscopes. It is used in conjunction with the rotating-drum camera drive on the schooner RELIANCE and enables location of the recorded shock pulse and calibrations at certain points on the camera film relative to the overlapping ends.

A master switch with the same positions as that in the master control panel* selects the operation desired. There is also one group delay switch for each of the three groups to determine the delay after firing of the respective group beam brightening pulses in terms of 180° rotations of the drive shaft.

The synchronizer consists of two sections, — the sequence brightening circuit (Fig. IX-1) controlling the beam brightening for the three separate groups, and the firing circuit (Fig. IX-2) controlling the firing of the charge.

The sequence brightening chassis contains a shaft driven by the rotating-drum drive, on which four cams rotate. Two of these cams (0° and 180° cams in Fig. IX-1) are constructed to ground a contact to the drive shaft over 10° of a revolution and are oriented 180° apart; a third (firing cam in Fig. IX-2) closes a contact over 10°; and the fourth insures a good continuous ground contact to the drive shaft. For use up to the present the 0° and firing cams have been aligned.

The brightening circuit contains a train of Type 2050 thyratrons, in which each, with the exception of the first, requires the previous one to be ignited before it can be tripped. This is obtained by making the positive rise on ignition across the cathode resistor of the preceding 2050 decrease the bias of the second grid of the 2050 in question, so that subsequent grounding of its first grid will trip it. The first 2050 is tripped in Q cal or V cal position by grounding its first grid through the shot switch (knife switch on panel) or in fire position by a positive pulse from the firing circuit. This sets the second 2050 so that it fires the next time its first grid is grounded by the 0° cam. The first grids of 2050's in the train after the initial 2050 are connected alternately to the 0° and 180° cams, so that the 2050's trip in sequence 180° apart as their grids are grounded. In this way, step pulses 180° apart over a range of 0° to 720° rotation from the origin may be obtained across the 2 K resistors in the 2050 cathodes.

The group delay switches, one for each group of oscilloscopes controlled, select two step pulses of desired delay and separation. These are applied to opposite grids of a cathode inverter stage, producing on one plate a beam brightening pulse of the selected delay and duration equal to the separation of the original pulse.

---

*See Section 7(ci).

The switches are arranged to give delays up to 360° although addition of more Type 2050 thyratrons in the train could extend this. The brightening duration for any delay setting is 360° for the FIRE position of the master switch, while the Q CAL positic gives brightening for the first 180° after the selected delay, and the V CAL position gives brightening for the second 180°. In this way, the Q CAL step will be conveniently located on the first half of the record film and the V CAL step on the second half.

The pulse to trip the stepper* for Q- and V-step calibrations is taken from the brightening output of the first group.

Manual brightening is produced by applying a step pulse through a microswitch on a cable to one of the inverter grids. The duration of the brightening is controlled by the time the switch is held closed.

The Type 2050 thyratrons must be reset after each operation by opening the B+ lead through the RESET microswitch which is connected by cable for convenience. Ignition of the RESET neon bulb indicates that the 2050's are reset.

The firing circuit utilizes a Sylvania type SN4 Strobotron which, when triggered, discharges 160 μf at 250 v through the firing line and charge. A transformer in series with the firing line produces a pulse at the time of firing for initiating the sequence brightening action.

The SN4 is triggered by a 2050 thyratron whose firing is controlled by the shot switch and firing cam. Normally the two grids are biased below firing potential; closing the shot switch connects the second grid to the cathode, so that the next time the firing cam shorts the first grid to the cathode, the tube will fire. The plate lead of the 2050 is run through the master switch so that the tube can fire only in FIRE position.

The firing circuit is completely insulated from the other equipment; experience has shown that serious pickup and ground loops can arise if this is not observed.

---

*See Section 7(c,iii).

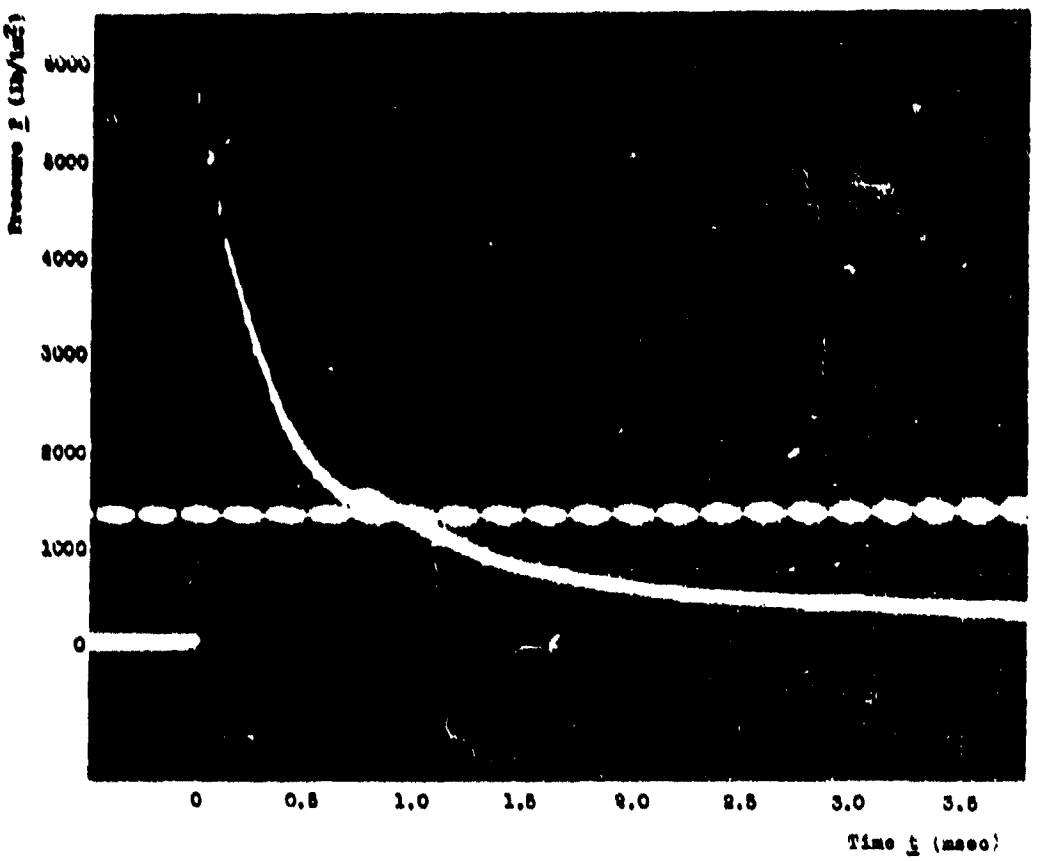
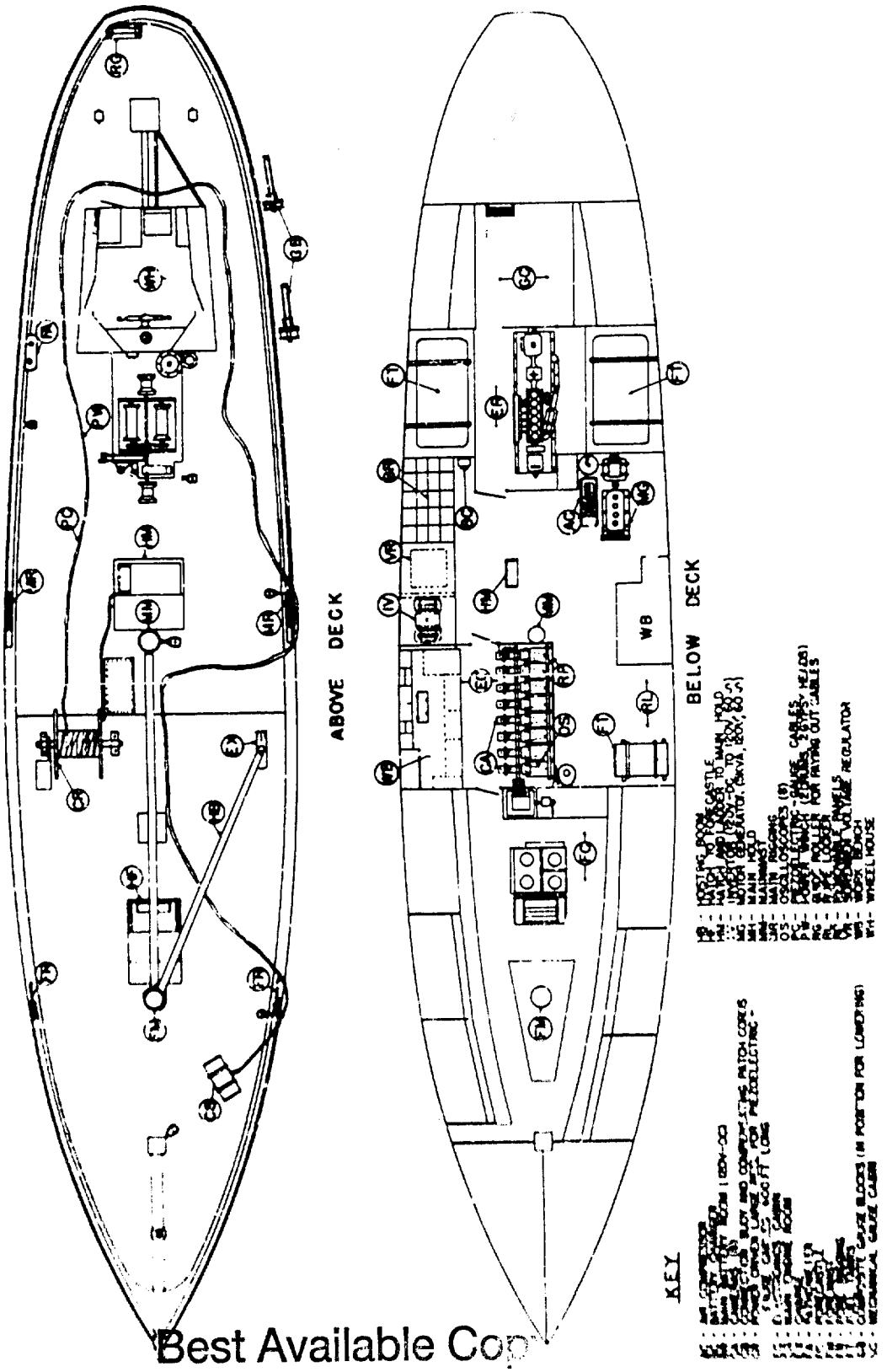


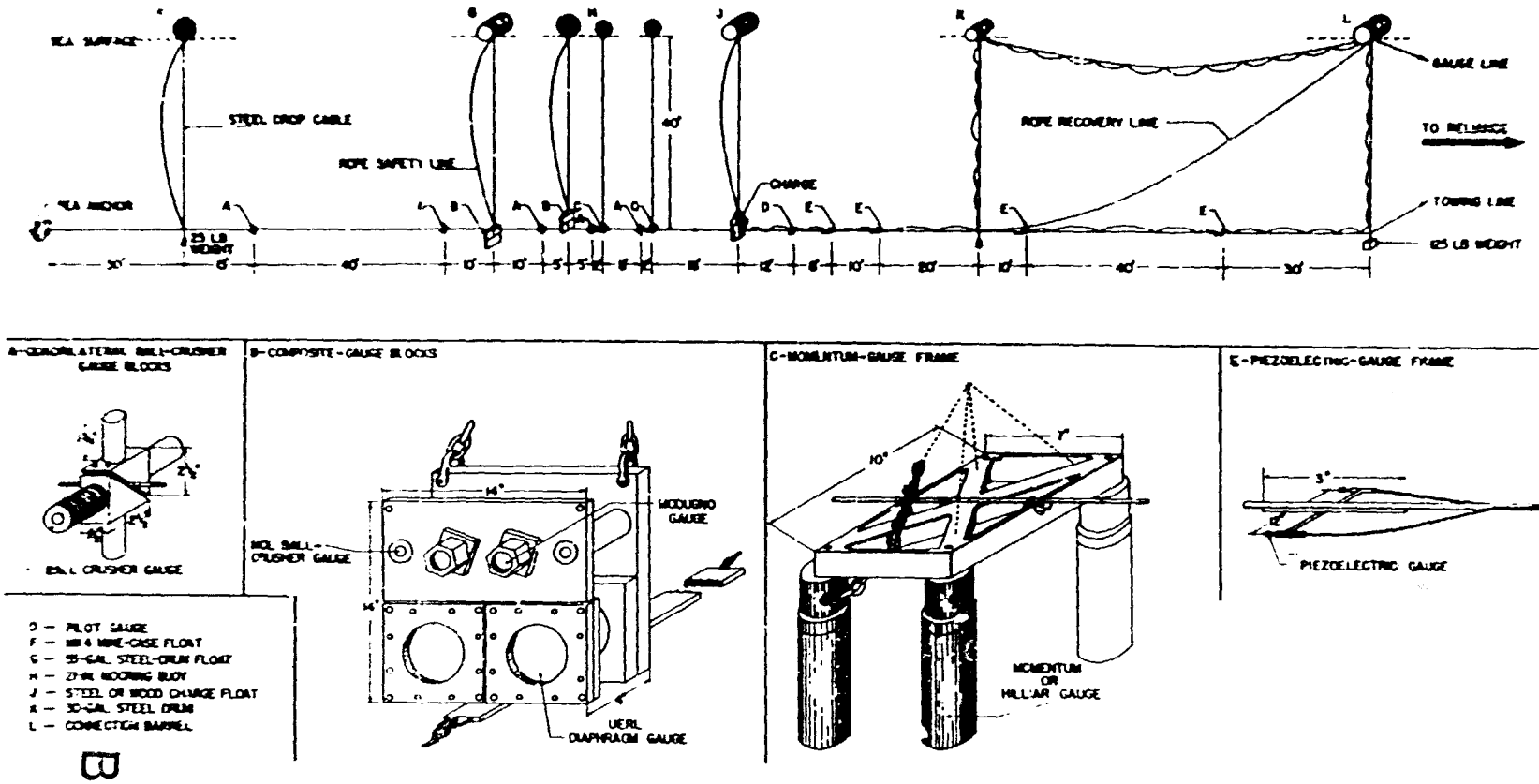
Fig. 1. The pressure-time curve from an underwater explosion.
Gauge 20 ft from charge. Timing frequency 5 kc/sec.
(Shot RE-111, film R-306.)

This is a photographic projection of an actual piezoelectric-gauge record. Note the base line at the left before the shock wave reaches the gauge, the instantaneous pressure rise to the "peak pressure", and the gradual decay of pressure with increasing time. The row of dots is the record of the time calibration and also serves to align the curve with respect to the axes.



Best Available Cop

FIG. 2. PLAN OF SCHOONER RELIANCE.



MODIFICATION D

FIG. 3. "ONE DIMENSIONAL" FORE AND AFT RIG USED FOR RELIANCE TESTS.

Best Available Copy

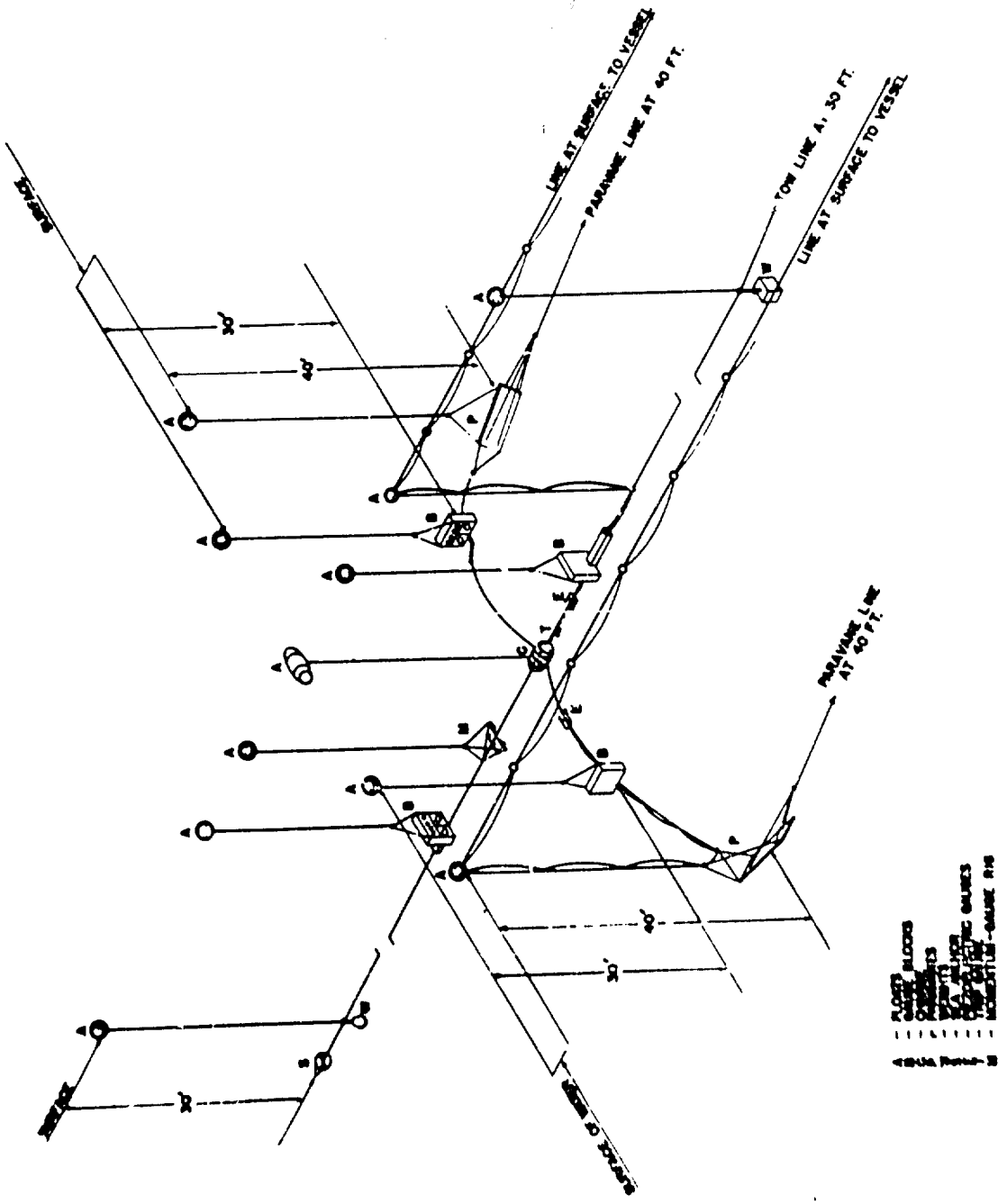
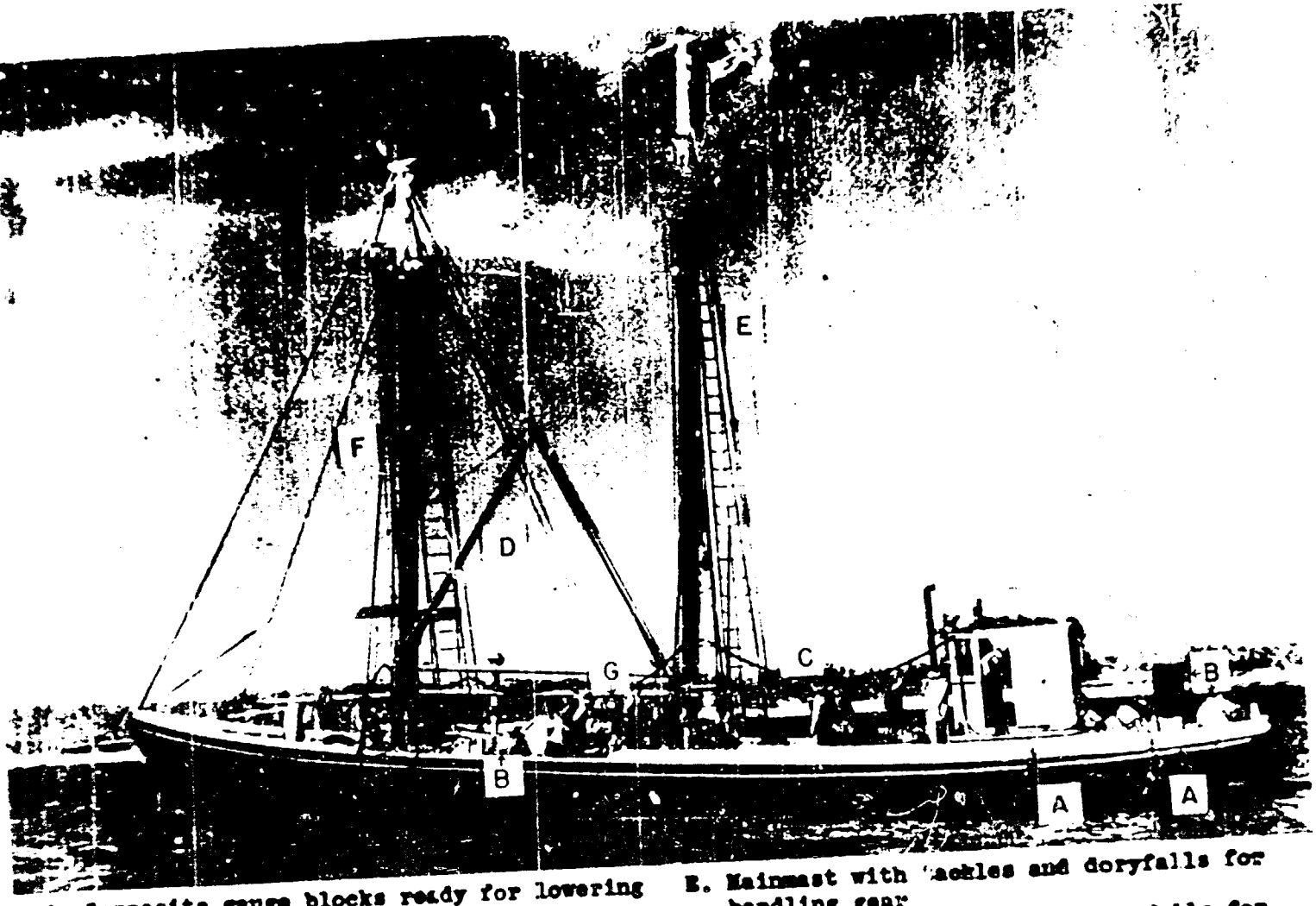


FIG. 4. THE "TWO-DIMENSIONAL" PARAVANE RIG.

Best Available Copy



A. Composite gauge blocks ready for lowering
B. Surface buoys
C. Piezoelectric gauge cables between connection buoy and large reel
D. Hoisting boom for lifting charge overboard
E. Mainmast with tackles and doryfalls for handling gear
F. Foremast with tackles and doryfalls for handling gear
G. Large reel for piezoelectric gauge cables

Fig. 5. Port side view of Reliance and gear.

Best Available Co

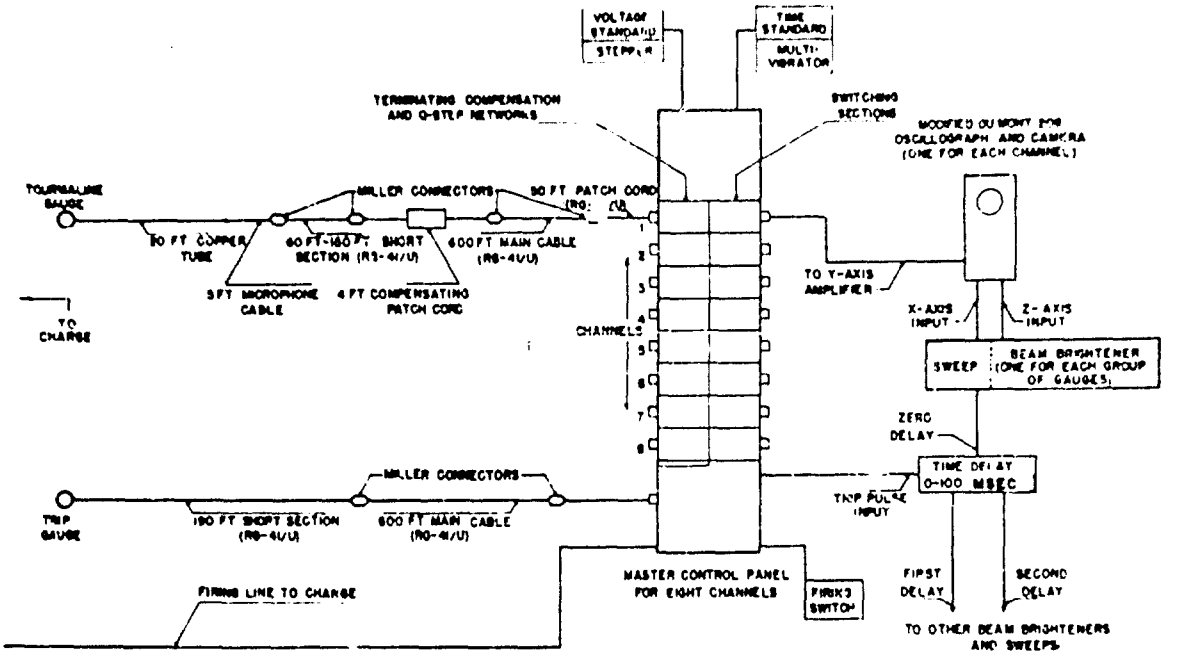
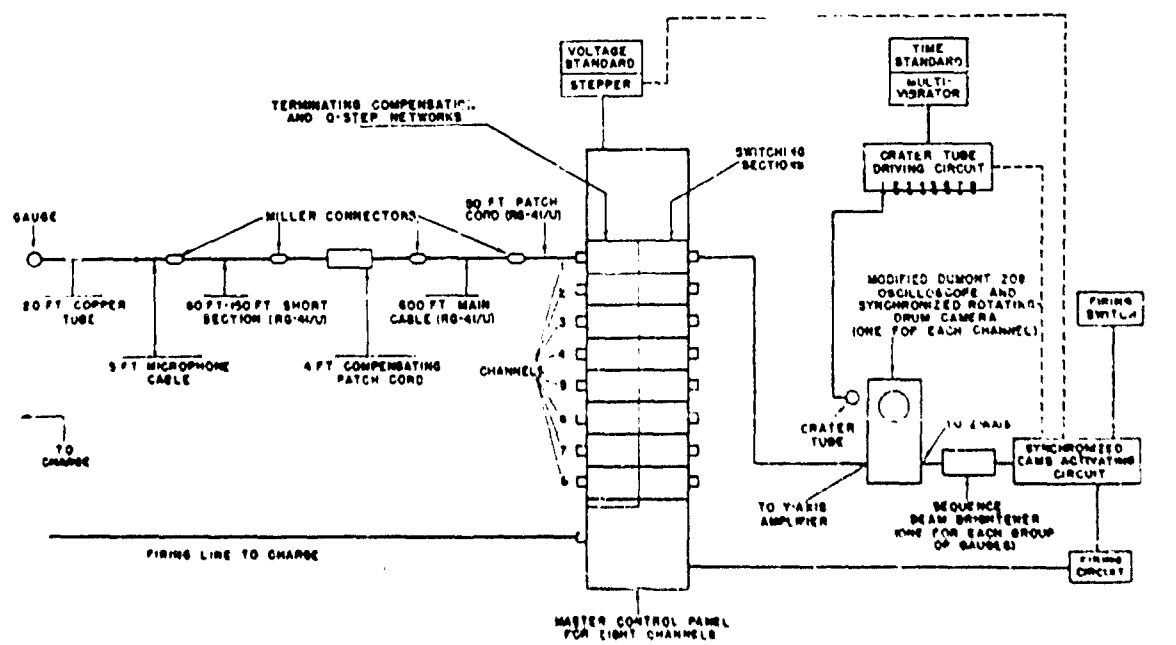


FIG. 6. BLOCK DIAGRAM OF COMPLETE PIEZOELECTRIC-GAUGE CHANNEL USING AN ELECTRONIC SWEEP AND STILL-FILM CAMERA.



Best Available Copy

FIG. 7. BLOCK DIAGRAM OF A COMPLETE PIEZOELECTRIC-GAUGE CHANNEL USING THE SYNCHRONIZED CAM-SEQUENCE ACTIVATOR AND ROTATING-DRUM CAMERA.

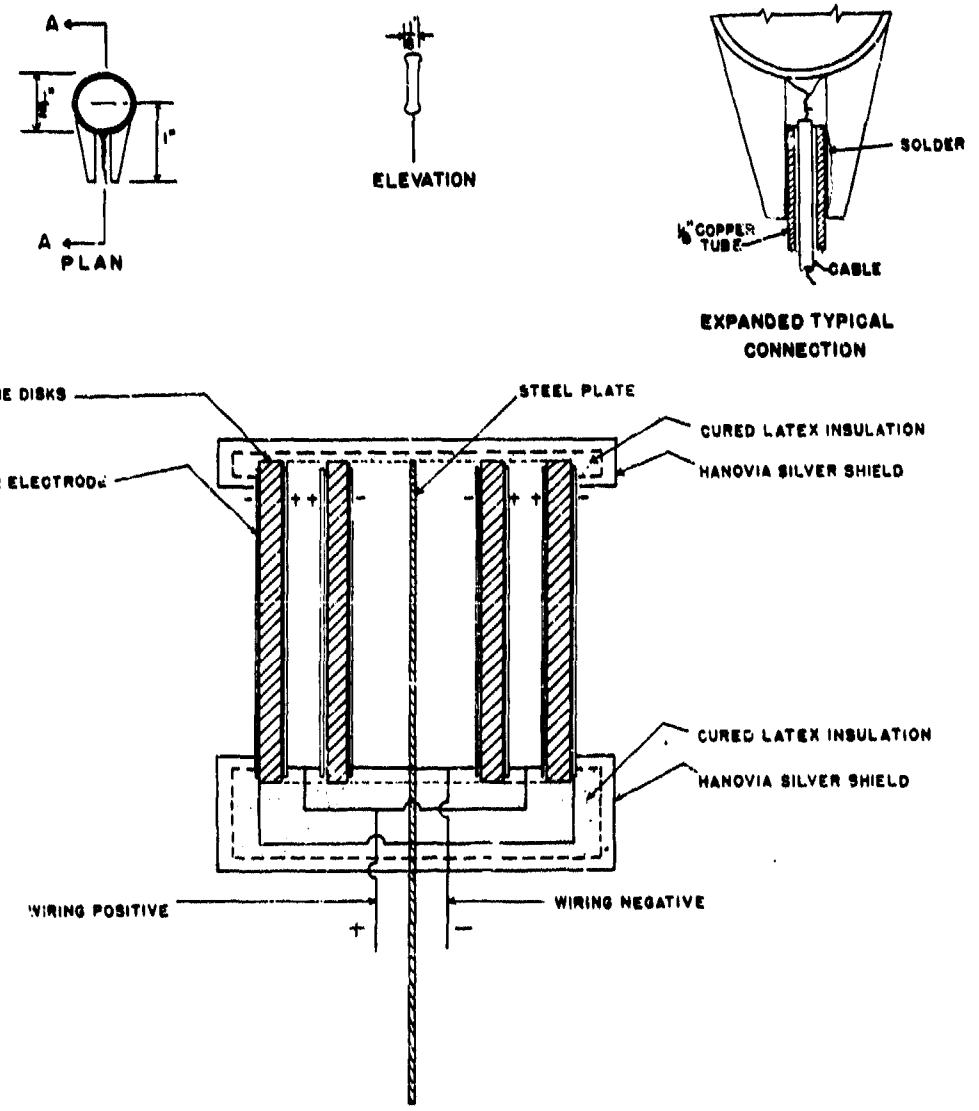
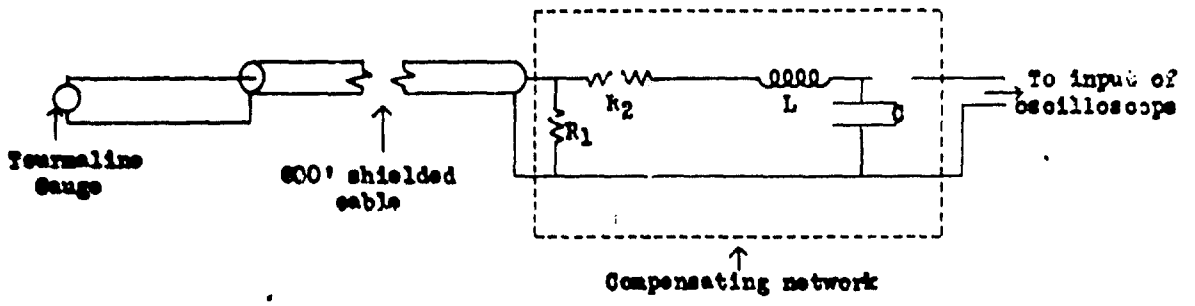


FIG. 8 DETAILS OF A PIEZOELECTRIC GAUGE (TYPE B).



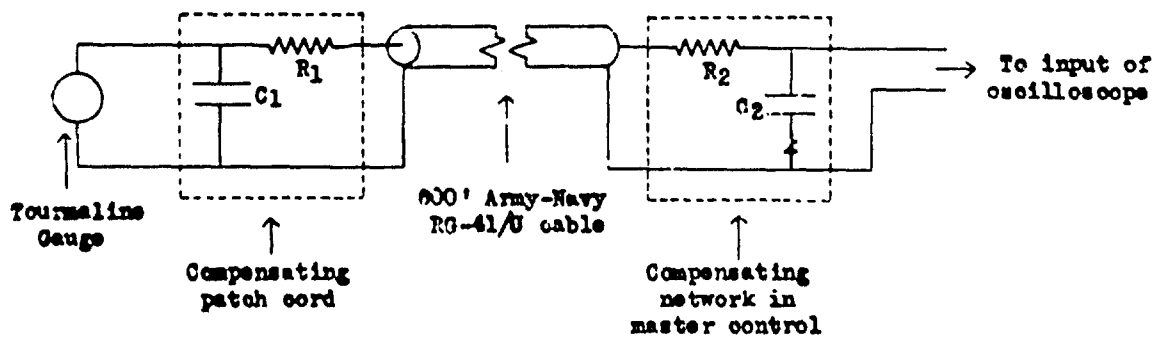
R_1 = 20 megohms resistor

R_2 = 100 ohms resistor

L = Inductance of 35 turns of #28 wire on $\frac{1}{2}$" coil

C = 0.05 μf capacitance

Fig. 9. Single-ended cable compensating network.



R_1 = 97 ohms resistor

R_2 = 56 ohms resistor

C_1 = C_2 = 15,300 $\mu\mu$f

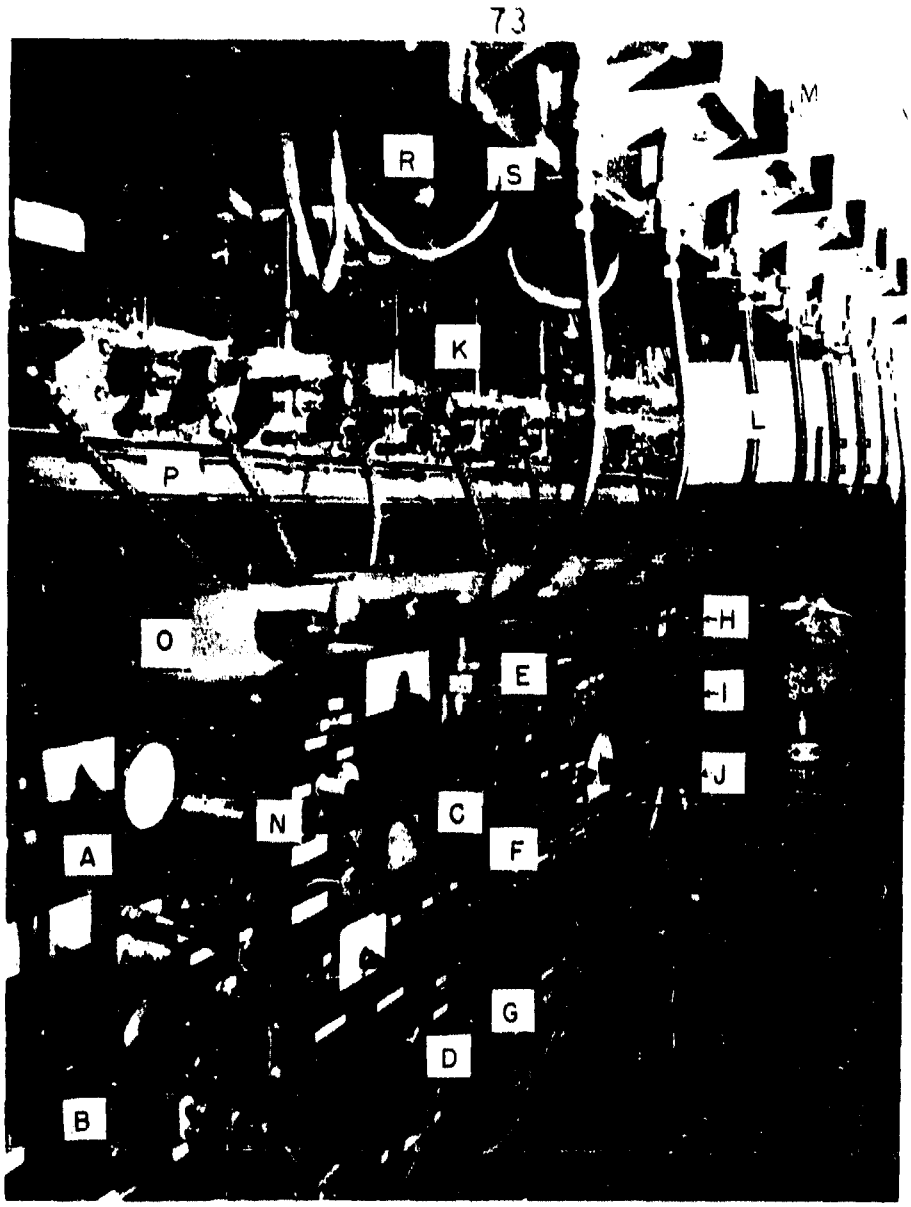
x = Point at which voltage step is applied when using the Q-step calibration [see Section 7 (c)(v)].

Fig. 10. Double-ended cable compensating network.

Best Available Copy

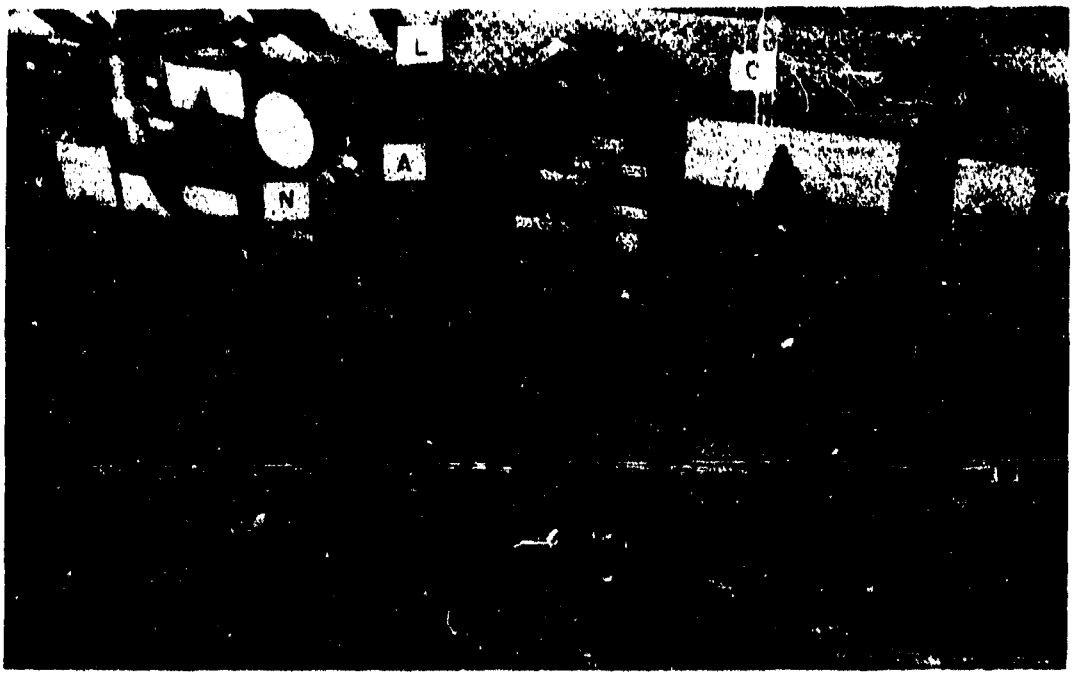
Fig. 11. Construction detail of compensating patch cord.

Best Available Copy



A. Sequence beam brightener, synchronising control cams, and tachometer
B. Capacity bridge
C. Master control
D. Crater (timing) tube power
E. Multivibrator frequency (timing) source
F. Voltage stepper
G. Sweep generator
H. Sweep generator
I. Time delay
J. Battery operated L-C oscillator
K. Modified Dumont 208 cathode-ray oscillograph
L. Flexible drive shaft to rotating-drum camera
M. Rotating-drum camera
N. Flexible drive shaft to control cams and tachometer
O. Main drive shaft and gear housing
P. Air duct for forced ventilation of oscillographs
R. Camera tube
S. Crater-tube connection

Fig. 12. Cathode-ray oscillographs and associated equipment for rotating-drum camera recording.



A. Sequence beam brightener, synchronising control cams, and tachometer
B. Capacitance bridge
C. Master control
D. Crater (timing) tube power
L. Flexible drive shaft to rotating-drum camera
N. Flexible drive shaft to control cams and tachometer
O. Main drive shaft and gear housing

Fig. 13. Master control panels, sequence brightener and firing control, crater-tube power, and capacitance bridge.

C. Master control
E. Multivibrator-frequency (timing) source
H. Sweep generator
K. Modified Dumont 208 cathode-ray oscillograph
L. Flexible drive shaft to rotating-drum camera
M. Rotating-drum camera
O. Main drive shaft and gear housing
P. Air duct for forced ventilation of oscillographs
Q. Intercom to wheel house, etc.
R. Camera tube
S. Crater-tube connection

Fig. 14. Synchronized rotating-drum cameras and drive.

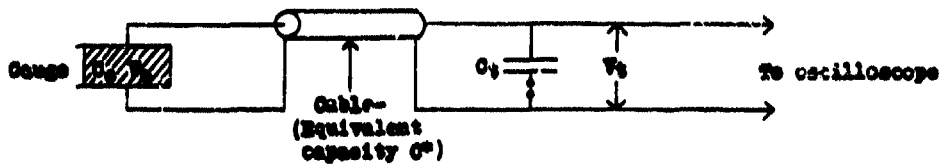
Best Available Co



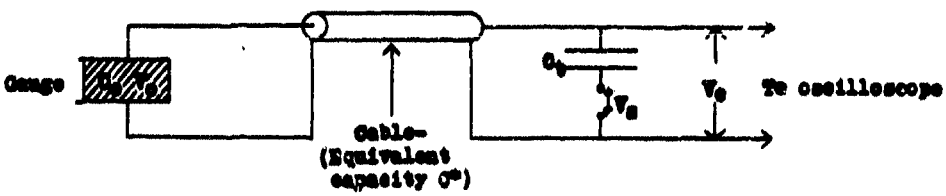


A. Voltage-calibration input
B. Pilot-gauge input
C. Stepper-trip input
D. Input for time calibration from multivibrator
E. Sweep-trip output
F. Patch cord to beam-brightener power supply
G. Outlet strips - 115 v regulated a.c.
H. Exhaust blower
I. Master control inputs from 600 ft sections
J. Master control outputs to scopes

Fig. 15. Back view of master control panel showing patch-cord connections.

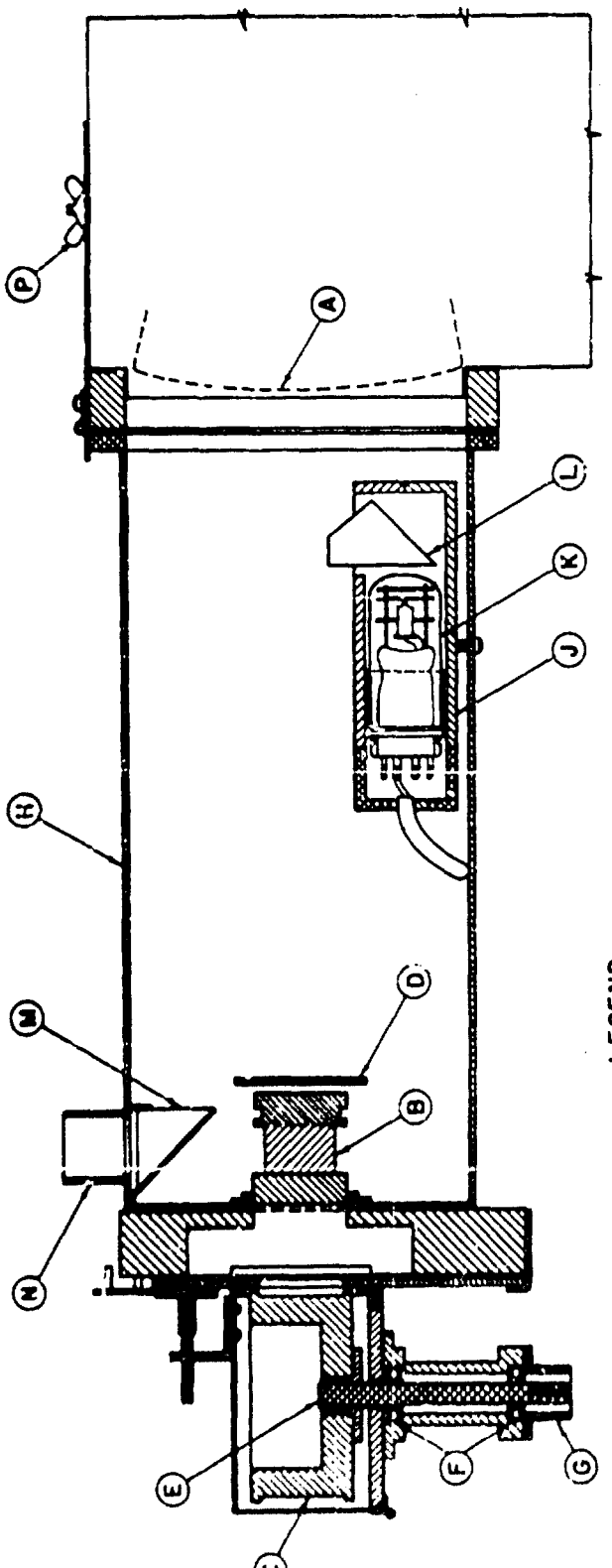


(a) CONNECTION FOR RECORDING SIGNALS.



(b) CONNECTION FOR CALIBRATING CABLE AND INDICATING INSTRUMENTS.

FIG. 16. Q-STEP CALIBRATION NETWORK.

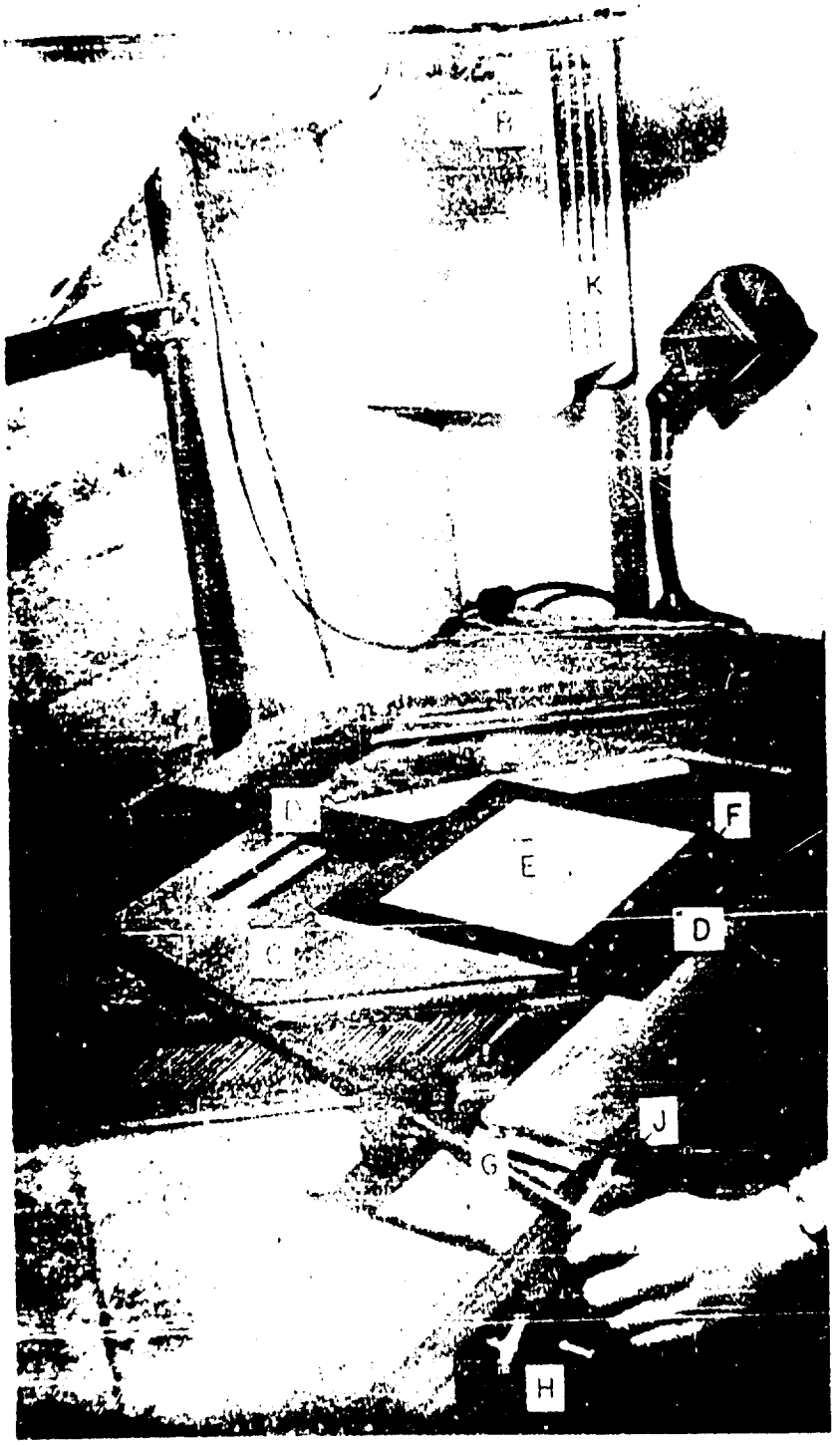


LEGEND

A - CATHODE-RAY TUBE SCREEN
B - f/2.0, 50 mm. LENS
C - CAMERA DRUM
D - MECHANICAL SHUTTER (FLAP TYPE)
E - CAMERA-DRUM SHAFT
F - BALL BEARINGS
G - COUPLING FOR FLEXIBLE SHAFT
H - CAMERA TUBE HOUSING
J - CRATER-TUBE R-1130B
K - CRATER TUBE PRISM
L - CRATER-TUBE PRISM
M - VIEWING AND IDENTIFICATION PROJECTION PRISM
N - VIEWING AND IDENTIFICATION PROJECTION TUBE
P - CAMERA-TUBE CLAMP TO SCOPE

FIG. 17. CRATER (TIMING)-TUBE MOUNTING AND ROTATING-DRUM CAMERA.

Best Available Copy



A. Projector
B. Projector lens
C. Adjustable horizontal grid
D. Fixed vertical grid
E. Platen for photographic paper
F. Slot and set screw for adjusting angle between horizontal and vertical grid lines
G. Spacing control for horizontal grid
H. X-axis displacement control
J. Y-axis displacement control
K. Extra fixed vertical grids with other spacings

...e "Warp".

Best Available Copy

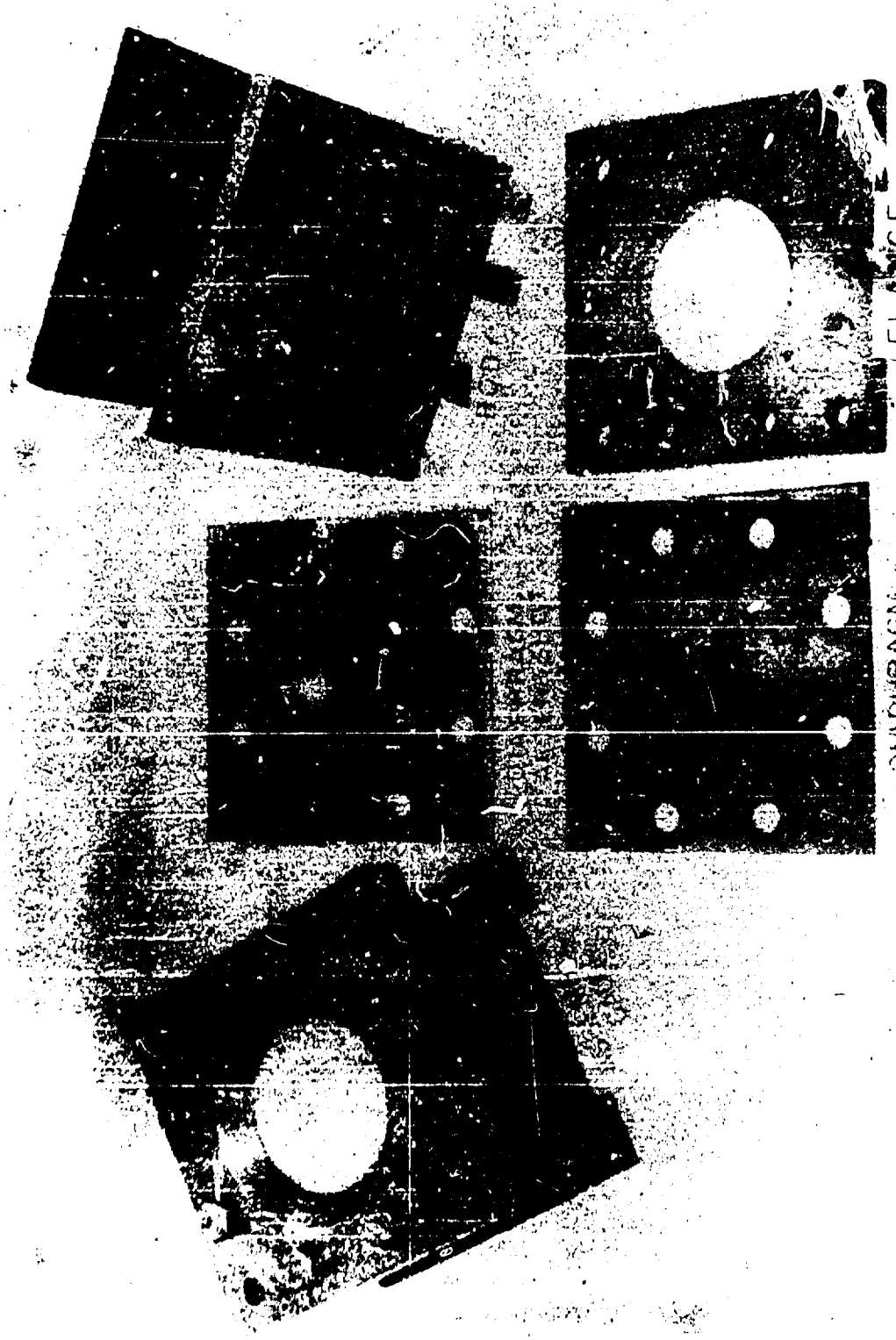


Fig. 19. The UHL diaphragm [illegible].

Best Available C

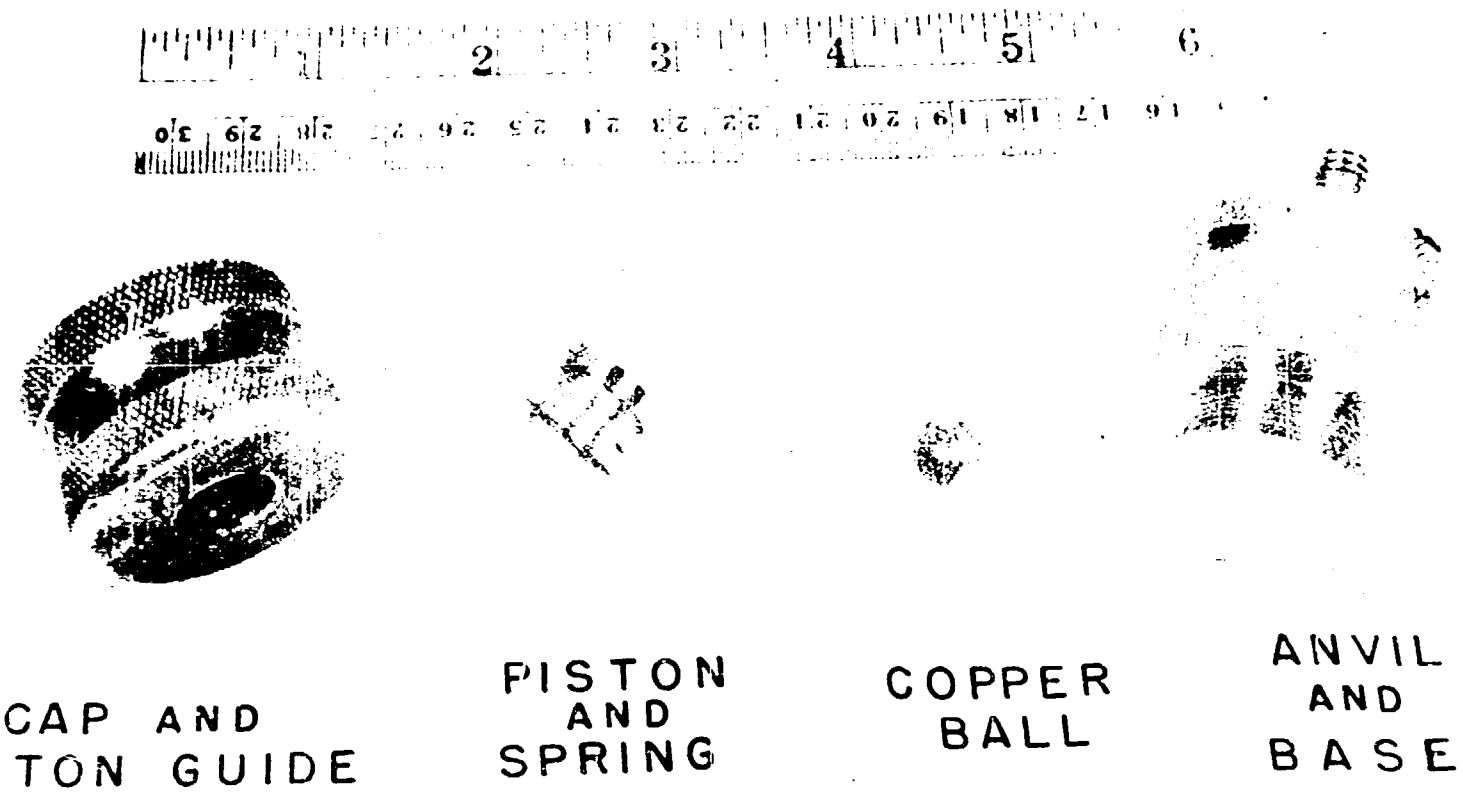


Fig. 20. The Naval Ordnance Laboratory ball-crusher gauge. (Spacer ring and centering washer not shown.)

781

Best Available Copy

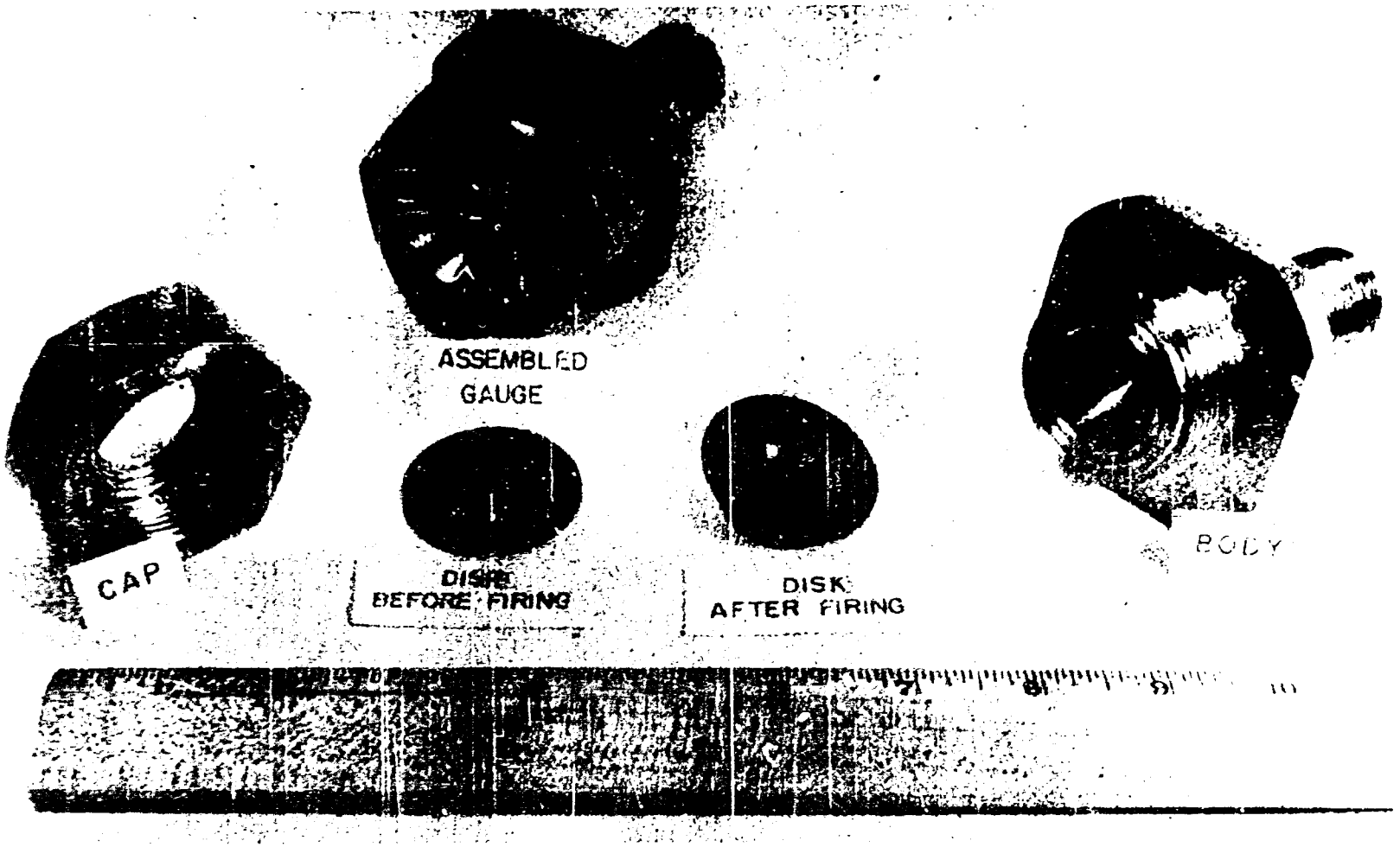


Fig. 21. The Bureau of Ships Mechgmo gauge.

Best Available Co

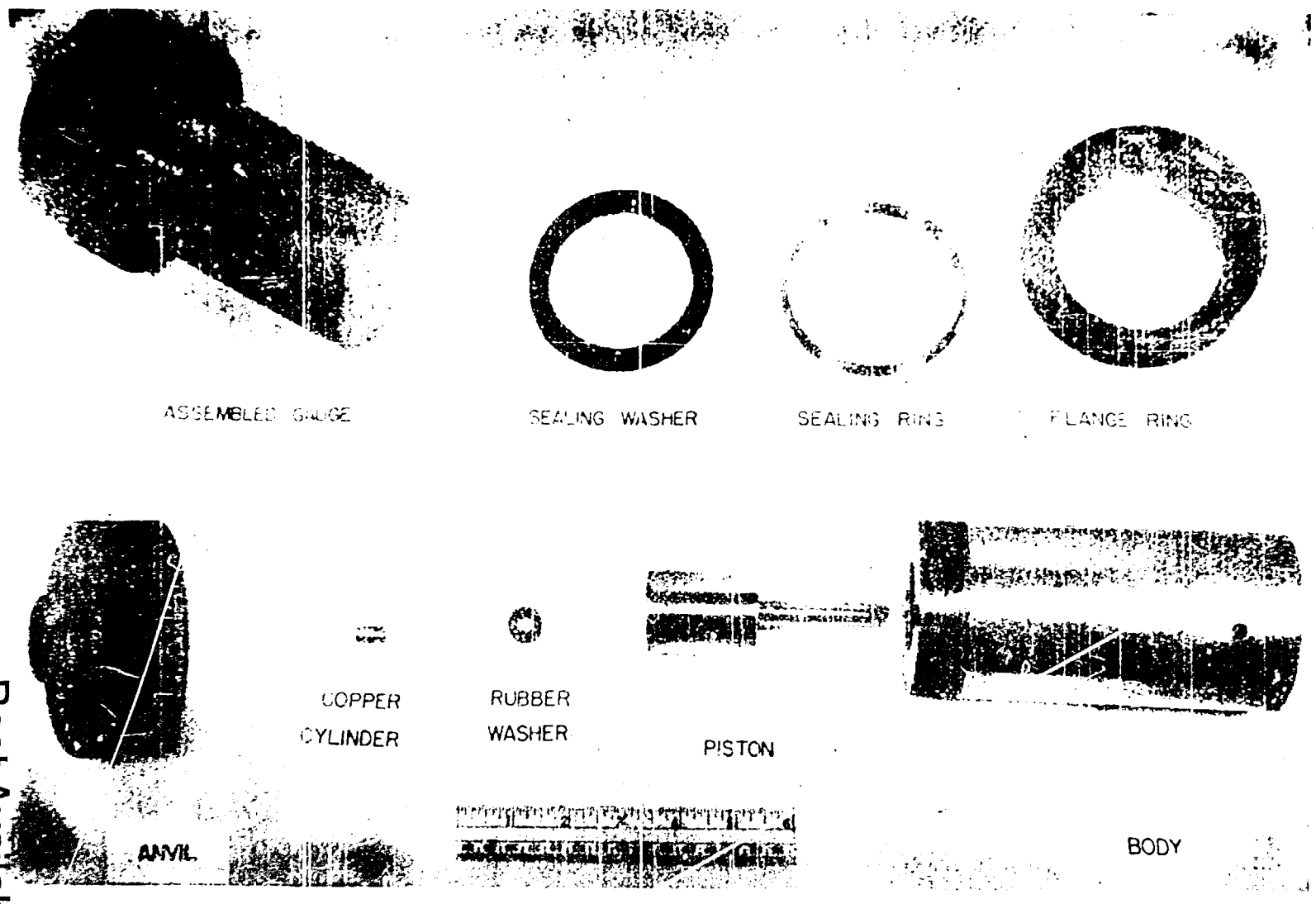


Fig. 22. Hartmann momentum gauge.

Best Available Copy



Fig. 23. The improved Hillier gauge, Mark 2. (3/8-in. copper ball and piston comprising ball-crusher gauge for central hole not shown.)

Best Available Copy

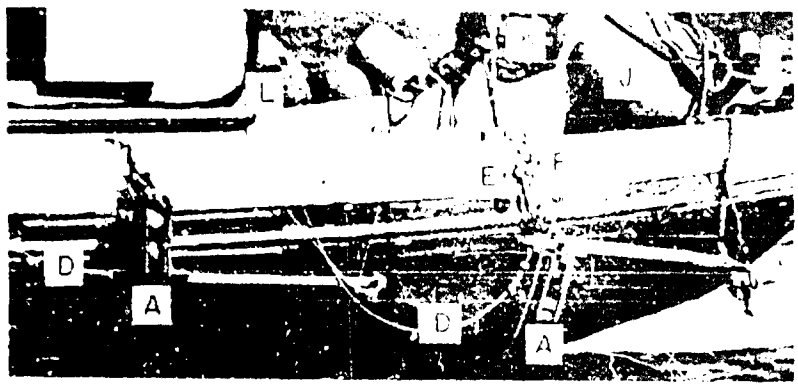


Fig. 24. Gauge blocks ready for lowering.

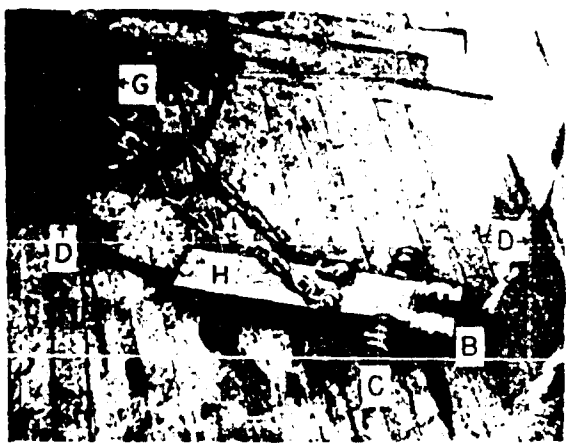


Fig. 25. Twenty-two lb side-on vs. face-on ball crusher gauge mount.

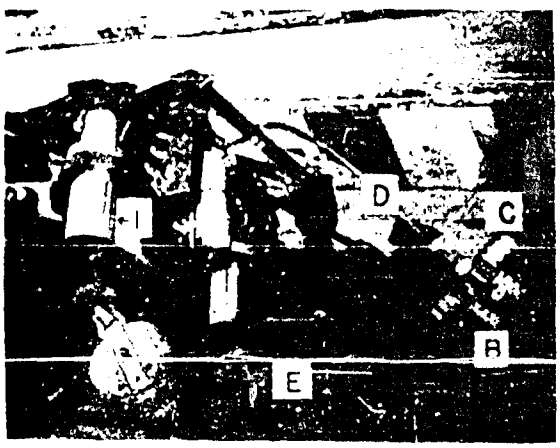
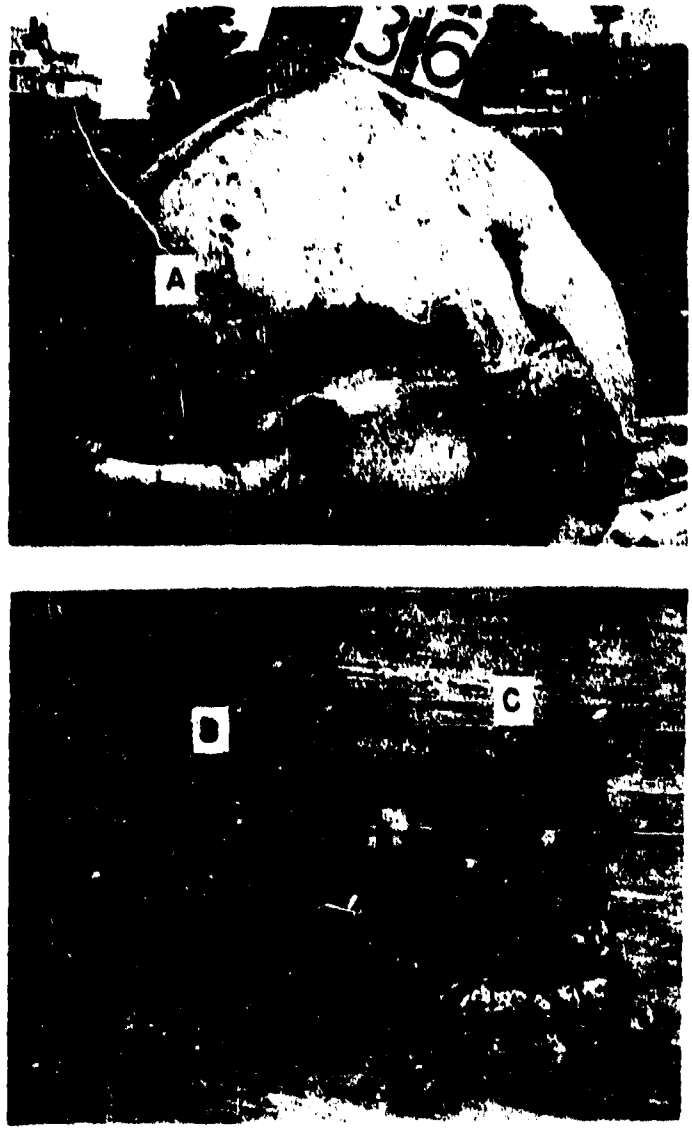


Fig. 26. Momentum gauge mount and 5 lb side-on vs. face-on ball crusher gauge mount.

A. Composite gauge blocks
B. Face-on ball crusher gauge
C. Side-on ball crusher gauge
D. Wire rope spacer line
E. Manilla snubber and safety recovery line to surface floats
F. Wire rope drop line to surface floats
G. Manilla drop line to surface floats
H. Small 22 lb face-on vs. side-on gauge mount (Section 13 (c)(iii))
I. Hartmann momentum gauge
J. Sea anchor buoy
K. Composite gauge block buoy
L. 14 in. buoy for electric cables

Best Available Copy



A. Mark 4 mine case after several shots
B. 30 gal oil drum, slightly damaged
C. 30 gal oil drum, severely damaged after the explosion of 700 lbs TNT 40 ft below surface and at a horizontal distance of 30 ft

Fig. 37. Surface floats showing typical damage.

Available Copy

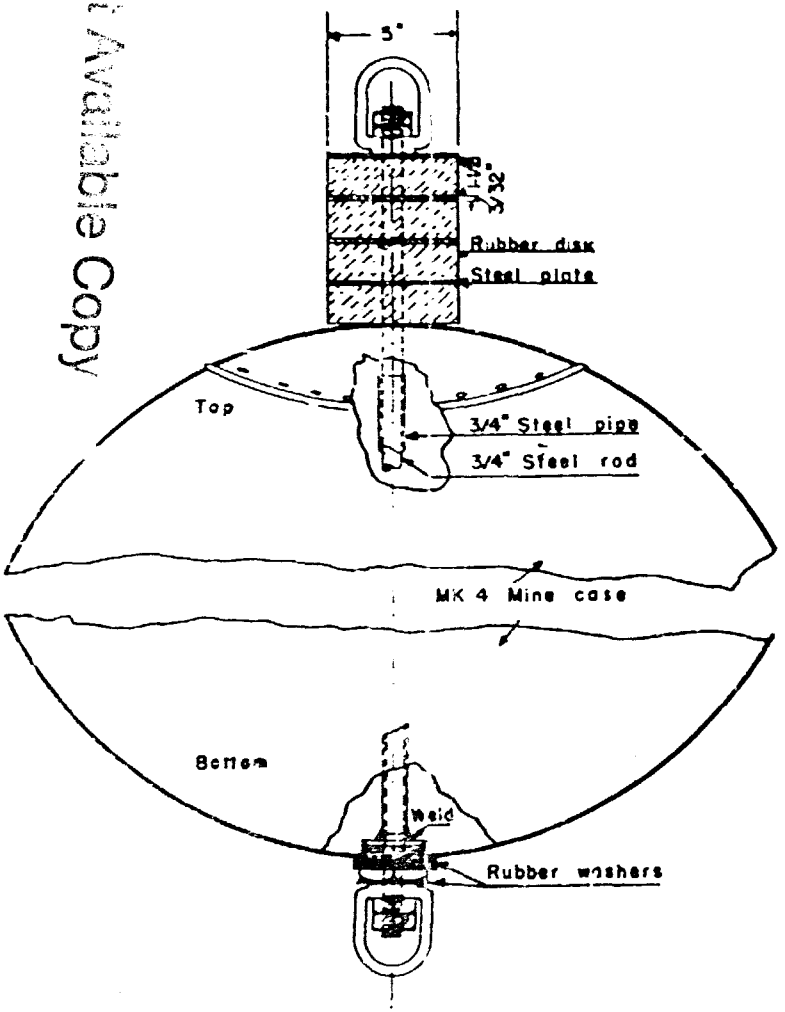


Fig 28a. Mark 4 mine case modifed to place load on top, with shock absorber.

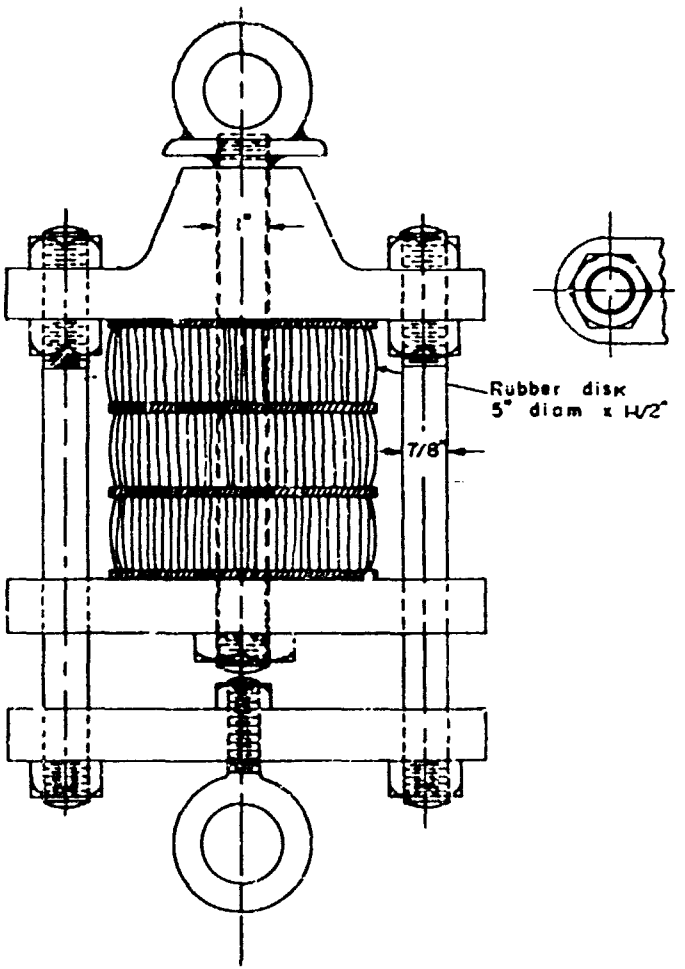


Fig 28b. Shock absorber for independant suspension.

Fig 28. Shock absorber connections for surface floats.

7187

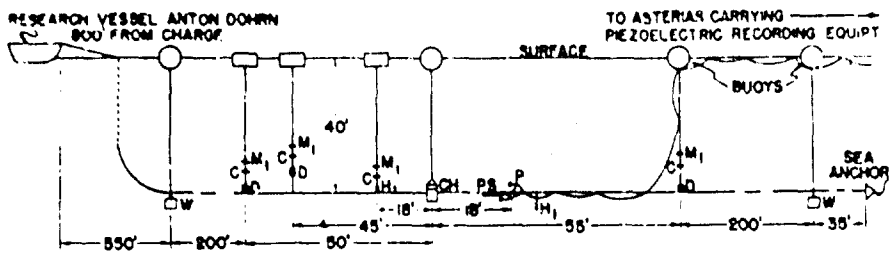


FIG. 29a. MODIFICATION A (PRE-RELIANCE)

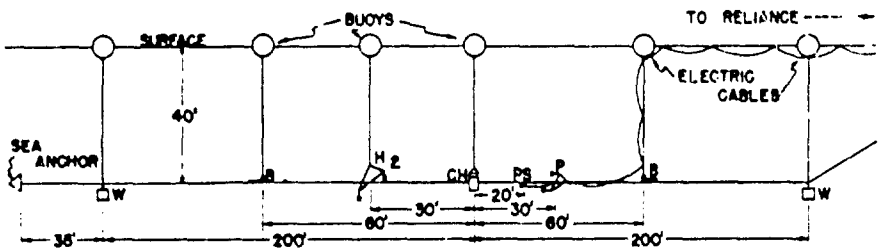


FIG. 29b. MODIFICATION B

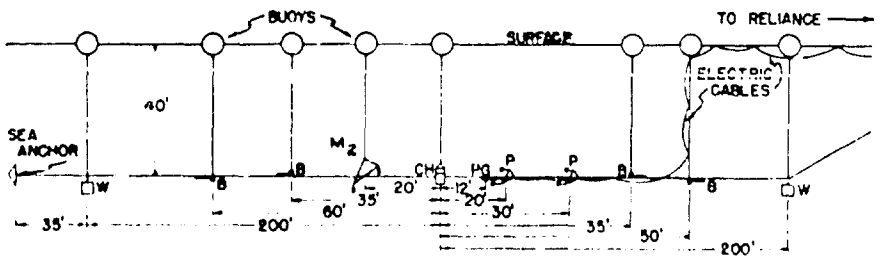


FIG. 29c. MODIFICATION C

LEGEND

B COMPOSITE GAUGE BLOCK [SEE FIG. 3B, AND SEC 13(a)]
C BALL-CRUSHER GAUGE, SUSPENDED FREE, FACE DOWN
CH CHARGE
D DIAPHRAGM GAUGES
H_1 HILLIAR GAUGE, SUSPENDED FREE, FACE DOWN
H_2 IMPROVED HILLIAR GAUGE
M_1 MODUGNO GAUGE, SUSPENDED FREE, FACE DOWN
M_2 HARTMANN MOMENTUM GAUGES
P PIEZOELECTRIC GAUGES
PJ PILOT GAUGE FOR TRIPPING
PS PRESSURE SWITCH (FOR TRIPPING)
W 200-LB WEIGHTS

Best Available Co

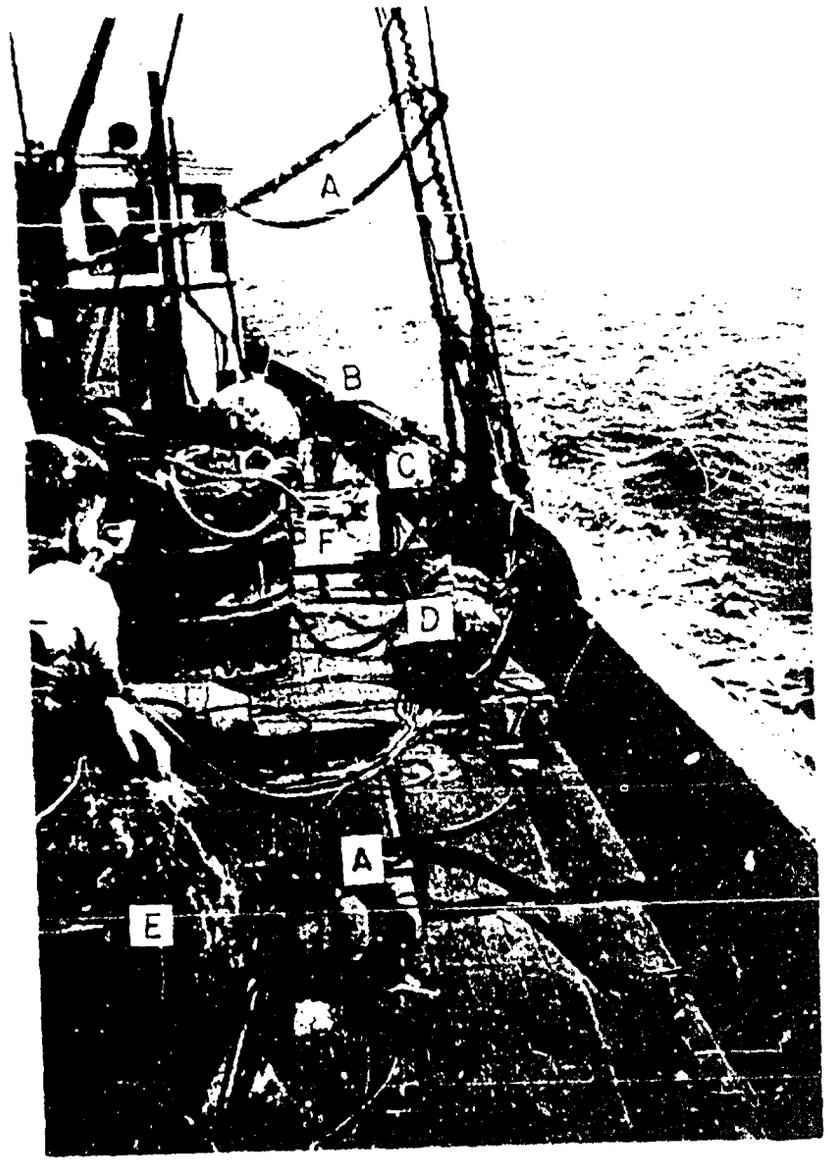
FIG. 29. "ONE-DIMENSIONAL" FORE-AND-AFT RIG.



A. Cables leading to connecting buoy
B. 50 ft patch cords leading to electronics cabin
C. Miller connectors for 8 piezoelectric gauge channels
D. Miller connector for pilot gauge channel
E. Jack and shorting switch for firing line (Note provision for locking safety cover over jack and switch.)

Fig. 30. Large power driven reel for piezoelectric gauge [illegible] ft sections).

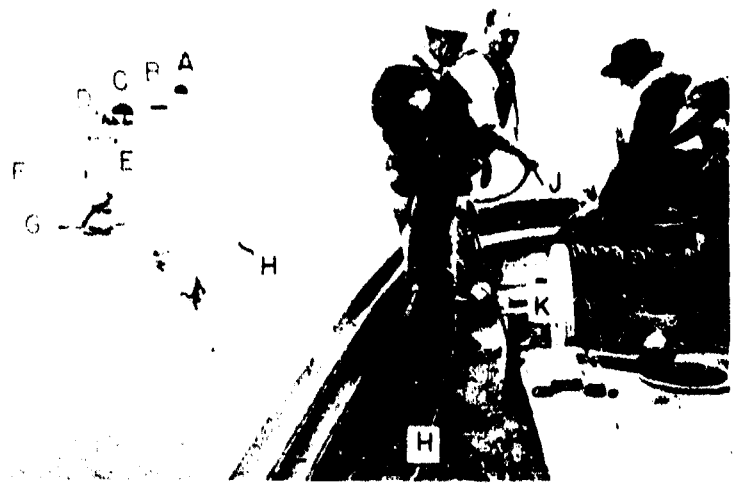
Best Available Copy



A. Piezoelectric gauge cables (600 ft section) leading to big reel
B. Composite gauge block
C. Momentum gauge frames
D. Charge
E. Surface float
F. Quadrilateral ball crusher gauge block

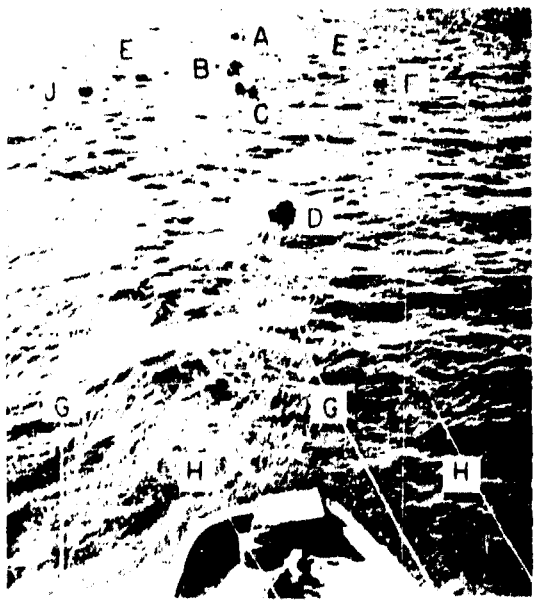
Best Available Copy

Fig. 31. Gear ("one dimensional" - modification C) laid out on deck ready for setting, looking toward stern.



A. Sea anchor buoy
B. Buoy for stern composite gauge block
C. Buoy for stern composite gauge block
D. Momentum gauge buoy
E. Charge buoy
F. Forward gauge block buoy
G. Forward gauge block and electric cable connection buoy
H. Manilla line supporting piezoelectric gauge cables
J. Piezoelectric cables (600 ft section)
K. Small reel for piezoelectric cables

Fig. 32. "One dimensional" gear (modification C) astern of Reliance.



A. Sea anchor buoy
B. Stern gauge block and connection buoy
C. Forward gauge block and connection buoy
D. Lead weight buoy
E. Side gauge block buoys
F. Port paravane buoy
G. Piezoelectric gauge cables
H. Steel towing cables for paravanes
J. Starboard paravane and connection buoy

Fig. 33. "Two dimensional" (paravane) gear astern of Reliance.

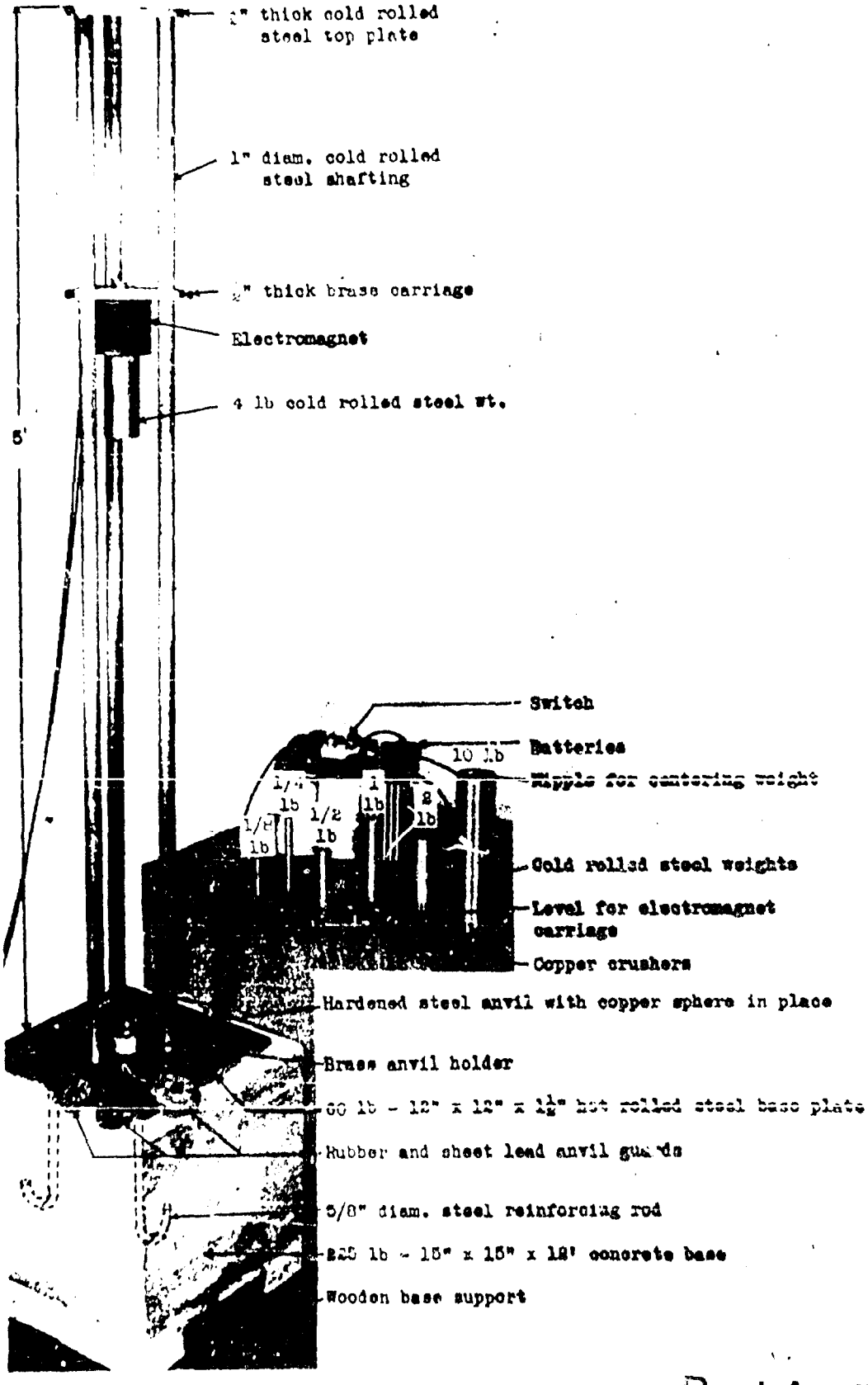


Fig. VII-1. Copper crusher calibration machine.

Best Available Copy

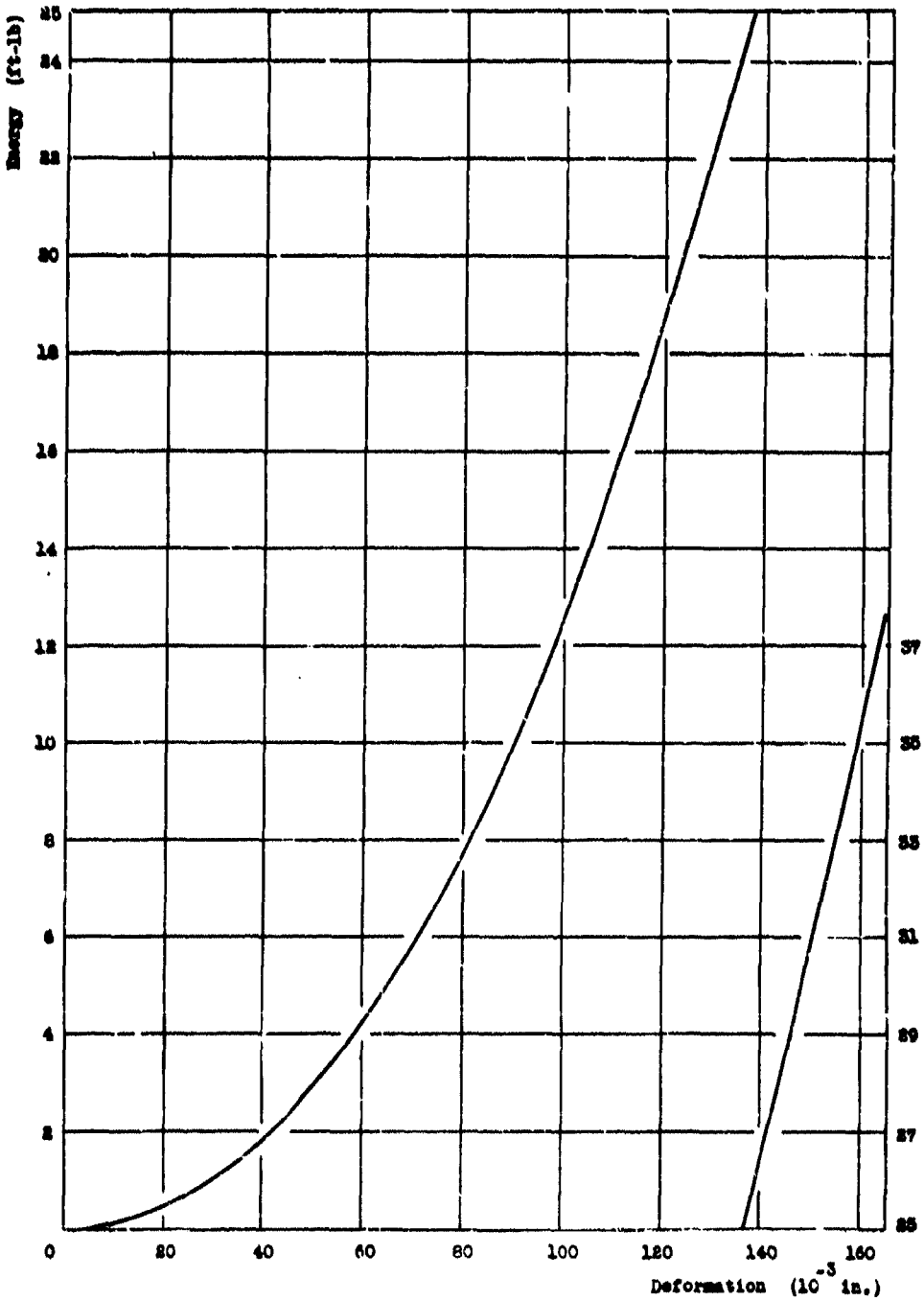


Fig. VII-2. Dynamic calibration of 0.3745-in. diameter copper spheres with freely falling weights.

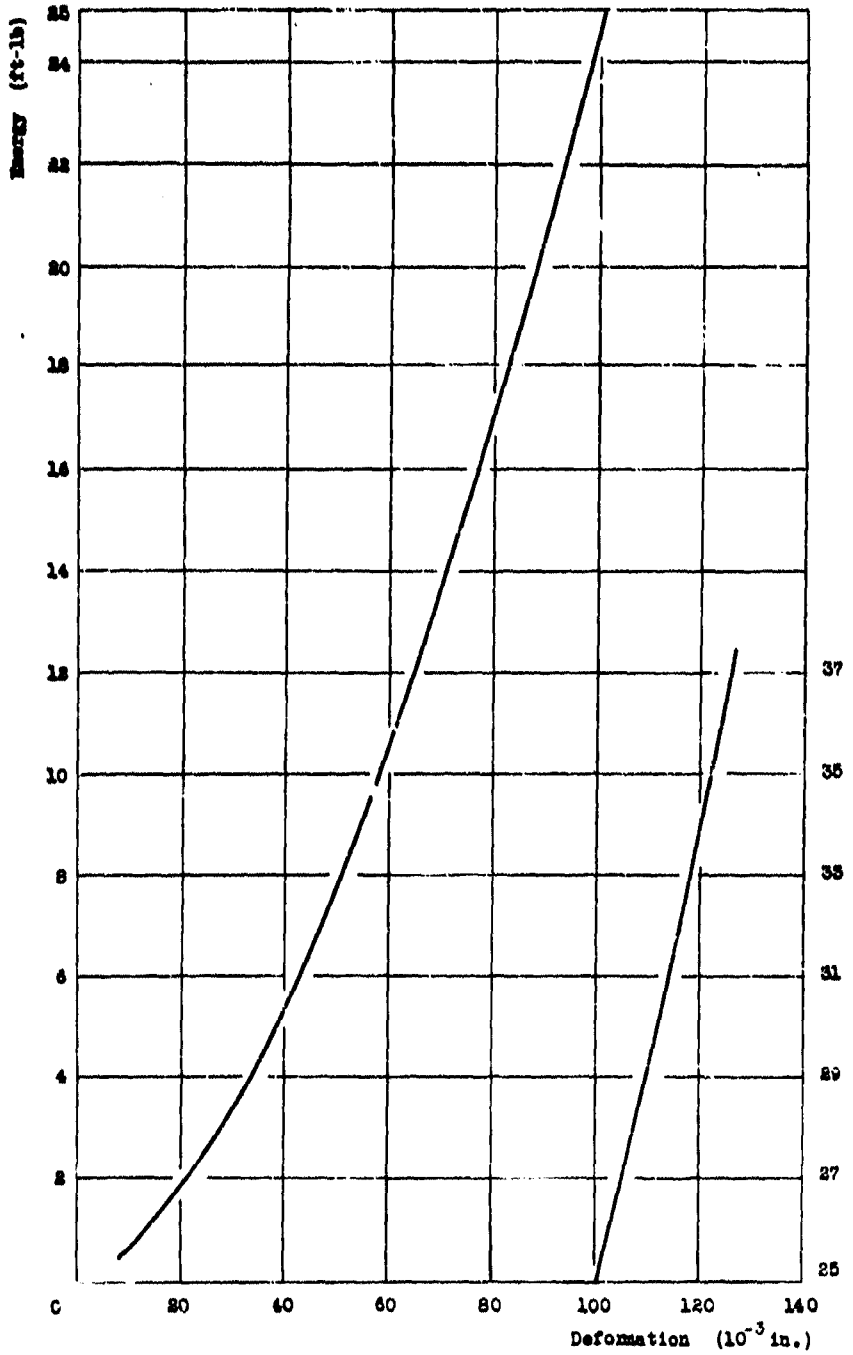


Fig. VII-3. Dynamic calibration of 0.5000-in. length, 0.3255-in. diameter copper cylinders with freely falling weights.

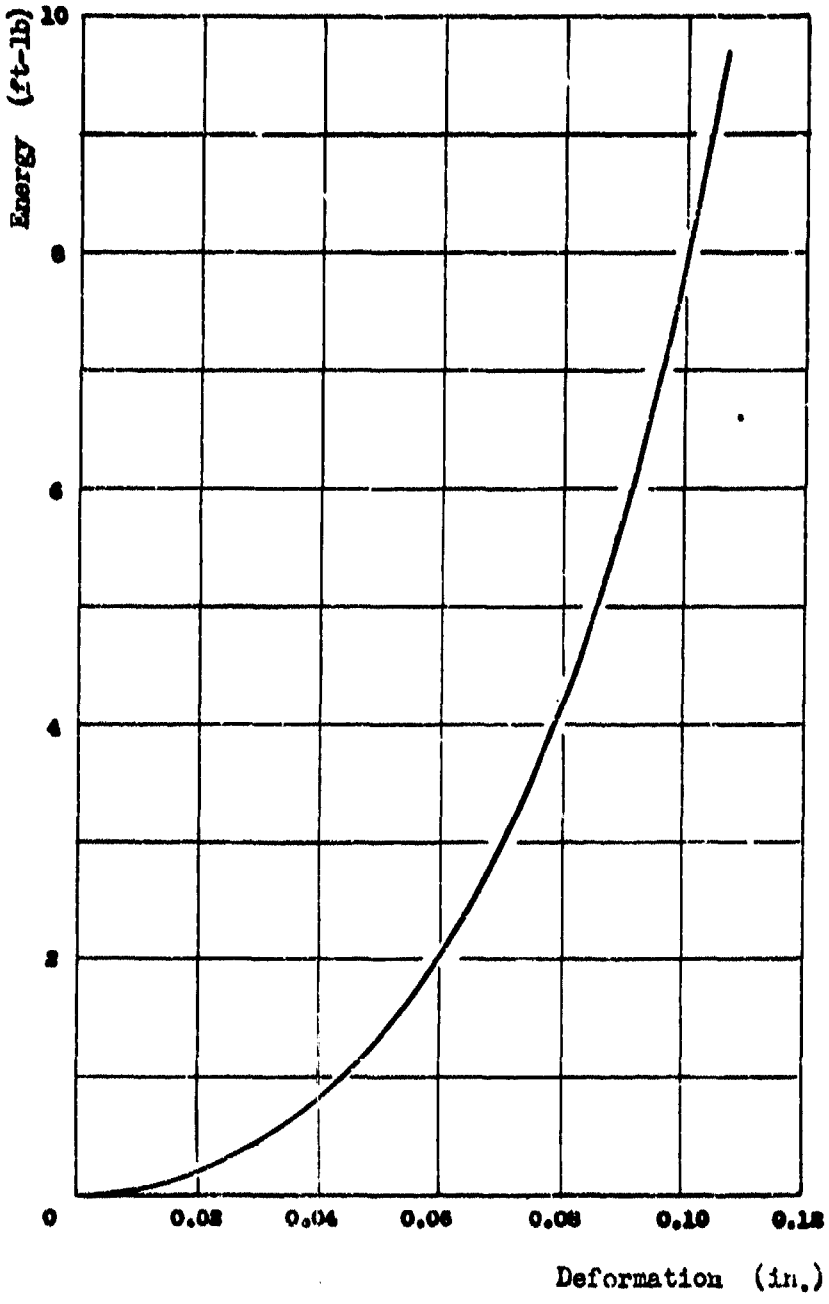


Fig. VII-4. Dynamic calibration of 0.1562-in. diameter copper spheres (lot of 2/6/46) with freely falling weights.

APPENDIX VIII. STATIC CALIBRATION CURVE, MODUGNO GAUGE DISKS.

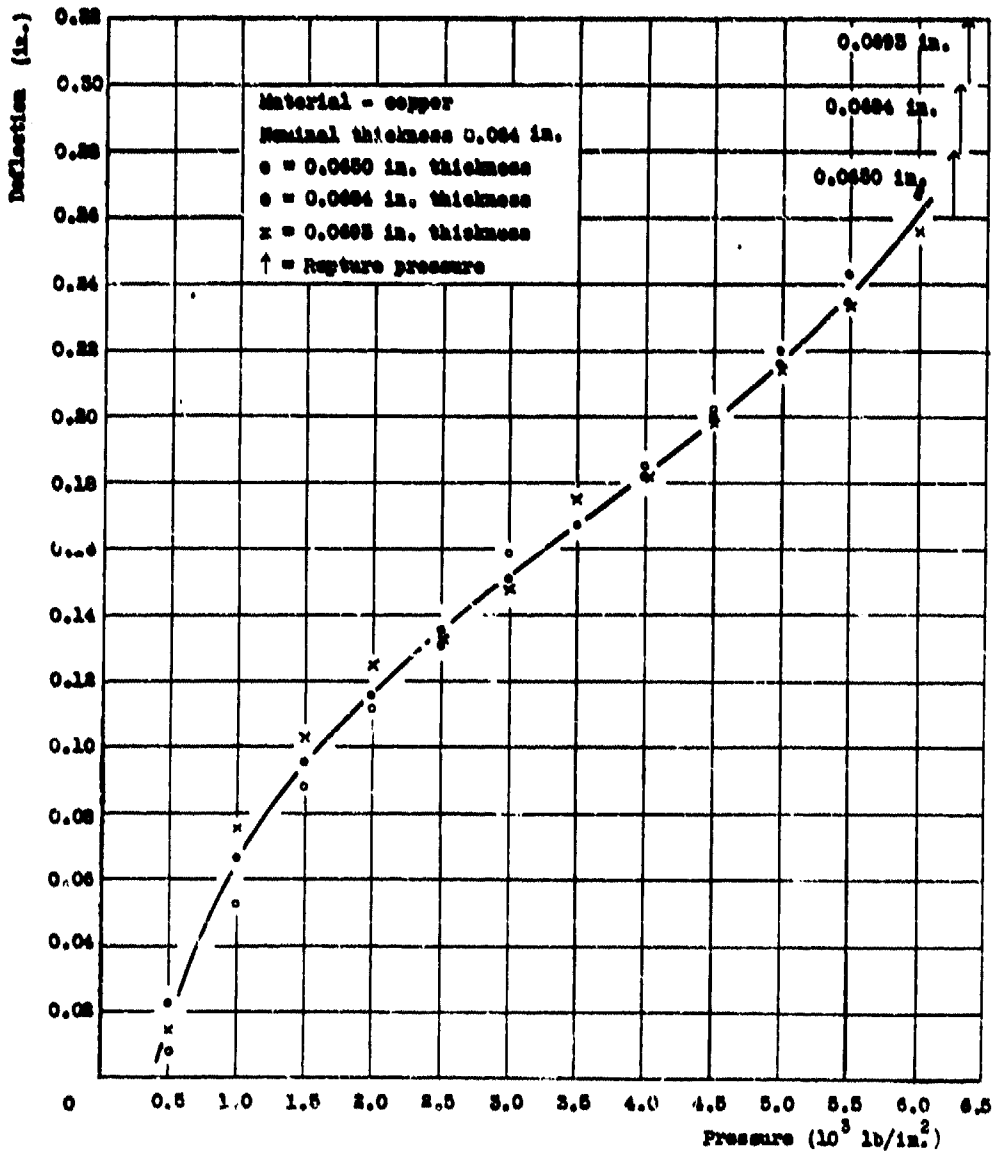


Fig. VIII-1. Static calibration curve for Modugno gauge disks (lot VD-1), Norfolk Navy Yard.

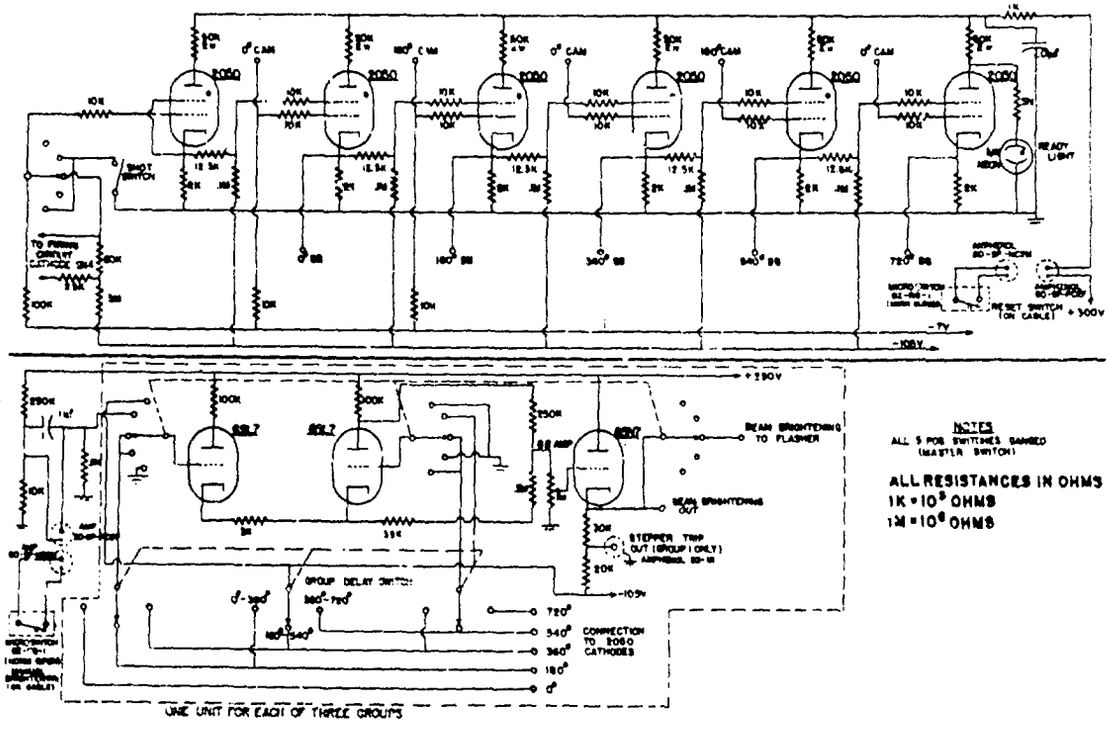


FIG. IX-1. BEAM BRIGHTENING AND FIRING SYNCHRONIZER; SEQUENCE BRIGHTENING CIRCUIT.

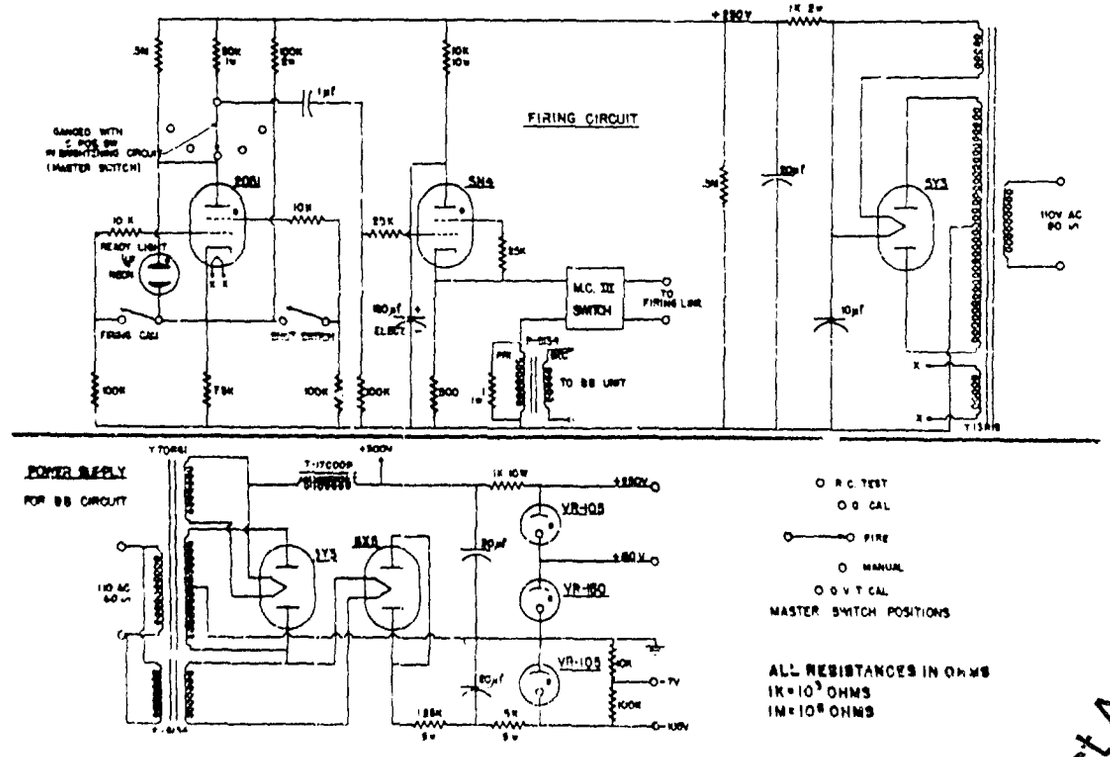


FIG. IX-2. BEAM BRIGHTENING AND FIRING SYNCHRONIZER; FIRING CIRCUIT AND POWER SUPPLY.

Best Available Copy

PIEZO-ELECTRIC GAUGES - DEVELOPMENT OF THE MINIATURE TYPE

A. H. Bebb, D. R. J. Wallace, and D. W. Taylor
Naval Construction Research Establishment
Rosyth, Scotland

British Contribution

May 1947

PIEZO-ELECTRIC GAUGES - DEVELOPMENT OF THE MINIATURE TYPE

A. H. Hebb, D. R. J. Wallace and D. W. Taylor

Naval Construction Research Establishment

May 1947

* * * * * * * *

SUMMARY

The development and experimental tests carried out with miniature tourmaline piezo-electric gauges involving different modes of construction are described in this report.

The effect of different thicknesses of electrodes, either cemented or sintered at high temperature to the crystal faces, of electrodes made from various materials, of many forms of insulation such as telecthene, rubber tape, paraffin wax-vaseline, rubberoid wax, cured natural latex and combinations of these insulators are described in some detail. Plates are included to illustrate the results obtained from the many constructional changes carried out.

To evolve a reliable gauge, the shots fired at it in various stages of progress consisted mainly of standard 1½ lb. T.N.T. blocks in standard canisters. Bare 1½ lb. T.N.T. charges as well as spherical P.E. charges have also been utilised.

It is believed that the design of the gauge is now completely satisfactory for recording pressure-time pulses resulting from underwater explosions, and work to this end in open water is now proceeding. The effects of the presence of targets, water-backed and air-backed, in the neighbourhood of the explosive charges, will also be studied in the near future. It is intended to use the miniature gauge close to explosive charges.

INTRODUCTION.

Descriptions have previously been given of the three types of piezo-electric gauges developed at this Establishment for the measurement of underwater explosion pressures, and also of a special wide-range amplifier for use with the gauges. At that time, no shots had been fired against the two small types of gauges, and whilst it had been proved that both were mechanically robust, it remained uncertain whether firing under controlled conditions would reveal certain improvements in design. Under static conditions of calibration, all three gauges had exhibited similar pressure-time records. In order to avoid a re-design of calibration pressure apparatus for the small gauges, the original was modified by fitting a solid brass cylinder up to the level of the non-return valve connecting the reinforced rubber hose from the pump to the pressure cylinder, and a new lid was constructed which enabled the gauge to be inserted into the steel cylinder without resort to the laborious method of threading the gauge and its long length of attached special signal-free cable through a gland.

The large type of gauge has been proved reliable in miscellaneous trials and whilst it must be accepted that due to its large size it can only enable the average pressure from an underwater explosion to be recorded, nevertheless for such tests as comparative efficiency of explosives, it meets a definite requirement.

This .....

This report therefore deals primarily with the development and re-design of the miniature gauge, and it is now believed that finality has been reached, although it is just possible that further trials may reveal minor improvements. It is hoped to measure peak pressures, momenta and energies resulting from an underwater explosion with high accuracy and very near to the exploding charge.

EXPERIMENTAL WORK: PREFACE

(i) Method of suspending charge and gauge.

The alteration in design of the small gauge has been brought about as a result of experimental work carried out during the last few months under controlled water conditions. The depth of water is about 36 feet, the surface area being 850 feet long and 120 feet wide. A boom, shown in Plate 1, was constructed to enable the charge and gauge to be suspended in the water about mid-way.

(ii) Distances and depths and sizes of charges.

The distance between charge and gauge was varied from approximately 8 to 14 feet, but mainly kept constant at about 10 feet, and the depth of gauge and charge was varied from 5 to 15 feet, but generally kept constant at about 10 feet. This report does not deal with actual magnitude of the pressures recorded but only with the form of the pressure-time signatures in order that reliable data for explosive charges may be ascertained in the future. The charges were generally 1¼ lb. blocks of T.N.T., but a considerable number of 14 oz. P.E. spherical charges were used latterly: the former charge was used without its case on many occasions.

(iii) Orientation of gauge.

After some initial experiments, means were provided to enable the small gauge to be either face-on or edge-on to the charge, the two faces and opposite edges being separately directed at the pressure wave. The length of cable attached to the gauge would naturally hang vertically, but later on provision was also made for the two faces of the crystal to be both parallel to the water surface and at right angles to it, the cable attached to the gauge being then parallel and leading away from the direction of the pressure wave. The above eight orientations were possible by fixing the cable and gauge to a T-bar about 25 feet long which was fixed to a rotating attachment on the boom.

(iv) Connection of gauge to amplifier.

The gauge was connected to the amplifier via a 150 to 200 feet length of non-signal cable developed at this Establishment(1) having a shunt capacity not less than 5 times that of the gauge and cable. A resistance equal to the surge impedance of the cable was inserted between the central conductor of the cable and the common point of the shunt condenser and the grid of the first valve. This method of connection shown in Appendix 1, is particularly useful to avoid end reflections when very long lengths of cable envisaged in field trials are being used.

EXPERIMENTAL WORK: PART I.

The numerous tests carried out and described below ran parallel with the development of perfecting the technique of construction of the miniature gauge. After a few early tests it was realised that thickness of electrodes should be reduced to a minimum, and that the best method was to spray conducting films on to the crystal faces. The effect of insulation, in giving distortion to the signature of the pressure-time pulse from an underwater explosion, soon manifested itself. The gauge construction finally developed is described in Appendix 2.

Best Available Co

The first .....

(a) The first miniature two-ply gauge.

This gauge had two tourmaline discs ½" in diameter and ¼" thick, a central steel electrode 0.013" thick and outer steel electrodes 1/16" thick, cemented with "gelva" to the crystal faces. The insulating layer was telecthene enveloping the gauge itself and connected to that surrounding the cable braid. Three layers of good quality rubber tape served as a further protective outer covering and this was joined to the rubber covering of the cable.

(b) Results of first shots against two-ply gauge.

The charges used for the first experimental tests were 1¼ lb. blocks of T.N.T. in standard cases. No attempt was made initially to orientate the gauge, and although there was similarity between some of the pressure-time records, the variations were considerable both in form and amplitude. Later, therefore, the gauge was orientated towards the pressure wave, and this resulted in consistent records being obtained with the gauge edge-on, and face-on respectively, but the types of records in the two directions differed considerably from each other.

Plate 2, Records 1 and 2, respectively show typical face-on and edge-on records with a sinusoidal 100 microsecond time base. Record 1 (face-on) has two peaks about 23 microseconds apart but the significance of this is not clear, and the spurious frequencies associated with both signatures mar the theoretical condenser discharge type of pressure-time signal normally associated with an underwater explosion. The time of rise of the face-on pressure pulse is slightly shorter than for the edge-on condition. Had the records been faithful ones, this feature would have been more pronounced, as will be shown later.

(c) A single crystal gauge.

This was of similar construction to the two-ply described briefly in paragraph (a) above, the two electrodes being of steel 1/16" thick.

(d) Results with single crystal gauge

Plate 2, Records 3 and 4 show face-on and edge-on records. These, except for minute details are very similar to the results discussed in paragraph (b) above. It was concluded that whatever the explanation for the curious form of the pressure-time signatures, in general the single-ply and two-ply gauges behaved with remarkable similarity, but for fundamental exploration, it was decided to continue firing against a single crystal gauge.

(e) Single crystal gauge with thin electrodes.

The construction remained the same as indicated in paragraphs (a) and (c), except that tinfoil 0.001" thick was used as electrodes.

(f) Results with the thin electrode single crystal gauge.

Plate 2, Records 5 and 6 are typical records for face-on and edge-on positions. There is still a tendency for the face-on record to show a double peak. The signatures are considerably cleaner, however, but the times of rise of the wave front are considerable. Moreover there was a difference (records not shown) between the recorded signatures for the opposite faces and edges.

It was noted also that the pressure amplitudes were considerably less than for the thick steel electrode single crystal under approximately similar firing conditions.

This gauge was reconstructed and only one layer of rubber used as the outer insulating cover. The records (not shown) were different, but not to a very marked degree. The inner insulation layer was still

telecthene .....

Best Available Copy

telcothene. The inference was that not only thickness of insulation, but thickness and material of electrodes had an effect on the pressure-time signatures.

(g) Original two-ply gauge with tinfoil electrodes.

The construction remained as hithorto except that the outer steel electrodes 1/16" thick were replaced by tinfoil 0.001" thick.

(h) Results with the two-ply gauge, having tinfoil outer electrodes.

Plate 3, Records 1a and 1b, 2a and 2b, were obtained with the gauge face-on (two opposite faces) and edge-on (two opposite edges) respectively. As pointed out under paragraph (f), the records for the two opposite faces are not identical nor are they identical for the two opposite edges. This can be accounted for partly by the fact that the gauge was not truly face-on nor truly edge-on in any one position, but as proved later, this is not the complete explanation.

It can be seen that with the two-ply gauge, the records obtained are cleaner than when thick steel outer electrodes are used. Moreover there is again confirmation that the amplitudes are less with thin tinfoil electrodes. The double peak has still a tendency to remain when the gauge is face-on to the pressure wave; and the wave front is less steep than expected.

(i) Single crystal with thin spring steel electrodes.

The construction remained as hithorto, except that the two electrodes were made from spring steel 0.0015" thick.

(j) Results with single crystal gauge, having steel foil electrodes.

The records obtained are shown on Plate 3, Records 3 and 4 with the gauge face-on and edge-on respectively with respect to the pressure wave. Records (not shown) were again somewhat different for the opposite face and edge.

(k) Alterations in amplifier.

During the above mentioned series of tests considerable temporary alterations were made to the amplifier used with a view to ascertaining the cause of the curious signatures recorded. These comprised changes in cable termination such as the shorting out of the inserted resistance equal in value to the surge impedance, the shorting out of the grid-inductance which reduced the flat response of the amplifier at the higher frequency range from 550,000 c/s to about 200,000 c/s. The conclusion reached was that the amplifier did not account for the distortions in the recorded pressure-time pulse.

(l) Firing against the cable.

A single crystal gauge was completed in the normal manner except that its electrodes were disconnected from the cable conductors. Two charges were fired against the cable with the circuit as normally connected to the amplifier and cathode ray tube. No movement of the cathode ray spot was obtained. This proved that the cable was free from pick-up due to pressure changes in the water.

(m) Two-ply gauge with three steel foil electrodes.

Best Available Copy

The construction was standard except that the three electrodes were made from spring steel 0.0015" thick.

(n) .....

(n) Results with two-ply gauge having steel foil electrodes.

Typical records are shown in Plate 4, Records 1a and 1b, 2a and 2b when the gauge was face-on (two opposite faces) and edge-on (two opposite edges) respectively to the pressure wave. The face-on records show double peaks with the second one larger than the first. The amplitude of the false peaks have been restored with the spring steel electrodes, with the restoration also of the spurious high frequencies.

(o) Single crystal gauge with thick steel electrodes.

The construction remained standard except that the steel electrodes were increased to 0.25" thick.

(p) Results with the single crystal gauge, having thick steel electrodes.

Typical face-on and edge-on records are shown on Plate 4, Records 3 and 4. Double peaks and increased oscillations appear, particularly in the face-on record.

(q) Two-ply gauge with thick steel electrodes.

For the purpose of continuity, it appeared reasonable to re-construct the two-ply gauge with thick steel outer electrodes 0.25" thick and a central electrode 0.0015" thick. Otherwise, the construction remained standard.

(r) Results with the two-ply gauge having thick steel electrodes.

Records 1 and 2 on Plate 5, face-on and edge-on types respectively, show the pronounced frequencies set up by the thick steel electrodes and their masking effect on the true pulse.

(s) Single crystal gauge with annealed copper electrodes.

Annealed copper foils 0.022" thick were now cemented by gelva onto the faces of the crystal, but otherwise the construction remained unaltered.

(t) Results with single-ply gauge having copper electrodes.

The face-on and edge-on signatures are shown on Plate 5, Records 3 and 4, respectively. The face-on (second face not shown) did not show such a pronounced second peak and was quite similar to the pair of edge-on records.

For the first time in this exploratory work with different thicknesses and materials of electrodes and insulation, the gauge was now arranged with its crystal faces parallel or perpendicular to the water surface and with the first few inches of the cable led horizontally away from the wave front. The pulses recorded are shown in Plate 5, Records 5 and 6.

These two records are similar, and similar to the ones obtained (not shown) for the opposite faces and edges in the parallel and perpendicular directions with respect to the water surface.

But it is still to be noted that whilst the records are cleaner than those obtained with the steel electrodes, they do exhibit markedly high frequency oscillations; moreover the steep wave front expected with the gauge face-on is not in evidence.

EXPERIMENTAL .....

EXPERIMENTAL WORK: PART 2.

It was realised that whilst the effects of thickness, material and method of attachment of electrodes were of fundamental importance, the fact that the steep front associated with the pressure wave from an underwater explosion had failed to manifest itself, indicated that the method of insulating the gauge with teleothene and rubber tape was unsatisfactory. It made the gauge into a mechanically robust unit, but at the expense of distortion of the pressure pulse. (The amplifier had been proved to be capable of dealing with a very sharp wave front).

When calibrating a piezo-electric gauge in the pressure pot, as previously described the record normally shows a time of rise of the order of a millisecond which is the duration associated with the bursting of the copper diaphragm but in the pressure pulse from a small underwater explosion, this time of rise is of the order of a microsecond. Hence, any insulation or electrode variations are not likely to reveal themselves during calibration.

Tests were therefore commenced with changes in the mode of insulating the gauge.

(a) Single-ply gauge without teleothene insulating layer

The gauge had annealed copper foil electrodes 0.022" thick, i.e. as used in 1(s) and 1(t) above, except that the insulation consisted of three coatings of good quality rubber tape only, the inner teleothene layer having been removed.

(b) Results with single-ply gauge, having only rubber insulation.

The records were still far from being satisfactory, and for comparison with Record 6 of Plate 5 with the gauge perpendicular to the water surface, Record 1, Plate 6, is shown. The only point to emphasise is that the teleothene layer had an effect on the form of the pressure pulse.

(c) Single-ply gauge with rubber solution as insulator.

The gauge had annealed copper foil electrodes 0.022" thick as for (a) and (b) above; the rubber tape was replaced by rubber solution. Mechanically it did not prove a satisfactory construction.

(d) Results with single-ply gauge having insulation of rubber solution.

Plate 6, Records 2 and 3, show the pressure pulse obtained with the gauge face-on and edge-on respectively whereas Record 4, Plate 6, shows the pulse when the gauge had its faces perpendicular to the water surface.

It will be apparent, for the first time, that the face-on record shows a tendency to a very steep front whereas the edge-on record and the record taken with the crystal face perpendicular to the water surface show somewhat equal and finite times of rise. Whilst the oscillations at the peak had yet to be eliminated, there was considerable improvement in the signatures.

EXPERIMENTAL WORK: PART 3.

Whilst evolving methods of sintering a metallic conductor on the surface of the tourmaline crystal and providing it with a thin rubberoid insulation, described later in Appendix 2, experimental tests proceeded with the insulation used in the large type of gauge, namely a mixture of 25% paraffin wax and 75% vaseline. The miniature gauge was insulated by dipping it in this hot mixture, and allowing the minimum thickness to adhere on cooling.

(a) .....

(a) Alteration in gauge thickness.

The investigation was continued with the single-ply gauge ½" in diameter, and ¼" thick, and in addition with single-ply gauge of thicknesses ⅛" and 1/16"

(b) Single-ply gauge with copper electrodes and wax-paraffin insulation layer.

For all three thicknesses of gauges, the electrodes consisted of the annealed copper foil 0.022" thick as used recently, the insulator being a thin layer of the paraffin wax-vaseline mixture.

(c) Results of single-ply gauges, having wax-paraffin insulation.

For comparison with previous records shown in this report, typical records are given only for the pressure pulse signatures obtained with the ¼" thick gauge. These are shown on Plate 7, Records 1, 2, 3 and 4. Records 1 and 2 were obtained with the gauge face-on and edge-on to the pressure wave respectively whereas in Records 3 and 4, the gauge had its faces parallel and perpendicular respectively to the water surface.

It will be observed that in Record 1, there is an overshoot and that the time of rise is certainly of the order of a microsecond. Whereas, with the remaining records, although Record 2 is slightly different in form from Records 3 and 4, the times of rise of the wave fronts have been measured and found to be about 8 microseconds, which is the time that the pressure wave takes to traverse the diameter of the gauge. In Record 1, the overshoot is due to the fact that the gauge was rigidly held, the tendency being to record a peak pressure double that of the incident wave. When the gauge is held face-on in a semi-rigid manner to the pressure wave, some intermediate but indeterminate value between the peak pressure and double the peak pressure value of the explosive wave would be expected. Therefore whilst a thin gauge held face-on to the pressure wave would be advantageous in giving extremely sharp times of rise provided the amplifier and recording film is capable of following and resolving the signatures, the better arrangement is to hold the gauge edge-on to the wave and preferably perpendicular to the water surface with the cable leading away in the direction of the motion of the pressure wave. Allowance has to be made for the effect of the reduction in peak pressure; this is brought about by averaging the pressure over the size of gauge. For a ½" gauge, it amounts to a 3% reduction in peak pressure.

On the whole it was found that the same features were exhibited with the thinner gauges.

(d) Gauges with sintered silver electrodes.

The method of sintering silver onto the crystal faces is described in Appendix 2 of this report. The silver is estimated to be only 0.0025" thick. The insulation is still a layer of paraffin wax-vaseline mixture. Three such gauges of thicknesses ¼", ⅛" and 1/16" respectively were tested.

(e) Results with single ply gauges, having silver electrodes and wax-vaseline insulation.

The connection between the electrodes and the cable leads was made by soldering annealed copper strips ½" long to the silver film. The records obtained are not given but in the main they are almost identical to those shown in Plate 7. It would appear therefore that sintering silver electrodes onto the crystal faces is not greatly superior to cementing metal foil electrodes of copper, although it is known that cementing metal other than steel with solva is not mechanically satisfactory for long durations.

(f) .....

(f) Repeat test - firing against cable.

This was similar to test 1(1), except that the end of the cable (a different sample) immersed in the water was sealed with a paraffin-wax vaseline insulator. The result on firing however was the same. The cable again proved itself immune to signals as a result of pressure changes in the water.

EXPERIMENTAL WORK: PART 4.

When this stage of the experimental work had been reached, the method of construction described in Appendix 2 had been evolved. Briefly this consists in sintering silver at a high temperature onto the crystal faces, soldering small connecting copper tags to the faces and enveloping the whole gauge in a very thin film of special rubberoid wax. The space between the cable end and the base of the gauge is filled with this wax, and the whole gauge after dipping in natural latex is cured at a moderately low temperature.

(a) Results with single-ply ½" gauge x ¼" thick.

Plate 8, Records 1 and 2 are typical face-on and edge-on records of the pressure pulse of the explosion wave. The only point to emphasise is the overshoot of the peak pressure in the face-on direction which amounts to about 68% of the true peak pressure for this relative large thickness of gauge.

(b) (i) Results with single-ply ½" gauge x ¼" thick.

Typical face-on and edge-on records are shown on Plate 3, Records 3 and 4, and attention is again drawn to the overshoot on the face-on record, which now amounts to about 20% only.

(ii) Amplifier changes.

Further face-on signatures are shown on Plate8, Records 5 and 6. In Record 5, a change was made in the amplifier, reducing the flatness of its high frequency response from 550 kc/s to about 300 kc/s, whereas in Record 6, the response was flat up to about 20 kc/s only.

An overshoot of about 15% is still present in Record 5; not only also is the peak rounded very considerably in Record 6, but the time of rise of the wave front is lengthened.

These records confirm that to avoid a reduction in the recording of peak pressures, the amplifier must have a suitably high frequency response; and, for faithful determination of peak pressures the gauge must not be directed face-on to the pressure wave.

(c) Results with single-ply ½" gauge x 1/16" thick.

Typical face-on and edge-on records are shown in Plate 9, Records 1 and 2 respectively.

(d) (i) Results with single-ply ½" gauge x ¼" thick from various charges.

On Plate 9, Records 3, 4 and 5 indicate the pressure-time pu[illegible] for a standard 1¼ lb. T.N.T. block charge in its standard case, a st[illegible]ard 1¼ lb. T.N.T. block bare charge without its case, and a 14 oz. P.E. spherical bare charge (fired without a primer) respectively. The gauge was directed face-on to the charges in all three cases. It will be observed that the tail of the signature is a little smoother for the spherical P.E. charge than for the T.N.T. charges, the bare T.N.T. charge being slightly smoother than the standard cased charge.

Best Available Co[illegible]

(b) (ii) .....

(ii) Result with single-ply ¼" x 1/16" gauge for a spherical charge.

On Plate 9, Record 6 is a typical signature obtained from a 14 oz. P.E. spherical bare charge. The extremely sharp rise, overshoot and fairly smooth decay is to be noted when the gauge is directed face-on to the pressure wave.

EXPERIMENTAL WORK: PART 5.

Although it now appeared that the most practical type of miniature gauge for general purposes was probably to be of dimensions ¼" in diameter and 1/16" in thickness, and that the construction would be similar to that given in Appendix 2, it was felt that in order not to lose sensitivity, a two-ply gauge would be necessary. A two-ply gauge had not yet been constructed with very thin silver electrodes sintered onto the crystal faces, and moreover the single-ply had not been really tested edge-on with the crystal faces perpendicular to the water surface and the cable leading away from and perpendicular to the pressure front. It was also felt that it would be worth exploring a gauge only 1/32" thick as well as a gauge 1" in diameter and ¼" thick. Circumstances might arise where this latter-sized gauge with double the thickness might be used. For example an approximate theoretical calculation revealed that whereas a 1½ lb. charge fired at a ¼" gauge edge-on caused a peak pressure to be recorded 3% less in value than the true peak pressure, the error would not be greater than about 15% for a 300 lb. charge fired at a 1" gauge edge-on. The tourmaline position being slightly precarious, it was thought worth while testing gauges ½" in diameter.

(a) The ½" diameter single crystal gauge.

Three such single-ply gauges were constructed, according to the description given in Appendix 2.

The gauges were of thicknesses ⅛", 1/16" and 1/32".

(b) Results with the ½" single-ply gauges.

There are no special features to emphasise for the normal face-on and edge-on records except that in the former case the time of rise is certainly not greater than 1 microsecond but with a definite tendency to overshoot at the peak, and the time of rise of the pressure pulse in the latter case is reduced to about 4 microseconds.

Plate 10, Records 1 to 6 illustrates the pressure pulses recorded with the gauges having their faces perpendicular to the water surface and the cable leading away from the pressure front. Record 1 was obtained with the ⅛" thick gauge, the explosive being the standard 1¼" lb. T.N.T. charge in its case. Records 2 and 3 were obtained with the 1/16" thick gauge, Record 3 being obtained from a spherical 14 oz. P.E. bare charge without a primer. Records 4, 5 and 6 were obtained with the 1/32" thick gauge, Record 6 from a spherical 14 oz. P.E. bare charge, and Record 5 from a bare 1½ lb. T.N.T. charge. The spherical charge gave a smoother tail to its pressure-time signature than either the cylindrical bare T.N.T. charge or the charge in its standard canister. The pressure pulse obtained from the standard charge in its case is also a little more disturbed in its contour than the pulse obtained from the bare charge.

(c) The 1" diameter single crystal gauge.

The construction of this gauge is similar to that given in Appendix 2, the thickness of the gauge being ⅛".

(d) Results with the 1" diameter single crystal gauge.

The records obtained from a 1½ lb. standard T.N.T. charge, with the gauge face-on and edge-on are shown on Plate 11, Records 1 and 2 respectively.

The .....

The face-on record shows the overshoot, accompanied by the almost instantaneous time of rise, whereas the time of rise in the case of the edge-on record is of the order of 16 microseconds.

On all edge-on records oscillations are apparent on the sloping time of rise, and when, as in the case of the 1" gauge, this time is relatively long the film speed makes them more pronounced. These are the natural oscillations set up in the tourmaline crystal, and their frequencies are dependent on the size of the gauge itself. In the case of the 1" crystal gauge the oscillations have frequencies of approximately 240,000 c/s. They are referred to here for the first time in this report, but of course close examination of the records obtained with the ½" and ¼" diameter gauges reveal similar oscillations in edge-on positions. The smaller the diameter of the gauges, the higher these frequencies become, the further reference to them appears in Appendix 1.

On Plate 11, Record 3, is exhibited the pressure-time pulses obtained from the 1" gauge with its crystal faces parallel to the water surface and the cable leading away from the pressure wave front. Plate 11, Records 4, 5 and 6 show similar pressure-time signatures with the crystal faces perpendicular to the water surface, Record 4 in the case of the 1½ lb. T.N.T. charge in its standard canister, Record 5 for a bare 1½ lb. T.N.T. charge, and Record 6 for a 14 oz. spherical bare P.E. charge without a primer. It will be seen that there are oscillations similar to those mentioned above, a finite time of rise of the pressure wave (16 microseconds) and that smoother contours are obtained with the bare charges, particularly the spherical types.

When the high frequency response of the amplifier was cut down from about 500,000 c/s to about 1/10th of this value, the sharp peak was rounded off and the amplitude reduced by about 20%.

EXPERIMENTAL WORK: PART 6.

This work constitutes the records finally obtained with the newly designed ½" gauge, both single-ply and twin-ply. The method of construction of twin-ply gauges was being developed simultaneously with this experimental work. This is described in Appendix 2. Here, there is only need to mention that the central electrode of silver foil only 0.0025" thick is strictly comparable with the burnished silver paste sintered and baked onto the outer crystal faces. Flat ligaments of annealed copper are soldered onto the outer silver films but the central electrode of silver foil is so cut as to provide its own silver tag for soldering onto the central core of the cable.

(a) The single-ply ½" gauge.

The construction is on similar lines to that given in Appendix 2, the thickness of crystal being 1/16".

(b) Results with the ½" single crystal gauge.

It was not considered necessary to repeat the normal face-on and edge-on records. Shots were fired therefore with the gauge having its faces parallel and perpendicular respectively to the water surface and the cable attached to the gauge leading away from the pressure front - these are edge-on records with the cable having its effect in distorting the pressure field reduced to its symmetric minimum.

On Plate 12, Records 1 and 2, are shown pressure-time records for a standard 1½ lb. T.N.T. charge and for a 14 oz. P.E. spherical bare charge respectively, with the gauge having its faces parallel to the water surface. On Plate 12, Records 3, 4 and 5, pressure time pulses are exhibited for a standard 1½ lb. T.N.T. charge in its standard case, for a 1½ lb. T.N.T. bare charge and for a spherical charge respectively, the gauge having its faces perpendicular to the water surface. The times of initial pressure

rise .....

rise for all these records is 8 microseconds and the oscillations exhibit twice the frequency registered by the 1" gauge. Bare and spherical charges again show smoother contours for the tails of the pressure time pulses than the standard charges in containers.

(c) The two-ply ¼" gauge.

The construction of this gauge is described in Appendix 2. It consists of two crystals 1/16" thick, the central silver foil electrode being connected to the central cores of the cable and the outer silver sintered faces being connected to the cable braid. Apart from the special rubberoid wax at the base of the gauge to remove all possibilities of trapping air cavities, the only insulation is a film of cured natural latex surrounding the gauge and blended into the rubber covering of the cable itself.

(d) Results with the two-ply ¼" gauge.

Three face-on pressure-time signatures are shown on Plate 13, Records 1, 2 and 3. These were obtained with the standard 1¼ lb. T.N.T. charge, the bare 1¼ lb. T.N.T. charge and the 14 oz. P.E. spherical charge (without primer) respectively.

In the case of the spherical charge, the smoothing effect on the tail of the signature is particularly noticeable. The overshoot and sharp times of rise are again predominant features for the face-on records of all three charges.

Further pressure-time pulses are shown on Plate 13, Records 4, 5 and Records 6, 7. In the case of Records 4 and 5, the faces of the crystals were parallel to the water surface, the gauge being turned through 180° for the second record. Similarly for Records 6 and 7, the faces of the crystals were perpendicular to the water surface, the gauge in the latter case being also turned through 180°. In Records 4, 5, 6 and 7, the cable of course was led away from the onset direction of the pressure front, the charge in all of these four records being a 1¼ lb. T.N.T. bare charge. For these edge-on records, the time of rise is 8 microseconds, and the natural oscillation frequencies of the crystals are clearly discernible.

DISCUSSION OF RESULTS AND CONCLUSIONS.

The constructional details of the three types of piezo-electric gauges developed at this Establishment have been described elsewhere. One of the objects in producing the medium type was to adhere to the principle of using the same type of construction and of gauge insulation (paraffin wax-vaseline mixture) as that for the well-tried large type of gauge. In fact only one short series of shots was fired against the medium type of construction, and the gauge itself was simply the original two-ply miniature type ¼" in diameter with thick steel outer electrodes 1/16" thick surrounded by a brass case and having wax-vaseline insulation. The pressure-time signatures recorded with the medium type of gauge were not satisfactory. This is partly due to the electrodes, as can be seen from this present report, partly due to oscillations set up by the brass case, and partly due to the type of insulation.

This report deals with the constructional modifications made to the miniature gauge from that given[1] in Appendix 2; the finalised design evolved as a result of a large number of tests.

The cable developed at this Establishment[1] has been used throughout these tests. The ratio cable signal/gauge signal has been proved to be a negligible quantity even in the case of the miniature gauge.

The telcothene and rubber tape formerly used in insulating the gauge into a robust unit has been abandoned, and the final design has simply a coating of cured natural latex.

The air .....

The air trapped underneath the telcothene, the thickness and composition of the telcothene as well as that of the thick rubber tape all contributed to distortion of the recorded pressure pulse from an underwater explosion.

The thick steel outer electrodes have been replaced by layers of silver sintered onto the crystal faces, and fine annealed copper tags are spot soldered to these to enable connections to be made to the cable braid. The central steel electrodes has also been replaced by a thin silver foil fused between the negative faces of the two crystals.

Thick metal electrodes have been shown to produce serious oscillations superimposed on the true pressure-time signature. These not only distort the pulse but give false peak pressures, and modify the time of rise of the steep wave front associated with the detonation wave from an underwater explosion.

Although the pressure pulses recorded from identical gauges when fine annealed copper electrodes "gelvaed" onto the crystal are not much, if any, inferior to those recorded with sintered silver electrodes, nevertheless mechanically the adherence of annealed copper electrodes is not sufficiently robust to record peak pressures of thousands of pounds per square inch, i.e. with charges close up to the gauge.

The total thickness of the complete two-ply miniature gauge is now $\frac{1}{8}$" and it consists of two tourmaline crystals $\frac{1}{4}$" in diameter. The thickness/diameter ratio of the gauge is, in part at least, defined by the strength and quality of the tourmaline discs. The gap between the copper tags at the base of the gauge adjacent to the central conductors and braid of the cable is filled with a molten rubberoid wax composition, and great care is taken to prevent air being trapped. As thin a film of natural latex as possible is then cured onto the gauge unit.

Experiment has proved that the more nearly the tourmaline gauge resembles the bare twin crystals, the more faithful the reproduction of the pressure-time pulse of the detonation wave.

For faithful reproduction, the gauge has to be directed edge-on to the pressure front with the cable leading away from the explosion wave, the faces of the crystals constituting the tourmaline gauge being at right angles to the water surface. For a 1½ lb. charge, the sharp time of rise of the steep-fronted wave is modified to about 8 microseconds which is the period taken by the wave to traverse the gauge diameter: this causes a peak pressure reduction of about 3% for this particular charge, but for a charge of about 30 lbs., the reduction is not greater than 1%. When the pressure pulse is travelling parallel to the plane of the gauge, it will be undisturbed by it so that the pressure on the plane will be equal to that in the pulse. The time of rise of the wave front as registered with the gauge face-on is of the order of 1 microsecond or less but a false peak pressure (described as an overshoot in the body of the report), is recorded, particularly with a thick gauge rigidly held towards the pressure wave. This peak pressure has been proved to lie somewhere between the true value of the incident wave pressure and twice this value when the reflected wave is in phase.

The amplifier developed for piezo-electric recording at this Establishment is capable of recording faithfully a steep fronted wave having a duration of only 1 or 2 microseconds, and this is about the limit of film resolution and writing speed with the present drum camera.

Experimental gauges having $\frac{1}{4}$" and 1" diameters respectively have also been used satisfactorily in the tests carried out and described in this report.

It is believed that except for the natural frequency oscillations set up in the tourmaline discs themselves, that the miniature gauge will

now .....

now record faithfully the pressure changes in open water as a result of an underwater explosion. Moreover it is confidently expected that the effect of changes brought about by the presence of water-backed and air-backed targets in the vicinity of exploding charges can be determined.

The simple theory of pressure measurement with a tourmaline gauge is given in Appendix 1, together with the theoretical effect of cable signal. A reference to the natural frequency oscillations set up in tourmaline discs is also given.

Work, involving exploration of the pressure field as near an underwater exploding charge as possible is now proceeding with the finalised type of miniature gauge described herein.

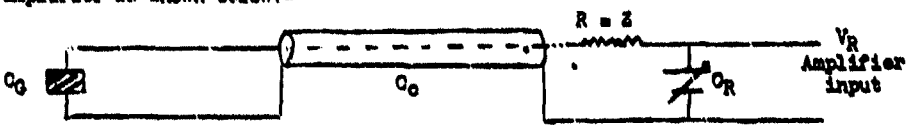
REFERENCE

(1) The electric potentials produced in the conductors of a submerged cable by underwater explosions. A.H. Bebb and R.V. Bundy.

APPENDIX 1.

1. PIEZO-ELECTRIC GAUGE THEORY.

The miniature gauge is connected to the input of the piezo-electric amplifier as shown below:-



The capacity of a n-ply gauge is given by

$$C_{G_n} = \frac{n\,k\,A}{4\pi d \times 9 \times 10^{11}} \text{ farads}$$

$$= \frac{n\,A}{d} \times 0.658 \times 10^{-12} \text{ farads.}$$

k = dielectric constant of tourmaline (7.44)
A = area of tourmaline disc in cms.^{2}
d = thickness of tourmaline disc in cms.
k = 4.5 for Quarts
5.6 for Rochi Salt

The charge developed by a n-ply gauge due to a pressure p dynes/cm^2 is given by

$$Q_{G_n} = n\,k'\,p\,A \text{ coulombs}$$

$$= 1.518\,n\,p\,A \times 10^{-12} \text{ coulombs (P = pressure in lbs./in}^2\text{).}$$

$$\therefore V_{G_n} = \frac{Q_{G_n}}{C_{G_n}} = 2.31\,Pd \text{ volts.}$$

k' = piezo-electric constant for tourmaline (2.20×10^{-17} coulombs/dyne)
p = pressure in dynes/cm^2.
A = area in cms.^{2}
P = pressure in lbs./in^2
d = thickness of disc in cms.

The special cable developed for use with piezo-electric gauges has a capacity of 18.5×10^{-12} farad per foot. Let total length of cable used with miniature gauge be L feet long.

$$\therefore C_c = 18.5\,L \times 10^{-12} \text{ farads.}$$

Hence voltage V_{R_n} developed across the amplifier input is given very closely by

$$V_{R_n} \doteq \frac{\frac{n\,A}{d} \times 0.658 \times 10^{-12}}{18.5\,L \times 10^{-12}} \times 2.31\,Pd \text{ volts (omitting the shunt capacity } C_R\text{)}$$

$$\doteq 0.0822\,\frac{n\,A\,P}{L} \text{ volts.}$$

n = number of tourmaline discs
P = pressure in lbs./in^2
A = area of tourmaline disc in cms^2.
L = length of cable in feet.

EXAMPLE.

Consider a two-ply miniature gauge, each tourmaline disc being $\frac{1}{8}$" in diameter and 1/16" thick.

Then. C 2 ply = 10.5 micromicrofarads
Q 2 ply = 3.85 P micromicrocoulombs
$\therefore$ V 2 ply = 0.367 P volts.

The voltage across the amplifier input is given by

$$V_R \text{ 2 ply} = 0.2086\,P/L$$

If L .....

If L = 750 feet, P = 1000 lbs./in^2

then V_R 2 ply = 0.278 volts.

2. CABLE SIGNAL.

The ratio Cable Signal/Gauge Signal:-

Let cable signal per foot of cable per lb./in^2 pressure per foot length of cable in circuit = v volts.

Then cable signal per foot of cable per lb./in^2 pressure per L feet of cable in circuit = $\frac{v}{L}$ volts.

And cable signal per foot of cable per P lbs./in^2 pressure per L feet of cable in circuit = $\frac{P\,v}{L}$ volts.

If 1 foot of this cable is immersed in the water and subjected to the same pressure as the miniature gauge, then the cable signal per 1 foot of cable per P lbs./in^2 pressure per L feet of cable in circuit = $\frac{P\,v\,l}{L}$ volts.

Hence percentage ratio,

$$\text{r of } \frac{\text{Cable signal}}{\text{Gauge signal}} = \frac{P\,v\,l}{L} \Big/ \frac{0.0822\,n\,A\,P}{L} \times 100\%$$

$$= 1216\,\frac{vl}{nA}\,\%$$

EXAMPLE:-

For a two-ply miniature gauge $\frac{1}{4}$" in diameter, assume that a trial is carried out where pressure measurements are required involving 30 feet of the cable immersed completely in water and therefore subjected to the same pressure as the gauge from the underwater explosion.

$\therefore$ r = 14380 v %

Now, with the special cable, experiment has shown that when 1 foot of the cable is subjected to a pressure of 1000 lbs./in^2 pressure in a circuit capacity of 2500 micromicrofarad (135 feet), the voltage developed is certainly less than $\frac{1}{4}$ of a millivolt, but taking this figure as an upper maximum,

$$\text{then } v = \frac{\frac{1}{4} \times .001 \times 135}{1000} = 45 \times 10^{-6}$$

$$\therefore r = 14380 \times 45 \times 10^{-6}\,\%$$

$$= 0.65\%$$

As described in the body of the report, firing against the cable has confirmed the fact that cable signal is not significant.

3. OSCILLATIONS IN TOURMALINE DISCS FROM SHOCK EXCITATION.

Various complex modes of vibrations may be set up in crystal discs of tourmaline when these are subjected to underwater explosions. It is very probable that with the present miniature gauge directed edge-on to the pressure wave, the pressure-time signature registered by the cathode ray oscillograph is so faithful that only resonant vibrations of the crystal slices remain superimposed on the pressure pulse. This is particularly noticeable in the case of the 1" diameter gauge where about 4 oscillations appear on the slope of the wave front (complete period 16 microseconds), giving therefore a frequency of oscillation of 250,000 c/s. Moreover, if the wave-length is assumed to be equal to the disc diameter, the frequency calculated is approximately in agreement with the observed frequency, assuming sound velocity for tourmaline to be 6000 meters per second.

APPENDIX 2

CONSTRUCTION OF TWO-PLY MINIATURE PIEZO-ELECTRIC TOURMALINE GAUGE AND CONNECTION TO SPECIAL CABLE.

by R.V. Bundy and G. Hendry.

1. The two tourmaline discs, ¼" in diameter and 1/16" thick are cleaned in benzene, and allowed to dry. Their resistances are then measured with a 2500 volt megger and only crystals showing a resistance greater than 10,000 megohms are accepted.

2. A very thin layer of silver paste (Burnish silver paste No. 38 purchased from Messrs. Baker Platinum Ltd.) is applied with a spatula to each crystal face, and the discs are placed vertically with their edges resting in a V-block, contact between the silvered surfaces and the block itself being avoided. The assembly is now put in a pre-heated muffle furnace, the temperature of which at this stage must not be higher than 100°C. Its temperature is then raised slowly to 550°C, and is maintained for 30 minutes. The furnace is now switched off and allowed to cool to room temperature. The crystals are removed, re-tested with a 2500 volt megger and carefully lapped flat on a large tourmaline slab completely immersed in petrol. The operations described above take about 3½ hours to complete.

3. The silvered discs are now tested for polarity and piezo-electric sensitivity, the positive faces being lightly marked. The crystals are once more cleaned in benzene or petrol.

4. Each positive face receives a second and slightly thicker coat of silver paste, and each disc placed, positive side up, in separate porcelain crucibles and re-heated as described in paragraph 2 above.

5. After this treatment, the resistance of each crystal is again checked, and the negative faces now receive their second coat of silver paste. On top of a steel pad ½" in diameter and ¼" thick, resting on a specially constructed end plate of a jig, one of the discs is now fitted with its negative face up; a silver electrode cut to the appropriate shape from silver foil 0.0025" thick is placed in contact with this negative face. The second disc is now fitted in the jig with its negative face also in contact with the silver electrode and a further steel pad is inserted on top. The second end plate of the jig is bolted on to force the component parts of the gauge and the steel pads into alignment. The pressure required to force the crystals and silver electrode together is applied by means of screws in the end plates bearing directly on the steel pads. The gauge is now returned to the pre-heated furnace and the temperature raised slowly to 550°C.

6. The gauge unit now consists of two silvered tourmaline discs fused to the silver electrode located between them. The outer or positive faces of the gauge are burnished and the resistance between them and the centre electrode measured. If this resistance is low, it is usually found possible to restore the high value by cleaning the edge of the unit with an abrasive such as bakelised diamond dust. This last step is in any case advisable. Two copper electrodes 0.4" long x 0.12" broad are cut from annealed copper foil 0.004" thick, and spot soldered to the outer faces of the unit.

7. The gauge unit is soldered to the cable described in reference 1, the cable end being suitably prepared. The copper electrodes from the gauge are connected to the braid, and the silver centre electrode to the centre conductor, so that the gauge is now secured with its under edge approximately 0.25" from the polyethene. The cable end and gauge unit is thoroughly washed in benzene or petrol, and the resistance of gauge and cable measured.

8. The gauge is now dipped in a special rubberised wax (I.C.I. Hot Melt Adhesive I.D. 5257) heated to a temperature of 130°C, the cable end being immersed to a depth of 0.1" approximately. The wax is allowed to cool, and dipping continued, until the gauge and cable end is embedded in a blob of wax. The wax is completely removed from the crystals and is tapered

back .....

Best Available Copy

back to the end of the cable, and the unit now appears to be fixed to the apex of a wax cone, with the base of this cone moulded to the cable end. The wax is reheated to 130°C and the unit dipped to give a smooth finished surface thereby finally leaving also a very thin wax film on the crystals.

9. The gauge is lightly washed in petrol, and approximately 1" of the outer rubber covering of the cable measured from the base of the wax cone, is also thoroughly cleaned with petrol or benzene prior to rubberising. The resistance of the gauge and cable is rechecked. The gauge and cable end is now dipped in 60% concentrated natural latex (North British Rubber Co.) and rotated by hand in order to obtain a uniform thickness. The rubber covering is allowed to dry until it changes from the milky white to the transparent state. The next step is to apply a ridge of latex to the sharp edge of the crystal faces to counteract the dilation of the rubber due to surface tension. When the ridge is dry this alternate process is repeated three times. It is important that each coat be allowed to dry before the next is added; failure to observe this condition may result in a gauge of low resistance. The gauge and about 6" of cable enters the oven through a modified vent-hole, and the rubber is cured by baking at a constant temperature of 47°C for a minimum period of 15 hours.

The total time taken for the construction and attachment to the cable of a miniature piezo-electric gauge is approximately 36 hours.

10. A photograph of the jig details is shown in Plate 14, and of the gauge before application of the special wax and natural latex, and after completion in Plate 15.

Best Available Co

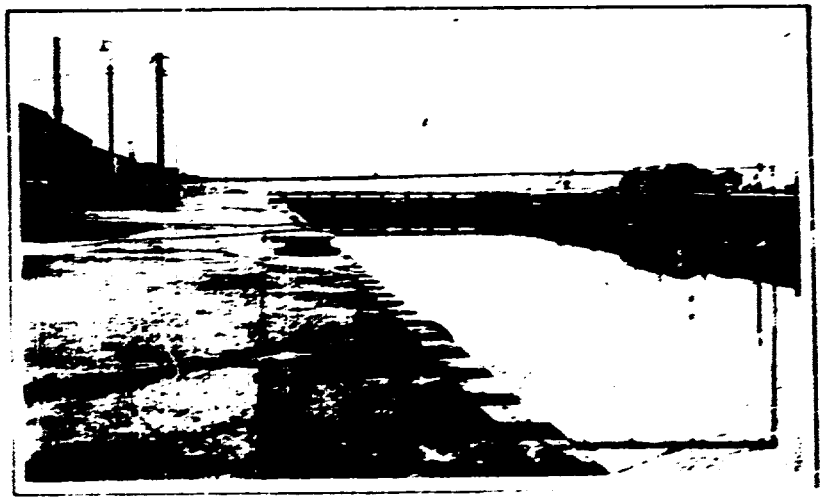
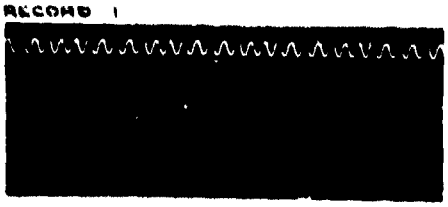


PLATE I

BOOM FOR SUSPENDING GAUGE AND CHAIN.

PLATE 2.

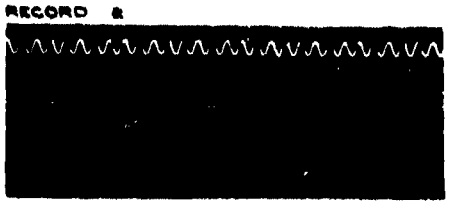
RECORD 1



FACE ON TO CHARGE.

8 PLY GAUGE 1/8"DIA. DISC. X 1/4"THICK EACH. OUTER ELECTRODES 1/16"THICK STEEL. CENTRAL ELECTRODE 0·013"THICK STEEL.

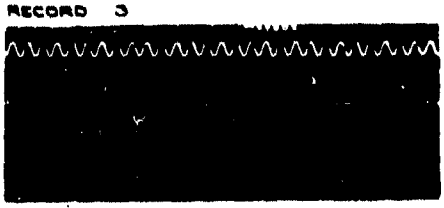
RECORD 2



EDGE ON TO CHARGE.

Do.

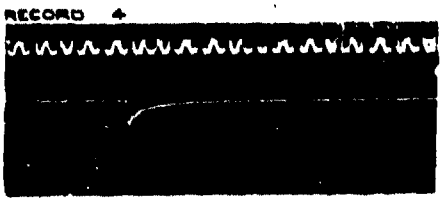
RECORD 3



FACE ON TO CHARGE.

SINGLE PLY GAUGE 1/2"DIA.X 1/4"THICK. OUTER ELECTRODES 1/16"THICK STEEL.

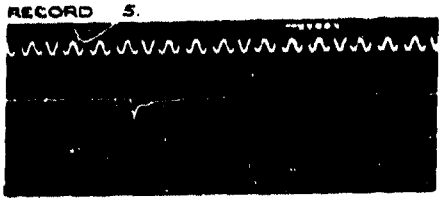
RECORD 4



EDGE ON TO CHARGE.

Do.

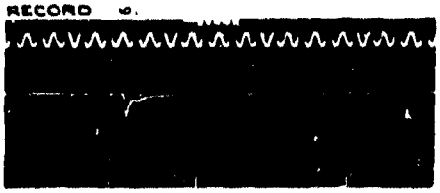
RECORD 5.



FACE ON TO CHARGE.

SINGLE PLY GAUGE 1/2"DIA.X 1/4"THICK. OUTER ELECTRODES '001" THICK TIN.

RECORD 6.



EDGE ON TO CHARGE.

Do.

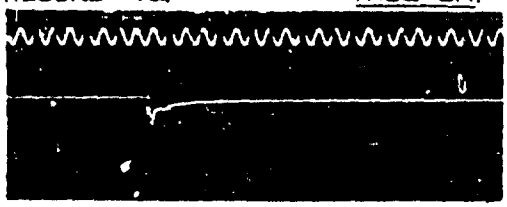
ELECTRODES CEMENTED WITH "GELVA."

INSULATION: LAYER OF TELCOTHENE AND 3LAYERS OF RUBBER TAPE.

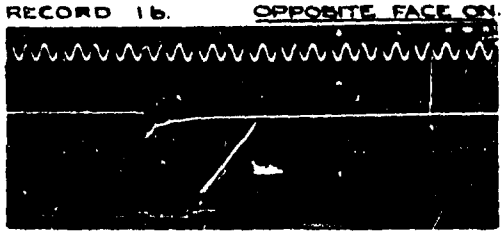
1 1/4 LBS. T.N.T. STANDARD CHARGE.

PLATE 3.

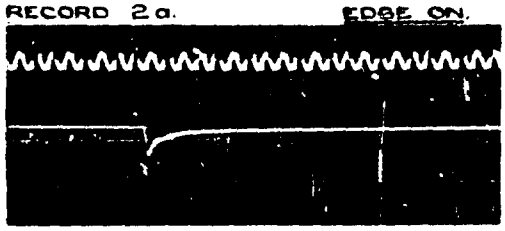
RECORD 1a. FACE ON.



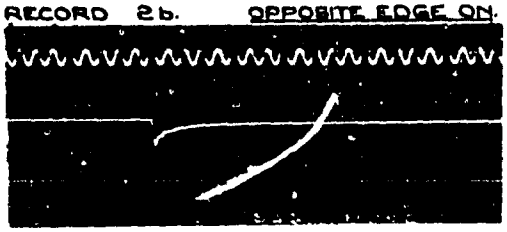
RECORD 1b. OPPOSITE FACE ON.



RECORD 2a. EDGE ON.

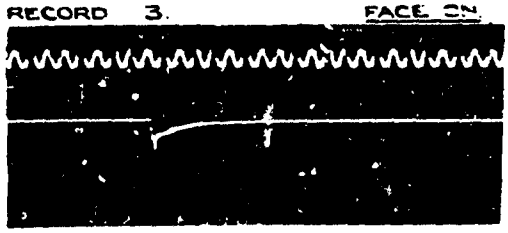


RECORD 2b. OPPOSITE EDGE ON.

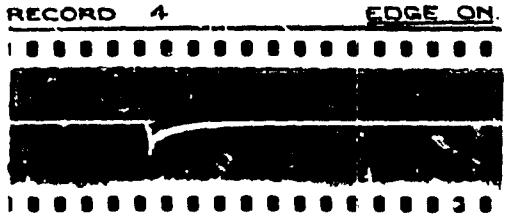


TWO PLY GAUGE ½" DIA. x ¼" THICK EACH.
OUTER ELECTRODES 0·001" TIN
CENTRAL ELECTRODE 0·015 STEEL

RECORD 3. FACE ON.



RECORD 4 EDGE ON.

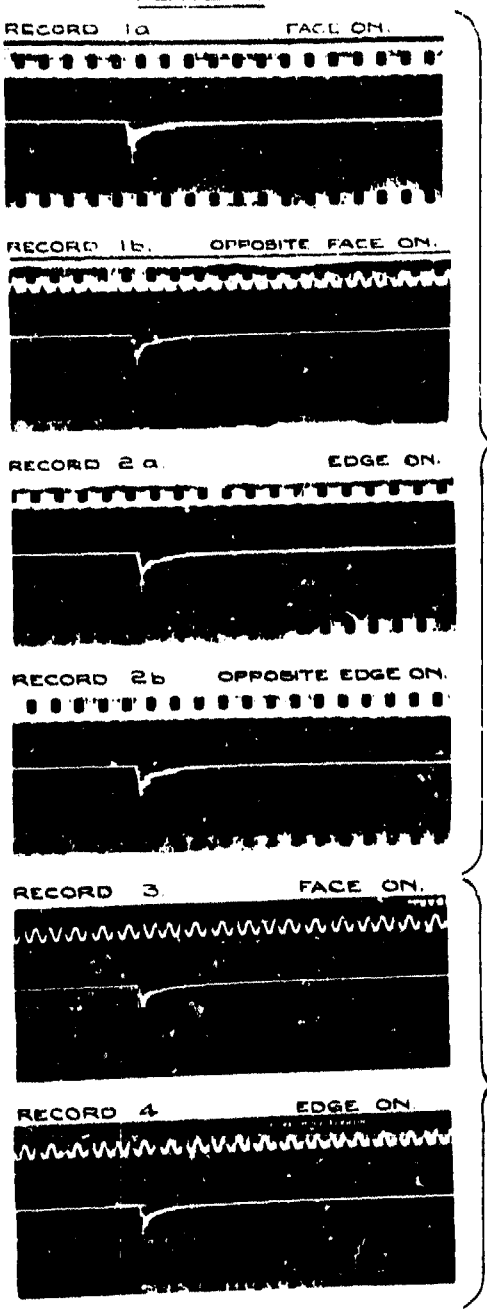


SINGLE PLY GAUGE ½" DIA. x ¼" THICK.
OUTER ELECTRODES
STEEL 0·001S."

ELECTRODES CEMENTED WITH "GELVA."
INSULATION: LAYER OF TELCOTHENE AND 3 LAYERS OF RUBBER TAPE.
1¼ LBS. T.N.T. STANDARD CHARGE.

Best Available Cop

PLATE 4



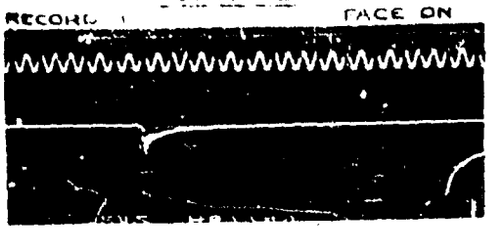
TWO PLY GAUGE 1/2"DIA. x 1/4"THICK EACH. OUTER AND CENTRAL ELECTRODES — STEEL 0·0015"THICK.

SINGLE PLY GAUGE 1/2"DIA x 1/4"THICK OUTER ELECTRODES 0·25"THICK STEEL.

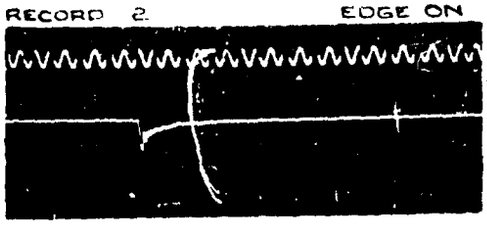
ELECTRODES CEMENTED WITH "GELVA"
INSULATION: LAYER OF TELCOTHENE AND 3 LAYERS OF RUBBER TAPE.
1 1/4 LBS. T.N.T. STANDARD CHARGE.

PLATE 5

RECORD 1 FACE ON

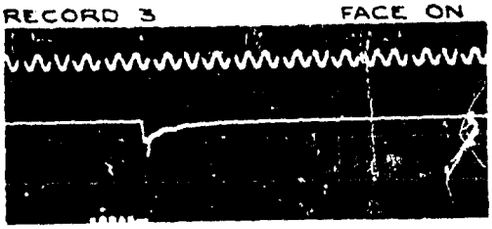


RECORD 2. EDGE ON

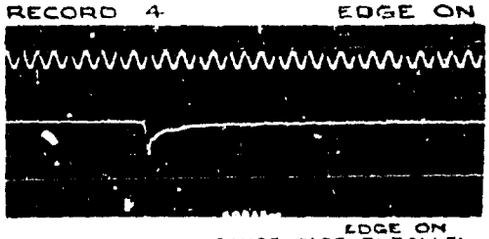


TWO PLY ½"DIA. x ¼"THICK EACH.
OUTER ELECTRODES 0·25" THICK STEEL.
CENTRAL ELECTRODE 0·0015" STEEL.

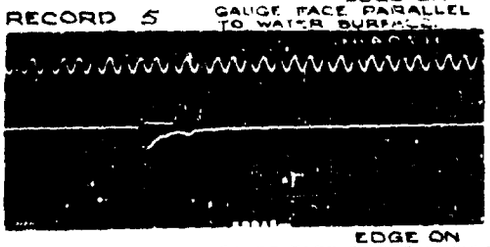
RECORD 3 FACE ON



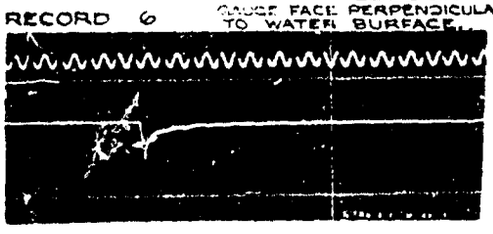
RECORD 4 EDGE ON



RECORD 5 EDGE ON GAUGE FACE PARALLEL TO WATER SURFACE



RECORD 6 EDGE ON GAUGE FACE PERPENDICULAR TO WATER SURFACE.



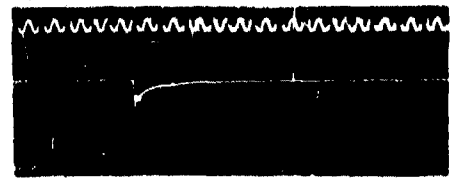
SINGLE PLY GAUGE ½"DIA. x ¼"THICK.
ANNEALED COPPER ELECTRODES 0·082"THICK.

Best Available Copy

ELECTRODES PRINTED WITH "GELVA"
INSULATION: LAYER OF TELCOTHENE AND 3 LAYERS OF RUBBER TAPE.
1/4 [illegible] STANDARD CHARGE.

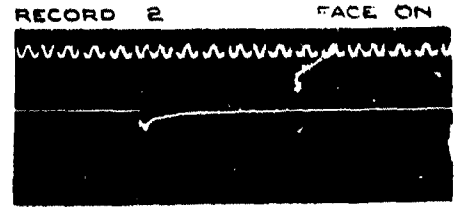
PLATE 6

RECORD 1 EDGE ON

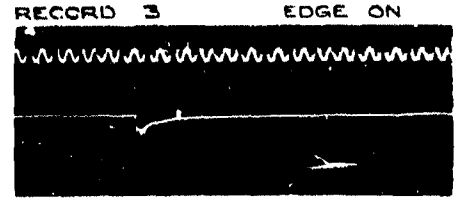


GAUGE FACE PERPENDICULAR TO WATER SURFACE
INSULATION: TELCOTHENE REMOVED - 3 LAYERS OF RUBBER TAPE ONLY.

RECORD 2 FACE ON

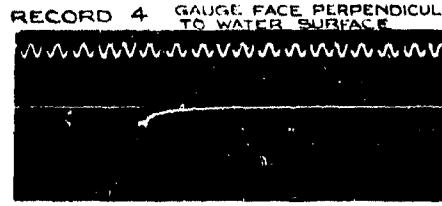


RECORD 3 EDGE ON



INSULATION: RUBBER SOLUTION ONLY

RECORD 4 EDGE ON GAUGE FACE PERPENDICULAR TO WATER SURFACE



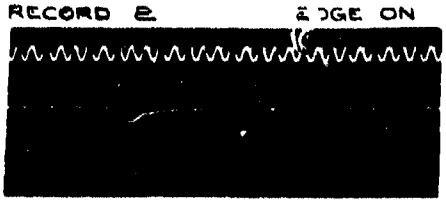
SINGLE PLY GAUGE ½" DIA. x ¼" THICK.
ANNEALED COPPER ELECTRODES 0·002" THICK
CEMENTED BY "GELVA"
ALL CHARGES 1¼ LBS STANDARD T.N.T.

PLATE 7.

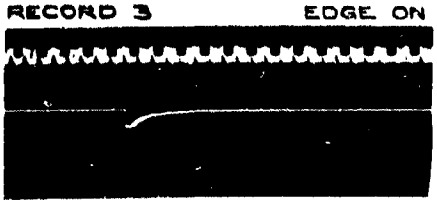
RECORD 1 FACE ON



RECORD 2. EDGE ON

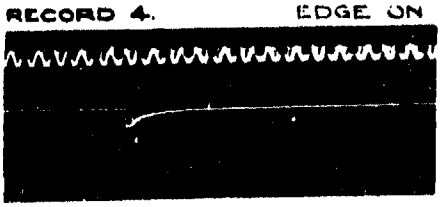


RECORD 3 EDGE ON



GAUGE FACE PARALLEL TO WATER SURFACE

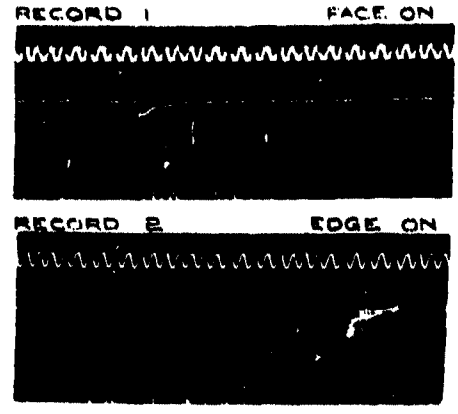
RECORD 4. EDGE ON



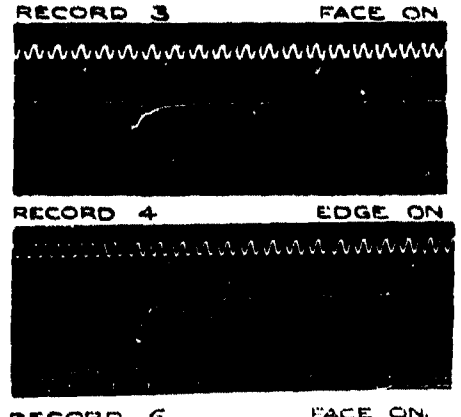
GAUGE FACE PERPENDICULAR TO WATER SURFACE.

SINGLE PLY GAUGE ½" DIA. x ¼" THICK.
ANNEALED COPPER ELECTRODES 0·08" THICK.
INSULATION: PARAFFIN WAX – VASELINE MIXTURE.
1¼ LBS. STANDARD T.N.T. CHARGES.

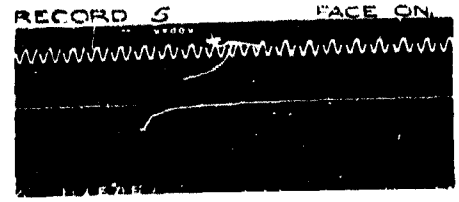
PLATE 8



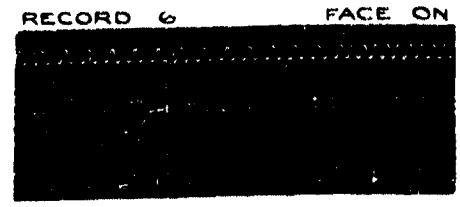
1¼ LBS. STANDARD T.N.T. SINGLE PLY GAUGE. ½" DIA. x ¼" THICK.



1¼ LBS. STANDARD T.N.T. SINGLE PLY GAUGE. ½" DIA. x ⅛" THICK.



H.F. RESPONSE OF AMPLIFIER REDUCED FROM 560 KC/S. TO 300 KC/S.

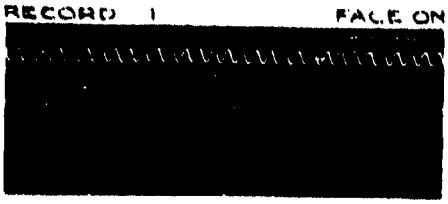


H.F. RESPONSE OF AMPLIFIER REDUCED FROM 550 KC/S TO 20 KC/S.

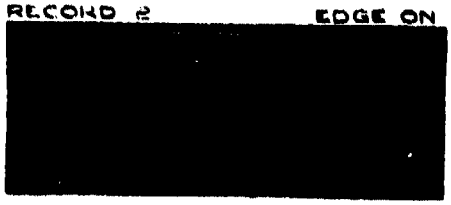
SINTERED OUTER SILVER ELECTRODES 0·0025" THICK.
INSULATION: RUBBEROID WAX AT BASE OF GAUGE WITH 4 VERY THIN LAYERS FROM DIPPING IN NATURAL LATEX AND CURING AT LOW TEMPERATURE.

PLATE 2

RECORD 1 FACE ON

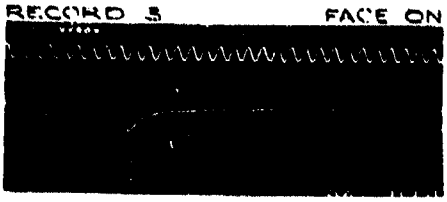


RECORD 2 EDGE ON



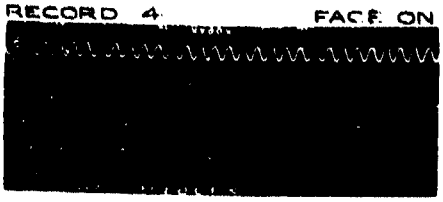
SINGLE PLY GAUGE.
1/2" DIA x 1/16" THICK.
1 1/4 LBS. T.N.T. STANDARD CHARGE

RECORD 3 FACE ON



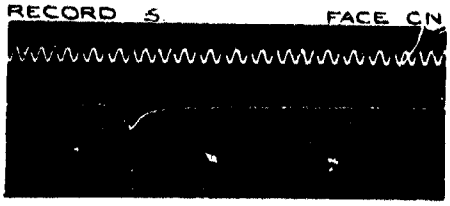
SINGLE PLY GAUGE.
1/2" DIA x 1/4" THICK.
1 1/4 LBS. T.N.T. STANDARD CHARGE

RECORD 4 FACE ON



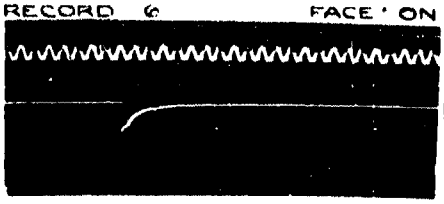
SINGLE PLY GAUGE.
1/2" DIA x 1/4" THICK
STANDARD 1 1/4 LBS T.N.T
CHARGE WITHOUT CANNISTER

RECORD 5 FACE ON



SINGLE PLY GAUGE.
1/2" DIA x 1/4" THICK.
1 4 OZ. P.E SPHERICAL CHARGE
(BARE)

RECORD 6 FACE ON



SINGLE PLY GAUGE.
1/2" x 1/16" THICK.
1 4 OZ BARE PE SPHERICAL
CHARGE

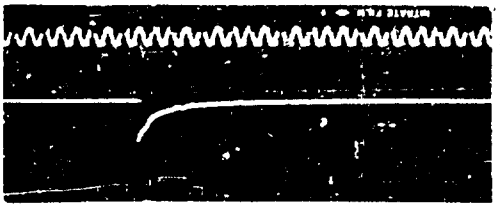
SINTERED OUTER SILVER ELECTRODES 0·0025" THICK
INSULATION: RUBBEROID WAX AT BASE OF GAUGE
WITH 4 VERY THIN LAYERS FROM DIPPING IN
NATURAL LATEX AND CURING AT LOW TEMPERATURE.

RECORD 1



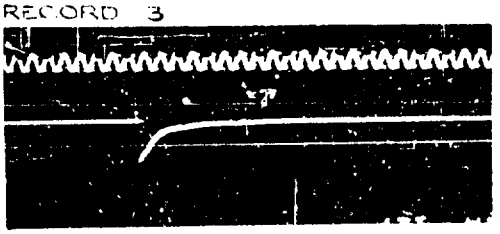
EDGE ON
GAUGE PERPENDICULAR TO
WATER SURFACE.
¼"DIA x ⅛" THICK GAUGE.
1¼ LBS TNT STANDARD CHARGE.

RECORD 2



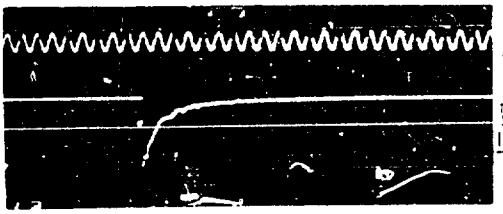
EDGE ON
GAUGE PERPENDICULAR TO
WATER SURFACE.
¼"DIA x 1/16" THICK GAUGE.
1¼ LBS STANDARD CHARGE TN T.

RECORD 3



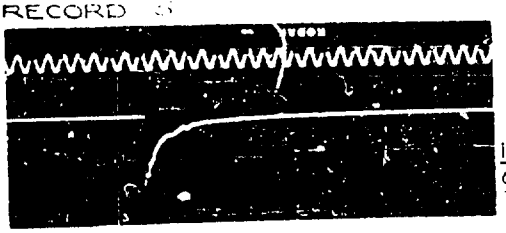
EDGE ON
GAUGE PERPENDICULAR TO
WATER SURFACE.
¼"DIA x 1/16" THICK GAUGE.
1-OZ. SPHERICAL PE. CHARGE.

RECORD 4



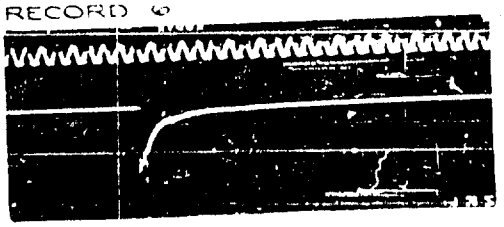
EDGE ON
GAUGE PERPENDICULAR TO
WATER SURFACE.
¼"DIA x 1/32" THICK GAUGE.
1¼ LBS STANDARD TN.T CHARGE

RECORD 5



EDGE ON.
GAUGE PERPENDICULAR TO
WATER SURFACE.
¼"DIA x 1/32" THICK GAUGE.
1¼ LBS. T.N.T WITHOUT
CANNISTER.

RECORD 6



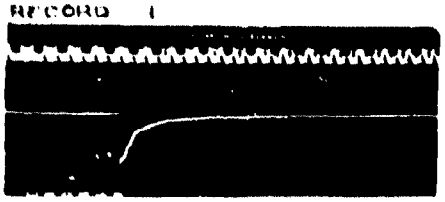
EDGE ON.
GAUGE PERPENDICULAR TO
WATER SURFACE.
¼"DIA x 1/32" THICK GAUGE.
1-OZ PE. SPHERICAL CHARGE.

Best Available Copy

SINGLE FOIL GAUGE. SINTERED SILVER ELECTRODES
0.0004" THICK
INSULATION BEHIND FOIL WAS AT BASE OF GAUGE
WITH A THIN LAYER FROM DIPPING IN
NATURAL RUBBER LATEX AT LOW TEMPERATURE

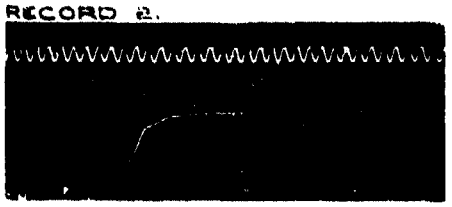
PLATE II

RECORD 1



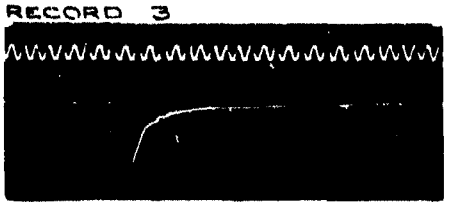
FACE ON.
STANDARD 1¼LBS. T.N.T.

RECORD 2.



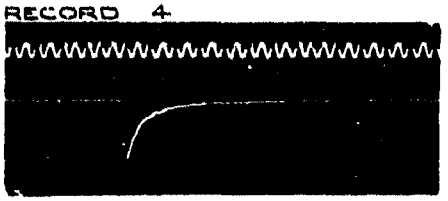
EDGE ON.
STANDARD 1¼LBS T.N.T.

RECORD 3



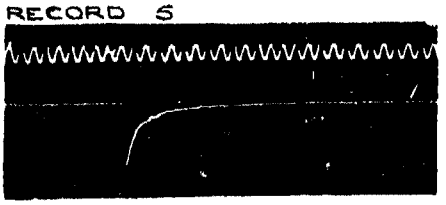
EDGE ON.
GAUGE FACE PARALLEL TO WATER SURFACE.
STANDARD 1¼LBS T.N.T.

RECORD 4



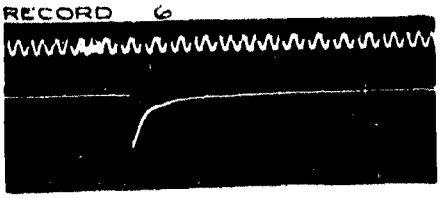
EDGE ON.
GAUGE FACE PERPENDICULAR TO WATER SURFACE.
STANDARD 1¼LBS. T.N.T.

RECORD 5



Dº.
BARE 1¼LBS. T.N.T.

RECORD 6

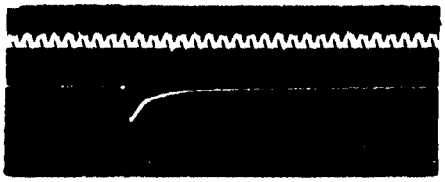


Dº.
SPHERICAL 14 OZ. P.E.

SINGLE PLY GAUGE 1"x ⅛"THICK SINTERED SILVER ELECTRODES 0·0025" THICK.
INSULATION: RUBBEROID WAX AT BASE OF GAUGE WITH 4 VERY THIN LAYERS FROM DIPPING IN NATURAL LATEX AND CURING AT LOW TEMPERATURE.

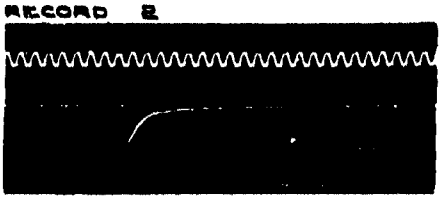
PLATE 12.

RECORD 1



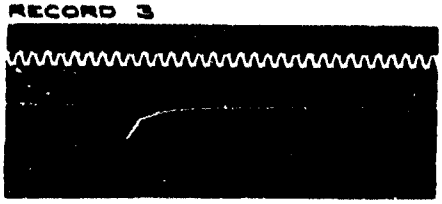
EDGE ON.
FACE PARALLEL TO WATER SURFACE.
STANDARD 1¼ LBS T.N.T CHARGE

RECORD 2



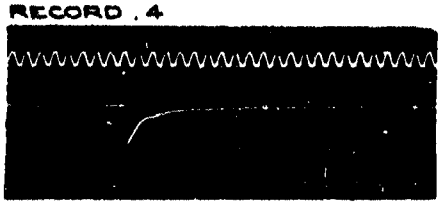
EDGE ON.
FACE PARALLEL TO WATER SURFACE.
1 4OZ SPHERICAL CHARGE.

RECORD 3



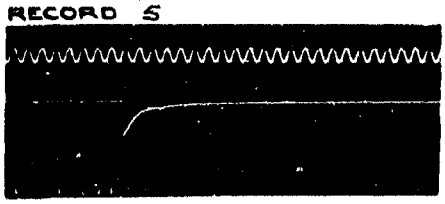
EDGE ON.
FACE PERPENDICULAR TO WATER SURFACE.
STANDARD 1¼ LBS T.N.T CHARGE

RECORD 4



Do.
BARE 1¼ LBS. T.N.T.

RECORD 5

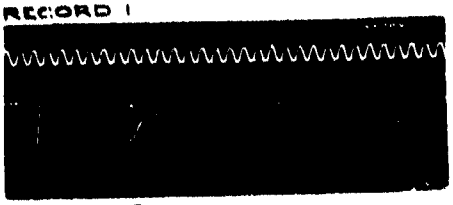


Do.
1 4OZ. SPHERICAL CHARGE

SINGLE PLY GAUGE ½" x 1/16" THICK.
SINTERED SILVER ELECTRODES 0·0025" THICK.
INSULATION: RUBBEROID WAX AT BASE OF GAUGE WITH 4 VERY THIN LAYERS FROM DIPPING IN NATURAL LATEX AND CURING AT LOW TEMPERATURE.

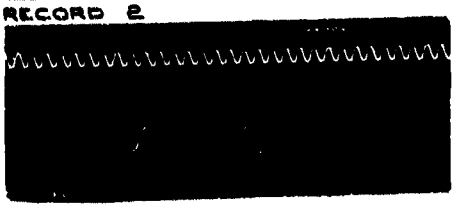
PLATE 13

RECORD 1



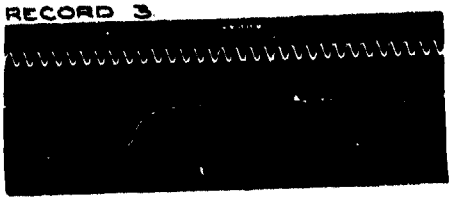
FACE ON.
1¼ LBS STANDARD T.N.T.

RECORD 2



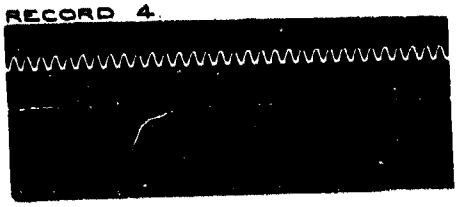
FACE ON.
BARE T.N.T.

RECORD 3

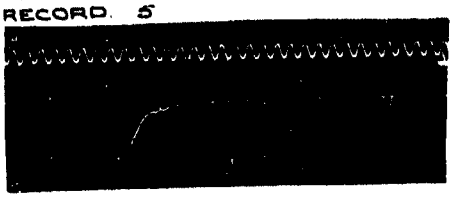


FACE ON.
14 OZ. SPHERICAL CHARGE.

RECORD 4.

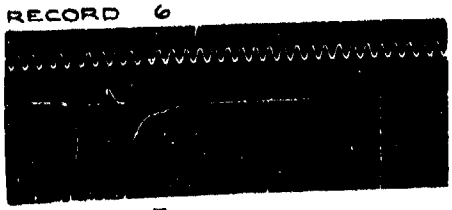


RECORD 5

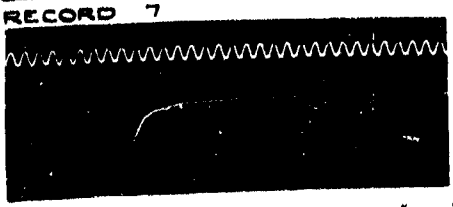


EDGE ON
FACES PARALLEL TO
WATER SURFACE.
BARE 1¼ LBS. T.N.T.

RECORD 6



RECORD 7



EDGE ON
FACES PERPENDICULAR
TO WATER SURFACE.
BARE 1¼ LBS. T.N.T.

TWO PLY GAUGES 1/2" DIA x 1/16" THICK EACH - SINTERED SILVER OUTER ELECTRODES 0·0025" THICK AND 0·0025" THICK CENTRAL ELECTRODE SILVER FOIL FUSED BETWEEN TWO CRYSTALS. INSULATION: RUBBEROID WAX AT BASE OF GAUGE WITH 4 VERY THIN LAYERS FROM DIPPING IN NATURAL LATEX AND CURING AT LOW TEMPERATURE.

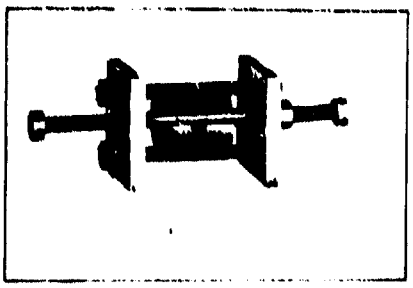


PLATE 14

JIG ASSEMBLY DETAILS IN CONSTRUCTION OF FINALISED MINIATURE GAUGE



PLATE 15.

MINIATURE GAUGE BEFORE APPLICATION OF RUBBEROID WAX AND NATURAL LATEX ALSO AFTER COMPLETION OF CURING PROCESS.

DESIGN AND USE OF PIEZOELECTRIC GAUGES FOR MEASUREMENT OF LARGE TRANSIENT PRESSURES

A. B. Arons and R. H. Cole
Underwater Explosives Research Laboratory
Woods Hole Oceanographic Institution

American Contribution

22 June 1948

Reprinted from THE REVIEW OF SCIENTIFIC INSTRUMENTS
Vol. 21, No. 1, pp. 31-38, January 1950

THE REVIEW OF SCIENTIFIC INSTRUMENTS VOLUME 21, NUMBER 1 JANUARY, 1950

Design and Use of Piezoelectric Gauges for Measurement of Large Transient Pressures*

A. B. Arons† and R. H. Cole‡
Underwater Explosives Research Laboratory, Woods Hole Oceanographic Institution, Woods Hole, Massachusetts

(Received June 22, 1948)

This report discusses the design and use of piezoelectric gauges for the measurement of rapidly varying hydrostatic pressures of large amplitude in gaseous and liquid media. Reasons are given for the selection of tourmaline in preference to other types of crystal. Fundamental principles of design are stated, and gauge construction is described in the light of these principles. A simplified theoretical analysis of transient response characteristics is presented.

I. INTRODUCTION

THE original suggestion that transient pressure waves could be recorded as functions of time by observing the trace of a cathode-ray oscilloscope as it was deflected by the signal from a piezoelectric crystal has been credited to J. J. Thomson. Early experiments using such apparatus to record shock waves from under water explosions of TNT were described by Keys in 1921.[1] Since that time, the technique has been applied to several types of large amplitude pressure measurement, the most common being pressure-time phenomena in internal combustion engines and in shock waves due to explosions in air and water.

During World War II, a group at the Underwater Explosives Research Laboratory of the Woods Hole Oceanographic Institution made a number of contributions to the technique of shock wave measurement, utilizing tourmaline crystal gauges. A discussion of the present status of this technique will be given in this report. The type of gauge developed at the Underwater Explosives Research Laboratory will be referred to in the following as the UERL gauge.¶

II. BASIC REQUIREMENTS FOR A PRESSURE-SENSITIVE DEVICE

It is illuminating to outline first the criteria which an ideal electromechanical pressure-measuring device should satisfy. Although in principle these criteria should apply to any magnitude or duration of applied pressure, in practice their relative importance depends on both characteristics. In this paper, we consider primarily the measurement of transient pressures lasting a fraction of a second at most and with amplitudes from one to hundreds of atmospheres, as opposed to static pressures or acoustic waves. The requirements for such purposes can be summarized as follows: linearity, freedom from hysteresis, thermal stability, freedom from extraneous signals, adequate high and low frequency response, minimum distortion of the pressure field, ruggedness, and simplicity.

The efforts of the UERL group were directed toward the development of a gauge affording a practicable compromise among these requirements.

III. SELECTION OF THE GAUGE MATERIAL

Of the many known piezoactive crystals, those that have been used and investigated most extensively are rochelle salt, ADP, quartz, and tourmaline. More recently, crystals such as barium titanate and its various modifications, lithium sulfate, and certain tartrates have been successfully prepared and utilized.

The most sensitive of these materials are rochelle salt, barium titanate, and ADP. The first two do not appear to be suitable for measurement of fairly large pressure amplitudes owing to a relaxation or hysteresis effect which causes them to produce a rising signal upon application of a step pressure. Rochelle salt and ADP exhibit further disadvantages in that they are not hydrostatically sensitive and not sufficiently rugged for the applications here intended. The other "synthetics" present various difficulties due to their solubility or the presence of water of crystallization.

An extensive survey of piezoelectric activity of minerals has been reported by Bond.[2] It is interesting to note that after listing all the known piezoactive, naturally occurring minerals, Bond concludes that only quartz and tourmaline are practical for any extensive piezoelectric work. All the other active minerals are very rare, occur in the form of exceedingly small crystals, or are very weak mechanically.

Quartz was rejected because of its lack of hydrostatic sensitivity. Because of its ruggedness, linearity, insolubility, and hydrostatic sensitivity, tourmaline appeared to offer most promise for the construction of small, simple gauges and was selected accordingly.

IV. DESIGN AND CONSTRUCTION OF TOURMALINE GAUGES

A. Basic Considerations of Design

Since the criteria listed in Section II are not all mutually consistent, the design of a gauge for a particular

* The work described in this report was initiated under contract with the OSRD in 1941 and after 1945 was continued under contract with the Navy Department, Bureau of Ordnance. Contribution from the Woods Hole Oceanographic Institution, No. 437.

† Present address: Department of Physics, Stevens Institute of Technology, Hoboken, New Jersey.
‡ Present address: Department of Chemistry, Brown University, Providence, Rhode Island.

[1] D. A. Keys, Phil. Mag. 42, 473 (1921).

¶ These gauges are now being produced commercially by the Cambridge Thermionic Corporation, Cambridge, Massachusetts.

[2] W. L. Bond, Bell System Tech. J. 22, 145 (1943).

application resolves itself into a search for a suitable compromise among these factors, and sometimes the final design cannot satisfy all the requirements to the extent desired. It has been established that tourmaline is satisfactory with respect to linearity, freedom from hysteresis, and stability of its pressure sensitivity, but there remains the problem of arriving at a design adequate from the points of view of sensitivity, frequency response, and ruggedness—all factors which are to some extent under the control of the designer.

Piezoelectric crystals develop polarization *charge* when subjected to pressure changes. This charge distributes itself over the capacitance which is in parallel with the gauge element, and consequently the amplitude of the voltage appearing at the amplifier input is not only directly proportional to the applied pressure change but also inversely proportional to the total capacitance parallel to the gauge element in the input circuit.

The necessary gauge sensitivity must therefore be evaluated in terms of the following controlling factors: (1) magnitude of pressure variations to be recorded, (2) total capacitance of the gauge circuit (this depends principally upon the length of cable required to connect the gauge to the amplifier or preamplifier), and (3) amplifier sensitivity.

A lower limit is sometimes placed upon the required sensitivity by the presence of spurious signal arising in the cable or the mounting of the gauge. In many applications, a piezoelectric gauge is connected to recording equipment by means of shielded cable, a certain length of which may be unavoidably exposed to the pressure wave as the latter advances from its source. Spurious signal arising in such cases is an integrated effect which generally introduces little error into the determination of initially discontinuous or rapidly changing pressures, but adds progressively more signal as the wave encounters more cable. It is evident that measurements of small pressures behind an initial high pressure region may thus become highly inaccurate and an effort to obtain reliable values of impulse by integration of the pressure-time curves may be entirely vitiated.

Experience has demonstrated that most ordinary commercial rubber microphone cables and polyethylene cables are completely inadequate since the signals they develop when subjected to pressure variations are very large and may even be, under some conditions, larger than those which would be produced by the gauge elements themselves.

A number of cables were developed which proved to be adequate, and one type—a copper tubing cable, originated at the David Taylor Model Basin—was used successfully for several years in under water studies. More recent developments have led to the production of a polyethylene cable (designated F.O. 5879 by the Simplex Wire and Cable Company) which appears to be superior to any other cables previously available and which is equally satisfactory for measurements in both gaseous and liquid media. However, even in this cable, the signal has not been completely eliminated (although it has been very greatly reduced) and one must always make sure that the gauge signal is large relative to the residual cable signal in each application.

Although much work in the past has been done with single-ended systems using coaxial cables,[3] it is well known that push-pull or balanced systems effect material reduction in residual cable signal by canceling out components which are symmetrical about ground. It seems unlikely, however, that such a system would eliminate the difficulty entirely, since there is no reason to expect the cable signal to be a perfectly symmetrical phenomenon.

The sensitivity of a piezoelectric gauge is directly proportional to the available sensitive area of crystal. In cases where spurious signal due to cable or gauge mounting is a significant factor, the permissible lower limit of sensitivity imposed by such signal places a lower limit upon the size of the gauge. On the other hand, the discussion of high frequency response and pressure-field distortion given in Section V shows that higher fidelity is obtained with *smaller* linear dimensions of the sensitive unit. Specific requirements as to accuracy with respect to high frequency response consequently put an upper limit on the linear dimensions of the gauge, particularly the dimension along the direction of propagation of the wave, and this upper limit must be reconciled with the lower limit indicated by the necessity of swamping spurious signal. In some cases the two requirements cannot be reconciled, and one or the other must be compromised in designing the gauge. This is particularly true where it is desired to measure very rapid pressure variations in liquid media. In gaseous media where the high frequency response requirements are usually less stringent, large gauges can be used and the above requirements can generally be reconciled.

In the actual construction of gauges, a given sensitivity can be obtained and the linear dimensions minimized by stacking two or more crystal plates in parallel. This feature has been utilized in all UERL gauges, but, except for a few special cases, it has not proved practicable to use gauges having more than four plates in the pile.

B. Construction of Gauges

The object of the UERL group was to develop a unit suitable for measurement of explosion-produced shock waves in air and water. Many of the basic principles, however, apply to measurement of transient pressure waves in general, and properly modified UERL-type gauges should be useful under a wide variety of circumstances.

The principal difficulties with the early gauge designs proved to be lack of stability of pressure sensitivity and prevalence of large systematic discrepancies between

[3] R. H. Cole, "The use of electrical cables with piezoelectric gauges." OSRD Report No. 4561.

gauges used on the same measurement, even when the sensitivity of each gauge appeared to be stabilized. These difficulties were largely overcome by adoption of an improved construction technique, the governing principle of which was to prevent disturbance of the electrodes during the later stages of gauge assembly and during subsequent use.

An assembly drawing of a single-ended UERL gauge is shown in Fig. 1, and a picture of the different stages of construction is shown in Fig. 2. Properly lapped tourmaline disks receive a coat of electrode material, such as Du Pont liquid silver No. 4391, and are baked for about an hour at 550°C. Four disks are then assembled in a pile, two on each side of a steel tab as shown in Fig. 1, and the pile is sweated together into a single, homogeneous unit by being placed in a spring clamp and again heated in an oven. Provision is made in this operation for electrode connection to the intermediate crystal faces.

The peripheral edges of the pile are insulated by the application of a thin layer of dielectric material such as pure latex which can be painted around the edges and cured *in situ* by baking at *ca.* 120°C. With the periphery properly insulated, contact can now be made between the outermost crystal faces and the grounded central tab. Originally this was accomplished by direct soldering to the electrodes, and the technique was revised because of the deleterious effect on the intimacy of electrode-crystal contact. The present technique is to make contact by means of a conducting silver paint which can be baked on at temperatures low enough to be compatible with the insulating material used around the edges of the unit.

In connecting a unit of this type to a length of electrical cable, it is only necessary to solder the central tab to the cable shield and spot solder the high electrode leads to the cable conductor. These connections can be made quickly, with a minimum of heating of the gauge element. In this manner the electrodes are afforded the greatest possible protection during mounting of the unit. (Elements of this type have also been mounted in threaded inserts which can be screwed into the wall of a container in which pressure variations are to be studied.)

Gauges of this design have been used to measure pressure, impulse, and energy flux in waves ranging in amplitude from 0.5 to 100,000 lb./in.^{2}.

It was originally feared that the introduction of the metal central tab might tend to introduce spurious mechanical oscillations on the pressure-time records. However, there has so far been no evidence of the presence of oscillations more serious than those ordinarily observed with gauges of earlier design which were not provided with central tabs.

The central tab principle is also vitally important because of the strength it gives the completed unit, particularly where measurements are to be made in gaseous media in which stresses caused by the exceedingly high particle velocities are capable of causing severe damage to unreinforced gauges.

The gauge design described is also well suited to the construction of push-pull units. If one pair of tourmaline disks is arranged with positive faces connected to one high potential lead while the pair on the opposite side of the central tab has negative faces connected to another high potential lead, the central tab and outer pair of faces can all be grounded to the shield of a two-conductor cable while the two high potential leads are connected to the two center conductors, respectively. This

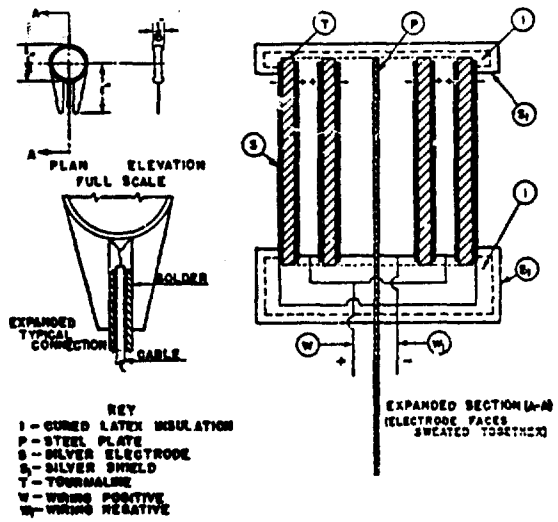


FIG. 1. Assembly drawing of UERL-type tourmaline gauge.

results in a perfectly symmetrical, completely shielded unit which develops signals balanced about ground. A less symmetrical, but more efficient push-pull gauge can be made by connecting a single-ended-type unit to the center conductors of a two-conductor cable without grounding any point within the gauge.

In the case of gauges intended for measurements in gaseous media, the serious effects of perturbation of the flow around the gauge[4] can be minimized by surrounding the gauge element with a streamlined housing or baffle of suitable shape and proportions. Various aspects of this design problem are still under investigation in several laboratories.

C. Coating of Gauges

After the gauge element is assembled and mounted, it is necessary to apply a waterproof coating, since contact with even minute quantities of moisture results in low gauge resistance with consequent impairment of the low frequency response.

Numerous coating techniques have been tested by the UERL group, and only a few have proved satisfactory. The most useful method has been the application of a

[4] J. K. L. MacDonald and S. A. Schaaf, "On the estimation of perturbations due to flow around blast gauges," OSRD Report No. 5639.

thin, tight winding of high grade rubber tape over a thin layer of rubber cement such as Bostik 292 (BB Chemical Company, Cambridge, Massachusetts).

Where the cable or other mounting is rigid (as in the case of copper tube cables), successful coatings have been obtained by dipping the unit several times into a molten mineral wax (such as Zophar Mills C276) and allowing a thin wax coating to be built up.

Successful, but fairly bulky coatings have been obtained by cold-molding of Thiokol (Minnesota Mining and Manufacturing Company). Molding in plastics has been unsuccessful because of the brittleness and poor adhesion of thin layers of these substances. Molding in rubber has proved impractical because the accompanying high temperatures damage the gauge elements.

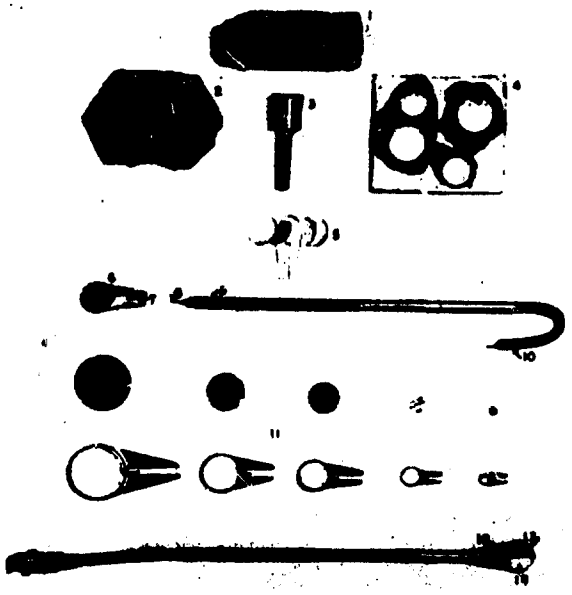


FIG. 2. Stages of construction of single-ended tourmaline blast gauges.

1—Raw tourmaline crystal. Cuts are made perpendicular to the principal (Z) axis.
2—Slab of tourmaline before dicing.
3—Dicing tool (periphery charged with diamond dust).
4—Tourmaline slabs cemented to glass plate for dicing operation.
5—Stacking of disks and central tab. (Silver electrodes have been applied.)
6—Element after being sweated together in oven.
7—High lead connecting intermediate pairs of faces.
8—Center conductor of cable.
9—Brass tube.
10—Special lead-sheathed microphone cable.
11—Various sizes of gauges which have been constructed. Diameters, left to right: 1½, 1¼, ¾, ½, and ¼ in. (½- and ¼-in. gauges are used for underwater measurements).
12—Central tab soldered to brass tube.
13—Latex edge insulation.
14—Painted silver shield providing contact between outer faces and ground.

In air or other gaseous media the coating serves an additional important purpose in that it provides a measure of thermal insulation to the crystal element, thus preventing serious pyroelectric interference from changes in ambient temperature and changes due to temperature rise of the gas on adiabatic compression in the shock wave.

V. TRANSIENT RESPONSE CHARACTERISTICS OF GAUGES

A. High Frequency Response

We shall first analyze the effect of the geometrical size of the gauge upon the fidelity of its peak pressure reading.

(1) Frequency response. Assume a simplified ideal case in which the gauge is represented by a circular disk of radius a, and negligible thickness, and assume the gauge to be oriented edgewise to the direction of propagation of a sinusoidal standing wave $P_0 \cos(2\pi x/\lambda)$, where x is the distance from an axis through the center of the gauge and λ is the wave-length.

If c is the velocity of propagation, it is readily shown, by integration over the surface of the gauge, that

$$R(f)=2J_1(2\pi fa/c)/(2\pi fa/c), \qquad (1)$$

where f is the frequency of the standing wave, $J_1(2\pi fa/c)$ is Bessel's function of the first kind, index one, and $R(f)$ is response of the gauge, defined as the ratio of the actual maximum force it experiences to the ideal maximum force given by the product of P_0 and the gauge area. $R(f)$ is plotted as a function of af/c in Fig. 3. It is seen that the response falls to zero at the frequency $f_0=0.61c/a$.

At higher frequencies the response undergoes successive reversals of phase and gradual decay. It should be noted that ordinary steady-state response measurements are insensitive to phase, and the negative portions of the curve would be measured as positive. This rectified form is indicated by the dashed curve of Fig. 3.

As a numerical example, the response in water of a gauge 12.6 mm in diameter will be half its static value at a frequency of about 60 kc/sec. and zero at a frequency of about 100 kc/sec.

A number of gauges were calibrated for the UERL group by the Columbia University Underwater Sound Reference Laboratories, the frequency-response curves being obtained at acoustic levels by using the gauge to pick up the signal of a standard projector previously calibrated by means of the reciprocity principle. A comparison of the theoretical calculation with experimental results is given in Fig. 4, and it is seen that the two are in generally good agreement. The hump in the experimental record for Gauge 5A53 has the characteristic appearance of a mechanical resonance and is probably due to a cantilever vibration of this particular gauge on its 5-in. length of copper tube cable.

(2) Step response. If a gauge is to be used for transient pressure measurements, it is desirable to analyze its performance in terms of its response to simple forms of traveling wave. The simplest useful case is that of a step

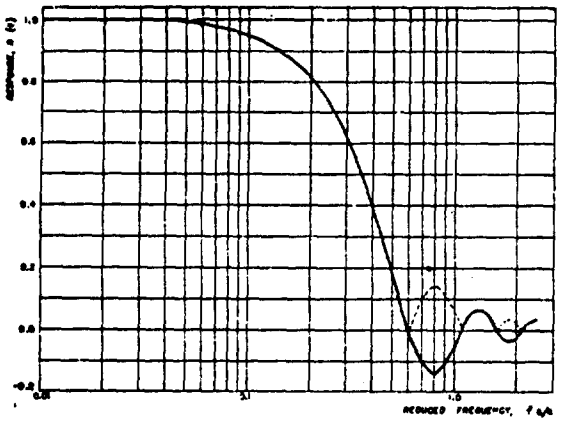


FIG. 3. Frequency response of a circular gauge of radius a oriented edge-on to an advancing pressure wave. (f is frequency, and c is velocity of wave propagation.)

pressure of value P_0, traveling with velocity c parallel to the faces of the disk. If the pressure discontinuity is at $x=0$ at time $t=0$, and the gauge of radius a has its center at $x=0$, the response of the gauge, $R(t)$, is readily shown from geometrical considerations to be given by:

$$R(t)=\begin{cases}0, & \text{when } t<-a/c\\ (\phi-\sin\phi\cos\phi)/\pi, & \text{when } -a/c<t<a/c,\\ 1, & \text{when } t>a/c\end{cases} \quad (2)$$

where

$$\phi=\cos^{-1}(-ct/a). \quad (3)$$

Equation (2) is plotted in Fig. 5 as a function of ct/a. From the symmetry, it is evident that the area under the response curve is the same as the area under the ideal curve if the integration is carried from $-a/c$ to times greater than $+a/c$. The interval $2a/c$ is obviously the time required for the pressure wave to cross the gauge. For a 12.6-mm diameter gauge in water, this crossing time is 8.4 μsec. It is apparent that a gauge of diameter $2a$ cannot be expected to give very detailed information about pressure changes occurring in time intervals of $2a/c$ or less.

(3) Response to saw-tooth wave. The response of a circular gauge to other arbitrary forms of transient can in principle be obtained either from Eq. (2) for the step response by use of the superposition theorem or from Eq. (1) for frequency response by use of the Fourier integral theorem. In many cases the practical difficulties of the calculations are considerable, and answers in closed form involving evaluated functions are not obtainable. In the special case of the type of wave encountered in shock-wave measurements, however, the nature of the response can be adequately illustrated by assuming a saw-tooth shape. If the incident wave is given by,

$$P(x,t)=\begin{cases}0, & \text{when } t<x/c\\ P_0[1-(1/\theta)(t-x/c)], & \text{when } t>x/c\end{cases} \quad (4)$$

the response of a circular gauge is shown to be,

$$S(t)=\begin{cases}0, & \text{when } t<-a/c\\ \phi/\pi-(\sin\phi\cos\phi)/\pi-(a/3\pi c\theta) & \\ \quad\times(3\sin\phi-3\phi\cos\phi-\sin^3\phi), & \text{when } -a/c<t<a/c\\ 1-t/\theta, & \text{when } t>a/c\end{cases} \quad (5)$$

where, as before, $\phi=\cos^{-1}(-ct/a)$.

The saw-tooth response of Eq. (5) is plotted in Fig. 6 as a function of t/θ for various values of the ratio $a/c\theta$. If this ratio is less than about $\frac{1}{5}$, the maximum response lies very nearly on the true response curve and is lower than the true maximum by the fraction $a/c\theta$. The time required for the gauge to give the maximum response is very nearly the crossing time $2a/c$. As a numerical example, consider a gauge 12.6 mm in diameter used to record a shock wave in water having a decay constant $\theta=400$ μsec. The time to cross the gauge is 8.4 μsec. and the indicated peak pressure will be approximately one percent low. If a gauge is to record a shock wave having $\theta=50$ μsec. with less than one percent error in peak pressure, its diameter should not exceed 1.5 mm.

The behavior of the saw-tooth response suggests that a measured value of peak pressure for a wave similar to a saw-tooth in form could be corrected for the effect of gauge size in either of two ways: (1) by adding a fraction $(a/c\theta)/(1-a/c\theta)$ of the maximum response to this value; (2) by extrapolating the initial decay of the response back an interval a/c along the time scale, determined either from the measured radius a or from the measured

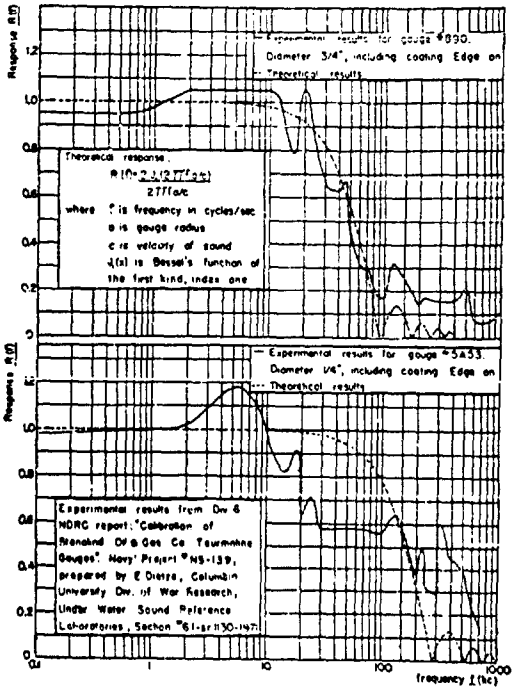


FIG. 4. Comparison of experimental and theoretical frequency response curves for two gauges. (Experimental calibrations performed in sinusoidal acoustic field.)

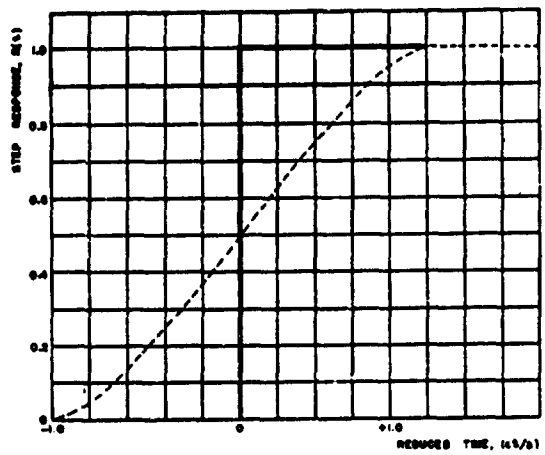


FIG. 5. Response of a gauge of radius a to a progressive step wave of velocity c.

time required for the gauge to give maximum response, this time being theoretically equal to $2a/c$.

The validity of such a correction involves the assumptions that distortion due to diffraction effects dies out sufficiently rapidly not to affect the curve after the maximum, and that the true pressure curve is sufficiently simple for a linear decay law to be a good approximation. It is reasonable, however, to expect that any diffraction effects will have the general character of damped transient oscillations about the gradual rise as the gauge is covered by the advancing wave and should not be significant after the gauge is covered. Whether or not the pressure curve is sufficiently simple to be represented by a straight line or smooth curve, depends, of course, on experimental conditions. Unless appreciable interference or reflections are combined in the resultant wave, the corrected maximum pressure may well be used as a significant measure of the wave.

This principle has been extensively applied by the UERL group in the interpretation of underwater shock wave records and the estimation of true peak pressures under conditions where the gauge size introduced appreciable error. It was found that the simplified theory provides adequate correction for amplitude effects up to about 10 to 15 percent, but then begins to show serious departures from observed values. It has also been found empirically that the gauge radius a which must be used in the theory is not the radius of the element alone, but rather the radius of the *complete* gauge *including* coating material.

B. Interference Effect

The analysis of the effect of gauge size on transient response neglected any disturbance of the pressure wave due to presence of the gauge in the field. Actually, of course, the gauge material is a medium through which sound waves can be transmitted. As a result, one can expect interference effects due to repeated internal reflections of the incident wave at the interfaces of the crystal. This would have roughly the character of a damped saw-tooth oscillation. The frequency of this oscillation cannot be calculated accurately, but it is probably of the order of 100 kc/sec. for the types of gauges described in this paper.

In order to examine the effect of interference on response of an actual gauge, we might consider a circular disk in either of two orientations: face-on and edge-on to the approaching pressure front. The Coulomb sensitivity of a disk of tourmaline depends only on the face area, not on the thickness, and, as a result, the travel time is obviously minimized and the natural frequency highest if a thin disk is oriented face-on. It is to be expected, however, that Bernoulli effects[4] will be much less if the same disk is edge-on.

To the extent that a single very thin disk is practical, the face-on orientation may appear preferable because of the inherently higher frequency characteristic. In actual practice there is a limit to the thinness possible, and in the interest of greater sensitivity, it is desirable to construct a gauge from a pile of disks; thus multiplying the effective area and sensitivity and obtaining a better electrical and mechanical design. Under such circumstances the face-on orientation would have much larger interference oscillations than the edge-on orientation and comparable transit time and flow effects.

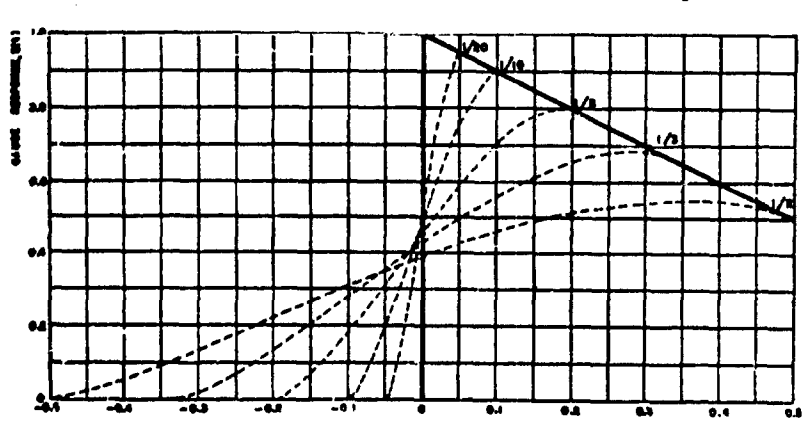


FIG. 6. Response of a gauge of radius a to a progressive saw-tooth wave of decay constant θ and velocity c. Solid line represents incident wave. Dotted curves show response for various values of $a/c\theta$.

Comparing the two possibilities, one might expect the edge-on gauge to have a much smoother rise in response to a step pressure, taking a longer time, but approaching the true curve more smoothly. Experimental tests have roughly indicated this state of affairs, and practical experience has also shown that records obtained with gauges in the edge-on orientation give about as much usable high frequency resolution as face-on gauges and are much cleaner and easier to analyze empirically.

C. Low Frequency Response

(1) Internal impedance. Although a piezoelectric crystal under ideal conditions develops a potential difference between its faces which persists as long as a force is applied to it, in practical use unavoidable leakage resistance and input resistance of recording equipment afford conducting paths by which the piezoelectric charge is gradually neutralized. As a result, the response to applied pressure falls off as the rate of change of pressure decreases. The electrical properties of a piezoelectric crystal are represented with sufficient accuracy for the present discussion by an e.m.f., V_0, proportional to applied pressure, in series with the capacitance, C_0, of the crystal. In actual use the gauge will be shunted by lead capacitance C and leakage or other resistance R.

The response of such a circuit to a step pressure P_0 is a negative exponential:

$$V_t=[KA/(C+C_0)]P_0\epsilon^{-t/\tau}, \qquad (6)$$

where V_t = terminal voltage; KA = gauge sensitivity expressed as charge developed per unit pressure change; and $\tau=R(C+C_0)$.

From Eq. (6) it is evident that the response in the limit of low frequencies or long times approaches zero. The useful lower limit is obviously increased by increasing the time constant τ. Therefore the input impedance and other resistances represented by R should be made as large as other considerations (for example, amplifier stability) permit. Likewise, the time constant can also be increased by use of larger values of C. (In practically all applications $C_0 \ll C$, and increase of crystal capacitance would have no appreciable effect on τ.)

Unfortunately, an increase in the value of the padding capacity C reduces the output voltage by the same proportion. If one is limited in allowable gauge sensitivity by high frequency considerations or by low pressure amplitudes, improvement of low frequency characteristics in this way requires increased sensitivity of the recording system. The best solution in difficult situations requires a compromise between gauge size, resistance of the circuit, and sensitivity of the recorder.

(2) Pyroelectric effect. A second factor that may affect the low frequency response of a piezoelectric gauge is the development of charge as a result of temperature changes in the crystal. Such charges can arise either directly from increased temperature due to adiabatic compression of the crystal, or, indirectly, from temperature changes in the surrounding medium or from radiation such as sunlight, explosion flashes etc.

The first effect has been shown to be negligible by Keys.[5] The second effect depends upon the amount of heat developed external to the crystal and the rate at which it can raise the crystal temperature by thermal conduction or radiation.

The pyroelectric sensitivity of tourmaline is such that a change in temperature of 1°C produces a charge equivalent to that developed by a pressure change of 200 lb./in.^{2}. In liquid media, however, the pressure wave durations are usually very short, and although the adiabatic temperature change of the liquid is appreciable, a gauge can hardly undergo more than a small fraction of the ultimately possible temperature change during such intervals, particularly in view of the thermal insulation afforded by the gauge coating.

In gaseous media, however, radiation effects, temperature changes due to adiabatic compression of the medium, and effects due to variations of ambient temperature become very much more pronounced. Special care must be taken to provide adequate thermal insulation by using coatings of sufficient thickness for the particular application. Excessive thickness of coating, however, has been found to affect the gauge properties by introducing spurious oscillations and other undesirable effects, and a suitable compromise must be found in difficult cases. Radiation effects can largely be protected against by the use of a bright coating, such as silver paint, on the outside of the gauge.

The longer the duration of the signal being measured, the more difficult it becomes to combat interference due to pyroelectric effect, and thus the applicability of the tourmaline gauge is more severely limited by its pyroelectric sensitivity than by the other natural limitations of input impedance, time constant, and piezoelectric sensitivity.

VI. REQUIREMENTS OF ASSOCIATED RECORDING EQUIPMENT

Detailed discussions relative to the design and construction of oscillographic recording equipment and cables for use with piezoelectric gauges will be found elsewhere.[3,6,7] It is the purpose here to discuss briefly only certain requirements of such equipment which are intimately associated with the selection and use of the piezoelectric gauges themselves.

From the foregoing considerations, it is obvious that the low frequency characteristics of an amplifier should be such that its over-all time constant is long relative to the duration of the phenomenon being recorded. In extreme cases this might require a d.c. amplifier. Input

[5] D. A. Keys, Phil. Mag. 46, 999 (1923).

[6] Cole, Stacey, and Brown, "Electrical instruments for study of underwater explosions and other transient phenomena," OSRD Report No. 6238; NDRC No. A-360.

[7] G. K. Fraenkel, "Apparatus for measurement of air-blast pressures by means of piezoelectric gauges," OSRD Report No. 6251; NDRC No. A-373.

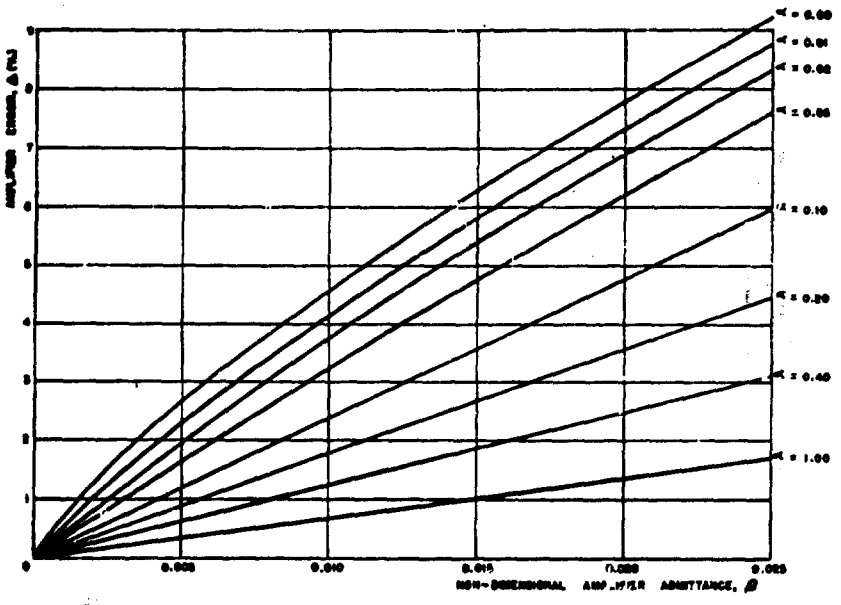


FIG. 7. Amplifier error *vs.* non-dimensional amplifier admittances β for incident waves of various α. (See text for explanation of notation.)

impedance can generally be made sufficiently high by use of cathode follower preamplifiers.

The situation with respect to high frequency requirements is slightly more complex in that a certain amount of high frequency distortion is unavoidably present because of the geometry of the gauge. (This effect was computed for some simple wave forms in Section V.)

In general, therefore, the demand upon amplifier response will be conditioned by the gauge response, and a useful quantitative calculation can be made for the special case of steep-fronted waves, where high frequency considerations are most important.

We assume that a saw-tooth wave is incident at the gauge and that the shape of the signal reaching the amplifier can be represented to a first approximation by a linear rise to a peak value followed by a linear decay, i.e.:

$$F(t)=\begin{cases}0 & \text{when } t<0\\ t/\gamma & \text{when } 0<t<\gamma,\\ 1-(t-\gamma)/\theta & \text{when } t>\gamma\end{cases} \qquad (7)$$

where θ is the decay constant of the wave and $\gamma=2a/c$, the transit time of the shock wave across the gauge.

The step response of the amplifier is assumed to have the form:

$$R(t)=1-\epsilon^{-t/\kappa}. \qquad (8)$$

Expressing the above relations in terms of dimensionless parameters with θ as the scaling factor ($\alpha=\gamma/\theta$, $\beta=\kappa/\theta$), and applying the superposition integral, it is shown that:

$$\Delta=\beta\ln[1+(1-\epsilon^{-\alpha/\beta})/\alpha], \qquad (9)$$

where Δ represents the fractional error introduced by the amplifier in reproducing the peak of the applied function, $F(t)$. $F(t)$, however, already contains an error $\alpha/2$, with respect to the peak pressure of the incident shock wave. Thus the total error introduced by the combined effects of gauge size and amplifier high frequency response is:

$$E=\Delta+\alpha/2 \qquad (10)$$

with respect to the incident shock wave peak pressure.

Figure 7 is a representation of Eq. (9) which should prove useful in estimating error due to a given frequency response for various gauge conditions or for design purposes where one seeks to find the frequency response necessary to keep the error below a certain selected limit.

The problem of calibrating piezoelectric gauges is a vital one, involving rather highly specialized instruments and techniques. Owing to fairly recent developments in the field, calibration will be discussed in a separate paper at some future date.

VII. ACKNOWLEDGMENTS

The knowledge and experience upon which this report is based could not have been accumulated were it not for the cooperative effort of a large number of individuals who participated in the work of the Underwater Explosives Research Laboratory. The authors are pleased to acknowledge in particular the significant contributions of Professor E. B. Wilson, Jr., Dr. W. D. Kennedy, Dr. W. G. Schneider, Dr. A. M. Shanes, and Dr. W. E. Gordon, and regret that space does not permit a more adequate identification of the contributions of each individual to the fundamental understanding of the use and design of piezoelectric gauges. Much credit for development of techniques of construction of the present gauge design is due Professor C. Frondel of the Department of Mineralogy, Harvard University. Earlier construction techniques were developed by Dr. D. Silverman and Mr. H. M. Lang of the Stanolind Oil and Gas Company.

A STUDY OF PIEZOELECTRIC GAUGE CABLE TERMINATION

Otto Meier, Jr.
Naval Ordnance Laboratory

American Contribution

14 November 1949

White Oak, Silver Spring 19, Maryland

NAVAL ORDNANCE LABORATORY MEMORANDUM 10467

14 November 1949

From: Otto Meier, Jr. (SE)

To: G. K. Hartmann (SE)

Via: E. Swift, Jr. (SE)

Subject: A Study of Piezoelectric Gauge Cable Termination. (Task NOL-37-Re2c-3-1).

Abstract: This memorandum gives data resulting from a study of the simple R-C cable compensation network developed by Lampson. Calculations and measurements are included for both the steady-state and step-transient response of the cable and termination. The steady-state response of a specified length of cable having known values of characteristic impedance and total capacitance can be predicted from these data, for wide ranges of terminating resistance and capacity. The corresponding step-transient response can also be predicted. For example, it is found that the initial overshoot of the transient response can be eliminated entirely by the proper choice of terminating resistance.

Foreword: The data and conclusions presented here are primarily for the use of the Explosives Division, but should be generally useful in the selection of the best values of piezoelectric gauge cable terminating resistance and capacity to be used with specified lengths of any cable having known constants. The interpretations herein are those of the author and are not necessarily views of the Naval Ordnance Laboratory.

Refs:
(a) OSRD 4561; "The Use of Electrical Cable with Piezoelectric Gauges", R. H. Cole; 12 December 1944.
(b) OSRD 1179, (NDRC Memo. A-63M); "Cable Compensation for Piezoelectric Gauges", C. W. Lampson; 18 January 1943.

Encls:
(A) Plate 2; Calculated Steady-State Cable Response, Terminating Capacity Equal to Cable Capacity.
(B) Plate 3; Calculated Steady-State Cable Response, Terminating Capacity Two Times Cable Capacity.
(C) Plate 4; Calculated Steady-State Cable Response, Terminating Capacity Four Times Cable Capacity.
(D) Plate 5; Calculated Steady-State Cable Response, Terminating Capacity Six Times Cable Capacity.

(E) Plate 6; Comparison of Measured and Calculated Steady-State Response of 955 ft. Simplex Cable with R-C Termination.
(F) Plate 7; Calculated Step-Transient Cable Response. Terminating Capacity Equal to Cable Capacity.
(G) Plate 8; Calculated Step-Transient Cable Response, Terminating Capacity Two Times Cable Capacity.
(H) Plate 9; Calculated Step-Transient Cable Response, Terminating Capacity Four Times Cable Capacity.
(I) Plate 10; Calculated Step-Transient Cable Response, Terminating Capacity Six Times Cable Capacity.
(J) Plate 11; Oscillograms of Step-Transient Response of Lampson Compensation Network.

The R-C Termination Circuit

1. The circuit dealt with here is the simple compensation network developed by Lampson (see reference b). It is shown in Plate 1. Double-ended compensation is not considered here because of the inconvenience of placing compensation network components at the gauge location in practical underwater field work. Moreover, the simple single-ended compensation network yields superior initial peak response and can be adjusted for satisfactory steady-state and transient response characteristics.

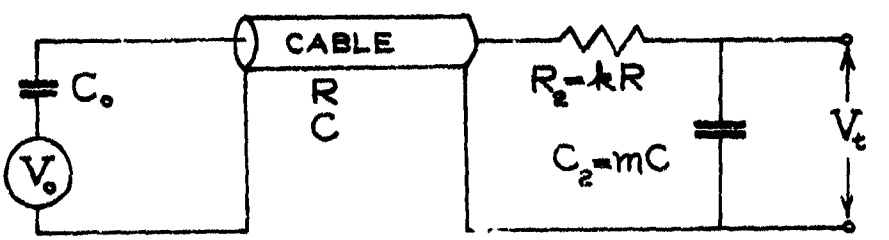


Plate 1. Lampson Compensation Network.

The notation is that given in reference (a). The cable is assumed to be ideal in the calculations, so that losses due to series resistance and shunt conductance are neglected. The cable constants are the characteristic impedance R and the capacity C of the total cable length. The voltage V_o and the small capacity C_o represent the gauge used at the input end of the cable. The terminating resistance R_2 is given as k times the characteristic impedance R of the cable. The terminating capacity C_2 is given as m times the cable capacity C for the total cable length. The output voltage is V_t.

2. All calculations and measurements are for single-ended circuits. In applications where double-ended or push-pull circuits are involved, the data presented here refer to one side only of the double-ended circuit, which

is assumed to be symmetrical. In particular, where twin coaxial cables are employed, the values given here apply to one coaxial line only of the twin coaxial cable.

Steady-State Response Calculations.

3. The steady-state response of the network of Plate 1 is given by

$$(1) \qquad \frac{V_t}{C_o V_o} = \frac{1}{C\,\frac{\sin RC\omega}{RC\omega}\,(1 + ikm\,RC\omega) + m\,C\cos RC\omega}$$

where $\omega = 2\pi f$ and f is the frequency in cycles per second. This is a complex expression and the absolute value is used in the calculations.*

As ω approaches zero, the limiting value of Eq. (1) becomes

$$(2) \qquad \left.\frac{V_t}{C_o V_o}\right]_{\omega \to o} = \frac{1}{C\,(1 + m)} = \frac{1}{C + C_2}$$

The response of the system at a given frequency relative to the limiting response at low frequencies is expressed as a relative amplitude which is obtained by dividing the absolute value of Eq. (1) by Eq. (2). Hence

$$(3) \qquad \text{Relative amplitude} = \frac{1 + m}{\left|\frac{\sin RC\omega}{RC\omega}\,(1 + ikm\,RC\omega) + m\cos RC\omega\right|}$$

The relative amplitudes are plotted as ordinates in Plates 2, 3, 4 and 5, against values of $RC\omega$ as abscissas. The use of the quantity $RC\omega$ permits the application of these curves to any cable of known values of R and C. The curves are therefore not limited to a particular type of cable

* It is to be noted that this expression is somewhat more general than Eq. (7) of reference (a) because of the use of the constants k and m. Moreover, Eq. (7) of reference (a) contains an error in the denominator, where the quantity given as $iRC_2\omega$ should read $iR_2C_2\omega$.

as would be the case if frequency were plotted along the axis of abscissas. Thus if the cable has a characteristic impedance of 50 ohms, a capacity of 30 micromicrofarads per foot, a length of 1000 feet, and if the frequency of interest is 100 kc, the numerical value of $RC\omega$ is 0.942. Then for $m = 2$ the curves of Plate 3 are used, and for $k = 1$ a value of 1.16 is obtained for the relative amplitude corresponding to the value of 0.942 for $RC\omega$.

The calculated steady-state cable response as given by the relative amplitude from Eq. (3) is plotted in Plate 2 for $m = 1$, and for $k = 0$, 1, 1.5, 2, 3 and 4. Similar curves are plotted in Plates 3, 4, and 5 for $m = 2$, 4, and 6 respectively.

4. From Eq. (2) it can be seen that greater sensitivity of the overall recording system can be achieved by using smaller values of the terminating capacity C_2. This corresponds to the use of smaller values of m and hence greater output voltage V_t in Eq. (2). A value of $m = 2$ has been used successfully in field work and the use of $m = 1$ will give even greater signal response. It is to be noted that after the value of m has been chosen, the corresponding value of k to be used will be determined by both the steady-state and transient responses desired. For example, for $m = 2$, from Plate 3, the use of $k = 1$ will give a steady-state relative amplitude of 1.62 for $RC\omega = 2$, but from Plate 8, the initial overshoot of the transient response will be on the order of 50 percent. As shown by Plate 8, this initial overshoot can be eliminated entirely by using $k = 2$ with $m = 2$, but the corresponding steady-state relative response from Plate 3, will be reduced from 1.62 to 0.82 for $RC\omega = 2$.

5. From Plates 2, 3, 4 and 5 it can be seen that if resonances are to be avoided in the steady-state response, the value of $RC\omega$ must not be appreciably greater than 2. Since C is proportional to the cable length and since $\omega = 2\pi f$, this condition places upper limits on the length of cable which may be used with a recording system capable of transmitting a given range of frequencies. For example a special Simplex twin coaxial cable has a capacity of 30.5 micromicrofarads per foot and a characteristic impedance of 50.4 ohms for one of the twin coaxial lines. For an upper frequency of 200 kc, the value of C is 31,600 micromicrofarads; hence the cable length should not exceed 1037 feet.

6. From Plates 2, 3, 4 and 5 it can also be seen that various desired degrees of steady-state compensation can be realized by suitable choices of m and k, after the length of cable to be used has been specified. For example, using 700 feet of the same special Simplex twin coaxial cable, and for an upper frequency of 200 kc, a value of 1.35 is obtained for $RC\omega$. Then for this value of $RC\omega$ and for $m = 2$, the curves of Plate 3 indicate a relative amplitude of 1.32 for $k = 1$, and by interpolation a relative amplitude of 1.14 for $k = 1.25$. The particular degree of compensation desired, and hence the relative amplitude desired, will of course be determined by the

limitations imposed by the steady-state frequency response characteristics of the other components of the overall recording system.

Steady-State Response Measurements.

7. Measurements were made using one coaxial line of a 955 - foot length of the special Simplex twin coaxial polyethylene cable for comparison with the calculated curves of Plates 2, 3, 4 and 5. Plate 6 is typical of the results obtained.

The input signal V_o was taken from a cathode-follower output amplifier of low output resistance. The signal sources used to supply this amplifier were a General Radio Type 605-B Standard Signal Generator and a Hewlett Packard Model 200C Audio Oscillator. For the input capacity C_o, a 100 micromicrofarad capacitor was used to represent the piezoelectric gauge. The input voltage V_o and the output voltage V_t were measured by a Hewlett Packard Model 400C VTVM. The input voltage V_o was held constant at 5 rms volts. The measured characteristic impedance of one of the twin coaxial lines of the cable was 50.4 ohms. The measured capacity of one of the coaxial lines was 30.46 micromicrofarads per foot.

In Plate 6 the calculated curve was obtained by using Eq. (3). At the higher frequencies the calculated curve exhibits sharper resonance peaks of greater magnitude than those of the measured curve. This is because Eq. (3) was derived from the theory of an ideal cable in which the series resistance loss and the dielectric loss are neglected. When allowance is made for the attenuation resulting from these losses, the measured and calculated curves are in good agreement.

Step-Transient Response Calculations

8. Following the mathematical procedure developed in reference (a) it can be shown that for the network of Plate 1 the first two terms in the equation for the transient response to an applied step voltage V_o are

$$(4)\qquad \frac{V_t}{C_o V_o} = \frac{2}{(1+k)mC}\, e^{-\frac{t-RC}{(1+k)mRC}} \qquad t \geq RC$$

$$+ \frac{2(k-1)}{(1+k)^2 mC}\, e^{-\frac{t-3RC}{(1+k)mRC}} \left[1 + \frac{2}{(k-1)} \cdot \frac{(t-3RC)}{(1+k)mRC} \right] + \cdots \qquad t \geq 3RC$$

In this expression, t is the time in seconds and all other quantities are the same as previously defined. This expression is a general one for the step-transient response of the network of Plate 1. It covers the special cases considered in reference (a)*.

In Eq. (4) the time required for a signal applied to the input of the cable to travel the length of the cable is given by the transit time RC. Hence the value of the response at the output of the cable is zero for all values of time from t = 0 to t = RC. The first term of Eq. (4) represents the direct signal at the output after one trip along the cable. The second term of Eq. (4) represents the reflected signal at the output after it has been reflected from the output end and again from the input end of the cable and has therefore made three trips along the cable. Thus for values of time between RC and 3RC the transient response is calculated by using only the first term of Eq. (4), and for values of time between 3RC and 5RC the transient response is calculated by using both terms of Eq. (4).

In the ideal case, the perfect response to an applied step voltage V_o would be a constant response equal to the final value of the response for all values of time greater than t = RC. In the actual case of the network of Plate 1 a high-impedance gauge represented by V_o and C_o is connected to a low-impedance cable and the transient response will oscillate about the final value and will be attenuated because of the cable losses. The magnitude of the initial response at time t = RC and the magnitude of the oscillations can be varied by proper selection of the terminating resistance and capacity.

The final value of the transient response can not be obtained from the two terms of Eq. (4). However, since the final value of the step-transient response after a long time has elapsed is equal to the steady-state response as the frequency approaches zero, it can be found from Eq. (2).

Hence the relative amplitude of the step-transient response was obtained by dividing the calculated values of Eq. (4) by Eq. (2). Calculated values of the relative amplitude of the step-transient cable response are plotted in Plates 7, 8, 9 and 10 for time values from zero to 5RC and for the same ranges of values of terminating resistance and capacity as were used for the calculated values of the steady-state response.

---

* It is to be noted that several errors occur in the numerical constants in Eq. (8) of reference (a) as published, for the special case considered there. The correct values of these numerical constants are given by Eq. (4) of this report.

9. From Plates 7, 8, 9 and 10 it can be seen that the amount of the initial overshoot (or "undershoot") of the step-transient response depends on the value of the terminating resistance R_2 employed with a constant value of terminating capacity C_2. The amount of this initial overshoot (or "undershoot") is particularly important in the faithful recording of an applied step signal and hence also in the faithful recording of an applied exponentially decaying signal having an initial rise time approaching zero. For example in Plate 8 for $m = 2$, the calculated initial value of the relative amplitude for $k = 0$ is 3.00 and therefore does not appear on the scale of Plate 8. This can be called an overshoot of 200 percent. As the value of k is increased for m constant, this overshoot decreases, becomes zero for a particular value of k, and then becomes an "undershoot". Plate 8 indicates an initial overshoot of 20 percent for $k = 1.5$, 9 percent for $k = 1.75$, zero percent for $k = 2$, and an initial "undershoot" of 25 percent for $k = 3$ (corresponding to a relative amplitude of 0.75 for $k = 3$). Similar results are plotted in Plates 7, 9, and 10.

From Eqs. (4) and (2) it can be shown that there will be zero overshoot (and also zero "undershoot") whenever k and m are selected to satisfy the condition.

$$(5) \qquad k = \frac{2 + m}{m}$$

10. Plates 7, 8, 9 and 10 also indicate the magnitude of the oscillations existing for time values up to $t = 5RC$. In general the oscillations are less in magnitude for those values of k and m which result in little or no overshoot. Hence for the optimum step-transient response for a given value of m, it is desirable to select a value of k which will yield little or no overshoot and therefore a reduced magnitude of oscillations.

Step-Transient Response Oscillograms

11. An experimental verification of the results indicated by the calculated step-transient response curves of Plates 7, 8, 9 and 10 was obtained by an oscillographic study using the same 955 ft length of special Simplex twin-coaxial cable as was used for the steady-state measurements. Typical oscillograms for $m = 2$ and various values of k are shown in Plate 11.

To obtain the oscillograms, a 10 kc sine wave from a Hewlett Packard Model 200 C Audio Oscillator was supplied to a Hewlett Packard Model 210A Square Wave Generator which was operated single ended. Since the output impedance of the square wave generator was 500 ohms from one side to ground, a 50 ohm resistor was connected across the output terminals so that the test wave form would be obtained from a low-impedance source. The output of the square wave generator was applied to the cable through an input capacity C_0 of 100 micromicrofarads. One coaxial line of the 955 ft Simplex twin coaxial cable was used and was terminated with the compensation network of Plate 1, using various values of k and m. The output voltage V_t of the

cable circuit was too small for direct application to the oscillograph and therefore was applied to the amplifier portion of a Hewlett Packard Model 400 C Voltmeter which served as a pre-amplifier for the DuMont Type 248 Cathode-Ray Oscillograph.

Plate 11(a) shows the wave form of the single-ended output of the square-wave generator when applied directly to the oscillograph. One period of the 10 kc wave is shown and hence the time base for the complete wave form shown is 100 microseconds.

Plate 11(b) shows the test wave form after it had passed through the pre-amplifier used with the oscillograph. This was obtained by passing the output of the square-wave generator through the pre-amplifier only before reaching the oscillograph. However the cable with its termination was also connected to the output terminals of the square-wave generator to serve as the normal load on the square-wave generator during this test.

Plate 11(c) for $k = 0$, $m = 2$, shows the extreme overshoot of the initial response and the violent oscillations that continue throughout the 50 microsecond time interval after the initial response for the case where the terminating resistance is zero. Similar oscillations throughout the 50 microsecond time interval were obtained for values of $m = 1$, 4, and 6, with $k = 0$ in each case.

Plate 11(d) for $k = 1$, $m = 2$, shows an initial overshoot of approximately 30 percent. The corresponding calculated curve of Plate 8 predicts an initial overshoot of 50 percent. The curve of Plate 8 also indicates the oscillations to be expected out to time $t = 5RC$, but yields no information after this time value because only two terms were retained in the series expansion for the relative amplitude. Plate 11(d) shows oscillations in close agreement with the calculated curve out to time $t = 5RC$, and also indicates that the oscillations are completely damped out after time $t = 5RC$. For Plate 11 the test length of 955 feet of special Simplex twin coaxial cable has a transit time RC of 1.47 microseconds. Since the initial response occurs at time $t = RC$, the oscillations predicted by Plate 8 and obtained by measurement in Plate 11(d) exist over a time interval from $t = RC$ to $t = 5RC$ or for 5.88 microseconds. This time interval can readily be identified in Plate 11(d) when it is remembered that the time base shown after the initial response is 50 microseconds.

Plate 11(e) for $k = 1.5$, $m = 2$, shows a greatly reduced initial overshoot which is not greater than 10 percent. This is to be compared with a 20 percent overshoot predicted by Plate 8. The oscillations are again evident for a time interval corresponding to the calculated interval of 5.88 microseconds, after which they are completely damped.

Plate 11(f) for $k = 2$, $m = .2$, shows the complete elimination of the initial overshoot. Indeed an "undershoot" on the order of 10 percent can be seen. This compares with zero overshoot predicted by Plate 8. The oscillations again exist only during the 5.88 microsecond time interval out to $t = 5RC$.

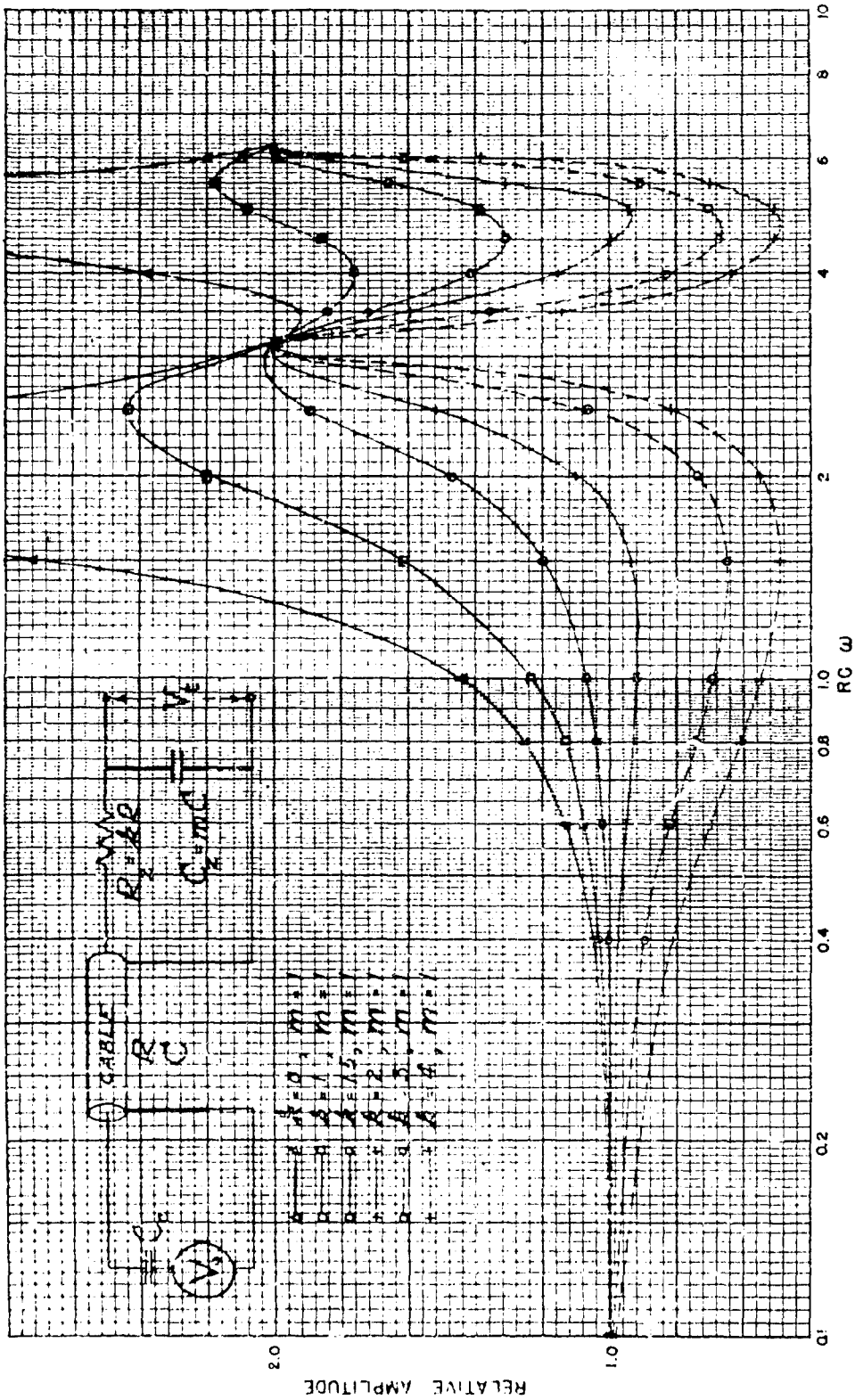
Plate 11(g) for k = 3, m = 2, clearly shows an "undershoot" for the initial response. The initial response is on the order of 80 percent of that of the test wave form of Plate 11(b). This can be called an "undershoot" of 20 percent and is to be compared with an "undershoot" of 25 percent predicted by Plate 8. The oscillations again exist only during the 5.88 microsecond time interval out to t = 5RC.

These oscillograms thus provide a very satisfactory confirmation of the transient response predicted by the calculated step-transient response curves of Plate 8. Similar confirmations were obtained for all other values of terminating capacity considered in Plates 7, 9, and 10.

12. From these results, selection of the most suitable cable terminating network may be made to satisfy various experimental requirements. Reference to these results should facilitate the determination of the optimum values of terminating network constants to be employed whenever modifications oto the recording equipment are considered.

Otto Meier, Jr.

PLATE 2

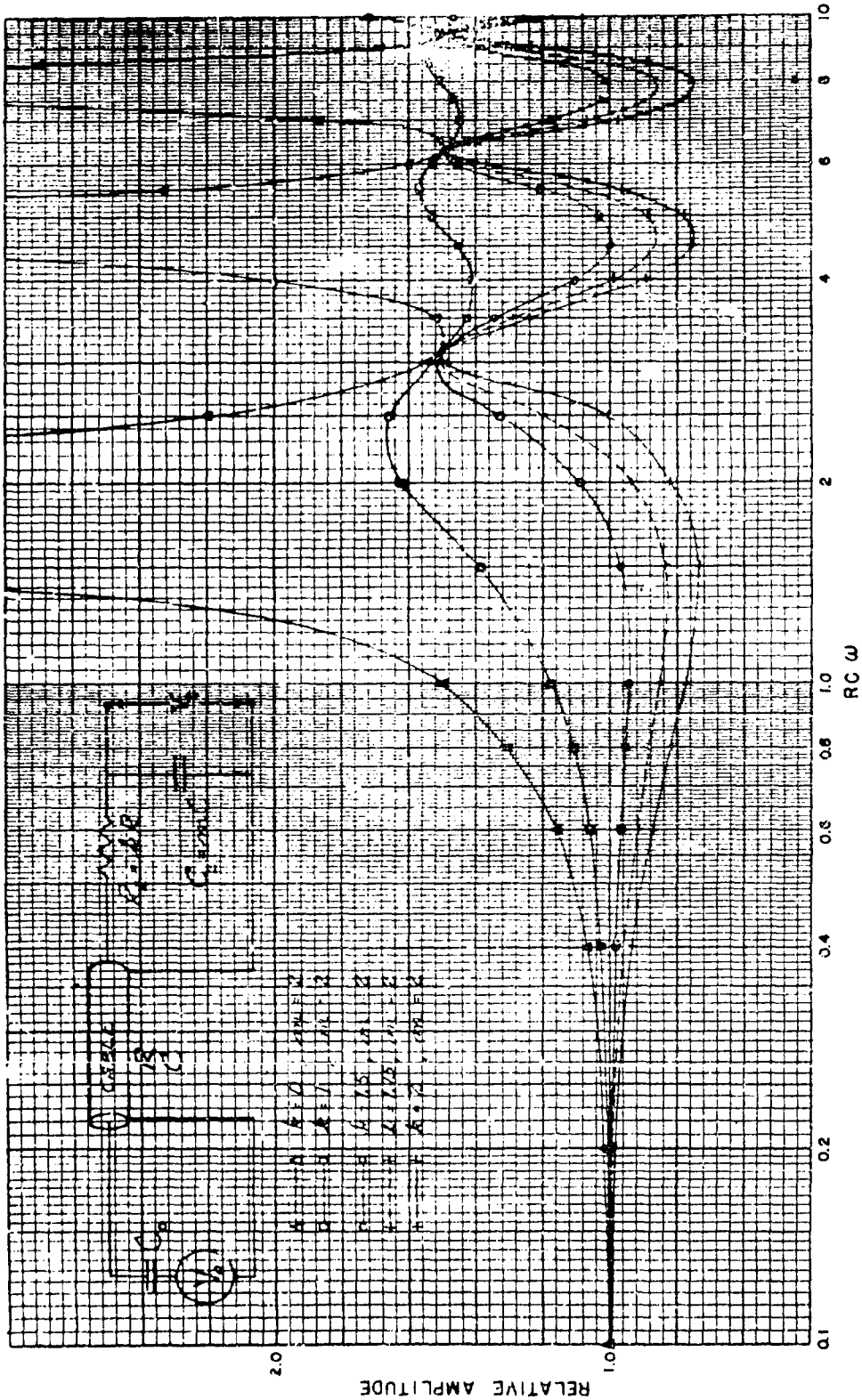


CALCULATED STEADY-STATE CABLE RESPONSE

TERMINATING CAPACITY EQUAL TO CABLE CAPACITY

NOLM 10467

PLATE 3

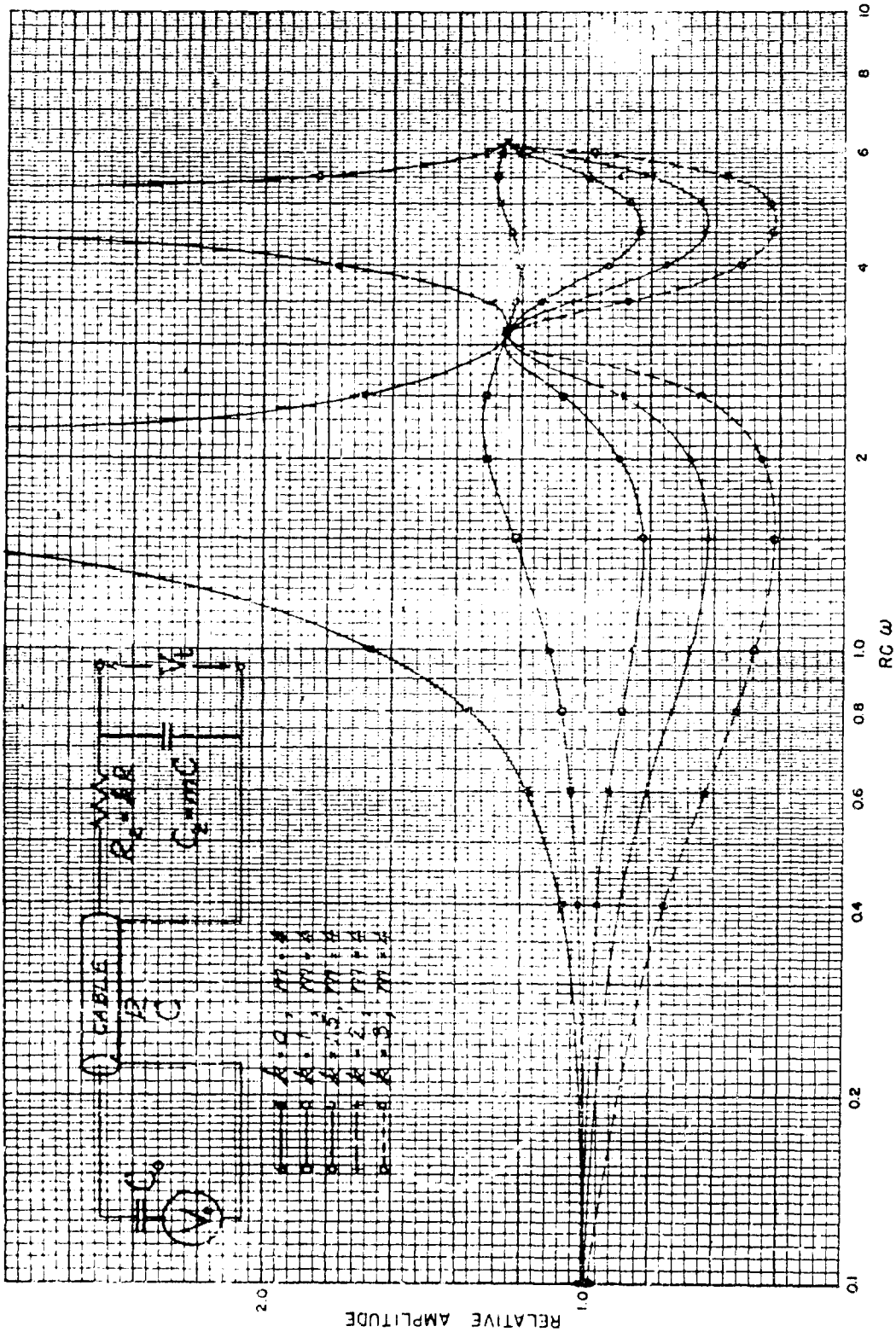


CALCULATED STEADY-STATE CABLE RESPONSE

TERMINATING CAPACITY TWO TIMES CABLE CAPACITY

NOLM 10467

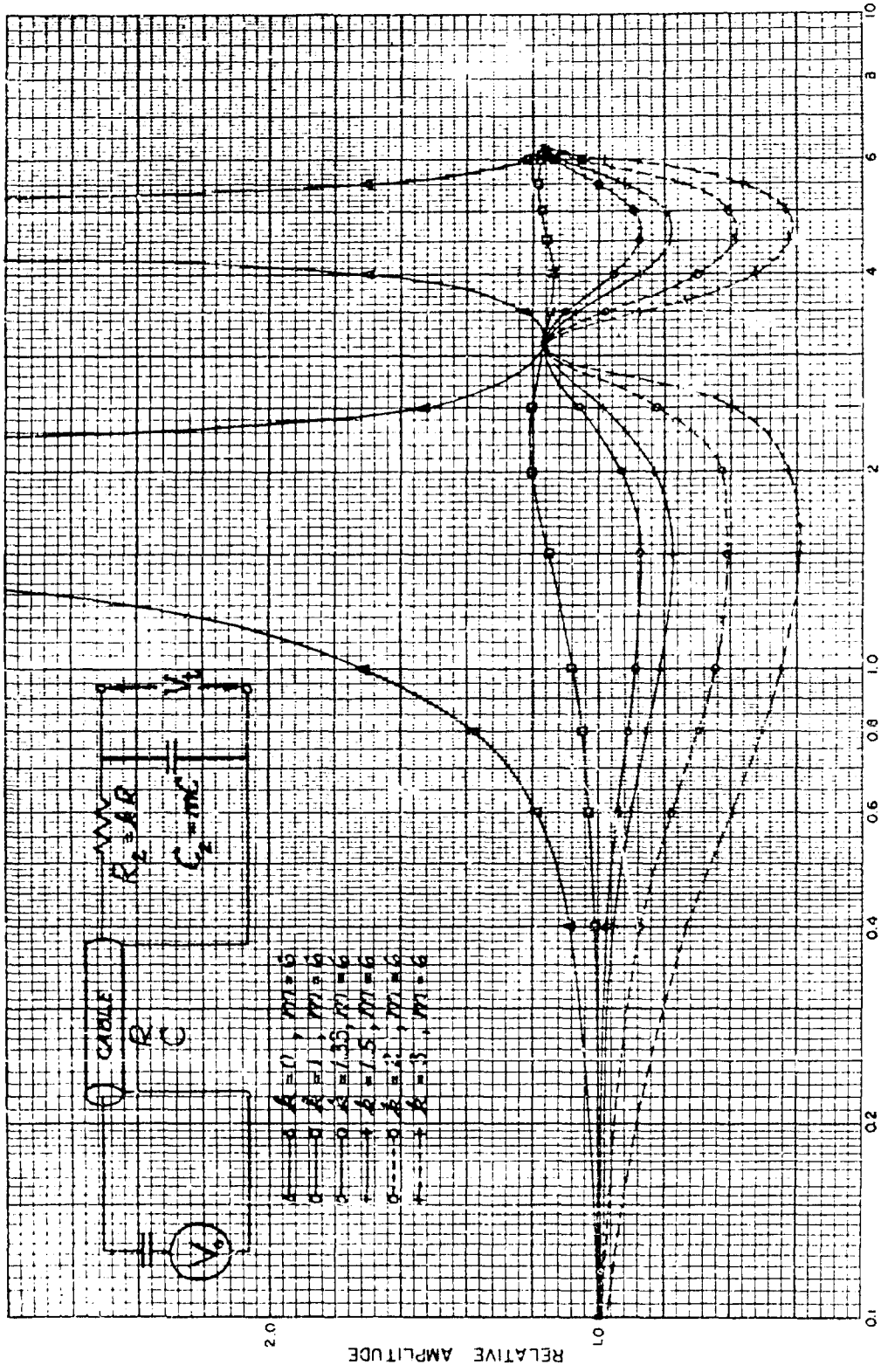
PLATE 4



CALCULATED STEADY-STATE CABLE RESPONSE

TERMINATING CAPACITY FOUR TIMES CABLE CAPACITY

PLATE 5

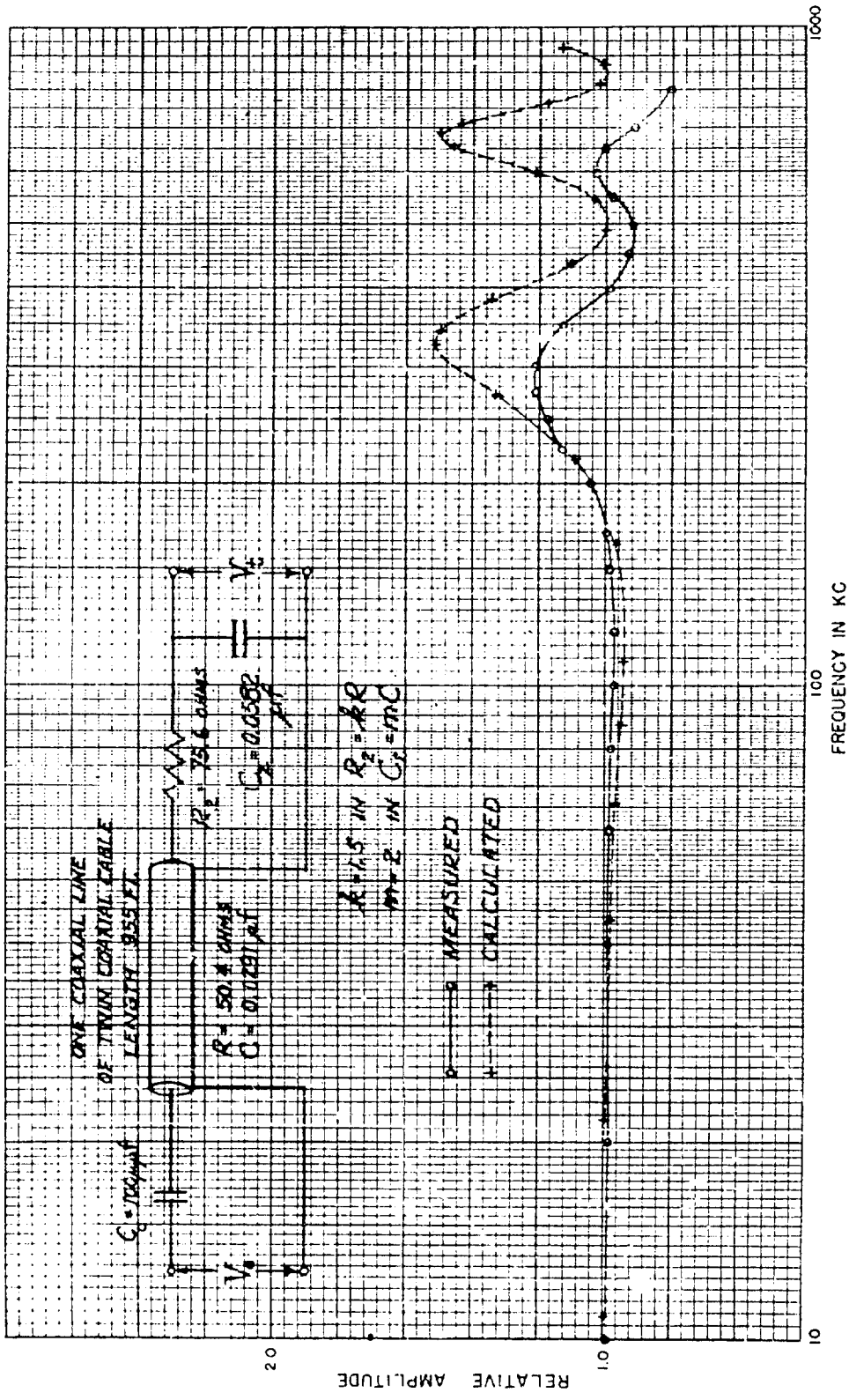


CALCULATED STEADY-STATE CABLE RESPONSE

TERMINATING CAPACITY SIX TIMES CABLE CAPACITY

NOLM 10467

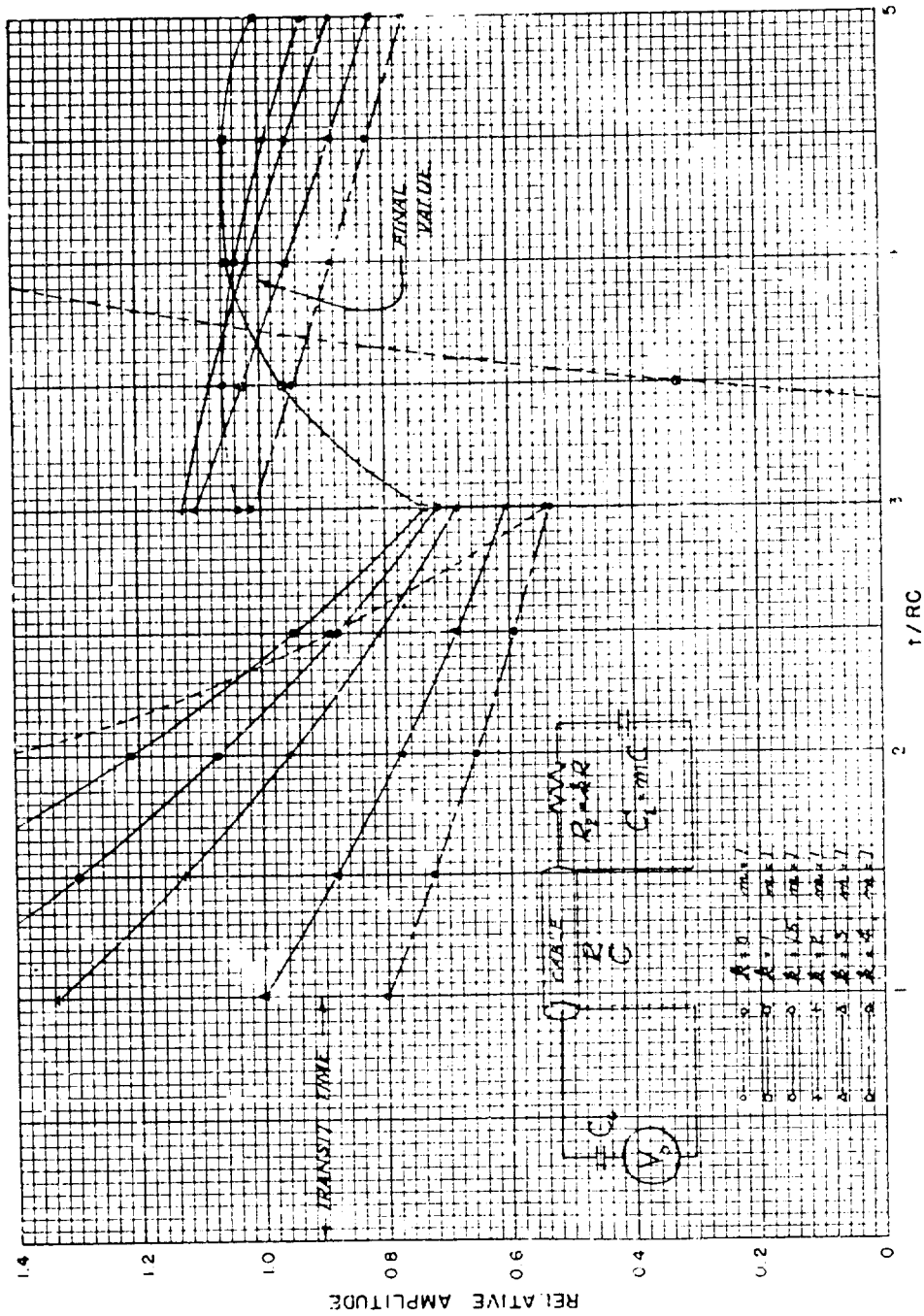
PLATE 6



COMPARISON OF MEASURED AND CALCULATED STEADY-STATE RESPONSE OF 955 FT SIMPLEX CABLE WITH R-C TERMINATION

NOLM 10467

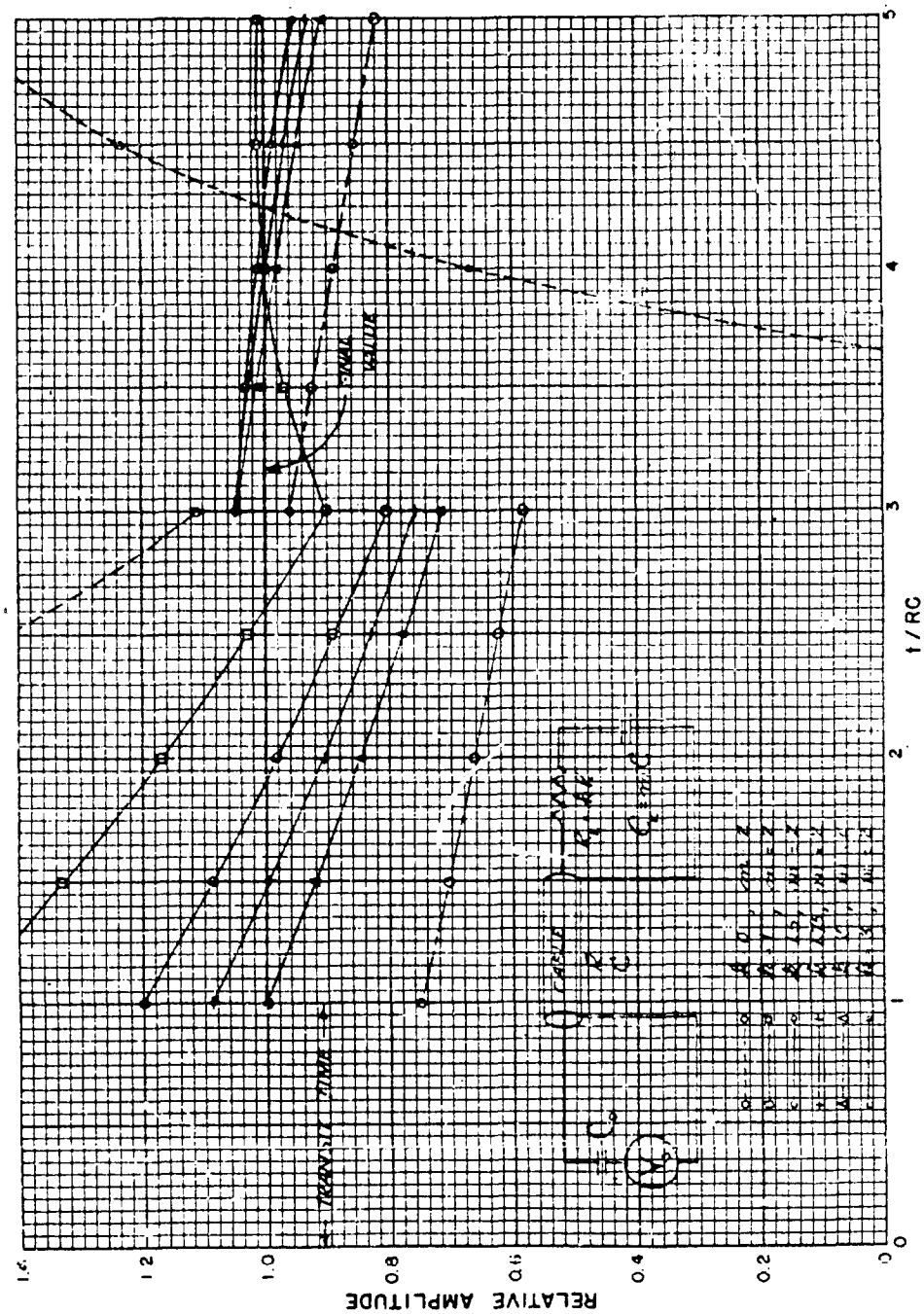
PLATE 7



CALCULATED STEP-TRANSIENT CABLE RESPONSE

TERMINATING CAPACITY EQUAL TO CABLE CAPACITY

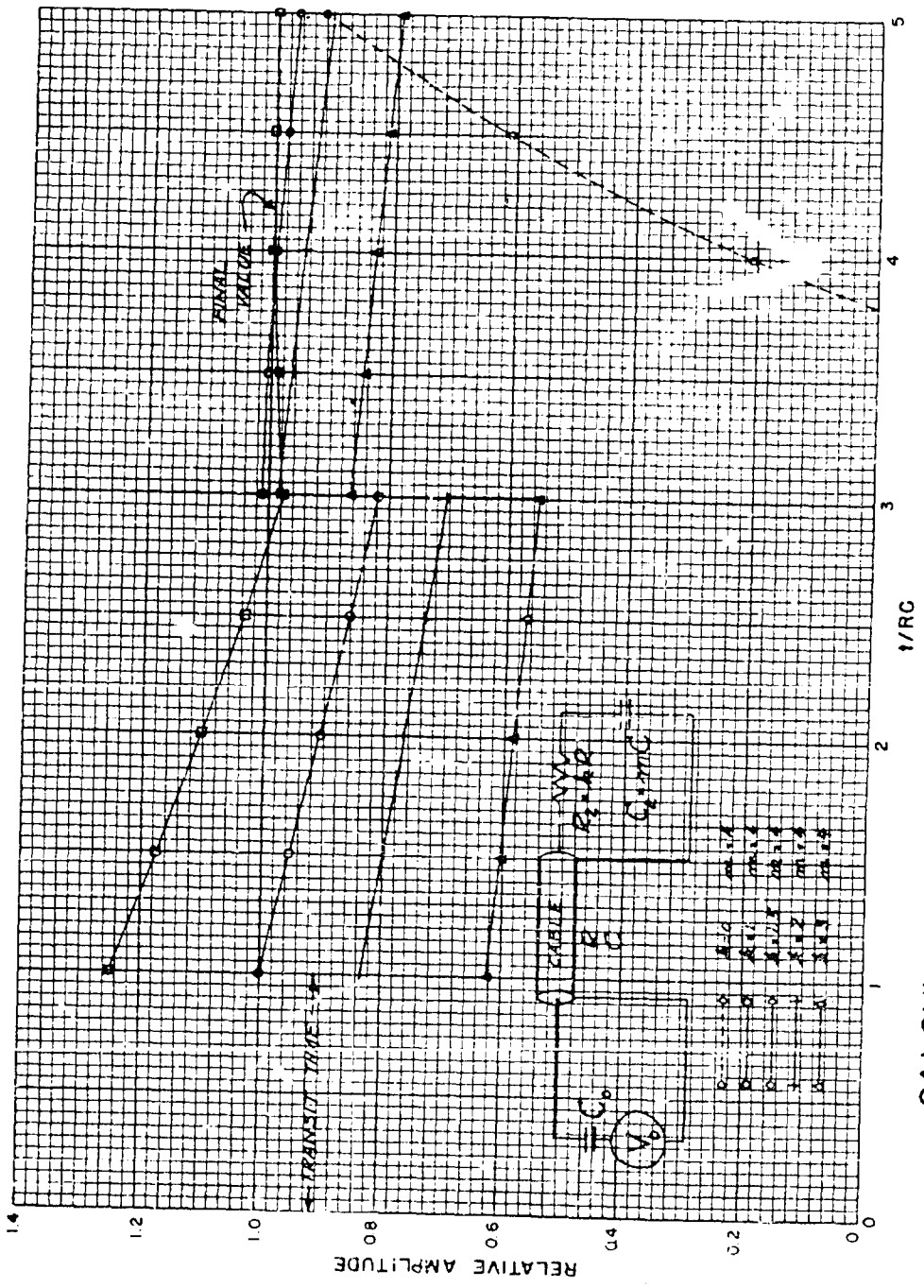
PLATE 8



CALCULATED STEP-TRANSIENT CABLE RESPONSE

TERMINATING CAPACITY TWO TIMES CABLE CAPACITY

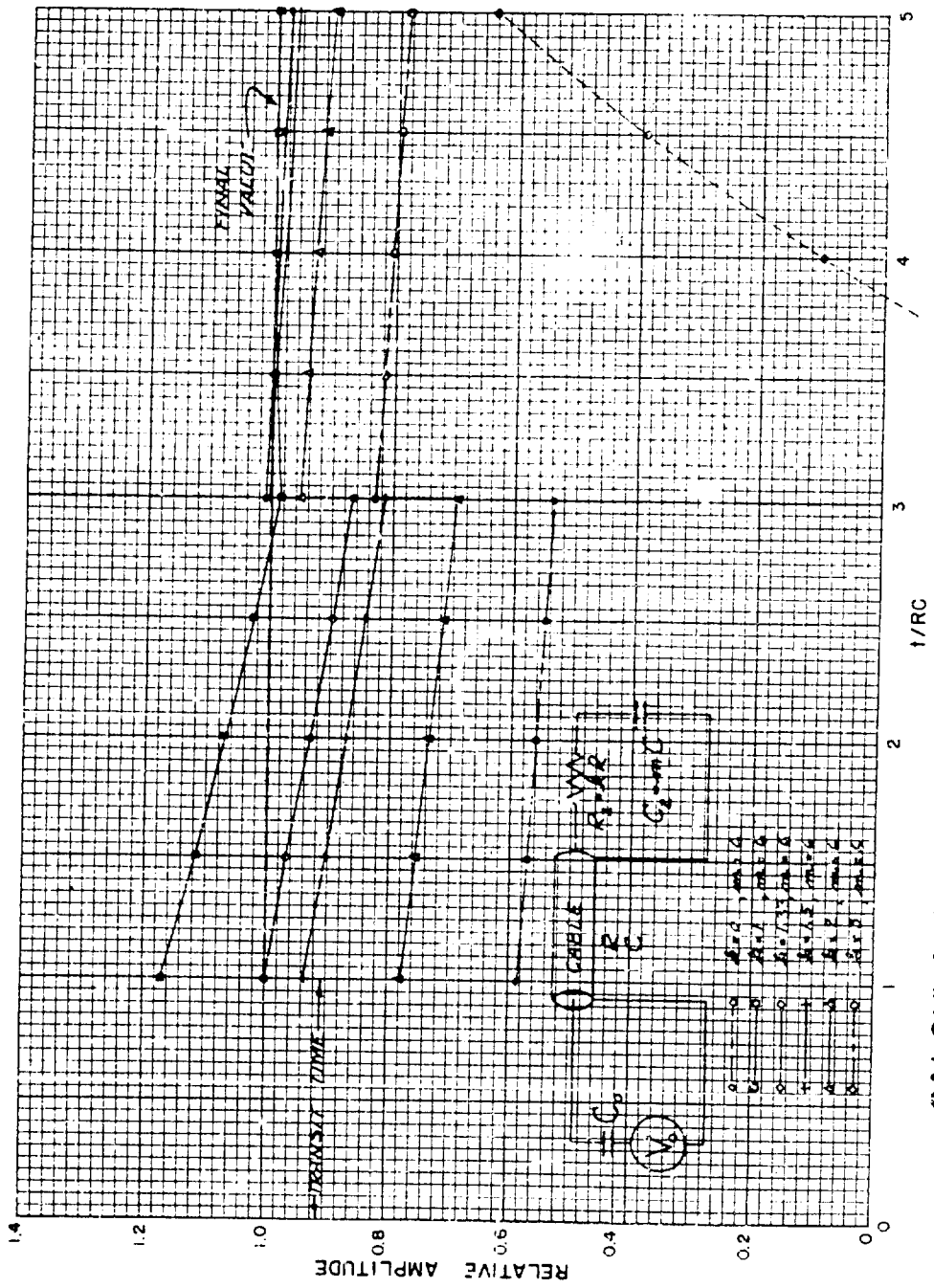
PLATE 9



CALCULATED STEP-TRANSIENT CABLE RESPONSE

TERMINATING CAPACITY FOUR TIMES CABLE CAPACITY

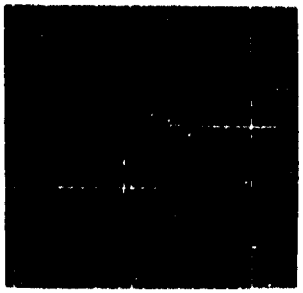
PLATE 10



CALCULATED STEP-TRANSIENT CABLE RESPONSE

TERMINATING CAPACITY SIX TIMES CABLE CAPACITY

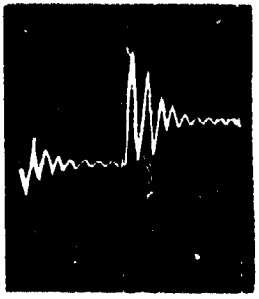
PLATE II



(a) SQUARE WAVE GENERATOR OUTPUT, 10 KC.



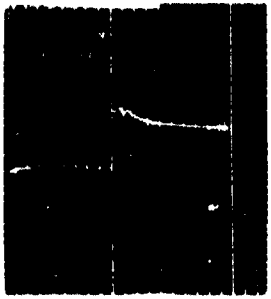
(b) SQUARE WAVE AS ALTERED BY PRE-AMPLIFIER. USED AS 10 KC TEST WAVE FORM.



(c) OUTPUT RESPONSE k = 0, m = 2.



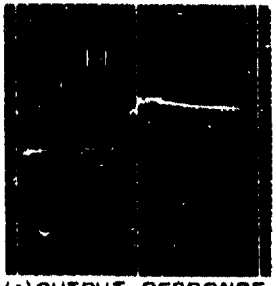
(d) OUTPUT RESPONSE k = 1, m = 2.



(e) OUTPUT RESPONSE k = 1.5, m = 2.



(f) OUTPUT RESPONSE k = 2, m = 2.



(g) OUTPUT RESPONSE k = 3, m = 2

OSCILLOGRAMS OF STEP-TRANSIENT RESPONSE OF LAMPSON COMPENSATION NETWORK

THE THEORY OF PISTON GAUGES

R. Finkelstein
Bureau of Ordnance, Navy Department

American Contribution

12 April 1944

ABSTRACT

In the Bureau of Ordnance the damaging effect of underwater weapons is at present measured by piston gauges. Since the difference in peak-pressure and impulse between the better explosives is only of the order of 30%, it is important to have a reliable theory of the gauges which are used to compare explosives and weapons. Therefore, the theory of piston gauges is considered here. It is now customary to use such a gauge in the "side-on" orientation, namely, with its pressure-sensitive face perpendicular to the face of the shock. In this position theoretical interpretation of the measurements is difficult because of diffraction and possible Mach reflection. In the same orientation experimental dispersion is larger than for the "head-on" position (where the shock is incident normally on the sensitive face of the gauge). Hence, in this report, the theory is given for the head-on orientation. The effect of rarefactions emitted by the recoiling pistons on themselves and on each other is calculated. This effect is small; it alters the pressure by only a few percent. On the other hand, the recoil of the front face of the block affects the pistons so much that it makes the head-on gauge useless if the block is not thick. Therefore, the block should be thick; the necessary thickness is estimated here. Another correction to be considered is due to the Bernoulli effect.

This may change the pressure behind a piston by a few percent, since a piston may recoil with high velocity. Cavitation and turbulence are shown to be unimportant in present gauges. The important affects, namely, recoil of pistons, recoil of block, and Bernoulli effect can be corrected, except for an uncertainty of about 2% in the pressure provided that the gauge is used in the head-on position. It is thus theoretically preferable to use a gauge in this position. If, for any reason, however, a gauge is used in the side-on position, it may be calibrated against a head-on gauge.

TABLE OF CONTENTS

I. Introduction

1. Purpose
2. Schematic description of piston gauges
3. Present theory of piston gauges
4. Diffraction effects
5. Irregular reflection
6. The head-on orientation
7. Method

II. The Pressure Field near a Gauge

8. Kirchhoff's theorem
9. Adaptation of Kirchhoff's theorem to problem
10. Validity of the acoustic approximation
11. The pressure variation at the center of the mouth of an orifice
12. The pressure at other points of the mouth

III. The Response of the Pistons

13. Equation of motion of a piston
14. Two approximations
15. Incompressive approximation
16. Comparison of the incompressive and central approximations
17. Estimate of the error in the incompressive approximation
18. The interaction between the motions of different pistons in the same gauge

IV. The Response of the Block and its Influence on the Pistons

19. The relief pressure from the block
20. The relief pressure from the water
21. The criterion for an immovable rigid block
22. The criterion for an infinitely thick soft block
23. Comparison between the preceding criteria
24. Dimensions of an ideal gauge
25. Softness and the motion of the front face of the block

V. Other Effects

26. Cavitation
27. Turbulence
28. The Bernoulli effect

VI. Summary

862

VII. Appendix

1. Statement of Kirchhoff's theorem
2. Application of Kirchhoff's theorem to a progressive wave
3. The wave incident on and thrown back from a gauge
4. The pressure field between the explosion and the gauge
5. Expression of total pressure in terms of incident pressure and motion of gauge
6. The mass M in equation (13.1)
7. Test of the incompressive and central approximations
8. Error in the incompressive approximation
9. Rarefaction coupling between two pistons
10. Thickness of an immovable rigid block
11. Two criteria for an infinitely thick baffle
12. Turbulence
13. The Bernoulli effect

TABLE OF PRINCIPAL NOTATION

A = face of piston or pistons, also area of piston.

A_o = A at time, $t = 0$, also face of piston number 0.

A_1 = face of piston number 1.

B = face of block in which pistons move.

B_o = B at time, $t = 0$.

C_o = $T_o - A_o - B_o$.

L = length of piston.

M = "effective" mass of piston and copper ball or pellet.

P = instantaneous total pressure at center of orifice.

P_e = mean value of incident pressure over face of orifice.

P_m = maximum value of incident pressure at a given point.

R = radius of piston, also Reynolds number.

R_b = radius of block.

T_o = infinite plane containing A_o and B_o.

$T = A + B + C_o$.

a_T = acceleration of fluid at surface of T. T can be specialized to A, B, or C_o.

b = distance of point from axis of orifice.

c = velocity of sound in water.

c_b = velocity of sound in block.

d = thickness of block.

d_r = thickness of effectively infinite, rigid block.

d_s = thickness of effectively infinite, soft block.

e = explosion.

g = gauge.

k = force constant of copper pellet connected for dynamic strain rate.

$m = \theta_g/\theta$.

$n = \theta_b/2\theta$.

p = instantaneous total pressure due to incident wave and wave thrown back by gauge (minus hydrostatic pressure).

p_e = instantaneous pressure of incident wave in absence of gauge

r = ratio of pressure at surface of rigid block to $2p_e$ = a measure of effect of recoil of block.

r = distance from a point in pressure field to an element of area.

s = distance between centers of two orifices in a gauge.

t = time.

$\vec{v}$ = material velocity of water.

v = magnitude of v.

v_b = velocity of block or baffle.

v_e = material velocity in incident wave.

z = coordinate normal to T_o, positive in direction of recoil.

z_T = z coordinate of surface T. T may be specialized to A, B, or C_o.

θ = time-constant of incident pulse, i.e., time required for pressure in incident pulse to decay to 1/e th of its peak value.

$\theta_b = R_b/c$ = diffraction time of block or baffle.

θ_c = cavitation time.

$\theta_d = \rho_b d/\rho c$ = damping time of block.

θ_g = time constant of gauge, i.e., time required for gauge to register.

$\theta_p = R/c$ = diffraction time of piston.

$\theta_s = 2d/C_b$ = time for sound to cross block twice.

$\theta_L = \rho_p L/\rho c$ = damping time of piston.

λ = resistance coefficient.

μ = coefficient of viscosity.

ρ = density of water.

ρ_b = density of block.

ρ_p = density of piston.

φ = angular coordinate.

ψ = velocity potential.

ψ_a = velocity potential of pressure field due to explosion.

ψ_g = velocity potential of pressure field due to gauge.

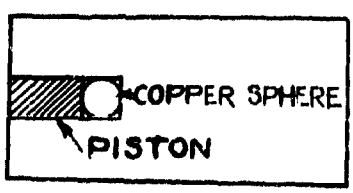
$\cdot = \frac{d}{dt}$

I. INTRODUCTION

1. A theory of diaphragm gauges has been developed by Kirkwood (1). A theory of piston gauges has been given by Hilliar (2) and by Hartmann (3), but their work ignores diffraction. This report gives a description of piston gauges which does not neglect diffraction. A piston gauge is to be interpreted as a ball-crusher gauge, a Hilliar gauge, or a Hartmann momentum gauge, and in these calculations there is no essential difference between them.

2. The essential element of a ball-crusher gauge (Fig. 1) contains a steel piston, one end of which touches a small copper sphere. The other end of the piston is exposed to the explosion. When the shock wave falls on it, the piston is driven forward and deforms the ball. The strength of the shock may be measured by the deformation of the ball. The Hilliar type of gauge is similar, but it may contain several pistons of different lengths. Each of these may have a different time of free travel before striking an anvil and deforming a cylindrical pellet, carried on its front face. The Hilliar gauge supplies information on the time-variation of pressure, since its pistons have different response times. Finally, a Hartmann momentum gauge contains a single piston of such long response time that it may measure the total momentum

Fig. 1

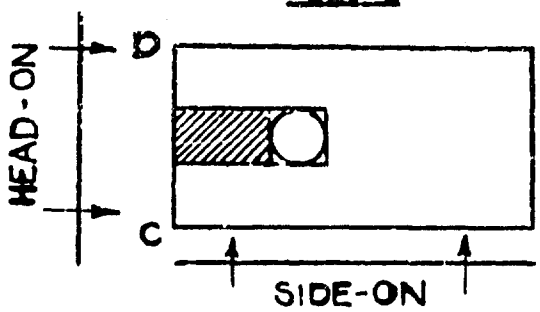


in a shock. Further details on these gauges are found in references (2), (4), and (5).

3. The theory of the Hillier gauge and the crusher gauge is given in references (2) and (3), under the assumption that the face of the piston is perpendicular to the face of the shock, (Fig. 2). This orientation of the gauge is here called "side-on". It is possible that the approximations made in references (2) and (3) are fair, but it is difficult to estimate the corrections which should be made for them. In particular, the diffracting effect of the gauge was not calculated, and the possibility of "irregular reflection" from the gauge face was neglected. These points will now be considered.

4. A side-on shock will cause a wave to be diffracted from the leading corner, C, of the block (Fig. 2). According to references (2) and (3) the pressure on the face CD is the same as in the incident shock (p). According to a well-known acoustical paradox, if CD is rigid and the wave diffracted from C is neglected, the pressure on CD is 2p, independent of the angle of incidence. Friedlander (6) has calculated the actual pressure on CD in the acoustic approximation without neglecting the disturbance from C and has shown that the wave diffracted from C is a mechanism for reducing the pressure from 2p to the neighborhood of p, the value which should be

Fig. 2



correct for glancing incidence. Although the pressure on CD is possibly close to p, as assumed in (2) and (3), it seems to be difficult to estimate it more accurately for the gages in current use.

5. A second neglect in (2) and (3) is the possibility of "irregular or Mach reflection" (see (7)). Since so-called regular reflection in water ceases at an angle of incidence near 65° for shocks of 300 atmospheres (8), Mach reflection from side-on gauges is also to be expected in the pressure range which interests us. In fact, the complete explanation of the doubling paradox referred to in the previous paragraph may depend upon non-linear theory, even for very weak waves (see von Neumann (7), page 8).

6. In order to avoid the unsolved theoretical problems associated with the side-on orientation, the case of normal incidence is considered here. In this position reflection is regular and the diffraction problem is much easier. There is also experimental, as well as theoretical, reason for preferring the head-on orientation, since dispersion is less there than for the side-on position. According to reference (9), page 20, the standard deviation is from 5 to 30% more in the side-on orientation. The increased dispersion is presumably due to the same causes: irregular reflection and diffraction.

7. The ultimate problem is to infer the pressure-time curve of a shock from the deformations of several copper pellets. To do this it is necessary to know the response of the pistons responsible for these deformations. This response is determined by

Best Available Copy

two conditions. First, the motion of any piston depends on the pressure over its exposed face. Second, and inversely, the pressure is a function of the motion of the piston itself, as well as of the motions of all other "nearby" parts of the gauge which recoil. (A moving element is to be regarded as "nearby" if sound has time to come from it before the gauge has completely registered.) We have to express the motion as a function of the total pressure, and the total pressure as a function of the motion, as well as of the incident pressure. These two conditions, taken together, lead to an integro-differential equation which is characteristic of this kind of problem, and which is sufficient to determine the motion of the piston (pistons).

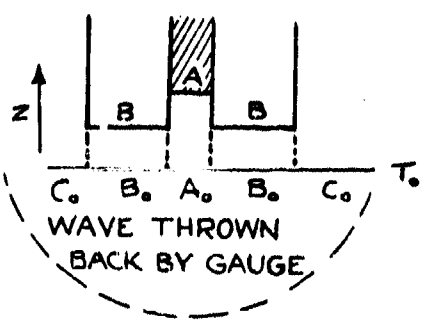
II. THE PRESSURE FIELD NEAR A GAUGE

8. We first express the total pressure as a function of the motion of the moving parts of the gauge and of the incident pressure, unperturbed by the gauge. The analytical method of doing this is provided by Kirchhoff's theorem. This theorem evaluates a solution of the wave equation at any point in an arbitrary, closed region in terms of retarded values of the function itself, and of its space-and time-derivatives on the boundary of this region. The data required in Kirchhoff's theorem are redundant. For example, in our problem, knowledge of only the retarded acceleration of the fluid over an infinite plane is sufficient to determine the pressure at any point in a certain region on one side of the plane. In paragraphs 1.-5. of the appendix the explicit expression

for the pressure in term of this information is calculated from Kirchhoff's theorem.

9. Before giving the adaptation of Kirchhoff's theorem just mentioned, it is convenient to introduce the following notation. The surface which the gauge presents to the shock consists essentially of two parts: the face, A, of the piston (pistons), and the face, B, of the block, in which it moves (see Fig. 3). B may be extended by a baffle. A, of course, moves rather rapidly while B moves much more slowly. At the time, t = 0, when the shock pulse first strikes the gauge, A is flush with B. Let the infinite plane containing A and B at t = 0 be T_o. At later values of t let the projections of A and B on T_o be A_o and B_o. Let the rest of T_o be C_o, so that

Fig. 3



$$(9.1)\quad T_o = A_o + B_o + C_o$$

Let the broken, moving surface, T, be defined by

$$(9.2)\quad T = A + B + C_o.$$

Then in terms of the surfaces, T_o and T, the fundamental expression for the pressure is (for proof see appendix, paragraphs 1. - 5.)

$$(9.3)\quad p = 2p_s - \frac{\rho}{2\pi}\int_{(T_o)} \frac{1}{r}\, a_r\left(t-\frac{r}{c}\right) dS$$

where

p = total pressure, excluding hydrostatic pressure, at any time on the plane T_o at any point which is behind the wave front thrown back by the gauge.

p_s = value of the pressure at this point if no gauge were present.

ρ = density of medium (water) in which gauge is immersed.

dS = element of area on T_o.

r = distance from dS to point at which p is evaluated.

c = velocity of sound in medium (water).

a_T = acceleration of the fluid at the projection of dS on T, the moving surface defined in (9.2).

The integral in (9.3) is to be extended over the infinite plane, T_o, but the retarded integrand makes it cut off at a finite distance. At the surface of the gauge a_T is the acceleration of A or of B. Elsewhere (C_o) it is not directly related to the motion of the gauge; but in our applications of (9.3) the surface B is usually taken so large that the integrand vanishes on C_o by retardation. Equation (9.3) is, therefore, the desired expression for the pressure at any time on the plane T_o in terms of the gauge motion and the incident pressure. The possibility of having a_T instead of a_{T_o} in the formula for p depends upon the very slight compressibility of water (appendix, paragraph 5.)

10. The equation (9.3) is, of course, acoustic and applicable only to "weak" shocks. Although the meaning of "weak" is not entirely clear at present, a shock of 300 atmospheres in water is probably well-described by acoustic theory if it impinges on the gauge at normal incidence. When a linear shock of 300 atmospheres is reflected from a rigid wall, the acoustic approximation is 3% too low on peak pressure and 2% too high on the momentum imparted to the wall (reference 10). Since we assume normal incidence, we

may use (9.3) and expect it to be error by not more than 2%.

11. With the help of (9.3) one may discuss the way in which the pressure changes at the mouth of the orifice left by a retreating piston. Consider a gauge which has a single, perfectly rigid piston and a completely immovable, infinite baffle, i.e.,

$$(11.1) \qquad z_T(b, \varphi, t) = z_A(t) \qquad b \leq R$$
$$z_T(b, \varphi, t) = 0 \qquad b > R$$

where z_T is the coordinate of a point on the surface T, and where (b, φ, z) is a cylindrical coordinate system whose origin is at the initial position of the center of the piston. R is the radius of the piston. By (9.3) and (11.1)

$$P = 2P_e - \rho \int_0^R \ddot{z}_A\left(t - \frac{r}{c}\right) dr$$

or
$$(11.2) \qquad P = 2P_e + \rho c\left[\dot{z}_A\left(t - \frac{R}{c}\right) - \dot{z}_A(t)\right]$$

where P is the value of the pressure at center of the orifice $(r = 0, z = 0)$, and z_A is the coordinate of the piston. Assume that all parts of the gauge are at rest before the shock wave strikes it. When the piston first begins to move, $\dot{z}_A(t - R/c)$ is zero, and it remains zero until $t = R/c$. During this period

$$(11.3) \qquad P = 2P_e - \rho c\, \dot{z}_A(t)$$

For large values of the time, on the other hand, P may be expanded in the following form.

$$(11.2)^1 \qquad P = 2P_e + \rho c\left[\ddot{z}_A(t)\left(-\frac{R}{c}\right) + \frac{\dddot{z}_A(t)}{2}\,\frac{R^2}{c^2} + \cdots\right]$$

It will be shown later that second and higher order terms in R/c

may be dropped. Then

$$(11.4) \qquad P = 2P_e - \rho R \ddot{z}_A(t)$$

By (11.3) the relief pressure (the decrease in pressure due to recoil) is at first proportional to the velocity of the piston and by (11.4) it later becomes proportional to its acceleration. At $t = 0$, the total pressure is $2P_e$. It then falls because of the recoil of the piston according to (11.3). This situation continues until $t = R/c$, at which time the pressure-increase propagated in from the edge of the orifice has reached its center. From then on (11.4) holds if R/c, or the third and higher derivatives of z_A are sufficiently small. The neglect of these terms is tested in the appendix, paragraph Z. Although (11.3), on the other hand, is perfectly correct, it holds only for a short time. For example, in all Bureau of Ordnance piston gauges $R = 1/4"$, $R/c \cong 4 \times 10^{-6}$ sec. The corresponding deformation time of a crusher gauge with a 5/32" ball is, however, of the order of 200×10^{-6} sec. (reference 3). Hence the initial motion, as described by (11.3), is short (4 microsec) compared to the total motion (200 microsec). The situation is even more exaggerated for Hilliar and for momentum gauges where the total motion may require 100-2000 microsec (depending on the piston) and about 4000 microsec, respectively. For diaphragms R/c has been called the "diffraction" time by Kirkwood. It is approximately the time at which (11.3) ceases to apply and at which (11.4) begins to be correct. The fact that the motion changes type in this way is an illustration of Kennard's "reduction

principle" (11), namely, that any motion approaches its incompressive approximation after a sufficiently long time (see paragraph 14.).

12. Only at the center of the orifice does the pressure vary exactly as just described. Near an edge waves coming from the direction of that edge spoil the proportionality of the relief pressure to the velocity in a shorter time than R/c; but, on the other hand, waves coming from the opposite edge take a longer time than R/c to arrive. The net effect is probably to make the pressure variation nearly the same for central and eccentric points.

III. THE RESPONSE OF THE PISTONS

13. In (9.3) the total pressure is written in terms of the motion and the incident pressure. The second condition, giving the motion as a function of the pressure, may now be stated. The response of any piston obeys the following equation

$$(13.1) \qquad (M + \rho A z_A)\,\ddot{z}_A + k z_A = \int_{(A_o)} p\, dS$$

where

M = effective mass of piston and copper ball or pellet

A = face of piston, also its area,

z_A = forward travel of piston,

k = force constant of pellet corrected for dynamic strain-rate,

p = pressure at mouth of orifice,

A_o = mouth of orifice.

Here M is the mass of the piston only if it is moving freely, as

in a Hillier gauge; it should be increased by 1/3 the mass of the copper pellet, if the pellet is always in contact with its anvil, as in a crusher gauge. (See Appendix, paragraph g.) The constant, k, is also different in these two cases; it vanishes for a freely moving piston. Since the pressure is integrated over the mouth of the orifice instead of over the face of the piston, the mass, M, must be augmented by that of the water following the piston into its cylinder. This water mass, $\rho A x_A$, is zero for a crusher gauge, since here the piston is always in contact with the ball, and the maximum value of x_A is negligible.

14. The equations (9.3) and (13.1) are the two conditions which determine the response of the gauge. These do not solve the problem completely, because the region of integration in (13.1) is A_o, while in (9.3) it is T_o; and, in general, knowledge of a_B and a_{G_o} is difficult to obtain. The problem is solved here for a gauge designed so that a_B is very small and so that a_{G_o} makes itself felt only after the gauge has registered. We combine the two equations by calculating the right hand member of (13.1) from (9.3). This will be done under two approximations: (a) that the velocity of sound is infinite, and (b) that the mean value of the pressure over the mouth of the orifice is equal to its value at the center of the same. The first approximation is generally called the <u>incompressive</u> one, and the second will here be called the <u>central</u> approximation. If the time required for sound to cross the orifice is small compared to the total time during which

the piston is in motion, one should expect these to be good approximations; it will be verified that they are.

15. Consider the incompressive, non-central, approximation first. Let the gauge have a rigid piston and an immovable, infinite baffle, as specified in (11.1). That is, the region B is infinite and $\ddot{z}_B = 0$. Then by (9.3) and (11.1)

$$(15.1) \qquad p = 2p_e - \frac{\rho}{4\pi} \int_{(A_o)} \frac{1}{R} \ddot{z}_A \, dS$$

where $\ddot{z}_A$ is not retarded, and A_o is the mouth of the orifice. After integration (15.1) gives for the pressure at the point (b, φ)

$$(15.2) \qquad p = 2p_e - \frac{2\rho R}{\pi} \ddot{z}_A \, E\left(\frac{\pi}{4}, \frac{\varphi}{4}\right)$$

where

$$E\left(\frac{\pi}{4}, k\right) = \int_0^{\frac{\pi}{4}} \left[1 - k^2 \sin^2\varphi\right]^{\frac{1}{2}} d\varphi$$

is an elliptic integral of the second kind. Equation (15.2) shows how the relief pressure according to the incompressive approximation decreases from the center ($E(0) = 1.57$) to the edge ($E(1) = 1$). To get the total force acting across A_o, the mouth of the orifice, integrate (15.2) over this area. Let P_e be the mean value of the incident pressure, p_e, over A_o. Then

$$(15.3) \qquad \int_{(A_o)} p \, dS = 2P_e A - \frac{8}{3} R^3 \rho \, \ddot{z}_A$$

since

$$\int_0^1 E(k) \, k \, dk = \frac{2}{3}$$

In the terminology of paragraph 14. the approximation (15.3) is

non-central. The required equation of motion of the piston is, by (15.3) and (13.1)

$$(15.4) \quad (M + A\rho\, z_A + \tfrac{8}{3} R^3 \rho)\, \ddot{z}_A + k z_A = 2AP_e$$

The additional mass, $8/3\ \rho\ R^3$, was calculated by Rayleigh (12) for the case of a disk vibrating with simple harmonic motion. The preceding calculation shows that the mass of the piston is augmented by the same amount when the motion is not periodic. This conclusion can also be deduced from Rayleigh's result by making a Fourier analysis of an arbitrary motion, and noting that the increase of mass for each frequency is independent of that frequency: but the above proof is more direct than Rayleigh's for our purpose. The equation (15.4) is similar to the one given in reference (3) for side-on incidence (but of course the pressure is not doubled in that case). We conclude from (15.4) that in the incompressive approximation the effect of the rarefaction emitted by a recoiling piston is simply to increase its effective mass.

16. In the nomenclature of paragraph 14, the equation (15.4) is correct for the incompressive, non-central approximation. In the appendix, paragraph 7., this is compared with the compressive, central and with the incompressive, central equations. There it is made clear that either the incompressive, or the central approximation, or both together, may be used without appreciable error. Equation (15.4), the incompressive, non-central approximation should be used, however, since it is as simple as the incompressive,

central solution and slightly more accurate.

17. It is also possible to give an upper bound to the error associated with the use of the incompressive equation (15.4). The calculation is made in the appendix, paragraph g., where it is shown that this approximation may be regarded as introducing an error in the effective mass of the piston. For a crusher gauge the relative error in effective mass is of the order of

$$(17.1)\quad \frac{11\,R^4}{M\theta_g} \times 10^{-3} \text{ per cent}$$

where R,M, and θ_g are radius of piston, effective mass of piston, and deformation time, all in cgs units. For a typical gauge this relative error is 0.5%. (Here R = 0.6 cm, M = 15g, and $\theta_g = 200 \times 10^{-6}$ sec). For a Hilliar piston the relative error is even less, namely,

$$(17.2)\quad \frac{4R^4}{M\theta} \times 10^{-3} \text{ per cent,}$$

where θ, the time-constant of the incident pulse, is generally much longer than the time-constant of a crusher gauge.

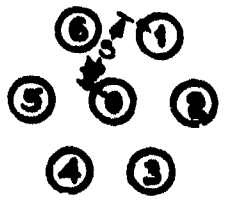
18. In the Hilliar type of gauge there are several pistons, all set in the same face of the gauge. There is thus the possibility, suggested by Hartmann, that the recoil of each piston will relieve the pressure on every other piston. A simple calculation of the effect may be made as follows: The force F_{10} which piston 1 exerts on piston 0 is by (9.3)

$$(18.1)\quad F_{10} = \frac{\rho}{4\pi} \int_{(A_1)} \int_{(A_0)} \frac{a_1\left(t - \frac{r}{c}\right)}{r}\, dS_1\, dS_0$$

where a_1 is the acceleration of piston 1, r is the distance between

dS_1 and dS_0, and the integration is carried out over the areas, A_1 and A_0, of the two orifices. This integral is calculated in the appendix, paragraph 9.; but F_{01} may be approximated with sufficient accuracy by its leading term, since its value is small in any case. As an example one may find the effect of the circumferential pistons on the central piston (the zero piston) in the Hartmann-Hilliar gauge. (See Fig. 4, and reference 5 for details. The zero piston is set in center of the gauge and is surround by 6 pistons, all at the distance, s, from it. The pistons are all of the same radius, R.) If the coupling (18.1) is included, the corrected equation of the zero piston of the Hartmann-Hilliar gauge is

Fig. 4



$$(18.2)\qquad (M + \tfrac{8}{3}\rho R^3)\,\ddot{z} + kz = 2AP_e\left[1 - \tfrac{5}{4}\frac{R^2}{s}\left(1 + \tfrac{1}{2}\frac{R^2}{s}\right)\sum_1^6 \frac{1}{m_1}\right]$$

The sum is carried out over the masses m_1 of the 6 circumferential pistons. The correction to be made in the deformation of the pellet is 1.4% in a typical case.

IV. THE RESPONSE OF THE BLOCK AND ITS INFLUENCE ON THE PISTONS

19. Consider a single piston at the center of a finite circular baffle. (The words baffle and block are interchangeable here.

In our schematic picture, the gauge consists of two parts: (a) the piston, and (b) the comparatively massive object in which the piston moves.) We have so far assumed the baffle to be infinite and at rest. Actually it will move, even if rigid, unless it is very heavy as well as rigid. Motion of the baffle will further diminish the pressure on the piston. In fact, the relief pressure due to the moving baffle is

$$\rho c \left[v_b(t - \theta_b) - v_b (t - \theta_p)\right] \tag{19.1}$$

where v_b is the velocity of the front face of the baffle; θ_p and θ_b are half the times required for sound to cross the piston and baffle, respectively. (19.1) is calculated in the same way as (11.2). If the action of the gauge is completed before $t = \theta_b$, the expression (19.1) becomes

$$-\rho c \; v_b \; (t - \theta_p) \tag{19.2}$$

In this case, while the gauge is responding, the relief pressure from the baffle is proportional to its velocity, but the relief pressure from the piston itself is proportional to its acceleration. Their difference in behavior is due to their different sizes: the time for sound to cross the piston is small compared to the response time of the gauge, while the baffle is so large that the time taken by sound to travel from its edge to its center exceeds the response time of the gauge. We shall usually assume that this is the situation, i.e.,

$$\theta_g \leqslant \theta_b \tag{19.3}$$

where θ_g is the response time of the gauge. This condition also enables us to ignore pressure waves which are propagated in toward the piston from water beyond the edge of the baffle; since these arrive too late to influence the gauge. Finally, it is not difficult to construct a gauge which satisfies (19.3).

20. If the condition (19.3) is not satisfied, there is a further reduction in pressure due to rarefactions travelling in from the region beyond the edge of the block. This region has been denoted by C_o (see Fig. 3). Let the incident wave be plane and neglect the perturbation caused by the block in the region C_o. Then the pressure there is p_e, the pressure of the incident wave. Let the corresponding velocity be v_e. If we assume that the velocity of flow across C_o is constant between the edge of the block and infinity, the relief pressure due to this moving water is

$$\rho c \left[v_e(t - \infty) - v_e (t - \theta_b)\right] = - \rho c\, v_e(t - \theta_b), \tag{20.1}$$

just as the pressure due to the finite baffle is given by (19.1). Since the incident wave is assumed to be plane, the material velocity is $p_e/\rho c$. By (20.1) the relief pressure due to the moving water becomes

$$- p_e(t - \theta_b) \tag{20.2}$$

The correction (20.2) has been made by Goranson in his experiments (13). There is, of course, more uncertainty in using a small baffle and applying the correction (20.2) than in using a baffle large enough to satisfy (19.3).

21. In order to take account of the rarefaction (19.2) it is necessary either to calculate the velocity of the front face of the recoiling block, or to make the block so heavy and so nearly rigid that this velocity is negligible. The procedure here is to suppose (19.2) decreased to a small value experimentally and to estimate this small quantity. The pressure (19.2) can be made small by choosing a nearly immovable block. Consider one which is rigid and laterally infinite, i.e., $R_b = \infty$. Let it be struck normally by an exponential pulse, namely, $p_e = P_m e^{-t/\theta}$. If the block is infinitely thick as well as wide, it does not recoil, and the pressure on its front face is always $2p_e$. If its inertia per unit area is finite, it recoils and the pressure on its front face is only a certain fraction of $2p_e$. Let it be $2p_e r$, where $r = 1$ for an immovable block, and r decreases when the thickness of the block decreases. In paragraph 10 of the appendix, r is calculated. There it may be seen that $r = 1$ at $t = 0$, and that r decreases as t increases. Its value is of no interest for values of the time longer than $t = \theta_g$, the deformation time of the gauge. In order that $r(\theta_g) = 0.99$, the block must be so thick that the following equation is satisfied.

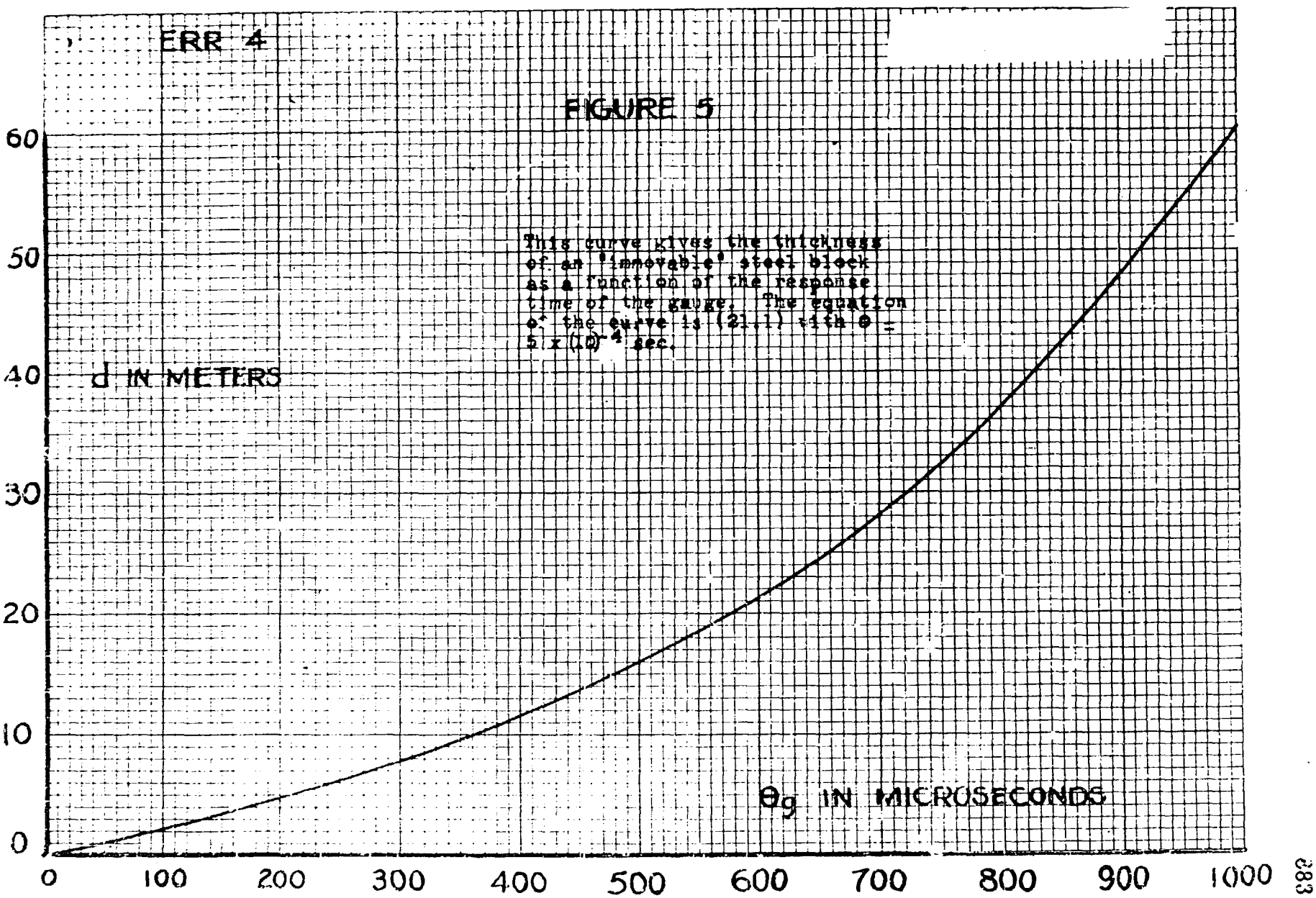
$$(21.1) \qquad m = \frac{n}{n-1} \ln (0.02n + 0.98),$$

where

$m = \theta_g/\theta$ $\qquad$ ρ_b = density of block

$n = \theta_d/2\theta$ $\qquad$ d = thickness of block

$\theta_d = \rho_b d/\rho c$


ERR 4
FIGURE 5
This curve gives the thickness of an 'immovable' steel block as a function of the response time of the gauge. The equation of the curve is (21.1) with θ = 5 x (10)^-4 sec.
d IN METERS
θg IN MICROSECONDS
0
10
20
30
40
50
60
0
100
200
300
400
500
600
700
800
900
1000

Here m is proportional to the gauge time, and n is proportional to the thickness of the block. A graph of d against θ_g is shown in Fig. 5. The values of d are seen to be very large. The equation (21.1), or Fig. 5, specifies the thickness of a rigid block for which the relief pressure due to recoil is not more than 1% of the total pressure during the response of the gauge.

22. It is next necessary to realize that the block is actually soft rather than rigid. One then arrives at a second criterion for an effectively infinite block. Let c_b = velocity of sound in the block, and let d = its thickness. A shock wave falling on the front face of the block does not return until a time, θ_s, has passed, where

$$\theta_s = \frac{2d}{c_b} \qquad (22.1)$$

If $\theta_s > \theta_g$ (the response time of the gauge), the gauge does not receive a signal from the back face until after it has registered. Hence the pellet deformations are the same as they would have been if the back face had been at infinity. Therefore a soft block is effectively infinite, if

$$\theta_g = \frac{2d}{c_b} \qquad (22.2)$$

23. In the appendix, paragraph 11, the two criteria, (21.1)

and (22.2) are compared. There it is shown that if a baffle must be of thickness d_r to satisfy the rigid-block criterion, (21.1), and of thickness d_s to satisfy the soft-block criterion, (22.2), then always

(23.1) $$d_r > d_s$$

This inequality is true only if $\rho_b c_b/\rho c < 200$; but this condition is always satisfied in practice, e.g., for steel, $\rho_b c_b/\rho c = 27$. That is, it is only necessary to satisfy the soft criterion (22.2). In so doing one fails to satisfy the rigid criterion (21.1); but, as remarked in the previous paragraph, one gains nothing by exceeding the thickness d_s. If it had turned out differently, i.e., if the result had been $d_r < d_s$, then it would be possible to use a thinner block than that specified in (22.2). As it is, an effectively infinite block should probably be determined experimentally with(22.2) as a guide. (A typical value of d_s is 50 cm, corresponding to a gauge time, θ_g, of 200 microsec).

24. It is then possible in principle to make the influence of the block on the piston negligible by giving the block a cylindrical form of length, d, and radius, R_b, where

(24.1) $$d = \frac{\theta_g c_b}{2}$$

(24.2) $$R_b = \theta_g c$$

Inertia and thickness having been considered, the principal remaining factor is the way the softness of the block allows the front face to move.

25. If the incident pressure is p_e, by ordinary acoustic theory the velocity of the front face is

$$(25.1) \qquad v = \frac{2\,p_e}{\rho_b c_b + \rho c}$$

This is correct only for times not exceeding $2d/c_b$; but by hypothesis the gauge action is over by then. The corresponding diminution in pressure due to softness is by (19.2), if θ_p/θ_g is made $<<$ 1,

$$(25.2) \qquad \frac{2\rho c\ p_e}{\rho_b c_b + \rho c}$$

If the block is steel, the correction is approximately 3.6% of $2p_e$. The expression (25.2) is correct only for a block of infinite radius. It supposes that all parts of the front face move inwards at the same velocity in response to the same pressure. This, of course, is not true, since the pressure, and hence the velocity, at the center are greater than the corresponding quantities at the edge, where they are diminished by diffraction. The expression (25.2) therefore gives an upper limit for the effect of softness.

V. OTHER EFFECTS

26. Some discussion will be given to show that there is no cavitation in front of the recoiling pistons. It will then appear that the same is true of the block. Conditions favorable for the development of cavitation are found in front of large, thin plates, which are given rather high velocities by impinging shocks. The retreating plates send out rarefactions which cause

tensions sufficient to break the water. The conditions near a piston gauge appear quite different. The pistons are of very small diameter and relatively thick. It has already been seen that the rarefactions which they produce are weak, and in addition they fall off as 1/r. The argument may be made quantitative in terms of the Kirkwood criterion (1), which predicts no cavitation if

$$\theta_p < \theta_c, \tag{26.1}$$

where

$$\theta_p = \frac{R}{c}$$

$$\theta_c = \frac{\theta\theta_L}{\theta - \theta_L} \ln \frac{\theta}{\theta_L}$$

$$\theta_L = \frac{\rho_p L}{\rho c} = \text{damping time of piston}$$

L = length of piston

ρ_p = density of piston

This criterion is based on the fact that the total pressure at the face of the piston does not become negative after the incompressive solution has begun to hold. Since this happens at the time θ_p, the pressure falls to zero, if it does at all, before θ_p. The time required during the compressive regime for the pressure to reach zero is θ_c. The condition for no cavitation, therefore, is that $\theta_p < \theta_c$. The constant θ_c has been called the cavitation time. This test is really only a test for "Taylor cavitation", i.e., cavitation at the liquid piston interface. The Kirkwood criterion is admittedly only rough, but it has been checked very well by the experiments reported in reference (14),

page 26. In the cases which interest us here θ_L/θ is very small. Assume $\theta_L/\theta = 0.10$. Then cavitation should not appear, according to (26.1) unless $R/L \geq 20$. Hence cavitation should be expected only for very thin, wafer shaped pistons, which are never used.

27. Effects of viscosity and turbulence in the fluid behind the recoiling pistons are usually small, but they may become appreciable in long bores of small diameter. In the appendix, paragraph 12., a short calculation on these points is given. Turbulence is to be expected in tubes when the Reynolds number (see appendix) reaches approximately 2000. Behind the recoiling pistons R, the Reynolds number, may be of the order of 10^5 - 10^6. Hence the flow may certainly become turbulent. At low velocities the pressure gradient necessary to maintain a given flow against viscosity is given by Poiseuille's law and is proportional to the velocity. When turbulence appears, resistance increases and the required pressure gradient is proportional nearly to the square of the velocity. According to the appendix, paragraph 12., however, the pressure necessary to overcome turbulence is not large - about 1 atmosphere for pistons of the usual diameter.

28. In references (5) and (11) the possibility of a non-negligible "Bernoulli pressure" has been pointed out. The reason it does not appear in the treatment given here is that the fundamental equation (9.3) is based on acoustic theory, which neglects non-linear terms in the hydrodynamical equations. In paragraph 10. it was remarked that the acoustic approximation is in error by not

not more than 2% in estimating the momentum of shocks of the strengths considered here when they are reflected from rigid walls. However, since the pistons, unlike rigid walls, recoil, the velocity of the fluid behind them may become high. This may be as large as 4×10^3 cm/sec for a shock of 300 atmospheres. (The corresponding material velocity in the wave is only 2×10^3 cm/sec). As a result, the force acting on a piston is less than the value calculated from linear theory by the amount $\rho \frac{u^2}{2} A$. For example, instead of (18.3) one has for the force on the piston

$$2P_0 A - \frac{8}{3} R^3 \rho \ddot{z}_A - \frac{1}{2} A \rho \dot{z}_A^2$$

This is shown in paragraph 13. of the appendix under the incompressive approximation. When the velocity of the piston is 4×10^3 cm/sec, the Bernoulli term is seen to be 8 atmospheres, or 2% of the total pressure.

VI. SUMMARY

Piston gauges are generally used in the side-on orientation. In this position interpretation of the measurements is difficult because of diffraction and irregular reflection; and in the same position, experimental dispersion is found to be larger than in the head-on orientation. Here the theory has been given for the head-on orientation. When a piston recoils it sends out a rarefaction. The effects of this rarefaction on the motion of its generating piston and on the motion of the other pistons in the gauge have been calculated (paragraphs 15. and 18.). These

effects are, in general, small. For example, in the Hartmann-Hilliar gauge the relief pressure from the circumferential pistons diminishes the pressure on the zero piston by less than 2%. Being small they can be found from the incompressive approximation, the error in which has been estimated in (17.1) and (17.2). The gauge block itself is the source of rarefactions for two reasons: (1) it recoils as a rigid body and (2) the front face retreats because it is really soft rather than rigid. These effects have been estimated (paragraphs 21. - 25.). The thickness of an "immovable" soft block is always less than the thickness of an "immovable" rigid block (paragraph 23). In general, the relief pressures due to gauge blocks in current use are proportional to their velocities and are rather large, while corresponding pressures from the pistons are proportional to their accelerations and quite small. According to the Kirkwood criterion there should be no cavitation in front of the pistons which are now used. Their small diameter insures both no cavitation and also accuracy in describing them with the incompressive approximation. Turbulence should be important only if the pistons are of small diameter and travel long distances. In most gauges the pressure necessary to overcome viscosity and turbulence does not exceed 1 atmosphere. Finally the high velocity of the recoiling pistons introduces an error into a description of their motion by linear theory, and makes it necessary to consider the Bernoulli effect, (paragraph 27.). The Bernoulli pressure may become of the order of 10 atmospheres.

Appendix

25

NOTE: An equation number which is underlined refers to an equation of the appendix.

1. Paragraphs 1.-8. of this appendix are devoted to a discussion of the fundamental expression for the pressure (9.3). A common starting point of the diffraction theory is Kirchhoff's theorem:

Let $\psi(\vec{r},t)$ be a solution of the wave equation,

$$\left(\nabla^2 - \frac{1}{c^2}\frac{\partial^2}{\partial t^2}\right)\psi = 0$$

whose partial derivatives of the first and second order are continuous within and on a closed surface S. Let $\vec{r}_1$ be a point inside of S. Then

$$(1.1) \qquad \psi(\vec{r}_1,t) = \frac{1}{4\pi}\int_{(S)}\left\{[\psi]\frac{\partial}{\partial n}\left(\frac{1}{r}\right) - \frac{1}{cr}\frac{\partial r}{\partial n}\left[\frac{\partial \psi}{\partial t}\right] - \frac{1}{r}\left[\frac{\partial \psi}{\partial n}\right]\right\} dS$$

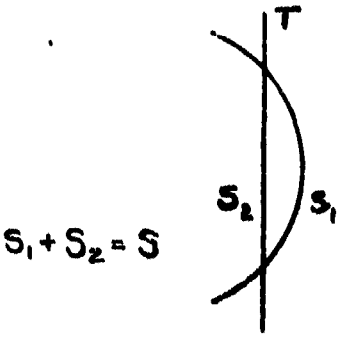
where r is the distance from $\vec{r}_1$ to dS, $\frac{\partial}{\partial n}$ denotes differentiation along the inward normal to S, and square brackets indicate retarded values, e.g., $[\psi(t)] = \psi\left(t - \frac{r}{c}\right)$. If, however, $\vec{r}_1$ lies outside S, the integral vanishes. The integrand in (1.1), which depends upon the position, $\vec{r}_1$, of the field point and the position, $\vec{r}_s$, of dS will be denoted by

$$\left\{\vec{r}_1, \vec{r}_s\right\}.$$

2. Kirchhoff's theorem may be applied to a progressive wave moving into an undisturbed medium. Let S_1 be that part of the wave front which has crossed a certain plane, T, and let S_2 be that part of T which the wave front has left behind. Let $S = S_1 + S_2$. Since the retarded quantities $[\psi]$, $\left[\frac{\partial \psi}{\partial n}\right]$, and $\left[\frac{\partial \psi}{\partial t}\right]$

892

Fig. 1



vanish on S_1, the integral in (1.1) extended over S_1 also vanishes. This is true for a point, $\vec{r}_1$, internal to S, and also for a point, $\vec{r}_2$, external to S. Hence the integral over S collapses to one over S_2, and one may write

$$(2.1) \qquad \psi(\vec{r}_1, t) = \frac{1}{4\pi} \int_{(S_2)} [\vec{r}_1, \vec{r}_2] \, dS$$

$$(2.2) \qquad 0 = \frac{1}{4\pi} \int_{(S_2)} [\vec{r}_2, \vec{r}_2] \, dS$$

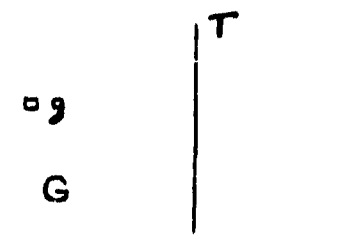
where $\vec{r}_1$, is any point inside of S and where $\vec{r}_2$ is its image in S_2. Addition of (2.1) and (2.2) gives

$$(2.3) \qquad \psi(\vec{r}_1, t) = -\frac{1}{2\pi} \int_{(S_2)} \frac{1}{n} \left[\frac{\partial \psi}{\partial n}\right] dS$$

The value of this integral is not changed if it is extended over all of T, since $\left[\frac{\partial \psi}{\partial n}\right]$ vanishes everywhere on T outside of S_2. Note that the gradient is taken opposite to the direction in which the wave front advances. (2.3) requires much less knowledge of the boundary conditions than (1.1).

3. Now divide space into two parts, G and E, by an infinite plane, T, on opposite sides of which are the gauge, g, and the source, e, of an explosion (Fig 2). The explosive wave starts out from e, strikes g, and is reflected and diffracted back into E. In

Fig. 2



the acoustic approximation the disturbance due to e may be described by a velocity potential, ψ, from which the pressure,

and the material velocity, $\vec{v}$, may be derived.

(3.1) $(\vec{v}, p) = (-\text{grad}\,\psi, \rho \frac{\partial \psi}{\partial t})$

ψ may be divided into two parts:

(3.2) $\psi = \psi_e + \psi_g$

where ψ_e is the disturbance produced by e in the absence of g, and where ψ_g is the perturbation due to the presence of g. Let the normal component of the fluid velocity across T toward g be v_z. Then

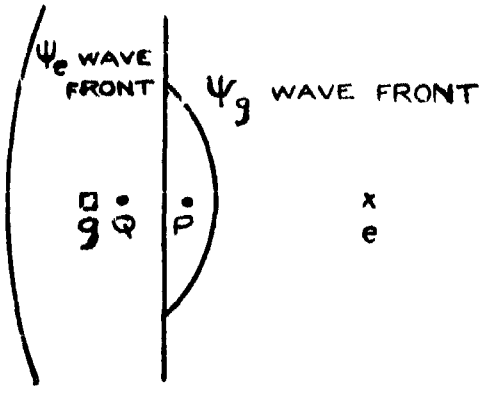
(3.3) $v_z = -\frac{\partial \psi_e}{\partial z} - \frac{\partial \psi_g}{\partial z}$

4. The velocity potential satisfies the wave equation. Hence (2.3) is applicable to ψ_e and ψ_g. (2.3) gives for the points P and Q in Fig. 3.

(4.1) $\psi_g(P) = \frac{1}{2\pi} \int_{(T)} \frac{1}{r} \left[\frac{\partial \psi_g}{\partial z}\right] dS$

(4.2) $\psi_e(Q) = -\frac{1}{2\pi} \int_{(T)} \frac{1}{r} \left[\frac{\partial \psi_e}{\partial z}\right] dS$

Fig. 3



(4.1) and (4.2) are valid on T itself inside of the ψ_g wave front. Let P and Q coincide on T behind the ψ_g wave front. Then by (4.1), (4.2), (3.2) and (3.3),

$$\psi(P) = \frac{1}{2\pi} \int_{(T)} \left\{ \frac{1}{r} \left[\frac{\partial \psi_g}{\partial z}\right] - \frac{1}{r} \left[\frac{\partial \psi_e}{\partial z}\right] \right\} dS$$

$$= \frac{1}{2\pi} \int_{(T)} \left\{ -\frac{1}{r} [v_z] - \frac{2}{r} \left[\frac{\partial \psi_e}{\partial z}\right] \right\} dS$$

$$(4.3) \qquad \psi(P) = 2\psi_2(P) - \frac{1}{2\pi}\int_{(T)} \frac{1}{n}[V_2]\,dS$$

where P is any point on T behind the ψ_g front. By (3.1) the total pressure at P is

$$(4.4) \qquad p = 2p_2 - \frac{\rho}{2\pi}\int_{(T)} \frac{1}{n}\left[\frac{\partial V_2}{\partial t}\right] dS$$

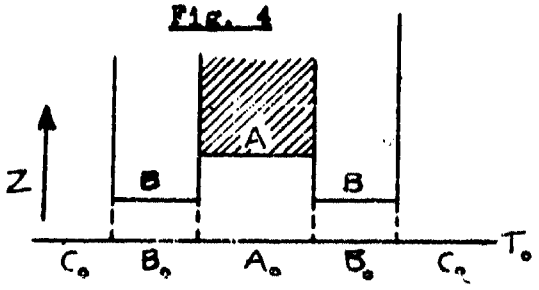
where p_e is the pressure due to e in the absence of g. The corresponding equation for the pressure in front of T follows similarly from (4.1), (4.2), (3.2), and (3.3). It is

$$(4.5) \qquad p(P) = p_2(P) + p_2(Q) - \frac{\rho}{4\pi}\int_{(T)} \frac{1}{n}\left[\frac{\partial V_2}{\partial t}\right] dS$$

where P is any point between T and the ψ_g wave-front and where Q is the mirror image of P in T.

5. The equations (4.4) and (4.5) express the pressure in terms of boundary conditions on any infinite plane dividing the gauge from the source of the explosion. However, what is really needed is an expression for this pressure in terms of the motion of the gauge. In order to obtain such an expression, choose the plane T of the preceding paragraph to be initially coincident with the face of the gauge. In the following, this plane is denoted by T_0 instead of T. In Fig. 4, let

Fig. 4



A = face of the piston (pistons),
B = face of block in which the piston moves,

A_o = projection of A on T_o,

B_o = projection of B on T_o.

Let C_o and T be defined as follows:

(5.1) $A_o + B_o + C_o = T_o$,

(5.2) $A + B + C_o = T$.

T is a moving, broken surface, which is only initially coincident with T_o. One would like to express the boundary conditions on T_o in terms of boundary conditions on T, because only the latter are directly related to the coordinates of the gauge. Fortunately, the displacement of the block is small. It is, therefore, assumed that

(5.3) $$\left(\frac{\partial V_z}{\partial t}\right)_{B_o} = \left(\frac{\partial V_z}{\partial t}\right)_B$$

Further, the flow behind the moving piston is nearly one-dimensional and incompressive. (In a shock of 300 atmospheres the density changes by about 1%.) If the flow is one-dimensional and incompressive between A_o and λ, then $\frac{\partial V_z}{\partial z} = 0$ there by the conservation of mass. Hence,

(5.4) $$\left(\frac{\partial V_z}{\partial t}\right)_{R_o} = \left(\frac{\partial V_z}{\partial t}\right)_R$$

by (5.1 - 4)

$$\left(\frac{\partial V_z}{\partial t}\right)_{T_o} = \left(\frac{\partial V_z}{\partial t}\right)_T$$

or

(5.5) $$\left(\frac{\partial V_z}{\partial t}\right)_{T_o} = \left(\frac{\partial V_z}{\partial t}\right)_T + \left(\frac{\partial V_z}{\partial z}\right)_T (V_z)_T \equiv a_T$$

where a_T is the acceleration of the fluid at T. The quadratic term in (5.5) vanishes in the acoustic approximation. Probably the only place where appeal to the acoustic approximation may be questioned is at the orifice where the material velocity may rather greatly exceed its value in the incident pulse; but here the flow is one-dimensional and nearly incompressive, hence $\frac{\partial V}{\partial x}$ is small, and therefore the quadratic term in (5.5) is small also. Then, by (5.5) and (4.4)

$$(5.6) \qquad p_{T_0} = 2p_2 - \frac{\rho}{2\pi}\int_{(T_0)} \frac{1}{r}\,[a_T]\,dS$$

where a_T is the acceleration of the fluid at the projection of dS on T. At the surface of the gauge a_T is the acceleration of A or of B. Elsewhere it is not directly related to the motion of the gauge; but in our applications of (5.6), the surface B is usually taken so large that its integral vanishes in C_0 by retardation. (5.6) is therefore the desired expression of the pressure in terms of gauge coordinates. The corresponding expression for the pressure at greater distances in front of the gauge is by (4.5)

$$(5.7) \qquad p(P) = p_2(P) + p_2(Q) - \frac{\rho}{2\pi}\int_{(T_0)} \frac{1}{r}\,[a_T]\,dS$$

The Mass M in Equation (13.1)

6. The factor, 1/3, is correct for a spring of uniform density, is probably satisfactory for a cylindrical pellet, and it is

customary to assume that it is also correct for a sphere. If it is intended to use ball crusher gauges with short time constants, and if it then becomes necessary to use a ball whose mass is comparable to that of the piston, this factor should be reexamined. In typical Bureau of Ordnance gauges with 5/32" and 3/8" balls, the masses of the spheres were respectively 2% and 28% that of the corresponding pistons. It should also be pointed out that ignorance of the plastic response of the copper ball or cylinder is now the cause of the main uncertainty in the theory of piston gauges.

Test of the Incompressive and Central Approximations

7. Equation (15.4) is the incompressive, non-central solution. We repeat it here.

(7.1) $$(M + A\rho z_A + \tfrac{2}{3}\rho R^3)\ddot{z}_A + k z_A = 2A P_a$$

The corresponding compressive, central equation follows from (11.2) and (13.1). It is

(7.2) $$(M + A\rho z_A)\ddot{z}_A + k z_A = 2A P_a + \rho c A\left[\dot{z}_A(t - \tfrac{R}{c}) - \dot{z}_A(t)\right]$$

This equation may be rewritten, when $\rho A z_A$ negligible, and the incident pulse is exponential, as

(7.2)' $$\ddot{z}_A + \theta_0^{-2} z_A = \alpha e^{-t/\theta} + \theta_1^{-1}\left[\dot{z}_A(t - \theta_1) - \dot{z}_A(t)\right]$$

where

$\alpha = 2AP_m/M$ = initial acceleration of piston,

$$\theta_0 = \sqrt{\frac{M}{k}} \qquad \theta_1 = \frac{M}{\rho A c} \quad , \quad \theta_2 = \frac{R}{c} \ .$$

Finally the two approximations may be made simultaneously to give the incompressive, central equation

(7.3) $$(M + \rho A z_R + \pi \rho R^3) \ddot{z}_R + k z_R = a A P_2$$

Since the radii of the pistons in current use are small, the differences between equations (7.1), (7.2), and (7.3) are also small. They were compared numerically for a crusher gauge with the following constants.

$M = 14.0$ g $\qquad \theta_0 = 82.0 \ 10^{-6}$ sec

$R = 0.60$ cm $\qquad \theta_1 = 82.4 \ 10^{-6}$ sec

$\theta_2 = 4.0 \ 10^{-6}$ sec

In the incident pulse, $\theta = 500 \ 10^{-6}$ sec

Equations (7.1) and (7.3) differ only in effective mass and in that by less than 1%. Numerical integration of (7.2)' gave a maximum displacement differing from the corresponding quantity for (7.3) also by less than 1%. This result also shows that it is legitimate to neglect the higher order terms in equation (11.2)'.

The Error in the Incompressive Approximation

8. During the action of the gauge, the acceleration of the piston is always decreasing, after its initial jump, since the pressure is falling, while mass and resistance are increasing. Hence at

times beginning with t = 2R/c, one has

(8.1) $a(t - 2R/c) \geq a(t - r/c) > a(t)$

where R is the radius of the piston, r is the distance between any two points on its face, and a is the acceleration of the piston. Therefore

(8.2) $$a(t - 2R/c)\int_{(R_0)} \frac{dS}{n} > \int_{(R_0)} a(t-\tfrac{n}{c})\frac{dS}{n} > a(t)\int_{(R_0)} \frac{dS}{n}$$

Again under the assumption of an infinite, immovable baffle equation (9.3) becomes

(8.3) $$p = 2p_a - \frac{\rho}{2\pi}\int_{(R_0)} \frac{1}{n}\, a(t-\tfrac{n}{c})\, dS$$

Let p_r be the correct relief pressure and let $\tilde{p}_n$ be the incompressive approximation to it. Then by (8.2) and (8.3)

$$p_n - \tilde{p}_n < \frac{\rho}{2\pi}\left[a(t-2R/c) - a(t)\right]\int_{(R_0)} \frac{dS}{n}$$

or

$$p_n - \tilde{p}_n < -\frac{Rf}{c\cdot\pi}\,\dot{a}(\tau)\int_{(R_0)} \frac{dS}{n} \quad \text{where} \quad t - 2R/c < \tau < t,$$

or

(8.4) $$\int_{(R_0)} (p_n - \tilde{p}_n)\, dS' = -\frac{16}{3}\frac{\rho}{c} R^4\, \dot{a}(\tau)$$

since

$$\iint_{(R_0)} \frac{dS\, dS'}{n} = \frac{16}{3}\pi R^3.$$

By (9.3) and (13.1) one has

$$(M + \rho R z_n)\ddot{z}_n + k z_n = \int 2p_a\, dS - \int \tilde{p}_n\, dS - \int (p_n - \tilde{p}_n)\, dS$$

900

or

$$(8.5)\quad \left(M + \rho R z_R + \frac{8}{3}\rho R^3\right)\ddot{z}_R + k z_R = \int a p_a \, dS - \int (p_n - \bar{p}_n)\, dS$$

By (8.5) and (8.4) one finds that the error in the effective mass, M, due to the incompressive approximation is not greater than the right side of the inequality:

$$(8.6)\quad \frac{\Delta M}{M} < \frac{16}{3}\,\frac{\rho R^4}{cM}\left|\frac{\dot{a}(\tau)}{a(t)}\right| \qquad \text{where} \qquad 0 < t - aR/c < \tau < t$$

For a crusher gauge (particularly for one subjected to a very heavy charge - see reference 3 page 4) we have $|\dot{a}/a| \cong \pi/\theta_g$ where θ_g is the time required for maximum displacement. Hence $\Delta M/M$ is in this case approximately

$$(8.7)\quad \frac{11R^4}{M\theta_g}\ 10^{-5}$$

in cgs units. For a freely moving piston, such as one in a Hilliar gauge, one would expect that $|\dot{a}/a| \cong 1/\theta$, where θ is the time constant of the incident pulse. Instead of (8.7) one would then have

$$(8.8)\quad \frac{4R^4}{M\theta}\ 10^{-5}$$

which is even smaller than (8.7).

Rarefaction Coupling between Two Pistons

9. The integral to be evaluated is

$$(9.1)\quad F_{10} = \frac{\rho}{2\pi}\int_{(R_1)}\int_{(R_0)} \frac{[a_1]}{r}\, dS_1\, dS_0$$

Expand $[a_1]$ as far as first order terms in r/c and expand 1/r about the centers of the two orifices. F_{10} is then calculated to be

$$(9.2) \quad F_{10} = \frac{\rho}{2\pi} A^2 \left\{ \frac{a_1}{s}\left(1 + \frac{1}{2}\frac{R^2}{s^2}\right) - \frac{\dot{a}_1}{c} \right\}$$

where s is the distance between centers. When R/s = 0.25, the error in F_{10} due to the expansion of 1/r is estimated at not more than 0.5% and that due to the expansion of [a] is believed to be not more than 0.1% for a 0.5 millisec pulse.

The Thickness of an Immovable Rigid Block

10. An estimate of the thickness of an immovable rigid block may be made as follows. Assume that the incident wave is plane, and that the block is infinitely wide as well as rigid; that is, neglect diffraction at its edges. Then the separate relief forces contributed by the front and back surfaces are equal and proportional to the velocity of the block, and the equation of motion is

$$(10.1) \quad (\rho_b d)\ddot{z} = 2 P_m e^{-t/\theta} - 2\rho c \dot{z} .$$

where

ρ_b = density of block,
d = thickness of block,
z = displacement of block,
P_m = peak pressure of incident wave,
θ = decay constant of incident wave.

We calculate the velocity of the baffle from (10.1) and then the relief pressure from (19.2). The result may be expressed as

the ratio, r, of the total pressure to $2P_m e^{-t/\theta}$, the value correct for a perfectly immovable, rigid, and infinitely wide block.

(10.2) $r(t) = 1 - \frac{1}{2}\frac{1}{n-1}\left[e^{(1-\frac{1}{n})\frac{t}{\theta}} - 1\right]$

where $n = \theta_d / 2\theta$, $\theta_d = \rho_s d / \rho c$.

n is a measure of the thickness of the block.

When t = o, r = 1; and as t increases, r decreases. The formula does not interest us for values of the time longer than $t = \theta_g$, the deformation time of the gauge. If the block has so much inertia that $r(\theta_g) = 0.99$, then its thickness must satisfy the equation.

(10.3) $m = \frac{n}{n-1} \ln (.02n + .98)$

$m = \theta_g / \theta$

The Two Criteria for an Infinitely Thick Baffle

11. The rigid block criterion is

(11.1) $m = \frac{n}{n-1} \ln (.02n + .98)$

The soft block criterion is by (22.2)

(11.2) $m = gn$

where

$g = 4\rho c / \rho_s c_s$

Suppose that the gauge constant, θ_g, and the pulse constant, θ, are fixed. Then m is fixed. Let the solutions of (11.1) and (11.2) for this value of m be n_R and n_g, respectively. It will be shown that $n_R > n_g$, if $g > 0.02$. (For steel $g = 0.15$.) Let

(11.3) $y = \ln (.02 n_R + .98)$,

(11.4) $z = g (n_R - 1)$

n_R and n_g are, of course, both positive.

Then, if $g > 0.02$,

$$z \lesseqgtr y, \text{ when } n_R \gtreqless 1.$$

Hence

(11.5) $$\frac{n_R \, z}{n_R - 1} \gtreqless \frac{n_R}{n_R - 1} y, \text{ when } n_R \gtreqless 1.$$

By (11.1-4)

$$n_R > n_g$$

Hence, if a block must be of thickness d_R to satisfy (11.1), and of thickness d_g to satisfy (11.2),

(11.6) $d_R > d_g$.

Turbulence

12. The Reynolds number, R, corresponding to flow in a tube, is

(12.1) $$R = \frac{v D \rho}{\mu}$$

where v = velocity of flow,
D = diameter of tube,
ρ = density of fluid,
μ = viscosity of fluid.

The pressure difference necessary to maintain turbulent flow along a tube of length, s, is

(12.2) $$\Delta p = \frac{\lambda s}{D} \frac{\rho}{2} v^2$$

where

λ = a resistance coefficient,

$\bar{v}$ = mean velocity of flow.

The following empirical expression for λ has been given by Blasius (see, for example, reference 16).

(12.3) $\lambda = .3(R)^{-.25}$

Let $\bar{v} = 10^4$ cm/sec, $R = 10^6$

$s = 1$ cm, $\lambda = 9.48 \times 10^{-3}$

$D = 1$ cm,

Then $\Delta p = .5$ atmospheres.

The Bernoulli Effect

13. The equations of continuity and motion are

(13.1) $\operatorname{div}(\rho \vec{u}) + \frac{\partial \rho}{\partial t} = 0$

(13.2) $-\operatorname{grad} p = \rho\left(\frac{\partial \vec{u}}{\partial t} + (\vec{u} \operatorname{grad})\vec{u}\right)$

It has been shown that the incompressive approximation introduces negligible error in the description of a single piston. Hence, assume that the fluid is incompressible. Then, if ψ is the velocity potential, equations (13.1) and (13.2) become

(13.3) $\nabla^2 \psi = 0$

(13.4) $\frac{\partial}{\partial s}\left(\frac{p}{\rho} - \frac{\partial \psi}{\partial t} + \frac{u^2}{2}\right) = 0$

respectively, where $\frac{\partial}{\partial s}$ indicates differentiation along a stream-

line. Hence, along a stream-line,

$$(13.5) \qquad p = \rho \frac{\partial \Psi}{\partial t} - \rho \frac{u^2}{2} + \text{constant}$$

In order to find the pressure one may determine Ψ from (13.3) and the given boundary conditions, and substitute in (13.5). The solution of (13.3) is the same in the linear and the non-linear approximations, and is given by Kirchhoff's equation in which c is made infinite. It then follows from (13.5) that the "acoustic pressure" may be corrected by subtracting $\rho \frac{u^2}{2}$ from it.

REFERENCES

1. The Plastic Deformation of Marine Structures by an Underwater Explosion Wave II, J.G. Kirkwood, O.S.R.D., 1115, 1942.

2. Experiments on the Pressure Wave Thrown out by Submarine Explosions, H.W. Hilliar, R.E. 142/19.

3. Theory of Crusher Gauges, G.K. Hartmann, BuOrd Re6b, Memorandum for File, 25 September 1942.

4. Construction and Performance of the NOL Crusher Gauge, N.O.L.R. No. 751, 1943.

5. Report on Hilliar Gauge, G.K. Hartmann, David Taylor Model Basin Report No. 531, 1944.

6. Diffraction of Blast Waves by an Infinite Wedge, F.G. Friedlander, R.C. 61, 1940.

7. Oblique Reflection of Shocks, J. von Neumann, BuOrd Re2c, Explosives Research Report No. 12, 1943.

8. Regular Reflections of Shocks in Water Like-Substances, BuOrd Re2c, H. Polachek and R.J. Seeger, Explosives Research Report No. 14, 1944.

9. Consistency of the N.O.L. Ball Crusher Gauge, R.H. Brown, BuOrd Re2c, Explosives Research Report, No.1, 1944.

10. The Normal Reflection of a Shock Wave in Water, R. Finkelstein, Explosives Research Report No. 1944.

11. The Effect of a Pressure Wave on a Plate or Diaphragm, E.H. Kennard, David Taylor Model Basin Report No. 527, 1944.

12. Theory of Sound Vol II, p 169, 2nd Ed., Rayleigh, 1896.

13. Progress Report, Circular Diaphragm Tests and Derived Damage Relations, Lt. Comdr. R.W. Gorenson, USNR, Underwater Explosion Report No. 1944-1.

14. Division 8 Interim Report, Underwater Explosives and Explosions, No. 16, 1944.

15. Aerodynamic Theory, W.F. Durand, Vol. III, Mechanics of Viscous Fluids, L. Prandtl, 1935.

RESPONSE OF THE BALL CRUSHER GAUGE TO VARIOUS DRIVING FUNCTIONS

A. B. Arons
Underwater Explosives Research Laboratory
Woods Hole Oceanographic Institution

American Contribution

1947

RESPONSE OF THE BALL CRUSHER GAUGE TO VARIOUS DRIVING FUNCTIONS

by

A. B. Arons
Woods Hole Oceanographic Institution

1. Introduction

The fundamental principles and theory of the ball crusher type gauge have been thoroughly discussed by several authors. It is the purpose of this appendix to present certain useful numerical results concerning the response of the ball crusher gauge to various types of driving functions which idealize conditions likely to occur in explosives work.

2. The Fundamental Equation of Motion

The equation of motion of the ball crusher gauge[a] is given by:

$$M\ddot{x} + G(x) = F(t) \qquad \text{(I-1)}$$

where:

M = equivalent mass of moving system

x = deformation of the ball = displacement of the piston

$\ddot{x} = \frac{d^2x}{dt^2}$ = acceleration of associated mass M

$G(x)$ = the "force function", i.e., the opposing force at deformation x

$F(t)$ = "driving function", i.e., applied force as a function of time t.

In the case of the ball crusher gauge, it has been shown[a,b,c] that, within certain limits, the force function is linear, allowing $G(x)$ in Eq. (I-1) to be represented by

$$G(x) = kx \qquad \text{(I-2)}$$

The equation of motion then becomes

$$M\ddot{x} + kx = F(t), \qquad \text{(I-3)}$$

an ordinary, linear differential equation readily soluble for various types of driving functions.

A brief discussion of the experimental determination of k will be found in the reference listed in footnote b of the preceding page.

Finkelstein[a] shows that for a rigidly mounted gauge[b] the associated mass

$$M = \text{mass of piston} + 1/3 \text{ mass of ball} + \frac{8}{3}\rho r^3 \qquad \text{(I-4)}$$

where:

ρ = density of fluid medium

r = radius of piston.

The last term in Eq. (I-4) represents the mass of fluid which becomes associated with the motion of the piston, thus adding to the inertia of the system. In the case of the NOL design of ball crusher gauge[c], used under water, this term constitutes about 4.5% of the total magnitude of M. When the gauges are used in air, the term is negligible.

The sensitivity of the gauge (i.e., the value of k) can be controlled by varying the size of the deformable copper ball. Two sizes, diameters 3/8 in. and 5/32 in., respectively, have become standard. Various numerical parameters pertinent to the two types of gauge are given in Section 13.

3. General Properties of the Equation of Motion

Letting $\omega = (k/M)^{1/2}$, Eq. (I-3) may be rewritten:

$$\ddot{x} + \omega^2 x = \frac{1}{M} F(t) \qquad \text{(I-5)}$$

This is familiar as the equation of motion of a spring obeying Hooke's law, and having a natural period

$$T = 2\pi\sqrt{M/k} = 2\pi/\omega$$

---

a) The Theory of Piston Gauges, by R. Finkelstein, Explosives Research Report No. 5, Navy Dept. BuOrd, April, 1944.

b) When the body of the gauge is free to move, correction must be made for the relative accelerations of piston and gauge body (see reference listed in footnote c of the preceding page).

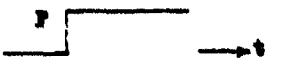
It is important to note, however, that in the case of the ball crusher gauge, the deformation is permanent[a] rather than elastic. Hence Eq. (I-5) does not represent the motion beyond the point of maximum deformation x_m.

In the problem of interest, the initial boundary conditions are:

$$x = 0, \quad \dot{x} = 0 \text{ at } t = 0 \tag{I-6}$$

It will be the purpose of the following sections to solve Eq. (I-5) for various forms of F(t) in the light of these boundary conditions.

4. Step Function: $F(t) = F\,H(t)$



Equation (I-5) may be rewritten in the notation of the Cauchy-Heaviside operational calculus:

$$x = \frac{1}{(D_t^2 + \omega^2)} \frac{F}{M} H(t) \tag{I-7}$$

where D_t is the operator $\frac{d}{dt}$, and H(t) is the unit step function.

$$x = \frac{F/M}{(D_t + i\omega)(D_t - i\omega) D_t} D_t H(t) \tag{I-8}$$

Separating Eq. (I-8) into partial fractions:

$$x = \left[\frac{1}{\omega^2 D_t} - \frac{1}{2\omega^2 (D_t - i\omega)} - \frac{1}{2\omega^2 (D_t + i\omega)}\right] \frac{F}{M} D_t H(t)$$

$$x = \left[\frac{1}{\omega^2} - \frac{1}{2\omega^2}(e^{i\omega t} + e^{-i\omega t})\right] \frac{F}{M} H(t) \tag{I-9}$$

$$x = \frac{F}{K}(1 - \cos \omega t) H(t)$$

To determine the maximum deflection x_m and the time of maximum deflection t_m:

---

a) For a discussion of corrections necessary for the slight amount of elastic recovery when working at low pressures.

$$\dot{x} = \frac{P_0}{k} \sin \omega t_m = 0,$$

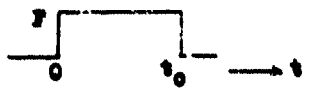
and hence

$$t_m = \frac{\pi}{\omega} = \pi \sqrt{M/k} \qquad \text{(I-10)}$$

Combining Eqs. (I-9) and (I-10),

$$x_m = \frac{2P}{k} \qquad \text{(I-11)}$$

5. **Square Wave:** $F(t) = P\,H(t) - P\,H(t - t_0)$



In this case, Eq. (I-5) becomes

$$x = \frac{1}{D_0^2 + \omega^2} \frac{P}{M} H(t) - \frac{1}{D_0^2 + \omega^2} \frac{P}{M} H(t - t_0) \qquad \text{(I-12)}$$

If $t_0 > \frac{\pi}{\omega}$ (see Eq. I-10), the situation reduces to that developed in Section 4 of this appendix, as the deformation of the gauge is complete before the time t_0 of pressure cut-off.

If $t_0 < \frac{\pi}{\omega}$,

$$x = \frac{P}{k} (1 - \cos \omega t)\, H(t) - \frac{P}{k} \left[1 - \cos \omega (t - t_0)\right] H(t - t_0) \qquad \text{(I-13)}$$

When $t > t_0$, Eq. (I-13) can be rewritten:

$$x = \frac{P}{k} \left[\cos \omega (t - t_0) - \cos \omega t\right]$$

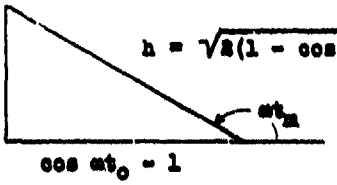
$$x = \frac{P}{k} (\cos \omega t \cos \omega t_0 + \sin \omega t \sin \omega t_0 - \cos \omega t) \qquad \text{(I-14)}$$

To find x_m and t_m:

$$\dot{x} = \frac{P_0}{k} \left[\sin \omega t_0 \cos \omega t_m - (\cos \omega t_0 - 1) \sin \omega t_m\right] = 0$$

$$\tan \omega t_m = - \frac{\sin \omega t_o}{\cos \omega t_o - 1} ; \quad t_m = \frac{1}{\omega} \tan^{-1} \frac{\sin \omega t_o}{\cos \omega t_o - 1} \tag{I-15}$$

Perform the following triangular substitution:



$$\sin \omega t_m = \frac{\sin \omega t_o}{h} \qquad \cos \omega t_m = \frac{\cos \omega t_o - 1}{h} \tag{I-16}$$

Combining Eqs. (I-14) and (I-16):

$$x_m = \frac{F}{kh} \left[\cos \omega t_o \ (\cos \omega t_o - 1) + \sin^2 \omega t_o - \cos \omega t_o + 1 \right]$$

$$x_m = \frac{1.414 \ F}{k} \sqrt{1 - \cos \omega t_o} \tag{I-17}$$

Since the response to a step function is 2F/k (Eq. I-11), the relative response

$$\gamma = 0.707 \sqrt{1 - \cos \omega t_o} \tag{I-18}$$

Consider Eq. (I-15):

$$\tan \omega t_m = \frac{\sin \omega t_o}{\cos \omega t_o - 1} \tag{I-15}$$

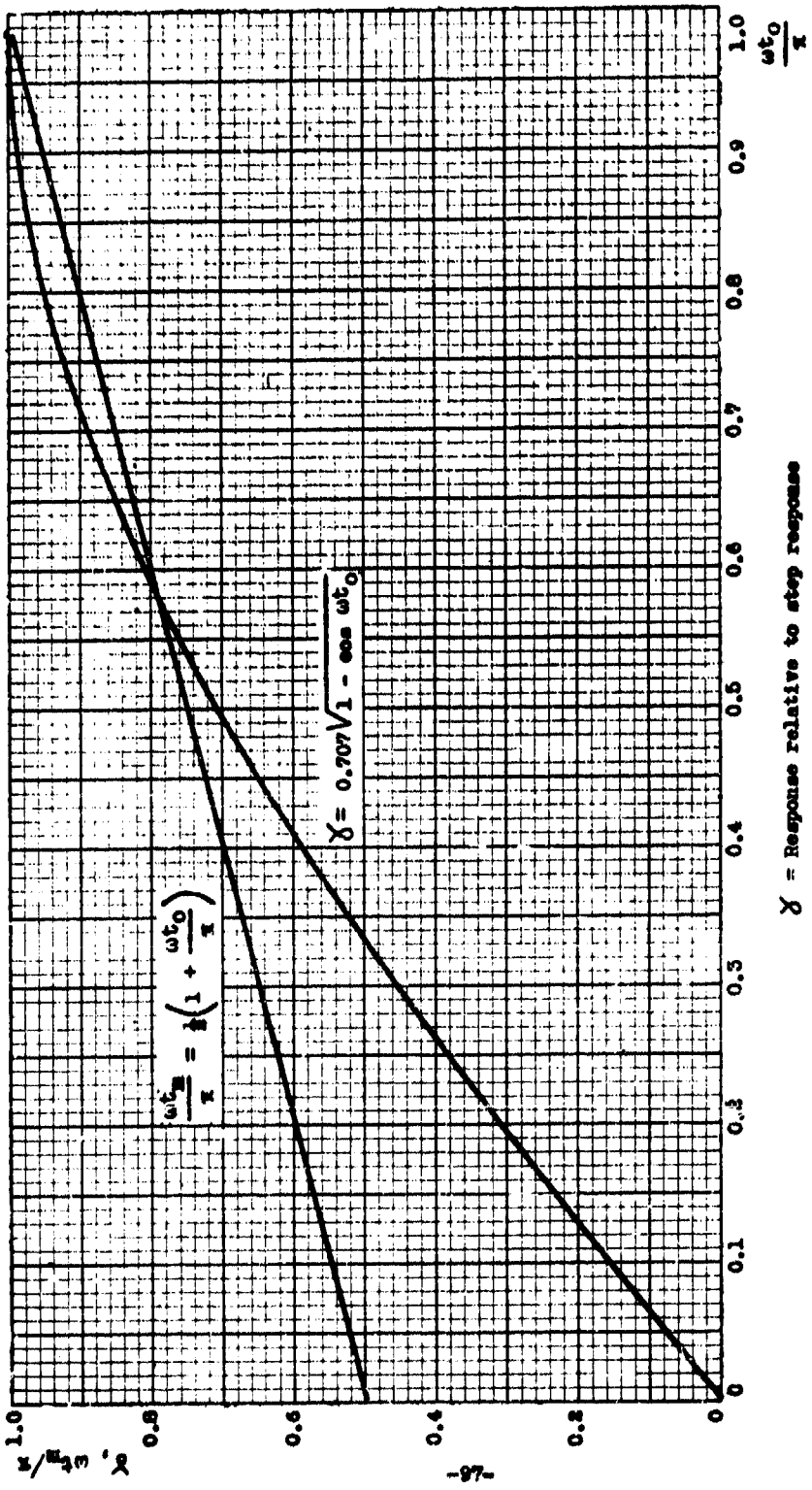
Since $\cot \frac{x}{2} = \frac{\sin x}{1 - \cos x}$

$$\tan \omega t_m = - \cot \frac{\omega t_o}{2} = \tan \left[\frac{\pi}{2} + \frac{\omega t_o}{2} \right]$$

Therefore

$$\omega t_m = \frac{\pi}{2} + \frac{\omega t_o}{2} \tag{I-19}$$

Figure I-1 consists of generalized plots giving γ and $\omega t_m / \pi$ as functions of $\omega t_o / \pi$.



γ = Response relative to step response

t_m = Time of maximum deformation

$\omega = (k/M)^{\frac{1}{2}}$

Fig. I-2.

Response of ball crusher gage to square wave of duration $t_o \leqslant \omega/\pi$.

From the data of Section 18 of this appendix (for the ball crusher gauge used under water):

$$\omega = 1.22 \times 10^4 \text{ sec}^{-1} \qquad \text{for 5/32 in. balls}$$

$$\omega = 1.88 \times 10^4 \text{ sec}^{-1} \qquad \text{for 3/8 in. balls}$$

Figures I-2 and I-3 show γ and t_m as functions of t_o for 5/32 in. and 3/8 in. balls.

It is interesting to note the extent to which the inertia of the system is instrumental in maintaining the amplitude of the response as the duration t_o falls below the step response time. γ is down only 10% when t_o is 89% less than the step response time.

6. Linear Decay: $F(t) = F(1 - \frac{t}{\theta})\, H(t)$



Substituting into Eq. (I-5):

$$x = \left[\frac{1}{(D_t^2 + \omega^2)\, D_t} - \frac{1}{\theta(D_t^2 + \omega^2)\, D_t^2}\right] \frac{F}{M} D_t\, H(t) \qquad \text{(I-30)}$$

$$x = \frac{F}{k}(1 - \cos \omega t)\, H(t) - \frac{F}{M\theta}\left[\frac{1}{(D_t + i\omega)2i\omega^3} + \frac{1}{(D_t - i\omega)(-2i\omega^3)} + \frac{1}{D_t^2 \omega^2}\right] D_t\, H(t)$$

$$= \frac{F}{k}(1 - \cos \omega t)\, H(t) - \frac{F}{\omega^2 M\theta}\left[\omega t - \frac{e^{i\omega t} - e^{-i\omega t}}{2}\right] H(t)$$

$$x = \frac{F}{k}(1 - \cos \omega t)\, H(t) - \frac{F}{k\omega\theta}\,(\omega t - \sin \omega t)\, H(t) \qquad \text{(I-31)}$$

To determine the maximum deformation:

$$\dot{x} = \frac{F}{k}\omega \sin \omega t_m - \frac{F}{k\theta} + \frac{F}{k\theta} \cos \omega t_m = 0$$

$$\omega\theta = \frac{1 - \cos \omega t_m}{\omega t_m} \qquad \text{(I-32)}$$

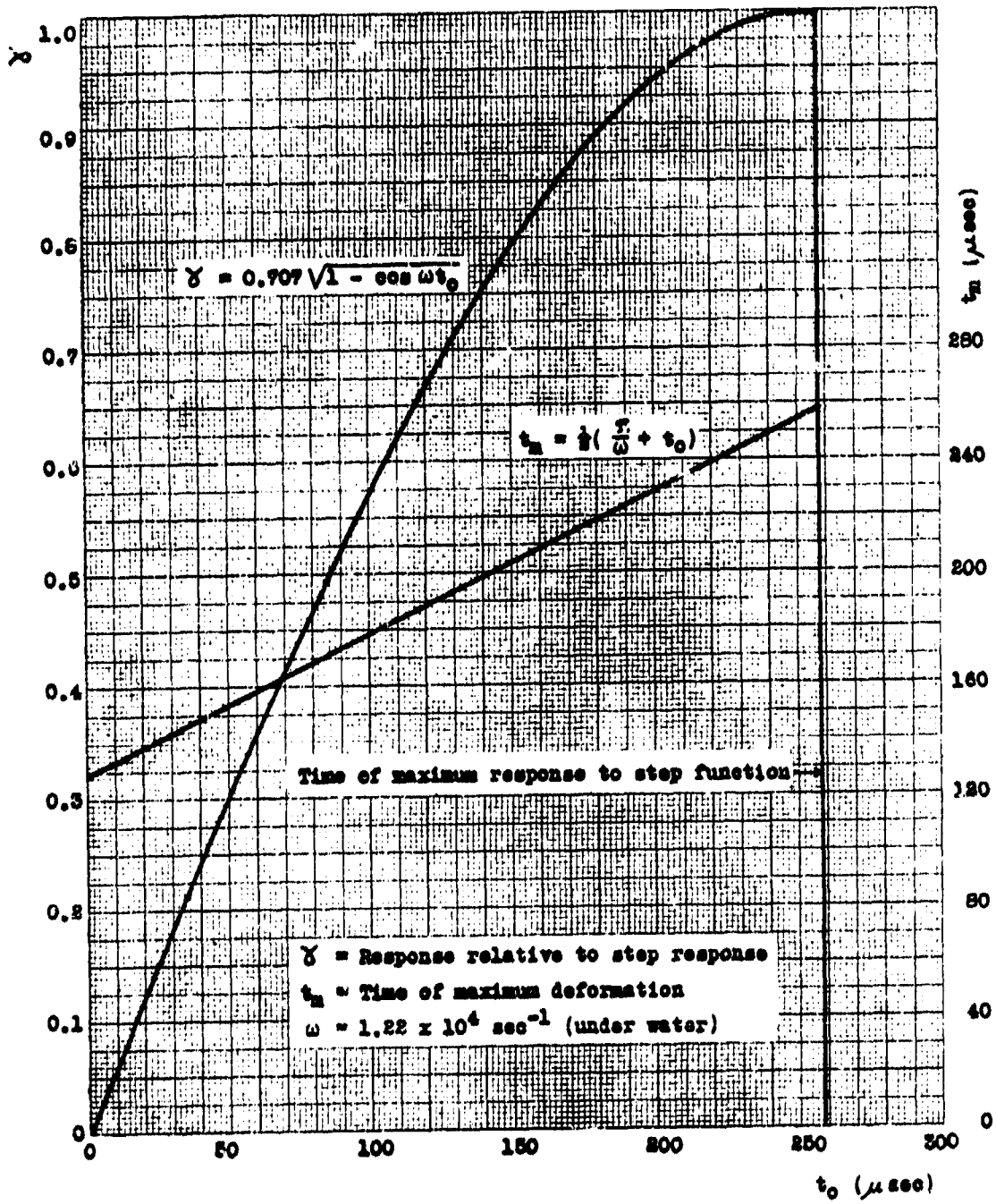


Fig. I-2.

Response of 5/32 in. ball crusher gauge to square wave of duration t_o.

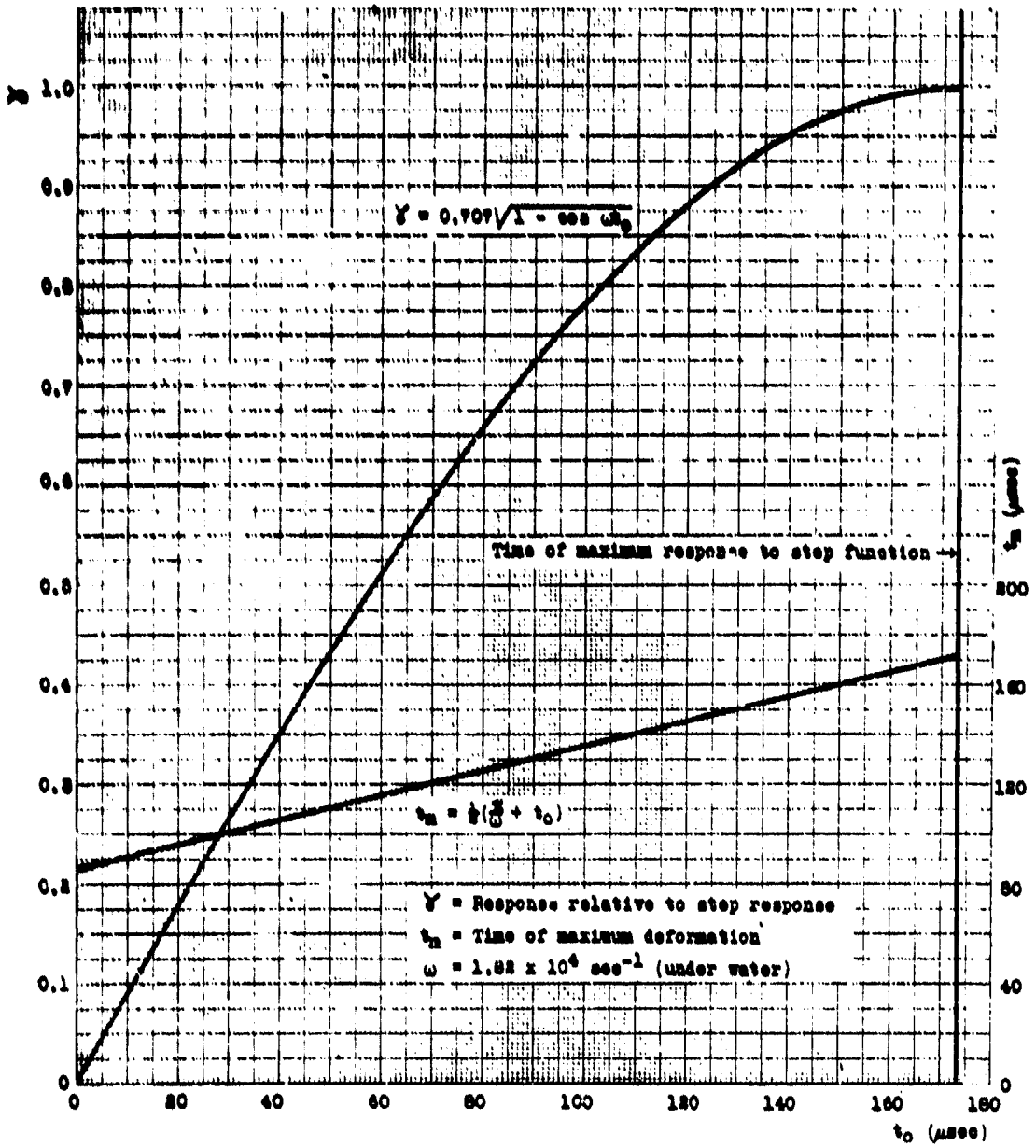


Fig. I-3.

Response of 5/8 in. ball crusher gauge to square wave of duration t_o.

Applying the following trigonometric relations:

$$\tan\frac{1}{2}x = \frac{1-\cos x}{\sin x}\,; \qquad \tan 2x = \frac{2\tan x}{1-\tan^2 x}\,,$$

and combining with Eq. (I-22)

$$\tan\frac{\omega t_m}{2} = \omega\theta$$

$$\tan\omega t_m = \frac{2\omega\theta}{1-\omega^2\theta^2}\,; \qquad t_m = \frac{1}{\omega}\tan^{-1}\frac{2\omega\theta}{1-\omega^2\theta^2} \tag{I-23}$$

Combining Eqs. (I-21) and (I-22):

$$x = \frac{F}{k}\left[1 - \frac{1-\omega^2\theta^2}{1+\omega^2\theta^2}\right] - \frac{F}{k\omega\theta}\left[\omega t_m - \frac{2\omega\theta}{1+\omega^2\theta^2}\right]$$

$$= \frac{F}{k}\left[\frac{2\omega^2\theta^2}{1+\omega^2\theta^2} - \frac{t_m}{\theta} + \frac{2}{1+\omega^2\theta^2}\right]$$

$$x = \frac{2F}{k}\left[1 - \frac{t_m}{2\theta}\right] \tag{I-24}$$

The response (relative to step response):

$$\gamma = 1 - \frac{t_m}{2\theta} \tag{I-25}$$

It should be noted that an additional consideration arises in cases of low θ where θ becomes $< t_m$. If the driving function actually continues to go negative for $t > \theta$, the above development is applicable. If, however, the driving function remains zero for $t > \theta$, it would be necessary to solve Eq. (I-5) with

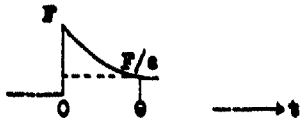
$$F(t) = F\left(1 - \frac{t}{\theta}\right) H(t) - F\left(1 - \frac{t}{\theta}\right) H(t - \theta) \qquad \text{(I-26)}$$

Since this consideration arises at values of θ lower than those normally encountered in the use of ball crusher gauges, the solution will not be carried out at this time.

A generalized plot of γ and $\omega t_m/\pi$ vs. $\omega\theta$ is given in Fig. I-4. Plots of γ and t_m vs. θ for 5/32 in. and 3/8 in. balls (used under water) are given in Figs. I-5 and I-6.

7. **Exponential Decay:**

A. $F(t) = F e^{-t/\theta} H(t)$



Substituting into Eq. (I-5):

$$x = \frac{e^{-t/\theta}}{D_t^2 + \omega^2} \frac{F}{M} H(t) = \frac{1}{(D_t + i\omega)(D_t - i\omega)\left(D_t + \frac{1}{\theta}\right)} \frac{F}{M} D_t H(t) \qquad \text{(I-27)}$$

$$= \left[\frac{1}{(D_t + i\omega)(-2i\omega)\left(\frac{1}{\theta} - i\omega\right)} + \frac{1}{(D_t - i\omega)(2i\omega)\left(\frac{1}{\theta} + i\omega\right)} + \frac{1}{\left(D_t + \frac{1}{\theta}\right)\left(i\omega - \frac{1}{\theta}\right)\left(-\frac{1}{\theta} - i\omega\right)} \right] \frac{F}{M} D_t H(t)$$

$$x = \left[\frac{-e^{-i\omega t}\left[\frac{1}{\theta} + i\omega\right]}{\left[\frac{1}{\theta^2} + \omega^2\right](2i\omega)} + \frac{e^{i\omega t}\left[\frac{1}{\theta} - i\omega\right]}{\left[\frac{1}{\theta^2} + \omega^2\right](2i\omega)} + \frac{e^{-t/\theta}}{\left[\frac{1}{\theta^2} + \omega^2\right]} \right] \frac{F}{M} H(t)$$

$$= \frac{F}{M\left[\frac{1}{\theta^2} + \omega^2\right]} \left[\frac{1}{2i\omega\theta} (e^{i\omega t} - e^{-i\omega t}) - \frac{1}{2} (e^{i\omega t} + e^{-i\omega t}) + e^{-t/\theta} \right] H(t)$$

$$x = \frac{F}{\frac{M}{\theta^2} + k}\left[\frac{1}{\omega\theta}\sin\omega t - \cos\omega t + e^{-t/\theta}\right]H(t) \qquad \text{(I-28)}$$

To obtain maximum deformation:

$$\dot{x} = \frac{F}{\frac{M}{\theta^2} + k}\left[\frac{1}{\theta}\cos\omega t_m + \omega\sin\omega t_m - \frac{1}{\theta}e^{-t/\theta}\right] = 0$$

$$e^{-t_m/\theta} = \cos\omega t_m + \omega\theta\sin\omega t_m \qquad \text{(I-29)}$$

The time of maximum deformation, t_m, must be obtained by solving Eq. (I-29). Since this is a transcendental equation, the solution must be carried out graphically or by successive approximation. A new solution is required for each new value of θ.

Putting Eq. (I-29) into Eq. (I-28):

$$x_m = \frac{F\theta^2}{M(1+\omega^2\theta^2)}\left[\frac{1}{\omega\theta}\sin\omega t_m + \omega\theta\sin\omega t_m\right] = \frac{F\theta}{\omega M}\sin\omega t_m$$

and hence

$$x_m = \frac{2F}{k}\,\frac{\omega\theta}{2}\sin\omega t_m \qquad \text{(I-30)}$$

The relative response γ is therefore:

$$\gamma = \frac{\omega\theta}{2}\sin\omega t_m \qquad \text{(I-31)}$$

Generalized plots of γ and $\omega t_m/\pi$ vs. $\omega\theta$ are given in Fig. I-4. Plots of γ and t_m vs. θ for 5/32 in. and 3/8 in. balls used under water are given in Figs. I-5 and I-6.

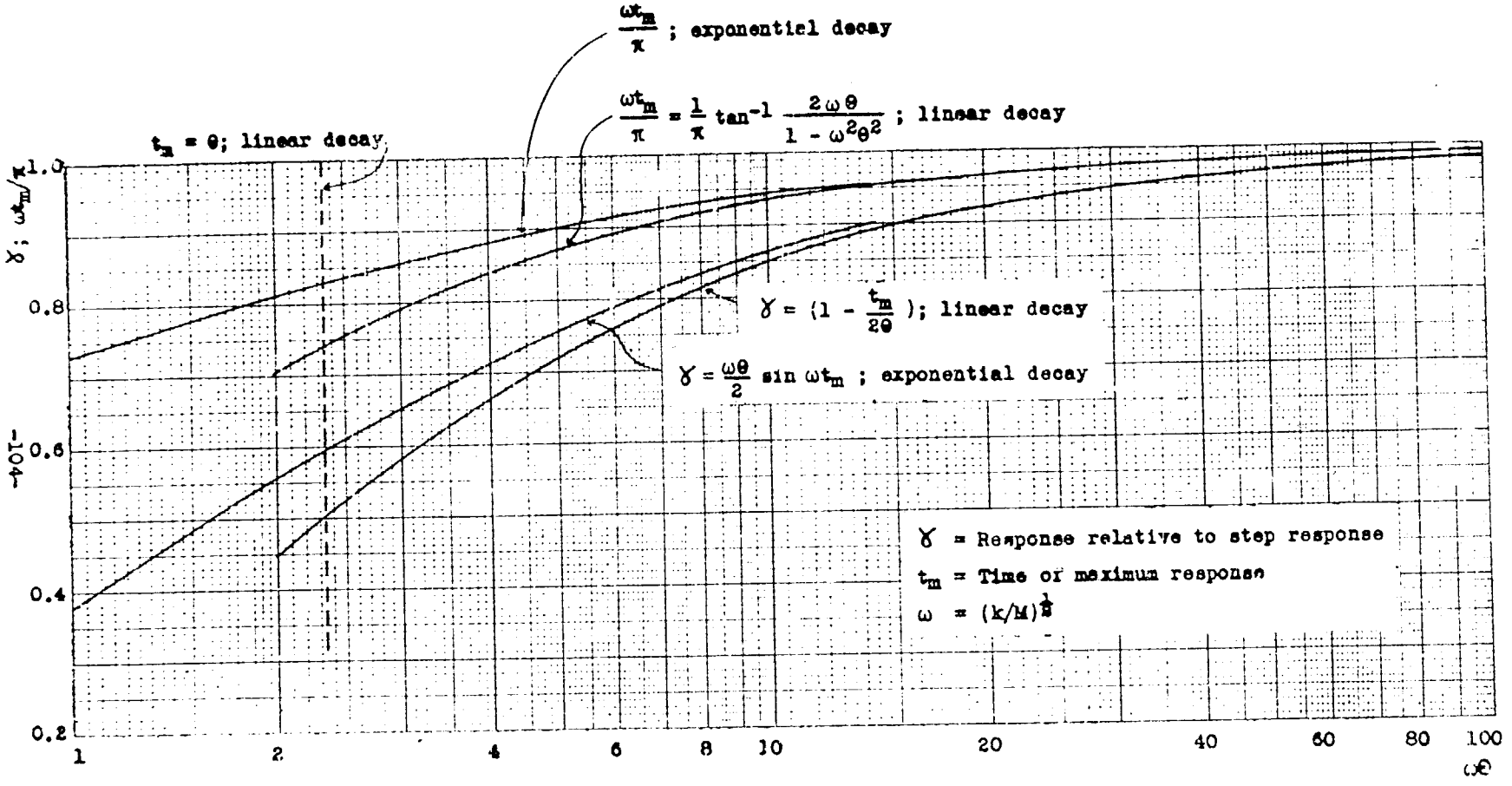


Fig. I-4.

Generalized response of ball crusher to linear and exponential decay driving functions: $F(t) = F(1 - t/\theta)$; $F(t) = Fe^{-t/\theta}$.

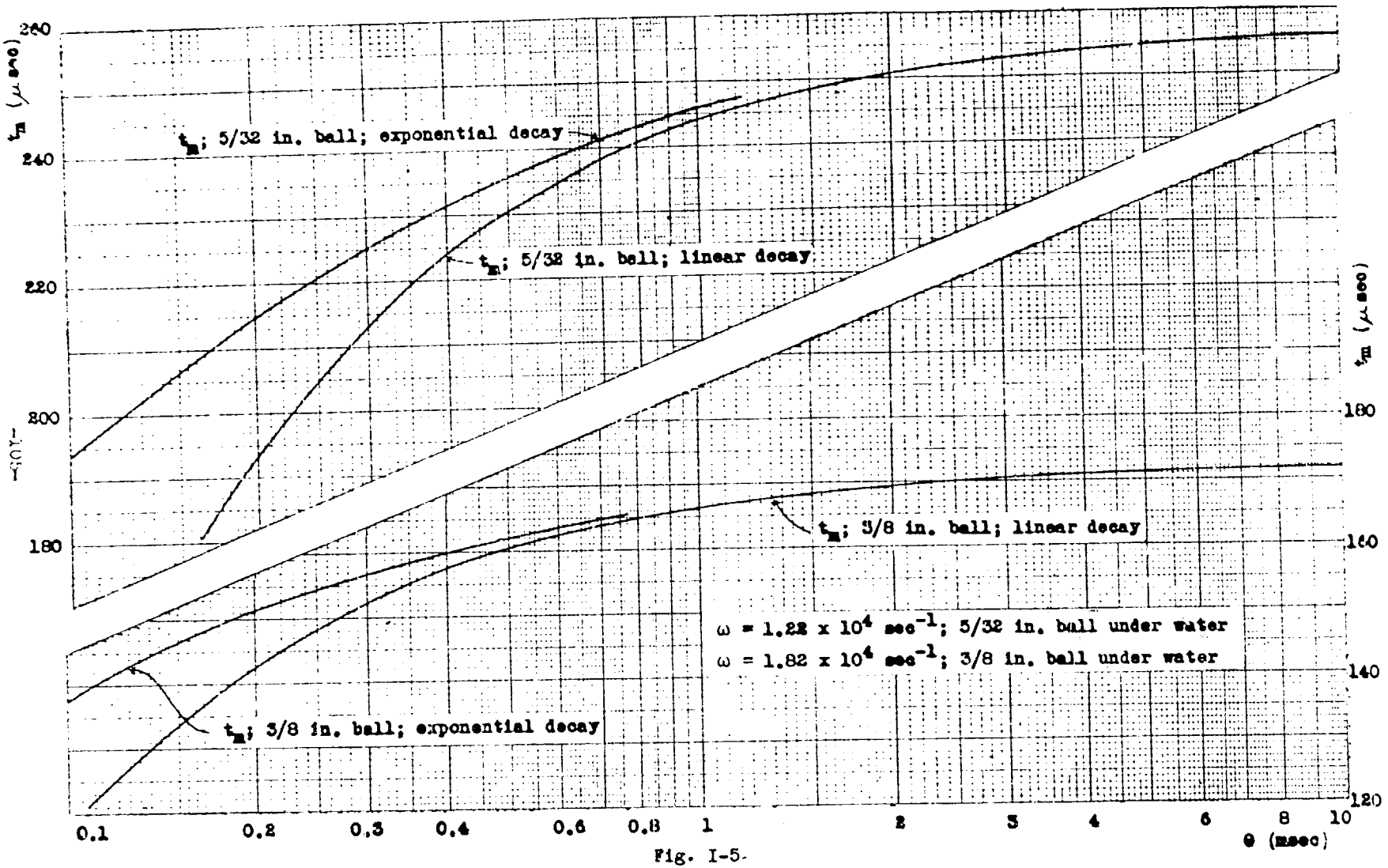


Fig. I-5.

Time of maximum response of 3/8 in. and 5/32 in. ball crusher gauges to linear and exponential decay driving functions: $F(t) = F(1 - t/\theta)$; $F(t) = Fe^{-t/\theta}$.

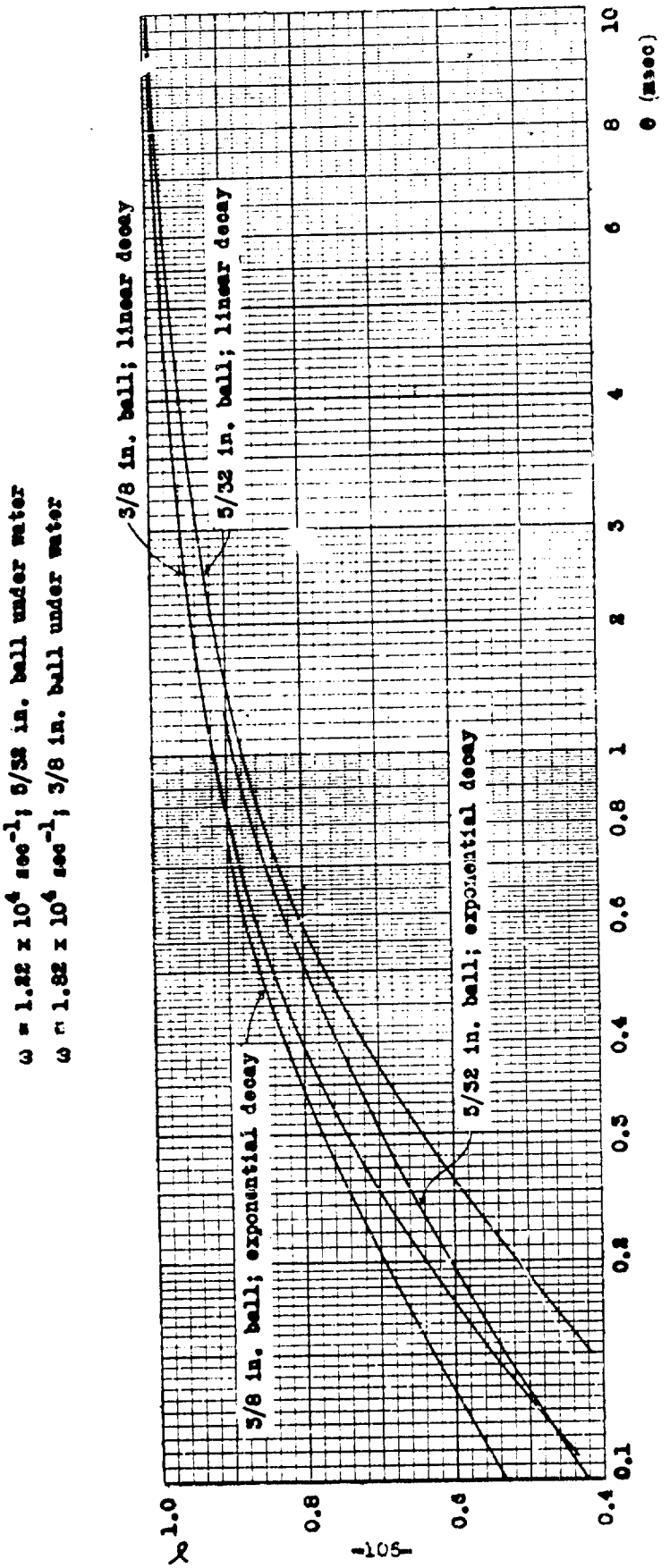
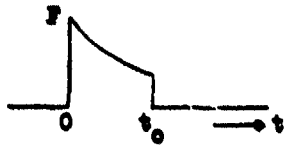


Fig. I-6.

Relative response of 5/32 in. and 3/8 in. ball crusher gauges to linear and exponential decay driving functions: $F(t) = F(1 - t/\theta)$; $F(t) = Fe^{-t/\theta}$.

B. Exponential Decay with Cut-Off.

$$F(t) = F\, e^{-t/\theta}\, H(t) - F\, e^{-t_o/\theta}\, e^{-\frac{t-t_o}{\theta}}\, H(t - t_o)$$



Substituting into Eq. (I-5), and following the development of Eq. (I-27):

$$x = \frac{F\,\theta^2}{M(1 + \omega^2\,\theta^2)} \left[\frac{1}{\omega\theta} \sin \omega t - \cos \omega t + e^{-t/\theta}\right] H(t)$$

$$- \frac{F\,\theta^2\, e^{-t_o/\theta}}{M(1 + \omega^2\,\theta^2)} \left[\frac{1}{\omega\theta} \sin \omega(t - t_o) - \cos \omega(t - t_o) + e^{-\frac{t-t_o}{\theta}}\right] H(t - t_o) \qquad \text{(I-31a)}$$

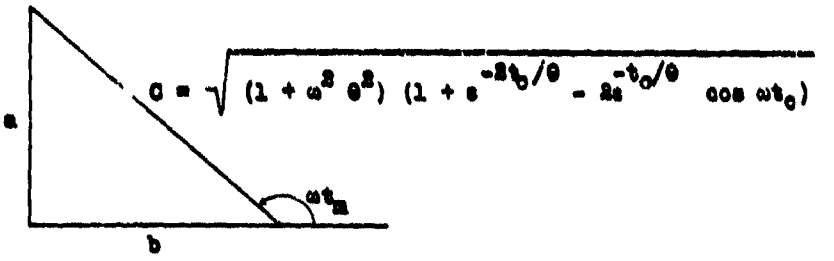
For $t_o < t < t_m$, Eq. (I-31a) becomes

$$x = \frac{F\,\theta^2}{M(1 + \omega^2\,\theta^2)} \left[\frac{1}{\omega\theta} \sin \omega t - \cos \omega t - \frac{e^{-t_o/\theta}}{\omega\theta} \sin \omega(t - t_o) + e^{-t_o/\theta} \cos \omega(t - t_o)\right] \qquad \text{(I-31b)}$$

Differentiating Eq. (I-31b), and solving for the time of maximum deformation:

$$\tan \omega t_m = \frac{1 - e^{-t_o/\theta} \cos \omega t_o + \omega\theta e^{-t_o/\theta} \sin \omega t_o}{e^{-t_o/\theta} \sin \omega t_o + \omega\theta e^{-t_o/\theta} \cos \omega t_o - \omega\theta} \qquad \text{(I-31c)}$$

Setting the numerator and denominator of Eq. (I-31c) equal to a and b respectively, and performing a trigonometric substitution:



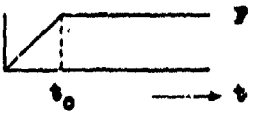
Expanding Eq. (I-31b), and substituting from the above triangle for cos ωt_m and sin ωt_m:

$$x_m = \frac{2F}{k} \cdot \frac{\omega\theta}{2} \left[\frac{1 + e^{-2t_o/\theta} - 2e^{-t_o/\theta} \cos \omega t_o}{1 + \omega^2 \theta^2} \right]^{1/2} \qquad \text{(I-31d)}$$

The relative response γ is therefore:

$$\gamma = \frac{\omega\theta}{2} \left[\frac{1 + e^{-2t_o/\theta} - 2e^{-t_o/\theta} \cos \omega t_o}{1 + \omega^2 \theta^2} \right]^{1/2} \qquad \text{(I-31e)}$$

8. Linear Rise to a Limiting Value



$$F(t) = F(t/t_o)\, H(t) - F(t/t_o)\, H(t - t_o) + F\, H(t - t_o)$$

$$= F(t/t_o)\, H(t) - F \frac{t - t_o}{t_o} H(t - t_o) \qquad \text{(I-32)}$$

Substituting in Eq. (I-6), and solving as in Eq. (I-20):

$$x = \frac{F}{kt_o\omega}\left[\omega t - \sin \omega t\right]H(t) - \frac{F}{kt_o\omega}\left[\omega(t - t_o) - \sin \omega(t - t_o)\right]H(t - t_o) \qquad \text{(I-33)}$$

When $t > t_o$,

$$x = \frac{F}{kt_o\omega}\left[\omega t_o - \sin \omega t + \sin \omega(t - t_o)\right] \qquad \text{(I-34)}$$

To obtain maximum deformation:

$$\dot{x} = \frac{F}{kt_o}\left[-\cos \omega t_m + \cos \omega(t_m - t_o)\right] = 0$$

$$\cos \omega t_m = \cos \omega t_o \cos \omega t_m + \sin \omega t_o \sin \omega t_m$$

$$\tan \omega t_m = \frac{1 - \cos \omega t_o}{\sin \omega t_o} = \tan \frac{\omega t_o}{2} \qquad \text{(I-35)}$$

Since t must be $> t_o$, the solution required by Eq. (I-35) is:

$$\omega t_m = \pi + \frac{\omega t_o}{2} \qquad \text{(I-36)}$$

Putting Eq. (I-36) into Eq. (I-34):

$$x_m = \frac{F}{kt_o\omega}\left[\omega t_o + 2 \sin \frac{\omega t_o}{2}\right]$$

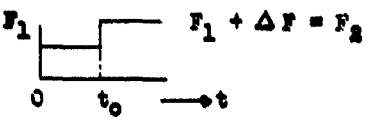
$$x_m = \frac{2F}{k}\left[\frac{1}{2} + \frac{1}{\omega t_o} \sin \frac{\omega t_o}{2}\right] \qquad \text{(I-37)}$$

and therefore

$$\gamma = \frac{1}{2} + \frac{1}{\omega t_o} \sin \frac{\omega t_o}{2} \qquad \text{(I-38)}$$

where γ is the response relative to step response. As $\omega t_o \longrightarrow 0$, $\gamma \longrightarrow 1$, i.e., approaches step response as expected. As $\omega t_o \longrightarrow \infty$, $\gamma \longrightarrow 1/2$. A plot of γ vs. ωt_o is given in Fig. I-7.

9. Successive Step Functions



$$F(t) = F_1 H(t) + \Delta F H(t - t_o) \tag{I-39}$$

$$x = \frac{1}{D_t^2 + \omega^2} \frac{F_1}{M} H(t) + \frac{1}{D_t^2 + \omega^2} \frac{\Delta F}{M} H(t - t_o) \tag{I-40}$$

Following the development leading from Eq. (I-8) to Eq. (I-9), the solution to Eq. (I-40) is:

$$x = \frac{F_1}{k} (1 - \cos \omega t) H(t) + \frac{\Delta F}{k} \left[1 - \cos \omega (t - t_o)\right] H(t - t_o) \tag{I-41}$$

If $t_o < \frac{\pi}{\omega}$, then for $t > t_o$:

$$x = \frac{F_1}{k} - \frac{F_1}{k} \cos \omega t + \frac{\Delta F}{k} - \frac{\Delta F}{k} (\cos \omega t \cos \omega t_o + \sin \omega t \sin \omega t_o)$$

$$x = \frac{F_2}{k} - \left[\frac{F_1}{k} + \frac{\Delta F}{k} \cos \omega t_o\right] \cos \omega t - \frac{\Delta F}{k} \sin \omega t_o \sin \omega t \tag{I-42}$$

$$\dot{x} = \frac{\omega}{k} (F_1 + \Delta F \cos \omega t_o) \sin \omega t - \frac{\omega}{k} \Delta F \sin \omega t_o \cos \omega t \tag{I-43}$$

For maximum deformation:

$$\tan \omega t_m = \frac{\Delta F \sin \omega t_o}{F_1 + \Delta F \cos \omega t_o}$$

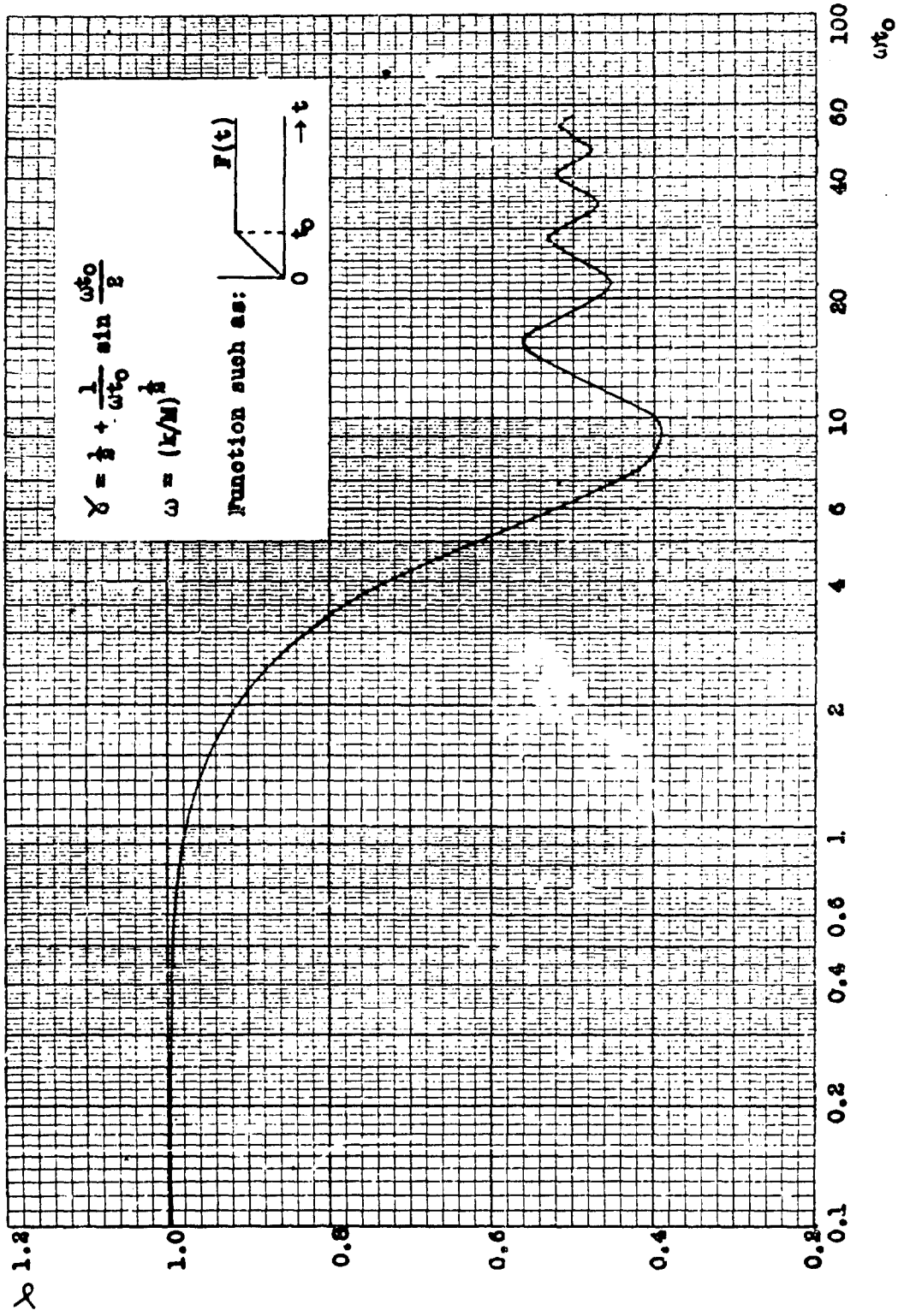
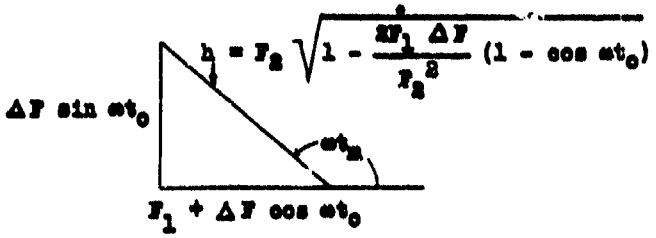


Fig. I-7.

Response of ball crusher gauge to linearly rising driving function.

As $\omega t_0 \longrightarrow 0$, $\omega t_m \longrightarrow \pi$. Perform the following trigonometric substitution:



$$kx_m = F_2 + \frac{(F_1 + \Delta F \cos \omega t_0)^2 - \Delta F^2 \sin^2 \omega t_0}{h}$$

$$= F_2 + h - \frac{2\Delta F^2 \sin^2 \omega t_0}{h}$$

$$x_m = \frac{2F_2}{k}\left[\frac{1}{2} + \frac{1}{2}\sqrt{1 - \frac{2F_1 \Delta F}{F_2^2}(1 - \cos \omega t_0)}\right.$$

$$\left. - \frac{\Delta F^2 \sin^2 \omega t_0}{F_2^2 \sqrt{1 - \frac{2F_1 \Delta F}{F_2^2}(1 - \cos \omega t_0)}}\right] \qquad \text{(I-44)}$$

To check Eq. (I-44):

$$\text{As } \omega t_0 \longrightarrow 0 , \quad x_m \longrightarrow \frac{2F_2}{k} ;$$

$$\Delta F \longrightarrow 0 , \quad x_m \longrightarrow \frac{2F_1}{k} ;$$

$$\omega t_0 \longrightarrow \pi , \quad x_m \longrightarrow \frac{2F_1}{k} ;$$

For the special case $F_2 = 2F_1$ (normal reflection from a rigid surface), Eq. (I-44) becomes:

$$x_m = \frac{2F_2}{k}\left[\frac{1}{2} + \frac{1}{2}\sqrt{1 - \frac{1}{2}(1 - \cos \omega t_o)} - \frac{\sin^2 \omega t_o}{4\sqrt{1 - \frac{1}{2}(1 - \cos \omega t_o)}}\right] \qquad \text{(I-45)}$$

If the gauge is oriented against the rigid surface as shown in Fig. I-8, t_o is approximately 25 microsec. Then

$$\omega t_o = 0.305 \quad \text{for 5/32 in. balls}$$
$$\omega t_o = 0.455 \quad \text{for 3/8 in. balls.} \qquad \text{(I-46)}$$

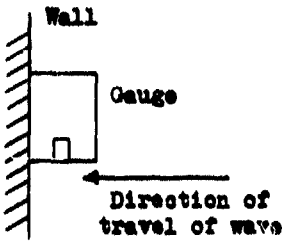


Fig. I-8.

Putting Eq. (I-46) into Eq. (I-45),

$$x_m = 0.971 \frac{2F_2}{k} \quad \text{for 5/32 in. balls}$$
$$x_m = 0.936 \frac{2F_2}{k} \quad \text{for 3/8 in. balls.}$$

10. Initial Deformation

Apply a step pressure wave F H(t) to a gauge in which the piston starts from rest in contact with a ball having initial deformation x_o.

The boundary conditions are given by $x = x_o$ and $\dot{x} = 0$ at $t = 0$, and the equation of motion becomes:

$$x = \frac{1}{D_t^2 + \omega^2}\frac{F}{M}H(t) + \frac{x_o D_t^2 H(t)}{D_t^2 + \omega^2} \qquad \text{(I-47)}$$

$$x = \frac{F}{k}(1 - \cos \omega t)\, H(t) + x_o \cos \omega t\, H(t) \qquad \text{(I-48)}$$

For maximum deformation:

$$\dot{x} = \frac{F\omega}{k} \sin \omega t_m - x_o \sin \omega t_m = 0$$

and hence

$$\omega t_m = \pi \tag{I-49}$$

Putting Eq. (I-49) into Eq. (I-48),

$$x_m = \frac{2F}{k} - x_o \tag{I-50}$$

Equation (I-50) is important in the interpretation of ball crusher gauge behavior, and will be considered in detail.

Reviewing preceding derivations, the deformation produced by a step wave F H(t) is given by Eq. (I-11):

$$x_m = \frac{2F}{k} \tag{I-11}$$

The deformation produced by a force F applied infinitely slowly is given by Eq. (I-37):

$$x = \frac{F}{k} \tag{I-37}$$

(This assumes that rate of strain is not significant in the production of the deformation. The assumption is manifestly incorrect, but a consideration of these idealized results is nevertheless illuminating.)

The deformation obtained under the dynamic conditions implicit in Eq. (I-11) is twice that obtained due to the same "static" force in Eq. (I-37). This is due to the fact that in the former case the piston acquires kinetic energy in the initial stages of deformation, causing it to "overshoot" and give a final deformation 2F/k.

Now returning to the consideration of Eq. (I-50): When an initial deformation exists, the piston cannot acquire kinetic energy in the initial stages; in fact, Eq. (I-50) shows that the piston cannot begin to move unless the applied force exceeds <u>twice</u> the step force which would originally have been necessary to produce the deformation x_o. In other words, if x_o had been produced initially by a step force F_1, so that

$$x_o = \frac{2F_1}{k} \tag{I-51}$$

then a step force exceeding $2F_1$ would be required to produce additional deformation.

From another point of view, the question arises as to how small initial deformations should be used in attempts to correct for their existence. Equation (I-50) shows that the correction is additive, i.e., the incident step force F must be calculated from the sum of the final and initial deformation:

$$F = \frac{k(x_m + x_0)}{2} \tag{I-52}$$

It is obvious that these results are highly idealized and stem from assumptions implicit in Eq. (I-1). The latter equation is simply an expression of Newton's second law and fails to account for phenomena associated with the propagation of the plastic wave through the copper sphere and subsequent reflections from the interfaces at piston and anvil, i.e., Eq. (I-1) assumes that the far end of the copper sphere is instantaneously conscious of events at the near end.

The theory developed in this section must consequently be regarded only as a first order treatment reliable only when the corrections are not large.

11. Gauge Not Rigidly Mounted

When the gauge is free to move under the influence of the pressure wave and is so mounted that the rear end of the gauge is not exposed to the pressure, the following force diagrams are applicable.

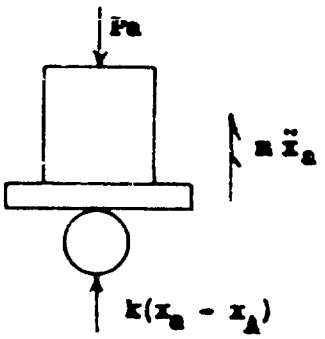


Fig. I-9. Piston and Ball.

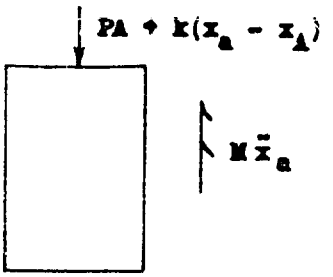


Fig. I-10. Gauge Body.

where:

P = applied pressure

a = piston area

A = area of gauge body

x_a = piston displacement

m = mass of piston + $\frac{1}{3}$ mass ball + $\frac{8}{3}\rho r^3$

M = mass of gauge body

x = deformation of copper ball

x_A = gauge body displacement

From Fig. I-9:

$$Pa = m\ddot{x}_a + k(x_a - x_A)$$

and

$$MPa = mM\ddot{x}_a + kM(x_a - x_A) \qquad \text{(I-53)}$$

From Fig. I-10:

$$PA = M\ddot{x}_A - k(x_a - x_A)$$

and

$$mPA = mM\ddot{x}_A - km(x_a - x_A) \qquad \text{(I-54)}$$

By definition:

$$x = x_a - x_A$$

and (I-55)

$$\ddot{x} = \ddot{x}_a - \ddot{x}_A$$

Combining Eqs. (I-53) and (I-54), substituting Eq. (I-55), and assuming P to be a function of time:

$$\frac{mM}{M + m}\ddot{x} + kx = \frac{Ma - mA}{M + m}P(t) \qquad \text{(I-56)}$$

Equation (I-56) may be written:

$$\mu\ddot{x} + kx = \beta P(t) \qquad \text{(I-57)}$$

where:

$$\mu = \frac{mM}{M + m}. \quad \text{(equivalent mass)} \qquad \text{(I-58)}$$

$$\beta = \frac{Ma - mA}{M + m} \quad \text{(equivalent area)} \qquad \text{(I-59)}$$

As $M \longrightarrow \infty$ (rigid mounting),

$$\mu \longrightarrow m \text{ and } \beta \longrightarrow a. \qquad \text{(I-60)}$$

12. The Force Function, G(x)

Copper spheres have been calibrated at UERL by measuring deformations produced by means of known weights dropped from known heights, i.e., measuring the energy E required to produce various deformations x. The force function is then given by:

$$G(x) = \frac{d}{dx} E(x) \tag{I-61}$$

It has been found empirically that over the initial region of deformation, the function E(x) is parabolic:

$$E(x) = \frac{k}{2} x^2 \tag{I-62}$$

$$G(x) = kx \tag{I-63}$$

From a series of calibrations (made Feb. 6, 1946) on spheres to be used on Operation Crossroads:

$$k_{5/32 \text{ in.}} = 1.51 \times 10^5 \text{ lb/ft} \tag{I-64}$$

$$k_{3/8 \text{ in.}} = 3.60 \times 10^5 \text{ lb/ft} \tag{I-65}$$

In the case of the 5/32 in. spheres, the force function is linear up to deformations of about 0.05 in. or 1600 lb/in.^{2} in a step wave. For the 3/8 in. spheres, the force function is linear to deformations of 0.09 in. or 7000 lb/in.^{2} in a step wave. Since the deviation from linearity is not very great in the region just above the values quoted, the systems can probably be considered linear, without appreciable error, to pressures of 2000 and 10,000 lb/in.^{2}, respectively.

The data of Section 13 of this appendix give:

$$\omega = \sqrt{k/M}$$

$$\omega_{5/32\ \text{in.}} = 1.22 \times 10^4\ \text{sec}^{-1} \qquad \text{(I-66)}$$

$$\omega_{3/8\ \text{in.}} = 1.82 \times 10^4\ \text{sec}^{-1} \qquad \text{(I-67)}$$

If $\gamma(\theta)$ = response (relative to step response) to an arbitrary shock wave having time parameter θ,

A = piston area

x_m = deformation of ball (in.)

P = peak pressure ($lb/in.^2$)

$$P = \frac{kx_m}{2A\,\gamma(\theta)} \qquad \text{(I-68)}$$

$$P_{5/32\ \text{in.}} = 3.19 \times 10^4\ \frac{x_m}{\gamma(\theta)} \qquad \text{(I-69)}$$

$$P_{3/8\ \text{in.}} = 7.62 \times 10^4\ \frac{x_m}{\gamma(\theta)} \qquad \text{(I-70)}$$

13. Gauge Constants[a)]

A. Constants for 5/32 in. Balls (Under water)

M = mass of piston + $\frac{1}{3}$ mass of ball + $\frac{8}{3}\rho r^3$

= 13.9 + 0.097 + 0.68 = 14.7 g = 1.01×10^{-3} slugs

Piston area = 0.197 $in.^2$ = 1.37×10^{-3} ft^2

B. Constants for 3/8 in. Balls

M = 13.9 + 1.3 + 0.68 = 15.88 g = 1.09×10^{-3} slugs

NOTE ON THE WATER FORMATION PRODUCED BY AN UNDERWATER EXPLOSION ON THE MODEL SCALE

A. J. Harris
Road Research Laboratory, London

British Contribution

August 1943

NOTE ON THE WATER FORMATION PRODUCED BY AN UNDERWATER EXPLOSION ON THE MODEL SCALE

A. J. Harris

Road Research Laboratory,
London

August 1943

* * * * * * * *

Summary.

Spark photographs have been taken of the vertical movement of water produced by the explosion of a No. 8 detonator at 1 inch below the water surface in a model tank.

Analysis of a drum camera "schlieren" record shows that the shock wave leaves the water surface with a velocity some 50 per cent greater than that of sound.

In order to throw light on the experimental results the transmission of shock waves through a water-air interface has been examined theoretically. The intensity of the shock wave in water has been evaluated from the velocity measurements and the effect of oblique incidence has been studied.

I. *EXPERIMENTAL*

Introduction.

Previous reports have been given of the "dome" and "plume" formation produced by the explosion of a No. 8 detonator in water, studied by means of a succession of photographs taken at ½ milliseconds intervals. The initial vertical velocity of the water formation has been measured with a rotating drum camera, a "schlieren" technique being used to show that the shock wave leaves the water surface at the instant at which it begins to move upwards. This present report deals in more detail with the movement of water and the accompanying shock wave from the explosion of a detonator 1 inch deep.

Experimental methods: Spark photography.

With a detonator 1 inch deep the initial movement of the water surface is about 1,000 ft./second – too rapid for the employment of the previous photographic method having a picture frequency of only 700 pictures/second. A number of spark photographs of the phenomena, i.e. movement of water surface and accompanying shock wave, were therefore obtained at intervals of about 100 microseconds corresponding to a picture frequency of about 10,000 pictures second. The experimental arrangement employed is shown in Figure 1 being that originally devised by Cranz and Schardin. Spark 1 is triggered through a thyratron by a diaphragm contact in the water near the detonator and the succeeding sparks are triggered in succession by suitable electric delay circuits. Spark 1 provides the illumination for the record given by camera 1 and so on; in this way up to nine shadow pictures can be obtained at intervals ranging from 2 to 200 microseconds depending on the characteristics of the delay circuits.

Drum camera record.

The drum camera record of the water front and of the shock wave front was obtained by the "schlieren" method described previously.

Results obtained.

A selection of the spark photographs obtained are given in Figures 2 and 3. Figure 2 shows successive stages in the water formation and Figure 3 shows a later stage more clearly.

Water .....

Water formation:

In the early stages of the water movement the water rises to form a shape somewhat similar to that formed when a pencil is pushed upwards into a sheet of rubber from beneath. This formation is then partially broken up by a rising spherical disturbance which an early drum camera record suggested might be hollow. It is believed that the shock wave first detaches a surface layer of water and flings it upwards and that the gas bubble then bursts through this layer.

Shock wave:

Figure 2 shows three successive stages in the development of the shock wave. It first rises from the water surface in the form of an arc, then two straight branches develop and finally a third wave develops where each straight branch joins the central arc. This bifurcation of the shock wave is shown more clearly in Figure 3. The photographs only show a section of the true shock wave formation, the true shape being a dome surmounting a cone, the whole formation being symmetrical about a vertical axis.

The photographic record produced by the dome is denser than that given by the cone (Figure 3) indicating that the dome is a more intense shock wave and is moving at a greater speed, the pressure and speed being possibly greatest at the top of the dome. The dome thus becomes more prominent as the shock wave system develops. The cone arises from the outward propagation of the explosion along the water surface. Thus if A and W are the velocities of propagation in air and water respectively then $A/W = \sin\alpha$ where α is the angle made by the cone and the water surface on a vertical plane through the centre of the explosion. A mean value of α from several records is 13.8° giving $W = 4.21A$. This is within 1 per cent of the ratio of the velocities of sound in air and water at 13°C (Smithsonian Tables) for sound $A = 1,110$ ft./second and $W = 4,730$ ft./second giving $W = 4.25A$. The reasons for the development of the bifurcation are not fully understood.

"Schlieren" record: velocity of shock wave:

Figure 4 shows a drum camera "schlieren" record giving the initial vertical velocities of the top of the dome and the accompanying shock wave, that is, the velocities of these disturbances in an upward vertical direction through the centre of the explosion. It will be seen that the "schlieren" record is curved. Measurement of this curvature shows that the shock wave leaves the water surface with a velocity some 50 per cent greater than that of sound. This matter is dealt with more fully in the following theoretical section.

II. THEORETICAL

Introduction.

In this section an evaluation is made of the intensity and velocity of the shock wave transmitted into air by a shock wave in water incident normally on the free surface. The velocity of the surface is also obtained and the results are compared with those found experimentally. The effect of oblique incidence is examined and it is found that a simple reflection theory does not reconcile the experimental results for oblique and normal incidence.

Theory.

We consider only the case of a plane shock wave. The results should apply to spherical waves or indeed to waves of any form since the effect of attenuation will be infinitesimal in comparison with the changes due to reflection and transmission.

In plane waves of finite amplitude the changes taking place may be regarded[1] as due to forward propagation of a quantity $P = f(p) + v$ with velocity $c + v$ and backward propagation of $Q = f(p) - v$ with velocity $c - v$, where

p = pressure in the medium
v = particle velocity
c = velocity of sound at point considered

$$f(p) = \int_{p_0}^{p} \frac{1}{\rho} \left(\frac{dp}{d\rho}\right)^{\frac{1}{2}} d\rho, \text{ i.e. Riemann's Function.}$$

We shall .....

We shall treat the shock wave in water as a wave of finite amplitude and neglect the irreversible heating at the shock front.

A shock wave in water of intensity p_w and particle velocity v_w strikes normally on the air water interface. Immediately afterwards the pressure and particle velocity at the interface are p_a and v_a while a shock wave of intensity p_a and particle velocity v_a has set out into the air. The law of propagation of the quantity v then gives us

$$f(p_w) + v_w = f(p_a) + v_a \qquad (1)$$

In shock waves the particle velocity immediately behind the front is a function of pressure so that we have two further relations

$$v_w = \phi_w (p_w) \qquad (2)$$

$$v_a = \phi_a (p_a) \qquad (3)$$

where ϕ_w and ϕ_a are the appropriate functions for water and air respectively. $\phi_w(p)$ and $f(p)$ for water have been computed by Tamney and Dasgupta and tabulated[2]. For air and for pressures not exceeding about six atmospheres $\phi_a(p)$ is the well known Hugoniot formula which has been tabulated by Taylor[3]. With the aid of these tables and equations (1), (2) and (3) the values of p_w and v_a may be found for a given value p_a. Table 1 shows the results together with U_w and U_a the velocities of the shock waves in water and air respectively. The table was constructed assuming a temperature of 20°C. and a pressure of one atmosphere. Pressures are absolute, not excess over one atmosphere.

TABLE 1.

p_w (tons/sq.in.)	p_a (lb./sq.in.)	v_a (ft./sec.)	U_w (ft./sec.)	U_a (ft./sec.)	p_a atmospheres
.0066	14.69	0	4800	1127	1.0
1.12	16.16	77	4880	1174	1.1
2.18	17.63	148	4950	1220	1.2
4.24	20.57	277	5080	1306	1.4
6.13	23.50	391	5200	1386	1.6
7.91	26.44	494	5310	1463	1.8
9.59	29.38	589	5400	1535	2.0
13.8	36.73	796	5620	1703	2.5
17.0	44.07	978	5800	1856	3.0
20.3	51.42	1132	5960	1997	3.5
23.4	58.76	1274	6100	2129	4.0
29.3	73.45	1527	6360	2370	5.0
34.8	88.14	1745	6590	2590	6.0

Comparison with experiment.

If the water velocity v_a or the intensity or velocity of the air shock wave is known then Table 1 enables us to determine the intensity p_w of the shock wave in water. A curve has been given showing the velocity with which the water surface moves when a No. 8 detonator is exploded beneath it at depths from one to eight inches. The present paper contains a record Figure 4 from which the velocity of the transmitted shock wave can be obtained when the detonator is at a depth of one inch. Measurement of this record gives the following figures.

Distance of wave from water surface (in.)	0	1	2	3	4	5	6
Velocity of wave in ft./second	1740	1700	1420	1360	1310	1280	1260

The intensity of the shock wave in water from a No. 8 detonator based on the water surface velocities is shown in Figure 5. It falls off much more rapidly than the reciprocal of the

distance .....

distance. At a distance of 1 inch the intensity is 20.6 tons/sq.in. The figure derived from the velocity of the shock wave is much lower, being only 14.2 tons/sq.in. The reason for this discrepancy is not clear, but it seems that the value based on the shock wave velocity entails fewer assumptions about the mechanism involved and is the more trustworthy provided the measurement of this velocity is sufficiently accurate. We have assumed that the drum camera records give the initial velocity of the surface but it is not certain that this is the case. It seems probable that a layer or several layers break away from the water and are projected upwards. If the first layer is very thin its velocity should be v_a as given in the table but the thickness depends on the tension at which cavitation occurs, while the tendency of the water to break up into droplets may also affect the measured velocity.

The effect of oblique incidence.

A simple theory based on geometrical reflection of the pressure wave as an equal tension wave shows that for an angle of incidence θ the surface velocity is $v_a \cos\theta$ where v_a is the velocity for normal incidence. The velocity of the water surface for angles of incidence 0° to 60° is obtained from Figure 2. Dividing these values by $\cos\theta$ we get v_a as a function of distance from the detonator. In Figure 6 these values are shown and it appears that the values of v_a deduced from the oblique reflection are considerably higher than those derived from normal incidence.

The reason for this discrepancy as also for the different intensities derived from water velocity and shock wave velocity is not apparent. The phenomenon of the rising water surface may be more complex than was supposed. Careful observation of the drum camera record for a detonator at 1 inch depth shows that the water surface immediately above the detonator is strongly decelerated for the first inch or so and then maintains a more or less constant speed or may even be accelerated.

References.

(1) Lamb's Hydrodynamics, 4th Edition, Ch. 10, p.477

(2) "Pressure-time curves for sub-marine explosions (Second paper)" by W.G. Penney and H.K. Dasgupta.

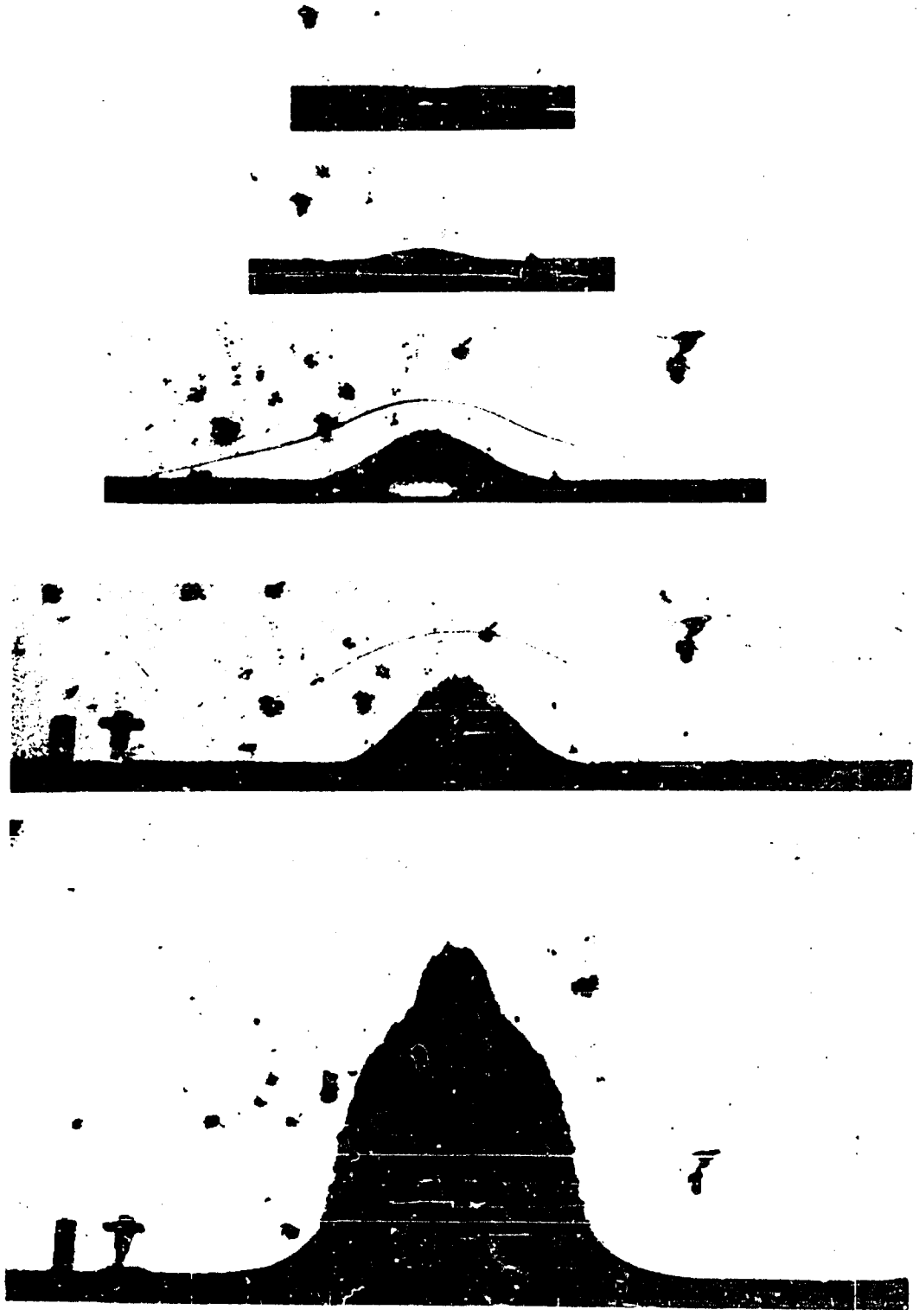


Fig. 2
Successive stages in the vertical movement of water produced by the explosion of a No. 8 detonator at 1 in. below the water surface in a model tank



Fig. 3

Bifurcation of shock wave: explosion of a No. 8 detonator at 1 in. below the water surface in a model tank



Fig. 4

Drum camera record showing curved "schlieren" record

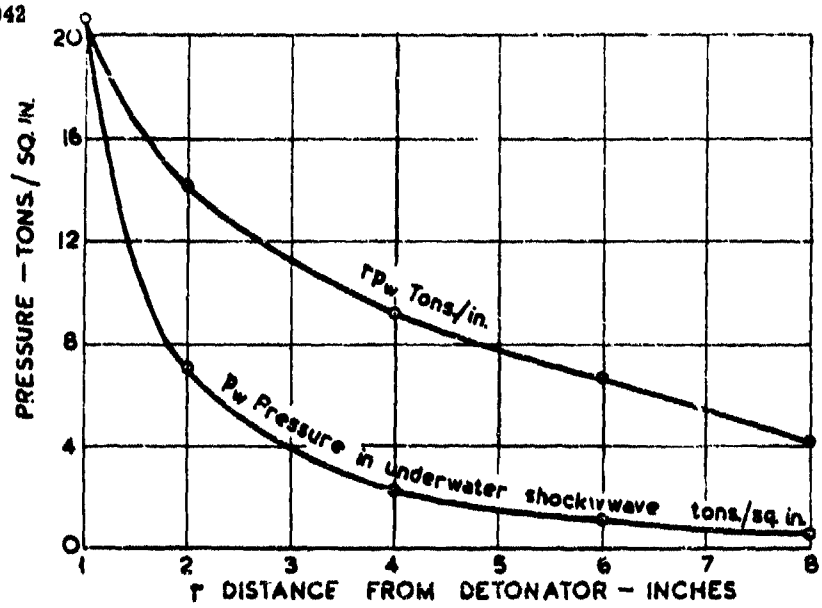


FIG. 5. PRESSURE DISTANCE GRAPH. No. 8. DETONATOR UNDERWATE

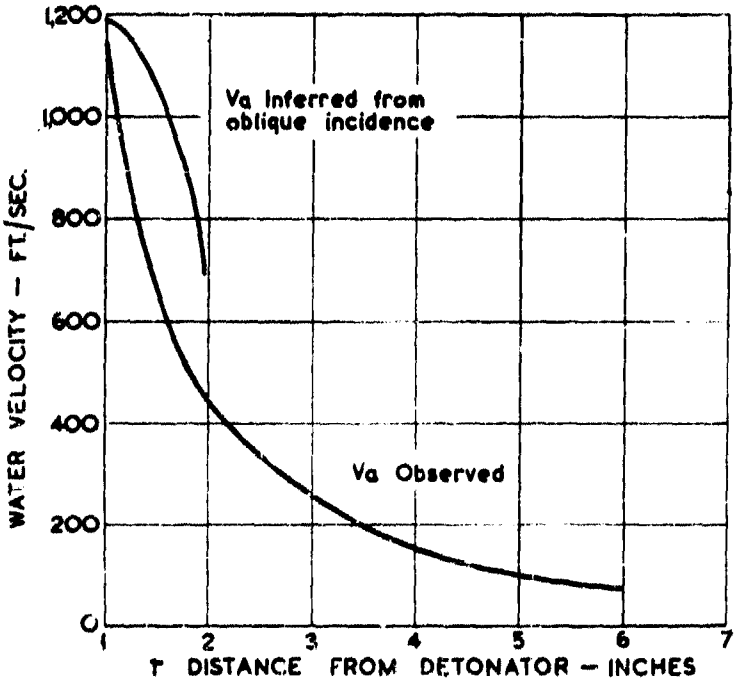


FIG. 6. RELATION BETWEEN DEPTH OF DETONATOR AND UPWARD VELOCITY Va OF WATER SURFACE IMMEDIATELY OVERHEAD. (a) AS OBSERVED AND (b) AS INFERRED FROM OBLIQUE INCIDENCE WITH DETONATOR 1in. DEEP

TRANSMISSION OF A SHOCKWAVE FROM WATER TO AIR AT NORMAL INCIDENCE

A. J. Harris
Road Research Laboratory, London

British Contribution

May 1944

TRANSMISSION OF A SHOCKWAVE FROM WATER TO AIR AT NORMAL INCIDENCE

A. J. Harris

Road Research Laboratory, London

May 1944

* * * * * * * * *

Summary.

A shock wave in water gives rise, whenever it meets the free surface, to a shock wave in the air. The case of normal incidence was discussed elsewhere[1]. In the present note the calculations are extended to an air shock wave pressure of 100 atmospheres, and are used to evaluate the pressure near ¼-oz. charges of C.E. from experimental data[2]. These pressures are compared with theoretical values[3].

In a previous investigation[1] the evaluation of the intensity of the transmitted air shock was not carried above 6 atmospheres, since the perfect gas equations there cease to be applicable. The work has now been extended to 100 atmospheres on the basis of the data given by Penney and Davies for shock waves in air at N.T.P. In perfect gases particle and shock wave velocities are proportional to the square root of the absolute temperature of the undisturbed gas. Now although air at pressures above 6 atmospheres departs from perfection the discrepancies in particle and wave velocities do not exceed 2.5% even when the pressure is 100 atmospheres, and in consequence it has been assumed that for shock waves in air at T° absolute, the velocities may be found quite accurately from those given by Penney and Davies by multiplying by $\sqrt{\frac{T}{273}}$.

Table 1 shows the results so derived for transmission from water at 20°C. to air at N.T.P. and to air at 20°C. and one atmosphere pressure. Differences of water temperature are likely to be less important than differences of air temperature since the effects on density and elasticity are much smaller in a liquid than in a gas.

Some measurements of the shock wave and spray velocities above a water surface when ¼ oz. of C.E. were exploded beneath it have been given[2] and from these the pressure in the water shock wave may be inferred with the help of Table 1. Both velocities usually fall off rather rapidly so that it is difficult to extrapolate back to the initial velocities with much accuracy, but on the basis of these extrapolated values the points in Figure 1 have been obtained. There is a difficulty about the records taken at 2 inch depth. The other records show the shock wave moving ahead of the spray but at 2 inch depth it cannot be distinguished separately. It is possible that the spray is moving faster than the shock wave but there is no evidence of this and it seems best to assume that the two velocities are equal. A single velocity measurement at 2 inch depth thus yields two water pressures; the higher value being obtained when the measured velocity is interpreted as spray velocity. It is difficult to see how the water surface can be in front of the shock wave unless the spray travels much faster than the surface from which it was formed or the shock wave is the more rapidly accelerated.

Penney and Dasgupta[3] have given a formula for the water shock wave pressure near T.N.T. an explosive about 5% less effective in producing peak pressure than C.E. They have assumed for T.N.T. a chemical energy release of 800 cals./gm. but suggest that 1000 cals./gm. would be a better value. To obtain from their results the pressures near C.E., the pressures for ¼ oz. T.N.T. were calculated from the formula of (3) and then increased in the ratio $1.05 \times \sqrt{\frac{1000}{800}}$. The calculated values are shown in Figure 1. There is reasonable agreement between the calculated pressures and those deduced from the velocity measurements at 4 inches and 6 inches but at 2 inches there is a considerable divergence especially if the measured velocity is interpreted as surface and not shock wave velocity. A possible source of disagreement between

theory .....

theory and experiment is the fact that close to the charge the shock wave is by no means spherical as assumed in the theory but concentrates along the polar axis and equatorial plane of the charge, possibly giving pressures in both of these directions higher than if the wave had been uniform.

TABLE 1.

Air shock atmospheres	WATER AT 20° TO AIR AT 20° Water Shock tons/sq.in.	Surface vel. ft./sec.	Vel. of air shock ft./sec.	Air shock atmospheres	WATER AT 20° TO AIR AT 0° Water Shock tons/sq.in.	Surface vel. ft./sec.	Vel. of air shock ft./sec.
1.0	0.0066	0	1128	1.0	0.0066	0	1089
1.2	2.2	148	1221	1.2	2.1	140	1184
1.4	4.2	277	1307	1.4	4.1	267	1261
1.6	6.1	391	1387	1.6	5.9	378	1339
1.8	7.9	495	1464	1.8	7.6	478	1413
2.0	9.6	589	1536	2.0	9.2	569	1483
2.5	13.4	797	1704	2.5	12.9	769	1645
3.0	17.0	975	1867	3.0	16.3	941	1793
3.5	20.3	1132	1998	3.5	19.5	1093	1929
4.0	23.4	1278	2130	4.0	22.5	1231	2056
5.0	29.3	1528	2372	5.0	28.1	1476	2290
6.0	34.8	1747	2590	6.0	33.3	1686	2500
15.0	77.0	3161	4040	15.0	74.0	3051	3900
30.0	137.0	4656	5680	30.0	130.0	4495	5480
50.0	207.0	6084	7310	50.0	196.0	5873	7050
65.0	260.0	7002	8290	65.0	245.0	6758	8010
100.0	378.0	8803	10200	100.0	357.0	8497	9840

References.

(1) Note on the water formation produced by an underwater explosion on the Model Scale. by A.J. Harris.

(2) Measurement of the shock wave velocity in air above a water surface, due to the detonation of a submerged charge. by D. Croney and R.D. Davis.

(3) Pressure time curves for Submarine Explosions. by W.G. Penney and H.K. Dasgupta.

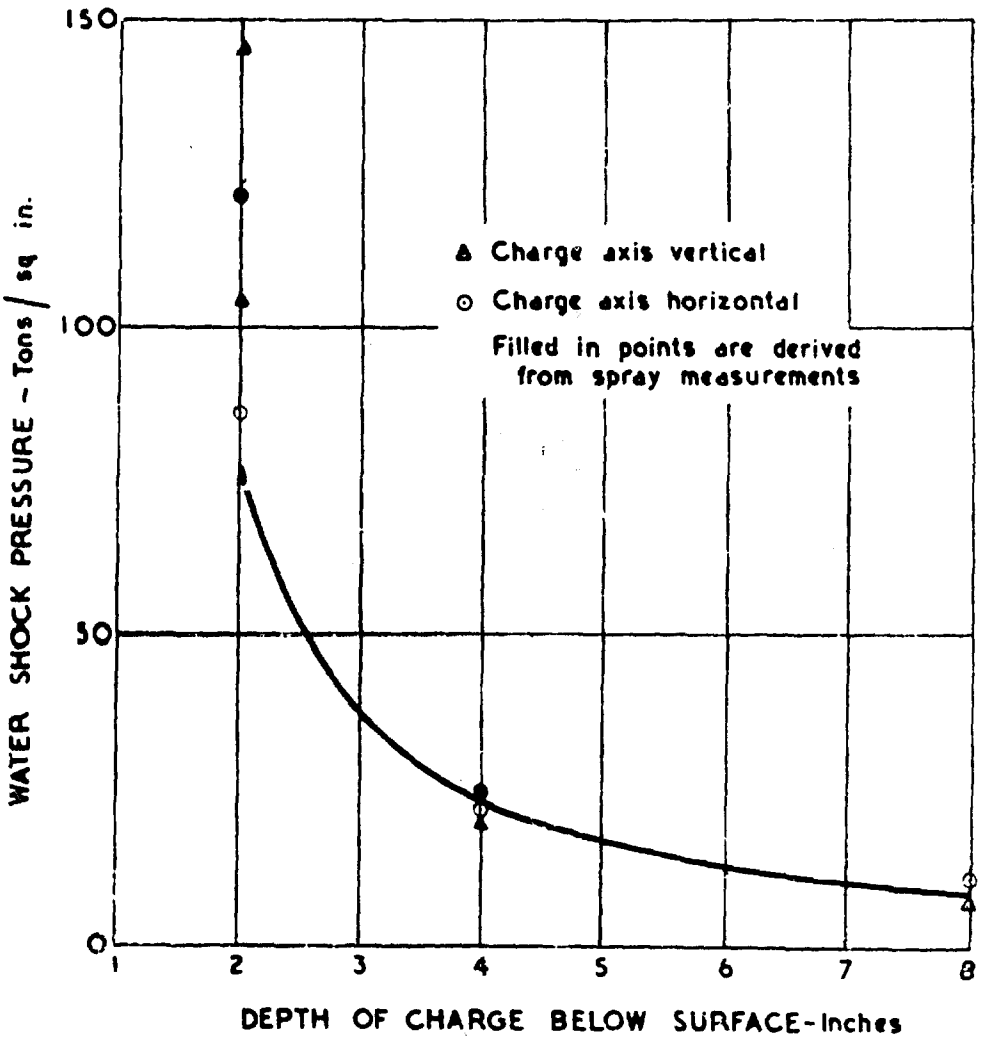


Fig. 1. PRESSURE AT WATER SURFACE IMMEDIATELY ABOVE CHARGE OF 4 oz. C.E.

THEORY OF PEAK PRESSURE AND TIME CONSTANT DETERMINATION FOR SHOCK WAVES BY THE METHOD OF OPTICAL DISTORTION

R. R. Halverson
Underwater Explosives Research Laboratory
Woods Hole Oceanographic Institution

American Contribution

24 March 1947

THEORY OF PEAK PRESSURE AND TIME CONSTANT DETERMINATION FOR SHOCK WAVES BY THE METHOD OF OPTICAL DISTORTION

R. R. Halverson

A theory has been developed for several sets of experimental conditions designed to measure the peak pressure of shock waves by the method of optical distortion. For one of these experimental arrangements (1 below), a method has also been developed for calculating the time constant. Since this arrangement has had considerable success experimentally, it will be discussed in detail.

1. Grid in plane of center of charge; charge off to the side; spherical shock wave

To study the distortion of light rays passing through the high pressure region behind the shock, an experimental arrangement as diagrammed in Figure 133 was used and the theory developed is based on these experimental conditions. E is the charge producing the shock wave S to be studied, C is the camera lens, F is a flash charge and G is a lucite sheet marked off in a uniform grid of 1/4 in. spacing. The grid is so placed that the grid lines intersect the shock wave diagonally in the portion of the shock studied. Two typical intersecting lines are shown in the front view in Figure 133. The charge was placed in the plane of the grid, and the line perpendicular to the grid passing through the center of the camera lens intersected the grid a short distance behind the shock, approximately 5% of the radius.

In the system of Cartesian coordinates shown in Figure 133 the position of the center of the camera lens is defined at (x_o, y_o, z_o). On the assumption that the grid acts as a source of diffuse illumination, a ray whose reverse path is the vector $\bar{M}$ from the camera to the shock front is considered. The intersection of this ray with the shock front is defined as (x,y,z). If there were no distortion, the ray would continue along the line $\bar{L}$ $\bar{M}$ and strike the grid at $(x'', 0, z'')$, but actually the ray follows some curved path $\bar{P}$ determined by the decay characteristics of the shock and strikes the grid at the point $(x', 0, z')$. Knowing the actual distance from the charge to a uniquely defined point on the grid, one obtains the radius of the shock wave from the photographic print by reference to this point after the scale factor of the print is determined from the undistorted part of the grid. The coordinates of the camera are also obtained by reference to this point. On the photographic print, the points $(x'', 0, z'')$, and $(x', 0, z')$ may be located, the latter being obtained by extending lines from the undistorted part of the grid until they intersect behind the shock.

(a) Peak pressure determination. -- As a first approximation, an average pressure may be calculated by assuming a step shock wave, that is, a constant pressure behind the front. With this approximation the curve $\bar{P}$ is replaced by the vector $\bar{N}$ (Figure 133) from (x,y,z) to $(x',0,z')$, and the step pressure calculated is, to this approximation, the pressure in the decaying wave on the spherical surface centered at $\bar{E}$ and passing through a point on $\bar{P}$ at which the tangent of $\bar{P}$ is parallel to $\bar{N}$. We define this index of refraction or pressure for a given intersection of grid lines as n_{av} or p_{av}, respectively.

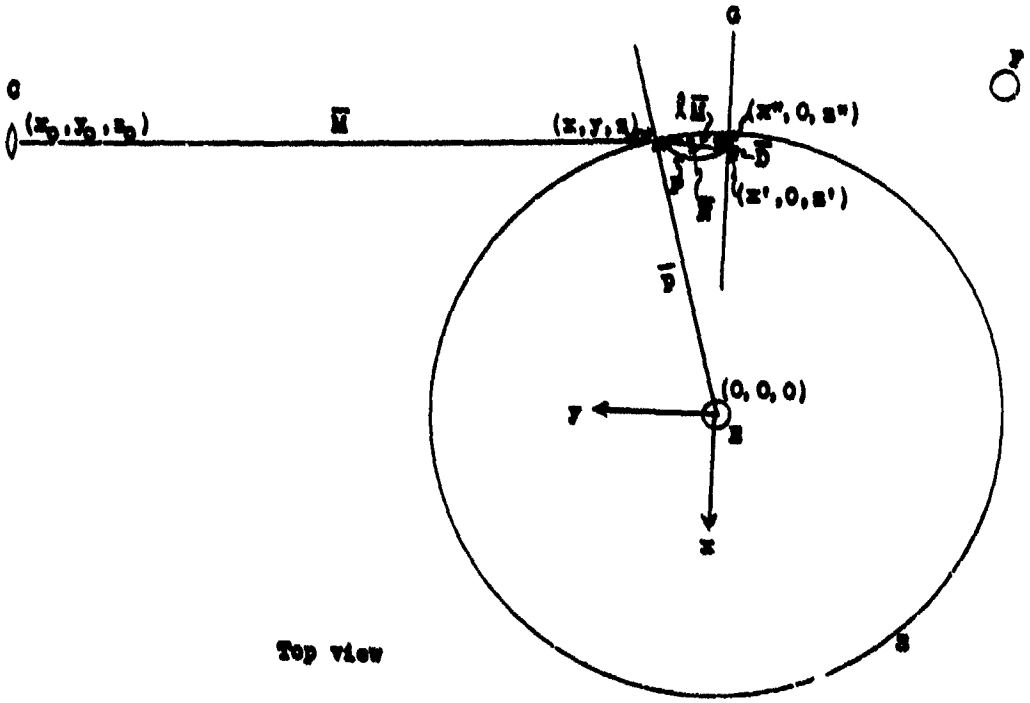
A very simple derivation of the index of refraction corresponding to this average pressure as a function of the distortion vector $\bar{D}$, (the vector from $(x'',0,z'')$ to $(x',0,z')$ for the given ray $\bar{M}$,) and the geometry of the experiment can be given in the system of coordinates discussed above. We are given (x_o,y_o,z_o), $(x'',0,z'')$, $(x',0,z')$ and R , the radius of the shock wave. The point (x,y,z) is readily obtained as the intersection of the line joining (x_o,y_o,z_o) and $(x'',0,z'')$ with the sphere of radius $|R|$.

The following vectors are defined.

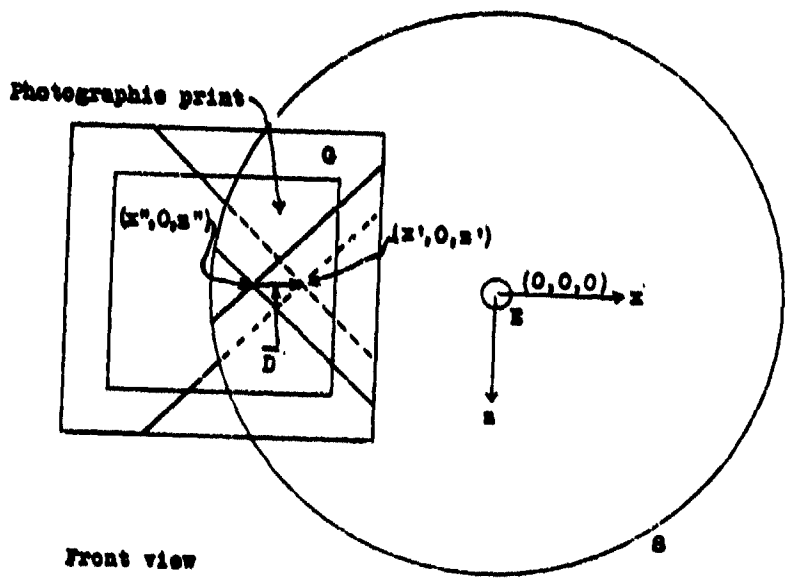
$$\bar{p} = xi + yj + zk,$$

$$\bar{M} = (x-x_o)i+(y-y_o)j+(z-z_o)k,$$

$$\bar{H} = (x''-x)i+(0-y)j+(z''-z)k,$$



Top view



Front view

Fig. 133. Experimental arrangement for optical distortion study.

$$\bar{M} = (x'-x)i+(0-y)j+(z'-z)k, \qquad \text{(II-1)}$$

$$\bar{D} = \bar{N} - \bar{M} = (x'-x'')i+(z'-z'')k$$

$$= D_x i+D_z k.$$

The magnitude of all vectors and distances is to be taken in units of $|R|$, i.e., $|p| = 1$.

Consider the following cross-product relations.

$$\left.\begin{aligned} \frac{\bar{M}\times\bar{p}}{|M|} &= \bar{q} \sin\theta, \\ \frac{\bar{N}\times\bar{p}}{|N|} &= \bar{q} \sin\theta', \end{aligned}\right\} \qquad \text{(II-2)}$$

where $\bar{q}$ is a unit vector perpendicular to the plane which contains $\bar{M}$, $\bar{p}$, $\bar{N}$ and $\bar{D}$ and θ and θ' are the angles of incidence and refraction respectively in this plane. This is not necessarily the plane shown in the top view in Figure 133. Applying Snell's Law,

$$\frac{\sin\theta}{\sin\theta'} = \frac{n_{av}}{n_o} = \nu,$$

where n_{av} is the index of refraction corresponding to the average pressure p_{av}, and n_o is the index of refraction of sea water at zero pressure, we obtain the relation,

$$\frac{\bar{N}\times\bar{p}}{|N|\nu} = \ell\frac{\bar{M}\times\bar{p}}{|M|}, \qquad \text{(II-3)}$$

From the last of (Eqs. II-1),

$$\frac{\bar{D}\times\bar{p}}{|N|} = \frac{\bar{M}\times\bar{p}}{|N|} - \frac{(\bar{M}\times\bar{p})}{|N|}, \qquad \text{(II-4)}$$

or using (Eq. II-3),

$$\bar{D}\times\bar{p} = \frac{|N|}{|M|}\left(\frac{1}{\nu} - \frac{\ell|M|}{|N|}\right)\bar{M}\times\bar{p}, \qquad \text{(II-5)}$$

which may be written,

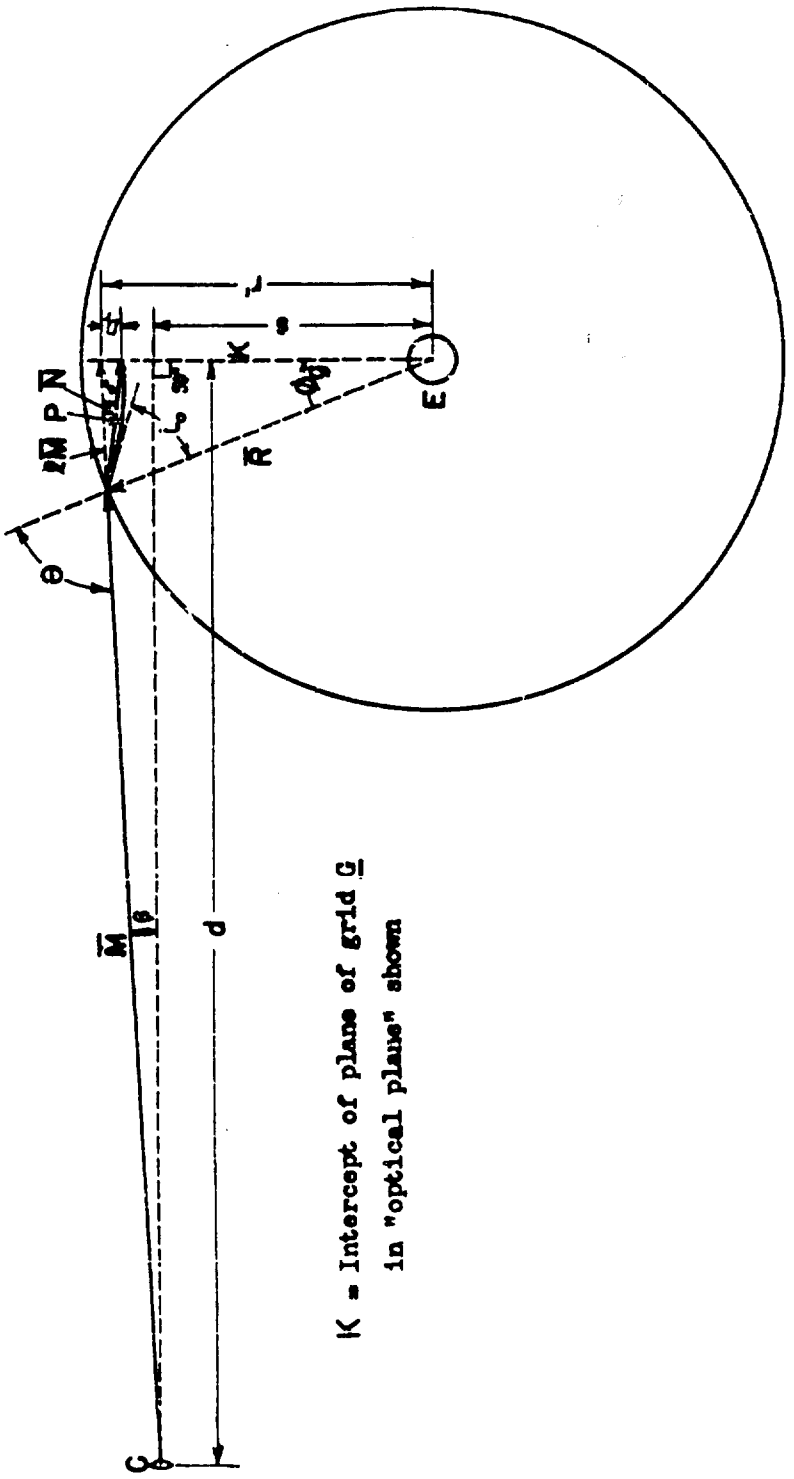
$$\left.\begin{aligned} \frac{|N|}{|M|}\left(\frac{1}{\nu} - \frac{\ell|M|}{|N|}\right)(z_o y - y_o z) &= -D_z y, \\ \frac{|N|}{|M|}\left(\frac{1}{\nu} - \frac{\ell|M|}{|N|}\right)(y_o x - x_o y) &= D_x y, \end{aligned}\right\} \qquad \text{(II-5')}$$

or,

$$\left.\begin{aligned} \frac{1}{\nu} &= -\frac{|M|}{|N|}\frac{D_z y}{(z_o y - y_o z)} + \frac{\ell|M|}{|N|} \\ \frac{1}{\nu} &= \frac{|M|}{|N|}\frac{D_x y}{(y_o x - x_o y)} + \frac{\ell|M|}{|N|} \end{aligned}\right\} \qquad \text{(II-5'')}$$

The distances $|M|$, $|N|$ and $\ell|M|$ can be readily obtained from the coordinates (x,y,z), (x_o,y_o,z_o), $(x',0,z')$, and $(x'',0,z'')$. Although two values of the index of refraction can be obtained from each distortion, they are not independent, and in general because of the coordinates chosen and the experimental arrangment used D_z was too small to be measured.

Given ν from the above and n_o for sea water, P_{av} can be obtained by applying the relationship between the index of refraction and pressure for water. This relationship is discussed later.



K = Intercept of plane of grid G
in "optical plane" shown

Fig. 134. Plan view of "optical plane".

Since the computational method outlined above is somewhat lengthy, a more direct method, again assuming a step shock but taking advantage of the planar nature of the probl ., was used in the actual calculations. The determination of the "optical plane", that containing $\bar{M}$, $\bar{P}$, $\bar{N}$, $\bar{D}$, E and C, is very simple when the charge is in the plane of the grid, for, in this case, the intercept of the optical plane in the plane of the grid contains $\bar{D}$ and E. Knowing the projection of the camera on the line containing $\bar{D}$ and E, and the perpendicular distance d of the camera from it, the optical plane is determined and can be represented as in Figure 134. The distance $|R|$ to which all other dimensions are referred is obtained as described above. r' and D_r are obtained directly from the print as above, whereas d and s are obtained from the known position of the camera relative to the grid. To derive the index of refraction from the distortion of the ray $\bar{M}$ in terms of these measurements using the symbols shown in Figure 134 the following relations are used.

$$\tan\beta = \frac{r' - s}{d} \quad , \tag{II-6}$$

where β may be positive or negative, and since $|R| = 1$,

$$\cos(\phi_g - \beta) = r' \cos\beta \quad . \tag{II-7}$$

Then using the law of cosines,

$$\ell/|M| = \sqrt{1+r'^2-2r'\cos\phi_g} \tag{II-8}$$

It can be shown, using the law of sines, that

$$\tan\delta = \frac{\frac{D_r}{\ell/|M|}\cos\beta}{1 - \frac{D_r}{\ell/|M|}\sin\beta} \tag{II-9}$$

On applying Snell's Law,

$$\nu = \frac{\sin\theta}{\sin\theta'} = \frac{\sin\theta}{\sin(\theta-\delta)} \quad , \tag{II-10}$$

$$\nu - 1 = \frac{n_{av}-n_o}{n_o} = \frac{\sin\theta\left[\frac{1}{\ell/|M|}-1\right] + \cos\theta\tan\delta}{\sin\theta - \cos\theta\tan\delta} \tag{II-11}$$

where $\theta = 90^\circ - (\phi_g - \beta)$

In order to convert n_{av} to p_{av}, data on the pressure coefficients of index of refraction for water are required.

Data were available for fresh water, and were assumed to hold for salt water as well. This assumption is felt to be valid to within a few percent as is indicated by some preliminary calculations. In Table VII the available data on the coefficients a and b in the equation,

$$n(p) - n_o = ap - bp^2 \quad , \tag{II-12}$$

are given together with the source of the data. For the calculations of p_{av} concerning a specific point, Eq. (II-12), of course, becomes

$$n_{av} - n_o = a\,p_{av} - b\,p_{av}^2 .$$

The type of film used in the experiments studied was Contrast Process Ortho, which is sensitive in a narrow range of wave length centered around ca. 4800 A.U. In order, then, to correct n_{av} to p_{av} it is necessary to obtain adiabatic values of a and b for a wave length of 4800 A.U. and for the proper temperature. The isothermal value of a was taken from the data Rontgen and Zehnder for a wave length of 5890 A.U. and the proper temperature for the given experiment. It was then

corrected for wave length from the data for various wave lengths of Röntgen and Zehnder, assuming the difference due to wave length is independent of temperature. It was then corrected to the adiabatic coefficient from the data of Raman and Venkataraman, assuming again that the difference between the isothermal and adiabatic a is independent of temperature. The value of b was taken directly from the isothermal data of Poindexter and Rosen by interpolating for the proper wave length. It was assumed independent of temperature. The error in b can be of the order of 30% and still make an error of only ca. 3% in the calculation of the pressure in the range of pressure studied (ca. 17,000 lb/in.^{2}).

Table VII. Coefficients a and b in $B(P) - B_0 = aP - bP^2$ for Pure Water

t (°C)	Wave Length (A.U.)	a x 10^6 (per atm.)	b x 10^6 (per atm.^{2})	Type of Pressure Change	Source of Data*
-0.78	5890	16.91	-	Isothermal	R and Z
0.06	"	16.87	-	"	"
0.42	"	16.78	-	"	"
1.05	"	16.68	-	"	"
2.62	"	16.51	-	"	"
2.67	"	16.52	-	"	"
2.92	"	16.48	-	"	"
3.10	"	16.44	-	"	"
4.95	"	16.26	-	"	"
8.95	"	15.87	-	"	"
9.00	"	15.91	-	"	"
13.05	"	15.56	-	"	"
13.28	"	15.56	-	"	"
17.83	"	15.26	-	"	"
18.01	"	15.26	-	"	"
18.03	"	15.25	-	"	"
23.27	"	14.97	-	"	"
23.1	"	14.98	-	"	R and V
18.0	4861	15.40	-	"	R and Z
18.0	6807	15.16	-	"	"
25.0	4060	15.02	.003182	"	P and R
25.0	4360	14.65	.002700 **	"	"
25.0	5460	14.75	.003132	"	"
25.0	5790	14.56	.002990	"	"
23.1	5890	14.66	-	Adiabatic	R and V

* R and Z - W. C. Röntgen, and L. Zehnder, Ann.d. Physik (Wied.) 44, 24-51 (1891) (low pressure study).

R and V - Sir Venkata Raman, F.R.S., and K.S. Venkataraman, Proc. Roy. Soc. (London), 171A, 137 (1939) (low pressure study).

P and R - F. E. Poindexter and J. S. Rosen, Phys. Rev. (2), 45, 760(A) (1934) (pressures up to 4800 kg/cm^2).

- - - -

- - - -

** This datum seems out of line with the rest.

The peak-pressure of the shock wave was then calculated from several values of p_{av} in the following manner. The assumption was made that p_{av} calculated from a given intersection of grid lines with a given value of r' was the pressure existing in the decaying spherical shock on a spherical surface of radius

$$r_{av} = \frac{|R| + (r' - D_r)}{2},$$

the average radius vector for the vector $\bar{N}$. p_{av} was then plotted against $|R| - r_{av}$ (see Figures 108, 109, 110 and 111) on semi-log paper. Within experimental scatter the points fell on a straight line which was extrapolated to $|R| - r_{av} = 0$, that is, to the shock front. The pressure at this point was taken to be the peak pressure of the shock wave. The error in the assumption as to what value of r_{av} the value of p_{av} applies should go to zero in the limit, $|R| = r_{av} = 0$.

(i) Technique of Measurement. Before the shot, the perpendicular distance from the camera lens to the grid was measured. A cross was marked on the lucite grid at the foot of this perpendicular, and the distance s (Figure 134) was measured from the center of the charge to the cross. An additional cross 10/ was marked on the lucite grid on the extension of the line joining the charge and the first cross about 4 in. (measured accurately) beyond the first cross. This second cross was placed so as to be ahead of the shock wave, and thus to appear undistorted in the final picture. It was from this measurement from the charge to the second cross that the radius of the shock wave was determined on the final photograph. The illumination was provided by a flash charge for which the firing was delayed by means of primacord from the firing of the charge which produced the shock wave to be studied.

The measurements were taken from prints of the original photograph. With a scale factor for the print determined from the undistorted part of the grid, the charge position was determined from the experimental measurements referred to the crosses marked on the grid. By use of this as a center, the shock front was drawn in on the print as a circle whose radius was such that it passed through the breaks in the lines of the undistorted and distorted parts of the grid. Several of the undistorted lines were extended behind the shock front giving intersections which are called "actual" intersections to which correspond the "apparent" intersections seen behind the shock. There was no difficulty in assigning any given actual intersection to an apparent intersection. Through each pair of intersections a radial line was drawn from the charge position, and was extended to intersect the shock front. This is the intercept of the optical plane in the plane of the grid. The distances r' and D_r (Figure 134) can be measured directly on this line. R , the radius of the shock front, was obtained on the print by reference to the crosses marked on the lucite grid. The distance d is obtained by measuring the perpendicular distance from the cross to the intercept line and using this measurement together with the experimental measurement of the distance from the camera lens to the lucite grid.

(b) Calculation Procedure for Time Constant (Exponential Decay Constant with Distance Behind Front). The path of a ray of light in a non-homogeneous medium has been treated very thoroughly by Richard Gans (see e.g. Handbuch der Experimental Physik, Volume 19, p. 341 ff. and Ann d Physik (4), 47, 709 (1915)). From his derivation based on Snell's law (see reference to Handbuch der Experimental Physik) for a medium in which the index of refraction is a function only of r, the radius in plane polar coordinates, the following differential equation is obtained for the path of a ray of light:

$$d\phi = \frac{n_R |R| \sin i_o \, dr}{r\sqrt{n^2 r^2 - n_R^2 |R|^2 \sin^2 i_o}} , \qquad \text{(II-13)}$$

where ϕ is the polar angle, |R| is the radius of the shock front, r is the length of the radius vector to any point on the path, i_o is the angle made by the ray of light and the radius vector to the point, $r = |R|$, $\phi = 0$ (see Fig. 134). ϕ is measured clockwise from the point of entry into the shock wave of the reverse vector $\bar{N}$ (Fig. 134) for the ray of light studied. In Fig. 134 ϕ_g, the polar angle at the grid, is shown. n_R is the index of refraction at $r = |R|$, and n is the index of refraction at r.

10/ The second cross is not necessary if the position of the first cross is corrected for optical distortion.

The method used in determining the time constant of the shock wave was to express n as a function of r in terms of the parameters of an assumed exponential shock wave (exponential with distance behind the front), the peak pressure and time constant. This may be done by writing p in Eq. (II-12) as a function of r,

$$p = p_{max} e^{-\frac{(|R| - r)}{\theta_r}} , \qquad \text{(II-14)}$$

where θ_r is expressed in units of length.

Substituting p from Eq. (II-14) into Eq. (II-12) gives

$$n(p) - n_o = a p_{max} e^{-\frac{(|R| - r)}{\theta_r}} - b p_{max}^2 e^{-\frac{2(|R| - r)}{\theta_r}} , \qquad \text{(II-15)}$$

where n_o (the index of refraction at zero pressure), a, and b are functions of the temperature for a given type of film, and p_{max} is the peak pressure for the given shot as determined by the method outlined in this Appendix I (a).

This function of r is then substituted for n in Eq. (II-13). In Eq. (II-13) n_R is obtained from Eq. (II-15) by putting $r = |R|$.

Eq. (II-13) is a function of the given ray of light on a given film, that is, of the pair of intersections (apparent and actual) of the pair of grid lines studied, because of the explicit presence of the angle i_o. This is obtained for each pair of intersections by the following equation:

$$\frac{\sin i_o}{\sin \theta} = \frac{n_o}{n_R} , \qquad \text{(II-16)}$$

where the angle θ (Fig. 134) is obtained for the given point (that is, for the given pair of intersections) in the calculation procedure for p_{av} for that point.

Thus all the parameters of Eq. (II-13) are determined except θ_r. Some general discussion of this equation is felt to be necessary. A statement of Snell's Law for spherical symmetry, in which case the path of a given ray of light, as was discussed previously, lies in a great circle, is given by the following:

$$n_R |R| \sin i_o = nr \sin i = C, \qquad \text{(II-17)}$$

where i is the angle made by the path of light and the radius vector r to a given point on the path, and n is the index of refraction at ra for some given θ_r in Eq. (II-15). Then in Eq. (II-13) the denominator vanishes at the point of total reflection, that is, at the point where sin i = 1.

The right hand side of Eq. (II-13), from physical arguments, has a finite integral from $r = |R|$ to $r = r_{min} - \epsilon$ where,

$$r_{min} \cdot n(r_{min}, \theta_r) = n_R |R| \sin i_o . \qquad \text{(II-18)}$$

By making ϵ sufficiently small, the integration can be carried up to within an infinitesimal distance from r_{min}. Then since the path of light is symmetrical about the radius vector of length r_{min}, the whole path is known from the point of entry into the shock wave to the point of exit from the shock wave.

The first step in the calculation of θ_r is to determine $\theta_{r,min}$ where

$$(r' - D_r) \cdot n(r' - D_r, \theta_{r,min}) = n_R |R| \sin i_o . \qquad \text{(II-19)}$$

Physically $\theta_{r,min}$ is the lowest value of the exponential decay constant which will allow the given ray of light studied to get as far into the shock wave as the point at which it is observed to strike the lucite grid, that is, at $r = r' - D_r$ (Fig. 134).

The procedure, then, for determining θ_r for a given point on a given film is to choose several values of θ_r $\theta_{r,min}$ and to calculate ϕ $(r'-D_r, \theta_r)$ by numerical integration.

$$\phi(r' - D_r, \theta_r) = \int_{|R|}^{r' - D_r} \frac{n_R |R| \sin i_o \, dr}{r\sqrt{n^2 r^2 - n_R^2 |R|^2 \sin^2 i_o}} , \qquad \text{(II-13a)}$$

where n is given as a function of θ_r and r in Eq. (II-15). ϕ is then plotted against θ_r and r in Eq. (II-15). ϕ is then plotted against θ_r at the value of $r' - D_r$ determined by the point studied. ϕ can easily be shown by physical arguments or by mathematical considerations to be a monotonically decreasing function of θ_r. The value of θ giving a value of $\phi = \phi_g$ (Fig. 134), that is, that value of ϕ obtained in the course of the calculation of p_{av} for the given point, is taken as the correct value of θ_r for the shock wave as determined by that point. If no value of θ_r $\theta_{r,min}$ gives a value of ϕ as large as ϕ_g, the ray of light studied is assumed to have passed through the point of total reflection after it left the diffuse light source, the lucite grid. In this case (Eq. II-13a) must be replaced by

$$\phi(r'-D_r,\theta_r) = \int_{|R|}^{r_{min}+} \frac{n_R |R| \sin i_o \, dr}{r\sqrt{n^2 r^2 - n_R^2 |R|^2 \sin^2 i_o}} + \int_{r_{min}+}^{r'-D_r} \frac{n_R |R| \sin i_o \, dr}{r\sqrt{n^2 r^2 - n_R^2 |R|^2 \sin^2 i_o}} \qquad \text{(II-13b)}$$

Again the integration is carried out numerically. In the numerical integration near r_{min}, the intervals chosen must, of course, be very small. Again a plot of ϕ vs. θ_r is made, and θ_r is then determined for the given point as that value which gives a $\phi = \phi_g$ for that point.

Values of θ_r are calculated for several points on a given film. The tacit assumption has been made that θ_r can be a function of the value of $r' - D_r$ for the point for which it is calculated. The conversion of this exponential decay constant with distance behind the shock front to an exponential decay constant with time behind the front is discussed below.

(c) Calculation Procedure for Time Constant (Exponential Decay Constant with Time Behind Front). In the conversion of θ_r to θ_t, the exponential parameter in

$$p_{p.E.}(t) = p_{max} e^{-\frac{t}{\theta_t}} , \qquad \text{(II-20)}$$

θ_t is assumed constant, but the possibility is admitted of dependence of θ_r on the value of $r' - D_r$ for the point for which θ_r is calculated. $p_{p.E.}(t)$ is the pressure that would have been recorded by a piezoelectric gage at time t after the passing of the shock front of peak pressure p_{max}. $p_{O.D.}(r)$ is the pressure at t = o and at a distance ($|R| - r$) behind the shock front of pressure p_{max} and radius $|R|$. That is,

$$p_{O.D.}(r) = p_{max} e^{-\frac{(|R| - r)}{\theta_r}} \qquad \text{(II-21)}$$

θ_r can be a function of r if it is necessary to make Eqs. (II-20) and (II-21) compatible.

The assumption is made that θ_t changes very little with $|R|$ over distances of length of the order of θ_r. Under this assumption, the decay of p_{max} with $|R|$ will follow the same law as the decay of p(r) (where $r = |R| - C$ and where C is a constant distance of the order of magnitude of θ_r) with R. That is, since for a given weight of some explosive,

$$\frac{P_{max}(|R|_1)}{P_{max}(|R|_2)} = \left(\frac{|R|_2}{|R|_1}\right)^{\alpha} , \qquad \text{(II-22)}$$

where $\alpha \approx 1$ is a function of the kind of explosive, then

$$\frac{P_{p.E.}(t)}{P_{O.D.}(r)} = \left(\frac{r}{|R|}\right)^{\alpha} , \qquad \text{(II-23)}$$

where the relation $|R| - r = ct$ exists, in which c is assumed to be a constant, ca. 0.0445 in./msec, for the pressures studied.

Elimination of $P_{p.E.}(t)$ and $P_{O.D.}(r)$ among Eqs. (II-20), (II-21) and (II-22) and rearranging leads to

$$\theta_t = \frac{1}{c}\left[\frac{1}{\frac{1}{\theta_r} + \frac{\alpha}{|R| - r}\ln\frac{|R|}{r}}\right] \qquad \text{(II-24)}$$

The value of r in $P_{O.D.}(r)$ is taken for a given point which resulted in a given θ_r as $r' = D_r$ at that point. The value of α is obtained from piezoelectric measurements at various values of $|R|$ and W (weight of explosive), that is, from a peak-pressure similarity curve for a given explosive. It can be taken as unity with little resulting error in θ_t. It is found by solving Eq. (II-23) for θ_r that the dependence of θ_r on r for a given θ_t is not great.

An alternative method of deriving an equation to convert θ_r into θ_t which is in essential numerical agreement with Eq. (II-24) has been suggested by Professor J. G. Kirkwood. Here θ_r and θ_t are defined only at the shock front as

$$\frac{1}{\theta_r} = \left(\frac{\partial \log p}{\partial r}\right)_t \quad \text{for } r = |R| \qquad \text{(II-25)}$$

and

$$\frac{1}{\theta_t} = -\left(\frac{\partial \log p}{\partial t}\right)_r \quad \text{for } r = |R| \text{ at } t = 0. \qquad \text{(II-26)}$$

If the logarithmic peak pressure vs. distance curve has a derivative $\frac{d \log P_{max}}{d R}$, then, exactly,

$$\frac{d \log P_{max}}{d |R|} = \left[\left(\frac{\partial \log p}{\partial r}\right)_t\right]_{r = |R|} + \frac{1}{c}\left[\left(\frac{\partial \log p}{\partial t}\right)_r\right]_{r = |R|} \qquad \text{(II-27)}$$

where c is the shock-front velocity at peak pressure P_{max}. By using Eqs. (II-25) and (II-26) and rearranging, Eq. (II-27) becomes

$$\theta_t = \frac{1}{c}\,\frac{1}{\frac{1}{\theta_r} - \frac{d \log P_{max}}{d |R|}} \qquad \text{(II-28)}$$

For a given weight of explosive,

$$P_{max} = \frac{P}{|R|^{\alpha}} \qquad \text{(II-29)}$$

where P is a constant depending on the weight and kind of explosive. Then,

$$\frac{d \log p_{max}}{d |R|} = - \frac{\alpha}{R} \quad , \tag{II-30}$$

and thus,

$$\theta_t = \frac{1}{\theta} \frac{1}{\frac{1}{\theta_2} + \frac{\alpha}{|R|}} \tag{II-31}$$

This latter treatment is a more direct approach, but in neither case is the variation of θ_t with $|R|$ stated. This is not an important factor however. Eqs. (II-24) and (II-31) are very nearly equivalent numerically, and in the applications Eq. (II-24) will be used.

(d) Possible Errors. The most apparent source of error in this method of measuring peak pressure and time constant is the possibility of mechanical distortion of the lucite grid by the impact of the shock wave. Preliminary measurements on the velocity of sound in lucite indicate a value of approximately 6.0 ft./msec. Thus the shock wave started at the center of the edge of the lucite grid travels faster in the lucite than the shock wave in the water, and the possibility for mechanical distortion of the lucite grid at the time of the photograph is increased.

Measurements on the photographs of the two shots reported in Sec. III, 3, a indicate that such mechanical distortion as well as lens distortion is very small, however. If the grid lines ahead of the shock are extended far behind the shock front, they coincide within drawing errors, with the apparent position of the grid lines in this region of "zero" optical distortion. Since the "direction" of the displacement due to optical distortion is the same as that due to mechanical distortion, that is, away from the charge, this result indicates a very small mechanical distortion. Also the fact that the edge of the lucite grid towards the charge appears as a straight line in the shot photographs indicates no mechanical distortion of the lucite grid in the interval between the time of impact of the edge of the grid and the time of the photograph. It should be mentioned that the curved contour at the left of the grid photograph (Fig. 107) is not the edge of the grid, but rather the edge of a paper diffusion screen behind the grid. The edge of the grid is the line in which the diagonal grid lines terminate. Although there may be some slight curvature to this line in the photograph published, the line on the original print from which this print was made is as close to a straight line as is measurable. Thus mechanical or lens distortion is felt to have little effect on the results obtained by the optical-distortion method.

Another source of error is in using the index of refraction-pressure coefficient measured in fresh water for the studies of pressure and time constant in salt water. Preliminary calculations based on the assumption that the difference in the index of refraction between fresh and salt water at high pressure is the same as it would be at zero pressure but at the concentration of salt per unit volume that the water would have at the high pressure have been made. These calculations indicate that the error involved in the assumption that the index of refraction-pressure coefficient is independent of the salinity is of the order of 2.5%. The direction of this error is such as to make the calculated pressure too great. The data necessary for these calculations on the effect of salinity are from a report by E. A. Brodsky and J. M. Soberschewer (Z. Phys. Chem., B, 21, 412 (1933)).

The possibility of error in the assumption that Snell's Law of Refraction holds in a non-homogeneous medium also deserves some consideration. Gans (Ann. d. Phys. (4), 47, 709 (1915)) studies in detail the case of refraction of a linearly-polarized light wave in a non-homogeneous medium by use of the electromagnetic-field equations. He assumes that $n = \sqrt{\epsilon}$, where n is the index of refraction of the medium and ϵ is the dielectric constant. This relation, of course, does not hold for water. He shows that under these assumptions Snell's Law holds over most of the light path, but very near the point of total reflection the ray of light deviates from the path predicted by Snell's Law and undergoes an angular discontinuity, "knick", at the point of total reflection. A short distance beyond the point of total reflection, the path again coincides with the path predicted by Snell's Law.

It is felt that this deviation from Snell's Law is not important for the case of non-polarized light in water. However, in order to make a quantitative statement as to the amount of possible error, a further analysis would have to be made.

An experimental argument for the assumption that this deviation from Snell's Law is not important for the case of the shock-wave study in water is that, in several calculations of the time constant based on rays of light which are observed to strike the lucite grid at varying distances from the point of total reflection, no systematic trend can be detected with the distance of the point of observation from the point of total reflection.

(c) Sample calculation of time-constant. -- As an example of the time-constant calculation, the data for Point 22, Film 536 (Fig. 111) will be developed.

The first step is to obtain n as a function of r for a given film. The data necessary for this are given in Table VIII which shows data from film No.'s 536 and 537 for comparison.

Table VIII Constants Necessary for Eq. (II-15)

	Film 536	Film 537
Kind of Film	Contrast Process Ortho	Contrast Process Ortho
Temperature	21.3° C.	17.1° C.
a	14.94×10^{-6} per atmosphere	15.18×10^{-6} per atmosphere
b	$.001578 \times 10^{-6}$ per atm.^{2}	$.001578 \times 10^{-6}$ per atm.^{2}
n_o	1.3435	1.3444
$\|R\|$	15.97 in.	15.99 in.
p_{max}	17,050 lb/in^2 = 1,160 atm.	17,050 lb/in^2 = 1,160 atm

When the proper values of n_o, a, b, and p_{max} from Table VIII for Film 536 are substituted in Eq. (II-15) it becomes

$$n = 1.3435 + .0173284\, e^{\frac{-(1-x)}{\psi}} - .00212286\, e^{-2\frac{(1-x)}{\psi}} \qquad \text{(II-32)}$$

where

$$x = \frac{r}{|R|} \quad \text{and} \quad \psi = \frac{\theta_r}{|R|}$$

since throughout all calculations, measurements in units of $|R|$ were used.

Then, since for any pair of intersections,

$$\frac{\sin i_o}{\sin \theta} = \frac{n_o}{n_R}$$

from Eq. (II-16) $n_R \sin i_o = n_o \sin \theta$. The value of n_o is known for a given film (Table VIII) and $\sin \theta$ was found for each point in the calculation for p_{av}. Thus, for Film 536, Pt. 22, $n_R \sin i_o = n_o \sin \theta = (1.3435)(.93154) = 1.25152$.

Substituting for n and for $n_R \sin i_o$ the values obtained in the preceding paragraphs, one obtains the differential equation of the path of the ray of light considered at point 22,

$$d\phi = \frac{1.25124}{\sqrt{x^2\left[1.3435 - 0.0173284\left(\frac{1-x}{\psi}\right) - 0.00212286\left(\frac{2(1-x)}{\psi}\right)^2\right] - (1.25124)^2}}\frac{dx}{x} \qquad \text{(II-33)}$$

This equation is then integrated numerically by use of Gregory's formula (see e.g. the Mathematics of Physics and Chemistry by Margenau and Murphy, D. van Nostrand Co. 1943, p. 459) from

$$x = 1 \text{ to } x = \frac{r'-D_r}{|R|} = 0.92429$$

(for the point) for several values of ψ greater than

$$\frac{\theta_{r,min}}{|R|} = 0.1835.$$

The results of these integrations are given in Table IX.

Table IX Results of Integration for ϕ as a Function of ψ. Value of ϕ_g as Obtained in Calculation for p_{av} is 0.4078 Radians (Point 22, Film 536).

ψ	ϕ (radians)
0.184	0.3813
.195	.3671
.230	.3528

The data in this table indicate that there is no value of ψ that will give a value of ϕ as great as ϕ_g. Thus, it is assumed that the ray of light considered for this point has gone through the point of total reflection after leaving the diffuse source of light, the lucite grid. For each of the three values of ψ, then, the value of r_{min} was calculated (Eq. (II-18)), and the numerical integration of Eq. (II-33) was carried out in two steps, first, from x = 1 up to $x = \frac{r_{min}}{R} + \epsilon$ and then up to x = 0.92429. The results of these integrations beyond the point of total reflection are given as a function of ψ in Table X.

Table X Results of Integration for ϕ Beyond Point of Total Reflection. Value of ϕ_g as Obtained in Calculation for p_{av} is 0.4078 radians (Point 22, Film 536).

ψ	ϕ (radians)
0.184	0.3907
.195	.4061
.230	.4232

A plot of these results is given in Fig. 135, from which the value of ψ to give a $\phi = \phi_g = 0.4078$ radian is found to be 0.197.

Since the value of |R| for this shot, Film 536, was 15.97 in., θ_r is obtained as 0.197 x 15.97 = 3.15 in.

To convert this to a value of θ_t, use is made of Eq. (II-24), where c is taken as 0.0645 in./μsec., α is taken as 1.23, |R| is taken as 15.97 in., and r is the value of r' - D_r for Point 22, Film 536 (=0.92429 x 15.97 = 14.76 in.). This leads to a value of θ_t = 39.1 μsec.

960

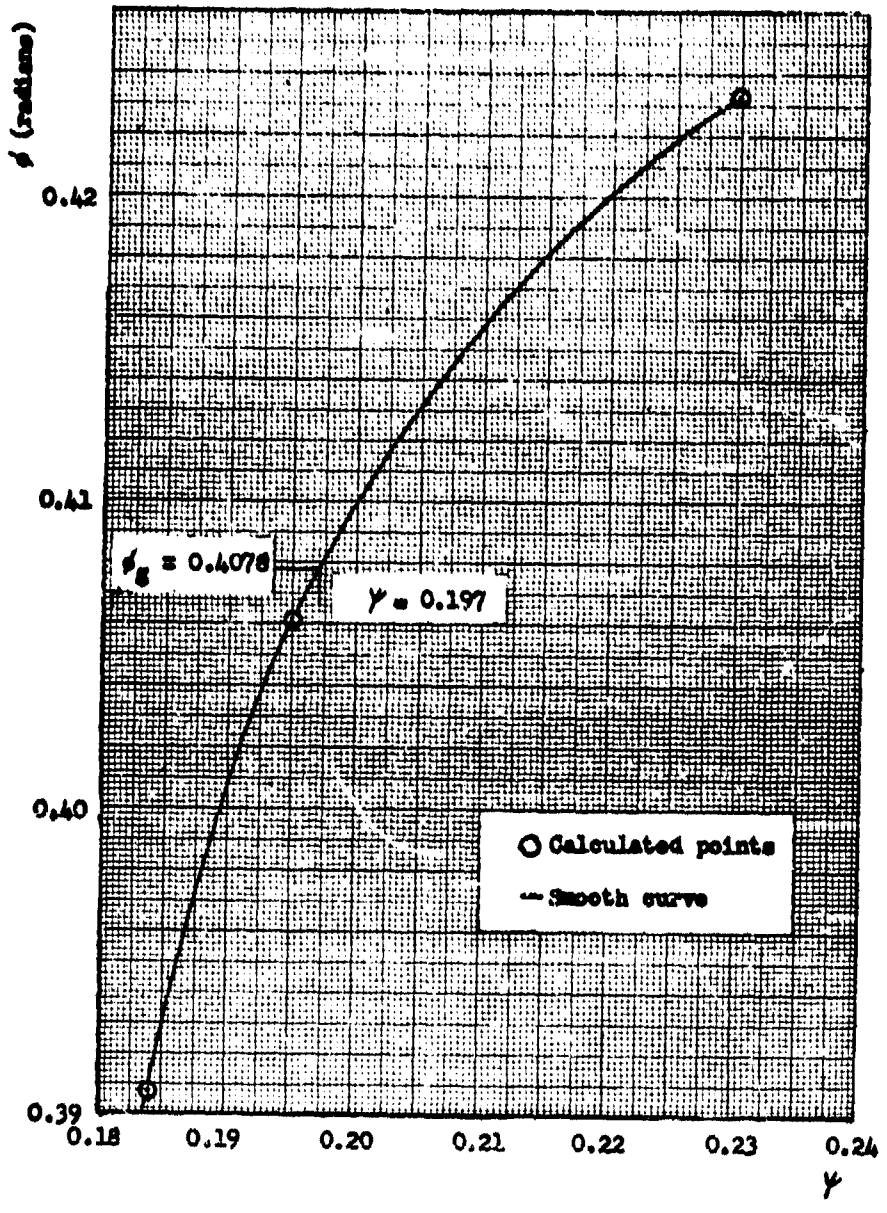


Fig. 135. ϕ vs. ψ obtained by integration beyond the point of total reflection. (ϕ_g = 0.4078 radians, point 22, film 536)

15518

Table XI Results in the evaluation of time constant

Film No.	Point No.	$\lvert R\rvert - r_{av}$ (in.)	θ_r (in.)	$r' - D_r$ (in.)	θ_t (μ sec)
536	22	0.61	3.15	14.76	39.1
537	5a	0.63	3.39	14.72	41.3
537	12	0.94	3.23	14.11	39.6
536	6	0.97	3.63	14.03	43.8
537	18	1.13	3.09	13.71	38.1

Av. θ_t=40.4 μ sec, average deviation from mean = ±1.7 μ sec.

It will be noted that there is no systematic trend of θ_t with distance of the point selected for calculation behind the shock front ($\lvert R\rvert - r_{av}$).

2. Grid in same plane with charge: charge directly in front of camera: spherical shock wave

If the experimental set-up is such that the plane of the grid is perpendicular to the optical axis of the camera with the center of the charge at this point of intersection, then the peak pressure of the shock wave may be calculated as follows: Referring to Fig. 136, C is the position of the camera; S is the shock wave; Q is the charge; QQ is the grid (perpendicular to the plane of the paper); R is the point at which the given light ray passes through the shock front; r and r' are the true and apparent points of intersection of a pair of grid lines, respectively. A construction line is drawn from Q perpendicular to Rr'. As in Sec. 1, (a), the assumption is made that the pressure from R to r is constant. ν is the ratio of the index of refraction over this range to the index of refraction outside the shock wave.

The quantities β, ϕ, θ, Rr', Rr, S, and δ are successively determined by the following equations:

$$\tan\beta = \frac{Or'}{CO} \tag{II-34}$$

$$QR\cos(\phi - \beta) = Or'\cos\beta \tag{II-35}$$

$$\theta = 180^\circ - (90^\circ + \phi - \beta) = 90^\circ - \phi + \beta \tag{II-36}$$

By the law of sines,

$$\frac{\sin\phi}{Rr'} = \frac{\sin(90^\circ - \beta)}{QR} \tag{II-37}$$

By the law of cosines,

$$Rr = \sqrt{(Qr)^2 + (rr')^2 - 2(Rr)(rr')\cos(90^\circ - \beta)} \tag{II-38}$$

Again by the law of sines,

$$\frac{\sin\delta}{rr'} = \frac{\sin(90^\circ - \beta)}{Rr} \tag{II-39}$$

By Snell's law,

$$\nu = \frac{\sin\theta}{\sin\theta'} = \frac{\sin\theta}{\sin(\theta - \delta)} \tag{II-40}$$

The corresponding pressure is then obtained from Table X. After calculations have been made for several grid line intersections, the peak pressure is determined by the method described in Section 1 of Appendix II; namely, by plotting the calculated pressures against corresponding distances of the mid-point of Rr from the shock front, and extrapolating to zero distance from the shock front.

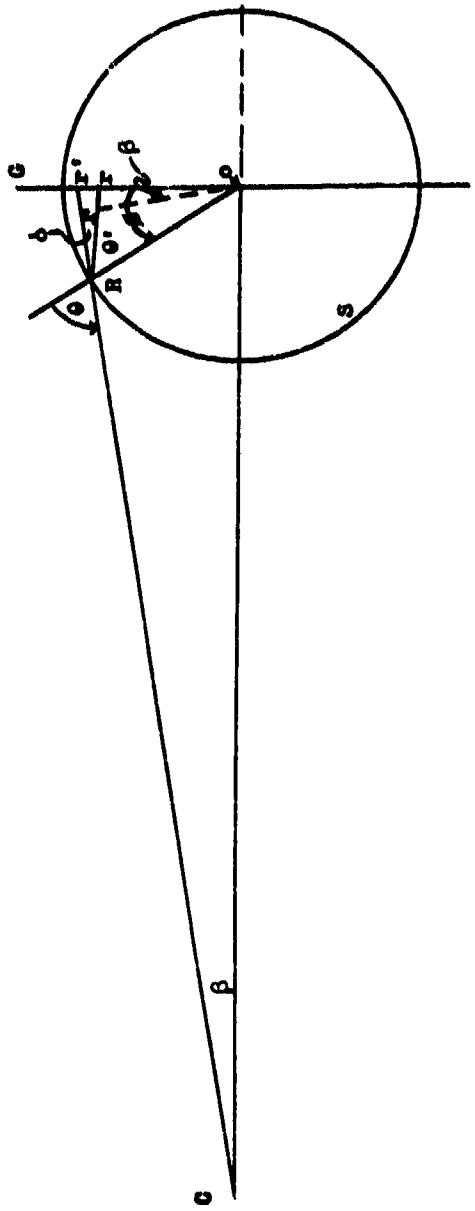


Fig. 136. Second experimental arrangement for determination of peak pressure by optical distortion.

It is to be noted that the shock wave photograph in this case probably does not show the intersection of the shock wave and the grid plane, but rather the intersection of the grid plane and a cone which has its apex at the camera lens and is tangent to the shock wave sphere. Thus, in determining the shock wave radius from the photograph, a corresponding correction should be applied to the apparent radius.

3. Grid in same plane with charge; charge directly in front of camera; non-spherical shock wave

If the experimental conditions meet the above requirements, the peak pressure of the shock wave may be calculated as follows: Referring to Fig. 137, C is the position of the camera; S is the shock wave; O is the charge; GG is the grid (perpendicular to the plane of the paper); R is the point at which the given light ray passes through the shock front; r and r' are the true and apparent points of intersection of a pair of grid lines, respectively; RG is the normal to the shock wave surface at R. As in section 1 of this Appendix, the assumption is made that the pressure from R to r is constant. μ is the ratio of the index of refraction over this range to the index of refraction outside the shock wave. Although the shock wave is not assumed spherical, it is assumed that the shock wave surface can be represented by some equation $f(x,y,z) = 0$, the exact form being determined from the photograph of the shock wave.

The solution proceeds according to the methods of analytic geometry. The charge is taken as the origin of the coordinate axes, X, Y, Z, and the various points in the experimental arrangement are assigned the coordinates given in Fig. 137.

The equation of ling OR is

$$\frac{x - 0}{x_4 - 0} = \frac{y - y_3}{0 - y_3} = \frac{z - z_3}{0 - z_3} , \qquad \text{(II-41)}$$

which simplifies to

$$\frac{x}{x_4} = \frac{y - y_3}{y_3} = - \frac{z - z_3}{z_3} \qquad \text{(II-41')}$$

These equations are combined with $f(x,y,z) = 0$ to obtain x_1, y_1, z_1. The direction components of OR are

$$\frac{\partial f}{\partial x_1} , \frac{\partial f}{\partial y_1} , \frac{\partial f}{\partial z_1} .$$

The direction components of CR are

$$x_4, -y_3, -z_3 .$$

$$\cos \theta_1 = \frac{x_4 \frac{\partial f}{\partial x_1} - y_3 \frac{\partial f}{\partial y_1} - z_3 \frac{\partial f}{\partial z_1}}{(x_4^2 + y_3^2 + z_3^2)^{1/2} \left[\left(\frac{\partial f}{\partial x_1} \right)^2 + \left(\frac{\partial f}{\partial y_1} \right)^2 + \left(\frac{\partial f}{\partial z_1} \right)^2 \right]^{1/2}} \qquad \text{(II-42)}$$

The equation of line Rr is

$$\frac{x - x_1}{0 - x_1} = \frac{y - y_1}{y_5 - y_1} = \frac{z - z_1}{z_5 - z_1} . \qquad \text{(II-43)}$$

The direction components of this line are

$$-x_1, y_5 - y_1, z_5 - z_1 .$$

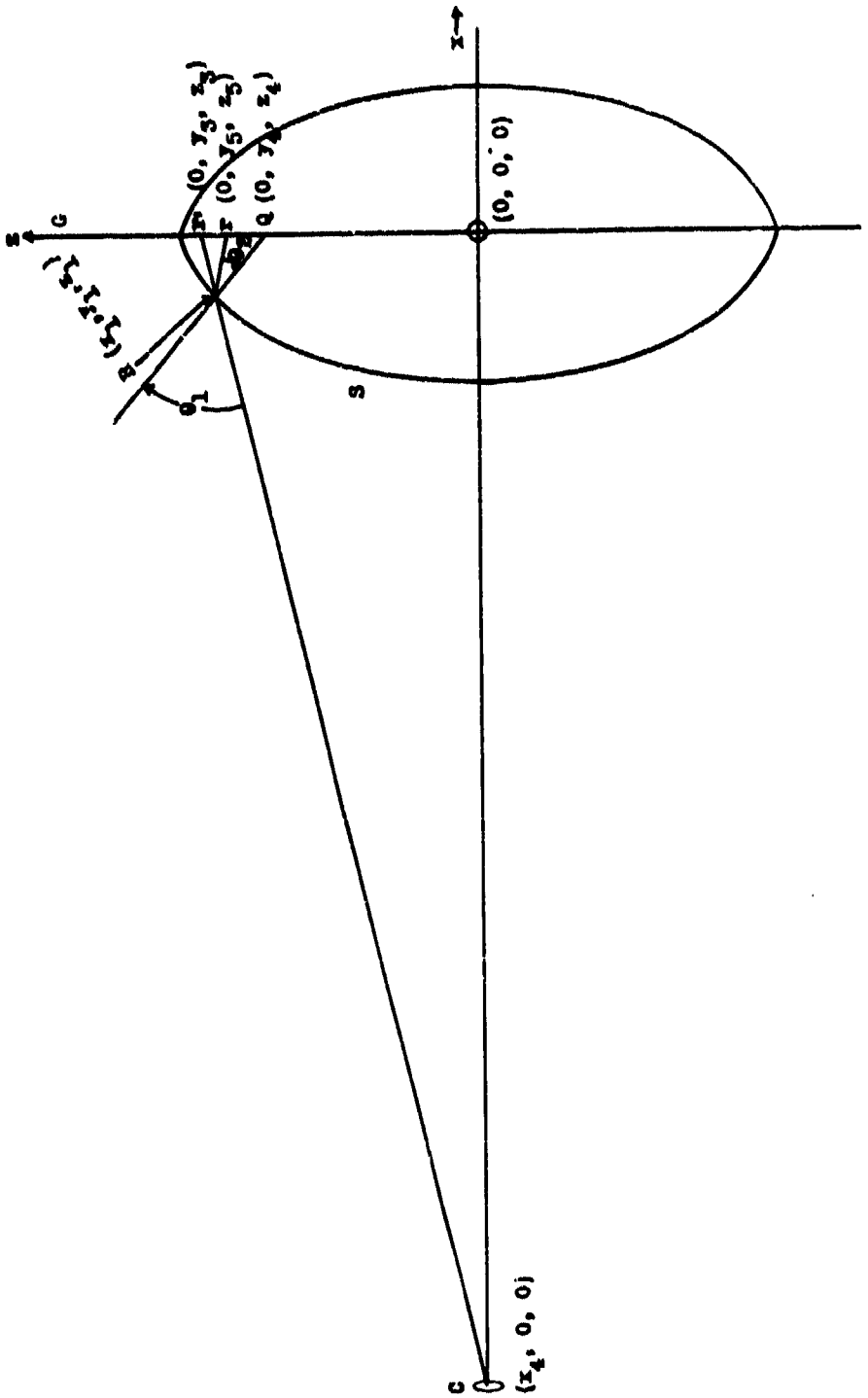


Fig. 137. Third experimental arrangement for determination of peak pressure by optical distortion.

15518

$$\cos\theta_2 = \frac{-x_1\frac{\partial f}{\partial x_1} + (y_5 - y_1)\frac{\partial f}{\partial y_1} + (z_5 - z_1)\frac{\partial f}{\partial z_1}}{\left[x_1^2 + (y_5 - y_1)^2 + (z_5 - z_1)^2\right]^{1/2}\left[\left(\frac{\partial f}{\partial x_1}\right)^2 + \left(\frac{\partial f}{\partial y_1}\right)^2 + \left(\frac{\partial f}{\partial z_1}\right)^2\right]^{1/2}} \qquad \text{(II-44)}$$

Having values now for θ_1 and θ_2, by Snell's law,

$$\nu = \frac{\sin\theta_1}{\sin\theta_2} \quad . \qquad \text{(II-45)}$$

The corresponding pressure is then obtained from Table VII.

After calculations have been made for several grid line intersections, the peak pressure is determined by the method described in Section 1; namely, by plotting the calculated pressures against corresponding distances of the mid-point of Rr from the shock front, and extrapolating to zero distance from the shock front. Since the shock wave is not spherically symmetric, the other grid line intersections must be chosen in the same general region behind the shock wave to obtain the peak pressure for that region.

Attention is called also to the last paragraph in Section 2 of this Appendix, which is applicable here.

4. Grid behind shock wave; charge directly in front of camera; spherical shock wave

If the experimental set-up meets the above requirements, the peak pressure of the shock wave may be calculated as follows: Referring to Fig. 138, C is the position of the camera; S is the shock wave; O is the charge; OH is the grid (perpendicular to the plane of the paper); R and Q are the points at which the given light ray passes through the shock front; r and r' are the true and apparent points of intersection of a pair of grid lines, respectively; OR and OQ are the normals to the shock wave surface at R and Q respectively. As in Section 1 of this Appendix, the assumption is made that the pressure from R to Q is constant. ν is the ratio of the index of refraction over this range to the index of refraction outside the shock wave.

The solution proceeds according to the methods of analytic geometry. The charge is taken as the origin of the coordinate axes x and y, and the various points in the experimental arrangements are assigned the coordinates given in Fig. 138. Due to the symmetry of the shock wave, the problem becomes planar for any single grid line intersection. x_3 and x_4 are obtained before the shot; and the radius of the shock wave OR, y_3 and y_4 are determined from the photograph.

The two equations

$$x_1^2 + y_1^2 = (OR)^2 \qquad \text{(II-46)}$$

and

$$\frac{y_1}{x_1 - x_4} = \frac{y_3}{x_3 - x_4} \qquad \text{(II-47)}$$

are solved simultaneously for x_1 and y_1, the roots x_2 and y_2 being discarded. Due to the circular symmetry of the shock wave in the x,y plane,

$$\tan\angle rQO = \tan\angle ORC \qquad \text{(II-48)}$$

If, now, the slope of any line AB is designated λ_{AB}, from Eq. (II-48),

$$\frac{\lambda_{Qr} - \lambda_{OQ}}{1 + \lambda_{Qr}\lambda_{OQ}} = \frac{\lambda_{OR} - \lambda_{CR}}{1 + \lambda_{OR}\lambda_{CR}} \qquad \text{(II-49)}$$

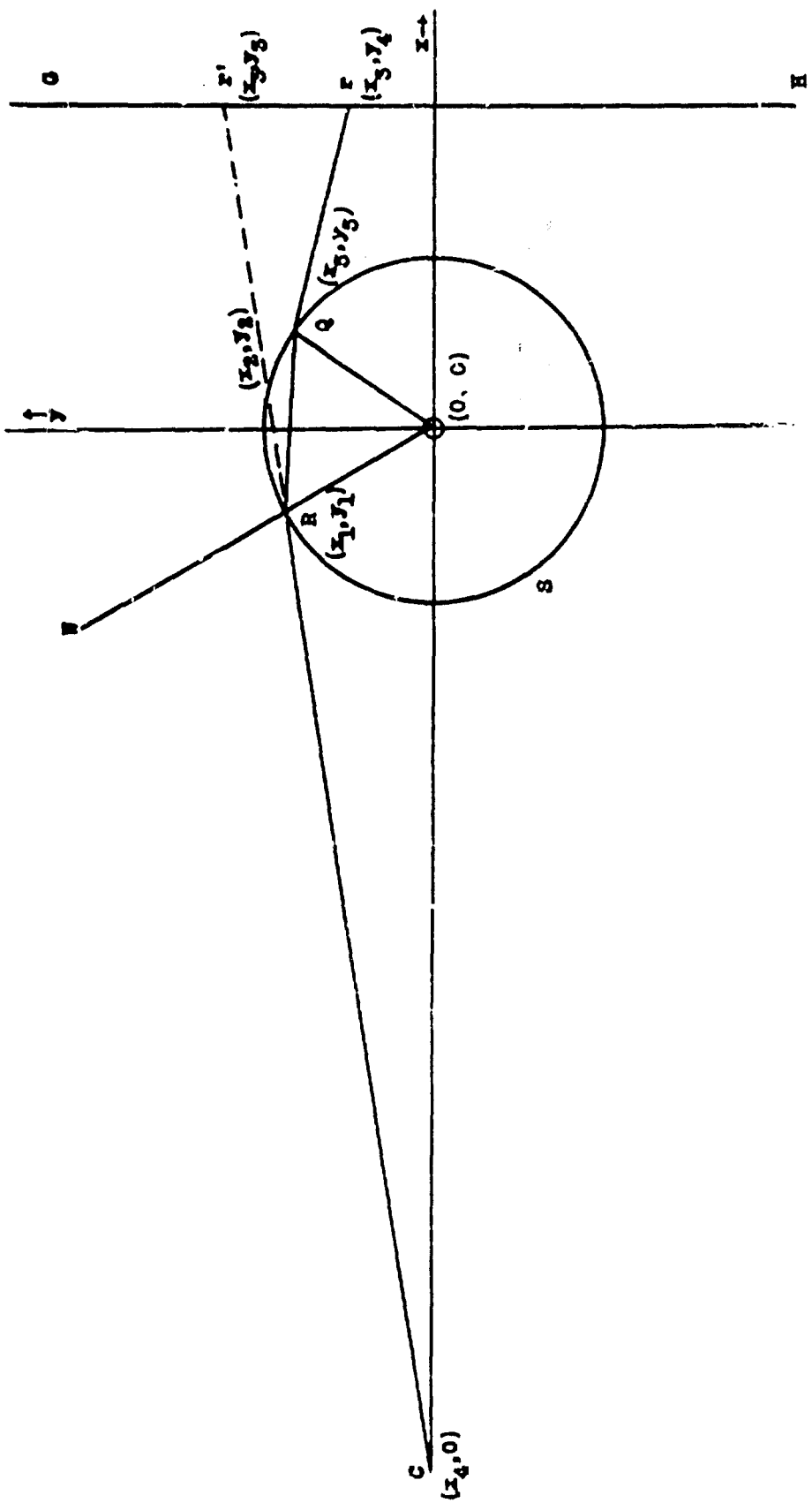


Fig. 138. Fourth experimental arrangement for determination of peak pressure by optical distortion.

But

$$\lambda_{QR} = \frac{y_4 - y_5}{x_3 - x_5} \qquad \text{(II-50)}$$

$$\lambda_{OR} = \frac{y_1}{x_1} \qquad \text{(II-51)}$$

$$\lambda_{OQ} = \frac{y_5}{x_5} \qquad \text{(II-52)}$$

$$\lambda_{CR} = \frac{y_3}{x_3 - x_4} \qquad \text{(II-53)}$$

Combining Eqs. (II-50), (II-51), (II-52), (II-53) with Eq. (II-49) results in an equation which reduces to

$$\frac{y_4 x_5 - x_5 y_5 - x_3 y_5 + x_5 y_5}{x_3 x_5 - x_5^2 + y_4 y_5 - y_5^2} = \frac{x_3 y_1 - x_4 y_1 - x_1 y_3}{x_1 x_3 - x_1 x_4 + y_1 y_3} = k \qquad \text{(II-54)}$$

where k is a constant for a given grid line intersection. Eq. (II-54) is combined with

$$x_5^2 + y_5^2 = (OQ)^2 = (OR)^2 \qquad \text{(II-55)}$$

to obtain values for x_5 and y_5, the extraneous roots being discarded.

$$\angle WRC = \tan^{-1}\left[\frac{\lambda_{CR} - \lambda_{RO}}{1 + \lambda_{CR}\lambda_{RO}}\right] \qquad \text{(II-56)}$$

and

$$\angle ORQ = \tan^{-1}\left[\frac{\lambda_{RQ} - \lambda_{RO}}{1 + \lambda_{RQ}\lambda_{RO}}\right] \qquad \text{(II-57)}$$

Combining

$$\lambda_{RQ} = \frac{y_5 - y_1}{x_5 - x_1} \qquad \text{(II-58)}$$

and Eqs. (II-50), (II-51), (II-52), (II-53), with Eqs. (II-56) and (II-57) results in the following equations:

$$\angle WRC = \tan^{-1}(-k) \qquad \text{(II-59)}$$

$$\angle ORQ = \tan^{-1}\left[\frac{x_1 x_5 - x_5 y_1}{x_1 x_5 - x_1^2 + y_1 y_5 - y_1^2}\right] \qquad \text{(II-60)}$$

Finally,

$$\nu = \frac{\sin \angle WRC}{\sin \angle ORQ}, \text{ (Snell's law)}, \qquad \text{(II-61)}$$

and the corresponding pressure is then obtained from Table VII.

After calculations have been made for several grid line intersections, the peak pressure is determined by the method described in Section 1 of the Appendix; namely by plotting the calculated pressures against corresponding distances of the mid-point of RQ from the shock front, and extrapolating to zero distance from the shock front.

Attention is again called to the fact that the apparent intersection of the shock wave and grid on the photograph is the projection on the grid of a cone with its apex at the camera lens and tangent to the shock wave sphere, and the shock wave radius must be calculated accordingly.

PHOTOGRAPHY OF UNDERWATER EXPLOSIONS, I

J. E. Eldridge, P. M. Fye, an . W. Spitzer
Underwater Explosives Resea ratory
Woods Hole Oceanographic a.. ..ution

American Contribution

24 March 1947

Table of Contents

Abstract / Section		Page
I.	INTRODUCTION	1
II.	EXPERIMENTAL METHODS AND EQUIPMENT	1
	1. Methods of flash photography	1
	(a) General information	1
	(b) Water transparency	1
	(c) Cameras for flash photography	2
	(i) Argus C-3	2
	(ii) Kodak "35"	2
	(iii) UERL camera	2
	(iv) Automatic photography	2
	(d) Light sources	2
	(i) Glass enclosed flash charges for depths down to 20 feet	7
	(ii) Conical flash charges for depths down to 10 feet	7
	(iii) Flash charges for depths down to 600 feet	10
	(iv) Other sources	10
	(e) Underwater equipment	10
	(f) Firing devices	10
	2. Methods of motion picture photography	10
	(a) Cameras for motion picture photography	10
	(i) Eastman high speed camera	10
	(ii) Jerome camera	15
	(iii) Victor camera	15
	(b) Associated equipment for underwater photography	15
	(i) Underwater gear	15
	(c) Light sources	15
	(i) Photoflash lamps	15
	(ii) Mercury arc	15
	(d) Timers	15
	(e) Power supply for cameras	15
III.	RESULTS OF EXPERIMENTS	20
	1. Cavitation	20
	(a) Minimum tension necessary to cause cavitation	20
	(b) Criterion for cavitation in front of steel diaphragm	20
	(c) Cavitation from objects other than plane surfaces	26
	(d) Disappearance of cavitation	26
	(e) Cavitation caused by oblique reflection of shock waves from air-water interfaces	26
	2. Investigation of the effect of shape of charge and point of detonation on shock wave and bubble	35

Table of Contents (Continued)

		Page
3.	Pressure and time-constant measurements of shock waves by optical distortion	43
	(a) Spherical shock wave; charge not on the optical axis; charge in grid plane	43
	(i) Peak pressure	43
	(ii) Time-constants	47
	(iii) Summary and remarks	48
	(b) Spherical shock wave; charge on the optical axis; charge in grid plane	48
	(c) Non-spherical shock wave; charge on the optical axis; charge in grid plane	48
	(d) Spherical shock wave; charge on the optical axis; charge in front of grid plane	48
4.	Cylinder damage	51
	(a) Introduction	51
	(b) Still pictures	51
	(c) Slow speed movies	51
	(d) High speed movies	51
5.	Miscellaneous experiments	51
	(a) Mach effect	51
	(b) Shock wave from 300 lb. charge	51
	(c) Pressure of shock wave determined from shock wave velocity	57
	(d) Experiments showing that the apparent position of the shock wave coincides closely with its actual position	57
	(e) Luminosity of charges exploded underwater	60
APPENDIX		
I.	Theory of pressure in front of an air-backed free plate accelerated by a shock wave	61
II.	Theory of peak pressure and time constant determination for shock waves by the method of optical distortion	66

Editor's note: This appendix, by R.R. Halverson, appears as a separately published paper in this volume, just preceding this paper.

Table of Contents (Continued)

		Page
III.	Circuit diagrams of camera timers	87
	1. Timer for high speed camera	87
	2. Timer for Jerome camera	87
IV.	Gaskets and stuffing boxes for camera cases	90

List of Tables

Table		Page
I.	Cavitation data for steel plates in UERL diaphragm gage	24
II.	Summary of results of studies of cavitation from simulated free plates	27
III.	Experimental conditions applying to the photographs of Figs. 39 - 49	27
IV.	Data of experiments on oblique reflection of shock waves from water-air interfaces	31
V.	Data of experiments on oblique reflection of shock waves from 20 in. by 10 in. water-air interface, and from ocean surface	33
VI.	Results on the evaluation of time constant	47
VII.	Coefficients of a and b in $n(p) = n_0 + ap - bp^2$ for pure water	71
VIII.	Constants necessary for Eq. (II-15)	77
IX.	Results of integration for ϕ as a function of ψ. Value of ϕ_g as obtained in calculation for p_{av} is 0.4078 radians (point 22, film 536)	78
X.	Results of integration for ϕ beyond point of total reflection. Value of ϕ_g as obtained in calculation for p_{av} is 0.4078 radians (point 22, film 536)	78

NOTATION OF MAJOR SYMBOLS

		Page*
a and b	pressure coefficients of index of refraction for water	70
c	velocity of sound in water	21
D_r	a distance r' - r	47
L	mass per unit area of the plate, $\rho_s a$	21
n_{av}	average index of refraction of that section of the shock wave being investigated	43
n_o	index of refraction of sea water at zero pressure	68
p	pressure at a distance x and at a time t	20
p_{av}	average pressure of that section of the shock wave being investigated	43
p_o	peak pressure of original shock front	20
P	p/p_o	20
r	true radial distance from center of charge to intersection of a pair of grid lines in the optical distortion discussion, also	47
R	radial distance from center of plate to diffracted shock front in cavitation theory	63
r'	apparent radial distance from center of charge to intersection of a pair of grid lines	47
r_{av}	an average radius vector $\frac{\lvert R\rvert + (r' - D_r)}{2}$	43
r_b	radius of bubble or particle	20
R	inside radius of pipe and/or radius of the diaphragm (or "plate")	21
$\lvert R\rvert$	shock wave radius	43
R_c	radius of cavitation region	21
R_o	outside radius of pipe	21
R_p	radius of steel plate	21
s	interfacial tension between water and the particles	20
t	time measured from the time the original wave strikes the plate	61
t_c	time corresponding to x_c (calculated)	21
t_p	interval of time between impact of shock wave on plate and time of photograph	26
T	t/θ	63
u	instantaneous velocity of the plate	61

*Page where symbol is first used

NOTATION OF MAJOR SYMBOLS (Continued)

		Page
x	the distance of any point measured positively out into the water from the initial position of the plate	61
x_c	farthest perpendicular distance of cavitation from plate	21
X	$x/c\theta$, i.e. distance in units of $c\theta$	20
X_c	$x_c/c\theta$	21
α	weight-distance exponent for peak pressure	75
α	p_{max} = constant x $(W^{1/3}/R)^{\alpha}$	75
β	θ/θ_1, $c\theta/a$	21
θ	time constant of shock wave	21
θ_c	cavitation time	21
θ_p	exponential decay constant of shock wave with respect to distance	47
θ_t	exponential decay constant of shock wave with respect to time	47
θ_1	$a/\rho c$	21
ν	a_{sw}/a_0	68
ρ	density of water	21
τ	interval of time between impact of shock wave on plate and beginning of diffracted shock wave from the edge	63

I. INTRODUCTION

Interesting photographs of underwater explosions in model tanks have been obtained by many investigators. Their experiments suffered almost universally from the drawback that it was impossible to shoot charges larger than a gram or even a tenth of a gram. A technique has been developed at UERL of shooting in the open ocean so that the charge size is limited essentially only by the transparency of the water rather than by the strength of tank.

This report discusses in detail the methods and apparatus used in obtaining the pictures and the results of some two years of experimentation. It indicates the usefulness of photographic techniques for studying underwater explosions.

II. EXPERIMENTAL METHODS AND EQUIPMENT

Two main types of picture have been taken; the flash photograph, in which a single picture of approximately one microsecond exposure was obtained, and the motion picture, which usually gave three or four to several hundred pictures in a single experiment. These latter pictures were taken at speeds up to 2500 per second and corresponding exposures down to 100 microseconds. The two methods will be taken up in detail.

1. Methods of flash photography

(a) General information. -- In taking short exposures of rapidly changing phenomena, the shutter of the still camera was opened, the explosion initiated, a short duration flash of light emitted, and the shutter closed. During the winter months, it was found possible to work in daylight by actuating the instantaneous shutter mechanism, set at 1/100 second, with a solenoid and synchronizing the explosion electrically. When the sun was brighter, however, this method caused a general fogging even at 1/200 second, and it was found necessary to work at night. This simplified the problem of synchronization inasmuch as it was possible to set the shutter on bulb, open it with the solenoid, fire the charge, and close the shutter.

In experiments in which it was necessary to "stop" shock waves, the light source was an explosive flash charge (Section II, 1, (d)). The delay between the time of detonation of the subject charge and the flash charge was obtained by the proper length of Ensign-Bickford Primacord whose detonation velocity is 0.248 inches per microsecond.

It is possible to obtain multiple exposures on a single plate by firing several flash charges in sequence, using primacord timing.

When extreme speed was not necessary, the flash charge was replaced by a photoflash bulb or Eastman Kodatron Speedlamp.

(b) Water transparency. -- One of the important variables in underwater photography in the open sea (near land at least) is the transparency of the water. Not only does the total amount of transmitted light from a constant light source decrease at lower transparency, but, since the lower transmission is due to turbidity, image sharpness decreases even if the proper exposure is made. To take this into account, a crude transparency measure is made by dropping a white disk eight inches in diameter through the water until it disappears from view. The depth of this disappearance is recorded as the "Secchi disk reading." 1/ As a rough rule of thumb, it may be stated that fairly good pictures can be taken with object-to-camera distances up to half the Secchi disk reading.

1/ Progress Report on Underwater Photography, by D.E. Kirkpatrick, J.L. Worzel, M. Ewing, NDRC Section C-4 (Division 6.1), May 4, 1942.

For most single flash photographs, Eastman Contrast Process Ortho film was used and developed in D-11. Typical lens openings with a 250 gm explosive flash charge at 8 ft. from the camera varied from f/3.5 to f/8 depending on water conditions.

(c) Cameras for flash photography. -- A variety of cameras were used for flash photography with approximately equal success. In order to keep the size of the equipment at a minimum, 35 mm still cameras were used.

(i) Argus C-3. Figure 1 shows the Argus C-3 camera and its water and explosion-proof case. This camera has an internal synchronizer which was sometimes used to set off explosions when the shutter was at its maximum opening. The case was constructed from 6 1/2 in. O.D. by 3/4 in. thick steel pipe and the window is of 1 in. thick "tempered" glass having a 2 1/8 in. diameter for the unsupported area. The case and window have successfully withstood the explosion of a 300 pound charge 50 ft. away, both charge and camera case being at a depth of 40 ft.

(ii) Kodak "35". Figures 2 and 3 show a Kodak "35" and case. This case which was made from a pipe coupling, has also survived the explosion of a 300 pound charge at 50 ft. The camera was later modified as shown in Figure 4 which shows a much smaller homemade camera using the lens and shutter of the Kodak 35. A smaller case would obviously have been built for this camera.

(iii) UERL camera. In the early stages of this work it was considered that commercial cameras might not be rugged enough for the work we were doing, and a camera with laboratory designation "Brute" was constructed. The "Brute" camera consisted merely of a solid brass cylinder with a heavy spring-driven rotary shutter, a hole for the lens, and another for the film. The camera also contained a "foolproof" synchronizer for firing the charge which consisted of a contact made by the shutter at any desired time in its travel. By using an SSS seismographic cap (No. 8) which explodes within a millisecond of the time the circuit is closed, the synchronizer could be set to close the circuit when the shutter was barely opened and the timing would then automatically be right.

Subsequent experience showed that the commercial shutters were sufficiently rugged so long as they were not immersed in sea water, and the "Brute" camera was rarely used.

The cameras were all mounted on rubber as a matter of principle.

(iv) Automatic photography. One photograph was obtained by means of an automatic rig. A charge was detonated which activated a pressure switch. The pressure switch closed a solenoid circuit which tripped the camera shutter. As the shutter opened, a synchronizing switch fired a cap in the flash charge. The battery required was enclosed in the camera case. The resulting photographic image is not reproduced. This method can be used in experiments in which external connections with the camera are undesirable or impossible.

(d) Light sources. -- Still close-up photography of explosion phenomena requires exposures of the order of a μsec and a light source of about a million candlepower. A satisfactory source of light was developed by the Explosives Research Laboratory at Bruceton, Pennsylvania 2/, utilizing a spherical cast explosive charge of pentolite mounted concentrically in a round bottom glass flask; the space between the charge and flask being filled with argon at atmospheric pressure. Duration and intensity of the light increased respectively with the thickness and area of the argon layer.

2/ The Flash Photography of Detonating Explosives to May 1, 1943, Explosives Research Laboratory, Bruceton, OSRD Report 1488.

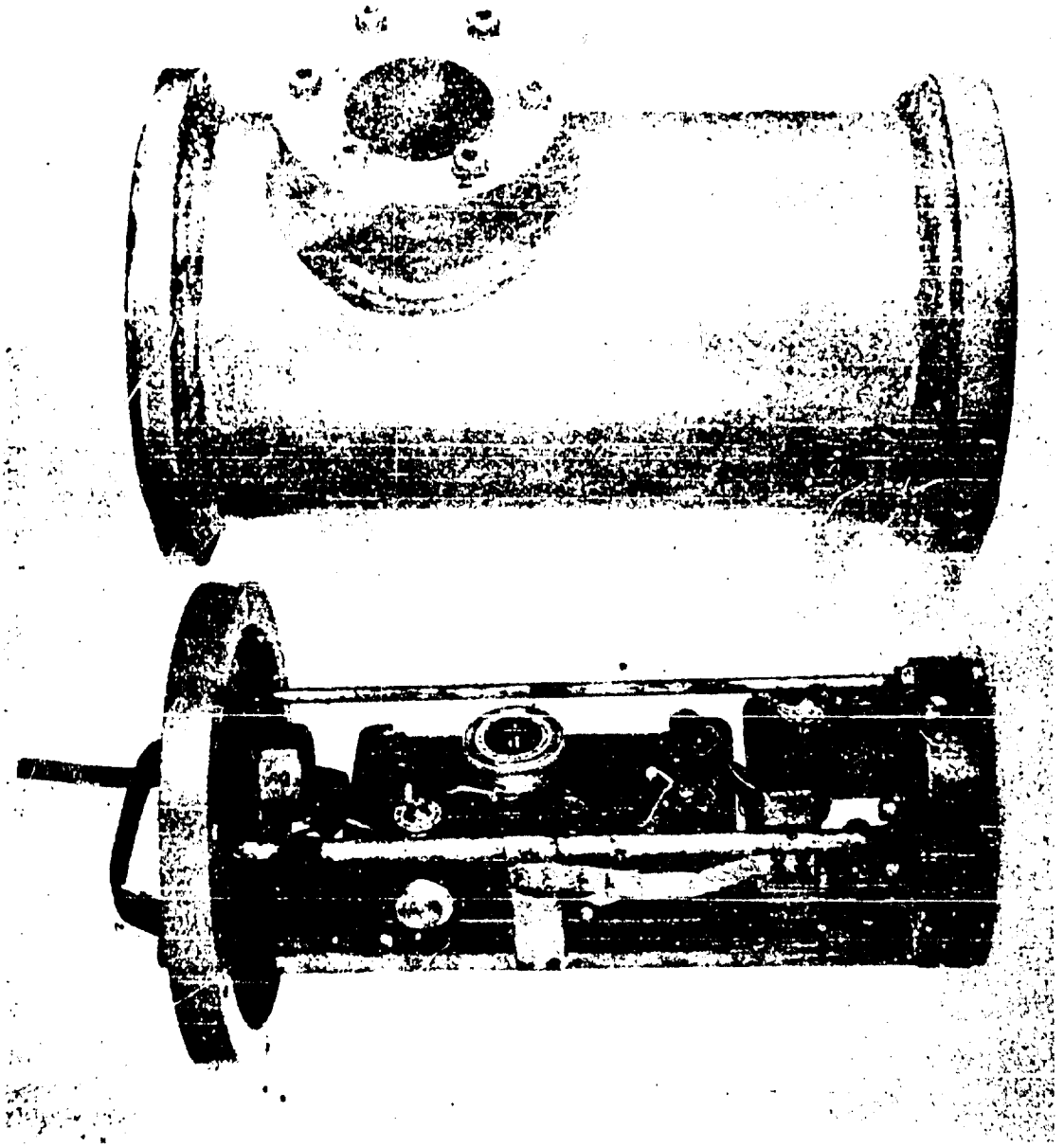


Fig. 1. Argus C-3 camera and case.

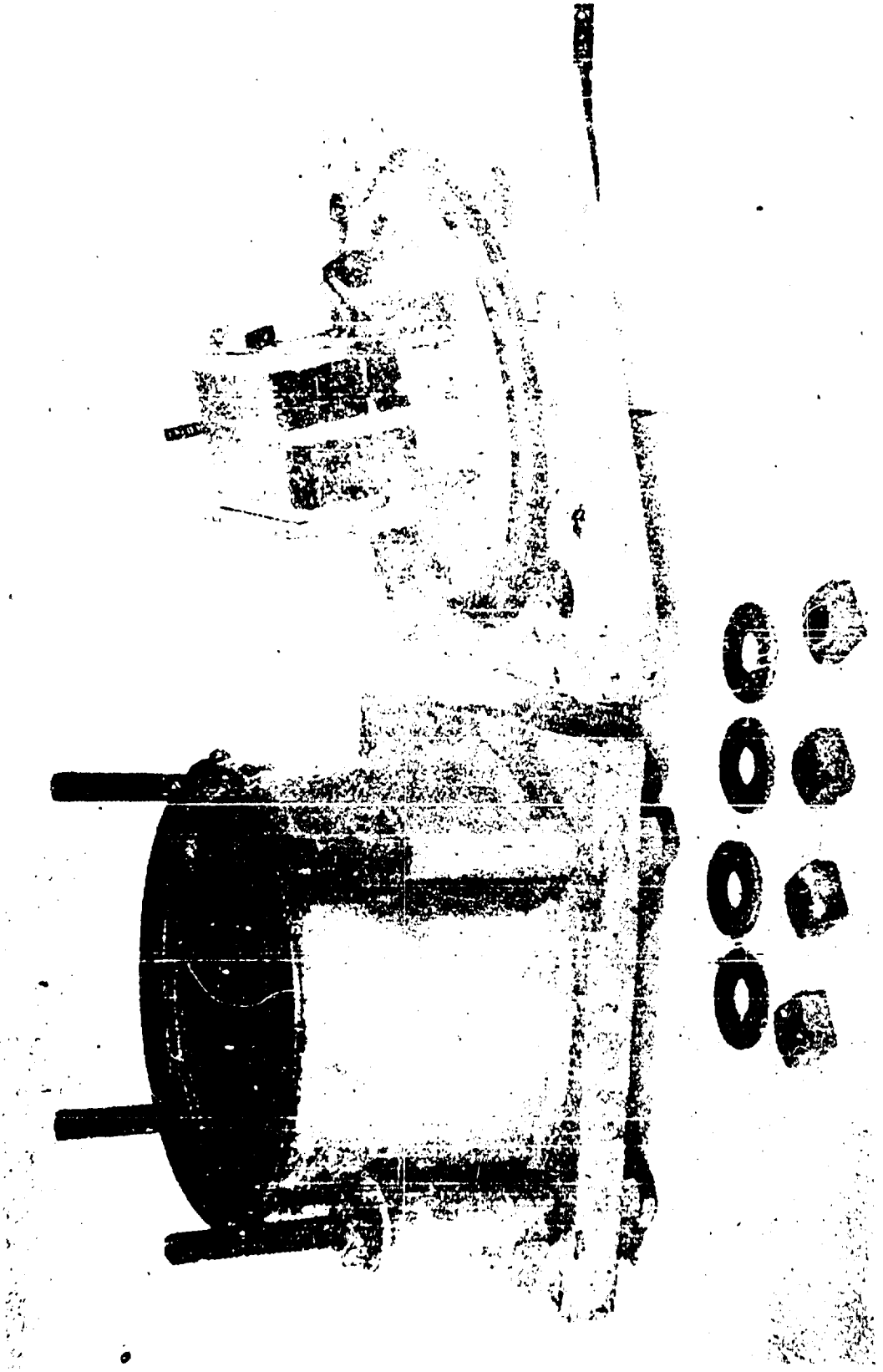


Fig. 2. Kodak "35" and case.



Fig. 3. Kodak "35" in case.

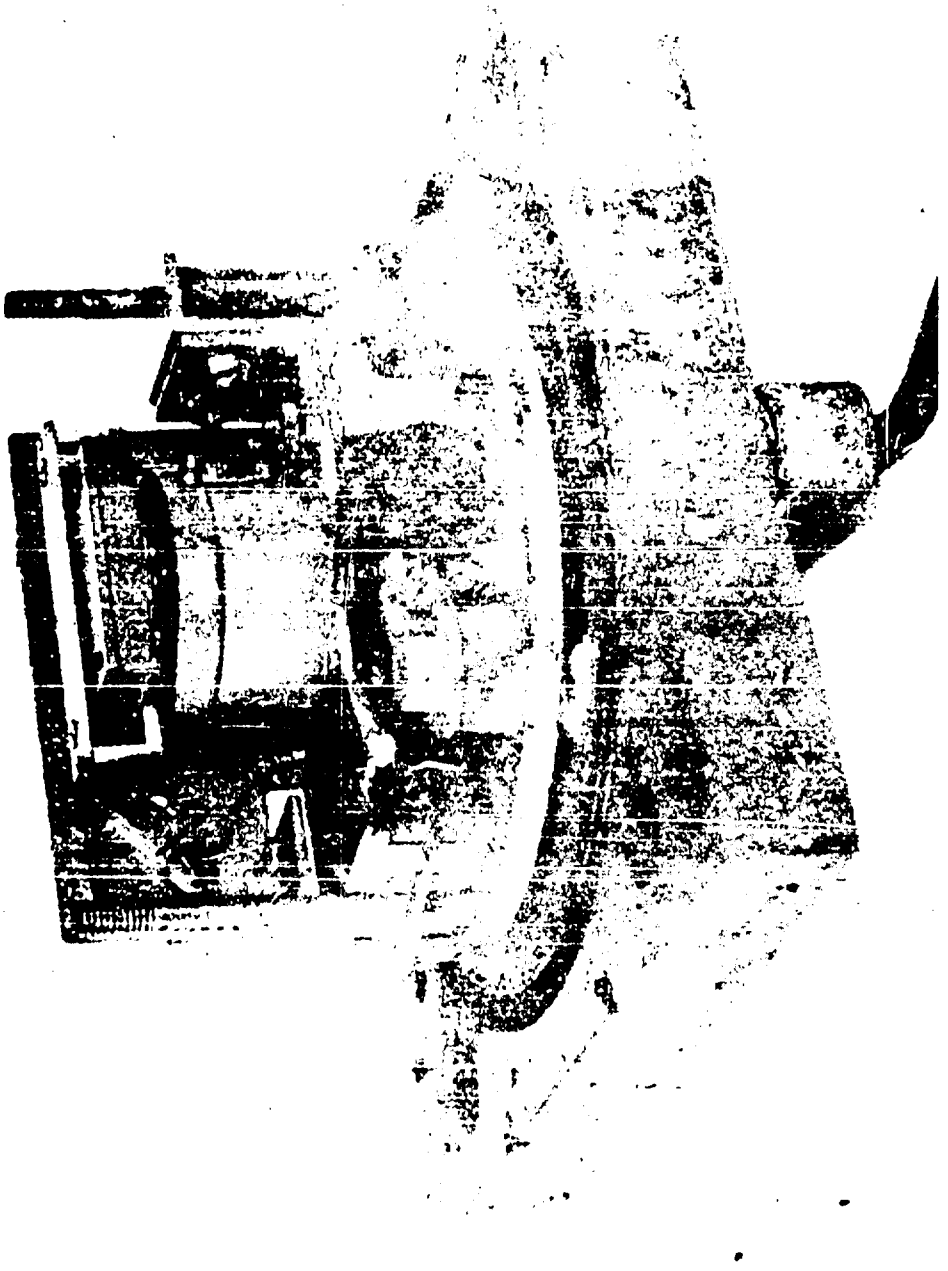


Fig. 4. Modified Kodak "35".

Argon-surrounded flash charges were adopted at UERL [3] for use underwater and proved satisfactory. By using conical rather than spherical charges it was possible to produce a given amount of useful light with less explosive. The amount of light emitted by the charges was about halved if the gas layer was air instead of argon. Tests were conducted with charges coated with mercurous chloride and sodium chloride (because of their emission spectra), but the results were erratic. The various types of flash charge prepared at UERL are illustrated in Figure 5.

(i) Glass enclosed flash charges for depths down to 20 feet. Since this type of flash charge was used most, its fabrication will be discussed in some detail. A primacord fuse is cut to the desired length and one end rolled tightly in a 2 x 2 x 1/32 in. sheet of lead with 1/8 in. of primacord projecting beyond the lead (see 1C of Figure 5). The function of the lead is to prevent detonation except that starting from the center of the sphere. To obtain maximum charge density and to minimuse segregation, all of the air should be driven out of the molten pentolite and the mix should be as cool as possible when poured. The charge is cast in a well-greased (e.g. petroleum jelly) plaster of paris mold (Figure 6) with the exposed end of primacord fuse in the center. The half molds are set over one another on their rims with the fuse in the groove provided and with the filling hole on top. Molten explosive is poured in up to the base of the filling hole and as the mix cools and shrinks, more is added to keep the level constant. When solid, the charge is easily removed by taking apart the molds. Molds may be cooled, regreased, and used again many times.

Charges may also be cast as two hemispheres. One hemisphere is cast with the primacord fuse in place and is removed from the mold when the explosive solidifies. Molten explosive is poured into the second mold up to the level of the fuse groove and the first half (with fuse) is placed on top. [4] The completed charge is easily removed from the mold when the second half solidifies.

The charge is next mounted in the round bottom glass flask which has been split into two halves (see 1B, 1C of Figure 5) by the hot wire technique familiar to glassblowers. Rubber tape is wrapped around the lead covered primacord fuse to provide a snug fit in the neck of the flask and to center the charge. There is a 3/16 in. space between the charge and the wall of the flask. A small chip of glass is removed from one of the split edges of the flask to provide a filling hole for the gas. The split halves of the flask are glued together with transparent tygon paint or Duco cement and the region over the seam is painted twice with the cement for waterproofing. Plaster of paris is poured into the neck of the flask to fix the charge in position, aid in waterproofing and minimize the leakage of gas. Bostik cement (a heavy-bodied rubber compound) or vaseline is placed over the plaster of paris to waterproof completely the mouth of the flask. Just before shooting, the charge is placed in a steel (for safety) vacuum desiccator, the air evacuated through the filling hole and argon allowed to flow in at atmospheric pressure. The filling hole is then resealed with a piece of scotch tape and Bostik.

(ii) Conical flash charges for depths down to 10 feet. Only a part of the light distributed by the shperical type flash charge described above is used in illuminating the field of view of the camera. The lighting efficiency may be improved by using a reflector behind the flash charge. However, there was little loss in light when the spherical charge was replaced by a conical

---

[3] Preparation of Charges for the Study of Explosion Phenomena at UERL, by P. Newmark and E. L. Paterson, NDRC Report A-381 (OSRD 6259); also The Preparation and Testing of High-Intensity, Short Duration Underwater Flares, by E. L. Patterson, NDRC Report A-382 (OSRD 6260).

[4] While this technique leads to some cavitation at the center of the cold charge, it was found in practice to make little or no difference for this purpose if the precautions noted above were taken.

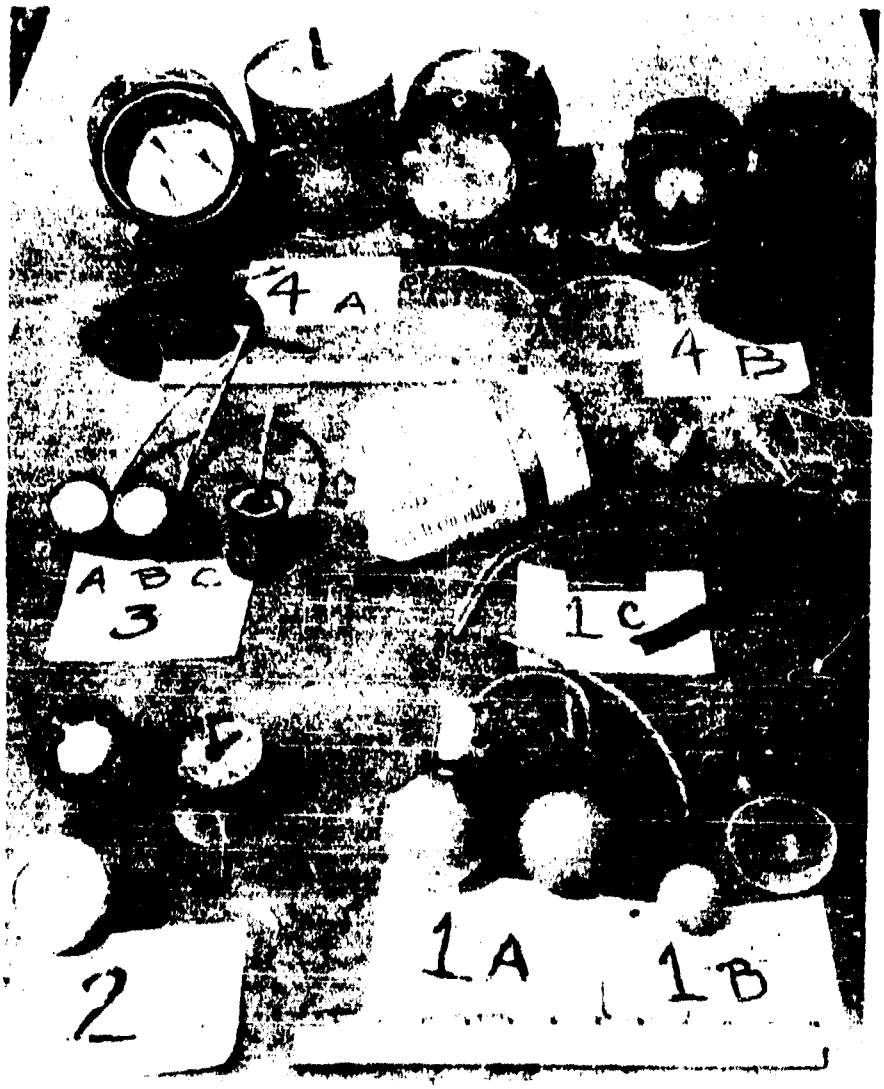


Fig. 5. Various types of flash charges prepared at UERL.

Data for Figure 5 - Various types of flash charges prepared at UERL.

1A 250 gm spherical pentolite flash charge - glass-cased and uncased. (See Figure 7).
1B 75 gm spherical pentolite flash charge - uncased.
1C Materials: primacord, 1/32 in. lead sheet, rubber tape, plaster f paris, and split flask (200 ml round bottom).
2 Conical flash charges. (see Figure 8).
3 Cylindrical tetryl flash charges (salt coated).
4 Flash charges for deep water. (see Figure 9).

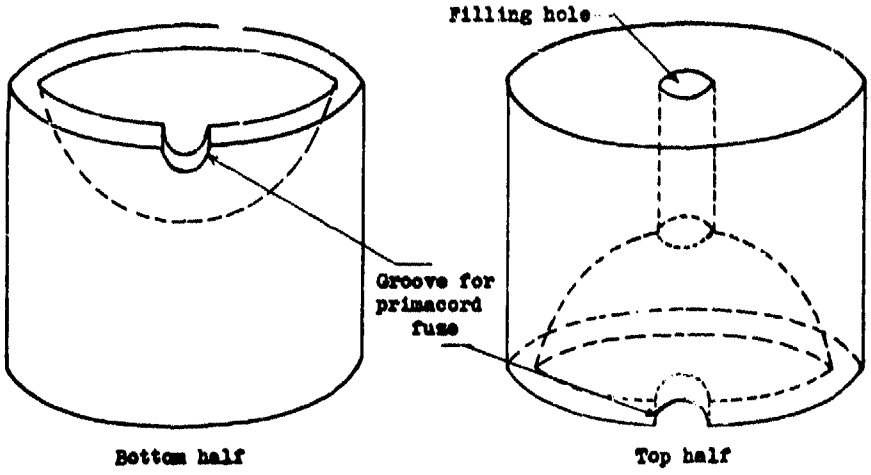


Fig. 6. Plaster of paris molds for casting spherical pentolite flash charges.

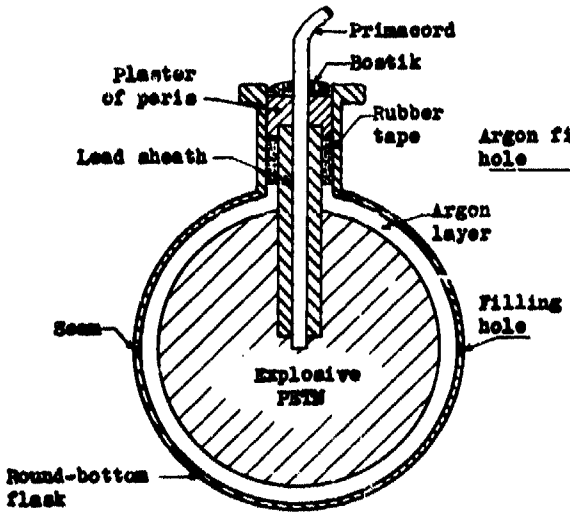


Fig. 7. Glass-enclosed spherical flash charge; a cross-sectional view.

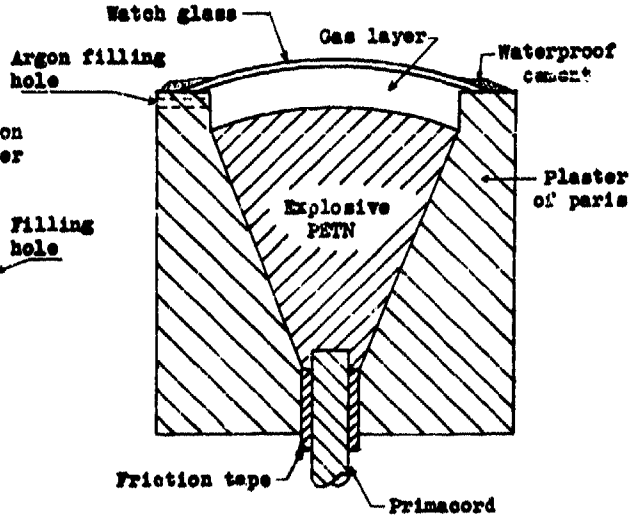


Fig. 8. Conical pentolite flash charge; a cross-sectional view.

charge which was actually a sector of a sphere. (See 2 of Figure 5). The fabrication is indicated by Figure 8. The advantage of this form was that about one-seventh the amount of explosive ($\sim$ 40 gm) was required which permitted the use of flash charges in areas where half-pound charges were too large.

(iii) Flash charges for depths down to 600 feet. The construction of a flash charge which would be waterproof in deep water and would not collapse under the hydrostatic pressure was accomplished by casting the pentolite in a tin can and using a thick (1/4 to 1/2 in.) disk of lucite for a window; Figure 9 shows the details. Photographs of this type of charge are given in Figure 5 (4a, 4b). The window is clamped against a rubber gasket and a 1/32 in. hole is drilled in the window for an argon filling hole. This hole was later closed with a tapered plug of wood and Bostik. A metal tube, closed at one end and soldered to the base of the tin can, projected into the explosive to comprise the detonator well. The charge was detonated by inserting primacord into the open end of a non-electric blasting cap, wrapping the junction carefully with rubber tape, inserting the blasting can into the detonator well, and initiating the primacord.

(iv) Other coverage. Some single pictures of damage to model structures were taken with a #22 photoflash lamp or with a gas-filled Kodatron flash tube. Both of these lamps had to be protected from the explosion by a metal case with lucite window. The usual explosive flash charge technique was not employed in this instance because the final damage to the model would have been affected by the explosion of the flash charge.

(e) Underwater equipment. -- Figure 10 shows a sketch and Figure 11 photographs of a typical experimental set-up for underwater photography. The majority of experiments were carried out in rings of this sort. While the circular shape is not the most convenient for the suspension of miscellaneous objects, it is generally less subject to destruction from the explosions. Lightweight objects, such as paper diffusing screens, were stayed from the ring by light line, while cameras, gauges and other heavy gear were fastened directly to the ring or to sturdy auxiliary structures bolted or welded to the ring.

(f) Firing devices. -- The flash charge and the target charge were generally fired a short time apart by connecting them with primacord. Since it was sometimes undesirable to have primacord extending between the two charges, a method was developed for simultaneously firing two charges which were separated in space. The method was to discharge a 40 microfarad condenser, charged to 600 - 1000 volts, through two No. S 833 seismographic caps connected in series. Under these conditions the caps detonated within a few microseconds of each other. Primacord was still necessary to obtain delays, but more control was obtainable over the geometrical configuration of the primacord since it was no longer necessary to have a continuous length between the two charges. Furthermore, this eliminated the necessity of having primacord in the field of view when photographing exploding charges.

2. Methods of motion picture photography.

Relatively slow phenomena, such as bubble growth and structural damage, can be photographed successfully using motion picture technique. We have used two conventional movie cameras and an Eastman High Speed camera, all of which require a continuous light source. For pictures in which a total duration of only 100 milliseconds is required, such as studies of damage from a 25 gm charge at 600 ft. depth, a single #31 photoflash lamp has been used. For longer durations it is possible to use several photoflash lamps tripped in series.

Eastman Super XX film or its equivalent has been used in all underwater movies.

(a) Cameras for motion picture photography. --

(i) Eastman high speed camera. Figure 12 shows the Eastman high speed electrically driven 16 mm camera with attached Lord vibration mounts. The mounts slide into the tracks shown inside the case, (Figure 13) and shock mounts

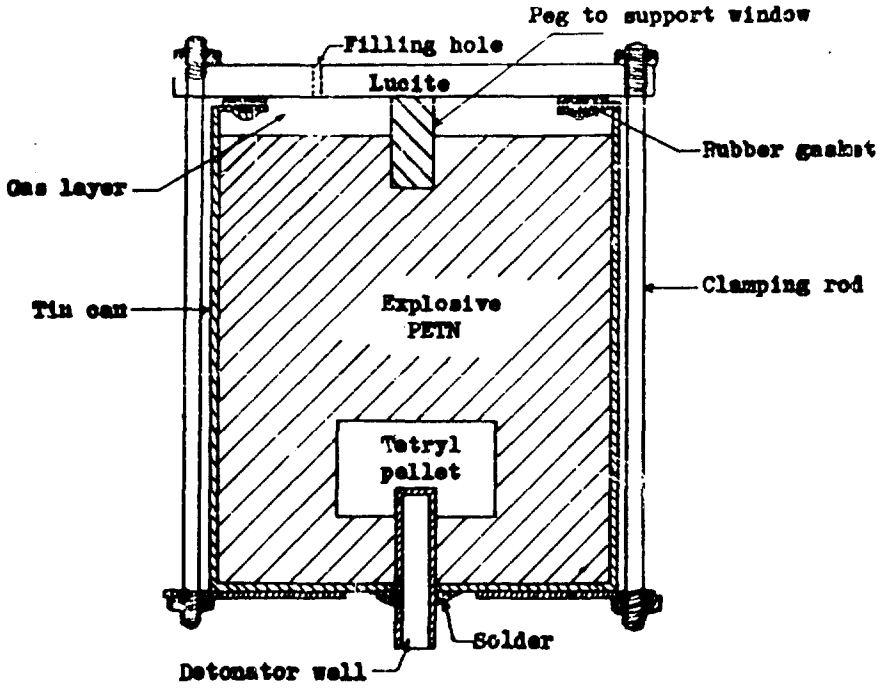
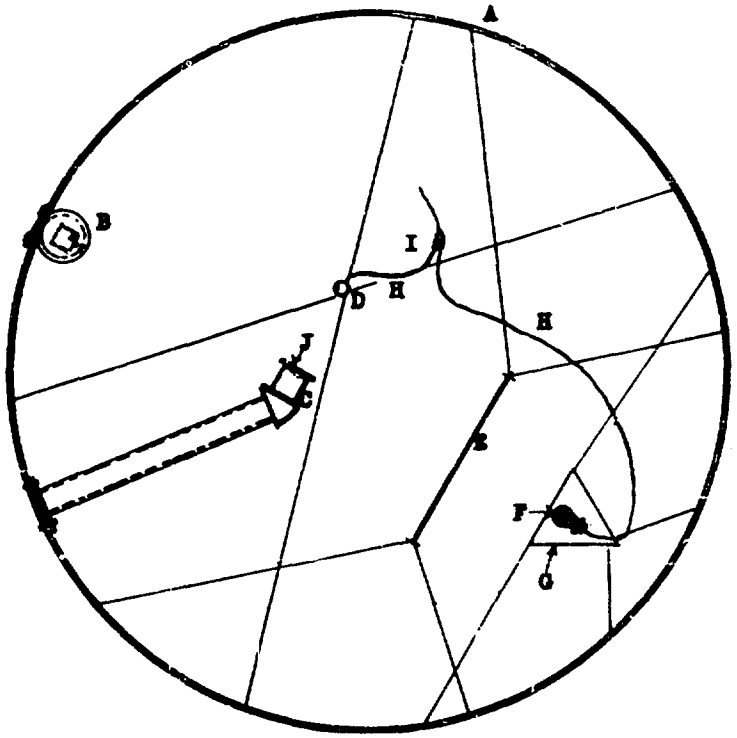
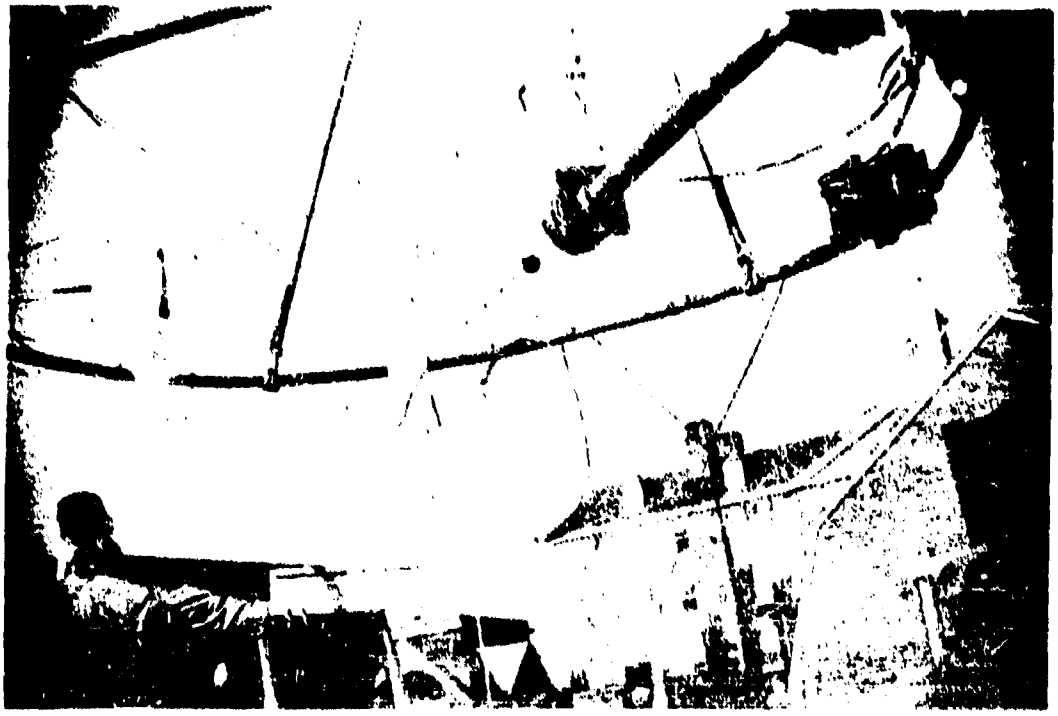


Fig. 9. Flash charge for deep water; a cross-sectional view.

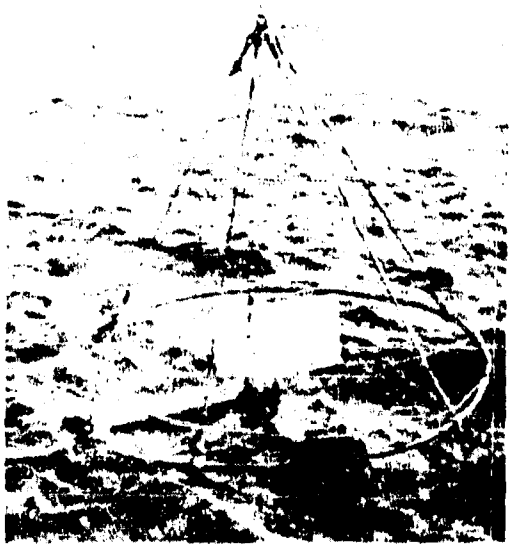


A.	Ring - 9 ft diameter	F.	Flash charge
B.	Camera	G.	Reflector
C.	Gauge	H.	Primacord
D.	Damaging charge	I.	Cap - No. 8
E.	Diffusing screen	J.	Diaphragm

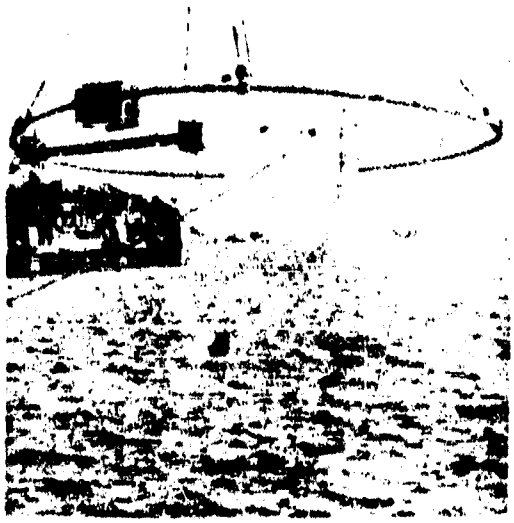
Fig. 10. Diagram of apparatus for underwater photography.



Close-up, showing camera, charge, diaphragm, diffusing screen, and flash charge reflector



Apparatus just entering water



Ring swung out over water preliminary to lowering

Fig 11 Steps in lowering equipment for single shot photograph of charge damaging diaphragm.

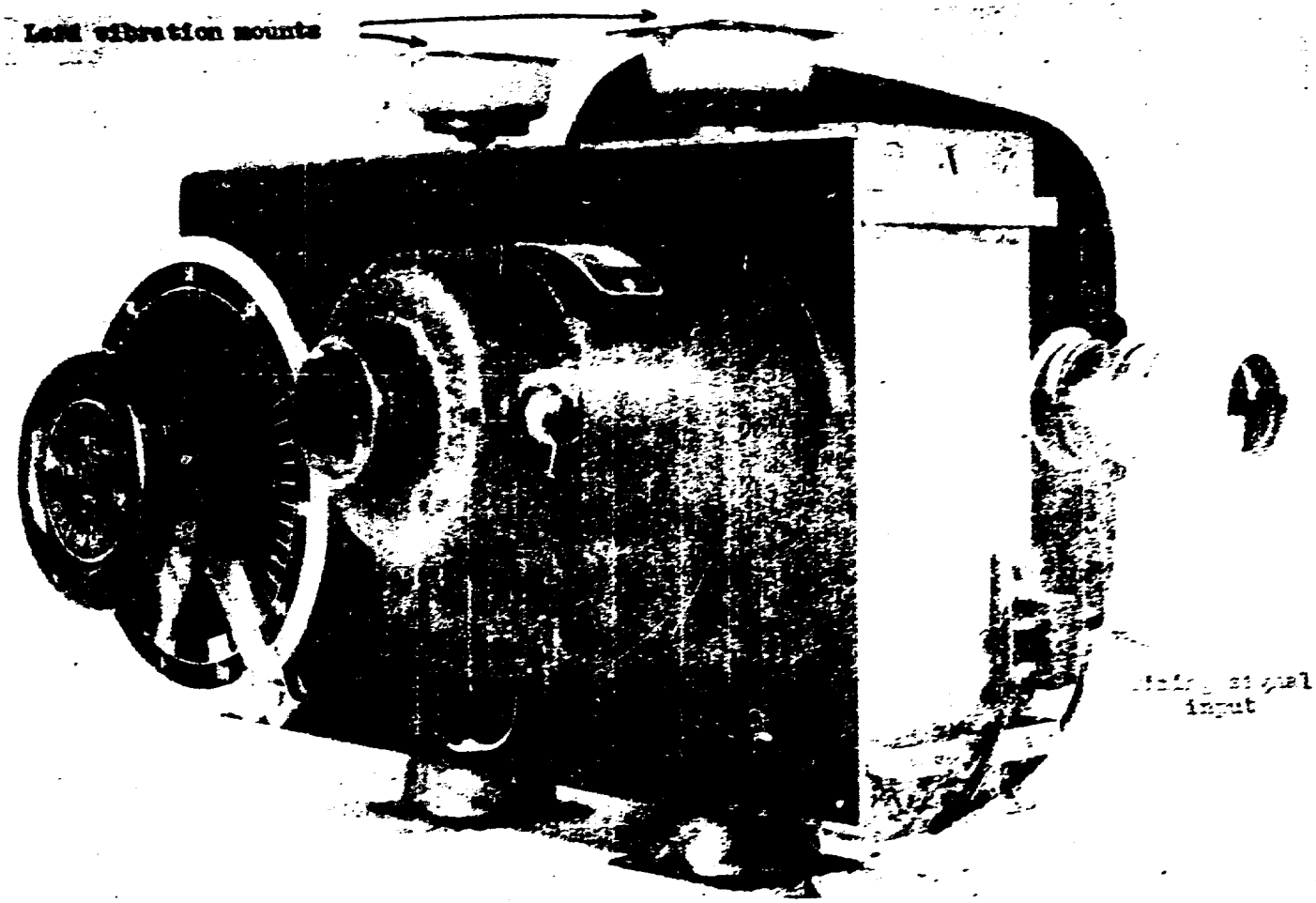
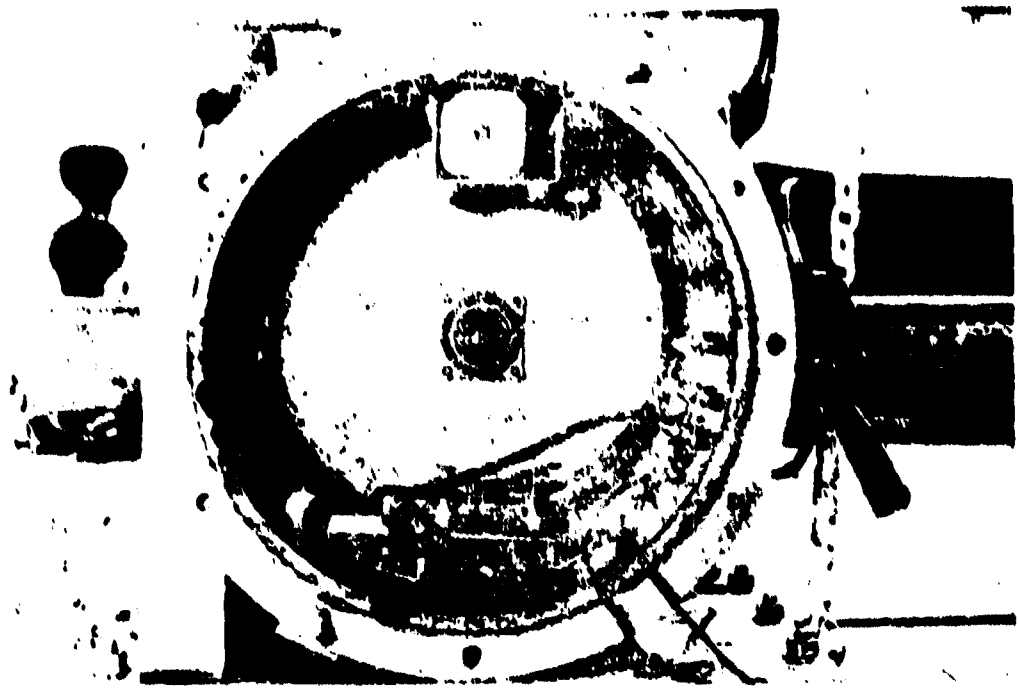
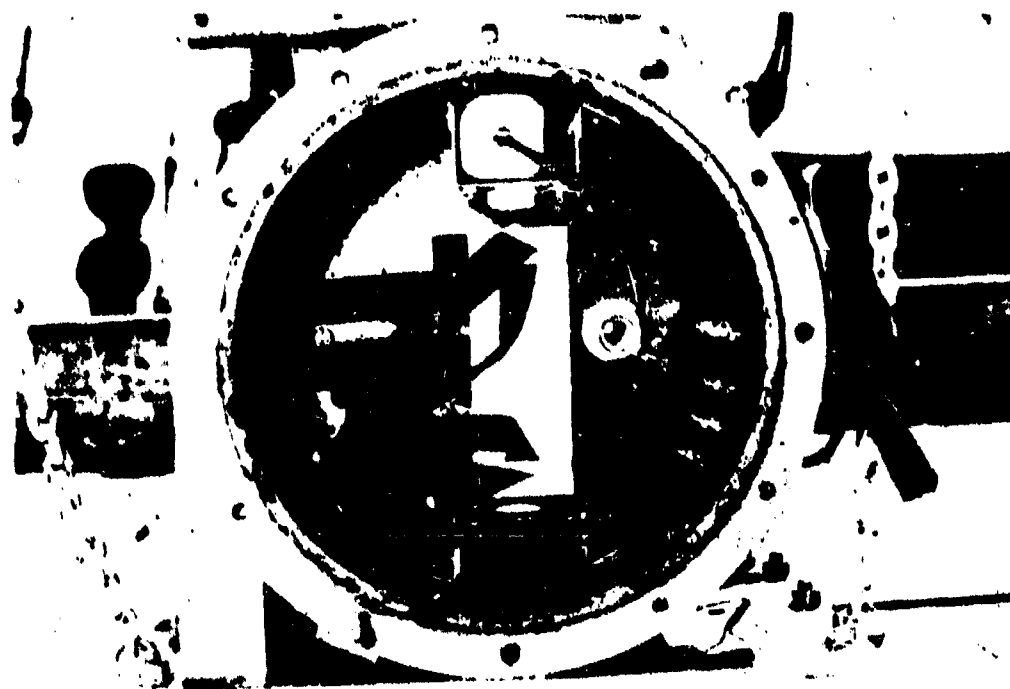


Fig. 12. Eastman high speed camera.



EMPTY CASE



CAMERA IN POSITION

FIG. 13

HIGH SPEED CAMERA AND "EXPLOSION PROOF" CASE

on the ends of the case prevent camera motion along the axis of the cylinder.

The case for this camera is made of standard 16 in. O.D. by 3/8 in. wall thickness steel tubing, and the ends are hot rolled steel 1 in. thick. We have never tested this case near its ultimate strength, but it was calculated that it would stand over 1000 lbs./in.^{2} static pressure and considerably more dynamic pressure of low time constant.

The high speed camera can be used at speeds up to 3000 frames per second. Due to the rotating four-sided prism that is interposed between the lens and the film, the ratio between exposure time and the time between frames is fixed at 1/4 and the minimum exposure time is 80 microseconds. Another effect of the optical system is that it requires long focal length lenses (63 mm minimum) with the result that the field of view is small (angle of view ca. 5°) at reasonable object distances. This feature is a drawback in underwater photography due to the further restriction of the field which results from the high index of refraction of water, and the severe limitations on object distances due to water turbidity.

(ii) Jerome camera. Figure 14 shows the Jerome 35 mm camera. This camera is of a conventional type, electrically driven, and is limited to speeds slower than 100 frames per second. The angular opening in the shutter is variable, so that exposures as short as one millisecond can be made. A 1 in. focal length lens was used to obtain the widest possible angle of view. The shock mounts shown in the figure engage tracks in the case.

(iii) Victor camera. Our first underwater movies were taken with an ordinary spring-wound 16 mm camera running at 64 frames per second, with an exposure time of approximately 1/130 second.

(b) Associated equipment for underwater photography.

(i) Underwater gear. One of the rigs used for photographing damage to cylindrical targets is shown in Figures 15 and 16. The photograph (Figure 15) shows the rig arranged for photographing by reflected light while the drawing (Figure 16) shows the set-up for silhouette. The parallel beams in this frame can be extended to obtain greater object distances. Figure 17 shows the firing circuit diagram.

(c) Light sources.

(i) Photoflash lamps. In order to increase the duration of the illumination used in these photographs, several photoflash lamps may be set off in sequence by means of the rotating commutator switch shown in Figure 18. The proper time interval to use between #31 photoflash lamps is 80-100 milliseconds. In the clear waters around the Bahamas, it was found that a good silhouette of a cylinder could be obtained at 2500 frames per second with the lens at f/11 using two #31 photoflashes 9 ft. from the camera.

(ii) Mercury Arc. The light source used with the Victor camera was a G. E. high pressure H-6 mercury arc. This proved satisfactory except that in a fair fraction of the experiments the light was extinguished by the shock wave. Furthermore the intensity is too low for high speed work, and 60 cycle fluctuation would be undesirable in short exposure pictures.

(d) Timers. -- Each camera is equipped with a small neon flasher which provides timing by marking the edge of the film at a frequency determined by tuning forks - 1000 cycles for the High Speed and 50 cycles for the Jerome. Circuit diagrams for the power supplies that operate these lamps are given in Appendix III.

(e) Power supply for cameras. -- The cameras must be brought up to speed gradually. The High Speed is equipped with an internal mechanism which cuts out a resistor and provides for gradual acceleration. The Jerome is accelerated by hand with a Variac. The High Speed requires about 1.5 kw (2 at starting) and the Jerome less than 1 kw.

990

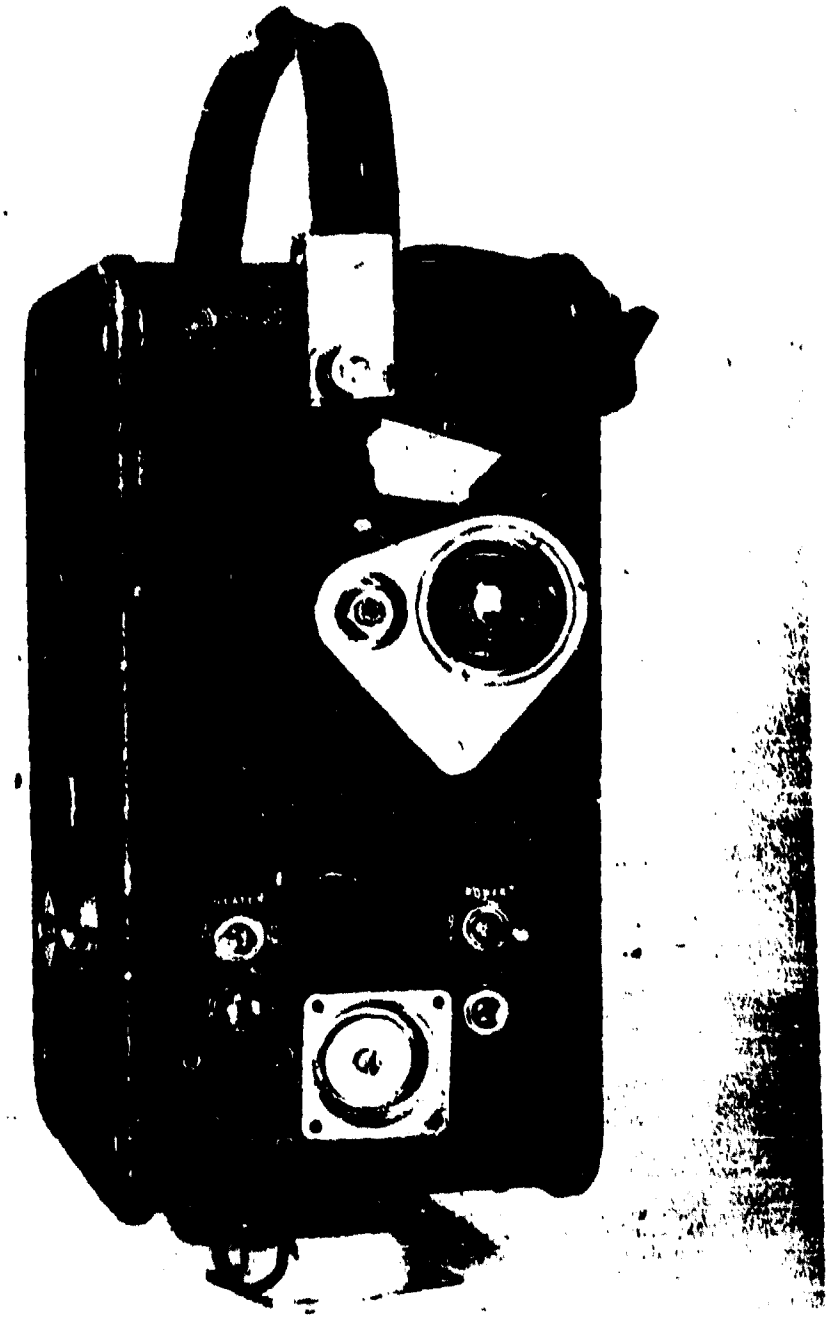


Fig. 14. Jerome camera showing shock mounts.

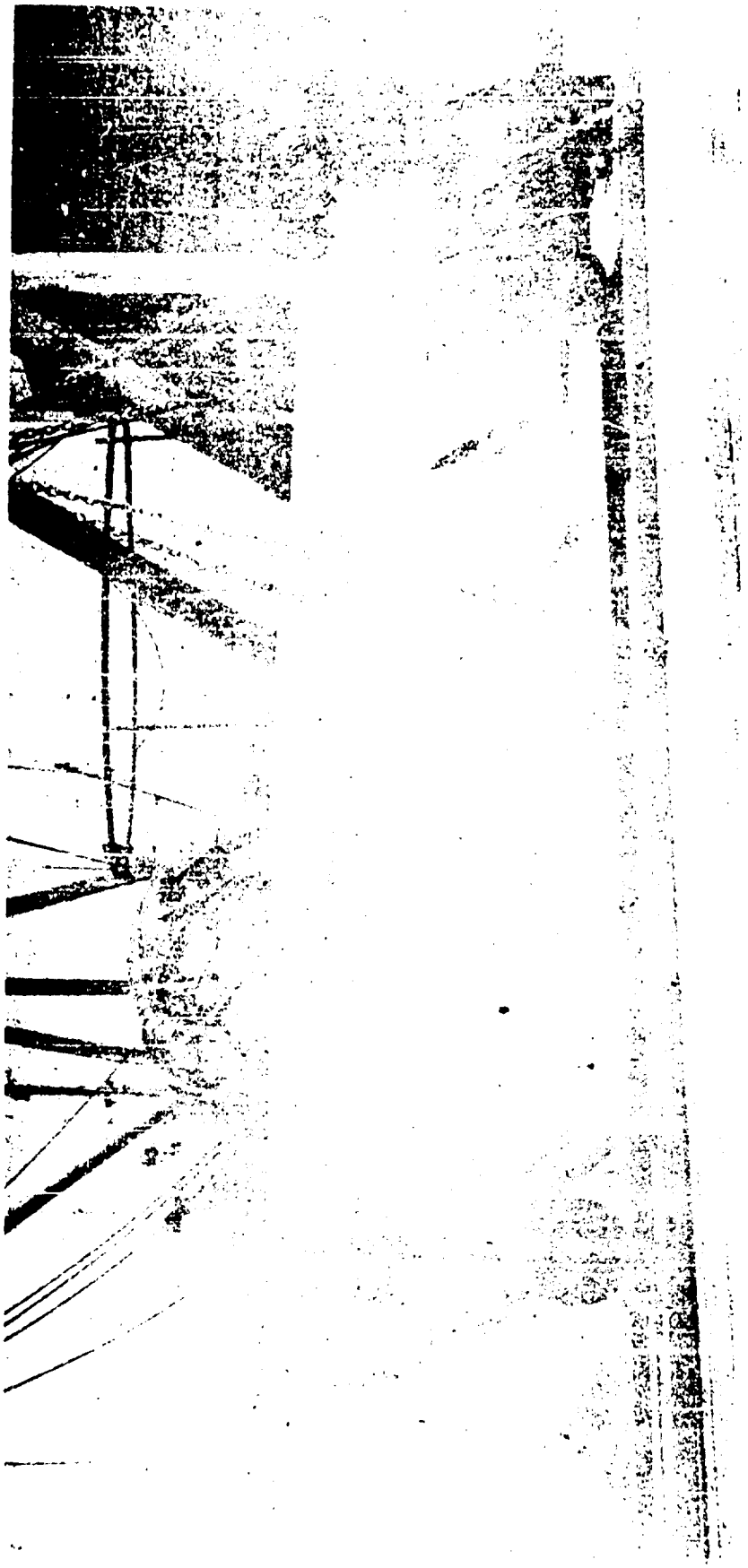
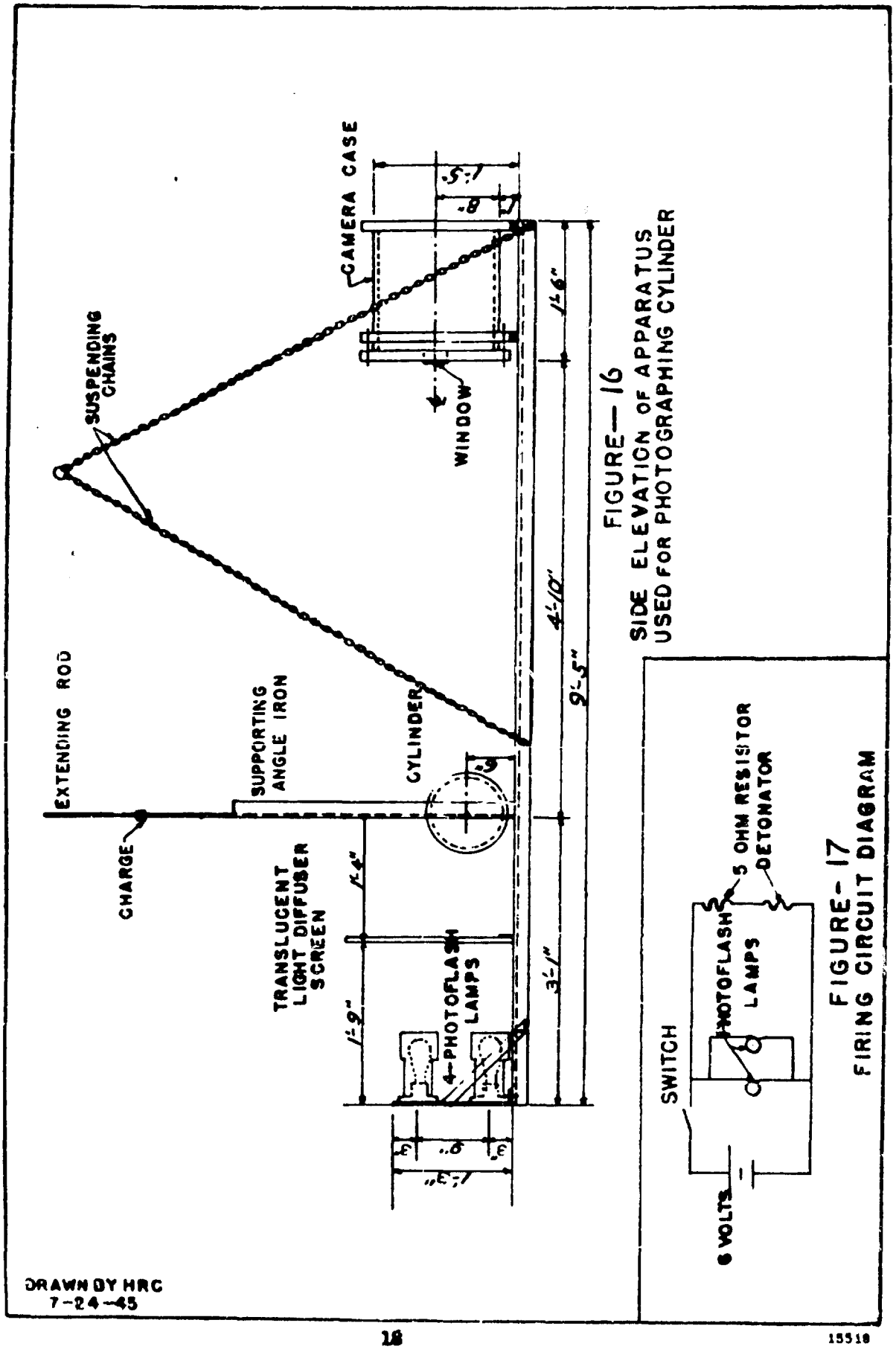


Fig. 15. Rig for high speed photography of cylinders.



FIGURE— 16
SIDE ELEVATION OF APPARATUS USED FOR PHOTOGRAPHING CYLINDER

FIGURE- 17
FIRING CIRCUIT DIAGRAM

15518

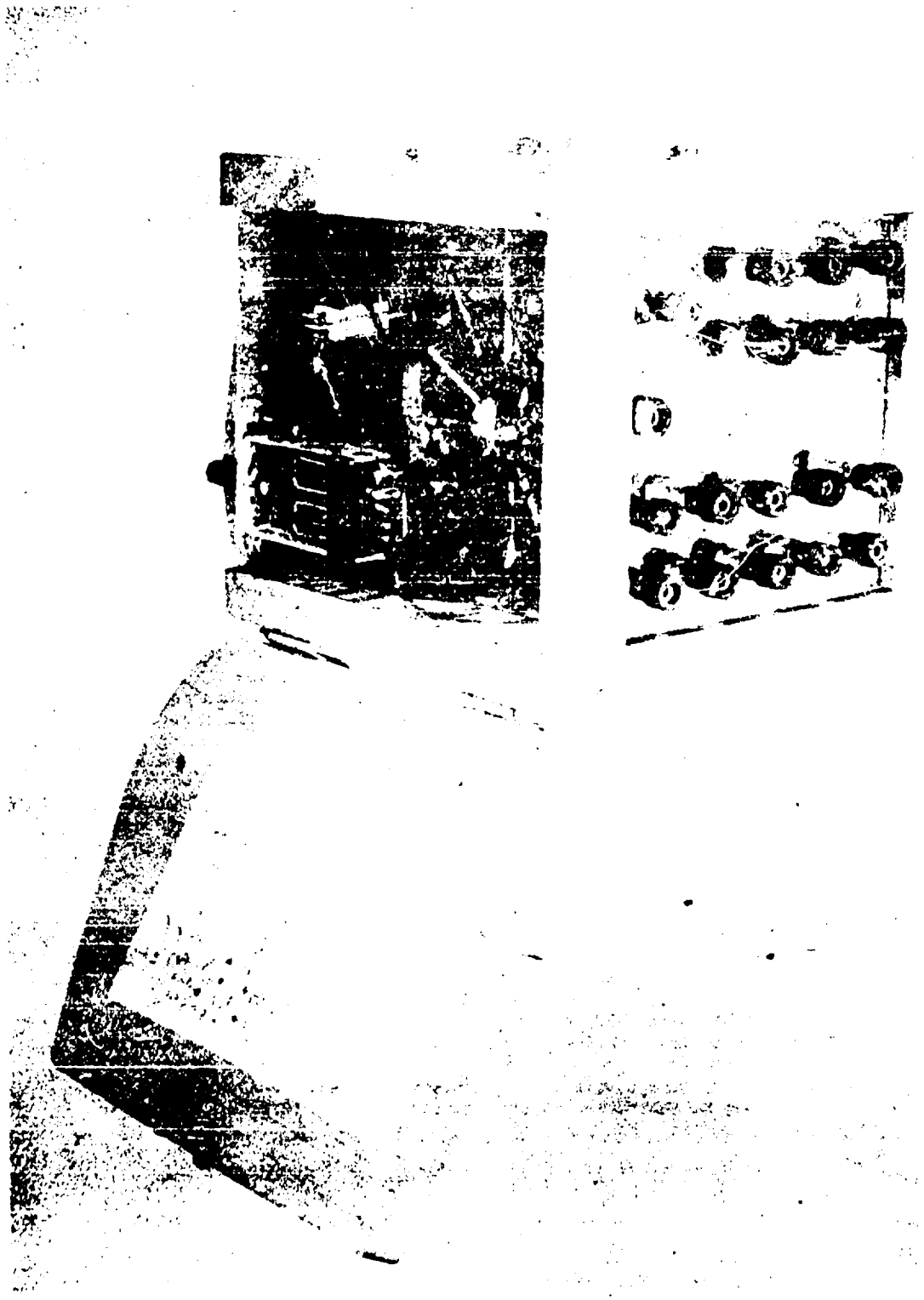


Fig. 18. Rotating commutator switch for firing photoflash lamps in sequence.

III. RESULTS OF EXPERIMENTS

1. Cavitation

Inasmuch as damage theories depend on the presence or absence of cavitation, it was considered important to investigate experimentally the more important factors influencing the production and decay of cavitation. The various divisions of this problem will be discussed separately.

(a) Minimum tension necessary to cause cavitation. -- While theoretical considerations lead to the expectation that very high negative pressures should be necessary to start cavitation in extremely pure (nucleus-free) water, it can be demonstrated that if bubbles or particles of radius r_b are present, cavitation should appear at $P = -2s/r_b$, where s is the interfacial tension between water and the particle. Inasmuch as seawater contains numerous suspended particles, some of considerable size, cavitation might be expected at small negative pressures (tensions).

In order to determine the minimum tension required for cavitation in seawater, the following experiment was carried out: A weak shock wave impinged on an air-backed cellulose acetate diaphragm 0.02 in. thick and 6 in. in diameter. At a known time after impact a photograph was taken and the position of the cavitating region noted. From the curves given in Appendix I, the tension was estimated at the minimum distance from the diaphragm at which cavitation occurred, since the magnitude of the tension is a direct function of the distance from the diaphragm, this value gives the minimum tension necessary for cavitation. It is possible that lower values can be found under other conditions.

Figure 19 shows cavitation in front of such a surface when a 10 gm charge of loose tetryl was fired 24 in. from the diaphragm. The peak pressure 24 in. from this charge is estimated to be 2700 lbs./in.^{2}. The charge used in making Figures 20, 21, and 22 was a three-foot piece of primacord stretched in a straight line perpendicular to the diaphragm at its center. For Figure 20 the closest end of the primacord was 8 in. from the surface of the diaphragm, in Figure 21 it was 10 in. and in Figure 22 it was 20 in. The peak pressures p_o in the shock fronts at the target are estimated to be 1100, 900, and 450 lbs./in.^{2} respectively. The letters A and B mark the positions of the primary and reflected shockwaves respectively as observed in the original negatives. It will be noted that cavitation is visible in all four pictures.

The theory of Appendix I has been used to estimate the pressures in the water in front of the diaphragm. This simple theory assumes that the shock front is planar, that the diaphragm acts as an incompressible free plate of infinite extent, and that the region ahead of the cavitation front is unaffected by the presence of the cavitation.

Cavitation is observed at least as close to the diaphragm as 1/8 in. From Figure 131 (Appendix I) it is estimated that the pressure at this point ($X = 0.04$) never falls below $P = 0.1$ or $p = -0.1\ p_o$. In the case photographed in Figure 22 this means, according to this theory, that the tension p near the diaphragm never exceeded 45 lbs./in.^{2}. We therefore conclude that cavitation in seawater can occur at 45 lbs./in.^{2} (or even less) on the basis of this interpretation of the experiment. Since the maximum tension possible in this experiment on any theoretical basis is 450 lbs./in.^{2} we conclude that this value represents an upper limit for the required tension. These values are estimated relative tensions, from which about 18 lbs./in.^{2} must be subtracted to correct for atmospheric plus hydrostatic pressure.

(b) Criterion for cavitation in front of a steel diaphragm. -- Kirkwood 5/ has

---

5/ The Plastic Deformation of Marine Structures by an Underwater Explosion Wave II, John G. Kirkwood, OSRD-1115, Serial No. 450, December 9, 1942.

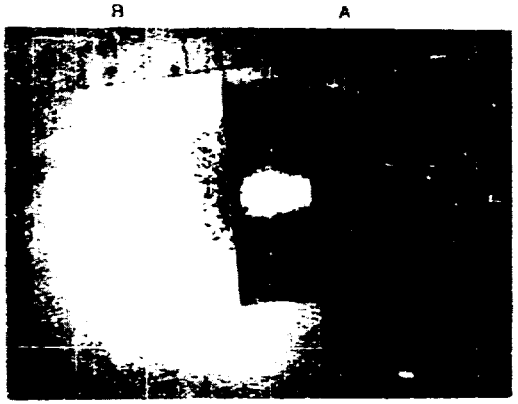


Fig 19

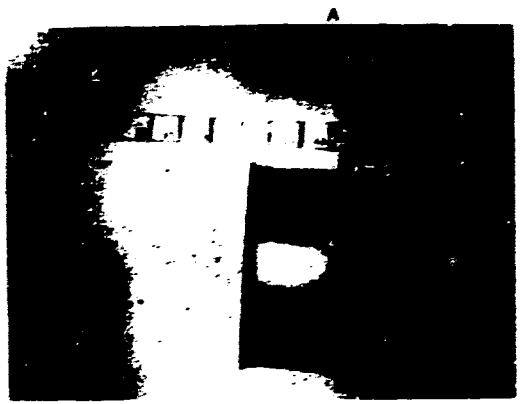


Fig 20

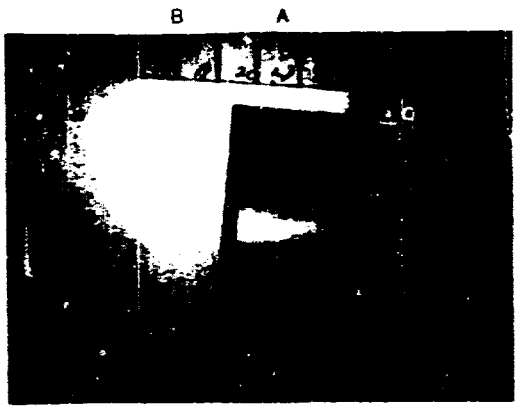


Fig 21



Figs 19-22 Cavitation produced by weak shock waves

A= Initial shock wave B= Reflected shock wave

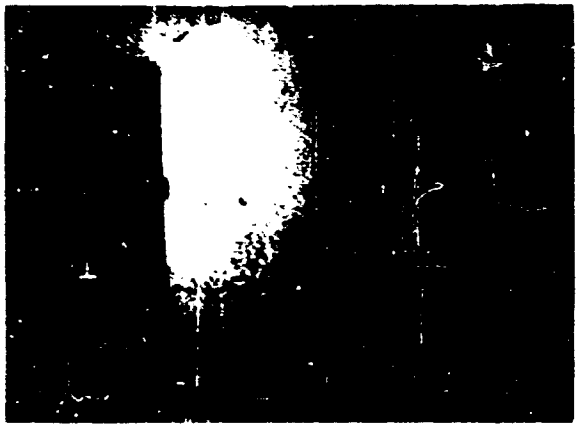


Fig 23

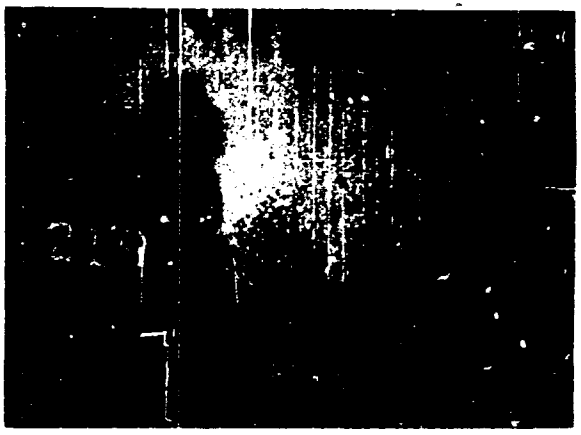


Fig. 24



Fig 25



Fig. 26

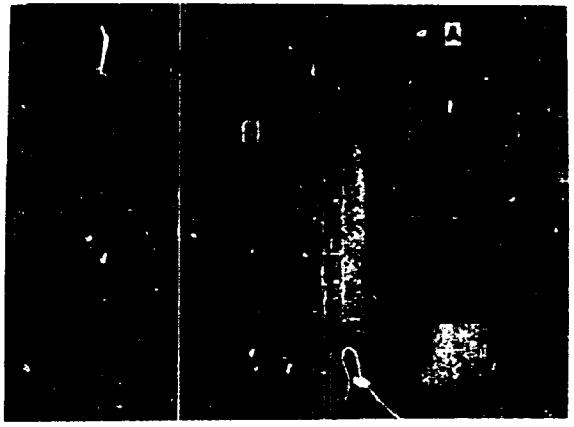


Fig. 27



Fig. 28

Figs. 23-28. Cavitation from circular diaphragms fixed at the edges.
A = Initial shock wave B = Reflected shock wave

postulated (See Appendix I) that cavitation at a particular point in front of the diaphragm will occur only if the cavitation time θ_c is less than the time for the diffracted wave to come in from the edge of the diaphragm and that the cavitation time can be calculated for an infinite rigid free plate by

$$\theta_c = \frac{\theta\,\theta_1}{\theta - \theta_1} \ln \frac{\theta}{\theta_1}$$

in which θ is the time constant of the shock wave and $\theta_1 = m/\rho c$, m being the mass per unit area of the plate, ρ and c the density and sound velocity of water, respectively. In order to test this hypothesis, two series of photographs were taken.

In one series, shock waves were reflected from a deformable steel diaphragm, the center of which should approximate the motion of a free plate in the initial part of its motion. In the other series, a closer approximation to a true free plate was made by supporting a steel disk on a weak backing of cellulose acetate or shim brass, and in a few pictures there was no support for the steel plate.

Figures 23, 24, 25, 26, and 27 show UERL diaphragm gages being damaged under the conditions given in Table I. The table shows that cavitation occurs only when θ_c is less than R/c, where R is the radius of the diaphragm. In a few cases, no cavitation occurred under this condition, but the condition was satisfied by only a slight margin. In Figure 25 the cavitation region does not extend back to the diaphragm. This is thought to be due to the increase in pressure caused by "reloading" or deceleration of the diaphragm.

The target used to obtain Figure 28 was a 0.013 in. thick steel diaphragm soldered over the mouth of a 6 in. pipe. Five other photographs were taken of similar targets in which the only experimental condition changed was the time lapse after impact of the shock wave from the 50 gm charge at a distance of 12 in. Cavitation occurred in all pictures except one in which this time lapse was approximately 8 μsec, whereas the calculated cavitation time (θ_c) is 6 μsec.

Figure 29 is a drawing of the target used in the second series of photographs to give a closer approximation to a free plate.

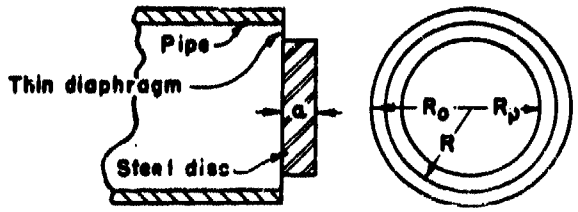


Figure 29. Target simulating free plate.

Typical photographs of cavitation from such a target are Figures 30, 31, and 32. Using this target, it is found that the position of the cavitation front is very close to the region of zero pressure calculated by the method of Appendix I.

Measurements were also made of the radius R_c of the cavitation region and of the maximum perpendicular distance from the plate that cavitation occurred, x_c. The time after impact at which the picture was taken, t_c was calculated from the value of x_c b/. These values are shown in Table II, together with the corresponding time

---

b/ The equation for this was developed from the theory of Appendix I.

$$t_c = \frac{\theta}{\beta - 1} \ln \frac{2\beta \cdot e^{\beta x_c/c\theta}}{(\beta + 1) \cdot e^{x_c/c\theta} - (\beta - 1) \cdot e^{-x_c/c\theta}}$$

where $\beta = \theta/\theta_1$

998

TABLE I. Cavitation data for steel plates in UERL diaphragm gage.

Fig. No.	Film No.	Charge Weight (gm)	Charge Distance (in.)	θ (μsec)	Plate Thickness (in.)	Cavitation Time θ_c (μ sec)	R/c (μ sec)	Cavitation Observed?
	2	50	12	35	0.013	6	29	yes
	3	50	14	35	.013	6	29	yes
23	1	50	24	40	.025	8	29	yes
	218	50	24	40	.040	12	29	yes
24	219	50	24	40	.039	12	29	yes
	220	500	48	80	.038	15	29	yes
	5	50	12	35	.074	17	29	yes
25	19	250	30	55	.073	20	29	yes
26	70	250	36	55	.076	20	29	yes
27	24	50	12	35	.156	28	29	no
	23	250	30	55	.156	34	29	no
	4	50	12	35	.500	45	29	no
	21	75	12	40	.500	48	29	no
	22	75	12	40	.500	48	29	no
	31	75	12	40	.500	48	29	no

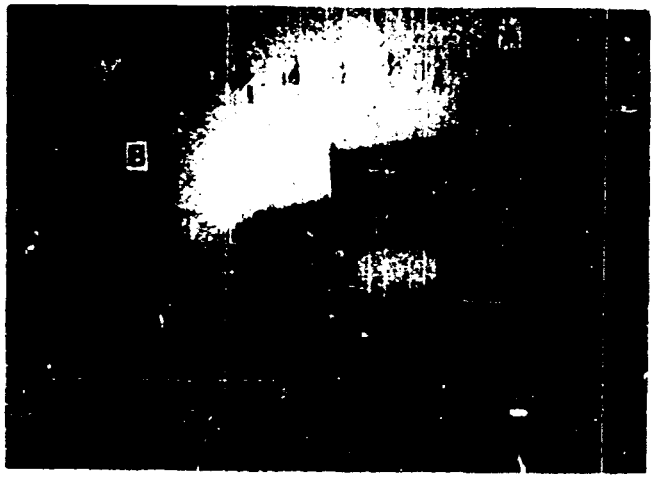


Fig. 30



Fig. 31

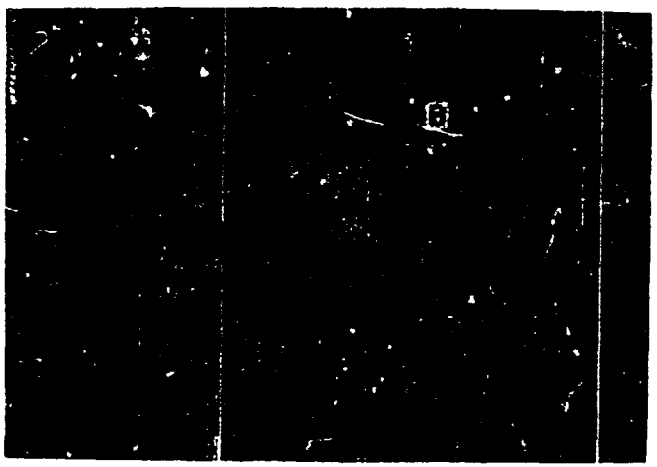


Fig. 32

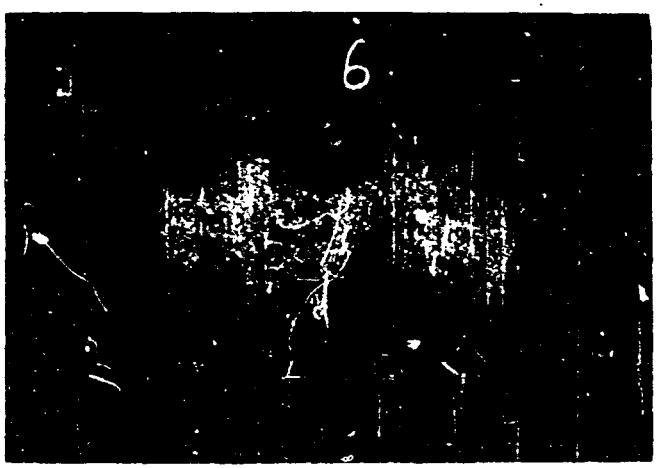


Fig. 33

Figs. 30-33. Cavitation from "free" plates.

A= Initial shock wave B= Reflected wave

t_s found from the shock wave position. The radius of the cavitation region R_c was also calculated and the values are shown in Table II together with the measured values. In the calculation it was assumed that cavitation takes place only in the region where the pressure drops to zero before the compressional diffraction wave from the edge of the plate arrives.[1]

It is assumed that once cavitation appears, it persists for some time after the diffraction wave from the edge of the plate has reached it. (See Section III, 1, d.) The rather good agreement of the calculated and observed results for both sets of values argues that the assumptions made in the calculations, including the low value for the tension necessary for cavitation, are roughly correct.

The target used to obtain Figure 33 was an essentially completely free plate which is illustrative of several experiments. A small can filled with air was hung with its open end down and the disk was supported at the air-water interface on small clips which offered no resistance to its motion. The fact that no essential difference is shown between these experiments and the type illustrated by Figure 29 indicates that plates mounted as in Figure 29 were essentially "free" plates.

(c) Cavitation from objects other than plane surfaces. -- A single photograph of an early UERL cylinder taken 200 μsec after impact of a shock wave from a 65 gm tetryl charge 30 in. distant showed a considerable region of cavitation. This is seen in Figure 34; the cylinder is not shown because of the restricted field of view. The cylinder axis is parallel to the plane of the photograph and the top edge of the cylinder is in view at the lower edge of the picture. Figure 35 shows cavitation off the side of a 4.5 x 5 x 0.011 in. paint can 129 μsec after being damaged by a 25 gm charge 48 in. away.

Figures 36, 37, and 38 demonstrate that no cavitation occurs when a 1/4 in. piezoelectric gage, or a Hartman type momentum gage or a 5 x 5 in. cylinder of steel is hit by a shock wave from 250 gm of tetryl at 30 in.

(d) Disappearance of cavitation. -- If the cavitation bubbles consist simply of water vapor, it seems hard to understand why these bubbles persist for long times after the pressure has returned to the hydrostatic level. In an attempt to cast some light on this problem, a series of experiments was performed in which cavitation was allowed to disappear spontaneously, while, in another series, auxiliary shock waves were passed into the cavitation region.

Figures 39, 40, 41, 42, and 43 show a series of photographs in each of which a 0.002 in. brass diaphragm supported by a 6 in. pipe was ruptured by a 25 gm charge 12 in. away. The picutres are taken at different times after the impact as shown. The finest bubbles begin to disappear by 125 μsec and there is only a trace of cavitation left at 400 μsec.

Figures 44, 45, 46, 47, 48, and 49 show the effect of an auxiliary shock wave. The auxiliary charge, data for which are given in Table III, is detonated at the same time as the charge causing cavitation either by means of primacord or the simultaneous cap method. It may be seen that increase in the pressure of the auxiliary shock wave results in more effective destruction of the cavitation, that increase in time constant has but little effect, and that the large bubbles are much more resistant than the fine bubbles.

(e) Cavitation caused by oblique reflection of shock waves from air-water interfaces. - Experiments were performed to discover whether there was a critical angle of reflection from a water-air interface beyond which no cavitation would occur. The

---

[1] In computing the time at which the diffraction wave relieves the tension in front of the plate, it must be remembered that the front of the diffraction wave may actually reduce the pressure in front of the plate and only in later stages raise it, since initially the pressure is higher in front of the plate than in the surrounding water. It is only when the plate is surrounded by an infinite baffle that the diffraction wave is always positive relative to the existing pressure.

Table II. Summary of results of studies of cavitation from simulated free plates.

Fig. No.	Film No.	Inside Radius of pipe (in.)	Thickness of disk (in.)	Radius of disk (in.)	Charge Weight (g)	Charge-plate distance (in.)	Time Constant of Shock Wave θ (microsec)	$\theta/\theta_{25/24}$	R_c(calc) (in.) radius of cavitation region	R_c(obs.) (in.)	x_c(obs) (in.) Length of cavitation region	t_c(calc) (microsec)	t_c(obs) (microsec)
	77	2.78	.154	1.65	25	24	32	1.59	1.98	1.5	2.0	47	48
	79	"	"	"	150	"	44	2.19	1.78	1.5	2.4	56	53
30	80	"	"	1.00	"	"	44	2.19	1.78	1.9	2.6	58	59
	83	1.78	"	1.65	25	12	24	1.20	1.12	1.1	1.8	42	46
31	85	"	"	"	150	24	44	2.19	0.78	0.6	3.2	69	76
32	88	2.63	.255	2.33	"	"	44	1.33	1.46	1.1	1.25	47	48
	93	1.55	.154	1.38	"	"	44	2.19	0.55	0.3	---	?	66
	95	1.55	"	"	250	"	51	2.54	0.46	None	---	No Cav.	74
	97	1.79	.382	1.66	150	"	44	0.88	0.48	0.3	1.8	59	67
	99	"	"	"	"	"	44	0.88	0.48	0.5	2.5	72	81
	100	1.55	.190	1.38	"	"	44	1.78	0.48	0.3	2.4	58	59
	201	2.63	.502	2.47	25	12	24	0.37	1.80	1.1	3.0	78	78
	202	1.80	.382	1.76	250	24	51	1.02	0.33	0.2	2.8	76	85
	203	1.55	.190	1.34	"	"	51	2.06	0.37	None	---		
	204	1.80	1.06	1.63	"	"	51	0.37	0.04	None	---	No Cav.	96
	214	1.60	0.150	1.55	25	12	24	1.20	0.95	0.90	2.2	48	54
33	216	"	"	"	"	"	24	1.20	0.95	1.0	1.2	41	38

Table III. Experimental conditions applying to the photographs of Figs. 39 - 49.

Target, .002 in. air-backed brass diaphragm over end of 6 in. pipe.
Cavitation produced by 25 g loose tetryl charge.
Distance from target to cavitation producing charges, 12 in.

Figure Number	Auxiliary charge and shock-wave data				Approximate time interval between impact of cavitation producing wave and picture (microsec)
	Charge Weight (g)	Charge to shock wave distance (in.)	Calc. Peak pressure (lb/in.^{2})	Calc. time constant (microsec)	
39	None				75
40	None				125
41	None				175
42	None				225
43	None				400
44	25	20.5	4400	30	125
45	150	40.	4000	49	235
46	150	35.	4600	48	125
47	250	44.	4400	60	125
48	250	14.5	13000	45	125
49	25	35.5	2500	35	90

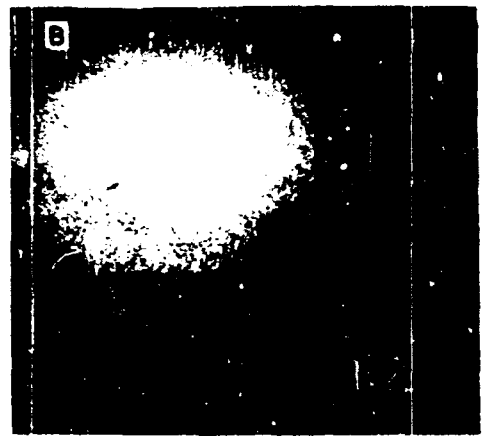


Fig. 34

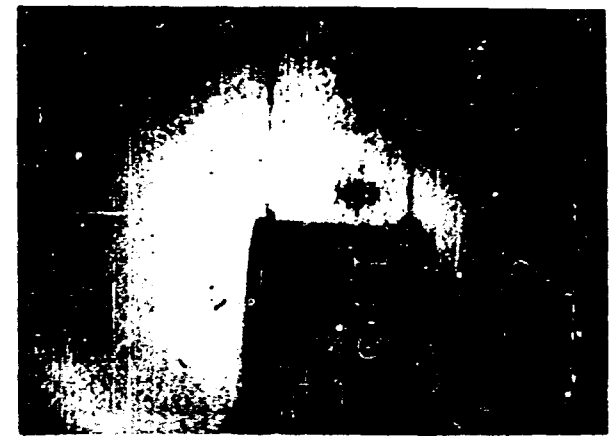


Fig. 35

Cavitation about collapsing cylinders

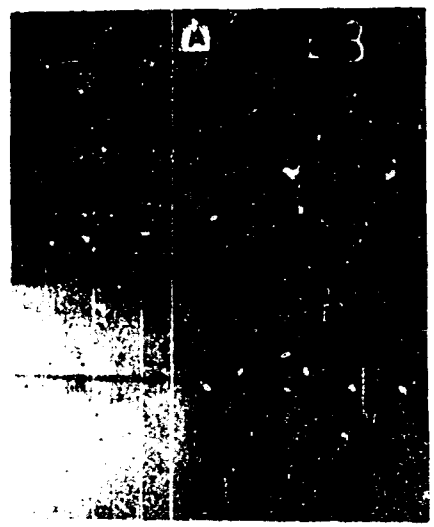


Fig. 36
Piezo electric gauge



Fig. 37
Momentum gauge

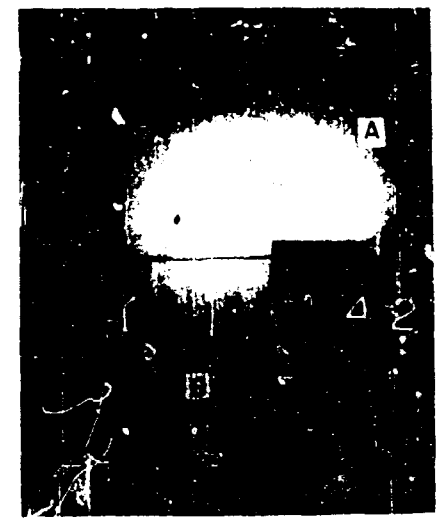


Fig. 38
Steel block

A= Initial shock wave B= Reflected wave

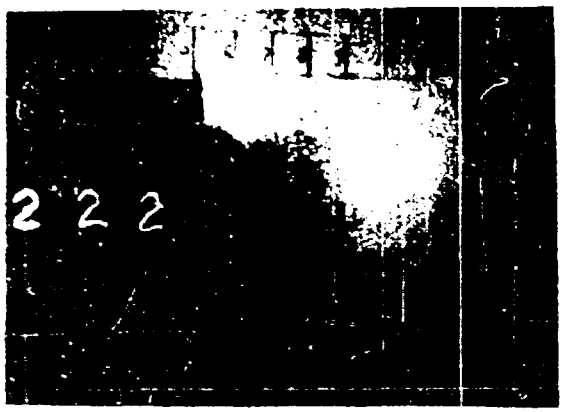


Fig 39
75 Microseconds

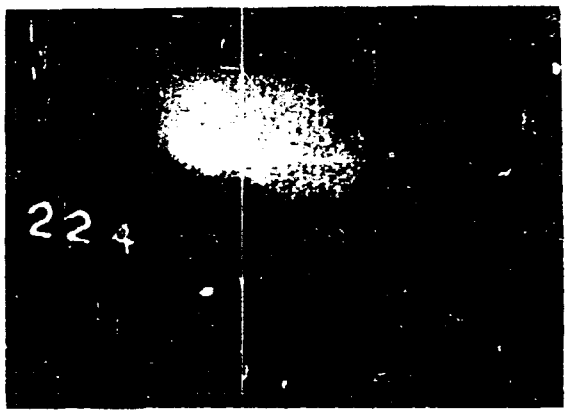


Fig. 40
125 Microseconds



Fig 41
175 Microseconds



Fig. 42
225 Microseconds

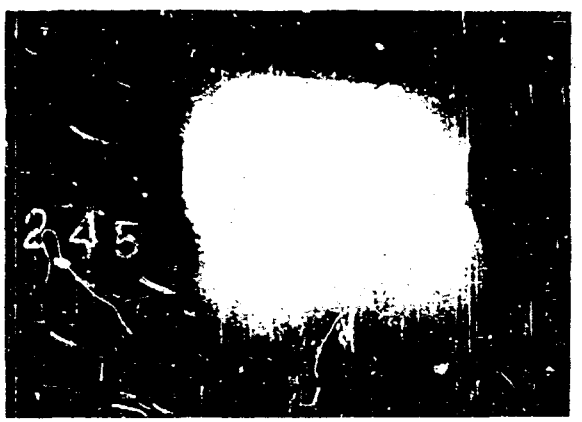


Fig 43
400 Microseconds

Figs 39-43 Spontaneous disappearance of cavitation at various times after impact of shock wave.

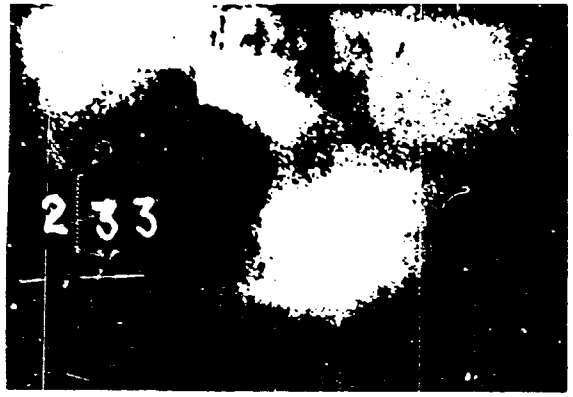


FIG. 44

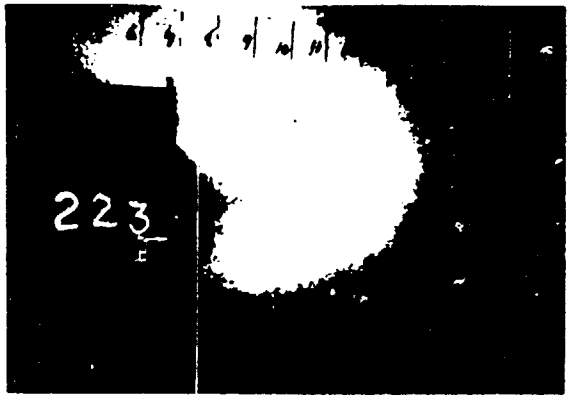


FIG. 45

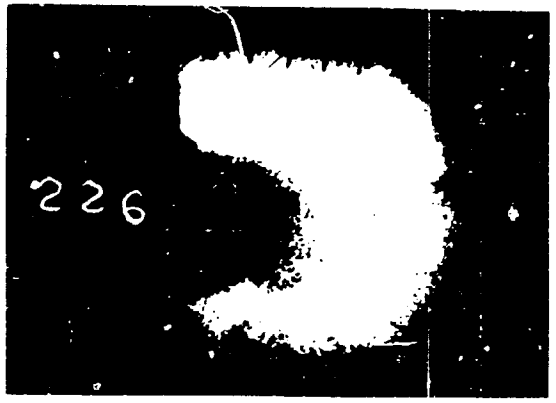


FIG. 46



FIG. 47



FIG. 48

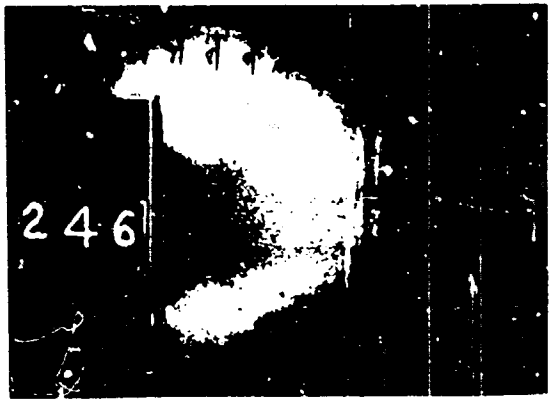


FIG. 49

DESTRUCTION OF CAVITATION BY SHOCK WAVES

[EXPERIMENTAL CONDITIONS IN TABLE III]

water-air interfaces were provided by filling with air to hydrostatic pressure a 6 in. pipe open on the bottom as shown in Figure 50. Other experiments were carried out substituting a 20 x 10 in. sheet metal trough for the pipe, and finally by using the surface of the sea on a calm night. It was found that such a critical angle existed and was greater for greater size of surface.

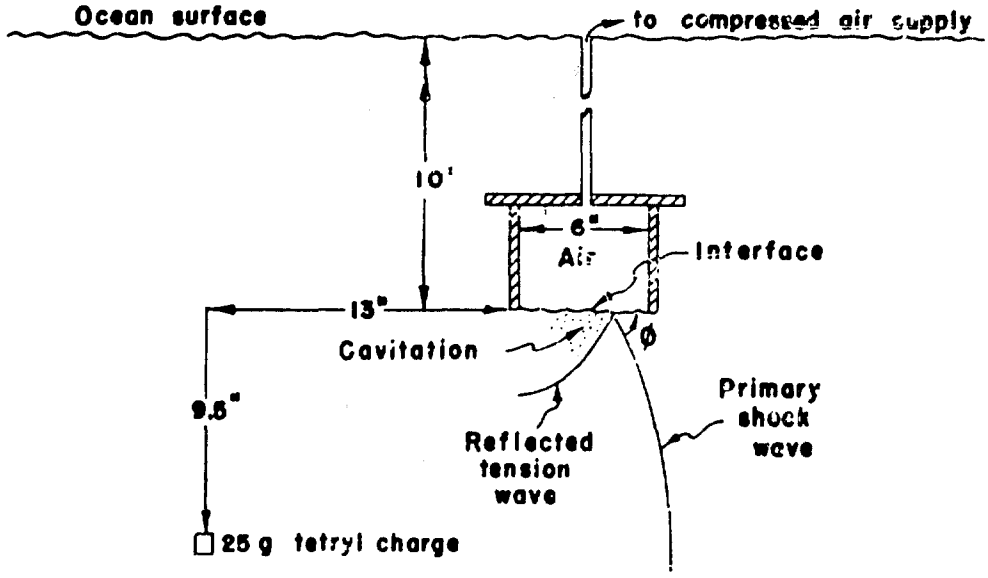


Figure 50. Sketch showing experimental arrangement for Figs. 51 - 56.

The results of the experiments with the six in. pipe are listed in Table IV, and six representative pictures are shown in Figures 51, 52, 53, 54, 55, and 56. The critical angle is about 70° for the conditions of these experiments.

Table IV Data of Experiments on Oblique Reflection of Shock Waves from Water-air Interfaces

Fig. No.	Film No.	Charge Weight (gms)	Distance, Charge to Shock Front (in.)	Angle of Incidence ϕ (degrees)	Estimated Peak Pressure (lbs/in.^{2})	Cavitation ?
51	256	25	23 1/2	0	3700	yes
52	270	250	45	45	4200	yes
-	258	25	22 1/2	50	3900	yes
-	261	25	19 1/2	56	4500	yes
53	264	25	19 1/2	62	4500	yes
54	265	250	45 1/2	69	4100	no
55	259	25	21	70	4200	no
-	267	25	20 1/2	71	4300	?
-	269	250	46	71	4100	no
56	257	25	23	90	3800	no

With the large trough, pictures have been taken up to 80° and, using the surface of the ocean, up to 83°. Cavitation was present in all cases, although it was much fainter at the larger angles. See Table V for complete data and Figures 57, 58, 59, and 60 for typical examples.

Table V. Data of experiments on oblique reflection of shock waves from 20 in. by 10 in. water-air interface, and from ocean surface.

Fig. No.	Film No.	Charge Weight (g)	Charge below surface (in.)	Charge-to-shock front (in.)	Estimated peak pressure at time of photograph (lb./in.^{2})	Angle of incidence (degrees)	Surface	Qualitative description of cavitation
57	281	25	6	20	4400	73	Trough	Heavy
	282	25	4	24	3800	81	"	Heavy (Fig. 58)
58	283	250	12	45	3700	75	"	Heavy
	284	250	8	46	3600	80	"	Light (Fig. 59)
	285	25	12	45	2000	75	"	Heavy (Fig. 57)
	286	25	12	50	1800	76	"	Moderate (Fig. 60)
59	288	25	12	68	1300	80	"	Light
	289	25	12	70	1300	80	"	Moderate (Fig. 60)
	297	25	12	73	1200	81	Ocean	Moderate (Fig. 60)
	401	25	8	75	1200	84	"	Light (Fig. 60)
60	402	25	14	74	1200	79	"	Moderate

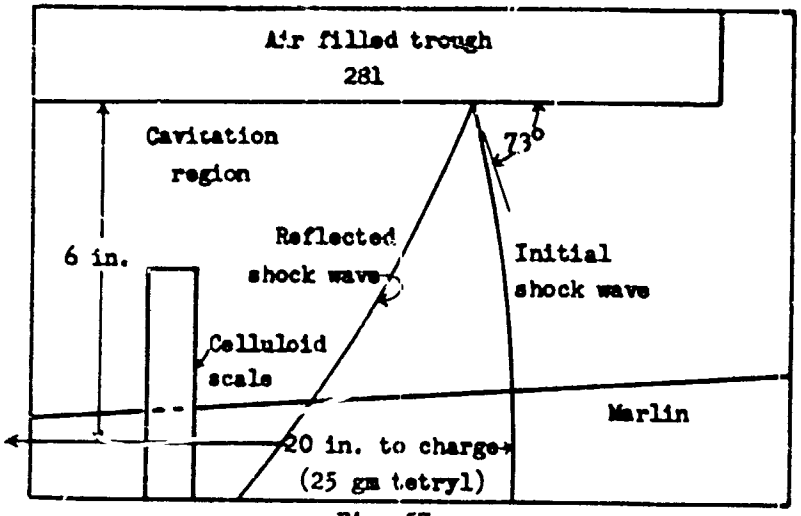


Fig. 57.

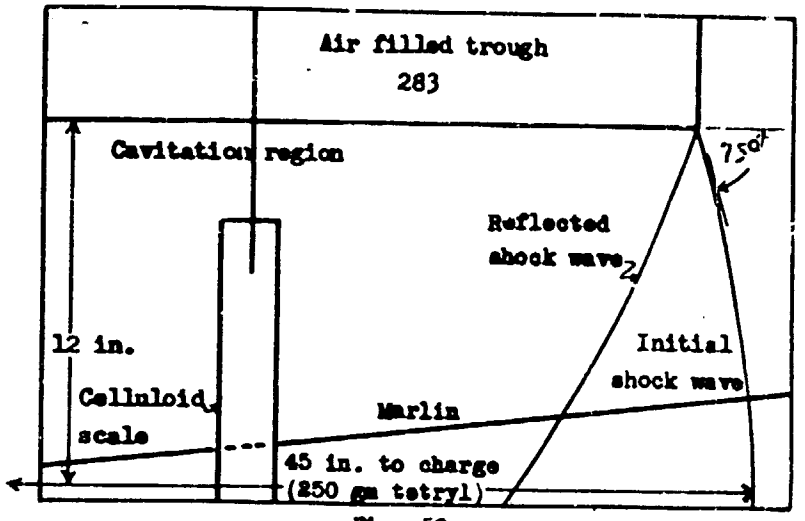


Fig. 58.

Celluloid scale - 1 in./unit

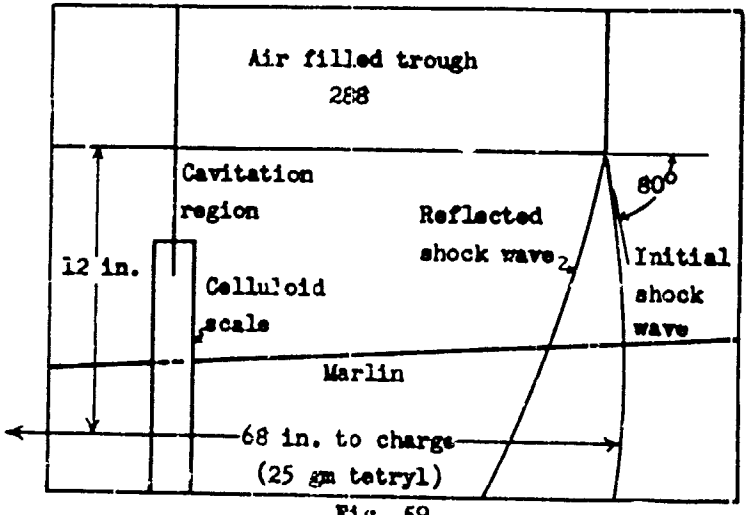


Fig. 59.

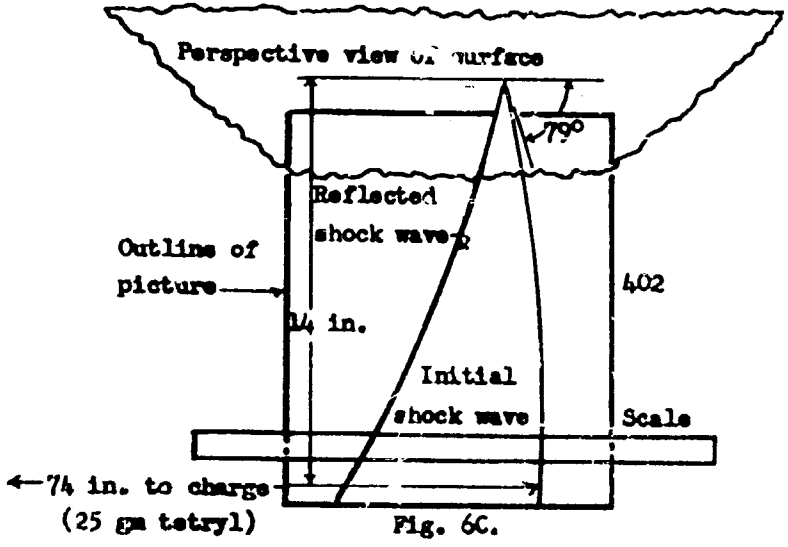


Fig. 60.

Schematic diagrams of Figs. 57, 58, 59, and 60.

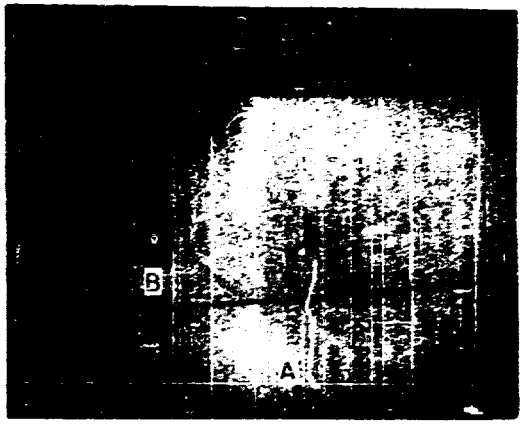


FIG. 57

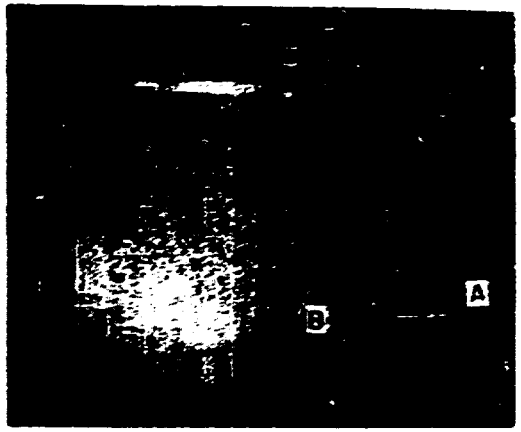


FIG. 58

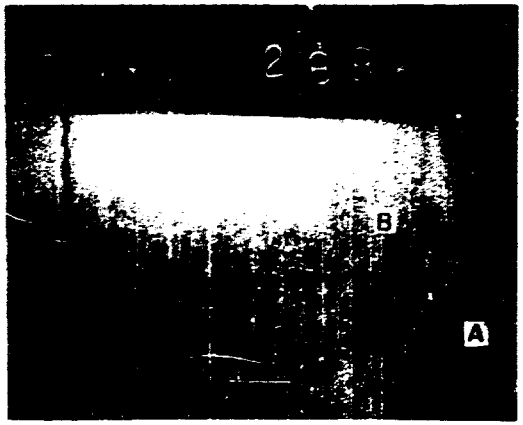


FIG. 59

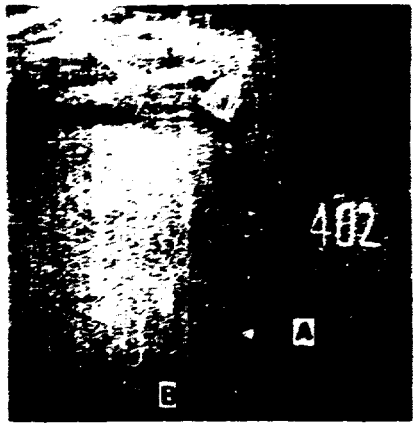


FIG. 60

CAVITATION PRODUCED BY OBLIQUE REFLECTION OF SHOCK WAVES FROM WATER-AIR INTERFACES.

A= Initial shock wave B= Reflected wave

2. Investigation of the effect of shape of charge and point of detonation on shock wave and bubble

Photographs (reproduced in Figures 61 to 103) of the shock wave and bubble surrounding spherical, cylindrical and conical charges weighing approximately 1/2 lb. have been taken at intervals ranging from 10 to 200 microseconds after the initiation of detonation at various points in the charges. It has been found that the shock wave tends rapidly to become spherical after it leaves the charge. A graph (Figure 105) giving bubble size as a function of shock wave radius for spherical charges of this type is also included.

The charges were all of cast pentolite and were bare except for a waterproof coating. The cylinders were cast in the following length-to-diameter ratios (keeping the weight constant): 1:1, 2:1, 4:1, 8:1. The cones were of the same weight as the cylinders and were equilateral. Timing of the detonation of the main charge and the flash charge was accomplished by the simultaneous firing of two No. 8 seismographic (SSS) DuPont caps connected in series, the delay interval being determined by a suitable length of primacord extending from one cap to the flash charge; the other cap was inserted in a well provided in the main charge. One cylinder of each shape was detonated at the center and another at one end. Of the cones, one was detonated at the apex, another at the center of the base and a third at the "center" defined as the point equidistant from the base and the conical wall. As control tests, photographs at the same time intervals were taken of cast pentolite spheres of the same weight and detonated from the center.

The experimental set-up for these shots consisted simply of the main charge, the flash charge, the camera, and occasionally a translucent diffusing screen. The main charge was suspended in front of the camera by strings cast in the charge; the flash charge was mounted on the line from the camera to the main charge, and behind the main charge as viewed from the camera. The diffusing screen, when used, was mounted between the flash charge and the main charge. For the 10 and 50 microsecond series, the distance from the camera to the main charge was about 60 in.; the distance from the main charge to the flash charge was about 24 in. For the 100 microsecond series, the distances were about 76 in. and 32 in. respectively, and for the 200 microsecond series, the distances were about 112 in. and 46 in. respectively.

In some of the spherical charge control shots, two straight steel rods 3/8" in diameter and about 6 ft. long were mounted perpendicular to the camera-charge axis and in the plane of the center of the main charge; the ends of these rods pointed toward the charge and were placed so as to be just outside the bubble at the instant of the photograph (Figures 62 - 64). Knowing the distance between the two ends, it was possible to obtain an estimate of the optical distortion of the bubble. The rods were sufficiently long so that the shock wave in the rod had not reached the far end of the rod at the instant of the photograph; hence, motion of the near end of the rod could not occur up to the instant of the photograph except by elastic compression of the rod. This amount is well under 0.1 in. in all cases. The ends of the rods were calculated from the photograph to be about 9% (2 to 8%, farther apart than they actually were which indicates that the diameter of the bubble must have been magnified by the shock wave by this amount.

The photographs are reproduced in Figures 61 to 100. The 50, 100 and 200 microsecond series are complete; the 10 microsecond series is not complete, but the pictures which are available for this time interval are presented and also some other photographs which are of interest although they do not fall into any of the four time groups. The data for each figure appear on the page opposite the figure, and include lengths of the vertical and horizontal axes of the shock wave and bubble as determined from measurements on the original negatives and the lens equations. From previous optical tests (See III, 5, d), it is believed that the shock wave axes thus determined are accurate to within one inch.

Each photograph is a double exposure due to the relatively weak flash of light given off by the main charge before detonation of the flash charge, the camera shutter being open during the whole interval. This causes an image of the original charge to appear on the film.

Data for Figs. 61 through 67.

Spheres, 2-5/8 in. diameter
Detonated at center

Fig.	61	62	63	64
Estimated time after detonation (μsec)	13	56	104	207
Shock wave axes (in.)				
Vertical	4.6	13.1	19.1	32.7
Horizontal	4.6	13.1	19.2	32.8
Bubble axes (in.)*				
Vertical	3.7	5.9	7.0	9.5
Horizontal	3.8	5.9	6.9	9.3
Distance between inside edges of scale markings (in.)	7	7	13	26

Cones, 3-1/2 in. equilateral
Detonated at center

Fig.	65	66	67
Estimated time after detonation (μsec)	59	132	199
Shock wave axes (in.)			
Vertical	13.2	23.0	31.7
Horizontal	13.2	23.0	31.9
Bubble axes (in.)*			
Vertical	5.9	7.8	9.5
Horizontal	6.0	7.7	9.1
Distance between inside edges of scale markings (in.)	7	13	26

* Uncorrected for optical distortion.

155:8

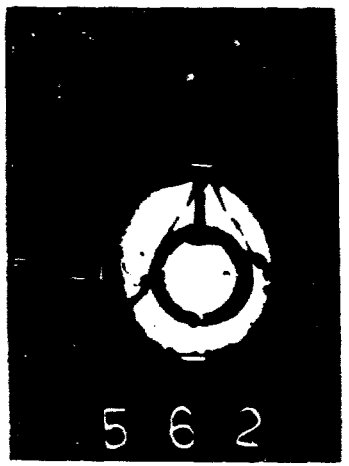


Fig 61

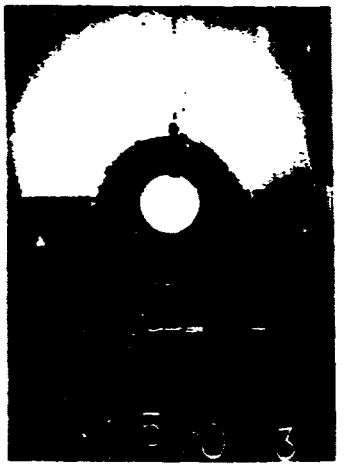


Fig 62



Fig 63



Fig 64

Figs 61-64 Spheres, 2 5/8 in diam, detonated at center



Fig 65

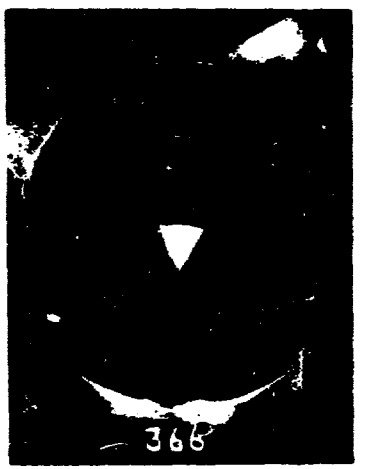


Fig 66

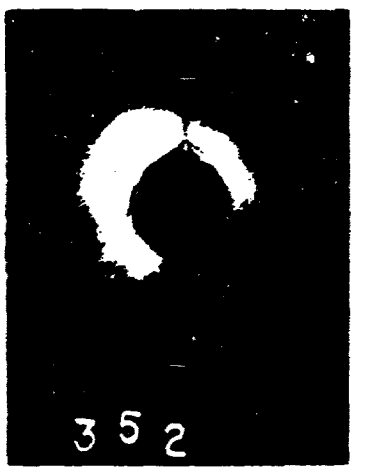


Fig 67

Figs 65-67 Cones, 3 1/2 in equilateral, detonated at "center"



Fig 68



Fig. 69
Detonated at apex

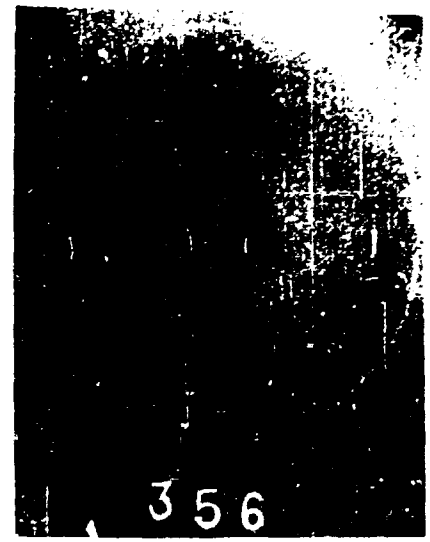


Fig. 70

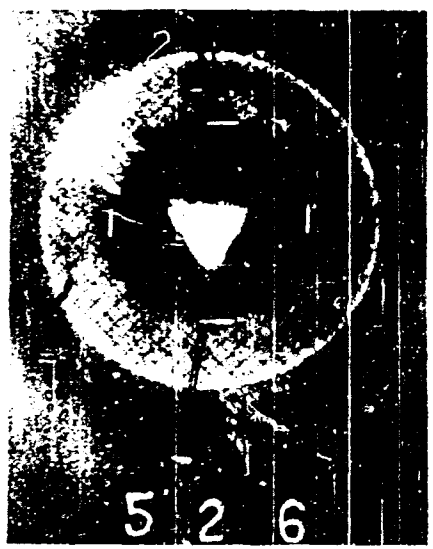


Fig 71

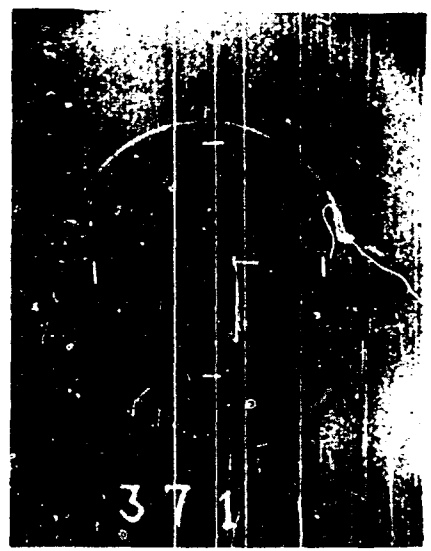


Fig. 72
Detonated at center of base



Fig. 73

Figs. 68-73 Cones, 3 1/2 in equilateral

Data for Figs. 68 through 73.

Cones, 3-1/2 in. equilateral Detonated at apex			
Fig.	68	69	70
Estimated time after detonation (μsec)	45	124	215
Shock wave axes (in.)			
Vertical	11.4	22.2	33.9
Horizontal	11.1	21.9	33.5
Bubble axes (in.)*			
Vertical	6.0	8.6	10.7
Horizontal	5.3	7.4	9.2
Distance between inside edges of scale markings (in.)	7	13	26

Cones, 3-1/2 in. equilateral Detonated at center of base			
Fig.	71	72	73
Estimated time after detonation (μsec)	52	87	195
Shock wave axes (in.)			
Vertical	12.1	17.1	31.2
Horizontal	12.2	17.0	31.2
Bubble axes (in.)*			
Vertical	5.8	7.0	9.8
Horizontal	6.4	6.9	9.3
Distance between inside edges of scale markings (in.)	7	13	26

* Uncorrected for optical distortion.

Data for Figs. 74 through 80.

Cylinders, 2-1/2 in. diameter, 2-1/2 in. long Detonated at center				
Fig.	74	75	76	77
Estimated time after detonation (μsec)	8	46	114	192
Shock wave axes (in.)				
Vertical	-	11.4	20.5	30.8
Horizontal	-	11.1	20.8	30.8
Bubble axes (in.)*				
Vertical	-	5.4	8.1	8.9
Horizontal	-	5.2	7.2	8.8
Distance between inside edges of scale markings (in.)		7	13	26

Cylinders, 2-1/2 in. diameter, 2-1/2 in. long Detonated at top end			
Fig.	78	79	80
Estimated time after detonation (μsec)	46	107	204
Shock wave axes (in.)			
Vertical	11.7	19.7	32.3
Horizontal	10.9	19.6	32.5
Bubble axes (in.)*			
Vertical	6.5	8.0	9.6
Horizontal	5.2	6.9	9.8
Distance between inside edges of scale markings (in.)	7	13	26

* Uncorrected for optical distortion.



Fig. 74



Fig. 75



Fig. 76



Fig. 77

Detonated at center



Fig. 78



Fig. 79.

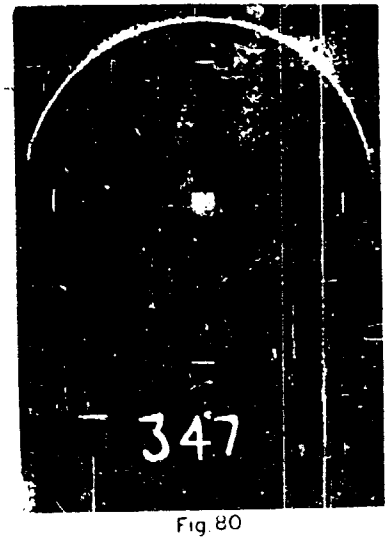


Fig. 80

Detonated at top end

Figs. 74-80 Cylinders, 2 1/2 in. diam, 2 1/2 in. long.

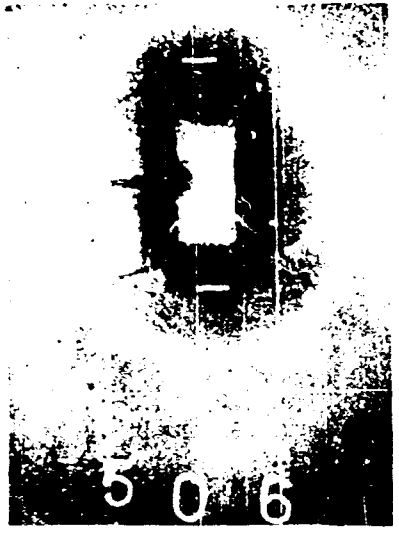


Fig. 81



Fig. 82
Detonated at center

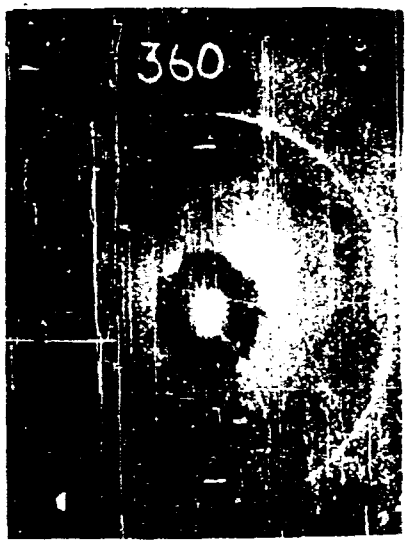


Fig. 83

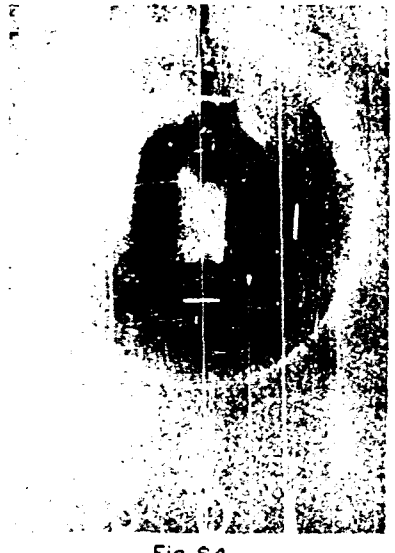


Fig. 84

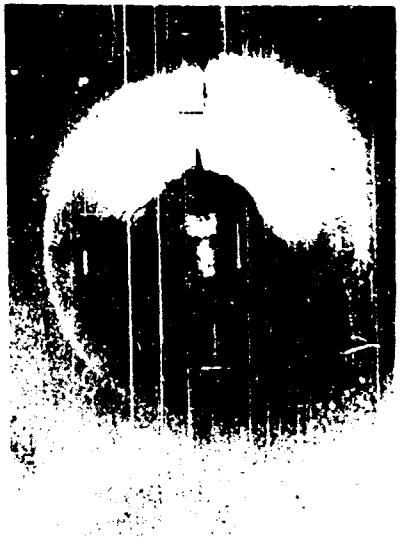


Fig. 85
Detonated at top end



Fig. 86

Figs. 81-86 Cylinders, 1 3/4 in. diam, 3 1/2 in. long

Data for Figs. 81 through 86.

Cylinders, 1-3/4 in. diameter, 3-1/2 in. long Detonated at center			
Fig.	81	82	83
Estimated time after detonation (μsec)	37	111	193
Shock wave axes (in.)			
Vertical	10.7	20.7	31.3
Horizontal	8.9	19.5	30.8
Bubble axes (in.)*			
Vertical	6.4	8.4	10.0
Horizontal	4.3	6.6	8.6
Distance between inside edges of scale markings (in.)	7	13	26

Cylinders, 1-3/4 in. diameter, 3-1/2 in. long Detonated at top end			
Fig.	84	85	86
Estimated time after detonation (μsec)	50	91	196
Shock wave axes (in.)			
Vertical	12.7	17.9	31.8
Horizontal	11.3	16.8	31.1
Bubble axes (in.)*			
Vertical	7.2	8.2	10.6
Horizontal	4.7	5.8	8.0
Distance between inside edges of scale markings (in.)	7	13	26

* Uncorrected for optical distortion.

Data for Figs. 87 through 93.

Cylinders, 1-7/16 in. diameter, 5-7/8 in. long
Detonated at center

Fig.	87	88	89
Estimated time after detonation (μsec)	61	107	207
Shock wave axes (in.)			
Vertical	15.5	21.1	33.7
Horizontal	11.8	18.0	31.7
Bubble axes (in.)*			
Vertical	9.3	10.4	11.8
Horizontal	4.4	5.7	8.2
Distance between inside edges of scale markings (in.)	7	13	26

Cylinders, 1-7/16 in. diameter, 5-7/8 in. long
Detonated at top end

Fig.	90	91	92	93
Estimated time after detonation (μsec)	10	54	101	207
Shock wave axes (in.)				
Vertical	-	14.4	20.2	33.7
Horizontal	2.4	10.5	17.5	31.8
Bubble axes (in.)*				
Vertical	-	9.6	9.8	12.6
Horizontal	-	4.0	5.2	7.4
Distance between inside edges of scale markings (in.)	7	7	13	26

* Uncorrected for optical distortion.



Fig. 87



Fig. 88



Fig 89

Detonated at center

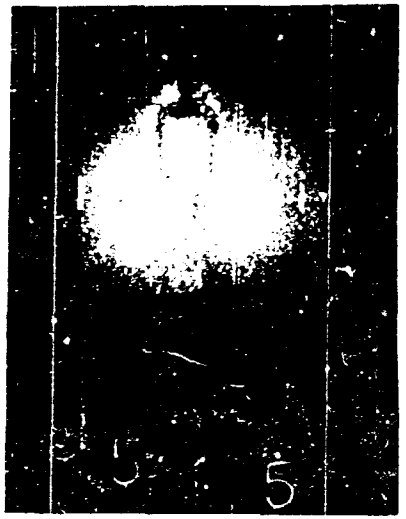


Fig 90



Fig 91

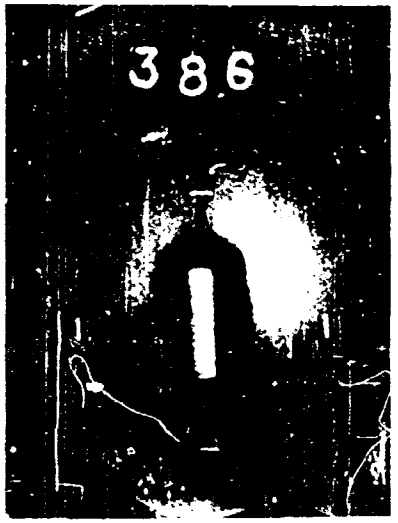


Fig 92



Fig 93

Detonated at top end

Figs 87-93 Cylinders, 1 7/16 in. diam., 5 7/8 in. long.



Fig 94

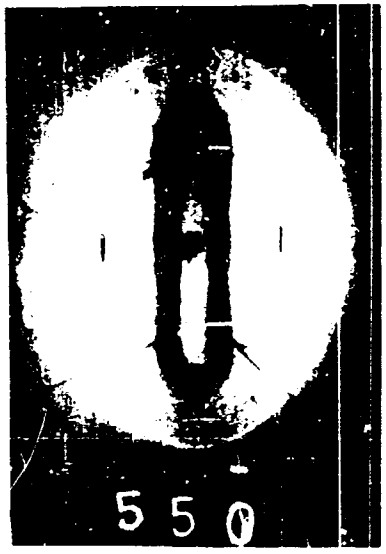


Fig 95



Fig 96



Fig 97

Detonated at center

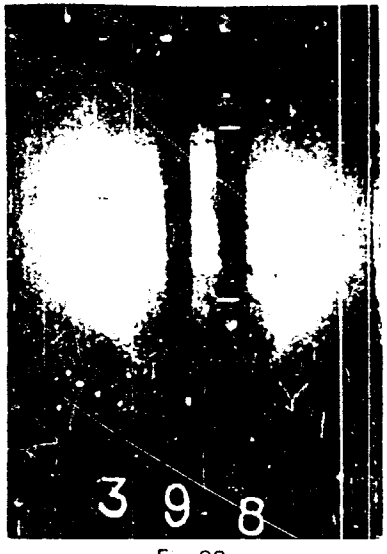


Fig 98

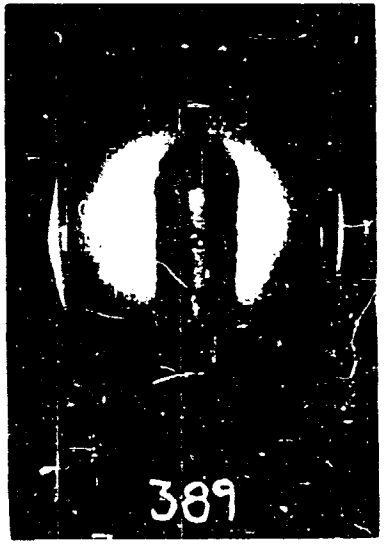


Fig 99



Fig 100

Detonated at top end

Figs 94-100 Cylinders, 1 1/8 in. diam, 9 in. long

Data for Figs. 94 through 100

Cylinders, 1-1/8 in. diameter, 9 in. long Detonated at center				
Fig.	94	95	96	97
Estimated time after detonation (μsec)	11	60	120	203
Shock wave axes (in.)				
Vertical	-	16.6	24.4	34.6
Horizontal	3.3	10.2	18.5	29.7
Bubble axes (in.)*				
Vertical	-	12.1	13.2	14.7
Horizontal	-	3.7	5.2	6.9
Distance between inside edges of scale markings (in.)	7	7	13	26

Cylinders, 1-1/8 in. diameter, 9 in. long Detonated at top end			
Fig.	98	99	100
Estimated time after detonation (μsec)	56	94	198
Shock wave axes (in.)			
Vertical	15.9	20.6	33.8
Horizontal	9.9	14.9	29.3
Bubble axes (in.)*			
Vertical	11.6	12.5	14.2
Horizontal	3.5	4.2	6.1
Distance between inside edges of scale markings (in.)	7	13	26

* Uncorrected for optical distortion.

Data for Figs. 101 through 104: Miscellaneous Photographs

Fig.	101	102
Cylinder; diameter (in.)	2-1/2	1-1/8
length (in.)	2-1/2	9
Detonated at center		
Estimated time after detonation (μsec)	25	83
Shock wave axes (in.)		
Vertical	8.0	19.4
Horizontal	7.7	13.1
Bubble axes (in.) *		
Vertical	4.9	12.7
Horizontal	5.4	4.2
Distance between inside edges of scale markings (in.)	7	13

Fig. 103

Cylinder; diameter (in.) 1-3/4.
length (in.) 3-1/2.

Detonated at top end.

Shock wave just emerging from top.

Fig. 104

Flash photograph following detonation of Ensign-Bickford primacord.

* Uncorrected for optical distortion.

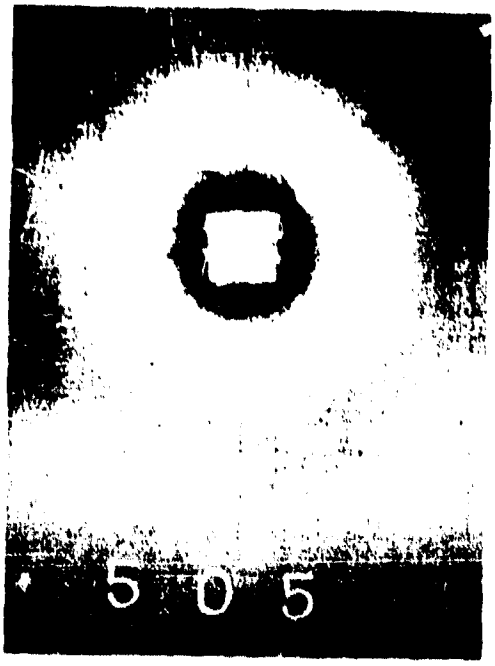


Fig 101



Fig. 102



Fig 103

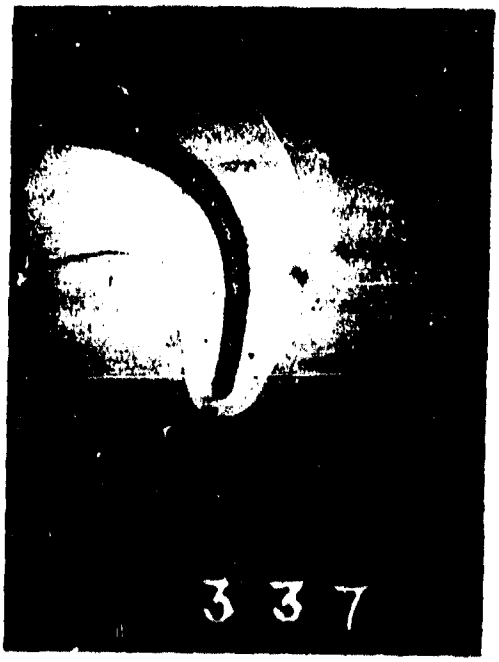


Fig 104

Figs 101-104 **Miscellaneous** photographs

Because of distortion occurring in reproduction, horizontal and vertical scales are provided in the photographs in the form of black or white lines drawn on the prints. The distances between the inside edges of the lines corresponds in the actual experiments to 7 in. in the 10 and 50 microsecond series pictures and the miscellaneous photographs, to 13 in. in the 100 microsec. series and to 26 in. in the 200 microsec. series.

The pieces of some of the longer cylindrical charges which had been broken in handling were rejoined after fusion at the points of fracture. It is interesting to note that the remelted parts are visible in the photographs. In many of the photographs, twine, pieces of detonator wire, and part of the detonator itself are visible in addition to the charge, bubble, and shock wave.

The focal length of the camera lens was determined at two distances by photographing a grid underwater so that calculations based on the lens equations could be made. In so doing, it was found that the lens used gave some "pincushion" distortion of rectangular objects, but this distortion is not sufficient to change the relative axial lengths by an amount greater than 0.6 in.

Figure 105 shows the relation between bubble radius and shock wave radius for 1/2 lb. spherical charges of cast pentolite. Since the time intervals for these shots can be estimated from the positions of the shock waves, an approximate time scale is also included.

Figure 106 indicates the rates at which the shock waves from the asymmetric cylindrical charges approach a spherical shape.

3. Pressure and time-constant measurements of shock waves by optical distortion.

Several photographic methods have been developed which allow calculation of the peak pressure of a shock wave, and for one of these methods the calculations have been extended to make possible an evaluation of the time constant of the shock wave. These methods make use of the fact that light rays passing through a shock wave at favorable angles are considerably distorted due to the increase of refractive index in the region of high pressure. A detailed theoretical discussion of these methods is to be found in Appendix II.

(a) Spherical shock wave; charge not on the optical axis; charge in grid plane. -- The arrangement with which most of the work has been done involves placing a transparent lucite grid marked off with lines 1/4 in. apart in front of the camera, and the shock-wave-producing charge off to one side and in the same plane with the grid. (See Figure 133, Appendix II.) A flash charge is placed behind the grid and is timed by means of primacord to go off when the shock wave from the main charge is crossing the grid. The results of both peak pressure and time-constant determinations from four shots using this method agree essentially with UERL piezoelectric results for similar conditions.

(1) Peak pressure. Two of these four shots were made with 250 gm tetryl as the main charge, and the photographs were taken when the shock wave radius was about 15 in. One of these photographs is reproduced in Figure 107. The theory (Appendix II.1) relates the amount of apparent displacement of an individual intersection of grid lines with the average refractive index of that section of the shock wave through which the corresponding light ray must pass. This average refractive index is then converted to the corresponding pressure, p_{av}. This calculation is made for several grid intersections at different radii. Plotting (or semi-log paper) log p_{av} against the corresponding distances of the mid-points of the refracted light rays behind the shock front, $(R - r_{av})$, a straight line is obtained to within the precision of measurement. Figure 108 is such a plot for a shock wave 14.9 in. from a 250 gm tetryl charge, while Figs. 109 and 110 are the results of measurements on two different prints of another shock wave 14.4 in. from 250 gm tetryl. The average deviations from the straight lines drawn are approximately 7%, 6%, and 3%, respectively. The peak pressure is assumed to be the extrapolation of this line to zero distance behind the front. Any errors introduced by assumption that the calculated p_{av}'s correspond to the

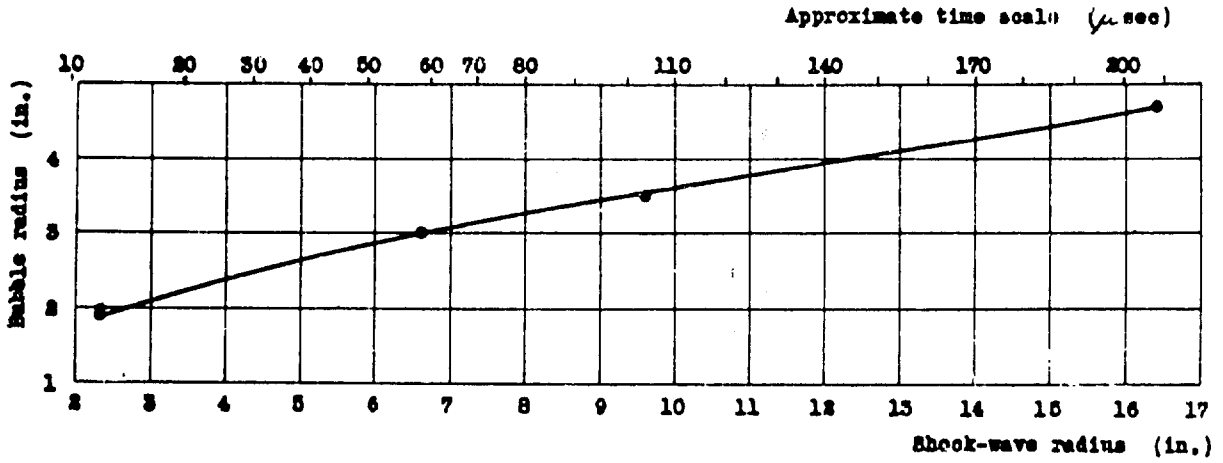


Fig. 105. Bubble radius vs. shock-wave radius for $\frac{1}{4}$ lb cast pentolite (spherical charge).

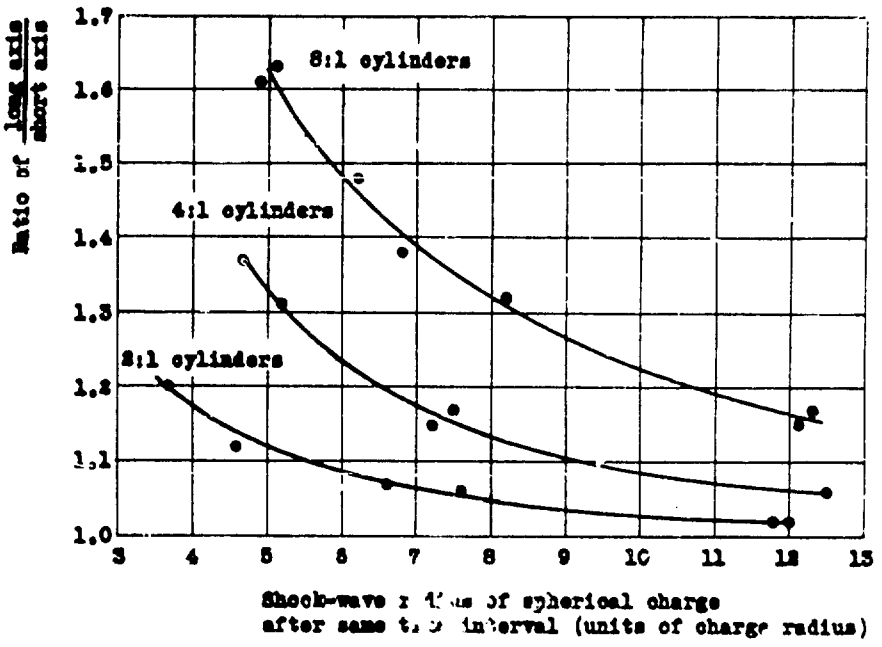


Fig. 106. Ratios of long axis to short axis of shock waves from asymmetric cylinders vs. shock-wave radius (in charge radii) for spherical charge of same weight and after same time.

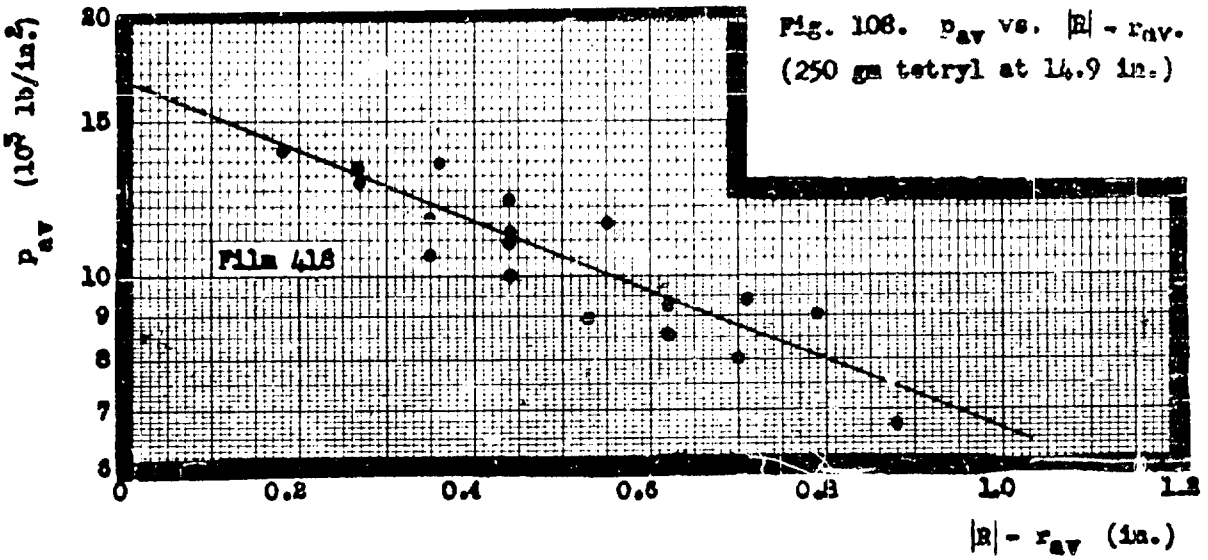


Fig. 108. p_{av} vs. $|R| - r_{av}$. (250 gm tetryl at 14.9 in.)

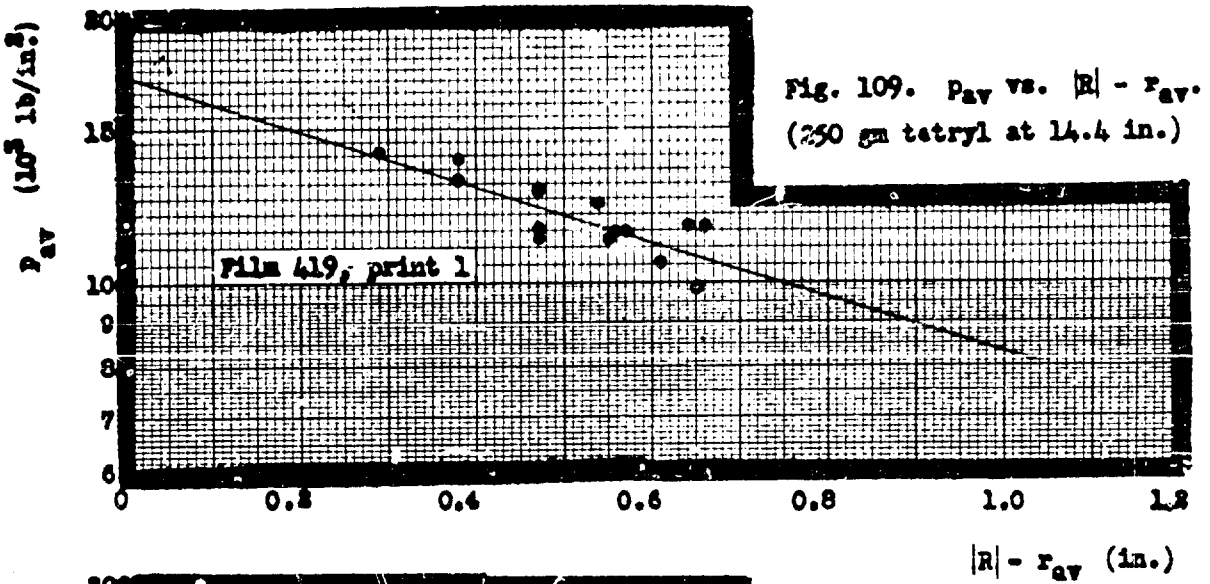


Fig. 109. p_{av} vs. $|R| - r_{av}$. (250 gm tetryl at 14.4 in.)

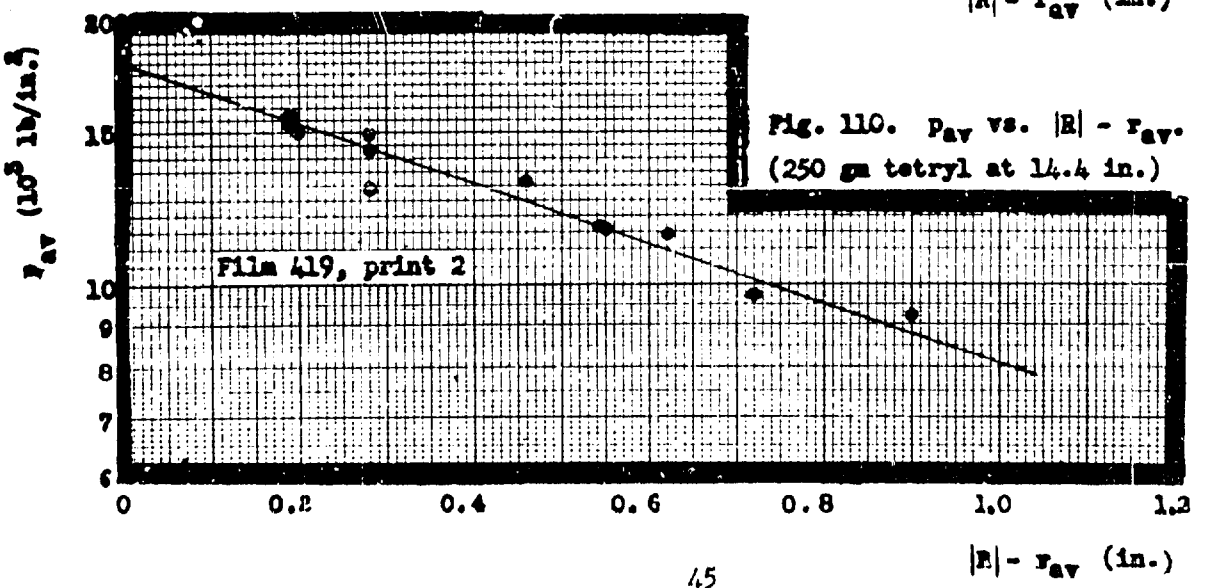


Fig. 110. p_{av} vs. $|R| - r_{av}$. (250 gm tetryl at 14.4 in.)

Fig. 107 Typical example of optical distortion photograph. Film 418 - 250 gm tetryl at 14.9 in.



points of mean distance of the light rays behind the shock front should go to zero in this limit. The peak pressure obtained from two prints of the same shot (Figures 109 and 110) agree to within 4.5% (17,200 and 18,000 lbs./in.^{2}). Correcting the result from Figure 108 (p_{max} = 16,700 lbs./in.^{2}) to a shock wave radius of 14.4 in., using a distance exponent of 1.13, one obtains a pressure of 17,400 lbs./in.^{2}, which agrees with the average of Figures 109 and 110 to within 1.5%.

This method of peak pressure determination was also applied successfully to the other two shots, consisting of ca. the equivalent of ca. 364 gm TNT and using a shock wave radius of ca. 16 in. Measurements were made at several pairs of grid line intersections for each of the two films. The values of log p_{av} were plotted against ($|R| - r_{av}$) as before and one straight line was drawn through the data from both films, since the value of $|R|$, the shock wave radius, for the two films was identical. Extrapolation of this line to $|R| - r_{av} = 0$ gave a value for p_{max} of 17,050 lbs./in.^{2}. This plot is given in Figure 111. The average deviation of the points from the straight line is ca 5.5%, with no systematic difference between the points for the two shots.

(ii) Time-constants. The results for the two torpex shots were also used for calculation of time-constants of the shock wave. Since the detailed development of the theory, together with a sample calculation, is given in Appendix II, only the results will be reported here. In general, the calculations are considerably more tedious than for the peak pressures.

Five points were used in the calculations, two from one shot and three from the other. The ones whose images were the clearest, and thus the most accurately measured, were selected. They were picked from the plot of Figure 111 at different values of ($|R| - r_{av}$) and at different deviations from the line. The results of the calculations are shown in Table VI.

Table VI. Results in the evaluation of time constant.

Film No.	Point No.	$\lvert R\rvert - r_{av}$ (in.)	Θ_r (in.)	$r' - D_r$ (in.)	Θ_t (μsec)
536	22	0.61	3.15	14.76	39.1
537	5a	0.63	3.39	14.72	41.3
537	12	0.94	3.23	14.11	39.6
536	8	0.97	3.68	14.03	43.8
537	18	1.13	3.09	13.71	38.1

Av. Θ_t = 40.4 μsec, average deviation from mean = 1.7 μsec.

It will be noted that there is no systematic trend of Θ_t with distance of the point selected for calculation behind the shock front ($|R| - r_{av}$).

(iii) Summary and remarks. As shown in Figure 111, the peak pressure of the shock wave produced by ca.364 gm TNT at 16.0 in. is 17,030 lbs./in.^{2}. The results for both peak pressure and time constant are in essential agreement with piezoelectric results obtained at UERL both for small bare charges and depth bombs (scaled down). The agreement is within the accuracy of either method for these experimental conditions (ca 10%).

This experimental method has the disadvantage that the results obtained are rather sensitive to the geometry of the experiment. For example, to obtain the desired accuracy for these shots, the point at which the line from the camera lens, perpendicular to the grid, intersected the grid had to be determined in the actual set-up to within 1/16 in. For this reason, a single rigid frame had to be used to support the camera, the main charge, and the grid. It has been demonstrated, however, that the method is satisfactory if the experiment is carefully set up.

Further experiments in fresh water for comparison with those made in salt water should be done.

(b) Spherical shock wave: charge on the optical axis: charge in grid plane. -- The theory for peak pressure determination has been worked out for an experimental arrangement similar to that of Section (a) except that now the charge is located directly in front of the camera (See Appendix II, 2). Figure 112 (Film 526) shows a photograph obtained according to this method.

(c) Non-spherical shock wave: charge on the optical axis: charge in grid plane. -- The theory for peak pressure determination has also been worked out for an experimental arrangement similar to that of Section 3(b) except that the shock wave surface is not required to be spherical, but expressible only by some definite equation of the form $f(x, y, z) = 0$ (See Appendix II, 3).

(d) Spherical shock wave: charge on the optical axis: charge in front of grid plane. -- Partly to increase the amounts of distortion measured on the photograph, and thus improve the precision of the measurements, and partly in an effort to find an experimental arrangement in which less precision would be necessary in setting up the apparatus, one photograph (reproduced in Figure 113 (Film 531)) has been taken in which the grid was mounted in back of the charge, as viewed from the camera. Inspection of Figure 138 in Appendix II, 4 will show how the measured distortion is increased by allowing the refracted ray, (considered as projected backwards) to traverse a greater distance than in the other experimental set-ups. Another evident advantage of this arrangement is that at the time of the photograph the shock wave need not have reached the grid, so that there is no danger of mechanical distortion of the grid.

In this particular shot, the charge was 250 gm cast pentolite and was placed 51 in. in front of the camera. The grid was positioned 8 in. behind the charge, and a flash charge 28 in. behind the grid. Since the charge and grid are at different distances from the camera, both the shock wave and the grid cannot be in perfect focus, but this is not likely to be troublesome if a reasonably small lens aperture is used.

Not enough work has been done using this method to warrant a comparison with the method described in Section III, 3, (a).

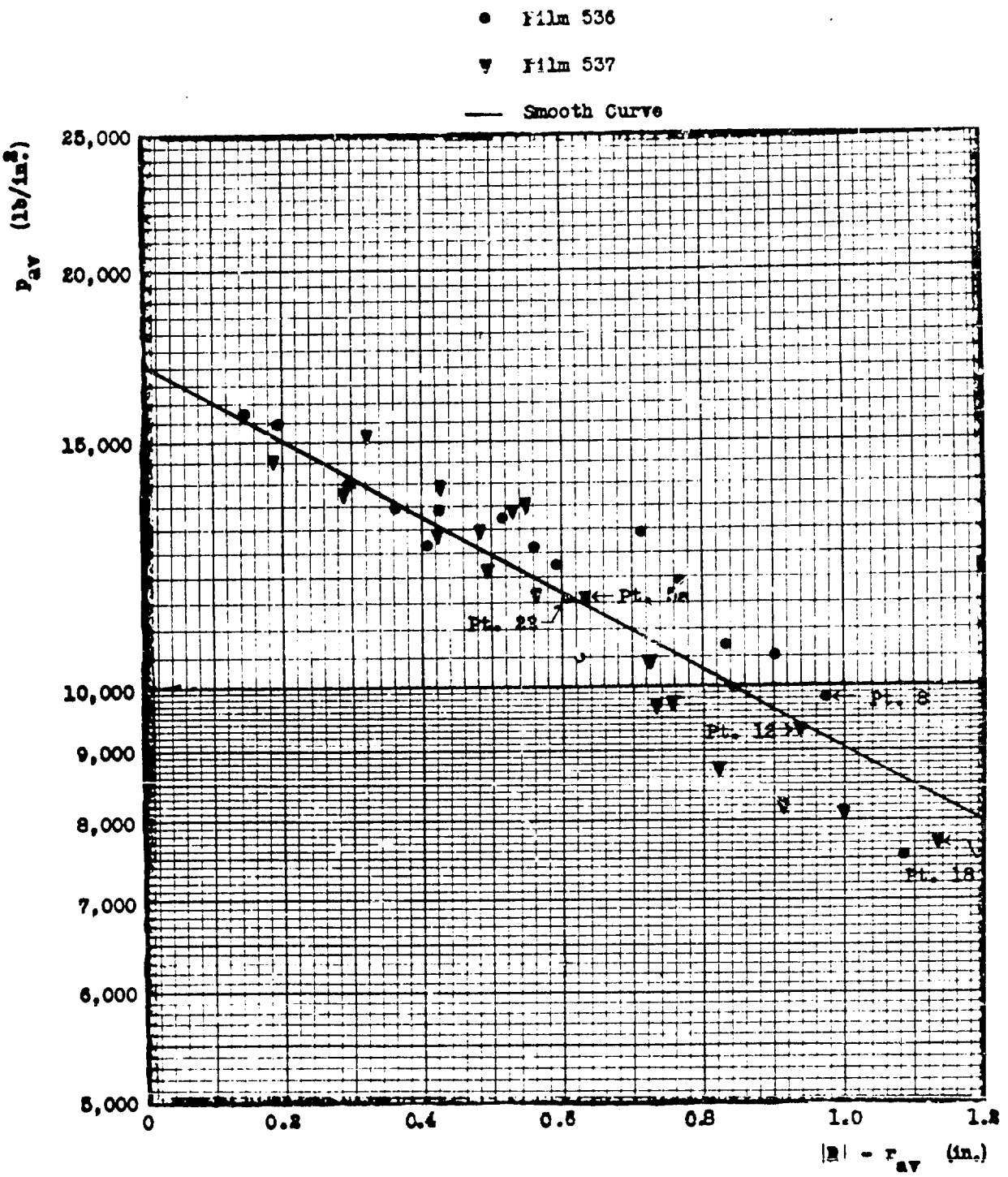
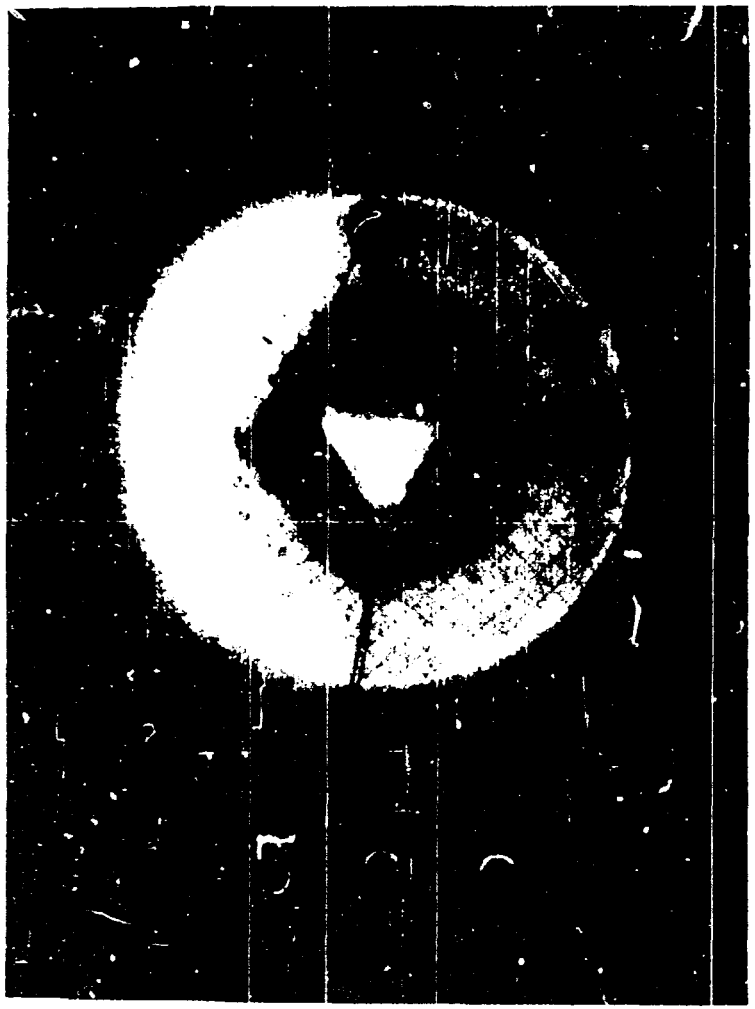
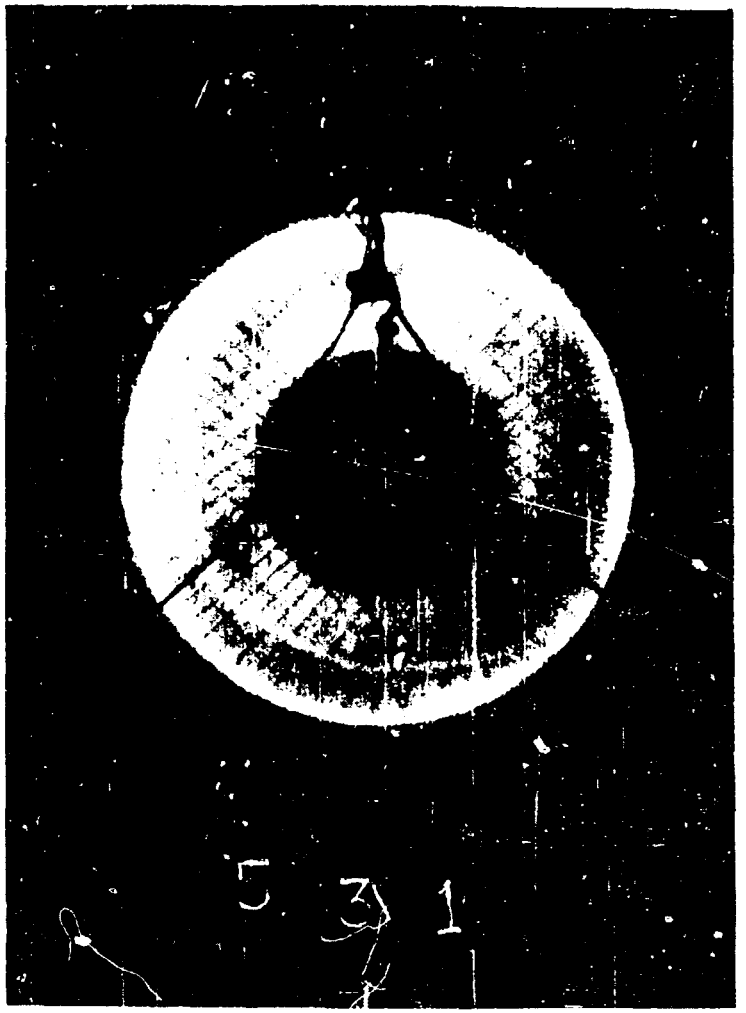


Fig. 111. p_{av} vs. |R| - r_{av} for shock waves produced by two charges of ca.364 gm TNT at a value of |R| of 16 in.





OPTICAL DISTORTION PHOTOGRAPHS

Fig. 112. Spherical shock wave; charge on the optical axis; charge in grid plane.

Fig. 113. Spherical shock wave; charge on the optical axis; charge in front of grid plane.

4. Cylinder Damage [8]

(a) Introduction. -- After some of the early UERL experiments on damage to cylindrical targets by explosions, it became apparent that bubble pressure was contributing to a considerable extent to the damage. Since bubble damage does not scale in the same manner as shock-wave damage and since the gross damage is the result of both bubble and shock wave damage, a preliminary step in the interpretation of the cylinder results is the separation of shock wave and bubble pulse damage. The easiest way to effect this separation is by photography.

(b) Still pictures. -- Preliminary still photographs taken between the time of impact of the shock wave and the first bubble pulse show i that damage was by no means complete compared with the final condition of the cylinder. These pictures, some of which are shown in Figures 114, 115, 116, were taken with a photoflash lamp so that the act of photographing the cylinders does not contribute to the damage.

(c) Slow speed movies. -- Some motion pictures were then taken with the Victor camera of 3 simple, small cylindrical shells of the S type [8] and one supported cylinder of the SA type being damaged by a 25 gm charge. These showed that the unsupported cylinder was practically undamaged until the time of the first bubble pulse and was damaged by both the first and second pulses. The supported cylinder, on the other hand, was damaged essentially completely by the shock wave.

(d) High speed movies. -- Still another series of experiments was performed with SD class cylinders at depths of 200, 400 and 580 ft. The photographs were taken with the Eastman high speed camera with #31 photoflash lamps for lighting. The apparatus shown in Figure 16 was used. A representative film is reproduced in Figure 117. It shows that the cylinder was relatively stable after it was damaged by the shock wave but collapsed completely soon after the bubble pulse. This sequence of events was not followed for closer shots; in some of the latter, instability resulted from shock wave damage.

The sharpness of this series is due to the unusual clarity of the Bahamas water in which the pictures were taken. The Secchi disk reading was about 135 ft.

A complete description of the cylinder results will be given in a forthcoming report. [8]

5. Miscellaneous experiments

(a) Mach effect. -- Three pictures were taken of intersecting shock waves having a peak pressure about 700 times hydrostatic pressure ($\sim$ 9,500 lb./in.^{2}). In two cases the intersection was obtained by reflecting the shock wave from a 50 gm tetryl charge off a 1/2 in. steel plate 12 in. away, and in the third case, by the shock waves from two appropriately placed 50 gm charges. (See Figure 118). In all three shots, the charges were approximately 12 in. from the point of intersection of the shock waves. The resulting pictures are Figures 119, 120, and 121. The angle of intersection of the shock waves shown is 64°, 71°, and 71° respectively. The Mach effect appears quite strongly in the last two cases. A fourth picture with an angle of intersection of 45° is presented for comparison in Figure 122. This angle is outside the Mach region and no Mach effect shows although the appearance of the shock waves is somewhat distorted due to refractive index discontinuity.

(b) Shock wave from 300 lb. charge. -- A single flash picture of the shock wave from a 300 lb. charge was taken in the Bahamas at a distance of 65 ft. and is presented in Figure 123 to show the possibilities for full scale photography in clear water. Although lack of time prevented us from following up this promising lead, it is

---

[8] These cylinders are described in a report by J. C. Decius and P. M. Fye, Damage to Thin Steel Cylindrical Shells by Underwater Explosions, NDRC Report No. A-369, OSRD No. 6247.

BEFORE BUBBLE PULSE



Fig 114 A

T≃55 T_B-T≃20

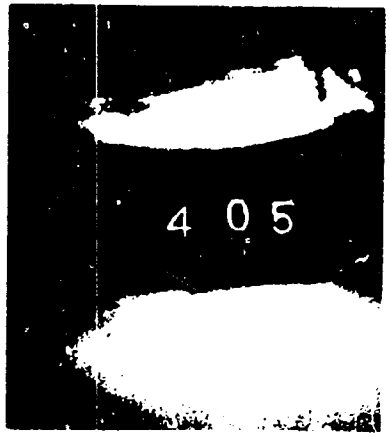


Fig 115 A

T≃40 T_B-T≃35

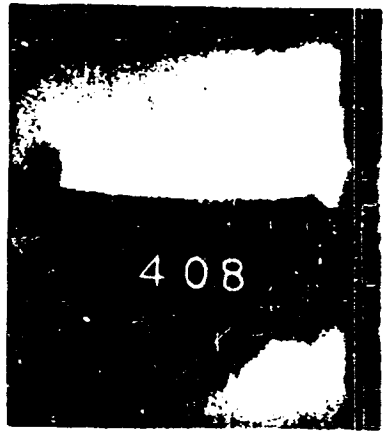


Fig 116 A

T≃65 T_B-T≃10

LONG AFTER BUBBLE PULSE

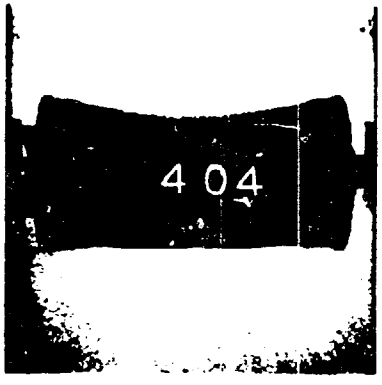


Fig 114 B

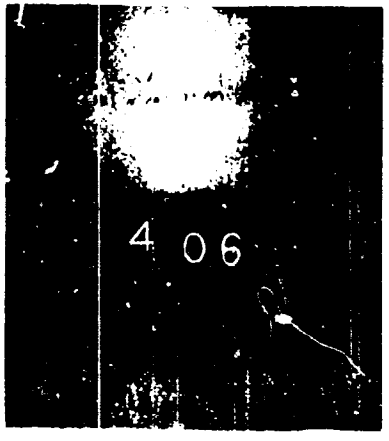


Fig 115 B

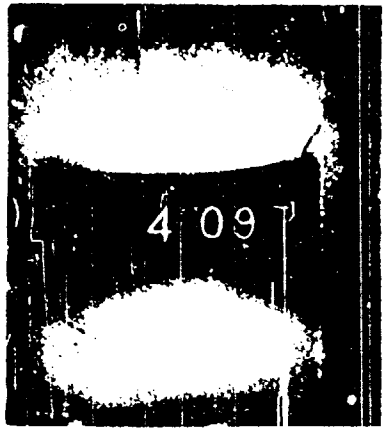


Fig 116 B

T= TIME AFTER EXPLOSION: MILLISEC. T_B=CALCULATED TIME OF BUBBLE PULSE. 75 MILLISEC.

DAMAGE TO CYLINDERS BEFORE AND AFTER CALCULATED TIME OF BUBBLE PULSE

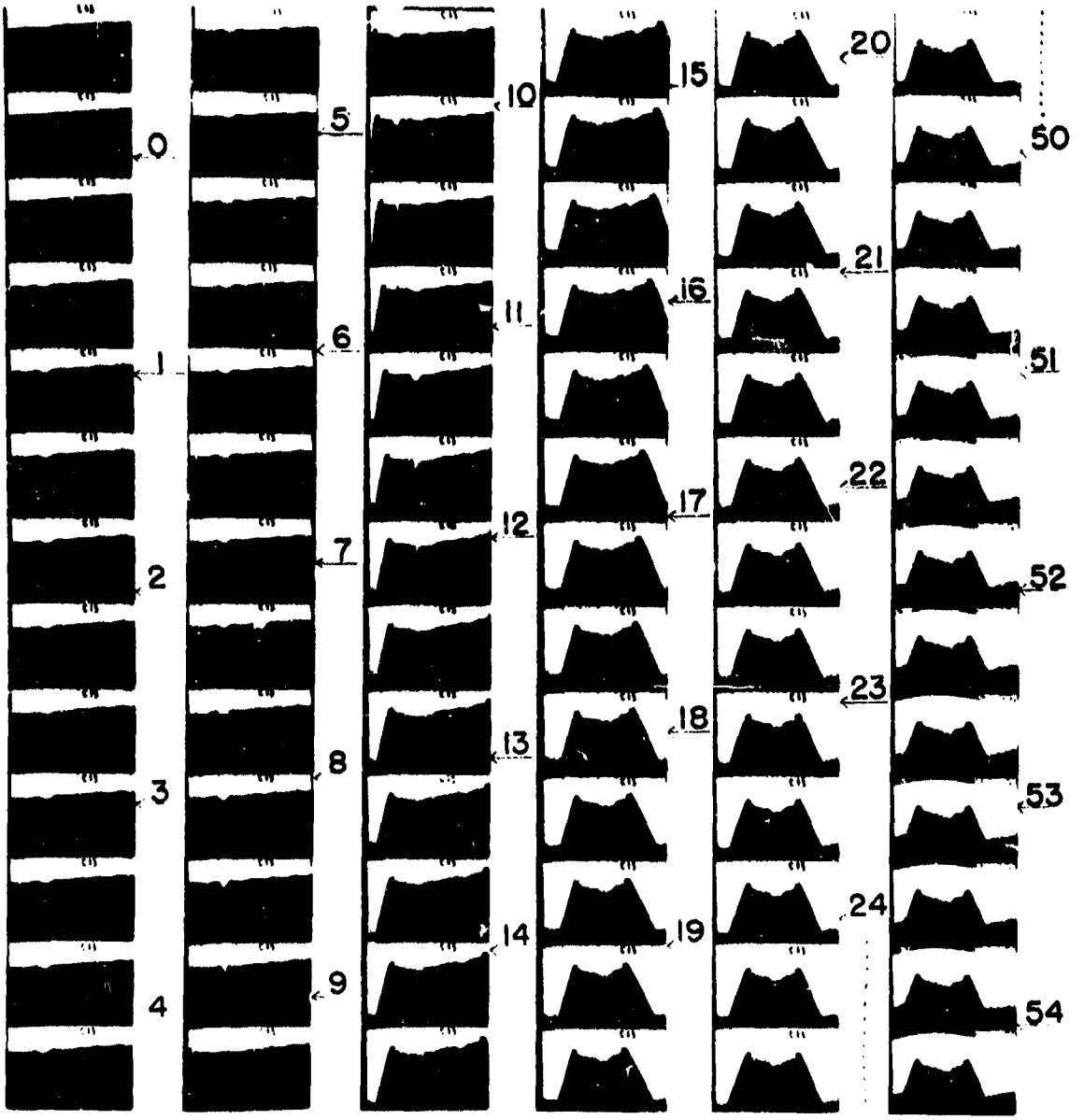


FIG. 117
CYLINDER NO SD-47-29C
CHARGE: 253 G PRESSED TETRYL
CYLINDER DEPTH: 580'
CHARGE DISTANCE: 28"
OOR: OVERALL = 0.26%, FRONT 90° = 0.12%
BUBBLE PERIOD: 7.9 MSEC
CAMERA SPEED: 2500 FRAMES/SEC

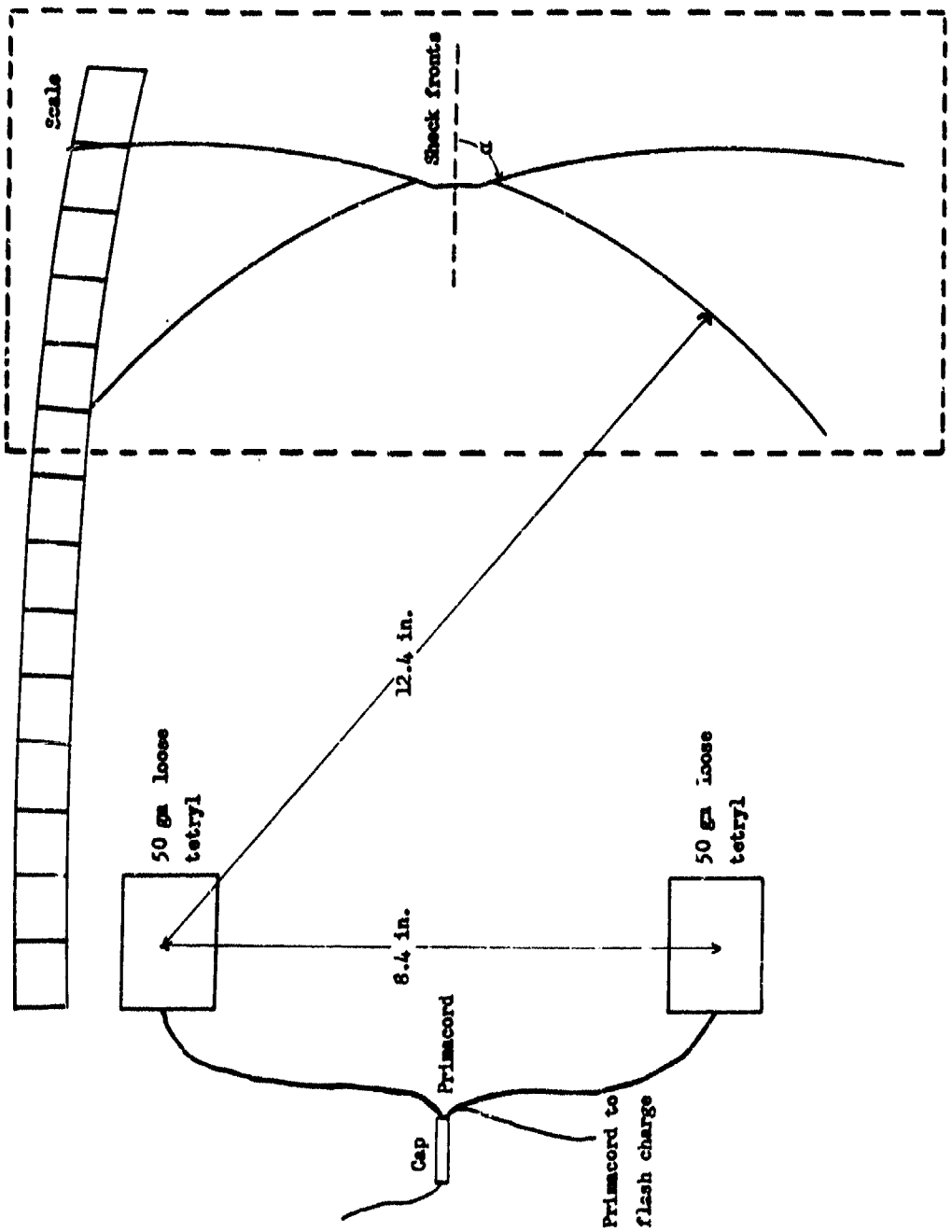


Fig. 118. Schematic view, from camera position, of arrangement for Fig. 121.

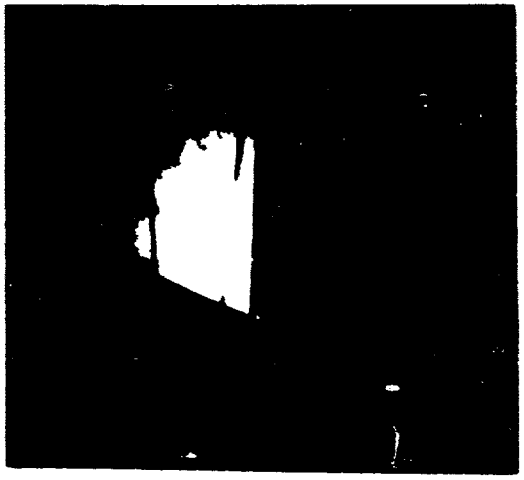


Fig. 119

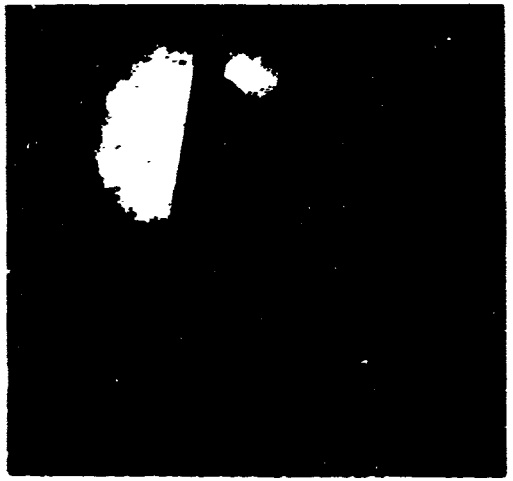


Fig. 120



Fig. 121

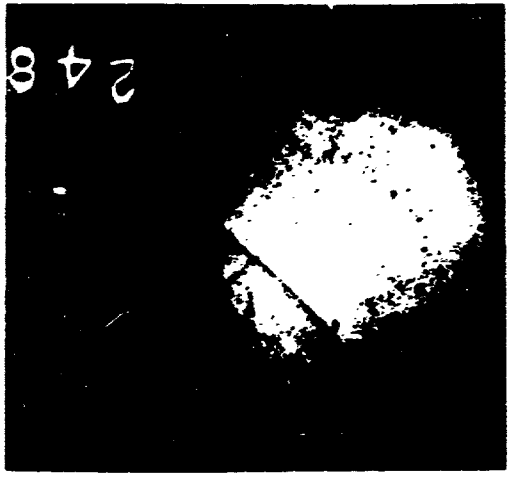


Fig. 122

Intersecting shock waves

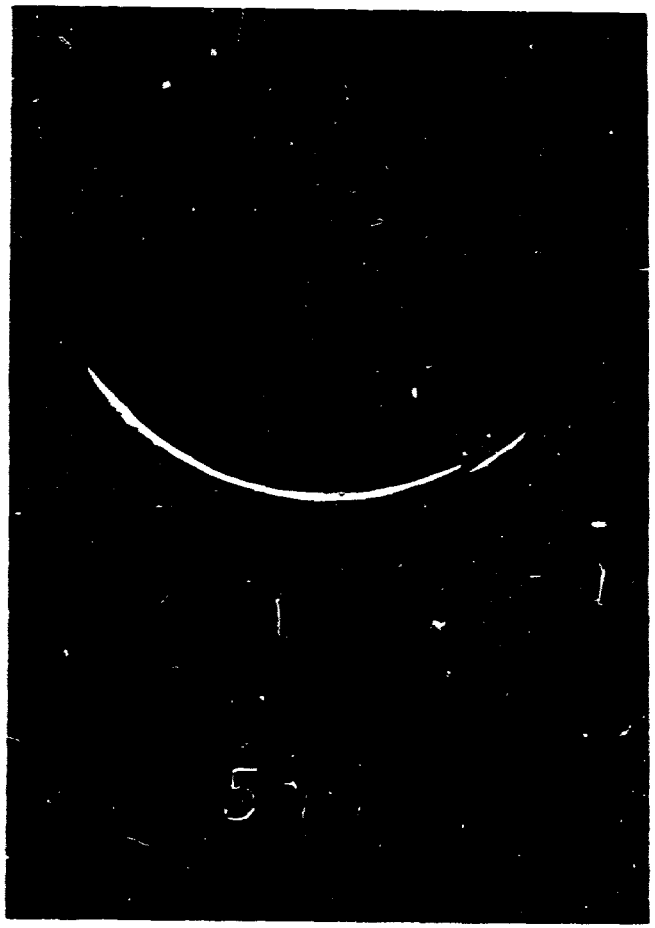


Fig. 123. Shock wave from 300 lb charge 65 ft from camera.

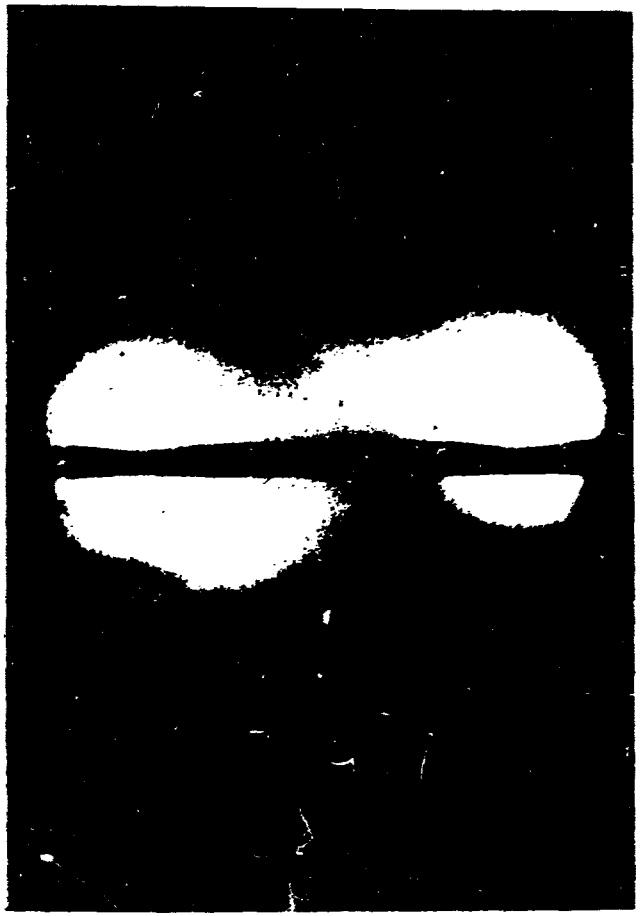


Fig. 124. Shock wave photographed at two positions by double exposure technique.

obvious that good pictures can be taken under these circumstances. A large edition of the conventional flash charge was used and the equipment, including flash charge, depth charge and camera was strung out on a line supported by floats. The line was stretched out by a small boat.

(c) Pressure of shock wave determined from shock wave velocity. -- One measurement of average shock wave velocity was made by a double exposure technique. Two flash charges were employed and set off about 246 μsec apart. It was intended to obtain this time difference accurately by means of piezoelectric gages strapped to the two flash charges and recording on an oscilloscope. This part of the experiment failed, and the time difference can be estimated only from the length of primacord used to delay the second flash charge. Figure 124 shows the shock wave at the two positions and a steel scale 15.66 in. long. The shock wave came from a third charge to the left of the field of view. The average velocity determined from this shot is about 5180 ft./sec., or about 270 ft./sec. greater than acoustic velocity for the conditions of the experiment. This corresponds to a pressure of about 8,000 lbs./in.^{2} averaged over the time interval. The average pressure over this period as determined from piezoelectric gage measurements under similar conditions is about 11,000 lbs./in.^{2}. Considering the inaccuracy of the time interval measurement, this agreement seems satisfactory. It is to be noted that since the excess velocity (over acoustic) determines the pressure of the shock wave, the accuracy of the measurement of the total velocity must be considerably greater than the accuracy desired for the pressure to be determined.

(d) Experiments showing that the apparent positions of the shock wave coincides closely with its actual position. -- Three experiments have shown that, under the conditions ordinarily employed at UERL, the position of an underwater shock wave is within 1/2 in. of the position indicated by its flash photograph.

In one experiment piezo gages were used to obtain the time interval between the time of the photographic flash and the time the shock wave reached a known radius. From the known velocity of the wave it was possible to calculate its true radius at the time of the photograph and compare it with the value computed from the photographic image.

The 250 gm sphere of cast pentolite which produced the shock wave to be photographed was detonated simultaneously with the initiation of a 46 in. length of primacord leading to the flash charge. The time of the photograph was thus about 185 μ sec after the start of the shock wave. A small tourmaline gage fastened to the shock wave charge served to turn on the oscillograph spot for a rotating drum camera, while a similar gage on the flash charge signalled the time of the photograph. A third gage 17 1/4 in. from the shock wave charge noted the arrival of the shock wave at this radius. The diagram shows the arrangement used.

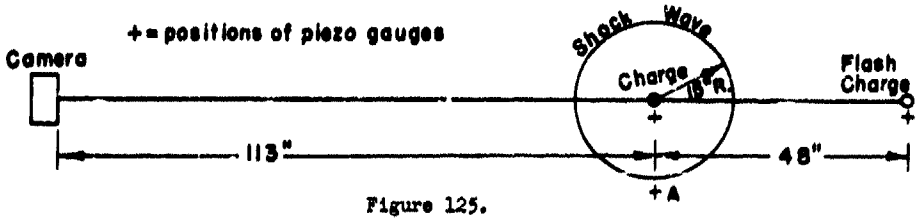


Figure 125.

The radius at the time of the photograph was 14.7 ± 0.2 in. as calculated from the positions of the gages and the measured time intervals. Values for the velocity of sound were taken from "Tables of the Velocity of Sound in Pure Water and Sea Water for use in Echo Sounding and Sound Ranging" (Second Edition) by D. J. Mathers. These were corrected for the effect of finite pressure in the

shock front by means of the data of Kirkwood and Montroll. 9/ Since the distance between the shock wave and the piezo gage at position A was only 2.25 in. at the instant of the photograph, these corrections amount to less than 0.25 in.

A similar experiment was carried out with the shock wave charge just out of the field of view and with a diffusion screen between the flash charge and shock wave. The whole set-up, shown in the diagram below,

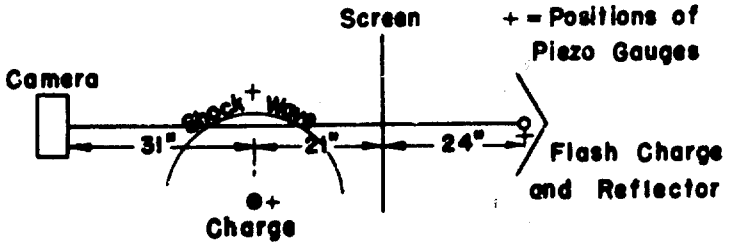


Figure 126

is similar to that used in this laboratory for cavitation studies. The resulting photograph is shown in Figure 129. From it one obtains a distance of 3.44 in. from the shock wave to the piezo gage as compared with a value of 3.36 in. calculated from the piezo records.

A third experiment compared the image of the shock wave with the projection of its shadow on a translucent screen. No piezo gages were involved. Two translucent paper screens were put in the same plane with the shock wave charge and perpendicular to the line from the camera to the charge. The charge and screens as viewed from the camera are sketched below:

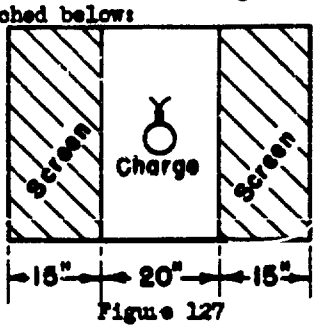


Figure 127

The whole set-up is shown from the top in the following sketch:

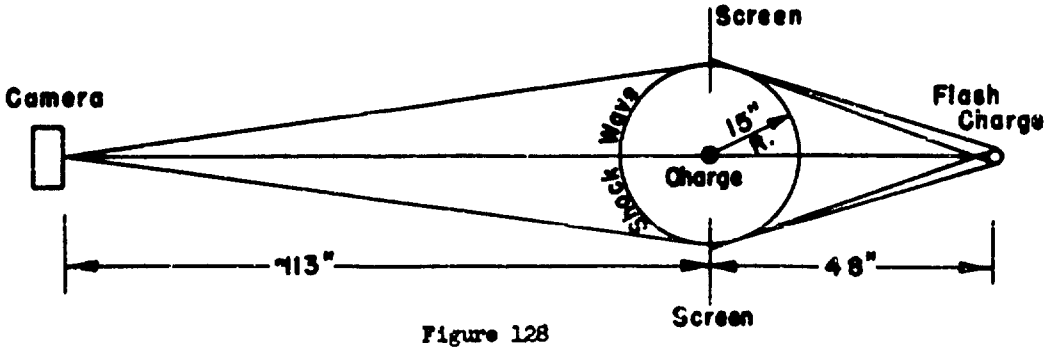


Figure 128

9/ The pressure wave produced by an underwater explosion II, July 1, 1942, by J. G. Kirkwood and E. W. Montroll, OSRD Report 670.

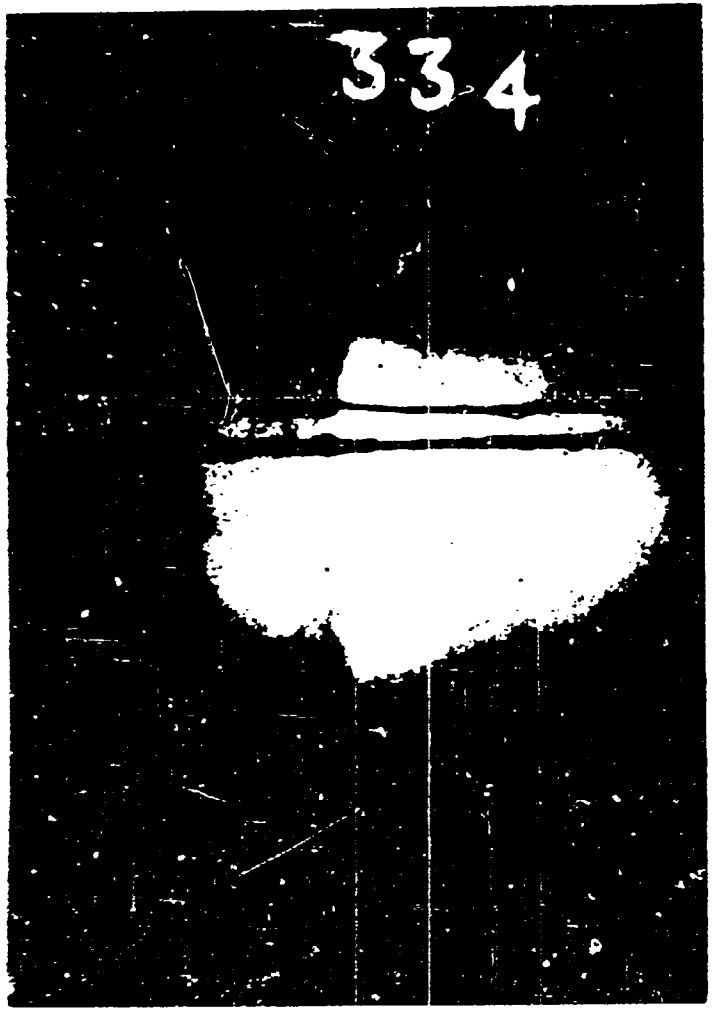


FIG. 129



FIG. 130

PHOTOGRAPHS FROM WHICH AGREEMENT BETWEEN TRUE AND APPARENT SHOCK-WAVE POSITIONS IS OBTAINED.

The resulting picture is reproduced in Figure 130. The image of the shock wave sphere and the image of the shadow projection of the shock wave sphere are seen nearly to coincide. On the average, however, the radius of the shadow projection appears greater than the radius of the shock wave by an amount corresponding to 0.25 in. The geometry of the experiment would require a radius difference of 0.65 in. The discrepancy is within the limits of experimental error.

(e) Luminosity of charges exploded underwater. -- It is shown elsewhere in this report (Sec. III, 2) that bare charges of cast pentolite were observed to emit light when detonated underwater. Photographs indicate this light to be of very short duration, probably less than 1 μsec, because of the detail visible (numbers on the charges, cracks, etc.) and because there is no blurring. Foreseeing possible uses for this flash of light (e.g., accurately signalling at a distant point by means of a photoelectric cell the time at which a charge detonates), several tests were conducted to determine if a cased charge would emit light on detonating underwater.

In all tests, the charge, weighing from 1/2 to 1 lb., was placed 5 ft. in front of the camera and the lens aperture was set at f:3.5. A short piece of primacord, to be detonated simultaneously with the charge, was also included in the field of view to serve as a standard for comparison, since primacord had been found to emit light on detonating underwater (See Figure 104). All tests were conducted at night.

The results showed that a heavy opaque casing reduced the emitted light to the extent that it was no longer detectable. For example, a charge wrapped with black rubber tape and detonated barely showed on the film, and a charge enclosed in a piece of steel pipe with pipe caps on the ends resulted in no image at all. Less heavy casings, however, such as 1/16 in. thick brass tubing, tin cans, and black lacquer resulted in weak but definite images of the charge and sometimes streamers of light emanating from the charge. There was some indication that aluminized explosives (torpex and minol) emitted more light than tetryl or pentolite under the same conditions, but the evidence is insufficient on this point.

APPENDIX I

THEORY OF PRESSURE IN FRONT OF AN AIR-BACKED FREE PLATE ACCELERATED BY A SHOCK WAVE

When a plane shock wave strikes a free air-backed plate head on, the pressure in the water in front of the plate first rises as the original wave passes through it, then rises still further as the reflected shock wave returns from the plate. The pressure on the plate causes it to begin to move and its motion reduces the pressure, sending out a rarefaction wave. Consequently, the pressure out in front of the plate, after rising twice, then falls and actually goes negative, provided that cavitation does not interfere. The pressure can be calculated under certain simplifying assumptions; namely, the plate is assumed to be made of an infinitely rigid material, to be of infinite extent (but finite thickness), i.e., a rigid body whose motion is restricted only by its inertia. It is also assumed that cavitation does not form and that acoustic (small amplitude) theory can be used.

The pressure at a point x (measured positively out into the water from the initial position of the plate) and at a time t (measured from the time the original wave strikes the plate) is the sum of three terms:

(1) The pressure due to the original shock wave (assumed to be exponential in shape)

$$p_o e^{-\frac{t+\frac{x}{c}}{\theta}} \quad , \text{ for } t > -\frac{x}{c} \ , \tag{I-1}$$

(2) The pressure due to the reflected wave

$$p_o e^{-\frac{t-\frac{x}{c}}{\theta}} \quad , \text{ for } t > \frac{x}{c} \ , \tag{I-2}$$

(3) The rarefaction wave from the motion of the plate

$$-\rho c u \qquad \text{for } t > \frac{x}{c} \ . \tag{I-3}$$

In the above, p_o is the peak pressure and θ the duration parameter of the original wave, m is the mass per unit area and u the instantaneous velocity of the plate, c the velocity of sound in water, and ρ the density of water. By Newton's law the sum of these pressures (acting at $x = 0$) will give the plate a velocity.

$$u = \frac{2 p_o \theta}{m (\beta - 1)} \left(e^{-t/\theta} - e^{-\beta t/\theta}\right) , \tag{I-4}$$

in which $\beta = \rho c\theta/m$. In inserting this value of u in the expression for the pressure at x the proper value of the time to use is $t-x/c$ because of the propagation time. It is convenient to measure pressure in terms of p_o, time in terms of θ, and distance in terms of $c\theta$; i.e., $P = p/p_o$, $T = t/\theta$, $X = x/c\theta$. Then the sum of the three terms becomes

$$P = e^{-(T+X)} - \frac{\beta+1}{\beta-1} e^{-(T-X)} + \frac{2\beta}{\beta-1} e^{-\beta(T-X)} \tag{I-5}$$

an equation valid only for $T \geq X$. These considerations naturally hold only so long as cavitation does not take place.

Figure 131 shows some of the contour lines for P plotted against time T and distance

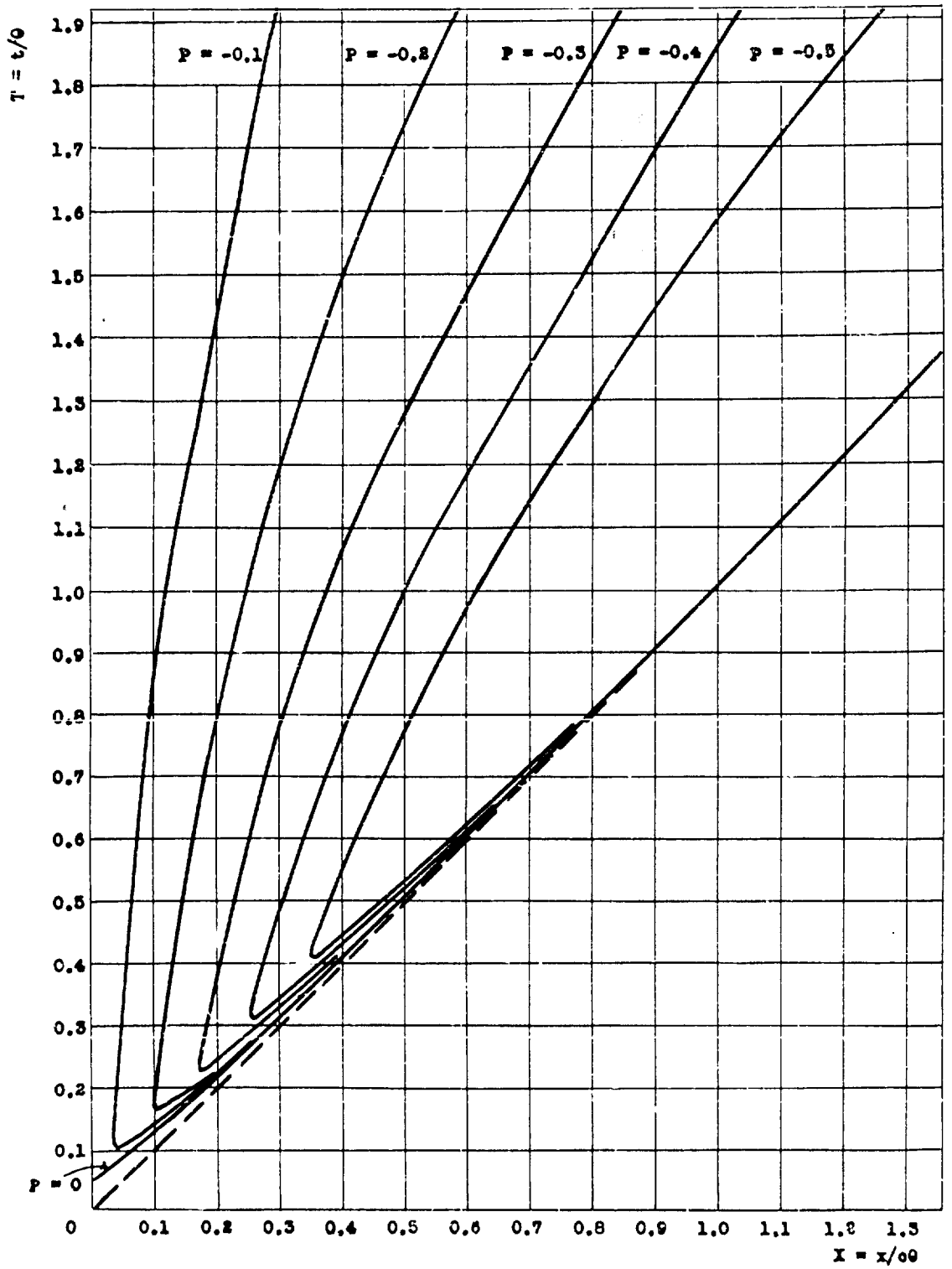


Fig. 131. Pressure before accelerated free plate.
Contours for $P = p/p_o$ vs. time and distance ($\beta = 83 = \rho c_0/m$).

15518

X, both in reduced units. $\beta = 83$ in this case, representing a very light plate, or a charge of great duration. The dashed line represents the front of the reflected wave. Below it the pressure is positive due to the original shock wave. Above it the pressure is at first positive and then falls steeply down into a valley of negative pressure. Except for the discontinuous rise and steep fall near the front of the reflected wave ($X = T$) the contours for this case closely approximate the case of a free surface.

Figure 132 shows similar contours for $\beta = 4$, a heavier plate (or smaller duration). In both cases it will be seen that the pressure falls to zero first at the plate, in a finite time $T = [1/(\beta-1)] \ln\beta$. It reaches negative vlaues first out in the water and below a certain limiting negative value the given contour never reaches the plate at all.

Assuming that the theory applies between the shock wave and the cavitation front, and that cavitation occurs at $p = 0$ we get, on solving Equation (I-5) for the time at which the pressure falls to Q at reduced distance X,

$$T = t/\theta = \frac{1}{\beta - 1} \ln \frac{2\beta\, e^{\beta X}}{(\beta+1)\, e^{X} - (\beta-1)\, e^{X}} \qquad \text{(I-6)}$$

In Table II, the measured values of x_0 (farthest distance of cavitation from plate) are substituted in Eq. (I-6) and the calculated values of T are compared with the times computed from the position of the shock wave.

In order to determine the radius of the cavitating region at the plate, it is necessary to take account of diffraction.

A very rough treatment of the effect of the diffraction wave is as follows. The same basic Eq. (I-1) can be used to compute the time τ at which the pressure in front of the plate has fallen from $2p_0$ to a value equal to that outside the plate, $p(\tau)$. For this purpose $X = 0$ (surafce of plate) and $p/p_0 = e^{-T}$ so

$$\tau = \frac{\theta}{\beta - 1} \ln \frac{2\beta}{\beta + 1} \qquad \text{(I-7)}$$

Beginning at time τ a pressure wave will spread inward from the edges because the pressure in front of the plate is being lowered by its motion. This pressure wave will reach a radius r at time $[\tau + (R-r)/c]$. If the pressure at r has fallen to zero before this time, it is postulated that cavitation will extend out to r, but if the diffraction wave reached r first then cavitation will not extend to r. Consequently, this theory predicts that the maximum radius of cavitation R_c will be determined by the equation

$$\tau + \frac{(R - R_c)}{c} = \theta_c \qquad \text{(I-8)}$$

where θ_c is the so-called cavitation time, i.e., time for p to fall to zero at the front of the plate. If $X = 0$ in Eq. (I-6) $t = \theta_c$ so

$$\theta_c = \frac{\theta}{\beta - 1} \ln\beta \qquad \text{(I-9)}$$

Combining Eqs. (I-7), (I-8), and I-9),

$$R_c = R - \frac{\theta\, c}{\beta - 1} \ln \frac{\beta + 1}{2}$$

or

$$\frac{R - R_c}{c\theta} = \frac{1}{\beta - 1} \ln \frac{\beta + 1}{2} \qquad \text{(I-10)}$$

The latter equation expresses the result in a dimensionless form, in which the distance in from the edge of the disk, $R - R_c$ is measured in terms of the length unit $c\theta$. In the case of a plate surrounded by an infinite rigid baffle, $\tau = 0$ and Eq. (I-10) becomes:

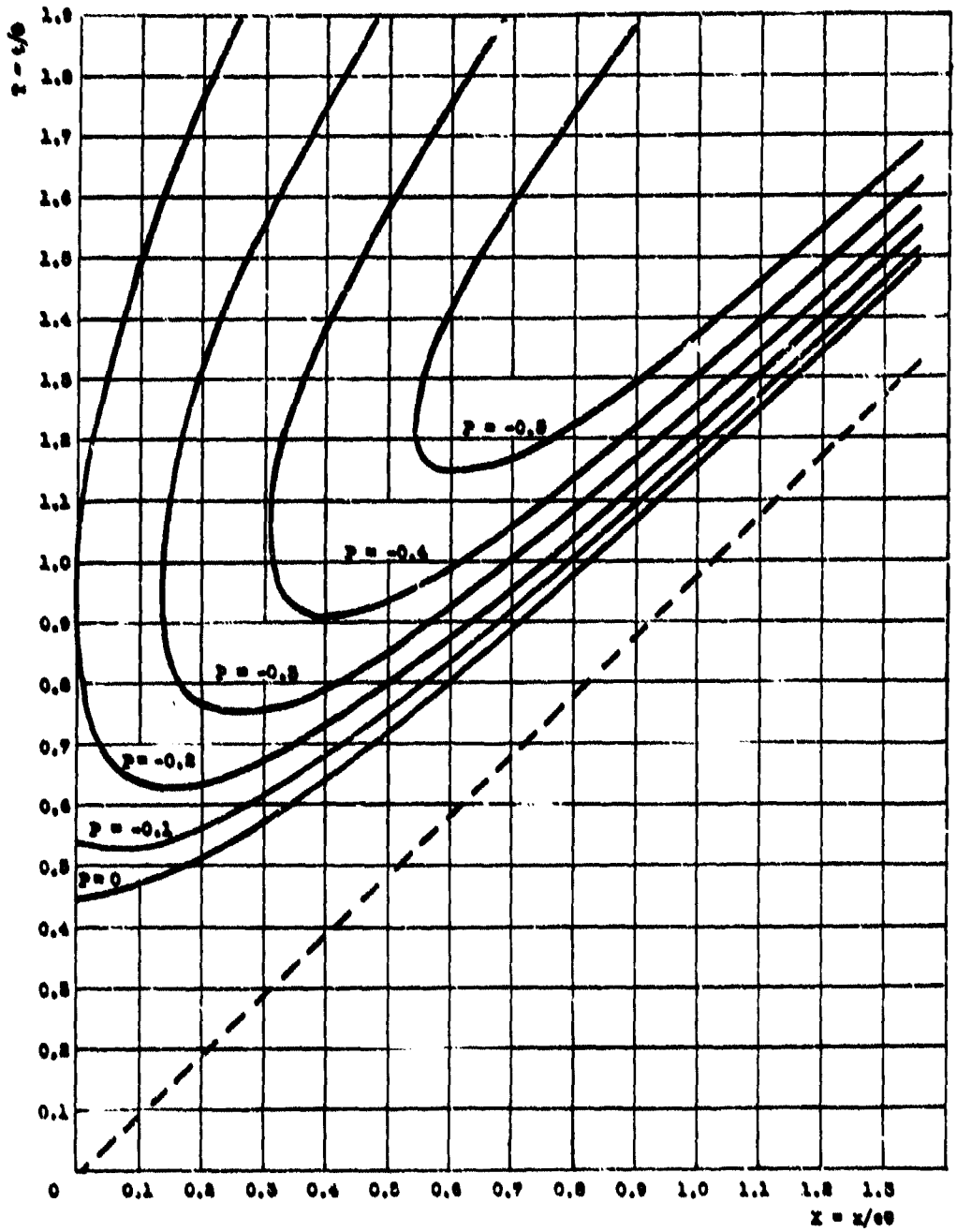


Fig. 158. Pressure before accelerated free plate.
Contours for $P = p/p_0$ vs. time and distance ($\beta = 4$ m/sec/m).

18518

$$\frac{R - R_c}{c\theta} = \frac{1}{\beta - 1} \ln \beta \qquad \text{(I-11.)}$$

This is the equation previously used as a cavitation criterion in connection with the photographs of the UERL diaphragm gage which is a baffled gage.

Editor's note: Appendix II, pages 66 to 86, by R.R. Halverson, appears as a separately published paper in this volume, just preceding this paper.

APPENDIX III

CIRCUIT DIAGRAMS OF CAMERA TIMERS

1. Timer for high speed camera [11]

Timing of the film speed of the Eastman High Speed Camera Model III is accomplished by photographing periodic light flashes from a small neon bulb synchronized with an oscillator. The bulb is mounted close to the film on the inside of the camera. The timing marks appear along the edge of the film and are photographed simultaneously with the recording of the phenomena under observation. Operating at 3000 frames per second, the maximum speed of the camera, the circuit shown schematically in Fig. 139 produces one mark on the film every third frame. Under these conditions the distance between two adjacent marks can be measured to one tenth of one per cent (i.e. to one μsec) by the use of an optical comparator.

The circuit was designed to operate from the output of a 1000 cycle per second tuning fork (General Radio Type 813A) although it can be used with other sinusoidal oscillators operating at different frequencies if slight changes are made in some of the circuit constants. The accuracy of the film speed determination depends on the accuracy of the oscillator frequency.

The essential parts of the circuit are a clipper (tubes T_2 and T_3) which converts the input sine wave into a square wave; a counter circuit (T_5 and T_6) which divides the input frequency by two; a short duration pulse generator (T_7 and T_8); a power output tube (T_9) to drive the neon flasher, and a tuning eye (T_1) to indicate the voltage of the sine wave from the oscillator.

The neon bulb operates satisfactorily when cables as long as 1000 ft. are used between the timer and the bulb; this is the greatest length of cable which has been employed. The current in the neon bulb is adjusted by the potentiometer in the cathode circuit of T_9 in order to control the intensity of the bulb; about 5 mamp is used at 1000 cps and 3 mamp at 500 cps.

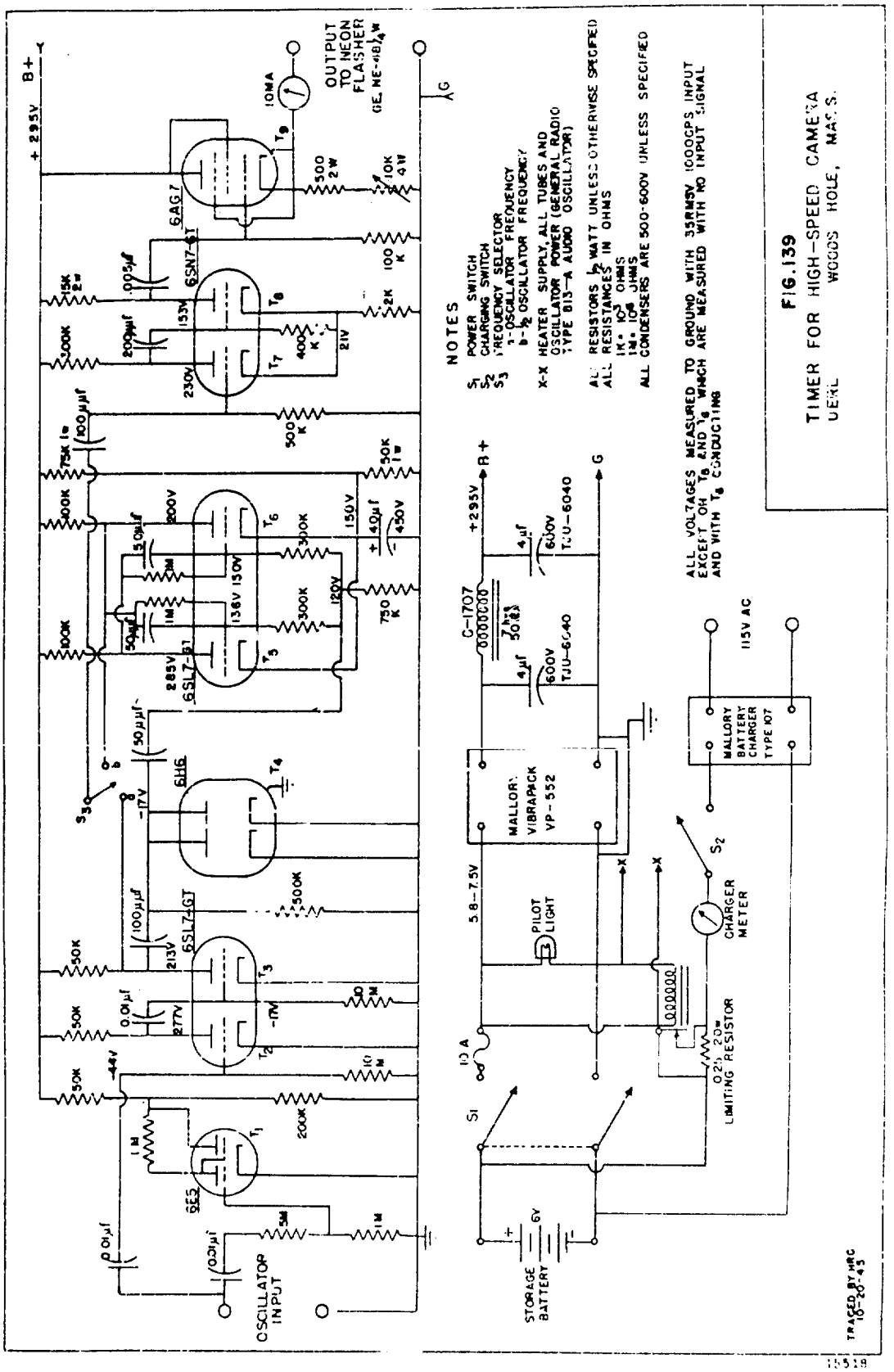
This circuit can be used with an external power supply operating from a power line and delivering 300-500 volts at 40 mamp, in addition to current for tube heaters, or from a 6-volt storage battery if other power is not available. It is desirable to use a different source of power for operating the circuit than that used for operating the camera because, when the camera starts, a very large surge is introduced which may affect the operation of the electronic circuit, particularly if the power is obtained from a small generator. A Mallory Type VP-552 vibrapack and a filter section are built into the unit for operation from a 6-volt battery and a Mallory Type 107 battery charger is included for charging the storage battery from a power line. The 1000 cps tuning fork, the vibrapack and the battery charger are included in a portable wooden carrying case which houses the electronic circuit.

2. Timer for Jerome camera

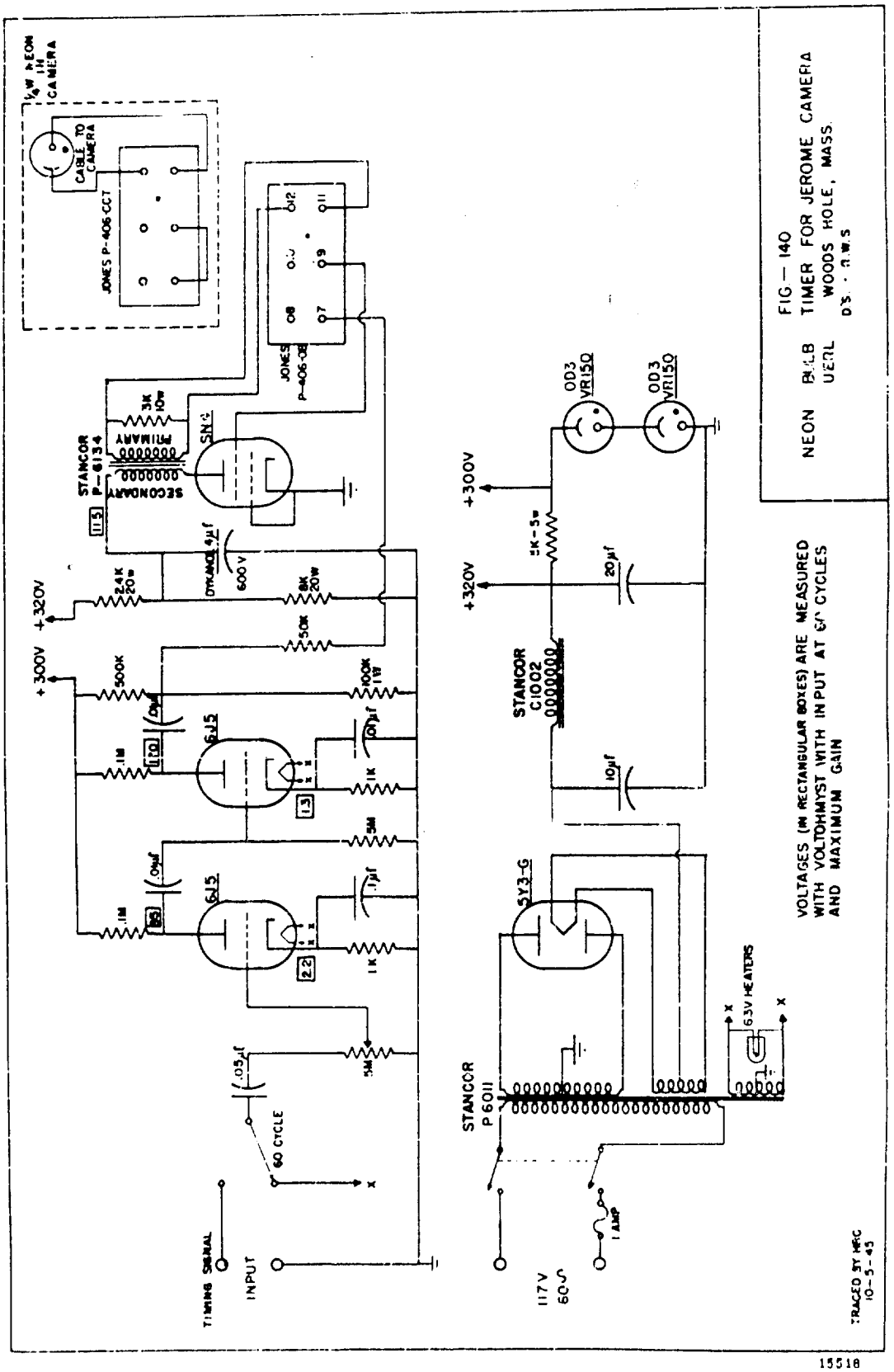
Inasmuch as the requirements for the Jerome camera were much less severe than those for the Eastman High Speed Camera because of the lower speed required, a simpler circuit shown in Fig. 140 was used to drive a neon lamp. A 50 cycle, single contact electrical tuning fork excites this unit. The signal from the fork is amplified and sharpened into short duration pulses in the first two stages and then applied to the grid of a Strobotron tube (SN4). The SN4 fires on each pulse, discharging the 4 μf condenser through the transformer in its plate circuit. The output of this transformer drives a 1/4 watt neon bulb mounted in the camera and connected to the timer unit through a cable. The short discharge time of the 4 μf condenser insures short duration light pulses from the neon bulb suitable for dotting the film.

---

[11] This is discussed in more detail by G. K. Fraenkel, Apparatus for the measurement of air burst pressures by means of piezoelectric gages, NDRC No. A-373, OSRD No. 6251, Chapter 9.3.


+295V B+
OUTPUT TO NEON FLASHER
OSCILLATOR INPUT
STORAGE BATTERY 6V
MALLORY VIBRAPACK VP-552
MALLORY BATTERY CHARGER TYPE 107
115V AC
PILOT LIGHT
CHARGER METER
LIMITING RESISTOR
NOTES
ALL VOLTAGES MEASURED TO GROUND WITH 35RMSV 1000CPS INPUT EXCEPT OH T6 AND T8 WHICH ARE MEASURED WITH NO INPUT SIGNAL AND WITH T6 CONDUCTING
FIG.139
TIMER FOR HIGH-SPEED CAMERA
USNL WOODS HOLE, MASS.
TRACED BY MRC 10-20-45

1050


1/4 W NEON IN CAMERA
CABLE TO CAMERA
JONES P-406-CCT
JONES P-406-CB
STANCOR P-6134
PRIMARY
SECONDARY
3K 10W
SN-2
600 V
2.4K 20W
8K 20W
5.0K
+320V
+300V
500K
100K 1W
.1M
6J5
1K
5M
1M
1µf
.05µf
60 CYCLE
INPUT
TIMING SIGNAL
+300V
+320V
2K-5W
20µf
10µf
STANCOR C1002
OD3 VR150
OD3 VR150
5Y3-G
STANCOR P-6011
6.3V HEATERS
1 AMP
117V 60~
NEON BULB USED
VOLTAGES (IN RECTANGULAR BOXES) ARE MEASURED WITH VOLTOHMYST WITH INPUT AT 60 CYCLES AND MAXIMUM GAIN
FIG — 140
TIMER FOR JEROME CAMERA
WOODS HOLE, MASS.
TRACED BY HRC 10-5-45
15518

APPENDIX IV

GASKETS AND STUFFING BOXES FOR CAMERA CASES

We have found that gasket and stuffing box design for our camera cases is not very critical. No special effort is made to achieve very close tolerances on gasket surfaces. However, whenever practical we put the gasket in a tongue and groove type of joint. The only gasket failures we have had have been due to static and not dynamic pressure. At a depth of 600 feet, for example, we found that we could not use our ordinary 1/8 to 1/16 inch rubber gasket because it squeezed out. Thin Vellumoid was found satisfactory in this instance.

We have used two types of stuffing boxes for electrical leads with equal success. In the first type (see Fig. 141) the wire cable led through a hole in the case which was packed with compressed rubber. In the second type (Fig. 142), an insulated metal jack was put through the case and electrical connections were made on both sides of the jack. The second method is perhaps preferable in deep water because there is no chance of water leaking into the case through a hole in the cable insulation.

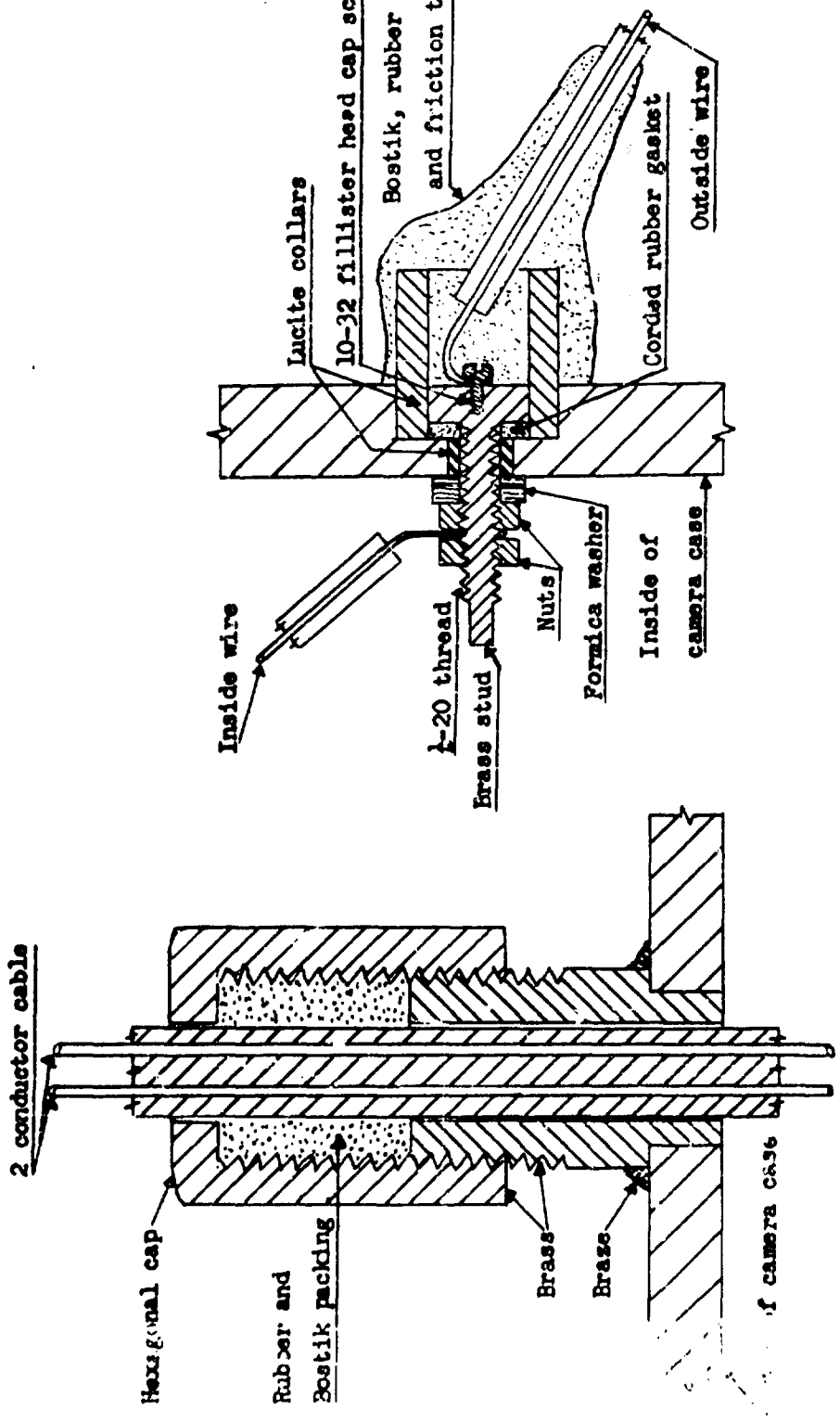


Fig. 142. Single wire lead-in connector.

Fig. 141. Stuffing box for electric cable.

15518

Best Available Copy

THE DECAY OF PLANE, CYLINDRICAL AND SPHERICAL SHOCK WAVES

A. J. Harris
Road Research Laboratory, London

British Contribution

September 1942

THE DECAY OF PLANE, CYLINDRICAL AND SPHERICAL SHOCK WAVES

A. J. Harris

Road Research Laboratory, London

September 1942

* * * * * * *

Summary:

Expressions are deduced connecting the rate of decay of the pressure at a shock front in a spherical cylindrical or plane wave with the space rates of change of pressure and particle velocity behind the shock front. It is suggested that these may be used to derive some idea of the thickness of a shock wave when its rate of propagation has been determined as a function of time.

We shall consider only the spherical wave, since the plane wave is merely a particular case of this more general type. Taylor(1) has given an approximate expression relating the rate of decay to the slope of the wave immediately behind the shock front. The present analysis results in a more accurate relation, moreover the corresponding results for spherical and cylindrical waves given here are new.

Assuming spherical symmetry in the wave we take spherical co-ordinates with origin at the centre of the shock front.

r = distance of point from origin of co-ordinates.
t = time.
u = particle velocity in direction of r increasing.
ρ = density of gas.
p = pressure in gas.
p_1 = pressure immediately behind shock front.
u_1 = velocity of particles immediately behind shock front.
v_1 = velocity of shock front.
ρ_1 = density of gas behind shock front.
R = radius of shock front sphere at time t.

Equations of motion and continuity are

$$\frac{\partial u}{\partial t} + u\frac{\partial u}{\partial r} = -\frac{1}{\rho}\frac{\partial p}{\partial r} \qquad (1)$$

$$\frac{\partial \rho}{\partial t} + \frac{1}{r^2}\frac{\partial}{\partial r}(r^2 \rho u) = 0 \qquad (2)$$

p_1 u_1 v_1 ρ_1 and R are functions of t only and we have

$$\frac{dp_1}{dt} = \frac{\partial p}{\partial t} + v_1\frac{\partial p}{\partial r} \text{ at } r = R \qquad (3)$$

$$\frac{d\rho_1}{dt} = \frac{\partial \rho}{\partial t} + v_1\frac{\partial \rho}{\partial r} \text{ at } r = R \qquad (4)$$

$$\frac{du_1}{dt} = \frac{\partial u}{\partial t} + v_1\frac{\partial u}{\partial r} \text{ at } r = R \qquad (5)$$

Let $\frac{D}{Dt}$ denote the rate of change associated with a particular gas particle, i.e. $\frac{D}{Dt} = \frac{\partial}{\partial t} + u\frac{\partial}{\partial r}$.

we have

$$\frac{Du}{Dt} = \frac{\partial u}{\partial t} + u \frac{\partial u}{\partial r} \qquad (6)$$

also $$\frac{D\rho}{Dt} = c^2 \frac{D\rho}{Dt} \qquad (7)$$

where c^2 is a function of ρ or s and the particular particle under consideration.

Then from (3) and (6)

$$\frac{\partial a}{\partial t} + \frac{Du}{Dt} = u \frac{\partial a}{\partial r} + b_1 \frac{\partial r}{\partial t} + (b_1 - u) \frac{\partial a}{\partial r} + c^2 \left(\frac{\partial \rho}{\partial t} + u \frac{\partial \rho}{\partial r} \right)$$

$$= (b_1 - u) \frac{\partial a}{\partial r} + c^2 \left(-\frac{1}{r^2} \frac{\partial}{\partial r} (r^2 \rho u) + u \frac{\partial \rho}{\partial r} \right) \text{ using (2).}$$

and finally

$$\frac{\partial a}{\partial t} + (b_1 - u) \frac{\partial a}{\partial r} - c^2 \rho \frac{\partial u}{\partial r} - \frac{2 \rho c^2 u}{r} \quad \text{where } r = R \qquad (8)$$

Again from (1) and (5) we have

$$\frac{\partial u}{\partial t} + u \frac{\partial u}{\partial r} + b_1 \frac{\partial u}{\partial r} = -u \frac{\partial u}{\partial r} - \frac{1}{\rho} \frac{\partial a}{\partial r} + b_1 \frac{\partial u}{\partial r}$$

$$= (b_1 - u) \frac{\partial u}{\partial r} - \frac{1}{\rho} \frac{\partial a}{\partial r} \quad \text{where } r = R \qquad (9)$$

Eliminating $\frac{\partial u}{\partial r}$ from (8) and (9) we have

$$(b_1 - u) \frac{da_1}{dt} - (b_1 - u)^2 \frac{\partial a}{\partial r} - c^2 \rho \left\{ \frac{du_1}{dt} + \frac{1}{\rho} \frac{\partial a}{\partial r} \right\} = \frac{2 \rho c^2 u}{r} (b_1 - u)$$

$$(b_1 - u) \frac{da_1}{dt} + c^2 \rho \frac{du_1}{dt} = \frac{\partial a}{\partial r} \{ (b_1 - u)^2 - c^2 \} - \frac{2 \rho c^2 u (b_1 - u)}{r}$$

where $r = R$ (10)

Since all terms in (10) refer to the point immediately behind the shock wave we may rewrite (10) as

$$(b_1 - u_1) \frac{da_1}{dt} + c_1^2 \rho_1 \frac{du_1}{dt} = \frac{\partial a}{\partial R} \{ (b_1 - u_1)^2 - c_1^2 \} - \frac{2 \rho_1 c_1^2 u_1 (b_1 - u_1)}{R} \qquad (11)$$

where c_1 is the value of c appropriate to gas just behind the shock wave.

The Rankine Hugoniot theory(1) of the shock waves gives

$$u_1 = \frac{2 b_1 (b_1 - a_0)}{(\gamma - 1) c_0 + (\gamma + 1) c_1} \qquad (12)$$

$$b_1 = c_0 \sqrt{\frac{(\gamma - 1) a_0 + (\gamma + 1) a_1}{2 \gamma a_0}} \qquad (13)$$

$$c_0 = \sqrt{\frac{\gamma p_0}{\rho_0}} \qquad (14)$$

$$c_1 = \sqrt{\frac{\gamma p_1}{\rho_1}} \qquad (15)$$

$p_1 = \ldots\ldots$

$$\rho_1 \quad \rho_0 \frac{(\gamma-1)\,a_0 + (\gamma+1)\,a_1}{(\gamma+1)\,a_0 + (\gamma-1)\,a_1} \qquad (16)$$

where the suffix o refers to the undisturbed gas.

Using (12)-(16) we can eliminate from (11) all quantities with the suffix 1 except a_1. When this is done we obtain the result

$$\frac{da_1}{dt} = -c_0 \frac{\gamma+1}{\sqrt{2\gamma}} \frac{(\gamma-1)\{\gamma+1+(\gamma-1)y\}\sqrt{\gamma-1+(\gamma+1)y}}{\{\gamma^2-1+y(5\gamma^2-\gamma+2)+y^2(2\gamma^2+\gamma-1)\}} \left\{ \frac{\partial \rho}{\partial R} + \frac{4\gamma}{\gamma+1} \frac{a_0 y}{R} \right\} \qquad (17)$$

where a_1/a_0 is denoted by y.

Since $dR = a_1 dt$ we may write (17) in the form

$$\frac{da_1}{dR} = -(\gamma+1) \frac{(\gamma-1)\{\gamma+1+(\gamma-1)y\}}{\{\gamma^2-1+y(5\gamma^2-\gamma+2)+y^2(2\gamma^2+\gamma-1)\}} \left\{ \frac{\partial \rho}{\partial R} + \frac{4\gamma}{\gamma+1} \frac{a_0 y}{R} \right\} \qquad (18)$$

The formula for plane waves is obtained by going to the limit as $R \to \infty$. The term containing R is simply dropped from equations (17) and (18). Taylor's formula for the plane wave is

$$\frac{da_1}{dt} = -(u_1 + c_1 - a_1) \frac{\partial \rho}{\partial x} \quad \text{or}$$

$$\frac{da_1}{dt} = -\frac{c_0}{\sqrt{2\gamma}} \sqrt{\frac{\gamma+1+(\gamma-1)y}{\gamma-1+(\gamma+1)y}} \{\sqrt{2\gamma y} - \sqrt{\gamma+1+(\gamma-1)y}\} \frac{\partial \rho}{\partial x} \qquad (19)$$

which differs from (17). The discrepancy is due to Taylor's assumption that a given value of pressure just behind the shock front is propagated forward with a velocity c_1 relative to the gas.

If instead of $\frac{\partial u}{\partial r}$ we had eliminated $\frac{\partial \rho}{\partial r}$ from (8) and (9) we should have found

$$\frac{da_1}{dt}\left[1 + \rho_1 (a_1 - u)\frac{du_1}{da_1}\right] = \rho_1 \frac{\partial u}{\partial R}\{(a_1 - u)^2 - c_1^2\} - \frac{2\rho_1 c_1^2 u_1}{r} \qquad (20)$$

or

$$\frac{da_1}{dt} = -\frac{\partial u}{\partial R} \cdot a_0 (\gamma+1) \frac{(\gamma-1)\{\gamma-1+(\gamma+1)y\}}{\{3y(\gamma+1)+5\gamma-3\}} - \frac{4\sqrt{2}}{R}\sqrt{\frac{c_0^3}{\rho_0}} \times$$

$$\times \frac{\gamma y (\gamma-1)\sqrt{\gamma-1+(\gamma+1)y}}{\{3y(\gamma+1)+5\gamma-3\}} \qquad (21)$$

or

$$\frac{da_1}{dR} = -\frac{\partial u}{\partial R} \cdot \frac{a_0}{c_0} \frac{(\gamma+1)(\gamma-1)\sqrt{2\gamma(\gamma-1+(\gamma+1)y}}{3y(\gamma+1)+5\gamma-3} - \frac{8}{R} \frac{a_0 \gamma y (\gamma-1)}{(3y(\gamma+1)+5\gamma-3)} \qquad (22)$$

If we omit from (18) and (22) the terms depending on the form of the wave, we obtain two different rates of decay. These agree, however, when a_1 is small, and reduce to the ordinary result for small waves. When a_1 is large, equation (18) gives

$$\frac{da_1}{dR} = -\frac{4\gamma(\gamma-1)}{(2\gamma-1)(\gamma+1)} \frac{a_0 y}{R}$$

Integrating .....

Integrating we obtain

$$y \propto R^{\frac{1}{\frac{4\gamma(\gamma-1)}{(2\gamma-1)(\gamma+1)}}} \quad \text{which becomes} \tag{22}$$

$$y \propto \frac{1}{R^{1.52}} \quad \text{for the case of air}$$

Equation (22) gives

$$y \propto R^{\frac{1}{\frac{4\gamma}{3(\gamma+1)}}} \quad \text{or} \quad y \propto \frac{1}{R^{1.5}} \quad \text{for air} \tag{23}$$

Since the blast waves from bombs decay much more rapidly at first than $R^{-1.5}$ it follows that most of the decay is due to the form of the wave. If the forepart of the wave could be flattened far less energy would be lost in the early stages of the blast.

Equations (17) (18) (21) and (22) may be used to find $\frac{db_1}{dR}$ as in (1), or they may be used to determine $\frac{\partial \rho}{\partial R}$ and $\frac{\partial u}{\partial R}$ when c_1 is known as a function of time. If the velocity of propagation of a shock wave can be recorded, the pressure can be calculated. The quantities $\frac{\partial \rho}{\partial R}$ and $\frac{\partial u}{\partial R}$ then give some indication of the thickness of the wave.

Expressing our equations directly in terms of b_1 and its rate of decay we get

$$\frac{\partial \rho}{\partial R} = -\frac{2\rho_0}{(\gamma+1)} \frac{\left[2(2\gamma-1)b_1^4 + (\gamma+3)b_1^2 c_0^2 - (\gamma-1)c_0^4\right]}{(b_1^2 - c_0^2)\left\{(\gamma-1)b_1^2 + 2c_0^2\right\}} \frac{db_1}{dt}$$

$$-\frac{4}{R}\frac{\rho_0}{(\gamma+1)^2}\left\{2\gamma b_1^2 - (\gamma-1)c_0^2\right\} \tag{24}$$

$$\frac{\partial u}{\partial R} = -\frac{2(3b_1^2 + c_0^2)}{(\gamma+1)b_1(b_1^2 - c_0^2)}\frac{db_1}{dt} - \frac{4}{R}\frac{\left\{2\gamma b_1^2 - (\gamma-1)c_0^2\right\}}{(\gamma+1)^2 b_1} \tag{25}$$

It may be noted that the case of cylindrical waves can be treated in the same manner. The equations which result are the same as for the spherical wave except that the coefficient of $\frac{1}{R}$ is only half what it is in the spherical case, e.g. for a cylindrical wave (24) becomes

$$\frac{\partial \rho}{\partial R} = -\frac{2\rho_0}{\gamma+1} \frac{\left[2(2\gamma-1)b_1^4 + (\gamma+3)b_1^2 c_0^2 - (\gamma-1)c_0^4\right]}{(b_1^2 - c_0^2)\left\{(\gamma-1)b_1^2 + 2c_0^2\right\}} \frac{db_1}{dt}$$

$$-\frac{2}{R}\frac{\rho_0}{(\gamma+1)^2}\left\{2\gamma b_1^2 - (\gamma-1)c_0^2\right\} \tag{26}$$

Reference.

(1) "The Propagation and Decay of Blast Waves". G.I. Taylor.

PRESSURES PRODUCED BY THE UNDERWATER EXPLOSION OF LINE CHARGES

G. Charlesworth
Road Research Laboratory, London

British Contribution

November 1943

PRESSURES PRODUCED BY THE UNDERWATER EXPLOSION OF LINE CHARGES

G. Charlesworth

November 1943

* * * * * * *

Summary.

Pressure-time curves have been obtained with piezo-electric gauges at points near to line charges consisting of lengths of Cordtex detonated under water. Measurements on the perpendicular bisectors of 30, 14 and 5 feet lengths of charge showed that the peak pressure was not appreciably affected by the length of the charge but that the impulse decreased with length of charge. Measurements were also made at points on the axes of 5 feet lengths of Cordtex with detonation towards and away from the gauges. At the same distance from the charge the maximum pressures were greatest at points on the perpendicular bisector and least on the axis in the direction of detonation of the charge. The rate of decay of pressure behind the wave front was less on the axis than at right angles to it. It is suggested that the enhanced peak pressure on the axis when detonation took place away from the gauge may have been partly due to the added effect of the detonator. The impulses on the axis were independent of the direction of detonation and about half those on the perpendicular bisector of the charge. This difference may have been partly due to the effect of the negative surface reflection reducing the impulses more at points on the axis than at right angles to it.

Introduction.

The object of the tests was to determine the form and magnitude of the pressures produced by underwater explosion of line charges.

Experimental.

Pressure measurement:- Pressures were measured by piezo-electric gauges recording photographically by means of cathode-ray oscillographs.

Charges:- The charges used consisted of various lengths of Cordtex containing about 2.3 gm. of P.E.T.N./ft. The charges were stretched in a straight line parallel to the water surface.

Site:- The tests were made in a concrete tank containing about 36,000 gallons of water, the depth of water being about 9 feet 6 inches. The charges and gauges were all about 3 feet 6 inches deep.

Arrangement of Tests.

Two sets of tests were made:-

(a) Pressures were measured at points on the perpendicular bisector of the line charge for charge lengths of 30 feet, 14 feet and 5 feet.

(b) Measurements were made along the axis of the charge, the charge being detonated towards the gauges in one case and away from them in the other.

The arrangements are shown diagrammatically in Figure 1.

Results .....

Results.

Typical pressure-time records obtained in the tests are reproduced in Figure 3(a), (b), (c), (d) and (e). It is seen that the records consist of a main pulse followed about 3 milliseconds later by reflections from the bottom and the sloping sides of the tank. The two lower records show further waves which occur 5 to 6 milliseconds after the initial wave. The origin of these waves is not known but they may be due to the bubble produced by the charge. The pulses were probably too small to be detected in the other records.

The main pulses in Figures 3(a), (b) and (c) are similar to those produced by a charge of normal shape, i.e. a cylindrical charge with height equal to diameter and have a shock front followed by a rapid decrease of pressure behind the front. In Figures 3(d) and (e), however, the rate of fall of pressure is much lower.

The variation of peak pressure and impulse with distance along the perpendicular bisector of the line charge are shown in Figures 4 and 5 for lengths of 30 feet, 14 feet and 5 feet of Cordtex. These figures also show the values for a 1 oz. charge of P.E.T.N. of normal shape. It is seen that in these tests the length of Cordtex did not appreciably affect the peak pressure at a given distance from it but that the impulse decreased with decreasing length of charge.

The velocity of detonation along the Cordtex is about 20,000 ft./sec. whilst the velocity of sound in water is only about 5,000 ft./sec. Hence the pressure-wave front in the water will resemble somewhat the bow wave produced by firing a bullet in air. The state of affairs will be approximately as represented in Figure 2 where $\sin\beta$ equals 0.25. The first part of the pressure wave to reach a point at a perpendicular distance d from the middle of the line charge thus comes from a point at a distance x from the centre of the Cordtex where $x = 0.26d$ approximately. For the lengths of Cordtex and the distances d used in the tests, x was less than half the length of the charge and it is therefore to be expected that the initial peak pressure will be independent of the length of the charge. This acoustic approximation is not strictly true for explosion waves but serves to indicate the nature of the effects involved. Since the tail of the wave is due to the cumulative effect of all the wavelets produced by all parts of the Cordtex, the impulse will decrease with length of charge, as was in fact observed.

The pressure and impulse values at points on the perpendicular bisector of the 14 feet charge were about the same as those from 1 oz. P.E.T.N. at equal distances from the centres of the charges. Thus at these points 1.63 oz. P.E.T.N in Cordtex is about equivalent to 1 oz. P.E.T.N. in a charge of normal shape.

In Figures 6 and 7 the variations of pressure and impulse at points round 5 feet of Cordtex are shown as functions of the shortest distance from the charge. It is seen that the pressure was greatest on the perpendicular bisector of the line charge and least on the axis when detonation was towards the gauge. The difference in peak pressure at points on the axis of the charge may have been due to the contribution of the detonator which contained about 1 gm. charge since the pressure was greater when the detonator was near the charge. This is indicated by the pressure-time curves (Figures 3(d) and (e)) where the initial peak pressure falls rapidly to about the same value in each case.

Figure 7 shows that under the test conditions at points at the same distance from the charge, the impulses along the axis of the charge were independent of the direction of detonation and were about half those on the perpendicular bisector. Reflection from the free surface, however, reduces the impulse along the axis. Figure 3(c) shows that perpendicular to the line charge the pressure-time curve is not appreciably affected by the surface reflection and the measured impulse is approximately the total impulse. On the axis of the charge where the rate of decay of pressure behind the shock front was less rapid, Figures 3(d) and (e) show that the negative surface reflection cuts off an appreciable part of the tail of the pulse. Consequently the measured impulse was probably considerably less than the total impulse produced by the charge in the water.

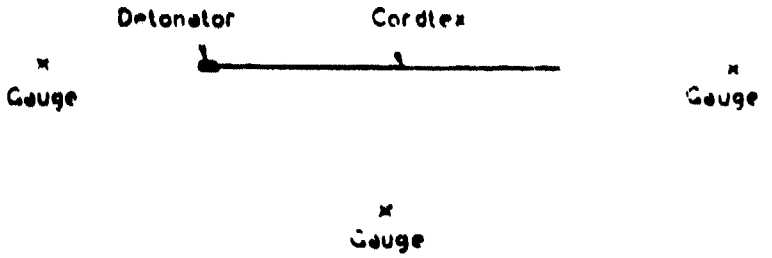


Fig.1 DIAGRAMMATICAL REPRESENTATION OF GAUGE POSITIONS ROUND THE CORDTEX

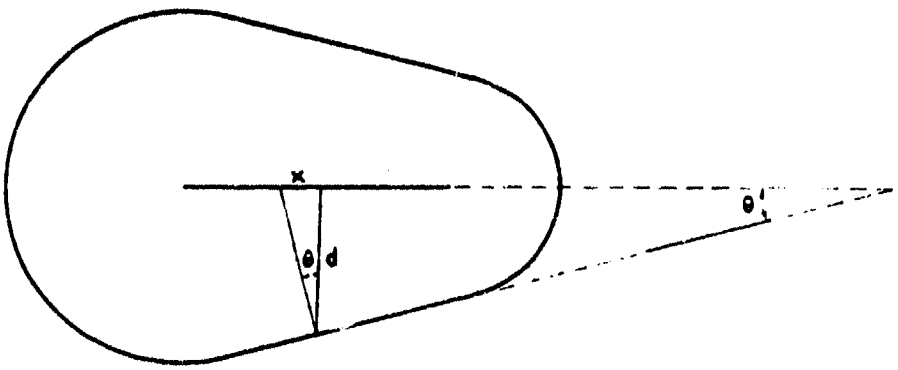
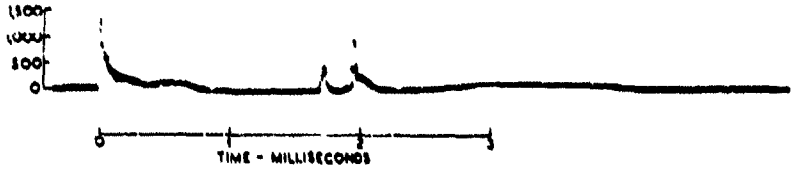
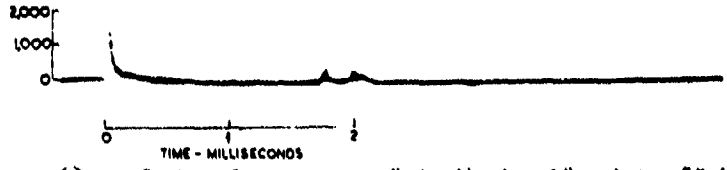


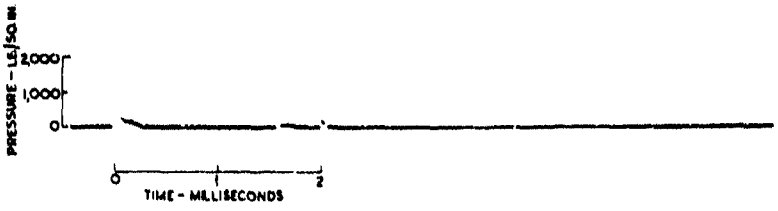
Fig.2. DIAGRAMMATICAL REPRESENTATION OF THE APPROXIMATE FORM OF THE WAVE FRONT PRODUCED IN THE WATER BY THE CORDTEX



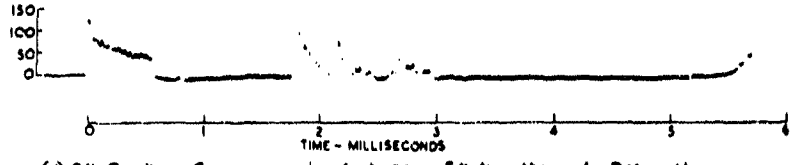
(a) 30ft. Cordtex. Gauge on perpendicular bisector of line charge, 5ft from the centre



(b) 14ft. Cordtex. Gauge on perpendicular bisector of line charge, 5ft. from the centre



(c) 5ft. Cordtex. Gauge on perpendicular bisector of line charge, 5ft. from the centre



(d) 5ft. Cordtex. Gauge on axis of charge, 5ft. from the end, Detonation towards the gauge



(e) 5ft. Cordtex. Gauge on axis of charge 5ft. from the end, Detonation away from the gauge

Fig. 3. Pressure-time curves produced by various lengths of Cordtex.

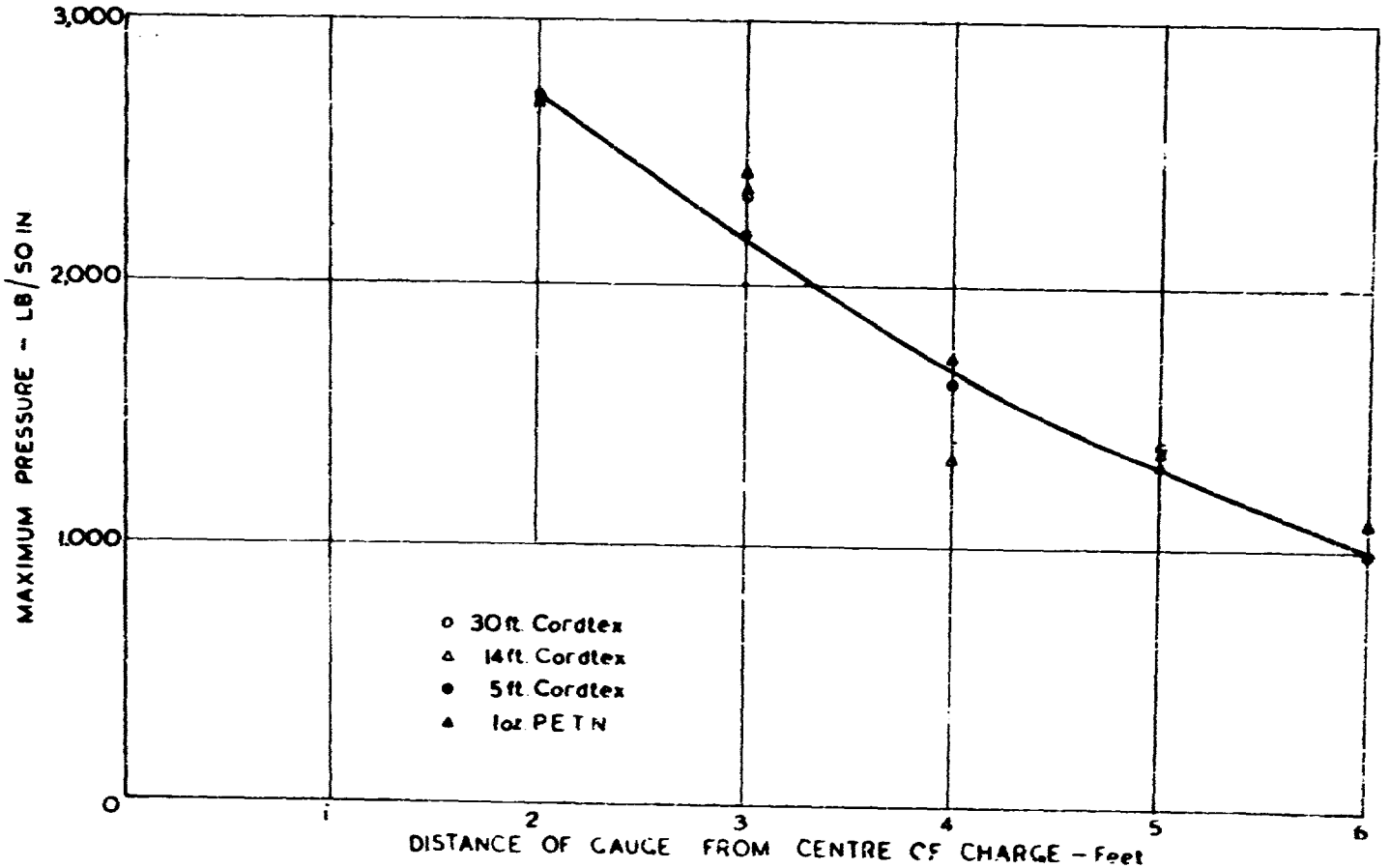
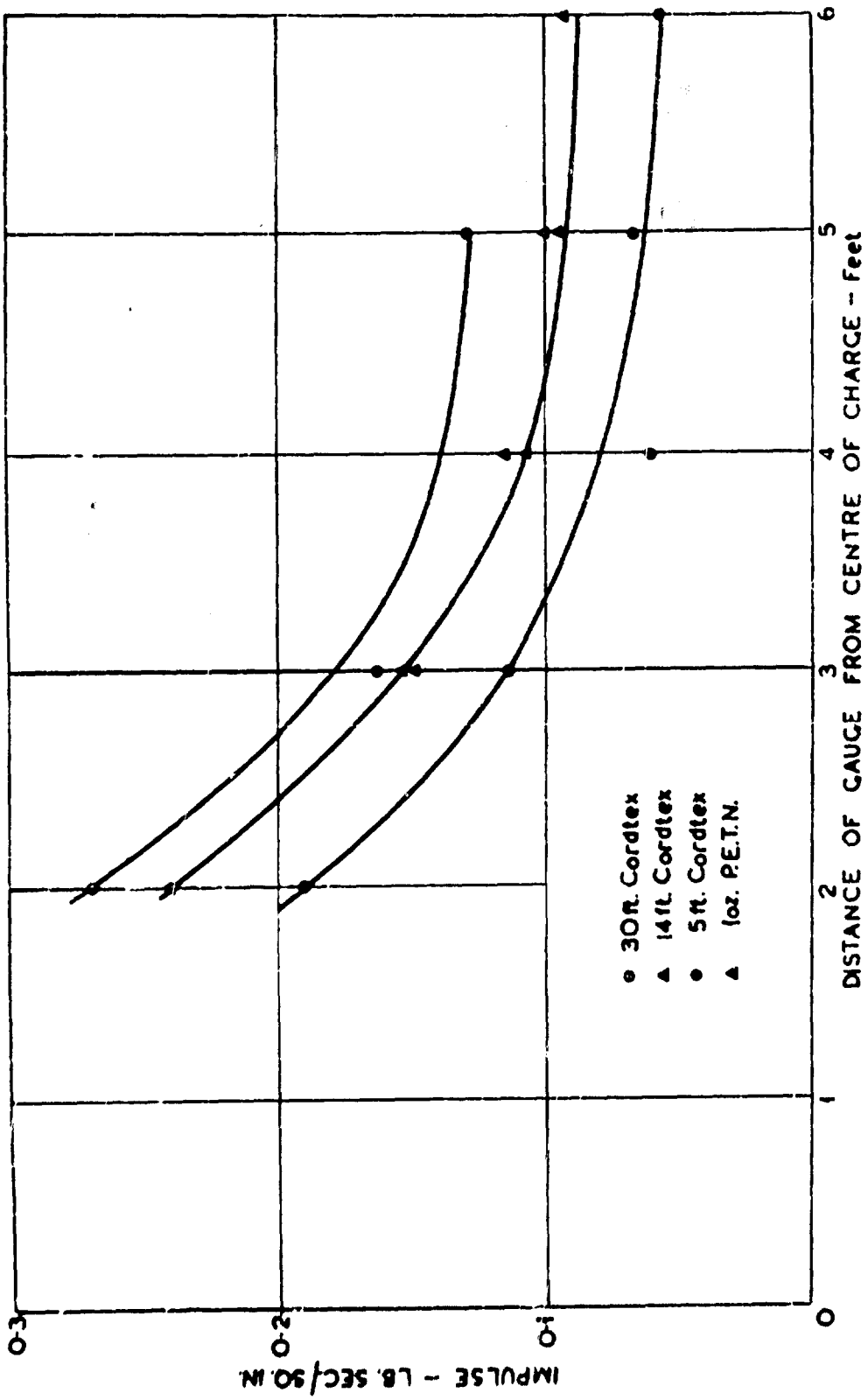


Fig 4. MAXIMUM PRESSURES AT POINTS ON THE PERPENDICULAR BISECTOR OF THE LINE CHARGE FOR VARIOUS LENGTHS OF CHARGE AND ALSO THE MAXIMUM PRESSURES AT VARIOUS DISTANCES FROM A 1oz CHARGE OF PETN. OF NORMAL SHAPE

1081



Figs. IMPULSES AT POINTS ON THE PERPENDICULAR BISECTOR OF THE LINE CHARGE FOR VARIOUS LENGTHS OF CHARGE, AND ALSO THE IMPULSES AT VARIOUS DISTANCES FROM A 1oz. CHARGE OF P.E.T.N. OF NORMAL SHAPE

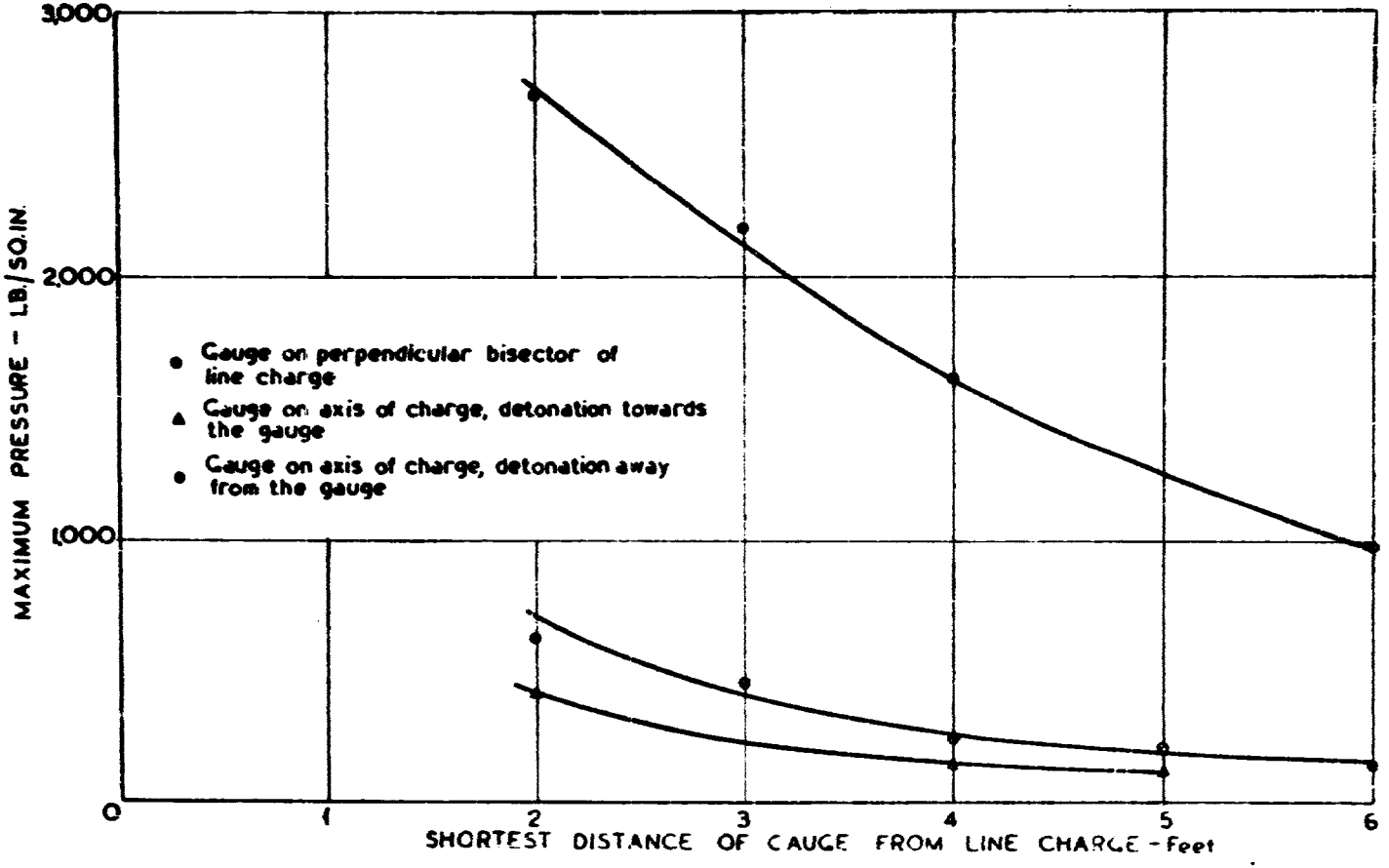
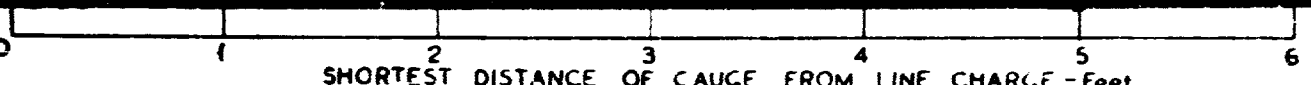


Fig.6. MAXIMUM PRESSURES AS FUNCTIONS OF THE SHORTEST DISTANCE OF THE CAUGE FROM THE CHARGE AT VARIOUS POINTS ROUND THE LINE CHARGE



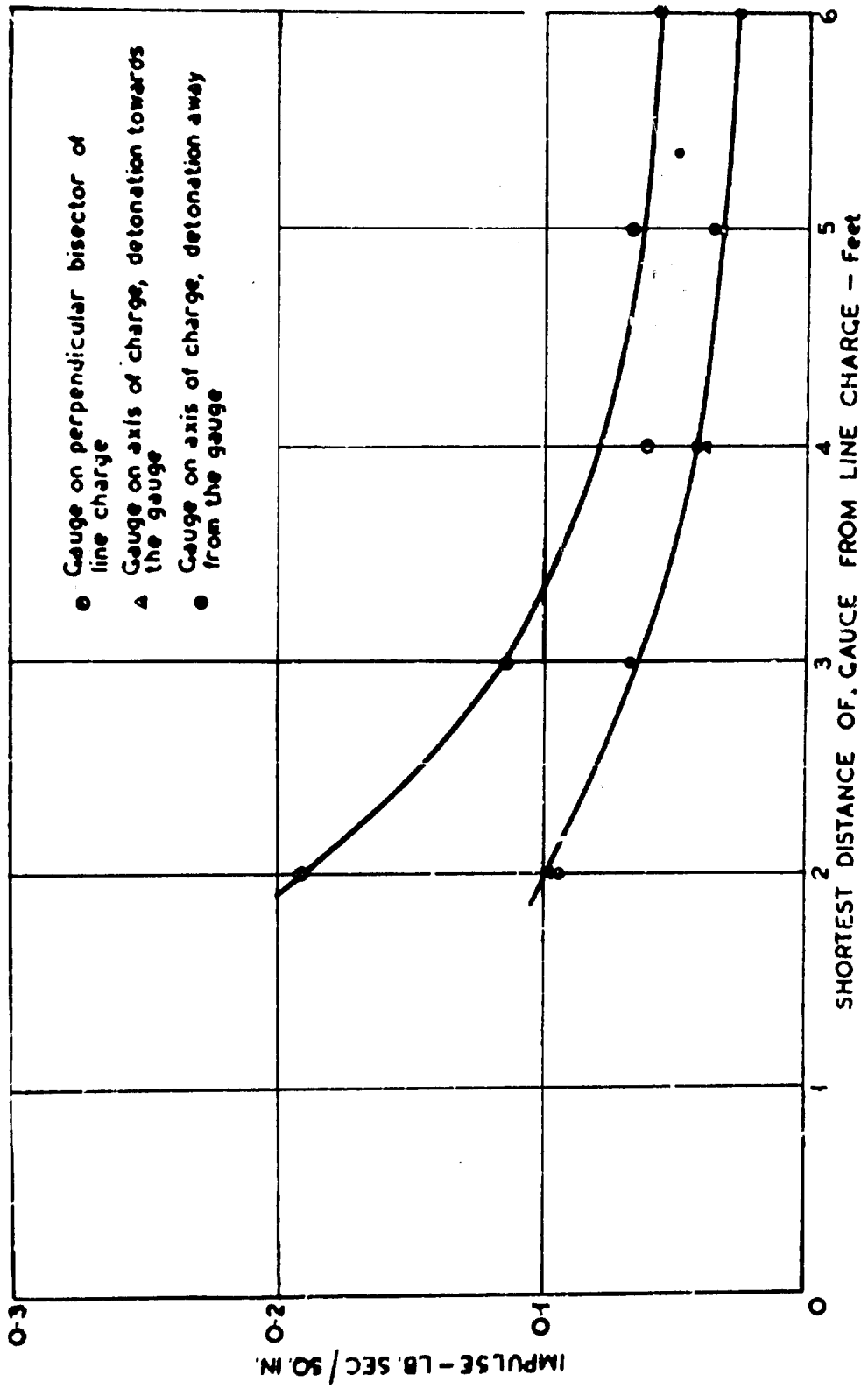


Fig 2. IMPULSES AS FUNCTIONS OF THE SHORTEST DISTANCE OF THE GAUGE FROM THE CHARGE AT VARIOUS POINTS ROUND THE LINE CHARGE

DECAY OF SHOCK WAVES IN WATER

A. J. Harris
Road Research Laboratory, London

British Contribution

December 1943

DECAY OF SHOCK WAVES IN WATER.

A. J. Harris

Road Research Laboratory,
London

December 1943

* * * * * *

Summary.

In O.S.R.D. 588, on certain assumptions, Kirkwood and Bethe have given a complete solution for the shock wave propagated into water from an explosive charge. There is, however, a manner in which the self consistency of the solution can be checked. Assuming that the pressure at the shock front decays with distance from the origin as in Kirkwood and Bethe's solution it is possible, through relations given in R.R.L. Note No. ID/17/AJH, to calculate the pressure gradient just behind the shock front, and to compare it with the gradient given in Kirkwood and Bethe's own solution. It is found that until the wave has moved outwards five or six charge radii those values of the gradient differ by about 30 per cent indicating some discrepancy between form of wave and rate of decay in the early stages.

A further application of the theory outlined in ID/17 indicates that the effect of wave shape on the rate of decay is much smaller than that due to the increasing distance from the origin, indeed if the effect of wave shape is entirely neglected the peak pressure at 12 charge radii from the origin is raised only by some 20 per cent.

The relation between the rate of decay of pressure at the shock front and the pressure gradient behind the shock front in a spherical wave has been given in R.R.L. Note No. ID/17/AJH; if the rate of decay is known the gradient can be calculated or vice versa. It was pointed out by W.G. Penney that this possibility provides a test of the self consistency of any theoretical wave solution which gives both the rate of decay and the gradient. Such a solution is that of Kirkwood and Bethe in O.S.R.D. 588, for a wave in water. The test of consistency used in this note is a comparison of the pressure gradient given in O.S.R.D. 588 with that evaluated from the rate of decay of pressure given in the same paper.

The solution for the shock wave in water given by Kirkwood and Bethe[D] may be written

$$\left.\begin{aligned} \Omega(R,t) &= \frac{\chi_0}{R}\,\Omega_1\, e^{-\frac{t'}{\theta}} \\ \theta &= \gamma\theta_1 \end{aligned}\right\} \qquad (1)$$

where Ω = kinetic enthalpy = enthalpy increment + $\frac{1}{2}u^2$

u = particle velocity

w = enthalpy increment = $\varepsilon + \frac{p}{\rho} - \varepsilon_0 - \frac{p_0}{\rho_0}$

ε = internal energy

p, ρ = pressure and density

t' = time measured from instant of arrival of the shock wave at the point.

χ and γ are parameters which can be calculated as functions of $\frac{R}{a_0}$, a_0 being the initial charge radius and R the distance from the centre of the charge.

Although .....

although it is not true generally that in (1) Ω is a function of θ only, it is true at the shock front and nearly true for a little distance behind. It has been assumed in the theory that u is a function of θ so that we are justified in regarding Ω as a function of pressure p, and therefore in using the symbol $\frac{\partial \Omega}{\partial p}$, the value of which we calculate from tables in O.S.R.D. 686.

Differentiating (1) w.r.t. respect to time t we get

$$\frac{\partial^2 \theta}{\partial t^2} = \frac{\partial \Omega}{\partial t} + \frac{\partial \Omega}{\partial \theta} \cdot \frac{\partial \theta}{\partial t} = -\frac{\Omega}{\theta} \tag{2}$$

or

$$\frac{\partial \theta}{\partial t} = -\frac{\Omega}{\theta \frac{\partial \Omega}{\partial \theta}} \tag{3}$$

As the wave passes over any given point the value of θ at that point changes because the wave is decaying in intensity and also because the pressure behind the shock front varies from point to point. Expressed in equation form, for points just behind the shock front.

$$\frac{\partial \theta}{\partial t} = \frac{d\theta}{dt} - U \frac{\partial \theta}{\partial R} \tag{4}$$

where U = velocity of shock wave

$\frac{d\theta}{dt}$ = rate of decay of peak pressure.

Eliminating $\frac{\partial \theta}{\partial t}$ from (3) and (4) we get

$$\frac{\partial \theta}{\partial R} = \frac{1}{U}\left(\frac{d\theta}{dt} + \frac{\Omega}{\theta \frac{\partial \Omega}{\partial \theta}} \right) = \frac{d\theta}{dR} + \frac{\Omega}{\theta \frac{\partial \Omega}{\partial \theta} U} \tag{5}$$

written in terms of $\frac{R}{R_0}$ this becomes

$$\frac{\partial \theta}{\partial \left(\frac{R}{R_0}\right)} = \frac{d\theta}{d\left(\frac{R}{R_0}\right)} + \frac{\Omega}{\frac{\partial \Omega}{\partial \theta} U} \tag{6}$$

In (6) all symbols refer to values just behind the shock front, i.e. to the peak values. From equation (1) we see that the peak value is given by

$$\Omega = \frac{\chi a_0}{R} \Omega_1 \tag{7}$$

χ and $\frac{a^2}{a_0^2}$ are calculated functions of $\frac{a}{a_0}$. Ω_1 is given in O.S.R.D. 686 for T.N.T. at density 1.60. Hence using the tabular relation (c) between Ω and θ we get θ as a function of $\frac{R}{R_0}$. Numerical differentiation then gives us $\frac{d\theta}{d\left(\frac{R}{R_0}\right)}$. It is possible therefore to evaluate the right-hand side of (6) numerically as a function of $\frac{R}{R_0}$.

The equation connecting rate of decay $\frac{dp}{dR}$ of a spherical shock wave and the space rate of change of pressure behind the shock front $\frac{\partial p}{\partial R}$ may be written[a]

$$\frac{dp}{dR} = \frac{\partial p}{\partial R}\left[\frac{-(U-u)^2 + c^2}{U\left[U - u + \frac{c^2}{V}\frac{\partial V}{\partial p}\right]} \right] - \frac{1}{R}\left[\frac{2c^2 u (U-u)}{VU\left[U - u + \frac{c^2}{V}\frac{\partial V}{\partial p}\right]} \right] \tag{8}$$

or for simplicity

$$\frac{dp}{dR} = A\frac{\partial p}{\partial R} - \frac{B}{R} \tag{9}$$

where .....

where v = specific volume of fluid just behind front

c = velocity of sound in fluid just behind front.

(9) gives us another expression for $\frac{\partial p}{\partial \left(\frac{R}{a_0}\right)}$

$$\frac{\partial p}{\partial \left(\frac{R}{a_0}\right)} = \frac{A}{B}\left[\frac{dp}{d\left(\frac{R}{a_0}\right)} + \frac{p}{\frac{R}{a_0}}\right] \qquad (10)$$

The coefficients A and B have been computed from the data of O.S.R.D. 676 and are given in Table 1. The two values of $\frac{\partial p}{\partial \left(\frac{R}{a_0}\right)}$ as derived from (6) and (9) are shown in Figure 1 where it is seen that until the wave has progressed some five charge radii there is a discrepancy of about 30 per cent between the two values. At distances less than seven charge radii the value from (10) is less than that from (6), beyond this distance the relation is reversed.

It may be worth while pointing out here that close to the charge the term $A\frac{\partial B}{\partial R}$ in (9) is not of much importance in comparison with $\frac{B}{R}$. Since B is a known function of p the equation is now integrable in the form

$$\frac{dp}{B} = -\frac{dR}{R}$$

$$\text{or} \quad \int_{p_1}^{p} \frac{dp}{B} = \log\left(\frac{a_0}{R}\right) \qquad (11)$$

where p_1 is the pressure in the wave at the moment of initiation.

In Figure 2 is shown the value of $\frac{pR}{a_0}$ as a function of $\frac{R}{a_0}$ derived from (11) together with the value derived from the theory of O.S.R.D. 588. It is seen that at first the effect of shape is to delay the attenuation, then at about 2.8 a_0 from the centre to increase it. The effect of shape is not very large, for example at 12 a_0 from the centre where the pressure has fallen to about 1/30 of the initial value the difference between the curves is some 22 per cent. This shows that the rate of decay near to an explosive of this type is not likely to depend much on anything but the initial peak value of the pressure.

TABLE 1.

p KILOBARS	A NON-DIMENSIONAL	B KILOBARS	p KILOBARS	A NON-DIMENSIONAL	B KILOBARS
0.0	0.0	0.0	12.5	- .377	16.8
1.0	- .0657	1.06	15.0	- .403	20.4
2.0	- .130	2.26	17.5	- .426	24.1
3.0	- .180	3.54	20.0	- .445	27.7
4.0	- .216	4.87	22.5	- .464	31.3
5.0	- .246	6.23	25.0	- .470	34.7
6.0	- .270	7.67	30.0	- .507	42.3
7.0	- .294	8.98	35.0	- .530	49.8
8.0	- .311	10.3	40.0	- .550	57.3
9.0	- .330	11.8	45.0	- .562	64.9
10.0	- .346	13.2	50.0	- .567	71.4

References.

(a) The Decay of Plane, Cylindrical and Spherical Shock Waves ID/17/AJH.

(b) Progress Report on "The Pressure Wave Produced by an Underwater Explosion I". J.G. Kirkwood and H.A. Bethe. O.S.R.D. 588.

(c) Progress Report on "The Pressure Wave Produced by an Underwater Explosion II". J.G. Kirkwood and E.W. Montroll. O.S.R.D. 676.

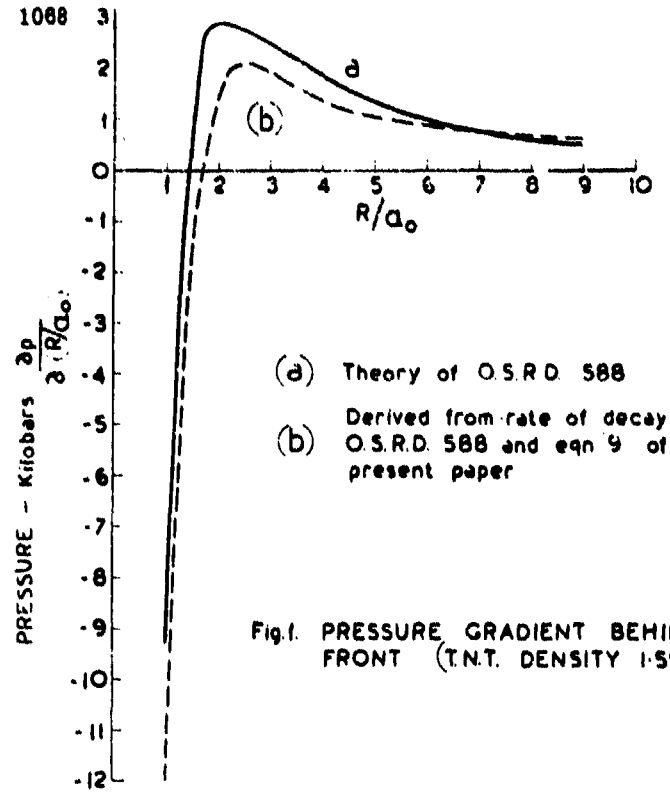


Fig.1. PRESSURE GRADIENT BEHIND SHOCK FRONT (T.N.T. DENSITY 1·59)

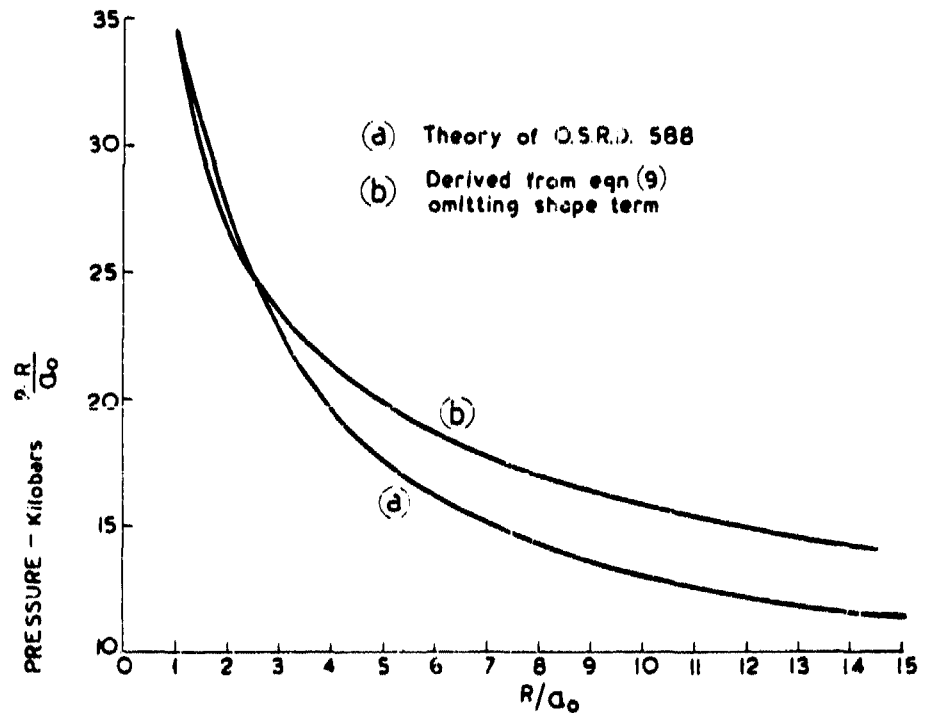


Fig.2. DECAY OF PRESSURE WAVE (T.N.T. DENSITY 1·59)

MEASUREMENT OF THE SHOCK-WAVE VELOCITY IN AIR ABOVE A WATER SURFACE, DUE TO THE DETONATION OF A SUBMERGED CHARGE

D. Croney and R. D. Davies
Road Research Laboratory, London

British Contribution

April 1944

MEASUREMENT OF THE SHOCK-WAVE VELOCITY IN AIR ABOVE A WATER SURFACE, DUE TO THE DETONATION OF A SUBMERGED CHARGE

D. Croney and R. D. Davies

Road Research Laboratory, London

April 1944

* * * * * * * *

Summary.

The velocities of the shock wave and water surface due to the detonation of submerged 4-oz. cylindrical charges of C.E., have been obtained over the first 5 ft. above the water surface from a determination with a rotating drum camera of the extinction times of a row of acetylene jets, situated in air vertically above the charge.

With the charge at a depth of 2 inches, the water surface and shock-wave velocities were indistinguishable vertically above the charge, the water surface velocity falling from about 4,800 ft./second at 3 inches, to about 2,600 ft./second at 3 ft. above the surface.

For charge depths of 4 inches and 8 inches, shock-wave velocities at 3 inches from the water surface were 1,900 and 1,450 ft./second respectively (axis vertical and horizontal), corresponding velocities at 3 ft. were 1,800 and 1,200 ft./second (axis vertical) and 1,280 and 1,150 ft./second respectively (axis horizontal).

Water-surface velocities for the 4 inches and 8 inches depths were 1,400 and 700 ft./second respectively (axis horizontal) at 3 inches above the surface and 1,100 and 500 ft./second respectively (axis horizontal) at 3 ft.

Description of charges used.

The charge used in each of the tests consisted of a 4-oz. cylindrical pellet of C.E., 2 inches in diameter, and 1¼ inches thick.

Experimental procedure.

The shock-wave velocity in air due to the detonation of a submerged charge was measured using acetylene flames, a row of small acetylene jets burning vertically above the charge being extinguished by the passage of the shock wave. The time interval between the extinction of successive flames was recorded by a rotating drum camera, the slit of which was focussed on the burners.

In the first series of experiments, the jets were spaced at 6 inches intervals, the lowest being 3 inches above the water surface. With this arrangement 6 tests were carried out, 3 with the axis of the charge vertical and its centre (a) 2 inches, (b) 4 inches and (c) 8 inches, below the surface and 3 with the charge axis horizontal, and the same 3 depths of immersion.

A further test was made with the charge axis vertical and depth of immersion 2 inches, but with the 8 jets used arranged at 1, 3, 5, 7, 9, 11, 24 and 36 inches respectively above the water surface.

Serious damage due to the dislaced water was sustained by the burners and their supporting framework during each experiment.

Records obtained.

Two records, typical of those obtained, are shown in Figures 1 and 2. The time scale for each record was calculated from the drum speed used, and the time interval between the

extinction .....

extinction of successive flames was obtained from direct measurements made on the negatives using a double-traverse microscope. Time-displacement curves were drawn from these figures and velocities deduced in the usual way by drawing tangents. The results are shown graphically in Figures 3 and 4.

Discussion of records.

On examination of Figures 1 and 2, a faint curved trace will be observed crossing both photographs. In Figure 1 the curve passes through the terminations of the jet trace. This trace, which is present on those records which were taken under bright weather conditions, is attributed to sunlight reflected into the camera lens from the atomised spray forming the apex of the water plume. If this explanation is correct the trace is, therefore, in effect a time-displacement curve for the rising water surface. Water surface velocities have been calculated from the records on which the trace is sufficiently distinct, and they are shown graphically in Figure 4.

A separate shock wave in air was not detected on any of the records taken with the charge 2 inches below the water surface, the jets being extinguished by the water plume. For this reason the velocities obtained at this depth have been plotted as water-surface velocities on Figure 4.

The comparatively small difference between the water surface and shock-wave velocities when the charge is detonated 4 inches below the surface, suggests that a detached shock wave would not be detected for depths of immersion much less than 4 inches.

The results obtained at the 2 inches depth from the two records taken with different jet arrangements were in very close agreement, and they have been plotted as a single curve in Figure 4.

Finally in Figure 2, the shape of the flame traces after deflection by the shock wave is of some interest. The abrupt changes in slope apparent in some of the flame traces may be taken as a measure of corresponding changes in particle velocity occurring in the air zone between the shock-wave front and the rising water surface.

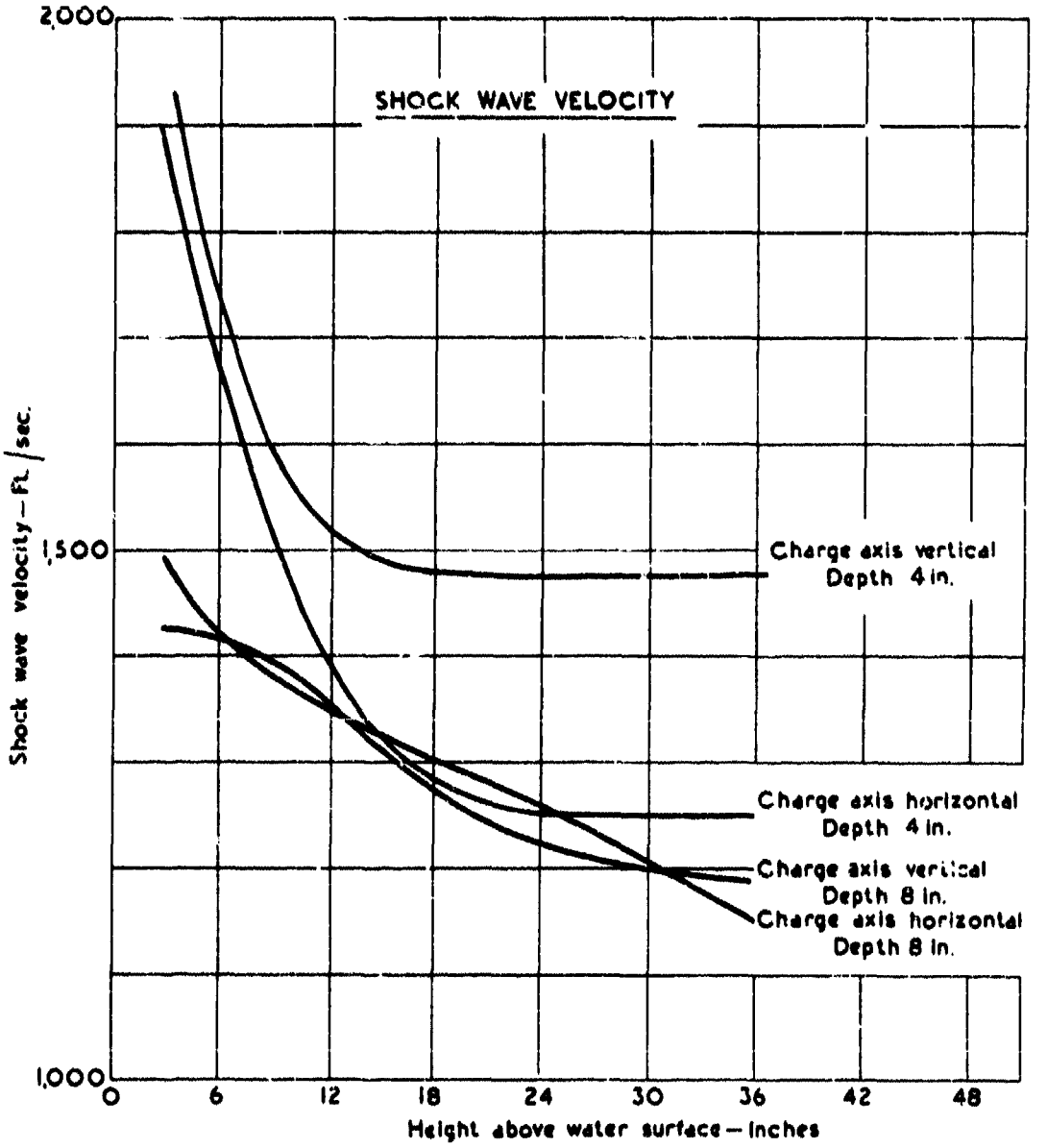


Fig. 3. SHOCK WAVE VELOCITY IN AIR DUE TO THE DETONATION OF A SUBMERGED 4 oz. CHARGE OF C.E.

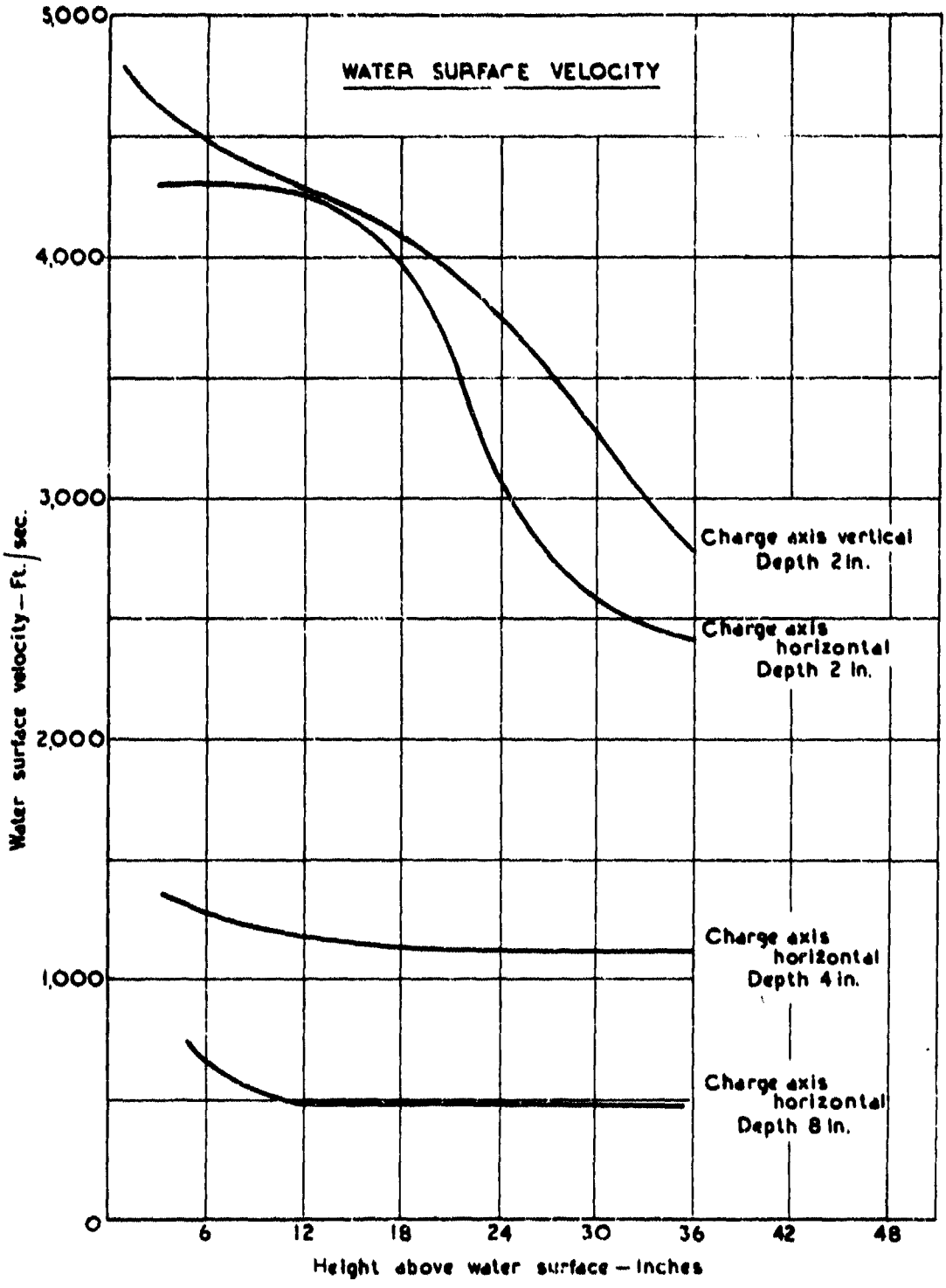


Fig. 4. VELOCITY OF WATER SURFACE DUE TO THE DETONATION OF A SUBMERGED 4 oz. CHARGE OF C.E.

MEASUREMENT OF THE SHOCK WAVE VELOCITY IN AIR ABOVE A WATER SURFACE DUE TO THE DETONATION OF 16-LB. SPHERICAL CHARGES OF T.N.T.

D. Croney
Road Research Laboratory, London

British Contribution

March 1946

MEASUREMENT OF THE SHOCK WAVE VELOCITY IN AIR ABOVE A WATER SURFACE DUE TO THE DETONATION OF 16-lb. SPHERICAL CHARGES OF T.N.T.

D. Croney

Road Research Laboratory, London

March 1946

Summary.

In a previous investigation the shock wave and water surface velocities due to the detonation of submerged 4-oz. charges of C.E. were measured by an acetylene jet method. The results were used to obtain values for the peak shock pressures in the water surface, and these values were compared with theoretical figures deduced from the formula given by Penney and Dasgupta.

It was decided to repeat the work on approximately four times the previous scale using 16-lb. spherical charges of T.N.T., fired at depths (measured to the charge centre of 8, 16 and 32 in. This investigation was not completed, but several exploratory charges were fired. The present report summarises the results obtained on these charges.

Some of the 4-oz. experiments have been repeated, the Marley high-speed camera working at about 6,000 frames/second being used to photograph the water plume. Water surface velocities and peak shock pressures in the water surface deduced from these records are compared with the values previously obtained.

Introduction.

Experimental data previously reported(1) was used(2) to obtain values for the water and air shock pressures associated with the detonation of submerged 4-oz. charges of C.E. In particular, the peak shock pressures in the water surface were compared with theoretical values obtained from the formula given by Penney and Dasgupta(3). A discrepancy between the calculated and experimental values in the case of the shallowest charges was in part attributed to the cylindrical shape of the explosive.

It was decided to repeat the work on four times the previous scale using 16-lb. spherical charges of T.N.T. fired at depths (measured to the charge centre) of 8, 16 and 32 in. This investigation was not completed, but the present note summarises the results obtained on several exploratory charges which were fired.

Some of the 4-oz. experiments have been repeated, and the Marley high-speed camera working at about 6,000 frames/second has been used to photograph the water plume. Water surface velocities and peak shock pressures in the water surface deduced from these records are compared with the values previously obtained.

Description of Charges.

16-lb. charges.

The 16-lb. charges were 8-in. diameter spheres of T.N.T. fitted with radial C.E. primers each 2 in. in diameter and 4 in. long. The charges were detonated with the primer axis vertical and the detonator uppermost.

4-oz. charges.

The 4-oz. charges were cylindrical pellets of C.E., 2 in. in diameter and 1½ in. long. Each charge was fired with its principal axis vertical.

Details .....

Details of charges fired.

16-lb. charges.

Three charges were fired; one each at depths (measured to the charge centre) of 8, 16 and 32 inches.

4-oz. charges.

Three charges were fired; one each at depths (measured to the charge centre) of 2, 4 and 8 inches.

Experimental procedure.

The tests were carried out in a disused gravel pit, in about 15 ft. of water.

16-lb. charges.

Figures 1(a) and 1(b) show in plan and elevation the layout used for the larger charges.

A row of photoflood bulbs fixed to a vertical pole and spaced as shown in figure 1(b) was viewed using a double mirror periscope through the horizontal slit of a drum camera. The lowest lamp and the centre of the lower periscope mirror were each set at approximately 3 in. from the water surface. The charge was arranged to lie in the plane containing the lamp standard and the lower periscope mirror. The method by which it was supported, and its height adjusted, will be apparent from figure 1(b). The length of the bamboo pole used in the charge mounting was approximately 10 ft. and the sealed cans used to provide the necessary buoyancy were about 4 ft. below the charge. Each charge was fired through a switch operated by the shutter of the drum camera.

The complete mechanism used for supporting the charge was destroyed by each shot.

4-oz. charges.

Figure 1(c) shows the arrangement used for the 4-oz. charges.

A lens cover plate provided with ¼ in. slots, together with a rotor having a single ¼ in. slot was used on the Marley camera. With this combination a sequence of 60 pictures is recorded during one complete revolution of the rotor, with a lens aperture of about f/12.

To record the plume with this aperture, artificial illumination was necessary. This was provided by the two flash bombs shown in figure 1(c), each consisting of a 2-oz. pellet of C.E. surrounded by 2 oz. of aluminium powder. During the tests the camera was shielded from the direct flash of these charges by cardboard screens.

The detonators used to fire the underwater charge and the flash bombs were wired in parallel. To ensure adequate illumination in the early stages of the explosion very short delay detonators were used in the flash bombs.

Records obtained.

16-lb. charges.

Figures 2, 3 and 4 show the records taken on the 16-lb. charges at depths of 8, 16 and 32 in. respectively.

The lamp images focussed on the moving film give rise to luminous traces. As a shock front rising between the camera and the lamp standard intercepts the light pencils subtended at the camera by each lamp, the rays are refracted momentarily out of the camera slit causing small breaks in the lamp traces. The traces are terminated as the lamps become obscured by the rising water surface.

Breaks marking the progress of the shock wave can be seen in figure 4, but they are absent in figure 2. This indicates that a shock wave travelling faster than the water surface was not detected with the charge centre 8 in. below the surface. With the charge 16 in. deep,

figure 3 .....

figure 3, there is evidence of a shock wave moving ahead of the spray. In the case of figures 3 and 4 the water surface, which was illuminated by bright sunlight, has recorded.

4-oz. charges.

Figures 6, 7 and 8 show selected frames from the Marley camera records.

Evaluation of records.

16-lb. charges.

The distance vertically above the charge which it was necessary for the shock wave or water plume to travel in order to intercept the light pencils subtended at the camera by the lamps was deduced from the geometry of the layout. A reduced distance scale corresponding to the position of the charge was obtained in this way. (The error in height introduced by assuming that the shock wave first cuts the light pencils vertically above the charge instead of slightly nearer to the camera, is very small).

From the records time-displacement curves have been plotted. In the case of records 3 and 4 the trace terminations were not sufficiently well defined to give a satisfactory displacement curve for the water surface.

Velocity curves have been plotted from the displacement curves and these are shown in figure 5, compared with the corresponding results in (1) scaled up.

4-oz. charges.

The distance scale for the Marley camera records was obtained by taking a record of a graduated pole supported vertically over charge position. From this scale time-displacement curves for the water surface have been plotted. Deduced velocity curves are shown in figure 9, compared with the corresponding acetylene jet results reported in (1).

Discussion of results.

In (2) a table was given in which water surface and air shock wave velocities were tabulated with the corresponding pressures in the water surface and the air shock wave. This data can be used in conjunction with the curves given in figure 5 to obtain values for the water and air shock pressures at various heights above the undisturbed water level.

As in the case of the previous 4-oz. charges the velocities fall off rapidly so that it is difficult to extrapolate back to initial velocities with much accuracy. On the basis of such extrapolated values however, the peak shock pressures in the water surface obtained are 135, 42 and 34 tons/sq.in at depths of 8, 16 and 32 in. respectively. The corresponding figures calculated from the Penney and Dasgupta formula for charges at depths of 2, 4 and 8 charge radii are 61, 19 and 7 tons/sq.in. and those calculated from the later work of Temperley and Craig are 81, 25 and 8 tons/sq.in

There is evidence to suggest that the detonation process in the T.N.T. was initiated near the detonator and not at the centre of the charge. This may in part account for the high experimental results at the shallow depths. The disagreement between theory and experiment at the 32-in. depth is probably attributable to the unsatisfactory character of the record (figure 4), interpretation of which is particularly difficult over the first 2 ft. above water level.

4-oz. charges.

The spray velocities obtained by the Marley camera technique, figure 9, are in reasonable agreement with the drum camera results given in (1), except at the 2-in. depth. Extrapolation gives initial spray velocities of approximately 3200, 1300 and 580 ft./sec. respectively for the 2, 4 and 8 in. depths corresponding to peak shock pressures in the water surface of 78, 24 and 9.5 tons/sq.in. respectively for the three depths.

If, as in (2), the charges are regarded as 2-in. diameter spheres of C.E. at depths of 2, 4 and 8 charge radii, the results agree closely with the theoretical values given above. (For comparison with T.N.T. the experimental results should be reduced by about 5%).

Conclusion .....

Conclusion.

The results given for the larger charges are, as they stand, based on incomplete experimental work. Before further work in connection with this investigation was abandoned, it was planned to use a second drum camera fitted with a telephoto lens to record a row of closely spaced lamps covering the first few feet above water level. It was also proposed to photograph the plume from the 16-lb. charges with the Marley camera. This procedure would have given more accurate time-displacement curves for both the shock wave and the water plume.

References.

(1) "Measurement of the shock wave velocity in air above a water surface, due to the detonation of a submerged charge". D. Cronoy and R.D. Davies.

(2) "Transmission of a shock wave from water to air at normal incidence". A.J. Harris.

(3) "Pressure-time curves for submarine explosions (Second paper)." W.G. Penney and H.K. Dasgupta.

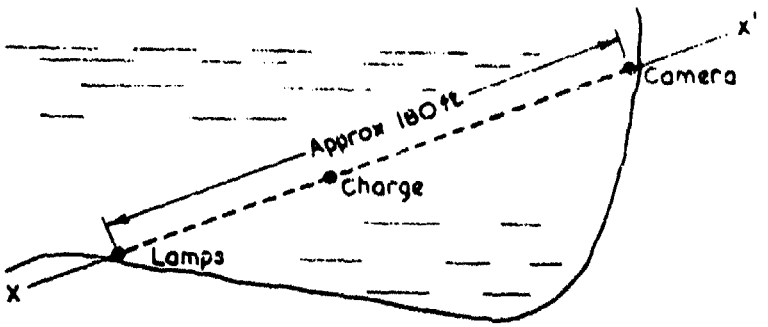


Fig. I.a. PLAN OF LAYOUT USED FOR 16-lb. CHARGES

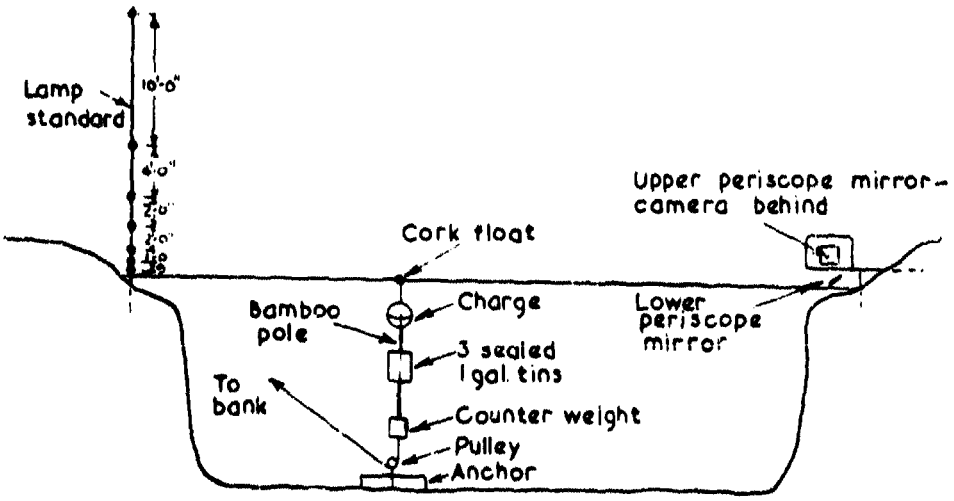


Fig. I.b SECTION ON XX' (Fig. I.a.)

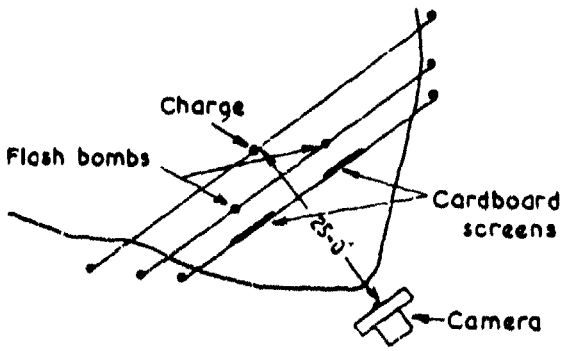


Fig. I.c. PLAN OF LAYOUT USED FOR 4-oz CHARGES

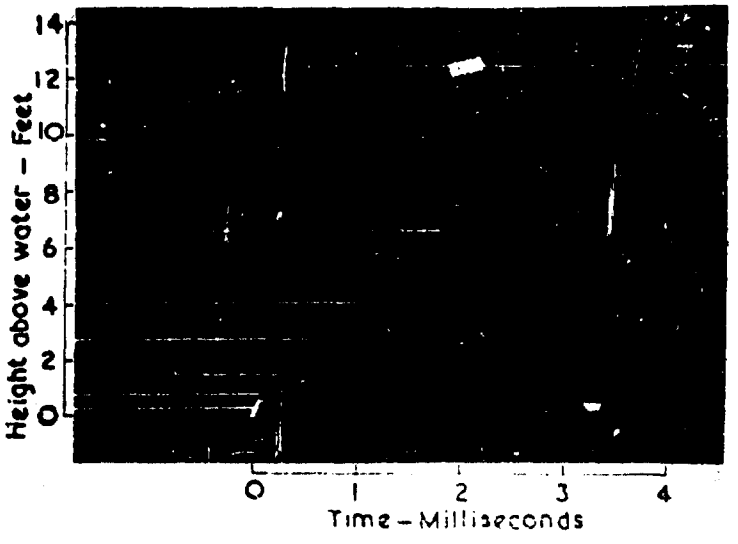


Fig.2. CENTRE OF CHARGE 8 in. BELOW WATER LEVEL

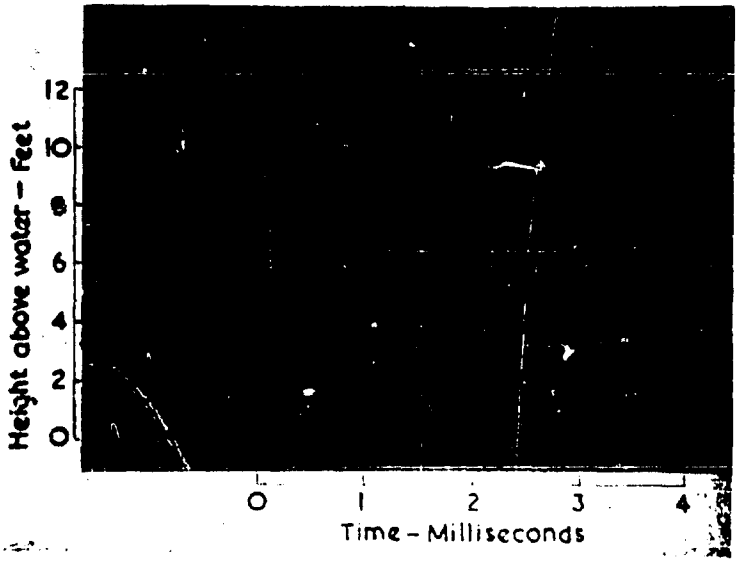


Fig.3. CENTRE OF CHARGE 16 in. BELOW WATER LEVEL

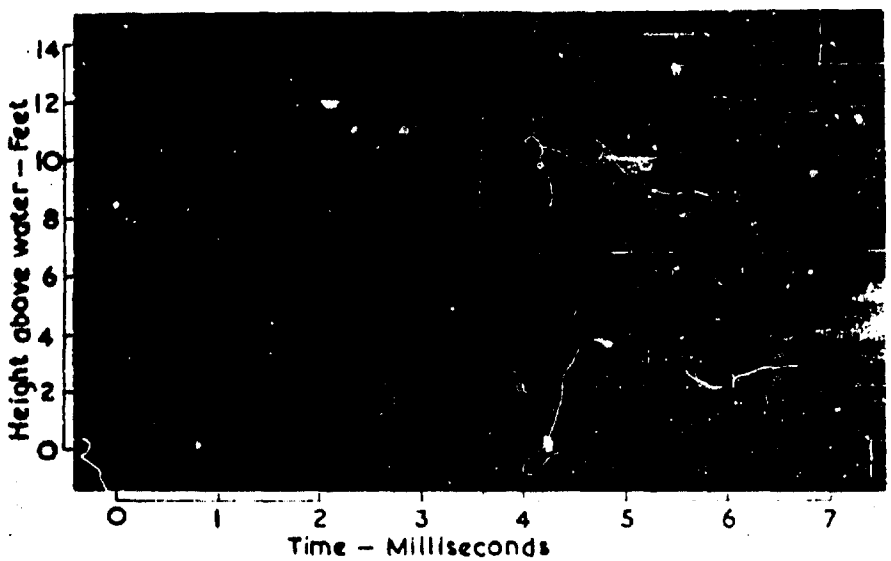


Fig.4. CENTRE OF CHARGE 32 in. BELOW WATER LEVEL
(Part only of record reproduced)

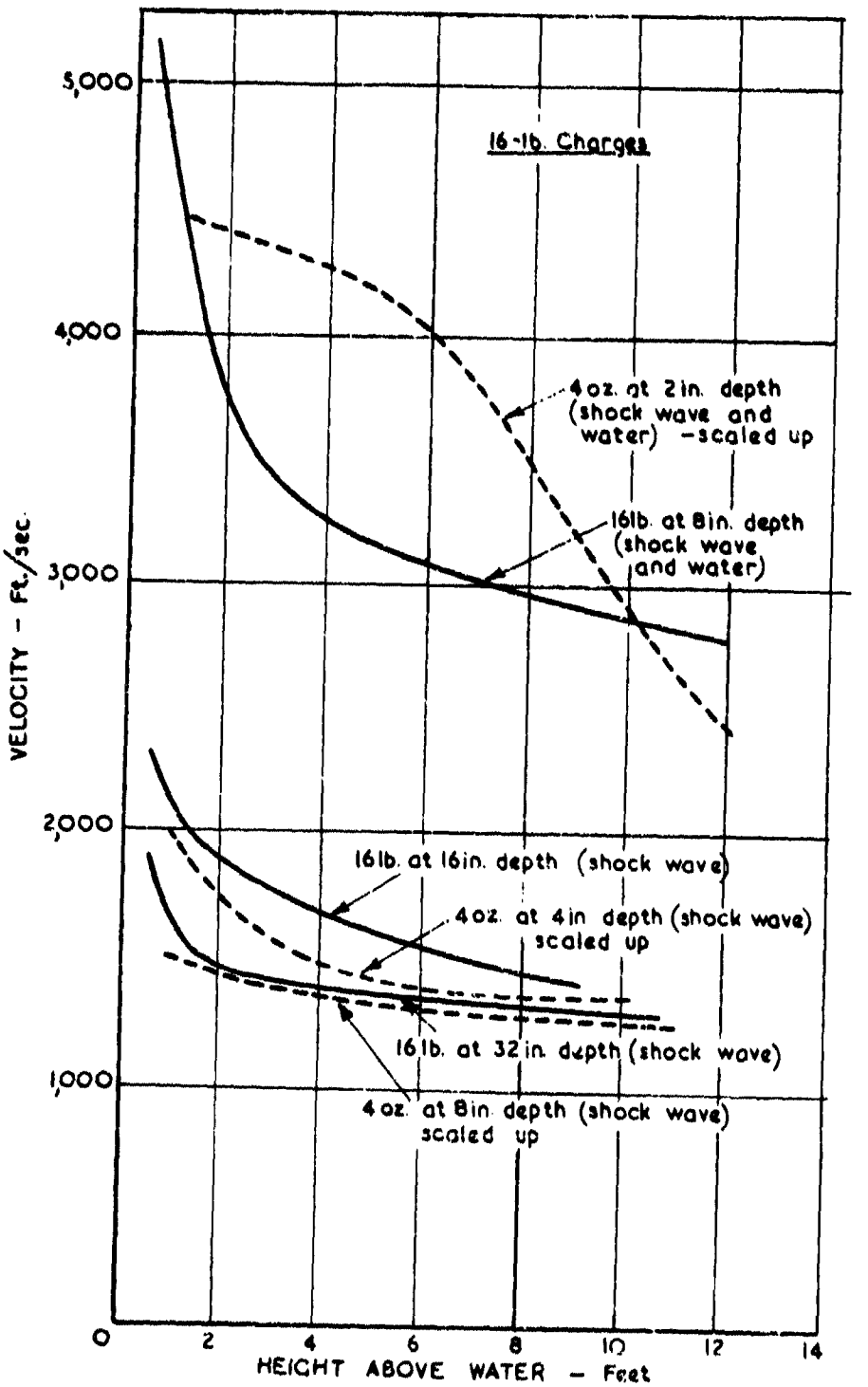
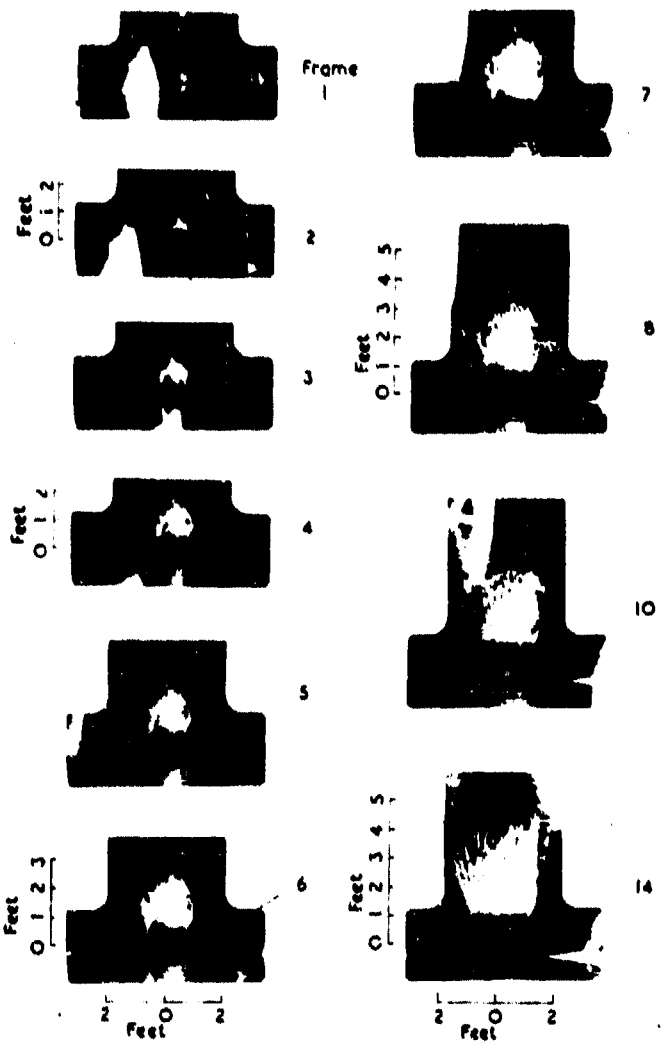
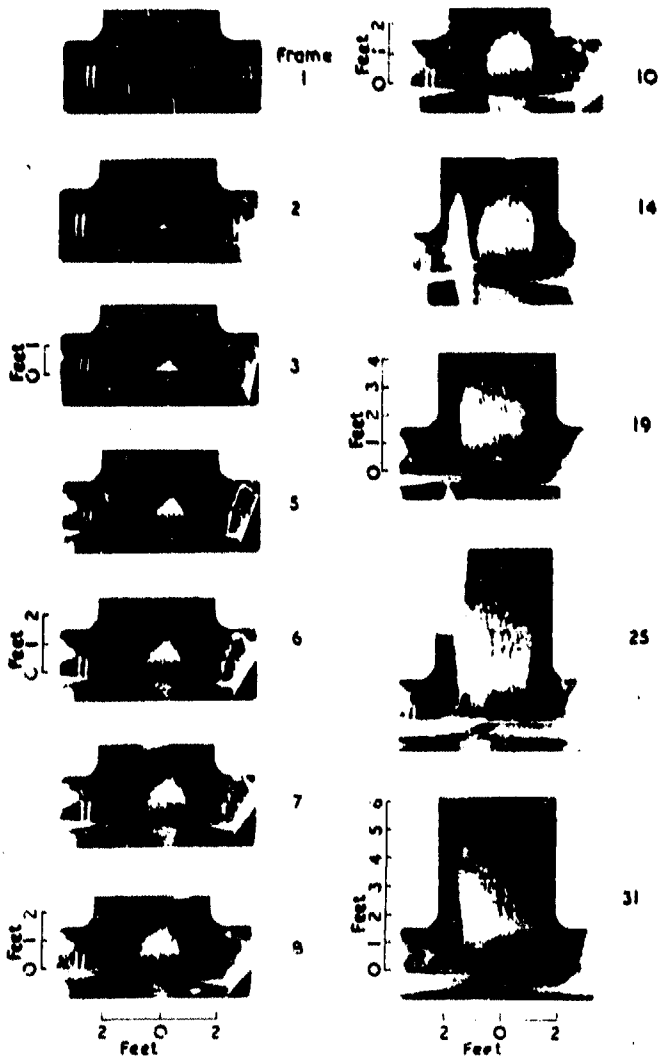


Fig. 5. SHOCK WAVE AND WATER PLUME VELOCITIES AT VARIOUS HEIGHTS ABOVE WATER LEVEL



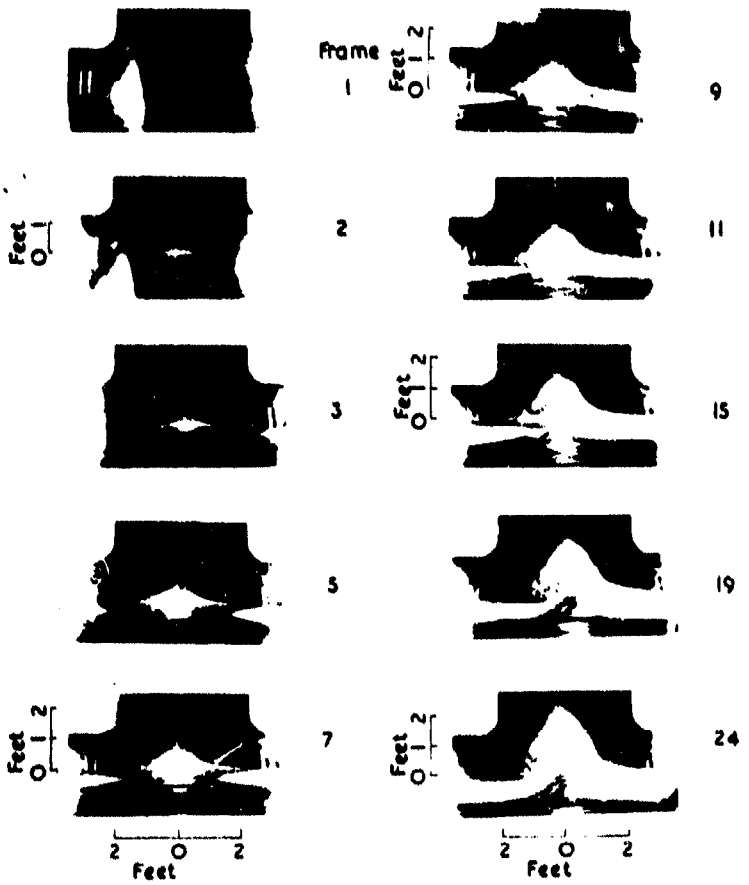
PLUME FROM SUBMERGED 4 oz. CHARGE OF C.E. ($1\frac{1}{2}$" x 2" dia.) CENTRE OF CHARGE 2 in. BELOW WATER SURFACE. SELECTED FRAMES FROM RECORD TAKEN AT 6,000 FRAMES/SECOND

Fig. 6.



PLUME FROM SUBMERGED 4oz. CHARGE OF C.E. ($1\frac{1}{2}$" x 2" dia.)
CENTRE OF CHARGE 4" BELOW WATER SURFACE SELECTED
FRAMES FROM RECORD TAKEN AT 6,000 FRAMES / SECOND

Fig. 7.



PLUME FROM SUBMERGED 4oz. CHARGE OF C.E. ($1\frac{1}{2}$" x 2" dia.) CENTRE OF CHARGE 8" BELOW WATER SURFACE. SELECTED FRAMES FROM RECORD TAKEN AT 6,000 FRAMES/SECOND

Fig. 8.

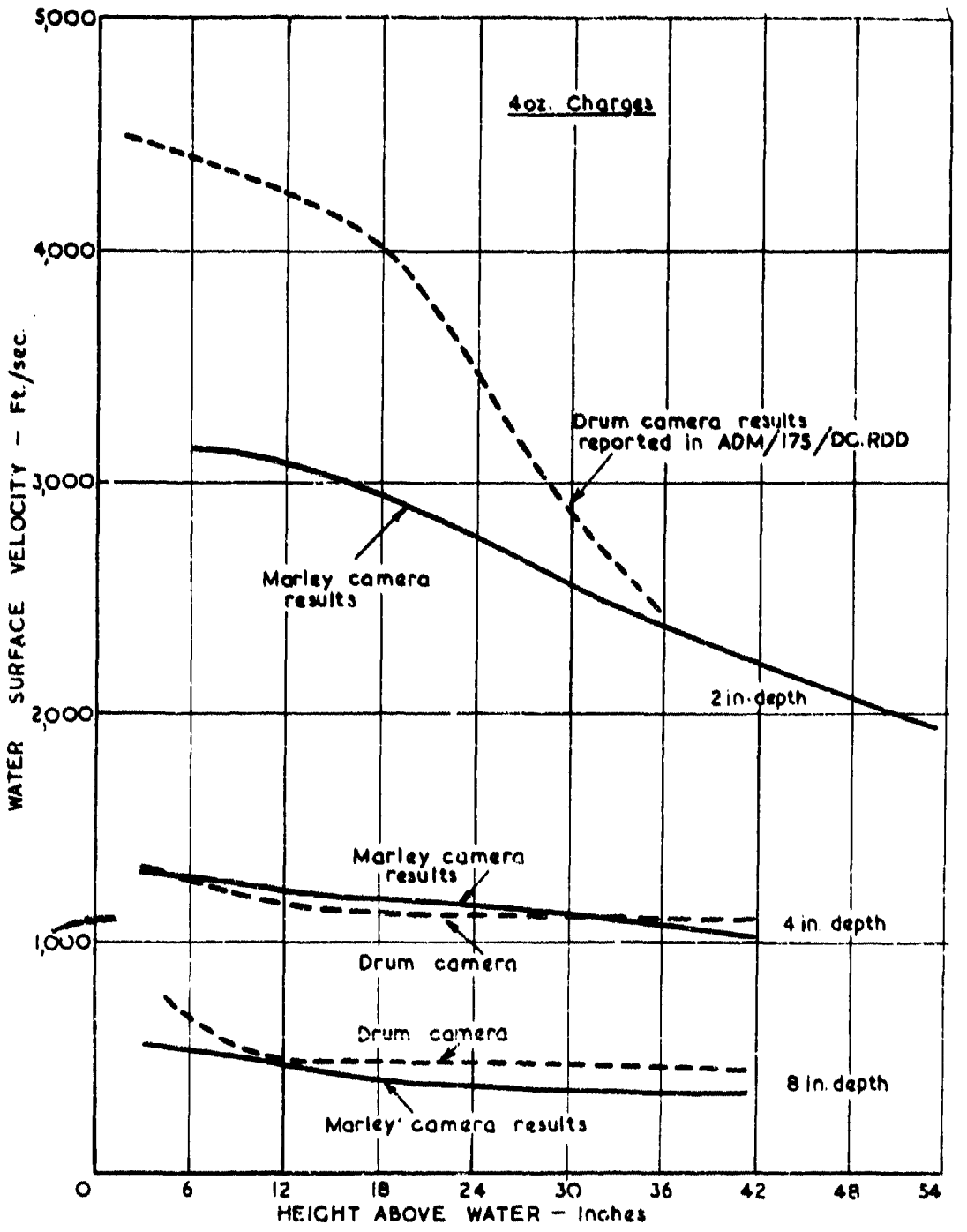


Fig.9. WATER PLUME VELOCITIES AT VARIOUS HEIGHTS ABOVE WATER LEVEL

SHOCK-WAVE PARAMETERS FROM SPHERICAL TNT CHARGES DETONATED UNDER WATER

J. S. Coles, E. A. Christian, J. P. Slifko,
C. R. Niffenegger, and M A. Rogers
Underwater Explosives Research Laboratory
Woods Hole Oceanographic Institution

American Contribution

1946

SHOCK-WAVE PARAMETERS FROM SPHERICAL TNT CHARGES DETONATED UNDER WATER

by J. S. Coles, E. A. Christian, J. P. Slifko, C. R. Niffenegger, and R. A. Rogers, Underwater Explosives Research Laboratory, Woods Hole, Massachusetts, 1946.

ABSTRACT

The similitude curves for peak pressure, momentum, time constant and energy of TNT have been determined from experiments with 12 and 14 inch diameter spherical charges. Data are presented from piezoelectric gauges, as well as from UERL diaphragm, Modugno, ball crusher and momentum mechanical gauges. Kirkwood's theoretical curves for TNT peak pressures, momentum and time constant have been calculated and are compared with the experimental values. Peak pressures calculated from ball crusher deformations show good agreement with piezoelectric gauge results for pressures below 8000 lb/in.^{2}.

I. INTRODUCTION

A series of spherical TNT charges has been shot at the Underwater Explosives Research Laboratory in Woods Hole, Massachusetts, to obtain the parameters of the explosive and to compare the results with Kirkwood's theoretical calculations

The charges were all fired from the schooner "Reliance" with the standard rig used on previous underwater work at this laboratory. The charge and gauges were suspended 40 feet below the surface in at least 80 feet of water. It was especially desired to obtain records in the high pressure region where the theoretical curve deviates from the empirical straight line on a log-log plot of pressures versus $W^{1/3}/R$ (cube root of the charge weight in pounds = $W^{1/3}$, and charge-to-gauge distance in feet = R). In order to obtain pressures over the range of 400 to 20,000 lb/in.^{2} with the charge weights used, the charge-to-gauge distances were varied from 100 to 5 feet, and consequently the range of $W^{1/3}/R$ was 0.036 to 0.86.

Results were obtained from UERL diaphragm, Modugno, ball crusher, and momentum mechanical gauges, and from piezoelectric gauges. Data from these gauges are given in Tables A-I, A-II, and A-III of the Appendix. Plots have been made of peak pressure, momentum/$W^{1/3}$, energy/$W^{1/3}$ and time constant (θ)/$W^{1/3}$ against $W^{1/3}/R$ (Figs. 2-8) and equations determined for the best straight line through the experimental points.

II. CHARGES

The TNT charges were cast into 14 gauge steel spheres of 12 inch and 14 inch diameters, resulting in average TNT charge weights of 48 pounds and 76 pounds (average loading density of TNT = 1.62). A 250 gram pentolite booster (spherical) was cast into the center of each charge. The charges were centrally detonated by U. S. Army Engineer's Special Electric Detonators (base charge 13.5 grains of PETN) inserted through a tube from the bottom of the charge as oriented for firing. Three eye-pads welded fore, aft, and topside of the sphere were used to position the charges (filling hole to one side) relative to the gauge lines. Six charges were fired, three of each weight.

III. INSTRUMENTATION AND RIG[1]*

The rig used for the tests is shown in Fig. 1. The charge and gauges were on a straight line 40 feet below and parallel to the surface of the water. This line was attached at the forward end to a tow line leading up to the vessel "Reliance", and a sea anchor at the aft end of the line served to maintain tension as the gear was towed through the water. The charge was at the center of this line, and the piezoelectric and mechanical gauges were located forward and aft of the charge respectively. All parts of the gear were suspended from surface buoys, and charge-to-gauge distances were determined by steel spacer cables.

The mechanical gauge instrumentation consisted of:

(1) Two heavy gauge blocks (Fig. 1B) each containing two UERL diaphragm gauges[2] two Modugno gauges[3] and two NOL ball crusher gauges[5]. All gauges are held face on to the charge by means of the strain of the spacer lines on a rigid tail extending 4 feet out from the back of the block. The ball crusher and Modugno gauges in these blocks were baffled by the face of the block (ca. 3.5 inches from center of the gauge to the nearest edge). The diaphragm gauges were unbaffled except by the faces of the gauges themselves. Lot V-B thin plates were used in the diaphragm gauges farthest from the charge, and lot V medium plates in those close to the charge.

(2) Five light ball crusher gauge blocks (Fig. 1A) each holding four NOL ball crusher gauges. These gauges were side-on to the charge, and were unbaffled except for the face of the gauge itself.

(3) One momentum gauge rig (Fig. 1C), holding two Hartmann type "M" and three Hartmann type "A" momentum gauges.

Piezoelectric gauges with $\frac{1}{4}$ inch and $\frac{1}{2}$ inch diameters were used; the smaller were 4 or 8 pile and the larger were 2 or 4 pile gauges. They were mounted on a 20 foot copper tube which served as a shield for the central conductor[8] and a cable attached to the end of the copper tube was run back to a compensating network located on a float barrel about 130 feet from the charge. From the float barrel the cable was led along the surface to the "Reliance", where it was terminated in a compensating network within the master control panel, then to the vertical amplifiers of modified DuMont 208 cathode-ray oscilloscopes. The main gauge cable used was Army-Navy type RG-41/U.

Previous tests had shown that in order to eliminate a jagged rise line which had been noted on gauges at large distances from the charge, it was necessary to: (1) run the cable from the two pairs of gauges nearest the charge to the surface separately from the cables for the other two pairs of gauges, and (2) position the pair of gauges farthest from the charge at least $2\frac{1}{2}$ feet from the cable. The three pairs of gauges nearest the charge were held about 6 inches from the cable by H-frames having a 1 foot crosstree (Fig. 1E), whereas the pair of gauges farthest from the charge were mounted on a larger frame which held them $2\frac{1}{2}$ feet from the cable by means of a 5 foot crosstree.

*The list of references has been deleted.

The charges were fired in three strings, one charge of each weight being fired in each string. Charge-to-gauge distances were varied for each string to obtain $W^{1/3}/R$ values over as wide a range as practicable.

IV. RESULTS OF TESTS

The data obtained are presented in Tables A-I, A-II, and A-III of the Appendix. The results are presented as the mean and percentage deviation from the mean of the readings of pairs of equivalent gauges, and the + or - sign refers to the deviation of the first gauge listed. Where no percentage follows the table entry, the value is obtained from a single gauge.

1. Piezoelectric Gauge Results

(a) Peak pressure:--The log of the peak pressure plotted as a function of log $W^{1/3}/R$ for spherical TNT charges is shown in Fig. 2. The best straight line through the experimental points may be represented by the following equation:

$$p = 2.16 \times 10^4 \, (W^{1/3}/R)^{1.13} \text{ lb/in.}^2$$

The standard deviation of the experimental points from this line is 8.9%. Values from Kirkwood's theory, which were calculated from Ref. 4 and are represented by the dotted line, are in better than 6% agreement with the above equation for values of $W^{1/3}/R < 0.2$, and differ by only 13% at the upper limit of the experimental curve. There is a slight tendency for the experimental curve to deviate upward at the highest pressure values obtained, but the theoretical line shows a much greater curvature than the experimental.

(b) Time constants:--Since the first portion of the pressure time curve fits reasonably closely an exponential of the form $p = p_o e^{-t/\theta}$ out to $t \leq \theta$, the time constant θ (i.e., the time required for the curve to fall to a pressure value = p_{max}/e) of the initial portion of the shock wave may be determined. Curves of experimental values of $\theta/W^{1/3}$ plotted against $W^{1/3}/R$ for TNT, and the line from Kirkwood's theoretical calculations for TNT are shown in Fig. 3. Though the theoretical line drops off sharply the best line through the experimental points is only very slightly curved downward at the high values of $W^{1/3}/R$ in each case, and might almost equally well be a straight line represented by the following equation:

$$\theta = 0.060 \, W^{1/3} (W^{1/3}/R)^{-0.18}$$

(c) Impulse:--Impulse values were obtained by integration of the pressure time curve to 6.7 times the nominal time constant which, for each particular value of $W^{1/3}/R$, was taken from the line representing $\theta/W^{1/3}$ versus $W^{1/3}/R$ shown in Fig. 3. The use of these faired time constants prevents the low precision of the measured time constants from introducing an unjustified scatter in the momentum and energy. Integration to a fixed multiple of the time constant, for each $W^{1/3}/R$, gives values which are more nearly proportional to the total momentum or total

energy than would be obtained by integrating to some fixed time which is independent of weight and distance.

Log $I/W^{1/3}$ (reduced impulse) is plotted against log $W^{1/3}/R$ in Fig. 4, and the empirical equations obtained from the best straight line through the experimental points and the standard deviation of the experimental points from the line is:

$$I = 1.46\ W^{1/3}\ (W^{1/3}/R)^{0.89},\ \sigma = 10.3\%$$

The experimental curves are not concave downward as is the theoretical curve, which is shown as a dotted line on Fig. 4. The spherical pentolite impulse curve[6] agreed with the theoretical curve in this respect, but the linearity of the TNT impulse curve is to be expected since the log time constant/$W^{1/3}$ - log $W^{1/3}/R$ relation is nearly linear.

(d) Energy:--The energy factor (E) reported here is defined as:

$$\frac{1}{\rho c_o}\ (1 - 2.3 \times 10^{-6}\ p_m) \int_0^{6.7\theta} p^2 dt$$

(where θ is the nominal time constant at the particular value of $W^{1/3}/R$) and contains the correction for finite amplitude[9] though the "afterflow" terms are omitted. Figure 5 is a plot of log $E/W^{1/3}$ versus log $W^{1/3}/R$ for TNT. The empirical equation for energy as a function of charge weight and charge-to-gauge distance obtained from the best straight line through the experimental points is:

From Fig. 5, for TNT,

$$E = 2.44 \times 10^3\ W^{1/3}\ (W^{1/3}/R)^{2.04}$$

with the standard deviation of the experimentally determined values from the line of 16.0%.

The total energy flux density per unit area is given by the equation:

$$F = \frac{1}{\rho c_o}\left[(1 - 2.3 \times 10^{-6}\ p_m) \int_0^{6.7\theta} p^2 dt + \frac{c_o}{R} \int_\theta^{6.7\theta} p \int_0^t p\,dt\,dt\right]$$

where F = total energy flux

p = pressure as a function of time in lb/in.^{2}

p_m = peak pressure in lb/in.^{2}

t = time in seconds

c_o = velocity of sound in sea water at given temperature in ft/sec

ρ_o = density of sea water at given temperature and salinity

$\rho_o{}^c{}_o$ = 5.58 + 0.0065 T, where T is temperature in degrees Centigrade

R = charge-to-gauge distance in ft.

The first term only of this equation is usually reported as the energy factor (see Sec. d), but in the case of a spherical shock wave the second term is not negligible when the charge-to-gauge distances are small. Figure 6 shows the second, or so-called "afterflow", term of the equation as a percentage of the first, or "primary", term plotted against $R/W^{1/3}$. A scale of charge radii for TNT is also shown in Fig. 6.

Charge-to-gauge distances (R) in Fig. 6 vary from 5 to 47 feet, and the importance of the afterflow term is seen to increase rapidly as $R/W^{1/3}$ decreases.

(e) The pressure time curves:--Average pressure time curve for TNT is shown in Fig. 7. The curve is based on ten records corrected to a $W^{1/3}/R$ value of 0.242. This curve falls off exponentially out to a time $t \leq \theta$, passes through a minimum (p_{min}, t_{min}) and a maximum (p_{max}, t_{max}) to form the "bump" characteristic of piezoelectric pressure time curves, and falls off again, at first exponentially and then more slowly.

Log-log plots of the quantities p_{min}, p_{max}, $t_{min}/W^{1/3}$, and $t_{max}/W^{1/3}$ versus $W^{1/3}/R$ are shown in Figs. 8 and 9. The p_{min} and p_{max} values follow the similitude law though their scatter is great, and the $t_{min}/W^{1/3}$ and $t_{max}/W^{1/3}$ quantities fall on a very nearly straight line with slight negative slope

2. Mechanical Gauge Results

Table A-II of the Appendix shows the deformations in inches for all the ball crusher gauges, and Table A-III of the Appendix contains the data from momentum, diaphragm and Kodugno gauges.

Ball crusher gauges were mounted in two ways; four to a block in side-on orientation at distances from 5 to 67 feet from the charge, and two to a block in face-on orientation at distances 15 to 60 feet from the charge. The deformations from the gauge blocks in side-on orientation have been interpreted in terms of peak pressure. Fig. 10 shows log peak pressure versus log $W^{1/3}/R$ for TNT and the best average line through the experimental points may be represented by the following empirical equation:

$$p = 1.92 \times 10^4 \, (W^{1/3}/R)^{1.08},$$

with a standard deviation of the experimental points from the line of 2.9%. Peak pressures from piezoelectric gauges are shown as dotted lines on the ball crusher peak pressure plots. The method of determining peak

pressures from ball crusher deformations used in this report is described in Ref. 7, Appendix I. The equation for peak pressures from 3/8 inch copper balls is

$$p = 7.62 \times 10^4 \frac{x_m}{\gamma(\theta)}$$

where x_m is an average deformation in inches of the four gauges in one block, and values for γ, the relative response (as defined in Ref. 7), are based on the θ obtained from piezoelectric results (see Fig. 3).

As can be seen from Fig. 10 the ball crusher peak pressures agree very well with the piezoelectric peak pressures in the lower portion of the curve, but they are about 11% lower than the piezoelectric at the highest pressures measured. Several considerations neglected in the above calculations may tend to lower the peak pressures calculated from large ball crusher deformations:

(1) The calibration curve for the copper spheres is assumed to be linear throughout, although it deviates appreciably from the linear for deformations above about 0.09 inches. For shock waves of the type discussed in this report, the time constant is of the order of 300 microseconds and the correction factor (γ) is approximately 0.80. Consequently, calculated pressure values above 8500 lb/in.^{2} would be lowered by the assumption of a linear calibration curve.

(2) The rate of strain increases with large deformations.

(3) It is possible that, under the velocities of the piston attained during deformation of the sphere, there could be an increase in the frictional effect sufficiently great to account for a part of this discrepancy.

V. SUMMARY

If the equations for peak pressure, impulse, and energy are represented by the equations;

$$p = X\,(W^{1/3}/R)^{\alpha} \qquad (1)$$

$$I = Y\,W^{1/3}(W^{1/3}/R)^{\beta} \qquad (2)$$

$$E = Z\,W^{1/3}(W^{1/3}/R)^{\delta} \qquad (3)$$

Table I shows a comparison of the parameters for TNT based on piezoelectric and ball crusher gauge results from tests on spherical charges. The constants for the Kirkwood theoretical curves for TNT are also shown.

TABLE I

SIMILITUDE LAW PARAMETERS OF TNT FOR UNDERWATER SHOCK-WAVE PEAK PRESSURE, MOMENTUM AND ENERGY

TNT		
Piezoelectric Gauges	Ball Crusher Gauges	Kirkwood Theoretical
2.16×10^4	1.92×10^4	2.34×10^4
1.13	1.08	1.16
1.46		1.59
0.89		0.89
2.44×10^3		
2.04		

APPENDIX I

TABLE A-I

PIEZOELECTRIC GAUGE RESULTS FROM SPHERICAL TNT CHARGES

Shot No. Sphere Diameter (in.) Explosive	Gauge Number	P_m $(lb/in.)^2$	Impulse[a] $(lb/in.^2\ sec)$	θ (msec)	Energy[a] $(in.\ lb/in.^2)$	Gauge Number	P_m $(lb/in.)^2$	Impulse[a] $(lb/in.^2\ sec)$	θ (msec)	Energy[a] $(in.\ lb/in.^2)$
Distance			10'					20'		
RE 385 14" TNT	AR-136 104-R	8185 +0.3%	3.21 -3.1%	0.30 0.30	2070 +2.1%	AR-52 S-857	3755 -5.2%	1.52 -12.5%	0.32 0.33	409 -15.2%
RE 386 12" TNT	AR-136 104-R	6595 -3.6%	2.26 -7.5%	0.28 0.27	1150 -4.5%	AR-52 S-857	3220 -5.6%	1.15 -5.2%	0.29 0.30	255 -15.5%
Distance			7'					17'		
RE 387 14" TNT	AR-136 AR-44	12,400 -0.8%	4.06	0.27	3970	AR-132 AR-84	4215 -3.7%	1.63 -11.1%	0.29 0.34	540 -13.7%
RE 389 12" TNT	AR-136 AR-46	9900 +3.1%	3.00 +2.4%	0.24 0.24	2280 +2.4%	AR-132 AR-90	3440 -4.1%	1.31 -8.0%	0.28 0.28	334 -9.6%
Distance			5'					15'		
RE 392 12" TNT	AR-132 AR-48	14,000	3.65	0.23	4200	AR-46 AR-80	3795 -7.5%	1.33 -11.7%	0.28 0.28	395 -12.3%
RE 393 14" TNT	AR-132 S-1114	18,950 -4.5%	5.62 -4.0%	0.26 0.26	8740 +1.7%	AR-46 AR-80	4530 -10.4%	1.97 -1.8%	0.35 0.32	733 -1.8%

a) Impulse and energy time of integration is 6.7 nominal θ.
b) Values for gauge AR-84 on shot Re-389 omitted because gauge was found to be faulty when removed and tested.

APPENDIX I

TABLE A-I

PIEZOELECTRIC GAUGE RESULTS FROM SPHERICAL TNT CHARGES

Gauge Number	P_m (lb/in.)^2	Impulse[a] (lb/in.^{2} sec)	θ (msec)	Energy[a] (in. lb/in.^{2})	Gauge Number	P_m (lb/in.)^2	Impulse[a] (lb/in.^{2} sec)	θ (msec)	Energy[a] (in. lb/in.^{2})
Distance		60'				100'			
AR-90	1066	0.59	0.44	44.1	AR-80	577	0.31	0.48	14.5
AR-84	-7.4%	-4.3%	0.43	-6.4%	AR-86	-1.9%	+3.3%	0.48	+4.3%
AR-90	923	0.42	0.34	26.7	AR-80	485	0.31	0.42	10.6
AR-84	-3.0%	-6.0%	0.33	-8.6%	AR-86	-3.6%	+3.3%	0.40	+3.4%
Distance		47'				87'			
S-857	1595	0.73	0.37	77.8	104-R	760	0.41	0.44	21.5
AR-48	+3.5%	-2.8%	0.34	-5.9%	AR-86	+2.7%	+8.6%	0.44	+14.0%
S-857	1190	0.58	0.34	49.2	104-R	603	0.32	0.39	13.1
AR-48[b]	+14.3%				AR-86	+9.6%	+6.3%	0.40	+12.3%
Distance		38'				78'			
S-857	1590	0.75	0.39	78.2	104-R	701	0.35	0.39	17.2
S-1106	-4.4%	+2.0%	0.41	+2.5%	AR-90	+7.9%	+1.5%	0.39	-4.6%
S-857	2115	0.98	0.35	136	104-R	814	0.49	0.43	28.6
S-1106	+1.7%	-7.2%	0.36	-12.2%	AR-90	+5.2%	+4.1%	0.44	+6.8%

APPENDIX

TABLE A-II

BALL CRUSHER GAUGE RESULTS FROM SPHERICAL TNT CHARGES

DEFORMATION IN INCHES x 10^2

	COMPOSITE GAUGE BLOCKS FACE ON		LIGHT BALL CRUSHER GAUGE BLOCKS SIDE ON									
	II	I	IX		VIII		VII		VI		V	
Shot No. and Explosive Loading	Ave. of Gauges 059 U16	Ave. of Gauges 055 058	Ave. of Gauges 319 U13	Ave. of Gauges 333 336	Ave. of Gauges U12 332	Ave. of Gauges 337 334	Ave. of Gauges 90 056	Ave. of Gauges U1 338	Ave. of Gauges 7 335	Ave. of Gauges U15 331	Ave. of Gauges 02 03	Ave. of Gauges 119 118
1st String Charge to Gauge Distance	20'	60'	10'		30'		40'		50'		67'	
RE 385 TNT	4.37 -0.5 %	1.28 +2.8 %	7.86 +0.4%	8.01 -0.2 %	2.48 0 %	2.52 -3.0 %	1.82 +2.5 %	1.88 -2.4 %	1.45 -3.5 %	1.55 -2.9 %	1.07 +3.8 %	1.07 -1.9 %
RE 386 TNT	3.59 -0.7 %	1.05 -1.0 %	6.53 +0.6 %	6.56 +0.5 %	2.04 -3.0%	2.08 0%	1.49 -0.7 %	1.43 -1.4 %	1.22 -6.6 %	1.25 -1.2 %	0.91 +3.3 %	0.81 -1.3 %
2nd String Charge to Gauge Distance	17'	47'	7'		27'		32'		42'		54'	
RE 387 TNT	5.18 -0.4 %	1.68 -2.7 %	11.31 -1.2%	11.60 +0.1%	2.88 -2.8 %	2.94 +1.4 %	2.31 +3.1 %	(2.20) (-6.8%)	1.76 -4.3 %	1.72 -2.4 %	1.34 +1.9 %	1.31 -3.5 %
RE 389 TNT	4.27 -2.7 %	(1.33) (-4.2 %)	9.42 +0.1 %	9.51 +1.1 %	2.38 -1.7 %	2.43 -2.1 %	1.87 +1.4 %	1.89 -5.3 %	1.43 +4.2 %	1.48 -4.8 %	1.13 +5.3 %	1.10 +1.4 %
3rd String Charge to Gauge Distance	15'	38'	5'		25'		30'		35'		45'	
RE 392 TNT	4.93 -0.3 %	1.63 +1.3 %	12.71 +1.7 %	12.83 +1.0 %	2.49 -0.8 %	2.55 +0.4 %	2.02 -1.5 %	2.05 -1.2 %	1.73 -2.6 %	1.78 -2.3 %	1.30 +1.6 %	1.29 -0.8 %
RE 393 TNT	6.00 -1.9 %	2.06 +2.5 %	14.80 -2.4 %	15.23 +0.2 %	3.07 +0.5 %	3.12 +0.5 %	2.47 -0.6 %	2.48 -0.6 %	2.15 -3.0 %	2.17 -2.6 %	1.68 +3.3 %	1.61 -1.6 %

Values in parentheses are not considered reliable because the deviation is greater than three times the standard deviation.

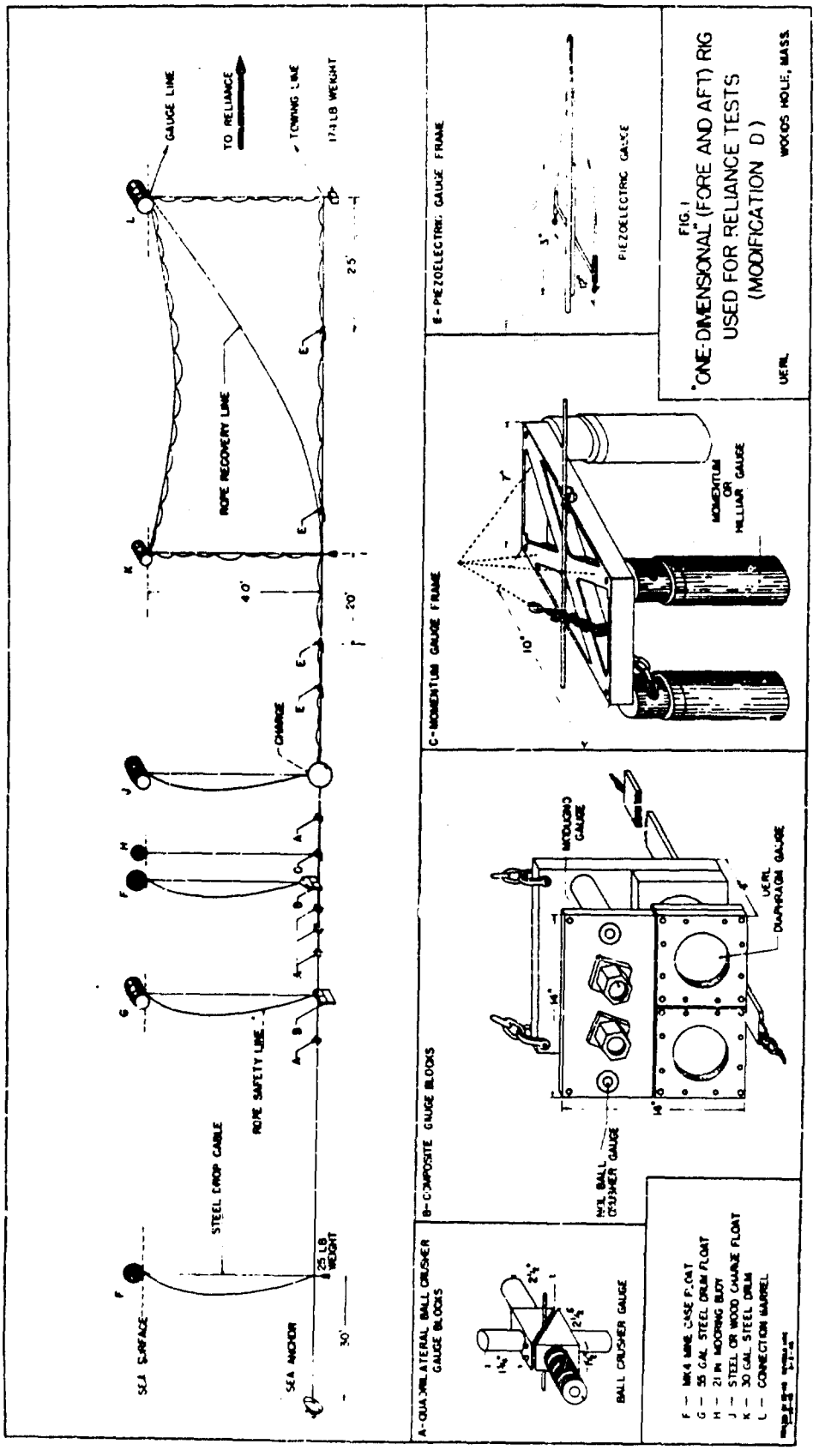
APPENDIX

TABLE A-III

DIAPHRAGM, MODUGNO, AND MECHANICAL MOMENTUM GAUGE RESULTS FROM SPHERICAL TNT CHARGES

		DIAPHRAGM GAUGE RESULTS (Deformations in in.x10^2)		MODUGNO GAUGE RESULTS (Deformations in in.x10^2)		HARTMANN MOMENTUM GAUGE RESULTS (PSI SEC)		
Shot No. and Explosive Loading	Net Weight of Loading and Diameter of Spherical Charge	Block II Average of Gauges 4 and 15	Block I Average of Gauges 14 and 20	Block II Average of Gauges 30 and 66	Block I Average of Gauges 55 and 65	Average of Gauges M1 and M4	Average of Gauges A38 and A39	Gauge A40 (Gauge A40 has Spring and Catch)
1st String Charge to Gauge Distance		20'	60'	20'	60'	15'	15'	15'
RE 385 TNT	75.4 lbs. 14 inches	54.0 +0.7 %	32.6 -0.8 %	13.7 +4.8 %	(0.9) (+18.7 %)	(1.71) (+24.8 %)	(1.85) (-27.3%)	
RE 386 TNT	48.4 lbs. 12 inches	42.5 +0.5%	26.7 -1.0 %	10.9 +6.9 %	0.3 0 %	2.31 +7.4 %	1.79 +4.5 %	
2nd String Charge to Gauge Distance		17'	47'	17'	47'	12'	12'	12'
RE 387 TNT	76.4 lbs. 14 inches	(62.1) (+6.2 %)	42.9 -1.4 %	17.4 +3.2 %	3.4 +8.8 %	2.93 +21.2 %	3.55 -5.7%	(2.23)
RE 389 TNT	48.1 lbs. 12 inches	51.9 +0.2 %	34.3 -1.0 %	13.6 +4.4 %	(2.2) (+18.2 %)	2.72 +9.4 %	3.05	(0.78)
3rd String Charge to Gauge Distance		15'	38'	15'	38'	10'	10'	10'
RE 392 TNT	48.2 lbs. 12 inches	59.7 +0.7 %	43.1 -0.7 %	16.1 +3.1 %	5.1 +10.8 %	3.60 -2.7 %	3.71 -0.2 %	(2.34)
RE 393 TNT	76 lbs. 14 inches	74.3 +1.1 %	53.2 +2.8 %	19.4 +4.1 %	(6.9) (+12.3 %)	2.83 +2.7 %	4.13 -0.1 %	3.33

Values in parentheses are not considered reliable because the deviation is more than three times the standard deviation.


SEA SURFACE
STEEL DROP CABLE
ROPE SAFETY LINE
25 LB WEIGHT
SEA ANCHOR
30'
CHARGE
40'
20'
ROPE RECOVERY LINE
GAUGE LINE
TO RELIANCE
TOWING LINE
17-LB WEIGHT
25'
A-QUASI-BILATERAL BALL CRUSHER GAUGE BLOCKS
BALL CRUSHER GAUGE
B-COMPOSITE GAUGE BLOCKS
MODIFIED GAUGE
NRL BALL CRUSHER GAUGE
UERL DIAPHRAGM GAUGE
C-MOMENTUM GAUGE FRAME
MOMENTUM OR IMPULSE GAUGE
E-PIEZOELECTRIC GAUGE FRAME
PIEZOELECTRIC GAUGE
F — MK4 MINE CASE FLOAT
G — 55 GAL STEEL DRUM FLOAT
H — 21 IN MOORING BUOY
J — STEEL OR WOOD GAUGE FLOAT
K — 30 GAL STEEL DRUM
L — CONNECTION BARREL
FIG. 1
"ONE-DIMENSIONAL" (FORE AND AFT) RIG USED FOR RELIANCE TESTS (MODIFICATION D)
UERL
WOODS HOLE, MASS.

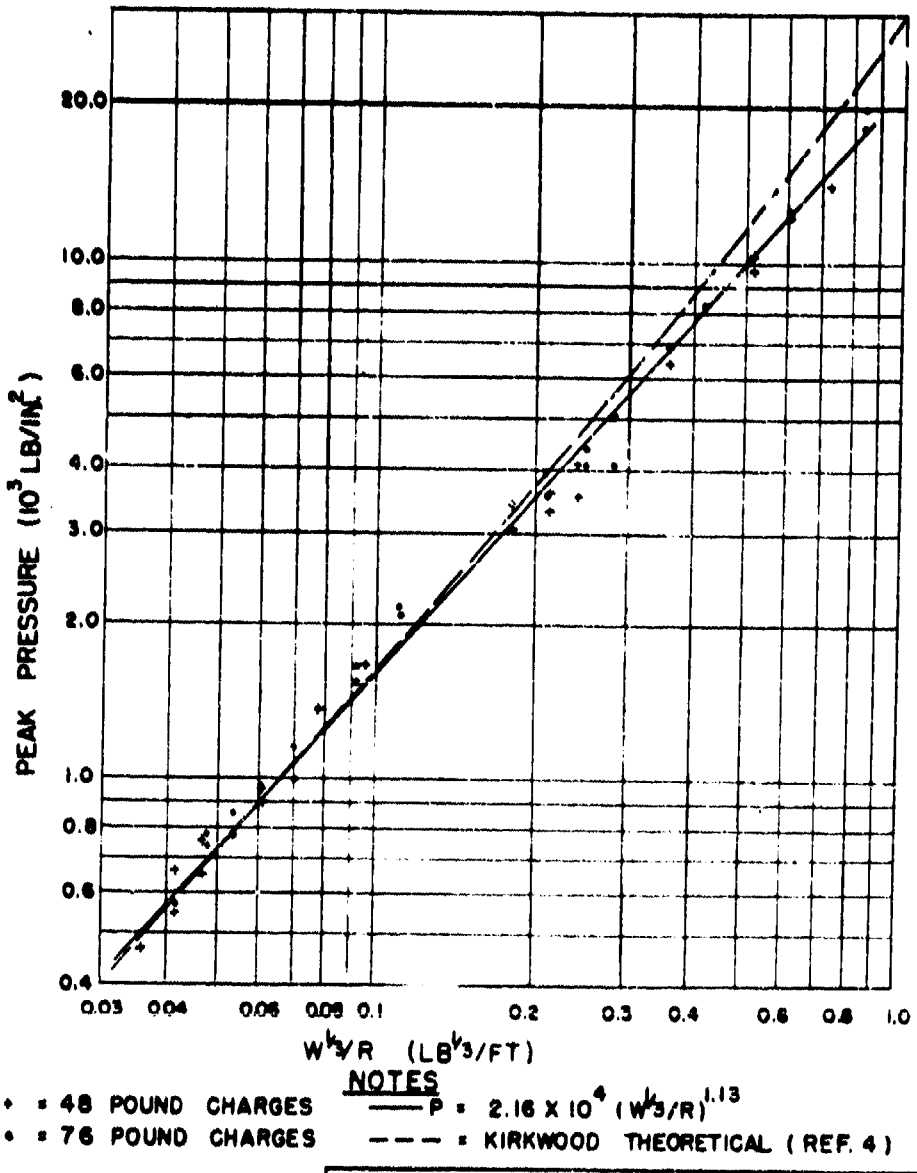
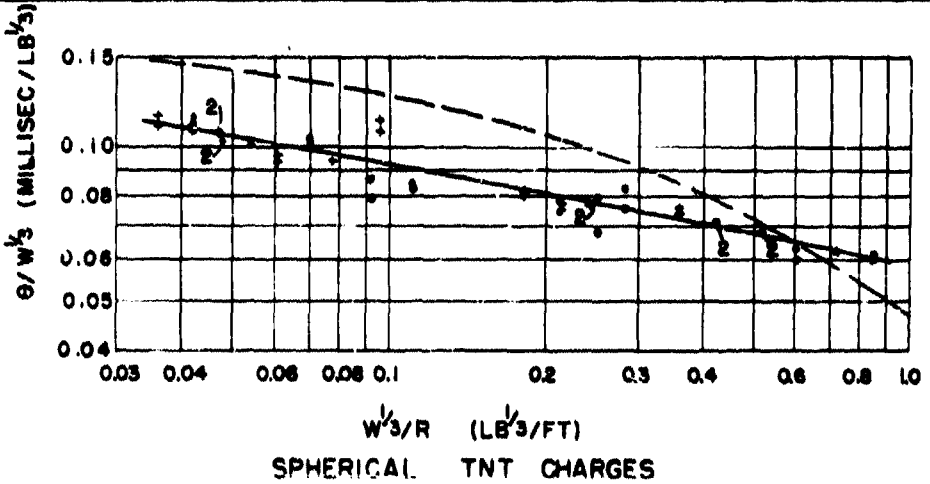


FIG 2
UNDERWATER PEAK PRESSURES VS $W^{1/3}/R$
FOR
SPHERICAL TNT CHARGES
(PIEZOELECTRIC RESULTS)
UERL WOODS HOLE, MASS.





SPHERICAL TNT CHARGES

NOTES

\+ = 48 POUND CHARGES

• = 76 POUND CHARGES

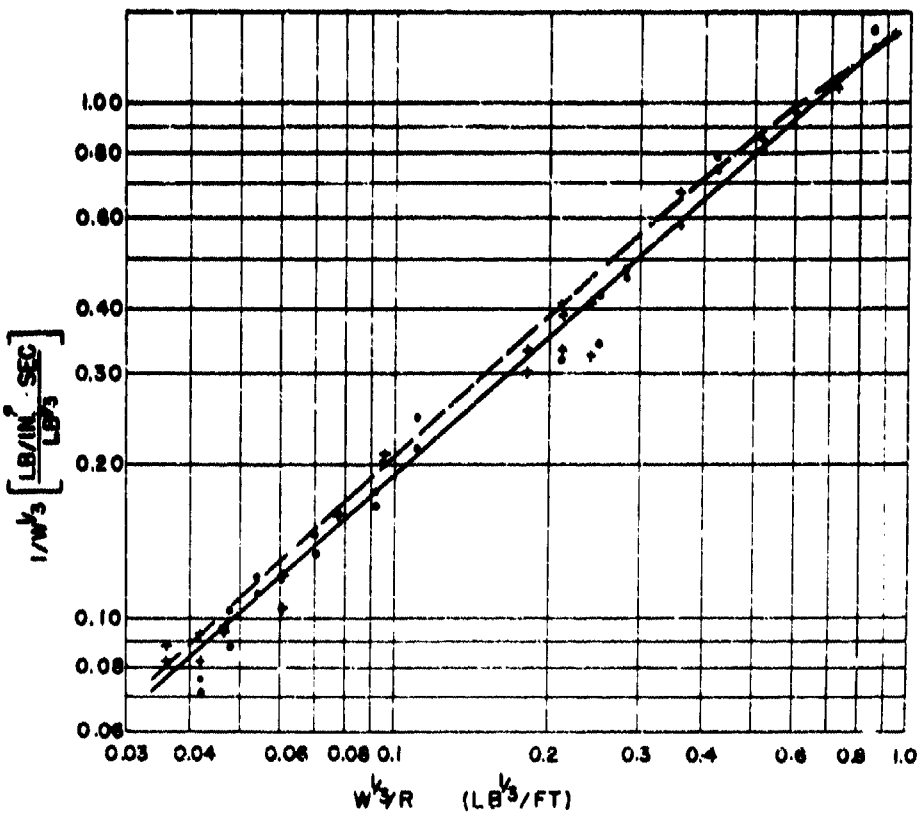
——— = KIRKWOOD THEORETICAL VALUES

FIG. 3

TIME CONSTANT / $W^{1/3}$ vs $W^{1/3}/R$ FOR SPHERICAL HBX AND TNT CHARGES

(PIEZOELECTRIC RESULTS)

UERL WOODS HOLE, MASS.



NOTES

—— I = 1.46 $W^{1/3}(W^{1/3}/R)^{.69}$

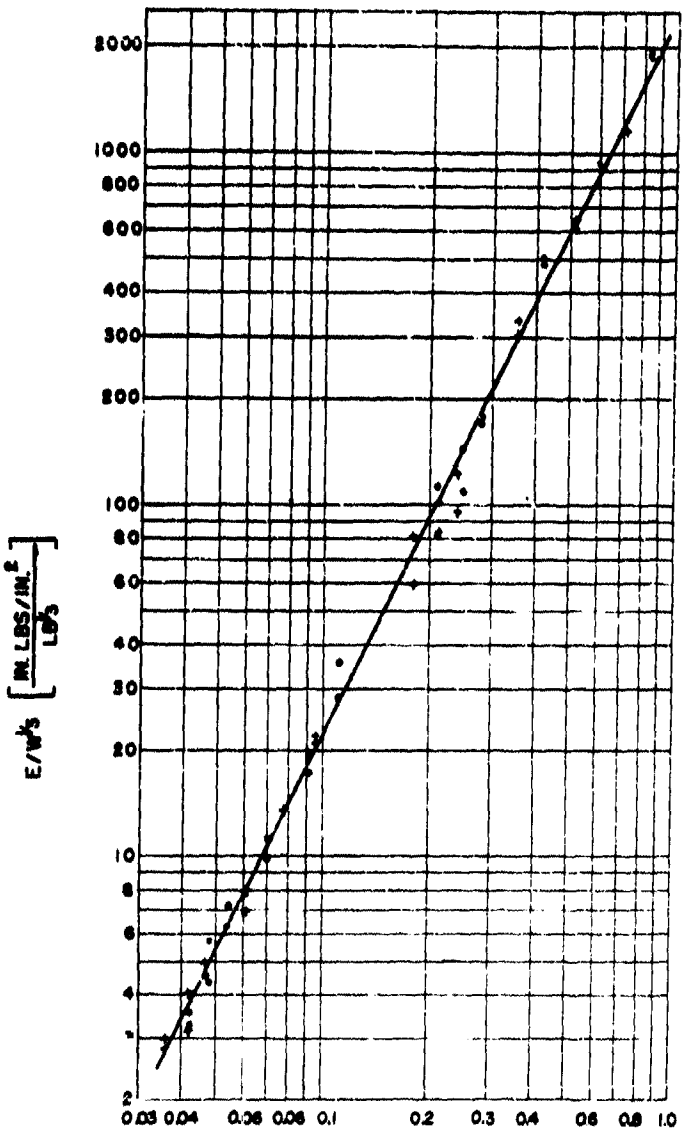
\+ = 48 POUND CHARGES

• = 76 POUND CHARGES

– – – = KIRKWOOD THEORETICAL (REF. 4)

FIG. 4

IMPULSE/$W^{1/3}$ (INTEGRATED TO 6.7 NOMINAL Θ)
VS
$W^{1/3}/R$ FOR SPHERICAL TNT CHARGES
(PIEZOELECTRIC RESULTS)
UERL WOODS HOLE, MASS.



NOTES

—— E = $2.44 \times 10^3 \, W^{1/3}(W^{1/3}/R)^{2.04}$

• = 48 POUND CHARGES

• = 76 POUND CHARGES

FIG. 5

ENERGY / $W^{1/3}$ (INTEGRATED TO 6.7 NOMINAL Θ)
VS
$W^{1/3}/R$ FOR SPHERICAL TNT CHARGES
(PIEZOELECTRIC RESULTS)

USRL WOODS HOLE, MASS

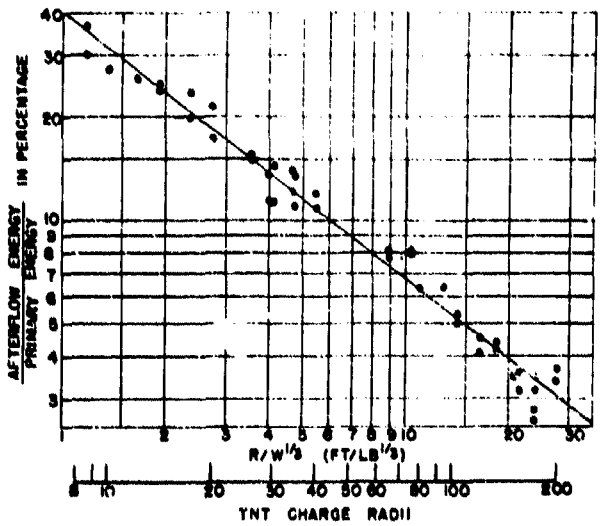


FIG. 6

AFTERFLOW ENERGY AS A PERCENTAGE OF PRIMARY ENERGY
VS
$R/W^{1/3}$ FOR SPHERICAL TNT



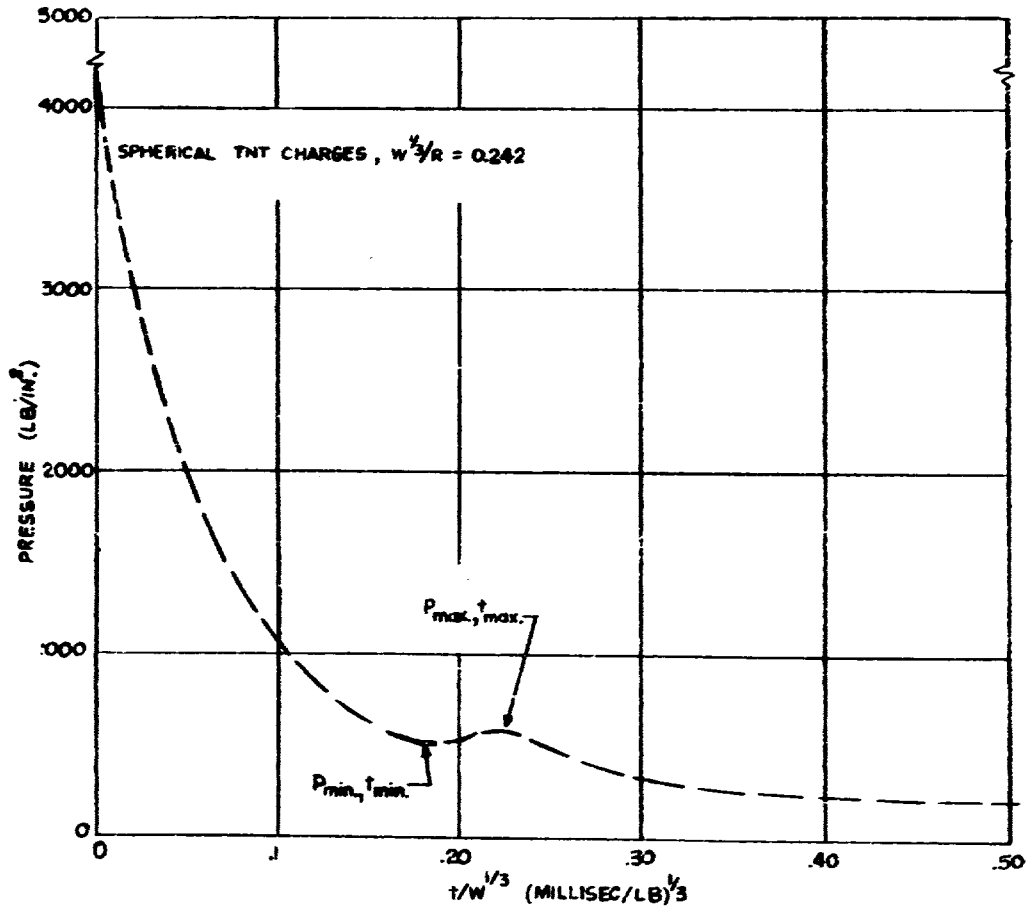


FIG. 7
COMPOSITE CURVE OF P vs. $t/W^{1/3}$ FOR SPHERICAL TNT CHARGE
VERL WOODS HOLE, MASS

VERL WOODS HOLE, MASS

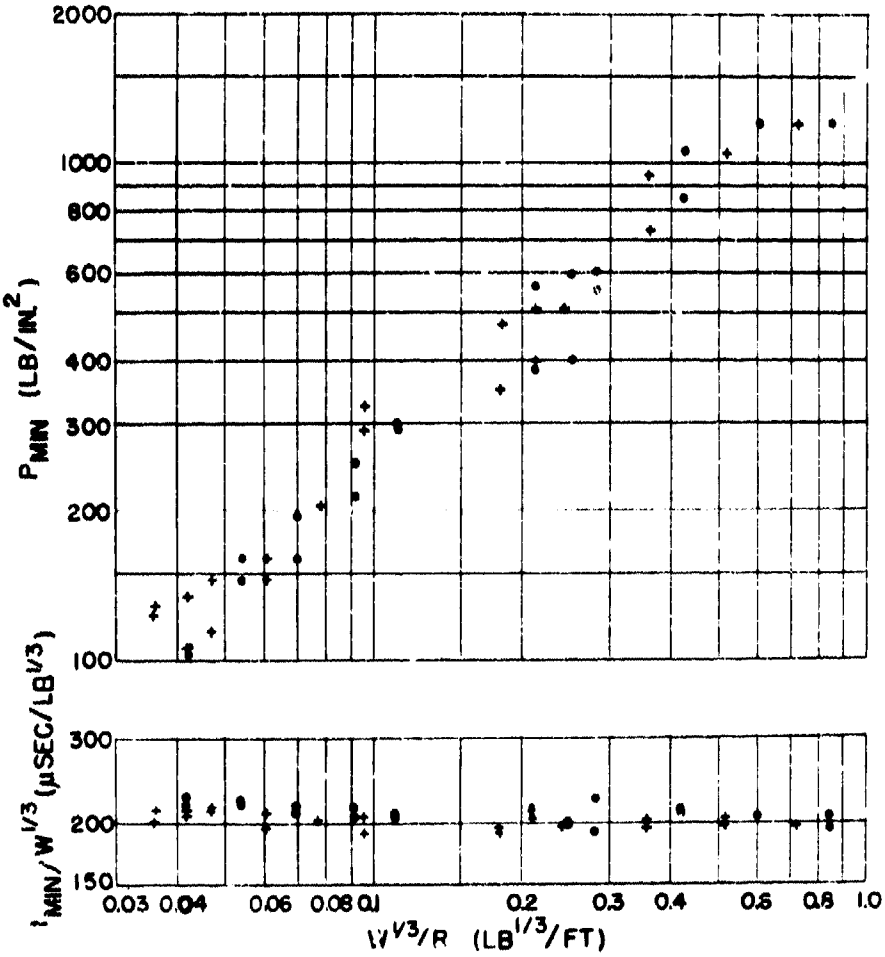


FIG 8

PRESSURE and REDUCED TIME OF MINIMUM IN PRESSURE TIME CURVE vs. $W^{1/3}/R$. SPHERICAL TNT CHARGES.

UERL WOODS HOLE, MASS.

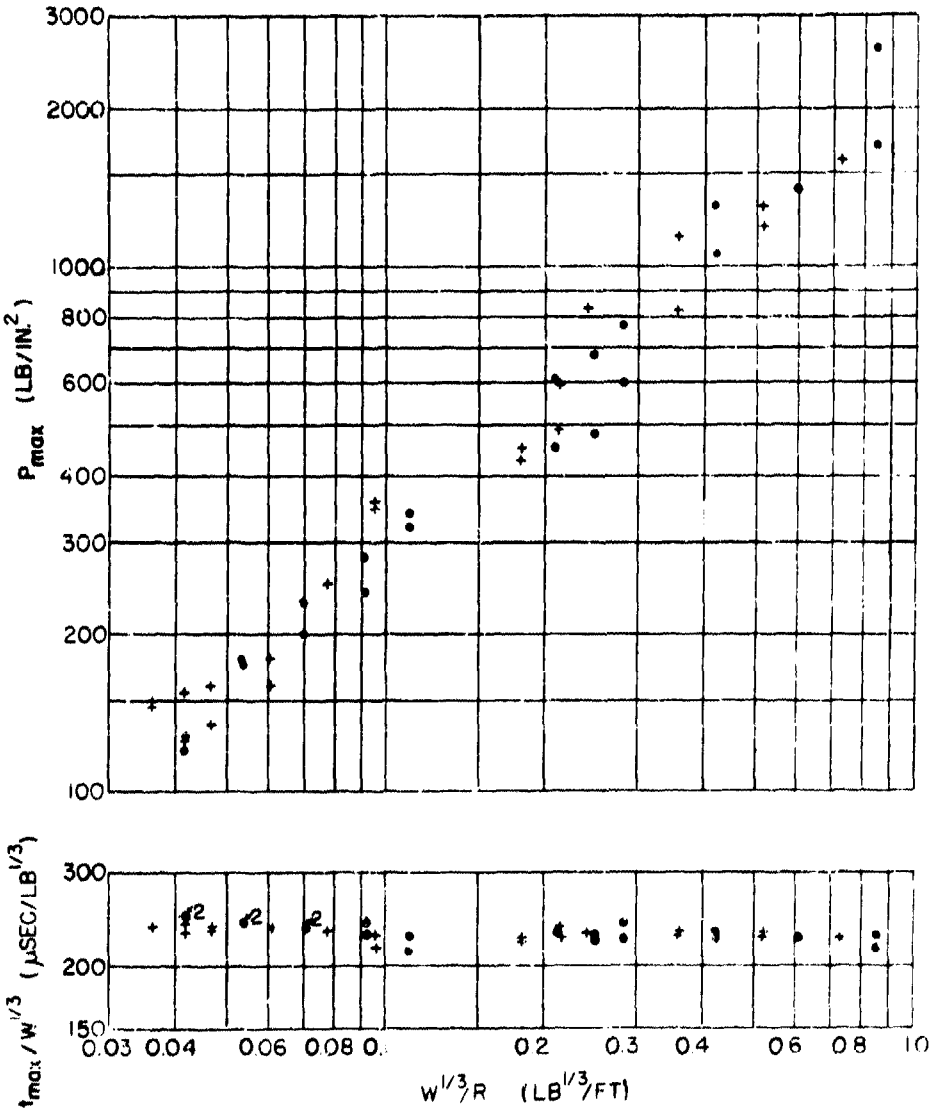
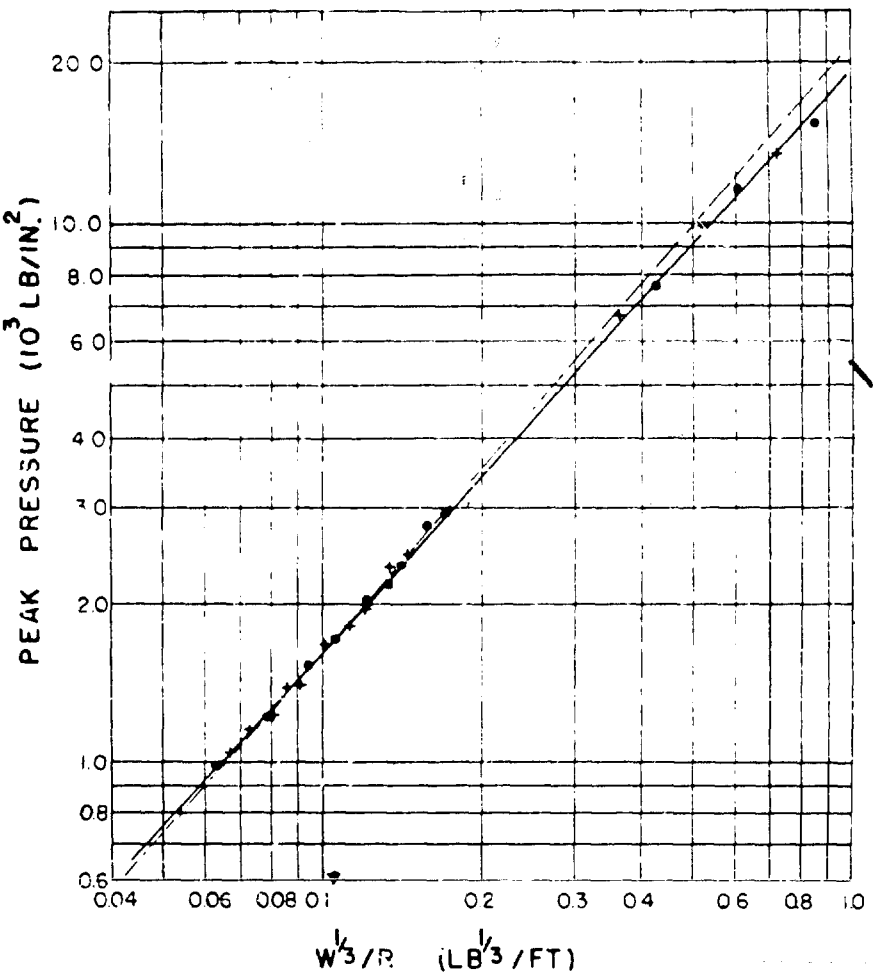


FIG. 9

PRESSURE and REDUCED TIME of MAXIMUM in PRESSURE TIME CURVE vs. $W^{1/3}/R$, SPHERICAL TNT CHARGES.

UERL WOODS HOLE, MASS



NOTES

\+ = 48 POUND CHARGES

• = 76 POUND CHARGES

——— $P = 1.92 \times 10^4 (W^{1/3}/R)^{1.08}$

— — — PIEZOELECTRIC GAUGE RESULTS

FIG. 10
UNDERWATER PEAK PRESSURES VS $W^{1/3}/R$
FOR
SPHERICAL TNT CHARGES
(BALL CRUSHER CALCULATED PRESSURES)
UERL WOODS HOLE, MASS.

SHOCK-WAVE PARAMETERS MEASURED OFF THE ENDS AND PERPENDICULAR BISECTOR OF LINE CHARGES 25 FT. LONG CONTAINING 50 LB. OF FLEXED TNT

J. S. Coles, R. H. Cole, P. C. Cross, J. P. Slifko,
C. R. Niffenegger, A. E. Christian, and M. A. Rogers
Underwater Explosives Research Laboratory
Woods Hole Oceanographic Institution

American Contribution

3 July 1947

TABLE OF CONTENTS

		Page
Glossary		
Abstract		
I.	INTRODUCTION	1
	1. Nature of Problem	1
II.	EXPERIMENTAL ARRANGEMENTS	1
	2. Charges	1
	3. Instrumentation	1
	4. Rig	4
III.	RESULTS	4
	5. Pressure-Time Curves	4
	6. Experimental Data	5
IV.	DISCUSSION	5
	7. Non-Linear Interaction of Shock Waves	5
	8. Time Phenomena	11
	A. Gauge Position A, on Charge Axis, Near Detonator	11
	B. Gauge Position B, on Charge Axis, Away from Detonator	12
	C. Gauge Position C, in Charge-Bisecting Plane. One End Detonated	12
	D. Gauge Position C, in Bisecting Plane, Both Ends Detonated Simultaneously	16
	9. Pressure, Impulse, and Energy Measurements	19
	10. Diaphragm Gauge Measurements	23
LIST OF REFERENCES		25

LIST OF TABLES

Table		Page
I	Piezoelectric Gauge Results from 50 lb TNT Line Charges	8-9
II	Diaphragm Gauge Results from 50 lb TNT Line Charges	10
III	Expressions for the Arrival Times at a Gauge of Shock Waves from Various Parts of a Line Charge	18

LIST OF FIGURES

Figure		Page
1	Longitudinal Cross-Section of Mark 8 Demolition Charge	2
2	Rigs for Long Cylindrical Charge Series	3
3	Gauge Positions Relative to Line Charge and Detonator	4
4	Photographic Reproductions of Typical Pressure-Time Curves from Piezoelectric Gauges on the Axis of a Long Cylindrical Charge at Various Distances	6
5	Photographic Reproductions of Typical Pressure-Time Curves from Piezoelectric Gauges on the Perpendicular Bisector of a Long Cylindrical Charge at Various Distances	7
6	Shock-Wave Durations vs Distance from a Line Charge on the Longitudinal Axis and in the Perpendicular Bisecting Plane	13
7	Difference $(t_x - t_i)$ in Time of Arrival at Gauge from Elements of Charge at Various Distances x from the Detonator End and the First Signal Reaching the Gauge vs x for Various Values of r_c	14
8	p_i and p_f vs $W^{1/3}/r$ for TNT Line Charges at Gauge Positions A, B, and C	20
9	Impulse/$W^{1/3}$ vs $W^{1/3}/r$ for TNT Line Charges at Gauge Positions A, B, and C	21
10	Energy/$W^{1/3}$ vs $W^{1/3}/r$ for TNT Line Charges at Gauge Positions A, B, and C	22
11	UERL Diaphragm Gauge Deformations vs Distance for 50 lb TNT Line Charges	24

LIST OF SYMBOLS

c	=	Velocity of sound in sea water (4.75 ft/millisec)
dx	=	Charge element at position x
E	=	Energy $\left(\frac{1}{\rho_o c}\int p^2 dt\right)$ (in. lb/in.^{2})
I	=	Impulse $\left(\int p dt\right)$ (lb sec/in.^{2})
ℓ	=	Charge length (ft)
p	=	Pressure at any time t (lb/in.^{2})
p_f	=	Pressure at time t_f (lb/in.^{2})
p_i	=	Pressure at time t_i (lb/in.^{2})
R	=	Shortest distance at which $t_i = t_o$ for gauge position C $\left[= \frac{\ell}{2c}(v^2 - c^2)^{\frac{1}{2}}\right]$ (ft)
R'	=	Distance at which $t_o = t_{\ell/2}$ for gauge position C, double-ended detonation $\left[= \frac{\ell}{4cv}(v^2 - c^2)\right]$ (ft)
r_A	=	Distance from detonator end of the charge to gauge position A (ft)
r_B	=	Distance from non-detonator end of the charge to gauge position B (ft)
r_C	=	Distance from center of charge to gauge position C (ft)
t_f	=	Arrival time of the signal from the charge element producing the final signal to reach the gauge (millisec)
t_i	=	Arrival time of the first signal to reach the gauge (millisec)
t_ℓ	=	Arrival time of the signal from the non-detonator end of the charge (millisec)
$t_{\ell/2}$	=	Arrival time of the signal from the midpoint of the charge (millisec)
t_o	=	Arrival time of the signal from the detonator end of the charge (millisec)
t_x	=	Arrival time of the signal from a charge element at distance x from the detonator (millisec)
v	=	Velocity of detonation of TNT (19 ft/millisec)
W	=	Charge weight (lb)
x	=	Distance measured along charge from detonator (ft)
x_i	=	Distance from the detonator to the charge element to produce the initial signal to reach the gauge (ft)
ρ_o	=	Density of sea water at a given temperature and salinity
$\rho_o c$	=	5.58 + 0.0065 t, where t is the temperature in degrees Centigrade (the acoustic impedance of sea water)

ABSTRACT

Pressure-time curves from piezoelectric gauges located on the extension of the longitudinal axis and in the bisecting plane of Mark 8 Demolition charges (25 ft hose filled with 50 lb TNT) fired under water are interpreted quantitatively in terms of time phenomena, and qualitatively in terms of pressure time phenomena by consideration of the geometry of the experiment, detonation velocity (v), and velocity of sound in sea water (c). For gauges off the initiating end, (gauge position A) $t_f - t_i = \ell(1/c + 1/v)$, where t_i is the arrival time of the first signal to reach the gauge, t_f the arrival time of the final signal to reach the gauge, and ℓ is the charge length. For gauges off the opposite (non-detonator) end of the charge (gauge position B), $t_f - t_i = \ell(1/c - 1/v)$. For gauges in the bisecting plane (gauge position C), at small charge-to-gauge distances (r_C) for which t_c, the arrival time of the signal from the detonator end of the charge, is greater than t_i,

$$t_i = (1/v)\ \ell/2 + (r_C/c)\ (v^2 - c^2)^{\frac{1}{2}} .$$

The arrival time of the signal from the opposite end of the charge is

$$t_\ell - t_f = \frac{1}{c}\left[r_C^2 + \left(\frac{\ell}{2}\right)^2\right]^{\frac{1}{2}} + \ell/v .$$

Pressures measured by gauges in position B are 20-40% greater than those measured in position A, and those measured in position C are several fold greater. These are so compensated by the durations that differences in impulse in the various orientations are not significant. Shock-wave energies obtained from position C are several fold greater than for positions A and B, which do not differ significantly from one another. These relative parameters off the ends and side of a cylindrical charge agree with the recent theoretical results of Polachek,[10]* and confirm earlier results obtained at UERL on somewhat more symmetrical cylindrical charges.

---

* Superscript numerals refer to List of References at the end of this report.

SHOCK-WAVE PARAMETERS MEASURED OFF THE ENDS AND PERPENDICULAR BISECTOR OF LINE CHARGES 25 FT LONG CONTAINING 50 LB OF FLEXED TNT

I. INTRODUCTION

1. Nature of Problem

A great many measurements of the primary shock wave have been made for large charges, usually of symmetrical cylindrical shape (i.e., height = diameter), although spherical charges have been used in certain experiments.[1,2] To develop a better understanding of the fundamental nature of shock waves as they are affected by charge shape, a number of different charge shapes must be used. Such studies have been carried out on small charges photographically[3] and with piezoelectric and diaphragm gauges[4] at UERL, on Cordtex (similar to primacord) by the British,[5] and have been investigated theoretically by Rice and Grinnel.[6,7] Owing to instrumental and experimental limitations, the Cordtex experiments did not yield as much information as was desired. To obtain more information, a number of measurements of the shock wave have been carried out at UERL with gauges on the extension of the longitudinal axis and also on the perpendicular bisector of 50 lb "flexed" TNT charges, 25 ft long. The results so obtained are in agreement with calculations made by considering the relative velocities of the detonation wave through the explosive and of the shock wave through water. They cannot be compared directly, however, with the calculations of Rice,[6,7] owing to his assumption of infinite detonation velocity and charge length.

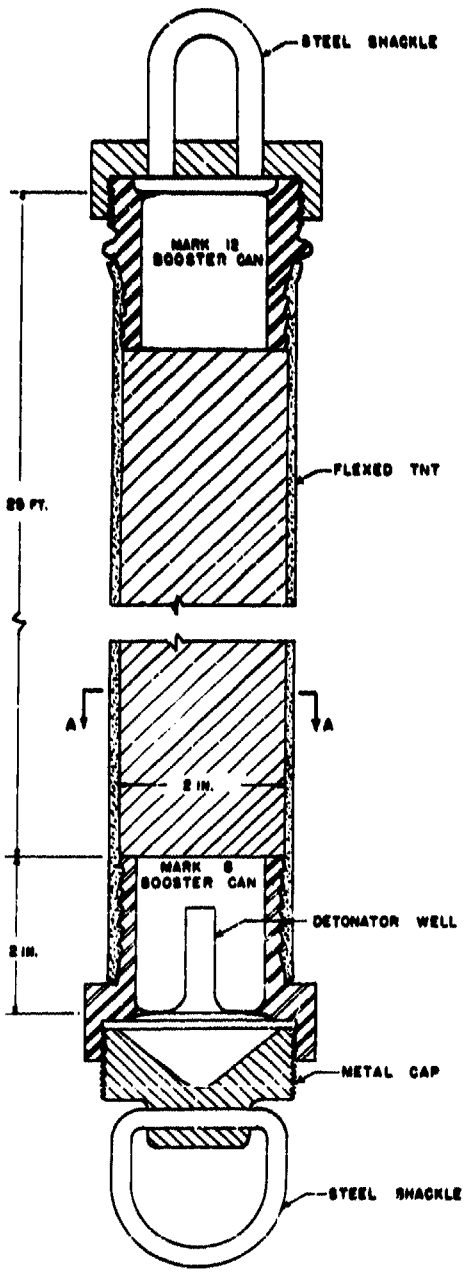
II. EXPERIMENTAL ARRANGEMENTS

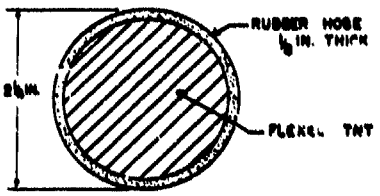
2. Charges

The charges used in these tests were US Navy Mark 8 demolition charges, which contained 50 lb of "flexed" TNT in a 2 in. inside diameter rubber hose 25 ft long. ("Flexed" TNT is prepared by pouring the molten TNT into the rubber hose, which is then subjected to continued flexing until the TNT has solidified in the form of densely packed crystals.) As will be noted in Fig. 1 a tetryl booster was cast into each end of the charge; the charges were detonated statically by means of a US Army Engineer's Special Electric Detonator placed in one or both of the ends of the charge, as desired.

3. Instrumentation

Four pairs of piezoelectric gauges were arranged at four distances from the charge, on a horizontal line 40 ft below and parallel to the water surface. These gauges were all forward of the charge as it was towed through the water. Two light gauge blocks, each mounting two





SECTION A-A

FIG. 1
LONGITUDINAL CROSS-SECTION OF
MARK 8 DEMOLITION CHARGE
UERL WOODS HOLE, MASS.

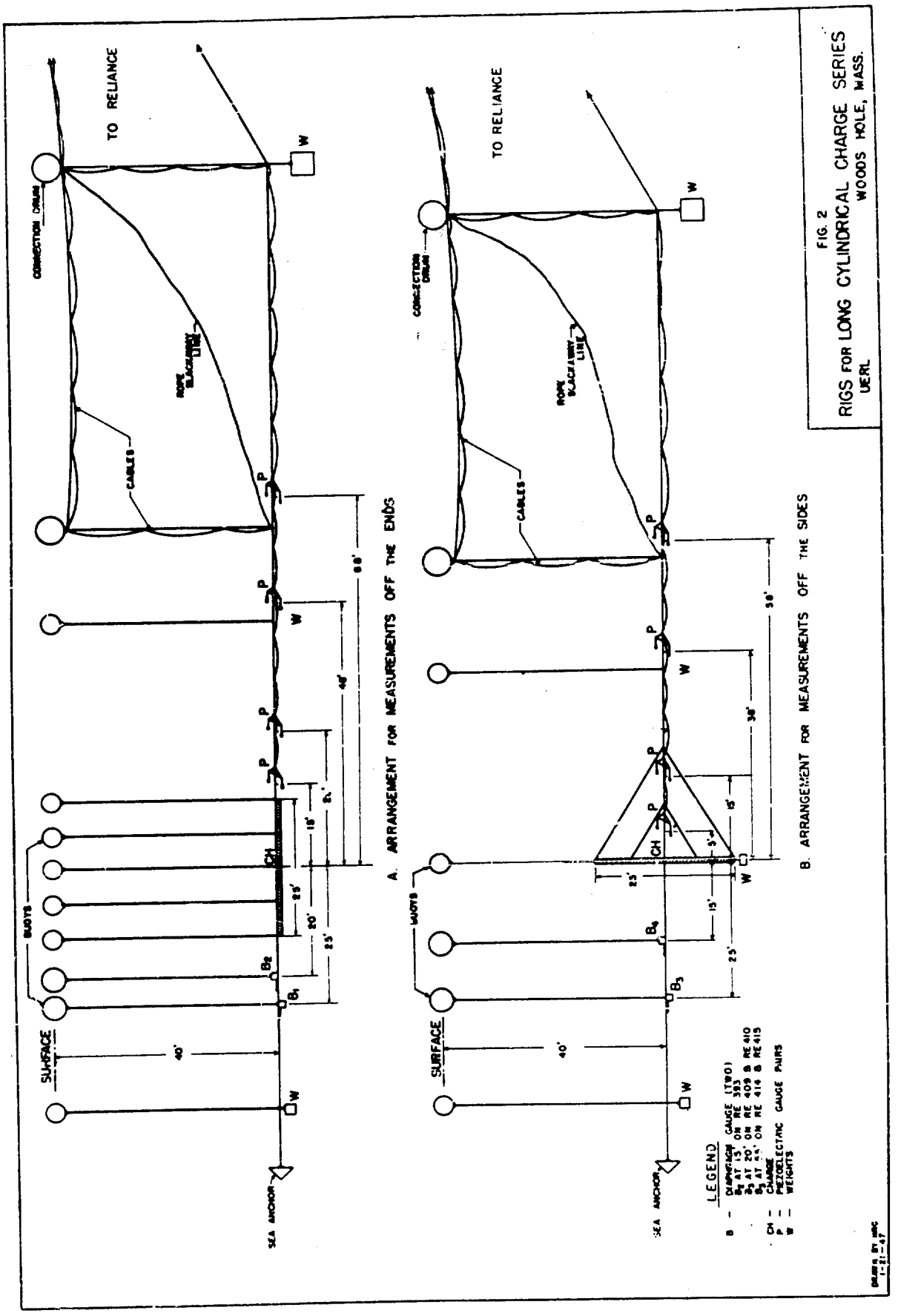


FIG. 2
RIGS FOR LONG CYLINDRICAL CHARGE SERIES
WOODS HOLE, MASS.
UERL

UERL diaphragm gauges, were similarly arranged at two distances aft of the charge. A full description of the types of instruments used has been reported previously in UERL reports.[2,8]

4. Rig

The various gauges were attached to one another and to the charge by steel spacer cables which were maintained taut by the drag of the sea anchor moving through the water at the extreme aft of the rig. When measurements were being made with gauges off either end of the charge, the charge was lashed along the steel spacer cable in the correct position. Five surface floats were affixed equidistant along the charge to maintain its alignment with respect to the gauges. This is shown in Fig. 2A. When measurements were being made with the gauges off the sides of the charge, the charge was lashed with its mid-point at the spacer cable to a vertical line running from a surface float to a 55 lb weight below the charge. In addition, the charge was bridled at four points forward to the spacer cable, as shown in Fig. 2B.

III. RESULTS

5. Pressure-Time Curves

To simplify the further consideration and discussion of this group of experiments, the various gauge positions and distances have been defined as indicated in Fig. 3. In practice only one of the gauge

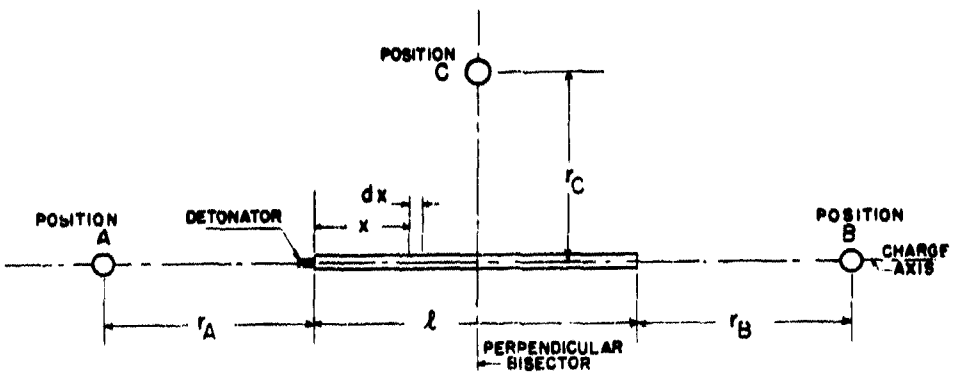


FIG 3
GAUGE POSITIONS RELATIVE TO LINE CHARGE AND DETONATOR

positions indicated by Position A, Position B, or Position C was obtained from a single shot, three different charges being fired to obtain data for all three positions. However, measurements at four different distances

along a given direction from the charge were obtained on each shot.

The pressure-time curves obtained from the ends (Positions A and B) of these long cylindrical charges were characteristically different from those of spherical charges or cylindrical charges with the ratio of length to diameter not greater than 2. In addition, the pressure-time curves with gauges off the detonator end, off the non-detonator end and off the sides, are distinctly different from one another (records from Position A, B, and C, respectively). The characteristics of pressure-time curves from various positions about long cylindrical charges are illustrated in Figs. 4 and 5, where t_i is the arrival time of the first signal to reach the gauge, t_f the arrival time of the signal from the charge element producing the final signal to reach the gauge, t_o the arrival time at the gauge of the signal from the detonator end of the charge, $t_{\ell/2}$ the arrival time of the signal from the midpoint of the charge, and t_ℓ the arrival time of the signal from the non-detonator end of the charge. The pressures corresponding to t_f and t_i are p_f and p_i. The actual time of detonation of the charge element at $x = 0$ is the zero point on the time scale. The pressure measured at the gauge between times t_i and t_f does not show the initial exponential decay obtained with spherical or more symmetrical charges, but is sustained by the finite detonation time of the charge. Not until detonation is complete, and no further contribution to the shock wave from detonating explosive is reaching the gauge, does the shock wave begin decaying more rapidly (at time t_f).

6. Experimental Data

Table I gives the experimental pressures (p_i and p_f), durations ($t_f - t_i$), and momenta ($\int p\,dt$) and energies ($1/\rho_o c \int p^2 dt$) together with their integration times for the various gauge positions and distances used. In Table II are presented the experimental data for the UERL diaphragm gauges, with thin (0.038 in. standard thickness) and medium (0.085 in. standard thickness) diaphragms at various distances from the charge for the three charge orientations.

IV. DISCUSSION

7. Non-Linear Interaction of Shock Waves

The treatment of the pressure-time function at a given point in space as a summation of the contributions of the elements of a line charge is extremely difficult because of the complicated non-linear manner in which shock waves of finite amplitude interact. A linear super-position theory would, under the conditions employed for the off-end shots in these experiments, fail to account for the observed initial peak pressure, but would predict instead a finite and measurable time of build-up to a maximum pressure. A more nearly correct theory is no doubt possible, but no quantitative discussion of the pressure-time relationships as a function of distance and orientation from the charge will be attempted here. The qualitative features which appear to be related to the times of detonation of each charge element and to the corresponding transit-time of the shock wave from each element to the gauge, as estimated by the acoustic approximation, will be discussed in detail.

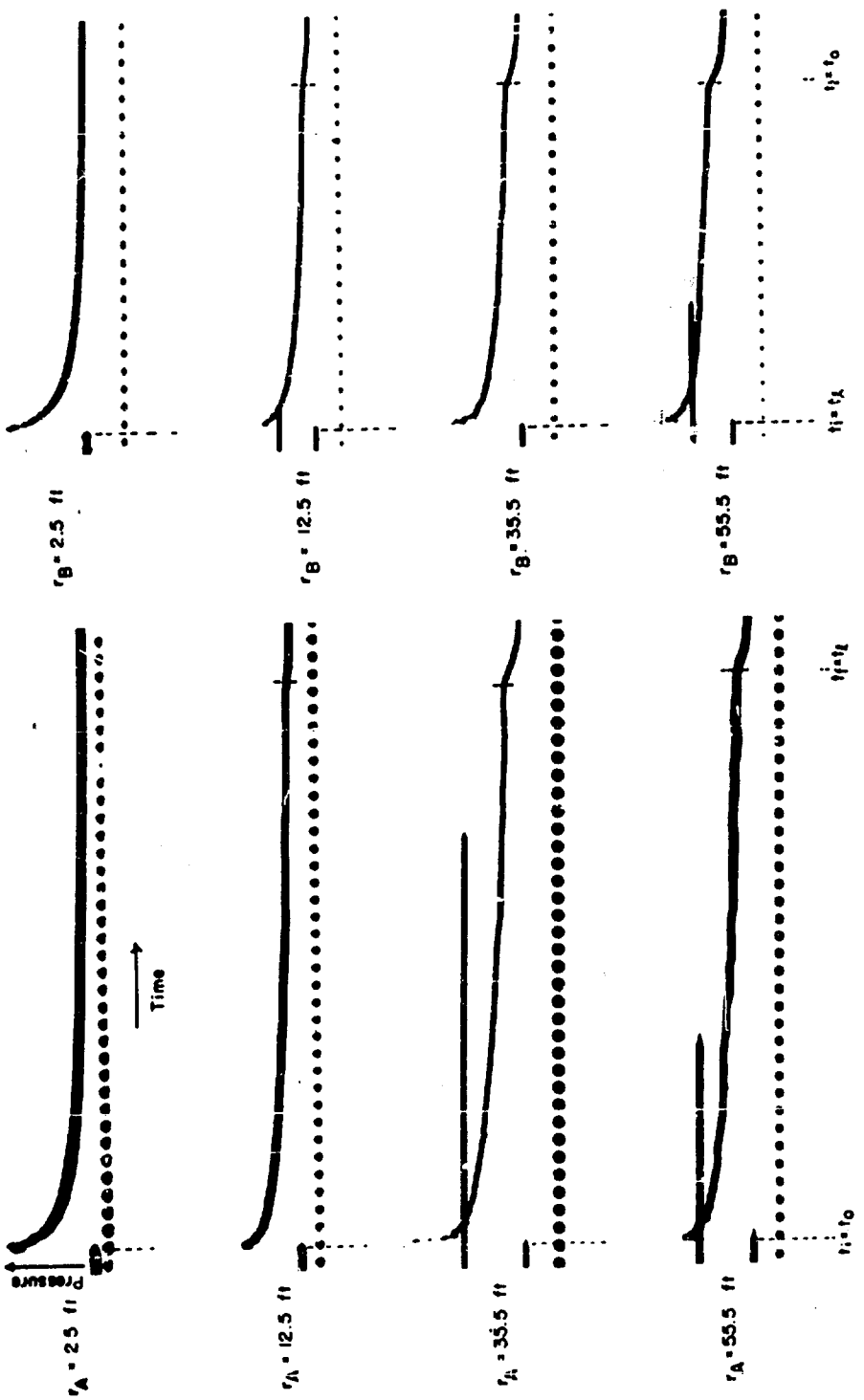


Fig. 4. Photographic reproductions of typical pressure time curves from piezoelectric gauges on the axis of a long cylindrical charge at various distances.

Notes: Timing dots are at intervals of 0.200 msec
a. Position A: Shot RE 398 (near detonator end)
b. Position B: Shot RE 403 (near non-detonator end)

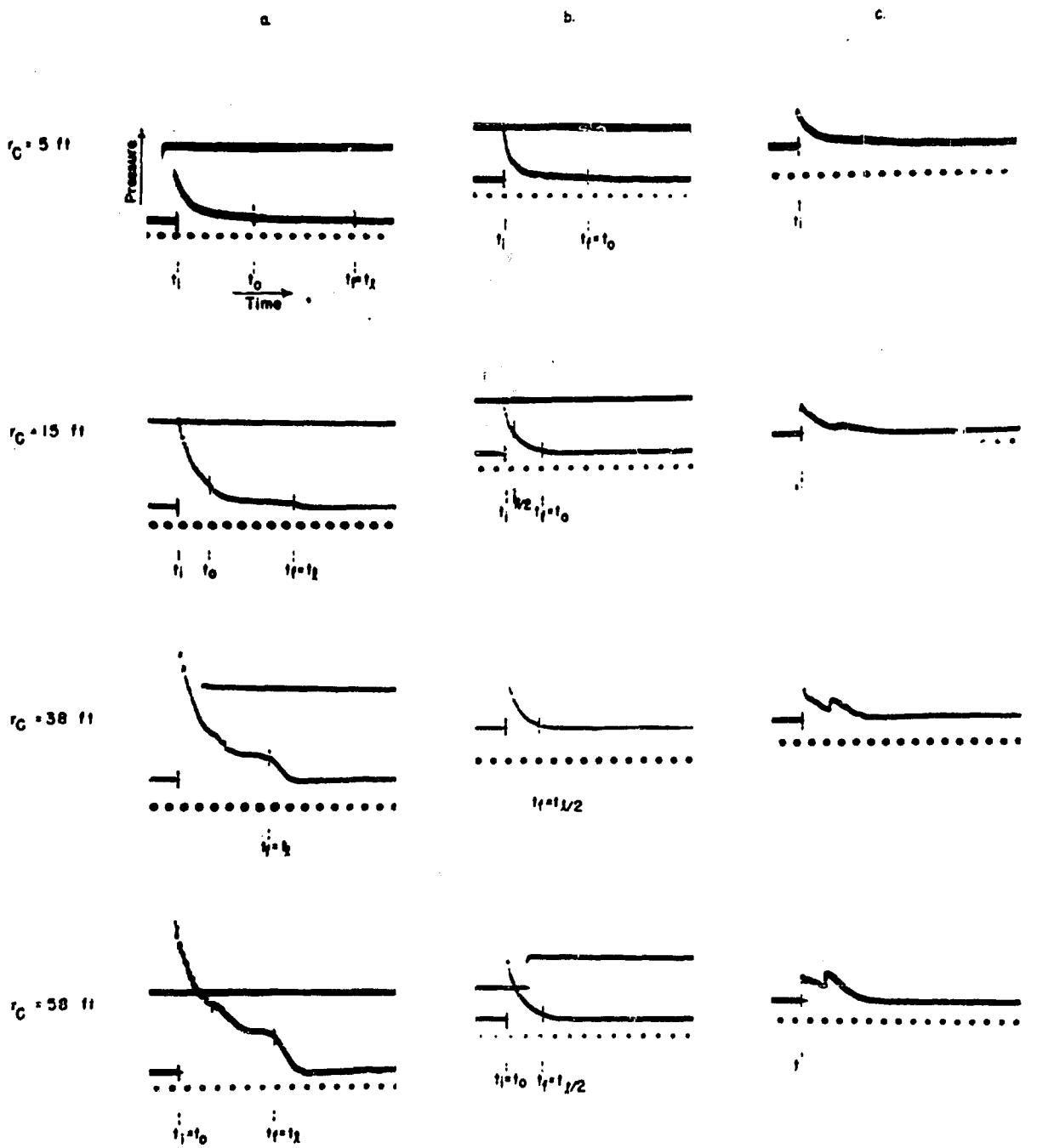


Fig. 5. Photographic reproductions of typical pressure time curves from piezo-electric gauges on the perpendicular bisector of a long cylindrical charge at various distances. (Position C).

Notes: Timing dots are intervals of 0.200 msec

a. Detonated from one end. Shot RE 409

b. Detonated from both ends. Shot RE 415

c. Detonated from both ends, but not simultaneously. Shot RE 414

TABLE I

PIEZOELECTRIC GAUGE RESULTS FROM 50 LB TNT LINE CHARGES

	Shot No. RE-	Channel	r_A (ft)	P_i (psi)	P_f (psi)	t_f-t_i (msec)	I (psi sec)	Integration Time for I (msec)	E (in. lb/in^2)	Integration Time for E (msec)
GAUGE POSITION A	398	1	2.5	4100	--	--	5.06	8.0	1198	8.0
	398	2	2.5	4400	--	--	5.09	8.0	1317	8.0
	399	1	2.5	3750	--	--	4.46	7.0	1001	7.0
	399	2	2.5	4000	--	--	4.50	7.0	1133	7.0
	400	1	2.5	4350	--	--	4.25	7.0	982	7.0
	400	2	2.5	3300	--	--	2.72	7.0	544	7.0
	Average		2.5	4067	--	--	4.35	7.3	1029	7.3
	398	3	12.5	760	100	6.5	1.45	6.5	75.8	8.0
	398	4	12.5	780	--	--	--	--	83.5	8.0
	399	3	12.5	780	40	6.5	1.37	6.5	74.4	7.0
	399	4	12.5	722	20	6.5	1.10	6.5	58.2	7.0
	400	3	12.5	810	80	6.5	1.51	6.5	86.0	7.0
	400	4	12.5	804	60	6.5	1.29	6.5	67.2	7.0
	Average		12.5	776	60	6.5	1.34	6.5	74.2	7.3
	398	5	35.5	270	60	6.3	0.638	6.3	13.5	8.0
	398	6	35.5	270	70	6.4	0.682	6.4	15.5	8.0
	399	5	35.5	260	35	--	--	--	--	--
	399	6	35.5	260	65	--	--	--	--	--
	400	5	35.5	295	40	6.4	0.598	6.4	12.1	7.0
	400	6	35.5	310	60	6.4	0.686	6.4	15.7	7.0
	Average		35.5	278	55	6.4	0.651	6.4	14.2	7.5
	398	7	55.5	180	45	6.4	0.452	6.4	6.65	8.0
	398	8	55.5	160	30	6.4	0.401	6.4	5.32	8.0
	399	7	55.5	153	50	--	--	--	--	--
	399	8	55.5	160	52	--	--	--	--	--
	400	7	55.5	190	41	6.3	0.440	6.3	6.26	7.0
	400	8	55.5	200	55	6.4	0.522	6.4	8.30	7.0
	Average		55.5	174	46	6.4	0.454	6.4	6.63	7.5
			r_B							
GAUGE POSITION B	397	1	2.5	6400	--	--	2.82	4.2	984	4.2
	397	2	2.5	7200	--	--	2.75	4.2	926	4.2
	403	1	2.5	6200	--	--	2.80	4.2	942	4.2
	403	2	2.5	7400	--	--	2.70	4.2	940	4.2
	Average		2.5	6800	--	--	2.77	4.2	948	4.2
	397	3	12.5	1130	90	3.96	1.16	3.96	80.6	4.2
	397	4	12.5	970	70	4.0	0.992	4.0	62.9	4.2
	403	3	12.5	900	170	3.9	1.30	3.9	91.8	4.2
	403	4	12.5	920	120	3.9	1.12	3.9	74.6	4.2
	Average		12.5	980	113	3.9	1.14	3.9	77.5	4.2
	397	5	35.5	390	95	3.85	0.588	3.85	18.0	4.2
	397	6	35.5	390	84	3.8	0.531	3.8	17.6	4.2
	403	5	35.5	370	80	3.8	0.540	3.8	16.0	4.2
	403	6	35.5	370	80	3.8	0.558	3.8	17.3	4.2
	Average		35.5	380	85	3.8	0.554	3.81	17.4	4.2
	397	7	55.5	245	70	3.8	0.383	3.8	7.64	4.2
	397	8	55.5	267	67	3.8	0.407	3.8	8.55	4.2
	403	7	55.5	237	67	3.8	0.384	3.8	7.73	4.2
	403	8	55.5	270	70	3.85	0.420	3.85	9.09	4.2
	Average		55.5	255	69	3.8	0.398	3.81	8.25	4.2

TABLE I

PIEZOELECTRIC GAUGE RESULTS FROM 50 LB TNT LINE CHARGES

	Shot No. RE-	Channel	r_c (ft)	p_i (psi)	p_f (psi)	$t_f - t_i$ (msec)	I (psi sec)	Integration Time for I (msec)	E (in. lb/in^2)	Integration Time for E (msec)
GAUGE POSITION C, SINGLE-ENDED DETONATION	409	1	5	11,600	1000	2.43	3.54	2.45	2438	2.45
	409	2	5	--	--	2.58	--	--	--	--
	411	1	5	12,700	1200	--	4.23	2.45	3023	2.45
	411	2	5	12,300	900	--	--	--	--	--
	412	1	5	10,500	1000	2.42	3.77	2.45	2725	2.45
	412	2	5	10,200	1000	2.42	3.19	2.45	2389	2.45
	Average		5	11,460	1020	2.46	3.63	2.45	2644	2.45
	409	3	15	4900	100	1.64	1.60	1.64	741.5	1.60
	409	4	15	4870	200	1.58	1.38	1.58	524	1.60
	411	3	15	5000	300	1.68	1.80	1.72	671	1.80
	411	4	15	4900	200	1.56	1.60	1.52	603	1.80
	412	3	15	5200	120	1.65	1.42	1.65	610	1.70
	412	4	15	4450	110	1.61	1.31	1.60	490	1.65
	Average		15	4870	172	1.62	1.52	1.62	607	1.69
	409	5	38	1210	230	1.30	0.633	1.30	75.8	1.60
	409	6	38	1570	260	1.20	0.695	1.20	100	1.40
	411	5	38	1750	125	1.30	---	--	---	--
	411	6	38	1920	365	1.08	0.723	1.04	113	1.60
	412	5	38	1730	250	1.23	0.676	1.20	103	1.50
	412	6	38	1800	290	1.10	0.724	1.10	126	1.35
	Average		38	1663	253	1.20	0.690	1.17	104	1.49
	409	7	58	835	200	1.30	0.461	1.30	34.9	1.60
	409	8	58	---	---	--	---	--	-	--
	411	7	58	925	265	0.98	0.450	1.00	42.5	1.40
	411	8	58	1000	290	1.04	0.430	0.96	40.9	1.40
	412	7	58	1025	275	0.83	0.429	0.825	49.6	1.20
	412	8	58	965	225	1.23	0.476	1.20	42.1	1.58
	Average		58	950	251	1.08	0.449	1.06	42.0	1.44
GAUGE POSITION C, DOUBLE-ENDED DETONATION	410	1	5	18,000	--	1.06	---	--	--	--
	410	2	5	18,000	1400	--	---	--	--	--
	413	1	5	18,000	1600	1.20	---	--	--	--
	413	2	5	19,000	1400	1.20	---	--	--	--
	415	1	5	20,400	--	--	---	--	--	--
	415	2	5	19,300	1700	1.13	3.16	1.15	3810	1.15
	Average			18,783	1525	1.15	3.16	1.15	3810	1.15
	410	3	15	7500	600	0.52	1.47	0.52	1136	0.72
	410	4	15	8400	400	0.47	1.22	0.50	914	0.56
	413	3	15	11,500	350	--	--	--	--	--
	413	4	15	10,000	400	--	--	--	--	--
	415	3	15	10,000	600	0.50	1.40	0.50	1057	0.63
	415	4	15	--	---	--	--	--	--	--
	Average		15	9480	470	0.50	1.36	0.51	1036	0.64
	410	5	38	3710	210	0.46	0.498	0.42	176	0.56
	410	6	38	3800	200	0.43	0.554	0.44	203	0.60
	413	5	38	3900	320	--	---	--	---	--
	413	6	38	--	---	--	---	--	---	--
	415	5	38	3630	250	0.49	0.616	0.49	218	1.80
	415	6	38	4650	300	0.42	0.634	0.42	277	0.60
	Average		38	3938	256	0.45	0.576	0.44	218	0.89
	410	7	58	2240	195	0.47	0.373	0.48	76.0	0.84
	410	8	58	2650	200	0.44	0.374	0.44	86.2	0.72
	413	7	58	1740	90	--	---	--	--	--
	413	8	58	1710	90	--	---	--	--	--
	415	7	58	2340	210	0.50	0.423	0.49	98.0	0.80
	415	8	58	1950	---	--	---	--	93.2	0.875
	Average		58	2105	157	0.47	0.390	0.47	88.4	0.81

TABLE II

DIAPHRAGM GAUGE RESULTS FROM 50 LB TNT LINE CHARGES

Plate deformation in inches x 100

		Shot No. RE-	DISTANCE FROM CENTER OF CHARGE (ft)			
			Thin Plates Standard Thickness = 0.038			Medium Plates Standard Thickness = 0.085
			55	25	20	15
GAUGE POSITION B		398		32.6 32.5	48.3 48.8	
		399		26.3 30.9	44.0 47.6	
		400		29.2 29.7	44.6 44.8	
		Average		30.2	46.4	
GAUGE POSITION A		397		26.5 26.3		
		403		25.4 25.0	39.3 39.0	
		Average		25.8	39.2	
GAUGE POSITION C	Single-Ended	409			99.2 01.3	60.0 57.5
		411		77.4 77.6		53.7 51.9
		412		65.9 66.4		54.0 52.1
		Average		71.8	100.2	54.9
	Double-Ended	410			Burst Burst	85.5 82.9
		413		Burst Burst		84.4 81.5
		415	52.0 53.0			92.2 89.4
		Average	52.5	(>100)	(>100)	86.0

8. Time Phenomena

The abrupt increase in the rate of decay of pressure with time, which was observed in the records of Figs. 4 and 5, may be qualitatively correlated with the termination of sustaining contributions to the pressure by the detonation of new elements of the explosive charge. The times at which these breaks should occur may be estimated from simple considerations involving the velocity, v, of detonation, the velocity, c, of the shock-wave transmission through the sea water (assumed acoustic as a first approximation), and the geometry of the gauge-charge system. Figure 3 shows the geometric arrangement for the three cases involving detonation at one end of the straight line charge.

Figures 4 and 5 are actual photographic reproductions of typical piezoelectric records for the various experimental conditions. In the shot illustrated by Fig. 5C, the detonations of the two ends of the charge were not simultaneous. It will be noted that the second peak, which is barely visible at $r_C = 5$ ft, is equal to the first peak when $r_C = 58$ ft. The records for this shot are included for interest only. No quantitative analysis of any sort was attempted.

It should be noted that the pressure scales in Figs. 4 and 5 are different for the various distances.

A. Gauge Position A, on Charge Axis, Near Detonator. Let $t = 0$ at the time of initiation of detonation. The first signal of the explosion then arrives at gauge A at the time

$$t_i = r_A/c \tag{1}$$

and the signal from the last element of charge contributing to the pressure arrives at the time

$$t_f = \ell/v + (\ell + r_A)/c \tag{2}$$

The difference

$$t_f - t_i = \ell(1/c + 1/v) \tag{3}$$

represents the time after the shock front that the gauge pressure-time record should show an increase in the decay rate. This "duration" for gauges on the charge axis is seen to be independent, in the acoustic

approximation, of the distance from charge to gauge. Figure 6 shows the comparison of observed durations with those calculated from Eq. (3) using the approximate velocities, v = 19 ft/millisec and c = 4.75 ft/millisec.

B. Gauge Position B, on Charge Axis, Away from Detonator. The first signal to arrive at gauge B is from the charge element at $x = \ell$, i.e., the explosive farthest from the detonator. In this case,

$$t_i = \ell/v + r_B/c \tag{4}$$

The final signal is from the charge element at x = 0, and

$$t_f = (\ell + r_B)/c \tag{5}$$

Thus the duration is

$$t_f - t_i = \ell(1/c - 1/v) \tag{6}$$

Comparison with observed durations in this gauge orientation are also included in Fig. 6.

It is interesting that the ratio of the durations at the two axial gauge orientations relative to the initiator end is independent of the charge length.

$$\frac{\text{duration near the detonator}}{\text{duration away from the detonator}} = \frac{v + c}{v - c} \simeq \frac{5}{3} \tag{7}$$

C. Gauge Position C, in Charge-Bisecting Plane, One End Detonated. This case is considerably more complicated to treat than are the cases in which the gauges are on the charge axis. The principal difficulty arises from the fact that the initial signal to reach the gauge at time t_i may come from a charge element, x_i, at $0 \leq x_i \leq \ell/2$, depending upon the distance r_C of the gauge from the charge center. This is illustrated in Fig. 7. For convenience $t_x - t_i$ is used in place of t_x (the time of arrival of a signal from a charge element x ft from the detonator) to reduce the scale of the graph. "Break points", or points

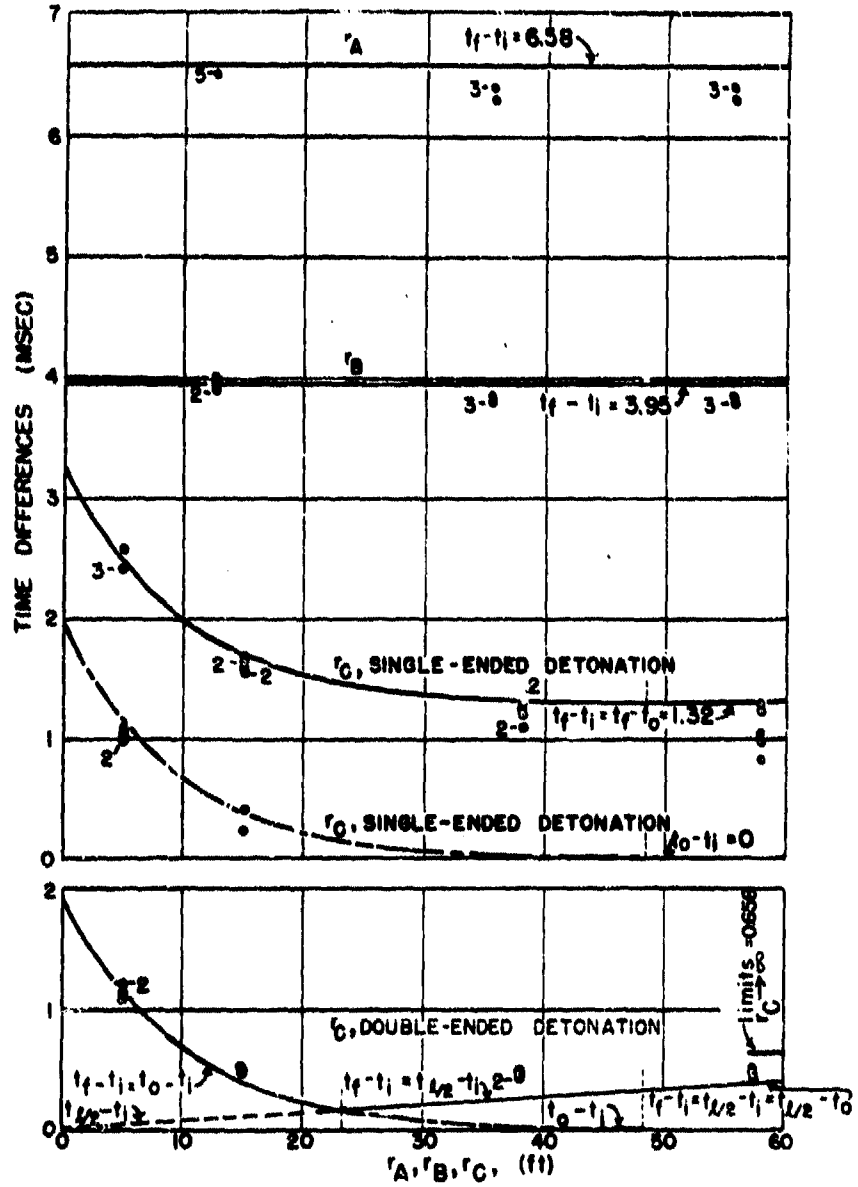


FIG. 6

SHOCK WAVE DURATIONS VS DISTANCE FROM A LINE CHARGE ON THE LONGITUDINAL AXIS AND IN THE PERPENDICULAR BISECTING PLANE.

NOTES: SMALL FIGURES INDICATE THE NUMBER OF OBSERVED POINTS IF MORE THAN ONE.
OBSERVED POINTS •
CALCULATED VALUES:
$t_f - t_i$ ———
$t_{1/2} - t_i$ — — —
$t_o - t_i$ —·—·—

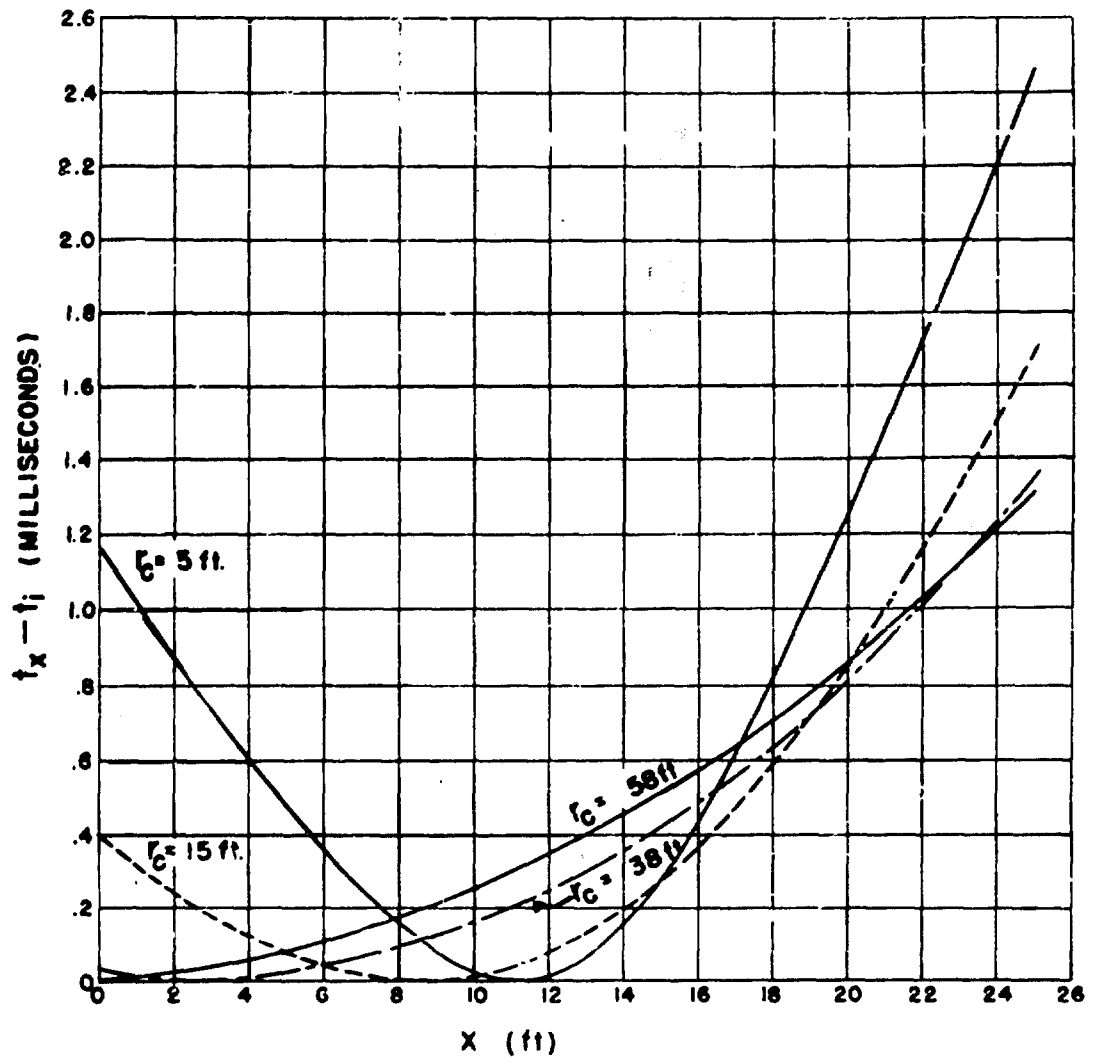


FIG. 7

DIFFERENCE ($t_x - t_i$) IN TIME OF ARRIVAL AT GAUGE FROM ELEMENTS OF CHARGE AT VARIOUS DISTANCES X FROM THE DETONATOR END AND THE FIRST SIGNAL REACHING THE GAUGE VS X FOR VARIOUS VALUES OF r_c (INTERCEPTS AT X=0 GIVE VALUES OF $t_o - t_i$ AND AT X=25 GIVE VALUES OF $t_c - t_i$)

at which the pressure-time curves might show increased decay rates related to the cessation of contributions from explosive elements on the <u>two sides</u> of x_1 may be expected to occur at t_o and t_ℓ, representing the contributions of charge elements at $x = 0$ and $x = \ell$, respectively. For $r_C > \ell(v^2 - c^2)^{\frac{1}{2}}/2c = R$, $t_1 = t_o$. The expressions for t_x, x_1, t_1, t_o, and t_ℓ are as follows:

$$t_x = \frac{x}{v} + \frac{1}{c}\left[r_C^2 + (\tfrac{\ell}{2} - x)^2\right]^{\frac{1}{2}} \qquad (8)$$

$$x_1 = \frac{\ell}{2} - cr_C\left[v^2 - c^2\right]^{-\frac{1}{2}} \quad \text{for } r_C \leq R \qquad (9)$$

$$x_1 = 0 \quad \text{for } r_C \geq R \qquad (10)$$

$$t_1 = \frac{1}{v}\left[\frac{\ell}{2} + \frac{r_C}{c}(v^2 - c^2)^{\frac{1}{2}}\right] \quad \text{for } r_C \leq R \qquad (11)$$

$$t_1 = t_o = \frac{1}{c}\left[r_C^2 + (\tfrac{\ell}{2})^2\right]^{\frac{1}{2}} \quad \text{for } r_C \geq R \qquad (12)$$

$$t_\ell = t_o + \frac{\ell}{v} = \frac{\ell}{v} + \frac{1}{c}\left[r_C^2 + (\tfrac{\ell}{2})^2\right]^{\frac{1}{2}} \qquad (13)$$

$$t_f - t_1 = \frac{1}{c}\left[r_C^2 + (\tfrac{\ell}{2})^2\right]^{\frac{1}{2}} + \frac{1}{v}\left[\frac{\ell}{2} - \frac{r_C}{c}(v^2 - c^2)^{\frac{1}{2}}\right]$$

$$\text{for } r_C \leq R \qquad (14)$$

$$t_f - t_1 = \ell/v \quad \text{for } r_C \geq R \qquad (15)$$

In this case, t_f, the time of arrival of the final signal at the gauge, is always equal to t_ℓ. The times of breaks on the pressure-time record as measured from the shock front, assumed to coincide with t_1,

are then given by the appropriate intervals $t_o - t_i$ and $t_\ell - t_i$. These are given in numerical form below as functions of r_C for the experimental conditions used in this study, i.e., the substitutions $\ell = 25$ ft, $v = 19$ ft/millisec and $c = 4.75$ ft/millisec ($v = 4c$) have been made.

$$t_o - t_i = -0.6580 - 0.2039\, r_C + \frac{1}{4.750}\left[r_C^2 + 156.25\right]^{\frac{1}{2}} \text{ millisec}$$

$$\text{for } r_C \leq R \qquad (16)$$

$$t_o - t_i = 0 \qquad \text{for } r_C \geq R \qquad (17)$$

$$t_f - t_i = t_\ell - t_i = 1.316 + t_o - t_i \qquad (18)$$

The line representing Eq. (18) is plotted in Fig. 6 (solid curve) and the observed break times corresponding to $t_f - t_i$ are shown to agree well with this simple calculation. The break times corresponding to $t_o - t_i$, which might be expected to occur when $r_C < R = 48.4$ ft, were, however, not distinguishable on all the records, since they usually occurred too close to the initial peak where the decay is extremely rapid. The points observed, however, agree well with the theoretical values (dash-dot curve of Fig. 6). The critical distance R is indicated by the short vertical dotted lines intersecting each curve at 48.4 ft. At distances greater than this critical distance the time differences are constant.

D. Gauge Position C, in Bisecting Plane, Both Ends Detonated Simultaneously. From the symmetry with respect to the time of signals from x and $\ell - x$, the time factors for this case can readily be derived as equivalent to those for the single-end initiation of a charge of length $\ell/2$ with the gauge in a plane perpendicular to the charge axis through $x = \ell/2$. The expressions for t_x, x_1 and t_o are the same as given under c. The additional term required, $t_{\ell/2}$, is

$$t_{\ell/2} = \frac{\ell}{2v} + \frac{r_C}{c} = 0.6580 + 0.2105\, r_C \qquad (19)$$

Break points are thus expected at

$$t_o - t_i = -0.6580 - 0.2039\, r_C + \frac{1}{4.75}\left[r_C^2 + 156.25\right]^{\frac{1}{2}} \text{ millisec}$$

$$\text{for } r_C \leq R \qquad (20$$

$$(t_o - t_i = 0 \qquad \text{for } r_C \geq R) \qquad (21)$$

as before, and at

$$t_{\ell/2} - t_i = 0.0066\, r_C \quad \text{for } r_C \leq R \qquad (22)$$

$$t_{\ell/2} - t_i = 0.6580 + 0.2105\left[r_C - (r_C^2 + 156.25)^{\frac{1}{2}}\right] \text{ millisec}$$

$$\text{for } r_C \geq R \qquad (23)$$

For double-ended detonation, there is a second critical distance R', at which $t_{\ell/2} = t_o$. When $r_C \leq R'$, $t_f = t_o$, and when $r_C \geq R'$, $t_f = t_{\ell/2}$. The theoretical lines for $t_f - t_i$, $t_o - t_i$, $t_{\ell/2} - t_i$, and $t_{\ell/2} - t_o$ are given in the lower portion of Fig. 6, and the observed values of $t_f - t_i$ are plotted. The critical distances R' = 23.4 ft, and R = 48.4 ft are indicated by vertical dotted lines. $t_f - t_i$ slowly approaches a limiting value of 0.658 millisec as r_C increases.

The theoretical expressions for t_o, t_i, t_ℓ, $t_{\ell/2}$, and t_f are summarized in Table III, and the appearance of these points on the pressure-time curves is indicated in Figs. 4 and 5.

For all charge orientations and conditions of firing, the observed time intervals fall further below the calculated time intervals as the charge-to-gauge distance increases. This is what one would expect from the assumption of constant shock-wave velocity in calculating the time intervals. Actually, the latter part of the pressure wave, travelling in a higher pressure region, has greater velocity, and gradually overtakes the shock front. The greater the distance from the charge, the more pronounced will be this overtaking effect.

TABLE III

EXPRESSIONS FOR THE ARRIVAL TIMES AT A GAUGE OF SHOCK WAVES FROM VARIOUS PARTS OF A LINE CHARGE

TIME	GAUGE POSITION			
	A	B	C	
			Single-ended Detonation	Double-ended Detonation
t_o =	$\frac{r_A}{c}$	$\frac{\ell + r_B}{c}$	$\frac{1}{c}\left[r_C^2 + (\frac{\ell}{2})^2 \right]^{\frac{1}{2}}$	Same as for single-ended detonation
t_ℓ =	$\frac{\ell}{v} + \frac{\ell + r_A}{c}$	$\frac{\ell}{v} + \frac{r_B}{c}$	$t_o + \frac{\ell}{v}$,	$t_{\ell/2} = \frac{\ell}{2v} + \frac{r_C}{c}$
t_i =	t_o	t_ℓ	$\frac{1}{v}\left[\frac{\ell}{2} + \frac{r_C}{c}(v^2 - c^2)^{\frac{1}{2}} \right]$, for $r_C < R^*$ t_o, for $r_C > R$	Same as for single-ended detonation
t_f =	t_ℓ	t_o	t_ℓ	t_o, for $r_C < R'$ ** $t_{\ell/2}$, for $r_C > R'$

* $R = \frac{\ell}{2c}(v^2 - c^2)^{\frac{1}{2}}$ ** $R' = \frac{\ell}{4cv}(v^2 - c^2)$

9. Pressure, Impulse, and Energy Measurements

The values for the initial pressure (p_i) for gauge positions A, B, and C, and for the final pressure (p_f) for gauge positions A and B, are plotted as a function of distance in Fig. 8. The dash-dot line shows for comparison the corresponding pressures from a spherical charge. Also, as mentioned previously, pressures at position A are about 20-40% lower than those at position B, and at both A and B the pressures are several fold lower than at position C. This is, of course, in part due to the way in which the various r's have been defined.

At position C, close to the charge the slope approaches the Rice-Ginnell theoretical[6,7] slope for an infinitely long line charge with infinite detonation velocity; at greater distances, the slope approaches that for spherical charges,[1,2,9] and is also at about the same absolute level. Even though the theoretical slope for line charges is in good agreement with the measured limiting slope close to the charge, it does not agree in absolute level, being about 30% higher than for a single-ended detonated charge and about 30% below a double-ended detonated charge. As the Rice-Ginnell theory assumes infinite detonation velocity, and it is reasonable to suppose that a double-ended charge approximates infinite detonation velocity more closely than a single-ended charge, it would appear that the theory would be even more than 30% below such experimental data as might be used to check it. (Note that although the data are plotted as p vs $W^{1/3}/r$ as is usually done for similitude, actually only 50 lb charges were fired. The relation found probably should hold for charges of different weights, provided the ratio of charge length to diameter were kept the same.)

The reduced impulse is plotted against $W^{1/3}/r$ (W = 50 lb) in Fig. 9. This impulse was obtained by integrating over roughly the interval $t_f - t_i$. Also plotted is the reduced impulse for spherical TNT charges, the integration time being 6.7θ, where θ is the time constant of the shock wave. In contrast with the pressure measurements, impulse measurements do not differ radically from one another. Considering the fact that the pressure-time curves were integrated over the interval $t_f - t_i$, which differed for positions and methods of detonation, the data indicates that the total shock-wave impulse is about the same for the different conditions and not widely different from that of a spherical charge. Since from acoustic theory the pressures at positions A and B are in the ratio $p_A/p_B = (c - v)/(c + v)$, and the durations are in the opposite ratio $(t_f - t_i)_A/(t_f - t_i)_B = (c + v)/(c - v)$, the impulse should be virtually the same at A and B, when $r_A = r_B$. The apparent agreement in absolute level with the reduced impulse for spherical charges plotted in Fig. 9 is partly fortuitous, owing to the arbitrary times of integration.

Reduced energy is plotted against $W^{1/3}/r$ for 50 lb charges in Fig. 10 and the same remarks made about pressure and impulse with regard to weight, integration times, etc., apply equally well here.

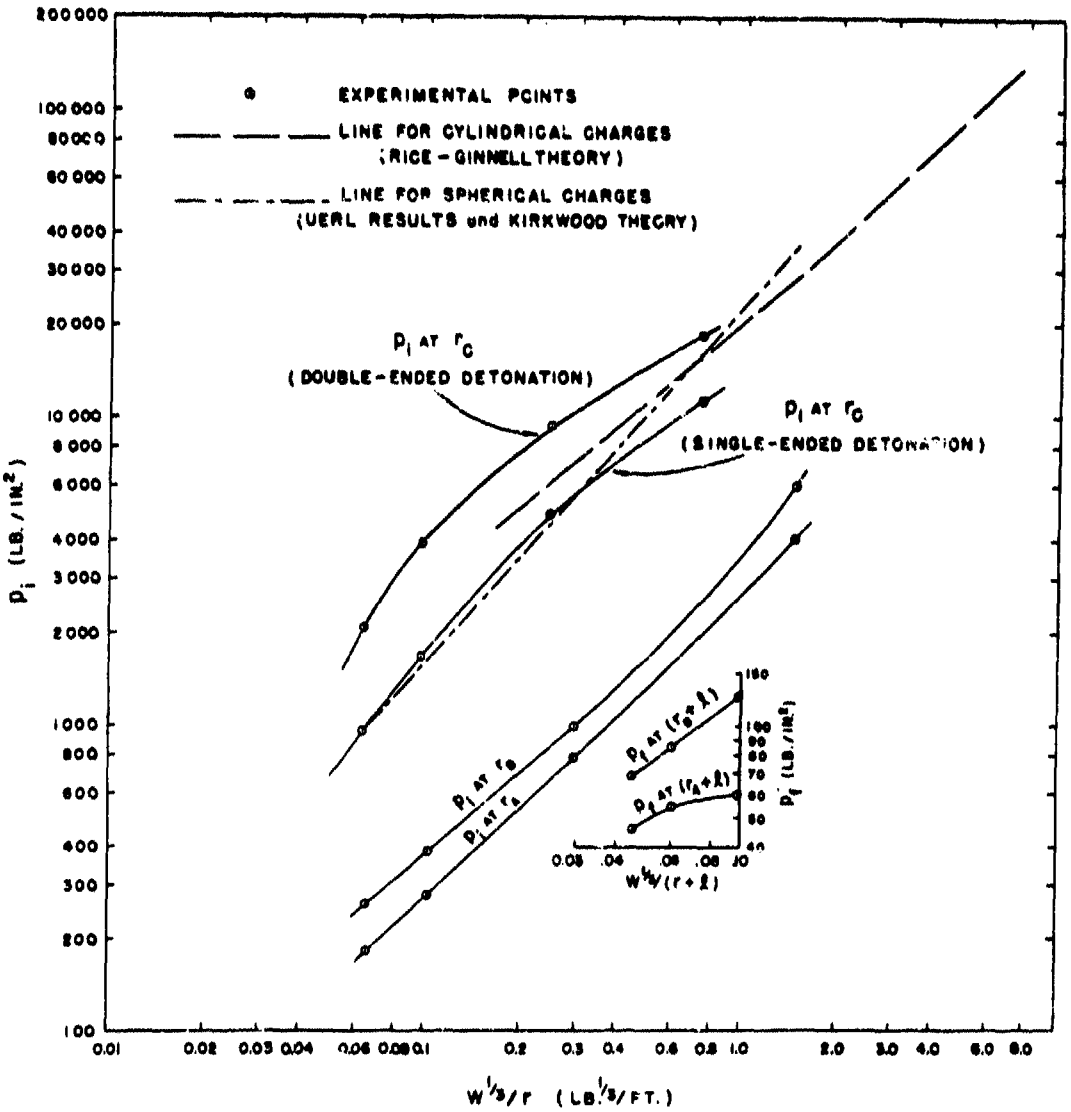


FIG. 8.

p_i and p_f vs $W^{1/3}/r$ FOR TNT LINE CHARGES AT GAUGE POSITIONS A, B, and C.
CHARGE WEIGHT (W) = 50 LB.

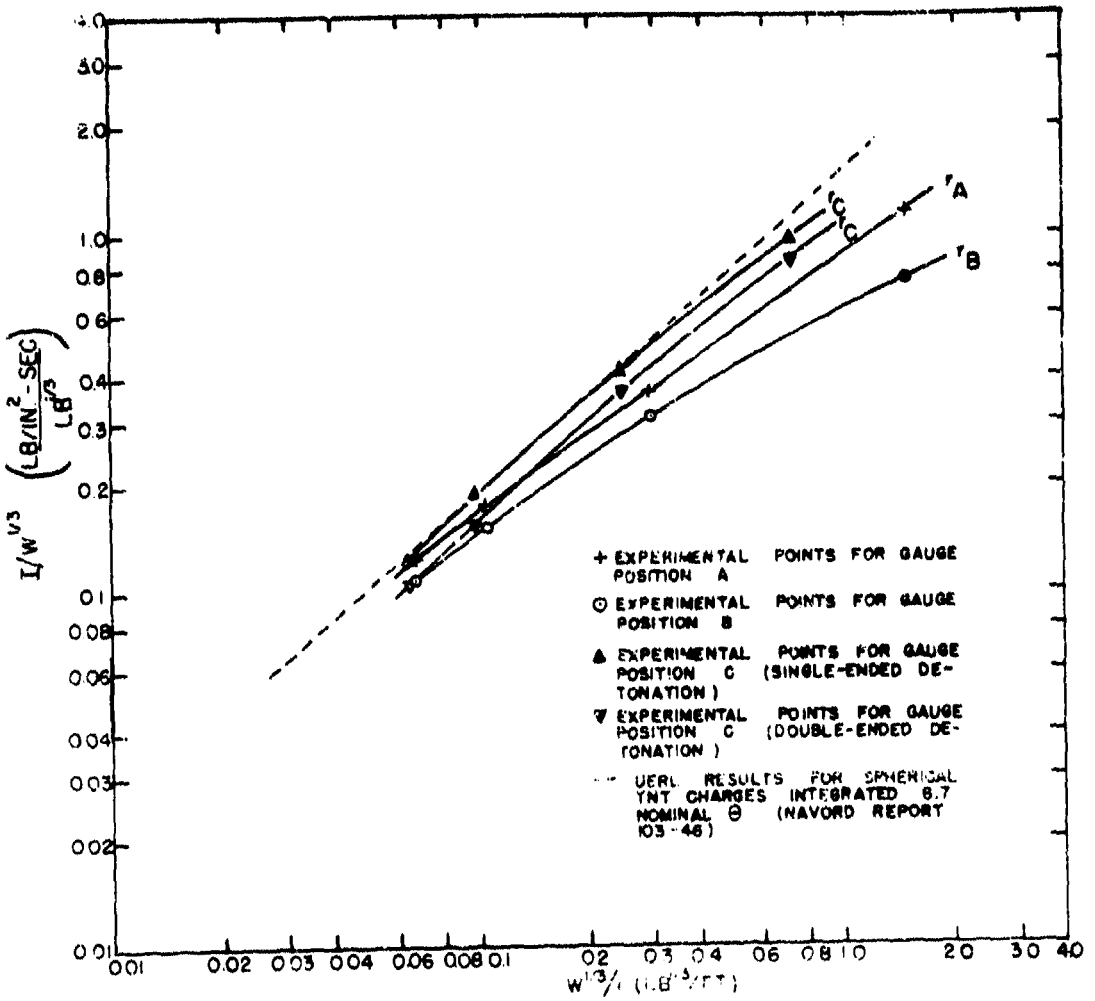


FIG. 9

IMPULSE/$W^{1/3}$ vs $W^{1/3}/r$ FOR TNT LINE CHARGES AT GAUGE POSITIONS A, B, and C
INTEGRATED FROM t_i TO t_f
CHARGE WEIGHT (W) = 50 LB

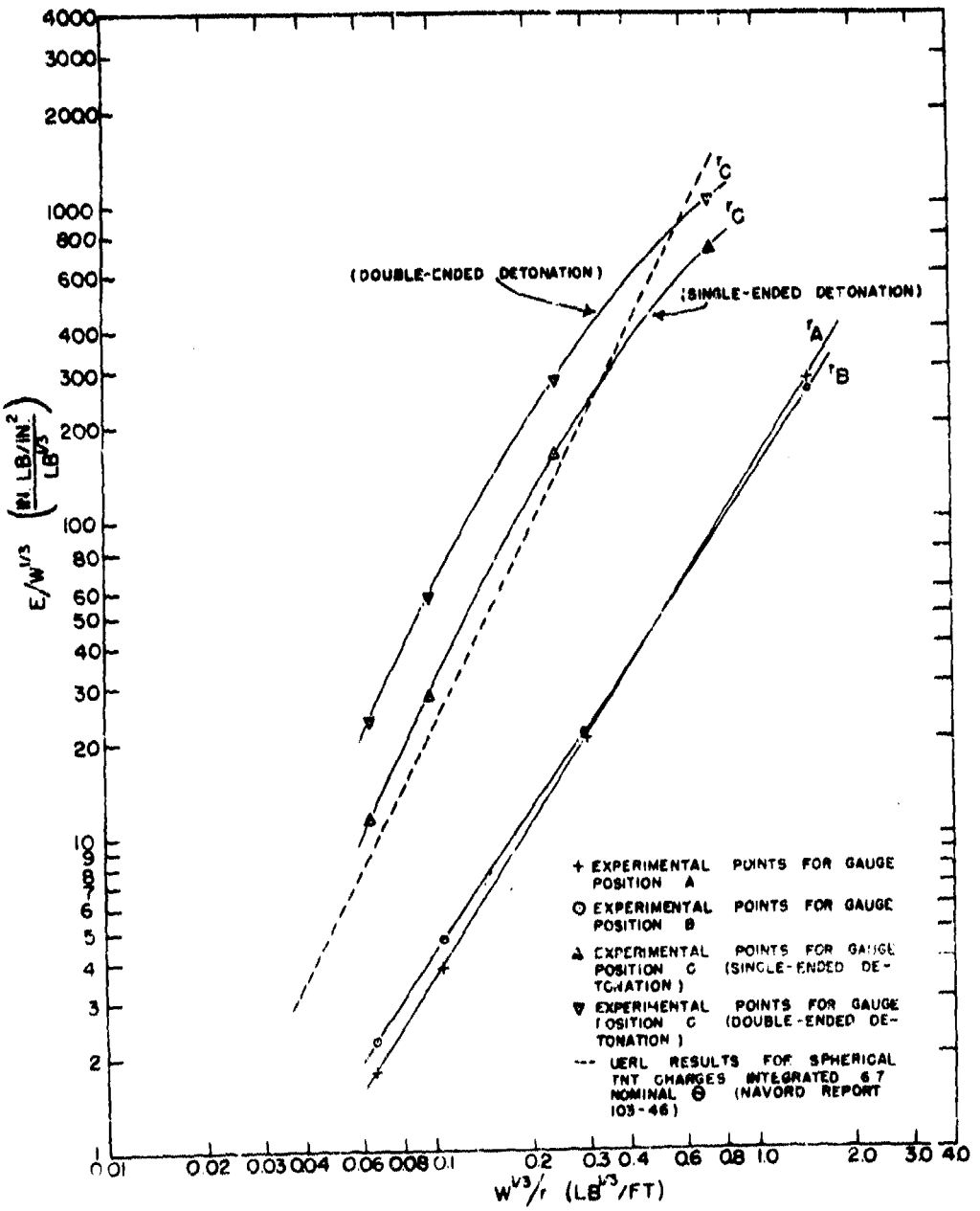


FIG 10

ENERGY/$W^{1/3}$ vs $W^{1/3}/r$ FOR TNT LINE CHARGES AT GAUGE POSITIONS A,B, and C
INTEGRATED FROM t_i TO t_f
CHARGE WEIGHT (W) = 50 LB

10. Diaphragm Gauge Measurements

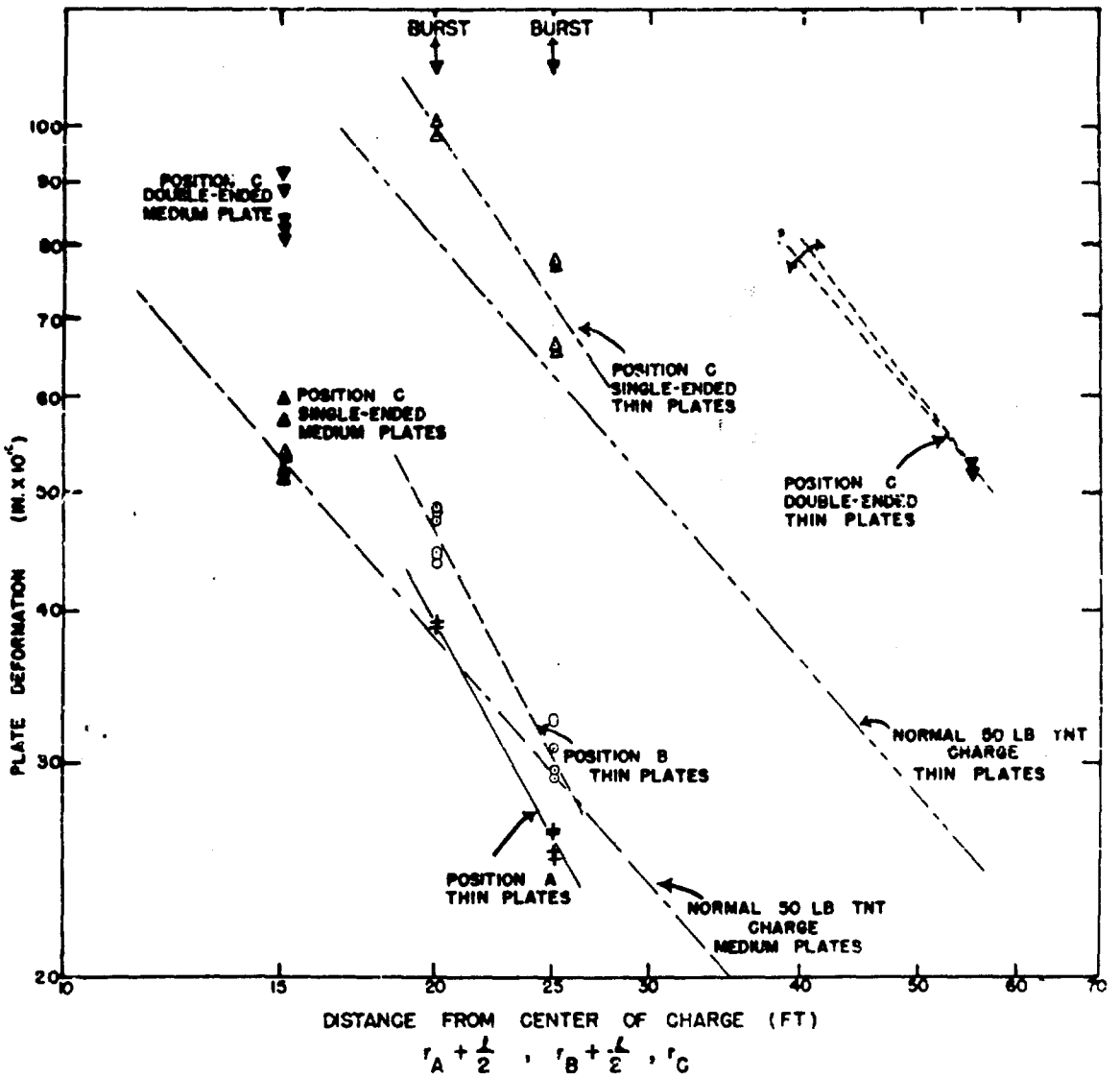
The deformations of the steel diaphragms used in the diaphragm gauges at various positions aft of the charge are given in Table II. (Note that the shot numbers for position A and position B are interchanged from those of piezoelectric gauges due to the diaphragm gauges being on the opposite end of the charge from the former.) These deformations have been plotted against distance (log-log) in Fig. 11, together with the deformation-distance relation for normal cylindrical 50 lb TNT charges (ratio of length/diameter = ca. 1.7).

The relative magnitude of the deformations for the various gauge positions with respect to the charge follows the relative magnitude of peak pressure (Fig. 8) rather than that for impulse (Fig. 9). This is in accord with previous observations at UERL wherein the diaphragm gauge deformations on large charges, owing to their short response time relative to the time constant of the pressure wave, follow peak pressure; for small charges, where the response time of the gauge is long compared with the time constant of the shock wave, the diaphragm gauge deformations follow the impulse. Deformations measured off the non-detonator end of the charge (position B) are greater than those off the detonator end (position A). Owing to the "piling-up" of the shock wave in position B, the pressure averaged over the reaction time of the gauge is thereby greater than that in position A. The same effect is noted for double-ended detonated charges compared with single-ended detonated charges with gauges in the bisecting plane of the charge (position C).

The slope of the log deformation-log distance curves for the positions off the ends of the charge is greater than that for positions in the bisecting plane, as the curves were plotted. This is probably due to the fact that the distances plotted were as measured from the center of the charge ($r_A + \ell/2$, or $r_B + \ell/2$). The gauges off the ends, therefore, are actually nearer the end of the charge than indicated, and the difference is relatively greater for the gauges closest to the charge, hence the greater slope. If deformations for more than two distances were available, this would be indicated by an upward curvature of the line at smaller distances. When these deformations are plotted against the distance to the nearest ends of the charge the slope diminishes to approximately that obtained in the bisecting plane (which is roughly equal to that from nearly symmetrically shaped cylindrical charges).

Compared with nearly symmetrical cylindrical charges of equal weight, the deformations measured off the ends of the line charges are much lower. Line charge deformations are about equal when measured in the bisecting plane of charges detonated from both ends. These data are in agreement with the piezoelectric gauge results.

1134



LEGEND	GAUGE POSITION	STANDARD PLATE THICKNESS (IN.)	SINGLE OR DOUBLE-ENDED DEFORMATION
+ ———	A	0.038	SINGLE-ENDED
● — —	B	0.038	SINGLE-ENDED
△ —·—	C	0.038	SINGLE-ENDED
▲	C	0.065	SINGLE-ENDED
▼ - - - - -	C	0.038	DOUBLE-ENDED
▼	C	0.065	DOUBLE-ENDED
——·——		0.038	NORMAL 50 LB TNT CHARGE
———·-		0.065	NORMAL 50 LB TNT CHARGE

FIG. 11.

UERL DIAPHRAGM GAUGE DEFORMATIONS vs DISTANCE FOR 50 LB TNT LINE CHARGES.

LIST OF REFERENCES

Summary of Underwater Explosives Comparisons, J. S. Coles, OSRD Report No. 6241, NDRC A-363, 1946.

Shock-Wave Parameters from Spherical HBX and TNT Charges Detonated Under Water, J. S. Coles, E. A. Christian, J. P. Slifko, C. R. Niffenegger, and M. A. Rogers, NavOrd Report 103-46, December 1946.

Photography of Underwater Explosions I, P. M. Fye, J. E. Eldridge, R. W. Spitzer, OSRD Report No. 6246, NDRC A-368, 1947.

Interim Reports on Underwater Explosives and Explosions, NDRC Div. 2 and 8:

(a) "Special Shape Charges" UE-8, p. 19, March 15-April 15, 1943.
(b) "Effect of Charge Shape and Orientation on the Pressure-time Curve for Small Charges" UE-15, p. 18, October 15-November 15, 1943.
(c) "Shock Wave from a Long Cylindrical Charge" UE-17, p. 11, December 15, 1943-January 15, 1944.
(d) "Submarine Mines (Case M3A1)" W. G. Schneider
I. Piezo Gauge Measurements of the Shock Wave in Various Directions from a 1/10 Scale-Model in Free Water, UE-19, p. 6, February 15-March 15, 1944.

II. Piezo Gauge Measurements of the Shock Wave in Various Directions above a 1/10 Scale-Model Resting on a Sandy Bottom, UE-20, p. 32, March 1944.

(Case M3A1-Top Firing Device)
III. Piezo Gauge Measurements in Various Directions in Free Water from a 1/10 Scale-Model, UE-21, p. 47, April 15-May 15, 1944.

(a) Pressures Produced by the Underwater Explosion of Line Charges, G. Charlesworth, Dept. of Scientific and Industrial Research, Road Research Laboratory, Report to the Admiralty, Note No. ADM/146/GC, November 1943, Undex 65.
(b) An Approximate Calculation of the Pressures Produced by Detonating Line Charges Underwater, ibid, Note No. ADM/153/GC.ARB, December 1943, Undex 66.
(c) The Pressures Produced by Explosions Underwater of Straight Line Charges of Cordtex 20 ft Long, ibid, Note No. ADM/172/GC, March 1944, Undex 90.

Interim Reports on Underwater Explosives and Explosions, NDRC Div. 2 and 8:

(a) Pressure Waves from Cylindrical Underwater Charges" O. K. Rice, UE-11, p. 26, June 15-July 15, 1943; UE-12, p. 20, July 15-August 15, 1943.
(b) Pressure-Time Curves for "Infinite" Cylindrical Charges of TNT, O. K. Rice and R. Ginnell, UE-16, p. 87, November 15-December 15, 1943.
(c) The Pressure Wave Produced by an Underwater Explosion. Asymptotic Equation for the Case of Cylindrical Symmetry, O. K. Rice and R. Ginnell, UE-18, p. 20, January 15-February 15, 1944.

LIST OF REFERENCES (Cont'd)

7. The Pressure Wave Produced by an Underwater Explosion, Part VI: The Case of Cylindrical Symmetry, O. K. Rice and R. Ginnell, OSRD Report No. 2023, November 13, 1943.

8. The Measurement of Underwater Explosions from Service Weapons at the Underwater Explosives Research Laboratory, J. S. Coles, OSRD Report No. 6240, NDRC A-362, March 1946.

9. The Pressure Wave Produced by an Underwater Explosion, Part V, J. G. Kirkwood, S. R. Brinkley, Jr., and J. M. Richardson, OSRD Report No. 2022, November 1943.

10. Underwater Explosion of a Cylindrical Charge, H. Polachek, Washington Meeting, American Physical Society, May 3, 1947.

ENERGY PARTITION IN UNDERWATER EXPLOSION PHENOMENA

A. B. Arons and D. R. Yennie
Underwater Explosives Research Laboratory
Woods Hole Oceanographic Institution

American Contribution

July 1948

Reprinted from REVIEWS OF MODERN PHYSICS
Vol. 20, No. 3, pp 519-536, July, 1948

Reprinted from REVIEWS OF MODERN PHYSICS, Vol. 20, No. 3, pp. 519–536, July, 1948
Printed in U. S. A.

Energy Partition in Underwater Explosion Phenomena*

A. B. ARONS AND D. R. YENNIE

Woods Hole Oceanographic Institution, Woods Hole, Massachusetts

and

Stevens Institute of Technology, Hoboken, New Jersey

Pressure-time curves, continuous from initial shock wave incidence through the second bubble pulse, are examined in the light of acoustic theory. Calculations of impulse and reversible and irreversible energy flux are made for the various phases of the phenomenon. An estimate has been made of the amount of energy dissipation associated with the propagation of the shock front. A tabulation of the energy partition is included, and it is shown that substantial quantities of energy are radiated or dissipated by mechanisms other than these taken into account in this discussion.

I. INTRODUCTION

1

MOST of the energy released by the detonation of an explosive charge is ultimately imparted to the surrounding medium and becomes distributed among the various phases of succeeding phenomena. It is the purpose of the present investigation to examine the distribution of this energy in underwater explosions, particularly from the point of view of making a complete interpretation of data now available in the form of pressure-time curves.

In general, underwater explosions are characterized by the emission of a shock wave followed by a series of pressure pulses caused by subsequent oscillations of the gas globe containing the products of detonation. A typical pressure-time record is reproduced in Fig. 1.

At the instant following detonation the released energy is present in the form of potential energy of exceedingly high pressure and temperature in the resulting volume of gas. As the gas proceeds to expand it transfers energy to the water. Part of this energy is "radiated" in the sense that it is not stored as reversible potential energy in the water. Rather, it is gradually dissipated by conversion into thermal energy which elevates the temperature of the fluid through which the pressure wave is propagated.

* This investigation was supported under contract with the Navy Department, Bureau of Ordnance. Contribution No. 449 from the Woods Hole Oceanographic Institution.

2

The remainder of the energy transferred to the water is imparted to it as kinetic energy, the water being pushed radially outward against the opposing hydrostatic pressure. The gas globe expansion continues until the energy available to this phase of the motion is stored as potential energy in the water. At this point the gas bubble has attained its maximum radius, and its internal pressure has fallen well below that of the surrounding hydrostatic level. The potential energy now stored in the water is given by

$$E_p = (4/3)\pi A_{M1}^3 P_0,$$

where A_{M1} is the maximum bubble radius and P_0 is the absolute hydrostatic pressure. This will be referred to as a "reversible" energy, since it is returned to the gas globe on the succeeding collapsing phase.

The collapse of the bubble and the following expansion are characterized by emission of the first bubble pulse, in which part of the energy E_p is again radiated "acoustically." Thus all the potential energy stored in the water is not returned to the bubble as compressional energy in the gas** at minimum bubble size. An additional

** If the charge is detonated under conditions such that the gas bubble undergoes appreciable migration because of the influence of gravity or boundary surfaces, a substantial part of E_p will be imparted irreversibly to vertical motion of the water. The condition principally considered in this report is that in which the bubble migration is negligibly small. This, however, has no bearing on considerations

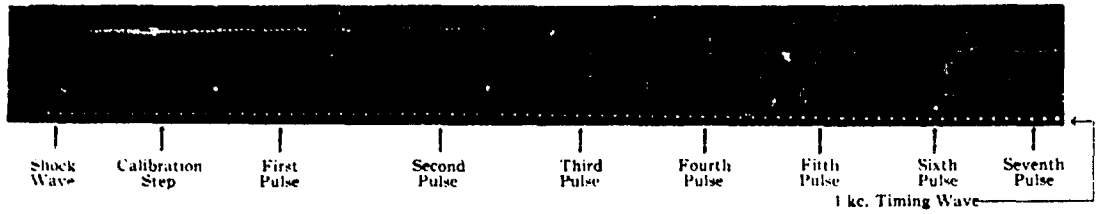


FIG. 1. Pressure-time record showing shock wave and bubble pulses. Charge: 0.505-lb. TNT; gauge dist: 2.25 ft.; depth: 500 ft.

loss occurs on re-expansion, resulting in a value A_{M4} (for the second maximum in the bubble radius) considerably smaller than A_{M1}.

3

In addition to the energy observed in waves of compression and in reversible interchange between the gas globe and the water, energy is also being continually dissipated because of various other factors such as:

(i) radiation and conduction from gas globe,
(ii) viscous loss in the water,
(iii) turbulent loss in the water.

4

An observer at a fixed point (radial distance R from the center of the charge) would see a "flow" of energy past his point in the positive or negative direction of R, depending upon the phase of the explosion phenomenon. Piezoelectric gauge measurements provide a record of pressure *vs.* time at just such a point of observation. In order to investigate the energy flux, it is necessary to have a relation between energy and the variables pressure and time. These relationships are developed in the following chapter.

The experimental results to be quoted subsequently were all obtained from measurements on TNT.

II. GENERAL EXPRESSIONS FOR ENERGY FLUX

5

In this report the energy flux will be defined as the amount of energy that passes through a unit area of surface during a given time interval. In the case of spherical symmetry this energy flux will be uniform over the surface of a sphere, and the total flow of energy through the spherical surface will be given by:

$$E=4\pi R^2 F. \tag{1}$$

The symbol E will be used to designate the total energy flow through the surface, and a component of the total will be indicated by attaching a suitable subscript. The symbol F will be used in a similar way to represent the energy flux.

In general, the energy flux will be found to consist of a number of components varying inversely as some power of the radius:

$$F=F_1/R^{n_1}+F_2/R^{n_2}+F_3/R^{n_3}+\cdots \text{ etc.} \tag{2}$$

If the value of an exponent n happens to be 2, Eq. (1) shows that the total energy flow, E, corresponding to that term will be the same at all radii and therefore the energy will be radiated away to infinity. If the value of n is greater than 2, the total energy flow will be smaller at larger radii, indicating that some energy has been left behind in the water. In some cases the energy left in the water is in the form of kinetic energy or other undissipated forms and therefore should be returned ultimately to the gas globe. In other cases it represents an energy which has been dissipated irreversibly and goes into heating of the water.

6

The general expression for what might be termed the "useful" total energy flow through a sphere of radius R relative to the center of the explosive charge is given by the following time integral:

$$E=4\pi R^2\int_0^{t_1}\left(\frac{\Delta p}{\rho}+\tfrac{1}{2}u^2+\Delta\eta\right)\rho u\,dt, \tag{3}$$

pertaining to events up to the first bubble maximum, since migration never becomes appreciable until the phase of bubble collapse.

where t = time measured from instant of incidence of the pressure wave, t_1 = arbitrary upper limit of integration, Δp = excess pressure $(p - P_0)$, a function of time, P_0 = absolute hydrostatic pressure level at point of detonation, u = particle velocity relative to the unperturbed fluid, ρ = density of the fluid at time t, $\Delta\eta$ = increase in internal energy of a unit mass of fluid relative to the initially unperturbed state.

The term in Δp represents a compressional energy capable of doing work against the fluid external to the sphere through which it passes. The second term represents the kinetic energy of the mass of fluid moving past the point of observation, while the third term in $\Delta\eta$ represents the increment of internal energy of this mass. It will be shown that at values of R which are large relative to the initial charge radius, the last two terms are both very small compared to the term in $\Delta\phi$.

7

The type of experimental data available for making an analysis of the energy flux consists mainly of pressure-time curves recorded by means of piezoelectric gauges.[1]

Such data have previously been available for the shock wave to times of the order of 10θ, where θ is the time constant of the initially exponential shock-wave decay. Additional data have recently been obtained from bubble pulse measurements,[2] making it possible to extend the pressure-time curve from 10θ through the second bubble pulse.

If u in Eq. (3) can be expressed in terms of the variables Δp and t, it becomes possible to evaluate energy transfer from the primary pressure-time data. A rigorous development would involve the exact solution of the hydrodynamical equations of motion. Such a solution would involve exceedingly laborious and complicated numerical integrations which are impractical except in a very few special cases.

Fortunately the compressibility of water is sufficiently low to make the so-called acoustic approximation useful (and probably adequate) for the treatment of pressure-time data in the region normally accessible to experimental measurement.

8

The acoustic approximation in a case of spherical symmetry yields the following relationship for the particle velocity, u:[3]

$$u = \frac{\Delta p}{\rho_0 C_0} + \frac{1}{\rho_0 R}\int_0^t \Delta p\, dt, \tag{4}$$

where

ρ_0 = the density of the unperturbed fluid,
$C_0 = (\partial P/\partial \rho_0)_{s_0}^{\frac{1}{2}}$, the velocity of sound in the fluid.

The second term on the right-hand side of Eq. (4) is frequently referred to as the afterflow term in the particle velocity.

Combining Eqs. (4) and (3) we find

$$E = 4\pi R^2 \left\{ \int_0^{t_1} \left(\frac{\Delta p}{\rho} + \tfrac{1}{2}u^2 + \Delta\eta \right) \frac{\rho \Delta p}{\rho_0 C_0}\, dt + \int_0^{t_1} \left[\frac{((\Delta p/\rho) + \frac{1}{2}u^2 + \Delta\eta)\rho}{\rho_0 R} \int_0^t \Delta p\, dt \right] dt \right\}. \tag{5}$$

The sum $(\frac{1}{2}u^2 + \Delta\eta)$ is small relative to $\Delta p/\rho$, as will be shown in Section 10; at low values of Δp it can be neglected entirely. A correction is justified at high values of Δp, but only the first term in Eq. (5) requires this correction since the second term is initially zero and does not acquire appreciable value until after the elapse of a certain amount of time, during which the pressure is decaying very rapidly.

The Rankine-Hugoniot conditions*** afford relationships for u, U, and $\Delta\eta$ in terms of Δp and the change in density across a shock front. (U represents the velocity of propagation of the shock.)

$\Delta\eta$ and u in the first term of Eq. (5) are then replaced by the appropriate Hugoniot relations

[1] J. S. Coles. OSRD Report No. 6240.
[2] A. B. Arons, J. P. Slifko, and A. Carter, J. Acous. Soc. Am. 20, 271 (1948), and A. B. Arons, ibid. 20, 277 (1948).
[3] H. Lamb, *Hydrodynamics* (University Press, Cambridge, 1932), p. 490.
*** The Rankine-Hugoniot conditions are obtained by application of the laws of conservation of mass, momentum, and energy at the shock front (see reference 3). These conditions are:

$$U = v_0((p - P_0)/(v_0 - v))^{\frac{1}{2}},$$
$$u = ((p - P_0)(v_0 - v))^{\frac{1}{2}},$$
$$\Delta\eta = \tfrac{1}{2}(P_0 + p)(v_0 - v),$$
$$\Delta H = \Delta\eta + \Delta(pv) = \tfrac{1}{2}(p - P_0)(v_0 + v).$$

and C_0 is replaced by the propagation velocity U. This is equivalent to treating the fluid at time t behind the shock front as though it had just passed from its unperturbed state through a shock front of corresponding amplitude Δp, i.e., directly along a Hugoniot curve from 0 to Δp. Strictly speaking this is not correct, since the particle of fluid under consideration has actually passed through a shock front of greater amplitude at a preceding time and has returned to the pressure Δp along an adiabatic. Also neglected is the effect of spherical divergence on the particle velocity, u. However, the above substitution is introduced as a first approximation, and since the correction is quite small for all practical cases, the approximation is probably adequate.

Making the substitution discussed above in the first term of Eq. (5) and neglecting $\frac{1}{2}u^2$ and $\Delta\eta$ in the second term, one obtains, after algebraic manipulation:

$$E=\frac{4\pi R^2}{\rho_0}\left\{\int_0^{t_1}\frac{(\Delta p)^2}{U-\dfrac{\Delta p}{\rho_0 U}}dt+\frac{1}{R}\int_0^{t_1}\left[\Delta p\int_0^{t}\Delta p\,dt\right]dt\right\}^{\dagger} \quad (6)$$

For comparison, it is convenient to state the result yielded by Eq. (5) if $\frac{1}{2}u^2$ and $\Delta\eta$ are neglected throughout and C_0 is not substituted by U:

$$E=4\pi R^2\left\{\frac{1}{\rho_0 C_0}\int_0^{t_1}(\Delta p)^2dt+\frac{1}{\rho_0 R}\int_0^{t_1}\left[\Delta p\int_0^{t}\Delta p\,dt\right]dt\right\}. \quad (7)$$

It will be shown in Section 10 that Eq. (6) differs from Eq. (7) only in that the first term contains a correction factor which does not depart from unity by more than a few percent at pressures as high as 20- or 30-thousand pounds per square inch.

† Note that the second integral of Eq. (6) may also be written in the form:

$$\frac{1}{2R}\left[\int_0^{t_1}\Delta p\,dt\right]^2,$$

this form being more useful for purposes of computation.

In acoustic theory Δp varies inversely as R, the distance from the origin. Inspection of Eq. (7) in the light of Eq. (2) therefore indicates that the first term on the right-hand side represents principally "radiated" energy associated with what will be termed the "irreversible energy flux," while the second term represents energy stored reversibly in the region covered by the shock wave. It should be noted that the small contributions made by $\frac{1}{2}u^2$ and $\Delta\eta$ to the first term are also reversible.

III. THE FIRST TERM FOR THE ENERGY FLUX IN THE SHOCK WAVE

To complete the development of expressions necessary for the interpretation of pressure-time data, we return to that part of the energy flux as given by the first term of Eq. (6):

$$F_1=\frac{1}{\rho_0}\int_0^{t_1}\frac{(\Delta p)^2}{U-(\Delta p/\rho_0 U)}dt. \quad (8)$$

The Rankine-Hugoniot conditions give a relation for U in terms of Δp at a shock front:

$$U=v_0(\Delta P_s/v_0-v)^{\frac{1}{2}}, \quad (9)$$

where ΔP_s is the excess pressure at the shock front and v_0 and v are the specific volumes of the fluid ahead and behind the shock front, respectively.

Combination of Eq. (9) with certain thermodynamic relations and with equation of state data[4] makes it possible to calculate U for corresponding arbitrary values of ΔP_s. Such calculations have been made for sea water at quite closely spaced values of ΔP_s, and the results can be represented empirically by the following approximate fit:

$$U=C_0[1+5.6\times10^{-6}\Delta P_s-17\times10^{-12}(\Delta P_s)^2], \quad (10)$$

where the excess pressure is expressed in lb./in.^{2}. For the purpose of obtaining a first-order correction to the energy flux, the propagation velocity may be represented approximately by the following linear relation:

$$U=C_0[1+\alpha\Delta P_s],$$
$$U=C_0[1+5.3\times10^{-6}\Delta P_s]. \quad (11)$$

[4] J. M. Richardson, A. B. Arons, and R. R. Halverson, J. Chem. Phys. 15, 785 (1947).

Equation (10) fits the results of reference (4) quite closely from zero to 60,000 p.s.i., while Eq. (11) represents a rough average fit of a straight line in the region from zero to 40,000 p.s.i. Equation (11) falls slightly below the true values at low and somewhat above at high pressures.

Inserting Eq. (11) into Eq. (8), and carrying the result to first-order terms, the following expression is obtained:

$$F_1 = \frac{1}{\rho_0 C_0}\int_0^{t_1} (\Delta p)^2\left[1-\left(\alpha-\frac{1}{\kappa}\right)\Delta p\right]dt, \quad (12)$$

where $\kappa = \rho_0 C_0^2$.

The same expression may be derived by applying first-order corrections directly to the general expression given in Eq. (5):

$$F_1 = \int_0^{t_1}\left(\frac{\Delta p}{\rho}+\tfrac{1}{2}u^2+\Delta\eta\right)\rho u\,dt, \quad (13)$$

where u is given by the Rankine-Hugoniot conditions

$$u = (\Delta p/\rho_0 U),$$

and the internal energy increment, $\Delta\eta$, is approximately the compressional energy of the fluid:

$$\Delta\eta = \tfrac{1}{2}(\Delta p)^2/\kappa\rho_0, \quad (14)$$

κ being the bulk modulus. The kinetic energy per unit mass is

$$\tfrac{1}{2}u^2 = \tfrac{1}{2}(\Delta p)^2/\rho_0^2 U^2 \approx \tfrac{1}{2}(\Delta p)^2/\rho_0^2 C_0^2 = \tfrac{1}{2}(\Delta p)^2/\rho_0\kappa = \Delta\eta. \quad (15)$$

Equation (12) is verified by substituting these relations in Eq. (13) and carrying the results to first-order terms.

In its present form, Eq. (12) is unwieldy because it requires integrations of both $(\Delta p)^2$ and $(\Delta p)^3$. The term in $(\Delta p)^3$, however, introduces only a small correction, and it is convenient to represent the average value of this correction in terms of one convenient parameter, such as the peak pressure of the shock wave. To do this, it is assumed that the shock-wave pressure varies exponentially with time.

$$\Delta p = P_m e^{-t/\theta}.$$

Although this is not a correct representation of the whole wave, it is true for times up to $t = \theta$, from which region most of the correction to the energy flux actually stems. Therefore, applying this approximation

$$\int_0^t (\Delta p)^2 dt = \frac{P_m^2\theta}{2},$$

$$\int_0^t (\Delta p)^3 dt = \frac{P_m^3\theta}{3} = \frac{2}{3}P_m\int_0^t (\Delta p)^2 dt$$

The first energy flux term then becomes

$$F_1 = \frac{1}{\rho_0 C_0}\left[1-\frac{2}{3}\left(\alpha-\frac{1}{\kappa}\right)P_m\right]\int_0^{t_1}(\Delta p)^2 dt. \quad (16)$$

The correction represented by the second term in the bracket is small (the order of a few percent), so that even though the correction itself might be subject to a large error because of the crudeness of various approximations, the final result for energy flux should not be greatly in error. For P_m in lb./in.^{2}, and F_1 in in. lb./in.^{2}, Eq. (16) may be written

$$F_1 = \frac{1}{\rho_0 C_0}[1-1.6\times10^{-6}P_m]\int_0^{t_1}(\Delta p)^2 dt. \quad (17)$$

Equation (17) is based on U as given by Eq. (11). This equation can now be used in the computation of the energy flux given by the first term of Eq. (5).

This approximation can easily be carried to second-order terms, although for most applications this is an unnecessary refinement. The result to second order is

$$F_1 = \frac{1}{\rho_0 C_0}[1-1.8\times10^{-6}P_m+4\times10^{-12}P_m^2]\times\int_0^{t_1}(\Delta p)^2 dt. \quad (18)$$

Equation (18) is based on U as given by Eq. (10).

If pressures are expressed in lb./in.^{2} and time in seconds, F_1 is obtained in in. lb./in.^{2} by using

$$\rho_0 C_0 = 5.58+0.0065T, \quad (19)$$

where T is temperature of the water in degrees centigrade.

The quantity $\rho_0 C_0$ is commonly called the acoustic impedance of the medium. Equation (19) applies specifically to sea water having a salinity of 32 parts per thousand.

10

It is now possible to investigate the relative magnitude of the terms for internal and kinetic energy in Eq. (3). The part of the energy flux given by these terms is

$$F_e = \int_0^{t_1} (\tfrac{1}{2}\rho u^2 + \rho\Delta\eta) u dt. \qquad (20)$$

From Eqs. (14) and (15)

$$\tfrac{1}{2}\rho u^2 = \rho\Delta\eta = \tfrac{1}{2}(\Delta p)^2/\kappa, \qquad (14), (15)$$

and the particle velocity is given by

$$u = \Delta p/\rho_0 C_0,$$

approximately.

Using the exponential approximation for the pressure *versus* time relation, the part of energy flux given by Eq. (20) becomes

$$F_e = \frac{1}{\rho_0 C_0}\left(\frac{2}{3}\frac{P_m}{\kappa}\right)\int_0^{t_1} (\Delta p)^2 dt$$

$$= \frac{1}{\rho_0 C_0}(2\times 10^{-6} P_m)\int_0^{t} (\Delta p)^2 dt, \qquad (21)$$

where pressures are in lb./in.^{2} and the energy flux is in in. lb./in.^{2}. The term $(2\times 10^{-6}P_m)$ represents a fractional part of the total energy flux given by Eq. (17). The contribution of the kinetic and internal energy terms to the flux F_1 is, therefore,

$$\frac{F_e}{F_1} = \frac{2\times 10^{-6} P_m}{1 - 1.8\times 10^{-6} P_m}\times 100 \text{ percent}$$

or approximately

$$(2\times 10^{-6} P_m) \text{ percent}. \qquad (22)$$

At the highest pressure levels so far investigated (*ca.* 30,000 to 40,000 lb./in.^{2}) this contribution is of the order of a few percent. For pressures below 10,000 lb./in.^{2} the contributions of the kinetic and internal energy terms are negligibly small.

IV. ENERGY DISSIPATION AT THE SHOCK FRONT

11

Acoustic theory, which does not admit dissipative effects, predicts that the pressure in a spherically divergent wave will decay as the inverse first power of the radial distance. It would naturally be expected that a finite amplitude wave should decay somewhat more rapidly, and this fact has been confirmed by experimental pressure-distance curves.

As noted in Section 5, a decay of this type implies that some energy is being left behind as thermal energy in the water through which the wave has passed. Most of this dissipation can probably be ascribed to the irreversible thermodynamic process occurring at the shock front.

As an element of fluid passes through the shock front, it undergoes a sudden non-isentropic compression, the final state being determined by the Rankine-Hugoniot conditions.[4] When the pressure later drops to the hydrostatic level, it is found that the element of fluid has suffered a net increase of enthalpy (and entropy). This increase of enthalpy, which depends on the magnitude of the pressure at the shock front, is known as the dissipated enthalpy increment and will be designated by the symbol h.

The dissipated enthalpy increment is approximately proportional to the cube of the shock-wave pressure for low and moderate pressures, the limiting law for low pressures being given by[5]

$$h = (1/12)(\partial^2 v/\partial P^2)_s (\Delta P_s)^3. \qquad (23)$$

Using the Ekman equation of state[4] for sea water and applying Eq. (23), it is found that

$$h = 1.52\times 10^{-10}(\Delta P_s)^3, \qquad (24)$$

where h is in in.-lb./lb. and ΔP_s is in lb./in.^{2}. Equation (24) holds quite well for pressures up to 5000 lb./in.^{2}.

12

For higher pressures a modified adiabatic Tait equation of state has been used:[4]

$$P = B(S)[(v_1/v)^n - 1], \qquad (25)$$

[5] J. G. Kirkwood and H. Bethe; J. G. Kirkwood and E. Montroll, OSRD Reports No. 588 and 676.

where $n = 7.15$ and $B(S) = 44{,}400$ lb./in.^{2}, v_1 is the final specific volume after return to hydrostatic pressure, and v is the specific volume immediately after the passage of the shock wave. This equation of state leads to the following formula[4] for the dissipated enthalpy increment:

$$h = \frac{Bv_1}{2}\left[\left(\frac{v_1}{v}\right)^n - \frac{n+1}{n-1}\left\{\left(\frac{v_1}{v}\right)^{n-1} - 1\right\} - \frac{v}{v_1}\right] - \frac{B(v_1 - v_0)}{2}\left[\left(\frac{v_1}{v}\right)^n - 1\right]. \quad (26)$$

The term v_0 appearing here is the specific volume of the fluid before the arrival of the shock front. The last term on the right is relatively small and may be neglected for shock pressures under 40,000 lb./in.^{2}.

Figure 2 shows a plot of h as a function of the shock pressure, as computed from Eq. (26).

13

In a spherical wave the energy dissipated between two spherical shells is given by

$$E_D = 4\pi\rho_0 \int_{R_1}^{R_2} R^2 h(\Delta P_s) dR, \quad (27)$$

where $h(\Delta P_s)$ is the dissipated enthalpy increment at pressure ΔP_s, and ΔP_s is the excess shock pressure at distance R from the origin.

This integral can be evaluated in the low pressure region by use of Eq. (25), and at higher pressure by use of Eq. (26), providing experimental data are available, giving ΔP_s as a function of the radial distance R.

Reliable pressure-distance data, based on piezoelectric measurements, are available up to pressures of 20 to 30 thousand lb./in.^{2}. A few experimental points based upon measurement of spray dome velocities are available at higher pressures, but values for the region between the surface of the charge and the 30,000 lb./in.^{2} pressure level must be based principally upon theoretical calculations such as those of Kirkwood, Bethe *et al.*,[5] or Brinkely and Kirkwood.[6]

Available estimates of the pressure in the water at the surface of the charge range from 30 to 50 kilobars. The calculations cited[5,6] both lead to values close to 36 kilobars.

In Fig. 3 the pressure-radius similarity curve for TNT is shown extrapolated back to two arbitrary values at the charge surface. The value of 36 kilobars or 520,000 lb./in.^{2} is considered to be the order of magnitude of the actual peak pressure. The similarity curve extrapolated to 1,000,000 lb./in.^{2} is given for purposes of comparison as a possible upper limit of error. Isolated experimental values from dome velocity measurements are plotted on the same figure.

Using values from Fig. 3, the integrand of Eq. (27) is shown plotted in Fig. 4. For the solid curve of this figure the empirical relation $x^2h = 1230x^{-1.23}$ (where $x = R/W^{\frac{1}{3}}$) satisfactorily represents the integrand between the limits of $x = 0.136$ and $x = 10$. The dashed curve represents an upper limit to the integrand based on a peak pressure of 1,000,000 lb./in.^{2} at the charge. This curve is drawn to indicate the possible extent of the error in calculating the energy dissipation.

From the empirical relation given above, the energy dissipated between any two spherical surfaces may be readily calculated:

$$\frac{E_D}{W} = 4\pi\rho_0 \int_{x_1}^{x_2} 1230x^{-1.23}dx = 4{,}300{,}000\left[(W^{\frac{1}{3}}/R_1)^{0.23} - (W^{\frac{1}{3}}/R_2)^{0.23}\right] \frac{\text{in.-lb.}}{\text{lb. chg.}}, \quad (28)$$

where W is charge weight in. lb. and R is in ft.

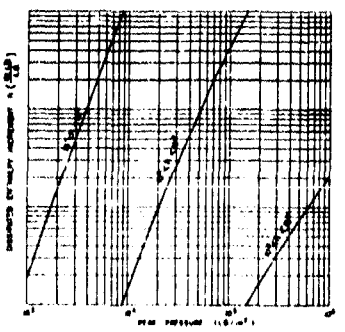


FIG. 2. Dissipated enthalpy increment, h, *versus* shock front pressure, ΔP_s.

[6] S. R. Brinkely and J. G. Kirkwood, Phys. Rev. 71, 606 (1947).

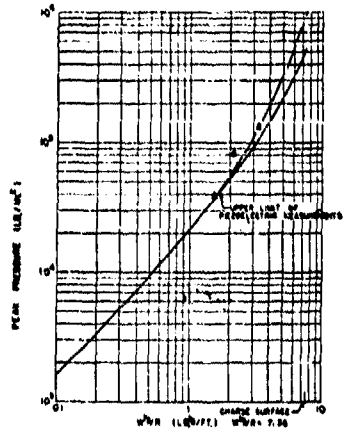


FIG. 3. Peak pressure similarity curve for TNT. Legend: ⚠ isolated experimental points based on measurement of spray dome velocity. ——— experimental curve based on piezoelectric measurements, extrapolated to a theoretical value at the charge surface based upon the results of reference 5, 6. – – – – similarity curve arbitrarily extrapolated to a value of 10^6 lb./in.^{2} at the charge surface.

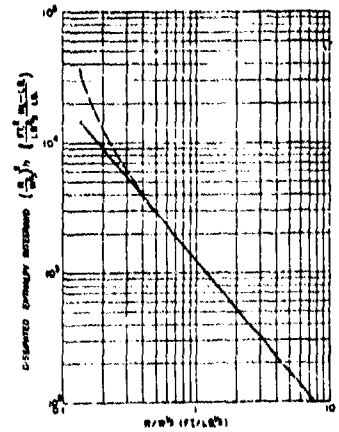


FIG. 4. Dissipated enthalpy integrand, $(R/W^{\frac{1}{3}})^2 h$, *versus* $R/W^{\frac{1}{3}}$ for TNT. Legend: ——— based on solid curve, Fig. 3. – – – – based on dashed curve, Fig. 3.

As an example, the amount of energy dissipated between the charge surface, $(W^{\frac{1}{3}}/R) = 7.35$, and a radius given by $R = W^{\frac{1}{3}}/0.352$ is approximately 3,400,000 in. lb. per pound of charge or 200 cal./g of charge.

A calculation based on the dashed curve of Fig. 4 for the same limits of integration would yield roughly 25 percent additional dissipated energy. The actual error is probably smaller than this, but the above value is an indication, at least, of the uncertainties involved in the assumption of the form of the pressure-radius curve in the region very close to the charge.

It must be remembered that an additional error, the magnitude of which cannot be estimated, is present because of uncertainty with respect to the equation of state data in the high pressure region. The equations used are based on extrapolation of experimental data[4] from pressures of 10 kilobars, and at high pressures actually imply applicability to metastable liquid water in the ice VII region.

14

It is now possible to compare the measured shock-wave energy flux at different radii with the loss caused by dissipation. Unfortunately, there is considerable scatter in the shock-wave data available, so that it is hard to state precisely what the energy flux is at a given radius. As a result, the total energy flow through a surface is known only to within about 5 to 10 percent, and although the total flow at a given radius may be known to within these limits, the experimentally measured dissipation, which is given by the small difference between flow at each of two radii, will be very appreciably in error.

To illustrate this, for TNT the flux at $W^{\frac{1}{3}}/R = 1$ is 2700 ± 250 in. lb./in.^{2} lb.$^{\frac{1}{3}}$, and at $W^{\frac{1}{3}}/R = 0.1$ it is 20.5 ± 1.5 in. lb./in.^{2} lb.$^{\frac{1}{3}}$. The total energy flow at $W^{\frac{1}{3}}/R = 1$ is then $4{,}900{,}000 \pm 450{,}000$ in. lb./lb. and at $W^{\frac{1}{3}}/R = 0.1$ it is $3{,}700{,}000 \pm 270{,}000$ in. lb./lb. The energy dissipated in the interval $W^{\frac{1}{3}}/R = 1$ to 0.1 calculated from these figures is $1{,}200{,}000 \pm 720{,}000$ in. lb./lb. The large uncertainty in the dissipated energy is immediately apparent. (These values are obtained from data taken at Woods Hole by J. S. Coles and his coworkers.)

By the use of Eq. (28), the energy loss resulting from dissipation between $W^{\frac{1}{3}}/R = 1$ and $W^{\frac{1}{3}}/R = 0.1$ would be 1,760,000 in. lb./lb. This value is to be compared with that of $1{,}200{,}000 \pm 720{,}000$ in. lb./lb. obtained above from the Woods Hole data. It will be noted that the two results agree within the limit of error of the experimental measurement. The calculated value,

based on a knowledge of the somewhat more accurate pressure-distance curve, is probably the better of the two.

V. IMPULSE AND ENERGY FLUX ASSOCIATED WITH THE SHOCK WAVE

15

The general character of the pressure wave emitted by an underwater explosion is illustrated by the oscilloscope trace reproduced in Fig. 1. The first portion is generally referred to as the shock wave, and this in turn is succeeded by the first, second, etc., bubble pulses. The pressure-time record is continuous, and naturally there is no sharply defined demarcation between the various portions of the wave. For convenience, an arbitrary demarcation will be introduced for the purposes of this report.

The shock wave will be defined as the portion of the wave lying between the shock front ($t=0$) and the first bubble maximum ($t=t_{M1}$) which occurs at the pressure minimum lying halfway between the shock front and the peak of the first bubble pulse. The first bubble pulse will be defined as the portion of the wave lying between the times of first and second bubble maxima (i.e., between $t=t_{M1}$ and $t=t_{M2}$), etc., for the succeeding pulses.

Usually, shock-wave pressure-time recording is carried only to times of the order of 10θ, where θ is the time constant of the initial exponential decay. Recently, a series of deep water measurements[7] has provided data making it possible to construct average or composite curves out to time t_{M1} as defined above. These curves are based on measurements with 0.50-, 2.50-, and 12.0-lb. charges of TNT at depths of 250 and 500 ft. Gauges were placed at such distances as to keep the value of $W^{\frac{1}{3}}/R$ constant at 0.352 for each charge size. The curves are shown in Figs. 5, 6, and 7.

16

The impulse delivered up to any time t is defined by

$$I=\int_0^t \Delta p\,dt. \tag{29}$$

The shock wave has an initial positive phase of relatively short duration and high amplitude followed by a long negative phase of low amplitude. The positive portion of the impulse is of principal interest as far as damage considerations are involved.

As the integration is carried to t_{M1}, the value of the integral becomes very small and in an incompressive system would become zero. In a compressive fluid the integral has a small positive residual at t_{M1}, as indicated in the following.

At t_{M1} the bubble has attained maximum radius, and the particle velocity at its surface is zero. In the acoustic approximation the particle velocity as a function of time at a point in the fluid is given by

$$u=\frac{\Delta p}{\rho_0 C_0}+\frac{1}{\rho_0 R}\int_0^t \Delta p\,dt. \tag{30}$$

If we make an observation at $R=A_{M1}$, where A_{M1} is the maximum bubble radius, then at

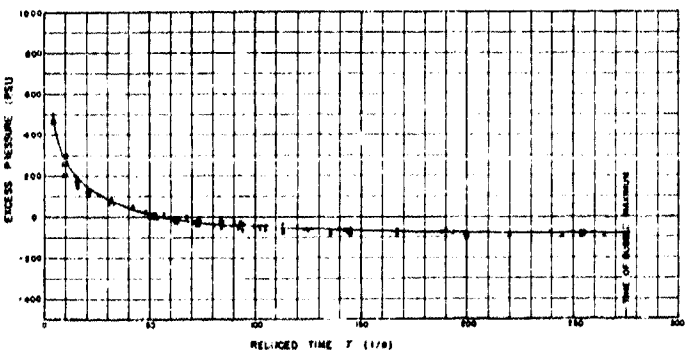


FIG. 5. Composite pressure-time curve for tail of shock wave. Explosive: TNT; charge depth: 250 ft.; distance from center of charge: $R=W^{\frac{1}{3}}/0.352$. Legend: θ time constant of initial shock wave decay, ●, × 0.5-lb. and 2.5-lb. charges from measurements of reference 2. Δ Points from shock-wave composites obtained by J. S. Coles *et al.*, Woods Hole.

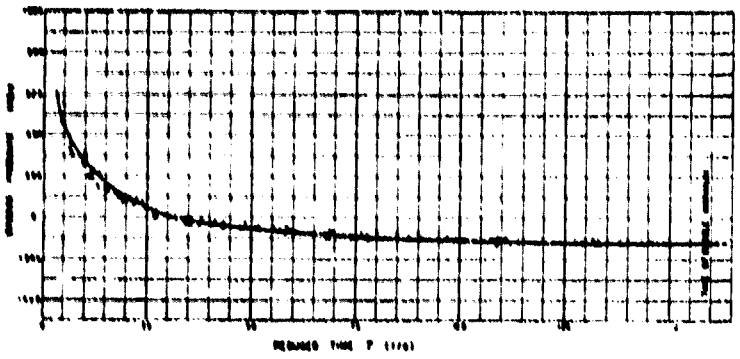


FIG. 6. Composite pressure-time curve for tail of shock wave. Explosive: TNT; charge depth: 500 ft.; distance from center of charge: $R = W^{\frac{1}{3}}/0.332$. Legend: θ time constant of initial shock-wave decay. ●, ×, ⊙ 0.5-, 2.5-, and 12.0-lb. charges based on measurements of reference 2. △ Points from shock-wave composites obtained by J. S. Coles *et al.*, Woods Hole.

$t = t_{M1}$, $u_{M1} = 0$ and from Eq. (30)

$$I_{M1} = \int_0^{t_{M1}} \Delta p\, dt = -\frac{A_{M1}\Delta p}{C_0}. \qquad (31)$$

Since Δ_s is negative in this region, I_{M1} is inherently positive. Its magnitude is very small compared to that of the total positive or negative impulse.

17

Combining Eqs. (6) and (17), the complete expression for total energy flow to time t becomes

$$E = \frac{4\pi R^2}{\rho_0 C_0}\left[(1 - 1.6\times 10^{-9} P_m)\int_0^t (\Delta p)^2 dt + \frac{C_0}{2R}\left(\int_0^t \Delta p\, dt\right)^2\right]. \qquad (32)$$

As previously indicated, the first term in the bracket increases monotonically with increasing time of integration and represents energy radiated acoustically, while the second or afterflow term represents energy which is stored reversibly in the water and returned at intervals to the gas bubble. This term attains a maximum at time t corresponding to the end of the positive phase and then decreases, becoming virtually zero at $t = t_{M1}$ since it involves the squaring of the small residual impulse given by Eq. (31). In the later stages of the positive phase at distances fairly close to the charge, the afterflow term predominates over the irreversible term.

Although in the limit of low pressures the afterflow term represents the contribution of essentially incompressive flow consequent upon the bubble expansion, it cannot be regarded as a purely incompressive term throughout the integration. Incompressive and compressive effects are not dissociable in the acoustic approximation, and in the region just behind the shock front the afterflow term represents principally a compressive contribution due to the radial divergence of the flow initiated by passage of the wave of compression.

18

Figures 5, 6, and 7 are composite pressure-time curves for TNT at the depths of 250 and 500 ft. and at a distance from the charge given by $W^{\frac{1}{3}}/R = 0.352$. Several charge sizes have been plotted on the same curve by scaling the time in terms of θ, the time constant of initial shock wave decay which is given by††

$$\theta = 0.060 W^{\frac{1}{3}}(W^{\frac{1}{3}}/R)^{-0.16} = 0.0725 W^{\frac{1}{3}} \text{ millisec. at } W^{\frac{1}{3}}/R = 0.352. \qquad (33)$$

Using this scale factor, the reduced time τ is defined by

$$\tau = t/\theta. \qquad (34)$$

τ is, of course, a dimensionless quantity. Any other scale factor proportional to $W^{\frac{1}{3}}$, such as the bubble period at the given depth, might equally well have been used.

From the pressure-time curves in Figs. 5, 6, and 7, certain quantities (listed below) have been

†† Equation (33) is an empirical fit of TNT data obtained at Woods Hole by J. S. Coles *et al.*

computed and plotted in Figs. 8, 9, and 10. Figure 8 shows curves for the initial positive phase, i.e., up to the time at which the excess pressure at the point of observation becomes zero following the arrival of the shock wave. This figure is for a charge depth of 500 ft. only, but a similar one for a depth of 250 ft. would not be very different. Figures 9 and 10 show the same curves extended to the time of first bubble maximum for depths of 250 ft. and 500 ft., respectively. They are essentially the same in form, the principal differences being due to the longer negative phase and smaller negative pressure at the 250-ft. depth. The functions plotted in Figs. 8, 9, and 10 are:

a. Irreversible energy flux, given by

$$F_1 = \frac{1}{\rho_0 C_0}[1 - 1.6\times10^{-6}P_m]\int_0^t (\Delta p)^2 dt. \quad (32a)$$

b. Afterflow: the afterflow energy flux should, according to the criterion of Section 5, average out to zero because it does not represent a radiated or an irreversibly stored energy. Afterflow energy flux is given by

$$F_A = \frac{1}{2\rho_0 R}\left(\int_0^t \Delta p dt\right)^2 = \frac{I^2}{2\rho_0 R}. \quad (32b)$$

Since the total impulse up to $t = t_{M1}$ is very small, the total afterflow energy up to this time is also very small. Physically what has happened is that the afterflow velocity was always outward, while the excess pressure was first positive, then negative. At one time the afterflow was with the pressure, later against it so that the total work done because of the motion has a net value that is very small, while each of its positive and negative components are large in magnitude.

c. Impulse: the impulse is defined by

$$I = \int_0^t \Delta p dt. \quad (29)$$

d. Particle velocity: the total particle velocity is given by

$$u = \frac{\Delta p}{\rho_0 C_0} + \frac{1}{\rho_0 R}\int_0^t \Delta p dt. \quad (30)$$

Separate curves for each component of the particle velocity have not been plotted, since their form may be obtained directly from the pressure-time and impulse-time curves. The form of the total particle velocity curve will change with the distance from the charge, since the two components vary as the first and second powers of the radius, respectively. The curves shown apply to the specific case where $R = W^{\frac{1}{3}}/0.352$.

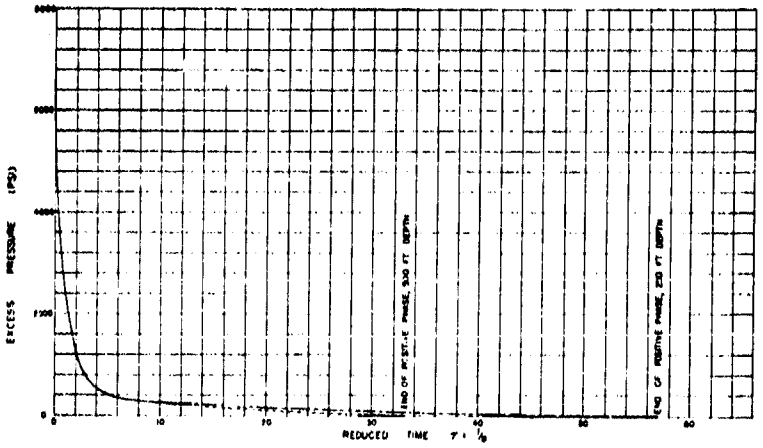


FIG. 7. Composite pressure-time curve for entire shock wave. Explosive: TNT; distance from center of charge: $R = W^{\frac{1}{3}}/0.352$. Legend: θ time constant of initial shock wave decay. ——— initial portion of shock wave from measurements by J. S. Coles *et al.*, Woods Hole. – – – – tail of curve from Fig. 5, 250-ft. depth. – – – – tail of curve from Fig. 6, 500-ft. depth.

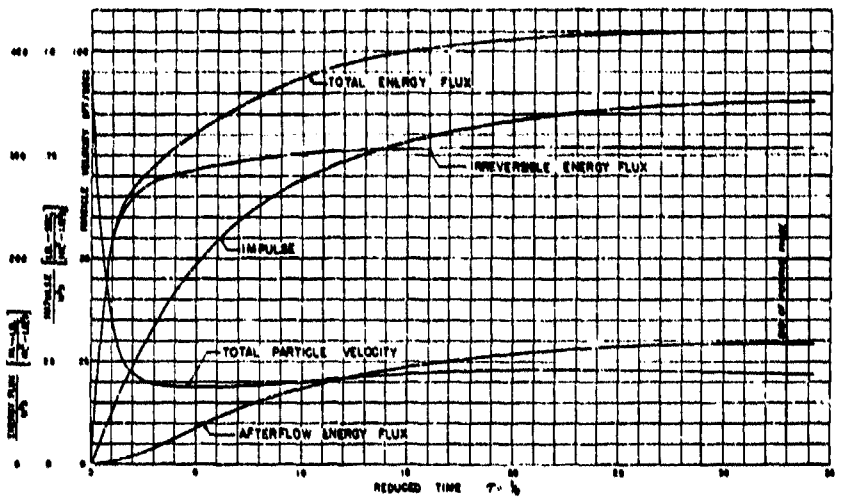


FIG. 8. Energy flux, impulse, and total particle velocity *versus* time for initial positive pressure phase of shock wave. Explosive: TNT; charge depth: 500 ft.; distance from center of charge: $R = W^{\frac{1}{3}}/0.352$. θ = time constant of initial shock-wave decay.

The total volume flow through a spherical surface may be expressed as

$$\Delta V = 4\pi R^2 \int_0^t u\,dt.$$

In the case under consideration, the total volume flow up to the time of bubble maximum is

$$\Delta V = 4\pi R^2 \int_0^{t_{M1}} \frac{\Delta p}{\rho_0 C_0} dt + 4\pi R^2 \int_0^{t_{M1}} \left[\int_0^t \frac{\Delta p}{\rho_0 R} dt \right] dt,$$

and since the first term on the right is very small,

$$\Delta V = \frac{4\pi R}{\rho_0} \int_0^{t_{M1}} \left[\int_0^t \Delta p\,dt \right] dt. \qquad (35)$$

Since ΔV is nearly independent of the radius, Eq. (35) should give us the total flow through the surface at the maximum bubble radius, i.e., the volume of the bubble at t_{M1}. This volume may also be calculated independently from experimental knowledge of the maximum radius.

From high speed photographic work carried out at Woods Hole by J. C. Decius and E. Swift, the following empirical equation relating maximum bubble radius to charge size and depth has been obtained:

$$A_{M1} = J_1 (W/Z_0)^{\frac{1}{3}}. \qquad (36)$$

A_{M1} is maximum bubble radius in feet, W is charge weight in pounds, Z_0 is the total hydrostatic head in feet (depth +33 ft.), and J_1 is a nearly constant factor which has a value of 12.6 for TNT over the range of depths under consideration.

At a depth of 500 ft. Eq. (35), utilizing the pressure-time curve of Fig. 6, gives a volume of 17 cu. ft. per lb. of explosive, while Eq. (36) gives 15.7 cu. ft. per lb. At 250 ft. the respective figures are 33.6 cu. ft. per lb. and 29.6 cu. ft. per lb. In each case the integrated particle velocity gives a greater volume change than the direct measurement of the radius by 8 and 13 percent, respectively. The error in the radius formula (36) is of the order of 2 percent, which could amount to an 8 percent error in the volume. The error in the double integration in Eq. (35) is of the order of 5 percent, because of base line inaccuracies, etc. (A base line shift of about 5 lb./in.^{2} in the pressure-time curve would

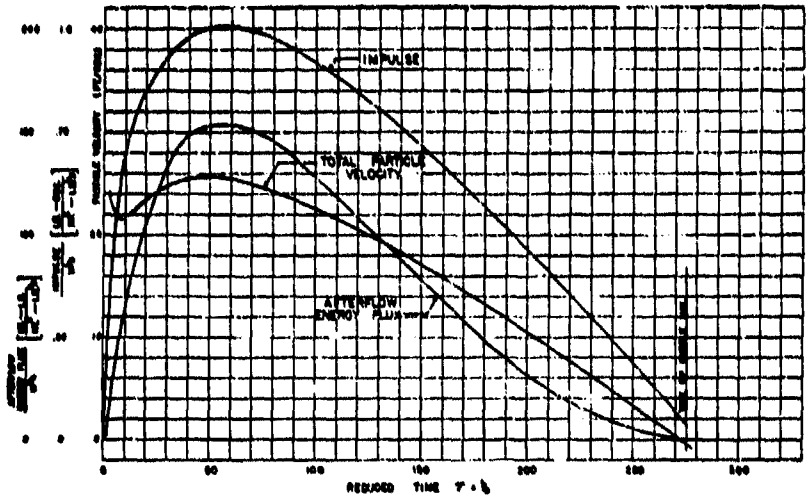


FIG. 9. Afterflow energy flux, impulse, and total particle velocity *versus* time to instant of first bubble maximum. Explosive: TNT; charge depth: 250 ft.; distance from center of charge: $R = W^{\frac{1}{3}}/0.352$; θ = time constant of initial shock-wave decay.

make the discrepancy in the volume almost negligible, while it would not seriously affect the impulse and afterflow energies, and a base line error of this magnitude could easily be present.) For these reasons it is impossible to say whether the discrepancy is due to inaccuracies in interpreting the experimental results or to inadequacy of the acoustic approximation.

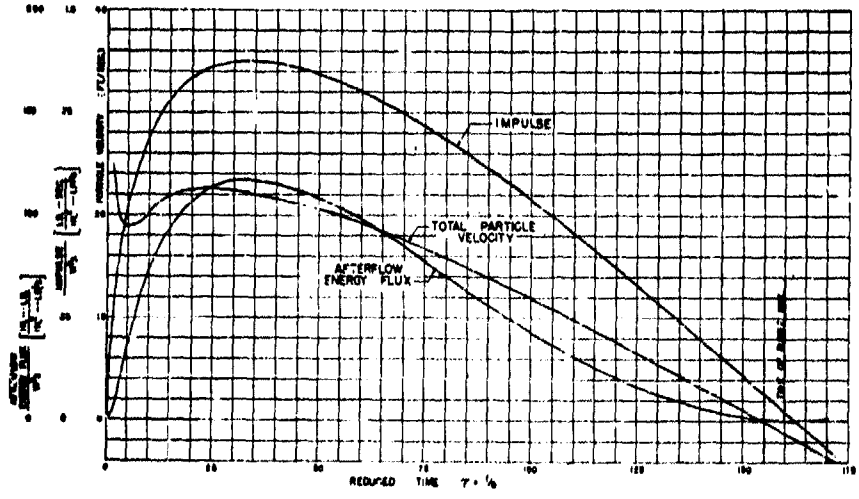


FIG. 10. Afterflow energy flux, impulse, and total particle velocity *versus* time to instant of first bubble maximum. Explosive: TNT; charge depth: 500 ft.; distance from center of charge: $R = W^{\frac{1}{3}}/0.352$; θ = time constant of initial shock-wave decay.

VI. IMPULSE AND ENERGY FLUX ASSOCIATED WITH THE BUBBLE PULSES

20

The bubble pulses have been defined as those parts of the pressure-time curve lying between times of successive bubble maxima. In practice, the times of bubble maxima are taken to be halfway between successive pressure peaks. This assumes that the time of expansion of the bubble is equal to the time of collapse. According to the theory of the bubble phenomenon,[7] the period (or half-period) is dependent on the amount of energy available for the oscillation. Since the bubble is continually radiating acoustic energy, the bubble expansion has more energy associated with it, and therefore actually lasts longer than the following contraction. Our approximation can be justified, however, because most of the radiation occurs in a relatively short length of time near the bubble minimum, and during the major portion of a cycle the bubble has nearly constant energy. The difference between the time of expansion and contraction should therefore be very small.

Composite curves of the first two bubble pulses from the series of measurements reported in reference (2) are reproduced in Fig. 11. The particular composites shown are for a depth of 500 ft. and $W^{\frac{1}{3}}/R$ equal to 0.352, the gauges being positioned to the side of the cylindrical charges used. The time scale has been reduced by the cube root of the charge size, thus:

$$z = t/W^{\frac{1}{3}}. \tag{37}$$

21

As in the case of the shock wave, it is possible to determine the nature of the net impulse delivered by a bubble pulse from theoretical considerations. At the time of a bubble maximum the following condition holds at the bubble surface:

$$u_M = 0 = \frac{\Delta P_M}{\rho_0 C_0} + \frac{1}{\rho_0 A_M} \int_0^{t_M} \Delta p dt, \tag{38}$$

where ΔP_M is the pressure in the gas bubble. The impulse as measured at A_M would therefore be:

$$I_{AM} = -(A_M \Delta P_M / C_0). \tag{39}$$

The impulse varies inversely as the radius (allowing for the time lag due to finite velocity of propagation), so that the impulse at radius R would be

$$I_R = -(A_M^2 \Delta P_M / RC_0). \tag{40}$$

The incremental impulse delivered at a radius R_1 between the times of first and second bubble maxima would therefore be

$$\Delta I_R = (-A_{M2}^2 \Delta P_{M2}/RC_0) - (-A_{M1}^2 \Delta P_{M1}/RC_0). \tag{41}$$

The terms in parentheses are inherently small and positive since the ΔP_M's are small and negative. The first term is smaller than the second in magnitude because both A_{M2} and ΔP_{M2} are smaller than the corresponding quantities in the second term. ΔI_R, which is the net impulse delivered between the first and second bubble maxima, should therefore be small and negative. The same statement is, of course, true for the second and succeeding bubble pulses. The negative impulses delivered in this manner should ultimately cancel the net positive impulse delivered by the shock wave (see Section 16).

This treatment neglects the finite amplitude of the wave and other effects such as turbulence and migration of the bubble. The effect of these factors on the impulse is difficult to ascertain, but it is believed that the results of the above discussion are in any case qualitatively correct.

Integrations of Fig. 11 show that the positive impulse delivered by the first bubble pulse is 1.076-lb. sec./in.^{2} lb.$^{\frac{1}{3}}$, while the net impulse for the whole pulse is +0.106-lb. sec./in.^{2} lb.$^{\frac{1}{3}}$. Although the net impulse appears to be positive in contradiction to Eq. (41), a base line shift of the order of 5 lb./in.^{2} in Fig. 11 could make the impulse come out zero or even negative. This is the order of magnitude of the error in originally determining the base line on the photographic records.

If the net volume flow from the time of first bubble maximum to second bubble maximum is calculated from Eq. (35),

$$\Delta V = \frac{4\pi R}{\rho_0} \int_{t_{M1}}^{t_{M2}} \left[\int_0^t \Delta p dt \right] dt, \tag{35}$$

[7] Bernard Friedman, *Theory of Underwater Explosion Bubbles*, Report IMM-NYU 166, Inst. for Math. and Mech., New York University, September 1947.

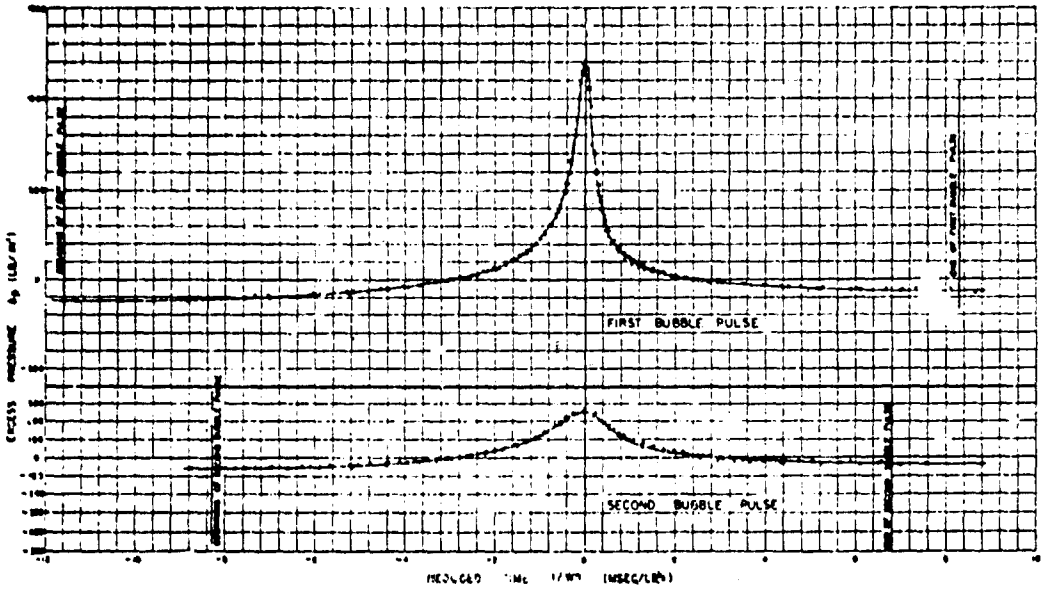


FIG. 11. Composite pressure-time curves for first and second bubble pulses. Explosive: TNT; charge depth: 500 ft.; distance from center of charge: $R = W^{\frac{1}{3}}/0.352$. (Based on measurements cited in reference 2.) Legend: ⊙ 0.5-lb. charges. × 2.5-lb. charges. ● 12.0-lb charges.

it is found, using the curve of Fig. 11, that the net flow is 9.7 cu. ft. per lb. *toward* the bubble. The ratio of the volume of the bubble at its second maximum to its volume at first maximum should therefore be

$$(17.0-9.7/17.0) \approx 0.43,$$

since the volume of 17.0 cu. ft. was found in Section 19 to be the total outward flow up to the time $t = t_{M1}$.

As in Section 19, we have at our disposal an equation giving the second bubble maximum in terms of the charge size and the depth:

$$A_{M2} = J_2(W/Z_0)^{\frac{1}{3}}, \tag{42}$$

where $J_2 = 8.5$.

The ratio of the first and second maximum volumes as obtained from direct bubble radius measurement is, therefore,

$$(A_{M2}/A_{M1})^3 = (J_2/J_1)^3 = 0.31.$$

This ratio is considerably lower than the value of 0.43 given above by Eq. (35), but the discrepancy is in the direction of the same type of base line error that probably caused the net impulse to be positive. In this case the effect would be somewhat exaggerated because of the cumulative effect of base line error upon the integration.

The impulse of the second bubble pulse will not be considered as the error in the base line in that region is excessive.

22

The radiated energy flux for the first bubble pulse is given by the equation

$$F_{R1} = \frac{1}{\rho_0 C_0} \int_{t_{M1}}^{t_{M1}} (\Delta p)^2 dt. \tag{43}$$

Integration of the energy flux from the composite of Fig. 11, yields

$F_{R1}/W^{\frac{1}{3}} = 139$(in.-lb./in.^{2} lb.$^{\frac{1}{3}}$) (at $R = W^{\frac{1}{3}}/0.352$)

and

$$E_{R1}/W = 121\text{(cal./g)}.$$

Similarly, for the second bubble pulse

$F_{R2}/W^{\frac{1}{3}} = 16.8$(in.-lb./in.^{2} lb.$^{\frac{1}{3}}$)
(at $R = W^{\frac{1}{3}}/0.352$),

$E_{R2}/W = 14.7$(cal./g).

The error in the energy flux of bubble pulses caused by error in the base line is very small

TABLE I. Reported detonation energies of TNT.

ΔH cal./g	Source
840	*Bericht über die Arbeitstagung Unterwassersprengwesen, Veranstaltet von der Amtsgruppe Mar Rust/FEP* im OKM am 28/29 Oktober 1943 im Harnackhaus im Berlin (experimental)
880	G. I. Taylor, *The Vertical Motion of a Spherical Bubble and the Pressure Surrounding It*, TMB 510, August 1943
950	G. D. Clift and B. T. Federoff, *A Manual for Explosives Laboratories* (Lefax, Inc., Philadelphia, 1942). This value seems to have been obtained from Soukharevsky and Pershakoff, Explosives, Moscow, 1932
1060	Private communication from S. R. Brinkley to W. D. Kennedy (theoretical)

TABLE II. Energy partition at time of first bubble maximum (W = charge weight in lb.; R = distance in ft.).

Acoustic energy flowing past $R = W^{1}/0.352$	275 cal./g
Energy dissipated at the shock front during propagation up to $R = W^{1}/0.352$ (calculated in Section 13)	200
Unaccounted for	95
Total energy associated with emission of shock wave (1050 − 480)	570
Potential energy stored in water at first bubble maximum as calculated from measured maximum bubble radius	385
Internal energy of gaseous products (referred to infinite adiabatic expansion: (480 − 385)	95
	1050

because of the fact that the calculated energy flux is near a minimum with respect to a base line shift. In this case an error of 10 lb./in.^{2} in the base line would cause less than 2 percent error in the energy, while it would cause a very large error in the impulse.

VII. PARTITION OF ENERGY IN AN UNDERWATER EXPLOSION

23. Energy of Detonation

At the present time there seems to be a lack of precise knowledge concerning the quantity of energy released in the detonation of various explosives. A wide range of values is quoted in the literature, and it is not always possible to ascertain the original source of the data. A summary of such results is given in Table I. Detonation energy is defined as the enthalpy change, ΔH, in calories per gram, with final products reduced to standard conditions.

In the theory of the gas bubble oscillation[7] it is customary to use as a zero energy reference the state of infinite adiabatic expansion of the product gases. Since it is our purpose to include bubble phenomena in the discussion of energy partition, it will be more convenient to adopt this reference rather than the standard state usually used for ΔH. The order of magnitude of the internal energy of the products at standard conditions (relative to infinite adiabatic expansion) is 100 cal./g, and this quantity should be added to the values given in Table I.

For purposes of further discussion, we shall arbitrarily adopt the value of 950 cal./g as the detonation energy of TNT, giving 1050 cal./g as the approximate detonation energy relative to infinite adiabatic expansion of the products. The uncertainty in this figure is at least of the order of ± 10 percent.

24. The Shock Wave

It is known that the total energy associated with the gas bubble at its first maximum is approximately 480 cal./g.[3] Of this quantity, 385 cal./g are stored as potential energy because of the formation of the cavity in the water, while the remainder is in the form of internal energy of the gaseous products (referred to an infinite adiabatic expansion). The value of the potential energy stored in the water is based on the experimental maximum radius as given by Eq. (36).

The net energy lost by the bubble up to the time of the first maximum is therefore 1050 minus 480, or about 570 cal./g.

The partition of this energy has been discussed in previous chapters and is summarized in Table II.

The unaccounted term should comprise losses resulting from turbulence, viscosity, conduction, etc. It should be noted that the magnitude of

TABLE III. Successive periods of bubble oscillation (TNT charges in free water)* at a depth of 500 ft.

$T_1/W^{1} = 23.2$ millisec./lb.^{1}
$T_2/W^{1} = 16.7$
$T_3/W^{1} = 13.5$

* See reference 3.

TABLE IV. Energy partition at time of second bubble maximum.

Acoustic radiation in first bubble pulse	120 cal./g
Potential energy in the water at time of second bubble maximum based on measured maximum radius	120
Internal energy of gas at second bubble maximum: (B_2-120)	60
Unaccounted for	180
Total energy associated with first maximum (B_1)	480 cal./g
Total loss during emission of first pulse (180+120)	300
Energy left for second pulse (B_2)	180

TABLE V. Energy partition at time of third bubble maximum.

Acoustic radiation in second bubble pulse	15 cal./g
Potential energy in the water at time of third bubble maximum	55
Internal energy of gas at third bubble maximum: (B_3-55)	40
Unaccounted for	70
Total energy associated with second bubble maximum (B_2)	180 cal./g
Total loss during emission of second pulse = 70+15	85
Energy left for succeeding pulses (B_3)	95

this portion (95 cal./g) is much smaller than the combined uncertainty in the detonation energy and in the energy dissipated at the shock front, and therefore even its order of magnitude is in doubt.

25. The Bubble Pulses

From the theory of the bubble pulsation it is known that the period is proportional to the cube root of the total energy associated with the oscillation as defined in Section 24. Since the periods of successive oscillations decrease progressively, it is evident that energy is lost between successive bubble maxima. Using the cube root law stated above, it is seen that the energy left after the emission of a bubble pulse is given by

$$B_{n+1}=B_n(T_{n+1}/T_n)^3, \qquad (44)$$

where B_n = total energy associated with the nth oscillation and T_n = period of nth oscillation.

The necessary period data[2] are summarized in Table III.

Using Eq. (44), the data of Table III, and the maximum radius data quoted in Sections 21 and 22, we obtain the energy partition for the first and second bubble pulses as given in Tables IV and V.

Since the total energy associated with an oscillation and the energy of acoustic radiation are both known to within ±3 percent, it is important to note the magnitude of the unaccounted terms in Tables IV and V.

A summary of energy partition data is given in Table VI. It is seen from Table VI that less than half the detonation energy is to be found in waves of compression, while somewhat more than half is lost in dissipative processes.

It is difficult to ascribe any appreciable portion of the unaccounted 345 cal./g to dissipation similar to that which was computed for the shock front. Figure 11 shows the pressure pulses to rise relatively slowly with time, and the resulting process should be very nearly isentropic on both compression and expansion. Furthermore the second pulse rises very much more slowly than the first, and yet the unaccounted portion in this pulse is an even greater *fraction* of the total energy loss than is the case in the first pulse.

Because of the shortness of the time intervals during which temperature and pressure in the gas bubble are high, it is doubtful that losses of such magnitude could be attributed to conduction or radiation of heat.

We conclude, therefore, that the unaccounted for energy losses are associated with some combination of the following factors:

(i) turbulence induced in the water surrounding the bubble,

(ii) chemical or physical changes in the gaseous products!

(iii) actual loss of gaseous products in the form of small bubbles in the water, perhaps due to high degree of turbulence at the periphery of the gas globe.

TABLE VI. Summary of energy partition tables.

Total acoustic radiation (through emission of second bubble pulse) at $R=W^{1}/0.352$	410 cal./g
Shock front dissipation up to $R=W^{1}/0.352$	200
Unaccounted losses	345
Total energy left at third bubble maximum	95

APPENDIX I

Summary of Notation

p = absolute pressure at any point as a function of time
P_0 = absolute hydrostatic pressure
Δp = excess pressure as a function of time $(p - P_0)$
P_m = excess peak pressure of an exponentially decaying shock wave
ΔP_s = excess pressure at any shock front
v = specific volume of the fluid at pressure p
ρ = density of the fluid $(\rho = 1/v)$
E = total energy flow through a spherical surface
F = energy flux (energy flow per unit area of a spherical surface)
R = radial distance
A = radius of the gas bubble
t = time measured from instant of incidence of the pressure wave
u = radial particle velocity relative to the unperturbed fluid
U = shock front propagation velocity
C_0 = sound velocity $(C_0 = (\partial P/\partial \rho)_{s_0}^{\frac{1}{2}})$
$\Delta \eta$ = internal energy increment of a unit mass of fluid relative to the initially unperturbed state
ΔH = enthalpy increment of a unit mass of fluid relative to the initially unperturbed state $(\Delta H = \Delta \eta + \Delta(pv))$
h = dissipated portion of the enthalpy increment ΔH, per unit mass of fluid
S = entropy per unit mass of fluid
κ = bulk modulus of the fluid $(\kappa = \rho_0 C_0^2)$
θ = time constant of initial exponential decay of shock wave
$B(S)$ = characteristic pressure parameter of the modified adiabatic Tait equation of state
n = exponent of Tait equation of state
x = reduced radius $(x = R/W^{\frac{1}{3}})$
I = impulse delivered—the time integral of the pressure
τ = reduced time defined by $\tau = t/\theta$
s = reduced time defined by $s = t/W^{\frac{1}{3}}$
T_n = period of nth oscillation, measured between successive pressure peaks
B_n = total energy associated with the nth oscillation.

THE PRESSURE AND IMPULSE OF SUBMARINE EXPLOSION WAVES ON PLATES

G. I. Taylor
Cambridge University

British Contribution

July 1941

THE PRESSURE AND IMPULSE OF SUBMARINE EXPLOSION WAVES ON PLATES

G. I. Taylor

July 1941

* * * * * * * * *

Summary.

Some work of F.G. Friedlander is summarised which describes the way in which the pressure due to reflection of a pulse from an explosion is built up during the passage of the pulse along a plane set obliquely to its direction of motion. The pressure ultimately attained at some distance from the point where the pulse first strikes the reflecting surface is twice that in the incident pulse when that surface is immovable, but when the reflecting surface is not fixed, as when it is a steel plate, the motion of the reflecting surface reduces the pressure acting on it. This reduction is greater for oblique than for normal incidence. For comparatively thin plates the pressure changes to tension in a time which is small compared with the duration of the pulse. If water can support tension the displacement of the plate is small compared with the displacement which occurs when no tension can be held. The amount of tension which water can support for periods of the order of 1 millisecond at a free surface can be estimated from observations of the radius of the circle over which spray is projected upwards from a submarine explosion. It seems likely that this tension could be applied to a surface which is wetted by water but experiments on this subject are desirable.

Though the amount of damage done to a ship must depend on the strength of the structure supporting the plate and other factors not included in the present analysis, the results give the relationship between weight of charge and distance for a given amount of damage. It is found that if water can support tension the charge weight for given damage is proportional to $(\text{distance})^{\frac{3}{2}}$. On the other hand if the water is incapable of withstanding any tension, the law of variation of charge weight with distance is not a simple power law. If, however, an attempt were made to represent experimental results by means of a formula

$$(\text{distance for given damage}) = \text{constant} \times (\text{charge weight})^{S},$$

S would have a value which in the extreme range of charges and plate thicknesses varies from $\frac{1}{3}$ to $\frac{2}{3}$. In the range covered by charges from 300 to 2,400 lb. of T.N.T. and plate thicknees $\frac{1}{4}$ inch to 3 inches, S varies from 0.38 to 0.54, the mean value of S being 0.46.

The reflection of sound waves both in air and water by an infinite rigid plane provides a simple mathematical problem. The amplitude of the reflected wave is equal to that of the incident wave, so that at the reflecting surface where the pressures due to the incident and reflected waves are in phase the pressure is double that due to the incident wave alone. This statement is correct whether the incident disturbance is a train of harmonic waves or a single pulse. It is also true for all angles of incidence.

When the reaction between a plate and a pulse is considered, certain limitations to the simple theory immediately appear. These are due to the two assumptions of the simple theory that the reflecting plane is infinite and that it is rigid and fixed. Neither of these assumptions is true when the reflecting plane is a finite flat or bent steel plate, though it is to be expected that in the limiting case when the plate is very thick and of very large area the simple theory will apply. The object of the present note is to explore the modifications which the reflected pulse will experience owing to the finite size and thickness of the plate and to describe the motion of the plate due to the incident pulse.

The .....

The inadequacy of the simple theory to represent the reflection conditions of a fixed finite plate may be seen by imagining the angle of incidence of the pulse to decrease to zero. As long as there is a finite angle of incidence the pressure on the plate is according to the simple theory twice the pressure in the pulse. On the other hand, when the pulse is travelling parallel to the plane it is undisturbed by it so that the pressure on the plane is equal to that in the pulse. This apparent discrepancy or paradox is resolved when the reflection of a pulse by a finite plane or wedge is considered. The change in a special type of pulse (chosen because it closely resembles the pulse produced by a submarine explosion of a high explosive charge) when it is reflected from a symmetrical wedge, the angle of which is 2θ, has been calculated by F.G. Friedlander. This pulse is a sound wave in which the pressure is zero till the arrival of shock wave in which the sudden pressure change is p_0. The pressure subsequently dies down exponentially so that the pressure p at time t after the onset of the wave is

$$p = p_0 e^{-nt} \qquad (1)$$

This pulse has a characteristic length $l = c/n$, (where c is the velocity of sound), in which the pressure dies down to 0.368 of its maximum value. The reflected wave and the pressure on the wedge is proportional to p_0 and is a function of θ, r/l and $n\left(t - \frac{r\cos\theta}{c}\right)$ where r is the distance of any point on the surface of the wedge from its vertex. The characteristic features of reflection by a wedge can be appreciated by reference to Figure 1, which shows the form of the wave fronts of the incident, reflected and diffracted waves. In Figure 1, O is the vertex of the wedge. The wave strikes the wedge symmetrically, the angle of incidence on each face being $90° - \theta$. The line A_0OB_0 is the position of the wave front at the moment of striking the vertex. After a time $r\cos\theta/c$ the incident wave front consists of the two parts A_1C_1, D_1B_1 above and below the wedge. The reflected wave front consists of the lines C_1E_1, D_1F_1 which are tangential to the circle described with centre O and radius $OG = OC_1\cos\theta = r\cos\theta$. The wave front of the diffracted disturbance is the part of the circle of radius r which lies outside the wedge, i.e. the segment HE_1KF_1LG.

Assuming that $\theta < 90°$, points on the wedge are reached first by the incident wave. In the section C_1H the pressure is double that due to the incident wave. The section OH is subject to the rear parts of the incident and reflected wave and also to the diffracted wave which is a suction wave when the incident wave is a pressure wave.

The time interval between the arrival of the wave front at the point C_1 and the arrival of the diffracted wave is $(1 - \cos\theta)r/c$. If therefore the incident pulse is limited so that it has passed any given point in a time interval τ after the passage of the wave front, then if r is greater than $c\tau/(1 - \cos\theta)$ the whole of the incident and reflected waves will have passed the point C_1 before the diffracted wave reaches it. At points further away from the vertex than $c\tau/(1 - \cos\theta)$ the pressure-time curve is as shown in Figure 2b, which shows the distribution for a square-topped pulse, i.e. an incident pulse in which the pressure suddenly increases by an amount p_0 and remains at this value for time τ when it suddenly returns to its initial value. As the wave proceeds the incident and reflected pulses remain constant in height but get further away from the region of the diffracted disturbance. The diffracted disturbance continually decreases in intensity but increases in the area covered, since it extends over the whole radius from the vertex to the diffraction wave front. Figure 2b shows the pressure-time curve calculated by Friedlander at distance 4 pulse lengths (i.e. $4c\tau$) from the vertex of a 90° wedge. Figure 2c shows the pressure-time curve for a point 10 pulse lengths from the vertex. The reduction of intensity in the diffracted wave as distance from the vertex increases may be noticed.

At points nearer to the vertex than $c\tau/(1 - \cos\theta)$ the incident and reflected waves are not separated from the diffracted wave. At such points the pressure-time curve is as shown in Figure 2a, which represents the state of affairs at distance $r = \frac{1}{2}c\tau$ from the vertex.

Friedlander has proved some interesting properties of the diffracted pulse. He shows for instance that its total impulse, (i.e. $\int_0^\infty p\ (\text{diffracted wave})\ dt$) is constant at all distances from the vertex.

Further, he finds that this constant is definitely related to the angle of incidence of the pulse $\frac{\pi}{2} - \theta$. If the impulse of the incident wave is I where $I = \int_0^\infty p_i\ dt$ and p_i is the pressure in the incident wave, the impulse applied at any point of the surface by the incident

and .....

and reflected beam is 2I. The impulse of the diffracted pulse is $-I\left(1-\frac{2\theta}{\pi}\right)$. Thus when $\theta = \frac{1}{2}\pi$ so that the wedge has such a wide angle as to become a single plane, the total impulse is 2I. When $\theta = 0$ so that the wedge is a semi infinite sheet the total impulse is $2I - I = I$.

It will be seen, therefore, that Friedlander's resolution of the apparent paradox with which this investigation started is that the total impulse of a pulse striking an inclined plane is always $\left(1+\frac{2\theta}{\pi}\right)I$, where I is the impulse of the incident pulse. On the other hand, at points far from the vertex the pressure pulse predicted by the simple theory of reflection at an infinite plane separates from the diffracted suction disturbance, the intensity of which becomes ultimately very small though its pulse remains constant.

When the incident pulse is not confined to a finite duration but extends indefinitely as does the exponential pulse represented by (1), the reflected and diffracted zones on the reflecting plane do not separate, so that the above discussion must be modified. A useful method for discussing the reflection of a pressure pulse of the type represented by (1) is to calculate the impulse of the part of the system where the pressure is positive. Its initial value near the vertex is equal to $I\left(1+\frac{2\theta}{\pi}\right)$, for this is the value of the total impulse and it is found that near the vertex no suction region is formed. At great distances from the vertex where the incident and refracted pulses have almost completely separated from the diffracted suction area, the positive pressure impulse tends to the limit 2I. The ratio of the positive pressure impulse to its limiting value 2I at any distance from the vertex may be taken as a measure of the completeness with which the true reflected pulse has established itself at this distance.

Figure 3 shows Friedlander's calculated values of

$$\alpha = \frac{\text{positive impulse on plane}}{\text{impulse of incident pulse}} \text{ as a function of } \frac{r}{l} = \frac{rn}{c} = \frac{\text{distance from vertex}}{\text{pulse length}}$$

for the pulse represented by (1). Here the "pulse length" is defined as c/n.

The calculations show the values for $\theta = 45^\circ$ and $\theta = 15^\circ$ and the results are plotted in Figure 3 with rn/c on a logarithmic scale. It will be seen that with a plane inclined at 45°, the reflected pulse is established to within 10 per cent. of its ultimate value when the incident pulse has moved about 10 pulse lengths up the plane.

When the angle of incidence is 15° the reflected pulse does not establish itself to this extent until the incident pulse has travelled a distance of 80 pulse lengths along the plane. In the first 10 pulse lengths the positive impulse has only risen from its initial value 1.08I to 1.24I. For smaller angles of incidence the positive impulse on the plane tends to 1.0I near the vertex and the distance from the vertex at which there is any appreciable increase over this value becomes very great, so that in the limit when θ tends to 0 no reflection takes place.

Reflection at curved surfaces.

The reflection of pulses at curved surfaces provides a difficult problem. In two cases however, namely, the paraboloid and the parabolic cylinder, the solution has been obtained. The method, originally due to Lamb, has been modified by Friedlander, who finds that, unlike the case of the reflecting plane, the pressure-time curve is identical at all points on the surface. This is true for all kinds of incident plane pulse or wave and the total time integral of the pulse is simply I, i.e. the positive contribution due to the reflected and diffracted wave system is exactly neutralised by their negative contribution. If, however, the integral of the positive pressure alone be taken, the positive pulse thus found depends on the ratio c/nf, f being the focal length and c/n the pulse length.

For very thin pulses this positive pulse is 2I and this corresponds with ... reflection of the ordinary type. When the pulse length is twice the focal length, i.e. c/n = ... of curvature of the parabolic cylinder at the vertex, the positive impulse is 1.3I. For very long pulses the positive impulse is 1.0I. Friedlander's results are shown in figure 4.

Reflection of a pressure pulse from a plate.

Normal incidence.

When the pulse is reflected perpendicularly from a plate which is not rigid and fixed the motion of the plate due to the combined action of the incident and reflected pulses gives rise to

modifications in the reflected wave. The pressure in the incident wave will first be taken as

$$p_i = p_0 e^{-n(t - x/c)} \tag{2}$$

where x is distance measured perpendicular to the plate in the direction of the oncoming wave. The pressure in the reflected wave will necessarily be of the form

$$p_r = p_0 \phi \left(t + \frac{x}{c}\right) \tag{3}$$

At the surface of the plate itself x = 0 and the total pressure is

$$\frac{p}{p_0} = e^{-nt} + \phi (t) \tag{4}$$

where $p = p_r + p_i$. If $c = \sqrt{dp/\rho}$ is the velocity of sound, the velocity of the water (or other medium of density ρ) in the incident wave is $p_i/\rho c$, while the velocity due to the reflected wave is $-\phi/\rho c$. If ξ is the displacement of the plate the equation of continuity at the surface is therefore

$$\frac{\rho c \dot{\xi}}{p_0} = e^{-nt} - \phi \tag{5}$$

where $\dot{\xi}$ is written for $d\xi/dt$ and ϕ for ϕ (t).

The motion of the plate is determined by its mass per unit area, m, by the pressure, p, and by external constraints such as the supporting framework. For simplicity it will be assumed that these constraints are equivalent to a spring which would cause the plate to oscillate freely (i.e. when not in contact with water) with a period $2\pi/\mu$. The equation of motion is

$$\frac{p}{m} = \ddot{\xi} + \mu^2 \xi \tag{6}$$

Eliminating ξ the equation for ϕ is

$$\ddot{\phi} + \frac{\rho c}{m} \dot{\phi} + \mu^2 \phi = \left(n^2 + \frac{n\rho c}{m} + \mu^2\right) e^{-nt} \tag{7}$$

The solution of (7) is

$$\phi = A e^{s_1 t} + B e^{s_2 t} + \frac{n^2 + \frac{n\rho c}{m} + \mu^2}{n^2 - \frac{n\rho c}{m} + \mu^2} e^{-nt} \tag{8}$$

where s_1 and s_2 are the roots of

$$s^2 + \frac{\rho c}{m} s + \mu^2 = 0 \tag{9}$$

The conditions at t = 0 are $\xi = 0$ and $\ddot{\xi} = p/m$. When expressed in terms of ϕ these become

$$\left.\begin{aligned} \phi &= 1 \\ (1 + \phi) \frac{\rho c}{m} + n + \dot{\phi} &= 0 \end{aligned}\right\} \quad \text{when } t = 0 \tag{10}$$

The equations for A and B are therefore

$$A + B = -\frac{2n\rho c}{m} \left(\frac{1}{n^2 - \frac{n\rho c}{m} + \mu^2}\right)$$

$$s_1 A + s_2 B = \frac{n\rho c}{m} \left(\frac{-\frac{n\rho c}{m} + \mu^2}{n^2 - \frac{n\rho c}{m} + \mu^2}\right)$$

Hence, using the relations implicit in (9), namely $\frac{\rho c}{m} = -s_1 - s_2$, $\mu^2 = s_1 s_2$,

A = ...

$$A = \frac{\rho c s_1 (s_1 + n)}{m (s_2 - s_1)(n^2 - \frac{\rho c}{m} s_1 + \mu^2)}$$

$$B = \frac{\rho c s_2 (s_1 + n)}{m (s_1 - s_2)(n^2 - \frac{\rho c}{m} s_2 + \mu^2)} \qquad (11)$$

and substituting these in (4), (5) and (6)

$$\frac{p}{p_0} = \frac{1}{n^2 - \frac{\rho c}{m} s + \mu^2} - \left[- \frac{\rho c s_1 (s_2 + n)}{m (s_1 - s_2)} e^{s_1 t} + \frac{\rho c s_2 (s_1 + n)}{m (s_1 - s_2)} e^{s_2 t} + (n^2 + \mu^2) e^{-nt} \right] \qquad (12)$$

and

$$\xi = \frac{2 p_0}{m(n^2 - \frac{\rho c}{m} s + \mu^2)} \left[e^{-nt} + \frac{s_2 + n}{s_1 - s_2} e^{s_1 t} - \frac{s_1 + n}{s_1 - s_2} e^{s_2 t} \right] \qquad (13)$$

Oblique incidence.

When the incident pulse falls obliquely on the plate it is no longer possible to consider the plate as though it were moving as a whole. The pressure pulse will in fact travel along the plate and give rise to a corresponding disturbance in the plate and it is possible to consider a variety of possible conditions of support which would give rise to corresponding motions. The simplest of these and the most closely analogous to the case of normal incidence already discussed is to assume that the plate has no stiffness in bending and that it is supported in such a way that each element of it can vibrate freely in a direction normal to its plane with frequency $\mu/2\pi$. It is shown in the first part of this report that the pressure on an oblique fixed and rigid plane only develops its final value (twice that in the incident pulse) at some distance from the leading edge where the pulse first strikes it. It would be difficult to take account of the finite mass of the plate as well as the distance from the leading edge; accordingly only the motion of the plate far from the leading edge will be considered. In this case the pressures in the incident and reflected pulses may be assumed in the forms

$$p_i = p_0 e^{-n \left(t - \frac{x \sin\theta}{c} - \frac{y \cos\theta}{c} \right)} \qquad (14)$$

$$p_r = p_0 \phi \left(t + \frac{x \sin\theta}{c} - \frac{y \cos\theta}{c} \right) \qquad (15)$$

where θ is the angle of incidence and y is measured parallel to the plate.

The pressure at $x = 0$ is therefore

$$p = p_0 \left\{ e^{-nt'} + \phi (t') \right\} \qquad (16)$$

where $t' = t - (y \cos\theta)/c$, (17)

The equation of continuity at the surface is now

$$p_0 \frac{\rho c}{2 \sin\theta} \dot{\xi} = e^{-nt'} - \phi (t') \qquad (18)$$

where ξ now represents $d\xi/dt'$.

With the above mentioned assumption that the plate has no stiffness in bending, the equation of motion is identical with (6) and the equation for ϕ assumes the form

$$\ddot{\phi} + \frac{\rho c}{m \sin\theta} \dot{\phi} + \mu^2 \phi = \left(n^2 + \frac{n \rho c}{m \sin\theta} + \mu^2 \right) e^{-nt'} \qquad (19)$$

which is identical with (7) except that $m \sin\theta$ is substituted for m and t' for t.

The .....

The expressions for p and ξ are

$$\frac{p}{p_0} = \frac{1}{n^2 - \frac{\rho c n}{m \sin\theta} + \mu^2} \left\{ - \frac{\rho c s_1 (s_2 + n)}{m \sin\theta (s_1 - s_2)} e^{s_1 t'} + \frac{\rho c s_2 (s_1 + n)}{m \sin\theta (s_1 - s_2)} e^{s_2 t'} + (n^2 + \mu^2) e^{-nt'} \right\} \qquad (20)$$

which is the same as (12) except that m sin θ is substituted for m, and

$$\xi = \frac{2 p_0 \sin\theta}{m \sin\theta (n^2 - \frac{\rho c n}{m \sin\theta} + \mu^2)} \left\{ e^{-nt'} + \frac{s_2 + n}{s_1 - s_2} e^{s_1 t'} - \frac{s_1 + n}{s_1 - s_2} e^{s_2 t'} \right\} \qquad (21)$$

which is similar to (13) except that m sin θ is substituted for m and a factor sin θ has appeared.

Numerical examples.

The pulse from a submarine explosion of 300 lb. of T.N.T. falls to half value in 0.3 milliseconds. This gives $n = 2.3 \times 10^3$ sec^{-1}. The motion which this pulse gives to a steel plate 0.25 inches (= 0.635 cm.) thick will first be calculated. Here m = 5.0 grammes per sq.cm. The velocity of sound in water is $c = 1.4 \times 10^5$ cm. per second. Taking $\rho = 1$, $\rho c/m = 2.8 \times 10^4$. In general μ is likely to be small compared with $\rho c/m$, even if, for instance, the plate is so rigidly supported that its period of vibration is 1/100th of a second, so that $\mu = 6.3 \times 10^2$, μ is only 1/45th of $\rho c/m$. In these circumstances the approximate solution of (9) is $s_1 = -\rho c/m$, $s_2 = -\mu^2 m/\rho c$. This gives for the $\frac{1}{4}$ inch plate

$$\frac{p}{p_0} = 2.19\, e^{-2.8 \times 10^4 t} - 0.012\, e^{-14t} - 0.18\, e^{-2.3 \times 10^{-7} t}$$

and

$$\frac{\xi}{p_0} = 0.677 \times 10^{-8} \left[0.082\, e^{-2.8 \times 10^4 t} + 0.918\, e^{-14t} - e^{-2.3 \times 10^3 t} \right]$$

If the same plate had been unsupported the motion would have been almost identical except that the terms $0.918\, e^{-14t}$ would be replaced by the constant 0.918. The displacement would have tended to a definite value of $0.667 \times 10^{-8}\, p_0\, (0.918)$.

The pressure-time curve for points on the surface of the $\frac{1}{4}$ inch plate is shown in Figure 5. Since p is proportional to p_0 values of p/p_0 depend only on t. The displacement of the plate is also shown in Figure 5, but in this case, though the displacement is also proportional to p_0, the result may be expressed more simply by assigning a definite value to p_0. The value chosen is 1 ton/square inch or 1.55×10^8 dynes/sq.cm. This corresponds with the pressure found at 50 feet from a submarine explosion of 300 lb. of T.N.T. The displacement-time curve for $\frac{1}{4}$ inch steel plate struck normally by this pressure wave is shown in Figure 5. It will be seen that the pressure vanishes and the maximum speed of 17 metres/second is attained after only 1/10th of a millisecond. At that time the displacement is only 1.3 millimetres. The pressure-time curve for the pulse is also shown in Figure 5. In Figure 5 the time-scale is chosen so that only one millisecond is covered in order that the form of the pressure-time curve may be visible. The plate goes on moving for a considerable time after the attainment of the maximum velocity. It will be seen later in fact that if the supporting structure exerted no restoring force the plate would come to a stop at a definite limiting displacement. The restoring force makes it return slowly to its original position. The displacement-time curves are shown in Figure 6 for plates $\frac{1}{4}$ inch and 1 inch thick, the restoring forces being such that in each case the plate would have a free period of 1/100th of a second when not in contact with the water. The $\frac{1}{4}$ inch plate reaches its maximum displacement of 0.96 cm. after two milliseconds, and after ten milliseconds it has only returned through 0.12 cm. to the value 0.84 cm. Figure 6 also shows the time-displacement curve for a plate 1 inch thick.

Approximate formula.

If the frequency of free vibration of the plate is small compared with the time constants n and $\rho c/m$, the formulae (20) and (21) can be written in approximate forms obtained by neglecting μ and writing $s_1 = -(\rho c)/(m \sin\theta)$, $s_2 = 0$

$\frac{p}{p_0}$.....

$$\frac{p}{p_0} = \frac{2}{\frac{\rho c}{m \sin\theta} - n} \left\{ \frac{\rho c}{m \sin\theta} e^{-\frac{\rho c t'}{m \sin\theta}} - n e^{-nt'} \right\}$$

$$\xi = \frac{2p_0}{mn \sin\theta \left[\frac{\rho c}{m \sin\theta} - n\right]} \left\{ 1 - \frac{mn \sin\theta}{\rho c} + \frac{mn \sin\theta}{\rho c} e^{-\frac{\rho c t'}{m \sin\theta}} - e^{-nt'} \right\}$$

Writing

$$\epsilon = \frac{\rho c}{mn \sin\theta} \tag{22}$$

these may be expressed in the simpler forms

$$\frac{p}{p_0} = \frac{2}{\epsilon - 1} \left(\epsilon e^{-n\epsilon t'} - e^{-nt'} \right) \tag{23}$$

$$\xi = \frac{2p_0}{mn^2 (\epsilon - 1) \epsilon} \left(\epsilon - 1 + e^{-n\epsilon t'} - \epsilon e^{-nt'} \right) \tag{24}$$

$$\dot{\xi} = \frac{2p_0}{mn (\epsilon - 1)} \left(e^{-nt'} - e^{-n\epsilon t'} \right) \tag{25}$$

The maximum velocity occurs when $p = 0$, i.e. when

$$nt' = \frac{1}{\epsilon - 1} \log_0 \epsilon, \tag{26}$$

and its value is

$$\dot{\xi}_{max} = \frac{2p_0}{mn} \epsilon^{-\frac{\epsilon}{\epsilon - 1}} \tag{27}$$

Some values of $\frac{\log_e \epsilon}{\epsilon - 1}$ are given in column 3 and of $\epsilon^{-\frac{\epsilon}{\epsilon - 1}}$ in column 4 in Table I.

Values of $\log_{10}\left[\frac{\log_e \epsilon}{\epsilon - 1}\right]$ and $\log_{10}\left[\epsilon^{-\frac{\epsilon}{\epsilon - 1}}\right]$ are shown as functions of $\log_{10} \epsilon$ in Figure 7. These curves can be used to find the maximum velocities with which a plate is projected at right angles to its plane by the pressure wave from a submarine explosion. A few examples of the use of these curves are shown in Table II. 300 lb. of T.N.T. gives a pressure wave which falls to half value in 0.3 milliseconds so that $n = 2.3 \times 10^3$ sec^{-1}. For plates of thickness $t = \frac{1}{8}$ inch, 1 inch, 3 inches and 6 inches, the values of $\rho c/mn$ are 12.1, 3.0, 1.0 and 0.5. These are the values of ϵ for these plates during normal incidence. Values of $\log_{10} \epsilon$ are given in column 2 and the values of $\log_{10} \epsilon^{\frac{\epsilon}{\epsilon - 1}}$ taken from Figure 7 in column 3. Values of $\epsilon^{-\frac{\epsilon}{\epsilon - 1}}$ are given in column 4.

At 50 feet from the explosion $p_0 = 1$ ton/square inch, so that

$$\frac{2p}{mn} = \frac{2 \times 1.54 \times 10^8}{m \times 2.3 \times 10^3} = \frac{1.34 \times 10^5}{m}$$

Values of $\dot{\xi}_{max} = \frac{2p_0}{mn} \epsilon^{-\frac{\epsilon}{\epsilon - 1}}$ are given in column 5 for normal incidence and in colume 9 for incidence $\theta = 10^0$. It will be seen that as the angle of incidence decreases the velocity with which the plate is thrown in the direction perpendicular to its surface decreases. This decrease, however, diminishes as the thickness of the plate increases. For extremely thick plates the steel would act as a perfect reflector and the pressure at its surface would be double that in the incident pulse, so that $\dot{\xi}_{max}$ would by independent of the angle of incidence. Values of t and $\dot{\xi}_{max}$ for normal incidence of plate at 50 feet from 300 lb. T.N.T. are also given in columns 6 and 7 of Table I.

Maximum displacement.

In the approximate formulae (23-25) the maximum displacement occurs when $\dot{\xi} = 0$, i.e. when t becomes very large. The maximum displacement is according to this formula, $2p_0/mn^2\epsilon$. With $\frac{1}{8}$ inch plate exposed normally at 50 feet from 300 lb. of T.N.T., $n = 2.3 \times 10^5$, $m = 5.0$ gms/sq.cm., $p_0 = 1$ ton/sq.inch $= 1.54 \times 10^6$ dynes/sq.cm., $\epsilon = 12.1$, this corresponds with a displacement of 0.99 cm. It might therefore be supposed that if a structure of which a $\frac{1}{8}$ inch plate forms an outer wall can be subjected to a sudden displacement of 0.99 cm. without injury it would necessarily be uninjured by the explosion of 300 lb. of T.N.T. at a distance of 50 feet. Such a deduction, though in agreement with the formulae so far developed, would probably not turn out to be justified in practice because the formulae assume that water can sustain tension as well as pressure. Referring to Figure 5 it will be seen that the positive pressure is maintained only for 1/10,000th of a second. During this time the plate acquires a velocity of about 17 metres/second, and moves through a distance of about 0.13 cm. The slowing down of the plate is due chiefly to the suction phase which, though far less intense than the pressure phase, continues for much longer. During the slowing down process the $\frac{1}{8}$ inch plate of Figure 6 suffers a further displacement of $0.958 - 0.13 = 0.83$ cm. The maximum suction in this case is 0.12 x (maximum pressure in the incident pulse) i.e. 0.12 tons/square inch or 269 lb./square inch or 18 atmospheres. It is this suction which in the foregoing theoretical treatment is responsible for the rapid deceleration of the plate. If the water is incapable of exerting suction the plate will leave the water as soon as the positive pressure vanishes. It is then moving at 17 metres/second and the distance it will move before being brought to rest depends on the nature of the structure which supports it. If, for instance, the supporting structure is elastic and is of such stiffness that the plate would execute $\mu/2\pi$ vibrations per second in the absence of the water (so that μ has the meaning assigned to it in equation (6)) the equation connecting displacement and velocity is

$$\xi^2 + \dot{\xi}^2/\mu^2 = A^2 \qquad (28)$$

where A is the amplitude of the vibration and is therefore the maximum displacement. If ξ_0 is the displacement when the plate leaves the water and $\dot{\xi}_0$ the velocity at this time

$$A^2 = \xi_0^2 + \dot{\xi}_0^2/\mu^2 \qquad (29)$$

If the frequency with which the $\frac{1}{8}$ inch plate vibrates owing to its own stiffness and that of its supports is 100 cycles per second, $\mu = 628$. Using $\xi_0 = 0.13$ cm., $\dot{\xi}_0 = 1700$ cm./sec., $A^2 = (.13)^2 + (2.7)^2$ so that $A = 2.7$ cm. In this case therefore the maximum displacement is nearly three times as great as it would be if the water had been assumed to be capable of exerting suction and 21 times as great as the displacement at the moment when it left the water. The displacement-time curve for the $\frac{1}{8}$ inch plate when it leaves the water on attaining maximum velocity is shown in Figure 6.

For this reason it is important to know what suction sea water will stand during the suction phase of a pulse and its reflection. Estimates based on the radius of the circle over which spray is thrown upwards when the pulse from a submarine explosion strikes the surface of the sea seem to show that water will stand a tension of about 200 or 300 lb./square inch for times of the order of 1 millisecond. It does not seem to be certain, however, whether this tension could be maintained at the surface between water and, say, paint or iron.

In connection with the formula (24) it seems worth while to give the expression for the displacement ξ_0 of a plate at the moment when the pressure changes to suction. In the case where the effect of the stiffness of the structure is neglected formula (24) gives

$$\xi_0 = \frac{2p_0}{mn^2\epsilon}\left\{1 - (\epsilon + 1)\,\epsilon^{-\frac{\epsilon}{\epsilon - 1}}\right\} \qquad (30)$$

In general this is small compared with the subsequent displacement whether the plate is assumed to leave the water or not. In the latter case, when water is assumed to be capable of exerting suction it will be seen that the ratio

$$\left[\frac{\text{Displacement when pressure changes to suction}}{\text{Maximum displacement when plate remains in contact with water}}\right] = \left[1 - (\epsilon + 1)\,\epsilon^{-\frac{\epsilon}{\epsilon - 1}}\right] \qquad (31)$$

Values of this ratio are given in column 8, Table 8, and are shown graphically in Figure 7. Its maximum value, 0.262, occurs when $\epsilon = 1$.

Damage .....

Damage to structure supporting the plate

Though the damage which the water pulse will do depends on the strength of the supporting structure, so that the actual amount of damage cannot be calculated, the foregoing analysis shows that for a given amount of damage the relationship between charge and distance can be determined. This will depend on whether (a) the plate remains in contact with the water or (b) it breaks contact.

(a) *The water remains in contact with the plate.*

In this case the plate is moved through a distance ξ_{max} and is brought to rest by the suction of the water. The true value of ξ_{max} will depend to a small extent on the stiffness of the structure but this effect will always be small compared with the effect of water suction in a structure of the type used in ship construction. In assessing the damage expected according to (a) it is necessary to compare the charges which will produce a given value of ξ_{max}. From (24) it will be seen that $\xi_{max} = \frac{2p_0}{mn^2\epsilon}$, or, inserting ϵ from (22),

$$\xi_{max} = \frac{2p_0 \sin\theta}{n\rho c} \tag{32}$$

For a given amount of destruction therefore a constant value of $p_0 \sin\theta/n$ is necessary. The maximum pressure at distance r from a submarine explosion of a mass M of explosive is $p_0 = AM^{1/3}/r$ where A is a constant depending on the composition of the explosive and a number of other factors which can be regarded as constant when the relationship between charge-weight and distance for a given amount of damage is being considered. The time constant n is proportional to $M^{-1/3}$ so that $n = BM^{-1/3}$; thus for a given amount of destruction according to hypothesis (a)

$$\left.\begin{aligned} &\left(\frac{M^{1/3}\sin\theta}{r}\right) M^{1/3} = \text{constant} \\ &\text{or } r \text{ is proportional to } M^{2/3}\sin\theta \\ &\text{and for normal incidence } r \text{ is proportional to } M^{2/3} \end{aligned}\right\} \tag{33}$$

(b) *The water breaks contact with the plate when the pressure ceases to be positive.*

In this case the plate is discharged from the water with velocity ξ_{max} where ξ_{max} is given by (27). In this case inserting the expressions $p_0 = AM^{1/3}/r$, $n = BM^{-1/3}$ in (27)

$$\xi_{max} = \frac{2A}{mB}\,\frac{M^{2/3}}{r}\,e^{-\frac{\epsilon}{\epsilon-1}} \tag{34}$$

To find how r varies with M the case of normal incidence may be considered. In that case $\epsilon = \rho c/mn$. For a given thickness of plate therefore ϵ is proportional to $M^{1/3}$. Though (34) shows that for a given amount of destruction r is not related to M by any simple power law, yet for practical purposes it may be convenient to find the power law which most nearly represents (34) over a limited range. Assuming this to be

$$r = (\text{constant})\, M^S \tag{35}$$

the value of S may be determined by logarithmic differentiation of (35) and (34), thus

$$\frac{dr}{r} = \frac{S\,dM}{M} \tag{36}$$

and

$$\frac{dr}{r} = \frac{2}{3}\,\frac{dM}{M} - \left(2\frac{\epsilon}{\epsilon-1}\right)\left(1 - \frac{\log_e \epsilon}{\epsilon-1}\right)\frac{d\epsilon}{\epsilon} \tag{37}$$

and since ϵ is proportional to $M^{1/3}$, $d\epsilon/\epsilon = \frac{1}{3}(dM/M)$. Hence comparing (36) and (37)

$$S = \frac{2}{3} - \frac{1}{3}\left(\frac{\epsilon}{\epsilon-1}\right)\left(1 - \frac{\log_e \epsilon}{\epsilon-1}\right) \tag{38}$$

Values .....

Values of S calculated from (38) are given in column 9, Table 1. It will be seen that S varies from $\frac{1}{3}$ for large values of ϵ (i.e. thin plates) to $\frac{2}{3}$ for small values of ϵ (i.e. thick plates). For the explosion pulse from 300 lb. of T.N.T. for instance ϵ varies from 12 to 0.5 as the plate thickness increases from 0.25 to 6.0 inches. The value of S varies from 0.38 to 0.54 in this range. With a charge of 2400 lb. of T.N.T. ϵ varies from 24 to 1.0 as the plate thickness varies from 0.25 to 6.0 inches. In this range S varies from 0.37 to 0.50. If, therefore the question "what is the relationship between charge-weight and distance necessary to produce a given amount to the structure of a ship" had been put in the form "what is the best exponent S to choose in an assumed power law of the form

$$\text{(radius of destruction) proportional to (charge-weight)}^{S} \qquad (39)$$

when the charge varies between 300 and 2400 lb. and the plate between 0.25 and 6.0 inches in thickness?" the answer given by the foregoing analysis would be that S varies between 0.37 and 0.54, the mean value being 0.46.

Comparing (a) and (b) it will be noticed that if this exponent is determined experimentally a value near 0.66 might indicate that the water remains in contact with the plate, whereas a value near 0.46 would indicate that the plate separates from the water.

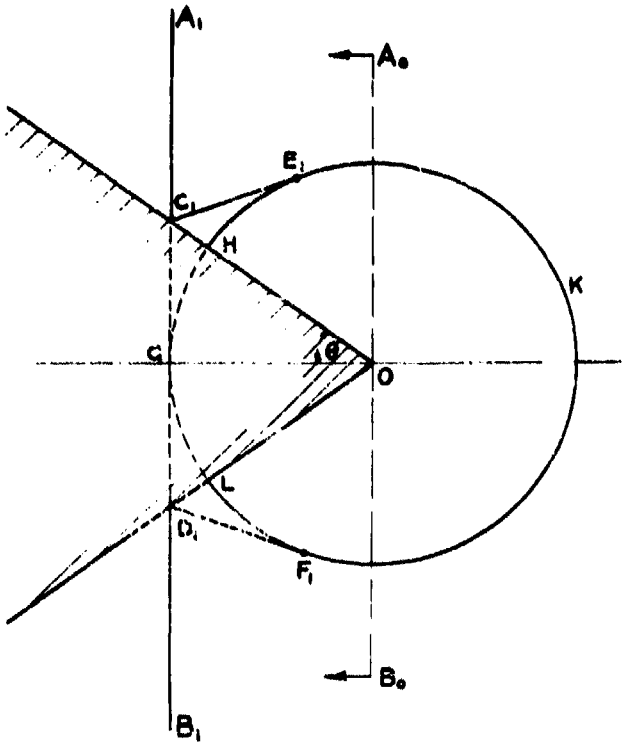


Fig. 1.

FRONTS OF { incident wave (A, C and B, D).
reflected wave (C, E, and D, F).
refracted wave (arc HE, KF, L) }

FIG. 2. Pressure time curve when square-topped pulse of duration τ reaches distance r from the vertex of a 90° wedge.
(a) $r = 0.5c\tau$, (b) $r = 4.0c\tau$, (c) $r = 10.0c\tau$

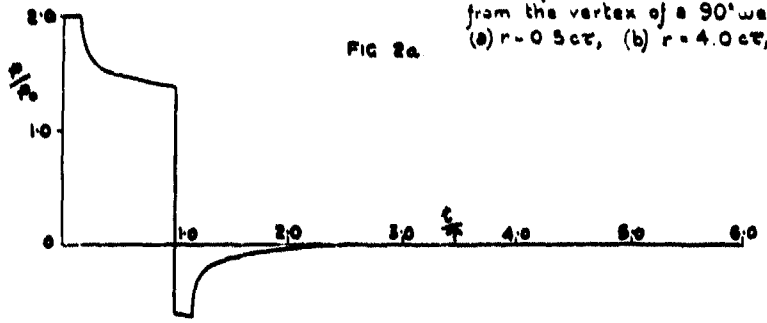


FIG. 2a.

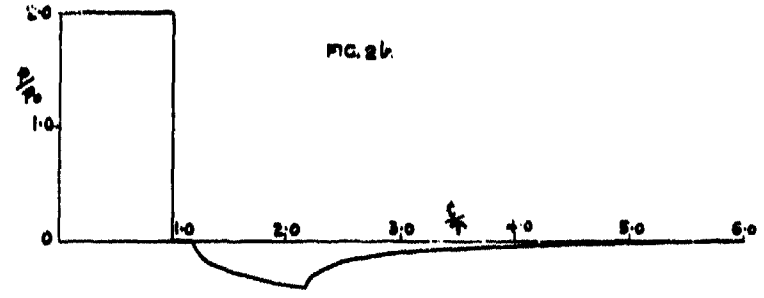


FIG. 2b.

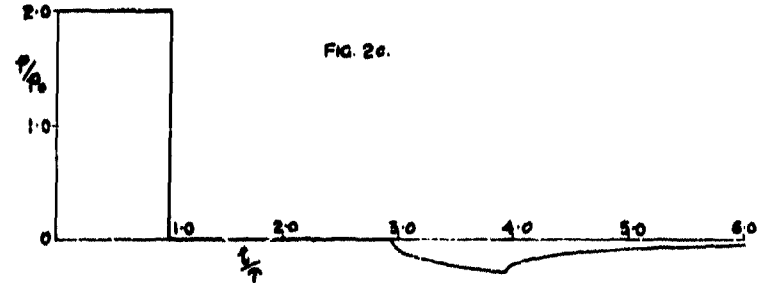
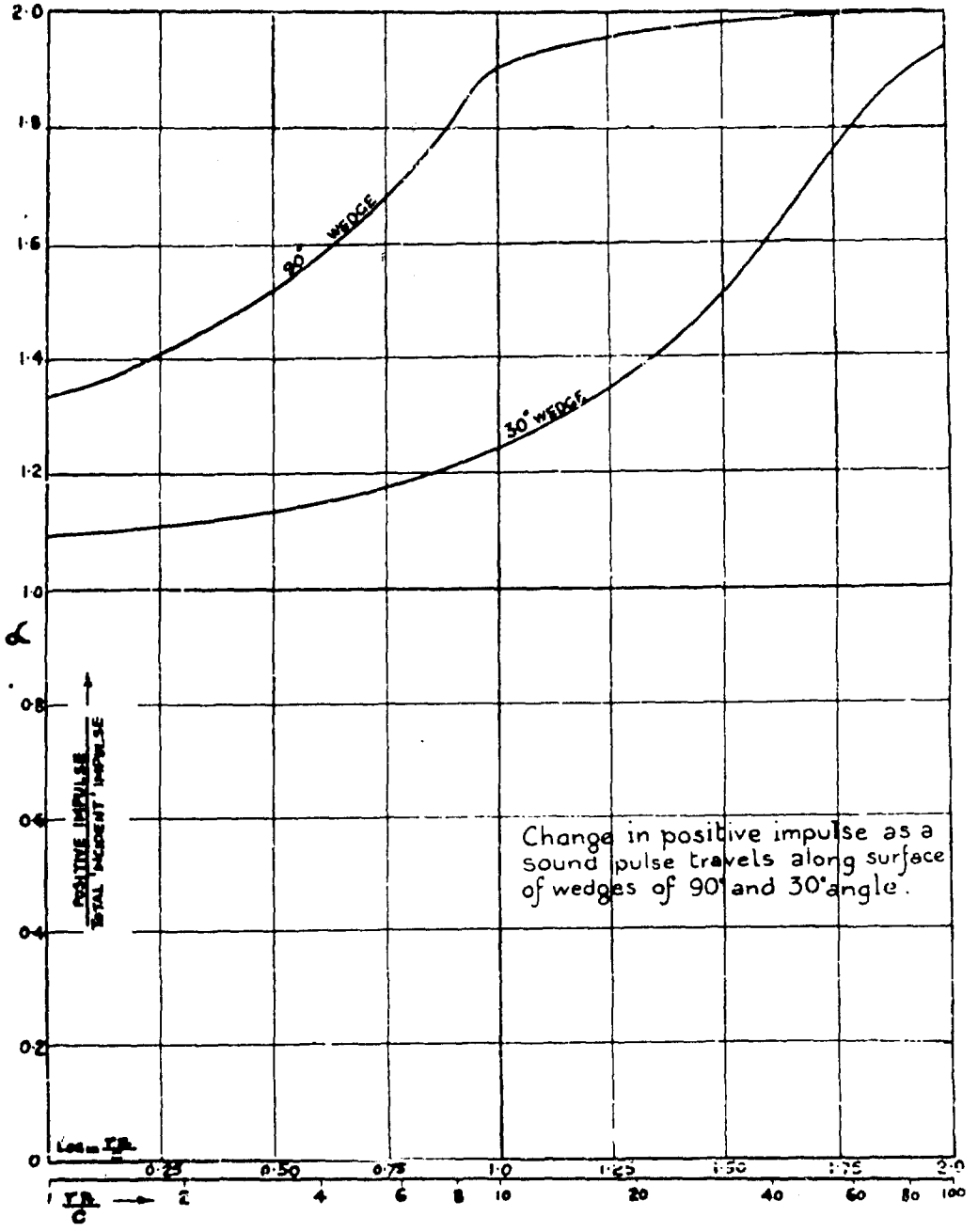


FIG. 2c.

FIG: 3


2·0
1·8
1·6
1·4
1·2
1·0
0·8
0·6
0·4
0·2
0
90° WEDGE
30° WEDGE
POSITIVE IMPULSE / TOTAL INCIDENT IMPULSE
0·25
0·50
0·75
1·0
1·25
1·50
1·75
2·0
2
4
6
8
10
20
40
60
80
100
Change in positive impulse as a sound pulse travels along surface of wedges of 90° and 30° angle.

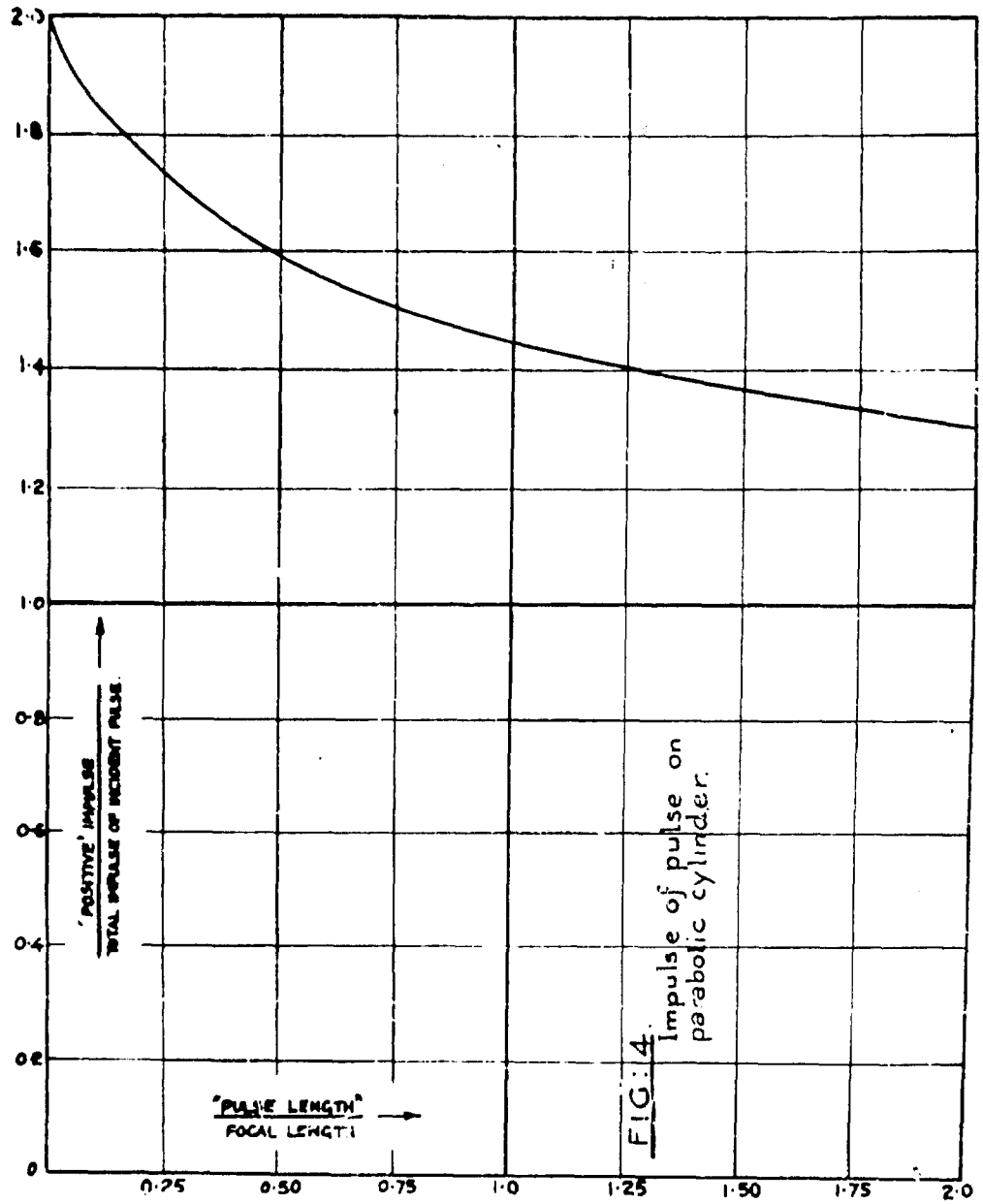


FIG: 4.
Impulse of pulse on parabolic cylinder.

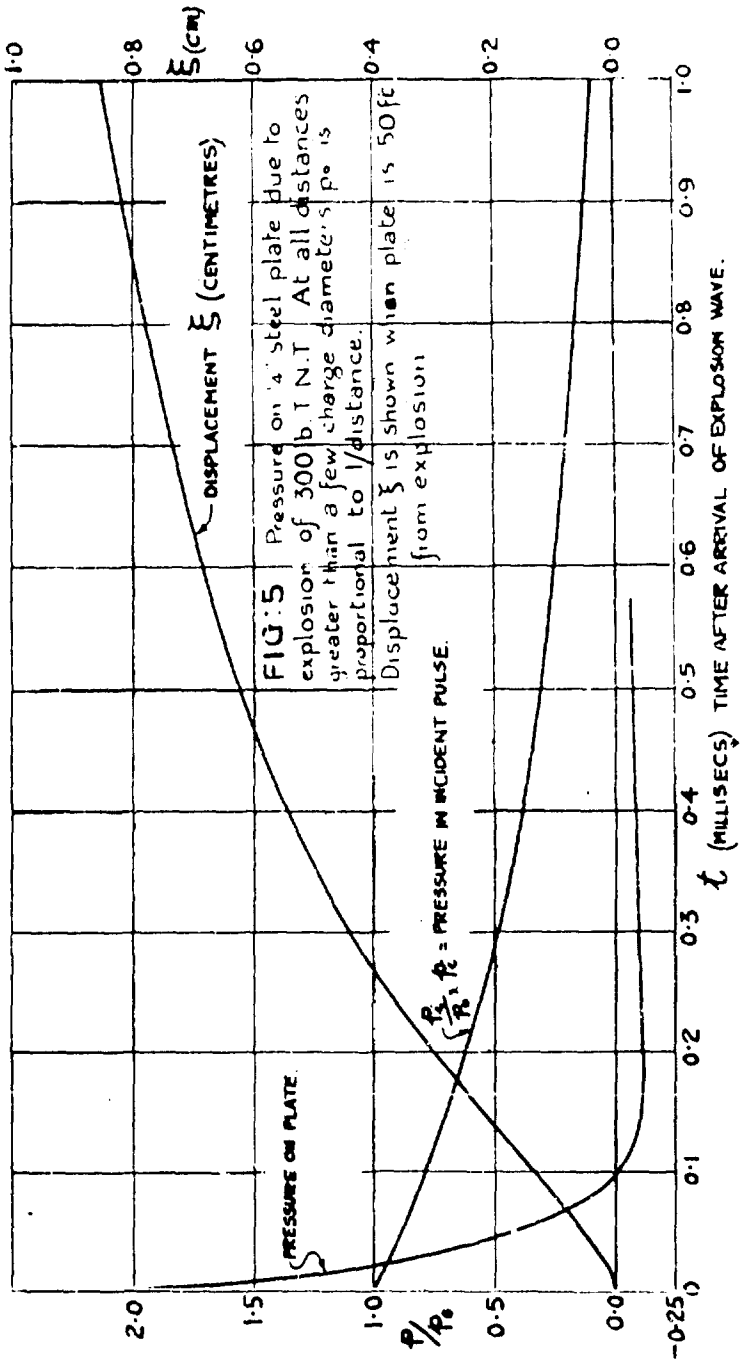


FIG:5 Pressure on 4" steel plate due to explosion of 300lb T N.T At all distances greater than a few charge diameters p0 is proportional to 1/distance.
Displacement ξ is shown when plate is 50ft from explosion

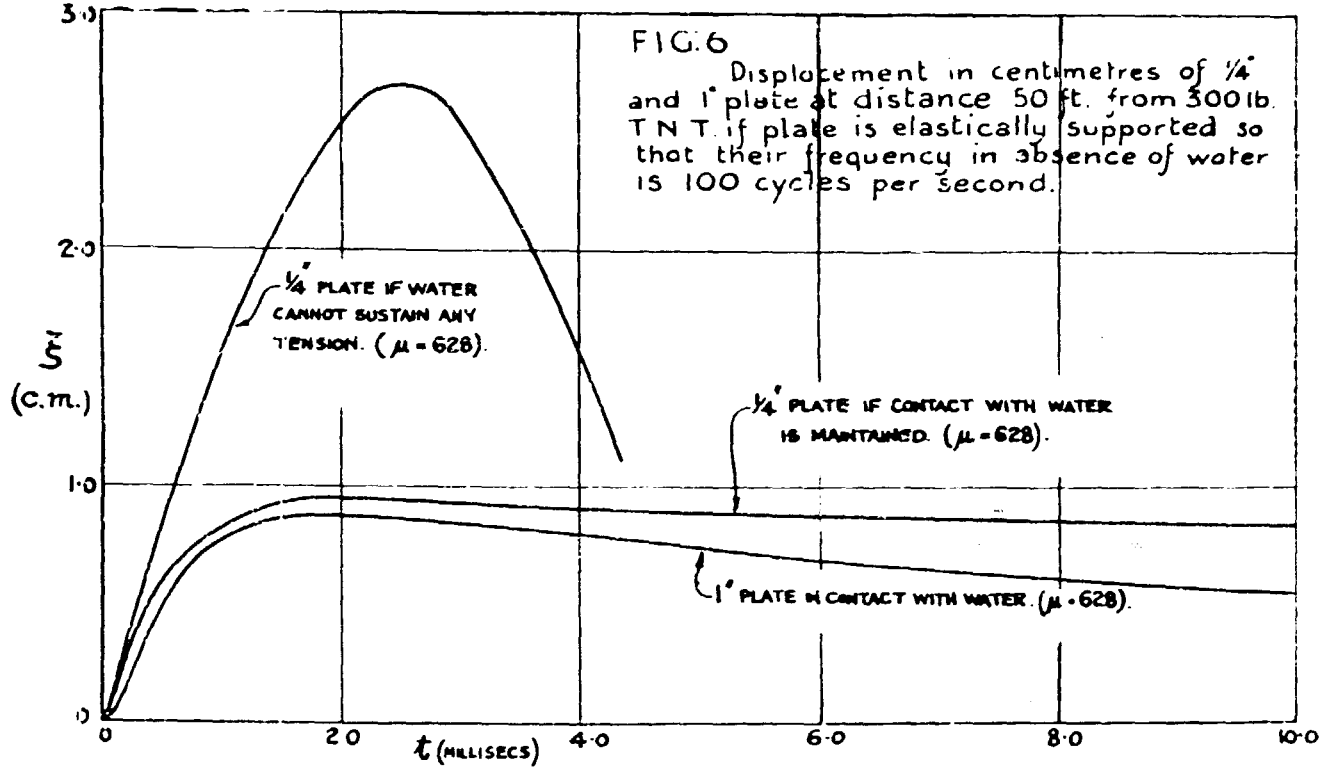


FIG. 6

Displacement in centimetres of ¼" and 1" plate at distance 50 ft. from 300 lb. T N T. if plate is elastically supported so that their frequency in absence of water is 100 cycles per second.

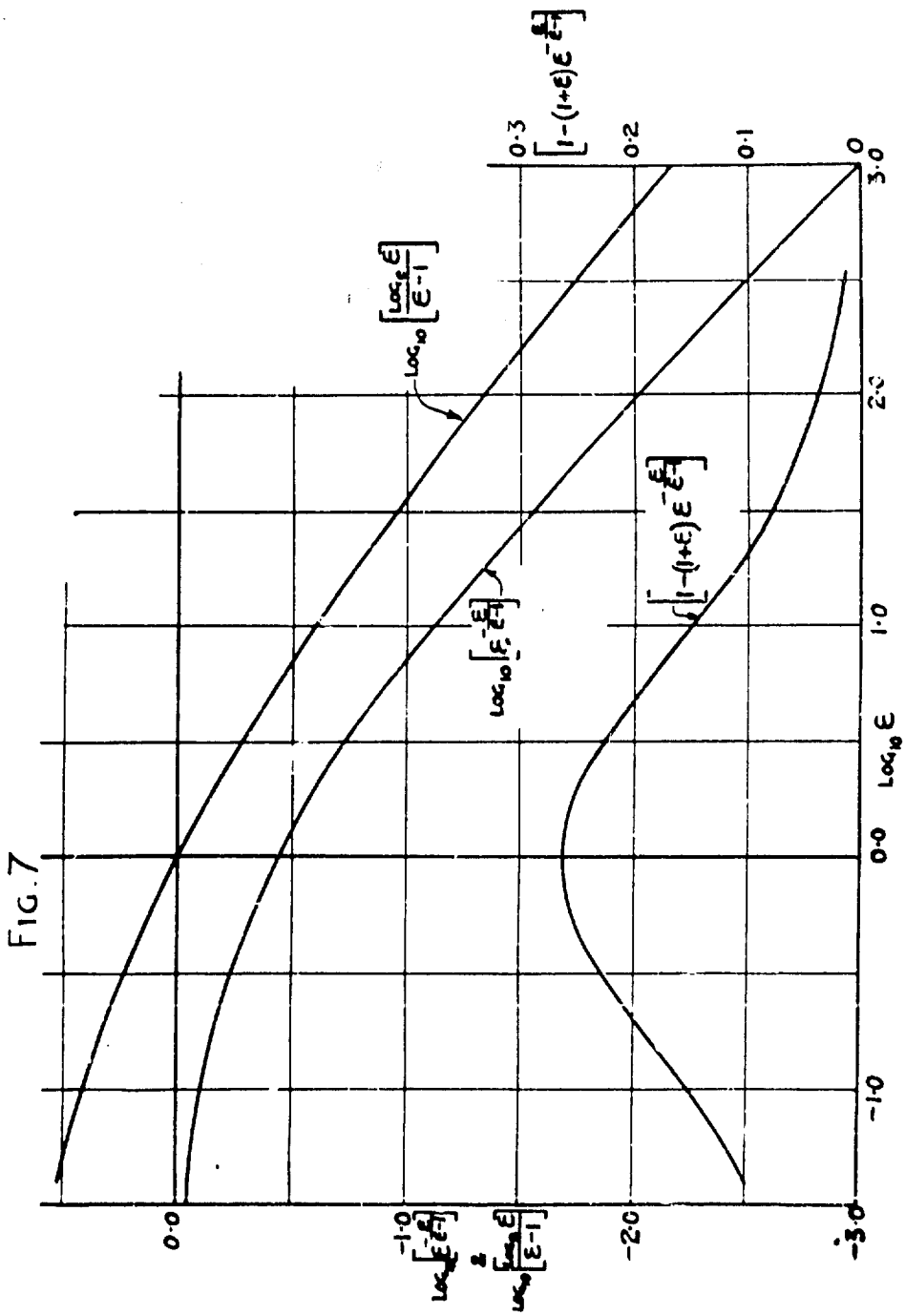

$\log_{10}\left[\frac{\log_e \varepsilon}{\varepsilon-1}\right]$
$\log_{10}\left[\frac{\varepsilon-1}{\varepsilon+1}\right]$
$\log_{10}\left[1-(1+\varepsilon)\varepsilon^{-\frac{\varepsilon}{\varepsilon+1}}\right]$
$\log_{10}\left[1-(1+\varepsilon)\varepsilon^{-\frac{\varepsilon}{\varepsilon+1}}\right]$
0·0
-1·0
-2·0
-3·0
0·3
0·2
0·1
0
3·0
2·0
1·0
0·0
-1·0
$\log_{10}\varepsilon$

FIG. 7

TABLE I.

1	2	3	4	5	6(a)	7(b)	8	9(c)
ε	$\log_{10}\varepsilon$	$\frac{\log_e \varepsilon}{\varepsilon - 1}$	$\varepsilon^{-\frac{\varepsilon}{\varepsilon-1}}$	$\log_{10} \varepsilon^{-\frac{\varepsilon}{\varepsilon-1}}$	t (inches)	$\frac{\dot{\xi}_{max}}{\text{cm. per sec.} \times 10^{-3}}$.	$1 - (\varepsilon+1)\varepsilon^{-\frac{\varepsilon}{\varepsilon-1}}$	S
1000	3.0	0.00692	0.0010	$\bar{3}.0$	0.0031	2.22	0	0.335
100	2.0	0.0465	0.0095	$\bar{2}.978$	0.031	2.11	0.040	0.346
50	1.6990	0.0799	0.0185	$\bar{2}.267$	0.06	2.05	0.059	0.354
20	1.3010	0.1577	0.0426	$\bar{2}.629$	0.15	1.89	0.106	0.372
10	1.0	0.256	0.0774	$\bar{2}.889$	0.31	1.72	0.149	0.384
5	0.6990	0.402	0.134	$\bar{2}.127$	0.62	1.49	0.198	0.417
4	0.6021	0.462	0.158	$\bar{1}.199$	0.76	1.4	0.210	0.427
3	0.4771	0.549	0.195	$\bar{1}.294$	1.02	1.31	0.225	0.441
2.5	0.3979	0.611	0.217	$\bar{1}.336$	1.22	1.20	0.240	0.451
2	0.3010	0.693	0.250	$\bar{1}.398$	1.53	1.11	0.250	0.462
1.5	0.1761	0.811	0.297	$\bar{1}.473$	2.04	0.985	0.258	0.478
1.0	0	1.000	0.369	$\bar{1}.567$	3.06	0.818	0.262	0.500
0.5	$\bar{1}.690$	1.385	0.500	$\bar{1}.699$	6.12	0.554	0.250	0.538
0.2	$\bar{1}.3010$	2.013	0.668	$\bar{1}.823$	15.3	0.296	0.200	0.582
0.1	$\bar{1}.0$	2.556	0.774	$\bar{1}.889$	30.6	0.172	0.150	0.612
0.04	$\bar{2}.602$	3.355	0.875	$\bar{1}.942$	76.5	0.088	0.100	0.631
0	$-\infty$	∞	1.0	0	∞	0	0	0.667

NOTES:

(a) Figures in col.6 refer to thickness of plate for ε as in col.1 when $n = 2.3 \times 10^{3}$ and $\theta = 90^{\circ}$.

(b) Figures in col.7 refer to maximum velocity of steel plate when $p_o = 1$ ton/sq.in., $\theta = 90^{\circ}$ and $n = 2.3 \times 10^{3}$.

(c) $S = \frac{2}{3} - \frac{1}{3}\left(\frac{\varepsilon}{\varepsilon - 1}\right)\left(1 - \frac{\log_e \varepsilon}{\varepsilon - 1}\right)$

TABLE II.

	Normal incidence $\theta = 90^\circ$				$\theta = 10^\circ$			
1	2	3	4	5	6	7	8	9
t (inches)	$\log_{10}\mathcal{E}$	$\log_{10}\mathcal{E}^{-\frac{\mathcal{E}}{\mathcal{E}-1}}$	$\mathcal{E}^{-\frac{\mathcal{E}}{\mathcal{E}-1}}$	$\dot{\varepsilon}_{max}$ metres/sec	$\log_{10}\mathcal{E}$	$\log_{10}\mathcal{E}^{-\frac{\mathcal{E}}{\mathcal{E}-1}}$	$\mathcal{E}^{-\frac{\mathcal{E}}{\mathcal{E}-1}}$	$\dot{\varepsilon}_{max}$ metres/sec
0.25	1.083	$\bar{2}.81$	0.064	17.2	1.843	$\bar{2}.13$	0.013	3.5
1.0	0.477	$\bar{1}.30$	0.200	13.4	1.237	$\bar{2}.67$	0.047	3.1
3.0	0.0	$\bar{1}.50$	0.363	8.1	0.760	$\bar{1}.08$	0.120	2.7
6.0	$\bar{1}.699$	$\bar{1}.70$	0.50	5.0	0.459	$\bar{1}.24$	0.174	1.9
30.0	$\bar{1}.000$	0.90	0.79	1.8	$\bar{1}.769$	$\bar{1}.65$	0.447	1.0

THE REFLECTION OF A SPHERICAL WAVE FROM AN INFINITE PLATE

E. N. Fox
Admiralty Index Works, Rosyth, Scotland

British Contribution

1942

THE REFLECTION OF A SPHERICAL WAVE FROM AN INFINITE PLATE

E. N. Fox

1942

* * * * * * * *

Introduction.

Consider a spherical wave propagated from centre A in a medium of density ρ with wave-velocity C. The medium is bounded by an infinite plate POQ distance a from A. The wave is assumed to be of sufficiently small amplitude for the ordinary sound-wave equations to hold while the plate is assumed to move normal to itself and to offer purely inertia resistance to such motion.

In the report "The pressure and impulse of submarine explosion waves on plates", hereafter called Report A, G.I. Taylor considered a similar plane wave problem with the more general boundary condition in which the plate offers also an elastic resistance to motion normal to itself. Since the frequency of vibration is usually relatively small in practice, Taylor gives approximate formulae which correspond to the exact solution for purely inertia resistance. The present problem is thus the spherical wave analogue of the plane wave problem whose solution is given by equations (22) to (27) of Report A.

General Solution.

If A' be the image of A in the plane POQ then the problem is one of axial symmetry about AA' and we shall use cylindrical co-ordinates x, r, with origin O and denote by R and R' the distancesof any point from A and A respectively. The zero of time t will be taken to correspond with the front of the incident wave leaving A and we are concerned only with the region $x \leq o$.

The pressure p satisfies the usual wave equation

$$\nabla^2 p = \frac{1}{c^2} \frac{\partial^2 p}{\partial t^2} \qquad (1)$$

while the incident wave from A is taken to be

$$p = \frac{f(ct - R)}{R} \qquad (2)$$

The boundary equation at the plate is

$$m \frac{dv}{dt} = p \qquad x = o \qquad (3)$$

where m is the mass of the plate per unit area and v is its velocity assumed normal to itself.

Now in terms of the velocity-potential ϕ we have

$$\left.\begin{aligned} v &= \frac{\partial \phi}{\partial x} \\ p &= -\rho \frac{\partial \phi}{\partial t} \end{aligned}\right\} \qquad (4)$$

and .....

and thus from (3) and (4) the boundary condition may be written in the form

$$\frac{1}{\beta}\frac{\partial p}{\partial x} + p = 0 \qquad x = 0 \tag{5}$$

where

$$\beta = \frac{\varrho}{m} \tag{6}$$

In order to solve the equation (1), (2) and (5) let us introduce a pressure p' defined by

$$p' = \frac{1}{\beta}\frac{\partial p}{\partial x} + p \tag{7}$$

then p' satisfies the wave equation, vanishes at x = o and contains the incident wave terms

$$p' = \frac{1}{\beta}\frac{\partial}{\partial x}\left\{\frac{f(ct - R)}{R}\right\} + \frac{f(ct - R)}{R} \tag{8}$$

The problem for p' is thus that of a wave source and doublet at A with a free surface at x = o. Hence by the addition of terms corresponding to a virtual source and doublet of appropriate signs a. the image point A' the solution for p' is

$$p' = \frac{1}{\beta}\frac{\partial}{\partial x}\left[\frac{f(ct - R)}{R}\right] + \frac{f(ct - R)}{R} + \frac{1}{\beta}\frac{\partial}{\partial x}\left[\frac{f(ct - R')}{R'}\right] - \frac{f(ct - R')}{R'} \tag{9}$$

From (7) and (9) we have

$$\frac{\partial p}{\partial x} + \beta p = \left(\frac{\partial}{\partial x} + \beta\right)\left[\frac{f(ct - R)}{R} + \frac{f(ct - R')}{R'}\right] - 2\beta\frac{f(ct - R')}{R'} \tag{10}$$

and the solution for p is obtained in the form

$$p = \frac{f(ct - R)}{R} + \frac{f(ct - R')}{R'} - 2\beta\int_{x_0}^{x}\frac{e^{-\beta(x-\lambda)}\, f(ct - R_2)\, d\lambda}{R_2} \qquad \left.\begin{array}{r} o \geq x \geq x_0 \\ ct \geq R' \geqslant R \end{array}\right\} \tag{11}$$

where

$$\left.\begin{aligned} R^2 &= r^2 + (x + a)^2 \\ R'^2 &= r^2 + (x - a)^2 \\ R_2^2 &= r^2 + (\lambda - a)^2 \\ x_0 &= a - \sqrt{c^2t^2 - r^2} \end{aligned}\right\} \tag{12}$$

It can be verified by direct substitution in (1) and (5) that (11) satisfied both these equations. For ct < R' the solution for p is of course given solely by the incident wave (2).

By .....

By change of integration variable to R_2 equation (11) can be written in the form

$$p = \frac{f(ct - R)}{R} + \frac{f(ct - R')}{R'} - \alpha\beta e^{-\beta(x-a)} \int_{R'}^{ct} \frac{e^{-\beta\sqrt{R_2^2 - r^2}} f(ct - R_2)\, dR_2}{\sqrt{R_2^2 - r^2}}$$

$$o \geq x \geq x_o \qquad (13)$$

$$ct \geq R' \geq R$$

The solution for the velocity potential ϕ is given simply by substituting $-f_1/\rho c$ for f in (13) where f_1 is defined by

$$f_1(\theta) = \int_o^\theta f(\theta)\, d\theta \qquad (14)$$

Application to underwater explosion wave.

For an underwater explosion wave we assume as in Report A that the incident wave has the form

$$f(ct - R) = p_o R_o e^{-n\left(t - \frac{R}{c}\right)} \qquad (15)$$

where p_o is the maximum pressure in the incident wave at distance R_o from the explosion. We shall consider only the pressure and velocity at the plate since this is the item of major practical importance.

Now from (13) and (15) we have at $x = o$,

$$\frac{p}{2p_o} = e^{-n\left(t - \frac{R_o}{c}\right)} - \beta R_o e^{-nt} + \beta a \int_{R_o}^{ct} \frac{e^{-\beta\sqrt{R_2^2 - r^2} + nR_2/c}\, dR_2}{\sqrt{R_2^2 - r^2}}$$

$$x = o, \quad t \geq \frac{R_o}{c}. \qquad (16)$$

where R_o is the distance of a point P of the plate from the explosion centre and is given by

$$R_o^2 = r^2 + a^2 \qquad (17)$$

The velocity v communicated to the plate is from (3) and (4) given by

$$mv = \int p\, dt = -\rho\phi \qquad (18)$$

and $-\rho c \phi$ is obtained by putting f_1 for f where from (14) and (15)

$$f_1(ct - R) = \frac{p_o R_o c}{n}\left\{1 - e^{-n\left(t - \frac{R}{c}\right)}\right\} \qquad (19)$$

Hence $-n\rho\phi + p$ is equal to the pressure when the incident wave is of constant pressure $p_o R_o$, i.e. when $n = o$ in (16). Hence

$$\frac{mv + p}{2p_o} \ldots\ldots$$

$$\frac{mv + \rho}{2\rho_0} = 1 - \beta\epsilon_c e^{\beta\epsilon} \int_{R_0}^{ct} \frac{e^{-\beta\sqrt{R_2^2 - r^2}}}{\sqrt{R_2^2 - r^2}} \, dR_2$$

$$x = 0, \quad t \geq R_0/C \tag{20}$$

The integrals in (16) and (20) cannot be integrated in terms of known tabulated functions and can at best be expressed in terms of an indefinite integral involving also a parameter. Numerical evalution of this integral for all possible combinations of upper limit and parameter would be extremely laborious and it is thus desirable to consider what approximations are possible.

Let us put

$$\left.\begin{aligned} t &= t' + R_0/C \\ R_2 &= R_0 + c \\ \epsilon &= \frac{\beta R_0 c}{n a} = \frac{\rho R_0 c}{m n a} \end{aligned}\right\} \quad \begin{aligned} ct &\geq R_2 \geq R_0 \\ t' &\geq \zeta \geq 0 \end{aligned} \tag{21}$$

so that t' is the time after arrival of the incident wave at a point P of the plate and ϵ is a non-dimensional quantity defined by the same equation as in Report A.

Now when t' and therefore ζ is small,

$$\sqrt{R_2^2 - r^2} = \sqrt{a^2 + 2R_0 c\zeta + c^2\zeta^2} = a + \frac{R_0 c\zeta}{a} + O\left[\frac{r^2c^2\zeta^2}{a^3}\right] \tag{22}$$

and thus if

$$\frac{R_0 ct'}{a^2} \text{ and } \frac{\beta r^2 c^2 t'^2}{a^3} \text{ are small} \tag{23}$$

and we neglect terms of these orders in (16) we obtain

$$\frac{p}{2\rho_0} = e^{-nt'} - \frac{\beta c R_0}{a} e^{-nt'} \int_0^{t'} e^{-\left(\frac{\beta R_0 c}{a} - n\right)\zeta} \, d\zeta \tag{24}$$

whence after integration

$$\frac{p}{2\rho_0} = \frac{1}{\epsilon - 1}\left(\epsilon e^{-n\epsilon t'} - e^{-nt'}\right), \qquad \begin{aligned} x &= 0 \\ t' &\geq 0 \end{aligned} \tag{25}$$

which is identical with equation (23) of Report A. The approximate expression for v will similarly agree with equation (25) of Report A.

Thus the solution given in Report A for an incident plane wave will hold as a good approximation for an incident spherical wave provided t' is small enough to satisfy the conditions (23) above.

It is of especial interest to consider whether these conditions hold up to the time when p changes from positive to negative since if so the solution and conclusions of Report A for the case where the plate leaves the water will hold with sufficient accuracy for the spherical wave case.

Now the time at which the water leaves the plate for an incident plane wave is from equation (26) of Report A given by

$$nt' = \frac{\log \epsilon}{\epsilon - 1} \tag{26}$$

and ....

and the corresponding velocity communicated to the plate is from equation (27) of Report A given by

$$v_m = \frac{2\rho_0}{mn} \epsilon^{-\frac{\epsilon}{\epsilon-1}} \qquad (27)$$

The above equations (26) and (27) will hold as a good approximation for the present case of a spherical wave provided (26) satisfies the conditions (23), i.e. provided

$$\frac{R_0 c}{n a^2} \frac{\text{Log } \epsilon}{\epsilon - 1} \text{ and } \frac{\beta r^2 c^2}{n^2 a^3} \left(\frac{\text{Log } \epsilon}{\epsilon - 1} \right)^2 \text{ are small}$$

and these conditions can be written in the form

$$\frac{1}{\beta a} \frac{\epsilon \text{ Log } \epsilon}{\epsilon - 1} \text{ and } \frac{r^2}{\beta a R_0^2} \left(\frac{\epsilon \log \epsilon}{\epsilon - 1} \right)^2 \text{ are small} \qquad (28)$$

Now in practice (see Appendix I) βa will be large and thus unless ϵ is large conditions (28) will hold and therefore equations (26) and (27) as in Report A.

Since ϵ can be large in practice, especially for small angles of incidence, an approximation to cover this case is obtained in the Appendix where it is shown that under the conditions βa and ϵ large, while $1 - \frac{c}{n} R_0$ of order unity, then, correct to fractional errors of order $\frac{1}{\epsilon}$ and $\frac{1}{\beta a}$, equation (16) becomes

$$\frac{\rho}{2\rho_0} = \frac{R_0}{ct} e^{-\beta \sqrt{c^2 t^2 - r^2 - a)}} - \frac{1}{\epsilon} \left(1 - \frac{c}{n R_0}\right) e^{-nt'} \qquad (29)$$

and ρ vanishes when

$$\left.\begin{aligned} nt' &= \frac{\text{Log } \alpha_1}{\epsilon} + \frac{1}{2} \frac{(\text{Log } \alpha_1)^2}{\beta a \epsilon} \\ \text{where } \alpha_1 &= \frac{\epsilon}{\left(1 - \frac{c}{n R_0}\right)} \end{aligned}\right\} \qquad (30)$$

The velocity given to the plate if it leaves the water is still given, however, by equation (27) correct to fractional errors of the first order.

Thus although when ϵ is large the conditions (23) do not hold up to the time when the plate leaves the water yet equation (27) is still a good approximation for the velocity given to the plate. The apparent anomaly is due of course to the fact that when ϵ is large the pressure on the plate decreases very rapidly at first so that practically the whole of the velocity given to the plate is communicated in the very early stages during which the conditions (23) are valid.

Now, as shown in the Appendix, the conditions (i) βa large and, (ii) $1 - \frac{c}{n} R_0$ positive of order unity, will usually hold in practice at distances from the explosion at which the explosion wave can be regarded as of small amplitude. We thus have finally that the velocity communicated by an underwater spherical wave to the plate if it leaves the water is given approximately, whether ϵ be large or not, by the same expression (27) as that obtained in Report A for an incident plane wave.

Summary.

A general solution is given for the problem of a spherical wave of small amplitude incident on an infinite plate which moves normally to itself and offers a purely inertia resistance to such motion.

The case of an underwater explosion wave is specifically considered and approximate formulae are obtained which will usually hold in practice at distances from the explosion for which the explosion wave may be expected to behave as one of small amplitude. It is shown in particular that

If no .....

if no tension can be sustained between plate and water so that the plate leaves the water when the pressure tends to become negative, then the velocity communicated to the plate is given to a good approximation by the same expression (27) as derived in Report A for an incident plane wave. It follows that the conclusions given by Taylor in Report A for the damage law to be expected if the plate leaves the water still hold when allowance is made for the spherical nature of an explosion wave.

Best Available Copy

APPENDIX

I. *Numerical values for underwater explosion waves.*

Let

p_o = maximum pressure in explosion wave, tons/square inch.

A = total impulse in explosion wave, lb.seconds/square inch.

W = weight of charge, lbs.

D = distance from charge, feet.

C = velocity of explosion wave, feet/second.

h = plate thickness (inches)

Then for distances at which $p_o \leq 2$ tons/square inch the following empirical relations have been established for T.N.T., amatol and guncotton.

$$p_o = \frac{7\,W^{1/3}}{D} \text{ tons/square inch} \qquad (31)$$

$$A = \frac{1.90\,W^{2/3}}{D} \text{ lb.second/square inch}$$

Since the experimental curve is not exactly of the exponential form assumed theoretically the value to be assigned to n will vary to a small extent according to the criteria used in fitting an exponential to the experimental curve. Since we are concerned here only with the order of quantities involving n it will be sufficient to take the simple criteria that theoretical and experimental curves have the same p_o and A. Then since $n = p_o/A$ for the theoretical curve, the same will hold for the experimental n remembering that p_o and A must be expressed in the same units. On this basis the empirical formulae (31) give

$$\frac{1}{n} = \frac{W^{1/3}}{8250} \text{ seconds} \qquad (32)$$

whence taking c = 4900 feet/second for a small amplitude wave we have

$$\frac{c}{n} = \frac{W^{1/3}}{1.68} \text{ feet} \qquad (33)$$

In order to decide on a reasonable value for the distance, D_o say, beyond which the explosion wave may be regarded as of small amplitude we note that the empirical relations (31) agree with the inverse distance law valid for a small amplitude wave. Since these relations have been established for $p_o \leq 2$ tons/square inch this suggests that D_o be taken as the distance for which $p_o = 2$ tons/square inch.

On this basis

$$D_o = 3.5\,W^{1/3} \text{ feet} \qquad (34)$$

For a spherical charge this value of D_o corresponds to about 13 charge diameters and for a charge of 390 lb. T.N.T. gives $D_o = 25.6$ feet = 780 cm. For this latter charge Penney has calculated the theoretical variation of $p_o D$ with D and from his paper we see that $D_o = 780$ cm. is a reasonable value for the distance beyond which $p_o D$ is constant. It may be noted that the equilibrium radius, D_1 say, of the bubble as given by Ramsauer's formula is

$$D_1 = \frac{4\,W^{1/3}}{\sqrt[3]{p_1}} \text{ feet} \qquad (35)$$

where .....

where w is weight of charge in lbs.
P is external hydrostatic pressure in atmospheres.

For depths from 0 to 90 feet, P_1 varies from 1 to 4 atmospheres and D_1 is much the same as D_0 given by (34).

Taking (34) therefore as a reasonable estimate of the distance D_0 beyond which the assumption of a small amplitude wave is justified we have from (33) and (34),

$$\left.\begin{aligned} \frac{n R_0}{c} &\geqslant 5.9 \\ R_0 &\geqslant D_0 \end{aligned}\right\} \qquad (36)$$

Considering now the order of the value to be expected for βa we have

$$\beta a = \frac{\rho a}{m} = \frac{a}{s h} \qquad (37)$$

where h is the plate thickness and s is the specific gravity of the plate relative to the water.

For steel plates relative to sea water we take s = 7.7, whence

$$\beta a = \frac{a}{7.7 h}$$

where h and a are in same units OR

$$\beta = \frac{1.56 a}{h}, \qquad \begin{matrix} a \text{ in feet} \\ h \text{ in inches} \end{matrix} \qquad (38)$$

For a small amplitude wave we thus have

$$\left.\begin{aligned} a &\geqslant D_0 \\ -\beta a &\geqslant \frac{5.5\, w^{1/3}}{h} \end{aligned}\right\} \qquad \begin{matrix} w \text{ in lbs.} \\ h \text{ in inches} \end{matrix} \qquad (39)$$

We thus see that except for small charges close to thick plates the value of βa will be large, of order 10 or greater. It may be noted that for the particular case considered in Report A of 300 lb. T.N.T. at 50 feet against ½ inch plate, $\beta a = 147$.

II. Approximate solution for βa and ϵ large.

Let u and w be functions of R_2 defined by

$$\left.\begin{aligned} u &= \frac{n}{c} R_2 - \beta \sqrt{R_2^2 - r^2} \\ w &= \beta R_2 - \frac{n}{c} \sqrt{R_2^2 - r^2} \end{aligned}\right\} \qquad (40)$$

Then .....

Then the following relations hold

$$\left.\begin{aligned} \frac{du}{dR_2} &= \frac{-w}{\sqrt{R_2^2 - r^2}} \\ w^2 - u^2 &= \left(\beta^2 - \frac{n^2}{c^2}\right) r^2 \\ \frac{dw}{du} &= \frac{u}{w} \\ \frac{d^2w}{du^2} &= \frac{1}{w} - \frac{u^2}{w^3} \end{aligned}\right\} \qquad (41)$$

The integral in equation (16) may now be integrated by parts to give

$$I = \int \frac{e^{\frac{n}{c} R_2 - \beta\sqrt{R_2^2 - r^2}}}{\sqrt{R_2^2 - r^2}} \, dR_2 = -\int \frac{e^u}{w} \, du$$

$$= -\left[\frac{e^u}{w} + \frac{e^u}{w^2}\frac{dw}{du}\right] - \int \frac{e^u}{w}\left\{\frac{2}{w^3}\left(\frac{dw}{du}\right)^2 - \frac{1}{w}\frac{d^2w}{du^2}\right\} du$$

Whence using the relations (41) we have

$$I = -\left[\frac{e^u}{w}\left(1 + \frac{u}{w^2}\right)\right] - \int \frac{e^u}{w}\left\{\frac{2}{w^2} - \frac{3\left(\beta^2 - \frac{n^2}{c^2}\right) r^2}{w^4}\right\} du \qquad (42)$$

Now putting as in (21)

$$R_2 = R_0 + c\zeta$$

$$\sqrt{R_2^2 - r^2} = \sqrt{a^2 + 2R_0 c\zeta + c^2\zeta^2}$$

we have since $R_0 \geq a$ the inequalities,

$$a + \frac{R_0 c\zeta}{a} \geq \sqrt{R_2^2 - r^2} \geq a + c\zeta \qquad (43)$$

whence

$$\beta(R_0 + c\zeta) - \frac{n}{c}\left(a + \frac{R_0 c\zeta}{a}\right) \leq w \leq \beta(R_0 + c\zeta) - \frac{n}{c}(a + c\zeta)$$

which may be written in the form

$$\beta R_0\left\{1 - \frac{1}{\epsilon} + \frac{c\zeta}{R_0} - \frac{n\zeta}{\beta a}\right\} \leq w \leq \beta R_0\left\{1 - \frac{1}{\epsilon} + \frac{c\zeta}{R_0} - \frac{n\zeta}{\beta R_0}\right\} \qquad (44)$$

Since $\zeta \leq t'$ we see that if $nt'/\beta a$ is small and ϵ large,

$$w \sim \beta R_0\left\{1 + \frac{c\zeta}{R_0}\right\} \qquad (45)$$

whence .....

whence since βa is large and $R_o > a$ we see that w is large of order βR_o or greater. Hence it can be shown that

$$\left| \frac{2}{w^2} - \frac{3(\beta^2 - n^2/c^2) r^2}{w^4} \right| = 0\left[\frac{1}{\beta^2 R_o^2}, \frac{1}{\epsilon^2 \beta^2 a^2} \right] \tag{46}$$

and we thus have from (42)

$$I = -\left[\frac{e^u}{w} \left(1 + \frac{u}{w^2} \right) \right] - \delta_1 I \tag{47}$$

where

$$|\delta_1| = 0\left[\frac{1}{\beta^2 R_o^2}, \frac{1}{\epsilon^2 \beta^2 a^2} \right] \text{ or less} \tag{48}$$

From equation (16) we have

$$(1 + \delta_1) \frac{p}{2 p_o} = (1 + \delta_1) e^{-nt'} - 2\beta R_o e^{-nt + \beta a} (1 + \delta_1) I$$

and thus from (47) we find after simplication

$$\frac{p}{2 p_o} = e^{-nt'} \left\{ -\frac{1}{\epsilon - 1} + \frac{\epsilon}{\epsilon - 1} \frac{\beta a - n R_o/c}{(\beta R_o - na/c)^2} + 0(\delta_1) \right\}$$

$$+ \frac{\beta k_o e^{-\beta \{\sqrt{c^2 t^2 - r^2} - a\}}}{\beta ct - n\sqrt{t^2 - r^2/c^2}} \left\{ 1 - \frac{\beta\sqrt{c^2 t^2 - r^2} - nt}{(\beta ct - n\sqrt{t^2 - r^2/c^2})^2} + 0(\delta_1) \right\} \tag{49}$$

Under the assumptions βa and ϵ large and $nt'/\beta a$ small the above equation (49) thus gives the solution correct to $0(\delta_1)$, i.e. the errors are of the second order.

If we now approximate further we obtain from (49)

$$\frac{p}{2 p_o} = \frac{R_o}{ct} e^{-\beta\sqrt{c^2 t^2 - r^2} + \beta a} - \frac{1}{\epsilon} \left(1 - \frac{c}{n R_o} \right) e^{-nt'} \tag{50}$$

which is correct to fractional errors in each term of the first order $\frac{1}{\epsilon}$, $\frac{1}{\beta a}$, provided $\left(1 - \frac{c}{n R_o}\right)$ is not small. As shown in Appendix I, $c/n R_o$ will usually be of order $\frac{1}{6}$ or less for underwater explosion waves of small amplitude and thus $(1 - c/n R_o)$ is positive of order unity. If equation (50) is true up to the time of maximum velocity corresponding to $p = o$ then this time is given by

$$\left.\begin{aligned} e^{-\beta\sqrt{c^2 t^2 - r^2} + \beta a + nt'} &= \frac{a_1 ct}{R_o} \\ \text{where} \quad a_1 &= \frac{\epsilon}{(1 - \frac{c}{n R_o})} \end{aligned}\right\} \tag{51}$$

In order to solve this implicit equation we assume ct'/R_o is small and retaining only the predominant terms, we obtain as solution

$$nt' = \frac{\log a_1}{\epsilon} + \frac{1}{2} \frac{(\log a_1)^2}{\beta a \epsilon} \tag{52}$$

since .. ..

since, for $1 - c/n R_0$ positive of order unity,

$$\left.\begin{aligned} \text{Log } a_1 &= 0\,(\text{Log } \epsilon) \\ \frac{ct'}{R_0} &= \frac{c}{n R_0}\, nt' \end{aligned}\right\} \qquad (53)$$

We thus see that for large ϵ and βa, then up to the time of maximum velocity the assumptions that $nt'/\beta a$ and ct'/R_0 are small are both justified, especially the former since nt' is itself small up to this time.

Corresponding to the approximation (50) for (16) we have a similar approximation for equation (20) given by

$$\frac{m n v + p}{2 p_0} = \frac{R_0}{ct}\, e^{-\beta\sqrt{c^2t^2 - r^2} + \beta a} + \frac{c}{\epsilon n R_0} \qquad (54)$$

whence

$$\frac{m n v}{2 p_0} = e^{-nt'} \left\{ \frac{1}{\epsilon} - \frac{c}{\epsilon n R_0} \right\} + \frac{c}{\epsilon n R_0}$$

$$+ e^{-\beta\sqrt{c^2t^2 - r^2} + \beta a} \left\{ 0\left(\frac{1}{\epsilon}\right) + 0\left(\frac{1}{\beta a}\right) \right\} \qquad (55)$$

Now at the time of maximum velocity we have from (51) and (52)

$$e^{-\beta\sqrt{c^2t^2 - r^2} + \beta a} = 0\left(\frac{1}{\epsilon}\right)$$

$$\frac{c}{\epsilon n R_0}\,(1 - e^{-nt'}) \sim \frac{c\, n t'}{\epsilon n R_0} = 0\left(\frac{1}{\epsilon}\right) \times 0\left(\frac{ct'}{R_0}\right)$$

$$nt' = \frac{\text{Log } \epsilon}{\epsilon} + 0\left(\frac{1}{\epsilon}\right) + 0\left(\frac{1}{\beta a}\right)$$

whence to the first order

$$\frac{m n v_m}{2 p_0} \sim \frac{1}{\epsilon}\, e^{-nt'} \sim \left(\frac{1}{\epsilon}\right) 1 - \frac{1}{\epsilon} \sim \left(\frac{1}{\epsilon}\right)^{\frac{\epsilon}{\epsilon - 1}} \qquad (56)$$

which is correct to small fractional errors of order $\frac{ct'}{R_0}$, $\frac{1}{\epsilon}$, $\frac{1}{\beta a}$.

Thus under the conditions βa large and $1 - \frac{c}{n R_0}$ positive of order unity, when ϵ is large the maximum velocity communicated to the plate is given approximately by the same expression (27) as for ϵ not large.

III. *Validity of solution when plate leaves the water.*

The solution has been obtained on the assumption implicit in the boundary condition (5) that the plate is in contact with the water. If the plate leaves the water at any point P then the solution will be valid at P up to this time provided no effect has by then reached P of earlier separation of plate and water at other points P' of the plate. Since the effect of such earlier separation will travel from P' to P with velocity C the solution will be valid provided the separation of plate and water travels over the plate with velocity greater than C.

Now .....

Now the time t at which the plate leaves the water is given by

$$t = \frac{R_0}{c} + t' \tag{57}$$

where t', if the solution is valid, is given by equation (52) or (26) according to whether ϵ is large or not. Equation (57) gives the relation for the time t at which the separation reaches a distance r from the centre of the plate and thus

$$\text{velocity of separation} = \frac{\partial r}{\partial t} \tag{58}$$

and from (57)

$$\frac{\partial t}{\partial r} = \left[\frac{1}{c} + \frac{\partial t'}{\partial R_0} \right] \frac{r}{R_0} \tag{59}$$

(i) ϵ not large.

Then from equation (26)

$$\frac{\partial t'}{\partial R_0} = \frac{\partial \epsilon}{\partial R_0} \frac{\partial t'}{\partial \epsilon} = \frac{\epsilon}{R_0} \frac{\partial t'}{\partial \epsilon} = -\frac{1}{n R_0} \left\{ \frac{\epsilon \operatorname{Log} \epsilon - \epsilon + 1}{(\epsilon - 1)^2} \right\} \tag{60}$$

It can easily be shown that as ϵ increases from 0 to ∞ the function in brackets in equation (60) decreases steadily from 1 to 0.

Hence

$$0 \geqslant \frac{\partial t'}{\partial R_0} \geqslant -\frac{1}{n R_0} \tag{61}$$

whence from (59)

$$\frac{1}{c} \geqslant \frac{r}{R_0 c} \geqslant \frac{\partial t}{\partial r} \geqslant \frac{r}{R_0} \left[\frac{1}{c} - \frac{1}{n R_0} \right] \geqslant 0 \tag{62}$$

provided $n R_0/c \geqslant 1$. As shown in Appendix I this latter is satisfied by small amplitude underwater explosion waves and thus from (62)

$$\frac{\partial r}{\partial t} \geqslant c \tag{63}$$

(ii) ϵ large.

From equation (51) regarding α_1 as a function of R_0 we have

$$\frac{\partial \alpha_1}{\partial R_0} = \frac{\beta c}{n a} \cdot \left\{ \frac{2}{1 - c/n R_0} - \frac{1}{(1 - c/n R_0)^2} \right\} = \frac{\epsilon \theta}{R_0} \tag{64}$$

defining θ which is of order unity since $n R_0/c$ is of order 6 or greater.

Hence from equation (52)

$$\frac{\partial t'}{\partial R_0} = -\frac{1}{n R_0} \left[\frac{\operatorname{Log} \alpha_1}{c} + \frac{(\operatorname{Log} \alpha_1)^2}{2 \beta a \epsilon} - \frac{\vartheta}{\alpha_1} - \frac{1}{\beta a} \frac{\operatorname{Log} \alpha_1}{\alpha_1} \right] \tag{65}$$

Since .....

Since α_1 is of order ϵ which is large the bracketed function in (65) is small and positive, whence equations (61) and (63) hold also for ϵ large.

Thus whether ϵ be large or not the velocity of separation is greater than C and the solution of this paper is valid at any point of the plate up to the time it leaves the water.

THE EFFECT OF STRATIFICATION OF SEA-WATER ON THE PROPAGATION OF AN EXPLOSION PULSE

H. N. V. Temperley
Admiralty Undex Works, Rosyth, Scotland

British Contribution

March 1944

THE EFFECT OF STRATIFICATION OF SEA-WATER ON THE PROPAGATION OF AN EXPLOSION PULSE.

H. N. V. Temperley

March 1944

* * * * * * * *

Summary

It is possible that the propagation of the pressure-pulse from an underwater explosion may be affected if the velocity of sound is different at different depths of water. The suggestion by Professor Taylor that energy may be concentrated near the surface by a layer of fresh water lying over salt water, and that shock damage may thus be caused to ships at abnormally great distances, is examined mathematically (using linear sound theory). It appears that the energy flow per unit area might be increased by a factor of the order of three if the top ten feet of water were fresh instead of salt provided that the explosion occurs in, or within a few feet of, this layer. The effect of temperature variations is concluded to be too small to produce an appreciable effect. The extent to which these conclusions are affected by the departures of explosion pulses from ordinary acoustic theory is uncertain.

1. *Introduction.*

It has been suggested that the propagation of the pressure pulse from an underwater explosion may be materially affected by the fact that, due to variations in temperature and salinity, the velocity of sound is different in different places. In particular, certain cases of shock damage to ships at unexpectedly large distances of the order of 1,000 yards might be accounted for by a concentration of energy by some such mechanism (1). An investigation of this point, following up suggestions made by Professor G. I. Taylor has been made. In order to make the mathematics manageable, it has been necessary to use ordinary sound theory, to neglect both the variation in the velocity of sound with pressure and the cavitation phenomena which occur when an explosion pulse is reflected at a free surface. This means that we cannot hope to obtain more than a semi-quantitative picture of what takes place, but the indications seem to be that isolated cases of shock damage at abnormally great distances can be accounted for in this way.

2. *The Physical Mechanism.*

Although one can think of a number of ways in which a concentration of energy might be caused, practical considerations seem to narrow down the field of choice. One might imagine a section of coast or sea-bottom acting as a concave mirror, or a large body of water, slightly different from its surroundings, acting like a converging lens (2). Such possibilities cannot be ruled out, but it is almost impossible to form an estimate of their probability or importance. We consider here a phenomenon that is definitely known to be appreciable, the refraction of sound by stratified sea-water. A little consideration shows that the general effect of refraction is to concentrate the flow of energy into those regions where the velocity of sound is least. We consider, therefore, the case of a "slow" layer of water lying

above .....

Best Available Copy

above a "fast" one and investigate the extent to which such a concentration is likely to occur. We need a numerical estimate of the likely difference of velocities. If we suppose that we are near a river-mouth, it is possible that a layer of fresh water will lie above the salt water for a considerable distance out to sea. The velocity of sound in fresh water is about 4% less than in salt which turns out to be of the right order of magnitude to give an observable effect of the type for which we are looking. If we attempt to attribute such effects to temperature variation in the water alone, we meet with a number of difficulties so serious as almost to rule out this possibility.

(a) The temperature difference between the two layers to give a velocity difference of 4% would have to be about 15° C., a large value.

(b) Even if such temperature differences were possible, the transition between the layers would not be as sharp as it can be between fresh and salt water, and reflection effects would be correspondingly reduced.

(c) In order that the energy should be concentrated near the surface, it would be necessary for the "slow" or cold layer to be above the hot. Such a state of affairs does sometimes occur, but it is rare, being essentially unstable, except in the region between 4° C. and zero, over which range the change in velocity is very small.

3.1. *Statement of the Mathematical Problem.*

To fix our ideas, consider a sea of salt water, with a ten-foot layer of fresh water above it. We wish to investigate the propagation of sound waves of various frequencies, and this being known we can infer the way in which a pulse of arbitrary shape will be propagated from a point source. For mathematical reasons, it is difficult to treat directly the case of an infinitely deep sea, so we consider the case of a ten-foot layer of fresh water above a hundred-foot layer of salt water resting on an acoustically rigid bottom. (This is probably not unlike the conditions that do in fact exist near a river-mouth). We first review two available methods for dealing with the corresponding problem in a uniform sea.

(a) The method of images. The effect of the surface and bottom is replaced by that of an infinite series of images of the source, and the effect at a distant point is computed as the sum of all these. The resulting series is very slowly convergent, but can be transformed in various ways, provided that we assume perfect reflection at bottom and surface. Application to the present problem, where we are concerned with a partially reflecting surface, would be difficult.

(b) The method of normal modes. We use cylindrical co-ordinates, the axis of symmetry being the vertical through the point source. Let the free surface be the plane $y = 0$ and let y be the distance below this surface. Let:

y_0 be the depth of the source;

h be the depth of the boundary between the two layers;

l be the thickness of the lower layer.

If the velocity of sound is uniform, a typical solution of the wave equation satisfying the boundary conditions at the free and rigid surface is:-

ϕ_n .....

$$\phi_n = \sin\left[\frac{(2n-1)\pi y}{2(h+1)}\right] J_0\left[\left(\frac{\omega^2}{c^2} - \frac{(2n-1)^2\pi^2}{4(h+1)^2}\right)^{\frac{1}{2}} r\right] e^{i\omega t} \quad (1)$$

We need a sine function of this type in order to satisfy $\frac{\partial\phi_n}{\partial y} = 0$ at the free surface, and $\frac{\partial\phi_n}{\partial y} = 0$ at the rigid surface. (The function J_0 could be replaced by Y_0). We solve the problem of a point source first by adding together such solutions in order to make the potential near $y = y_0$ agree with that of a point source. We could then add up these solutions for various frequencies to make a pulse of the form we wish to study. For the present we confine ourselves to a single frequency source. The appropriate solution for this case can be shown to be:- (3)

$$p = \rho\frac{\partial\phi}{\partial t} = \frac{\rho q_0 \omega c}{4}\sum_{n=1}^{n=\infty}\frac{\sin(\gamma_n y)\sin(\gamma_n y_0)}{\int_0^{h+1}\sin^2(\gamma_n y)\,dy} H_0^{(1)}\left[\left(\frac{\omega^2}{c^2} - \gamma_n^2\right)^{\frac{1}{2}} r\right] e^{i\omega t} \quad (2)$$

where $\gamma_n = \frac{(2n-1)\pi}{2(h+1)}$ and $H_0^{(1)}$ is the first Hankel function. At large distances this function may be written $H_0^{(1)}(x) \sim \frac{e^{-\frac{\pi i}{4} - ix}}{\sqrt{\frac{\pi}{2}x}}$

and therefore represents, if x is real, a wholly outgoing wave, the factor $\frac{1}{\sqrt{x}}$ being the familiar one associated with cylindrical spreading. If x is imaginary, this function represents a decreasing exponential, and will die away to a very small value in a distance r of the order of h + 1. Thus, at distances great compared with the depth, the contributions of those modes for which $\gamma_n > \frac{\omega}{c}$ will be negligible so that the pressure will fall off as $\frac{1}{\sqrt{r}}$, the sound being continually reflected between surface and bottom. As we approach to distances of the order h + 1 the contributions of these "exponential-like" modes become appreciable until finally very near the source, we find that the pressure is falling off according to the familiar inverse distance law $\frac{1}{(r^2+y^2)^{\frac{1}{2}}}$. For brevity, we shall describe those modes for which $\gamma_n < \frac{\omega}{c}$, which alone are important at great distances, as the "carrier" modes.

The mathematical problem is now quite clear: we have to repeat the work we have just summarised, using normal modes appropriate to conditions when the velocity in the two layers is different.

3.2. *The New Normal Modes.*

Let c_1 be the velocity in the upper layer, and c that in the lower layer. By continuity considerations, we should expect our normal modes to be similar to those that occur in the uniform case. We therefore try solutions of the wave equation of the following types.

$$\begin{aligned}\phi_n &= e^{i\omega t}\sin py\, H_0^{(1)}\left[r\left(\frac{\omega^2}{c_1^2} - p^2\right)^{\frac{1}{2}}\right] && \text{in top layer}\\ &= e^{i\omega t}\left(B_n e^{qy} + C_n e^{-qy}\right) H_0^{(1)}\left[r\left(\frac{\omega^2}{c^2} + q^2\right)^{\frac{1}{2}}\right] && \text{in lower layer,}\end{aligned} \quad (3)$$

where for the present we leave open the question of whether p and q are real or imaginary. We use a sine in the top layer in order that $\frac{\partial\phi}{\partial t}$ may vanish

at .....

at the free surface y = 0. From the conditions that the pressure and normal velocity are continuous at the boundary y = h, we obtain:-

$$p^2 + q^2 = \frac{\omega^2}{c_1^2} - \frac{\omega^2}{c^2} = \frac{1}{L^2} \text{ say.} \quad \text{(L is always real since } c_1 < c\text{)} \tag{4}$$

$$\sin p h = B_n e^{qh} + C_n e^{-qh} \quad \text{(Pressure continuous at boundary)} \tag{5}$$

$$p \cos p h = q (B_n e^{qh} - C_n e^{-qh}) \quad \text{(Normal velocity continuous at boundary)} \tag{6}$$

B_n and C_n are related by the fact that the normal velocity at the bottom must be zero. This makes:-

$$B_n e^{q(h+1)} = C_n e^{-q(h+1)} \tag{7}$$

Eliminating B_n and C_n we obtain the following relation between p and q:-

$$\tan p h + \frac{p}{q} \operatorname{cotn} q l = 0 \tag{8}$$

and the following form for the typical normal mode:-

$$\phi_n = e^{i\omega t} \sin p y \, H_0^{(1)}\left[\left(\frac{\omega^2}{c_1^2} - p^2\right)^{\frac{1}{2}} r\right] \quad \text{in top layer}$$

$$\phi_n = e^{i\omega t} \frac{\sin p h \cosh q (y - h - l)}{\cosh q l} H_0^{(1)}\left[\left(\frac{\omega^2}{c_1^2} - p^2\right)^{\frac{1}{2}} r\right] \quad \text{in bottom layer.} \tag{9}$$

It can be shown without difficulty that these functions are orthogonal if two distinct ones are multiplied together, and integrated from y = 0 to y = h + l. They can therefore be treated exactly like Fourier series in every respect but one. In equation (2) the normalisation factor is independent of γ_n and is simply $\frac{h+l}{2}$. For normal modes of type (9) the expression is:-

$$\int_0^h \sin^2 p y \, dy + \int_h^{h+l} \frac{\sin^2 p h \cosh^2 q (y - h - l)}{\cosh^2 q l} \, dy$$

$$= \frac{h}{2} - \frac{\sin^2(p h)}{4 l^2 p q^2} + 1 - \frac{\cos^2 p h}{q^2 l^2} \cdot \frac{(d - h)}{2} = K_n \tag{10}$$

which has to be computed separately for each mode. Repeating the work that led to equation (2), we have to replace

$$\frac{\sin(\gamma_n y_0)}{\int_0^{h+l} \sin^2(\gamma_n y) \, dy}$$

by $\frac{\sin(p y_0)}{K_n}$ or by $\frac{\cosh q (y_0 - h - l) \sin p h}{K_n \cosh q l}$ according to whether the source is in the top layer or the lower layer. Our problem is now solved if we can determine p and q for each mode.

3.2.1.....

3.2.1. *The Solutions of Equations (4) and (8)*

We consider various possibilities:-

(a) p imaginary. This would only be possible if $c_1 > c$ (L imaginary). For L real Equation (4) implies that q must be real, and there is then no solution of equation (8).

(b) p real, q real. This corresponds to a mode which oscillates with y in the top layer, and dies away exponentially in the bottom layer, so that most of the energy is carried by the top layer. We call this type of mode a "canalised" one.

(c) p real, q imaginary. This corresponds to a mode which oscillates with y in both layers. We call this type of mode "non-canalised".

A rather troublesome problem is to prove that the canalised and non-canalised modes together form a complete set, so that we need not consider complex values of p and q. Perhaps the best argument is the physical one. If we allow l to approach zero, our problem goes over into that of uniform sound velocity and it can be shown that the modes of types (b) and (c) go over smoothly into the Fourier Series for the uniform medium, which is known to be a complete set. The introduction of complex values of p and q would lead to modes which would go over into something of the type sin [(a + i b) y] which would be redundant in a Fourier expansion.

There are only a finite number of canalised modes. From equation (8), if p and q are both real, tan p h must be negative, which means that p h can only take certain values between $\frac{\pi}{2}$ and π, between $\frac{3\pi}{2}$ and 2π, and so on. As p is less than $\frac{1}{L}$ by equation (4), this implies that $\frac{1}{L}$ must be greater than $\frac{\pi}{2h}$ for a canalised mode to exist. This implies a lower limit to the frequency for which such a mode can exist. As the frequency rises, two things happen. First, q, for any given mode, increases steadily from zero, which means that the exponential decay in the bottom layer becomes more and more rapid. Secondly, more and more modes of the canalised type appear as $\frac{1}{L}$ passes the values $\frac{3\pi}{2h}$, $\frac{5\pi}{2h}$, etc., so that we might reasonably infer an increasing concentration of energy in the upper layer, as the frequency rises. However, a rise in the frequency also increases the number of non-canalised modes (p real, q imaginary) for which $\frac{\omega}{c_1} > p$ and which therefore remain important at great distances (say of the order of 500 feet). We therefore investigate the energy flow for a few frequencies in a typical case.

3.3. *Results of Calculations.*

We assume the following conditions:-

Thickness of top layer 10 feet, velocity in this layer 5,000 feet/ second.
Thickness of bottom layer 100 feet, velocity in this layer 5,200 feet/ second.

Whence we have $\frac{1}{L} = 5.49 \times 10^{-4}$ (11)

the critical value of ω is given by $\tan \frac{10}{L} = -\frac{100}{L}$, which, solves by successive

approximations .....

approximations, gives us $\omega_c = 2.97 \times 10^3$. For a very large depth of water c takes the slightly smaller value 2.86×10^3 for the same thickness of top layer. We now calculate p and q by successive approximations from equations (4) and (8) and then calculate K_n from equation (10). This was done for some typical modes for the following three frequencies $\omega = 10^3$, 10^4 and 1.82×10^4, the first being below the critical, and the other two above it. As it was found that these three frequencies gave a sufficiently good physical picture of the situation, no further calculations were carried out. Some specimen results are tabulated below.

TABLE 1. $\omega = 10^3$. Total number of carrier modes = 7

Number and Type of Mode	1 N	2 N	3 N	4 N
p	.0958	.0495	.0335	.1130
q	.0144	.0424	.0708	.0992
K_n	630	110	68.9	58.3
q for uniform water	.0143	.0428	.0714	.0995

TABLE 2. $\omega = 10^4$. Total number of carrier modes = 69.

Number and Type of Mode	1 C	2 C	5 N	7 N	14 N	23 N
p	.264	.510	.555	.568	.674	.853
q	.481	.205	.0791	.143	.390	.652
K_n	5.15	8.94	1437	559	135	69.2
q for uniform water	-	-	.0714	.120	.329	.595

TABLE 3. $\omega = 1.82 \times 10^4$. Total number of carrier modes = 125

Number and Type of Mode	1 C	2 C	3 C	12 N	24 N	30 N	40 N
p	.283	.568	.842	1.034	1.192	1.319	1.547
q	.959	.823	.539	.254	.648	.860	1.180
K_n	5.51	5.61	5.94	325	130	100	89
q for uniform water	-	-	-	.243	.587	.760	1.045

C stands .....

C stands for a canalised mode, N for a non-canalised mode.

K_n would take the value 55 for all modes in 110 feet of uniform water.

The values of "q for uniform water" are calculated on the assumption that the speed of sound is the same as in the lower layer. If we took it equal to the speed in the upper layer, extra modes, corresponding to the canalised modes, would appear. p is always real, q is real for a canalised mode, imaginary for a non-canalised mode.

The K_n (the normalising factors) are all calculated on the basis of the amplitude of the sine wave in the top layer being unity. We therefore have three possible cases:-

(a) A very large value of K_n indicates that the amplitude of the sine-wave in the lower layer is large compared with that in the top layer.

(b) A value of K_n of the order of 5 indicates that the mode is practically confined to the top layer (a canalised mode).

(c) A value of K_n of the order of 55 indicates that the amplitude of the mode in the two layers is practically equal.

By generalising equation (2), we find that the extent to which any given mode is stimulated is proportional to the expression obtained by putting $y = y_0$ (where y_0 is the depth of our source) in equation (9), and then dividing by K_n. We thus see that, for a source in the top layer, modes of type (b) (canalised modes) will be strongly stimulated, modes of type (c) moderately stimulated, and modes of type (a) will be weak. For a source in the bottom layer, the stimulation of the canalised modes will be weak (due to the exponential decay), while modes of types (a) and (c) will be moderately stimulated. In other words, we should expect a canalisation effect if the source is in the top layer due to reflection at the boundary tending to confine the sound, but, if the source is in the bottom layer, the sound will be transmitted very much as if the top layer were not present at all. We therefore confine our attention to sources in the top layer. The stimulation factor of every mode will then be of the order of magnitude $\frac{1}{K_n}$. Strictly speaking it is $\frac{\sin p y_0}{K_n}$, but we are not concerned with calculations of pressure fields due to sources at particular depths, but we want rather a rough average over sources at all depths within the top layer. In the same way, it is permissible to average the Hankel functions (provided that their arguments are real) over a distance of the order of a wave-length, so that we neglect the oscillating property of the function and simply retain the factor $\frac{1}{\sqrt{r}}$. Of course, we may not do this if the argument is imaginary.

Expressed more precisely, what we are really doing is to estimate the energy residing in a hollow cylinder of large radius due to point sources distributed along the r axis at all depths in the top layer. To do this, we take an expression of the type (2) for the pressure, substitute in it normal modes given by equation (9), square and then integrate over the whole depth of water. All the cross-terms then vanish owing to the orthogonality, and the contribution of all except the carrier modes is negligible owing to the exponential decay of the others with r. We have therefore simply to estimate how the energy of each mode divides itself between the upper and lower layer, and how much each contributes to the energy. The energy residing in the upper layer is proportional to $\frac{\int_0^h \phi_n^2 \, dy}{K_n^2}$ and that in the lower layer

to .....

to $\frac{\int_h^{h+l} \phi_n^2 \, dy}{K_n^2}$. Proceeding on these lines, we obtain the following final results, comparing this case with the one for uniform water:-

$\omega = 10^3$ No change in flow of energy due to stratification.

$\omega = 10^4$ Energy flow in top layer increased by factor of 2.5
Energy flow in bottom layer reduced by about 15%

$\omega = 1.82 \times 10^4$ Energy flow in top layer increased by factor of 2.9
Energy flow in bottom layer reduced by about 20%

} by stratification

These results were not obtained by a very accurate method, as it was only desired to calculate the order of magnitude of the effect. Since the pressure pulse from a large charge is represented approximately by t^{-n} and n is of the order of 10^3, it is clear that only the higher frequencies, making up the head of the pulse, can be canalised.

3.4. *Extension to other Depths of Water.*

The difficulties that stand in the way of applying this theory to infinite depths are fairly obvious. Not only does the number of carrier modes become infinite, so that we have an integral to deal with instead of a sum, and the processes we have adopted (while clearly justifiable for a finite series) may not be so for an integral, but we have to take account of the remaining modes as well. It can, however, be shown without difficulty that if we are 1,000 feet away, the figures we have given for initial frequency and energy flow would hardly be altered up to depths of 1,000 feet, so that our investigation seems to cover most of the situations that are ever likely to occur at a river mouth.

4. *Conclusions.*

It appears that the canalisation mechanism suggested by Professor Taylor is in principle capable of accounting for freak cases of "shock damage" in such places as river mouths where fresh water is likely to lie above salt. It also seems that this mechanism is not capable of accounting for freak cases of damage to ships' plating, because only part of the pressure pulse is transmitted in this special way. It also seems that stratification due to temperature differences is too small an effect to be of importance in this connection. The extent to which the conclusions must be modified in order to take account of the differences between sound and explosion pulses is uncertain. The factor found for the higher frequencies is about three in the energy flow, which would give a factor three in the maximum distance for damage caused by these frequencies.

MEASUREMENTS ON PRESSURE WAVES IN REGION OF TWO OBLIQUELY INTERSECTING UNDERWATER SHOCK WAVES

A. M. Shanes
Underwater Explosives Research Laboratory
Woods Hole Oceanographic Institution

American Contribution

May 1944

MEASUREMENTS ON PRESSURE WAVES IN REGION OF TWO OBLIQUELY INTERSECTING UNDERWATER SHOCK WAVES

A. M. Shanes
Underwater Explosives Research Laboratory
Woods Hole Oceanographic Institution
Woods Hole, Massachusetts

Introduction. When two equal waves intersect, elementary theory indicates that the maximum pressure should be approximately twice that of one of the shocks alone. By more advanced methods, Von Neumann (Bureau of Ordnance, Explosives Research Report No. 12, 1943) has shown that when the finite amplitude of the waves is considered, the pressure in water should exceed the sum of the components by an amount which increases as the waves intersect more and more obliquely, i.e., less head-on. At a certain critical angle, however, the phenomenon changes qualitatively, the two waves merging into one in a certain region (Mach region) about the intersection plane of the two shocks. It has been postulated that in this region the pressure at first increases and then falls to a relatively low value as the intersection becomes more and more oblique, approaching glancing incidence.

Experiments on the underwater shock waves from two simultaneous explosions have now confirmed this picture, at least qualitatively. Pressure-time curves in the region of intersection of the shock waves from the two charges were obtained with 4 small piezo gauges. Two of the gauges were located on the perpendicular bisector of the line joining the charges. The gauge-to-charge distances for these gauges were kept constant but the angle of intersection at the gauges was varied by changing the charge-to-charge distance.

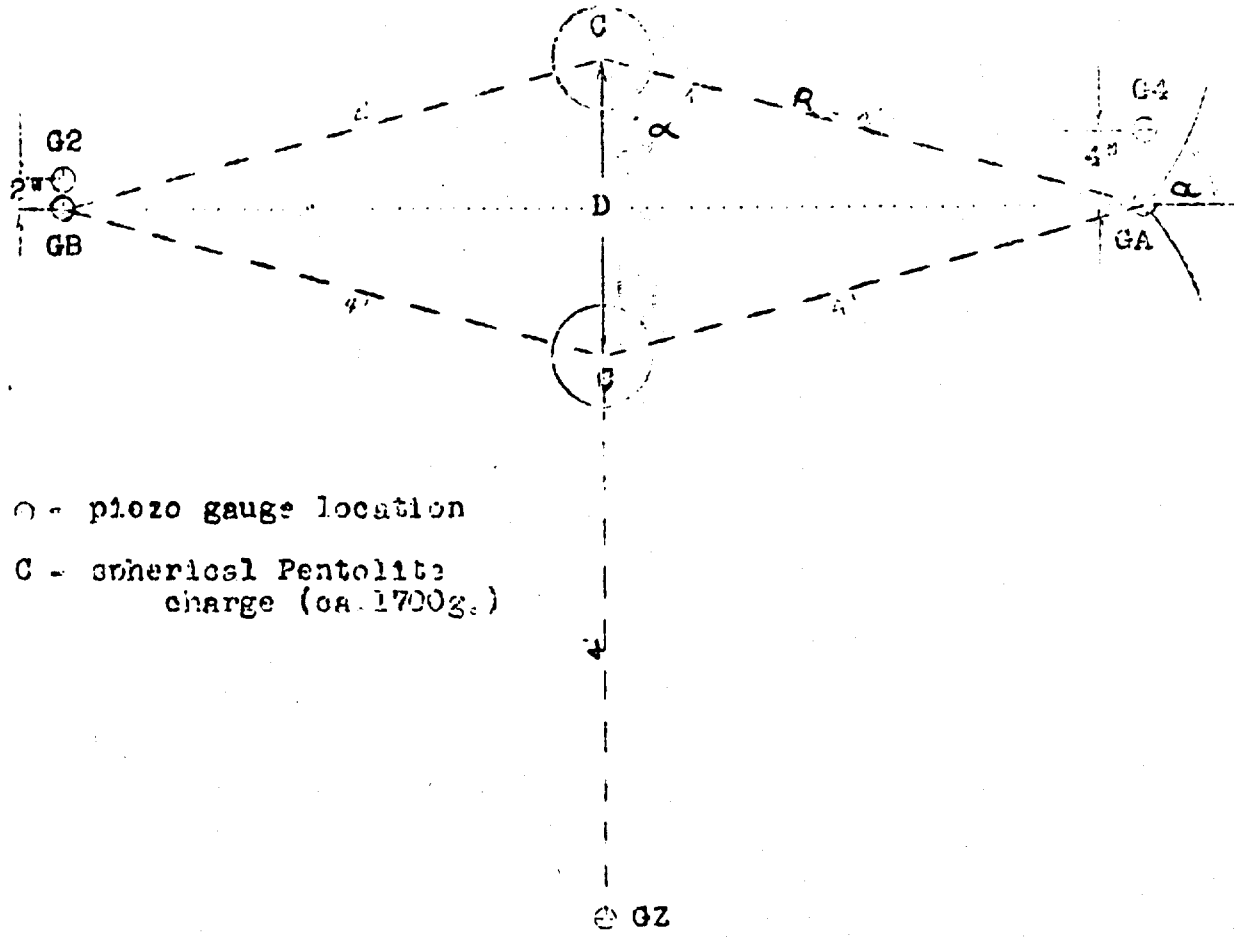
The pressure versus angle curves show the expected maximum (Figs. 1, 3, 4). This is more pronounced if the observed peak pressures are corrected in the customary way for the finite response time of the gauges.

The impulse integral $\int p\,dt$ and the energy integral $\frac{1}{\rho c}\int p^2 dt$ were also evaluated (Figs. 5-10).

From the practical viewpoint these results indicate that a given weight of charge should be more effective in certain directions if divided into two (or more) equal parts fired simultaneously. For damage tests with double charges see UE-18, p. 68 and UE-19, p. 21.

A gauge on the line through the charges showed the expected strong shielding of one explosion by the gas bubble of the other.

Method. The shock waves studied were generated by the simultaneous detonation of the two ca. 1700 g. spherical cast pentolite charges and recorded by 0.22" diameter doublet piezo gauges. The arrangement of charges (C) and gauges (G-A, G-B, G-2, G-4, G-Z) is shown in the following sketch.



The distance D was varied from zero (a single charge) to 66 inches, R being kept constant at 4 feet. Throughout this report the separation is expressed in terms of the angle α which is also the half angle of shock wave intersection which, in the absence of a Mach effect, would be expected at G-A and G-B. Displaced slightly from the plane of intersection were gauges G-4 (4 inches from G-A) and G-2 (2 inches from G-B).

To obtain records of the screening effect of the gas bubble from one charge on the shock wave from the other charge, gauge G-Z was placed along the line of the charges as shown in the sketch.

Simultaneous detonation was obtained by discharging dykanol condensers totalling 36 microfarads capacity, charged to ca. 1000 volts, through the 2 Dupont "SSS" seismograph caps connected in serie

Prior to adoption of the above technique for simultaneous detonation of caps, a more extensive series was run in which pairs

of 50 g. loose tetryl charges were detonated with one cap by means of equal lengths of primacord. Two gauges were employed, both in the intersection plane. The results on peak pressure, the only ones obtainable because of the interference of the primacord waves, are in agreement with those obtained with the larger charges.

Results; Peak Pressure. Table I and Figs. 1, 3 and 4 summarize the peak pressure data. In particular, Fig. 1 shows the results obtained in the intersection plane for the 1700 g. charges, corrections having been applied for systematic gauge differences and for the response time of the gauges (see below). It is seen that the initial shape of the curve follows the theory (H. Polachek and R. J. Seeger; Bureau of Ordnance, Explosives Research Report No. 14, 1944) but that the quantitative agreement is not perfect.

It is important to note that the correction for finite frequency response was made by extrapolating the pressure-time curve to zero time on a semi-log plot. Normally this plot is a straight line for a time of the order of the time constants, indicating an initially exponential decay. In the region near the pressure maximum (α = 62-72°), the initial decay was not exponential, and the semi-log plot showed a pronounced upward curvature in the initial portion. This causes the extrapolated values in this region to be considerably higher than the uncorrected values. In fact, the uncorrected peak pressures (Fig. 3) do not show a very pronounced maximum. Although the exact value of the correction for finite gauge size may not be obtained by this extrapolation procedure, there is no doubt that such a correction is required and that it will be largest in the region indicated, where the pressure is decaying abnormally rapidly with time.

The peak pressure curve obtained with 50 g. charges is shown in Fig. 4. If extrapolation had been possible, presumably the level of pressure, particularly in the Mach region, would have been greater. The maximum pressures occur at larger angles than for the 1700 g. charges, as would be expected from the larger α_{MACH} predicted for the lower pressure levels obtained from the 50 g. charges.

The gauges G-2 and G-4 show a qualitatively different behavior from those in the intersection plane. For small angles (α) G-2 and G-4 show two distinct peaks, corresponding to the waves from the two charges. G-A and G-B do not show two peaks because the waves arrive at the same time. At about α = 72°, G-2 begins to show only one peak, indicating that it has come within the Mach region, while G-4 does not show single peaks until α = 80.8°. As a rough estimate, a linear extrapolation to the intersection plane can be made, which indicates that the critical angle for the onset of the Mach effect at this pressure (8900 psi) is of the order of 63°, which is comparable with the theoretical value of 57½°.

The pressures measured outside the plane of intersection were the same as those within for 80.8° and higher. At smaller angles

Table I. Peak Pressures, direct and extrapolated, obtained in the region of intersection of shock waves from two 1700 g. pentolite charges. All values corrected for systematic differences observed among the gauges with single 1700 g. pentolite charges. Pressures are in lb./in^2

α = half angle of shock wave intersection (c.f. sketch above).
p = directly read pressure; p_1 = first or only peak; p_2 = second peak.
P = extrapolated pressure; P_1 = first or only peak; P_2 = second peak.
G-A, G-B = gauges in the plane of intersection.
G-3 = gauge 3" from intersection plane.
G-4 = gauge 4" from intersection plane.

α	G-A		G-B		G-2				G-4			
	p	P	p	P	p_1	P_1	p_2	P_2	p_1	P_1	p_2	P_2
90°*	11,000	11,450			10,150	10,750			10,650	11,300		
90°**			8,010	8,510	8,010	8,510			8,830	9,170		
90°**	8,360	8,870	8,460	9,270	7,950	9,080			8,370	8,970		
90°**	8,070	8,650			9,040	8,700			8,450	8,670		
87°	11,700	12,600			11,900	12,500			12,300	12,950		
87°	11,300	12,000	11,700	12,030	10,600	11,450			12,100	12,700		
80.8°	15,780	16,800			15,700	16,680			15,800	16,800		
80.8°	15,000	16,800	15,000	16,800	13,700	14,900			15,900	17,230		
72°	18,400	23,300			16,900	18,500			8,620		7,150	(8,090)/
67°	19,050	26,250			8,330	9,250	9,450	10,150	8,630	9,300	8,900	9,300
62°	18,300	22,100			8,430	8,820	9,780	10,520	8,240	8,770	9,360	10,700
62°	17,930	20,700	17,640	21,400	8,250	8,820	8,760	9,000	8,490	9,210	9,920	10,450
57°	18,200	20,500			8,170	8,410	9,550	10,056	8,380	9,430	8,650	9,020
57°	17,660	18,670	17,000	21,700	8,130	8,400	8,530	9,270	7,910	9,340	8,660	8,770
45°	16,980	18,200	17,100	18,600	8,170	8,850	9,080	9,540	8,010	9,410	8,730	9,020

* Single 3400 g. charge. ** Single 1700 g. charge.
/ Inaccurate because of extremely short duration of 1st pulse.

the appearance of two peaks requires a less direct comparison, viz., that of the total pressure which would obtain in the absence of the exponential decay of pressure and if the waves were plane. This may be obtained by adding the second increment in pressure to the first peak, correcting both pressures to the same distance from the charges. From analogy to the reflection case, the pressure so obtained is equivalent to the total pressure behind the shock front upon reflection of a plane, step shock wave incident upon a rigid wall. This pressure, relative to the incident wave (i.e., to the shock front from a single charge), is given in Table II. It may be seen that even in the absence of Mach interaction ($\alpha < \alpha_{EXTREME}$) the pressures from the two charges do not simply add acoustically, the ratios being greater than 2.

The gauges outside the plane of intersection indicate the width of the Mach region. Thus the disappearance of the second peak for G-2 at 72° and for G-4 at 80.8° means that the Mach zone was at least 4 inches wide in the former case and over 8 inches wide in the latter. It must be borne in mind, however, that a second peak would have escaped observation if it had been less than about 5 microseconds behind the first peak.

The observed effective time constants are given in Fig. 2. They were obtained from the initial slope of the semi-log plots. The low values obtained in the range of α in which maximum pressures occur are a measure of the abnormally rapid decay in this critical region.

Momentum Integral. The evaluation of the momentum integral $\int p dt$ is complicated by a "cut-off" in most of the pressure-time curves (See Fig. 11). This cut-off is believed to be due to the arrival at the gauge of a rarefaction wave produced by the reflection of the shock wave from one charge off the gas bubble of the other. In Table III this hypothesis is applied to the observed cut-off times in order to roughly estimate bubble radii. The radii were calculated by assuming that all waves traveled with sound velocity. The results are consistent with the bubble radii from smaller charges (See Section 2).

Because of this complication, the impulse integral was evaluated out to both 218 and 560 microseconds, the former time being the shortest cut-off observed. Figs. 5, 7 and 9 show the values observed for $\int p dt$ within, 2" outside, and 4" outside the plane of intersection, respectively. See also Table IV. At the shorter integration time, the gauges in the plane of intersection show no maximum, but instead a steady decline as the charges are brought together. The other gauges show a slight small maximum but this is probably due to the smaller contribution of the wave from the second charge at smaller angles because of the arbitrary limitation of the integration to 218 microseconds. The slight minimum in the 560 microsecond curves is believed to be due to the early cut-off when the charges are close together (see Fig. 11).

Energy Function. The quantity $\frac{1}{\rho c} \int p^2 dt$ is plotted in Figs. 6, 8 and 10. Only the integrations to 560 microseconds are given since those to 218 microseconds give essentially the same general curves. It is apparent that this energy function does not pass through any

Table II. Finite Amplitude Effect as illustrated by the ratios $(P_1 + P_2)/P_1$ (=D) for double shocks and P/P_s (=S) for single shocks (t is the interval between successive peaks in microseconds).

P_1 = Peak pressure at first (incident) shock, evaluated at time of measurement of P_2.
P_2 = Pressure increase at second (reflected) shock.
P = Peak pressure at single (Mach) shock.
P_s = Peak pressure 4 feet from single 1700 g. charge.

α (degrees)	In the plane of intersection	2" to the side of the intersection R	2" to the side of the intersection t	4" to the side of the intersection R	4" to the side of the intersection t
90*	1.31 (S)	1.33 (S)	-	1.29 (S)	-
87	1.44 (S)	1.43 (S)	0	1.48 (S)	0
87	1.37 (S)	1.31 (S)	0	1.45 (S)	0
80.8	1.90 (S)	1.90 (S)	0	1.92 (S)	0
80.8	1.90 (S)	1.70 (S)	0	1.97 (S)	0
72	2.66 (S)	2.10 (S)	0	1.94 (D)	12
67	2.99 (S)	2.13 (D)	32	2.06 (D)	41
62	2.52 (S)	2.24 (D)	33	2.30 (D)	58
62	2.36 (S)	2.06 (D)	27	2.21 (D)	45
57	2.34 (S)	2.24 (D)	26	2.04 (D)	62
57	2.13 (S)	2.14 (D)	26	2.02 (D)	70
45	2.08 (S)	2.16 (D)	51	2.08 (D)	95

* Single 3400 g. charge.

Table III. Calculated and Measured Times of Pressure Cut-off and Approximate Bubble Radii*

Distance between charge surfaces (in.)	Measured time (t_1, microsec)	Calculated time (t_2, microsec)	Approximate bubble radius ≯ (in.)
11.0	76.2	183	5.8
11.0	74 0	183	
24.5	287	408	6.2
32.5	402	542	6.7
40.0	522	667	7.5
40.0	473	667	
47.0	565	783	9.1

* Shock front velocity v assumed 0.0607 in./sec.
≯ $\frac{1}{2}(t_2-t_1)v + 2\frac{1}{2}$ ($2\frac{1}{2}$ in. = charge radius.)

Table IV. **Values of the Impulse and Energy Integrals in the Region of Two Obliquely Intersecting Shock Waves.**

Location of gauges G-A, G-B, G-2, and G-4 shown in sketch.

α	Impulse $\int p\,dt$, psi-sec., to time indicated (microseconds)								Energy $\frac{1}{\rho c}\int p^2\,dt$, in.lb./in.^{2}, to 560 microseconds			
	at intersection				2 in. from intersection		4 in. from intersection		at intersection		2 in. from intersection	4 in. from intersection
	G-A		G-B		G-2		G-4		G-A	G-B	G-2	G-4
	218 μs.	560 μs.	218 μs.	550 μs.	218 μs.	560 μs.	218 μs.	560 μs.				
90°*	1.17	1.67					1.20	1.68	1570			1605
90°**					0.818	1.06	0.880	1.22			807	920
90°**	0.811	1.19	0.852	1.17	0.833	1.16	0.835	1.15	801	864	551	805
90°**	0.832	1.10			0.847	1.08	0.855	1.15	818		820	832
87°	1.16	1.62			1.11	1.56	1.18	1.66	1630		1605	1605
87°	1.12	1.61	1.16	1.68	1.17	1.68	1.25	1.79	1600	1570	1580	1790
80.8°	1.35	1.62			1.33	1.59	1.47	1.71	2560		2510	2740
80.8°	1.36	1.50	1.38	1.64	1.28	1.54	1.42	1.72	2260	2355	2105	2920
72°	1.56	1.76			1.57	1.78	1.63	1.88	2950		3070	3130
67°	1.50	1.90			1.63	2.04	1.70	2.24	2940		2900	3080
62°	1.73	2.02			1.65	2.30	1.58	2.25	3600		3170	2680
62°	1.52	2.03	1.56	2.02	1.65	2.20	1.59	2.14	2880	2890	2970	2740
57°					1.55	2.42					2820	
57°	1.55	2.12	1.60	2.28	1.52	2.19	1.53	2.39	3030	3075	2670	2390
45°	1.63	2.29	1.67	2.30	1.58	2.20	1.48	2.18	3320	3330	2880	2370

* Single 3400 g. charge ** Single 1700 g. charge $\frac{1}{\rho c}$ has been taken as 5.38 lb.sec./in.^{3}

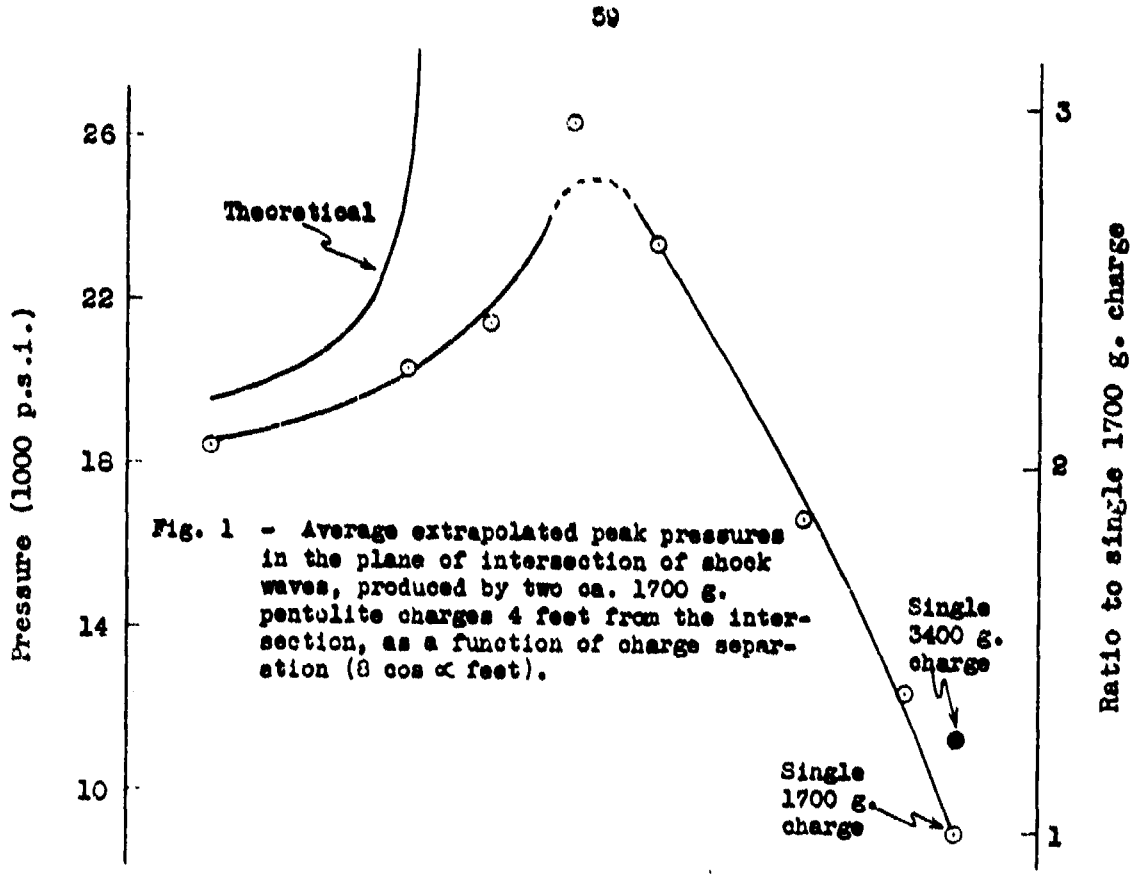


Fig. 1 - Average extrapolated peak pressures in the plane of intersection of shock waves, produced by two ca. 1700 g. pentolite charges 4 feet from the intersection, as a function of charge separation (8 cos ∝ feet).

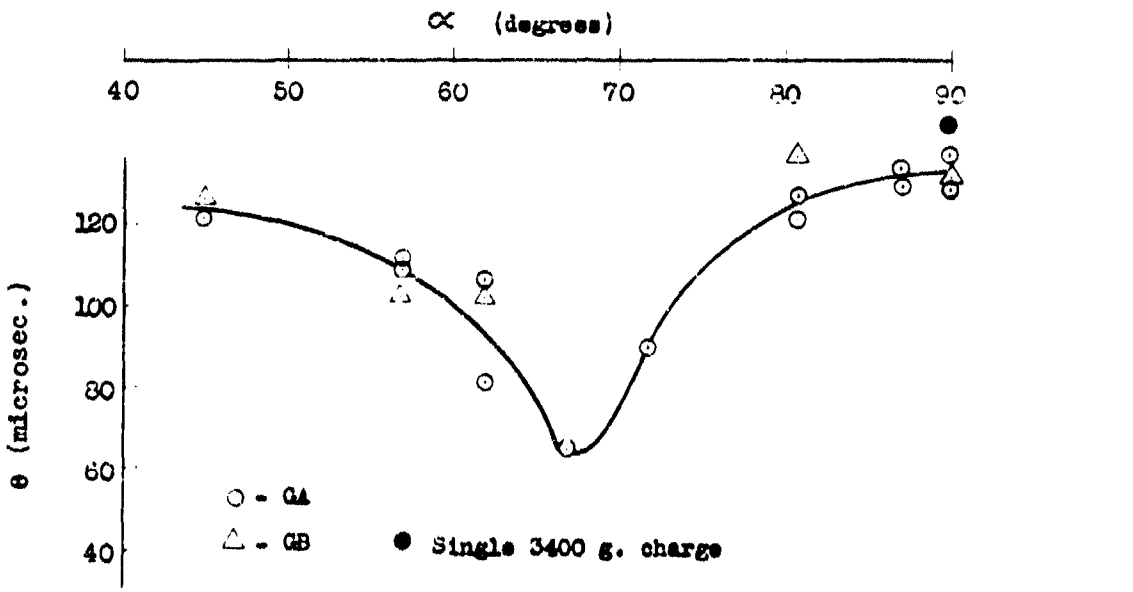


Fig. 2 - The effective time constant (see text) obtained under the same conditions as in Fig. 1.

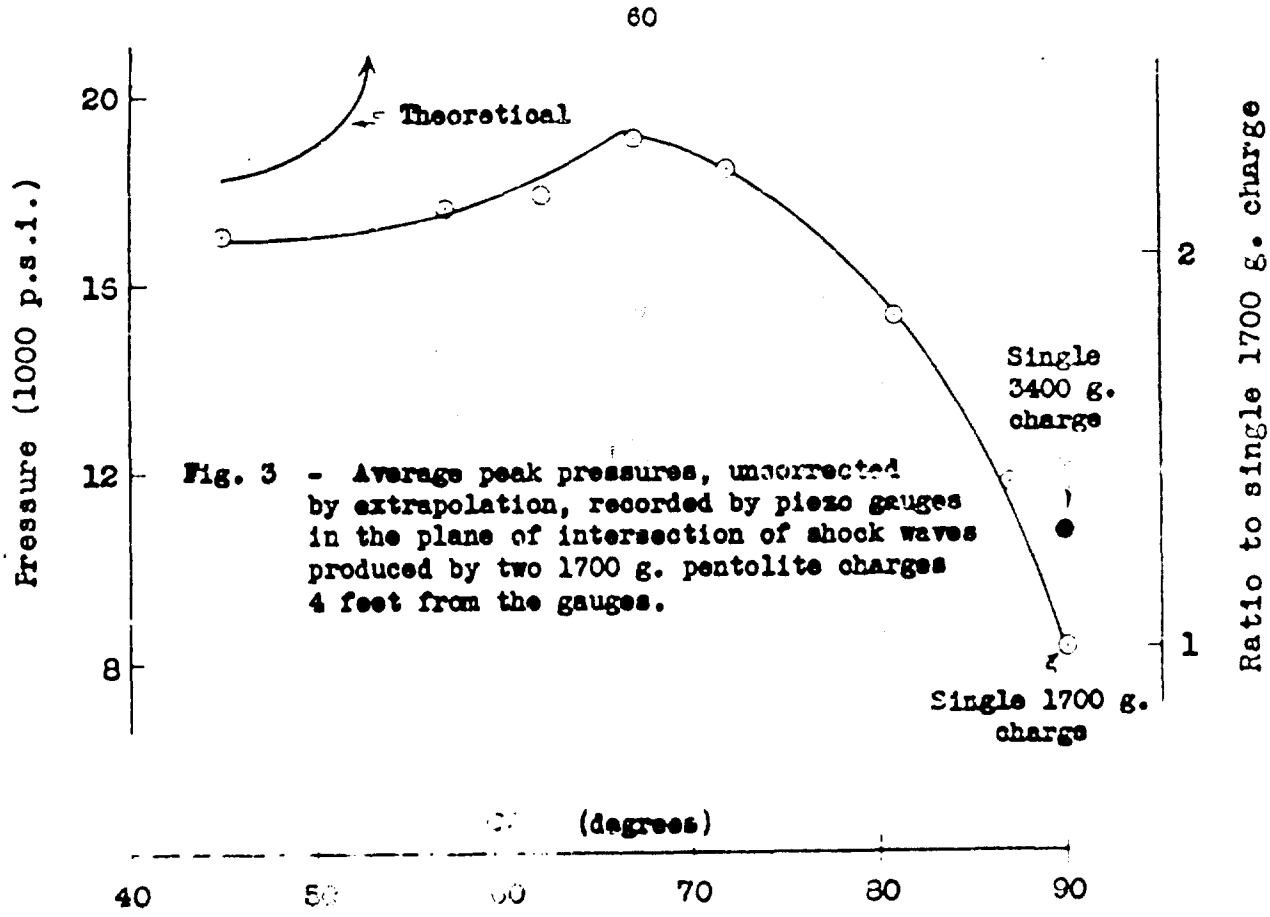


Fig. 3 - Average peak pressures, uncorrected by extrapolation, recorded by piezo gauges in the plane of intersection of shock waves produced by two 1700 g. pentolite charges 4 feet from the gauges.

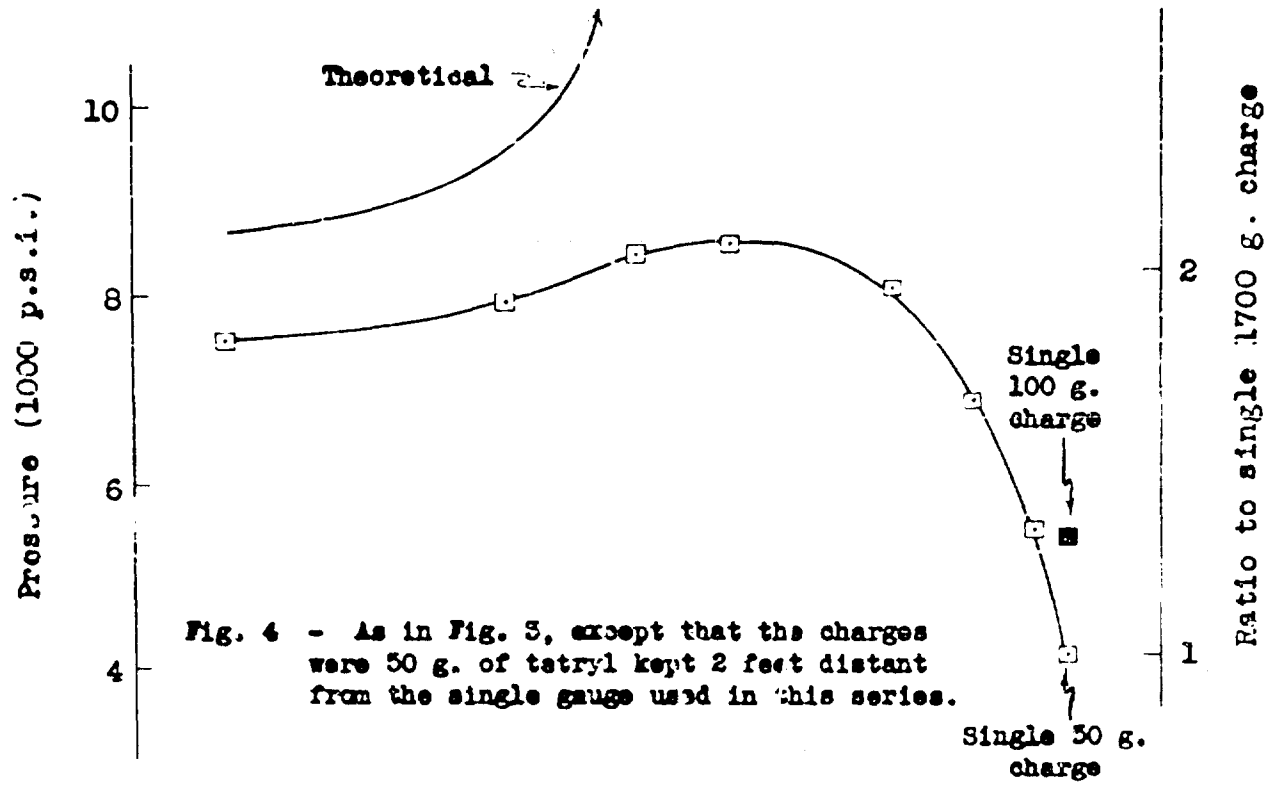


Fig. 4 - As in Fig. 3, except that the charges were 50 g. of tetryl kept 2 feet distant from the single gauge used in this series.

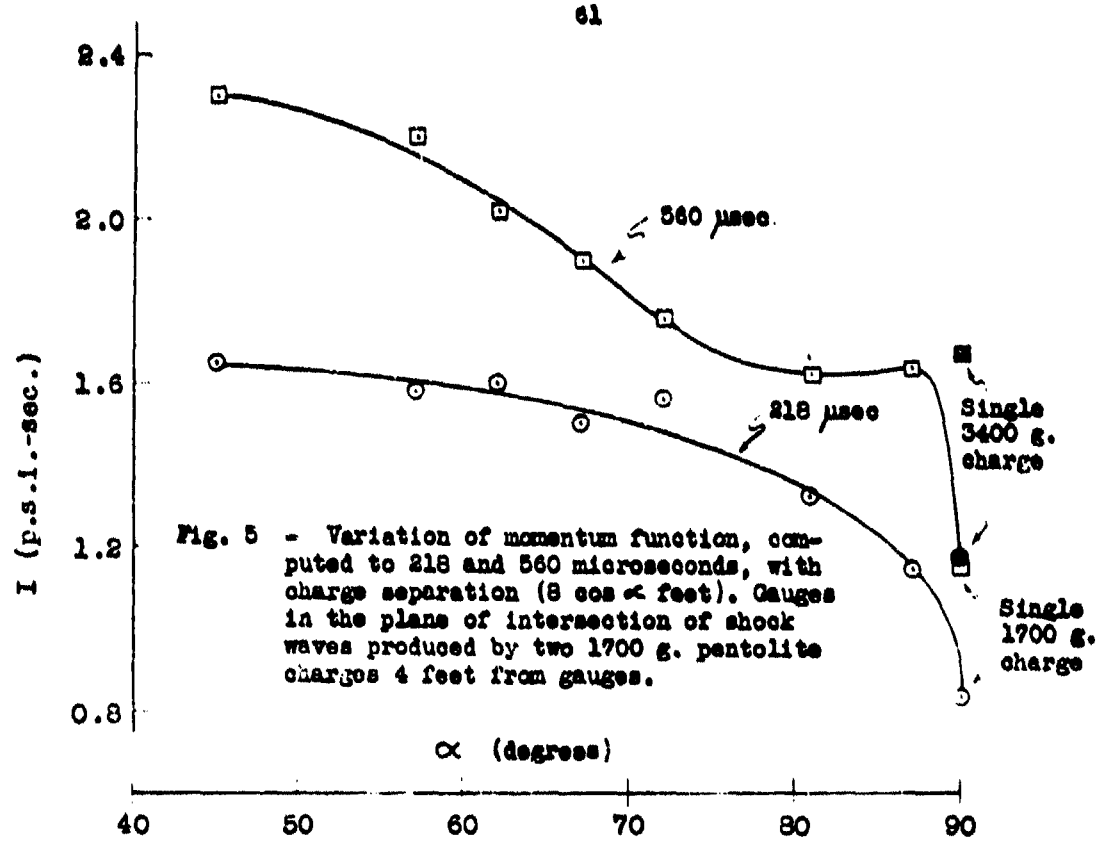


Fig. 5 - Variation of momentum function, computed to 218 and 560 microseconds, with charge separation (8 cos ∝ feet). Gauges in the plane of intersection of shock waves produced by two 1700 g. pentolite charges 4 feet from gauges.

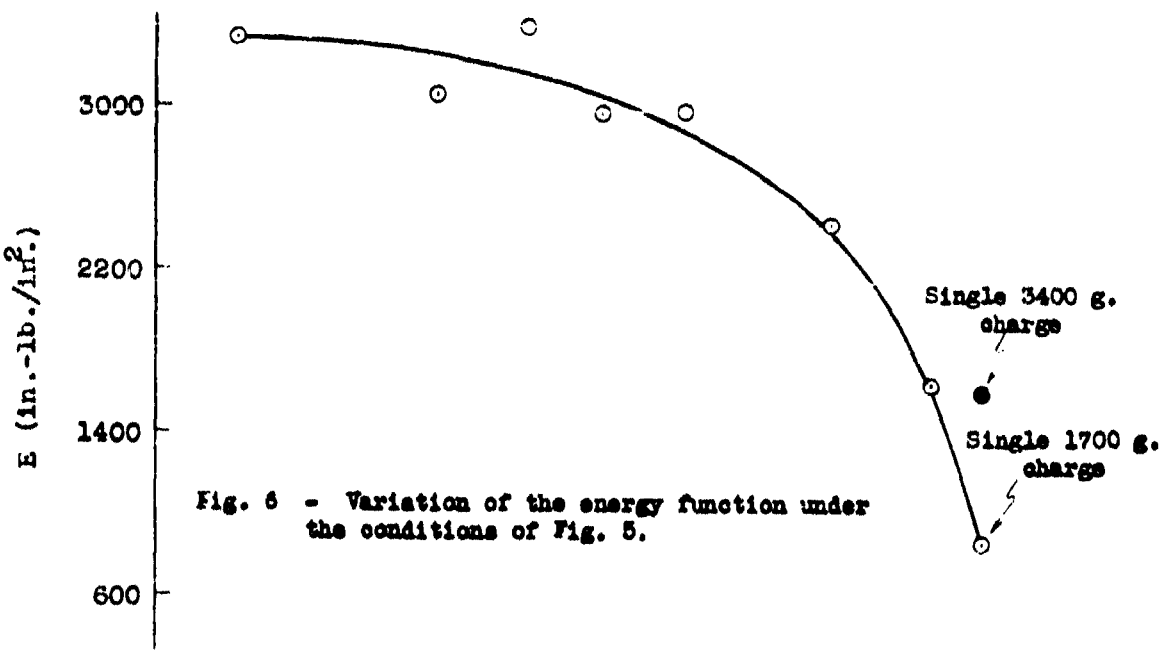


Fig. 6 - Variation of the energy function under the conditions of Fig. 5.

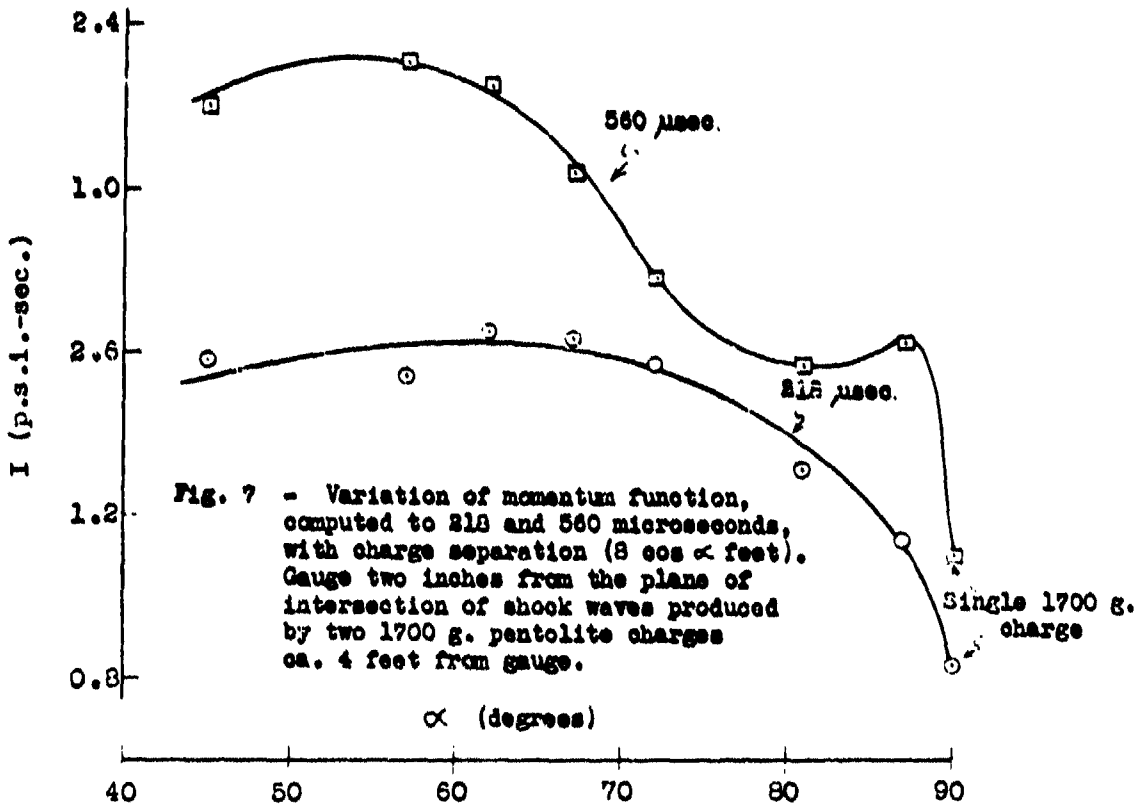


Fig. 7 - Variation of momentum function, computed to 218 and 560 microseconds, with charge separation (8 cos ∝ feet). Gauge two inches from the plane of intersection of shock waves produced by two 1700 g. pentolite charges ca. 4 feet from gauge.

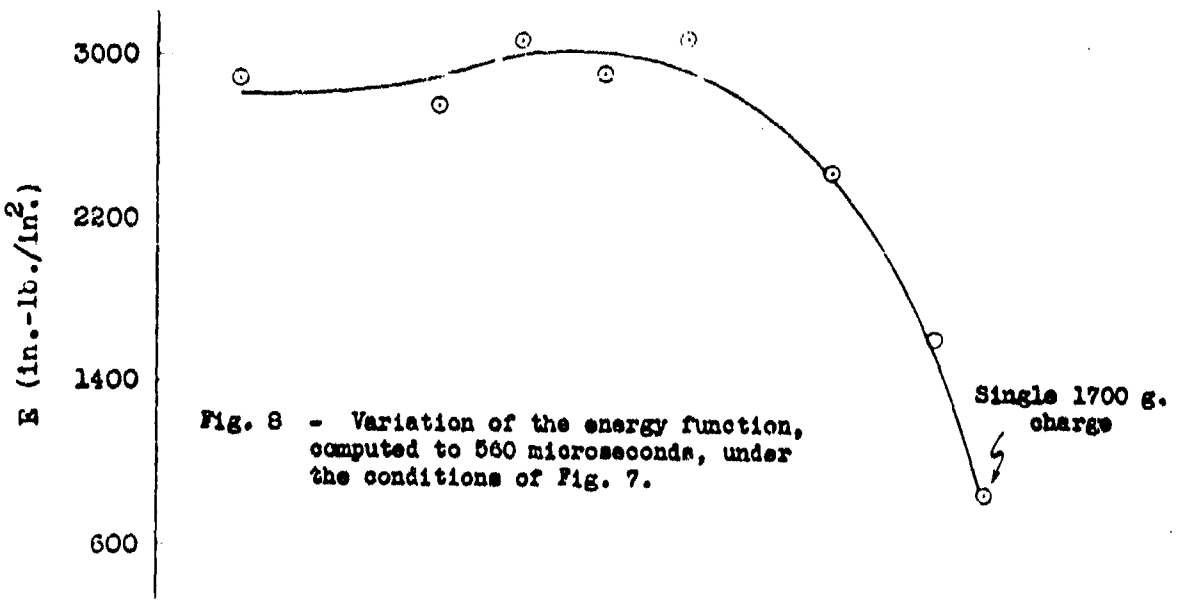


Fig. 8 - Variation of the energy function, computed to 560 microseconds, under the conditions of Fig. 7.

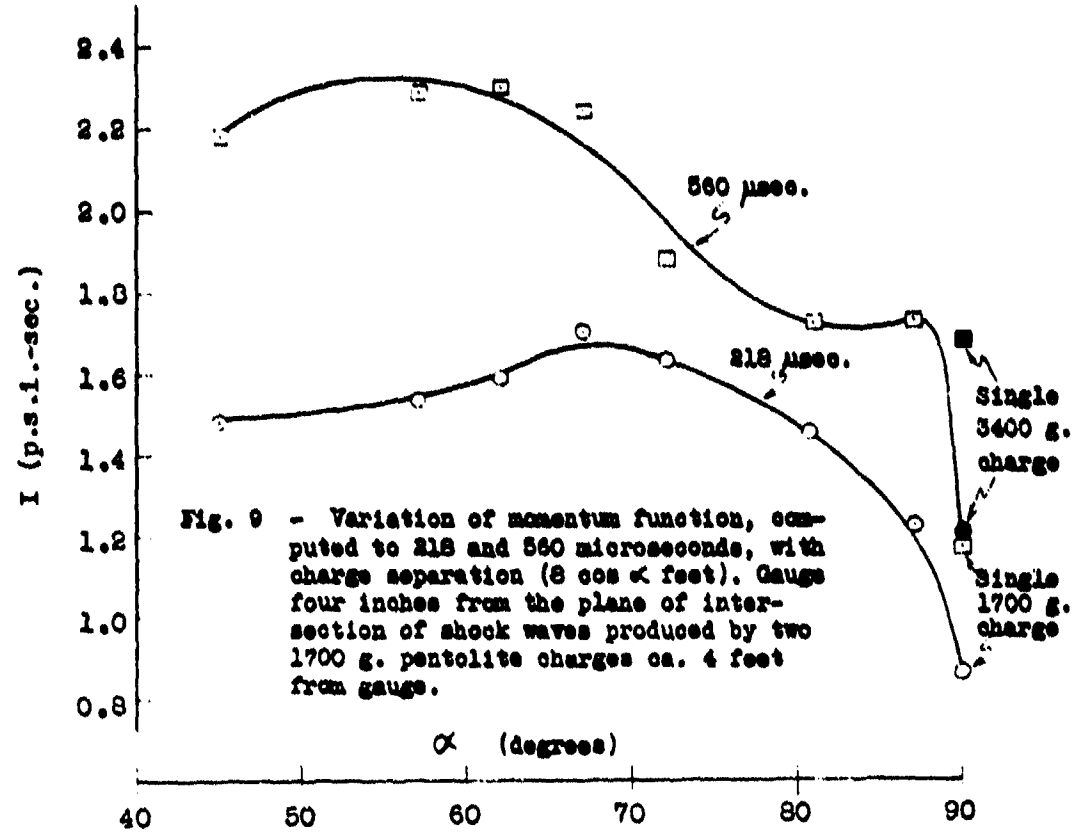


Fig. 9 - Variation of momentum function, computed to 218 and 560 microseconds, with charge separation (8 cos α feet). Gauge four inches from the plane of intersection of shock waves produced by two 1700 g. pentolite charges ca. 4 feet from gauge.

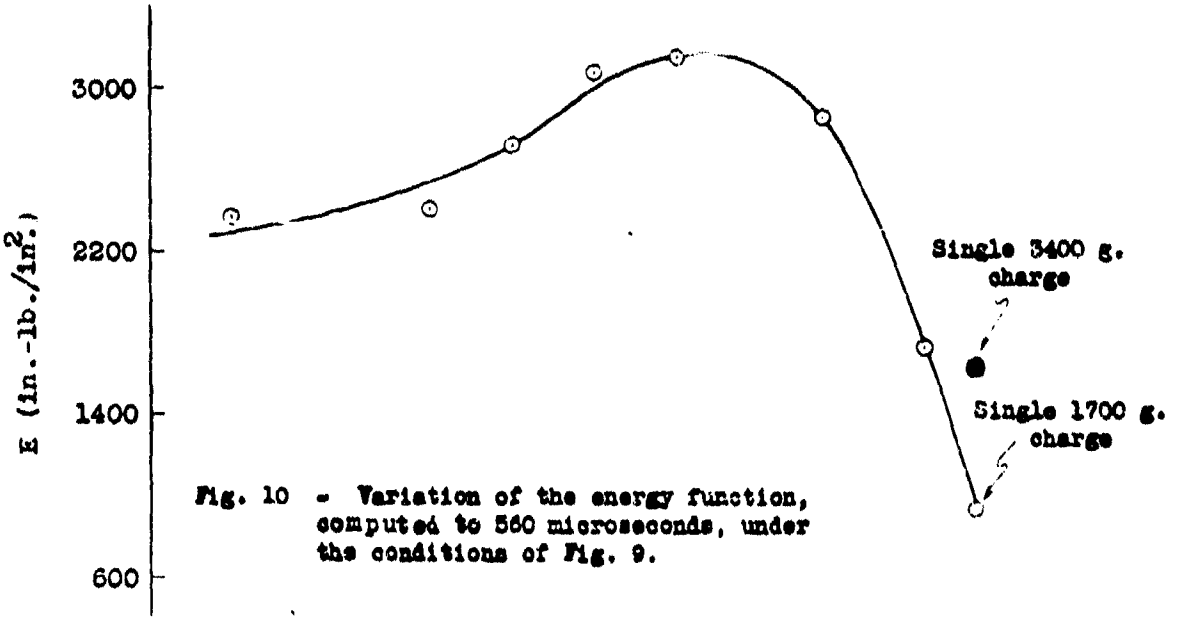


Fig. 10 - Variation of the energy function, computed to 560 microseconds, under the conditions of Fig. 9.

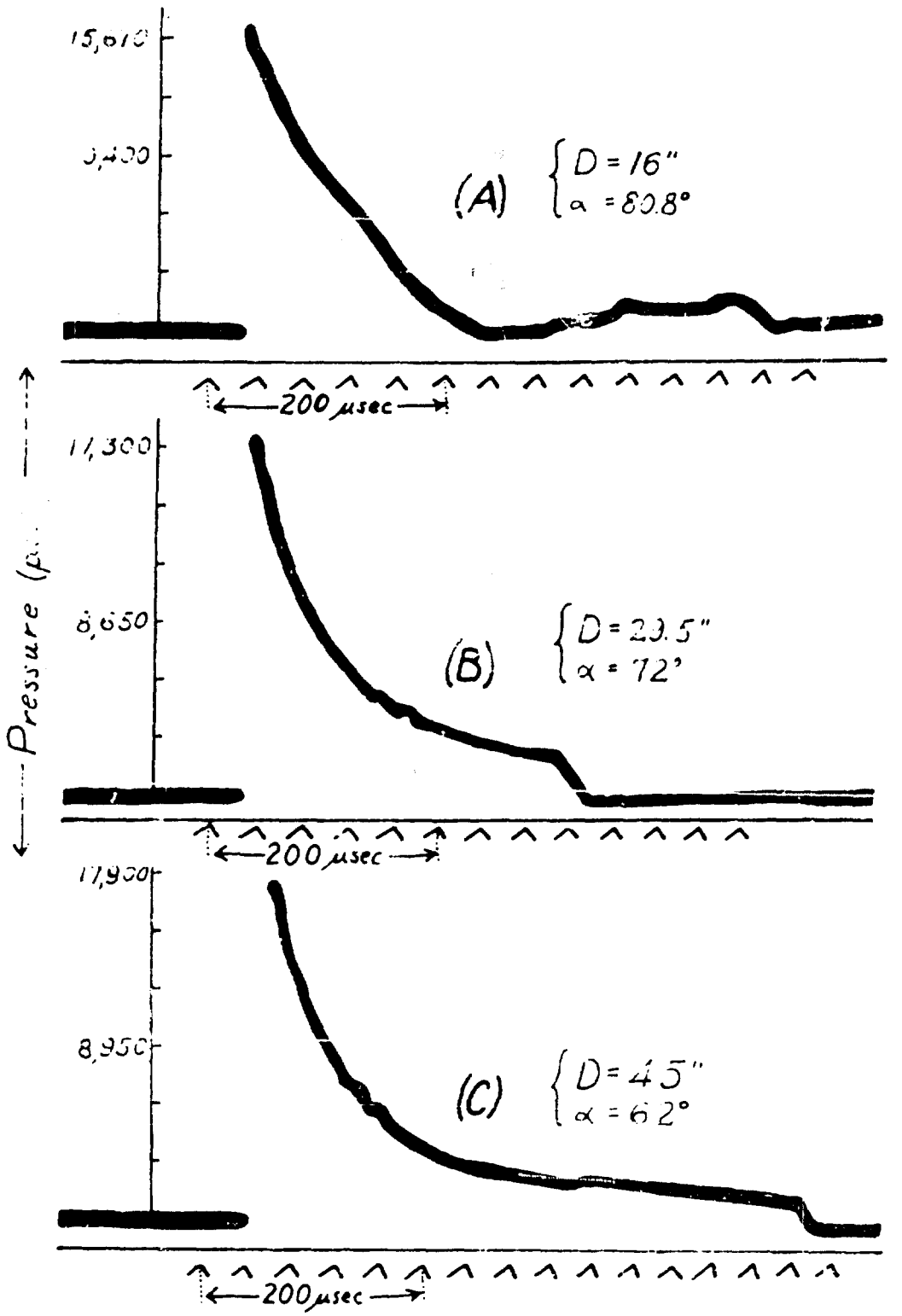


Fig. 11. Typical Pressure Time Records Obtained at the Intersection of Shock Waves.
Gauges 4 ft. from two 1700 g. pentolite charges separated by (A), 16 in.; (B), 29.5 in., and (C), 45 in.

maximum in the plane of intersection but decreases steadily and greatly as the charges are brought together. Outside the plane of intersection, on the other hand, the curves show maxima, again to be explained on the basis of the late arrival, for the smaller α's, of the wave from the more distant charge.

Shielding of One Explosion by Bubble from Another. The gauge at G-2 recorded the shock wave from the more distant charge as affected by the presence of the gas bubble from the nearer charge. The observed pressure was found to be ½ to 1/3 the value expected in the absence of "screening". Furthermore, the pulse arrived later than would have been the case without the screening.

THE MULTIPLE CHARGE EFFECT

A. G. Booker and C. Harrington
Mine Design Department, Admiralty

British Contribution

July 1944

THE MULTIPLE CHARGE EFFECT

A. G. Booker and C. Harrington

Mine Design Department,
Admiralty

July 1944

* * * * * *

Summary.

The report discusses an effect, called the multiple charge effect, by which an enhanced explosive effect is obtained in a certain direction. Trials have proved that a multiple charge of weight 3½ lbs. T.N.T. produces a maximum pressure along a given line equal to that from a normal charge of weight 7½ lbs.

Theoretical considerations suggest that larger gains in efficiency are possible.

Introduction.

In connection with the development of a weapon employing sympathetic detonation as a means of initiating a second charge it was necessary to devise a means of recording the detonation of the second charge. Small scale trials were carried out in Horsea Lake with two 1½ lb. T.N.T. charges, one detonated sympathetically by the other, to find if the double detonation is distinguishable by piezo-electric gauges recording on a cathode ray oscillograph and photographed by a camera running at approximately 100 inches a second. During these trials the effect reported was discovered.

Trials have been carried out elsewhere in which one 2 oz. charge detonated electrically, operated a pressure switch, which fired a second 2 oz. charge at 3 ft. distance from the first. The time lag between the firing of these two charges was of the order of 2 or 3 milliseconds, and were of no use in relation to the present investigation. Sympathetic detonation on the other hand can reduce the time lag between the firing of the charges to the order of 100 microseconds, and this is the order of magnitude of the interval which must not be exceeded if the phenomena discussed here are to be studied.

Experimental details.

Two 1½ lb. T.N.T. charges, each fitted with a ½ oz. C.E. primer and a detonator in 1½ lb. demolition tins were slung 7 ft. deep and 6 inches apart, (i.e. there was 6 inches of water between the nearest points of the charges - see Plate 1, Figure 1). The live charge was fired electrically and the target charge detonated sympathetically. Piezo-electric gauges were slung 7 ft. deep, one on either side of the multiple charge in the plane containing the axes of the charges. (See Plate 1, Figure 1). The piezo-electric gauge A, on the live charge side showed two distinct pressure pulses. Gauge C on the target charge side recorded one pressure pulse with a maximum pressure about 60% higher than for a single charge; there was no suggestion of a double kick.

Three 1½ lb. T.N.T. charges, each fitted with a ½ oz. C.E. primer and a detonator were slung 7 ft. deep and with 6 inches water gaps between the charges. The charge at one end, the line charge, was fired electrically, and the two target charges detonated sympathetically. Piezo-electric gauge A on the live charge side showed three distinct pulses (See Plate III, Figure 5). Gauge C on the target charge side recorded one pressure pulse with a maximum pressure about 80% higher than that of a single charge and again there was no indication of multiple kicks.

A series of shots with multiple charges composed of 2, 3 and 4 times 1½ lb. T.N.T. charges, and comparison single charges were fired alternately. In general the distance between the charges was 6 inches but for two shots the distance was 3 inches and for another it was 9 inches.

The results are given in Table 1. The maximum pressure, momentum (area under the pressure-time curve) energy ($\int p^2 dt$) and 1/n, the exponential time constant (the time taken for

the .....

Available Copy

the pressure to fall to 1/e of the maximum pressure) are given as percentages of the values for the single charge. The equivalent weight of the charge is the weight of a normal charge which would produce the same effect as the multiple charge, using the laws.

$$\left.\begin{aligned} \text{Maximum pressure} &= K_1 W^{1/3} \\ \text{Momentum} &= K_2 W^{2/3} \\ \text{Energy} &= K_3 W \end{aligned}\right\} \quad W = \text{weight of charge}$$

TABLE 1. Value of maximum pressure, momentum and energy for multiple charge of 2, 3 and 4 times 1½ lbs. T.N.T.

No. of units in Multiple charge	Dist. between units ins.	Maximum pressure		Momentum ($\int p.dt$)		Energy ($\int p^2 dt$)		
		%	Equiv. weight of charge	%	Equiv. weight of charge	%	Equiv. weight of charge	%
One	-	100	W(= 1½ lbs.)	100	W	100	W	100
Two	6	134		154		264		344
	"	147		158		236		139
	"	141		162		286		170
	"	161		164		340		186
Two	3	144		142		214		92
Two	9	189		154		184		83
	Mean	159	4.0 W	157	2.0 W	271	2.7 W	
Three	6	192		207		500		98
	"	170		207		465		164
	Mean	181	5.9 W	207	3.0 W	482	4.8 W	
Four	6	197	7.6 W	246	3.9 W	683	6.8 W	172
Four*	3	170	4.9 W	220	3.8 W	460	4.6 W	136

* It is considered possible that only 3 of these charges detonated.

Theoretical considerations.

The pressure pulse from an explosive charge consists of a very rapid rise to a maximum pressure followed by a more gradual fall of pressure to zero. As a fair approximation the pulse at distance D ft. from W lbs. of T.N.T. may be taken to be

$$\left.\begin{aligned} p &= p_0 e^{-nt}, \; p = p_0, \; t = 0 \\ p &= 0 \qquad\qquad t = 0 \end{aligned}\right\} \quad \text{with} \quad p_0 = \frac{K W^{1/3}}{D} \text{ and } n = c/W^{1/3} \qquad (1)$$

where p is the pressure, t the time, W the weight of charge, D the distance from the charge to the point in question and K, c are constants.

If the charge of weight W is replaced by a charge of weight 8 W the pulse becomes

$$p = 2 p_0 e^{-\frac{n}{2} t} \qquad p = p_0; \; t = 0$$

i.e. .....

Best Available Co

i.e., the maximum pressure is doubled and the time constant of the exponential (1/n in the first case) is also doubled.

Suppose the charge of weight W is now replaced by 8 single charges of weight W spaced on the circumference of a circle (Plate 1, Figure 3) and the charges are detonated simultaneously. At the point O, if the pressures are additive, the pulse is still exponential with the same time constant as for the single charge (1/n) but with a maximum pressure eight times that of the single charge. The effect is illustrated in Plate 1, Figure 4.

Table 2 gives the maximum pressure, momentum and energy in the 3 cases.

TABLE 2. Maximum pressure, momentum and energy in the pressure pulse at a point distance D from a multiple charge and a normal charge.

Charge	Maximum Pressure	Momentum	Energy
Single charge of Weight W	p_0	p_0/n	$p_0^2/2n$
Multiple charge, 8 separate charges of Weight W	$8p_0$	$8p_0/n$	$64p_0^2/2n$
Normal charge of Weight 8W	$2p_0$	$4p_0/n$	$8p_0^2/2n$

The multiple charge has a much enhanced effect at the point in question over the normal charge of equal weight. The multiple charge effect is equivalent to an interference effect, the separate pulses reinforcing each other in a certain direction and interfering in the geometrically opposite direction. For a normal charge the energy is propagated equally in all directions; for a multiple charge an excess of the energy is directed towards the point in question.

The figures of the exponential time constant 1/n given in Table 1 suggest why the actual gain in efficiency is not as great as the theoretical maximum. With absolute coincidence of the arrival of the pressure pulses the time constant should be equal to that of the single charge (i.e. should = 100%). Generally the experimental time constants are of the order of 150% and for shots in which the time constant is low the equivalent weight of the multiple charge is high, e.g. the double charge with 9 inches between the units has a freak time constant of 83% and an equivalent weight of 6.7 W as against a mean time constant of 125% and an equivalent weight of 4.0 W.

It is of interest to find the lag in the arrival of the pulses from a double charge which would give the maximum pressure actually obtained (159%). Taking $\frac{7800}{W^{1/3}} = 6900$ for the 1½ lb. T.N.T. charge the lag is 75 microseconds. Similarly for a triple charge in which the pulses arrive at time 0, t, 2t the maximum pressure obtained (181%) corresponds to t = 92 microseconds. If, however, it is assumed that the time lag of arrival of the first two pulses is 75 microseconds (i.e. the value for a double charge) then the time lag between the arrival of pulses two and three becomes approximately 100 microseconds.

The graphs Plates IV and V illustrate how the maximum pressure and equivalent weight of charge vary with the time lag between the arrival of the multiple pulses. The multiple charges fired at Horsea had lags of the order of 75 to 100 microseconds between kicks. If these lags can be cut down say by 30% then a triple charge of actual weight 3 W would have an equivalent weight of over 10 W, i.e. a gain of over 3 : 1 as against the 2 : 1 obtained.

Conclusion.

The report discusses an effect, called the multiple charge effect, by which an enhanced explosive efficiency is obtained in a certain direction. Trials have proved that a multiple charge of weight 3½ lbs. T.N.T. produces a maximum pressure along a given line equal to that from a normal charge of weight 7½ lbs.

Theoretical considerations suggest that larger gains in efficiency are possible.

Best Available Copy

APPENDIX

THE MECHANISM AND TIMING OF THE MULTIPLE PULSE EFFECT BY SYMPATHETIC DETONATION

An attempt is made below to describe how the multiple pulse effect is obtained by sympathetic detonation.

Assume that the charge X (see Plate 1, Figure 1) detonates instantaneously. The 'rays' of the pressure pulse travel radially outwards from the charge through the water at a velocity greater than 5,000 ft. per second, and strike the charge Y along the line L M, and, until detonation, travel through that charge with the velocity of sound through T.N.T. (about 6,000 ft. per second - see Wood, S.S. Report No. 1064). At some time t_o after the rays arrive at L M the charge Y is detonated sympathetically. During detonation the detonation wave travels from the point of initiation in all directions through the charge at approximately 20,000 ft. per second (the velocity of detonation for T.N.T.). On reaching the far side of charge Y at (= Q) the pulse then travels through the water with a velocity which soon drops to approximately 5,000 ft. per second.

Two pulses therefore arrive at gauge C, one from X diffracted round the charge Y, which travels through the water at 5,000 ft. per second (approximately) and the other originating from Y t seconds after the X pulse arrives at L M, which travels to the = Q side of Y at 20,000 ft. per second, and then travels through the water at a velocity soon falling to 5,000 ft. per second.

Consider the times of arrival of the two pulses at C. That due to the charge Y has, as compared with that due to X, a lag t seconds and gains (1) due to the detonation wave travelling at 20,000 ft. per second through part of the charge Y (as compared with 5,000 ft. per second) (2) due to the point of initiation of the charge Y not being at the edge of the charge, along L M, but at some point in the interior of the charge.

If the lag t_o is equal to the sum of the gains the two pulses arrive at C simultaneously. As discussed in the report the difference between the lag t_o and the two gains is of the order of 75 microseconds.

Gauge A recorded the multiple pulses separately (see Plate 3, Figure 3). The time lag between the arrival of the peaks was always slightly more than is accounted for by the pulse travelling at 5,000 ft. per second from X to the edge of Y (at L M) and back to the point in space which was originally the centre of the charge X. The extra time is not necessarily the time lag t_o between the arrival of the pulse at L M and the sympathetic detonation, because the return pulse arrives at the Gauge A after travelling through the gas bubble from X and the velocity of the pulse on the return path may drop below 5,000 ft. per second in passing through the gas bubble.

Best Available Copy

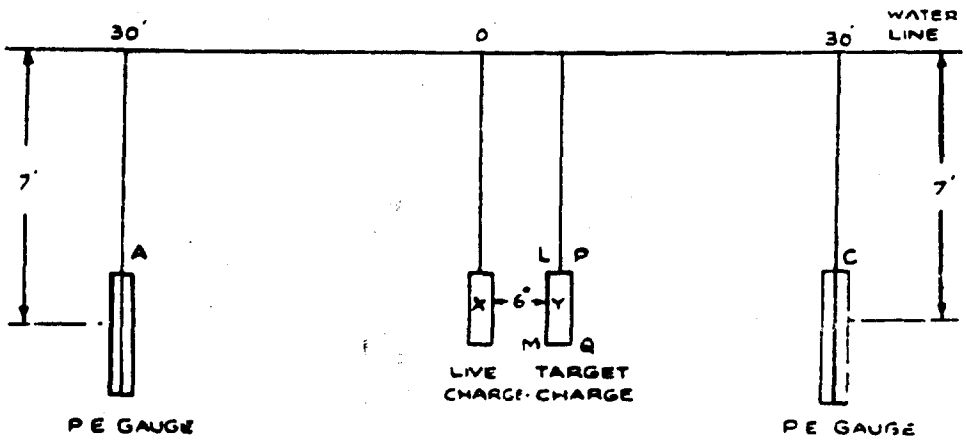


FIG 1. LAY OUT OF TROT

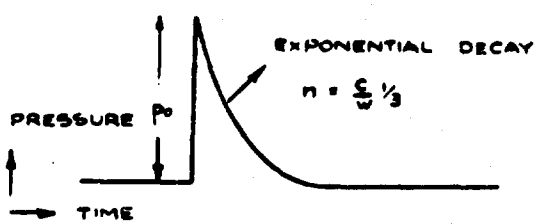


FIG 2. THE PRESSURE PULSE AT A POINT DUE TO AN EXPLOSIVE CHARGE

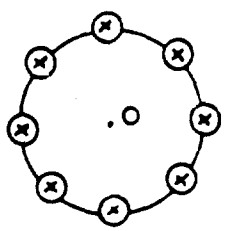


FIG. 3 ILLUSTRATING THE MULTIPLE CHARGE EFFECT

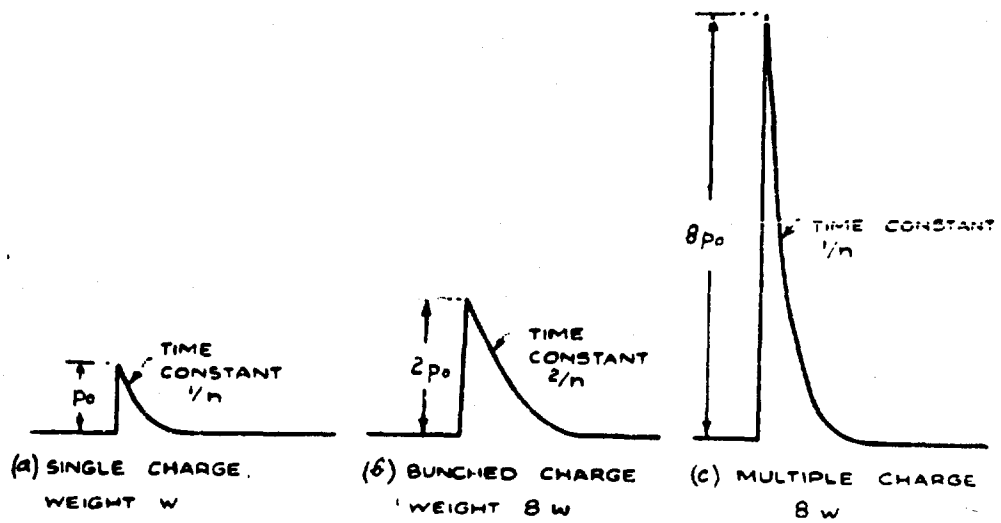


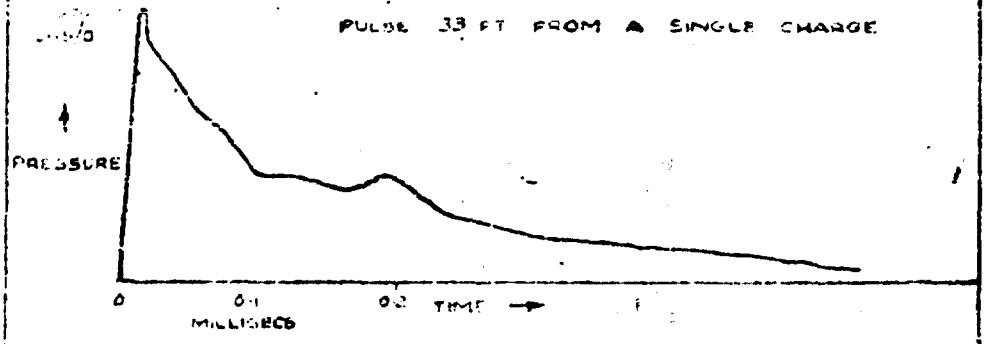
FIG 4 THE BUNCHED CHARGE EFFECT (b) AND THE MULTIPLE CHARGE EFFECT (c)

PLATE II

PRESSURE PULSES FROM MULTIPLE CHARGES

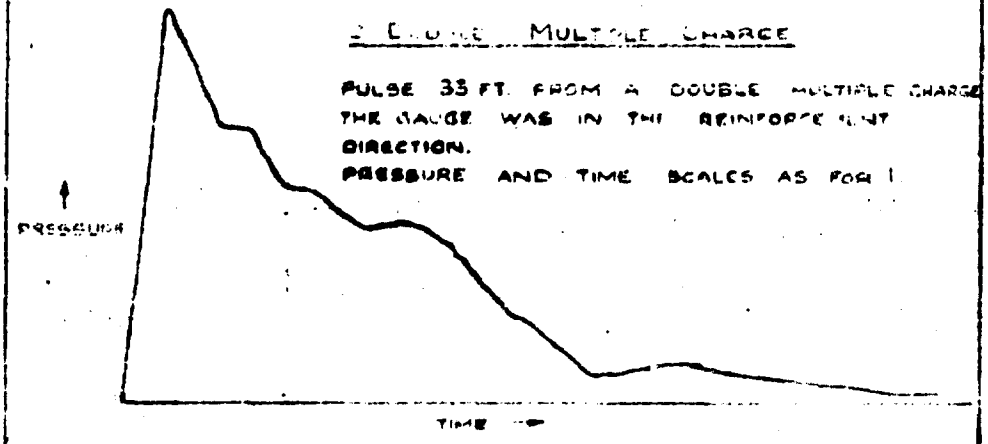
1 SINGLE CHARGE

PULSE 33 FT FROM A SINGLE CHARGE



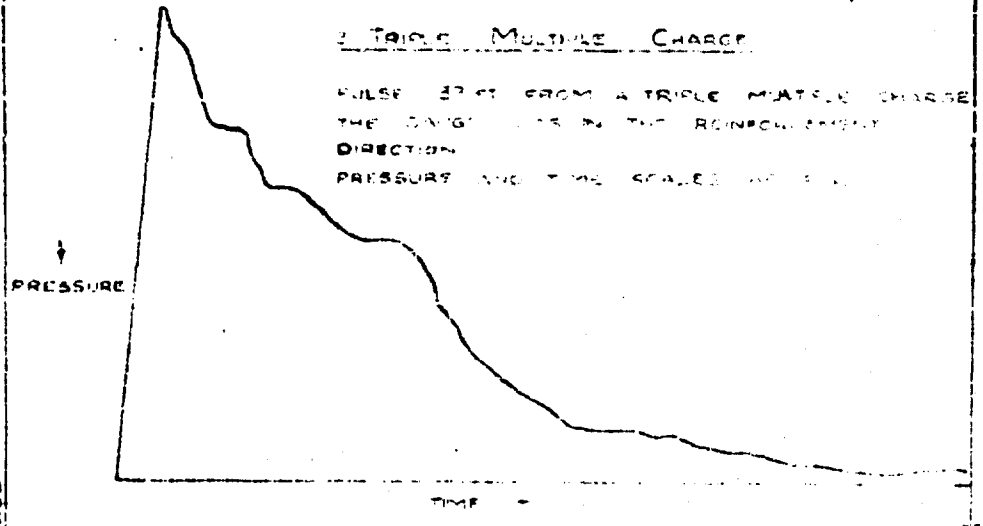
2 DOUBLE MULTIPLE CHARGE

PULSE 33 FT. FROM A DOUBLE MULTIPLE CHARGE
THE GAUGE WAS IN THE REINFORCEMENT
DIRECTION.
PRESSURE AND TIME SCALES AS FOR 1



3 TRIPLE MULTIPLE CHARGE

PULSE 33 FT FROM A TRIPLE MULTIPLE CHARGE
THE GAUGE WAS IN THE REINFORCEMENT
DIRECTION
PRESSURE AND TIME SCALES AS FOR 1



Best Available Copy

1. QUADRUPLE MULTIPLE CHARGE

PRESSURE

TIME

2. TRIPLE MULTIPLE CHARGE

THE PULSES FROM A TRIPLE MULTIPLE CHARGE IN THE INTERFERENCE CHAMBER (DIRECTED ON THE LOW CHARGE SIDE)

3RD PULSE

2ND PULSE

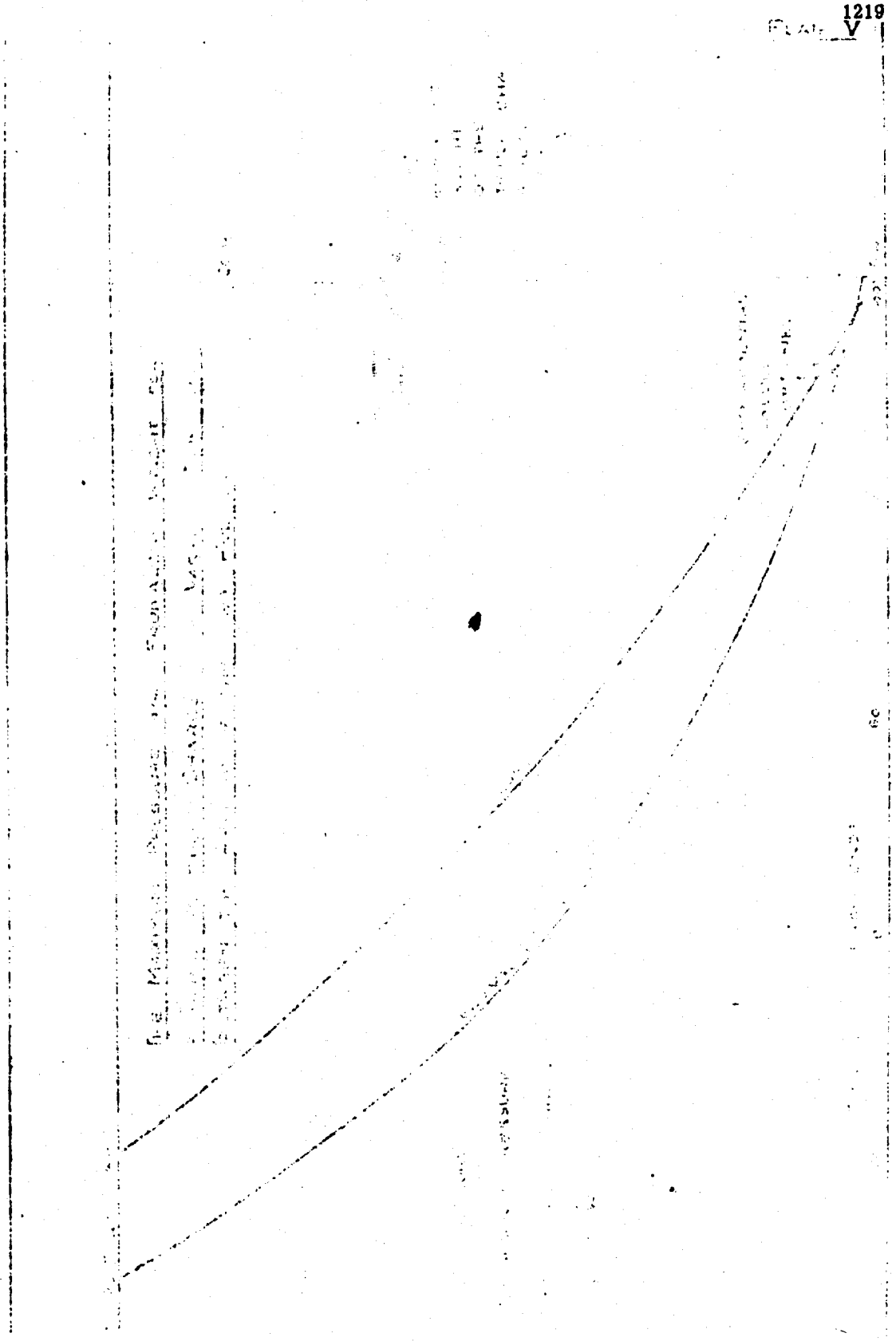
1ST PULSE

TIME

Best Available Copy

Best Available Copy

PLATE V



Best Available Copy

THE MULTIPLE CHARGE EFFECT, PART III

A. G. Booker and C. Harrington
Mine Design Department, Admiralty

British Contribution

July 1945

THE MULTIPLE CHARGE EFFECT, PART III

A. G. Booker and C. Harrington

Mine Design Department,
Admiralty.

July 1945

* * * * * * *

Introduction.

A previous paper (1) described trials on the Multiple Charge Effect by which an enhanced explosive effect is obtained in certain directions. The effect was obtained by means of sympathetic detonation. A new method of initiation using cordtex has been developed and is found to give a more efficient charge as well as being easier of application to explosive weapons.

Types of multiple charge used in the trial.

Experiments were carried out on two essentially different types of multiple charge (see Figures 1 and 2). They both consist of two 1½ lb. T.N.T. charges each with a ½ oz. C.E. primer and fitted in the 1½ lb. demolition charge tin. One of the 1½ lb. charges, called the initiator charge, is fitted with a detonator No. 21 Mark VII and is fired electrically. The second 1½ lb. charge called the target charge, has no detonator and is initiated by means of a length of cordtex running from the initiator charge. One end of the cordtex is attached to the outside of the initiator charge parallel to the axis of the charge, the other end runs through the primer of the target charge which is placed in the charge in the reverse direction and the end of the cordtex is knotted to prevent the cordtex pulling out of the primer.

The sequence of events in the detonation of the multiple charge is as follows:-

(1) The detonator of the initiator charge is fired electrically.

(2) From the detonator, the detonation wave travels through the primer and the T.N.T. to the cordtex strapped on the outside of the initiator charge.

(3) The detonation wave travels through the cordtex to the end which passes through the primer of the target charge.

(4) The primer and the T.N.T. of the target charge are detonated.

The target charge is detonated by the firing of the initiator charge but after a time lag determined by the time for the detonation wave to travel from the detonator of the initiator charge to the primer of the target charge. This time lag can be varied by varying the length of cordtex.

In Multiple Charge types 1A and 1B the two 1½ lb. charges are fixed by small pieces of wood with axes vertical and with a 6 inch water separation between them (Figure 1). It is known from the trials reported in (1) that sympathetic detonation does not occur with a water separation of 3 inches or more. 6 inch water separation was chosen for type 1 as a compromise between the minimum possible separation (which may be 1 inch or less) and a large separation (e.g. 1 ft.) which is best for experimental reasons since experimental errors in the measurement of distances and angles are thereby rendered less important. Although sympathetic detonation occurs at 2 inch separation and less a multiple charge with a separation less than the sympathetic detonation range may still be initiated by cordtex if the time for the detonation wave to travel through the cordtex is less than the time for sympathetic detonation to occur.

Multiple Charges type 1A and 1B differ only in the length of cordtex used. Type 1A has 40 inches of cordtex from the bung of one charge to the bung of the other charge, i.e. there is 40 inches of cordtex completely surrounded by water. This corresponds to a distance which the detonation wave has to travel of 47 inches of cordtex and 1½ inches of primer and T.N.T.

Type 1B .....

Type 1B has 12 inches of cordtex from the bung of one charge to the bung of the other charge, corresponding to a distance which the detonation wave has to travel of 19 inches of cordtex and 1½ inches of primer and T.N.T.

In Multiple Charge type 2 (see Figure 2) the two 1½ lb. T.N.T. charges are fixed by small pieces of wood with axes horizontal, with the primer end of the two charges pointing in the same direction and the primer end of the target charge nearer to the initiator charge. There is 6 inches of water between the two charges and 6 inches of cordtex between the bung of the target charge and the end of the initiator charge, corresponding to a distance which the detonation wave has to travel of 5 inches of charge and 10 inches of cordtex.

Multiple Charge type 1A is more efficient than Multiple Charges type 1B and 2. Trials were carried out on the latter two charges to clear up points of interest which arose. The charge type 1A is found to have a high efficiency within a cone of 90 degrees semi-vertical angle about the 0 degree direction as axis (throughout the report the 0 degree direction is the horizontal line from the centre of the initiator charge to the centre of the target charge and all directions quoted are directions in the horizontal plane through the 0 degree direction). Within the cone the pressure pulses from the two constituent charges combine to form a Mach wave. Charge type 1B was investigated because it was already known that the Mach wave from such a charge extended to the 90 degree direction at least. Theoretical considerations suggest that where the constituent charges detonate simultaneously the Mach wave angle is centred about the 90 degree direction. Multiple Charge type 2 was chosen as being one in which the detonations were nearly simultaneous, it being impossible to cut down the length of cordtex in the Type 1 charges below 12 inches without introducing right angle bends.

Since the distance between the centre of gravity of the constituent charges in Type 1 is 8½ inches as compared with 15 inches in Type 2 no comparison between 'vertical' and 'horizontal' charges is possible.

Experimental details.

Preliminary trial.

As a preliminary trial the length of cordtex in Multiple Charge Type 1 was varied and the efficiency with each length of cordtex measured by four piezo-electric pressure gauges. The gauges, with axes vertical and one side facing the charge were slung at the same depth as the charge, 7 ft. in Horsea Lake as follows (see Figure 3):-

(1) Pear Gauge (crystal area 2 sides x ⅜ inches diameter) 15 ft. from the charge in the direction 0 degrees.

(2) A third size strip gauge (crystal area 2 sides x 5 inches x 1¼ inches) 30 ft. from the charge in the direction 30 degrees.

(3) A full size strip gauge (crystal area 2 sides x 18 inches x 1¼ inches) 55 ft. from the charge in the direction 45 degrees.

(4) A full size strip gauge 37 ft. from the charge in the direction 90 degrees.

The gauge was placed at 90 degrees to give an approximate value for the time interval between the detonation of the initiator and target charges, the argument being that since the gauge is equidistant from the two charges the pulses from the initiator and target charges would travel to the gauge in equal times and hence the time between the arrivals of the two pulses at the gauge is the time lag between the detonations themselves. This argument is only approximately true because the pressure pulse from the target charge may travel in part through water which is already at a high pressure due to the initiator charge. Again the measurements show that when the target charge detonates a small but finite time (e.g. 20 microseconds) after the initiator charge the 90 degree gauge records not two but one pulse only which on the above argument implies that the two charges detonate simultaneously whereas in fact simultaneous detonation is not possible. This method of time interval measurement fails in such circumstances due to the formation of a Mach wave.

The results of the preliminary trial are given in Table 1 and in Figures 6 and 7. A normal 2½ lb. T.N.T. charge consisting of two 1¼ lb. T.N.T. charges strapped together was fired at regular intervals and Table 1 gives the maximum pressure and momentum of the Multiple Charge 1 with lengths of cordtex varying from 8 inches to 50 inches given as percentages of the

maximum .....

maximum pressure and momentum for the standard charge.

Measurement of the efficiency of multiple charges Types 1A, 1B and 2.

Four piezo electric gauges were slung 7 ft. deep in Horsea Lake in two directions from the charge making 15 degrees with each other and with one gauge at 15 ft. and one at 25 ft. in each direction. The gauges were kept fixed and the charges which were also slung 7 ft. deep, were rotated about a vertical axis relative to the gauges so that the pressure pulse was measured for all three types of Multiple Charge at all angles from 0 degrees to 180 degrees in steps of 15 degrees.

The measurements were repeated with the two gauge directions at 30 degrees with each other and with the gauges 37 ft. and 50 ft. from the charge. The charges were rotated relative to the gauge directions so that the pressure pulse was measured for all three types of charge at all angles from 0 degrees to 180 degrees in steps of 30 degrees.

A normal 2½ lb. T.N.T. charge consisting of two 1¼ lb. T.N.T. charges strapped together was fired at regular intervals and the result for the three types of Multiple Charge given in Tables 2, 3 and 4 are expressed as percentages of the results for this standard charge.

Results.

The preliminary trial results show that in the 0 degree direction the most efficient Multiple Charge Type 1 (two 1¼ lb. T.N.T. charges, axes vertical, 6 inches water separation) has a length of cordtex of 40 inches. This is the reason why Multiple Charge 1A was chosen with 40 inches of cordtex.

The explosive efficiency measurements of Multiple Charges Types 1A, 1B and 2 have been plotted in polar co-ordinate form in Figures 8 to 16. In the maximum pressure graphs Figures 8, 11, 14 the value of the maximum pressure on the four iso-lines drawn is the value of the maximum pressure 15, 25, 37 and 50 ft. from the standard 2½ lb. T.N.T. charge. In the momentum graphs Figures 9, 12, 15 the value of the momentum on the four iso-lines drawn is the value of the momentum at 15, 25, 37 and 50 ft. from the standard 2½ lb. T.N.T. charge. In the energy graphs Figures 10, 13, 16 the value of the energy on the four iso-lines drawn is the value of the energy at 15, 25, 37 and 50 ft. from the standard 2½ lb. T.N.T. charge. It has been assumed that for the Multiple Charges the maximum pressure and momentum obey the inverse distance law and the energy obeys the inverse distance squared law. The maximum pressure momentum and energy from the normal 2½ lb. T.N.T. charge have been obtained from the following empirical laws:-

$$\text{Maximum pressure} = 20{,}400 \left[\frac{W^{1/3}}{R}\right]^{1.14} \text{ lbs. per square inch.}$$

$$\text{Momentum} = 1.30 \left[\frac{W^{1/3}}{R}\right]^{0.842} \times W^{1/3} \text{ lbs. seconds per square inch.}$$

$$\text{Energy} = 2.79 \times 10^{4} \left(\frac{W}{R^2}\right) \text{ ft. lbs. per square ft.}$$

Figure 17 gives the maximum pressure, momentum and energy 15 ft. from the Multiple Charge Type 1A expressed as a ratio of the maximum pressure momentum and energy 15 ft. from the normal 2½ lb. T.N.T. charge.

Mach wave effects.

Colonel Libessart of M.O.M.S. and MacDougall of the U.S.A. and others have obtained photographs showing that when the pulse from a charge strikes a boundary geometrical reflection breaks down when the pressure in the pulse is sufficiently high and the reflection near to grazing incidence; the point of junction of the direct and reflected pulses leaves the boundary and a Mach shock wave is formed between the intersection and the boundary, i.e. some points near the boundary are traversed not by two distinct pulses, the direct and reflected pulses, but by one only, the Mach wave. A similar effect has also been observed when two charges detonate simultaneously; some points near the right bisector of the two charges are traversed by one wave only, the Mach wave.

In the elementary acoustic theory when two pulses meet at an angle they pass through the point of intersection and continue in their original direction each unaffected by the other.

Von Neumann .....

Von Neumann (Bureau of Ordnance Explosives Research Report No. 12: Oblique Reflection of Shocks) has shown theoretically that when two shock waves meet at an angle then if the intensities of the waves are large and the angle between their two directions sufficiently small the two waves merge into one, known as the Mach wave (see Figure 5).

Figures 18 and 19 are pressure pulse records at angles from 180 degrees to 0 degrees and at distances of 37 ft. and 50 ft. from the Multiple Charge Type 1A. As the angle of measurement decreases from 180 degrees the time interval between the two distinct pulses recorded decreases from 300 microseconds to about 5 microseconds at 60 degrees. At angles of less than 60 degrees the two pulses merge into one.

Consider Figure 4 in which A and B represent the initiator and target charges respectively. Charge A is fired electrically at time 0 and as noted previously charge B detonates after the time the detonation wave requires to travel through 12 inches of C.E. primer and T.N.T. charge and through 47 inches of cordtex. The time interval between the detonation of charges A and B as measured by the gauge at 90 degrees is approximately 90 microseconds. The pressure pulses from A and B initiated at times 0 and 90 microseconds respectively travel in all directions with the velocity of propagation of the pressure pulse in water. For the gauge in the 180 degree direction the pulse from A leads the pulse from B by 90 microsoconds plus the time for the B pulse to travel BA (including the extra time the B pulse requires to traverse or diffract round the gas bubble of A). For the gauges at 150 degrees the pulse from A leads by 90 microseconds plus the time for the B pulse to travel the extra distance AB cos 30°. For the gauges at 60 degrees the pulse from A leads by 90 microseconds minus the time for the A pulse to travel the extra distance AB cos 60°. For the gauges at 0 degrees the pulse from A leads by 90 microseconds minus the time for the A pulse to travel the extra distance AB.

The reasoning in the preceding paragraph explains why, for Multiple Charge Type 1A, the time interval between the two distinct pulses recorded decreases as the angle of measurement decreases from 180 degrees to 60 degrees. At less than 60 degrees the two pulses merge into a Mach wave.

For Multiple Charge Type 1B the Mach zone extends from 0 degrees to 100 degrees. For Multiple Charge Type 2 the Mach zone extends from 60 degrees to 95 degrees approximately. Table 5 analyses the results from a Mach wave standpoint.

Figure 5 illustrates the formation of the Mach wave zone for the Multiple Charge Type 2.

Charge B detonates approximately 30 microseconds after charge A. Consider the hyperbola, foci A and B, whose difference in focal distances PA minus PB is equivalent to 30 microseconds. This hyperbola is the locus of intersection of the pulses from A and B. Let P_1 be the point of intersection nearest to the charges. If the angle AP_1B is sufficiently small for the intensity of the intersecting pressure pulses a Mach wave will be formed. If AP_1B is too large the two pulses will continue in their original directions undisturbed. It may be for some other point on the hyperbola, that corresponding to the intensity of the constituent pulses at that point, the angle APB is small enough for a Mach wave to be formed. Suppose P_2 is the point at which the Mach wave is formed and P_2L_1 and P_2M_1 are positions of the wave fronts from the charges A and B respectively. At a later time the wave front from charge A is at Q_2L_2, the wave front from charge B is at R_2M_2 and the Mach wave front is R_2Q_2. The position of the three wave fronts at an even later time are Q_3L_3, R_3M_3 and R_3Q_3 respectively and the Mach zone is the area bounded by the lines $P_2R_2R_3$ —— and $P_2Q_2Q_3$ ——.

When the time interval between the detonation of the charges is zero the hyperbola of intersection becomes the straight line in the 90 degrees direction and the Mach zone is formed symmetrically about that line. When the time interval between the detonation of the charges is equivalent to the time for the pressure pulse to travel from A to B then the hyperbola of intersection becomes the straight line in the 0 degrees direction and the Mach zone is formed symmetrically about that line. The equations of the asymptotes to the hyperbola of intersection are

$$y = \pm \frac{\sqrt{b^2 - \delta^2}}{\delta} \quad x$$

where the x axis is the 0 degree direction

the y axis is the 90 degree direction

$2b$ = effective distance between the charges

2δ = distance lag of the two pulses.

For .....

For Multiple Charges Types 1A and 1B the distance between the centres of the two charges is 4½ inches, i.e. b = 4½ inches. For Multiple Charge Type 2 the distance between the centre of the charges is 18 inches, i.e. b = 9 inches. These values are only very approximate since "the effective distance" between the charges may be the distance between the centre of gravity of the two charges or it may be the water separation between the charges or some distance between the two. Any estimations of the distance lag of the two pulses, i.e. the distance travelled to the point of intersection by the pulse from the initiator charge above that travelled by the target charge is even more approximate involving as it does a knowledge of the time lag between the detonations of the two charges and the velocity of the two pressure pulses. An estimate has been made as follows. The velocity of the detonation wave through cordtex is about four times the velocity of the pressure pulse when the two velocities settle down to their steady value, i.e at some distance from the initiating charge. As a rough estimation therefore the distance lag 2 δ is taken to be one quarter of the distance the detonation wave has to travel through C.E., T.N.T. and cordtex, i.e. b = 6, 2½ and 2 inches for Multiple Charge Types 1A, 1B and 2 respectively. The corresponding directions of the asymptotes are 0, 50 and 75 degrees respectively, i.e. the Mach zones for the charges should be centred about these directions, respectively. These calculated values agree with the experimental results.

For Multiple Charge Type 1A the Mach zone is centred about the 0 degrees direction and extends 50 degrees in any plane from that direction. The intensity of the pulse in this Mach wave cone is higher than the intensity in the other directions and is greater than that of a normal 2½ lb. charge. Figures 8, 9 and 10 show that within the Mach zone the intensity is almost constant with a slight increase in the 0 degree direction.

For Multiple Charge Type 1B the Mach zone is centred about the 50 degree direction and extends 50 degrees in any plane from that direction. Since the charge is symmetrical about 0 degrees there is a Mach zone at -50 degrees which also extends 50 degrees in any plane from that direction. Therefore the two Mach zones at the charge merge into a cone of semivertical angle 100 degrees centred about the 0 degrees direction. Figures 11, 12 and 13 show that within the Mach zone the intensity shows maximum value in directions about 50 to 60 degrees, i.e. in the direction about which the Mach zone is centred. Hence the preceding theory gives an explanation of the greater efficiency at 50-to 60 degrees in Figures 11, 12 and 13.

For Multiple Charge Type 2 the Mach zone is centred about the 75 degrees direction and extends 25 degrees in any plane from that direction. Since the charge is symmetrical about 0 degrees there is a Mach zone from -50 degrees to -100 degrees. The intensity of the charge is higher in the Mach zone than in any other direction and is greater than that from a normal 2½ lb. charge. Figures 14, 15 and 16 show that within the Mach zone the intensity is not constant but has a maximum value in the 75 degrees direction. Whilst for the previous two Multiple Charges 1A and 1B the angular spread of the Mach zone is the same at all distances measured from 15 ft. to 50 ft. the results for this charge give a Mach zone at 60 degrees for 37 and 50 ft. distance but a normal zone in the same direction at 15 and 25 ft. This may be due to experimental error in orienting the charge relative to the trot. These orientations are considered only accurate to ± 5 degrees.

A.H. Shanes of U.S.A., as reported previously, found that for two intersecting underwater pressure pulses with peak pressures 8900 p.s.i. at the point of intersection the critical angle between the two pulse directions for the onset of the Mach effect is 54 degrees, i.e. if the two pulses intersect at less than 54 degrees they form a Mach wave. The angle of intersection of the two pulses for Multiple Charge Type 2 is less than 54 degrees for all points on the hyperbola of intersection 1 ft. and more from the point midway between the two charges. At 1 ft. the peak pressure is much greater than 8900 p.s.i. Therefore the Mach wave extends back to within 1 ft. and nearer of the charge. The same reasoning applies to a Multiple Charge Types 1A and 1B. Thus for all practical purposes the Mach zones can be said to extend back to the charge itself.

To summarise: Multiple Charges Types 1A, 1B and 2 form Mach wave zones within volumes which are, to a first degree of approximation at least, cones with semi-vertical angles 50, 100 and 25 degrees respectively, the vertex of the cone being at the charge. Within the Mach zone the intensity of the pressure pulse is greater than in other directions and is greater than that from a normal charge with equal weight of T.N.T. For Multiple Charge Type 2 the intensity within the Mach zone varies appreciably and is greater in the direction of the axis of the Mach zone cone. For Multiple Charge Type 1A the Mach zone has a greater volume and whilst the variation of intensity within the zone is not so great the intensity is still much greater than that outside the Mach zone. For Multiple Charge Type 1B the Mach zone is of even greater volume extending over more than a hemisphere, the variation of intensity within the zone is again small and the intensity within the zone is not much greater than that outside the zone.

Summary .....

Summary of results.

For Multiple Charge Type 1A, at 15 ft. distance, the Mach zone extends 50 degrees either side of the 0 degree direction and the maximum pressure, momentum and energy in this zone are 140%, 158% and 212% respectively of the corresponding values at the same distance from a normal charge with equal weight of explosive. The 2½ lb. Multiple Charge 1A thus produces at 15 ft. a maximum pressure, momentum and energy equal to those from normal charges of weights 7 lbs., 5 lbs. and 5.25 lbs. respectively, i.e. this Multiple Charge has the explosive efficiency of a normal charge containing at least double its own weight of explosive.

For Multiple Charge Type 1B, at 15 ft. distance, the Mach zone extends 100 degrees either side of the 0 degree direction. The charge has highest explosive efficiency in the directions between 60 and 80 degrees where the maximum pressure, momentum and energy are 140%, 135% and 135% respectively of the corresponding values at the same distance from a normal charge with equal weight of explosive, i.e. Multiple Charge Type 1B produces at 15 ft. in the directions between 60 and 80 degrees a maximum pressure momentum and energy equal to those from normal charges of weights 7 lbs., 4 lbs. and 3.8 lbs. respectively.

For Multiple Charge Type 2, at 15 ft. distance, the Mach zone extends from about 50 to 100 degrees. The charge has highest explosive efficiency at about 75 degrees where the maximum pressure, momentum and energy are 165%, 155% and 195% respectively of the corresponding values at the same distance from a normal charge with equal weight of explosive, i.e. Multiple Charge Type 2 produces at 15 ft. in the 75 degree direction a maximum pressure, momentum and energy equal to those from normal charges of weights 11 lbs., 5 lbs. and 5 lbs. respectively.

Conclusions.

A further trial has been carried out on the Multiple Charge Effect using a new method of initiating the charge by means of cordtex. Pressure measurements have been made at four different distances and in various directions from three types of Multiple Charge each consisting of two 1½ lb. T.N.T. demolition charges. A 2½ lb. T.N.T. Multiple Charge gives within a cone of 50 degrees semi-vertical angle a maximum pressure, momentum and energy equal to that from normal charges of weight 7 lbs., 5 lbs. and 5.25 lbs. respectively.

The effect is found to be closely connected with the Mach wave effect.

Reference.

(1) "The Multiple Charge Effect", by A.G. Booker and C. Harrington.

TABLE 1. Multiple Charge 1. Effect of varying the length of Cordtex.

Two 1½ lb. T.N.T. charges axes vertical, 6 inches water separation. Results expressed as percentage of results for normal 2½ lb. T.N.T. charge.

No.	Length of Cordtex (bung to bung) ins.	Time interval between detonations of A and B as measured by 90° gauge	PRESSURE PULSE MEASUREMENTS					
			Gauge at 0°		Gauge at 30°		Gauge at 45°	
			Maximum Pressure %	Momentum %	Maximum Pressure %	Momentum %	Maximum Pressure %	Momentum %
1	8	0	106	113	111	105	115	113
2	20	28	113	120	116	114	116	114
3	30	63	121	128	132	124	126	126
4	40	113	136	141	136	132	134	134
5	80	170	136	136	140	136	130	130

TABLE 2. The pressure field round Multiple Charge 1A.

Two 1½ lb. T.N.T. charges, axes vertical, 6 inches water separation 40 inches cordtex.

Results expressed as percentages of results for normal 2½ lb. T.N.T. charge.

Angle degrees	AT 15 ft.			AT 25 ft.			AT 37 ft.			AT 80 ft.		
	Max. Press.	Momentum	Energy	Max. Press.	Momentum	Energy	Max. Press.	Momentum	Energy	Max. Press.	Momentum	Energy
0	131	144	212	130	127	165	132	149	170	125	130	174
15	130	176	196	136	127	166						
18							147	148	193	123	115	141
30	129	134	242	143	133	180	143	126	167	127	125	167
45	140	136	216	141	146	215						
48							136	99	129	137	117	125
54	118	136	172	128	130	172						
60	137	133	178	146	115	151	140	146	204	118	141	184
69	105	124	149	111	108	133						
75	121	115	143	138	136	180						
90	112	114	121	115	116	128	105	123	139	110	123	144
105	75	104	68	100	110	90						
120	83	97	86	70	94	84	83	80	63	74	73	52
135	83	89	78	69	67	45						
150	84	67½	48	78	72	57	78	86	70	59	57	44
165	79	66	48	77	66	47						
180	70	72	55	78	71	55	72	81	59	70	65	45

TABLE 3. The pressure field round Multiple Charge 1B.

Two 1½ lb. T.N.T. charges, axes vertical, 6 inches water separation, 12 inches cordtex.

Results expressed as percentages of results for normal ½ lb. T.N.T. charge.

Angle degrees	AT 13 ft.			AT 25 ft.			AT 37 ft.			AT 50 ft.		
	Max. press.	Mom-entum	En-ergy	Max. press.	Mom-entum	En-ergy	Max. press.	Mom-entum	En-ergy	Max. press.	Mom-entum	En-ergy
0	112	109	124	110	98	101	106	107	110	103	103	118
15	104	119	134	118	113	120						
18							106	117	136	103	107	128
30	100	101	103	110	105	117	120	114	130	107	104	104
45	113	123	146	130	104	118						
48							112	108	128	110	100	102
60	132	113	134	128	120	150	120	114	142	139	101	143
75	143	134	160	144	173	143						
90	119	108	131	128	118	130	124	117	147	110	128	129
105	100	142	143	111	161	133						
120	78	87	73	78	69	76	81	91	79	66	67	71
135	86	103	77	78	122	94						
150							80	98	78	89	70	69
165	84	87	63	72	980	539						
180	73	74	58	80	89	74	69	73	49	74	49	48

TABLE 4. The pressure field round Multiple Charge 2.

Two 1½ lb. T.N.T. charges axes horizontal 6 inches water separation 6 inches cordtex.

Results expressed as percentages of results for normal ½ lb. T.N.T. charge.

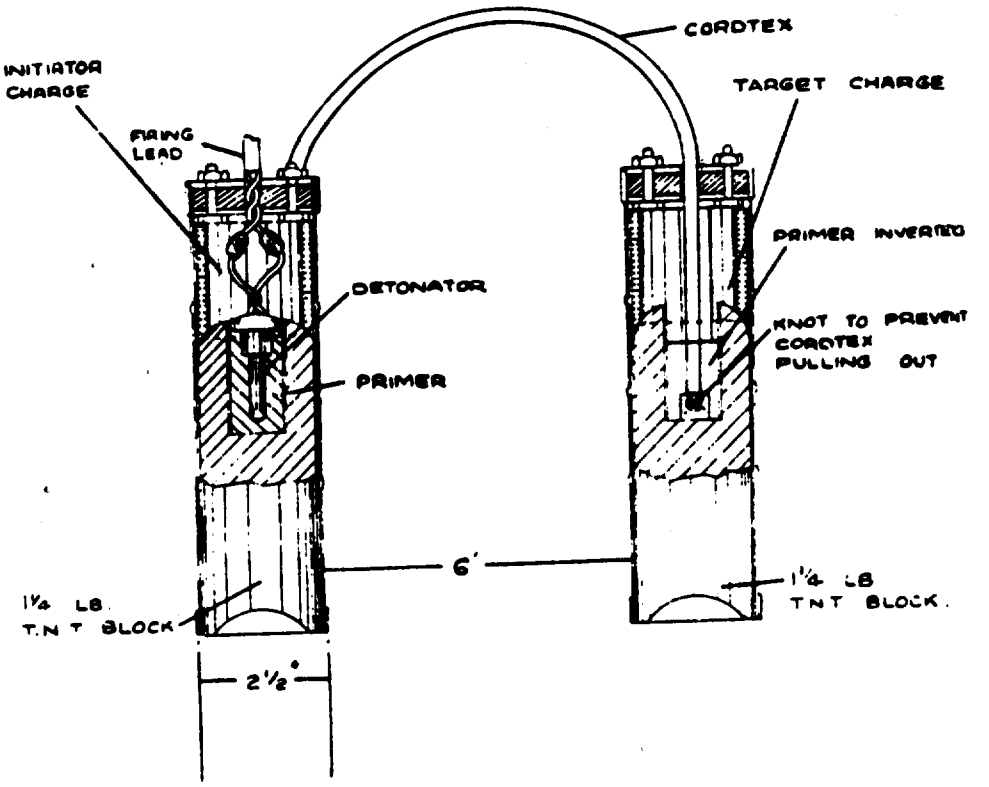
Angle degrees	AT 13 ft.			AT 25 ft.			AT 37 ft.			AT 50 ft.		
	Max. press.	Mom-entum	En-ergy	Max. press.	Mom-entum	En-ergy	Max. press.	Mom-entum	En-ergy	Max. press.	Mom-entum	En-ergy
0	69	79	70	82	86	74	70	86	66	82	66	81
15	69	77	65	70	120	68						
30	67	84	72	75	99	84	72	99	79	111	125	134
45	98	115	94	92	144	101						
60	94	103	97	110	105	119	127	129	190	111	122	141
75	162	145	116	136	196	196						
90	129	150	202	142	153	219	131	124	188	113	131	149
105	76	88	100	115	110	107						
120	102	118	120	93	102	89	68	92	69	78	86	69
135				70	94	80						
150				88	81	89	90	100	79	87	82	80
165	68	115	112	84	70	66						
180	65	86	80	80	82	58	64	77	54	79	78	80

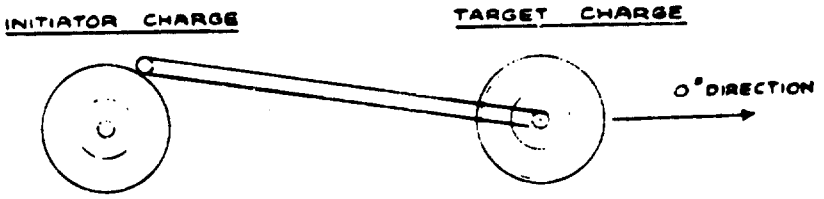
TABLE 5. Formation of Mach waves from the three types of Multiple Charge.

'M' indicates that a Mach wave was recorded.
'N' indicates that a normal double pulse was recorded.

Angle	MULTIPLE CHARGE TYPE 1A				MULTIPLE CHARGE TYPE 1B				MULTIPLE CHARGE TYPE 2			
	18'	28'	37'	50'	18'	28'	37'	50'	18'	28'	37'	50'
0	M	M	M	M	M	M	M	M	M	M	M	M
15	M	M			M	M	M	M	M	M		
30	M	M	M	M	M	M	M	M	M	M	M	M
45	M	M			N	M	M	M	M	M		
54	M	M										
60	M	M	M	M	M	M	M	M	M	M	M	M
69	M	M										
75	M	M			M	M			M	M		
90	M	M	M	M	M	M	M	M	M	M	M	M
105	M	M			M	M			M	M		
120	M	M	M	M	M	M	M	M	M	M	M	M
129	M	M			M	M			M	M		
150	M	M	M	M	M	M	M	M	M	M	M	M
165	M	M			M	M			M	M		
180	M	M	M	M	M	M	M	M	M	M	M	M

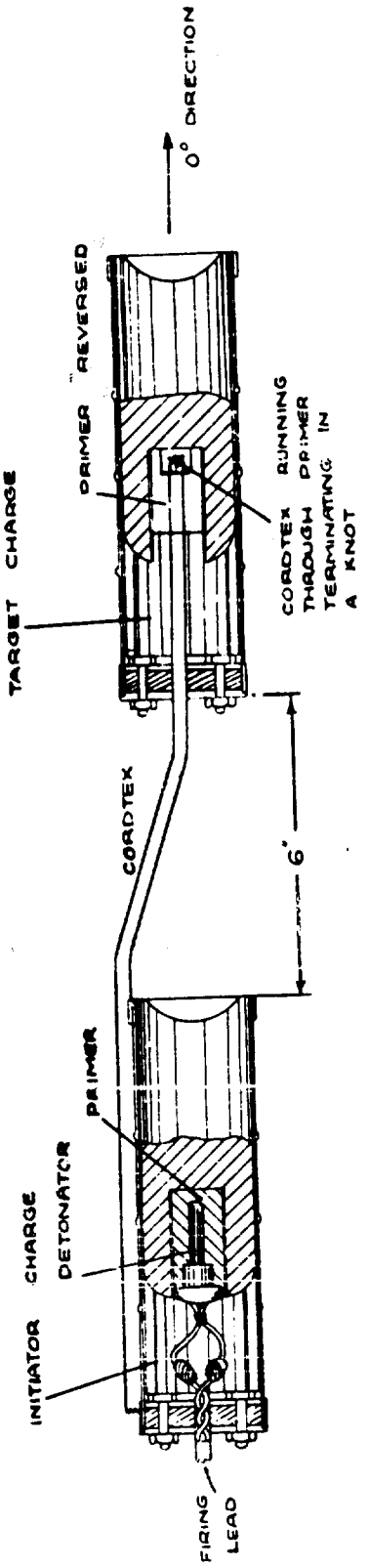
FIG. 1





MULTIPLE CHARGE TYPE 1.

FIG. 2



MULTIPLE CHARGE TYPE 2

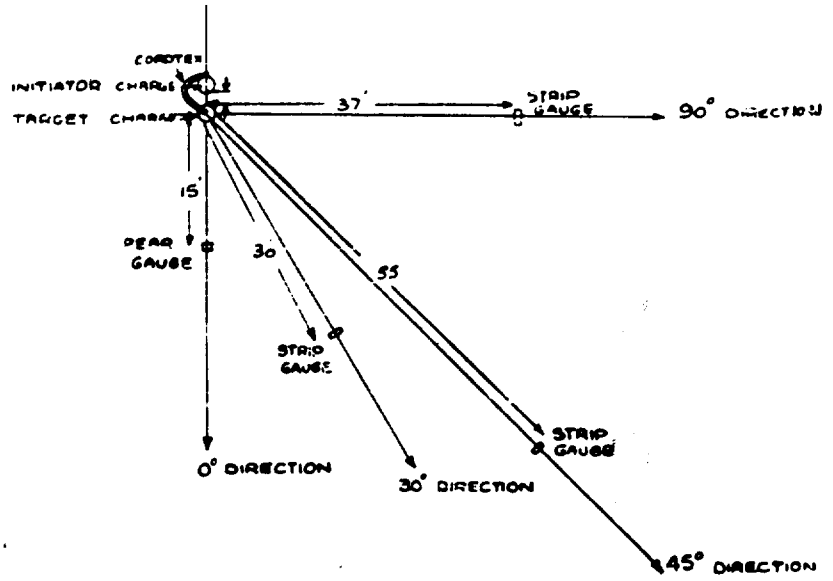


FIG 3 PLAN OF GAUGE & CHARGE LAY-OUT FOR PRELIMINARY TRIAL WITH VARYING LENGTHS OF CORDTEX

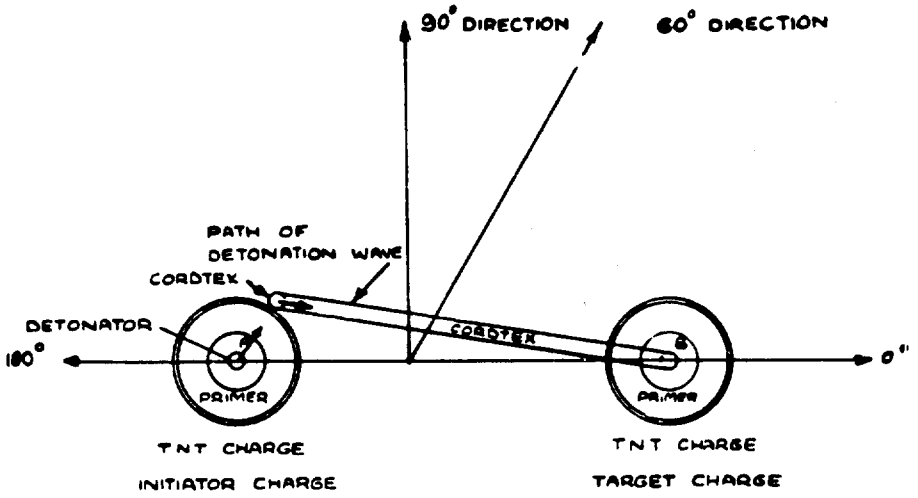


FIG 4 PLAN OF MULTIPLE CHARGE TYPE 1

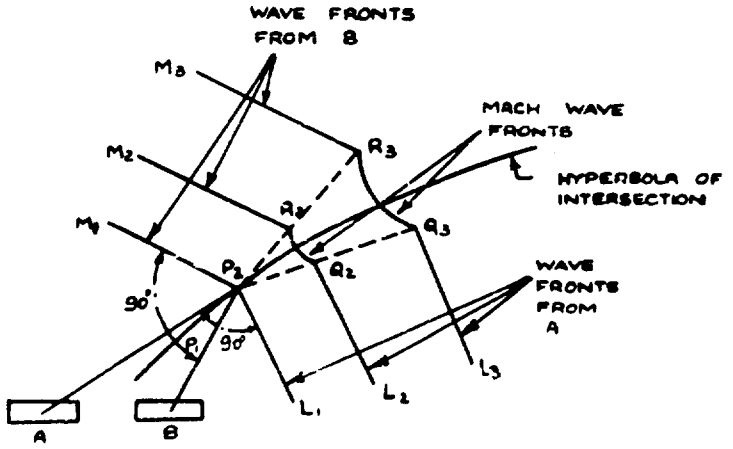


FIG 5 SHOWING FORMATION OF MACH WAVE FOR MULTIPLE CHARGE TYPE 2

MULTIPLE CHARGE TYPE 1

(TWO 1¼ LB T.N.T. CHARGES, AXES VERTICAL, 6 INS WATER SEPARATION)

THE EFFECT ON THE MAXIMUM PRESSURE AND MOMENTUM OF VARYING THE LENGTH OF CORDTEX

FIG 6 MAX PRESSURE

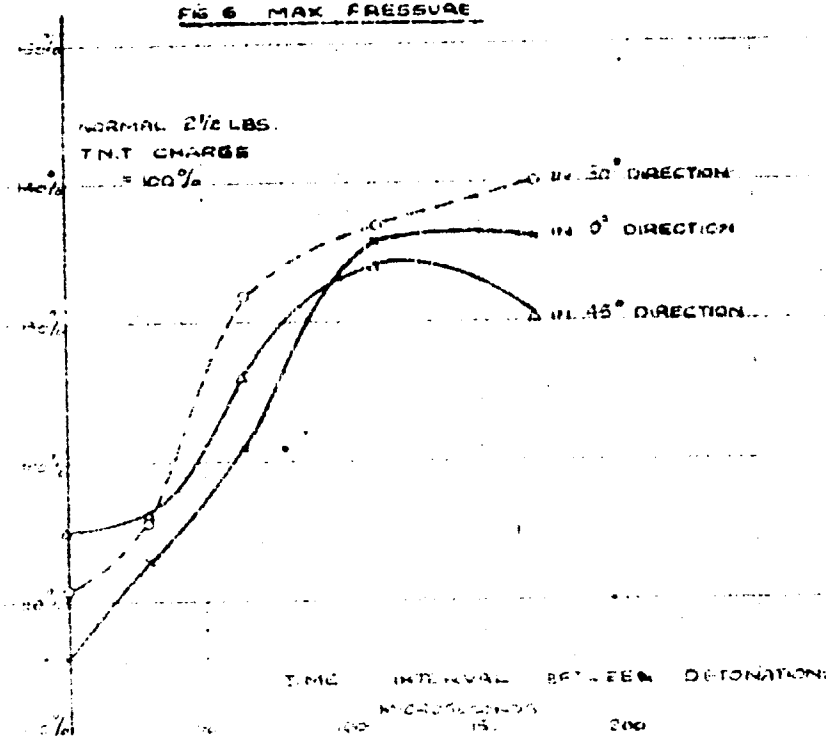
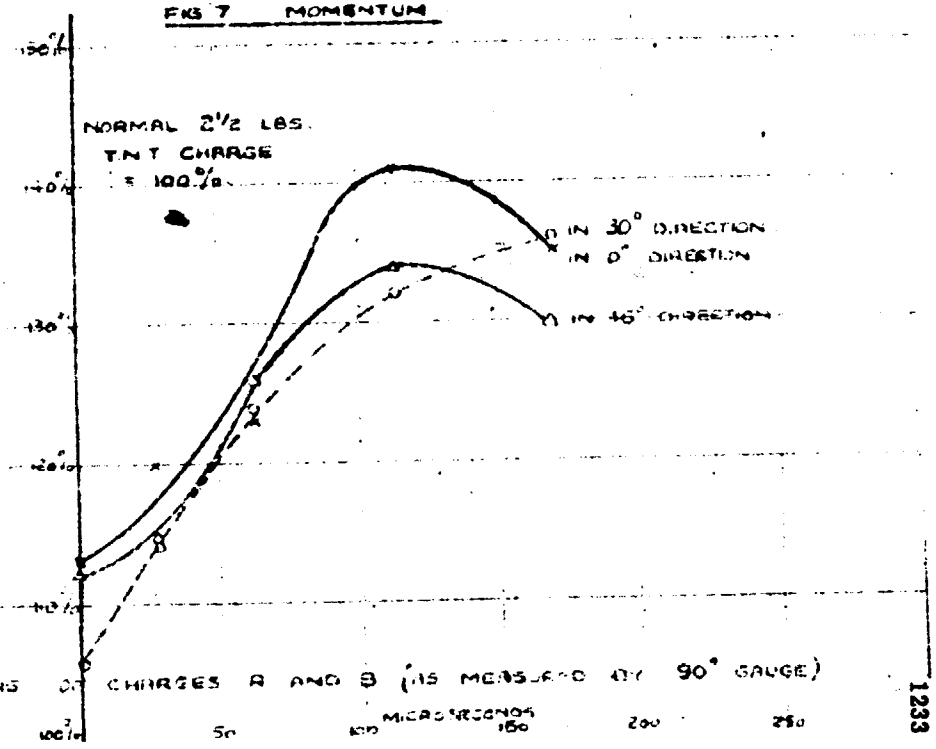


FIG 7 MOMENTUM

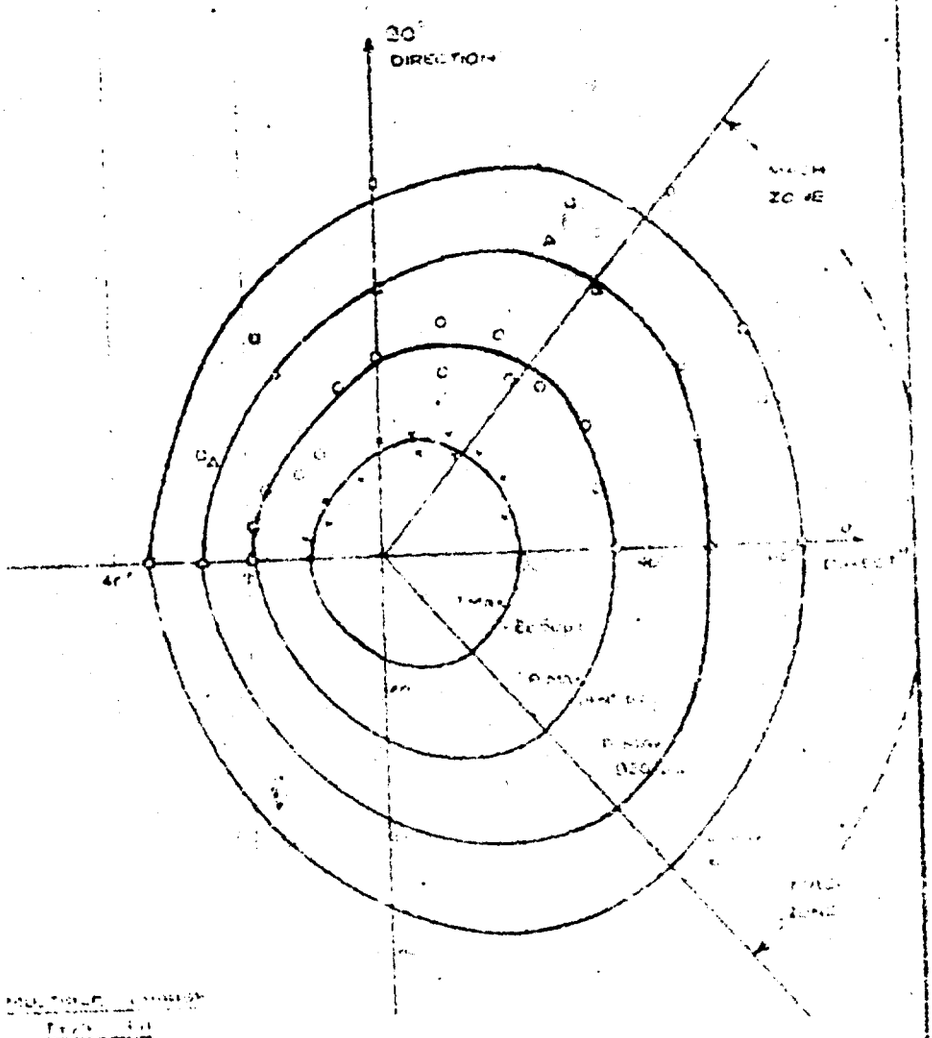


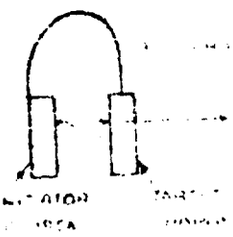
1233

Best Available Copy

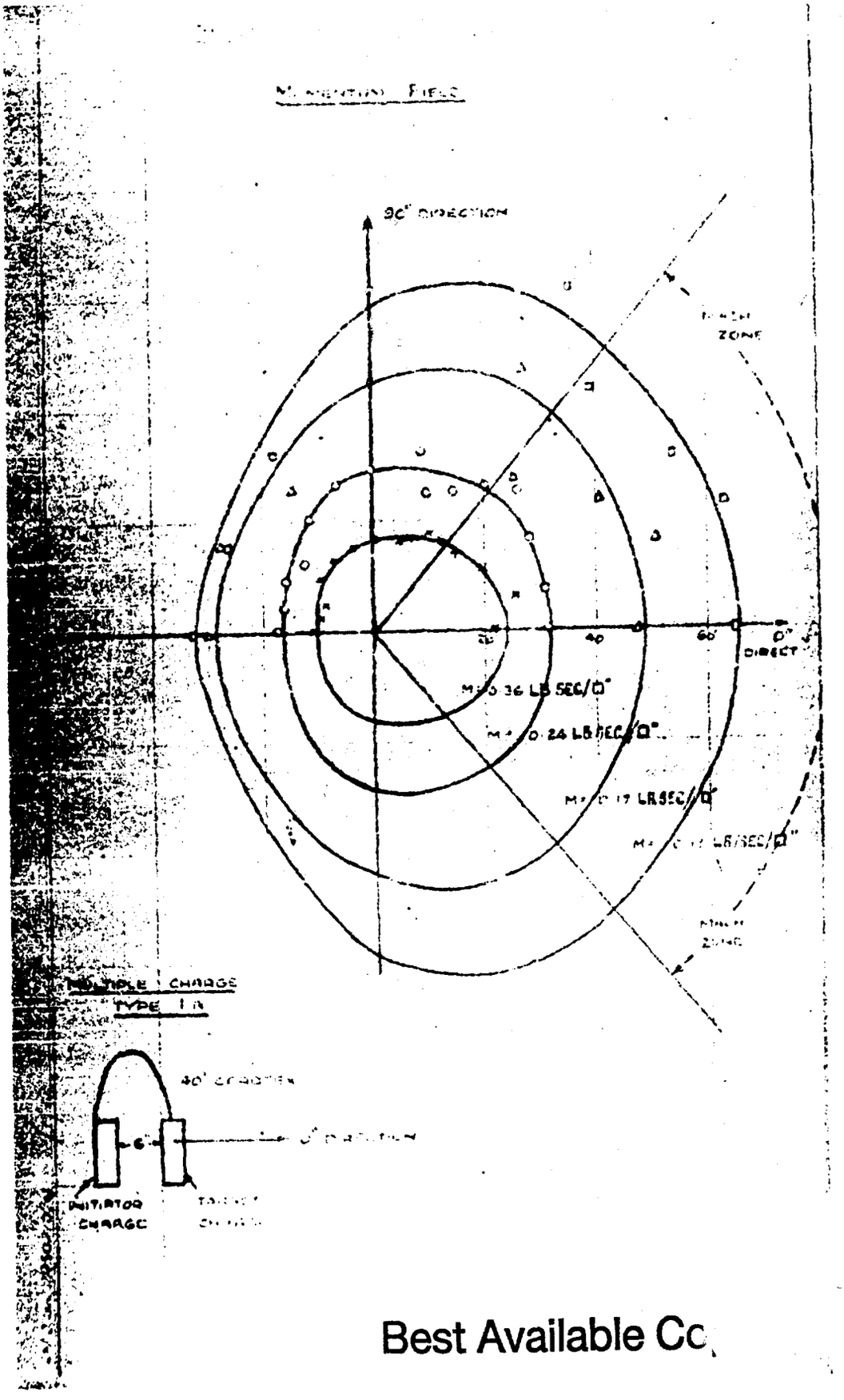
1234

MAXIMUM PRESSURE FIELD

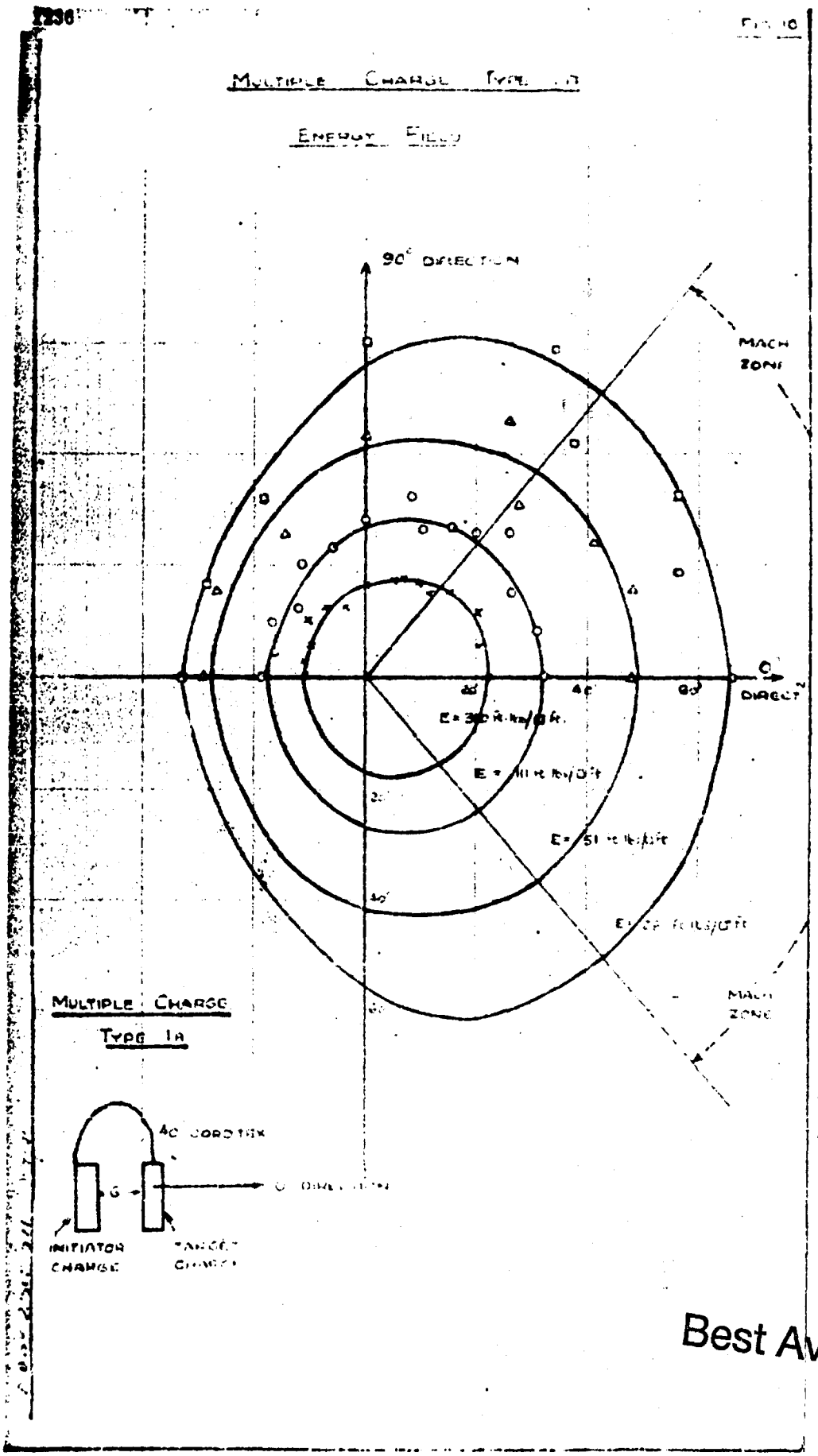




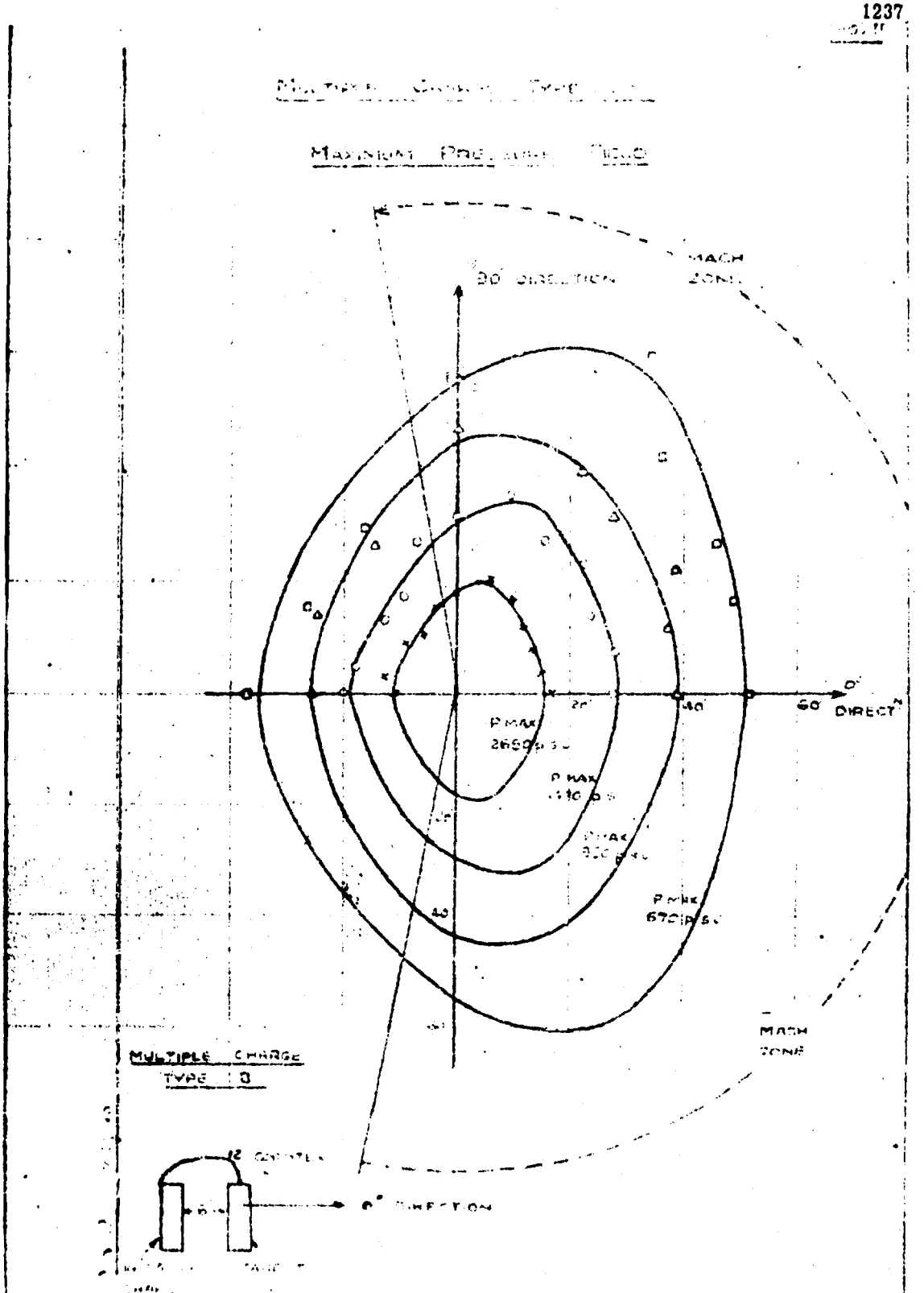
Best Available Cop



Best Available Cc

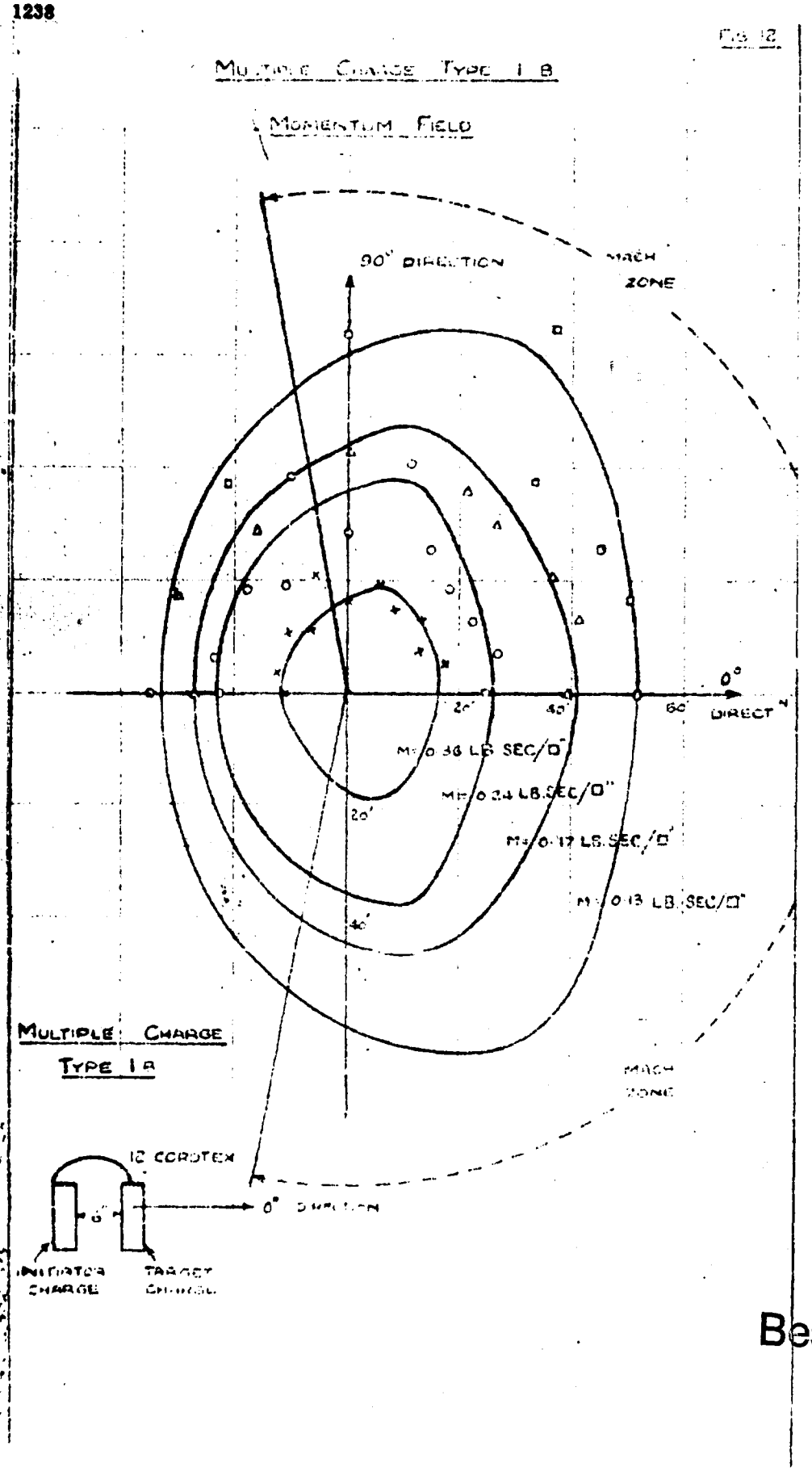


Best Available Copy

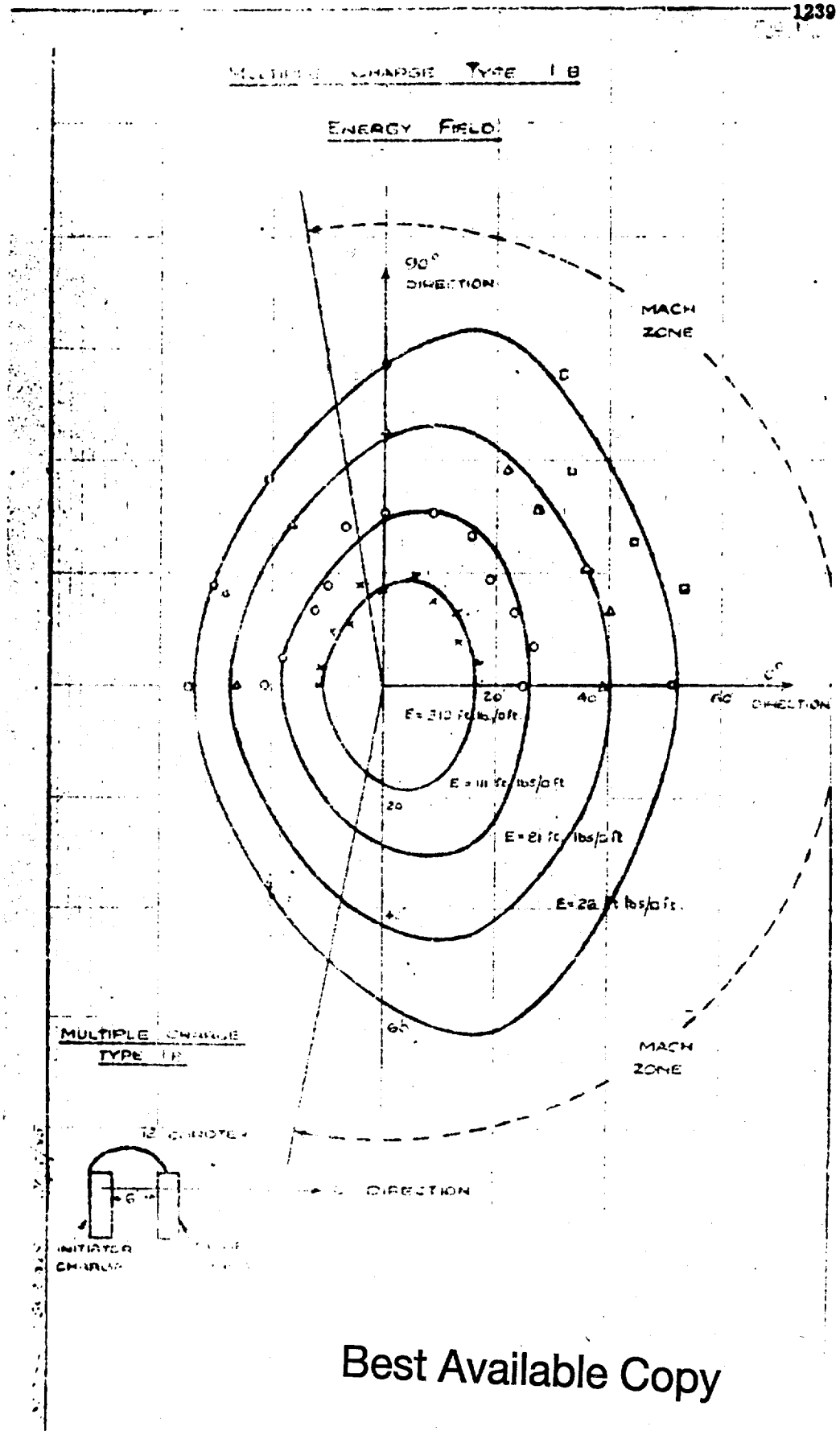


Best Available Copy

Fig 12.

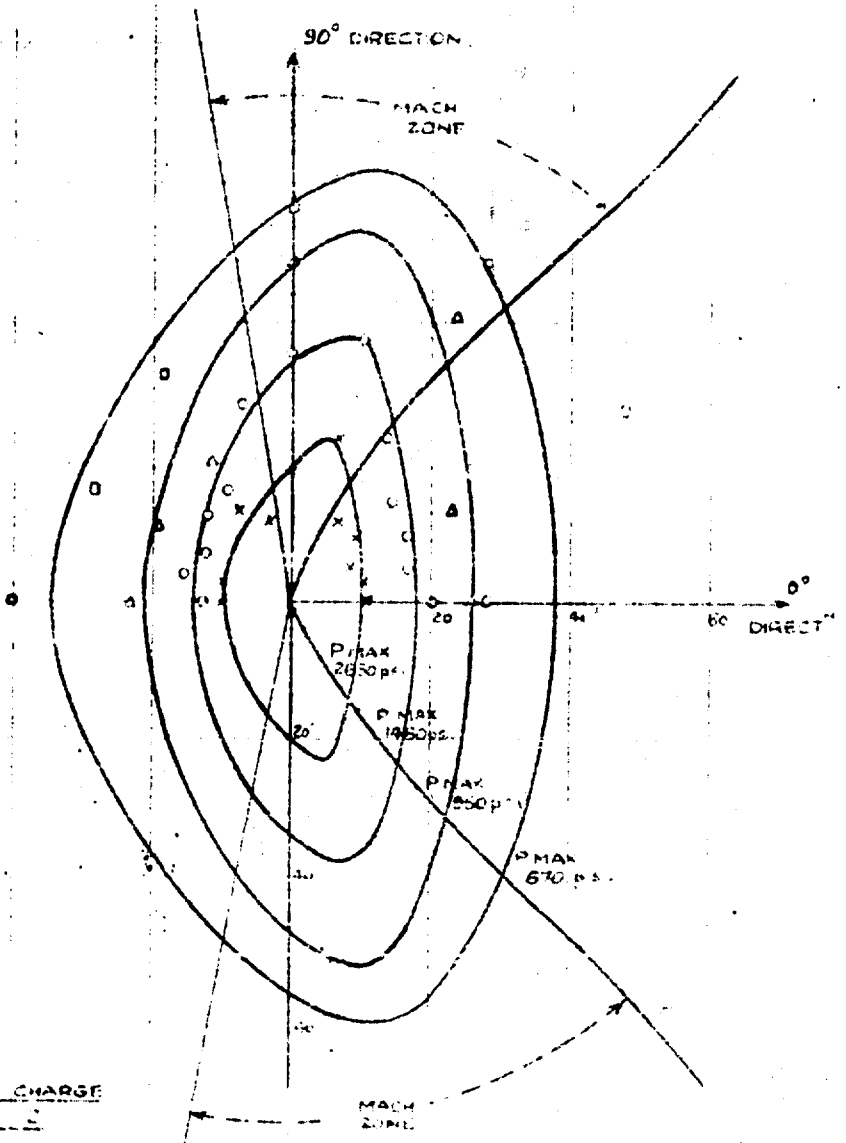


Best Available Copy



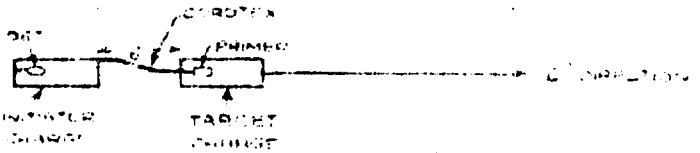
Best Available Copy

MAXIMUM PRESSURE FIELD

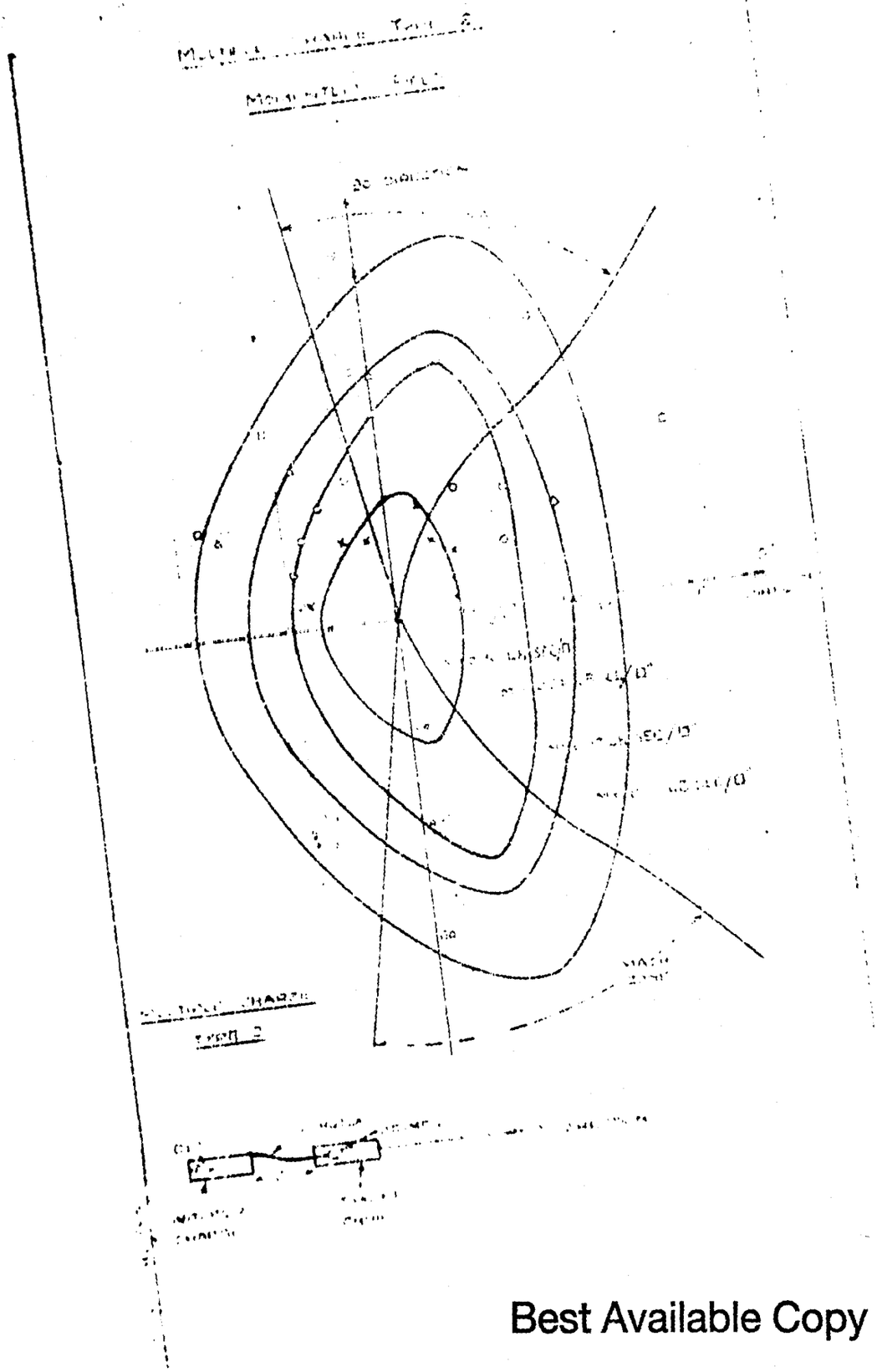


MULTIPLE CHARGE

TYPE 2

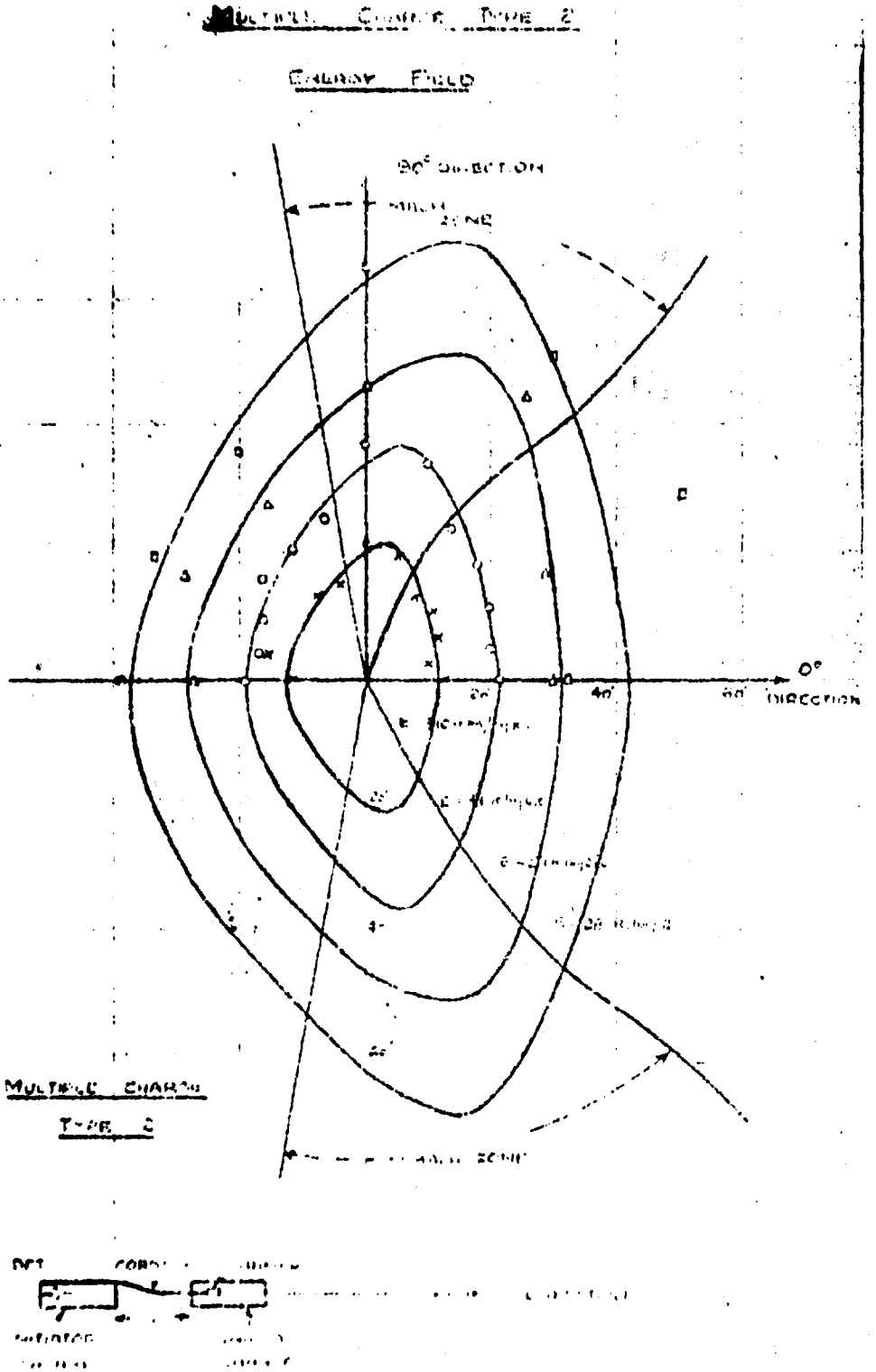


Best Available Copy

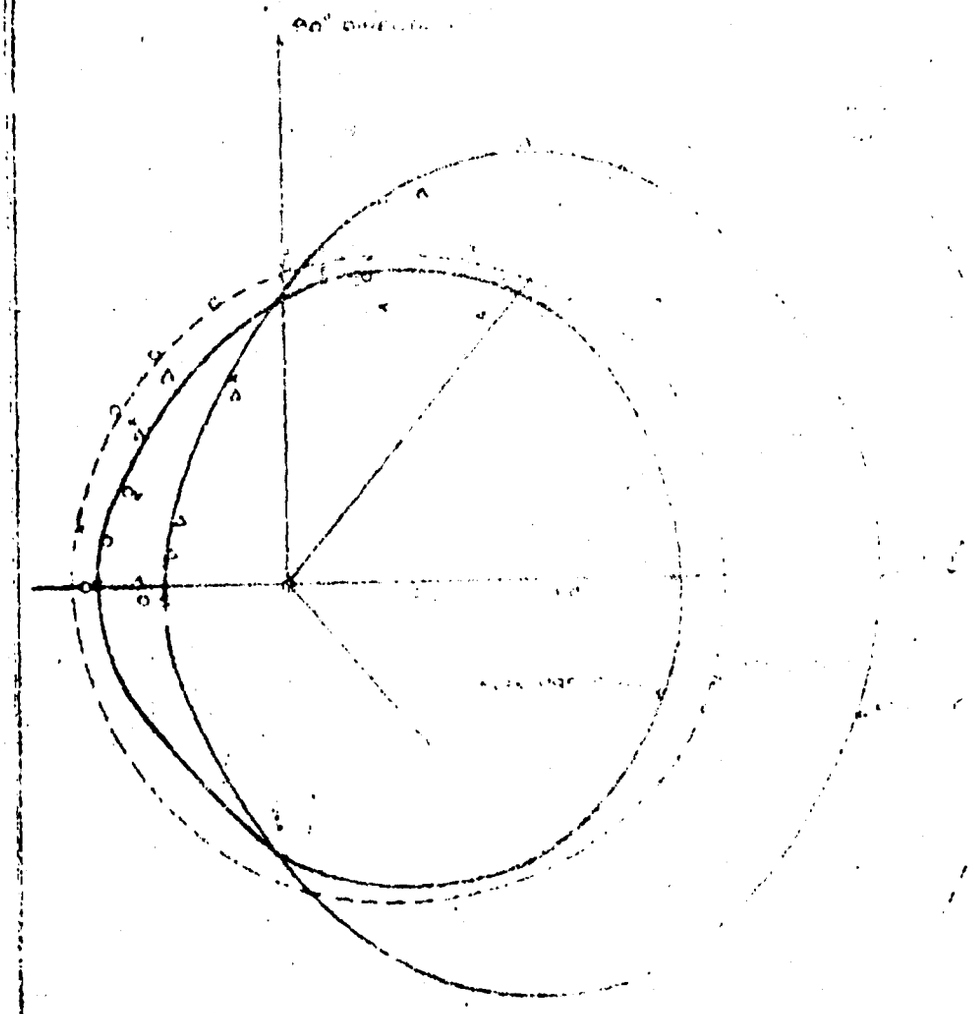


Best Available Copy

FIG 16



Best Available Copy



Best Available Copy

MULTIPLE CHARGE TYPE IA PRESSURE PULSE RECORDS

AT 37 FT AND 50 FT IN 0° AND 30° DIRECTIONS

COMPARED WITH NORMAL 2½ LBS T.N.T. CHARGE

Best Available Copy

Best Available Copy

MULTIPLE CHARGE TYPE 1A PRESSURE PULSE RECORDS

IN THE 60°, 90°, 150° AND 180° DIRECTIONS AT 37 FT. AND 50 FT

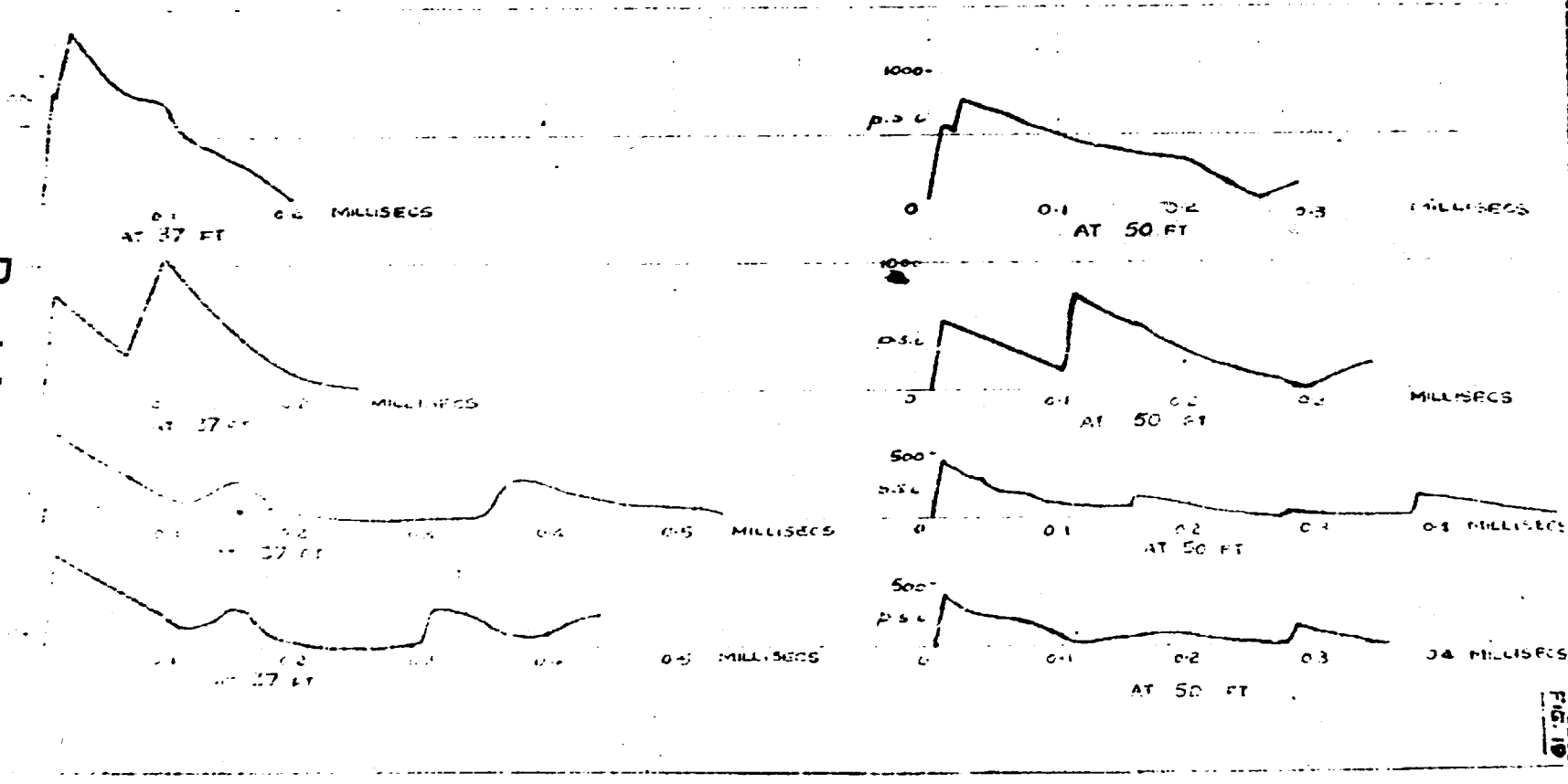


FIG. 19 — 1245

THE NORMAL REFLECTION OF A SHOCK WAVE

R. Finkelstein
Bureau of Ordnance, Navy Department

American Contribution

17 August 1944

ABSTRACT

When a shock collides with a structure, the resulting damage depends upon the duration of the blow as well as upon the initial pressure due to it. In spite of this commonly appreciated fact no theoretical attempt (going beyond acoustic theory) has been made to find the complete pressure-time curve at a reflecting surface except in one calculation by Chandrasekhar. He treated the case of normal reflection from a rigid surface in air and obtained his results by a numerical method. In the present report, too, normal reflection from a rigid surface is considered, but the numerical method is replaced by an analytical one and the work is extended to pressure-time curves in other gases and in water. Now the pressure-time curve at a wall can be roughly described by three characteristics, namely: (1) its peak pressure, (2) its curvature, and (3) its duration. It is well-known that in all media the initial overpressure caused by normal reflection at a rigid wall exceeds the acoustic value (which is double the overpressure in the incident pulse). In this report it is found that the correct theoretical pressure-time curves at the wall are, in typical fluids, concave upward more strongly than their acoustic approximations. With respect to the third of the above properties, however, gases and water are here found to behave differently. In gases the blow is prolonged and the impulse delivered to a rigid wall exceeds the value predicted by acoustic theory. In water, on the other hand, the blow is shorter and the impulse is less than one would expect from

the acoustic approximation. For shocks of 1500 atmospheres in water, duration and impulse are respectively 1% and 8% less than the predictions of acoustic theory. In air for shocks of corresponding strength, namely 0.5 atmosphere overpressure, duration and impulse are respectively 10% and 4% greater than their acoustic approximations. Results of this report may be applied to current damage theories to estimate errors introduced by the use of the acoustic approximation. These errors may be very large if the target is close to the charge (e.g., contact mine, torpedo, depth charge, or a near-miss bomb), although they may be negligible if the target is attacked by a distant charge, such as one in an influence mine.

TABLE OF CONTENTS

I. General Description of Problem and Results.

1. Purpose
2. Specification of the incident pulse
3. Remarks on this specification
4. Qualitative description of reflection
5. Duration of reflection
6. Decay during reflection
7. Equation of state
8. Numerical and analytical methods
9. Comparison between reflection in various fluids
10. Typical pressure-time curves
11. Momentum in the reflected shock

II. The Analytical Solution

12. A geometrical representation
13. Formulation of the problem
14. Differential equations
15. Shock equations
16. Initial conditions
17. Units
18. Initial pressure distribution
19. Solution in M_o
20. Method of finding D
21. Assumption of no decay during reflection

22. Determination of D

23. Solution in M

24. Determination of Q at the wall

25. Determination of the pressure at the wall

26. Summary of method for computing the pressure-time curve

III. The Numerical Solution

27. Brief description of this method

PRINCIPAL NOTATION

a velocity of sound in undisturbed fluid

c velocity of sound in disturbed fluid

$e = \frac{1}{2}\frac{\gamma+1}{\gamma-1}$

$e_o = 1 - e$

i subscript referring to incident shock

k constant in equation of adiabatic = effective pressure at unit density

p overpressure

$\bar{p}$ effective pressure $= p + \pi$

$\bar{p}_m$ maximum value of $\bar{p}$ in incident shock

q_i defined in equations (22.8 - 22.10) for $i = 0, 1, 2$

r subscript referring to reflected shock

s velocity of shock wave

t time

u material velocity

v specific volume

x distance of an arbitrary point from the wall

B maximum material velocity

D shock discontinuity in x,t - plane (Fig. 8

I impulse in shock

L length of shock pulse

M_o region of x,t-plane between D and x-axis (Fig. 8

M region of x,t-plane between D and t-axis (Fig. 8

P Riemann function $\frac{2}{\gamma-1} c + u$

Q Riemann function $\frac{2}{\gamma-1} c - u$

S shock

T tail of pulse

W wall

α, β defined in equations (22.3 and 22.4)

γ adiabatic constant

ζ ratio of the greater to the lesser "effective" pressure on the two sides of a shock discontinuity

λ average slope of a Q characteristic in M

π constant in equation of state = 1 atmosphere for gases, 3×10^3 atmospheres for water

ρ density

I. GENERAL DESCRIPTION OF PROBLEM AND RESULTS

1. When a finite shock-wave in a fluid is reflected from a solid body, the pressure on the body at first rises nearly instantaneously and then decays to its initial value when the reflection is completed. In theoretical studies of reflection attention has been directed mainly toward the initial increase in pressure. No attempt has yet been made to determine the subsequent decrease in pressure when the incident wave falls obliquely on the reflecting surface. When, however, the incident wave is reflected normally, the situation is much simpler. In this case Chandrasekhar [1] has worked out the complete pressure-time curve for air by a numerical method based on Riemann's treatment of motions of finite amplitude. The purpose of this report is to extend his work to other fluids, particularly water. In so doing it has been found possible to replace his numerical method by an analytical one.

2. Let a laterally infinite, rigid wall be struck by a normally incident, plane shock. (An exactly equivalent hydrodynamical situation is presented by the head-on collision of two equal shocks, and so results obtained here are applicable to such a collision.) Since the wave incident on the wall is plane, it is able to propagate in only two directions - forward and backward. In order to describe this wave completely it is necessary to

specify the pressure, material velocity, and entropy distribution in it. The customary experimental description of a shock in terms of pressure alone is therefore incomplete. In this report it is assumed that the entropy is constant on both sides of the shock front, and that it is continuous across this front. Three particular kinds of incident pulses are considered here. At the instant the wall is first struck, they may be described as follows:

(a) Both the pressure and the velocity fall off linearly behind the shock;

(b) they both fall off exponentially;

(c) the velocity falls off linearly and the shape of the pressure pulse is determined by the condition that the wave is progressive, i.e., by the condition that the incident disturbance propagates only toward the wall, rather than both toward it and away from it. (It will be shown in par. 16 how the progressive assumption fixes the pressure.)

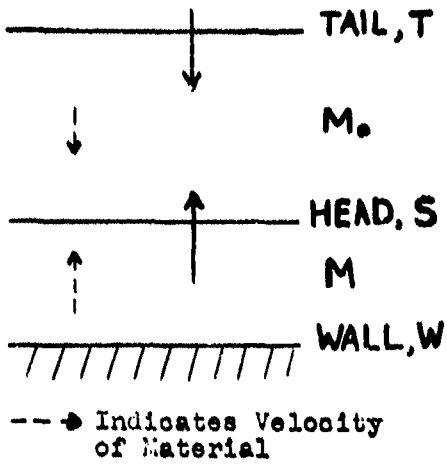
Some remarks will now be made about these assumptions.

3. Although a continuous wave of finite amplitude can propagate without increase of length, the same is no longer true as soon as it has evolved into a shock (See for example, reference 2). After it has become a shock,

reflection of the continuous portion of the pulse from the discontinuity begins; as a result the disturbance propagates backward, as well as forward, and the peak pressure steadily decreases. This phenomenon is called "decay" of the shock-wave. Hence the progressive assumption (c) can not be rigorously satisfied by a shock any time after it is formed. It is, however, a good approximation; in fact, shocks of the type (a) and (b), of the strengths considered here (pressure-ratio across shock ≤ 1.6) are very nearly progressive. Further, one may verify that a shock of type (c) has a pressure distribution which is nearly linear. That is, the difference between types (a) and (c) is insignificant for shocks of the strengths considered here. It may also be remarked that the descriptions (a), (b), and (c) apply to the incident shock only at the moment the wall is first struck. Before and after this time (a) is not linear, (b) is not exponential, and (c) is not progressive, again because of decay.

4. The general course of a reflection may be described qualitatively. When a normally incident wave strikes a rigid wall, the overpressure on the wall is at first increased to more than twice the peak overpressure previously existing in the wave. (In the limiting case of a weak shock the overpressure is exactly doubled.) After the instant of impact the head of the wave reverses direction and begins to travel toward its tail (fig. 1.)

Fig. 1



Just after impact the overpressure in the region, M, between the shock front, S, and the wall, W, is nearly 2p, where p is the peak overpressure before collision; in the region, M_o, the overpressure is slightly less than p just in front of S and it decreases to zero at the tail, T. Now when S reverses direction the medium in front of it changes from M to M_o. Therefore, as soon as S has reversed direction, the pressure has increased immediately in front of it and behind it by about the same amount (p). At the same time the medium M_o, now in front of S, is still travelling toward the wall. The net result, in the examples considered in this report, is that the velocity of S relative to the wall is subsonic in air and supersonic in water (where "sonic" refers to undisturbed fluid). Now as soon as S has been reversed by the wall, the total disturbance may be regarded as an approximate superposition of two waves of finite amplitude. One of these moves toward the wall and is bounded by T and W. The other moves away from the wall and is bounded by W and S. These two waves penetrate each other until T reaches the wall and

thereby marks the end of the reflection. During this interpenetration S is moving away from the wall with one speed, and T is moving toward it with another speed, namely, a, the speed of sound in undisturbed fluid. When S and T meet, the original pulse is very much compressed. Since both head, S, and tail, T, travel at nearly sonic velocity, a, the pulse has about half its initial thickness when they meet. At this instant the entire region of disturbance is contained in M, and the fluid here is at high and nearly uniform pressure. After passing through S, the tail of the incident wave travels relative to M with the new velocity, c, that of sound in M. Its velocity with respect to the wall is c-u, where u is the material velocity in M away from the wall. The velocity c-u may be either greater than or less than a. In our examples $c-u < a$ in air; $c-u > a$ in water. When T reaches the wall, the pressure at the wall has fallen to its value before the impact, the incident pulse has reversed its direction, and the reflection is finished.

5. Let L be the initial length of the pulse. Then the time from the start of reflection until head and tail meet is nearly L/2a, since the velocity of both is nearly sonic for shocks of the strength considered here. The time for the tail to reach the wall after it has passed through the head is approximately $L/2(\overline{c-u})$, where $\overline{c-u}$ is the average velocity of the tail in M.

Hence the total time required for the reflection, or the duration of the pressure on the wall, is approximately $L/2a + L/2(\overline{c-u})$. On the other hand, the duration of the pulse in free fluid is L/a. Hence, if $\overline{c-u} < a$, as in air, the pressure on the wall lasts for a longer time than the pressure in the incident pulse. Moreover the reflected pulse is in this case longer than the incident one. In water, where $\overline{c-u} > a$, opposite remarks are true. (The difference between the behavior of air and water may be conveniently referred to the difference of material velocity, u, in the two fluids; in air u is large and in water it is small.) The result is that in air the duration of the pressure on a wall and the impulse given to the wall are both greater than the acoustic approximation would indicate, and in water they are both less than the predictions of acoustic theory. These qualitative considerations are corroborated by the detailed calculations, the results of which are given in par. 9 and 10.

6. One other general remark may be made. Since the velocity of the shock S with respect to M_o is greater than its velocity with respect to the wall, the wall may be regarded as a piston which helps to sustain the shock. For this reason and because the total time of reflection is short, the assumption that decay during reflection is negligible may be a good approximation. The importance of this point will be seen in par. 21.

7. To compare different fluids it is convenient to

neglect entropy changes. It is then possible to write for certain fluids the following common equation of state[3]

$$\bar{p}\, v^{\gamma} = k \qquad (7.1$$

Here $\bar{p} = p + \pi$. $\bar{p}$ is an effective pressure, p is the overpressure, and π is a constant, characteristic of the fluid (for example, in perfect gases π = 1 atmosphere and in water, $\pi = 3 \times 10^3$ atmospheres); v is the specific volume; γ is also characteristic of the fluid (for gases it is the adiabatic constant, lying between 1 and 5/3, and for water it is approximately 7.15[3]); k is another constant characteristic of the fluid. The constants appearing in (7.1) are actually functions of the entropy. Here it is assumed that the entropy is a constant on both sides of the shock front and that it is continuous across this front. It will be shown later (par. 9) that this approximation is adequate for the problem at hand. Hence (7.1) is assumed to hold everywhere in this report.

8. In this report two methods are used. One method[1] is numerical; it is described in part III. The other method is analytical; it is described in part II. The numerical method allows the entropy to change across the shock front, but nowhere else. Except for this approximation it is completely rigorous. In the analytical method, on the other hand, there are several approximations which are discussed in part II. These approximations are

apparently satisfactory, however, because agreement between the methods is good, as one can see in the next paragraph.

9. In fig. 2 - 4 five examples [4] of a pressure-time curve are given. These curves show the pressure at the wall during reflection. The three linear cases were worked out by both the numerical and the analytical methods. The two exponential cases, however, were computed by the numerical method only. The exponential cases were calculated because the experimental pressure-time curves are more nearly exponential than straight. The underwater shocks were chosen of the strengths indicated, because their strengths probably bound the range of most interest. A shock of 300 atmospheres is of about the violence ordinarily measured by underwater gauges. On the other hand, it would be difficult to realize the reflection of a shock of strength exceeding 2000 atmospheres from a rigid surface, because no surface would remain rigid under such a blow for long. (The elastic limit of mild steel is not more than 2000 atmospheres.) Calculations like the ones in this report for shocks of greater strengths than 2000 atmospheres can be interpreted, however, as relating to collisions of equal and opposite shocks, rather than to impacts between a single shock and a rigid surface. The curves in fig. 2 - 4 are described in the following table.

TABLE 1

Medium	Incident Pulse			Pressure-Time Curve at Wall		Fig.
	Shape	Peak Pressure (atm)	ζ	Impulse / Acoustic Impulse Numerical	Analytical	
Water (γ=7.15)	Linear	300	1.10	0.98	0.98	2
	Linear	1800	1.60	0.92	0.92	2a
	Expon.	300	1.10	0.97	----	3
	Expon.	1800	1.60	0.90	----	3a
Air (γ=1.40)	Linear	1.50	1.50	1.04	1.04	4

Here ζ is the ratio of the greater to the lesser effective pressure on the two sides of the incident shock. In this table "impulse" means the time-integral of the overpressure at the wall. In computation of impulse the duration of an exponential pulse was arbitrarily taken to be the time required to fall to an overpressure of three atmospheres. The impulse is normalized by dividing it by the "acoustic impulse", i.e., $2 \int p_i \, dt$, where p_i is the value the overpressure would have at the position of the wall, if the wall were absent and all parts of the incident wave moved forward with the velocity of sound in undisturbed fluid. In fig. 2, 2a, and 4, the points obtained by the numerical method are circled, and the curve calculated by the analytical method is drawn in. The agreement is seen to be good. Fig. 4 provides a test not only of the analytical method, but also of the adiabatic assumption mentioned in par. 7, inasmuch as the circled points in this fig. were calculated by Chandrasekhar

under the Rankine-Hugoniot rather than the adiabatic assumption. In each of these figures is also drawn (as a dashed curve) the acoustic approximation, $2\,p_i$. When the acoustic approximations are straight, the correct pressure-time curves are seen to be concave upward, and in the exponential cases the correct pressure-time curves are more concave than the acoustic ones.

10. Probably the most interesting feature of the curves in fig. 2 - 4 is the difference in behavior shown by air and water. In terms of the γ defined in (7.1) the influence of the fluid is shown in fig. 5. Here the impulse given to the wall is plotted as a function of γ for three values of the strength, $\mathfrak{s}$, of the incident shock. In fig. 5 the incident pulse is always of type (c), that is, it is progressive and its velocity decreases linearly behind the shock front. As remarked before, the pressure in this case is also approximately linear. The impulse in fig. 5 is normalized as in fig. 2 - 4. In this graph all gases lie between $\gamma = 1$ and $\gamma = 5/3$. The limiting value $\gamma = 1$ may be interpreted as relating either to an isothermal reflection or to reflection in a gas whose polyatomic molecules have infinitely many inner degrees of freedom; $\gamma = 5/3$ describes a monatomic gas. The curves show that in gases and water the impulse given to a rigid wall is respectively more and less than acoustic theory predicts. The essential reason for this was indicated in par. 6, namely, in gases the tail of the in-

cident wave travels slowly after passing through the head of the reflected wave on its way to the wall. Consequently the reflection is prolonged and the impulse is increased.

11. The momentum in the reflected pulse is easily found from such pressure-time curves as are shown in fig. 2 - 4. The equation of momentum transfer for one-dimensional flow is (fig. 6)

$$(p_1 + \rho_1 u_1^2) - (p_2 + \rho_2 u_2^2) = \frac{\partial}{\partial t}\int_{x_1}^{x_2} \rho u \, dx \qquad (11.1$$

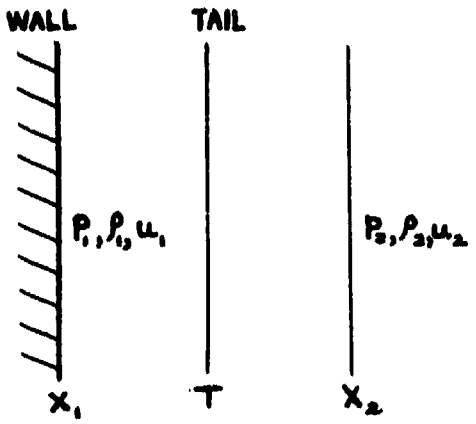


Fig. 6

where the subscripts refer to two planes perpendicular to the motion and separated by the distance $x_2 - x_1$. p, u, and ρ are pressure, velocity, and density. Choose the plane x_1 at the rigid wall and the plane x_2 in undisturbed fluid. Then (11.1) becomes

$$p_1 = \frac{\partial}{\partial t}\int_{x_1}^{x_2} \rho u \, dx,$$

and after integration one has

$$\int_0^t p_1 \, dt = \left[\int_{x_1}^{x_2} \rho u dx \right]_0^t \qquad (11.2$$

Let t be the time required for the reflection. Let I_i and I_r be the impulses of the incident and reflected shocks. It follows from (11.2) that

$$I_r = I_i + \int_0^t p_1 \, dt, \qquad (11.3$$

where

$$I_i = \int_{x_1}^{x_2} \rho_i \, u_i \, dx,$$

$$I_r = \int_{x_1}^{x_2} \rho_r \, u_r \, dx.$$

II. THE ANALYTICAL SOLUTION

12. Consider a plane shock, S, impinging on a rigid wall, W, at normal incidence (fig. 7). Let the plane of the wall be $x = 0$, and let the x-axis be directed toward the oncoming shock. Let the position of any element of the fluid be $x = x(t)$, where t is the time measured from the moment at which S strikes W. The situation is represented in the x, t-plane shown in fig. 8. Here D is the world line of the shock front after the time $t = 0$. The world line of a typical element, initially at x_0, is shown with a

Fig. 7

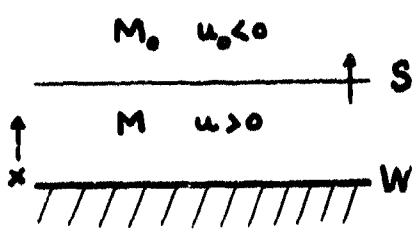
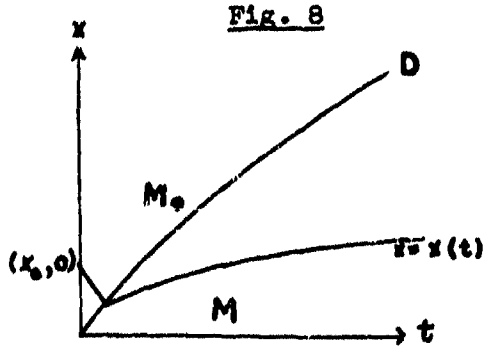


Fig. 8



discontinuity in velocity where it crosses D. M_0 and M are the regions between D and the x-axis and t-axis respectively.

13. The problem may be stated in this way. The following conditions are given:

(A) Boundary conditions on axes and on D.

(1. Distribution of pressure, p_1 and velocity, u_1, on x-axis. This is the distribution of pressure and velocity behind the shock front when it strikes the wall.

(2. u = 0 on t-axis, since the wall is rigid.

(3. The shock equations across the discontinuity, D,

(a conservation of mass.

(b conservation of momentum

(c conservation of entropy (an approximation)

(B Equations to be satisfied in M_0 and in M

(1. conservation of mass.

(2. conservation of momentum

(3. conservation of entropy (an approximation)

We wish to find the pressure, p, and velocity, u, as functions of x and t in both regions, M_0 and M. In addition, we shall find the equation of the curve D, which separates them.

14. The conditions B may be expressed by the following equations:

$$\frac{\partial}{\partial x}(\rho u) + \frac{\partial \rho}{\partial t} = 0 \qquad (14.1$$

$$\frac{\partial p}{\partial x} = -\rho\left(\frac{\partial u}{\partial t} + u\frac{\partial u}{\partial x}\right) \qquad (14.2$$

$$\bar{p} = k\rho^{\gamma} \qquad (14.3$$

where ρ = density. Equations (14.1) and (14.2) are the conservation equations for mass and momentum, respectively. (14.3) may be regarded as an empirical equation of state, which is correct for adiabatic processes. It is assumed that motion is entirely adiabatic so that (14.3) is true in both M and M_0 and that k is the same in both regions. By Riemann's method the equations (14.1) - (14.3) are rewritten.

$$\frac{\partial P}{\partial t} = -(c + u)\frac{\partial P}{\partial x}, \qquad (14.4$$

$$\frac{\partial Q}{\partial t} = (c - u)\frac{\partial Q}{\partial x}, \qquad (14.5$$

where P and Q are the Riemann functions, which are defined in this report as

$$P = \frac{2}{\gamma - 1}c + u \qquad (14.6$$

$$Q = \frac{2}{\gamma - 1}c - u \qquad (14.7$$

where $c = \left(\frac{dp}{d\rho}\right)^{\frac{1}{2}}$ = velocity of sound. (14.8

The conditions B are now contained in the equations (14.4)

and (14.5) in the form to be used here.

15. On the other hand, the conditions A-3 are equivalent to the following equations:

$$s = u_o + v_o \left[\frac{p - p_o}{v_o - v}\right]^{1/2} \qquad (15.1$$

$$u = u_o + \left[(p - p_o)\,(v_o - v)\right]^{1/2} \qquad (15.2$$

$$\bar{p}_o\, v_o^{\gamma} = \bar{p}\; v^{\gamma} \qquad (15.3$$

where s is the shock velocity (s = slope of D) and v is the specific volume. The variables in these equations are, of course, to be evaluated on D. Variables with and without subscript refer to the regions M_o and M respectively of the x,t-plane. The first two equations, (15.1) and (15.2), again express the conservation of mass and of momentum, respectively. The third equation supposes no entropy change in crossing D. It is convenient to rewrite (15.1) and (15.2) with the aid of (15.3) and (14.8) in terms of these five variables: c, u, c_o, u_o, and s.

$$s = u_o + \frac{c_o}{\sqrt{\gamma}} \left[\frac{\left(\frac{c}{c_o}\right)^{\frac{2}{\gamma-1}} - 1}{1 - \left(\frac{c}{c_o}\right)^{-\frac{2}{\gamma-1}}}\right]^{1/2} \qquad (15.4$$

$$u = u_o + \frac{c_o}{\sqrt{\gamma}} \left[\left(\left(\frac{c}{c_o}\right)^{\frac{2}{\gamma-1}} - 1\right)\left(1 - \left(\frac{c}{c_o}\right)^{-\frac{2}{\gamma-1}}\right)\right]^{1/2} \qquad (15.5$$

The equations (15.4) and (15.5) may be simplified if the

shock is not too strong. They become respectively, to the first order in $c/c_o - 1$,

$$s = u_o + ec + e_o c_o, \qquad (15.6$$

$$Q = Q_o \qquad (15.7$$

where the following abbreviations have been introduced,

$$e = \frac{1}{2}\,\frac{\gamma + 1}{\gamma - 1},$$

$$e_o = 1 - e$$

(The first higher order term neglected in (15.7) is quite small. In fact one finds

$$\frac{Q - Q_o}{Q_o} = -\frac{(\gamma+1)^2(\gamma-1)}{192\,\gamma^3}\left(\frac{\bar{p} - \bar{p}_o}{\bar{p}_o}\right)^3 + \cdots$$

for a shock moving into undisturbed fluid. Here $\bar{p}$, Q represent quantities on the high pressure side of the discontinuity. For a shock in which $\bar{p}/\bar{p}_o = 1.6$ one has, as far as third order terms,

$$\frac{Q - Q_o}{Q_o} = -0.0009, \quad \text{in air}$$

$$\frac{Q - Q_o}{Q_o} = -0.0012, \quad \text{in water.}$$

It was pointed out in reference (5) that Q is nearly constant across a shock front in air, even without neglect of the entropy change.) The procedure in this report has been to use the equations (15.4) and (15.5) in the numerical integration and to use (15.6) and (15.7) in the analytical

integration. As already seen (cf. par. 9) the two methods lead to nearly the same results.

16. Only the condition A-1 remains to be formulated. As stated above (cf. par. 2), three types of incident pulse are considered in this report. Incident pulses of type (a) and (b) were treated numerically and the results were given in Table I, par. 9. We now consider an incident shock of type (c), in which the velocity pulse is linear, and the pressure distribution is determined by the condition that the wave is progressive. From equations (14.4) and (14.5) the progressive condition follows. For according to these equations, P and Q travel in opposite directions with the velocities c + u and c - u respectively. The condition, therefore, for a progressive wave is that either P or Q be constant; and in this case, it must be P, since the pulse is travelling in the direction of - ∞. The boundary conditions A-1 on the velocity, $u_o(x,t)$, and on the Riemann function, $P_o(x,t)$, are then

$$u_o(x,0) = -B + A\,x, \qquad x \leq B/A \qquad (16.1$$

$$u_o(x,0) = 0 \qquad , x > B/A \qquad , B > 0$$

$$P_o(x,0) = \frac{2}{\gamma - 1}\, a. \qquad (16.2$$

Here B is the peak velocity and B/A is the length of the incident pulse. The velocity, a, is the value of c in undisturbed fluid ($\bar{p} = \bar{w}$). Equation (16.2), together with (14.3) and (14.8), determines the pressure as the following

function of the velocity.

$$\bar{p} = \pi \left[1 - \frac{\gamma-1}{2} \frac{u}{a}\right]^{\frac{2\gamma}{\gamma-1}} \qquad (16.3$$

As already remarked in par. 3, the pressure pulse computed from (16.3) and (16.1) is very nearly linear for shocks, whose $\bar{p}/\pi \leq 1.6$. From this it follows that the kind of pulse considered here, type (c), is essentially equivalent to a pulse of type (a).

17. It is convenient to choose units of length and time so that $a = 1$ and so that the initial length of the incident pulse is also unity. Then the boundary conditions (16.1) and (16.2) become

$$u_o(x,0) = -B + Bx, \qquad x \leq 1 \qquad (17.1$$

$$u_o(x,0) = 0, \qquad x > 1$$

$$p_o(x,0) = \frac{2}{\gamma-1} \qquad (17.2$$

18. One could specify the initial pressure-distribution instead of the initial velocity-distribution, as has been done here. In fact, this would be desirable, since gauges are usually interpreted to give pressures rather than velocities. The reason for adopting the opposite procedure here is that it is analytically more convenient to regard the velocity as given. Since, however, the experimental data generally concern pressure, it is necessary to have

a way of determing the maximum velocity, B, from the given peak pressure. This can be done by means of the following formula, which follows from (15.2)

$$B = \frac{1}{\sqrt{\gamma}} \left[(\zeta - 1)(1 - \zeta^{-\frac{1}{\gamma}}) \right]^{1/2} \qquad (18.1$$

where $\zeta = \bar{p}_m / \pi$

$\bar{p}_m$ = effective peak pressure in incident pulse.

It may be noted that equation (16.3) provides a relation between $\bar{p}_m$ and B which is not consistent with (18.1). Equation (18.1) is for a shock, whereas (16.3) is the progressive condition; as mentioned before (par. 3) they are not compatible, and decay must always be expected. The procedure followed here is this: ζ is regarded as given. From (18.1) B is found. From (17.1) u is found. (17.1) and (17.2) then completely determine the wave. $\bar{p}_m$ is the given effective peak pressure. Let $\tilde{p}_m$ be the approximate effective peak pressure computed from (16.3). The difference $(\tilde{p}_m - \bar{p}_m)/\bar{p}_m$ is shown in Table 2; it is seen to be unimportant.

TABLE 2

ζ	Air (γ = 1.40)	Water (γ = 7.15)
1.1	0.0005	0.0002
1.5	0.0020	0.0008

19. The differential equations (14.4) and (14.5) can at once be solved in M_o subject to the boundary conditions (17.1) and (17.2) if the approximation is introduced that the

disturbance in M_o remains progressive. One may verify that the error so introduced is negligible by comparing the analytic solution so obtained with the result of the Riemann type of numerical integration. Therefore, let the disturbance everywhere in M_o be progressive so that

$$P_o(x,t) = \frac{a}{\gamma-1} \qquad (19.1$$

Let $$\Delta = a_o - u_o. \qquad (19.2$$

Then by (19.1), (19.2), (14.5), (14.6), and (14.7) it follows that

$$\frac{\partial \Delta}{\partial t} = \Delta \frac{\partial \Delta}{\partial x} \qquad (19.3$$

The solution of (19.3) is

$$\Delta t + x = w(\Delta) \qquad (19.4$$

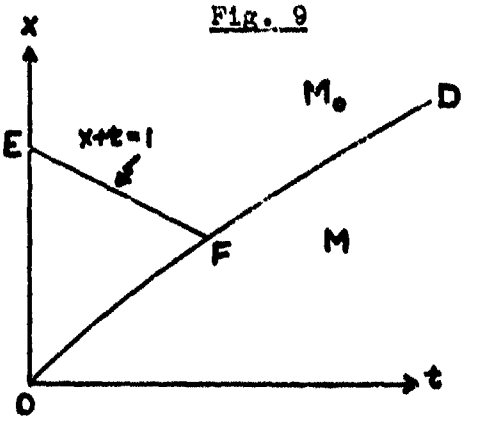
where w is a function to be determined by the boundary conditions. When these conditions are (17.1) and (17.2), then

$$\Delta = \frac{-Bx + D + \frac{2}{\gamma+1}}{Bt + \frac{2}{\gamma+1}}, \quad x < 1 - t \qquad (19.5$$

$$= 1 \qquad , \quad x > 1 - t$$

The discontinuity in the derivatives of Δ along the line $x + t = 1$ (see fig. 9) has its origin in the discontinuity at the tail of the initial pulse (equation (17.1)). The straight line EF is the world line of the tail of the incident shock, and F represents its intersection with the head of

Fig. 9



the reflected shock. Here we are interested only in the part OEF of the region M_0; and so only the first representation of Δ in (19.5) will be carried. The quantities u_0, c_0, and Q_0 are now readily found.

$$u_0 = \frac{x + t - 1}{\frac{1}{B} + \frac{\gamma+1}{2} t} \qquad x < 1-t \qquad (19.6$$

$$c_0 = 1 - \frac{\gamma-1}{2} \frac{x + t - 1}{\frac{1}{B} + \frac{\gamma+1}{2} t} \qquad x<1-t \qquad (19.7$$

$$Q_0 = 2\left[\frac{1}{\gamma-1} - \frac{x + t - 1}{\frac{1}{B} + \frac{\gamma+1}{2} t}\right] \qquad x<1-t \qquad (19.8$$

With these expressions the problem is solved in M_0.

20. The situation in the region M is more difficult; for although the boundary conditions on D are known, the position of D is unknown. In the approximate form which is adequate here the shock equations are (15.6) and (15.7). These two equations contain five variables: u_0, c_0, u, c, and s. Now u_0 and c_0 have been found in (19.6) and (19.7). There is

still one more condition needed to fix u, c, and s. The additional condition is easily available only at the wall, where u vanishes. Elsewhere the approximation is made that the line D is a characteristic of P, i.e.,

$$P(g(t),t) = P(0,0) \qquad (20.1$$

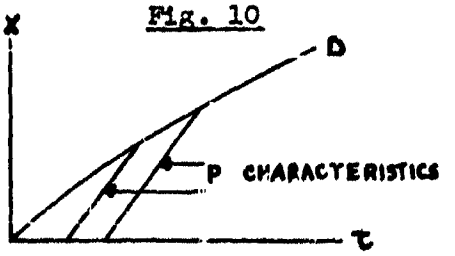
where

$$x = g(t) \qquad (20.2$$

is the equation of D. The required additional condition is (20.1); its accuracy will be discussed in the next paragraph.

21. The best arguments for the condition (20.1) are that the decay of P along D, computed by the rigorous numerical method, is small and that the pressure-time curve, obtained on the basis of (20.1), agrees very closely with the corresponding curve computed according to the numerical method (as shown in par. 9.). In fig. 10 the characteristics of P are actually steeper than D. In this figure two such characteristics are shown. That these lines must be steeper than D may be shown as follows. By (15.6)

Fig. 10



$$s = u_o + ec + e_o c_o < u_o + c,$$

since $c_o < c$, because c is on the high pressure side of D. Since $u_o < 0$, and $u > 0$,

$$s < c < c + u.$$

But s is the slope of D and c + u is the slope of a P-characteristic. Hence D is intersected by successive values of P. Since these values decrease, the result is that P decays at the shock front. Since any shock will decay if not supported from behind, the physical meaning of the approximation (20.1) is that this decay is negligible during the period of reflection. Aside from its numerical success, this assumption has in its favor two facts which make it plausible: first, the time of reflection is short; and second, since the shock travels faster with respect to M_o than with respect to the wall, the wall behaves as a sustaining piston behind the shock.

22. The equations (15.6), (15.7), (19.6), (19.7), and (20.1) lead to a differential equation for the shock front. This equation is

$$\frac{dx}{dt} = \frac{f + hx + jt}{\frac{1}{B} + \frac{\gamma+1}{2} t}$$

where

$$f = \frac{1}{B} + \frac{1}{4}(3\gamma - 5)$$

$$h = \frac{3-1}{2}$$

$$j = 2 + \frac{B}{8}(\gamma + 1)^2$$

The solution of this differential equation is

$$x = \left[\frac{2}{\gamma-1} \frac{1}{B} + \frac{5\gamma-3}{4(\gamma-1)}\right]\left[1 - (1 + \frac{\gamma+1}{2} Bt)^{\frac{3-\gamma}{1+\gamma}}\right] + \\ + \frac{2}{\gamma-1}\left[1 + \frac{B}{4}(\frac{\gamma+1}{2})^2\right] t \qquad (22.1$$

(22.1) is the equation of D from O to F in fig. 9. It is more convenient and numerical comparison with the complete equation shows that it is little less accurate to use only the first two terms of the expansion of (22.1) in powers of t.

$$x = \alpha t + \beta t^2, \qquad (22.2$$

where

$$\alpha = \frac{3\gamma - 5}{4} B + 1 \qquad (22.3$$

$$\beta = \frac{3 - \gamma}{4}\left[\frac{5\gamma - 3}{4} B^2 + 2B\right] \qquad (22.4$$

The equation (22.2) fixes the boundary D. The boundary conditions on it are

$$P(x,t) = P(0,0) \qquad (22.5$$

$$Q(x,t) = Q_0(x,t) \qquad (22.6$$

Q_0 is given by (19.8) and (22.2). If the value of Q_0 so obtained is put in (22.6), one gets

$$Q(x,t) = q_0 + q_1 t + q_2 t^2, \qquad (22.7$$

where

$$q_0 = 2\left(\frac{1}{\gamma - 1} + B\right) \qquad (22.8$$

$$q_1 = -4B\left(\frac{5\gamma - 3}{8} B + 1\right) \qquad (22.9$$

$$q_2 = B^2 (3\gamma - 1)\left(\frac{5\gamma - 3}{8} B + 1\right) \qquad (22.10$$

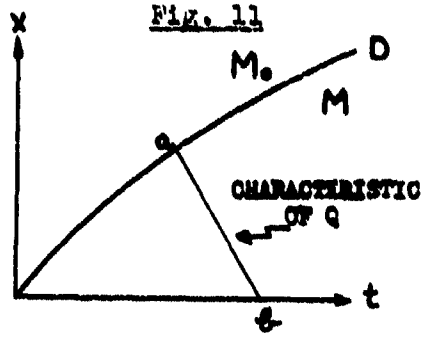
In (22.7) higher order terms in t were again dropped (the error was found to be small in this case, too). One also has

$$P(x,t) = P(0,0) = Q(0,0) = q_0 \qquad (22.11$$

The boundary conditions are most convenient in the forms (22.7' nd (22.11).

23. The boundary D, and the boundary conditions on it having been fixed, one can solve the equations (14.4) and (14.5) in M. Here numerical integration shows that it is accurate enough to assume that the characteristics of Q are straight. Now the actual slope of a Q characteristic is c - u. Let the assumed constant slope be $-\lambda$, which is defined as follows:

Fig. 11



$$2\lambda = (c-u)_a + (c-u)_b \qquad (23.1$$

where the points a and b are shown in fig. 11. One then finds

$$(c-u)_b = c_b = \frac{\gamma-1}{2} Q_b = \frac{\gamma-1}{2} Q_a,$$

and by (22.11) $(c-u)_a = \frac{\gamma-3}{4} P_a + \frac{\gamma+1}{4} Q_a = \frac{\gamma-3}{4} q_0 + \frac{\gamma+1}{4} Q_a$

Hence
$$\lambda = \frac{\gamma-3}{8} q_0 + \frac{3\gamma-1}{8} Q_a \qquad (23.2$$

Then the equation of a characteristic passing through $(0, t_b)$ is

$$x - \lambda (t_b - t), \qquad (23.3$$

where λ is given by the preceding equation (23.2).

24. One may now find Q_b as a function of t_b. To do this it is convenient to regard t_a as the independent variable. The relationship between Q_b and t_b is then given by the parametric equations:

$$Q_b = q_0 + q_1 t_a + q_2 t_a^2 \qquad (24.1$$

$$t_b = t_a + \frac{x(t_a)}{\lambda(t_a)} \qquad (24.2$$

according to (22.7) and (23.3), where,

$$x(t_a) = \alpha t_a + \beta t_a^2$$

$$\lambda(t_a) = \frac{\gamma-3}{8} q_0 + \frac{3\gamma-1}{8} Q_a(t_a),$$

according to (22.2) and (23.2), respectively. The time t_a is a retarded value of the time t_b, since $t_b - t_a$ is the time required for a given value of Q to propagate itself from the shock front to the wall. If the shock and Q both travelled with the velocity of sound (unity), then one would have exactly $t_a = 0.5\ t_b$. This relation is nearly satisfied in any case.

25. Our aim is to calculate $p(0,t_b)$ from t_b. For this purpose it is sufficient to find $Q(0,t_b)$; because at the wall, where $u = 0$,

$$c = \frac{\gamma-1}{2} Q, \qquad (25.1$$

and from c the pressure follows according to the equation

$$\bar{p} = \pi c^{\frac{2\gamma}{\gamma-1}} \qquad (25.2$$

as one may calculate from (14.3) and (14.8). It is convenient to combine (25.1) and (25.2)

$$\bar{p} = \pi\left[\frac{\gamma-1}{2} Q\right]^{\frac{2\gamma}{\gamma-1}} \qquad (25.3$$

Since $Q(0,t_b)$ is known from the preceding paragraph, this equation completes the determination of $p(0,t_b)$ as a function of t_b. The problem will be carried no further here, but it is possible to determine all quantities of interest in the complete region, M, by similar methods.

26. In this paragraph all formulas necessary for the calculation of the pressure-time curve on the wall are

gathered together. The incident shock is specified by its pressure-ratio, ξ , The maximum material velocity, B, is first found

$$B = \frac{1}{\sqrt{\gamma}} \left[(\xi - 1)(1 - \xi^{-\frac{1}{\gamma}}) \right]^{1/2} \qquad (18.1$$

The following constants are functions of B and γ :

$$q_0 = 2\left(\frac{1}{\gamma - 1} + B\right) \qquad (22.8$$

$$q_1 = -4B\left(\frac{5\gamma - 3}{8} B + 1\right) \qquad (22.9$$

$$q_2 = -\frac{B}{4} (3\gamma - 1)\, q_1 \qquad (22.10$$

$$\alpha = \frac{3\gamma - 5}{4} B + 1 \qquad (22.3$$

$$\beta = \frac{3 - \gamma}{4} \left[\frac{5\gamma - 3}{4} B^2 + 2B \right] \qquad (22.4$$

These constants determine the auxiliary functions:

$$x(t_a) = \alpha t_a + \beta t_a^2 \qquad (22.2$$

$$Q(t_a) = q_0 + q_1 t_a + q_2 t_a^2 \qquad (22.7$$

$$\lambda(t_a) = \frac{\gamma - 3}{8} q_0 + \frac{3\gamma - 1}{8} Q\,(t_a) \qquad (22.3$$

In terms of these functions the parametric equations of the pressure-time curve at the wall are

$$t = t_a + \frac{x\,(t_a)}{\lambda\,(t_a)} \qquad (24.2$$

$$\bar{p} = \pi \left(\frac{\gamma - 1}{2} Q\,(t_a) \right)^{\frac{2\gamma}{\gamma - 1}} \qquad (25.3$$

The duration of the pressure on the wall is determined by putting $Q = \frac{2}{\gamma - 1}$ in (22.7), and then using (24.2).

III. THE NUMERICAL SOLUTION

27. The numerical method, as applied to this problem, is described in reference (1). Briefly, the method is as follows: If the initial distributions of pressure and of velocity are given, then the initial values of P and Q can be found from equations (14.6), (14.7), (14.3), and (14.8). If P and Q are known at any time t, they can be found at the later time $t + \Delta t$ since P moves with the velocity $c + u$, and Q moves with the velocity $c - u$, according to (14.4) and (14.5). These new values may be found by a simple deformation of the P,x and Q,x curves. This process is carried out in both regions, M and M_o. On the M_o side of the shock P_o and Q_o are always known. On the M side, however, Q travels away from the shock, and so a gap in the Q distribution develops after each deformation. Since P_o, Q_o, and P are known, by means of the shock equations one can fill the gap, and determine the shock velocity at each step. Similarly at the wall a gap appears in the P curve, and this has to be filled by the relation

$$P_{(wall)} = Q_{(wall)}$$

References

1. The Normal Reflection of a Blast Wave, S. Chandrasekhar, Ballistic Research Laboratory Report No. 439.
2. The Propagation and Decay of Blast Waves, G. I. Taylor, R.C. 39.
3. The Pressure Wave Produced by an Underwater Explosion III, J. G. Kirkwood and J. M. Richardson, O.S.R.D. No. 813 (This report gives an average value of γ for the range 0-25,000 atmospheres. We have used this value (7.15) although it is slightly too low for the pressure range considered here.)
4. The computations and graphs in this report were made by F. N. Hord, BuOrd, Re2c.
5. On the Decay of Plane Shock Waves, S. Chandrasekhar, Ballistic Research Laboratory Report No. 423.

Best Available Copy

FIGURE 2a

Best Available Copy

FIGURE 3

PRESSURE–TIME CURVE AT WALL IN WATER

ERR 6

Best Available Copy

FIGURE 3a
PRESSURE-TIME CURVE AT WALL IN WATER

Best Available Copy

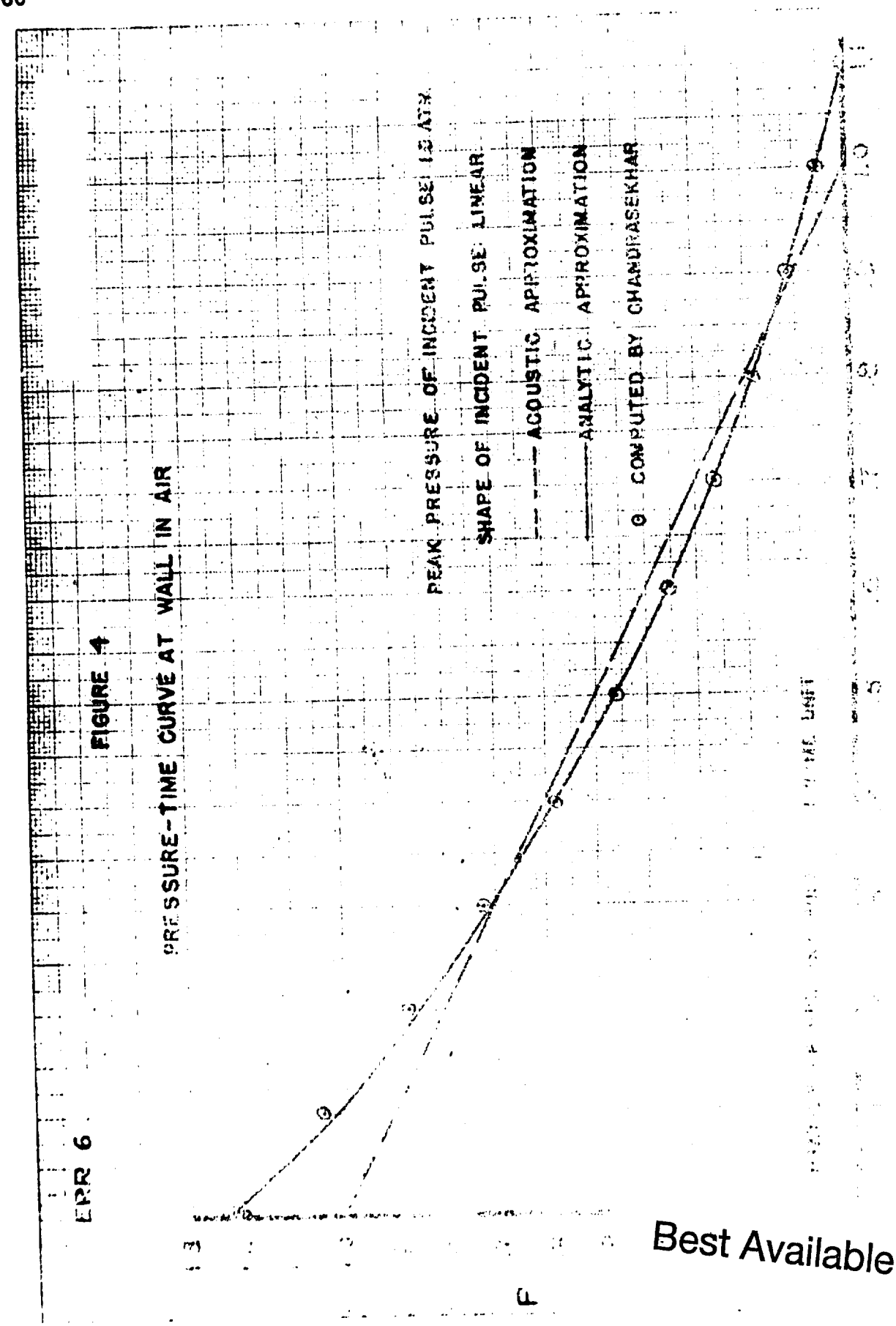


FIGURE 4

PRESSURE-TIME CURVE AT WALL IN AIR

Best Available Copy

FIGURE 5

VARIATION OF IMPULSE WITH

Best Available Copy

37

INTERACTION OF SHOCK-WAVES IN WATER-LIKE SUBSTANCES

H. Polacheck and R. J. Seeger
Bureau of Ordnance, Navy Department

American Contribution

14 August 1944

ABSTRACT

The best utilization of the pressure and momentum produced by an explosion need not be for head-on impact of the shock-wave. Theory predicts that the pressure produced by oblique impact may exceed that obtained by head-on impact of the same shock. The theoretical investigations have been summarized by J. von Neumann in ERR No. 12 on "Oblique Reflection of Shocks."

The present report deals primarily with the reflection of plane shock-waves in water-like substances. It is shown that in the case of water the pressure for any oblique, "regular" reflection of a given shock is greater than that for head-on reflection. A complete set of graphs for quantities involved in regular reflection is furnished for γ, the adiabatic exponent, equal to 7.15 for water and 2.00 (also certain ones for $\gamma = 1.40$ — for comparison with the Rankine-Hugoniot values). For convenience there are included essential formulae and tables of various functions used in the discussion of the propagation of plane shock-waves in water-like substances with $\gamma = 7.15$ and 2.00.

To complete the theoretical discussion the one-dimensional interaction of shock-waves and rarefaction-waves has been considered, as well as the so-called "simple" theory of three-shock intersections. The latter may be of value in the interpretation of the Mach phenomenon, which occurs when regular reflection ceases. Graphs of the parameters needed to specify three-shock configurations in water are accordingly given. In this

connection the essential differences between water-like substances and ideal gases are noteworthy.

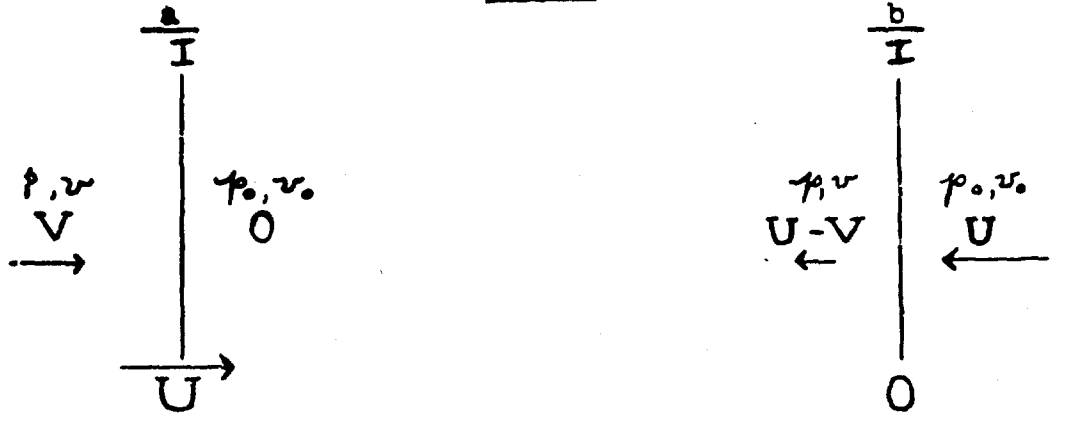
The experimental evidence is still fragmentary, but for water it shows definitely the existence of the expected higher-than-head-on pressures for oblique, regular reflection and of the Mach effect. There is included a brief survey of the experimental work done to date at Oxford, England, at the David Taylor Model Basin, Carderock; at the Explosives Research Laboratory, Bruceton; and at the Underwater Explosives Research Laboratory, Woods Hole.

INTERACTION OF SHOCK-WAVES IN WATER-LIKE SUBSTANCES

I. PLANE SHOCK-WAVES IN WATER-LIKE SUBSTANCES

It is desired to determine the interaction [1] of shock-waves colliding in a water-like substance. The following theoretical discussion will be restricted to constant, plane shocks in liquids of negligible viscosity and thermal conductivity; it can also be applied, however, in the neighborhood of the line of contact for shock-waves that are not too curved. For convenience the usual development of the equations for a plane shock will be repeated here.

Fig. 1



The plane shock-wave I (cf. fig. 1a) is moving with constant velocity in a liquid that is initially at rest. Let the state of the undisturbed liquid be specified by its pressure p_0 and its specific volume* v_0. The state of the liquid behind the shock-front will, in turn, be determined by its pressure p and its specific volume* v. Let V designate

* density: $\rho = \frac{1}{v}$, $\rho_0 = \frac{1}{v_0}$.

the resulting velocity of the liquid. It is convenient to consider the flow of the liquid relative to the shock-front (cf. fig. 1b). By the conservation of mass we have

$$\frac{1}{v_o} U = \frac{1}{v} (U-V)$$

The conservation of momentum states that

$$p-p_o = \frac{1}{v_o} U.V$$

Eliminating V from these two equations we obtain for the velocity of the shock relative to the medium in front of it.

$$U = v_o \sqrt{\frac{p-p_o}{v_o-v}} \qquad (1$$

The substitution of this value for U in the second of the two original equation then gives

$$V = \sqrt{(p-p_o)(v_o-v)} \qquad (2$$

Thus the velocity of the shock relative to the medium behind it is given by

$$U-V = v \sqrt{\frac{p-p_o}{v_o-v}} \qquad (2a$$

Finally, the conservation of energy requires that

$$E-E_o = \frac{1}{2} (p+p_o)(v_o-v) \qquad (3$$

where E is the intrinsic energy per unit mass of the liquid behind the shock and E_o is the intrinsic energy per unit mass of that in front.

Tammann's[2] equation of state, which is sometimes used for liquids at high pressures, is

$$(p+\pi)(v-b) = KT$$

where T is the absolute temperature and π, b, K are all constants. In this case we find that

$$E-E_o = \bar{c}_v\,(T-T_o) + \pi\,(v-v_o) \qquad (4$$

where $\bar{c}_v$, the average specific heat at constant volume, is given by

$$\bar{c}_v = \frac{\int_{T_o}^{T} c_v\, d\,T}{T-T_o}$$

Using the equation of state to eliminate the temperature from equation (4) we obtain

$$E-E_o = \frac{\bar{c}_v}{K}\left[(p+\pi)(v-b) - (p_o+\pi)(v_o-b)\right] + \pi\,(v-v_o)$$

The substitution of this expression in equation (3) gives

$$\frac{v-b}{v_o-b} = \frac{\left(\frac{2\bar{c}_v}{K}+1\right)\frac{p_o+\pi}{p+\pi}+1}{\left(\frac{2\bar{c}_v}{K}+1\right)+\frac{p_o+\pi}{p+\pi}}$$

Put $$\xi \equiv \frac{p_o+\pi}{p+\pi} = \frac{\bar{p}_o}{\bar{p}}$$

and $$\eta \equiv \frac{v-b}{v_o-b}$$

and $$\gamma \equiv 1+\frac{K}{\bar{c}_v}$$

Then the so-called Rankine-Hugoniot dynamic adiabatic is given by

$$\eta = \frac{(\gamma+1)\xi+(\gamma-1)}{(\gamma-1)\xi+(\gamma+1)} \qquad (3'$$

In terms of the variable ξ equation (1) can be written

$$M \equiv \frac{U-V_o}{c_o} = \sqrt{\frac{(\gamma+1)\frac{1}{\xi} + (\gamma-1)}{2\gamma}} \qquad (1'$$

where $$c_o \equiv \sqrt{\frac{\gamma(p_o+\pi)\, v_o}{v_o-b}}$$

Likewise from equation (2a) we obtain

$$\sigma \equiv \frac{U-V}{c} = \sqrt{\frac{(\gamma+1)\xi + (\gamma-1)}{2\gamma}} \qquad (2a'$$

where $$c \equiv \sqrt{\frac{\gamma(p+\pi)\, v}{v-b}}$$

The functions c_o and c represent the speed of sound in front of the shock and behind it, respectively. It is to be noted that the equations (1'), (2a'), and (3') are identical with those for an ideal gas having the same value of γ.

If the change in entropy across the shock-front is small, the pressure-volume relation is expressed approximately by the static adiabatic, viz.,

$$\eta = \xi^{\frac{1}{\gamma}} \qquad (3''$$

In this instance equations (1) and (2a) become respectively:

$$M \equiv \frac{U}{c_o} = \xi^{-\frac{\gamma+1}{2\gamma}} \sqrt{\frac{1-\xi}{\gamma(\xi^{-\frac{1}{\gamma}}-1)}} \qquad (1''$$

and $$\sigma \equiv \frac{U-V}{c} = \sqrt{\frac{1-\xi}{\gamma(\xi^{-\frac{1}{\gamma}}-1)}} \qquad (2a''$$

For values of ξ slightly less than unity equations (3') and (3") both reduce to

$$\eta \sim 1 - \frac{1-\xi}{\gamma} \qquad (3'''$$

Likewise equations (1') and (1") become

$$M \sim 1 + \frac{\gamma+1}{4\gamma}(1-\xi), \qquad (1"'$$

and equations (2a') and (2a") give

$$\sigma \sim 1 - \frac{\gamma+1}{4\gamma}(1-\xi) \qquad (2a"'$$

Thus for weak shocks ($\xi \sim 1$) a water-like substance characterized by the adiabatic equation behaves apparently like an ideal gas that would have the same value of the adiabatic exponent γ [1,3]. (We shall note later that this conclusion is not generally valid.) The adjective weak connotes here that $p \ll \pi$ (and hence $p_o \ll \pi$, too).

We are particularly interested in water. Here the parameters take on the following average values [4] in the domain of physical interest: π = 3,000 atomospheres, b = 0, and γ = 7.15. In fig. 2 there is shown a comparison of the static adiabatic for these water constants with the rigorous Rankine-Hugoniot curves computed by various individuals [4,5]. For the purposes of the present discussion it will be adequate to use the simple adiabatic as an approximation. It is convenient to introduce two more expressions which are functions of the pressure-ratio ξ and which become for b = 0

$$\tau \equiv \frac{U}{c} = \xi^{-\frac{1}{\gamma}} \sqrt{\frac{1-\xi}{\gamma(\xi^{-\frac{1}{\gamma}}-1)}} \qquad (4$$

where τ represents the velocity of the shock relative to the medium in front of it (τ differs from M in the sound-velocity that is taken for reference), and

$$-\upsilon = \frac{V-0}{c} = \pm \sqrt{\frac{(1-\xi)(\xi^{-\frac{1}{\gamma}}-1)}{\gamma}} \qquad (5$$

where υ signifies the change in the material velocity across the shock-front (the sign of $-\upsilon$ corresponds to that of $(1-\xi)$). It is to be noted that

$$\tau = \sigma - \upsilon$$

and

$$\eta = \frac{\sigma}{\tau}$$

In addition, it is of theoretical interest to consider the so-called hydraulic jump [6] in the case of water flowing in an open, shallow channel. This phenomenon is somewhat analogous to the propagation of a plane shock-wave in water. The height h of the incompressible water corresponds to the density of a compressible fluid; the "sound velocity" is equal to $\sqrt{gh}$. Hence there is an analogous "adiabatic equation", viz.,

$$\eta = \xi^{1/2}$$

Thus γ has effectively the value 2, which can be immediately substituted in the above equations.

Table 1 [7] gives ξ as a function of M for $\gamma = 2.00$ and 7.15 (in this case p/p_o also).

The same formulae hold for normalization n with respect to either region provided that ξ is defined as $\bar{p}/\bar{p}_n$. In either case η is the density-ratio $\frac{v_n-b}{v-b}$, σ is the shock-velocity relative to the fluid in the normalized region, τ is the shock-velocity relative to the region not normalized, υ is the increase in material velocity across the shock relative

TABLE 1

M	$\frac{F}{\gamma = 2.00}$	$\frac{F}{\gamma = 7.15}$	$\frac{p/p_o}{\gamma = 7.15}$
1.000	1.00000	1.0000	1.00
1.001	0.9973	0.9965	11.54
1.002	.9947	.9930	22.10
1.003	.9920	.9896	32.69
1.004	.9894	.9861	43.29
1.005	0.9868	0.9827	53.92
1.006	.9842	.9793	64.57
1.007	.9816	.9759	75.24
1.008	.9790	.9725	85.92
1.009	.9764	.9691	96.64
1.010	0.9738	0.9658	107.4
1.011	.9713	.9624	118.1
1.012	.9687	.9591	128.9
1.013	.9662	.9558	139.7
1.014	.9637	.9525	150.5
1.015	0.9611	0.9493	161.3
1.016	.9586	.9460	172.2
1.017	.9561	.9428	183.1
1.018	.9536	.9396	194.0
1.019	.9512	.9364	204.9
1.020	0.9487	0.9332	215.9
1.021	.9462	.9300	226.8
1.022	.9438	.9269	237.8
1.023	.9413	.9237	248.8
1.024	.9389	.9206	259.8
1.025	0.9364	0.9175	270.9
1.026	.9340	.9144	282.0
1.027	.9316	.9113	293.1
1.028	.9292	.9082	304.2
1.029	.9268	.9052	315.3
1.030	0.9244	0.9022	326.5
1.031	.9221	.8991	337.7
1.032	.9197	.8961	348.9
1.033	.9174	.8931	360.1
1.034	.9150	.8902	371.3
1.035	0.9127	0.8872	382.6
1.036	.9103	.8842	393.9
1.037	.9080	.8813	405.2
1.038	.9057	.8784	416.5
1.039	.9034	.8755	427.9

TABLE 1 (cont.)

M	F		P/P₀
	$\gamma = 2.00$	$\gamma = 7.15$	$\gamma = 7.15$
1.039	0.9034	0.8755	427.9
1.040	0.9011	0.8726	439.2
1.041	.8988	.8697	450.6
1.042	.8965	.8668	462.1
1.043	.8943	.8640	473.5
1.044	.8920	.8611	484.9
1.045	0.8898	0.8583	496.4
1.046	.8875	.8555	507.9
1.047	.8853	.8527	519.4
1.048	.8830	.8499	531.0
1.049	.8808	.8471	542.6
1.05	0.8786	0.8444	554.1
1.06	.8569	.8174	671.2
1.07	.8360	.7917	790.4
1.08	.8159	.7672	911.8
1.09	.7964	.7437	1035.
1.10	0.7776	0.7212	1161.
1.11	.7595	.6997	1289.
1.12	.7419	.6791	1419.
1.13	.7250	.6594	1551.
1.14	.7086	.6404	1686.
1.15	0.6928	0.6223	1823.
1.16	.6774	.6049	1962.
1.17	.6626	.5881	2103.
1.18	.6482	.5720	2246.
1.19	.6343	.5566	2392.
1.20	0.6208	0.5417	2540.
1.21	.6077	.5274	2690.
1.22	.5951	.5137	2842.
1.23	.5828	.5005	2997.
1.24	.5709	.4877	3154.
1.25	0.5593	0.4754	3313.
1.26	.5481	.4635	3474.
1.27	.5372	.4521	3638
1.28	.5266	.4411	3804.
1.29	.5164	.4304	3972.

TABLE 1 (cont.)

	ξ		p/p_0
M	$\gamma = 2.00$	$\gamma = 7.15$	$\gamma = 7.15$
1.29	0.5164	0.4304	3972.
1.30	0.5064	0.4202	4143.
1.4	.4205	.3343	5976.
1.5	.3545	.2717	8043.
1.6	.3028	.2248	10350.
1.7	.2615	.1888	12900.
1.8	.2280	.1605	15690.
1.9	.2005	.1380	18740.
2.0	0.1777	0.1199	22040.
2.1	.1585	.1050	25590.
2.2	.1423	.0926	29400.
2.3	.1284	.0823	33460.
2.4	.1164	.0736	37790.
2.5	0.1060	0.0661	42390.
2.6	.0970	.0597	47250.
2.7	.0890	.0542	52380.
2.8	.0820	.0494	57770.
2.9	.0758	.0452	63440.
3.0	0.0703	0.0415	69390.
3.1	.0653	.0382	75600.
3.2	.0609	.0353	82090.
3.3	.0569	.0327	88860.
3.4	.0532	.0303	95910.
3.5	0.0499	0.0282	103200.
3.6	.0469	.0264	110900.
3.7	.0442	.0246	118700.
3.8	.0417	.0231	126900.
3.9	.0394	.0217	135400.
4.0	0.0373	0.0204	144100.

to the normalized region (same sign as (ξ -1)), and c/c_n the velocity of sound in the region not normalized. Tables 2a, b give these quantities for γ = 7.15 (cf. fig. 3a,b) and 2.00, respectively.

TABLE 2a

$\gamma = 7.15$

ξ	η	σ	τ	$-v$	ρ/ρ_0
			∞	∞	0
0.00	0	0	0.7498	0.3159	0.1859
0.02	0.5796	0.4338	.7622	.2763	.2505
0.04	.6375	.4859	.7740	.2518	.2982
0.06	.6747	.5222	.7846	.2335	.3375
0.08	.7024	.5511			
0.10	0.7247	0.5756	0.7943	0.2187	0.3715
0.12	.7434	.5971	.8032	.2061	.4018
0.14	.7596	.6165	.8116	.1951	.4293
0.16	.7739	.6341	.8194	.1853	.4547
0.18	.7868	.6505	.8268	.1763	.4783
0.20	0.7984	0.6657	0.8338	0.1681	0.5005
0.22	.8092	.6801	.8405	.1604	.5214
0.24	.8191	.6937	.8469	.1532	.5413
0.26	.8283	.7066	.8530	.1465	.5603
0.28	.8369	.7189	.8589	.1401	.5784
0.30	0.8450	0.7306	0.8646	0.1340	0.5958
0.32	.8527	.7402	.8701	.1282	.6126
0.34	.8599	.7529	.8755	.1226	.6288
0.36	.8669	.7634	.8806	.1173	.6444
0.38	.8734	.7736	.8857	.1121	.6596
0.40	0.8797	0.7834	0.8905	0.1071	0.6743
0.42	.8857	.7930	.8953	.1023	.6886
0.44	.8915	.8023	.8999	.0976	.7025
0.46	.8971	.8114	.9045	.0931	.7161
0.48	.9024	.8202	.9089	.0887	.7293
0.50	0.9076	0.8288	0.9132	0.0844	0.7422
0.52	.9126	.8372	.9174	.0802	.7549
0.54	.9174	.8455	.9216	.0761	.7672
0.56	.9221	.8535	.9256	.0721	.7793
0.58	.9266	.8614	.9296	.0682	.7911
0.60	0.9310	0.8693	0.9335	0.0644	0.8028
0.62	.9353	.8767	.9373	.0606	.8142
0.64	.9395	.8842	.9411	.0570	.8254
0.66	.9435	.8915	.9448	.0533	.8364
0.68	.9475	.8986	.9484	.0498	.8472
0.70	0.9513	0.9057	0.9520	0.0463	0.8578
0.72	.9551	.9126	.9556	.0429	.8682
0.74	.9588	.9195	.9590	.0396	.8785
0.76	.9623	.9262	.9624	.0362	.8887
0.78	.9658	.9328	.9658	.0330	.8987
0.80	0.9693	0.9393	0.9691	0.0298	0.9085

TABLE 2a (cont.)

$\gamma = 7.15$

ξ	η	σ	τ	$-v$	c/c_n
0.80	0.9693	0.9393	0.9691	0.0298	0.9085
0.82	.9726	.9458	.9724	.0266	.9182
0.84	.9759	.9521	.9756	.0235	.9278
0.86	.9791	.9584	.9788	.0204	.9372
0.88	.9823	.9645	.9819	.0174	.9465
0.90	.9854	0.9706	0.9851	0.0144	0.9557
0.92	.9884	.9767	.9881	.0115	.9648
0.94	.9914	.9826	.9911	.0085	.9737
0.96	.9943	.9885	.9941	.0057	.9826
0.98	.9972	.9943	.9971	.0028	.9913
1.00	1.0000	1.0000	1.0000	0.0000	1.0000
1.10	1.013	1.028	1.014	-0.0136	1.042
1.20	1.026	1.054	1.028	.0265	1.082
1.30	1.037	1.079	1.040	.0389	1.119
1.40	1.048	1.103	1.052	.0507	1.156
1.50	1.058	1.126	1.064	-0.0621	1.191
1.60	1.068	1.148	1.075	.0731	1.224
1.70	1.077	1.170	1.086	.0837	1.256
1.80	1.086	1.191	1.097	.0940	1.288
1.90	1.094	1.211	1.107	.1040	1.318
2.00	1.102	1.230	1.117	-0.1137	1.347
2.10	1.109	1.249	1.126	.1231	1.376
2.20	1.117	1.268	1.135	.1324	1.404
2.30	1.124	1.286	1.144	.1414	1.431
2.40	1.130	1.303	1.153	.1502	1.457
2.50	1.137	1.321	1.162	-0.1589	1.483
2.60	1.143	1.337	1.170	.1673	1.508
2.70	1.149	1.354	1.178	.1756	1.533
2.80	1.155	1.370	1.186	.1837	1.557
2.90	1.161	1.386	1.194	.1917	1.581
3.00	1.166	1.401	1.202	-0.1996	1.604
3.10	1.171	1.417	1.209	.2073	1.627
3.20	1.177	1.432	1.217	.2149	1.649
3.30	1.182	1.446	1.224	.2224	1.671
3.40	1.187	1.461	1.231	.2298	1.693
3.50	1.191	1.475	1.238	-0.2371	1.714
3.60	1.196	1.489	1.245	.2442	1.735
3.70	1.201	1.503	1.251	.2513	1.755
3.80	1.205	1.516	1.258	.2583	1.776
3.90	1.210	1.530	1.265	.2651	1.796

TABLE 2a (cont.)

$\gamma = 7.15$

ξ	η	σ	τ	$-v$	σ/σ_n
3.90	1.210	1.530	1.265	.2651	1.796
4.00	1.214	1.543	1.271	-0.2719	1.815
4.10	1.218	1.556	1.277	.2787	1.835
4.20	1.222	1.569	1.284	.2853	1.854
4.30	1.226	1.581	1.290	.2918	1.873
4.40	1.230	1.594	1.296	.2983	1.891
4.50	1.234	1.606	1.302	-0.3047	1.910
4.60	1.238	1.619	1.307	.3111	1.928
4.70	1.242	1.631	1.313	.3174	1.946
4.80	1.245	1.643	1.319	.3236	1.963
4.90	1.249	1.654	1.325	.3297	1.981
5.00	1.252	1.666	1.330	-0.3358	1.998
5.10	1.256	1.678	1.336	.3418	2.015
5.20	1.259	1.689	1.341	.3478	2.032
5.30	1.263	1.700	1.347	.3537	2.049
5.40	1.266	1.711	1.352	.3596	2.065
5.50	1.269	1.722	1.357	-0.3654	2.082
5.60	1.272	1.733	1.362	.3712	2.098
5.70	1.276	1.744	1.367	.3769	2.114
5.80	1.279	1.755	1.372	.3825	2.130
5.90	1.282	1.766	1.377	.3881	2.145
6.00	1.285	1.776	1.382	-0.3937	2.161
6.10	1.288	1.787	1.387	.3992	2.176
6.20	1.291	1.797	1.392	.4047	2.192
6.30	1.294	1.807	1.397	.4102	2.207
6.40	1.296	1.817	1.402	.4156	2.222
6.50	1.299	1.827	1.407	-0.4209	2.237
6.60	1.302	1.837	1.411	.4262	2.251
6.70	1.305	1.847	1.416	.4315	2.266
6.80	1.307	1.857	1.420	.4368	2.281
6.90	1.310	1.867	1.425	.4420	2.295
7.00	1.313	1.877	1.430	-0.4471	2.309
7.10	1.315	1.886	1.434	.4523	2.323
7.20	1.318	1.896	1.438	.4574	2.337
7.30	1.321	1.905	1.443	.4625	2.351
7.40	1.323	1.915	1.447	..4675	2.365
7.50	1.326	1.924	1.452	-0.4725	2.379
7.60	1.328	1.933	1.456	.4775	2.392
7.70	1.330	1.942	1.460	.4824	2.406
7.80	1.333	1.952	1.464	.4873	2.419
7.90	1.335	1.961	1.468	.4922	2.432

TABLE 2a (cont.)

$\gamma = 7.15$

ξ	η	σ	τ	$-v$	c/c_n
7.90	1.335	1.961	1.468	.4922	2.432
8.00	1.338	1.970	1.473	-0.4971	2.446
8.10	1.340	1.979	1.477	.5019	2.459
8.20	1.342	1.987	1.481	.5067	2.472
8.30	1.344	1.996	1.485	.5114	2.485
8.40	1.347	2.005	1.489	.5162	2.497
8.50	1.349	2.014	1.493	-0.5209	2.510
8.60	1.351	2.022	1.497	.5256	2.523
8.70	1.353	2.031	1.501	.5302	2.535
8.80	1.355	2.040	1.505	.5349	2.548
8.90	1.358	2.048	1.509	.5395	2.560
9.00	1.360	2.056	1.512	-0.5441	2.573
9.10	1.362	2.065	1.516	.5486	2.585
9.20	1.364	2.073	1.520	.5532	2.597
9.30	1.366	2.081	1.524	.5577	2.609
9.40	1.368	2.090	1.528	.5622	2.621
9.50	1.370	2.098	1.531	-0.5667	2.633
9.60	1.372	2.106	1.535	.5711	2.645
9.70	1.374	2.114	1.539	.5755	2.657
9.80	1.376	2.122	1.542	.5800	2.669
9.90	1.378	2.130	1.546	.5843	2.680
10.00	1.380	2.138	1.549	-0.5887	2.692

TABLE 2b

$\gamma = 2.00$

ξ	η	σ	τ	$-v$	c/c_n
0.00	0.0000	0.0000	∞	∞	0.0000
0.02	.1414	.2841	2.009	1.7248	.3761
0.04	.2000	.3464	1.732	1.3856	.4472
0.06	.2449	.3905	1.594	1.2036	.4949
0.08	.2828	.4259	1.506	1.0800	.5318
0.10	0.3162	0.4562	1.443	0.9864	0.5623
0.12	.3464	.4829	1.394	.9111	.5886
0.14	.3742	.5070	1.355	.8481	.6117
0.16	.4000	.5292	1.323	.7937	.6325
0.18	.4243	.5497	1.296	.7459	.6514

TABLE 2b (cont.)

$\gamma = 2.00$

ξ	η	σ	τ	$-\nu$	σ/σ_n
0.18	0.4243	0.5497	1.296	0.7459	0.6514
0.20	0.4472	0.5689	1.272	0.7032	0.6687
0.22	.4690	.5870	1.251	.6644	.6849
0.24	.4899	.6041	1.233	.6290	.6999
0.26	.5099	.6204	1.217	.5964	.7141
0.28	.5292	.6361	1.202	.5600	.7274
0.30	0.5477	0.6510	1.189	0.5376	0.7401
0.32	.5657	.6655	1.176	.5109	.7521
0.34	.5831	.6794	1.165	.4857	.7636
0.36	.6000	.6928	1.155	.4619	.7746
0.38	.6164	.7058	1.145	.4392	.7851
0.40	0.6325	0.7185	1.136	0.4175	0.7953
0.42	.6481	.7308	1.128	.3968	.8050
0.44	.6633	.7427	1.120	.3770	.8144
0.46	.6782	.7544	1.112	.3579	.8235
0.48	.6928	.7658	1.105	.3395	.8324
0.50	0.7071	0.7769	1.099	0.3218	0.8409
0.52	.7211	.7878	1.092	.3047	.8492
0.54	.7348	.7984	1.086	.2881	.8572
0.56	.7483	.8088	1.081	.2720	.8651
0.58	.7616	.8190	1.075	.2564	.8727
0.60	0.7746	0.8290	1.070	0.2412	0.8801
0.62	.7874	.8389	1.065	.2265	.8874
0.64	.8000	.8485	1.061	.2121	.8944
0.66	.8124	.8580	1.056	.1981	.9013
0.68	.8246	.8674	1.052	.1845	.9081
0.70	0.8367	0.8765	1.048	0.1711	0.9147
0.72	.8485	.8856	1.043	.1581	.9212
0.74	.8602	.8945	1.040	.1453	.9275
0.76	.8718	.9033	1.036	.1328	.9337
0.78	.8832	.9119	1.033	.1206	.9398
0.80	0.8944	0.9204	1.029	0.1086	0.9457
0.82	.9055	.9289	1.026	.0970	.9516
0.84	.9165	.9372	1.023	.0854	.9573
0.86	.9274	.9453	1.019	.0740	.9630
0.88	.9381	.9534	1.016	.0629	.9685
0.90	0.9487	0.9614	1.013	0.0520	0.9740
0.92	.9592	.9693	1.011	.0413	.9794
0.94	.9695	.9771	1.008	.0307	.9847
0.96	.9798	.9848	1.005	.0203	.9898
0.98	.9899	.9925	1.003	.0101	.9950

TABLE 2b (cont.)

$\gamma = 2.00$

ξ	η	σ	τ	$-v$	c/c_n
0.98	0.9899	0.9925	1.003	0.0101	0.9950
1.00	1.0000	1.0000	1.000	-0.0000	1.0000
1.10	1.049	1.037	0.9883	.0482	1.024
1.20	1.095	1.071	.9780	.0933	1.047
1.30	1.140	1.105	.9688	.1358	1.068
1.40	1.183	1.136	.9605	.1760	1.088
1.50	1.225	1.167	0.9530	-0.2142	1.107
1.60	1.265	1.197	.9462	.2507	1.125
1.70	1.304	1.226	.9399	.2856	1.142
1.80	1.342	1.253	.9342	.3192	1.158
1.90	1.378	1.280	.9288	.3515	1.174
2.00	1.414	1.307	0.9239	-0.3827	1.189
2.10	1.449	1.332	.9193	.4129	1.204
2.20	1.483	1.357	.9149	.4421	1.218
2.30	1.517	1.381	.9109	.4705	1.231
2.40	1.549	1.405	.9071	.4982	1.245
2.50	1.581	1.428	0.9035	-0.5250	1.257
2.60	1.612	1.451	.9000	.5512	1.270
2.70	1.643	1.474	.8968	.5768	1.282
2.80	1.673	1.496	.8938	.6018	1.294
2.90	1.703	1.517	.8908	.6262	1.305
3.00	1.732	1.538	0.8881	-0.6501	1.316
3.10	1.761	1.559	.8854	.6735	1.327
3.20	1.789	1.579	.8829	.6965	1.337
3.30	1.817	1.599	.8805	.7190	1.348
3.40	1.844	1.619	.8782	.7411	1.358
3.50	1.871	1.639	0.8759	-0.7628	1.368
3.60	1.897	1.658	.8738	.7841	1.377
3.70	1.924	1.677	.8717	.8051	1.387
3.80	1.949	1.695	.8698	.8257	1.396
3.90	1.975	1.714	.8679	.8460	1.405
4.00	2.000	1.732	0.8660	-0.8660	1.414
4.10	2.025	1.750	.8643	.8857	1.423
4.20	2.049	1.768	.8625	.9051	1.432
4.30	2.074	1.785	.8609	.9243	1.440
4.40	2.098	1.802	.8593	.9432	1.448
4.50	2.121	1.820	0.8577	-0.9618	1.456

TABLE 2b (cont.)

$\chi = 2.00$

ξ	η	σ	τ	$-v$	σ/σ_n
4.50	2.121	1.820	0.8577	-0.9618	1.456
4.60	2.145	1.836	.8562	0.9802	1.468
4.70	2.168	1.853	.8548	0.9983	1.482
4.80	2.191	1.870	.8534	1.0162	1.496
4.90	2.214	1.886	.8520	1.0340	1.508
5.00	2.236	1.902	0.8507	-1.0515	1.521
5.10	2.258	1.918	.8494	1.0688	1.534
5.20	2.280	1.934	.8481	1.0859	1.547
5.30	2.302	1.950	.8469	1.1028	1.560
5.40	2.324	1.965	.8457	1.1195	1.572
5.50	2.345	1.981	0.8445	-1.1360	1.585
5.60	2.366	1.996	.8434	1.1524	1.598
5.70	2.387	2.011	.8423	1.1686	1.610
5.80	2.408	2.026	.8412	1.1847	1.622
5.90	2.429	2.041	.8401	1.2006	1.634
6.00	2.449	2.055	0.8391	-1.2163	1.646
6.10	2.470	2.070	.8381	1.2319	1.658
6.20	2.490	2.084	.8371	1.2473	1.670
6.30	2.510	2.099	.8362	1.2626	1.682
6.40	2.530	2.113	.8352	1.2778	1.693
6.50	2.550	2.127	0.8343	-1.2928	1.705
6.60	2.569	2.141	.8334	1.3077	1.716
6.70	2.588	2.155	.8326	1.3225	1.727
6.80	2.608	2.169	.8317	1.3371	1.738
6.90	2.627	2.183	.8309	1.3516	1.749
7.00	2.646	2.196	0.8300	-1.3661	1.760
7.10	2.665	2.210	.8292	1.3804	1.771
7.20	2.683	2.223	.8285	1.3945	1.781
7.30	2.702	2.236	.8277	1.4086	1.792
7.40	2.720	2.249	.8269	1.4226	1.802
7.50	2.739	2.263	0.8262	-1.4364	1.813
7.60	2.757	2.276	.8255	1.4502	1.823
7.70	2.775	2.289	.8247	1.4638	1.833
7.80	2.793	2.301	.8240	1.4774	1.843
7.90	2.811	2.314	.8233	1.4908	1.853
8.00	2.828	2.327	0.8227	-1.5042	1.862

TABLE 2b (cont.)

$\gamma = 2.00$

ξ	η	σ	τ	$-v$	c/c_n
8.00	2.828	2.327	0.8227	-1.5042	1.682
8.10	2.846	2.339	.8220	1.5174	1.687
8.20	2.864	2.352	.8213	1.5306	1.692
8.30	2.881	2.364	.8207	1.5437	1.697
8.40	2.898	2.377	.8201	1.5567	1.702
8.50	2.915	2.389	0.8195	-1.5696	1.707
8.60	2.933	2.401	.8188	1.5825	1.712
8.70	2.950	2.413	.8182	1.5952	1.717
8.80	2.966	2.426	.8176	1.6079	1.722
8.90	2.983	2.438	.8171	1.6205	1.727
9.00	3.000	2.449	0.8165	-1.6330	1.732
9.10	3.017	2.461	.8159	1.6454	1.737
9.20	3.033	2.473	.8154	1.6578	1.742
9.30	3.050	2.485	.8148	1.6701	1.746
9.40	3.066	2.497	.8143	1.6823	1.751
9.50	3.082	2.508	0.8138	-1.6944	1.756
9.60	3.098	2.520	.8132	1.7065	1.760
9.70	3.114	2.531	.8127	1.7185	1.765
9.80	3.130	2.543	.8122	1.7304	1.769
9.90	3.146	2.554	.8117	1.7423	1.774
10.00	3.162	2.565	0.8112	-1.7541	1.778

II. ONE-DIMENSIONAL INTERACTION

The one-dimensional interaction of shock-waves, rarefaction waves, and contact-discontinuities (density alone discontinuous) can be conveniently discussed for water-like substances in the manner used by Courant and Friedrichs for ideal gases.[8] One considers the change in material velocity in terms of the characterizing pressure-ratio ξ.

Consider a plane shock-wave. Let V_n be the material velocity of the normalized region and V the material velocity of the other one. Then we have from the definition of v

(cf. equation (5)).

$$V_n = V - c_n \upsilon(\bar{p})$$

Put $$\Phi_n(\bar{p}) = c_n \upsilon(\bar{p})$$

Then $$V = V_n + \Phi_n(\bar{p}) \qquad (6a$$

If the sense of the direction from left to right be always positive, the equation (6a) applies to fig. 1a. Such a forward shock-wave will be designated $\underset{\rightarrow}{S}$. On the other hand, a backward shock traveling toward the left will be indicated by $\underset{\leftarrow}{S}$ and will satisfy the following relation.

$$V = V_n - \Phi_n(\bar{p}) \qquad (6b$$

The various shocks that are possible for a given value of V or of V_n may be conveniently represented on a $V,\bar{p}$ diagram (fig. 4a,b). It is to be noted that if a point k is given on a $V,\bar{p}$ diagram, a single infinity of curves $V = V_k + \Phi_\mu(\bar{p})$ can be drawn through that point, since $\Phi_\mu(\bar{p})$ is a function of $\bar{p}$ and of ρ_k. If ρ_k, however, is also fixed, then the curve through k is determined.

Fig. 4

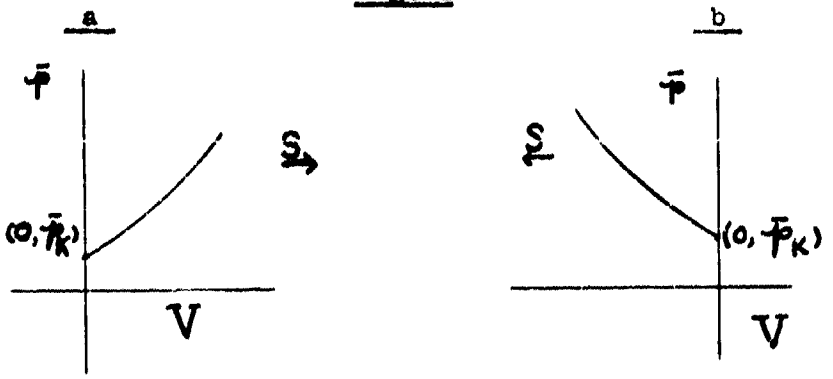
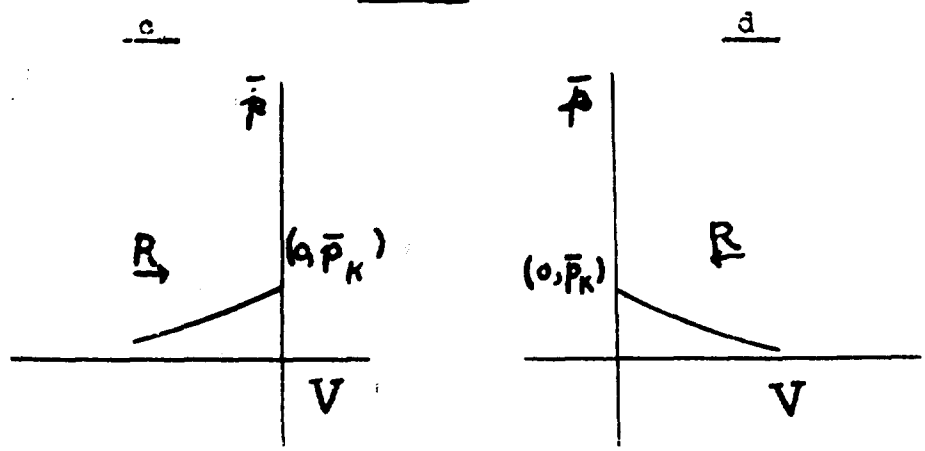


Fig. 4



Consider a finite rarefaction wave $\underrightarrow{R}$ (continuous, adiabatic change) moving toward the right. As before, let V_n be the material velocity of the normalized region and V that of the region not normalized (i.e., on either side of the rarefaction). Then we have from Riemann's argument

$$V - \frac{2}{\gamma-1}\, c = V_n - \frac{2}{\gamma-1}\, c_n$$

Put $$\Psi_n(\bar{p}) \equiv -\frac{2c}{\gamma-1}\left(\frac{c_n}{c} - 1\right)$$

Then $$V = V_n + \Psi_n(\bar{p}) \qquad (7a$$

In the case of such a rarefaction wave $\underleftarrow{R}$ traveling to the left

$$V = V_n - \Psi_n(\bar{p}) \qquad (7b$$

The $V,\bar{p}$ diagrams for such rarefaction waves are shown in fig. 4c,d.

The functions $\Phi_n(\bar{p})$ and $\Psi_n(\bar{p})$ represent physically the absolute change in material velocity across a shock-

wave and a rarefaction-wave of finite amplitude, respectively. They possess certain intrinsic properties (cf. proofs in Appendix A), namely,

$$\Phi_n(\bar{p}) = \Psi_n(\bar{p}) = 0 \qquad \bar{p} = \bar{p}_n \qquad (8a$$

$$\Phi_n(\bar{p}) \gtrless \Psi_n(\bar{p}) \qquad \bar{p} \gtrless \bar{p}_n \qquad (8a'$$

$$\Phi_n'(\bar{p}) = \Psi_n'(\bar{p}) = \frac{c_n}{\gamma} \qquad \bar{p} \to \bar{p}_n \qquad (8b$$

$$\Phi_n'(\bar{p}) \lessgtr \Psi_n'(\bar{p}) \qquad \bar{p} \lessgtr \bar{p}_n \qquad (8b'$$

$$\Phi_n'(\bar{p}),\ \Psi_n'(\bar{p}) \text{ positive} \qquad \text{all } \bar{p} \qquad (8b''$$

$$\Phi_n''(\bar{p}) = \Psi_n''(\bar{p}) = -\frac{(1+\gamma)c_n}{2\gamma^2}, \qquad \bar{p} \to \bar{p}_n \qquad (8c$$

$$\Phi_n''(\bar{p}),\ \Psi_n''(\bar{p}) \text{ negative} \qquad \text{all } \bar{p} \qquad (8c'$$

If $\rho_i \lessgtr \rho_j$ and $\bar{p}_i < \bar{p}_j$

then $\Phi_i(\bar{p}) > \Phi_j(\bar{p}) \qquad \bar{p} \geq \bar{p}_i \qquad (8d$

If $\frac{\bar{p}_i^{\frac{1}{\gamma}}}{\rho_i} \leqslant \frac{p_j^{\frac{1}{\gamma}}}{\rho_j}$ and $\bar{p}_i < \bar{p}_j$

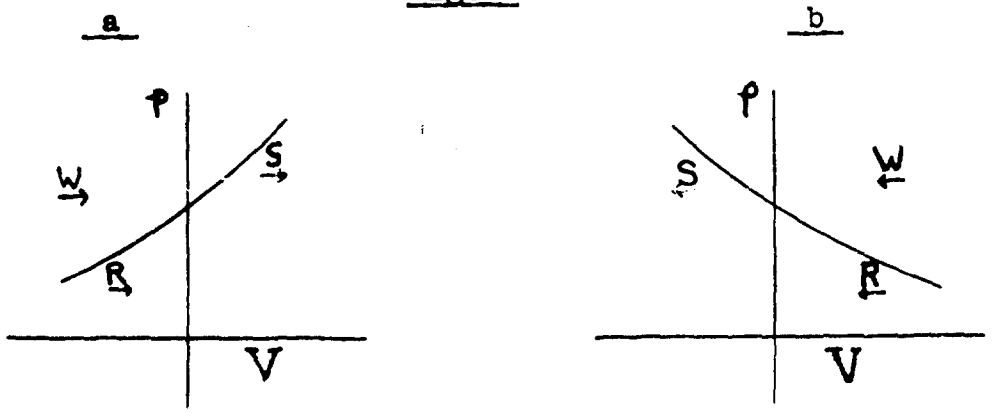
then $\Psi_i(\bar{p}) > \Psi_j(\bar{p}) \qquad \bar{p} \leqslant \bar{p}_j \qquad (8d'$

$$\Phi_i(\bar{p}_k) > \Phi_i(\bar{p}_j) + \Phi_j(\bar{p}_k), \quad \bar{p}_i < \bar{p}_j < \bar{p}_k \qquad (8e$$

$$\Psi_i(\bar{p}_k) = \Psi_i(\bar{p}_j) + \Psi_j(\bar{p}_k), \text{ all } p_i, p_j, p_k \qquad (8e'$$

It is useful in discussing interaction on the basis of these theorems to construct for any given state a $\underrightarrow{W}$ transition-curve for waves toward the right (cf. fig. 5a) and a $\underleftarrow{W}$ transition-curve for those to the left (cf. fig. 5b).

Fig. 5



For example, let us now consider the head-on collision of two shocks S_1 and S_2. It is required to determine the final state of the intermediary region, given its initial state (p_0, ρ_0, V_0) and the strengths ξ_1 and ξ_2 (for definiteness ξ_1 is taken less than ξ_2). Evidently (cf. the illustrative example for water in fig. 6a) a common V_0' and p_0' exists only for the intersection of the upper branches of the W transition-curves through the initial V,p points. In other words, the original colliding shocks result in two new shocks receding from each other. Thus symbolically we may write

$$\underrightarrow{S_1}\ \ \underleftarrow{S_2} \rightarrow \underleftarrow{S_3}\ \ \underrightarrow{S_4}$$

It is to be noted that because of the assumption of no entropy change the condition of pressure equality between two regions implies density equality also, i.e., no contact-discontinuity can exist in this case.[8] In a similar fashion

1312
ERR 14

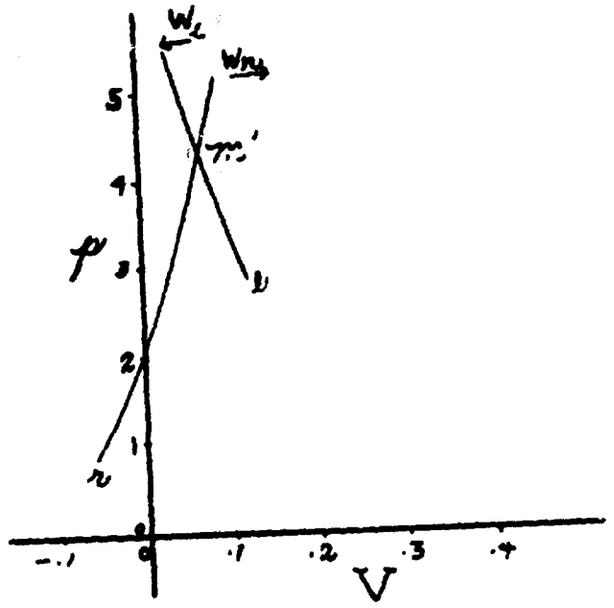
FIGURE 6
WATER $\gamma = 7.15$

ONE-DIMENSIONAL INTERACTION

$$S_1 S_2 \xrightarrow{a} S_3 S_4$$

S_1	BEFORE	S_2
$p_1 = 3.002$	$p_m = 0.001$	$p_r = 1.001$
$c_1 = 1.347$	$c_m = 1.000$	$c_r = 1.131$
$V_1 = 0.114 \rightarrow$	$V_m = 0.000$	$V_r = .043 \leftarrow$

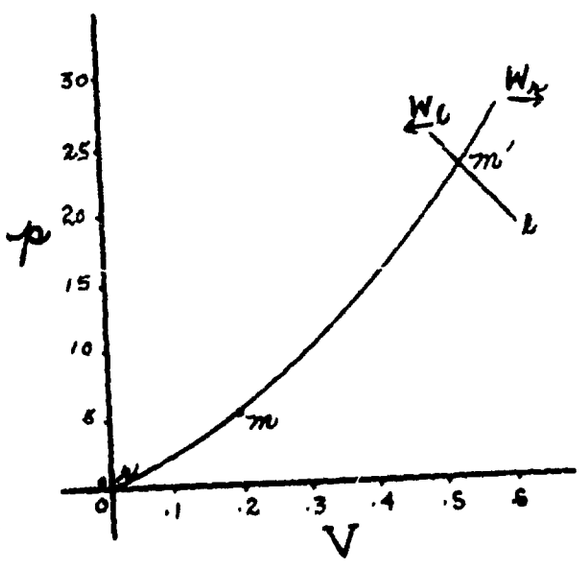
S_3	AFTER	S_4
$p_1 = 3.002$	$p_m = 4.450$	$p_r = 1.001$
$c_1 = 1.347$	$c_m = 1.478$	$c_r = 1.131$
$V_1 = 0.114 \rightarrow$	$V_m = .0708 \rightarrow$	$V_r = .043 \leftarrow$



$$S_1 S_2 \xrightarrow{b} R S_3$$

S_1	BEFORE	S_3
$p_1 = 24.009$	$p_m = 6.003$	$p_r = .001$
$c_1 = 2.573$	$c_m = 1.604$	$c_r = 1.000$
$V_1 = 0.520 \rightarrow$	$V_m = 0.200 \rightarrow$	$V_r = 0\ 000$

$R \leftarrow$	AFTER	$S_3 \rightarrow$
$p_1 = 24.009$	$p_m = 23.150$	$p_r = 0.001$
$c_1 = 2.573$	$c_m = 2.538$	$c_r = 1.000$
$V_1 = 0.520 \rightarrow$	$V_m = 0.531 \rightarrow$	$V_r = 0\ 000$



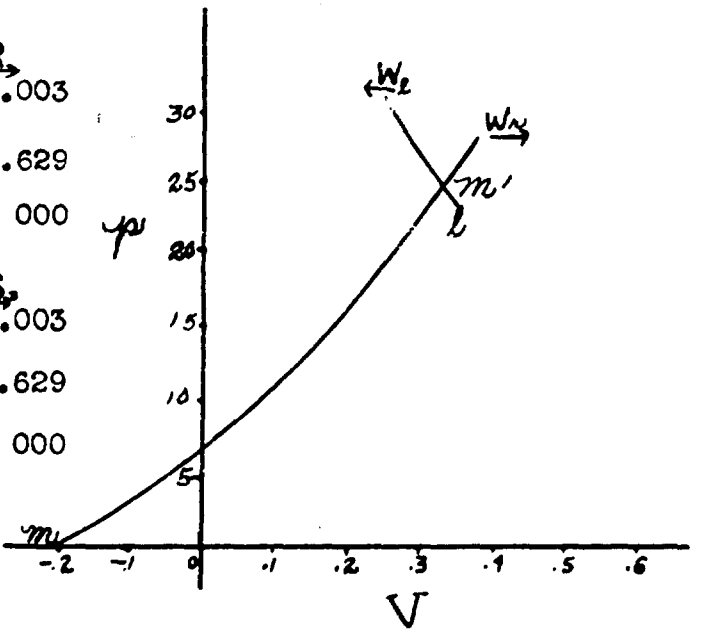
ERR 14

FIGURE 6
WATER $\gamma = 7.15$

ONE-DIMENSIONAL INTERACTION

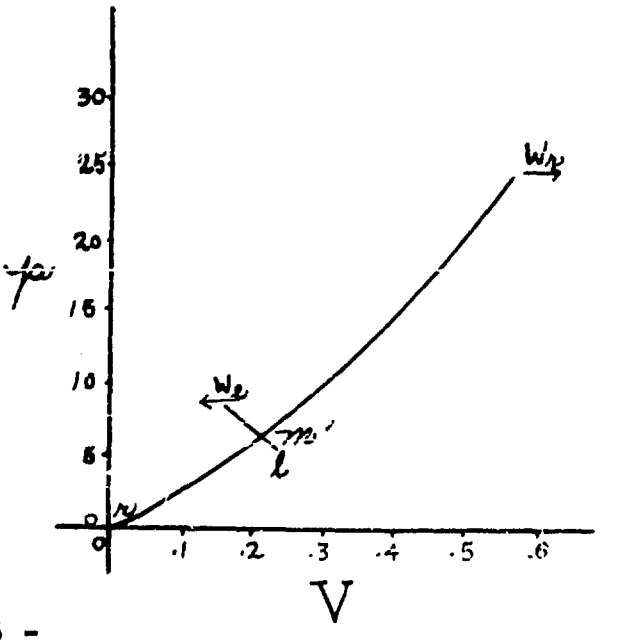
$$S_1 R \xrightarrow{c} S_2 S_3$$

	BEFORE	
S_1		R
$p_1 = 24.009$	$p_m = 0.001$	$p_r = 6.003$
$c_1 = 2.573$	$c_m = 1.000$	$c_r = 1.629$
$V_1 = 0.340$	$V_m = -.204$	$V_r = 0\ 000$
S_2	AFTER	S_3
$p_1 = 24.009$	$p_m = 24.600$	$p_r = 6.003$
$c_1 = 2.573$	$c_m = 2.609$	$c_r = 1.629$
$V_1 = 0.340$	$V_m = 0.333$	$V_r = 0\ 000$



$$R S_1 \xrightarrow{d} S_2 S_3$$

	BEFORE	
R		S_1
$p_1 = 6.003$	$p_m = 24.009$	$p_r = 0.001$
$c_1 = 1.605$	$c_m = 2.573$	$c_r = 1.000$
$V_1 = 0.229$	$V_m = 0.544$	$V_r = 0\ 000$
S_2	AFTER	S_3
$p_1 = 6.003$	$p_m = 6.600$	$p_r = 0.001$
$c_1 = 1.605$	$c_m = 1.649$	$c_r = 1.000$
$V_1 = 0.229$	$V_m = 0.215$	$V_r = 0\ 000$



other types of interaction can be discussed (cf. Appendix B for proofs of two interesting results); they are summarized in Table 3, which includes also the ideal gas results for comparison. It is significant that a water-like substance does not always behave like an ideal gas (fictitious for $\gamma > 5/3$) having the same value of γ. For example, in the case of water the overtaking of one shock-wave by another results always in a rarefaction being reflected, whereas there may be a reflected shock for the analogous ideal gas. Then, too, for a rarefaction overtaking a shock-wave the reflected wave is always a shock in water, but it may be a rarefaction in the ideal gas. Moreover, the kinds of phenomena that occur in water-like substances are independent of the value of γ, not so in the gamut of so-called ideal gases where $\gamma = 5/3$ is a peculiar mathematical boundary. Typical instances of interactions in water-like substances are illustrated in fig. 6a, b, c, and d.

III. OBLIQUE REFLECTION OF SHOCKS

The oblique collision of two similar shock-waves is mathematically equivalent to the oblique reflection of a single shock. Hence consider a plane shock-wave I (cf. fig. 7a) moving with constant velocity in a water-like substance and incident at an angle α on an infinitely wide, plane rigid wall. The reflection is said to be "regular" [1] if

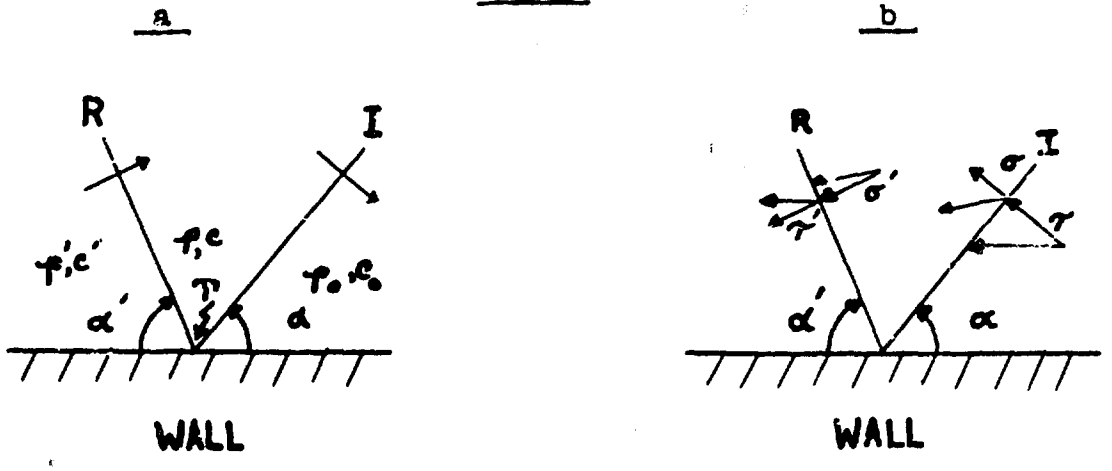
TABLE 3

Water-like Substance	Ideal Gas [8]	
$\underset{\rightarrow}{S}\ T_{<} \rightarrow \underset{\leftarrow}{S}\ T\ \underset{\rightarrow}{S}$	$\underset{\rightarrow}{S}\ T_{<} \rightarrow \underset{\leftarrow}{S}\ T\ \underset{\rightarrow}{S}$	
$\underset{\rightarrow}{S}\ T_{>} \rightarrow \underset{\leftarrow}{R}\ T\ \underset{\rightarrow}{S}$	$\underset{\rightarrow}{S}\ T_{>} \rightarrow \underset{\leftarrow}{R}\ T\ \underset{\rightarrow}{S}$	
$\underset{\rightarrow}{R}\ T_{<} \rightarrow \underset{\leftarrow}{R}\ T\ \underset{\rightarrow}{R}$	$\underset{\rightarrow}{R}\ T_{<} \rightarrow \underset{\leftarrow}{R}\ T\ \underset{\rightarrow}{R}$	
$\underset{\rightarrow}{R}\ T_{>} \rightarrow \underset{\leftarrow}{S}\ T\ T\ \underset{\rightarrow}{R}$	$\underset{\rightarrow}{R}\ T_{>} \rightarrow \underset{\leftarrow}{S}\ T\ T\ \underset{\rightarrow}{R}$	
$\underset{\rightarrow}{S}\ \underset{\leftarrow}{S} \rightarrow \underset{\leftarrow}{S}\ \underset{\rightarrow}{S}$	$\underset{\rightarrow}{S}\ \underset{\leftarrow}{S} \rightarrow \underset{\leftarrow}{S}\ T\ \underset{\rightarrow}{S}$	
$\underset{\rightarrow}{S}\ \underset{\leftarrow}{R} \rightarrow \underset{\leftarrow}{R}\ \underset{\rightarrow}{S}$	$\underset{\rightarrow}{S}\ \underset{\leftarrow}{R} \rightarrow \underset{\leftarrow}{R}\ T\ T\ \underset{\rightarrow}{S}$	
$\underset{\rightarrow}{R}\ \underset{\leftarrow}{R} \rightarrow \underset{\leftarrow}{R}\ \underset{\rightarrow}{R}$	$\underset{\rightarrow}{R}\ \underset{\leftarrow}{R} \rightarrow \underset{\leftarrow}{R}\ \underset{\rightarrow}{R}$	
$\underset{\rightarrow}{S}\ \underset{\rightarrow}{S} \rightarrow \underset{\leftarrow}{R}\ \underset{\rightarrow}{S}$	$\underset{\rightarrow}{S}\ \underset{\rightarrow}{S} \rightarrow \underset{\leftarrow}{R}\ T\ \underset{\rightarrow}{S}$	all γ
	$\underset{\rightarrow}{S}\ \underset{\rightarrow}{S} \rightarrow \underset{\leftarrow}{S}\ T\ \underset{\rightarrow}{S}$	$\gamma > 5/3$
	$\underset{\rightarrow}{S}\ \underset{\rightarrow}{S} \rightarrow\ T\ \underset{\rightarrow}{S}$	$\gamma > 5/3$
$\underset{\rightarrow}{R}\ \underset{\rightarrow}{S} \rightarrow \underset{\leftarrow}{S}\ \underset{\rightarrow}{R}$	$\underset{\rightarrow}{R}\ \underset{\rightarrow}{S} \rightarrow \underset{\leftarrow}{S}\ T\ T\ \underset{\rightarrow}{R}$	
$\underset{\rightarrow}{R}\ \underset{\rightarrow}{S} \rightarrow \underset{\leftarrow}{S}$	$\underset{\rightarrow}{R}\ \underset{\rightarrow}{S} \rightarrow \underset{\leftarrow}{S}\ T\ T\ \underset{\rightarrow}{S}$	
$\underset{\rightarrow}{R}\ \underset{\rightarrow}{S} \rightarrow \underset{\leftarrow}{S}\ \underset{\rightarrow}{S}$	$\underset{\rightarrow}{R}\ \underset{\rightarrow}{S} \rightarrow \underset{\leftarrow}{R}\ T\ T\ \underset{\rightarrow}{S}$	
	$\underset{\rightarrow}{R}\ \underset{\rightarrow}{S} \rightarrow \underset{\leftarrow}{R}\ T\ T\ \underset{\rightarrow}{R}$	$\gamma \leq 5/3$
	$\underset{\rightarrow}{R}\ \underset{\rightarrow}{S} \rightarrow \underset{\leftarrow}{S}\ T\ T$	$\gamma \leq 5/3$
	$\underset{\rightarrow}{R}\ \underset{\rightarrow}{S} \rightarrow\ T\ T$	$\gamma \leq 5/3$
	$\underset{\rightarrow}{R}\ \underset{\rightarrow}{S} \rightarrow \underset{\leftarrow}{R}\ T\ T$	$\gamma \leq 5/3$
$\underset{\rightarrow}{S}\ \underset{\rightarrow}{R} \rightarrow \underset{\leftarrow}{S}\ \underset{\rightarrow}{S}$	$\underset{\rightarrow}{S}\ \underset{\rightarrow}{R} \rightarrow \underset{\leftarrow}{S}\ T\ T\ \underset{\rightarrow}{S}$	
$\underset{\rightarrow}{S}\ \underset{\rightarrow}{R} \rightarrow \underset{\leftarrow}{S}$	$\underset{\rightarrow}{S}\ \underset{\rightarrow}{R} \rightarrow \underset{\leftarrow}{S}\ T\ T$	$\gamma \leq 5/3$
$\underset{\rightarrow}{S}\ \underset{\rightarrow}{R} \rightarrow \underset{\leftarrow}{S}\ \underset{\rightarrow}{R}$	$\underset{\rightarrow}{S}\ \underset{\rightarrow}{R} \rightarrow \underset{\leftarrow}{S}\ T\ T\ \underset{\rightarrow}{R}$	$\gamma \leq 5/3$

Note: $T_{<}$ signifies a density-discontinuity with the density of the region on the left less than that on the right. T T signifies a contact-zone of constant pressure through which there is a monotonic change of density.

the line of contact T between the reflected plane shock R and the incident one is always on the wall. The phenomenon is evidently stationary for an observer moving with the line of contact (cf. fig. 7b) so that it is determined by the

Fig. 7



kinematical condition that the relative flow of the fluid is parallel to the wall both initially and finally. Now the only changes in material velocity are normal to the shocks, viz., v at the incident shock of strength ξ and v' at the reflected shock of strength ξ'. Since the total change of material velocity normal to the wall must be zero, for normalization in the region between the two shocks,

$$v \cos \alpha + v' \cos \alpha' = 0 \qquad (9a$$

Furthermore, the total change of material velocity parallel to the wall must be equal to the difference between the initial parallel velocity and the final one, i.e.,

$$v \sin \alpha - v' \sin \alpha' = \frac{\tau'}{\sin \alpha'} - \frac{\tau}{\sin \alpha} \qquad (9b$$

Now τ and υ are both functions of ξ : τ' and υ' are both functions of ξ'. Hence equations (9a) and (9b) are sufficient to determine the strength ξ' of the reflected shock and its angle of reflection α' in terms of the known strength ξ of the incident shock and its angle of incidence α. For computational purposes it is convenient to combine these equations in a single quadratic equation as follows:

$$L X^2 + M X + N = 0 \qquad (9$$

$$X \equiv \cos^2 \alpha$$

$$L \equiv \upsilon^2 \{(\tau'^2 - \sigma'^2) - (\tau^2 - \sigma^2)\}$$

$$M \equiv \upsilon'^2 \{(\tau^2 - \sigma^2) + \sigma'^2\} - \upsilon^2 \{(\tau'^2 - \sigma'^2) + \sigma^2\}$$

$$N \equiv \upsilon'^2 (\sigma^2 - \sigma'^2)$$

The graphical representations of typical numerical solutions are shown here for $\gamma = 7.15$ and 2.00; $\alpha'(\alpha)$ for given ξ (or p/p_0) in fig. 8a, b and $\xi'(\alpha)$ for given ξ in fig. 9a, b. As in the case of ideal gases [13] there are, in general, two solutions ξ', α' for given ξ, α : one with large ξ' and large α': the other with relatively small ξ' and small α'. For certain "extreme" values, however, the two solutions merge into one, while for still higher values of α no solutions at all exist. The "extreme" values are determined by the condition that the derivative $\frac{\partial \xi'}{\partial \alpha}$ or $\frac{\partial \upsilon'}{\partial \alpha}$ becomes infinite (cf. fig. 9a, b). Subject to this condition equations (9a), (9b) give for $\alpha'_{extr.}$ ($\xi'_{extr.}$)

TABLE 4a

"Extreme" Solutions

$\gamma = 7.15$

$\log_{10}(p/p_0)$*	ξ	$\xi'_{extr.}$	$\alpha_{extr.}$	$\alpha'_{extr.}$
0	1.0000	1.000	90°00	90°00
1.0	0.9970	1.006	85°28	87°64
1.6	0.9872	1.026	80°29	85°14
1.8	0.9797	1.041	77°81	83°89
2.0	0.9681	1.065	74°80	82°37
2.2	0.9501	1.102	71°17	80°52
2.4	0.9230	1.159	66°90	78°34
2.6	0.8831	1.247	62°02	75°82
2.8	0.8265	1.378	56°66	73°02
3.0	0.7502	1.569	51°05	70°05
3.2	0.6545	1.838	45°48	67°07
3.4	0.5444	2.197	40°24	64°24
3.6	0.4299	2.651	35°57	61°70
3.8	0.3224	3.190	31°59	59°53
4.0	0.2308	3.795	28°31	57°71
4.2	0.1592	4.442	25°65	56°23
4.4	0.1067	5.112	23°53	55°01
4.6	0.0701	5.793	21°84	54°00
4.8	0.0454	6.478	20°49	53°15
5.0	0.0291	7.167	19°42	52°41
6.0	0.0030	10.759	16°43	49°78

* p_0 = 1 atm.

TABLE 4b

"Extreme" Solutions

	$\gamma = 2.00$			$\gamma = 1.40$		
ξ	$\xi'_{extr.}$	$\alpha_{extr.}$	$\alpha'_{extr.}$	$\xi'_{extr.}$	$\alpha_{extr.}$	$\alpha'_{extr.}$
0	∞	90°00	0	∞	90°00	0
0.1	5.291	34°36	42°31	5.455	41°72	35°08
0.2	3.874	35°17	46°87	3.845	40°34	40°96
0.3	3.118	36°66	50°48	3.051	40°42	45°52
0.4	2.605	38°59	53°80	2.537	41°27	49°63
0.5	2.218	40°98	57°10	2.160	42°76	53°62
0.6	1.905	43°98	60°55	1.862	44°95	57°69
0.7	1.641	47°87	64°35	1.612	48°10	62°08
0.8	1.410	53°27	68°83	1.395	52°83	67°12
0.9	1.200	61°83	74°76	1.195	60°97	73°63
1.0	1.000	90°00	90°00	1.000	90°00	90°00

$$\tan^2 \alpha'_{extr.} = \left(\frac{\tau'}{v'} \frac{dv'}{d\sigma'}\right)^*_{extr.}$$

Table 4a, b lists these "extreme" solutions $\xi'_{extr.}$, $\alpha'_{extr.}$ for $\gamma = 7.15$ and for $\gamma = 2.00$, 1.40 (included for comparison with air) respectively. Comparative graphs (cf. fig. 10a, a', b, c) show that unless the shocks are very strong the limits of regular reflection for water-like substances are similar to those for ideal gases having corresponding values of γ and obeying the Rankine-Hugoniot adiabatic.

The vanishing of the discriminant of equation (9) is sufficient

* $\tan^2 \alpha'_{extr.} = \frac{1}{\beta^2} \frac{1+\xi}{1-\xi}$

$f(\xi) = \frac{\xi'-1}{\nu\xi'(\xi'+1)}$

to determine the value of $\alpha_{min.}$ for which the reflected pressure $\bar{p}$ is a minimum for given $\bar{p}$. Thus

$$\cos^2 \alpha_{min.} = -\frac{M}{2L}$$

with $$M = 2\sqrt{LN}$$

The minimum solutions for $\gamma = 2.00$ and 1.40 are given in Table 5; those that exist for $\gamma = 7.15$ are not in the region of physical interest. The limiting value or $\alpha_{min.}$ for weak shocks ($\bar{p} \to 1$) is the same as that for an ideal gas [3] having the same γ, namely

$$\sin^2 \alpha_{min.} \to 1 - \frac{\sqrt{\gamma+1}}{2}$$

TABLE 5

"Minimum" Solutions

	$\gamma = 2.00$			$\gamma = 1.40$		
$\bar{p}$	$\bar{p}'_{min.}$	$\alpha_{min.}$	$\alpha'_{min.}$	$\bar{p}'_{min.}$	$\alpha_{min.}$	$\alpha'_{min.}$
0.1	4.393	26°92	20°95	4.946	38.73	22°64
0.2	3.139	24°90	20°87	3.371	35°35	24°00
0.3	2.504	23°83	20°86	2.622	33°44	24°87
0.4	2.094	23°14	20°88	2.156	32°16	25°55
0.5	1.796	22°64	20°94	1.850	31°17	26°12
0.6	1.568	22°27	21°02	1.585	30°39	26°63
0.7	1.385	22°00	21°11	1.393	29°76	27°10
0.8	1.234	21°79	21°22	1.237	29°22	27°54
0.9	1.108	21°58	21°32	1.108	28°78	27°96
1.0	1.000	21°47	21°47	1.000	28°34	28°34

The angle of reflection α' is an increasing montonic function of the angle of incidence α in the range $0 \leq \alpha' \leq \frac{\pi}{2}$

It is to be noted from equation (9a) that the angle of incidence is equal to the angle of reflection provided

$$\nu' = -\nu \qquad \text{(10a}$$

TABLE 6a

"Head-on" Solutions

$\gamma = 7.15$

$\log_{10}(p/p_o)$*	ξ'
0	1.000
1.0	1.003
1.6	1.013
1.8	1.020
2.0	1.032
2.2	1.051
2.4	1.080
2.6	1.125
2.8	1.192
3.0	1.291
3.2	1.431
3.4	1.620
3.6	1.860
4.0	2.472
5.0	4.344
6.0	6.449

* p_o = 1 atm.

TABLE 6b

"Head-on" Solutions

ξ	$\gamma = 2.00$ ξ'	$\gamma = 1.40$ ξ'
0.0	∞	∞
0.1	6.171	4.634
0.2	3.806	3.229
0.3	2.823	2.548
0.4	2.258	2.116
0.5	1.882	1.808
0.6	1.610	1.574
0.7	1.404	1.388
0.8	1.241	1.235
0.9	1.109	1.108
1.0	1.000	1.000

Now this relation always holds for the one-dimensional case of "head-on" reflection ($\alpha = \alpha' = 0$). The "head-on" values are given for $\gamma = 7.15$ in Table 6a and for $\gamma = 2.00$, 1.40 in Table 6b. Furthermore, substituting relation (10a) in equation (9b) we find that these angles are equal also for an angle of incidence α_0 given by

$$\sin^2 \alpha_0 = \frac{\tau' - \tau}{-v} \qquad (10b$$

Inasmuch as υ is intrinsically negative for $0 \leq \mathfrak{F} \leq 1$, no such angle exists for $\tau > \tau'$; hence the limiting condition is given by $\tau' = \tau$, for which $\alpha_s = 0$. It is seen that the magnitude of α_s varies in general not only with the value of γ, as is the case for ideal gases [1,3], but also with the strength $\mathfrak{F}$ of the incident shock. The situation is shown qualitatively in fig. 11 where $\upsilon'(\mathfrak{F}')$ is plotted against $\tau'(\mathfrak{F}')$ and $-\upsilon(\mathfrak{F})$ against $\tau(\mathfrak{F})$ for $\gamma = 1.40$, 2.00 and 7.15. It is to be noted that for $\gamma \leq 3$ the curves intersect at a point $\tau' = \tau$, $\upsilon' = -\upsilon$ only for weak shocks, i.e., $\tau' \sim \tau \sim 1$. Furthermore, in this γ range $\tau' > \tau$ so that the angle α_s exists for all strengths $\mathfrak{F}$. On the other hand, for $\gamma > 3$ (e.g., $\gamma = 7.15$) the curves start out in a reversed position so that τ' is initially less than τ; in other words, there is no such angle α_s. At some lower value $\mathfrak{F}_{\infty}$, however, the curves cross over so that then $\tau' > \tau$ and α_s exists. For example, for $\gamma = 7.15$ the weakest shock for which $\alpha = \alpha'$ is $\mathfrak{F}_{\infty} = 8.481\ (10)^{14}$, i.e., $p_{\infty}/p_0 = 3.538\ (10)^{16}$ outside the domain of interest. Finally, it is seen that for $\gamma = 3$ the curves form a vertical cusp in the neighborhood of weak shocks. Let $\mathfrak{F} \to 1$. Then

$$-\upsilon \sim 1 - \frac{1 - \mathfrak{F}}{\gamma}$$

and

$$\tau \sim 1 - \frac{\gamma - 3}{4\gamma}\ (1 - \mathfrak{F})$$

hence $\frac{d(-\upsilon)}{d\tau} \sim \frac{4}{\gamma - 3}$, which becomes infinite for $\gamma = 3$.

For angles of incidence greater than α_s or 0, if α_s does not exist, the reflected pressure actually exceeds the

"head-on" value. In fig. 12a, a', b, c, the ratio of $\varphi_{extr.}$ to $\varphi'_{head\text{-}on}$ is plotted as a function of φ for $\gamma = 7.15$, 2.00, 1.40, respectively.

It may be that the extreme value of φ' coincides with the "head-on" value for a particular strength φ_1 of the incident shock. In that case "head-on" reflection gives higher values of φ' than any oblique reflection for all stronger incident shocks ($\varphi < \varphi_1$). Table 7 gives φ_1 for $\gamma = 7.15$, 2.00, 1.40.

TABLE 7

"Extreme-Head-on" Equality

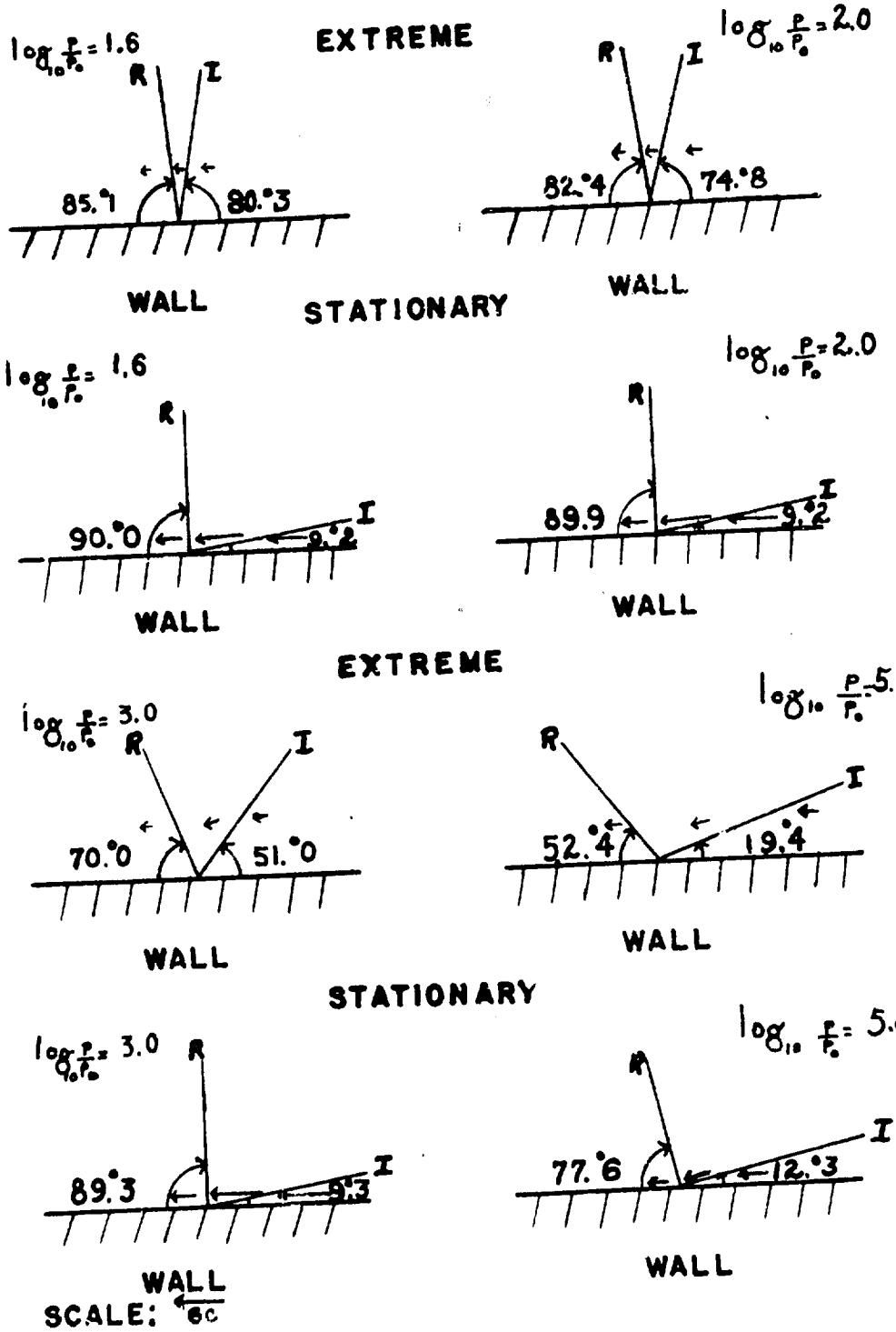
γ	$\varphi_{1(extr.head)}$	$\varphi'_{1(extr.head)}$	$\alpha_{1(extr.head)}$	$\alpha'_{1(extr.head)}$
7.15	$6.243 \times (10)^{-25}$	3563	31°.08	31°.08
2.00	0.02345	0.083	35°.80	35°.80
1.40	0.1889	3.965	40°.39	40°.39

Typical cases of material flow are shown in fig. 13a, b, c. For a given strength $\varphi_{stat.}$ of the incident shock I there is always one angle of incidence $\alpha_{stat.}$ for which the pressure and flow-direction of the material behind the reflected shock R are identical with those corresponding to a "simple" three-shock intersection (cf. Section IV). For example, suppose the wall in fig. 7b is replaced by fluid having the same pressure as that of the neighboring fluid which had been in contact with the wall. This can be accomplished by having a third shock M (cf. fig. 14) with its front normal to the contact-surface.

ERR 14

FIGURE 13 a.
WATER $\gamma = 7.15$

MATERIAL FLOW



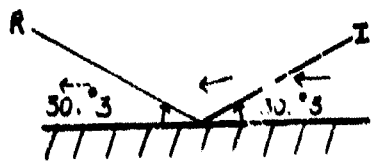
ERR 14

FIGURE 13b
WATER-LIKE
SUBSTANCE $\delta = 2.00$

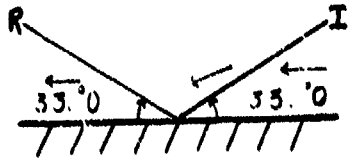
MATERIAL FLOW

HEAD-ON

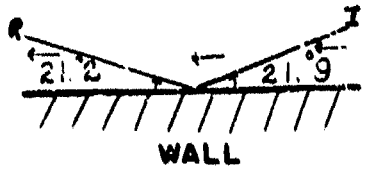
$\xi = 0.75$

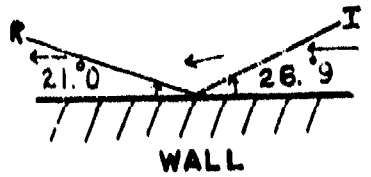


$\xi = 0.10$

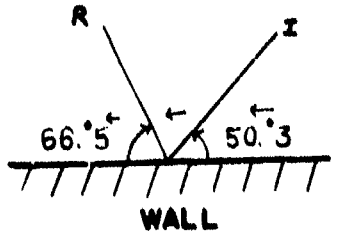


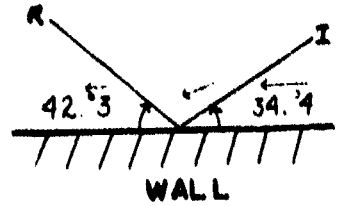
MINIMUM



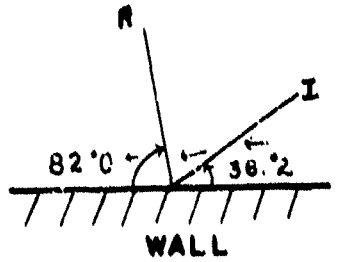


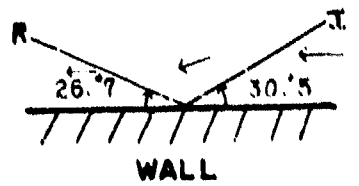
EXTREME





STATIONARY





SCALE: $\overleftarrow{yc}$

ERR 14

FIGURE 13a
WATER-LIKE
SUBSTANCE $\gamma = 1.40$

MATERIAL FLOW

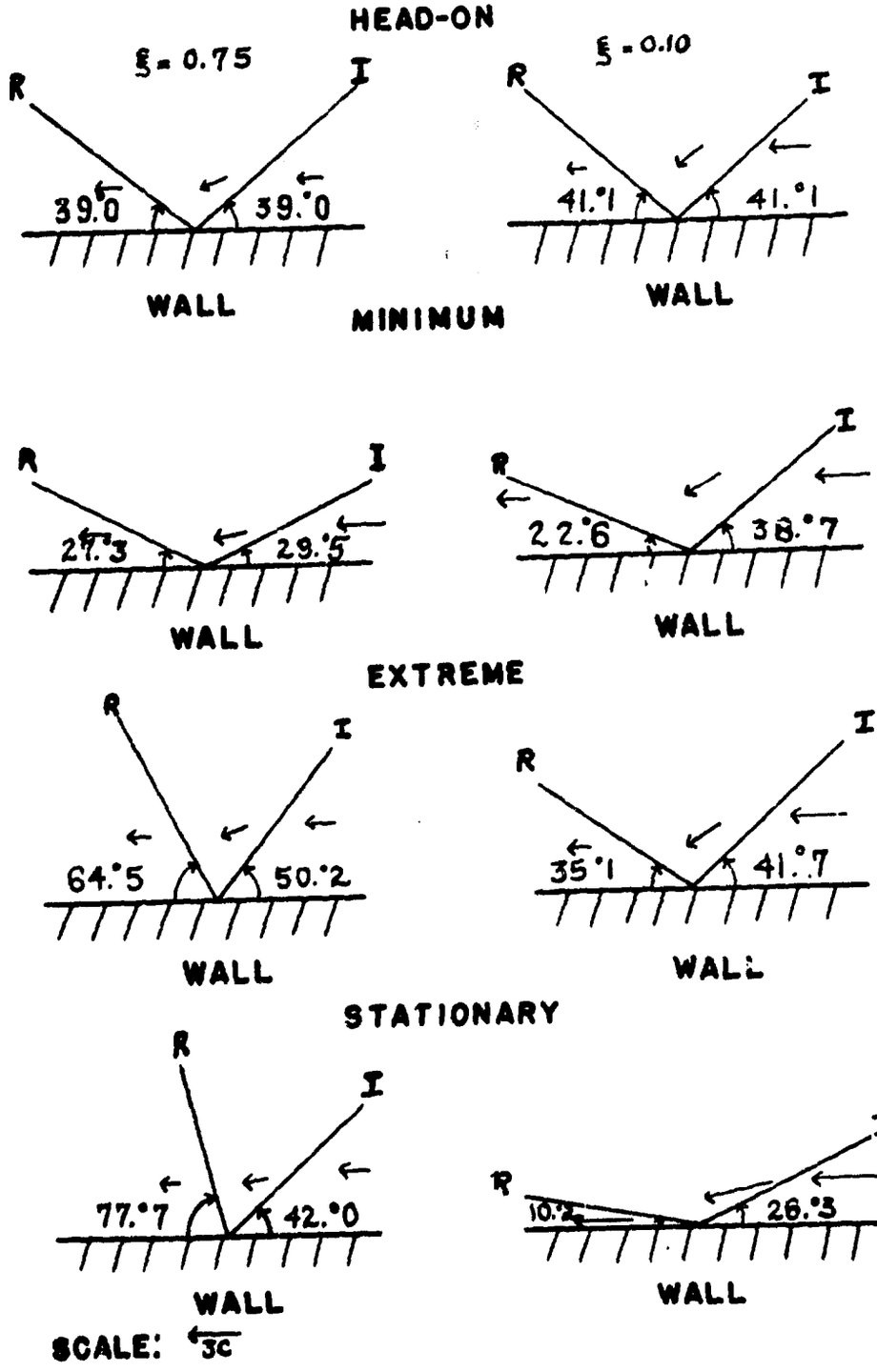
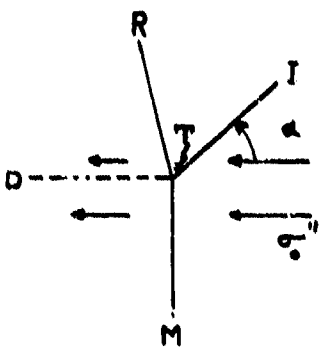


Fig. 14



A density-discontinuity, however, will exist in the region between the shocks M and R. Let $\bar{p}''(=\bar{p}')$ be the pressure behind the shock M and $\sigma_o'' = \bar{p}_o/\bar{p}'' = \frac{1}{\sigma''}$. Then by (2a") we have for normalisation with respect to the region in front of M

$$\sigma''(\sigma'') = M(\sigma) \operatorname{cosec} \alpha$$

or

$$\sigma''\left(\frac{1}{\sigma''}\right) = \sigma\left(\frac{1}{\sigma}\right) \operatorname{cosec} \alpha \qquad (11$$

Thus in addition to equations (9a) and (9b) we now have relation (11) holding for the variables (σ', σ , α). Hence for a given value of σ an angle $\alpha_{stat.}$ is determined. In the limiting case $\sigma \to 1$ equation (11) reduces to

$$\sin \alpha_{stat.} \to \sqrt{\frac{\gamma}{2(2\gamma - 1)}}$$

where

$$\sigma'_{stat.} \to 2^{\gamma}$$

Tables 8a, b give these so-called "stationary" values for γ = 7.15 and 2.00, 1.40 respectively.

This "quasi-stationary" flow corresponds to the regular-reflection solution with low-valued σ' for weak incident shocks, but with the high-valued σ' for strong incident shocks. The critical strength σ_2 that separates these two classes of quasi-stationary solutions is that particular one which is identical with an "extreme" solution (cf. fig. 10a, a', b, c).

J. von Neumann [10] has determined the "extreme-stationary" contact by means of an asymptotic expansion for relatively strong shocks ($\xi \sim 0$) in which terms like ξ are neglected, but not terms such as $\xi^{\frac{1}{\gamma}}$. It turns out that $\xi'_{\text{extr.-stat.}}$ must satisfy the following equations:

$$\frac{\left(F\,\xi'^{\frac{\gamma+1}{\gamma}} - \left(F\,\xi'^{\frac{1}{\gamma}} - 1\right)\right)^2}{F\,\xi'^{\frac{1}{\gamma}} - 1} = \frac{4\,\xi'^{\frac{\gamma+2}{\gamma}}\,(\xi' - 1)}{\left(\xi'^{\frac{1}{\gamma}} - 1\right)(1+f)\left\{\xi'^{\frac{1}{\gamma}}(1-f) + (1+f)\right\}}$$

where $$f(\xi') \equiv \frac{\xi' - 1}{\gamma\,\xi'\left(\xi'^{\frac{1}{\gamma}} - 1\right)}$$

and $$F(\xi') \equiv \frac{(1-f)\left(\xi'^{\frac{1}{\gamma}} - 1\right)\xi'}{\xi'^{\frac{1}{\gamma}}(1-f) + (1+f)} + \frac{\xi'^{\frac{\gamma+1}{\gamma}} - 1}{\xi'^{\frac{1}{\gamma}}(\xi' - 1)} = \xi^{-\frac{1}{\gamma}}$$

for $\gamma = 7.15$ one obtains thus the asymptotic value (cf. Table 9) $\xi_{\text{extr.-stat.}} = 0.0001435$, $\xi'_{\text{extr.-stat.}} = 16.395$, $\alpha_{\text{extr.-stat.}} = 15.^{\circ}24$, $\alpha'_{\text{extr.-stat.}} = 47.^{\circ}46$. The existence of such a contact for all γ in the case of water-like substances is still another respect in which these behavs differently from the analogous ideal gases [1,3].

As yet, there is not sufficient experimental evidence to direct the theoretical understanding of the region beyond the validity of "regular reflection", where the so-called Mach effect [1,3] occurs. In this connection it is desirable to consider as a first approximation the "simple" theory of three-shock intersections.

TABLE 8a

"Stationary" Solutions

$\gamma = 7.15$

$\log_{10}(p/p_o)^*$	$\nu'_{stat.}$
0.0	142.0
1.0	141.8
1.6	141.1
1.8	140.6
2.0	139.8
2.2	138.5
2.4	136.6
2.6	133.7
2.8	129.5
3.0	123.7
3.2	116.0
3.4	106.4
3.6	95.57
3.8	84.10
4.0	72.87
4.2	62.53
4.4	53.46
4.6	45.77
4.8	39.41
5.0	34.23
6.0	20.35

* p_o = 1 atm

TABLE 8b

"Stationary" Solutions

	$\gamma = 2.00$	$\gamma = 1.40$
ξ	$\xi'_{stat.}$	$\xi'_{stat.}$
0.0	∞	∞
.1	4.441	5.444
.2	3.583	3.373
.3	3.379	2.729
.4	3.361	2.496
.5	3.418	2.422
.6	3.509	2.418
.7	3.619	2.450
.8	3.740	2.502
.9	3.868	2.567
1.0	4.000	2.639

Table 9 contains the values of ξ_2 for $\gamma = 7.15, 2.00, 1.40$.

TABLE 9

"Extreme-Stationary" Contact

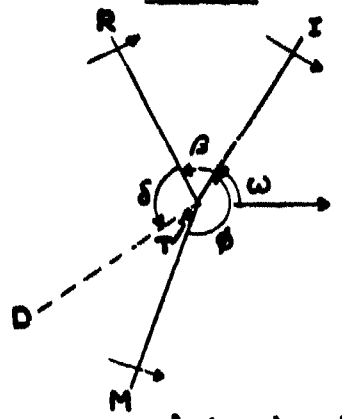
γ	ξ_2(extr.stat.)	ξ'_2(extr.stat.)	α_2(extr.stat.)	α'_2(extr.stat.)
7.15	0.0001435	16.3948	15°.24	47°.46
2.00	0.2514	3.442	35°.87	48°.78
1.40	0.4137	2.479	41°.44	50°.18

IV. THREE-SHOCK INTERSECTIONS

Three-shock intersections in air are not yet understood,[11] although the so-called "simple" theory [3] offers a first approximation for strong shocks. The requirement here is that the pressure be uniform between adjacent shocks. It can be satisfied, however, only if there is a discontinuity D in tangential material-velocity (and density) in one of the regions (cf. fig. 15).

The same method [3] has been used to survey three-shock configurations for water-like substances.

Fig. 15



For the limiting value $\xi \to 1$ the various conditions result in a cubic equation for $\cos\beta_1$, viz.,

$$\{4\sigma'\cos\beta_1 - [(\gamma+1)r\sigma' - 2(\gamma-1)\sigma'^2][\sigma'^2 - \tau'^2]\cos^2\beta_1 - 2\sigma'\cos\beta_1 + (\tau'^2+1)\} - [(m\sigma'^2+n)\cos^2\beta_1 - 2m\sigma'\cos\beta_1 + (m-n)] = 0$$

where $m \equiv (\gamma+1)s\sigma' + 2(\gamma-1)\sigma'\tau'$

and $n \equiv \sigma'\tau'\{(\gamma+1)r\sigma' - 2(\gamma-1)\sigma'^2 - 4\}$

and $r \equiv \frac{+4\gamma}{\gamma+1}\xi' \cdot \frac{d\sigma'}{d\xi'}$

and $$\pi = -\frac{4}{\gamma+1}\mathfrak{F}'\frac{d\tau'}{d\mathfrak{F}'}$$

The other angles are then given by

$$\delta_1 = \pi - \cot^{-1}\left(\frac{\tau'\cos\beta_1 - 1}{\tau'\sin\beta_1}\right)$$

and $$\phi_1 = \pi - \beta_1$$

and $$\omega_1 = \cot^{-1}\left(\frac{\tau' - \cos\beta_1}{\sin\beta_1}\right)$$

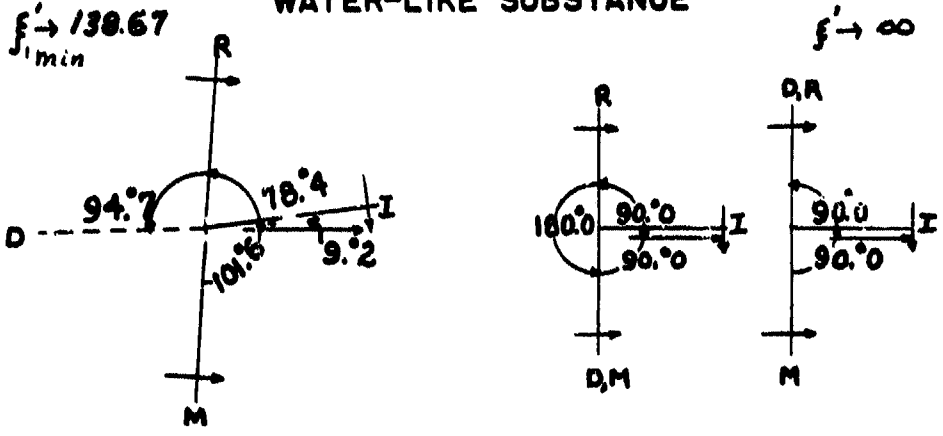
The solutions are surprising. Even though the one shock is very weak ($\mathfrak{F}\to 1$) the minimum resultant pressure $\mathfrak{F}'_{min.}$ may be many times greater, e.g., $\mathfrak{F}'_{min.} = 2.0234$ for $\gamma = 1.40$, $\mathfrak{F}'_{min.} = 3.3175$ for $\gamma = 2.00$, and $\mathfrak{F}'_{min.} = 138.67$ for $\gamma = 7.15$ (cf. fig. 17d_a, d_b, d_c). In other words, for weaker resultant pressures $\mathfrak{F}'_1$ no three-shock configurations exist at all; they do exist, however, for an ideal gas with the same value of γ. It can be shown that this peculiarity is independent of γ (cf. Appendix C). Thus we have another characteristic difference between water-like substances and ideal gases! The configurations for limiting cases are shown in fig. 16a, b.

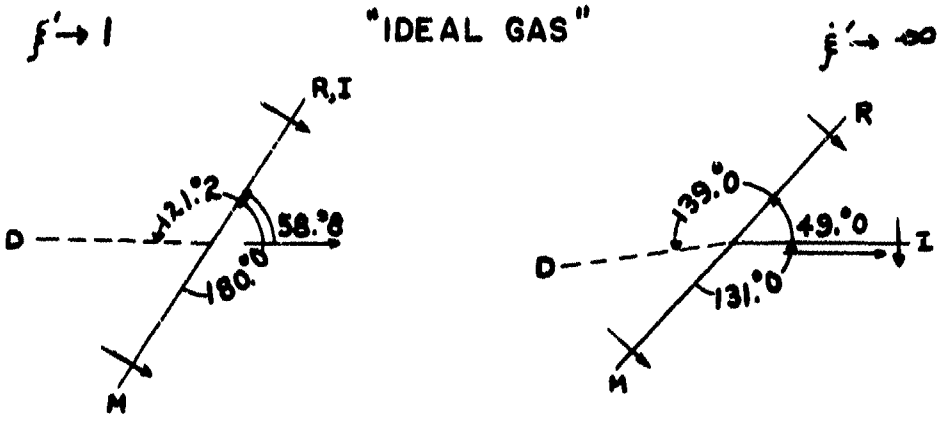
Numerical results for $\gamma = 7.15$ are shown graphically for given values of $\mathfrak{F}$; namely $\mathfrak{F}\to 1$, $\mathfrak{F} = 0.75$ and 0.10; e.g., $\beta(\phi)$ in fig. 17a, $\sigma(\phi)$ in fig. 17b, $\omega(\phi)$ in fig. 17c, $\mathfrak{F}'(\phi)$ in fig. 17d_a, d_a' and $\omega(\beta)$ in fig. 17e. Here, too, for each value of $\mathfrak{F}$ is a minimum resultant pressure $\mathfrak{F}'_{min.}$ (e.g., $\mathfrak{F}'_{min.} = 120.2$ for $\mathfrak{F} = 0.75$ and $\mathfrak{F}'_{min.} = 48.1$ for $\gamma = 0.10$) in contrast to the three-shock solutions for the analogous ideal gas, where configurations with $\mathfrak{F}$ in the neighborhood of unity always exist. It is to be remarked also how close the various curves are to the limiting one for $\mathfrak{F}\to 1$, which is accordingly a good approximation for qualitative

ERR 14

FIGURE 16a

LIMITING THREE-SHOCK CONFIGURATIONS
$\gamma = 7.15$, $\xi \to 1$
WATER-LIKE SUBSTANCE





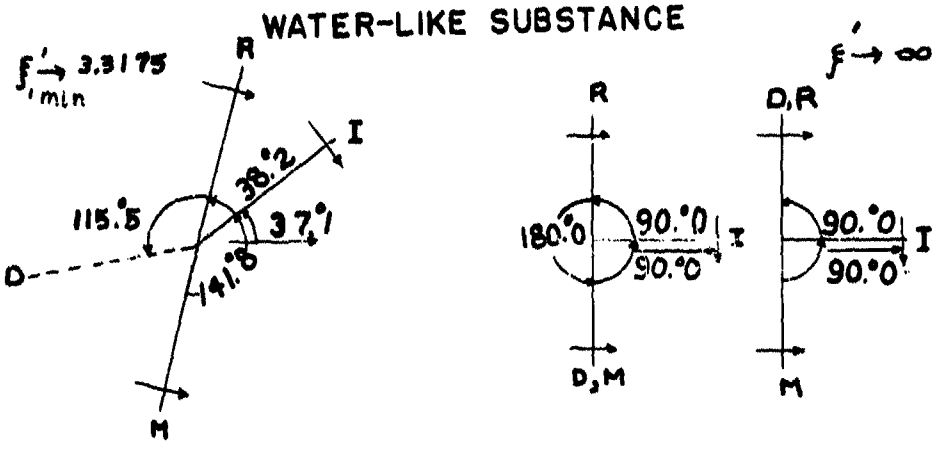
ERR 14

FIGURE 16 b

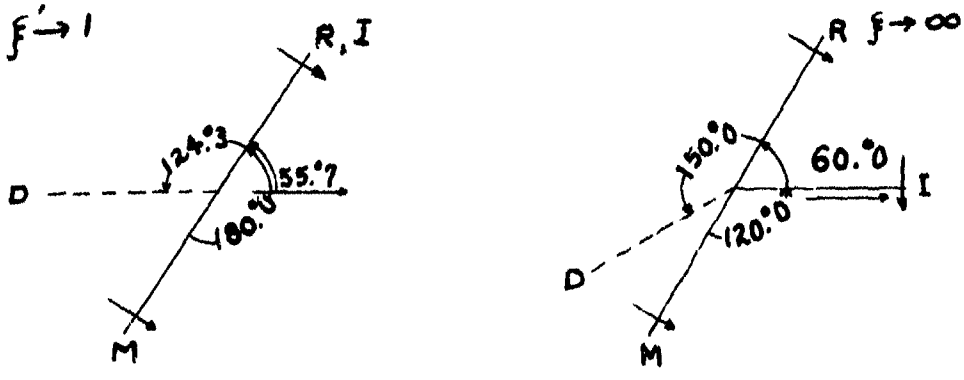
LIMITING THREE-SHOCK CONFIGURATIONS

$\gamma = 2.00$, $f \to 1$

WATER-LIKE SUBSTANCE



"IDEAL GAS"



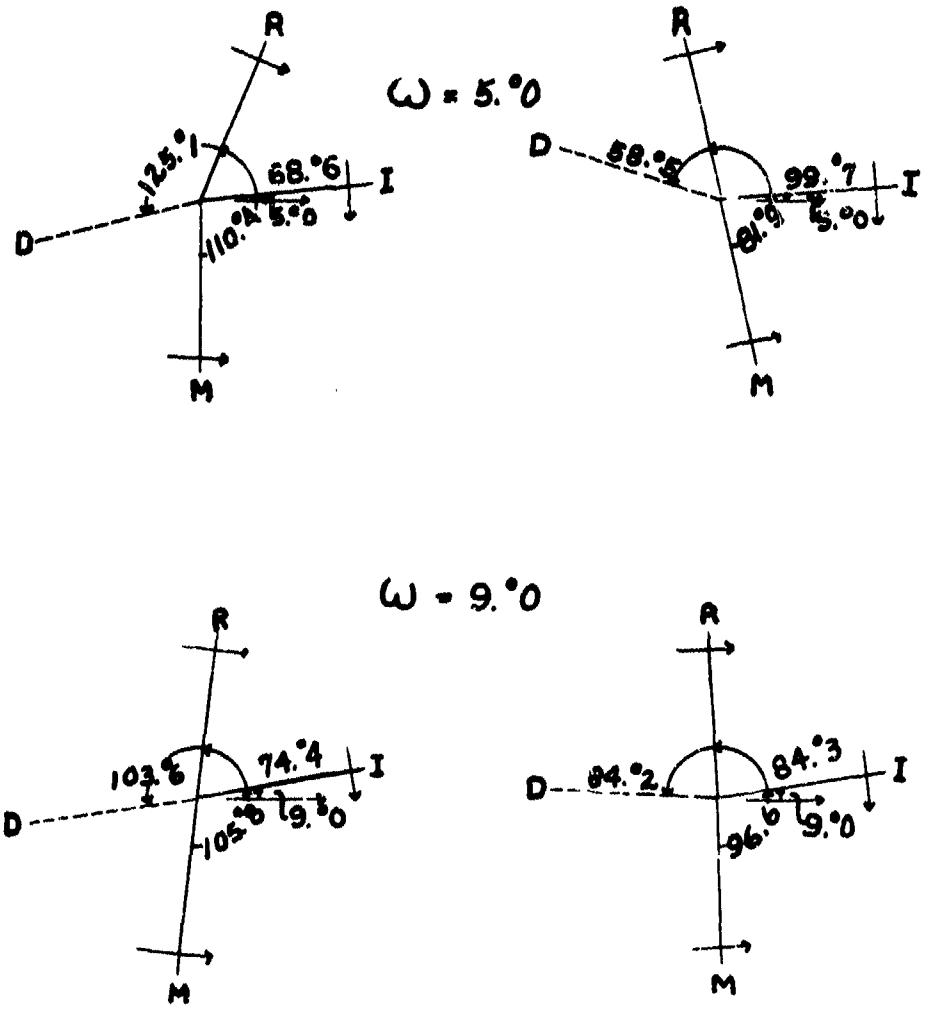
ERR 14

FIGURE 18 a

THREE-SHOCK CONFIGURATIONS

WATER-LIKE SUBSTANCE

$\gamma = 7.15$ $\xi = .75$



ERR 14

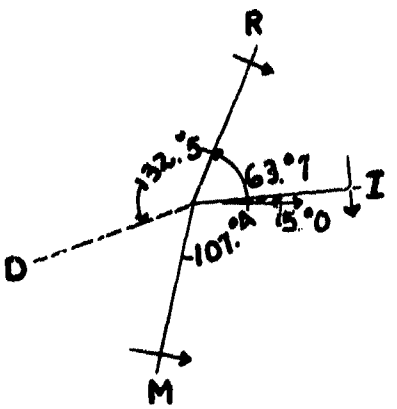
FIGURE 18a'

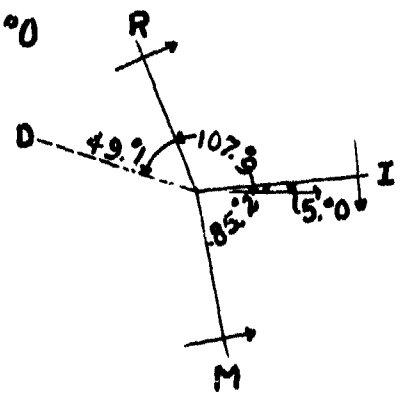
THREE-SHOCK CONFIGURATIONS

WATER-LIKE SUBSTANCE

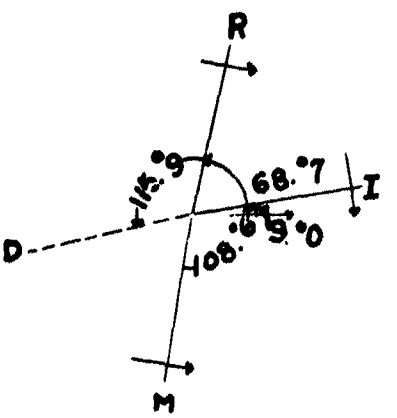
$\gamma = 7.15 \quad \beta = .10$

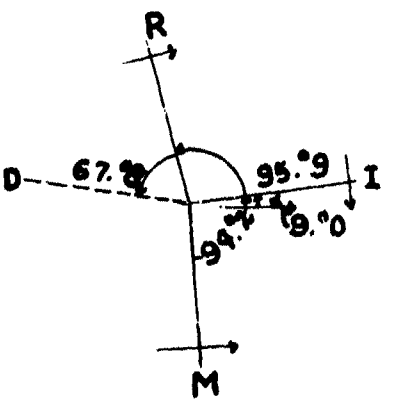
$\omega = 5.°0$





$\omega = 9.°0$





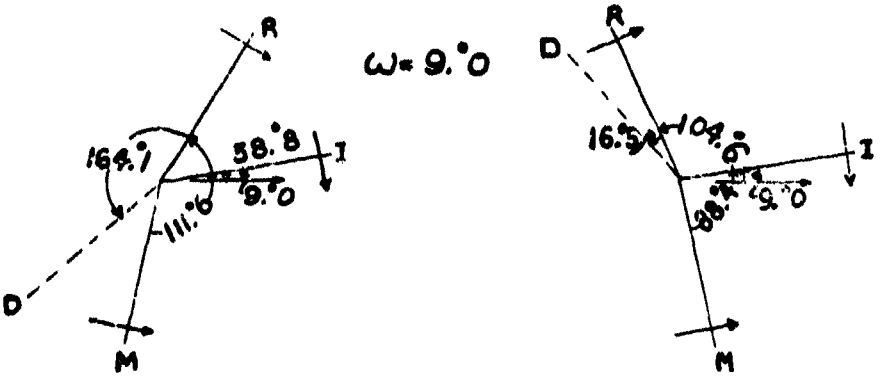
ERR 14

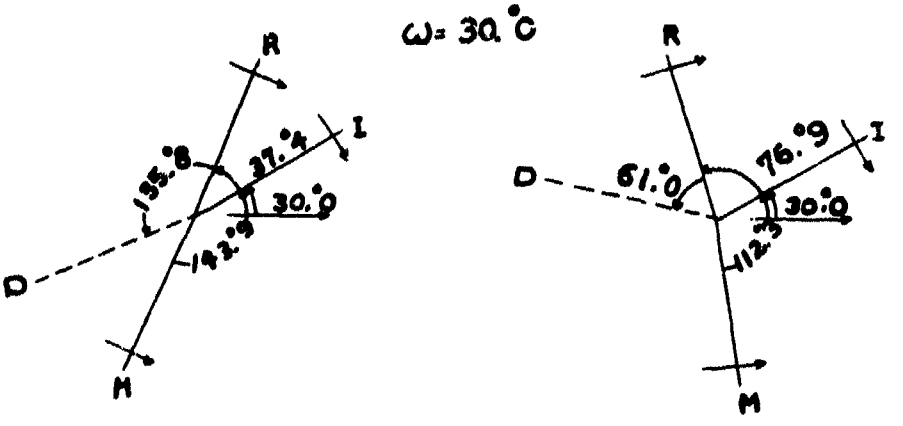
FIGURE 18b

THREE-SHOCK CONFIGURATIONS

WATER-LIKE SUBSTANCE

$\gamma = 2.00$ $\xi = .75$





ERR 14

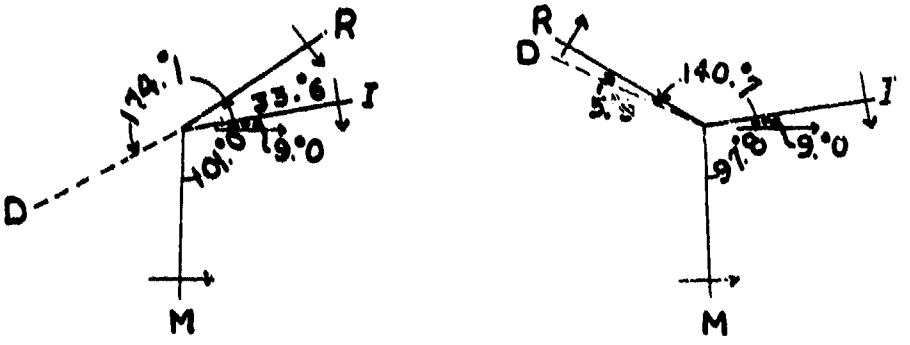
FIGURE 186'

THREE-SHOCK CONFIGURATIONS

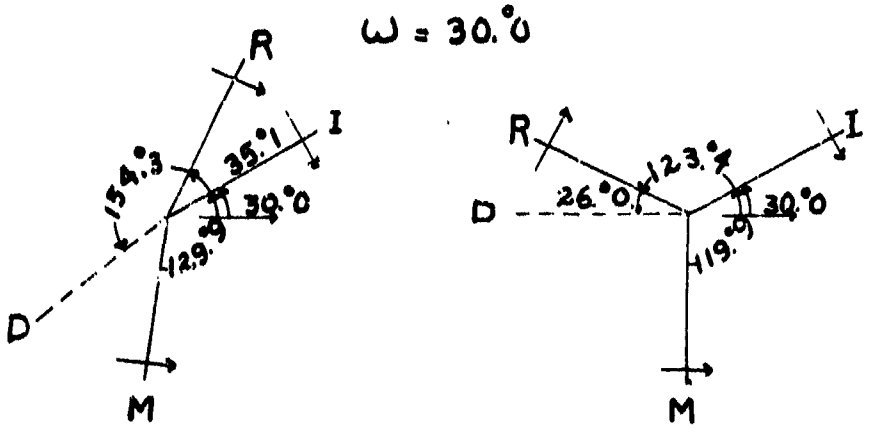
WATER-LIKE SUBSTANCE

$\gamma = 2.00$ $f = .10$

$\omega = 9.^\circ 0$



$\omega = 30.^\circ 0$



description. In each case the limiting curve $\xi \to 1$ for the analogous ideal gas is given for comparison. The two apparent families of solutions which are usually distinct for an ideal gas are undoubtedly physical regions of one double-valued family in the case of water-like substances. Typical three-shock configurations for given values of ξ and of ω are shown in the diagrams of fig. 18a, a'. The influence of γ is illustrated in the comparative cases of fig. 18b, b'.

V. EXPERIMENTAL EVIDENCE

The interaction of shock-waves in water was first studied by P. Libessart [12] at Oxford, England. In fig. 19, Plate I, a spherical shock-wave produced by No. 8 detonator is shown reflected obliquely from a wall. From the four exposures we observe how "regular reflection" develops into "Mach reflection" (incipient at 3rd exposure). In fig. 20, Plate I, shock-waves from two No. 8 detonators, fired simultaneously from opposite ends of an ebonite cylinder, have interacted to produce a Mach effect. It is likely that the central band is the region included between two surfaces of density-discontinuity (the optics of such photographs require further study).

(See page 74 for insert.)

D. P. Mac Dougall, G. H. Messerly, and E. M. Boggs[14] of the Explosives Research Laboratory, Bruceton, Pa., have investigated the oblique collision of two intense shock-waves produced by the detonation of an inclined pair of pentolite sticks (1" diameter) in water. Figure 23, Plate III, illustrates a

"regular" collision. For β in the neighborhood of 0.174 and for $\alpha = 20.^{\circ}8$ the measured value of α' is $23.^{\circ}5$ [15] - greater than α, as the theory predicts. Figure 24, Plate III, shows a Mach effect. The measured angle $\alpha = 39^{\circ}$ is beyond the range of "regular" values (cf. fig. 10a, where $\alpha_{extr.}$ for $\beta = 0.174$ is about $26.^{\circ}6$).

The most complete quantitative investigation [16] has been carried out experimentally at the Underwater Explosives Research Laboratory, Woods Hole, Mass. In general, two equal charges are exploded simultaneously at a variable distance apart. The resultant effect of the shock-waves is registered by a piezo-electric or diaphragm gauge at some point equidistant from the two charges (it is convenient for this distance to be kept constant). Figure 25, Plate IV shows a "regular" collision produced by the spherical shock-waves from two 50-g tetryl charges [17], while figure 26 illustrates a Mach effect. The measurements were made primarily in the case of two ca. 1700-g spherical, cast, pentolite charges. In fig. 27 a typical plot is given. The average experimental curve indicates the predicted increase of resultant pressure β' with increasing angle of incidence α. The quantitative discrepancy is of the order of magnitude of the observational error. (Exact agreement is hardly to be expected in view of the above theoretical assumption of constant pressure behind the incident shocks and in view of the experimental uncertainty of determining the peak pressure by a method of extrapolation.) Furthermore, the

"damage" [18] as indicated by a diaphragm gauge and by a cylindrical shell-target shows a maximum beyond the "extreme" angle similar to that found for the peak pressure.

More data, including values of α', as well as β' over a wide range, are required before any statement can be made regarding the quantitative satisfactoriness of the theory.

ERR 14

PLATE A

SHOCK WAVES IN WATER
OXFORD

Fig. 19 - Development of Reflection

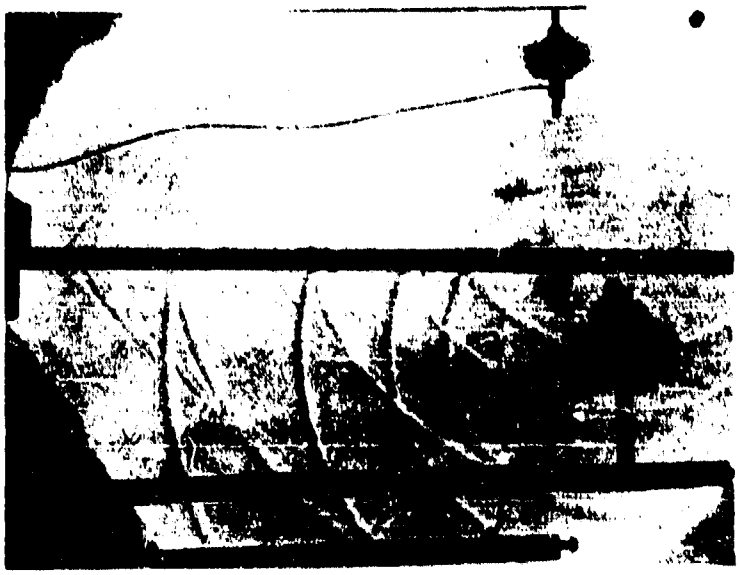


Fig. 20 - Mach Intersection

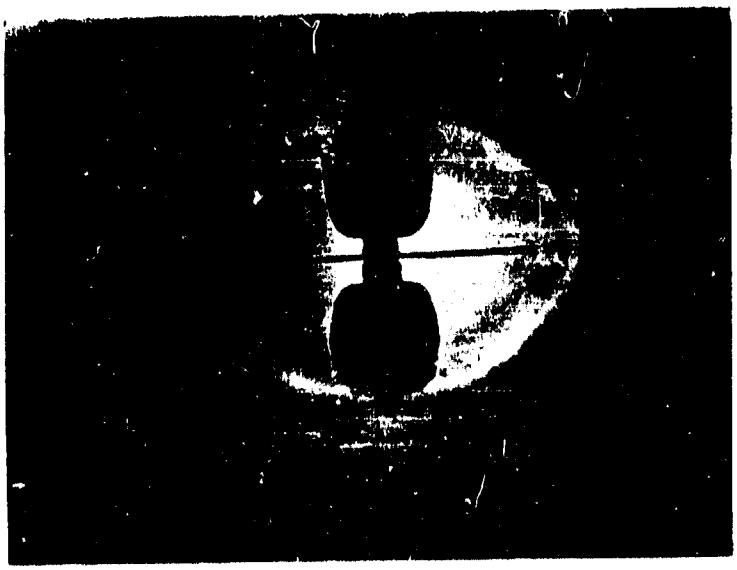


PLATE II

SHOCK COLLISIONS IN WATER
DAVID TAYLOR MODEL BASIN

Fig. 21 - Regular Intersection

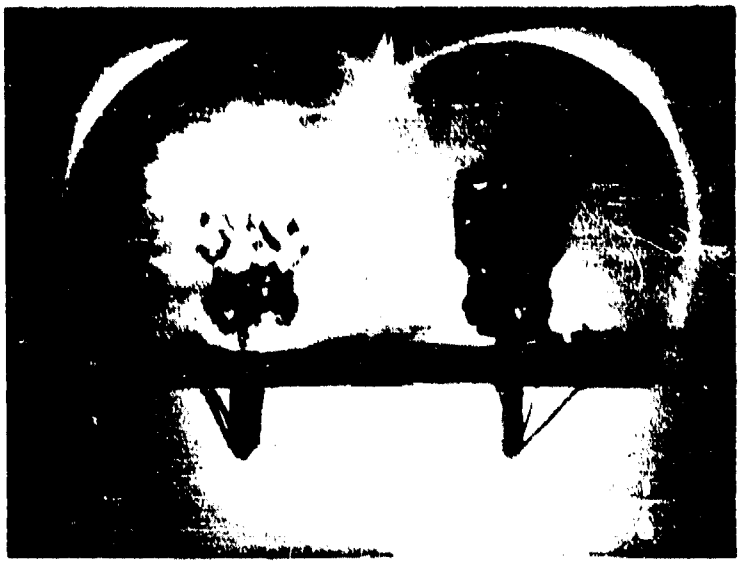


Fig. 22 - Mach Intersection

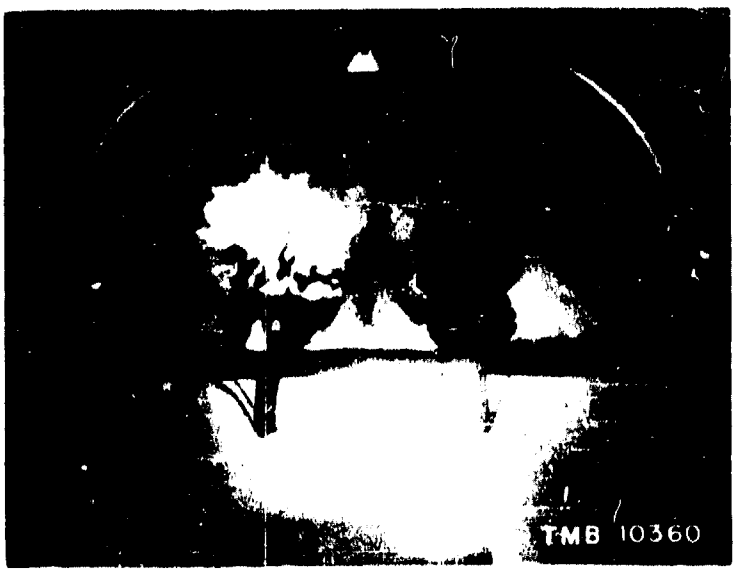


PLATE III

SHOCK COLLISIONS IN WATER
ERL BRUCETON

Fig. 23 - Regular Intersection

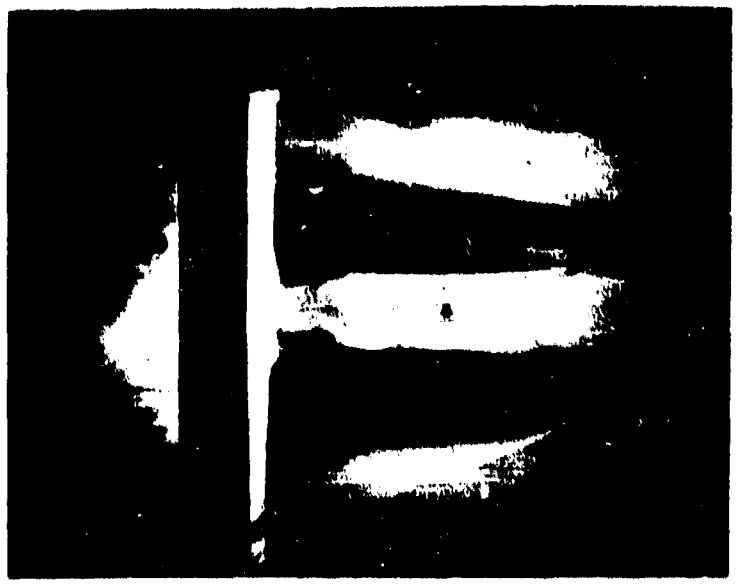


Fig. 24 - Mach Intersection

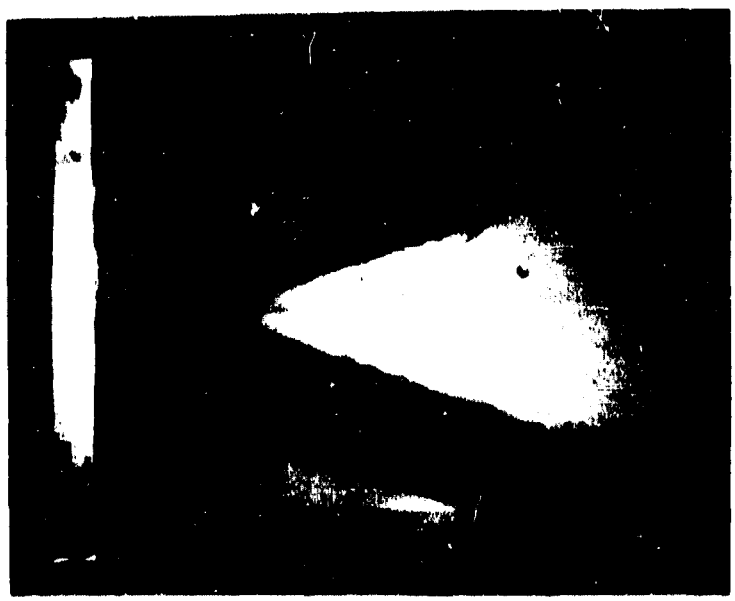


PLATE IV

SHOCK COLLISIONS IN WATER
UERL WOODS HOLE

Fig. 25 - Regular Intersection

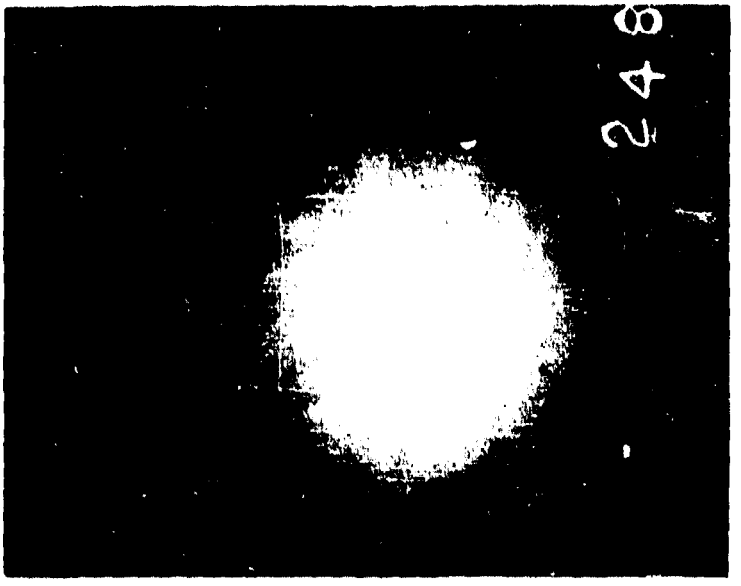
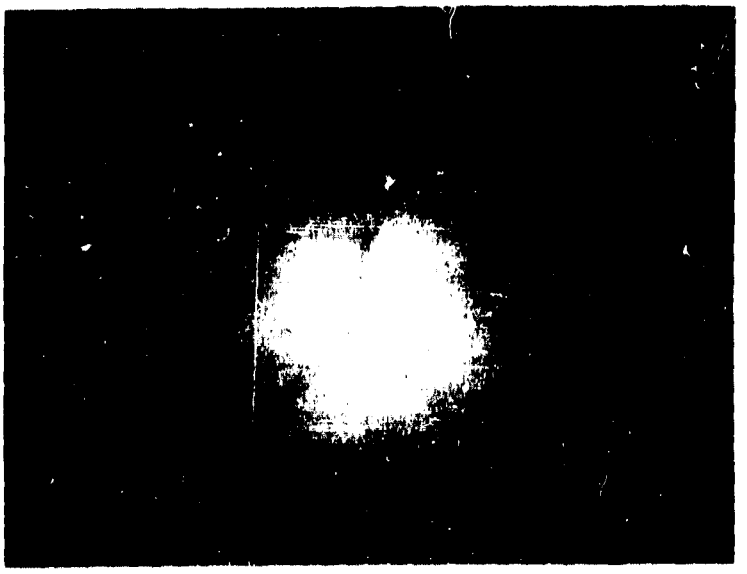


Fig. 26 - Mach Intersection



APPENDIX A

PROPERTIES OF $\Phi_n(\bar{p})$ AND $\Psi_n(\bar{p})$ FUNCTIONS

1. The basic equations for the functions $\Phi_n(\bar{p})$ and $\Psi_n(\bar{p})$ and their derivatives are as follows:

$$\Phi_n(\bar{p}) = c_n v(\frac{\bar{p}}{p_n}) = \pm\frac{c_n}{\sqrt{\gamma}}(\xi-1)^{1/2}(1-\xi^{-\frac{1}{\gamma}})^{1/2} \qquad (1a$$

($\pm$, the sign of $(\xi-1)$)

$$\Phi_n'(\bar{p}) = c_n v'(\frac{\bar{p}}{p_n}) = \frac{c_n}{2\sqrt{\gamma}\cdot\gamma}\frac{(\xi-1)\xi^{-\frac{1+\gamma}{\gamma}} + \gamma(1-\xi^{-\frac{1}{\gamma}})}{(\xi-1)^{1/2}(1-\xi^{-\frac{1}{\gamma}})^{1/2}} \qquad (1a'$$

$$\Phi_n''(\bar{p}) = c_n v''(\frac{\bar{p}}{p_n}) = \frac{c_n}{2\gamma^2 v(\xi)}\left\{\frac{\gamma-1}{\gamma}\xi^{-\frac{1+\gamma}{\gamma}} + \frac{\gamma+1}{\gamma}\xi^{-\frac{1+2\gamma}{\gamma}} - 2\gamma^2[v'(\xi)]^2\right\} \qquad (1a''$$

Also

$$\Psi_n(\bar{p}) = \frac{2c_n}{\gamma-1}\left(\xi^{\frac{\gamma-1}{2\gamma}} - 1\right) \qquad (1b$$

$$\Psi_n'(\bar{p}) = \frac{c_n}{\gamma}\xi^{-\frac{1+\gamma}{2\gamma}} \qquad (1b'$$

$$\Psi_n''(\bar{p}) = -\frac{(1+\gamma)c_n}{2\gamma^2}\xi^{-\frac{1+3\gamma}{2\gamma}} \qquad (1b''$$

2. Proof of (8a'), (8b')

For any real, non-zero value of A, B

$A^2 - 2AB + B^2 > 0$

Let $A^2 \equiv (\xi-1)\xi^{-\frac{1+\gamma}{\gamma}}$, $B^2 \equiv \gamma(1-\xi^{-\frac{1}{\gamma}})$

then, $(\xi-1)\xi^{-\frac{1+\gamma}{\gamma}} - 2\sqrt{\gamma}(\xi-1)^{1/2}(1-\xi^{-\frac{1}{\gamma}})^{1/2}\xi^{-\frac{1+\gamma}{2\gamma}} + \gamma(1-\xi^{-\frac{1}{\gamma}}) > 0$

or $\{(\xi-1)\xi^{-\frac{1+\gamma}{\gamma}}+\gamma(1-\xi^{-\frac{1}{\gamma}})\}c_n > 2\gamma\sqrt{\gamma}(\xi-1)^{\frac{1}{2}}(1-\xi^{-\frac{1}{\gamma}})^{\frac{1}{2}}\frac{\xi^{-\frac{1+\gamma}{2\gamma}}c_n}{\gamma}$

(a) For values of $0<\xi<1$ the expression $2\gamma\sqrt{\gamma}(\xi-1)^{\frac{1}{2}}(1-\xi^{-\frac{1}{\gamma}})^{\frac{1}{2}}$ is negative, by the rule of signs of equation (1a), hence

$$\frac{\{(\xi-1)\xi^{-\frac{1+\gamma}{\gamma}}+\gamma(1-\xi^{-\frac{1}{\gamma}})\}c_n}{2\gamma\sqrt{\gamma}(\xi-1)^{1/2}(1-\xi^{-\frac{1}{\gamma}})^{1/2}} < \frac{\xi^{-\frac{1+\gamma}{2\gamma}}c_n}{\gamma}$$

or $$\Phi_n'(\bar{p}) < \Psi_n'(\bar{p})$$

(b) For values of $\infty>\xi>1$ the expression $2\gamma\sqrt{\gamma}(\xi-1)^{\frac{1}{2}}(1-\xi^{-\frac{1}{\gamma}})^{\frac{1}{2}}$ is positive, hence

$$\frac{(\xi-1)\xi^{-\frac{1+\gamma}{\gamma}}+\gamma(1-\xi^{-\frac{1}{\gamma}})}{(\xi-1)^{1/2}(1-\xi^{-\frac{1}{\gamma}})^{1/2}}\quad\frac{c_n}{2\gamma\sqrt{\gamma}} > \frac{\xi^{-\frac{1+\gamma}{2\gamma}}}{\gamma}c_n$$

or $$\Phi_n'(\bar{p}) > \Psi_n'(\bar{p})$$

Since $\Phi_n(\bar{p}) = \Psi_n(\bar{p})$ and $\Phi_n'(\bar{p}) = \Psi_n'(\bar{p})$ for $\bar{p}\to\bar{p}_n$ [(8a), (8b)] it follows that $\Phi_n(\bar{p}) \gtrless \Psi_n(\bar{p})$ for $\bar{p} \gtrless \bar{p}_n$.

3. Proof of (8a), (8b), (8c), (8b"), (8c")

As $\bar{p}\to\bar{p}_n$, $\xi\to 1$. It is evident that $\Phi_n(\bar{p}) = \Psi_n(\bar{p}) = 0$ for $\xi\to 1$. It also follows from equations (1a') and (1b') that $\Phi_n'(\bar{p}) = \Psi_n'(\bar{p}) \to \frac{c_n}{\gamma}$, and from equations (1a") and (1b") that $\Phi_n''(\bar{p}) = \Psi_n''(\bar{p}) \to -\frac{(1+\gamma)c_n}{2\gamma^2}$

From equations (1b') and (1b") it follows that $\Psi_n'(\bar{p}) > 0$ and that $\Psi_n''(\bar{p}) < 0$. It remains to prove that $\Phi_n'(\bar{p}) > 0$ and that $\Phi_n''(\bar{p}) < 0$

for all values of $\bar{p}$. We shall first prove the former statement.

(a) For values of $0 < \frac{p}{p_c} < 1$: the expression

$$\phi_n'(\bar{p}) = \frac{c_n}{2\gamma\sqrt{\gamma}} \frac{\left(\frac{p}{p_c}-1\right)\frac{p}{p_c} - \frac{1+\gamma}{\gamma} + \gamma\left(1-\frac{p}{p_c}-\frac{1}{\frac{p}{p_c}}\right)}{\left(\frac{p}{p_c}-1\right)^{1/2}\left(1-\frac{p}{p_c}-\frac{1}{\frac{p}{p_c}}\right)^{1/2}}$$

is always positive, since the numerator is always negative, and the denominator is always negative by the rule of signs of equation (1).

(b) For $\frac{p}{p_c} \to 1$: we have noted that $\phi_n'(\bar{p}) \to \frac{c_n}{\gamma}$, which is positive.

(c) For values of $\infty > \frac{p}{p_c} > 1$; it is sufficient to show that $\phi_n'(\bar{p}) > \gamma\psi_n'(\bar{p})$, since we have noted that $\psi_n'(\bar{p})$ is always greater than zero. This has been shown in the preceding section.

We will now prove that $\phi_n''(\bar{p}) < 0$ for all values of $\bar{p}$.

$$\phi_n''(\bar{p}) = \frac{c_n}{2\gamma^2 v(\frac{p}{p_c})}\left\{\frac{\gamma-1}{\gamma}\left(\frac{p}{p_c}\right)^{-\frac{1+\gamma}{\gamma}} + \frac{\gamma+1}{\gamma}\left(\frac{p}{p_c}\right)^{-\frac{1+\gamma}{\gamma}}\left(\frac{p}{p_c}\right)^{-1} - 2\gamma^2[v'(\frac{p}{p_c})]^2\right\}$$

(a') For values of $0 < \frac{p}{p_c} < 1$; (1) v is negative from equation (1a), (2) $v'(\frac{p}{p_c}) < \gamma\left(\frac{p}{p_c}\right)^{-\frac{1+\gamma}{2\gamma}}$ or $\gamma^2 v'^2 < \left(\frac{p}{p_c}\right)^{-\frac{1+\gamma}{\gamma}}$ from preceding section. To prove that $\phi_n''(\bar{p}) < 0$ it remains to show that

$$2\gamma^2[v'(\frac{p}{p_c})]^2 < \left(\frac{p}{p_c}\right)^{-\frac{1+\gamma}{\gamma}}\left\{\frac{\gamma-1}{\gamma} + \frac{\gamma+1}{\gamma}\,\frac{1}{\frac{p}{p_c}}\right\}$$

or $$2\left(\frac{p}{p_c}\right)^{-\frac{1+\gamma}{\gamma}} < \left(\frac{p}{p_c}\right)^{-\frac{1+\gamma}{\gamma}}\left\{\frac{\gamma-1}{\gamma} + \frac{\gamma+1}{\gamma}\,\frac{1}{\frac{p}{p_c}}\right\}$$

or $$2 < \frac{\gamma-1}{\gamma} + \frac{\gamma+1}{\gamma}\,\frac{1}{\frac{p}{p_c}}$$, which is true.

(b') For $\frac{p}{p_c} \to 1$; $\phi_n''(\bar{p}) \to -\frac{(1+\gamma)c_n}{2\gamma^2}$, which is negative.

(c') For values of $\infty > \frac{p}{p_c} > 1$; (1) v is positive from equation (1a),

(2) $v'(\xi) > \frac{1}{\gamma}\,\xi^{-\frac{\gamma+1}{2\gamma}}$ or $\gamma^2\,[v'(\xi)]^2 > \xi^{-\frac{\gamma+1}{\gamma}}$

To prove that $\phi_n''(\bar{p}) < 0$ it remains to show that

$$2\gamma^2[v'(\xi)]^2 > \xi^{-\frac{\gamma+1}{\gamma}}\left\{\frac{\gamma-1}{\gamma} + \frac{\gamma+1}{\gamma}\,\frac{1}{\xi}\right\}$$

or $$2\,\xi^{-\frac{\gamma+1}{\gamma}} > \xi^{-\frac{\gamma+1}{\gamma}}\left\{\frac{\gamma-1}{\gamma} + \frac{\gamma+1}{\gamma}\,\frac{1}{\xi}\right\}$$

or $$2 > \left\{\frac{\gamma-1}{\gamma} + \frac{\gamma+1}{\gamma}\,\frac{1}{\xi}\right\}$$, which is true.

4. Proof of (8d)

We have

$$\phi_i(\bar{p}) = c_i\, v\left(\frac{\bar{p}}{\bar{p}_1}\right) = \sqrt{\frac{\bar{p}_1}{\rho_i}\left(\frac{\bar{p}}{\bar{p}_i} - 1\right)\left(1 - \left(\frac{\bar{p}}{\bar{p}_1}\right)^{-\frac{1}{\gamma}}\right)} =$$

$$= \sqrt{\frac{1}{\rho_i}\,(\bar{p} - \bar{p}_1)\left(1 - \left(\frac{\bar{p}}{\bar{p}_1}\right)^{-\frac{1}{\gamma}}\right)}$$

$$\phi_j(\bar{p}) = c_j\, v\left(\frac{\bar{p}}{\bar{p}_j}\right) = \sqrt{\frac{\bar{p}_1}{\rho_j}\left(\frac{\bar{p}}{\bar{p}_j} - 1\right)\left(1 - \left(\frac{\bar{p}}{\bar{p}_j}\right)^{-\frac{1}{\gamma}}\right)} =$$

$$= \sqrt{\frac{1}{\rho_j}\,(\bar{p} - \bar{p}_j)\left(1 - \left(\frac{\bar{p}}{\bar{p}_j}\right)^{-\frac{1}{\gamma}}\right)}$$

If $\bar{p} = \bar{p}_1$, $\phi_i(\bar{p}) = 0$ and $\phi_j(\bar{p})$ is negative; hence theorem (8d) is true. If $\bar{p} = \bar{p}_j$, $\phi_i(\bar{p})$ is positive and $\phi_j(\bar{p}) = 0$. If $\bar{p}_1 < \bar{p} < \bar{p}_j$, $\phi_i(\bar{p})$ is positive while $\phi_j(\bar{p})$ is negative. Finally, if $\bar{p}_1 < \bar{p}_j < \bar{p}$, both $\phi_i(\bar{p})$ and $\phi_j(\bar{p})$ are positive. In this case, however, the factors for the expression $\phi_i(\bar{p})$ are each either greater than or equal in absolute value to the

corresponding factors of $\Phi_j(\bar{p})$. Hence in each case $\Phi_i(\bar{p}) > \Phi_j(\bar{p})$, algebraically.

5. Proof of (8d')

We have

$$\Psi_i(\bar{p}) = \frac{2c_i}{\gamma-1}\left\{\left(\frac{\bar{p}}{\bar{p}_i}\right)^{\frac{\gamma-1}{2\gamma}} - 1\right\} =$$

$$= \frac{2\sqrt{\gamma}}{\gamma-1}\sqrt{\frac{\bar{p}_i^{\frac{1}{\gamma}}}{\rho_i}}\left\{\bar{p}^{\frac{\gamma-1}{2\gamma}} - \bar{p}_i^{\frac{\gamma-1}{2\gamma}}\right\}$$

$$\Psi_j(\bar{p}) = \frac{2c_j}{\gamma-1}\left\{\left(\frac{\bar{p}}{\bar{p}_j}\right)^{\frac{\gamma-1}{2\gamma}} - 1\right\} =$$

$$= \frac{2\sqrt{\gamma}}{\gamma-1}\sqrt{\frac{\bar{p}_j^{\frac{1}{\gamma}}}{\rho_j}}\left\{\bar{p}^{\frac{\gamma-1}{2\gamma}} - \bar{p}_j^{\frac{\gamma-1}{2\gamma}}\right\}$$

If $\bar{p} = \bar{p}_i$, $\Psi_i(\bar{p}) = 0$ and $\Psi_j(\bar{p})$ is negative; hence theorem (8d') is satisfied. If $\bar{p} = \bar{p}_j$, $\Psi_i(\bar{p})$ is positive while $\Psi_j(\bar{p}) = 0$. If $\bar{p}_i < \bar{p} < \bar{p}_j$, $\Psi_i(\bar{p})$ is positive and $\Psi_j(\bar{p})$ is negative. Finally, if $\bar{p} < \bar{p}_i < \bar{p}_j$ both $\Psi_i(\bar{p})$ and $\Psi_j(\bar{p})$ are negative. In this case, however, the factors for the expression $\Psi_i(\bar{p})$ are each either less than or equal in absolute value to the corresponding factors of $\Psi_j(\bar{p})$. Hence in each case $\Psi_i(\bar{p}) > \Psi_j(\bar{p})$, algebraically.

6. Proof of (8e)

We are to prove that

$$\upsilon\left(\frac{\bar{p}_k}{\bar{p}_i}\right) c_i > \upsilon\left(\frac{\bar{p}_i}{\bar{p}_i}\right) c_i + \upsilon\left(\frac{\bar{p}_k}{\bar{p}_j}\right) c_j$$

or

$$\upsilon\left(\frac{\bar{p}_k}{\bar{p}_j} \div \frac{\bar{p}_i}{\bar{p}_j}\right)\frac{c_i}{c_j} > \upsilon\left(\frac{1}{\bar{p}_i/\bar{p}_j}\right)\frac{c_i}{c_j} + \upsilon\left(\frac{\bar{p}_k}{\bar{p}_j}\right)$$

Let $\xi \equiv \frac{\bar{p}_i}{\bar{p}_j}$ and $\xi' \equiv \frac{\bar{p}_k}{\bar{p}_j}$, then $0 < \xi < 1 < \xi' < \infty$

Since $\frac{c_i}{c_j} = \left(\frac{p_i}{p_j}\right)^{\frac{\gamma-1}{2\gamma}} = \xi^{\frac{\gamma-1}{2\gamma}}$

the above is equivalent to

$$v\left(\frac{\xi'}{\xi}\right)\xi^{\frac{\gamma-1}{2\gamma}} > v\left(\frac{1}{\xi}\right)\xi^{\frac{\gamma-1}{2\gamma}} + v(\xi')$$

Substituting the value of v, we obtain

$$\{(\xi'-\xi)(\xi^{-\frac{1}{\gamma}}-\xi'^{-\frac{1}{\gamma}})\}^{\frac{1}{2}} > \{(1-\xi)(\xi^{-\frac{1}{\gamma}}-1)\}^{\frac{1}{2}} + \{(\xi'-1)(1-\xi'^{-\frac{1}{\gamma}})\}^{\frac{1}{2}}$$

This may be proved by a method similar to that used in section

2. For any real, non-zero value of A,B

$$A^2 - 2AB + B^2 > 0$$

Let $A^2 \equiv (\xi'-1)(\xi^{-\frac{1}{\gamma}}-1)$, $B^2 \equiv (1-\xi)(1-\xi'^{-\frac{1}{\gamma}})$

then $(\xi'-1)(\xi^{-\frac{1}{\gamma}}-1) - 2\{(1-\xi)(1-\xi'^{-\frac{1}{\gamma}})\}^{\frac{1}{2}}\{(\xi'-1)(\xi^{-\frac{1}{\gamma}}-1)\}^{\frac{1}{2}} +$
$+ (1-\xi)(1-\xi'^{-\frac{1}{\gamma}}) > 0$

or $(\xi'-1)(\xi^{-\frac{1}{\gamma}}-1) + (1-\xi)(1-\xi'^{-\frac{1}{\gamma}}) + (\xi'-1)(1-\xi'^{-\frac{1}{\gamma}}) +$
$+ (1-\xi)(\xi^{-\frac{1}{\gamma}}-1) > (1-\xi)(\xi^{-\frac{1}{\gamma}}-1) + (\xi'-1)(1-\xi'^{-\frac{1}{\gamma}}) +$
$+ 2\{(1-\xi)(\xi^{-\frac{1}{\gamma}}-1)\}^{\frac{1}{2}}\{(\xi'-1)(1-\xi'^{-\frac{1}{\gamma}})\}^{\frac{1}{2}}$

or $\{(\xi'-1)+(1-\xi)\}\{(\xi^{-\frac{1}{\gamma}}-1) + (1-\xi'^{-\frac{1}{\gamma}})\} > (1-\xi)(\xi^{-\frac{1}{\gamma}}-1) +$
$+ (\xi'-1)(1-\xi'^{-\frac{1}{\gamma}}) + 2\{(1-\xi)(\xi^{-\frac{1}{\gamma}}-1)\}^{\frac{1}{2}}\{(\xi'-1)(1-\xi'^{-\frac{1}{\gamma}})\}^{\frac{1}{2}}$

Hence

$$(\bar{p}' - \bar{p})(\bar{p}^{-\frac{1}{2}} - \bar{p}'^{-\frac{1}{2}}) > \{[(1-\bar{p})(\bar{p}^{-\frac{1}{2}}-1)]^{\frac{1}{2}} + [(\bar{p}'-1)(1-\bar{p}'^{-\frac{1}{2}})]^{\frac{1}{2}}\}^2$$

Taking the square root of each side we obtain

$$\{(\bar{p}' - \bar{p})(\bar{p}^{-\frac{1}{2}} - \bar{p}'^{-\frac{1}{2}})\}^{\frac{1}{2}} > \{[(1-\bar{p})(\bar{p}^{-\frac{1}{2}}-1)]^{\frac{1}{2}} + [(\bar{p}'-1)(1-\bar{p}'^{-\frac{1}{2}})]^{\frac{1}{2}}\}$$

which is what we set out to prove.

7. Proof of (8e')

This relation may be seen to be true by considering three points on a forward rarefaction wave $x_i < x_j < x_k$ with effective pressures $\bar{p}_i$, $\bar{p}_j$, and $\bar{p}_k$ and material velocities V_i, V_j, and V_k. The theorem simply states that

$$(V_k - V_i) = (V_j - V_i) + (V_k - V_j).$$

APPENDIX B

TWO PROOFS OF ONE-DIMENSIONAL INTERACTIONS

Table 3 in the text outlines the results of one-dimensional interaction of shock-waves and rarefaction waves. In this section we will discuss in detail several instances of wave interactions, in which the differences between ideal gases and water-like substances are most striking.

We shall first recall some relations existing between the effective pressure, material velocity, and density in front and behind a shock-wave or a rarefaction wave. Consider the shock or rarefaction wave moving along an x-axis. The x-axis will thus be divided in two parts. The effective pressure, material velocity, and density on the right of the wave-front will be designated $\bar{p}_r$, V_r, and ρ_r; those on the left, $\bar{p}_1$, V_1, and ρ_1, respectively. The material velocity will be considered positive if it is moving in a positive direction along this x-axis, and negative if it is moving in the negative direction. A shock or rarefaction wave moving in a forward or positive direction relative to the undisturbed material will be designated $\underrightarrow{S}$ and $\underrightarrow{R}$, respectively; in the opposite direction, $\underleftarrow{S}$ and $\underleftarrow{R}$. On the basis of the above conventions the following inequalities hold

$$\begin{aligned}
&\bar{p}_1 > \bar{p}_r,\ \rho_1 > \rho_r && \text{for } \underrightarrow{S} \\
&\bar{p}_1 < \bar{p}_r,\ \rho_1 < \rho_r && \text{for } \underleftarrow{S} \qquad \text{(A} \\
&V_1 > V_r && \text{for } \underrightarrow{S} \text{ or } \underleftarrow{S}
\end{aligned}$$

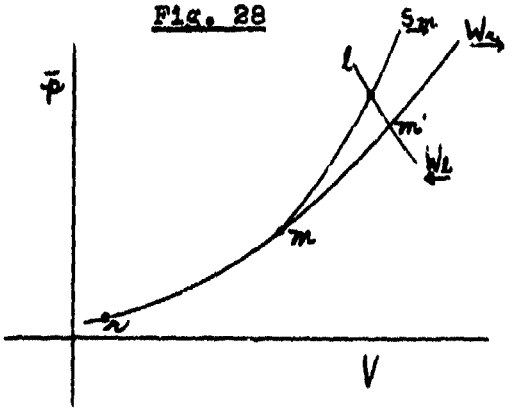
$$\begin{aligned}
&\bar{p}_1 < \bar{p}_r,\ \rho_1 < \rho_r && \text{for } \underrightarrow{R} \\
&\bar{p}_1 > \bar{p}_r,\ \rho_1 > \rho_r && \text{for } \underleftarrow{R} \qquad \text{(A'} \\
&V_1 < V_r && \text{for } \underrightarrow{R} \text{ or } \underleftarrow{R}
\end{aligned}$$

1. $S_2 S_2$

From relations (8b") and (8c') it follows that $\Phi_n(\bar{p})$ and $\Psi_n(\bar{p})$ are monotonically increasing functions of $\bar{p}$, while their slopes are monotonically decreasing functions of $\bar{p}$. Before proceeding we would like to call to attention that $\Phi_r(\bar{p}_1) = -\Phi_1(p_r)$ and $\Psi_r(\bar{p}_1) = -\Psi_1(\bar{p}_r)$, each of which simply states that the difference of material velocity $(V_1 - V_r) = -(V_r - V_1)$, for a shock-wave or for a rarefaction-wave, respectively.

Let us consider the case of two forward shocks following each other. These will divide the x-axis into three regions, left, middle, and right which we will designate l, m, and r. From (A) we have the inequalities $\bar{p}_1 > \bar{p}_m > \bar{p}_r$ and $V_1 > V_m > V_r$. These will indicate the relative positions of l, m, and r on the V , $\bar{p}$ diagram. After the interaction

Fig. 28



has taken place the regions l and r remain unchanged, while a new region m' appears at the center to take the place of m. The region m' is connected to region l by a backward wave, W_l.

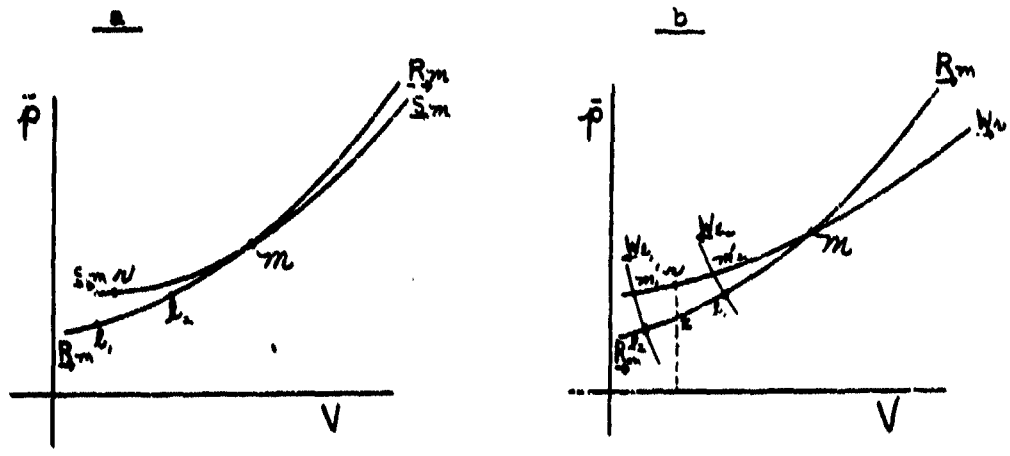
and to region r by a forward wave, $\overrightarrow{W}$. If we draw a $\overrightarrow{W}_l$ curve (cf. fig. 28) through l and a $\overrightarrow{W}_r$ curve through r, m' will be determined by the intersection of these two curves. We wish to show that m' is on the shock branch of $\overrightarrow{W}_r$, but on the rarefaction-wave portion of $\overrightarrow{W}_l$.

Since m was connected to r by a shock the curve $\overrightarrow{W}_r$ passes through the point m. From the disposition of the point l and the slope of $\overrightarrow{W}_l$ it is evident that m' is on the shock branch of $\overrightarrow{W}_r$. Hence the forward wave connecting m' with the region r will be a shock. We will now draw $\overrightarrow{S}_m$ through l and m. It follows from relations (8e) that $\overrightarrow{S}_m$ will lie on the left of $\overrightarrow{W}_r$ for values of $\bar{p} > \bar{p}_m$. Hence m' will lie on the rarefaction branch of $\overrightarrow{W}_l$.

2. $\overrightarrow{R}$ $\overrightarrow{S}$

Let us consider a forward shock overtaken by a forward rarefaction-wave. The inequalities (A) and (A') yield the following relations for the effective pressures and material velocities in regions l, m, and r: $\bar{p}_l < \bar{p}_m > \bar{p}_r$ and $V_l < V_m > V_r$. The points l and r will lie on the $\overrightarrow{R}_m$ and $\overrightarrow{S}_m$ curves, respectively (cf. fig. 29a). Now for $\bar{p} < \bar{p}_m$, $\sqrt{\rho_m}(\bar{p}) < \sqrt{\rho_m}(\bar{p})$ (cf. 8a'). Hence the curve $\overrightarrow{S}_m$ will lie above $\overrightarrow{R}_m$. It may be shown that $\overrightarrow{W}_r$ will also lie above $\overrightarrow{R}_m$ for values of $\bar{p}$ below $\bar{p}_m$. It follows that the point m' will fall on the $\overrightarrow{S}_l$ branch of the $\overrightarrow{W}_l$ curve, resulting in a weak reflected shock. On the other hand, m' may fall either on the $\overrightarrow{S}_r$ or $\overrightarrow{R}_r$ branch of $\overrightarrow{W}_r$ curve depending on the original position of 1 on the $\overrightarrow{R}_m$ curve (cf. fig. 29b).

Fig. 29



Thus for a strong shock and a weak rarefaction-wave a shock will be transmitted, while the reverse is true for a weak shock and a strong rarefaction-wave. It remains to be shown that $\underset{\rightarrow}{W}_r$ will lie above $\underset{\rightarrow}{R}_m$ for values of $\bar{p}$ below $\bar{p}_m$. The transition-curve $\underset{\rightarrow}{W}_r$ consists of two branches. It is composed of $\underset{\rightarrow}{S}_r$, from r to m and of $\underset{\rightarrow}{R}_r$ for values of $\bar{p}$ less than $\bar{p}_r$. It follows from (8e) that $\underset{\rightarrow}{S}_r$ must lie above $\underset{\rightarrow}{S}_m$ from r to m, hence this portion is also above $\underset{\rightarrow}{R}_m$. Also, if we draw a vertical line through r we pass through some point t on $\underset{\rightarrow}{R}_m$. Relation (8e') implies that $\underset{\rightarrow}{R}_t$ coincides with $\underset{\rightarrow}{R}_m$. But $\bar{p}_t < \bar{p}_r$ and

$$\frac{\bar{p}_t^{\frac{1}{\gamma}}}{\rho_t \psi_t(\bar{p})} = \frac{\bar{p}_r^{\frac{1}{\gamma}}}{\rho_r \psi_r(\bar{p})}$$

, hence it follows from relations (8d') that $\psi_t(\bar{p}) < \psi_r(\bar{p})$ for $\bar{p} \leq \bar{p}_r$. Consequently $\underset{\rightarrow}{R}_r$ lies above $\underset{\rightarrow}{R}_t \equiv \underset{\rightarrow}{R}_m$.

APPENDIX C

THREE-SHOCK CONFIGURATIONS FOR WEAK SHOCKS

In the case of weak reflected shocks, $\sigma \to 1$, a quadratic equation has been derived for ideal gases in terms of the cosine of the limiting angle β_1'[3]. The analogous equation for water-like substances is

$$\sigma\{\sigma^2(\tau-\sigma)-(3\sigma+\tau)\}\cos^2\beta_1' + 4\sigma(\sigma^2+1)\cos\beta_1' + \{\sigma\tau(1-\sigma^2)-(1+3\sigma^2)\}=0$$

As is the case for ideal gases ϕ_1' approaches π as a limit, and the limiting angles ω_1', δ_1' are given by

$$\tan\omega_1' = \frac{\tau}{\csc\beta_1' - \sigma\cot\beta_1'}$$

and

$$\cot\delta_1' = \csc\beta_1' - \cot\beta_1'$$

The distinction between ideal gases and water-like substances becomes apparent when one considers a value of σ slightly less than one. Let this correspond to a value of $\sigma = 1 - \epsilon$, where ϵ is a small positive quantity. The discriminant of the above quadratic equation is then given, in terms of a power series in ϵ, by the expression

$$16\epsilon^4\left\{\left[\left(\frac{\gamma-3}{\gamma+1}\right) - 1\right] + \text{terms in } \epsilon\right\}$$

which is negative for a sufficiently small value of ϵ and $\gamma > 1$. Hence, for a value of σ sufficiently near one there is always a region where no real three-shock solutions can be found in the case of water-like substances.

For ideal gases on the other hand, the discriminant is

given by the expression

$$64\epsilon^4\left[(\gamma^2-1) - 2(\gamma-1)^2\epsilon\right]$$

which is positive for a sufficiently small value of ϵ and $\gamma > 1$. In this instance for a value of γ sufficiently near one there is always a region where real three-shock solutions must exist. In fact, as $\gamma \to 1$, $\Delta_1' \to 0$, $\phi_1' \to \pi$, $\tan\omega_1' \to \sqrt{1 \pm 2\sqrt{\frac{\gamma-1}{\gamma+1}}}$, while $\sigma_1' \to \pi - \omega_1'$.

REFERENCES

1. J. von Neumann: "Oblique Reflection of Shocks" - BuOrd, Explosives Research Report No. 12 (1943).
2. G. Tammann: "Über Zustandsgleichungen im Gebiete kleiner Volumen", Ann. d Physik 37, 975 (1912).
   R. Becker: "Stosswelle und Detonation", Zs. für Physik 8, 321 (1922).
   H. Weyl: "A Scheme for the Computation of Shock Waves in Gases and Fluids," Applied Mathematics Panel, NDRC, Memorandum 38.7 (1943)
   Note: For $\eta' = 0$ this equation reduces to Abel's simplified equation of state for explosion gases, where molecular cohesion is negligible because of the high temperatures.
3. H. Polachek and R.J. Seeger: "Regular Reflection of Shocks

in Ideal Gases" - BuOrd, Explosives Research Report No. 13 (1944).

4. J. G. Kirkwood and H. A. Bethe: "The Pressure Wave Produced by an Underwater Explosion I", OSRD 588 (1942).
J. G. Kirkwood and J. M. Richardson: "The Pressure Wave Produced by an Underwater Explosion III", OSRD 813 (1942).
Note: The use of a mean value for γ causes the sound-velocities for low pressures to be slightly in error. (Shock-wave velocities for low pressures are given in notes prepared at UERL by A. B. Arons.)

5. W. G. Penney and H. K. Dasgupta: "Pressure-Time Curves for Submarine Explosions" II, R.C. 333, S.W. 20 (1942).
P. Libessart: "Interim Report on Microëxplosions", R.C. 375, S.W. 30 (1943).

6. E. Preiswerk: "Andwendung gasdynamischer Methoden auf Wasserströmunger mit freier Oberfläche." Mitteilungen aus dem Institut für Aerodynamik No. 7, Parts I and II, Zürich (1938). B. A. Bakhmeteff: "Hydraulics of Open Channels" (1932).

7. Various numerical results cited in this report are taken largely from tables prepared specifically for the Bureau of Ordnance under the Mathematical Tables Project of the Applied Mathematics Panel, NDRC.

8. R. Courant and K. Friedrichs: "Interaction of Shock and Rarefaction Waves in One-Dimensional Motion", OSRD 1567 (1943).

9. J. von Neumann: "Report on the Theory of Shock Waves", OSRD, 1140 (1942).

10. J. von Neumann: Private Communication to R. J. Seeger, 24 Nov. (1943).

11. P. C. Keenan and R. J. Seeger: "Analysis of Data on Shock Intersections - Progress Report I", BuOrd, Explosives Research Report No. 15 (1944).

12. P. Libessart: "Spark Photographs of the Mach Effect", R.C. 417, May (1944).

13. D.C. Campbell: "Experiments in the Production and Photography of Intersection Underwater Shock Waves" TMB Report R - 203 (1943).
TMB Conf. ltr. C-S81-3, C-S85-2, C-A9-14A10/2, to BuOrd: "Intersecting Shock Waves" - 3 Jan. (1944).

14. D. P. MacDougall and G. H. Messerly: "Flash Photography of Underwater Shock-Waves" - Underwater Explosives and Explosions No. 15 p. 3 - 4, Division 8 NDRC, Interim Report (1943).
D. P. MacDougall, G. H. Messerley, E. M. Boggs: "Note on Mach Reflection in Water"- Underwater Explosives and Explosions No. 20, p. 10 - 11, Division 8, NDRC, Interim Report (1944).

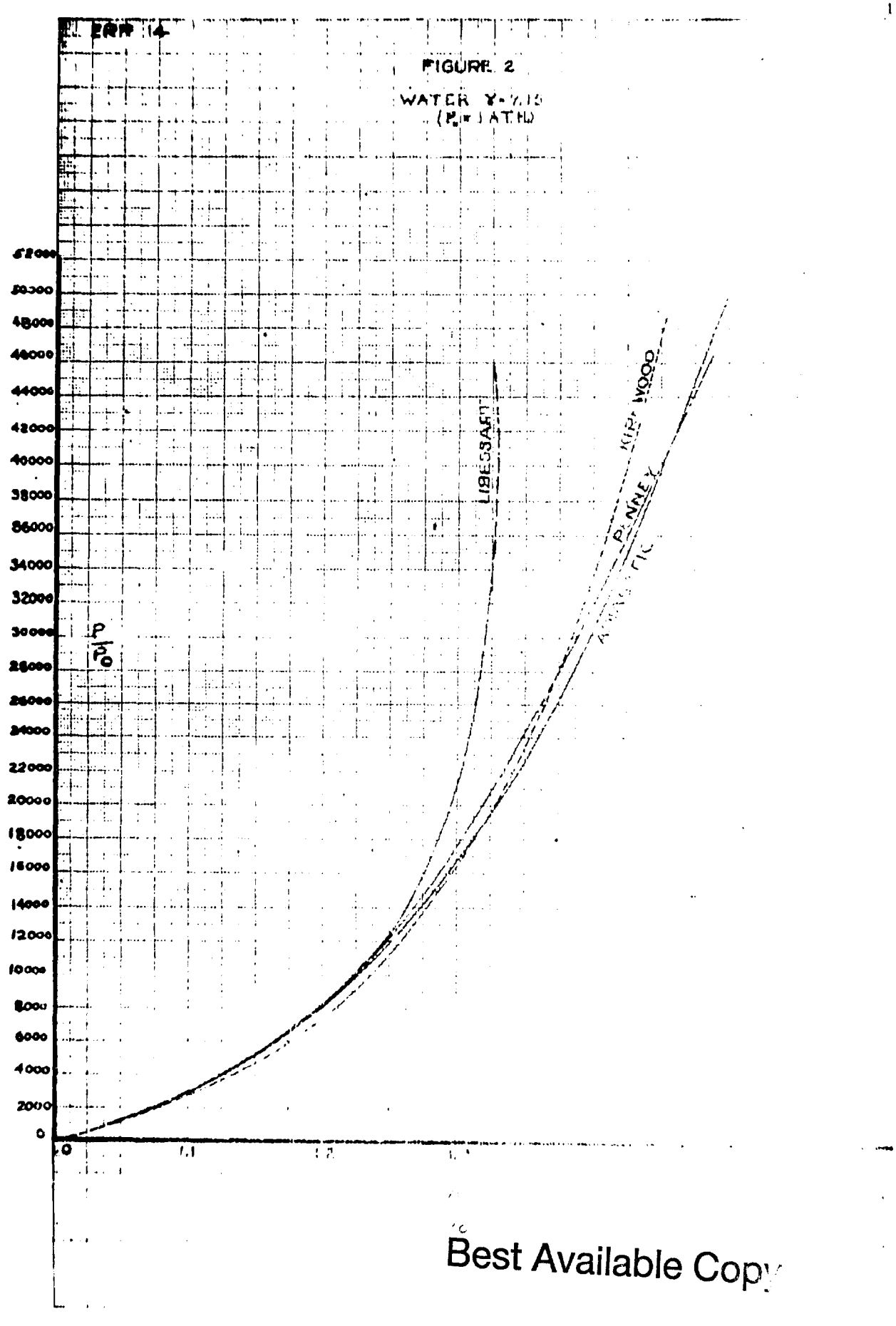
15. E. M. Boggs: Private Communication to R. J. Seeger 14 June (1944).

16. A. M. Shanes: "Measurements on Pressure Waves in Region of Two Obliquely Intersecting Underwater Shock Waves" - Underwater Explosives and Explosions No. 21, p. 52 - 65, Division 8, NDRC, Interim Report (1944).

17. R. W. Spitzer and R. S. Price: "Photographs of Intersecting Shock Waves (Mach Effect)" - Underwater Explosives and Explosions No. 16, p. 26 - 29, Division 8, NDRC, Interim Report (1943).

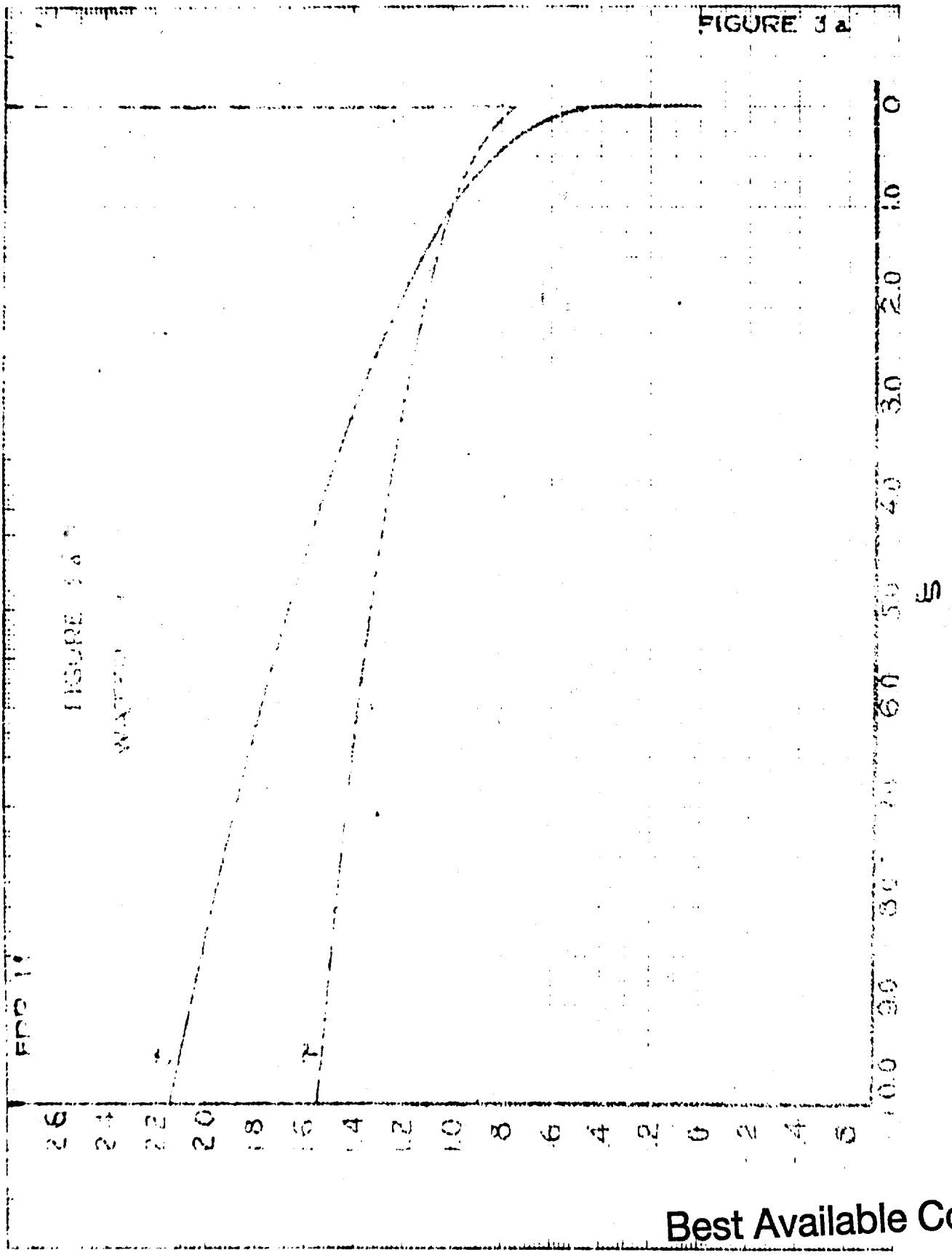
18. J. E. Eldrige: "Increased Damage to Diaphragm Gauges in the Mach Region Underwater Explosives and Explosions No. 18, p. 68 - 69, Division 8, NDRC, Interim Report (1944).
T. Zandstra and V. Kumin: "Mach Effect Underwater, Effect of Intersecting Shock Waves on Cylindrical Shell Target" - Underwater Explosives and Explosions No. 19, p. 21 - 24, Division 8, NDRC, Interim Report (1944).

E.C. Campbell, and C.W. Wyckoff of the David Taylor Model Basin have similarly taken photographs [13] of two simultaneously detonated Hercules caps as sources of shock waves. The collision shown in fig. 21, Plate II, is certainly "regular", whereas that in fig. 22 is probably Mach, (the optical effects are not completely understood).



Best Available Copy

FIGURE 3 a.



Best Available Copy

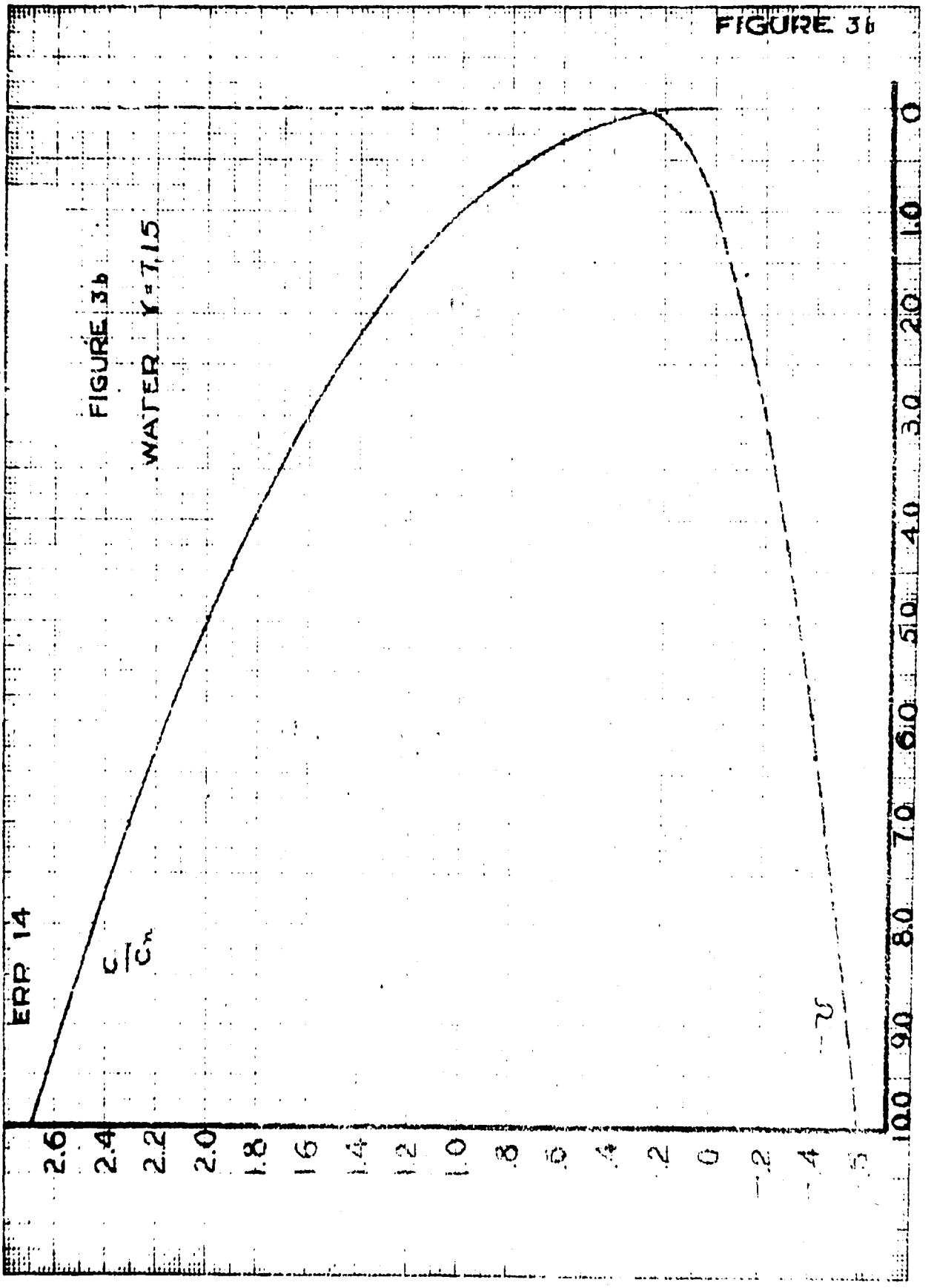
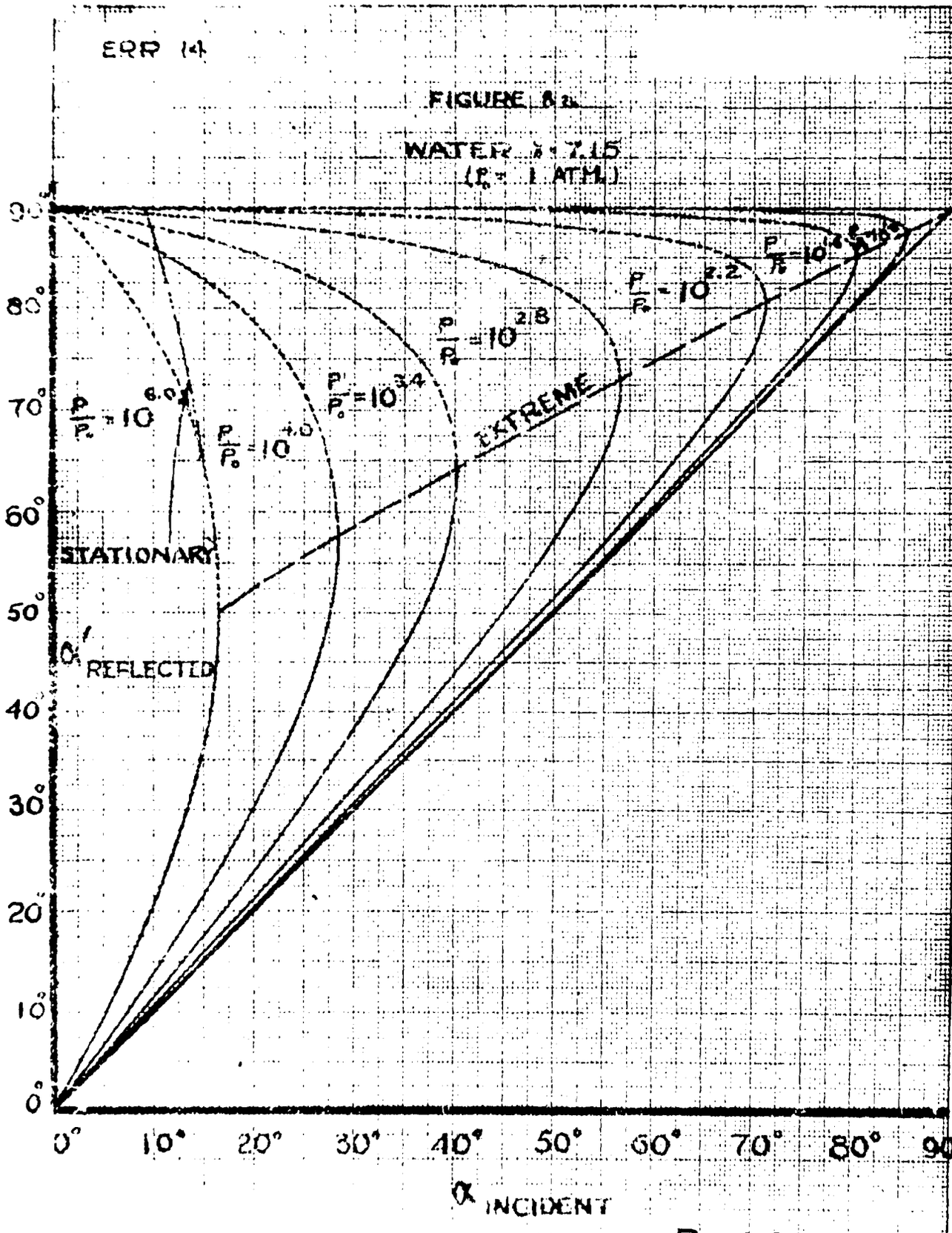
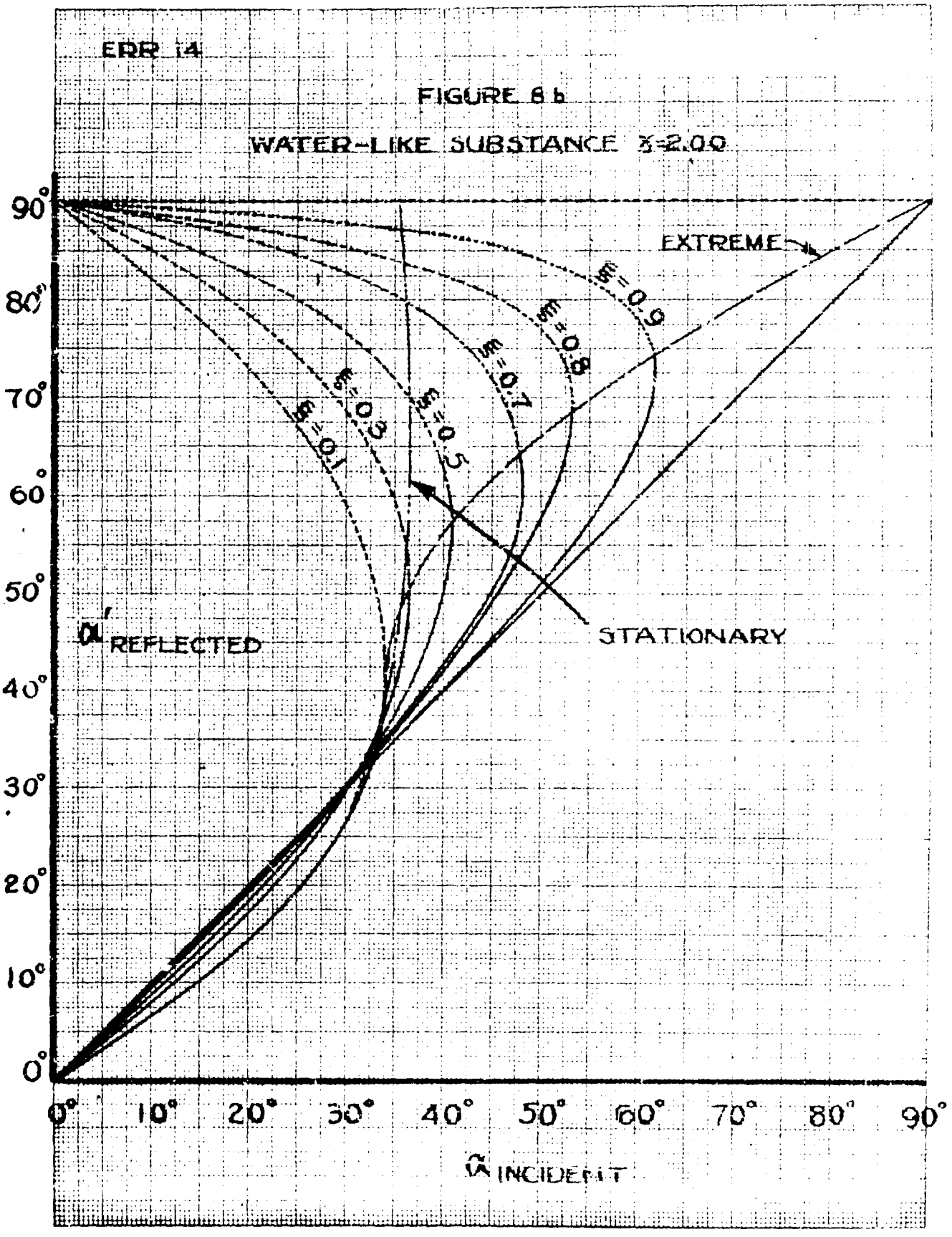
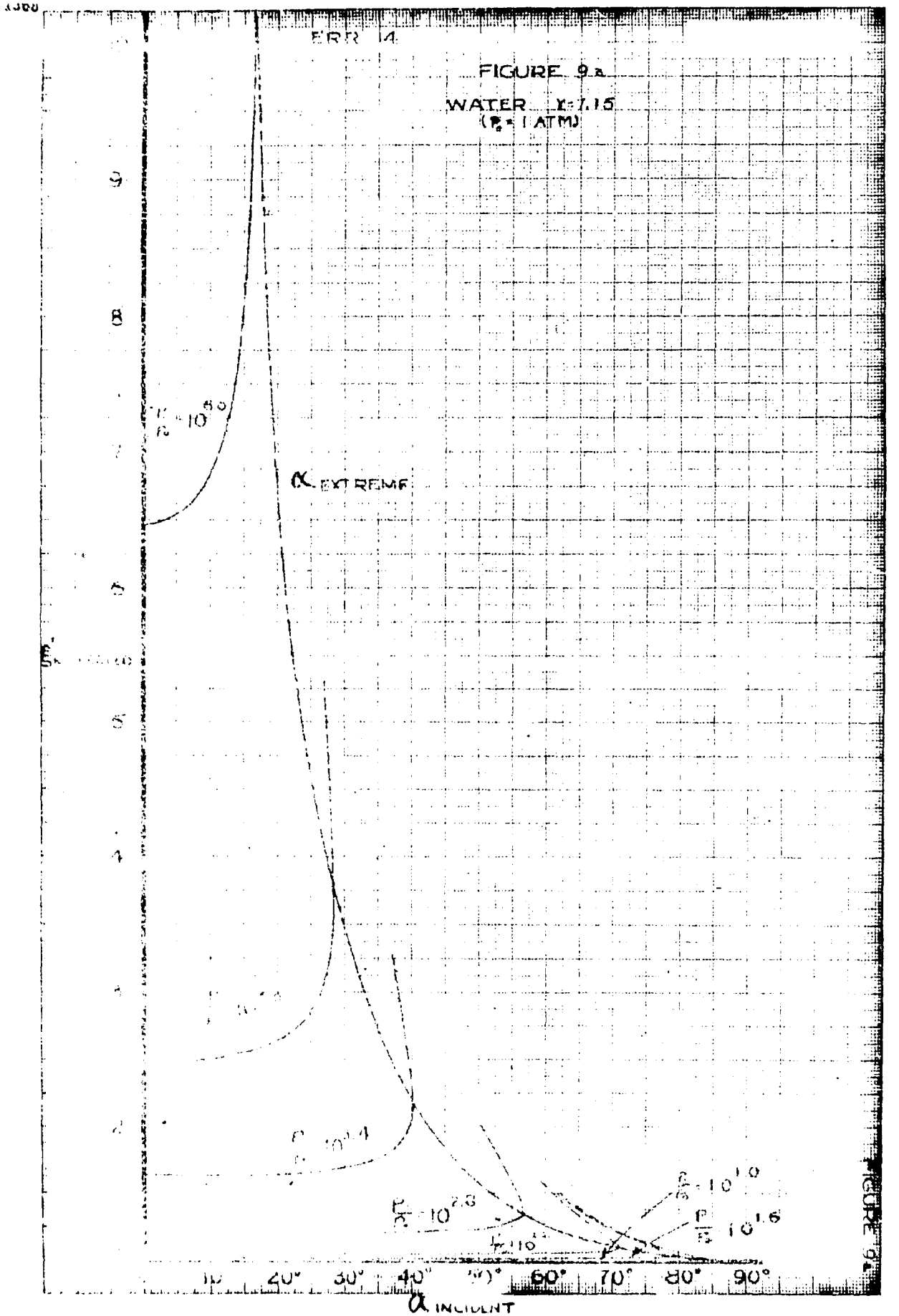

FIGURE 3b
WATER Y=7.15
ERR 14
C/C∞
2.6
2.4
2.2
2.0
1.8
1.6
1.4
1.2
1.0
.8
.6
.4
.2
0
-.2
-.4
100
90
80
70
60
50
40
30
20
10
0

FIGURE 3b

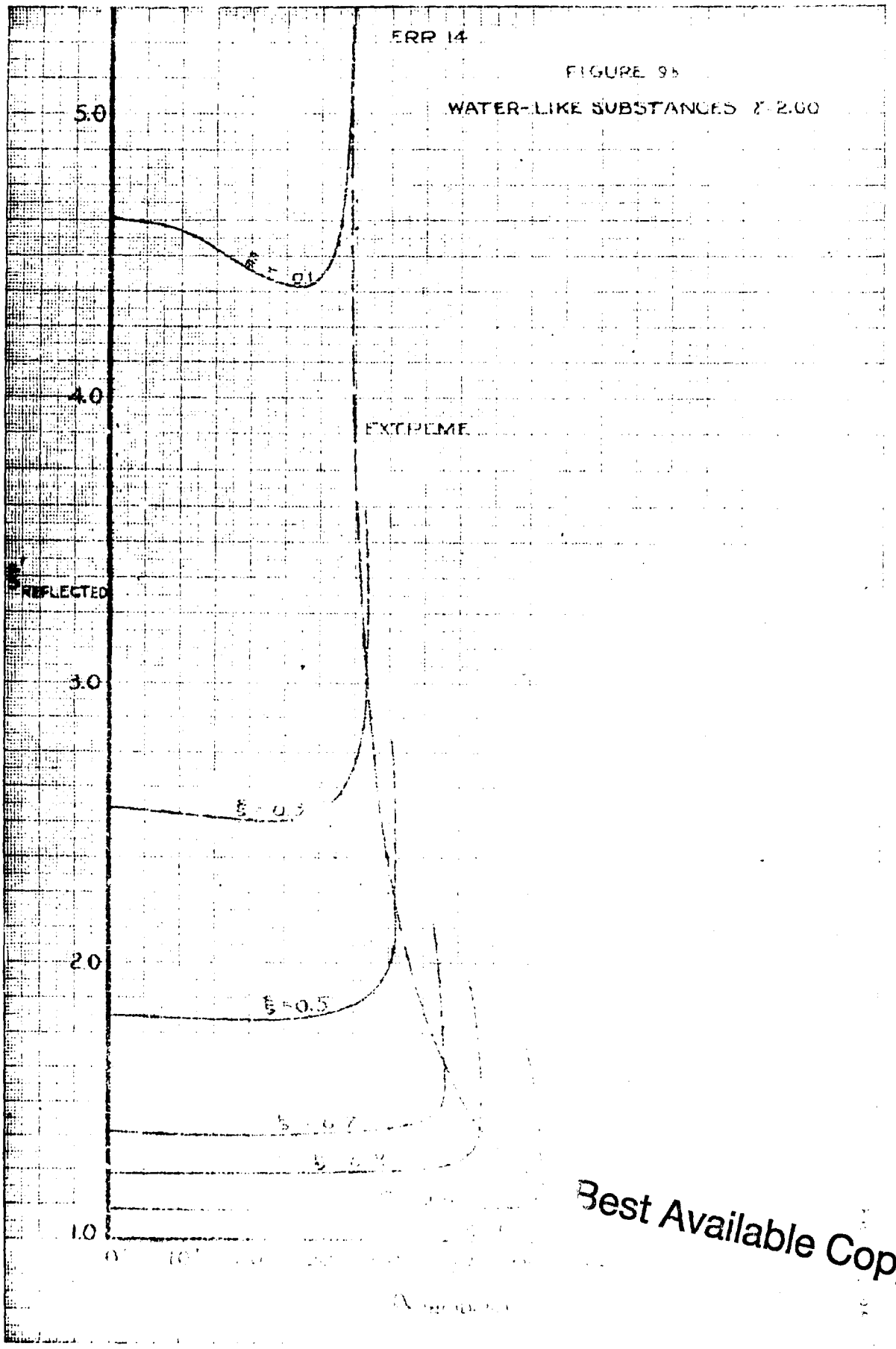


Best Available Copy

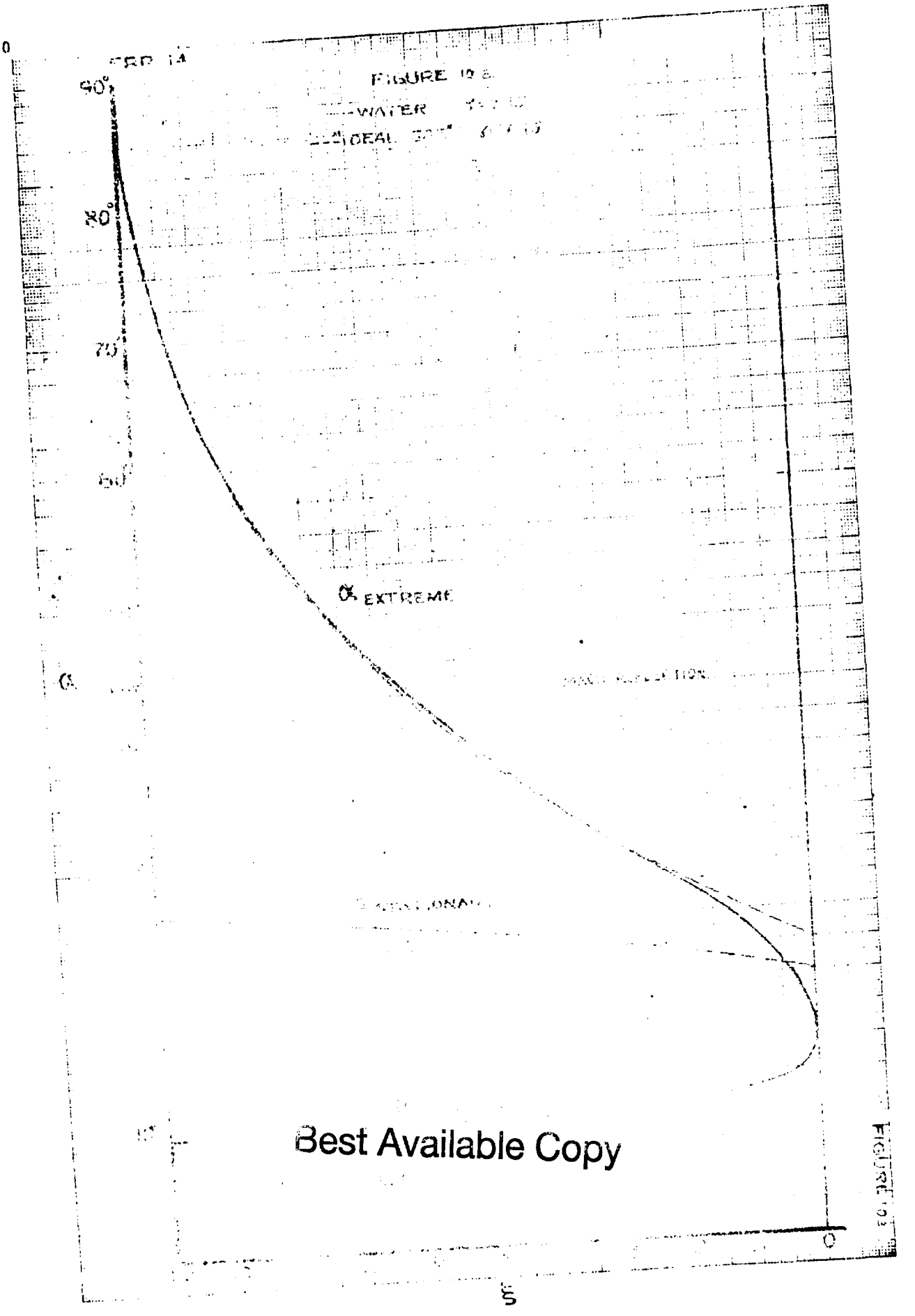

ERR 14
FIGURE 8 b
WATER-LIKE SUBSTANCE x=2.00
90°
80°
70°
60°
50°
40°
30°
20°
10°
0°
EXTREME
m = 0.9
m = 0.8
m = 0.7
m = 0.5
m = 0.3
m = 0.1
STATIONARY
α' REFLECTED
0° 10° 20° 30° 40° 50° 60° 70° 80° 90°
α INCIDENT



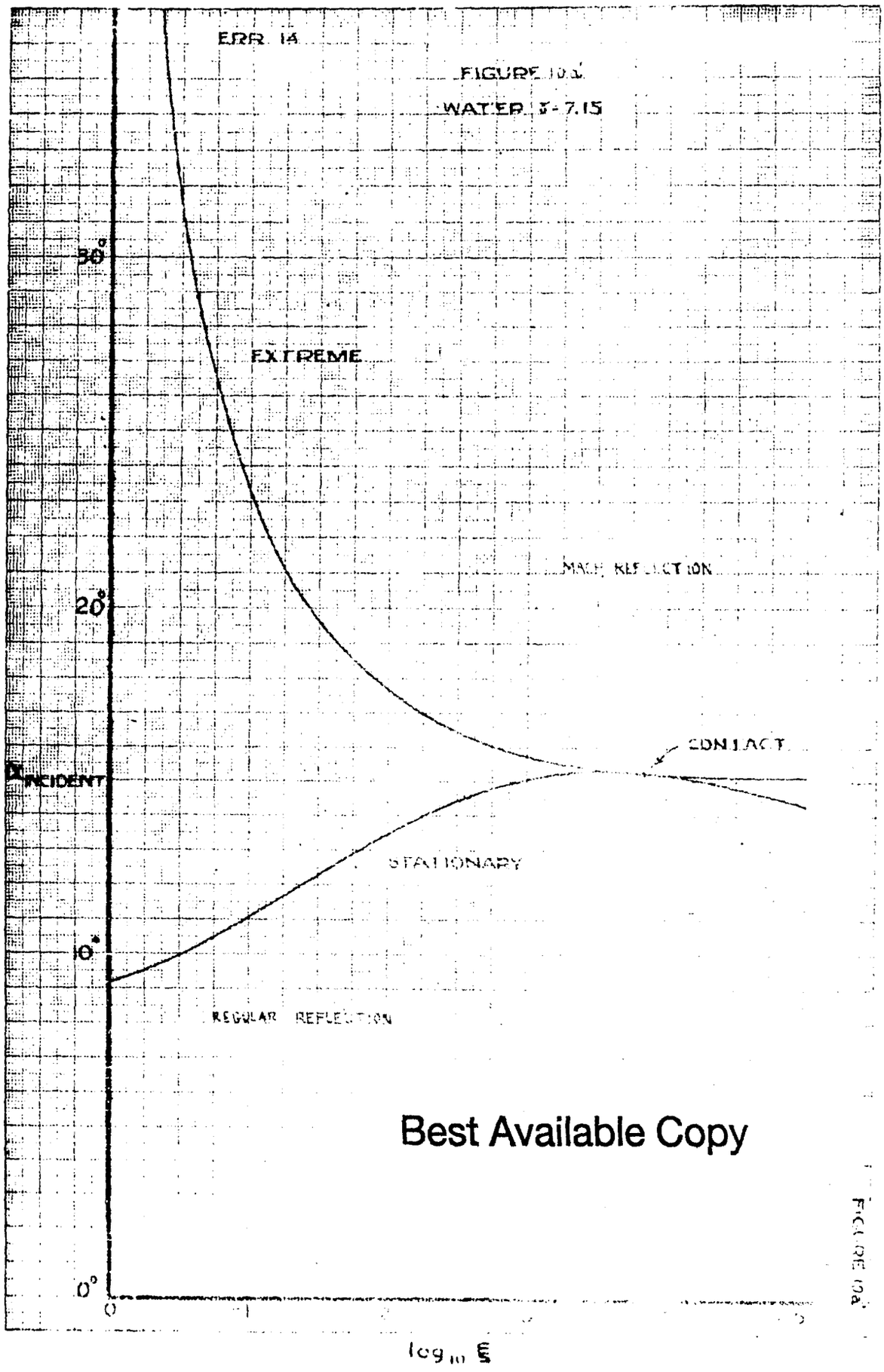
Best Available Copy



Best Available Copy



Best Available Copy



Best Available Copy

FIGURE 10.2

ERR .14

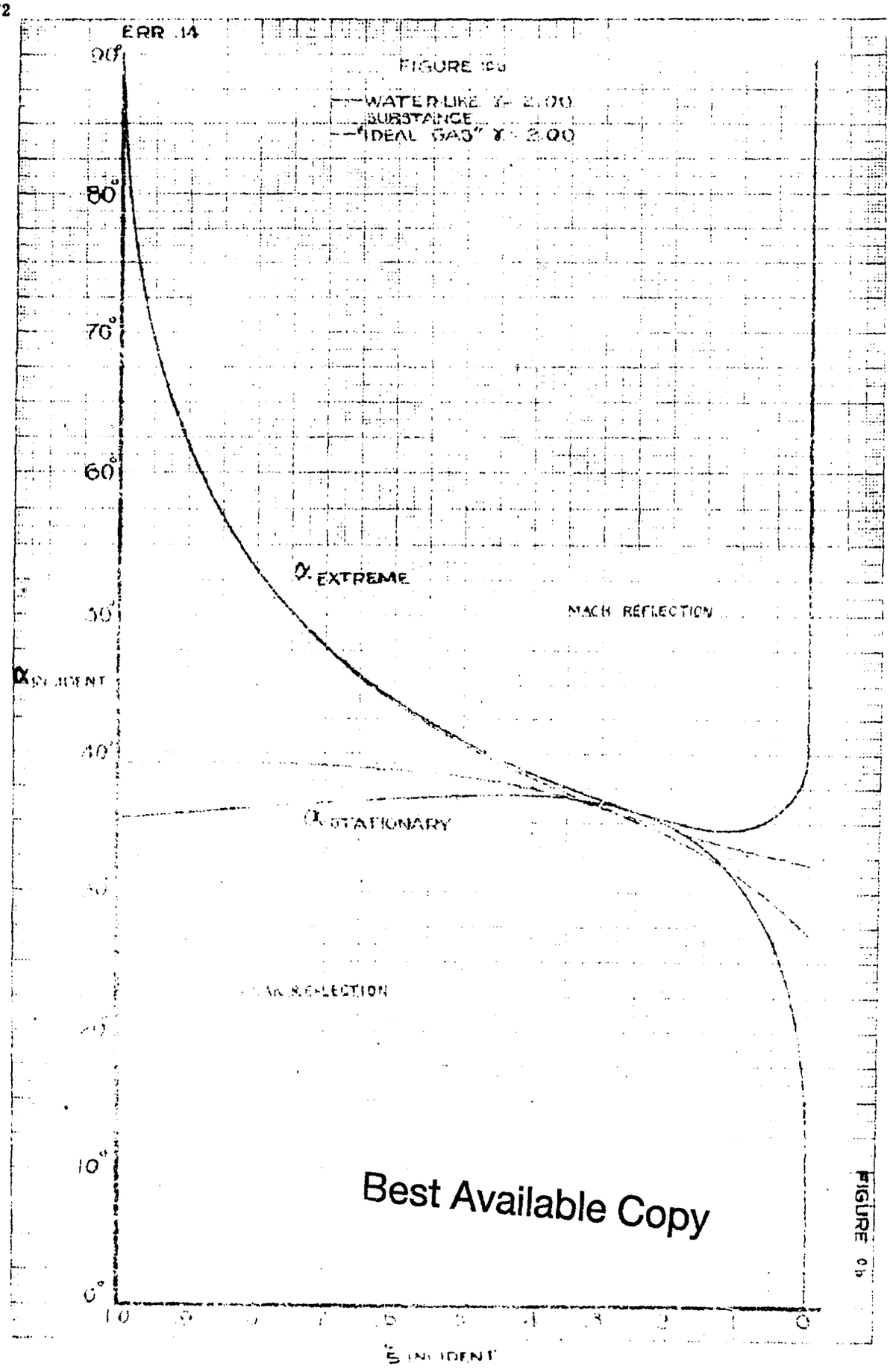
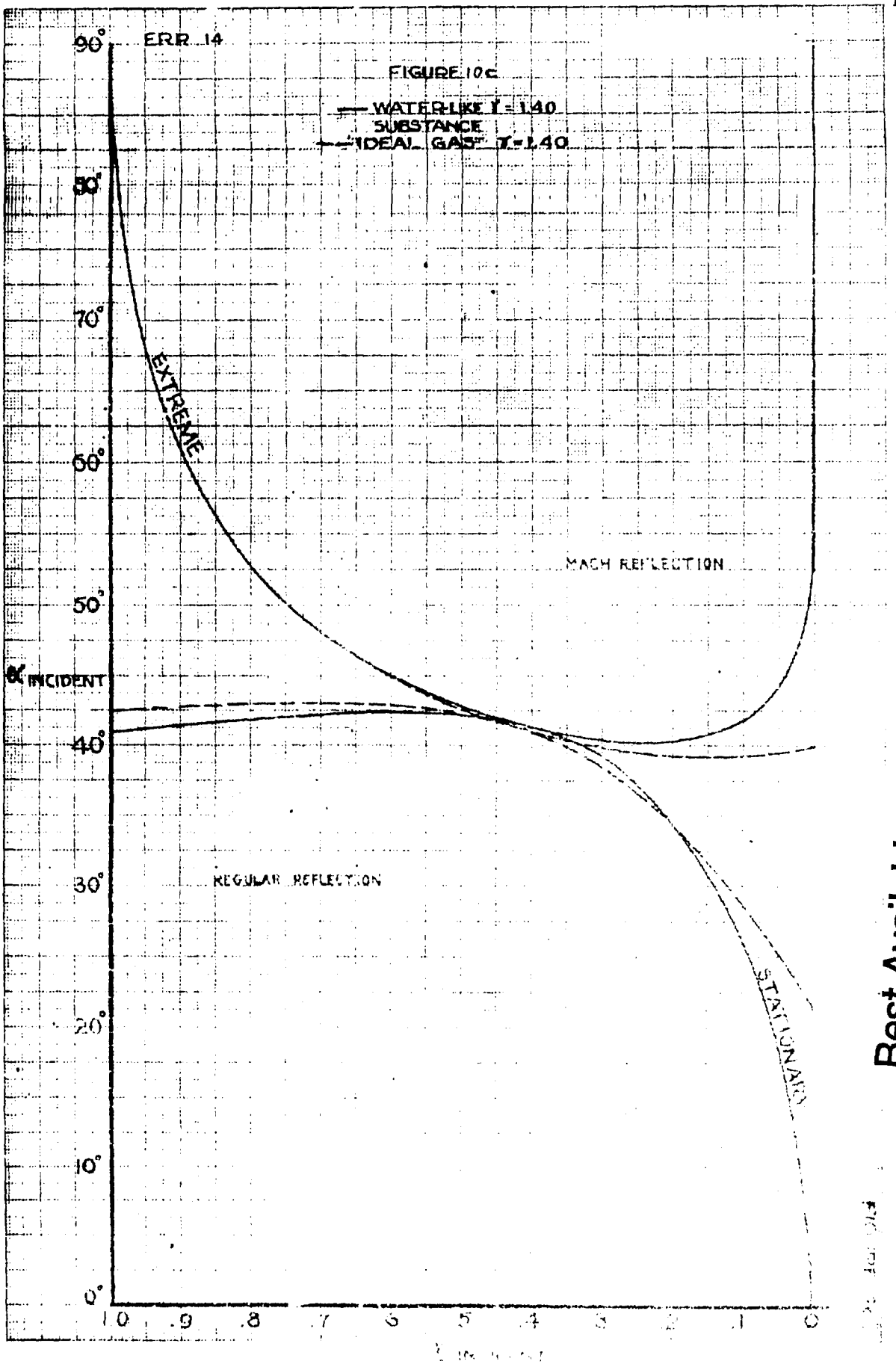


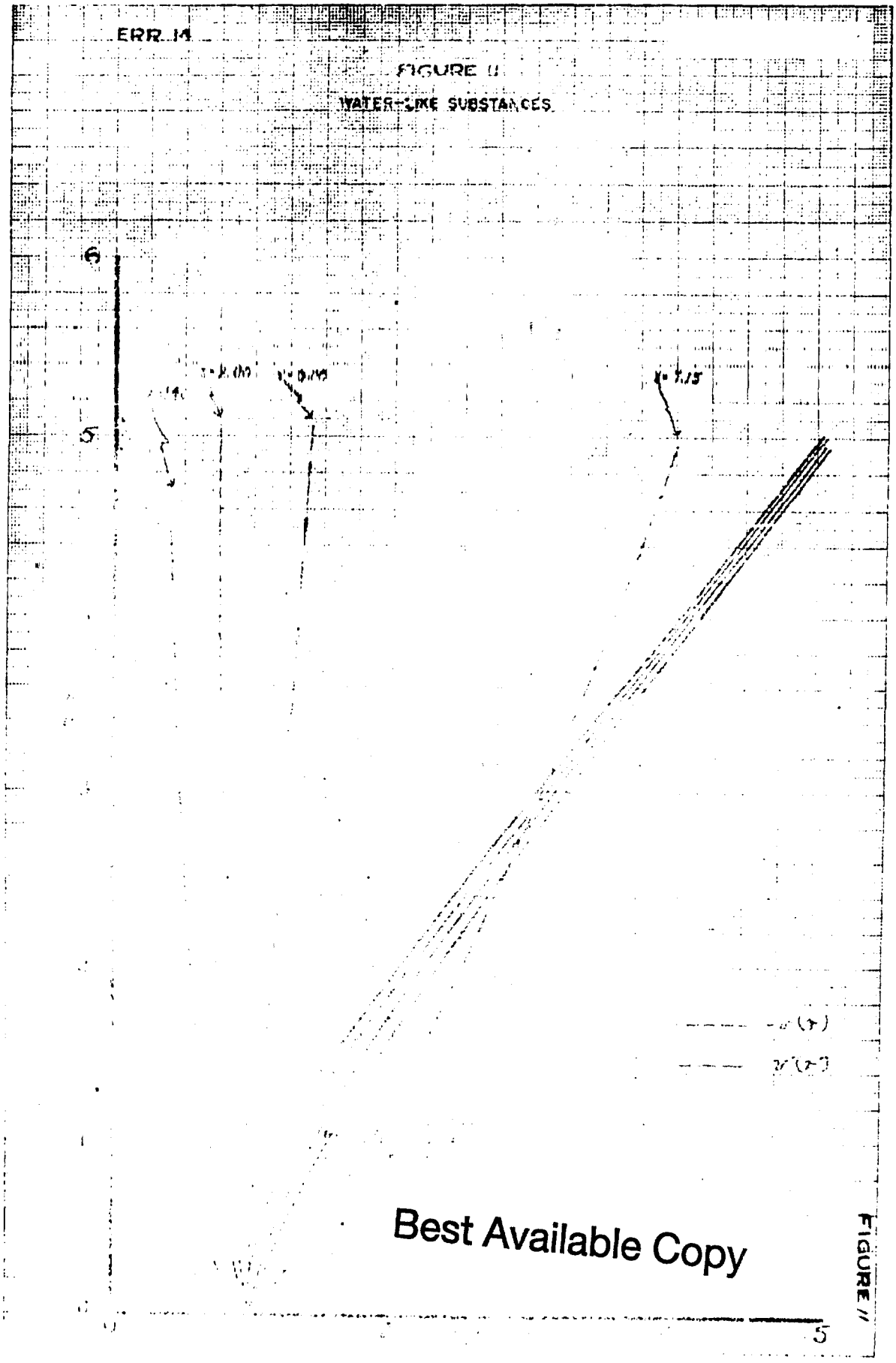
FIGURE 9a

Best Available Copy



Best Available Copy

1374

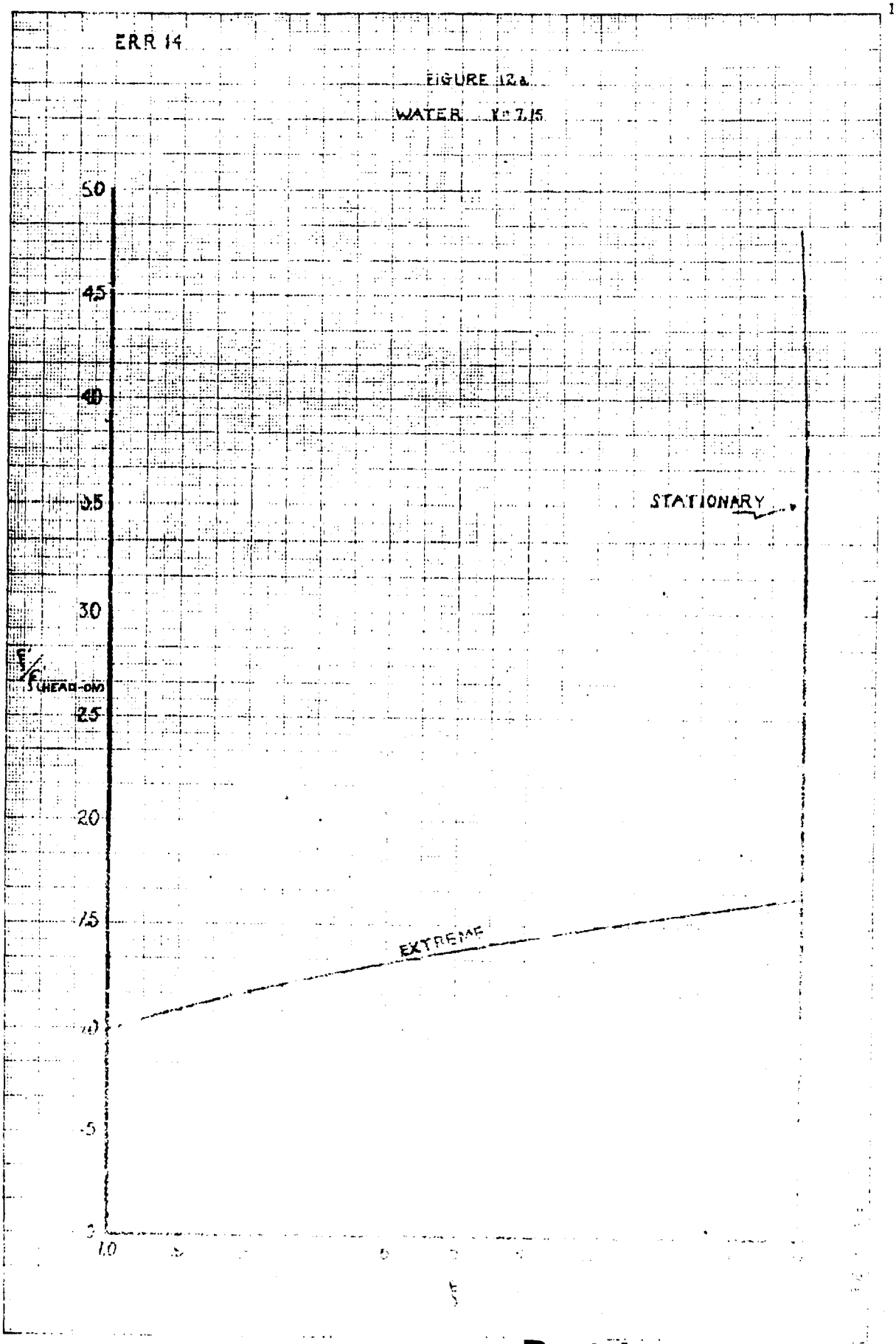


Best Available Copy

ERR 14

FIGURE 12a

WATER $\gamma = 7.15$



Best Available Copy

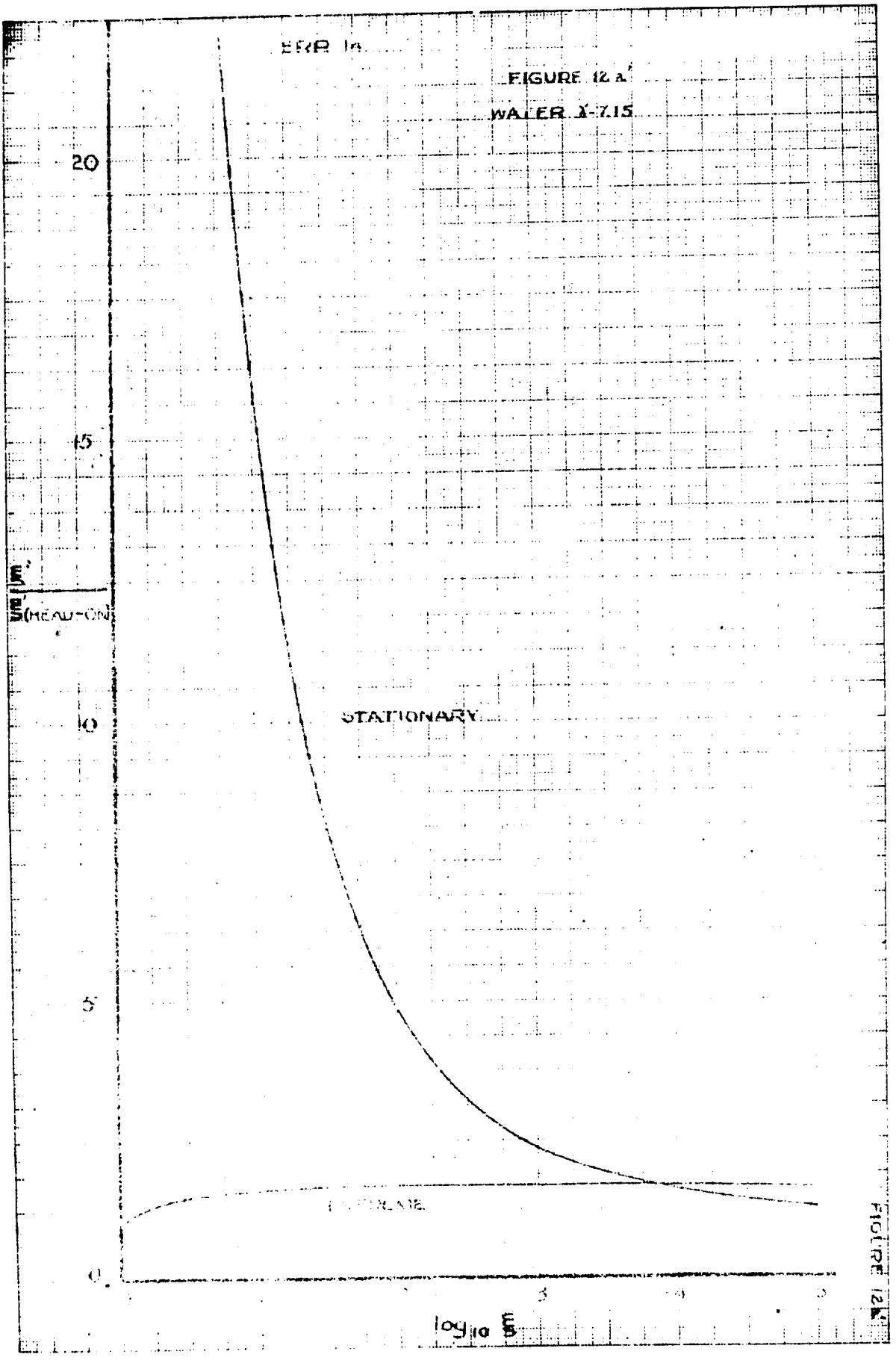


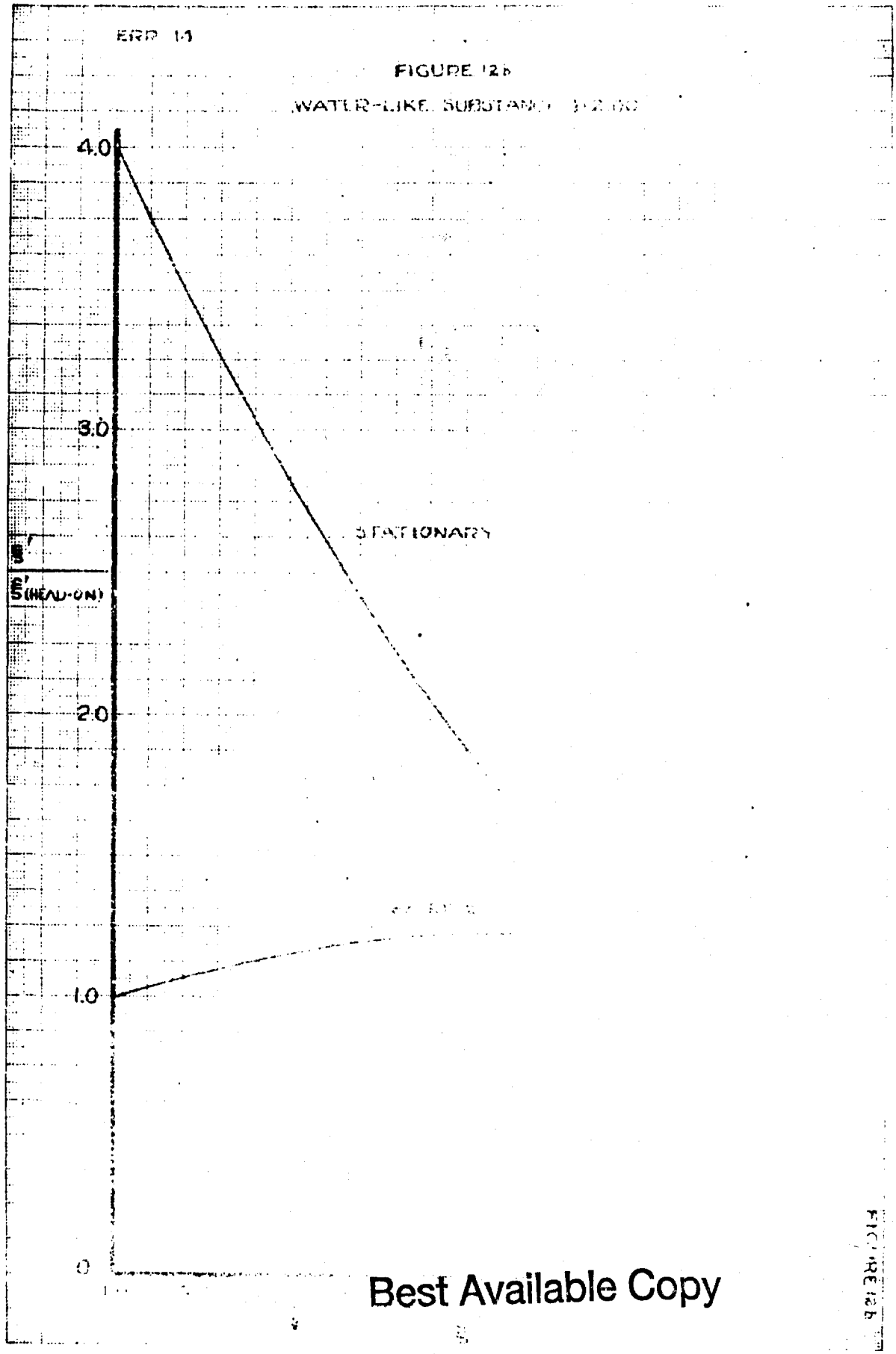
FIGURE 12b

Best Available Copy

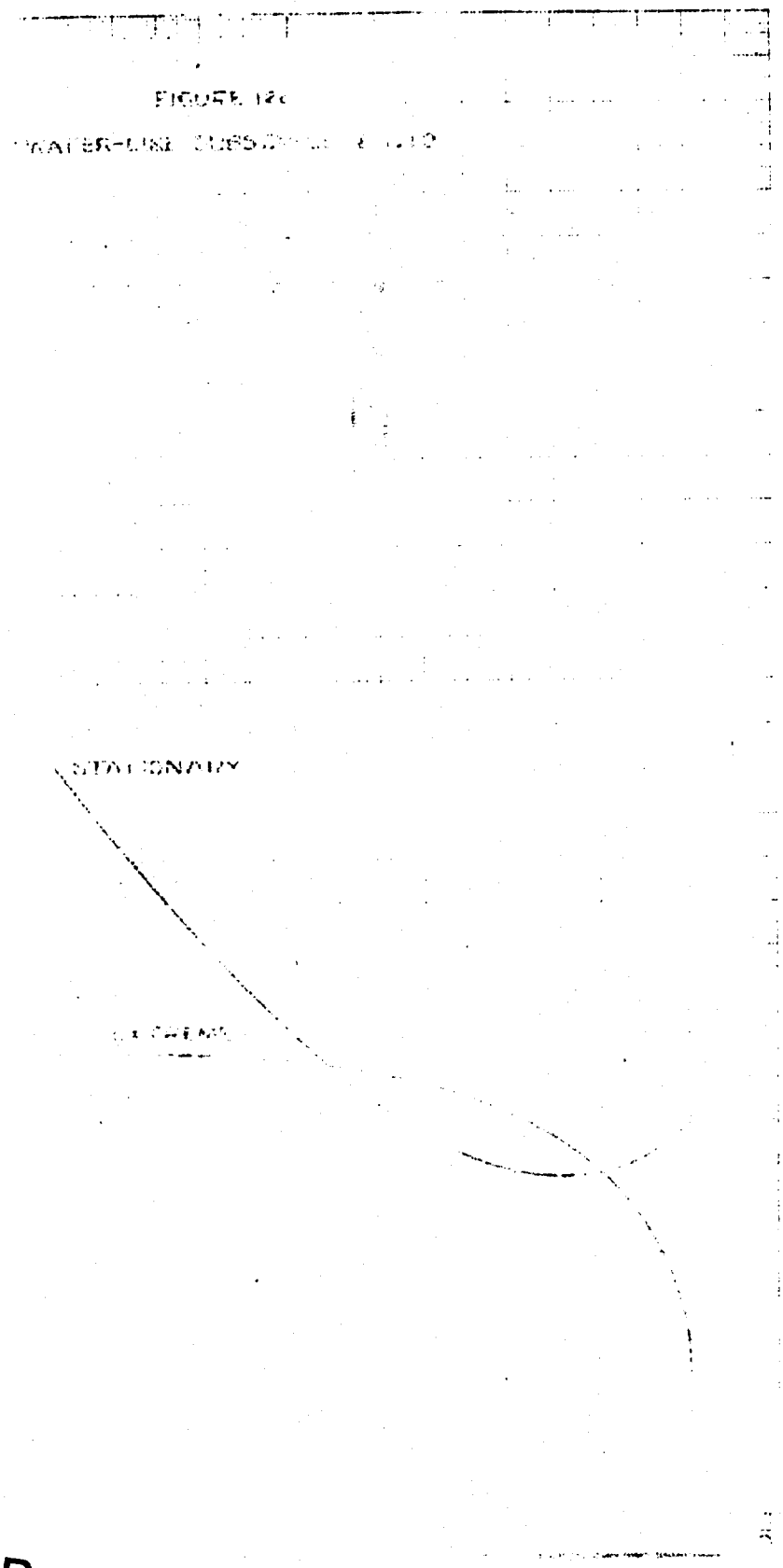
ERR 14

FIGURE 12b

WATER-LIKE SUBSTANCE



Best Available Copy



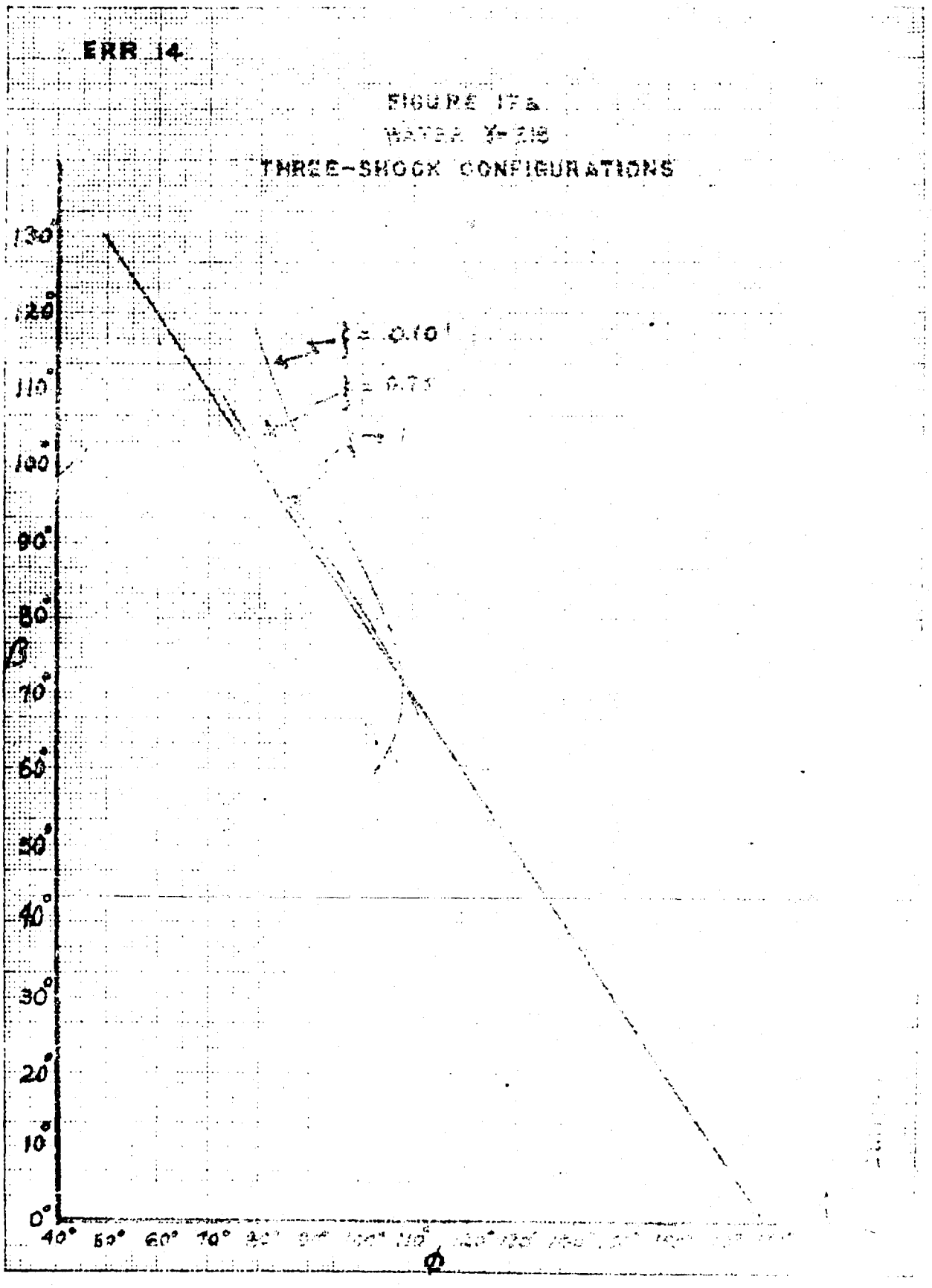
Best Available Copy

ERR 14.

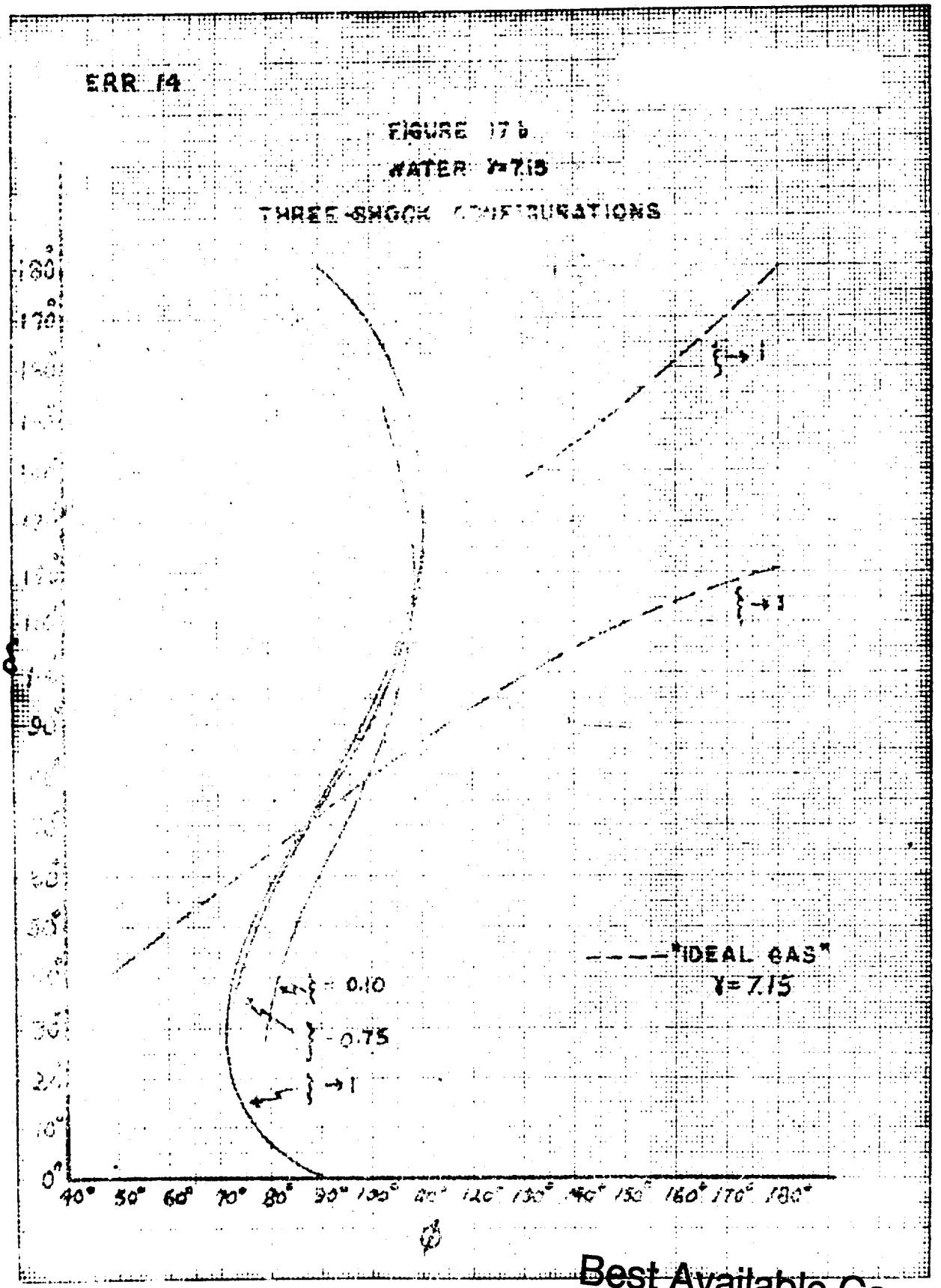
FIGURE 17a.

WATER $\gamma = 2.15$

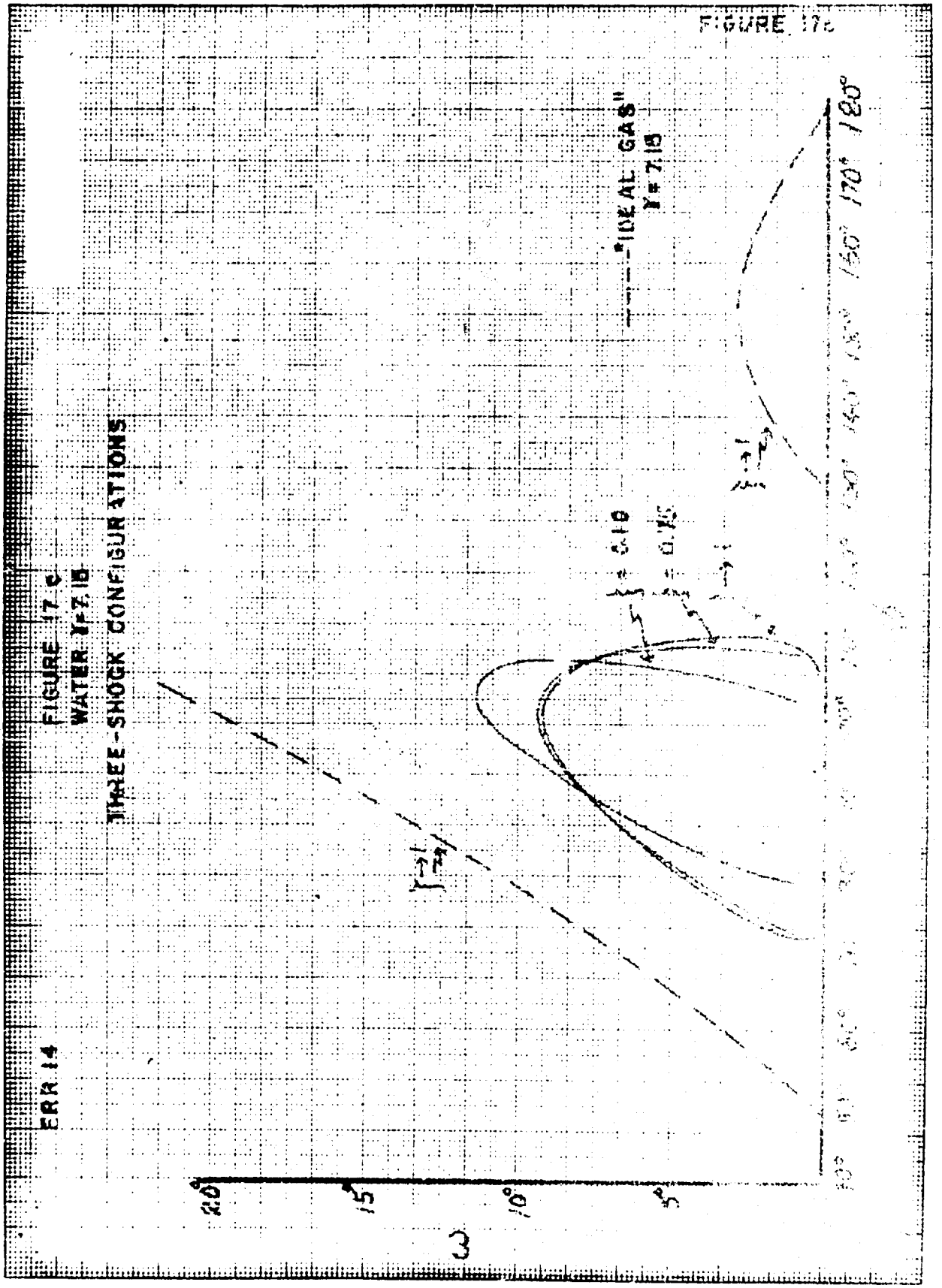
THREE-SHOCK CONFIGURATIONS



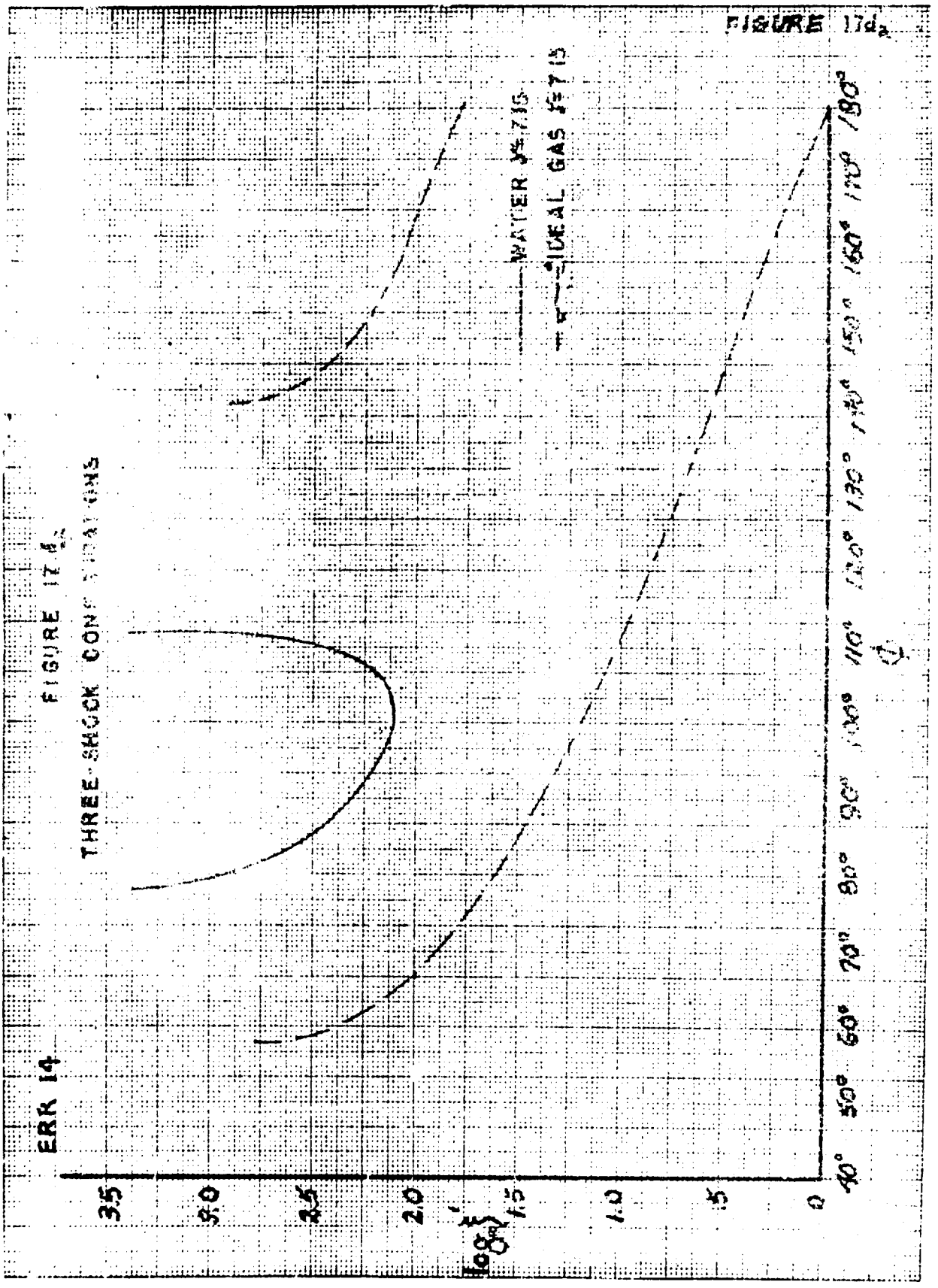
Best Available Copy



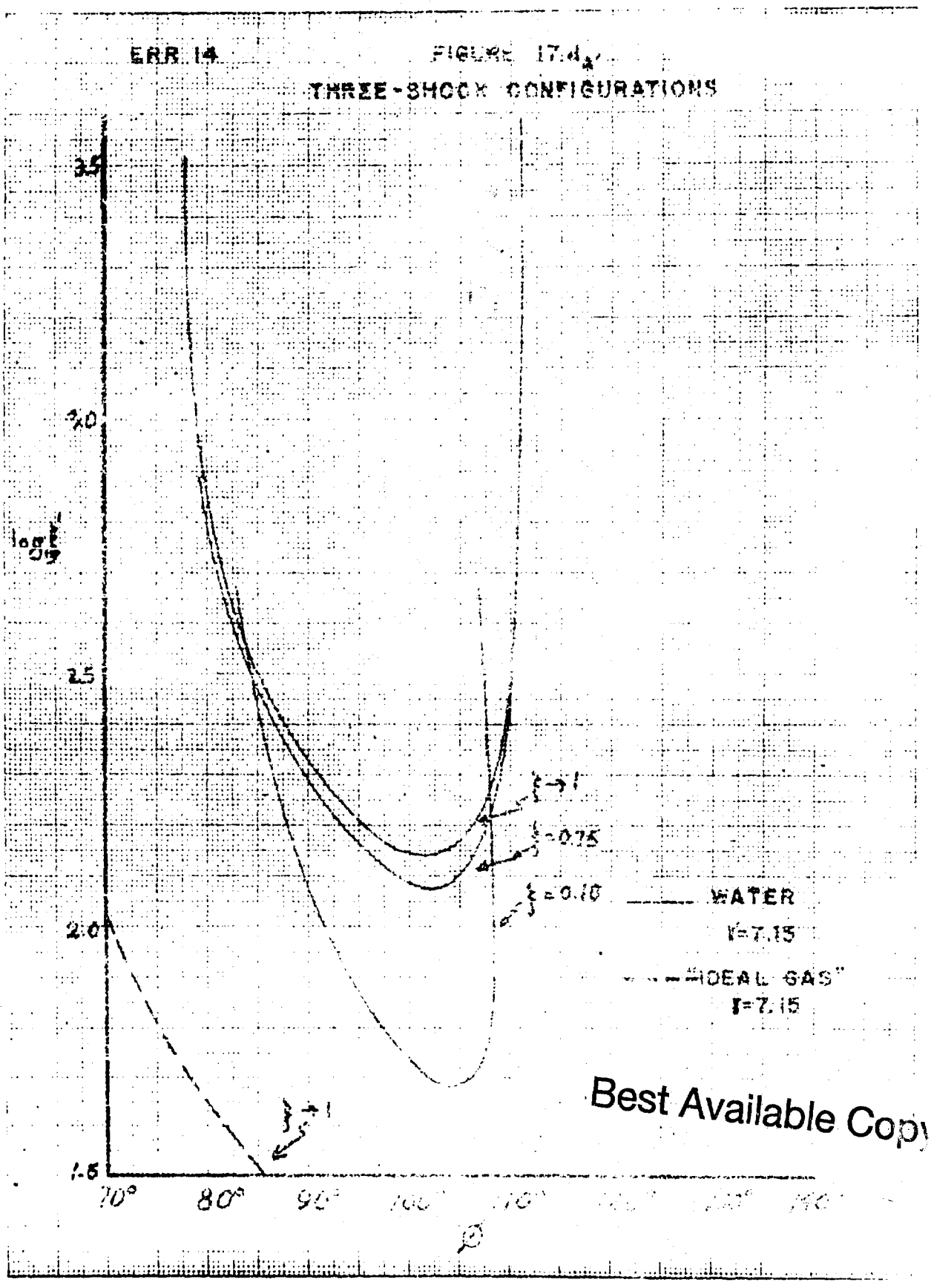
Best Available Co



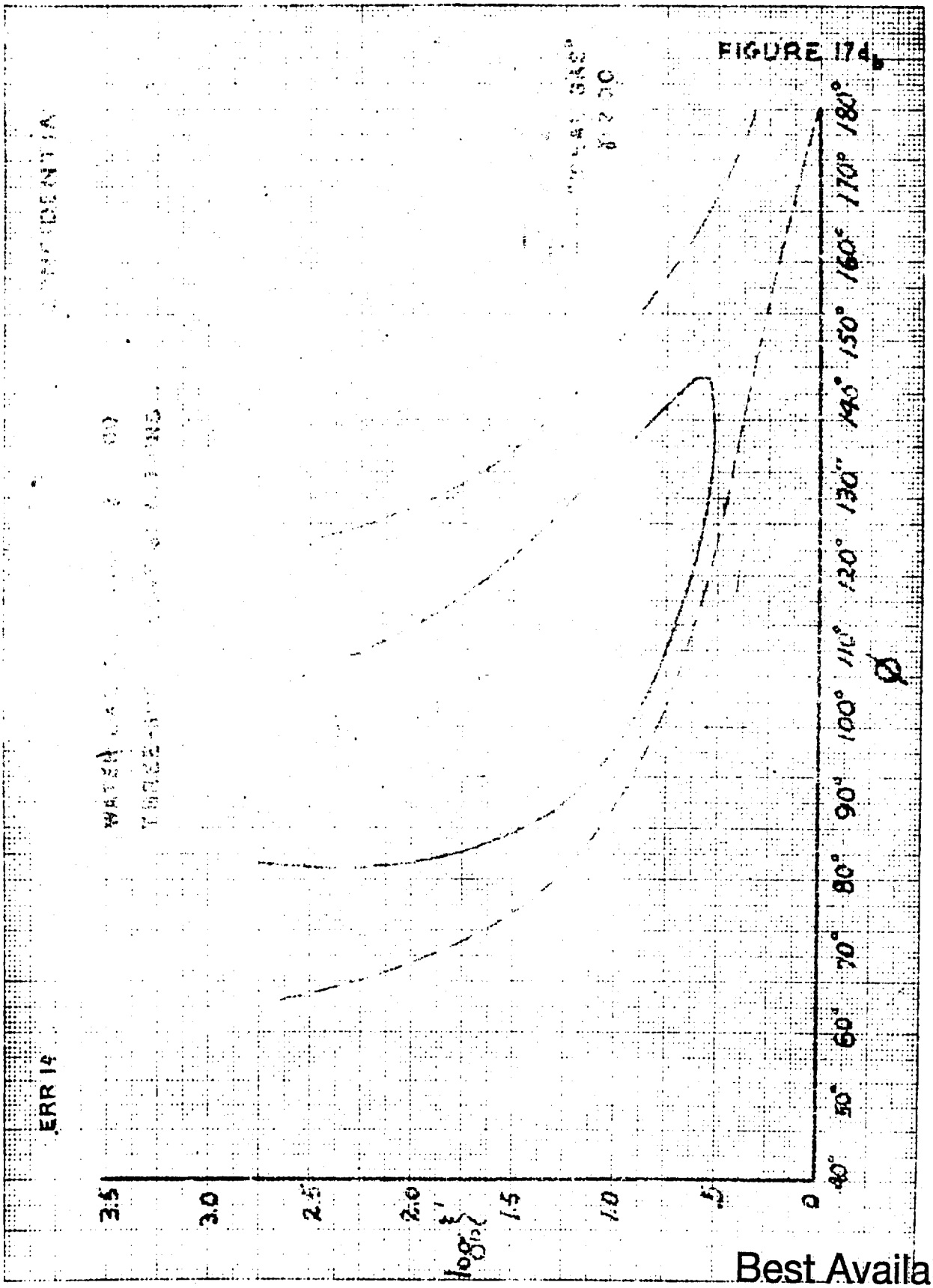
Best Available Copy



Best Available Copy

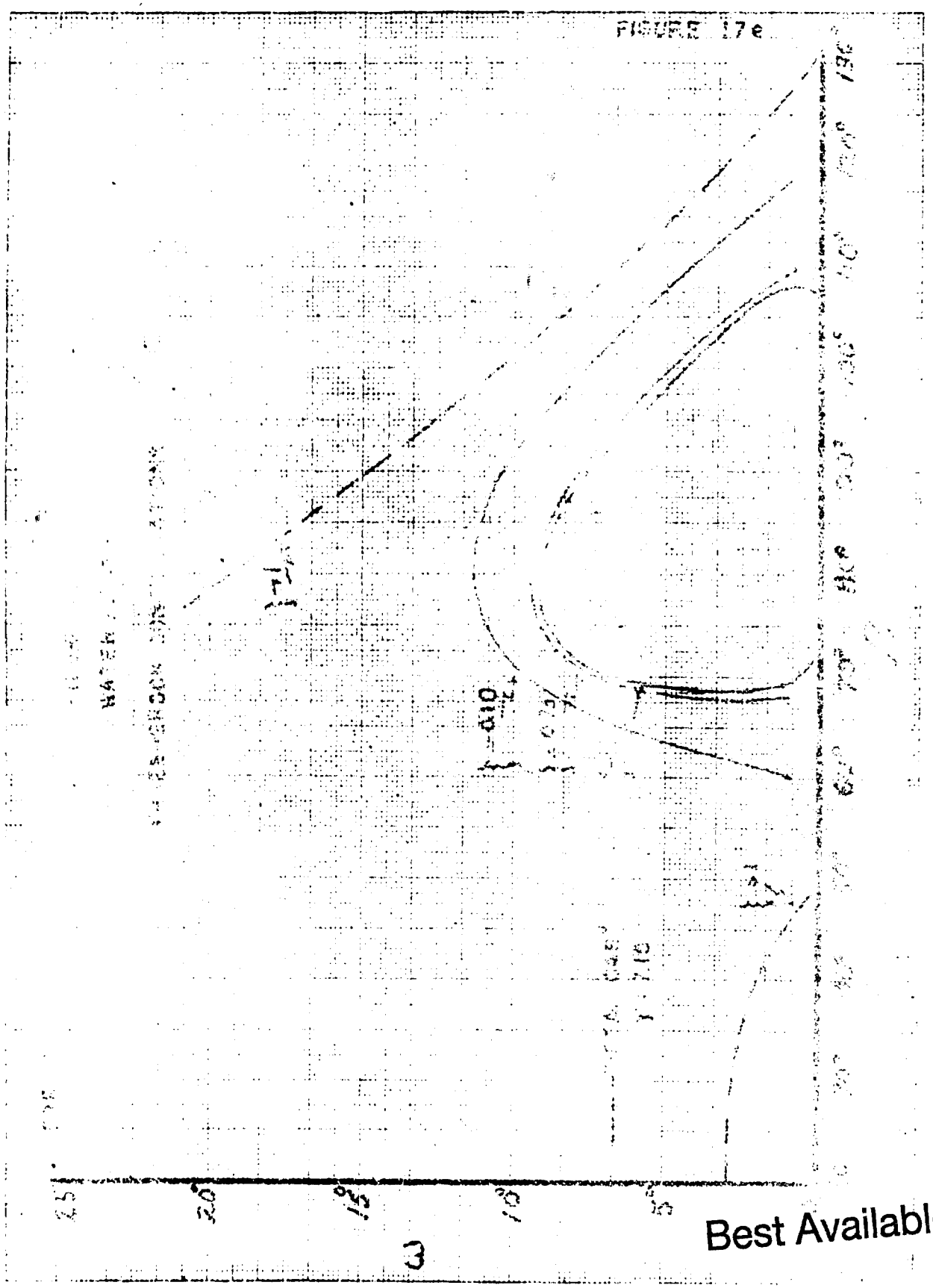


Best Available Copy



Best Available Copy

Best Available Co



Best Available Copy

Best Available Copy

THE REFLECTION OF SMALL-CHARGE SHOCK WAVES FROM A FREE SURFACE

G. M. Sokol
Underwater Explosives Research Laboratory
Woods Hole Oceanographic Institution

American Contribution

15 December 1947

CONTENTS

		Page
Abstract		
Glossary		
I.	INTRODUCTION	1
II.	OUTLINE OF SHOOTING PROGRAM	2
III.	INSTRUMENTATION	4
IV.	ANALYSIS OF RECORDS	5
	1. Photographic Records	5
	2. Pressure Measurements	5
	3. Time Duration Measurements	6
V.	RESULTS	8
	4. Low Pressure Series	8
	5. High Pressure Series	10
	A. Varying Gauge and Charge Depths	10
	B. Constant Charge Depth and Varying Gauge Depths	14
	C. Constant Charge and Gauge Depth and Varying $W^{1/3}/R$	15
VI.	CONCLUSIONS	15
LIST OF REFERENCES		29

LIST OF FIGURES

Figure		Page
1	Schematic diagram of shooting rigs	3
2	Pressure-time curve for 250 gm of Pentolite in free water	6
3	Schematic diagram of surface reflection shock-wave paths	7
4	Pressure-time curves	7
5	Graph of peak pressure vs. charge depths for constant charge-to-gauge distance	12
6	Graph of duration vs. charge depth for constant charge-to-gauge distance	13
7	Graph of peak pressure vs. $W^{1/3}/R$ for charges close to surface	17
8	Graph of duration vs. $W^{1/3}/R$ for charges close to surface	18
9-13	Piezoelectric records of surface reflections at low pressures	20-24
14-15	Piezoelectric records for varying depths	25-26
16	Piezoelectric records for varying gauge depths	27
17	Piezoelectric records for varying $W^{1/3}/R$	28

LIST OF TABLES

Table		Page
I	Gauge Crossing Times	8
II	Summary of Piezoelectric Gauge Results for Oblique Surface Incidence at Pressures below 8200 psi	9
III	Pressure and Duration for Varying Charge and Gauge Depths at Constant Pressure Level	11
IV	Comparison of Results for Gauge Depths of 4 and 33 in., with Charge Depth 4 in. and Charge-to-Gauge Distance 45 in. in Both Cases	14
V	Pressure and Duration for Varying $W^{1/3}/R$ for 250 gm Pentolite with Charge and Gauge 4 in. below Surface	16

GLOSSARY OF SYMBOLS

P_m	Peak pressure at gauge position as obtained from Kirkwood's similitude curves (OSRD 3949) for free water (psi)
P_A	Apparent peak pressure of shock wave at gauge position: the highest visible point on photographic record (psi)
P_D	Derived peak pressure: an approximation to extrapolated peak pressure (psi)
P_S	Peak pressure at a given point on the water's surface, as obtained from Kirkwood's similitude curves (OSRD 3949) for free water (psi)
t	Calculated shock-wave duration time between the arrival of the directly propagated pressure wave and the subsequent arrival of the reflected tension wave (microsec)
T	Experimental shock-wave duration time as measured on the piezoelectric record (microsec)
T_G	Gauge crossing time of the positive shock wave (microsec)
T_D	Gauge crossing time of the reflected tension wave (microsec)
D	Depth from the center of the charge or gauge to the surface (ft or in., as specified)
R	Charge-to-gauge distance (ft or in., as specified)
S	Surface point of incidence of that part of the shock front which is reflected in such a way as to strike the gauge, assuming equal angles of incidence and reflection
$W^{1/3}/R$	Scaling constant for similitude curves in terms of charge weight, W, and charge-to-gauge distance, R ($lb^{1/3}/ft$)
α	Angle of incidence of shock front at point S (degrees) (angle between ocean surface and the line from S to the charge)
θ	Time constant; time required for pressure to drop to $1/\theta$ of its initial value (microsec)
σ	Standard deviation of a single observation from the mean (%)

ABSTRACT

This report presents the results of piezoelectric measurements of underwater explosion pressure waves generated and observed near the free water surface. The charge-surface-gauge positions were such that the rarefaction wave resulting from reflection of the compression wave at the surface was propagating in the moving and compressed medium not far behind the shock front. Under these conditions, the interaction with the surface deviates from the predictions of simple acoustic theory.

If the angle of incidence is defined as $\alpha = \tan^{-1} (D_c + D_g)/R$, where D_c and D_g are the charge and gauge depths and R is their horizontal separation, one finds that the deviations from acoustic theory become more pronounced as α decreases at constant pressure level (at the point of reflection on the surface) or as the pressure level is increased at constant α.

The deviations readily observed by the methods employed in this investigation are 1) a falling-off of the peak pressure from the value obtained in free water at the same charge-to-gauge distance, and 2) a change in the character of the rarefaction cut-off to zero pressure. The rarefaction becomes less steep-fronted and, in extreme cases, would appear to have penetrated to the shock front. The decay of pressure behind the shock front becomes non-exponential and the pressure-time records become convex upward. The total duration of the positive pressure phase, however, becomes longer than predicted by acoustic theory for the cut-off to zero pressure on the arrival of a negative reflected front.

THE REFLECTION OF SMALL-CHARGE SHOCK WAVES FROM A FREE SURFACE

I. INTRODUCTION

The phenomena accompanying the oblique incidence of shock waves upon a free surface have already been described.[5,6]* However, the theoretical descriptions generally available apply only to that part of the pressure field in which the angle of incidence is large and the pressure level comparatively low, less than 15,000 psi. Under such conditions, the normal acoustic laws of propagation offer a satisfactory description of the direct shock wave and of the tension wave which is reflected from the surface. Experimental evidence previously obtained at this laboratory has been seen to indicate that for very small angles of incidence and for cases in which either the charge or the gauge is very close to the surface, the acoustic theory no longer offers an adequate explanation of the observed results.[6]

These earlier results showed that, at points very close to the surface, the shock wave duration (the time interval between the arrival of the directly propagated wave at the gauge and the subsequent arrival of the reflected negative wave) is greater than simple acoustic theory predicts. Furthermore, pressures measured near the surface were found to be much lower than the similitude values obtained for free water, although for a given charge fired near the surface this attenuation is less pronounced beneath the charge than near the surface. And even before the arrival of the negative wave, the decay of pressure with time differs from the exponential decay of free-water pressure fields.

The study here described was undertaken to obtain a more nearly complete picture of these surface-reflection phenomena. A program was set up to study shock waves near the surface for various charge and gauge depths, as well as for varying pressure levels at a given depth. Experimental results are presented with a minimum of interpretation, in the hope that the additional information will be of assistance in the development of a satisfactory theory for free surface shock-wave phenomena. The present foundation for such theoretical development is naturally based on the Meyer Corner theory and the work of Prandtl and Mach[9], but, except for a brief mention by Cole[7], the general literature does not reveal any extension of this work to cover explosive propagation under the conditions here investigated.

---

* All such numbers refer to the List of References at the end of this report.

II. OUTLINE OF SHOOTING PROGRAM

For the shooting which is here reported, pentolite was chosen because of its availability and the ease with which it may be cast in spherical molds. Spherical charges were used throughout to obtain pressure fields as nearly symmetrical as possible. The first series of shots, with 250 gm charges, was done in sea water immediately off the Oceanographic Institution dock at Woods Hole. A horizontal boom (Fig. 1A) was suspended above the surface and from it a vertical rod was projected down into the water. On this rod were mounted three piezoelectric gauges, 1, 2, and 3 ft below the surface. Farther along the boom, a pair of movable spreaders held the charge 2 ft below the surface at any desired horizontal distance from the gauges. With this rig, shots were fired at horizontal charge-to-gauge distances that varied from 4 to 45 ft.

During this series, the surface of the water was somewhat rippled even on the very calmest days, and therefore the depth measurements could seldom be made with an accuracy better than 3 or 4 in. This was one of the reasons that subsequent shooting was done at a fresh-water pond on Nonamessett Island. Because of the shelter afforded by nearby high ground, a good calm prevailed on the pond and, except on the windiest days, the ripple was less than an inch high.

At the pond, charges and gauges were mounted on a ring (Fig. 1B). Three uprights were bolted to the ring to serve as depth indicators. Brightly colored lengths of thin wire were strung between the uprights and drawn as tight as possible. Gauges and charge were mounted any desired number of inches below the wire, and the ring was lowered into the pond until the wire just broke the surface. Because the wire was light and tightly strung, there was no appreciable sagging, and the gauge and charge depths could be measured accurately to within one quarter of an inch.

With this rig, a series of shots was made with charge and gauges all at the same depth, with the depth varying from 4 to 12 in. beneath the surface, and a charge-to-gauge distance of 45 in. A second series consisted of shots at the 4 in. depth with gauge distances of 30, 45, and 60 in. All of these shots were made with 250 gm charges. One group of 500 gm charges was also used, at a depth of 5 in. and a gauge distance of 19 in.

It was further desired to observe the pressure directly below the explosive source, but this would have required extensive revision of the existing set-up. Instead, a vertical support was mounted on the ring and extended 3 ft beneath it By means of this support a gauge could be mounted off to one side and about 30 in. deeper than the charge.

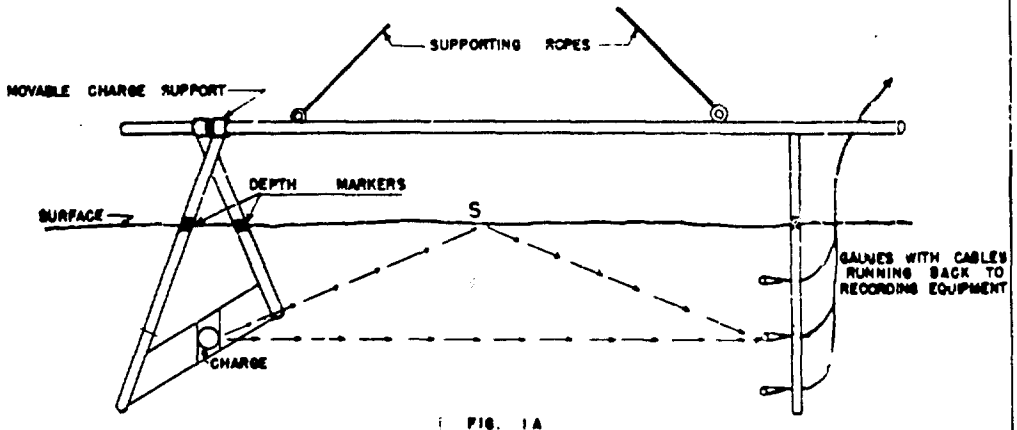
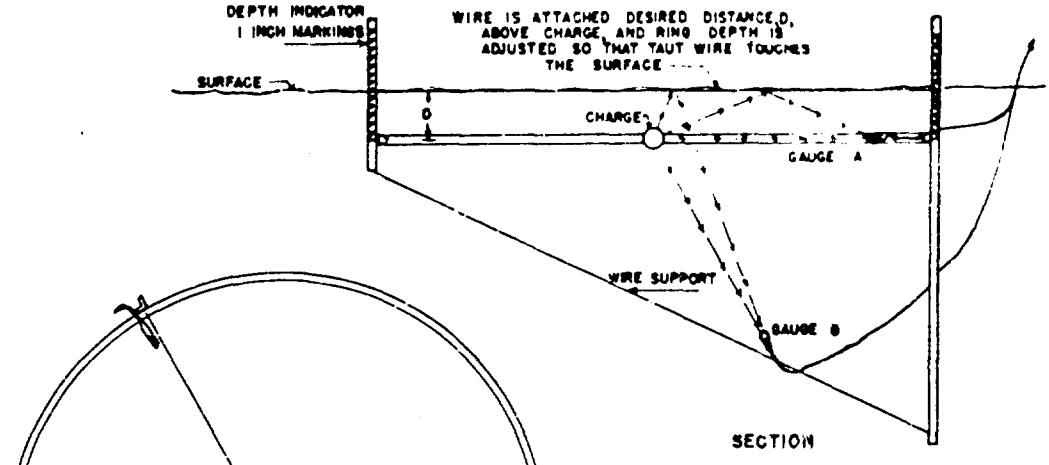
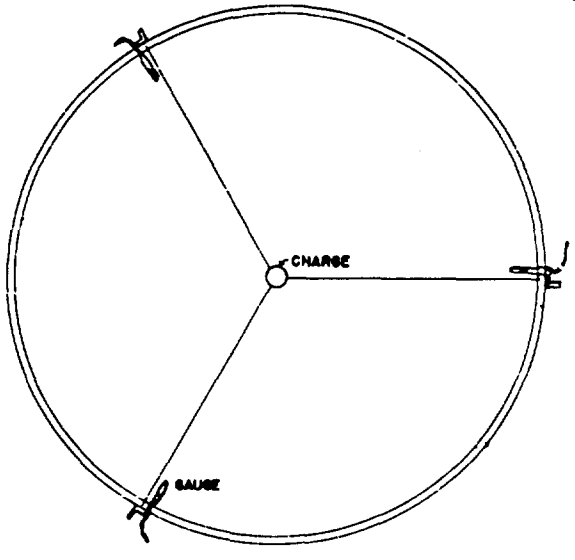


FIG. 1A

BOOM USED TO OBSERVE OBLIQUE REFLECTION PHENOMENA AT LOW PRESSURES (535 TO 8200 PSI) AT SURFACE POINT, S. THE CHARGE-TO-GAUGE DISTANCE, R, MAY BE VARIED FROM 4 TO 45 FT.





TOP VIEW

FIG 1B

RING USED IN VERY SHALLOW SHOOTING AT SURFACE PRESSURES FROM 6900 TO 75,900 PSI. DEPTH, D, CAN BE VARIED FROM 4 IN. TO 12 IN.

FIG. 1.

SCHEMATIC DIAGRAM OF SHOOTING RIGS

UERL WOODS HOLE, MASS.

III. INSTRUMENTATION

Experimental results in this program were obtained with UERL Type B gauges[1], the initial work being done with 3/8 in. diameter gauges and the pond shooting with 1/4 in. gauges. These gauges were mounted on 5 ft lengths of wax-filled copper tubing chosen for low cable signal. The tubing was in turn spliced to 75 ft lengths of copolene cable. To record the gauge signals, four DuMont 208 Cathode Ray Oscilloscopes were used as previously modified at this laboratory, and further modified as will be described below. The cameras which were used in photographing the oscilloscope screens are of the rotating-drum type, accommodating a 10 in. strip of 35 mm film. The associated electronic equipment used to fire the charge, to synchronize the oscilloscope beam brightening with the detonation, and to obtain voltage and timing calibrations is essentially the same as has been previously described.[2]

The time resolution required in the study of small-charge shock waves imposed severe demands upon the above equipment, particularly since the surface-reflection phenomena are of durations as short as 10 microsec. The necessary resolution required a writing speed of at least 0.7 millisec per in., more than twice the fastest drum speed for which the equipment had been designed. The high speed was obtained by running the camera motors, which were Elinco Midget Type F-78 6-volt D.C. motors, from a 12-volt supply. Variable drum speeds corresponding to writing speeds of from 0.7 to 1.0 millisec per in. were thus obtained.

At these writing speeds further modification of the existing equipment was necessary to obtain readable photographic records. The intensifier voltage on the 5LP5 cathode ray tubes was increased from the 1000-volt value indicated in OSRD Report No. 6238 to 3000 volts, giving a total voltage across each tube of 4000 volts. Although the deflection sensitivity was thus slightly decreased, the gain provided by the amplifiers continued to be more than adequate for input voltages of more than 0.5 volts.

With increased intensity, satisfactory photography of the scope faces was possible with an f:1.4 Zeiss Biotar lens and Eastman Kodak PF402 green-sensitive Photoflure film. However, the necessity for recording a time scale simultaneously with the piezoelectric record imposed stricter requirements on the film. Timing marks were obtained from a crater tube (Sylvania type R-1130B) mounted inside each camera hood, just as described for other UERL equipment.[2] Because the crater-tube flashes are red, the Photoflure is relatively insensitive to them, and at the drum speeds needed here the timing pips did not show up at all. Therefore, it was necessary to use Eastman LP421 Linograph Pan recording film, which is panchromatic but also particularly sensitive to the blue-green cathode ray tube light. By force-developing the films thus obtained for 20 minutes in D-19, readable records were obtained.

IV. ANALYSIS OF RECORDS

1. Photographic Records

Representative piezoelectric pressure-time records are shown in Figs. 9-17 for all shooting conditions for which results are presented in this report. Immediately underneath each record is a time scale which was recorded simultaneously on the film. Two different timing methods were used. When possible a separate cathode ray tube was utilized since it simplified photographic problems. Otherwise the crater tube flasher provided timing dots. In both cases the timing signal came from the same source, a multivibrator which, operating from a standard 100 kilocycle crystal, gave a 10 kilocycle output and 100 microsec markers.

2. Pressure Measurements

Pressure-time records obtained in this shooting series were measured to find values of peak pressure, P_m, and the duration, T, of the compression wave. Because these shots were shallow, the reflected rarefaction or tension wave arrived at the gauge a very short time after the initial shock front. Therefore, normal extrapolation procedure was not possible, and to derive a pressure P_D, which approximates extrapolated peak pressure, the following method was used.

It was assumed first of all that the initial compression wave arrives at the gauge unaffected by surface reflections. The first few microseconds of the record, therefore, yield a value for apparent peak pressure, P_A, that starts to decay at the normal free-water rate until the arrival of the tension wave. From work done at this laboratory with pentolite in free water[7], a value may be obtained for $\theta/W^{1/3}$, where θ is the decay time-constant in microseconds and W the charge weight in pounds. If θ is taken as 62.6 microsec for a 250 gm charge, at a value of $W^{1/3}/R$ equal to 0.216, the extrapolated peak pressure in free water is 4000 psi and the pressure-time curve is as shown in Fig. 2, plotted on a semi-log grid so that the exponential decay appears as a straight line.

The solid line shows the pressure-time curve as it would be observed by a gauge of infinitesimal size, rising to true peak pressure, P_m, then decaying exponentially. The gauges used in this study have a diameter of more than 1/4 in. including the waterproof wrapping. This finite diameter results in the recording of a finite rise time and therefore a lower apparent peak pressure, P_A. As seen in Table I, the average rise time for the gauges used in this study is about 8 microsec, shown by the dotted line in Fig. 2. Zero time is defined as the time at which the shock wave passes the center of the gauge. For these gauges the expected P_A is seen to be 3750 psi in free water

and the ratio P_m/P_A is 1.07. The ratio remains roughly the same for all values of $W^{1/3}/R$ used in this study, and it was therefore concluded that, had extrapolation been possible in the results here presented, the values of P_m would have been 7 per cent higher than the values of P_A obtained. A derived peak pressure, $P_D = 1.07\ P_A$, is therefore presented as an approximation of P_m.

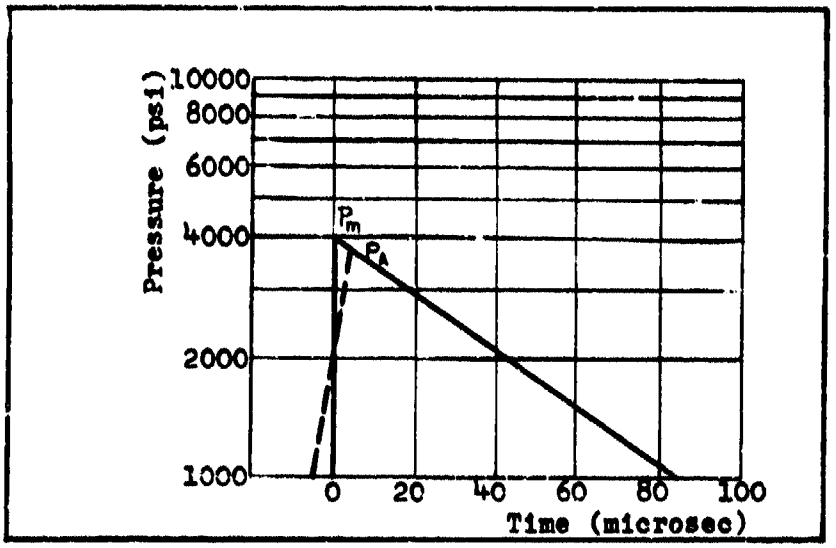


Fig. 2. Free-Water Pressure-Time Curve for 250 gm Pentolite Charge.

3. Time Duration Measurements

In the accompanying tables, computed values of shock-wave duration, t, are given as derived from acoustic theory. These values were obtained from the geometric configuration of the rig, as shown in Fig. 3, and are derived from the differences in path length traveled by the direct shock wave and the reflected tension wave, assuming that both travel with the speed of sound. The experimental measurement corresponding to this value is called T and is taken as the time interval between the top of the rise line, at which instant the gauge is recording the apparent peak pressure, and the point at which the pressure returns to the hydrostatic value. For gauges small relative to the thickness of the shock wave, this corresponds to the time between the arrival of the shock wave at the edge of the gauge farthest from the charge and the subsequent arrival of a steep-fronted rarefaction wave at that point.

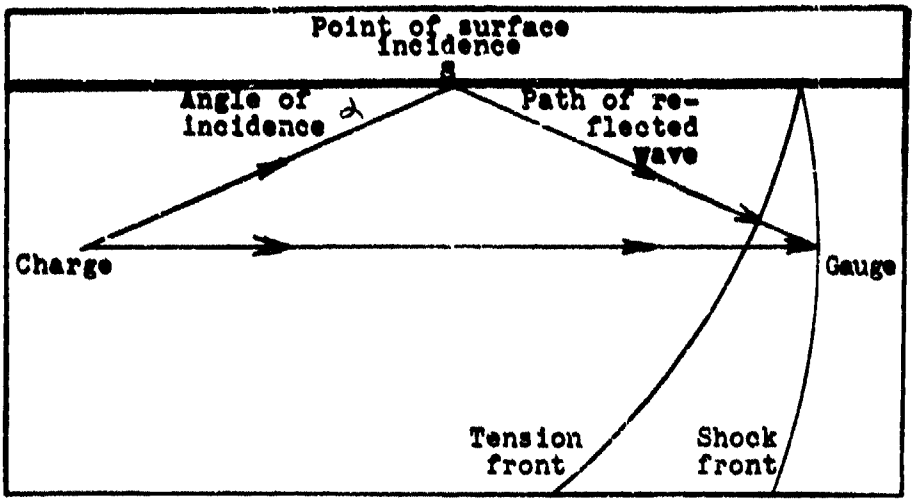


Fig. 3. Schematic Diagram of Surface-Reflection Shock-Wave Paths.

This measurement was chosen in preference to the time between the arrival of the wave fronts at the front edge of the gauge because the drop-off due to the tension wave becomes gradual for increasingly oblique incidence and the choice of the point at which the normal free-water decay ceases becomes correspondingly unreliable.

Even in the acoustic region, the time, T_D, of the tension cut-off is longer than the crossing time, T_G, of the initial pressure wave.

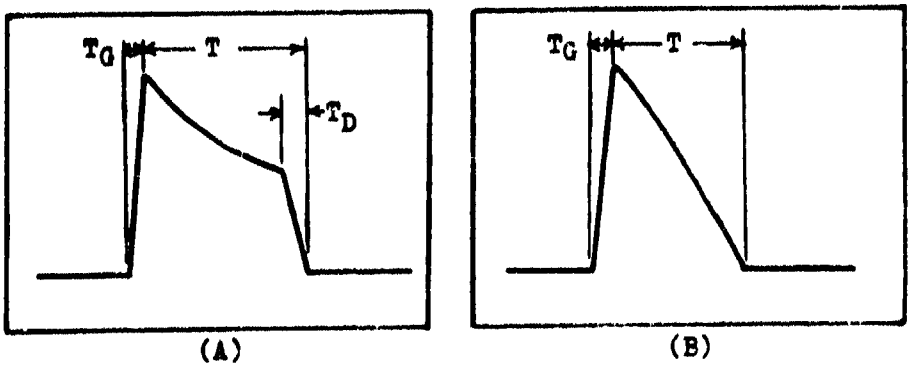


Fig. 4. Typical Pressure-Time Curves

Figure 4A shows, for example, a typical shock-wave record in the acoustic region, while Fig. 4B shows the record at the same pressure level for a much more oblique incidence. Here, no measurement of T_D may be made since there is no apparent rarefaction front. With charge and gauges at the same depth, D, results were obtained for varying D. These are shown in Table I for those angles of incidence at which measurements of T_D were possible.

TABLE I

GAUGE CROSSING TIMES

D (in.)	α (degrees)	Average T_G		Average T_D		Ratio T_D/T_G
		(microsec)	σ(%)	(microsec)	σ(%)	
10	23.9	8.0	24	11.1	20	1.39
9	21.7	8.4	11	12.6	13	1.50
8	19.5	7.3	11	13.0	19	1.78
7	17.2	6.9	22	20.0	30	3.34

V. RESULTS

4. Low-Pressure Series

Because the first series of shots was made in sea water with surface ripple always present, a charge depth of 2 ft and gauge depths of 1, 2, and 3 ft were used, these being the shallowest values at which depth variations due to ripple could be considered negligibly small. At such depths relatively large charge-to-gauge distances were required, to obtain small incident angles, α in Fig. 3, and the pressure levels at the point of incidence, S, were consequently quite low. Values for $W^{1/3}/R$ at point S varied from 0.364 (corresponding to a free water similitude pressure of 8200 psi) at an angle, α, of 51.2° down to 0.024 (535 psi) at α = 3.8°.

Experimental pressure and duration results obtained under these conditions show no great deviation from the values predicted by Kirkwood for pressure in free-water, or from the durations predicted by the acoustic theory. As shown in Table II, the only duration measurement that shows a significant difference from the acoustic value was obtained for the smallest angle of incidence in the series and the lowest surface pressure. On the other hand, the individual pressure-time records, of which representative examples are shown in Figs. 9-13 reveal curves that deviate considerably from the free water exponential decay pattern. Note, for example, how the decay curve varies for a 2 ft gauge depth as the charge-to-gauge distance is increased,

TABLE II

SUMMARY OF PIEZOELECTRIC GAUGE RESULTS FOR OBLIQUE SURFACE INCIDENCE AT PRESSURES BELOW 8200 PSI

α	P_S	R	P_m	P_A		P_D	Ratio P_D/P_m	Gauge Depth D	t	Average T		Ratio T/t
(°)	(psi)	(ft)	(psi)	(psi)	σ (%)	(psi)		(ft)	(microsec)	(microsec)	σ (%)	
3.80	535	45	248	190	15.6	204	0.823	1	19	28	2.1	1.47
5.08								2	37	38	1.5	1.03
6.33								3	56	55	8.2	0.98
7.43	1147	23	496	470	7.7	503	1.07	1	34	37	0.5	1.03
9.87								2	73	71	3.5	0.98
12.27								3	108	110	16.2	1.02
11.32	1845	15	878	880	19.9	940	1.07	1	55	48	11.9	0.87
14.92								2	110	109	3.8	0.99
18.43								3	164	165	1.3	1.01
23.15	4365	7	2150	2240	12.8	2400	1.07	1	115	141	22.7	1.22
29.75								2	223	247	12.1	1.11
35.53								3	322	358	9.2	1.11
36.87	8190	4	3920	3840	15.2	4000	1.02	1	165	220	10.0	1.19
45.0								2	349	379	9.2	1.12
51.3								3	480	523	7.3	1.09

causing $W^{1/3}/R$ and α to decrease. In Figs. 9 and 10, α is large and the records show a sharp pressure peak and a decay which is definitely exponential. For a smaller α (Figs. 11, 12, and 13) the positive peak is rounded off so that for the shorter durations the exponential nature of the decay is completely obscured. For shallow gauge positions the decays are even more difficult to reconcile with the usual records. Note the double peak on record 57-2 (Fig. 12) and the more nearly normal cut-off on 61-1, a subsequent record obtained with a different gauge. At such very short durations the finite diameter of the gauge must introduce some error and variations from gauge to gauge may be responsible for such differences.

5. High-Pressure Series

To obtain higher pressures at equally small angles of incidence, it was necessary to detonate charges much closer to the surface, and therefore all subsequent shooting was done at a sheltered fresh-water pond where the surface was generally perfectly calm. Here it was possible to maintain accurate charge depths as small as 4 in. Charge-to-gauge distances were then feasible such that $W^{1/3}/R$ at the surface point varied from 1.78 (similitude pressure, 75,900 psi) at $\alpha = 46.4°$ down to 0.326 (pressure, 6900 psi) at $\alpha = 7.6°$.

A. Varying Gauge and Charge Depths. With a constant charge-to-gauge distance of 45.6 in. a series of shots as completed for charge and gauges at the same depth, D, which was varied from 4 to 10 in. The value of $W^{1/3}/R$ at the surface point half way between charge and gauge varied from 0.382 to 0.429 over this range of depths corresponding to a free-water pressure variation from 9400 to 10,200 psi. Thus, while the pressure did not change more than 8%, the angle of incidence was varied from 10.1° to 23.9°. Table III contains a summary of pressure and duration results thus obtained, and Figs. 5 and 6 represent the results graphically.

From these results it may be seen that at a depth of 4 in. and for an angle of incidence of 10.1° the derived peak pressure at the gauge is only 0.70 of the free-water similitude value for the same $W^{1/3}/R$. For increasing angles of incidence, the pressure gradually increases to about 93% of the free-water value at 10 in. and 23.9°. Under the same conditions the measured duration at 10.1° is 1.59 times higher than the acoustic theory predicts and as the angle is increased the duration approaches the theoretical value. For angles larger than 17° the experimental results approximate the acoustical values rather well.

Figures 14 and 15 show typical piezoelectric records for this series of shots. These photographs show much less rounding off of peaks than was seen for the low pressure shots. The difference is doubtless due to the smaller diameter gauges used. These figures show how the decay curve becomes more and more exponential as is increased.

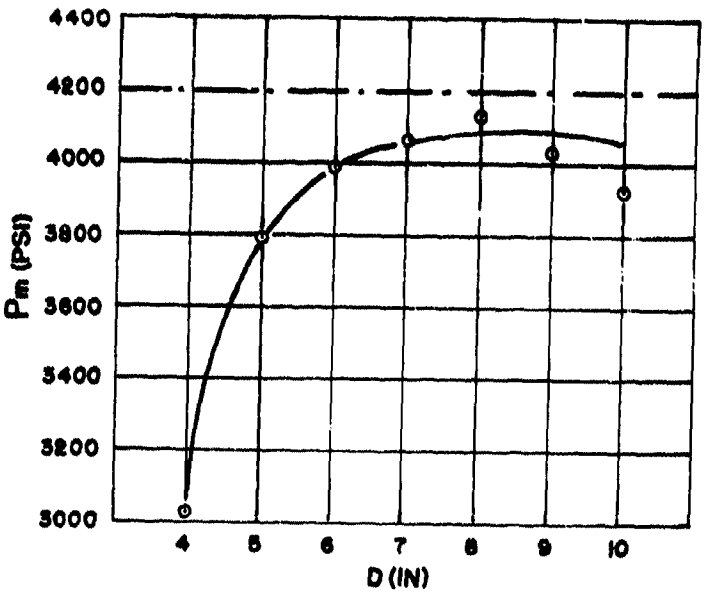
TABLE III

PRESSURE AND DURATION FOR VARYING CHARGE AND GAUGE DEPTHS AT CONSTANT PRESSURE LEVEL

Charge 250 gm Pentolite at R = 45.6 in. At gauge, $W^{1/3}/R = 0.216$ ($P_m = 4200$).

α	P_S	Depth D	Average P_A		P_D	Ratio P_D/P_m	t	Average T		Ratic T/t
(°)	(psi)	(in.)	(psi)	σ (%)	(psi)		(microsec)	(microsec)	σ (%)	
10.1	10,200	4	2830	6.8	3030	0.684	11.7	18.6	5.8	1.59
12.5	10,100	5	3540	1.3	3790	0.904	18.2	23.4	10.5	1.29
14.9	10,000	6	3730	4.9	3990	0.950	26.0	32.3	6.2	1.24
17.2	9,900	7	3800	4.3	4060	0.966	35.1	38.0	6.0	1.08
19.5	9,800	8	3860	4.2	4130	0.984	45.5	53.0	4.9	1.16
21.7	9,600	9	3760	2.2	4030	0.959	57.2	56.3	2.4	0.99
23.9	9,400	10	3660	6.0	3920	0.934	70.0	71.7	4.2	1.02

1403



—o—o— DERIVED PEAK PRESSURE FOR 250 GM PENTOLITE CHARGE.

—·—·—·— FREE WATER SIMILTUDE PRESSURE (KIRKWOOD OSRD 3949)

FIG. 5

PEAK PRESSURE, P_m, PLOTTED AGAINST DEPTH, D, FOR CONSTANT CHARGE-TO-GAUGE DISTANCE, 45.6 IN. ($W^{1/3}/R = 0.216$)

UERL WOODS HOLE, MASS.

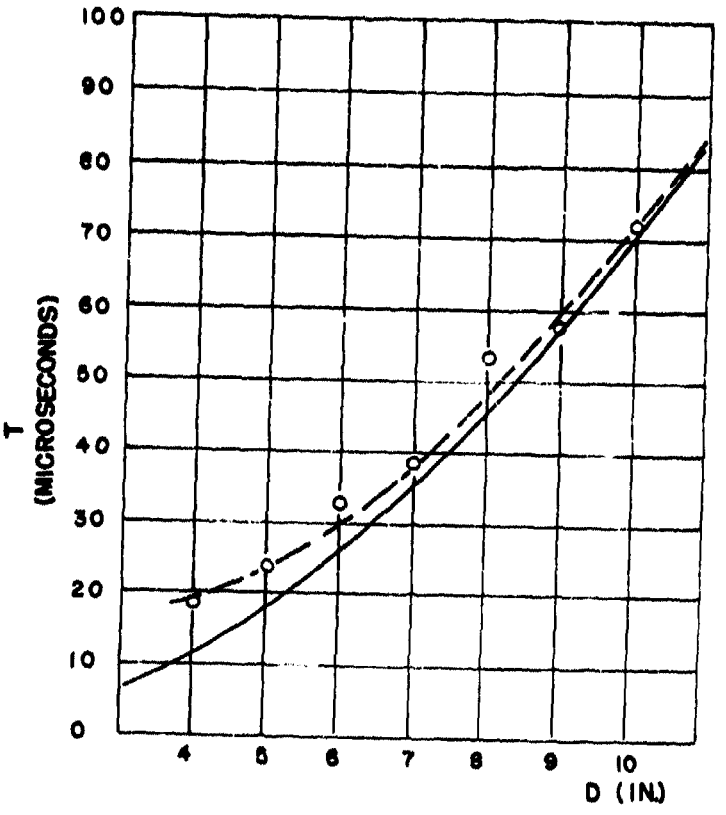


FIG. 6

DURATION, T, PLOTTED AGAINST DEPTH, D,
FOR
CONSTANT CHARGE-TO-GAUGE DISTANCE, 45.6 IN.
($W^{1/3}/R = 0.216$)

UERL WOODS HOLE, MASS.

B. Constant Charge Depth and Varying Gauge Depths. Because the deviation from predicted pressure and duration values is greatest at very shallow charge depths, there remains the possibility that part of the deviation, at least, is due to venting effects rather than to surface reflection phenomena. To shed some light on these effects, further shooting was done with the charge maintained 4 in. beneath the surface and with several different gauge positions. It would have been advisable to obtain records from gauges placed directly underneath the charge. The mechanical difficulties involved prevented such a rig at this time, and instead gauges were mounted off to one side of the charge and 29 in. below it, as shown in position B in Fig. 1B. Records thus obtained are compared, in Table III, with those from gauges at the 4 in. depth. As is noted in the figure the point of surface in evidence for that part of the reflected wave which strikes the deeper gauge is much closer to the charge than the similar point for the shallower gauge. Therefore, the angle of incidence and the pressure are both considerably higher than for the 4 in. gauge position.

In both cases the gauge pressures are lower than similitude values, but for the 33 in. gauge depth the measured duration is not significantly higher than the theoretically predicted value. This is particularly interesting in view of the fact that Table II indicates that, for changing angles and constant pressure, the duration starts to deviate from the theory at larger angles than does the pressure.

TABLE IV

COMPARISON OF RESULTS FOR GAUGE DEPTHS OF 4 AND 33 IN. WITH CHARGE DEPTH 4 IN., AND CHARGE-TO-GAUGE DISTANCE 45 IN. IN BOTH CASES

$W^{1/3}/R$ = 0.216 at gauge (similitude P_m = 4300 psi)

Gauge Depth D (in.)	α (°)	P_S (psi)	Average P_A (psi)	σ (%)	P_D (psi)	Ratio P_D/P_m	t (microsec)	Average T (microsec)	σ (%)	Ratio T/t
4	10.1	9,700	2820	18.4	3040	0.718	11.7	20.7	15.9	1.77
33	46.4	75,900	3150	9.4	3370	0.784	91.2	98.1	6.5	1.07

It may be noted that since the duration time of 90 microsec was ample, normal extrapolation techniques could be applied. Extrapolated peak pressure was 3300 psi, differing from derived peak pressure by only 1.2%, and thus affording a check on the procedure outlined in the analysis section. Shock-wave time constants could also be obtained from the extrapolation plots, and the average value obtained for this group of shots was 59.1 microseconds

with a standard deviation of 6.4 %. The time constant for the same charge in free water has been observed to be 65.6 microsec.[7] Typical pressure-time records are shown in Fig. 16.

C. Constant Charge and Gauge Depth and Varying $W^{1/3}/R$. Additional investigation into the nature of surface reflection phenomena from very shallow charges consisted of a series of shots made with both charge and gauge 4 in. beneath the surface but with charge-to-gauge distances changing from 60 in. to an effective 15 in., corresponding to a variation in $W^{1/3}/R$ at the gauge from 0.164 to 0.657. The 0.657 value was actually obtained with 500 gm at a 5 in. depth and 19 in. charge-to-gauge distance, these dimensions being obtained by appropriate use of scaling laws to obtain the desired angle of incidence and peak pressure at the incident point. Typical records for this shooting are shown in Fig. 17.

Results, as shown in Table V and Figs. 7 and 8, indicate that for high values of $W^{1/3}/R$ the measured duration approximates the theoretical value rather well, but for decreasing $W^{1/3}/R$ (and this involves a decreasing angle of incidence as well as a decreasing peak pressure) the measured duration becomes higher and higher compared with the acoustic value. Pressure deviates in much the same way from the similarity curve for free water, except that the deviation does not become as noticeable until $W^{1/3}/R$ drops to about 0.3. This is what might be expected from the results of Sec. A above, where, as the incidence becomes oblique the duration begins to deviate from acoustic theory, and only when the incidence becomes even more oblique does the pressure begin to deviate from free water similitude values.

VI. CONCLUSIONS

Several conclusions may be drawn from the above experimental measurements of shock-wave peak pressure and duration, as measured by a piezoelectric gauge at some point beneath the surface in the path of propagation of both the direct shock wave and the reflected negative wave.

(i) When the peak pressure at the point of surface incidence is low, 5000 psi or less, the shock-wave peak pressure conforms reasonably well to free water similarity law predictions, even for the smallest angles of incidence observed. The duration satisfactorily approximates the computed values obtained from the geometrical structure, assuming the shock waves to travel with the speed of sound.

(ii) For higher pressures, at the same angles of incidence, peak pressures are appreciably less than the similarity values and the difference increases with decreasing angles. Durations are larger than acoustic predictions, and the difference again increases for decreasing angle.

TABLE V

PRESSURE AND DURATION FOR VARYING $W^{1/3}/R$ FOR 250 GM PENTOLITE*

WITH CHARGE AND GAUGE 4 IN. BELOW SURFACE

α	P_S	$W^{1/3}/R$ at gauge	Average P_A		P_D	Ratio P_D/P_m	t	Average T		Ratio T/t
(°)	(psi)	($lb^{1/3}$/ft)	(psi)	σ (%)	(psi)		(microsec)	(microsec)	σ (%)	
28	27,500	0.657	14,500	12.6	15,500	0.896	43.4	44.4	9.6	1.07
15	16,500	0.328	5,860	7.4	6,260	0.895	17.5	24.3	13.2	1.39
10	9,700	0.216	2,920	9.5	3,120	0.726	11.7	17.1	7.4	1.46
7.6	6,900	0.164	1,880	9.6	2,010	0.674	8.8	14.8	6.2	1.70

* For $W^{1/3}/R = 0.657$, 500 gm charges were used and all distances were scaled accordingly.

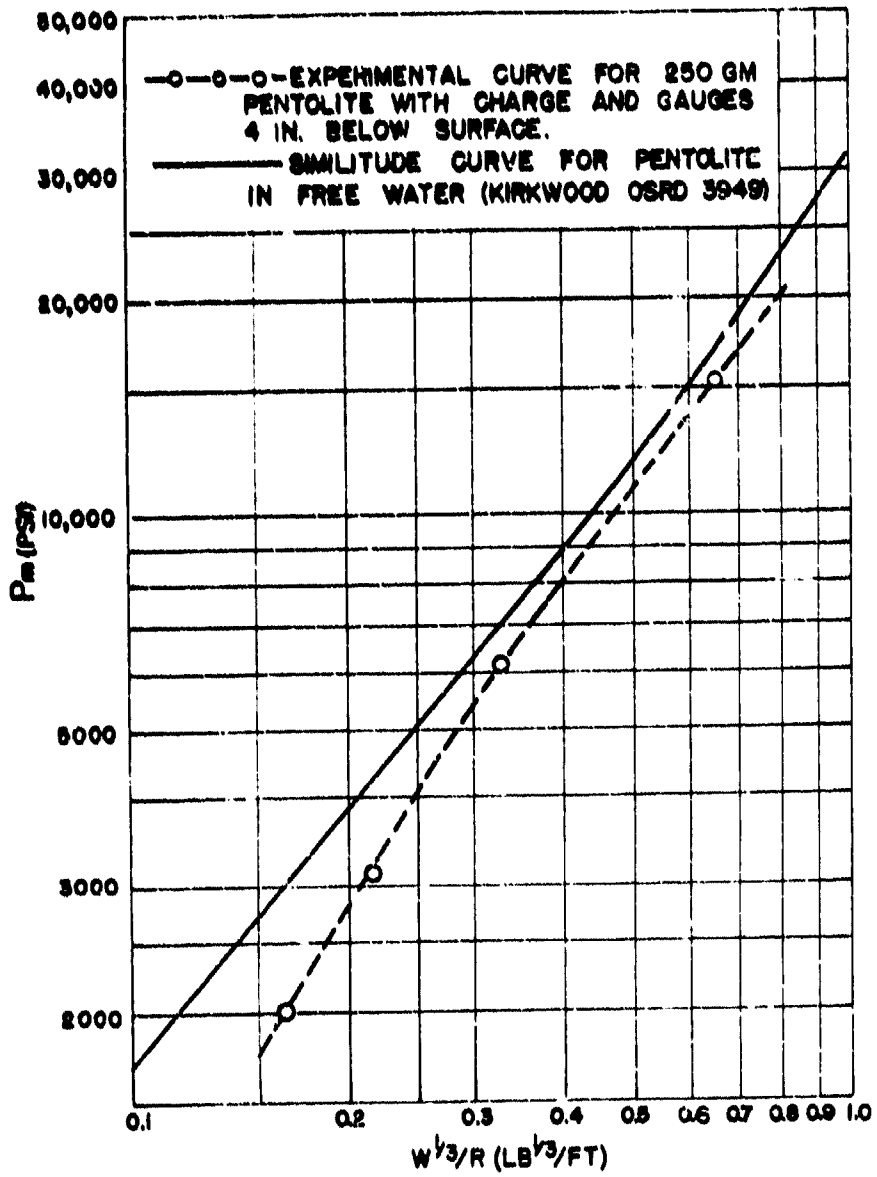


FIG. 7

PEAK PRESSURE FOR VARYING $W^{1/3}/R$ WITH CHARGE AND GAUGES CLOSE TO THE SURFACE

UERL WOODS HOLE, MASS.

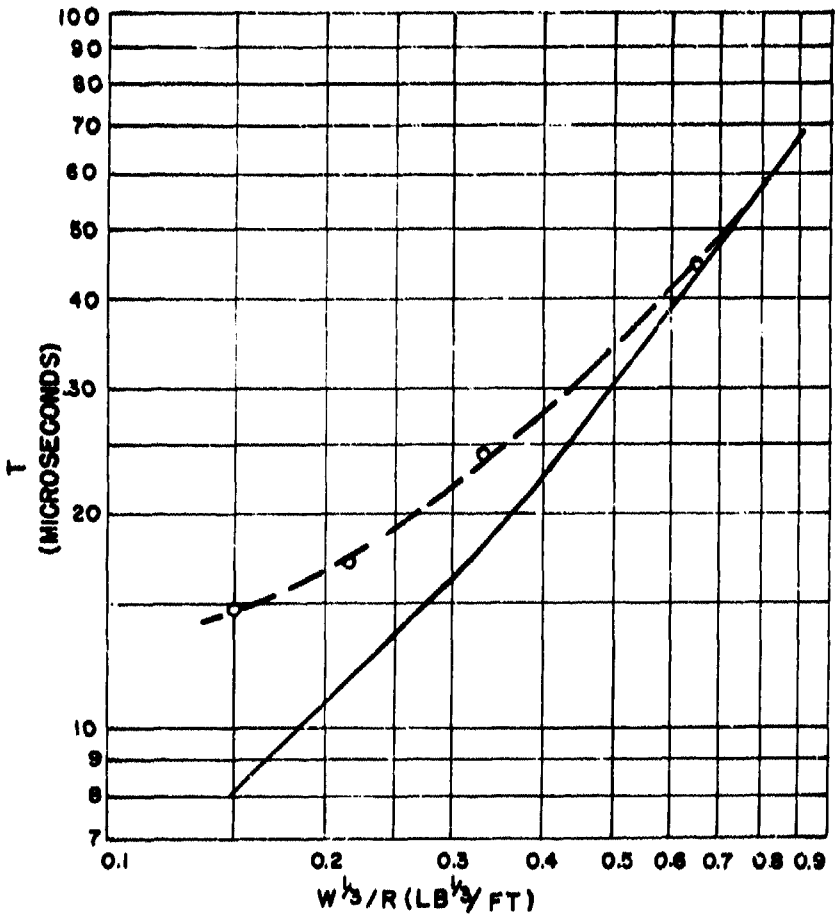


FIG. 8
DURATION, T, FOR VARYING $W^{1/3}/R$
WITH
CHARGE AND GAUGES 4 IN. BELOW SURFACE
UERL WOODS HOLE, MASS.

(iii) As the angle is decreased, durations first begin to deviate from the theoretical predictions, and only when the angle is further decreased does pressure deviation become significant.

(iv) If the charge is very close to the surface, there is a diminution of peak pressure even when the rarefaction cut-off is steep. This may possibly indicate that some of the pressure effects might be due to venting of the gaseous explosion products.

Although there is no theoretical formulation which covers these conclusions at this time, the general manner in which deviations from ordinary acoustic theory occur is in agreement with the description of finite amplitude effects presented by Cole[5], and the deviations are in the direction that Cole indicates.

Throughout the results presented above, standard deviations appear which are higher than might have been expected. This would seem to indicate that the methods of measuring depths were not so accurate as was believed, or simply that the number of shots was so limited that significant results could not be expected. In any case, the need for further investigation is apparent. For example, additional work may enable one to define the boundaries of the non-acoustic region, and to describe the nature of the shock wave emitted by shallow explosions.

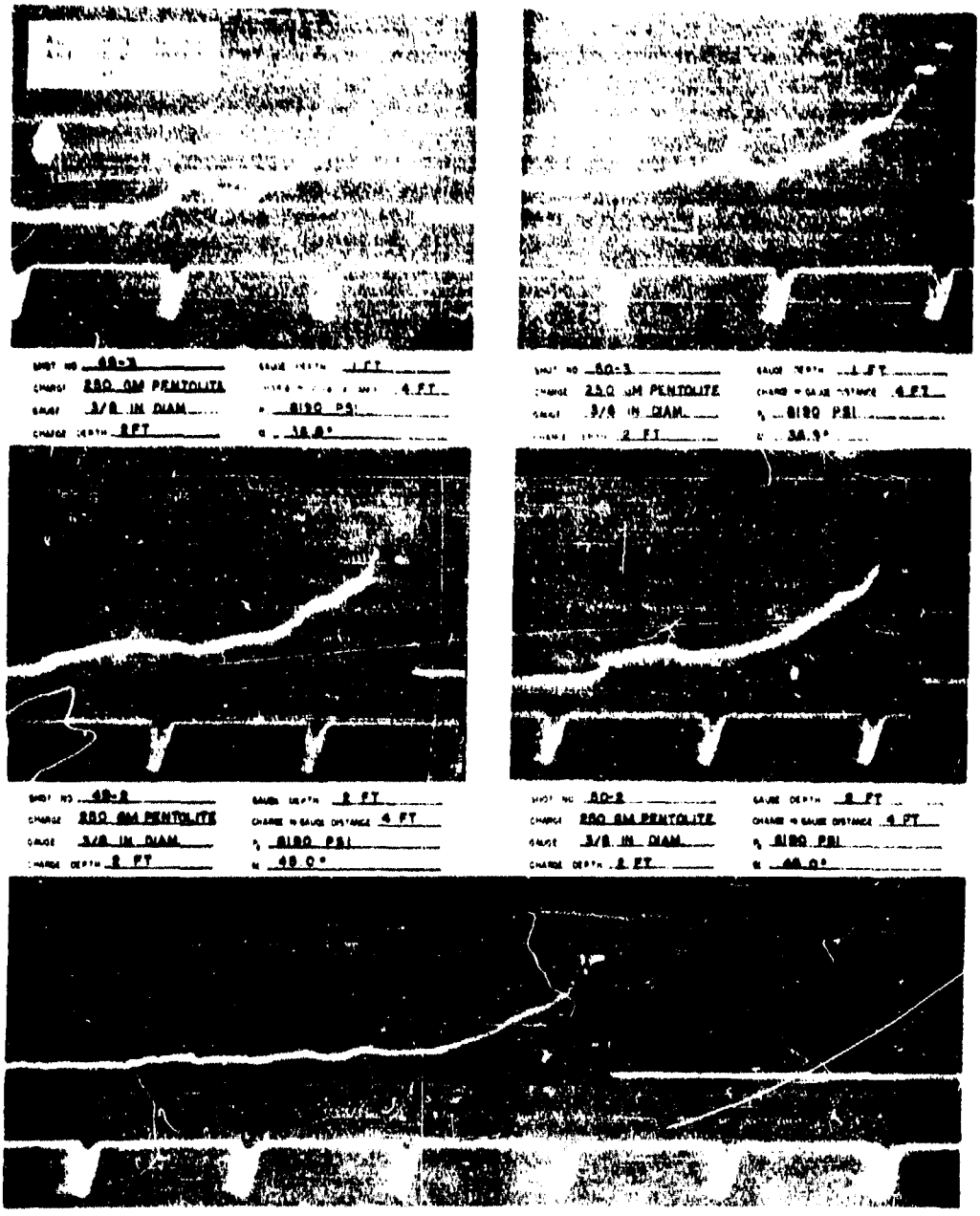


FIG 9

PIEZOELECTRIC GAUGE RECORDS FOR LOW PRESSURE LEVELS

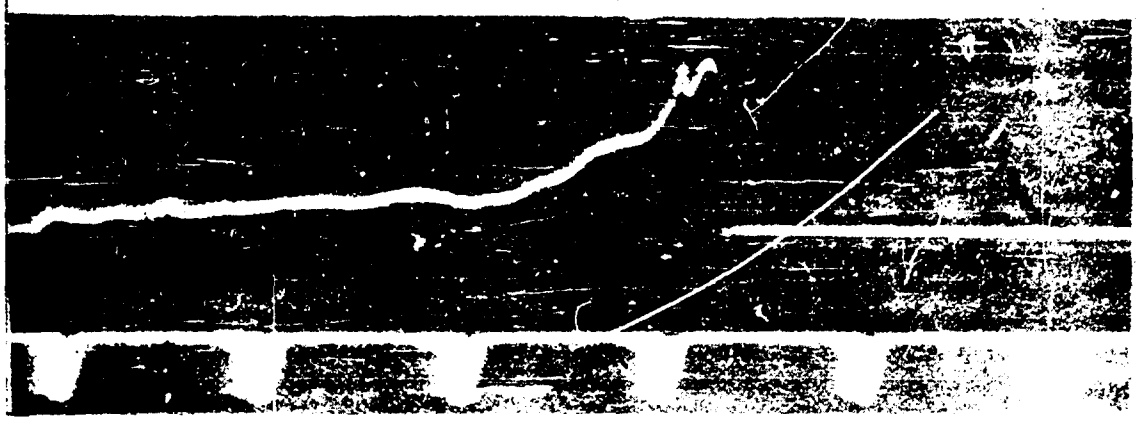
I W[illegible] AT GAUGE [illegible]



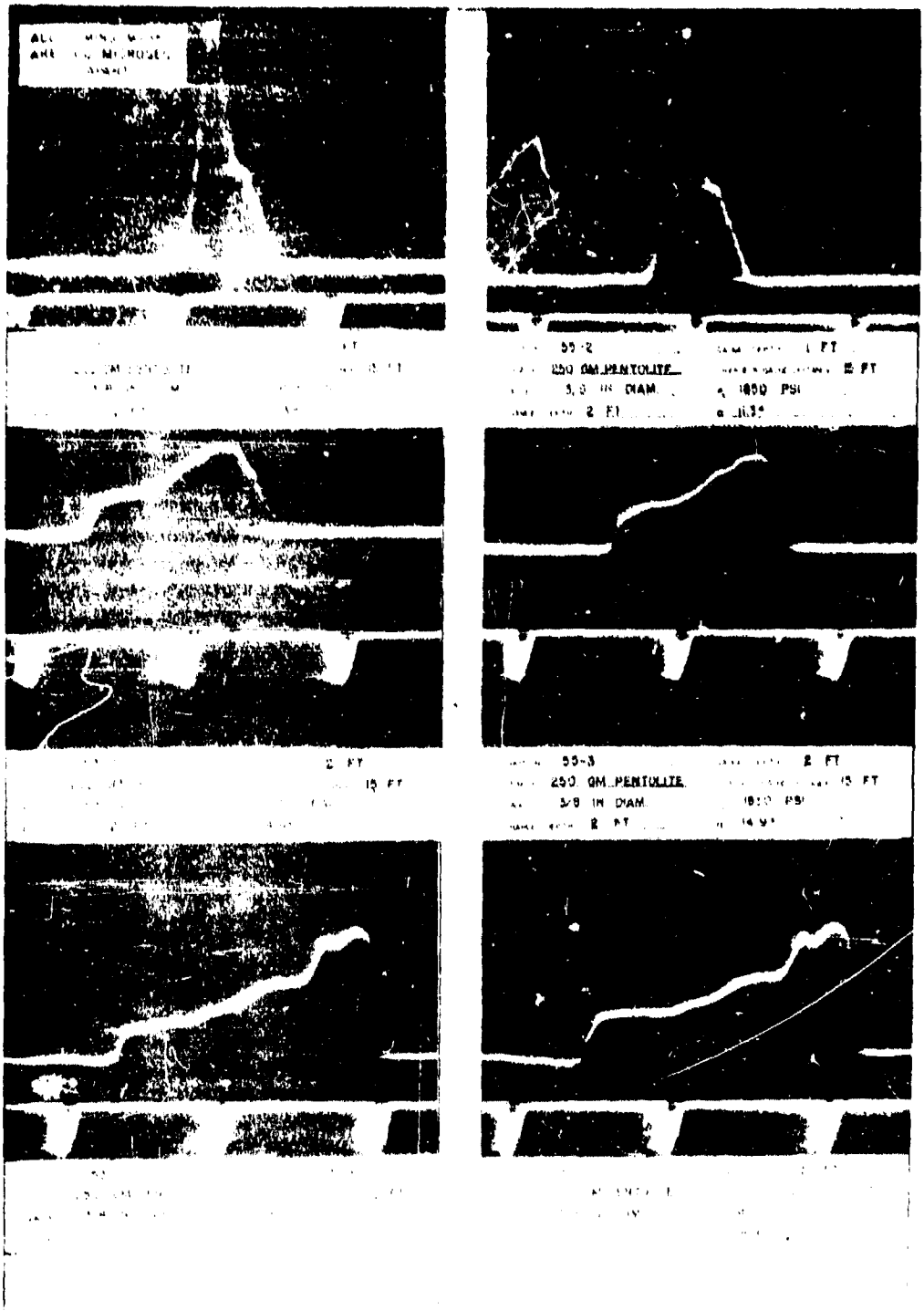
52-2 1 FT
250 GM PENTOLITE
3/8 IN DIAM 4370 PSI
23.2°

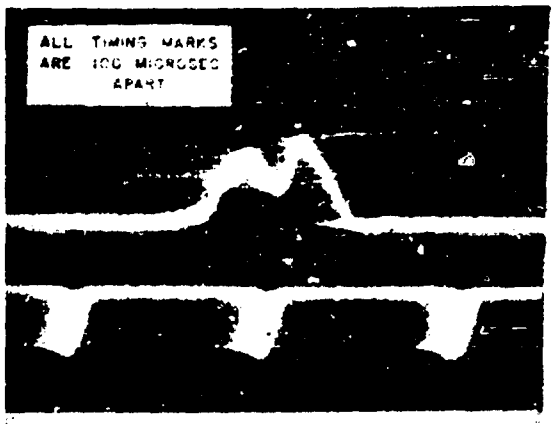


51-3 2 FT
250 GM PENTOLITE
3/8 IN DIAM 4370 PSI
2 FT



Best Available Copy





SHOT NO. 57-2 GAUGE DEPTH 1 FT
CHARGE 250 GM PENTOLITE CHARGE TO GAUGE DISTANCE 23 FT
GAUGE 3/8 IN DIAM. P 1150 PSI
CHARGE DEPTH 2 FT α 7.4°



SHOT NO. 61-1 GAUGE DEPTH 1 FT
CHARGE 250 GM PENTOLITE CHARGE TO GAUGE DISTANCE 23 FT
GAUGE 3/8 IN DIAM. P 1150 PSI
CHARGE DEPTH 2 FT α 7.4°

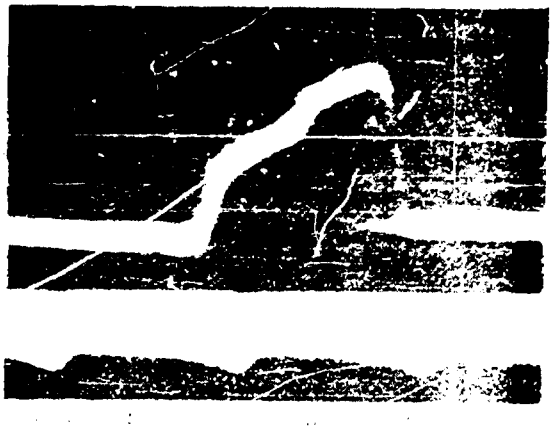


SHOT NO. 57-3 GAUGE DEPTH 2 FT
CHARGE 250 GM PENTOLITE CHARGE TO GAUGE DISTANCE 23 FT
GAUGE 3/8 IN DIAM. P 1160 PSI
CHARGE DEPTH 2 FT α 9.9°



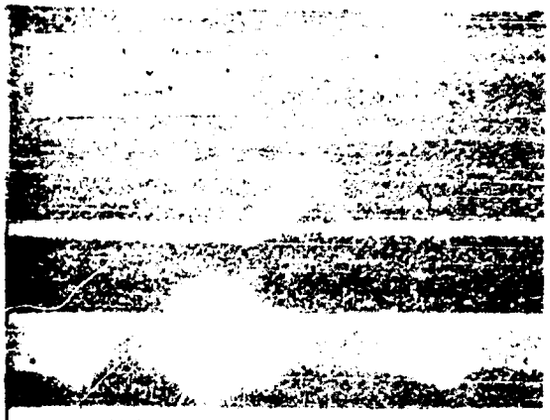
SHOT NO. 61-2 GAUGE DEPTH 2 FT
CHARGE 250 GM PENTOLITE CHARGE TO GAUGE DISTANCE [illegible]
GAUGE 3/8 IN DIAM. P 1150 PSI
CHARGE DEPTH 2 FT α 9.9°



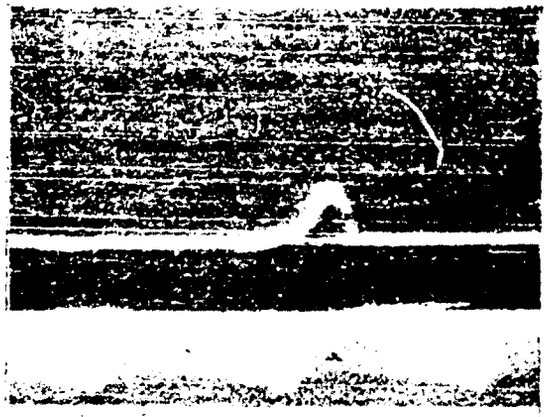


5'
250 GM PENTOLITE

Best Available Cop



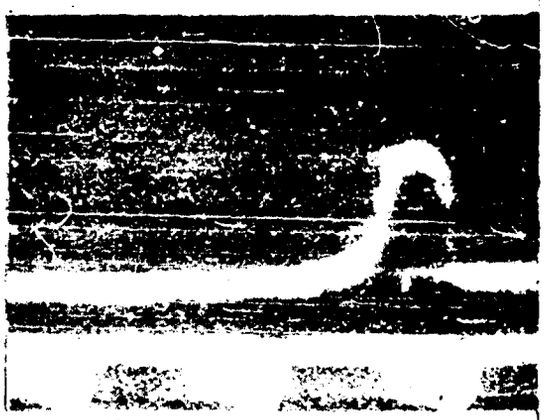
95-1 1 FT
250 GM PENTOLITE 45 FT
3/8 IN DIAM. 535 PSI
12 FT 3.9*



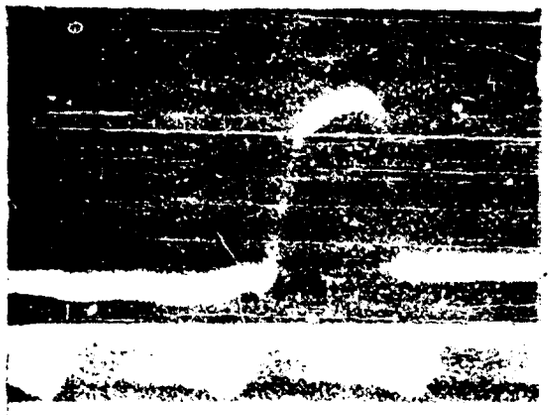
FT
250 GM PENTOLITE 45 FT
3/8 IN DIAM. 535 PSI
2 FT

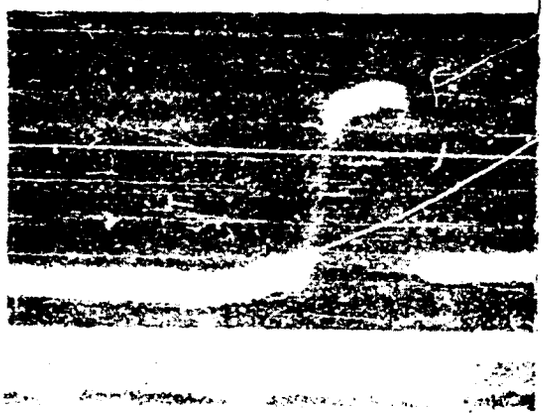


95-2 2 FT
250 GM PENTOLITE 45 FT
3/8 IN DIAM 535 PSI
6 FT 5.1*

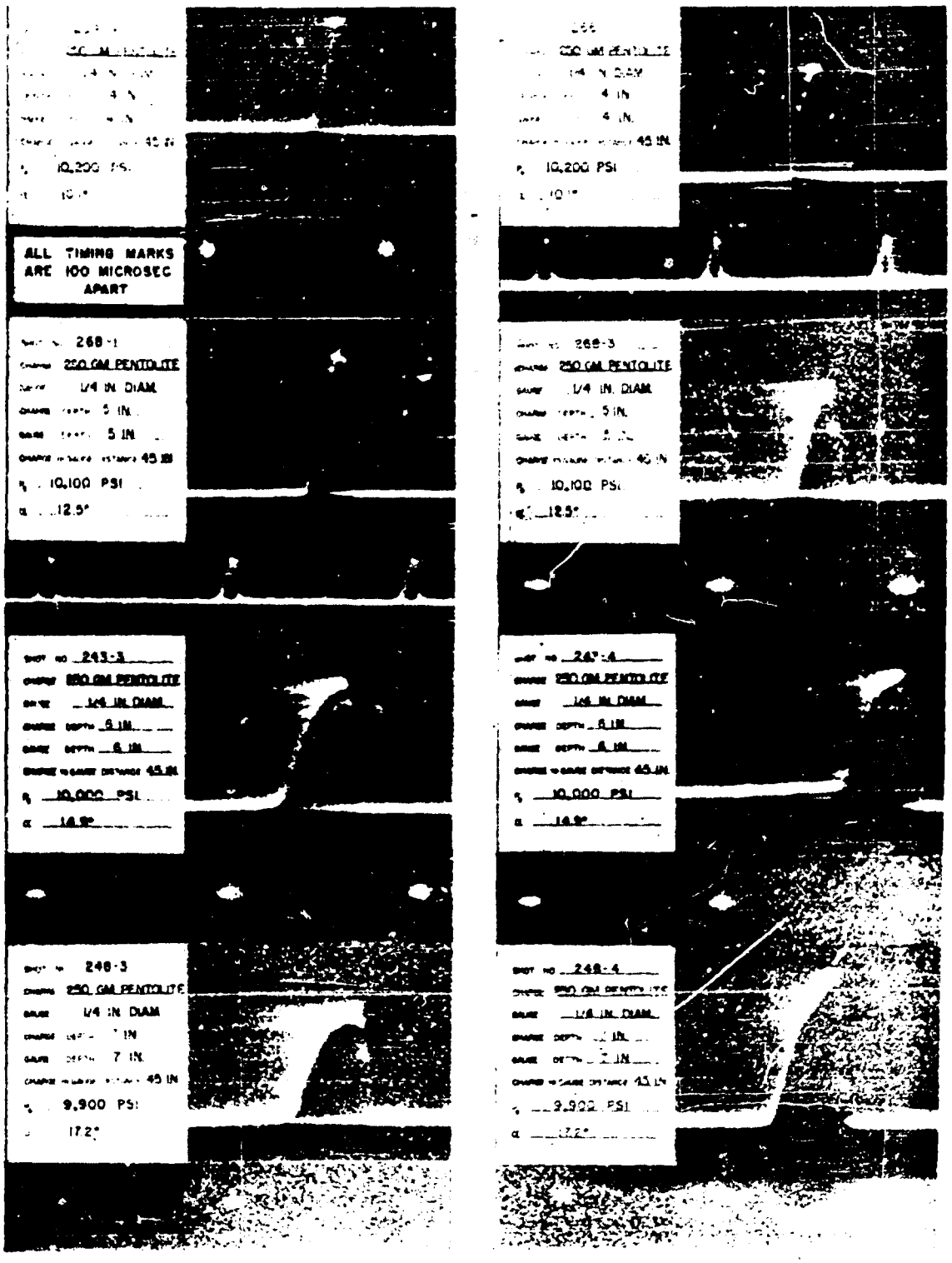


2 FT
45 FT





Best Available Copy



PIEZOE[illegible] SURFACE REFLECTION PHENOMENA
[illegible] AND A CONSTANT [illegible]
[illegible] 216)

Best Available Copy

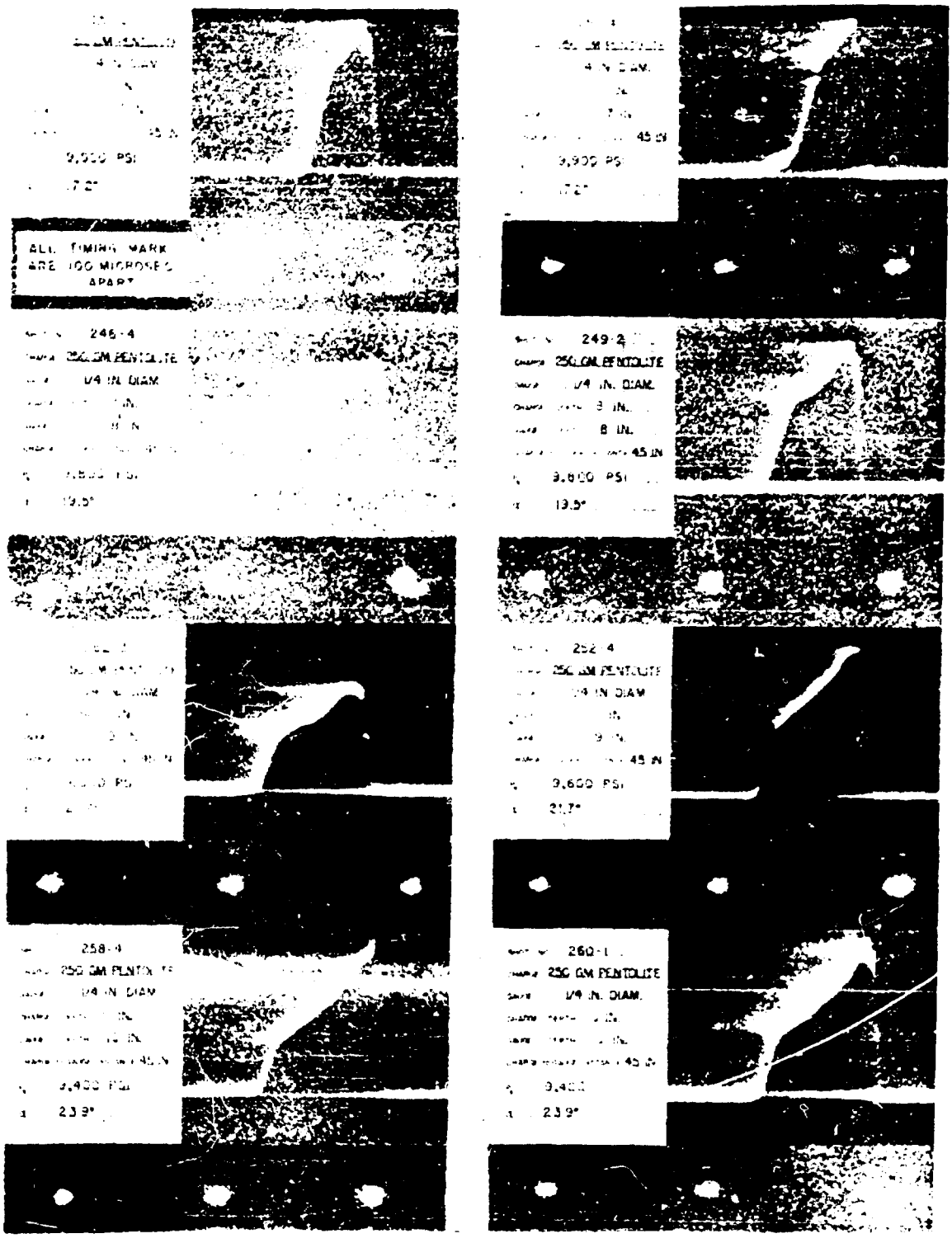
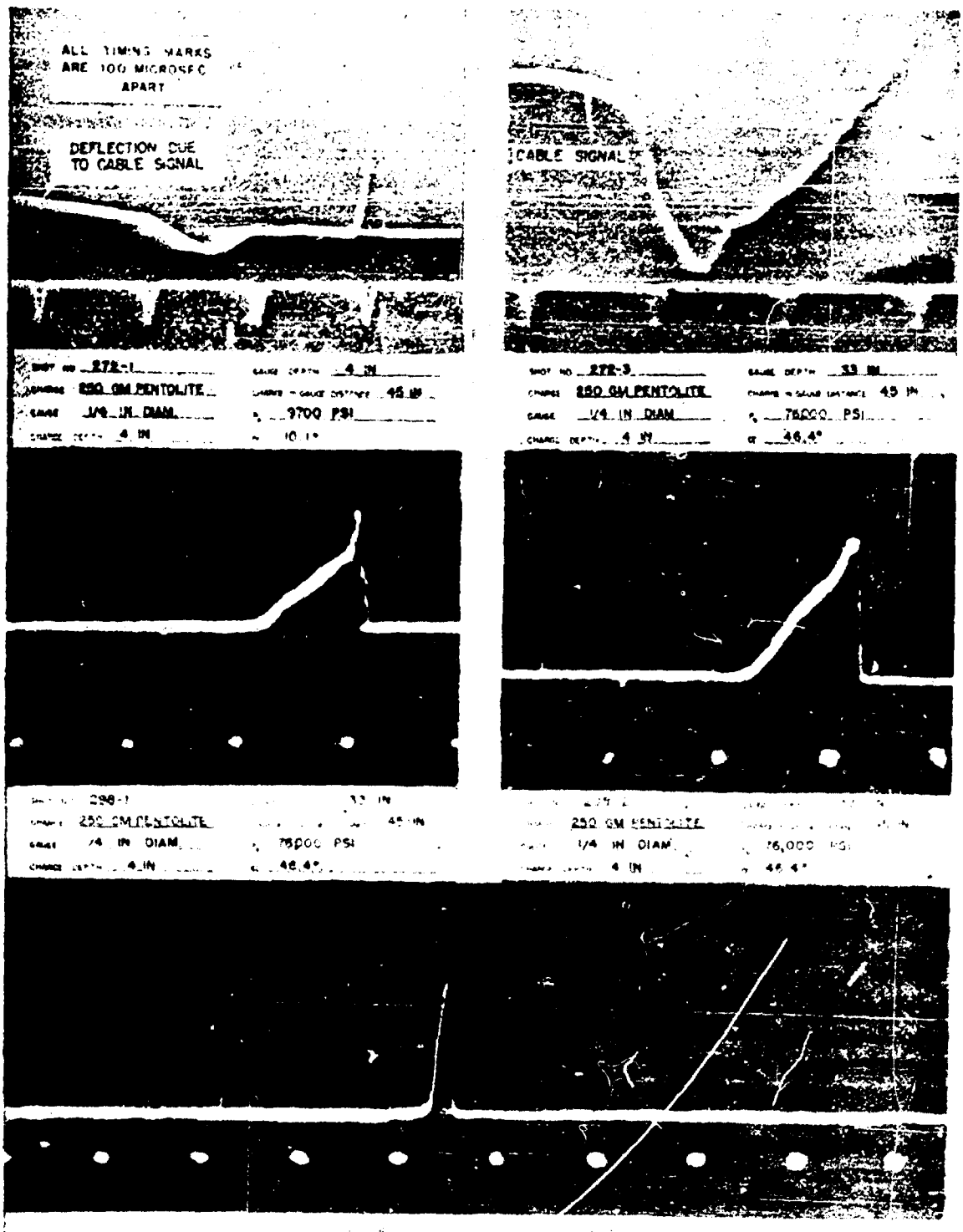


FIG. 15

Best Available Copy



Best Available Copy

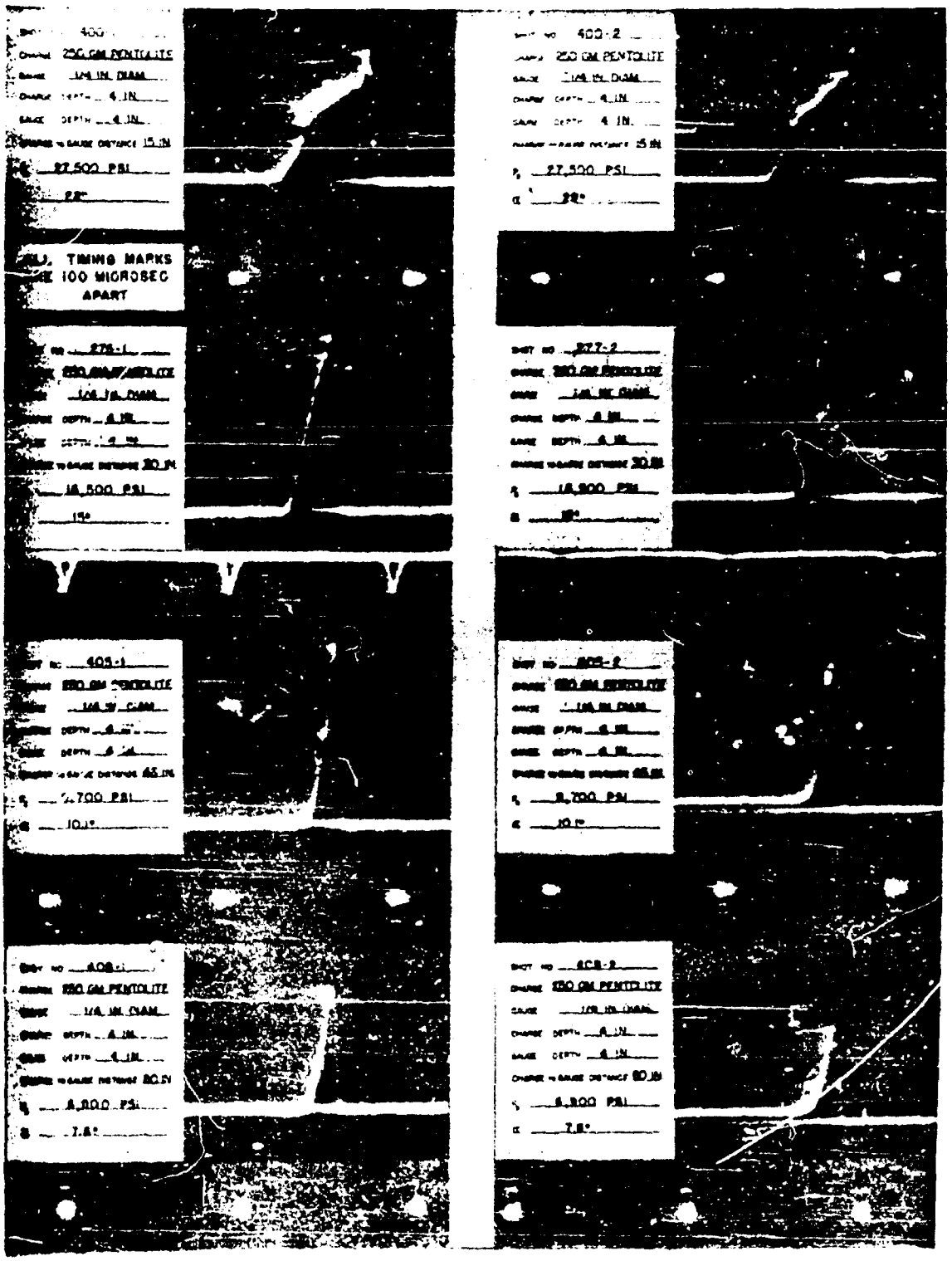


FIG. 17

PIEZO... SHOWING SURFACE REFLECTION ... MARK
FOR A CHARGE ... DEPTH OF 4 IN AND VARYING CHARGE ... GAUGE
VALUES OF ... ARE GIVEN TOP TO BOTTOM, RESPECTIVELY
RECORDS 4 ... ARE FULLY OBTAINED WITH ... ARE SCALED ...

Best Available Copy

LIST OF REFERENCES

1. NavOrd 104-46.

2. Electrical Instruments for Study of Underwater Explosions and Other Transient Phenomena, R.H. Cole, D. Stacey, and R.M. Brown, OSRD Report No. 6238, NDRC A-360, November 1945.

3. OSRD Report No. 624C, NDRC No. A-362.

4. Oblique Reflections of Shocks. J. von Neumann, Explosives Research Report No. 12 (Re2c), October 1943.

5. Underwater Explosives and Explosions, R.H. Cole, Princeton University Press (in press).

6. Measurement of Underwater Explosions Near the Surface and Bottom of the Ocean, J.S. Coles, C.R. Niffenegger, E.A. Christian, J.P. Slifko, M.R. Reynolds, and P.C. Cross, NavOrd Report No. 105-46.

7. UE-32, OSRD Report No. 4874.

8. OSRD Report No. 3949.

9. A general survey of work on this problem appears in "Aerodynamic Theory", W.F. Durant. Guggenheim Fund, 1934, Vol. III, Sec. H, "The Mechanics of Compressible Fluids".

Distribution List

Chief of the Bureau of Ordnance (Ad6c) (20)
Chief of Naval Research (2)
Chief, Bureau of Aeronautics (2)
Chief, Bureau of Ships (2)
CO, Naval Ordnance Test Station, Inyokern, Calif. (4)
CO, Naval Proving Ground, Dahlgren, Va. (2)
CO, Norfolk Naval Shipyard, Attention: Code 227 (3)
OinC, Naval Ordnance Laboratory, Naval Gun Factory, Washington, D.C. (5)
OinC, Naval Powder Factory, Indian Head, Maryland (2)
Director, David Taylor Model Basin, Carderock, Maryland (3)
Director, Naval Research Laboratory, Washington 20, D.C. (2)
ChOrd, War Department, Washington, D.C. (4)
OinC, Ballistic Research Laboratory, Aberdeen Proving Ground, Maryland (2)
CO, Picatinny Arsenal, Dover, New Jersey (2)
Director, Woods Hole Oceanographic Institution, Woods Hole, Mass. (10)
British Commonwealth Scientific Office, 1785 Massachusetts Ave., N.W., Washington, D.C. (5)
British Admiralty Delegation, 1025 Vermont Ave., Washington, D.C. (5)
Director, Institute for Mathematics and Mechanics, New York University, 45 Fourth Ave., New York 3, N.Y. (3)
Chief of the Bureau of Ordnance (Re2c) (5)

BOUNDARY OF DISTURBANCE FOR NON-LINEAR REFLECTION OF UNDERWATER SHOCK WAVES AT A FREE SURFACE

Alfred H. Keil
Underwater Explosions Research Unit
Norfolk Naval Shipyard

American Contribution

1948

ABSTRACT

The surface reflection of underwater shockwaves is a problem of non-linear mechanics of compressible fluids. The fact that the speed of sound behind the shock front is larger than the propagation velocity of the shock front is the reason that for certain conditions of reflection, that is for certain angles of incidence, the attenuation of the reflected (rarefraction) wave propagates along the initial wave front, thus producing a range of distortion of the initial wave.

It is shown that this range of distortion exists for any charge weight and charge depth, and that the geometrical conditions of this range are subject to the well known law of similitude of underwater explosions.

The critical distance from charge to the point of the surface where this disturbance starts to travel along the initial wavefront is derived as function of the charge depth, expressing all distances in charge radii, that is in a non-dimensional scale. The boundary between this surface disturbance and the undistorted propagation is calculated for a series of charge depths and a general rule is formulated which readily permits the derivation of this boundary for any charge depth.

The comparison between this theory and the small number of experimental results evince agreement between theory and experiment.

The investigations of the surface reflection for an underwater shockwave and of the condition where the Mayer corner solution fails to describe the reflection are in certain ways similar to the investigations of the Mach effect. There the conditions, under which the reflection of a shockwave by a rigid surface can no longer be described by the two shock conditions of incident and reflected wave, have to be determined. The mathematical relation between the critical angles of incidence for both cases is derived in the last section.

BOUNDARY OF DISTURBANCE FOR NON-LINEAR REFLECTION OF UNDERWATER SHOCKWAVES AT A FREE SURFACE

CONTENTS

Section 1. Introduction

2. Basic theoretical relations for shockwaves in water

3. Experimental pressure distance relations for explosion shockwaves in water

4. The critical angle

5. The critical distance

6. The range of peak pressure distortion

7. Comparison with experimental results

8. The relation to the critical angle for reflection at a rigid surface

REFERENCES

1. Oblique Reflection of Shocks; by John von Neumann, Explosive Research Report No. 12, BuOrd, 1943.

2. Zustandsgleichung fuer Wasser bei sehr hohen Drucken und die Geschwindigkeit einer Stosswelle in Wasser (Equation of state for water at very high pressures and velocity of a shockwave in water); by G. Burkhardt, Ballistisches Institut, Berlin-Gatow, 1942.

3. Temperature-Pressure-Volume and Phase Relations for Water; by Roy W. Goranson, Papers from the Geophysical Laboratory, Carnegie Institute of Washington, No. 1057.

4. Measurements of Shockwaves in Water with the High Speed Spark Camera; by Dr. A. Keil, TMB Translation 213, September 1947.

5. Beitraege zur Theorie der Detonation (Contribution to the Theory of Detonation); by W. Doering and G. Burkhardt, Ballistisches Institut, Berlin-Gatow, 1944. (Technical Intelligence Center Report O-846-47.)

6. Energy Partition in Underwater Explosion Phenomena; by A.B. Arons and D.R. Yennie, NavOrd Report 406, October 1947.

7. (a) The Determination of Peak Pressure of an Underwater Explosion from a Study of the Initial Dome Velocity; by D.A. Wilson, Barbara A. Cotter, and R.S. Price, Navord Report 15-47, May 1947.

   (b) "Multiple Charge Effect" from Two 500 GM Pentolite Charges Underwater; by E.A. Christian, J.P. Slifko, U.R. Niffenegger, A.H. Carter, P.M. Fye, P.C. Cross, J.S. Coles, M.R. Reynolds, M. Gifford; NavOrd Report 405, 5 Dec. 1947.

8. "The Mechanics of Compressible Fluids"; by G.I. Taylor and I.W. MacColl, Division H in Volume III of W.F. Durand's "Aerodynamic Theory", Guggenheim Fund.

9. Calculations by Dr. Penney, information furnished the author by Bureau of Ships, Code 423.

10. The Reflection of Small Charge Shockwaves from a Free Surface; by G.M. Sokol, NavOrd Report 410.

11. Measurements of Pressure Distribution around Cylindrical Charges in Water; by Dr. A.H. Keil, Underwater Explosions Research Unit, Norfolk Naval Shipyard, Report 1-48.

NOTATIONS

v = specific volume

ρ = $\frac{1}{v}$ = density

t = temperature

τ = temperature difference, passing the shockfront

p = pressure

π = pressure difference, passing the shockfront

c_p = specific heat at constant pressure

α = $\frac{\partial v}{\partial \tau}$

k = $-\frac{\partial v}{\partial \pi}$

β = $\frac{\partial^2 v}{\partial \pi \partial \tau}$

ℓ = $-\frac{1}{2}\frac{\partial^2 v}{\partial \pi^2} - \frac{1}{2}\frac{\partial k}{\partial \pi}$

γ = $\frac{1}{2}\frac{\partial^2 v}{\partial \tau^2}$

μ = $-\frac{\ell}{2k}$

D = velocity of shockwave with amplitude π

a_0 = speed of sound in medium in front of shockwave

a = speed of sound in medium behind shockfront

u = speed of flow of medium behind shockfront

r	=	distance from charge
r_o	=	charge radius
W	=	charge weight
π_o	=	see Formula 9
$\bar{r}$	=	distance in charge radii
Θ	=	angle between wavefront and normal to the surface
Θ_{crit}	=	critical angle
r_{crit}	=	critical distance
$\bar{r}_{crit}$	=	critical distance in charge radii
d	=	charge depth
$\bar{d}$	=	charge depth in charge radii
y	=	depth of boundary of disturbance in a distance r from charge
$\bar{y}$	=	y, expressed in charge radii

I. INTRODUCTION

The reflection phenomena are complicated problems in acoustics or more general in the theory of waves. The usual solution for the linearized equations and infinitely extended plane waves being reflected by an infinite baffle is simple and well known. However, the exact solution of the reflection of spherical acoustical waves by the plane boundary of two materials requires a complicated mathematical investigation.

The situation is more complicated for waves of finite amplitudes and shockwaves owing to the fact that the hydrodynamic equation can no longer be linearized. Exact solutions can be derived for the free propagation of plane shockwaves. The waves of practical interest, however, are spherical shockwaves; they cannot be treated without simplifying assumptions (Bethe, Kirkwood, Brinkley).

The exact treatment of reflection phenomena of plane shockwaves presents considerable difficulities. The case of plane shockwaves, reflected by a rigid surface, has been investigated by J. von Neumann (Ref. 1) and some calculations concerning the reflection of plane shockwaves from a free water surface have been carried out by Dr. Penney.

A partial but interesting solution for the reflection of the spherical shockwave at a free water surface is given in the following. Only shockwaves produced by an underwater explosion

are considered, using the reliable experimental results obtained for the pressure distance decay of these waves (Section III) and the available theoretical investigation for the relation between velocity and amplitude for shockwaves in water (Section II).

II. BASIC THEORETICAL RELATIONS FOR SHOCKWAVES IN WATER

Prior to formulating any discussion concerning shockwaves in water, the relation between pressure, temperature, and specific volume must be known. This relation is usually described by the equation of state which, in the case of water, is difficult to derive. Usually an approximate equation of state is applied, such as the one given by J. von Neumann in Ref. 1. For extremely high pressures an equation of state was derived theoretically for water by G. Burkhardt (Ref. 2) and correlated to the measurements of Bridgman. However, it is often possible to use initially the experimental data as presented, for instance, in Ref. 3 and derive the relation mentioned above.

In Ref. 4 the following equation of state is used to derive the speed D of a shockwave in water:

$$v = v_0(1 + \alpha t - k\pi + \beta\pi\tau - l\pi^2 + \gamma\tau^2) \qquad (1)$$

The values for α, k, β, l, and γ are given in Ref. 4 and have been derived from the original measurements of Bridgman. π is the difference between the pressure in the medium behind and in front of the shockwave, τ the corresponding difference in temperature. It was found

$$D = a_0\left(1 - \frac{l}{2k}\pi\right) = \alpha_0(1 + \mu\pi) \qquad (2)$$

with a_0 as speed of sound in the undisturbed medium and

$$\mu = -\frac{\ell}{2k} - \frac{1}{4k}\frac{\partial k}{\partial \pi} \sim 8.75 \times 10^{-5}\ at^{-1} \qquad (3)$$

In Ref. 4 a numerical value of 1.1×10^{-4} at $^{-1}$ was given for μ using earlier measurements only.

In addition to D, the value for speed of sound in the medium behind the shockwave is needed. It can be derived in the following way:

The temperature rise behind the shockwave front (see Ref. 4, page 9) can be derived

$$\tau = \frac{\alpha T_0 v_0}{c_p}\,\pi$$

and therefore the medium behind the first shockwave can be described by the equation of state:

$$v = v_0\left[1 + \left(\frac{\alpha^2 T_0 v_0}{c_p} - k\right)\pi + \left(\frac{\alpha\beta T_0 v_0}{c_p} - \ell\right)\pi^2\right]$$

Since $a^2 = v^2 / \frac{\partial v}{\partial p}$, there is

$$\frac{a^2}{a_0^2} = \frac{v^2}{v_0^2}\,\frac{1 - \frac{\alpha^2 T_0 v_0}{k c_p}}{1 - \frac{\alpha^2 T_0 v_0}{k c_p} - 2\left(\frac{\alpha\beta T_0 v_0}{k c_p} - \frac{\ell}{k}\right)\pi}$$

and with the above mentioned relation between v and v_0:

$$a = a_0\left\{1 + (2\mu - k)\pi\right\} \qquad (4)$$

The speed of flow behind the shockwave with an amplitude π can be found easily with the relation $\pi = \rho_0 a_0 u$;

$$u - \frac{\pi}{\rho_0 a_0} - \pi a_0 \left(k - \frac{\alpha^2 T_0 v_0}{c_p}\right) \simeq \pi a_0 k \qquad (5)$$

It further is of general interest to know the speed of a shockwave propagating in the medium behind the primary shock. Designating the data behind the primary wave with a_1, α_1, etc., and those behind the second wave with a_2, α_2, etc., the velocity D^1 of the second wave can be derived:

$$D^1 = a_1 (1 + \mu_1 \pi^1)$$

with π^1 as pressure difference between behind and in front of the second wave.

Therefore

$$D^1 = a_0 \{ 1 + (2\alpha - k)\pi \} \{ 1 + (\mu + \frac{\partial \mu}{\partial \pi} \pi) \pi' \}$$

because $\mu_1 = \mu + \frac{\partial \mu}{\partial \pi} \pi$. Neglecting terms $\pi \pi^1$ we get:

$$D^1 = a_0 \{ 1 + (2\mu - k)\pi + \mu \pi' \} \qquad (6)$$

and for $\pi = \pi^1$

$$D^1 = a_0 (1 + (3\mu - k) \pi) \qquad (7)$$

Attention is called to the fact that D^1 and a are speeds relative to the medium behind the first shockwave. Since this medium flows with a velocity u these velocities related to the medium in front of the first shockwave are obtained by vectorially adding u to D^1 and a.

The approximations used above are only correct for "small compressions", that means for pressures $\tilde{\pi} \leqq$ 500 at. as can be derived from the experimental data. But it will be seen that these relations are useful for handling the problems which shall be investigated.

For higher pressures (500 at. $< \tilde{\pi}$) the calculations are more difficult. Based on the theoretical equation of state derived in Ref. 2 the relation between shockwave velocity D or flow velocity u behind the shockfront and the amplitude $\tilde{\pi}$ of the shockwave were calculated by G. Burkhardt (Refs. 2 and 5) and later by W. Doering (Ref. 5). These relations are repoated in the following table:

$\tilde{\pi}$ at	T	v	D/a_o	u/a_o	$-\frac{\partial v}{\partial \tilde{\pi}}$ bar$^{-1} \times 10^5$	a/a_o
0	15	1.0007	1.000	0	4.54	1.000
1000	16.6	0.962	1.072	0.042	3.455	1.102
2000	19	0.9324	1.145	0.078	2.763	1.195
3000	22.1	0.9091	1.206	0.110	2.23	1.286
5000	29	0.8735	1.322	0.168	1.69	1.430
7500	39	0.8403	1.447	0.230	1.255	1.597
10000	51	0.8183	1.564	0.285	0.97	1.769

TABLE 1: Amplitude and propagation velocity of a shockwave in water, as well as temperature T, specific volume v, velocity of flow u, compressibility of water and sound velocity a of medium behind the shockfront.

In addition to these data, Table 1 gives the compressibility of the medium behind the shockwave. This compressibility was derived from the tables presented in Ref. 3 for the different conditions given by τ, T_0 and v in each line of Table 1. The last column of Table 1 gives the value of speed of sound in the medium behind the shockwave; this velocity was calculated by using the derived data for $\frac{\partial v}{\partial p}$ and v for each shock pressure.

All these data for D, a, and u are plotted in Fig. 1 as functions of the amplitude of the shockwave. The approximation formulas (2), (4), and (5) are plotted as broken lines. This diagram proves that the agreement between the approximations and the exact data is good for pressures up to 500 at.

III. EXPERIMENTAL PRESSURE DISTANCE RELATION FOR EXPLOSION SHOCKWAVES IN WATER

The whole problem investigated here concerns underwater explosion shockwaves and their reflection by a free water surface. For that reason it is necessary to go into some details of these special shockwaves. The theoretical treatment of spherical shockwaves is complicated and only approximate solutions exist. However, a great number of experimental investigations have been carried out to measure the shockwave parameters as a function of charge weight and distance from the charge. An important result of both investigations is the fact that a law of similitude exists which permits the pressure-distance relation to be plotted for any charge weight in a non dimensional scale, as for instance in expressing the distance from the charge in charge radii.

The results for pentolite have been summarized in Ref. 7. The experimental results derived from early piezo-electric measurements in the range from 1000 to 40,000 psi were described by the formula

$$P = 22500 \left(\frac{W^{\frac{1}{3}}}{r}\right)^{1.13} \qquad \begin{array}{l} W \ldots lbs \\ r \ldots feet \\ P \ldots psi \end{array} \qquad (8)$$

This formula is plotted in Fig. 2.

In addition, the results of the spray dome method and of newer piezo-electric measurements for Pentolite (Ref. 7) are plotted in Fig. 2. The high pressure range had already been

measured using the spark camera (Ref. 4) and the results of this investigation are also presented in Fig. 2.

All results are in good agreement. The solid line drawn in Fig. 2 therefore is considered as a pretty reliable overall peak pressure-distance relation for the underwater shockwave of pentolite.

The results for TNT, which were summarized in Ref. 6, Diagram 4, are replotted in Fig. 2 also. They show that the estimation of the high pressure part by A.B. Arons and D.R. Yennie agrees well with the obtained overall behavior of this relation for pentolite. This curve therefore will be used to derive results for TNT.

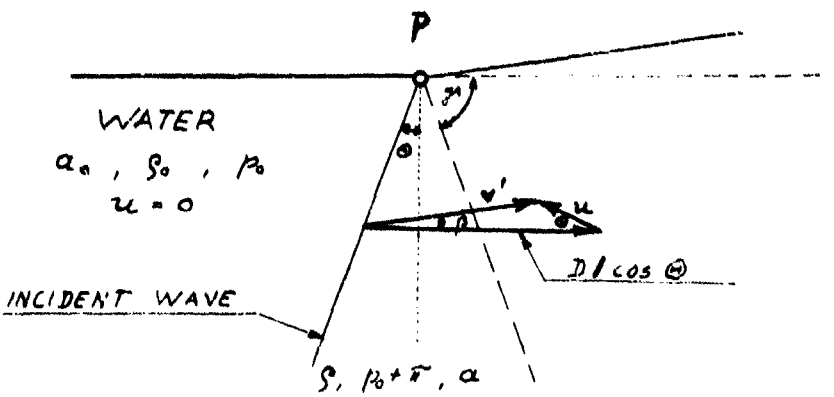
The pressure range from 5000-20000 psi for pentolite is presented by formula (8) and a similar formula exists for TNT. However, because of the curvature of the pressure distance curve, the experimental results in the range of distances corresponding to the approximation formulas (2) and (4) can be described with adequate accuracy by the simple formulas

$$\text{Pentolite} \qquad \bar{\pi} = \bar{\pi}_0 \frac{r_0}{r} = \frac{\bar{r}_0}{\bar{r}} = \frac{160\,000}{\bar{r}} \text{ (psi)} \qquad (9a)$$

$$\text{TNT} \qquad \tilde{\pi} = \tilde{\pi}_0 \frac{r_0}{r} = \frac{\tilde{r}_0}{\tilde{r}} = \frac{135\,000}{\tilde{r}} \text{ (psi)} \qquad (9b)$$

IV. THE CRITICAL ANGLE

If an infinite plane shockwave is subjected to an oblique reflection at an infinite plane free surface, the effect is usually steady if we move with a velocity of $D/\cos\Theta$ parallel to the surface. Herein D is the speed of the shockwave and Θ the angle between wavefront and a normal to the free surface.



The undisturbed medium flows from the left to the right side with velocity $D/\cos\Theta$. The stream lines in the undisturbed medium are deflected through an angle β when passing the incident wavefront. In the pictured diagram the flow velocity along the streamline is $D/\cos\Theta$ in the undisturbed medium and v^1 in medium behind the incident wave. v^1 usually is larger than the speed of sound in the medium behind the shockwave as further investigations show. Therefore the part of flow to the right of the incident wave in the above sketch corresponds to supersonic

flow around a corner P, which is known as Meyer-corner (Prandtl and Meyer, see Ref. 8, page 243). The reflected wave therefore is a Machwave produced at point P.

The problem which will be investigated here is not so much the pressure distribution behind this reflected wave but rather at what angles of incidence this whole assumption ceases to be correct. It can be derived

$$v' = u \sin\Theta \frac{1}{\sin\beta}$$

and therefore as conditions for the Mach angle $M = \beta + \gamma'$

$$\sin(\beta+\gamma') = \frac{a}{V'} = \frac{a \sin\beta}{u \sin\Theta} \tag{10}$$

It further can be found

$$\tan\beta = \frac{u \sin\Theta}{D/\cos\Theta - u\cos\Theta}. \tag{11}$$

From (10) and (11) an equation for γ' can be derived

$$(D - u\cos^2\Theta)^2 \sin\gamma' - (u \sin\Theta\cos\Theta)\cos\gamma' = a\cos\Theta \tag{12}$$

This is a quadratic equation for $\sin\gamma'$ and real solutions will exist with the exception of the case when the expression under the square root in the solution becomes negative. The boundary between both cases is given by:

$$\tan \Theta_{crit} = \frac{a}{D} \sqrt{1 - \left(\frac{D-u}{a}\right)^2} \qquad (13)$$

Θ_{crit} is the critical value of Θ derived here, and shall be called the critical angle. As can be derived from (12), the normal solutions exist for $\Theta > \Theta_{crit}$. There are only imaginary solutions for $\Theta < \Theta_{crit}$ which means that conditions for $\Theta < \Theta_{crit}$ may not be considered steady. The physical sense behind that condition is that for $\Theta < \Theta_{crit}$ the reflected wave behind the incident wave is so fast that it propagates into the wavefront of the first one.

In a pressure range $0 \leq \bar{\pi} \leq 500$ atm the approximations (2), (4), and (5) for D, a, and u can be applied. Therefore Θ_{crit} can be determined here by an explicit function. Combining (2), (4), and (5) with (13) gives

$$\tan \Theta_{crit} = \frac{1+(2\mu-k)\bar{\pi}}{1+\mu\bar{\pi}} \sqrt{1-\left(\frac{1+(\mu-k)\bar{\pi}}{1+(2\mu-k)\bar{\pi}}\right)^2} \approx \sqrt{2\mu\bar{\pi}} \qquad (14)$$

Considering the small value of $\tan \Theta_{crit}$ in that range of pressures, $\tan \Theta_{crit}$ can be approximated by Θ_{crit} and it is found

$$\Theta^{o}_{crit} = \sqrt{2\mu\bar{\pi}} \qquad (14a)$$

$$\Theta^{o}_{crit} = 0.20\sqrt{\bar{\pi}} \qquad (\bar{\pi} \text{ in psi}) \qquad (14b)$$

This formula agrees with the one derived by Dr. Penney (Ref. 9) who gives

$$\Theta^{\circ}_{crit} = 0.21\sqrt{\pi} \qquad (\pi \text{ in psi})$$

For higher pressures, Θ_{crit} can be derived directly for each pressure from (13) in using the data given in Table 1. The results which were obtained that way are summarized in Table 2:

π (at)	500	1000	2000	3000	5000	7500	10000
Θ°_{crit}	16.1	20	25.1	29.2	32.5	35.5	38

TABLE 2: Critical angle Θ_{crit} as function of shock pressure.

These results are plotted in Fig. 3 and can be compared with the approximation (14). The curves show that the approximation is adequate (5% difference) up to 500 at.

V. THE CRITICAL DISTANCE

It is necessary to remember that all investigations in Section IV concerning the critical angle Θ_{crit} were carried out assuming plane waves. The case which is of direct interest for underwater explosion shockwaves is the propagation of a spherical wave. A small section of such a wave shall be approximated by a plane wave so that the results of Section IV can be applied.

A spherical shockwave in water produced by a charge in the distance d from the surface propagates and hits the surface at first under $\Theta = 90^{\circ}$. This angle of incidence decreases during the further propagation, the pressure in the wave decreasing also. Thus the intersection of wave and surface travels at first with $c' = \infty$, this speed c' decreasing to velocity of sound for $\Theta = o$. In a certain distance corresponding to the critical angle the reflected wave will begin to travel along the primary wavefront and thus attenuate the peak pressure, if a critical angle exists.

Before going into further details the critical case shall be investigated to determine if it always occurs for any charge weight and any charge depth. For this purpose a spherical shockwave whose decay is given by Fig. 2 shall be considered. The critical angle defined by (14) is

$$\tan \Theta_{crit} = \frac{a}{D}\sqrt{1-\left(\frac{D-u}{a}\right)^2} = f(\pi)$$

which means that Θ_{crit} is a single valued function of the pressure in the shockwave. Assuming a chargeweight W with a charge radius r_0 and a charge depth d, there is

$$\sin \Theta_{crit} = \frac{d}{r_{crit}}$$

with r_{crit} as critical distance corresponding to the critical angle Θ_{crit}. Therefore the above equation for Θ_{crit} can be modified:

$$\frac{d}{r_{crit}} = f(\bar{\pi}) \quad \text{with} \quad \bar{\pi} = g(r_{crit}) \tag{16}$$

wherein g(r) is given by Fig. 2. This is the equation to determine the critical distance, that is, the distance from the charge to that point of the surface where the reflected (attenuation) wave just starts to propagate along the primary wave front.

A general remark shall be stated first. The critical distance given by the general equation (15) meets the conditions of the general law of similitude, applied in underwater explosion research. If all linear dimensions are changed by the same factor n, then the pressure field for a charge with the weight W and n^3W are the same.

Starting with a charge in a greater depth, the pressure at the surface is low enough so that the approximations can be used:

$$\frac{d}{r_{crit}} = \sqrt{2\mu\bar{\pi}} \quad \text{and} \quad \bar{\pi} = \bar{\pi}_0 \frac{r_0}{r_{crit}}$$

Herefrom the critical distance is easily determined as

$$r_{crit} = \frac{d^2}{2\mu \bar{\pi}_0 r_0} \longrightarrow \bar{r}_{crit} = \frac{\bar{d}^2}{2\mu \bar{\pi}_0} \qquad (16)$$

Applying (9a) and (9b) it will be obtained

Pentolite $\bar{r}_{crit} = 0.5\, \bar{d}^{2}$ (16a)

TNT $\bar{r}_{crit} = 0.6\, \bar{d}^{2}$ (16b)

These formulas show that there exists a critical distance even for large depths, that is, for small pressures at the surface. If the charge weight is kept constant and the depth d is decreased, this critical distance decreases much faster because $r_{crit} \backsim d^2$. Therefore we quickly approach a range where the approximations are no longer correct.

For this reason it is necessary to control the range where (16) may be used. This is simply obtained in checking the assumptions. Formula (16) is correct as long as $\bar{\pi} = g(r_{crit}) \leq 500$ at.

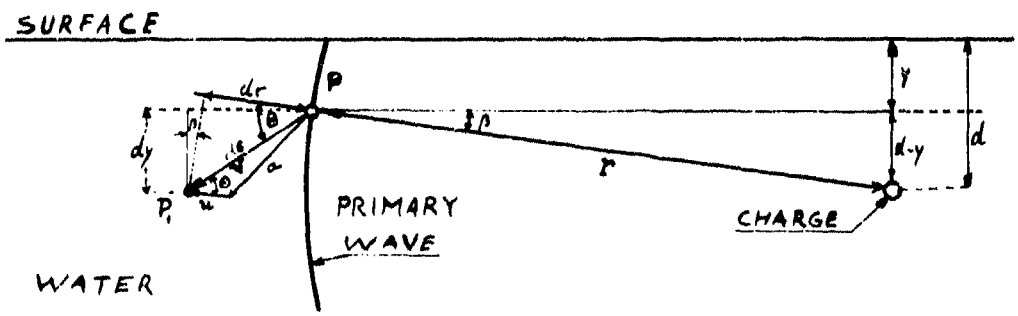
If the initial peak pressure at the critical distance is larger, a general consideration is necessary. This general calculation for r_{crit} as function of the depth d is not difficult if the pressure-distance relations (Fig. 2) and the relations between φ_{crit} and the pressure (Fig. 3) are used. The relation between φ_{crit} and r_{crit} is given by $\sin \varphi_{crit} = d/r_{crit}$. All calculations will now be carried out in expressing all distances in charge radii. The way of obtaining the derived relation between $\bar{r}_{crit}$ and $\bar{d}$ is as follows: Starting with a certain

value of $\bar{r}_{crit}$ the corresponding pressure $\bar{p}$ is derived from Fig. 2. φ_{crit} corresponding to this pressure $\bar{p}$ is taken from Fig. 3. The value which finally corresponds to the used value of r_{crit} is derived as $\bar{d} = \bar{r}_{crit} \sin \varphi_{crit}$. The results thus obtained are plotted in Fig. 4. They show that the approximation formulae (16a) and (16b) are adequate for describing this relation for depths larger than 10 charge radii. This corresponds to a pressure at the critical distance of about 1000 at, which is about twice the limit given above.

Regarding the initial question "if a critical distance always exists for any charge weight in any depth", it has been found that this critical distance always exists for the shockwave of an underwater explosion thus giving a range of distance between charge and surface from this critical distance on to infinity, wherein the reflected wave propagates along the primary wavefront and attenuates its peak pressure.

VI. THE RANGE OF DISTORTION

For distances larger than the initial distance the attenuation (rarefaction wave-reflected wave) is traveling along the primary wavefront of the considered spherical shockwave. This attenuation will propagate farther as the shockwave propagates. For getting the mathematical formulation of this distortion the following case will be considered:



The shockwave is produced by a charge in a depth $\bar{d}$ (expressed in charge radii). The primary wave has travelled over a distance $\bar{r}$ (expressed in charge radii). A point P in a depth $\bar{y}(\bar{y} < \bar{d})$ shall be considered on the original wavefront and it is assumed that this point P just defines a point on the boundary between distorted and undisturbed peak pressure.

The undistorted propagation of the peak pressure during a certain time interval dt is $dr = Ddt$. In that time the

disturbance travelling with speed a of sound in the medium behind the shockfront which flows with flow velocity u has propagated from P to P_1 and this distance ds can be determined as

$$ds = V dt = dt \left\{ u \cos \Theta + \sqrt{a^2 - u^2 \sin^2 \Theta} \right\}$$

The angle Θ between ds and dr just has to be the critical angle, derived in Section IV; if a free surface would have been produced along ds, the attenuation by the reflected wave would just have the same speed of propagation in this direction as the point of intersection between incident wave and the imagined surface. Therefore it is easy to derive the following equations:

$$\frac{d\bar{y}}{d\bar{r}} = \tan \Theta \cos\beta - \sin\beta \tag{17}$$

$$\frac{\bar{d} - \bar{y}}{\bar{r}} = \sin\beta \; , \quad \tan \Theta = \frac{a}{D} \sqrt{1 - \left(\frac{D-u}{a}\right)^2} \tag{17a}$$

Since a, u, and D are known as functions of the pressure $\bar{\pi}$, equation (17) can be considered as differential equation for $y = y(r)$, that is, for the boundary of the range of distortion; the charge depth d is acting as parameter.

A general solution of (17) will be difficult. However, simpler solutions can be obtained for the case $\bar{\pi} < 500$ at, because the approximations (2), (4), and (5) can be used. If (9) and (14)

are applied, it will be seen:

$$\frac{d\bar{y}}{d\bar{r}} = \sqrt{\frac{2\mu\bar{\pi}_0}{\bar{r}}}\cos\beta - \sin\beta$$

and if $\bar{y} \ll d$, it is possible to simplify

$$\cos\beta \sim 1 - \frac{\bar{d}^2}{d\bar{r}^2} \quad ; \quad \sin\beta = \frac{\bar{d}}{\bar{r}}$$

and therefore:

$$\frac{d\bar{y}}{d\bar{r}} = \sqrt{2\mu\bar{\pi}_0}\cdot\bar{r}^{-\frac{1}{2}} - \frac{\bar{d}}{\bar{r}} \tag{18}$$

This can be integrated and gives

$$\bar{y} = 2\sqrt{2\mu\bar{\pi}_0}\,\bar{r}^{\frac{1}{2}} - \bar{d}\ln\bar{r} + C'$$

Considering the condition $\bar{y}(\bar{r}_{crit}) = 0$, it will be derived

$$\bar{y} = 2\bar{d}\left\{\sqrt{n} - 1 - \ln\sqrt{n}\right\} \tag{19}$$

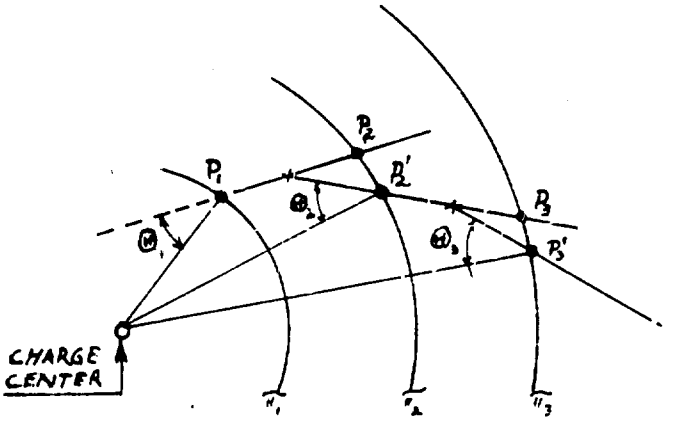
with $n = \bar{r}/\bar{r}_{crit}$ (19a)

It should be remembered that this formula holds only for pressures $\bar{\pi} \leq 500$ at at the critical distance and for depths of that boundary of surface disturbance which are small compared with the charge depth ($\bar{y} \ll \bar{d}$).

For smaller charge depths, that is, for the range of small depths where the pressures are too high and the approximations therefore are no more correct, the boundary of the range of disturbance can be derived directly. This is not difficult if the

relation between charge depth d and critical distance (Fig. 4) together with the relations plotted in Fig. 2 and Fig. 3 are used.

However, it is more convenient to investigate the following case first: A spherical shockwave, produced by an underwater explosion, will be considered in infinitely extended water with a sudden disturbance (attenuation) produced at one point P_1 of the shockfront. The shockfront is chosen to correspond to about the highest pressure π_1 for which the critical angle is known. According to the above investigations, the disturbance begins to propagate in a direction differing by that critical angle Θ_1 from the direction toward the charge. If a series of spheres of equal pressures $\pi_i < \pi_1$ are constructed, the sphere r_2 is soon hit in P_2 if we followed the direction given by $\Theta_1 = \Theta_{crit}(\pi_1)$.



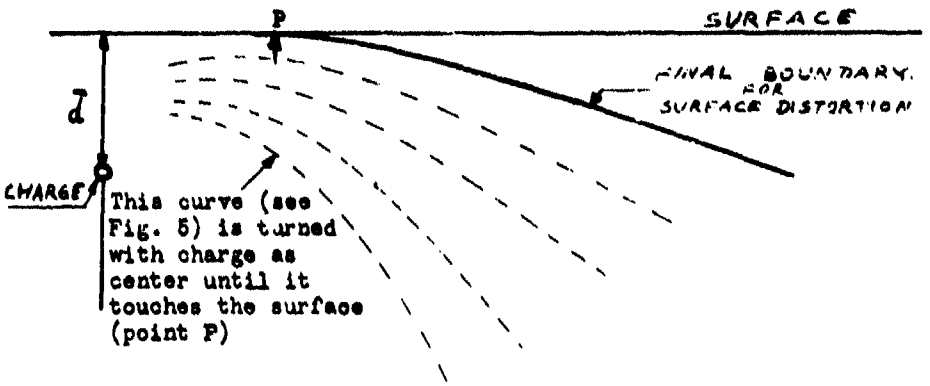
At P_2 we would have to follow a direction inclined by $\Theta_2 = \Theta_{crit}(\pi_2)$ against the connection to the charge. However, this would not be the best approximation. We have

to choose a point P_2' on the wavefront $\mathcal{W}_2$ so that starting with Θ_2 in P_2' against the radius of the shockwave, this direction just intersects with the line P_1P_2 in the center between P_1 and P_2. Following this direction through P_2' outward gives the intersection P_3 with the wavefront corresponding to $\mathcal{W}_3$. Now P_3' has to be chosen so that the direction Θ_3 against the connection of P_3' with the charge just hits the connection $P_2'P_3$ in its center. In this way a boundary of the undistorted propagation is derived in non-dimensional scale because all distances were expressed in charge radii. This result is presented in Fig. 5, both for Pentolite and TNT. It can be seen that the range of disturbance gets greater for Pentolite than for TNT due to its higher pressure.

Another way of obtaining these two curves could have been accomplished by using the fact that the pressure-distance relation for Pentolite and TNT as plotted in Fig. 2 is described by two nearly parallel curves. Therefore, if the pressure for a TNT charge of a certain weight W is given by $\mathcal{W}_{TNT} = f(r/r_o)$, the pressure relation for a Pentolite charge of the same weight W would be given by $\mathcal{W}_P = f'(r/nr_o)$ with $n > 1$, thus permitting the substitution of a Pentolite charge W by a TNT charge n^3W. However this would not be simpler than the way used here.

With the curves Fig. 5 available it is now easy to determine the boundaries of the peak pressure attenuation for different charge depths. The fact that the well known law of similitude is correct

for that case here, also permits the elimination of the parameter "Charge weight" in expressing all distances in charge radii. The desired group of boundaries can be derived from Fig. 5 in putting the center (charge location) in different charge depths $\bar{d}$ and in



turning the construction Fig. 5 until the boundary curve given there just touches the surface. The group of boundaries obtained that way are plotted in Fig. 6.

VII. COMPARISON WITH EXPERIMENTAL RESULTS

There is experimental evidence for small charge depths that the reflection of the underwater explosion shockwave is unusual (Ref. 10). There is a certain range of distortion wherein the peak pressure is smaller and the reflected wave arrives later than expected. The boundary between that range of disturbance and the free water propagation can be found for two conditions which were investigated in Ref. 10.

In Fig. 7A the results of Fig. 5 of Ref. 10 are replotted. They were obtained for 250 gm Pentolite with a charge gauge distance of 45.6" ($\bar{r}$ = 34.8) and different depths; charge and gauge were in the same depth. Using Fig. 6 the fact can easily be derived that the disturbance should reach the gauge only for depths $\bar{d}$ = 7.5 , that is for d = 4.6" under the test conditions. The results of Fig. 7A seem to give a larger depth; however, these measurements scatter considerably and were not obtained with the last gauge type (page 10 of Ref. 10). An estimated curve considering this scattering of the peak pressures is plotted as a broken line in Fig. 10 and gives a critical depth of about 5", which does not differ greatly from the calculated value of 4.6".

In Fig. 7B the results of Fig. 7 of Ref. 10 are replotted. These results were obtained for 250 gm Pentolite with gauge and charge in constant depth of 4" ($\bar{d}$ = 3.06) and different distances between charge and gauge. From Fig. 6 it was derived that the

disturbance should reach the gauge for $\bar{r} = 26.3$, that is for 34.1" under the test condition. This corresponds to $\bar{W}^{1/3}/r = 0.56$ which is marked in Fig. 7B and is in fair agreement with the experimental results.

A much better check of the calculations is possible if the following experimental result is considered which was presented in Ref. 4 and which is repeated in Fig. 8. A spherical shockwave propagates from the lower side of the picture. A plate out of plastic material, hard sponge ebonite with cellular construction containing air bubbles and an overall density < C.1, is arranged above the charge (see Fig. 8). When the spherical shockwave hits the plate, a sudden disturbance (attenuation) is produced in the shockfront which should propagate according to the theory described above.

The observed wavefronts at that test are drawn as thin lines in Fig. 7; they are no longer circles but are additionally curved near the material presenting the surface. The attenuation propagates along the wavefront decreasing the peak pressure, thus decreasing the speed of propagation. The evaluation of these wavefronts results in the curves of equal peak pressure, which are drawn on Fig. 8 as solid lines. They show that a range of distortion exists which increases with increasing distance from the charge.

With the undistorted peak pressure known for different distances by the spherical behavior of the undistorted curves of

equal pressure, and using the known relation between critical angle and pressure (Fig. 5), it is possible to determine the theoretical boundary of the disturbance. This boundary is plotted in Fig. 8 as a broken line; the agreement between this theoretical curve and the observed facts is surprising.

There is another test recorded with the spark camera which permits a comparison with the calculated boundary of the disturbance. The test arrangement is shown in Fig. 9 which is an enlargement of a single picture of the taken series of 24 pictures. A charge is exploded in water below the center of a horizontally suspended bar out of the same hard sponge ebonite mentioned above. The sudden attenuation of the initial shockfront at the points where the shockwave hits the sides of the bar must propagate along the initial wavefront during the further propagation of the shockwave. The range of the disturbance should be in agreement with the calculations which were carried out in the above section.

Enlargements of the single pictures of the taken series were prepared and the spherical shockwave drawn on each of them. The radius was chosen to fit the outer parts of the wavefront (Fig. 9). The range of disturbance must show up in these pictures as deviation from the spherical shockfront because the lower pressures in the range of disturbance correspond to a smaller velocity of propagation. These points where the observed shockfronts begin to deviate from the circles were marked on each enlargement and all of them transferred to Fig. 10. They determine

the boundary between disturbance and undistorted propagation. It should be noted that a more complete determination of that boundary over the curves of equal pressure was not possible for this test because a time scale had not been recorded.

The theoretical curve is drawn also in Fig. 10. It was derived from the known charge weight and the distances assuming a spherical charge (instead of the cylindrical charge which was used) and neglecting the difference between Pentolite and the used Tetryl. The agreement is good.

It is interesting that the consideration concerning the range of disturbance can be applied to another problem. In Ref. 11 the pressure distribution around a cylindrical charge in water has been determined. It could be shown that the curves of equal pressure initially are parallel to the charge surface and that this parallel part gradually becomes smaller for smaller pressures due to the propagation of disturbances produced at both ends of the charge and propagating along the wavefront. A theoretical boundary for the propagation of the disturbance could not be derived because the critical angle has only been calculated for pressures up to 10000 at. (pressured up to 50000 at. occur here), but mainly because of the fact that the detonation wave has to propagate over a certain length of the cylindrical charge before the detonation becomes steady.

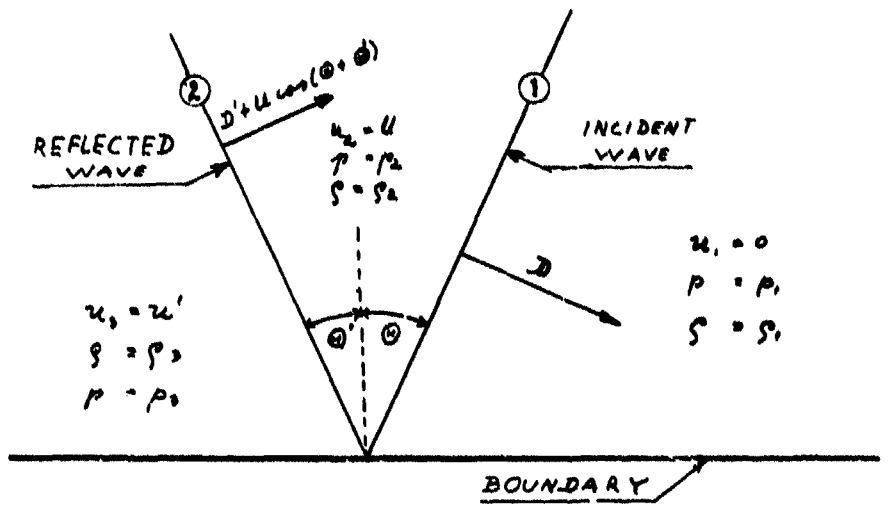
VIII. THE RELATION TO THE CRITICAL ANGLE FOR REFLECTION AT A RIGID SURFACE

The conditions for the beginning of the surface attenuation of the initial shockwave are due to the failure of the Mayor corner solution. The treatment of the reflections of a shockwave at a rigid boundary is similar: the condition has to be found when the reflected shockwave just begins to travel along the initial shockfront; that is, when the usual assumption of incident and reflected wave are no more correct.

The difference in solving the two problems arises from the fact that for a surface reflection the propagation velocity of the reflected wave can be assumed to be the sound velocity of the medium behind the incident wave. For the reflection from a rigid wall the pressure behind the reflected wave and therefore its velocity of propagation is unknown. For this reason an additional condition has to be applied: the flow behind the reflected wave must be parallel to the boundary.

The problem can be solved in using the following picture. The incident wave (1) with an amplitude $\overline{\pi} = p_2 - p_1$ and a velocity D has an angle of incidence ω, the reflected wave (2) with an amplitude $\overline{\pi}' = p_3 - p_2$ and a velocity D' in the medium behind the incident wave has an angle ω between wavefront and a normal to the boundary. The initial conditions are p_1, ρ_1, and flow velocity $u_1 = 0$. Behind the incident shockfront there exists p_2, ρ_2 and flow velocity u in direction

vertical to the incident wave; behind the reflected shockwave there is $p = p_3$, $\rho = \rho_3$ and $u_3 = u'$ vertical to the front of the reflected wave.



The two conditions, which have to be satisfied, shall be considered now.

(a) The velocity of the intersection between incident wave (1) and boundary has to be equal to the velocity of the intersection between reflected wave (2) and boundary. The reflected wave travels in a medium which flows with a velocity + u cos(Θ + Θ') vertical to the reflected wave. The velocity for the observer at rest therefore is D' + u cos(Θ + Θ') and therefore

$$\frac{D' + u\cos(\Theta+\Theta')}{\cos\Theta'} = \frac{D}{\cos\Theta} \qquad (20)$$

(b) The second condition is that the medium behind the reflected wave flows parallel to the boundary also:

$$u \sin \Theta = u' \sin \Theta' \tag{21}$$

All investigations for this effect shall only concern low pressure ($\pi < 500$ at). Then these two conditions can be combined with the relations (3), (4), and (5). If we designate

$$\begin{aligned} p_2 - p_1 &= \pi \\ p_3 - p_2 &= \pi' \end{aligned} \tag{22}$$

it will be found

$$\begin{aligned} D &= a_0(1+\mu\pi) \; ; \quad D' = a_0(1+(2\mu-k)\pi+\mu\pi') \\ u &= a_0 k \pi \; ; \quad u' = a_0 k \pi'(1-(2\mu+k)\pi) \end{aligned} \tag{23}$$

Combination of (23) with (20) and (21) together with the fact that Θ and Θ' for that range are small, gives:

$$\frac{1+(2\mu-k)\pi+\mu\pi'+k\pi\left(1-\frac{(\Theta+\Theta')^2}{2}\right)}{1-\frac{\Theta'^2}{2}} = \frac{1+\mu\pi}{1-\frac{\Theta^2}{2}} \tag{20a}$$

$$\pi\Theta = \pi'\Theta'(1-(2\mu+k)\pi) \tag{21a}$$

(20a) can be transformed and finally gives:

$$\mu(\pi+\pi') - \frac{\Theta^2}{2}(1+\cancel{k\pi}+\cancel{\mu\pi}) - \frac{\Theta'^2}{2}(1-\cancel{k\pi}+\cancel{\mu\pi}) - k\pi\Theta\Theta' = 0 \tag{24}$$

wherein the noted terms can be neglected:

$$\mu\tilde{\pi} + \mu\pi' - \frac{\Theta^2}{2} + \frac{\Theta'^2}{2} = 0 \tag{25}$$

Making the same neglection as for deriving (25), it is found from (21a)

$$\Theta' = \frac{\bar{\pi}}{\bar{\pi}'} \Theta \tag{26}$$

These two equations (25) and (26) correspond to (20) and (21) and combining them, the following equation for Θ' as function of Θ is found:

$$\Theta'^2 - \Theta\Theta' + 2\mu\pi = 0 \tag{27}$$

which has only real solutions as long as

$$\frac{\Theta^2}{4} - 2\mu\pi \geq 0$$

Therefore the assumption for these calculations, that is the incident and the reflected shockwave, is only correct for $\Theta \leq \Theta_M$ with

$$\Theta_M = 2\sqrt{2\mu\pi} \tag{28}$$

Combining (28) with the formula (14a) for the critical angle at a free surface reflection, it will be found

$$\Theta_M = 2\,\Theta_{crit} \tag{29}$$

This is in good agreement with the result of J. von Neumann (Ref. 1) who gives

$$\Theta_M^0 = 1.51 \sqrt{\bar{r}_{at}}$$

while it was derived here

$$\Theta_M^0 = a + \sqrt{\bar{r}_{max}} = 1.51 \sqrt{\bar{r}_{at}}$$

According to the critical distance r_{crit} for reflection of an underwater explosion shockwave at a free surface, a critical distance can be derived for the reflection at a rigid boundary:

$$r = \tfrac{1}{4} r_{crit} \qquad (30)$$

which is correct only for small pressures ($\bar{\pi} \leq 500$ at) also.

A general result, which was derived by J. von Neumann in Ref. 1 can easily be reproduced here:

Combining (25) and (26) gave (27), and it was found

$$\Theta' = \frac{\Theta}{2} + \sqrt{\frac{\Theta^2}{4} - 2\mu\bar{\pi}}$$

The minus sign for the root gives no physical sense and is neglected. This result can be transformed with (28) and gives

$$\Theta' = \frac{\Theta}{2}\left(1 + \sqrt{1 - \left(\frac{\Theta_M}{\Theta}\right)^2}\right)$$

and

$$\bar{\pi}' = \frac{2}{1 + \sqrt{1 - \left(\frac{\Theta_M}{\Theta}\right)^2}} \cdot \bar{\pi}$$

For a plane shockwave with a fixed small amplitude ($\pi < 500$ at) and smaller angles of incidence it therefore can be derived that $\pi' \leq \pi$ and $\Theta' \geq \Theta$ as long as Θ is much larger than Θ_M, that is, as long as Θ is far off from the critical Mach angle. The more Θ approaches Θ_M, the more Θ' falls off compared with Θ and the more π' increases. For $\Theta = 2\,\Theta_M$ the difference is still only 10%. But for the critical case $\Theta = \Theta_M$ it is found $\Theta' = \frac{\Theta_M}{2}$ and $\pi' = 2\pi$. The derived theory no more holds for $\Theta > \Theta_M$, that is for the range when a Mach wave (Bridge wave) occurs.

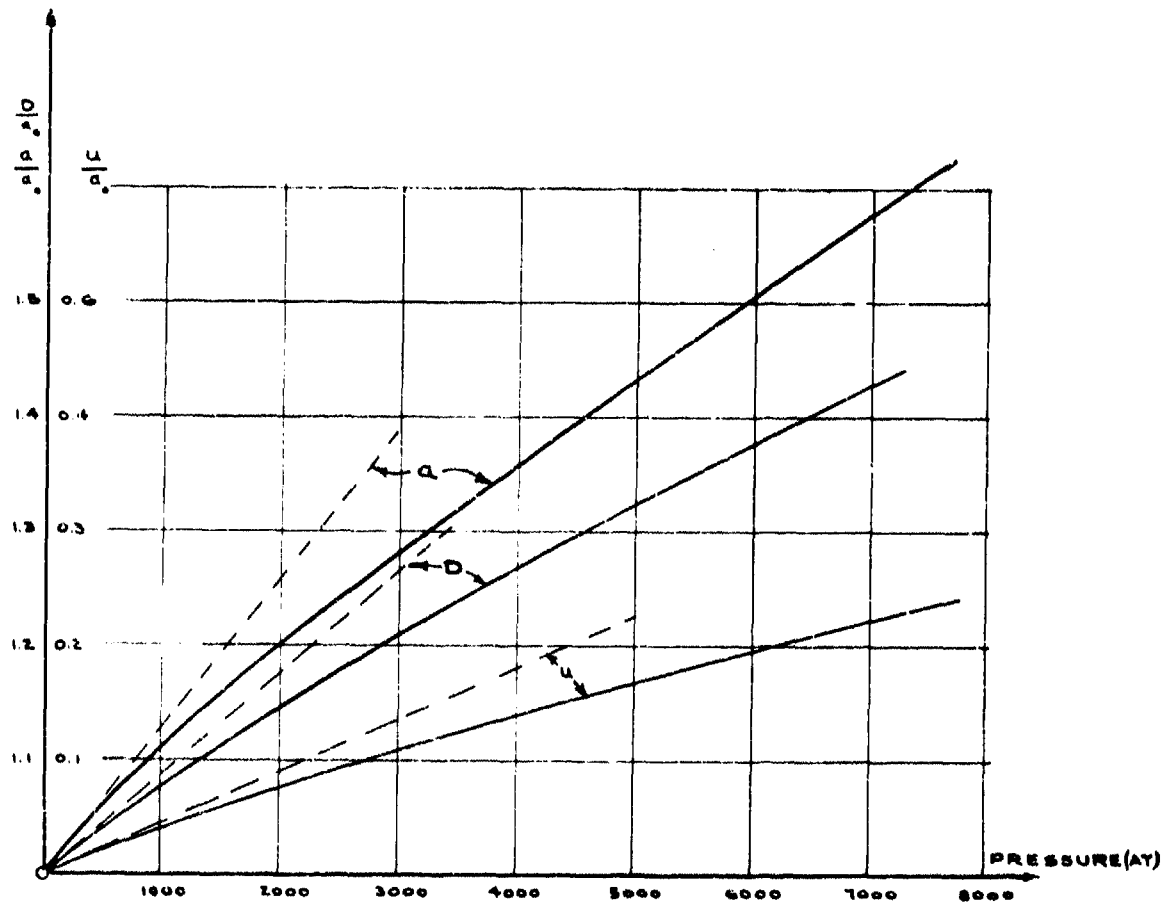
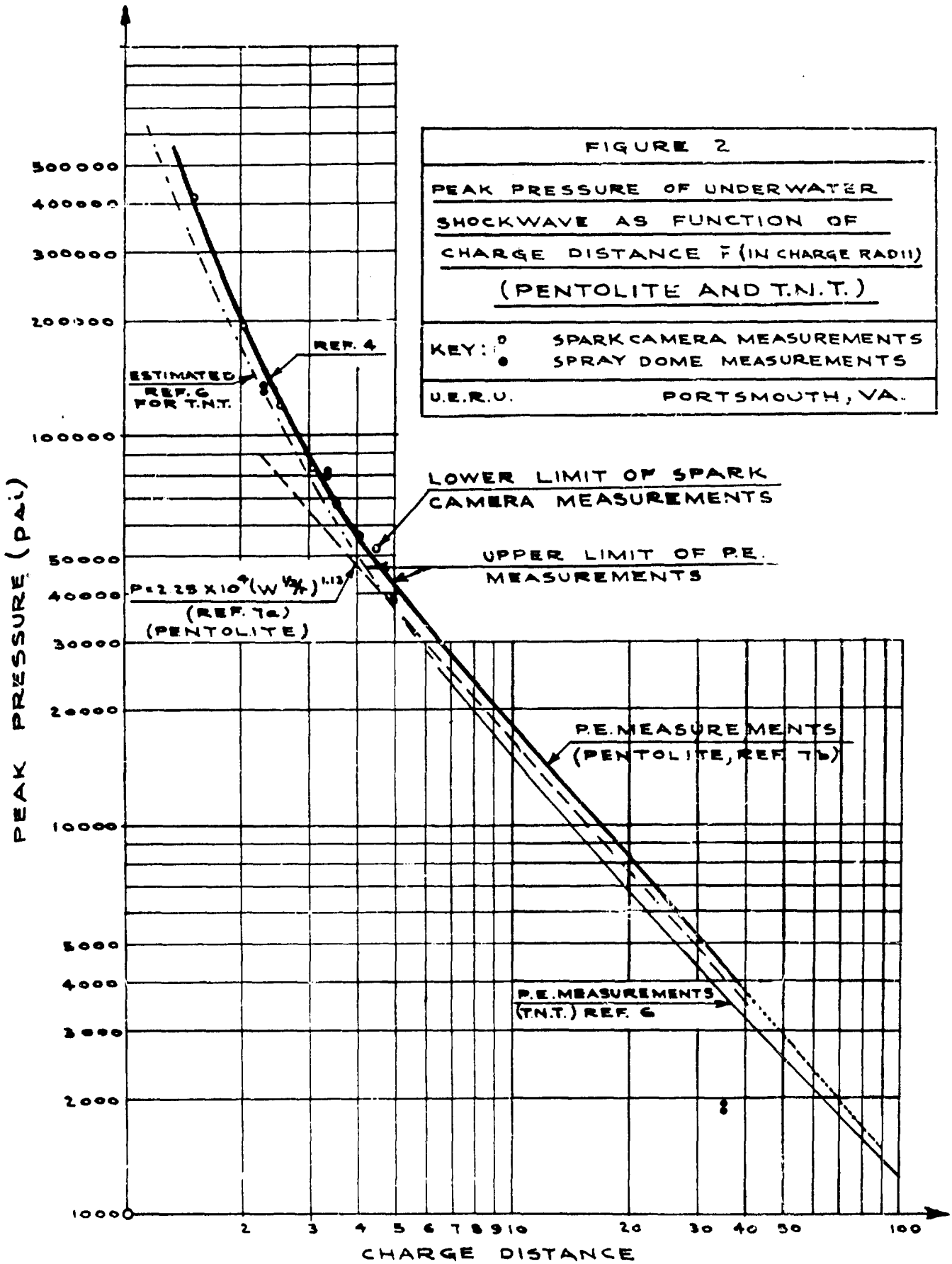


FIGURE 1

VELOCITY D OF SHOCKWAVE IN WATER; FLOW VELOCITY u AND SOUND VELOCITY a OF MEDIUM BEHIND SHOCK FRONT

KEY: - - - - APPROXIMATION
——— EXACT CALCULATION

U.E.R.U. PORTSMOUTH, VA.


FIGURE 2
PEAK PRESSURE OF UNDERWATER SHOCKWAVE AS FUNCTION OF CHARGE DISTANCE F (IN CHARGE RADII)
(PENTOLITE AND T.N.T.)
KEY: ○ SPARK CAMERA MEASUREMENTS
● SPRAY DOME MEASUREMENTS
U.E.R.U. PORTSMOUTH, VA.
PEAK PRESSURE (psi)
500000
400000
300000
200000
100000
50000
40000
30000
20000
10000
5000
4000
3000
2000
1000
REF. 4
ESTIMATED REF. 6 FOR T.N.T.
LOWER LIMIT OF SPARK CAMERA MEASUREMENTS
UPPER LIMIT OF P.E. MEASUREMENTS
P = 2.25 X 10^4 (W^1/3 / R)^1.13
(REF. 7a)
(PENTOLITE)
P.E. MEASUREMENTS (PENTOLITE, REF. 7b)
P.E. MEASUREMENTS (T.N.T.) REF. 6
2
3
4
5
6
7
8
9
10
20
30
40
50
100
CHARGE DISTANCE

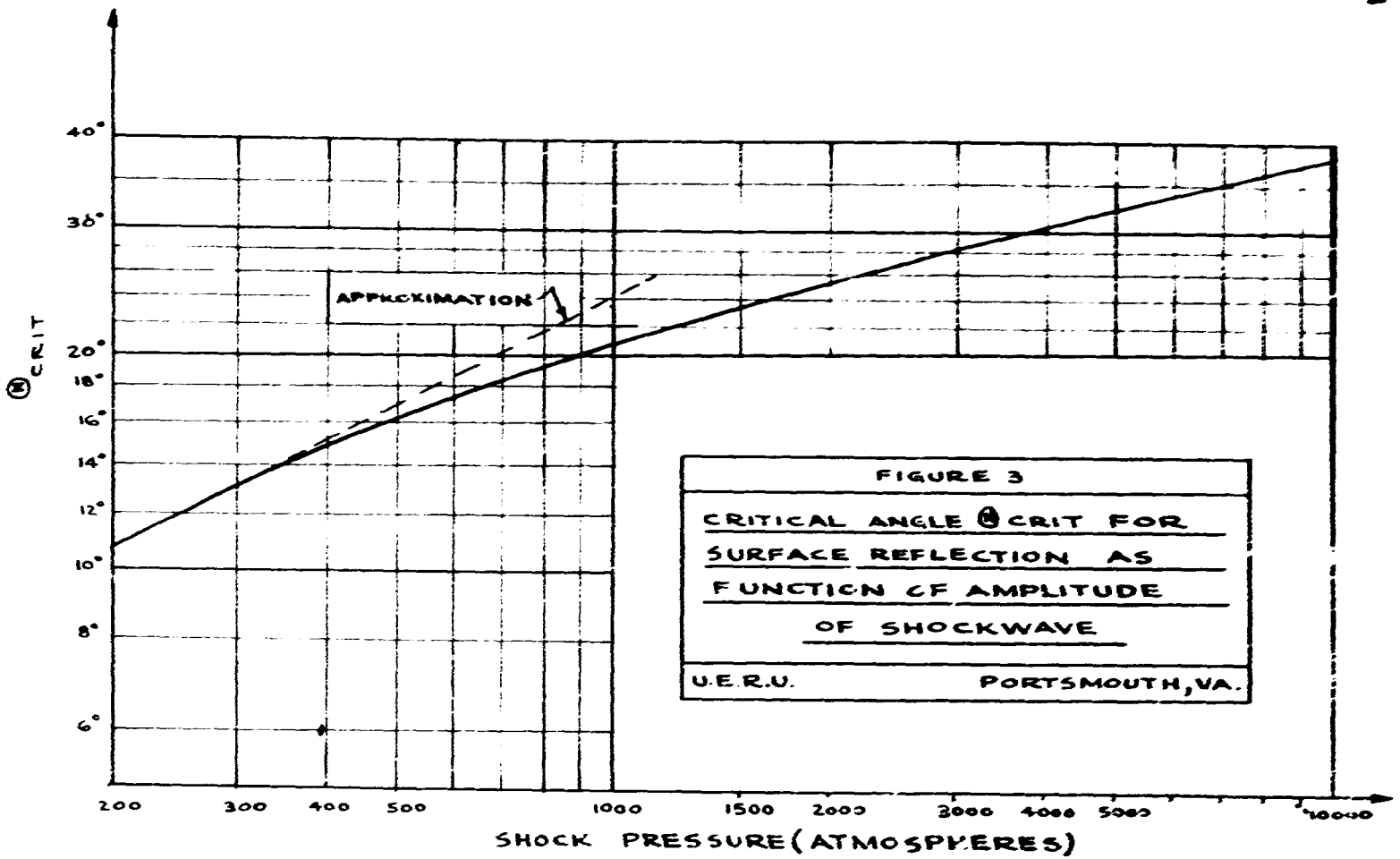


FIGURE 3

CRITICAL ANGLE θ CRIT FOR SURFACE REFLECTION AS FUNCTION OF AMPLITUDE OF SHOCKWAVE

U.E.R.U. PORTSMOUTH, VA.

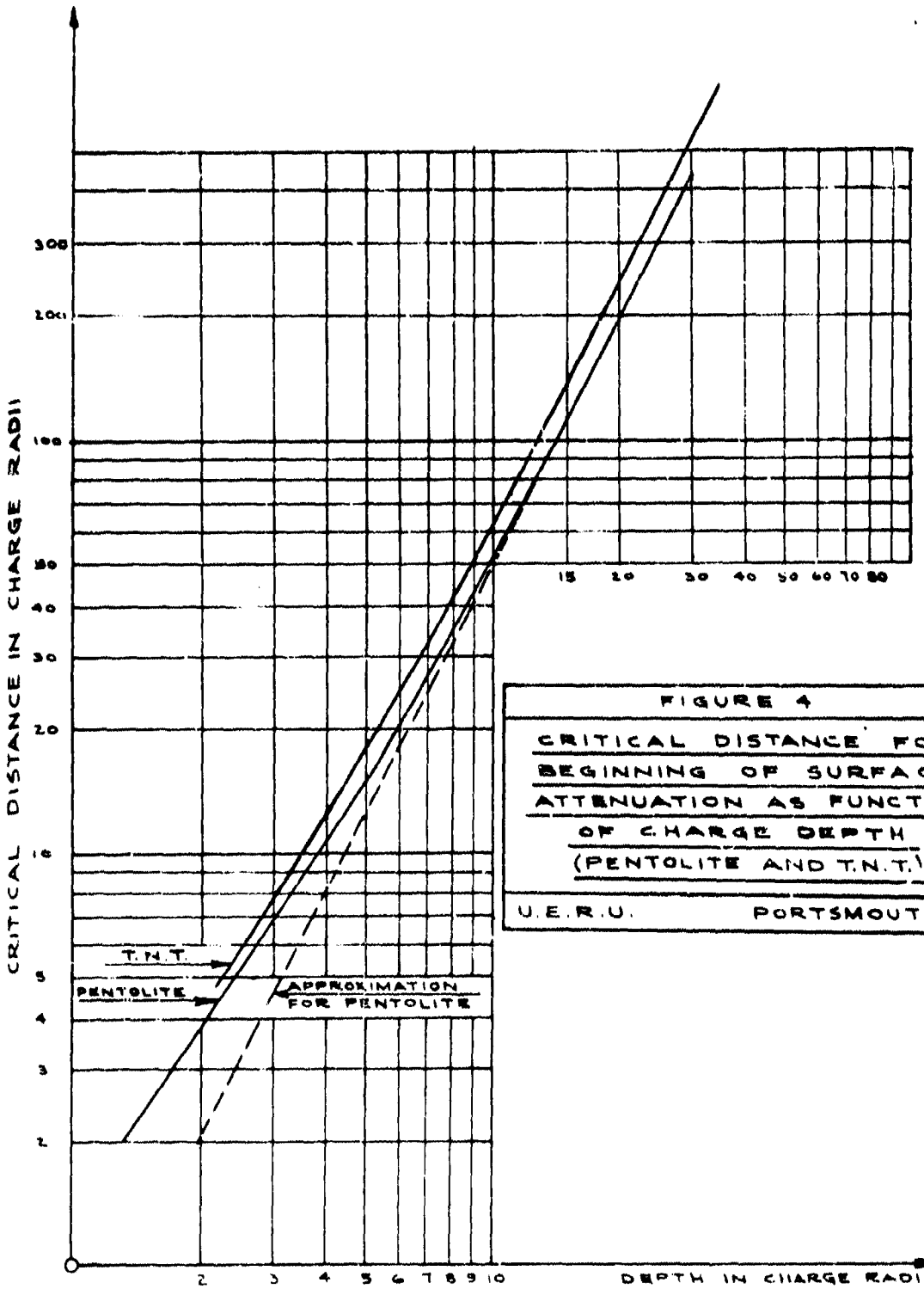


FIGURE 4

CRITICAL DISTANCE FOR BEGINNING OF SURFACE ATTENUATION AS FUNCTION OF CHARGE DEPTH (PENTOLITE AND T.N.T.)

U.E.R.U. PORTSMOUTH, VA.

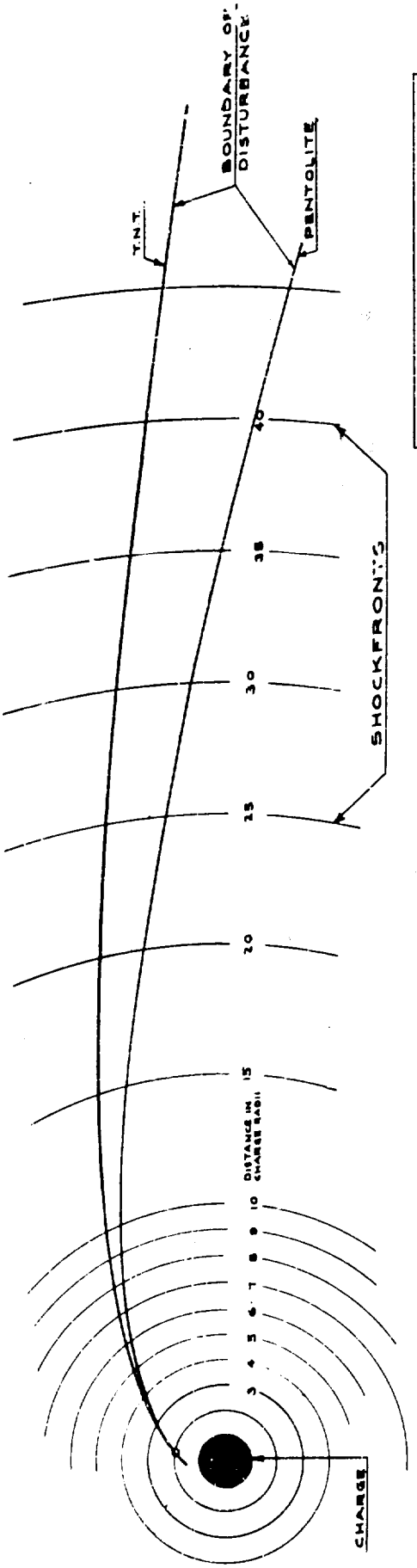


FIGURE 5

CALCULATED BOUNDARY FOR PROPAGATION OF A SMALL DISTURBANCE ALONG THE SHOCKFRONT OF AN UNDERWATER EXPLOSION

U.E.R.U. PORTSMOUTH, VA.

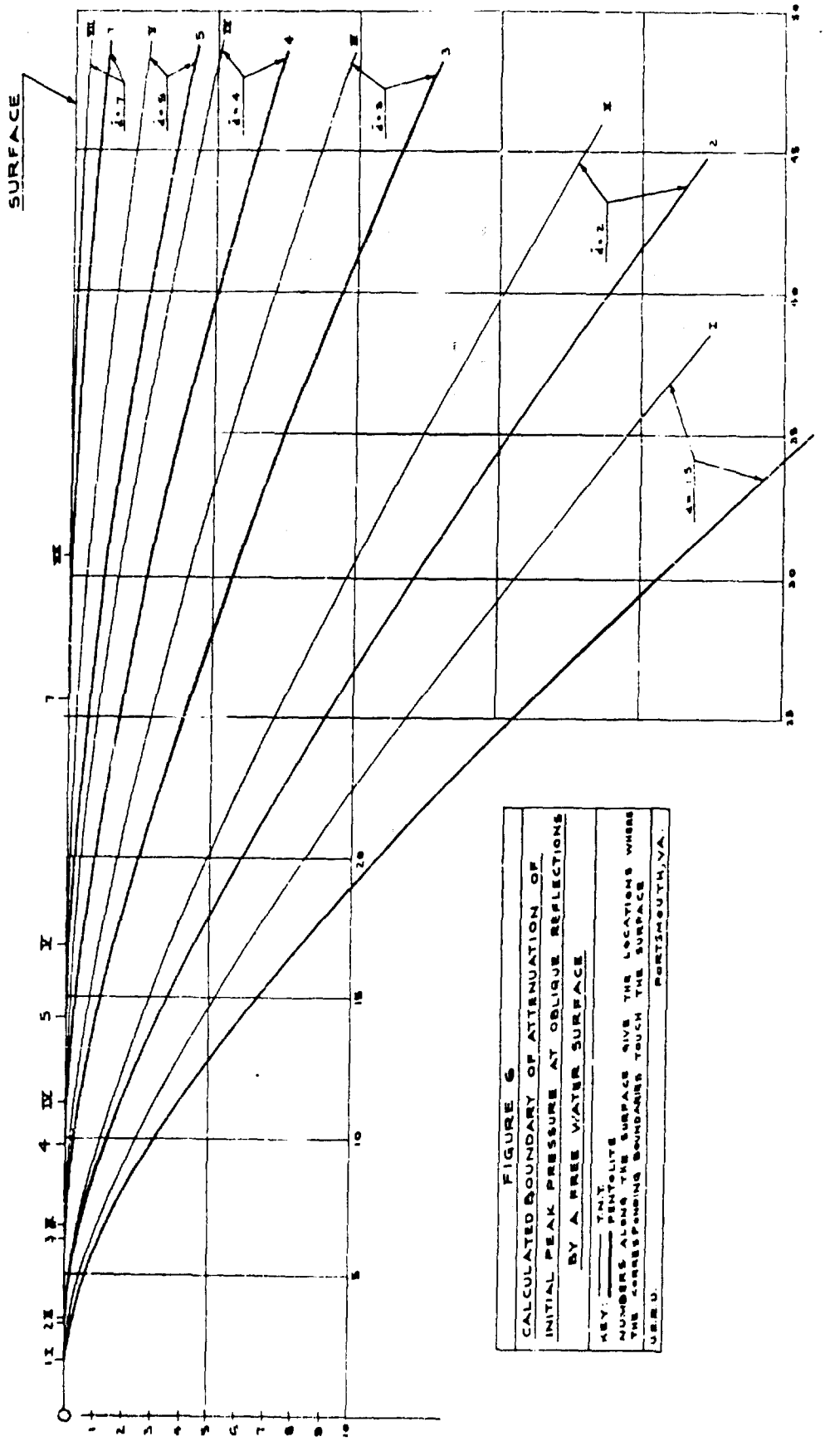


FIGURE 6

CALCULATED BOUNDARY OF ATTENUATION OF INITIAL PEAK PRESSURE AT OBLIQUE REFLECTIONS BY A FREE WATER SURFACE

KEY: —— T.N.T.
- - - - PENTOLITE
NUMBERS ALONG THE SURFACE GIVE THE LOCATIONS WHERE THE CURVES BOUNDING BOUNDARIES TOUCH THE SURFACE

U.S.N.O. PORTSMOUTH, VA.

FIGURE 7A

PEAK PRESSURE AS FUNCTION OF DEPTH FOR CONSTANT CHARGE-TO-GAUGE DISTANCE OF 45.6"; 250G PENTOLITE (REPLOTTED FROM FIG. 5 OF REF. 10)

U.E.R.U. PORTSMOUTH, VA.

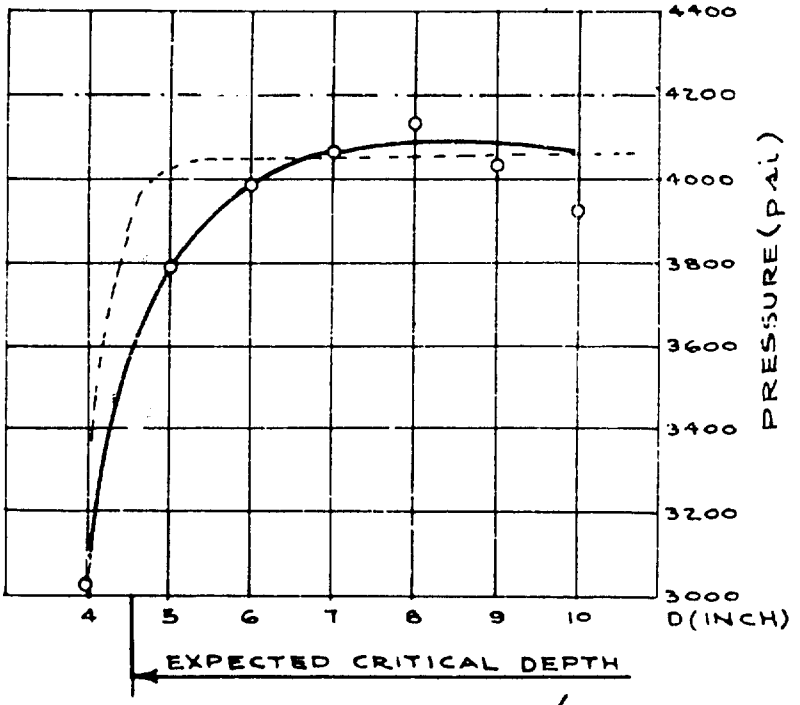
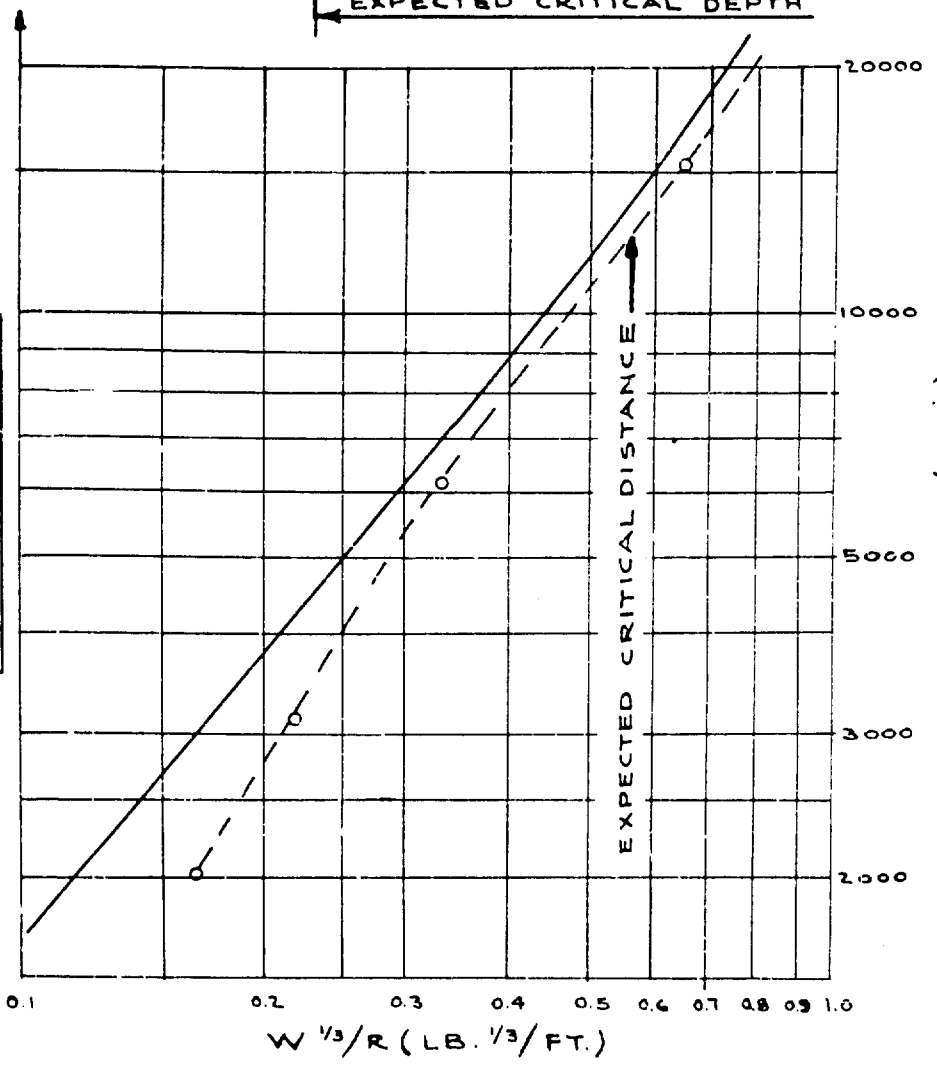


FIGURE 7B

PEAK PRESSURE FOR VARYING $W^{1/3}/R$ WITH CHARGE AND GAUGE 4" DEEP. CHARGE WEIGHT 250 G. (REPLOTTED FROM FIG. 7 OF REF. 10)

U.E.R.U. PORTSMOUTH, VA.



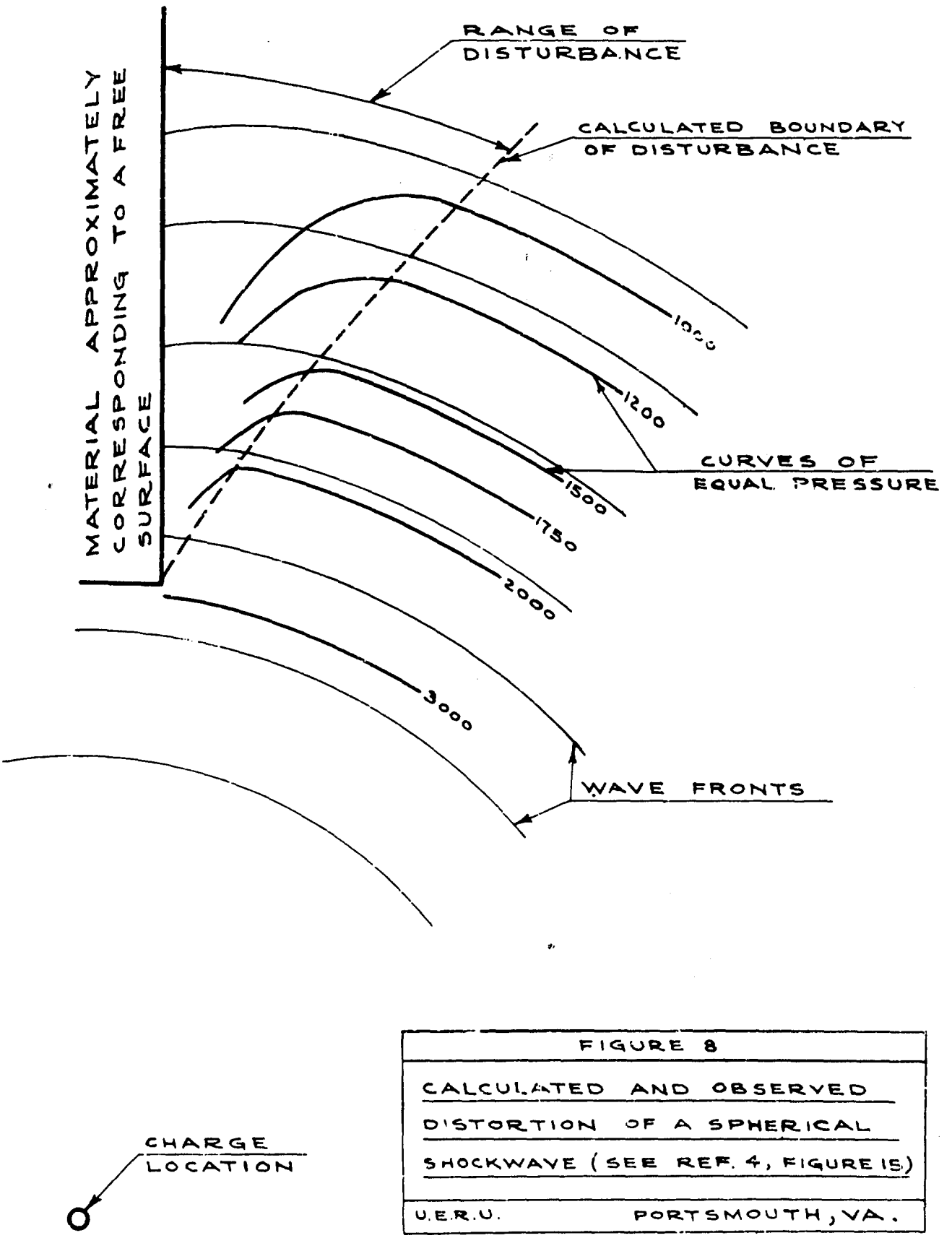
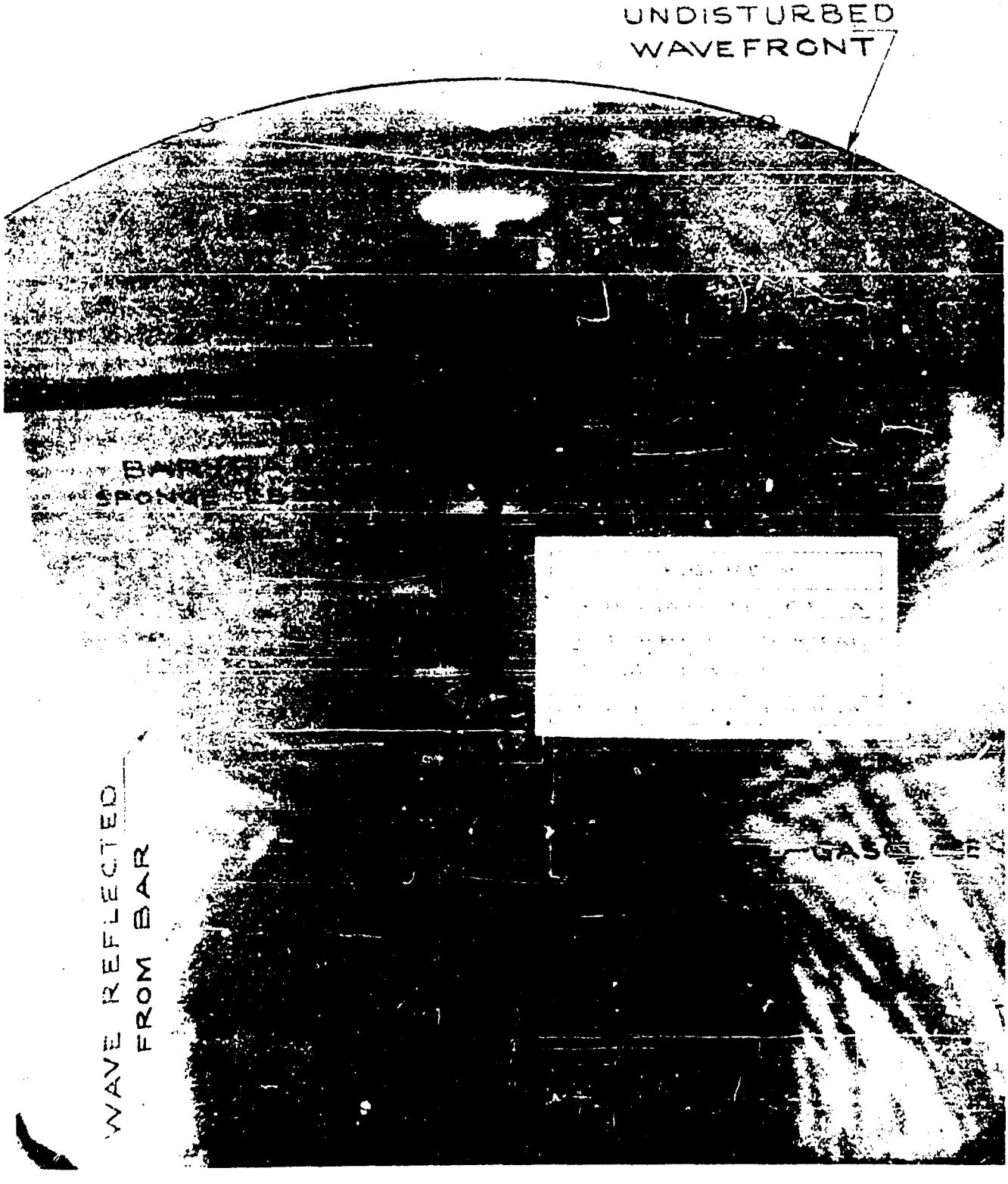


FIGURE 8

CALCULATED AND OBSERVED DISTORTION OF A SPHERICAL SHOCKWAVE (SEE REF. 4, FIGURE 15)

U.E.R.U. PORTSMOUTH, VA.


UNDISTURBED
WAVEFRONT
WAVE REFLECTED
FROM BAR

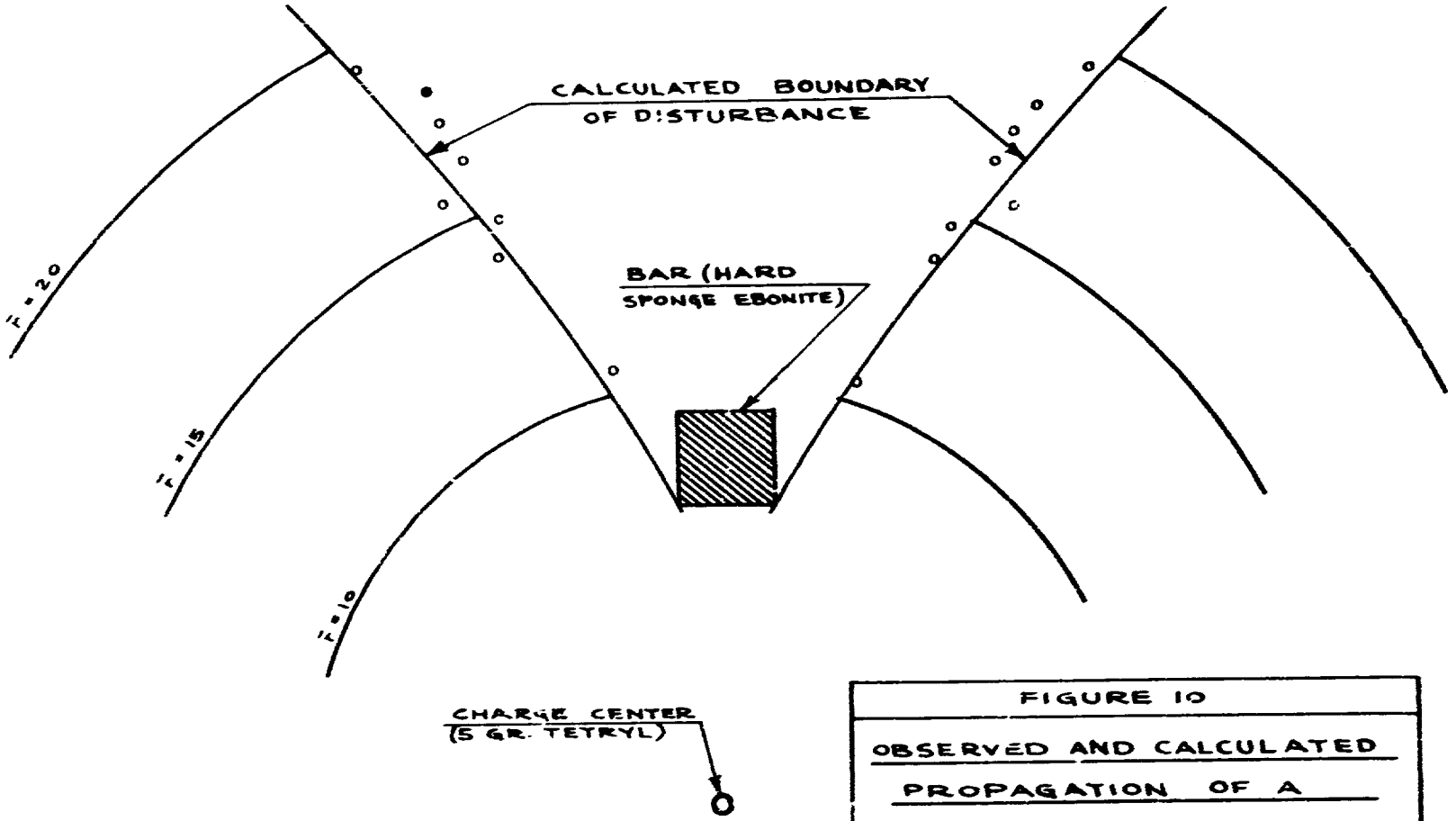


FIGURE 10
OBSERVED AND CALCULATED PROPAGATION OF A DISTURBANCE ALONG A SPHERICAL SHOCKWAVE
KEY: ooo OBSERVATION
U.E.R.U. PORTSMOUTH, VA.

1471

LONG RANGE SHOCK PROPAGATION IN UNDERWATER EXPLOSION PHENOMENA II

A. B. Arons, D. R. Yennie and T. P. Cotter, Jr.
Underwater Explosives Research Laboratory
Woods Hole Oceanographic Institution

American Contribution

26 October 1949

TABLE OF CONTENTS

		Page
LIST OF FIGURES		iv
LIST OF TABLES		v
ABSTRACT		vi
I.	PHASE DISTORTION ASSOCIATED WITH OBLIQUE REFLECTIONS FROM THE SEA BED	1
1.	Introduction	1
2.	Revised theory of critical angle reflection of transient waves	1
3.	Experimental verification of the character of the phase distortion	9
4.	Alternative treatment of plane wave reflection as a boundary value problem	20
5.	Reflection of spherical waves	29
6.	Comments with respect to oblique reflection of strong shocks	37
II.	THE EFFECT OF VISCOUS ATTENUATION ON EXPONENTIAL SHOCK WAVES	38
7.	Introduction	38
8.	The effect of viscosity alone on a low amplitude exponential shock	39
9.	Correction of the preceding theory for certain finite amplitude effects	51
10.	Effects of Gauge Size on rise time and shape of shock wave which has undergone viscous attenuation	64
III.	ENERGY FLUX AND DISSIPATION	
11.	Extension of the similarity curves for shock wave impulse and energy flux	69
12.	Ratio of reflected and incident energy flux for bottom reflections up to the critical angle of incidence	69
13.	Energy loss due to viscous effects	74
14.	Slope of the peak pressure similarity curve	84

		Page
IV.	DISTORTION ASSOCIATED WITH REFLECTION FROM THE SEA SURFACE	86
	15. Introduction	86
	16. Bulk cavitation	88
	17. Sharpness of the negative wave front	98
V.	ACKNOWLEDGMENTS	100
APPENDIX		
I.	AN IMPROVED MICROCOULOMETER FOR THE CALIBRATION OF PIEZOELECTRIC GAUGES	100
	1. Introduction	100
	2. Description of the circuit	100
	3. Sensitivity	102
	4. Further modification and improvements	103
	5. Use of a speedomax or brown recorder as a detecting device	103
REFERENCES		106, 107
DISTRIBUTION LIST		108

LIST OF FIGURES

Number		Page
1.	Oblique reflection of a plane wave at a plane interface	2
2.	Comparison of the experimental and theoretical pressure-time curves including higher order reflections	10, 11
3a.	Pressure-time records showing distortion of bottom reflection with increasing angle of incidence	12
3b.	Theoretical pressure-time curves for bottom reflection of an exponential shock wave	12
4.	Simple geometrical arrangement of source and receiver	31
5.	Distorted reflection of plane exponential shock wave	34

6.	Branch point and path of integration	42
7.	Theoretical effect of viscous attenuation of an exponential shock wave (Finite amplitude effects neglected)	48
8.	Theoretical reduced rise time (β_r) as a function of the reduced distance parameter (α) from an exponential shock wave subject to viscous attenuation alone	49
9.	X - R plane for equation (109)	57
10.	"Equivalent viscous distance", X_r, as a function of ranges for various charge sizes, (Results of numerical integration of equation (108))	60
11.	Pressure-time curves for 0.5 lb. charges at various ranges, showing expected combined effect of viscous attenuation and finite amplitude sharpening	61
12.	Pressure-time curves for 8 lb. charges at various ranges, showing expected combined effect of viscous attenuation and finite amplitude sharpening	62
13.	Theoretical rise time vs range for various charge sizes	63
14.	Pressure-time curves for 8 lb. charges at ranges of 6000 & 20,000 ft.	67
15.	Energy flux and impulse vs $W^{1/3}/R$ for pentolite	70
16.	Illustration of the behavior of the amplitude parameter π_m	80
17.	Ratio of pressure drop of reflected wave to peak pressure of direct wave vs range	91
18.	Cavitation region for a 0.5 lb. pentolite charge at 40 ft. depth	93
19.	Microcoulometer	101

LIST OF TABLES

Number		Page
I.	Impulse and energy flux for 0.5 lb. pentolite charge	71
II.	Ratio of reflected to incident energy flux (E_r/E_1) for bottom reflections at various angles	73
III.	Shock wave energy dissipation over the interval $W^{1/3}/R = 0.0053$ to $W^{1/3}/R = 0.00022$	81
IV.	Comparison of gauge calibrations with various instruments	105

Abstract

The theory of oblique reflection of low amplitude exponential shock waves is considered in more detail than in the preceding report (NavOrd 424) and is extended to include higher order reflections in shallow water. Errors arising from use of the plane wave approximation are discussed.

Recently published data on the attenuation of harmonic sound waves in sea water are used to develop a theory of the effect of viscous attenuation on the front of a shock wave propagating over long ranges. Crude correction is made for the compensating effects of finite amplitude.

Experimental data on impulse and energy flux at long ranges are reported. The energy dissipation is analyzed in terms of the theory of viscous attenuation and an attempt is made to account for the slope of the pressure-distance curve.

Experimental data on negative gauge pressures in surface reflections are reported and analyzed in terms of a new treatment of the expected region of bulk cavitation. The data indicate a very low value of the "breaking tension" of sea water.

An improved microcoulometer circuit for the calibration of piezoelectric gauges is described.

I. Phase distortion associated with oblique reflection from the sea bed.

1. Introduction.

1.1 A preliminary discussion of critical angle effects and phase distortion of low amplitude exponential shock waves upon reflection from the sea bed was given in NavOrd Report No. 424. Since publication of this report, the theoretical analysis has been improved, extended to include multiple reflections, and examination of the experimental records has been completed. The results of these investigations are described below.

2. Revised theory of critical angle reflection of transient waves.

2.1 Figure 1 defines the notation for angles of incidence and reflection, properties of the adjacent media, pressure wave parameters, etc. Using the notation and development given in Sections 4.4 through 4.7 of NavOrd 424, we have for the incident, reflected, and transmitted waves at angles exceeding the critical:

$$p_i = P_i \exp\left[i\omega(t-\alpha_1 x+\beta_1 y)\right] \qquad (1)$$

$$p_r = P_r \exp\left[i\omega(t-\alpha_1 x-\beta_1 y)\right] \qquad (2)$$

$$p_2 = P_2 \exp\left[i\omega(t-\alpha_1 x)+|\omega|\beta_{2r} y\right] \qquad (3)$$

It will be recalled that since region 2 is one in which

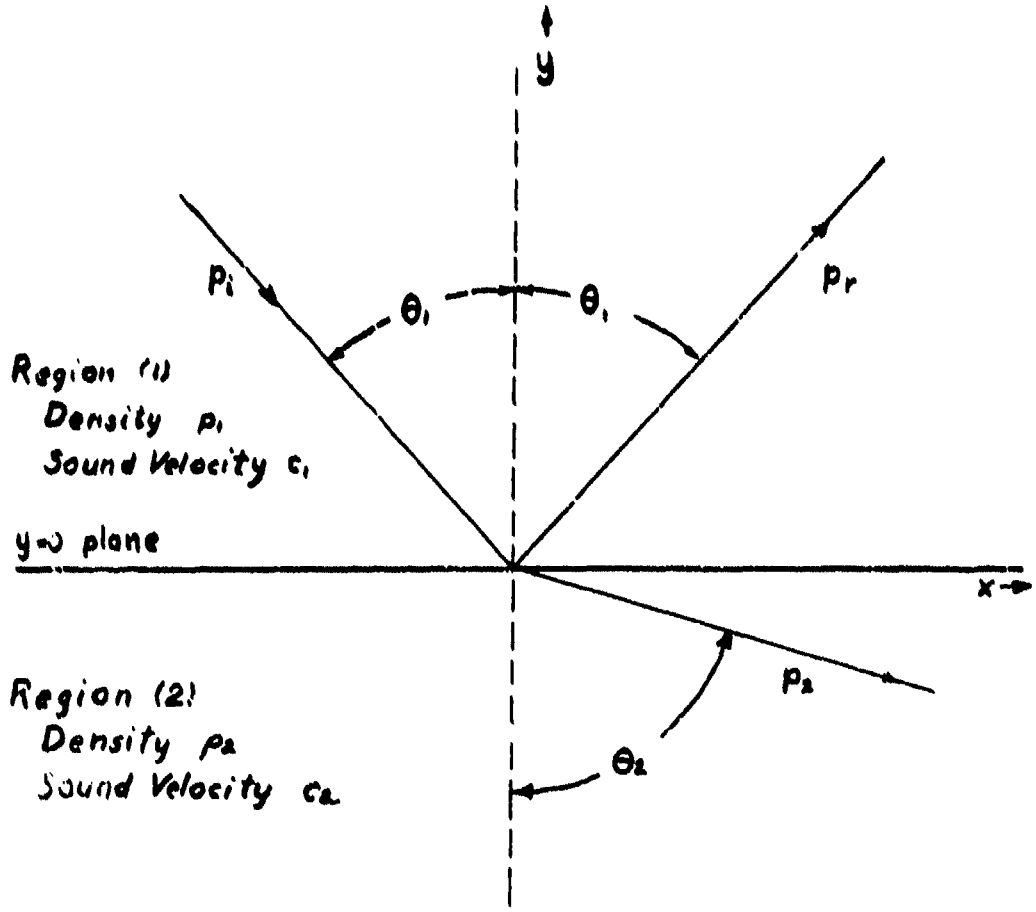


Fig. 1

Oblique reflection of a plane wave at a plane interface.

θ_1 = angle of incidence and reflection.

θ_2 = angle of refraction

p_i, p_r, p_t incident, reflected and refracted wave trains respectively.

y is always negative, β_2 was set equal to $-i\beta_{2r}$ to make the real exponential term of eq. (3) tend to zero as $y \to -\infty$. For the same reason one must then use $|\omega|$ rather than ω in the same term.

The boundary conditions to be satisfied are:

$$p_1 = p_i + p_r \tag{4}$$

$$\frac{1}{\rho_1}\frac{\partial p_1}{\partial y} = \frac{1}{\rho_2}\frac{\partial p_2}{\partial y} \tag{5}$$

at $y = 0$

2.2 Application of these boundary conditions leads to the following expressions for the incident and transmitted waves:

$$p_r = P_i \exp\left[i\omega(t-\alpha_1 x-\beta_1 y) + i\,2|\omega|\varepsilon/\omega\right] \tag{6}$$

$$p_2 = 2P_i \cos\varepsilon \exp\left[i\omega(t-\alpha_1 x) + i|\omega|\varepsilon/\omega + |\omega|\beta_{2r} y\right] \tag{7}$$

It will be seen that the factor $|\omega|/\omega$ enters through the differentiations with respect to y in equation (5). This factor is simply set equal to unity in Rayleigh's treatment[1] and in NavOrd 424 since in the consideration of harmonic wave trains negative values of ω have no physical significance.

In the present treatment, however, we wish to apply the phase shift of equation (6) to the Fourier spectrum of an exponential transient and to do this by utilizing the general

complex Fourier integral in which integration over the parameter ω is carried from minus to plus infinity. For this treatment we may no longer regard ω as a simple positive quantity and must take account of the change in sign of the phase shift indicated by equation (6) for negative values of ω.

2.3 Suppose the incident wave is now given by the general form:

$$p_i(t) = (2\pi)^{-1/2} \int_{-\infty}^{\infty} \varphi(\omega) \exp(i\omega t)\, d\omega \qquad (8)$$

where

$$\varphi(\omega) = (2\pi)^{-1/2} \int_{-\infty}^{\infty} p_i(\tau) \exp(-i\omega\tau)\, d\tau \qquad (9)$$

Applying the phase shift indicated by equation (6),

$$p_r(t) = (2\pi)^{-1/2} \int_{-\infty}^{\infty} \varphi(\omega) \exp(i\omega t + i2|\omega|\varepsilon/\omega)\, d\omega \qquad (10)$$

From which it follows, upon substitution of the trigonometric form of $\exp(i2|\omega|\varepsilon/\omega)$, that:

$$p_r(t) = p_i(t) \cos 2\varepsilon + F(t) \sin 2\varepsilon \qquad (11)$$

where

$$F(t) \equiv (2\pi)^{-1/2} \int_{-\infty}^{\infty} \frac{i|\omega|}{\omega} \varphi(\omega) \exp(i\omega t)\, d\omega \qquad (12)$$

The problem is further simplified by replacing the term $|\omega|/\omega$ with the Dirichlet discontinuous factor expressed in the form

$$\frac{|\omega|}{\omega} = \underset{\sim}{P}\,(\pi i)^{-1}\int_{-\infty}^{\infty} x^{-1}\exp(i\omega x)\,dx = \begin{cases} -1, & \omega < 0 \\ 0, & \omega = 0 \\ +1, & \omega > 0 \end{cases} \tag{13}$$

The symbol $\underset{\sim}{P}$ stands for "principal value."[2] Equation (12) then becomes

$$F(t) = (2\pi^3)^{-1/2}\,\underset{\sim}{P}\int_{-\infty}^{\infty}\frac{dx}{x}\int_{-\infty}^{\infty}\varphi(\omega)\exp\left[i\omega(t+x)\right]d\omega \tag{14}$$

and the problem reduces to the evaluation of the double integral F (t) for specific cases in which $\varphi(\omega)$ is available.

In the case of an exponentially decaying shock wave

$$p_i(t) = \begin{cases} 0 & , t < 0 \\ P_i\,\epsilon^{-\lambda t} & , t > 0 \end{cases} \tag{15}$$

$$\varphi(\omega) = \frac{P_i}{(2\pi)^{1/2}(\lambda + i\omega)} \tag{16}$$

Substitution of (16) into (14) and evaluation of the complex integral in ω by standard methods of contour integration

gives:

$$F(t) = P_i \pi^{-1} \epsilon^{-\lambda t} \underset{\sim}{P} \int_{-t}^{\infty} \frac{\epsilon^{-\lambda x}}{x} dx \qquad (17)$$

The principal value of the integral in equation (17) is identical with the negative of the "exponential integral" defined and tabulated in reference 3. Thus

$$F(t) = -P_i \pi^{-1} \epsilon^{-\lambda t} \overline{E_i}(\lambda t) \qquad (18)$$

If a higher order reflection undergoes more than one reflection from the bottom at the same angle of incidence, the total phase shift to be applied in equation (10) becomes $2N\varepsilon / \omega / / \omega$ where N is the number of times the wave has been reflected from the bottom at an angle of incidence corresponding to the shift ε. Each time the wave is reflected from the free surface it undergoes a complete inversion; thus if M is the number of times the wave has been reflected from the surface, the general expression for higher order reflections becomes, analagous to equation (11),

$$p_{MNr}(t) = (-1)^M \left[P_i(t) \cos 2N\varepsilon + F(t) \sin 2N\varepsilon \right] \qquad (19)$$

2.4 Conservation of energy. The energy flux in the incident wave is given by

$$E_i = (\rho_1 c_1)^{-1} \int_{-\infty}^{\infty} p_i^2 \, dt \qquad (20)$$

or, using Plancherel's theorem[4],

$$E_i = (\rho_1 c_1)^{-1} \int_{-\infty}^{\infty} |\varphi(\omega)|^2 \, d\omega \qquad (21)$$

Using equation (10), the energy flux in the reflected wave is given by

$$E_r = (\rho_1 c_1)^{-1} \int_{-\infty}^{\infty} |\varphi(\omega) \exp(i 2|\omega|\varepsilon/\omega)|^2 \, d\omega$$

$$= (\rho_1 c_1)^{-1} \int_{-\infty}^{\infty} |\varphi(\omega)|^2 \, d\omega \qquad (22)$$

Comparing equations (21) and (22) it is seen that:

$$E_i = E_r .$$

Equation (22) also shows that despite the distortion of the shape of the pulse, the distribution of energy in the Fourier spectrum remains unaltered upon reflection.

2.5 The preceding development, leading to equation (18) is simply a more elegant and rigorous treatment of the material

covered in NavOrd 424. The derivation of equation (19) extends the treatment to include higher order reflections.

3. Experimental verification of the character of the phase distortion.

3.1 Experimental pressure - time curves were obtained by cathode ray oscilloscope recording of signals from tourmaline piezoelectric gauges[5]. The overall, effective high frequency response of the system depends upon the size of the gauge, which in turn is selected on the basis of expected pressure amplitude and corresponding sensitivity requirements. Gauge diameters varied from 1/2 to 1 inch, and it is estimated that the frequency at which the response would be down to 70% of midband would be 30 and 15 kc. respectively. (The high frequency response of the amplifiers was known to be much higher than that of the gauges.)

Cathode follower preamplifiers were used to obtain high input impedance. The low frequency response was determined by the overall time constant of the oscilloscope amplifier and is estimated to be down to 70% of midband at 0.1 cycle per sec.

The experiments were performed with 1/2 lb. pentolite charges and 25 and 55 lb. TNT charges in Vineyard Sound off Naushon Island near Woods Hole. Gauges were placed at a depth of about 25 ft. below the surface; charges at about 40 ft. Heavy tidal currents in this region insure rapid mixing of the water, which was always found to be very nearly isothermal over its average depth of about 70 ft.

The bottom of Vineyard Sound in this region is of firmly packed sand and is relatively smooth. Fathometer traverses show fairly gradual rise and fall of the order of 5 to 10 ft. over horizontal distances of the order of a few hundred feet.

The range, or horizontal distance between charge and gauges, was obtained by timing the interval between charge detonation and arrival of the primary shock wave at the gauge position. This time interval was then converted to distance by using the value of sound velocity in sea water of the salinity and temperature obtaining at the time of the experiment.

3.2 Sample experimental records for a variety of conditions are shown in Figures 2 and 3. The first event on all of these records is the incident exponential shock wave; the subsequent disturbances are reflections of successively higher order. In Figure 3, the emphasis is placed upon the comparison of theoretical and experimental curves for the first bottom reflection, denoted by BR, for various angles of incidence. It is believed that the critical angle for total reflection (θ_{1c}) is about 58° for these experiments. Taking the density ratio ρ_2/ρ_1 to be about 2.7*, the velocity ratio C_2/C_1 appears to be roughly 1.15.

The theoretical curves in Figure 3b are plotted at 15° intervals of the angle ε. The adjacent experimental curves

---

* Information supplied by Dr. Henry Stetson of the Woods Hole Oceanographic Institution.

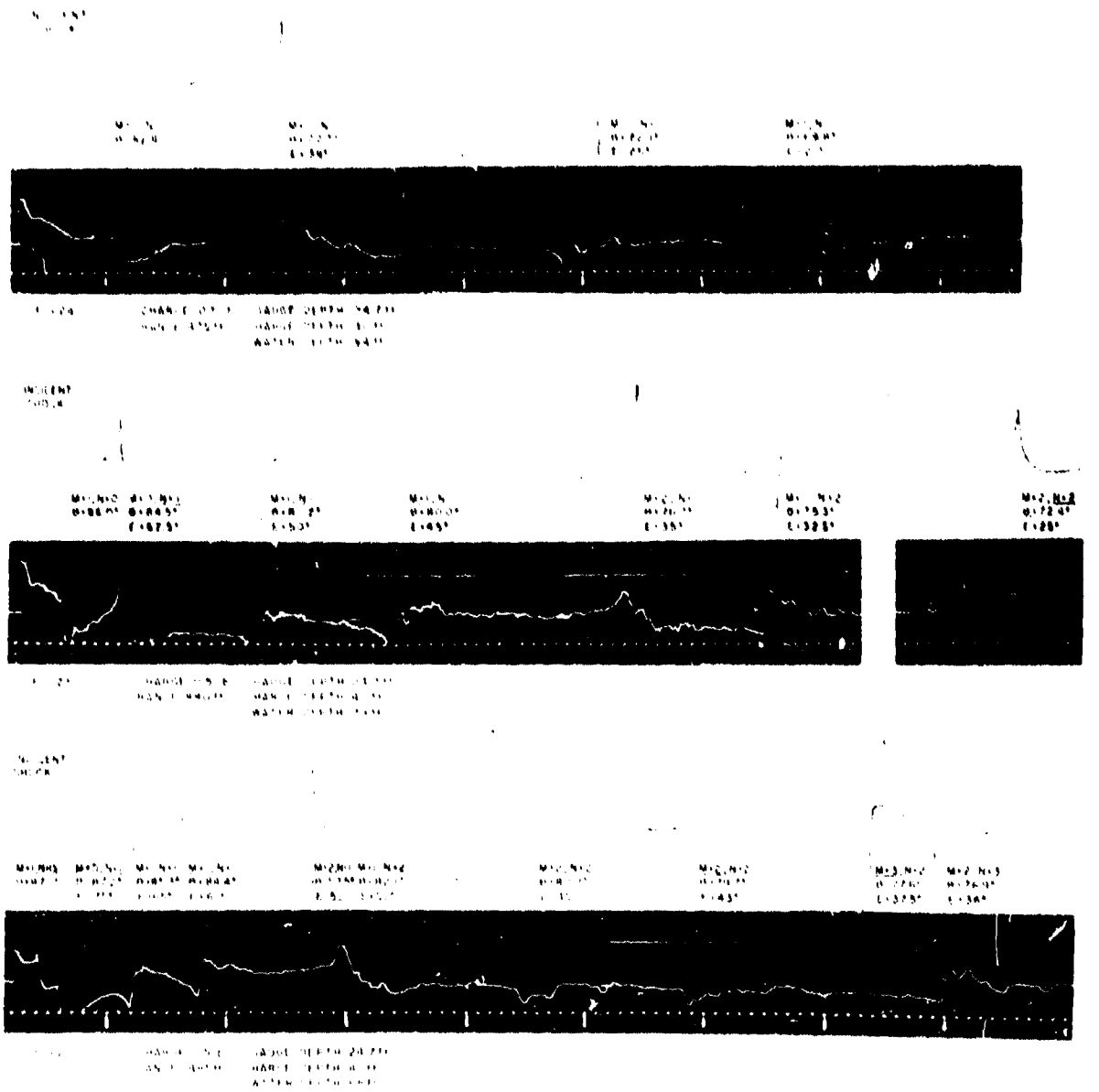


FIGURE 2

COMPARISON OF EXPERIMENTAL AND THEORETICAL PRESSURE-TIME CURVES INCLUDING HIGHER ORDER REFLECTIONS.

DATA TIMING WAVE ON EXPERIMENTAL RECORDS = 10 kc

THEORETICAL RECORDS ASSUMED DENSITY RATIO, $\frac{\rho_2}{\rho_1}$ = 2.7 ASSUMED VELOCITY RATIO, $\frac{C_2}{C_1}$ = 1.15

UNDERLINING M OR N INDICATES THAT THE FIRST REFLECTION OF THE SEQUENCE TOOK PLACE AT THE SURFACE OR BOTTOM, RESPECTIVELY

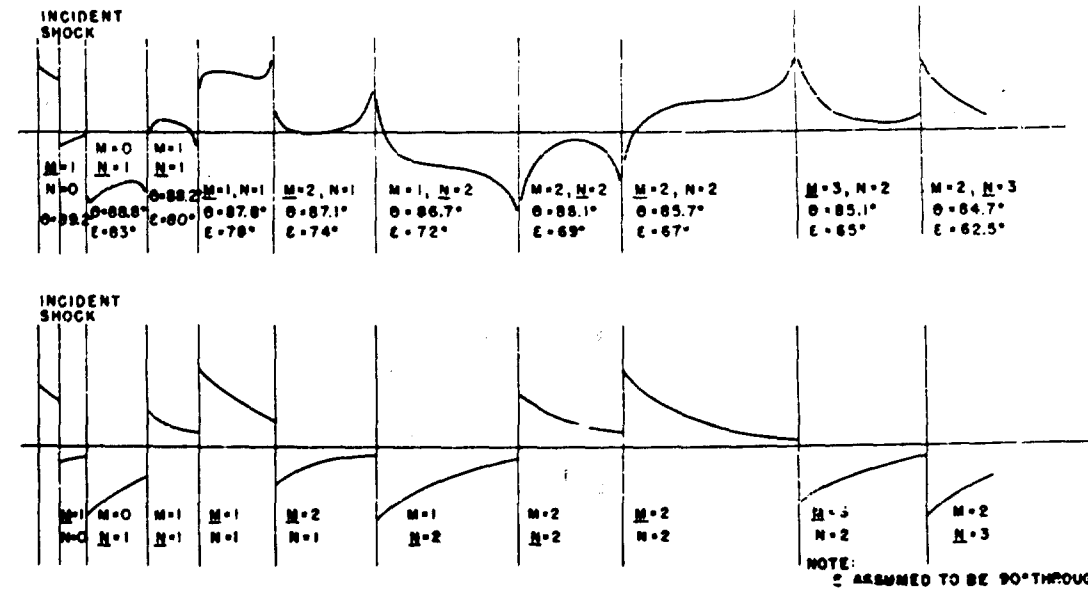




FIG. 2d CHARGE: 0.5 lb. RANGE: 4475 ft. GAUGE DEPTH: 24.7 ft. CHARGE DEPTH: 40 ft. WATER DEPTH: 80 ft.

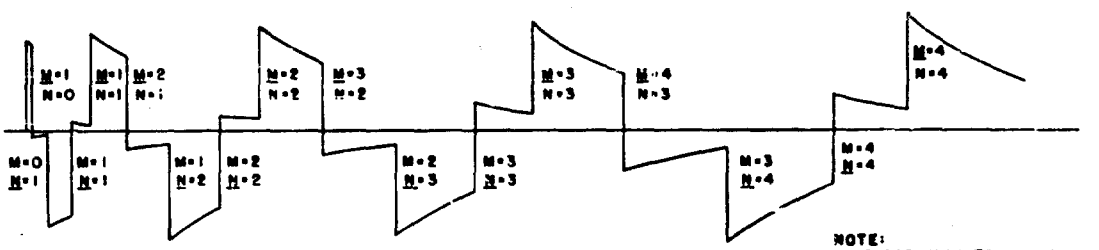




FIG. 2e CHARGE: 25 lb. RANGE: 9115 ft. GAUGE DEPTH: 24.7 ft. CHARGE DEPTH: 42 ft. WATER DEPTH: 92 ft.

FIGURE 2 (cont'd.)

COMPARISON OF EXPERIMENTAL AND THEORETICAL PRESSURE–TIME CURVES INCLUDING HIGHER ORDER REFLECTIONS.

DATA: TIMING WAVE ON EXPERIMENTAL RECORDS = 10 kc

THEORETICAL RECORDS: ASSUMED DENSITY RATIO, $\frac{\rho_2}{\rho_1} = 2.7$ ASSUMED VELOCITY RATIO, $\frac{c_2}{c_1} = 1.15$

UNDERLINING M OR N INDICATES THAT THE FIRST REFLECTION OF THE SEQUENCE TOOK PLACE AT THE SURFACE OR BOTTOM, RESPECTIVELY.

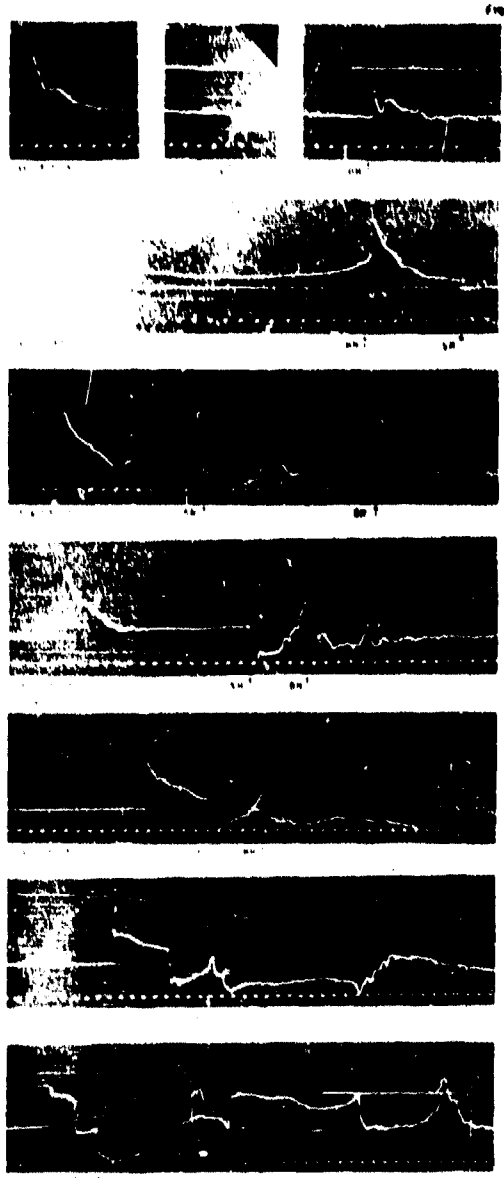


FIGURE 8a.

PRESSURE-TIME RECORDS SHOWING DISTORTION OF BOTTOM REFLECTION WITH INCREASING ANGLE OF INCIDENCE

θ ANGLE OF INCIDENCE AT THE SEA BED
BR BOTTOM REFLECTION
SR SURFACE REFLECTION
TIMING WAVE 10 KC

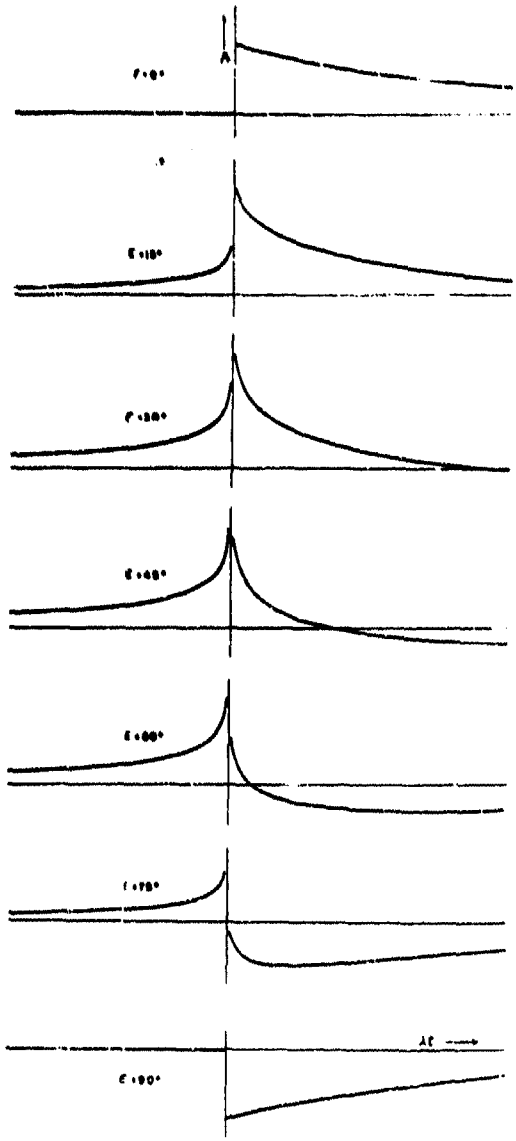


FIGURE 8b.

THEORETICAL PRESSURE-TIME CURVES FOR BOTTOM REFLECTION OF AN EXPONENTIAL SHOCK WAVE.

INCIDENT WAVE: $p_i = e^{-\lambda t}$

REFLECTED WAVE $p_r = P \cos 2\epsilon + P \sin 2\epsilon$

PHASE SHIFT FOR VARIOUS ANGLES OF INCIDENCE ϵ

were selected because of their resemblance to the theoretical ones rather than on the basis of known apriori values of $\mathcal{E}$. An objective mathematical method of analyzing the experimental curve to obtain the experimental $\mathcal{E}$ has not been successfully developed, and at this time it is only possible to guess at the angles by qualitative comparison of the shapes of the experimental and theoretical curves.

Figure 3 illustrates the very close agreement between theory and experiment as to the progressively changing shape of the first bottom reflection with increasing angle of incidence, including the complete phase inversion predicted at glancing angles.

Figure 2 compares theoretical and experimental curves for an entire record of several milliseconds duration. Here account is taken in the theoretical curves of the superposition of the various reflections which follow closely upon each other and of the cumulative phase shifts taking place in higher order reflections undergoing more than one incidence at the bottom.

The theoretical curves are calculated using the assumed values of 2.7 for ρ_2/ρ_1, 1.15 for C_2/C_1, and the values of θ_i for the various reflections to establish the values of $\mathcal{E}$. The values of θ_i for each reflection are obtained from the geometry of the particular experiment. (The shapes of the curves are not critically sensitive to the value adopted for C_2/C_1 so that a comparison of experimental results with theoretical shapes

would not afford a good, critical method of selecting the velocity ratio.)

3.3 The striking measure of agreement between theoretical and experimental curves in Figure 2 affords added confirmation of the predicted effects of the phase distortion. It must be remembered that the theoretical analysis assumed (1) plane rather than spherical waves, (2) smooth, plane, horizontal, fluid bottom rather than the actual sloping, undulating semi-solid one, (3) purely exponential decay of the primary shock wave, whereas it is known that the decay is exponential only for an interval equal to the time constant and then proceeds much more slowly.

It is not surprising, therefore, that various discrepancies can be detected upon closer examination of Figure 2. Some reflections seem to disappear on the experimental records; others differ appreciably from the predicted shape; in some cases there are appreciable discrepancies in arrival times. All of these discrepancies could reasonably stem from errors in our knowledge of depths and ranges and from deviations from the idealized model assumed in the theoretical analysis. As would be expected, agreement between experimental and theoretical curves becomes poorer with increasing order of reflection.

Many records were obtained in which the peak of the first bottom reflection was considerably higher than that of the incident shock, and much of the true peak may actually be

lost because of the limited high frequency response of the recording system. The theoretical peak pressure of the reflected wave is infinite since, in equation (18), $p_r \to \infty$ as $t \longrightarrow 0$. This singularity is associated with the assumption of a mathematical discontinuity (perfect shock) in the incident pressure wave. For a shock with a finite rise time, the reflected peak would be finite. Even in the case of mathematical discontinuity treated above, energy conservation is not violated since the function p_r is of integrable square as shown in Section 2.4.

The high experimental peaks attest to the effect of the steepness of the shock front even though the rise time is actually finite.

The slowly rising precursor which leads the peak of the reflection is associated with the propagation of a certain amount of energy through the reflecting medium at a velocity higher than that of the primary medium. In the plane wave treatment, the precursor starts rising at -00 since the plane wave must essentially be considered as originating at an infinite distance (or time) from the point of observation. For a spherical wave originating at a given point source, the precursor would start at a finite time before arrival of the reflected peak, the time interval being determined by the least time path connecting the origin and point of observation.

3.4 In cases of shallow layer propagation, successive higher

order reflections from both boundaries will follow the primary wave. The case of interest here is one in which the lower boundary is a plane, horizontal sea bed as treated above, and the upper boundary is the free surface of the water. Since the sound velocity in air is lower than that in water, the surface reflection does not involve any critical angles or phase shifts other than the usual acoustic inversion at the free surface. (Finite amplitude effects introduce their own complications, which are not considered in this treatment.)

The various higher order reflections will in general undergo more than one reflection from the sea bed. For example, the reflection designated by the notation M = 1, N = 2 undergoes the following sequence before reaching the point of observation: reflection from the bottom, reflection of this wave from the surface, and again a reflection from the bottom. The reflections all take place at the same angle of incidence, and the resulting pressure wave is given by equation (19).

Equation (19) makes apparent the cumulative nature of the successive phase shifts. For example in the case of reflection M = 1, N = 2, cited above, equation (19) becomes

$$p_{1,2r}(t) = -p_i(t)\cos 4\varepsilon - F(t)\sin 4\varepsilon \qquad (23)$$

If the geometry and acoustic properties are such that $\varepsilon = 45^\circ$, equation (23) reduces to

$$p_{1,2r}(t) = p_i(t) \,, \qquad (24)$$

and this particular reflection is identical in form and amplitude with the incident wave, the various phase shifts and inversions having neutralized each other exactly. In general, of course, the cumulation will be such as to give more or less distorted forms depending upon the geometry and other parameters.

The experimental record in Figure 2b illustrates a case in which cumulative phase shift produces a reflection, $\underline{M = 1, N = 2}$, which is an almost perfect reconstruction of the incident shock wave.

3.5 The changing character of the wave with increasing range is also illustrated by the sequence in Figure 2. It is seen how the reflections become more distorted and how they increasingly interfere more strongly with each other and with the primary shock wave as all the superposed disturbances get closer and closer together.

The increasing interference is, of course, a consequence of the spherical nature of the waves, since in the case of truly plane waves "range" would have no meaning and the time intervals would be fixed by Θ_1 and the position of the point of observation.

At very large ranges so many higher order reflections would overlap and interfere with each other that the simple treatment developed above would no longer be useful and the resultant wave would be better described in terms of the normal mode analysis of Pekeris[6].

Figures 2d and 2e illustrate this increasing complexity at very long ranges. (One theoretical curve in Figure 2d and the theoretical curve in Figure 2e are plotted on the assumption that all orders of reflection take place at glancing incidence, without entering into the detailed calculations required to account for the actually expected phase shifts.) It is evident that even in Figure 2e, where many processes have probably participated in changing the character of the wave, there is still a general correspondence between the principal features of the experimental and theoretical curves. In the experimental record, the primary shock wave shows evidence of having been cut down by the finite amplitude effects discussed by Keil[15]; viscous attenuation and gauge size have also played their parts, and as a result the initial portion is very much lower in amplitude than the linear theory predicts. The higher order reflections, however, are of the expected amplitude and show the gradually increasing amplitude of oscillation predicted by the theory.

The marked rounding and smoothing of the wave which is apparent in the experimental record in Figure 2e is too strong to be ascribed entirely to viscous attenuations and gauge size effects. At least part of it must probably be ascribed to absorption or inelastic losses in the various reflections, etc.

The treatment developed in this paper affords a detailed description of the progressive changes taking place in the pressure wave during shallow water propagation between the region close to the charge, discussed by R. H. Cole[7], and the very long range effects treated theoretically by Pekeris[6], and experimentally by Ewing[6] and his co-workers at Columbia University and the Woods Hole Oceanographic Institution.

It should also be noted that when acoustic pulses are reflected from media of greater sound velocity at angles exceeding the critical, it is no longer possible to attach meaning to any single quantity described by the term "reflection coefficient." The reflection of the pulse so distorts its shape and amplitude that descriptions in terms of reflection coefficients become virtually useless.

It is somewhat surprising to find that the naive approximation of the bottom as a fluid medium proves as successful as it does in predicting the experimental curves. In this connection it is interesting to note Dr. Ewing's observation (privately communicated to the authors) that even limestone bottoms are more successfully treated as fluids than as solids in his very long range experiments.

4. Alternative treatment of plane wave reflection as a boundary value problem.

4.1 It will be noted in the harmonic wave solutions (equations (6) and (7)) that t and x always appear in the combination $(t - \alpha_1 x)$ where $\alpha_1 = C_1^{-1} \sin\theta_1$. Thus the wave pattern as a whole moves in the direction of increasing x with a velocity $C_1/\sin\theta_1$.

Since we are interested in pulses rather than in harmonic wave trains, we are led to investigate the conditions under which a more general pressure field may be propagated with constant velocity parallel to the surface of discontinuity. Such a pressure field may be written in the form:

$$\begin{aligned} p_i + p_r \equiv p_1 &= f(y, C_1 t - \gamma x) = f(y, u) \\ \text{and} \quad p_2 &= g(y, C_1 t - \gamma x) = g(y, u) \end{aligned} \tag{25}$$

where $u \equiv C_1 t - \gamma x$

The pressure fields in regions 1 and 2 must satisfy the wave equations:

$$\begin{aligned} \nabla^2(p_i + p_r) &= \frac{1}{C_1^2} \frac{\partial^2 (p_i + p_r)}{\partial t^2} \\ \nabla^2 p_2 &= \frac{1}{C_2^2} \frac{\partial^2 p_2}{\partial t^2} \end{aligned} \tag{26}$$

Combining equations (25) and (26) we have:

$$\frac{\partial^2 f}{\partial y^2} + (\gamma^2 - 1)\frac{\partial^2 f}{\partial u^2} = 0 \qquad (27)$$

$$\frac{\partial^2 g}{\partial y^2} + \left(\gamma^2 - \frac{c_1^2}{c_2^2}\right)\frac{\partial^2 g}{\partial u^2} = 0 \qquad (28)$$

4.2 Considering the situation in which $c_2 > c_1$, there are three distinct cases for which the equations must be solved:

Case (1) : $1 > c_1/c_2 > \gamma$

Case (2) : $1 > \gamma > c_1/c_2$

Case (3) : $\gamma > 1 > c_1/c_2$

Comparison with the previous derivations shows that γ corresponds to the sine of the angle of incidence, i.e. $\gamma = \sin\theta_1$. In case (1) both equations (27) and (28) are of the hyperbolic type; physically this corresponds to the situation in which θ_1 is less than the critical angle since γ is less than c_1/c_2. The solution for case (1) must therefore prove to be the usual undistorted acoustic reflection.

In case (2) equation (27) is hyperbolic while equation (28) is elliptic. This corresponds to the situation in which θ_1 lies between the critical angle and $\pi/2$, and the solution corresponds to that developed in Section 2 above.

In case (3) both equations (27) and (28) are elliptic, and do not describe any real physical situation since $\sin\theta_1$ exceeds unity. (It can be shown also that the only

possible mathematical solution for this case is the trivial one of zero pressure throughout the system.) We are therefore concerned only with cases (1) and (2).

4.3 Mathematical solution of case (1): Since both equations (27) and (28) are hyperbolic, a general progressive wave solution may be written down at once.

$$f(y,u) = f_1(u+\mu_1 y) + f_2(u-\mu_1 y) \tag{29}$$

$$g(y,u) = g_1(u+\mu_2 y) + g_2(u-\mu_2 y) \tag{30}$$

where

$$\mu_1^2 + \gamma^2 = 1 \tag{31}$$

$$\mu_2^2 + \gamma^2 = c_1^2/c_2^2 \tag{32}$$

and where f_1, f_2, g_1 and g_2 are arbitrary functions.

Making use of the boundary conditions given by equations (4) and (5):

$$f_1(u) + f_2(u) = g_1(u) + g_2(u) \tag{33}$$

$$\frac{\mu_1}{\rho_1}\left[\frac{df_1(u)}{du} - \frac{df_2(u)}{du}\right] = \frac{\mu_2}{\rho_2}\left[\frac{dg_1(u)}{du} - \frac{dg_2(u)}{du}\right] \tag{34}$$

Integrating equation (34):

$$\frac{\mu_1}{\rho_1}\left[f_1(u) - f_2(u)\right] = \frac{\mu_2}{\rho_2}\left[g_1(u) - g_2(u)\right] \tag{35}$$

The constant of integration in equation (35) has been set equal to zero since it does not represent any progressive wave solutions.

Equations (33) and (35) provide two relations among the four functions f_1, f_2, g_1 and g_2. Thus two of these functions may be arbitrarily assigned and the remaining two expressed in terms of them. To realize the condition of plane wave reflection under discussion, we set $g_2 = 0$ and let f_1 represent the incident pulse given by

$$p_i = f_1(C_1 t - \gamma x + \mu_1 y) \tag{36}$$

The reflected and transmitted waves are then obtained by simultaneous solution of equations (33) and (35):

$$p_r(C_1 t - \gamma x - \mu_1 y) = f_2 = \frac{\mu_1\rho_2 - \mu_2\rho_1}{\mu_1\rho_2 + \mu_2\rho_1} f_1 \tag{37}$$

$$p_2(C_1 t - \gamma x + \mu_2 y) = g_1 = \frac{2}{1 + \frac{\mu_2\rho_1}{\mu_1\rho_2}} f_1 \tag{38}$$

where
$$\mu_1 = \cos\theta_1$$
$$\mu_2 = \frac{C_1}{C_2}\cos\theta_2 \tag{39}$$

These are the familiar results of conventional acoustic reflection theory and have been developed principally in order to illustrate the nature of the present mathematical treatment.

If we were interested in the case of a plane wave progressing from a medium of high to low sound velocity, we could set $f_1 = 0$ and express g_1 and f_2 in terms of g_2. The results would be analagous to equations (37) and (38).

4.4 We now consider case (2) where equation (27) is hyperbolic while equation (28) is elliptic. The latter equation does not have a progressive wave solution, and the problem is somewhat more complicated than in case (1). Under such circumstances, if we specify the pressure along the surface $y = o$, then the solution is completely determined in the region $y < o$, provided that we require it to remain finite as $y \longrightarrow -\infty$. This pressure field can be expressed in terms of the Fourier integral:

$$g(y,u) = (2\pi)^{-1}\int_{-\infty}^{\infty} d\omega \int_{-\infty}^{\infty} g(0,v)\, \exp[i\omega(u-v) + i|\omega|\nu y]\, dv \qquad (40)$$

where

$$\nu^2 \equiv \gamma^2 - C_1^2/C_2^2 \qquad (41)$$

from equation (28).

The boundary conditions (4) and (5) determine the pressure and normal derivative of the pressure at the surface of discontinuity. This completely fixes the solution in the hyperbolic region, where we can again write the progressive wave

solution

$$f(y,u) = f_1(u+\mu, y) + f_2(u-\mu, y) \qquad (29)$$

Application of the boundary conditions and equation (40) gives:

$$\left.\begin{aligned} f_1(u) + f_2(u) &= g(0,u) \equiv A(u) \\ A(u) &= (2\pi)^{-1} \int_{-\infty}^{\infty} d\omega \int_{-\infty}^{\infty} g(0,v) \exp[i\omega(u-v)]\, dv \end{aligned}\right\} \qquad (42)$$

and

$$\frac{\mu_1}{\rho_1}\left[\frac{df_1(u)}{du} - \frac{df_2(u)}{du}\right] = \frac{\nu}{2\pi\rho_2} \int_{-\infty}^{\infty} d\omega \int_{-\infty}^{\infty} g(0,v)\, |\omega| \exp[i\omega(u-v)]\, dv \qquad (43)$$

Integrating with respect to u, equation (43) becomes:

$$\left.\begin{aligned} \frac{\mu_1}{\rho_1}\left[f_1(u) - f_2(u)\right] &= \frac{\nu}{2\pi i \rho_2} \int_{-\infty}^{\infty} d\omega \int_{-\infty}^{\infty} g(0,v)\, \frac{|\omega|}{\omega} \exp[i\omega(u-v)]\, dv \\ &\equiv \nu B(u)/\rho_2 \end{aligned}\right\} \qquad (44)$$

Equations (42) and (44) serve to define the functions A (u) and B (u). Solving for f_1 and f_2 in terms of A and B, we have:

$$\frac{2\mu_1}{\rho_1} f_1(u) = \frac{\mu_1}{\rho_1} A + \frac{\nu}{\rho_2} B \qquad (45)$$

$$\frac{2\mu_1}{\rho_1} f_2(u) = \frac{\mu_1}{\rho_1} A - \frac{\nu}{\rho_2} B \qquad (46)$$

For convenience, at this point we define the phase angle ε by:

$$\tan\varepsilon \equiv \frac{\nu\rho_1}{\mu_1\rho_2} = \frac{\rho_1}{\rho_2}\left(\frac{\gamma^2 - c_1^2/c_2^2}{1-\gamma^2}\right)^{1/2} \tag{47}$$

This is identical with the angle previously identified as the phase shift in the simple harmonic treatment. Also let

$$M \equiv \left(\frac{\mu_1^2}{\rho_1^2} + \frac{\nu^2}{\rho_2^2}\right)^{1/2} \tag{48}$$

We now express A and B in terms of the Fourier transforms of A:

$$A(u) = (2\pi)^{-1/2}\int_{-\infty}^{\infty} \psi(\omega)\exp(i\omega u)\,d\omega \tag{49}$$

$$B(u) = (2\pi)^{-1/2}\int_{-\infty}^{\infty} \frac{|\omega|}{i\omega}\psi(\omega)\exp(i\omega u)\,d\omega \tag{50}$$

where,

$$\psi(\omega) = (2\pi)^{-1/2}\int_{-\infty}^{\infty} g(0,v)\exp(-i\omega v)\,dv \tag{51}$$

Dividing equation (45) by M and utilizing (47), (49), and (50), we have:

$$\frac{2\mu_1}{\rho_1 M} f_1(u) = A\cos\varepsilon + B\sin\varepsilon$$
$$= (2\pi)^{-1/2}\int_{-\infty}^{\infty}\psi(\omega)\exp\left[i\omega u - i|\omega|\varepsilon/\omega\right]d\omega \tag{52}$$

Similarly from equation (46):

$$\frac{2\mu_1}{\rho_1 M} f_2(u) = A\cos\varepsilon - B\sin\varepsilon$$
$$= (2\pi)^{-1/2}\int_{-\infty}^{\infty} \psi(\omega)\exp\left[i\omega u + i|\omega|\varepsilon/\omega\right] d\omega \tag{53}$$

Since we shall denote the known incident wave by f_1, it will be convenient to determine ψ in terms of f_1 or its Fourier transform. Expressing f_1 as a Fourier integral:

$$f_1(u) = (2\pi)^{-1/2}\int_{-\infty}^{\infty} \varphi(\omega)\exp(i\omega u)\, d\omega \tag{54}$$

where

$$\varphi(\omega) = (2\pi)^{-1/2}\int_{-\infty}^{\infty} f_1(v)\exp(-i\omega v)\, dv \tag{55}$$

Comparing equations (52) and (54), we see that:

$$\psi(\omega) = \frac{2\mu_1}{\rho_1 M}\varphi(\omega)\exp(i|\omega|\varepsilon/\omega) \tag{56}$$

and combining equations (53) and (56):

$$f_2(u) = (2\pi)^{-1/2}\int_{-\infty}^{\infty} \varphi(\omega)\exp\left[i\omega u + i\,2|\omega|\varepsilon/\omega\right] d\omega \tag{57}$$

From here on the solution becomes identical with that of equation (10) in section 2 above.

4.5 The purpose of this alternative development has been to show that the distortion of an acoustic pulse on oblique reflection can be treated directly as a boundary value problem without recourse to the initial harmonic wave treatment developed by Rayleigh[1] and described in section 2. The phase angle $2\mathcal{E}$ defined in equation (47) can a posteriori be identified as the phase shift which is applied to the Fourier spectrum components of the incident pulse, but it is not a priori introduced as such.

4.6 A few remarks may be made at this point concerning the pressure field, p_2, in the bottom. An expression for p_2 may be obtained in section 2 by combining equations (7) and (9) or from the treatment in this section by combining equations (40), (51), and (56). In either case, one obtains the form:

$$p_2 = 2\cos\mathcal{E}\,(2\pi)^{-1/2}\int_{-\infty}^{\infty}\varphi(\omega)\exp\left[i\omega u + i\frac{\mathcal{E}}{\omega}|\omega| + |\omega|\nu y\right]d\omega$$

$$= 2\cos^2\mathcal{E}\,(2\pi)^{-1/2}\int_{-\infty}^{\infty}\varphi(\omega)\exp\left[i\omega u + |\omega|\nu y\right]d\omega$$

$$+ \sin 2\mathcal{E}\,(2\pi)^{-1/2}\int_{-\infty}^{\infty}\frac{i|\omega|}{\omega}\varphi(\omega)\exp\left[i\omega u + |\omega|\nu y\right]d\omega$$

where ν is identical with the quantity θ_{2r} defined in section 2.

It will be seen that the integrand in the expression for p_2 is not analytic because of the presence of the

term $\exp(i\omega/\nu y)$. (One can easily demonstrate this by showing that the Cauchy - Riemann conditions are not satisfied.) For this reason, it is not possible to evaluate an expression for P_2 by means of the usual methods of contour integration, which are only applicable to analytic functions. It is felt that whatever additional information might be gained would probably not be sufficiently valuable to justify further laborious manipulation of the complex integrals involved.

5. Reflection of spherical waves.

5.1 The preceding discussions (section 3 in particular) have been based on certain simplifying assumptions which may be restated briefly as follows:

1. The ray approximation was used to calculate the paths along which energy passed from the source to the receiver. These rays included direct transmission through the water and various orders of reflection from the surface and bottom.

2. The shape of the individual reflections was obtained by using the plane wave theory of Section 2.

3. The effect of the point source was allowed for by assuming that the amplitude of the wave was subject to normal spherical attenuation ($\sim 1/R$). No other effects due to propagation from a point source were taken into account.

As will be seen later, these approximations represent the first order term in an asymptotic expansion of the spherical wave solution. Before proceeding to this asymptotic expansion,

we shall illustrate by means of a simple example how these approximations must fall down for angles of incidence near the critical angle.

5.8 The example is sketched in Figure 4. Path ABC is the normal path of a reflected ray, making equal angles of incidence and reflection (θ) with the bottom. The angle θ would be used in calculating the phase shift ε for this wave. Path AB'B"C is the path of a ray entering and leaving the bottom at the critical angle of incidence (θ_c), and traveling just within the bottom from B' to B".

We seek to calculate the difference in time of propagation along the two paths and also to show that AB'B"C is the least time path for all rays from A to C which touch the bottom. To this end we make the following constructions: In order to show that AB'B is a least time path, consider a varied path AbB. Extend AB' and drop a perpendicular bD to it from b. Then we have:

$$\sin \theta_c = \frac{B'd}{B'b} = \frac{C_1}{C_2} \qquad (58)$$

This expression shows that propagation from B' to d at velocity C_1 takes the same time as propagation from B' to b at velocity C_2. Hence the difference in time between the two

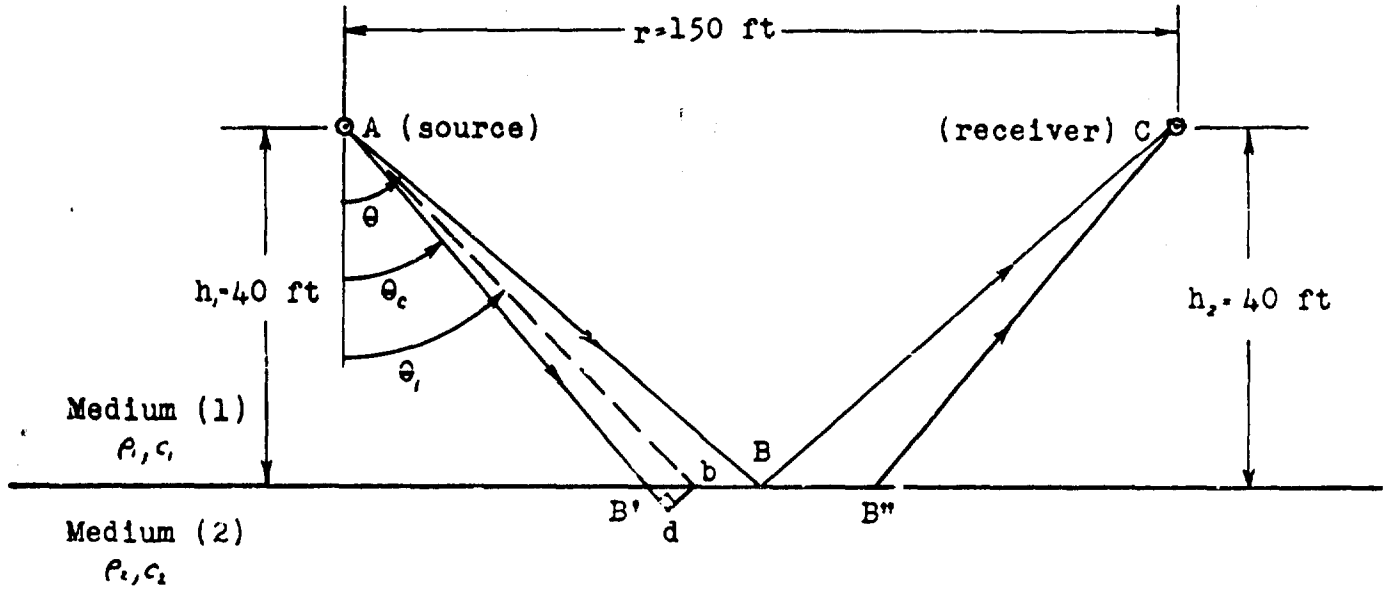


Fig. 4

Simple geometrical arrangement of source and receiver.

$c_1 = 5000$ ft/sec

$c_2 = 1.15c_1 = 5750$ ft/sec

angle of incidence, $\theta = \arctan(75/40) = 61.93°$

critical angle, $\theta_c = \arcsin(1/1.15)$

paths AbB and AB'B is:

$$\Delta t_b = \frac{Ab}{C_1} - \frac{Ad}{C_1} = \frac{Ab}{C_1}\left[1 - \cos(\theta_1 - \theta_c)\right] \qquad (59)$$

where

$$Ab = h_1 \sec \theta_1 \qquad (60)$$

This expression obviously has a minimum of zero for $\theta_1 = \theta_c$ and AB'B"C is then the least time path as was to be proved. The total difference in time of propagation for ABC and AB'B"C is now:

$$\Delta t = 2\frac{AB}{C_1}\left[1 - \cos(\theta - \theta_c)\right] \qquad (61)$$

$$\cong \frac{AB(\theta - \theta_c)^2}{C_1}, \quad \text{(for small } \theta - \theta_c\text{)} \qquad (62)$$

(Note: in case that $h_1 \neq h_2$, it would be necessary to replace AB by $\frac{1}{2}$ (AB + BC), in this expression.)

5.3 For the geometry assumed in Figure 4:

$$\theta - \theta_c = .0267 \text{ radians}$$

$$\Delta t = .012 \text{ milliseconds}$$

To see how this affects the reflected wave, we consider a particular case where the source is emitting an exponential shock wave of time constant .150 milliseconds, which corresponds roughly to an explosion of about 0.5 lbs. of TNT. The theoretical pressure time curve using the plane wave reflection theory(which

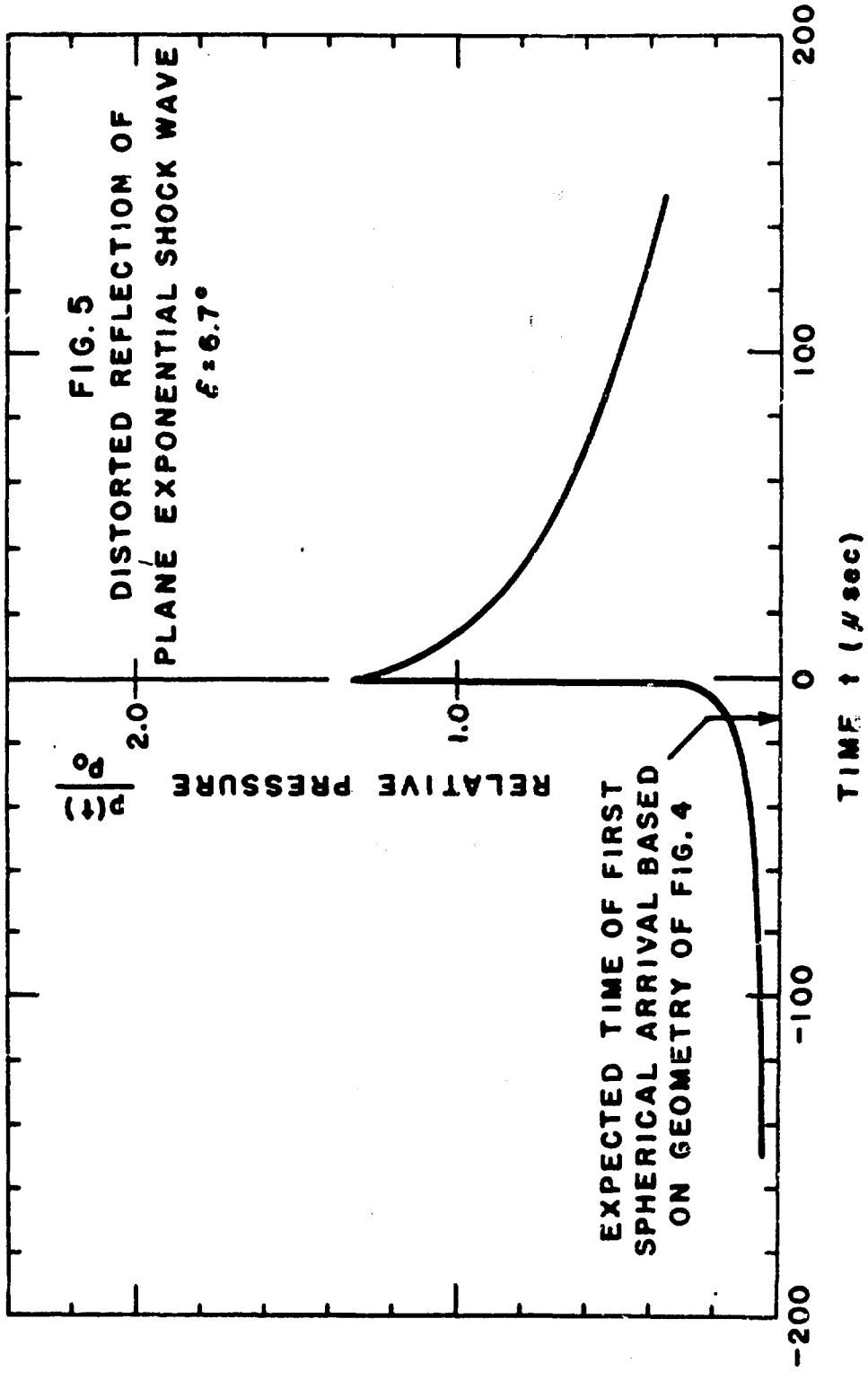
gives $\mathcal{E} = 6.71^{\circ}$) is shown in Figure 5. In this figure the origin of time is the instant of arrival of a wave which has traveled along the path ABC. The arrow indicates the expected arrival time of sound which has traveled along path AB'B"C. Since this is the earliest instant at which sound should begin to arrive at the receiver, we can see from the plot that the plane wave approximation is in considerable error. It is also qualitatively evident that the major errors occur in the treatment of the lower frequency components.

If the range is increased from 150 ft. to 200 ft., the difference of time between the two paths increases to about 0.4 milliseconds. This is due principally to the fact that $\theta-\theta_c$ increases to .136 radians, that is by a factor of 5.1 over the previous value, and Δt varies as $(\theta-\theta_c)^2$. This value of Δt is nearly three times as large as the time constant of the wave, so the plane wave approximation should be fairly good for ranges exceeding 200 ft. under the assumed conditions.

5.4 It is possible to give a more exact treatment of the reflection of a spherical wave from a surface of discontinuity[6,8]. Here we shall merely quote some of the pertinent results from ref. (6) p. 49. Pekeris gives the following asymptotic expression for the "reflection coefficient" at a given angular frequency ω :

$$\left\{\frac{\cos\theta-b\delta}{\cos\theta+b\delta}-\frac{iC_1b\nu^2}{\omega R\delta^3(\cos\theta+b\delta)^3}\left[\sin^2\theta\cos^2\theta+2\delta^2(1+b\delta\cos\theta)+3b\delta\sin^2\theta\cos\theta\right]\right.$$
$$\left.+O\left(C_1^2/\omega^2R^2\right)\right\} \qquad (63)$$

1510


FIG. 5
DISTORTED REFLECTION OF
PLANE EXPONENTIAL SHOCK WAVE
ε=6.7°
RELATIVE PRESSURE
$\frac{p(t)}{p_0}$
2.0
1.0
200
100
0
-100
-200
TIME t (μ sec)
EXPECTED TIME OF FIRST
SPHERICAL ARRIVAL BASED
ON GEOMETRY OF FIG. 4

where $R = \left[r^2 + (h_1 + h_2)^2\right]^{1/2}$; $\delta = \left(\frac{C_1^2}{C_2^2} - \sin^2\theta\right)^{1/2}$

$\nu = \left(\frac{C_1^2}{C_2^2} - 1\right)^{1/2}$; $\cos\theta = \frac{h_1 + h_2}{R}$

$b = \rho_1/\rho_2$

(Note that δ becomes imaginary if $\theta > \theta_c$). In addition a spherical attenuation proportional to $1/R$ is to be applied to the amplitude of the wave.

The first term of this expansion is the familiar reflection coefficient for plane waves incident at an angle θ . The second term is frequency dependent and represents a correction term which will be small for high frequencies, that is provided $C_1/\omega_1 R\delta^3 = \lambda/2\pi R\delta^3$ is small compared to unity (λ is the wave length corresponding to angular frequency ω). For angles not too close to the critical angle (which makes $\delta = 0$), the requirement is essentially that R be much greater than a wave length.

For the geometry assumed in Figure 4, we have

$$|\delta| \cong .15$$

Taking as a typical wave length the distance a signal would travel in twice the time constant:

$$\lambda = 1.5 \text{ ft.},$$

we have

$$\lambda/2\pi R|\delta|^3 \cong .41$$

This confirms that the plane wave approximation is poor for the case of Figure 4, and in general when the angle of incidence is near the critical angle.

5.5 It is evident from the preceding discussion that the plane wave approximation fails in two principal respects. (a) It does not give a reflected pressure time curve with a precursor starting at a finite time prior to arrival of the reflected peak as would be expected on the basis of the ray picture, but instead shows a precursor starting at $-\infty$. This is evidence of error in the treatment of the low frequency components. (b) Equation (63) shows that in the general spherical case, the phase shift at a given ω is a complicated function of ω instead of being independent of ω as in the plane wave theory. This means that the shapes of reflections based on plane wave theory would be somewhat in error even in the neighborhood of the peak, where the higher frequency components dominate. That this error is not very serious at reasonably large distances from the charge is demonstrated by the general agreement between theory and experiment in Figures 2 and 3.

The rigorous calculation of the shape of the reflected pulse when an incident exponential is subjected to the shifts implied in equation (63) would be an exceedingly difficult problem.

6. Comments with respect to oblique reflection of strong shocks.

6.1 The theory developed in the foregoing sections is purely linear, applicable only to pressure waves which do not deviate appreciably from the restrictions of the acoustic approximations, and it is not possible to discuss the oblique reflection of strong shocks (such as air blast reflected from ground or water surfaces) in the same terms.

Many workers have discussed the strong shock problem, but the theory has so far met with rather limited success. In view of the results described above, one is led to question whether present theories take proper account of the interactions occurring at the boundary surface and to speculate as to the type of experimental investigation which might cast some light on the problem.

One suggestion (made by Dr. W. D. Kennedy) is the systematic comparison of pressure time curves obtained at the plane which is the perpendicular bisector of the line connecting two simultaneously detonated charges, with curves obtained close to a rigid boundary (such as a piece of armor plate), the charge being detonated at a perpendicular distance from this surface equal to half the charge spacing in the first experiment. Such an experiment would essentially provide a test of the hypothesis that the rigid plane boundary can be replaced by an image charge to satisfy the boundary conditions at the surface of discontinuity.

Furthermore, it is conceivable that various departures

from expected scaling laws which have been observed under conditions of Mach reflection near the ground in air blast studies may be at least partly associated with distortions originating in interaction with the reflecting medium as well as with the afterburning effects to which all of the deviations are now generally ascribed.

The development of an accurate theory of the pressure-time curve of an obliquely reflected strong shock wave presents an extremely difficult if not insoluble problem, and it is felt that the most fruitful approach at the present time lies in further experimental investigation of pressure-time curves in air blast and in shock tubes. Results of such investigations may in turn provide fresh assumptions and starting points for theoretical development.

II. The effect of viscous attenuation on exponential shock waves.

Introduction

7.1 In view of the fact that shock wave measurements at relatively large distances from the origin of the explosion are now becoming available, it seems appropriate to examine the effect of viscous attenuation upon exponential shock waves. It is a familiar result of acoustic theory[9] that harmonic waves would be subject to an exponential attenuation of amplitude with increasing range of propagation, and that the attenuation coefficient depends upon the viscous forces and the square of the frequency of the harmonic wave.

Liebermann[10] has recently reported accurately measured experimental values of the attenuation coefficient as a function of frequency for harmonic waves in sea water, and it is our object to apply these results to an analysis of effects one might expect to observe in the long range propagation of low amplitude shock waves.

7.2 It should be noted at this point that the object of this analysis is not that of determining the so called "thickness of a shock front" which many investigators have discussed[7]. We start with the essential result of these investigations, that the shock front thickness is vanishingly small at large amplitudes, and proceed to investigate the change in shape which might be expected due to selective attenuation of the higher frequency components in accordance with Liebermann's empirical data.

The analysis contains a number of rough approximations and is obviously open to criticism on that account, but we feel that the present status of knowledge and interest in this field does not justify expenditure of the time and effort which a more refined theory would require.

8. The effect of viscosity alone on a low amplitude exponential shock.

8.1 The propagation of plane sound waves in a viscous medium is governed by the equation[9]:

$$\frac{\partial^2 p}{\partial t^2} = c^2 \frac{\partial^2 p}{\partial x^2} + \frac{4}{3} \nu \frac{\partial^3 p}{\partial x^2 \partial t} \qquad (64)$$

where the notation is that adopted by Lamb. This equation may be reduced to an ordinary differential equation in x by carrying out a Laplace transformation with respect to the time. The transformation is given by the reciprocal formulae[11].

$$P(x,\gamma) = \int_0^\infty p(x,t)\, \exp(-\gamma t)\, dt \quad , \quad Re\,\gamma > \alpha \tag{65}$$

$$p(x,t) = \frac{1}{2\pi i} \int_{\sigma-i\infty}^{\sigma+i\infty} P(x,\gamma)\, \exp(\gamma t)\, d\gamma \quad , \quad \sigma > \alpha \tag{66}$$

The transforms of the derivatives are given by

$$\left.\begin{aligned} \int_0^\infty \frac{\partial p}{\partial t} \exp(-\gamma t)\, dt &= \gamma P(x,\gamma) - p(x,0) \\ \int_0^\infty \frac{\partial^2 p}{\partial t^2} \exp(-\gamma t)\, dt &= \gamma^2 P(x,\gamma) - \gamma p(x,0) - \frac{\partial p(x,0)}{\partial t} \end{aligned}\right\} \tag{67}$$

The physical case of interest here is the propagation of a transient wave which vanishes everywhere for $t \leq 0$ and is then a known function of the time at $x = 0$. These conditions require:

$$\left.\begin{aligned} p(x,0) &= 0 \\ \frac{\partial p(x,0)}{\partial t} &= 0 \end{aligned}\right\} \quad \text{for } x \neq 0 \tag{68}$$

Then the propagation equation (64) becomes, upon use of equations (67) and (68):

$$\frac{\partial^2 P}{\partial x^2} = b^2 P \tag{69}$$

where

$$b^2 \equiv \gamma^2 / (c^2 + \tfrac{4}{3}\nu\gamma) \qquad (70)$$

The general solution of this equation is:

$$P = A(\gamma)\exp(-bx) + B(\gamma)\exp(bx) \qquad (71)$$

The functions A and B are to be determined from the boundary conditions.

8.2 The function $b = \gamma / (c^2 + \tfrac{4}{3}\nu\gamma)^{1/2}$

has a branch point in the complex γ-plane (Fig. 6) at $\gamma = -3c^2/4\nu$. From this branch point, a cut is made to $\gamma = -\infty$. The upper sheet of the Riemann surface so formed is chosen so that b is real and positive if γ is real and greater than $-3c^2/4\nu$. The integration in equation (65) will be taken on the upper sheet of the surface. The integrand of (66) is:

$$A(\gamma)\exp(\gamma t - bx) + B(\gamma)\exp(\gamma t + bx)$$

For $x > 0$, the second term becomes infinite as $\gamma \to \sigma \pm i\infty$, since $\mathrm{Re}\,(\gamma t + bx) \to \sigma t + (3|\gamma|/8\nu)^{1/2} x \to +\infty$. The first term approaches zero strongly because

$$\mathrm{Re}\,(\gamma t - bt) \to \sigma t - (3|\gamma|/8\nu)^{\frac{1}{2}} x \to -\infty.$$

We accordingly set B = 0, and obtain A from the conditions at x = o:

$$A(\gamma) = \int_0^\infty p(0,t)\exp(-\gamma t)\,dt, \qquad \text{analytic for } \mathrm{Re}\,\gamma > \alpha \qquad (72)$$

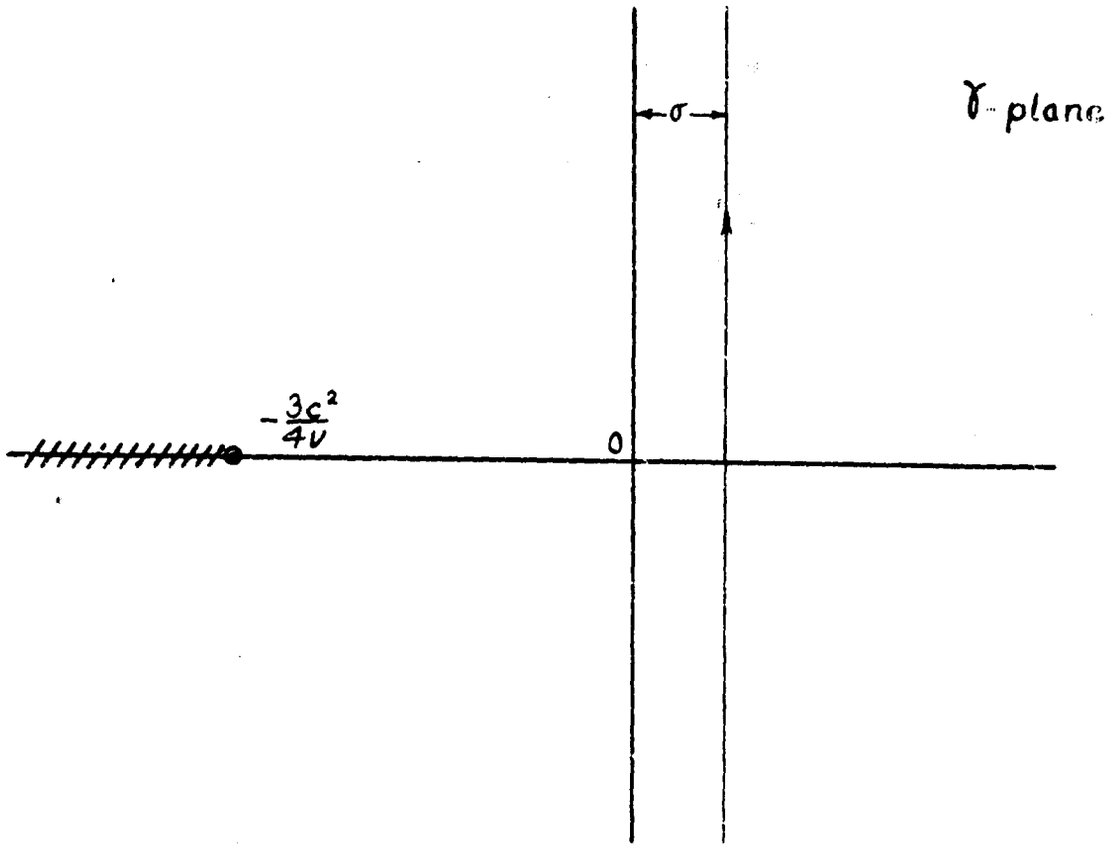


Fig. 6

Branch point and path of integration for equation (66)

Then

$$p(x,t) = \frac{1}{2\pi i}\int_{\sigma-i\infty}^{\sigma+i\infty} A(\gamma)\exp(\gamma t - bx)\,d\gamma\,, \quad \sigma > \alpha \tag{73}$$

8.3 For $t \leq 0$, $x \neq 0$, the path of integration of (73) may be closed by an infinite arc in the right half plane. The contribution of this arc will be zero, and since no poles of A will be enclosed, we have

$$p(x,t) = 0 \qquad \text{for} \quad t \leq 0\,,\ x \neq 0\,.$$

For an exponential shock wave, we have:

$$\left.\begin{aligned} p(0,t) &= 0\,, \quad t < 0 \\ p(0,t) &= \exp(-\lambda t)\,, \quad t > 0 \end{aligned}\right\} \tag{74}$$

and

$$A(\gamma) = \int_0^\infty \exp\left[-(\lambda+\gamma)t\right]dt = \frac{1}{\lambda+\gamma}\,, \quad \alpha = -\lambda\,. \tag{75}$$

Then

$$p(x,t) = \frac{1}{2\pi i}\int_{\sigma-i\infty}^{\sigma+i\infty} \frac{\exp(\gamma t - bx)}{\gamma+\lambda}\,d\gamma \tag{76}$$

Since ν, the coefficient of viscosity, is small, we approximate b by a series expansion:

$$b = \frac{\gamma}{c} - \frac{2}{3}\frac{\nu}{c^3}\gamma^2 + \ldots. \tag{77}$$

This expansion is valid in the region which gives the major contribution to the integral (76). Since the integrand is small outside this region, we can use the first two terms of the expansion over the entire range. Taking $\sigma = 0$, equation (76) becomes

$$p(x,t) \cong \frac{1}{2\pi i}\int_{-i\infty}^{i\infty} \frac{\exp\left[\gamma(t-x/c) + 2\nu\gamma^2 x/3c^3\right]}{\gamma+\lambda}\, d\gamma \tag{78}$$

For convenience, we define the parameters:

$$\left.\begin{aligned} a^2 &\equiv 2\nu x/3c^3 \\ \tau &\equiv t - x/c \\ I &\equiv \int_{-i\infty}^{i\infty} \frac{\exp(\gamma\tau + a^2\gamma^2)}{\gamma+\lambda}\, d\gamma \end{aligned}\right\} \tag{79}$$

Combining equations (78) and (79):

$$2\pi i\, p(x,t) = I \tag{80}$$

Differentiating I with respect to τ it is evident that:

$$\lambda I + \frac{dI}{d\tau} = \int_{-i\infty}^{i\infty} \exp(\gamma\tau + a^2\gamma^2)\, d\gamma \tag{81}$$

and completing the square of the exponent in the integrand:

$$\lambda I + \frac{dI}{d\tau} = \exp(-\tau^2/4a^2)\int_{-i\infty}^{i\infty} \exp\left[a^2(\gamma + \tau/2a^2)^2\right] d\gamma \tag{82}$$

Setting $\gamma = i\omega$ in equation (82):

$$\lambda I + \frac{dI}{d\tau} = i \exp(-\tau^2/4a^2) \int_{-\infty}^{\infty} \exp\left[-a^2(\omega - i\tau/2a^2)^2\right] d\omega$$

$$\lambda I + \frac{dI}{d\tau} = \frac{i\pi^{1/2}}{a} \exp(-\tau^2/4a^2) \tag{83}$$

Also:

$$\lambda I + \frac{dI}{d\tau} = \exp(-\lambda\tau) \frac{d}{d\tau}\left[I \exp(\lambda\tau)\right] \tag{84}$$

Combining equations (83) and (84):

$$\frac{d}{d\tau}\left[I \exp(\lambda\tau)\right] = \frac{i\pi^{1/2}}{a} \exp(\lambda\tau - \tau^2/4a^2) \tag{85}$$

Integrating equation (85) and using equation (80):

$$p(\tau) = \frac{I}{2\pi i} \cong \frac{\exp(-\lambda\tau)}{2a\pi^{1/2}} \int_{-x/c}^{\tau} \exp(\lambda\tau - \tau^2/4a^2)\, d\tau \tag{86}$$

the lower limit being $-x/c$ since $p = 0$ at $t = 0$.

Completing the square of the exponent of the integrand in equation (86):

$$p(\tau) \cong \frac{\exp(-\lambda\tau + \lambda^2 a^2)}{\pi^{1/2}} \int_{\lambda a - \tau/2a}^{\lambda a + x/2ac} \exp(-y^2)\, dy \tag{87}$$

where

$$y \equiv (\tau/2a) - \lambda a \tag{88}$$

8.4 Since a is very small (it will be shown to be of the order of $10^{-7} \times \frac{1}{2}$ for length units in feet), the upper limit of integration in equation (87) can be considered + ∞ for all practical purposes. Using this approximation, and introducing the parameters $\alpha \equiv \lambda a$; $\beta \equiv \tau/a$, equation (87) becomes:

$$p(\rho) \cong \frac{\exp(\alpha^2 - \alpha\beta)}{\pi^{1/2}} \int_{\alpha - \beta/2}^{\infty} \exp(-y^2)\, dy \tag{89}$$

In order to plot curves and perform computations with equation (89) it is convenient to introduce the form of the probability integral which is generally tabulated:

$$Pi(y) \equiv \frac{2}{\pi^{1/2}} \int_{0}^{y} \exp(-y^2)\, dy \tag{90}$$

Noting that

$$\int_{0}^{\infty} \exp(-y^2)\, dy = \pi^{1/2}/2$$

equation (89) takes the form:

$$p(\rho) = \begin{cases} \dfrac{\exp(\alpha^2 - \alpha\beta)}{2} \left[1 - Pi(\alpha - \beta/2)\right], & \alpha > \beta/2 \\ \dfrac{\exp(\alpha^2 - \alpha\beta)}{2} \left[1 + Pi(\beta/2 - \alpha)\right], & \alpha < \beta/2 \end{cases} \tag{91}$$

Equation (91) is then the most convenient form for plotting the function $p(\sigma)$, which, in terms of reduced parameters, represents the shape imposed upon an exponential shock wave by viscous attenuation after propagation over various distances, $\mathcal{N}$. For spherical waves, one would simply introduce the factor 1/R, where R is the distance of the point of observation from the origin of the wave.

Figure 7 shows a family of curves of $p(\beta)$ vs β for various values of α, based upon equation (91). Increasing α corresponds to increasing range of propagation.

8.5 It will be noted that all the curves in Fig. 7 can be considered as originating at $\beta = -4$, and that they attain maxima at values of β which increase with decreasing α. We shall define β_r as the reduced rise time, i.e. the total time in units of β for a curve to rise from essentially zero at $\beta = -4$ to its maximum in Fig. 7. Figure 8 shows a plot of the quantity $(\beta_r - 4)$ vs. α based on values obtained from Fig. 7, and it is found that β_r can be empirically represented by:

$$\beta_r = 4 + 0.655 \ln \frac{3.30}{\alpha} \qquad (92)$$

The actual rise time τ_r would then be given by:

$$\tau_r = 4a + 0.655 a \ln \frac{3.30}{\alpha} \qquad (93)$$

Thus, although the reduced rise time β_r increases with decreasing α (or decreasing range), the actual rise time decreases and

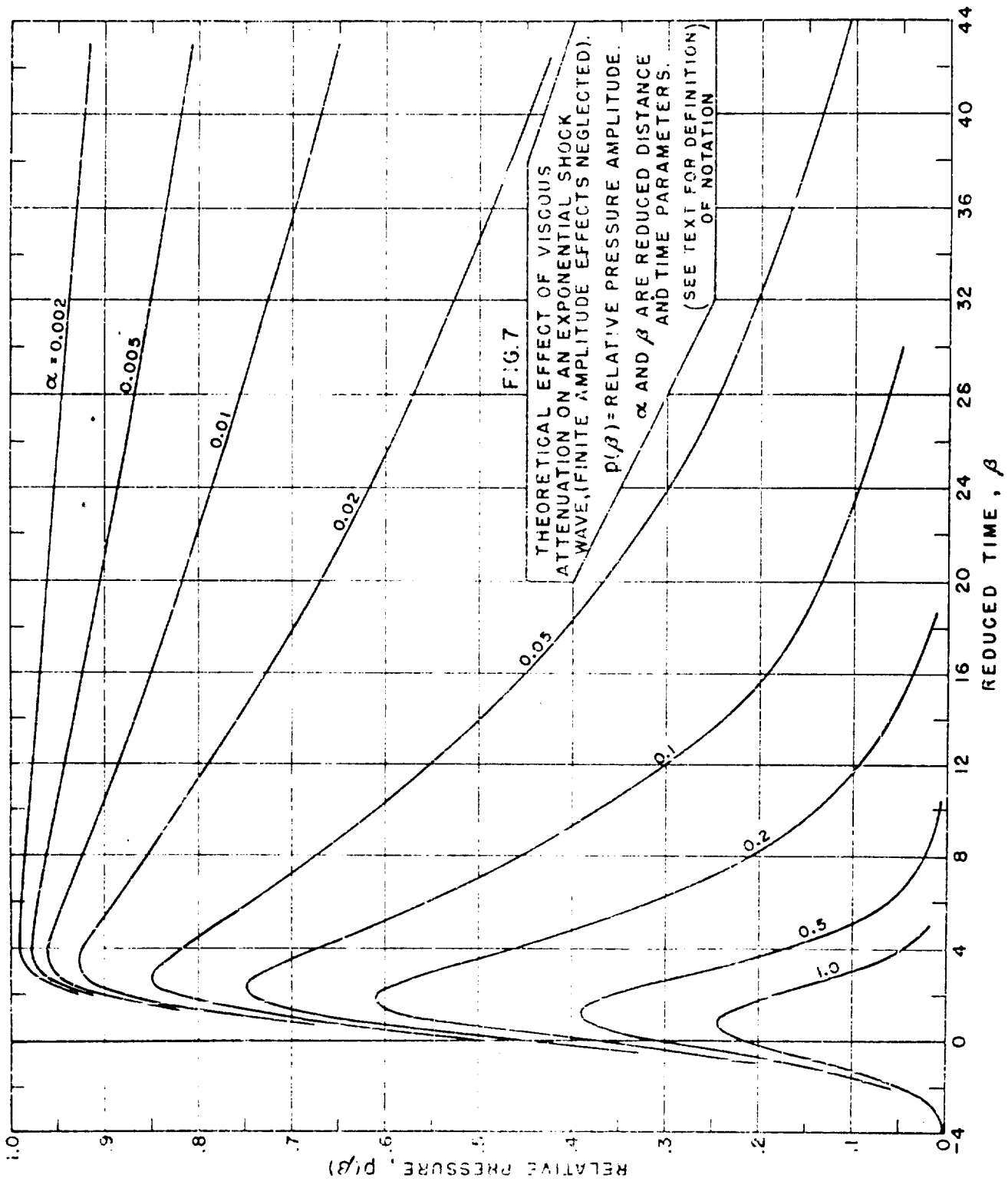


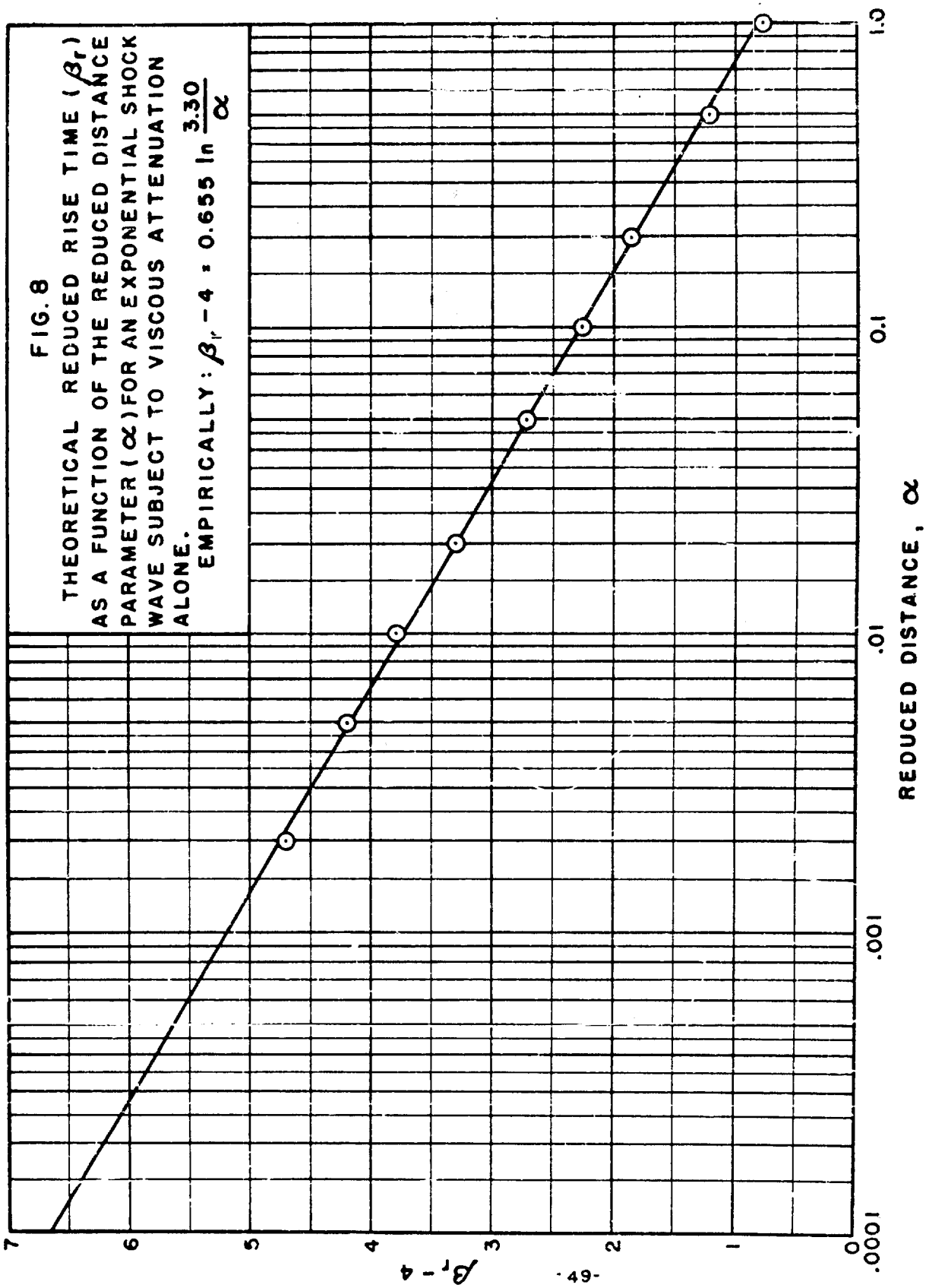
FIG. 7

THEORETICAL EFFECT OF VISCOUS ATTENUATION ON AN EXPONENTIAL SHOCK WAVE, (FINITE AMPLITUDE EFFECTS NEGLECTED).

$p(\beta)$ = RELATIVE PRESSURE AMPLITUDE.

α AND β ARE REDUCED DISTANCE AND TIME PARAMETERS.

(SEE TEXT FOR DEFINITION OF NOTATION)


FIG. 8
THEORETICAL REDUCED RISE TIME (β_r) AS A FUNCTION OF THE REDUCED DISTANCE PARAMETER (α) FOR AN EXPONENTIAL SHOCK WAVE SUBJECT TO VISCOUS ATTENUATION ALONE.
EMPIRICALLY: $\beta_r - 4 = 0.655 \ln \frac{3.30}{\alpha}$
$\beta_r - 4$
0
1
2
3
4
5
6
7
.0001
.001
.01
0.1
1.0
REDUCED DISTANCE, α

tends to zero when $\alpha \to 0$, as would be expected.

8.6 In order to use the above results to predict rise times and wave shapes for actual cases of interest, one must be able to estimate the value of $\underline{a}$ and consequently α . For this purpose we use the attenuation coefficients for sea water reported by Liebermann[10]:

$$2\gamma = \frac{A\omega^2\theta}{1+\omega^2\theta^2} + B\omega^2 \qquad (94)$$

where $A = 2.9 \times 10^{-10}$ sec/cm

$B = 1.8 \times 10^{-17}$ sec^2/cm

$\theta = 1.1 \times 10^{-8}$ sec.

(Liebermann uses α to denote the attenuation coefficient, and we replace it by γ to prevent confusion in notation.)

Instead of simply relying upon classical values of shear viscosity to calculate $\underline{a}$ from equation (79), we adopt Liebermann's results, which include the effects of dilational viscosity as well as shear, and evaluate $\underline{a}$ on the basis that

$$a^2 = \gamma x/\omega^2 \qquad (95)$$

A rigorous evaluation, using equation (94) for γ would be extremely difficult because of the manner in which it would complicate the integral in equation (78). In order to utilize the simplified results already obtained, we neglect the relaxation effect indicated in (94) and approximate by setting:

$$\gamma \cong \frac{A\theta + B}{2}\omega^2 \qquad (96)$$

This approximation has the effect of subjecting frequencies higher than 30 or 40 kilocycles to too severe an attenuation, but since in any case the very high frequency components rapidly cease to contribute appreciably to the pulses in which we are interested, the approximation is probably justified.

Using equations (95) and (96) together with the numerical values of A, B, and ρ, and converting to ft., sec. units, we obtain:

$$a = 7.11 \, (10^{-8}) \, x^{\frac{1}{2}} \qquad (97)$$

Liebermann argues convincingly that all the attenuation in underwater sound propagation is ascribable to viscosity, thermal conduction effects being negligible. Thus, if finite amplitude effects are entirely neglected, one can use estimates of $\underline{a}$ based on (97) together with the known λ of the shock wave under consideration, to predict rise times and wave shapes for various distances x by use of equations (91) and (93).

9. Correction of the preceding theory for certain finite amplitude effects.

9.1 The theory developed in the preceding section treated the effect of viscous attenuation on purely acoustic pressure waves and completely neglected the effect of finite amplitude in modifying the shape of the wave. Finite amplitude modifications enter our problem in two principal aspects: (a) spread of the profile (b) "sharpening effect" at the front.

The spread of the profile makes λ(the reciprocal of the time constant) in the above theory a function of distance of propagation. We take this effect roughly into account in the ultimate numerical calculations by using an average value of the time constant over the region of propagation to determine λ, but continue to treat λ as a constant in the mathematical analysis.

The sharpening effect is more significant in modifying the shape of the front of the wave, and we attempt in this section to make some correction for it.

9.2 Assuming that the front of the wave has developed a finite rise time, we see (as a result of the theory of finite amplitude waves) that the initial portion of the wave will propagate at the velocity of sound C_0 while the peak of the wave will propagate approximately at the velocity $C+u$, where C is the local velocity of sound and u the particle velocity. Since $(C+u) > C_0$, it is evident that the effect of finite amplitude is opposite to that of viscous attenuation in that it tends to decrease the rise time and sharpen the front. From a slightly different point of view, we can regard this approximately as a process of restoration of higher frequency components to the spectrum of the pulse.

An outline of the correction proceedure follows: We calculate the rate at which the rise time is increasing with distance from the origin owing to viscous attenuation and also the rate at which it is decreasing owing to finite amplitude.

The net rate of increase of the rise time is then used as a basis for a numerical integration which ultimately yields rise time as a function of distance. It is then assumed that the shape of the wave is approximately that given by Figure 7 for the resultant rise time. Thus we introduce the rather crude approximation that the compensating effect of finite amplitude affects the resultant rise time without appreciable modification of the fundamental mathematical shape as given by equation (91) and plotted in Figure 7.

However, the errors thus introduced should not be too serious at long ranges, and in general, one should obtain correctly the rough magnitudes of the changes involved. A more refined analysis does not seem worth while at the present time.

9.3 To calculate the effect of pressure on the rise time we write:

$$\left(\frac{d\tau_r}{dR}\right)_p = \frac{1}{C+u} - \frac{1}{C_0} \tag{98}$$

Using the results summarized by Cole (ref. 7, p. 14):

$$C+u \cong C+\sigma = C_0(1+2\beta\sigma) \tag{99}$$

$$U = C_0(1+\beta\sigma) \tag{100}$$

where U is the shock propagation velocity as obtained by application of the Rankine-Hugoniot conditions.

Empirically, the lower pressure range results of Arons and Halverson[12] can be expressed in the form[13]:

$$U = C_o \left(1 + 5.6 \times 10^{-6} P\right) \tag{101}$$

where P is the shock wave peak pressure in lb./in^2.

Comparing equations (99), (100), and (101), we obtain:

$$2\beta\sigma = 11.2 \times 10^{-6} P \tag{102}$$

Combining equations (98) and (99) and expanding to first order terms:

$$\left(\frac{d\tau_r}{dR}\right)_p \cong -\frac{2\beta\sigma}{C_o} = -2.24 \times 10^{-9} P \text{ sec./ft.} \tag{103}$$

The empirical pressure-distance relation for TNT is[14]:

$$P = 2.16 \,(10^4)\left(\frac{W^{1/3}}{R}\right)^{1.13} \tag{104}$$

where W is charge weight in pounds and R is distance in feet.

Substituting (104) into (103):

$$\left(\frac{d\tau_r}{dR}\right)_p = -4.84 (10^{-5})\left(\frac{W^{1/3}}{R}\right)^{1.13} \text{ sec./ft.} \tag{105}$$

9.4 A complication is now introduced into our consideration of the viscous effect on the rate of change of rise time with distance. The variable χ which in section 8 was simply

regarded as the independent distance variable can no longer be treated as such, or associated directly with R. We shall use χ to represent the "equivalent viscous distance", i.e. the distance of propagation which would have produced a given rise time with viscous attenuation acting alone. Thus χ will be a complicated function of R and in the case of compression waves will be less than R at any given point because of the restoring effect of finite amplitude. The rate of increase of rise time with χ is obtained by differentiating equation (93), making use of the relation between a and χ in equation (97):

$$\left(\frac{d\tau_r}{d\chi}\right)_v = \left[4a + 0.655a \ln\frac{3.30}{a} - 0.655a\right]\frac{1}{2\chi}$$

$$= \left[\tau_r - 4.65(10^{-8})\chi^{1/2}\right]\frac{1}{2\chi} \qquad (106)$$

The overall rate of change of rise time with R is obtained by means of a similar operation:

$$\frac{d\tau_r}{dR} = \left[\tau_r - 4.65(10^{-8})\chi^{1/2}\right]\frac{1}{2\chi}\frac{d\chi}{dR} \qquad (107)$$

We assume that to a first approximation:

$$\frac{d\tau_r}{dR} = \left(\frac{d\tau_r}{d\chi}\right)_v + \left(\frac{d\tau_r}{dR}\right)_p \qquad (107a)$$

and combining (105), (106), and (107), and solving for $d\chi/dR$:

$$\frac{d\chi}{dR} = 1 - \frac{9.68(10^{-5})\chi}{\tau_r - 4.65(10^{-8})\chi^{1/2}}\left(\frac{W^{1/3}}{R}\right)^{1.13} \qquad (108)$$

with τ_r to be expressed as a function of χ by means of (93) and (97).

We can now use equation (108) to determine the "equivalent viscous distance," χ_r, by numerical integration for any value of R. As indicated previously, χ_r represents the propagation distance which would have led to the rise time existing at this value of R if only viscous effects had been present. Having χ_r as a function of R, it is then possible to compute the effective $\underline{a}$ at any given R and from it in turn the rise time τ_r and the form of the wave from equation (91) or Figure 7.

9.5 In order to effect the numerical integration of (108), it is necessary to select an appropriate starting point, i.e. fix the value of χ_r at some initial value of R. To do this, we first examine the general behavior of equation (108) in some detail. We write the equation in more concise form:

$$\frac{d\chi}{dR} = 1 - \frac{f(\chi)}{R^{1.13}} \qquad (109)$$

and examine its properties in the χ-R plane, a schematic sketch of which is shown in Figure 9.

The family of curves (shown as solid lines in Fig. 9) defined by:

$$1 - \frac{f(\chi)}{R^{1.13}} = m \qquad (110)$$

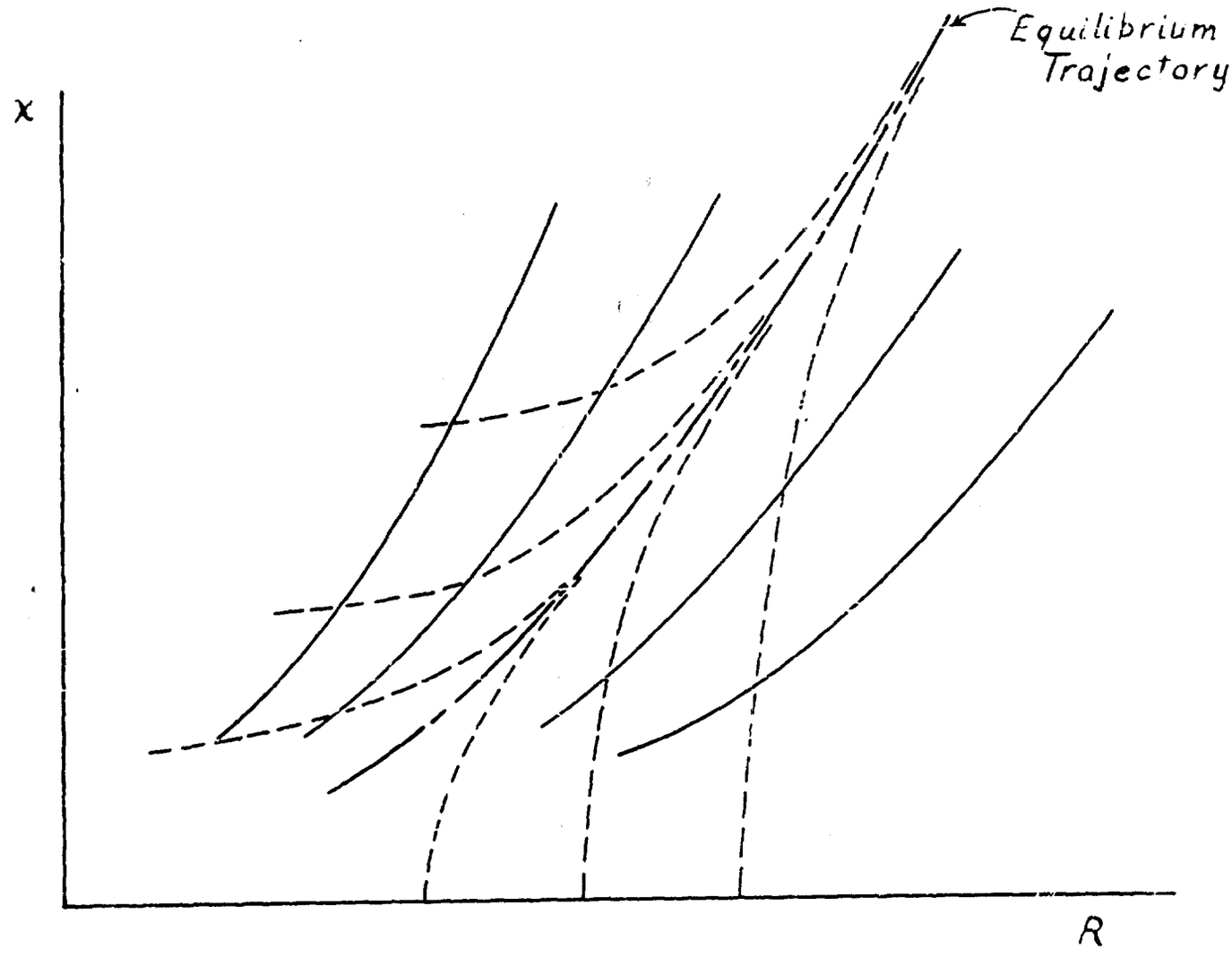


Fig. 9

x - R plane for equation (109)

Solid Lines: loci of constant slope, equation (110)

Dotted Lines: "trajectories", or solutions of equation (109) for various boundary conditions.

are the loci of constant slope of the solutions of (109), while the dotted trajectories are the solutions themselves for various arbitrary starting points (or boundary conditions) of x_r and R.

Examination of Figure 9 shows that all the trajectories, regardless of their initial starting point, tend at larger values of R to approach very close to a certain central trajectory which has been denoted as the "equilibrium trajectory." It seems reasonable therefore, in view of the lack of any well known, a priori boundary condition, to select this equilibrium trajectory as the solution of equation (109) which is appropriate to our particular problem.

Thus, differentiating equation (110) we have along any of the loci of constant slope:

$$\frac{1.13\, f(x)}{R} - f'(x)\,\frac{dx}{dR} = 0 \qquad (111)$$

But for the solution we seek, dx/dR in (111) is given by equation (109). Therefore

$$\frac{1.13\, f(x)}{R} - f'(x)\left[1 - \frac{f(x)}{R^{1.13}}\right] = 0 \qquad (112)$$

is the equation of the equilibrium trajectory, and we could obtain x_r as a function of R by graphical solution of (112) at a succession of points.

For practical purposes, it is more convenient to solve equation (112) once in order to obtain an appropriate starting

point and then proceed to integrate (108) numerically by means of the Runge-Kutta method. This proceedure was used to obtain the results shown for a few representative charge sizes in Figure 10.

9.6 The results summarized in Figure 10 are then used to obtain expected wave shapes for various specific cases by using χ_r for a given R and charge size to calculate a from equation (97) and α from the definition $\alpha \equiv \lambda a$. The resulting α is then used in equation (91) to obtain the wave shape or (92) to obtain an estimate of the rise time.

Some typical results for 0.5 and 8 lb. charges are shown in Figures 11 and 12. Curves of rise time vs R for 0.5, 8, 25 and 300 lb charges are shown in Figure 13.

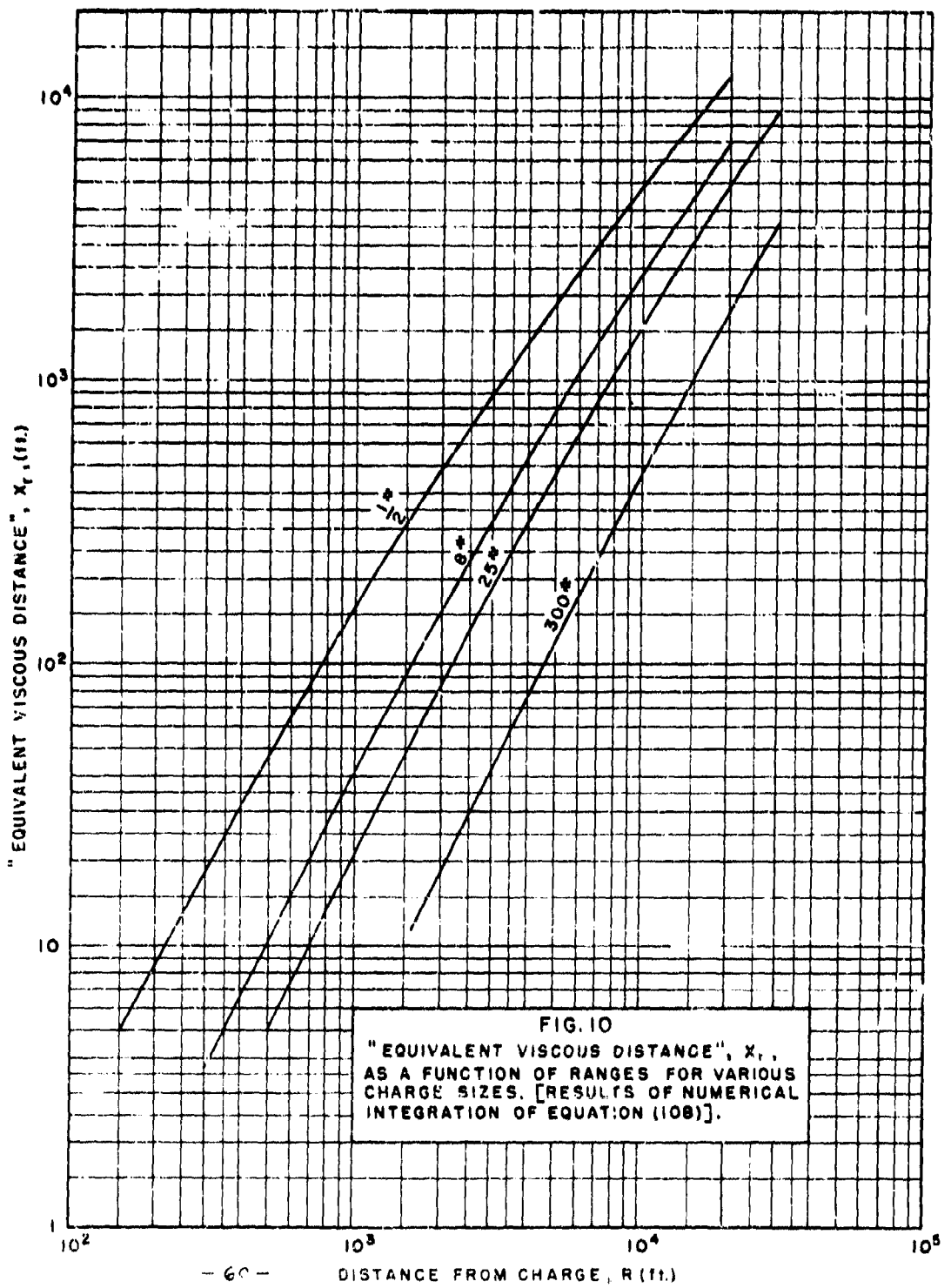


FIG. 10
"EQUIVALENT VISCOUS DISTANCE", X_r, AS A FUNCTION OF RANGES FOR VARIOUS CHARGE SIZES. [RESULTS OF NUMERICAL INTEGRATION OF EQUATION (108)].

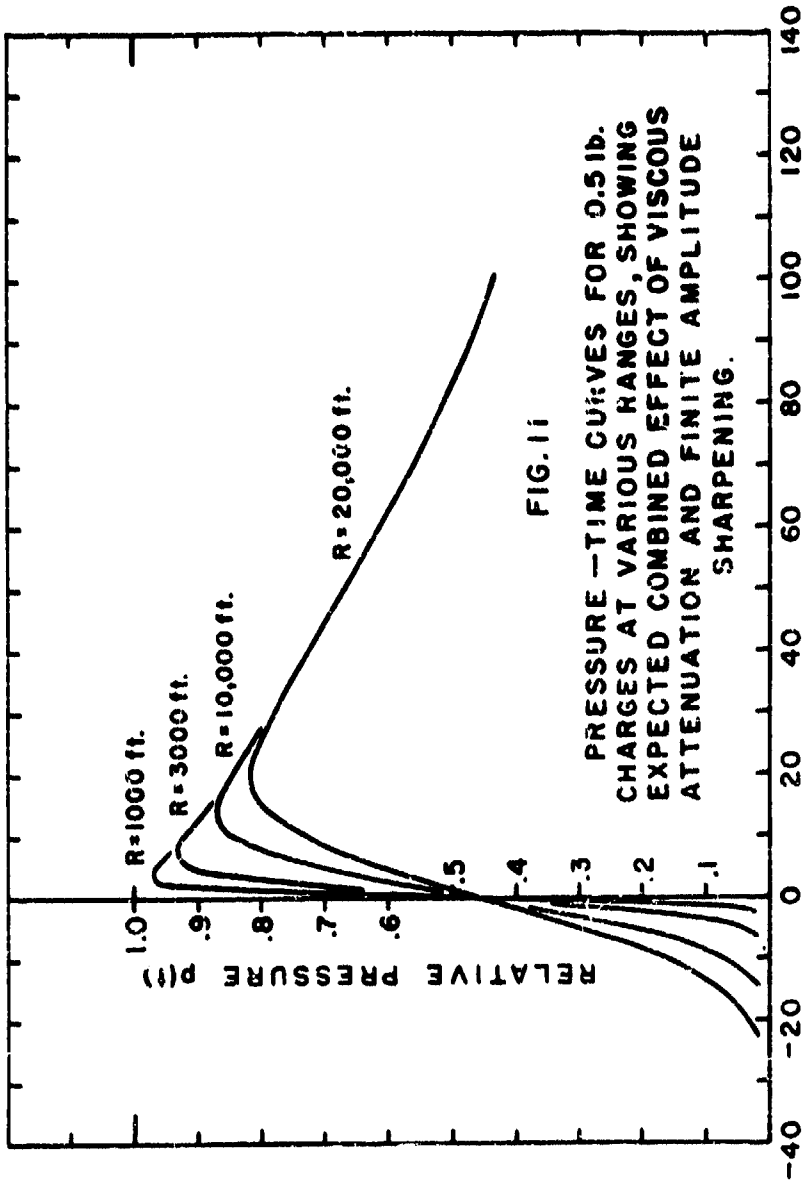


FIG. 11

PRESSURE—TIME CURVES FOR 0.5 lb. CHARGES AT VARIOUS RANGES, SHOWING EXPECTED COMBINED EFFECT OF VISCOUS ATTENUATION AND FINITE AMPLITUDE SHARPENING.

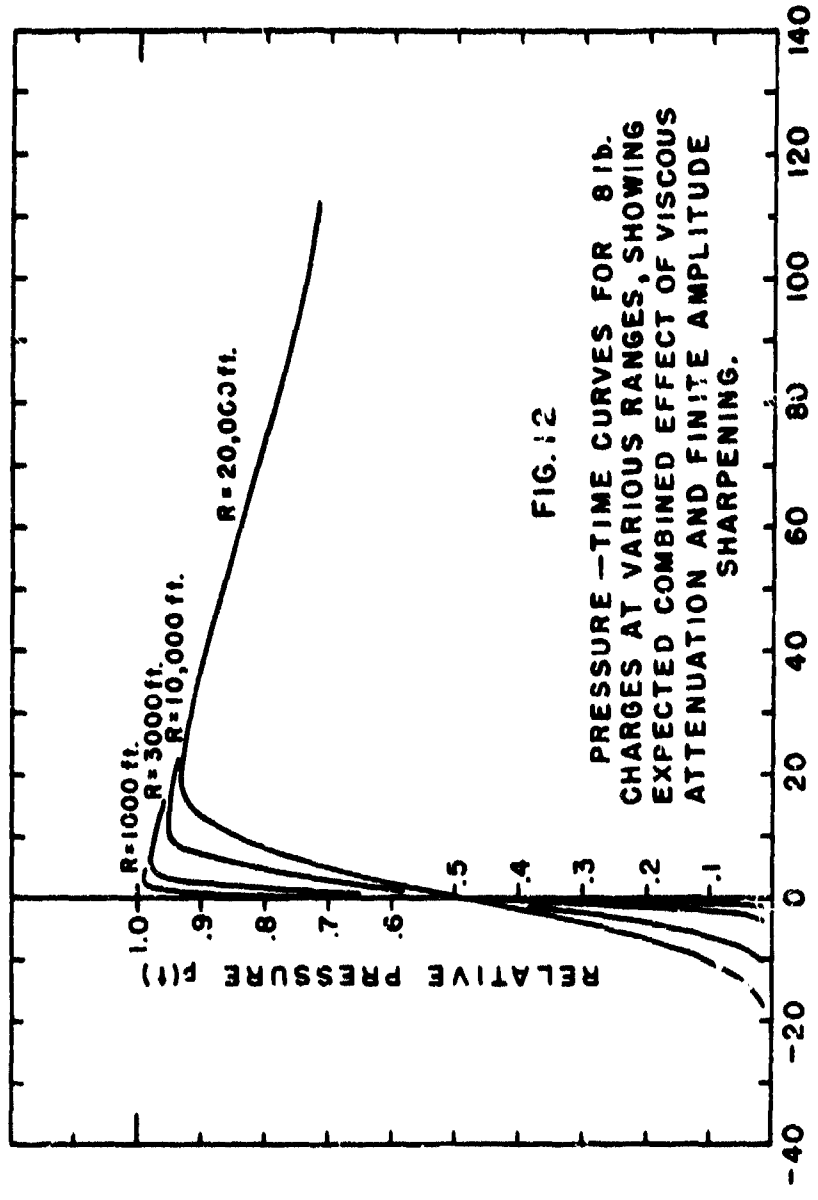
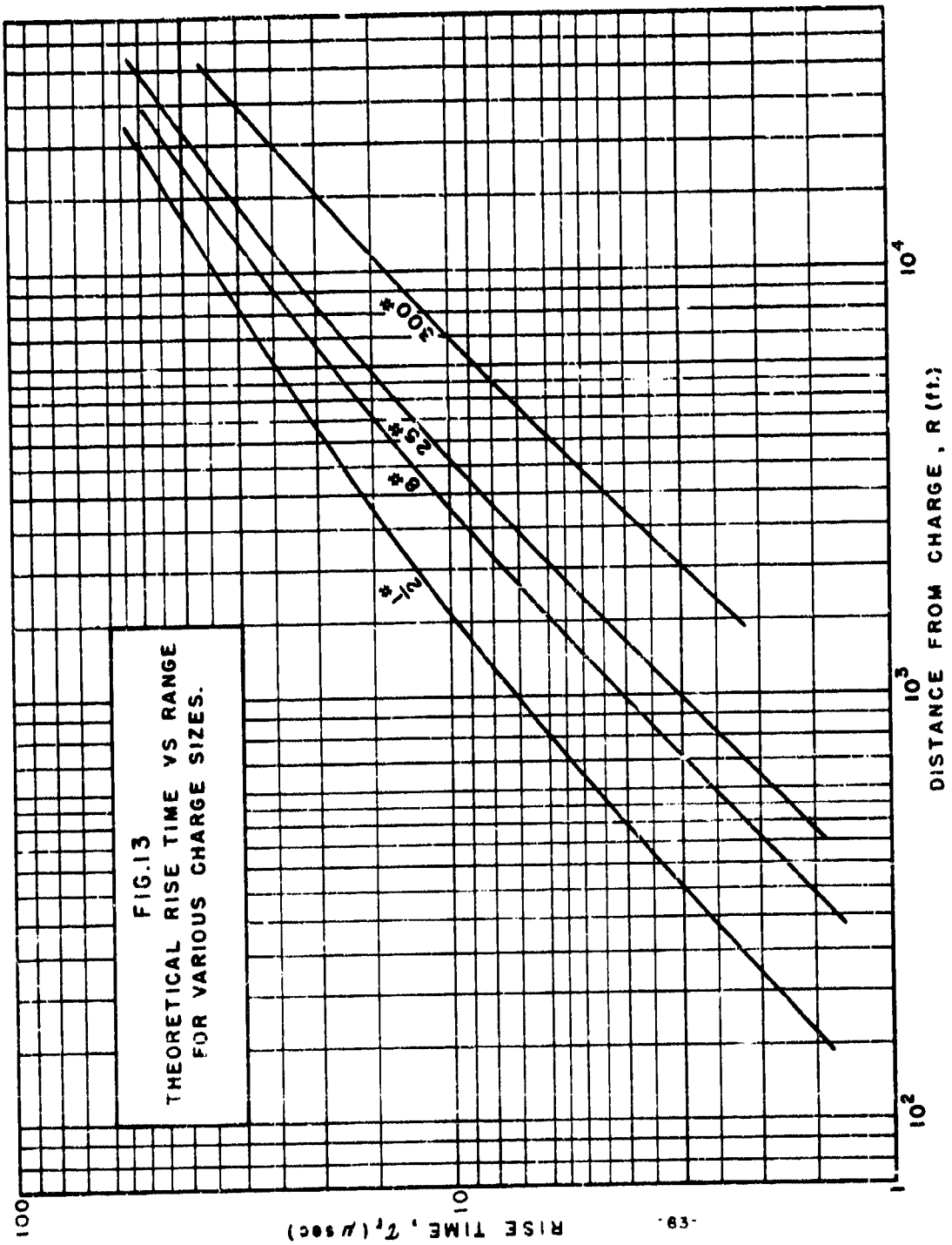


FIG. 12

PRESSURE—TIME CURVES FOR 8 lb. CHARGES AT VARIOUS RANGES, SHOWING EXPECTED COMBINED EFFECT OF VISCOUS ATTENUATION AND FINITE AMPLITUDE SHARPENING.


FIG.13
THEORETICAL RISE TIME VS RANGE
FOR VARIOUS CHARGE SIZES.
½*
9*
25*
300*
RISE TIME, τ_1 (μsec)
DISTANCE FROM CHARGE, R (ft.)
100
10
1
10^2
10^3
10^4

10. Effect of gauge size on rise time and shape of shock wave which has undergone viscous attenuation.

10.1 Owing to the low pressure amplitudes obtaining at ranges where viscous effects have become apparent, experimental measurements must be made with sensitive (and consequently large) gauges. It is desirable, therefore, to examine the effect of gauge size in distorting waves of the type illustrated in Figures 11 and 12.

In view of the approximations already introduced into the theory, it is not worthwhile carrying out the analysis rigorously in terms of circular gauge shapes and equation (91); we rather introduce simplified forms for the step response and incident wave as follows:

Relative step response of gauge, $$R(t) = \begin{cases} 0 & , -\infty < t < 0 \\ t/m & , 0 < t < m \\ 1 & , m < t < \infty \end{cases} \quad (113)$$

Relative pressure of incident wave, $$p_i(t) = \begin{cases} 0 & , -\infty < t < 0 \\ t/n & , 0 < t < n \\ 1-\lambda(t-n), & n < t < \lambda \end{cases} \quad (114)$$

Thus the step response is assumed to have a linear rise of duration $\underline{m}$ where $\underline{m}$ is the transit time of the pressure wave across the gauge, and the incident wave is approximated by a saw tooth shape with a linear rise of duration $\underline{n}$ and a decay-constant λ .

To obtain the expected response of the finite gauge

to the incident wave we use the superposition integral[11] in the form:

$$p(t) = p_i(0)\,R(t) + \int_0^t p_i'(\tau)\,R(t-\tau)\,d\tau \qquad (115)$$

The results of integration for various cases of interest are summarized below. (t_m denotes time of maximum response)

For $n > m$:

$$p(t) = \begin{cases} t^2/2mn & , \ 0 < t < m \\ t/n - m/2n & , \ m < t < n \\ -t^2\left(\lambda/2m + 1/2mn\right) + t\left(\frac{1}{m} + \frac{\lambda n}{m} + \frac{1}{n}\right) - \left(\frac{\lambda n^2}{2m} + \frac{n}{2m} + \frac{m}{2n}\right) & , \ n < t < m+n \\ 1 - \lambda t + \lambda n + \frac{\lambda m}{2} & , \ m+n < t < 1/\lambda \end{cases} \qquad (116)$$

$$t_m = n + m/(1+n\lambda) \qquad (117)$$

For $n < m$

$$p(t) = \begin{cases} t^2/2mn & , \ 0 < t < n \\ -\frac{\lambda t^2}{2m} + t\left(\frac{1}{m} + \frac{\lambda n}{m}\right) - \left(\frac{n}{2m} + \frac{\lambda n^2}{2m}\right) & , \ n < t < m \\ -t^2\left(\frac{\lambda}{2m} + \frac{1}{2mn}\right) + t\left(\frac{\lambda n}{m} + \frac{1}{m} + \frac{1}{n}\right) - \left(\frac{\lambda n^2}{2m} + \frac{n}{2m} + \frac{m}{2n}\right) & , \ m < t < m+n \\ 1 - \lambda t + \lambda n + \frac{\lambda m}{2} & , \ m+n < t < 1/\lambda \end{cases} \qquad (118)$$

$$t_m = n + m/(1+n\lambda) \qquad (119)$$

For $m = n$

$$p(t) = \begin{cases} t^2/2m^2 & , \ 0 < t < m \\ -t^2\left(\frac{\lambda}{2m} + \frac{1}{2m^2}\right) + t\left(\lambda + \frac{2}{m}\right) - \left(\frac{\lambda m}{2} + 1\right) & , \ m < t < 2m \\ 1 - \lambda t + \frac{3\lambda m}{2} & , \ 2m < t < 1/\lambda \end{cases} \qquad (120)$$

$$t_m = m(2 + m\lambda)/(1 + m\lambda) \qquad (121)$$

It will be noted for cases in which $1/\lambda$ is large relative to the rise time of the incident wave, the rise time of the response, t_m, becomes essentially equal to m+n. Thus the rise time of the recorded trace would be nearly equal to the sum of the rise time of the wave and the transit time across the gauge.

These results are applied to two of the curves of Figure 12 to illustrate the effect produced by a 2½ inch diameter gauge, and the resulting curves are plotted in Figure 14.

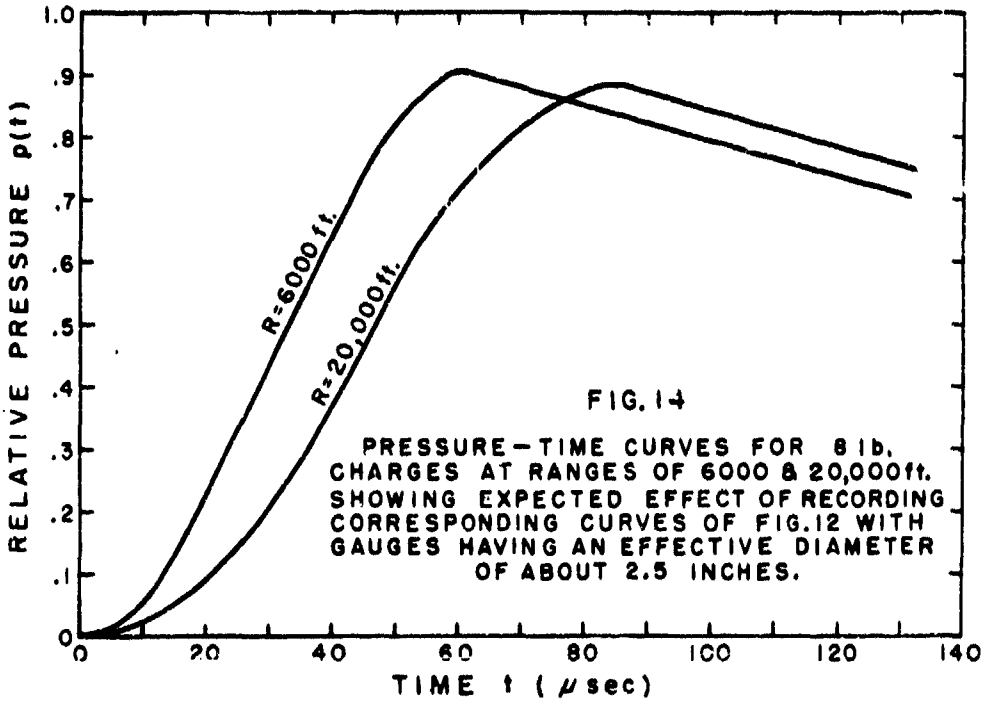


FIG. 14

PRESSURE—TIME CURVES FOR 8 lb. CHARGES AT RANGES OF 6000 & 20,000 ft. SHOWING EXPECTED EFFECT OF RECORDING CORRESPONDING CURVES OF FIG. 12 WITH GAUGES HAVING AN EFFECTIVE DIAMETER OF ABOUT 2.5 INCHES.

10.2 The experimental records obtained in this program unfortunately do not provide an adequate test of the theory developed above. The ranges are such that the expected rise times would be somewhat less than the transit time across the gauge, and the recording speed was such that the rise of the record is not highly resolved. Furthermore, it proved very difficult to keep the oscilloscope tubes rigidly aligned so as to make the spot deflection accurately normal to the plane of rotation of the film drum. Thus, the measured rise time on many records is grossly in error because of the presence of a slight tilt of the "vertical" axis and in general the scatter is extremely large. One can only conclude from the records that the recorded rise time is of the order of the transit time across the gauge, but it is impossible to obtain values precise enough to justify subtraction of the gauge transit in order to estimate the actual rise time of the pressure wave.

There now exist very long range data, obtained during the Spring of 1949 by Dr. E. Swift's group of the Naval Ordnance Laboratory Explosives Division. Some preliminary tracings which Dr. Swift kindly supplied the authors seem to correspond to the wave shapes of Figure 14, and the rise times are of the order predicted by the theory, but these remarks are based on the examination of a few isolated records rather than on an analysis of all the data now available. It is possible that a complete analysis of the NOL records will afford a more critical test of the theoretical results than the data so far available.

III. Energy Flux and Dissipation

11. Extension of the similarity curves for shock wave impulse and energy flux.

11.1 Certain of the 0.5 lb. pentolite charges were fired at ranges and depths such that the primary shock wave was not distorted by arrival of the first reflection until after it had decayed to negligibly small amplitude. The resulting records have been integrated to obtain the impulse and energy flux for the primary shock, and the data are shown in Figure 15. Impulse was calculated as:

$$I = \int_0^{6.7\theta} p\,dt \qquad (122)$$

where θ is the average decay constant at the given $W^{1/3}/R$ obtained from Figure 2 of NavOrd 424[22]. Energy flux was calculated from the purely acoustic equation:

$$E = \frac{1}{\rho c}\int_0^{\infty} p^2\,dt \qquad (123)$$

The numerical results used in Figure 15 are summarized in Table I.

It was not practicable to obtain similar data for greater ranges or for any of the TNT shots because of interference resulting from the arrival of the first reflection.

12. Ratio of reflected and incident energy flux for bottom reflections up to the critical angle of incidence.

12.1 A few records were available in which it was possible to

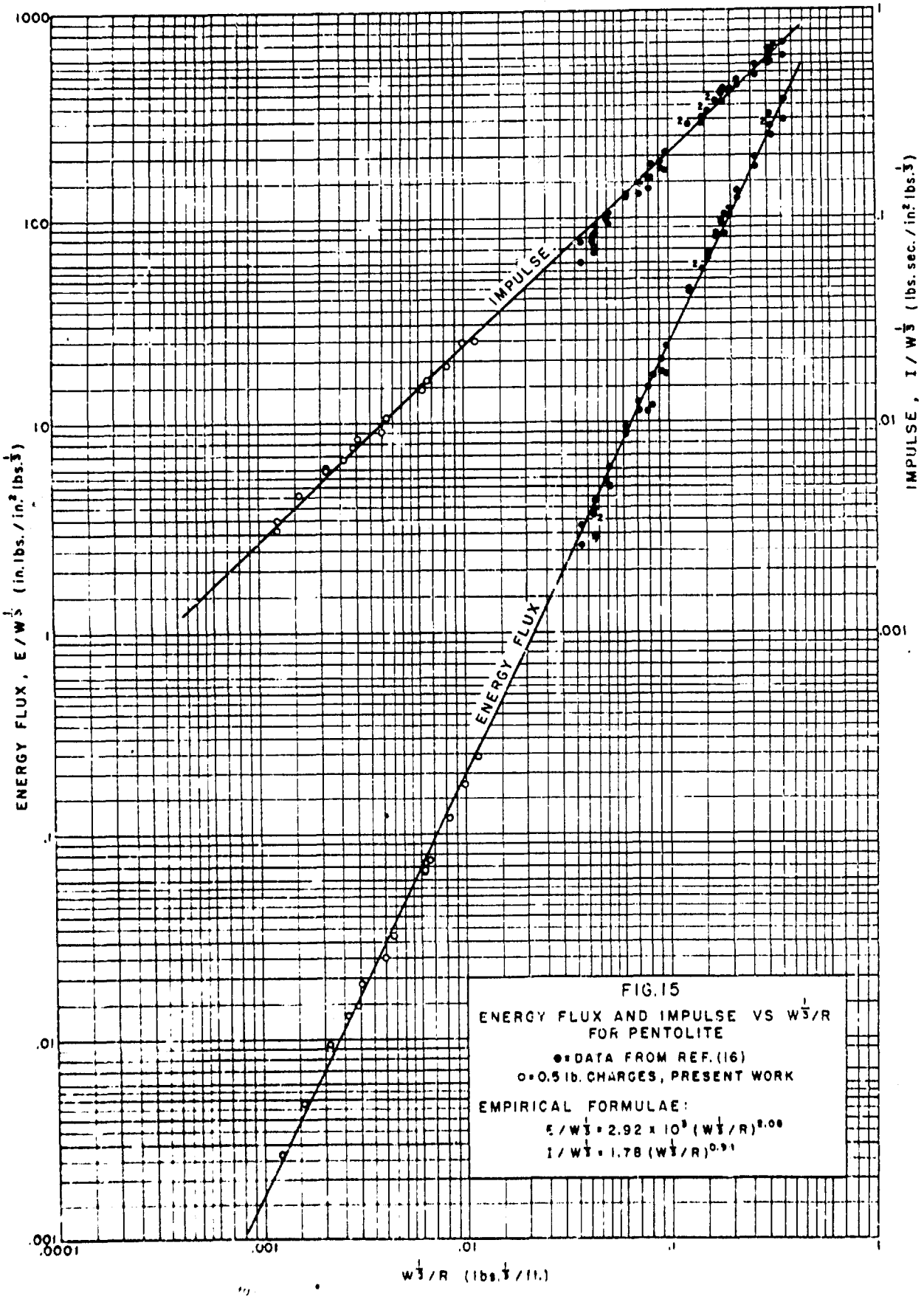


FIG. 15

ENERGY FLUX AND IMPULSE VS $W^{\frac{1}{3}}/R$ FOR PENTOLITE

● = DATA FROM REF. (16)

○ = 0.5 lb. CHARGES, PRESENT WORK

EMPIRICAL FORMULAE:

$$E/W^{\frac{1}{3}} = 2.92 \times 10^{3} (W^{\frac{1}{3}}/R)^{2.08}$$

$$I/W^{\frac{1}{3}} = 1.78 (W^{\frac{1}{3}}/R)^{0.91}$$

Table I

Impulse and Energy Flux for 0.5 lb.

Pentolite Charges

$$E = \frac{1}{\rho c}\int_0^\infty p^2\,dt$$

$$I = \int_0^{6.7\theta} p\,dt$$

Shot No.	$W^{1/3}/R$	$E/W^{1/3}$	$I/W^{1/3}$
	$(lb)^{1/3}/ft.$	$in.\ lb/lb.^{1/3} in.^2$	$lb.sec./in.^2 lb.^{1/3}$
214	.0114	.242	.0247
218	.00993	.176	.0243
230	.00836	.120	.0188
240	.00662	.0748	.0160
231	.00635	.0723	.0146
232	.00635	.0667	.0145
233	.00635	.0656	.0142
235	.00443	.0320	.0107
239	.00399	.0249	.00920
241	.00306	.0187	.00850
242	.00290	.0146	.00766
243	.00262	.0130	.00678
253	.00213	.00870	.00597
250	.00210	.00845	.00607
258	.00157	.00478	.00463
259	.00123	.00262	.00348
261	.00122	.00266	.00312

measure the energy flux of both the incident wave and the bottom reflection for various angles of incidence up to the critical. The flux in the bottom reflection was corrected to the same radius as the incident flux, and the measured ratios of E_r/E_i are given in Table II. The observed ratios are compared with theoretical ratios based on the result of acoustical theory:

$$\text{Theoretical } E_r/E_i = \left[\frac{\frac{\rho_2 C_2}{\rho_1 C_1}\cos\theta_1 - \left(1 - \frac{C_2^2}{C_1^2}\sin^2\theta_1\right)^{1/2}}{\frac{\rho_2 C_2}{\rho_1 C_1}\cos\theta_1 + \left(1 - \frac{C_2^2}{C_1^2}\sin^2\theta_1\right)^{1/2}}\right]^2 \qquad (124)$$

In accordance with the discussion of Chapter I, ρ_2/ρ_1 was taken as 2.7 and C_2/C_1 as 1.15.

It is evident in Table II that the observed ratio E_r/E_i is in general significantly lower than that given by equation (124). This could be adjusted at lower angles of incidence by using somewhat lower values of ρ_2/ρ_1, but such an adjustment would not serve to explain the fact that the observed ratio remains less than unity even when the critical angle is approached or exceeded. It is probable that the low values of observed E_r/E_i indicate substantial energy loss to inelastic processes and absorption occurring at the reflecting interface.

12.2 Energy flux ratios were measured rather than amplitude ratios in order to take advantage of the smoothing or averaging afforded by the integration process. An average amplitude ratio

Table II

Ratio of reflected to incident energy flux (E_r/E_i) for bottom reflections at various angles of incidence.

Theoretical E_r/E_i calculated by means of equation (124) with $\rho_2/\rho_1 = 2.7$ and $C_2/C_1 = 1.15$.

Shot No.	Angle of Incidence, θ_1 (degrees)	Theoretical		Observed	
		E_r/E_i	$(E_r/E_i)^{\frac{1}{2}}$	E_r/E_i	$(E_r/E_i)^{\frac{1}{2}}$
214	0	.26	.51	.10	.32
218	0	.26	.51	.09	.30
230	46	.34	.58	.26	.51
240	51	.40	.63	.45	.67
231	52	.40	.63	.28	.53
232	57	.52	.72	.45	.67
233	60	.82	.91	.47	.68
235	64*	1.0	1.0	.48	.69
239	64*	1.0	1.0	.65	.81

*Critical angle exceeded

can be obtained indirectly by extracting the square root of E_r/E_i, and these square roots are also given in Table II for comparison. It will be noted that the amplitude ratio near the critical angle is about 0.7 to 0.8 rather than 1.0. The amplitude ratio has no meaning at angles lying between θ_c and glancing incidence. At glancing incidence, however, the bottom reflection is simply the inverted image of the incident wave, and from the point of view of the idealized theory, the amplitude ratio would be unity. Examination of the experimental records shows that the observed ratio again lies in the neighborhood of 0.7 to 0.8.

13. Energy loss due to viscous effects.

13.1 We shall now proceed to extend the theory of sections 8 and 9 in an effort to estimate the energy losses which may be ascribed to viscous dissipation. Making use of equation (66), supposing $\alpha < 0$ and taking $\sigma = 0$, we have:

$$\int_0^\infty p^2 dt = \frac{1}{2\pi i} \int_0^\infty \int_{-i\infty}^{i\infty} p(x,t)\, P(x,\gamma) \exp(\gamma t)\, d\gamma\, dt \qquad (125)$$

The integration with respect to t gives $P(x, -\gamma)$ if Re $(-\gamma) > \alpha$. Since Re $(\gamma) = 0$ for the integration over γ, and $\alpha < 0$, this condition is satisfied. Therefore:

$$\int_0^\infty p^2 dt = \frac{1}{2\pi i} \int_{-i\infty}^{i\infty} P(x,\gamma)\, P(x,-\gamma)\, d\gamma \qquad (126)$$

For an exponential shock wave we have, as in equation (76):

$$P(x,\gamma) = \frac{\exp(-bx)}{\lambda + \gamma} \tag{127}$$

Using the expansion for b in equation (77), the definition $a^2 \equiv 2\nu\chi/3C^3$, and setting $\gamma = i\omega$, equation (126) becomes:

$$\int_0^\infty p^2 dt = \frac{1}{2\pi}\int_{-\infty}^{\infty} \frac{\exp(-2a^2\omega^2)}{\lambda^2+\omega^2}\, d\omega \tag{128}$$

The integral on the right hand side of equation (128) can be transformed in a manner very similar to that employed in obtaining equation (89) from equation (78). We set $u = 2a^2$ and define

$$I \equiv \int_{-\infty}^{\infty} \frac{\exp(-u\omega^2)}{\lambda^2+\omega^2}\, d\omega = \exp(u\lambda^2)\, J \tag{129}$$

where

$$J \equiv \int_{-\infty}^{\infty} \frac{\exp\left[-u(\lambda^2+\omega^2)\right]}{\lambda^2+\omega^2}\, d\omega \tag{130}$$

Then

$$\frac{dJ}{du} = -\int_{-\infty}^{\infty} \exp\left[-u(\lambda^2+\omega^2)\right] d\omega = -\frac{\pi^{1/2}\exp(-u\lambda^2)}{u^{1/2}} \tag{131}$$

Integrating equation (131) with respect to u; and noting that $J = 0$ when $u \rightarrow \infty$,

$$J = \pi^{1/2} \int_u^\infty \frac{\exp(-u\lambda^2)}{u^{1/2}}\, du \qquad (132)$$

Transforming the variable of integration in (132) by setting $y^2 = 2a^2\lambda^2$, we have from equations (128) and (129):

$$\int_0^\infty p^2\, dt = \frac{\exp(2a^2\lambda^2)}{\pi^{1/2}\lambda} \int_{\sqrt{2}\,\lambda a}^\infty \exp(-y^2)\, dy \qquad (133)$$

Adopting the notation of section 8 with $\alpha = \lambda a$,

$$\int_0^\infty p^2\, dt = \frac{\exp(2\alpha^2)}{2\lambda}\left[1 - P_i(\alpha\sqrt{2})\right] \qquad (134)$$

13.2 The total energy flow through a spherical surface of radius R surrounding the charge would then be given by

$$E(R) = \frac{4\pi R^2 \Pi_m^2}{\rho C} \frac{\exp(2\alpha^2)}{2\lambda}\left[1 - P_i(\alpha\sqrt{2})\right] \qquad (135)$$

where Π_m is an amplitude parameter, which at small values of a is essentially the peak pressure of the shock wave.

Thus if we consider an ideal case in which finite amplitude effects are absent, and changes in shape of the shock wave are due only to viscous attenuation, the dissipation parameter χ is zero at some initial low value of the range denoted by R_0 where the rise time is assumed negligibly small, and then increases with R in the manner:

$$\chi = R - R_0 \qquad (136)$$

To calculate the energy dissipated over any arbitrary interval between R_1 and R_2, we would substitute the appropriate values of α_1 and α_2 into equation (135) and obtain the energy loss by taking the difference $E(R_1) - E(R_2)$. The quantity $R^2 \pi_m^2$ would be a constant, the value of which would be given by $R_0^2 P_0^2$, where P_0 is the peak pressure of the shock wave at R_0.

From a slightly different point of view for the same ideal case, we could consider the rate of energy loss with respect to R by differentiating equation (135) in the light of (136):

$$\frac{dE}{dR} = \frac{4\pi R^2 \pi_m^2}{\rho C} \frac{d}{d\alpha} \left\{ \frac{\exp(2\alpha^2)}{\lambda \pi^{1/2}} \int_{\alpha\sqrt{2}}^{\infty} \exp(-y^2)\, dy \right\}$$

$$= \frac{4\pi R^2 \pi_m^2}{\rho C} \left\{ 2\lambda k^2 \frac{\exp(2\alpha^2)}{\pi^{1/2}} \int_{\alpha\sqrt{2}}^{\infty} \exp(-y^2)\, dy - \frac{k_2 x^{-1/2}}{(2\pi)^{1/2}} \right\} \quad (137)$$

where $\alpha = k x^{\frac{1}{2}}$ and $k = 7.11\ (10^{-8})$ in accordance with equation (97).

Since α is generally small, the first term in the brackets of equation (137) is of the order λk^2, and the ratio of this term to the second term is therefore of the order $(2\pi)^{\frac{1}{2}} \alpha$ which is also small. We therefore neglect the first term and write approximately:

$$\frac{dE}{dR} = -\frac{4\pi R^2 \pi_m^2}{\rho C} \frac{k_2 x^{-1/2}}{(2\pi)^{1/2}} \quad (138)$$

To the degree of approximation involved, this expression gives

the rate of energy loss with respect to R for the case in which viscous effects alone are present.

13.3 In order to estimate the energy losses in the case where we take account of the sharpening effect of finite amplitude, we make use of equation (138) as an expression for the rate of energy loss, and integrate it over the range under consideration, using for $\varkappa$ the results of Figure 10 rather than equation (136). It would not be correct to evaluate (135) at R_1 and R_2 by substituting the corresponding values of $\varkappa_{r_1}$ and $\varkappa_{r_2}$ from Figure 10 and taking the difference to measure the energy loss. This method would not take into account the fact that the sharpening effect causes the wave to travel a given range with a shorter average rise time, and therefore greater viscous dissipation, than it would have had if only viscous effects were present. By using (138) as a measure of the rate of dissipation per foot of propagation for a given value of $\varkappa$, we can apply the results of section 9 to estimate the total energy loss.

There remains the problem of selecting appropriate values for the amplitude parameter Π_m. As indicated above, an upper bound can be set by taking Π_m as the peak pressure of the wave at some relatively low value of the range, R_o, where viscous effects have not appreciably rounded off the front and thereafter setting $R\Pi_m$ equal to the constant R_oP_o. This method would be strictly correct only for the case in which change of shape is due solely to viscous effects. The situation

which develops when we include the sharpening effects of finite amplitude is illustrated schematically in Figure 16. The initial, steep fronted shock has a peak pressure Π_{m1}; in the course of propagation, viscous effects would produce the rounding and lower peak value as shown. Finite amplitude effects would, in turn, sharpen the front of this rounded wave without affecting the resulting peak pressure (tc a first approximation). The final wave in which viscous and finite amplitude effects have been superposed has a lower value of Π_m as shown in Figure 16.

Thus we can set a lower bound to the amplitude parameter Π_m by equating it to the actual peak pressure as given by the similarity curve (equation (104)) for various values of R. In the calculations to be made below, we shall compute the upper and lower limits of the expected energy dissipation in accordance with the above methods of selecting Π_m. Substituting the appropriate numbers into equation (138):

$$\frac{d\mathcal{E}}{dR} \cong -9.17\,(10^{-6})\,R^{4}\Pi_m^{2}\chi^{-1/2} \qquad \text{inch.lb./ft.} \quad (139)$$

where R and χ are in ft. and Π_m in lb/in^2. In equation (139) χ is obtained as a function of R by use of Figure 10. The results of numerical integration of (139) for various cases are given in Table III, where we have calculated $\Delta\mathcal{E}_v$ (the viscous dissipation) over the interval $W^{1/3}/R = 0.0053$ to $W^{1/3}/R = 0.00022$ for charge sizes of 0.5, 8, and 300 lb.

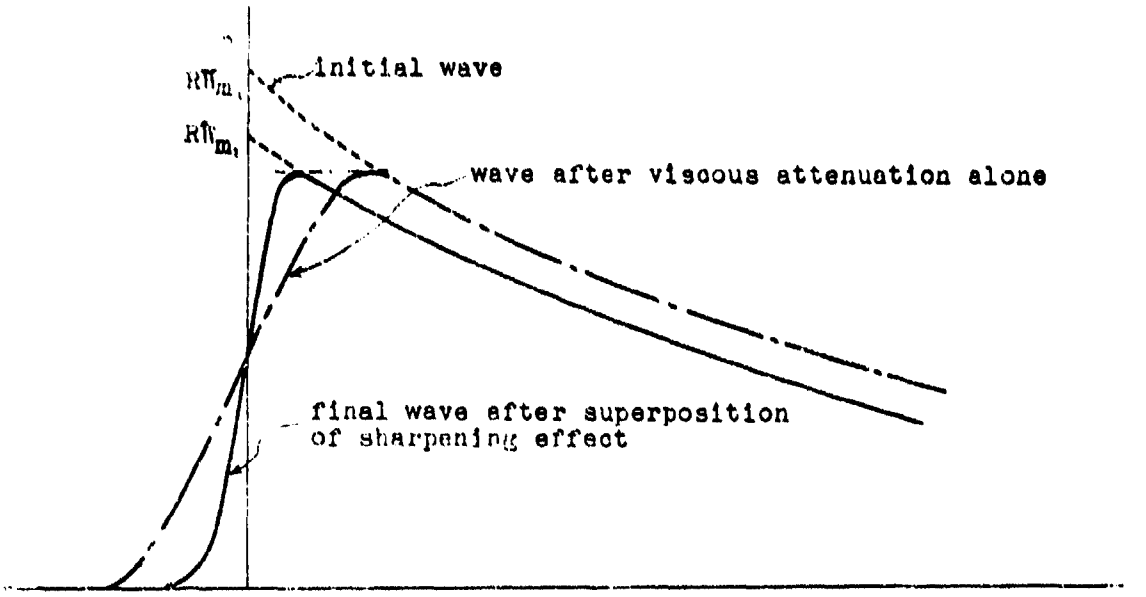


Fig. 16

Illustration of the behavior of the amplitude parameter Π_m.

Table III

Shock wave energy dissipation over the interval $W^{1/3}/R = 0.0053$ to $W^{1/3}/R = 0.00022$.

Charge Size W (lb.)	$\Delta E_v \times 10^{-6}$ (in. lb)		$\overline{\Delta E_v} \times 10^{-6}$ (in. lb.)	$\Delta E_s \times 10^{-6}$ (in. lb.)	$(\Delta E_s + \overline{\Delta E_v}) \times 10^{-6}$ (in. lb.)	$\Delta E \times 10^{-6}$ (in. lb.) from Fig. 15, extrapolated	$\Delta E \times 10^{-6}$ (in. lb.) From eq. (142)
	Upper Limit $R\,\Pi_m$ = const.	Lower Limit $\Pi_m = P_m$					
0.5	0.20	0.15	0.17	0.14	0.31	0.27	~ 0.2
8	2.4	1.6	2.0	2.3	4.3	4.2	~ 3
300	46	50	48	87	140	150	~ 130

1557

13.4 If we assume that the rise of the front is sufficiently abrupt to justify our continued use of the Rankine-Hugoniot conditions, we may calculate the irreversible shock loss by use of equation (36) of NavOrd 406[13], which after some manipulation leads to the form:

$$\Delta E_s = 3.15(10^6)\, W \left[\left(\frac{W^{1/3}}{R}\right)_1^{0.39} - \left(\frac{W^{1/3}}{R}\right)_2^{0.39} \right] \qquad (140)$$

Values of ΔE_s calculated by means of equation (140) are also given in Table III, together with the sum $\Delta E_s + \overline{\Delta E_v}$ where $\overline{\Delta E_v}$ is the average of the upper and lower limits of the viscous dissipation. This sum is compared with the quantity ΔE as calculated over the same interval of $W^{1/3}/R$ from the energy curve of Figure 15 extrapolated to $W^{1/3}/R = 0.00022$. The uncertainty in this calculation is large since ΔE is a small residual of a subtraction of large numbers.

Another rough estimate of ΔE may be obtained by use of the peak pressure and time constant similarity curves and calculating $\Delta (P_m^2 \theta / 2 \rho C)$, on the assumption that the pressure wave is purely exponential from t = o to ∞. The empirical equation for the time constant as obtained from Figure 2 of Nav Ord 424[22] is approximately:

$$\theta \cong 58\ (10^{-6})\ W^{1/3} \left(\frac{W^{1/3}}{R}\right)^{-0.22} \text{ sec.} \qquad (141)$$

Then, making use of equations (104) and (141),

$$\Delta E \cong \frac{P_m^2 \theta}{2\rho C} \cong 4.36\,(10^6)\, W^{1.01}\, R^{-0.04} \text{ (in. lb.)} \qquad (142)$$

Results obtained by use of equation (142) are exceedingly rough, not only because of the exponential approximation but because of the large uncertainty in the exponent of R. Values are quoted in Table III to one significant figure.

13.5 It is apparent from Table III that the observed energy loss over the interval considered is approximately accounted for by the sum of the estimated viscous and shock front dissipations, if it is assumed that one may correctly use the shock dissipation results for waves having rise times of the order of 10 to 20 microseconds. Furthermore, it is apparent that the predicted losses are such that one would not expect to observe significant departures (relative to the present experimental precision) from similarity scaling of the energy flux out to values of $W^{1/3}/R$ of the order of 10^{-4}.

14. Slope of the peak pressure similarity curve.

14.1 We can use a method very similar to that of section 13 in order to estimate the peak attenuation due to viscous effects. Combining equations (89) and (92), the relative peak pressure is given by

$$p(\beta_r) = \frac{\exp\left[\alpha^2 - \alpha(\beta_r - 4)\right]}{\pi^{1/2}} \int_{\alpha - (\beta_r - 4)/2}^{\infty} \exp(-y^2)\, dy \qquad (143)$$

Then, as in section 13, we differentiate equation (143) with respect to χ and account for the sharpening effect by setting the resulting expression equal to $dp(\beta_r)/dR$ and obtaining χ as a function of R from Figure 10. The result of differentiation, making use of equations (92) and (97), is

$$\frac{dp(\beta_r)}{dR} = \frac{\exp\left[\alpha^2 - \alpha(\beta_r - 4)\right]}{2} \left\{1 + Pi\left[\frac{(\beta_r - 4)}{2} - \alpha\right]\right\} \frac{\alpha}{2\chi} \left[2\alpha + 0.655 - (\beta_r - 4)\right]$$

$$- \frac{\exp\left[-(\beta_r - 4)^2/4\right]}{\pi^{1/2}} \left(\frac{\alpha + 0.328}{2\chi}\right) \qquad (144)$$

In these calculations $\alpha^2 << \alpha(\beta_r - 4)$, and $1 + Pi\left[\frac{(\beta_r - 4)}{2} - \alpha\right]$ is always very nearly equal to 2. Therefore equation (144) may be somewhat simplified:

$$\frac{dp(\beta_r)}{dR} \cong \frac{-\alpha \exp\left[-\alpha(\beta_r - 4)\right]}{2\chi} \left[(\beta_r - 4) - 0.655 - 2\alpha\right]$$

$$- \frac{\exp\left[-(\beta_r - 4)^2/4\right]}{\pi^{1/2}} \left(\frac{\alpha + 0.328}{2\chi}\right) \qquad (145)$$

Numerical integration of equation (145) was carried out for two charge sizes: 0.5 and 300 lb. over the $W^{1/3}/R$ interval 0.0053 to 0.00022. The resulting relative pressures were plotted against

R on logarithmic paper and were found to be approximately represented by power functions of average slope -0.11 and -0.08 respectively. (The lines actually show a slight downward curvature.) These calculations probably overestimate the viscous effect somewhat because of the approximation involved in equation (96).

The asymptotic shock propagation theory of Kirkwood and Bethe (see reference 7, p. 126) predicts a peak pressure - distance dependence at long ranges of the form

$$P_m \sim \frac{a_0}{R}\left(\log \frac{R}{a_0}\right)^{-1/2} \qquad (146)$$

where a_0 is the charge radius. The logarithmic term in equation (146) measures the departure of the distance decay law from the R^{-1} law of spherical sound waves, and represents, essentially, the effect upon the peak pressure of the continued spread of the profile of the wave. (Note that the quantity $P_m^2\Theta/2\rho C$ as calculated from equations 4.20 and 4.22 of reference 7 represents the energy flux of the shock wave and varies as R^{-2}, the logarithmic terms in the pressure and the time constant just serving to annul each other.)

The effect of the logarithmic term in equation (146) can be ascertained by plotting on log-log paper, and it is found that this term contributes an average slope of about -0.06 to the P_m vs. R curve in the region between $W^{1/3}/R = 0.0053$ and 0.00022. (The line actually shows a slight upward curvature.)

If we now combine the effects of viscous attenuation

and spread of the profile and add the spherical effect of R^{-1}, we would expect a pressure-distance dependence of the form

$$P_m \sim R^{-1.17} \quad \text{for 0.5 lb. charges}$$
$$P_m \sim R^{-1.14} \quad \text{for 300 lb. charges} \qquad (147)$$

This calculation omits a small contribution from the residual Rankine-Hugoniot dissipation.

Most experimental peak pressure similarity curves have been found to have exponents of 1.13 to 1.15, and the results reported in NavOrd 424[22] show that this slope persists into the low pressure region to which the calculations leading to equations (147) apply.

Our interpretation of this result is that in the high pressure region the contribution of 0.13 to 0.15 to the exponent comes from the combined effects of spread of profile and Rankine-Hugoniot shock dissipation. As the range increases, the Rankine-Hugoniot effects drop off, and the slope would tend toward the magnitude of 1.06 as given by the asymptotic theory; but it is in this region that viscous effects become appreciable, and apparently take over most of the role initially played by Rankine-Hugoniot dissipation in such a way as to make departures from the straight line on log-log paper undetectable within experimental error.

IV. Distortion associated with reflection from the sea surface.

15. Introduction

15.1 In the derivation of equation (19) it was tacitly assumed that the wave reflected from the sea surface was simply inverted without distortion or attenuation. This

ideal behavior may not be realized at the receiving gauge owing to: (a) non-linear reflection (b) transmission to the air (c) sea-surface roughness (d) cavitation near the sea surface (e) propagation with finite amplitude (f) viscous attenuation.

15.2 Keil has shown[15] that for any charge weight and charge depth, if the angle of incidence at the surface is sufficiently oblique, the reflected wave propagates along the initial wave front, producing a range of distortion in both waves. In all shots of the series reported here, at ranges less than 5000 ft., the direct and reflected waves are clearly resolved on the records, so that non-linear reflection plays no part in these cases. However, the few shots at extreme ranges (~10,000 ft.) exhibit gross attenuation of the direct shock wave and show nothing directly identifiable as a reflected wave. (See Figure 2e.) If a half-pound charge of pentolite is detonated at a depth of 40 feet, distortion should begin to occur (according to reference 15) at the surface approximately 8000 feet from the charge, and will then travel along the initial wave front, influencing it for example, to a depth of about 7 feet from the surface at a range of 20,000 feet. In the case of Figure 2e where the receiving gauges were at a depth of 25 feet, and at a range of 9100 ft. the distortion already appears quite pronounced, while the theory indicates that it should not have set in. We are, however, close enough to the border line so that small changes in the parameters could reverse this prediction, and we can probably consider this as within the margin of error of the theory. Thus it is not unreasonable to ascribe, tentatively, at

least part of the observed attenuation at very long ranges to non-linear reflection.

15.3 It was pointed out previously that when an acoustic wave in water is reflected from a water-air interface, in view of the higher sound velocity in the water, reflection is regular for all angles of incidence. The reflected wave is undistorted but is slightly attenuated due to a very small transmission of sound into the air. Even in the extreme case of normal incidence this amounts to a decrease of less than 0.01% in amplitude. Thus no observable attenuation can be attributed to this cause.

15.4 Roughness in the sea surface (which prevailed to some extent during all the measurements) undoubtedly produces some incoherent scattering of the reflected wave due to the essentially chaotic character of surface wave motion considered on the scale pertinent here. However, the remarkable sharpness of the front of all reflected waves measured up to ranges of 5000 feet (see Figure 2) makes it clear that scattering due to surface roughness is not an important means of producing distortion of the surface reflection in these particular measurements.

16. Bulk cavitation

16.1 The phenomenon called by Kennard[17] "bulk cavitation" has a most important effect on the structure of the reflected wave. If the negative pressure of the reflection is great enough the water experiences an insupportable tension and is torn into many bubbles, giving rise to a region of cavitation which has a rapid

subsequent history of expansion and contraction. The cavitation occurs within a space lying near the surface and having a large horizontal extent. This distorts and attenuates the reflected wave which is causing it to an extent depending on the vigor of the cavitation. A quantitative theoretical description of the character of the reflected wave both during the cavitation and after it emerges into homogeneous water is very difficult, involving as it does, wave propagation through a medium containing randomly-distributed time-dependent inhomogeneities which have been initiated under conditions not yet adequately described.

16.2 The surface reflections in the present series of experiments frequently show the following characteristics: first, a sharp drop, of duration approximately equal to the transit time across the gauge; this forms the leading side of a brief, but strong negative pressure spike; the pressure then rises somewhat and oscillates erratically at a constant level for a few tenths of a millisecond and eventually merges into the succeeding event. In his theory of bulk cavitation, Kennard assumes that cavitation occurs whenever the pressure in the water falls to a characteristic fixed "breaking pressure", then instantly becomes equal to a characteristic "cavity pressure" which cannot be less than the breaking pressure, and finally cavitation disappears instantly when the pressure rises above the cavity pressure. Our observations seem to support this qualitative picture. Whether or not the breaking and cavity pressures are fixed magnitudes however, cannot be determined.

It is believed that the oscillations noted in the tail of the reflected wave do not originate in the gauge response or recording system, nor in the immediate vicinity of the gauge, for in some cases a striking qualitative correlation has been observed in the detail of the oscillation as recorded by the several channels. It is felt that these small pulses originate in or near the cavitation region and may be associated with the formation and collapse of bubbles.

The pressure drop in the reflected wave is always less than that to be expected ideally. In Figure 17 the measured ratios of reflected to direct peak pressures from 0.5 pound pentolite charges are plotted against range, both for the drop to the tip of the negative spike and the drop to the level region smoothed through the oscillations. The scatter of the data is considerable, but the trend is clear. The reflected wave has an amplitude of but a few tenths of the direct shock at short ranges and increases to an appreciable fraction of it at large ranges. On the same plot is shown the ratio to be expected if there were no drastic attenuation due to cavitation. This curve is not horizontal because account has been taken of the extra distance traveled by the reflected wave in its passage to the gauge. Also displayed is a curve showing the ratio to be expected when a crude account of cavitation is taken by the method described below.

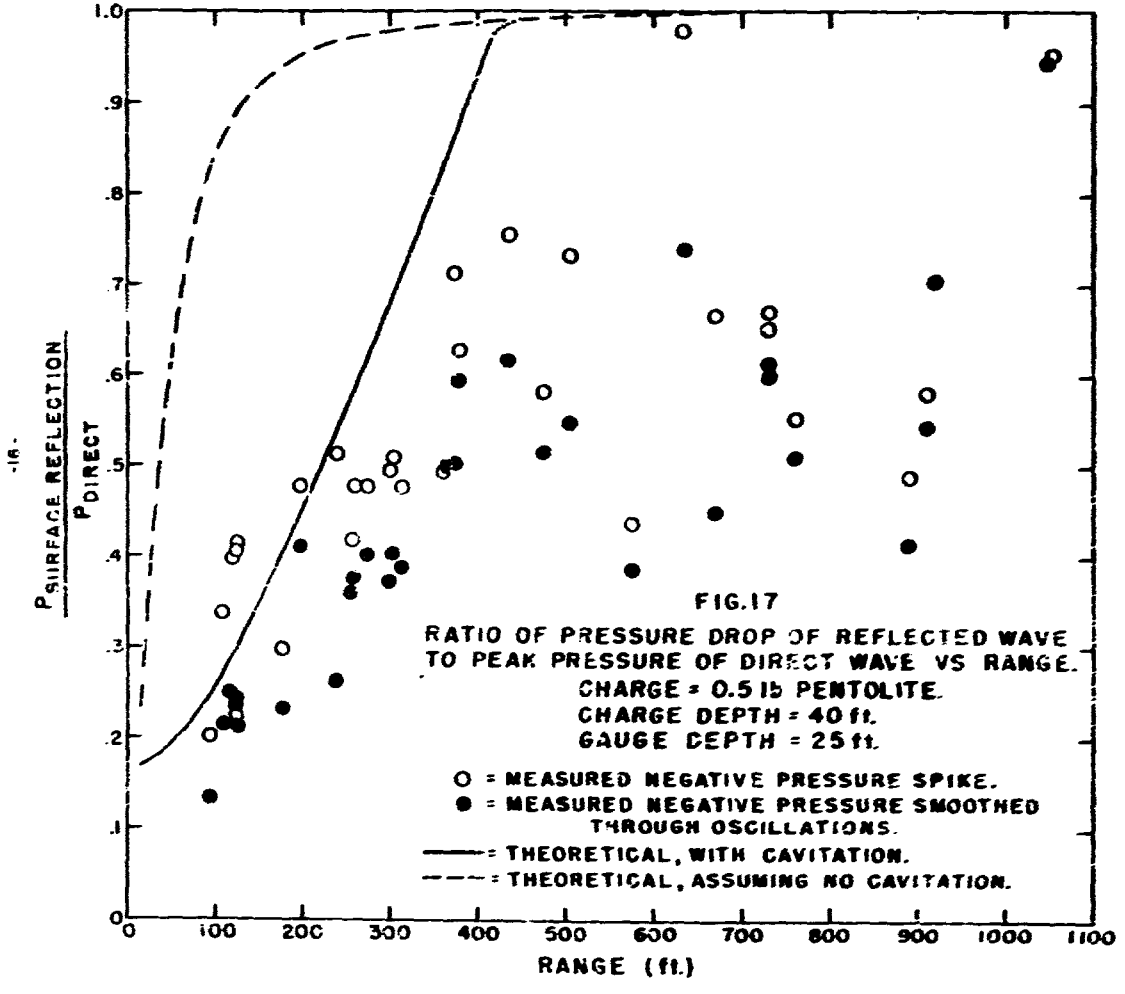


FIG.17

RATIO OF PRESSURE DROP OF REFLECTED WAVE TO PEAK PRESSURE OF DIRECT WAVE VS RANGE.
CHARGE = 0.5 lb PENTOLITE.
CHARGE DEPTH = 40 ft.
GAUGE DEPTH = 25 ft.

ADVT

16.3 When an explosion takes place near the sea surface we will assume that:

(a) Cavitation begins when the pressure in the water drops to a fixed value, p_c , the cavitation pressure. We will take $p_c = 0$ p. s. i. This assumption will be examined later.

(b) The pressure at a point on the front of the reflected wave can be described as emanating from an image charge above the surface, having a variable apparent weight, W_i, so adjusted as to account for the pressure diminution due to cavitation.

(c) W_i is a continuous <u>non-increasing</u> function of distance along a ray away from the image charge, being equal to the true charge weight W, before any cavitation takes place, decreasing monotonically in regions of cavitation, and remaining constant in regions of no cavitation.

The assumptions (b) and (c) imply that cavitation propagates as long as the spherically expanding negative reflected wave is decaying in amplitude less rapidly than is the positive pressure region into which it is propagating in accordance with the criterion given by Kennard.[23] The assumptions, however, take no account of the effects of pressure gradients along the wave front.

Referring to Figure 18c, where the origin of coordinates is taken at the image charge, the total pressure at a point (R_1,θ) on the front of the reflected wave is the sum of the hydro-static head at this point, $p_s(R_1,\theta)$, the pressure at distance R_2 from a charge of weight W at a reduced time τ (associated with propagation through the distance x) behind its front, $p\left(\frac{W^{1/3}}{R_2}, \tau\right)$, and the pressure at the front of a negative wave at a distance R_1 from a charge of apparent weight W_i, $-p\left(\frac{W_i^{1/3}}{R_1}, 0\right)$. If cavitation is

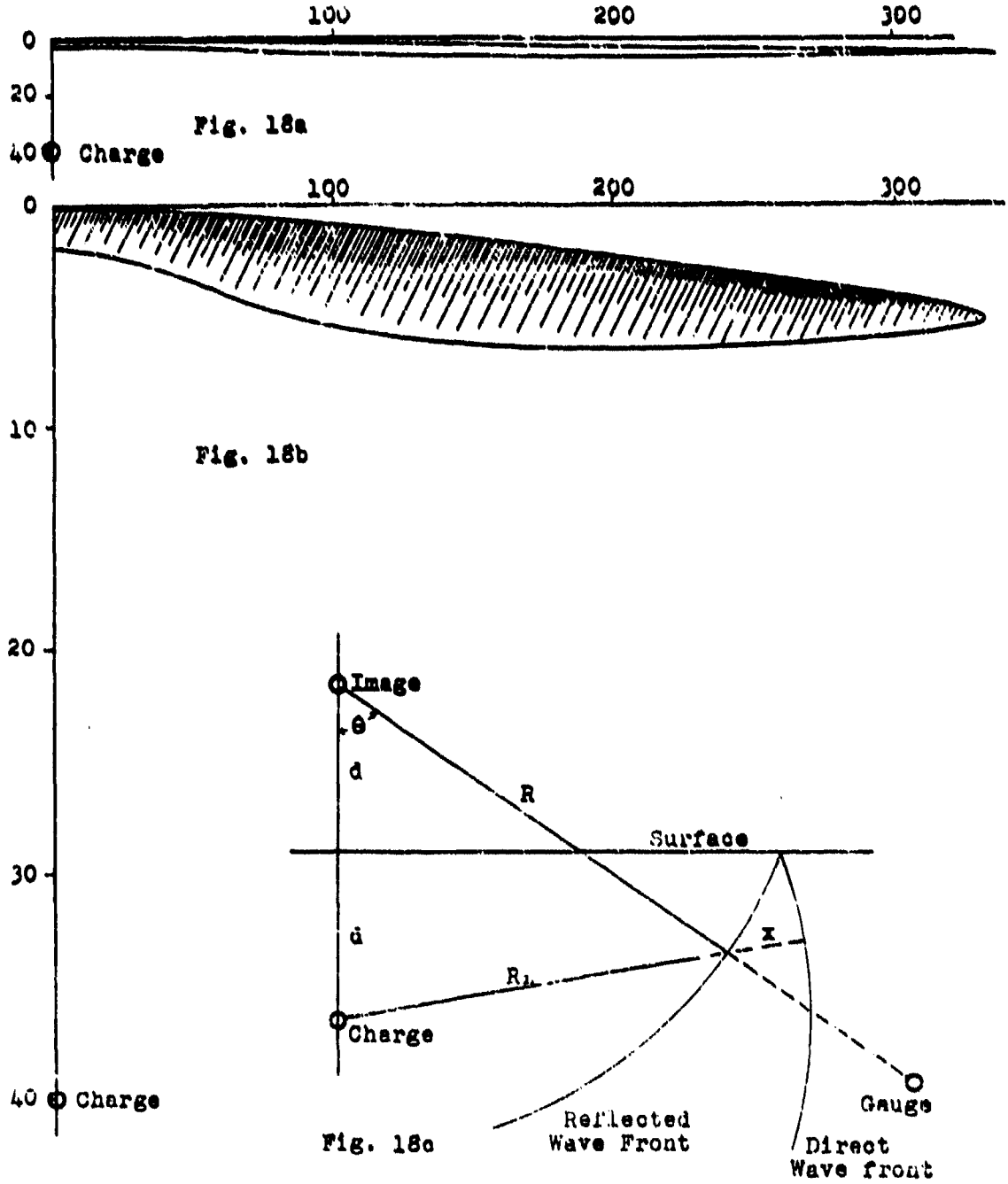


Fig. 18

Cavitation region for a 0.5 lb. Pentolite charge at 40 ft. depth.

occurring at (R_1, θ) then the total pressure must equal the cavitation pressure:

$$P_A(R_1,\theta) + p\left(\frac{W_1^{1/3}}{R_2}, \tau\right) - p\left(\frac{W_1^{1/3}}{R_1}, 0\right) = p_c \qquad (148)$$

W_1 is defined by this equation in the region of cavitation and by assumption (c) elsewhere. To make (148) explicit for calculation using empirical data, we note from the geometry of Figure 18c that

$$\begin{aligned} \chi &= R_1 - R_2 \\ R_2 &= R_1^2 + 4d^2 - 4dR_1 \cos\theta \end{aligned} \qquad (149)$$

If p_a is the atmospheric pressure and H is the vertical hydrostatic pressure gradient, then

$$P_A(R_1,\theta) = p_a + H(R_1 \cos\theta - d) \qquad (150)$$

Letting $f(\tau)$ be the fraction of the peak pressure which obtains at reduced time τ we can write

$$p\left(\frac{W^{1/3}}{R_2}, \tau\right) = f(\tau)\, p\left(\frac{W^{1/3}}{R_2}, 0\right) \qquad (151)$$

The function $f(\tau)$ is obtained from a composite curve of pressure versus reduced time at some particular reduced distance[13] and the function $p\left(\frac{W^{1/3}}{R}, 0\right)$ from a similarity curve[14].

The reduced time τ is related to the distance χ, and the sound velocity C by an empirical relation[14] valid for TNT or pentolite

$$\tau = \frac{\chi}{0.060\, C\, W^{1/3} \left(\frac{W^{1/3}}{R_2}\right)^{-0.18}} \qquad (152)$$

where weight is in pounds, distance in feet, and time in milliseconds. Inserting (150), and (151) into (148):

$$p_a + W(\kappa_1 \cos\theta - d) + f(\tau)\, p\left(\frac{W^{1/3}}{R_1}, 0\right) - p\left(\frac{W_i^{1/3}}{R_1}, 0\right) = p_c \qquad (153)$$

To find W_i at any point (R_1, θ) one calculates R_2 and $\varkappa$ by (149), τ by (152), and finally W_i from (153). The limits of the cavitation region are found by varying R_1 at a fixed θ; the value of R_1 which makes $W_i = W$ determines a point on the upper boundary of cavitation and that which makes W_i a minimum, W_{min}, determines a point on the lower boundary. On this particular ray, according to (e) we then set $W_i = W$ above the cavitation and $W_i = W_{min}$. below. The process is repeated for other values of θ until the cavitation region is mapped to the degree desired.

The cavitation region found in this way, due to the explosion of a 0.5 lb. pentolite charge 40 feet below the surface is shown in true scale in Figure 18a. It is seen to be a thin layer of wide extent near the surface, though never touching it. In 18b the same region is shown with an eight-fold magnification in depth scale. Here the shading is meant to imply qualitatively that the cavitation is most vigorous along the top side of the region and gradually dies out to nothing along the bottom and at the outer tip.

The pressure drop in the reflected wave arriving at the gauge is taken to be $p\left(\frac{W_i^{1/3}}{R}, 0\right)$, computed for the gauge position. The theoretical curve of Figure 17 was obtained in this way. In no case was the receiving gauge theoretically in the region of cavitation in this particular series of measurements. At small ranges

the agreement between theory and experiment is quite good, in view of the scatter of the data, but at higher ranges there is considerable attenuation still to be accounted for. If the cavitation pressure had been chosen as an actual tension of some magnitude rather than zero, the theoretical curve would be moved upward resulting in even poorer agreement with the observations. This gives some support to the assignment of a low breaking pressure for initiation of cavitation.

16.4 Any complete quantitative theory of bulk cavitation must take explicit account of the conditions and process of its initiation. The theory must go on to describe the way in which the bubbles abstract and scatter energy through the pressure field. It has been the view that sea-water possesses a unique breaking tension and that this essentially static pressure condition is the criterion for the initiation of bulk cavitation and the formation of spray domes due to transient pressure waves. Observations of cavitation[18] have led to the assignment of breaking tensions smaller by at least an order of magnitude (0-100 psi) than those deduced from photographs of the spray dome[24] (400-6000 psi).

Breaking tensions obtained by spray dome measurements vary over an order of magnitude depending upon the smoothness of the sea-surface, the surface tension of the water, the dynamic structure of the pressure wave incident at the surface, and even upon the particular aspect of the phenomenon from which the breaking tension is deduced. We are dealing here with the disintegration of a liquid surface into droplets, the onset of which is intimately connected with the condition of the surface.

It is felt that bulk cavitation is not simply another direct manifestation of the same property of sea water as that controlling the formation of a spray dome, but depends on something like this property in an entirely different way. The nucleation of a new phase in the bulk of a metastable medium has been treated statistically[19]. It is found that over a small range of increasing static tensions the rate of formation of stable nuclei increases enormously. This effect makes the notion of a unique breaking tension a useful one at least under static conditions, but in the rapidly varying pressure field of a shock wave it may be that more detailed account must be taken of the nucleation process. Photographs of cavitation (Ref. 18, 20 21) suggest that cavitation bubbles continue to grow for some distance behind the front of a negative wave and can become quite large and occur in such numbers as to occupy a considerable volume fraction when the cavitation is severe. One hopeful feature seen in photographs of bulk cavitation is the considerable uniformity of bubble size in regions which presumably have had the same pressure history. At the other extreme, when the pressures encountered are relatively small, as in our measurements, cavitation can still seriously modify a negative wave even though the cavitation would appear only as a slightly increased turbidity of sea water.

16.5 In order to illuminate some of the patent obscurities that still remain connected with bulk cavitation, it would be most useful, as a start, to make photographic observations of the intensity and

Best Available Copy

propagation of the cavitation itself and simultaneous piezoelectric measurements outside of the region of cavitation.

One interesting consequence of the assumptions (a), (b), and (c) is that there should be no cavitation vertically below any charge at any depth, although the cavitation may extend deeper than the charge off to the side. Thus it should be possible to avoid the obscuration due to cavitation encountered in photography of shallow explosions[21] by observing from directly below the charge. This would have the additional advantage of giving a well lighted silhouett picture.

17. Sharpness of the negative wave front.

17.1 It is frequently asserted that negative shocks are unstable and would tend to spread "rapidly". (see reference 7, p. 25, and reference 25, p. 181). It is interesting to examine the available experimental records in the light of this prediction, remembering, of course, that the minimum "fall time" which can be resolved is the transit time across the gauge. Examination of the records reproduced in Figures 2 and 3 (and of the other existing records as well) shows that the "fall" of the negative wave is equally sharp at all ranges, i.e. of the order of magnitude of the gauge transit time of 20 to 30 microseconds, and that any spread of the front due to the combined effects of finite amplitude and viscous attenuation must be smaller than this magnitude.

It is possible to make a theoretical prediction of the expected spread by application of the methods of section 9.3. In the case of the negative wave, the viscous and finite amplitude effects both tend to spread the front instead of opposing each other as in

the positive wave. The counterpart of equation (108) thus becomes

$$\frac{dx}{dR} = 1 + \frac{9.68(10^{-5})x}{\tau_r - 4.65(10^{-8})x^{1/2}}\left(\frac{W^{1/3}}{R}\right)^{1.13}, \qquad (154)$$

an equation differing from (108) only in sign but having an entirely different character. The differential equation (154) possesses no "equilibrium trajectory," so that it is necessary to select an appropriate starting point by some other means. It is natural to carry out the integration for the positive wave by (108) up to the point of reflection and subsequently by (154) for the negative wave up to the point of interest, using the condition of continuity of the "equivalent viscous distance" at the point of reflection. The results of such integrations show that the fall time of the reflected wave is greater than the rise time of the direct wave only by an amount too small to be successfully distinguished by our measuring equipment. For example the fall time of the reflected wave from a $\frac{1}{2}$ lb. charge which reflects at 2000 ft. from the charge and then propagates for an additional 2000 ft. is 32μsec. The rise time of the direct shock which travels the same total distance is 19μsec. Both of these figures are of the order of magnitude of the transit time for the gauges used at this range. On the average, the observed fall times appear to be larger than the rise times, but for the reasons outlined in section 10.2 it is not possible to obtain reliable absolute values of these small intervals to test the theory quantitatively.

V. Acknowledgments

The authors wish to acknowledge the assistance of G. Wertheim and C. Wingate in the analysis of the data.

Appendix I

An Improved Microcoulometer for the Calibration of Piezoelectric Gauges

by

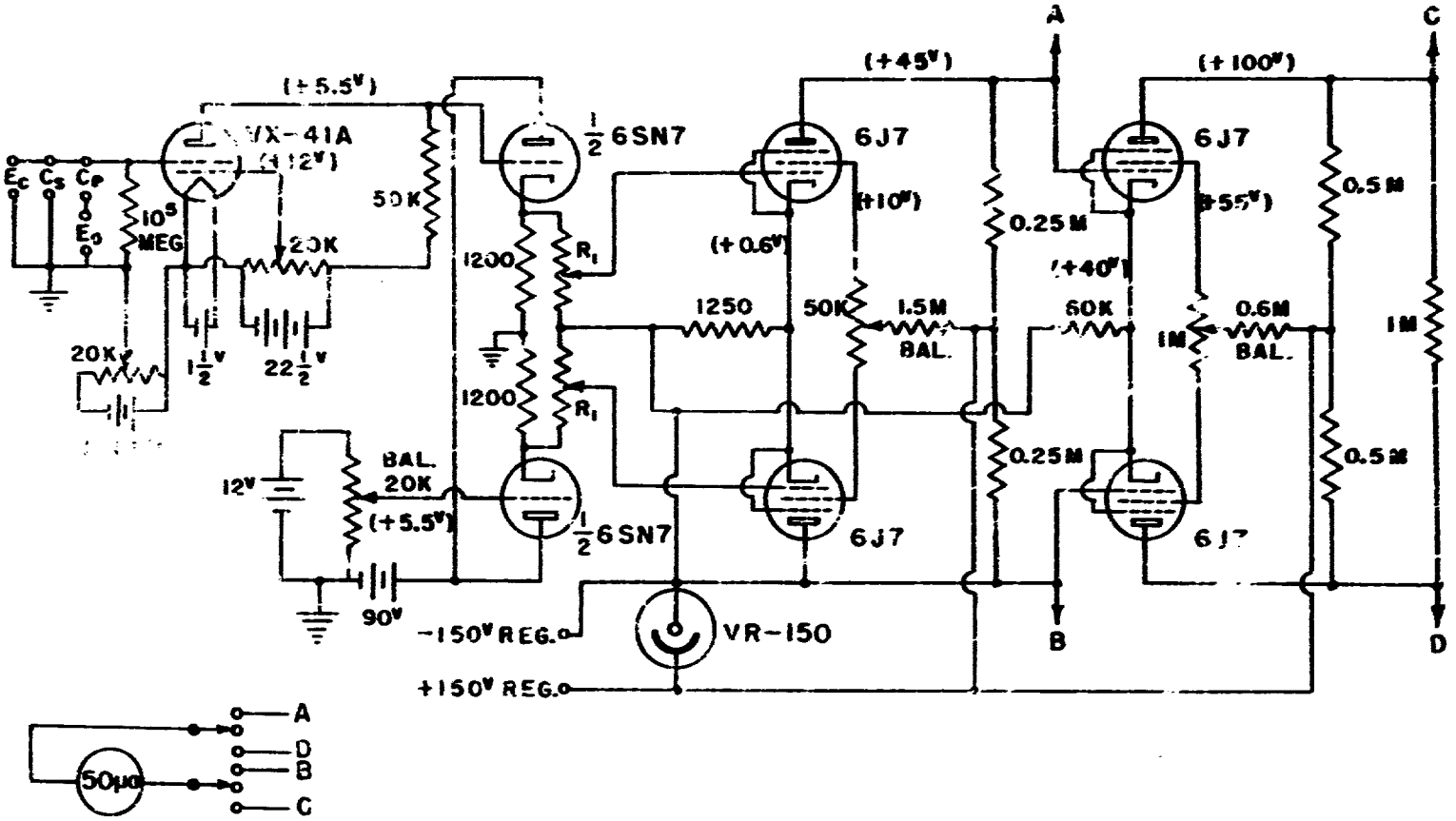
A. B. Arons and W. Grube

1. Introduction

1.1 The a.c. powered microcoulometer which has been used for several years by this laboratory [5,26] for the calibration of piezoelectric gauges has frequently proved inadequate when stability and high sensitivity were required. It was the object of this program to design a new instrument of suitable stability and sensitivity, capable of operating with very high input resistance, by taking advantage of recent developments in electrometer tubes and electrometer circuits.

2. Description of the circuit

2.1 A diagram of the new microcoulometer circuit (designated LH) is shown in Figure 19. The input stage utilizes the Victoreen VX-41A electrometer tetrode, the input grid resistor being 10^5 megohms. The electrometer output feeds one side of a push-pull cathode follower stage, the other side of which can be positioned by control of its grid bias in such a way as to set an initial balanced condition of zero potential across



NOTE:
ALL RESISTANCES ARE WIRE WOUND
R_1 = 2500 Ω BLEEDER TAPPED AT
50, 150, 300, 600, 1000 & 1500 OHMS

FIG 19

MICROCOULOMETER
TYPE LH

W.H.O.I. 8/25/49

the output points R_1 R_1. A signal applied to the input them appears as a voltage change across R_1 R_1 which is measured by the detecting circuit consisting of two push-pull amplification stages, using 6J7 (or 6SJ7) tubes.

The detecting circuit is a modified version of an instrument described by Lyons and Heller[27] in 1939. The output is read by noting the swing of a 50 microampere meter placed across the points AB for low gain operation or CD for high gain. Various normal operating voltages are indicated on the circuit diagram. Any well regulated a.c. operated power supply is adequate for the B^+ and B^- voltages.

3.2 This circuit has been found to be very stable and linear in its operation. Some typical calibration results are shown in Table IV and are compared with measurements made at the Cambridge Thermionic Corporation by means of the old microcoulometer.

3. Sensitivity

3.1 The sensitivity of the low gain range of the new instrument is such as to give full scale deflection of the meter for an input signal of 0.5V. The high gain range gives full scale deflection for an input signal of 0.05V.

On the high gain range it would therefore be possible to calibrate small gauges having sensitivities of the order of 0.1 micro micro coulomb per psi. by using pressure differentials of about 4000 psi. and total input capacity of 10,000 micro microfarads.

3.2 The instrument becomes quite sensitive to pick-up if the input capacity is made very low (ca. 1000 $\mu\mu$ fds.), but this difficulty could

be overcome by means of careful shielding. It would then be possible to take advantage of the increased effective sensitivity afforded by lower input capacity, and one could probably adapt the instrument to measure sensitivities as low as 0.01 $\mu\mu$ coul. per psi.

4. Further modifications and improvements.

4.1 The diagram of Figure 19 shows the present stage of development of the microcoulometer. Various modifications and improvements suggest themselves for future versions of the device: (a) Use RCA long life (red base) 6SJ7 and 6SN7 tubes. (b) The 6J7 screen balance controls affect the sensitivity slightly. These variables should be removed and all balancing done by means of the 6SN7 grid control. (c) Obtain the 6SN7 plate voltage by putting two VR 75's in series across the 150V regulated supply, and use a 75V plate voltage instead of the 90V battery. (d) Install 6E5 or 6U5 shadow tube to permit ready balancing of voltage across R_1 R_1 before connecting 50 μ amp. meter.

4.2 Fairly elaborate precautions must be taken in order to maintain an effective resistance of 50 to 100 thousand megohms at the input. The entire input stage should be carefully dried and then dipped or cast in polystyrene to minimize the effects of surface moisture films. Guard rings should also be installed at the input and connected to a suitable point in the circuit so as to rise and fall with the input voltage. Grid bias of the VX-41A must be carefully adjusted for minimum grid current.

5. Use of a Speedomax or Brown recorder as a detecting device.

5.1 Several experiments were conducted in which a Speedomax recorder was used to record the signal appearing across R_1 R_1 at the 6SN7 output. (The recorder was made available through the cooperation of Mr. A. Bunker's meteorological group.) The Speedomax has ample sensitivity and stability for this purpose, and the results were very promising. Calibrations could be carried out rapidly and conveniently, with pressure signals and standard voltage signals being rapidly and continuously recorded on the moving paper. The record can be conveniently read and the results computed after the paper strip is removed from the recorder. One man operation is possible.

The response time of the recorder is roughly the same as that of the Sensitive Research University model microammeters which have usually been used in this work. The error due to pyroelectric effect (which is greater the longer the response time) would therefore not be any more serious with the recorder than with previous devices. It is therefore suggested that the most efficient and convenient calibration technique would be to use the electrometer and cathode follower stages of Figure 19 to feed a Speedomax or Brown recorder as described above.

Results of calibrations with the Speedomax are shown in Table IV and are found to agree well with the values obtained by CTC and by means of microcoulometer LH.

In the preliminary experiments, it was not possible to connect the electrometer ground and the Speedomax. This led to some difficulty with pick-up when the operator touched the pressure chamber. The pick-up was made negligible by careful isolation of the grounds and insulation of the operator. In a permanent set-up, suitable modifications could probably be introduced to eliminate the grounding difficulties.

Table IV

Comparison of Gauge Calibrations with Various Instruments

KA = Sensitivity in $\mu\mu$ coul./psi.

CTC : Cambridge Thermionic Corp. calibrations

LH : New microcoulometer calibrations

S : Speedomax calibrations

Gauge No.	CTC KA	LH KA			S KA	
116	2.03	2.05	2.08	2.07	2.07	2.06
117	1.94	1.93	1.97	1.95	1.96	1.94
118	1.98	1.99	1.99			
120	1.85	1.86	1.87			
129	4.31	4.32	4.32	4.37	4.38	4.40
130	4.33	4.29	4.28	4.35	4.32	4.32
131	4.14	4.15	4.20			
132	4.17	4.26				
133	4.21	4.23				
143	8.54	8.63				
145	8.25	8.28	8.17		8.25	8.28
151	24.8	25.2				
153	24.8	25.1				

References

1. Rayleigh. Theory of Sound. Dover, 1945 V2, p 78-85.
2. Whittaker and Watson. Modern Analysis. Macmillan, p 75.
3. Jahnke and Emde. Tables of Functions. Dover, 1943, p 1-8.
4. Kemble, E. C. Fundamental Principles of Quantum Mechanics. McGraw Hill, 1937, p 36.
5. Arons, A. B. and Cole, R.H. Design and Use of Tourmaline Gauges for Piezoelectric Measurement of Underwater Explosion Pressure. OSRD Report No. 6239, March 1946.
6. Propagation of Sound in the Ocean. Memoir 27. Geological Society of America. October 1948. (Papers by Ewing and Worzel, and by Pekeris.)
7. Cole, R.H. Underwater Explosions. Princeton University Press, 1948.
8. Ott, H. Ann. d. Phys. (5 Folge) 41, 443 (1942.)
9. Lamb, H. Hydrodynamics. Dover, 1945, p 647.
10. Liebermann, L.N. J. Acoust. Soc. of Am. 20, 868 (1948).
11. Gardner and Barnes. Transients in Linear Systems. Wiley, 1942.
12. Richardson, J. M.; Arons, A.B.; Halverson, R.R. Hydrodynamic Properties of Sea Water at the Front of a Shock Wave. J. Chem. Phys. 11 785 (1947). or OSRD No. 6577
13. Arons, A. B.; Yennie, D. R. Energy Partition in Underwater Explosion Phenomena. Rev. Mod. Phys. 20, 519 (1948). or NavOrd 406.
14. Coles, J. S. et.al. Shock Wave Parameters from Spherical HBX and TNT Charges Detonated Under Water. NavOrd. 103-46, December 1946.
15. Keil, A.H. Boundary of Disturbance for Non-Linear Reflection of Underwater Shock Waves at a Free Surface. Report No. 3-48, Underwater Explosions Research Unit, Norfolk Naval Shipyard, Portsmouth, Va.

16. Coles, J. S. et. al. Underwater Shock Wave Measurements of Pressure, Momentum, Energy, and Decay Constant for Spherical Pentolite (50/50) Charges. NORC Division 2 Interim Report on Underwater Explosives and Explosions. U.E. Series Report no. 32, OSRD Report No. 4784, April, 1945.

17. Kennard, E.H. Explosive Load on Underwater Structures as Modified by Bulk Cavitation. Taylor Model Basin Report No. 511, May 1943.

18. Eldridge, J. E.; Fye, P. M.; Spitzer, R.W. Photography of Underwater Explosions I. NavOrd Report No. 9-47, March, 1947.

19. Fisher, The Fracture of Liquids. J. App. Phys. 19, 1062 (1948).

20. Swift, E. et.al. Photography of Underwater Explosions II. NavOrd Report No. 95-46. December, 1946.

21. Decius, J. C. et. al. Photography of Underwater Explosions III. NavOrd Report No. 96-46, February, 1947.

22. Arons, A.B.; Yennie, D.R. Long Range Shock Propagation in Underwater Explosion Phenomena. I. NavOrd Report No. 424. April, 1949.

23. Kennard, E.H. Cavitation in an Elastic Liquid. Phys. Rev. 63, 172 (1943).

24. Wilson, D. A. et. al. The Determination of Peak Pressure of an Underwater Explosion from a Study of the Initial Dome Velocity. NavOrd Report No. 13-47. May, 1947.

25. The Physics of Sound in the Sea. Summary Technical Report of Division 6, NDRC. Vol 8, 1946.

26. Fraenkel, G. K. Apparatus for Measurement of Air Blast Pressure by means of Piezoelectric Gauges. OSRD Report No. 6251.

27. Lyons, W. Heller, R. Electronics. Nov. 1939, p. 25.

INDEX OF AUTHORS

	Page
Arons, A. B.	373, 831, 907, 1137, 1473
Bebb, A. H.	623, 799
Booker, A. G.	1211, 1221
Brinkley, Stuart R., Jr.	383
Brown, R. M.	635
Bryant, A. R.	301
Bundy, R. V.	623
Charlesworth, G.	301, 1057
Christian, E. A.	1085, 1107
Cole, R. H.	835, 831, 1107
Coles, J. S.	703, 1085, 1107
Cotter, T. P., Jr.	1473
Craig, J.	347
Croney, D.	1069, 1073
Cross, P. C.	1107
Dasgupta, H. K.	289
Davies, R. D.	1069
Davies, R. M.	549
Eldridge, J. E.	969
Finkelstein, R.	859, 1247
Fox, E. N.	1, 1475
Fye, P. M.	969
Greenfield, M. A.	569
Halford, R. S.	209
Halverson, R. R.	373, 947
Harrington, C.	1211, 1221
Harris, A. J.	939, 947, 1053, 1065
Hilliar, H. W.	85
Jones, M.	263
Keil, Alfred H.	1423
Kennard, E. H.	159
Kirkwood, John G.	383
Kistiakowsky, G. B.	209
Meier, Otto, Jr.	839
Niffinegger, C. R.	1085, 1107
Penney, W. G.	273, 289
Polachek, H.	1289
Richardson, J. M.	373
Rogers, M. A.	1085, 1107
Seeger, R. J.	1289
Shanes, A. M.	1197
Shapiro, M. M.	569
Slifko, J. P.	1085, 1107
Sokol, G. M.	1389
Spitzer, R. W.	969
Stacey, David	635
Taylor, D. W.	799
Taylor, G. I.	263, 549, 1155
Temperley, H. N. V.	7, 1189
Von Neumann, John	311
Wallace, D. R. J.	799
Wilson, E. Bright, Jr.	209
Wood, A. B.	497
Yennie, D. R.	1137, 1473

Best Available Copy

DEPARTMENT OF THE NAVY
OFFICE OF NAVAL RESEARCH
800 NORTH QUINCY STREET
ARLINGTON, VA 22217-5660

IN REPLY REFER TO
5510/6
Ser 43/655
4 Sep 03

From: Chief of Naval Research
To: Commanding Officer, Naval Research Laboratory (NRL 5996.3)

Subj: PUBLIC RELEASE APPROVAL

Ref: (a) Your e-mail to me of 14 Jul 2003

Encl: (1) Underwater Explosion Research, Volume I - The Shock Wave, 1950 (AD 006 841)
(2) Underwater Explosion Research, Volume II - The Gas Globe, 1950 (AD 037 466)
(3) Underwater Explosion Research, Volume III - The Damage Process, 1950 (AD 037 467)

1. In response to reference (a), enclosures (1), (2) and (3) are approved for public release; distribution is unlimited. They are returned for your use.

2. Questions may be directed to the undersigned on (703) 696-4619.

PEGGY LAMBERT
By direction

Copy to:
DTIC-OCQ (Larry Downing)